Initial Reports of the Deep Sea Drilling Project

Volume LXXXVI

Honolulu, Hawaii to Yokohama, Japan
May—June 1982

NATIONAL SCIENCE FOUNDATION
National Ocean Sediment Coring Program

NSFSP—86

November 1985

86

Drilling locations

Leg	Location	Sites
Phase 1 1968–1970		
1	North Atlantic	1–7
2	North Atlantic	8–12
3	South Atlantic	13–22
4	Central Atlantic	23–31
5	North Pacific	32–43
6	North Pacific	44–60
7	Central Pacific	61–67
8	Central Pacific	68–75
9	Central Pacific	76–84
Phase 2 1970–1972		
10	Gulf of Mexico	85–97
11	North Atlantic	98–108
Re-entry trials		109–110
12	North Atlantic	111–119
13	Mediterranean	120–134
14	Central Atlantic	135–144
15	Caribbean	146–154
16	Central Pacific	155–163
17	Central Pacific	164–171
18	North Pacific	172–182
19	North Pacific	183–193
20	North Pacific	194–202
21	Coral Sea	203–210
22	Indian Ocean	211–218
23	Arabian Sea	219–230
24	Indian Ocean	231–238
25	Indian Ocean	239–249
Phase 3 1972–1975		
26	Indian Ocean	250–258
27	Indian Ocean	259–263
28	Antarctic	264–274
29	Tasman Sea	275–284
30	South Pacific	285–289
31	North Pacific	290–302
32	North Pacific	303–313
33	North Pacific	314–318
34	South Pacific	319–321
35	South Pacific	322–325
36	South Atlantic	326–331
37	North Atlantic	332–335
38	Arctic	336–352
39	Atlantic	353–359
40	South Atlantic	360–365
41	South Atlantic	366–370
42A	Mediterranean	371–378
42B	Black Sea	379–381
43	North Atlantic	382–387
44	North Atlantic	388–392
44A	North Atlantic	393–394
IPOD I 1975–present		
45	North Atlantic	395–396
46	North Atlantic	396A–396B
47	North Atlantic	397–398
48	North Atlantic	399–406
49	North Atlantic	407–414
50	North Atlantic	415–416
51A	North Atlantic	417–417A
51B	North Atlantic	417B–417D
52	North Atlantic	417D–418A
53	North Atlantic	418A–418B
54	Central Pacific	419–429
55	North Pacific	430–433
56	North Pacific	434–437
57	North Pacific	438–441
58	North Pacific	442–446
59	North Pacific	447–451
60	North Pacific	452–461
61	Central Pacific	462
62	North Pacific	463–466
63	North Pacific	467–473
64	Gulf of California	474–481
65	Gulf of California	482–485
66	Central Pacific	486–493
67	Central Pacific	494–500
68	Central Pacific	502–503
69	Central Pacific	504–505, 501
70	Central Pacific	506–510, 504B
71	South Atlantic	511–514
72	South Atlantic	515–518
73	South Atlantic	519–524
74	South Atlantic	525–529
75	South Atlantic	530–532
76	North Atlantic	533–534
77	Caribbean	535–540
78	North Atlantic	541–543, 395A, B
79	North Atlantic	544–547
80	North Atlantic	548–551
81	North Atlantic	552–555
82	North Atlantic	556–564
83	Central Pacific	504B
84	Central Pacific	565–570
85	Central Pacific	571–575
86	North Pacific	576–581

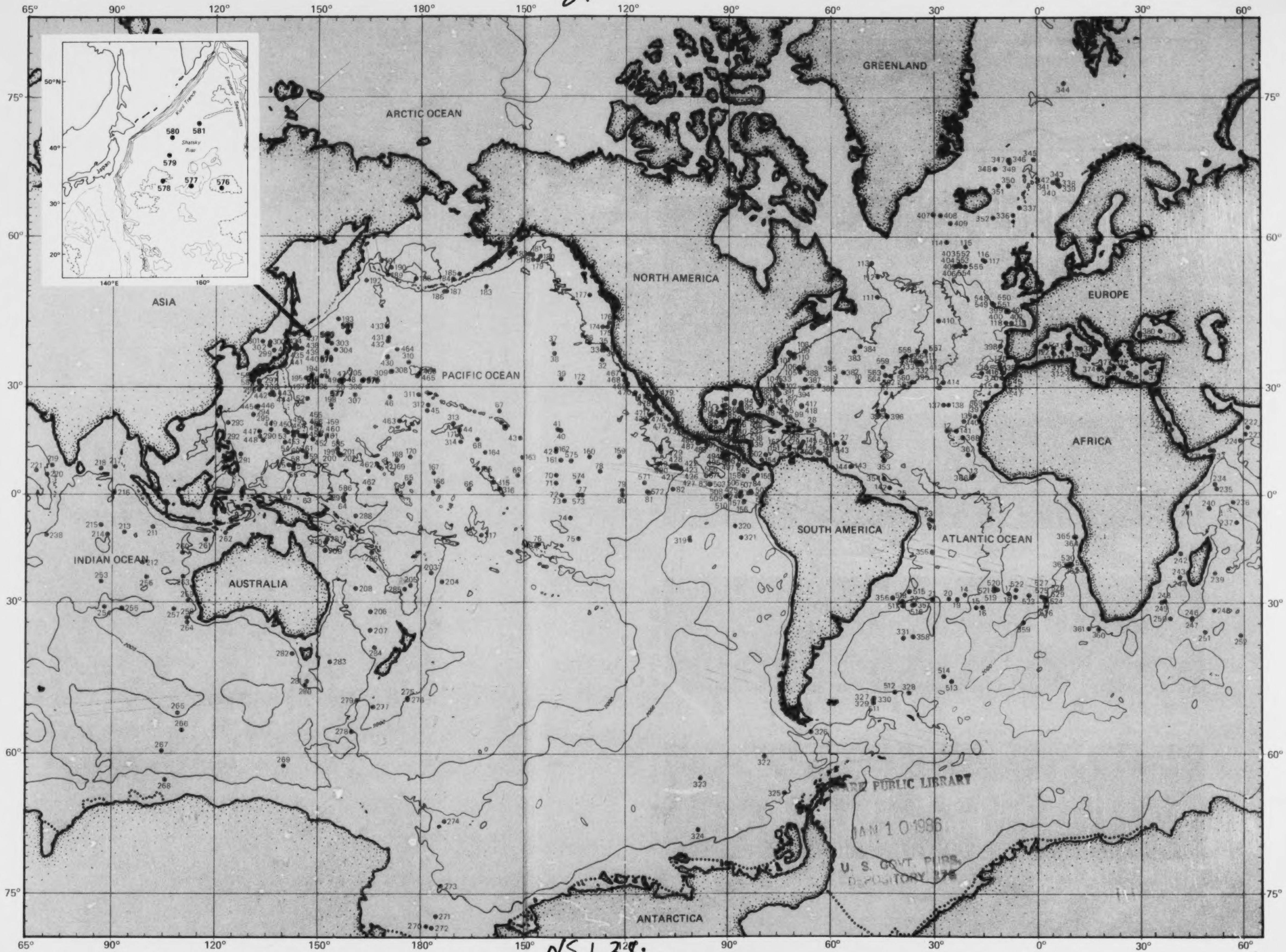

65°
90°
120°
150°
180°
150°
120°
90°
60°
30°
0°
30°
60°
75°
60°
30°
0°
30°
60°
75°
50°N
40°
30°
20°
140°E
160°
Japan
Kuril Trench
Emperor Seamounts
Shatsky Rise
580
581
579
578
577
576
ARCTIC OCEAN
GREENLAND
ASIA
NORTH AMERICA
EUROPE
PACIFIC OCEAN
AFRICA
INDIAN OCEAN
AUSTRALIA
SOUTH AMERICA
ATLANTIC OCEAN
ANTARCTICA

...ARD PUBLIC LIBRARY
JAN 1 0 1986
U. S. GOVT. PUBS.
DEPOSITORY

NS 1.38:

DEEP SEA DRILLING PROJECT

READEX
FICHE

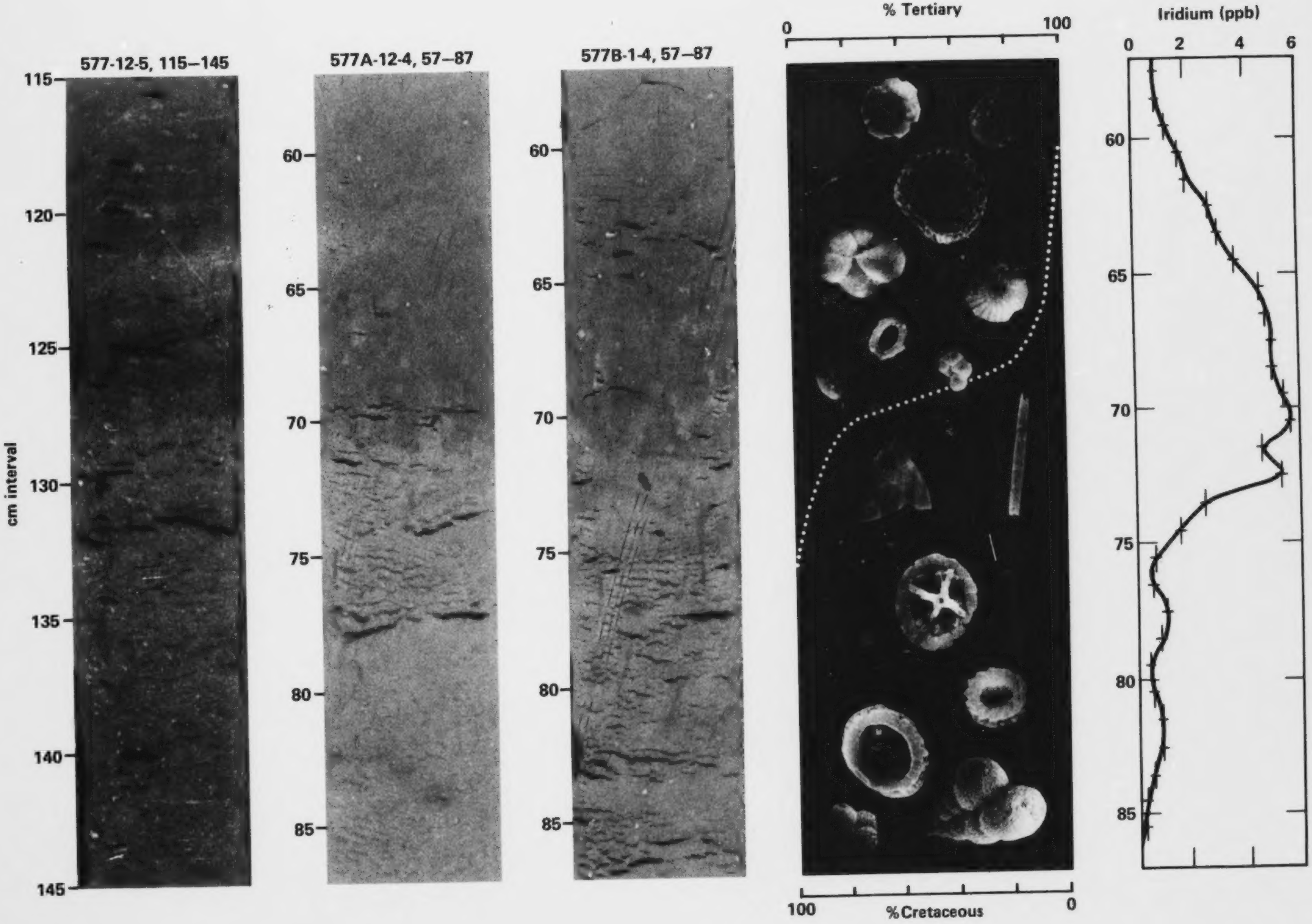
577-12-5, 115–145
577A-12-4, 57–87
577B-1-4, 57–87
% Tertiary
0
100
Iridium (ppb)
0
2
4
6
cm interval
115
120
125
130
135
140
145
60
65
70
75
80
85
100
% Cretaceous
0

Initial Reports of the Deep Sea Drilling Project

A Project Planned by and Carried Out With the Advice of the
JOINT OCEANOGRAPHIC INSTITUTIONS FOR DEEP EARTH SAMPLING (JOIDES)

VOLUME LXXXVI

covering Leg 86 of the cruises of the Drilling Vessel *Glomar Challenger*
Honolulu, Hawaii, to Yokohama, Japan
May–June 1982

PARTICIPATING SCIENTISTS

G. Ross Heath, Lloyd H. Burckle, Anthony E. D'Agostino, Ulrich Bleil,
Ki-iti Horai, Robert D. Jacobi, Thomas R. Janecek, Itaru Koizumi,
Lawrence A. Krissek, Simonetta Monechi, Nicole Lenôtre,
Joseph J. Morley, Peter Schultheiss, and Audrey A. Wright

SHIPBOARD SCIENCE REPRESENTATIVE

Audrey A. Wright

EDITOR

Katie L. Turner

Prepared for the
NATIONAL SCIENCE FOUNDATION
National Ocean Sediment Coring Program
Under Contract C-482
By the
UNIVERSITY OF CALIFORNIA
Scripps Institution of Oceanography
Prime Contractor for the Project

This material is based upon research supported by the National Science Foundation under Contract No. C-482.

Any opinions, findings, and conclusions or recommendations expressed in this publication are those of the author(s) and do not necessarily reflect the views of the National Science Foundation.

It is recommended that reference to the whole or to part of this volume be made in one of the following forms, as appropriate:

Heath, G. R., Burckle, L. H., et al., 19__. *Init. Repts. DSDP*, 86: Washington (U.S. Govt. Printing Office).

McDuff, R. E., 19__. The chemistry of interstitial waters, Deep Sea Drilling Project Leg 86. *In* Heath, G. R., Burckle, L. H., et al., *Init. Repts. DSDP*, 86: Washington (U.S. Govt. Printing Office), ___-___.

Effective Publication Dates of DSDP *Initial Reports*

According to the International Code of Zoological Nomenclature, the date of publication of a work and of a contained name or statement affecting nomenclature is the date on which the publication was mailed to subscribers, placed on sale, or when the whole edition is distributed free of charge, mailed to institutions and individuals to whom free copies are distributed. The mailing date, ***not the printed date***, is the correct one.

Mailing dates of the more recent *Initial Reports of the Deep Sea Drilling Project* are as follows:

Volume 77—September, 1984
Volume 78A,B—August, 1984
Volume 79—November, 1984
Volume 80—March, 1985
Volume 81—January, 1985
Volume 83—April, 1985

Printed November 1985

Library of Congress Catalog Card Number 74—603338

For sale by the Superintendent of Documents, U.S. Government Printing Office
Washington, D.C. 20402

Stock number 038-000-00559-6

Foreword

The world's first major oceanographic expedition took place between 1872 and 1876. This expedition, aboard the H.M.S. *Challenger* covering nearly 70,000 nautical miles and gathering oceanographic data from 362 stations, expanded our knowledge of the ocean and provided a solid foundation for future studies in marine geology. A century later, another vessel also named *Challenger* continued to expand our knowledge of the world's ocean and helped revolutionize our concepts of how the seafloor and the continents form and change. The drilling vessel *Glomar Challenger* sailed the same waters as its historic counterpart, seeking answers to new questions concerning the history of our planet and the life it supports. The continued advancement of knowledge about the fundamental processes and dynamics of the earth is leading to a greater understanding of our planet and more intelligent use of its resources.

Since 1968, the Deep Sea Drilling Project (DSDP) has been supported by the National Science Foundation, primarily through a contract with the University of California which, in turn, subcontracted to Global Marine Incorporated for the services of the D/V *Glomar Challenger*.

Through contracts with Joint Oceanographic Institutions, Inc. (JOI, Inc.), the National Science Foundation supported the scientific advisory structure for the project and funded predrilling geophysical site surveys. Scientific planning was conducted under the auspices of the Joint Oceanographic Institutions for Deep Earth Sampling (JOIDES). The JOIDES advisory group consisted of over 250 members who made up 24 committees, panels, and working groups. The members were distinguished scientists from academic institutions, government agencies, and private industry all over the world.

In 1975, the International Phase of Ocean Drilling (IPOD) began. The IPOD member nations, Federal Republic of Germany, Japan, United Kingdom, Soviet Union, and France, partially supported the project. Each member nation actively participated in the scientific planning of the project through membership in JOIDES. Scientists from these countries also took part in the field work aboard the D/V *Glomar Challenger* and postcruise scientific studies.

The first ocean coring operations for the Deep Sea Drilling Project began on August 11, 1968. During the ensuing years of drilling operations in the Atlantic, Pacific, and Indian oceans, the Gulf of Mexico, Caribbean Sea, Mediterranean Sea, and Antarctic waters, the scientific objectives that had been proposed were successfully accomplished. Primarily, the age of the ocean basins and their processes of development were determined. The validity of the hypothesis of seafloor spreading was firmly demonstrated and its dynamics studied. Emphasis was placed on broad reconnaissance and testing the involvement of mid-oceanic ridge systems in the development of the ocean basin. Later legs of the *Challenger's* voyages concentrated on the nature of the oceanic crust, the sedimentary history of the passive ocean margins, sediment dynamics along active ocean margins, and other areas of interest. The accumulated results of this project have led to major new interpretations of the pattern of sedimentation and the physical and chemical characteristics of the ancient oceans.

Technological advances have provided new tools which in turn have opened new dimensions of scientific discovery. The introduction of the Hydraulic Piston Corer in 1979 permitted virtually undisturbed cores of soft sediment layers to be obtained. This technological advance has greatly enhanced the ability of scientists to study ancient ocean environments, as recorded by sediment characteristics and flora and fauna preserved in these deposits.

A second major advance has been the use of the hole after drilling. The project routinely logged holes and performed geophysical and geochemical studies before, during, and after drilling. Long-term downhole geophysical seismic monitoring devices have been implanted successfully in DSDP holes. These new listening devices and geophysical studies have provided valuable information about the origin and nature of the dynamic processes of plate tectonics.

These reports contain the results of the initial studies of the recovered core material and the associated geophysical information. All the world's people benefit either directly or indirectly from this fundamental research. Knowledge about past and present conditions and processes are the foundations for future predictions and developments. Both short- and long-term benefits are obtained by advances in drilling technology and instrumentation. Information is being obtained about the origin and geographic distribution of natural resources. Just as the H.M.S. *Challenger* had a profound impact on scientific thought for over a century, this second *Challenger* expedition has given a greater understanding of the oceans and the processes that form and shape the earth.

Erich Bloch,
Director

Washington, D.C.

Preface

Recognizing the need in the oceanographic community for scientific planning of a program to obtain deep sedimentary cores from the ocean bottoms, four of the major oceanographic institutions that had strong interests and programs in the fields of marine geology and geophysics formed, in May 1964, the Joint Oceanographic Institutions for Deep Earth Sampling (JOIDES). This group, Lamont-Doherty Geological Observatory; Rosenstiel School of Marine and Atmospheric Science, University of Miami; the Scripps Institution of Oceanography, University of California at San Diego; and the Woods Hole Oceanographic Institution, expressed an interest in undertaking scientific planning and guidance of the sedimentary drilling program. It was the purpose of this group to foster programs to investigate the sediments and rocks beneath the deep oceans by drilling and coring. The membership of this original group was later enlarged in 1968 when the University of Washington became a member, and again in 1975 when University of Hawaii Institute of Geophysics, the Oregon State University School of Oceanography, the University of Rhode Island Graduate School of Oceanography, and Texas A&M University Department of Oceanography became members. In accordance with international agreements, institutions of participating nations became members of JOIDES. Thus, during 1974 to 1976, the Bundesanstalt für Geowissenschaften und Rohstoffe of the Federal Republic of Germany, the Centre National pour l'Exploitation des Océans of France, the Natural Environment Research Council of the United Kingdom, the University of Tokyo of Japan, and Academy of Sciences of the USSR became JOIDES members.

Through discussions sponsored by the JOIDES organization, with support from the National Science Foundation, Columbia University's Lamont-Doherty Geological Observatory operated a drilling program in the summer of 1965, on the Blake Plateau region off Jacksonville, Florida.

With this success in hand, planning began for a more extensive deep sea effort. This resulted in the award of a contract by the National Science Foundation to the Scripps Institution of Oceanography, University of California at San Diego for an eighteen-month drilling program in the Atlantic and Pacific oceans, termed the Deep Sea Drilling Project (DSDP). Operations at sea began in August 1968, using the now-famous drilling vessel, the *Glomar Challenger*.

The goal of the Deep Sea Drilling Project is to gather scientific information that will help determine the age and processes of development of the ocean basins. The primary strategy is to drill deep holes into the ocean floor, relying largely on technology developed by the petroleum industry.

Through the efforts of the principal organizations and of the panel members, who were drawn from a large cross section of leading earth scientists and associates, a scientific program was developed.

Cores recovered from deep beneath the ocean floor provide reference material for a multitude of studies in fields such as biostratigraphy, physical stratigraphy, and paleomagnetism that afford a new scope for investigating the physical and chemical aspects of sediment provenance, transportation, deposition, and diagenesis. In-hole measurements, as feasible, provide petrophysical data to permit inference of lithology of intervals from which no cores were recovered.

A report, describing the core materials and information obtained both at sea and in laboratories onshore, is published after the completion of each cruise. These reports are a cooperative effort of shipboard and shore-based scientists and are intended primarily to be a compilation of results which, it is hoped, will be the starting point for many future new and exciting research programs. Preliminary interpretations of the data and observations taken at sea are also included.

Core materials and data collected on each cruise will be made available to qualified scientists through the Curator of the Deep Sea Drilling Project, following a Sample Distribution Policy (p. xvii) approved by the National Science Foundation.

The advent of *Glomar Challenger*, with its deep-water drilling capability, is exceedingly timely. It has come when geophysical investigation of the oceans has matured through 20 to 30 years of vigorous growth to the point where we have some knowledge about much of the formerly unknown oceanic areas of our planet. About one million miles of traverses have been made which tell us much about the global pattern of gravity, magnetic and thermal anomalies, and about the composition, thickness, and stratigraphy of the sedimentary cover of the deep sea and continental margin. The coverage with such data has enabled the site selection panels to pick choice locations for drilling. The knowledge gained from each hole can be extended into the surrounding area. Detailed geophysical surveys were made for most of the selected locations prior to drilling.

The earth sciences have recently matured from an empirical status to one in which substantial theories and hypotheses about major tectonic processes are flourishing. Theories about the origin of magnetic fields and magnetic reversals, about ocean floor spreading and continental drift, and about the thermal history of our planet have led to specific predictions that could be tested best by an enlightened program of sampling of deep sea and continental margin sediments and underlying rocks.

In October 1975, the International Phase of Ocean Drilling (IPOD) began. This international interest, and the true participation of both the scientists and governments of a number of nations, are eloquent testimony to the importance of the work being done by the Deep Sea Drilling Project.

The members of JOIDES and DSDP and the scientists from all interested organizations and nations who have served on the various advisory panels are proud to have been of service and believe that the information and core materials that have been obtained will be of value to students of earth sciences and to all humanity for many years to come.

Deep Sea Drilling Project

MEMBER ORGANIZATIONS OF THE JOINT OCEANOGRAPHIC INSTITUTIONS FOR DEEP EARTH SAMPLING (JOIDES):[1]

Bundesanstalt für Geowissenschaften und Rohstoffe, Federal Republic of Germany

University of California at San Diego, Scripps Institution of Oceanography

Centre National pour l'Exploitation des Océans, Paris

Columbia University, Lamont-Doherty Geological Observatory

University of Hawaii, Hawaii Institute of Geophysics

University of Miami, Rosenstiel School of Marine and Atmospheric Science

Natural Environment Research Council, London

Oregon State University, School of Oceanography

University of Rhode Island, Graduate School of Oceanography

Texas A&M University, Department of Oceanography

University of Tokyo, Ocean Research Institute

University of Washington, Department of Oceanography

U.S.S.R. Academy of Sciences[2]

Woods Hole Oceanographic Institution

OPERATING INSTITUTION:

Scripps Institution of Oceanography
University of California at San Diego
La Jolla, California
W. A. Nierenberg, Director

DEEP SEA DRILLING PROJECT

Dr. M. N. A. Peterson
Principal Investigator
Project Manager

Mr. Robert S. Bower
Assistant Project Manager for
Administration and Contracts

Dr. Yves Lancelot
Chief Scientist

Mr. Ed Dean
Finance Administrator

Ms. Sue Strain
Personnel Officer

---

[1] Includes member organizations during time of cruise.
[2] This institution and its committees and panel members were noncontributing members of JOIDES at time of cruise.

Participants aboard
GLOMAR CHALLENGER for Leg Eighty-six

Dr. G. Ross Heath
Co-Chief Scientist
School of Oceanography
Oregon State University
Corvallis, Oregon 97331

Dr. Lloyd H. Burckle
Co-Chief Scientist
Lamont-Doherty Geological Observatory
Palisades, New York 10964

Mr. Anthony E. D'Agostino
Paleontologist (foraminifers)
ARCO Exploration Company
Houston, Texas 77056

Dr. Ulrich Bleil
Paleomagnetist
Institut für Geophysik
Ruhr-Universität Bochum
Federal Republic of Germany

Dr. Ki-iti Horai
Heat Flow Specialist
Lamont-Doherty Geological Observatory
Palisades, New York 10964

Dr. Robert D. Jacobi
Sedimentologist and Seismic Stratigrapher
Department of Geological Sciences
State University of New York at Buffalo
Amherst, New York 14226

Mr. Thomas R. Janecek
Sedimentologist
Department of Atmospheric and
Oceanic Science
University of Michigan
Ann Arbor, Michigan 48109

Dr. Itaru Koizumi
Paleontologist (diatoms)
College of General Education
Osaka University
Osaka 560, Japan

Dr. Lawrence A. Krissek
Sedimentologist
School of Oceanography
Oregon State University
Corvallis, Oregon 97331

Dr. Nicole Lenôtre
Sedimentologist
Bureau de Recherches Géologiques et Minières
Centre Océanologique de Bretagne
B. P. 6009
45060 Orléans Cedex, France

Dr. Simonetta Monechi
Paleontologist (nannofossils)
Geological Research Division
Scripps Institution of Oceanography
La Jolla, California 92093

Dr. Joseph J. Morley
Paleontologist (radiolarians)
Lamont-Doherty Geological Observatory
Palisades, New York 10964

Dr. Peter Schultheiss
Physical Properties Specialist
Institute of Oceanographic Sciences
Wormley, Godalming
United Kingdom

Dr. Audrey A. Wright
Sedimentologist/Staff Science Representative
Deep Sea Drilling Project
Scripps Institution of Oceanography
La Jolla, California 92093

Mr. Michael Storms
Cruise Operations Manager
Deep Sea Drilling Project
Scripps Institution of Oceanography
La Jolla, California 92093

Mr. Melvin Fields
Weatherman
Deep Sea Drilling Project
Scripps Institution of Oceanography
La Jolla, California 92093

Captain Joseph A. Clarke
Master of the Drilling Vessel
Global Marine, Inc.
San Diego, California 92111

Mr. James A. Ruddell
Drilling Superintendent
Global Marine, Inc.
San Diego, California 92111

Mr. Ted B. Gustafson
Laboratory Officer
Deep Sea Drilling Project
Scripps Institution of Oceanography
La Jolla, California 92093

Ms. Amy B. Altman
Curatorial Representative
Deep Sea Drilling Project
Scripps Institute of Oceanography
La Jolla, California 92093

Mr. James S. Pine
Chemist
Deep Sea Drilling Project
Scripps Institution of Oceanography
La Jolla, California 92093

Mr. Robert R. Current
Electronics Technician
Deep Sea Drilling Project
Scripps Institution of Oceanography
La Jolla, California 92093

Mr. Michael C. Reitmeyer
Electronics Technician
Deep Sea Drilling Project
Scripps Institution of Oceanography
La Jolla, California 92093

Mr. Bradley de Flon Julson
Marine Technician
Deep Sea Drilling Project
Scripps Institution of Oceanography
La Jolla, California 92093

Mr. Blair McKay
Marine Technician
Deep Sea Drilling Project
Scripps Institution of Oceanography
La Jolla, California 92093

Mr. William M. Meyer
Marine Technician
Deep Sea Drilling Project
Scripps Institution of Oceanography
La Jolla, California 92093

Mr. Thomas W. Witte
Marine Technician
Deep Sea Drilling Project
Scripps Institution of Oceanography
La Jolla, California 92093

Mr. Donald F. Marsee
Photographer
Deep Sea Drilling Project
Scripps Institution of Oceanography
La Jolla, California 92093

Ms. Louise Henry
Yeoperson
Deep Sea Drilling Project
Scripps Institution of Oceanography
La Jolla, California 92093

Deep Sea Drilling Project Publications Staff

Publications Manager
Jan H. Blakeslee

Editors
Marian G. Bailey
Susan Orlofsky
Katie L. Turner
Elizabeth Whalen

Production Manager
Raymond F. Silk

Production Assistants
Elaine Bruer
Madeleine A. Mahnken

Production Coordinators
Carolina Bertling
Mary A. Young

Art-Photo Supervisor
Virginia L. Roman (this volume)

Illustrators
Aileen Bobryk
Vicki Cypherd
Kathleen Sanderson
Alice N. Thompson (this volume)

JOIDES Advisory Groups[1]

Executive Committee

Dr. D. James Baker, Jr.
University of Washington

Prof. Dr. Friedrich Bender
Bundesanstalt für Geowissenschaften und Rohstoffe

Dr. G. Ross Heath
Oregon State University

Dr. Charles E. Helsley
Hawaii Institute of Geophysics

Sir Peter Kent, F.R.S.
Natural Environment Research Council

Dr. John A. Knauss
University of Rhode Island

Dr. Noriyuki Nasu
University of Tokyo

Dr. William A. Nierenberg, Chairman
Scripps Institution of Oceanography

Dr. M. N. A. Peterson (ex-officio)
Scripps Institution of Oceanography

M. Gerard Piketty
Centre National pour l'Exploitation des Océans

Dr. Barry Raleigh
Lamont-Doherty Geological Observatory

Prof. Robert D. Reid
Texas A&M University

Dr. Alexander V. Sidorenko
U.S.S.R. Academy of Sciences

Dr. John Steele
Woods Hole Oceanographic Institution

Dr. Edward L. Winterer (ex-officio Planning Committee Representative)
Scripps Institution of Oceanography

Dr. Warren Wisby
Rosenstiel School of Marine and Atmospheric Science

Planning Committee

Dr. Jean Aubouin
Université Pierre et Marie Curie

Dr. Helmut Beiersdorf
Bundesanstalt für Geowissenschaften und Rohstoffe

Dr. William R. Bryant
Texas A&M University

Dr. Joe R. Cann
University of Newcastle-upon-Tyne

Dr. John B. Corliss
Oregon State University

Dr. Joe S. Creager
University of Washington

Mr. John I. Ewing
Woods Hole Oceanographic Institution

Dr. Dennis E. Hayes
Lamont-Doherty Geological Observatory

Dr. Jose Honnorez
Rosenstiel School of Marine and Atmospheric Science

Dr. James P. Kennett
University of Rhode Island

Dr. Kazuo Kobayashi
University of Tokyo

Dr. Yves Lancelot (ex-officio)
Scripps Institution of Oceanography

Dr. Ralph Moberly
Hawaii Institute of Geophysics

Dr. Lev Nikitin
U.S.S.R. Academy of Sciences

Dr. Edward L. Winterer, Chairman
Scripps Institution of Oceanography

Advisory Panel on Sedimentary Petrology and Physical Properties

Dr. Richard Bennett
National Oceanic and Atmospheric Administration

Dr. John W. Handin
Texas A&M University

Dr. George deVries Klein, Chairman
University of Illinois, Urbana

Dr. Leland Kraft
McClelland Engineers, Inc.

Dr. I. Nick McCave
University of East Anglia

Dr. Frédéric Mélières
Université Pierre et Marie Curie

Dr. Ralph Moberly (ex-officio)
Hawaii Institute of Geophysics

Dr. Orrin H. Pilkey
Duke University

Dr. Peter Rothe
Universität Mannheim

Dr. Matthew Salisbury (ex-officio)
Scripps Institution of Oceanography

Dr. Peter Timofeev
U.S.S.R. Academy of Sciences

Advisory Panel on Organic Geochemistry

Dr. Earl W. Baker
Florida Atlantic University

Dr. Simon C. Brassell
University of Bristol

Dr. John B. Corliss (ex-officio)
Oregon State University

---

[1] Membership at time of cruise.

Dr. William T. Coulbourn (ex-officio)
Scripps Institution of Oceanography

Dr. Gordon Erdman
Phillips Petroleum Company

Dr. Eric Galimov
U.S.S.R. Academy of Sciences

Dr. John M. Hunt
Woods Hole Oceanographic Institution

Dr. Keith Kvenvolden
U.S. Geological Survey

Dr. Philip A. Meyers
University of Michigan

Dr. Bernd R. Simoneit, Chairman
Oregon State University

Dr. Colin P. Summerhayes
Exxon Production Research Company

Dr. Bernard Tissot
Institut Français du Pétrole

Dr. Dietrich Welte
Lehrstuhl für Geologie, Geochemie und Lagerstätten des Erdöls und der Kohle

Advisory Panel on Information Handling

Dr. Daniel E. Appleman, Chairman
Smithsonian Institution

Dr. Joe S. Creager (ex-officio)
University of Washington

Dr. John C. Hathaway
U.S. Geological Survey

Dr. Alfred Loeblich, Jr.
University of California, Los Angeles

Dr. Michael S. Loughridge
National Oceanic and Atmospheric Administration

Dr. Marthe Melguen
Centre Océanologique de Bretagne

Mrs. Judit Nowak
Bundesanstalt für Geowissenschaften und Rohstoffe

Mr. Peter Woodbury (ex-officio)
Scripps Institution of Oceanography

Industrial Liaison Panel

Mr. R. L. Adams
Conoco Inc.

Prof. Nikolai P. Budnikov
Ministry of Geology of the U.S.S.R.

Mr. Melvin J. Hill
Gulf Oil Exploration and Production Company

Dr. Ing. Guenter Peterson
Gewerkschaft Walter

Mr. W. A. Roberts, Chairman
Energy Concepts, Inc.

Dr. Gilbert Rutman
Société Nationale des Pétroles d'Aquitaine

Mr. G. Williams
United Kingdom Offshore Operators Association, Ltd.

Advisory Panel on Ocean Crust

Dr. Roger N. Anderson
Lamont-Doherty Geological Observatory

Dr. Henri Bougault
Centre Océanologique de Bretagne (CNEXO)

Dr. John B. Corliss (ex-officio)
Oregon State University

Prof. Dr. Rolf Emmermann
Universität Karlsruhe

Dr. Paul J. Fox, Chairman
University of Rhode Island

Dr. Paul Johnson
University of Washington

Dr. Ralph Moberly (ex-officio)
Hawaii Institute of Geophysics

Dr. James Natland (ex-officio)
Scripps Institution of Oceanography

Dr. Minoru Ozima
University of Tokyo

Dr. Paul Robinson
Dalhousie University

Dr. Hans Schouten
Woods Hole Oceanographic Institution

Dr. Ralph Stephen
Woods Hole Oceanographic Institution

Dr. John Tarney
The University of Leicester

Dr. Andrei A. Tsvetkov
U.S.S.R. Academy of Sciences

Advisory Panel on Ocean Margin (Active)

Dr. Peter F. Barker
The University of Birmingham

Dr. Jean-Paul Cadet
Université d'Orléans

Dr. Darrel Cowan
University of Washington

Dr. Joe S. Creager (ex-officio)
University of Washington

Dr. Yury I. Dmitriev
U.S.S.R. Academy of Sciences

Dr. Dennis E. Hayes (ex-officio)
Lamont-Doherty Geological Observatory

Dr. Donald M. Hussong, Chairman
Hawaii Institute of Geophysics

Dr. Daniel Karig
Cornell University

Dr. John W. Ladd
Lamont-Doherty Geological Observatory

Dr. Kazuaki Nakamura
University of Tokyo

Dr. James Natland (ex-officio)
Scripps Institution of Oceanography

Dr. Roland von Huene
U.S. Geological Survey

Dr. Hansjust Walther
Bundesanstalt für Geowissenschaften und Rohstoffe

Advisory Panel on Ocean Margin (Passive)

Dr. Mikhail E. Artemiev
U.S.S.R. Academy of Sciences

Dr. Arnold H. Bouma
Gulf Science and Technology Company

Dr. William R. Bryant (ex-officio)
Texas A&M University

Dr. Karl Hinz
Bundesanstalt für Geowissenschaften und Rohstoffe

Dr. Hideo Kagami
University of Tokyo

Dr. Charlotte Keene
Geological Survey of Canada

Dr. Yves Lancelot (ex-officio)
Scripps Institution of Oceanography

Dr. Lucien Montadert
Institut Français du Pétrole

Dr. David G. Roberts, Chairman
British Petroleum Co., Ltd.

Dr. William B. F. Ryan
Lamont-Doherty Geological Observatory

Dr. Sigmund Snelson
Shell Oil Company

Dr. Jørn Thiede
Universitetet i Oslo

Dr. Brian E. Tucholke
Woods Hole Oceanographic Institution

Dr. Peter R. Vail
Exxon Production Research Company

Dr. Jan E. van Hinte
Vrije Universiteit

Dr. Edward L. Winterer (ex-officio)
Scripps Institution of Oceanography

Advisory Panel on Pollution Prevention and Safety

Dr. Nikolai I. Beliy
Ministry of Gas Industry, U.S.S.R.

Dr. Rustum Jean Byramjee
Compagnie Français des Pétroles

Dr. George Claypool
U.S. Geological Survey

Mr. Brian E. Davies
Sohio Petroleum Company

Dr. Louis E. Garrison, Chairman
U.S. Geological Survey

Dr. Arthur E. Green
Exxon Production Research Company

Prof. A. J. Horn
Atherton, California

Dr. Ernst Hotz
Deminex, Essen, Federal Republic of Germany

Dr. Yves Lancelot (ex-officio)
Scripps Institution of Oceanography

Dr. David B. MacKenzie
Marathon Oil Company

Dr. Geoffrey D. Taylor
British Petroleum Company, Ltd.

Dr. Edward L. Winterer (ex-officio)
Scripps Institution of Oceanography

Advisory Panel on Inorganic Geochemistry

Dr. Joe R. Cann (ex-officio)
University of Newcastle-upon-Tyne

Dr. Henry Elderfield
University of Leeds

Dr. Michel Hoffert
Université Louis Pasteur

Dr. Miriam Kastner, Acting Chairman
Scripps Institution of Oceanography

Dr. Margaret Leinen
University of Rhode Island

Dr. Igor D. Ryabchikov
U.S.S.R. Academy of Sciences

Dr. Sam Savin
Case Western Reserve University

Dr. Fred L. Sayles
Woods Hole Oceanographic Institution

Dr. Karl-Heinz Wedepohl
Universität Göttingen

Stratigraphic Correlations Panel

Dr. Ivan Basov
U.S.S.R. Academy of Sciences

Dr. Lloyd H. Burckle
Lamont-Doherty Geological Observatory

Dr. William Coulbourn (ex-officio)
Scripps Institution of Oceanography

Dr. Joe S. Creager (ex-officio)
University of Washington

Dr. D. Graham Jenkins
The Open University, Buckinghamshire

Prof. Dr. Erlend Martini
Universität Frankfurt

Dr. Catherine Nigrini
La Habra Heights, California

Dr. Richard Poore, Chairman
U.S. Geological Survey

Dr. John B. Saunders
Naturhistorisches Museum Basel

Downhole Measurements Panel

Dr. Heinz Beckmann
Technische Universität Claustahl

Mr. Robert E. Boyce (ex-officio)
Scripps Institution of Oceanography

Dr. William Bryant (ex-officio)
Texas A&M University

Dr. Nikolas I. Christensen
University of Washington

Dr. Timothy J. G. Francis
Natural Environment Research Council

Dr. Roy Hyndman
Department of Energy, Mines and Resources, British Columbia

Mr. Alfred H. Jageler
Amoco Production Research Company

Dr. Hajimu Kinoshita
Chiba University

Dr. Mark Mathews
Los Alamos National Laboratory

Dr. Yury Neprochnov
U.S.S.R. Academy of Sciences

Dr. Lev Nikitin (ex-officio)
U.S.S.R. Academy of Sciences

Dr. Vincent Renard
Centre National pour l'Exploitation des Océans

Dr. Richard P. Von Herzen, Chairman
Woods Hole Oceanographic Institution

Advisory Panel on Ocean Paleoenvironment

Dr. Helmut Beiersdorf (ex-officio)
Bundesanstalt für Geowissenschaften und Rohstoffe

Dr. Hervé Chamley
Université des Sciences et Techniques de Lille

Dr. Robert G. Douglas, Chairman
University of Southern California

Dr. Dieter Fütterer
Universität Kiel

Dr. Robert E. Garrison
University of California, Santa Cruz

Dr. James D. Hays
Lamont-Doherty Geological Observatory

Dr. James P. Kennett (ex-officio)
University of Rhode Island

Dr. Robert B. Kidd
Natural Environment Research Council

Dr. Yves Lancelot (ex-officio)
Scripps Institution of Oceanography

Dr. Seymour O. Schlanger
Northwestern University

Dr. Yokichi Takayanagi
Tohoku University

Dr. Fritz Theyer
Hawaii Institute of Geophysics

Dr. Peter P. Timofeev
U.S.S.R. Academy of Sciences

Advisory Panel on Site Surveying

Dr. Helmut Beiersdorf (ex-officio)
Bundesanstalt für Geowissenschaften und Rohstoffe

Dr. LeRoy M. Dorman
Scripps Institution of Oceanography

Dr. Dennis Hayes (ex-officio)
Lamont-Doherty Geological Observatory

Dr. E. John W. Jones, Chairman
University College, London

Dr. Shozaburo Nagumo
University of Tokyo

Dr. Philip Rabinowitz (ex-officio)
Lamont-Doherty Geological Observatory

Dr. Vincent Renard
Centre National pour l'Exploitation des Océans

Dr. Matthew Salisbury (ex-officio)
Scripps Institution of Oceanography

Dr. Alexander A. Schreider
U.S.S.R. Academy of Sciences

Dr. Wilfried Weigel
Universität Hamburg

SAMPLE DISTRIBUTION POLICY *

Distribution of Ocean Drilling Program and of Deep Sea Drilling Project samples is undertaken in order to (1) provide support to shipboard scientists in achieving the scientific objectives of their cruise, and support shorebased investigators who are preparing contributions to DSDP and ODP reports; (2) provide individual investigators with materials to conduct detailed studies beyond the scope of ODP reports; (3) provide paleontological reference centers with samples for reference and comparison purposes; and (4) provide educators with samples for teaching purposes.

Funding for sample-related activities must be secured by the investigator independently of requesting the samples.

The Ocean Drilling Program Curator is responsible for distributing samples and for preserving and conserving core material. The Curator, who may accept advice from chairmen of the appropriate JOIDES advisory panels, is responsible for enforcing the provisions of this sample distribution policy. He is responsible for maintaining a record of all samples that have been distributed, both onboard ship and subsequently from the repositories, indicating the recipients and the nature of investigations proposed. This information is available to interested investigators on request.

Every sample distributed from the ship or from a repository is labeled with a standard identifier, which includes leg number, hole number, core and section numbers, and interval within the section from which the sample was removed. It is imperative that this standard identifier be associated with all data reported in the literature, and that residues of the sample remain labeled throughout their lives, so that later workers can relate the data to the cores.

Distribution of sample materials is made directly from the repositories (Lamont-Doherty Geological Observatory, Scripps Institution of Oceanography, or Texas A&M University) by the Curator or his designated representative.

1. *Distribution of Samples for Research Leading to Contributions to ODP Reports*

Any investigator who wishes to contribute to the reports of a scheduled cruise may write to the Curator, Ocean Drilling Program, Texas A&M University, College Station, Texas 77843-3469, U.S.A., in order to request samples from that cruise. Requests for a specific cruise must be received by the Curator at least TWO MONTHS in advance of the departure of that cruise, in order to allow time for the review of the request in conjunction with other requests, so that a suitable shipboard sampling program can be assembled. The request should include a statement of the nature of the proposed research, size and approximate number of samples required to complete the study, and any particular sampling technique or equipment which may be required. Requests will be reviewed by the staff representative and co-chief scientists of the cruise and by the Curator. Approval/disapproval will be based upon the scientific requirements of the cruise as determined by the appropriate JOIDES advisory panel(s). The scope of a request must be such that samples can be processed, that proposed research can be completed, and that the paper can be written in time for submission to the relevant ODP cruise report.

Except for rare, specific instances involving ephemeral properties, the total volume of samples removed during a cruise-related sampling program will not exceed one-quarter of the volume of core recovered, and no interval will be depleted. One-half of all recovered materials will be retained in the archives in as pristine a condition as is practicable. Investigators requesting shipboard samples of igneous materials may receive a maximum of 100 igneous samples per cruise.

Because many sample requests are received for shipboard work and because the time of the shipboard party is at a premium, co-chief scientists are strongly urged to limit shipboard sampling to the minimum necessary to accomplish the cruise objectives. Shore-based investigators whose requests for cruise-related samples are approved should expect that they will receive the samples after the cores are returned to the repository, and should schedule research activities accordingly.

Co-chief scientists may invite investigators who are not cruise participants to perform special studies of selected core samples in direct support of shipboard activities. If this occurs, the names and addresses of these investigators and details of all samples loaned or distributed to them must be forwarded to the Curator, via the ODP Staff Representative to that cruise, immediately after the cruise. These investigators are expected to contribute to the cruise reports as though they had been cruise participants. All requirements of the Sample Distribution Policy apply.

Any publication of results other than in ODP reports within twelve (12) months of completion of the cruise must be approved and authored by the whole shipboard party and, where appropriate, shorebased investigators. After twelve months, individual investigators may submit related papers for open publication provided they have already submitted their contributions to ODP reports. Investigations which are not completed in time for inclusion in ODP reports for a specific cruise may be published in a later edition of ODP reports; however, they may not appear in another journal until the ODP report for which they were intended has been published.

---

*Revised October 1984

2. *Distribution of Samples for Research Leading to Publication Outside of the DSDP and ODP Reports*

   A. Researchers who wish to use samples for studies beyond the scope of the DSDP or ODP reports should obtain sample request forms from the Curator, Ocean Drilling Program, Texas A&M University, College Station, Texas 77843-3469, U.S.A. Requestors are required to specify the quantities and intervals of core required, to make a clear statement of the nature of the proposed research, to state the time which will be required to complete the work and to submit results for publication, and to specify funding status and the availability of equipment and space for the research.

      Additionally, if the requestor has received samples from ODP or from DSDP previously, he/she will be required to account for the disposition of those samples by citing published works, six (6) copies of which must be sent to the Curator. If no report has been published, this requirement can be fulfilled by sending a brief (two or three page) report of the status of the research. Unused and residual samples should be returned and data should be sent to the Curator if the project has terminated. Paleontological materials may be returned either to the Curator at ODP or to one of the designated paleontological reference centers. If material is returned to a reference center, notify the Curator when it is sent.

      Requests for samples from researchers in industrial laboratories will be honored in the same manner as those from academic organizations. Industrial investigators have the same obligations as other investigators to publish all results promptly in the open literature and to provide the Curator with copies of all reports published and of all data acquired in their research.

      In order to ensure that all requests for highly desirable but limited samples can be considered together, approval of requests and distribution of samples will be delayed until twelve (12) months after completion of the cruise or two (2) months after official publication of the core descriptions, whichever occurs earlier. The only exceptions to this policy will be made for specific requests involving ephemeral properties. Requests for samples may be based on core descriptions published in ODP reports produced by the shipboard party, copies of which are on file at various institutions throughout the world. Copies of original core logs and data are kept on open file at ODP, and at the repositories at Lamont-Doherty Geological Observatory and at Scripps Institution of Oceanography.

   B. Most investigations can be accomplished handily with sample volumes of 10 ml or less. Investigators must provide explicit justification of requests for larger sample sizes or for frequent intervals within a core. Requests which exceed reasonable size or frequency limits will require explicit justifications and more time to process, and are unlikely to be granted in their entirety.

      Requests for samples from thin layers, from stratigraphically important boundaries, from sections which are badly depleted or in unusually high demand may be delayed in order to coordinate requests from several investigators or while the Curator seeks advice from the community. Investigators who submit such requests may expect to receive suggestions for alternative sampling programs or that they join a research consortium which will share the samples. In any event, such exceptional requests will require more time for processing than will more routine requests.

      Investigators who wish to study ephemeral properties may request a waiver of the waiting period; however, such requests will be referred automatically to the relevant co-chiefs. If approved, the investigator will join the shore-based contributors to the shipboard science effort, and will incur the obligations thereof (see section 1).

   C. Samples will not be provided until the requestor assures the Curator that funding for the proposed research is available or unnecessary. If a sample request is dependent in any way upon proposed funding, the Curator is prepared to provide the proposed funding organization with information on the availability (or potential availability) of suitable samples.

D. Investigators who receive samples incur the following obligations:

(1) To publish significant results promptly; however, no contribution may be submitted for publication prior to twelve (12) months following the termination of the relevant leg unless it is approved and authored by the entire shipboard party.

(2) To acknowledge in all publications that the samples were supplied through the assistance of the international Ocean Drilling Program and others as appropriate.

(3) To submit six (6) copies of reprints of all published works to the Curator, Ocean Drilling Program, Texas A&M University, College Station, Texas 77843-3469, U.S.A. These reprints will be distributed to the repositories, to the ship, to the National Science Foundation, and to the Curator's reprint file.

(4) To submit all final analytical data obtained from the samples to Data Base Manager, Ocean Drilling Program, Texas A&M University, College Station, Texas 77843-3469, U.S.A. Please consult recent issues of the JOIDES Journal or call (409-845-2673) for information on acceptable data formats. Investigators should be aware that they may have other data obligations under NSF's Ocean Science Data Policy or under relevant policies of other funding agencies which require submission of data to national data centers.

(5) To return all unused or residual samples, in good condition and with a detailed explanation of any processing they may have experienced, upon termination of the proposed research. In particular, all thin sections and smear slides manufactured onboard the vessel or in the repositories are to be returned to the Curator. Paleontological materials may be returned either to the Curator at ODP or to one of the designated paleontological reference centers.

Failure to honor these obligations will prejudice future applications for samples.

E. Cores are available for examination by interested parties at the repositories. Investigators are welcome to visit the repositories in order to inspect cores and to specify sample locations when that is required for their research; however, time and space in the workrooms are limited, so advance appointments are required. Occasionally, the space may be fully booked several weeks in advance, so investigators are urged to call for appointments well ahead in order to avoid disappointment. Only the Curator or his delegate may actually remove samples from the cores.

F. A reference library of thin sections, smear slides, and archive photographs is maintained in the repositories for the use of visting investigators. All thin sections and smear slides produced onboard the ship or in the repositories belong to this library.

3. *Distribution of Samples to Paleontological Reference Centers*

As a separate and special category of repository activity, selected samples are being distributed to paleontological reference centers, where the prepared material may be studied by visitors. As of this writing (mid-1984), Foraminifera and Calcareous Nannofossils can be viewed; Radiolaria and Diatoms will be prepared in the future. The present centers are Scripps Institution of Oceanography, California (W. R. Riedel, tel. 619-452-4386); Basel Natural History Museum, Switzerland (J. B. Saunders, tel. 061-25.82.82); and New Zealand Geological Survey, Lower Hutt, New Zealand (A. R. Edwards, tel. 699.059). Future centers are likely to include Texas A&M University, College Station, Texas (S. Gartner, tel. 409-845-8479); Smithsonian Institution, Washington, D.C.; Lamont-Doherty Geological Observatory, Palisades, New York; and an as yet undesignated center in Japan.

Further details concerning the paleontological reference centers are reported periodically in the JOIDES Journal.

4. *Distribution of Samples for Educational Purposes*

Samples may be available in limited quantities to college-level educators for teaching purposes. Interested educators should request application forms from the Curator, Ocean Drilling Program, Texas A&M University, College Station, Texas 77843-3469, U.S.A. Requestors are required to specify preferred sample size and location, to make a very clear statement of the nature of the coursework in which the samples will be used, to explain how the core samples will be prepared and how they will be used in the classroom, to explain in detail why they cannot use similar materials derived from outcrops or dredge hauls (it is NOT acceptable to argue that it requires less effort for the requestor to obtain samples from ODP than to assemble them from other sources), and to certify that funds are available to prepare the materials for classroom use. In general, only samples of materials which are abundant in the collection and which are in little demand for research purposes should be requested for educational purposes. The Curator will not ap-prove requests for materials which are limited in supply or for which demand (real or potential) is great, including most paleontological materials.

5. *Distribution of Data*

The Deep Sea Drilling Project and the Ocean Drilling Program routinely capture much of the data generated onboard ship and published in Program reports. Additionally, data supplied by investigators who have received samples are incorporated into the data bases, so data sets which are larger than can be published are available to investigators. Magnetics, downhole logging, seismic reflection, bathymetric data, and other data collected by the drilling vessel become available for distribution to investigators at the same time as core samples.

At least through mid-1986, DSDP data will continue to be distributed by the Data Base Manager, Deep Sea Drilling Project, A-031, University of California, San Diego, California 92093, U.S.A. A charge will be made to recover expenses in excess of $50.00 incurred in filling individual requests. If required, estimates of charges can be furnished before the work is performed. As DSDP phases down, DSDP data will be available primarily from the National Geophysical Data Center, Boulder, Colorado.

Requests for ODP data should be addressed to the Data Base Manager, Ocean Drilling Program, Texas A&M University, College Station, Texas 77843-3469, U.S.A. Many varieties of DSDP data will be included in ODP data bases. Information on sources of DSDP data will be available from the ODP Data Base Manager.

CONTENTS

Chapter Page

ACKNOWLEDGMENTS 1

PART I: INTRODUCTION, SEISMIC STUDIES, AND SITE REPORTS

1. INTRODUCTION, CRUISE SUMMARY, AND EXPLANATORY NOTES: DEEP SEA DRILLING PROJECT LEG 86, WESTERN NORTH PACIFIC 5
A. A. Wright

2. HIGH-RESOLUTION SEISMIC STUDIES AND SITE SURVEY RESULTS NEAR DEEP SEA DRILLING PROJECT SITES 576 AND 578, NORTHWEST PACIFIC 23
R. D. Jacobi, D. E. Hayes, and J. E. Damuth

3. SITE 576 51
Shipboard Scientific Party, with a contribution by P. S. Doyle

4. SITE 577 91
Shipboard Scientific Party

5. SITE 578 139
Shipboard Scientific Party, with a contribution by P. S. Doyle

6. SITE 579 175
Shipboard Scientific Party

7. SITE 580 209
Shipboard Scientific Party

8. SITE 581 241
Shipboard Scientific Party

PART II: BIOSTRATIGRAPHIC AND PALEOCEANOGRAPHIC STUDIES

9. NEOGENE DIATOM BIOSTRATIGRAPHY OF THE MIDDLE LATITUDE WESTERN NORTH PACIFIC, DEEP SEA DRILLING PROJECT LEG 86 269
I. Koizumi and Y. Tanimura

10. CAMPANIAN TO PLEISTOCENE CALCAREOUS NANNOFOSSIL STRATIGRAPHY FROM THE NORTHWEST PACIFIC OCEAN, DEEP SEA DRILLING PROJECT LEG 86 301
S. Monechi

Chapter Page

11. FORAMINIFERS AND COARSE DETRITUS FROM FIVE DEEP-WATER SITES, DEEP SEA DRILLING PROJECT LEG 86, NORTHWEST PACIFIC 337
A. D'Agostino

12. ICHTHYOLITH BIOSTRATIGRAPHY OF WESTERN NORTH PACIFIC PELAGIC CLAYS, DEEP SEA DRILLING PROJECT LEG 86 349
P. S. Doyle and W. R. Riedel

13. LATE CENOZOIC SILICOFLAGELLATES FROM THE NORTHWEST PACIFIC, DEEP SEA DRILLING PROJECT LEG 86: PALEOTEMPERATURE TRENDS AND TEXTURE CLASSIFICATION 367
D. Bukry and S. Monechi

14. RADIOLARIANS FROM THE NORTHWEST PACIFIC, DEEP SEA DRILLING PROJECT LEG 86 399
J. J. Morley

15. LATE PLEISTOCENE (BRUNHES) DIATOM RECORD AT SITE 580 423
C. Sancetta

16. LATE NEOGENE PALEOCEANOGRAPHY IN THE WESTERN NORTH PACIFIC 429
I. Koizumi

PART III: PALEOMAGNETIC AND GEOCHEMICAL STRATIGRAPHIC STUDIES

17. THE MAGNETOSTRATIGRAPHY OF NORTHWEST PACIFIC SEDIMENTS, DEEP SEA DRILLING PROJECT LEG 86 441
U. Bleil

18. PALEOMAGNETISM AND ACCUMULATION RATES OF SEDIMENTS AT SITES 576 AND 578, DEEP SEA DRILLING PROJECT LEG 86, WESTERN NORTH PACIFIC 459
G. R. Heath, D. H. Rea, and S. Levi

19. CARBON-ISOTOPE STRATIGRAPHY, SITE 577 503
N. J. Shackleton, M. A. Hall, and U. Bleil

Chapter Page

20. STABLE ISOTOPE AND TRACE ELEMENT GEOCHEMISTRY OF CARBONATE SEDIMENTS ACROSS THE CRETACEOUS/TERTIARY BOUNDARY AT DEEP SEA DRILLING PROJECT HOLE 577, LEG 86 513
J. C. Zachos, M. A. Arthur, R. C. Thunell, D. F. Williams, and E. J. Tappa

21. ELEMENTAL PROFILE OF IRIDIUM AND OTHER ELEMENTS NEAR THE CRETACEOUS/TERTIARY BOUNDARY IN HOLE 577B 533
H. V. Michel, F. Asaro, W. Alvarez, and L. W. Alvarez

22. ^{10}Be DISTRIBUTIONS IN DEEP SEA DRILLING PROJECT SITE 576 AND SITE 578 SEDIMENTS STUDIED BY ACCELERATOR MASS SPECTROMETRY 539
T. L. Ku, J. R. Southon, J. S. Vogel, Z. C. Liang, M. Kusakabe, and D. E. Nelson

PART IV: SEDIMENTOLOGIC AND GEOCHEMICAL STUDIES

23. MINERALOGY AND DIAGENESIS: THEIR EFFECT ON ACOUSTIC AND ELECTRICAL PROPERTIES OF PELAGIC CLAYS, DEEP SEA DRILLING PROJECT LEG 86 549
J. Schoonmaker, F. T. Mackenzie, M. Manghnani, R. C. Schneider, D. Kim, A. Weiner, and J. To

24. CLAY STRATIGRAPHY AT DEEP SEA DRILLING PROJECT SITES 576 AND 578, LEG 86 (WESTERN NORTH PACIFIC) 571
N. Lenôtre, H. Chamley, and M. Hoffert

25. QUARTZ CONTENT OF NORTHWEST PACIFIC HOLE 576A AND IMPLICATIONS FOR CENOZOIC EOLIAN TRANSPORT 581
M. Leinen

26. EOLIAN SEDIMENTATION IN THE NORTHWEST PACIFIC OCEAN: A PRELIMINARY EXAMINATION OF THE DATA FROM DEEP SEA DRILLING PROJECT SITES 576 AND 578 589
T. R. Janecek

Chapter Page

27. ELEMENTAL COMPOSITION OF CENOZOIC PELAGIC CLAYS FROM DEEP SEA DRILLING PROJECT SITES 576 AND 578, WESTERN NORTH PACIFIC 605
G. R. Heath, R. B. Kovar, C. Lopez, and G. L. Campi

28. THE OCCURRENCE, ABUNDANCE, AND COMPOSITION OF ICE-RAFTED DEBRIS IN SEDIMENTS FROM DEEP SEA DRILLING PROJECT SITES 579 AND 580, NORTHWEST PACIFIC 647
L. A. Krissek, J. J. Morley, and D. K. Lofland

29. GEOCHEMISTRY OF SEDIMENTS AT SITES 579, 580, AND 581, DEEP SEA DRILLING PROJECT LEG 86, WESTERN NORTH PACIFIC 657
G. R. Heath, R. B. Kovar, and C. Lopez

30. LIPID GEOCHEMISTRY OF THE CRETACEOUS/TERTIARY BOUNDARY SEDIMENTS, HOLE 577, DEEP SEA DRILLING PROJECT LEG 86 671
B. R. T. Simoneit and H. R. Beller

31. THE CHEMISTRY OF INTERSTITIAL WATERS, DEEP SEA DRILLING PROJECT LEG 86 675
R. E. McDuff

PART V: IGNEOUS PETROLOGY

32. PETROLOGY AND GEOCHEMISTRY OF BASALTS FROM DEEP SEA DRILLING PROJECT LEG 86, SITE 581 691
J. C. Fountain, R. D. Jacobi, and T. J. Fahey

PART VI: PHYSICAL PROPERTIES AND GEOTHERMAL STUDIES

33. PHYSICAL AND GEOTECHNICAL PROPERTIES OF SEDIMENTS FROM THE NORTHWEST PACIFIC: DEEP SEA DRILLING PROJECT LEG 86 701
P. J. Schultheiss

34. GEOTECHNICAL PROPERTIES OF NORTHWEST PACIFIC PELAGIC CLAYS: DEEP SEA DRILLING PROJECT LEG 86, HOLE 576A 723
The Marine Geotechnical Consortium

Chapter Page

35. MEASUREMENT OF HEAT FLOW ON LEG 86 OF THE DEEP SEA DRILLING PROJECT 759
K. Horai and R. P. Von Herzen

PART VII: SYNTHESES AND SUMMARIES

36. ASSESSMENT OF DIATOM AND RADIOLARIAN HIGH- AND LOW-LATITUDE ZONATIONS IN NORTHWEST PACIFIC SEDIMENTS: COMPARISON BASED UPON MAGNETOSTRATIGRAPHY 781
L. H. Burckle, J. J. Morley, I. Koizumi, and U. Bleil

37. MAGNETOBIOCHRONOLOGY OF LATE CRETACEOUS-PALEOGENE AND LATE CENOZOIC PELAGIC SEDIMENTARY SEQUENCES FROM THE NORTHWEST PACIFIC (DEEP SEA DRILLING PROJECT, LEG 86, SITE 577) 787
S. Monechi, U. Bleil, and J. Backman

Chapter Page

38. SUMMARY OF CRETACEOUS/TERTIARY BOUNDARY STUDIES, DEEP SEA DRILLING PROJECT SITE 577, SHATSKY RISE 799
A. A. Wright, U. Bleil, S. Monechi, H. V. Michel, N. J. Shackleton, B. R. T. Simoneit, and J. C. Zachos

BACK POCKET FOLDOUTS

CHAPTER 9: TABLE 2. STRATIGRAPHIC OCCURRENCES OF NEOGENE DIATOMS IN HOLE 578.

CHAPTER 9: TABLE 3. STRATIGRAPHIC OCCURRENCES OF NEOGENE DIATOMS IN HOLES 579 AND 579A.

CHAPTER 9: TABLE 4. STRATIGRAPHIC OCCURRENCES OF NEOGENE DIATOMS IN HOLE 580.

ACKNOWLEDGMENTS

The Scientific Party of Leg 86 gratefully acknowledges the assistance of Captain Joseph Clark and his crew in making our cruise a success. We thank Mike Storms for resolving many difficult drilling problems in our favor and Gus Gustafson and his Deep Sea Drilling Project (DSDP) technical crew for their excellent logistical and technical support. Without the advice and support of Jim Hays, Connie Sancetta, Joseph Morley, and Bob Douglas, we would never have located such excellent sites or been given the opportunity to drill them.

The production staff of DSDP has been very helpful in managing the publication of this volume. Special thanks go to Elaine Bruer and Madeleine Mahnken for typesetting and drafting the barrel sheets, to Katie Turner for editing our site chapters and manuscripts, to illustrators Virginia Roman and Alice Thompson for drafting numerous figures, to Lola Boyce for typing our site chapters, and to Carol Bertling for coordinating volume production.

Papers included in the second part of the volume were greatly improved by the thoughtful reviews of Michael Arthur, John Barron, William Berggren, Jim Brooks, Kirk Cochran, E. Davis, Roger Flood, Joris Gieskes, Howard Harper, Jim Hein, Thomas Janecek, David Kadko, Ansis Kaneps, Miriam Kastner, Gerta Keller, Dennis Kent, LaVerne Kulm, Frank Kyte, Ed Laine, James Lawrence, Margaret Leinen, Bill Levy, William Lowrie, Mitchell Lyle, Chad McCabe, Larry Mayer, Ron Merrill, Ted Moore, Jr., Katherine Perch-Nielsen, Cathy Nigrini, Charles Orth, Nick Pisias, Bob Prindle, Joseph Prospero, David Rea, William Riedel, Michael Riggins, Constance Sancetta, Sy Schlanger, Peter Scholle, Jane Schoonmaker, Hans Schrader, Nick Shackleton, Hans Thierstein, Victor Vacquier, Philip Valent, Jeanne Westberg, and Jean Whelan.

Special kudos must be given to King Neptune for deflecting all hurricanes from our path and to the Great-Seafloor-Spreader-in-the-Sky for arranging to have the Falkland Islands/Malvinas form in the South Atlantic rather than at the antipodes.

Finally, we would like to acknowledge, *in nostris cordibus*, the person who, in calculating our total time at sea, forgot about the international date line. We are pleased to know that Affirmative Action includes hiring members of the Flat Earth Society.

PART I: INTRODUCTION, SEISMIC STUDIES, AND SITE REPORTS

1. INTRODUCTION, CRUISE SUMMARY, AND EXPLANATORY NOTES: DEEP SEA DRILLING PROJECT LEG 86, WESTERN NORTH PACIFIC[1]

Audrey A. Wright, Deep Sea Drilling Project, Scripps Institution of Oceanography[2]

INTRODUCTION AND OBJECTIVES

One of the long-standing goals of the Deep Sea Drilling Project (DSDP) has been to study the oceanic paleoenvironment of the western Pacific through deep sea drilling. Two complementary legs were planned to address this problem: Leg 86 in the western North Pacific and Leg 90 along the Lord Howe Rise in the western South Pacific (Kennett, von der Borch, et al., in press).

The primary objective of Leg 86 was to drill a north-south transect of four sites across the Kuroshio Current system, from subtropical to subarctic waters (Staff Scientific Party, 1982). The late Neogene sections recovered at these sites would help to unravel the preglacial and Quaternary paleoceanographic history of the Kuroshio Current system and to determine whether the Miocene onset of biosiliceous sedimentation in the region was synchronous or diachronous. Hydraulic piston coring (HPC) of two holes at each site was planned to allow a high-resolution late Neogene midlatitude stratigraphy using paleomagnetics, tephrachronology, stable isotopes (when possible), and biostratigraphy.

Secondary objectives of Leg 86 included the following: First, to hydraulic piston core the Cretaceous/Tertiary boundary at the Shatsky Rise for midlatitude calcareous biostratigraphic, paleomagnetic, and geochemical studies. The late Neogene carbon and oxygen isotope record determined at this site would be compared with the noncalcareous (siliceous) sites drilled to the north. Second, to recover a "type" North Pacific red clay section for geochemical, paleomagnetic, and geotechnical studies. The low biogenic and terrigenous yield at this site would allow assessment of the nature and history of authigenic and eolian sedimentation during the Late Cretaceous and Cenozoic. The nature of the red clay/chert boundary could also be assessed, particularly in terms of enhanced diagenesis of the basal clay. Third, to determine the thickness and character of sediments at the site of the proposed Defense Advanced Research Projects Agency (DARPA) downhole seismometer experiment (Leg 88) to allow design of casing strings. A fourth objective, that of recovering a late Quaternary section of the Japanese continental margin to study water-mass boundary migration, was not met because of time constraints.

SUMMARY OF RESULTS

Eleven holes at six sites, Sites 576 through 581, were occupied during Leg 86 (Table 1). Locations of these six sites are shown in Figure 1 and generalized lithologic sections are shown in Figure 2.

Site 576, located beneath the central water mass east of Shatsky Rise in 6,217 m water depth (Fig. 1), recovered a "type" red clay section in each of three HPC holes. One complete section was stored vertically, unopened, for shore-based geotechnical studies (Marine Geotechnical Consortium, this volume). Fifty-five meters of Pleistocene to Cretaceous pelagic clay overlies about 20 m of interbedded Cretaceous carbonate turbidites and pelagic clay overlying chert (Fig. 2). The upper 20 to 30 m of the pelagic clay is yellowish brown, silty, and slightly biosiliceous. Underlying that, down to the interbedded turbidites and clay, is a classic dark brown "red clay" section. By analogy with North Pacific clay sections farther east, we infer that the upper part of the section is dominated by eolian debris from Asia, the flux of which increased from the late Miocene or early Pliocene as the site moved farther into the influence of the westerlies and as an increase in global aridity associated with the onset of Northern Hemisphere glaciation made large amounts of material available for wind transport (Janecek, this volume; Leinen, this volume). The underlying clays include a large authigenic component; they accumulated at 4 m/m.y. or less.

Site 577 is located on the west side of Shatsky Rise close to Site 47 in 2678 m of water (Fig. 1). An unusually good late Cenozoic sequence, a Paleogene sequence, and an undisturbed record of the Cretaceous/Tertiary boundary were recovered at this site. The sediments recovered are all nannofossil oozes ranging from white to light gray to pale brown in color and from late Pleistocene to latest Maestrichtian in age (Fig. 2). The percentage of radiolarians and diatoms decreases downcore. A major unconformity separates late Miocene from middle Eocene sediments at approximately 61 m below the seafloor. This unconformity was previously reported at Site 47 (Heezen et al., 1971) and was expected. Foraminifers and nannofossils indicate two minor hiatuses, one in the middle Eocene and the other in the middle Paleocene. Both physical properties and heat flow measurements seem to "sense" the late Miocene/middle Eocene unconformity. There is a sudden increase in bulk density (and decrease in water content) just below the unconformity, as well as a rapid increase in compressional wave velocity (1.48 to 1.53 km/s; Schultheiss, this vol-

---

[1] Heath, G. R., Burckle, L. H., et al., *Init. Repts. DSDP*, 86: Washington (U.S. Govt. Printing Office).

[2] Address: Ocean Drilling Program, 500 University Drive West, Texas A&M University, College Station, Texas 77843.

Table 1. DSDP Leg 86 drill sites.

Hole	Dates (1982)	Latitude (N)	Longitude (E)	Water depth (m)	Penetration (m)	No. of cores	Length cored (m)	Length recovered (m)	Average recovery (%)
576	16–18 May	32°21.36′	164°16.54′	6217	69.2	8	69.2	68.52	99
576A	18–19 May	32°21.38′	164°16.52′	6217	65.7	7	65.7	66.20	101
576B	19–20 May	32°21.37′	164°16.52′	6217	74.8	9	74.8	74.07	99
577	23 May	32°26.51′	157°43.40′	2675	118.8	13	118.8	111.07	93
577A	24 May	32°26.53′	157°43.39′	2675	123.4	13	123.4	110.64	90
577B	25 May	32°26.48′	157°43.39′	2675	113.9	1	9.5	9.63	101
578	27–30 May	33°55.56′	151°37.74′	6010	176.8	20	167.8	165.02	98
579	1 June	38°37.68′	153°50.17′	5736.6	17.9	2	17.9	16.90	94
579A	2–4 June	38°37.61′	153°50.28′	5736.6	149.5	15	135.5	115.87	86
580	6–8 June	41°37.47′	153°58.58′	5375	155.3	17	155.3	140.74	91
581	10–13 June	43°55.62′	159°47.76′	5476	352.5	19	172.0	77.59	45
						124	1109.9	956.25	86

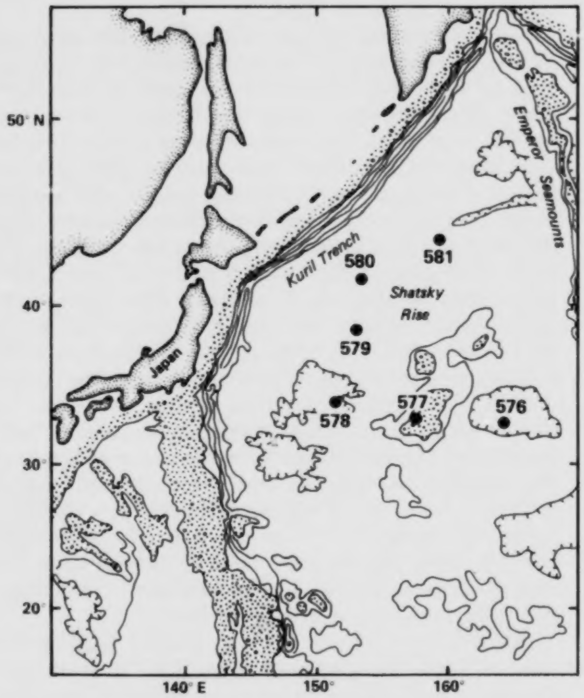

Figure 1. Location map of sites drilled on DSDP Leg 86. Areas shallower than 4 km stippled, 5-km contour plain, 6-km contour hachured.

ume). The heat flow data show a linear increase with depth until the level of the unconformity, at which point there is an apparent temperature reversal (Horai and von Herzen, this volume). A complete, continuous, and undisturbed Cretaceous/Tertiary boundary sequence was recovered in each of the three holes drilled at Site 577. The boundary is defined by the first appearance of several Tertiary nannofossil taxa (*Biscutum romeinii, Thoracosphaera, Cyclagelosphaera*) (Monechi, this volume; Monechi et al., this volume). It is located at a sub-bottom depth of about 109.6 m (Samples 577-12-5, 130 cm, 577A-12-4, 72 cm, and 577B-1-4, 72 cm). Small primitive globigerinid foraminifers appear about 40 cm below the boundary, unlike the section at Gubbio, where they first appear at the boundary (Heath, Burckle, et al., 1982).

Sites 578 through 581 were drilled as a transect of four sites from 34°N to 44°N centered about 155°E, primarily to investigate the paleoceanography of the northwest Pacific. Site 578, the southernmost (most subtropical) site of the transect, is located on the west side of Shatsky Rise in 6,010 m of water (Fig. 1). A complete section from Pleistocene to Late Cretaceous (Maestrichtian–Campanian) overlying a basal chert was recovered (Fig. 2). The uppermost part of the sediment section consists of 125 m of biosiliceous clay and radiolarian-diatom ooze with abundant ash layers. The upper 76 m of these biosiliceous clays are suboxic to anoxic (gray and olive gray in color) with many pyrite-cemented layers; from 76 to 125 m the clays are oxidized (yellow brown and brown in color) with rare ferromanganese nodules. From 125 to 176 m, underlying the biosiliceous unit and overlying the chert, the section is entirely "slick" dark brown to very dark brown, very homogenous pelagic clay that includes a substantial authigenic component. Sedimentation rates drop from almost 40 m/m.y. at the surface to about 8 m/m.y. at the base of the biosiliceous section; the pelagic clays accumulated at an average rate of 0.8 m/m.y., if deposition was continuous. This pelagic clay section complements those recovered at Site 576 and LL44-GPC3 and provides the basis for preparing an east–west profile of Paleogene authigenic sedimentation (Janecek, this volume).

Site 579 lies near the southern margin of the transition zone between the subtropical and subarctic gyres (Fig. 1). It forms an important link between the more siliceous subarctic sites to the north and the calcareous/siliceous subtropical sites to the south, and it should therefore record the most extreme southerly excursions of the subarctic front. Site 580 lies near the present-day subarctic front (42° N) and the northern margin of the transition zone between the subarctic and subtropical gyres (Fig. 1). It therefore serves as the reference point for the modern subarctic/subtropical gyre boundary and should provide a Plio-Pleistocene record of fluctuations in the position of the front. Similar sections of gray and gray green biosiliceous clay and ooze with abundant ash layers were recovered at both Sites 579 and 580 (Fig. 2). Site 579 bottomed in biosiliceous clay of early Pliocene age; Site 580 bottomed in biosiliceous clay of late Pliocene age. Although neither site penetrated the base of the siliceous section, the oldest sediments at Site 579 predate the green to yellow brown biosiliceous clay transition at Site 578, so at least that boundary is diachronous along the transect.

Site 581 was drilled both as the northernmost site of the Leg 86 paleoceanographic transect and as a pilot hole for the DARPA downhole seismometer experiment to be carried out on Leg 88 (Fig. 1). Because of time constraints, HPC sampling of the softer sediments at Site 581 was deferred until Leg 88 (and was dropped from the Leg 88 itinerary by them; see Duennebier, Stephen, et al., in press). Hole 581 was rotary cored from 181.5 m sub-bottom into basaltic basement rocks (Fig. 2). From 181.5 to 223.6 m, the section is reduced (gray and green) late Miocene to earliest Pliocene biosiliceous clay to ooze, similar to but less ashy and pyritic than the sections at Sites 579 and 580. Presumably, the uncored section above is similar, but with more ash and pyritic layers toward the surface. From 223.6 to 244.8 m, the sediment is oxidized (yellow brown) latest middle Miocene to late Miocene biosiliceous clay, which accumulated at about one-sixth the rate of the overlying sediments. The biosiliceous clay is underlaid by "slick," fine-grained, brown to dark brown pelagic clay of presumed middle Miocene age from 244.8 to 276.5 m. From 276.5 to 344 m, we recovered only chert and porcellanite fragments, although the drilling rate suggests that most of the section is soft sediment (clay?). The chert ranges from off-white to bright reds and yellows and dark brown in color; most of it looks like silicified dark brown pelagic clay. Diatoms from a small vug in a chert fragment at about 287 m are middle Miocene in age. Medium-gray aphyric basalt was sampled from 344 to 352.5 m. Most fragments have prominent alteration rinds and fractures that are filled with iron oxides and calcite. There is a small amount of fresh-looking glass. If it is primary oceanic crust, it should be about 115 m.y. old (between Mesozoic magnetic Anomalies M-3 and M-4). Additional basalts were drilled at Site 581 during Leg 88 (Holes 581A, 581B, and 581C) and are described in the Leg 88 *Initial Reports* volume (see Duennebier, Stephen, et al., in press).

By comparing drilling results from Sites 578 and 581, it is clear that the base of the reduced sediments (at 77 m, 2.75 m.y. old at Site 578 and at 224 m, 6.5 m.y. old at Site 580), as well as the base of the underlying yellow brown biosiliceous clay (at 125 m, 8 m.y. old at Site 578 and at 245 m, 12 m.y. old at Site 581) is markedly diachronous from south to north.

A successful first on Leg 86 was the test of the miniature microprocessor-based heat flow unit, designed at Woods Hole Oceanographic Institution (WHOI), that fits into the wall of the core nose of the hydraulic piston corer. It records a temperature with each core at virtually no cost in time. Temperature data were collected at all sites except Site 581; the results are given in Horai and von Herzen (this volume).

EXPLANATORY NOTES

These explanatory notes are intended to aid the reader in understanding the Leg 86 site chapters that follow. Although procedures followed by the Leg 86 shipboard party were by and large standard DSDP procedures, every DSDP cruise has procedural peculiarities that result from the personalities and scientific priorities involved. This section outlines standard DSDP shipboard procedures and details the Leg 86 deviations from those procedures.

Responsibility of Authorship

Site summary chapters are coauthored by the entire shipboard scientific party; ultimate responsibility lies with the two co-chief scientists. These chapters are organized into the following sections, with authors' names in parentheses.

Site Summary and Principal Results (Heath, Burckle)
Background and Objectives (Heath, Burckle)
Operations (Storms)
Lithostratigraphy (Jacobi, Janecek, Krissek, Lenotre, Wright)
Seismic Correlations (Jacobi)
Biostratigraphy (D'Agostino, Koizumi, Monechi, Morley)
Paleomagnetics (Bleil)
Sediment Accumulation Rates (Bleil, D'Agostino, Koizumi, Monechi, Morley)
Physical Properties (Schultheiss)
Inorganic Geochemistry (Heath, Pine)
Heat Flow (Horai)
Summary and Conclusions (Heath, Burckle)

The interpretations of individual authors have been retained in the sections for which they are responsible. As a result, differences between interpretations in a particular section and those in the conclusions sometimes occur. In addition, interpretations in the site summary chapters reflect knowledge gleaned only from shipboard and initial postcruise analysis. Results of the more detailed shore-based work presented in the manuscripts in the second portion of this *Initial Reports* volume may necessitate changing these preliminary site chapter interpretations to some extent.

Survey and Drilling Data

The survey data used for specific site selections are discussed in each site chapter. En route between sites, continuous observations were made of depth, magnetic field, and sub-bottom structure. Short surveys using a precision echo sounder, seismic profiles, and magnetometer were made on *Glomar Challenger* before dropping the beacon.

While we were under way, depths were continuously recorded on a Gifft precision graphic recorder. The depths

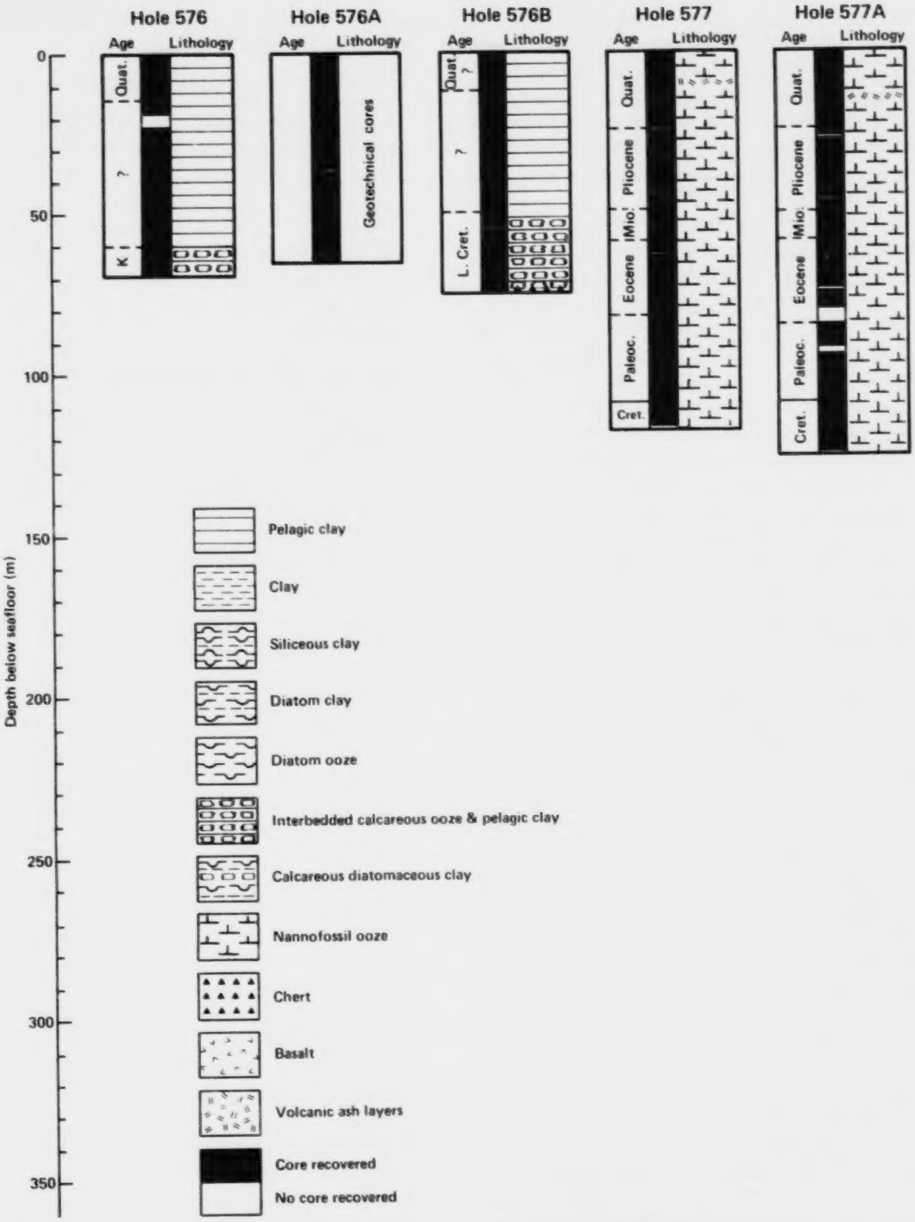
Hole 576
Age
Lithology
Quat.
?
K
Hole 576A
Age
Lithology
Geotechnical cores
Hole 576B
Age
Lithology
Quat.
?
?
L. Cret.
Hole 577
Age
Lithology
Quat.
Pliocene
Mio.
Eocene
Paleoc.
Cret.
Hole 577A
Age
Lithology
Quat.
Pliocene
Mio.
Eocene
Paleoc.
Cret.
Depth below seafloor (m)
0
50
100
150
200
250
300
350
Pelagic clay
Clay
Siliceous clay
Diatom clay
Diatom ooze
Interbedded calcareous ooze & pelagic clay
Calcareous diatomaceous clay
Nannofossil ooze
Chert
Basalt
Volcanic ash layers
Core recovered
No core recovered

Figure 2. Age, core recovery, and generalized lithologic sections of Leg 86 drill sites.

were read on the basis of an assumed 1463 m/s sounding velocity. The water depth (in meters) at each site was corrected (1) according to the tables of Matthews (1939) and (2) for the depth of the hull transducer (6 m) below sea level. In addition, any depths referring to the drilling platform have been calculated on the assumption that this level is 10 m above the water line.

The seismic-profiling system consisted of two Bolt air guns, a Scripps-designed hydrophone array, Bolt amplifiers, two band-pass filters, and two Edo recorders, usually recording at two different filter settings.

Drilling Characteristics

Because water circulation down the hole is open, cuttings are lost on the seabed and cannot be examined. The only available information about sedimentary stratification in uncored or unrecovered intervals, other than from seismic data, is from an examination of the behavior of the drill string as observed on the drill platform. The harder the layer being drilled, the slower and more difficult it usually is to penetrate. There are, however, a number of other variable factors that determine the rate

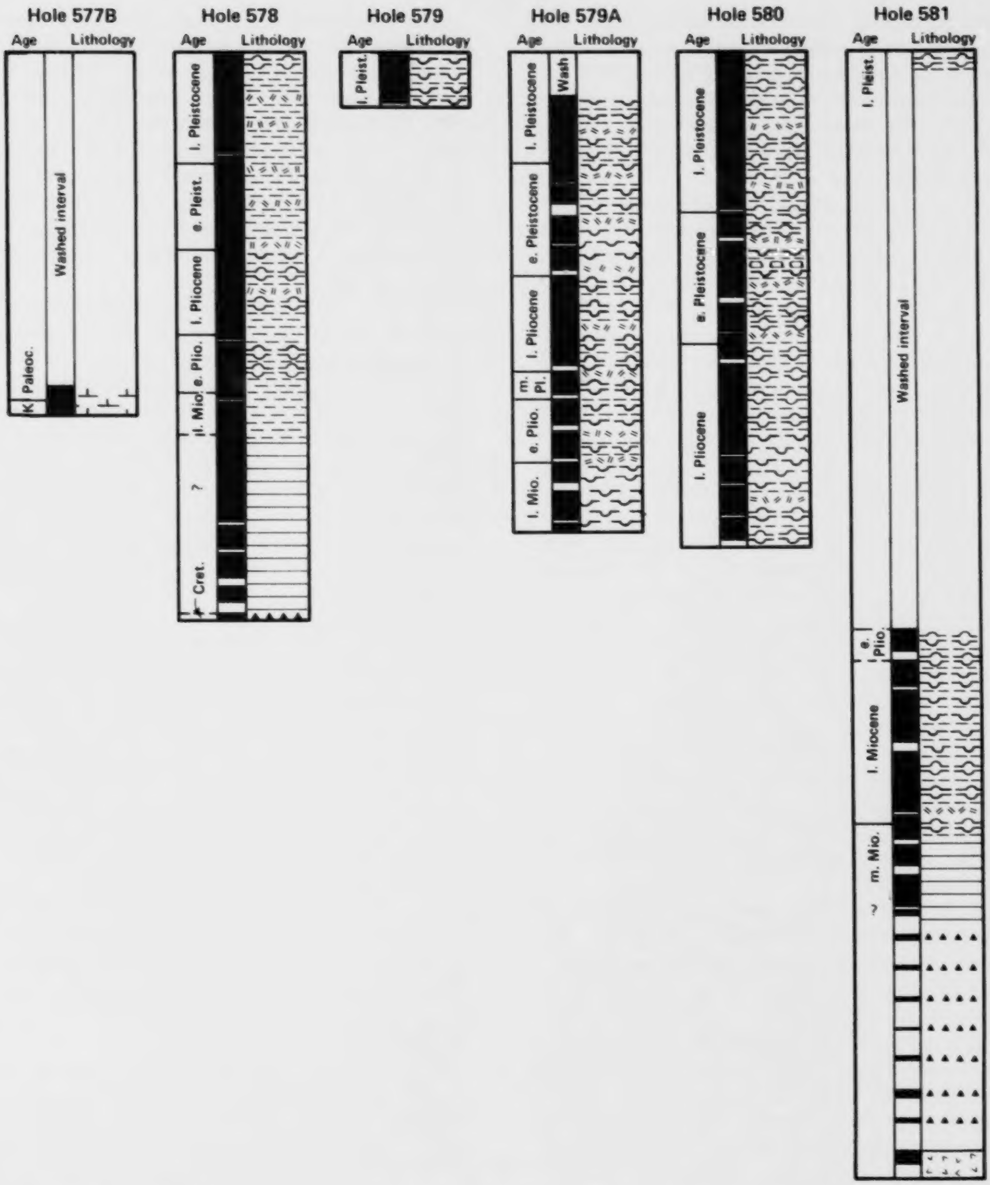
Hole 577B
Age
Lithology
K
Paleoc.
Washed interval
Hole 578
Age
Lithology
l. Pleistocene
e. Pleist.
l. Pliocene
e. Plio.
l. Mio.
?
Cret.
Hole 579
Age
Lithology
l. Pleist.
Hole 579A
Age
Lithology
l. Pleistocene
Wash
e. Pleistocene
l. Pliocene
m. Pl.
e. Plio.
l. Mio.
Hole 580
Age
Lithology
l. Pleistocene
e. Pleistocene
l. Pliocene
Hole 581
Age
Lithology
l. Pleist.
Washed interval
e. Plio.
l. Miocene
m. Mio.
?

Figure 2. (Continued).

of penetration, so it is not always possible to relate it directly to the hardness of the layers. The parameters of bit weight and revolutions per minute are recorded on the drilling recorder and influence the rate of penetration.

Drilling Deformation

When cores are split, many show signs of significant sediment disturbance. Such signs include the concave-downward appearance of originally horizontal bands, the haphazard mixing of lumps of different lithologies, and the near-fluid state of some sediments recovered from tens to hundreds of meters below the seabed. It seems reasonable to suppose that this deformation occurred during or after the cutting of the core. Three different stages during which the core may suffer stresses sufficient to alter its physical characteristics are cutting, retrieval (with accompanying changes in pressure and temperature), and core handling.

Shipboard Scientific Procedures

Numbering of Sites, Holes, Cores, and Samples

DSDP drill sites are numbered consecutively from the first site drilled by *Glomar Challenger* in 1968. Site numbers are slightly different from hole numbers. A site number refers to one or more holes drilled while the ship is positioned over a single acoustic beacon. These holes can be within a radius as great as 900 m from the beacon. Several holes may be drilled at a single site by pulling the drill pipe above the seafloor (out of one hole), moving the ship 100 m or more from the previous hole, and then drilling another hole.

The first (or only) hole drilled at a site takes the site number. A letter suffix distinguishes each additional hole at the same site. For example: the first hole takes only the site number; the second takes the site number with suffix A, the third takes the site number with suffix B, and so forth. It is important, for sampling purposes, to distinguish the holes drilled at a site, because recovered sediments or rocks from cores with the same site number but from different holes usually do not come from equivalent positions in the stratigraphic column.

The cored interval is measured in meters below the seafloor. The depth interval of an individual core is the depth below seafloor that the coring operation began to the depth that the coring operation ended. Each coring interval is generally 9.5 m long, which is the nominal length of a core barrel. The coring interval may, however, be shorter. "Cored intervals" are not necessarily adjacent to each other, but may be separated by "drilled intervals." In soft sediment, the drill string can be "washed ahead" with the core barrel in place, but not recovering sediment, by pumping water down the pipe at high pressure to wash the sediment out of the way of the bit and up the space between the drill pipe and wall of the hole; however, if thin, hard rock layers are present, it is possible to get "spotty" sampling of these resistant layers within the washed interval, producing a cored interval greater than 9.5 m.

Cores taken from a hole are numbered serially from the top of the hole downward. Full recovery for a single core is normally 9.28 m of sediment or rock, which is in a plastic liner (6.6 cm I.D.), plus about a 0.2-m-long sample (without a plastic liner) in a core catcher. The core catcher is a device at the bottom of the core barrel that prevents the core from sliding out when the barrel is being retrieved from the hole. The sediment core, which is in the plastic liner, is then cut into 1.5-m-long sections that are numbered serially from the top of the sediment core (Fig. 3). When full recovery is obtained, the sections are numbered from 1 through 7, the last section being shorter than 1.5 m. The core catcher sample is placed below the last section when the core is described, and labeled "Core Catcher" (CC); it is treated as a separate section (for sediments only).

When recovery is less than 100%, and if the sediment is contiguous, the recovered sediment is placed at the top of the cored interval, and then 1.5-m-long sections are numbered serially, starting with Section 1 at the top. There will be as many sections as needed to accommodate the length of the core recovered (Fig. 3); for example, 3 m of core sample in a plastic liner will be divided into two 1.5-m-long sections. Sections are cut starting at the top of the recovered sediment, and the last section may be shorter than the normal 1.5-m length.

When recovery is less than 100%, the original stratigraphic position of the sediment in the cored interval is unknown; we conventionally assign the top of the recovered sediment to the top of the cored interval. This is done for convenience in data handling and for consistency. If recovery is less than 100% and core fragments are separated, and if shipboard scientists believe that the fragments were not originally contiguous, then sections are numbered serially and the intervening sections are noted as void, whether the fragments as found were contiguous or not.

Samples are designated by distances in centimeters from the top of each section to the top and bottom of the sample interval in that section. A full identification number for a sample consists of the following information (1) Leg, (2) Site, (3) Hole, (4) Core Number, (5) Section, (6) Interval in centimeters. For example, the sample identification number "86-577A-6-3, 98-100 cm" means that a sample was taken between 98 and 100 cm below the top of Section 3 of Core 6, from the second hole drilled at Site 577 during Leg 86. A sample from the core catcher of this core might be designated "86-577A-6,CC (8-9 cm)."

The depth below the seafloor for a sample numbered "86-577A-6-3, 98-100 cm" is the sum of the depth to the top of the cored interval for Core 6 (47.4 m) plus the 3 m included in Sections 1 and 2 (each 1.5 m long) plus the 98 cm below the top of Section 3. The sample in question is therefore located at 51.38 m sub-bottom, which in principle is the sample sub-seafloor depth (sample requests should refer to a specific interval within a core section, rather than the depth below seafloor). Sub-seafloor depths for Leg 86 sediments drilled at Site 576 were adjusted by matching paleomagnetic reversals and distinct lithologic changes recovered in Holes 576, 576A, and 576B. Details for computing adjusted sub-seafloor depths for these sediments are given in Heath et al. (this volume); these adjusted depths supercede those given in the "Operations" section of the Site 576 chapter (this volume).

Two types of coring systems were used on the *Glomar Challenger* during Leg 86: (1) the standard DSDP rotary-coring system, and (2) the hydraulic piston coring (HPC) system. Conventions regarding the cataloguing of the HPC cores are the same as those for the rotary cores. A full HPC core, therefore, consists of six sections, each 1.5-m long, a seventh section of variable length, and a core catcher as much as 0.2 m long. For details regarding the HPC operation, the core orientation, and the special HPC features, see Prell, Gardner, et al. (1982).

Handling of Cores

Cores were normally cut into 1.5-m sections, sealed, and labeled; the sections were then brought into the shipboard core laboratory for processing. Continuous wet-bulk density determinations using the Gamma Ray Attenuation Porosity Evaluator (GRAPE) were made before the sections were split.

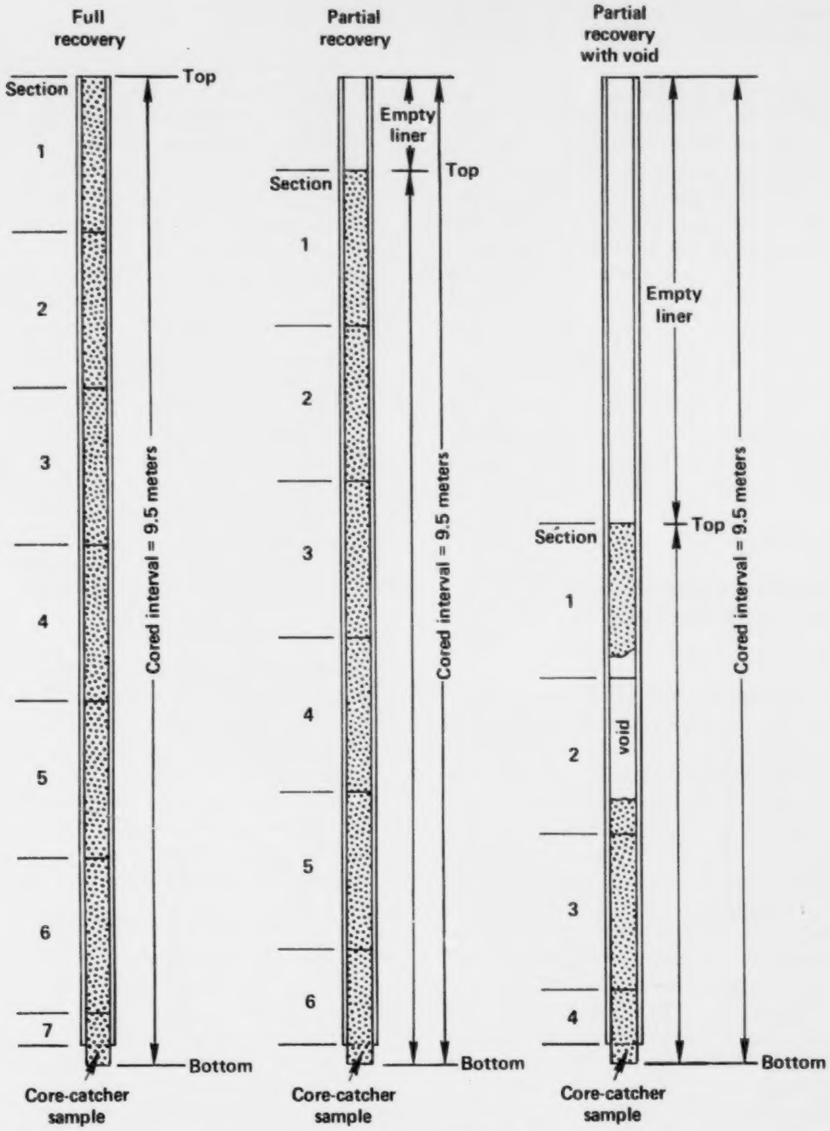

Figure 3. Diagram showing procedure in cutting and labeling of core sections.

The cores were then split longitudinally into "work" and "archive" halves with the wire cutter. All sections from a given HPC core were oriented relative to each other with the result that all archive halves are from the same side of the hole; their orientation relative to the Earth's magnetic north is, however, unknown. Compressional and shear wave velocity, vane shear, and thermal conductivity measurements were made on the split work halves. Samples subsequently extracted from the work half include those for measurement of wet-bulk density by GRAPE and gravimetric techniques (Boyce, 1976), measurement of calcium carbonate percentage with the carbonate bomb (Müller and Gastner, 1971), and geochemical, paleontological, paleomagnetic, geotechnical, sedimentologic, and petrologic studies.

The color, texture, structure, physical disturbance by the drill bit, and composition of the various lithologically different parts of each archive half were described on standard visual core description sheets (one per section). Any unusual features were noted. One or more smear slides were made from the sediments recovered in each core and examined by petrographic microscope. The archive half of the core section was then photographed.

After the cores were sampled and described, both the "work" and "archive" halves were maintained in cold storage aboard *Glomar Challenger* until they were transferred to the DSDP repository. Whole core sections removed for organic geochemistry studies were frozen immediately on board ship and kept frozen. All Leg 86 cores are presently stored at the Ocean Drilling Program (ODP) West Coast Repository (Scripps Institution of Oceanography).

Visual core description sheets, smear slide descriptions, and carbonate bomb (percentage $CaCO_3$) determinations (all done aboard ship) provide the data for the summary core descriptions or "barrel sheets" presented at the end of the site chapters in this volume (Fig. 4). Locations of smear slide and carbonate bomb samples are shown with a symbol on these barrel sheets.

Cores collected on Leg 86 from Hole 576A were intended for shore-based geotechnical studies and were therefore handled differently. They were cut into 1.5-m sections, sealed, labeled, and GRAPEd, but not split. Instead, they were stored in vertical position in cold storage aboard the *Glomar Challenger*, shipped to the West Coast Repository, and subsequently sampled by shore-based scientists for detailed geotechnical studies (Marine Geotechnical Consortium, this volume).

Description of Sediments

Sediments and Sedimentary Rocks Core Description Form

Drilling Disturbance

Recovered rocks, particularly soft sediments, may be extremely disturbed. This mechanical disturbance is a result of the coring technique, which uses a 25-cm-diameter bit with a 6-cm-diameter opening for the core sample. Symbols for the five disturbance categories used for soft and firm sediment on Leg 86 are shown on the core description form in the column entitled "Drilling Disturbance" (Fig. 4). The disturbance categories are defined as follows: (1) Slightly deformed: bedding contacts are slightly bent. (2) Moderately deformed: bedding contacts have undergone extreme bowing. Firm sediment is fractured. (3) Very deformed: bedding is completely disturbed or homogenized by drilling, sometimes showing symmetrical diapir-like structure. (4) Soupy: water-saturated intervals that have lost all aspects of original bedding. (5) Breccia: indurated sediments broken into angular fragments by the drilling process, perhaps along preexisting fractures.

Sedimentary Structures

It may be extremely difficult to distinguish between natural structures and structures created by the coring process in sediment cores. Consequently, the description of sedimentary structures was optional. Locations and types of structures appear as graphic symbols in the column entitled "Sedimentary Structures" on the core description form (Fig. 4). Figure 5 gives the key to the symbols used for sedimentary structures recognized in sediments recovered on Leg 86.

Color

Colors of the core samples were determined with Munsell Soil Color Charts. Colors were determined immediately after the cores were split and still wet.

Lithology

Recovered lithologies are represented on the core description forms by a single symbol or by a grouping of two or more symbols (Fig. 6) in the column entitled "Graphic Lithologies" (Fig. 4). The symbols in a grouping correspond to end-members of sediment constituents, such as clay or nannofossil ooze. The symbol for the terrigenous constituent appears on the right-hand side of the column, the symbol for the biogenic constituent(s) on the left-hand side of the column. The abundance of any component approximately equals the percentage of the width of the graphic column its symbol occupies. For example the left 20% of the column may have a nannofossil ooze symbol, whereas the right 80% may have a clay symbol, indicating sediment composed of 80% clay and 20% nannofossils.

Because of the difference in the length-to-width ratio between the actual sediment core and the graphic lithologic column, it is not possible to reproduce structures as they appear in the core; in the graphic representation they are highly flattened and distorted. The same is true for rock fragments or pebbles in the cores.

Shipboard Analyses

Smear slide compositions and carbonate bomb analyses determined on board are listed below the written core descriptions on the core description forms. The locations of these samples in the core are given in the column entitled "Samples" (Fig. 4). Locations and intervals of organic geochemistry (OG), interstitial water (IW), physical property (PP), and geotechnical consortium (GTP) whole core samples are given in the "Graphic Lithology" column on the core description forms.

Lithologic Classification of Sediments

The basic classification system used on Leg 86 was devised by the Joint Oceanographic Institutions for Deep Earth Sampling (JOIDES) Sedimentary Petrology and Physical Properties Panel (SP4) and adopted for use by the JOIDES Planning Committee in March, 1974.

This classification is descriptive rather than generic, and categories are based on sediment parameters measured on board ship. Sediment names are those in common usage, defined within the limits of existing definitions. We treat lithologic types not covered in this classification as a separate category termed "special rock types." A brief outline of the conventions and descriptive data used to construct this classification follows.

Conventions and Descriptive Data

In this classification scheme, composition and texture are the only criteria used to define the type of sediment or sedimentary rock recovered. Composition is more important for describing sediments deposited in the open ocean, while texture becomes significant for hemipelagic and nearshore sediments. These data come principally from visual estimates of component percentages in smear slides, examined using a petrographic microscope. These data are estimates of areal abundance and

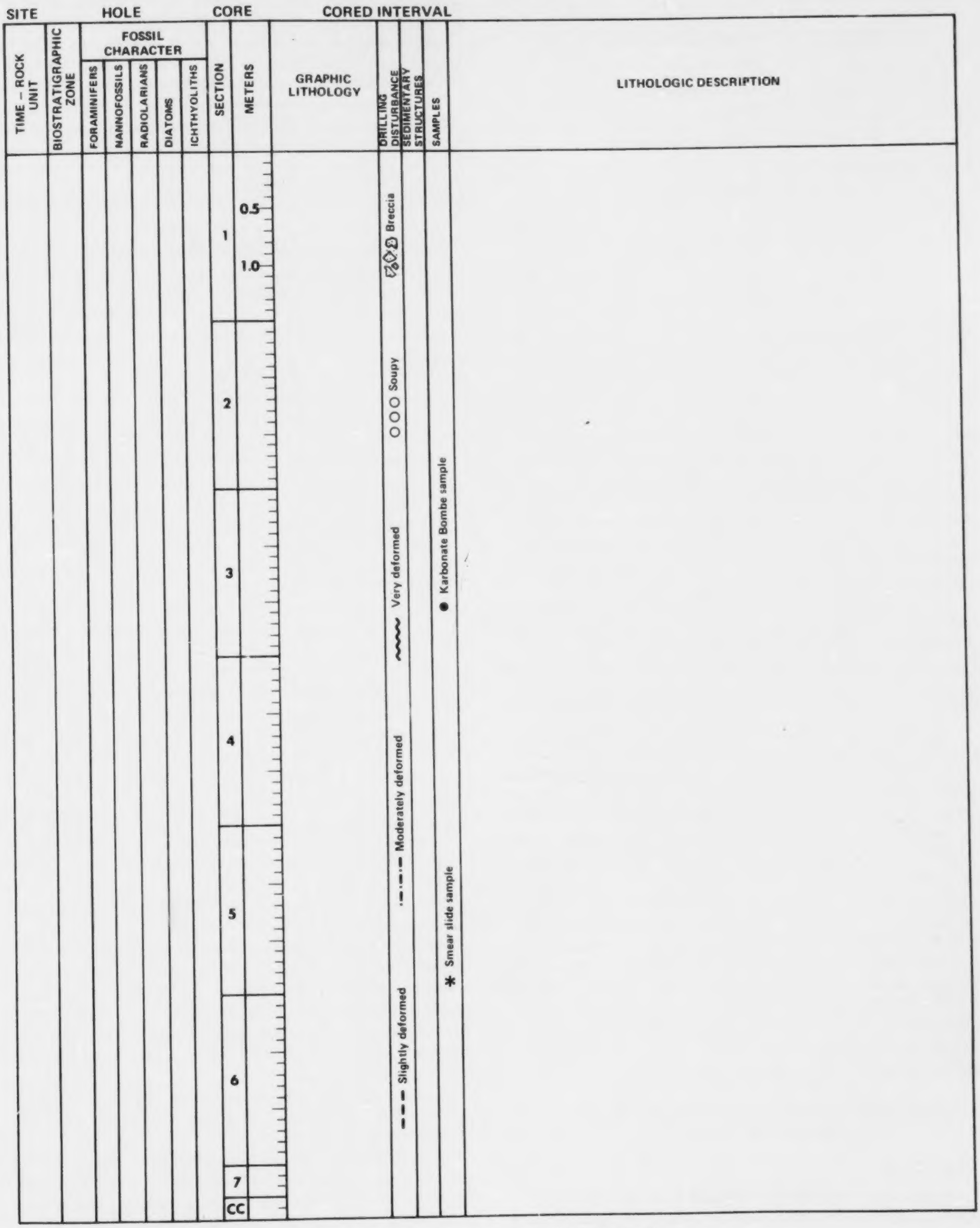
SITE
HOLE
CORE
CORED INTERVAL
TIME – ROCK UNIT
BIOSTRATIGRAPHIC ZONE
FOSSIL CHARACTER
FORAMINIFERS
NANNOFOSSILS
RADIOLARIANS
DIATOMS
ICHTHYOLITHS
SECTION
METERS
GRAPHIC LITHOLOGY
DRILLING DISTURBANCE
SEDIMENTARY STRUCTURES
SAMPLES
LITHOLOGIC DESCRIPTION
0.5
1.0
1
2
3
4
5
6
7
CC
Breccia
Soupy
Very deformed
Moderately deformed
Slightly deformed
Karbonate Bombe sample
Smear slide sample

Figure 4. Sample core form for description of sediments and sedimentary rocks ("barrel sheets").

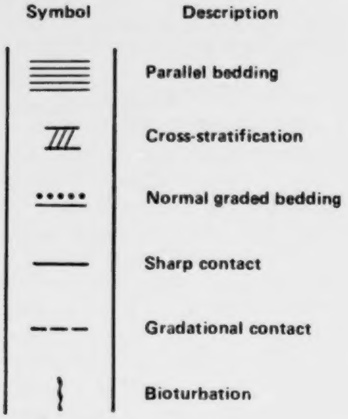
Symbol
Description
Parallel bedding
Cross-stratification
Normal graded bedding
Sharp contact
Gradational contact
Bioturbation

Figure 5. Standard symbols for sedimentary structures recognized in sediments recovered during Leg 86. These symbols are shown in the "Sedimentary Structure" column of the DSDP core description forms.

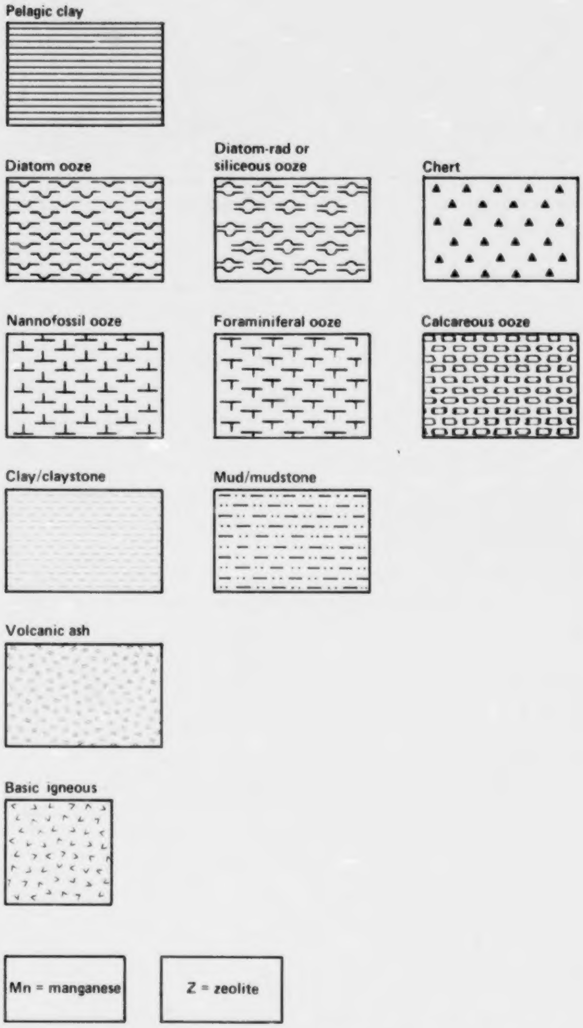
Pelagic clay
Diatom ooze
Diatom-rad or siliceous ooze
Chert
Nannofossil ooze
Foraminiferal ooze
Calcareous ooze
Clay/claystone
Mud/mudstone
Volcanic ash
Basic igneous
Mn = manganese
Z = zeolite

Figure 6. Standard symbols for lithologies drilled during Leg 86. These symbols are shown in the "Graphic Lithology" column of the DSDP core description forms.

size components on the slide and may differ somewhat from more accurate analyses of grain size, carbonate content, and mineralogy. Past experience indicates that quantitative estimates of distinctive minor components are accurate to within 1 to 2%, but that accuracy for major constituents is poorer, 10%. Smear slide data are verified by carbonate content data determined using the carbonate bomb available on board ship.

Where applicable, one or several modifiers are used in naming the type of sediment encountered. In all cases the dominant component appears last in the name; minor components precede, with the least common constituent listed first. Minor constituents occurring in amounts less than 10% are not included in the name.

The degree of induration or lithification of the recovered sediment is reflected in the sediment name. Calcareous sediments and sedimentary rocks are divided into three categories of induration after Gealy and others (1971). (1) *Oozes* are soft calcareous sediments with little strength that readily deform under the pressure of a finger or the broad blade of a spatula. (2) *Chalks* are firm, partially lithified calcareous oozes that are readily scratched with a fingernail or the edge of a spatula. (3) *Limestones* are hard, well lithified and cemented calcareous sedimentary rocks that are resistant or impossible to scratch with a fingernail or the edge of a spatula. Noncalcareous sediments are called by the sediment name if the material is soft enough for the core to be split with a wire cutter (e.g., silty clay), or by the sediment name plus the suffix *stone* if the core must be cut with a band saw or diamond saw (e.g., silty claystone).

Types of Sediments, Sedimentary Rocks, and Compositional Boundaries

Pelagic Clay

Pelagic clay is principally composed of authigenic pelagic material that accumulated at very slow rates. This type of sediment has also often been termed "brown clay" or "red clay."

1. Boundary of pelagic clay with terrigenous sediments is where authigenic components (Fe/Mn micronodules, zeolites), fish debris, etc., become common (more than 10%) in smear slides, indicating pelagic clay. Because the accumulation rates of pelagic clay and terrigenous sediments are very different, transitional deposits are exceptional.
2. Boundary of pelagic clay with siliceous biogenic sediments is the point at which there is less than 30% identifiable siliceous remains.
3. Boundary of pelagic clay with calcareous biogenic sediment is uncommon. Generally this facies passes from pelagic clay through siliceous ooze to calcareous ooze, with one important exception: At the base of many

oceanic sections, black, brown, or red clays occur directly on basalt, overlaid by or grading up into calcareous sediments. Most of the basal clayey sediments are rich in iron, manganese, and other metallic trace elements. For proper identification they require more elaborate geochemical work than is available on board. These sediments are placed in the "Special Rock" category, and care is taken to distinguish them from ordinary pelagic clay.

Siliceous Biogenic Sediment

Siliceous biogenic sediments are distinguished from pelagic clay because they contain common siliceous microfossils. Siliceous biogenic sediments are distinguished from a calcareous category by a calcium carbonate content of less than 30%.

There are two categories of siliceous biogenic sediments: (1) pelagic siliceous biogenic sediments, which contain greater than 70% siliceous microfossils and less than 30% silt and clay, and (2)transitional siliceous biogenic sediments, which contain between 10 and 70% siliceous microfossils and greater than 30% silt and clay. Soft pelagic siliceous biogenic sediments are termed *siliceous oozes* (radiolarian ooze or diatom ooze, depending on the dominant fossil component). Hard pelagic siliceous biogenic sediments include radiolarite, porcellanite, diatomite, and chert. Soft transitional siliceous biogenic sediments with less than 50% siliceous microfossils were termed *siliceous* (or *diatomaceous*, if diatoms were the dominant fossil component) *clays* or *silty siliceous* (*diatomaceous*) *clays* by the Leg 86 scientific party. Soft transitional siliceous biogenic sediments with greater than 50% siliceous microfossils were termed *clayey diatom ooze*. The standard DSDP classification scheme terms these transitional siliceous biogenic sediments *siliceous muds* and *muddy diatom oozes*, respectively, but the Leg 86 scientific party preferred to avoid use of the term *mud* in their sediment classification.

Calcareous Biogenic Sediment

Calcareous biogenic sediment is distinguished by a biogenic $CaCO_3$ content in excess of 30%. There are two classes: (1) pelagic calcareous biogenic sediments which contain 60 to 100% biogenic $CaCO_3$ (less than 30% silt and clay) and (2) transitional calcareous biogenic sediments which contain 30 to 60% $CaCO_3$ (greater than 30% silt and clay). Only pelagic biogenic calcareous sediments were recovered on Leg 86 (Sites 576 and 577). These sediments were soft sediments and are therefore termed *calcareous oozes* (nannofossil or foraminiferal oozes, depending on the dominant fossil component).

Terrigenous Sediments

Terrigenous sediments are distinguished by a terrigenous component in excess of 30% and by siliceous and authigenic components each less than 10%. Sediments in this category are subdivided into textural groups by smear slide estimation of the relative proportions of sand, silt, and clay. The size limits are those defined by Wentworth (1922) (Fig. 7). Five major textural groups were recognized by the Leg 86 scientific party and are shown in a triangular diagram (Fig. 8). These groups are defined according to the abundance of clay (>90%, 90-10%, <10%) and the ratio of sand to silt (>1 or <1). The term *mud* was not favored by the Leg 86 party; the terms *silty clay* and *sandy clay* were used instead.

	Grain size (mm)		ϕ	Wentworth size class
	2.00	2	-1.0	Granule
Sand	1.68		-0.75	
	1.41		-0.5	Very coarse sand
	1.19		-0.25	
	1.00	1	0.0	
	0.84		0.25	
	0.71		0.5	Coarse sand
	0.59		0.75	
	0.50	1/2	1.0	
	0.42		1.25	
	0.35		1.5	Medium sand
	0.30		1.75	
	0.25	1/4	2.0	
	0.210		2.25	
	0.177		2.5	Fine sand
	0.149		2.75	
	0.125	1/8	3.0	
	0.105		3.25	
	0.088		3.5	Very fine sand
	0.074		3.75	
	0.0625	1/16	4.0	
Silt	0.053		4.25	
	0.044		4.5	Coarse silt
	0.037		4.75	
	0.031	1/32	5.0	
	0.0156	1/64	6.0	Medium silt
	0.0078	1/128	7.0	Fine silt
	0.0039	1/256	8.0	Very fine silt
Mud	0.0020		9.0	
	0.00098		10.0	Clay
	0.00049		11.0	
	0.00024		12.0	
	0.00012		13.0	
	0.00006		14.0	

Figure 7. Grade scales for terrigenous sediments (from Wentworth, 1922).

Volcanogenic Sediments

Pyroclastic rocks are described according to the textural and compositional scheme of Wentworth and Williams (1932). The textural groups are (1) volcanic breccia: more than 32 mm in size; (2) volcanic lapilli: between 4 and 32 mm in size; and (3) volcanic ash: less than 4 mm in size (tuff when indurated). The composition of these pyroclastic rocks is described as vitric

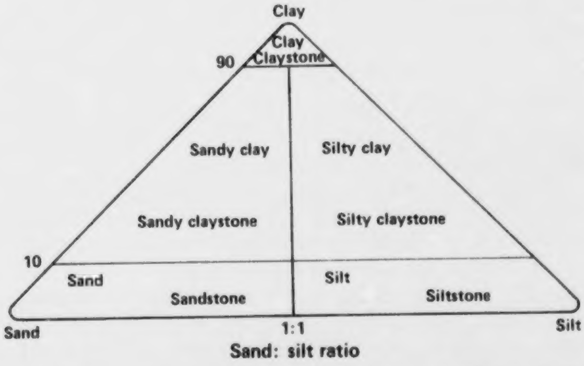

Figure 8. Triangular diagram showing classification scheme for terrigenous sediments used on DSDP Leg 86.

(glass), crystalline, or lithic. Volcanic ash layers were recovered at all sites drilled on Leg 86; no volcanic breccia or lapilli layers were encountered.

Special Rock Types

The definition and nomenclature of sediment and rock types not included in the system described above are left to the discretion of shipboard scientists, with the recommendation that they adhere as closely as practical to conventional terminology. In this category fall such rocks as intrusive and extrusive igneous rocks, evaporites, shallow water limestones, dolomites, gravels, conglomerates, breccias, metalliferous brown clays, and concretions. Special rock types encountered by the Leg 86 scientific party included manganese nodules and basalts.

Basement Description Conventions

Core Handling

Basalt basement rocks were recovered only in Core 19 of Hole 581 on Leg 86. These basalts were split using a rock saw with a diamond blade into "archive" and "work" halves. Styrofoam spacers were taped between basalt pieces inside the liner, and each piece was numbered sequentially from the top of each section, beginning with the number 1. Pieces were labeled on the rounded, not the sawed, surface. Pieces that could be fitted together before splitting were given the same number, but were consecutively lettered 1A, 1B, 1C, etc. Spacers were placed between pieces with different numbers, but not between those with different letters and the same number.

All pieces that are cylindrical and longer than the liner diameter have orientation arrows pointing to the top of the section, both on archive and working halves. Special procedures were used to ensure that orientation was preserved through every step of the sawing and labeling process. Since the pieces are rotated during drilling, it is not possible to sample for declination studies.

Additional Site 581 basalts were recovered during Leg 88 at Holes 581A, 581B, and 581C. Description and sampling of all of the Site 581 basalts was deferred until after Leg 88. Detailed descriptions and results of shore-based studies of these basalts are presented in the Leg 88 *Initial Reports* volume (Duennebier, Stephen, et al., in press).

Igneous Rock Classification

Classification of basalts is based mainly on mineralogy and texture. Thin-section work in general adds little new information to the hand-specimen classification.

Basalts are termed aphyric, sparsely phyric, moderately phyric, or phyric, depending on the proportion of phenocrysts visible with the binocular microscope (about × 12). Basalts are called aphyric if phenocrysts are absent. For practical purposes, this means that if one piece of basalt is found with a phenocryst or two in a section where all other pieces lack phenocrysts, and no other criteria such as grain size or texture distinguish this basalt from the others, then it is described as aphyric. A note of the rare phenocrysts is included in the general description, however. This approach enables us to restrict the number of lithologic units to those with clearly distinctive and persistent visible differences.

Sparsely phyric basalts are those with 1 to 2% phenocrysts in almost every piece of a given core or section. Clearly contiguous pieces without phenocrysts are included in this category and the lack of phenocrysts is again noted in the general description.

Moderately phyric basalts contain 2 to 10% phenocrysts. Aphyric basalts within a group of moderately phyric basalts are separately termed aphyric basalts.

Phyric basalts contain more than 10% phenocrysts. No separate designation is made for basalts with more than 20% phenocrysts; the proportion indicated in the core forms should be sufficient to guide the reader.

The basalts are further classified by phenocryst type, and a modifying term precedes the terms phyric, sparsely phyric, etc. For example, a plagioclase–olivine moderately phyric basalt contains 2 to 10% phenocrysts, most of them plagioclase, but with some olivine.

Biostratigraphy, Paleomagnetics, and Basis for Age Determination

Microfossil zonations of sediments cored on Leg 86 were based on the scheme outlined in Figure 9. The foraminifera zonation was based on Blow (1969), Stainforth et al. (1975) as modified and correlated by Berrgren, Kent, and Flynn (in press), and Pessagno (1967). The nannofossil zonation was constructed from Martini (1971), Bukry (1973, 1981), van Hinte (1976), Verbeek (1977), Roth (1978), Okada and Bukry (1980), and S. Monechi and H. Thierstein (pers. comm., 1984). The radiolarian zonation was constructed from Hays (1970), Foreman (1975), and Riedel and Sanfilippo (1970, 1971, 1978). The diatom zonation was modified from Burckle (1972), Koizumi (1973, 1975), Burckle and Opdyke (1977), and Barron (1980), as shown in Koizumi and Tanimura (this volume). The pelagic clay intervals recovered at Sites 576, 578, and 581 were dated by ichthyoliths (Doyle, this volume).

The geomagnetic time scale is from Berggren, Kent, and Flynn (in press). The numbering schemes are based on LaBrecque et al. (1977) for numbering marine magnetic anomalies, on Theyer and Hammond (1974) and Opdyke et al. (1974) for geomagnetic epochs, and on Tauxe et al. (1984) for geomagnetic chrons. All age boundaries except the Miocene/Pliocene agree with those given by Palmer (1983). The Leg 86 shipboard party uses an age of 5.1 m.y. for the Miocene/Pliocene boundary in the site chapters (this volume), whereas Palmer (1983) places an age of 5.3 m.y. on this boundary.

Downhole sedimentation rates were calculated on board ship from biostratigraphic and paleomagnetic results and are presented in the site chapters.

The following letters are used on core description forms to indicate fossil abundance:

A = abundant (many species and specimens),
C = common (many species, easy to make age assignment),
R = rare (enough for age assignment), and
B = barren.

Letters used to designate fossil preservation are

E = excellent (no dissolution or abrasion),
G = good (very little dissolution or abrasion),
M = moderate (dissolution and/or abrasion and/or recrystallization very noticeable), and
P = poor (substantial or very strong evidence of dissolution and/or abrasion, and/or recrystallization).

Shipboard Geochemical Measurements

Carbonate Bomb

Percent $CaCO_3$ was determined on board ship by the carbonate bomb technique of Müller and Gastner (1971). In this simple procedure, a sample is dried in an oven, ground to powder, and treated with HCl in a closed cylinder. Any resulting CO_2 pressure is proportional to the $CaCO_3$ content of the sample. Application of the calibration factor to the manometer reading (× 100) yields percent $CaCO_3$. Percent error can be as low as 1% for sediments high in $CaCO_3$; in general an accuracy of about 2 to 5% can be obtained.

Carbonate bomb samples were run from the calcareous (turbidite) layers at Holes 576 and 576B, at frequent intervals throughout Holes 577 and 577A, and from the section in Hole 578, Core 20 containing silicified foraminifers. These data are presented on the core description sheets (Fig. 4). The sample interval is designated by two numbers: the section number, followed by the top of the sample interval. For example, a sample from Section 2, 11-12 cm, with 90% calcium carbonate will be represented on the core description sheet as "2,11 cm = 90%."

Interstitial Water

Interstitial water samples were routinely analyzed for pH, alkalinity, salinity, calcium, magnesium, and chlorinity on board ship. One sample was analyzed from every core in Hole 576A, and from every third core at Sites 577 through 581. In addition, three *in situ* pore water samples from Site 576 were analyzed. Data from all these analyses are given in the site chapters (this volume). Sediments are squeezed using a stainless steel press. The water collects in plastic syringes and is then filtered through 0.45-μm, 1-inch millipore filters. Interstitial waters collected with the *In Situ* Pore Water Sampler are filtered through 0.4-μm, 13-mm filters prior to analysis.

pH is determined using a Corning Model 130 pH meter and a Markson combination electrode. The pH meter is calibrated with 4.01 and 7.42 buffer standards. Readings are originally made in millivolts and are later converted to pH. All pH measurements are made in conjunction with alkalinity measurements.

Alkalinity is determined potentiometrically. Five to 10 ml samples are first tested for pH and then titrated with 0.1 *N* HCl. Near the end point, acid is added in 0.01-ml or 0.005-ml increments. Millivolt readings are noted for each increment. The exact end point is then calculated using the Gran Factor method (Gieskes and Rogers, 1973).

Salinity is calculated from the fluid refractive index, as measured by a Goldberg optical refractometer, using this expression:

$$\text{Salinity (‰)} = 0.55 \times \Delta N,$$

where ΔN is the refractive index multiplied by 10^4. The refractometer's calibration is checked periodically using a IAPSO seawater standard and deionized water.

Calcium is determined by titrating a 0.5-ml sample with EGTA (a complexing agent) using GHA as an indicator. To sharpen the end point, the calcium-GHA complex is extracted into a layer of butanol. No correction is made for strontium, which is also included in the result.

Magnesium is determined by titrating a buffered 0.5-ml sample to an Ereochrome Black-T end point using EDTA (sodium salt) as a titrant. This method analyzes all alkaline earths, including calcium, magnesium, strontium, and magnesium; concentrations are obtained by subtracting the calcium (which includes strontium) from this analysis.

Chlorinity is determined by titrating a 0.1-ml sample diluted with 1 ml deionized water with silver nitrate to a potassium chromate end point.

Methods and equipment are checked and standardized at each site using IAPSO standard seawater. As a further check, a surface seawater sample is also analyzed and archived. This sample is also used to test for possible drill water contamination of the interstitial water samples.

Physical Properties Procedures

Physical properties measured on board the *Glomar Challenger* during Leg 86 included the following: (1) saturated bulk density measured with a Gamma Ray Attenuation and Porosity Evaluator (GRAPE), (2) saturated bulk density and water content using gravimetric analyses, (3) compressional wave velocity, using the Hamilton Frame, (4) shear wave velocities, using specially built transducers, and (5) shear strength values, using both a mechanical and a hand-held device.

Physical properties measurements were generally all made within a 30-cm length of a section that appeared to be undisturbed. Occasional measurements were taken in obviously disturbed regions to examine the effects of disturbance. The frequency of measured intervals varied greatly from approximately one per section at Site 576 to one per core at Site 581. Measurements were made more frequently around lithologic boundaries.

Most of the methods and techniques used to assess the physical properties on Leg 86 are discussed in detail by Boyce (1976, 1977). Consequently, only a brief review of the methods is given here.

GRAPE

The Gamma Ray Attenuation and Porosity Evaluator (GRAPE) was used to assess the saturated bulk density of sediments from all the sites drilled during Leg 86. GRAPE analysis compares the attenuation of gamma rays through a sediment sample of unknown bulk densi-

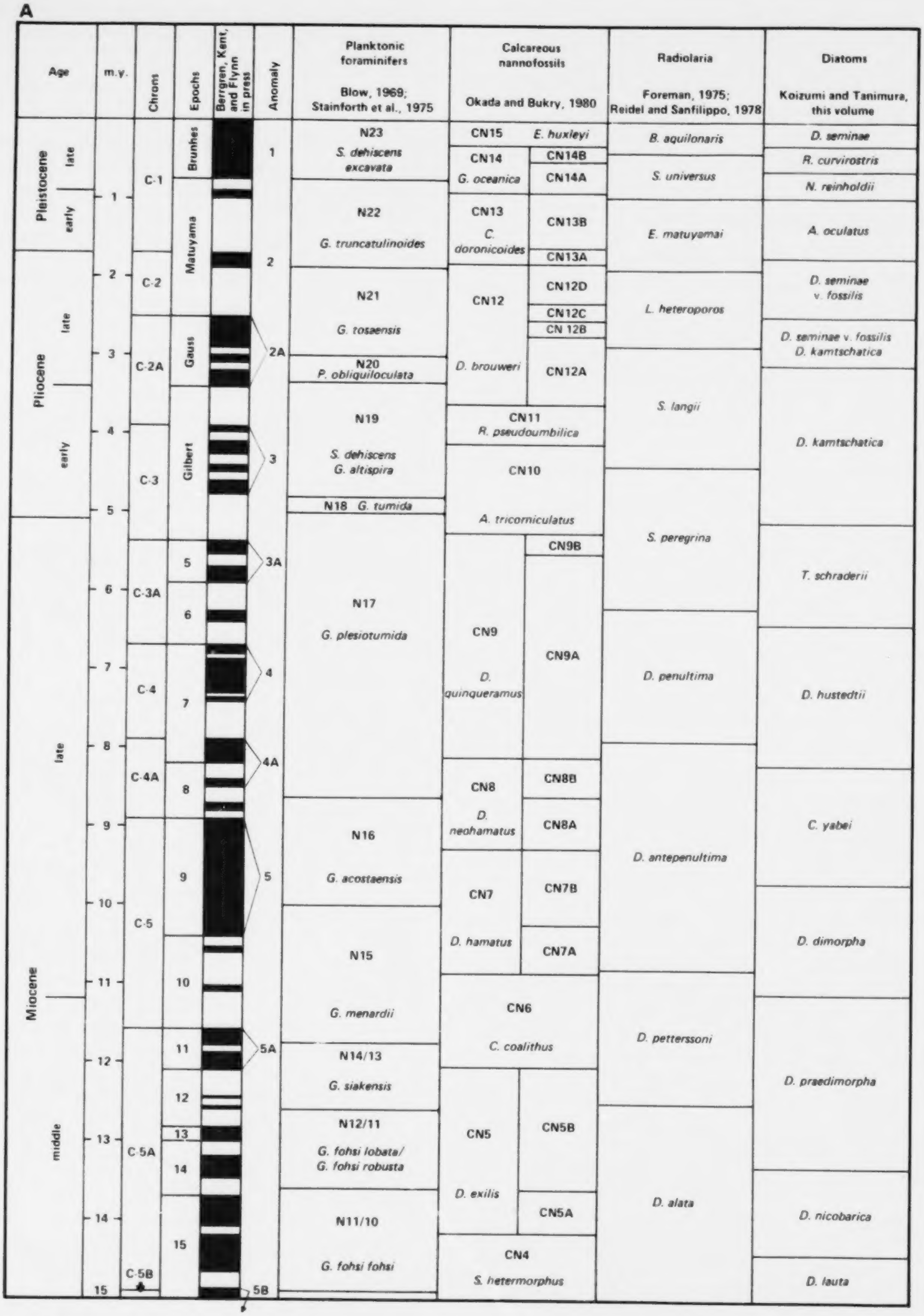

Figure 9. Biostratigraphic zonations for microfossil groups used to date Leg 86 cores. A. Recent through middle Miocene zonations. B. Middle Miocene through Cretaceous zonations. The tie to the paleomagnetics is, in part, by second-order correlation.

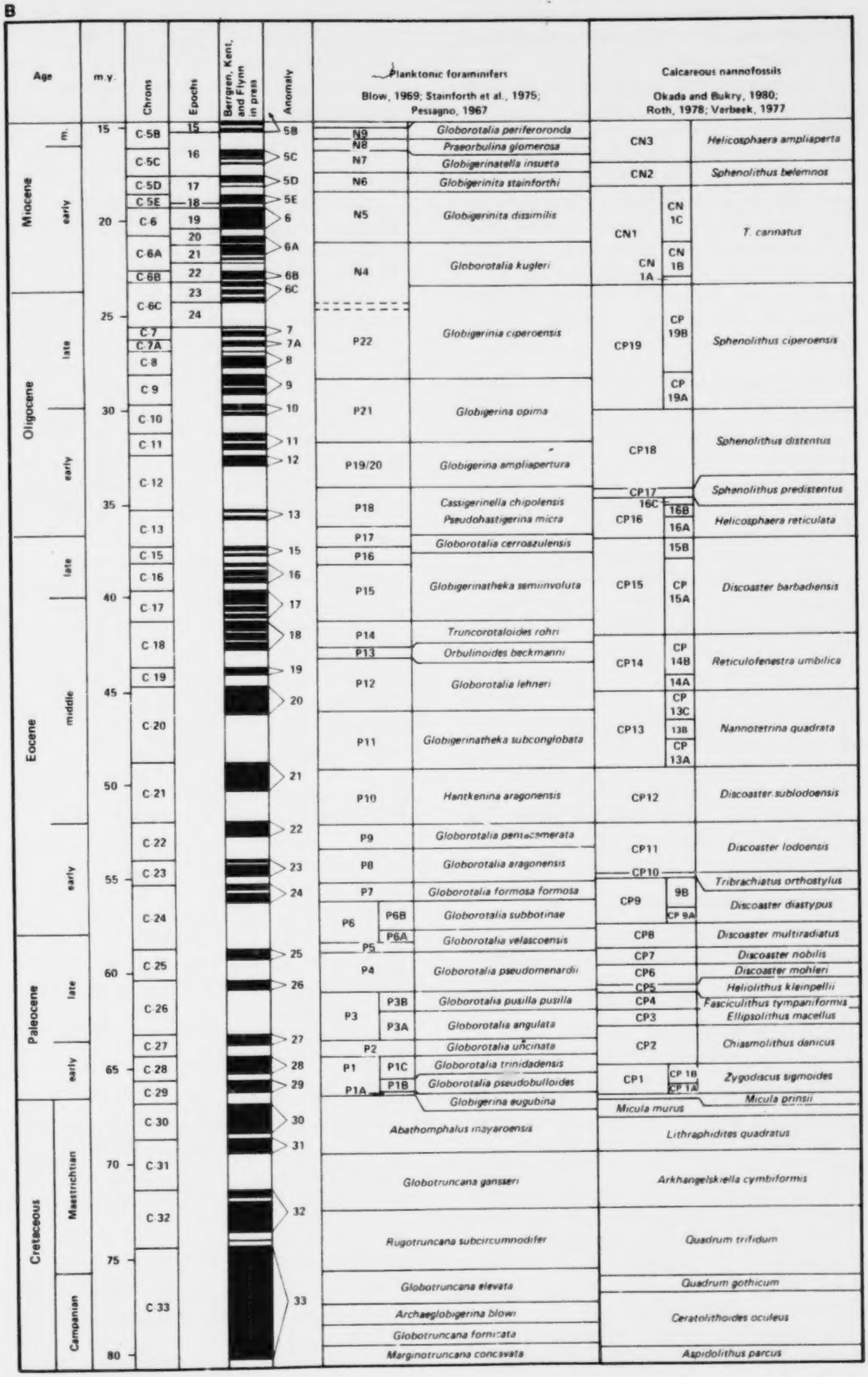

Figure 9. (Continued).

ty with that of a reference sample of known density. The main problem with assessing density from gamma ray attenuation measurements is that attenuation coefficients vary for different mineral types.

Two GRAPE techniques were employed: (1) continuous GRAPE in which the entire, unsplit 1.5-m sections were scanned providing a continuous analog record of approximate bulk density, and (2) 2-min. GRAPE, in which the gamma count was measured through a sediment sample contained in a 1-inch high, 1-inch diameter stainless steel cylinder capped by plexiglass end caps. The longer count times over an accurately known sediment thickness provide more reliable gamma counts. The calibration and calculation procedures are given in Boyce (1976). The 2-min. GRAPE samples were later used as samples for shipboard gravimetric analyses.

Gravimetric Measurements

Two samples were taken adjacent to each other using the 1-inch high, 1-inch diameter stainless steel cylinders. One sample was subjected to the 2-min. GRAPE test before being weighed, dried at 105°C, and then reweighed. The second sample was packed and returned to a shore-based laboratory as a check on the shipboard measurements. The metal cylinders (referred to sometimes as "Boyce cylinders") were inserted into the split section. To minimize the disturbance caused by this insertion, a 20-25 V dc voltage was applied between the cylinder (cathode) and a nearby platinum anode (placed in the sediment). The ease of insertion and subsequent lack of disturbance results from the electro-osmotic effect which continuously lubricates the steel cathode with water, preventing the sediment from sticking to the cylinder. From the wet and dry weights of the sediment sample and the volume of the sample, the bulk density, water content, porosity, and void ratio were calculated. Salt corrections were made assuming 35‰ salinity and a water density of 1.024 g/cm^3.

Velocity Measurements

Compressional wave velocities were measured at 400 kHz using the Hamilton Frame Velocimeter. The apparatus was calibrated using various standards, including distilled water. It was found for nearly all the cores taken on Leg 86 that it was appropriate to measure the velocity on the split core through the liner. This proved very accurate because the HPC cores filled the liners so no errors were introduced by uncertain sediment thicknesses. Velocities were measured immediately after the core had been split longitudinally, which was at least 4 hr. after recovery. This time period was to allow the core temperature to reach that of the laboratory. Temperature was measured at the same time the velocity measurement was made, and all reported velocities are corrected to 20°C using standard seawater velocity/temperature tables. It was found that a resolution of less than 2 m/s was possible when carefully calibrated.

Shear wave velocities were measured by timing a shear wave pulse between two specially designed transducers that were pushed into the split section. The technique employed piezoelectric bender elements; the transmitter was driven with the rising edge of a 10-V square wave, while the received signal was high-pass filtered to remove extraneous noise. Shear wave velocity measurements are not normally performed on DSDP cores, and the reader is referred to Schultheiss (this volume) for more details.

Shear Strength Measurements

Vane shear strengths were measured at all sites on Leg 86 using the modified Wykeham-Farrance Vane Shear Apparatus. The theory and operation of this device is described by Boyce (1976). A four-blade vane is inserted into the split section and a motor rotates it via a torsion spring. The sediment cylindrically shears around the vane. The shear strength is given as a function of the vane size, the spring stiffness, and the amount of torque at failure.

A Torvane hand-held device was also used. This operates on the same principle as the Wykeham-Farrance device, except the test is not as well controlled. However, it is a very quick test to perform and it was interesting to compare the data from the two devices.

Heat Flow

A new heat flow instrument, developed by R.P. von Herzen and others at WHOI, was used for the first time to record bottom hole temperatures. The instrument is specifically designed for use in a modified HPC nose cone. It consists of a temperature sensor (thermistor), a recorder, and batteries that are inserted as a unit into a slot opening in the metal wall of the HPC nose cone shoe so that the temperature sensor is placed close to the shoe's tip. The recorder is a minicomputer, energized by the batteries, that stores data of measured temperatures as a function of time at intervals specified by a program that is loaded into the computer prior to operation. Because of the short time constant of the instrument (10-s intervals), a recording time of 5 min. appears to be sufficient for estimating the undisturbed temperature of the sediment by extrapolation of the cooling curve. This instrument thus provides an efficient way of measuring undisturbed sediment temperature without interfering with the coring process. Heat flow measurements were made at all Leg 86 sites except Site 581 (Horai and von Herzen, this volume).

Photography

Black and white photos of all cores collected during Leg 86 are printed in the site chapters (this volume). In addition, both color core slides and black and white closeups are archived at DSDP and are available for consultation.

Obtaining Samples

Potential investigators who wish to obtain samples should refer to the NSF Sample Distribution Policy for DSDP and ODP. Sample request forms may be obtained from the Curator, Ocean Drilling Program, Texas A&M University, College Station, Texas 77843. Requests must be as specific as possible: include site, hole, core, section, interval within a section, and volume of sample required.

REFERENCES

Barron, J. A., 1980. Lower Miocene to Quaternary diatom biostratigraphy of Leg 57, off northeastern Japan, Deep Sea Drilling Project. *In* Scientific Party, *Init. Repts. DSDP*, 56, 57, Pt. 2: Washington (U.S. Govt. Printing Office), 641–686.

Berggren, W. A., Kent, D. V., and Flynn, J. J., in press. Paleogene geochronology and chronostratigraphy. *In* Snelling, N. J. (Ed.), *Geochronology and the Geological Record*. Geol. Soc. London Spec. Pap.

Blow W. H., 1969. Late middle Eocene to Recent planktonic foraminiferal biostratigraphy. *In* Bronnimann, P., and Renz, H. H., (Eds.), *Proc. Int. Conf. Planktonic Microfossils, 1st*, Leiden (Brill), 6: 199–421.

Boyce, R. E., 1976. Definitions and laboratory techniques of compressional sound velocity parameters and wet-water content, wet bulk density, and porosity parameters by gravimetric and gamma ray attenuation techniques. *In* Schlanger, S. O., Jackson, E. D., et al., *Init. Repts. DSDP*, 33: Washington (U.S. Govt. Printing Office), 931–958.

________, 1977. Deep Sea Drilling Project procedures for shear strength measurement of clayey sediment using modified Wykeham Farrance Laboratory Vane Apparatus. *In* Barker, P. F., Dalziel, I. W. D., et al., *Init. Repts. DSDP*, 36: Washington (U.S. Govt. Printing Office), 1059–1068.

Bukry, D., 1973. Low-latitude coccolith biostratigraphic zonation. *In* Edgar, N. T., Saunders, J. B., et al., *Init. Repts. DSDP*, 15: Washington (U.S. Govt. Printing Office), 685–704.

________, 1981. Cenozoic coccoliths from the DSDP. *The Deep Sea Drilling Project: A Decade of Progress*. Soc. Econ. Paleontol. Mineral. Spec. Publ., 32:335–353.

Burckle, L., 1972 Late Cenozoic planktonic diatom zones from the eastern equatorial Pacific. *Nova Hedwigia Beih.*, 39:217–246.

Burckle, L., and Opdyke, N. D., 1977. Late Neogene diatom correlations in the Circum-Pacific. *Proc. Int. Congr. Pacific Neogene Stratigraphy, 1st*, Tokyo (Kaiyo Shuppan), pp. 255–284.

Duennebier, R. K., Stephen, R. A., et al., in press. *Init. Repts. DSDP*, 88: Washington (U.S. Govt. Printing Office).

Foreman, H. P., 1975. Radiolaria from the North Pacific, Deep Sea Drilling Project, Leg 32. *In* Larson, R. L., Moberly, R., et al., *Init. Repts. DSDP*, 32: Washington (U.S. Govt. Printing Office), 579–676.

Gealy, E. L., Winterer, E. L., and Moberly, R. M., Jr., 1971. Methods, conventions, and general observations. *In* Winterer, E. L., Riedel, W. R., et al., *Init. Repts. DSDP* 7, Pt. 1: Washington (U.S. Govt. Printing Office), 9–26.

Gieskes, J. M., and Rogers, W. C., 1973. Alkalinity determination in interstitial waters of marine sediments. *J. Sediment. Petrol.*, 43: 272–277.

Hays, J. D., 1970. Stratigraphy and evolutionary trends of Radiolaria in North Pacific deep-sea sediments. *In* Hays, J. D. (Ed.), *Geological Investigations of the North Pacific*. Mem. Geol. Soc. Am. 126: 185–218.

Heath, G. R., Burckle, L. H., Wright, A. A., Bleil, U., D'Agostino, A., et al., 1982. *Glomar Challenger* at the Cretaceous-Tertiary boundary. *Nature (London)*, 299:208.

Heezen, B. C., Fischer, A. G., Boyce, R. E., Bukry, D., Douglas, R. G., et al., 1971. Site 47. *In* Fischer, A. G., Heezen, B. C., et al., *Init. Repts. DSDP*, 6: Washington (U.S. Govt. Printing Office), 67–143.

Kennett, J., von der Borch, C., et al., in press. *Init. Repts. DSDP*, 90: Washington (U.S. Govt. Printing Office).

Koizumi, I., 1973. The Late Cenozoic diatoms of Sites 183–193, Leg 19, Deep Sea Drilling Project. *In* Creager, J. S., Scholl, D. W., et al., *Init. Repts. DSDP*, 19: Washington (U.S. Govt. Printing Office), 805–856.

________, 1975. Neogene diatoms from the western margin of the Pacific Ocean, Leg 31, Deep Sea Drilling Project. *In* Karig, D. E., Ingle, J. C., Jr., et al., *Init. Repts. DSDP*, 31: Washington (U.S. Govt. Printing Office), 779–819.

LaBrecque, J. L., Kent, D. V., and Cande, S. C., 1977. Revised magnetic polarity time scale for Late Cretaceous and Cenozoic time. *Geology*, 5:330–335.

Martini, E., 1971. Standard Tertiary and Quaternary calcareous nannoplankton zonation. *Plankt. Conf., Roma, 2nd*, pp. 739–785.

Matthews, D. J., 1939. *Tables of the Velocity of Sound in Pore Water and in Seawater.* London: Admiralty (Hydrographic Department).

Müller, G., and Gastner, M., 1971. The "Karbonat Bombe", a simple device for the determination of the carbonate content in sediments, soils and other materials. *Neues. Jahrb. Mineral. Monatsh.*, 10: 466–469.

Okada, K., and Bukry, D., 1980. Supplementary modification and introduction of code numbers to the low-latitude coccolith biostratigraphic zonation (Bukry, 1973, 1975). *Mar. Micropaleontol.* 5: 321–325.

Opdyke, N. D., Burckle, L. H., and Todd, A., 1974. The extension of the magnetic time scale in sediments of the central Pacific Ocean. *Earth Planet. Sci. Lett.*, 22:300–306.

Palmer, A. R., 1983. The decade of North American Geology 1983 geological time scale. *Geology*, 11(9):503–504.

Pessagno, E. A., 1967. Cenomanian–Turonian stratigraphy in the western Gulf coastal plain area. *In* Brönniman, P., and Ranzrenz, H. H. (Eds.), *Proc. Int. Conf. Planktonic Micrcforaminifera, 1st*, 2: 509–525.

Prell, W. L., Gardner, J. V., and Shipboard Scientific Party, 1982. Leg 68: Introduction, explanatory notes, and conventions. *In* Prell, W. L., Gardner, J. V., et al., *Init. Repts. DSDP*, 68: Washington (U.S. Govt. Printing Office), 5–13.

Riedel, W. R., and Sanfilippo, A., 1970. Radiolaria, Leg 4, Deep Sea Drilling Project. *In* Bader, R. G., Gerard, R. D., et al., *Init. Repts. DSDP*, 4: Washington (U.S. Govt. Printing Office), 503–575.

________, 1971. Cenozoic Radiolaria from the western tropical Pacific, Leg 7. *In* Winterer, E. L., Riedel, W. R., et al., *Init. Repts. DSDP*, 7, Pt. 2: Washington (U.S. Govt. Printing Office), 1529–1672.

________, 1978. Stratigraphy and evolution of tropical Cenozoic radiolarians. *Micropaleontology*, 24:61–96.

Roth, P. R., 1978. Cretaceous nannoplankton biostratigraphy and oceanography of the northwestern Atlantic Ocean. *In* Benson, W. E., Sheridan, R. E., et al., *Init. Repts. DSDP*, 44: Washington (U.S. Govt. Printing Office),731–759.

Staff Scientific Party, 1982. On Leg 86, *Challenger* investigates NW Pacific. *Geotimes*, 27(11):20–22.

Stainforth, R. M., Lamb, J. L., Luterbacher, H., Beard, J. H., and Jeffords, R. M., 1975. Cenozoic planktonic foraminiferal zonations and characteristics of index forms. *Univ. Kans. Paleontol. Contrib. Pap.* 62:1–425.

Tauxe, L., Tucker, P., Petersen, N. P., and LaBrecque, J. L., 1984. Magnetostratigraphy of Leg 73 sediments. *In* Hsü, K. J., LaBrecque, J. L., et al., *Init. Repts. DSDP*, 73: Washington (U.S. Govt. Printing Office), 609–621.

Theyer, F., and Hammond, S. R., 1974. Cenozoic magnetic time scale in deep-sea cores: completion of the Neogene. *Geology*, 2: 487–492.

van Hinte, J. E., 1976. Cretaceous time scale. *Am. Assoc. Pet. Geol. Bull.*, 60(4):269–287.

Verbeek, J. W., 1977. Calcareous nannoplankton biostratigraphy of middle and upper Cretaceous deposits in Tunisia, southern Spain and France. *Utrecht Micropaleont. Bull.*, 16:1–157.

Wentworth, C. K., 1922. A scale of grade and class terms of clastic sediments. *J. Geol.*, 30:377–390.

Wentworth, C. K., and Williams, H., 1932. The classification and terminology of the pyroclastic rocks. *Rep. Comm. Sedimentation, Bull. Nat Res. Council, U.S.*, 80:10–53.

Date of Initial Receipt: 18 December 1983
Date of Acceptance: 10 August 1984

2. HIGH-RESOLUTION SEISMIC STUDIES AND SITE SURVEY RESULTS NEAR DEEP SEA DRILLING PROJECT SITES 576 AND 578, NORTHWEST PACIFIC[1]

Robert D. Jacobi, SUNY at Buffalo and Lamont-Doherty Geological Observatory of Columbia University
and
Dennis E. Hayes and John E. Damuth, Lamont-Doherty Geological Observatory of Columbia University[2]

ABSTRACT

The seafloor near Deep Sea Drilling Project Site 576 (study Area E_2) has a strong northwest to southeast lineation, parallel to the strike of the Mesozoic magnetic lineations. High-resolution (3.5-kHz) seismic profiles show four prominent reflectors (R_2–R_5). Two strong, continuous reflectors (R_2 and R_3) overlie a semitransparent section. These reflectors correspond to an ~1.3 m.y. old volcanic ash and an ~7.2 m.y. old horizon. Reflector R_4 is a discontinuous reflector within the semitransparent section and is ~25 m.y. old. Reflector R_5 corresponds to ~70-m.y.-old carbonate turbidites in bathymetric lows and to pelagic carbonates or cherts in bathymetric highs. Isopach maps of all seismic intervals between these reflectors reveal local thinning and thickening and can be used to measure variations in sediment-accumulation rate. The local sediment distribution suggests that bottom water has flowed southeast or southwest across Area E_2 for the past 70 m.y. This direction is counter to the present net flow of the Pacific Bottom Water and may indicate the existence of a persistent local bottom gyre caused by bathymetric barriers to the west, north, and east of Area E_2. Dramatic thinning of all seismic intervals in the northeast corner of Area E_2 may be related to constricted Pacific Bottom Water accelerating through a gap in the barrier. Anomalous sedimentation suggests that the bottom currents were relatively sluggish from ~25 to 7 m.y. ago. All seismic intervals reveal very small mass-wasting features; these features are more prevalent in intervals R_1–R_2 and R_4–R_5.

The seafloor around Site 578 (study Area B_1) has an east–west lineation that also parallels Mesozoic lineations. The local relief is low, less than 80 m. High-resolution seismic profiles show several continuous, parallel reflectors that generally correspond to volcanic ash layers: Reflectors R_2 (~0.47 m.y. ago), R_3 (~0.97 m.y. ago), R_4 (~2.44 m.y. ago), R_5 (5–6 m.y. ago), and R_6. All reflector intervals increase dramatically (roughly 10 times) in thickness over a south–north distance of only 80 km. This abrupt increase appears to mark a major boundary separating a province with uniformly high sedimentation rates (typically about 50 mm/1000 yr. in the upper intervals) to the north from a large province with relatively low sedimentation rates (typically about 5–10 mm/1000 yr.) to the south. The sedimentation boundary has remained virtually stationary for ~6 m.y. and perhaps for more than 20 m.y. Although the sharpness and spatial stability of the boundary remain an enigma, we believe that the sedimentation boundary is the consequence of bottom-water flow modulating an otherwise more gradual north–south sedimentation gradient. South of Area B_1, sedimentation anomalies indicate that the Pacific Bottom Water flows north or northwest, but within Area B_1, sedimentation variations suggest an eastward flow. A period of higher velocity flow between ~ 2.44 and 5–6 m.y. ago (R_4–R_5 times) is consistent with results from Area E_2, indicating that bottom-water velocity has also apparently increased there since ~7 m.y. ago.

INTRODUCTION

The Northwest Pacific Basin is bounded on the south by the Mid-Pacific Seamounts, on the west and north by the Japan–Kuril–Aleutian trench system, and on the east by the Emperor and Hawaiian seamount chains (Fig. 1). The scarcity of ship tracks compared to the immensity of the Northwest Pacific Basin has precluded all but regional studies of the basin. The bathymetry has been mapped by Chase et al. (1971), Iwabuchi (1979), and Udintsev (1980). M-sequence magnetic lineations, indicating crust of late Mesozoic age, have been mapped throughout most of the Northwest Pacific (e.g., Larson and Hilde, 1975; Larson et al., 1983).

Regional piston-core studies of the upper 10–20 m of sediment show that two distinct sediment types predominate in seafloor depths greater than 5000 m: brown clay in the southeast and siliceous clays and oozes in the northwest (e.g., Horn et al., 1970; Damuth et al., 1983). Volcanic ash layers are prevalent in the upper parts of the piston cores raised near the Japan/Kuril arcs (Horn et al., 1969; Hays and Ninkovich, 1970; Ninkovich and Robertson, 1975). Deeper sediment sections were studied at 12 previously drilled Deep Sea Drilling Project (DSDP) sites (see inside cover, this volume). At these sites, the base of the siliceous clay and ooze is generally middle to late Miocene in age, whereas the base of the brown clay is generally Late Cretaceous in age. Upper Cretaceous chert interbedded with porcellanite and brown clay usually comprises the sedimentary section beneath the homogeneous brown clays (e.g., Damuth et al., 1983).

Regional studies of bottom-water circulation show that the dominant bottom-water mass in the northwest Pacific is Pacific Bottom Water (PBW) (Reid and Lynn, 1971; Warren, 1973; Gordon and Gerard, 1970; Craig and Gordon, 1965, Mantyla, 1975). This bottom water flows northward into the Central Pacific through the Samoan Passage (Reid and Lonsdale, 1974; Lonsdale and Spiess, 1977) and enters the Northwest Pacific Basin

---

[1] Heath, G. R., Burckle, L. H., et al., *Init. Repts. DSDP*, 86: Washington (U.S. Govt. Printing Office).

[2] Addresses: (Jacobi) Department of Geological Sciences, SUNY at Buffalo, 4240 Ridge Lea Road, Amherst, NY 14226 and Lamont-Doherty Geological Observatory of Columbia University, Palisades, NY 10964; (Hayes) Lamont-Doherty Geological Observatory of Columbia University, Palisades, NY 10964; (Damuth, present address) Mobil Research & Development Corp., Dallas Research Laboratory, P.O. Box 819047, Dallas, TX 75381.

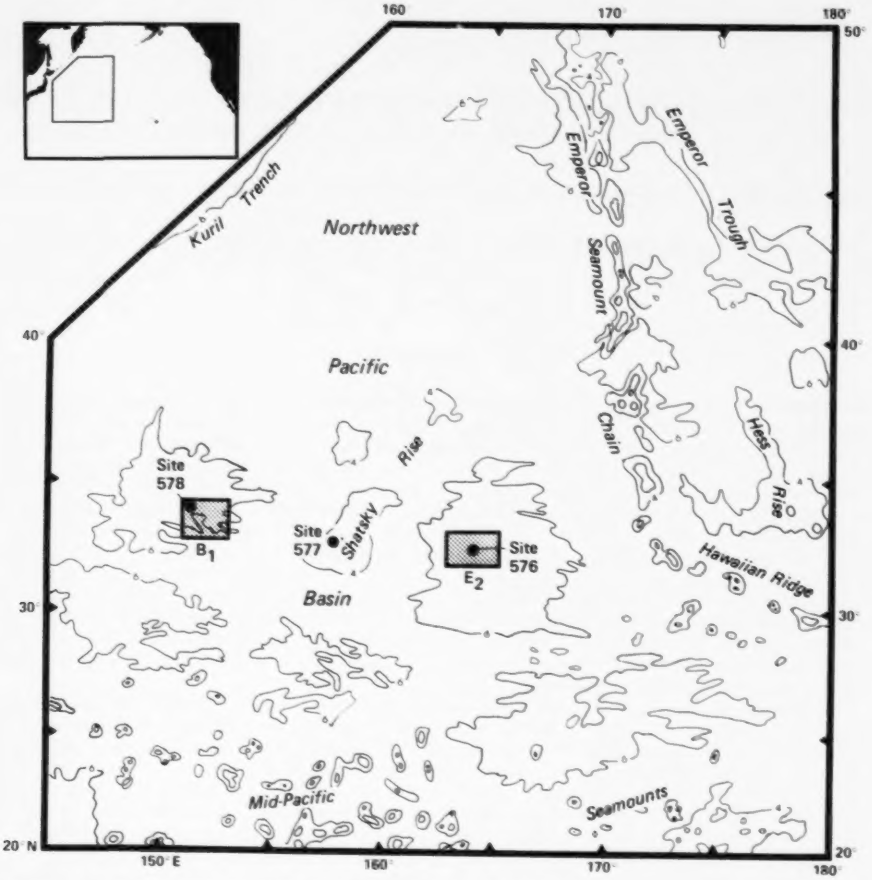

Figure 1. Location of study Areas E_2 (DSDP Site 576) and B_1 (DSDP Site 578). Generalized bathymetric contours (2-km contour interval) are redrawn from General Bathymetric Chart of the Oceans (GEBCO) Maps 5-06 (Iwabuchi, 1979) and 5-02 (Udintsev, 1980). Figure is after Damuth et al., 1983.

through deeps between the Mid-Pacific seamounts (Mantyla, 1975; Lonsdale and Smith, 1980). Two branches of the PBW flow through the Northwest Pacific Basin: (1) the western branch, which flows into and northeast along the Japan Trench and (2) the eastern branch, which generally flows northeast from east of the Shatsky Rise to the Emperor Seamount Chain (e.g., Gordon and Gerard, 1970; Mantyla, 1975).

Damuth et al. (1983) conducted echogram studies in order to define the sedimentation processes of the entire basin and to evaluate the potential of selected study sites for subseabed disposal of high-level nuclear waste. In the southeast, transparent sediment (with a few reflectors near the top) overlies a strong prolonged reflector (echo Type II, Damuth et al., 1983). In contrast, continuous, multiple reflectors occur in the northwest (echo Type I; Damuth et al., 1983). Although the areal extent of these two echo types corresponds very generally to the areal extent of the two predominant sediment types (brown clay and siliceous clay), most of the multiple reflectors probably correspond to volcanic ash layers. Two large areas with echo types characteristic of relatively fast bottom-water flow occur: (1) along the north side of the Mid-Pacific Seamounts where the PBW enters the Northwest Pacific Basin and (2) west of the Emperor Seamount Chain and north of the Shatsky Rise.

In 1980, *Vema* Cruise V3612 surveyed in detail three ~1° × 1° (latitude and longitude) candidate areas (designated B_1, E_2, and C_1) to study further the subseabed option for disposal of high-level nuclear waste (Damuth et al., 1980). Area E_2 is located east of the Shatsky Rise on oceanic crust of Early Cretaceous age (~130 m.y. ago; magnetic Lineation M-13). This area has subdued seafloor relief with a Type II echo character. Area B_1 is located west of the Shatsky Rise on oceanic crust of Late Jurassic age (~150 m.y. ago; magnetic Lineation M-21 or M-23/M-25). This area has subdued bathymetry and a Type I echo character. Site 576 was drilled in Area E_2 and Site 578 in Area B_1 during DSDP Leg 86 (Fig. 1).

During *Vema* Cruise 3612, we recovered eight piston cores and conducted five heat-flow and six sonobuoy refraction experiments at Area E_2 (Fig. 2, Tables 1-3). All the cores contained brown clay (Table 1); the digitized heat flow values (DHF) were typically ~55 mW/m^2 except in the northeastern part of Area E_2, where DHF Station 55 had a higher heat flow of 78 mW/m^2 (Table 2). Essentially linear thermal gradients were seen throughout (except at DHF Station 55, Hayes et al., 1983) and

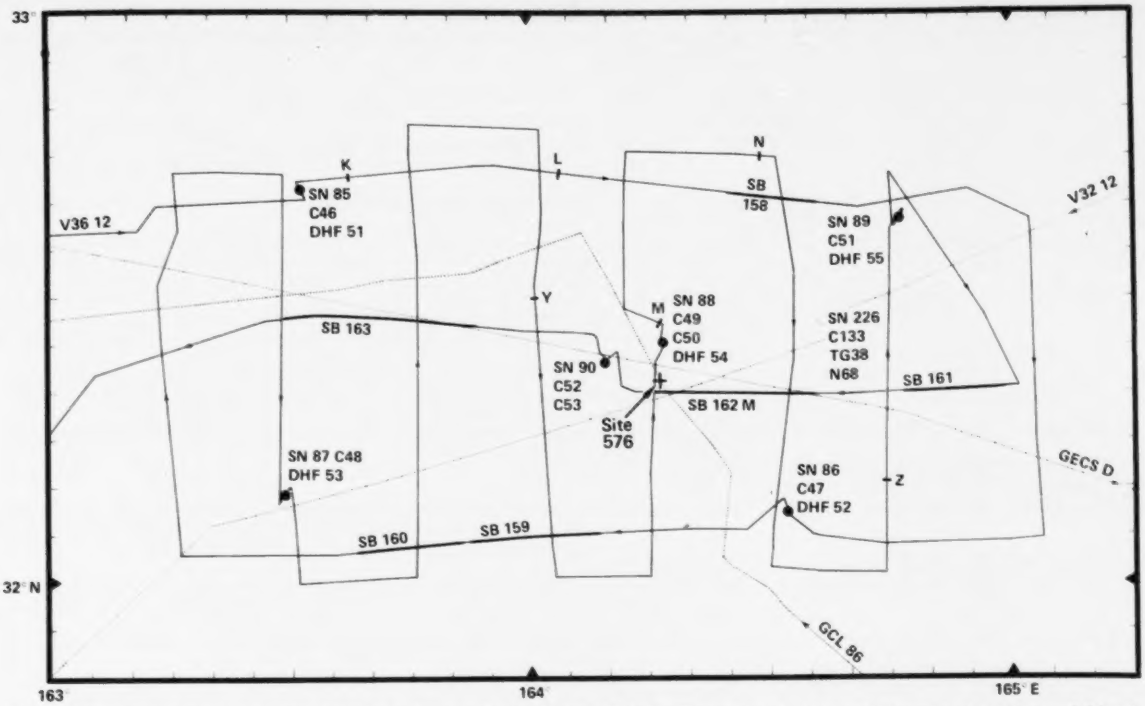

Figure 2. Cruise track lines and station location index map for study Area E_2 (after Damuth et al., 1980 and Hayes et al., 1982); track identification as follows: V = *Vema*, GCL = *Glomar Challenger*, GECS = Geosecs cruise. Sonobuoy (SB) and ship station (SN) locations are shown (C = core, DHF = digital heat-flow measurement, N = nephelometer measurement, TG = thermograd measurement). The ~100-Hz seismic reflection Profile Y–Z is shown in Figure 3; 3.5-kHz echogram Profiles K–L and M–N are shown in Figure 6. Location of DSDP Site 576 is shown.

argue against any significant recent erosion, high-velocity bottom-water flow, or hydrothermal circulation within the sediments for the area as a whole. Single-channel (~100 Hz) seismic-reflection profiles collected throughout Area E_2 reveal a three-part seismic section (Fig. 3): Unit I, a thin, relatively transparent section (brown clay layer); Unit II, an underlying, more reverberant section (carbonate and chert interbedded with brown clay); and Unit III, oceanic basement. The sonobuoy studies show that the sedimentary layer is ~0.5-km thick. Oceanic Layer 2 extends to ~8.3 km below sea level (bsl), and Moho lies at 10.1 km bsl (Table 3).

At Area B_1, we raised six piston cores and conducted four heat-flow and five sonobuoy experiments (Fig. 4, Tables 1–3). The cores are predominantly gray pelagic to siliceous clay with a brown clay layer at the top (Table 1). The heat-flow values range from ~43 to 57 mW/m^2 (Table 2). All thermal gradients were linear except at DHF Station 47, where the nonlinear gradient could be caused by recent erosion or bottom-current fluctuation. Single-channel (~100 Hz) seismic-reflection profiles were collected throughout the area. The three-part seismic section consists of an upper unit (I) of relatively transparent siliceous and brown clay, a more reverberant middle unit (II) of carbonate and chert interbedded with brown clay, and a lower unit (III) consisting of oceanic basement (Fig. 5). The upper unit exhibits dramatic northward thickening. The sonobuoy studies show that the total sediment layer increases in thickness from 0.36 km in the south to 0.63+ km in the northeast. Layer 2 extends to 8.09 km bsl, and the Moho lies at ~10.66 km bsl (Table 3).

This chapter presents geophysical survey results of study Areas E_2 and B_1 and focuses on the detailed bathymetry and near-surface sediment distribution maps primarily derived from 3.5-kHz echograms from *Vema* Cruise 3612. Determining areal variations in sediment-accumulation rates and the factors that may be controlling the rates is the primary goal of our study. In our discussion, the terms "sedimentation rate" and "sediment-accumulation rate" are used synonymously, recognizing that the two are not necessarily equivalent.

Although various factors may contribute to the present sediment disposition, systematic regional variations in sedimentation in the mid-gyre regions probably record significant fluctuations in bottom-water circulation. We therefore use the following simple model (e.g., Roberts et al., 1974) to interpret the major sediment-distribution patterns in terms of the present and past bottom-water circulation in Areas E_2 and B_1. It is commonly assumed that bottom water flowing past bathymetric highs will result in sediment thinning (e.g., moats) on their up-current sides and sediment thickening (drifts) on their down-current sides. Furthermore, looking downstream, the Coriolis force will accelerate the flow to the left of an obstruction and deaccelerate the flow to the right of it (in the Northern Hemisphere). Preferential sediment thinning and thickening should occur accordingly as a con-

Table 1. General description and location of cores raised from study Areas E_2 and B_1 on Cruise V3612[a].

Area	Core	Core location (lat., long.)	Length of core (cm)	General description
E_2	V36/12-C46	32°41.12′N, 163°31.7′E	1265	Yellowish brown silt above 2 cm. Generally yellowish brown mottled clayey silt to silty clay below 2 cm. Two yellowish brown silt layers at 623–633 cm and 920–968 cm. One volcanic ash layer at 1105–1113 cm.
E_2	V36/12-C47	32°05.95′N, 164°32′E	1262	Generally brown to yellowish brown mottled clayey silt to silty clay. Brown to yellowish brown silt above 35 cm and below 904 cm.
E_2	V36/12-C48	32°09′N, 163°29′E	1268.5	Yellowish brown silt with some laminations 0–91 cm. Yellowish brown mottled clayey silt to silty clay: 91–627 cm and 1065–1224 cm. Yellowish brown mottled silt: 627–1065 cm (coarse grained at 674–726 cm) and below 1224 cm. One volcanic ash layer at 1060–1065 cm.
E_2	V36/12-C49	32°24′N, 164°16′E	1192.5	Generally yellowish brown to brown clayey silt to silty clay above 552 cm, between 670–690, 780–820, and 859–974 cm; laminations present at 24–35 cm. Yellowish brown mottled silt at 552–648, 690–780, 842–859, 977–992, and 1014–1164 cm. One volcanic ash layer at 974–977 cm.
E_2	V36/12-GC50	32°24′N, 164°16′E	289	Same as above.
E_2	V36/12-C51	32°24′N, 164°46′E	1271	Yellowish brown mottled clayey silt: 0–305 cm with yellowish brown gravel layer at 17–28 cm. Yellowish brown mottled silt: 305–1059 cm. Brown clayey mottled clayey silt: 1059–1208 cm. Brown mottled silt: 1230–1256 cm. Numerous Mn nodules.
E_2	V36/12-C52	32°21.48′N, 164°11.15′E	1244	Yellowish brown to brown mottled clayey silt and lesser amounts of silty clay throughout core. Volcanic ash layer at 934–936 cm.
E_2	V36/12-GC53	32°24.74′N, 164°08.89′E	289	Same as above.
B_1	V36/12-C40	33°39.119′N, 152°13.194′E	—	—
B_1	V36/12-C41	33°21.12′N, 152°03.05′E	1266	Laminated olive brown silt: 0–9 cm interbedded yellowish brown to brown silty clay and clayey silt with brown silt (590–692 cm): 9–919 cm, brown clay and yellowish brown–brown silty clay: 919–1178 cm. Yellowish brown silt: 1200–1240 cm. Numerous volcanic ash layers.
B_1	V36/12-GC42	33°17.84′N, 152°02.80′E	46	Same as above.
B_1	V36/12-C43	33°45.03′N, 151°45.81′E	1247	Primarily gray-olive gray silt 0–49 cm. Interbedded gray/olive gray and gray/olive brown silty clay and clayey silt: 49–815 cm. Gray-olive gray silt at 605–641, 815–1028, and 1198–1226 cm. Gray-black clayey silt and silty clay 1028–1174 cm. Numerous volcanic ash layers.
B_1	V36/12-C44	33°23.09′N, 152°02.86′E	1258	Interbedded brown, yellowish brown, and grayish brown clayey silt: 0–604, 698–1258, and 604–690 cm. Brown silt.
B_1	V36/12-C45	33°05.63′N, 152°16.38′E	1264	Brown-yellowish brown silt; 0–9, 107–143, 445–594, and 907–1057 cm. Yellowish brown clayey silt: 12–107 cm. Interbedded yellowish brown and brown clayey silt and silty clay: 143–423 cm. Yellowish brown silty clay: 616–714 cm. Interbedded brown, yellowish brown, olive brown clayey silt and silty clay 736–1228 cm.

Note: C = piston core, GC = gravity core. For location of E_2 cores, see Figure 2; for location of B_1 cores, see Figure 4.

[a] Compilation of data from Heath (1981).

Table 2. V3612 revised heat-flow summaries for study Areas E_2 and B_1.[a]

DHF station	Latitude (N)	Longitude (S)	Water depth (m)	Probe penetration (m)	Number of probes	Thermal gradient (m°C/m)	Heat flow, Q (mW/m^2)
Area B_1[b]							
47-V36	33°39.6′	152°13.0′	5978	4.0	2	≥69	≥57.0[d]
48-V36	33°21.1′	152°03.1′	6003	12.7	4	56	45.6
49-V36	33°45.0′	151°45.9′	6021	12.7	3	57	46.5
50-V36	33°05.6′	152°16.4′	5888	12.7	5	52	42.7
Area E_2[c]							
51-V36	32°41.0′	163°31.5′	6162	12.7	5	61	52.5
52-V36	32°06.7′	164°33.2′	6117	12.7	5	61	52.4
53-V36	32°08.9′	163°28.5′	6081	12.7	5	66	57.0
54-V36	32°24.2′	164°16.4′	6200	11.9	5	68	59.0
55-V36	32°38.1′	164°45.7′	6269	12.7	5	90	78.0[e]

Note: For locations of E_2 heat-flow experiments, see Figure 2; for location of B_1 experiments, see Figure 4.

[a] From Hayes et al. (1983).

[b] Conductivity $K = 0.818$.

[c] Conductivity $K = 0.863$.

[d] Nonlinear.

[e] Slightly nonlinear.

sequence of bottom-water flow around local bathymetric highs. Thus, by comparing the mapped patterns of anomalous sediment thickness to the bathymetry, the bottom-water circulation patterns can be inferred for each time period defined by discrete reflector intervals.

Many mapped seismic-reflector intervals are defined by reflectors that correspond to cored volcanic ash layers; each of which is an isochron. The ages of these individual ash horizons were calculated from magnetostratigraphic and biostratigraphic sedimentation rates determined from Sites 576 and 578 (see Site 576 and 578 chapters, this volume).

BATHYMETRY AND ISOPACH METHODOLOGY

For survey Areas E_2 (Site 576) and B_1 (Site 578), the bathymetric and isopach maps of the various reflector

Table 3. V3612 sonobuoy summaries for study Areas E_2 and B_1.[a]

Area	Sonobuoy	Latitude (N)	Longitude (E)	Layer	Time (s)	Depth below seafloor (km)	Velocity (km/sec)	Refraction intercept	Layer thickness (km)	Layer thickness (s)
B_1	153-V36	33°51.0′	152°15.0′	1	7.96		1.50^b		5.970	
				2	8.54	0.63	2.20^b		0.63	0.58
				3	8.87	1.46	5.0	8.11	0.83	0.33
				4	9.22	2.49	5.8	8.39	1.03	0.35
				5	9.67	3.99	6.8	8.72	1.50	0.45
				6	9.85	4.69	7.5	9.01	0.70	0.18
				7			8.6	9.29		
B_1	156-V36	33°20.4′	151°51.0′	1	7.90		1.50^b		5.925	
				2	8.23	0.36	2.20^b		0.36	0.33
				3	8.57	1.23	5.0	7.83	0.87	0.34
				4	8.75	1.74	5.75	8.10	0.51	0.18
				5			6.45	8.29		
B_1	157-V36	33°7.8′	151°43.2′	1	7.939		1.50^b		5.954	
				2	8.288	0.36	2.08		0.36	0.35
				3	8.55	0.82	3.50^b		0.46	0.26
				4	9.03	2.19	5.75	8.20	1.37	0.48
				5			6.45	8.49		
E_2	158-V36	32°41.4′	164°25.2′	1	8.260		1.50^b		6.195	
				2	8.65	0.43	2.20^b		0.43	0.39
				3	9.23	2.18	6.0	8.36	1.75	0.58
				4	9.72	3.94	7.25	8.78	1.76	0.49
				5			8.25	9.13		
E_2	159-V36	32°5.4′	164°9.0′	1	8.013		1.50^b		6.01	
				2	8.41	0.43	2.17		0.43	0.40
				3	8.55	0.66	3.50^b		0.23	0.14
				4	8.81	1.37	5.30	8.15	0.71	0.26
				5	9.19	2.55	6.15	8.39	1.18	0.38
				6			6.80	8.66		
E_2	160-V36	32°4.2′	163°53.4′	1	8.055		1.50^b		6.042	
				2	8.62	0.70	2.50^b		0.70	0.56
				3	8.73	0.97	4.80	8.13	0.27	0.11
				4	9.19	2.30	5.80	8.35	1.33	0.46
				5	9.61	3.67	6.60	8.66	1.37	0.42
				6			8.15	9.11		
E_2	161-V36	32°20.4′	164°58.8′	1	8.173		1.50^b		6.130	
				2	8.66	0.40	1.61		0.40	0.50
				3	8.67	0.407	2.50^b		0.007	0.003
				4	9.12	1.737	5.85	8.38	1.33	0.45
				5			6.30	8.59		
E_2	162-V36	32°19.8′	164°35.4′	1	8.091		1.50^b			
				2	8.55	0.63	2.70		0.63	0.466
				3	8.63	0.73	3.00^b		0.10	0.07
				4	8.80	1.08	4.050	7.91	0.35	0.17
				5	9.16	1.99	5.050	8.28	0.91	0.36
				6	9.59	3.22	5.800	8.59	1.23	0.43
				7			6.250	8.84		
E_2	163-V36	32°27.0′	163°53.4′	1	8.082		1.50^b		6.061	
				2	8.55	0.42	1.78		0.42	0.472
				3	8.57	0.44	2.50^b		0.02	0.016
				4	8.90	1.29	5.20	8.20	0.85	0.33
				5	9.11	1.90	5.85	8.43	0.61	0.21
				6	9.57	3.50	6.90	8.69	1.60	0.46
				7			7.40	8.92		

Note: For location of E_2 sonobuoys, see Figure 2; for location of B_1 sonobuoys, see Figure 4.

[a] From Hayes et al. (1983).

[b] '*D* velocities are assumed.

intervals are based primarily on 3.5-kHz echogram data collected from *Vema* Cruise 3612. The seafloor and distinctive sub-bottom reflectors were digitized at 1-min. intervals from the original 3.5-kHz echograms. Additional data were digitized from the various cruises shown in Figures 2 and 4. For the bathymetric maps, the digitized two-way travel times were converted to corrected meters by using Carter's correction tables (Carter, 1980). For isopach maps, the digitized two-way travel times to individual reflectors were converted to meters below seafloor (bsf) by using an assumed sediment velocity of 1550 m/s. This velocity is consistent both with DSDP/

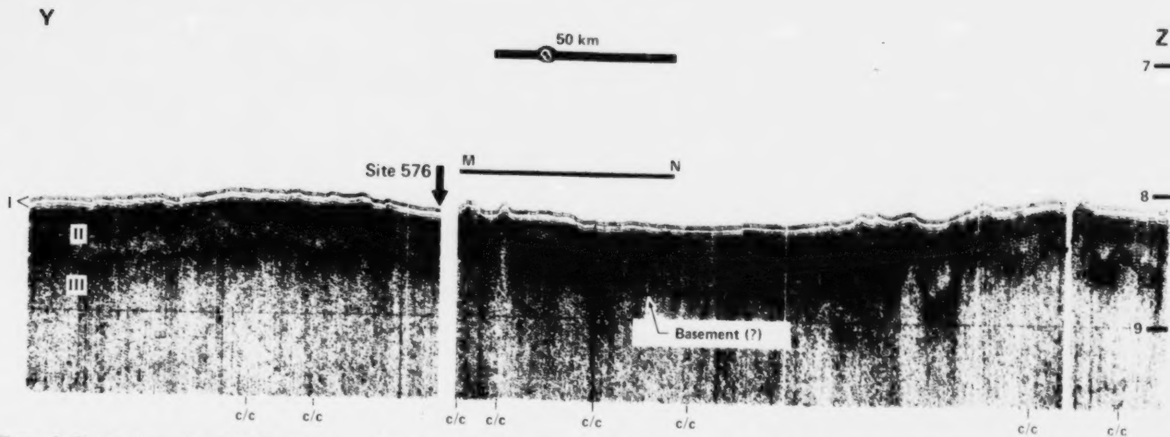

Figure 3. Single-channel, ~100-Hz seismic reflection Profile Y–Z (location shown in Fig. 2). The locations of the 3.5-kHz echogram Profile M– (displayed in Fig. 6) and DSDP Site 576 are shown. C/C = change course. Vertical exaggeration is 50:1.

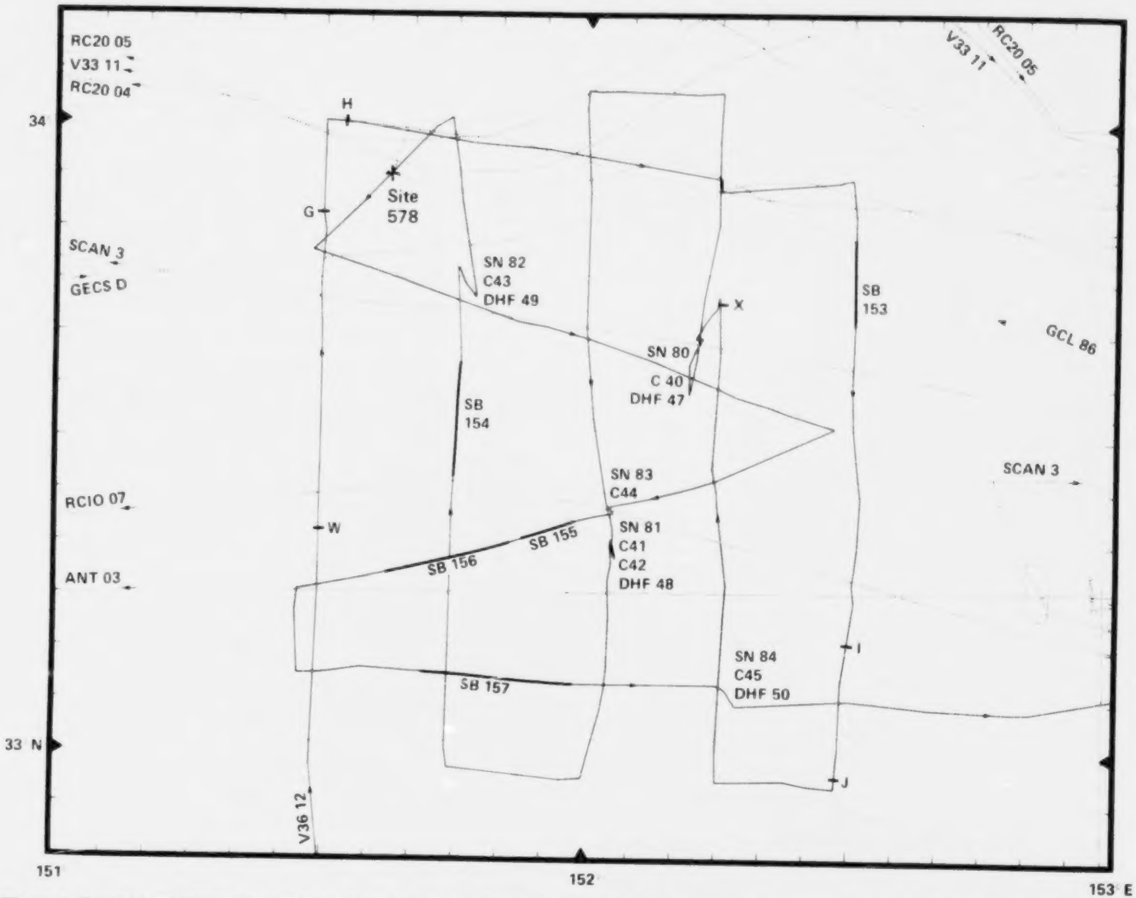
RC20 05
V33 11
RC20 04
34
33 N
151
152
153 E
SCAN 3
GECS D
RC10 07
ANT 03
V36 12
GCL 86
H
G
Site
578
SN 82
C43
DHF 49
X
SN 80
C 40
DHF 47
SB
153
SB
154
SN 83
C44
SN 81
C41
C42
DHF 48
W
SB 155
SB 156
SB 157
SN 84
C45
DHF 50
I
J

Figure 4. Cruise track lines and station-location index map for study Area B_1 (after Damuth et al., 1980 and Hayes et al., 1983); track identification as follows: V = *Vema*, RC = *Robert D. Conrad*, GCL = *Glomar Challenger*, ANT = Antipode cruise, SCAN = *ARGO*, GEOS = Geosecs cruise on *Melville*. Sonobuoy (SB) and ship station (SN) locations are shown (C = core, DHF = digital heat-flow measurement). The ~100-Hz seismic reflection Profile W–X is shown in Figure 5; 3.5-kHz echogram Profiles G–H and I–J are shown in Figure 11.

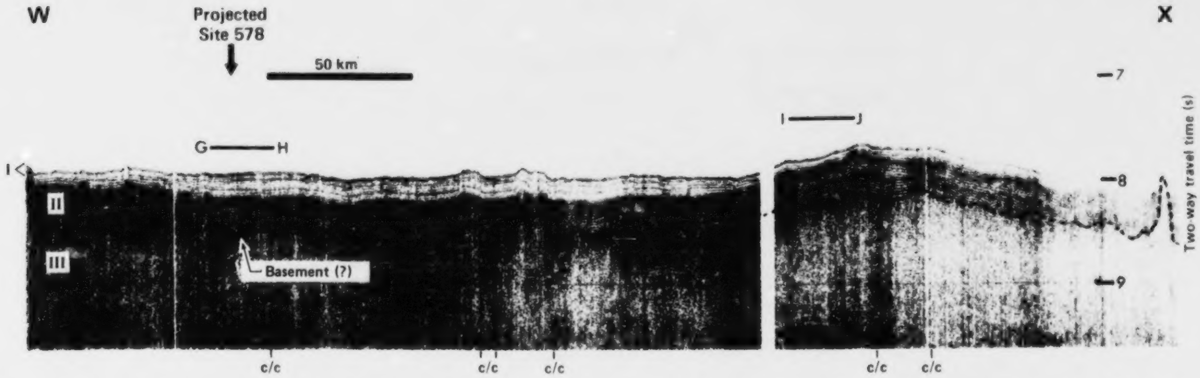

Figure 5. Single-channel ~100-Hz seismic reflection profile W–X (from Damuth et al., 1980 and Hayes et al., 1983); for location of Profile W–X, see Figure 4. Location of 3.5-kHz echogram Profiles G–H and I–J are shown, as well as the projected location of DSDP Site 578. Note the dramatic northward thickening of the relatively transparent upper section from W to H and both thickening and thinning in the region of Profile I–J. C/C = change course. Vertical exaggeration is 50:1.

IPOD Leg 86 shipboard velocity profiles (see site chapters, this volume) and with velocity studies of piston cores and 3.5-kHz hydrophone-pinger studies in these areas (Flood, pers. comm., 1983; Hayes et al., 1983). We estimate the digitization error to be ~1 m. Depth and sediment thickness crossover errors at intersecting tracks were calculated in order to assess the internal consistency of the data. Crossover errors may be caused by problems in navigation, reflector misidentification, and instrumentation errors. The average crossover error of Reflector R_1 (seafloor) for the V3612 survey at study Area E_2 is ~3 m and is ~6 m at study Area B_1. Average crossover errors for other cruises with respect to the V3612 surveys are greater, as much as ~30 m for *Glomar Challenger* Leg 86. At study Areas E_2 and B_1, digitized reflectors from the V3612 survey are internally consistent to within 1 m for shallow reflectors and 2 m for deep reflectors (e.g., R_5). For other cruises, the errors with respect to the V3612 survey are greater (up to 10 m). For all reflectors, selected tracks of cruises other than V3612 were adjusted by adding constant corrections to the recorded depths.

STUDY AREA E_2—SITE 576

Seismic Section

At Area E_2, 3.5-kHz echograms reveal that two seismic subunits (Fig. 6) comprise the seismic Unit 1 defined by 100-Hz seismic profiles (Fig. 3). The uppermost subunit, Reflector R_1 (seafloor) to Reflector R_3, consists of continuous, multiple, sharp and parallel reflectors. This subunit corresponds to a section of brown clay with a few volcanic ash layers. A few small areas with relatively steep gradients return hyperbolic reflections (Fig. 6). Two strong, continuous reflectors, R_2 and R_3, occur at ~12 m bsf and ~22 m bsf, respectively. Reflector R_2 corresponds to an ~1.295 m.y. old volcanic ash layer cored at 12.18 m bsf in Hole 576. Reflector R_3 does not correspond to any observed major lithologic change in either Hole 576 or Hole 576B. However, at the expected depth of the reflector, a large void occurs in Core 576-3 and highly disturbed intervals occur in Sections 4 and 5 of Core 576B-3. Thus, Reflector R_3 could represent a lithologic boundary (a volcanic ash layer?) that was unsampled. The reflector might also be caused by the sharp decrease in porosity in the DSDP cores at about the depth of the reflector (Flood, pers. comm., 1983). The interpolated age of such a boundary is ~7.2 m.y. Both Reflectors R_2 and R_3 are regional in extent and can be traced at least 190 km to the southeast of Site 576. Reflector R_3 can be traced ~380 km westward to the eastern flank of the Shatsky Rise, where it disappears. Although Reflector R_2 is discontinuous on the eastern flank of the Shatsky Rise, its distinct character is very similar to that of Reflector 1-e observed on the Shatsky Rise at Site 577. Volcanic ash layers cored at the level of Reflectors 1-e and R_2 at both sites have essentially identical ages. A weaker, but continuous, sharp reflector occurs between Reflectors 2 and 3 (Fig. 6) at ~16 m bsf. This reflector probably corresponds to a series of thin, closely spaced ash layers cored in Hole 576B that have ages ranging from 1.79 m.y. to ~2.37 m.y.

Although the reflectors in the upper subunit are generally parallel, detailed examination of the echograms (e.g., Fig. 6) reveals local variations in the subunit thickness near abyssal hills. The character of the reflectors in the areas of the thickened sections (commonly at the base of steep slopes) suggests that they represent sediment-slide deposits (e.g., areas A and B in Fig. 6). In contrast, a gradual thinning of both intervals R_1–R_2 and R_2–R_3 occurs over many abyssal hills (e.g., Area C on Fig. 6). Very localized thinning is also observed at the base of steep slopes and is probably caused by accelerated bottom-water flow in some areas (e.g., Area D, Fig. 6). In other areas (possibly part of Area E, Fig. 6) the thinning may represent slide scars. In Figure 6, both thinning and thickening appear to be more prevalent in the interval R_1–R_2 (0–1.3 m.y. ago) than in the interval R_2–R_3 (1.3–7.2 m.y. ago).

The lower subunit of seismic Unit 1 is primarily a thick transparent section with discontinuous, sharp to slightly prolonged reflectors (Fig. 6). The transparent section corresponds to brown clay. Reflector R_4 (the prevalent discontinuous reflector) occurs about two-thirds of

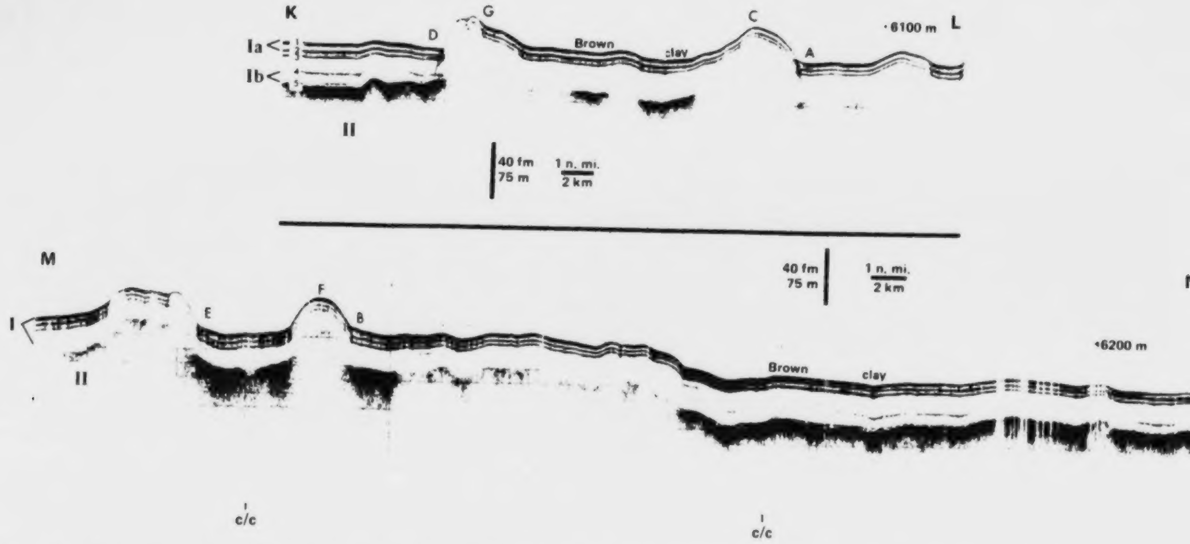

Figure 6. High-resolution seismic Profiles (3.5-kHz echograms) K–L and M–N in study Area E_2 (locations in Fig. 2). Digitized reflectors are numbered and R_2 is 1.295 m.y. old, R_3 = ~7.2 m.y. old, R_4 = ~25 m.y. old, and R_5 is ~70 m.y. old. Areas A and B show localized, near-surface sediment slide deposits; Area C exhibits gradual thinning of reflector intervals on the slope and also illustrates the diffuse character of R_5 on relative highs; Area D shows gradual thinning at the margin of the trough caused by accelerated bottom-water flow; Area E exhibits thinning and thickening caused by buried sediment slide scar and deposit; and Areas F and G illustrate the diffuse character of R_5 on highs. C/C = course change. Profile K–L: vertical exaggeration is 46:1; Profile M–N: vertical exaggeration is 42:1.

the way down the lower subunit and at Site 576 its age is assumed to be ~25 m.y. It is possible that R_4 does not represent a single lithologic unit. Reflector R_4 does not correlate with any observed lithologic change in the Site 576 cores; the cause of the discontinuous reflectors thus remains a puzzle.

Seismic Unit II consists of several different 3.5-kHz echo types. On abyssal hills these echoes are generally diffuse, weak, and prolonged (e.g., Areas C, F, and G in Fig. 6). A few weak hyperbolic reflections are observed along the steep slopes of abyssal hills (e.g., Area G in Fig. 6). In contrast, areas of smoother slopes and lower gradients between abyssal hills return strong, sharp to prolonged echoes. In some of these areas, multiple strong echoes can be discerned, and at Site 576 these appear to onlap the more diffuse echoes returned from abyssal hills. The relatively smooth, strong echoes probably correspond to the Campanian to early Maestrichtian (~70 m.y. ago) carbonate turbidites interbedded with brown clay cored at Site 576. The weak diffuse echoes on the abyssal hills have several possible sources: (1) carbonate layers equivalent to those cored at Site 576, (2) a discontinuous chert layer at ~55 m bsf that was not cored at Site 576, and (3) a single, generally continuous chert layer, but with considerably more relief than the seafloor (note that the chert was cored at 76 m bsf whereas the diffuse echo commonly occurs elsewhere at 55 m bsf). Reflector 5 is the first prolonged echo encountered at the base of the transparent seismic Unit I and defines "acoustic basement" on 3.5-kHz echograms.

Bathymetry (Reflector R_1)

The seafloor at Area E_2 has a regional slope from the southwest (6017 m) to the northeast (6267 m, Fig. 7). Small ridges and isolated abyssal hills occur throughou the area; the shoalest abyssal hill reaches a depth o 5865 m and has relief of 305 m. The seafloor is characterized by a series of lineated ridges that trend northwes to southeast (~130°). This trend is parallel to observed seafloor-spreading magnetic lineations in Area E_2 and strongly suggests that the ridges are related to mid-ocean ridge rifting phenomena (e.g., fault blocks, scarps, and volcanic ridges).

The study area can be divided into six bathymetric provinces (Fig. 8, Table 4): a northeast province with very subdued bathymetry (A), a southeast province with lineated and relatively steep ridges and valleys (B), a northwest-trending central valley and ridge (C), a province southwest of the central valley with subdued relief (D), and provinces of abyssal hills along the southern margin of D and in the northwestern corner of the site survey (Provinces E and F, respectively). Computer-generated, perspective drawings of the seafloor at Site E_2 (Fig. 9) provide a better "sense" of the very low relief within the study area.

Intervals R_1–R_2 and R_2–R_3

The regional and local variations in the R_1–R_2 interval thicknesses are similar to those of the R_2–R_3 interval (Figs. 10A and 10B). The thickness of interval R_1–R_2 is generally 12 m (sedimentation rate = 9.2 mm/1000 yr.) in the central and western areas but decreases to a minimum of 3 m (2.32 mm/1000 yr.) in the northeast. The thickness of interval R_2–R_3 varies from 10 to 11 m (1.79 mm/1000 yr.) in the southwest to ~4 m (0.68 mm/1000 yr.) in the northeast. The thinning to the northeast is also observed in the other reflector intervals. Local variations in these interval thicknesses generally range from 1

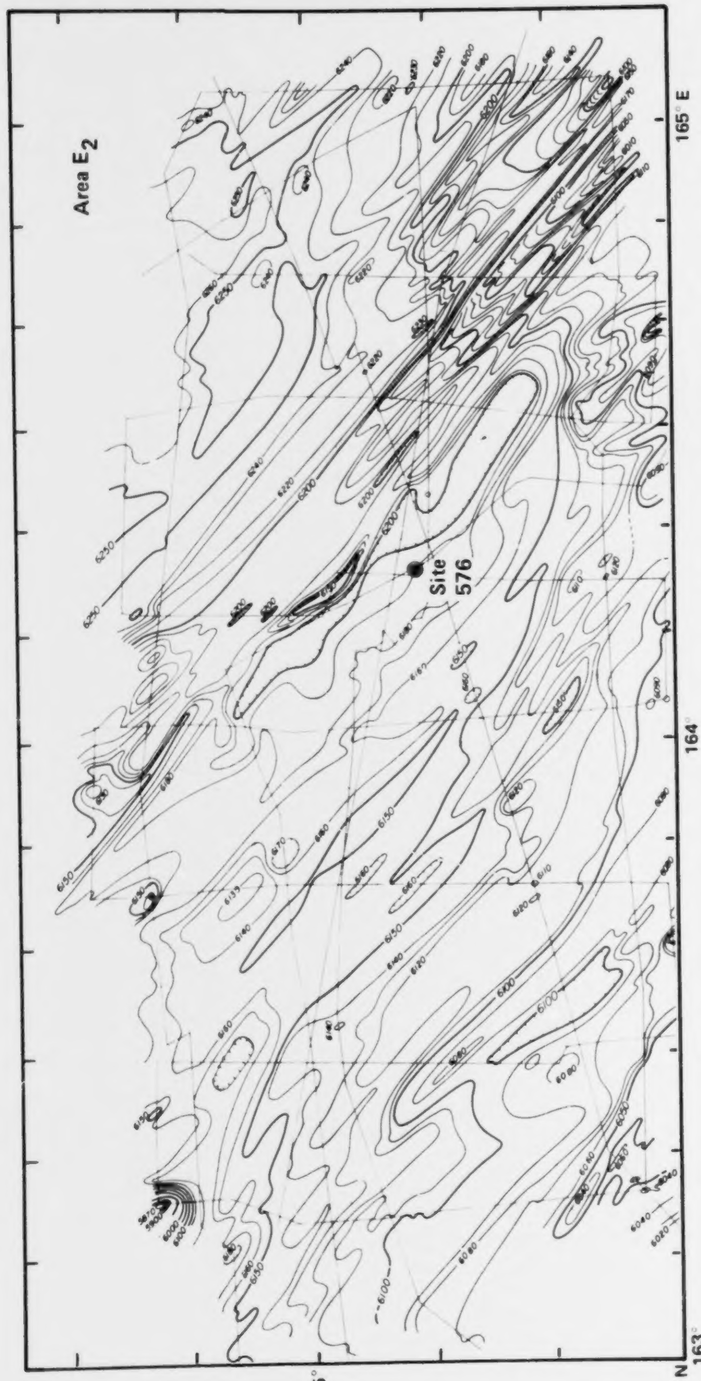
Area E_2
Site 576
163°
164°
165° E
32° N
32.5°
6250
6240
6220
6200
6150
6100
6080
6060
6040
6020

Figure 7. Bathymetry of study Area E_2. Depths are in corrected meters, using the correction tables of Carter (1980). Primary contour interval is 10 m.

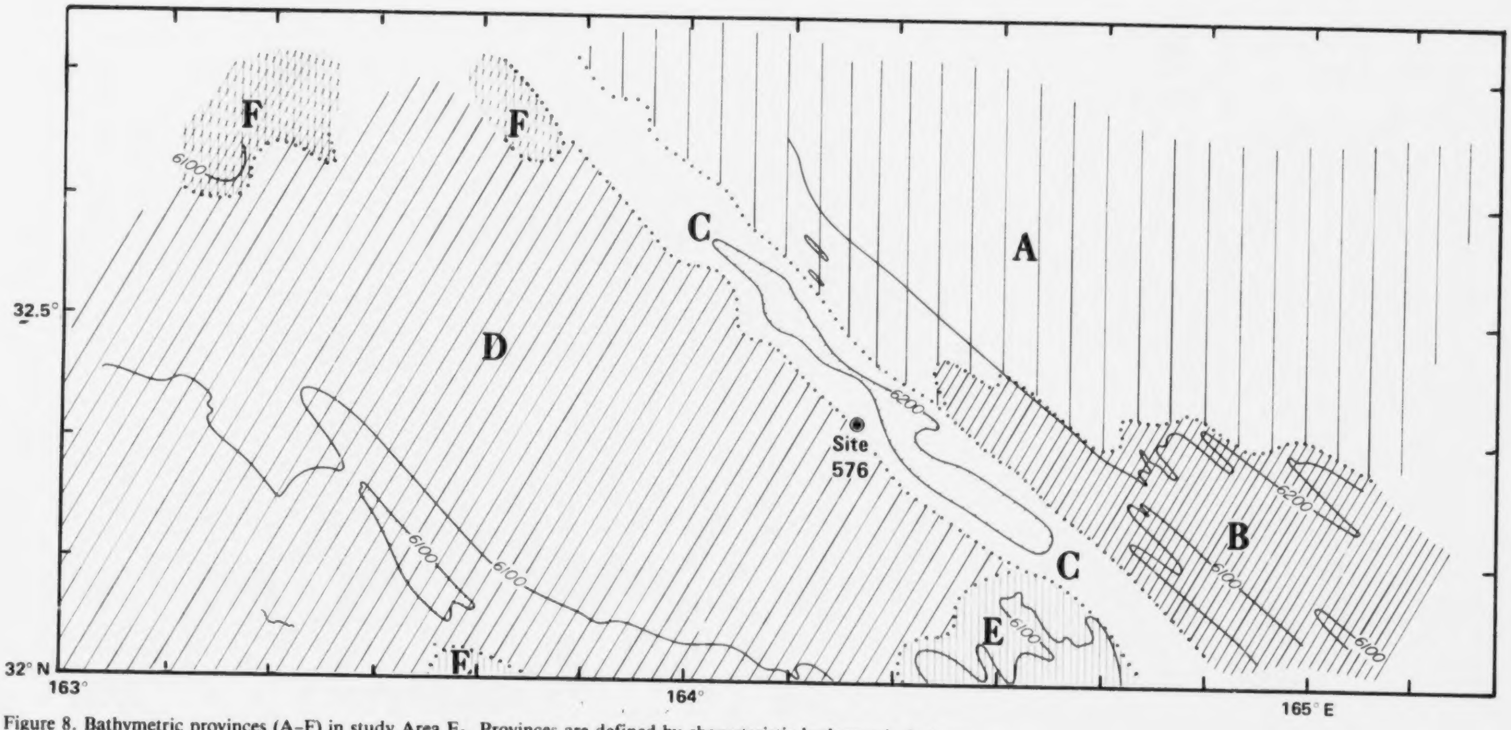
A
B
C
C
D
E
F
F
F
6100
6200
Site 576
32.5°
32° N
163°
164°
165° E

Figure 8. Bathymetric provinces (A–F) in study Area E_2. Provinces are defined by characteristic bathymetric features.

Table 4. Characteristics of bathymetric features in provinces of study Area E_2[a].

Province	Depth range (m)	Relief (m)		Slope (°)		Wavelength (km)
		General	Maximum	General range	Maximum	
A	6200-6267		38	0.1-0.5	~1.5	3-9
B	6010-6220		160	0.5-3	8	Common: 4-5 Maximum: 9-10
C	~6150-6200	30-40	58	<3	6	5-11
D		<50	<80	0.1-1.0	2-3	7-23
E						
Western	6035-6073		38	4		
Eastern	6043-6140	30	42	0.5-1.5	3	
F	5863-6170	17-44	307	0.5-2	4.5	

[a] Based on Figure 7.

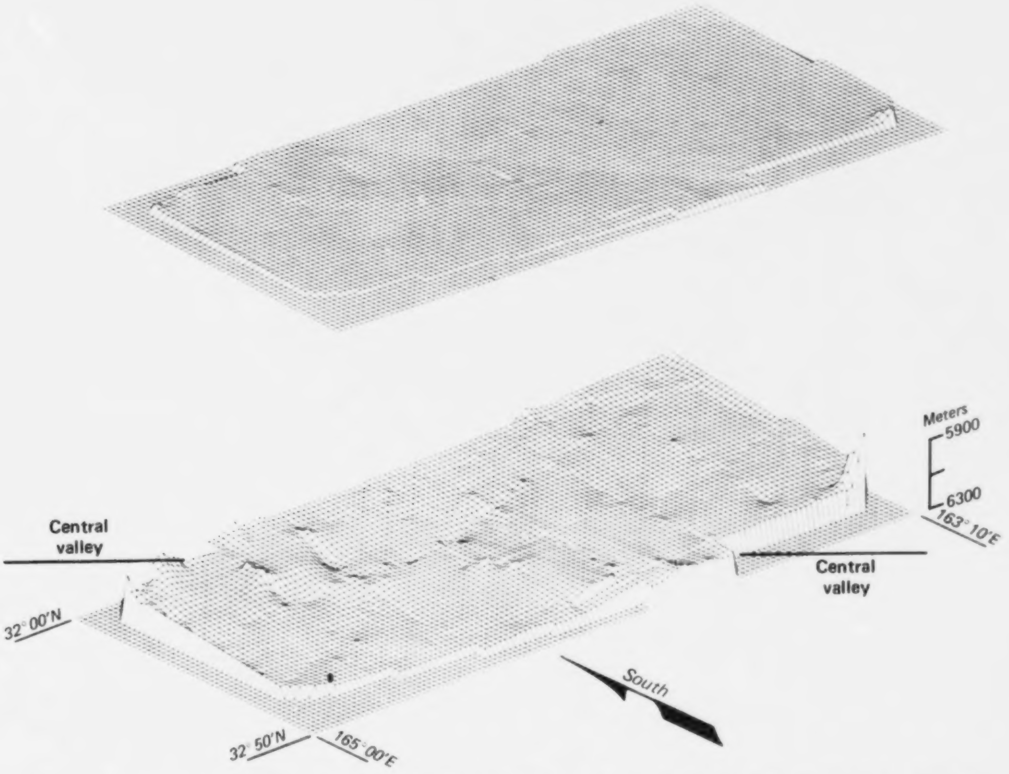

Figure 9. Three-dimensional south-looking view of the seafloor at study Area E_2. Upper plot with smaller vertical exaggeration (10:1) has same coordinates as lower plot (vertical exaggeration is 50:1). Note northwest-trending central valley and the abyssal hills along the borders of E_2.

to 4 m and are commonly <2 m. However, in moats the R_1–R_2 thicknesses decrease as much as 6 m and the R_2–R_3 thickness may vary by as much as 10 m (Province B).

Variations in sedimentation rate are related to the direction, steepness, and extent of seafloor slopes. If anomalous sections were primarily the result of unidirectional bottom-water flow, one would expect that one slope direction would consistently have a thinner sediment section while the opposing slope would be consistently thicker. Because anomalously thick and thin zones can be observed in any hill, slope, or trough setting (Table 5) factors other than regional bottom-water flow (e.g., mass wasting) must contribute to anomalous sedimentation. However, within regions characterized by relatively steep seafloor slopes, it is clear that anomalously thin sedimentary sections occur preferentially: (1) on northeast facing slopes (e.g., eastern portion of Province F; southwest portion of Province D) and (2) along the margins of small basins and troughs. These relationships strongly suggest that bottom-water flow does play an im-

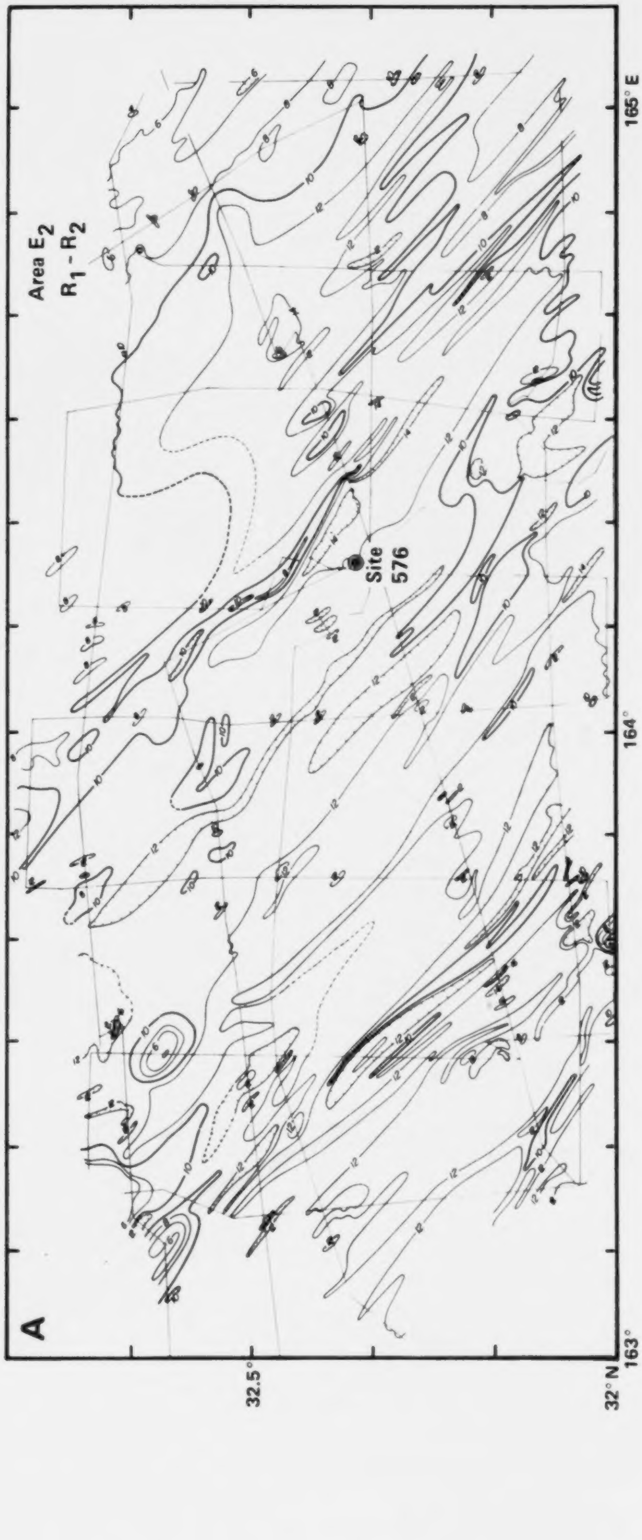
A
Area E$_2$
R$_1$ - R$_2$
Site 576
165° E
164°
163°
32.5°
32° N

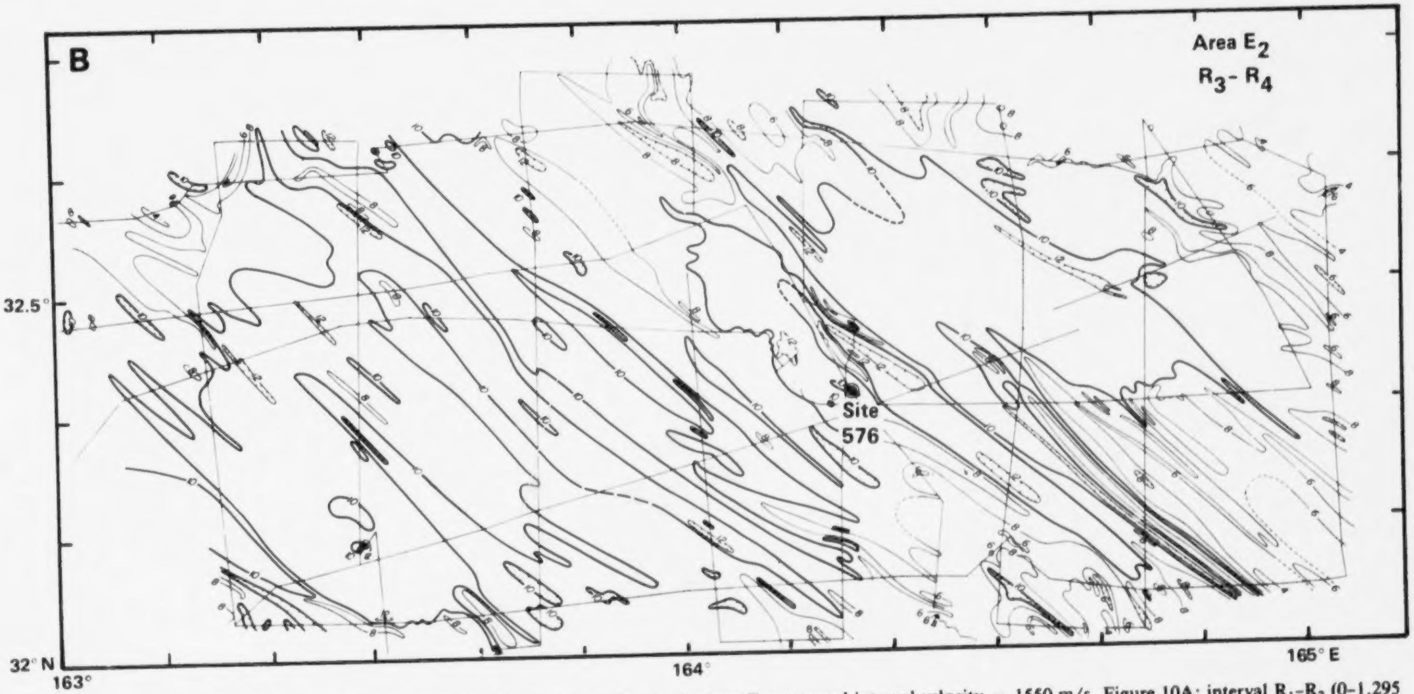
B
Area E_2
R_3- R_4
Site
576
32.5°
32° N
163°
164°
165° E

Figure 10. Isopach maps for the various 3.5-kHz seismic reflector intervals in study Area E_2; assumed interval velocity = 1550 m/s. Figure 10A: interval R_1–R_2 (0–1.295 m.y.), Figure 10B: interval R_2–R_3 (1.295–7.2 m.y.), Figure 10C: R_3–R_5 (7.2–~70 m.y.). Contour interval is 2 m for Figures 10A and 10B and the primary contour interval for Figure 10C is 4 m.

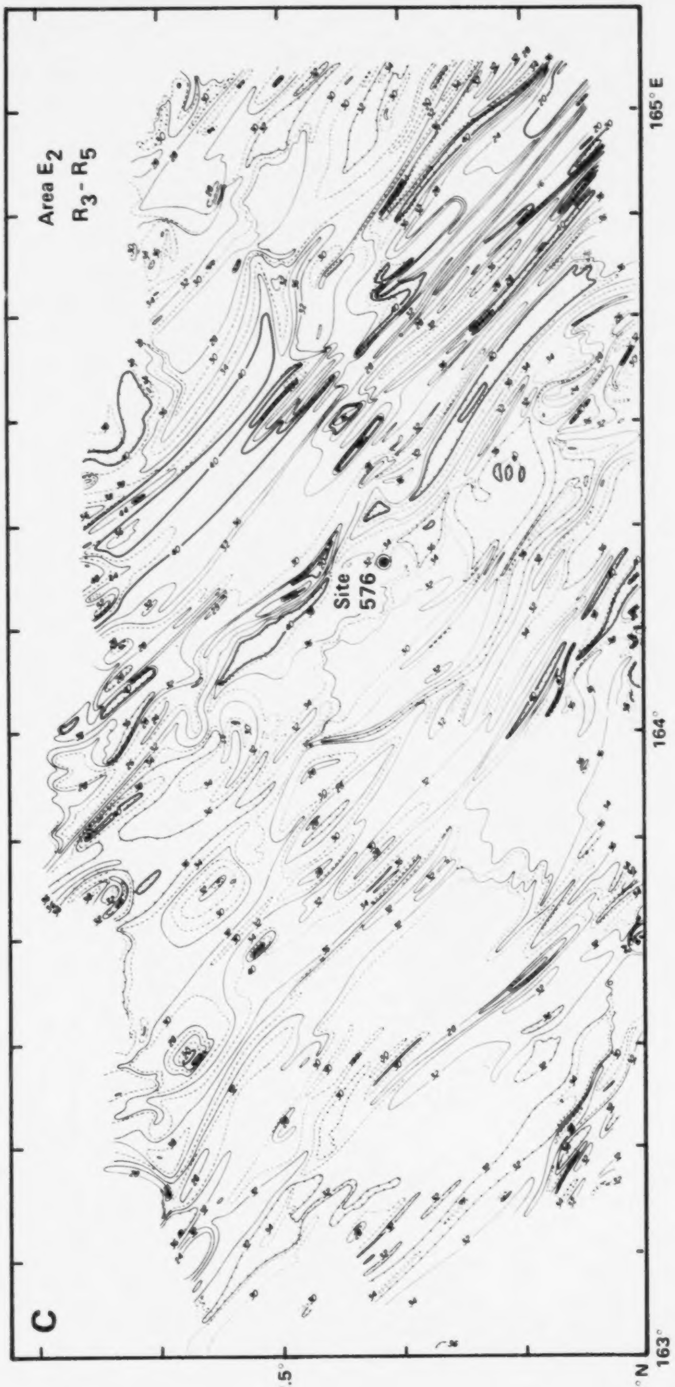
C
Area E_2
R_3 - R_5
Site 576
163°
164°
165° E
32° N
32.5°

Figure 10. (Continued).

Table 5. Nature of the seafloor slope in areas with anomalous sediment accumulation rates.[a]

Reflector interval	Seafloor slopes to NE (%)	Seafloor slopes to SW (%)	Centered on seafloor low (%)	Centered on seafloor high (%)	At base of NE slope (%)	At base of SW slope (%)
Anomalously thin zones						
R_1-R_2	55 (n = 47)	23 (n = 20)	22 (n = 19)			
R_2-R_3	38 (n = 31)	17 (n = 14)	5 (n = 4)	28 (n = 23)	7 (n = 6)	5 (n = 4)
R_3-R_5	42 (n = 40)	16 (n = 15)	4 (n = 4, moat)	29 (n = 28)	7 (n = 7)	2 (n = 2)
Anomalously thick zones						
R_1-R_2	40 (n = 36)	12 (n = 11)	25 (n = 22)	7 (n = 6)	6 (n = 5)	10 (n = 9)
R_2-R_3	24 (n = 25)	10 (n = 10)	30 (n = 31)	7 (n = 7)	12 (n = 12)	17 (n = 17)
R_3-R_5	30 (n = 37)	9 (n = 11)	27 (n = 34)	5 (n = 6)	19 (n = 24)	10 (n = 13)

Note: n = number of observations, % = $(n/\Sigma n) \times 100$ for each horizontal series.

[a] Based on comparison of Figure 10 with Figure 7.

portant role in effecting the ultimate sediment disposition. According to our simple model, bottom-water flow either to the southwest or southeast is indicated.

Two "basins" at ~32.6°N, 163.2°E and at 32.6°N, 163.5°E have anomalously thin sediment sections and may actually be moats around seamounts that were undetected by the survey.

Interval R_3-R_5

Interval R_3-R_5 is the integral of intervals R_3-R_4 and R_4-R_5. The uncertainty involved in correlating R_4 from one occurrence to another precludes detailed analysis of regional sedimentation rate variations within interval R_3-R_5. Reflectors 3 and 5 occur throughout most of the site survey and therefore show a spatially complete picture of the variations in sedimentation rate during R_3-R_5 times (Fig. 10C). The regional interval thickness decreases northeastward from ~32 m in the southwest to ~28 m in the northeast. Province C has an average thickness of 38–39 m in the central valley.

The local variations in thickness of R_3-R_5 are similar to the upper intervals (Table 5). Both anomalously thick and thin zones occur primarily on northeast-sloping seafloor. Anomalously thin zones are also centered on bathymetric highs and a few occur along the margins of troughs. Thick zones are also centered on bathymetric lows, margins of troughs, and bathymetric highs. The relatively high proportion of R_3-R_4 thick zones at the margins of troughs (compared to R_1-R_2 and R_2-R_3) may suggest a greater debris flow/turbidity flow or less bottom-water influence on the sedimentation in R_3-R_4 time (~25–7 m.y. ago).

Like the upper intervals, the relationships of thin zone/northeast slope, thick zone/southwest slope are observed in interval R_3-R_5 in regions of steep seafloor gradients (e.g., the ridges in Province B); these relationships also suggest bottom-water flow to the southeast or southwest. However, R_4-R_5 thickness minima occur along the northeast margins of troughs and therefore suggest opposite flow direction. Because of the small number of observations of R_4-R_5, the resolution of this apparent discrepancy is unclear. The R_4-R_5 observations may simply record local flow directions.

STUDY AREA B_1—SITE 578

Seismic Section

In the southern part of study Area B_1, there are four sets of strong, continuous, and generally parallel 3.5-kHz reflectors (Fig. 11), all within the 100-Hz seismic Unit I (Fig. 5). The uppermost group includes the seafloor (R_1). Because the uppermost reflector of the second group is not continuous throughout Area B_1, the lower, stronger reflector of the second group was defined as Reflector R_2. The uppermost reflector of the third group is defined as R_3 and commonly is weaker than the underlying reflectors in the third group. The uppermost reflector of the fourth group (composed of a series of strong, continuous reflectors) is defined as R_4; the weak, somewhat discontinuous reflector at the base of the fourth group is defined as R_5 (the fourth reflector below R_4). Because this reflector merges with the overlying reflectors in some areas and fades out in a few areas, the intervals involving R_5 are not as well defined as the overlying intervals. Reflector R_6 is the relatively strong, continuous reflector that is separated from R_5 by a thick semitransparent section.

Within Area B_1 all reflectors become progressively deeper and more separated to the north, illustrating pronounced increases in sedimentation rates (Fig. 11). Thus, many reflectors within each group that are masked in the condensed section in the south become quite pronounced to the north.

Most of the continuous reflectors are caused by volcanic ash layers that were cored at Site 578. Reflector R_2 is equivalent to Reflector 1-f as defined at Site 578 (see Site 578 chapter, this volume) and probably corresponds to volcanic ash Layer #8 (~0.475 m.y. ago). Reflector R_3 is equivalent to Reflector 2-a at Site 578; this reflector does not correlate with any major observed lithologic change. The depth of R_3 corresponds to a magnetostratigraphic age of ~0.975 m.y. Reflector R_4 is Reflector 3-g at Site 578; this reflector correlates with volcanic ash Layer #50, which is ~2.44 m.y. old. At Site 578 horizons corresponding to Reflectors R_5 and R_6 are below the depth of penetration of the 3.5-kHz echograms; hence positive correlations of these deep reflectors with volcanic ashes cored at Site 578 are not possible. Extrapolation of R_5 to Site 578 yields an inferred R_5 age of ~5–6 m.y.

Bathymetry (Reflector R_1)

The seafloor in study Area B_1 generally slopes north and ranges in depth from 5740 m on the southern margin of the area to 6040 m in the northern part (Fig. 12). Abyssal hills occur primarily in the northern half of the site survey. The maximum local relief in the study area is only 79 m on an abyssal hill located at 33.7°N, 152.25°E.

The study area can be divided into three distinct bathymetric provinces: the southern Province A, with a very regular north–northeast-sloping seafloor, the central Prov-

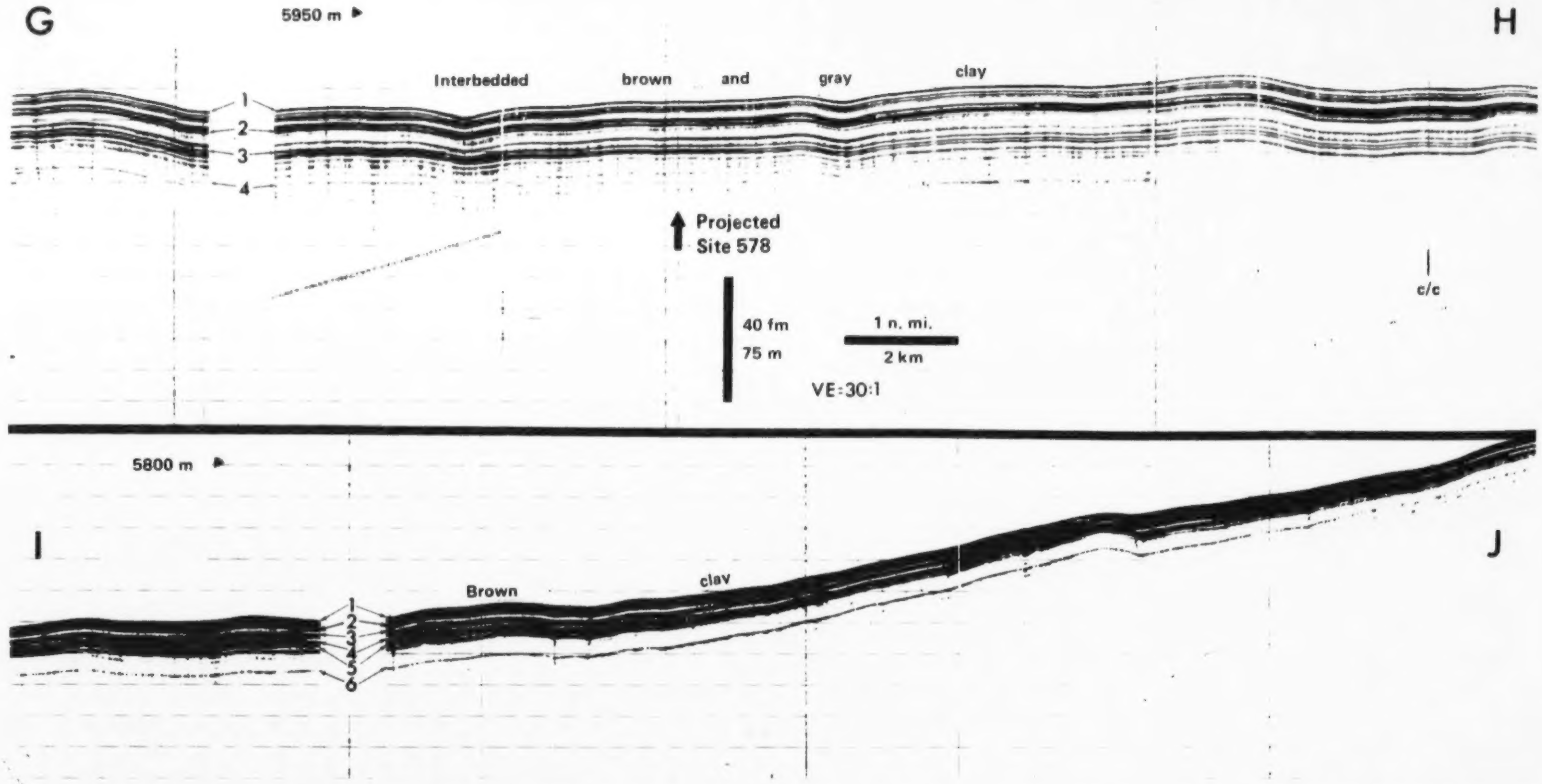

Figure 11. High-resolution seismic Profiles (3.5-kHz echograms) G–H and I–J in study Area B_1 (after Damuth et al., 1980 and Hayes et al., 1983). Profiles are located in Figure 4. Digitized reflectors are labeled and R_2 is 0.475 m.y. old, R_3 is 0.975 m.y. old, R_4 is ~2.44 m.y. old, and R_5 = ~5–6 m.y. old. Profile G–H was recorded in the northern part of B_1 where the sedimentation rate is relatively high, whereas Profile I–J was recorded in the southern part of B_1 where the sedimentation rate is relatively low. In Profile I–J, note the southward thinning of reflector intervals (toward J). Site 578 is projected westward onto Profile G–H. C/C = course change. Vertical exaggeration is 30:1.

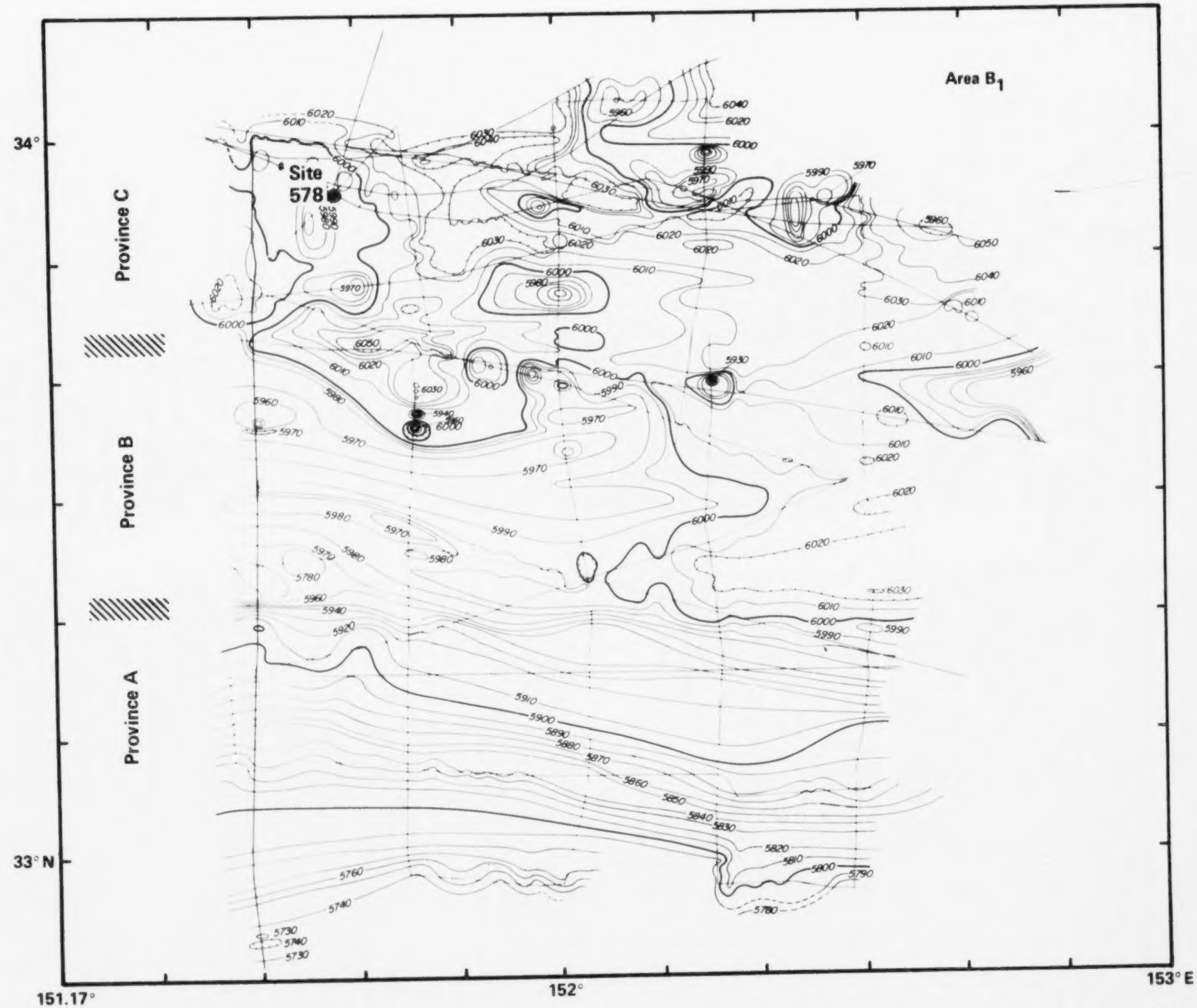
Area B_1
Site 578
Province C
Province B
Province A
34°
33° N
151.17°
152°
153° E

Figure 12. Bathymetry of study Area B_1. Depths are in corrected meters utilizing the correction tables of Carter (1980). Primary contour interval is 10 m. Boundaries are noted for the approximately east–west trending bathymetric provinces.

ince B, with subdued ridges, troughs, and locally relatively steep slopes, and the northern Province C, which has many small abyssal hills (see Fig. 12 and Table 6).

The Province A/Province B boundary consists of a relatively steep, north-northeast facing slope (commonly 1-2°) with 60-70 m relief. In Province B, broad, low ridges and troughs generally trend west to west-northwest. The southern flanks of these ridges slope gently while the northern flanks slope steeply.

Province C has a large number of abyssal hills with relatively steep slopes (Table 6). Because the ship's track spacing is typically large, it is not possible in most cases to determine if the abyssal hills have a preferred orientation. In the northernmost part of the survey area, where the track spacing is smaller, abyssal hills appear to have both north-south and east-west trends. The magnetic lineations trend west-northwest throughout most of Area B_1 suggesting that the west-northwest bathymetric trend is a relict fabric originally created at a spreading center active ~155 m.y. ago. The seafloor becomes younger to the north; thus, the relatively steep slopes that face north are probably surface expressions of buried fault scarps of the rift mountains. The regional seafloor gradient is opposite to that predicted by empirical age/depth cooling curves (e.g., Parsons and Sclater, 1977). The age of the seafloor at study Area B_1 predicts a relatively flat age-crustal depth curve; therefore, factors other than crustal cooling may control the regional gradient at Area B_1 (e.g., bordering volcanic edifices).

Intervals R_1-R_2, R_2-R_3, and R_3-R_4

The local and regional variations in interval thicknesses and sedimentation rate are summarized in Table 7 and Figures 13 and 14. Each interval thickness within R_1-R_4 generally decreases northward from the southern border of study Area B_1 to a minimum value in the west central part of Province A. Interval thicknesses then increase northward to maximum values along the northern border of Area B_1 (Figs. 13 and 14). This 8- to 13-fold increase in sediment accumulation in all intervals occurs over a distance of only ~80 km (see Table 7).

Anomalously thin zones in Province A commonly occur on relatively steep, north-facing slopes (e.g., the northern border of Province A, the west central anomaly, and the southeast corner of Province A). In contrast, a zone of anomalously thick sediment is located in the east central part of Province A where the seafloor gradient is distinctly lower than the surrounding area. Some relatively steep north-facing slopes have anomalously thick R_1-R_2 sediment sections (e.g., 33.13°N, 152.23°E) and may result from mass wasting. In the southern part of Province A, most of the north-south tracks display similar R_2-R_3 and R_3-R_4 variations along track that appear to form east-west trending waves of 2- to 3-km wavelengths and amplitudes of ≤ 2 m. Bottom-water flow that is independent of the local slope may cause some of these local variations. The sediment-interval thickness that characterizes Province A extends southward only to a large abyssal hill at 32.75°W, 151.50°E (just south of study Area B_1). Southward from this abyssal hill to at least 32°N, each of the intervals R_1-R_2, R_2-R_3, and R_3-R_4 is consistently ~5 m, while to the north of this abyssal hill, interval thicknesses increase abruptly to ~8 m.

Table 6. Characteristics of bathymetric features in provinces of study Area B_1.[a]

	Local relief (m)		Local slopes (°)	
Province	Typical	Maximum	Typical range	Maximum range
A		4	0.25-0.5	0.09-0.6 and few 2
B	30-40	30-70	1.5-2	0.2-3
C	40-50	10-79	0.5-2	0.25-9

[a] Based on Figure 12.

Table 7. Seismic interval thicknesses and sedimentation rates in study Area B_1.

		Province A		Province B		Province C	
Interval	Value[a]	Typical	Maximum	Minimum	Typical	Typical	Maximum
R_1-R_2	A	6-8		3-5	8	22.5	28-30
	B	12.6	16.8	6.3-10.5			59.9-63.2
	C	2			3	9	16
	D	4.2			6.3	18.9	33.7
R_2-R_3	A	6-8		2-4	10.5	20	24-26
	B	12-19		4-8			48-52
	C	2-3	4		2-3	2[b]	7
	D	4-6	8		4-6	4	14
R_3-R_4	A	7-8		3-5			28-29
	B	4.7-5.4		2.0-3.4			18.9-19.6
	C	1	2		3	2[b]	7
	D	0.68	1.35		2	4	14

[a] A = regional thickness of reflector interval (m), B = regional sedimentation rate (mm/1000 yr.), C = local thickness variations (m), D = local sedimentation rate variations (mm/1000 yr.).

[b] Very local anomalies.

In Province B most of the anomalously thick zones occur on south-facing slopes, while the steeper north-facing slopes generally have anomalously thin zones (e.g., the northwest boundary of Province B). Other zones of thick sediment occur on gentle north-facing slopes, on tops of ridges, and in small basins.

In Province C, the regional thickness increases from south to north by a factor of more than two, but this gradient is less uniform than in the other provinces. North slopes of abyssal hills and ridges generally have anomalously thin zones, south slopes have thick zones. A few abyssal hills exhibit the opposite relationship. East slopes have primarily thick zones and west slopes have thin zones for intervals R_1-R_2 and R_2-R_3. Other thin zones occur on tops of ridges and in gaps.

The general case of north and west slopes/thin sediment indicate bottom-water flow to the south or east, but the anomalous abyssal hills provide a warning that the bottom-water circulation may be more complicated or our data may be inadequate. We view the rapid increase in sedimentation rate as delineating the southern boundary of a major sediment drift deposit. The extent and cause of this sediment drift remain uncertain. The drift extends north to at least the northern margin of the study area (34.3°N) and possibly much farther.

Although most major R_3-R_4 anomalies are similar in extent to those in intervals R_1-R_2 and R_2-R_3, some are different. In Province A, the southern part of the west-central thin zone is much smaller for R_3-R_4 times than for later times. Similarly, the northern part of the east-central R_3–R_4 thick zone is not observed for R_1–R_3. Thus, the central area of Province A appears to have experienced a slightly faster bottom-water flow during R_1–R_3 times than during R_3–R_4 times. In contrast, the width of the thin zone along the northwest boundary of Province B contracted by at least 5 km for R_3–R_4 to R_1–R_3 time. This observation suggests that the bottom-water flow decreased from R_3–R_4 to R_1–R_3 in Province B. That the inferred sense of change of bottom-water flow is opposite for adjacent provinces indicates that anomalous thicknesses can be controlled in Area B_1 by very local flow conditions.

In Provinces B and C, a few thickness anomalies appear to shift south from R_3–R_4 times to R_2–R_3 times (e.g., the thick zone at 33.5°N, 152.3°E shifts 2 km downslope). In contrast, the small anomaly at 33.7°N, 152.2°E appears to shift north (upslope) 1 km from R_3–R_4 times to R_2–R_3 times. These observations also suggest that the flow conditions varied on a very local scale from R_3–R_4 times to R_2–R_3 times.

Intervals R_4–R_5 and R_5–R_6

Reflectors R_5 and R_6 are too deep to be observed on 3.5-kHz echograms in Province C and the north and eastern parts of Province B (Fig. 13D and 13E). However, the regional variations of intervals R_4–R_5 and R_5–R_6 that are observed suggest that the sedimentation during R_4–R_6 times was similar to that in later times (Fig. 14). The regional thickness for interval R_4–R_5 and R_5–R_6 decreased by about a factor of two from the southern boundary of Province B_1 to the west-central part of Province A. The regional thickness then increases rapidly northward for both intervals. The thickness of R_5–R_6, R_4–R_5, and R_3–R_4 all increase by about 100% over the same distance of only ~12 km. It is therefore probable that like R_3–R_4, the R_5–R_6 and R_4–R_5 interval thicknesses continue to increase northward beyond the northern limits of their observation.

In Province A, east-west trending, prominent thin zones occur on relatively steep, north-facing slopes. The major examples occur along the northern boundary of Province A and in the zone extending from the west central to the southeast corner of Province A. In contrast, a thick zone lying between these two thin zones is most prominent over the areas of relatively low seafloor gradients in the east-central part of Province A. As in the overlying units, WNW-trending waves in the R_4–R_6 interval thicknesses occur along the southern part of Province A with ~1 m amplitude and 1.5- to 2-km wavelengths. The southern extent of the major variations of R_4–R_6 characteristic of Province A is marked by the abyssal hill just south of Area B_1 for interval R_5–R_6 and is ~14 km south of the abyssal hill for R_4–R_5.

In Province B, spatially prominent thin zones occur on relatively steep north-facing slopes (e.g., R_4–R_5: north flank of the ridge from 33.5°N, 151.5°E to 33.4°N, ~152°E). Well-developed thick zones occur on south-facing slopes of abyssal hills and, for R_4–R_5, on tops of abyssal hills and in areas of low seafloor gradients.

In Province C, R_5 is observed only at the two abyssal hills located at 33.6°N, 152.75°E, where thick zones occur on the south sides of the hills.

Although intervals R_4–R_5 and R_5–R_6 are observed over a limited extent, the pattern of anomalies is similar to that of the more extensive, overlying units (e.g., Fig. 14), suggesting bottom-water flow to the south or east for R_4–R_6 times. The major flow components appear to have remained spatially stable from R_4–R_6 times to R_3–R_4 times because the major sediment drift in central and northern B_1, as well as most other anomalies, is located in the same area for these reflector intervals. Locally the southern boundaries of the thin zones migrated south through time (R_5–R_6 to R_4–R_5 times), expanding the thin zones at the expense of the thick zones. The expanding thin zones might suggest that the strength of the bottom-water circulation increased locally from R_5–R_6 times to R_4–R_5 times.

SUMMARY AND CONCLUSIONS

The bathymetry in Area E_2 has a northwest-southeast lineation that is parallel to the magnetic lineations and may be a consequence of original rift tectonics. The local relief is generally ≤50 m except in the southeastern part (bathymetric Province B) and along the northern and southern borders of Area E_2, where relief up to 305 m is observed.

Two continuous, sharp reflectors in the upper part of the 3.5-kHz seismic section are observed throughout the area; the upper reflector (R_2) corresponds to an ~1.3 m.y. old volcanic ash layer and the other reflector (R_3) is ~7.2 m.y. old (Fig. 6). Isopach maps of these seismic intervals reveal local variations in sediment thickness that can be attributed to sediment slides and probably also to variations in the bottom-water flow. Localized areas with either diminished or increased sedimentation occur commonly on northeast slopes. However, on the steep slopes of abyssal hills and ridges, the northeast slopes generally show anomalously thin sediments. This relationship could arise from any pattern of bottom-water flow with a strong southerly component (with a range from southeast to southwest). Sediment slide deposits appear to be less prominent in the 1.3 to 7.3 m.y. ago interval than in more recent times. Although sediment slides are apparent in association with some small, localized bathymetric highs, such deposits occupy only a very minor fraction of the study area. The overall pattern of recent sedimentation, as revealed by the 3.5-kHz echograms and piston cores, indicates that Area E_2 records a low energy and remarkably stable sedimentation environment.

Reflector R_4 is discontinuous throughout the study area and where observed, may not always represent the same geologic horizons. At Site 576, the age of R_4 is ~25 m.y. The most distinct difference between seismic interval R_3–R_4 and all other digitized seismic intervals is the lack of "mini-moats" along the margins of troughs. This may indicate a decrease in the intensity of bottom-water flow during the period from ~7.2 to ~2.5 m.y. ago. However, the overall relationship between seafloor

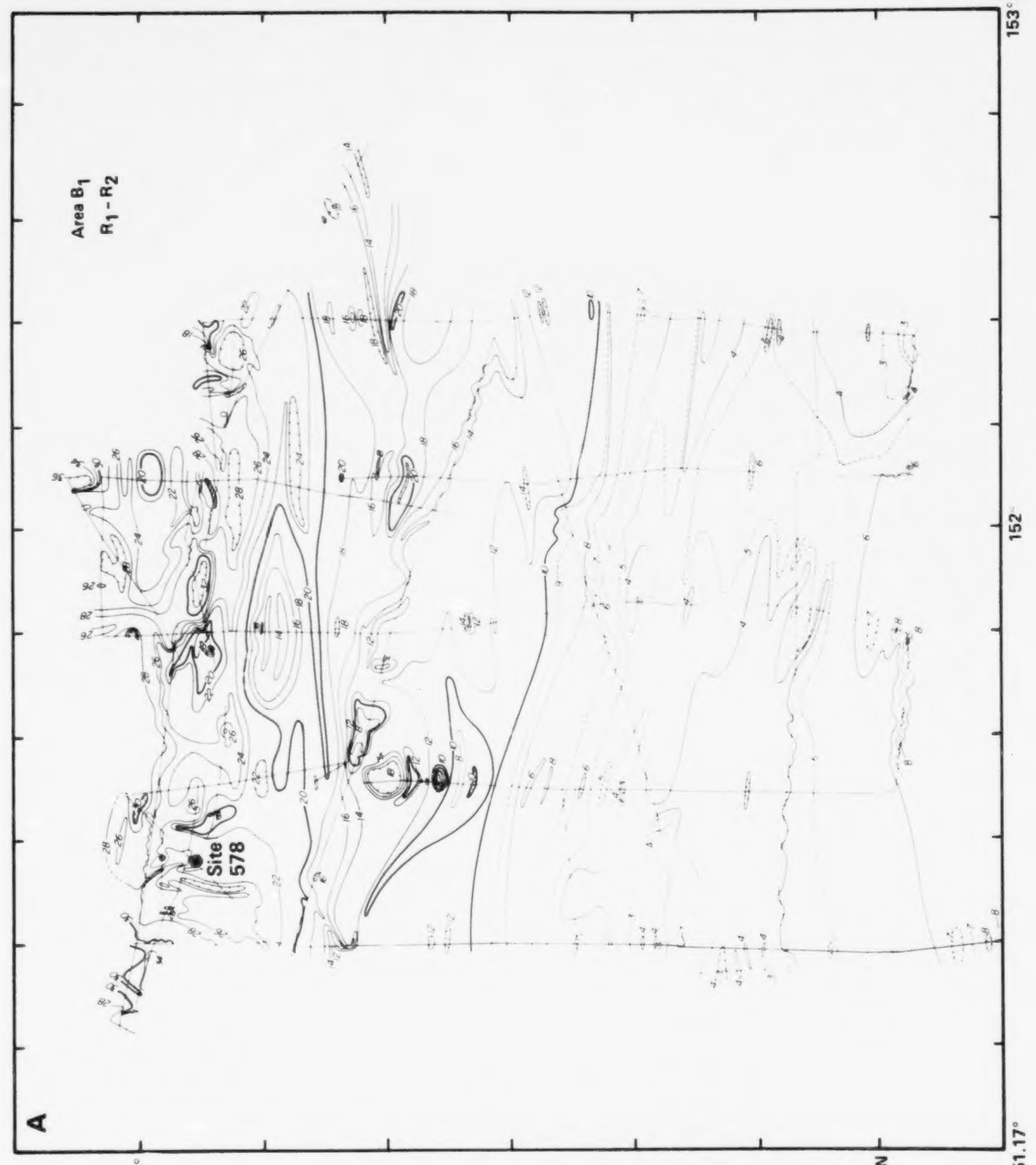
A
Area B$_1$
R$_1$ - R$_2$
Site 578
34°
33° N
151.17°
152°
153° E

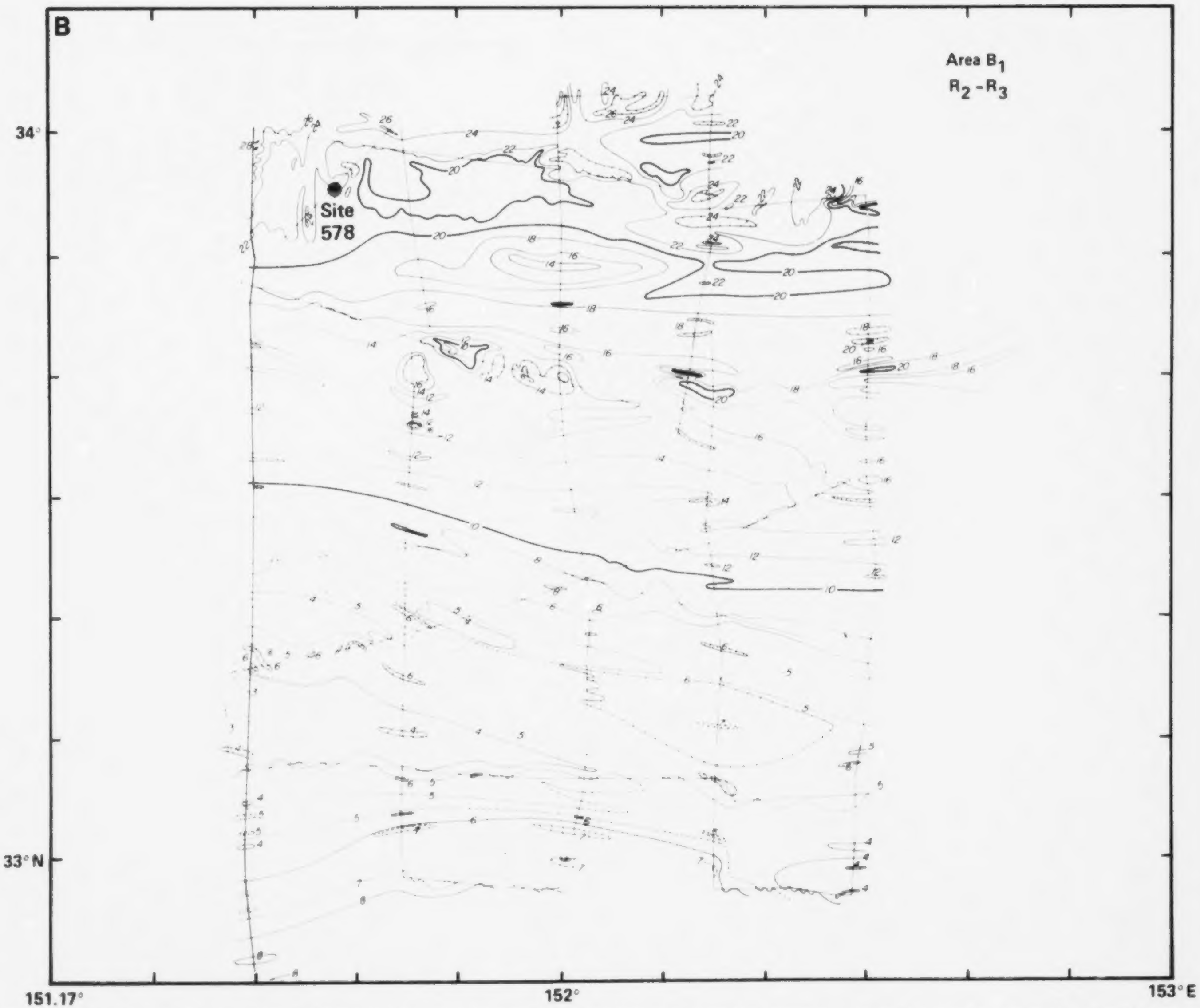
B
Area B1
R2 - R3
Site
578
34°
33° N
151.17°
152°
153° E

Figure 13. Isopach maps for the various 3.5-kHz seismic reflector intervals in study Area B_1. Figure 13A: interval R_1–R_2 (0–0.475 m.y.), Figure 13B: interval R_2–R_3 (0.475–0.975 m.y.), Figure 13C: interval R_3–R_4 (0.975–2.44 m.y.), Figure 13D: interval R_4–R_5 (2.44–~5–6 m.y.), Figure 13E: interval R_5–R_6.

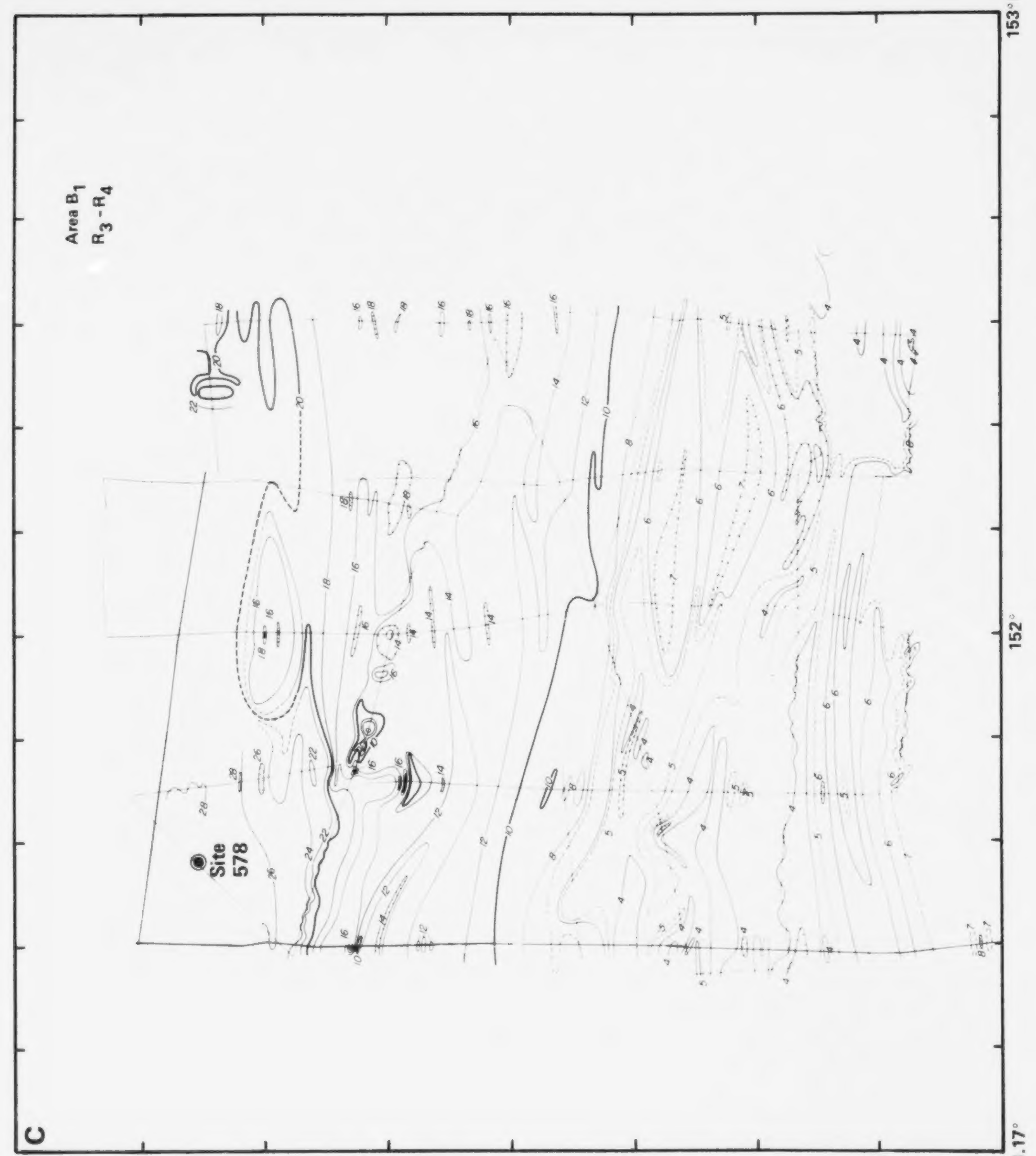
C
Area B_1
$R_3 - R_4$
Site 578
34°
33°N
151.17°
152°
153°E

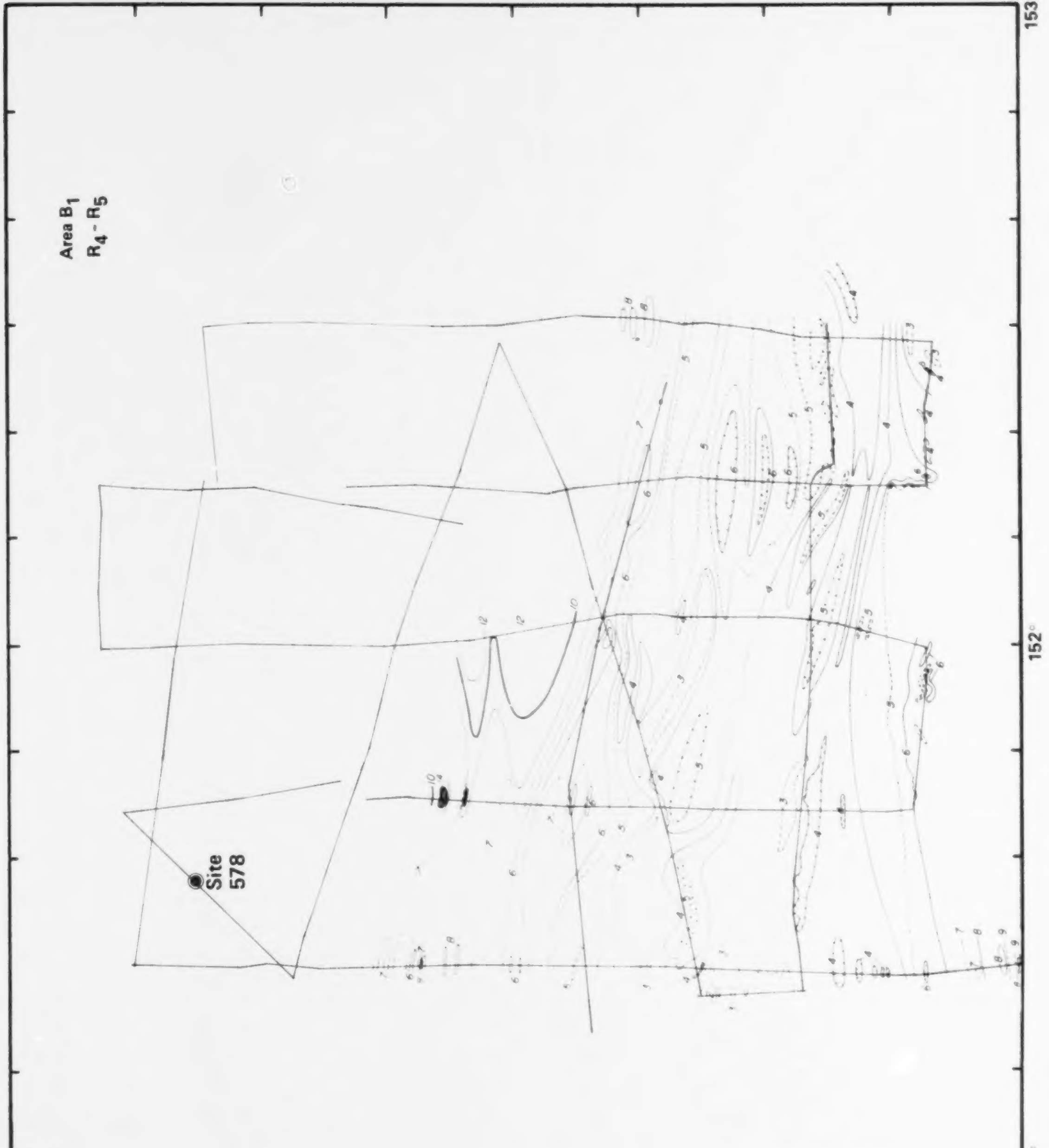
D
Area B_1
$R_4 - R_5$
Site 578
34°
33° N
151.17°
152°
153° E

Figure 13. (Continued).

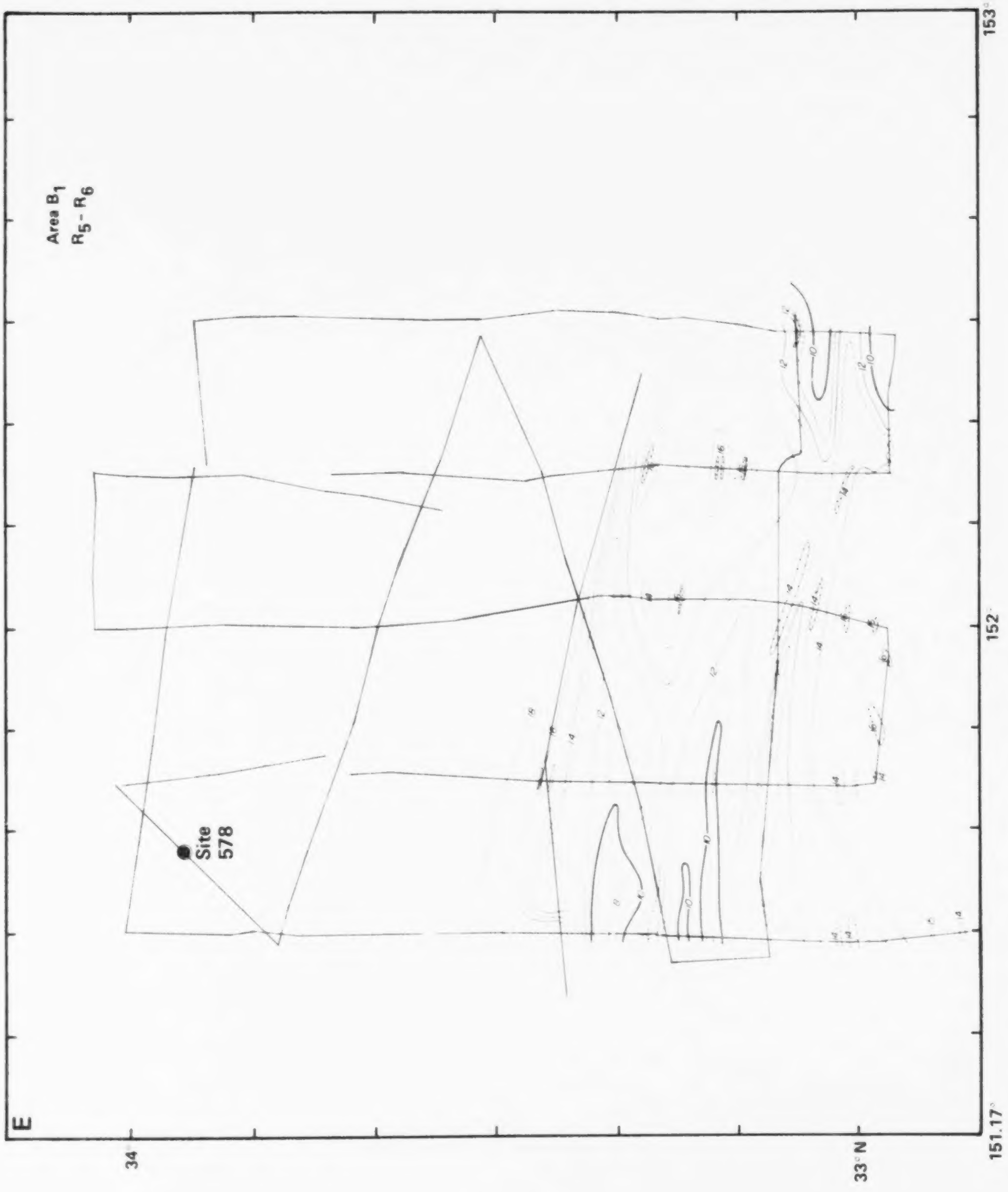
E
Area B_1
$R_5 - R_6$
Site 578
34
33° N
151.17°
152°
153° E

Figure 13. (Continued).

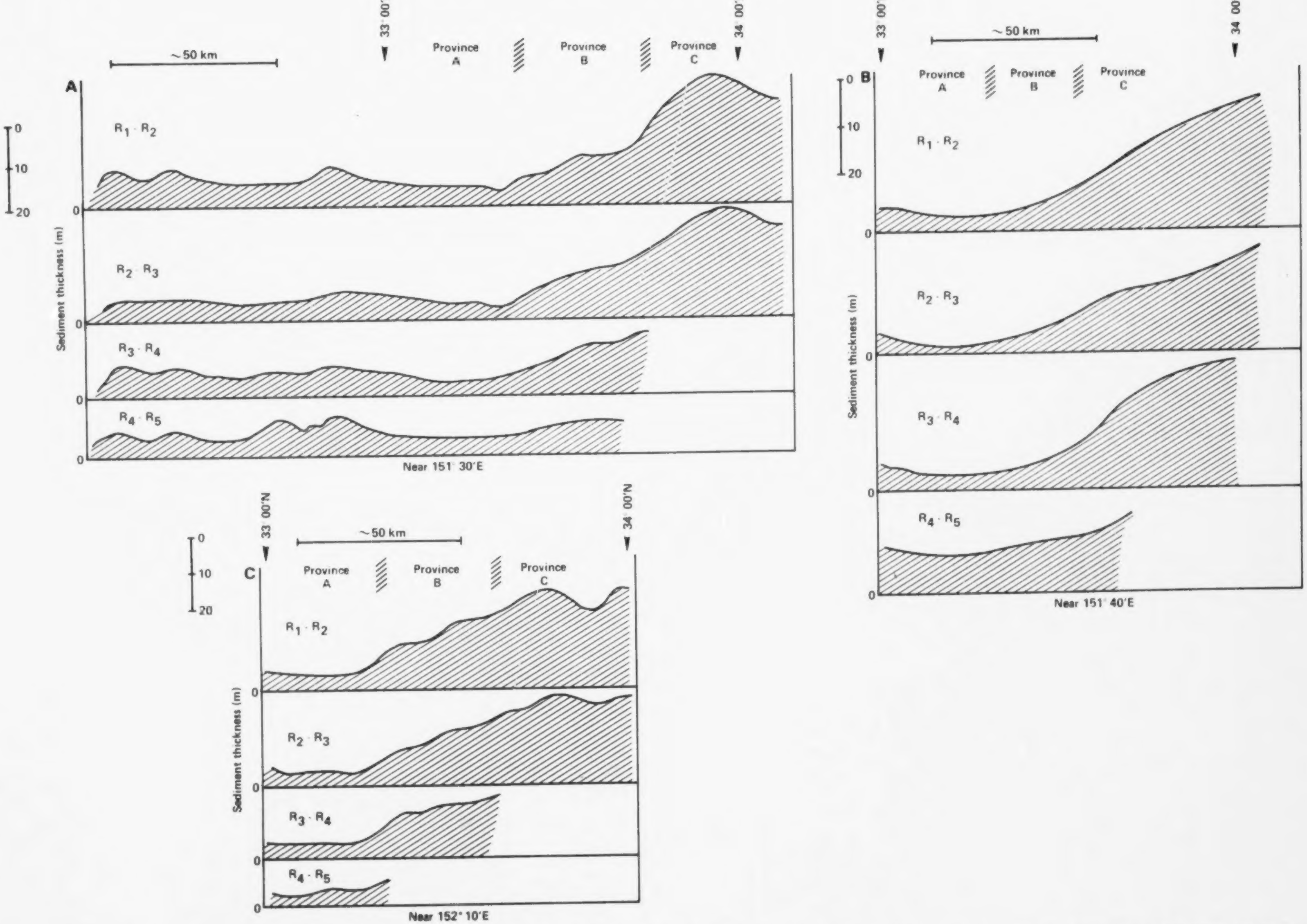

Figure 14. North–south profiles displaying the northward increase in all reflector interval thicknesses. Figures 14A, 14B, and 14C are located along north–south tracks near 151.50°E, 151.67°E, and 152.17°E, respectively (see Fig. 4).

relief and anomalous sediment accumulation rates in R_3-R_4 is similar to that observed in the overlying intervals. Thus, direction of the bottom-water flow probably remained roughly constant for the past 25 m.y.

Acoustic basement (R_5) on the 3.5-kHz echograms (Fig. 6) corresponds to ~70 m.y. old carbonate turbidites and pelagic sediments interbedded with brown clay in "basement" lows; pelagic carbonate or chert probably mark the "basement" highs. Seismic interval R_4–R_5 exhibits thin zones along the margins of troughs, suggesting increased bottom-water flow compared to R_3–R_4 time. These thin zones generally lie along the northeast margins of troughs and could result from northward bottom-water flow. However, the larger population of observations from entire interval R_3–R_5 is inconsistent with this hypothesis, and therefore any inference of northward bottom-water flow during the interval R_4–R_5 should be regarded as very tentative. The integrated seismic interval, R_3–R_5, shows relationships of seafloor slope to anomalous sediment accumulation similar to those of the overlying units. It is probable, therefore, that the overall circulation pattern of bottom-water at Area E_2 has remained relatively stable for the past 70 m.y. The inferred southward flow is contrary to the regional flow direction thought to exist for the PBW in this area (Mantyla, 1975). This apparent contradiction suggests either that accurate regional flow directions cannot be ascertained from local, small variations in sediment-accumulation rate or that local bottom-water flow in this area was counter to the overall PBW circulation.

The dramatic thinning of all seismic intervals in the northeast corner of study Area E_2 suggests that bottom-water flow was accelerated in this area. This hypothesis is consistent with the Area E_2 piston cores, which reveal coarser sediments in this area (generally silt size in Core 51 versus silty clay and clayey silt in all other cores, see Table 1). The consistent sedimentation pattern for the past 70 m.y. suggests that flow here has been controlled by bathymetric features. North and east of Area E_2, a barrier to the northeastward flow of PBW is formed by the intersection of northwest to southeast trending bathymetric highs with the Shatsky Rise (fig. 2 in Damuth et al., 1983). An apparent gap in this barrier occurs at 32.83°N, 166.83°E; northeast of this gap the seafloor returns echoes typical of areas with accelerated bottom-water flow (Damuth et al., 1983). The sediment thinning at the northeast corner of Area E_2 may be the expression of constricted and accelerated bottom-water flow through this gap. The bathymetric barrier may also cause a local bottom "gyre" within the generally northeast flowing PBW and could explain the apparent southerly flow directions at Area E_2.

At study Area B_1, the bathymetry is extremely subdued in Province A, with a maximum local relief of only 4 m. In the remainder of Area B_1, abyssal hills and ridges occur with a maximum local relief of 79 m. The east–west trend of many of the bathymetric features is parallel to the magnetic lineations, suggesting that much of the bathymetry is related to rifting phenomena. The linear, steeper slopes generally face north toward younger seafloor and may be surface expressions of buried fault scarps generated at rift mountains. The regional gradient of the seafloor at Area B_1 slopes to the north toward younger seafloor (opposite to slope predicted by empirical age/depth cooling curves).

The 3.5-kHz seismic section in Area B_1 contains several continuous, parallel reflectors that correspond to volcanic ash layers. All seismic intervals defined by these reflectors exhibit similar regional and local variations in the sediment-accumulation rate. The thickness of reflector interval R_1–R_2 (0–0.475 m.y. ago) shows a dramatic 10-fold increase from the center of Area B_1 to its northern border, a distance of only 80 km. Over the same distance, interval R_2–R_4 thickness (0.975–2.44 m.y. ago) increases by eight times (Fig. 14). Intervals R_4–R_5 and R_5–R_6 show similar increases where observed. This sharp gradient in sedimentation rates appears to mark the boundary between the two major regional sediment provinces in the Northwest Pacific Basin. These provinces are distinguished by both sediment thickness and type (Table 1 and Fig. 14). Northward from the boundary, the sedimentation rate remains high to near the Kuril Trench. For example, 500 km north of Site 578, at Site 579, the sedimentation rate is comparable to that found at Site 578. Southward from the boundary, the sedimentation rate remains low to at least 31°N.

The cause of the abrupt change in sedimentation rate is an enigma. The southern border of the Kuroshio Current is presently located over study Area B_1. However, this surface current alone cannot be the direct cause of the abrupt sedimentation rate change because it did not remain fixed in its present position during Pleistocene glacials and interglacials. We therefore believe that bottom-water flow directed by bathymetric features has persistently localized and accentuated any expected "normal" gradient in sedimentation rate.

We have attempted to determine the flow direction and relative flow strength from the relationship between seafloor slope and variations in sedimentation rate. A moat on the south side of a major abyssal hill at 32.75°N, 151.50°E (south of study Area B_1) clearly suggests bottom-water flow to the north or west. A northward flow is consistent with the proposed flow of the western branch of the PBW (Mantyla, 1975). However, within study Area B_1, all seismic intervals typically exhibit anomalously thin zones on north-facing slopes and thick zones on south-facing slopes. These relationships suggest bottom-water flow to the east or south. The east–west strike of the sharp sedimentation "front" suggests that eastward bottom-water flow is more plausible. Eastward flow is not in accord with the proposed regional northward flow of PBW. Either a local bottom "gyre" operated in the immediate area of B_1 or our observed sedimentation rate variations are not good indicators of bottom-water flow. A long-term current instrument moored at 4000 m depth at 33.77°N, 151.98°E (#7003, Schmitz et al., 1982) suggests that eastward and southward flow maxima predominate at this location, confirming the inferred flow direction and "gyre."

Although most of the zones of anomalous sedimentation remain spatially fixed through time, the positions of some anomalous zones change with time, suggesting waxing and waning of the bottom current. The predominant change in bottom-water flow appears to have occurred during R_4–R_5 times (2.44 to 5–6 m.y. ago). It was only during this time interval that the southern boundaries of thin zones migrated significantly southward, enlarging their area. Thus the inferred higher bottom-water velocity acting during R_4–R_5 times did not persist into R_3–R_4 times. At Site 578 the sedimentation rate, computed from paleomagnetics and paleontology, increases dramatically at about 2.5 m.y. ago and remains high to the present (see Site 578 chapter, this volume), and independently argues for a higher velocity bottom current in earlier times. At study Area E_2, the velocity of the bottom water increased at R_3 times ($\sim$7.2 m.y. ago) but the duration of this increase is unknown. The gross similarity in the timing of bottom-water velocity changes at both Sites 576 and 578 suggests that in the northwest Pacific Basin the eastern and western branches of the PBW have experienced roughly contemporaneous perturbations.

ACKNOWLEDGMENTS

We thank the officers, crew, and scientists aboard the *Vema* and *Glomar Challenger* for able assistance in gathering the data presented herein. We acknowledge the important contribution of R. Flood, M. Coffin, and J. Kostecki during *Vema* Cruise V36-12. Alison Gold and Norma Iturrino assisted in the digitization of the seismic records and David Johnson drafted most of the figures. R. Flood, E. Laine, and A. Wright critically reviewed the manuscript and provided many helpful suggestions. Doris Millholland and Carol Elevitch typed the manuscript. This study was supported by Sandia Contract No. SL475693.

REFERENCES

Carter, D. J. T., 1980. *Echo-Sounding Correction Tables:* Taunton, England (Hydrographic Dept., Ministry of Defense).

Chase, T. E., Menard, H. W., and Mammerickx, J., 1971. Topography of the North Pacific. *Scripps Inst. Oceanogr., Inst. Mar. Resources, Tech. Rept. Ser.*, TR-17.

Craig, H., and Gordon, A. L., 1965. Isotopic oceanography: Deuterium and oxygen 18 variations in the ocean and the marine atmosphere. *Mar. Geochem., Proc. Symp., Univ. Rhode Isl., Narragansett Mar. Lab., Occas. Publ.*, 3:277–374.

Damuth, J. E., Jacobi, R. D., Flood, R. D., and Hayes, D. E., 1980. Evaluation of the North Pacific subseabed for disposal of high-level nuclear waste. III. Preliminary results of geological/geophysical surveys of three 1° × 1° candidate disposal sites. *Trans. Am. Geophys. Union*, 61:989. (Abstract)

Damuth, J. E., Jacobi, R. D., and Hayes, D. E., 1983. Sedimentation processes in the Northwest Pacific Basin revealed by echo-character mapping studies. *Geol. Soc. Am. Bull.*, 94:381–395.

Gordon, A. L., and Gerard, R. D., 1970. North Pacific bottom potential temperature. *In* Hays, J. D. (Ed.), *Geological Investigations of the North Pacific*. Mem. Geol. Soc. Am., 126:23–39.

Hayes, D. E., Damuth, J. E., Jacobi, R. D., and Flood, R. D., 1982. Analysis of geological and geophysical data from study locations C_1, B_1, and E_2 in the Northwest PAC 1 study region. *In* Hinga, K. R. (Ed.), *Subseabed Disposal Program Annual Report January to September 1981* (Vol. 2, Pt. 1): Albuquerque (Sandia National Laboratories), 191–206.

________, 1983. Analysis of geological and geophysical data from study locations C_1, B_1, and E_2 in the northwest PAC 1 study region. *In* Shephard, L. (Ed.), *1982 Subseabed Disposal Program Annual Report: Site Assessment October 1981 to September 1982:* Albuquerque (Sandia National Laboratories) Sandia Report SAND82-2711, pp. 17–43.

Hays, J. D., and Ninkovich, D., 1970. North Pacific deep-sea ash chronology and age of present Aleutian underthrusting. *In* Hays, J. D. (Ed.), *Geological Investigations of the North Pacific*. Mem. Geol. Soc. Am., 126:263–290.

Heath, G. R., 1981. Site qualification and multibarrier assessment, 1980. Appendix R *In* Hinga, K. R. (Ed.), *Subseabed Disposal Program Annual Report January to December 1980* (Vol. II, Pt. 2), Albuquerque (Sandia National Laboratories), Rept. SAND81-1095, pp. 50–145.

Horn, D. R., Delach, M. H., and Horn, B. M., 1969. Distribution of volcanic ash layers and turbidites in the North Pacific. *Geol. Soc. Am. Bull.*, 80:1715–1724.

Horn, D. R., Horn, B. M., and Delach, M. N., 1970. Sedimentary provinces of the North Pacific. *In* Hays, J. D. (Ed.), *Geological Investigations of the North Pacific*. Mem. Geol. Soc. Am., 126: 1–21.

Iwabuchi, Y., 1979. *General Bathymetric Chart of the Oceans (GEBCO):* Otfawa, Canada (Canadian Hydrographic Service), Map 5-06.

Larson, R. L., Cande, S. C., Dewey, J. F., Golovchenko, X., Haxby, W. F., LaBrecque, J. L., and Pitman, W. C. III, 1983. The bedrock geology of the world. *Trans. Am. Geophys. Union*, 64:863. (Abstract)

Larson, R. L., and Hilde, T. W. C., 1975. A revised time scale of magnetic reversals for the Early Cretaceous and Late Jurassic. *J. Geophys. Res.*, 80:2586–2594.

Lonsdale, P., and Smith, S. M., 1980. "Lower insular rise hills" shaped by a bottom boundary current in the Mid-Pacific. *Mar. Geol.*, 34: M19–M25.

Lonsdale, P., and Spiess, F. N., 1977. Abyssal bedforms explored with a deeply-towed instrument package. *Mar. Geol.*, 23:57–75.

Mantyla, A. W., 1975. On the potential temperature in the abyssal Pacific Ocean. *J. Mar. Res.*, 33:341–354.

Ninkovich, D., and Robertson, J. H., 1975. Volcanogenic effects on the rates of deposition of sediments in the Northwest Pacific Ocean. *Earth Planet. Sci. Lett.*, 27:127–136.

Parsons, B., and Sclater, J. G., 1977. An analysis of the variation of ocean floor bathymetry and heat flow with age. *J. Geophys. Res.*, 82:803–827.

Reid, J. L., and Lonsdale, P. F., 1974. On the flow of water through the Samoan Passage. *J. Phys. Oceanogr.*, 4:58–73.

Reid, J. L., and Lynn, R. J., 1971. On the influence of the Norwegian-Greenland and Weddell Seas upon the bottom waters of the Indian and Pacific Oceans. *Deep Sea Res.*, 19:1063–1088.

Roberts, O. G., Hogg, N. G., Bishop, D. G., and Flewellen, C. G., 1974. Sediment distribution around a moated seamount in the Rockall Trough. *Deep Sea Res.*, 21:175–184.

Schmitz, W. J., Niiler, P. P., Bernstein, R. L., and Holland, W. R., 1982. Recent long-term moored instrument observations in the Western North Pacific. *J. Geophys. Res.*, 87:9425–9440.

Udintsev, G., 1980. General bathymetric chart of the oceans (GEBCO): Ottawa, Canada (Canadian Hydrographic Service), Map 5-02.

Warren, B. A., 1973. Transpacific hydrographic sections at lats. 43°S and 28°S: the SCORPIO Expedition—II. Deep water. *Deep Sea Res.*, 20:9–38.

Date of Initial Receipt: 27 February 1984
Date of Acceptance: 26 August 1984

3. SITE 576[1]

Shipboard Scientific Party, with a contribution by Patricia Doyle[2]

HOLES 576, 576A, 576B

Date occupied: 16–18 May (576);
18–19 May (576A);
19–20 May (576B)

Date departed: 21 May 1982

Time on site: 4 days, 16 hr.

Position (latitude; longitude): 32°21.36′N; 164°16.54′E (576)
32°21.38′N; 164°16.52′E (576A)
32°21.37′N; 164°16.52′E (576B)

Water depth (sea level; corrected m, echo-sounding): 6217

Water depth (rig floor; corrected m, echo-sounding): 6227

Bottom felt (m, drill pipe): 6220.3 (576);
6218.0 (576A);
6219.3 (576B)

Penetration (m): 69.2 (576);
65.7 (576A);
74.8 (576B)

Number of cores: 8 (567);
7 (576A);
9 (576B)

Total length of cored section (m): Same as penetration (above)

Total core recovered (m): 68.52 (576);
66.20 (576A);
74.07 (576B)

Core recovery (%): 99 (576);
101 (576A);
99 (576B)

Oldest sediment cored:
Depth sub-bottom (m): 73
Nature: Nannofossil ooze–pelagic clay
Age: Campanian
Measured velocity (km/s): 1.43–1.50

Basement: Not reached

Principal results: Site 576 met all of its objectives. The surface ("transparent") acoustic layer was completely cored three times, with essentially full recovery. One complete section (Hole 576A) was stored vertically, unopened, for shore-based geotechnical studies.

The section cored consists of three lithologic units, with the top unit divisible into two subunits as follows:

Subunit IA (0 to 28 m, contact gradational over several meters) is a yellowish brown to brown pelagic clay of Pliocene and Quaternary age (based on paleomagnetics). Sedimentation rate decreases from 10 m/m.y. in the Brunhes Epoch to less than 3 m/m.y. at the base of the Matuyama Epoch. Based on earlier studies and the abundance of silt-sized quartz, we infer that this unit is largely of eolian origin.

Subunit IB (28 to 55 m) is a dark brown "slick" pelagic clay, zeolitic in part. This material is extremely homogeneous, very fine grained, and manganese rich. If deposition has been continuous, the average sedimentation rate decreased from about 1 m/m.y. during the late Neogene to about 0.35 m/m.y. at about 40 m.y. ago, before increasing to 0.6 m/m.y. (uncorrected for compaction) during the Late Cretaceous. Shore-based studies of ichthyoliths should further constrain these rates. By analogy with similar North and South Pacific pelagic clays, we infer that this subunit contains a large authigenic component.

Lithologic Unit II (55 to 76 m sub-bottom) is an interbedded dark brown pelagic clay similar to Subunit IB and pale brown nannofossil ooze of Campanian age. At the base of the unit, the clay layers also include pink bands and mottles. Several of the carbonate layers are graded and have sharp erosional basal contacts; these are turbidites. Other layers may be pelagic. The absence of microfossils younger than Campanian age and the results of earlier Deep Sea Drilling Project (DSDP) drilling in this region suggest that the components of the carbonate and clay layers are essentially contemporaneous. Whether the carbonate reflects enhanced biogenic deposition due to higher productivity (at the lower latitude of the site 70 m.y. ago) or to fluctuations in the carbonate compensation depth (CCD) is unclear.

Lithologic Unit III (76 m) consists of one small glassy chert chip and a few small fragments of off-white porcellanite. This unit forms the prominent reflector at the base of the "transparent" layer in the northwest Pacific.

Progressive consolidation of the pelagic clays of lithologic Units I and II yielded striking physical properties profiles. Both shear wave velocity and vane shear strength increased with depth (from 6 to 127 m/s and less than 20 to more than 1000 g/cm^2, respectively) without regard to the lithologic change from Subunit IA to IB. LL44-GPC3 at 30°N, 158°W showed similar trends.

The new Woods Hole Oceanographic Institution (WHOI) core-nose heat flow unit worked well on 7 of 11 deployments.

BACKGROUND AND OBJECTIVES

Site 576 (target Site NW-9) was proposed by the JOIDES Ocean Paleoenvironment, Sedimentary Petrology and Physical Properties, and Inorganic Geochemistry Panels as a "type" North Pacific red clay site. The general location was chosen to be far enough west to lie in an area of uniform pelagic sedimentation between Shatsky Rise and the Emperor Seamounts, but far enough east to minimize the fraction of the section occupied by ash layers. Our operational objectives were to recover a complete section above Cretaceous(?) chert by triple hydraulic piston coring (HPC), with the cores from one entire hole to be returned to shore unopened for detailed geotechnical studies.

---

[1] Heath, G. R., Burckle, L. H., et al., *Init. Repts. DSDP*, 86: Washington (U.S. Govt. Printing Office).

[2] Addresses: (Shipboard Scientific Party) G. Ross Heath (Co-Chief Scientist) School of Oceanography, Oregon State University, Corvallis OR 97331 (present address: College of Ocean and Fishery Sciences, University of Washington, Seattle, WA 98195); Lloyd H. Burckle (Co-Chief Scientist) Lamont-Doherty Geological Observatory, Palisades, NY 10964; Anthony E. D'Agostino, ARCO Exploration Company, Houston, TX 77056; Ulrich Bleil, Institut für Geophysik, Ruhr-Universität Bochum, D-4630 Bochum Querenburg, Federal Republic of Germany; Ki-iti Horai, Lamont-Doherty Geological Observatory, Palisades, NY 10964 (present address: Meteorological College, Chiba University, Chiba 277, Japan); Robert D. Jacobi, Department of Geological Sciences, SUNY Buffalo, Amherst, NY 14226; Tom Janecek, Department of Atmospheric & Oceanic Science, University of Michigan, Ann Arbor, MI 48109 (present address: Lamont-Doherty Geological Observatory, Palisades, NY 10964); Itaru Koizumi, College of General Education, Osaka University, Osaka 560, Japan; Lawrence A. Krissek, School of Oceanography, Oregon State University, Corvallis, OR 97331 (present address: Department of Geology and Mineralogy, Ohio State University, Columbus, OH 43210); Nicole Lenôtre, Bureau de Recherches Géologiques et Minières, Centre Océanologique de Bretagne, 45060 Orléans Cedex, France; Simonetta Monechi, Geological Research Division, Scripps Institution of Oceanography, La Jolla, CA 92093 (present address: Dipartimento di Scienze della Terra, Università di Firenze, 4 Via La Pira, 50121 Firenze, Italy); Joseph J. Morley, Lamont-Doherty Geological Observatory, Palisades, NY 10964; Peter Schultheiss, Institute of Oceanographic Sciences, Surrey GU8 5UB, United Kingdom; Audrey A. Wright, Deep Sea Drilling Project, Scripps Institution of Oceanography, La Jolla, CA 92093 (present address: Ocean Drilling Program, 500 University Drive West, Texas A&M University, College Station, TX 77843). (Doyle) Geological Research Division, Scripps Institution of Oceanography, La Jolla, CA 92093.

Our specific scientific objectives were

1. To recover a very long-term record of North Pacific red clay sedimentation;
2. To assess the nature and history of authigenic sedimentation during the Late Cretaceous and Cenozoic;
3. To determine the Late Cretaceous and Cenozoic history of eolian sedimentation for comparison with the LL44-GPC3 record at 30°N, 158°W;
4. To collect an oriented undisturbed red clay section for paleomagnetic studies;
5. To determine the consolidation history of a "type" red clay section by detailed geotechnical studies;
6. To assess the nature of the red clay/chert boundary, and particularly to determine if the transition is marked by an increase in the content of opaline silica or enhanced diagenesis of the basal red clays.

Geologic and Topographic Setting

The regional seafloor morphology and echo character of the near-surface sediments of the northwest Pacific has been mapped by Damuth et al. (1983) using all available Lamont-Doherty, Scripps, and Hawaii Institute of Geophysics 3.5-kHz reflection records. Site 576 lies east of Shatsky Rise in an area of continuous, acoustically transparent sediment, 20 to 60 m thick, with a few continuous reflectors in the upper 15 m.

The area around Site 576 was surveyed in detail on R/V *Vema* Cruise 36-12. Based on bathymetric and isopach maps prepared from this survey, a drill site was selected at 32°20′N, 164°15′E. This area is characterized by gently rolling topography, with a northwesterly grain and local relief of less than 50 m over distances of tens of kilometers. There is a regional deepening of 100 m over 100 km from southwest to northeast across the site.

The site lies close to the magnetic bight, probably on Anomaly M13. Thus, the basement age is about 129 m.y.

The 3.5-kHz records show about 55 m of largely transparent sediment overlying a strongly reverberating reflector thought to be chert. The upper 20 m of section contain three strong and several weaker continuous reflectors. There is a weaker continuous reflector at 30 m and an intermittent weak reflector at about 50 m. On the basis of the *Vema*-36 piston cores, these reflectors were believed to be thin beds of volcanic ash. They allow precise correlations of piston and HPC cores.

The site selected for drilling is typical of the surrounding area for thousands of square kilometers.

OPERATIONS

We arrived at Site 576 after steaming for 10 days from Honolulu. This long transit provided an opportunity to check over the lab gear and process test "wash down" sections of core to iron out procedural questions in the lab. Air-gun and 3.5-kHz records collected en route to the site are of superior quality.

The D/V *Glomar Challenger* entered the E-2 survey area of R/V *Vema* Cruise 36-12 on 15 May 1982 (Z). Because of the detail of the *Vema* survey and uniformity of the surficial "transparent" layer, we pulled the air guns and magnetometer as we approached the site from the south and dropped the beacon at 2059Z on the basis of the 3.5-kHz profile.

Drill pipe run-in began at 2200Z on 15 May, with the first 9.5-m HPC core on deck at 1845Z on 16 May. The mud line at Hole 576 was established at 6220.3 m. Coring proceeded uneventfully for eight cores (Table 1), with significant time lost (7 hr.) only when the sand line parted during lowering of Core 7. The problem was attributed to "floating" of the core barrel because of the narrow clearance afforded by the undersize drift of the drill pipe and to omission of a swivel above the corer, again because of clearance problems. Fortunately the broken line caught in the first joint of pipe at the rig floor, thereby minimizing lost time. Because of this incident, however, the lowering speed was reduced for subsequent cores, thereby increasing on-site time.

Conventional heat flow/*in situ* pore water probe lowerings were made on three occasions in Hole 576. The heat flow system had equipment problems and did not generate usable data. The pore water appears to be seawater, probably because the sediment was not strong enough to support the bottom-hole assembly (BHA) and keep the probe in the sediment.

We had better luck with the new WHOI core nose temperature probe. Despite teething problems (the unit would not fit into its slot, even though the core nose sub had been at WHOI for some time, and the wires from the battery pack to the electronics unit break very easi-

Table 1. Site 576 coring summary (drilling depths).

Core	Date (May 1982)	Local time	Depth from drill floor (m)	Depth below seafloor (m)	Length cored (m)	Length recovered (m)	Percent recovered
Hole 576							
1	17	0545	6220.3-6223.0	0.0-2.7	2.7	2.71	100
2	17	0813	6223.0-6232.5	2.7-12.2	9.5	9.78	103
3	17	1031	6232.5-6242.0	12.2-21.7	9.5	6.64	70
4	17	1445	6242.0-6251.5	21.7-31.2	9.5	10.05	106
5	17	1655	6251.5-6261.0	31.2-40.7	9.5	9.81	103
6	17	2120	6261.0-6270.5	40.7-50.2	9.5	10.07	106
7	18	0805	6270.5-6280.0	50.2-59.7	9.5	9.78	103
8	18	1130	6280.0-6289.5	59.7-69.2	9.5	9.68	102
					69.2 (total)	68.52 (total)	99 (avg.)
Hole 567A							
1	18	1530	6218.0-6227.5	0.0-8.7	8.7	8.68	100
2	18	1802	6227.5-6237.0	8.7-18.2	9.5	9.28	98
3	18	2045	6237.0-6246.5	18.2-27.7	9.5	9.77	102
4	19	0000	6246.5-6256.0	27.7-37.2	9.5	9.11	96
5	19	0335	6256.0-6265.5	37.2-46.7	9.5	9.75	103
6	19	0540	6265.5-6275.0	46.7-56.2	9.5	9.75	103
7	19	0820	6275.0-6284.5	56.2-65.7	9.5	9.86	104
					65.7 (total)	66.20 (total)	101 (avg.)
Hole 576B							
1	19	1105	6219.3-6227.5	0.0-8.2	8.2	8.21	100
2	19	1400	6227.5-6237.0	8.2-17.7	9.5	9.59	101
3	19	1625	6237.0-6246.5	17.7-27.2	9.5	9.70	102
4	19	1845	6246.5-6256.0	27.2-36.7	9.5	9.73	102
5	19	2130	6256.0-6265.5	36.7-46.2	9.5	8.98	95
6	20	0000	6265.5-6275.0	46.2-55.7	9.5	9.27	98
7	20	0305	6275.0-6284.5	55.7-65.2	9.5	9.71	102
8	20	0600	6284.5-6294.0	65.2-74.7	9.5	8.87	93
9	20	0810	6294.0-6294.1	74.7-74.8	0.1	0.01	10
					74.8 (total)	74.07 (total)	99 (avg.)

ly), the unit worked on 7 of 11 attempts. Unfortunately, we could not "ground truth" the new instrument with the conventional probe at this location.

Holes 576A (seven cores which were all left upright and unopened for shore-based geotechnical studies) and 576B (nine cores before terminating in chert) proceeded smoothly, with the final core on deck at 2110Z on 19 May (Table 1).

Examination of the cores from Holes 576 and 576B revealed several points of concern:

1. "Flow-in" within cores. On several occasions, cores contained intervals of flow-in separated by intervals of normal looking sediment. The gross layering in the flow-in suggests that the HPC barrel was moving ahead as the piston was moving up (due to heave of the ship?). Thus, the sedimentary section is intermittently stretched, presumably with the loss of an equivalent amount of section from the bottom of the cored interval. This phenomenon introduces substantial uncertainties in the exact depths sampled

2. The interbedded clay–nannofossil ooze at the base of the section could be correlated in detail between the two holes. However, the sub-bottom depths were offset by 10 m, a displacement that is not evident in the 3.5-kHz records and that seems excessive given all the indications of laterally uniform post-chert deposition in the area. It is tempting to assume a one-stand (9.5-m) bookkeeping error during drilling of one of the holes, but we have no evidence of this. We hope that shore-based studies will allow the uniform dark brown clays that form the middle part of the cored section to be correlated in detail, thereby throwing additional light on this problem.

3. Shear strength profiles show a systematic decrease from the bottom of one core to the top of the next, even though all the sediments appear undisturbed. Whether this effect is due to progressive artificial consolidation, or to decreasing disturbance downcore is unclear. We favor the latter. It does indicate, however, that HPC samples must be used with caution for geotechnical studies.

Correlation of Holes 576 and 576B

The lithologic units recovered in Holes 576 and 576B are essentially identical (see Lithostratigraphy section that follows). However, the nominal sub-bottom depth (based on the drilling records) to the base of the clay unit (lithologic Unit I) is more than 10 m deeper in Hole 576 than in Hole 576B. In addition, the pattern of magnetic reversals in Cores 576-2 and -3 looks peculiar, and Hole 576B seems to be missing the Jaramillo Event. The remarkable depositional uniformity indicated by the *Vema*-36 piston cores and all the 3.5-kHz acoustic records near the site suggest that the differences in the nominal sub-bottom depths of lithologic boundaries in the two holes are spurious.

We have, therefore, attempted to adjust the core depths and location of "good" core (brecciated and flow-in material excluded) within cored intervals so as to minimize the differences between the two holes. The following "rules" and comments define what we did:

1. The top of Core 576-1 was placed at 4.5 m because of the short Brunhes record relative to Hole 576B and the presence of radiolarians older than 400,000 yr. in the uppermost sediments.

2. Based on the presence of the same volcanic ash bed and duplication of a portion of the magnetic record, we believe that Cores 576-2 and -3 sampled essentially the same early Matuyama section.

3. The absence of the Jaramillo Event in Hole 576B and the correlations of the Brunhes/Matuyama boundary and Olduvai Event between the two holes indicate that there is a gap of 3.4 m between Cores 576B-1 and -2.

4. Similarly, the correlations of the Olduvai Event and "friable"/"slick" boundary between the two holes indicates a gap of 2.4 m between Cores 576-2 and -4 (this interval corresponds to the incomplete recovery in Core 3).

5. To align the zeolitic interval of Subunit IB, and the Unit I/II boundary in the two holes, we have shortened Core 576-5 by 3 m. We hypothesize that the bumper subs may have closed at this point.

6. Intervals of no recovery, drilling brecciation, or flow-in are assigned to the bottoms of cores, unless a correlation is enhanced by attributing part of the defective interval to a core top or to its original position in the core (in the case of flow-in).

7. Except for the case described in (2) above, the adjustments do not lead to overlap of sections of "good" core within a hole.

8. Except for the case described in (5) above, the drillers' core lengths have been conserved. Only the sub-bottom depths have been adjusted.

For Hole 576B, the revisions are rather minor, but the interpretation of Hole 576 is significantly different. We have no simple explanation for the discrepancies, but feel that small topographic variations around the drill site, perhaps in combination with procedural adjustments accompanying the drilling of what was the first hole on Leg 86, may be responsible.

We believe that the section constructed from the adjusted core depths is a good first approximation to the *in situ* stratigraphy. Thus, although the acoustic profiler data were not used in the adjustments, the resultant depth of 55 m for the lithologic Unit I/II boundary is exactly as predicted from 3.5-kHz records. Small discrepancies undoubtedly remain. For example, we suspect that the ash at 12.5 m in Hole 576 lies in the gap between Cores 576B-1 and -2 (ash was found at the very top of Core 2), whereas the thicker ash at 16 m in Hole 576B should lie in the gap between Cores 576-2 and -4.

Table 2 allows depths in the core sections as labeled by DSDP to be converted to the new adjusted sub-bottom depth. Table 3 shows the depths drilled and "good" core recovered in Holes 576 and 576B in terms of the adjusted scale.

It is clear that the nominal 100% core recovery in each of the two continuously cored sections is somewhat misleading. In fact, the recovery of relatively undeformed core is closer to 80%. Fortunately, with the exception of about 2 m at an adjusted depth of 30 m, we managed to recover virtually the entire sediment section.

We departed the site at 1322Z on 20 May, steaming southeast and streaming the gear before profiling across the site en route to Site 577.

Table 2. Key to convert section depths in Holes 576 and 576B to sub-bottom depths in centimeters (see text for discussion).

Section	Depth (cm)	Adjusted sub-bottom depth (cm)	Comments
Hole 576			0–450 cm not recovered
1-1	0	450	Magnetics (B/M)
1-2	0	600	
1,CC	0	707	
2-1	0	720	Assumes no gap between Cores 1 and 2
2-2	0	870	
2-3	0	1020	
2-4	0	1170	
2-5	0	1320	
2-6	0	1470	
2-7	0	1620	
2,CC	0	1670	
3-1	0	960	Repeat of Core 2 ash and magnetics
3-2	0	1110	
3-3	0	1260	
3-4	0	1410	
3-5	0	1560	
3,CC	0	1592	
			1695–1980 cm not recovered
4-1	70	1980	Correlation of "rough-smooth" boundary
4-2	0	2060	
4-3	0	2210	
4-4	0	2360	
4-5	0	2510	
4-6	0	2660	
4-7	0	2810	
4,CC	0	2858	
5-1	40	2860	40 cm of cave-in debris
			2970–3158 cm not recovered
5-5	48	3158	Correlation of zeolitic clay
5-6	0	3260	
5-7	0	3410	
5,CC	0	3459	
			3459–3510 cm not recovered
6-3	70	3510	
6-4	0	3590	
6-5	0	3740	
6-6	0	3890	
6-7	0	4040	
6,CC	0	4085	
	40	4115	
			4125–4460 cm not recovered
7-1	0	4460	
7-2	50	4610	
7-3	0	4710	
7-4	0	4860	
7-5	0	5010	
7-6	0	5160	
7-7	0	5310	
7,CC	0	5360	
			5385–5425 cm not recovered
8-1	15	5425	
8-2	0	5560	
8-3	0	5710	
8-4	0	5860	
8-5	0	6010	
8-6	0	6160	
8-7	0	6310	
8,CC	0	6353	
	8	6358	
			Hole 576, 6379 cm total depth sampled
Hole 576B			
1-1	0	0	
1-2	0	150	
1-3	0	300	
1-4	0	450	
1-5	0	600	
1-6	0	750	
Hole 576B (Cont.)			
1,CC	0	807	
			820–1165 cm not recovered
2-1	5	1165	
2-2	0	1310	
2-3	0	1460	
			1560–1645 cm disturbed
2-4	35	1645	
2-5	0	1760	
2-6	0	1910	
2-7	0	2060	
2,CC	0	2098	
3-1	0	2110	
3-2	0	2260	
3-3	0	2410	
3-6	21	2470	
3-7	0	2599	
3,CC	0	2649	
			2671–3410 cm not recovered
4-3	100	3410	
4-4	0	3460	
4-5	0	3610	
4-6	0	3760	
4-7	0	3910	
4,CC	0	3962	
			3982–4010 cm not recovered
5-2	0	4010	
5-3	0	4160	
5-4	0	4310	
5-5	0	4460	
5-6	0	4610	
5,CC	2	4735	
			4755–5070 cm not recovered
6-1	110	5070	
6-2	0	5110	
6-3	0	5260	
6-4	0	5410	
6-5	0	5560	
6-6	0	5710	
6,CC	10	5852	
			5887–5913 cm not recovered
7-1	5	5913	
7-2	0	6058	
7-3	108	6208	
7-4	0	6250	
7-5	0	6400	
7-6	0	6550	
7-7	0	6700	
7,CC	0	6734	
			6771–6860 cm not recovered
8-1	115	6860	
8-2	0	6895	
8-3	0	7045	
8-4	0	7195	
8-5	0	7345	
8-6	0	7495	
			7500–7610 cm not recovered
9,CC	0	7610	Hole 576B, 7610 cm total depth sampled

LITHOSTRATIGRAPHY

The sediments recovered at Site 576 can be divided into three lithologic units based on macroscopic core descriptions, smear slide analyses, and carbonate content data. The lithostratigraphic succession observed in Holes 576 and 576B consists of a pelagic clay unit overlying an interbedded pelagic clay–nannofossil or nannofossil–foraminifer ooze unit which in turn overlies a chert unit (Fig. 1, Table 4).

Table 3. Adjusted sub-bottom depths (in meters, see text for discussion) of Site 576 cores and intervals of good quality core.

	Hole 576		Hole 576B	
Core	Length drilled (m)	Length recovered (m)	Length drilled (m)	Length recovered (m)
1	4.50–7.20	4.50–7.20	0.00–8.20	0.00–8.20
2	7.20–16.70	7.20–16.95	11.60–21.10	11.65–21.10
3	9.60–19.10	9.60–16.22	21.10–30.60	21.10–26.71
4	19.10–28.60	19.80–28.60	30.60–40.10	34.10–39.82
5	28.60–35.10[a]	28.60–29.70 31.58–34.97	40.10–49.60	40.10–47.55
6	35.10–44.60	35.10–41.25	49.60–59.10	50.70–58.87
7	44.60–54.10	44.60–53.85	59.10–68.60	59.15–67.71
8	54.10–63.60	54.25–63.77	68.60–76.10	68.60–75.00
9			76.10–76.20	76.10–76.11

[a] 3 m short—bumper subs closed?

Unit I: Pelagic Brown Clay

Lithologic Unit I is a pelagic brown clay recovered in both Holes 576 and 576B. It is divided into two subunits as follows.

Subunit IA

Subunit IA is a pelagic yellowish brown to brown, visibly burrowed clay found in Samples 576-1-1, 0 cm to 576-4-6, 53 cm and 576B-1-1, 0 cm to 576B-3-6, 150 cm. This subunit is composed of alternating yellowish brown and dark yellowish brown to brown highly mottled clay with burrows. The abundance of visible burrows decreases downhole. With the exception of Core 576-1, which is a silty clay containing 20–45% quartz, this subunit contains greater than 80% clay-size material and less than 15% visible quartz. Hole 576 contains two layers of volcanic ash in this subunit; each is 1 cm thick. Hole 576B contains three volcanic ash layers in this subunit; they range in thickness from 1 to 3 cm. This subunit contains no nannofossils or foraminifers and less than 10–12% siliceous microfossils (diatoms and radiolarians). Sponge spicules and silicoflagellates are present in only trace amounts. The abundance of siliceous organisms decreases with depth.

Subunit IB

Subunit IB is an unburrowed, homogeneous dark brown pelagic clay found in Samples 576-4-6, 53 cm to 576-8-2, 8 cm and 576B-3-6, 150 cm to 576B-6-4, 121 cm. Zeolites, principally phillipsite, are present in abundances of up to 10% in Sections 576-5-4 to 576-5-6 and 576B-4-1 to 576B-4-5. These two zeolite-rich zones appear to be stratigraphically correlative. Traces of fish debris are found throughout this subunit. The boundary between the two Subunits IA and IB is gradational over several meters.

Unit II: Interbedded Calcareous Ooze and Pelagic Brown Clay

Lithologic Unit II is composed of interbedded calcareous oozes and brown pelagic clays found in Samples 576-8-2, 8 cm to 576-8,CC and 576B-6-4, 121 cm to 576B-8,CC. The thickness of the calcareous ooze intervals ranges from 0.10 to 3.0 m; that of the clay intervals ranges from 0.10 to 1.10 m. The carbonate content in the oozes ranges from 80–98%. The calcareous oozes in these intervals are predominantly nannofossil oozes; foraminifers are present and increase in abundance downcore to 15% in Sample 576-8-6, 64–72 cm.

The interbedded calcareous oozes and pelagic clays in Hole 576 can be correlated layer-by-layer with those in Hole 576B (Fig. 2). Such a correlation indicates that the bottom of Hole 576 corresponds to Sample 576B-7-4, 110 cm. The thicknesses of the correlative layers are almost identical (Fig. 3) with the exceptions of the interval from Section 576-8-1 to the top of 576-8-2 and from Section 576B-6-4 to the top of 576B-6-5. In the latter hole the units are about 9% thicker (Fig. 4). In addition, the thickest calcareous ooze layer is 3.48 m thick in Hole 576, but 4.30 m thick in Hole 576B. This 0.82-m difference in layer thickness is likely due to "flow-in" in Hole 576B.

Contacts between the calcareous ooze and pelagic clay layers range from gradational to sharp. The base of each calcareous ooze layer is marked by a sharp contact, whereas the bases of the pelagic clay layers vary from very gradational to sharp.

Normal graded bedding is observed in the uppermost calcareous ooze layers in Samples 576-8-2, 8–21 and 34–66 cm and 576B-6-4, 121–132 and 150 cm to 576B-6-5, 40 and 60–80 cm. Normal graded bedding and small-scale crossbedding are also observed in the lower 20 cm of the thickest calcareous ooze layer in both holes (Samples 576-8-4, 25 cm to 576-8-6, 73 cm correlative to Samples 576B-7-1, 5 cm to 576B-7-3, 135 cm). These calcareous ooze layers all have sharp bottom contacts with the pelagic clay layers below. The graded bedding, small-scale cross bedding, and sharp basal contacts observed in these calcareous ooze layers suggest that they are turbidites. The other calcareous ooze layers lack these macroscopic features. It is uncertain, therefore, whether these deposits are also turbidites.

Unit III: Chert

Lithologic Unit III is a chert and/or silicified clay unit. It was not reached in Hole 576 and is only poorly recovered as small chips in Sample 576B-9,CC.

SEISMIC CORRELATIONS

High resolution seismic reflection profiles (3.5 and 12 kHz) and 100-Hz reflection profiles were recorded at Site 576. Both hull-mounted and near-bottom sound sources were utilized; the near-bottom transducer (3.5 and 5.25 kHz) was mounted on the drill string 99 m above the face of the drill bit. The quality of the 3.5-kHz echograms was substantially improved by repairing a factory-produced error in the booster for the hull-mounted transducer.

The 3.5-kHz echograms from the hull-mounted transducer revealed a three-part seismic section (Figs. 5 and 6, Table 5). The upper seismic section extends to 0.025 s below the seafloor (about 18 m, Reflector 2) and consists of several parallel sub-bottom reflectors. The middle seismic section has a base with variable sub-bottom

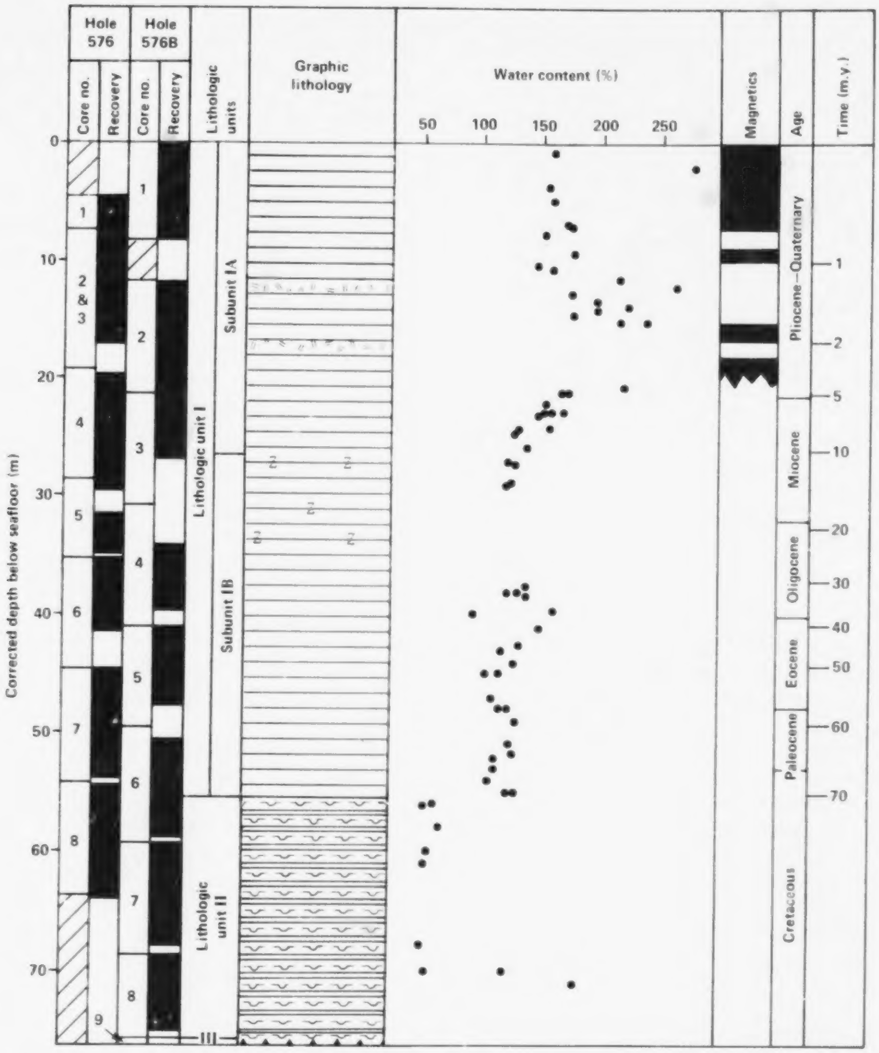

Figure 1. Site summary diagram showing Site 576 core numbers, core recovery, lithologic units, graphic lithology, water content (%), magnetostratigraphy, and age versus adjusted sub-bottom depths. Adjusted depths of cored and recovered intervals are given in Table 3. Symbols used in graphic lithology column are defined in Introduction and Explanatory Notes (this volume).

Table 4. Site 576 lithostratigraphic units.

Lithologic units		Core interval		Adjusted sub-bottom depth (m)	
		Hole 576	Hole 576B	Hole 576	Hole 576B
I	Pelagic brown clay	1-1 to 8-2, 8 cm	1-1 to 6-4, 121 cm	4.5-55.7	0-55.3
	Subunit IA: Pelagic yellowish brown to brown burrowed clay	1-1 to 4-6, 53 cm	1-1 to 3-6, 150 cm	4.5-27.1	0-26.2
	Subunit IB: Unburrowed dark brown pelagic clay	4-6, 53 cm to 8-2, 8 cm	3-6, 150 cm to 6-4, 121 cm	27.1-55.7	26.2-55.3
II	Interbedded calcareous ooze and pelagic brown clay	8-2, 8 cm to end of hole	6-4, 121 cm to 8,CC	55.7-63.8	55.3-76.1
III	Chert	—	9	—	76.1

Note: — indicates no data.

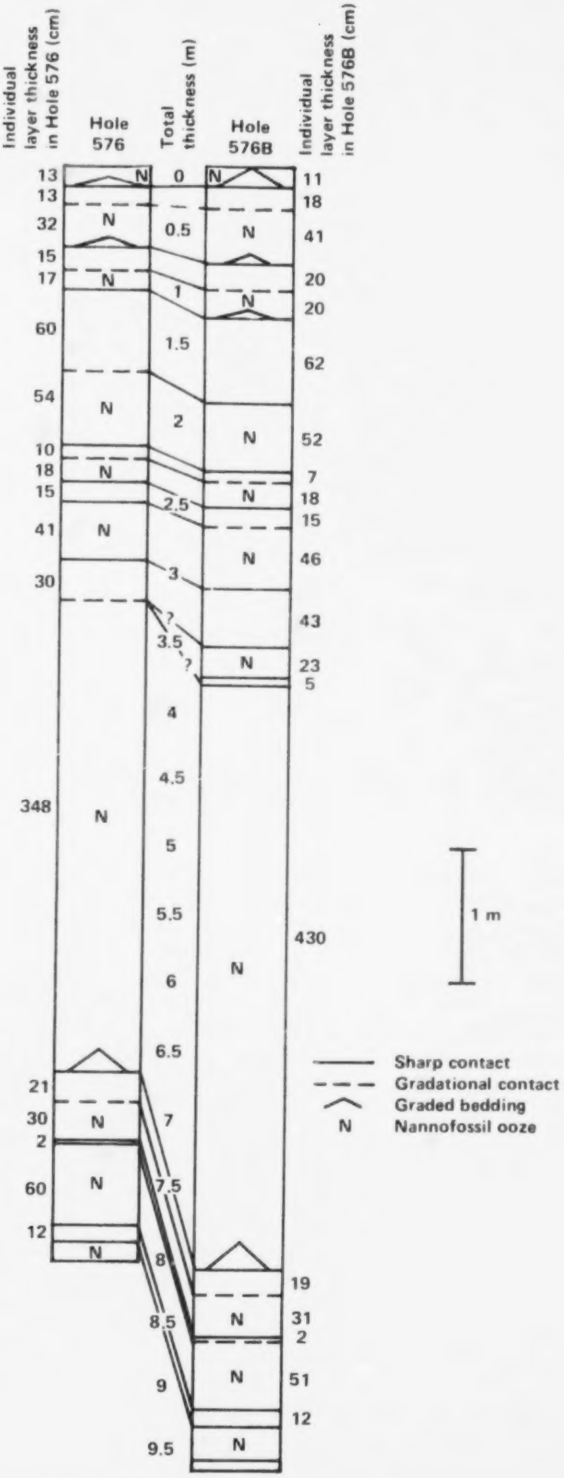

Figure 2. Correlation of interbedded calcareous ooze and pelagic clay layers in lithologic Unit II at Holes 576 and 576B.

depth (0.07-0.08 s, ~53-60 m) and consists of the essentially transparent section above Reflector 4. The lower seismic section consists of a strong, prolonged echo and a slightly deeper and weaker intermittent prolonged echo.

In the upper seismic section, strong echoes occur at 0.0053 s (~4 m), 0.016 s (~11.5 m, Reflection 1), and 0.025 s (~18 m, Reflector 2). Reflector 1 at about 11.5 m is probably the first ash layer (1.4 m.y. ago) encountered in Holes 576 and 576B. Reflector 2 at about 18 m probably represents the third ash layer recovered in Hole 576B. The interval thickness between Reflectors 1 and 2 (~6.5 m) is very similar to the observed thickness between the first and third cored ash layers in Samples 576B-2-1, 8 cm and 576B-2-5, 40 cm.

The middle transparent seismic section corresponds to the monotonous brown and reddish brown pelagic clay section cored between the ash layers and the interbedded pelagic clay and nannofossil ooze unit. Reflector 2a is closely associated with the transition between lithologic Subunits IA and IB (Fig. 6).

Reflector 3 (Figs. 5 and 6) is a strong, slightly prolonged echo that occurs 0.0695 s below the seafloor (~51.0 m). It is restricted to localized lows in Reflector 4 and has a ponded character. Although the ponded nature of Reflector 3 is consistent with the interpretation that it represents the calcareous turbidites of lithologic Unit II, the seismic interval thickness between the ash (Reflector 2) and Reflector 3 is about 33 m, whereas the interval thicknesses between the ash and the nannofossil oozes (turbidites) is 39 m.

Reflector 4 (Fig. 6, Table 5) defines the top surface of the lowest seismic section. The local relief on this surface suggests that Reflector 4 is not similar to the overlying ponded turbidites (Reflector 3). Reflector 4 may be a composite echo from turbidites in the local lows and chert on the local highs or it may represent single layers of relatively high density and viscosity. In either case, the thickness of the cored turbidite section (20.5 m) and the sub-bottom depth of the chert encountered at Site 576 (~76 m) do not permit positive correlation of the chert with the strong prolonged echo at Site 576. In order to correlate Reflector 4 with the cored chert, an improbable interval velocity of 2155 m/s would be necessary.

Reflectors 1 (ash), 2 (ash?), 4, and the intervening transparent layer can all be traced westward to the slopes of the Shatsky Rise and eastward for at least 400 km. Site 576 therefore provides control for not only regional lithologic but also time-stratigraphic correlations of Late Cretaceous and younger sediments.

The transducer mounted on the drill string returned weak seafloor echoes similar to those produced by the hull-mounted transducer, but Reflector 5 was more evident on the record of the drill string mounted pinger. The pinger-to-seafloor travel time showed that the Carter Correction Tables were 2 m too deep in this area (i.e., the seafloor depth is 6209, not 6211 m).

The 100-Hz records also reveal a three-part seismic section (Fig. 7): (1) weak, generally parallel reflections from 0 to about 0.05 s below seafloor, (2) strong, parallel echoes from 0.05 s to variable depths of 0.3 to 0.55 s

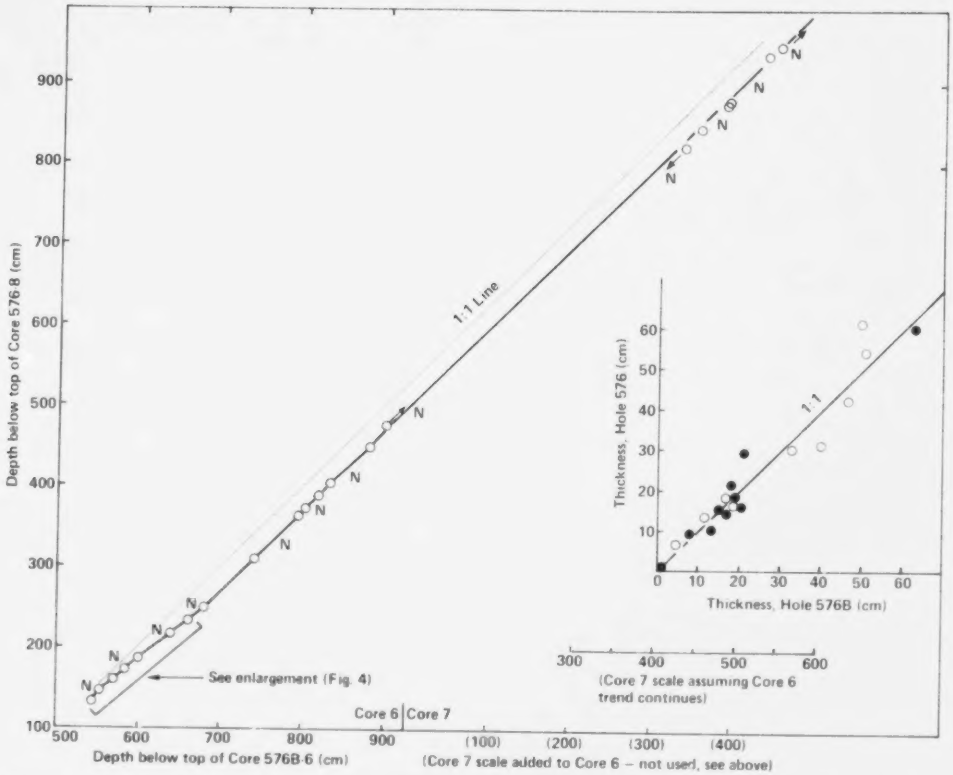

Figure 3. Graph comparing thickness of correlated calcareous ooze and pelagic clay layers at Holes 576 and 576B. N = nannofossil ooze layer. Inset: comparison of layer thicknesses, ● = red clay, ○ = nannofossil ooze.

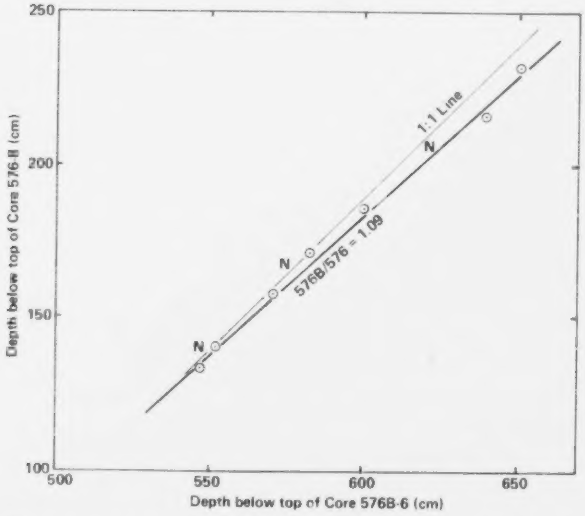

Figure 4. Graph comparing thickness of correlated calcareous ooze and pelagic clay layers in Holes 576 and 576B. (Expansion of lower part of graph shown in Figure 3.) N = nannofossil ooze layer.

below seafloor, and (3) very strong echoes that define a surface with very high relief. The upper section has a variable thickness of 0.05 to 0.07 s; the unit appears to "pond" in troughs of the underlying middle section. The upper section may represent sediments above the Cretaceous chert, since the seismic thickness is about 75 m at the site and the cored thickness to chert is 74 m at Hole 576B. The middle section with variable thickness of 0.23–0.5 s consists of an upper unit (2a) of parallel reflectors with variable thickness that overlie a lower semitransparent unit (2b) of relatively constant thickness. Section 2 represents the Cretaceous nannofossil oozes and interbedded cherty sediments. The lowest section with very high relief is the echo off Cretaceous basement of M13 age (about 129 m.y.).

BIOSTRATIGRAPHY

Site 576 recovered 74 m of sediment ranging in age from late Quaternary through Late Cretaceous (Fig. 8). The sequence consists of 55 m of pelagic brown to yellowish brown clay overlying a unit composed of interbedded calcareous ooze and brown pelagic clays. A chert unit underlies this sequence.

Ichthyoliths, which were found throughout the clay interval, vary from rare to abundant in all samples. Nannofossils are restricted to the calcareous ooze layers where an abundant, moderately preserved Late Cretaceous assemblage is present. The brown clays are barren of foraminifers except for those few specimens that have been replaced by manganese oxide. The calcareous ooze layers contain abundant, well-preserved Upper Cretaceous

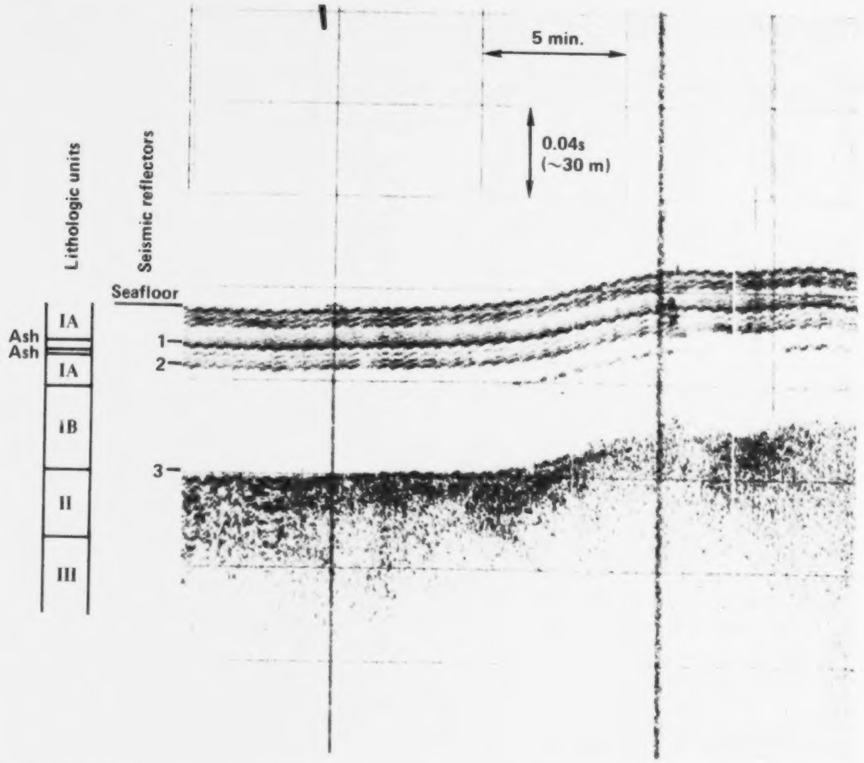

Figure 5. 3.5-kHz echogram from the hull-mounted transducer at Site 576 showing the three-part seismic section and reflectors described in the text. Sub-bottom depths to seismic reflectors are given in Table 5.

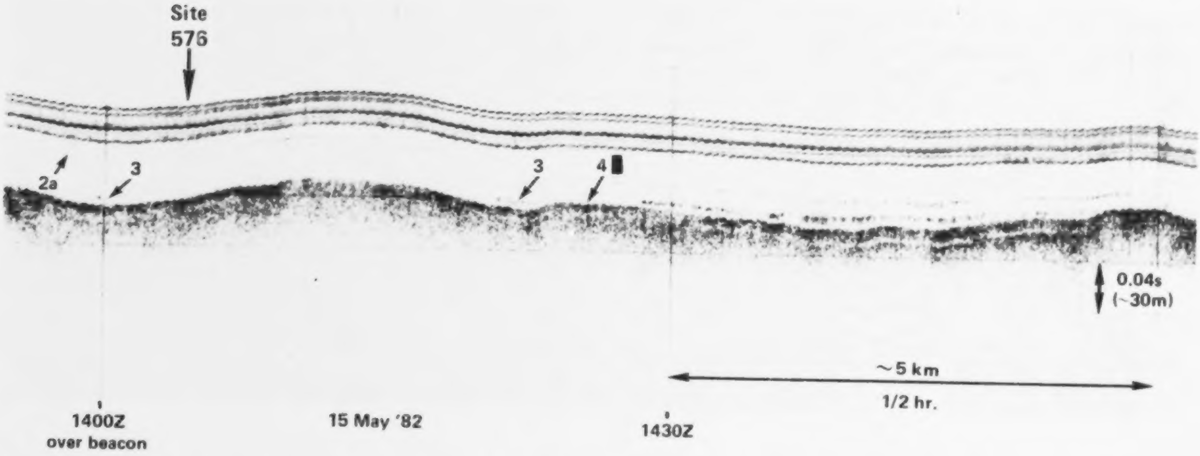

Figure 6. 3.5-kHz echogram from the hull-mounted transducer at Site 576 showing Reflectors 2a, 3, and 4 (Table 5) described in the text.

foraminifers. Although Quaternary-late Pliocene diatoms and radiolarians were found in the first several cores, they are abundant and well preserved only in the upper portion of Core 1 of each of the three holes.

The generally poor preservation and low abundance of each of the major microfossil groups precludes assignment of age boundaries to specific core sections at this site. Ichthyolith determinations indicate that the Oligocene/Miocene boundary lies between 32 and 35 m, the Eocene/Oligocene between 38.6 and 41.6 m, the Paleocene/Eocene between 44.6 and 51 m, and the Cretaceous/Tertiary boundary between 51 and 55 m.

Table 5. 3.5-kHz seismic correlations, Site 576.

Reflector	Relative strength[a]	Sub-bottom depth (s)	Depth (m)			
			1440 m/s	1500 m/s	1550 m/s	1574 m/s
	S	0.00526	3.8	3.9	4.08	4.1
1	S	0.0158	11.3	11.85	12.24	12.43
	W	0.0200	14.39	14.92	15.49	15.73
	W	0.0210	15.1	15.75	16.28	16.57
2	S	0.0247	17.78	18.50	19.10	19.47
2a	W	0.0358-0.0389	25.78-28.01	26.85-29.18	27.74-30.15	28.17-30.61
3	S	0.0695	50.04	52.12	53.86	54.70
4	S	0.0705-0.0800	50.77-57.53	52.80-59.90	54.60-57.90	55.49-62.90

[a] S = strong; W = weak.

Calcareous Nannofossils

The first seven cores recovered at Hole 576 were barren of calcareous nannofossils. Coccoliths are present only in samples from Core 8, where they occur in the calcareous ooze layers interbedded with pelagic brown clays. The common and moderately well preserved coccolith assemblages belong to the *Quadrum trifidum* Zone (upper Campanian).

The first five cores recovered at Hole 576B were barren of calcareous nannofossils. From Section 576B-6-4 to Sample 576B-9,CC, poorly to moderate preserved nannofossils of the Campanian *Q. trifidum, Ceratolithoides aculeus*, and *Broinsonia parca* Zones occur (Thierstein, 1976).

Foraminifers

Core-catcher samples were examined from all eight cores of Hole 576. Foraminifers were found in two Tertiary samples (576-3,CC and 576-4,CC). The individuals were completely replaced by manganese oxide and were difficult to distinguish from micronodules. This phenomenon was recorded by Thompson (1980) in the Japan Trench. The replaced foraminifers were abundant in Sample 576-3,CC, rare in Sample 576-4,CC and absent in Samples 576-1, -2, -5, -6, and -7,CC. Species included: *Globigerina dutertrei, G. linaperta, Pseudohastigerina wilcoxensis, Lagena* spp., and *Pullenia* spp. Rare specimens of the agglutinate form *Reophax difflugiformis* were found in Samples 576-1-1, 56-58 cm and 576-1,CC.

Abundant, moderately preserved foraminifers of Campanian age from the *Globotruncana fornicata-G. stuartiformis* Zone (Pessagno, 1967) were found in Sample 576-8,CC. Species include: *Globotruncana lapparenti, G. bulloides, G. angusticarinata, Globigerinelloides asperus, G. prairiehillensis, Hedbergella planispira, Hastigerina watersi, Heterohelix* spp., *Lagena* spp., and *Gyroidina* spp.

Samples from Hole 576A were not examined.

Samples 576B-1,CC to 576B-5,CC were barren of any foraminifers. Rare Mn-replaced specimens were found in Samples 576B-2-4, 130-132 cm; 576B-3-1, 92-94 cm; and 576B-3-4, 92-94 cm. Rare benthic foraminifers were found in Sample 576B-6,CC. These were: three specimens of *Anomalinoides pinguis* and two *Gavelinella* cf. *velascoensis*. Rare specimens from Sample 576B-7,CC were caught on the 149-μm sieve. Three agglutinate species were observed including: *Paratrochomminoides vitreus, Praecystammina globigerinaeformis*, and the torus-shaped solution remnants of a third species. Other species include: *Anomalinoides pinguis, Gavelinella* cf. *velascoensis*, and *Globigerina eugubina*.

Samples 576B-8,CC and 576B-9,CC were barren in the fraction larger than 149 μm. The 62.5- to 149-μm fraction of both samples contained an abundant, well-preserved Upper Cretaceous fauna (zone uncertain). Representative species include: *Globigerinelloides volutus, G. subcarinatus, G. multispinus, Heterohelix striata, H. navarroensis, H.* cf. *globocarinata*, and *Hastigerina* spp. Preliminary examination has revealed no specimens of *Globotruncana*. This genus is most important for the identification of Upper Cretaceous zones.

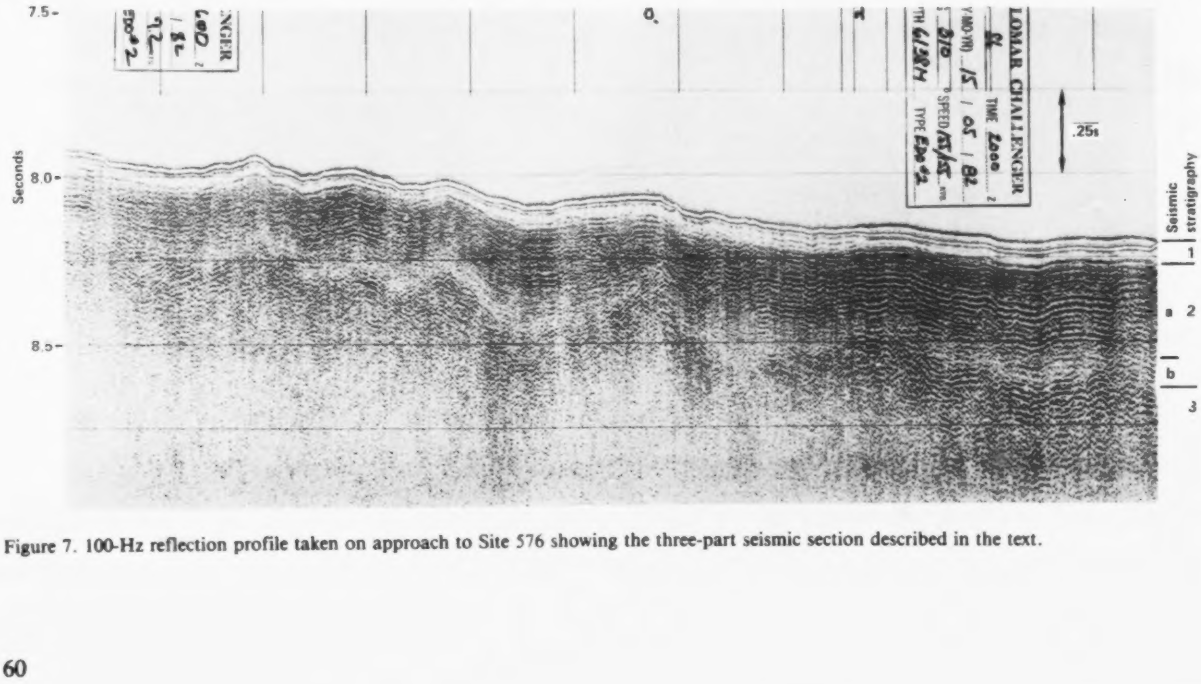

Figure 7. 100-Hz reflection profile taken on approach to Site 576 showing the three-part seismic section described in the text.

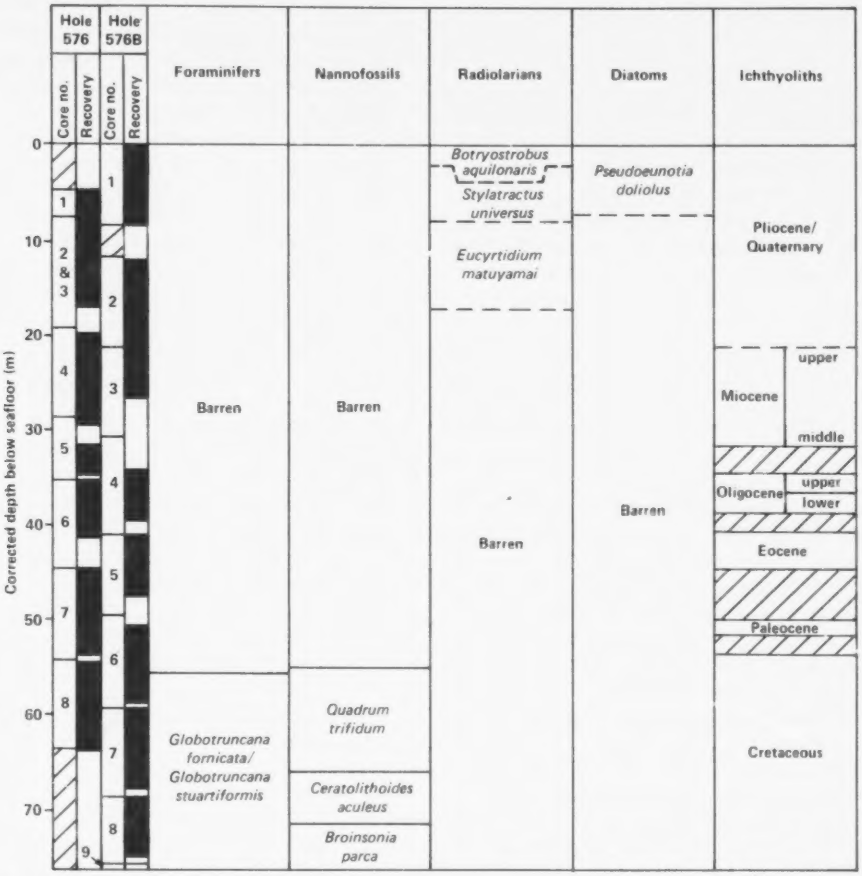

Figure 8. Site 576 biostratigraphic summary.

Radiolarians

Radiolarians are present in the first three cores at Site 576 (Section 576-1-1; Samples 576-1,CC; 576-2,CC; and 576-3,CC). The sediments in Core 576-1 are Pleistocene in age, with species characteristic of the *Botryostrobus aquilonaris* Zone (Hays, 1970) and the *Stylatractus universus* Zone (Hays, 1970) in sediments from the top and bottom of Core 576-1, respectively. Poorly preserved specimens are present in the core-catcher samples from Cores 576-2 and 576-3. Radiolarians are absent in core-catcher samples from Cores 576-4 through 8. A calcareous sequence in Core 576-8 from this hole contains poorly preserved Upper Cretaceous radiolarians.

Core 576A-1 contains common, moderately well-preserved radiolarians belonging to the *S. universus* Zone (Sample 576-1,CC) with only a few specimens present in Core 2 (Sample 576-2,CC). Core-catcher samples from subsequent cores are barren (Samples 576-3,CC through 576-7,CC).

The radiolarian fauna in Core 576B-1 (Section 576B-1-1; Sample 576B-1,CC) is Pleistocene in age with preservation decreasing rapidly from good at the core top to poor at the base. Core 576B-2 (Sample 576B-2,CC) from this hole contains only a few specimens and Core 576B-3 (Sample 576B-3,CC) is barren.

Diatoms

Diatoms become increasingly less abundant between Cores 576-1 and 3 and are absent from Cores 576-4 to 8. The presence of *Pseudoeunotia doliolus* and the absence of *Nitzschia reinholdii* and *N. fossilis* in Core 576-1 places the sample in the middle to late Quaternary *P. doliolus* Zone (Brunhes Normal Epoch, 0–0.73 m.y. ago; Burckle, 1977). Rare to few specimens and fragments of specimens of a moderately preserved Neogene species, *N. reinholdii, Nitzschia* spp., and *Coscinodiscus* spp., were recovered in Cores 576-2 and 3 from this hole. These assemblages consist of diatom taxa that are commonly found in warm water regions.

Only fragments of some Neogene species, *N. reinholdii, Thalassiosira lineata*, and *T. oestrupii*, were recovered in Cores 576A-1 through -3. In Core 576A-1, however, many fragments of moderately preserved *Ethmodiscus rex* were encountered. Diatoms were not found below Core 576A-4.

Core 576B-1 contains only a few fragments of some Neogene species, *Coscinodiscus* sp., *E. rex, T. lineata*, and *Thalassiothrix longissima*. Diatoms are absent from Cores 576B-2 to 9.

Ichthyoliths

Ichthyoliths are present throughout Hole 576A. Their abundance ranges from rare in the rapidly accumulating sediments in the top two cores to a peak abundance typically found near the Paleocene/Eocene boundary. Ichthyoliths in Cores 576A-1 and 2 are late Miocene or younger based on the coherent range of *Narrow triangle ragged base*. Core 576A-3 and Sections 576A-4-1 and -3 are Miocene with a rich and diverse assemblage of characteristic taxa. Representative subtypes are: *Two triangles, Triangle sinuous inline, Elliptical with line across*, and *Triangle irregular base*. Section 576A-3-3 contains an aberrant, very sparse assemblage of foraminifers, radiolarians, diatoms, and ichthyoliths. The ichthyoliths indicate only that the sample is Miocene.

The Oligocene/Miocene boundary falls between Sections 576A-4-3 and -4-5 based on the first occurrence of *Triangle with high inline apex* in Section 576A-4-5 and the first occurrence of *Small triangle long striations*, as well as the first occurrences of the discriminating Miocene taxa listed above, in Section 576A-4-3. The first appearance of *Rounded apex triangle* and *Flexed triangle shallow in base* in Section 576A-5-1 correlates with an early Oligocene age.

The Eocene/Oligocene boundary lies between Sections 576A-5-1 and -5-3. Sections 3 and 5 of that core are Eocene, most probably early and middle Eocene based on the absence of younger taxa and the presence of subtypes characteristically found in abundance in the Eocene: *Triangle with triangular projection, Triangle pointed margin ends*, and *Triangle medium wing*.

The Paleocene/Eocene boundary is between Sections 576A-6-1 and -6-3 and the Cretaceous/Tertiary boundary is between Sections 576A-6-3 and -6-5. The Cretaceous assemblages in Sections 576A-6-5 and -7 include subtypes *Striated blunt triangle, Triangle long inline, Triangle square inline*, and *Wide triangle projection*.

In Hole 576, the Cretaceous/Tertiary boundary is below Sample 576-8-1, 25 cm. In Hole 576B, the boundary is below Section 576B-6-3.

PALEOMAGNETICS

Detailed paleomagnetic studies of Site 576 samples are reported in a later chapter (see Heath, Rea, and Levi, this volume). Initial results indicate that the Brunhes/Matuyama boundary (0.73 m.y.) lies at 7.05 m sub-bottom and the Matuyama/Gauss boundary (2.47 m.y.) at 18.21 m sub-bottom. The Jaramillo boundaries (0.91 and 0.98 m.y.) were found at 8.95 and 9.85 m sub-bottom, and the Olduvai boundaries (1.66 and 1.68 m.y.) at 14.85 and 16.3 m sub-bottom, respectively. These levels correlate well with reversals recorded in *Vema*-36 cores collected near Site 576.

SEDIMENT ACCUMULATION RATES

An accurate shipboard determination of sedimentation rates at regular intervals throughout the sediment sequence recovered at Site 576 is difficult because calcareous and siliceous microfossils are not present in most of the cores. The age of the top of the hole is based on radiolarian stratigraphy with paleomagnetic data providing input for rates through the last 2.5 m.y. Ichthyolith stratigraphic ranges constrain ages in the least fossiliferous clays, but not very precisely (Fig. 9). Through the upper 18 m, the sedimentation rate decreased from 9.7 m/m.y during the Brunhes to about 2 m/m.y. at the base of the Matuyama (Fig. 10). A smooth sedimentation rate curve from 2.5 to 70 m.y. yields rates of about 1 m/m.y. at 5 m.y., decreasing to about 0.35 m/m.y. at about 40 m.y., and then increasing slightly to about 0.6 m/m.y. in the Late Cretaceous.

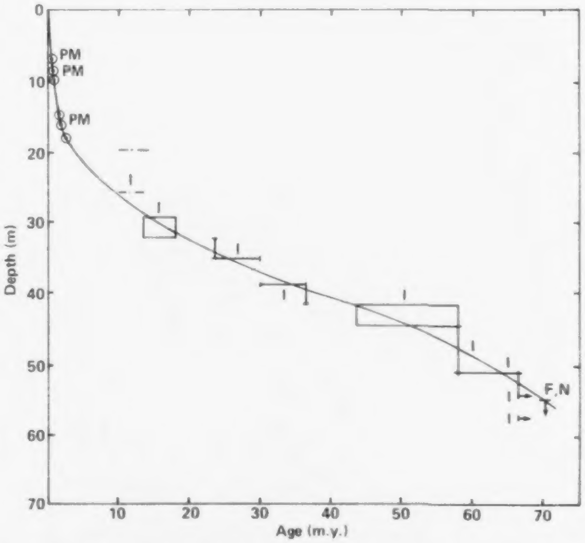

Figure 9. Age-depth curve for Site 576. PM = paleomagnetics, I = ichthyoliths, F = foraminifers, N = nannofossils.

PHYSICAL PROPERTIES

Physical properties measurements at Site 576 were performed using mainly standard DSDP methods (Boyce, 1976a, b; Introduction and Explanatory Notes, this volume). Table 6 summarizes the properties that were measured at Holes 576 and 576B. Cores from Hole 576A were left unopened and used exclusively for detailed shore-based laboratory geotechnical tests (Marine Geotechnical Consortium, this volume). Figures 11, 12, and 13 show profiles of shear strength, compressional and shear wave velocity, and saturated bulk density and water content, respectively.

Measurements were taken at approximately 1.5-m intervals throughout the cores in Holes 576 and 576B. A full discussion of the physical properties of the recovered sediment, including tables of the data, is given by Schultheiss (this volume). However, some of the more interesting features of the data are highlighted here:

1. Shear strengths and shear wave velocities in the carbonate layers are generally much less than in the brown clay. This does not necessarily mean that the *in situ*

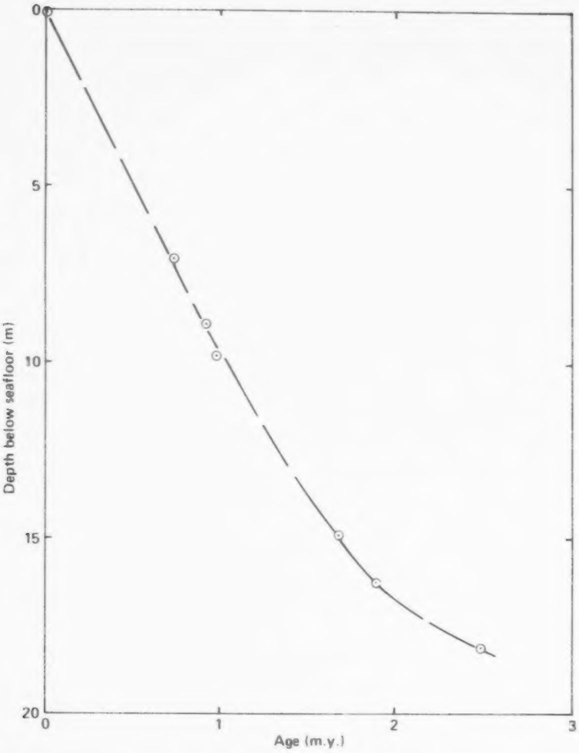

Figure 10. Age–depth curve for near-surface Site 576 sediments based on magnetic reversals.

Table 6. Physical properties measurements made at Site 576.

	Hole 576	Hole 576B
Shear strength		
Hand operated vane	x	x
Motorized vane	x	x
Wave velocity		
Shear wave	x	x
Compressional wave	x	x
Water content/bulk density		
Shipboard analysis	x	—
Shore-based analysis	x	x
Bulk density by 2 min. GRAPE	x	—

strengths vary by this amount; rather, it is probably caused by different forms of stress disturbance in the different lithologies.

2. Where there is a large amount of visual disturbance ("flow-in"), the shear strength in the brown clay is markedly reduced whereas the shear wave velocity is only slightly reduced.

3. The large increase in the shear strength and shear wave velocities in the brown clay below 65 m in Hole 576B may be indicative of the onset of diagenesis (Figs. 11 and 12).

4. The compressional wave velocity profile shows no obvious trend through the brown clay section and is always less than the water velocity. Peaks in the compressional wave velocity correspond to ash and carbonate layers (Fig. 12).

5. The uniformity of shear wave velocities measured parallel and perpendicular to the core axis indicates a total lack of anisotropy within any of the lithologies.

6. Water content increases markedly by up to 220% between 11 and 20 m in the brown clay unit before it gradually decreases to 110% at 50 m (Fig. 13). The cause of this is not known but a change in mineralogy, similar to that found in LL44-GPC3, is suspected. The increase in water content is consistent with a decrease in shear strength around 16 m as shown in Figure 11. Higher frequency fluctuations in water content (on a scale of approximately 0.5 m) occur in the brown clay and reflect subtle changes in lithology which are not yet understood.

INORGANIC GEOCHEMISTRY

Seven squeezed core samples from Hole 576A and three *in situ* pore water samples (PW-1, PW-2, and PW-3) from Hole 576 were analyzed for the standard suite of components: pH, alkalinity, salinity, calcium, magnesium, and chlorinity (Table 7). The squeezed samples show very little variability downcore, as would be expected from the very slow deposition rate of the pelagic clays which allows diffusional equilibration (Fig. 14).

The *in situ* samples look much like surface seawater, apparently somewhat diluted with distilled water (from the sampler) in the case of Sample PW-3. In all three cases, the Mg/salinity and chlorinity/salinity ratios are so close to surface seawater that contamination by drilling fluid is suspected. We assume that this was caused by the sediments being too weak to support the BHA, thereby allowing the heave of the ship to move the probe into and out of the sediment as it was drawing a sample. Mechanically, the operation of the probe with an HPC BHA did not cause any problems.

HEAT FLOW

A new heat flow instrument, developed by R. P. Von Herzen and others at WHOI, was used for the first time to record bottom hole temperatures. The instrument, specifically designed for use with the HPC, consists of a temperature sensor (thermistor), a recorder, and a battery pack that are inserted as a unit into a slot opened in the metal wall of the corer's shoe so that the temperature sensor is placed close to the shoe's tip. The recorder is a battery powered minicomputer that stores data of measured temperatures as a function of time at intervals specified by a program that is loaded into the computer prior to the operation. This instrument, which provides an efficient way of measuring undisturbed sediment temperature without interfering with the core-sampling process, was used throughout Leg 86.

Out of 11 test runs made at Site 576 (5 in Hole 576, 3 in Hole 576A, and 3 in Hole 576B), 7 (2 in Hole 576, 3 in Hole 576A, and 2 in Hole 576B) were successful. The reasons for the unsuccessful runs varied from case to case. However, either electrical disconnection between the recorder and the battery or problems with computer programming due to inexperienced operators (as the instrument is totally new) generally were responsible.

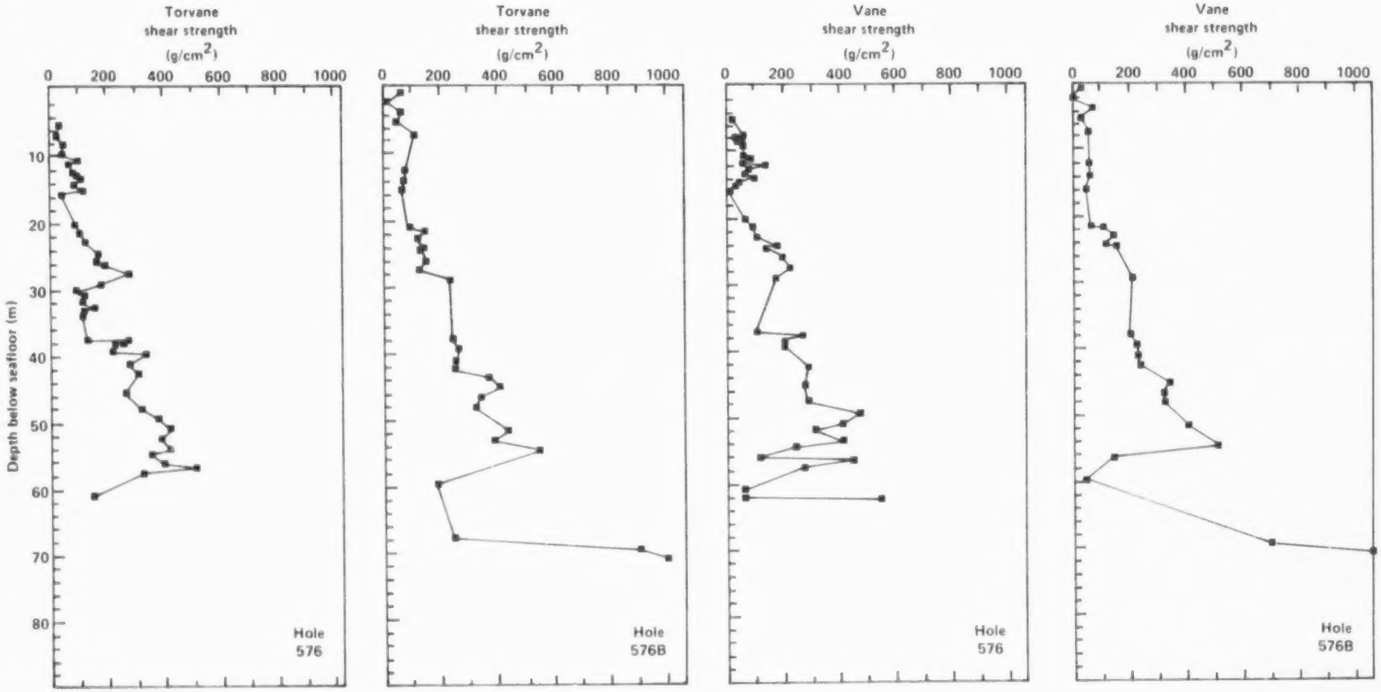

Figure 11. Plot of shear strength versus sub-bottom depth for Site 576.

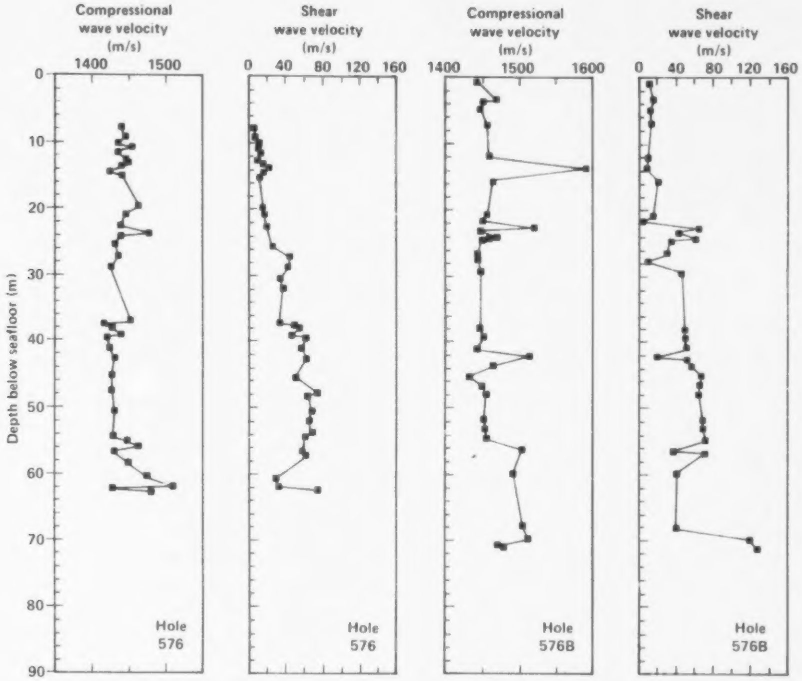

Figure 12. Plot of compressional and shear wave velocities versus sub-bottom depth for Site 576.

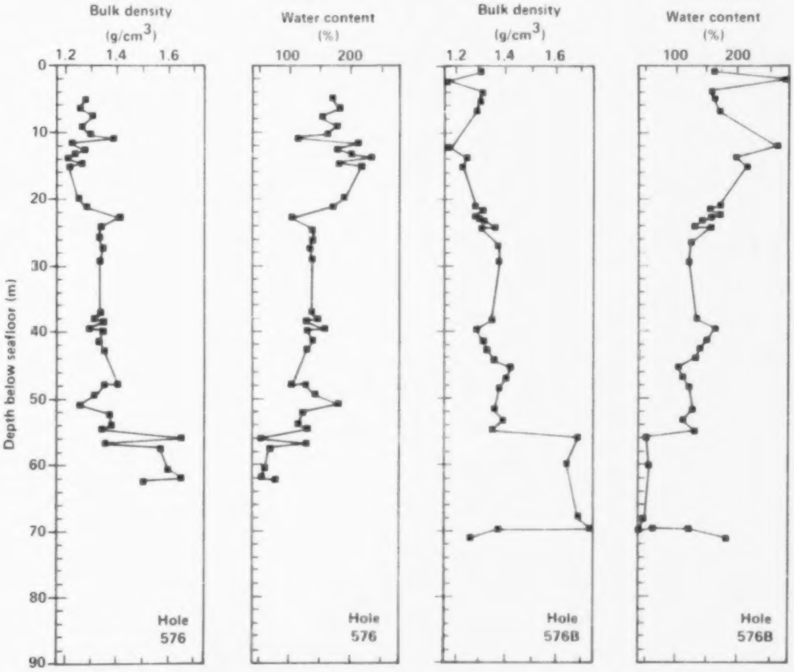

Figure 13. Profiles of saturated bulk density and water content versus sub-bottom depth for Site 576.

Table 7. Inorganic geochemistry measurements at Site 576.

Sample	pH	Alkalinity (mEq/l)	Salinity (‰)	Calcium m*M*	Magnesium m*M*	Chlorinity (‰)
IAPSO	7.74	2.59	35.2	10.55	53.99	19.376
SSW	8.22	2.46	35.2	10.15	53.79	19.174
PW-1	8.26	3.00	35.5	9.79	54.93	19.309
PW-2	8.30	2.53	35.2	9.96	53.31	19.073
PW-3	8.39	2.78	33.8	10.51	51.19	18.264
576A-1-4, 140-150 cm	7.11	2.63	35.2	10.37	53.62	18.871
576A-2-4, 140-150 cm	7.14	2.63	35.5	10.56	53.61	19.208
576A-3-5, 130-140 cm	7.19	2.84	35.5	10.65	51.29	19.174
576A-4-4, 140-150 cm	7.19	2.97	35.5	11.24	51.97	19.342
576A-5-4, 140-150 cm	7.34	3.14	35.5	10.96	53.03	19.376
576A-6-5, 130-140 cm	7.52	3.14	35.5	11.07	53.29	19.275
576A-6-5, 130-140 cm	7.29	2.71	35.8	10.06	53.45	19.275
576A-7-4, 130-140 cm	7.51	2.85	35.5	10.67	53.27	19.140

Temperature data for the successful runs, taken at 10-s intervals for a duration of more than 5 min., clearly show the changing thermal environment at the tip of the HPC. The portion of the cooling curve resulting from the dissipation of frictional heat generated by the HPC as it entered the sediment is most important for estimating the undisturbed sediment temperature. Analyses of the data from all successful runs yield a good estimate of the temperature profile in the unlithified sediments at Site 576 (see Horai and Von Herzen, this volume).

Thermal conductivity measurements on the recovered cores form an integral part of the heat flow study. Measurements were made on 211 samples selected from the cores of Holes 576, 576A, and 576B. These data are combined with the temperature measurements to compute the heat flow at Site 576 (see Horai and Von Herzen, this volume).

SUMMARY AND CONCLUSIONS

Site 576 sampled about 55 m of pelagic clay overlying 20 m of interbedded carbonate turbidites and pelagic clay, before terminating on chert at 76 m.

The upper 25-30 m of clay is yellowish brown, silty, and slightly biosiliceous. It yields a consistent natural remanent magnetization (NRM) record that fits the standard geomagnetic time scale. By analogy with other North Pacific clay sections, we infer that this section is dominated by eolian debris from Asia that increased from the late Miocene or early Pliocene to the late Pleistocene as the onset of northern hemisphere glaciation made large amounts of material available for wind transport. The rate of accumulation of the yellow brown clay has increased from about 2 m/m.y. in the Pliocene to almost 10 m/m.y. during the Brunhes.

The lower dark brown pelagic clays (about 28 to 55 m sub-bottom) are very homogeneous, "slick," and fine grained. Again, by analogy with other North Pacific sections, we infer that much of this material is authigenic. Preliminary ichthyolith dates suggest that the accumulation rate decreased from about 0.6 m/m.y. during the Late Cretaceous to 0.35 m/m.y. at 40 m.y. ago, then increased to about 1 m/m.y. at 2.5 m.y. ago.

Below 55 m, the pelagic clay is interbedded with nannofossil and foraminifer-nannofossil oozes, some, if not all, of which show the graded bedding characteristic of turbidites. The absence of fossils younger than Campanian in the ooze beds suggests that the clays are at least that old and may well be contemporaneous with the

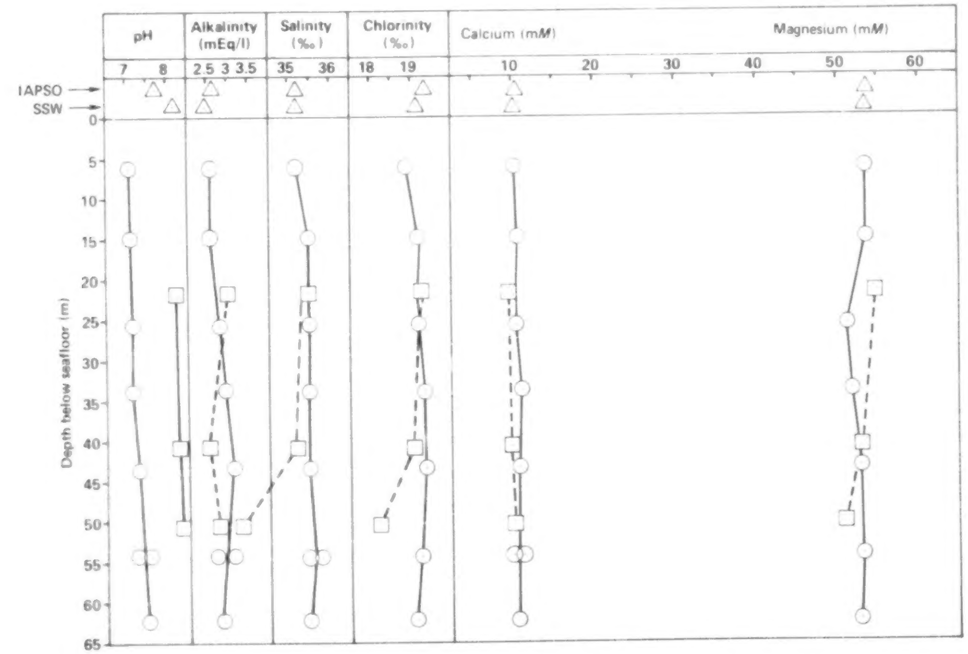

Figure 14. Profiles of pH, alkalinity (mEq/l), salinity (‰), chlorinity (‰), calcium (m*M*), and magnesium (m*M*) versus sub-bottom depth (m) from interstitial water samples analyzed at Site 576. Symbols are as follows: ▲ = IAPSO and SSW standards; ⊙ = samples from Hole 576A; ⊡ = *in situ* pore water samples from Hole 576.

ooze. If so, the carbonate may be of local derivation, having slumped off nearby hills during a period of enhanced carbonate deposition due either to depression of the calcite compensation depth or increased carbonate productivity or both.

Drilling was terminated by a chert layer that stopped the HPC. The few chips recovered are "flinty" chert and light gray porcellanite typical of silicified pelagic carbonates.

Most of the physical properties of the pelagic clays change fairly monotonically downcore. Both the shear wave velocity and vane shear strength increase by more than an order of magnitude from the surface to 70 m. The deeper clays interbedded with the carbonates are significantly more indurated than the shallower beds. Whether this reflects enhanced diagenesis due to the enclosing carbonate or proximity to the chert remains to be determined. In contrast to the shear wave velocities, the compressional wave values in the clays hover in the vicinity of 1440 m/s. Carbonate values range up to 1510 m/s, explaining why the clay/ooze boundary is such a good acoustic reflector. The water content values peak at about 15-20 m sub-bottom. We attribute this to an increase in the abundance of smectite relative to illite at the base of the eolian-dominated section and continuing downcore. This hypothesis will be tested in shore-based studies.

Site 576 met its objective of recovering a "type" northwestern Pacific pelagic ("red") clay section. If, as suggested by the preliminary results, deposition has been continuous throughout the Cenozoic, this section will provide a record of eolian and authigenic deposition comparable to that in LL44-GPC3.

REFERENCES

Boyce, R. E., 1976a. Definitions and laboratory techniques of compressional and sound velocity parameters and wet-water content, wet-bulk density, and porosity parameters by gravimetric and gamma ray attenuation techniques. *In* Schlanger, S. O., Jackson, E. D., et al., *Init. Repts. DSDP*, 33: Washington (U.S. Govt. Printing Office), 931-958.

_______, 1976b. Deep Sea Drilling Project procedures for shear strength measurements of clayey sediment using modified Wykeham Farrance Laboratory Vane Apparatus. *In* Barker, P., Dalziel, I. W. D., et al., *Init. Repts. DSDP*, 36: Washington (U.S. Govt. Printing Office), 1059-1068.

Burckle, L. H., 1978. Early Miocene to Pliocene diatom datum levels for the equatorial Pacific. *Geol. Res. and Dev. Centre, Repub. of Indonesia, Special Publ.*, 1:25-44.

Damuth, J. E., Jacobi, R. D., and Hayes, D. E., 1983. Sedimentation processes in the Northwest Pacific Basin revealed by echo character mapping studies. *Geol. Soc. Am. Bull.*, 94:381-395.

Hays, J. D., 1970. Stratigraphy and evolutionary trends of Radiolaria in North Pacific deep-sea sediments. *In* Hays, J. D. (Ed.), *Geological Investigations of the North Pacific*. Mem. Geol. Soc. Am. 126: 185-218.

Pessagno, E. A., 1967. Upper Cretaceous planktonic foraminifera from the western Gulf Coastal Plain. *Paleontographica Americana*, 5(37): 245-445, pls. 48-101.

Thierstein, H., 1976. Mesozoic calcareous nannoplankton biostratigraphy of marine sediments. *Mar. Micropaleontol.*, 1:325-362.

Thompson, P. R., 1980. Foraminifers from Deep Sea Drilling Project Sites 434, 435, and 436, Japan Trench. *In* Scientific Party, *Init. Repts. DSDP*, 56, 57, Pt. 2: Washington (U.S. Govt. Printing Office), 775-807.

SITE 576 HOLE CORE 1 CORED INTERVAL 6220.3–6223.0 mbsl; 0.0–2.7 mbsf

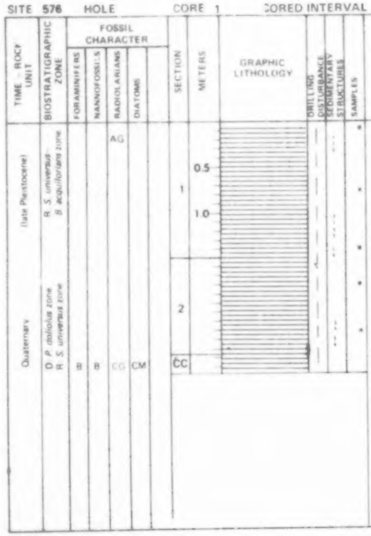
TIME – ROCK UNIT
BIOSTRATIGRAPHIC ZONE
FOSSIL CHARACTER
FORAMINIFERS
NANNOFOSSILS
RADIOLARIANS
DIATOMS
SECTION
METERS
GRAPHIC LITHOLOGY
DRILLING DISTURBANCE
SEDIMENTARY STRUCTURES
SAMPLES
(late Pleistocene)
Quaternary
R. S. universus–B. aquilonaris zone
D. P. doliolus zone
R. S. universus zone
AG
B
B
CG
CM
1
2
CC
0.5
1.0

LITHOLOGIC DESCRIPTION

PELAGIC CLAY

- Dominant colors: dark yellow brown (10YR 4/4) yellowish brown (10YR 5/4), light yellowish brown (10YR 6/4), yellowish brown (10YR 5/6), and brownish yellow (10YR 6/6).
- Core is slightly deformed throughout.
- Bioturbation evident, especially in lighter-colored intervals.

SMEAR SLIDE SUMMARY (%)

	1, 10 D	1, 80 D	1, 140 D	2, 30 D	2, 85 D
Texture:					
Sand	0	3	0	0	0
Silt	25	40	10	10	10
Clay	75	57	90	90	90
Composition:					
Quartz	25	35	45	30	20
Feldspar	2	3	–	–	Tr
Mica	1	1	–	–	–
Heavy minerals	1	1	–		
Clay	60	50	50	60	70
Volcanic glass	2	2		Tr	Tr
Micronodules	2	1	–	1	1
Foraminifers	1	2	–	–	–
Diatoms	–	–	1	2	3
Radiolarians	2	5	2	3	5
Sponge spicules	3	–	2	–	–
Silicoflagellates	–	–	–	1	–

SITE 576 HOLE CORE 2 CORED INTERVAL 6223.0–6232.5 mbsl; 2.7–12.2 mbsf

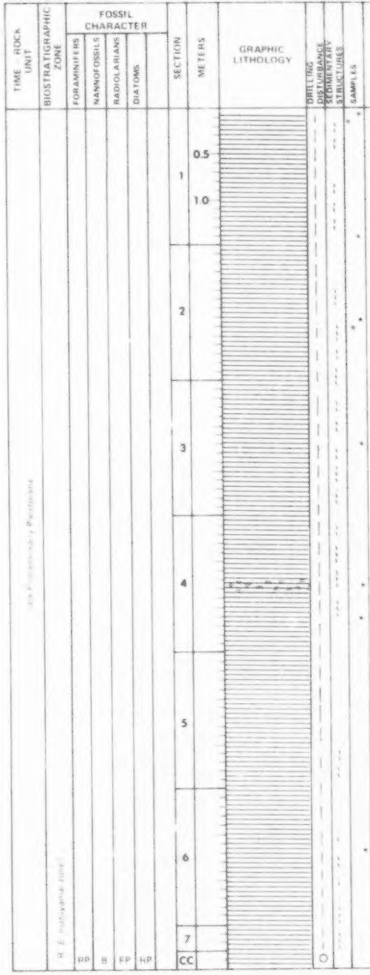
TIME – ROCK UNIT
BIOSTRATIGRAPHIC ZONE
FOSSIL CHARACTER
FORAMINIFERS
NANNOFOSSILS
RADIOLARIANS
DIATOMS
SECTION
METERS
GRAPHIC LITHOLOGY
DRILLING DISTURBANCE
SEDIMENTARY STRUCTURES
SAMPLES
late Pleistocene–early Pleistocene
R. E. matuyamai zone
RP
B
FP
HP
1
2
3
4
5
6
7
CC
0.5
1.0

LITHOLOGIC DESCRIPTION

PELAGIC CLAY

- Dominant colors: dark yellow brown (10YR 4/4) and yellowish brown (10YR 5/4) with dark brown (10YR 3/3), brown (7.5YR 5/4), brownish yellow (10YR 6/6), dark brown (10YR 4/3), and yellow brown (10YR 5/6) intervals. Minor colors: light gray (10YR 7/2) ash.
- Core is slightly deformed throughout.
- Much of this core has been extensively burrowed. Trace to minor amounts of volcanic ash are dispersed throughout the core, with one distinct ash layer in Section 4, 73–74 cm.

SMEAR SLIDE SUMMARY (%)

	1, 7 D	1, 15 D	1, 140 D	2, 86 D	2, 95 D	3, 70 D	4, 74 M	4, 116 D	6, 70 D
Texture:									
Sand	0	1	1	1	1	Tr	30	1	Tr
Silt	5	10	7	7	10	5	68	1	6
Clay	95	89	92	92	89	95	2	98	94
Composition:									
Quartz	4	15	6	6	5	3	3	1	3
Feldspar	1	2	Tr	1	4	Tr	1	–	1
Mica	–	–	Tr	–	Tr	Tr	–	1	Tr
Heavy minerals	Tr	Tr	Tr	Tr	Tr	–	Tr	Tr	Tr
Clay	85	80	87	87	82	87	2	94	85
Volcanic glass	–	Tr	–	Tr	3	5	93	1	5
Palagonite	–	Tr	–	–		–	–		–
Micronodules	5	1	1	2	1	Tr	1	1	2
Diatoms	1		2	Tr	1	1	–	1	1
Radiolarians	3	7	3	3	3	3	–	2	3
Sponge spicules	1	–	Tr	Tr	Tr	Tr	–	Tr	Tr
Silicoflagellates	–	–	–	Tr	–	–	–	–	–

Information on core description sheets, for ALL sites, represents field notes taken aboard ship under time pressure. Some of this information has been refined in accord with post-cruise findings, but production schedules prohibit definitive correlation of these sheets with subsequent findings. Thus the reader should be alerted to the occasional ambiguity or discrepancy.

SITE 576 HOLE CORE 3 CORED INTERVAL 6232.5–6242.0 mbsl; 12.2–21.7 mbsf

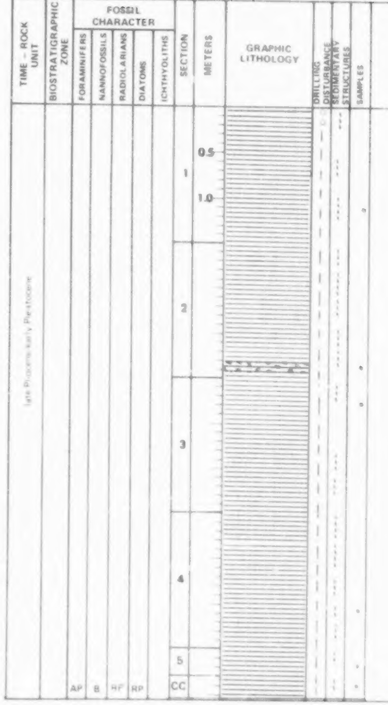
TIME – ROCK UNIT
BIOSTRATIGRAPHIC ZONE
FOSSIL CHARACTER
FORAMINIFERS
NANNOFOSSILS
RADIOLARIANS
DIATOMS
ICHTHYOLITHS
SECTION
METERS
GRAPHIC LITHOLOGY
DRILLING DISTURBANCE
SEDIMENTARY STRUCTURES
SAMPLES
late Pliocene-early Pleistocene
AP
B
RP
RP
0.5
1.0
1
2
3
4
5
CC

LITHOLOGIC DESCRIPTION

PELAGIC CLAY

- Dominant colors: dark yellow brown (10YR 4/4), yellowish brown (10YR 5/4), and yellowish brown (10YR 5/6) with dark brown (10YR 3/3) and light yellowish brown (10YR 6/4) intervals. Minor colors: light gray (10YR 7/2) ash.

  Core is slightly deformed throughout.

- Much of this core has been extensively burrowed. There is one distinct, but discontinuous ash layer in Section 2, 137–139 cm.

SMEAR SLIDE SUMMARY (%)

	1, 110 D	2, 139 M	3, 30 D	4, 100 D	5, 20 D	CC D
Texture:						
Sand	1	60	1	5	2	0
Silt	7	40	6	15	14	20
Clay	92	0	93	80	84	80
Composition:						
Quartz	4	10	3	10	10	15
Feldspar	1	—	1	3	3	5
Mica	Tr	—	Tr			
Heavy minerals	Tr	Tr	Tr	1	1	—
Clay	87	—	87	80	84	80
Volcanic glass	3	90	4	1	1	
Micronodules	Tr	—	Tr	—		
Diatoms	1		1			
Radiolarians	4		4	5	1	
Sponge spicules	Tr		Tr	—	—	

SITE 576 HOLE CORE 4 CORED INTERVAL 6242.0–6251.5 mbsl; 21.7–31.2 mbsf

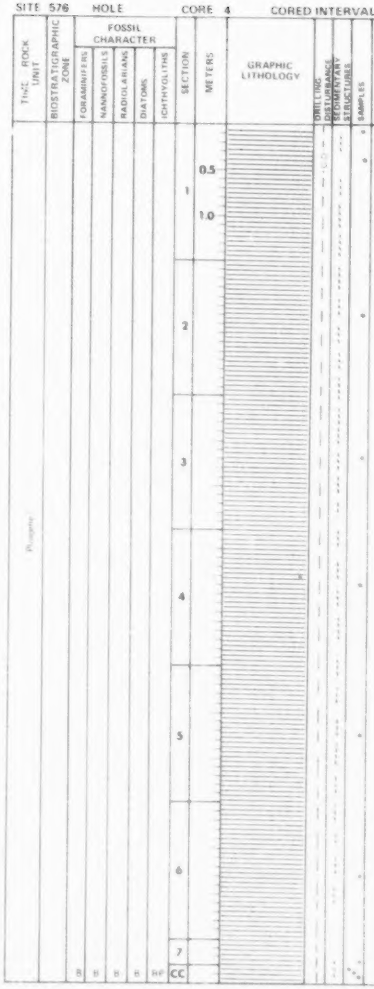
TIME – ROCK UNIT
BIOSTRATIGRAPHIC ZONE
FOSSIL CHARACTER
FORAMINIFERS
NANNOFOSSILS
RADIOLARIANS
DIATOMS
ICHTHYOLITHS
SECTION
METERS
GRAPHIC LITHOLOGY
DRILLING DISTURBANCE
SEDIMENTARY STRUCTURES
SAMPLES
Pliocene
B
B
B
B
RP
0.5
1.0
1
2
3
4
5
6
7
CC

LITHOLOGIC DESCRIPTION

PELAGIC CLAY

- Dominant colors: yellowish brown (10YR 5/4) and dark yellowish brown (10YR 4/4) with brown (7.5YR 5/6) burrows. Grades to brown (10YR 4/3) clay with yellowish brown (10YR 6/6) burrows at Section 2, 90–110 cm. Grades to dark brown (10YR 3/3) with yellowish (10YR 5/6) burrows below Section 6, 53 cm.

- Core is slightly deformed, with moderately deformed portions restricted to Section 1, 0–86 cm.

- This core has been extensively bioturbated, containing large burrows up to 3 cm in diameter. Sections 5, 6, and Core Catcher contain small nodules (less than 0.5 cm in diameter) and specks of MnO_2 that cover up to 3% of the core surface. Zeolites first appear in trace amounts in Section 3.

SMEAR SLIDE SUMMARY (%)

	1, 10 D	1, 40 D	2, 80 D	3, 70 D	4, 80 D	5, 75 D
Texture:						
Sand	1	1	2	0	0	3
Silt	15	11	9	7	18	12
Clay	84	88	89	93	82	85
Composition:						
Quartz	10	7	7	6	15	7
Feldspar	3	3	3	1	2	3
Heavy minerals	1	2	1	—	—	—
Clay	84	86	88	93	82	88
Volcanic glass	1	1	1	—	—	
Pyrite	—	—	—	Tr	—	—
Zeolite	—	—	—	Tr		
Carbonate unspec.	—	—	—	—	—	Tr
Radiolarians	1	1	—	—	—	—
Fish remains	—	—	—	Tr	1	1
Plant debris		—	—	—	—	1

	6, 80 D	7, 25 D	CC, 1 D	CC, 2 D	CC, 3 D
Texture:					
Sand	0	Tr	2	3	2
Silt	3	6	10	7	10
Clay	97	94	88	90	88
Composition:					
Quartz	Tr	4	8	7	7
Feldspar	Tr	2	2	2	5
Mica	1	Tr	—	—	—
Heavy minerals	—	Tr	—	1	
Clay	95	92	90	90	88
Volcanic glass	—	Tr	—	—	—
Micronodules	Tr	2	—	—	—
Zeolite	4	—	—	—	—

SITE 576 HOLE CORE 5 CORED INTERVAL 6251.5–6261.0 mbsl; 31.2–40.7 mbsf

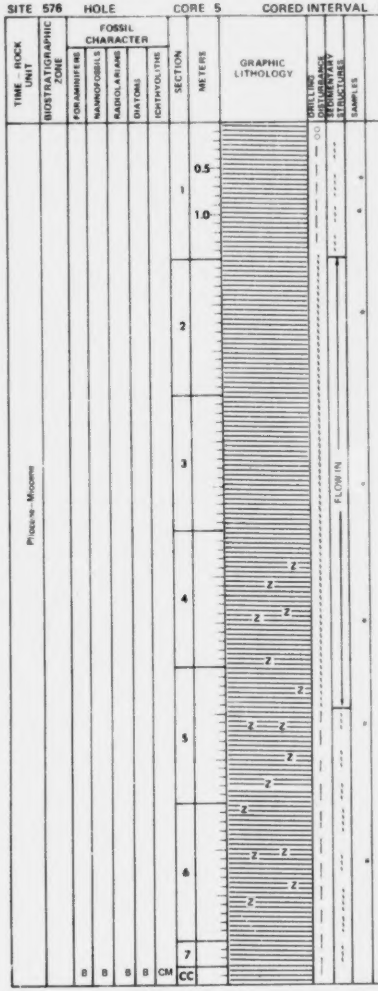
TIME – ROCK UNIT
BIOSTRATIGRAPHIC ZONE
FOSSIL CHARACTER
FORAMINIFERS
NANNOFOSSILS
RADIOLARIANS
DIATOMS
ICHTHYOLITHS
SECTION
METERS
GRAPHIC LITHOLOGY
DRILLING DISTURBANCE
SEDIMENTARY STRUCTURES
SAMPLES
Pliocene–Miocene
B
B
B
B
CM
0.5
1.0
1
2
3
4
5
6
7
CC
Z
FLOW IN

LITHOLOGIC DESCRIPTION

PELAGIC CLAY (Zeolitic clay in Sections 4 through 6.)

- Dominant colors: dark yellow brown (10YR 4/4) in Section 1, dark brown (10YR 3/3) in Sections 2 through 5, 49 cm, except for the lower portion of Section 3 which is dark yellowish brown (10YR 3/4). Below Section 5, 49 cm, the core is very dark grayish brown (10YR 3/2).
- Section 1 and core below Section 5, 49 cm is slightly deformed. The interval from Sections 2 to 5, 49 cm is very deformed, resulting from flow in of drilled material.
- This core has been extensively bioturbated. Burrows in Sections 1 and 6 have "reaction rims" around them. The percentage of zeolites seen in smear slides increases downcore to approximately 10% in Section 4.

SMEAR SLIDE SUMMARY (%):

	1, 63 D	1, 100 D	2, 66 D	3, 100 D	4, 100 D	5, 65 D	6, 62 D
Texture:							
Sand	0	1	0	0	0	0	0
Silt	4	6	5	4	11	7	10
Clay	96	93	95	96	89	93	90
Composition:							
Quartz	3	4	4	4	4	2	Tr
Feldspar	Tr	Tr	1	Tr	Tr	Tr	
Mica	Tr	Tr	Tr	Tr	—	—	Tr
Clay	97	92	94	94	86	93	90
Volcanic glass	Tr	1	Tr	Tr	Tr	Tr	Tr
Pyrite	—	—	Tr	—	—	—	—
Micronodules	Tr	1	1	1	Tr	Tr	Tr
Zeolite	—	2		1	10	5	10

SITE 576 HOLE CORE 6 CORED INTERVAL 6261.0–6270.5 mbsl; 40.7–50.2 mbsf

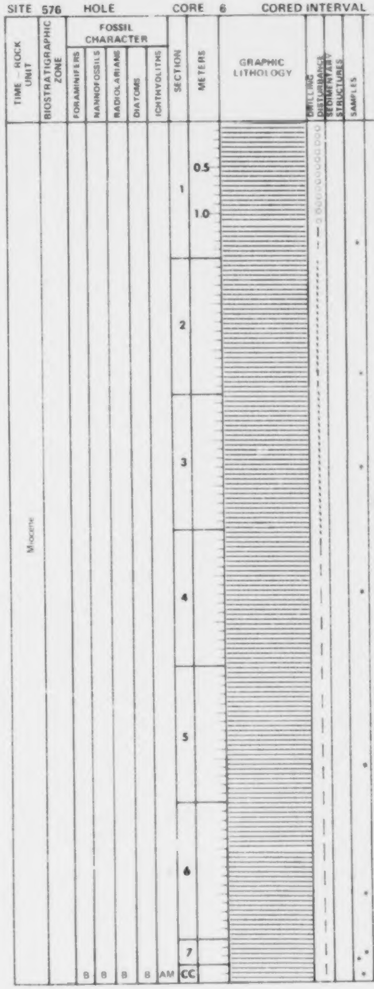
TIME – ROCK UNIT
BIOSTRATIGRAPHIC ZONE
FOSSIL CHARACTER
FORAMINIFERS
NANNOFOSSILS
RADIOLARIANS
DIATOMS
ICHTHYOLITHS
SECTION
METERS
GRAPHIC LITHOLOGY
DRILLING DISTURBANCE
SEDIMENTARY STRUCTURES
SAMPLES
Miocene
B
B
B
B
AM
0.5
1.0
1
2
3
4
5
6
7
CC

LITHOLOGIC DESCRIPTION

PELAGIC CLAY

- Dominant colors: dark brown (7.5YR 3/2) throughout, except for dark reddish brown (5YR 3/2) interval in Section 3 and dark reddish brown (5YR 3/3) interval in Section 7 and Core Catcher.
- The top meter of Section 1 is soupy, and Sections 2 and 3 are very deformed. The rest of the core is slightly deformed.
- This core contains very homogeneous pelagic clay. There are 2 burrows in Section 4. Zeolites are found in trace amounts, but are much less abundant than in Core 4.

SMEAR SLIDE SUMMARY (%):

	1, 135 D	2, 130 D	3, 80 D	4, 70 D	5, 110 D	6, 100 D	7, 20 D	7, 30 D	CC D
Texture:									
Sand	Tr	1	1	1	Tr	Tr	1	2	0
Silt	3	4	2	3	2	2	7	15	7
Clay	97	95	97	96	98	98	92	83	93
Composition:									
Quartz	Tr	1	1	2	1	2	5	7	5
Feldspar	—	—	—	Tr	—	1	2	3	1
Mica	Tr	—	—	Tr	Tr	—	—	—	—
Clay	96	95	98	96	93	92	92	83	93
Volcanic glass	Tr	1	1	1	Tr	1	—	2	Tr
Palagonite	—	—	—	—	—	—	—	3	—
Micronodules	Tr	Tr	—	1	6	4	—	—	—
Zeolite	3	3	—	—	—	Tr	—	—	1
Opaques	—	—	—	—	—	—	1	2	—

SITE 576 HOLE CORE 7 CORED INTERVAL 6270.5–6280.0 mbsl; 50.2–59.7 mbsf

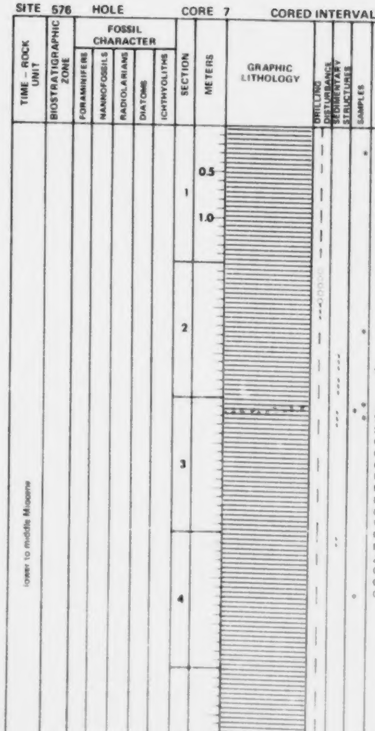
TIME – ROCK UNIT
BIOSTRATIGRAPHIC ZONE
FOSSIL CHARACTER
FORAMINIFERS
NANNOFOSSILS
RADIOLARIANS
DIATOMS
ICHTHYOLITHS
SECTION
METERS
GRAPHIC LITHOLOGY
DRILLING DISTURBANCE
SEDIMENTARY STRUCTURES
SAMPLES
lower to middle Miocene
0.5
1.0
1
2
3
4
5
6
7
CC
B
B
B
B
FM

LITHOLOGIC DESCRIPTION

PELAGIC CLAY

* Dominant colors: dark reddish brown (5YR 3/3) and dark reddish brown (5YR 3/2). Minor colors: Sections 2 and 3 contain reddish brown (5YR 4/4) mottles. Section 3 contains a yellowish red (5YR 4/6) layer at 16–18 cm. Section 6 contains four continuous (at 80, 84, 103, and 111 cm) and two discontinuous (at 57.5 and 76 cm) thin dark reddish brown to reddish brown (5YR 3/4–5YR 4/3) layers. The Core Catcher has brown (7.5YR 5/6) strong vertical streaks.

* Core is slightly deformed throughout, except for one soupy section in the upper 50 cm of Section 2.

* This core contains homogeneous, undeformed clay with very restricted intervals of mottled clay. The distinct layers in Sections 3 and 6 are also clay.

SMEAR SLIDE SUMMARY (%)

	1, 30 D	2, 75 D	3, 10 D	3, 16 D	3, 24 D	4, 70 D	5, 70 D	6, 90 D	6, 111 D	CC D
Texture										
Sand	2	0	0	3	1	1	1	2	1	1
Silt	10	10	4	7	7	7	10	3	4	2
Clay	88	90	96	90	92	92	89	95	95	97
Composition										
Quartz	5	8	2	3	3	5	3	Tr	Tr	Tr
Feldspar	2	1	1	2	2	2	3	Tr	Tr	Tr
Mica	–	–	–	–	–	–	–	–	Tr	1
Heavy minerals	–	–	–	1	1	–	–	–	–	–
Clay	88	90	96	90	90	88	91	94	95	95
Volcanic glass	–	1	1	2	1	3	3	3	2	3
Pyrite	–	–	1	2	3	Tr	–	–	–	–
Micronodules	–	–	–	–	–	–	1	3	1	–
Zeolite		Tr	–	–	–	–	–	–	Tr	
Carbonate unspec.			–	–	–	–	Tr	–	–	
Calc. nannofossils			–	–	–	Tr	–	–	–	–
Opaques	5	Tr	Tr	Tr	Tr	Tr	–	2	–	Tr

SITE 576 HOLE CORE 8 CORED INTERVAL 6280.0–6289.5 mbsl; 59.7–69.2 mbsf

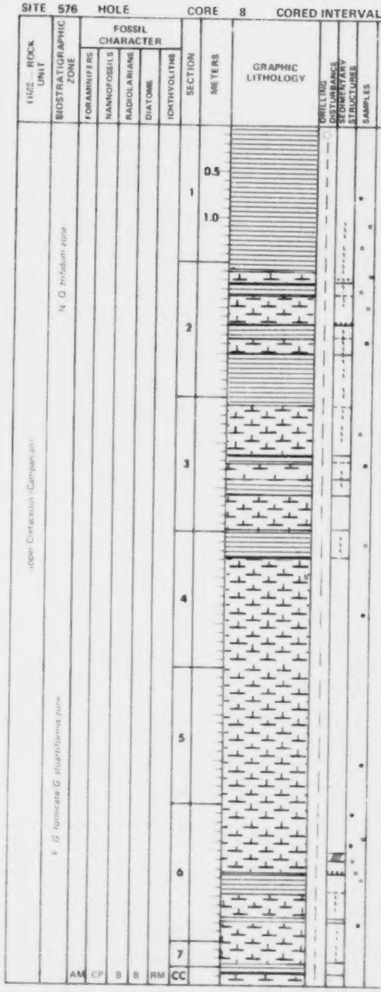
TIME – ROCK UNIT
BIOSTRATIGRAPHIC ZONE
FOSSIL CHARACTER
FORAMINIFERS
NANNOFOSSILS
RADIOLARIANS
DIATOMS
ICHTHYOLITHS
SECTION
METERS
GRAPHIC LITHOLOGY
DRILLING DISTURBANCE
SEDIMENTARY STRUCTURES
SAMPLES
upper Cretaceous (Campanian)
N. G. trifidum zone
E. G. fornicata-G. stuartiformis zone
0.5
1.0
1
2
3
4
5
6
7
CC
AM
CP
B
B
RM

LITHOLOGIC DESCRIPTION

INTERBEDDED PELAGIC CLAY AND NANNOFOSSIL OOZE, with proportion of nannofossil ooze increasing downcore.

* Dominant colors: clay intervals are dark brown (7.5YR 3/2), except for the clay in Section 1 which is dark reddish brown (5YR 3/2). The nannofossil ooze intervals are yellow (10YR 7/6), reddish yellow (7.5YR 6/8), light yellowish brown (10YR 6/4), and yellowish brown (10YR 5/6) in Sections 2 and 3; changing to very pale brown (10YR 7/4 and 10YR 8/4) in Sections 4, 5, and 6; changing to yellow (10YR 7/6) in the base of Section 6, Section 7, and the Core Catcher. Minor colors: white (10YR 8/2) and pink (7.5YR 8/4) nannofossil ooze layers approximately 1 cm thick in Section 6.

* This core is slightly deformed throughout.

* This core consists of interbedded dark brown pelagic clay with either gradational or sharp basal contacts and lighter colored nannofossil ooze layers with sharp basal contacts. Much of the core is bioturbated. Several of the nannofossil ooze layers are normally graded. The base of the nannofossil ooze layer in Section 6 is crossbedded.

SMEAR SLIDE SUMMARY (%)

	1, 110 D	1, 138 D	2, 13 D	2, 30 D	2, 60 D	3, 40 D
Texture						
Sand	0	0	Tr	Tr	0	Tr
Silt	3	2	2	5	1	2
Clay	97	98	98	95	99	98
Composition						
Quartz	Tr	Tr	Tr	Tr	Tr	–
Feldspar	Tr	Tr	–	–	–	–
Mica	–	–	–	Tr	–	–
Clay	94	–	5	94	4	2
Volcanic glass	3	1	1	2	Tr	1
Micronodules	1	1	1	1	Tr	Tr
Foraminifers	–	–	Tr	–	Tr	Tr
Calc. nannofossils	–	97	92	–	95	96
Opaques	2	1	1	3	1	1

	4, 13 D	6, 40 D	6, 64 D	6, 73 D	6, 84 D
Texture					
Sand	1	1	15	15	Tr
Silt	5	1	2	5	3
Clay	94	98	83	80	97
Composition					
Quartz	Tr	–	–	–	Tr
Feldspar	Tr	–	–	–	–
Clay	1	1	–	2	95
Volcanic glass	3	1	2	5	2
Micronodules	Tr	Tr	Tr	–	Tr
Foraminifers	–	1	15	15	–
Calc. nannofossils	96	97	83	78	1
Fish remains	–	–	–	Tr	–
Opaques	–	–	Tr	–	2

$CaCO_3$ data
1, 80 cm = 3%
2, 90 cm = 82%
3, 77 cm = 83%
4, 90 cm = 86%
5, 106 cm = 82%
6, 15 cm = 87%
6, 45 cm = 85%
6, 135 cm = 85%

SITE 576 HOLE A CORE 1 CORED INTERVAL 6218.0–6227.5 mbsl, 0.0–8.7 mbsf

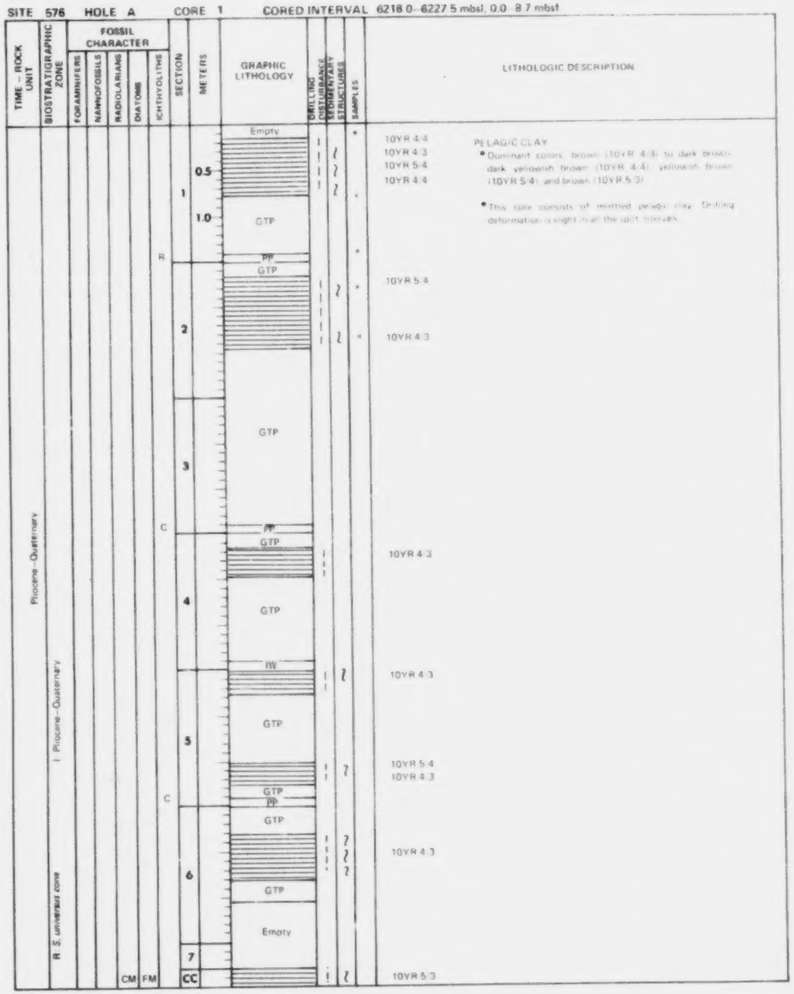
TIME – ROCK UNIT
BIOSTRATIGRAPHIC ZONE
FOSSIL CHARACTER
FORAMINIFERS
NANNOFOSSILS
RADIOLARIANS
DIATOMS
ICHTHYOLITHS
SECTION
METERS
GRAPHIC LITHOLOGY
DRILLING DISTURBANCE
SEDIMENTARY STRUCTURES
SAMPLES
LITHOLOGIC DESCRIPTION
Pliocene–Quaternary
I: Pliocene–Quaternary
R: S. universus zone
R
C
C
CM
FM
1
2
3
4
5
6
7
CC
0.5
1.0
Empty
GTP
PP
GTP
GTP
PP
GTP
GTP
IW
GTP
GTP
PP
GTP
GTP
Empty
10YR 4/4
10YR 4/3
10YR 5/4
10YR 4/4
10YR 5/4
10YR 4/3
10YR 4/3
10YR 4/3
10YR 5/4
10YR 4/3
10YR 4/3
10YR 5/3

PELAGIC CLAY

- Dominant colors: brown (10YR 4/3) to dark brown, dark yellowish brown (10YR 4/4), yellowish brown (10YR 5/4), and brown (10YR 5/3).
- This core consists of mottled pelagic clay. Drilling deformation is slight in all the split intervals.

SITE 576 HOLE A CORE 2 CORED INTERVAL 6227.5–6237.0 mbsl, 8.7–18.2 mbsf

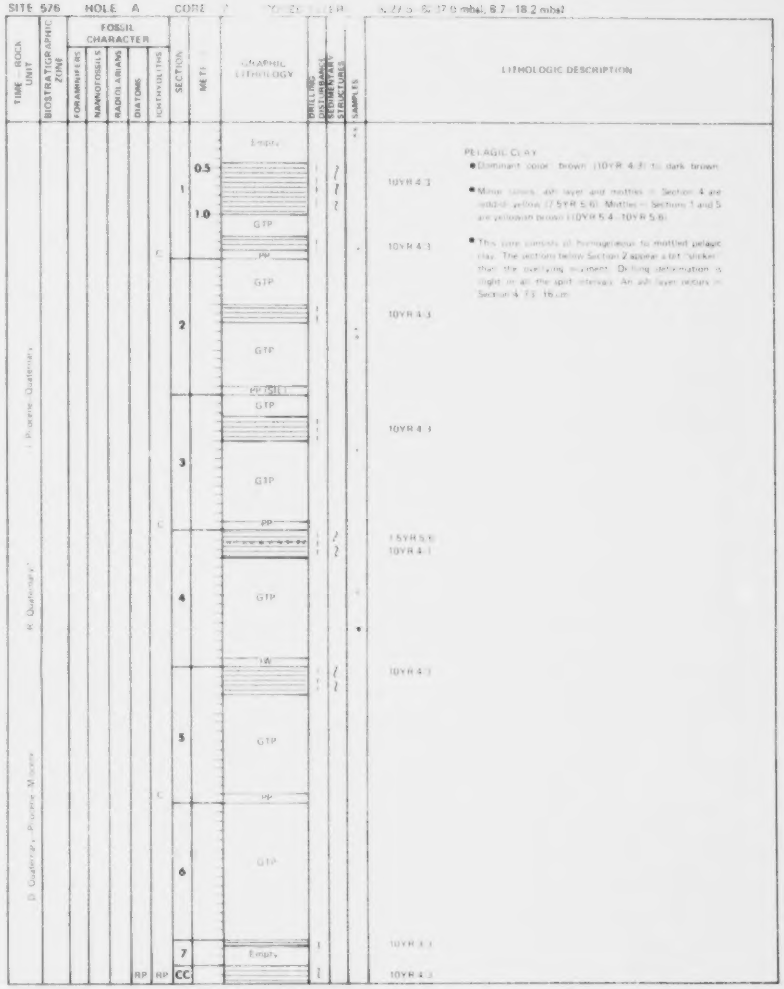
TIME – ROCK UNIT
BIOSTRATIGRAPHIC ZONE
FOSSIL CHARACTER
FORAMINIFERS
NANNOFOSSILS
RADIOLARIANS
DIATOMS
ICHTHYOLITHS
SECTION
METERS
GRAPHIC LITHOLOGY
DRILLING DISTURBANCE
SEDIMENTARY STRUCTURES
SAMPLES
LITHOLOGIC DESCRIPTION
I: Pliocene–Quaternary
R: Quaternary
D: Quaternary–Pliocene–Miocene
C
C
C
RP
RP
1
2
3
4
5
6
7
CC
0.5
1.0
Empty
GTP
PP
GTP
GTP
PP/SILT
GTP
GTP
PP
GTP
IW
GTP
PP
GTP
Empty
10YR 4/3
10YR 4/3
10YR 4/3
10YR 4/3
7.5YR 5/6
10YR 4/3
10YR 4/3
10YR 3/3
10YR 4/3

PELAGIC CLAY

- Dominant color: brown (10YR 4/3) to dark brown.
- Minor colors: ash layer and mottles in Section 4 are reddish yellow (7.5YR 5/6). Mottles in Sections 1 and 5 are yellowish brown (10YR 5/4–10YR 5/6).
- This core consists of homogeneous to mottled pelagic clay. The sections below Section 2 appear a bit "stickier" than the overlying sediment. Drilling deformation is slight in all the split intervals. An ash layer occurs in Section 4, 13–16 cm.

SITE 576 HOLE A CORE 3 CORED INTERVAL 6237.0–6246.5 mbsl; 18.2–27.7 mbsf

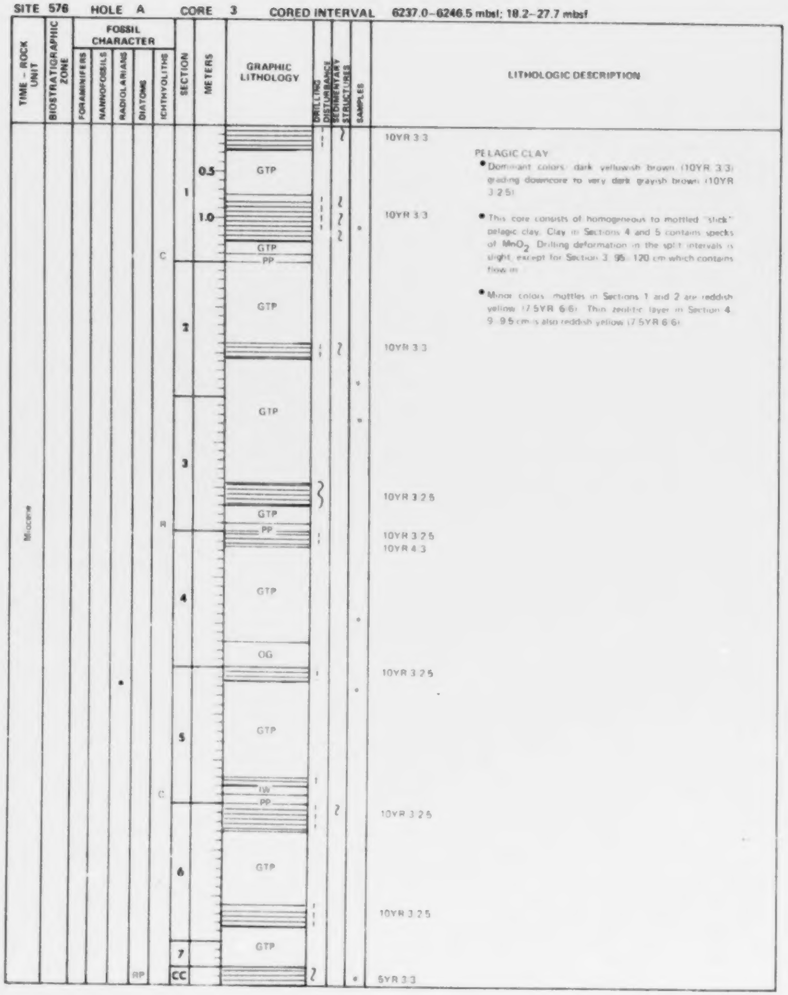
TIME – ROCK UNIT
BIOSTRATIGRAPHIC ZONE
FOSSIL CHARACTER
FORAMINIFERS
NANNOFOSSILS
RADIOLARIANS
DIATOMS
ICHTHYOLITHS
SECTION
METERS
GRAPHIC LITHOLOGY
DRILLING DISTURBANCE
SEDIMENTARY STRUCTURES
SAMPLES
LITHOLOGIC DESCRIPTION
Miocene
C
R
C
RP
1
2
3
4
5
6
7
CC
0.5
1.0
GTP
PP
OG
IW
10YR 3/3
10YR 3/3
10YR 3/3
10YR 3/2.5
10YR 3/2.5
10YR 4/3
10YR 3/2.5
10YR 3/2.5
10YR 3/2.5
5YR 3/3

PELAGIC CLAY

- Dominant colors: dark yellowish brown (10YR 3/3) grading downcore to very dark grayish brown (10YR 3/2.5).
- This core consists of homogeneous to mottled "slick" pelagic clay. Clay in Sections 4 and 5 contains specks of MnO_2. Drilling deformation in the split intervals is slight, except for Section 3, 95–120 cm which contains flow-in.
- Minor colors: mottles in Sections 1 and 2 are reddish yellow (7.5YR 6/6). Thin zeolitic layer in Section 4, 9–9.5 cm is also reddish yellow (7.5YR 6/6).

SITE 576 HOLE A CORE 4 CORED INTERVAL 6246.5–6256.0 mbsl; 27.7–37.2 mbsf

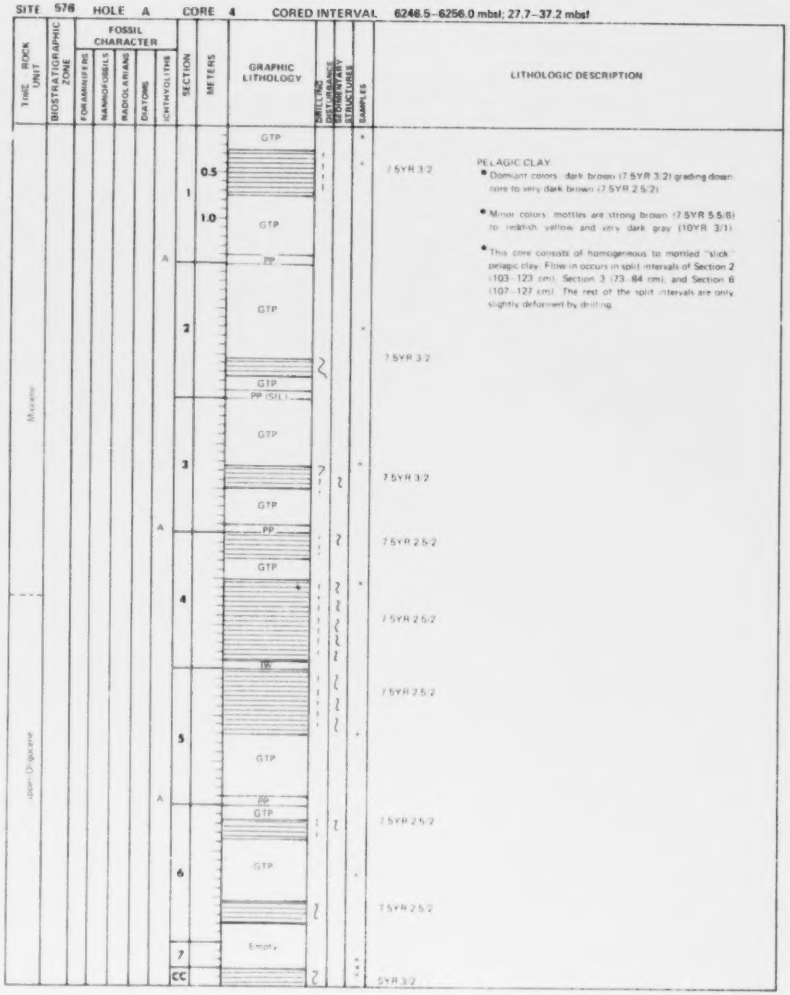
TIME – ROCK UNIT
BIOSTRATIGRAPHIC ZONE
FOSSIL CHARACTER
FORAMINIFERS
NANNOFOSSILS
RADIOLARIANS
DIATOMS
ICHTHYOLITHS
SECTION
METERS
GRAPHIC LITHOLOGY
DRILLING DISTURBANCE
SEDIMENTARY STRUCTURES
SAMPLES
LITHOLOGIC DESCRIPTION
Miocene
upper Oligocene
A
A
A
1
2
3
4
5
6
7
CC
0.5
1.0
GTP
PP
PP (SIL)
IW
Empty
7.5YR 3/2
7.5YR 3/2
7.5YR 3/2
7.5YR 2.5/2
7.5YR 2.5/2
7.5YR 2.5/2
7.5YR 2.5/2
7.5YR 2.5/2
5YR 3/2

PELAGIC CLAY

- Dominant colors: dark brown (7.5YR 3/2) grading downcore to very dark brown (7.5YR 2.5/2).
- Minor colors: mottles are strong brown (7.5YR 5.5/6) to reddish yellow and very dark gray (10YR 3/1).
- This core consists of homogeneous to mottled "slick" pelagic clay. Flow-in occurs in split intervals of Section 2 (103–123 cm), Section 3 (73–84 cm), and Section 6 (107–127 cm). The rest of the split intervals are only slightly deformed by drilling.

SITE 576 HOLE A CORE 5 CORED INTERVAL 6256.0–6265.5 mbsl, 37.2–46.7 mbsf

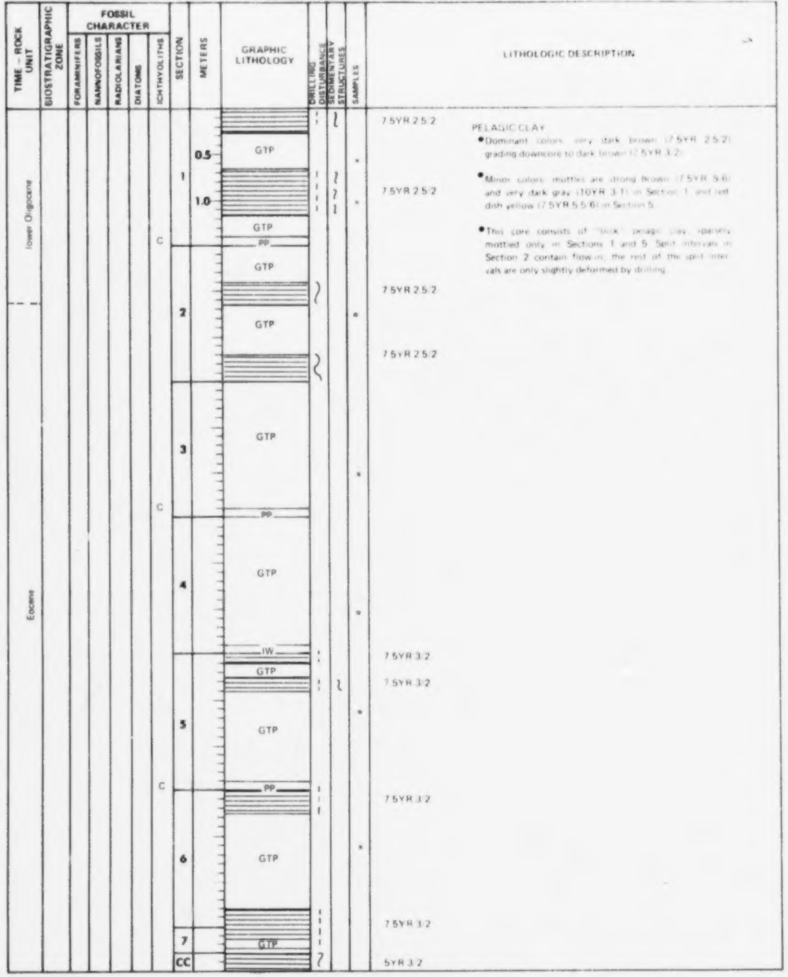
TIME – ROCK UNIT
BIOSTRATIGRAPHIC ZONE
FOSSIL CHARACTER
FORAMINIFERS
NANNOFOSSILS
RADIOLARIANS
DIATOMS
ICHTHYOLITHS
SECTION
METERS
GRAPHIC LITHOLOGY
DRILLING DISTURBANCE
SEDIMENTARY STRUCTURES
SAMPLES
LITHOLOGIC DESCRIPTION
lower Oligocene
Eocene
C
C
C
0.5
1.0
1
2
3
4
5
6
7
CC
GTP
PP
IW
7.5YR 2.5/2
7.5YR 2.5/2
7.5YR 2.5/2
7.5YR 2.5/2
7.5YR 3/2
7.5YR 3/2
7.5YR 3/2
7.5YR 3/2
5YR 3/2

PELAGIC CLAY

- Dominant colors: very dark brown (7.5YR 2.5/2) grading downcore to dark brown (7.5YR 3/2).
- Minor colors: mottles are strong brown (7.5YR 5/6) and very dark gray (10YR 3/1) in Section 1, and reddish yellow (7.5YR 5.5/6) in Section 5.
- This core consists of "slick" pelagic clay, sparsely mottled only in Sections 1 and 5. Split intervals in Section 2 contain flow-in; the rest of the split intervals are only slightly deformed by drilling.

SITE 576 HOLE A CORE 6 CORED INTERVAL 6265.5–6275.0 mbsl, 46.7–56.2 mbsf

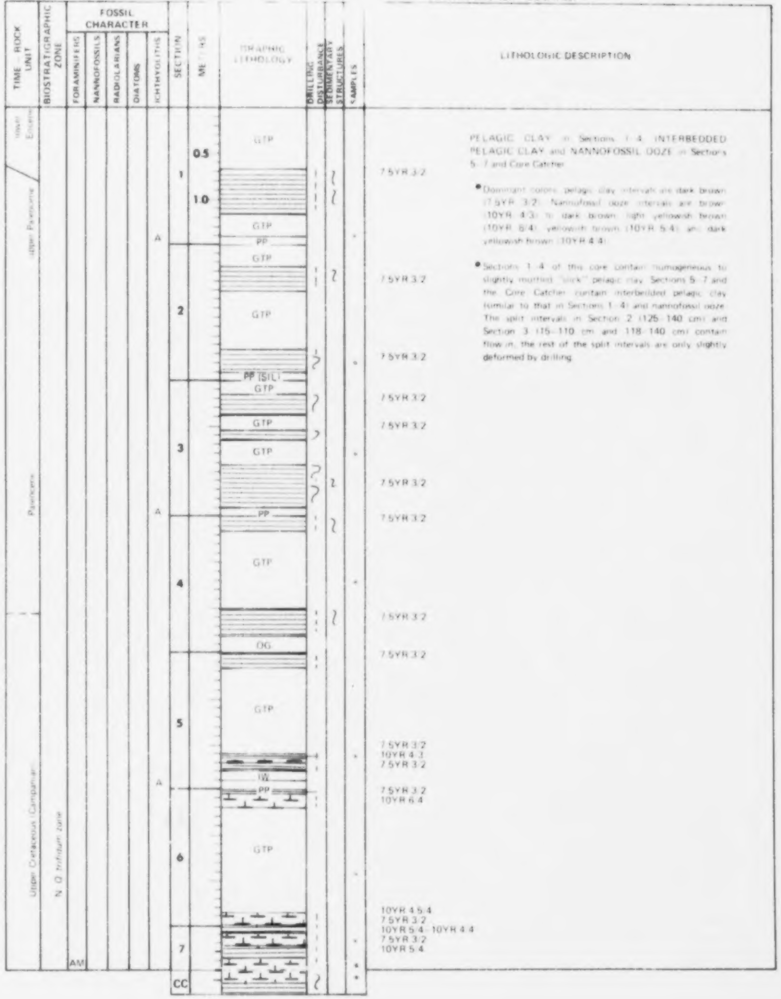
TIME – ROCK UNIT
BIOSTRATIGRAPHIC ZONE
FOSSIL CHARACTER
FORAMINIFERS
NANNOFOSSILS
RADIOLARIANS
DIATOMS
ICHTHYOLITHS
SECTION
METERS
GRAPHIC LITHOLOGY
DRILLING DISTURBANCE
SEDIMENTARY STRUCTURES
SAMPLES
LITHOLOGIC DESCRIPTION
lower Eocene
upper Paleocene
Paleocene
Upper Cretaceous (Campanian)
N. Q. trifidum zone
AM
A
A
A
0.5
1.0
1
2
3
4
5
6
7
CC
GTP
PP
PP (SIL)
DG
IW
7.5YR 3/2
7.5YR 3/2
7.5YR 3/2
7.5YR 3/2
7.5YR 3/2
7.5YR 3/2
7.5YR 3/2
7.5YR 3/2
7.5YR 3/2
7.5YR 3/2
10YR 4/3
7.5YR 3/2
7.5YR 3/2
10YR 6/4
10YR 4.5/4
7.5YR 3/2
10YR 5/4 10YR 4/4
7.5YR 3/2
10YR 5/4

PELAGIC CLAY in Sections 1–4. INTERBEDDED PELAGIC CLAY and NANNOFOSSIL OOZE in Sections 5–7 and Core Catcher.

- Dominant colors: pelagic clay intervals are dark brown (7.5YR 3/2). Nannofossil ooze intervals are brown (10YR 4/3) to dark brown, light yellowish brown (10YR 6/4), yellowish brown (10YR 5/4), and dark yellowish brown (10YR 4/4).
- Sections 1–4 of this core contain homogeneous to slightly mottled "slick" pelagic clay. Sections 5–7 and the Core Catcher contain interbedded pelagic clay (similar to that in Sections 1–4) and nannofossil ooze. The split intervals in Section 2 (125–140 cm) and Section 3 (15–110 cm and 118–140 cm) contain flow-in; the rest of the split intervals are only slightly deformed by drilling.

SITE 576 HOLE A CORE 7 CORED INTERVAL 6275.0–6284.5 mbsl; 56.2–65.7 mbsf

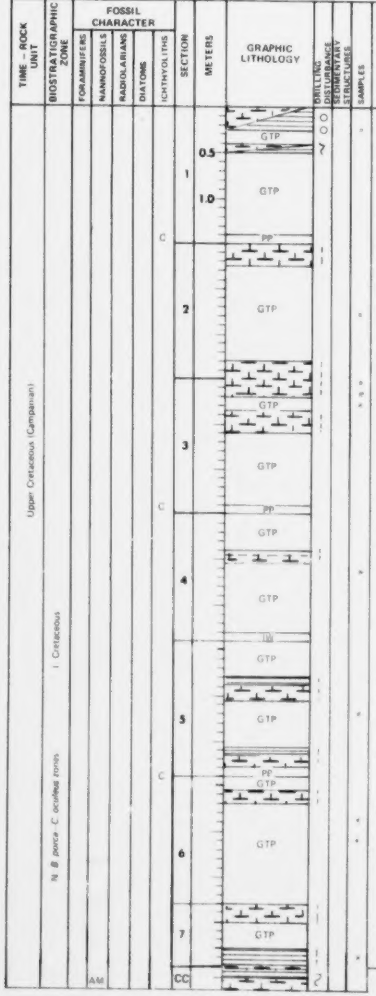
TIME – ROCK UNIT
BIOSTRATIGRAPHIC ZONE
FOSSIL CHARACTER
FORAMINIFERS
NANNOFOSSILS
RADIOLARIANS
DIATOMS
ICHTHYOLITHS
SECTION
METERS
GRAPHIC LITHOLOGY
DRILLING DISTURBANCE
SEDIMENTARY STRUCTURES
SAMPLES
Upper Cretaceous (Campanian)
I. Cretaceous
N. B. porca – C. oculeus zones
AM
C
C
C
1
2
3
4
5
6
7
CC
0.5
1.0
GTP
PP
10YR 7.5/4
10YR 7.5/4
10YR 7.5/4
10YR 7.5/4
10YR 3/2
10YR 7/3
10YR 3/2
10YR 6/4
10YR 7/3
10YR 7/3
10YR 3/2

LITHOLOGIC DESCRIPTION

INTERBEDDED PELAGIC CLAY and NANNOFOSSIL OOZE

- Dominant colors: pelagic clay intervals are very dark grayish brown (10YR 3/2). Nannofossil ooze intervals are very pale brown (10YR 7.5/4), very pale brown (10YR 7/3–7/4), and light yellowish brown (10YR 6/4).
- This core consists of interbedded homogeneous pelagic clay and nannofossil ooze. Split intervals in Section 1 are very deformed by drilling; the rest of the split intervals are only slightly deformed.

NOTE that Sections 4 and 6 of this core were mistakenly cut to only 140 cm total length onboard ship. Core section dividers on this barrel sheet have been adjusted accordingly.

SITE 576 HOLE B CORE 1 CORED INTERVAL 6219.3–6227.5 mbsl; 0.0–8.2 mbsf

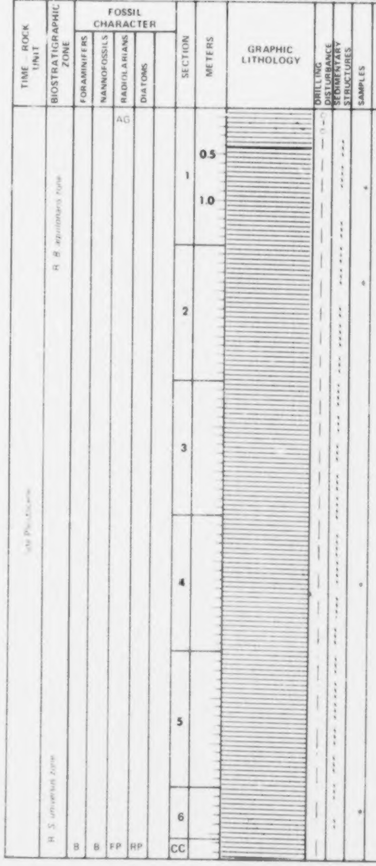
TIME – ROCK UNIT
BIOSTRATIGRAPHIC ZONE
FOSSIL CHARACTER
FORAMINIFERS
NANNOFOSSILS
RADIOLARIANS
DIATOMS
SECTION
METERS
GRAPHIC LITHOLOGY
DRILLING DISTURBANCE
SEDIMENTARY STRUCTURES
SAMPLES
R. B. aquilonaris zone
R. S. universus zone
AG
B
B
FP
RP
1
2
3
4
5
6
CC
0.5
1.0

LITHOLOGIC DESCRIPTION

PELAGIC CLAY

- Dominant colors: yellowish brown (10YR 5/6), yellowish brown (10YR 5/4), and dark yellowish brown (10YR 4/4) with intervals of light yellowish brown (10YR 6/4) and dark brown (7.5YR 4/4).
- Sections 1 to 4 are slightly deformed; Sections 5 and 6 are moderately deformed.
- This core is composed of pelagic clay, both homogeneous and with varying amounts of mottles and burrows. MnO_2 streaks are present in some sections. Four pumice(?) pebbles were cored in Section 2, 117 cm.

SMEAR SLIDE SUMMARY (%):

	1, 90	2, 40	4, 75	6, 20
	D	D	D	D
Texture:				
Sand	5	5	3	1
Silt	15	20	12	10
Clay	80	75	85	89
Composition:				
Quartz	8	10	12	12
Feldspar	2	Tr	Tr	Tr
Clay	79	75	81	84
Volcanic glass	4	4	5	3
Micronodules	1	Tr	Tr	Tr
Diatoms	2	Tr	Tr	Tr
Radiolarians	5	5	2	1
Sponge spicules	Tr	Tr	Tr	Tr
Silicoflagellates	Tr	Tr	Tr	–
Opaques	–	1	–	–

SITE 576 HOLE B CORE 2 CORED INTERVAL 6227.5–6237.0 mbsl; 8.2–1/./ mbsf

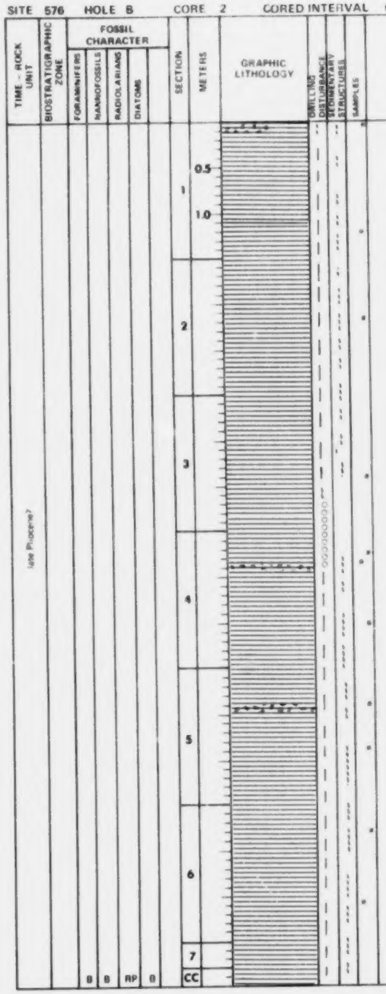
TIME – ROCK UNIT
BIOSTRATIGRAPHIC ZONE
FOSSIL CHARACTER
FORAMINIFERS
NANNOFOSSILS
RADIOLARIANS
DIATOMS
SECTION
METERS
GRAPHIC LITHOLOGY
DRILLING DISTURBANCE
SEDIMENTARY STRUCTURES
SAMPLES
late Pliocene?
B
B
RP
B
0.5
1.0
1
2
3
4
5
6
7
CC

LITHOLOGIC

PELAGIC CLAY

*Dominant colors: brown (10YR 5/3) and brown (7.5YR 5/4) in Sections 1 to 5, changing to brown (10YR 4/3) to dark brown at the base of Section 5. Reddish yellow (7.5YR 6/6) and brownish yellow (10YR 6/8) mottles. Minor colors: gray (10YR 6/1) ash in Section 5, 40 cm.

*This core is slightly deformed throughout, except for a soupy section in the base of Section 3 and top of S tion 4.

*This core is composed of pelagic clay darkening in color downcore with abundant mottles. Two ash layers were cored at Section 4, 40 cm and Section 5, 40 cm.

SMEAR SLIDE SUMMARY (%)

	1, 3 M	1, 120 D	2, 70 D	3, 96 D	4, 30 D	4, 40 M
Texture:						
Sand	20	5	1	2	1	15
Silt	60	20	15	10	12	65
Clay	20	75	84	88	87	20
Composition:						
Quartz	7	10	15	10	10	5
Feldspar	3	1	5	2	Tr	2
Heavy minerals	2	–	Tr	Tr	–	–
Clay	–	75	75	88	87	2
Volcanic glass	88	1	Tr	Tr	3	90
Micronodules	–	–	–	–	Tr	–
Zeolite	–	–	Tr	Tr	–	1
Diatoms	–	1	Tr	–	–	–
Radiolarians	–	10	6	Tr	–	–
Sponge spicules	–	1	Tr	–	–	–
Opaques	–	1	–	–	–	Tr

	4, 100 D	5, 40 M	5, 90 D	6, 30 D	6, 110 D
Texture:					
Sand	Tr	20	2	0	Tr
Silt	10	60	12	6	10
Clay	90	20	86	94	90
Composition:					
Quartz	7	3	10	4	7
Feldspar	1	1	1	Tr	Tr
Clay	90	5	85	95	90
Volcanic glass	2	90	3	1	3
Micronodules	Tr	–	Tr	Tr	Tr
Zeolites	–	1	–	–	–
Radiolarians	Tr	–	–	–	–
Opaques	–	–	1	Tr	–

SITE 576 HOLE B CORE 3 CORED INTERVAL 6237.0–6246.5 mbsl; 17.7–27.2 mbsf

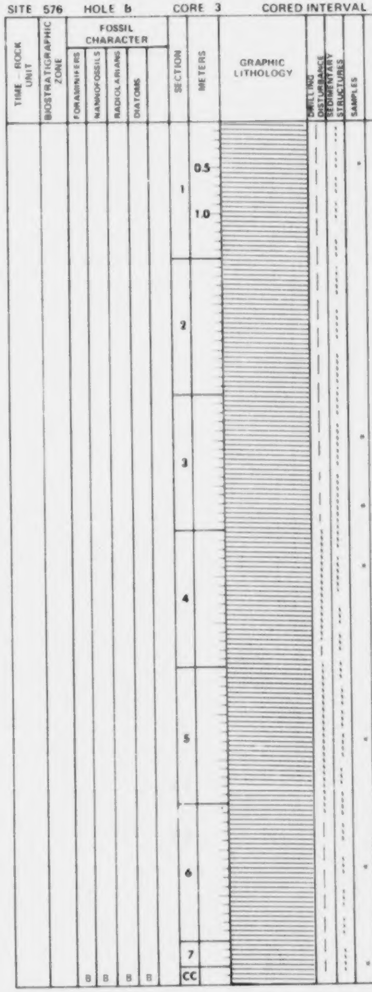
TIME – ROCK UNIT
BIOSTRATIGRAPHIC ZONE
FOSSIL CHARACTER
FORAMINIFERS
NANNOFOSSILS
RADIOLARIANS
DIATOMS
SECTION
METERS
GRAPHIC LITHOLOGY
DRILLING DISTURBANCE
SEDIMENTARY STRUCTURES
SAMPLES
B
B
B
B
0.5
1.0
1
2
3
4
5
6
7
CC

LITHOLOGIC DESCRIPTION

PELAGIC CLAY

*Dominant colors: dark brown (10YR 4/3) and dark yellowish brown (10YR 3/4) clay grading to dark brown (7.5YR 3/2) clay below Section 6.

*This core has been slightly deformed, except for Sections 4 and 5 which were very deformed.

*This core has been bioturbated throughout, with abundant burrows and mottled zones. MnO_2 specks and streaks are common.

SMEAR SLIDE SUMMARY (%)

	1, 50 D	3, 50 D	3, 124 D	4, 40 D	5, 80 D	6, 70 D	7, 30 D
Texture:							
Sand	1	2	1	Tr	Tr	Tr	0
Silt	9	15	7	10	8	7	12
Clay	90	83	92	90	92	93	88
Composition:							
Quartz	7	6	5	7	7	6	5
Feldspar	Tr	Tr	Tr	Tr	Tr	Tr	–
Mica	–	2	2	Tr	–	1	–
Clay	90	83	91	89	89	90	85
Volcanic glass	2	2	–	1	1	Tr	Tr
Micronodules	1	1	1	1	2	1	Tr
Zeolite	–	7	–	–	–	–	7
Fish remains	–	–	Tr	–	–	–	–
Opaques	Tr	Tr	1	2	1	2	3

SITE 576 HOLE B CORE 4 CORED INTERVAL 6246.5–6256.0 mbsl; 27.2–36.7 mbsf

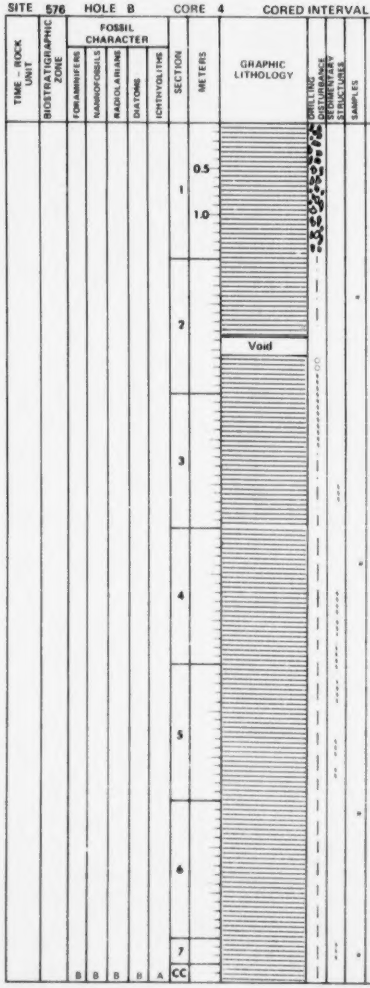
TIME – ROCK UNIT
BIOSTRATIGRAPHIC ZONE
FOSSIL CHARACTER
FORAMINIFERS
NANNOFOSSILS
RADIOLARIANS
DIATOMS
ICHTHYOLITHS
SECTION
METERS
GRAPHIC LITHOLOGY
DRILLING DISTURBANCE
SEDIMENTARY STRUCTURES
SAMPLES
0.5
1.0
1
2
3
4
5
6
7
CC
Void
B
B
B
B
A

LITHOLOGIC DESCRIPTION

PELAGIC CLAY

*Dominant colors: dark brown (7.5YR 3/2) and dark reddish brown (5YR 2/2). Burrows are dark brown (7.5YR 4/4) and strong brown (7.5YR 5/6).

*Sections 4 to 7 of this core are slightly deformed. Section 1 is brecciated; Sections 2 and 3 are soupy and moderately to very deformed. Section 2 contains a void from 85–105 cm.

*This core consists of homogeneous brown pelagic clay with minor burrows and mottled zones.

SMEAR SLIDE SUMMARY (%)

	2, 40 D	4, 40 D	6, 16 D	7, 20 D
Texture:				
Sand	Tr	0	1	0
Silt	10	8	2	4
Clay	90	92	97	96
Composition:				
Quartz	2	6	1	3
Feldspar	Tr	Tr	Tr	Tr
Mica	Tr	Tr	Tr	Tr
Clay	88	89	97	96
Volcanic glass	1	2	1	1
Micronodules	Tr	Tr	–	Tr
Zeolite	5	5	Tr	–
Hematite	4	3	1	—

SITE 576 HOLE B CORE 5 CORED INTERVAL 6256.0–6265.5 mbsl; 36.7–46.2 mbsf

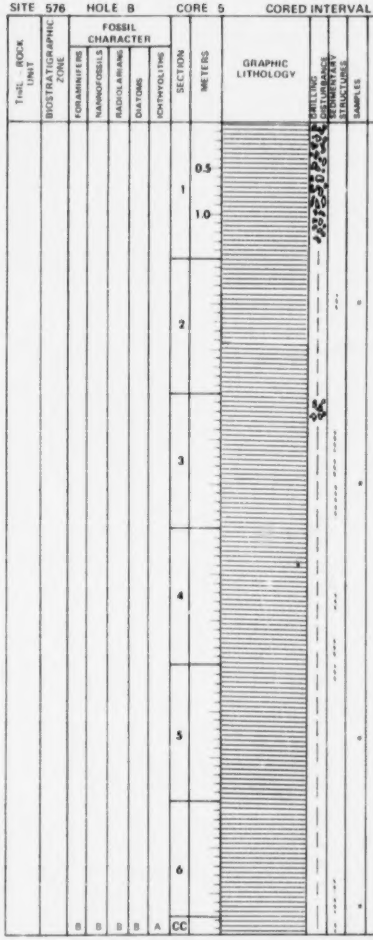
TIME – ROCK UNIT
BIOSTRATIGRAPHIC ZONE
FOSSIL CHARACTER
FORAMINIFERS
NANNOFOSSILS
RADIOLARIANS
DIATOMS
ICHTHYOLITHS
SECTION
METERS
GRAPHIC LITHOLOGY
DRILLING DISTURBANCE
SEDIMENTARY STRUCTURES
SAMPLES
0.5
1.0
1
2
3
4
5
6
CC
B
B
B
B
A

LITHOLOGIC DESCRIPTION

PELAGIC CLAY

*Dominant colors: dark brown (7.5YR 3/2) and dark reddish brown (5YR 3/2). Burrows are dark reddish brown (5YR 3/4).

*Section 1 is brecciated and soupy. The rest of the core is slightly deformed.

*This core consists of homogeneous brown pelagic clay with only minor small burrows and mottled zones.

SMEAR SLIDE SUMMARY (%):

	2, 50 D	3, 100 D	5, 80 D	6, 116 D
Texture:				
Sand	1	Tr	Tr	2
Silt	6	7	5	2
Clay	93	93	95	96
Composition:				
Quartz	2	Tr	Tr	1
Feldspar	Tr	Tr	Tr	Tr
Mica	Tr	Tr	Tr	–
Clay	92	96	95	96
Volcanic glass	1	1	1	2
Micronodules	1	1	1	1
Zeolite	–	Tr	Tr	–
Radiolarians	Tr	–	–	–
Opaques, Hematite	4	2	3	Tr

SITE 576 HOLE B CORE 6 CORED INTERVAL 6265.5–6275.0 mbsl; 46.2–55.7 mbsf

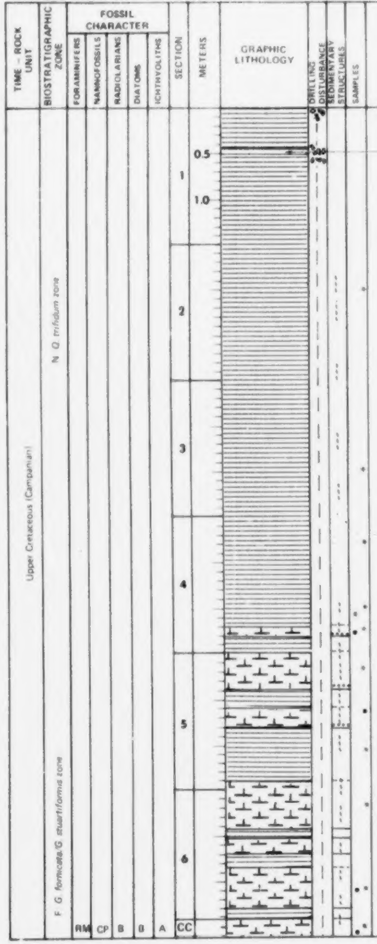
TIME – ROCK UNIT
BIOSTRATIGRAPHIC ZONE
FOSSIL CHARACTER
FORAMINIFERS
NANNOFOSSILS
RADIOLARIANS
DIATOMS
ICHTHYOLITHS
SECTION
METERS
GRAPHIC LITHOLOGY
DRILLING DISTURBANCE
SEDIMENTARY STRUCTURES
SAMPLES
Upper Cretaceous (Campanian)
N. Q. trifidum zone
F. G. fornicata/G. stuartiformis zone
RM
CP
B
B
A
1
2
3
4
5
6
CC
0.5
1.0
Void

LITHOLOGIC DESCRIPTION

INTERBEDDED PELAGIC CLAY AND NANNOFOSSIL OOZE

- Dominant colors: clay intervals are dark brown (7.5YR 3/2) grading downcore into brown (7.5YR 4/4) in Section 4, and to dark yellowish brown (10YR 3/4) in Section 5. Nannofossil ooze intervals are light brownish yellow (10YR 6/4), yellowish brown (10YR 5/8, yellowish brown (10YR 5/6), and brownish yellow (10YR 6/8). Burrows are dark reddish brown (5YR 3/4) and dark brown (7.5YR 4/4).
- Except for the brecciated and soupy portions of Section 1, this core is slightly deformed throughout.
- This core contains interbedded homogeneous brown pelagic clay and brownish yellow mottled nannofossil ooze. Several of the ooze layers are normally graded, indicating deposition by turbidity currents.

Note: Core Catcher is 30 cm in length.

SMEAR SLIDE SUMMARY (%)

	2, 50 D	3, 100 D	4, 30 D	4, 100 D	4, 110 D	4, 125 D
Texture:						
Sand	2	1	2	0	0	1
Silt	4	2	10	5	10	14
Clay	94	97	88	96	90	85
Composition:						
Quartz	1	1	5	5	2	5
Feldspar	—	—	3	3	2	2
Clay	94	97	78	85	89	10
Volcanic glass	2	2	4	2	2	Tr
Palagonite	—	Tr	—	—	—	—
Micronodules	2	Tr	—	—	—	—
Foraminifers	—	—	—	—	Tr	Tr
Calc. nannofossils	—	—	—	—	2	81
Radiolarians	—	—	—	—	Tr	—
Hematite	1	Tr	10	5	3	2

	5, 20 D	5, 105 D	6, 20 D	6, 110 D	CC D
Texture:					
Sand	0	0	0	1	1
Silt	50	10	40	9	19
Clay	50	90	60	90	80
Composition:					
Quartz	5	5	7	3	2
Feldspar	—	—	—	1	—
Heavy minerals	2	—	—	—	—
Clay	15	83	20	10	2
Volcanic glass	2	—	5	1	1
Glauconite	1	—	—	—	—
Zeolite	Tr	2	3	—	—
Carbonate unspec.	5	—	15	—	—
Foraminifers	70	—	—	Tr	—
Calc. nannofossils	—	5	50	85	95
Hematite	—	5	—	Tr	—

CaCO$_3$ data:
4, 129 cm = 83%
5, 167 cm = 88%
6, 110 cm = 84%
CC, 30 cm = 88%

SITE 576 HOLE B CORE 7 CORED INTERVAL 6275.0–6284.5 mbsl; 55.7–65.2 mbsf

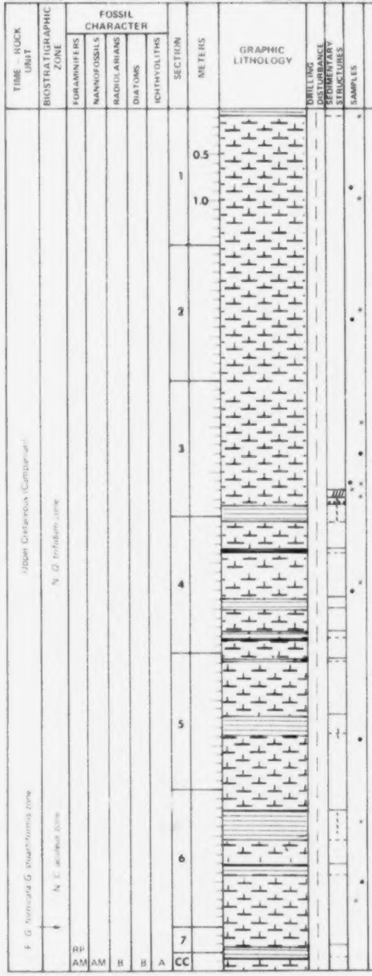
TIME – ROCK UNIT
BIOSTRATIGRAPHIC ZONE
FOSSIL CHARACTER
FORAMINIFERS
NANNOFOSSILS
RADIOLARIANS
DIATOMS
ICHTHYOLITHS
SECTION
METERS
GRAPHIC LITHOLOGY
DRILLING DISTURBANCE
SEDIMENTARY STRUCTURES
SAMPLES
Upper Cretaceous (Campanian)
N. Q. trifidum zone
N. C. aculeus zone
F. G. fornicata/G. stuartiformis zone
RP
AM
AM
B
B
A
1
2
3
4
5
6
7
CC
0.5
1.0

LITHOLOGIC DESCRIPTION

INTERBEDDED PELAGIC CLAY AND NANNOFOSSIL OOZE

- Dominant colors: clay is dark brown (10YR 3/3) changing to dark yellowish brown (10YR 3/4) below Section 3. Nannofossil ooze is very pale brown (10YR 7/4). Minor colors: clay contains brown (7.5YR 5/4) and brown (10YR 5/3) mottles. Section 3 contains laminations of nannofossil ooze colored very pale brown (10YR 7/4), pink (7.5YR 8/4), light gray (10YR 7/2), white (10YR 8/2), and gray (10YR 6/1).
- Core is slightly deformed throughout.
- Thick nannofossil ooze layer in Sections 1 to 3 is normally graded and crossbedded at lower 20 cm with sharp bottom contact with underlying pelagic clay layer, thus appears to have been deposited by a turbidity current. Rest of ooze layers have sharp bottom contacts, but no obvious grading.

SMEAR SLIDE SUMMARY (%)

	1, 4 D	1, 100 D	2, 76 D	3, 50 D	3, 115 D
Texture:					
Sand	3	0	1	0	5
Silt	12	10	19	40	15
Clay	85	90	80	60	80
Composition:					
Quartz	7	5	7	5	4
Feldspar	2	3	3	—	1
Clay	10	10	10	20	10
Volcanic glass	2	2	Tr	2	5
Pyrite	—	—	—	1	—
Micronodules	—	—	—	1	—
Carbonate unspec.	—	—	—	1	—
Foraminifers	3	—	—	—	5
Calc. nannofossils	73	80	80	70	75
Opaques –					
Hematite and Goethite	3	—	Tr	—	—

	3, 120 D	3, 130 D	4, 75 D	6, 35 D	6, 125 D
Texture:					
Sand	6	3	0	0	0
Silt	20	17	50	15	60
Clay	74	80	50	85	40
Composition:					
Quartz	7	5	20	5	10
Feldspar	2	3	—	—	—
Clay	15	7	10	82	10
Volcanic glass	3	5	2	—	2
Pyrite	—	—	1	Tr	—
Micronodules	—	—	1	Tr	—
Zeolite	—	—	1	—	1
Foraminifers	5	—	Tr	—	2
Calc. nannofossils	67	80	65	3	75
Opaques –					
Hematite and Goethite	1	—		10	Tr

CaCO$_3$ data:
1, 86 cm = 91%
2, 86 cm = 91%
3, 86 cm = 92%
3, 119 cm = 84%
4, 80 cm = 89%
5, 94 cm = 96%
6, 100 cm = 98%

SITE 576 HOLE B CORE 8 CORED INTERVAL 6284.5–6294.0 mbsl; 65.2–74.7 mbsf

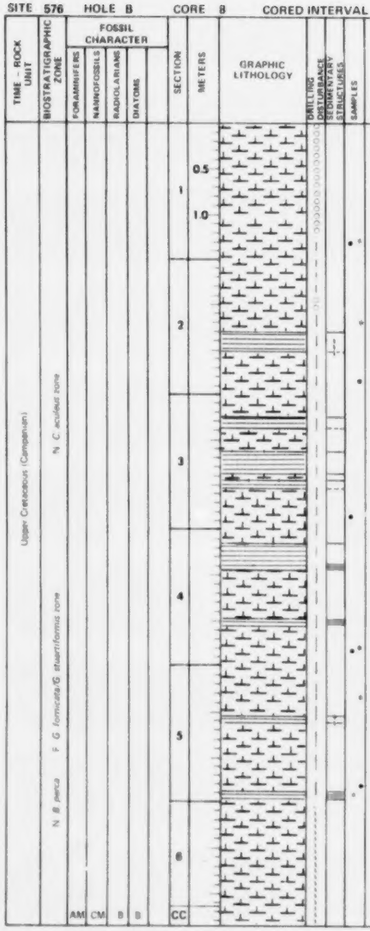
TIME – ROCK UNIT
BIOSTRATIGRAPHIC ZONE
FOSSIL CHARACTER
FORAMINIFERS
NANNOFOSSILS
RADIOLARIANS
DIATOMS
SECTION
METERS
GRAPHIC LITHOLOGY
DRILLING DISTURBANCE
SEDIMENTARY STRUCTURES
SAMPLES
Upper Cretaceous (Campanian)
N. C. aculeus zone
F. G. fornicata/G. stuartiformis zone
N. B. parca
AM
CM
B
B
1
2
3
4
5
6
CC
0.5
1.0

LITHOLOGIC DESCRIPTION

INTERBEDDED PELAGIC CLAY AND NANNOFOSSIL OOZE

- Dominant colors: clay is dark brown (10YR 3/3) grading to dark yellowish brown (10YR 3/4) in Section 3. Nannofossil ooze is light yellowish brown (10YR 6/4), very pale brown (10YR 7/4), brownish yellow (10YR 6/6), yellowish brown (10YR 5/6), and yellow (10YR 7/6). Minor colors: clay contains dark yellowish brown (10YR 4/4), strong brown (7.5YR 5/6), and black mottles and very dark brown to black and brown (10YR 5/3–10YR 3/3) laminations. Ooze in Section 2 contains white (10YR 8/2) zones.
- Section 1 is soupy. Section 6 is very deformed. The rest of the core is slightly deformed.
- The nannofossil ooze in this core is homogeneous, with no obvious grading or crossbedding. The clay ranges from homogeneous to mottled to laminated.

SMEAR SLIDE SUMMARY (%):

	1, 130 D	2, 70 D	4, 130 D	5, 35 D	5, 141 D
Texture:					
Sand	7	4	0	5	0
Silt	23	15	60	25	25
Clay	70	81	40	70	75
Composition:					
Quartz	5	5	5	7	10
Feldspar	2	3	—	3	—
Clay	25	4	5	8	50
Volcanic glass	Tr	2	5	2	5
Palagonite	—	—	1	—	—
Glauconite	—	—	1	—	1
Micronodules	—	—	1	—	—
Zeolite	—	—	1	—	2
Carbonate unspec.	—	—	—	—	10
Foraminifers	7	3	1	3	1
Calc. nannofossils	61	80	80	77	20
Hematite and Goethite	Tr	3	—	—	—

$CaCO_3$ data:
1, 135 cm = 94%
2, 135 cm = 90%
3, 135 cm = 93%
4, 135 cm = 91%
5, 135 cm = 89%

SITE 576 HOLE B CORE 9 CORED INTERVAL 6294.0–6294.1 mbsl; 74.7–74.8 mbsf

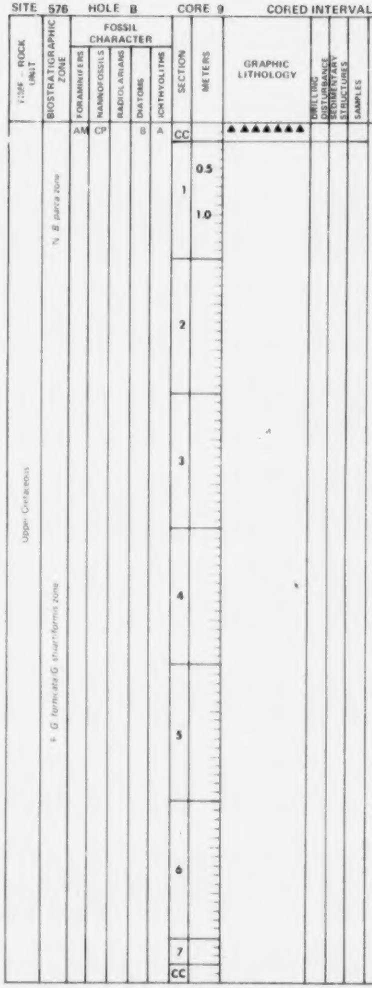
TIME – ROCK UNIT
BIOSTRATIGRAPHIC ZONE
FOSSIL CHARACTER
FORAMINIFERS
NANNOFOSSILS
RADIOLARIANS
DIATOMS
ICHTHYOLITHS
SECTION
METERS
GRAPHIC LITHOLOGY
DRILLING DISTURBANCE
SEDIMENTARY STRUCTURES
SAMPLES
Upper Cretaceous
N. B. parca zone
F. G. fornicata/G. stuartiformis zone
AM
CP
B
A
CC
1
2
3
4
5
6
7
CC
0.5
1.0

LITHOLOGIC DESCRIPTION

Core Catcher contained ~~several small~~ chert and silicified clay chips of a brownish yellow (10YR 6/6) color.

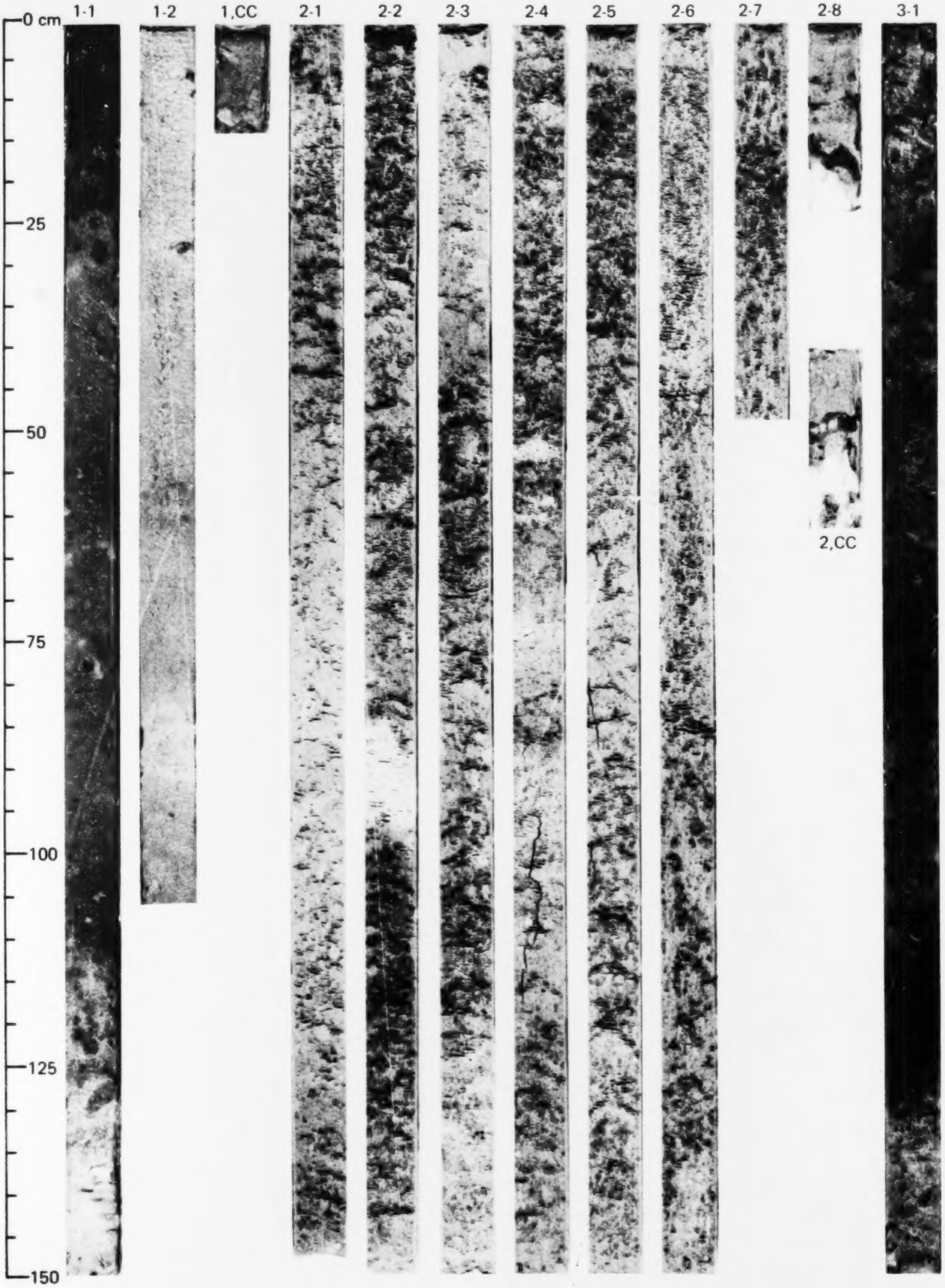
0 cm
25
50
75
100
125
150
1-1
1-2
1,CC
2-1
2-2
2-3
2-4
2-5
2-6
2-7
2-8
2,CC
3-1

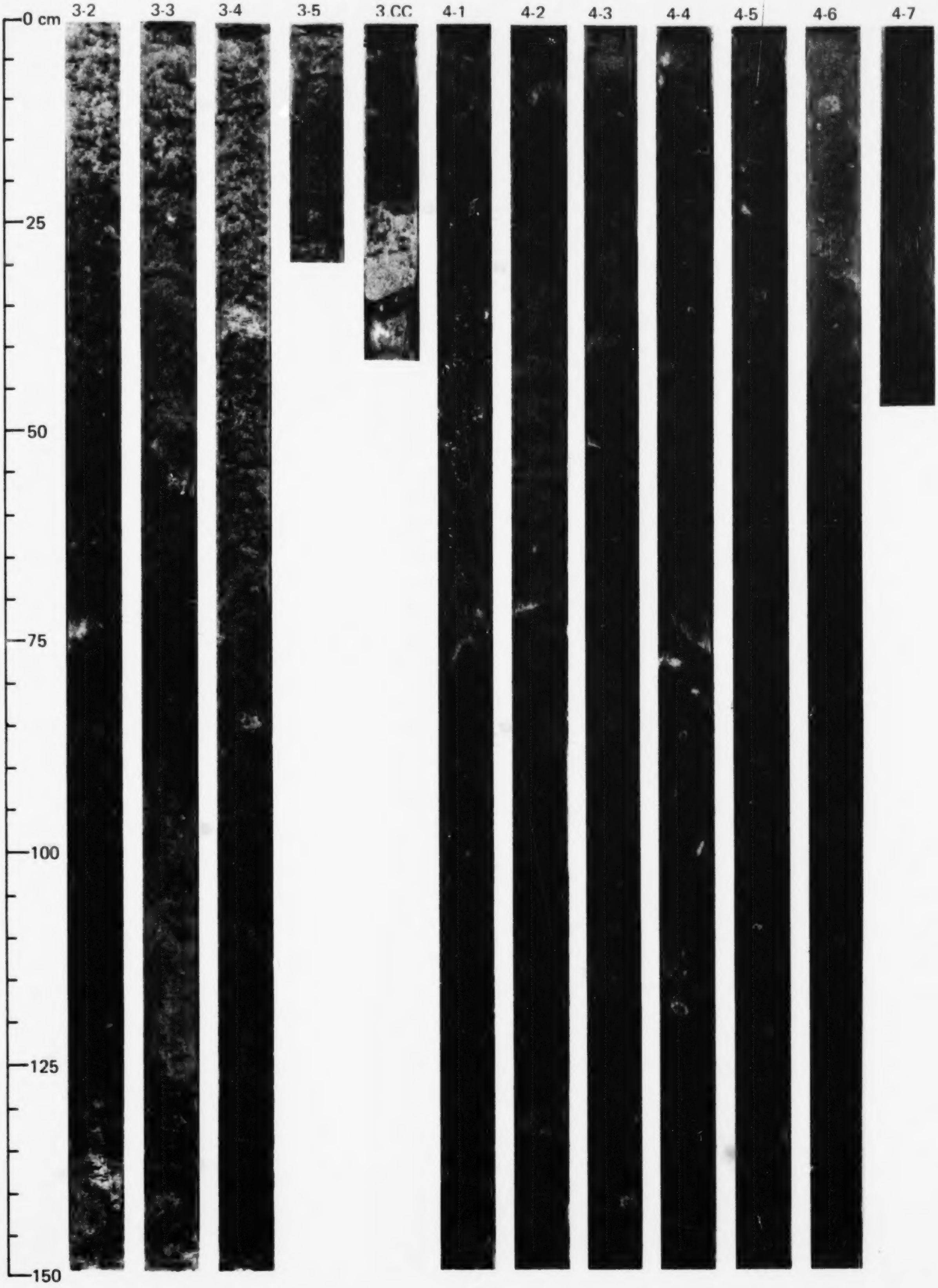
0 cm
25
50
75
100
125
150
3-2
3-3
3-4
3-5
3 CC
4-1
4-2
4-3
4-4
4-5
4-6
4-7

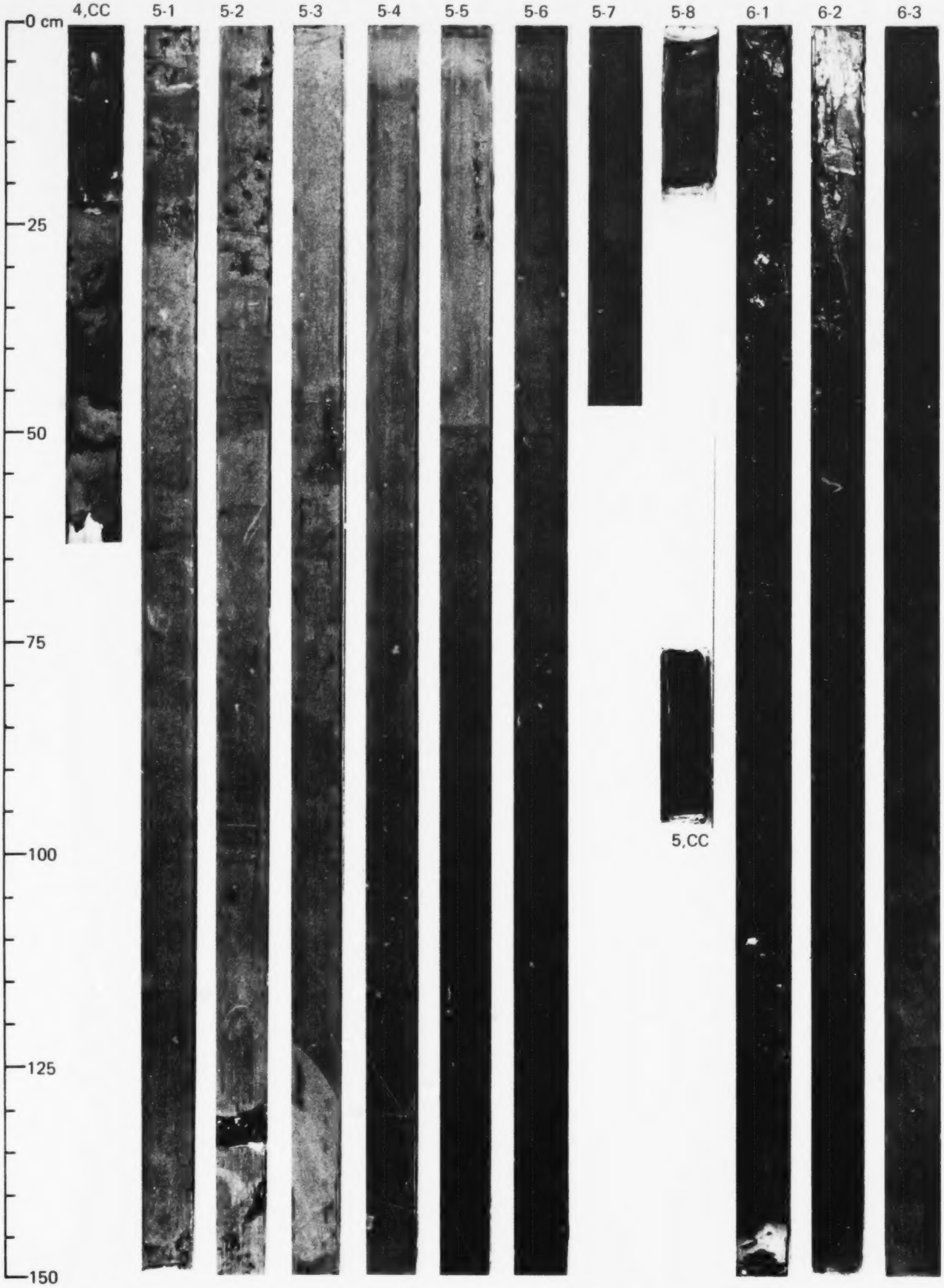
4,CC
5-1
5-2
5-3
5-4
5-5
5-6
5-7
5-8
6-1
6-2
6-3
0 cm
25
50
75
100
125
150
5,CC

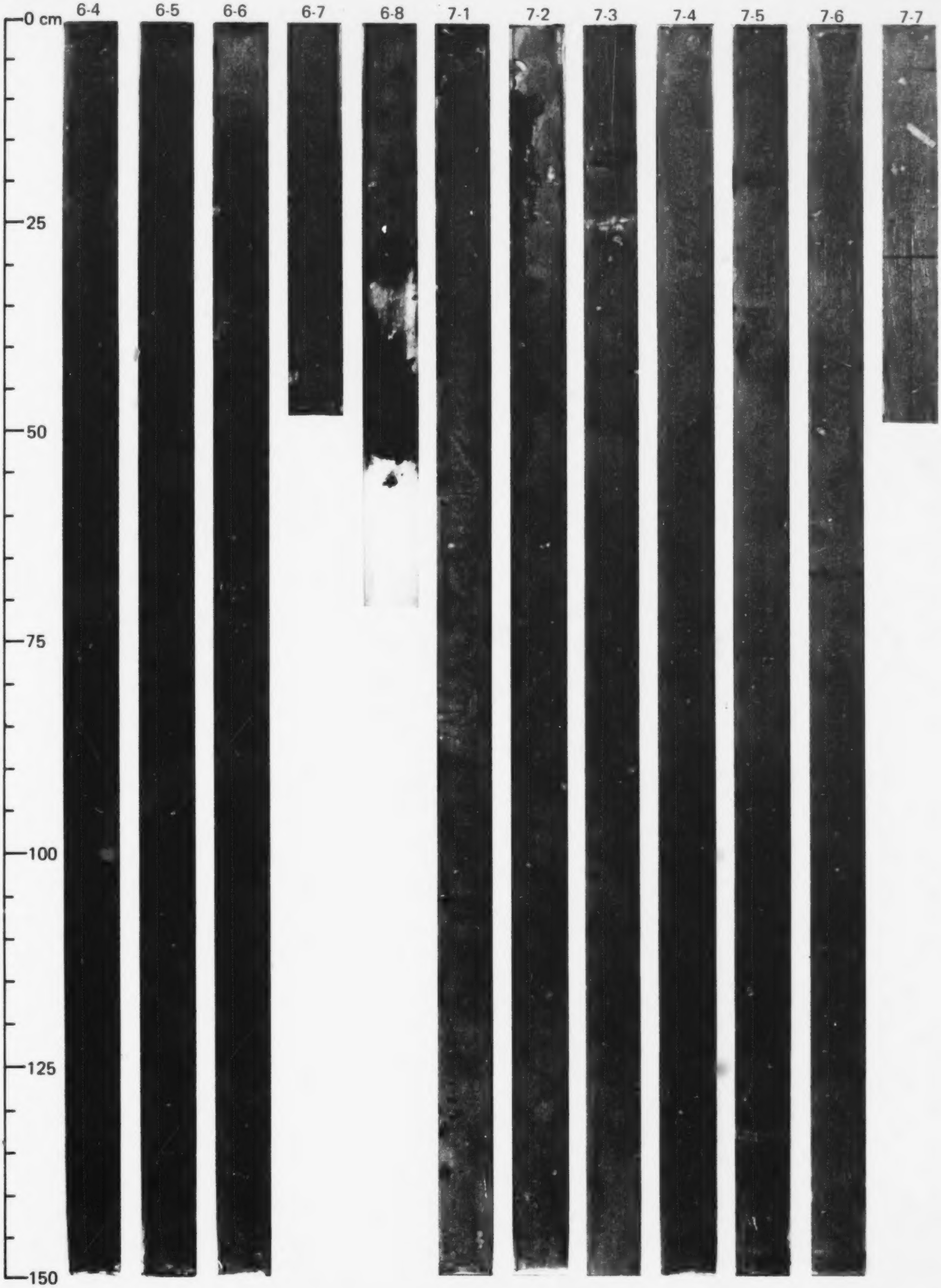
0 cm
25
50
75
100
125
150
6-4
6-5
6-6
6-7
6-8
7-1
7-2
7-3
7-4
7-5
7-6
7-7

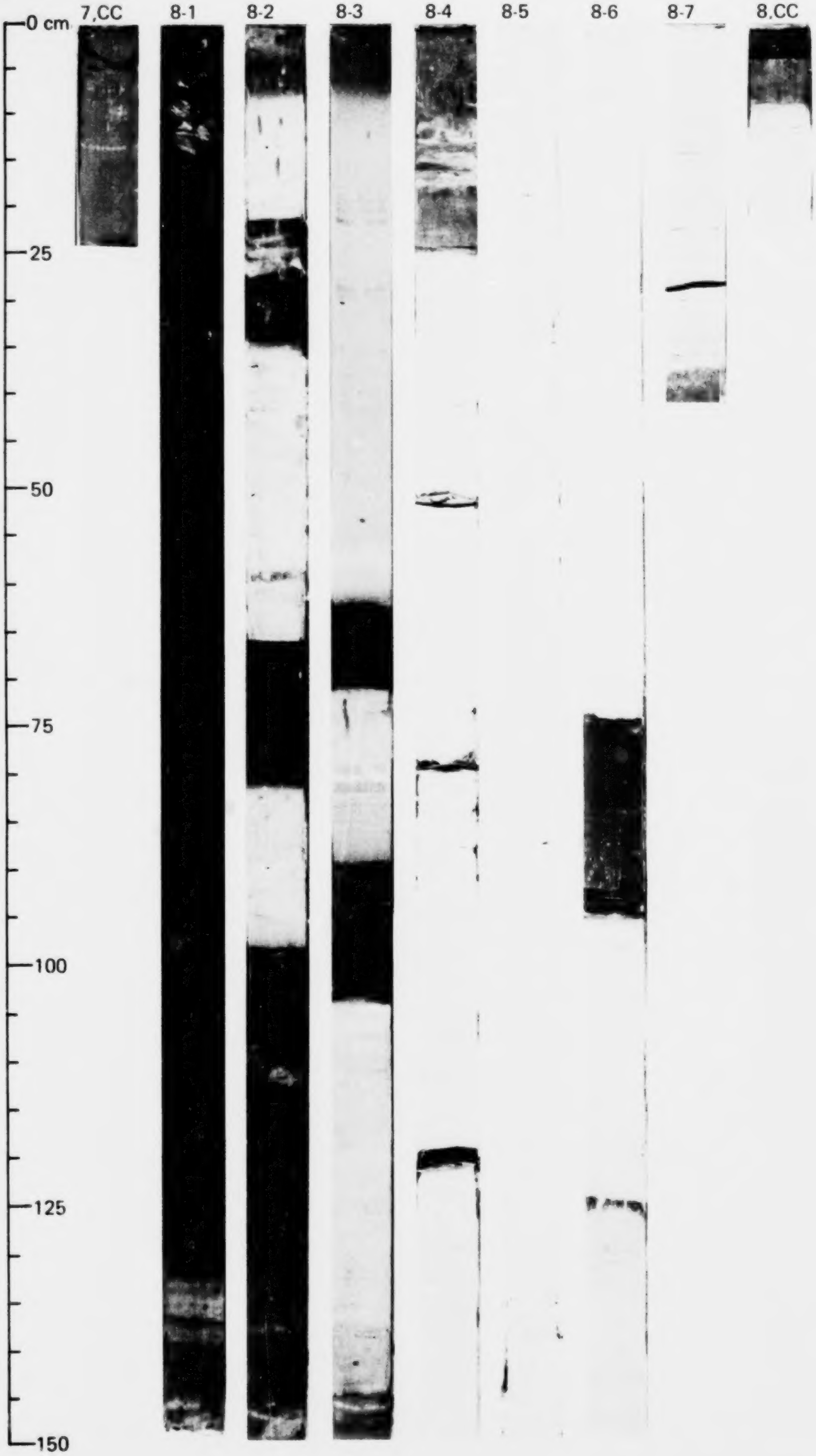
7,CC
8-1
8-2
8-3
8-4
8-5
8-6
8-7
8,CC
0 cm
25
50
75
100
125
150

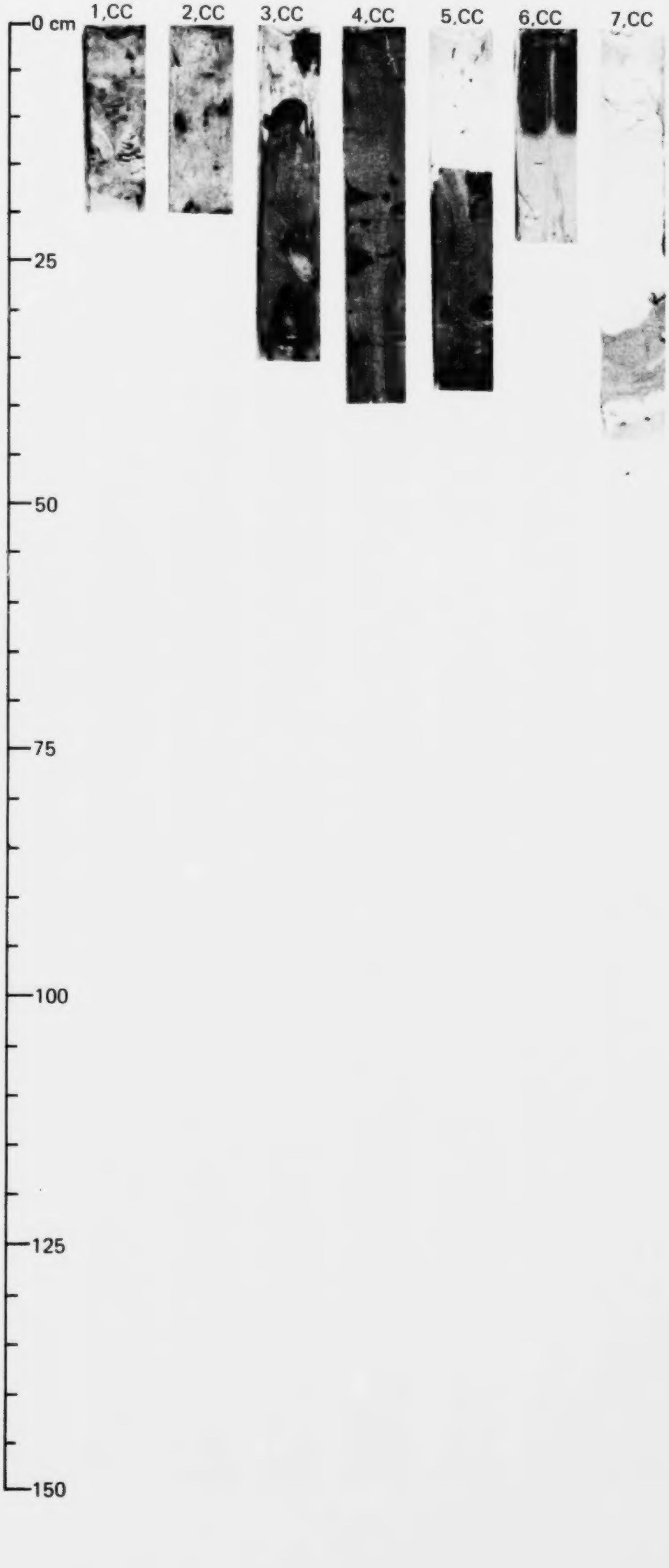
0 cm
25
50
75
100
125
150
1,CC
2,CC
3,CC
4,CC
5,CC
6,CC
7,CC

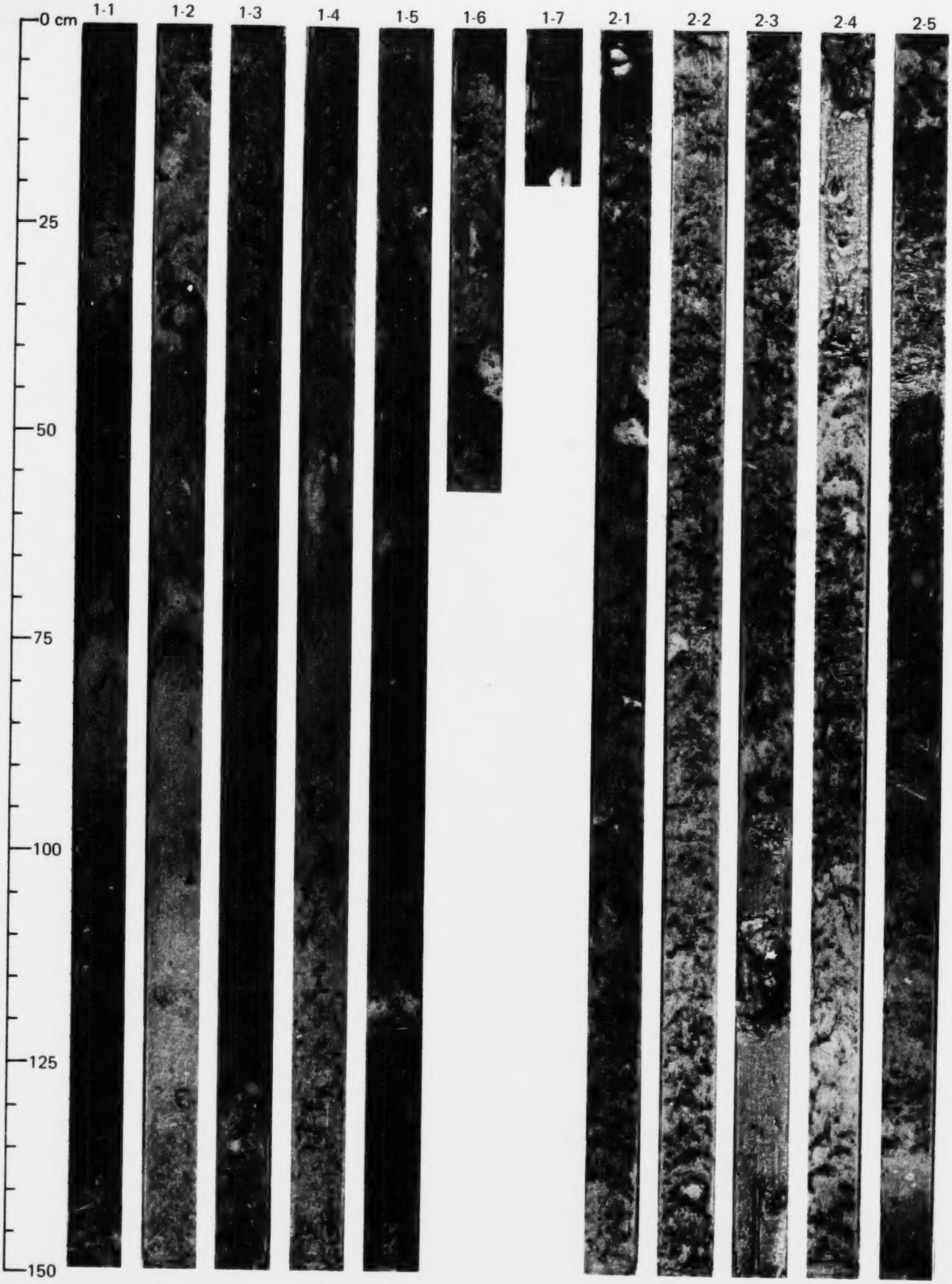
0 cm
25
50
75
100
125
150
1-1
1-2
1-3
1-4
1-5
1-6
1-7
2-1
2-2
2-3
2-4
2-5

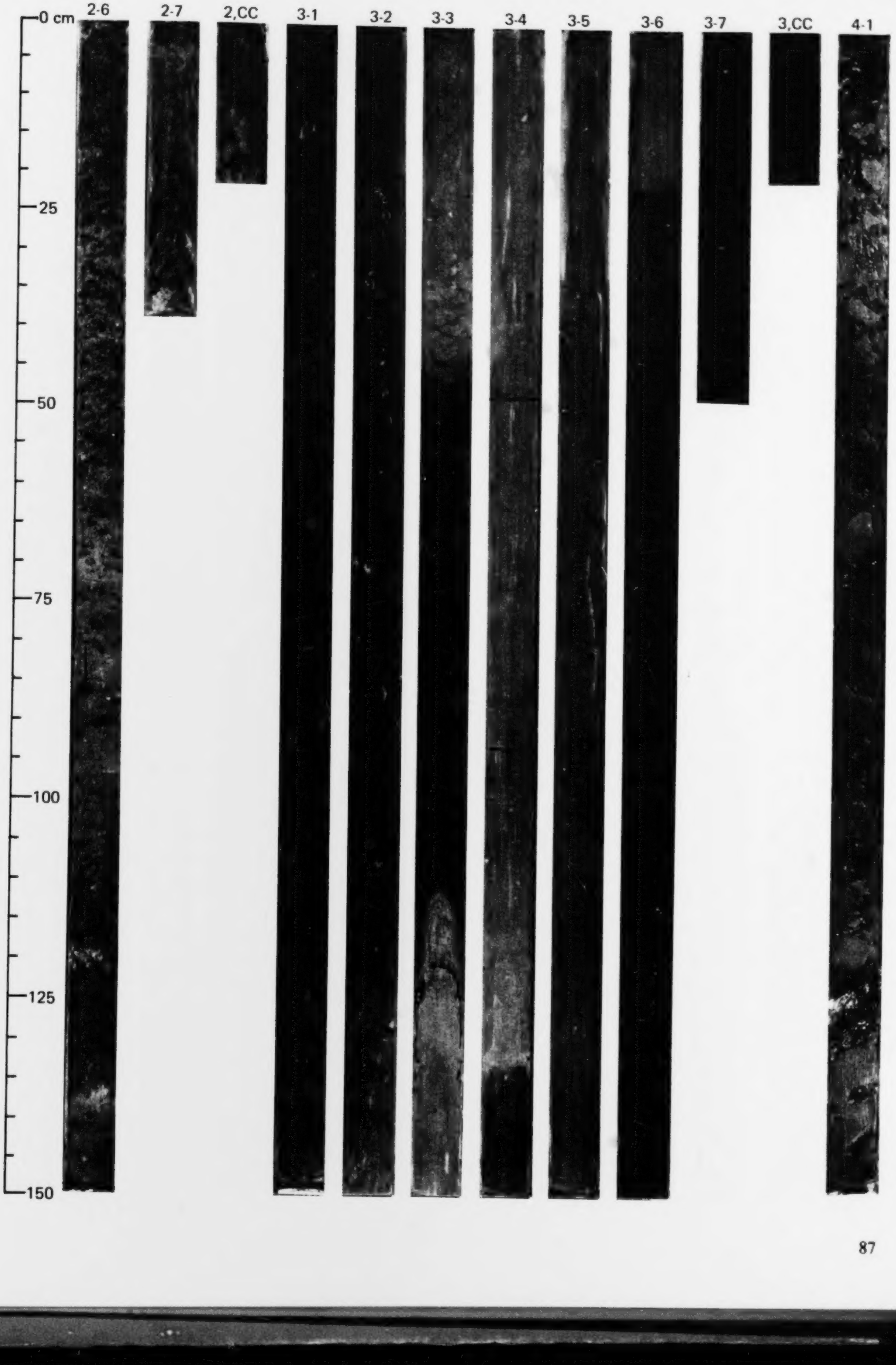
0 cm
25
50
75
100
125
150
2-6
2-7
2,CC
3-1
3-2
3-3
3-4
3-5
3-6
3-7
3,CC
4-1

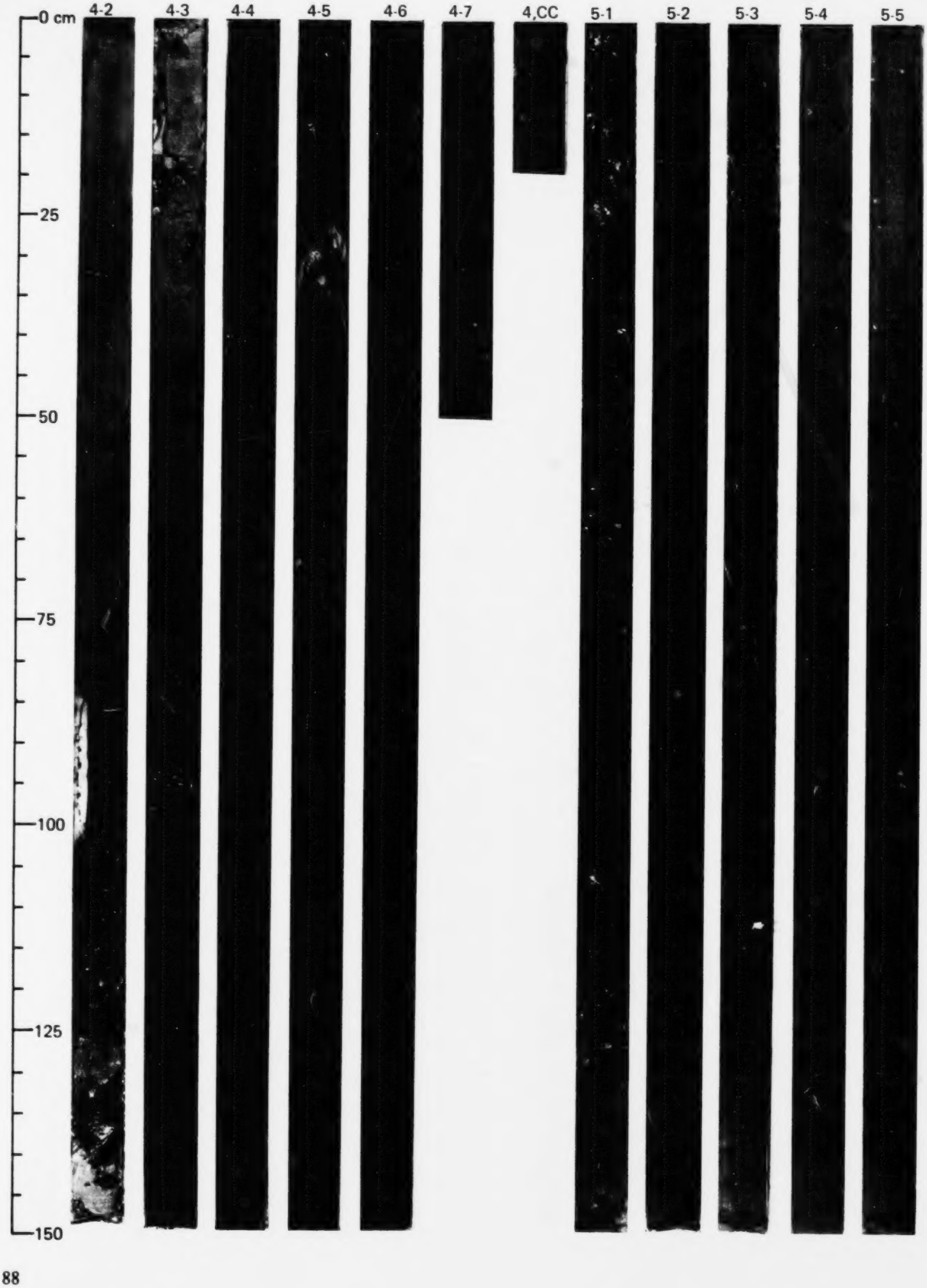
0 cm
25
50
75
100
125
150
4-2
4-3
4-4
4-5
4-6
4-7
4,CC
5-1
5-2
5-3
5-4
5-5

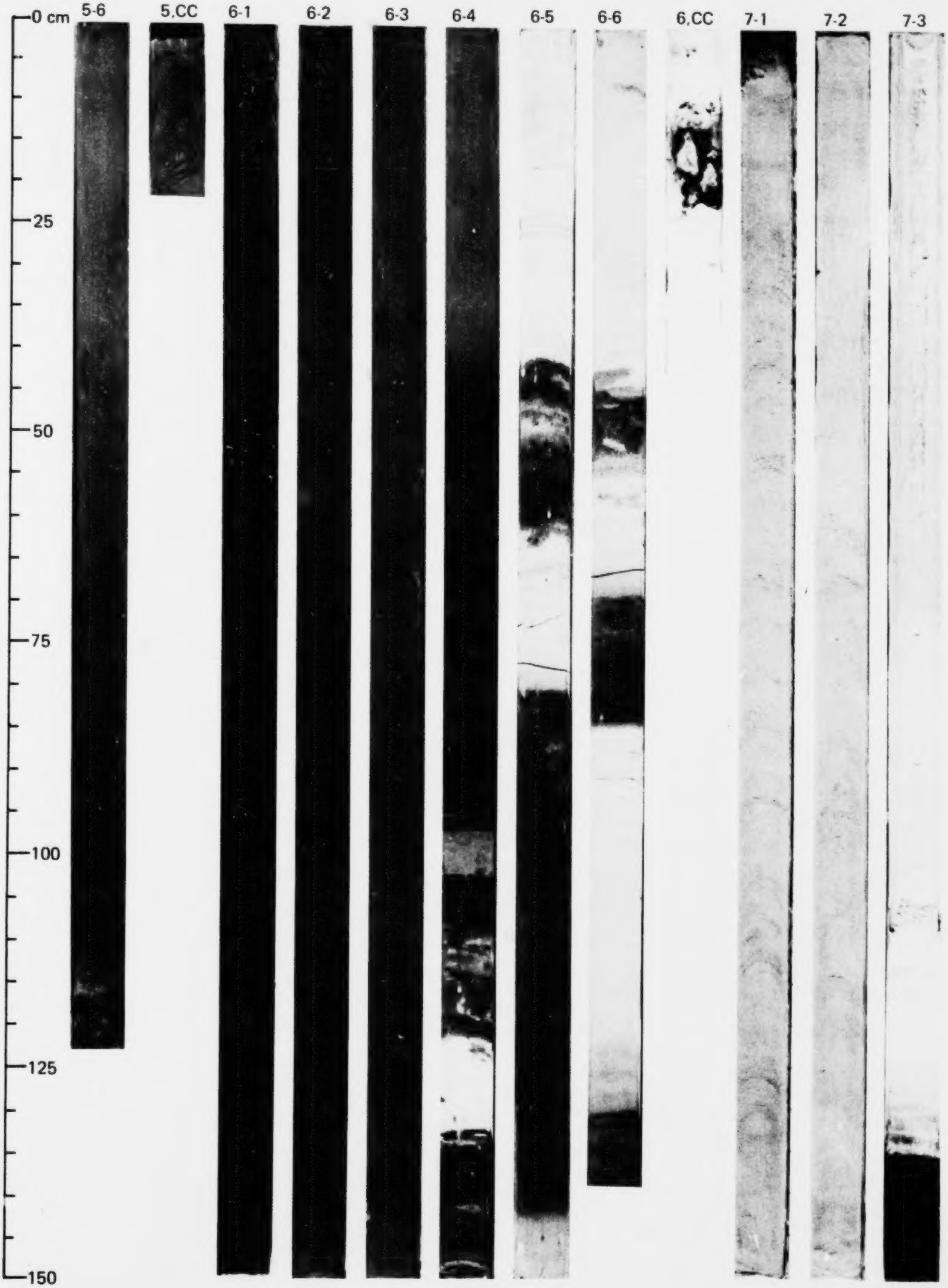
0 cm
25
50
75
100
125
150
5-6
5,CC
6-1
6-2
6-3
6-4
6-5
6-6
6,CC
7-1
7-2
7-3

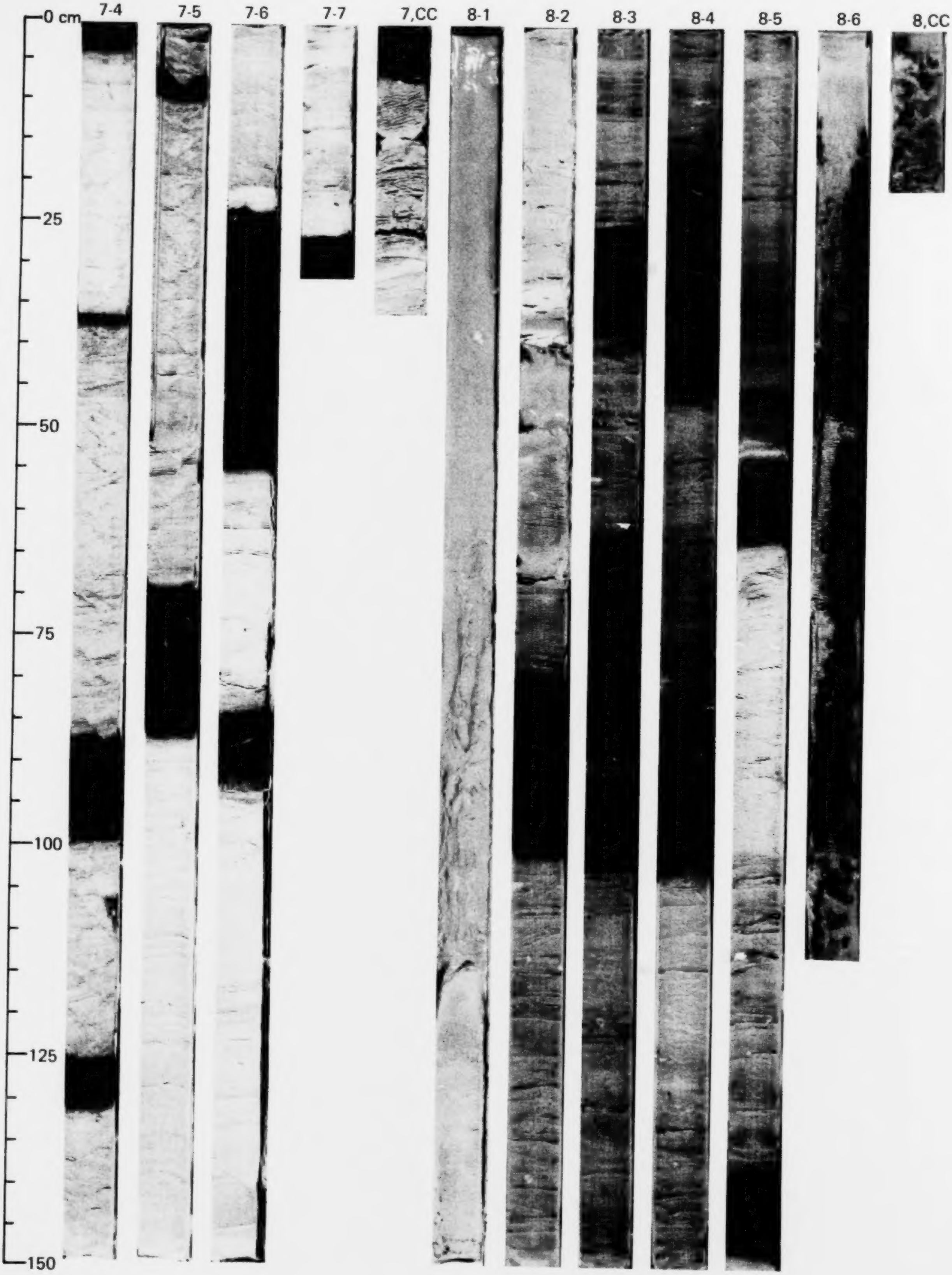
0 cm
25
50
75
100
125
150
7-4
7-5
7-6
7-7
7,CC
8-1
8-2
8-3
8-4
8-5
8-6
8,CC

4. SITE 577[1]

Shipboard Scientific Party[2]

HOLES 577, 577A, 577B

Date occupied: 23 May 1982 (577), 24 May (577A), 25 May (577B)

Date departed: 25 May 1982

Time on site: 2 days, 19 hr., 27 min.

Position (latitude; longitude): 32°26.51′N; 157°43.40′E (577)
32°26.53′N; 157°43.39′E (577A)
32°26.48′N; 157°43.39′E (577B)

Water depth (sea level; corrected m, echo-sounding): 2675

Water depth (rig floor; corrected m, echo-sounding): 2685

Bottom felt (m, drill pipe): 2678.2 (577), 2677.6 (577A), 2782.0 (577B)

Penetration (m): 118.8 (577), 123.4 (577A), 113.9 (577B)

Number of cores: 13 (577), 13 (577A), 1 (577B)

Total length of cored section (m): 118.8 (577), 123.4 (577A), 9.5 (577B)

Total core recovered (m): 111.07 (577), 110.64 (577A), 9.63 (577B)

Core recovery (%): 93 (577), 90 (577A), 101 (577B)

Oldest sediment cored:
Depth sub-bottom (m): 123.4
Nature: calcareous nannofossil ooze
Age: Cretaceous (Maestrichtian)
Measured Velocity (km/s): 1.52

Basement: Not reached

Principal results: An unusually good late Cenozoic sequence, a Paleogene sequence, and an undisturbed record of the Cretaceous/Tertiary boundary were recovered at Site 577. The former two sections were recovered in two holes, while the latter was recovered in three holes. A paleomagnetic reversal record was determined for the Neogene but, since the magnetization of the Cretaceous and Paleogene sediments was within the noise level of the shipboard magnetometer, detailed magnetostratigraphy had to await shore-based analysis. Although the sediments recovered are all nannofossil oozes, they can be divided into three lithologic units.

Unit I (0–53.5 m) is a white to light gray nannofossil ooze. It is divided into two subunits based on a downcore decrease in the percentage of foraminifers, radiolarians, and diatoms. The lower subunit carries only a few percent foraminifers and traces of radiolarians and diatoms.

Unit II is a white to pale brown nannofossil ooze. This unit is characterized by high percentages (60–90%) of coccoliths. It is further divided into two subunits, with the upper one being pale brown in color and the lower one characterized by alternating white and pale brown colors.

The deepest lithologic unit (Unit III) is a calcareous nannofossil ooze, white in color, and Latest Cretaceous in age. It is found in the lower 20 m of the hole. Penetration was stopped by a hard layer, presumably chert.

Sediment accumulation rates were highest in the late Cenozoic (11.6 m/m.y.) and markedly less below the late Miocene/middle Eocene unconformity (3 m/m.y.). Late Cretaceous rates were on the order of 10 m/m.y.

Both the measurements of physical properties and heat flow seemed to "sense" the late Miocene/middle Eocene unconformity at approximately 60 m. There is a sudden increase in bulk density just below this boundary as well as a rapid increase in compressional wave velocity at this level (1.48 to 1.53 km/s). The heat-flow data show a linear increase with depth until the level of the unconformity at which point there is an apparent temperature reversal.

All in all, this was a highly successful site, highlighted by three separate holes in which we recovered undisturbed and complete Cretaceous/Tertiary boundary sequences.

BACKGROUND AND OBJECTIVES

Site 577 (target Site NW-8B) is the middle member of the suite of three sites taken along an east–west track between 32°N, 164°E and the west side of the Shatsky Rise. It is located as near as possible to Site 47 on the flank of the Shatsky Rise. Its proximity to the western edge of the subtropical gyre and the water depth (<3000 m) permit the preservation of calcareous microfossils. In addition to standard biostratigraphic treatment of this site, we expected to establish good stratigraphic control using stable isotopes (oxygen and carbon). At the same time, at least marginal preservation of siliceous microfossils allows us to correlate the Neogene sequences in this site with the more siliceous sequences to the north (Sites 578–581). Such a strategy will result in high resolution stratigraphic control for Neogene sediments from the equatorial Pacific to the northwest Pacific and is a natural prelude to any broad, regional paleoceanographic or paleoenvironmental study.

The location of this site is an excellent complement to Site 576 and LL44-GPC3 in that it reflects input of eolian sediments from the Asian mainland.

Our specific scientific objectives were

1. To obtain a detailed paleoceanographic record for the western edge of the subtropical gyre during the late Neogene, principally using foraminifers and calcareous nannofossils.

2. To recover a late Neogene carbon and oxygen isotope record for comparison with the noncalcareous (siliceous) sites to the north.

---

[1] Heath, G. R., Burckle, L. H., et al., *Init. Repts. DSDP*, 86: Washington (U.S. Govt. Printing Office).

[2] Addresses: G. Ross Heath (Co-Chief Scientist) School of Oceanography, Oregon State University, Corvallis, OR 97331 (present address: College of Ocean and Fishery Sciences, University of Washington, Seattle, WA 98195); Lloyd H. Burckle (Co-Chief Scientist) Lamont-Doherty Geological Observatory, Palisades, NY 10964; Anthony E. D'Agostino, ARCO Exploration Company, Houston, TX 77056; Ulrich Bleil, Institut für Geophysik, Ruhr-Universität Bochum, D-4630 Bochum Querenburg, Federal Republic of Germany; Ki-iti Horai, Lamont-Doherty Geological Observatory, Palisades, NY 10964 (present address: Meteorological College, Chiba University, Chiba 277, Japan); Robert D. Jacobi, Department of Geological Sciences, SUNY Buffalo, Amherst, NY 14226; Tom Janecek, Department of Atmospheric & Oceanic Science, University of Michigan, Ann Arbor, MI 48109 (present address: Lamont-Doherty Geological Observatory, Palisades, NY 10964); Itaru Koizumi, College of General Education, Osaka University, Osaka 560, Japan; Lawrence A. Krissek, School of Oceanography, Oregon State University, Corvallis, OR 97331 (present address: Department of Geology and Mineralogy, Ohio State University, Columbus, OH 43210); Nicole Lenôtre, Bureau de Recherches Géologiques et Minières, Centre Océanologique de Bretagne, 45060 Orléans Cedex, France; Simonetta Monechi, Geological Research Division, Scripps Institution of Oceanography, La Jolla, CA 92093 (present address: Dipartimento di Scienze della Terra, Università di Firenze, 4 Via La Pira, 50121 Firenze, Italy); Joseph J. Morley, Lamont-Doherty Geological Observatory, Palisades, NY 10964; Peter Schultheiss, Institute of Oceanographic Sciences, Surrey GU8 5UB, United Kingdom; Audrey A. Wright, Deep Sea Drilling Project, Scripps Institution of Oceanography, La Jolla, CA 92093 (present address: Ocean Drilling Program, 500 University Drive West, Texas A&M University, College Station, TX 77843).

3. To establish a high-resolution stratigraphy for the late Neogene and Quaternary, using paleomagnetics, stable isotopes, tephrachronology, and biostratigraphy (chiefly foraminifers and calcareous nannofossils, but also siliceous microfossils).

4. To determine the late Neogene history of eolian sedimentation for comparison with other sites along the east-west track.

5. To recover the Cretaceous/Tertiary boundary for midlatitude calcareous biostratigraphy and for paleomagnetic and geochemical studies.

OPERATIONS

We arrived at Site 577 after approximately 1 1/2 days steaming from Site 576. Air-gun, 3.5, and 12-kHz records were taken en route. We passed over the proposed site at 1534 hr., after which the gear was retrieved and the ship was positioned over the beacon. After a 1-hr. delay (slips did not hold) we began running pipe at 2400 hr. and, by 0400 hr., 24 May, were ready to take the first hydraulic piston core (HPC) at Site 577. This went off without a hitch, with the first core coming up at 0500 hr. and then at 1 hr., 15 min. to 1 hr., 30 min. intervals after that (Table 1). At 2335 hr. (24 May), Hole 577A was spudded in and the first core came up at 2400 hr. This operation also went off without a hitch (Table 1). However, when Site 577 cores were opened, we discovered considerable coring disturbance in some parts of the section, particularly the Paleogene. An effort was made to rectify this by modifying the shear pin assembly to allow the equivalent of one additional shear pin. It was believed that the shallow water depth at this site coupled with premature yielding of shear pins resulted in slow penetration rates on some cores, resulting in increased disturbance. The character of the sediments (a clay-poor nannofossil ooze) may have contributed to this problem. At Hole 577B (0035 hr., 25 May), we washed down to just above the approximate level of the Cretaceous/Tertiary boundary and recovered one core of the boundary (Table 1).

Table 1. Site 577 coring summary.

Core	Date (May 1982)	Local time	Depth from drill floor (m)	Depth below seafloor (m)	Length cored (m)	Length recovered (m)	Percent recovered
Hole 577							
1	23	0505	2678.2-2685.0	0.0-6.8	6.8	6.81	100
2	23	0615	2685.0-2694.5	6.8-16.3	9.5	8.84	93
3	23	0730	2694.5-2704.0	16.3-25.8	9.5	8.15	86
4	23	0845	2704.0-2713.5	25.8-35.3	9.5	8.62	91
5	23	0958	2713.5-2723.0	35.3-44.8	9.5	7.99	84
6	23	1110	2723.0-2732.5	44.8-54.3	9.5	9.69	102
7	23	1225	2732.5-2742.0	54.3-63.8	9.5	8.24	87
8	23	1350	2742.0-2751.5	63.8-73.3	9.5	9.33	98
9	23	1505	2751.5-2761.0	73.3-82.8	9.5	8.80	93
10	23	1610	2761.0-2770.5	82.8-92.3	9.5	9.61	101
11	23	1800	2770.5-2780.0	92.3-101.8	9.5	9.21	97
12	23	1910	2780.0-2789.5	101.8-111.3	9.5	9.39	99
13	23	2020	2789.5-2797.0	111.3-118.8	7.5	6.39	85
					118.8 (total)	111.07 (total)	93 (avg.)
Hole 577A							
1	24	0001	2677.6-2687.0	0.0-9.4	9.4	9.39	100
2	24	0119	2687.0-2696.5	9.4-18.9	9.5	8.70	92
3	24	0245	2696.5-2706.0	18.9-28.4	9.5	7.08	75
4	24	0356	2706.0-2715.5	28.4-37.9	9.5	9.72	102
5	24	0705	2715.5-2725.0	37.9-47.4	9.5	8.78	92
6	24	0815	2725.0-2734.5	47.4-56.9	9.5	9.85	104
7	24	1120	2734.5-2744.0	56.9-66.4	9.5	8.90	94
8	24	1230	2744.0-2753.5	66.4-75.9	9.5	8.13	86
9	24	1520	2753.5-2763.0	75.9-85.4	9.5	3.80	40
10	24	1650	2763.0-2772.5	85.4-94.9	9.5	8.15	86
11	24	1802	2772.5-2782.0	94.9-104.4	9.5	9.26	97
12	24	1938	2782.0-2791.5	104.4-113.9	9.5	9.62	101
13	24	2058	2791.5-2801.0	113.9-123.4	9.5	9.26	97
					123.4 (total)	110.64 (total)	90 (avg.)
Hole 577B							
1	25	0035	2782.0-2791.5	104.4-113.9	9.5	9.63	101
					9.5 (total)	9.63 (total)	101 (avg.)

While coring Holes 577A and 577B, it was noticed that several connections were breaking with a torque of 8000/ft. lbs. or less. This problem has occurred on previous legs and, since no rotation is imparted to drill pipe during HPC coring, it was decided to retorque all connections on new pipe while coming out of Hole 577B.

The heat flow shoe was deployed nine times, six of which were successful. However, the three unsuccessful runs were not due to any inadequacies of the unit. Two failures were due to an undiscovered broken wire; the third occurred when the unit was plugged into the computer before the recording cycle was completed and the data were dumped.

LITHOSTRATIGRAPHY

The sediments in Holes 577, 577A, and 577B at Site 577 are nannofossil oozes that can be divided into three units based on color variations: (I) a white to light gray unit, (II) a white to pale brown unit, (III) a white unit. The upper two units can be further subdivided on the basis of color variation (Fig. 1, Table 2). Carbonate contents of these sediments, determined by the shipboard Carbonate Bomb, are included in Figure 1.

Unit I: White to Light Gray Nannofossil Ooze

This unit is characterized by high percentages (60–97%) of nannofossils and is further divided into two subunits as follows.

Subunit IA

Subunit IA is an alternating white to light gray (2.5Y and 5Y), lightly mottled nannofossil ooze that extends from the top of Cores 1 through 5 in both Holes 577 and 577A. This subunit contains 60–95% nannofossils with subordinate amounts of foraminifers (0–20%), radiolarians (0–7%), and diatoms (0–3%). Sponge spicules are present in trace amounts. With the exception of Cores 577-1 and 577A-1, terrigenous material generally accounts for less than 15% of the sediment; in Cores 577-1 and 577A-1, terrigenous concentrations of up to 35% occur. The dominant terrigenous components are quartz (0–10%), feldspar (0–5%) and clay (0–15%). Volcanic ash is generally present in concentrations of 2% or less.

Hole 577 contains three ash layers in Subunit IA (ash greater than 50%), one in Sample 577-2-5, 60 cm; one in Sample 577-2-6, 103 cm; and one in Sample 577-3-1, 39 cm. Hole 577A contains two ash layers, one in Sample 577A-2-3, 105 cm and another in Sample 577A-2-4, 136 cm. An ash-rich horizon (ash concentrations 20–30%) is also found in Sample 577A-4-4, 76–80 cm. The ash layer in Sample 577-2-5, 60 cm is likely correlated with the one in Sample 577A-2-3, 105 cm. The ash layer in

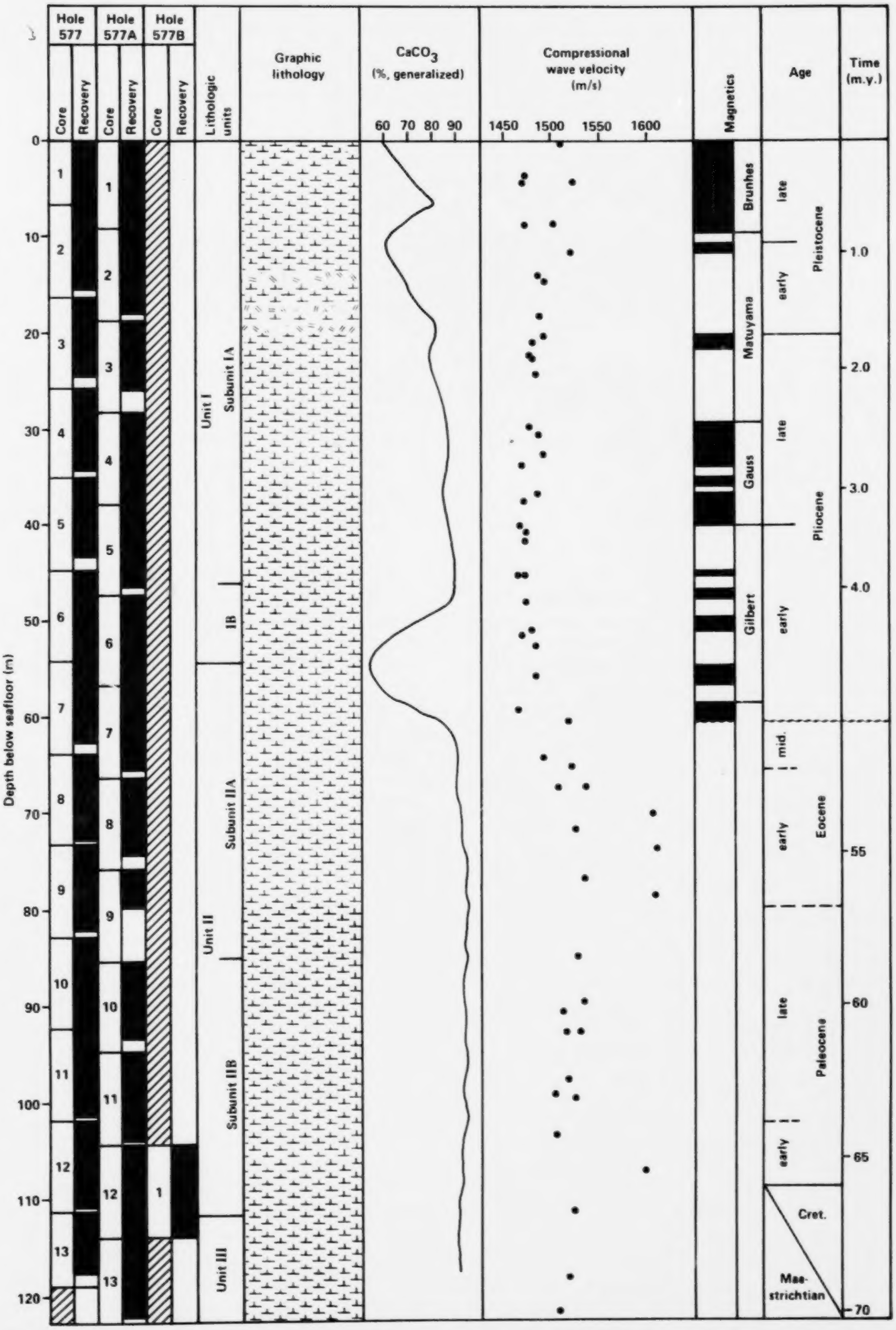

Figure 1. Site summary diagram showing Site 577 core numbers, core recovery, lithologic units, graphic lithology, carbonate percentages (generalized), compressional wave velocities (m/s), magnetostratigraphy, and age. Symbols used in graphic lithology column are defined in Introduction and Explanatory Notes (this volume).

Table 2. Site 577 lithostratigraphic units.

		Core interval			Sub-bottom depth (m)		
	Lithologic unit	Hole 577	Hole 577A	Hole 577B	Hole 577	Hole 577A	Hole 577B
I	White to light gray nannofossil ooze						
	Subunit IA (2.5Y to 5Y color)	1-1, 0 cm to 5,CC	1-1, 0 cm to 5,CC		0–44.8	0–47.4	
	Subunit IB (10YR color)	6-1, 0 cm to 6,CC	6-1, 0 cm to 6-5, 150 cm		44.8–54.3	47.4–53.5	
II	White to pale brown nannofossil ooze						
	Subunit IIA (pale brown)	7-1, 0 cm to 9,CC	6-6, 0 cm to 10-2, 150 cm		54.3–82.8	53.5–88.4	
	Subunit IIB (white to pale brown)	10-1, 0 cm to 12-7, 50 cm	10-3, 0 cm to 12-6, 150 cm	1-1, 0 cm to 1-5, 150 cm	82.8–111.1	88.4–111.9	104.4–111.9
III	White nannofossil ooze	12,CC to 13,CC	12-7, 0 cm to 13,CC	1-6, 150 cm to 1,CC	111.1–118.8	111.9–123.4	111.9–113.9

Sample 577A-2-4, 136 cm may be correlative with either the layer in Sample 577-2-6, 103 cm or Sample 577-3-1, 39 cm. Hole 577 does not contain an ash-rich horizon correlative to that found in Sample 577A-4-4, 76–80 cm.

Subunit IB

Subunit IB is an alternating white to light gray (10YR) nannofossil ooze that extends from the top of Core 577-6 to the top of Core 577-7 and from the top of Core 577A-6 through Section 577A-6-5. This subunit contains 90–97% nannofossils with only a few percent foraminifers. Siliceous microfossils are present in trace amounts. Combined quartz, feldspar, and clay concentrations are less than 5%. Volcanic ash generally constitutes less than 2% of the sediment. An ash layer in Sample 577A-6-4, 60 cm does not appear to have a correlative layer in Hole 577.

Unit II: White to Pale Brown Nannofossil Ooze

This nannofossil ooze unit is characterized by high percentages (60–90%) of nannofossils and is divided into two subunits as follows.

Subunit IIA

Subunit IIA is a pale brown (10YR) nannofossil ooze that extends from the top of Cores 577-7 through 577-9 and from the top of Sections 577-6-6 through 577A-10-2. This subunit contains 80–90% nannofossils with only trace amounts of foraminifers and siliceous microfossils. Quartz (0–5%), feldspar (0–2%), clay (0–10%), and volcanic ash (0–2%) constitute the remaining sediment.

Subunit IIB

Subunit IIB is characterized by alternating white and pale brown (10YR) nannofossil oozes found in Sections 577-10-1 through 577-12-7, 577A-10-3 through 577A-12-6, and 577B-1-1 through 577B-1-5. Nannofossils comprise 65–95% of the sediment; foraminifer concentrations range up to 35%. Combined quartz, feldspar, clay, and ash concentrations are generally less than 10%.

Unit III: White Nannofossil Ooze Unit

This white (10YR) nannofossil unit extends from Sections 577-12,CC through 577-13,CC, 577A-12-7 through 577A-13,CC, and 577B-1-6 through 577B-1,CC. Core 577-13 struck a hard layer, presumably chert, and coring in that hole was discontinued. Holes 577A and 577B did not reach this layer. Unit III is comprised of 80–90% nannofossils with foraminifers and siliceous microfossils present in trace amounts. Quartz and clay concentrations each comprise 0–5% of the sediment; feldspar and ash are present in abundances of less than 2%.

SEISMIC CORRELATIONS

High-resolution seismic reflection profiles (3.5 and 12 kHz) and about 100-Hz reflection profiles were recorded at Site 577. Both hull-mounted and near-bottom sound sources were utilized. The near-bottom transducer (3.5 and 5.25 kHz) was mounted on the drill string 253 m above the face of the drill bit.

The 3.5-kHz echograms over Site 577 reveal a four-part seismic section (Fig. 2, Table 3). Seismic Unit 1 extends to 0.032 s (23.8 m below seafloor, assuming a velocity of 1485 m/s) and consists of strong, multiple, parallel sub-bottom reflectors at 0.008 s (5.9 m, Reflector 1a), 0.011 s (7.9 m, Reflector 1b), 0.015 s (11.4 m, Reflector 1c), 0.019 s (14.4 m, Reflector 1d), and 0.023 s (16.8 m, Reflector 1e) below the seafloor. The strongest reflectors are 1b, 1c, and especially 1e; Reflectors 1a and 1d are somewhat intermittent. A relatively thin transparent layer separates Reflector 1e from the underlying seismic Unit 2. The source of these reflectors is unclear, but the interval thickness between Reflectors 1d and 1e (2.4 m) and the depth below seafloor of these reflectors (1d = 14.4 m, 1e = 16.8 m) are similar to those of the ash layers encountered in Core 2 of Holes 577 and 577A (577: 2.0 cm thickness, 13.5 and 15.5 m depth; 577A: 1.5 cm thickness, 13.5 and 15 m depth). The shallower depths recorded between the cored ashes and seafloor suggests that the HPC did not retrieve the uppermost 1 to 1.5 m of sediment.

Seismic Unit 2 is composed of two parallel reflectors of medium strength overlying a transparent section. The uppermost reflector (2a) occurs at 0.032 s (23.8 m) below seafloor; the lowest reflector (2b) occurs at 0.039 s (29.2 m) below seafloor. The source of these reflectors is unknown.

Seismic Unit 3 consists of a transparent section with its top defined by a weak, generally continuous reflector (Reflector 3a at 0.059 s, 43.5 m below seafloor assuming

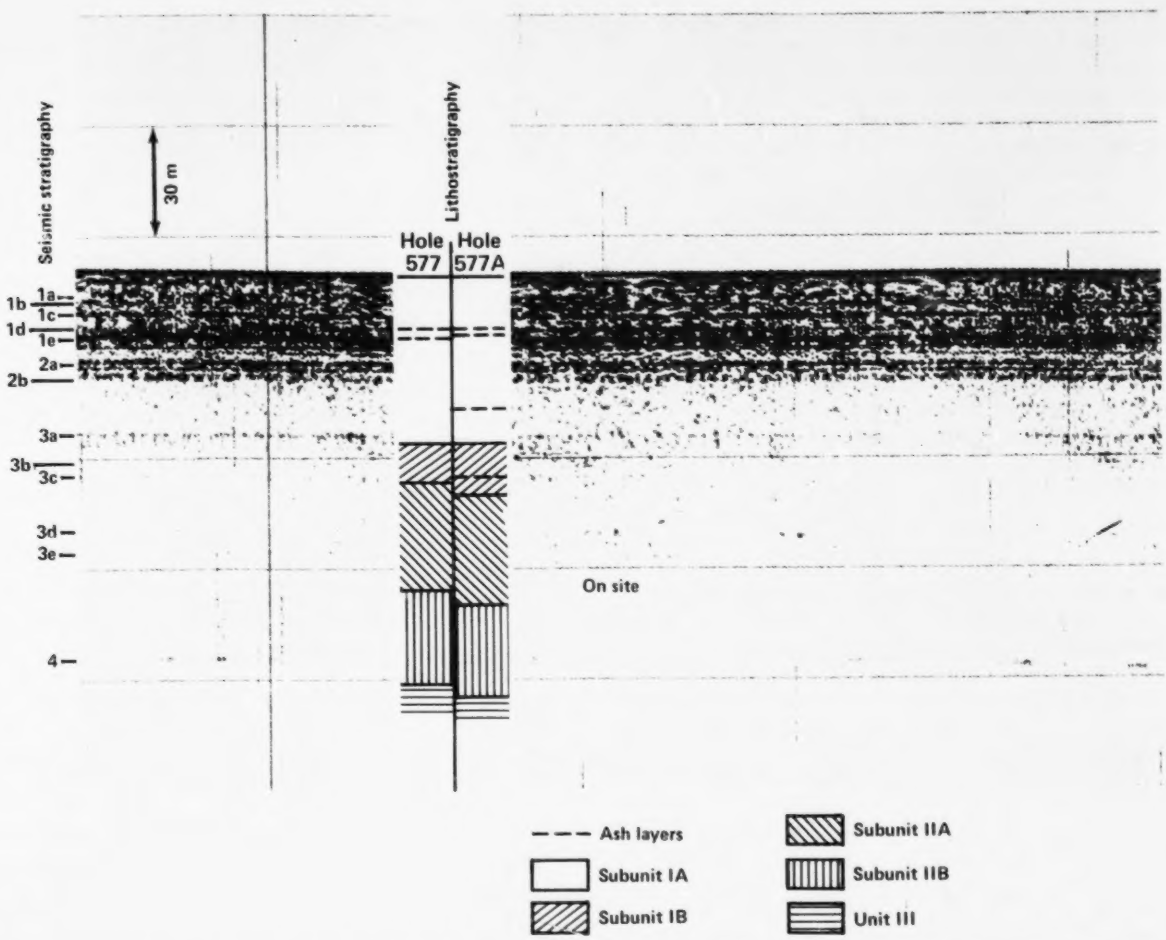

Figure 2. 3.5-kHz echogram over Site 577 showing the four-part seismic section described in the text. Sub-bottom depths to seismic reflectors are given in Table 3.

Table 3. 3.5-kHz seismic correlations, Site 577.

Reflector	Relative strength[a]	Sub-bottom depth (s)	Sub-bottom depth (m)[b]
1a	I	0.00795	5.9
1b	S	0.0106	7.9
1c	S	0.0153	11.4
1d	I	0.0194	14.4
1e	S	0.0226	16.8
2a	M	0.0320	23.8
2b	M	0.0393	29.2
3a	W	0.0587	43.5
3b	W, I	0.0694	51.4
3c	W, I	0.0733	54.3
3d	W, I	0.0932	69.3
3e	W, I	0.102	76.3
4	W-M, I	0.140	104.8

[a] I = intermittent, M = medium, S = strong, W = weak.

[b] Assuming 0–30 m = 1485 m/s, 30–60 m = 1475 m/s, 60+ m = 1520 m.

1475 m/s below 30 m depth). The transparent section is punctuated by weak, intermittent reflectors at 0.069 s (51.4 m, Reflector 3b), 0.073 s (54.3 m, Reflector 3c), 0.093 s (69.3 m, Reflector 3d), and 0.102 s (76.4 m, assuming a velocity of 1520 cm/s below 60 m, Reflector 3e). The generally transparent section between Reflectors 3a and 3e reflects the homogenous nature of the nannofossil oozes. The transparent intervals below Reflector 3e correlate with the uncored clay(?) section.

The sources for the sparse reflectors are unclear. An angular unconformity is observed on both the 3.5-kHz echograms and 100-Hz seismic reflection profiles on the ship's departure track between 0300Z and 0330Z (Figs. 3 and 4). This unconformity is observed around a seamount on top of the Shatsky Rise and on the margins of the top of the Rise. The unconformity separates parallel reflectors with relatively little local relief above the unconformity from parallel reflectors with relatively high local relief below the unconformity (e.g., Reflectors 3e and 4). The weak, intermittent reflector that marks the unconformity is about 8 m below Reflector 3a and probably is Reflector 3b/3c at Site 577. This unconformity is

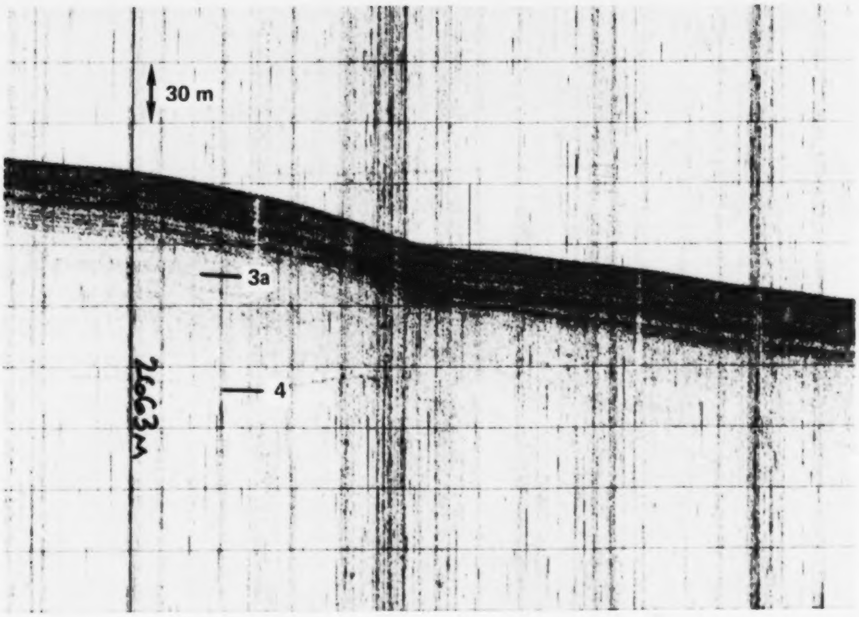

Figure 3. 3.5-kHz echogram collected on ship's departure track from Site 577 (0300Z to 0330Z on 25 May 1982) showing angular unconformity discussed in the text.

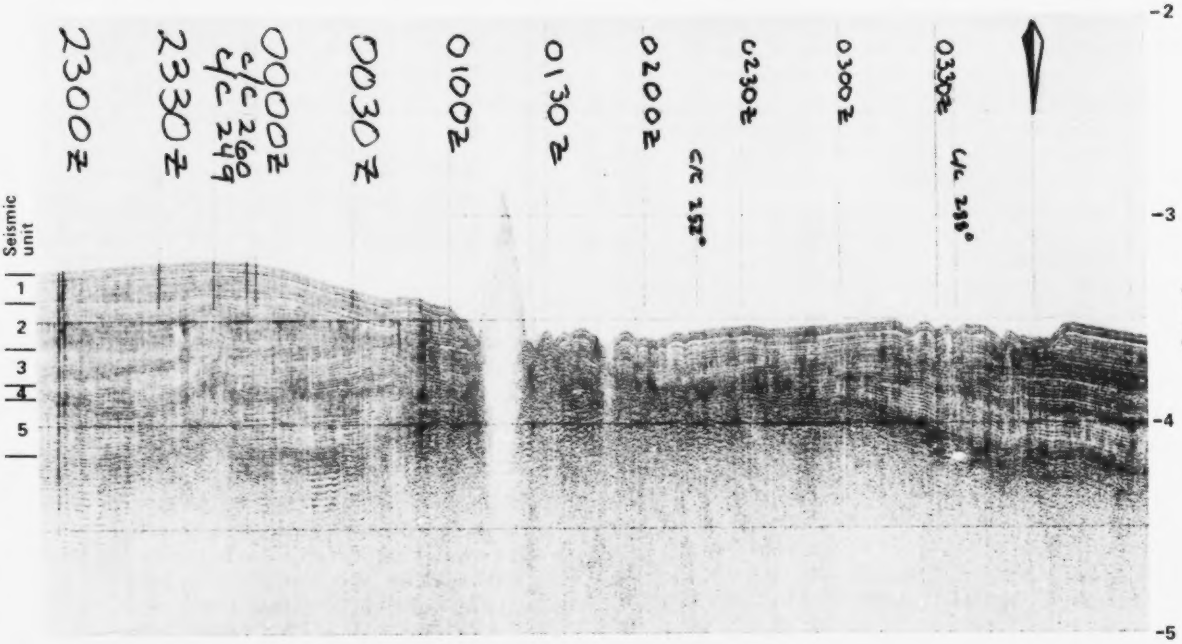

Figure 4. 100-Hz reflection profile near Site 577 showing the five-part seismic section described in the text.

the upper Miocene/middle Eocene unconformity observed in the upper part of Core 7 of Hole 577A. However, Reflectors 3b and 3c are 51.4 and 54.3 m below the seafloor, respectively, at Site 577, while the cored unconformity occurs at about 57.5 and 61 m below seafloor. This discrepancy suggests that (1) the assumed velocities deduced from shipboard velocity measurements are too low, or (2) the cores were actually retrieved from shallower depths. If Reflector 3c marks the unconformity, then Reflector 3a is probably the ash layer cored at about 53 m below seafloor in Hole 577A.

Reflector 4 of seismic Unit 4 is a weak, generally continuous reflector at 0.140 s (104.8 m) below the seafloor. Before coring, this reflector was thought to be a chert horizon, but its depth below seafloor is more consistent with the top of sedimentary Unit III at 111–114 m or the Cretaceous/Tertiary boundary at about 110 m. In either proposed correlation, velocities deduced from shipboard measurements appear to low. The doubt concerning the velocity structure and core depths does not allow a more precise correlation.

The 100-Hz seismic reflection profiles reveal a five-part seismic section (Fig. 4). The uppermost unit (Unit 1) in the seismic section is a packet of strong, parallel reflectors. On the relatively flat areas at the top of the Shatsky Rise, Unit 1 consists of conformable reflectors down to a relatively transparent zone at approximately 0.16 to 0.17 s (about 120 m) below seafloor. The interval thickness suggests that Unit 1 includes all the sediment above the Cretaceous chert layer. However, along the margins of the top of Shatsky Rise and near seamounts at the top, Unit 1 consists of two sections: an upper section of strong reflectors parallel to the seafloor and a lower section that has strong reflectors with dips divergent from those of the upper section. On both the site approach and departure tracks, it is clear that the upper section cuts downsection, thinning the lower section to a "0" isopach. This angular unconformity at about 0.085 s below seafloor is the upper Miocene/middle Eocene unconformity cored in Holes 577 and 577A. Because of the interference of the "bubble pulse," it is not possible to identify precisely the reflector that marks this unconformity.

Each of the succeeding three lower seismic units (Units 2, 3, and 4) consists of weak reflectors forming a relatively semitransparent zone that grades downward into strong parallel reflectors. At the maximum sediment thickness near Site 577, Unit 2 occurs from 0.17 to 0.38 s below seafloor, Unit 3 extends to about 0.52 s below seafloor, and Unit 4 extends to about 0.68 s below seafloor. Unit 5 consists of only a semitransparent section and extends to about 0.88 s below seafloor. The deepest reflector (the base of Unit 5) is probably basement. A minor unconformity is observed near seamounts on the Shatsky Rise where Unit 2 crosscuts Unit 3 and possibly Unit 4.

BIOSTRATIGRAPHY

A total thickness of 251.7 m of nannofossil ooze was recovered from three holes at Site 577. The sediment is rich in calcareous microfossils throughout and provides a high-resolution biostratigraphy (Fig. 5).

A late Miocene through Quaternary sequence was recovered down to Section 577A-7-3. There is a major hiatus at approximately 61 m representing the late Eocene, the Oligocene, and the early and middle Miocene. Below this, a Late Cretaceous through middle Eocene sequence was recovered. Foraminifers and nannofossils indicate two minor hiatuses in the Paleogene. The Cretaceous/Tertiary boundary was recovered intact in Sections 577-12-5, 577A-12-4, and 577B-1-4.

Preservation and Abundance

Radiolarians are abundant and moderately to well preserved through Core 577A-6, below which the samples are barren. Diatoms are rare to few and their preservation is poor to moderate through Cores 577-5 and 577A-5, below which the samples are barren. In general, calcareous nannofossils are common to abundant and moderately to well-preserved throughout. Near the Cretaceous/Tertiary boundary, nannofossils are abundant but preservation is poor to moderate. Nannofossils in Cores 577-5 through 577-8 also show poor to moderate preservation. Foraminifers are abundant throughout. In the upper Tertiary intervals, effects of dissolution are light to moderate and moderate test breakage is common. In the middle Eocene interval (Cores 577-7 and 577A-7), test breakage is heavy, the samples are flooded with fragments, but dissolution effects on the survivors are light. The assemblage is limited to the subspherical forms *Globigerinatheca index index* and *G. barri*, which make their outlines more spherical and abrasion resistant by adding bullae over their sutural apertures. The Paleocene and Upper Cretaceous samples contain moderately to well-preserved foraminiferal faunas.

Stratigraphic Record and Hiatuses

The biostratigraphic record is summarized in Figure 5. An upper Miocene to lower Pleistocene sequence was defined by all four fossil groups. Calcareous nannofossils and foraminifers define an Upper Cretaceous through middle Eocene sequence. There is a lengthy middle Tertiary hiatus between Cores 577-6, -7 and 577A-6 and -7. Cores 577-7 and 577A-7 contain middle Eocene sediments which were not reported at nearby Site 47. Calcareous nannofossils suggest additional hiatuses in the middle Eocene and the middle Paleocene. The foraminifers also suggest the possibility of an earliest Eocene–latest Paleocene hiatus and a hiatus in the middle Paleocene.

Three core sections (577-12-5, 577A-12-4, and 577B-1-4) contain an undisturbed Cretaceous/Tertiary boundary. There is no significant lithologic change at the boundary. The most distinctive feature is a color change from white below the boundary to pale brown above. Mottling attributed to bioturbation is visible in the pale brown earliest Paleocene ooze.

Calcareous Nannofossils

The stratigraphic sequence of this site ranges from Quaternary to Late Cretaceous (Maestrichtian). The calcareous nannofossil assemblages are abundant and diversified. Their preservation ranges from poor to moderate. Calcareous nannofossils are significantly overgrown near the Cretaceous/Tertiary boundary and in the lower-middle Eocene. A significant hiatus is noted from the late Eocene to the late Miocene.

Diverse and well-preserved Pleistocene nannofossil assemblages were found in Core 577-1 through Section 577-3-4, and in Core 577A-1 through Section 577A-3-2. They represent the *Emiliania huxleyi* (CN15), *Gephyrocapsa oceanica* (CN14), and *Crenalithus doronicoides* (CN13) Zones (Bukry, 1973, 1975; Okada and Bukry, 1980). Abundant and generally well preserved Pliocene nannofossil assemblages occur between Samples 577-3-5, 44 cm and 577-5-4, 60 cm and between Samples 577A-3-3, 60 cm and 577A-5-5, 15 cm. All the subzones of the *Dis-*

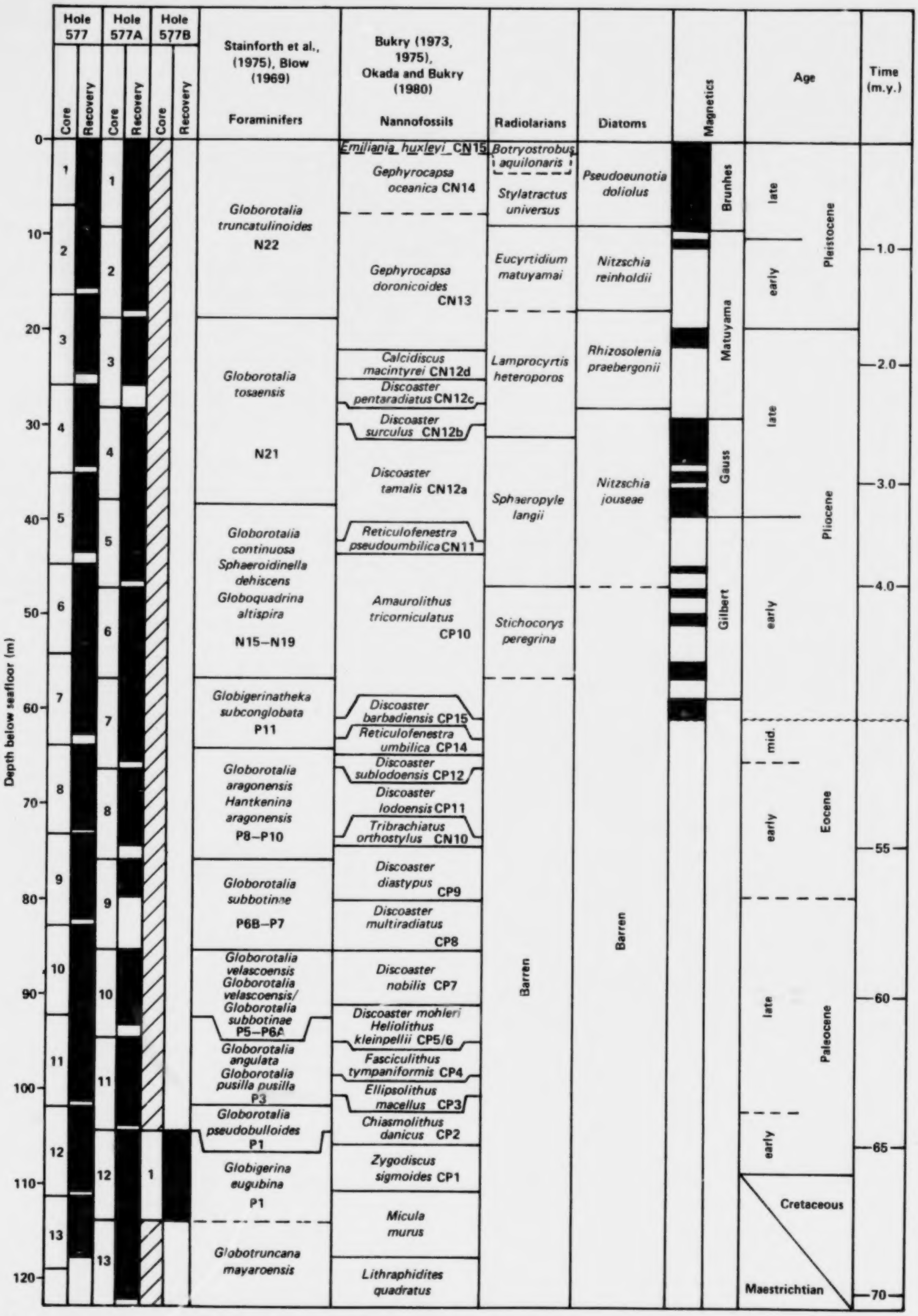

Figure 5. Site 577 biostratigraphic and magnetostratigraphic summary.

coaster brouweri Zone (CN12) are recognized. In Cores 577-5, -6 and 577A-5, -6 a moderately well preserved assemblage belongs to the *Amaurolithus tricorniculatus* (CN10) Zone. The absence of *Triquetrorhabdulus rugosus* indicates that the lower part of the *A. tricorniculatus* Zone is missing. An important hiatus is found in Cores 577-7 and 577A-7 separating assemblages of the *A. primus* (CN9b) Subzone from the *D. barbadiensis* (CP15) Zone. Most of the lower Eocene and Paleocene zonal markers were found with these exceptions: *Tribrachiatus contortus* was not found and *D. mohleri* and *Heliolithus kleinpellii* have the lowest occurrence in the same samples.

The Cretaceous/Tertiary boundary is located in Samples 577-12-5, 130 cm, 577A-12-4, 72 cm, and 577B-1-4, 72 cm. The boundary is recognized by the appearance of common *Thorascosphaera* and *Biscutum* sp. The oldest assemblage recovered from Hole 577 is moderately well preserved and belongs to the *Micula murus* Zone of latest Maestrichtian age. Holes 577A and 577B extend just below the appearance level of *M. murus*.

Planktonic Foraminifers

Abundant foraminifers were recovered from all cores taken at Site 577. Preliminary examination of core-catcher samples has revealed an upper Miocene–Pliocene–lower Pleistocene sequence, a long hiatus in the middle Tertiary and an Upper Cretaceous through middle Eocene sequence. Preliminary zonations are shown in Figure 5.

Samples 577-1,CC and -2,CC and 577A-1,CC and -2,CC contain an abundant early Pleistocene fauna typical of the *Globorotalia truncatulinoides* Zone (Stainforth et al., 1975) or N22 (Blow, 1969). Representative taxa include: *Globorotalia acostaensis, G. hirsuta, G. humerosa, G. inflata, G. menardii* (ex. gr., sinistral), *G. ronda, G. tosaensis, G. triangula, Globigerina dutertrei*, and *Globigerinoides conglobatus*. Core catchers from 577-3, -4 and 577A-3, -4 contain an upper Pliocene fauna of the *G. tosaensis* Zone (N21). This diverse fauna includes: *Globorotalia praehirsuta, G. menardii* (ex. gr., dextral), *G. crassaformis, Globigerina venezuelana, Globigerinoides conglobatus*, and many of the long-ranging taxa found in Zone N22. Samples 577-5,CC, -6,CC, 577A-5,CC, and -6,CC contain a mixed assemblage that spans the upper Miocene and lower Pliocene *Globorotalia continuosa* Zone to *G. margaritae* Zone or N15–N19. The assemblage includes: *G. acostaensis, G. humerosa, G. obesa, G. multicamerata, G. tosaensis, G. margaritae, G. scitula, Globigerinoides obliquus, G. quadrilobatus trilobus*, and *G. sacculifer*. Sample 577-7,CC contains a middle Eocene fauna of the *Globigerinatheka subconglobata* Zone (P11). The fauna is composed entirely of *G. barri* and *G. index index*. A fauna found in Samples 577-8,CC -9,CC and 577A-7,CC and -8,CC characterizes the *Globorotalia aragonensis* Zone to the *Hantkenina aragonensis* Zone (P8–P10). Taxa comprising this fauna include: *Globigerina primitiva, G. soldadoensis soldadoensis, G. soldadoensis angulosa, Globorotalia pseudotopilensis, G. wilcoxensis, G. subbotinae, G. formosa formosa, G. formosa gracilis*, and *G. aragonensis*. Sample 577A-9,CC contains taxa characteristic of the earliest Eocene, *G. subbotinae* Zone or P6B. This fauna is similar to the younger P7 fauna, but excludes *G. soldadoensis angulosa* and includes *G. velascoensis*.

The upper Paleocene is identified in Sample 577-10,CC by the combined *Globorotalia velascoensis* Zone and *G. velascoensis/G. subbotinae* Zone or P5 to P6A. The characteristic taxa are *Globorotalia subbotinae, G. aequa, G. pusilla pusilla, G. velascoensis, G. angulata*, and *Globigerina mckannai*. Samples 577A-10,CC and 577-11,CC represent the middle Paleocene. They contain species found in the *Globorotalia angulata* Zone through *G. pusilla pusilla* Zone or P3. These are *G. aequa, G. pusilla pusilla, G. angulata, G. occlusa, G. pseudobulloides, G. compressa, Globigerina mckannai, G. nitida, G. triloculinoides*, and *G. velascoensis*. The *Globorotalia pseudobulloides* Zone or the middle portion of P1 was recognized in Sample 577A-11,CC. The earliest Paleocene, *Globigerina eugubina* Zone (P1) was identified in Samples 577-12,CC and 577A-12,CC. This fauna is typified by *Globorotalia pseudobulloides, Globigerina eugubina, G. sabina, G. trinidadensis*, and *Chiloguembelina taurica*. The next sample downhole is problematic and will require further detailed study because of proximity to the Cretaceous/Tertiary boundary. Sample 577A-12,CC contains *G. eugubina* and *G. sabina* and other primitive globigerinids in roughly equal abundance with many Cretaceous taxa. The samples are below the boundary (Samples 577-12-5, 130 cm and 577A-12-4, 72 cm) as identified by nannofossils, the extinction of Cretaceous forms, and a change in maximum diameter of *G. eugubina*. We hope that close-spaced sampling in Core 12 will explain this occurrence. Samples 577-13,CC and 577A-13,CC contain a distinctive Upper Cretaceous fauna of the *Globotruncana mayaroensis* Zone including: *Globotruncana mayaroensis, G. stuarti, G. contusa, Globotruncanella petaloides, Rugoglobigerina rotundata, R. rugosa, Pseudotextularia varians*, and *P. carseyae*.

Radiolarians

Holes 577 and 577A contain abundant radiolarians from the top of Sections 1-1 through 6,CC. Radiolaria are not found in Sections 7-4 through 13,CC. The results of the preliminary biostratigraphic survey of the sediments recovered at Site 577 are summarized in Figure 5.

The species in the uppermost samples from Holes 577 and 577A are representative of the *Botryostrobus aquilonaris* Zone (Hays, 1970), indicating that sediment younger than 400,000 yrs. was recovered at this site. The sediment sequence from the lower half of Cores 577-1 and 577A-1 is assigned to the *Stylatractus universus* Zone (Hays, 1970) based on the presence of *S. universus* and *Druppatractus acquilonius* and the absence of *Eucyrtidium matuyamai*. Based on the presence of the radiolarian species *E. matuyamai*, the *E. matuyamai* Zone (Hays, 1970; Foreman, 1973) extends from Core 2 through the upper half of Core 3. This zone was somewhat difficult to define since the southern limit of *E. matuyamai's* habitat nearly coincides with this site's position. The absence of *E. matuyamai* and *Stichocorys peregrina* from the lower half of Core 577-3 through the upper half of

Core 577-4 indicates that this sequence belongs to the *Lamprocyrtis heteroporos* Zone (Hays, 1970; Foreman, 1975). The top of the *Sphaeropyle langii* Zone (Foreman, 1975), based on the presence of *Stichocorys peregrina*, is located in a core-catcher sample of Core 577-4 and in Section 577A-4-5. The fauna in Core 577-5 and 577A-5 is representative of the *Sphaeropyle langii* Zone. The oldest radiolarian-bearing sediment at this site belongs to the *Stichocorys peregrina* Zone (Riedel and Sanfilippo, 1970; Foreman, 1975) and is confined to Cores 577-6 and 577-A-6.

Diatoms

Cores 577-1 through 577-6 contain few to rare diatoms with moderate preservation, but diatoms are absent below Core 7. Core 1 belongs to the *Pseudoeunotia doliolus* Zone. Core 2 is placed in the *Nitzschia reinholdii* Zone by the presence of *N. reinholdii*. Core 3 is correlated with the *Rhizosolenia praebergonii* Zone by the presence of *R. praebergonii* and the absence of *P. doliolus*. Cores 4 and 5 correlate with the middle Pliocene *N. jouseae* Zone, which ranges from the lower part of the Gauss Epoch to the Sidufjall Event of the Gilbert Epoch, by the presence of *N. jouseae* and *Thalassiosira convexa*, and the absence of *R. praebergonii* (Burckle and Opdyke, 1977; Burckle, 1978).

Diatoms are few to rare and preservation is moderate above Core 577A-6. Core 1 belongs to the *P. doliolus* Zone, Core 2 to the *N. reinholdii* Zone, and Core 3 to the *R. praebergonii* Zone. Cores 4 and 5 belong to the *N. jouseae* Zone. In Core 6, no age-diagnostic species were found.

Diatoms are completely absent from Core 577B-1.

PALEOMAGNETICS

Paleomagnetic analyses were performed on 475 samples from the sedimentary sequences recovered in Holes 577 and 577A at this site. The details of this study are given in a separate chapter (see Bleil, this volume).

The intensity of the natural remanent magnetization (NRM) in both holes decreases systematically from about 1.5×10^{-5} Gauss near the top to about 1×10^{-6} Gauss in the lower parts. The variability of the NRM intensities, both between and within cores, is less at this site than at the more northern sites drilled during Leg 86. The magnetic stability displays just the opposite characteristic. In the upper 60 m of both holes median destructive field (MDF) determinations yielded extremely variable results, with an average high level of about 400 Oe. At greater depths, consistently lower MDF values, mostly in the range of about 200 Oe, were observed. Over several zones, MDF values of less than 100 Oe indicate poor magnetic stability.

Alternating field (AF) demagnetization resulted in large changes in magnetization directions not only for the majority of samples from lower parts of both holes, but also for many samples from the upper 60 m. The relatively large scatter in directional data likely indicates that the stable directions defined are not always true primary single component magnetizations, but also include some secondary components that could not be erased completely by AF demagnetization.

The downhole pattern of stable magnetization directions at a number of levels is further complicated by large amounts of physical disturbances introduced during the coring operation. All samples from below about 60 m sub-bottom in both holes show clear evidence of a strong artificial magnetic overprinting. A discussion of the complex results from these sections is given elsewhere (see Bleil, this volume).

In the upper part of the cored sections, the downhole sequence of stable magnetization directions yields an unequivocal reversal stratigraphy for the last 5.5 m.y. that includes all major reversals of the Earth's magnetic field since the beginning of the Gilbert Epoch (Fig. 5). However, because of the limited recovery or badly disturbed sediment in some cores of both holes, exact sub-bottom depths are difficult to define for a number of the reversals. For the same reason, some short polarity events (such as the Jaramillo in Hole 577A and the Cochiti in Hole 577A) are missing in one hole but could be recognized in the other. A comparison of the depth data for several well-defined reversals in both holes reveals variable degrees of mutual offsets amounting to at least ± 1 m downhole.

Down to about 60 m sub-bottom, the inclination data scatter around the axial dipole value for the present latitude of the site (51.8°). A hiatus of about 35 m.y. is revealed by the biostratigraphy at this level. Below the hiatus, the range of stable inclinations abruptly changes to about 20–30°. a reflection of the northward motion of the Pacific Plate. Using the most recent polarity time scale of Berggren et al. (in press) the sedimentary column above the hiatus accumulated at a remarkably average rate of about 11 m/m.y.

SEDIMENT ACCUMULATION RATES

The average sediment accumulation rate through the Neogene portion of Holes 577 and 577A was 11.6 m/m.y. The rate in the Paleogene portion averaged 3.0 m/m.y. This is in stark contrast to the rate of accumulation in the Late Cretaceous, which was 10.0 m/m.y. An age versus depth plot is given in Figure 6. Age determinations are based on nannofossil correlations calibrated according to Berggren et al. (in press) below the hiatus at a sub-bottom depth of 60 m. Age determinations for the first 5 m.y. are based on magnetostratigraphy according to Berggren et al. (in press).

PHYSICAL PROPERTIES

Physical properties measurements at Site 577 were performed using mainly standard Deep Sea Drilling Project (DSDP) methods (Boyce, 1976a, b; see Introduction and Explanatory Notes, this volume). Table 4 summarizes the properties that were measured in sediments from Holes 577 and 577A. Measurements were taken at approximately 3-m intervals throughout Hole 577. Measurements were taken at approximately 4.5-m intervals in Hole 577A. Figures 7, 8, and 9 show profiles for Holes 577 and 577A of shear strength, compressional and shear wave veloci-

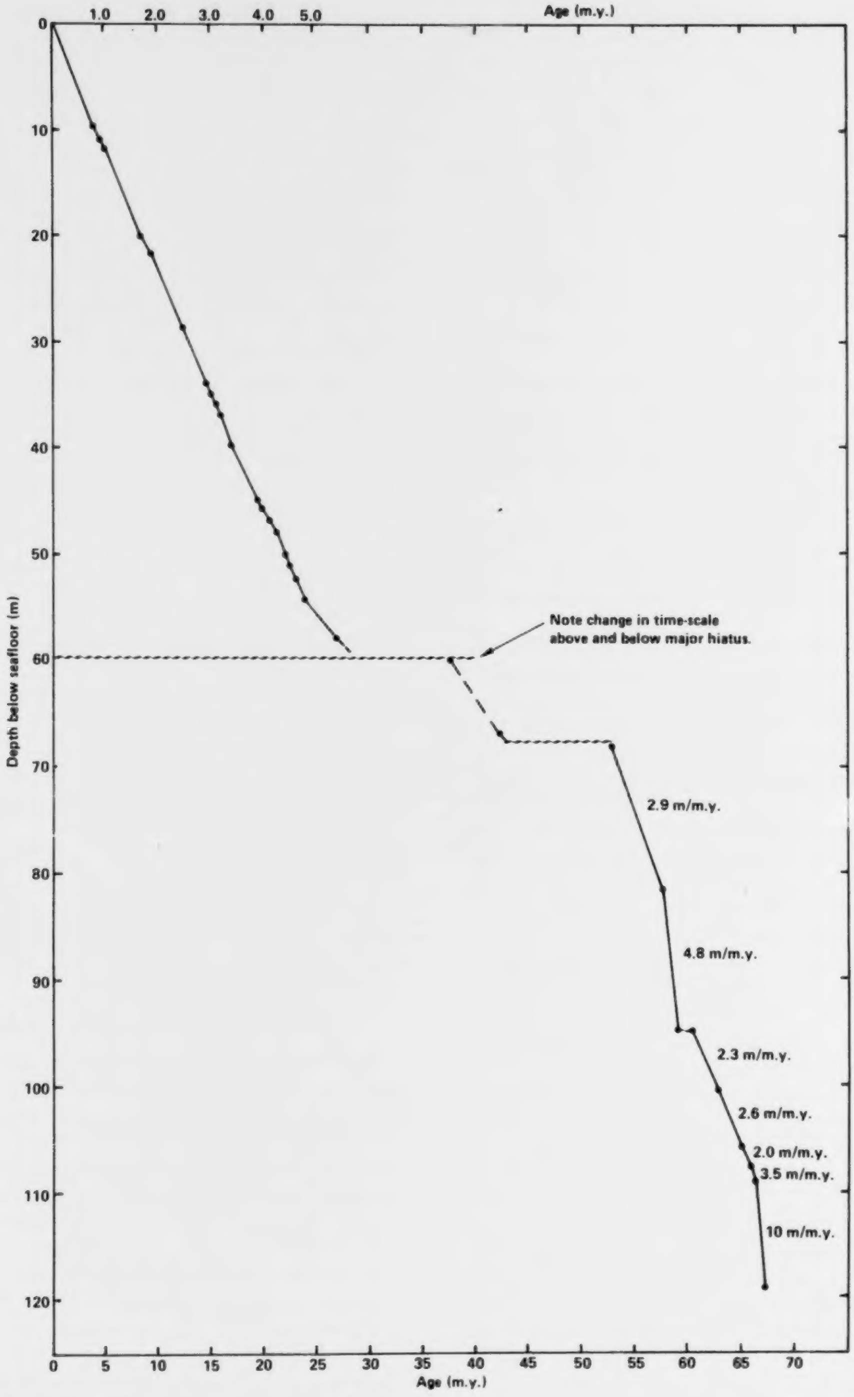

Figure 6. Site 577 sediment accumulation rates.

ty, and saturated bulk density and water content, respectively. A full discussion of the physical properties of the recovered sediment, including tables of the data, is given by Schultheiss (this volume). However, some of the more interesting features of the data are highlighted here.

1. There are wide variations in the shear strength measurements down to 50 m, below which there is a rapid decrease in strength which remains consistently low (Fig. 7). The reduction in shear strength correlates with the boundary of lithologic Units I and II, and is thought to occur

Table 4. Physical properties measurements made at Site 577.

	Hole 577	Hole 577A
Shear strength:		
Hand-operated vane	x	x
Motorized vane	x	x
Wave velocity:		
Shear wave	x	x
Compressional wave	x	x
Water content/bulk density:		
Shipboard analysis	x	—
Shore-based analysis	x	x
Bulk density by 2-min. GRAPE	x	—

as a result of the changing carbonate content (Fig. 1). It is postulated that, at carbonate contents in excess of 90 to 95%, the sediment strength is drastically reduced by the coring process (the interparticulate bonding may be more brittle).

2. The shear wave velocity data show no distinct trends throughout the two holes, the velocity varies between 20 and 70 m/s (Fig. 8). Poor signal quality in most of these cores limits the accuracy of these measurements to ± 10 m/s.

3. A sudden increase in bulk density (and decrease in water content) at about 60 m is the major feature that occurs just below the lithologic boundary between Units I and II (Fig. 9). This corresponds to a possible 30-m.y. missing section in the mid-Tertiary (see Biostratigraphic summary), which at sedimentation rates of 3.0 m/m.y. would represent 90 m of missing sediment. The rapid change in water content suggests that this may have been an erosional event because the material may be overconsolidated. Laboratory consolidation data from Hole 577A may be able to indicate whether this was a nondepositional or an erosional hiatus.

4. The compressional wave velocity profile (Fig. 8) also shows a major discontinuity at 60 m. The velocity increases rapidly from around 1480 to 1530 m/s. The corresponding impedance changes using bulk density values of 1590 and 1720 kg/m^3, respectively, are 2.35×10^6 and 2.63×10^6 kg $m^{-2}S^{-1}$ (a change of more than 10%). However, this depth does not correspond to any distinct reflector on the 3.5-kHz seismic record.

INORGANIC GEOCHEMISTRY

Six squeezed core samples, three from Hole 577 and three from 577A, were analyzed for the standard suite of components: pH, alkalinity, salinity, calcium, magnesium, and chlorinity (Table 5). The two data sets agree well (Fig. 10) and show a slight downcore increase in alkalinity and an overall drop in Mg, but otherwise little variation with depth.

No *in situ* samples were taken.

HEAT FLOW

Downhole temperature measurements were made with the new WHOI heat flow instrument. Of 15 runs (6 in Hole 577 and 9 in Hole 577A), 10 (4 in Hole 577 and 6 in Hole 577A) were successful. Of the unsuccessful runs, the cause of failure could be more specifically diagnosed than for the previous runs at Site 576. For example, the first run at this site appeared to fail because of a loose interface connection in the shipboard Apple computer that was used for loading the program into, and recovering data from, the heat flow instrument's temperature recorder. The recorder was designed to be capable of delaying the starting time of data collection by an amount specified by the program. It appeared, however, that the delay time circuit of all the recorders was not functioning properly. Recorder WHOI-4A connected to battery pack NTLT-3, which had functioned correctly on nine previous deployments, failed on its fifth run at this site when the delay time was set to 30 min., as well as on the eleventh run at Site 576, when the delay time also had been set to a nonzero value (60 min.). A check of the log book revealed that all successful runs at Sites 576 and 577 were made with zero delay times. Use of a nonzero delay time always resulted in failure or an unsatisfactory record. All measurements in subsequent sites of this cruise were made by setting the delay time equal to zero. It was also found that measurement results from recorder WHOI-2A were not satisfactory.

For the first time during this cruise, the new WHOI heat flow instrument was compared with the conventional ERI-type heat flow instrument. In Hole 577A, a combined run was made by attaching the shoe containing the WHOI instrument to the ERI-type heat flow rig. Unfortunately, only one out of three such runs was successful. The result of that successful run showed, however, that the ERI-type instrument recorded a temperature 3.5°C higher than the WHOI instrument. The difference appears to be too large to be accounted for by the measurement error at a single downhole depth. A detailed comparison of the two measurements is in progress at the time of this writing.

Thermal conductivity data were taken on 240 samples selected from the cores of Holes 577 and 577A (see Horai and Von Herzen, this volume).

SUMMARY AND CONCLUSIONS

Site 577 is located at 32°26.51′N and 157°43.40′E in 2678 m of water on the flank of the Shatsky Rise. Over this part of the Rise sediments reach a thickness of 0.88 s.

The objective at this site—to obtain an expanded late Miocene to Quaternary record for detailed paleoceanographic and isotopic analyses, to determine the late Cenozoic history of eolian sedimentation, and to recover the Cretaceous/Tertiary boundary for mid-latitude calcareous biostratigraphy and for paleomagnetic and geochemical analysis—was achieved in two holes. In an additional hole (577B), we washed down to basal Paleocene sediments and took one core to recover a third Cretaceous/Tertiary boundary sequence. Hole 577 (HPC) penetrated to a maximum depth of 118.8 m sub-bottom depth and terminated in a hard layer.

The sediments recovered in Holes 577, 577A, and 577B are nannofossil oozes that can be divided into three units based upon color changes. Lithologic Unit I is a white to light gray nannofossil ooze characterized by high percentages of nannofossils. It is further divided into two subunits: an alternating white to light gray lightly mot-

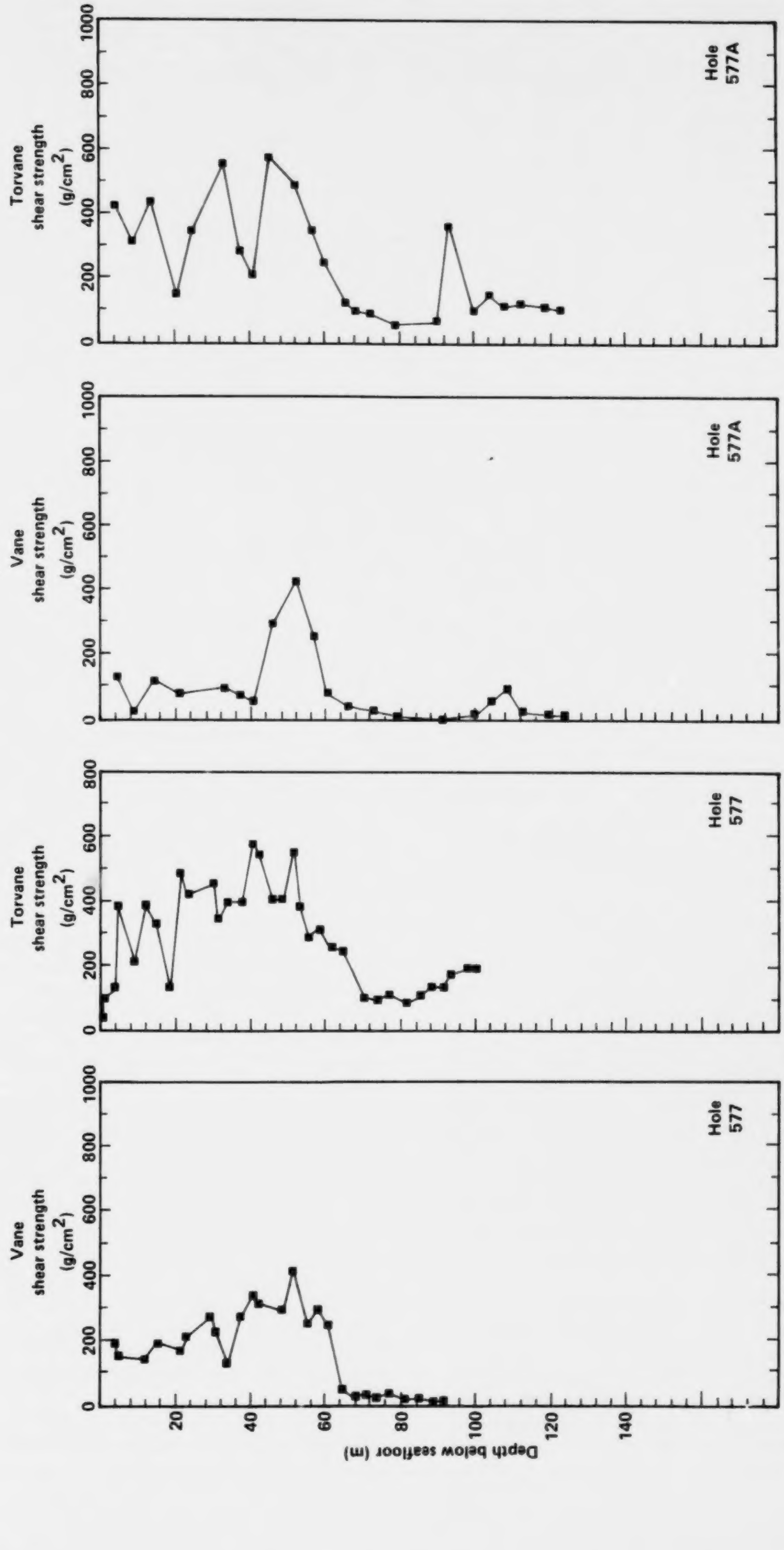

Figure 7. Plot of shear strength versus sub-bottom depth for Site 577.

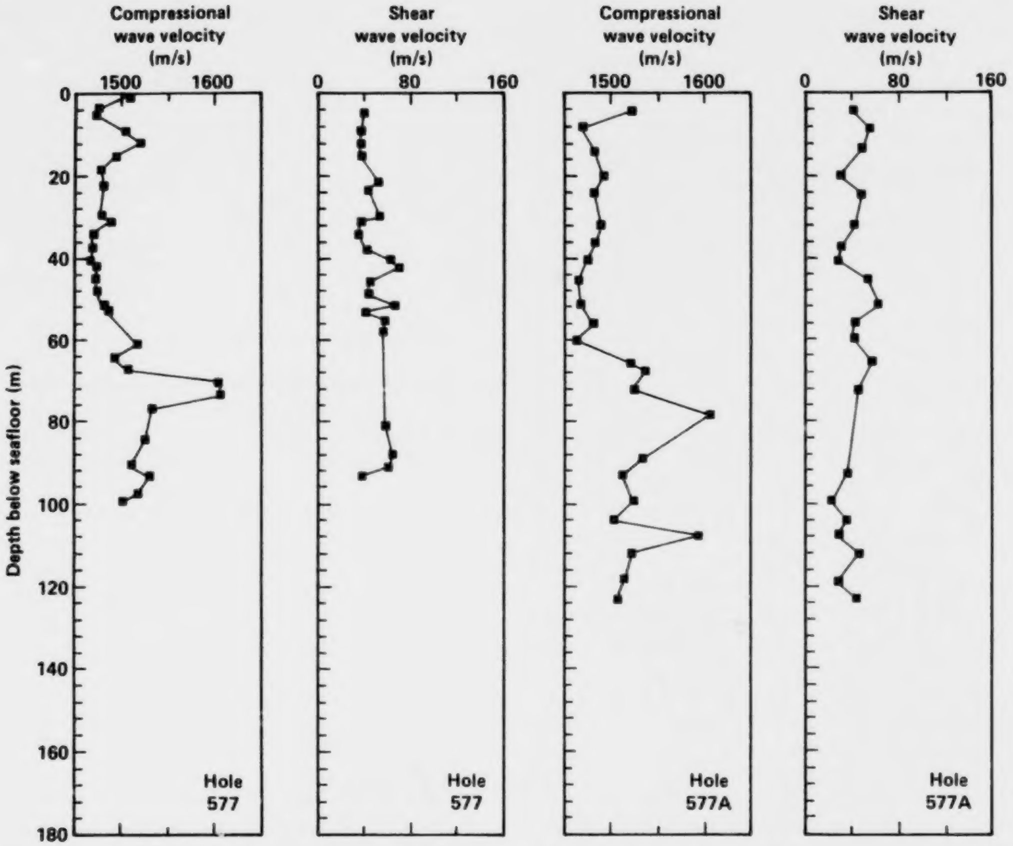

Figure 8. Plot of compressional and shear wave velocities versus sub-bottom depth for Site 577.

tled nannofossil ooze (Subunit IA) and a white nannofossil ooze (Subunit IB) that contains up to 97% calcareous nannofossils.

Lithologic Unit II is a white to pale brown nannofossil ooze that is divided into two subunits: Subunits IIA is a pale brown nannofossil ooze; Subunit IIB is characterized by alternating white and pale brown nannofossil ooze layers and contains the Cretaceous/Tertiary boundary. Lithologic Unit III is a white nannofossil ooze unit.

An apparently complete Miocene to Quaternary section was recovered in Holes 577 and 577A. Late Cenozoic sediments are primarily nannofossil ooze, but foraminifers are also present. Well-preserved and diverse radiolarian assemblages occur in the late Cenozoic sediments but tend to drop off, both in abundance and in degree of preservation, in the latest Miocene. Diatoms are present in Pliocene-Pleistocene sediments but are never abundant or well preserved. They are essentially absent below the Pliocene

A major unconformity at approximately 60 m sub-bottom depth separates late Miocene from middle Eocene sediments. This unconformity was previously reported in Site 47 and was expected. Paleogene sediments are also nannofossil oozes with minor (but diverse and moderately well preserved) foraminifers. No diatoms or radiolarians were found from this part of the section. Part of this Paleogene section was disturbed, mostly by flow-in and/or disturbed bedding. This disturbance was likely due to a number of factors: (1) the absence or near absence of clay in this part of the section resulting in a less cohesive lithology, and (2) premature yielding of the HPC shear pins causing reduced penetration rates and, thus, increased disturbance. The increased disturbance in the Paleogene section means that one of our objectives—to recover an expanded Paleogene section for paleoenvironment analysis—was not entirely met. This, however, can be more properly assessed by shore-based studies.

The Cretaceous/Tertiary boundary was recovered in Sections 577-12-5; 577A-12-4, and 577B-1-4 and at a sub-bottom depth of approximately 109.6 m. Lithologically, the basal Paleocene-Upper Cretaceous sequence is an undisturbed white to light brown nannofossil ooze. Moderate to well-preserved foraminifers are present, but diatoms and radiolarians are absent. Except for a minor color change just below it, the Cretaceous/Tertiary boundary is essentially featureless with no obvious signs of sediment disruption or nondeposition. The biostratigraphic data yield sedimentation rates of 11.6 m/m.y. (for the Neogene), 3 m/m.y. (for the Paleogene), and 10 m/m.y. (for the Cretaceous).

Physical properties were measured on the entire section (Quaternary to Cretaceous). However, some sections were skipped because obvious coring disturbance and/

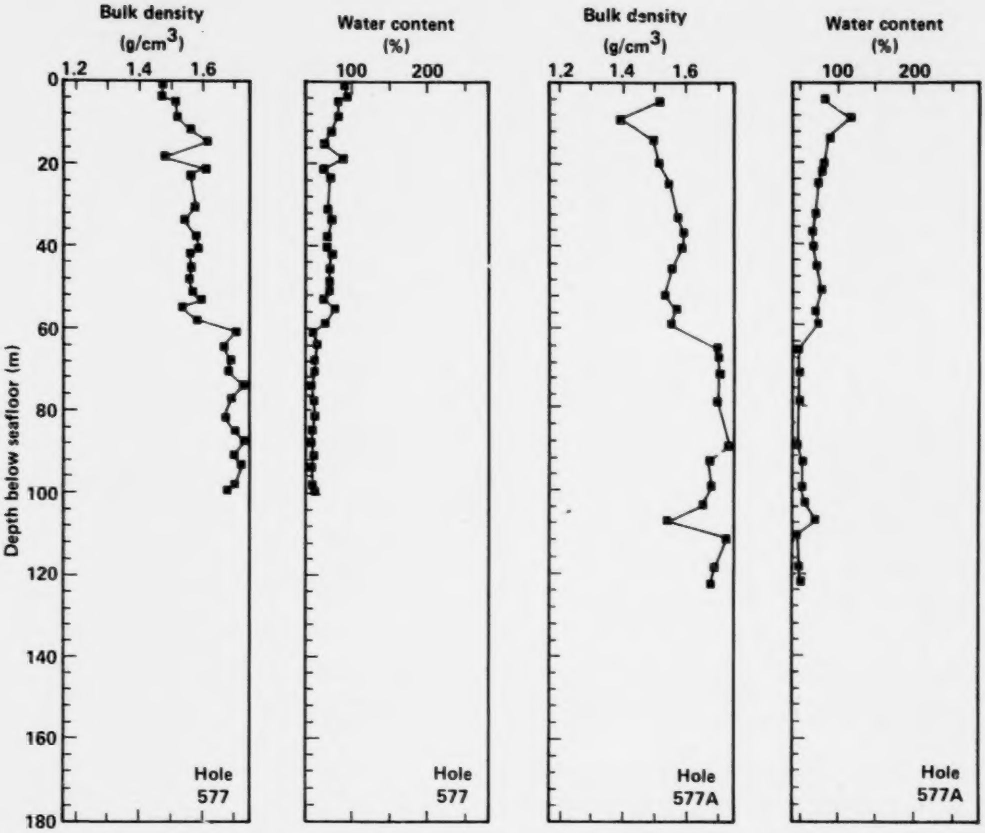

Figure 9. Profiles of saturated bulk density and water content versus sub-bottom depth for Site 577.

Table 5. Inorganic geochemical measurements from Site 577.

Sample	pH	Alkalinity (mEq/l)	Salinity (‰)	Calcium (m*M*)	Magnesium (m*M*)	Chlorinity (‰)
IAPSO	8.00	2.45	35.2	10.55	53.99	19.38
SSW	8.08	2.37	35.2	10.34	52.98	19.14
577-2-5, 140–150 cm	7.39	2.64	35.2	10.32	51.16	19.51
577-6-4, 140–150 cm	7.31	2.89	35.5	10.51	51.95	19.58
577-10-5, 140–150 cm	7.42	3.17	35.5	11.14	51.99	19.44
577A-4-5, 140–150 cm	7.35	2.60	35.2	9.88	52.09	19.54
577A-8-5, 140–150 cm	7.16	3.27	35.5	10.78	52.35	19.48
577A-13-5, 140–150 cm	7.29	3.15	35.5	10.57	52.32	19.38

or excess water at these levels made measurements unreliable. Shear strength, water content, bulk density, and compressional wave velocity data all show a major discontinuity at about 60 m sub-bottom depth. This is the approximate boundary between lithologic Units I and II and represents a major unconformity in which late Eocene to early Miocene sediments are missing. Bulk density data suggest that, given the measured 3.9 m/m.y. sedimentation rate for this hole, this unconformity may represent as much as 156 m of missing sediments. Further studies on shore (laboratory consolidations tests) may be useful in indicating whether this is an erosional or a nondepositional hiatus.

The 3.5-kHz echograms reveal a four-part seismic section. The uppermost unit consists of strong, multiple, parallel reflections that are tentatively correlated with volcanic ash layers. The second unit is composed of three parallel reflectors of medium strength which overlie a transparent section. The source of these reflectors is not immediately obvious from the lithology. The third seismic unit is a transparent section with its top defined by a weak, although generally continuous, reflector. Within this unit are several weak, discontinuous reflectors. The source of these weaker reflectors is unclear, but the transparent section reflects the homogeneous nature of the nannofossil ooze. The lowermost unit and its source lithology is uncertain. Because of uncertainty concerning velocity structure and core depth, this reflector may be a chert layer or may be within the sediment sequence.

Downhole temperature measurements were made with the new WHOI heat flow instrument. Of 15 runs, 10 were successful. The data show a linear increase with depth to the level of the Eocene/Miocene unconformity. Below the unconformity, the data indicate a temperature reversal.

Samples for paleomagnetic studies were taken throughout Holes 577 and 577A, with particularly dense sampling across the Cretaceous/Tertiary boundary. Because magnetic intensities were usually close to or within the noise level of the shipboard instrument, no attempt was made to identify specific magnetic reversals below the

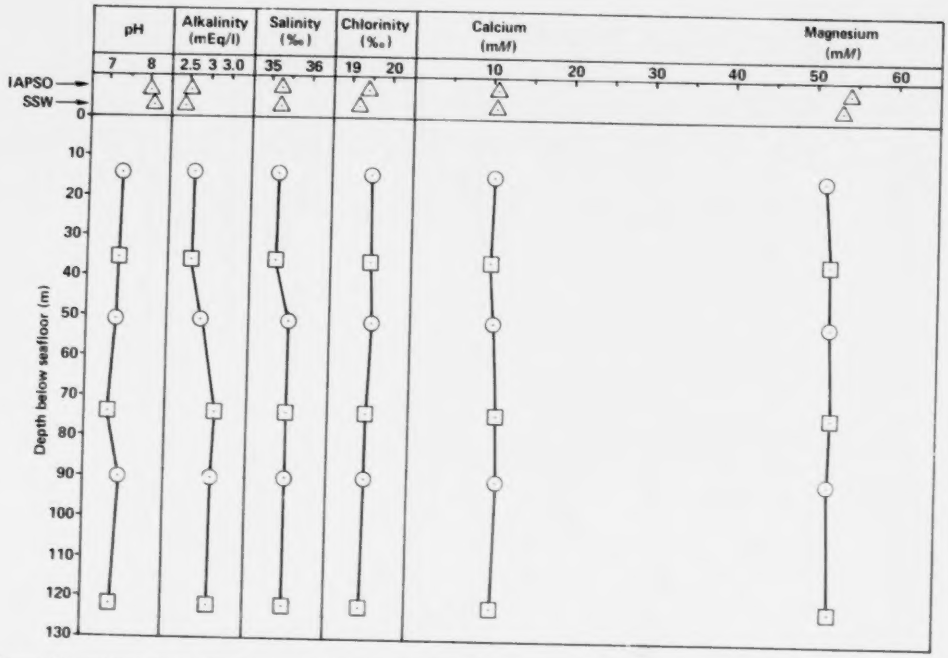

Figure 10. Profiles of pH, alkalinity, salinity (‰), chlorinity (‰), calcium (m*M*), and magnesium (m*M*), versus subbottom depth from interstitial water samples analyzed at Site 577. Symbols are as follows: △ = IAPSO and SSW standards; ⊙ = samples from Hole 577; ⊡ = samples from Hole 577A.

Eocene/Miocene unconformity. Study of this part of the section requires shore-based AF demagnetization experiments.

REFERENCES

Berggren, W. A., Kent, D. V., and Flynn, J. J., in press. Paleogene geochronology and chronostratigraphy. *In* Snelling, N. J. (Ed.), *Geochronology and the Geological Record.* Geol. Soc. London Spec. Paper.

Blow, W. H., 1969. Late middle Eocene to Recent planktonic foraminiferal biostratigraphy. *In* Bronnimann, P. and Renz, H. H. (Eds.), *Proc. First Int'l. Conf. Planktonic Microfossils* (Vol. 6): Leiden (Brill), 199–421.

Boyce, R. E., 1976a. Definitions and laboratory techniques of compressional and sound velocity parameters and wet-water content, wet-bulk density, and porosity parameters by gravimetric and gamma ray attenuation techniques. *In* Schlanger, S. O., Jackson, E. D., et al., *Init. Repts. DSDP*, 33: Washington (U.S. Govt. Printing Office), 931–958.

————, 1976b. Deep Sea Drilling Project procedures for shear strength measurements of clayey sediment using modified Wykeham Farrance Laboratory Vane Apparatus. *In* Barker, P., Dalziel, I. W. D., et al., *Init. Repts. DSDP*, 36: Washington (U.S. Govt. Printing Office), 1059–1068.

Bukry, D., 1973. Low latitude coccolith biostratigraphic zonation. *In* Edgar, N. T., Saunders, J. B., et al., *Init. Repts. DSDP*, 15: Washington (U.S. Govt. Printing Office), 685–703.

————, 1975. Coccolith and silicoflagellate stratigraphy, northern Pacific Ocean, DSDP Leg 32. *In* Larson, R. L., Moberly, R., et al., *Init. Repts. DSDP*, 32: Washington (U.S. Govt. Printing Office), 677–701.

Burckle, L. H., 1978. Early Miocene to Pliocene diatom datum levels for the equatorial Pacific. *Geol. Res. and Dev. Centre, Repub. of Indonesia, Spec. Publ.*, 1:25–44.

Burckle, L. H., and Opdyke, N. D., 1977. Late Neogene diatom correlations in the circum-Pacific. *Proc. 1st Int'l. Congr. Pac. Neogene Strat.*: Tokyo (Kaiyo Shuppan), pp. 255–284.

Foreman, H. P., 1973. Radiolaria from DSDP Leg 20. *In* Heezen, B. C., MacGregor, I. D., et al., *Init. Repts. DSDP*, 20: Washington (U.S. Govt. Printing Office), 249–305.

————, 1975. Radiolaria from the North Pacific, Deep Sea Drilling Project, Leg 32. *In* Larson, R. L., Moberly, R., et al., *Init. Repts. DSDP*, 32: Washington (U.S. Govt. Printing Office), 578–701.

Hays, J. D., 1970. Stratigraphy and evolutionary trends of Radiolaria in North Pacific deep-sea sediments. *In* Hays, J. D. (Ed.), *Geological Investigations of the North Pacific.* Mem. Geol. Soc. Am., 126:185–218.

Okada, H., and Bukry, D., 1980. Supplementary modification and introduction of code numbers to the low-latitude coccolith biostratigraphic zonation (Bukry, 1973, 1975). *Mar. Micropaleontol.*, 5: 321–325.

Riedel, W. R., and Sanfilippo, A., 1970. Radiolaria, Leg 4, Deep Sea Drilling Project. *In* Bader, R. G., Gerard, R. D., et al., *Init. Repts. DSDP*, 4: Washington (U.S. Govt. Printing Office), 503–575.

Stainforth, R. M., et al., 1975. Cenozoic planktonic foraminiferal zonations and characteristics of index forms. *Univ. Kans. Paleontol. Contrib. Pap.*, 62:1–425.

SITE 577 HOLE CORE 1 CORED INTERVAL 2678.2–2685.0 mbsl; 0.0–6.8 mbsf

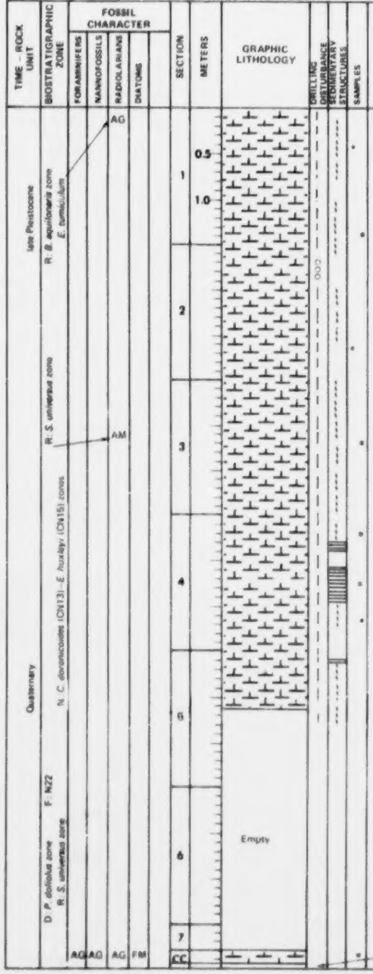
TIME – ROCK UNIT
BIOSTRATIGRAPHIC ZONE
FOSSIL CHARACTER
FORAMINIFERS
NANNOFOSSILS
RADIOLARIANS
DIATOMS
SECTION
METERS
GRAPHIC LITHOLOGY
DRILLING DISTURBANCE
SEDIMENTARY STRUCTURES
SAMPLES
late Pleistocene
Quaternary
R: B. aquilonaris zone
E. tumidulum
R: S. universus zone
N: C. doronicoides (CN13)–E. huxleyi (CN15) zones
F: N22
D: P. doliolus zone
R: S. universus zone
AG
AM
AG AG AG FM
0.5
1.0
1
2
3
4
5
6
7
CC
OOO
Empty
Empty

LITHOLOGIC DESCRIPTION

NANNOFOSSIL OOZE

* Dominant colors: grayish brown (2.5Y 5/2) and light brownish gray (2.5Y 6/2) in Section 1; olive gray (5Y 5/2) in Section 2; gray (5Y 5/1), gray (5Y 6/1), and light gray (5Y 7/1) in the rest of the core with olive gray (5Y 5/2) and white (2.5Y 8/0) intervals. Minor colors: gray (5GY 5/1), gray (5GY 7/1), and gray (5B 6/1) laminations in Section 4.

This core is slightly deformed, except for one soupy interval in Section 2, 20–40 cm.

* This core contains mottled and homogeneous nannofossil ooze layers, with thin laminations locally present in Section 4. It contains a 0.5 cm diameter pumice(?) pebble in Section 4, 86 cm.

SMEAR SLIDE SUMMARY (%):

	1, 140 D	3, 70 D	4, 20 D	4, 72 D	CC D
Texture:					
Sand	5	3	2	2	0
Silt	30	32	28	28	30
Clay	65	65	70	70	70
Composition:					
Quartz	7	7	7	5	7
Feldspar	5	3	5	2	3
Heavy minerals	3	5	Tr	1	–
Clay	15	10	5	5	5
Volcanic glass	5	3	2	2	–
Carbonate unspec.	–	–	2	2	–
Foraminifers	2	1	–	–	Tr
Calc. nannofossils	60	69	79	83	85
Diatoms	2	2	Tr	–	–
Sponge spicules	1	Tr	Tr	–	–

$CaCO_3$ data
1, 45 cm = 57%
2, 115 cm = 61%
4, 119 cm = 77%

SITE 577 HOLE CORE 2 CORED INTERVAL 2685.0–2694.5 mbsl; 6.8–16.3 mbsf

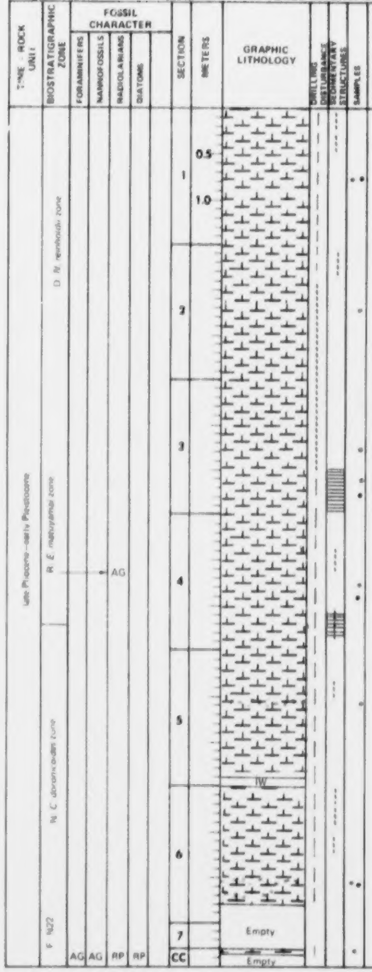
TIME – ROCK UNIT
BIOSTRATIGRAPHIC ZONE
FOSSIL CHARACTER
FORAMINIFERS
NANNOFOSSILS
RADIOLARIANS
DIATOMS
SECTION
METERS
GRAPHIC LITHOLOGY
DRILLING DISTURBANCE
SEDIMENTARY STRUCTURES
SAMPLES
late Pliocene–early Pleistocene
D: N. reinholdii zone
R: E. matuyamai zone
N: C. doronicoides zone
F: N22
AG
AG AG RP RP
0.5
1.0
1
2
3
4
5
6
7
CC
IW
Empty
Empty

LITHOLOGIC DESCRIPTION

NANNOFOSSIL OOZE WITH ASH LAYERS

* Dominant colors: white (2.5Y 8/0), white (5Y 8/1), light gray (2.5Y 7/0–2.5Y 7/1), light gray (5Y 7/1), gray (10YR 6/1), and medium gray (5Y 6/1). Minor colors: medium to dark (5Y 5/1–5Y 4/1), light gray (5Y 7/1), and gray (2.5Y N5) ash layers.

* Very deformed portions of Sections 2 and 3 result from flow in. The rest of the core is slightly deformed.

* This core consists of homogeneous to slightly mottled nannofossil ooze. There is a large pumice cobble in Section 3, 153–157 cm. Sections 3 and 4 contain intervals of 3–4 cm laminations with gradational contacts. Ash layers occur in Section 5, 57–60 cm; Section 6, 102.5–103.5 cm; and, Section 6, 114.5 cm.

SMEAR SLIDE SUMMARY (%):

	1, 80 D	2, 75 D	3, 80 D	3, 114 D	4, 80 D	5, 60 M	6, 103 M	CC D
Texture:								
Sand	0	0	0	0	10	40	45	5
Silt	17	15	10	25	40	50	5	25
Clay	83	85	90	75	50	10	50	70
Composition:								
Quartz	5	5	5	5	2	5	Tr	1
Feldspar	2	1	1	1	1	2	–	2
Mica	–	–	–	1	–	–	–	–
Heavy minerals	–	1	–	–	–	–	–	–
Clay	5	3	5	3	5	5	5	20
Volcanic glass	5	6	7	7	7	85	45	3
Palagonite	–	–	–	–	–	1	–	–
Micronodules	–	–	–	–	–	–	Tr	–
Zeolite	–	1	–	–	–	–	–	–
Carbonate unspec.	–	–	–	–	5	–	2	–
Foraminifers	5	3	–	Tr	20	–	Tr	2
Calc. nannofossils	71	73	82	83	60	–	48	72
Diatoms	Tr	1	Tr	–	–	–	Tr	–
Radiolarians	7	5	–	–	–	–	Tr	–
Sponge spicules	–	1	Tr	Tr	–	–	–	–
Opaques	–	–	–	–	–	2	–	–

$CaCO_3$ data
1, 80 cm = 67%
3, 130 cm = 56%
4, 93 cm = 73%
6, 110 cm = 84%

SITE 577 HOLE CORE 3 CORED INTERVAL 2694.5–2704.0 mbsl; 16.3–25.8 mbsf

TIME-ROCK UNIT	BIOSTRATIGRAPHIC ZONE	FORAMINIFERS	NANNOFOSSILS	RADIOLARIANS	DIATOMS
late Pliocene–early Pleistocene	D. R. praetergidus zone R. E. matuyamai zone N. D. brouweri zone–C. doronicoides zone R. L. heteroporos zone F. N21	AG	AG	AG CM	RP

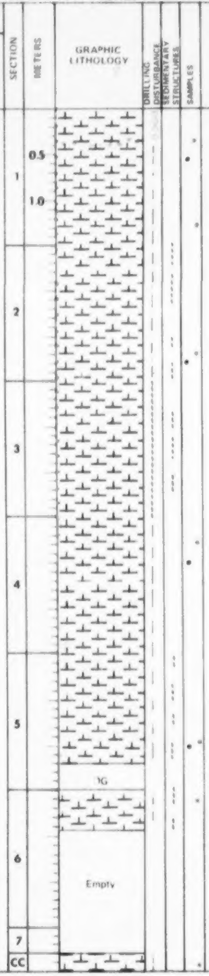

LITHOLOGIC DESCRIPTION

NANNOFOSSIL OOZE

- Dominant colors: medium gray (5Y 6/1), light gray (5Y 7/1), light gray (2.5Y N7), and white (2.5Y N8). Minor colors: thin layers of medium gray (5Y 6/1), light olive gray (5Y 6/2), and light green (5G 7/1). Gray (2.5Y N6) ash.
- Moderately to very deformed portions of Sections 2 and 3 result from flow-in. Rest of the core is slightly deformed.
- This core consists of nannofossil ooze. Thin (0.1–0.2 cm), distinct light green layers of nannofossil ooze occur in Section 5 and the Core Catcher. There is a discontinuous ash layer in Section 1, 39–40 cm.

SMEAR SLIDE SUMMARY (%):

	1, 39 M	1, 130 D	2, 120 D	4, 30 D	5, 94 D	6, 15 D	CC D
Texture:							
Sand	93	10	10	5	Tr	5	2
Silt	5	2	3	3	5	5	30
Clay	2	88	87	92	95	90	68
Composition:							
Quartz	7	—	—	—	—	—	5
Clay	7	5	10	3	30	10	10
Volcanic glass	91	—	—	Tr	Tr	Tr	2
Glauconite	—	—	—	Tr	—	—	—
Micronodules	Tr	1	—	3	—	—	—
Carbonate unspec.	—	Tr	—	1	1	Tr	3
Foraminifers	—	10	15	5	7	5	—
Calc. nannofossils	—	82	74	87	60	80	80
Diatoms	—	Tr	Tr	Tr	1	3	—
Radiolarians	—	2	1	Tr	1	1	—
Silicoflagellates	—	Tr	Tr	—	Tr	1	—
Opaques	—	—	—	1	—	—	—

$CaCO_3$ data: 1, 60 cm = 84%
2, 130 cm = 84%
4, 50 cm = 84%
5, 100 cm = 81%

SITE 577 HOLE CORE 4 CORED INTERVAL 2704.0–2713.5 mbsl; 25.8–35.3 mbsf

TIME-ROCK UNIT	BIOSTRATIGRAPHIC ZONE	FORAMINIFERS	NANNOFOSSILS	RADIOLARIANS	DIATOMS
late Pliocene	D. N. jouseae zone N. D. brouweri zone (CN13); R. S. langii zone; L. heteroporos zone F. N21	AG	AG	CM	RP

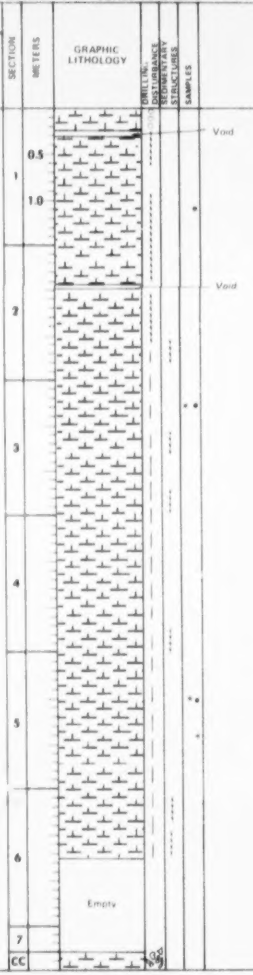

LITHOLOGIC DESCRIPTION

NANNOFOSSIL OOZE

- Dominant colors: light grey (2.5Y N7), white (2.5Y N8), medium gray (5Y 6/1), and light gray (5Y 5/1) gradually changing to light gray (7.5YR N7) and white (7.5YR N8) below Section 5. Minor colors: thin layers of light green (5G 7/1) and light green (5GY 7/1).
- Core is very deformed in Section 1 and Section 2, 0–112 cm. Rest of the core is slightly deformed.
- This core consists of homogeneous nannofossil ooze. Section 1 and Section 2, 0–112 cm are very deformed, resulting from flow-in. Sections 5 and 6 contain thin (0.2 cm), distinct layers of light green nannofossil ooze. All downcore color changes are gradational.

SMEAR SLIDE SUMMARY (%):

	3, 30 D	5, 62 D	5, 97 D
Texture:			
Sand	7	5	3
Silt	3	2	2
Clay	90	93	95
Composition:			
Quartz	Tr	Tr	—
Clay	15	25	10
Volcanic glass	Tr	Tr	—
Carbonate unspec.	Tr	1	Tr
Foraminifers	10	5	5
Calc. nannofossils	75	68	83
Diatoms	Tr	1	1
Radiolarians	Tr	Tr	1
Sponge spicules	Tr	—	Tr
Silicoflagellates	—	—	Tr

$CaCO_3$ data: 1, 116 cm = 83%
3, 30 cm = 87%
5, 55 cm = 87%

SITE 577 HOLE CORE 5 CORED INTERVAL 2713.5–2723.0 mbsl; 35.3–44.8 mbsf

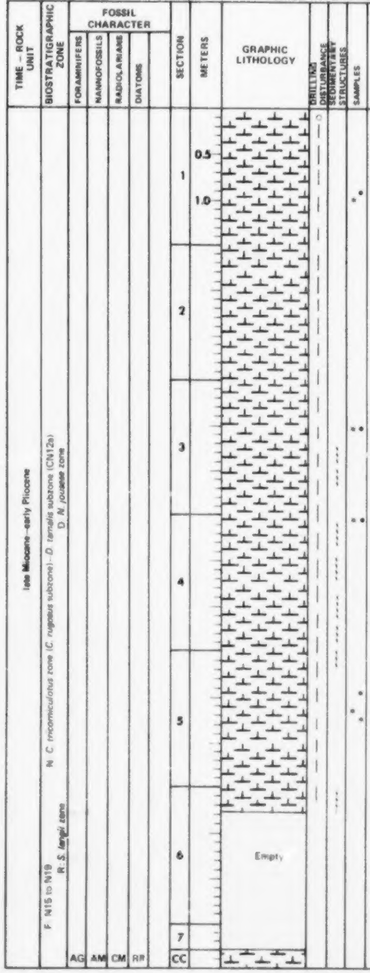
TIME – ROCK UNIT
BIOSTRATIGRAPHIC ZONE
FOSSIL CHARACTER
FORAMINIFERS
NANNOFOSSILS
RADIOLARIANS
DIATOMS
SECTION
METERS
GRAPHIC LITHOLOGY
DRILLING DISTURBANCE
SEDIMENTARY STRUCTURES
SAMPLES
late Miocene–early Pliocene
F: N15 to N19
N: C. tricorniculatus zone (C. rugosus subzone)–D. tamalis subzone (CN12a)
R: S. langii zone
D: N. jouseae zone
AG
AM
CM
RP
0.5
1.0
1
2
3
4
5
6
7
CC
Empty

LITHOLOGIC DESCRIPTION

NANNOFOSSIL OOZE

- Dominant colors: alternating intervals of white (2.5Y N8), white (7.5YR N8), and light gray (5Y 7/1). Minor colors: grayish brown (2.5Y 5/2) pebble.
- Core is slightly deformed throughout.
- This core consists of fairly homogeneous nannofossil ooze. Sections 3 and 4 are lightly burrowed and mottled. Section 5 contains a pebble at 125 cm.

SMEAR SLIDE SUMMARY (%):

	1, 100 D	3, 53 D	4, 7 D	5, 47 D	5, 66 D	5, 78 D
Texture:						
Sand	2	1	10	15	4	0
Silt	3	2	6	7	1	1
Clay	95	97	84	78	95	99
Composition:						
Quartz	–	–	–	12	Tr	Tr
Feldspar	Tr	–	–	Tr	–	
Mica	–	–	–	Tr	–	1
Clay	5	2	7	2	1	3
Volcanic glass	Tr	1	–	2	Tr	–
Glauconite	–	–	–	Tr	–	–
Micronodules	Tr	Tr	–	2	–	–
Carbonate unspec.	–	–	Tr	–	–	–
Foraminifers	–	4	3	–	5	–
Calc. nannofossils	95	93	77	80	94	96
Diatoms	Tr	–	2	–	–	Tr
Radiolarians	Tr	–	1	2	–	–
Sponge spicules	–	–	Tr	–	–	–
Silicoflagellates	–	–	Tr	–	–	–
Opaques	–	–	10	–	–	–

$CaCO_3$ data
1, 96 cm = 87%
3, 53 cm = 93%
4, 8 cm = 90%

SITE 577 HOLE CORE 6 CORED INTERVAL 2723.0–2732.5 mbsl; 44.8–54.3 mbsf

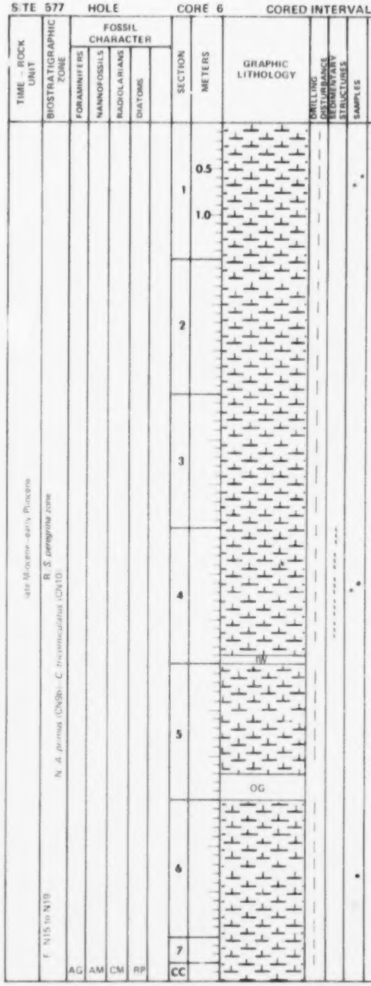
TIME – ROCK UNIT
BIOSTRATIGRAPHIC ZONE
FOSSIL CHARACTER
FORAMINIFERS
NANNOFOSSILS
RADIOLARIANS
DIATOMS
SECTION
METERS
GRAPHIC LITHOLOGY
DRILLING DISTURBANCE
SEDIMENTARY STRUCTURES
SAMPLES
late Miocene–early Pliocene
F: N15 to N19
N: A. primus (CN9b)–C. tricorniculatus (CN10)
R: S. peregrina zone
AG
AM
CM
RP
0.5
1.0
1
2
3
4
5
6
7
CC
IW
OG

LITHOLOGIC DESCRIPTION

NANNOFOSSIL OOZE

- Dominant colors: alternating layers of light gray (10YR 7/1) and white (10YR 8/1). Section 7 and the Core Catcher contain intervals of white (10YR 8/2).
- Core is slightly deformed throughout.
- This core consists of very homogeneous nannofossil ooze. Section 4 is lightly mottled. All downcore color changes are gradational.

SMEAR SLIDE SUMMARY (%):

	1, 70 D	4, 70 D
Texture:		
Sand	3	1
Silt	6	3
Clay	91	96
Composition:		
Quartz	1	1
Mica	–	1
Foraminifers	2	1
Calc. nannofossils	95	97
Diatoms	2	Tr
Radiolarians	Tr	Tr
Hematite	–	Tr

$CaCO_3$ data
1, 64 cm = 91%
4, 67 cm = 76%
6, 82 cm = 94%

SITE 577 HOLE CORE 7 CORED INTERVAL 2732.5–2742.0 mbsl; 54.3–63.8 mbsf

TIME – ROCK UNIT	BIOSTRATIGRAPHIC ZONE	FORAMINIFERS	NANNOFOSSILS	RADIOLARIANS	DIATOMS
middle–upper Eocene to late Miocene	F: P11 N: *D. barbadiensis* (CP15)–*A. primus* (CN9b)	AM	CP	B	B

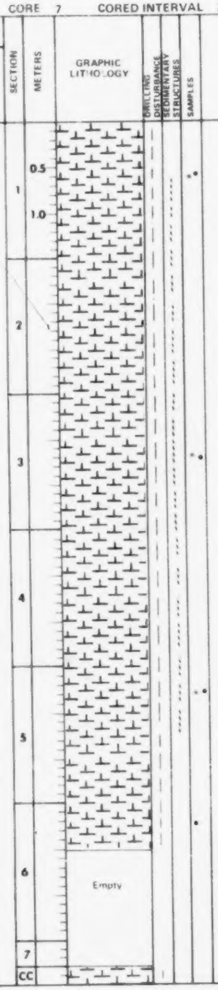
SECTION
METERS
GRAPHIC LITHOLOGY
DRILLING DISTURBANCE
SEDIMENTARY STRUCTURES
SAMPLES
0.5
1
1.0
2
3
4
5
6
Empty
7
CC

LITHOLOGIC DESCRIPTION

NANNOFOSSIL OOZE

- Dominant colors: white (10YR 8/2), very pale brown (10YR 7/3–10YR 8/3), and pale brown (10YR 6/3) mottled with the same colors and brown (10YR 4/3). Minor colors: Section 5 contains a light gray (10YR 7/2) interval.
- Section 2, 72 cm to Section 3, 40 cm is moderately deformed, perhaps resulting from flow-in. The rest of the core is slightly deformed.
- This core consists of slightly mottled nannofossil ooze. All do[illegible]ore color changes are gradational.

SMEAR [illegible] SUMMARY (%):

	1, 60	3, 70	5, 30	6, 30
	[illegible]	D	D	D
Texture:				
Sand	[illegible]	[illegible]	2	2
Silt	[illegible]	[illegible]	38	38
Clay	[illegible]	[illegible]	60	60
Composition:				
Quartz	5	[illegible]	[illegible]	7
Feldspar		[illegible]	[illegible]	2
Heavy minerals		[illegible]	[illegible]	[illegible]
Clay	5	5	[illegible]	[illegible]
Volcanic glass	2	2	[illegible]	[illegible]
Foraminifers	5	–	[illegible]	[illegible]
Calc. nannofossils	78	77	68	[illegible]
Diatoms	2	Tr	–	[illegible]
Radiolarians	Tr	–	–	–
Discoasters	3	5	10	15

$CaCO_3$ data
1, 60 cm = 83%
3, 69 cm = 83%
5, 28 cm = 59%
6, 22 cm = 96%

SITE 577 HOLE CORE 8 CORED INTERVAL 2742.0–2751.5 mbsl; 63.8–73.3 mbsf

TIME – ROCK UNIT	BIOSTRATIGRAPHIC ZONE	FORAMINIFERS	NANNOFOSSILS	RADIOLARIANS	DIATOMS
early–middle Eocene	N: *D. sublodoensis* zone (CP11)–*R. umbilica* zone (CP14) F: P8–P10	AM	CM	B	B

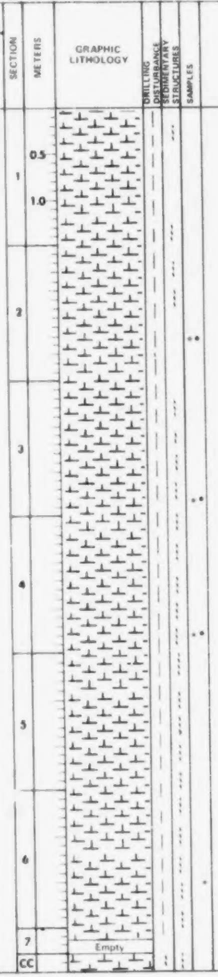
SECTION
METERS
GRAPHIC LITHOLOGY
DRILLING DISTURBANCE
SEDIMENTARY STRUCTURES
SAMPLES
0.5
1
1.0
2
3
4
5
6
7
Empty
CC

LITHOLOGIC DESCRIPTION

NANNOFOSSIL OOZE

- Dominant colors: pale brown (10YR 6/3) and very pale brown (10YR 7/3–10YR 8/3) with white (10YR 8/2) intervals in Section 2.
- This core is slightly deformed throughout.
- This core consists of mottled nannofossil ooze. All downcore color changes are gradational.

SMEAR SLIDE SUMMARY (%):

	2, 100	3, 132	4, 130	6, 100
	D	D	D	D
Texture:				
Sand	2	2	1	1
Silt	48	48	44	44
Clay	50	50	55	55
Composition:				
Quartz	5	7	7	7
Feldspar	2	–	2	2
Heavy minerals	2	5	Tr	1
Clay	5	5	5	5
Volcanic glass	3	2	1	2
Carbonate unspec.	5	–	–	–
Calc. nannofossils	63	66	70	68
Radiolarians	Tr	–	–	–
Discoasters	15	15	15	15

$CaCO_3$ data
2, 105 cm = 99%
3, 132 cm = 99%
4, 130 cm = 97%

SITE 577 HOLE CORE 9 CORED INTERVAL 2751.5–2761.0 mbsl; 73.3–82.8 mbsf

TIME – ROCK UNIT: late Paleocene–early Eocene

BIOSTRATIGRAPHIC ZONE: F D. multiradiatus (CP8)–T. orthostylus (CP10); F P6B–P7

FOSSIL CHARACTER: FORAMINIFERS AG; NANNOFOSSILS AM; RADIOLARIANS B; DIATOMS B

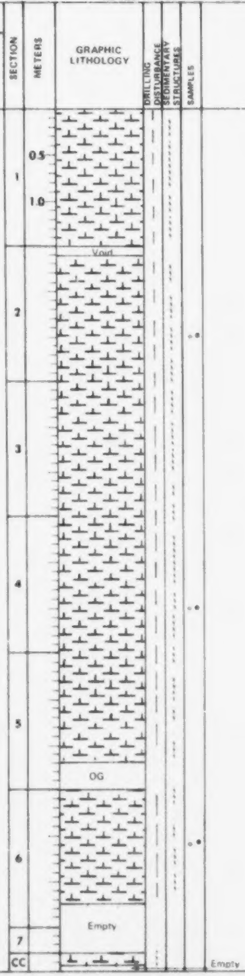
SECTION
METERS
GRAPHIC LITHOLOGY
DRILLING DISTURBANCE
SEDIMENTARY STRUCTURES
SAMPLES
1
0.5
1.0
Void
2
3
4
5
OG
6
Empty
7
CC
Empty

LITHOLOGIC DESCRIPTION

NANNOFOSSIL OOZE

*Dominant colors: very pale brown (10YR 8/3). Minor colors: pale brown (10YR 6/3), very pale brown (10YR 7/3), white (10YR 8/2), and black mottles.

*Core is slightly deformed throughout.

*This core consists of homogeneous white nannofossil ooze with infrequent small mottles in all sections.

SMEAR SLIDE SUMMARY (%):

	2, 100 D	4, 100 D	6, 60 D
Texture:			
Sand	1	2	1
Silt	34	38	34
Clay	65	60	65
Composition:			
Quartz	7	5	8
Feldspar	2	2	2
Heavy minerals	2	1	1
Clay	5		4
Volcanic glass	2	2	2
Carbonate unspec.	–	2	
Foraminifers	–	1	–
Calc. nannofossils	77	82	76
Discoasters	5	5	7

CaCO$_3$ data 2, 100 cm = 100%
4, 100 cm = 100%
6, 60 cm = 97%

SITE 577 HOLE CORE 10 CORED INTERVAL 2761.0–2770.5 mbsl; 82.8–92.3 mbsf

TIME – ROCK UNIT: late Paleocene

BIOSTRATIGRAPHIC ZONE: N D. mohleri–D. nobilis (CP6–CP7); F P5 P6A

FOSSIL CHARACTER: FORAMINIFERS AG; NANNOFOSSILS AM; RADIOLARIANS B; DIATOMS B

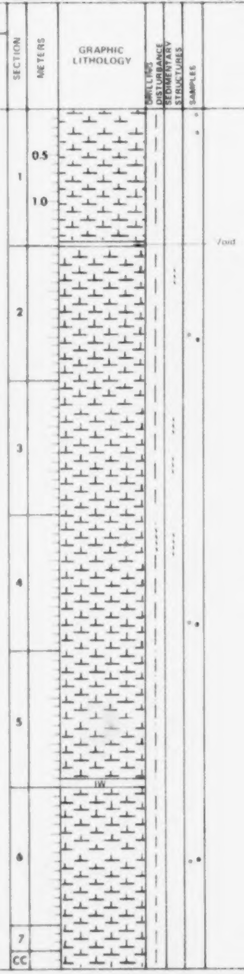
SECTION
METERS
GRAPHIC LITHOLOGY
DRILLING DISTURBANCE
SEDIMENTARY STRUCTURES
SAMPLES
1
0.5
1.0
Void
2
3
4
5
IW
6
7
CC

LITHOLOGIC DESCRIPTION

NANNOFOSSIL OOZE

*Dominant colors: white (10YR 8/2) with minor very pale brown (10YR 7/3–10YR 8/3), light gray (7.5YR 7/0), and pale brown (10YR 6/3) zones and mottles.

*Except for the very disturbed zone in Section 2, 0–40 cm, this core is slightly to moderately deformed. The very deformed zone in Section 2 is due to the fact that an O-ring was dragged through the section when the core was split.

*This core consists of homogeneous white nannofossil ooze with minor mottles.

SMEAR SLIDE SUMMARY (%):

	1, 2 D	1, 30 D	2, 100 D	4, 120 D	6, 80 D
Texture:					
Sand	7	1	0	1	0
Silt	28	39	25	38	20
Clay	65	60	75	60	80
Composition:					
Quartz	5	5	5	5	3
Feldspar	1	1	2	2	–
Heavy minerals	1	2	1	1	–
Clay	5	5	5	5	1
Volcanic glass	2	2	2	Tr	Tr
Carbonate unspec.	3	3	–	–	5
Foraminifers	5	2	–	–	1
Calc. nannofossils	78	75	82	84	90
Diatoms		Tr	Tr	–	–
Radiolarians	Tr	Tr	–	–	–
Discoasters	–	5	3	3	–

CaCO$_3$ data 2, 102 cm = 100%
4, 120 cm = 97%
6, 80 cm = 98%

SITE 577 HOLE CORE 11 CORED INTERVAL 2770.5–2780.0 mbsl; 92.3–101.8 mbsf

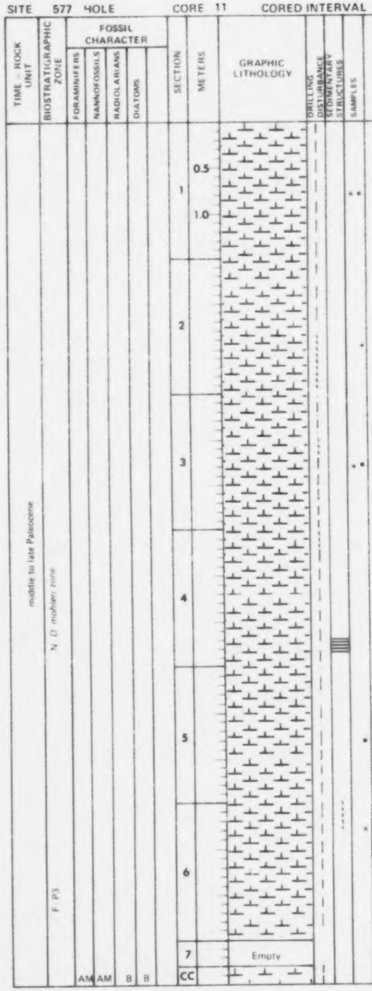
TIME – ROCK UNIT
BIOSTRATIGRAPHIC ZONE
FOSSIL CHARACTER
FORAMINIFERS
NANNOFOSSILS
RADIOLARIANS
DIATOMS
SECTION
METERS
GRAPHIC LITHOLOGY
DRILLING DISTURBANCE
SEDIMENTARY STRUCTURES
SAMPLES
middle to late Paleocene
N. D. mohleri zone
F. P3
0.5
1.0
1
2
3
4
5
6
7
CC
Empty
AM
AM
B
B

LITHOLOGIC DESCRIPTION

NANNOFOSSIL OOZE

*Dominant colors: white (10YR 8/2), very pale brown (10YR 7/3–10YR 8/3), and very pale brown (10YR 7/4) with minor white (10YR 8/1) patches and mottles.

*Section 2, 80 cm to Section 3, 62 cm and Section 4, 0–22 cm are moderately to very deformed, probably due to splitting the core sections. The rest of the core is slightly deformed.

*This core consists of homogeneous to slightly mottled nannofossil ooze. Several thin laminations are present near the base of Section 4.

SMEAR SLIDE SUMMARY (%):

	1, 80 D	2, 92 D	3, 80 D	6, 30 D
Texture:				
Sand	0	0	1	4
Silt	20	20	39	36
Clay	80	80	60	60
Composition:				
Quartz	2	3	7	5
Feldspar	–	–	1	1
Heavy minerals	–	–	Tr	1
Clay	1	2	7	5
Volcanic glass	1	–	Tr	2
Zeolite	1	1	–	–
Carbonate unspec.	5	3	–	–
Foraminifers	5	2	–	3
Calc. nannofossils	85	89	85	83

CaCO$_3$ data: 1, 80 cm = 96%
3, 80 cm = 94%
5, 80 cm = 95%

SITE 577 HOLE CORE 12 CORED INTERVAL 2780.0–2789.5 mbsl; 101.8–111.3 mbsf

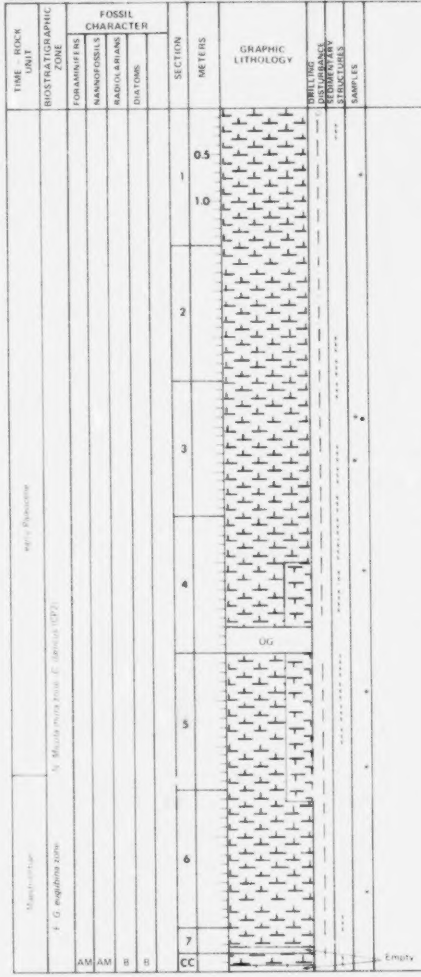
TIME – ROCK UNIT
BIOSTRATIGRAPHIC ZONE
FOSSIL CHARACTER
FORAMINIFERS
NANNOFOSSILS
RADIOLARIANS
DIATOMS
SECTION
METERS
GRAPHIC LITHOLOGY
DRILLING DISTURBANCE
SEDIMENTARY STRUCTURES
SAMPLES
early Paleocene
Maastrichtian
N. Micula mura zone C. danicus (CP2)
F. G. eugubina zone
0.5
1.0
1
2
3
4
5
6
7
CC
OG
Empty
AM
AM
B
B

LITHOLOGIC DESCRIPTION

NANNOFOSSIL OOZE

*Dominant colors: very pale brown (10YR 7/3–10YR 7/4), very pale brown (10YR 8/3–10YR 8/4), white (10YR 8/1–10YR 8/2), yellow (10YR 7/6), and light yellowish brown (10YR 6/4) in Sections 1 through 4. Sections 5, 6, 7, and the Core Catcher are white (10YR 8/1–10YR 8/2) with minor zones of very pale brown (10YR 7/3–10YR 8/3).

*This core is slightly deformed, except for a moderately deformed zone in Section 2. Deformation in Section 2 is due to the process of splitting the core.

*This core consists of homogeneous to slightly mottled nannofossil ooze. The Cretaceous Tertiary boundary is located in Section 5, 114–116 cm.

SMEAR SLIDE SUMMARY (%):

	1, 75 D	3, 43 D	3, 90 D	4, 60 D	5, 40 D	5, 125 D	6, 115 D
Texture:							
Sand	7	2	1	25	10	25	0
Silt	33	2	3	2	25	2	20
Clay	60	96	96	73	65	73	80
Composition:							
Quartz	5	–	–	–	–	–	5
Feldspar	1	–	Tr	–	–	–	1
Mica	–	Tr	–	–	–	–	–
Heavy minerals	Tr	–	–	–	–	–	–
Clay	10	Tr	–	–	–	–	2
Volcanic glass	2	1	1	–	Tr	–	–
Zeolite	–	–	–	–	–	–	2
Carbonate unspec.	–	–	–	–	–	–	5
Foraminifers	5	1	2	25	35	25	Tr
Calc. nannofossils	77	97	96	75	65	74	85
Radiolarians	–	Tr	–	–	–	–	–
Sponge spicules	–	–	–	–	–	–	Tr
Hematite	–	–	1	–	–	1	–

CaCO$_3$ data: 3, 44 cm = 93%

SITE 577 HOLE CORE 13 CORED INTERVAL 2789.5–2797.0 mbsl, 111.3–118.8 mbsf

TIME – ROCK UNIT	BIOSTRATIGRAPHIC ZONE	FORAMINIFERS	NANNOFOSSILS	RADIOLARIANS	DIATOMS	SECTION
Late Cretaceous (late Maestrichtian)	N. M. murus zone F. G. mayaroensis zone	AM		B	B	1, 2, 3, 4, 5, 6, 7, CC

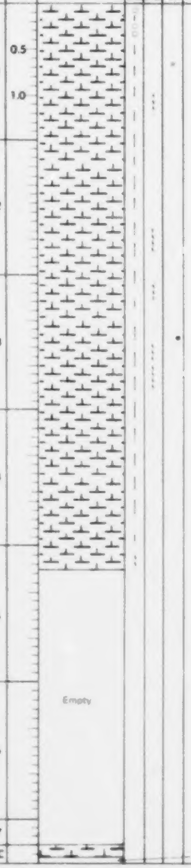

LITHOLOGIC DESCRIPTION

NANNOFOSSIL OOZE

- * Dominant colors: white (10YR 8/2). Minor colors: white (10YR 8/1) and very pale brown (10YR 8/3) mottles.
- * Core is slightly deformed throughout.
- * This core consists of uniform, white nannofossil ooze. Sections 1 through 3 are slightly mottled.

SMEAR SLIDE SUMMARY (%):

	1, 70
Texture:	
Sand	0
Silt	5
Clay	95
Composition:	
Quartz	5
Feldspar	2
Heavy minerals	Tr
Clay	2
Volcanic glass	1
Carbonate unspec.	3
Calc. nannofossils	87

$CaCO_3$ data: 3, 70 cm = 94%

SITE 577 HOLE A CORE 1 CORED INTERVAL 2677.6–2687.0 mbsl; 0.0–9.4 mbsf

TIME – ROCK UNIT	BIOSTRATIGRAPHIC ZONE	FORAMINIFERS	NANNOFOSSILS	RADIOLARIANS	DIATOMS	SECTION
late Pleistocene	R. S. universus–R. B. aquilonaris zone F. N22 N. C. doronicoides (CN13)–E. huxleyi (CN15) zone	AG	AG	AG AM AG	B	1, 2, 3, 4, 5, 6, 7, CC

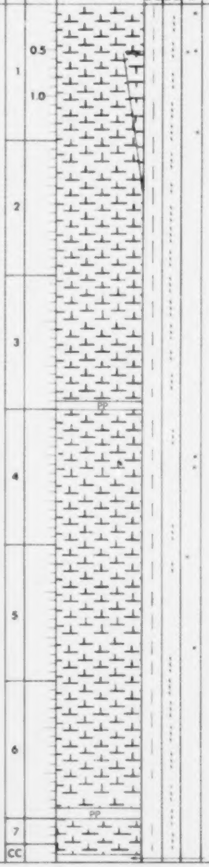

LITHOLOGIC DESCRIPTION

NANNOFOSSIL OOZE

- * Dominant colors: grayish brown (2.5Y 5/2), pale brown (10YR 6/3) grading to light gray (5Y 7/1), medium gray (5Y 6/1), and light gray (10YR 7/1) at the base of Section 1. Core contains white (2.5Y N8) intervals in Sections 3, 4, and 5. Minor colors: Thin (less than or equal to 0.1–0.2 cm) distinct layers of olive gray (5Y 4/2) in Section 2, and light green (5G 7/1) to green (5GY 5/1–5GY 6/1) in Sections 3 and 4.
- * This core is slightly deformed throughout.
- * This core contains mottled and burrowed nannofossil ooze, with thin layers of greenish ooze in Sections 3 and 4.

SMEAR SLIDE SUMMARY (%):

	1, 10	1, 50	1, 140	4, 66	5, 12
	D	D	D	D	D
Texture:					
Sand	7	20	15	7	7
Silt	3	5	3	3	3
Clay	90	75	82	90	90
Composition:					
Quartz	–	1	3	1	1
Feldspar	–	Tr	1	Tr	Tr
Clay	5	7	3	15	3
Volcanic glass	–	1	1	1	1
Micronodules	Tr	Tr	–	Tr	–
Carbonate unspec.	1	Tr	1	–	1
Foraminifers	7	20	14	7	5
Calc. nannofossils	83	69	74	73	87
Diatoms	1	1	2	2	1
Radiolarians	3	1	Tr	1	1
Sponge spicules	Tr	Tr	–	Tr	Tr
Silicoflagellates	Tr	Tr	–	Tr	–

$CaCO_3$ data: 1, 50 cm = 59%
4, 55 cm = 78%
5, 111 cm = 87%

SITE 577 HOLE A CORE 2 CORED INTERVAL 2687.0–2696.5 mbsl; 9.4–18.9 mbsf

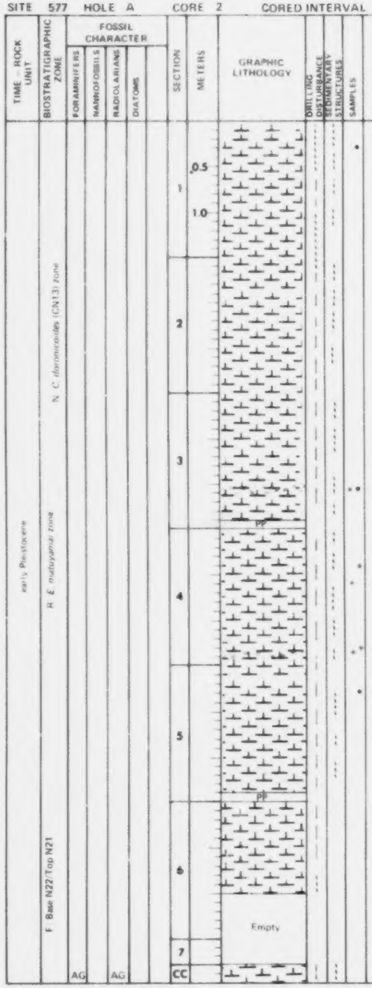
TIME – ROCK UNIT
BIOSTRATIGRAPHIC ZONE
FOSSIL CHARACTER
FORAMINIFERS
NANNOFOSSILS
RADIOLARIANS
DIATOMS
SECTION
METERS
GRAPHIC LITHOLOGY
DRILLING DISTURBANCE
SEDIMENTARY STRUCTURES
SAMPLES
early Pleistocene
N C. doronicoides (CN13) zone
R E. matuyamai zone
F Base N22/Top N21
AG
AG
0.5
1.0
1
2
3
4
5
6
7
CC
PP
Empty

LITHOLOGIC DESCRIPTION

NANNOFOSSIL OOZE

- Dominant colors: medium gray (5Y 6/1), light gray (5Y 7/1), white (2.5Y N8), and white (7.5YR N7) in all sections. Minor colors: thin distinct layers of light green (5G 7/1) ooze; dark gray (5Y 4/1) ash; gray (2.5Y N5) pyritiferous nanno ooze crust.
- This core is slightly deformed in Sections 2 to 6, and very deformed in Section 1.
- This core contains mottled and burrowed nannofossil ooze with thin (0.1–0.2 cm) layers of light green ooze in Sections 3 to 6. An ash layer was recovered in Section 3, 103–105.5 cm. Pumice fragments and pebbles up to 3 cm in diameter occur at Section 3, 22.5–23 cm, Section 3, 88–91 cm, and Section 4, 54–55 cm. The base of Section 4 contains a gray, hard crust of pyritiferous nannofossil ooze.

SMEAR SLIDE SUMMARY (%):

	3, 105	4, 40	4, 61	4, 130	4, 136
	M	D	D	D	M
Texture:					
Sand	80	7	7	7	75
Silt	15	2	3	10	20
Clay	5	91	90	83	5
Composition:					
Quartz	15		–	–	10
Feldspar	1	–	–	–	Tr
Clay	–	10	10	3	–
Volcanic glass	75	3	1	2	86
Pyrite	3	–	–	7	–
Micronodules	1	Tr	–	–	1
Carbonate unspec.	Tr	1	Tr	–	–
Foraminifers	–	5	10	7	1
Calc. nannofossils	5	81	77	80	1
Diatoms	–	Tr	1	1	–
Radiolarians	–	Tr	1	Tr	–
Opaques	–	–	–	–	1

$CaCO_3$ data 1, 30 cm = 65%
3, 108 cm = 37%
5, 30 cm = 86%

SITE 577 HOLE A CORE 3 CORED INTERVAL 2696.5–2706.0 mbsl; 18.9–28.4 mbsf

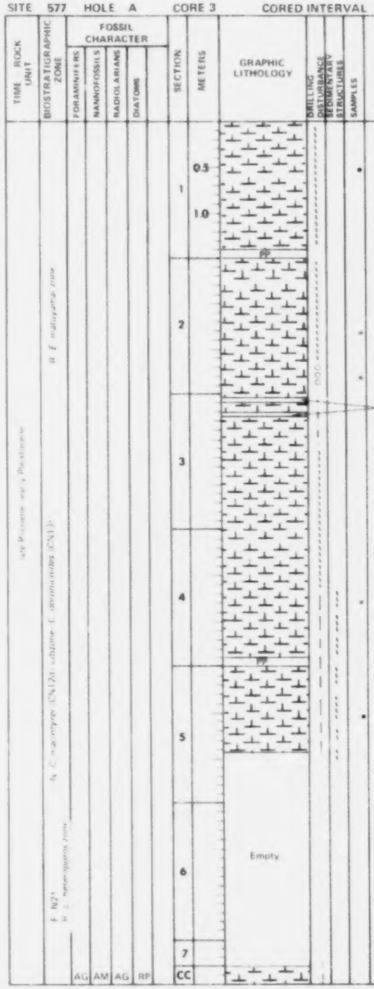
TIME – ROCK UNIT
BIOSTRATIGRAPHIC ZONE
FOSSIL CHARACTER
FORAMINIFERS
NANNOFOSSILS
RADIOLARIANS
DIATOMS
SECTION
METERS
GRAPHIC LITHOLOGY
DRILLING DISTURBANCE
SEDIMENTARY STRUCTURES
SAMPLES
late Pliocene–early Pleistocene
N C. macintyrei (CN12d) subzone – C. doronicoides (CN13)
R E. matuyamai zone
F N21
AG
AM
AG
RP
0.5
1.0
1
2
3
4
5
6
7
CC
PP
Void
Empty

LITHOLOGIC DESCRIPTION

NANNOFOSSIL OOZE

- Dominant colors: white (2.5Y N8), white (7.5YR N8), light gray (2.5Y N7), light gray (5Y 7/1), medium gray (5Y 6/1), gray (5Y 8/1), gray (2.5Y N5), and gray (2.5Y N6).
- This core is very disturbed in Sections 1 to 4, 65 cm. Section 2, 95–150 cm is soupy. Section 4, 65 cm to the end of the core is slightly deformed.
- This core contains nannofossil ooze. The upper portions of Sections 1 and 2, Section 3, 49–150 cm, and Section 4, 0–65 cm are very disturbed to soupy, resulting from flow in.

SMEAR SLIDE SUMMARY (%):

	2, 86	2, 132	4, 62
	D	D	D
Texture:			
Sand	5	5	7
Silt	6	10	4
Clay	89	85	89
Composition:			
Quartz	–	–	Tr
Clay	15	10	25
Volcanic glass	Tr	Tr	Tr
Pyrite	–	7	–
Micronodules	–	Tr	–
Carbonate unspec.	–	–	1
Foraminifers	7	5	10
Calc. nannofossils	74	76	64
Diatoms	1	Tr	Tr
Radiolarians	1	Tr	Tr
Sponge spicules	2	–	Tr
Silicoflagellates	Tr	1	–
Opaques	–	1	–

$CaCO_3$ data 1, 53 cm = 73%
5, 53 cm = 86%

SITE 577 HOLE A CORE 4 CORED INTERVAL 2706.0–2715.5 mbsl; 28.4–37.9 mbsf

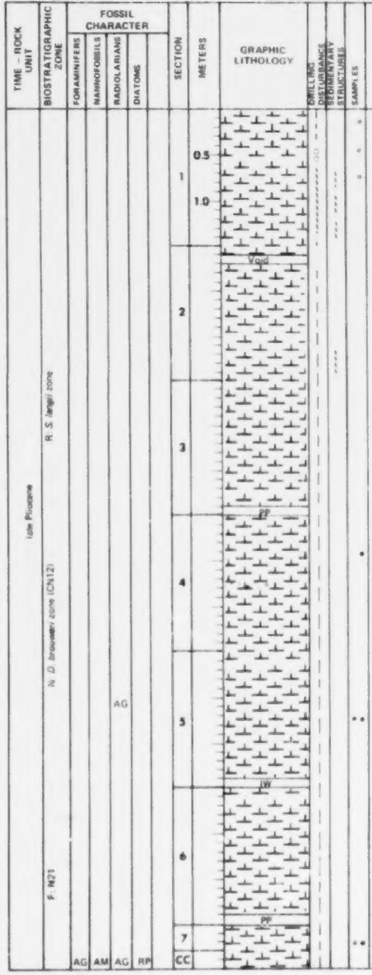
TIME – ROCK UNIT
BIOSTRATIGRAPHIC ZONE
FOSSIL CHARACTER
FORAMINIFERS
NANNOFOSSILS
RADIOLARIANS
DIATOMS
SECTION
METERS
GRAPHIC LITHOLOGY
DRILLING DISTURBANCE
SEDIMENTARY STRUCTURES
SAMPLES
late Pliocene
R: S. langii zone
N: D. brouweri zone (CN12)
F: N21
AG
AG AM AG RP
0.5
1.0
1
2
3
4
5
6
7
CC
Void
PP
IW
PP

LITHOLOGIC DESCRIPTION

NANNOFOSSIL OOZE

- Dominant colors: white (7.5YR N8), white (10YR 8/1), light gray (7.5YR N7), light gray (5Y 7/1), and medium gray (5Y 6/1). Minor colors: gray (7.5YR N6) pyritiferous crust and gray (10YR 6/1) ashy layer.
- This core is slightly deformed throughout, except for the very deformed to soupy portion of Section 1. The very deformed material at Section 1, 104–150 cm is flow in.
- This core contains homogeneous to slightly burrowed nannofossil ooze. The number of burrows decreases downcore. Section 2 contains a burrow filled with gray pyritiferous crust at 130 cm. Pumice pebbles are found at Section 3, 24 and 78 cm, and Section 5, 58 cm. Section 4, 78–80 cm consists of a gray ashy layer (see smear slide summary below).

SMEAR SLIDE SUMMARY (%)

	1, 15 D	4, 46 D	4, 78 M	5, 76 D	7, 20 D
Texture:					
Sand	1	9	20	6	3
Silt	5	4	15	4	2
Clay	94	87	65	90	95
Composition:					
Quartz	Tr	–	Tr	Tr	Tr
Mica	–	Tr	–	1	Tr
Clay	7	Tr	–	–	2
Volcanic glass	Tr	1	20	–	–
Carbonate unspec.	Tr	–	–	–	–
Foraminifers	2	9	15	8	4
Calc. nannofossils	87	90	64	91	94
Diatoms	2	–	–	Tr	–
Radiolarians	2	Tr	1	–	–
Sponge spicules	Tr	–	–	–	–
Silicoflagellates	Tr	–	–	–	–

$CaCO_3$ data: 4, 46 cm = 86%
5, 78 cm = 86%
7, 20 cm = 85%

SITE 577 HOLE A CORE 5 CORED INTERVAL 2715.5–2725.0 mbsl; 37.9–47.4 mbsf

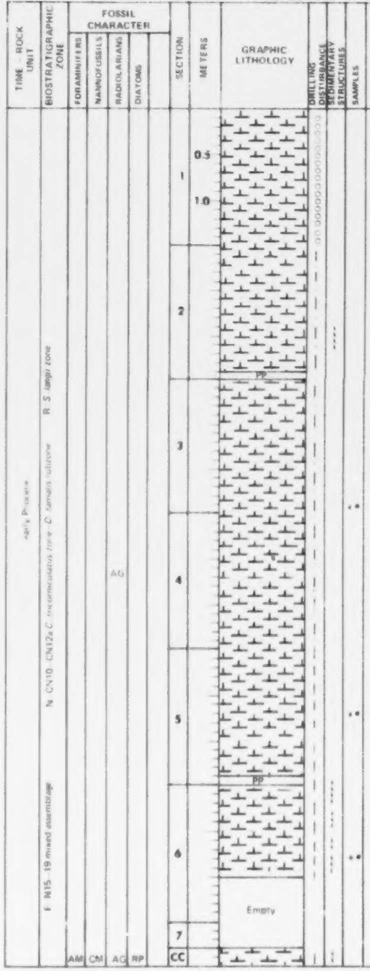
TIME – ROCK UNIT
BIOSTRATIGRAPHIC ZONE
FOSSIL CHARACTER
FORAMINIFERS
NANNOFOSSILS
RADIOLARIANS
DIATOMS
SECTION
METERS
GRAPHIC LITHOLOGY
DRILLING DISTURBANCE
SEDIMENTARY STRUCTURES
SAMPLES
early Pliocene
R: S. langii zone
N: CN10–CN12a C. tricorniculatus zone–C. tamalis subzone
F: N15–19 mixed assemblage
AG
AM CM AG RP
0.5
1.0
1
2
3
4
5
6
7
CC
PP
PP
Empty

LITHOLOGIC DESCRIPTION

NANNOFOSSIL OOZE

- Dominant colors: white (7.5YR N8) and light gray (2.5Y N7) with intervals of white (2.5Y N8), white (10YR 8/1), light gray (5Y 7/1), and gray (5Y 6/1). Core Catcher is white (5Y 8/1–5Y 8/2). Minor colors: burrow in Section 1 is gray (2.5Y N5).
- Section 1 of this core is soupy, Section 2 is moderately deformed and appears to be flow-in; Sections 3 and 4 are moderately deformed. Sections 5, 6, and Core Catcher are slightly deformed.
- This core contains homogeneous nannofossil ooze. There is a single gray burrow in Section 1, 95–96 cm.

SMEAR SLIDE SUMMARY (%)

	3, 146 D	5, 71 D	6, 80 D
Texture:			
Sand	2	3	4
Silt	2	10	7
Clay	96	87	89
Composition:			
Quartz	1	Tr	1
Mica	1	1	-
Clay	–	1	Tr
Volcanic glass	–	–	Tr
Pyrite	–	–	4
Foraminifers	2	3	5
Calc. nannofossils	96	96	90
Diatoms	–	Tr	–

$CaCO_3$ data: 3, 146 cm = 91%
5, 70 cm = 75%
6, 80 cm = 51%

SITE 577 HOLE A CORE 6 CORED INTERVAL 2725.0–2734.5 mbsl; 47.4–56.9 mbsf

TIME – ROCK UNIT	BIOSTRATIGRAPHIC ZONE	FORAMINIFERS	NANNOFOSSILS	RADIOLARIANS	DIATOMS	SECTION	METERS
late Miocene–early Pliocene	N. D. quinqueramus (CN9)–A. tricorniculatus (CN10) zones R. S. peregrina zone F N15–N19 mixed assemblage	CP	CM	AG AG	RP	1 2 3 4 5 6 7 CC	0.5 1.0

GRAPHIC LITHOLOGY

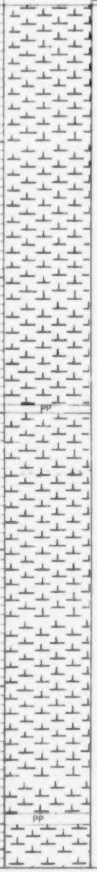

DRILLING DISTURBANCE

SEDIMENTARY STRUCTURES

SAMPLES

LITHOLOGIC DESCRIPTION

NANNOFOSSIL OOZE

*Dominant colors: white (10YR 8/1–10YR 8/2), white (5Y 8/2), white (2.5Y N8), white (7.5YR N8), and white (7.5YR 8/1) with intervals of light gray (5Y 7/1) and light gray (10YR 7/2); color changes below Section 5 to pale brown (10YR 6/3), very pale brown (10YR 7/3–10YR 7/4), very pale brown (10YR 8/3), and light yellowish brown (10YR 6/4). Minor colors: light brownish gray (10YR 6/2) ash.

*Sections 1 to 6, 60 cm are slightly deformed. Core below Section 6, 60 cm is very deformed, resulting from flow-in.

*This core contains nannofossil ooze lightly mottled below Section 2. All downcore color changes are gradational. Section 4, 66–68 cm is an ash layer (see smear slide summary below).

SMEAR SLIDE SUMMARY (%):

	1, 6 D	4, 68 M	6, 30 D
Texture:			
Sand	5	40	0
Silt	10	40	35
Clay	85	20	65
Composition:			
Quartz	1	2	5
Mica	Tr	—	—
Clay	1	3	10
Volcanic glass	—	50	10
Palagonite	—	5	—
Pyrite	5	—	—
Carbonate unspec.	—	5	3
Foraminifers	7	—	10
Calc. nannofossils	85	35	50
Diatoms	1	—	—
Sponge spicules	—	—	2
Discoasters	—	—	10

$CaCO_3$ data: 1, 5 cm = 72%
4, 68 cm = 56%
6, 28 cm = 65%

SITE 577 HOLE A CORE 7 CORED INTERVAL 2734.5–2744.0 mbsl; 56.9–66.4 mbsf

TIME – ROCK UNIT	BIOSTRATIGRAPHIC ZONE	FORAMINIFERS	NANNOFOSSILS	RADIOLARIANS	DIATOMS	SECTION	METERS
early Eocene–late Miocene	N. subbotinae (CP12) zone–A. primus (CN8b) subzone F P8–P10	AG	AM	B	B	1 2 3 4 5 6 7 CC	0.5 1.0

GRAPHIC LITHOLOGY

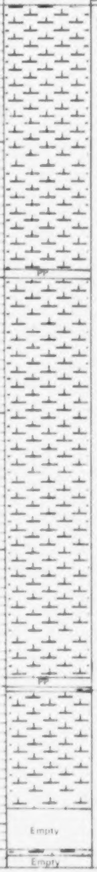

DRILLING DISTURBANCE

SEDIMENTARY STRUCTURES

SAMPLES

LITHOLOGIC DESCRIPTION

NANNOFOSSIL OOZE

*Dominant colors: Sections 1 to 4, 90 cm are white (10YR 8/2), very pale brown (10YR 7/3–10YR 8/3) pale brown (10YR 6/3), and yellowish brown (10YR 5/4). Section 4, 90 cm through Section 5 is light gray (2.5Y 7/2). Section 6 and the Core Catcher are white (10YR 8/2) and very pale brown (10Y 7/3).

*Sections 1 to 4, 90 cm are very deformed or soupy, resulting from flow-in. The rest of the core is moderately or slightly deformed, some or all of which may have resulted from flow-in.

*This core contains nannofossil ooze with mottled zones in Sections 1 and 5.

SMEAR SLIDE SUMMARY (%):

	1, 10 D	5, 100 D	6, 70 D
Texture:			
Sand	0	0	1
Silt	30	10	15
Clay	70	90	84
Composition:			
Quartz	4	3	5
Feldspar	Tr	—	–
Heavy minerals	1	—	–
Clay	Tr	7	5
Volcanic glass	Tr	10	2
Glauconite	—	—	Tr
Zeolite	—	—	1
Carbonate unspec.	—	—	10
Foraminifers	5	—	—
Calc. nannofossils	70	75	65
Sponge spicules	—	—	2
Discoasters	20	5	10

$CaCO_3$ data: 1, 10 cm = 81%
5, 100 cm = 96%
6, 68 cm = 94%

SITE 577 HOLE A CORE 8 CORED INTERVAL 2744.0–2753.5 mbsl; 66.4–75.9 mbsf

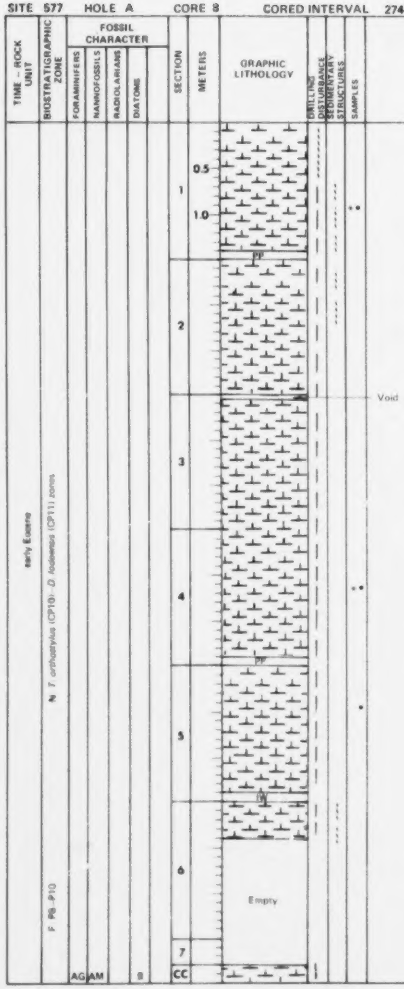
TIME – ROCK UNIT
BIOSTRATIGRAPHIC ZONE
FOSSIL CHARACTER
FORAMINIFERS
NANNOFOSSILS
RADIOLARIANS
DIATOMS
SECTION
METERS
GRAPHIC LITHOLOGY
DRILLING DISTURBANCE
SEDIMENTARY STRUCTURES
SAMPLES
early Eocene
N T. orthostylus (CP10)–D. lodoensis (CP11) zones
F P8–P10
AG
AM
B
1
2
3
4
5
6
7
CC
0.5
1.0
PP
IW
Void
Empty

LITHOLOGIC DESCRIPTION

NANNOFOSSIL OOZE

- Dominant colors: very pale brown (10YR 7/3–10YR 8/3). Minor colors: Section 1, 0–60 cm is light gray (2.5Y 7/2) with very pale brown (10YR 7/3–10YR 8/3) and white (10YR 8/1) distorted laminations. Section 1, 60–150 cm has small black mottles. Section 2 contains large white (10YR 8/2) mottles. Sections 2 through 5 contain faint thin (0.5 cm) black layers and zones.
- This core has been slightly deformed, except for Section 1, 0–60 cm which is very deformed and consists of flow in.
- This core contains nannofossil ooze with common thin black layers and zones.

SMEAR SLIDE SUMMARY (%):

	1, 95	4, 70
	D	D
Texture:		
Sand	0	0
Silt	50	50
Clay	50	50
Composition:		
Quartz	1	2
Clay	3	5
Volcanic glass	1	–
Carbonate unspec.	5	5
Foraminifers		Tr
Calc. nannofossils	85	85
Discoasters	5	3

CaCO$_3$ data 1, 95 cm = 94%
4, 68 cm = 96%
5, 46 cm = 94%

SITE 577 HOLE A CORE 9 CORED INTERVAL 2753.5–2763.0 mbsl; 75.9–85.4 mbsf

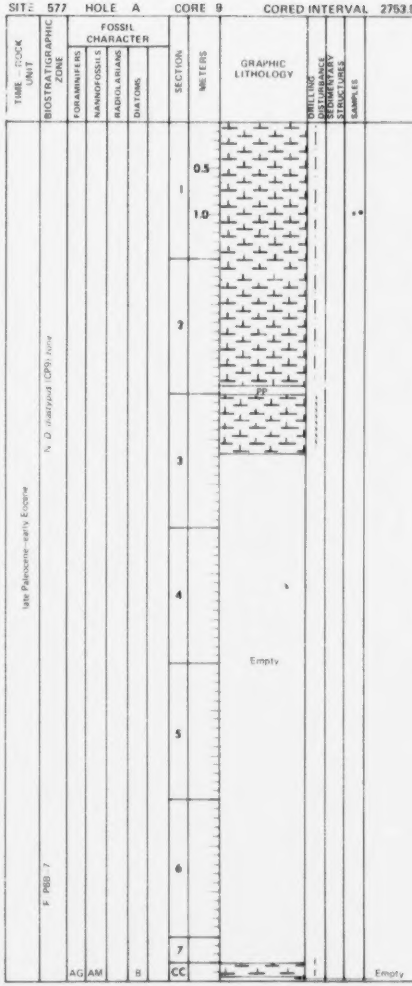
TIME – ROCK UNIT
BIOSTRATIGRAPHIC ZONE
FOSSIL CHARACTER
FORAMINIFERS
NANNOFOSSILS
RADIOLARIANS
DIATOMS
SECTION
METERS
GRAPHIC LITHOLOGY
DRILLING DISTURBANCE
SEDIMENTARY STRUCTURES
SAMPLES
late Paleocene–early Eocene
N D. diastypus (CP9) zone
F P6B–7
AG
AM
B
1
2
3
4
5
6
7
CC
0.5
1.0
PP
Empty
Empty

LITHOLOGIC DESCRIPTION

NANNOFOSSIL OOZE

- Dominant colors: very pale brown (10YR 8/3), very pale brown (10YR 7/4), and white (10YR 8/2). Minor colors: white (2.5Y 8/0) pumice cobble.
- Sections 1 and 2 of this core are moderately deformed; Section 3 is very deformed.
- This core consists of homogeneous nannofossil ooze, with small, infrequent mottles in Section 2. Section 1, 0–4 cm contains a single white pumice cobble 3 cm in diameter.

SMEAR SLIDE SUMMARY (%):

	1, 100
	D
Texture:	
Sand	0
Silt	40
Clay	60
Composition:	
Quartz	2
Clay	3
Volcanic glass	3
Glauconite	5
Carbonate unspec.	3
Calc. nannofossils	81
Discoasters	3

CaCO$_3$ data 1, 100 cm = 97%

SITE 577 HOLE A CORE 10 CORED INTERVAL 2763.0–2772.5 mbsl; 85.4–94.9 mbsf

TIME – ROCK UNIT	BIOSTRATIGRAPHIC ZONE	FORAMINIFERS	NANNOFOSSILS	RADIOLARIANS	DIATOMS
early Paleocene	N F. tympaniformis (CP4) D. nobilis (CP7) zone F P3	AM	AM		B

SECTION: 1, 2, 3, 4, 5, 6, 7, CC

METERS: 0.5, 1.0

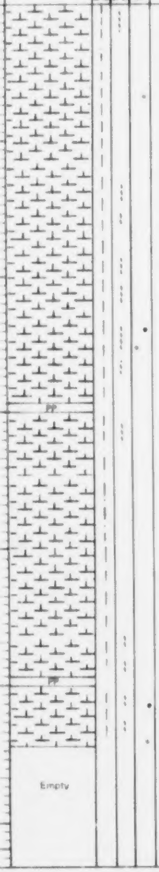

LITHOLOGIC DESCRIPTION

NANNOFOSSIL OOZE

- Dominant colors: white (10YR 8/2) with white (10YR 8/1) and very pale brown (10YR 7/3) mottles. Very pale brown (10YR 7/3–10YR 8/3) with white (10YR 8/2) and light yellowish brown (10YR 6/4) mottles. Sections 5 and 6 contain intervals of light yellowish brown (10YR 6/4) nannofossil ooze.
- This core is slightly deformed, except for Section 4 which is moderately deformed.
- This core consists of homogeneous nannofossil ooze with infrequent mottles. All downcore color changes have gradational contacts.

SMEAR SLIDE SUMMARY (%)

	1, 100	3, 80	6, 60
	D	D	D
Texture:			
Sand *	3	0	1
Silt	37	30	39
Clay	60	70	60
Composition:			
Quartz	5	3	5
Feldspar	2	—	2
Heavy minerals	1		1
Clay	5	3	5
Volcanic glass	2	2	2
Glauconite		1	
Zeolite		1	
Carbonate unspec.	—	4	
Foraminifers	Tr	—	—
Calc. nannofossils	80	86	85
Discoasters	5	—	—

CaCO$_3$ data: 3, 60 cm = 90%
6, 24 cm = 96%

SITE 577 HOLE A CORE 11 CORED INTERVAL 2772.5–2782.0 mbsl; 94.9–104.4 mbsf

TIME – ROCK UNIT	BIOSTRATIGRAPHIC ZONE	FORAMINIFERS	NANNOFOSSILS	RADIOLARIANS	DIATOMS
early Paleocene	N C. danius (CP2)–F. tympaniformis (CP4) zones F P1 G. pseudobulloides	AM	AM		B

SECTION: 1, 2, 3, 4, 5, 6, 7, CC

METERS: 0.5, 1.0

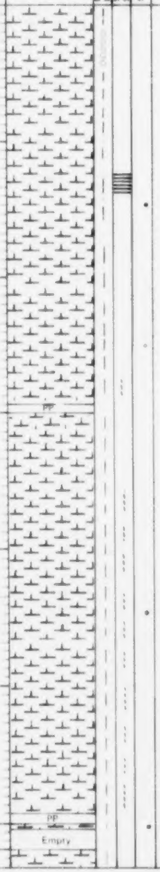

LITHOLOGIC DESCRIPTION

NANNOFOSSIL OOZE

- Dominant colors: white (10YR 8/2), and very pale brown (10YR 7/3–10YR 8/3) with interval of very pale brown (10YR 7/4) in Section 6. Sections 3 through 6 contain white (10YR 8/1) mottles.
- This core is slightly deformed, except for Section 2 which is moderately deformed. Section 1 contains a soupy interval from 30–70 cm.
- This core consists of homogeneous to slightly mottled nannofossil ooze.

SMEAR SLIDE SUMMARY (%)

	3, 75
	D
Texture:	
Sand	0
Silt	50
Clay	50
Composition:	
Quartz	3
Clay	3
Volcanic glass	2
Glauconite	1
Carbonate unspec.	3
Calc. nannofossils	88

CaCO$_3$ data: 2, 70 cm = 97%
5, 70 cm = 98%
7, 3 cm = 92%

SITE 577 HOLE A CORE 12 CORED INTERVAL 2782.0–2791.5 mbsl; 104.4–113.9 mbsf

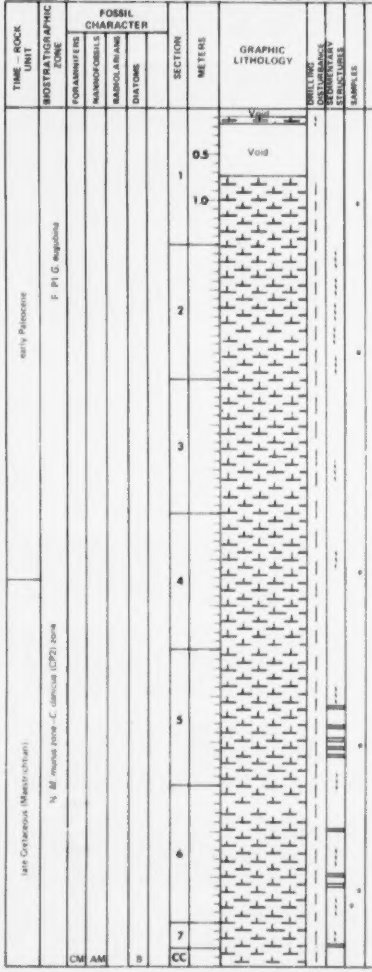
TIME – ROCK UNIT
BIOSTRATIGRAPHIC ZONE
FOSSIL CHARACTER
FORAMINIFERS
NANNOFOSSILS
RADIOLARIANS
DIATOMS
SECTION
METERS
GRAPHIC LITHOLOGY
DRILLING DISTURBANCE
SEDIMENTARY STRUCTURES
SAMPLES
early Paleocene
late Cretaceous (Maestrichtian)
F P1 G. eugubina
N M. murus zone–C. danicus (CP2) zone
CM
AM
B
Void
Void
0.5
1.0
1
2
3
4
5
6
7
CC

LITHOLOGIC DESCRIPTION

NANNOFOSSIL OOZE

- Dominant colors: very pale brown (10YR 7/3–10YR 7/4), very pale brown (10YR 8/3), white (10YR 8/1–10YR 8/2), and light yellowish brown (10YR 6/4). Sections 4 through the Core Catcher are dominantly white (10YR 8/1–10YR 8/2).
- Core is slightly deformed throughout.
- This core consists of homogeneous to slightly mottled nannofossil ooze. Sections 5 and 6 contain thin (1 cm) laminations of light yellowish brown nannofossil ooze. All downcore color changes are gradational contacts.

SMEAR SLIDE SUMMARY (%):

	1, 107 D	4, 70 D	5, 105 D	6, 117 D	6, 132 D
Texture:					
Sand	0	0	0	0	0
Silt	20	20	20	30	30
Clay	80	80	80	70	70
Composition:					
Quartz	2	2	2	2	2
Clay	3	5	3	3	5
Volcanic glass	2	3	2	2	2
Palagonite	1	–	–	–	–
Glauconite	1	–	2	–	1
Carbonate unspec.	5	5	7	7	3
Foraminifers	1	–	Tr	–	Tr
Calc. nannofossils	85	85	84	86	87
Sponge spicules	–	–	–	–	Tr

$CaCO_3$ data: 2, 120 cm = 96%

SITE 577 HOLE A CORE 13 CORED INTERVAL 2791.5–2801.0 mbsl; 113.9–123.4 mbsf

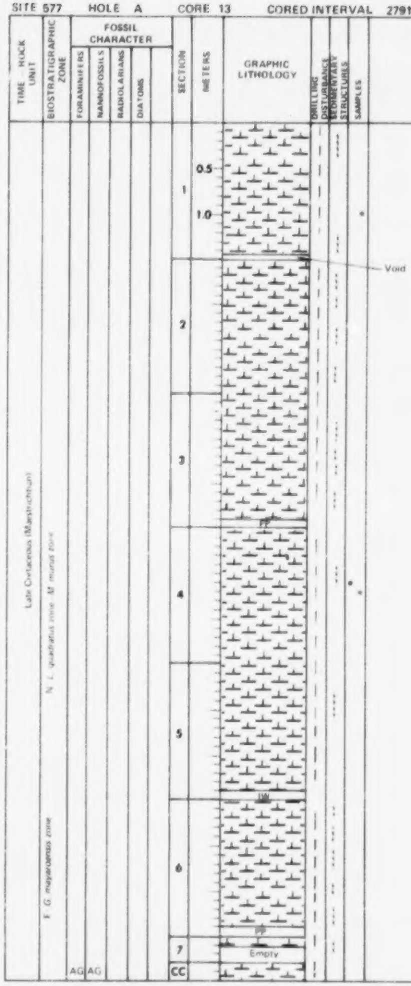
TIME – ROCK UNIT
BIOSTRATIGRAPHIC ZONE
FOSSIL CHARACTER
FORAMINIFERS
NANNOFOSSILS
RADIOLARIANS
DIATOMS
SECTION
METERS
GRAPHIC LITHOLOGY
DRILLING DISTURBANCE
SEDIMENTARY STRUCTURES
SAMPLES
Late Cretaceous (Maestrichtian)
N L. quadratus zone–M. murus zone
F G. mayaroensis zone
AG
AG
Void
Empty
0.5
1.0
1
2
3
4
5
6
7
CC

LITHOLOGIC DESCRIPTION

NANNOFOSSIL OOZE

- Dominant colors: white (10YR 8/2). Minor colors: white (10YR 8/1) and very pale brown (10YR 7/3–10YR 8/3) mottles.
- Core is slightly deformed throughout.
- This core consists of uniform, white nannofossil ooze with minor mottles.

SMEAR SLIDE SUMMARY (%):

	1, 100 D	4, 75 D
Texture:		
Sand	2	0
Silt	38	40
Clay	60	60
Composition:		
Quartz	5	2
Feldspar	2	–
Heavy minerals	1	–
Clay	5	3
Volcanic glass	2	2
Glauconite	–	1
Carbonate unspec.	5	5
Calc. nannofossils	80	87

$CaCO_3$ data: 4, 60 cm = 97%

SITE 577 HOLE B CORE 1 CORED INTERVAL 2782.0–2791.5 mbsl; 104.4–113.9 mbsf

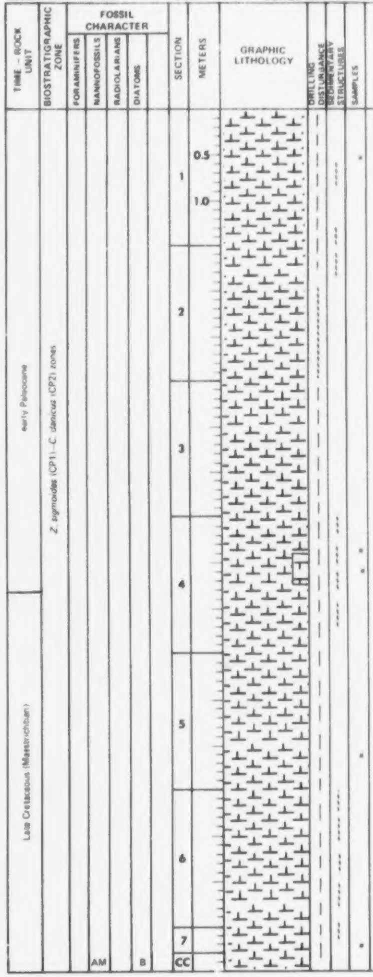
TIME – ROCK UNIT
BIOSTRATIGRAPHIC ZONE
FOSSIL CHARACTER
FORAMINIFERS
NANNOFOSSILS
RADIOLARIANS
DIATOMS
SECTION
METERS
GRAPHIC LITHOLOGY
DRILLING DISTURBANCE
SEDIMENTARY STRUCTURES
SAMPLES
early Paleocene
Late Cretaceous (Maastrichtian)
Z. sigmoides (CP1)–C. danicus (CP2) zones
AM
B
0.5
1.0
1
2
3
4
5
6
7
CC

LITHOLOGIC DESCRIPTION

NANNOFOSSIL OOZE

*Dominant colors: very pale brown (10YR 7/4–10YR 8/4), very pale brown (10YR 7/3–10YR 8/3), and light yellowish brown (10YR 6/4) changing to white (10YR 8/1–10YR 8/2) at base of Section 3. Sections 4 through 6 contain thin intervals of very pale brown (10YR 7/4), yellowish brown (10YR 5/4), and light gray (2.5Y N7).

*Section 2, 32–150 cm is very deformed flow in. The rest of the core is slightly deformed.

*This core consists of homogeneous to slightly mottled nannofossil ooze. Downcore color changes are gradational.

SMEAR SLIDE SUMMARY (%):

	1, 80	4, 40	4, 65	5, 116	7, 25
	D	D	D	D	D
Texture:					
Sand	5	15	20	1	1
Silt	2	5	5	0	0
Clay	93	80	75	99	99
Composition:					
Quartz	Tr	Tr	Tr	Tr	Tr
Feldspar	–	–	–	–	Tr
Clay	25	3	15	25	10
Volcanic glass	1	3	–	Tr	–
Carbonate unspec.	1	2	–	1	–
Foraminifers	7	15	25	Tr	1
Calc. nannofossils	66	77	60	74	89
Sponge spicules	–	–	–	–	Tr

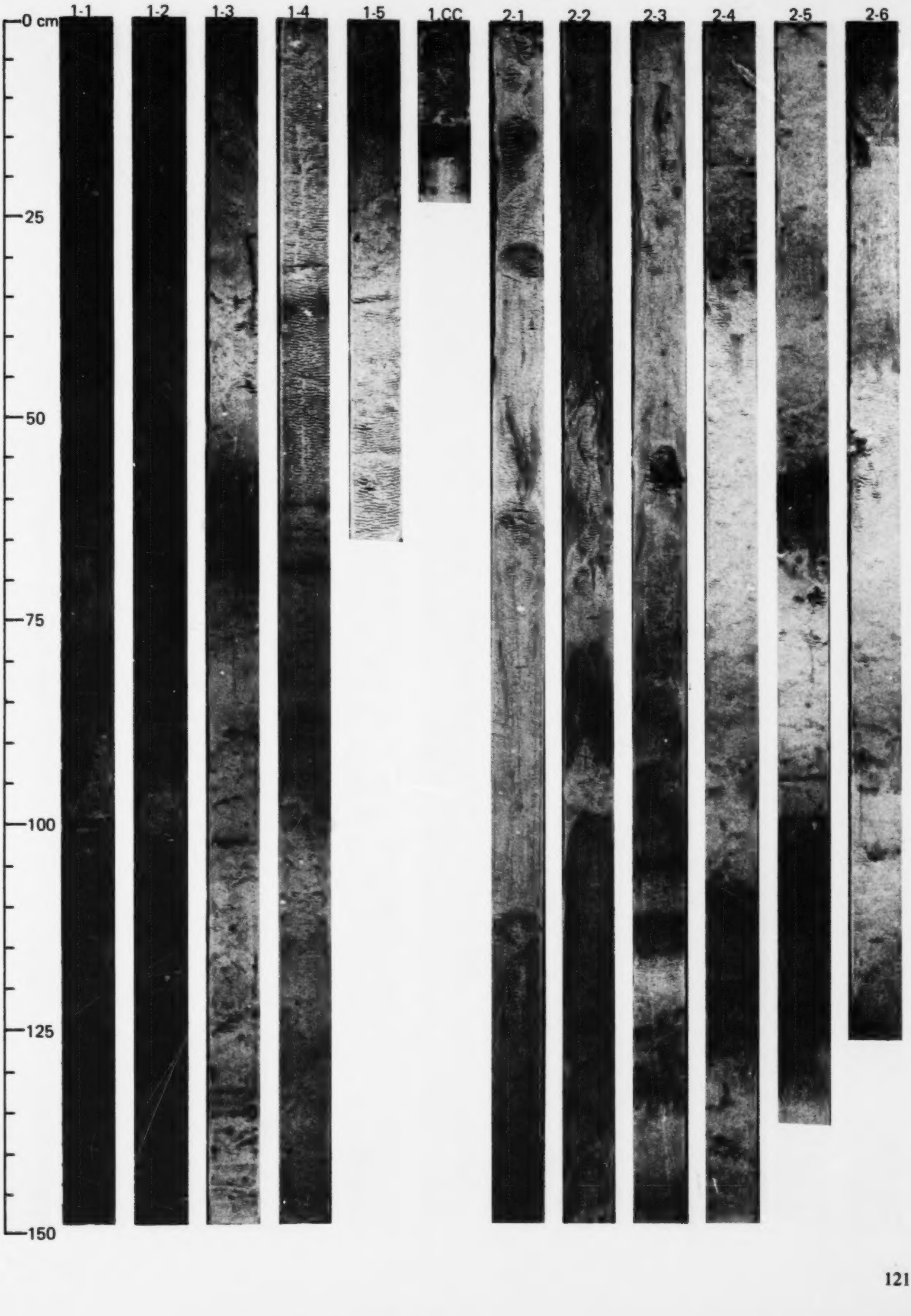
0 cm
25
50
75
100
125
150
1-1
1-2
1-3
1-4
1-5
1,CC
2-1
2-2
2-3
2-4
2-5
2-6

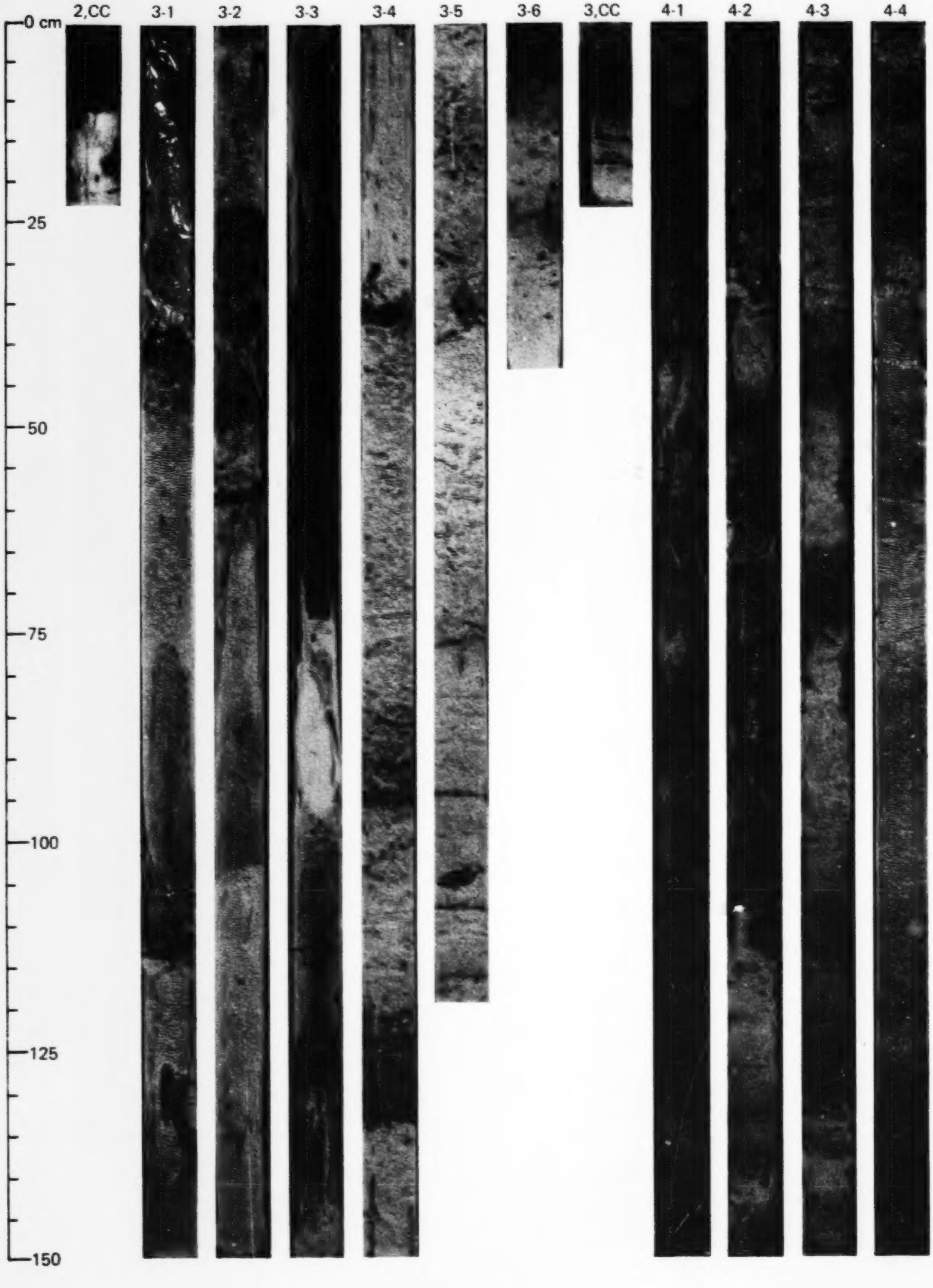
2,CC
3-1
3-2
3-3
3-4
3-5
3-6
3,CC
4-1
4-2
4-3
4-4
0 cm
25
50
75
100
125
150

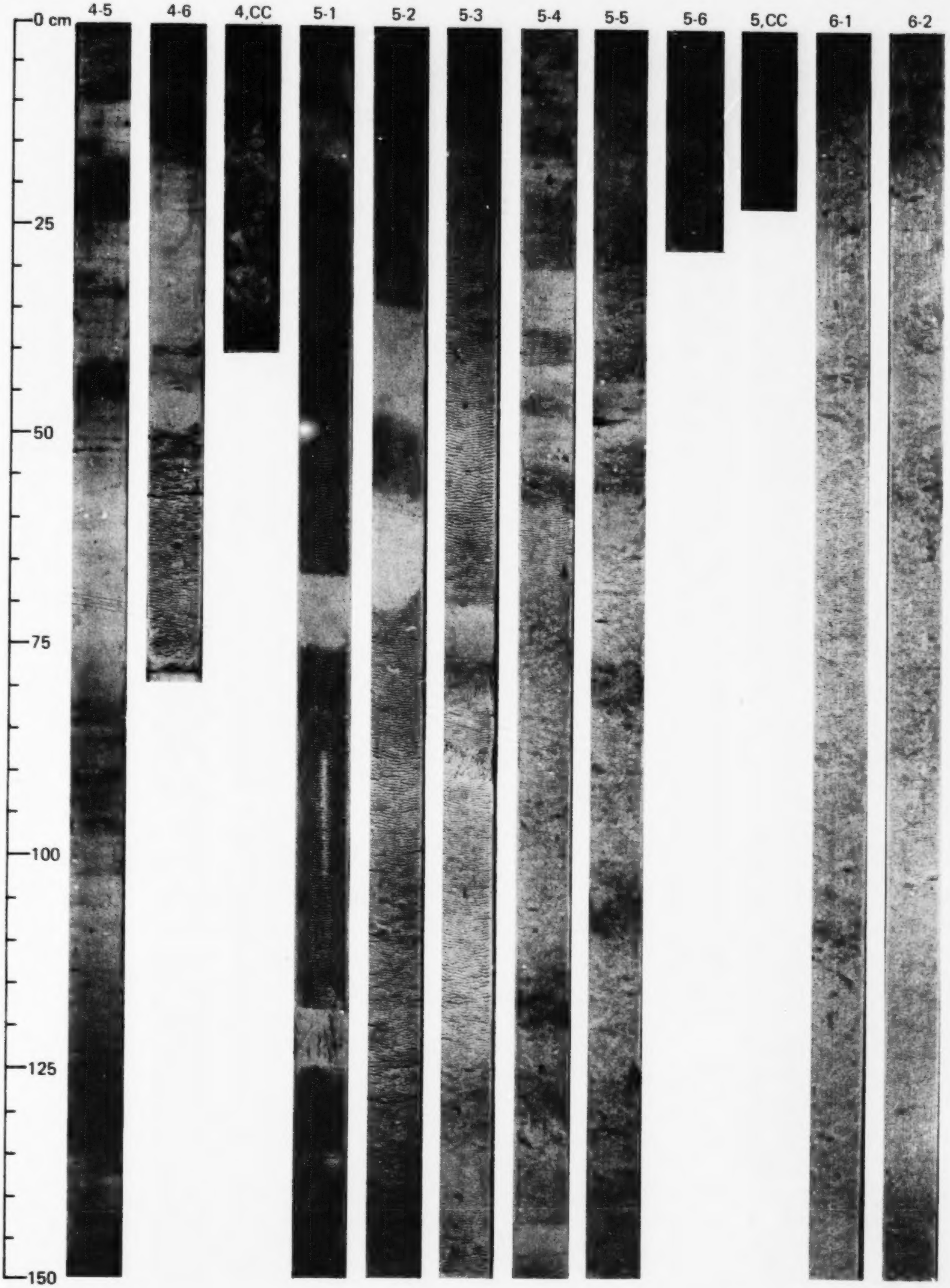
0 cm
25
50
75
100
125
150
4-5
4-6
4,CC
5-1
5-2
5-3
5-4
5-5
5-6
5,CC
6-1
6-2

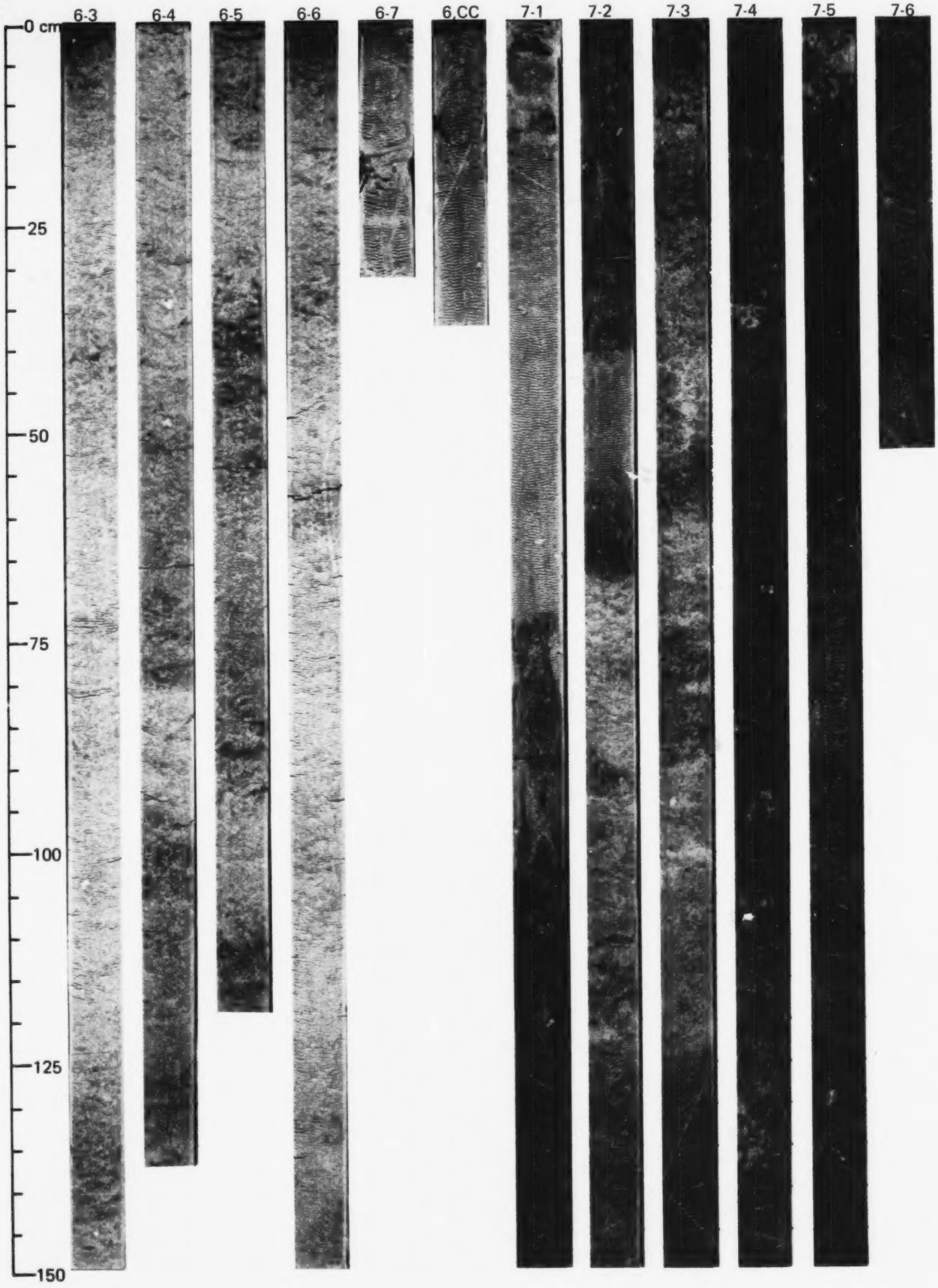
6-3
6-4
6-5
6-6
6-7
6,CC
7-1
7-2
7-3
7-4
7-5
7-6
0 cm
25
50
75
100
125
150

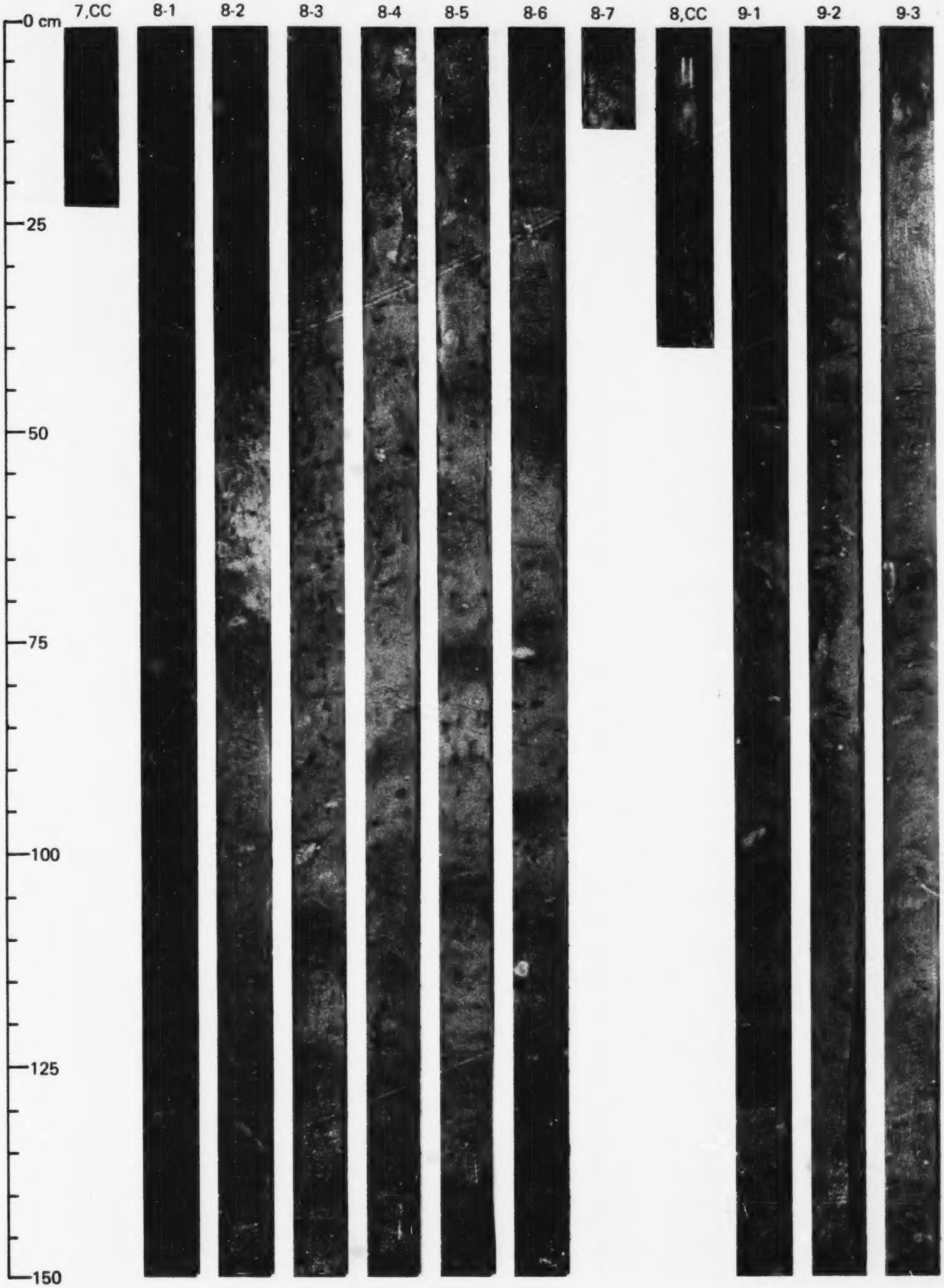
7,CC
8-1
8-2
8-3
8-4
8-5
8-6
8-7
8,CC
9-1
9-2
9-3
0 cm
25
50
75
100
125
150

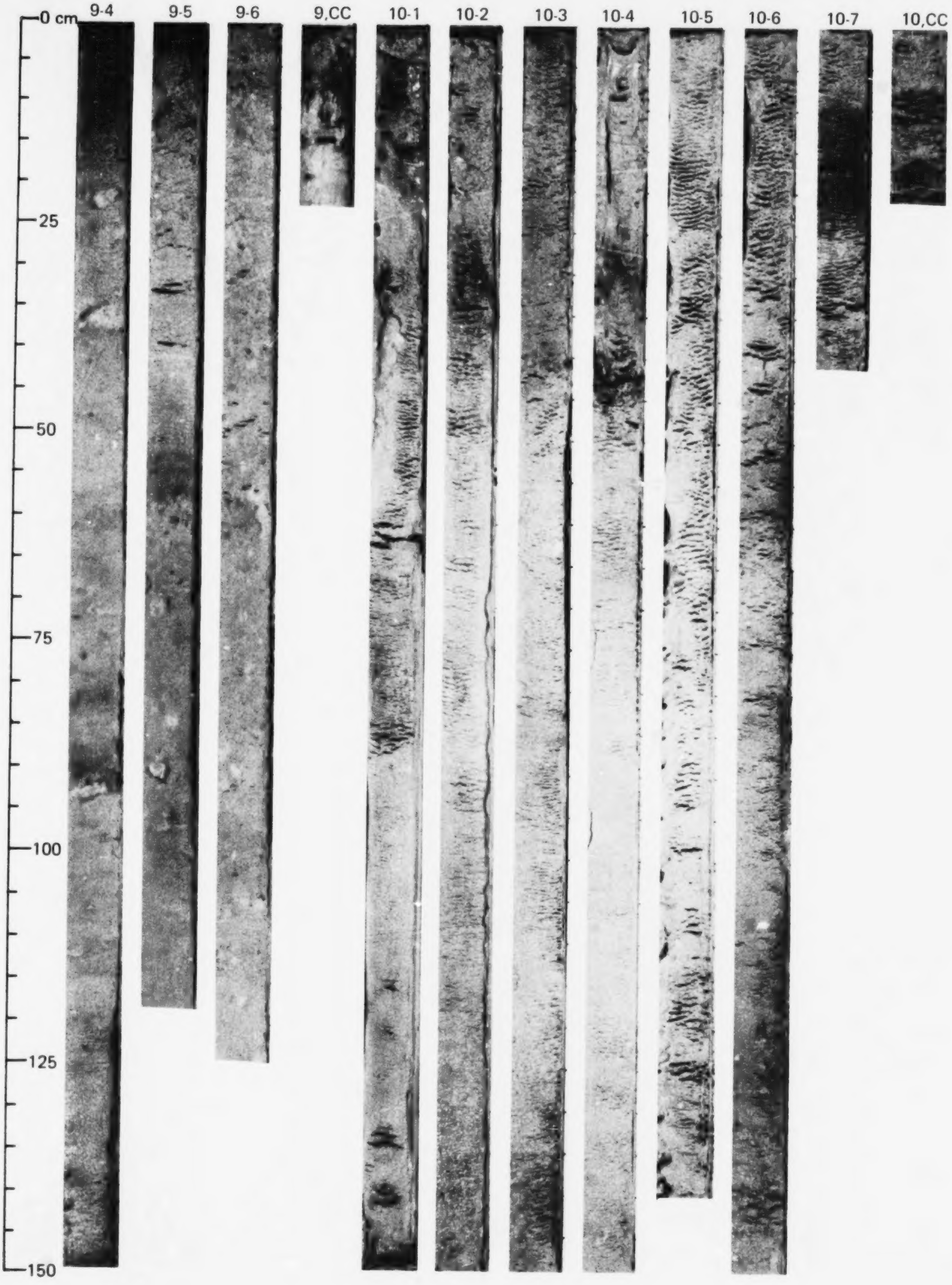
0 cm
25
50
75
100
125
150
9-4
9-5
9-6
9,CC
10-1
10-2
10-3
10-4
10-5
10-6
10-7
10,CC

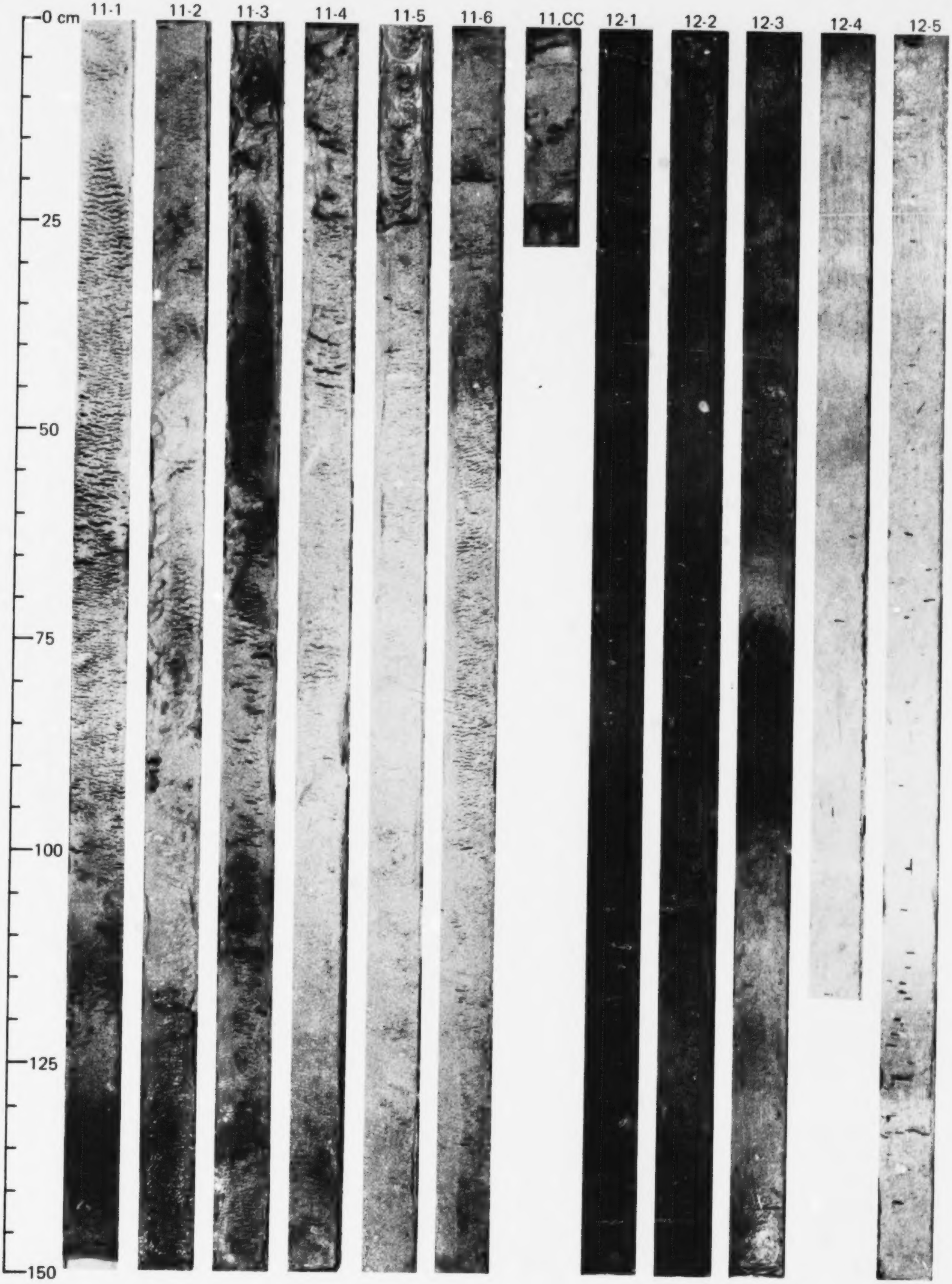
0 cm
25
50
75
100
125
150
11-1
11-2
11-3
11-4
11-5
11-6
11.CC
12-1
12-2
12-3
12-4
12-5

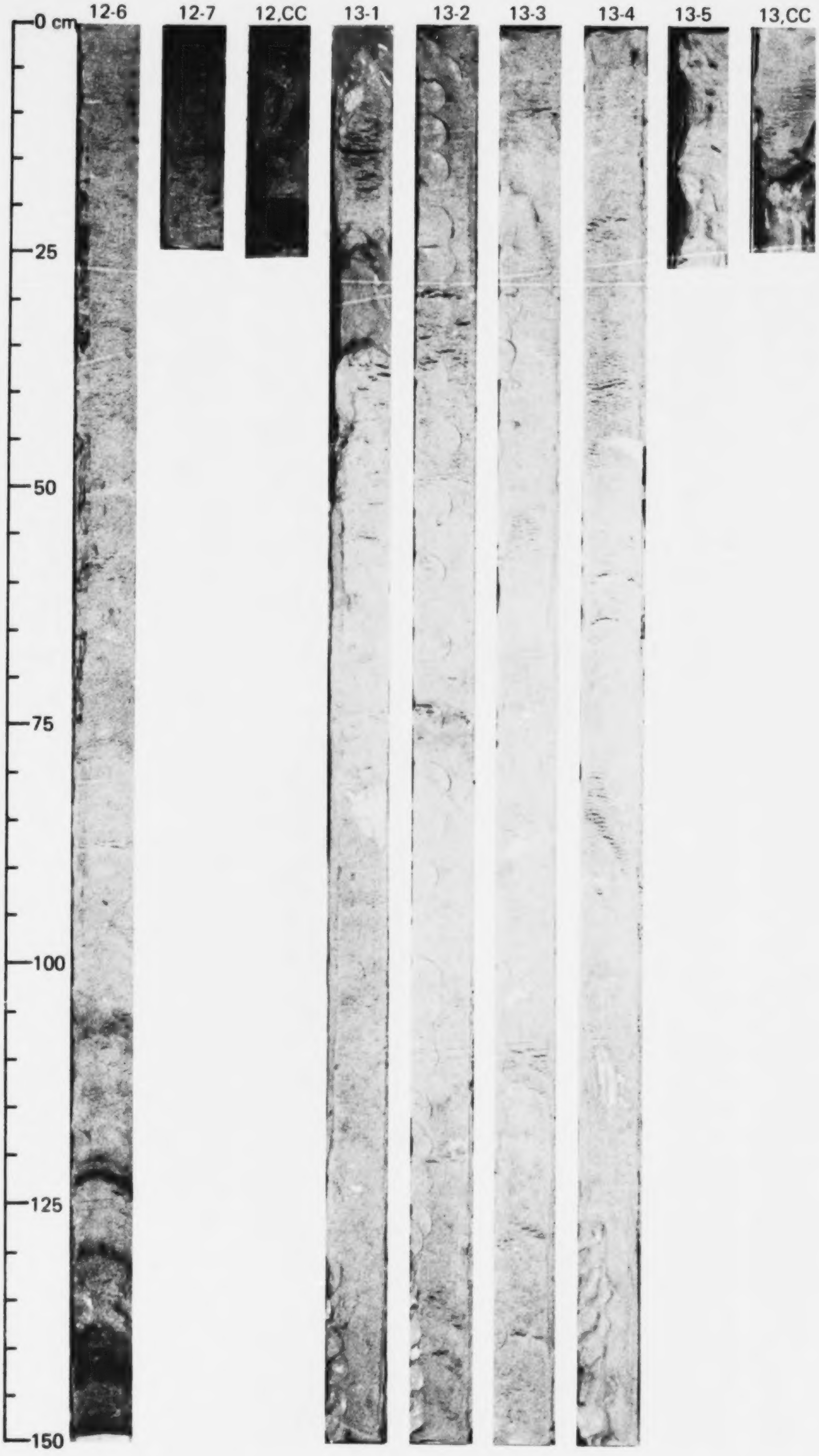
0 cm
25
50
75
100
125
150
12-6
12-7
12,CC
13-1
13-2
13-3
13-4
13-5
13,CC

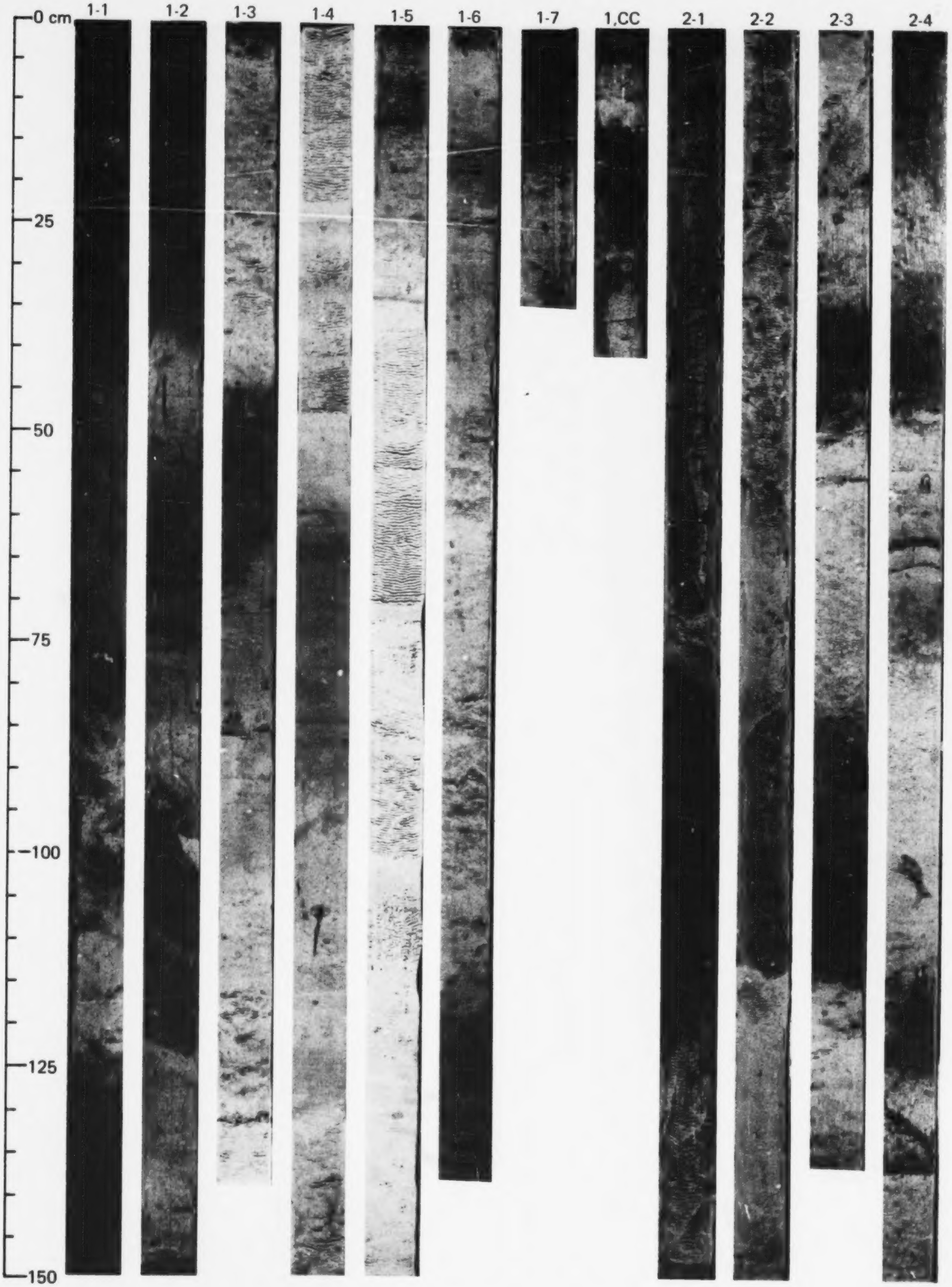
0 cm
25
50
75
100
125
150
1-1
1-2
1-3
1-4
1-5
1-6
1-7
1,CC
2-1
2-2
2-3
2-4

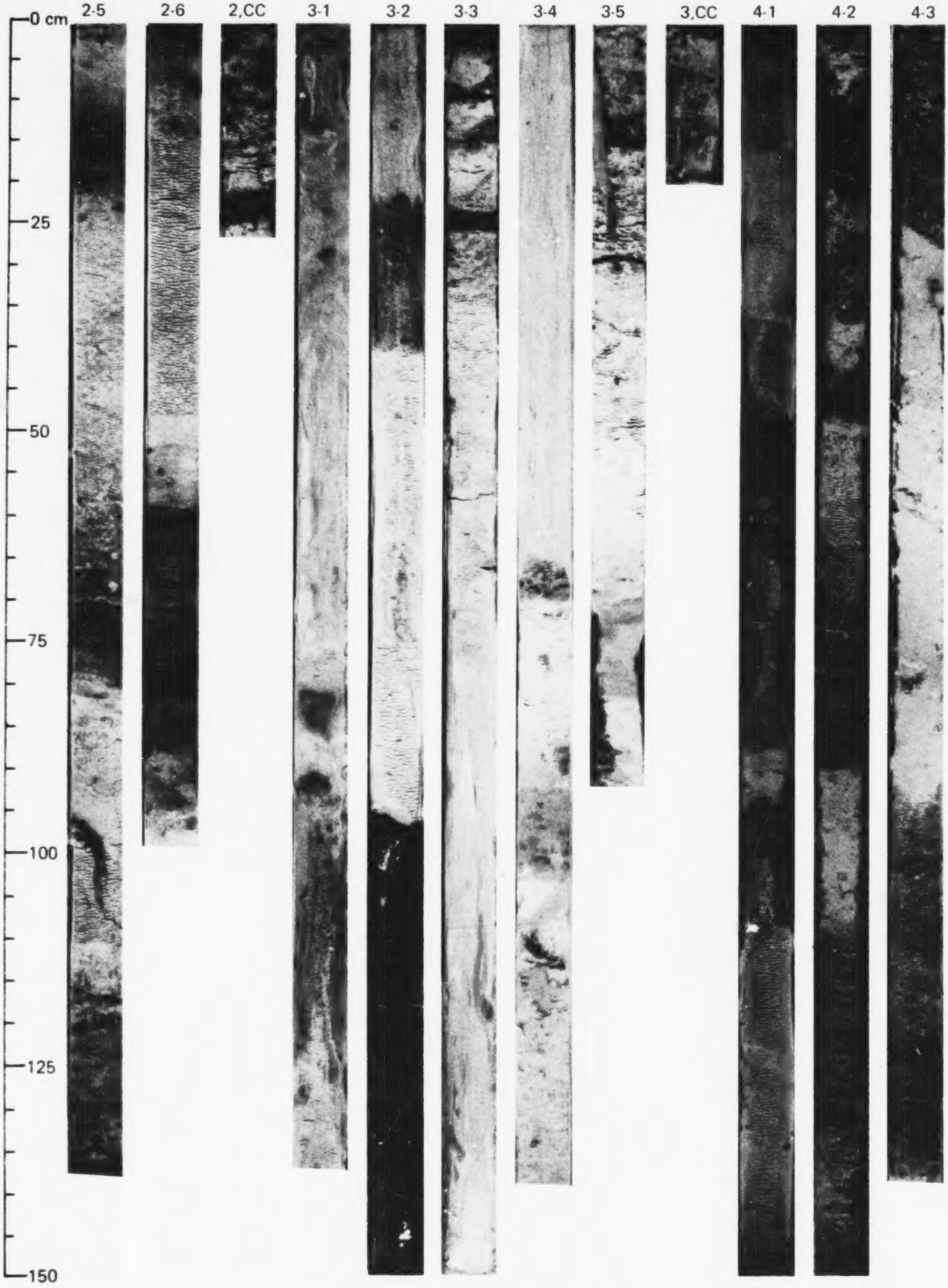
0 cm
25
50
75
100
125
150
2-5
2-6
2,CC
3-1
3-2
3-3
3-4
3-5
3,CC
4-1
4-2
4-3

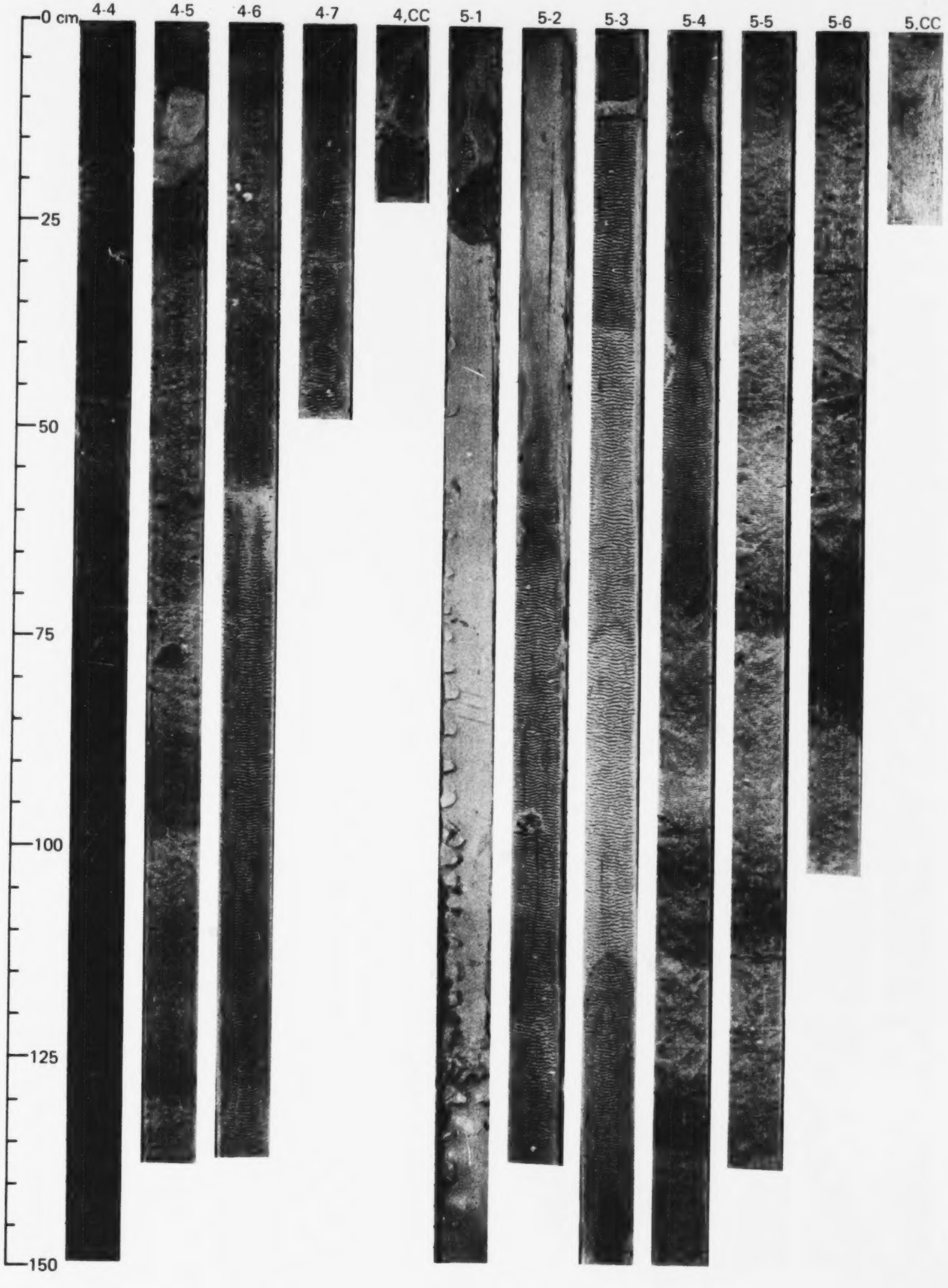
0 cm
25
50
75
100
125
150
4-4
4-5
4-6
4-7
4,CC
5-1
5-2
5-3
5-4
5-5
5-6
5,CC

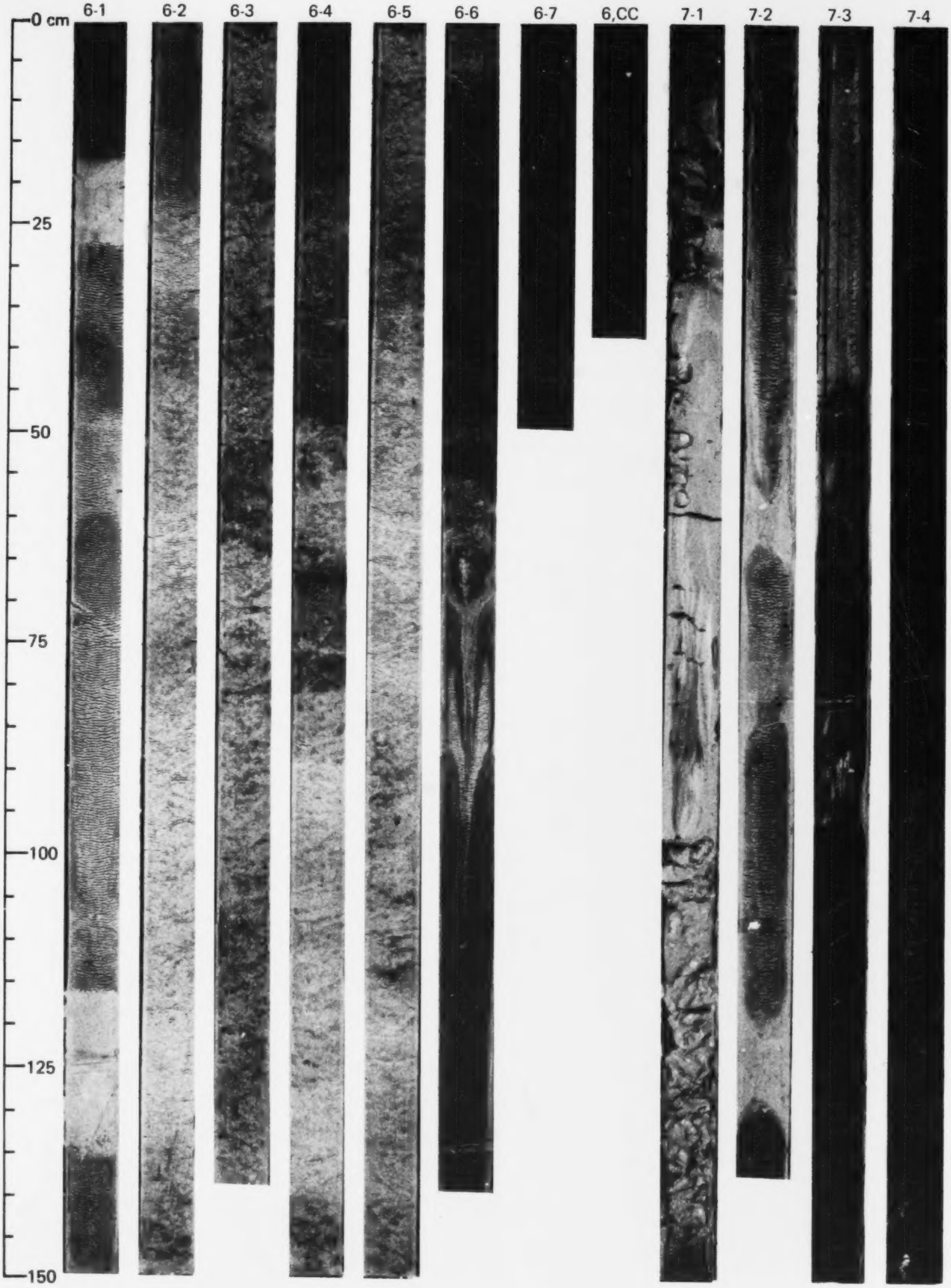
0 cm
25
50
75
100
125
150
6-1
6-2
6-3
6-4
6-5
6-6
6-7
6,CC
7-1
7-2
7-3
7-4

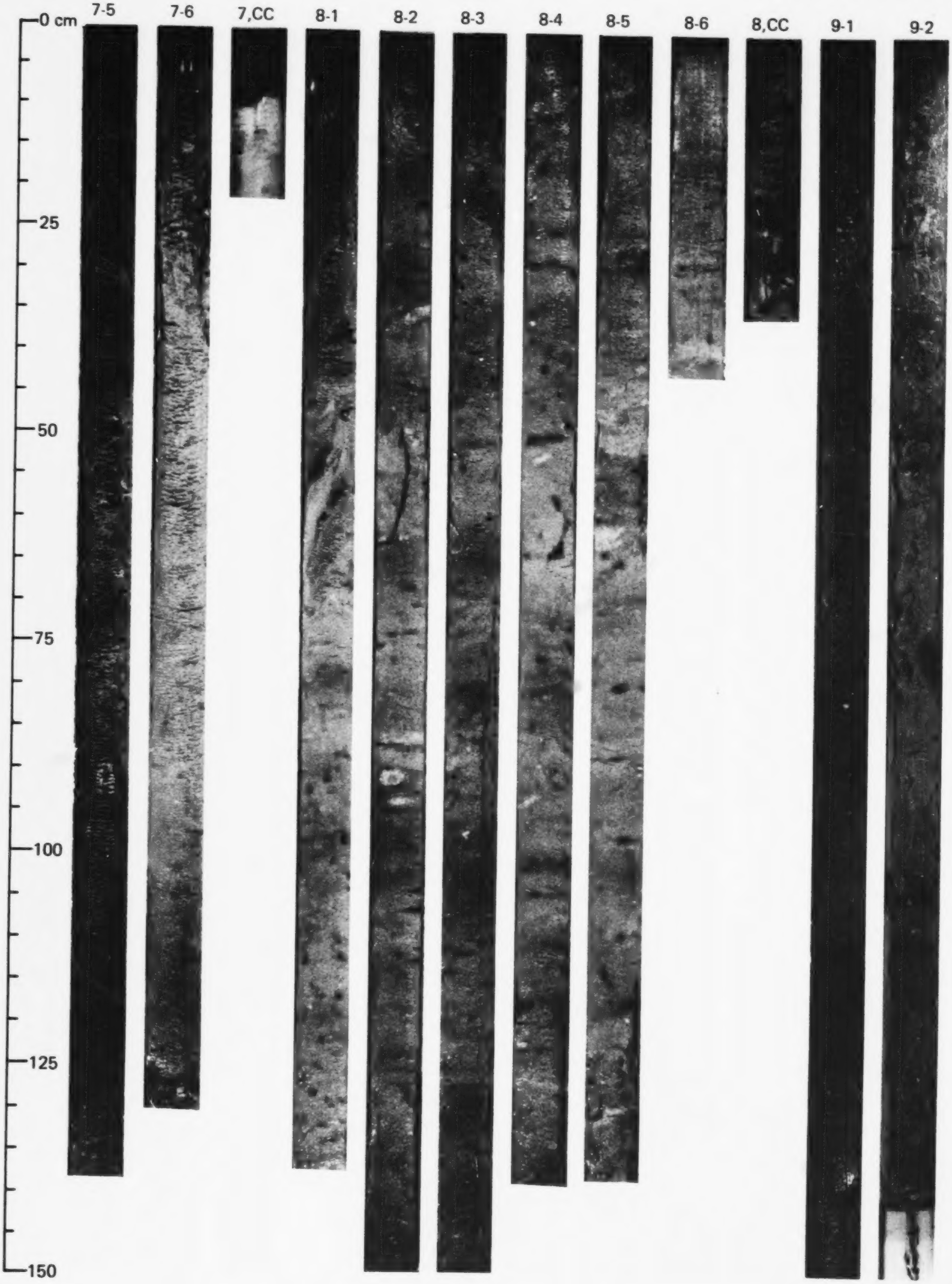
0 cm
25
50
75
100
125
150
7-5
7-6
7,CC
8-1
8-2
8-3
8-4
8-5
8-6
8,CC
9-1
9-2

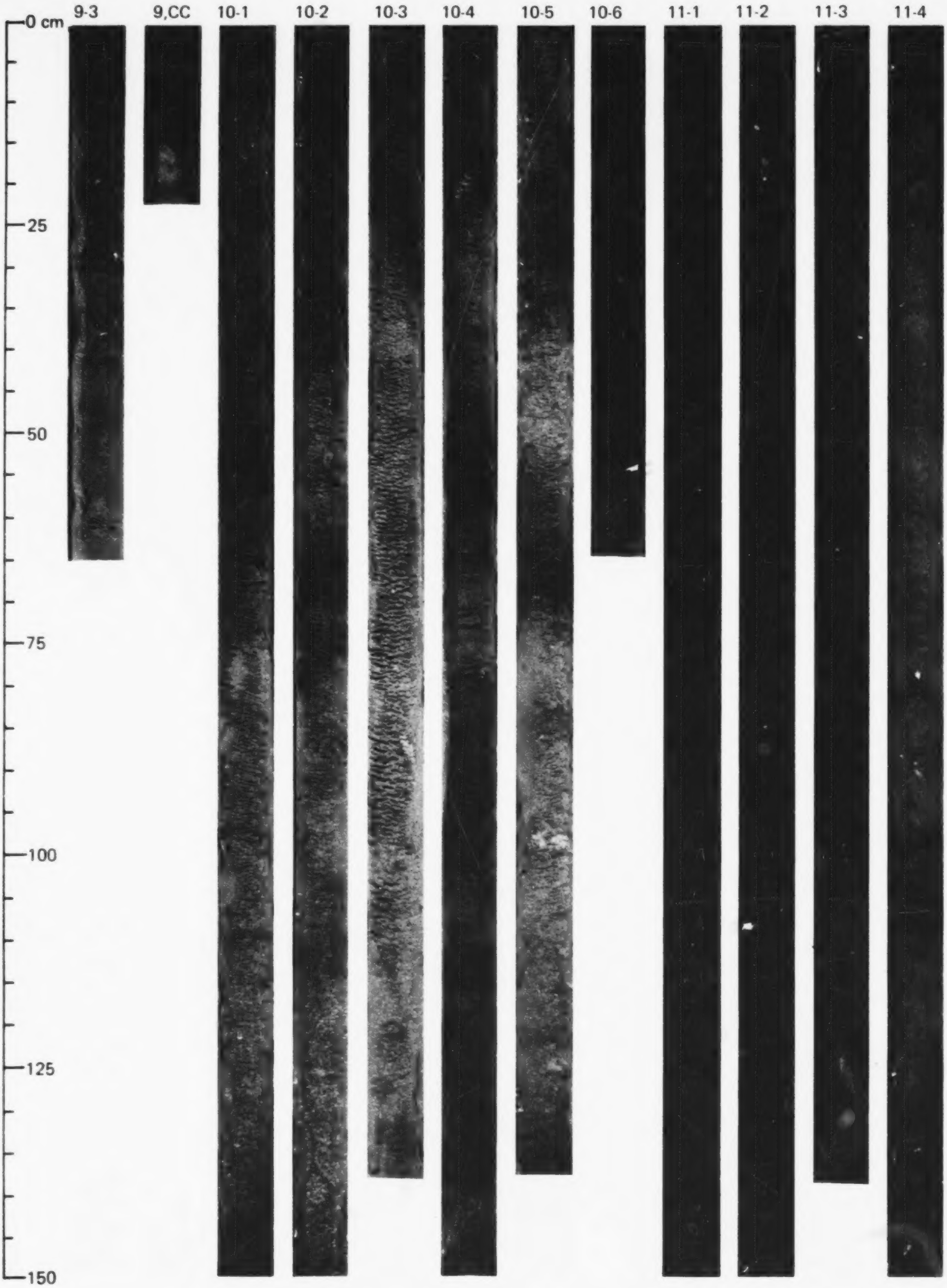
9-3
9,CC
10-1
10-2
10-3
10-4
10-5
10-6
11-1
11-2
11-3
11-4
0 cm
25
50
75
100
125
150

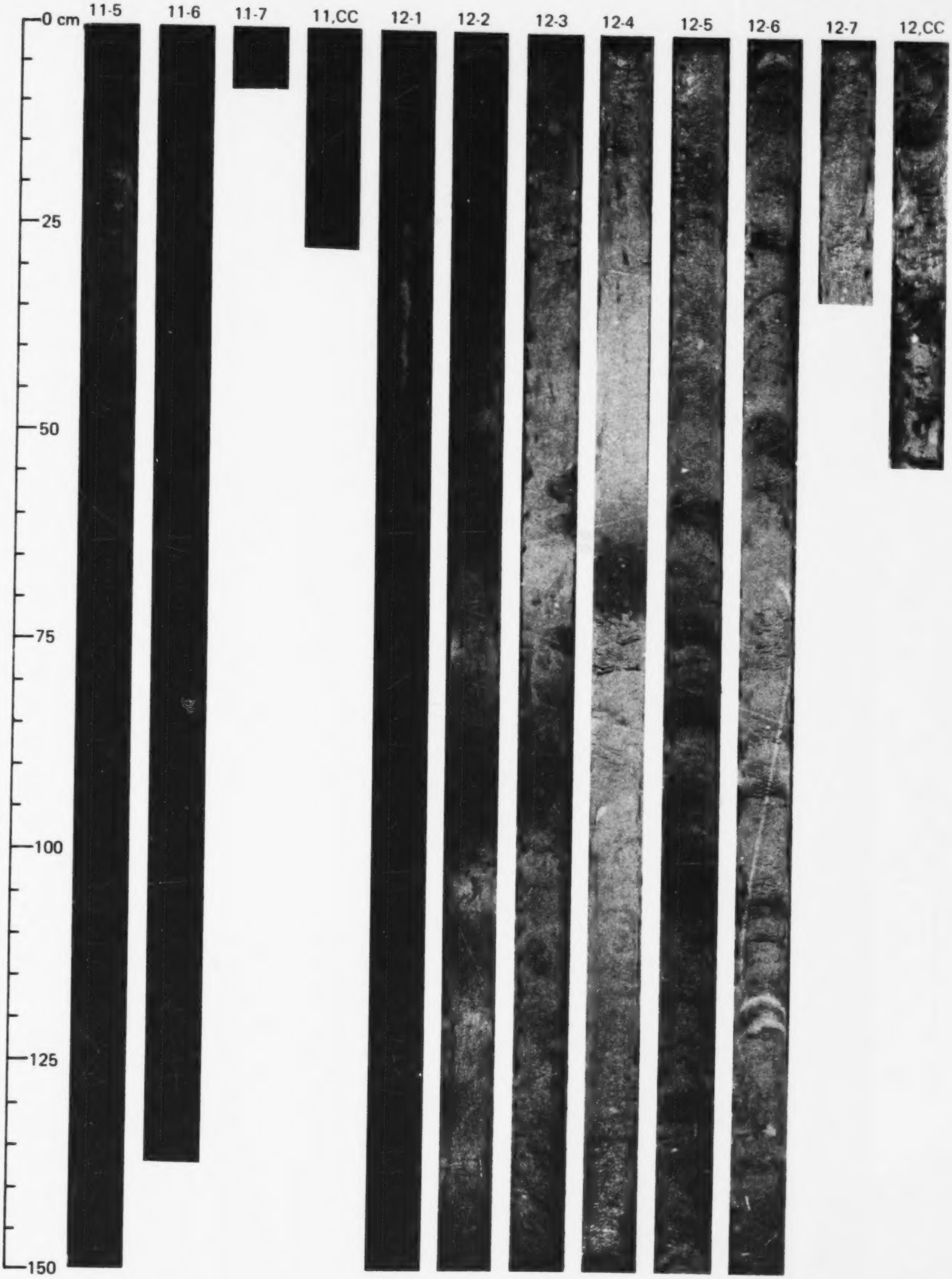
0 cm
25
50
75
100
125
150
11-5
11-6
11-7
11,CC
12-1
12-2
12-3
12-4
12-5
12-6
12-7
12,CC

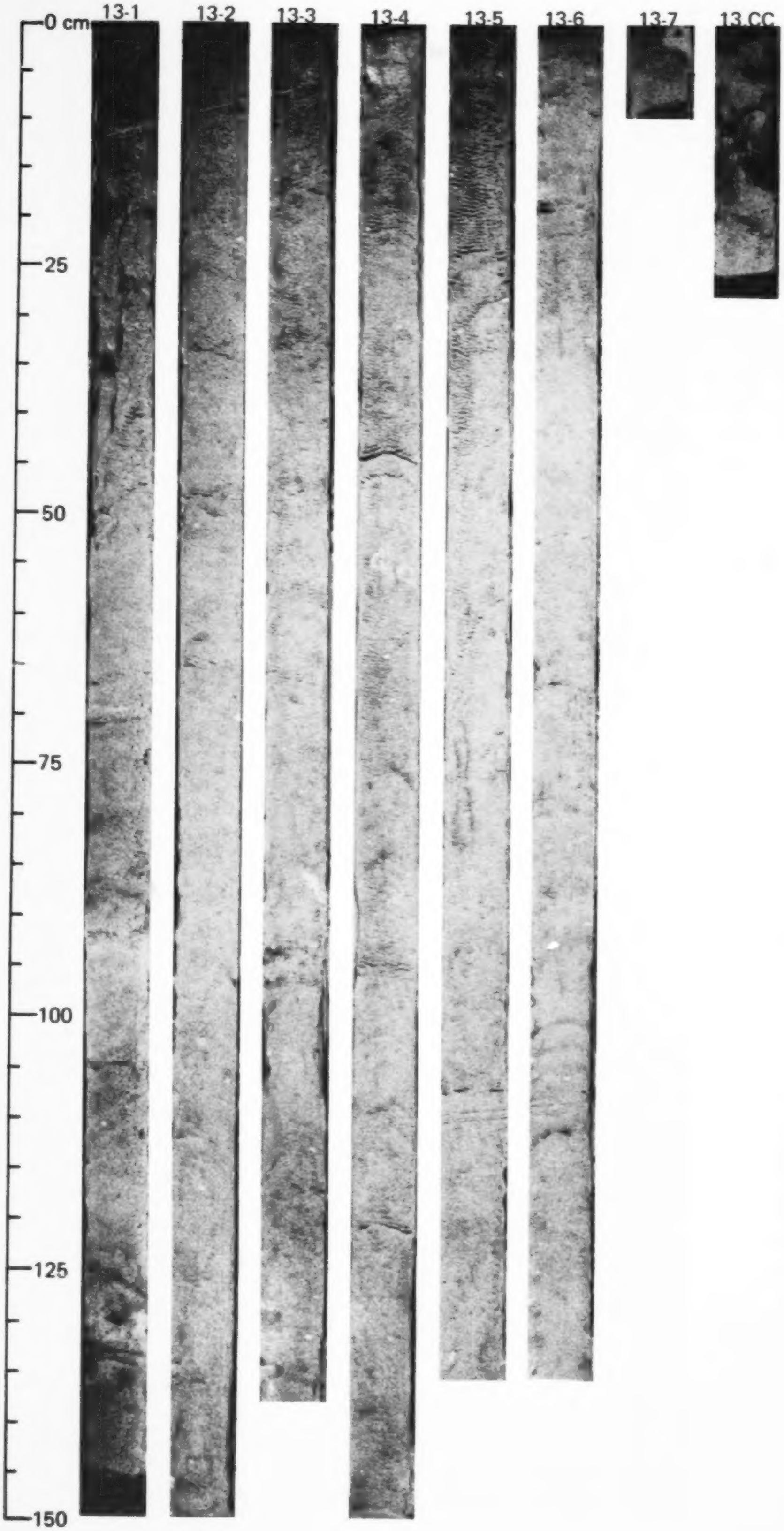
0 cm
25
50
75
100
125
150
13-1
13-2
13-3
13-4
13-5
13-6
13-7
13,CC

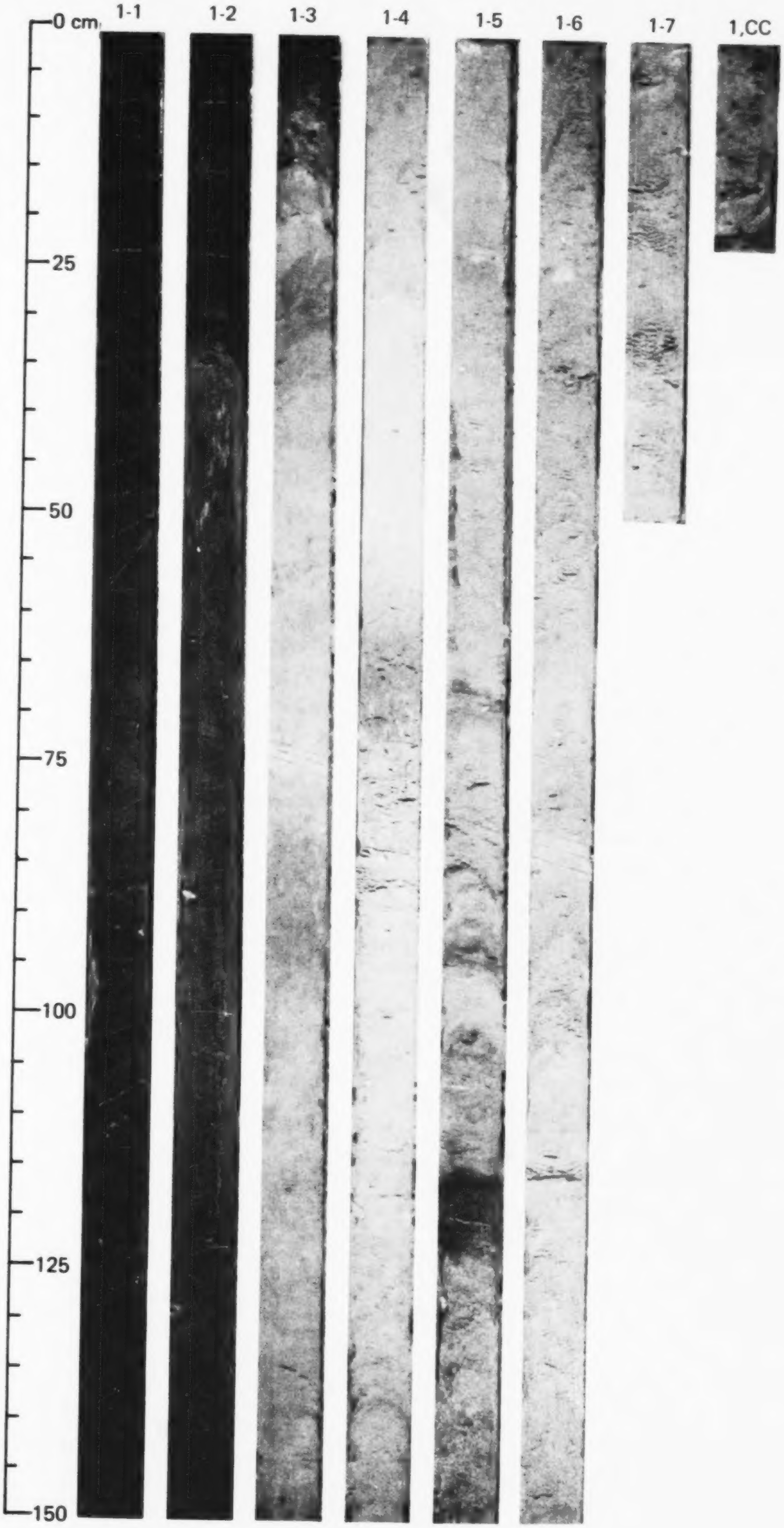
0 cm
25
50
75
100
125
150
1-1
1-2
1-3
1-4
1-5
1-6
1-7
1,CC

5. SITE 578[1]

Shipboard Scientific Party, with a contribution by Patricia Doyle[2]

HOLE 578

Date occupied: 27 May 1982

Date departed: 30 May 1982

Time on hole: 2 days, 6½ hr.

Position (latitude; longitude): 33°55.56′N: 151°37.74′E

Water depth (sea level; corrected m, echo-sounding): 6010

Water depth (rig floor; corrected m, echo-sounding): 6020

Bottom felt (m, drill pipe): 6005

Penetration (m): 176.8

Number of cores: 20

Total length of cored section (m): 167.8

Total core recovered (m): 165.02

Core recovery (%): 98

Oldest sediment cored:
  Depth sub-bottom (m): 176.6
  Nature: Chert and silicified chalk
  Age: Campanian to Maestrichtian
  Measured velocity (km/s): 1.52 (clay immediately above chert)

Basement: Not reached

Principal results: Hole 578 recovered a thick section of late Neogene siliceous clays. Siliceous microfossils are well represented in the late Quaternary and late Miocene–Pliocene portion of the section. The paleomagnetic stratigraphy is exceptionally good. All major events back to the middle of Epoch 5 can be identified even from the shipboard natural remanent magnetization (NRM) inclinations.

The upper 76.6 m of clay and siliceous clay (0–2.4 m.y. ago) is anoxic (gray and olive gray in color) with many pyrite-cemented layers. From 76.6 to 124.5 m (2.4 to 9–9.5 m.y. ago), the clays are oxidized (yellow brown and brown in color) with rare ferromanganese nodules. These two units contain 72 clearly visible ash layers, 24 of which are more than 5 cm thick (the thickest is 17 or 27 cm if adjoining 17 and 10 cm white and green ash beds formed from a single eruption).

From 124.5 to 176 m (9–9.5 to about 70 m.y. ago), the pelagic clay is "slick," predominantly dark to very dark brown, and very homogeneous. At its base, the clay is very stiff, with a shear strength approaching 2 kg/cm^2 (the 9.5 m core at a depth of 170 m penetrated only a little over 4 m). Drilling was stopped by chert at 176.8 m. Silicified foraminifers immediately above the chert are late Campanian to Maestrichtian in age (about 70 m.y.).

Sedimentation rates drop from almost 40 m/m.y. at the surface to about 25 m/m.y. from 1 to 2.4 m.y. ago, where they decrease abruptly to 15 m/m.y. and then gradually to about 8 m/m.y. at the base of the fossiliferous section. If deposition was continuous, the pelagic clays accumulated at less than 1 m/m.y. from about 10 to 70 m.y. ago. The rapid late Pliocene–Pleistocene sedimentation rates were unexpected. Further work is required to determine whether a change in provenance or transport was responsible for the 70% rate increase 2.4 m.y. ago.

BACKGROUND AND OBJECTIVES

Site 578 (target site NW-8A) lies at the join of the east–west and north–south traverses that make up most of Leg 86. On the east–west traverse, the site complements Site 576 because of its proximity to the Asian source of eolian debris and to the western boundary current of the North Pacific. For most of the Cenozoic, the pelagic clay section at Site 578 complements those at Site 576 and LL44-GPC3 to define the history of authigenic sedimentation in this large region.

On the north–south traverse, Site 578 provides the most subtropical paleoceanographic end member. The abrupt thickening of the "transparent" acoustic layer immediately to the south of the site may mark the southern limit of the Kuroshio return flow—the extreme southern limit of transition water in this area.

Our specific scientific objectives at Site 578 were

1. To obtain a detailed paleoceanographic record of the northern edge of the subtropical water mass for the late Cenozoic.
2. To determine the time of onset of significant biosiliceous accumulation.
3. To interrelate tephrachronology, paleomagnetic stratigraphy, and biostratigraphy for a northwest Pacific late Cenozoic subtropical section.
4. To assess the nature and history of authigenic sedimentation during the late Cretaceous and Paleogene.
5. To determine the late Cretaceous and Cenozoic history of eolian sedimentation for comparison with the more distal Site 576 and LL44-GPC3.
6. To assess the nature of the red clay–chert boundary, particularly in terms of enhanced diagenesis of the basal clay.

Geologic and Topographic Setting

The regional seafloor morphology and echo character of the near-surface sediments of the northwest Pacific have been mapped by Damuth et al. (1983), using all available Lamont-Doherty, Scripps, and Hawaii Institute of Geophysics 3.5-kHz reflection records. Site 578 lies west of Shatsky Rise in a large area of gently rolling seafloor underlain by a section of continuous parallel subbottom reflectors up to several hundred meters thick above Cretaceous chert and chalk.

---

[1] Heath, G. R., Burckle, L. H., et al., *Init. Repts. DSDP*, 86: Washington (U.S. Govt. Printing Office).

[2] Addresses: (Shipboard Scientific Party) G. Ross Heath (Co-Chief Scientist) School of Oceanography, Oregon State University, Corvallis OR 97331 (present address: College of Ocean and Fishery Sciences, University of Washington, Seattle, WA 98195); Lloyd H. Burckle (Co-Chief Scientist) Lamont-Doherty Geological Observatory, Palisades, NY 10964; Anthony E. D'Agostino, ARCO Exploration Company, Houston, TX 77056; Ulrich Bleil, Institut für Geophysik, Ruhr-Universität Bochum, D-4630 Bochum Querenburg, Federal Republic of Germany; Ki-iti Horai, Lamont-Doherty Geological Observatory, Palisades, NY 10964 (present address: Meteorological College, Chiba University, Chiba 277, Japan); Robert D. Jacobi, Department of Geological Sciences, SUNY Buffalo, Amherst, NY 14226; Tom Janecek, Department of Atmospheric & Oceanic Science, University of Michigan, Ann Arbor, MI 48109 (present address: Lamont-Doherty Geological Observatory, Palisades, NY 10964); Itaru Koizumi, College of General Education, Osaka University, Osaka 560, Japan; Lawrence A. Krissek, School of Oceanography, Oregon State University, Corvallis, OR 97331 (present address: Department of Geology and Mineralogy, Ohio State University, Columbus, OH 43210); Nicole Lenôtre, Bureau de Recherches Géologiques et Minières, Centre Océanologique de Bretagne, 45060 Orléans Cedex, France; Simonetta Monechi, Geological Research Division, Scripps Institution of Oceanography, La Jolla, CA 92093 (present address: Dipartimento di Scienze della Terra, Università di Firenze, 4 Via La Pira, 50121 Firenze, Italy); Joseph J. Morley, Lamont-Doherty Geological Observatory, Palisades, NY 10964; Peter Schultheiss, Institute of Oceanographic Sciences, Surrey GU8 5UB, United Kingdom; Audrey A. Wright, Deep Sea Drilling Project, Scripps Institution of Oceanography, La Jolla, CA 92093 (present address: Ocean Drilling Program, 500 University Drive West, Texas A&M University, College Station, TX 77843). (Doyle) Geological Research Division, Scripps Institution of Oceanography, La Jolla, CA 92093.

The area around Site 578 was surveyed in detail on R/V *Vema* Cruise 36-12. Based on the piston cores and 3.5-kHz records from the survey, a drill site was selected at 33°56′N, 151°38′E, a location typical of the northwestern quadrant of the area. The topography is very subdued, with local relief of tens of meters over distances of tens of kilometers. The air gun 100-Hz reflection profiles show about 160 m of layered sediment above chert(?). From the V-36 piston cores, we suspected that a significant number of the laterally continuous shallow reflectors were ash beds.

The site lies in the magnetic bight, possibly on Anomaly M21. If so, the basement age is about 145 m.y.

OPERATIONS

From Site 577 we steamed east, across the west side of Shatsky Rise for 1½ days to Site 578 (target Site NW-8A). The air-gun, 3.5-, and 12-kHz records collected underway are of excellent quality.

The vessel entered the B-1 survey area of R/V *Vema* Cruise 36-12 on 26 May 1982(Z). The site was selected some 19 miles west-northwest of the original target Site NW-8A because shipboard assessment of the V-36 air-gun records indicated slightly more lateral uniformity at the alternate site. Because of the detail of the *Vema* survey and the acoustic uniformity of the upper part of the sediment section, the *Challenger* steamed directly to the site, dropped the beacon at 1900Z, and immediately retrieved the magnetometer and seismic gear.

Drill pipe run-in began at 2015Z on 26 May, with the first successful 9.5-m hydraulic piston corer (HPC) core on deck at 1326Z on 27 May. Despite good returns from both the ship's 3.5-kHz transducer and a 3.5-kHz pinger attached 251 m above the bit, the first core contained only water. We are unable to account for the large discrepancy (18% in the case of the pinger) between the acoustic and drill pipe depths. The location of the pinger on the string was rechecked on retrieval and found to be correct.

Coring proceeded without mishap for 20 cores (Table 1). Cores 17 to 20 did not stroke out completely due to the stiffness of the red clay below 150 m. We washed down 9.5 m between cores 17 to 20 to conserve time.

The overall quality of the HPC cores at this site was substantially better than the quality of those at Sites 576 and 577. We attribute this to the addition of an extra shear pin to the HPC which allowed it to fully pressure up before firing. We suspect that the intermittent flow-in seen in cores from the earlier sites resulted from premature shear pin failure followed by slow penetration of the HPC, which allowed the heave of the ship to move the piston as the core was being taken. Mike Storms' efforts to solve this problem are greatly appreciated.

The core nose heat-flow unit worked well, with seven successful deployments out of eight.

Table 1. Site 578 coring summary.

Core	Date (May 1982)	Local time	Depth from drill floor (m)	Depth below seafloor (m)	Length cored (m)	Length recovered (m)	Percent recovered
1	28	0226	6004.7-6009.5	0.0-4.8	4.8	4.77	99
2	28	0451	6009.5-6019.0	4.8-14.3	9.5	8.25	87
3	28	0707	6019.0-6028.5	14.3-23.8	9.5	9.70	102
4	28	0925	6028.5-6038.0	23.8-33.3	9.5	9.01	95
5	28	1150	6038.0-6047.5	33.3-42.8	9.5	9.63	101
6	28	1412	6047.5-6057.0	42.8-52.3	9.5	10.00	105
7	28	1640	6057.0-6066.5	52.3-61.8	9.5	9.68	102
8	28	1905	6066.5-6076.0	61.8-71.3	9.5	9.76	103
9	28	2132	6076.0-6085.5	71.3-80.8	9.5	9.75	103
10	29	0003	6085.5-6095.0	80.8-90.3	9.5	8.93	94
11	29	0231	6095.0-6104.5	90.3-99.8	9.5	9.44	99
12	29	0453	6104.5-6114.0	99.8-109.3	9.5	9.06	95
13	29	0725	6114.0-6123.5	109.3-118.8	9.5	9.48	100
14	29	0940	6123.5-6133.0	118.8-128.3	9.5	10.18	107
15	29	1204	6133.0-6142.5	128.3-137.8	9.5	9.76	103
16	29	1420	6142.5-6152.0	137.8-147.3	9.5	8.36	88
17	29	1642	6152.0-6160.0	147.3-155.3	8.0	7.68	96
Wash	29		6160.0-6161.5	155.3-156.8	—	—	—
18	29	1925	6161.5-6168.0	156.8-163.3	6.5	6.20	95
Wash	29		6168.0-6171.0	163.3-166.3	—	—	—
19	29	2200	6171.0-6176.0	166.3-171.3	5.0	4.57	91
Wash	29		6176.0-6180.5	171.3-175.8	—	—	—
20	30	0027	6180.5-6181.5	175.8-176.8	1.0	0.81	81
					167.8 (total)	165.02 (total)	98 (avg.)

Two holes originally were scheduled for Site 578. Because of the excellent recovery and core quality in Hole 578, however, we cancelled the second hole to recover some of the time lost due to the reduced lowering speed of the HPC assembly necessitated by the undersize bore of the drill pipe.

We departed the site at 0245Z on 30 May, steaming south and streaming the seismic gear before profiling northward across the site en route to Site 579.

LITHOSTRATIGRAPHY

The lithostratigraphy of Site 578 is based on macroscopic core descriptions and smear slide analyses. The recovered section consists of four units (Fig. 1, Table 2): (1) a gray to olive gray clay-siliceous clay, (2) a yellowish brown to brown clay-siliceous clay, (3) a brown to dark brown pelagic clay, and (4) a basal chert overlain by an interbedded silicified foraminiferal ooze and clay unit.

Unit I: Gray Clay

Lithologic Unit I is a gray to olive gray clay and siliceous clay. This unit is divided into four subunits as follows.

Subunit IA

This subunit is a siliceous clay (radiolarian clay), predominantly homogeneous gray to dark gray (5Y) in color. The upper 0.71 m of this subunit is a dark yellowish brown (10YR) oxidized layer. Subunit IA extends from Section 578-1-1 through Sample 578-2-3, 20 cm (0–8.0 m sub-bottom depth). These sediments are composed of 30–60% clay, 5–10% quartz, 15–20% radiolarians, and 5–10% diatoms. This subunit contains four volcanic ash layers with an average thickness of 2.5 cm and a maximum thickness of 5 cm. Several thin (0.2–0.5 cm), indurated, dark, pyritic clay layers are found in this subunit.

Subunit IB

Subunit IB is a clay unit that extends from Samples 578-2-3, 20 cm through 578-6,CC (8.0–52.3 m sub-bot-

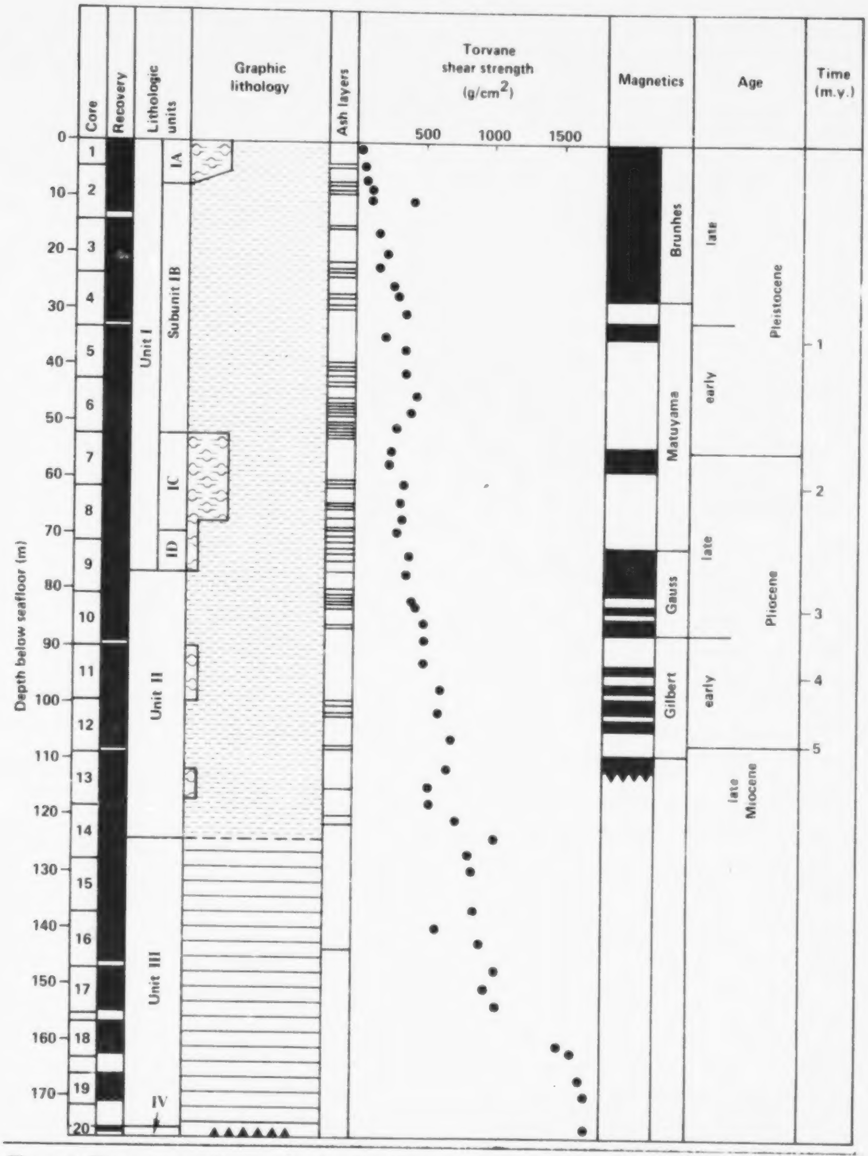

Figure 1. Site summary diagram showing Site 578 core numbers, core recovery, lithologic units, graphic lithology, ash layer locations, torvane shear strength (g/cm²), magnetostratigraphy, and age. Symbols used in graphic lithology column are defined in Introduction and Explanatory Notes (this volume).

tom depth). In the interval from Samples 578-2-3, 20 cm to 578-4-5, 20 cm, this subunit is gray to dark gray (5Y) interlayered with olive gray; an olive gray color is predominant from Samples 578-4-5, 20 cm through 578-6,CC. The sediments are composed of 85% clay, 5-10% quartz, and generally less than 5% biogenic silica. Thirty ash layers were cored in Subunit IB. Their average thickness is 3.0 cm, with a maximum thickness of 17 cm. No ash layers were found between Samples 578-4-4, 140 cm and 578-5-5, 20 cm. Thin, stiff, dark, indurated, pyritic clay layers occur throughout the subunit, but are significantly less abundant in the interval that lacks ash layers.

Subunit IC

Subunit IC is a siliceous clay that extends from Section 578-7-1 through Sample 578-8-6, 50 cm (52.3-69.75 m sub-bottom depth). This subunit is predominantly olive gray (5Y) in color, with a few layers of green gray (5G), gray (5Y), and olive (5Y). The sediments are composed of 25-30% diatoms, 5-15% radiolarians, and 30-55% clay. The quartz content increases downsection to a maximum of 15%.

Fourteen ash layers occur in Subunit IC; the average thickness is 4.3 cm. The thickest ash layer is 12 cm. No ash layers and relatively few dark, pyritic, indurated clay

Table 2. Site 578 lithostratigraphic units.

	Lithologic unit	Cored interval	Sub-bottom depth (m)
I:	Gray to olive gray clay to siliceous clay	1-1,0 cm to 9-4,80 cm	0–76.60
	Subunit IA: Siliceous clay (radiolarian clay)	1-1,0 cm to 2-3,20 cm	0–8.00
	Subunit IB: Clay	2-3,20 cm to 6,CC	8.00–52.30
	Subunit IC: Siliceous clay	7-1,0 cm to 8-6,50 cm	52.30–69.75
	Subunit ID: Clay	8-6,50 cm to 9-4,80 cm	69.75–76.60
II:	Yellow brown to brown clay (transitional biogenic mud)	9-4,80 cm to 14-4,120 cm	76.60–124.50
III:	Brown to dark brown pelagic clay	14-4,120 cm to 20-1,20 cm	124.50–176.00
IV:	Dark brown pelagic clay and chert	20-1,20 cm to 20,CC	176.00–176.80

layers occur between Samples 578-7-1, 40 cm and 578-7-6, 70 cm.

Subunit ID

This subunit extends from Samples 578-8-6, 50 cm through 578-9-4, 80 cm (69.35–76.6 m sub-bottom depth). It consists of interbedded layers of yellowish brown to dark brown (10YR) and olive gray (5Y) clay above Sample 578-9-2, 120 cm and olive gray (5Y) and olive (5Y) clay below Sample 578-9-2, 120 cm. These sediments contain approximately 55–68% clay, 15% quartz, 5–10% diatoms, and 0–8% radiolarians. In general, the brown layers have more clay and less biogenic silica than the olive gray and gray layers.

Six ash layers are found in Subunit ID. The average thickness of these layers is 5.7 cm; maximum thickness is 10 cm. The only thin indurated, dark pyritic clay layer in this subunit occurs in Sample 578-9-2, 20 cm.

Unit II: Yellowish Brown and Brown Clay

This unit extends from Samples 578-9-4, 80 cm through 578-14-4, 120 cm (from 76.6 to 124.5 m sub-bottom depth). The upper 14 m of this unit consists of interbedded yellowish brown (10YR) and brown (10YR) clay layers 40–60 cm thick. The lower 34.5 m of this unit consists of uniform yellowish brown (10YR) clay with minor amounts of siliceous microfossils. The sediments consist of 50–89% clay, 2–20% quartz, and 2–20% biogenic silica. Isolated manganese nodules occur within this unit.

Unit II contains 19 ash layers with an average thickness of 5 cm; maximum thickness is 17 cm. The abundance of ash layers decreases rapidly below Sample 578-10-2, 30 cm. No thin, indurated, dark pyritic layers occur in Unit II.

Unit III: Dark Brown Pelagic Clay

This unit extends from Samples 578-14-4, 120 cm through 578-20-1, 20 cm (from 124.5 to 176.0 m sub-bottom depth) and consists of a uniform dark brown (10YR) to very dark grayish brown (10YR) pelagic clay. The sediment in Unit III is composed of 90% or more clay and 1–7% quartz. Biogenic silica is virtually absent through the unit. Only one ash layer occurs in Unit III.

Unit IV: Dark Brown Pelagic Clay and Chert

This unit extends from Samples 578-20-1, 20 cm through 578-20,CC (from 176.0 to 176.8 m sub-bottom depth). The top 30 cm of Unit IV consists of dark brown to brown (10YR–7.5YR) pelagic clay with laminations 0.1 to 0.5 cm thick. Below the laminated clay is a 13-cm-thick sequence of interbedded very pale brown (10YR) siliceous clay and dark grayish brown (10YR) pelagic clay. The siliceous clay contains 77% clay, 15–20% silicified foraminifers, and 3% quartz. The lowermost lithology recovered consists of angular chert fragments (Sample 578-20,CC). These chert fragments exhibit the same vitreous reddish centers and white chalky rinds described for cherts recovered elsewhere (e.g., Fischer, Heezen, et al., 1971).

SEISMIC CORRELATIONS

High resolution seismic reflection profiles (3.5 and 12 kHz) and 100-Hz reflection profiles were recorded at Site 578. Both hull-mounted and near-bottom sound sources were utilized; the near bottom transducer (3.5 and 5.25 kHz) was mounted on the drill string 251 m above the drill bit.

The 3.5-kHz echograms over Site 578 reveal a three-part seismic section (Fig. 2, Table 3). The upper Unit 1 extends to 0.0433 s below seafloor (30.7 m, assuming a velocity of 1420 m/s) and consists of strong, continuous, multiple, parallel sub-bottom reflectors. A thin transparent layer separates seismic Unit 1 from the underlying seismic Unit 2. Seismic Unit 2 consists of parallel reflectors of weak–intermediate strength and extends to 0.0641 s below the seafloor (45.5 m, assuming a velocity of 1420 m/s). A thin transparent layer separates the deepest reflector in seismic Unit 2 from the top of seismic Unit 3. Seismic Unit 3 consists of parallel multiple reflectors that are commonly intermittent and weak; only the top reflector has intermediate strength.

The source of these reflectors was difficult to determine because of (1) the high number of relatively equally spaced reflectors, (2) the best fit of reflectors to lithostratigraphy utilizes an anomalously low velocity throughout the section (1420 m/s), and (3) both ash layers and thin, indurated, pyritic clay layers have anomalously high P-wave velocities. Some of the seismically transparent intervals correspond to sections of core without ash layers but with indurated, thin pyritic clays. Therefore, we attribute most of the reflectors to ash layers (Table 3). Only Reflector 3c is probably caused by a thin, pyritic clay layer; Reflectors 2a and 2b are probably caused by locally anomalous brown clay. The remainder of the reflectors account for all the ash layers of significant thickness cored to a depth of about 70 m below the seafloor. The proposed correlation matches the ash layer stratigraphy well below seismic Unit 1d, but a mismatch above this reflector suggests (1) inaccurate interval velocities, or (2) sources other than ash layers for the reflectors, or (3) poor control on the sub-bottom depth of the cored

Diatom assemblages in Cores 4 through 7 are placed in the *N. reinholdii* Zone. Core 4 can definitely be placed

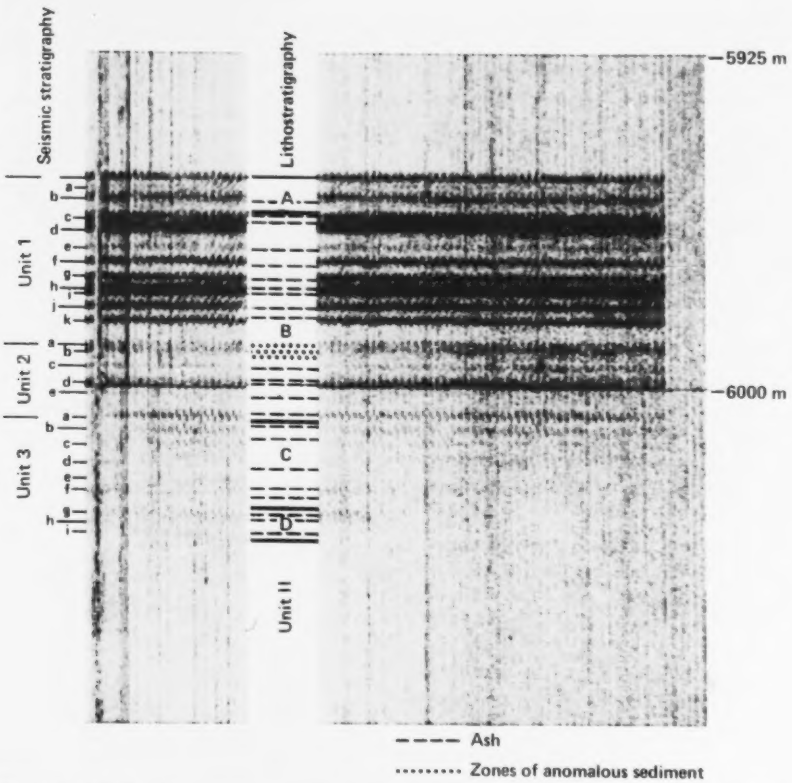

Figure 2. 3.5-kHz echogram near Site 578 showing the three-part seismic sequence described in the text.

ashes because of "intermittent flow-in" (i.e., discrete zones of "flow-in" at one or more depths within the length of a single core).

The 100-Hz seismic reflection profile over Site 578 (Fig. 3) is characterized by a three-part section. The uppermost unit (1) extends 0.23 s below the seafloor (176 m at 1520 m/s) and consists of strong, multiple sub-bottom reflectors. The strong reflectors parallel the seafloor and appear to "overprint" a few weaker, slightly divergent reflectors. Therefore, some of these strong reflectors may be "ringing" and not represent true lithologic changes. Seismic Unit 1 correlates with lithostratigraphic Units I, II, III. Seismic Unit 1 thus includes all the Cretaceous and younger sediments lying above the Cretaceous chert of lithostratigraphic Unit IV.

Seismic Unit 2 consists of strong, discontinuous, slightly divergent reflectors that form a dense "hackly" appearance on the reflection profiles. The thickness of Unit 2 is variable—from near zero on seamounts to more than 0.23 s. Unit 2 corresponds to the Cretaceous cherts and other interbedded sediments lying above basement and below lithostratigraphic Unit III.

Seismic Unit 3 consists of typical basement reflections and occurs at variable depths (less than 0.03 s on the slopes of seamounts, to about 0.5 s [378 m at 1520 m/s] elsewhere) below the seafloor.

BIOSTRATIGRAPHY

The sediments recovered at Site 578 range in age from late Quaternary to Late Cretaceous. No nannofossils were found except a few specimens in Section 578-16-2 which do not allow any age assignment. The sediments were also barren of foraminifers except for Samples 578-18,CC (18–20 cm), 578-20-1, 64–66 cm and 578-20,CC. The foraminifers found in Core 18 are of early middle Eocene age whereas the samples from Core 20 contained an upper Campanian to Maestrichtian assemblage. Ichthyoliths in Samples 578-17-4, 140–150 cm and 578-19-2, 140–150 cm have tentatively been dated as early Oligocene and Eocene in age, respectively. The upper 128 m of cored sediments contained rare to abundant diatoms and radiolarians varying in degree of preservation from good to poor.

No major hiatuses were detected in the late Miocene through Quaternary sequence. The absence of siliceous or calcareous microfossils through most of the interval between 125 and 175 m (Cores 14 through 19) at this site precludes the identification of any gaps in the record over this period. Based on the radiolarian and diatom biostratigraphy (Fig. 4), the Pliocene/Pleistocene boundary lies near the base of Core 7, with the Miocene/Pliocene boundary present in Core 12.

Table 3. 3.5-kHz seismic correlations, Site 578.

Reflector	Relative strength[a]	Sub-bottom depth (s)	Sub-bottom depth[b] (m)	Depth below seafloor of corresponding lithology (m)	Source
1a	W	0.00269	1.91		
1b	I	0.00608	4.32	4.75	Ash #2
1c	VS	0.0120	8.52	7.6?	Ash #3
1d	VS	0.0153	10.86	8.9	Ash #5
				9.1	Ash #6
1e	W	0.021	14.91	15.0	Ash #7
1f	S	0.025	17.75	18.75	Ash #8
1g	S	0.0302	21.44	21.5	Ash #9
1h	VS	0.0331	23.50	23.0	Ash #10-#11
1i	VS	0.0353	25.06	24.0	Ash #12
1j	S	0.0391	27.76	27.5	Ash #13
1k	S	0.0433	30.7	29.5	Ash #15-#16
2a	W	0.0496	35.2	34.5	Brown pelagic clay
2b	W	0.0516	36.6	35.6-36.75	Brown pelagic clay
2c	IT-W	0.0560	39.8	40.0	Ash #16A-#18
2d	I-S	0.0610	43.3	42.75	Ash #20
				43.3	Ash #21
2e	IT	0.0641	45.5	46.4	Ash #23
				46.6	Ash #24
3a	I	0.0713	50.6	50.2	Ash #29-#32
3b	IT	0.0744	52.8	52.5	Ash #35-#37
3c	IT	0.0786	55.8	55.0-55.75	Pyritic, indurated clay
3d	IT-W	0.0847	60.1	61.3	Ash #38-?#42
3e	IT	0.0905	64.25	65.2	Ash #43-#45
3f	IT-W	0.0930	66.0	67.2	Ash #46
3g	IT-W	0.0992	70.4	71.5	Ash #50
3h	IT	0.1025	72.8	72.45	Ash #51
3i	IT	0.1054	74.8	74.75	Ash #53
3j	IT	0.143	101.5	101.6	Ash #65 and #66

[a] IT = intermittent, weak; W = weak, but generally continuous; I = intermediate; S = strong; VS = very strong.
[b] Assuming a velocity of 1420 m/s.

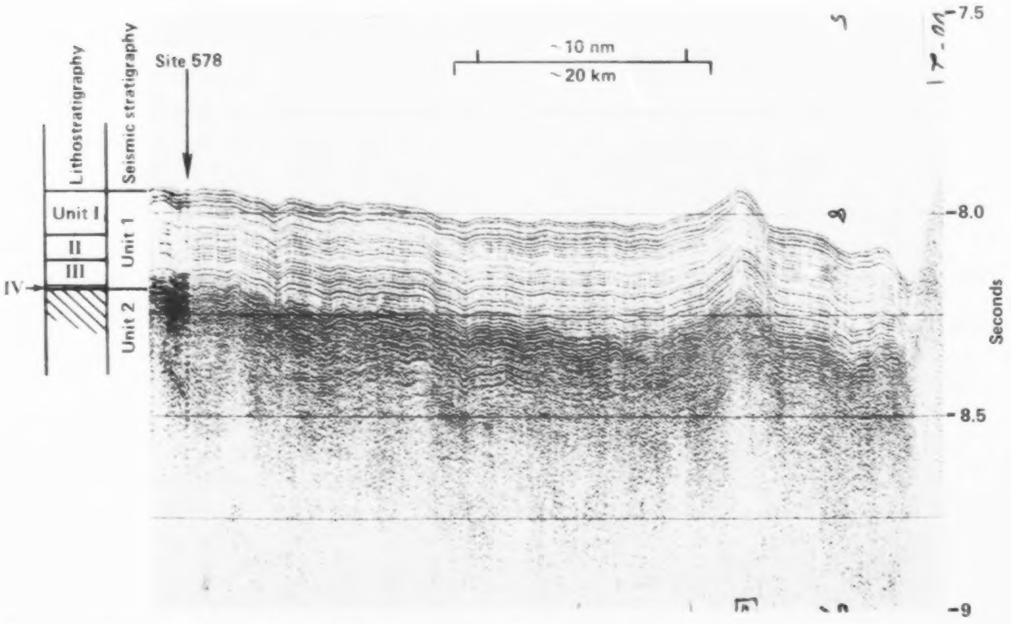

Figure 3. 100-Hz reflection profile over Site 578 showing the three-part seismic sequence described in the text.

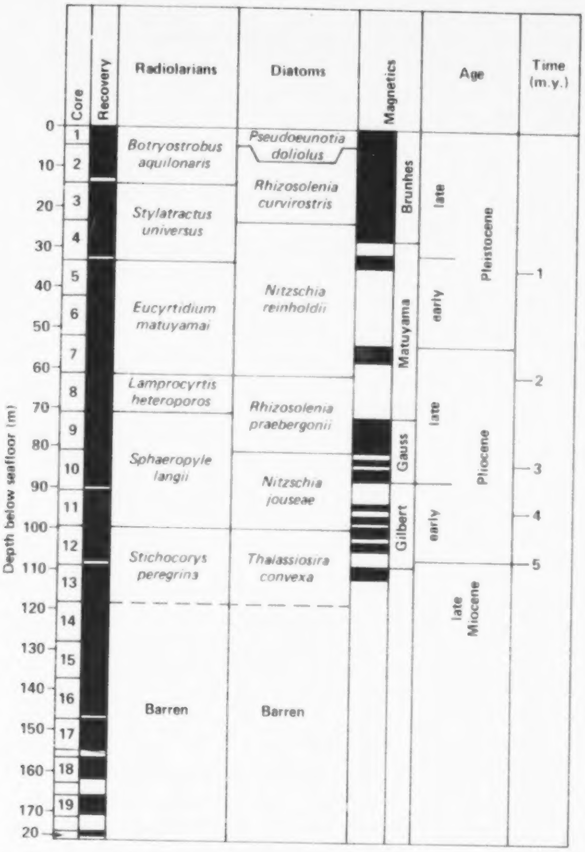

Figure 4. Site 578 biostratigraphic and magnetostratigraphic summary.

Calcareous Nannofossils

No calcareous nannofossils were found in cores recovered from this site with the exception of one assemblage in Sample 578-16-2. Rare and poorly preserved specimens include *Watznaueria barnesae, Braarudosphaera bigelowi, Zygodiscus* sp., *Coccolithus pelagicus, Coccolithus* sp., and *Discoaster* sp.

Planktonic Foraminifers

Core-catcher samples were examined from all 20 cores recovered at Site 578. In addition, two samples (578-16-5, 7–8 and 138–139 cm) from light colored layers within the dark pelagic muds were examined on board. Shore-based analysis revealed foraminifers in Samples 578-18,CC (18–20 cm) and 578-20-1, 64–66 cm. All samples except these two and Sample 578-20,CC (examined aboard ship) were barren of foraminifers. Sample 578-18,CC (18–20 cm) contained rare specimens of *Globorotalia spinulosa* and *G. broedermanni*. These two species alone indicate an interval spanning the *G. pentacamerata* Zone to the *Globigerinatheca subconglobata* Zone of Stainforth et al. (1975) or P9-P11 of Blow (1969). The samples from Core 20 contained a fauna of upper Campanian to Maestrichtian age. Typical species include *Globotruncana contusa, G. arca, G. fornicata, G. tricarinata, G. stuarti, G. stuartiformis, G. lapparenti, Heterohelix striata, Hedbergella planispira, Globigerinelloides asperus, G. prairiehillensis*, and *Rugoglobigerina rugosa*. These forms are common to the Upper Cretaceous as reported by Olsson (1964), Pessagno (1967), and Postuma (1971). The fauna found in Core 20 is similar in age to that found just above the impenetrable chert layer at Site 576, with the addition of some Maestrichtian forms. At Site 578, however, all the specimens were silicified after undergoing some dissolution. Such silicification was not seen at Site 576.

Radiolarians

Sediments from Site 578 contain Quaternary through late Miocene radiolarians. The preservation of individual specimens varied from good to poor in Samples 578-1,CC through 578-13,CC. No radiolarians were found in core-catcher samples from Cores 14 through 20. The radiolarian biostratigraphy for Site 578 is shown in Figure 4.

Radiolarians representative of the late Pleistocene are present in samples 578-1,CC through 578-4,CC with the first 14 m (Cores 1 and 2) at Site 578 containing an assemblage characteristic of the *Botryostrobus aquilonaris* Zone (Hays, 1970). The presence of *Stylatractus universus* and the absence of *Eucyrtidium matuyamai* in Samples 578-3,CC and 578-4,CC indicate that sediments recovered in this interval correlate with the *Stylatractus universus* Zone (Hays, 1970). The identification of the radiolarian species *E. matuyamai* in Samples 578-5,CC through 578-7,CC indicates that the sediments in these cores are early Pleistocene in age. Because of the relatively small width of the *E. matuyamai* specimens in Sample 578-7,CC, which is indicative of the beginning of its lineage, the Pliocene/Pleistocene boundary is probably very close to the bottom of Core 7. The species in Sample 578-8,CC are a typical late Pliocene assemblage characteristic of the *Lamprocyrtis heteroporos* Zone (Hays, 1970; Foreman, 1975). The presence of *Stichocorys peregrina, S. delmontensis*, and *Sphaeropyle langii* in Samples 578-9,CC through 578-11,CC indicate that this sequence belongs to the *S. langii* Zone (Foreman, 1975). Species characteristic of the *Stichocorys peregrina* Zone (Riedel and Sanfilippo, 1970; Foreman, 1975) are present in Samples 578-12,CC and 578-13,CC with the Miocene/Pliocene boundary occurring within Core 12.

Diatoms

Early Pliocene to Quaternary diatoms were recovered at Site 578 (Fig. 4). Diatoms are common to few and preservation is moderate except for Cores 5 and 13 where diatoms are rare and poorly preserved. Diatoms are absent below Core 13. Core 1 belongs to the lower latitude *Pseudoeunotia doliolus* Zone of Burckle et al. (1978) and the higher latitude *Denticulopsis seminae* Zone of Koizumi (1973) based upon the absence of *Rhizosolenia curvirostris*. Cores 2 and 3 are placed in the middle Pleistocene *R. curvirostris* Zone (the middle and lower part of the Brunhes Epoch) by the presence of *P. doliolus* and *R. curvirostris* and the absence of *Nitzschia reinholdii*.

around the Jaramillo Event of the Matuyama Epoch. The silicoflagellate *Mesocena quadrangula* is present in this core. The stratigraphic position of the base of Core 5 is less certain because of poor preservation. The top of Core 5 (Section 578-5-1) is near the Jaramillo Event, based upon the presence of *Rhizosolenia matuyamai* which ranges into the lower part of the Jaramillo.

Cores 8 and 9 are placed in the uppermost part of the Pliocene *R. praebergonii* Zone, based on the presence of *Thalassiosira convexa* and the absence of *Nitzschia jouseae*. Core 9 bottoms in the upper part of the Gauss Epoch as indicated by the presence of *T. convexa* and the absence of *N. jouseae* and *Denticulopsis kamtschatica*. Cores 10 and 11 are placed in the early to middle Pliocene *N. jouseae* Zone based upon the co-occurrence of *N. jouseae* and *T. convexa*. Core 12 is placed in the *T. convexa* Zone (magnetic Epoch 5) by the presence of *Nitzschia miocenica, T. convexa,* and *T. miocenica*. The Miocene/Pliocene boundary, therefore, lies between Cores 11 and 12 based on the occurrence of *N. miocenica* and *T. miocenica*. Core 13 is also placed in the *T. convexa* Zone (uppermost part of magnetic Epoch 6) by the co-occurrence of *T. convexa* and *T. praeconvexa*.

Ichthyoliths

Samples were taken from Cores 578-11 through 578-19 for a preliminary investigation of ichthyoliths. Ichthyoliths range in abundance from rare in the late Miocene-Pliocene siliceous sediments (Cores 578-11 through 578-13) to very abundant in pelagic clays of the Oligocene (Section 578-17-5) and the Paleocene/Eocene boundary (Core 578-19).

Core 578-12 through Section 578-17-4 is judged to be Miocene on the basis of the coherent range of *Small triangle long striations*. Section 578-14-2 is late Miocene on the basis of the concurrence of *Long triangle short inline* and *Long ellipse*. The presence of *Circular with line across* and *Short rectangular with striations* in Section 578-16-2 indicates a middle Miocene age.

The Oligocene/Miocene boundary falls between Sections 578-17-4 and 578-17-5; the Eocene/Oligocene boundary between Sections 578-17-5 and 578-18-1. The Oligocene is identified on the presence of *Rounded apex triangle* and *Triangle with base angle* and the absence of *Small triangle long striations*. It is not possible to tell from the available data whether some part of the Oligocene and early Miocene is missing or if sediment accumulation was very slow.

Core 578-18 and Section 578-19-1 are Eocene. On the basis of the absence of *Triangle curved based* in the top part of the sequence and its presence in the bottom, Sections 578-18-1 and 578-18-3 are middle to late Eocene. Section 578-18-4 and Section 578-19-1 are early to middle Eocene.

The Paleocene/Eocene boundary is between Sections 578-19-1 and 578-19-3. The presence of *Beveled triangle concave margins* in Section 578-19-2, as well as *Triangle radiating inline* and *Narrow straight triangle* suggests that this section is Paleocene, but the distribution of typically Paleocene forms in earliest Eocene has not been studied sufficiently to allow a confident Paleocene age assignment to this sample. The presence of *Triangle medium wing* and *Triangle curved base* in Section 578-19-3, together with the Paleocene forms listed above, indicates a late Paleocene age.

PALEOMAGNETICS

Excellent recovery of an undisturbed section with NRM intensities on the order of 50 × 10^6 G allowed us to establish a nearly complete magnetostratigraphy from the late Miocene to the Quaternary at this site.

Detailed shore-based magnetic results are described in a later chapter (see Heath, Rea, and Levi, this volume). The average NRM inclinations above 110 m are independent of the polarity and are close to the centered axial dipole value for the present latitude of the drill site (53°). Thus, they can be used to establish the polarity sequence down to Epoch 5 (Table 4), using the magnetic terminology of McDougall (1977).

SEDIMENT ACCUMULATION RATES

The sedimentation rates for this site are based on a combination of radiolarian, diatom, ichthyolith, foraminiferal, and paleomagnetic stratigraphies. In constructing the age-depth plot (Fig. 5), it is assumed that the Campanian-Maestrichtian silicified foraminiferal sediments found below 175 m are contemporaneous with the clays directly overlying them. Sedimentation rates during the late Pleistocene decreased from almost 40 m/m.y. at the surface to less than 30 m/m.y. at depth. Rates were close to 25 m/m.y. during the early Pleistocene and late Pliocene (Figs. 5 and 6). Early Pliocene rates de-

Table 4. Paleomagnetic reversals at Site 578 (shipboard NRM inclinations).

Age[a] (m.y.)	Age[b] (m.y.)	Age[c] (m.y.)	Depth in hole (m)	Boundary/Event
0.73	0.72	0.72	26.9	Brunhes/Matuyama
0.91	0.91	0.89	31.8	Jaramillo
0.98	0.97	0.94	34.5	
1.66	1.66	1.62	54.2	Olduvai
1.88	1.87	1.91	58.0	
	2.12	2.07	61.7	X (Reunion)
	2.14		62.1	
2.47	2.47	2.47	72.9	Matuyama/Gauss
2.92	2.91	2.91	80.4	Kaena
2.99	2.98	3.00	82.4	
3.08	3.07	3.07	83.6	Mammoth
3.18	3.17	3.17	85.0	
3.40	3.40	3.41	87.7	Gauss/Gilbert
3.88	3.86	3.82	93.4	Cochiti
3.97	3.98	3.92	94.7	
4.10	4.12	4.07	96.4	Nunivak
4.24	4.26	4.25	97.7	
4.40	4.41	4.44	99.1	Sidufjall
4.47	4.49	4.57	101.6	
4.57	4.59	4.72	102.6	Thvera
4.77	4.79	4.94	104.6	
5.35	5.41	5.44	109.0	Gilbert/Epoch 5

[a] Time scale of Berggren et al. (in press).
[b] Time scale of Ness et al. (1980).
[c] Time scale of McDougall (1977).

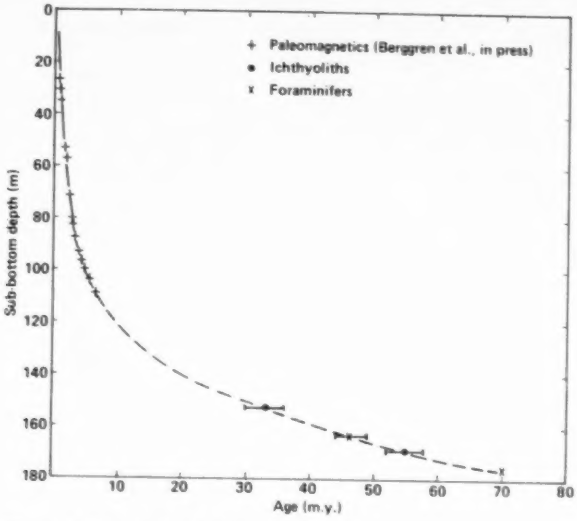

Figure 5. Age-depth curve for Site 578.

creased to less than 12 m/m.y. The very dark brown pelagic clay below 130 m accumulated at an average rate of 0.8 m/m.y., 50 times slower than the late Quaternary deposits. The oldest deposits (170–180 m) accumulated at the lowest rates (approximately 0.45 m/m.y.).

A marked increased in sedimentation rate occurs in the late Miocene–early Pliocene if the time scale of Berggren et al. (in press) for the magnetic event is adopted. The ages assigned to these events by McDougall (1977) produce a curve that indicates a more uniform decrease in the sedimentation rate through this interval.

PHYSICAL PROPERTIES

Physical properties measurements at Site 578 were performed using mainly standard Deep Sea Drilling Project (DSDP) methods (Boyce, 1976a, b; see Introduction and Explanatory Notes, this volume). Table 5 summarizes the properties that were measured at Hole 578. Measurements were taken at approximately 3-m intervals through Hole 578. Figures 7, 8, and 9 show profiles of compressional and shear wave velocity, saturated bulk density and water content, and shear strength, respectively. A full discussion of the physical properties of the recovered sediment, including tables of the data, is given by Schultheiss (this volume). However, some of the more interesting features of the data are highlighted here.

1. The compressional wave profile (Fig. 7) is dominated by high velocity layers of pyrite-indurated clay and ash beds superimposed on a constant velocity profile down to 160 m. Not all of the numerous layers were measured, but it can be assumed that they all have higher velocities. Below 160 m there is an indication that a

Table 5. Physical properties measurements made at Site 578.

	Hole 578
Shear strength:	
Hand-operated vane	x
Motorized vane	x
Wave velocity:	
Shear wave	x
Compressional wave	x
Water content/bulk density:	
Shipboard analysis	x
Shore-based analysis	x
Bulk density by 2-min. GRAPE	x

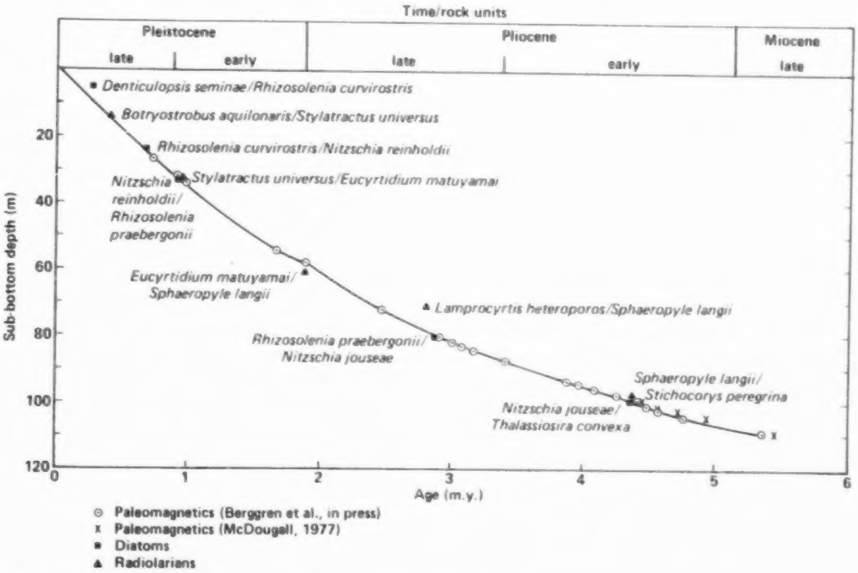

Figure 6. Age-depth curve for the upper 110 m at Site 578.

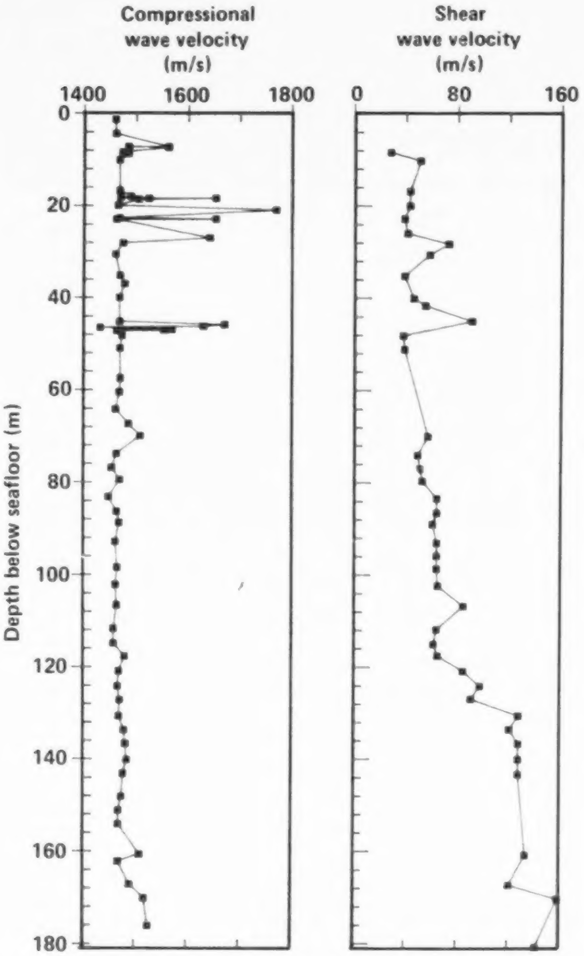

Figure 7. Plot of compressional and shear wave velocities versus sub-bottom depth at Site 578.

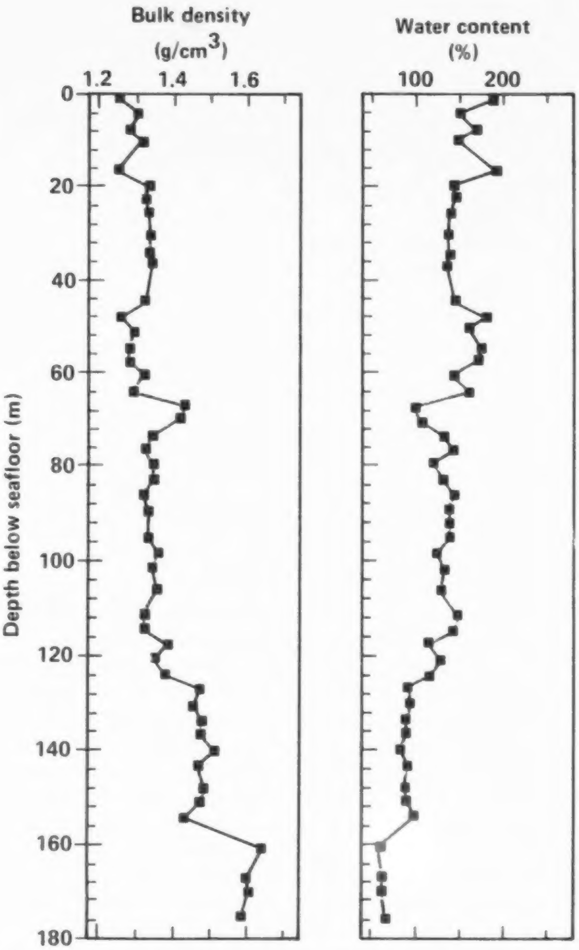

Figure 8. Profiles of saturated bulk density and water content versus sub-bottom depth at Site 578.

positive velocity gradient is developing in the very dark pelagic clay.

2. Shear wave velocities increase slowly up to 65 m/s at a depth of 120 m (Fig. 7). A rapid increase up to 128 m/s occurs between 120 and 130 m, below which the velocity remains essentially constant. This transition coincides with the lithologic boundary between Units II (clay) and III (pelagic clay).

3. The lithologic boundary between Units II and III is also characterized by a reduction in water content from 120 to 90% with a corresponding increase in the bulk density from 1.37 to 1.47 g/cm^3 (Fig. 8). Another significant change in water content occurs between Cores 17 and 18 (155–160 m sub-bottom depth) where it falls rapidly from 90 to 60%. This transition does not coincide with any obvious lithological boundary.

4. The shear strength profiles (Fig. 9) show the strength increasing with depth from 0 at the seafloor to around 1500 g/cm^2 at 176 m in Core 20. Recovery from Cores 17, 18, 19, and 20 were progressively poorer, with Core 20 being only 0.81-m long. These shear strengths in pelagic brown clays obviously represent the operational limits of the HPC in its present configuration. It is also interesting to note that the high lateral stresses within the core prevented any flow-in occurring (presumably water must have flowed around the piston during pull out).

The two discontinuities of water content at 120–130 and 155–160 m discussed above are also revealed by rapid increases in the shear strength profiles. At 123 m (boundary of Units II/III) there is a rapid increase from 500 to 1100 g/cm^2 according to the motorized vane measurements (a less pronounced step is revealed by the hand-held vane). At 157 m the hand-held vane shows an increase from 1050 to 1500 gm/cm^2 (a less pronounced step is revealed in this case by the motorized vane).

INORGANIC GEOCHEMISTRY

Six squeezed core samples from Hole 578 were analyzed for the standard suite of components: pH, alkalinity, salinity, calcium, magnesium, and chlorinity (Ta-

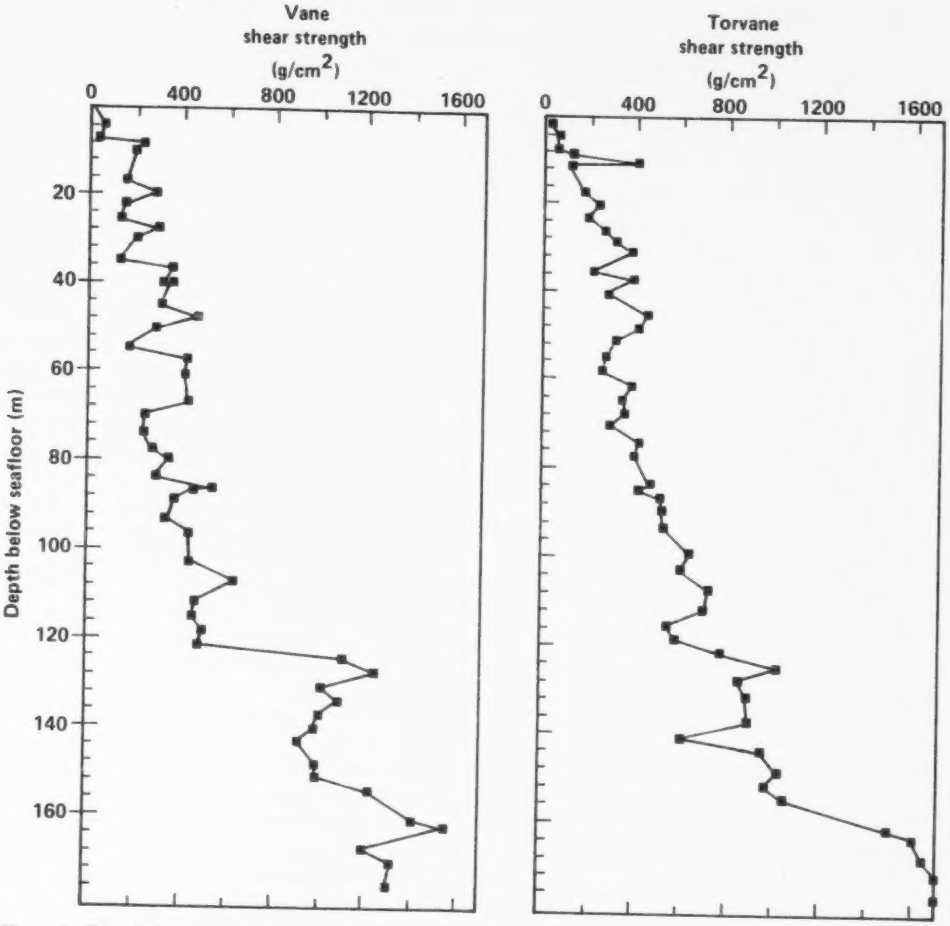

Figure 9. Plot of shear strength versus sub-bottom depth at Site 578.

ble 6). No *in situ* samples were taken. At least three trends are evident (Fig. 10):

1. Calcium increases linearly with depth throughout the cored interval. We suspect that this is a diffusion profile between the carbonate section beneath the chert (as sampled at Site 304, for example) and the seafloor.

2. Alkalinity and pH decrease within the anoxic sediments above 76 m (and possibly in the uppermost oxidized siliceous clays, although our sample spacing cannot resolve this), but are virtually constant in the highly oxidized pelagic clay section. Sulphide oxidation and alteration of volcanic ashes are reactions in the reduced sediments that could affect these parameters. The slight increase in alkalinity at 150 m may reflect the influence of carbonate dissolution beneath the cored section.

Table 6. Inorganic geochemistry measurements made at Site 578.

Sample	pH	Alkalinity (mEq/l)	Salinity (‰)	Calcium (mM)	Magnesium (mM)	Chlorinity (‰)
IAPSO	8.00	2.47	35.2	10.55	53.99	19.38
SSW	8.01	2.37	35.2	10.49	53.93	18.48
578-2-5, 140–150 cm	7.75	3.91	35.5	11.33	49.95	19.24
578-5-6, 140–150 cm	7.84	3.36	35.5	12.26	49.08	19.31
578-8-5, 140–150 cm	7.40	2.42	35.5	12.93	47.93	19.18
578-11-6, 140–150 cm	7.11	1.87	35.5	13.43	47.85	19.24
578-14-6, 140–150 cm	7.01	1.88	34.6	14.46	49.11	18.91
578-17-3, 140–150 cm	7.06	2.35	35.2	15.15	47.33	19.11

3. The slight decrease in magnesium in the upper 70 m (in the reduced sediments) may again reflect the alteration of the abundant volcanic ash in this section to smectite. Diagenesis of biogenic opal would have a similar effect.

We have no explanation for the low salinity value at 128 m.

HEAT FLOW

Downhole temperature measurements using the new Woods Hole Oceanographic Institution (WHOI) heat flow instrument were made at this site. All but one of eight deployments were successful. The failure of the eighth run at this site was attributed to a malfunction of the computer when loading the program. All runs were made by one recorder, WHOI-4A, connected to battery pack NTLT-2.

The quality of the temperature data improved substantially at this site, owing mainly to the Cruise Operations Manager's suggestion that tension in the sand line

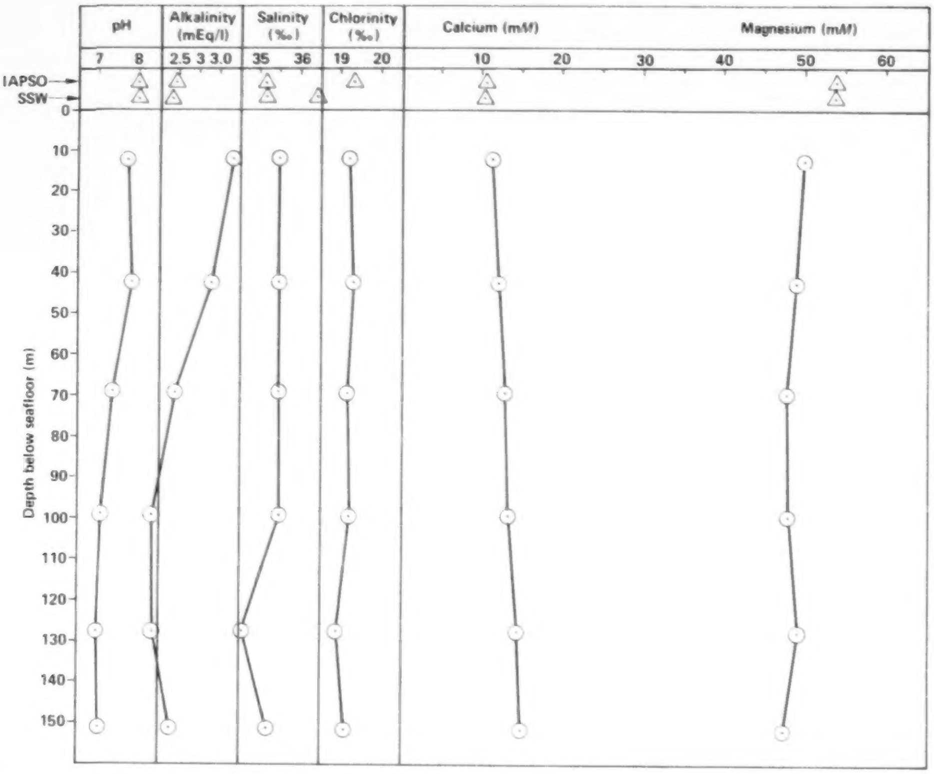

Figure 10. Profiles of pH, alkalinity, salinity (‰), chlorinity (‰), calcium (mM), and magnesium (mM) versus sub-bottom depth from interstitial water samples analyzed at Site 578. Symbols are as follows: △ = IAPSO and SSW standards; ⊙ = samples from Hole 578.

be released during the measurement. This eliminated propagation of the ship's motion through the sand line to the HPC (which generates frictional heat) resulting in a smoother cooling curve than in previous records.

Thermal conductivity values were measured at 200 locations in Hole 578. These data, combined with the downhole temperature measurements, yield a useful estimate of the heat flow at Site 578 (see Horai and Von Herzen, this volume).

SUMMARY AND CONCLUSIONS

The stratigraphic section recovered in Hole 578 and the major lithologic units, summarized in Figure 1, are as follows.

Unit I: 0-76.6 m

Gray and olive gray anoxic clay grading to siliceous clay, of late Pliocene and Quaternary age (0-2.4 m.y.). There are thin oxidized layers at the surface, at 35 and at 70 m. Siliceous microfossils are most abundant in the latest Quaternary and late Pliocene to early Pleistocene deposits (preservation also is good across the Miocene/Pliocene boundary). The youngest sediments accumulated at almost 40 m/m.y., but from about 1 to 2.4 m.y. ago, the rate was close to 25 m/m.y. This unit contains numerous ash beds (Fig. 1).

Unit II: 76.6-124.5 m

Mainly yellow brown, with some brown above 90 m, oxidized pelagic clay with locally abundant radiolarians and diatoms, of late Miocene to late Pliocene age (2.4 to about 9 m.y.). Below 90 m, the sediments are very uniform in appearance, with only ash beds (decreasing downsection) and rare ferromanganese nodules to break the monotony. Within this unit, the accumulation rate decreases steadily from 14 m/m.y. at the top to about 5 m/m.y. at the base.

Units I and II carry a strong remanent magnetization. Based on shipboard NRM analyses, the first four magnetic epochs and virtually all their events can be recognized (Fig. 4). The paleomagnetic data, which are consistent with the biostratigraphy, provide a detailed time scale for the past 5 m.y.

Unit III: 124.5-176 m

Mainly dark to very dark brown, fine-grained ("slick"), homogeneous pelagic clay, with dark yellow brown and yellow brown intervals above 129 m. The age limits of about 9 and 70 m.y. are defined by the bounding units; no diagnostic siliceous or calcareous microfossils occur near the boundaries of Unit III. This highly oxidized unit contains rare ferromanganese nodules and only one ash bed. If deposition was continuous, the sedimentation rate decreased from 4.3 m/m.y. at the top to 0.45 m/m.y. at the base. More detailed studies of ichthyoliths are needed to determine whether this rate varied uniformly through time.

Unit IV: 176.8 m

Hole 578 terminated in chert. The few fragments in the catcher of Core 20 consist of glassy flintlike chert and light gray porcellanite containing internal molds and quartz replacements of Campanian to Maestrichtian foraminifers. The age of this chert is close to that at Site 576, but may be slightly younger.

Lithologic Unit I is problematic. The very high deposition rate, which decreases very rapidly to the southeast (*Vema*-36 Cores 41PC, 44PC, and 45PC) is not due to a flood of biogenous opal, but rather to terrigenous debris. Whether this reflects near-bottom circulation (we may be seeing the initiation of a "drift" deposit), or the injection of large amounts of loess to the western North Pacific by east Asian rivers following the onset of northern hemisphere glaciation, is unclear. Shore-based grain size and mineralogical studies may throw light on this question.

The excellent paleomagnetic record induced us to critically compare the time scale of McDougall (1977) with those of other authors. The differences are small, but our data are better fitted by the McDougall values, particularly for the top of the Olduvai Event and for the boundaries of the Sidufjall and Thvera Events. We have used McDougall's dates for our sedimentation rate calculations.

Lithologic Units II and III are comparable to units at Site 576. Unit III is manganese rich and we infer that it includes a substantial authigenic component. Unit II reflects the onset of biosiliceous deposition as the site began to encounter the western boundary current system of the North Pacific. This unit also may have received more eolian material as the climate deteriorated during the late Neogene.

Overall, Site 578 was highly successful. The excellent quality of the cores and virtually full recovery, as well as the rapid sedimentation rate during the past 5 m.y., provide excellent records of ash deposition and magnetic reversals during this period. This site also fixes the onset of biosiliceous sedimentation at the southern limit of the north-south transect from Sites 578 to 581. The deeper pelagic clay section complements those at Site 576 and LL44-GPC3, and provides the basis for an east-west profile of Paleogene authigenic sedimentation.

REFERENCES

Berggren, W. A., Kent, D. V., and Flynn, J. J., in press. Paleogene geochronology and chronostratigraphy. *In* Snelling, N. J. (Ed.), *Geochronology and the Geological Record.* Geol. Soc. London Spec. Pap.

Blow, W. H., 1969. Late middle Eocene to Recent planktonic foraminiferal biostratigraphy. *In* Bronnimann, P. and Renz, H. H. (Eds.), *Proc. First Int'l. Conf. Planktonic Microfossils* (Vol. 6): Leiden (Brill), 199-421.

Boyce, R. E., 1976a. Definitions and laboratory techniques of compressional and sound velocity parameters and wet-water content, wet-bulk density, and porosity parameters by gravimetric and gamma ray attenuation techniques. *In* Schlanger, S. D., Jackson, E. D., et al., *Init. Repts. DSDP*, 33: Washington (U.S. Govt. Printing Office), 931-958.

———, 1976b. Deep Sea Drilling Project procedures for shear strength measurements of clayey sediment using modified Wykeham Farrance Laboratory Vane Apparatus. *In* Barker, P., Dalziel, I. W. D., et al., *Init. Repts. DSDP*, 36: Washington (U.S. Govt. Printing Office), 1059-1068.

Burckle, L. H., Hammond, S. R., and Seyb, S. M., 1978. A stratigraphically important new diatom from the Pleistocene of the North Pacific. *Pac. Sci.*, 32(2):209-214.

Damuth, J. E., Jacobi, R. D., and Hayes, D. E., 1983. Sedimentation processes in the northwest Pacific Basin revealed by echo character mapping studies. *Geol. Soc. Am. Bull.*, 94:381-395.

Fischer, A. G., Heezen, B. C., et al., 1971. Site 47, *In* Fischer, A. G., Heezen, B. C., et al., *Init. Repts. DSDP*, 6: Washington (U.S. Govt. Printing Office), 67-144.

Foreman, H. P., 1975. Radiolaria from the North Pacific, Deep Sea Drilling Project, Leg 32. *In* Larson, R. L., Moberly, R., et al., *Init. Repts. DSDP*, 32: Washington (U.S. Govt. Printing Office), 579-701.

Hays, J. D., 1970. Stratigraphy and evolutionary trends of Radiolaria in North Pacific deep-sea sediments. *In* Hays, J. D. (Ed.), *Geological Investigations of the North Pacific.* Mem. Geol. Soc. Am., 126:185-218.

Koizumi, I., 1973. The late Cenozoic diatoms of Sites 183-193, Leg 19, Deep Sea Drilling Project. *In* Creager, J. S., Scholl, D. W., et al., *Init. Repts. DSDP*, 19: Washington (U.S. Govt. Printing Office), 805-855.

McDougall, I., 1977. The present status of the geomagnetic polarity time scale. Research School of Earth Sciences. *A.N.U. Publ.*, No. 1288.

Ness, G., Levi, S., and Couch, R., 1980. Marine magnetic anomaly time scales for the Cenozoic and Late Cretaceous: a precis, critique, and synthesis. *Rev. Geophys. Space Phys.*, 18:753-770.

Olsson, R. K., 1964. Late Cretaceous planktonic foraminifera from New Jersey and Delaware. *Micropaleontology*, 10(2):157-188.

Pessagno, E. A., 1967. Upper Cretaceous planktonic foraminifera from the western Gulf Coastal Plain. *Paleontographica Americana*, 5(37):245-444.

Postuma, J. A., 1971. *Manual of Planktonic Foraminifera:* Amsterdam (Elsevier).

Riedel, W. R., and Sanfilippo, A., 1970. Radiolaria, Leg 4, Deep Sea Drilling Project. *In* Bader, R. G., Gerard, R. D., et al., *Init. Repts. DSDP*, 4: Washington (U.S. Govt. Printing Office), 503-575.

Stainforth, R. M., et al., 1975. Cenozoic planktonic foraminiferal zonation and characteristics of index forms. *Univ. Kans. Paleontol. Contrib. Pap.*, 62:1-425.

SITE 578 HOLE CORE 1 CORED INTERVAL 6004.7–6009.5 mbsl; 0.0–4.8 mbsf

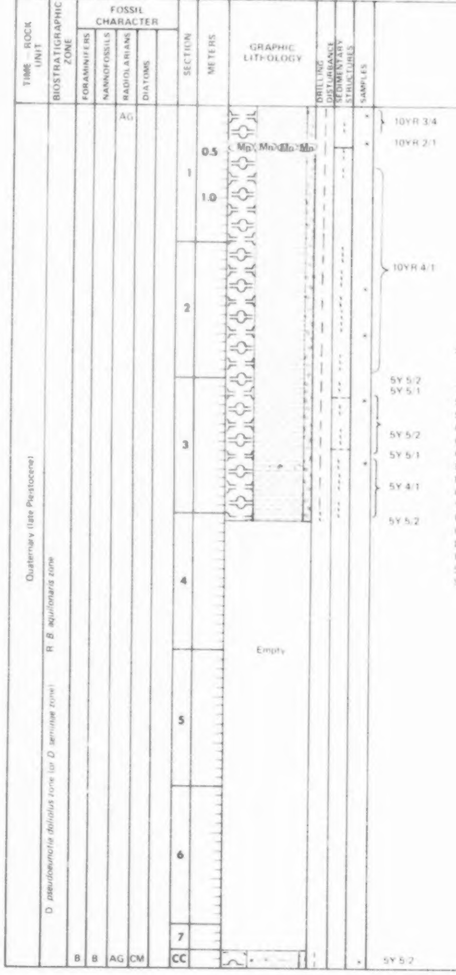
TIME – ROCK UNIT
BIOSTRATIGRAPHIC ZONE
FOSSIL CHARACTER
FORAMINIFERS
NANNOFOSSILS
RADIOLARIANS
DIATOMS
SECTION
METERS
GRAPHIC LITHOLOGY
DRILLING DISTURBANCE
SEDIMENTARY STRUCTURES
SAMPLES
Quaternary (late Pleistocene)
D. pseudoeunotia doliolus zone (or D. seminae zone)
R B. aquilonaris zone
AG
B
B
AG
CM
0.5
1.0
1
2
3
4
5
6
7
CC
Mn
Mn
Mn
Mn
Empty
10YR 3/4
10YR 2/1
10YR 4/1
5Y 5/2
5Y 5/1
5Y 5/2
5Y 5/1
5Y 4/1
5Y 5/2
5Y 5/2

LITHOLOGIC DESCRIPTION

SILICEOUS CLAY

*Dominant colors: dark yellowish brown (10YR 3/4) and dark gray (10YR 4/1) changing to olive gray (5Y 5/2), gray (5Y 5/1), and olive gray (5Y 4/1) at the base of Section 2. Minor colors: black (10YR 2/1) zone in Section 1.

*Core is slightly disturbed, except for Section 2, 0–53 cm which had a O-ring dragged through it during splitting and is moderately disturbed.

*This core consists of siliceous clay mottled with dark grayish brown to black specks and blebs. The small, mottled black zone in Section 1, 42–46 cm has a sharp bottom contact and is Mn-enriched. The Core Catcher contains two olive gray, sandy ash patches at 7–9 cm and 12–18 cm.

SMEAR SLIDE SUMMARY (%):

	1, 15	1, 45	2, 55	2, 106	3, 24	3, 96	CC
	D	D	D	D	D	M	M
Texture:							
Sand	10	10	5	5	5	5	50
Silt	40	50	35	35	40	70	40
Clay	50	40	60	60	55	25	10
Composition:							
Quartz	7	10	5	5	7	15	1
Feldspar	3	3	—	2	3	5	
Heavy minerals	3	25	1	1			
Clay	47	30	60	50	55	30	2
Volcanic glass	10	5	5	10	5	45	97
Foraminifers	Tr			Tr			
Calc. nannofossils	—	Tr					
Diatoms	10	7	10	10	15	5	
Radiolarians	20	15	15	20	15		
Sponge spicules			1	1			
Silicoflagellates		5	3	1			

SITE 578 HOLE CORE 2 CORED INTERVAL 6009.5–6019.0 mbsl; 4.8–14.3 mbsf

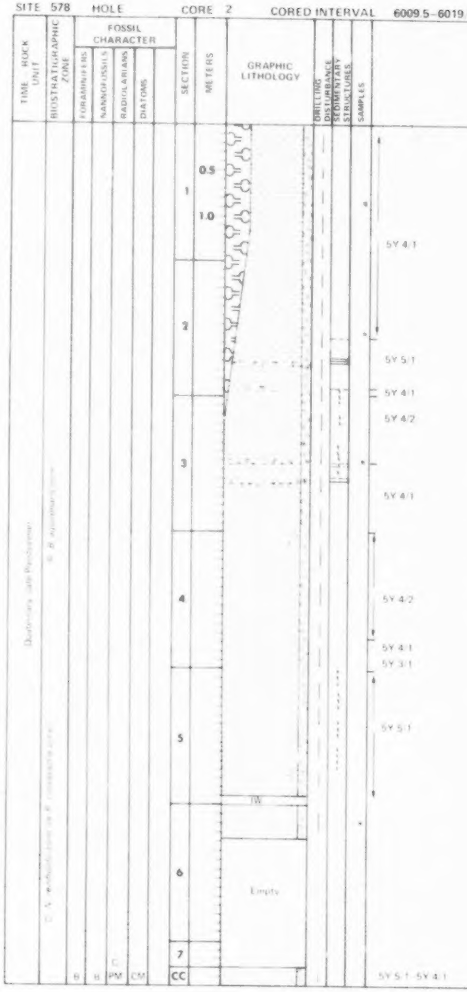
TIME – ROCK UNIT
BIOSTRATIGRAPHIC ZONE
FOSSIL CHARACTER
FORAMINIFERS
NANNOFOSSILS
RADIOLARIANS
DIATOMS
SECTION
METERS
GRAPHIC LITHOLOGY
DRILLING DISTURBANCE
SEDIMENTARY STRUCTURES
SAMPLES
Quaternary (late Pleistocene)
R B. aquilonaris zone
B
B
C
PM
CM
0.5
1.0
1
2
3
4
5
6
7
CC
IW
Empty
5Y 4/1
5Y 5/1
5Y 4/1
5Y 4/2
5Y 4/1
5Y 4/2
5Y 4/1
5Y 3/1
5Y 5/1
5Y 5/1–5Y 4/1

LITHOLOGIC DESCRIPTION

SILICEOUS CLAY CHANGING TO CLAY WITH VOLCANIC ASH LAYERS BELOW SECTION 1

*Dominant colors: dark gray (5Y 4/1), gray (5Y 5/1), and olive gray (5Y 4/2). Minor colors: Section 4 contains an interval of very dark gray (5Y 3/1). Ash layers are gray (5Y 5/1), dark gray (10YR 4/1) to black, and black (5Y 2/1).

*Entire core is slightly deformed by drilling. Section 5, 0–84 cm is gouged due to rock located at 5, 84 cm being dragged through core when it was split.

*This core consists of siliceous clay to clay with thin, stiff clay zones. Sections 2 and 3 have minor black mottles. The core contains three distinct ash layers: a dark gray ash layer at 2, 109–114 cm with fine (0.1 cm thick) internal lamination; a gray layer at 3, 75–78 cm; and, a black ash layer at 3, 92–95 cm. The two ash layers in Section 3 have sharp bottoms and gradational tops. In addition, there is an ash pocket at 2, 134 cm.

SMEAR SLIDE SUMMARY (%):

	1, 95	2, 80	3, 76	6, 20
	D	M	M	D
Texture:				
Sand	15	2	70	3
Silt	35	48	20	35
Clay	50	50	10	60
Composition:				
Quartz	7	50	10	15
Feldspar	—	10	2	5
Heavy minerals	1	—	—	—
Clay	50	15	18	63
Volcanic glass	10	15	70	10
Diatoms	10	10	Tr	5
Radiolarians	20	Tr	—	2
Sponge spicules	1	—	—	—
Silicoflagellates	1	—	—	—

SITE 578 HOLE CORE 3 CORED INTERVAL 6019.0–6028.5 mbsl; 14.3–23.8 mbsf

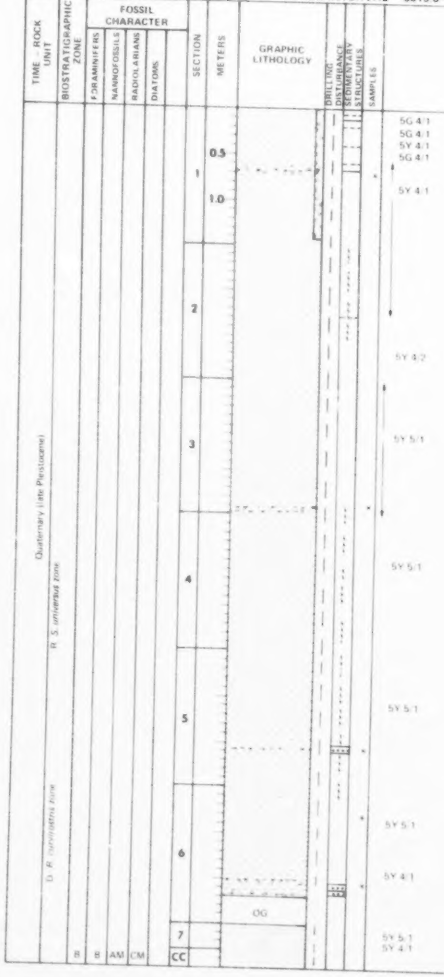
TIME – ROCK UNIT
BIOSTRATIGRAPHIC ZONE
FOSSIL CHARACTER
FORAMINIFERS
NANNOFOSSILS
RADIOLARIANS
DIATOMS
SECTION
METERS
GRAPHIC LITHOLOGY
DRILLING DISTURBANCE
SEDIMENTARY STRUCTURES
SAMPLES
Quaternary (late Pleistocene)
R. S. universus zone
D. R. curvirostris zone
B
B
AM
CM
1
2
3
4
5
6
7
CC
0.5
1.0
OG
5G 4/1
5G 4/1
5Y 4/1
5G 4/1
5Y 4/1
5Y 4/2
5Y 5/1
5Y 5/1
5Y 5/1
5Y 5/1
5Y 4/1
5Y 5/1
5Y 4/1

LITHOLOGIC DESCRIPTION

CLAY WITH VOLCANIC ASH LAYERS

- Dominant colors: dark gray (5Y 4/1) and olive gray (5Y 4/2) grading to gray (5Y 5/2) below Section 2. Sections 6, 7, and the Core Catcher contain intervals of dark gray (5Y 4/1). Minor colors: clay layers of dark greenish gray (5GY 4/1), and dark olive gray (5Y 3/2). Dark gray (5Y 4/1), gray (5Y 6/1), gray (2.5Y N5), and grayish brown (2.5Y 5/2) ash layers.
- Entire core is slightly deformed by drilling.
- This core consists of mottled clay with thin greenish layers of clay to pyritic clay. Five ash layers are found in this core: (1) 1, 60–65 cm is a dark gray ash layer with sharp bottom and gradational top; (2) 3, 141–141.5 cm is a gray ash layer; (3) 5, 106–111 cm is a normally graded gray ash layer; (4) 6, 107–111 cm is a grayish brown normally graded ash layer; and, (5) 6, 112–114 cm is a grayish brown normally graded ash layer.

SMEAR SLIDE SUMMARY (%):

	1, 70 D	3, 142 M	5, 110 M	6, 35 D	6, 108 M
Texture					
Sand	2	80	95	5	80
Silt	33	20	5	6	20
Clay	65	0	0	89	0
Composition					
Quartz	13	10	10	7	10
Feldspar	5	2	Tr	Tr	1
Clay	70	—		89	5
Volcanic glass	7	85	90	1	82
Pyrite	—	1	Tr	3	—
Diatoms	5	—		—	—
Radiolarians	Tr	Tr		Tr	Tr
Opaques	—	2		—	2

SITE 578 HOLE CORE 4 CORED INTERVAL 6028.5–6038.0 mbsl; 23.8–33.3 mbsf

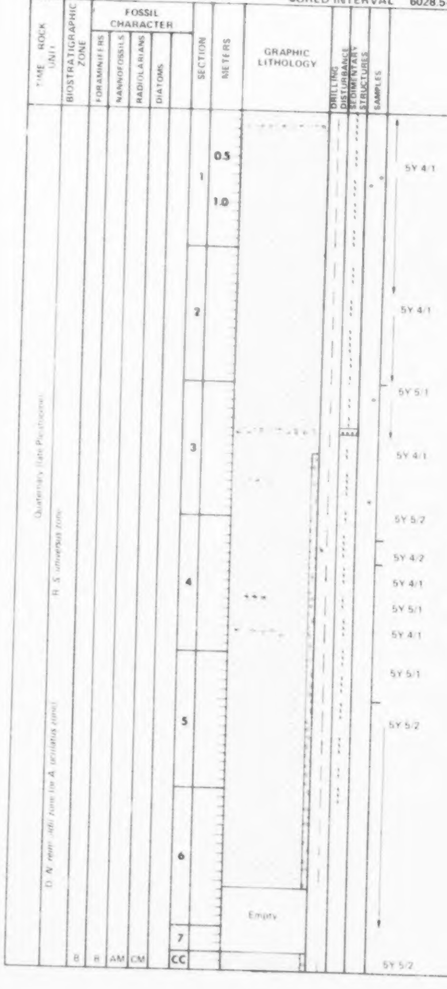
TIME – ROCK UNIT
BIOSTRATIGRAPHIC ZONE
FOSSIL CHARACTER
FORAMINIFERS
NANNOFOSSILS
RADIOLARIANS
DIATOMS
SECTION
METERS
GRAPHIC LITHOLOGY
DRILLING DISTURBANCE
SEDIMENTARY STRUCTURES
SAMPLES
Quaternary (late Pleistocene)
R. S. universus zone
D. N. reinholdii zone (or A. oculatus zone)
B
B
AM
CM
1
2
3
4
5
6
7
CC
0.5
1.0
Empty
5Y 4/1
5Y 4/1
5Y 5/1
5Y 4/1
5Y 5/2
5Y 4/2
5Y 4/1
5Y 5/1
5Y 4/1
5Y 5/1
5Y 5/2
5Y 5/2

LITHOLOGIC DESCRIPTION

CLAY WITH VOLCANIC ASH LAYERS

- Dominant colors: dark gray (5Y 4/1) with intervals of gray (5Y 5/1) and olive gray (5Y 4/2) changing to olive gray (5Y 5/2) at Section 5, 43 cm. Minor colors: green (5GY 4/1) clay layers. Gray (5Y 5/1) and light gray (2.5Y N7) ash layers.
- Entire core is slightly deformed by drilling.
- This core consists of mottled clay with thin (0.5–1.0 cm) green clay layers. Continuous ash layers occur at 1, 14–21 cm and 3, 51–56 cm. The continuous ash layer in Section 3 is normally graded. Discontinuous ash layers occur at 3, 110–110.5 cm; 4, 88 cm; and, 4, 124.5 cm.

SMEAR SLIDE SUMMARY (%):

	1, 70 D	1, 76 D	3, 20 D	3, 130 D
Texture				
Sand	5	2	5	10
Silt	13	20	13	13
Clay	82	78	82	77
Composition				
Quartz	10	15	10	7
Feldspar	Tr	Tr	Tr	Tr
Heavy minerals	—	—	—	Tr
Clay	82	78	81	77
Volcanic glass	3	1	5	10
Pyrite	Tr	1	—	—
Diatoms	2	2	1	1
Radiolarians	3	3	3	5
Sponge spicules	Tr	Tr	Tr	Tr
Silicoflagellates	Tr	Tr	—	Tr

SITE 578 HOLE CORE 5 CORED INTERVAL 6038.0–6047.5 mbsl; 33.3–42.8 mbsf

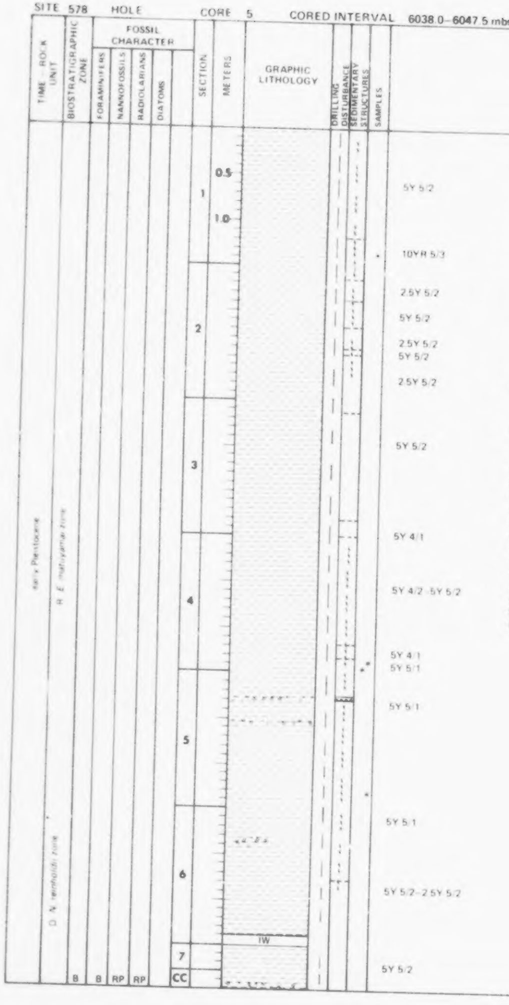
TIME – ROCK UNIT
BIOSTRATIGRAPHIC ZONE
FOSSIL CHARACTER
FORAMINIFERS
NANNOFOSSILS
RADIOLARIANS
DIATOMS
SECTION
METERS
GRAPHIC LITHOLOGY
DRILLING DISTURBANCE
SEDIMENTARY STRUCTURES
SAMPLES
early Pleistocene
R. E. matuyamai zone
D. N. reinholdii zone
B
B
RP
RP
1
2
3
4
5
6
7
CC
0.5
1.0
IW
5Y 5/2
10YR 5/3
2.5Y 5/2
5Y 5/2
2.5Y 5/2
5Y 5/2
2.5Y 5/2
5Y 5/2
5Y 4/1
5Y 4/2–5Y 5/2
5Y 4/1
5Y 5/1
5Y 5/1
5Y 5/1
5Y 5/2–2.5Y 5/2
5Y 5/2

LITHOLOGIC DESCRIPTION

CLAY WITH VOLCANIC ASH LAYERS

* Dominant colors: dark gray (5Y 4/1), gray (5Y 5/1) olive gray (5Y 4/2–5Y 5/2), grayish brown (2.5Y 5/2) and brown (10YR 5/3). Minor colors: green (5GY 4/1) to olive gray (5Y 4/2) clay layers. Medium gray (10YR 6/1) and very dark grayish brown (2.5Y 3/2) ash layers.

*Entire core is slightly deformed by drilling.

* This core consists of fairly homogeneous to lightly mottled clay with trace amounts of siliceous microfossils. It contains common, thin (0.2–1.0 cm) indurated green to olive gray clay layers. Continuous very dark grayish brown ash layers occur at 5, 28–29.5 cm; 5, 54–54.5 cm; 5, 55.2–56 cm; and, Core Catcher, 13–18 cm. The ash layer at 5, 28–29.5 cm is normally graded. A discontinuous medium gray ash layer occurs at 6, 37.2–37.7 cm.

SMEAR SLIDE SUMMARY (%)

	1, 140	4, 140	4, 143	5, 135
	D	D	D	D
Texture:				
Sand	5	5	1	1
Silt	14	7	12	20
Clay	81	88	87	79
Composition:				
Quartz	7	7	10	5
Feldspar	Tr	Tr	Tr	Tr
Clay	81	88	86	79
Volcanic glass	5	2	2	1
Pyrite	Tr	Tr	–	–
Micronodules	–	Tr	–	–
Diatoms	2	1	Tr	–
Radiolarians	3	1	Tr	–
Sponge spicules	1	1	2	Tr
Silicoflagellates	1	Tr	–	–
Opaques	–	–	–	15

SITE 578 HOLE CORE 6 CORED INTERVAL 6047.5–6057.0 mbsl; 42.8–52.3 mbsf

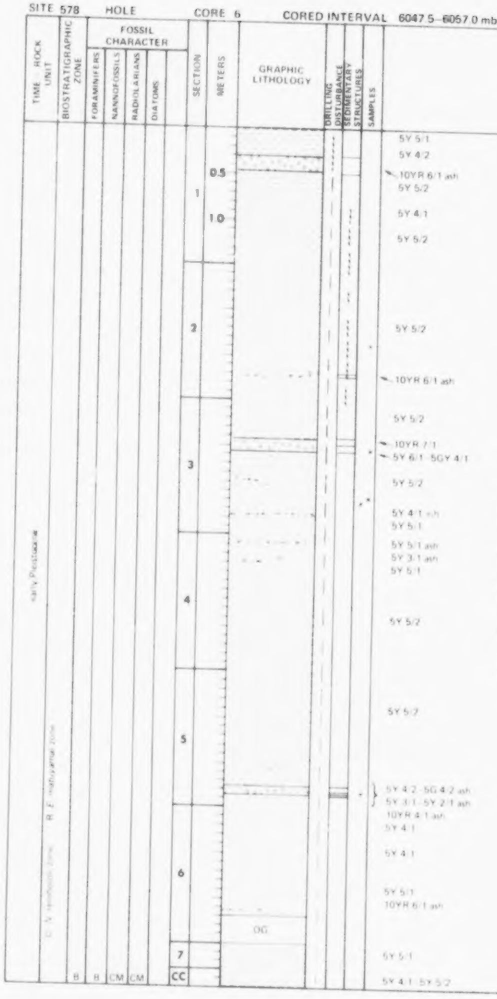
TIME – ROCK UNIT
BIOSTRATIGRAPHIC ZONE
FOSSIL CHARACTER
FORAMINIFERS
NANNOFOSSILS
RADIOLARIANS
DIATOMS
SECTION
METERS
GRAPHIC LITHOLOGY
DRILLING DISTURBANCE
SEDIMENTARY STRUCTURES
SAMPLES
early Pleistocene
R. E. matuyamai zone
D. N. reinholdii zone
B
B
CM
CM
1
2
3
4
5
6
7
CC
0.5
1.0
OG
5Y 5/1
5Y 4/2
10YR 6/1 ash
5Y 5/2
5Y 4/1
5Y 5/2
5Y 5/2
10YR 6/1 ash
5Y 5/2
10YR 7/1
5Y 6/1–5GY 4/1
5Y 5/2
5Y 4/1 ash
5Y 5/1
5Y 5/1 ash
5Y 3/1 ash
5Y 5/1
5Y 5/2
5Y 5/2
5Y 4/2–5G 4/2 ash
5Y 3/1–5Y 2/1 ash
10YR 4/1 ash
5Y 4/1
5Y 4/1
5Y 5/1
10YR 6/1 ash
5Y 5/1
5Y 4/1–5Y 5/2

LITHOLOGIC DESCRIPTION

CLAY WITH VOLCANIC ASH LAYERS

* Dominant colors: olive gray (5Y 4/2–5Y 5/2), dark gray (5Y 4/1), and gray (5Y 5/1). Minor colors: thin layers of dark gray (5Y 4/1), olive gray (5Y 4/2), and green (5GY 4/1–5/1). Black (5Y 2/1), very dark gray (5Y 3/1), dark gray (5Y 4/1), gray (5Y 5/1), medium gray (5Y 6/1), light gray (10YR 7/1), olive gray (5Y 4/2), green (5GY 4/1), and green (5G 4/2) ash layers.

* Entire core is slightly deformed by drilling.

* This core consists of homogeneous to mottled and burrowed clay with common, thin (0.1–0.5 cm), well indurated layers of greenish to olive gray clay. Continuous ash layers occur at 1, 30–47 cm; 2, 121–122 cm; 3, 43–48.5 cm; 3, 48.8–57 cm; 3, 129–130.5 cm; 4, 7–8 cm; 5, 127–133 cm; 5, 133–134.5 cm; 5, 134.5–135.5 cm. The ash layer at 5, 133–134.5 cm is a well indurated, pyritic clay (see smear slide summary below). Discontinuous ash layers occur at 3, 86–87 cm; 4, 26.3–26.8 cm; and, 6, 113–115 cm. Section 4, 5.5–5.8 cm contains a small pumice pebble.

SMEAR SLIDE SUMMARY (%)

	2, 90	3, 56	3, 112	3, 118	5, 133
	D	M	D	D	M
Texture:					
Sand	2	80	2	5	40
Silt	7	20	10	6	55
Clay	91	0	88	89	5
Composition:					
Quartz	3	5	3	3	3
Feldspar	Tr	–	Tr	–	Tr
Clay	91	–	88	89	5
Volcanic glass	3	95	–	7	75
Pyrite	–	–	–	–	15
Micronodules	–	–	–	Tr	–
Diatoms	1	–	1	Tr	–
Radiolarians	2	–	3	1	–
Sponge spicules	Tr	–	2	Tr	–
Silicoflagellates	Tr	–	1	Tr	–
Opaques	Tr	Tr	–	–	2

SITE 578 HOLE CORE 7 CORED INTERVAL 6057.0–6066.5 mbsl; 52.3–61.8 mbsf

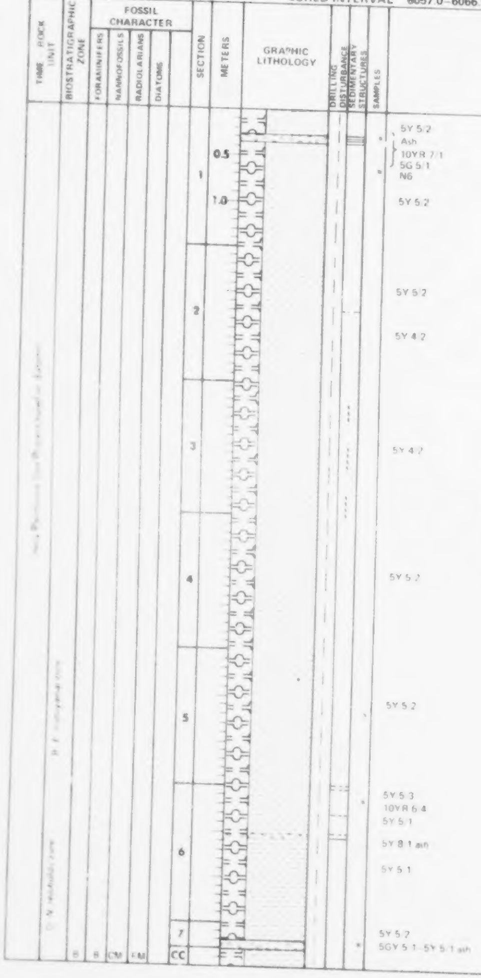
TIME – ROCK UNIT
BIOSTRATIGRAPHIC ZONE
FOSSIL CHARACTER
FORAMINIFERS
NANNOFOSSILS
RADIOLARIANS
DIATOMS
SECTION
METERS
GRAPHIC LITHOLOGY
DRILLING DISTURBANCE
SEDIMENTARY STRUCTURES
SAMPLES
0.5
1.0
1
2
3
4
5
6
7
CC
B
B
CM
FM
5Y 5/2
Ash
10YR 7/1
5G 5/1
N6
5Y 5/2
5Y 5/2
5Y 4/2
5Y 4/2
5Y 5/2
5Y 5/2
5Y 5/3
10YR 6/4
5Y 5/1
5Y 8/1 ash
5Y 5/1
5Y 5/2
5GY 5/1–5Y 5/1 ash

LITHOLOGIC DESCRIPTION

SILICEOUS CLAY WITH VOLCANIC ASH LAYERS

- Dominant colors: olive gray (5Y 4/2–5Y 5/2), and gray (5Y 5/1). Minor colors: thin layers of greenish gray (5GY 5/1), green (5G 4/2), olive (5Y 4/4), and dark olive gray (5Y 3/2). Ash layers are light gray (10YR 7/1), greenish gray (5G 5/1), gray (5GY 5/1), light gray (N6), and white (5Y 8/1).
- Entire core is slightly deformed by drilling.
- This core consists of homogeneous to lightly mottled siliceous clay with thin (0.5–1.0 cm), stiff greenish to olive gray clay layers. Ash layers occur at 1, 26–33 cm, 6, 49–53 cm, 7, 20–23 cm, and 7, 26–35 cm. The ash layer in Section 1 consists of three distinctly colored laminae, each 2–3 cm thick. The ash layer at 6, 49–53 cm is olive gray at the top and grades to white at the bottom.

SMEAR SLIDE SUMMARY (%)

	1, 30 M	1, 70 D	5, 70 D	6, 19 D	7, 23 M
Texture:					
Sand	70	7	7	7	70
Silt	20	33	33	38	20
Clay	10	60	60	55	10
Composition:					
Quartz	2	5	15	15	10
Feldspar		2	3	5	3
Heavy minerals			Tr	2	Tr
Clay	5	55	47	43	15
Volcanic glass	93	3	5	5	72
Diatoms	Tr	30	25	25	
Radiolarians		5	5	5	

SITE 578 HOLE CORE 8 CORED INTERVAL 6066.5–6076.0 mbsl; 61.8–71.3 mbsf

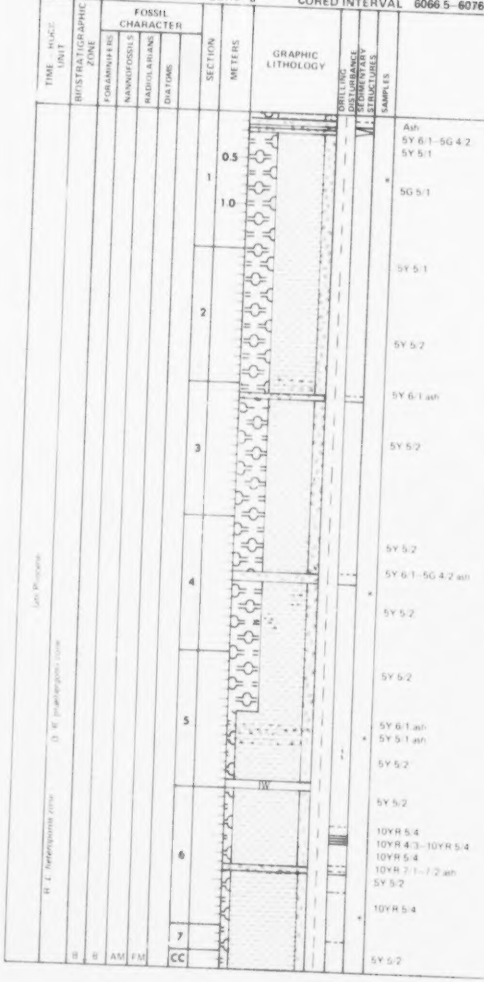
TIME – ROCK UNIT
BIOSTRATIGRAPHIC ZONE
FOSSIL CHARACTER
FORAMINIFERS
NANNOFOSSILS
RADIOLARIANS
DIATOMS
SECTION
METERS
GRAPHIC LITHOLOGY
DRILLING DISTURBANCE
SEDIMENTARY STRUCTURES
SAMPLES
Late Pliocene
R. L. heteroporos zone
0.5
1.0
1
2
3
4
5
6
7
CC
B
B
AM
FM
IW
Ash
5Y 6/1–5G 4/2
5Y 5/1
5G 5/1
5Y 5/1
5Y 5/2
5Y 6/1 ash
5Y 5/2
5Y 5/2
5Y 6/1–5G 4/2 ash
5Y 5/2
5Y 5/2
5Y 6/1 ash
5Y 5/1 ash
5Y 5/2
5Y 5/2
10YR 5/4
10YR 4/3–10YR 5/4
10YR 5/4
10YR 7/1–7/2 ash
5Y 5/2
10YR 5/4
5Y 5/2

LITHOLOGIC DESCRIPTION

SILICEOUS CLAY TO CLAY WITH VOLCANIC ASH LAYERS

- Dominant colors: olive gray (5Y 5/2) and gray (5Y 5/1). Greenish gray (5G 5/1) in Section 1. Sections 6 and 7 contain intervals of yellowish brown (10YR 5/4) and dark brown (10YR 4/3). Minor colors: thin layers of greenish gray (5G 4/1) in Sections 1, 2, and 3. Ash layers are gray (5Y 5/1), medium gray (5Y 6/1), greenish gray (5G 4/2), gray (5YR 5/1), and light gray (10YR 7/1–10YR 7/2).
- Entire core is slightly deformed by drilling.
- This core consists of siliceous clay to clay with thin (1.0 cm), greenish-gray layers of clay. Ash layers occur at 1, 5–11 cm; 1, 13–18.5 cm; 3, 10–15 cm; 5, 58–70 cm; 5, 86–87 cm; 5, 90–91 cm; and, 6, 81–87 cm. The ash layers have gradational top and sharp bottom contacts. Ash puckets occur at 2, 148 to 3, 3 cm; 5, 82–84 cm; and, 4, 116 cm. There is a small pebble at 1, 20 cm.

SMEAR SLIDE SUMMARY (%)

	1, 70 D	4, 80 D	5, 90 M	6, 140 D
Texture:				
Sand	20	15	60	5
Silt	50	45	20	30
Clay	30	40	20	65
Composition:				
Quartz	30	20	10	15
Feldspar	–	–	–	5
Clay	30	33	15	68
Volcanic glass	5	7	75	5
Diatoms	25	25	Tr	5
Radiolarians	10	15	Tr	2

SITE 578 HOLE CORE 9 CORED INTERVAL 6076.0–6085.5 mbsl; 71.3–80.8 mbsf

TIME–ROCK UNIT	BIOSTRATIGRAPHIC ZONE	FORAMINIFERS	NANNOFOSSILS	RADIOLARIANS	DIATOMS	SECTION	METERS
late Pliocene						1	0.5 1.0
						2	
						3	
						4	
						5	
						6	
						7	
		B	B	AM	CM	CC	

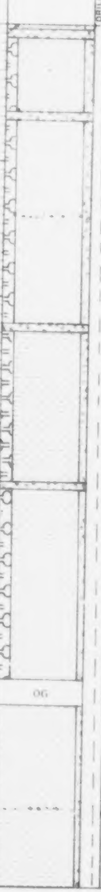

DRILLING DISTURBANCE / SEDIMENTARY STRUCTURES / SAMPLES

Ash 5Y 5/1
5Y 5/2
Ash 5Y 5/1
5Y 6/2
5Y 6/2
Ash 5Y 2/1
5Y 5/2
Ash 10YR 5/2
5Y 5/3
5Y 5/3
10YR 6/1
Ash 10YR 7/1
10YR 5/2
10YR 6/4
10YR 5/3
10YR 5/3
10YR 5/4
10YR 5/3
10YR 5/3
10YR 4/3
10YR 5/4
10YR 4/3
Ash 10YR 5/3
10YR 5/2
10YR 5/4

LITHOLOGIC DESCRIPTION

SILICEOUS CLAY TO CLAY WITH VOLCANIC ASH LAYERS

- Dominant colors: olive gray (5Y 5/2) and olive (5Y 5/3) in Sections 1 to 4, 56 cm. Section 4, 56 cm to the Core Catcher are pale brown (10YR 6/3), grayish brown (10YR 5/2), brown (10YR 4/3, 10YR 5/3), and light yellowish brown to yellowish brown (10YR 6/4, 10YR 6/4). Minor colors: thin layers of olive gray (5Y 4/2) in Sections 1 and 2. Ash layers are gray (5Y 5/1), black (5Y 2/1), grayish brown (10YR 5/2), light gray (10YR 7/1), and brown (10YR 5/3).
- Entire core is slightly deformed by drilling.
- This core consists of siliceous clay to clay with volcanic ash layers. Sections 1 through 3 contain frequent, thin, stiff, olive gray clay layers. Ash layers occur at 1, 4–14 cm; 1, 95–102 cm; 2, 59–60 cm; 3, 30–37 cm; 4, 56–61 cm; and 6, 111–114 cm. Ashy patches and mottles are found at 2, 51–96 cm and in Section 6. The ash layer at 6, 111–114 cm is graded. There is a distinct color change at 4, 56 cm, with uniform olive to olive gray above and mottled brown below.

SMEAR SLIDE SUMMARY (%)

	1, 60	3, 110	5, 80	7, 18
	D	D	D	M
Texture:				
Sand	15	7	9	25
Silt	35	20	26	50
Clay	60	73	65	25
Composition:				
Quartz	15	16	20	20
Feldspar	5	1	Tr	1
Mica	—	Tr	—	
Clay	55	62	63	28
Volcanic glass	10	10	5	15
Foraminifers			3	3
Calc. nannofossils	—	2		
Diatoms	10	4	3	1
Radiolarians	3	3	3	2
Sponge spicules		1	2	
Silicoflagellates		2	1	Tr
Opaques	2			

SITE 578 HOLE CORE 10 CORED INTERVAL 6085.5–6095.0 mbsl; 80.8–90.3 mbsf

TIME–ROCK UNIT	BIOSTRATIGRAPHIC ZONE	FORAMINIFERS	NANNOFOSSILS	RADIOLARIANS	DIATOMS	SECTION	METERS
early Pliocene						1	0.5 1.0
						2	
						3	
						4	
						5	
						6	
						7	
		B	B	AM	FM	CC	

Mn
Mn
Mn
Empty
4B

DRILLING DISTURBANCE / SEDIMENTARY STRUCTURES / SAMPLES

10YR 5/3
10YR 5/4
Ash 10YR 5/3
10YR 4/3
10YR 5/3
10YR 5/4
10YR 5/4
10YR 4/2
10YR 5/4
10YR 5/3
10YR 5/3
10YR 5/4
10YR 5/3
10YR 5/4
10YR 4/3 layers
10YR 5/4
10YR 5/3
10YR 6/4
10YR 5/3
10YR 5/4
10YR 5/3
10YR 5/4
10YR 3/2 layers
10YR 6/3
10YR 5/3

LITHOLOGIC DESCRIPTION

CLAY WITH FEW VOLCANIC ASH LAYERS
ASH LAYERS

- Dominant colors: brown (10YR 5/3) and yellowish brown (10YR 5/4) with interval of dark grayish brown (10YR 4/2) in Section 2. Minor colors: thin medium brown (10YR 4/3) layers in Section 4; thin very dark grayish brown (10YR 3/2) layers in Section 5. Ash layers in Section 1 are brown (10YR 4/3, 10YR 5/3).
- Entire core is slightly deformed by drilling.
- This core consists of mottled clay. Ash layers occur at 1, 49–54 cm and 1, 60–70 cm. The medium brown layers at 4, 64–66 cm and 4, 67–69 cm are ashy clay layers. Manganese nodules occur at 2, 25–28 cm and 2, 58–59 cm.

SMEAR SLIDE SUMMARY (%)

	3, 80	4, 68	5, 141
	D	M	D
Texture:			
Sand	7	15	5
Silt	15	40	10
Clay	78	45	85
Composition:			
Quartz	12	5	2
Feldspar	Tr		
Clay	79	48	73
Volcanic glass	2	40	3
Pyrite			10
Micronodules			10
Foraminifers	1	Tr	1
Diatoms	3	3	1
Radiolarians	Tr	3	Tr
Silicoflagellates	3	1	

SITE 578 HOLE CORE 11 CORED INTERVAL 6095.0–6104.5 mbsl; 90.3–99.8 mbsf

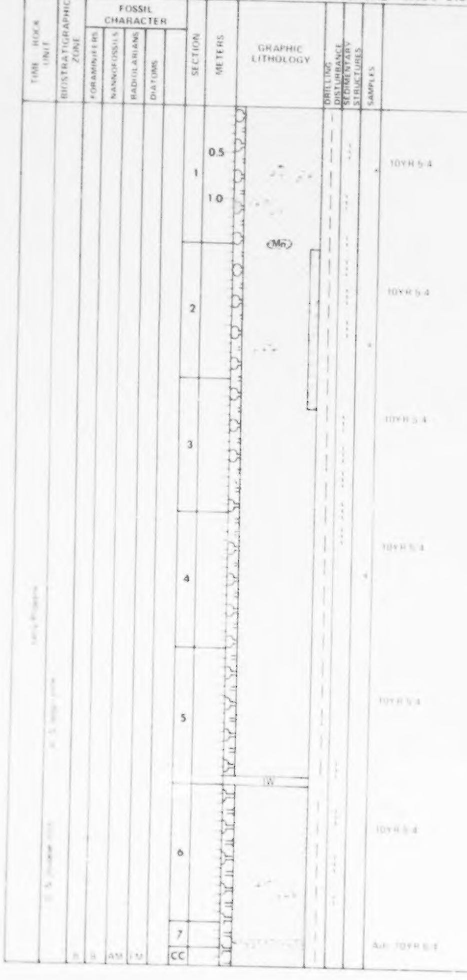
TIME-ROCK UNIT
BIOSTRATIGRAPHIC ZONE
FOSSIL CHARACTER
FORAMINIFERS
NANNOFOSSILS
RADIOLARIANS
DIATOMS
SECTION
METERS
GRAPHIC LITHOLOGY
DRILLING DISTURBANCE
SEDIMENTARY STRUCTURES
SAMPLES
0.5
1.0
1
2
3
4
5
6
7
CC
Mn
IW
B
B
AM
FM
10YR 5/4
10YR 5/4
10YR 5/4
10YR 5/4
10YR 5/4
10YR 5/4
Ash 10YR 6/4

LITHOLOGIC DESCRIPTION

SILICEOUS CLAY TO CLAY

- *Dominant colors: yellow brown (10YR 5/4) with intervals of brown (10YR 4/3), brown (10YR 5/3), dark grayish brown (10YR 4/2). Minor colors: light yellowish brown (10YR 6/4) ash in Section 2.
- *Entire core is slightly deformed by drilling.
- *This core consists of homogeneous yellowish brown siliceous clay with 2–20 cm thick intervals of brown to dark grayish brown mottled and burrowed siliceous clay. Sections 1, 2, and 6 contain small ashy patches. A light yellowish brown ash layer occurs at 7, 24–27 cm. A manganese nodule three cm long is found in Section 1, 142–148 cm.

SMEAR SLIDE SUMMARY (%)

	1, 70	2, 112	4, 70
	M	D	D
Texture:			
Sand	35	20	12
Silt	25	16	23
Clay	40	65	65
Composition:			
Quartz	10	10	10
Feldspar	Tr	Tr	—
Mica	—	—	1
Clay	30	65	66
Volcanic glass	45	15	3
Diatoms	1	1	1
Radiolarians	4	1	12
Silicoflagellates	1	—	1

SITE 578 HOLE CORE 12 CORED INTERVAL 6104.5–6114.0 mbsl; 99.8–109.3 mbsf

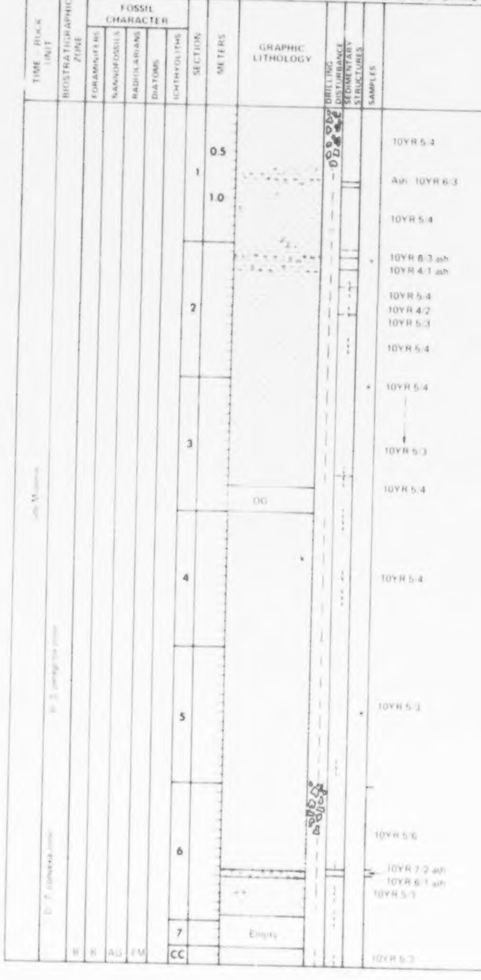
TIME-ROCK UNIT
BIOSTRATIGRAPHIC ZONE
FOSSIL CHARACTER
FORAMINIFERS
NANNOFOSSILS
RADIOLARIANS
DIATOMS
ICHTHYOLITHS
SECTION
METERS
GRAPHIC LITHOLOGY
DRILLING DISTURBANCE
SEDIMENTARY STRUCTURES
SAMPLES
late Miocene
0.5
1.0
1
2
3
4
5
6
7
CC
OG
Empty
B
R
AU
FM
10YR 5/4
Ash 10YR 6/3
10YR 5/4
10YR 6/3 ash
10YR 4/1 ash
10YR 5/4
10YR 4/2
10YR 5/3
10YR 5/4
10YR 5/4
10YR 5/3
10YR 5/4
10YR 5/4
10YR 5/3
10YR 5/6
10YR 7/2 ash
10YR 6/1 ash
10YR 5/3
10YR 6/3

LITHOLOGIC DESCRIPTION

CLAY WITH FEW VOLCANIC ASH LAYERS

- *Dominant colors: brown (10YR 5/3), yellowish brown (10YR 5/4) and dark grayish brown (10YR 4/2). Minor colors: pale brown (10YR 6/3), dark gray (10YR 4/1), 10YR 7/2, and gray (10YR 6/1) ash layers.
- *Core is slightly deformed by drilling, with brecciated intervals in Sections 1 and 6.
- *This core consists of homogeneous to lightly mottled clay. Ash layers occur at 1, 81–85 cm, 2, 5–15 cm, 2, 15–32 cm, and, 6, 96–102 cm. Small (0.5 cm diameter) pebbles occur at 4, 31–32 cm and 5, 29 cm.

SMEAR SLIDE SUMMARY (%)

	2, 20	3, 10	5, 70
	M	D	D
Texture:			
Sand	80	12	8
Silt	20	8	7
Clay	0	80	85
Composition:			
Quartz	6	7	6
Feldspar	—	Tr	—
Mica	—	2	1
Clay	—	79	85
Volcanic glass	94	5	5
Diatoms	—	1	Tr
Radiolarians	—	5	3
Silicoflagellates	—	1	—

SITE 578 HOLE CORE 13 CORED INTERVAL 6114.0–6123.5 mbsl; 109.3–118.8 mbsf

TIME–ROCK UNIT	BIOSTRATIGRAPHIC ZONE	FORAMINIFERS	NANNOFOSSILS	RADIOLARIANS	DIATOMS	ICHTHYOLITHS
late Miocene	R. S. peregrina zone D. T. convexa zone	B	B	AM	RP	

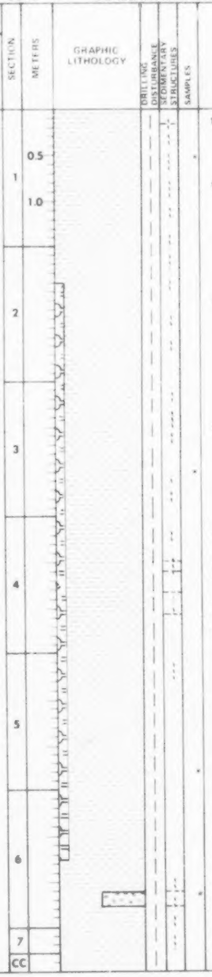

10YR 5/3
10YR 6/4
10YR 5/6
10YR 5/4
10YR 5/4
10YR 4/4
10YR 5/4
10YR 4/4
10YR 5/4
10YR 5/4
10YR 5/4
10YR 4/4
10YR 5/4
10YR 5/4

LITHOLOGIC DESCRIPTION

SILICEOUS CLAY TO CLAY

- Dominant colors: light yellowish brown (10YR 6/4) in Section 1, grading to yellowish brown (10YR 5/6) in Section 2, grading to yellowish brown (10YR 5/4) below Section 2. Minor colors: dark yellowish brown layers (10YR 4/4) in Sections 4 and 6.
- Entire core is slightly deformed by drilling.
- This core consists of homogeneous to lightly mottled siliceous clay to clay. Mottles are faint and black. Section 6, 112–125 cm is mottled with discrete patches of sand-sized black ash and altered ash (see smear slide summary below).

SMEAR SLIDE SUMMARY (%):

	1, 51 D	3, 100 D	5, 130 D	6, 118 D
Texture:				
Sand	2	3	2	60
Silt	8	27	28	30
Clay	90	70	70	10
Composition:				
Quartz	6	15	15	5
Feldspar				2
Mica	1			
Clay	89	70	73	36
Volcanic glass	1	5	3	55
Diatoms	Tr	10	7	2
Radiolarians	1	Tr	1	Tr
Opaques	3		2	

SITE 578 HOLE CORE 14 CORED INTERVAL 6123.5–6133.0 mbsl; 118.8–128.3 mbsf

TIME–ROCK UNIT	BIOSTRATIGRAPHIC ZONE	FORAMINIFERS	NANNOFOSSILS	RADIOLARIANS	DIATOMS	ICHTHYOLITHS
late Miocene		B	B	B	B	

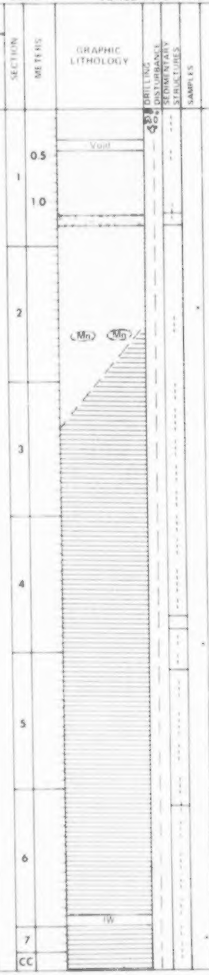

10YR 5/4
10YR 5/6
Ash: 10YR 8/1–10YR 6/1
10YR 5/6
10YR 5/6
10YR 5/6
10YR 5/6
10YR 4/4
10YR 5/4
10YR 5/6
10YR 5/4
10YR 3/3
10YR 3/4

LITHOLOGIC DESCRIPTION

CLAY

- Dominant colors: yellowish brown (10YR 5/6) and yellowish brown (10YR 5/4) grading to dark yellowish brown (10YR 3/3–10YR 3/4) at Section 6, 22 cm. Section 4, 114–125 cm contains a dark yellowish brown (10YR 4/4) layer. Minor colors: white (10YR 8/1) grading to gray (10YR 6/1) ash layer in Section 1.
- Entire core is slightly deformed by drilling.
- This core consists of lightly mottled to homogeneous clay. There is an ash layer in Section 1, 114–128 cm. Two 3 cm diameter manganese concretions occur in Section 2 at 93–100 cm.

SMEAR SLIDE SUMMARY (%):

	2, 70 D	4, 140 D	7, 20 D
Texture:			
Sand	7	2	1
Silt	33	28	24
Clay	60	70	75
Composition:			
Quartz	7	7	5
Feldspar	5	2	2
Heavy minerals	1		
Clay	70	87	84
Volcanic glass	15	7	2
Radiolarians	Tr	Tr	
Opaques	2	2	7

SITE 578 HOLE CORE 15 CORED INTERVAL 6133.0–6142.5 mbsl; 128.3–137.8 mbsf

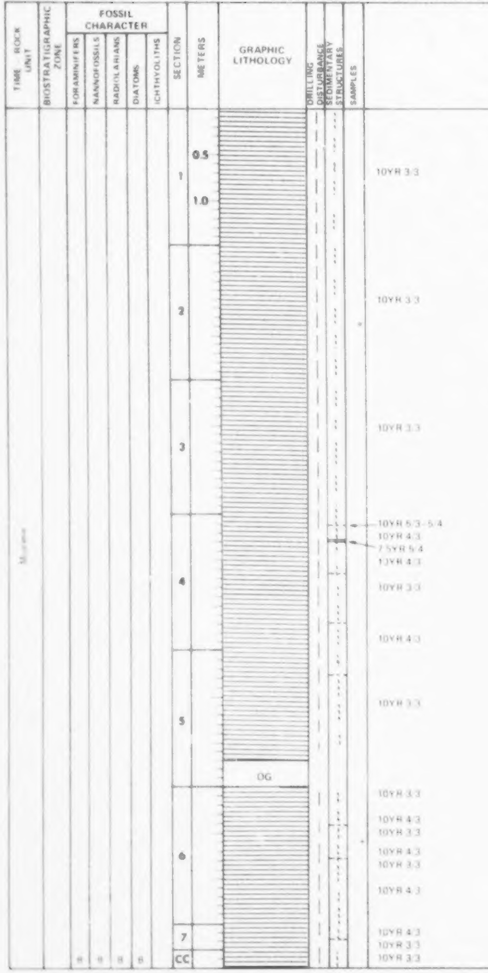
TIME-ROCK UNIT
BIOSTRATIGRAPHIC ZONE
FOSSIL CHARACTER
FORAMINIFERS
NANNOFOSSILS
RADIOLARIANS
DIATOMS
ICHTHYOLITHS
SECTION
METERS
GRAPHIC LITHOLOGY
DRILLING DISTURBANCE
SEDIMENTARY STRUCTURES
SAMPLES
Miocene
B B B B
0.5
1.0
1
2
3
4
5
6
7
CC
OG
10YR 3/3
10YR 3/3
10YR 3/3
10YR 5/3–5/4
10YR 4/3
7.5YR 5/4
10YR 4/3
10YR 3/3
10YR 4/3
10YR 3/3
10YR 3/3
10YR 4/3
10YR 3/3
10YR 4/3
10YR 3/3
10YR 4/3
10YR 4/3
10YR 3/3
10YR 3/3

LITHOLOGIC DESCRIPTION

PELAGIC CLAY

*Dominant colors: dark brown (10YR 3/3) and brown (10YR 4/3) to dark brown. Minor colors: Section 4 contains a thin brown (7.5YR 5/4) and a yellowish brown to brown (10YR 5/3–10YR 5/4) layer. Mottles in the core are yellowish brown (10YR 5/6) in Sections 1, 5, 6, and 7, brown (7.5YR 5/4) in Sections 2 and 3, and reddish yellow (7.5YR 6/6) in Section 4.

*Entire core is slightly deformed by drilling.

*This core consists of pelagic clay with tiny, faint black mottles and larger reddish yellow to yellowish brown to brown mottles.

SMEAR SLIDE SUMMARY (%):

	2, 90	6, 60
	D	D
Texture:		
Sand	0	0
Silt	15	10
Clay	85	90
Composition:		
Quartz	7	5
Feldspar	2	1
Heavy minerals	3	
Clay	84	88
Volcanic glass	3	2
Palagonite	1	
Opaques		4

SITE 578 HOLE CORE 16 CORED INTERVAL 6142.5–6152.0 mbsl; 137.8–147.3 mbsf

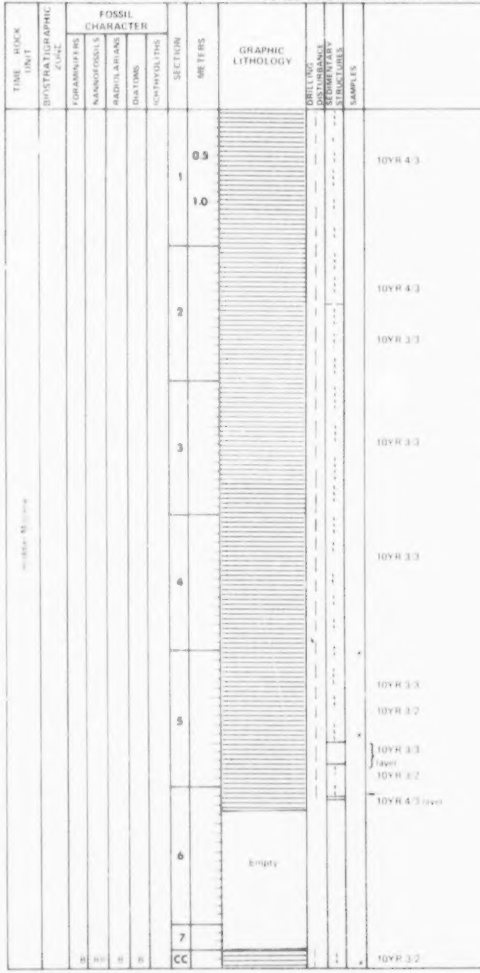
TIME-ROCK UNIT
BIOSTRATIGRAPHIC ZONE
FOSSIL CHARACTER
FORAMINIFERS
NANNOFOSSILS
RADIOLARIANS
DIATOMS
ICHTHYOLITHS
SECTION
METERS
GRAPHIC LITHOLOGY
DRILLING DISTURBANCE
SEDIMENTARY STRUCTURES
SAMPLES
middle Miocene
B RP B B
0.5
1.0
1
2
3
4
5
6
7
CC
Empty
10YR 4/3
10YR 4/3
10YR 3/3
10YR 3/3
10YR 3/3
10YR 3/3
10YR 3/2
10YR 3/3 layer
10YR 3/2
10YR 4/3 layer
10YR 3/2

LITHOLOGIC DESCRIPTION

PELAGIC CLAY

*Dominant colors: Section 1 to Section 2, 64 cm is brown (10YR 4/3) to dark brown with brown (7.5YR 5/4) to brown (10YR 5/3) mottles. Section 2, 64 cm to Section 5, 125 cm is dark brown (10YR 3/3) with brown (10YR 5/3) and yellowish brown (10YR 5/4) mottles. Section 5, 125 cm to the Core Catcher is very dark grayish brown (10YR 3/2). Faint black mottles are present throughout the core.

*Core is slightly deformed by drilling.

*This core consists of lightly mottled pelagic clay.

SMEAR SLIDE SUMMARY (%):

	5, 7	5, 95	CC
	D	D	D
Texture:			
Sand	2	1	5
Silt	5	7	1
Clay	93	92	94
Composition:			
Quartz	2	5	5
Feldspar	1	—	—
Mica	Tr	2	—
Clay	93	92	94
Volcanic glass	Tr	1	Tr
Palagonite	—	Tr	—
Micronodules	—	—	1
Opaques	5	—	—

SITE 578 HOLE CORE 17 CORED INTERVAL 6152.0–6160.0 mbsl; 147.3–155.3 mbsf

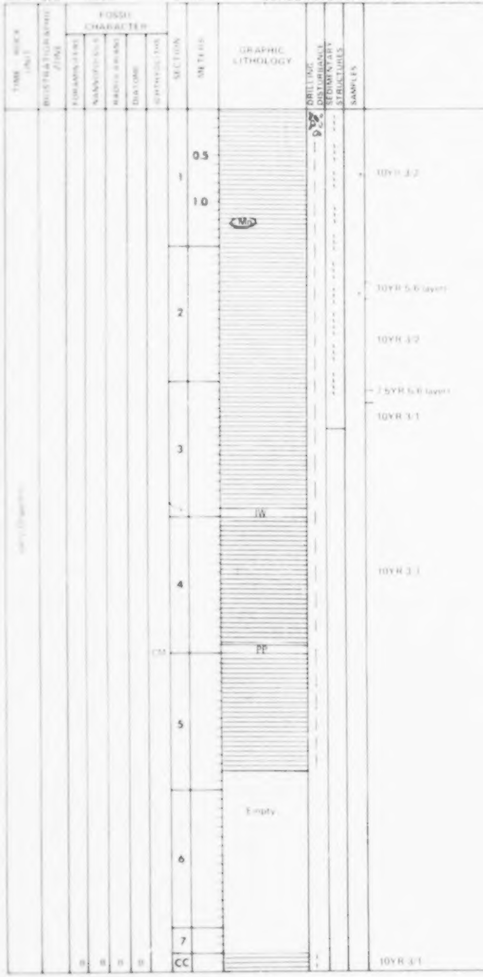
TIME-ROCK UNIT
BIOSTRATIGRAPHIC ZONE
FOSSIL CHARACTER
FORAMINIFERS
NANNOFOSSILS
RADIOLARIANS
DIATOMS
ICHTHYOLITHS
SECTION
METERS
GRAPHIC LITHOLOGY
DRILLING DISTURBANCE
SEDIMENTARY STRUCTURES
SAMPLES
0.5
1.0
1
2
3
4
5
6
7
CC
Mn
IW
PP
Empty
CM
B
B
B
B
10YR 3/2
10YR 5/6 layers
10YR 3/2
7.5YR 5/6 layers
10YR 3/1
10YR 3/1
10YR 3/1

LITHOLOGIC DESCRIPTION

PELAGIC CLAY

- Dominant colors: Sections 1 to 3, 53 cm are very dark grayish brown (10YR 3/2) with yellowish brown (10YR 5/4) mottles. Core below Section 3, 53 cm is very dark gray (10YR 3/1). Minor colors: Section 2, 45–64 cm contains thin yellowish brown (10YR 5/6) layers; Section 3, 12–21 cm contains thin strong brown (7.5YR 5/6) layers.
- Entire core is slightly deformed by drilling.
- This core consists of mottled to homogeneous pelagic clay. Section 1, 112–118 cm contains a manganese nodule 0.5 cm in diameter.

SMEAR SLIDE SUMMARY (%):

	1, 74	2, 55	4, 70
	D	D	D
Texture:			
Sand	5	0	0
Silt	25	7	2
Clay	70	93	98
Composition:			
Quartz	2	3	1
Mica		1	
Clay	85	88	96
Volcanic glass	1	1	1
Palagonite	1		
Micronodules	1		2
Zeolite	10	3	
Diatoms		4	

SITE 578 HOLE CORE 18 CORED INTERVAL 6161.5–6168.0 mbsl; 156.8–163.3 mbsf

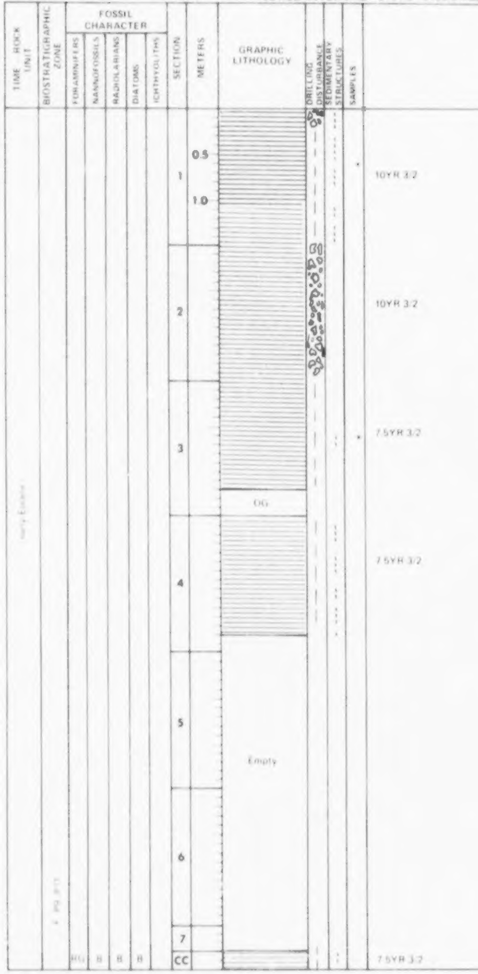
TIME-ROCK UNIT
BIOSTRATIGRAPHIC ZONE
FOSSIL CHARACTER
FORAMINIFERS
NANNOFOSSILS
RADIOLARIANS
DIATOMS
ICHTHYOLITHS
SECTION
METERS
GRAPHIC LITHOLOGY
DRILLING DISTURBANCE
SEDIMENTARY STRUCTURES
SAMPLES
early Eocene
0.5
1.0
1
2
3
4
5
6
7
CC
OG
Empty
RG
B
B
B
10YR 3/2
10YR 3/2
7.5YR 3/2
7.5YR 3/2
7.5YR 3/2

LITHOLOGIC DESCRIPTION

PELAGIC CLAY

- Dominant colors: Sections 1 and 2 are very dark grayish brown (10YR 3/2). Sections 3, 4, and the Core Catcher are dark brown (7.5YR 3/2) with yellowish red (5YR 4/6) and reddish brown (5YR 4/4) mottles.
- Section 2 of this core is slightly brecciated. The rest of the core is slightly deformed by drilling.
- This core consists of mottled pelagic clay. Section 1, 56–57 cm contains a fish tooth.

SMEAR SLIDE SUMMARY (%):

	1, 60	3, 69
	D	D
Texture:		
Sand	0	0
Silt	1	7
Clay	99	93
Composition:		
Quartz	Tr	2
Mica	–	1
Clay	99	93
Volcanic glass	1	3
Palagonite	–	1
Micronodules	Tr	–

SITE 578 HOLE CORE 19 CORED INTERVAL 6171.0–6176.0 mbsl; 166.3–171.3 mbst

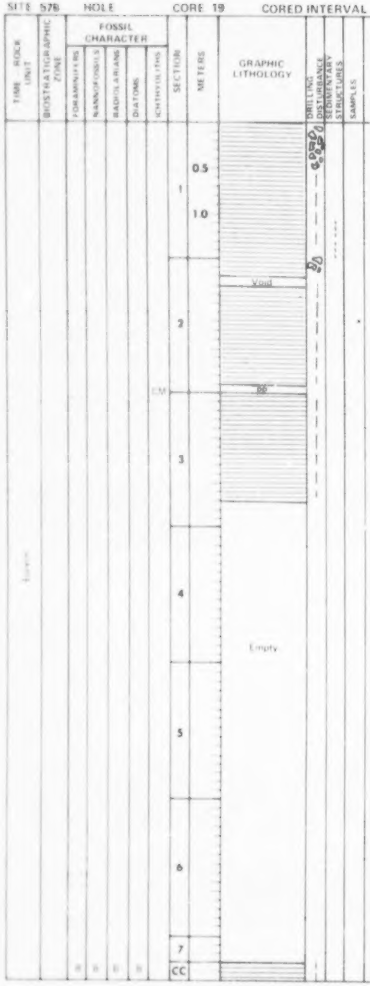
TIME-ROCK UNIT
BIOSTRATIGRAPHIC ZONE
FOSSIL CHARACTER
FORAMINIFERS
NANNOFOSSILS
RADIOLARIANS
DIATOMS
ICHTHYOLITHS
SECTION
METERS
GRAPHIC LITHOLOGY
DRILLING DISTURBANCE
SEDIMENTARY STRUCTURES
SAMPLES
0.5
1.0
1
2
3
4
5
6
7
CC
CM
Void
Empty
B
B
B
B

LITHOLOGIC DESCRIPTION

7.5YR 3/2

10YR 3/2

10YR 3/2

10YR 3/2

PELAGIC CLAY

- Dominant colors: Section 1 is dark brown (7.5YR 3/2) with reddish brown (5YR 4/4) mottles. Rest of the core is very dark grayish brown (10YR 3/2).
- Core is slightly deformed by drilling, with brecciated portions restricted to the tops of Sections 1 and 2.
- This core consists of homogeneous to slightly mottled pelagic clay. Mottling is confined to Section 1, 111–150 cm.

SMEAR SLIDE SUMMARY (%):

	2, 70 D
Texture:	
Sand	0
Silt	4
Clay	96
Composition:	
Quartz	1
Mica	1
Clay	96
Volcanic glass	2

SITE 578 HOLE CORE 20 CORED INTERVAL 6180.5–6181.5 mbsl; 175.8–176.8 mbsf

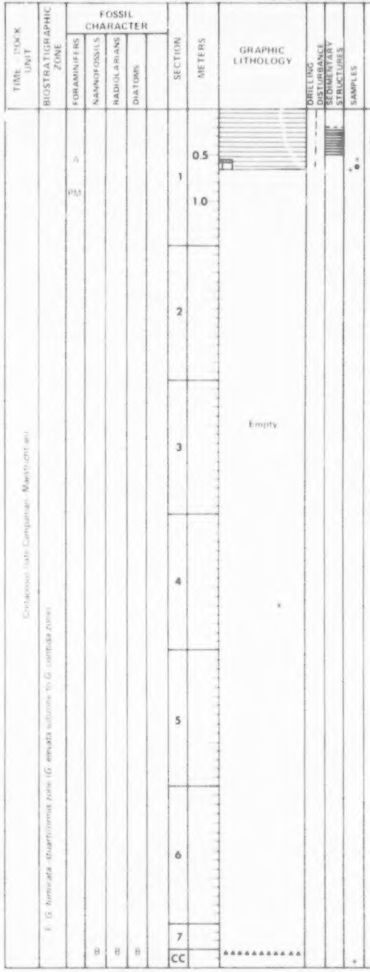
TIME-ROCK UNIT
BIOSTRATIGRAPHIC ZONE
FOSSIL CHARACTER
FORAMINIFERS
NANNOFOSSILS
RADIOLARIANS
DIATOMS
SECTION
METERS
GRAPHIC LITHOLOGY
DRILLING DISTURBANCE
SEDIMENTARY STRUCTURES
SAMPLES
Cretaceous (late Campanian–Maestrichtian)
F: G. havanensis–Gluembelina? zone (G. elevata subzone to G. contusa zone)
A
PM
B
B
B
0.5
1.0
1
2
3
4
5
6
7
CC
Empty

LITHOLOGIC DESCRIPTION

10YR 3/2
10YR 4/4
Laminations
10YR 3/3, 10YR 4/3,
7.5YR 4/4, 7.5YR 5/4
10YR 3/2 and 10YR 7/4

PELAGIC CLAY GRADING TO LAMINATED PELAGIC CLAY GRADING TO FORAMINIFERAL CLAY INTERBEDDED WITH CHERT

- Colors: Section 1, 0–20 cm is very dark grayish brown (10YR 3/2) grading to dark yellowish brown (10YR 4/4); 1, 20–52 cm is laminated layers of dark brown (10YR 3/3), brown (10YR 4/3), dark brown (7.5YR 4/4), and brown (7.5YR 5/4); 1, 52–65 cm contains very dark grayish brown (10YR 3/2) clay and very pale brown (10YR 7/4) foraminiferal clay.
- Core disturbance is slight in upper portions of Section 1 to moderate at base.
- This core consists of pelagic clay from 0–20 cm, laminated pelagic clay from 20–52 cm, and interbedded clay, foraminiferal clay, and chert in the Core Catcher. The laminated section contains laminations 0.1–0.5 cm thick. The forams in the foraminiferal clay layers are silicified. "Chalky" rinds of angular chert fragments are porcellanite with silicified forams.

SMEAR SLIDE SUMMARY (%):

	1, 53	1, 67	CC
Texture:			
Sand	70	20	—
Silt	20	5	—
Clay	10	75	—
Composition:			
Quartz	10	3	—
Mica	—	1	—
Clay	37	77	—
Volcanic glass	50	4	—
Foraminifers (silicified)	3	15	30
Chert	—	—	70

$CaCO_3$ data: 1, 56 cm = 0%

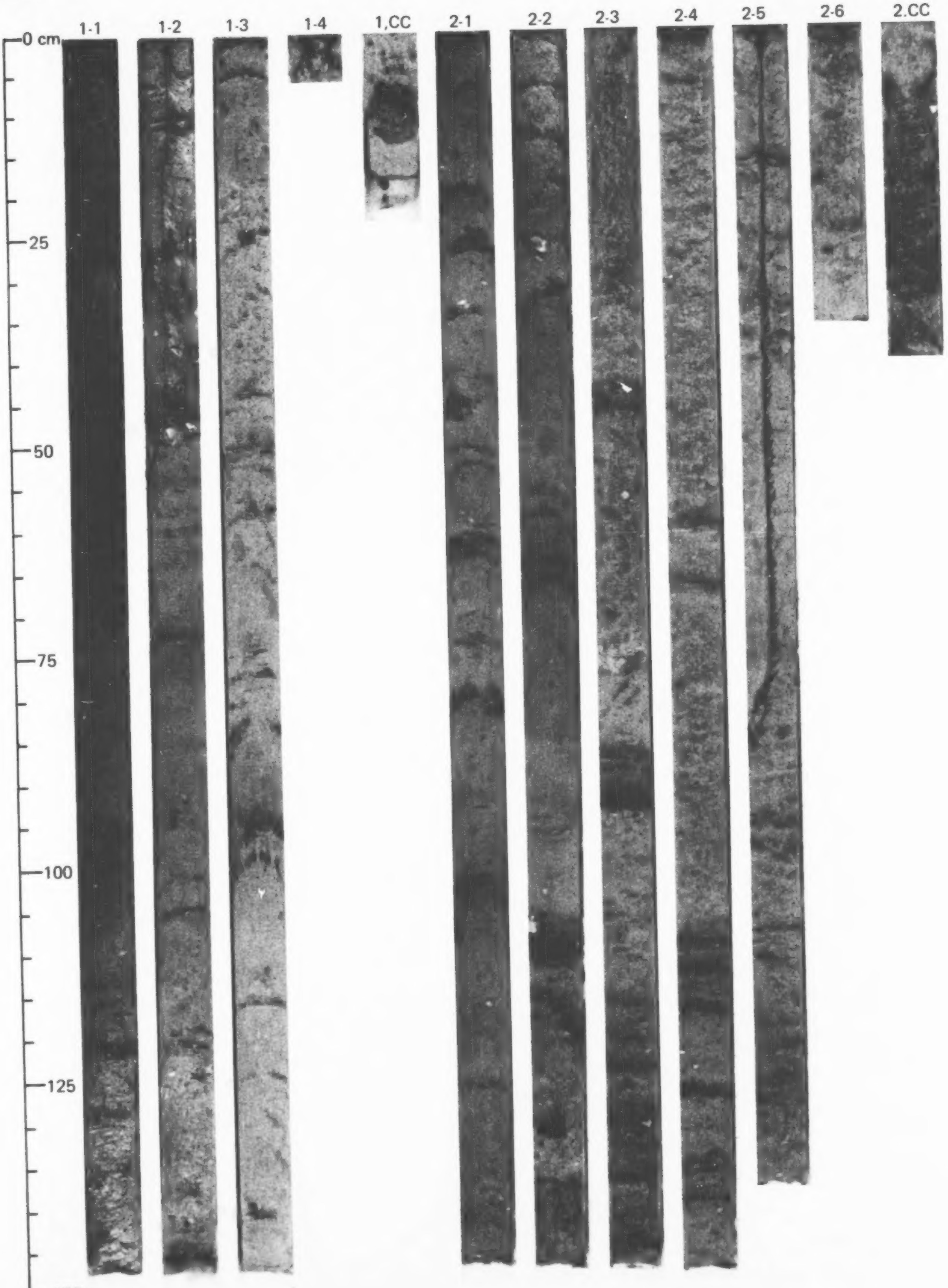
1-1
1-2
1-3
1-4
1,CC
2-1
2-2
2-3
2-4
2-5
2-6
2.CC
0 cm
25
50
75
100
125
150

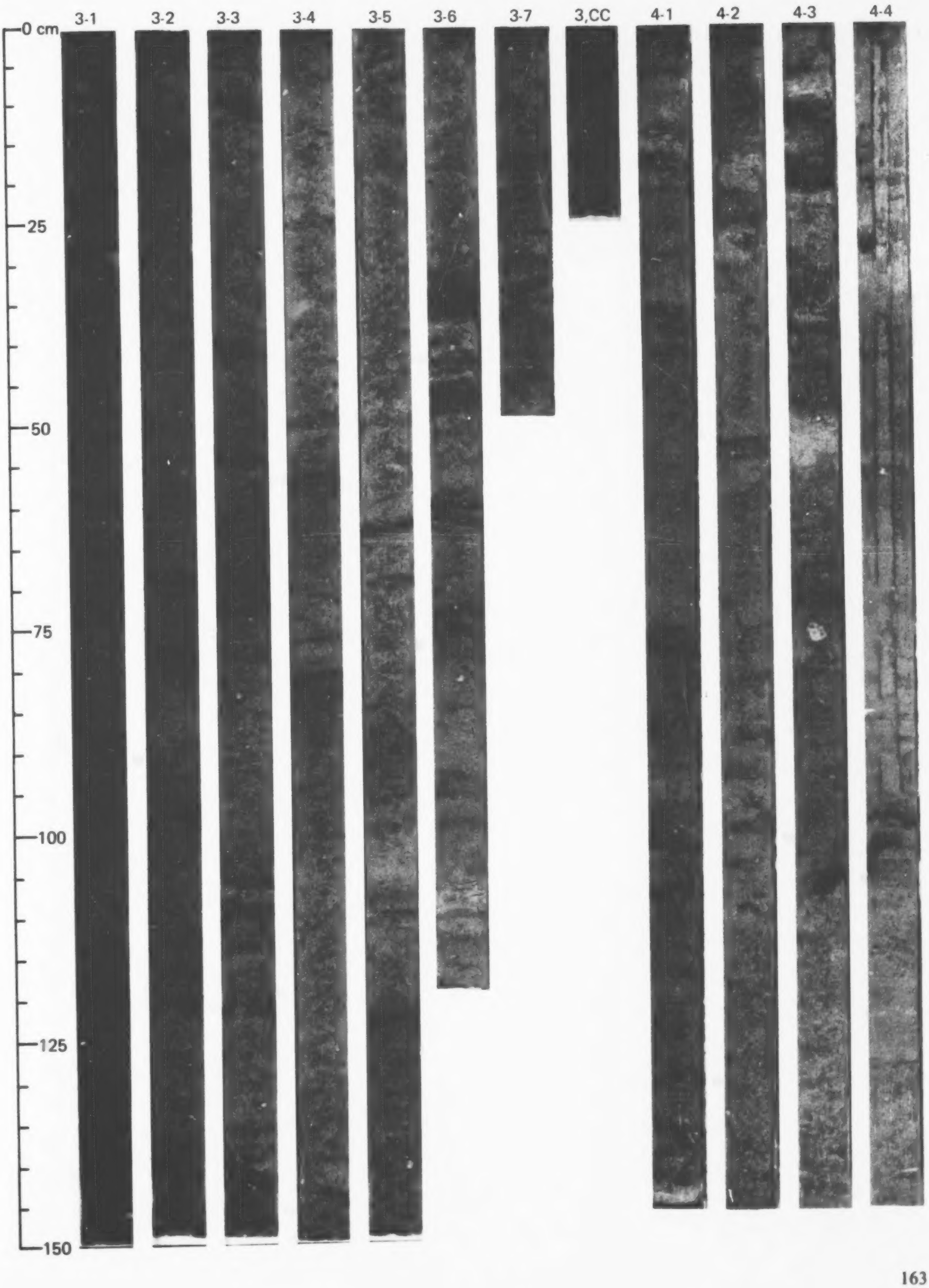
3-1
3-2
3-3
3-4
3-5
3-6
3-7
3,CC
4-1
4-2
4-3
4-4
0 cm
25
50
75
100
125
150

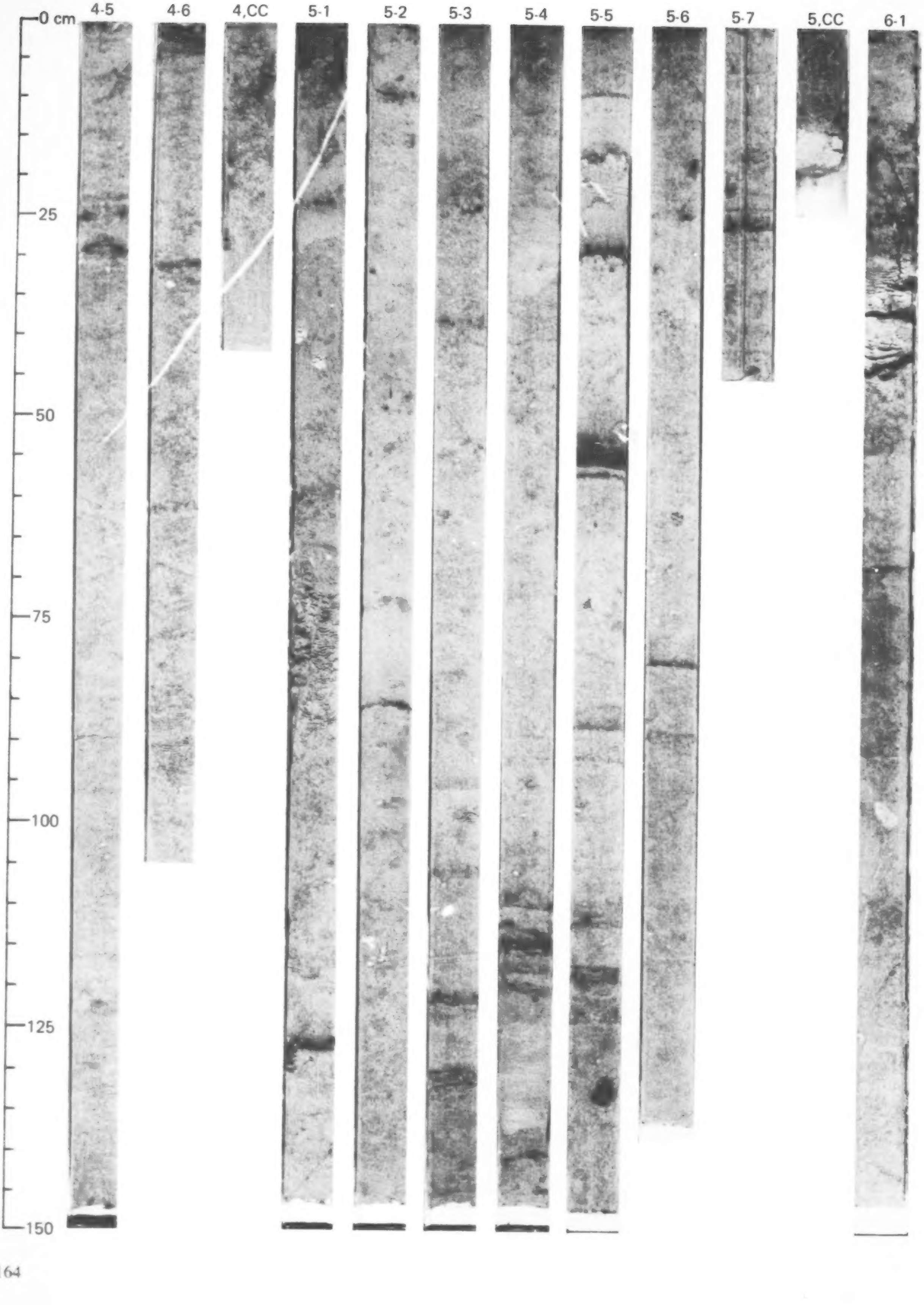
0 cm
25
50
75
100
125
150
4-5
4-6
4,CC
5-1
5-2
5-3
5-4
5-5
5-6
5-7
5,CC
6-1

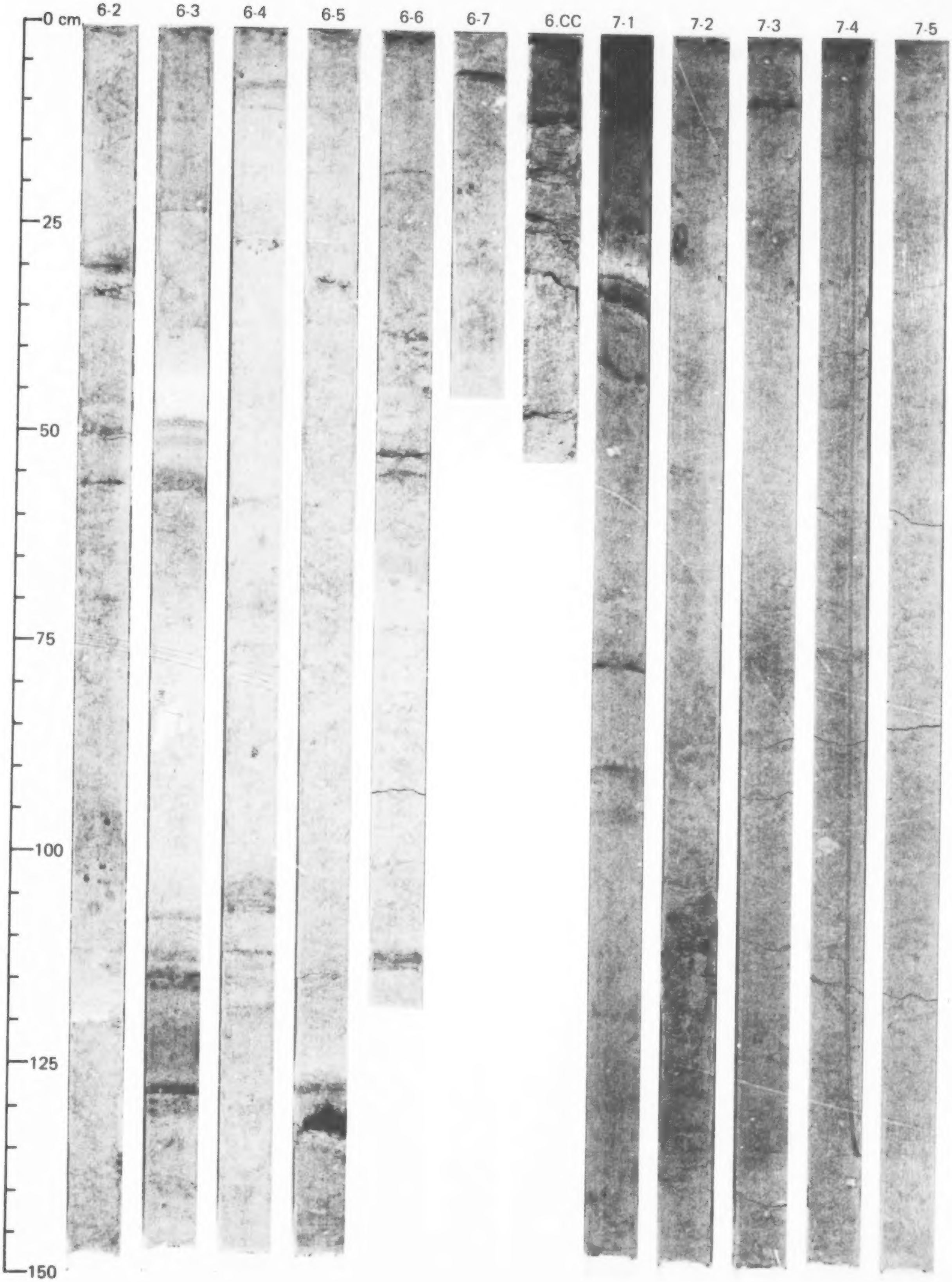
0 cm
25
50
75
100
125
150
6-2
6-3
6-4
6-5
6-6
6-7
6.CC
7-1
7-2
7-3
7-4
7-5

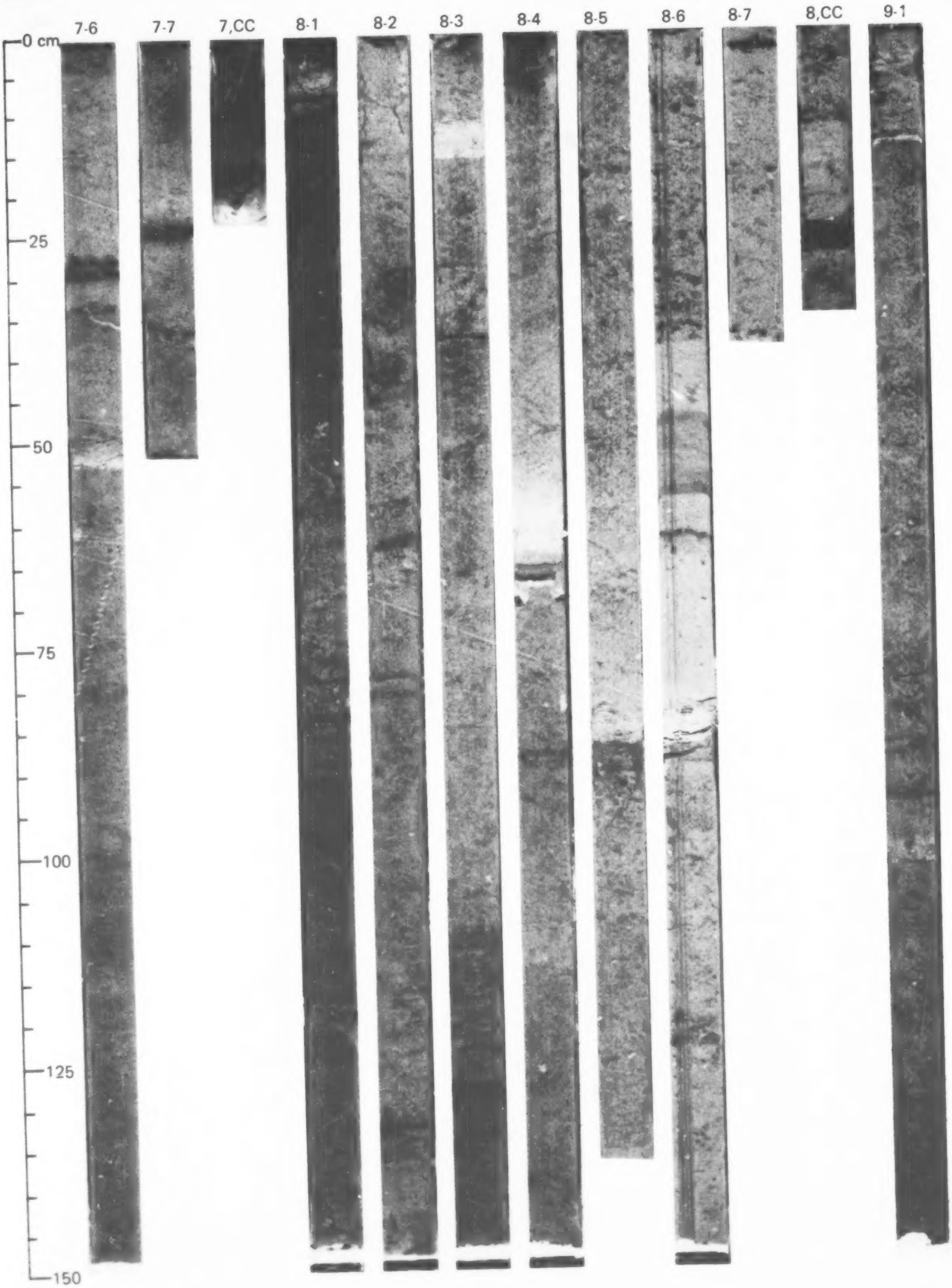
7-6
7-7
7,CC
8-1
8-2
8-3
8-4
8-5
8-6
8-7
8,CC
9-1
0 cm
25
50
75
100
125
150

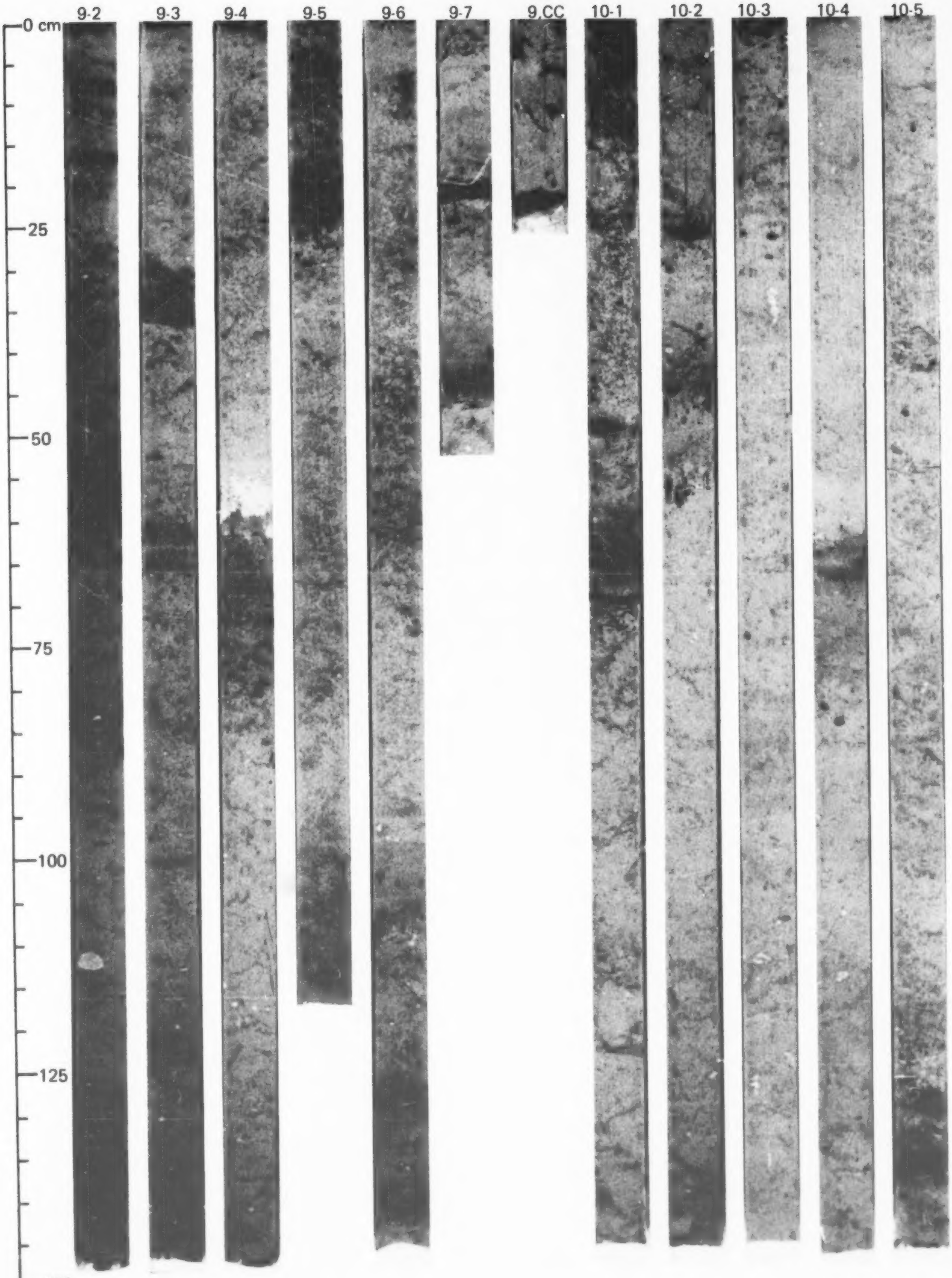
9-2
9-3
9-4
9-5
9-6
9-7
9,CC
10-1
10-2
10-3
10-4
10-5
0 cm
25
50
75
100
125
150

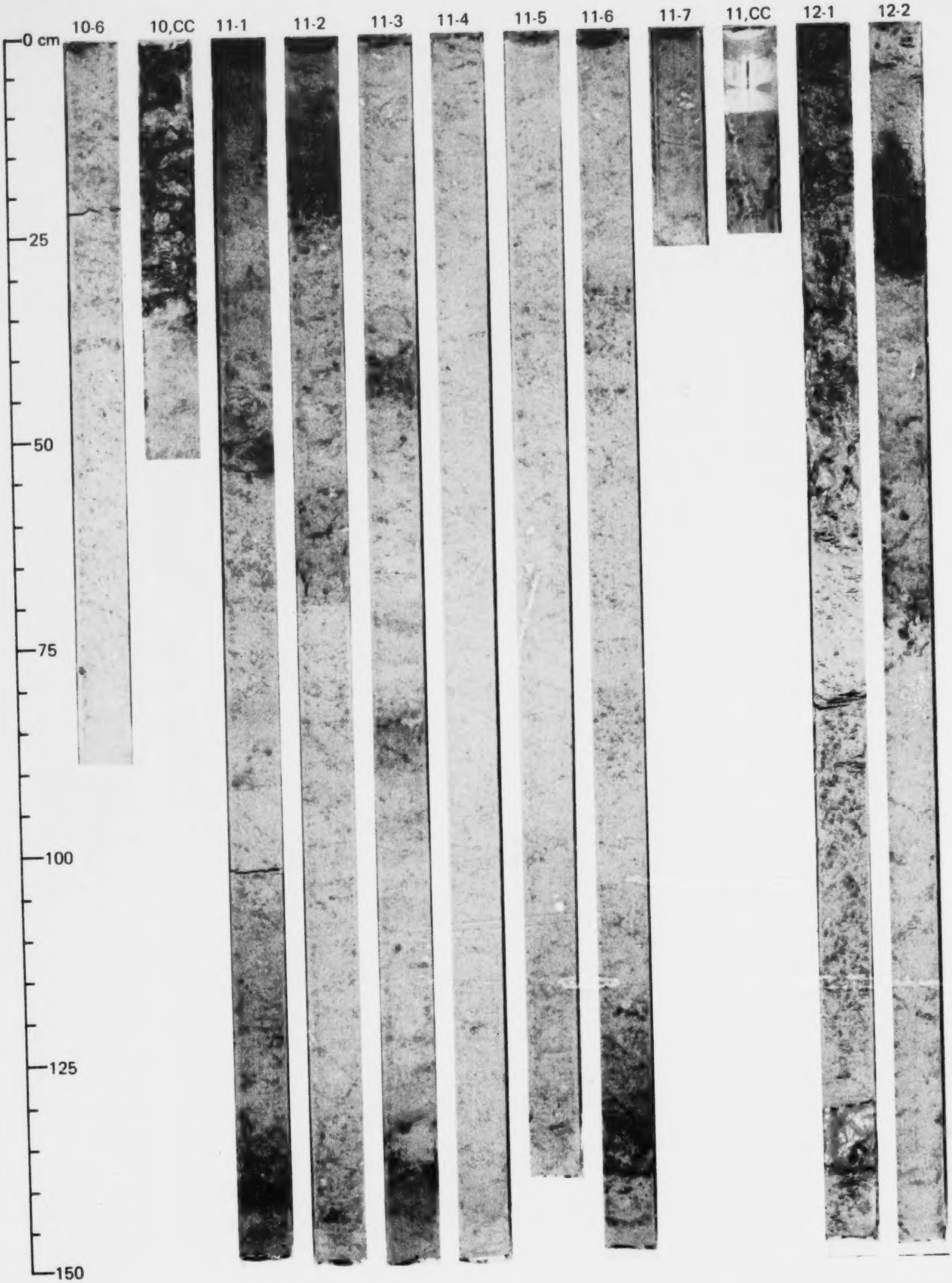
10-6
10,CC
11-1
11-2
11-3
11-4
11-5
11-6
11-7
11,CC
12-1
12-2
0 cm
25
50
75
100
125
150

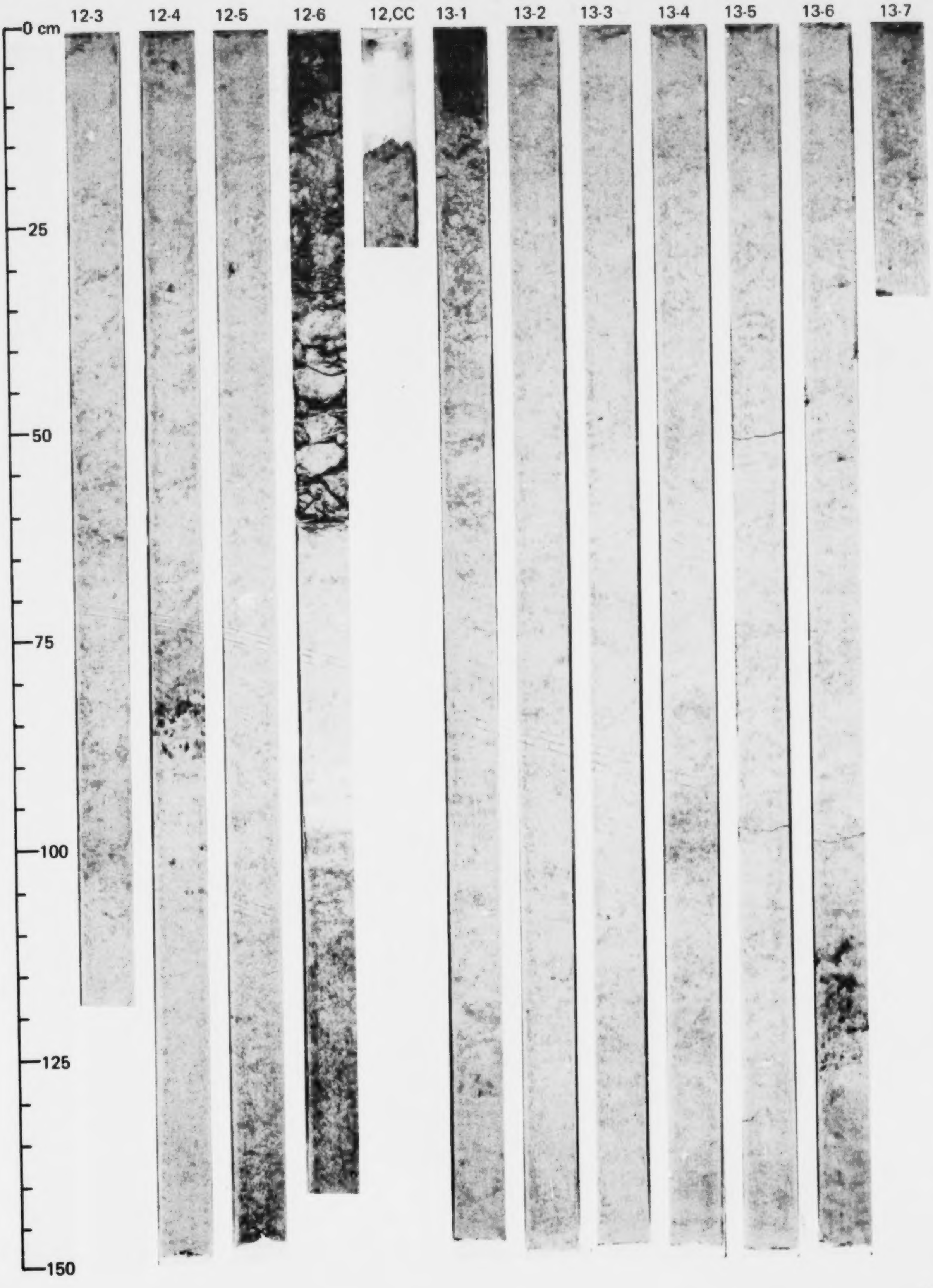
12-3
12-4
12-5
12-6
12,CC
13-1
13-2
13-3
13-4
13-5
13-6
13-7
0 cm
25
50
75
100
125
150

READEX FICHE

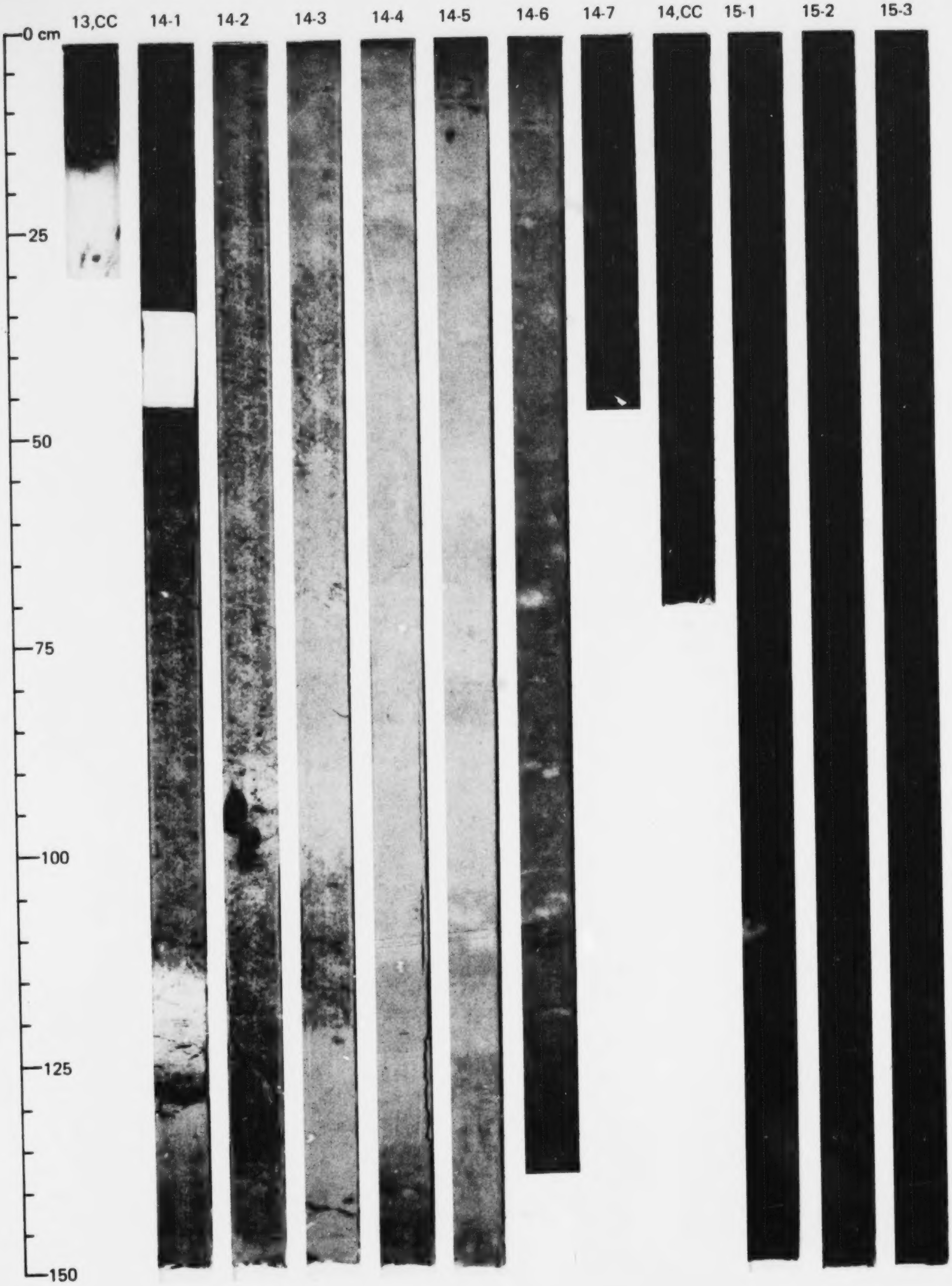
13,CC
14-1
14-2
14-3
14-4
14-5
14-6
14-7
14,CC
15-1
15-2
15-3
0 cm
25
50
75
100
125
150

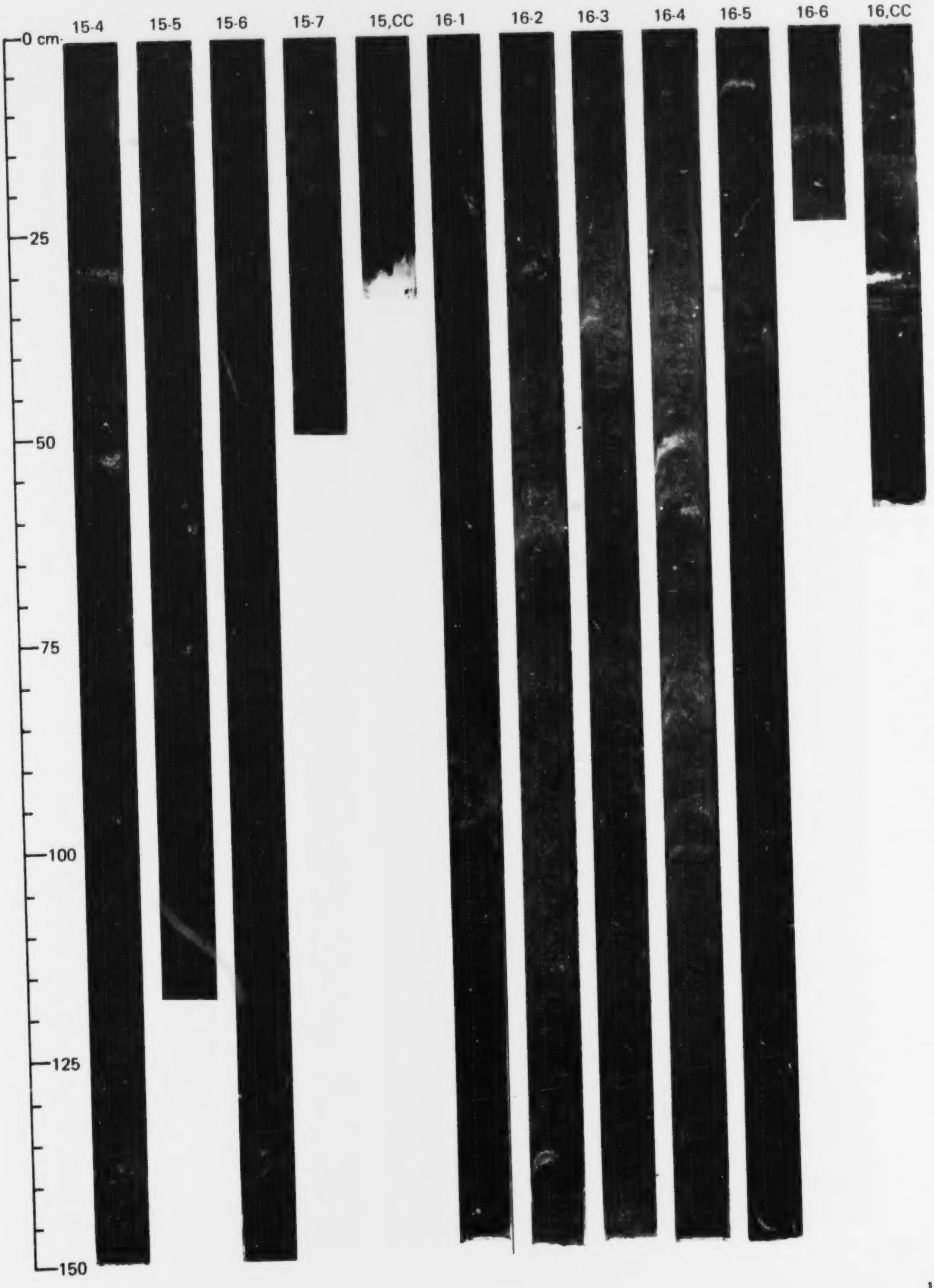
15-4
15-5
15-6
15-7
15,CC
16-1
16-2
16-3
16-4
16-5
16-6
16,CC
0 cm
25
50
75
100
125
150

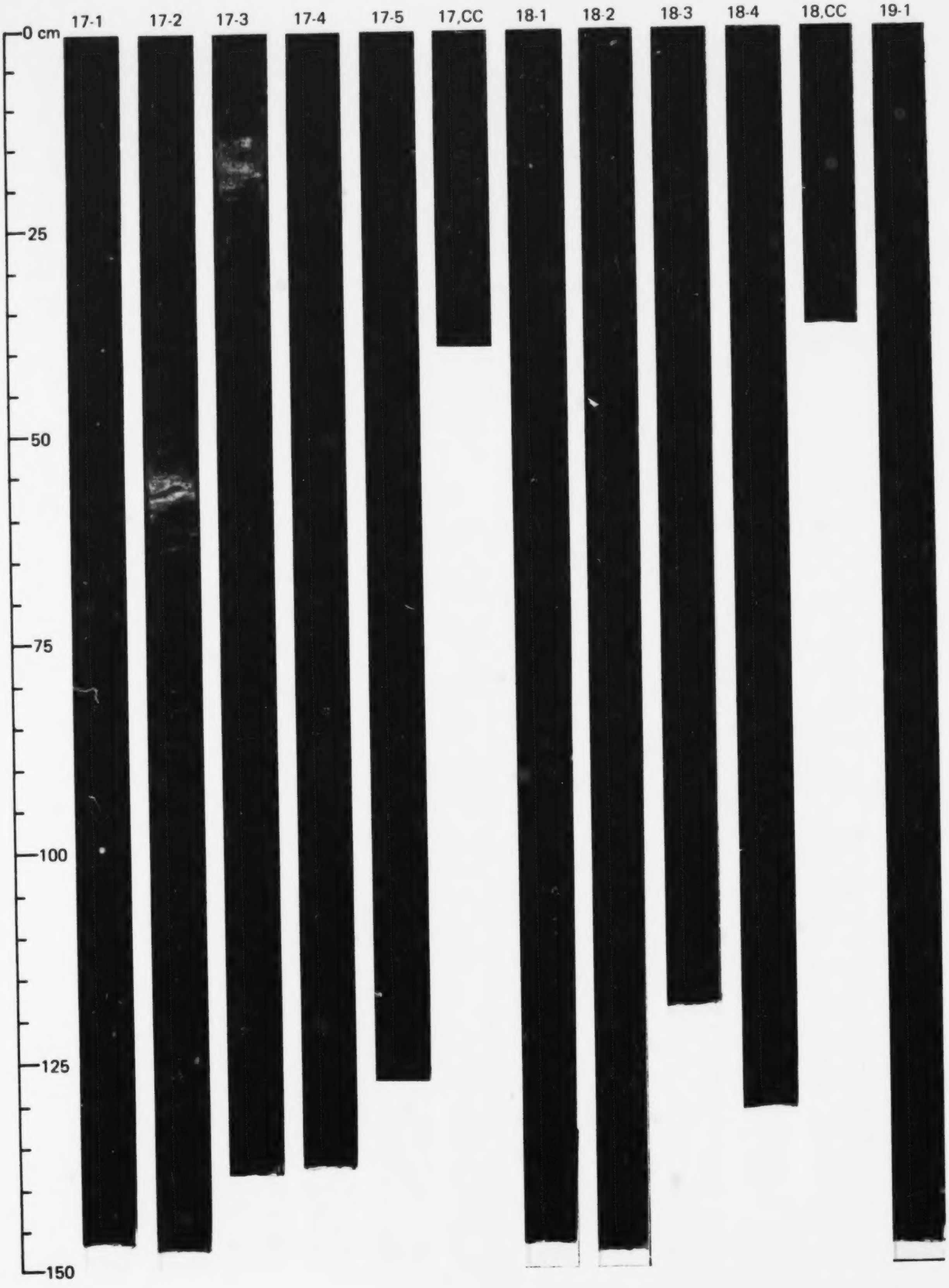
17-1
17-2
17-3
17-4
17-5
17,CC
18-1
18-2
18-3
18-4
18,CC
19-1
0 cm
25
50
75
100
125
150

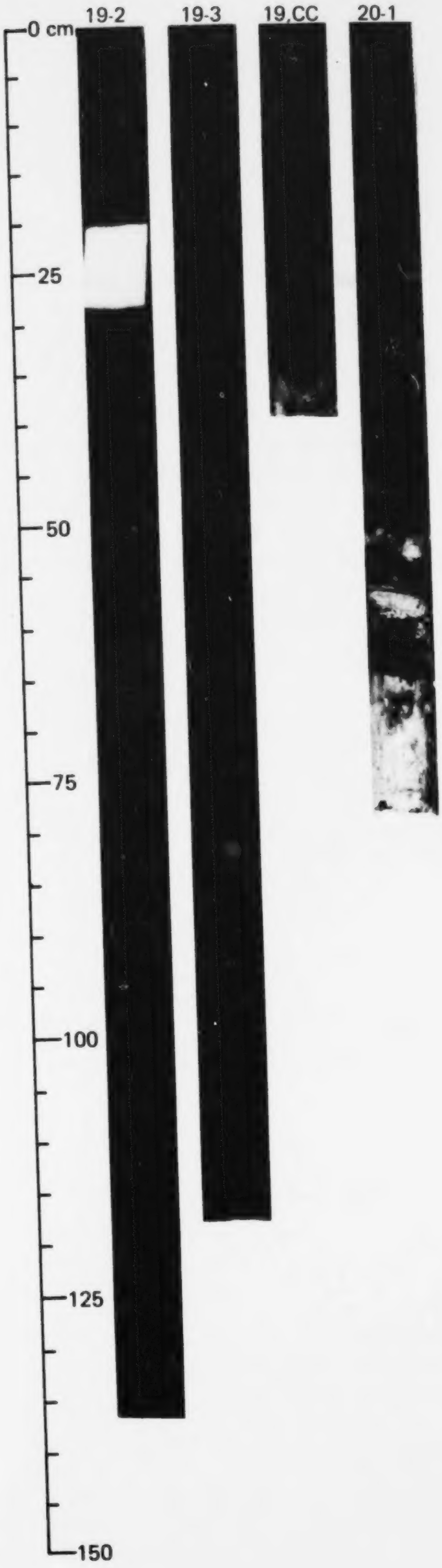
19-2
19-3
19,CC
20-1
0 cm
25
50
75
100
125
150

6. SITE 579[1]

Shipboard Scientific Party[2]

HOLES 579, 579A

Date occupied: 1 June 1982 (579), 2–4 June (579A)

Date departed: 4 June 1982

Time on site: 2 days, 17 hr., 6 min.

Position (latitude, longitude): 38°37.68′N; 153°50.17′E (579)
38°37.61′N; 153°50.28′E (579A)

Water depth (sea level; corrected m, echo-sounding): 5736.6

Water depth (rig floor; corrected m, echo-sounding): 5746.6

Bottom felt (m, drill pipe): 5746.6 (579), 5755.0 (579A)

Penetration (m): 17.9, (579), 149.5 (579A)

Number of cores: 2 (579), 15 (579A)

Total length of cored section (m): 17.9 (579), 135.5 (579A)

Total core recovered (m): 16.90 (579), 115.87 (579A)

Core recovery (%): 94 (579), 86 (579A)

Oldest sediment cored:
Depth sub-bottom (m): 149.5
Nature: siliceous clay
Age: early Pliocene
Measured velocity (km/s): 1.5

Basement: Not reached

Principal results: A thick section of early Pliocene to Quaternary siliceous clay was recovered from two holes at Site 579. Siliceous microfossils (diatoms and radiolarians) are generally abundant and well preserved throughout much of the section. An interpretable and complete magnetic stratigraphy can be identified back to the middle of the Gilbert Reversed Epoch (early Pliocene).

One hundred and forty-nine meters of sediment were cored. Except for ash layers, the recovered sediments are relatively uniform in color being gray, dark gray, olive gray, and greenish gray. Although burrow mottles are abundant, the sediment lacks any depositional sedimentary structures. Based upon these data, the entire sedimentary section recovered at Site 579 is placed into one single lithologic unit. However, based upon variations in biogenic and inorganic sediment compounds, three subunits can be recognized: a siliceous clay containing diatoms and radiolarians in approximately equal proportions, a clayey siliceous ooze with radiolarians somewhat more abundant than the diatoms, and a clayey diatom ooze.

The upper lithologic Subunit IA consists of 60 m of siliceous clay with 15–30% quartz. Twenty-seven ash layers and 83 thin, stiff, dark grayish green layers occur in this subunit. Subunit IB is a clayey siliceous ooze with 5–15% quartz and 5% or less disseminated volcanic glass. Twenty-four ash layers and 126 thin, indurated grayish green layers occur in this subunit. Lowermost lithologic Unit IC is approximately 46 m thick and contains from 3 to 25% quartz. There are only 10 ash layers in this subunit and 116 well-indurated dark grayish green layers.

Sedimentation rates are uniformly about 40 m/m.y., except for the interval near the Pliocene/Pleistocene boundary where the rates decrease to about 20 m/m.y.

Marginal weather prevented completion of the entire heat flow program. Measurements were not possible until Core 9. However, seven successful measurements were made between Cores 9 and 15 (~100–150 m sub-bottom depth). The temperature data clearly show a linear increase with depth. No temperature reversals were observed.

BACKGROUND AND OBJECTIVES

Site 579 (target Site NW-7A) lies near the southern margin of the transition zone between the subtropical and subarctic gyres. Because of its location, it forms an important link between the more siliceous, subarctic sites to the north and the calcareous-siliceous subtropical sites to the south. For this reason, it should record the most extreme southerly excursions of the subarctic front during the Neogene and Quaternary. When this information is combined with a study of the eolian input from the Asian mainland, a detailed paleoclimatic-paleoceanographic picture for this site should result.

Since this site is north of the abrupt thickening of the transparent acoustic layer, we may be able to learn something of the character of this layer.

Our specific scientific objectives were

1. To recover a detailed paleoceanographic record of the subtropical-subarctic transition zone for the late Neogene and Quaternary.
2. To establish a high-resolution midlatitude stratigraphy using paleomagnetics, tephrachronology, and biostratigraphy.
3. To determine the time of onset of significant biogenic silica accumulations for comparison with sites to the north and south.
4. To determine the late Cenozoic history of eolian input from the Asian mainland for comparison with the history of north-south migrations of the subarctic front.

OPERATIONS

After leaving Site 578, *Glomar Challenger* steamed northward to Site 579 (target Site NW-7A). Our passage was delayed somewhat due to strong head wind from a over the beacon. We immediately began running pipe and spudded in at 1428 hr. (0328Z). Two cores were recovered at Hole 579 before deteriorating weather forced us to pull clear of the mud line at 1920 hr. (0820Z) and insert heavy-wall joints. A gale which, at times, reached Force 7 prevented us from respudding the hole until 1625 hr. (0525Z), 2 June. This hole is now designated 579A. Taking advantage of a weather window, we completed coring at Hole 579A down to 149.5 m sub-bottom depth (Table 1).

---

[1] Heath, G. R., Burckle, L. H., et al., *Init. Repts. DSDP*, 86: Washington (U.S. Govt. Printing Office).

[2] Addresses: G. Ross Heath (Co-Chief Scientist) School of Oceanography, Oregon State University, Corvallis, OR 97331 (present address: College of Ocean and Fishery Sciences, University of Washington, Seattle, WA 98195); Lloyd H. Burckle (Co-Chief Scientist) Lamont-Doherty Geological Observatory, Palisades, NY 10964; Anthony E. D'Agostino, ARCO Exploration Company, Houston, TX 77056; Ulrich Bleil, Institut für Geophysik, Ruhr-Universität Bochum, D-4630 Bochum Querenburg, Federal Republic of Germany; Ki-iti Horai, Lamont-Doherty Geological Observatory, Palisades, NY 10964 (present address: Meteorological College, Chiba University, Chiba 277, Japan); Robert D. Jacobi, Department of Geological Sciences, SUNY Buffalo, Amherst, NY 14226; Tom Janecek, Department of Atmospheric & Oceanic Science, University of Michigan, Ann Arbor, MI 48109 (present address: Lamont-Doherty Geological Observatory, Palisades, NY 10964); Itaru Koizumi, College of General Education, Osaka University, Osaka 560, Japan; Lawrence A. Krissek, School of Oceanography, Oregon State University, Corvallis, OR 97331 (present address: Department of Geology and Mineralogy, Ohio State University, Columbus, OH 43210); Nicole Lenôtre, Bureau de Recherches Géologiques et Minières, Centre Océanologique de Bretagne, 45060 Orléans Cedex, France; Simonetta Monechi, Geological Research Division, Scripps Institution of Oceanography, La Jolla, CA 92093 (present address: Dipartimento di Scienze della Terra, Università di Firenze, 4 Via La Pira, 50121 Firenze, Italy); Joseph J. Morley, Lamont-Doherty Geological Observatory, Palisades, NY 10964; Peter Schultheiss, Institute of Oceanographic Sciences, Surrey GU8 5UB, United Kingdom; Audrey A. Wright, Deep Sea Drilling Project, Scripps Institution of Oceanography, La Jolla, CA 92093 (present address: Ocean Drilling Program, 500 University Drive West, Texas A&M University, College Station, TX 77843).

Because of swell conditions, heat flow measurements were not made until we were well down in Hole 579A. The core nose unit operated successfully on each attempt, becoming a routine procedure. The heavy swell also affected core recovery. Unlike the previous Site 578, which had excellent recovery coupled with unusually calm weather, Site 579 experienced frequent heavy swells that resulted in sometimes distorted, stretched, or otherwise disturbed cores. Inserting extra shear pins seemed to help, but weather remained a factor in dictating good core recovery.

Due to increasingly poor recovery (2.37 m in Core 15) in well indurated clayey diatom ooze, coring was terminated and the drill string was retrieved. The ship was secured from its drilling mode at 1755 hr., 4 June, and proceeded north to Site 580 (target Site NW-5A).

LITHOSTRATIGRAPHY

The lithostratigraphy of sediments recovered at Site 579 was determined by visual inspection of the split cores and by smear slide analyses with a petrographic microscope. Except for ash layers, these sediments are relatively uniform in color, ranging from gray (5Y 5/1), dark gray (5Y 4/1), and olive gray (5Y 5/2 or 5Y 4/2) to greenish gray (5GY 5/1 or 5G 5/1). Mottles are abundant and range from faint to intense; the sediments lack depositional sedimentary structures. On the basis of these data, the entire sedimentary section recovered at Site 579 (Holes 579 and 579A) is classified as a single lithologic unit. However, this unit can be divided into three subunits based on the abundances of biogenic and inorganic sediment components determined from smear slide analyses (Fig. 1, Table 2). These three subunits are a siliceous clay (Subunit IA), a clayey siliceous ooze with radiolarians slightly more abundant than diatoms (Subunit IB), and a clayey diatom ooze (Subunit IC).

Table 1. Site 579 coring summary.

Core	Date (June, 1982)	Local time	Depth from drill floor (m)	Depth below seafloor (m)	Length cored (m)	Length recovered (m)	Percent recovered
Hole 579							
1	1	1625	5746.6–5755.0	0.0–8.4	8.4	8.44	100
2	1	1845	5755.0–5764.5	8.4–17.9	9.5	8.46	89
					17.9	16.90	94
Hole 579A							
1	2	1832	5760.6–5770.1	14.0–23.5	9.5	9.30	98
2	2	2045	5770.1–5779.6	23.5–33.0	9.5	9.70	102
3	2	2310	5779.6–5789.1	33.0–42.5	9.5	8.88	93
4	3	0137	5789.1–5798.6	42.5–52.0	9.5	5.36	56
5	3	0400	5798.6–5808.1	52.0–61.5	9.5	9.03	95
6	3	0630	5808.1–5817.6	61.5–71.0	9.5	7.94	84
7	3	0855	5817.6–5827.1	71.0–80.5	9.5	8.27	87
8	3	1105	5827.1–5836.6	80.5–90.0	9.5	9.66	102
9	3	1335	5836.6–5846.1	90.9–99.5	9.5	7.68	81
10	3	1620	5846.1–5855.6	99.5–109.0	9.5	7.59	80
11	3	1840	5855.6–5865.1	109.0–118.5	9.5	7.30	77
12	3	2116	5865.1–5874.5	118.5–128.0	9.5	8.34	88
13	4	0015	5874.5–5884.1	128.0–137.5	9.5	6.95	73
14	4	0250	5884.1–5893.6	137.5–147.0	9.5	7.50	79
15	4	0510	5893.6–5896.1	147.0–149.5	2.5	2.37	95
					135.5 (total)	115.87 (total)	86 (avg.)

Volcanic ash layers are found throughout the entire sedimentary section, but they occur less frequently below Core 11 in Hole 579A. A total of 61 ash layers were identified. In addition, a large number (about 325) of thin (<0.5 cm), stiff to indurated, dark greenish gray (5G 4/1) layers were observed throughout the cores. Smear slide analysis of these layers showed no significant compositional difference from the adjacent "soft" sediments. Therefore, the genesis of these layers is unknown at this time. The distribution of ash layers with depth in Holes 579 and 579A is shown in Figure 1.

The three lithologic subunits are characterized as follows.

Subunit IA

This subunit is a siliceous clay that occurs in Core 579-1 and Section 579-2,CC (0.0–17.9 m sub-bottom), and in Sections 579A-1-1 through 579A-5-4 (14.0–60.0 m sub-bottom). It contains 15–30% quartz, 2–25% diatoms, and 0–15% radiolarians, with average values of approximately 20% quartz, 15% diatoms, and 7% radiolarians. Feldspar and volcanic glass abundances are each generally less than 5%; mica and heavy minerals, if present, have abundances of 2% or less. Clays form the remainder of the sediment, averaging approximately 45%. Twenty-seven ash layers and pockets occur in this subunit, with thicknesses ranging from 2 to 19 cm. Eighty-three of the thin, stiff, dark grayish-green layers occur within this interval.

Subunit IB

This subunit is a clayey siliceous ooze that occurs in Sections 579A-5-5 through 579A-10-2 (60.0–102.5 m sub-bottom). It contains 5–15% quartz, 4–30% diatoms, and 13–35% radiolarians, with average values of approximately 10% quartz, 20% diatoms, and 22% radiolarians. Disseminated volcanic glass abundances are generally 5% or less, and feldspar forms 2% or less of the sediments. Heavy minerals, when present, occur only in trace amounts. The remainder of the sediment, averaging approximately 40%, is composed of clays. Twenty-four ash layers and pockets and 126 of the thin, stiff, dark grayish green layers occur within this interval. The ash layers range in thickness from 1.5 to 13.0 cm.

Subunit IC

This subunit is a clayey diatom ooze that occurs in Sections 579A-10-3 through 579A-15,CC (102.5–149.5 m sub-bottom). It contains 3–25% quartz, 25–60% diatoms, and 2–30% radiolarians, with average values of approximately 10% quartz, 40% diatoms, and 8% radiolarians. Volcanic glass and feldspar abundances are generally 2–5%; heavy minerals, when present, occur only

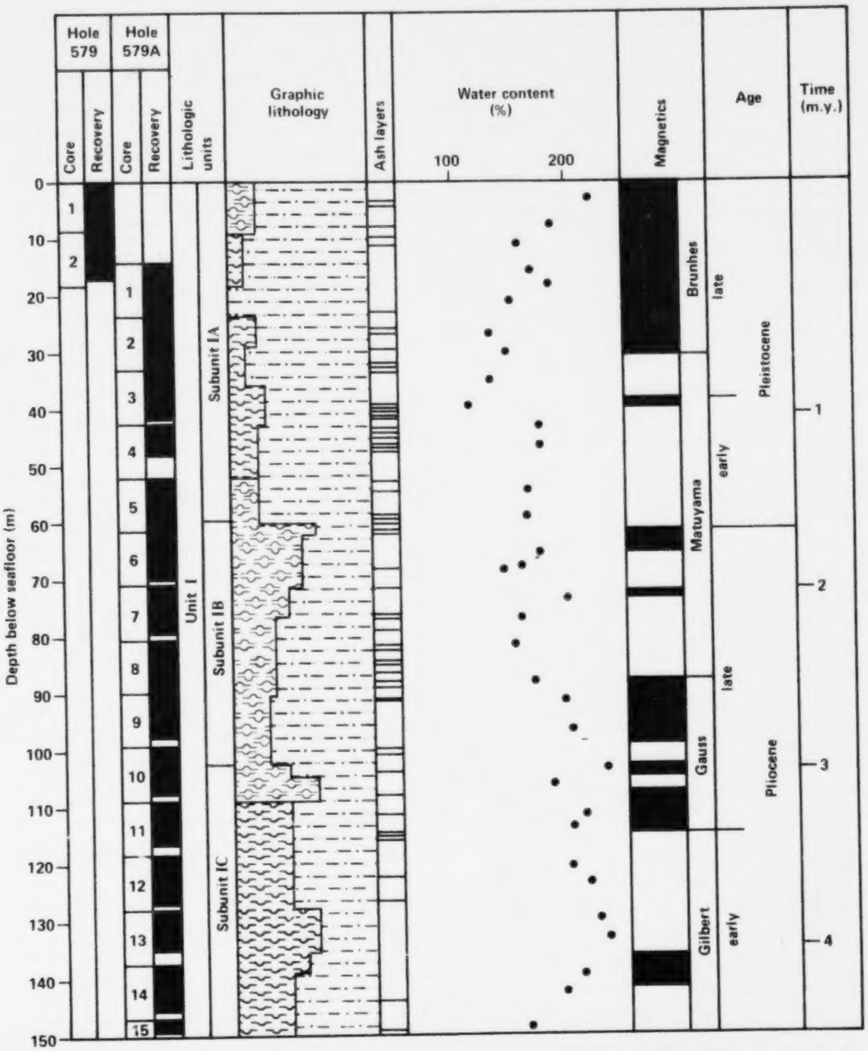

Figure 1. Site summary diagram showing Site 579 core numbers, core recovery, lithologic units, graphic lithology, ash layer locations, water content (%), magnetostratigraphy, and ages. Symbols used in graphic lithology column are defined in Introduction and Explanatory Notes (this volume).

Table 2. Site 579 lithostratigraphic units.

Lithologic unit	Cored interval		Sub-bottom depth (m)	Composition (%)		
	Hole 579	Hole 579A		Quartz	Diatom	Radiolarians
I: Siliceous clay						
Subunit IA: Siliceous clay	1-1, 0 cm to 2,CC	1-1, 0 cm to 5-4, 150 cm	0.0–60.0	15–30	2–25	0–15
Subunit IB: Clayey siliceous ooze		5-5, 0 cm to 10-2, 150 cm	60.0–102.5	5–15	4–30	13–35
Subunit IC: Clayey diatom ooze		10-3, 0 cm to 15,CC	102.5–149.5	3–25	25–60	2–30

frontal passage. On 1 June, shortly after midnight (0006 hr. local time, 1306Z), the beacon was dropped over the drill site, gear was retrieved, and the ship positioned in trace amounts. The remainder of the sediments, averaging approximately 38%, is composed of clays. Ten ash layers and pockets and 116 of the thin, stiff, dark grayish green occur within this interval. The ash layers range in thickness from 3 to 11 cm.

SEISMIC CORRELATIONS

High resolution seismic reflection profiles (3.5 and 12 kHz) and 100-Hz reflection profiles were recorded at Site

579. Only a hull-mounted 3.5-kHz sound source was utilized. The 3.5-kHz echograms over Site 579 reveal a fairly uniform seismic section of parallel sub-bottom reflectors (Fig. 2). This seismic section can be divided into a four-part sequence based primarily on gaps in the reflector sequence (Table 3).

The uppermost seismic unit (seismic Unit I) consists of strong reflectors and extends to 0.0268 s below the seafloor (20.3 m at 1513 m/s; 19.0 m at 1420 m/s). A thin transparent layer below the deepest reflector in seismic Unit 1 differentiates it from the top of seismic Unit 2. Seismic Unit 2 consists of three strong reflectors and extends to 0.0459 s below the seafloor (34.7 m at 1513 m/s; 32.6 m at 1420 m/s). A thin transparent layer at the base of seismic Unit 2 distinguishes it from the top of seismic Unit 3. Seismic Unit 3 consists of five intermediate-strong reflectors and extends to 0.0654 s below the seafloor (49.4 m at 1513 m/s; 46.4 m at 1420 m/s). Seismic Unit 4 consists of generally weak and discontinuous reflectors; only the top reflector is of intermediate strength. It extends to 0.0945 s below the seafloor (71.4 m at 1513 m/s; 67.1 m at 1420 m/s).

Identifying the source of these reflectors proved to be especially difficult at this site for two major reasons: (1) The moderate to heavy seas during the coring operation resulted in cores with a relatively high percentage of discrete "flow-in" zones. The uncertainty in the possible depths of most ashes because of this "flow-in" is quite large (up to 3 m). (2) A large number of equally strong and closely spaced reflectors occurs in the upper 70 m of the sediment section. The range of possible velocities results in a range of computed depths for most reflectors that overlaps with the depths of the adjacent reflectors. The combination of unknown depths for both seismic reflectors and lithologic units results in particularly difficult correlations. The seismically transparent layers, the variable strength of reflection signals, and the precise depths of some lithologic units do, however, allow some relatively reliable correlations (i. e., Reflectors 1b, 1e, 1f, 3a, 3d, 3d′, 4b, 4d, and 4e; Table 3). As at Site 578, the seismically transparent layers correlate with lithologic sections that lack ash layers. No such correlation is observed with the thin, pyritic, dark green layers which have anomalously high velocities like those of the ash layers. The source of the reflectors appears to be ash layers (Table 3).

Based on the proposed correlations, the top of seismic Unit 2 is probably the ash layer observed in Sample 579A-1-6, 56-75 cm (ash #3). The top of seismic Unit 3 is the ash layer located in Sample 579A-2-6, 106-129 cm (ash #8). The top of seismic Unit 4 may be located in Sample 579A-4-3, 55-60 cm (ash #15). Seismic Unit 4 may extend to ash #22 in Sample 579A-6-5, 59.5-67 cm. The top of lithologic Subunit IB may be associated with seismic Reflector 4c′.

The 100-Hz seismic reflection profiles reveal a four-part seismic section at Site 579 (Fig. 3). The uppermost seismic unit (Unit 1) extends to about 0.12 s below the

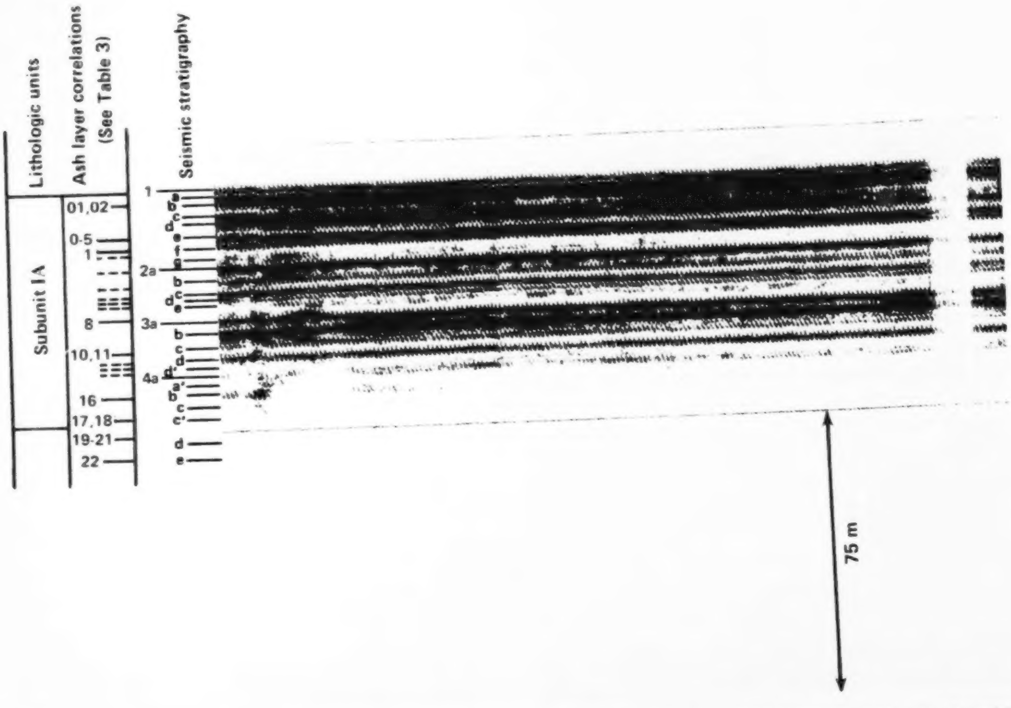

Figure 2. 3.5-kHz echogram near Site 579 showing the four-part seismic sequence described in the text. Lithostratigraphic correlations made assuming a velocity of 1480 m/s.

Table 3. 3.5-kHz seismic correlations, Site 579.

Reflector	Relative strength[a]	Depth below seafloor (s)	Depth below seafloor (m)		Depth in core (m)		Source
			1513 m/s	1420 m/s	Observed	Corrected for possible "flow-in"	
1a	I	0.00310	2.34				
1b	I-S	0.00569	4.31	3.95	3.35 3.6		Ash 01 Ash 02
1c	W-S	0.00886	6.7	6.29			
1d	VS	0.0124	9.35	8.78			
1e	S	0.0169	12.78	12.00	11.7		Ash 0-5
1f	S-VS	0.020	15.12	14.2	14.7		Ash 1
1g	IT-W	0.0241	18.24	17.13	16.1		Ash 2?
2a	VS	0.0268–0.0279	20.26–21.04	19.03–19.76	22.8	19.8	Ash 3?
2b	S	0.0319	24.08	22.61	25.7–26.4	24.7–25.4	Ash 4?
2c	S	0.0360	27.20	25.54	29.15	27.1	Ash 5?
2d	IT-W	0.0386	29.15	27.38	31.6	28.6	Ash 6??
2e	IT-W	0.0400–0.0412	30.24–31.18	28.4–29.28	31.9	28.9	Ash 7??
3a	S	0.0459	34.71	32.60	32.4	29.4	Ash 8
3b	VS	0.0503	38.03	35.72	39.75	37.25	Ash 9?
3c	S	0.0552	41.77	39.23	40.75	38.25	Ash 10, 11?
3d	S	0.0594	44.89	42.16	43.9	No flow-in	Ash 12
3d′	IT	0.0619	46.76	43.92	45.1	No flow-in	Ash 14
4a	I	0.0654	49.41	46.40	46.3	No flow-in	Ash 15?
4a′	IT	0.0682	51.60	48.46	Missing section		Missing section
4b	W-I	0.0711	53.78	50.51	52.4	No flow-in above ash	Ash 16
4c	IT-W	0.0742–0.0752	56.12–56.82	52.70–53.36	58.25 58.85	53.29 53.85	Ash 17, 18??
[4c′	IT	0.0784	59.31	55.70]	Missing section from flow-in		
4d	IT	0.0880	66.56	62.51	62.25–62.6–62.75	No flow-in above ash	Ash 19 Ash 20 Ash 21
4e	IT	0.0945	71.44	67.09	68.1		Ash 22

[a] IT = intermittent, weak; W = weak, but generally continuous; I = intermediate; S = strong; VS = very strong.

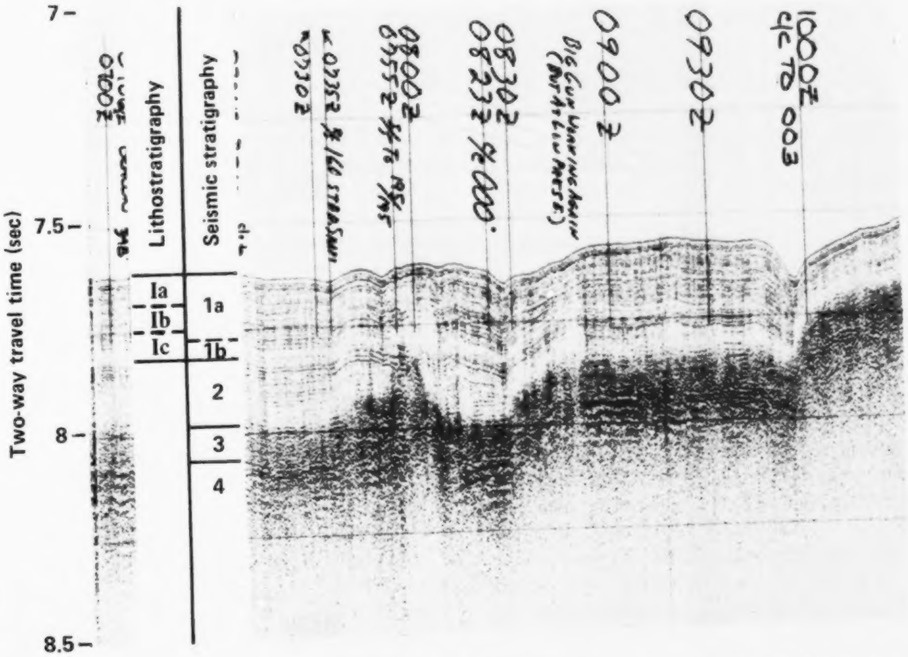

Figure 3. 100-Hz reflection profile over Site 579 showing the four-part seismic sequence described in the text.

seafloor (90 m, 1500 m/s) and consists of two subunits. The upper seismic subunit (Subunit 1a) is composed of strong, parallel, and continuous reflectors and extends to about 0.1 s below the seafloor (75 m at 1500 m/s). Seismic Subunit 1b occurs between 0.1 and 0.12 s (75 and 90 m at 1500 m/s) and consists of weak, discontinuous reflectors and transparent zones. The base of seismic Unit 1 is fairly close to the base of lithostratigraphic Subunit IB, at 102.5 m below the seafloor.

Seismic Unit 2 consists of strong, continuous, parallel reflectors to about 0.18 s below the seafloor (135 m at 1500 m/s) and a slightly transparent zone with weak, discontinuous echos to about 0.21 s below the seafloor (157.5 m at 1500 m/s). Seismic Unit 3 consists of strong, incoherent echoes that extend to 0.27 s below the seafloor. Seismic Unit 3 probably represents Cretaceous chert and associated sedimentary rocks. Seismic Unit 4 consists of a very strong, prolonged echo and probably is basalt basement.

BIOSTRATIGRAPHY

At Site 579 we cored 149.5 m of late Quaternary through early Pliocene sediment. No calcareous microfossils were found in any of the core catcher samples from the two holes taken at this site. Abundant, well preserved diatoms were found in all Pleistocene samples except for Sample 579A-4,CC where they were only moderately well preserved. Specimens in the early Pliocene were only moderately to poorly preserved. The shipboard diatom and radiolarian analyses did not detect any major hiatuses in the interval cored. A preliminary shipboard analysis of the moderately to well preserved silicoflagellates in samples from Hole 579A was also made (see Bukry and Monechi, this volume).

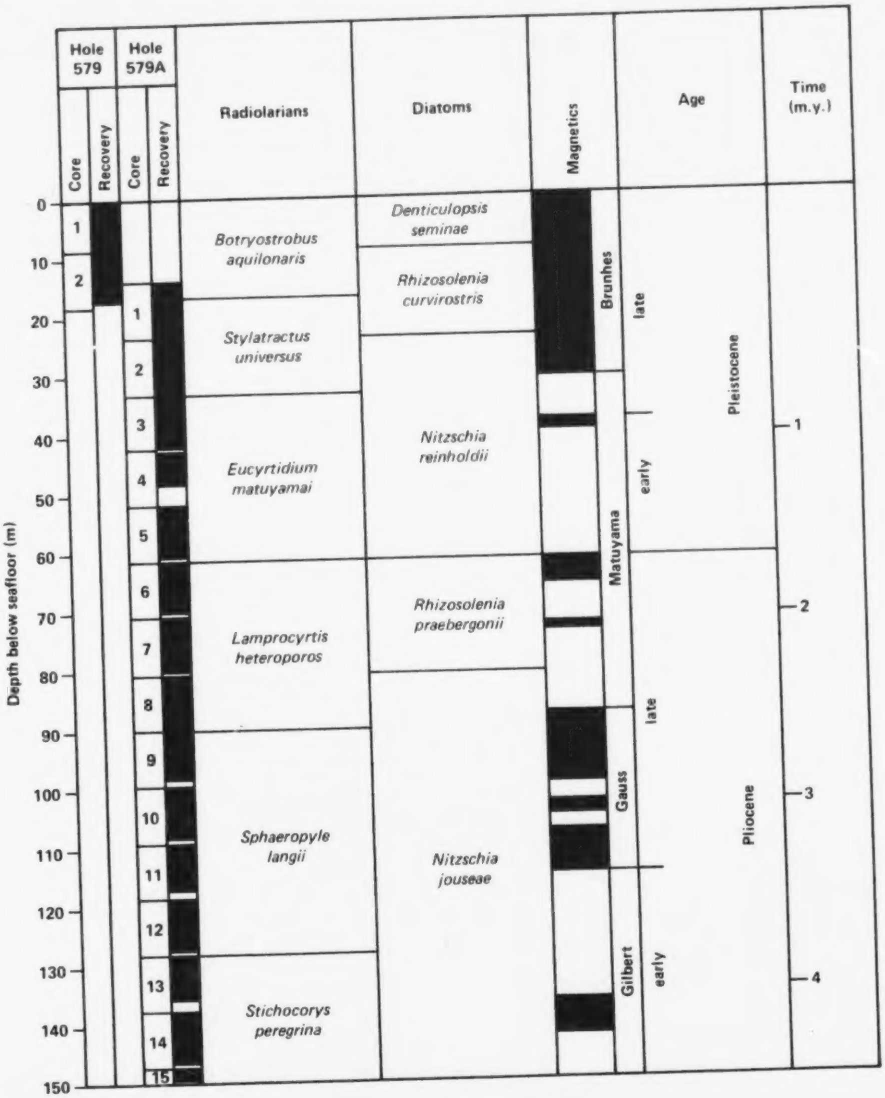

Figure 4. Site 579 biostratigraphic and magnetostratigraphic summary.

The diatom and radiolarian biostratigraphy is shown in summary form in Figure 4. According to this stratigraphy, the boundary between early and late Pleistocene falls within Core 579A-3. The Pliocene/Pleistocene boundary occurs in Core 579A-6.

Nannofossils

No calcareous nannofossils were found in any of the cores recovered at Site 579.

Planktonic Foraminifers

Seventeen core-catcher samples from two holes (579 and 579A) were examined. Hole 579 consisted of only two cores, and both core-catcher samples were barren of foraminifers. All 15 samples from Hole 579A were also barren of any foraminifers.

Radiolarians

Late Quaternary through early Pliocene radiolarians occur in sediment samples from Site 579 (Holes 579 and 579A). The preliminary radiolarian biostratigraphy for each of these holes is shown in Figure 4.

The entire sediment sequence from Hole 579 is late Quaternary in age containing an abundant, well preserved radiolarian fauna characteristic of the *Botryostrobus aquilonaris* Zone (Hays, 1970). The absence of *Lychnocanoma grande* in the first section (Sample 579-1-1, 2-3 cm) indicates that the sediments at the top of Hole 579 are less than 50,000 yr. old. In the core-catcher sample from Core 2, the presence of *Stylatractus universus* places this faunal assemblage within the *S. universus* Zone (Hays, 1970).

Radiolarians were present in all core catcher samples from Hole 579A, ranging in age from late Quaternary (Sample 579A-1,CC) through early Pliocene (Sample 579A-15,CC). Samples 579A-1,CC and 579A-2,CC contained an abundant, well preserved radiolarian fauna characteristic of the late Quaternary *S. universus* Zone (Hays, 1970). The top of Sample 579A-1-1, 5-7 cm did not contain *S. universus* and was assigned to the *B. aquilonaris* Zone. Comparing these results with those from Hole 579, it would appear that the base of the *B. aquilonaris* Zone (Hays, 1970) occurs somewhere in the middle of Core 579A-1. Radiolarians in Samples 579A-3,CC through 579A-6,CC were abundant and well preserved, except for Sample 579A-4,CC where preservation was only moderate. The presence of *Eucyrtidium matuyamai* in the core-catcher samples from Cores 3 through 5 indicates that the sediment sequence is early Pleistocene in age (*E. matuyamai* Zone [Hays, 1970; Foreman, 1973]) with the Pliocene/Pleistocene boundary occurring in the upper portion of Core 6. The abundant, well-preserved radiolarian fauna in Samples 579A-6,CC through 579A-8,CC did not contain *E. matuyamai* or *Stichocorys peregrina*, indicating that this sediment sequence is late Pliocene in age (*Lamprocyrtis heteroporos* Zone [Hays, 1970; Foreman, 1975]). The *Sphaeropyle langii* Zone (Foreman, 1975), based on the presence of *Stichocorys peregrina* and *Sphaeropyle langii*, extends from Cores 9 through 12. The boundary between late and early Pliocene is located within Core 11. The absence of *S. langii, Didymocyrtis penultima,* and *Diartus hughesi* in the fauna from Samples 579A-13,CC through 579A-15,CC places this sediment sequence in the early Pliocene *Stichocorys peregrina* Zone (Riedel and Sanfilippo, 1970; Foreman, 1975).

Diatoms

Early Pliocene to Pleistocene diatoms occur in Holes 579 and 579A. Six diatom zones were observed in Holes 579 and 579A. The assemblages alternate between a dominance of warm water species and cold water species. Diatoms are abundant to common and well preserved.

Core 579-1 belongs to the latest Quaternary *Denticulopsis seminae* Zone (Koizumi, 1973). Cores 579-2 and 579A-1 are assigned to the late Quaternary *Rhizosolenia curvirostris* Zone. The base of this zone is tentatively defined by the last occurrence of *Nitzschia reinholdii*. Diatom assemblages in Cores 579A-2 through 579A-5 are placed in the *N. reinholdii* Zone. The last occurrence of the silicoflagellate *Mesocena quadrangula* in Core 2 indicates this sample is placed around the Jaramillo Event of the Matuyama Epoch. Cores 6 and 7 are correlated with the late Pliocene *R. praebergonii* Zone. The Pliocene/Pleistocene boundary, therefore, is placed somewhere within Core 6. The middle to early Pliocene *N. jouseae* Zone occurs in Cores 8 through 15. Core 8 is placed in the upper part of the Gauss Epoch by the co-occurrence of *R. praebergonii* and *Cussia tatsunokuchiensis*. Core 12 is placed in the middle part of the Gilbert Epoch by the presence of *Cosmiodiscus insignis*. These two diatom events argue for correlation with the lower part of the *N. jouseae* Zone (early Pliocene) in Cores 12 through 13.

PALEOMAGNETICS

Paleomagnetic determinations were made on a total of 298 samples from the sediment cores recovered at the two holes drilled at Site 579. The results are briefly summarized here and documented in detail in a separate report (see Bleil, this volume).

The intensity of the natural remanent magnetization (NRM) is highly variable throughout the entire section recovered (varying from about 2×10^{-7} to about 5×10^{-5} emu/cm^3). There is no consistent downhole trend in the NRM intensities. However, higher values are generally observed for normally polarized samples, indicating the presence of at least some overprinting by viscous components. With but a few exceptions, the magnetic stability was high; median destructive field (MDF) measurements typically yielded values of 300 ± 50 Oe. Lower MDF values and related larger directional changes of the magnetization directions upon AF demagnetization were more frequent in core sections showing clear evidence of drilling disturbance.

The polarity pattern derived from the stable magnetization directions is shown in Figure 4. In some cases, the quality of the reversal chronology is limited by incomplete recovery or badly disturbed zones. The two cores recovered from Hole 579 acquired their remanent magnetization during the present normal geomagnetic Brunhes Epoch. Therefore the sediments at the base of this hole (17.9 m) are younger than 0.73 m.y. An almost complete reversal sequence for the last 4.5 m.y. was obtained in Hole 579A. The Brunhes/Matuyama boundary was recognized at a sub-bottom depth of 30.65 m (Sample 579A-2-5, 115 cm), the Jaramillo Event between 38.65 and 39.85 m (Samples 579A-3-4, 115 cm to 579A-3-5, 85 cm), indicating an average sedimentation rate of about 40.7 m/m.y. for the last 1 m.y. The Olduvai and one of the Reunion events can be identified in the older part of the Matuyama Epoch. The Matuyama/Gauss boundary was identified at 87.95 m sub-bottom (Sample 579A-8-5, 145 cm). Both the Kaena and Mammoth events are present, indicating that the geomagnetic record is also continuous and complete during the normal geomagnetic Gauss Epoch. The deepest clearly identifiable magnetic boundary at this site is the Gauss/Gilbert transition at about 115.01 m sub-bottom (Sample 579A-11-5, 1 cm). Between this depth and the base of the hole the paleomagnetic measurements revealed only one additional zone of positive polarity (136.38 to 141.95 m sub-bottom; Samples 579A-13-5, 88 cm to 579A-14-3, 145 cm). Assuming that no drastic increase in accumulation rate occurred at this level, the interval has been identified as the Nunivak Event. The youngest normal event in the Gilbert Epoch, the Cochiti, apparently lies in the 2.5-m gap between the base of Core 13 and the top of Core 14.

On the basis of the most recent polarity time scale of Berggren et al. (in press), the extrapolated absolute age of the base of Hole 579A is no more than 4.40 m.y. The average accumulation rate over the period of time represented by the entire sedimentary sequence at Site 579 thus was about 30.8 m/m.y. Compared to the other sites drilled on Leg 86, sedimentation rates at Site 579 were more variable, apparently due to real fluctuations in the supply of sediment.

SEDIMENT ACCUMULATION RATES

Paleomagnetic reversal boundaries were used to calculate the sedimentation rate at Site 579. According to the age-depth plot (Fig. 5) for this site, the sedimentation rate for the late Quaternary averages about 40 m/m.y. This rate decreases to approximately 20 m/m.y. near the Pliocene/Pleistocene boundary, but the rate increases again to 40 m/m.y. during the late early and late Pliocene. Changes in sedimentation rate do not appear to be related to lithologic type.

PHYSICAL PROPERTIES

Physical properties measurements at Site 579 were performed using mainly standard Deep Sea Drilling Project (DSDP) methods (Boyce, 1976a, b; see Introduction and Explanatory Notes, this volume). Table 4 summarizes the properties measured at Holes 579 and 579A. Measurements were taken at approximately 4.5-m intervals throughout the core. Figures 6, 7, and 8 show profiles of compressional and shear wave velocity, shear strength, and saturated bulk density and water content, respectively. A full discussion of the physical properties of the recovered sediments is given by Schultheiss (this volume), but some of the more interesting features are highlighted here:

1. The compressional wave velocity profile is dominated by many (61) high velocity ash layers and numerous (~325) thin (<0.5 cm), stiff to indurated dark greenish gray layers. Velocities measured in a few ash layers are typically about 1600 m/s. The thin indurated green layers also have higher velocities but they tend to be variable, one was as high as 1770 m/s. Velocities in the siliceous clay and ooze are remarkably uniform throughout the site at 1480 m/s (Fig. 6).
2. Shear wave velocity measurements show no distinct trends down to 73 m sub-bottom depth (Fig. 6). The transducer broke at this point, preventing further measurements.
3. Shear strength measurements (Fig. 7), although exhibiting a large amount of scatter, show increasing strength down the hole. A major discontinuity exists in Section 579A-9-5, with very high shear strengths relative to shallower sections. Values decrease again in Core 579A-10, however. This maximum cannot be explained by any visible lithological changes.
4. A good example of "flow-in" is found in the bottom of Core 579A-6-5 (Fig. 7). Measurements with both the hand-held and motorized vane showed that the remolded flow-in section had decreased in strength by a factor of about four from 380 g/cm^2 in the "undisturbed" region to 100 g/cm^2 in the section containing "flow-in."
5. The water-content profile (Fig. 8) can be split into three units. Unit I (from 0 to 41 m sub-bottom depth) has a decreasing water content from 220 to 111%, which is probably caused by normal consolidation processes. Unit II (from 41 to 134 m sub-bottom depth) has slowly increasing water content from around 170 to 228%, with a rapid change occurring at the boundary between Units I and II. Unit III, below 134 m sub-bottom depth, shows a decreasing water content down to 158% at 149 m sub-bottom.

These units do not correlate with the lithological units based on visual descriptions. It is probable that changes in clay mineralogy are responsible for the strength variations observed.

INORGANIC GEOCHEMISTRY

Five squeezed core samples, one from Hole 579 and four from Hole 579A, were analyzed for the standard suite of components: pH, alkalinity, salinity, calcium, magnesium, and chlorinity (Table 5). No *in situ* samples were taken.

Calcium increases linearly with depth (Fig. 9), suggesting diffusion between a source below the drilled section (presumably carbonate associated with the strong chert reflector) and the sink formed by the overlying ocean waters. Magnesium decreases through the cored interval, probably due to the formation of smectite by alteration of the abundant volcanic ash in the section. The slight initial increase in alkalinity may reflect sulfate reduction (to oxidize organic matter), but the trend reverses below 60 m, again probably because of ash alteration.

HEAT FLOW

Bad weather prevented the collection of a full profile of downhole temperature measurements by the new Woods Hole Oceanographic Institution (WHOI) heat flow instrument at this site. Heat flow measurements were not

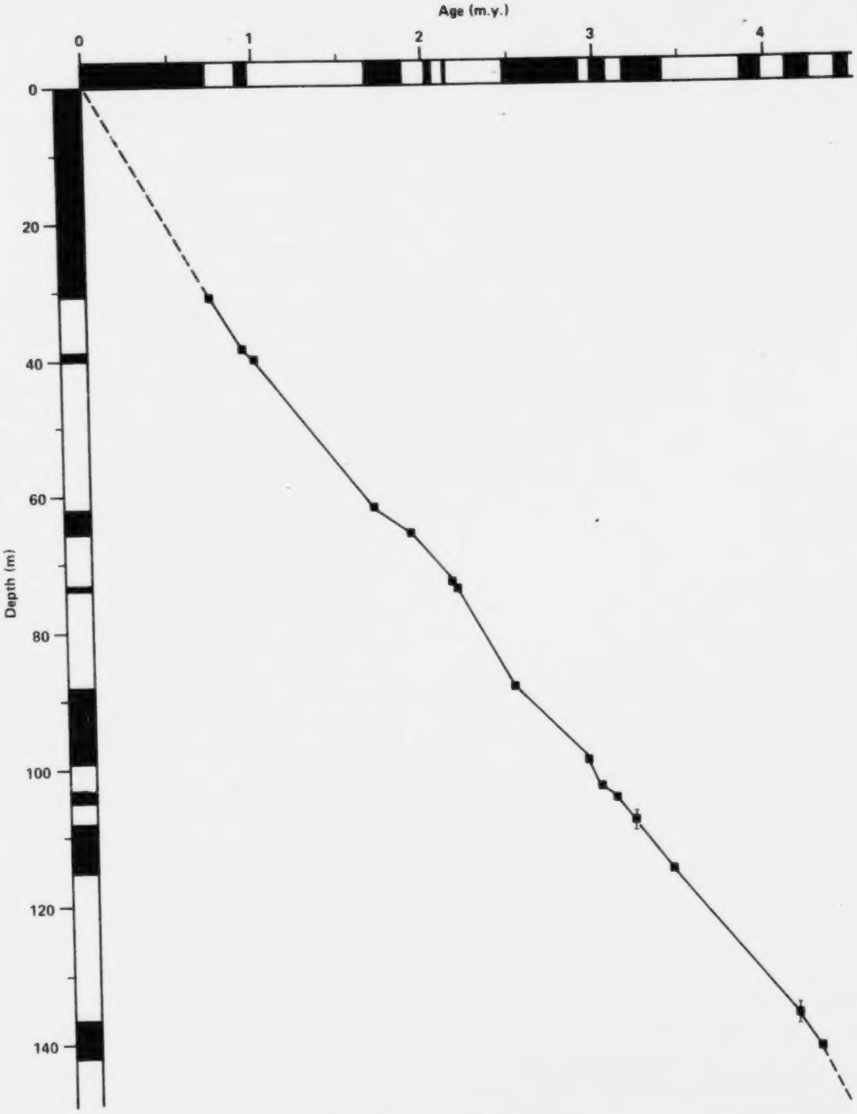

Figure 5. Site 579 sediment accumulation rates derived from the paleomagnetic reversal record.

Table 4. Physical properties measurements made at Site 579.

Physical property	Holes 579 and 579A
Shear strength:	
Hand-operated vane	x
Motorized vane	x
Wave velocity:	
Shear wave	x
Compressional wave	x
Water content/bulk density	
Shipboard analysis	x
Shore-based analysis	x
Bulk density by 2-min. GRAPE	x

possible until Core 579A-9, when weather and sea-surface conditions permitted operation of the core-nose temperature probe. Subsequent measurements were satisfactory. All seven runs, made at every core from Cores 579A-9 through 579A-15, were successful. Two recorders, WHOI-01 and WHOI-4A, connected to battery packs TILT-2 and NTLT-2, respectively, were used alternately throughout the operation. The thermal gradient seems to be constant for the measured interval.

The constant thermal gradient combined with the thermal conductivity data, which were taken at 155 locations in Holes 579 and 579A, yielded a reliable heat flow value (see Horai and Von Herzen, this volume).

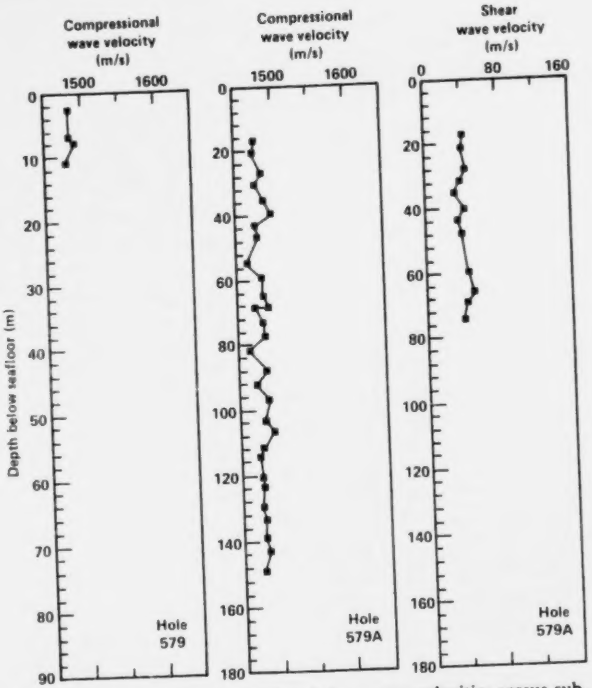

Figure 6. Plot of compressional and shear wave velocities versus subbottom depth at Site 579.

SUMMARY AND CONCLUSIONS

Some of the results of Site 579 are summarized in Figure 1. Only one major lithologic unit is recognized in this site. However, it is divided into three subunits as follows.

1. Subunit IA (0.0–60.0 m) is a siliceous clay, gray and gray green in color containing 15–30% quartz, 2–25% diatoms, and 0–15% radiolarians. Feldspar and disseminated volcanic ash are also present but usually in abundances of less than 5%. Approximately 45% clay forms the remainder of the sediment. Twenty-seven ash layers occur in this subunit, with thicknesses ranging from 2 to 19 cm. Also present are 83 thin, well indurated dark grayish green layers. These "green layers" are lithologically unlike the adjacent softer gray siliceous clay. Their origin is uncertain.

2. Subunit IB (60.0–102.5 m) is a clayey biosiliceous ooze. It contains 5–15% quartz, 4–30% diatoms, and 13–35% radiolarians. Disseminated volcanic glass forms less than 5%, and feldspar 2% or less, of the total sediment. The remainder (40%) is composed of clays. The subunit is differentiated from Subunits IA and IC by an increase in the percentage of radiolarians. Twenty-four ash layers and 126 indurated dark grayish green layers occur in this subunit.

3. Subunit IC (102.5–149.5 m) is a clayey diatom ooze, differentiated from the overlying subunit by a decrease in the radiolarian content. It contains 3–25% quartz, 25–60% diatoms, and 2–30% radiolarians. Disseminated volcanic ash and feldspar make up approximately 2–5% of the sediment. The remainder, about 38%, is composed of clays. This subunit contains 116 dark grayish green indurated layers, and fewer ash layers (10) than the overlying subunits.

Figure 4 summarizes the paleomagnetics and biostratigraphy for this site. Although there were some problems in obtaining a coherent magnetic reversal record (intensities were only slightly above the noise level of the machine), an adequate record was obtained for at least the Quaternary and middle to late Pliocene. The interpretation of the paleomagnetics was supported by the radiolarian and diatom biostratigraphy. Biostratigraphic evidence suggests that early Pliocene sediments were penetrated at this site: Hole 579A terminated in the lower part of the *Nitzschia jouseae* diatom zone and the *Stichocorys peregrina* radiolarian zone.

The presence of numerous ash layers at Site 579 prompted us to plot numbers of ash layers/m.y. as has been done for other DSDP sites in the circum-Pacific. Figure 10 presents these data and shows that there is a general increase in ash layer density to the present day. This generally agrees with the results of Furuta and Arai (1980), who attribute this increase to plate motion rather than to episodic volcanicity.

The great volume of ash, contributed mainly from the Japanese Islands, together with the high productivity in this region, have contributed to a high sedimentation rate, particularly for the late Pliocene and Pleistocene. Figure 5 summarizes the relevant data from paleomagnetic determinations in an age-depth diagram. Rates as high as 40–45 m/m.y. were achieved in the Quaternary. Rates were lower, however, around the Pliocene/Pleistocene boundary, but were high again in the late Pliocene.

In spite of the numerous ash layers and semi-indurated green layers recovered at this site, it was difficult to pinpoint the source of the seismic reflections. This was partially due to the sea state when the site was occupied, resulting in frequent distorted bedding and flow-in. A second consideration, however, was the large number of distinct, but closely spaced reflectors in the upper 70 m of the hole. In spite of this, we feel that we can identify some ash layers as discrete reflectors. Interestingly, it appears that only the ash horizons serve as seismic reflectors; there is no evidence that the indurated green layers show up on the seismic records, in spite of the fact that spikes in the compressional wave velocity profile are produced by both the ash and the green layers. Typical ash velocities are on the order of 1.6 km/s whereas the velocities in the green layers, although variable, range as high as 1.77 km/s. Other changes in sediment physical properties are likely due to changes in clay mineralogy.

The sea-state prevented us from making heat flow measurements in the upper part of Hole 579A. Observations began at 100 m and continued to 160 m, with the temperature data clearly showing a linear increase with depth.

The objectives at this site—to recover a detailed paleoceanographic record of the subtropical-subarctic transition zone for the late Cenozoic, to establish a high resolution, multitaxa stratigraphy for the late Cenozoic northwest Pacific, to determine the time of onset of significant biosiliceous accumulation, and to determine the late Cenozoic history of eolian input for comparison

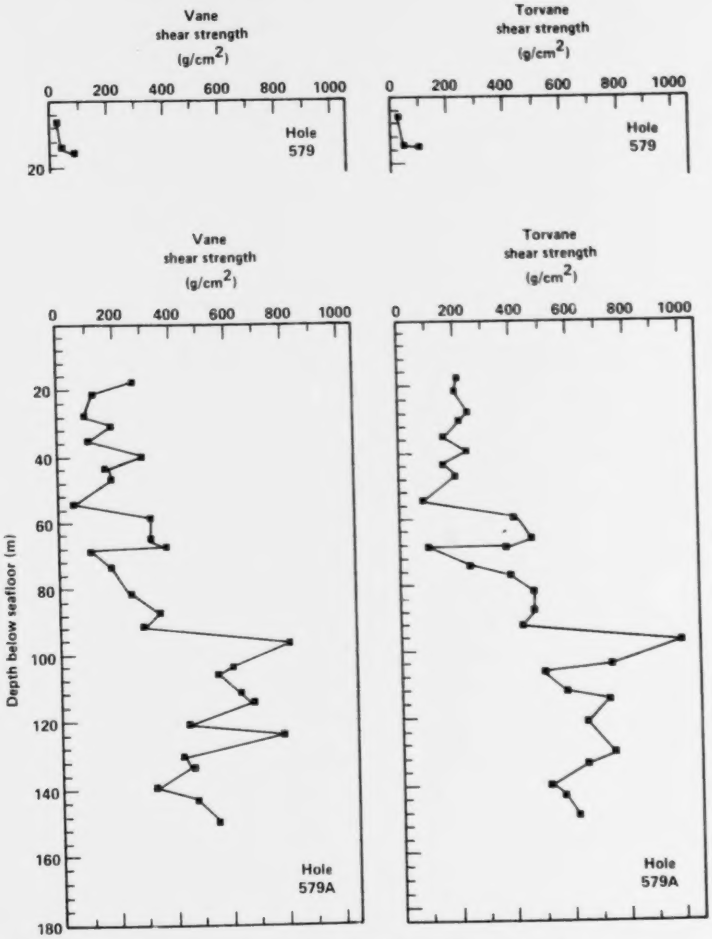

Figure 7. Plot of shear strength versus sub-bottom depth at Site 579.

with the history of north-south migration of the subarctic front—were largely achieved. Further, we obtained an excellent record of late Cenozoic ash falls on the northwest Pacific to complement the record from Site 578.

Because of time limitations coupled with increasingly poor penetration, we were unable to reach the transition from biosiliceous sediments into the underlying red clay as we had at Site 578.

REFERENCES

Berggren, W. A., Kent, D. V., and Flynn, J. J., in press. Paleogene geochronology and chronostratigraphy. *In* Snelling, N. J. (Ed.), *Geochronology and the Geological Record.* Geol. Soc. London Spec. Pap.

Boyce, R. E., 1976a. Definitions and laboratory techiniques of compressional and sound velocity parameters and wet-water content, wet-bulk density, and porosity parameters by gravimetric and gamma ray attenuation techniques. *In* Schlanger, S. O., Jackson, E. D., et al., *Init. Repts. DSDP*, 33: Washington (U.S. Govt. Printing Office), 931-958.

_______, 1976b. Deep Sea Drilling Project procedures for shear strength measurements of clayey sediment using modified Wykeham Farrance Laboratory Vane Apparatus. *In* Barker, P., Dalziel, I. W. D., et al., *Init. Repts. DSDP*, 36: Washington (U.S. Govt. Printing Office), 1059-1068.

Burckle, L. H., 1972. Late Cenozoic planktonic diatom zones from the eastern equatorial Pacific. *Nova Hedwigia Beih*, 39: 217-246.

Foreman, H. P., 1973. Radiolaria from DSDP Leg 20. *In* Heezen, B. C., MacGregor, I. D., et al., *Init. Repts. DSDP*, 20: Washington (U.S. Govt. Printing Office), 249-305.

_______, 1975. Radiolaria from the North Pacific, Deep Sea Drilling Project, Leg 32. *In* Larson, R. L., Moberly, R., et al., *Init. Repts. DSDP*, 32: Washington (U.S. Govt. Printing Office), 579-701.

Furuta, T., and Arai, F., 1980. Petrographic properties of tephras, Leg 56, Deep Sea Drilling Project. *In* Scientific Party, *Init. Repts. DSDP*, 56, 57, Pt. 2: Washington (U.S. Govt. Printing Office), 1043-1048.

Hays, J. D., 1970. Stratigraphy and evolutionary trends of Radiolaria in North Pacific deep-sea sediments. *In* Hays, J. D. (Ed.), *Geological Investigations of the North Pacific.* Mem. Geol. Soc. Am., 126:185-218.

Koizumi, I., 1973. The late Cenozoic diatoms of Sites 183-193, Leg 19, Deep Sea Drilling Project. *In* Creager, J. S., Scholl, D. W., et al., *Init. Repts. DSDP*, 19: Washington (U.S. Govt. Printing Office), 805-855.

Riedel, W. R., and Sanfilippo, A., 1970. Radiolaria, Leg 4, Deep Sea Drilling Project. *In* Bader, R. G., Gerard, R. D., et al., *Init. Repts. DSDP*, 4: Washington (U.S. Govt. Printing Office), 503-575.

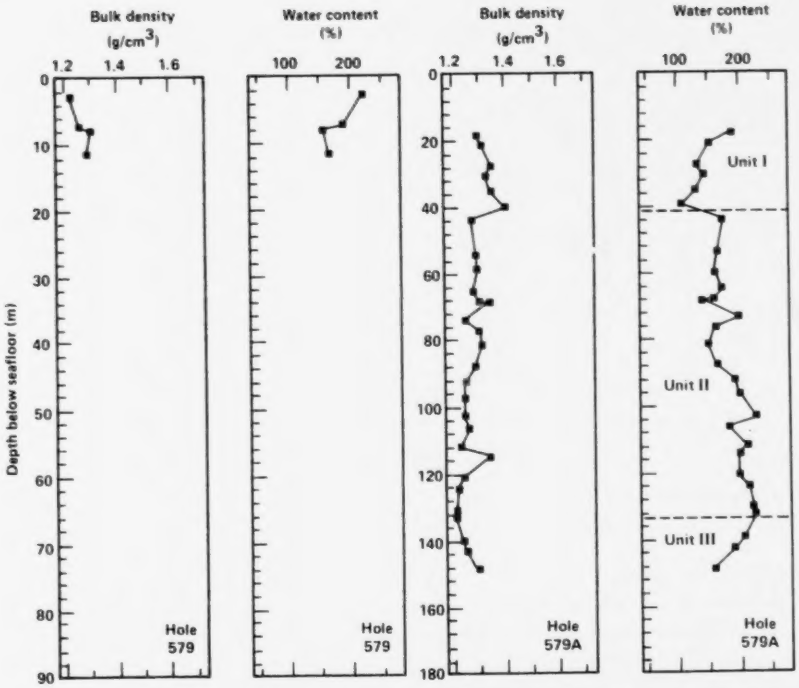

Figure 8. Profiles of saturated bulk density and water content versus sub-bottom depth at Site 579. Physical properties Units I, II and III are discussed in the text.

Table 5. Inorganic geochemical measurements made at Site 579.

Sample	pH	Alkalinity (mEq/l)	Salinity (‰)	Calcium (m*M*)	Magnesium (m*M*)	Chlorinity (‰)
IAPSO	8.62	2.45	35.2	10.55	53.99	19.38
SSW	8.74	2.36	34.9	10.37	53.03	19.07
579-2-5, 140–150 cm	8.37	5.13	35.2	10.77	50.71	19.34
579A-5-5, 140–150 cm	8.28	5.87	36.3	11.51	48.71	19.54
579A-8-5, 140–150 cm	8.42	5.73	35.2	11.92	47.52	19.41
579A-11-4, 140–150 cm	8.54	5.40	34.9	12.51	47.17	19.51
579A-14-4, 140–150 cm	8.27	4.85	34.9	12.85	45.63	19.44

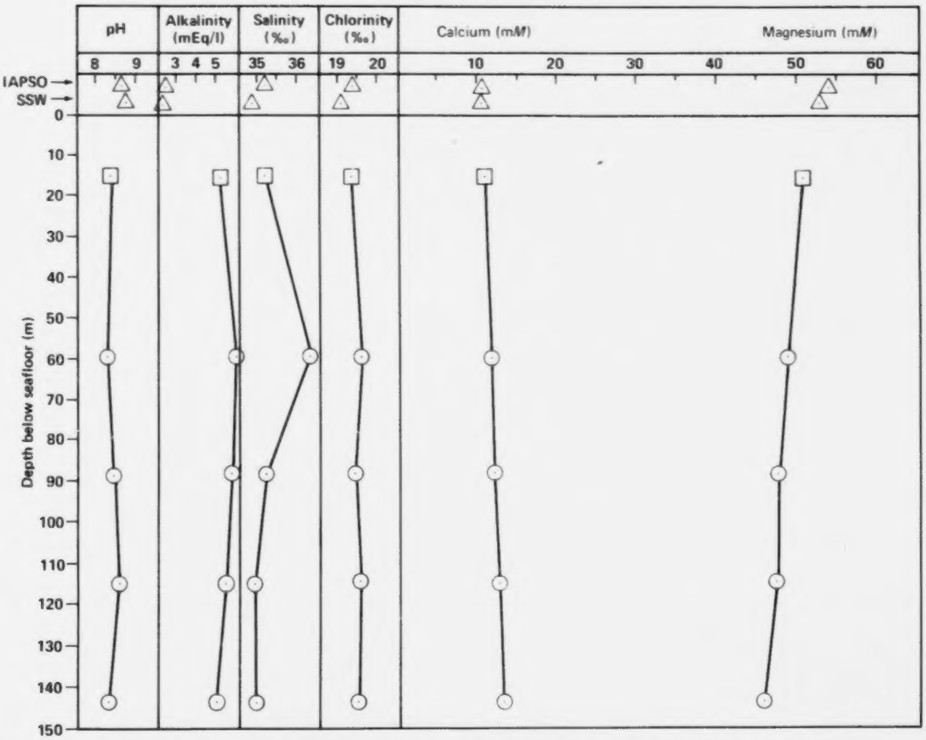

Figure 9. Profiles of pH, alkalinity, salinity (‰), chlorinity (‰), calcium (m*M*), and magnesium (m*M*) versus sub-bottom depth from interstitial water samples analyzed at Site 579. Symbols are as follows: △ = IAPSO and SSW standards; ⊡ = samples from Hole 579; ⊙ = samples from Hole 579A.

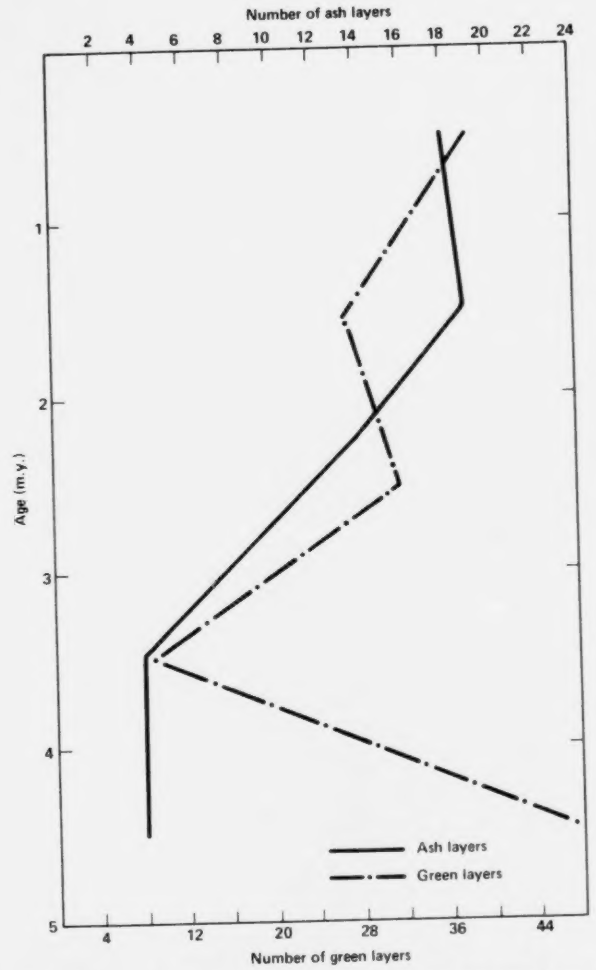

Figure 10. Plot of numbers of ash layers and indurated green layers/m.y. at Site 579.

SITE 579 HOLE CORE 1 CORED INTERVAL 5746.6–5755.0 mbsl; 0.0–8.4 mbsf

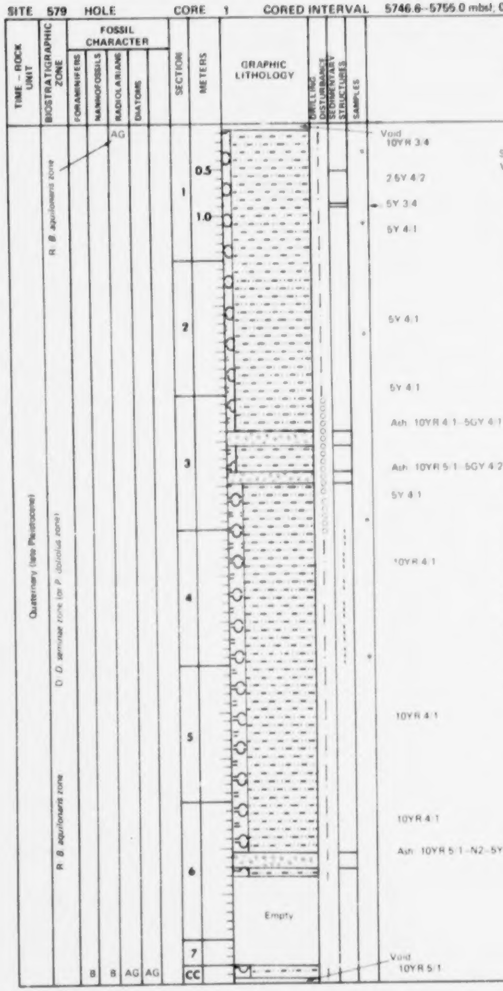
TIME – ROCK UNIT
BIOSTRATIGRAPHIC ZONE
FOSSIL CHARACTER
FORAMINIFERS
NANNOFOSSILS
RADIOLARIANS
DIATOMS
SECTION
METERS
GRAPHIC LITHOLOGY
DRILLING DISTURBANCE
SEDIMENTARY STRUCTURES
SAMPLES
Quaternary (late Pleistocene)
R. B. aquilonaris zone
D. D. seminae zone (or P. doliolus zone)
R. B. aquilonaris zone
AG
B
B
AG
AG
0.5
1.0
1
2
3
4
5
6
7
CC
Empty
Void
10YR 3/4
2.5Y 4/2
5Y 3/4
5Y 4/1
5Y 4/1
5Y 4/1
Ash 10YR 4/1–5GY 4/1
Ash 10YR 5/1–5GY 4/2
5Y 4/1
10YR 4/1
10YR 4/1
10YR 4/1
Ash 10YR 5/1–N2–5Y 3/2
Void
10YR 5/1

LITHOLOGIC DESCRIPTION

SILTY SILICEOUS CLAY (SILICEOUS MUD) WITH VOLCANIC ASH LAYERS

- Dominant colors: dark gray (5Y 4/1) and dark gray (10YR 4/1). Section 1, 0–87 cm contains layers of dark yellowish brown (10YR 3/4), dark grayish brown (2.5Y 4/2), and olive (5Y 3/4). Core Catcher is gray (10YR 5/1). Minor colors: thin layers of green (5GY 4/1) and olive gray (5Y 3/2). Ash layers in Section 3 are gray (10YR 4/1–5/1) to green (5GY 4/1–4/2); ash layers in Section 6 is gray (10YR 5/1) grading to black (N2) grading to dark olive gray (5Y 3/2).
- Section 3 of this core is soupy; the rest of the core is moderately deformed by drilling.
- This core consists of silty siliceous clay (siliceous mud) with thin (0.5–2.0 cm), stiff, green to olive gray clay layers present in Sections 1, 2, 5, and the Core Catcher. Ash layers occur at 3, 40–55 cm, 3, 85–97 cm and, 6, 55–71 cm. Section 4 has olive gray to dark gray mottles. The Core Catcher contains a pumice pebble from 10–13 cm.

SMEAR SLIDE SUMMARY (%)

	1, 35 D	1, 110 D	2, 80 Tr	3, 146 D	4, 140 D
Texture					
Sand	3	18	1	20	15
Silt	30	30	30	30	25
Clay	67	52	69	50	60
Composition					
Quartz	20	20	20	20	15
Feldspar	1	–	1	–	Tr
Mica	1	2	2	3	1
Clay	65	55	65	46	60
Volcanic glass	5	5	4	5	7
Diatoms	4	12	5	18	10
Radiolarians	4	5	3	7	6
Sponge spicules	–	–	Tr		
Silicoflagellates	Tr	1	Tr	1	1

SITE 579 HOLE CORE 2 CORED INTERVAL 5755.0–5764.5 mbsl; 8.4–17.9 mbsf

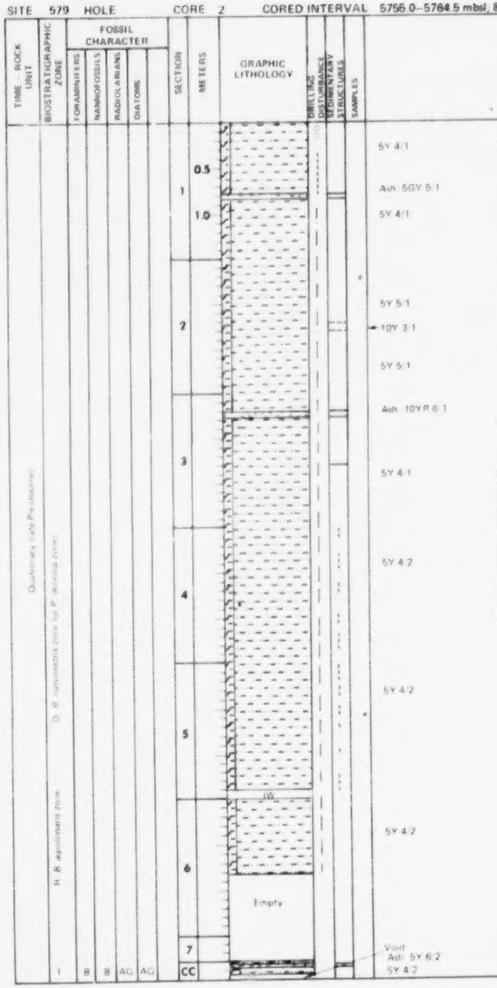
TIME – ROCK UNIT
BIOSTRATIGRAPHIC ZONE
FOSSIL CHARACTER
FORAMINIFERS
NANNOFOSSILS
RADIOLARIANS
DIATOMS
SECTION
METERS
GRAPHIC LITHOLOGY
DRILLING DISTURBANCE
SEDIMENTARY STRUCTURES
SAMPLES
Quaternary (late Pleistocene)
D. R. curvirostris zone (or P. doliolus zone)
R. B. aquilonaris zone
I
B
B
AG
AG
0.5
1.0
1
2
3
4
5
6
7
CC
Empty
5Y 4/1
Ash 5GY 5/1
5Y 4/1
5Y 5/1
10Y 3/1
5Y 5/1
Ash 10YR 6/1
5Y 4/1
5Y 4/2
5Y 4/2
5Y 4/2
Void
Ash 5Y 6/2
5Y 4/2

LITHOLOGIC DESCRIPTION

SILTY SILICEOUS CLAY (SILICEOUS MUD) WITH VOLCANIC ASH LAYERS

- Dominant colors: dark gray (5Y 4/1) and gray (5Y 5/1) in Sections 1 through 3. Olive gray (5Y 4/2) in Sections 4 through Core Catcher. Minor colors: Sections 1 through 3 and Section 5 contain thin green (5GY 4/1), dark olive gray (5Y 3/2–5Y 4/2) to olive gray, and very dark gray (5Y 3/1) stiff laminations. Section 2 contains a dark reddish gray (10Y 3/1) layer from 73–80 cm. Ash layers are green (5GY 5/1), gray (10YR 6/1), and light olive gray (5Y 6/2).
- Sections 1 and 2 are moderately to very deformed by drilling, the rest of the core is only slightly deformed.
- This core consists of silty siliceous clay (siliceous mud). Sections 1 through 3 and Section 5 contain thin(0.5–0.4 cm), stiff olive gray to green siliceous clay layers. Sections 4 and 5 have abundant faint black specks and mottles. Ash layers occur at 1, 75–81 cm, 3, 19–26 cm, and Core Catcher, 2–5 cm. There are two pebbles in 2, 46–49 cm.

SMEAR SLIDE SUMMARY (%)

	2, 26 D	5, 80 D
Texture		
Sand	10	15
Silt	25	17
Clay	65	68
Composition		
Quartz	15	15
Feldspar	2	2
Mica	–	Tr
Clay	65	68
Volcanic glass	Tr	Tr
Diatoms	10	10
Radiolarians	5	2
Sponge spicules	1	2
Silicoflagellates	2	1

SITE 579 HOLE A CORE 1 CORED INTERVAL 5760.6–5770.1 mbsl; 14.0–23.5 mbsf

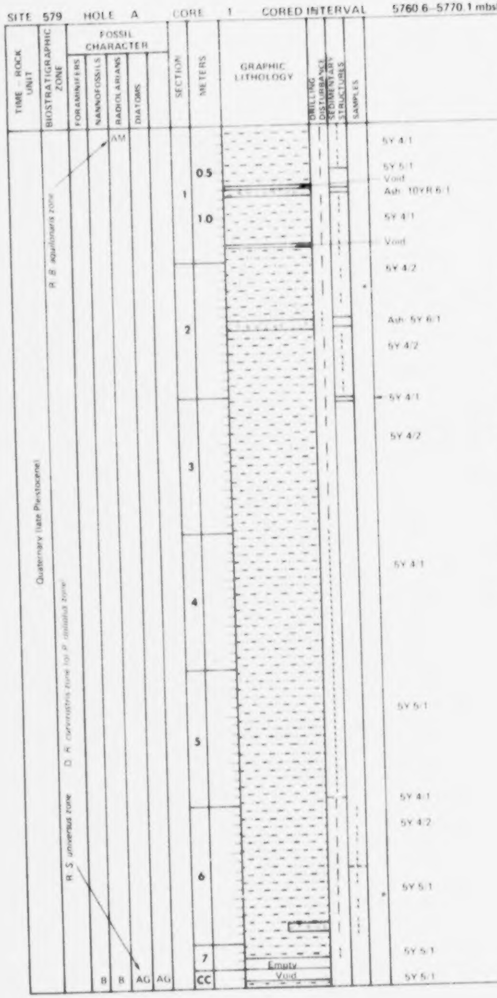
TIME – ROCK UNIT
BIOSTRATIGRAPHIC ZONE
FOSSIL CHARACTER
FORAMINIFERS
NANNOFOSSILS
RADIOLARIANS
DIATOMS
SECTION
METERS
GRAPHIC LITHOLOGY
DRILLING DISTURBANCE
SEDIMENTARY STRUCTURES
SAMPLES
Quaternary (late Pleistocene)
R. B. aquilonaris zone
D. R. curvirostris zone (or P. doliolus zone)
R. S. universus zone
AM
B
B
AG
AG
0.5
1.0
1
2
3
4
5
6
7
CC
Empty
Void
5Y 4/1
5Y 5/1
Void
Ash: 10YR 6/1
5Y 4/1
Void
5Y 4/2
Ash: 5Y 6/1
5Y 4/2
5Y 4/1
5Y 4/2
5Y 4/1
5Y 5/1
5Y 4/1
5Y 4/2
5Y 5/1
5Y 5/1
5Y 5/1

LITHOLOGIC DESCRIPTION

SILTY CLAY WITH VOLCANIC ASH LAYERS

- Dominant colors: dark gray (5Y 4/1), gray (5Y 5/1), and olive gray (5Y 4/2). Minor colors: thin layers of dark greenish gray (5G 4/1) clay. Ash layers are gray (10YR 6/1) and gray (5Y 6/1).
- Sections 1 through 3 and 5, 138 cm through 6 are slightly deformed by drilling. Sections 4 through 5, 138 cm and 7 through the Core Catcher are very deformed resulting from flow in.
- This core consists of homogeneous to mottled silty clay. Sections 2 and 6 have abundant faint black specks and mottles. Sections 3, 5, and 6 have thin (0.5–1.0 cm), indurated greenish-gray clay layers. Distinct ash layers occur at 1, 69–75 cm and 2, 66–75 cm. There is a dispersed ash layer at 6, 128–139 cm and a large pumice pebble at 1, 2–5 cm.

SMEAR SLIDE SUMMARY (%)

	2, 30 D	6, 100 D
Texture:		
Sand	2	3
Silt	33	32
Clay	65	65
Composition:		
Quartz	25	20
Feldspar		1
Mica	—	2
Heavy minerals	Tr	1
Clay	70	66
Volcanic glass	2	3
Diatoms	3	5
Radiolarians	Tr	2
Sponge spicules	Tr	—

SITE 579 HOLE A CORE 2 CORED INTERVAL 5770.1–5779.6 mbsl; 23.5–33.0 mbsf

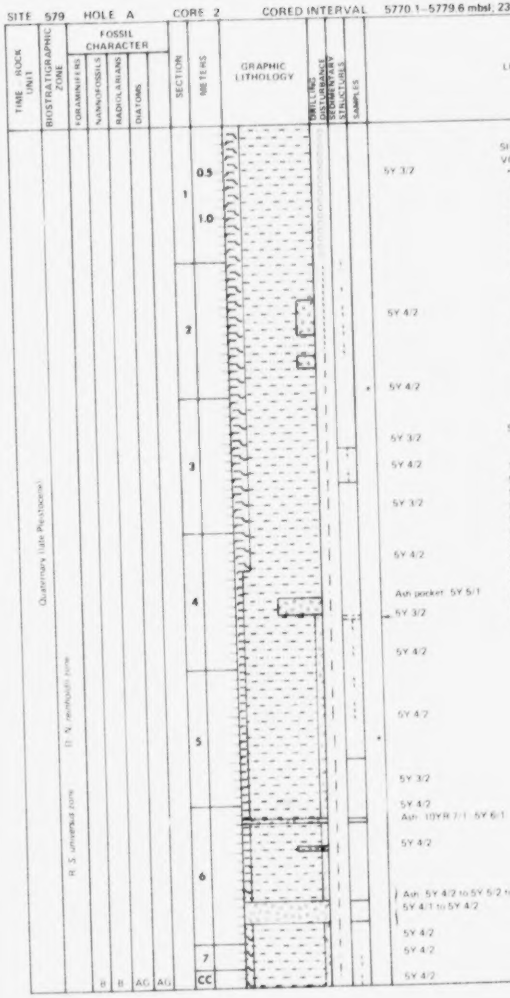
TIME – ROCK UNIT
BIOSTRATIGRAPHIC ZONE
FOSSIL CHARACTER
FORAMINIFERS
NANNOFOSSILS
RADIOLARIANS
DIATOMS
SECTION
METERS
GRAPHIC LITHOLOGY
DRILLING DISTURBANCE
SEDIMENTARY STRUCTURES
SAMPLES
Quaternary (late Pleistocene)
D. N. reinholdii zone
R. S. universus zone
B
B
AG
AG
0.5
1.0
1
2
3
4
5
6
7
CC
5Y 3/2
5Y 4/2
5Y 4/2
5Y 3/2
5Y 4/2
5Y 3/2
5Y 4/2
Ash pocket: 5Y 5/1
5Y 3/2
5Y 4/2
5Y 4/2
5Y 3/2
5Y 4/2
Ash: 10YR 7/1 – 5Y 6/1
5Y 4/2
Ash: 5Y 4/2 to 5Y 5/2 to 5Y 4/1 to 5Y 4/2
5Y 4/2
5Y 4/2
5Y 4/2

LITHOLOGIC DESCRIPTION

SILTY SILICEOUS CLAY (SILICEOUS MUD) WITH VOLCANIC ASH LAYERS

- Dominant colors: dark olive (5Y 3/2) gray and olive gray (5Y 4/2). Minor colors: thin layers of dark greenish gray (5G 4/1) clay in Sections 2, 3, 5, and 6. Ash pockets are gray (5Y 5/1, 5Y 6/1). Ash layer at 6, 16–19 cm is light gray (10YR 7/1) grading to gray (5Y 6/1) below 18 cm; ash layer at 6, 106–129 cm is olive gray (5Y 4/2) grading to olive gray (5Y 5/2) grading to dark gray and olive gray (5Y 4/2).
- Section 1 is soupy. Section 2, 0–122 cm is very deformed by drilling. The rest of the core is slightly to moderately deformed.
- This core consists of homogeneous to lightly mottled silty siliceous clay (siliceous mud). Dark olive gray (5Y 3/2) sections have thin (0.5–1.0 cm), indurated dark greenish gray clay layers. Ash pockets occur at 2, 80–87 cm, 2, 106–120 cm, 4, 72–91 cm; and, 6, 47–50 cm. Ash layers occur at 6, 16–19 cm and 6, 106–129 cm. There is a pumice cobble at 6, 40–42 cm.

SMEAR SLIDE SUMMARY (%)

	2, 146 D	5, 80 D
Texture:		
Sand	7	4
Silt	38	31
Clay	55	65
Composition:		
Quartz	25	20
Feldspar	5	3
Heavy minerals	Tr	Tr
Clay	35	52
Volcanic glass	3	10
Diatoms	25	13
Radiolarians	7	2
Silicoflagellates	Tr	—

SITE 579 HOLE A CORE 3 CORED INTERVAL 5779.6–5789.1 mbsl; 33.0–42.5 mbsf

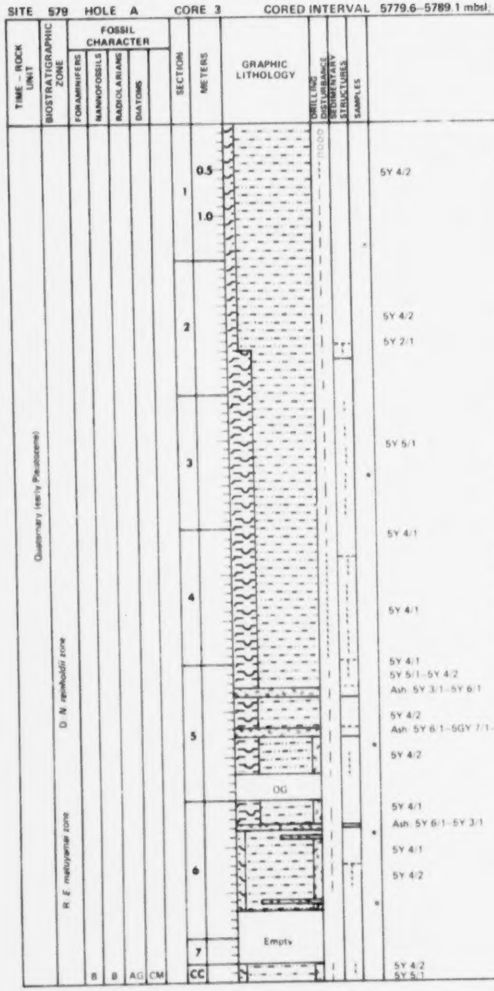
TIME – ROCK UNIT
BIOSTRATIGRAPHIC ZONE
FOSSIL CHARACTER
FORAMINIFERS
NANNOFOSSILS
RADIOLARIANS
DIATOMS
SECTION
METERS
GRAPHIC LITHOLOGY
DRILLING DISTURBANCE
SEDIMENTARY STRUCTURES
SAMPLES
Quaternary (early Pleistocene)
D. N. reinholdii zone
R. E. matuyamai zone
0.5
1.0
1
2
3
4
5
6
7
CC
B
B
AG
CM
OG
Empty
5Y 4/2
5Y 4/2
5Y 2/1
5Y 5/1
5Y 4/1
5Y 4/1
5Y 4/1
5Y 5/1–5Y 4/2
Ash: 5Y 3/1–5Y 6/1
5Y 4/2
Ash: 5Y 6/1–5GY 7/1–5G 4/1
5Y 4/2
5Y 4/1
Ash: 5Y 6/1–5Y 3/1
5Y 4/1
5Y 4/2
5Y 4/2
5Y 5/1

LITHOLOGIC DESCRIPTION

SILTY DIATOMACEOUS CLAY (DIATOMACEOUS MUD) WITH VOLCANIC ASH LAYERS

- Dominant colors: dark gray (5Y 4/1), gray (5Y 5/1) and olive gray (5Y 4/2). Minor colors: 5Y 2/1 moderately deformed black mottle at 2, 90–110 cm. Thin dark greenish gray (5G 4/1) laminations. Ash layers :re 5, 26–35 cm and 6, 27–31 cm are gray (5Y 6/1) grading to very dark gray (5Y 3/1); 5, 70–78 cm is gray (5Y 6/1) grading to interbedded light greenish gray (5GY 7/1) and dark greenish gray (5G 4/1). Ashy zones in Section 6 are dark gray (5Y 4/1) to gray (5Y 5/1).
- Section 1, 0–60 cm is soupy to very deformed. Section 2, 60–150 cm is moderately deformed and may be flow-in. Section 4, 32–144 cm is very deformed, resulting from flow-in. The rest of the core is slightly deformed.
- This core consists of homogeneous to lightly mottled silty diatomaceous clay (diatomaceous mud) with thin (0.5–1.0 cm), stiff greenish gray laminations, ash layers, and ashy zones. Ash layers occur at 5, 26–35 cm, 5, 70–78 cm, and 6, 27–31 cm. Ash-rich zones occur at 6, 37–41 cm and 6, 108–113 cm (see smear slide summary below).

SMEAR SLIDE SUMMARY (%)

	1, 135	3, 90	5, 90	6, 39	6, 111
	D	D	D	M	M
Texture:					
Sand	3	10	10	60	80
Silt	30	35	35	30	15
Clay	67	55	55	10	5
Composition:					
Quartz	20	20	25	10	13
Feldspar	3	5	5	—	—
Heavy minerals	2	Tr	—	—	2
Clay	60	43	30	15	5
Volcanic glass	5	7	10	50	75
Diatoms	8	20	25	20	5
Radiolarians	2	5	5	5	Tr

SITE 579 HOLE A CORE 4 CORED INTERVAL 5789.1–5798.6 mbsl; 42.5–52.0 mbsf

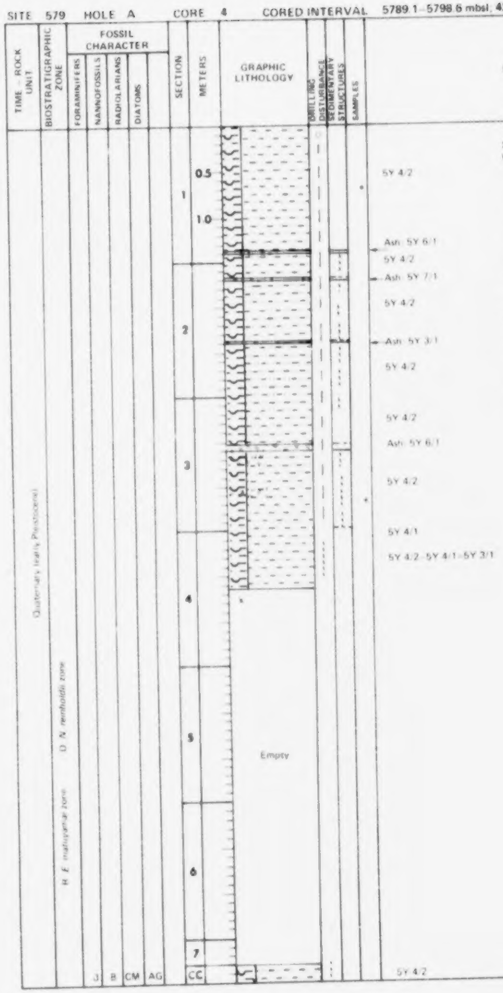
TIME – ROCK UNIT
BIOSTRATIGRAPHIC ZONE
FOSSIL CHARACTER
FORAMINIFERS
NANNOFOSSILS
RADIOLARIANS
DIATOMS
SECTION
METERS
GRAPHIC LITHOLOGY
DRILLING DISTURBANCE
SEDIMENTARY STRUCTURES
SAMPLES
Quaternary (early Pleistocene)
D. N. reinholdii zone
R. E. matuyamai zone
0.5
1.0
1
2
3
4
5
6
7
CC
3
B
CM
AG
Empty
5Y 4/2
Ash: 5Y 6/1
5Y 4/2
Ash: 5Y 7/1
5Y 4/2
Ash: 5Y 3/1
5Y 4/2
5Y 4/2
Ash: 5Y 6/1
5Y 4/2
5Y 4/1
5Y 4/2–5Y 4/1–5Y 3/1
5Y 4/2

LITHOLOGIC DESCRIPTION

SILTY DIATOMACEOUS CLAY (DIATOMACEOUS MUD) WITH VOLCANIC ASH LAYERS

- Dominant colors: olive gray (5Y 4/2) grading to dark gray (5Y 4/1) at the base of Section 3. Flow-in material in Section 4 and the Core Catcher is olive gray (5Y 4/2), dark gray (5Y 4/1), and very dark gray (5Y 3/1). Minor colors: dark greenish gray (5G 4/1), and dark gray (5Y 4/1) laminations and mottles. Ash layers and pockets are gray to light gray (5Y 6/1), light gray (5Y 7/1), and very dark gray.
- Section 4, 6–64 cm and the Core Catcher are very deformed, resulting from flow-in. The rest of the core is slightly to moderately deformed.
- This core consists of homogeneous to light mottled silty diatomaceous clay (diatomaceous mud) with stiff dark greenish gray and dark gray laminations, zones, and mottles. Ash layers occur at 1, 127–130 cm, 2, 18–20 cm, 2, 88–90 cm, and 3, 55–60 cm. These ash layers have gradational top and sharp bottom contacts. Small pockets of ash occur at 2, 20–63 cm, 3, 63–68 cm, and 3, 106–107 cm.

SMEAR SLIDE SUMMARY (%)

	1, 70	3, 120
	D	D
Texture:		
Sand	7	5
Silt	33	30
Clay	60	65
Composition:		
Quartz	20	20
Feldspar	5	5
Heavy minerals	Tr	Tr
Clay	45	41
Volcanic glass	5	7
Diatoms	20	25
Radiolarians	5	2

SITE 579 HOLE A CORE 5 CORED INTERVAL 5798.6–5808.1 mbsl; 52.0–61.5 mbsf

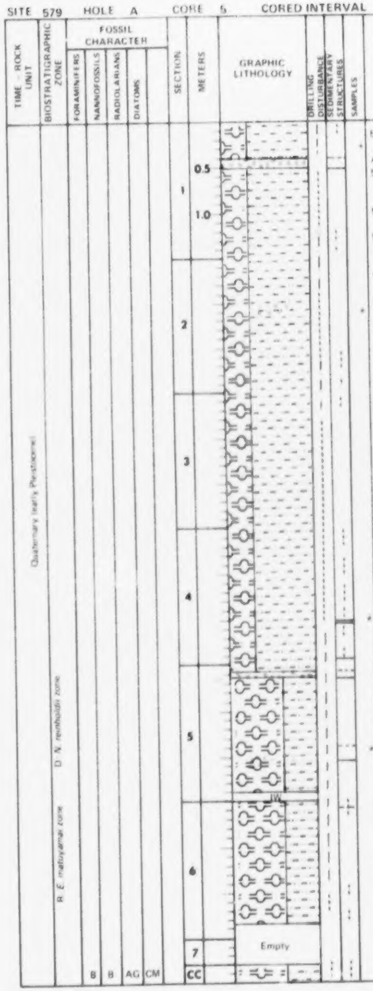
TIME – ROCK UNIT
BIOSTRATIGRAPHIC ZONE
FOSSIL CHARACTER
FORAMINIFERS
NANNOFOSSILS
RADIOLARIANS
DIATOMS
SECTION
METERS
GRAPHIC LITHOLOGY
DRILLING DISTURBANCE
SEDIMENTARY STRUCTURES
SAMPLES
Quaternary (early Pleistocene)
R: E. matuyamai zone
D: N. reinholdii zone
B
B
AG
CM
0.5
1.0
1
2
3
4
5
6
7
CC
Empty
5Y 4/1–5Y 4/2
Ash: 5Y 4/1–5Y 6/1–5G 4/1
5Y 4/2
5Y 4/1–5Y 4/2
5Y 5/1–5Y 4/2
5Y 4/2
5Y 5/1
5Y 5/1
5Y 5/1, 5Y 4/2, 5G 4/1, and 5Y 2/1
5Y 4/1
5Y 2/1
5Y 4/1
5Y 3/1
Ash: 5Y 5/1
5Y 4/2
5Y 5/1
5Y 3/1
5Y 5/1
5Y 4/1
5Y 3/2
5GY 4/1
5GY 4/1

LITHOLOGIC DESCRIPTION

SILTY SILICEOUS CLAY (SILICEOUS MUD) TO CLAYEY SILICEOUS OOZE WITH VOLCANIC ASH LAYERS

- Dominant colors: very dark gray (5Y 3/1), dark gray (5Y 4/1), gray (5Y 5/1), dark olive gray (5Y 3/2), olive gray (5Y 4/2–5/2). Minor colors: several layers of black (5Y 2/1). Dark greenish gray (5G 4/1) laminations. Ash layer at 1, 40–50 cm is dark gray (5Y 4/1) grading to dark greenish gray (5G 4/1). Ash layer at 5, 7–13 cm is gray (5Y 5/1). Other ash is dark olive gray (5Y 3/2) or gray (5Y 6/1).
- Very deformed portions of this core at 1, 50–106 cm, 2, 30–105 cm, 3, 30 cm to 4, 100 cm, 6, 98–132 cm, and the Core Catcher have vertically distorted flow features resulting from flow-in. The rest of the core is slightly to moderately deformed by drilling.
- This core consists of homogeneous to lightly mottled silty siliceous clay (siliceous mud) to clayey siliceous ooze with dark greenish gray laminations. Ash layers occur at 1, 40–50 cm, and 5, 7–13 cm. There are small ash patches at 5, 96–102 cm. A lithified mudstone cobble at 2, 57–58 cm is surrounded by dark olive gray ash.

SMEAR SLIDE SUMMARY (%)

	1, 30 D	2, 60 M	4, 101 D	5, 92 D
Texture:				
Sand	15	70	20	30
Silt	50	20	50	50
Clay	35	10	30	20
Composition:				
Quartz	20	30	30	10
Feldspar	3	—	—	—
Heavy minerals	1	2		
Clay	35	10	30	20
Volcanic glass	5	48	10	7
Diatoms	20	Tr	15	25
Radiolarians	15	—	10	35
Sponge spicules	—		2	—
Silicoflagellates	1		3	3
Opaques		10		

SITE 579 HOLE A CORE 6 CORED INTERVAL 5808.1–5817.6 mbsl; 61.5–71.0 mbsf

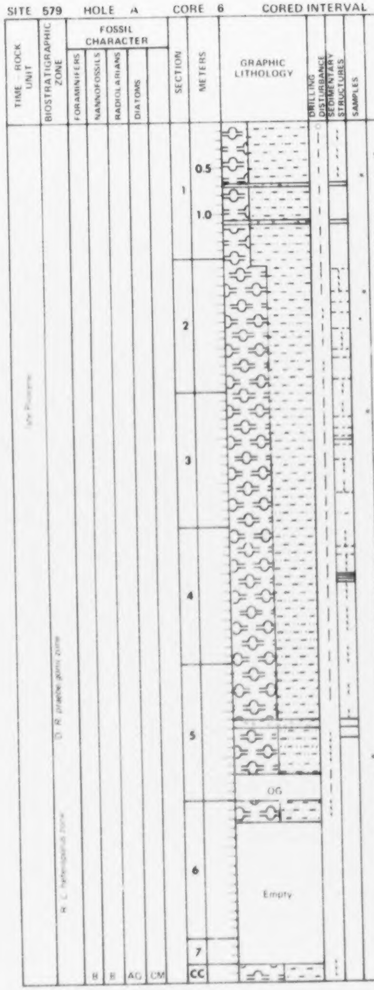
TIME – ROCK UNIT
BIOSTRATIGRAPHIC ZONE
FOSSIL CHARACTER
FORAMINIFERS
NANNOFOSSILS
RADIOLARIANS
DIATOMS
SECTION
METERS
GRAPHIC LITHOLOGY
DRILLING DISTURBANCE
SEDIMENTARY STRUCTURES
SAMPLES
late Pliocene
R: C. heteroporus zone
D: R. praebergonii zone
B
B
AG
CM
0.5
1.0
1
2
3
4
5
6
7
CC
OG
Empty
5Y 4/1
Ash: 5Y 6/1–5Y 5/1
5GY 5/1
Ash: 2.5Y 6/2
5Y 4/2
5Y 5/1
5Y 5/1
5GY 5/1
5Y 4/1
5GY 4/1
5Y 5/1
5Y 4/1
5Y 4/2
5Y 5/1
5Y 5/1
5Y 4/1
5GY 4/1
5Y 4/1
5Y 4/1
5Y 5/1–5Y 5/1
5Y 3/1
5Y 5/1
5Y 4/1–5/1
5Y 4/2
Two layers of 5P 3/1
5Y 5/1
5Y 5/1
Ash: 5Y 5/1 with 5Y 3/1 and 5GY 5/1 layers
5GY 4/1–5Y 4/1
5Y 5/1
5Y 5/1

LITHOLOGIC DESCRIPTION

CLAYEY SILICEOUS OOZE WITH VOLCANIC ASH LAYERS

- Dominant colors: very dark gray (5Y 3/1), dark gray (5Y 4/1), gray (5Y 5/1), olive gray (5Y 4/2), and greenish gray (5GY 4/1–5/1). Minor colors: ash layer at 1, 75–79 cm is gray (5Y 5/1) grading to light gray (5Y 6/1) to gray. Ash layer at 1, 106–109.5 cm is light brownish gray (2.5Y 6/2). Ash layer at 5, 59.5–67 cm is gray (5Y 5/1) with very dark gray (5Y 3/1) and green (5GY 5/1) laminae. Core contains greenish gray (5GY 4/1) and greenish gray (5G 4/1) laminae.
- Section 2, 55–73 cm, 2, 110–128 cm, and Sections 5 through the Core Catcher are very deformed, resulting from flow-in. The rest of the core is moderately to slightly deformed by drilling.
- This core consists of homogeneous to mottled clayey siliceous ooze with thin (0.1–0.3 cm), indurated laminae of greenish gray to green siliceous clay. Ash layers occur at 1, 75–79 cm, 1, 106–109.5 cm, and 5, 59.5–67 cm.

SMEAR SLIDE SUMMARY (%)

	1, 60 D	2, 40 D	3, 27 D	5, 102 D
Texture				
Sand	10	30	10	20
Silt	33	34	60	53
Clay	57	36	30	27
Composition				
Quartz	10	7	10	5
Feldspar	Tr	—	—	Tr
Clay	57	36	30	27
Volcanic glass	1	1	1	Tr
Diatoms	10	25	25	30
Radiolarians	20	31	30	35
Sponge spicules	—	—	1	—
Silicoflagellates	2	1	3	3

SITE 579 HOLE A CORE 7 CORED INTERVAL 5817.6–5827.1 mbsl; 71.0–80.5 mbsf

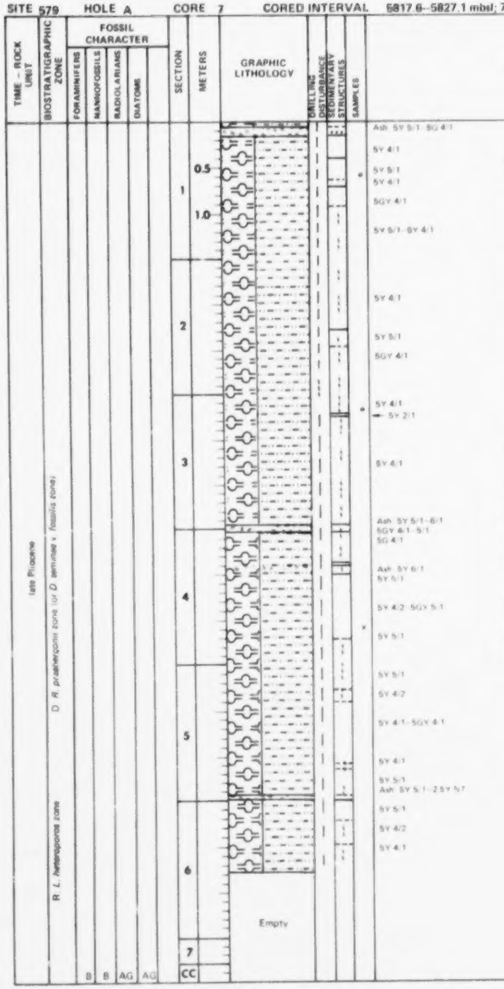
TIME – ROCK UNIT
BIOSTRATIGRAPHIC ZONE
FOSSIL CHARACTER
FORAMINIFERS
NANNOFOSSILS
RADIOLARIANS
DIATOMS
SECTION
METERS
GRAPHIC LITHOLOGY
DRILLING DISTURBANCE
SEDIMENTARY STRUCTURES
SAMPLES
late Pliocene
D R. praebergonii zone (or D. seminae v. fossilis zone)
R L. heteroporos zone
B
B
AG
AG
1
2
3
4
5
6
7
CC
0.5
1.0
Empty
Ash 5Y 5/1–5G 4/1
5Y 4/1
5Y 5/1
5Y 4/1
5GY 4/1
5Y 5/1–5Y 4/1
5Y 4/1
5Y 5/1
5GY 4/1
5Y 4/1
5Y 2/1
5Y 4/1
Ash 5Y 5/1–6/1
5GY 4/1–5/1
5G 4/1
Ash 5Y 6/1
5Y 5/1
5Y 4/2–5GY 5/1
5Y 5/1
5Y 5/1
5Y 4/2
5Y 4/1–5GY 4/1
5Y 4/1
5Y 5/1
Ash 5Y 5/1–2.5Y N7
5Y 5/1
5Y 4/2
5Y 4/1

LITHOLOGIC DESCRIPTION

SILTY SILICEOUS CLAY (SILICEOUS MUD) WITH VOLCANIC ASH LAYERS

- Dominant colors: dark gray (5Y 4/1), gray (5Y 5/1), olive gray (5Y 4/2), and greenish gray (5GY 4/1–5/1). Minor colors: greenish gray (5G 4/1), green (5GY 4/1), and very dark gray (5Y 3/1) laminations. Section 3, 18–21 cm contains a black (5Y 2/1) layer. Ash layers are gray (5Y 5/1) and greenish gray (5G 4/1) at 1, 5.5–15 cm, gray (5Y 5/1–6/1, green (5GY 4/1–5/1, and greenish gray (5G 4/1) at 3, 144 cm to 4, 3 cm, light gray (5Y 6/1) to gray at 4, 37–38.5 cm, and, gray (5Y 5/1) to light gray (2.5Y N7) at 5, 145 cm to 6, 1.5 cm.
- Entire core is slightly deformed by drilling.

This core consists of mottled silty siliceous clay (siliceous mud) with thin (0.2–2.0 cm), indurated laminations and layers. Section 3, 18–21 cm is a black, quartz-rich pyritic clay layer. Ash layers occur at 1, 5.5–15 cm, 3, 144 cm to 4, 3 cm, 4, 37–38.5 cm, and 5, 145.5 cm to 6, 1.5 cm. The ash layer at 1, 5.5–15 cm is normally graded; the one at 4, 37–38.5 cm is very burrowed.

SMEAR SLIDE SUMMARY (%):

	1, 60 D	3, 20 M	4, 110 D
Texture			
Sand	20	15	20
Silt	30	35	20
Clay	50	50	60
Composition			
Quartz	7	30	10
Feldspar	–	–	Tr
Clay	49	43	57
Volcanic glass	Tr	–	Tr
Pyrite	–	20	–
Diatoms	20	1	15
Radiolarians	20	1	15
Sponge spicules	1	–	2
Silicoflagellates	3	Tr	1

SITE 579 HOLE A CORE 8 CORED INTERVAL 5827.1–5836.6 mbsl; 80.5–90.0 mbsf

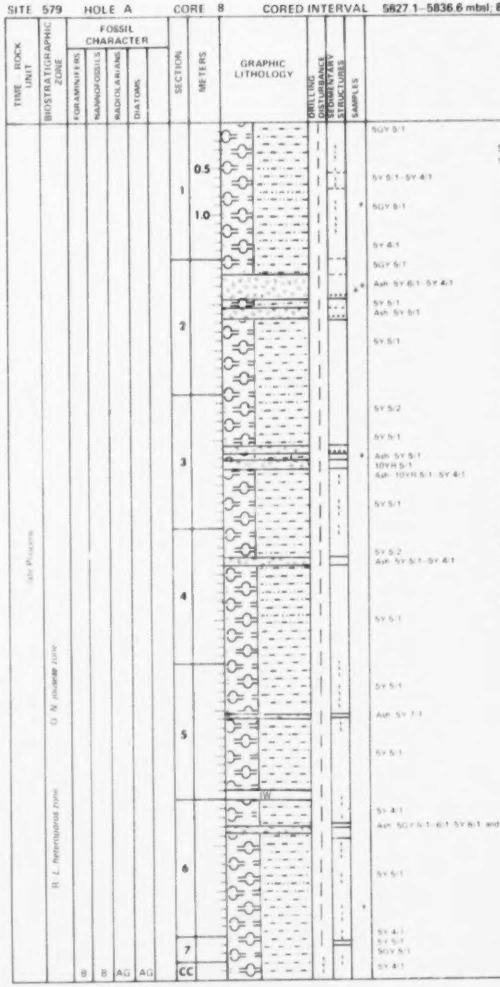
TIME – ROCK UNIT
BIOSTRATIGRAPHIC ZONE
FOSSIL CHARACTER
FORAMINIFERS
NANNOFOSSILS
RADIOLARIANS
DIATOMS
SECTION
METERS
GRAPHIC LITHOLOGY
DRILLING DISTURBANCE
SEDIMENTARY STRUCTURES
SAMPLES
late Pliocene
D N. jouseae zone
R L. heteroporos zone
B
B
AG
AG
1
2
3
4
5
6
7
CC
0.5
1.0
W
5GY 5/1
5Y 5/1–5Y 4/1
5GY 6/1
5Y 4/1
5GY 5/1
Ash 5Y 6/1–5Y 4/1
5Y 5/1
Ash 5Y 6/1
5Y 5/1
5Y 5/2
5Y 5/1
Ash 5Y 5/1
10YR 5/1
Ash 10YR 5/1–5Y 4/1
5Y 5/1
5Y 5/2
Ash 5Y 5/1–5Y 4/1
5Y 5/1
5Y 5/1
Ash 5Y 7/1
5Y 5/1
5Y 4/1
Ash 5GY 5/1–6/1 5Y 6/1 and 5Y 3/1
5Y 5/1
5Y 4/1
5Y 5/1
5GY 5/1
5Y 4/1

LITHOLOGIC DESCRIPTION

SILTY SILICEOUS CLAY (SILICEOUS MUD) WITH VOLCANIC ASH LAYERS

- Dominant colors: dark gray (5Y 4/1), gray (5Y 5/1), olive gray (5Y 5/2), and greenish gray (5GY 5/1). Minor colors: laminations of green (5GY 4/1) and thin layers of dark gray (5Y 4/1). Ash layers are light gray (5Y 7/1) light gray (5Y 6/1) to gray, gray (5Y 5/1), dark gray (5Y 4/1), very dark gray (5Y 3/1), and greenish gray (5GY 5/1–5GY 6/1)
- The Core Catcher is very deformed. The rest of the core is slightly deformed by drilling.
- This core consists of homogeneous to lightly mottled silty siliceous clay (siliceous mud) with thin (0.5–1.0 cm), indurated greenish gray siliceous clay laminations. Ash layers occur at 2, 19–45 cm; 2, 53–88 cm; 3, 57–60 cm; 3, 72–85 cm; 4, 32–40 cm; 5, 57–60 cm, and 6, 30–37 cm. The ash layers in Sections 2 and 3, 57–60 cm are normally graded.

SMEAR SLIDE SUMMARY (%):

	1, 90 D	2, 31 M	2, 38 M	3, 70 D	6, 120 D
Texture					
Sand	35	60	80	40	20
Silt	20	20	15	20	25
Clay	45	20	5	40	55
Composition					
Quartz	10	7	10	7	15
Feldspar	–	–	–	–	Tr
Mica	–	–	–	–	2
Clay	44	20	5	37	55
Volcanic glass	1	50	72	20	1
Diatoms	20	20	3	15	15
Radiolarians	20	1	5	20	12
Sponge spicules	5	2	–	–	–
Silicoflagellates	Tr	–	–	1	–
Opaques	–	–	5	–	–

SITE 579 HOLE A CORE 9 CORED INTERVAL 5836.6–5846.1 mbsl; 90.0–99.5 mbsf

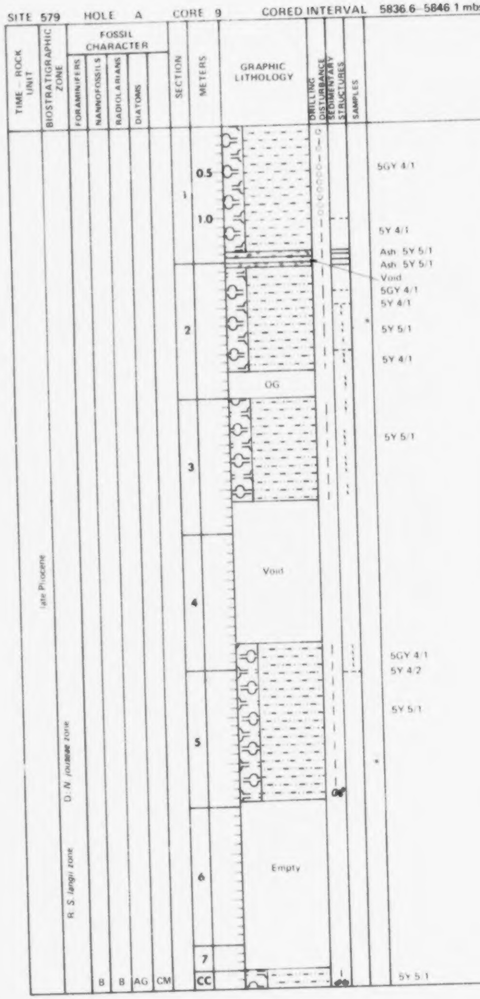
TIME – ROCK UNIT
BIOSTRATIGRAPHIC ZONE
FOSSIL CHARACTER
FORAMINIFERS
NANNOFOSSILS
RADIOLARIANS
DIATOMS
SECTION
METERS
GRAPHIC LITHOLOGY
DRILLING DISTURBANCE
SEDIMENTARY STRUCTURES
SAMPLES
late Pliocene
D: N. jouseae zone
R: S. langii zone
B
B
AG
CM
0.5
1.0
1
2
3
4
5
6
7
CC
OG
Void
Empty
5GY 4/1
5Y 4/1
Ash: 5Y 5/1
Ash: 5Y 5/1
Void
5GY 4/1
5Y 4/1
5Y 5/1
5Y 4/1
5Y 5/1
5GY 4/1
5Y 4/2
5Y 5/1
5Y 5/1

LITHOLOGIC DESCRIPTION

SILTY SILICEOUS CLAY (SILICEOUS MUD)

- Dominant colors: dark gray (5Y 4/1), gray (5Y 5/1), olive gray (5Y 4/2), and dark greenish gray (5GY 4/1). Minor colors: several black (5Y 2.5/1) to very dark gray (5GY 4/1) layers. Dark greenish gray (5GY 4/1) laminations. Ash layers are gray (5Y 5/1).

*Core contains a large void space from 3, 115 cm to 4, 120 cm. Parts of Section 1 are soupy, the rest of the core is slightly deformed by drilling.

*This core consists of homogeneous to lightly mottled silty siliceous clay (siliceous mud) with thin (0.2–0.5 cm), greenish gray laminae of siliceous clay. Ash layers occur at 1, 138.5–144 cm and 2, 1–4 cm. These two ash layers are separated by a void space at the base of Section 1 and are therefore likely adjacent portions of one and the same ash layer.

SMEAR SLIDE SUMMARY (%):

	2, 20	5, 100
	D	D
Texture:		
Sand	25	20
Silt	25	30
Clay	50	50
Composition:		
Quartz	15	18
Feldspar	1	
Mica	Tr	2
Clay	49	47
Volcanic glass	10	2
Diatoms	4	18
Radiolarians	20	13
Silicoflagellates	1	

SITE 579 HOLE A CORE 10 CORED INTERVAL 5846.1–5855.6 mbsl; 99.5–109.0 mbsf

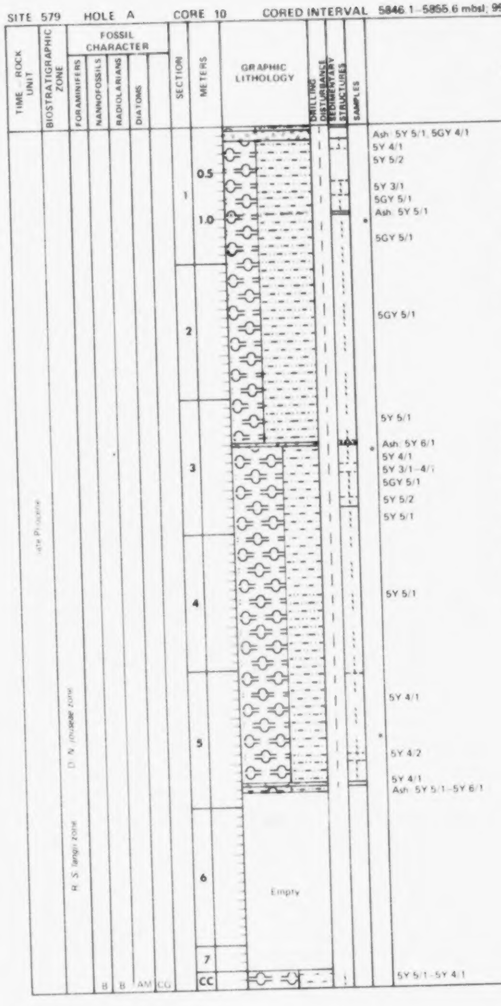
TIME – ROCK UNIT
BIOSTRATIGRAPHIC ZONE
FOSSIL CHARACTER
FORAMINIFERS
NANNOFOSSILS
RADIOLARIANS
DIATOMS
SECTION
METERS
GRAPHIC LITHOLOGY
DRILLING DISTURBANCE
SEDIMENTARY STRUCTURES
SAMPLES
late Pliocene
D: N. jouseae zone
R: S. langii zone
B
B
AM
CG
0.5
1.0
1
2
3
4
5
6
7
CC
Empty
Ash: 5Y 5/1, 5GY 4/1
5Y 4/1
5Y 5/2
5Y 3/1
5GY 5/1
Ash: 5Y 5/1
5GY 5/1
5GY 5/1
5Y 5/1
Ash: 5Y 6/1
5Y 4/1
5Y 3/1–4/1
5GY 5/1
5Y 5/2
5Y 5/1
5Y 5/1
5Y 4/1
5Y 4/2
5Y 4/1
Ash: 5Y 5/1–5Y 6/1
5Y 5/1–5Y 4/1

LITHOLOGIC DESCRIPTION

SILTY SILICEOUS CLAY (SILICEOUS MUD) TO CLAYEY SILICEOUS OOZE WITH VOLCANIC ASH LAYERS

- Dominant colors: dark gray (5Y 4/1), gray (5Y 5/1), olive gray (5Y 4/2–5Y 5/2), and greenish gray (5GY 5/1). Minor colors: several black (5Y 2/1) to very dark gray (5Y 3/1) layers. Dark greenish gray (5GY 4/1) laminations. Ash layers are gray (5Y 5/1–5Y 6/1). The ash layer at 1, 2–15 cm contains a lamination of dark greenish gray (5GY 4/1) ash.

*Entire core is slightly deformed by drilling.

*This core consists of mottled silty siliceous clay (siliceous mud) to clayey siliceous ooze with thin (0.3–1.0 cm), greenish gray, indurated siliceous clay laminae. Ash layers occur at 1, 2–15 cm; 1, 96–98 cm; 3, 47–50 cm; and, 5, 124.5–128 cm. The ash layer at 3, 47–50 cm is normally graded.

SMEAR SLIDE SUMMARY (%):

	1, 110	3, 60	5, 78
	D	D	D
Texture:			
Sand	40	39	40
Silt	10	30	27
Clay	50	31	33
Composition:			
Quartz	5	3	4
Feldspar	Tr	–	–
Clay	48	31	33
Volcanic glass	2	2	Tr
Pyrite	–	–	5
Diatoms	20	40	25
Radiolarians	20	20	30
Sponge spicules	5	3	3
Silicoflagellates	–	1	–

SITE 579 HOLE A CORE 11 CORED INTERVAL 5855.6–5865.1 mbsl; 109.0–118.5 mbsf

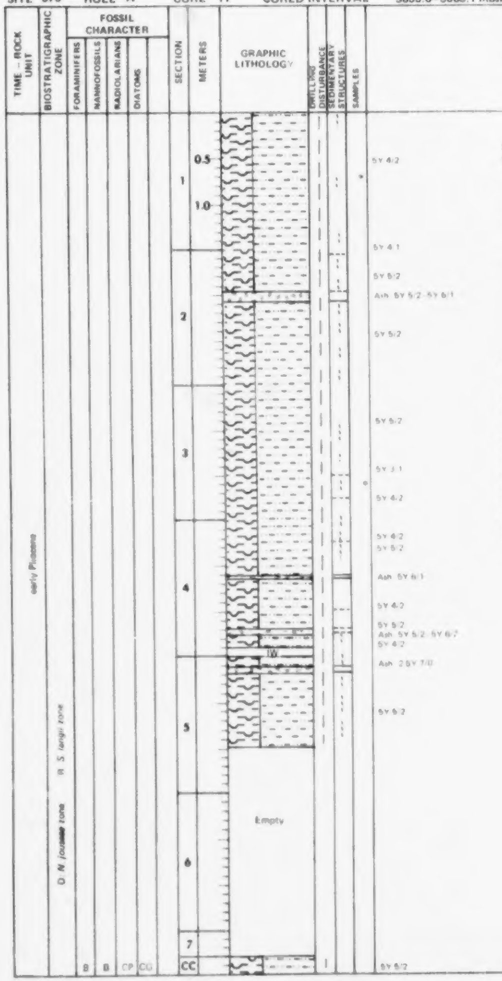
TIME – ROCK UNIT
BIOSTRATIGRAPHIC ZONE
FOSSIL CHARACTER
FORAMINIFERS
NANNOFOSSILS
RADIOLARIANS
DIATOMS
SECTION
METERS
GRAPHIC LITHOLOGY
DRILLING DISTURBANCE
SEDIMENTARY STRUCTURES
SAMPLES
early Pliocene
D. N. jouseae zone
R. S. langii zone
B
B
CP
CG
1
2
3
4
5
6
7
CC
0.5
1.0
IW
Empty
5Y 4/2
5Y 4/1
5Y 5/2
Ash 5Y 5/2–5Y 6/1
5Y 5/2
5Y 5/2
5Y 3/1
5Y 4/2
5Y 4/2
5Y 5/2
Ash 5Y 6/1
5Y 4/2
5Y 5/2
Ash 5Y 5/2–5Y 6/7
5Y 4/2
Ash 2.5Y 7/0
5Y 6/2
5Y 5/2

LITHOLOGIC DESCRIPTION

SILTY DIATOMACEOUS CLAY (DIATOMACEOUS MUD) WITH VOLCANIC ASH LAYERS

*Dominant colors: olive gray (5Y 4/2–5Y 5/2), very dark gray (5Y 3/1), and dark gray (5Y 4/1). Minor colors: core contains a few thin dark greenish gray (5G 4/1) laminations. Ash layers at 2, 45–56 cm and 4, 118–123 cm are olive gray (5Y 5/2) grading to gray (5Y 6/1) to light gray. Other ash layers are gray (5Y 6/1) to light gray and light gray (2.5Y 7/0).

*Entire core is slightly deformed by drilling.

• This core consists of lightly mottled to homogeneous silty diatomaceous clay (diatomaceous mud) with several thin laminations of greenish gray siliceous clay. Ash layers occur at 2, 45–56 cm, 4, 60–63 cm, 4, 118–123 cm, and 5, 11–16 cm.

SMEAR SLIDE SUMMARY (%)

	1, 75	3, 110
	D	D
Texture		
Sand	15	20
Silt	40	50
Clay	45	30
Composition		
Quartz	25	20
Feldspar		3
Heavy minerals	Tr	Tr
Clay	40	30
Volcanic glass	3	5
Diatoms	25	30
Radiolarians	7	12

SITE 579 HOLE A CORE 12 CORED INTERVAL 5865.1–5874.5 mbsl; 118.5–128.0 mbsf

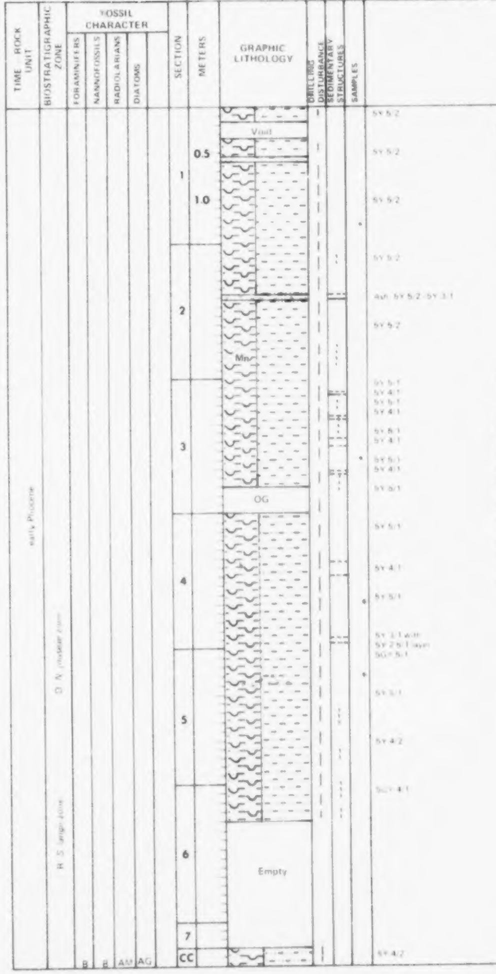
TIME – ROCK UNIT
BIOSTRATIGRAPHIC ZONE
FOSSIL CHARACTER
FORAMINIFERS
NANNOFOSSILS
RADIOLARIANS
DIATOMS
SECTION
METERS
GRAPHIC LITHOLOGY
DRILLING DISTURBANCE
SEDIMENTARY STRUCTURES
SAMPLES
early Pliocene
D. N. jouseae zone
R. S. langii zone
B
B
AM
AG
1
2
3
4
5
6
7
CC
0.5
1.0
Void
Mn
OG
Empty
5Y 5/2
5Y 5/2
5Y 5/2
5Y 5/2
Ash 5Y 5/2–5Y 3/1
5Y 5/2
5Y 5/1
5Y 4/1
5Y 5/1
5Y 4/1
5Y 6/1
5Y 4/1
5Y 5/1
5Y 4/1
5Y 6/1
5Y 5/1
5Y 4/1
5Y 5/1
5Y 3/1 with
5Y 2.5/1 layer
5GY 5/1
5Y 5/1
5Y 4/2
5GY 4/1
5Y 4/2

LITHOLOGIC DESCRIPTION

SILTY DIATOMACEOUS CLAY (DIATOMACEOUS MUD)

*Dominant colors: olive gray (5Y 4/2–5Y 5/2), gray (5Y 5/1), dark gray (5Y 4/1), and dark greenish gray (5GY 4/1–5GY 5/1). Minor colors: thin laminations of dark greenish gray (5G 4/1), very dark gray (5Y 3/1), greenish gray (5GY 5/1), and grayish green (5G 4/2). Ash layer at 2, 66–71 cm grades from olive gray (5Y 5/2) to very dark gray (5Y 3/1). Ashy patches in Section 5 are very dark gray (5Y 3/1) and black (5Y 2/1).

*Entire core is slightly deformed by drilling.

• This core consists of homogeneous to very lightly mottled silty diatomaceous clay (diatomaceous mud) with thin (0.3–2.0 cm) greenish-gray laminations. An ash layer occurs at 2, 66–71 cm. Section 5, 25–31 cm contains several patches of ash. A manganese nodule occurs at 2, 121–123 cm, and a gray pebble about 1 cm in diameter at 4, 131 cm.

SMEAR SLIDE SUMMARY (%)

	1, 130	3, 90	4, 100	5, 30
	D	D	D	M
Texture				
Sand	15	20	20	50
Silt	50	45	40	35
Clay	35	35	40	15
Composition				
Quartz	15	25	15	10
Feldspar	5	3	5	5
Heavy minerals	—	Tr	Tr	—
Clay	36	25	35	20
Volcanic glass	5	5	5	29
Diatoms	35	35	30	5
Radiolarians	5	7	10	1
Silicoflagellates	—	Tr	—	—
Opaques	—	—	—	30

SITE 579 HOLE A CORE 13 CORED INTERVAL 5874.5–5884.1 mbsl; 128.0–137.5 mbsf

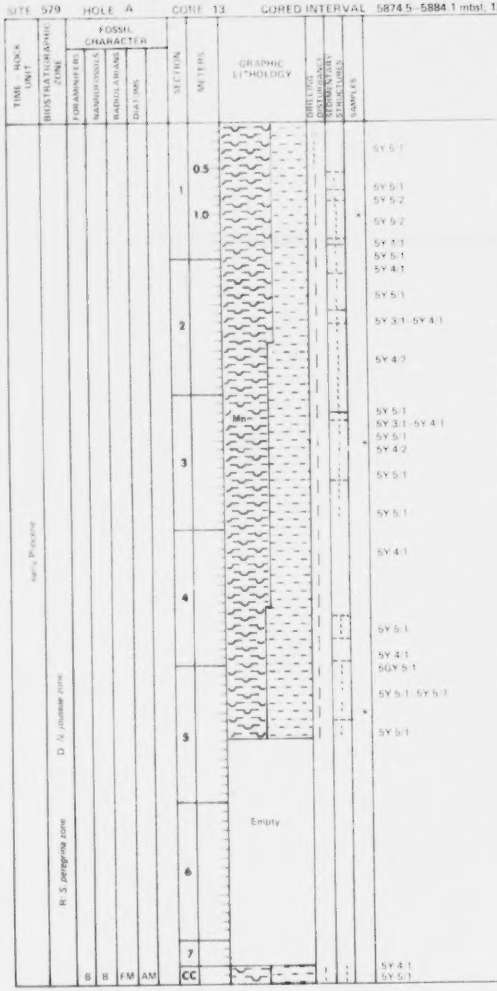
TIME – ROCK UNIT
BIOSTRATIGRAPHIC ZONE
FOSSIL CHARACTER
FORAMINIFERS
NANNOFOSSILS
RADIOLARIANS
DIATOMS
SECTION
METERS
GRAPHIC LITHOLOGY
DRILLING DISTURBANCE
SEDIMENTARY STRUCTURES
SAMPLES
early Pliocene
D: N. jouseae zone
R: S. peregrina zone
B
B
FM
AM
1
2
3
4
5
6
7
CC
0.5
1.0
Mn
Empty
5Y 5/1
5Y 5/1
5Y 5/2
5Y 5/2
5Y 4/1
5Y 5/1
5Y 4/1
5Y 5/1
5Y 3/1–5Y 4/1
5Y 4/2
5Y 5/1
5Y 3/1–5Y 4/1
5Y 5/1
5Y 4/2
5Y 5/1
5Y 5/1
5Y 4/1
5Y 5/1
5Y 4/1
5GY 5/1
5Y 5/1–5Y 5/2
5Y 5/1
5Y 4/1
5Y 5/1

LITHOLOGIC DESCRIPTION

CLAYEY DIATOM OOZE

*Dominant colors: dark gray (5Y 4/1), gray (5Y 5/1), olive gray (5Y 4/2–5Y 5/2) with layers of very dark gray (5Y 3/1) and greenish gray (5GY 5/1). Minor colors: dark greenish gray (5G 4/1) and greenish gray (5GY 5/1) laminations.

*Section 1, 0–54 cm is soupy to very deformed. Rest of the core is slightly deformed by drilling.

*This core consists of lightly mottled clayey diatom ooze with thin (0.5–1.0 cm) greenish gray laminations and zones. There is a manganese(?) nodule at 3, 24–25 cm.

SMEAR SLIDE SUMMARY (%):

	1, 100 D	3, 50 D	5, 50 D
Texture:			
Sand	20	15	10
Silt	50	50	50
Clay	30	35	40
Composition:			
Quartz	10	10	10
Feldspar	2	3	2
Clay	22	30	30
Volcanic glass	3	2	3
Diatoms	60	50	50
Radiolarians	3	5	2
Silicoflagellates			3

SITE 579 HOLE A CORE 14 CORED INTERVAL 5884.1–5893.6 mbsl; 137.5–147.0 mbsf

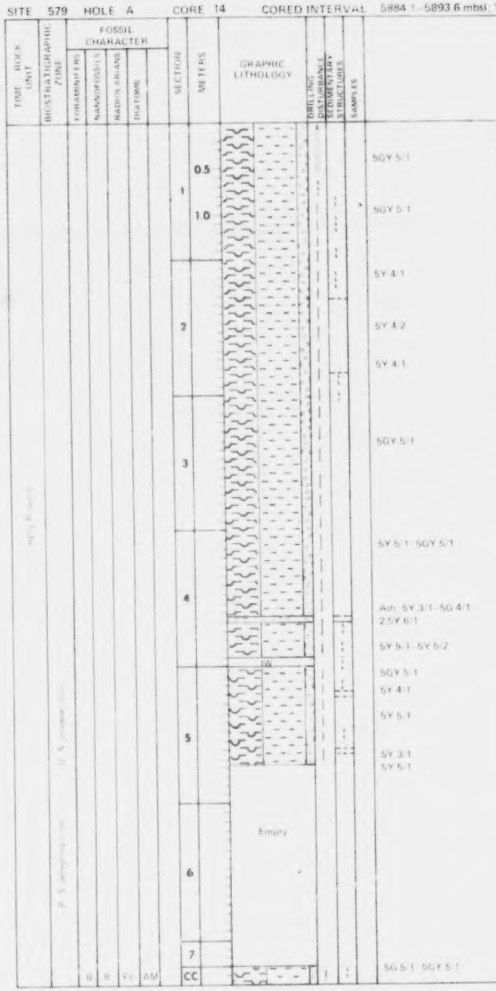
TIME – ROCK UNIT
BIOSTRATIGRAPHIC ZONE
FOSSIL CHARACTER
FORAMINIFERS
NANNOFOSSILS
RADIOLARIANS
DIATOMS
SECTION
METERS
GRAPHIC LITHOLOGY
DRILLING DISTURBANCE
SEDIMENTARY STRUCTURES
SAMPLES
early Pliocene
D: N. jouseae zone
R: S. peregrina zone
B
B
FM
AM
1
2
3
4
5
6
7
CC
0.5
1.0
IW
Empty
5GY 5/1
5GY 5/1
5Y 4/1
5Y 4/2
5Y 4/1
5GY 5/1
5Y 5/1–5GY 5/1
Ash: 5Y 3/1–5G 4/1–2.5Y 6/1
5Y 5/1–5Y 5/2
5GY 5/1
5Y 4/1
5Y 5/1
5Y 3/1
5Y 6/1
5G 5/1–5GY 5/1

LITHOLOGIC DESCRIPTION

CLAYEY DIATOM OOZE

*Dominant colors: greenish gray (5GY 5/1), dark gray (5Y 4/1), gray (5Y 5/1), and olive gray (5Y 4/2–5Y 5/2). Minor colors: dark greenish gray (5G 4/1) and very dark gray to dark gray (5Y 3/1–5Y 4/1) laminations and zones. Ash layer is gray (5Y 5/1) grading to dark greenish gray (5G 4/1) grading to gray (2.5Y 6/1) to light gray.

*Section 1, 0–75 cm is soupy to very deformed; vertically deformed flow structures indicate that it is likely flow-in. The rest of the core is slightly deformed by drilling.

*This core consists of homogeneous to lightly mottled clayey diatom ooze with commun dark gray and greenish gray, thin (0.5–1.0 cm) laminations. An ash layer occurs at 4, 94–100 cm.

SMEAR SLIDE SUMMARY (%):

	1, 94 D
Texture:	
Sand	15
Silt	50
Clay	35
Composition:	
Quartz	10
Feldspar	3
Clay	31
Volcanic glass	10
Diatoms	40
Radiolarians	3
Silicoflagellates	3

SITE 579 HOLE A CORE 15 CORED INTERVAL 5893.6–5896.1 mbsl; 147.0–149.5 mbsf

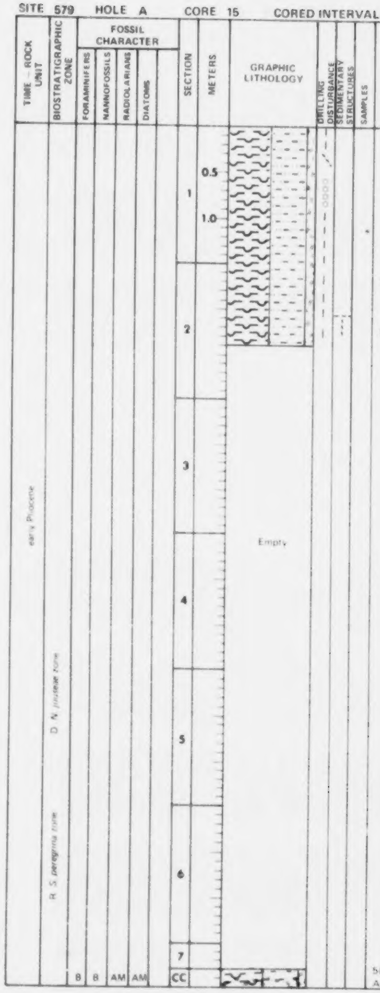
TIME – ROCK UNIT
BIOSTRATIGRAPHIC ZONE
FOSSIL CHARACTER
FORAMINIFERS
NANNOFOSSILS
RADIOLARIANS
DIATOMS
SECTION
METERS
GRAPHIC LITHOLOGY
DRILLING DISTURBANCE
SEDIMENTARY STRUCTURES
SAMPLES
early Pliocene
D. N. jouseae zone
R. S. peregrina zone
B
B
AM
AM
1
2
3
4
5
6
7
CC
0.5
1.0
Empty
5GY 5/1
5GY 5/1
5Y 4/1
5GY 4/1
Ash 5Y 6/1

LITHOLOGIC DESCRIPTION

CLAYEY DIATOM OOZE

*Dominant colors: greenish gray (5GY 5/1), dark greenish gray (5GY 4/1), and dark gray (5Y 4/1). Minor colors: dark greenish gray (5G 4/1) zones and laminations in Section 2, 60–88 cm. Ash in the Core Catcher is gray (5Y 6/1) to light gray.

*Section 1, 0–71 cm is soupy to very deformed. The rest of the core is slightly deformed by drilling.

*This core consists of clayey diatom ooze. The greenish gray portions of Section 1 and Section 2, 0–60 cm are homogeneous. The dark gray portion at 2, 60–88 cm is mottled and contains greenish gray laminations. An ash layer occurs in the Core Catcher at 46–49 cm.

SMEAR SLIDE SUMMARY (%)

	1, 110
	D
Texture:	
Sand	10
Silt	50
Clay	40
Composition:	
Quartz	7
Feldspar	3
Clay	27
Volcanic glass	10
Diatoms	45
Radiolarians	5
Silicoflagellates	3

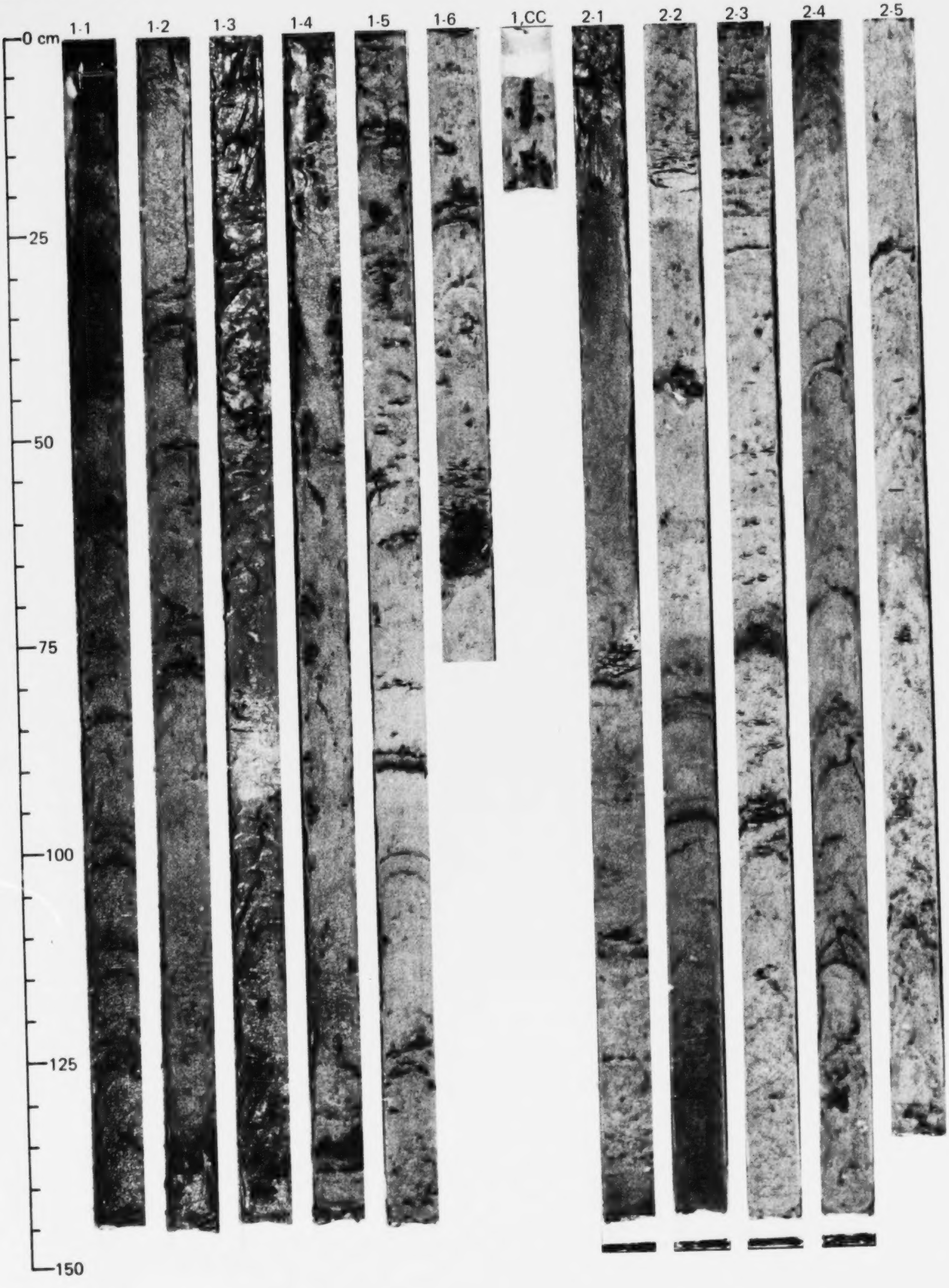
1-1
1-2
1-3
1-4
1-5
1-6
1,CC
2-1
2-2
2-3
2-4
2-5
0 cm
25
50
75
100
125
150

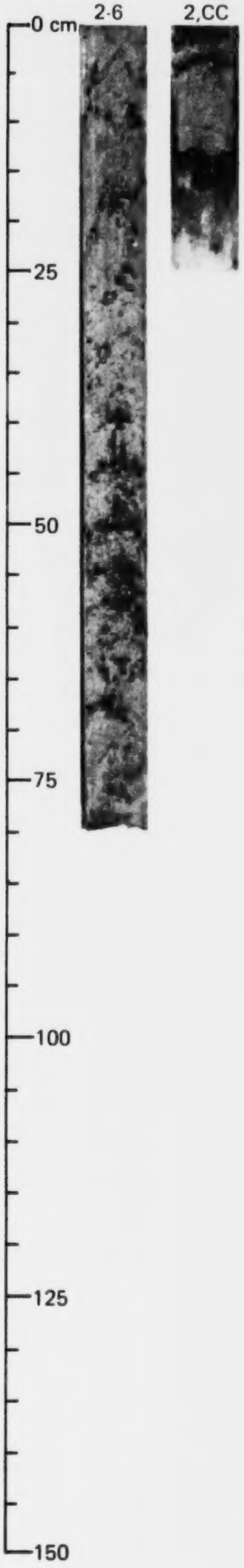
2-6
2,CC
0 cm
25
50
75
100
125
150

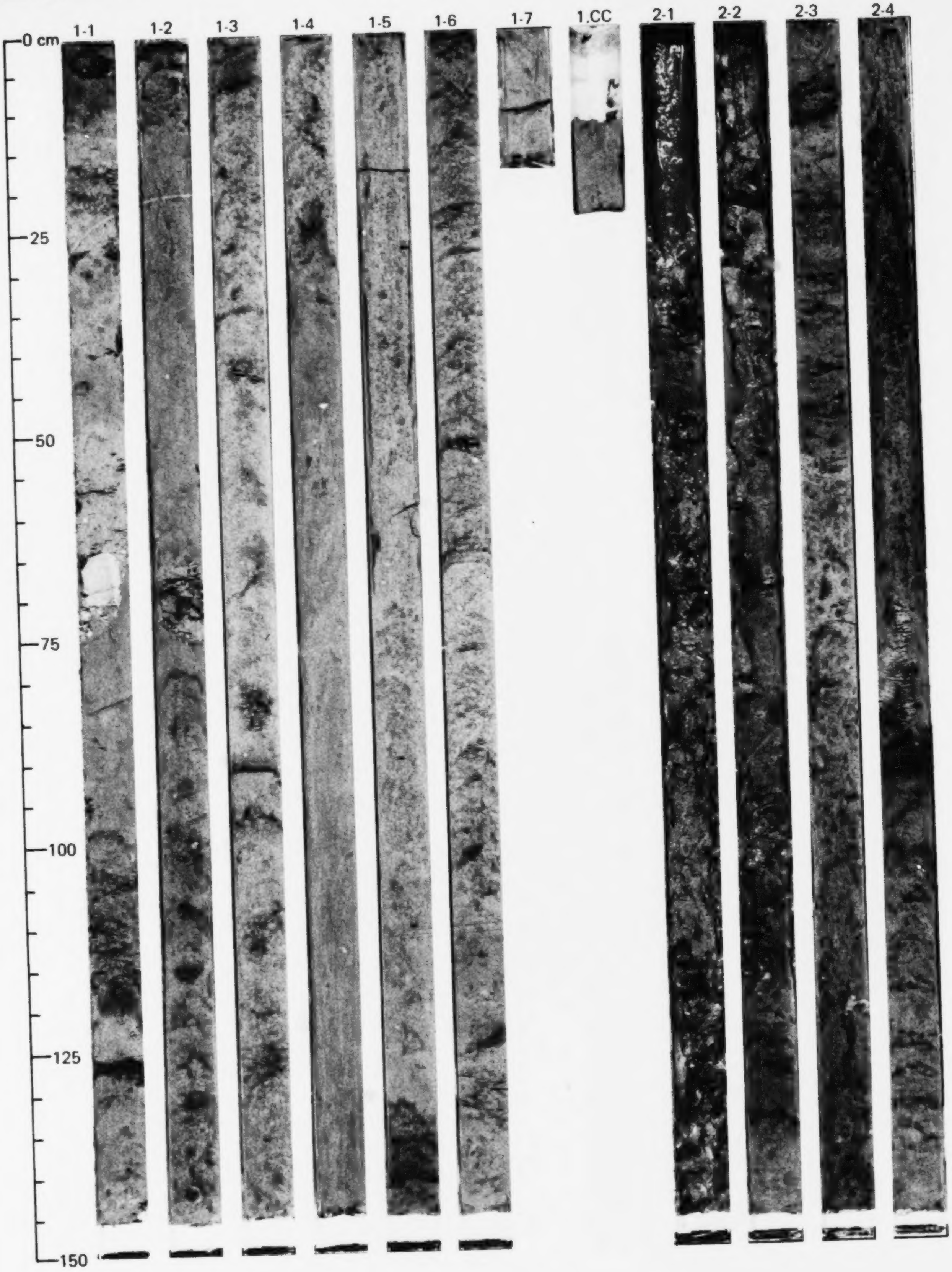
1-1
1-2
1-3
1-4
1-5
1-6
1-7
1.CC
2-1
2-2
2-3
2-4
0 cm
25
50
75
100
125
150

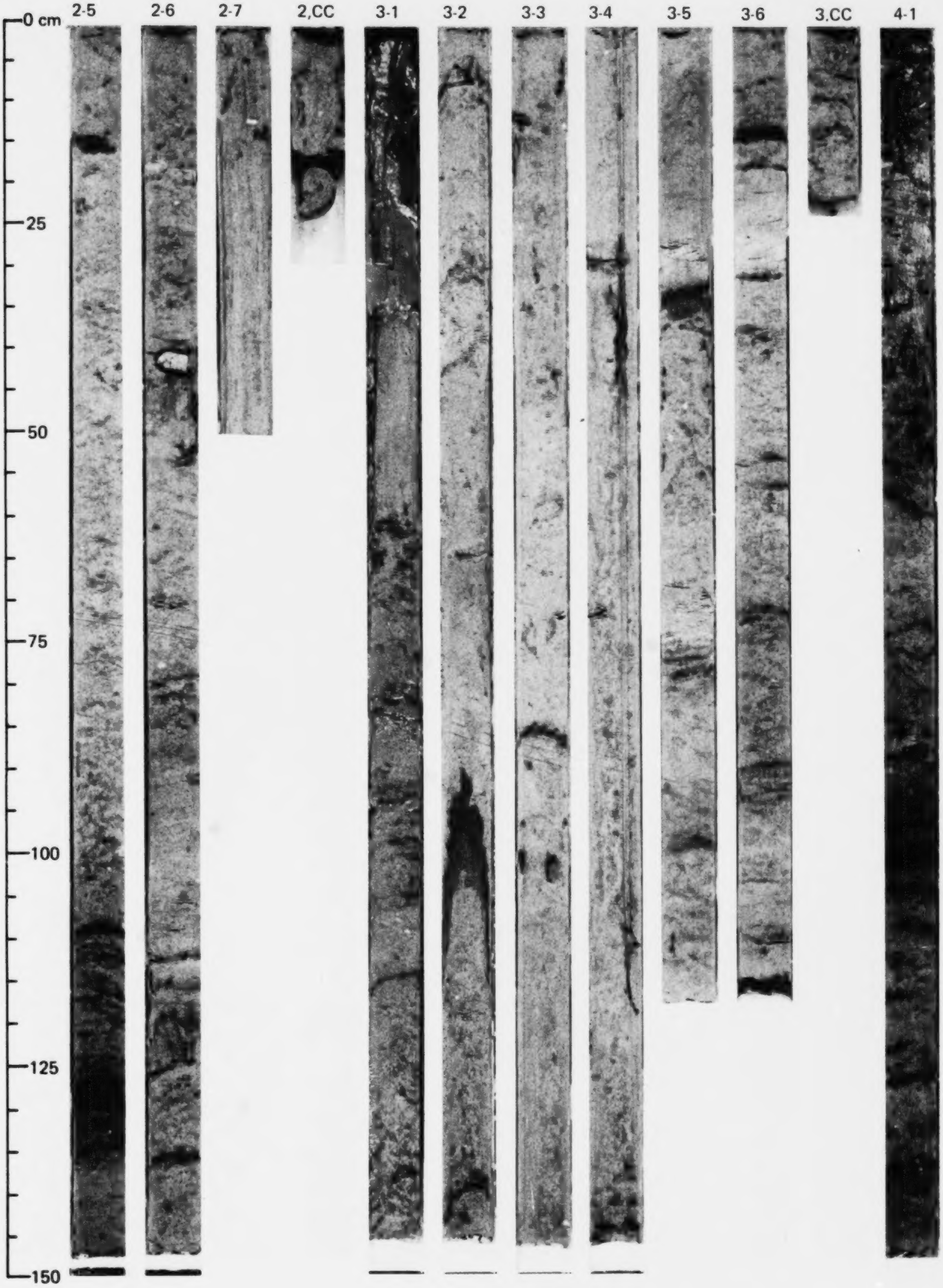
0 cm
25
50
75
100
125
150
2-5
2-6
2-7
2,CC
3-1
3-2
3-3
3-4
3-5
3-6
3,CC
4-1

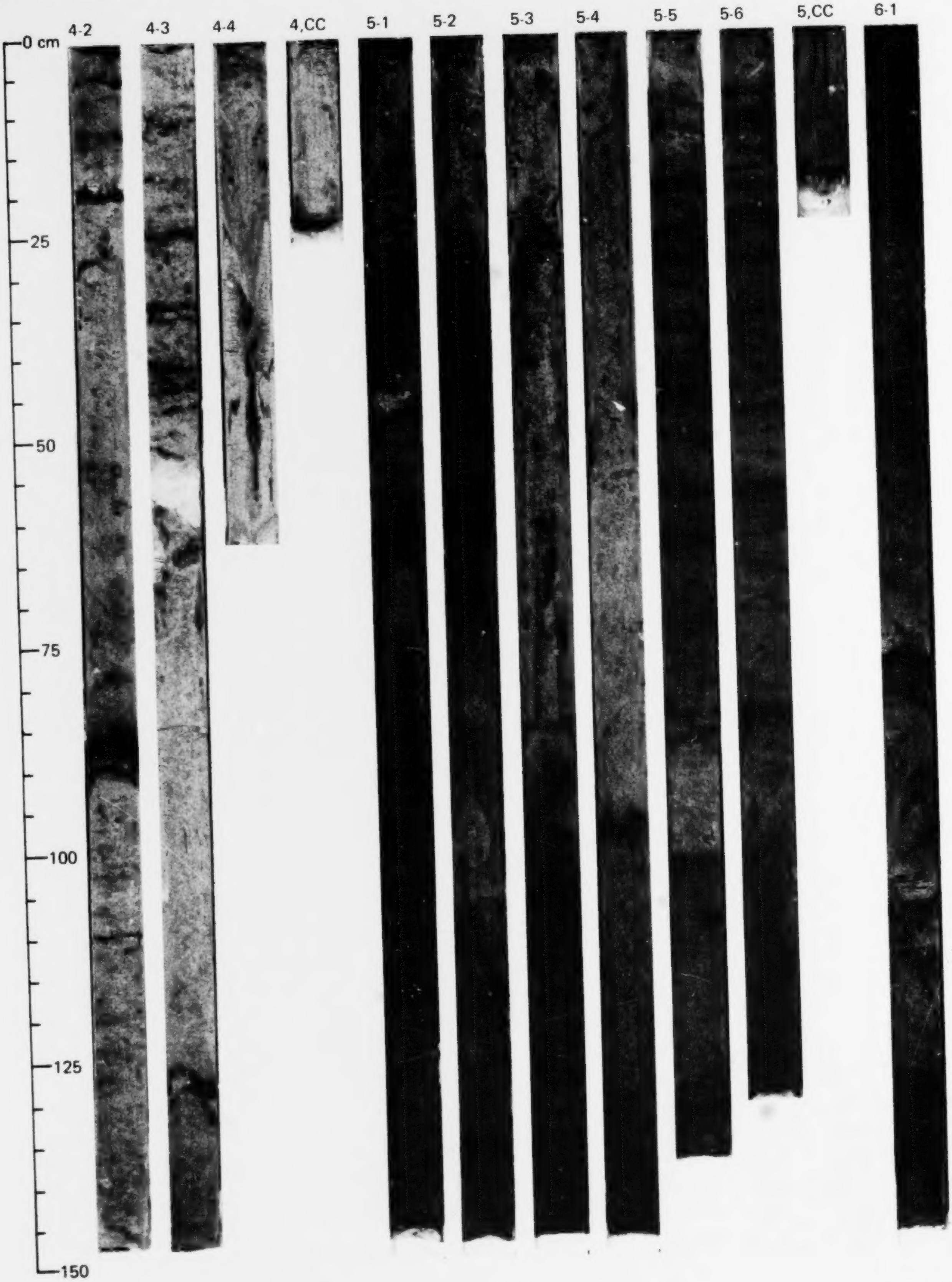
4-2
4-3
4-4
4,CC
5-1
5-2
5-3
5-4
5-5
5-6
5,CC
6-1
0 cm
25
50
75
100
125
150

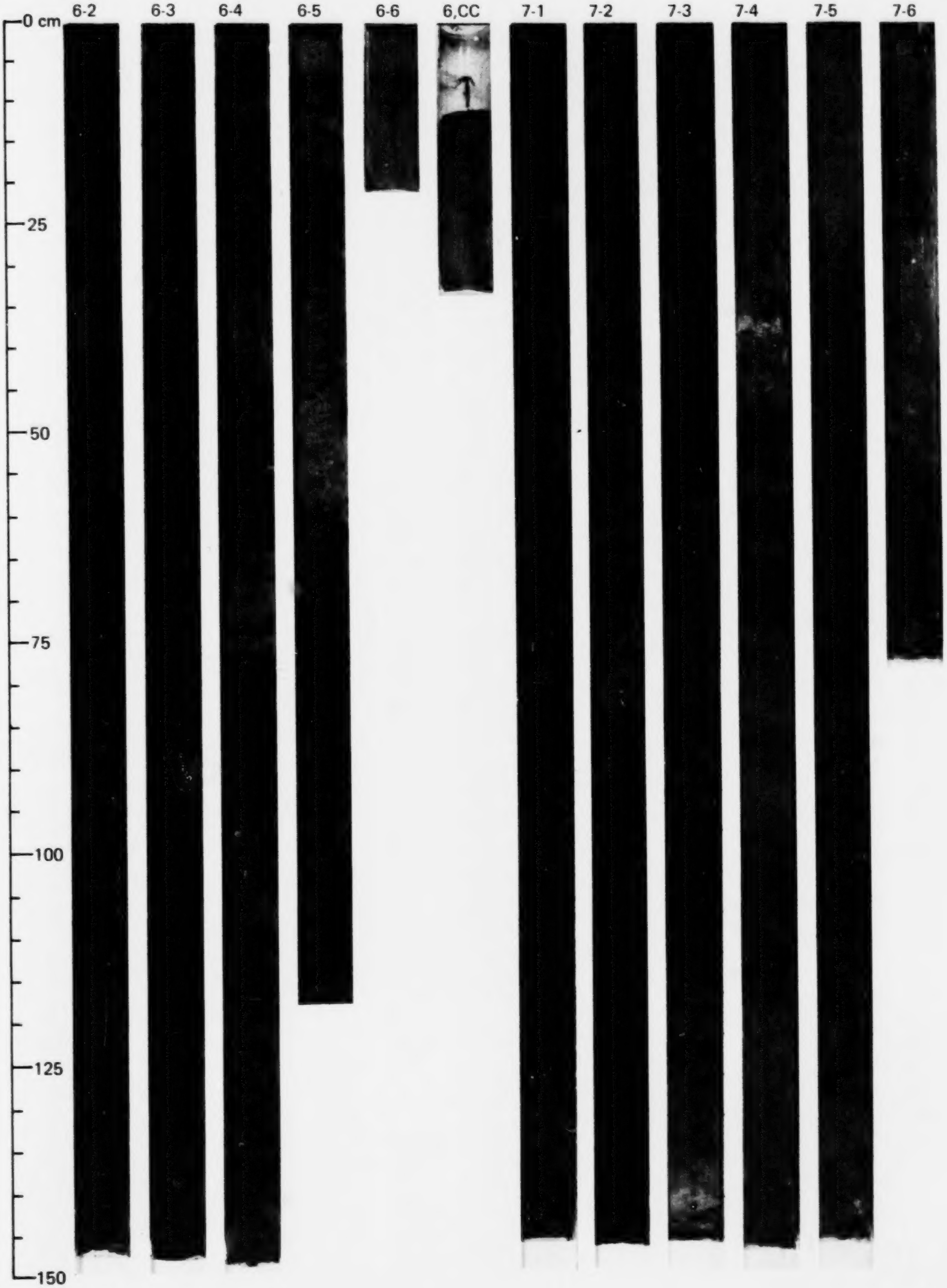
6-2
6-3
6-4
6-5
6-6
6,CC
7-1
7-2
7-3
7-4
7-5
7-6
0 cm
25
50
75
100
125
150

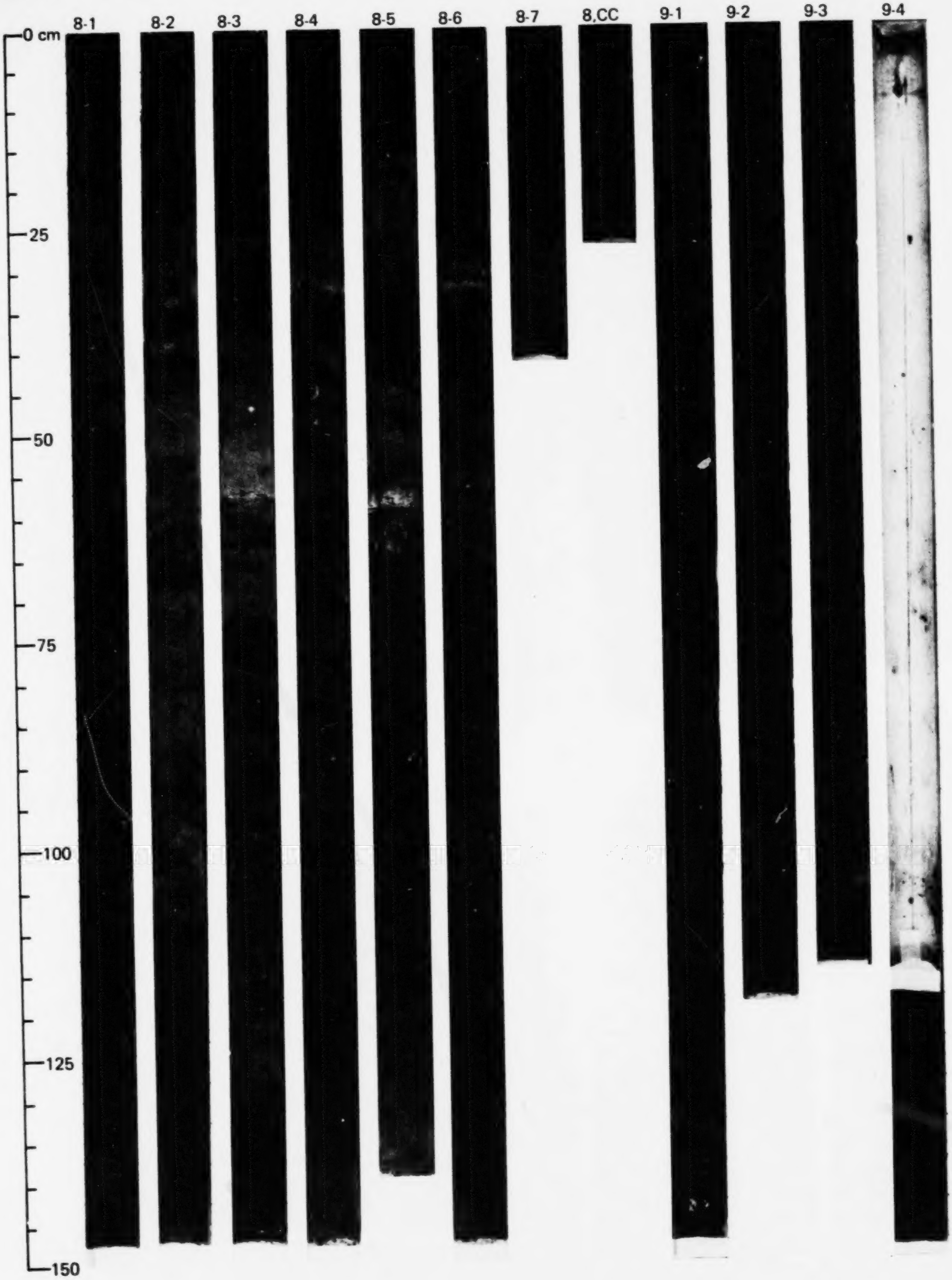
8-1
8-2
8-3
8-4
8-5
8-6
8-7
8,CC
9-1
9-2
9-3
9-4
0 cm
25
50
75
100
125
150

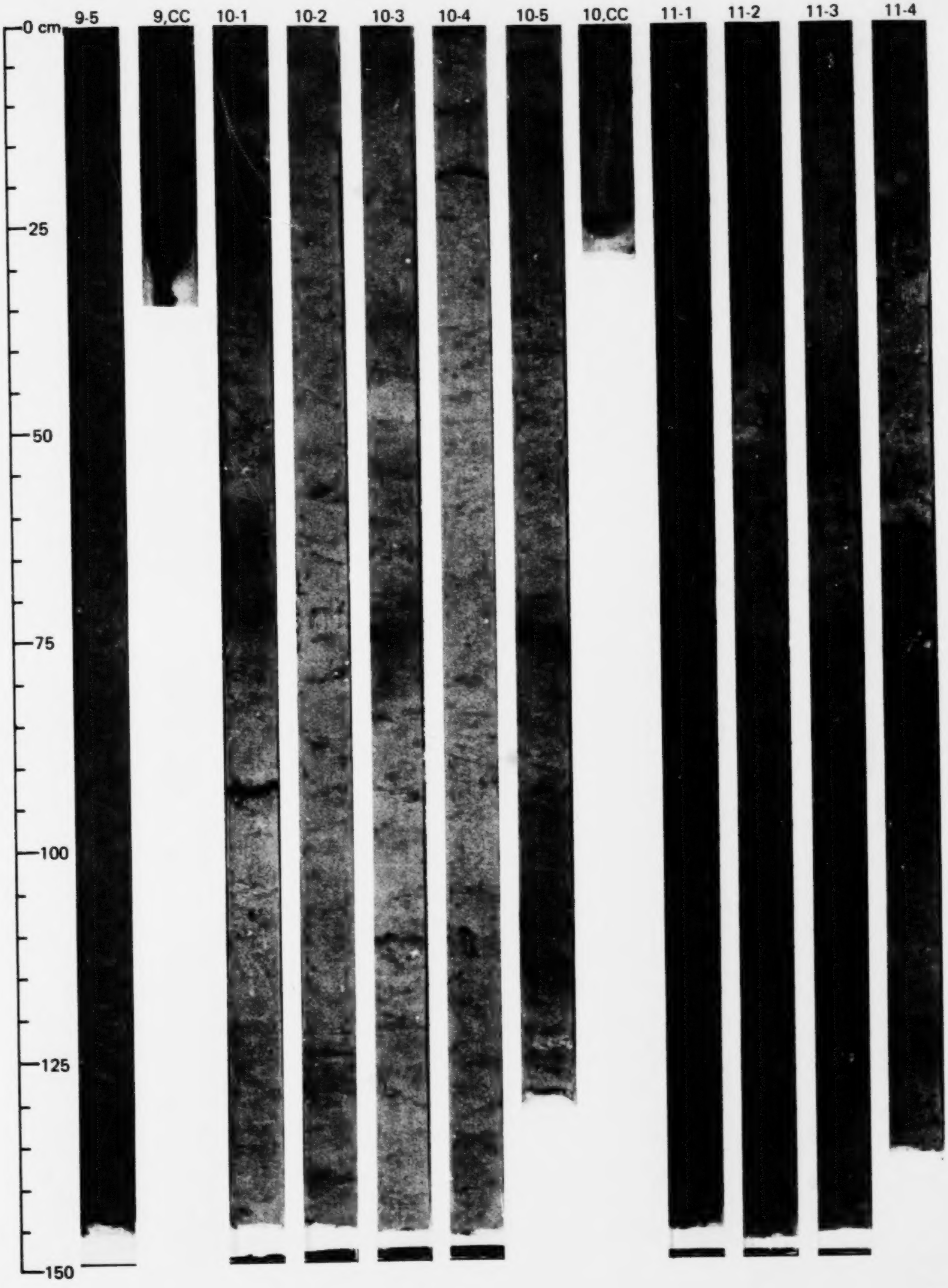
0 cm
25
50
75
100
125
150
9-5
9,CC
10-1
10-2
10-3
10-4
10-5
10,CC
11-1
11-2
11-3
11-4

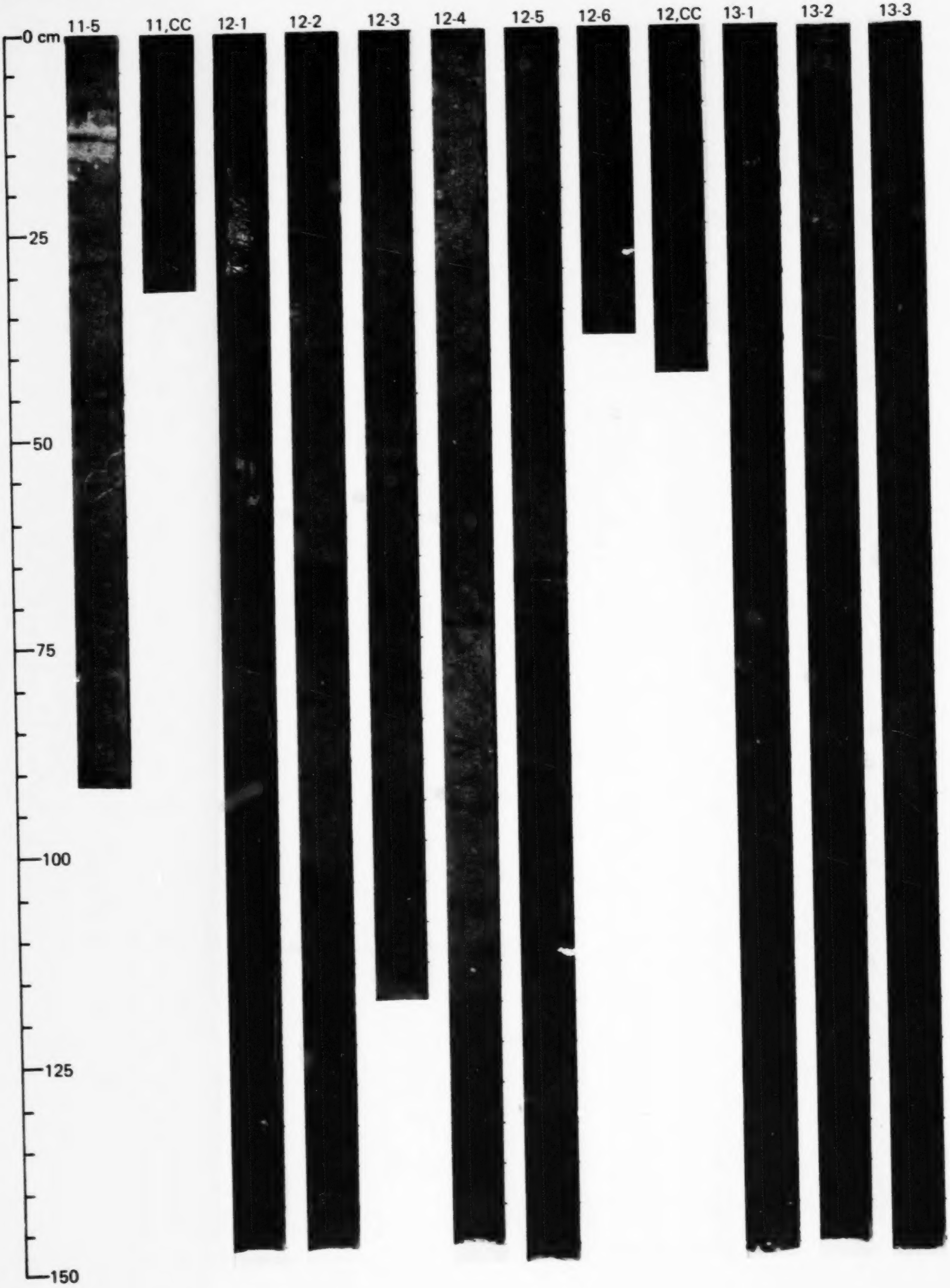
11-5
11,CC
12-1
12-2
12-3
12-4
12-5
12-6
12,CC
13-1
13-2
13-3
0 cm
25
50
75
100
125
150

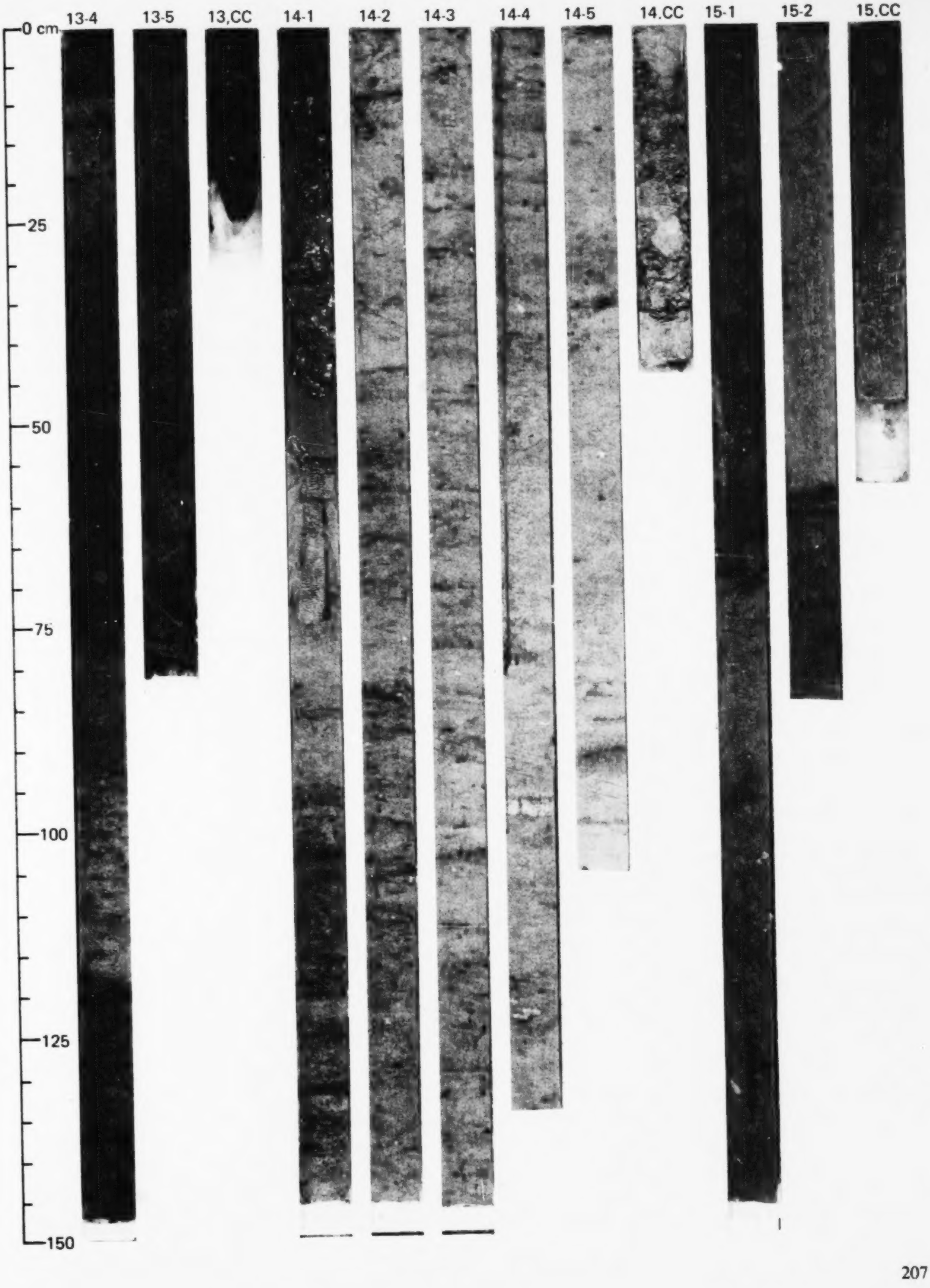
13-4
13-5
13,CC
14-1
14-2
14-3
14-4
14-5
14.CC
15-1
15-2
15.CC
0 cm
25
50
75
100
125
150

7. SITE 580[1]

Shipboard Scientific Party[2]

HOLE 580

Date occupied: 6 June 1982

Date departed: 8 June 1982

Time on hole: 2 days, 3 hr.

Position (latitude; longitude): 41°37.47′N; 153°58.58′E

Water depth (sea level; corrected m, echo-sounding): 5375

Water depth (rig floor; corrected m, echo-sounding): 5385

Bottom felt (m, drill pipe): 5386.7

Penetration (m): 155.3

Number of cores: 17

Total length of cored section (m): 155.3

Total core recovered (m): 140.74

Core recovery (%): 91

Oldest sediment cored:
Depth sub-bottom (m): 155.3
Nature: siliceous clay
Age: late Pliocene
Measured velocity (km/s): 1.5

Basement: Not reached

Principal results: A thick sequence of Pleistocene and late Pliocene sediments was recovered at Site 580. Siliceous microfossils (diatoms and radiolarians) are generally abundant and moderately to well preserved. An excellent magnetic reversal record can be identified back to the middle of the Gauss Normal Epoch.

One hundred and fifty-five meters of sediment were penetrated. Except for the numerous ash layers and indurated darkish green layers, these sediments are a remarkably uniform gray, olive gray, and dark gray color. Based on these data, the entire sedimentary sequence recovered at Site 580 is placed in one lithologic unit. However, based on changes in biosiliceous components and clay-sized carbonate, five subunits are recognized.

The upper subunit (Subunit IA) extends from 0 to 60.3 m sub-bottom and is predominantly a siliceous clay. Underlying this (Subunit IB) and extending from 60.3 to 79.3 m sub-bottom is a calcareous siliceous clay, characterized by up to 25% clay-sized carbonate material. Subunit IC (79.3–117.3 m sub-bottom) is similar lithologically to Subunit IA. Subunit ID (117.3–136.3 m sub-bottom) is a clayey diatom ooze, characterized by up to 60% diatoms. The lowest subunit (Subunit IE), extending from 136.3 to 155.3 m sub-bottom, is similar to Subunit IA.

Sedimentation rates are unusually high for the Pleistocene and late Pliocene, averaging 50 m/m.y. No unconformities or abrupt changes in sedimentation rate were encountered.

The heat-flow program operated normally. The temperature data clearly show a linear increase with depth. No temperature reversals were recorded.

BACKGROUND AND OBJECTIVES

Site 580 (target Site NW-5A) lies near the present-day subarctic front (42°N) and the northern margin of the transition zone between the subarctic and subtropical gyres. The transition zone defines the convergence of the Kuroshio and Oyashio currents and is marked by high biological productivity. Because of its location, this site will be the reference point for the modern subarctic/subtropical gyre boundary. This site is thought to be the northernmost limit of the subarctic front during the late Neogene and Quaternary.

Our specific scientific objectives were

1. To obtain a detailed paleoceanographic record in the subtropical/subarctic gyre transition zone for the late Miocene to Recent and, in particular, to document the north–south migration of the frontal zone with time.
2. To determine a midlatitude stratigraphy using paleomagnetics, tephrachronology, and biostratigraphy (chiefly siliceous).
3. To determine the time of onset of significant biosiliceous accumulation for comparison with the more southerly Sites 578 and 579.
4. To determine the timing and nature of the onset of the mid-Pliocene and Pleistocene climatic deterioration.
5. To assess the role of orbital forcing in determining pre-Pleistocene paleoclimatic oscillations.
6. To assess the nature and history of authigenic sedimentation in pre-biosiliceous (older than mid-Miocene) sediments.
7. To determine the Cenozoic history of eolian sedimentation for comparison with sites to the south and east.

OPERATIONS

From Site 579, we steamed northward for approximately 1 day, toward Site 580 (target Site NW-5A). Good quality 3.5- and 12-kHz records were collected while underway. The vessel entered the region of NW-5A at approximately 1400 hr. local time (0300Z). Because of the hummocky nature of the bottom topography and because of uncertainties concerning the nature of the topography at the target site, the core site was selected some 6 miles short of our target where our air-gun records indicated a reasonably smooth bottom. The beacon was dropped at 1436 local time (0336Z) and gear was retrieved as the vessel passed over the site. At 1630 hr. (0530Z) drill pipe run-in began but was halted at 2130 hr. (1030Z) when the drawworks shorted out. Troubleshooting indicated a problem with a faulty brush holder, which was replaced by 2400 hr. (1300Z). Running in hole continued until 1104 hr. (0004Z), when the corer reached bottom and spudding was attempted. This proved unsuccessful, as the first core recovered only water, and a second attempt was made. This was successful and the first core was recovered shortly thereafter. Following these initial mishaps, the station was occupied without any further problems. Unusually calm seas insured almost complete recovery and relatively little sediment disturbance. The heat-flow shoe was run seven times, all successful. Unfortunately, a combination heat-flow shoe–heat-flow probe–pore water–pressure measurement test failed when a tubing connector on line to the lower pressure port leaked while running in hole. The system was flooded.

---

[1] Heath, G. R., Burckle, L. H., et al., *Init. Repts. DSDP*, 86: Washington (U.S. Govt. Printing Office).

[2] Addresses: G. Ross Heath (Co-Chief Scientist) School of Oceanography, Oregon State University, Corvallis, OR 97331 (present address: College of Ocean and Fishery Sciences, University of Washington, Seattle, WA 98195); Lloyd H. Burckle (Co-Chief Scientist) Lamont-Doherty Geological Observatory, Palisades, NY 10964; Anthony E. D'Agostino, ARCO Exploration Company, Houston, TX 77056; Ulrich Bleil, Institut für Geophysik, Ruhr-Universität Bochum, D-4630 Bochum Querenburg, Federal Republic of Germany; Ki-iti Horai, Lamont-Doherty Geological Observatory, Palisades, NY 10964 (present address: Meteorological College, Chiba University, Chiba 277, Japan); Robert D. Jacobi, Department of Geological Sciences, SUNY Buffalo, Amherst, NY 14226; Tom Janecek, Department of Atmospheric & Oceanic Science, University of Michigan, Ann Arbor, MI 48109 (present address: Lamont-Doherty Geological Observatory, Palisades, NY 10964); Itaru Koizumi, College of General Education, Osaka University, Osaka 560, Japan; Lawrence A. Krissek, School of Oceanography, Oregon State University, Corvallis, OR 97331 (present address: Department of Geology and Mineralogy, Ohio State University, Columbus, OH 43210); Nicole Lenôtre, Bureau de Recherches Géologiques et Minières, Centre Océanologique de Bretagne, 45060 Orléans Cedex, France; Simonetta Monechi, Geological Research Division, Scripps Institution of Oceanography, La Jolla, CA 92093 (present address: Dipartimento di Scienze della Terra, Università di Firenze, 4 Via La Pira, 50121 Firenze, Italy); Joseph J. Morley, Lamont-Doherty Geological Observatory, Palisades, NY 10964; Peter Schultheiss, Institute of Oceanographic Sciences, Surrey GU8 5UB, United Kingdom; Audrey A. Wright, Deep Sea Drilling Project, Scripps Institution of Oceanography, La Jolla, CA 92093 (present address: Ocean Drilling Program, 500 University Drive West, Texas A&M University, College Station, TX 77843).

A total depth of 155.3 m was reached in one hole at this site. Seventeen cores were recovered, most with full, or close to full, penetration (Table 1).

We departed the site at 0700Z, 7 May, steaming north toward Site 581 (target Site MSS-82C).

LITHOSTRATIGRAPHY

The lithostratigraphy of sediments recovered at Site 580 is based on macroscopic descriptions of the cores and on smear slide analyses with a petrographic microscope. The sediments cored at Site 580 are similar to those cored at Site 579.

The sediments recovered at Site 580 are relatively uniform in color, ranging from gray (5Y 5/1) and dark gray (5Y 4/1) to olive gray (5Y 4/2–5Y 5/2). Smear slide analyses indicate that downhole abundances of siliceous microfossils range from 10 to 70%, averaging about 30%. Quartz abundances average 5%, but range up to 15%. A large number of thin, stiff to indurated, dark greenish gray (5GY 4/1 or 5G 4/1) layers are observed throughout the hole. Smear slide analyses of these layers indicates that they are composed of the same material as the adjacent sediment. Dark gray to black (5Y 3/1, 5Y 3/2, and 5Y 2/1) layers of clay are commonly found immediately below the indurated greenish-gray layers. Volcanic ash layers are common throughout the hole. A total of 89 volcanic ash layers, ranging in thickness from 0.5 to 18.5 cm, were identified (Fig. 1).

Table 1. Site 580 coring summary.

Core	Date (June 1982)	Local time	Depth from drill floor (m)	Depth below seafloor (m)	Length cored (m)	Length recovered (m)	Percent recovered
1	6	1428	5386.7–5390.0	0.0–3.3	3.3	3.32	101
2	6	1639	5390.0–5399.5	3.3–12.8	9.5	8.39	88
3	6	1855	5399.5–5409.0	12.8–22.3	9.5	8.62	91
4	6	2105	5409.0–5418.5	22.3–31.8	9.5	8.88	93
5	6	2334	5418.5–5428.0	31.8–41.3	9.5	9.14	96
6	7	0204	5428.0–5437.5	41.3–50.8	9.5	8.80	93
7	7	0440	5437.5–5447.0	50.8–60.3	9.5	7.74	81
8	7	0720	5447.0–5456.5	60.3–69.8	9.5	9.27	98
9	7	0945	5456.5–5466.0	69.8–79.3	9.5	7.51	79
10	7	1200	5466.0–5475.5	79.3–88.8	9.5	8.65	91
11	7	1425	5475.5–5485.0	88.8–98.3	9.5	7.30	77
12	7	1640	5485.0–5494.5	98.3–107.8	9.5	9.29	98
13	7	1850	5494.5–5504.0	107.8–117.3	9.5	9.08	96
14	7	2117	5504.0–5513.5	117.3–126.8	9.5	9.14	96
15	8	0330	5513.5–5523.0	126.8–136.3	9.5	8.45	89
16	8	0620	5523.0–5532.5	136.3–145.8	9.5	8.97	94
17	8	0902	5532.5–5542.0	145.8–155.3	9.5	7.72	81
					155.3 (total)	140.74 (total)	91 (avg.)

Unit I: Siliceous Clay

On the basis of these data, the sedimentary section recovered at Site 580 is classified as a single siliceous clay unit (lithologic Unit I). However, this siliceous clay unit can be subdivided into five subunits (Fig. 1, Table 2).

Subunit IA

This subunit occurs in Cores 1 through 7 and is a siliceous clay containing 2–25% diatoms, 0–15% radiolarians, and 3–15% quartz, with an average composition of approximately 20% diatoms, 10% radiolarians, and 7% quartz. Feldspar and heavy minerals are present in abundances of less than 2%. Volcanic glass contents outside of recognizable ash layers range from 2 to 10%, but are generally greater than 5%. The remainder of the sediment, averaging approximately 56%, is clay material. This subunit contains 43 identifiable ash layers.

Subunit IB

This subunit occurs in Cores 8 and 9, and is a calcareous siliceous clay characterized by 3–25% unspecified clay-sized carbonate material, 10–25% diatoms, 5–7% radiolarians, and 5–10% quartz. Average composition is approximately 10–15% carbonate, 17% diatoms, 6% radiolarians, and 7% quartz. Feldspar abundances are less than 2%, and dispersed ash contents range from 3 to 7%. The remainder of the sediment, averaging approximately 55%, is clay. This subunit contains seven identifiable ash layers.

Subunit IC

This subunit occurs in Cores 10 through 13, and is a siliceous clay similar to Subunit IA. Maximum diatom abundance in Subunit IC is 35%, slightly greater than in Subunit IA, but the approximate average composition of Subunit IC (20% diatoms, 7% radiolarians, 6% quartz) is very similar to that of Subunit IA. Eighteen recognizable ash layers occur in this subunit.

Subunit ID

This subunit occurs in Cores 14 and 15 and is a clayey diatom ooze containing 50–60% diatoms, 2–10% radiolarians, and 5–10% quartz. Average composition of this interval is approximately 52% diatoms, 6% radiolarians, and 7% quartz. Feldspar abundances are a constant 2% throughout this subunit, and dispersed volcanic ash abundances range from 5 to 10%. The remainder of the sediment, averaging approximately 27%, is clay. This subunit contains seven ash layers.

Subunit IE

This subunit occurs in Cores 16 and 17 and is another siliceous clay subunit. It is slightly enriched in siliceous microfossils relative to Subunits IA and IC, with an av-

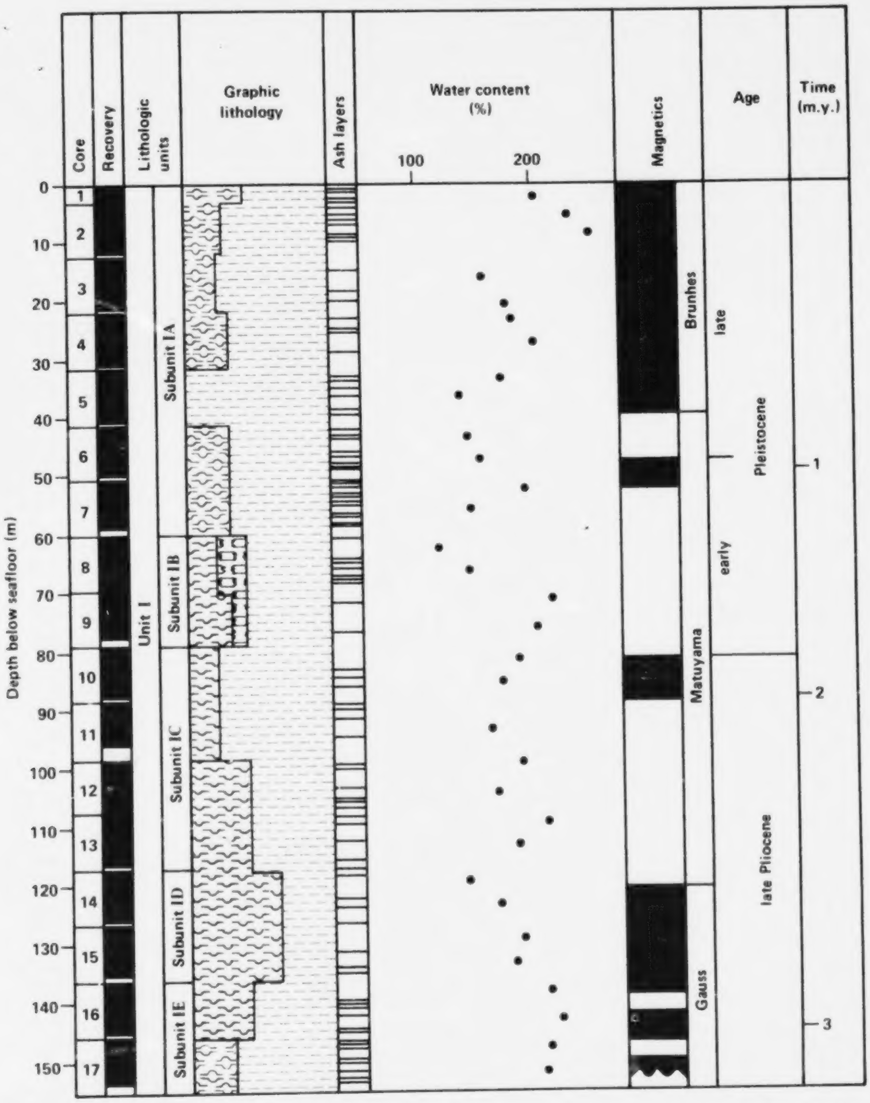

Figure 1. Site summary diagram showing Site 580 core numbers, core recovery, lithologic units, graphic lithology, ash layer locations, water content (%), magnetostratigraphy, and age. Symbols used in graphic lithology column are defined in Introduction and Explanatory Notes (this volume).

Table 2. Site 580 lithostratigraphic units.

Lithologic unit	Cored interval	Sub-bottom depth (m)
I: Siliceous clay		
Subunit IA: siliceous clay	1-1, 0 cm to 7,CC	0.0-60.3
Subunit IB: calcareous siliceous clay	8-1, 0 cm to 9,CC	60.3-79.3
Subunit IC: siliceous clay	10-1, 0 cm to 13,CC	79.3-117.3
Subunit ID: clayey diatom ooze	14-1, 0 cm to 15,CC	117.3-136.3
Subunit IE: siliceous clay	16-1, 0 cm to 17,CC	136.3-155.3

erage composition of approximately 27% diatoms and 8% radiolarians. Feldspar is rare to absent, quartz averages 7%, and dispersed volcanic glass abundances range from 2 to 10%, averaging approximately 5%. The remainder of the sediment, averaging approximately 53%, is clay. This subunit contains 14 recognizable ash layers.

SEISMIC CORRELATION

High-resolution seismic reflection profiles (3.5 and 12 kHz) and 100-Hz reflection profiles were recorded at Site 580. Only a hull-mounted 3.5-kHz sound source was utilized. The 3.5-kHz echograms over Site 580 reveal a fairly uniform seismic section of parallel sub-bottom reflectors (Fig. 2). This seismic section can be divided into a four-part sequence based on gaps in the reflector sequence and relative strength of the return signals (Table 3).

The uppermost seismic unit consists of three strong reflectors and extends to 0.0166 s below the seafloor

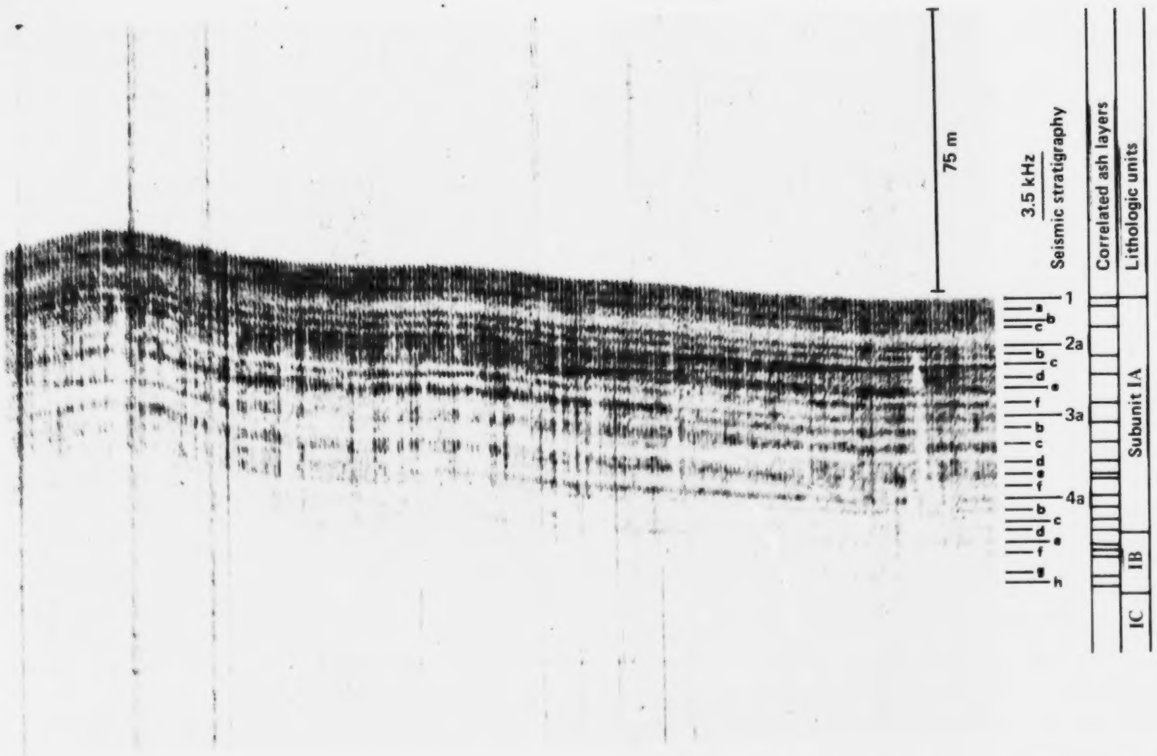

Figure 2. 3.5-kHz echogram near Site 580 showing the four-part seismic sequence described in the text. Sub-bottom depths and sources of seismic reflectors are given in Table 3.

Table 3. 3.5-kHz seismic correlations, Site 580.

			Sub-bottom depth (m)			Source		
Reflector	Relative strength[a]	Sub-bottom depth (s)	1440 m/s	1480 m/s	1504 m/s	Depth (m)	Lithology	Thickness (cm)
1a	S	0.00269	1.94	1.99	2.02	2.25	Ash 2	10.5
b	S	0.00662	4.76	4.90	4.98			
c	S	0.0108	7.78	7.96	8.12	7.7	Ash 8	15
2a	S	0.0166	11.95	12.24	12.48		No core	
b	S	0.0200	14.4	14.77	15.04	15.34	Ash 11,12	6,6
c	S	0.0228	16.42	16.836	17.15			
d	S	0.0269	19.39	19.90	20.23	19.8	Ash 16	2
e	S	0.0310	22.32	22.96	23.3	24.6	Ash 18?	6
f	S	0.0362	26.06	26.78	27.22	27.8	Ash 19?	6
3a	I	0.0413	29.74	30.53	31.06			
b	I	0.0447	32.18	33.06	33.61	32.8	Ash 20	8
c	I	0.0506	36.43	37.42	38.05			
d	IT-I	0.0568	40.90	42.01	42.71	42.75	Ash 27	14
						42.8	Ash 28	9
e	W-I	0.0612	44.06	45.30	46.02	45.45	Ash 32?	5
						46.4	Ash 33?	16
f	W	0.0642	46.22	47.52	48.28	47.25	Ash 35	5
4a	W-I	0.0685	49.32	50.66	51.51	51.6	Ash 37	11
b	IT-I	0.0724-0.0732	52.13-52.70	53.57-54.18	54.44-55.05	54.3	Ash 42	13
c	IT	0.0765	55.08	56.63	57.53	57.7	Ash 46	3
d	IT-W	0.0796-0.0807	57.31-58.10	58.92-59.69	59.86-60.69	60.4	Ash 49	6
e	IT-W	0.0839-0.0848	60.41-61.06	62.06-62.75	63.09-63.77	64.0	Ash 50	6
f	IT-W	0.0888	63.94	65.66	66.78	65.6	Ash 52	13
						67.5	Ash 53?	5
g	IT	0.0954	68.69	70.63	71.74	72.2	Ash 56	11
h	IT	0.0998	71.86	73.88	75.05	75.8	Ash 57	9

[a] S = strong; I = Intermediate; IT = intermittent, but weak; W = weak, but generally continuous.

(12.5 m at 1504 m/s). A thin transparent layer below the deepest reflector in seismic Unit 1 separates that unit from the top of seismic Unit 2. Seismic Unit 2 consists of six strong reflectors and extends to 0.413 s below the seafloor (31.1 m at 1504 m/s). A very thin transparent layer at the base of seismic Unit 2 separates that unit from the top of seismic Unit 3. Seismic Unit 3 consists of six reflectors of variable strengths and extends to 0.0685 s below the seafloor (51.5 m at 1504 m/s). Seismic Unit 4 consists of generally weak and discontinuous reflectors; only the top reflector is of intermediate strength. Unit 4 extends to 0.0998 s below the seafloor (75.0 m at 1504 m/s).

The source of these reflectors was difficult to determine primarily because of the large number of close equally spaced ash layers and indurated clay layers. In general, the reflectors correlate with ash layers, especially below about 45 m sub-bottom depth (Fig. 2, Table 3). However, several strong reflectors in the upper 45 m correlate with sections of core that do not contain ash layers. These strong reflectors could result from interference effects due to the ubiquitous thin, indurated pyritic clay layers. Alternatively, ash layers displaced in the core by unrecognized zones of "flow-in" or ash layers assigned incorrect depths because of inaccurate depth to the top of the core could account for the reflectors. The top of lithostratigraphic Subunit IB (60.3 m sub-bottom) is near Reflector 4d (~59.8–60.7 m, Table 3).

The 100-Hz seismic reflection profiles reveal a four-part seismic section at Site 580 (Fig. 3). The uppermost seismic unit (Unit 1) extends to 0.295 s below the seafloor (221 m at 1500 m/s) and consists of four subunits. The uppermost seismic subunit (1a) is composed of strong, parallel, and continuous reflectors. Subunit 1a extends to 0.01 s below the seafloor (75 m at 1500 m/s), corresponds with the entire 3.5-kHz seismic section (Fig. 2, seismic Units 1, 2, 3, and 4), and correlates with lithostratigraphic Units IA, IB, and perhaps the very top of IC. Seismic Subunit 1b occurs between 0.01 and 0.195 s (146.2 m at 1500 m/s) and is a zone of weak, discontinuous reflectors that wedge out away from the site. It correlates with lithostratigraphic Units IC and ID. Seismic Subunit 1c extends to 0.22 s below the seafloor (165 m at 1500 m/s) and consists of strong, continuous, and parallel reflectors. It may correlate with lithostratigraphic Subunit IE. Seismic Subunit 1d extends to 0.295 s below the seafloor (221.2 m at 1500 m/s) and is a transparent layer.

Seismic Unit 2 is divided into two subunits. Seismic Subunit 2a consists of strong, continuous, parallel reflectors extending to about 0.36 s below the seafloor (270 m at 1500 m/s). Seismic Subunit 2b is a transparent zone extending to 0.50 s below the seafloor (375 m at 1500 m/s).

Seismic Unit 3 consists of strong, slightly incoherent echoes that extend to 0.57 s below the seafloor. Seismic

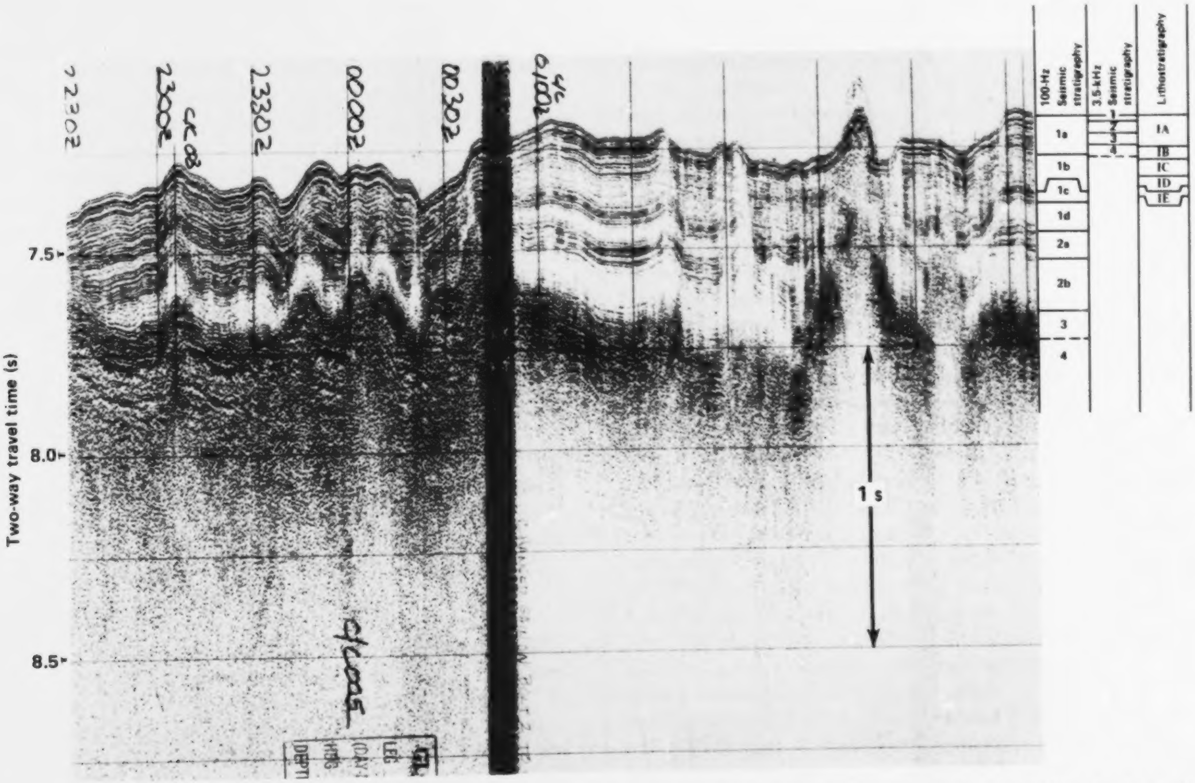

Figure 3. 100-Hz reflection profile over Site 580 showing the four-part seismic sequence described in the text and correlative 3.5-kHz seismic stratigraphic units and lithostratigraphic units.

Unit 3 is conformable with seismic Unit 4 underlying it, but unconformable with the overlying seismic units; both seismic Units 1 and 2 downlap Unit 3 over bathymetric highs. The source of seismic Units 2b and 3 is equivocal but based on the unconformity, the echo character, and the sub-bottom depth, it is probable that seismic Unit 2b is pelagic clay and seismic Unit 3 is Cretaceous chert and associated sedimentary rocks.

Seismic Unit 4 consists of a strong, slightly prolonged reflector and probably is basaltic "basement."

BIOSTRATIGRAPHY

About 155 m of Quaternary and late Pliocene sediments were recovered at Site 580. Abundant, well-preserved diatoms were found in all samples examined. Radiolarians were also common to abundant and well preserved in most sections. Rare to common silicoflagellates were noted in all core-catcher samples. In four core-catcher samples, poorly to moderately preserved foraminifers were recovered. Common, poorly preserved calcareous nannofossils were found in one core-catcher sample (580-13,CC).

The biostratigraphic summary based on three groups of microfossils is shown in Figure 4. The boundary between early and late Pleistocene occurs near the base of Core 6, and the Plio-Pleistocene boundary falls near the top of Core 11 based on the radiolarian and diatom biostratigraphic data.

Calcareous Nannofossils

Only one sample (580-13,CC) contained calcareous nannofossils. The poorly preserved assemblage includes *Crenalithus doronicoides, Coccolithus pelagicus, Calcidiscus macintyrei, Cyclococcolithus leptoporus, Emiliania ovata, Ceratolithus rugosus, Discoaster brouweri*, and *Reticulofenestra* sp. This assemblage indicates a probable Pliocene age.

Foraminifers

Core-catcher samples from all 17 cores recovered at Hole 580 were examined. Four core-catcher samples contained foraminifers (580-1,CC; 580-2,CC; 580-5,CC; 580-13,CC). Samples 580-1,CC, 580-2,CC, and 580-5,CC contained a Pleistocene assemblage typical of the *Glo-*

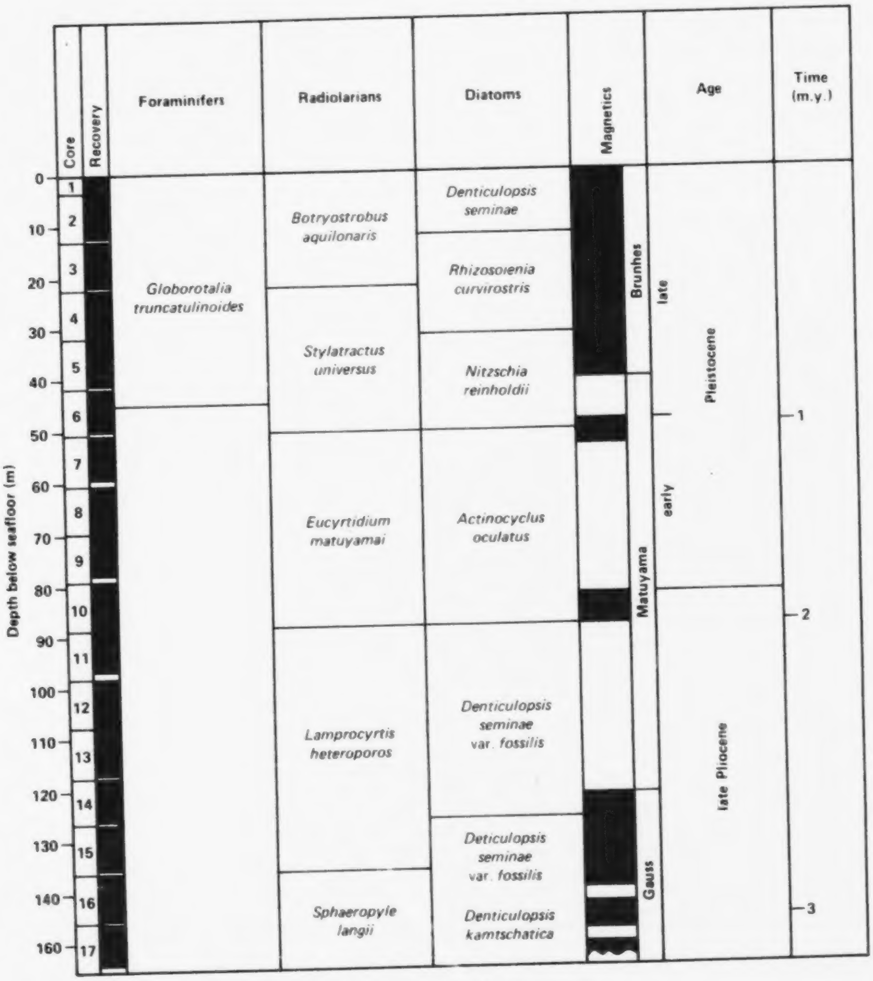

Figure 4. Site 580 biostratigraphic and magnetostratigraphic summary.

borotalia truncatulinoides Zone (Stainforth et al., 1975) or Zone N22 (Blow, 1969). The fauna included *G. truncatulinoides* (580-1,CC only), *G. humerosa, G. acostaensis, G. continuosa, G. obesa, G. inflata*, and *Neogloboquadrina pachyderma* (sinistral). Samples 580-1,CC and 580-2,CC contain rare benthic species such as *Pullenia quinqueloba, Cibicides pseudoungerianus, Melonis affinis, M. pompilioides, Gyroidina neosoldanii*, and *Parafissurina* spp. Shore-based studies have shown that this Pleistocene planktonic fauna can be found as deep as 44.9 m (Sample 580-6-3, 60 cm). Sample 580-13,CC contained an upper Pliocene fauna indicative of the upper part of the *Pulleniatina obliquiloculata* Zone equivalent to N21. The fauna consists of *Globorotalia humerosa, G. acostaensis, G. obesa, G. venezuelana, G. crassaformis*, and *Pulleniatina primalis*.

Preservation of all the specimens was poor to moderate. All show heavy but uniform dissolution effects. The tests are fragile and appear chalky. Features such as pores and apertures are commonly enlarged. Where present, the abundance of foraminifers in Hole 580 was low with only about 30–50 specimens per 10–15 cm^3 sample.

Radiolarians

Sediment samples from Hole 580 contain late Quaternary through late Pliocene radiolarians. Figure 4 shows the shipboard radiolarian biostratigraphy for this site.

All core-catcher samples from Hole 580 contain radiolarians. Common, well-preserved radiolarians characteristic of the late Pleistocene *Botryostrobus aquilonaris* Zone (Hays, 1970) are found in Samples 580-1,CC through 580-3,CC. Samples 580-4,CC through 580-6,CC contain generally well-preserved common to abundant radiolarians. The presence of *Stylatractus universus* and the absence of *Eucyrtidium matuyamai* in these cores (Cores 4 through 6) indicate that this sediment sequence belongs to the *S. universus* Zone (Hays, 1970). The *E. matuyamai* Zone (Hays, 1970; Foreman, 1973) is represented in sediment from this hole in Samples 580-7,CC through 580-10,CC based on the presence of the radiolarian species *E. matuyamai*. The sediment sequence in Samples 580-11,CC through 580-15,CC is assigned to the *Lamprocyrtis heteroporos* Zone (Hays, 1970; Foreman, 1975) based on the absence of *E. matuyamai* and *Stichocorys peregrina*. The radiolarians found in Samples 580-16,CC and 580-17,CC are late Pliocene in age, based on the presence of *S. peregrina*. The faunal assemblage in these cores (Cores 16 and 17) is characteristic of the mid to upper portion of the *Sphaeropyle langii* Zone (Foreman, 1975) since *Lamprocyrtis heteroporos* in addition to *Stichocorys peregrina* is present in these sediment samples.

Diatoms

A thick Quaternary and late Pliocene diatom biostratigraphic section was recovered at Site 580 and is suitable, in conjunction with Site 579, for a study of north–south migrations of the cold-water Oyashio Current and the warm-water Kuroshio Current from late Pliocene to Recent time. As cold-water species are dominant, the diatom zonation of Koizumi (1973) is applied to this section. Diatoms are abundant and well preserved.

Cores 1 and 2 belong to the latest Quaternary *Denticulopsis seminae* Zone, and Cores 3 and 4 to the late Pleistocene *Rhizosolenia curvirostris* Zone. Cores 5 and 6 are assigned to the middle Pleistocene *Nitzschia reinholdii* Zone. The last occurrence of the silicoflagellate *Mesocena quadrangula*, which is around the Jaramillo Event of the geomagnetic Matuyama Epoch, occurs in Core 6. The early Pleistocene *Actinocyclus oculatus* Zone occurs in samples from Cores 7 to 10. The Pliocene/Pleistocene boundary is placed between *Coscinodiscus pustulatus* and *Thalassiosira zabelina* in Core 11. Cores 11 through 14 are assigned to the late Pliocene *D. seminae* var. *fossilis* Zone by the presence of *D. seminae* var. *fossilis* and the absence of *D. kamtschatica*. Core 13 is placed in the lower Matuyama Epoch between the Olduvai Event and the top of the Gauss Epoch by the presence of *Thalassiosira convexa* and the absence of *D. kamtschatica*. Diatom assemblages in Cores 15 through 17 are placed in the *D. seminae* var. *fossilis–D. kamtschatica* Zone. Core 17 is estimated to be more than 2.7 m.y. old because of the presence of *N. jouseae*.

PALEOMAGNETICS

Paleomagnetic analyses using stepwise alternating field (AF) demagnetization techniques were made on 358 samples from the 155.3 m of sediments penetrated at Site 580.

In the upper part of the hole, the intensities of the natural remanent magnetization (NRM) show a systematic overall decrease from about 6×10^{-5} Gauss near the top of the hole to about 6×10^{-7} Gauss at about 120 m sub-bottom. Below this level, to the base of the hole, NRM intensities were somewhat higher again. Within virtually all the cores, NRM values vary by at least one order of magnitude. In contrast, the magnetic stability remains remarkably constant throughout. Median destructive field (MDF) measurements typically fall within the range of 300 ± 50 Oe. The directional changes between NRM and stable directions upon AF demagnetization are generally small.

The polarity pattern derived from the downhole variation of the stable magnetization directions is shown in Figure 4. The Brunhes/Matuyama boundary was identified at 40.00 m sub-bottom (Sample 580-5-6, 70 cm), and the Matuyama/Gauss boundary at 121.44 m sub-bottom (Sample 580-14-3, 114 cm). The Jaramillo and Olduvai events in the reversed Matuyama Epoch as well as the Kaena and Mammoth events in the normal Gauss Epoch are clearly recognizable in the record. In addition, one of the short events of the Reunion series and a yet unnamed event between the Jaramillo and Olduvai were found. The base of the hole, at 155.30 m sub-bottom, did not reach the Gauss/Gilbert boundary. Using the most recent polarity time scale of Berggren et al. (in press), the extrapolated absolute age at the base of the hole is about 3.30 m.y. The sediment column at this site accumulated at a remarkably constant average rate of about 46.5 m/m.y.

Above a sub-bottom depth of about 120 m (corresponding roughly to the Matuyama/Gauss boundary at 2.47 m.y.), the stable inclinations measured scatter around the axial dipole value for the present latitude of the site (60.6°). Only below this depth does the stable inclination record gradually become shallower, reflecting the northward component of the Pacific Plate motion.

The general variation in the inclination data throughout the hole apparently results from a normal range of secular paleofield variation. In contrast, the stable declination pattern is much more complex as it frequently includes variable amounts of disturbances introduced by the coring process.

SEDIMENT ACCUMULATION RATES

Nine radiolarian and diatom biostratigraphic zonal boundaries identified in the cores of Site 580 (Fig. 4), in addition to the paleomagnetic stratigraphy, were used to estimate the sediment accumulation rates at this site. The resulting curve (Fig. 5) shows a remarkably constant rate of deposition of almost 50 m/m.y. for the Quaternary through late Pliocene.

PHYSICAL PROPERTIES

Physical properties measurements at Site 580 were performed using mainly standard Deep Sea Drilling Project (DSDP) methods (Boyce, 1976a,b; see Introduction and Explanatory Notes, this volume). Table 4 summarizes the properties that were measured in Hole 580. These measurements were generally taken at 4.5-m intervals throughout the core. Detailed compressional wave velocity profiles were made on selected ash layers to determine the fine-scale velocity structure. Figures 6, 7, and 8 show profiles of compressional wave velocity, saturated bulk density and water content, and shear strength, respectively.

A full discussion of the physical properties of the recovered sediment, including tables of the data, is given by Schultheiss (this volume). Some of the more interesting features of the data are highlighted here:

1. As at Sites 578 and 579, the velocity profile for Site 580 (Fig. 6) is dominated by high velocity pyrite-indurated clay and ash beds. Velocities in the siliceous clays and oozes rise gradually downhole from about 1470 m/s

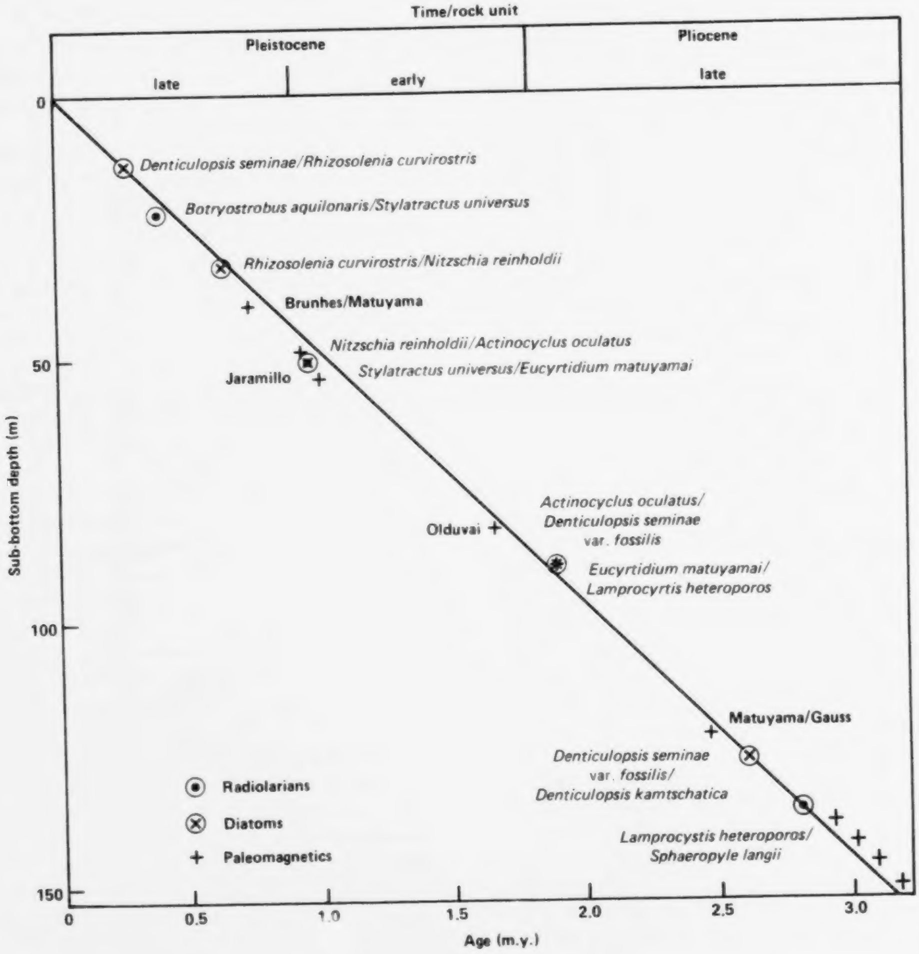

Figure 5. Site 580 sediment accumulation rates.

Table 4. Physical properties measurements made at Site 580.

	Hole 580
Shear strength	
Hand-operated vane	x
Motorized vane	x
Compressional wave velocity	x
Water content/bulk density	
Shipboard analysis	x
Shore-based analysis	x
Bulk density by 2-min. GRAPE	x

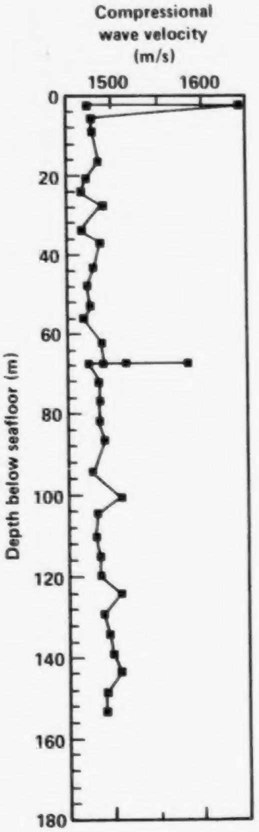

Figure 6. Plot of compressional wave velocity versus sub-bottom depth at Site 580.

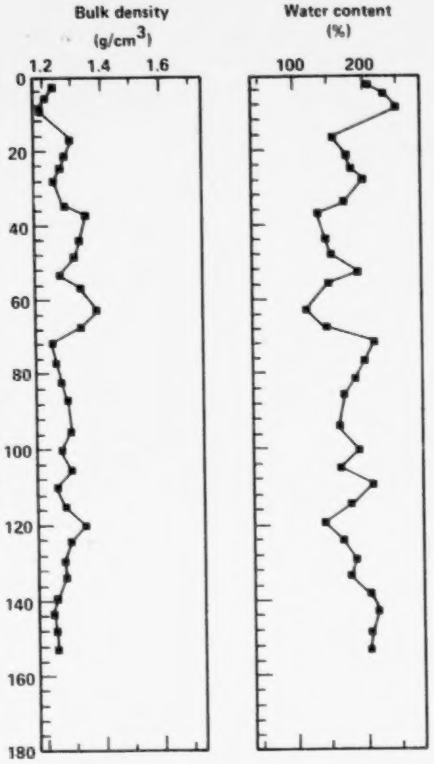

Figure 7. Plot of saturated bulk density and water content versus sub-bottom depth at Site 580.

in Core 1 to 1490 m/s in Core 17 at a sub-bottom depth of 150 m.

2. A detailed velocity structure was obtained from five ash layers by taking measurements at 1 or 2 cm intervals through the beds. Some of these examples clearly showed that the sharp basal contact produced a maximum velocity near or at the bottom of the ash layer. The velocities tend to decrease more slowly up through the layers.

3. The velocity structure in these ash beds is primarily governed by their bulk density structure. A comparison of the GRAPE record with the measured velocity profile for Section 580-2-2 illustrated the close relationship between the two profiles. This type of detailed profile may prove useful for modeling acoustic reflectors for correlation with seismic sections.

4. The water-content profile (Fig. 7) shows an erratic decrease from around 230% at the seafloor to 120% at 63 m sub-bottom. This roughly corresponds to lithologic Subunit IA (siliceous clay). An increase of up to 212% in water content occurs in Subunit IB (calcareous siliceous clay, 60.3–79.3 m). In Subunit IC (79.3–117.3 m), which is lithologically similar to Subunit IA, the water content is essentially constant at about 180%. Lithologic Subunit ID (diatom ooze) initially exhibits a decrease in water content to 140% but then increases slowly through Subunit ID before decreasing again in Subunit IE (which is lithologically similar to IA and IC).

5. The shear strength measurements (Fig. 8) show a nearly linear increase with depth up to 800 g/cm^2 at 150 m sub-bottom.

INORGANIC GEOCHEMISTRY

Six squeezed core samples from Hole 580 were analyzed for the standard suite of components: pH, alkalinity, salinity, chlorinity, calcium, and magnesium (Table 5). No *in situ* samples were taken.

As at the two prior sites, calcium increases linearly with depth (Fig. 9), suggesting diffusion from a carbonate source beneath the drilled section to the seafloor. Magnesium decreases nonlinearly with depth, probably

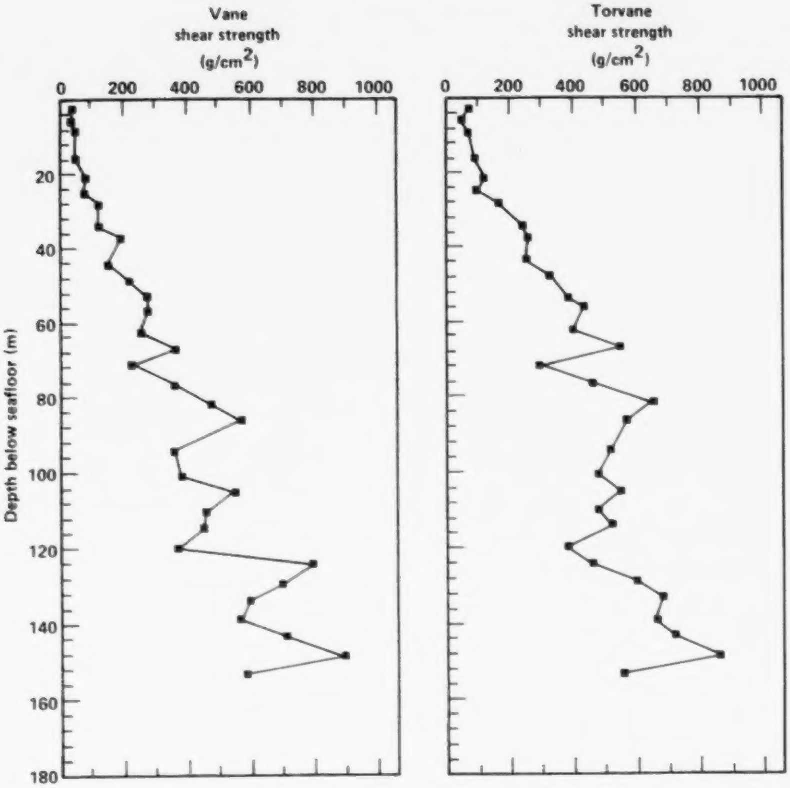

Figure 8. Plot of shear strength versus sub-bottom depth at Site 580.

Table 5. Inorganic geochemistry measurements made at Site 580.

Sample	pH	Alkalinity (mEq/l)	Salinity (‰)	Calcium (mM)	Magnesium (mM)	Chlorinity (‰)
IAPSO	7.81	2.45	35.2	10.55	53.99	19.376
SSW	7.96	2.33	34.1	10.15	51.62	18.58
580-2-5, 140-150 cm	7.61	5.85	35.2	10.61	51.22	19.36
580-5-5, 140-150 cm	7.59	7.87	35.2	11.22	49.12	19.16
580-8-5, 140-150 cm	7.49	8.44	35.2	11.41	47.45	19.39
580-11-4, 140-150 cm	7.55	8.64	34.9	11.79	46.42	19.46
580-14-5, 140-150 cm	7.57	8.59	34.9	12.16	46.04	19.36
580-17-5, 140-150 cm	7.64	8.43	34.9	12.29	45.68	19.36

due to uptake by the abundant altering ash in the drilled section. Alkalinity increases with depth to about 60 m, presumably due to oxidation of organic matter by sulfate-reducing bacteria, which must outweigh the effects of the alteration of volcanic ash.

HEAT FLOW

Measurements of sediment temperature using the new Woods Hole Oceanographic Institution (WHOI) heat-flow instrument were made at 11 locations in Hole 580. All runs were successful. Recorder WHOI-4A, connected either to battery pack NTLT-2 or NTLT-3, was used at every other core starting with Core 3 throughout the hole. At the sub-bottom depth interval of 60 to 100 m, where temperature distributions were most complex at the two previous sites, auxiliary measurements were made by recorder WHOI-01 connected to battery pack TILT-3. A comparison run with the conventional ERI-type heat flow instrument was made using the same recorder–battery unit. The comparison was unsuccessful owing to a failure on the part of the ERI-type instrument. The data from the new WHOI instrument were, however, useful and are valuable in providing a detailed temperature profile in a relatively shallow sediment section. The temperature data, combined with a detailed thermal conductivity profile constructed from 250 measurements on cores recovered from Hole 580, provided an estimate of heat flow at this site (see Horai and Von Herzen, this volume).

Past DSDP heat-flow studies have measured downhole temperatures at typical intervals of 100 m in deep holes. Oceanic heat-flow studies from ordinary research vessels have measured near-surface temperature to a depth of 10 to 15 m at intervals of 1 to 2 m. The field tests made on this leg demonstrated that the new WHOI hydraulic piston core (HPC) core-nose heat-flow instrument can be deployed successively to yield detailed temperature profiles in soft oceanic sediments.

SUMMARY AND CONCLUSIONS

At Site 580, we recovered a thick sequence of Quaternary and late Pliocene sediments. Siliceous microfossils (diatoms and radiolarians) are generally abundant and moderately to well preserved. An excellent magnetic reversal record can be identified back to the middle of the Gauss Normal Epoch.

One hundred and fifty-five meters of sediment were penetrated. Except for the numerous ash layers, these

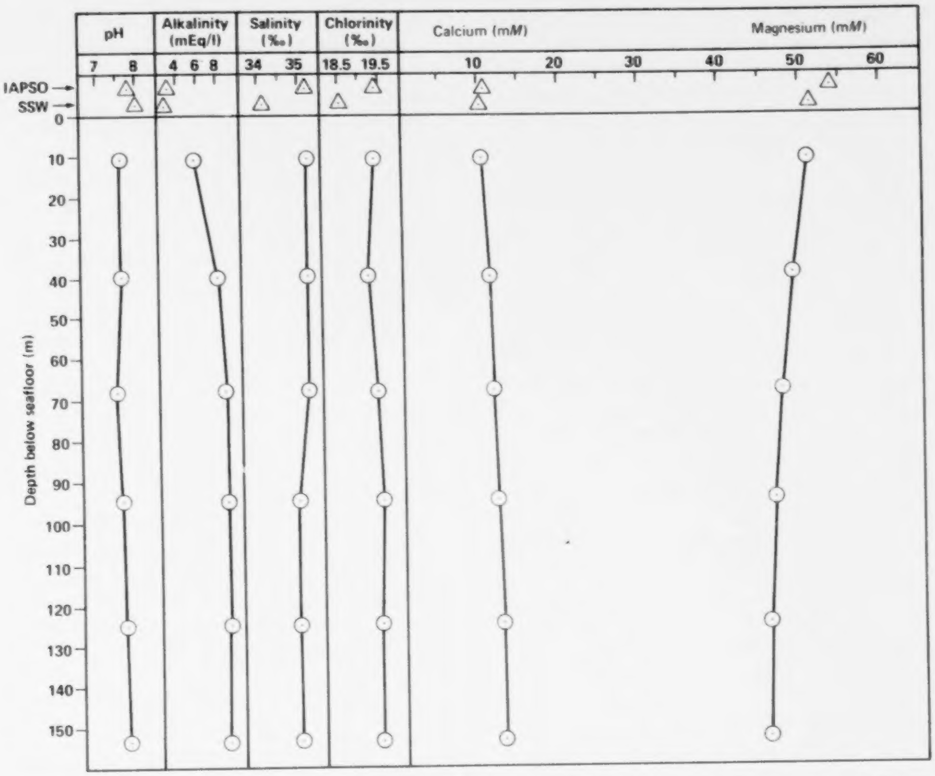

Figure 9. Profiles of pH, alkalinity, salinity (‰), chlorinity (‰), calcium (mM), and magnesium (mM) versus sub-bottom depth for interstitial water samples analyzed at Site 580. Symbols are as follows: △ = IAPSO and SSW standards; ⊙ = samples from Hole 580.

sediments are relatively uniform in color and texture. As at Site 579, we encountered numerous thin, well indurated, dark grayish green layers that were lithologically dissimilar from the adjacent, soft biosiliceous clay. Unlike Site 579, thin, dark gray to black layers of clay are commonly found immediately below the indurated layers.

The sediments from this site are placed into one lithologic unit, which is characterized as a siliceous clay, gray to dark gray to olive gray in color, with variable abundances of biogenic silica ranging from 10 to 70%. Based on these discrete changes in lithology and on the unexpected occurrence of clay-sized carbonate in one section of the hole, we can subdivide lithologic Unit I as follows:

Subunit IA (0-60.3 m) is a siliceous clay that is gray, olive gray, to dark gray in color. It contains 2-25% diatoms, 0-15% radiolarians, and 3-15% quartz. Feldspar and heavy minerals are present in abundances of less than 2%, while disseminated ash ranges from 2 to 10% in abundance. The remainder of the sediment (56%) is clay. The subunit contains 43 ash layers.

Subunit IB (60.3-79.3 m) is a calcareous biosiliceous clay. The distinguishing characteristic is the presence of 3 to 25% unspecified clay-sized carbonate. Additionally, the subunit contains 10-25% diatoms, 5-7% radiolarians, and 5-10% quartz. Quartz abundance ranges up to 10%, while feldspar is usually less than 2% and disseminated ash ranges from 3 to 7%. The remainder of the sediment (55%) is composed of clay. The subunit contains seven recognizable ash layers.

Subunit IC (73.9-117.3 m) is a siliceous clay with average composition similar to that of Subunit IA. Eighteen recognizable ash layers occur in this unit.

Subunit ID (117.3-136.3 m) is a clayey diatom ooze containing 50-60% diatoms, 2-10% radiolarians, and 5-10% quartz. Feldspar abundances are a constant 2% throughout this layer and disseminated ash ranges from 5 to 10%. The remainder of the sediment (~27%) is clay. This subunit contains seven ash layers.

Subunit IE (136.3-155.3 m) is another siliceous clay similar in composition to Subunits IA and IC except that it is slightly more enriched in diatoms. The bulk of the sediment (~53%) is clay. This subunit contains 14 ash layers.

Although the stiff greenish gray layers were present throughout all seventeen cores recovered, their locations were not recorded in the same detail as the ash layers.

Figure 4 summarizes the paleomagnetics and biostratigraphy for this site. Because of good weather, excellent recovery was achieved with minimum flow-in or coring disturbance. Thus, an excellent paleomagnetic reversal record was obtained at this site. Additionally, there was unusually fine preservation of the siliceous microfossils, making it possible to verify the magnetic reversal record via biostratigraphy. Both of the major siliceous microfossil groups (radiolarians and diatoms) were used to verify that the hole bottomed in the middle part of the Gauss. This excellent stratigraphic control permitted us to determine, in detail, sedimentation rates during the interval of time covered by this hole. Figure 5 is an age-depth curve for the interval sampled. Sedimentation rates are high (on the order of 50 m/m.y.) in the Pleistocene and late Pliocene.

Figure 10 shows the numbers of ash layers accumulated per million year interval. There is a high of 48 ash layers during the late Pleistocene and only 18 during the early Pleistocene and latest Pliocene. This does not conform with the pattern that we saw at Sites 578 and 579 or with what Furuta and Arai (1980) observed at Site 436. Since this site has been well within the range of ash falls during the entire depositional history of this hole, changes in the number of ash layers accumulated per unit time may well represent evidence for episodicity.

Because of the large number of ash layers at this site it was difficult to determine the sources of the seismic reflections. In general, the reflectors correlated with the ash layers below 45 m sub-bottom depth. However, there were several strong reflectors in the upper 45 m that definitely did not correlate with ash layers. It is entirely possible that these strong reflectors may result from the ubiquitous, indurated to semi-indurated gray-green layers. The 100-Hz seismic reflection profiles indicate a four-part seismic section at this site. The uppermost seismic unit (0-221 m at a velocity of 1.5 km/s) includes the interval cored at this site and is subdivided into four subunits. Subunits 1a and 1c contain distinct, continuous reflectors while Subunit 1b contains indistinct, discontinuous reflectors. It is interesting that the number of ash layers/m.y. roughly correlates with these subunits (see Fig. 10).

As we found at Sites 578 and 579, the compressional wave velocity profile for Site 580 is dominated by high velocity, semi-indurated greenish clay and ash layers. Velocities rise gradually downhole from 1.47 to 1.49 km/s in the siliceous clays and oozes. Detailed velocity profiles obtained on five ash layers clearly show that, for some layers, the maximum velocity occurs at or near the sharp, basal contact.

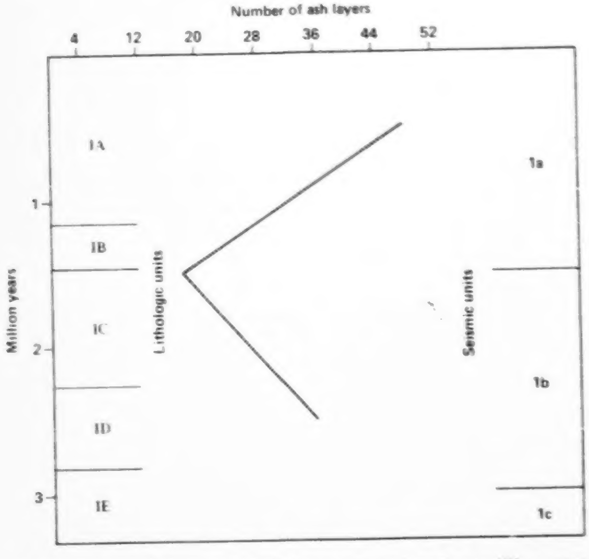

Figure 10. Plot of number of ash layers accumulated per million years at Site 580.

A total of eleven heat flow measurements were taken at Site 580. Measurements began at 22.3 m sub-bottom depth and continued to a sub-bottom depth of 155.3 m. Except for one anomalous point at 70 m, the data show a fairly linear increase in temperature with depth.

The objectives for this site—to obtain a detailed paleoceanographic record in the subtropical-subarctic gyre transition zone for the late Cenozoic; to refine the mid-latitude stratigraphy using paleomagnetics, tephrachronology, and biostratigraphy; to determine the time of onset of significant biosiliceous accumulation; to determine the timing and nature of the onset of the mid-Pliocene and Pleistocene climatic deterioration; to assess the nature and history of authigenic sedimentation in pre-biosiliceous sediments; and to determine the Cenozoic history of eolian sedimentation for comparison with sites to the south and north—was only partly achieved. Because of time limitations, we were unable to core as deep as our objectives required.

REFERENCES

Berggren, W. A., Kent, D. V., and Flynn, J. J., in press. Paleogene geochronology and chronostratigraphy. *In* Snelling, N. J. (Eds.), *Geochronology and the Geological Record*. Geol. Soc. London Spec. Pap.

Blow, W. H., 1969. Late middle Eocene to Recent planktonic foraminiferal biostratigraphy. *In* Brönnimann, P., and Renz, H. H. (Eds.) *Proc. First Int'l. Conf. Planktonic Microfossils* (Vol. 6): Leiden (Brill), 199-422.

Boyce, R. E., 1976a. Definitions and laboratory techniques of compressional and sound velocity parameters and wet-water content, wet-bulk density, and porosity parameters by gravimetric and gamma ray attenuation techniques. *In* Schlanger, S. O., Jackson, E. D., et al., *Init. Repts. DSDP*, 33: Washington (U.S. Govt. Printing Office), 931-958.

_______, 1976b. Deep Sea Drilling Project procedures for shear strength measurements of clayey sediment using modified Wykeham Farrance Laboratory Vane Apparatus. *In* Barker, P. F., Dalziel, I. W. D., et al., *Init. Repts. DSDP*, 36: Washington (U.S. Govt. Printing Office), 1059-1068.

Foreman, H. P., 1973. Radiolaria from DSDP Leg 20. *In* Heezen, B. C., MacGregor, I. D., et al., *Init. Repts. DSDP*, 20: Washington (U.S. Govt. Printing Office), 249-305.

_______, 1975. Radiolaria from the North Pacific, Deep Sea Drilling Project, Leg 32. *In* Larson, R. L., Moberly, R., et al., *Init. Repts. DSDP*, 32: Washington (U.S. Govt. Printing Office), 579-701.

Furuta, T., and Arai, F., 1980. Petrographic properties of tephras, Leg 56, Deep Sea Drilling Project. *In* Scientific Party, *Init. Repts. DSDP*, 56, 57, Pt. 2: Washington (U.S. Govt. Printing Office), 1043-1048.

Hays, J. D., 1970. Stratigraphy and evolutionary trends of Radiolaria in North Pacific deep-sea sediments. *In* Hays, J. D. (Ed.), *Geological Investigations of the North Pacific*. Mem. Geol. Soc. Am., 126:185-218.

Koizumi, I., 1973. The late Cenozoic diatoms of Sites 183-193, Leg 19, Deep Sea Drilling Project. *In* Creager, J. S., Scholl, D. W., et al., *Init. Repts. DSDP*, 19: Washington (U.S. Govt. Printing Office), 805-855.

Stainforth, R. M., Lamb, J. L., Luterbacher, H., Beard, J. H., and Jeffords, R. M., 1975. Cenozoic planktonic foraminiferal zonation and characteristics of index forms. *Univ. Kans. Paleontol. Contrib. Pap.*, 62:1-425.

SITE 580 HOLE CORE 1 CORED INTERVAL 5386.7–5390.0 mbsl; 0.0–3.3 mbsf

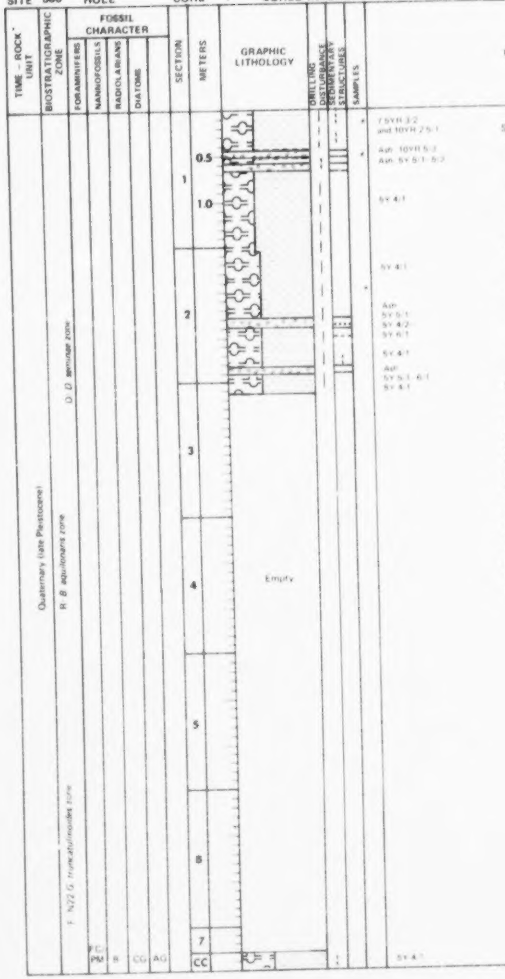
TIME – ROCK UNIT
BIOSTRATIGRAPHIC ZONE
FOSSIL CHARACTER
FORAMINIFERS
NANNOFOSSILS
RADIOLARIANS
DIATOMS
SECTION
METERS
GRAPHIC LITHOLOGY
DRILLING DISTURBANCE
SEDIMENTARY STRUCTURES
SAMPLES
Quaternary (late Pleistocene)
D. D. seminae zone
R. B. aquilonaris zone
F. N22 G. truncatulinoides zone
F/C
PM
B
CG
AG
0.5
1.0
1
2
3
4
5
6
7
CC
Empty
7.5YR 3/2 and 10YR 2.5/1
Ash 10YR 5/3
Ash 5Y 5/1–5/2
5Y 4/1
5Y 4/1
Ash 5Y 5/1
5Y 4/2
5Y 6/1
5Y 4/1
Ash 5Y 5/1–6/1
5Y 4/1
5Y 4/1

LITHOLOGIC DESCRIPTION

SILICEOUS CLAY WITH VOLCANIC ASH LAYERS

- Dominant colors: Section 1, 0–43 cm is dark brown (7.5YR 3/2) and black (10YR 2.5/1). Rest of the core is dark gray (5Y 4/1). Minor colors: small patches and thin layers of dark greenish gray (5G 4/1), dark greenish gray (5GY 4/1) and very dark gray (5Y 3/1). Ash layers in Section 1 are brown (10YR 5/3) and gray (5Y 5/1) grading to olive gray (5Y 5/2). Ash layers in Section 2 are gray (5Y 5/1–5Y 6/1).
- Section 1, 50–66 cm and the Core Catcher are very deformed; the rest of the core is slightly deformed by drilling.
- This core consists of homogeneous siliceous clay with local small patches and thin layers of greenish gray and very dark gray clay. The dark brown to black top 43 cm of Section 1 is mottled. Ash layers occur at 1, 43–50 cm; 1, 57–66 cm; 2, 77.5–88 cm; and, 2, 131–138.5 cm. The ash layer at 2, 77.5–88 cm is normally graded.

SMEAR SLIDE SUMMARY (%):

	1, 15 D	1, 50 M	2, 50 D
Texture:			
Sand	20	70	28
Silt	20	30	20
Clay	60	0	52
Composition:			
Quartz	5	27	7
Feldspar	Tr	—	Tr
Clay	60	—	52
Volcanic glass	1	73	1
Pyrite	—	2	1
Diatoms	20	—	25
Radiolarians	10	—	10
Sponge spicules	3	—	3
Silicoflagellates	1	—	1

SITE 580 HOLE CORE 2 CORED INTERVAL 5390.0–5399.5 mbsl; 3.3–12.8 mbsf

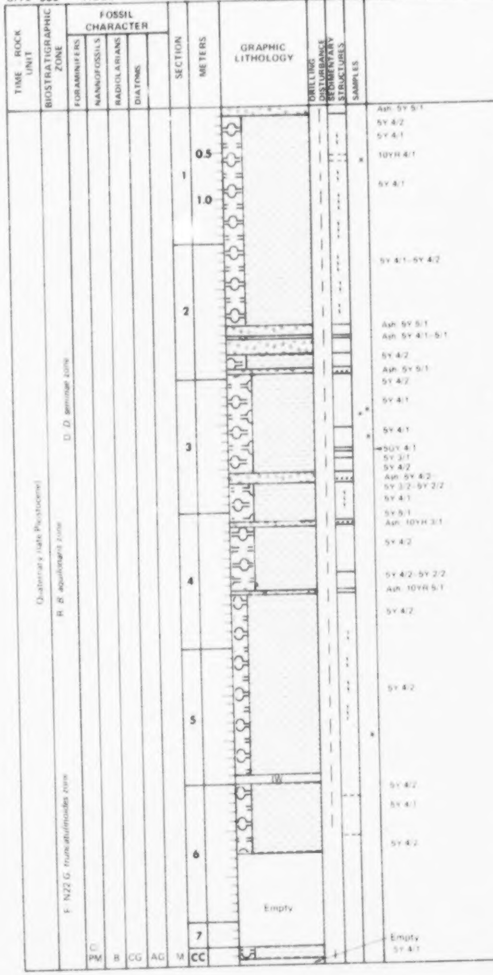
TIME – ROCK UNIT
BIOSTRATIGRAPHIC ZONE
FOSSIL CHARACTER
FORAMINIFERS
NANNOFOSSILS
RADIOLARIANS
DIATOMS
SECTION
METERS
GRAPHIC LITHOLOGY
DRILLING DISTURBANCE
SEDIMENTARY STRUCTURES
SAMPLES
Quaternary (late Pleistocene)
D. D. seminae zone
R. B. aquilonaris zone
F. N22 G. truncatulinoides zone
C/PM
B
CG
AG
M
0.5
1.0
1
2
3
4
5
6
7
CC
Empty
Ash 5Y 5/1
5Y 4/2
5Y 4/1
10YR 4/1
5Y 4/1
5Y 4/1–5Y 4/2
Ash 5Y 5/1
Ash 5Y 4/1–5/1
5Y 4/2
Ash 5Y 5/1
5Y 4/2
5Y 4/1
5Y 4/1
5GY 4/1
5Y 3/1
5Y 4/2
Ash 5Y 4/2
5Y 3/2–5Y 2/2
5Y 4/1
5Y 5/1
Ash 10YR 3/1
5Y 4/2
5Y 4/2–5Y 2/2
Ash 10YR 5/1
5Y 4/2
5Y 4/2
5Y 4/2
5Y 4/1
5Y 4/2
Empty
5Y 4/1

LITHOLOGIC DESCRIPTION

SILTY SILICEOUS CLAY WITH VOLCANIC ASH LAYERS

- Dominant colors: dark gray (5Y 4/1), olive gray (5Y 4/2–5Y 5/2). Minor colors: thin indurated layers and small patches of dark greenish gray (5GY 4/1), very dark gray (5Y 3/1), and black (5Y 2/1). Ash layers in Sections 1 and 2 are gray (5Y 5/1) and dark gray (5Y 4/1). The ash layer at 3, 103–118 cm is olive gray (5Y 4/2) grading down to dark olive gray (5Y 3/2) grading down to black (5Y 2/2). Ash layers in Section 5 are very dark gray (10YR 3/1) and gray (10YR 5/1).
- Entire core is slightly deformed by drilling.
- This core consists of homogeneous to lightly mottled silty siliceous clay with thin indurated layers and small patches of greenish gray and very dark gray siliceous clay. Ash layers occur at 1, 0–9.5 cm; 2, 90.5–101.5 cm; 2, 103.5–122 cm; 2, 138–142.5 cm; 3, 103–118 cm; 4, 10–13.5 cm; and, 4, 87.5–89 cm. Several of the ash layers are normally graded.

SMEAR SLIDE SUMMARY (%):

	1, 63 D	3, 40 D	3, 48 D	3, 70 D	5, 100 D
Texture:					
Sand	24	20	20	20	15
Silt	20	27	20	24	15
Clay	56	53	60	56	70
Composition:					
Quartz	16	10	10	10	10
Feldspar	—	Tr	—	Tr	—
Clay	56	53	61	56	70
Volcanic glass	2	1	2	1	2
Pyrite	—	Tr	Tr	2	—
Carbonate unspec.	—	Tr	Tr	—	Tr
Diatoms	15	20	15	20	10
Radiolarians	10	15	10	10	7
Sponge spicules	1	1	Tr	1	—
Silicoflagellates	Tr	Tr	2	Tr	1

SITE 580 HOLE CORE 3 CORED INTERVAL 5399.5–5409.0 mbsl; 12.8–22.3 mbsf

TIME-ROCK UNIT	BIOSTRATIGRAPHIC ZONE	FORAMINIFERS	NANNOFOSSILS	RADIOLARIANS	DIATOMS
Quaternary (late Pleistocene)	D. R. curvirostris zone (0.27–0.68 m.y.) R. B. aquilonaris zone (age between 310,000 and 425,000 yrs. BP) S. D. octangulatus zone	B	B	AG	AG

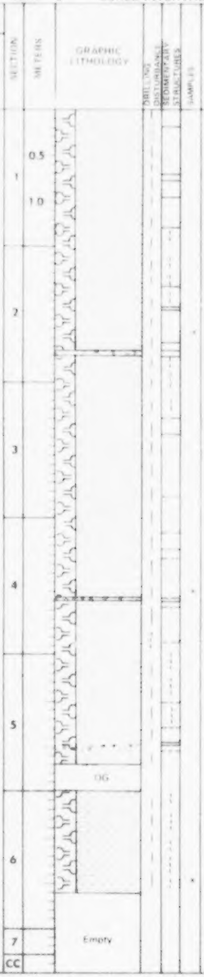

LITHOLOGIC DESCRIPTION

SILTY SILICEOUS CLAY WITH VOLCANIC ASH LAYERS

- *Dominant colors: dark gray (5Y 4/1), gray (5Y 5/1), olive gray (5Y 4/2), and greenish gray (5GY 5/1) with layers of very dark gray (5Y 3/1) and black (5Y 2/1). Minor colors: thin indurated layers and small patches of dark greenish gray (5GY 4/1) and dark greenish gray (5G 4/1). Ash layer in Section 2 is olive gray (5Y 4/2) grading to gray (5Y 6/1). Ash layer in Section 4 is dark gray (5Y 4/1) grading to black (5Y 2/2). Ash layer in Section 5 is dark gray (5Y 4/1).
- *Top of Section 1 is empty; rest of the core is slightly deformed by drilling.
- *This core consists of homogeneous to lightly mottled silty siliceous clay with thin (0.2–3.0 cm) indurated layers and small patches of greenish gray siliceous clay. Ash layers occur at 2, 114–120 cm, 4, 87–90 cm, and 5, 96–97 cm.

SMEAR SLIDE SUMMARY (%)

	2, 100	4, 80	6, 100
	D	D	D
Texture:			
Sand	20	20	20
Silt	29	27	25
Clay	51	53	55
Composition:			
Quartz	10	10	5
Feldspar	Tr	Tr	Tr
Clay	51	53	55
Volcanic glass	1	5	3
Pyrite	Tr	2	2
Carbonate unspec.	Tr	Tr	—
Diatoms	20	15	25
Radiolarians	10	10	10
Sponge spicules	2	Tr	—
Silicoflagellates	1	Tr	Tr

SITE 580 HOLE CORE 4 CORED INTERVAL 5409.0–5418.5 mbsl; 22.3–31.8 mbsf

TIME-ROCK UNIT	BIOSTRATIGRAPHIC ZONE	FORAMINIFERS	NANNOFOSSILS	RADIOLARIANS	DIATOMS
Quaternary (late Pleistocene)	D. R. curvirostris zone R. B. aquilonaris zone S. D. octangulatus zone	B	B	CG	AG

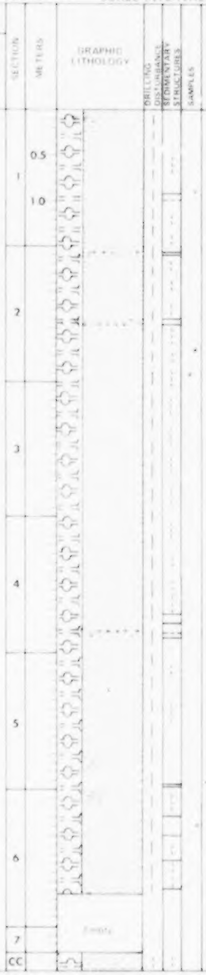

LITHOLOGIC DESCRIPTION

SILICEOUS CLAY WITH VOLCANIC ASH LAYERS

- *Dominant colors: dark gray (5Y 4/1), gray (5Y 5/1), olive gray (5Y 4/2), and greenish gray (5GY 5/1). Minor colors: thin, indurated layers and small patches of dark greenish gray (5G 4/1) and very dark gray (5Y 3/1). Ash layers are very light gray (5Y 7/1) (2, 4–6 cm), gray (5Y 6/1) (2, 78–84 cm), and olive gray (5Y 4/2) grading to dark greenish gray (5G 4/1) (4, 124–130 cm). The ash pocket in Section 1 is very dark gray (5Y 3/1).
- *Entire core is slightly deformed by drilling.
- *This core consists of lightly mottled siliceous clay with thin (0.5–1.0 cm), indurated greenish gray siliceous clay layers. Ash layers occur at 2, 4–6 cm, 2, 78–84 cm, and 4, 124–130 cm. Section 1, 11–14 cm contains a small ash pocket.

SMEAR SLIDE SUMMARY (%)

	1, 92	2, 120	2, 145	6, 40
	D	D	D	D
Texture:				
Sand	5	5	7	10
Silt	40	45	43	35
Clay	55	50	50	55
Composition:				
Quartz	7	7	8	5
Feldspar	1	1	1	1
Heavy minerals	1	1	1	—
Clay	59	47	48	57
Volcanic glass	2	3	10	3
Foraminifers	Tr	Tr	—	—
Diatoms	20	25	20	25
Radiolarians	10	15	10	7
Silicoflagellates	—	1	2	2

SITE 580 HOLE CORE 5 CORED INTERVAL 5418.5–5428.0 mbsl, 31.8–41.3 mbsf

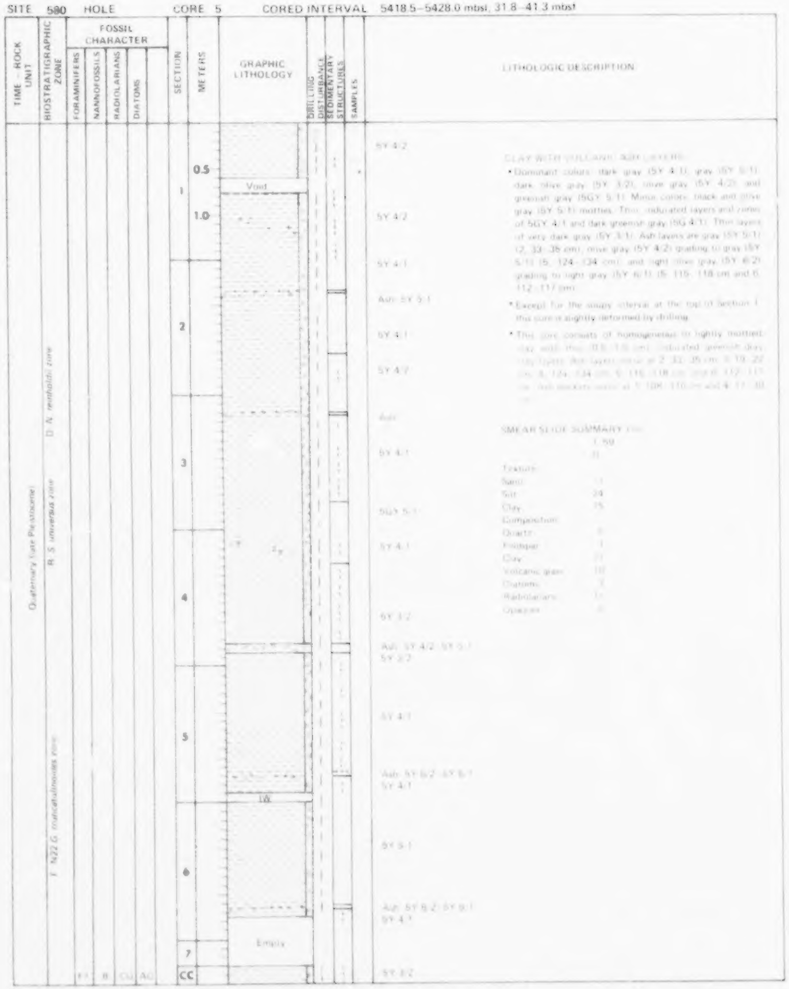
TIME – ROCK UNIT
BIOSTRATIGRAPHIC ZONE
FOSSIL CHARACTER
FORAMINIFERS
NANNOFOSSILS
RADIOLARIANS
DIATOMS
SECTION
METERS
GRAPHIC LITHOLOGY
DRILLING DISTURBANCE
SEDIMENTARY STRUCTURES
SAMPLES
LITHOLOGIC DESCRIPTION
Quaternary (late Pleistocene)
D. N. reinholdii zone
R. S. universus zone
F. N22 G. truncatulinoides zone
F? B CG AG
0.5
1.0
1
2
3
4
5
6
7
CC
Void
Empty
IW
5Y 4/2
5Y 4/2
5Y 4/1
Ash: 5Y 5/1
5Y 4/1
5Y 4/2
Ash
5Y 4/1
5GY 5/1
5Y 4/1
5Y 3/2
Ash: 5Y 4/2–5Y 5/1
5Y 3/2
5Y 4/1
Ash: 5Y 6/2–5Y 6/1
5Y 4/1
5Y 5/1
Ash: 5Y 6/2–5Y 6/1
5Y 4/1
5Y 3/2

CLAY WITH VOLCANIC ASH LAYERS

- Dominant colors: dark gray (5Y 4/1), gray (5Y 5/1), dark olive gray (5Y 3/2), olive gray (5Y 4/2), and greenish gray (5GY 5/1). Minor colors: black and olive gray (5Y 5/1) mottles. Thin, indurated layers and zones of 5GY 4/1 and dark greenish gray (5G 4/1). Thin layers of very dark gray (5Y 3/1). Ash layers are gray (5Y 5/1) (2, 33–36 cm), olive gray (5Y 4/2) grading to gray (5Y 5/1) (5, 124–134 cm), and light olive gray (5Y 6/2) grading to light gray (5Y 6/1) (5, 115–118 cm and 6, 112–117 cm).
- Except for the soupy interval at the top of Section 1, this core is slightly deformed by drilling.
- This core consists of homogeneous to lightly mottled clay with thin (0.5–1.0 cm) indurated greenish gray clay layers. Ash layers occur at 2, 33–35 cm; 3, 19–22 cm; 4, 124–134 cm; 5, 116–118 cm; and 6, 112–117 cm. Ash pockets occur at 1, 108–110 cm and 4, 17–30 cm.

SMEAR SLIDE SUMMARY (%):

	1, 59
	D
Texture:	
Sand	1
Silt	24
Clay	75
Composition:	
Quartz	8
Feldspar	1
Clay	71
Volcanic glass	10
Diatoms	7
Radiolarians	Tr
Opaques	3

SITE 580 HOLE CORE 6 CORED INTERVAL 5428.0–5437.5 mbsl, 41.3–50.8 mbsf

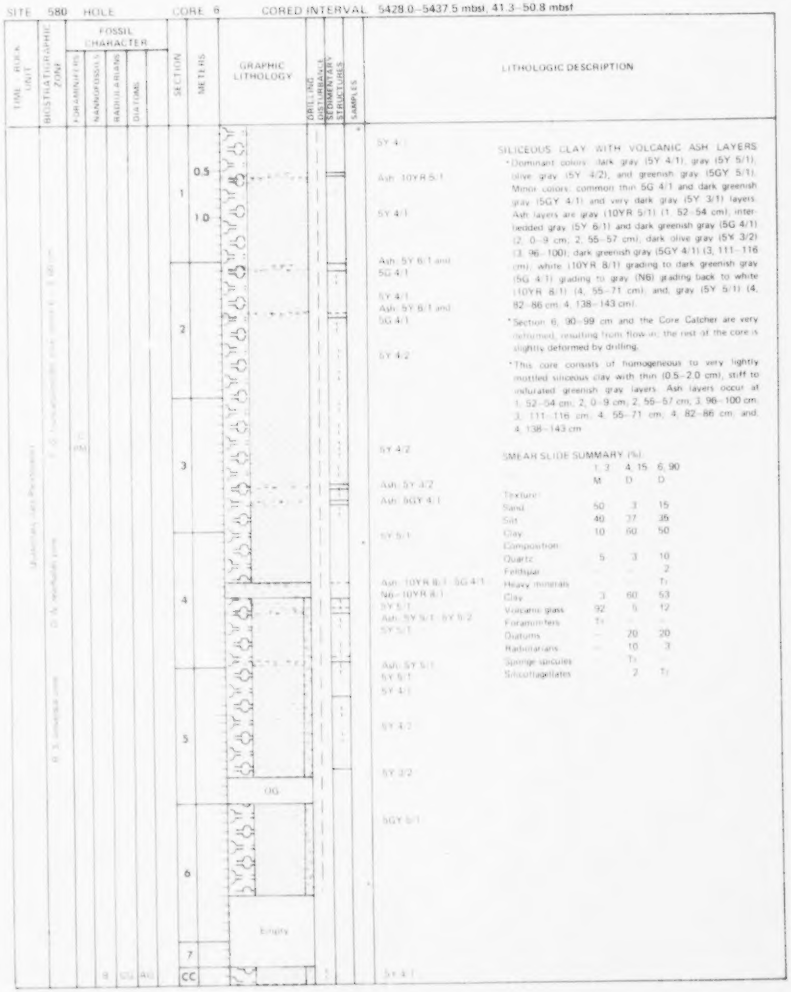
TIME – ROCK UNIT
BIOSTRATIGRAPHIC ZONE
FOSSIL CHARACTER
FORAMINIFERS
NANNOFOSSILS
RADIOLARIANS
DIATOMS
SECTION
METERS
GRAPHIC LITHOLOGY
DRILLING DISTURBANCE
SEDIMENTARY STRUCTURES
SAMPLES
LITHOLOGIC DESCRIPTION
Quaternary (late Pleistocene)
F. G. truncatulinoides zone
D. N. reinholdii zone
R. S. universus zone
C
PM
B CG AG
0.5
1.0
1
2
3
4
5
6
7
CC
OG
Empty
5Y 4/1
Ash: 10YR 5/1
5Y 4/1
Ash: 5Y 6/1 and 5G 4/1
5Y 4/1
Ash: 5Y 6/1 and 5G 4/1
5Y 4/2
5Y 4/2
Ash: 5Y 4/2
Ash: 5GY 4/1
5Y 5/1
Ash: 10YR 8/1–5G 4/1–N6–10YR 8/1
5Y 5/1
Ash: 5Y 5/1–5Y 5/2
5Y 5/1
Ash: 5Y 5/1
5Y 6/1
5Y 4/1
5Y 4/2
5Y 3/2
5GY 5/1
5Y 4/1

SILICEOUS CLAY WITH VOLCANIC ASH LAYERS

- Dominant colors: dark gray (5Y 4/1), gray (5Y 5/1), olive gray (5Y 4/2), and greenish gray (5GY 5/1). Minor colors: common thin 5G 4/1 and dark greenish gray (5GY 4/1) and very dark gray (5Y 3/1) layers. Ash layers are gray (10YR 5/1) (1, 52–54 cm), interbedded gray (5Y 6/1) and dark greenish gray (5G 4/1) (2, 0–9 cm; 2, 55–57 cm), dark olive gray (5Y 3/2) (3, 96–100); dark greenish gray (5GY 4/1) (3, 111–116 cm); white (10YR 8/1) grading to dark greenish gray (5G 4/1) grading to gray (N6) grading back to white (10YR 8/1) (4, 55–71 cm); and, gray (5Y 5/1) (4, 82–86 cm; 4, 138–143 cm).
- Section 6, 90–99 cm and the Core Catcher are very deformed, resulting from flow-in; the rest of the core is slightly deformed by drilling.
- This core consists of homogeneous to very lightly mottled siliceous clay with thin (0.5–2.0 cm), stiff to indurated greenish gray layers. Ash layers occur at 1, 52–54 cm; 2, 0–9 cm; 2, 55–57 cm; 3, 96–100 cm; 3, 111–116 cm; 4, 55–71 cm; 4, 82–86 cm; and 4, 138–143 cm.

SMEAR SLIDE SUMMARY (%):

	1, 3	4, 15	6, 90
	M	D	D
Texture:			
Sand	50	3	15
Silt	40	37	35
Clay	10	60	50
Composition:			
Quartz	5	3	10
Feldspar	—	—	2
Heavy minerals	—	—	Tr
Clay	3	60	53
Volcanic glass	92	5	12
Foraminifers	Tr	—	—
Diatoms	—	20	20
Radiolarians	—	10	3
Sponge spicules	—	Tr	—
Silicoflagellates	—	2	Tr

SITE 580 HOLE CORE 7 CORED INTERVAL 5437.5–5447.0 mbsl; 50.8–60.3 mbsf

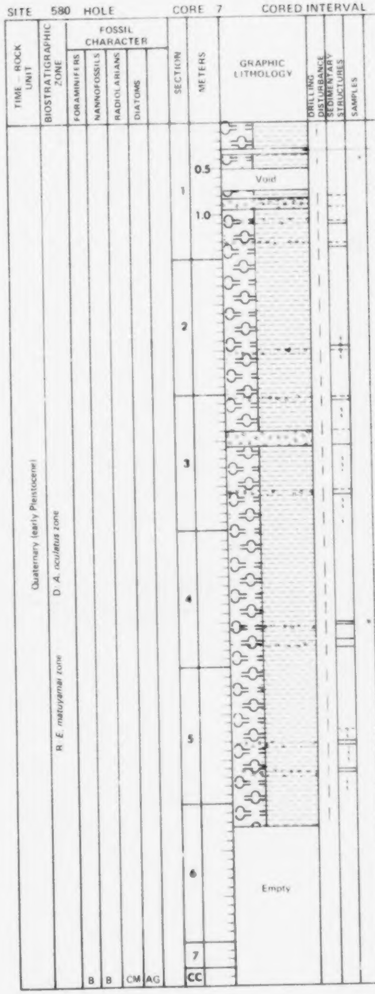
TIME – ROCK UNIT
BIOSTRATIGRAPHIC ZONE
FOSSIL CHARACTER
FORAMINIFERS
NANNOFOSSILS
RADIOLARIANS
DIATOMS
SECTION
METERS
GRAPHIC LITHOLOGY
DRILLING DISTURBANCE
SEDIMENTARY STRUCTURES
SAMPLES
Quaternary (early Pleistocene)
R. E. matuyamai zone
D. A. oculatus zone
B
B
CM
AG
1
2
3
4
5
6
7
CC
0.5
1.0
Void
Empty

LITHOLOGIC DESCRIPTION

5GY 5/1
Void
5GY 5/1
Ash: 5GY 5/1–5Y 7/1
5G 4/1–5GY 5/1
Ash: 5Y 6/1
5GY 5/1
Ash: 5GY 5/1
5GY 5/1
5Y 4/1
Ash: 5G 4/1 and 5Y 3/1
5Y 4/1
Ash: 5Y 4/2
5GY 5/1
Ash: 5Y 3/2 and 5Y 6/1
5GY 5/1
Ash: 2.5Y 3/2
5Y 4/2
5Y 4/2
Ash: 5Y 6/1
5Y 4/2
Ash: 5Y 5/1
5Y 4/1
5GY 5/1
5Y 4/2
Ash: 2.5Y 3/2
5Y 4/2
Ash: 10YR 3/1
5Y 4/2
5Y 4/1

SILICEOUS CLAY WITH VOLCANIC ASH LAYERS

*Dominant colors: dark gray (5Y 4/1), olive gray (5Y 4/2), and greenish gray (5GY 5/1). Minor colors: thin dark greenish gray (5G 4/1) and very dark gray (5Y 3/1) layers. Ash layers are gray (5Y 5/1–5Y 6/1) (1, 109–112 cm; 4, 100–101 cm; 4, 118–126 cm); greenish gray (5GY 6/1) (1, 131–136 cm); olive gray (5Y 4/2) (3, 2–5 cm); dark grayish brown (2.5Y 3/2) (3, 106–110 cm; 5, 80–83 cm); very dark gray (10YR 3/1) (5, 112–114 cm); olive gray (5Y 5/2) and gray (5Y 6/1) (3, 40–53 cm); mottled dark greenish gray (5G 4/1) and very dark gray (5Y 3/1) (2, 95–99 cm); and, interbedded greenish gray (5GY 5/1) light gray (5Y 7/1), and dark greenish gray (5G 4/1) (1, 81–92 cm).

*The top of Section 1 has void spaces and is moderately deformed; the rest of the core is slightly deformed by drilling.

*This core consists of homogeneous to very lightly mottled siliceous clay with thin (0.5–2.0 cm), stiff to indurated greenish gray layers. Ash layers occur at 1, 81–92 cm; 1, 109–112 cm; 1, 131–136 cm; 2, 95–99 cm; 3, 2–5 cm; 3, 40–53 cm; 3, 106–110 cm; 4, 100–101 cm; 4, 118–126 cm; 5, 80–83 cm; and 5, 112–114 cm.

SMEAR SLIDE SUMMARY (%)

	1, 40 D	4, 103 D
Texture		
Sand	5	5
Silt	45	45
Clay	50	50
Composition		
Quartz	10	7
Feldspar	—	1
Clay	50	40
Volcanic glass	—	7
Foraminifers	Tr	3
Diatoms	25	25
Radiolarians	10	10
Sponge spicules	Tr	
Silicoflagellates	5	2
Opaques	—	5

SITE 580 HOLE CORE 8 CORED INTERVAL 5447.0–5456.5 mbsl; 60.3–69.8 mbsf

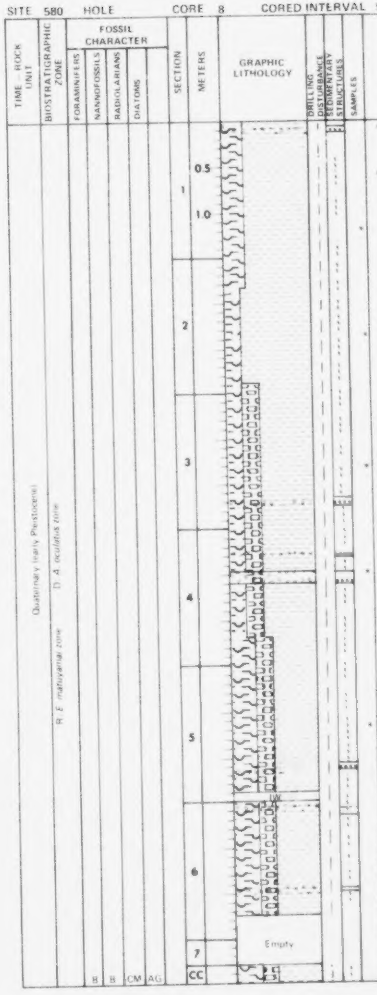
TIME – ROCK UNIT
BIOSTRATIGRAPHIC ZONE
FOSSIL CHARACTER
FORAMINIFERS
NANNOFOSSILS
RADIOLARIANS
DIATOMS
SECTION
METERS
GRAPHIC LITHOLOGY
DRILLING DISTURBANCE
SEDIMENTARY STRUCTURES
SAMPLES
Quaternary (early Pleistocene)
R. E. matuyamai zone
D. A. oculatus zone
B
B
CM
AG
1
2
3
4
5
6
7
CC
0.5
1.0
IW
Empty

LITHOLOGIC DESCRIPTION

Ash: 5Y 6/1
5Y 5/1
5Y 5/1
5Y 5/1
Ash: 5Y 5/1 and 5G 4/1
5Y 5/1
Ash: 10YR 6/1
5Y 5/1
Ash: 10YR 6/1–5GY 5/1
5Y 5/1
5Y 5/1
Ash: 5Y 5/1 and 5GY 4/1
5Y 5/1
Ash: 5Y 4/1
5Y 4/1
5Y 5/1
Ash: N5
5Y 5/1
5Y 5/1

SILTY SILICEOUS (DIATOMACEOUS) CLAY BECOMING CALCAREOUS SILICEOUS (DIATOMACEOUS) CLAY IN SECTION 2

*Dominant colors: gray (5Y 5/1). Minor colors: thin, indurated greenish gray (5G 4/1) layers. Thin dark gray (10YR 4/1) and very dark gray (5Y 3/1) layers. Ash layers are 5Y 6/1, 10YR 6/1, and gray (N6), dark gray (5Y 4/1), gray (5Y 5/1) with interbedded 5G 4/1 or dark greenish gray (5GY 4/1), and, gray (10YR 6/1) grading to greenish gray (5GY 5/1).

*With the exception of the top of Section 1, which is moderately deformed, the majority of the core is slightly deformed by drilling.

*This core consists of mottled and burrowed siliceous to calcareous siliceous clay with common, thin (0.5–1.0 cm), indurated greenish gray layers. The calcareous component ranges in abundance up to 25%, composed of unspecified clay-size carbonate. Ash layers occur at 1, 5–11 cm; 3, 117.5–123 cm; 4, 28–30 cm; 4, 47–60 cm; 5, 108–113 cm; 6, 6–12 cm; and 6, 95–98 cm. The thicker ash layers are normally graded.

	1, 120 D	2, 86 D	3, 87 D	4, 50 M	5, 70 D
Texture					
Sand	25	20	20	20	25
Silt	20	10	5	80	25
Clay	55	70	75	0	50
Composition					
Quartz	7	7	5	7	7
Feldspar	1	1	Tr	Tr	Tr
Mica	3	3	2	—	Tr
Clay	56	67	43	—	37
Volcanic glass	6	3	7	93	5
Carbonate unspec. (clay fragments)	—	—	25	—	15
Diatoms	20	12	10	—	25
Radiolarians	5	7	7	—	7
Silicoflagellates	2	Tr	1	—	4

SITE 580 HOLE CORE 9 CORED INTERVAL 5456.5-5466.0 mbsl, 69.8-79.3 mbsf

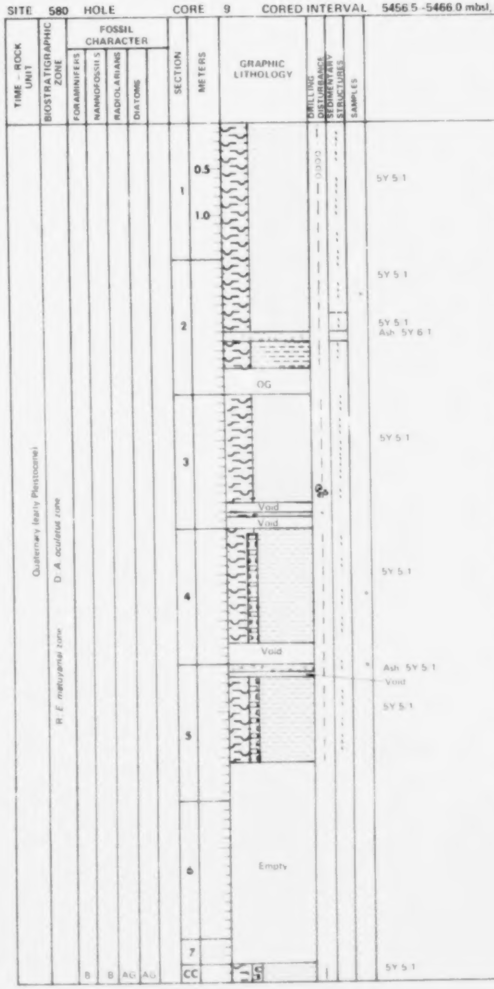
TIME – ROCK UNIT
BIOSTRATIGRAPHIC ZONE
FOSSIL CHARACTER
FORAMINIFERS
NANNOFOSSILS
RADIOLARIANS
DIATOMS
SECTION
METERS
GRAPHIC LITHOLOGY
DRILLING DISTURBANCE
SEDIMENTARY STRUCTURES
SAMPLES
Quaternary (early Pleistocene)
R. E. matuyamai zone
D. A. oculatus zone
B
B
AG
AG
1
2
3
4
5
6
7
CC
0.5
1.0
OG
Void
Void
Void
Empty
5Y 5/1
5Y 5/1
5Y 5/1
Ash 5Y 6/1
5Y 5/1
5Y 5/1
Ash 5Y 5/1
Void
5Y 5/1
5Y 5/1

LITHOLOGIC DESCRIPTION

SILICEOUS (DIATOMACEOUS) CLAY TO CALCAREOUS siliceous (DIATOMACEOUS) CLAY WITH VOLCANIC ASH LAYERS

- Dominant colors: Gray (5Y 5/1). Minor colors: thin indurated 5G 4/1 and dark greenish gray (5GY 4/1) layers. Thin layers of very dark gray (5Y 3/1) and dark gray (10YR 4/1). Ash layers are 5Y 5/1 and gray (5Y 6/1).
- Core contains several void spaces. Top of Section 1 is moderately deformed to soupy; rest of the core is slightly deformed by drilling.
- This core consists of mottled siliceous (diatomaceous) clay to calcareous siliceous (diatomaceous) clay with common, thin (0.5–1.0 cm) indurated greenish gray siliceous clay layers. The calcareous component ranges in abundance up to 10%, composed of unspecified clay-size carbonate. Ash layers occur at 2, 79–90 cm and 5, 0–9 cm.

SMEAR SLIDE SUMMARY (%):

	2, 40 D	4, 75 D	5, 4 M
Texture:			
Sand	20	15	70
Silt	30	20	30
Clay	50	65	0
Composition:			
Quartz	10	10	5
Feldspar	Tr		
Mica	3	1	
Clay	44	54	
Volcanic glass	5	2	95
Carbonate unspec. (clay size)	3	10	
Diatoms	25	17	Tr
Radiolarians	7	5	Tr
Silicoflagellates	3	1	

SITE 580 HOLE CORE 10 CORED INTERVAL 5466.0-5475.5 mbsl, 79.3-88.8 mbsf

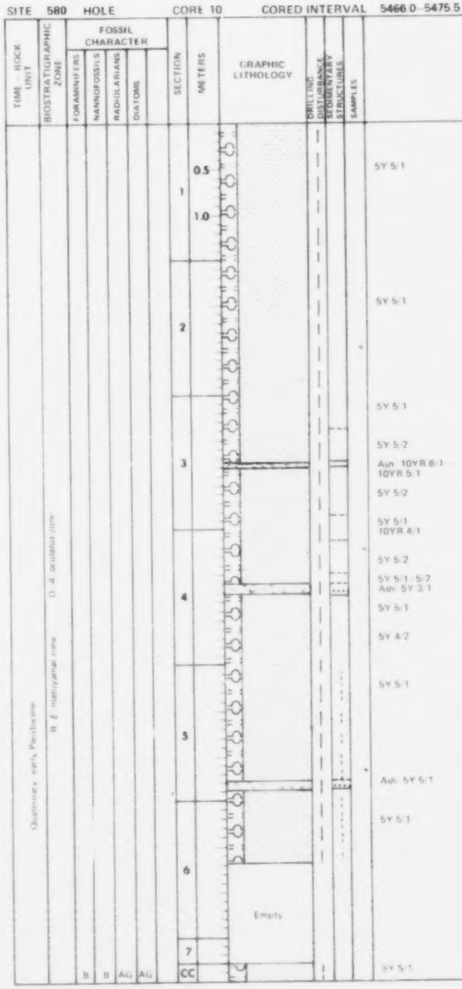
TIME – ROCK UNIT
BIOSTRATIGRAPHIC ZONE
FOSSIL CHARACTER
FORAMINIFERS
NANNOFOSSILS
RADIOLARIANS
DIATOMS
SECTION
METERS
GRAPHIC LITHOLOGY
DRILLING DISTURBANCE
SEDIMENTARY STRUCTURES
SAMPLES
Quaternary, early Pleistocene
R. E. matuyamai zone
D. A. oculatus zone
B
B
AG
AG
1
2
3
4
5
6
7
CC
0.5
1.0
Empty
5Y 5/1
5Y 5/1
5Y 5/1
5Y 5/2
Ash 10YR 6/1
10YR 5/1
5Y 5/2
5Y 5/1
10YR 4/1
5Y 5/2
5Y 5/1-5/2
Ash 5Y 3/1
5Y 5/1
5Y 4/2
5Y 5/1
Ash 5Y 5/1
5Y 5/1
5Y 5/1

LITHOLOGIC DESCRIPTION

SILICEOUS CLAY WITH VOLCANIC ASH LAYERS

- Dominant colors: gray (5Y 5/1), olive gray (5Y 4/2–5Y 5/2). Minor colors: Top of Section 4 is dark gray (10YR 4/1). All sections have thin, indurated dark greenish gray (5G 4/1–5G 5/1) or dark greenish gray (5GY 4/1) layers and thin dark gray (10YR 4/1), dark gray (N4), very dark gray (10YR 3/1), or very dark gray (5Y 3/1) layers. Ash layers are gray (10YR 6/1), gray (10YR 5/1), gray (5Y 5/1), and very dark gray (5Y 3/1).
- Entire core is slightly deformed by drilling.
- This core consists of siliceous clay with common, thin (0.5–1.0 cm), indurated greenish gray clay layers. Sections 5 and 6 are lightly mottled. Ash layers occur at 3, 74–79 cm, 4, 60–71 cm, and, 5, 128–139.5 cm. The two lower ash layers are normally graded with gradational top and sharp bottom contacts. The ash layer in Section 3 has sharp top and bottom contacts.

SMEAR SLIDE SUMMARY (%):

	2, 100 D	4, 25 D	5, 120 D
Texture:			
Sand	20	15	10
Silt	10	25	20
Clay	70	80	70
Composition:			
Quartz	5	7	7
Mica	1	1	–
Clay	68	59	69
Volcanic glass	5	5	5
Carbonate unspec.	–	2	–
Diatoms	9	16	13
Radiolarians	10	7	5
Silicoflagellates	2	4	1

SITE 580 HOLE CORE 11 CORED INTERVAL 5475.5–5485.0 mbsl; 88.8–98.3 mbsf

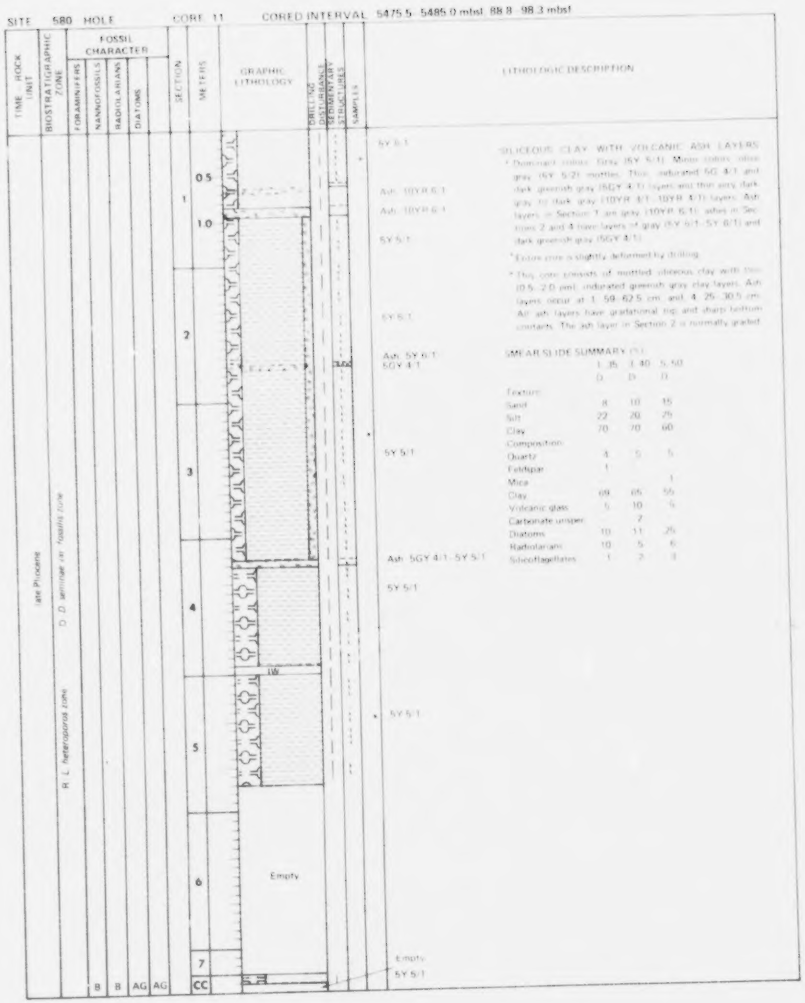
TIME-ROCK UNIT
BIOSTRATIGRAPHIC ZONE
FOSSIL CHARACTER
FORAMINIFERS
NANNOFOSSILS
RADIOLARIANS
DIATOMS
SECTION
METERS
GRAPHIC LITHOLOGY
DRILLING DISTURBANCE
SEDIMENTARY STRUCTURES
SAMPLES
LITHOLOGIC DESCRIPTION
late Pliocene
D. D. seminae var. fossilis zone
R. L. heteroporos zone
B
B
AG
AG
0.5
1.0
1
2
3
4
5
6
7
CC
IW
Empty
5Y 6/1
Ash: 10YR 6/1
Ash: 10YR 6/1
5Y 5/1
5Y 6/1
Ash: 5Y 6/1
5GY 4/1
5Y 5/1
Ash: 5GY 4/1–5Y 5/1
5Y 5/1
5Y 5/1
Empty
5Y 5/1

SILICEOUS CLAY WITH VOLCANIC ASH LAYERS

- Dominant colors: Gray (5Y 5/1). Minor colors: olive gray (5Y 5/2) mottles. Thin, indurated 5G 4/1 and dark greenish gray (5GY 4/1) layers and thin very dark gray to dark gray (10YR 3/1–10YR 4/1) layers. Ash layers in Section 1 are gray (10YR 6/1); ashes in Sections 2 and 4 have layers of gray (5Y 6/1–5Y 6/1) and dark greenish gray (5GY 4/1).
- Entire core is slightly deformed by drilling.
- This core consists of mottled siliceous clay with thin (0.5–2.0 cm), indurated greenish gray clay layers. Ash layers occur at 1, 59–62.5 cm and 4, 25–30.5 cm. All ash layers have gradational top and sharp bottom contacts. The ash layer in Section 2 is normally graded.

SMEAR SLIDE SUMMARY (%):

	1, 35	3, 40	5, 50
	D	D	D
Texture:			
Sand	8	10	15
Silt	22	20	25
Clay	70	70	60
Composition:			
Quartz	4	5	5
Feldspar	1		
Mica			1
Clay	69	65	55
Volcanic glass	5	10	5
Carbonate unspec.		2	
Diatoms	10	11	25
Radiolarians	10	5	6
Silicoflagellates	1	2	3

SITE 580 HOLE CORE 12 CORED INTERVAL 5485.0–5494.5 mbsl; 98.3–107.8 mbsf

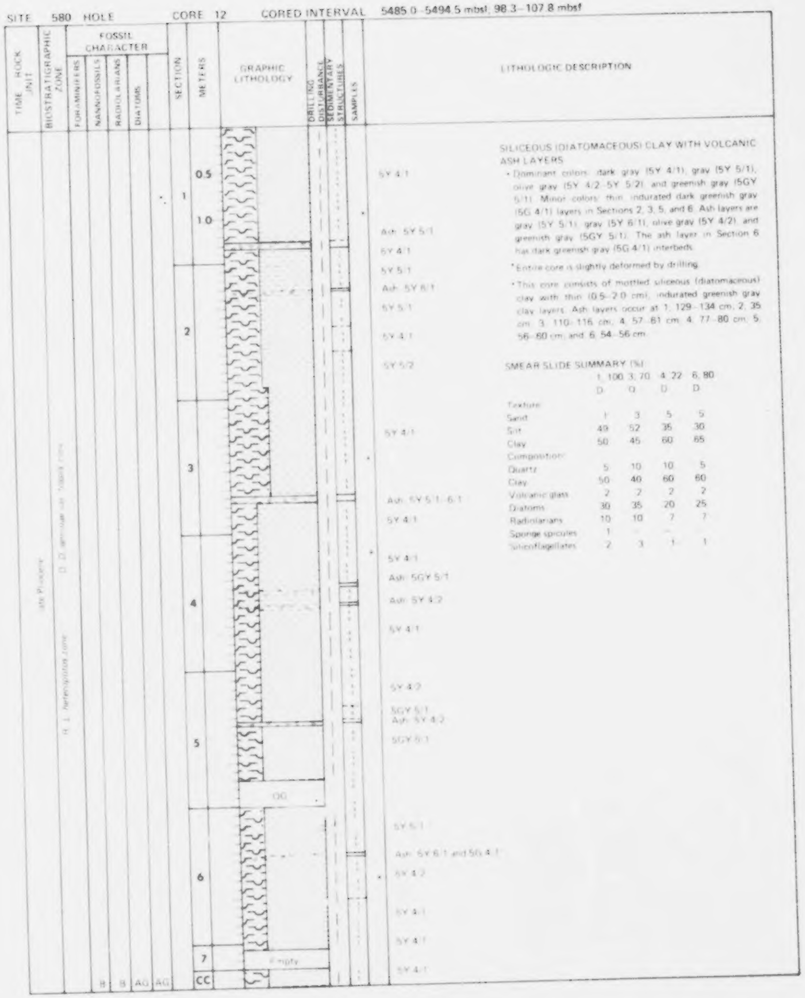
TIME-ROCK UNIT
BIOSTRATIGRAPHIC ZONE
FOSSIL CHARACTER
FORAMINIFERS
NANNOFOSSILS
RADIOLARIANS
DIATOMS
SECTION
METERS
GRAPHIC LITHOLOGY
DRILLING DISTURBANCE
SEDIMENTARY STRUCTURES
SAMPLES
LITHOLOGIC DESCRIPTION
late Pliocene
D. D. seminae var. fossilis zone
R. L. heteroporos zone
B
B
AG
AG
0.5
1.0
1
2
3
4
5
6
7
CC
OG
Empty
5Y 4/1
Ash: 5Y 5/1
5Y 4/1
5Y 5/1
Ash: 5Y 6/1
5Y 5/1
5Y 4/1
5Y 5/2
5Y 4/1
Ash: 5Y 5/1–6/1
5Y 4/1
5Y 4/1
Ash: 5GY 5/1
Ash: 5Y 4/2
5Y 4/1
5Y 4/2
5GY 5/1
Ash: 5Y 4/2
5GY 5/1
5Y 5/1
Ash: 5Y 6/1 and 5G 4/1
5Y 4/2
5Y 4/1
5Y 4/1
5Y 4/1

SILICEOUS (DIATOMACEOUS) CLAY WITH VOLCANIC ASH LAYERS

- Dominant colors: dark gray (5Y 4/1), gray (5Y 5/1), olive gray (5Y 4/2–5Y 5/2), and greenish gray (5GY 5/1). Minor colors: thin, indurated dark greenish gray (5G 4/1) layers in Sections 2, 3, 5, and 6. Ash layers are gray (5Y 5/1), gray (5Y 6/1), olive gray (5Y 4/2), and greenish gray (5GY 5/1). The ash layer in Section 6 has dark greenish gray (5G 4/1) interbeds.
- Entire core is slightly deformed by drilling.
- This core consists of mottled siliceous (diatomaceous) clay with thin (0.5–2.0 cm), indurated greenish gray clay layers. Ash layers occur at 1, 129–134 cm; 2, 35 cm; 3, 110–116 cm; 4, 57–61 cm; 4, 77–80 cm; 5, 56–60 cm; and 6, 54–56 cm.

SMEAR SLIDE SUMMARY (%):

	1, 100	3, 70	4, 22	6, 80
	D	O	D	D
Texture:				
Sand	1	3	5	5
Silt	49	52	35	30
Clay	50	45	60	65
Composition:				
Quartz	5	10	10	5
Clay	50	40	60	60
Volcanic glass	2	2	2	2
Diatoms	30	35	20	25
Radiolarians	10	10	7	7
Sponge spicules	1	–	–	–
Silicoflagellates	2	3	1	1

SITE 580 HOLE CORE 13 CORED INTERVAL 5494.5–5504.0 mbsl; 107.8–117.3 mbsf

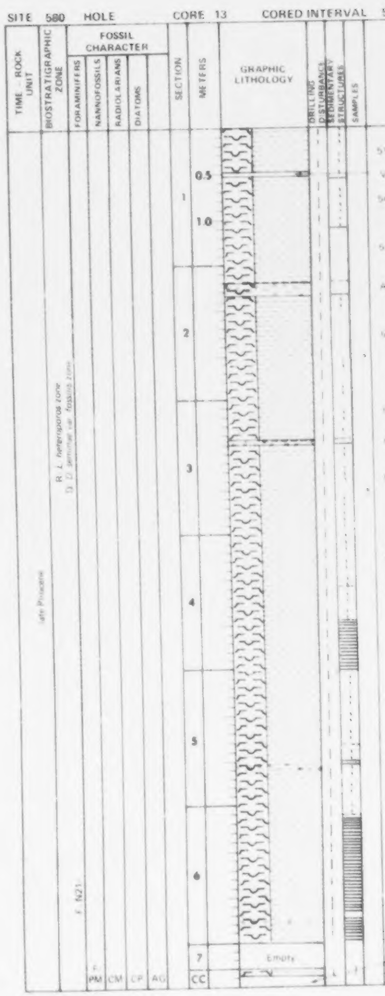
TIME – ROCK UNIT
BIOSTRATIGRAPHIC ZONE
FOSSIL CHARACTER
FORAMINIFERS
NANNOFOSSILS
RADIOLARIANS
DIATOMS
SECTION
METERS
GRAPHIC LITHOLOGY
DRILLING DISTURBANCE
SEDIMENTARY STRUCTURES
SAMPLES
late Pliocene
R. L. heteroporos zone
D. D. seminae var. fossilis zone
F. N21
F/PM
CM
CP
AG
1
2
3
4
5
6
7
CC
0.5
1.0
Empty

5Y 4/1
Void
5GY 5/1
5Y 4/1
Ash: 5Y 5/1
5GY 5/1
5Y 5/1
Ash: 5Y 5/1
5Y 4/1
5Y 5/1
5GY 4/1
5Y 4/1
5Y 5/2
Ash: 5Y 6/1
5Y 5/1
5Y 4/2
5Y 6/1
Empty
5Y 5/2

LITHOLOGIC DESCRIPTION

SILICEOUS (DIATOMACEOUS) CLAY WITH VOLCANIC ASH LAYERS

- Dominant colors: dark gray (5Y 4/1), gray (5Y 5/1), olive gray (5Y 4/2–5Y 5/2), dark greenish gray (5GY 4/1), and greenish gray (5GY 5/1). Minor colors: dark greenish gray (5G 4/1) lamination and thin stiff layers; very dark gray (5Y 3/1) laminations. Ash layers are gray (5Y 5/1) and gray (5Y 6/1).
- Entire core is slightly deformed by drilling.
- This core consists of homogeneous to lightly mottled siliceous (diatomaceous) clay with local thin (0.5–1.0 cm), stiff greenish gray clay layers. Section 4, 83–150 cm and Section 6, 11–150 cm have faint greenish gray laminations spaced approximately every 3–5 cm. Ash layers occur at 2, 29–33 cm; 3, 44–49 cm; 5, 101–103 cm; and 6, 124 cm.

SMEAR SLIDE SUMMARY (%)

	2, 100 D	3, 100 D
Texture		
Sand	1	5
Silt	49	45
Clay	50	50
Composition		
Quartz	6	5
Clay	54	48
Volcanic glass	3	5
Carbonate unspec.		1
Diatoms	25	30
Radiolarians	10	10
Silicoflagellates	1	2

SITE 580 HOLE CORE 14 CORED INTERVAL 5504.0–5513.5 mbsl; 117.3–126.8 mbsf

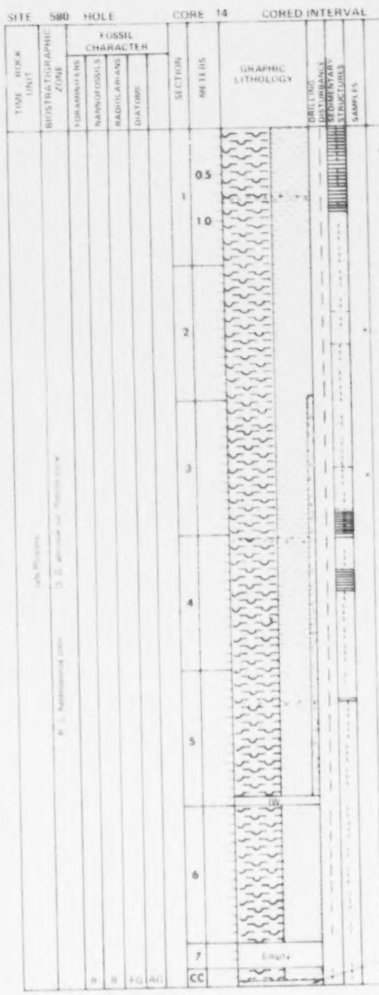
TIME – ROCK UNIT
BIOSTRATIGRAPHIC ZONE
FOSSIL CHARACTER
FORAMINIFERS
NANNOFOSSILS
RADIOLARIANS
DIATOMS
SECTION
METERS
GRAPHIC LITHOLOGY
DRILLING DISTURBANCE
SEDIMENTARY STRUCTURES
SAMPLES
late Pliocene
D. D. seminae var. fossilis zone
R. L. heteroporos zone
R
R
FG
AG
1
2
3
4
5
6
7
CC
0.5
1.0
IW
Empty

5Y 4/2
Ash: 5Y 3/1
5Y 4/2
5Y 4/2
5Y 5/1
5Y 4/1
5Y 4/1
5GY 5/1
5GY 4/1
Ash: 5Y 6/1
5Y 4/2
5Y 4/1
Ash: 5Y 5/1
5Y 4/1
5GY 5/1
Empty
5Y 4/2

LITHOLOGIC DESCRIPTION

CLAYEY DIATOM OOZE WITH VOLCANIC ASH LAYERS

- Dominant colors: dark gray (5Y 4/1), gray (5Y 5/1), olive gray (5Y 4/2), dark greenish gray (5GY 4/1), and greenish gray (5GY 5/1). Minor colors: dark greenish gray and very dark gray (5Y 3/1) laminations. Ash layers are very dark gray (5Y 3/1) and gray (5Y 5/1–5Y 6/1).
- Entire core is slightly deformed by drilling.
- This core consists of mottled clayey diatom ooze with laminated intervals at 1, 0–90 cm; 3, 124–150 cm; and, 4, 41–67 cm. Laminations are mostly very dark gray and spaced approximately one (1) cm apart. Ash layers occur at 1, 78 cm; 4, 1–3 cm; and, 5, 35–37 cm.

SMEAR SLIDE SUMMARY (%)

	2, 80 D	3, 87 D
Texture		
Sand	15	15
Silt	50	50
Clay	35	35
Composition		
Quartz	7	10
Mica	—	2
Clay	37	26
Volcanic glass	3	10
Diatoms	50	50
Radiolarians	3	2

SITE 580 HOLE CORE 15 CORED INTERVAL 5513.5–5523.0 mbsl, 126.8–136.3 mbsf

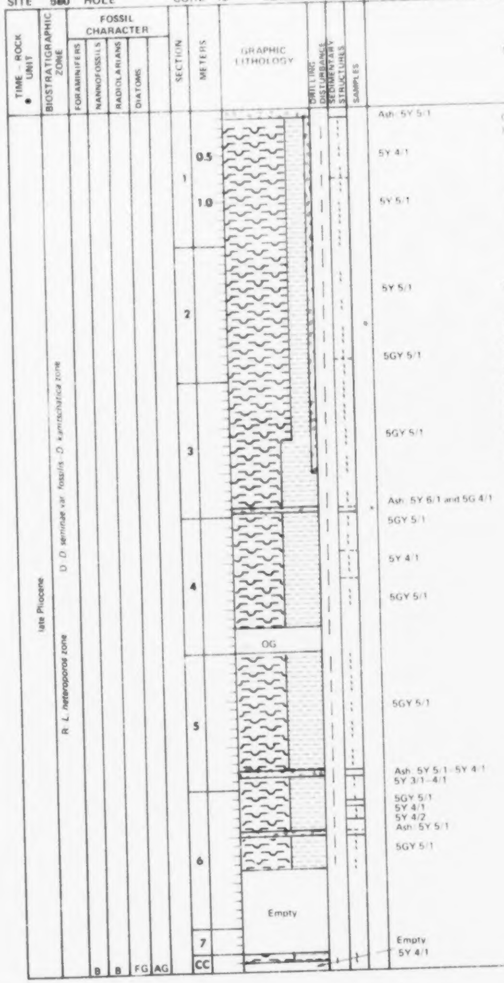
TIME – ROCK UNIT
BIOSTRATIGRAPHIC ZONE
FOSSIL CHARACTER
FORAMINIFERS
NANNOFOSSILS
RADIOLARIANS
DIATOMS
SECTION
METERS
GRAPHIC LITHOLOGY
DRILLING DISTURBANCE
SEDIMENTARY STRUCTURES
SAMPLES
late Pliocene
D D. seminae var. fossilis–D. kamtschatica zone
R L. heteroporos zone
B
B
FG
AG
0.5
1.0
1
2
3
4
5
6
7
CC
OG
Empty
Ash: 5Y 5/1
5Y 4/1
5Y 5/1
5Y 5/1
5GY 5/1
5GY 5/1
Ash: 5Y 6/1 and 5G 4/1
5GY 5/1
5Y 4/1
5GY 5/1
5GY 5/1
Ash: 5Y 5/1–5Y 4/1
5Y 3/1–4/1
5GY 5/1
5Y 4/1
5Y 4/2
Ash: 5Y 5/1
5GY 5/1
Empty
5Y 4/1

LITHOLOGIC DESCRIPTION

CLAYEY DIATOM OOZE WITH VOLCANIC ASH LAYERS

*Dominant colors: greenish gray (5GY 5/1), gray (5Y 5/1), and dark gray (5Y 4/1). Minor colors: zones and thin layers of dark greenish gray (5G 4/1) and very dark gray (5Y 3/1). Ash layers are dark gray (5Y 4/1), gray (5Y 5/1), and gray (5Y 6/1).

*Entire core is slightly deformed by drilling.

*This core consists of lightly mottled clayey diatom ooze. Ash layers occur at 1, 0–7 cm; 3, 139–144 cm; 5, 128–134 cm; and 6, 45–49 cm.

SMEAR SLIDE SUMMARY (%):

	2, 90 D	3, 148 D
Texture:		
Sand	25	15
Silt	40	50
Clay	35	35
Composition:		
Quartz	5	5
Feldspar	–	2
Clay	15	31
Volcanic glass	10	5
Diatoms	60	50
Radiolarians	10	7

SITE 580 HOLE CORE 16 CORED INTERVAL 5523.0–5532.5 mbsl; 136.3–145.8 mbsf

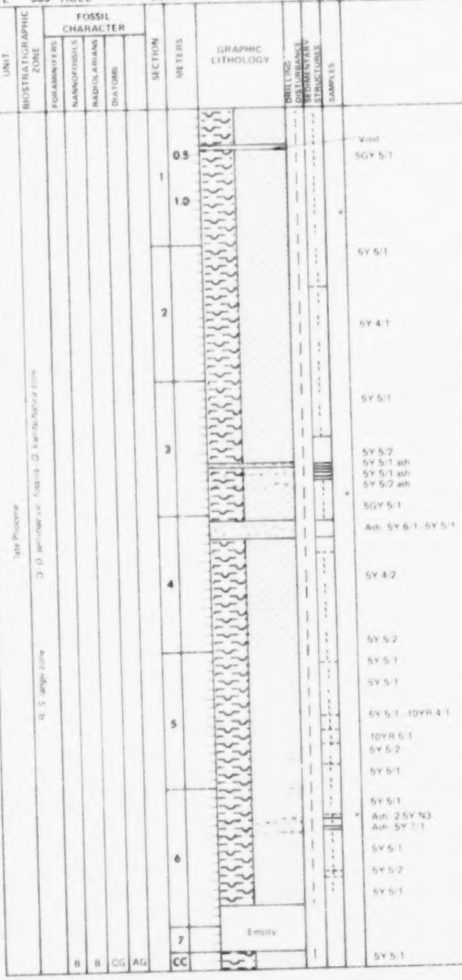
TIME – ROCK UNIT
BIOSTRATIGRAPHIC ZONE
FOSSIL CHARACTER
FORAMINIFERS
NANNOFOSSILS
RADIOLARIANS
DIATOMS
SECTION
METERS
GRAPHIC LITHOLOGY
DRILLING DISTURBANCE
SEDIMENTARY STRUCTURES
SAMPLES
late Pliocene
D D. seminae var. fossilis–D. kamtschatica zone
R S. langii zone
B
B
CG
AG
0.5
1.0
1
2
3
4
5
6
7
CC
Empty
Void
5GY 5/1
5Y 5/1
5Y 4/1
5Y 5/1
5Y 5/2
5Y 5/1 ash
5Y 5/1 ash
5Y 5/2 ash
5GY 5/1
Ash: 5Y 6/1–5Y 5/1
5Y 4/2
5Y 5/2
5Y 5/1
5Y 5/1
6Y 5/1–10YR 4/1
10YR 5/1
5Y 5/2
5Y 5/1
5Y 5/1
Ash: 2.5Y N3
Ash: 5Y 7/1
5Y 5/1
5Y 5/2
5Y 5/1
5Y 5/1

LITHOLOGIC DESCRIPTION

SILICEOUS CLAY WITH VOLCANIC ASH LAYERS

*Dominant colors: dark gray (5Y 4/1), gray (5Y 5/1), olive gray (5Y 4/2–5Y 5/2), greenish gray (5GY 5/1). Minor colors: Section 5 has layers of gray (10YR 4/1–10YR 5/1). Core contains local, thin, stiff dark greenish gray (5G 4/1) layers and zones. Ash layers are gray (5Y 5/1), gray (5Y 6/1), light gray (5Y 7/1), olive gray (5Y 5/2), and very dark gray (2.5Y N3).

*Entire core is slightly deformed by drilling.

*This core consists of mottled siliceous clay with local, thin (0.5–1.0 cm), stiff greenish gray clay layers. Ash layers occur at 3, 92–95 cm; 3, 99–101 cm; 3, 101–110 cm; 5, 6–24 cm; 6, 32–36 cm; and 6, 39–42 cm.

SMEAR SLIDE SUMMARY (%):

	1, 120 D	3, 130 D	6, 37 D
Texture:			
Sand	25	25	20
Silt	25	25	40
Clay	50	50	40
Composition:			
Quartz	5	7	7
Mica	1	Tr	1
Clay	52	48	40
Volcanic glass	3	5	10
Diatoms	30	30	35
Radiolarians	8	10	7
Silicoflagellates	1	–	–

SITE 580 HOLE CORE 17 CORED INTERVAL 5532.5–5542.0 mbsl; 145.8–155.3 mbsf

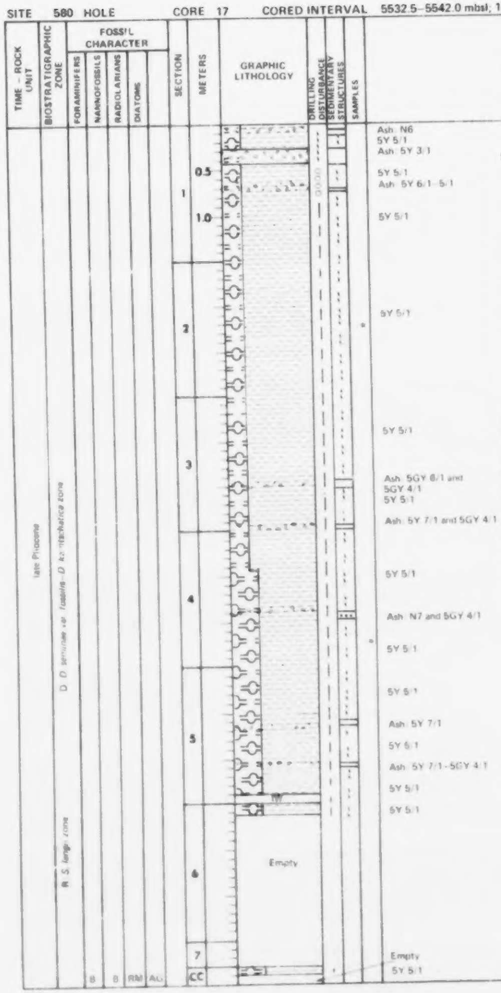
TIME – ROCK UNIT
BIOSTRATIGRAPHIC ZONE
FOSSIL CHARACTER
FORAMINIFERS
NANNOFOSSILS
RADIOLARIANS
DIATOMS
SECTION
METERS
GRAPHIC LITHOLOGY
DRILLING DISTURBANCE
SEDIMENTARY STRUCTURES
SAMPLES
late Pliocene
D. D. seminae var. fossilis–D. kamtschatica zone
R. S. langii zone
B
B
RM
AG
1
2
3
4
5
6
7
CC
0.5
1.0
Empty
Ash: N6
5Y 5/1
Ash: 5Y 3/1
5Y 5/1
Ash: 5Y 6/1–5/1
5Y 5/1
5Y 5/1
5Y 5/1
Ash: 5GY 6/1 and 5GY 4/1
5Y 5/1
Ash: 5Y 7/1 and 5GY 4/1
5Y 5/1
Ash: N7 and 5GY 4/1
5Y 5/1
5Y 5/1
Ash: 5Y 7/1
5Y 5/1
Ash: 5Y 7/1–5GY 4/1
5Y 5/1
5Y 5/1
Empty
5Y 5/1

LITHOLOGIC DESCRIPTION

SILICEOUS CLAY WITH VOLCANIC ASH LAYERS

*Dominant colors: gray (5Y 5/1). Minor colors: 5Y 5/2 mottles. Core contains thin layers of very dark gray (5Y 3/1) and dark greenish gray (5GY 4/1). Ash layers are light gray (5Y 7/1), light gray (N7), gray (5Y 6/1), gray (N6), gray (5Y 5/1), and very dark gray (5Y 3/1). Ash layers in Sections 3, 4, and 5 contain interbeds of dark greenish gray (5GY 4/1).

*Upper 75 cm of Section 1 is soupy or very deformed; rest of core is slightly deformed by drilling.

*This core consists of mottled siliceous clay. Ash layers occur at 1, 4–12 cm; 1, 24–41 cm; 1, 69–71 cm; 3, 91–99 cm; 3, 144–147 cm; 4, 87–94.5 cm; 5, 59–62 cm; and, 5, 103–106 cm. The ash layer in Section 4 is normally graded. A pebble of indurated ash(?) 2 cm in length is located in Section 1, 10–11 cm.

SMEAR SLIDE SUMMARY (%)

	2, 75	4, 128
	D	D
Texture		
Sand	10	25
Silt	20	15
Clay	70	60
Composition		
Quartz	7	5
Mica	Tr	–
Clay	69	57
Volcanic glass	2	2
Diatoms	15	5
Radiolarians	7	30
Silicoflagellates	—	1

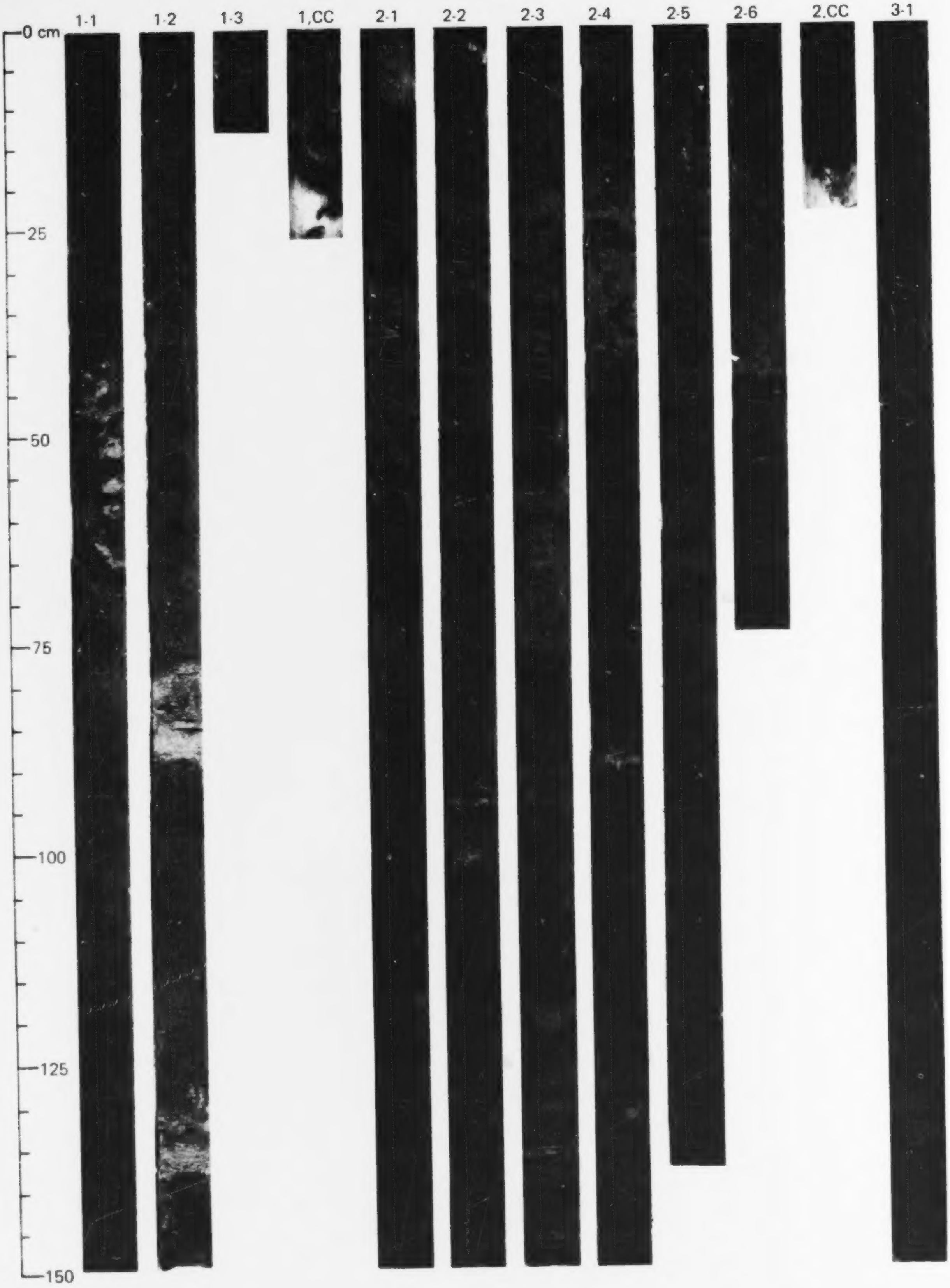
1-1
1-2
1-3
1,CC
2-1
2-2
2-3
2-4
2-5
2-6
2,CC
3-1
0 cm
25
50
75
100
125
150

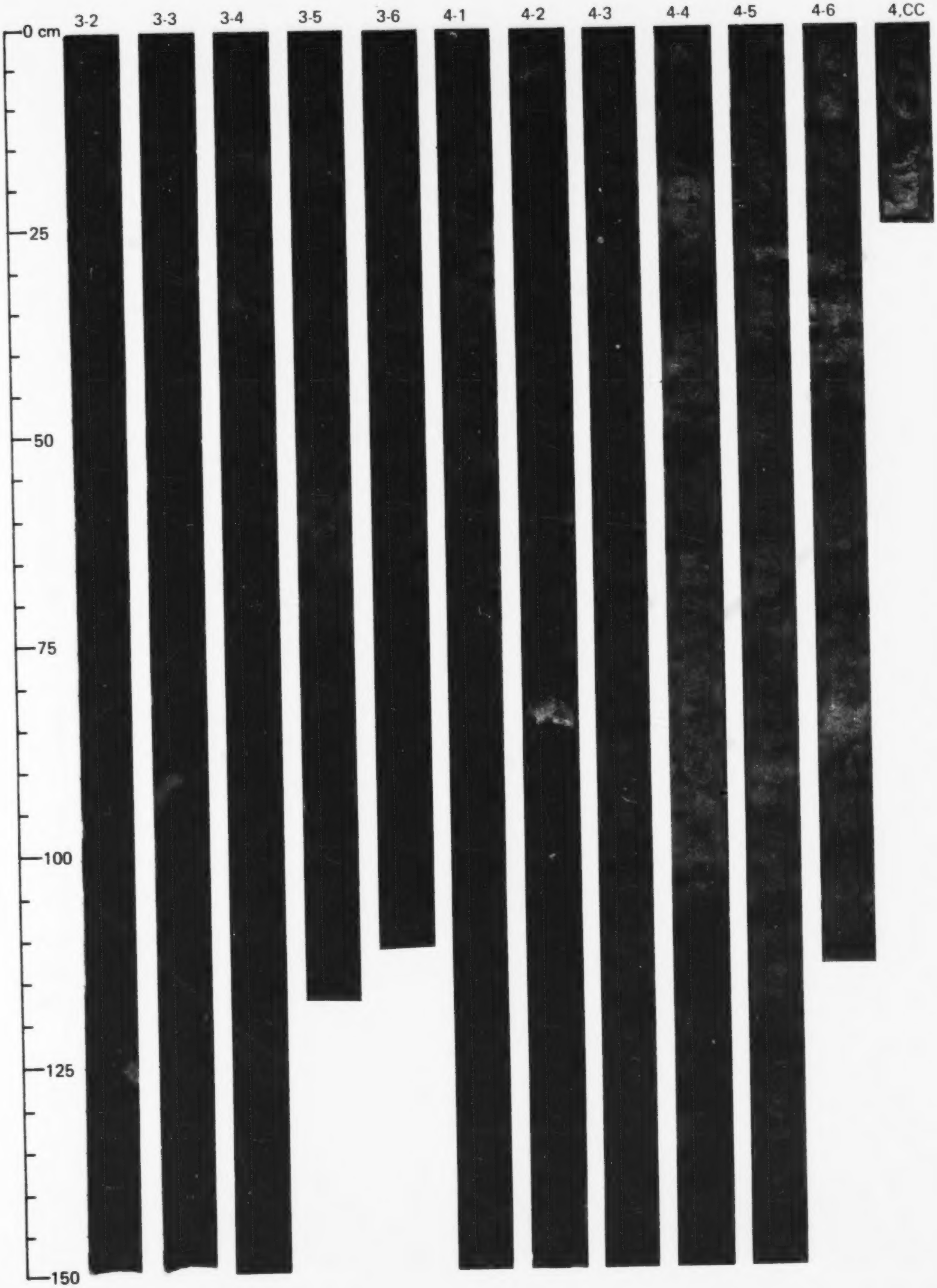
3-2
3-3
3-4
3-5
3-6
4-1
4-2
4-3
4-4
4-5
4-6
4,CC
0 cm
25
50
75
100
125
150

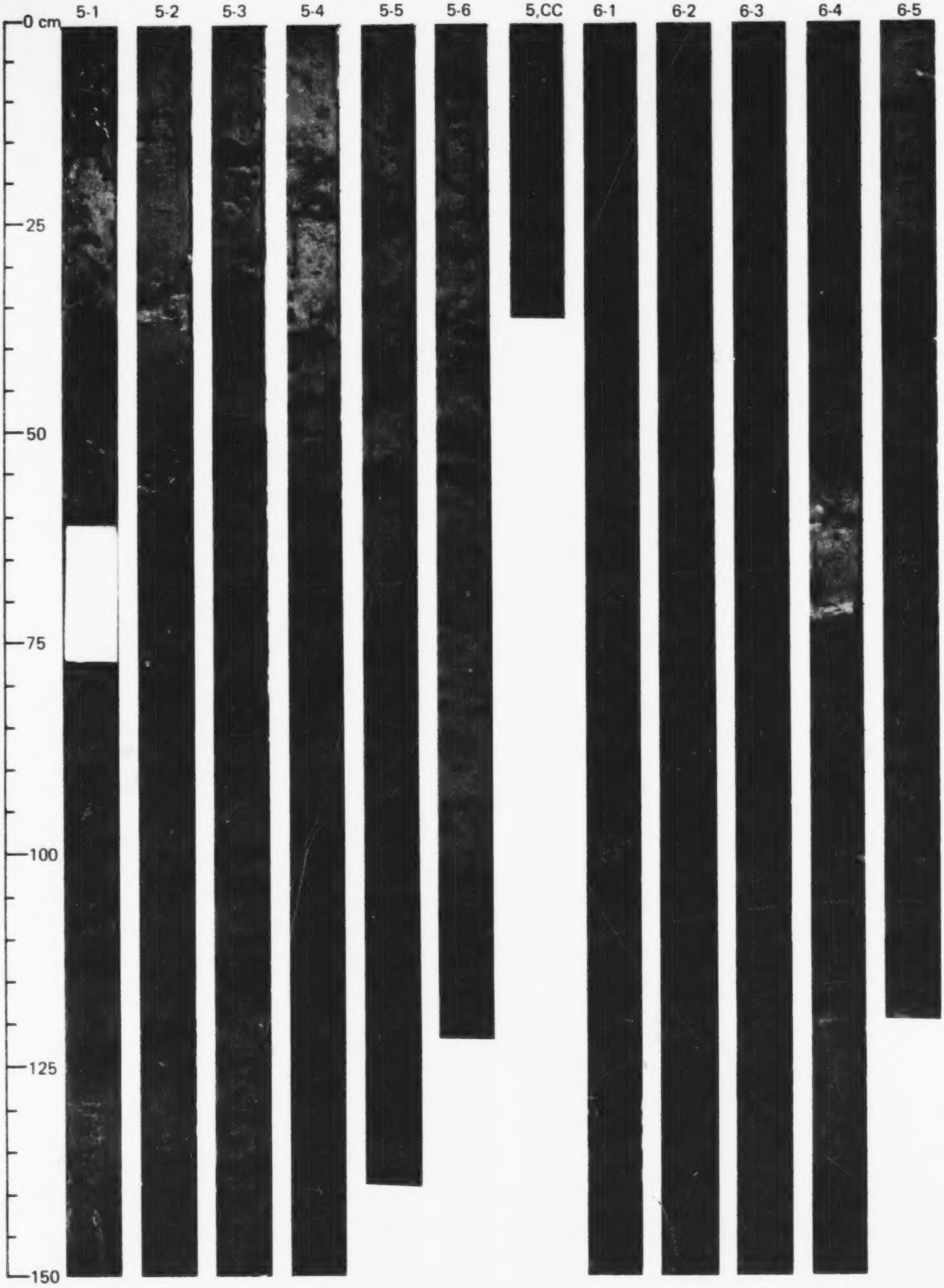
5-1
5-2
5-3
5-4
5-5
5-6
5,CC
6-1
6-2
6-3
6-4
6-5
0 cm
25
50
75
100
125
150

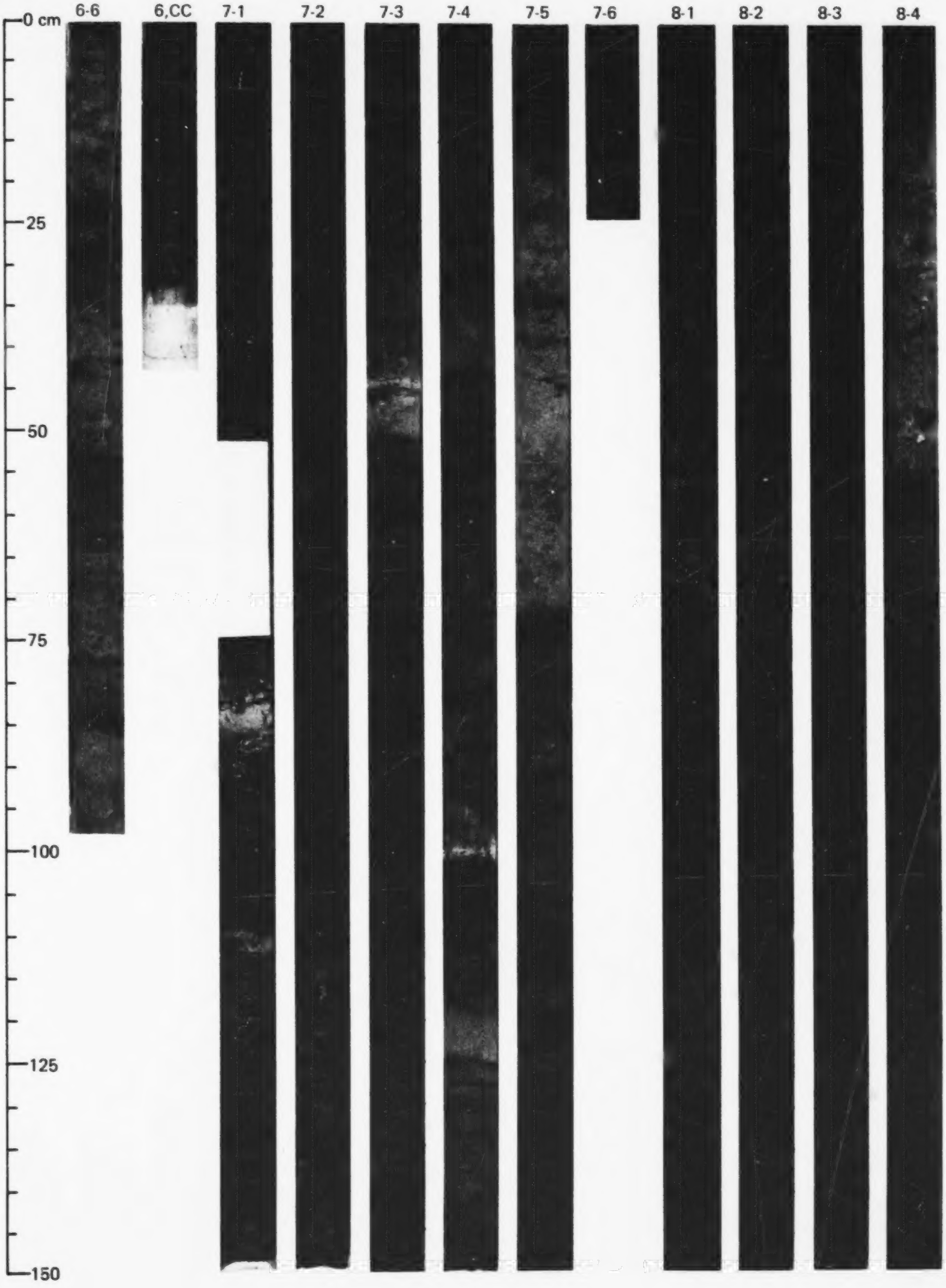
0 cm
25
50
75
100
125
150
6-6
6,CC
7-1
7-2
7-3
7-4
7-5
7-6
8-1
8-2
8-3
8-4

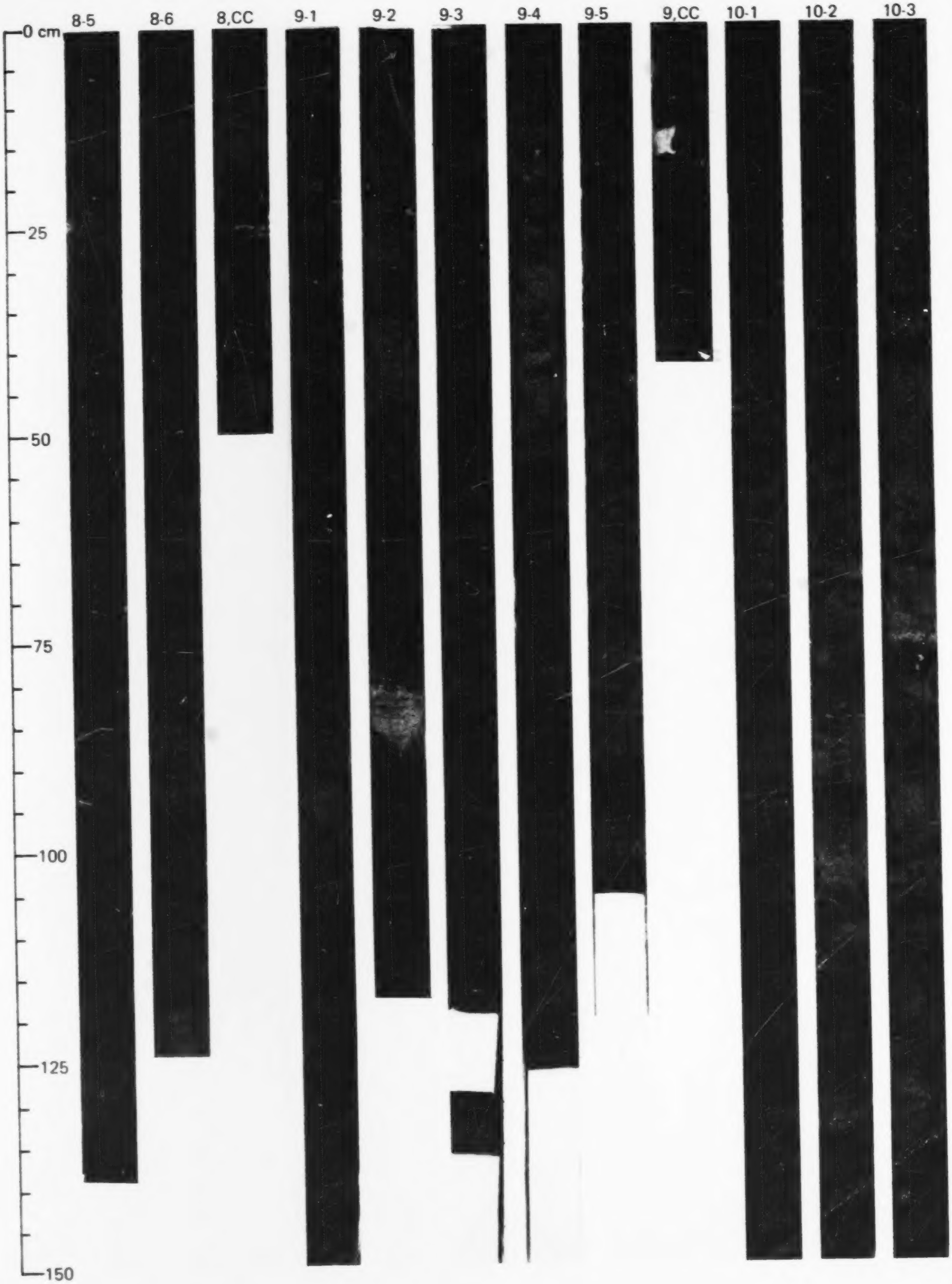
8-5
8-6
8,CC
9-1
9-2
9-3
9-4
9-5
9,CC
10-1
10-2
10-3
0 cm
25
50
75
100
125
150

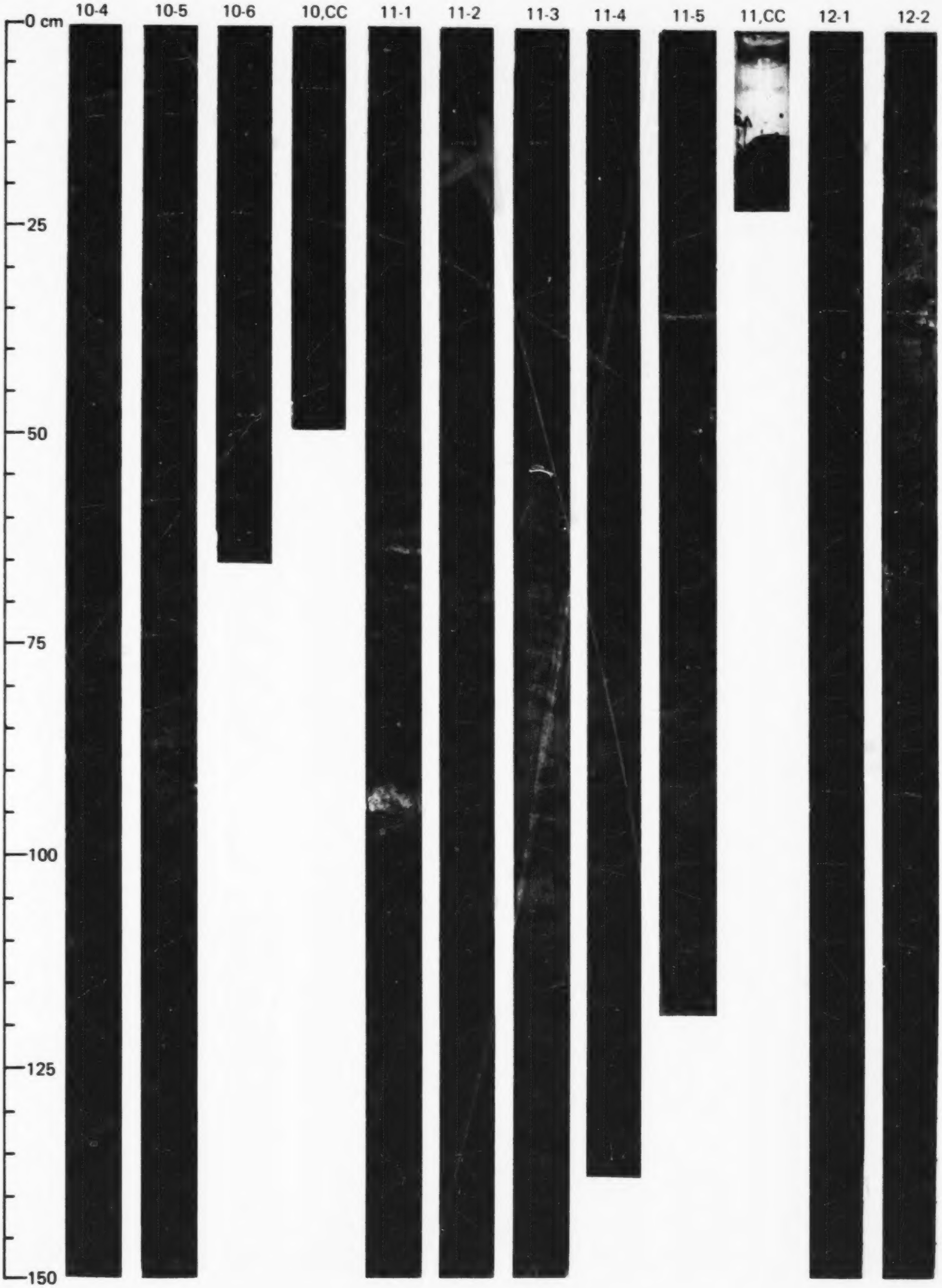
10-4
10-5
10-6
10,CC
11-1
11-2
11-3
11-4
11-5
11,CC
12-1
12-2
0 cm
25
50
75
100
125
150

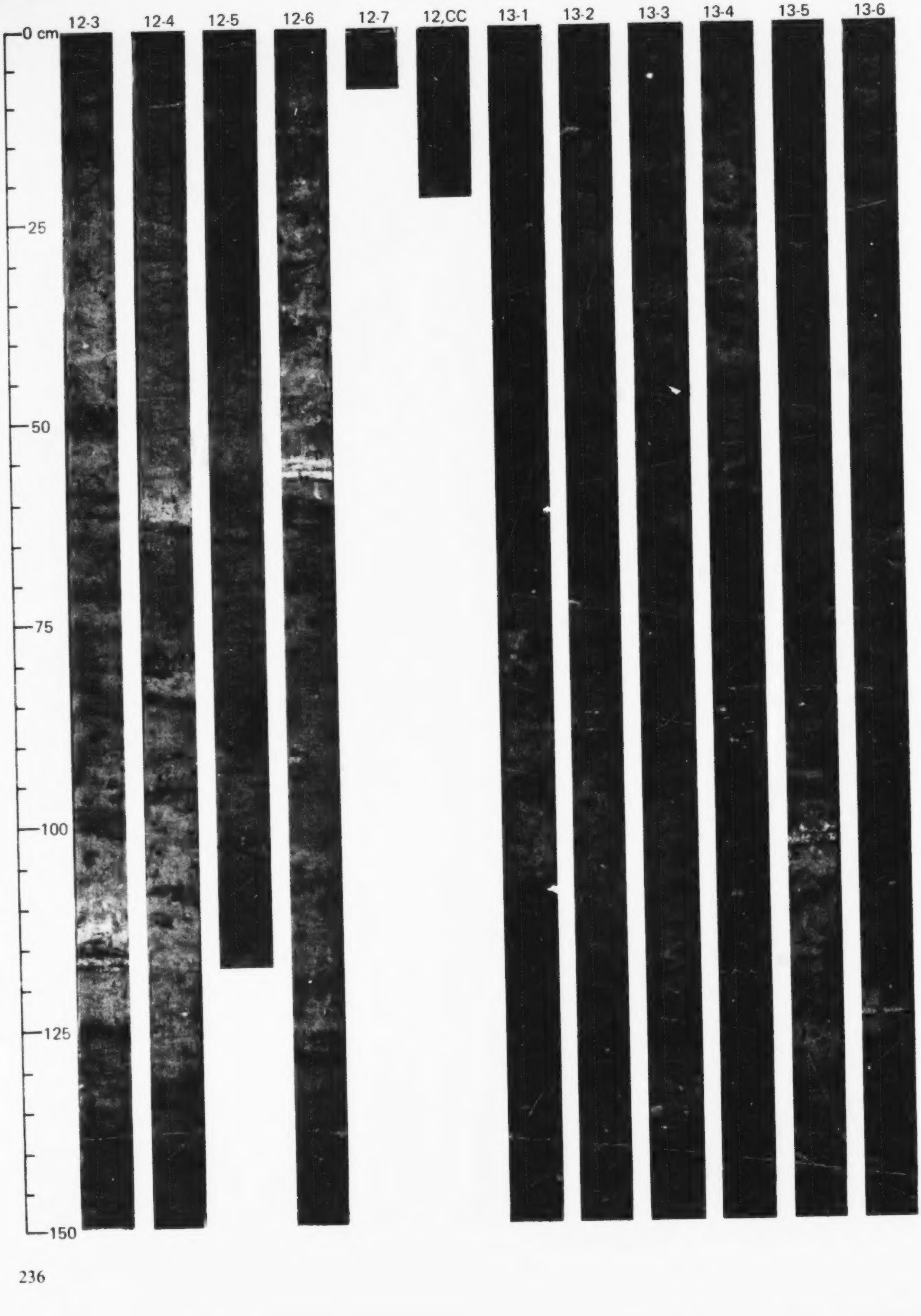
12-3
12-4
12-5
12-6
12-7
12,CC
13-1
13-2
13-3
13-4
13-5
13-6
0 cm
25
50
75
100
125
150

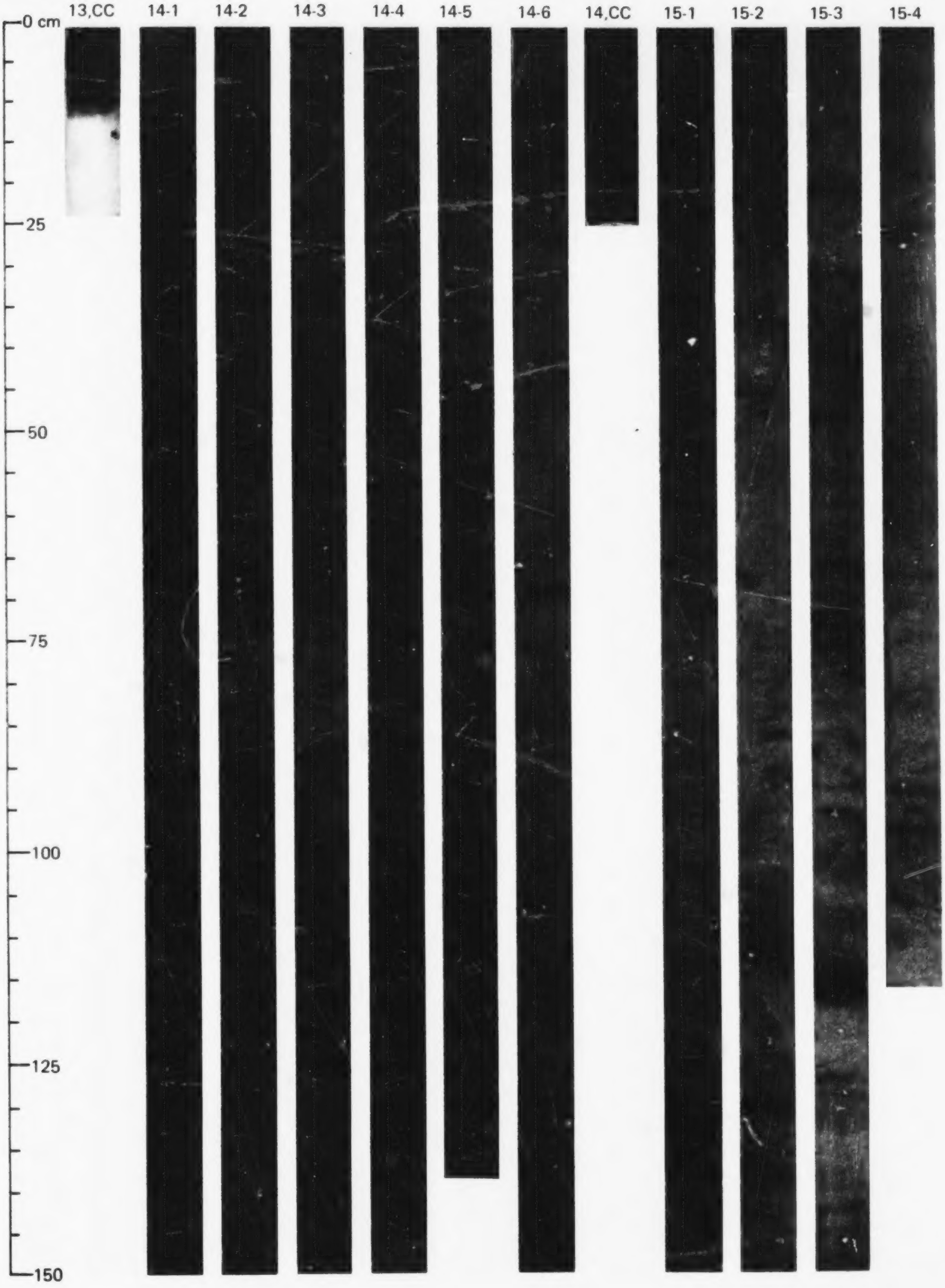
0 cm
25
50
75
100
125
150
13,CC
14-1
14-2
14-3
14-4
14-5
14-6
14,CC
15-1
15-2
15-3
15-4

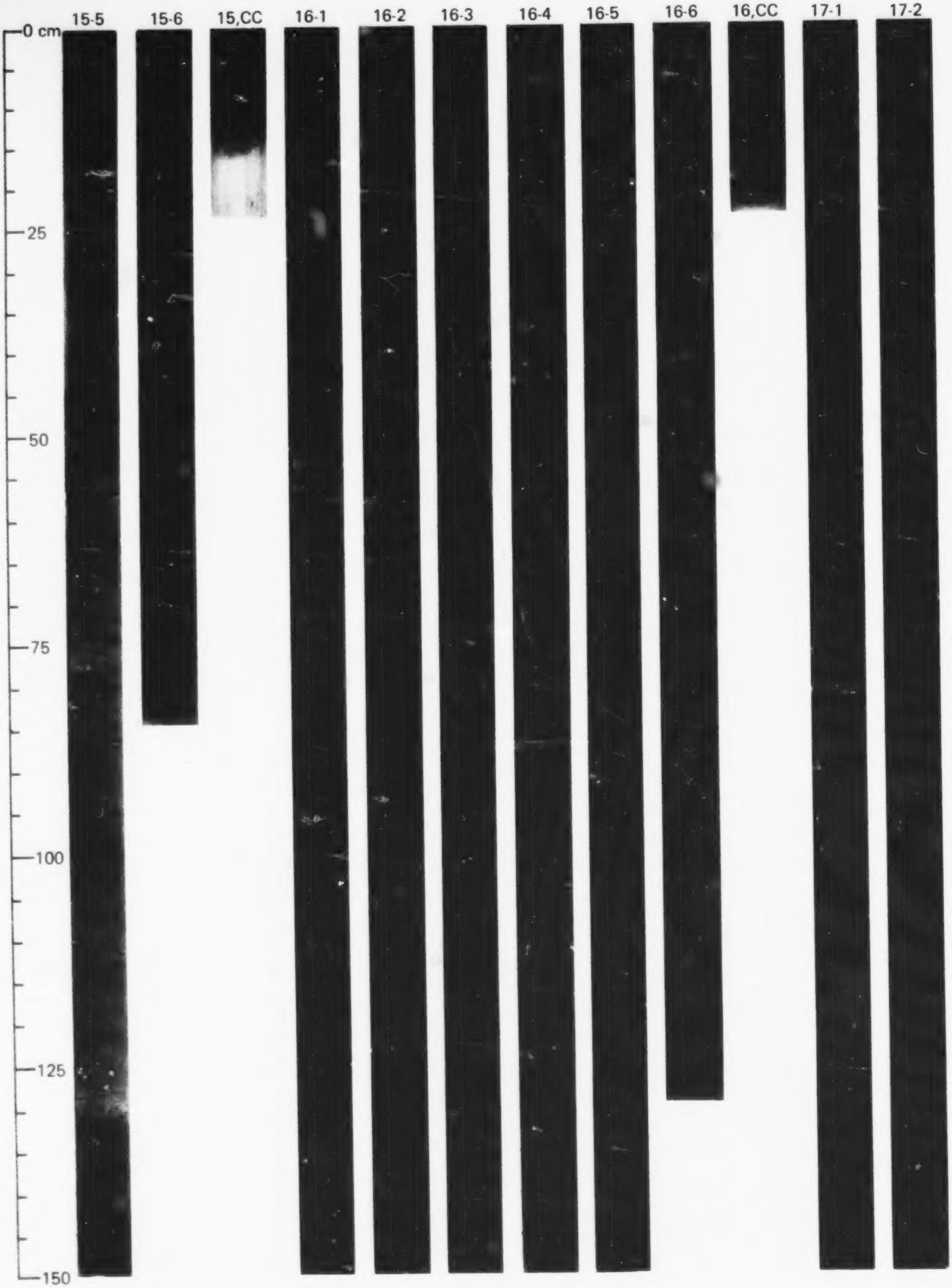
15-5
15-6
15,CC
16-1
16-2
16-3
16-4
16-5
16-6
16,CC
17-1
17-2
0 cm
25
50
75
100
125
150

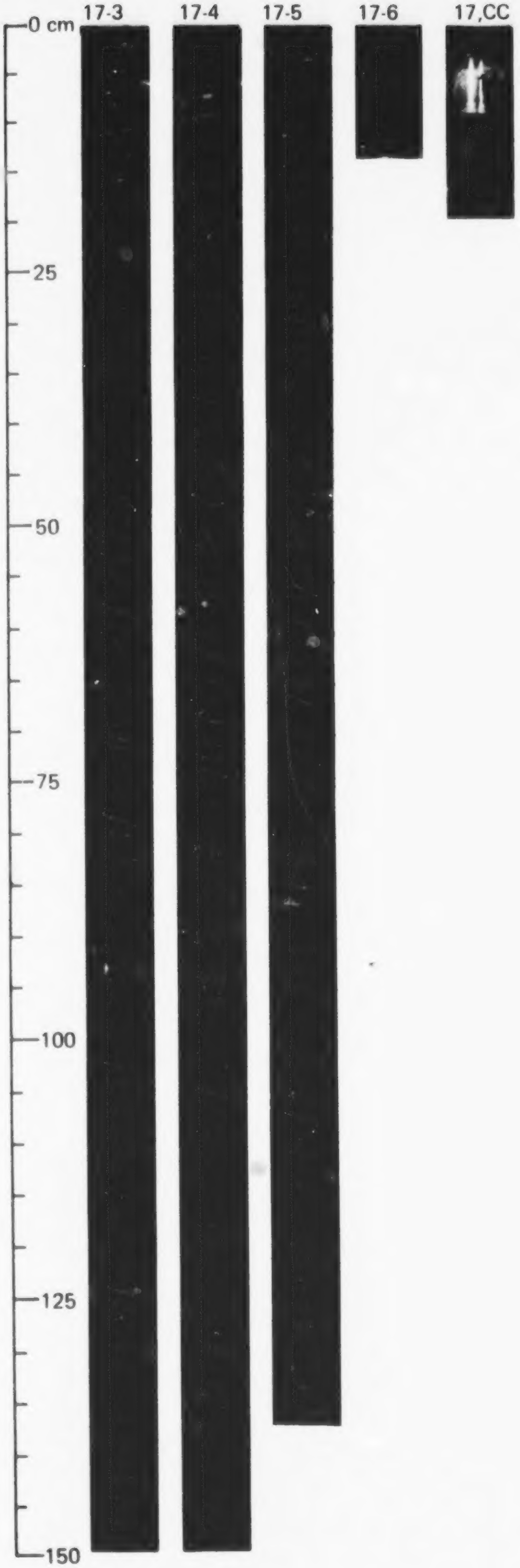
17-3
17-4
17-5
17-6
17,CC
0 cm
25
50
75
100
125
150

8. SITE 581[1]

Shipboard Scientific Party[2]

HOLE 581

Date occupied: 10 June 1982

Date departed: 13 June 1982

Time on hole: 3 days, 8 hr.

Position (latitude; longitude): 43°55.62′N; 159°47.76′E

Water depth (sea level; corrected m, echo-sounding): 5476

Water depth (rig floor; corrected m, echo-sounding): 5486

Bottom felt (m, drill pipe): 5487.5

Penetration (m): 352.5

Number of cores: 19

Total length of cored section (m): 172.0

Total core recovered (m): 77.59

Core recovery (%): 45

Oldest sediment cored:
Depth sub-bottom (m): 343.0
Nature: Chert
Age: Unknown
Measured velocity (km/s): 5.4

Basement:
Depth sub-bottom (m): 344
Nature: Basalt
Velocity range (km/s): 4.8–5.3

Principal results: Because of the limited time available and the need to drill to basement to allow participants on Leg 88 to plan their casing program, hydraulic piston core (HPC) sampling of the softer sediments at Site 581 was deferred until Leg 88 (which, unfortunately, did not accomplish this objective). Apart from a mud line core, we did not sample the interval above 181.5 m.

From 181.5 to 223.6 m, section is reduced (gray and green) late Miocene to earliest Pliocene biosiliceous clay to ooze, similar to but less ashy and pyritic than the sections at Sites 579 and 580. Presumably, the uncored section above is similar, but with more ash and pyritic layers toward the surface.

From 223.6 to 244.8 m, the sediment is oxidized (yellow brown) latest middle Miocene to late Miocene biosiliceous clay, which accumulated at about one fifth the rate of the overlying sediments.

From 244.8 to 276.6 m, the sediment is "slick," fine-grained pelagic clay of presumed middle Miocene age and older, which grades down from brown to very dark brown in color. From 276.6 to 343.0 m, we recovered nothing but chert fragments, even though the drilling rate suggests that most of the section is soft sediment (?clay). The chert ranges from off-white to bright reds and yellows and dark brown in color. Most of it looks like silicified dark brown pelagic clay. Diatoms from a small vug in a fragment near the top of the sequence are early late Miocene in age (younger than the overlying sediments), and, therefore, may have been introduced during the coring process.

The hole was terminated after drilling from 343 to 352.5 m in medium gray aphyric basalt containing calcite and iron oxide-lined fractures and alteration rinds. Because no soft sediment was recovered below 276.6 m, the age of the basalt is unknown.

BACKGROUND AND OBJECTIVES

Site 581 (target Site MSS-82C) was a late selection for this leg. It was designed to meet the goals of Site NW-6 (which was too close to Soviet territory for PCOM approval) for a very high resolution late Neogene record, as well as to serve as a pilot hole for the Defense Advance Research Projects Agency (DARPA) downhole seismometer experiment to be carried out on Leg 88.

Our operational objectives were to carry out a brief site survey to define further the area of smooth terrain crossed by *Vema*-21 profiler records 872 and 873 and then to drill to basalt to establish the section to be cased on Leg 88. Because of time constraints, the original plan to HPC the upper part of the section had to be deferred to Leg 88, which did not, in fact, accomplish this objective. Our drilling program involved collection of a mud line core, washing without rotation to establish the surface casing program, washing as far as possible with rotation (estimated to be about 170 m sub-bottom), and then continuous rotary coring to basalt.

The scientific objectives that remained after deletion of the HPC coring were

1. To date the transition from oxic to anoxic deposition (if deeper than washed depth) for comparison with Site 578.
2. To date the transition from pelagic clay to biosiliceous clay, again for comparison with Site 578.
3. To collect the Cretaceous–Neogene pelagic clay section above chert for geotechnical and geochemical comparisons with Sites 576 and 578. Geotechnical comparison was of particular interest because the clay sections at Sites 576, 578, and 581 should be of comparable age, but have been subjected to progressively greater overburden loads from Sites 576 to 578 to 581.

---

[1] Heath, G. R., Burckle, L. H., et al., *Init. Repts. DSDP*, 86: Washington (U.S. Govt. Printing Office).

[2] Addresses: G. Ross Heath (Co-Chief Scientist) School of Oceanography, Oregon State University, Corvallis, OR 97331 (present address: College of Ocean and Fishery Sciences, University of Washington, Seattle, WA 98195); Lloyd H. Burckle (Co-Chief Scientist) Lamont-Doherty Geological Observatory, Palisades, NY 10964; Anthony E. D'Agostino, ARCO Exploration Company, Houston, TX 77056; Ulrich Bleil, Institut für Geophysik, Ruhr-Universitat Bochum, D-4630 Bochum Querenburg, Federal Republic of Germany; Ki-iti Horai, Lamont-Doherty Geological Observatory, Palisades, NY 10964 (present address: Meteorological College, Chiba University, Chiba 277, Japan); Robert D. Jacobi, Department of Geological Sciences, SUNY Buffalo, Amherst, NY 14226; Tom Janecek, Department of Atmospheric & Oceanic Science, University of Michigan, Ann Arbor, MI 48109 (present address: Lamont-Doherty Geological Observatory, Palisades, NY 10964); Itaru Koizumi, College of General Education, Osaka University, Osaka 560, Japan; Lawrence A. Krissek, School of Oceanography, Oregon State University, Corvallis, OR 97331 (present address: Department of Geology and Mineralogy, Ohio State University, Columbus, OH 43210); Nicole Lenôtre, Bureau de Recherches Géologiques et Minieres, Centre Oceanologique de Bretagne, 45060 Orléans Cedex, France; Simonetta Monechi, Geological Research Division, Scripps Institution of Oceanography, La Jolla, CA 92093 (present address: Dipartimento di Scienze della Terra, Università di Firenze, 4 Via La Pira, 50121 Firenze, Italy); Joseph J. Morley, Lamont-Doherty Geological Observatory, Palisades, NY 10964; Peter Schultheiss, Institute of Oceanographic Sciences, Surrey GU8 5UB, United Kingdom; Audrey A. Wright, Deep Sea Drilling Project, Scripps Institution of Oceanography, La Jolla, CA 92093 (present address: Ocean Drilling Program, 500 University Drive West, Texas A&M University, College Station, TX 77843).

Geologic and Topographic Setting

The only data for the region were the echo character map of Damuth et al. (1983) and a *Vema*-21 air-gun profile. The regional topography is irregular, with about 300 m of relief at a length scale of 10-20 km. The proposed site lies in a 40-km section of smoother topography that forms a broad depression with about 100 m of relief. This depression may be part of the Hokkaido Fracture Zone. The profiler section shows about 300 m of layered sediment (ash-bearing siliceous clay overlying pelagic clay, based on the lithologic sections recovered at our earlier sites) above about 60 m of presumed chert-carbonate, resting on basalt.

OPERATIONS

From Site 580, we steamed northeast to Site 581 (target Site MSS-82C). The quality of the air-gun records, particularly approaching Site 581, was not as good as those collected earlier in the leg, because of adverse sea conditions and minor equipment problems. Because the DARPA downhole-seismometer experiment required an area of about 10 km by 30 km of fairly smooth and level topography, we had been asked by the Deep Sea Drilling Project (DSDP) to supplement the existing north-south *Vema*-21 track by one or two east-west lines to define further the structure and topography of the site. Unfortunately we did not have underway data from Scripps' *Zetes*-3 cruise track across the area, which would have helped us lay out a more effective survey. We began the survey at 1552Z, 9 June and completed an east-west cross line of the V-21 track before running west and selecting the drill site (Fig. 1). Neither of our crossings show the smooth topography seen in the V-21 crossing. The site appears to lie within a fracture zone trending west-northwest across the "M" series of magnetic anomalies. The area drilled is fairly smooth for more than 10 km east-west, but the northwest-southeast extent (along the inferred fracture zone) is not well defined. We were forced by time constraints to limit our survey. Basement appears to be faulted parallel to the fracture zone trend with a relief of 1 or 2 km.

The beacon was dropped at 2052Z, 9 June 1982. After retrieving the geophysical gear and running pipe, we spudded in at 1120Z, 10 June. Because time was running short, we elected to take a mud line core and then wash as far as possible before beginning to rotary core. HPC sampling of the softer sediments for studies of Neogene paleoceanography, one of our prime objectives, had to be deferred to Leg 88, which ran out of time before they could accomplish this goal.

From 181.5 to 267 m sub-bottom (Cores 1-10), the quality of the cores was good (for rotary drilling), and the recovery was fair to good (Table 1). From Core 11 on, however, the increased circulation required to penetrate the stiff clay from 267 to 276.5 m and the chert from 276.5 to 343 m washed away any unconsolidated sediment; we recovered nothing but chert for an interval of 66.5 m. The hole was terminated at 1204Z, 12 June at a depth of 352.5 m, after penetrating about 8 m into basalt.

Retrieval and securing of the drill string was completed at 0632Z on 13 June. We then headed east to stream the gear before running west across the beacon and for an additional 10 miles prior to heading for Yokohama and the conclusion of the leg.

LITHOSTRATIGRAPHY

The sediments recovered at Site 581 can be divided into four units based on macroscopic descriptions of the split cores and on smear slide analyses with a petrographic microscope. These units are (I) biogenic siliceous clay, (II) pelagic brown clay, (III) chert, and (IV) basalt. The first unit is divided into two subunits on the basis of color and abundance of biogenic siliceous material (Fig. 2, Table 2).

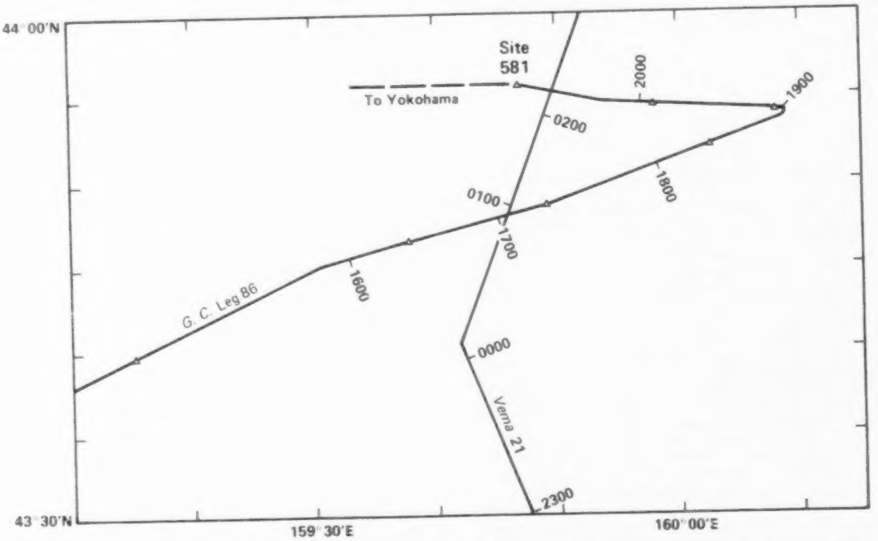

Figure 1. Track line map showing locations of north-south *Vema*-21 track and east-west *Glomar Challenger* Leg 86 track in vicinity of Site 581. Open triangles on *Challenger* track represent satellite fixes.

Table 1. Site 581 coring summary.

Core	Date (June 1982)	Local Time	Depth from drill floor (m)	Depth below seafloor (m)	Length cored (m)	Length recovered (m)	Percent recovered
1	11	0017	5487.5-5488.5	0.0-1.0	1.0	0.93	93
Wash			5488.5-5669.0	1.0-181.5			
2	11	0547	5669.0-5678.5	181.5-191.0	9.5	6.38	67
3	11	0740	5678.5-5688.0	191.0-200.5	9.5	8.52	90
4	11	0945	5688.0-5697.5	200-5-210.0	9.5	9.45	99
5	11	1135	5697.5-5707.0	210.0-219.5	9.5	5.32	56
6	11	1339	5707.0-5716.5	219.5-229.0	9.5	9.44	99
7	11	1543	5716.5-5726.0	229.0-238.5	9.5	8.98	95
8	11	1750	5726.0-5735.5	238.5-248.0	9.5	7.59	80
9	11	1953	5735.5-5745.0	248.0-257.5	9.5	5.48	58
10	11	2216	5745.0-5754.5	257.5-267.0	9.5	8.52	90
11	12	0022	5754.5-5764.0	267.0-276.5	9.5	0.40	4
12	12	0430	5764.0-5773.5	276.5-286.0	9.5	0.35	4
13	12	0758	5773.5-5783.0	286.0-295.5	9.5	0.16	2
14	12	1002	5783.0-5792.5	295.5-305.0	9.5	0.27	3
15	12	1220	5792.5-5802.0	305.0-314.5	9.5	0.55	6
16	12	1423	5802.0-5811.5	314.5-324.0	9.5	0.18	2
17	12	1632	5811.5-5821.0	324.0-333.5	9.5	1.07	11
18	12	1843	5821.0-5830.5	333.5-343.0	9.5	0.35	4
19	12	2304	5830.5-5840.0	343.0-352.5	9.5	3 65	38
					172.0 (total)	77.59 (total)	45 (avg.)

Unit I: Biogenic Siliceous Clay

This unit is a biosiliceous clay characterized by a high percentage of diatoms and radiolarians. It is divided into two subunits as follows.

Subunit IA

This subunit is dark gray to greenish gray (5Y and 5GY) biosiliceous clay characterized by abundant (up to 65%) diatoms and radiolarians. It extends from the top of Section 581-1-1, through Sample 581-6-3, 108 cm. Diatoms (20–60%) and radiolarians (5–15%) are the primary biosiliceous components with subordinate amounts of silicoflagellates (0–2%). Clay (30–65%) and quartz (3–5%) constitute the terrigenous component. Volcanic glass never reaches abundances greater than 5%, except in ash layers. Subunit IA contains four ash layers that range in thickness from 3 to 16 cm. Although this subunit is very similar in color and composition to the siliceous clay found at Sites 579 and 580, only ten indurated dark greenish gray layers were seen in Hole 581. In comparison, several hundred of these layers are found at both Sites 579 and 580.

Subunit IB

This subunit is a light yellowish brown to yellowish brown (10YR) biosiliceous clay with diatoms and radiolarians comprising up to 25% of the sediment. It extends from Samples 581-6-3, 108 cm to 581-8-5, 30 cm. Diatoms (7–20%) and radiolarians (7–20%) are the primary siliceous components, together with minor amounts of silicoflagellates (TR–5%). Clay (65–85%) and quartz (3–5%) comprise the terrigenous fraction of this subunit. Volcanic glass is present in abundances of 2% or less. Subunit IB contains only one ash layer, which is approximately 8 cm thick.

Unit II: Pelagic Brown Clay

This unit is characterized by a brown to dark brown (10YR) nonbiogenic clay extending from Samples 581-8-5, 30 cm to 581-12-1, 10 cm. The clay is moderately to heavily mottled in Cores 8 and 9 and moderately to lightly

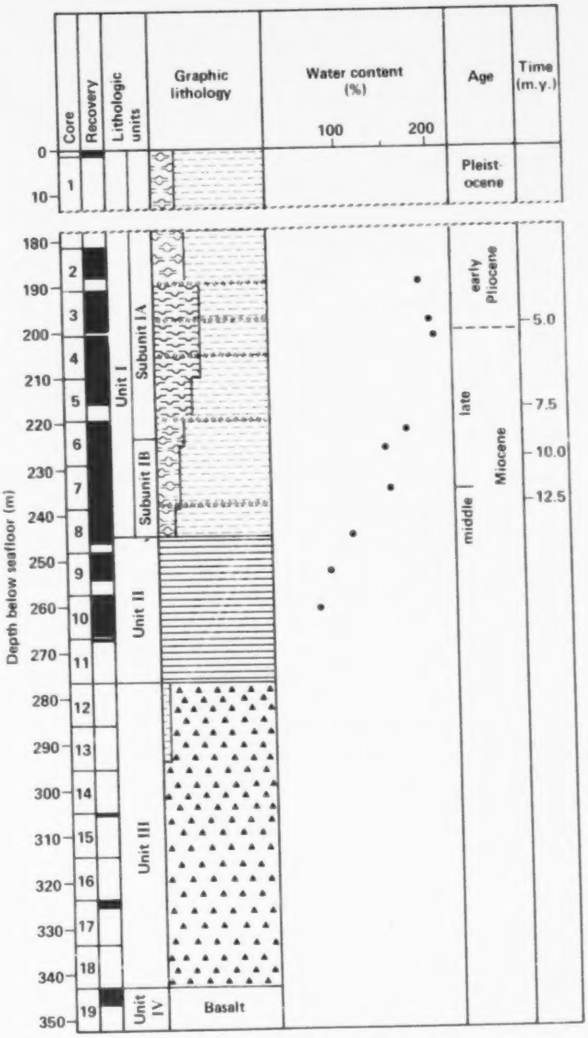

Figure 2. Site summary diagram showing Site 581 core numbers, core recovery, lithologic units, graphic lithology, water content (%), and age. Symbols used in graphic lithology column are defined in Introduction and Explanatory Notes (this volume).

Table 2. Site 581 lithostratigraphic units.

	Lithologic unit	Cored interval	Sub-bottom depth (m)
I	Biogenic siliceous clay	1-1,0 cm to 8-5,30 cm	0.0–1.0 and 181.5–244.8
	Subunit 1A: Dark gray to greenish gray siliceous clay.	1-1,0 cm to 6-3,108 cm	0.0–1.0 and 181.5–223.6
	Subunit 1B: Light yellowish brown to yellowish brown siliceous clay	6-3,108 cm to 8-5,30 cm	223.6–244.8
II	Pelagic brown clay	8-5,30 cm to 12-1,10 cm	244.8–276.6
III	Chert	12-1,10 cm–18,CC	276.6–343.0
IV	Basalt	19-1,0 cm–19-4,60 cm	343.0–348.1

mottled in Cores 10, 11, and 12. Clay is the dominant component of this unit, generally comprising more than 90% of the sediment. Biogenic siliceous material is absent. Quartz (2-3%), volcanic glass (0-3%), opaques (0-3%), and micronodules (0-7%) comprise the remaining fraction of the sediment.

Unit III: Chert

This unit consists of chert and comprises Sample 581-12-1, 10 cm through Core 581-18. Recovery never exceeded 11% of the cored interval and only chert fragments were obtained. These fragments vary in size from several millimeters up to 7 cm across the longest axis. Colors range from grayish and yellowish brown to yellowish red, pink, reddish black, and black. Most chert fragments exhibit conchoidal surface fractures. Quartz veins and laminations of porcellanite are common in the larger fragments.

Unit IV: Basalt

Unit IV consists of aphyric medium gray basalt. Coring was terminated following recovery of 3.65 m of this material in Core 19. Iron oxide coatings were found along most cracks. Calcite veins up to 0.5 cm thick and vugs up to 2 cm across were present in several of the fragments. Talc and altered glass were common in cracks and in several veins in the basalt fragments. Several fragments revealed a transition from unaltered glass exteriors to slightly altered glass to fine-grained aphyric basalt interiors. This alteration rind also included interlayered calcite, talc, and possible chlorite. These basalts, and those drilled at Holes 581A, 581B, and 581C on Leg 88, are described in detail in the Leg 88 Site 581 chapter (see Duennebier, Stephen, et al., in press).

SEISMIC CORRELATION

High-resolution seismic reflection profiles (3.5 and 12 kHz) and 100-Hz reflection profiles were recorded at Site 581. Only a hull-mounted 3.5-kHz sound source was utilized. The 3.5-kHz echograms reveal a fairly uniform seismic section of parallel sub-bottom reflectors near Site 581 and a three-part sequence based on transparent sections at the site (Fig. 3). Because the upper 181.5 m were not cored at this site, these 3.5-kHz reflectors cannot be correlated with lithologic units.

The uppermost unit (seismic Unit 1) at Site 581 consists of a generally transparent section extending to about 0.0095 s below the seafloor (14.2 m, 1500 m/s). The top reflector of the unit is a slightly prolonged, weak to strong echo. The morphology of this unit and its echo character suggest that it is a debris flow deposit.

Seismic Unit 2 extends to 0.0195 s below the seafloor (29.25 m, 1500 m/s) and is composed of six parallel and equally spaced reflectors. Drilling results from earlier sites on Leg 86 suggest that most of these reflectors correspond to volcanic ash layers. Seismic Unit 3 is a transparent zone and may represent another debris flow.

The 100-Hz reflection profiles over Site 581 reveal a four-part seismic section (Fig. 4). The uppermost unit (seismic Unit 1) extends to 0.1 s depth below the seafloor (75 m at 1500 m/s) and consists of strong, multiple, and parallel reflectors. Near the site, seismic Unit 1 also contains local transparent sections that probably represent buried debris flows. At these localities the reflectors above the transparent section are divergent from those below the transparent section.

Seismic Unit 2 is of variable thickness: at Site 581 it extends to 0.362 s below the seafloor (271.5 m at 1500 m/s). Unit 2 consists of parallel reflectors of weak to intermediate strength. Relatively transparent intervals occur between 0.17 and 0.2 s below the seafloor (127.5 m and 150 m at 1500 m/s) and between 0.295 and 0.362 s below seafloor (271 and 271.5 m at 1500 m/s). Varying thicknesses of the section of Unit 2 above the upper transparent interval accounts for the variable thickness of the unit as a whole. The lower transparent interval is conformable with the underlying seismic Unit 3 and has a constant thickness in the area immediately surround-

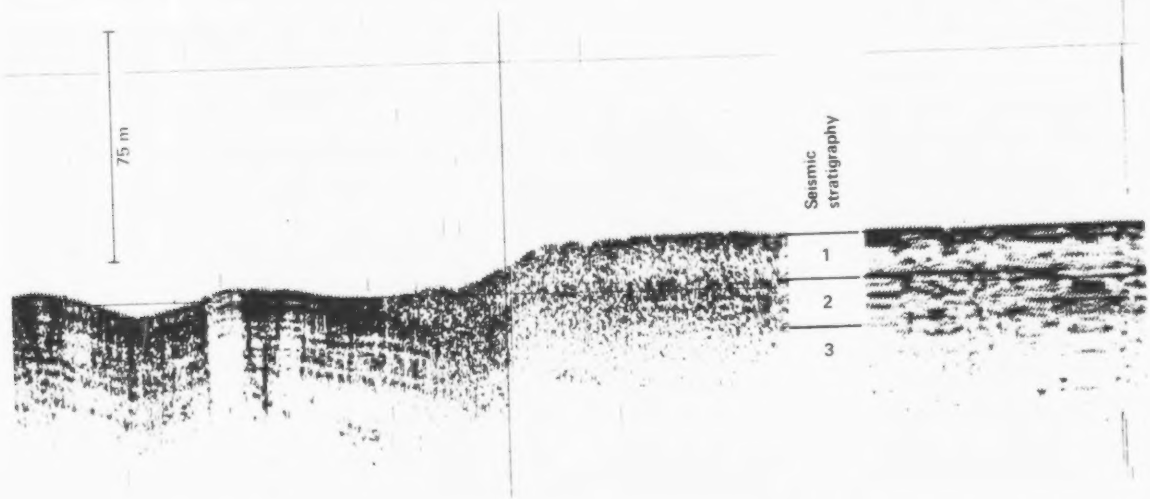

Figure 3. 3.5-kHz echogram near Site 581 showing the three seismic units described in the text.

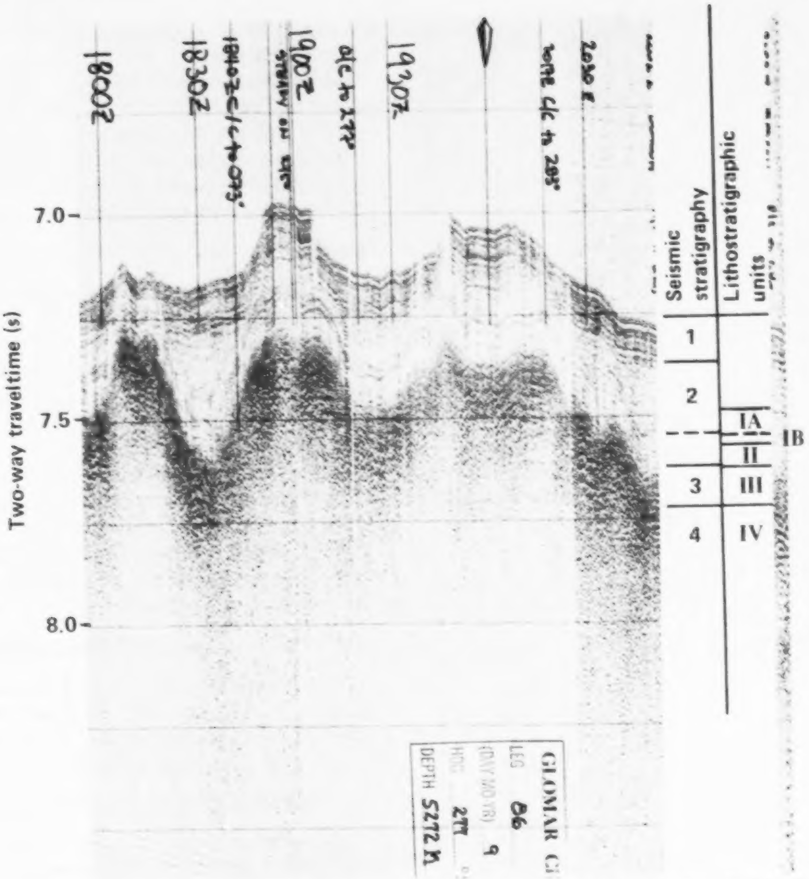

Figure 4. 100-Hz reflection profile over Site 581 showing the four seismic units described in the text.

ing Site 581. The lower transparent interval in Unit 2 correlates with lithostratigraphic Units IB and II (yellowish brown siliceous clay and pelagic brown clay, respectively). Seismic Unit 2 above the lower transparent interval correlates in part with lithostratigraphic Unit IA (gray to greenish gray siliceous clay).

Seismic Unit 3 is of constant thickness and extends from 0.362 s to about 0.46 s below the seafloor (345 m at 1500 m/s). This unit is characterized by a strong, incoherent echo. Unit 3 correlates with lithostratigraphic Unit III (chert and interbedded sediments).

Seismic Unit 4 is difficult to distinguish from Unit 3; it consists of a slightly stronger, less prolonged echo typical of "basement" and correlates with lithostratigraphic Unit IV (basalt).

BIOSTRATIGRAPHY

After Core 1 of late Quaternary age was recovered at the mud line (0–1.0 m sub-bottom), an interval of 180.5 m of sediment was washed at Site 581. Cores 2 through 9 (181.5–257.5 m below the seafloor) are early Pliocene through middle Miocene in age. No calcareous microfossils were found in any of the core-catcher samples. However, common to abundant siliceous microfossils consisting of radiolarians, diatoms, and silicoflagellates were found in Cores 1 through 8. In Core 9, radiolarians are rare in abundance, but diatoms and silicoflagellates are very rare. No siliceous microfossils were found below Core 9.

The biostratigraphic summary for Site 581, based on two groups of siliceous microfossils, is shown in Figure 5. Based on radiolarian biostratigraphy, the Miocene/Pliocene boundary falls within Core 3 with the boundary between middle and late Miocene occurring within Core 7. A sediment sample taken from a vug in the uppermost chert layer contained early late Miocene diatoms.

Radiolarians

Late Quaternary through middle Miocene radiolarians occur in sediments recovered at Site 581. The abundant Pleistocene radiolarian fauna is well preserved, but the preservation decreases from good in the early Pliocene to poor in the middle Miocene. Sediments older than middle Miocene (Samples 581-10,CC and 581-11,CC) do not contain radiolarians. The radiolarian biostratigraphy for Site 581 is shown in Figure 5.

Sections 581-1-1 and 581-1,CC contain radiolarians representative of the *Stylatractus universus* Zone (Hays, 1970). The fauna in Sections 581-2-1 and 581-2,CC is representative of the *Sphaeropyle langii* Zone (Foreman,

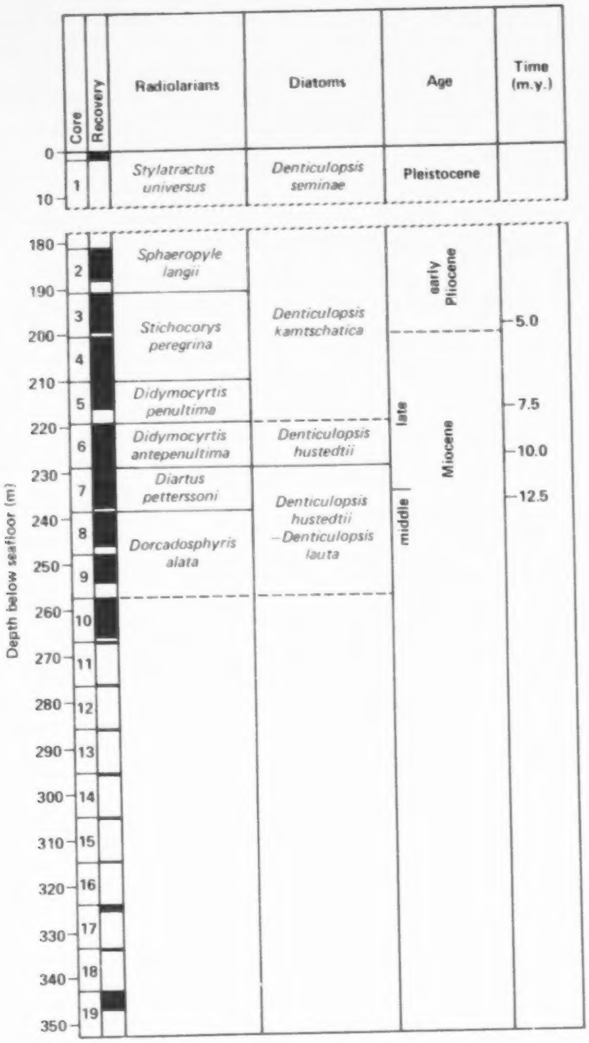

Figure 5. Site 581 biostratigraphic summary.

1975) with both *S. langii* and *Lamprocyrtis heteroporos* present in the assemblage. The sediment sequence in Sections 581-3,CC and 581-4,CC is assigned to the *Stichocorys peregrina* Zone (Riedel and Sanfilippo, 1970; Foreman, 1975), based on the presence of *S. peregrina* and *S. delmontensis* and the absence of *L. heteroporos* and *Sphaeropyle langii*. Examination of this sequence indicates that the Miocene/Pliocene boundary occurs in Core 3. The presence of *Didymocyrtis penultima* in Section 581-5,CC places this sediment within the late Miocene *D. penultima* Zone (Riedel and Sanfilippo, 1970). The radiolarian assemblage in Section 581-6,CC is representative of the *D. antepenultima* Zone (Riedel and Sanfilippo, 1970; Riedel and Sanfilippo, 1978) since *D. laticonus*, *D. antepenultima*, and *Diartus hughesi* are present whereas *Cyrtocapsella cornuta* and *C. tetrapera* are absent. The sediment sequence in Section 581-7,CC is assigned to the *D. petterssoni* Zone (Riedel and Sanfilippo, 1970; Riedel and Sanfilippo, 1971) based on the presence of *D. petterssoni* and the absence of *Didymocyrtis penultima*, *D. antepenultima*, and *C. cornuta*. The middle Miocene/late Miocene boundary occurs within Core 7. The oldest radiolarian-bearing sediment recovered at this site is middle Miocene in age (*Dorcadospyris alata* Zone [Riedel and Sanfilippo, 1970; Riedel and Sanfilippo, 1971]) based on the presence of *C. cornuta* and *C. tetrapera* and the absence of *Diartus petterssoni*.

Diatoms

A late to middle Miocene diatom biostratigraphy typical of the subarctic region was recovered at Site 581. Diatoms are abundant and well preserved in Cores 1 through 8. In Core 9, they are rare and only solution-resistant valves were recovered. Diatoms are absent below Core 9.

Core 1 belongs to the late Quaternary *Denticulopsis seminae* Zone. Cores 2 through 5 are assigned to the early Pliocene to latest Miocene *D. kamtschatica* Zone. Core 6 is placed in the late Miocene *D. hustedtii* Zone. Cores 7 and 8 are correlated with the late middle Miocene Subzone C of the *D. hustedtii*-*D. lauta* Zone by the presence of *D. dimorpha*.

PALEOMAGNETICS

Paleomagnetic analyses of a limited number of sediment and basalt samples have been carried out to determine the paleolatitudinal history of this site. Results are reported by Bleil (this volume).

SEDIMENT ACCUMULATION RATES

Radiolarian zonal boundaries and the boundaries of time-rock units are used to estimate the sediment accumulation rates for Site 581 (Fig. 6). Late Miocene rates are about 5 m/m.y. Assuming no stratigraphic breaks in the uncored section, the average Pliocene-Pleistocene accumulation rate was about 40 m/m.y., very close to the value at Sites 579 and 580.

PHYSICAL PROPERTIES

Physical properties measurements at Site 581 were performed using mainly standard DSDP methods (Boyce, 1976a, b; see Introduction and Explanatory Notes, this volume). Table 3 summarizes the properties measured at Site 581.

These measurements were taken approximately once per core in the unconsolidated sediments. A number of compressional wave velocity measurements were taken on the chert and basalt samples.

Figures 7, 8, and 9 show profiles of shear strength, compressional wave velocity, and water content and bulk density profiles, respectively. Shear strength measurements were hampered by the brittle nature of the semi-indurated sediments. This resulted in major cracks developing either upon initial insertion of the vane or during the test. If this happens the test is invalid because the failure plane is no longer a cylinder described by the vane blades.

In an attempt to overcome this problem, a minimum amount of confining pressure was applied by using two strips of angle aluminum held together by G clamps on either side of the split core. This eliminated the gap be-

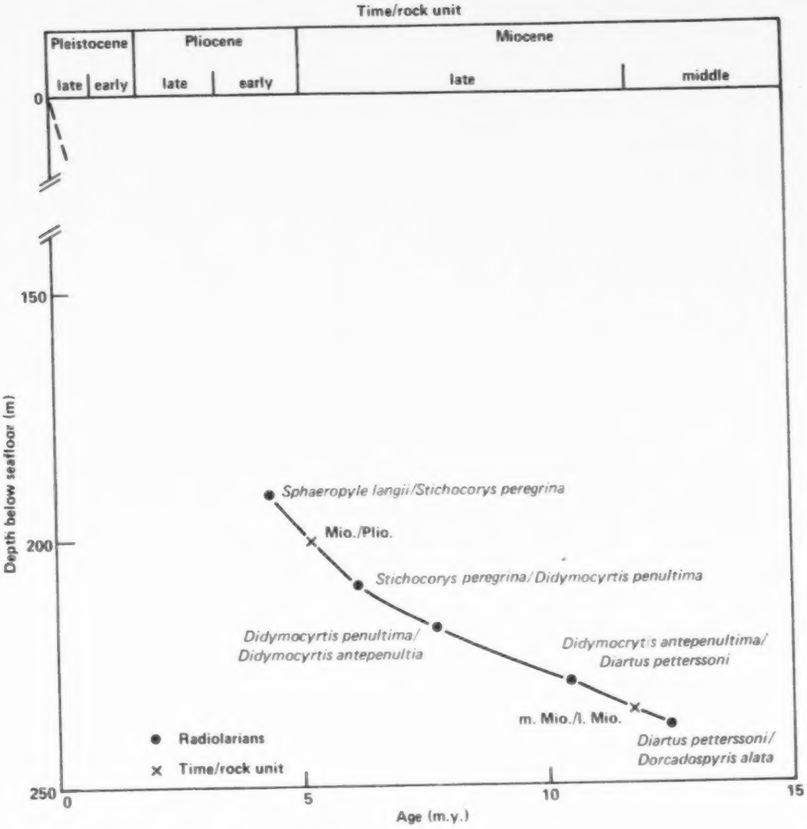

Figure 6. Site 581 sediment accumulation rates.

Table 3. Physical properties measurements made at Hole 581.

	Hole 581
Shear strength:	
Hand operated vane	x
Motorized vane	x
Compressional wave velocity	x
Water content/bulk density:	
Shipboard analysis	x
Shore-based analysis	x
Bulk density by 2-min. GRAPE	x

tween the liner and the sediment and prevented the cracking described earlier.

A full discussion of the physical properties of the recovered sediments, including tables of the data, is given by Schultheiss (this volume). However, some of the more interesting features of the data are highlighted here:

1. The shear strength measurements (Fig. 7) should be viewed with even more caution than usual. Rotary coring causes significantly more structural disturbance than the HPC. This is true even when the stratigraphic sequence looks undisturbed. Much of the material in Cores 1-7 consisted of alternating layers of soft and stiff sediments, probably a result of intermittent "rotation" and "punch" coring (rotation causing the most disturbance and hence the softer layers). Measurements were made in the largest sections of stiff material that could be found in each core. The first few readings were taken without the G-clamp modification and show comparatively low strengths. In the remaining sections of unconsolidated sediments, the shear strengths lie between 600 and 1300 g/cm^2.

2. Compressional wave measurements (Fig. 8) show a small decrease in velocity below 240 m which correlates with the boundary of lithologic Units I and II (biosiliceous clay-pelagic brown clay). Some measurements were made on selected chert and basalt samples and these varied between 4000 and 5500 m/s.

3. The water content and bulk-density profiles (Fig. 9) show a rapid change below 200 m. Water contents drop abruptly from 200 to 75% at 262 m. This corresponds to a rapid increase in clay content through lithologic Units IA, IB, and II. The water content in the pelagic brown clay (lithologic Unit II) is 75% at a sub-bottom depth of 262 m, whereas at Sites 576 and 578 water contents as low as 60% were found in similar sediment at sub-bottom depths of 60 and 170 m, respectively.

INORGANIC GEOCHEMISTRY

Only two samples from Hole 581 were squeezed and analyzed for the standard suite of components: pH, alkalinity, salinity, calcium, magnesium, and chlorinity (Table 4). No *in situ* samples were taken.

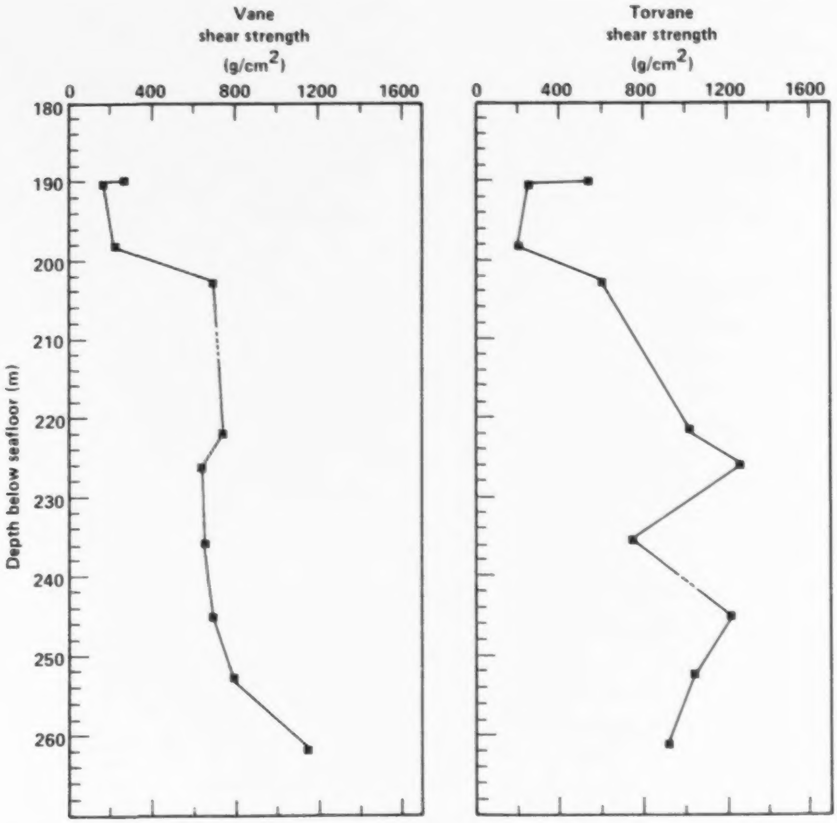

Figure 7. Plot of shear strength versus sub-bottom depth at Site 581.

The squeezed samples show the calcium and alkalinity increases and magnesium decrease (Fig. 10) evident at Sites 579 and 580, presumably for the same reasons (diffusion of calcium from a deeper source, oxidation of organic matter by sulfate reduction, and alteration of volcanic ash, respectively). However, the absence of samples above 181 m and the failure to recover sediment from the chert-bearing section below 276 m preclude any serious attempt to unravel the diagenetic processes at this site.

HEAT FLOW

No heat-flow measurements were made at this site, as the decision to defer HPC sampling to Leg 88 precluded use of the Woods Hole Oceanographic Institution (WHOI) core-nose temperature probe.

SUMMARY AND CONCLUSIONS

The stratigraphic section and major lithologic units recovered at Site 581 are described below.

0–223.6 m

Gray green reduced biosiliceous clay of late Miocene to late Quaternary age. By analogy with Sites 579 and 580, we infer that similar sediment, with ash beds and pyrite-indurated layers, makes up the washed interval from 1 to 181.5 m. Four ash beds were recovered between 181.5 and 224 m. The average accumulation rate for this unit was about 34 m/m.y.

223.6–244.8 m

Yellow brown oxidized biosiliceous clay, with common moderately preserved diatoms, radiolarians, and silicoflagellates of middle to late Miocene age, and a single ash layer.

244.8–276.6 m

Brown grading down to dark brown "slick" pelagic clay of middle Miocene age based on radiolarians in the top of the unit and diatoms in the underlying chert.

244.8–343 m

Chert and porcellanite, mostly brown to dark brown (looking like silicified pelagic clay), but with intervals of bright yellows and reds near 285 and 305 m. From the behavior of the drill, it appears that the chert forms layers a few centimeters thick separated by tens of centimeters of soft sediment. From the color of the chert, we infer that much, if not all, of the intervening sediment is pelagic brown clay, but none was recovered because of the circulation required to keep the hole clear of chert cuttings. A small vug in a chert fragment at about 286 m sub-bottom contained diatoms of early late Miocene age

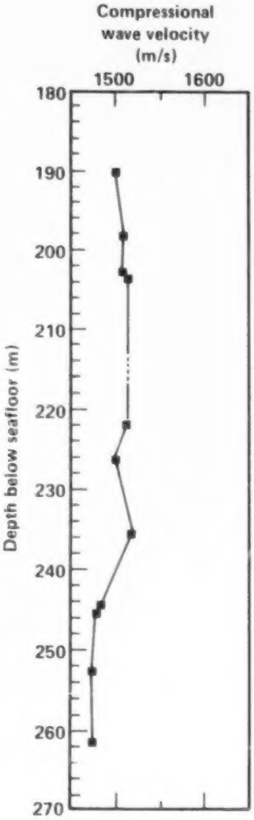

Figure 8. Plot of compressional wave velocity versus sub-bottom depth at Site 581.

(younger than the overlying sediment), but otherwise this unit is unfossiliferous.

343-352.5 m

Medium gray somewhat altered aphyric basalt with veins and fracture fillings of calcite and iron oxide. Minor amounts of fairly fresh-looking glass were recovered. From the linear magnetic anomalies, the crust at Site 581 should be Barremian (115 m.y., between Anomalies M-3 and M-4). We have no data to confirm or oppose this age.

REFERENCES

Boyce, R. E., 1976a. Definitions and laboratory techniques of compressional and sound velocity parameters and wet-water content, wet-bulk density, and porosity parameters by gravimetric and gamma ray attenuation techniques. *In* Schlanger, S. O., Jackson, E. D., et al., *Init. Repts. DSDP*, 33: Washington (U.S. Govt. Printing Office), 931-958.

________, 1976b. Deep Sea Drilling Project procedures for shear strength measurements of clayey sediment using modified Wykeham Farrance Laboratory Vane Apparatus. *In* Barker, P. F., Dalziel, I. W. D., et al., *Init. Repts. DSDP*, 36: Washington (U.S. Govt. Printing Office), 1059-1068.

Damuth, J. E., Jacobi, R. D., and Hayes, D. E., 1983. Sedimentation processes in the northwest Pacific Basin revealed by echo character mapping studies. *Geol. Soc. Am. Bull.*, 94:381-395.

Dunnebier, F. K., Stephen R. A., et al., in press. *Init. Repts. DSDP*, 88: Washington (U.S. Govt. Printing Office).

Foreman, H. P., 1975. Radiolaria from the North Pacific, Deep Sea Drilling Project, Leg 32. *In* Larson, R. L., Moberly, et al., *Init. Repts. DSDP*, 32: Washington (U.S. Govt. Printing Office), 579-701.

Hays, J. D., 1970. Stratigraphy and evolutionary trends of Radiolaria in North Pacific deep-sea sediments. *In* Hays, J. D. (Ed.), *Geological Investigations of the North Pacific*. Mem. Geol. Soc. Am., 126:185-218.

Riedel, W. R., and Sanfilippo, A., 1970. Radiolaria, Leg 4, Deep Sea Drilling Project. *In* Bader, R. G., Gerard, R. D., et al., *Init. Repts. DSDP*, 4: Washington (U.S. Govt. Printing Office), 503-575.

________, 1971. Cenozoic Radiolaria from the western tropical Pacific, Leg 7. *In* Winterer, E. L., Riedel, W. R., et al., *Init. Repts. DSDP*, 7, Pt. 2: Washington (U.S. Govt. Printing Office), 1529-1672.

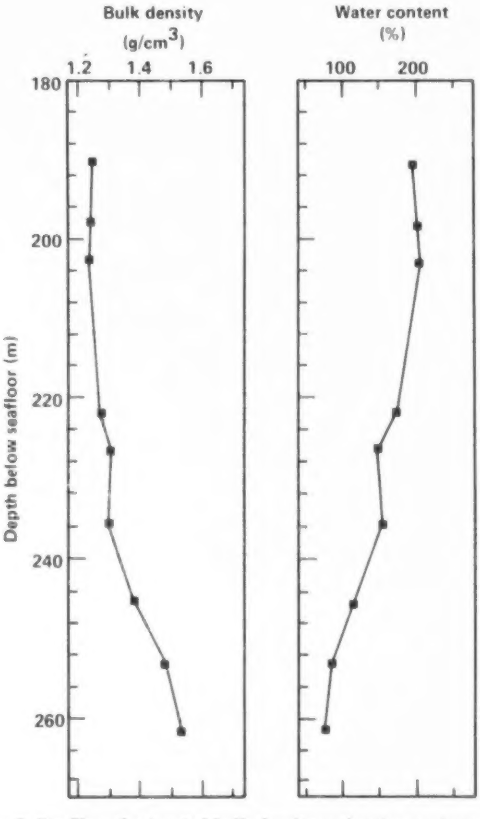

Figure 9. Profiles of saturated bulk density and water content versus sub-bottom depth at Site 581.

Table 4. Inorganic geochemistry measurements at Site 581.

Sample	pH	Alkalinity (mEq/l)	Salinity (‰)	Calcium (m*M*)	Magnesium (m*M*)	Chlorinity (‰)
IAPSO	7.86	2.43	35.2	10.55	53.99	19.38
SSW	7.81	2.32	33.6	10.05	50.76	18.48
581-5-3, 140-150 cm	7.72	4.14	35.2	11.91	46.83	19.33
581-8-4, 140-150 cm	7.00	3.26	35.2	12.25	47.26	19.22

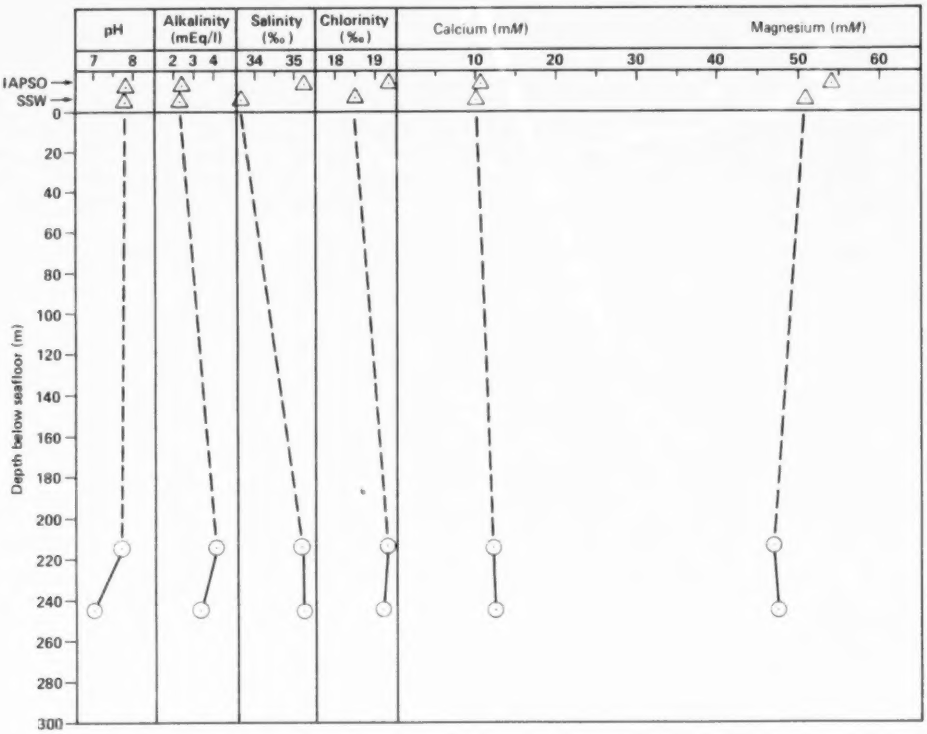

Figure 10. Profiles of pH, alkalinity, salinity (‰), chlorinity (‰), calcium (m*M*), and magnesium (m*M*), versus sub-bottom depth from interstitial water samples analyzed at Site 581. Symbols are as follows: △ = IAPSO and SSW standards; ⊙ = samples from Hole 581.

SITE 581 HOLE CORE 1 CORED INTERVAL 5487.5–5488.5 mbsl; 0.0–1.0 mbsf

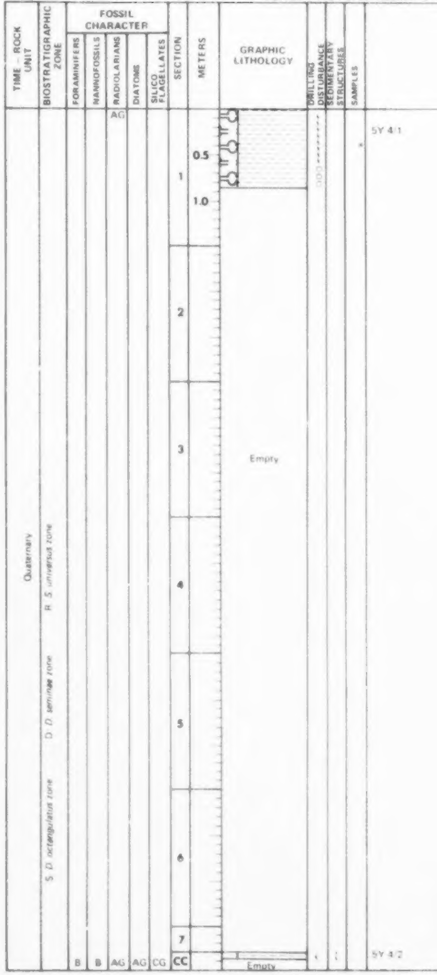
TIME – ROCK UNIT
BIOSTRATIGRAPHIC ZONE
FOSSIL CHARACTER
FORAMINIFERS
NANNOFOSSILS
RADIOLARIANS
DIATOMS
SILICO FLAGELLATES
SECTION
METERS
GRAPHIC LITHOLOGY
DRILLING DISTURBANCE
SEDIMENTARY STRUCTURES
SAMPLES
Quaternary
S. D. octangulatus zone
D. D. seminae zone
R. S. universus zone
AG
B
B
AG
AG
CG
1
2
3
4
5
6
7
CC
0.5
1.0
Empty
Empty
5Y 4/1
5Y 4/2

LITHOLOGIC DESCRIPTION

SILICEOUS CLAY

- *Dominant colors: dark gray (5Y 4/1). Core Catcher is olive gray (5Y 4/2).
- *Entire core is soupy or very deformed by drilling.
- *This core consists of homogeneous siliceous clay. The Core Catcher is mottled.

SMEAR SLIDE SUMMARY (%)

	1, 40
	D
Texture:	
Sand	5
Silt	30
Clay	65
Composition:	
Quartz	7
Feldspar	1
Clay	65
Volcanic glass	5
Diatoms	15
Radiolarians	7

SITE 581 HOLE CORE 2 CORED INTERVAL 5669.0–5678.5 mbsl; 181.5–191.0 mbsf

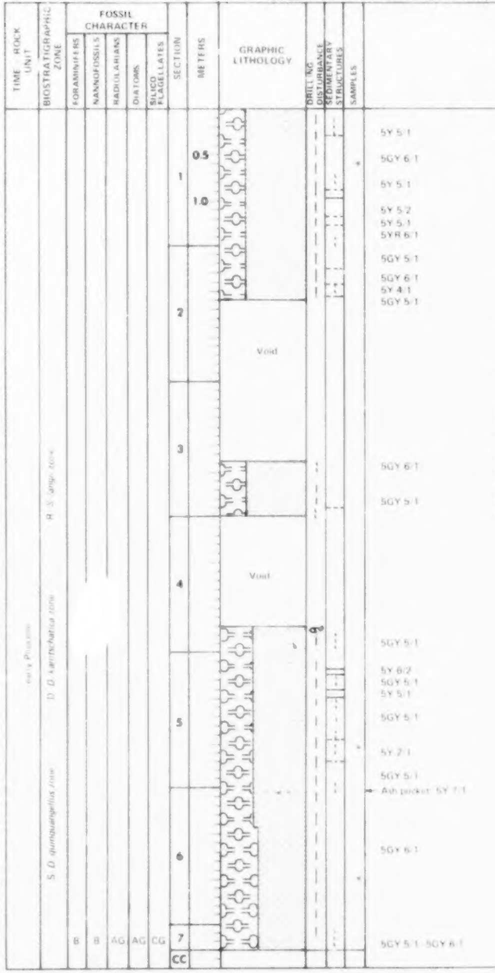
TIME – ROCK UNIT
BIOSTRATIGRAPHIC ZONE
FOSSIL CHARACTER
FORAMINIFERS
NANNOFOSSILS
RADIOLARIANS
DIATOMS
SILICO FLAGELLATES
SECTION
METERS
GRAPHIC LITHOLOGY
DRILLING DISTURBANCE
SEDIMENTARY STRUCTURES
SAMPLES
early Pliocene
S. D. quinquangellus zone
D. D. kamtschatica zone
R. S. langii zone
B
B
AG
AG
CG
1
2
3
4
5
6
7
CC
0.5
1.0
Void
Void
5Y 5/1
5GY 6/1
5Y 5/1
5Y 5/2
5Y 5/1
5YR 6/1
5GY 5/1
5GY 6/1
5Y 4/1
5GY 5/1
5GY 6/1
5GY 5/1
5GY 5/1
5Y 6/2
5GY 5/1
5Y 5/1
5GY 5/1
5Y 2/1
5GY 5/1
Ash pocket: 5Y 7/1
5GY 6/1
5GY 5/1–5GY 6/1

LITHOLOGIC DESCRIPTION

SILICEOUS (DIATOMACEOUS) CLAY

- *Dominant colors: greenish gray (5GY 5/1–5GY 6/1) and gray (5Y 5/1). Minor colors: local intervals of black (5Y 2/1), dark gray (5Y 4/1), gray (5Y 5/1), olive gray (5Y 5/2), light olive gray (5Y 6/2), and greenish gray (5YR 6/1). Minor zones and mottles of dark gray (10YR 4/1), very dark gray (5Y 3/10, and dark greenish gray (5G 5/1–5GY 4/1). One light gray (5Y 7/1) ash pocket.
- *This core is slightly to very deformed by drilling. Large void spaces occur at 2, 60 cm to 3, 88 cm and 4, 0–120 cm.
- *This core consists of homogeneous to lightly mottled siliceous (diatomaceous) clay. A small ash pocket occurs at 6, 0–3 cm.

SMEAR SLIDE SUMMARY (%)

	1, 60	5, 110	6, 100
	D	D	D
Texture:			
Sand	5	15	15
Silt	30	35	35
Clay	65	50	50
Composition:			
Quartz	5	3	5
Clay	63	50	47
Volcanic glass	2	5	3
Diatoms	20	30	35
Radiolarians	10	10	10
Silicoflagellates	—	2	—

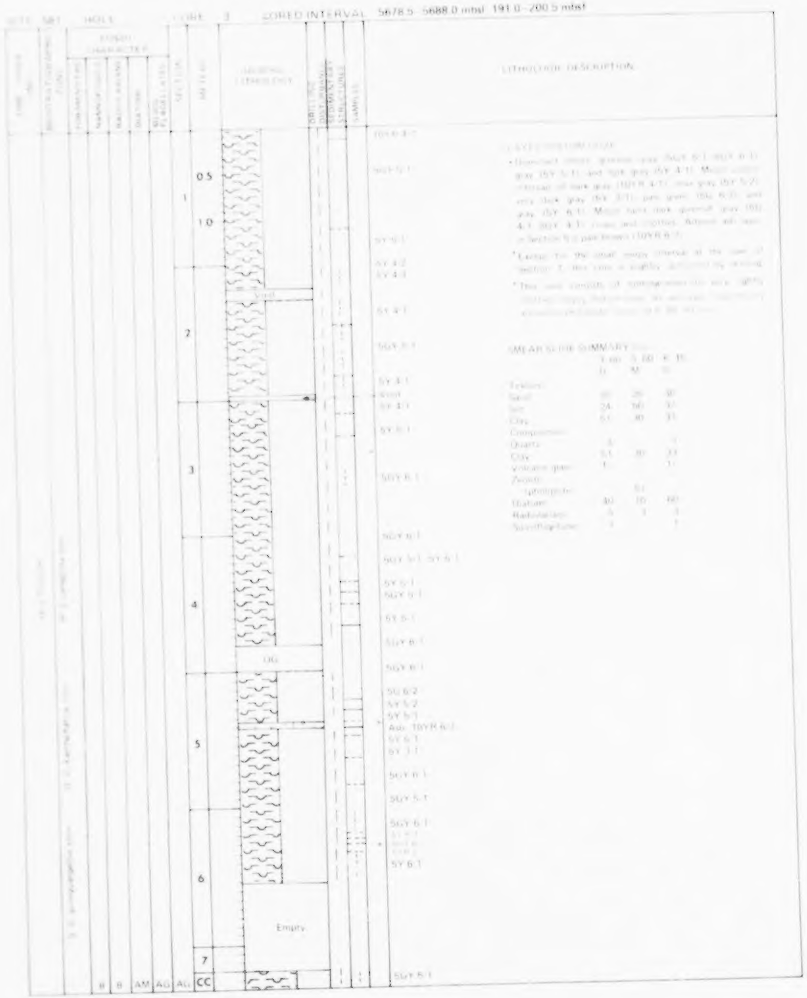
SITE 581 HOLE CORE 3 CORED INTERVAL 5678.5–5688.0 mbsl 191.0–200.5 mbsf
TIME-ROCK UNIT
BIOSTRATIGRAPHIC ZONE
FOSSIL CHARACTER
FORAMINIFERS
NANNOFOSSILS
RADIOLARIANS
DIATOMS
SILICOFLAGELLATES
SECTION
METERS
GRAPHIC LITHOLOGY
DRILLING DISTURBANCE
SEDIMENTARY STRUCTURES
SAMPLES
LITHOLOGIC DESCRIPTION
0.5
1.0
1
2
3
4
5
6
7
CC
B
B
AM
AG
AG
Void
OG
Empty
10YR 6/3
5GY 5/1
5Y 6/1
5Y 4/2
5Y 4/1
5Y 4/1
5GY 5/1
5Y 4/1
Void
5Y 4/1
5Y 6/1
5GY 6/1
5GY 6/1
5GY 5/1, 5Y 6/1
5Y 5/1
5GY 5/1
5Y 5/1
5GY 6/1
5GY 6/1
5G 6/2
5Y 5/2
5Y 5/1
Ash 10YR 6/3
5Y 6/1
5Y 3/1
5GY 6/1
5GY 5/1
5GY 6/1
5Y 6/1
5GY 5/1

CLAYEY DIATOM OOZE

- Dominant colors: greenish gray (5GY 6/1, 5GY 6/1), gray (5Y 5/1), and light gray (5Y 4/1). Minor colors: streaks of dark gray (10YR 4/1), olive gray (5Y 5/2), very dark gray (5Y 3/1), pale green (5G 6/2), and gray (5Y 6/1). Minor faint dark greenish gray (5G 4/1, 5GY 4/1) streaks and mottles. Altered ash layer in Section 5 is pale brown (10YR 6/3).
- Except for the small empty interval at the base of Section 2, this core is slightly deformed by drilling.
- This core consists of homogeneous to very slightly [illegible] [illegible] [illegible]

SMEAR SLIDE SUMMARY (%)

	3, 80	5, 80	6, 15
	D	M	D
Texture:			
Sand	25	20	30
Silt	24	50	37
Clay	51	30	33
Composition:			
Quartz	3	—	[illegible]
Clay	51	30	33
Volcanic glass	1	—	Tr
Zeolite (phillipsite)	—	51	—
Diatom	40	10	60
Radiolarians	5	3	3
Silicoflagellates	1	—	1

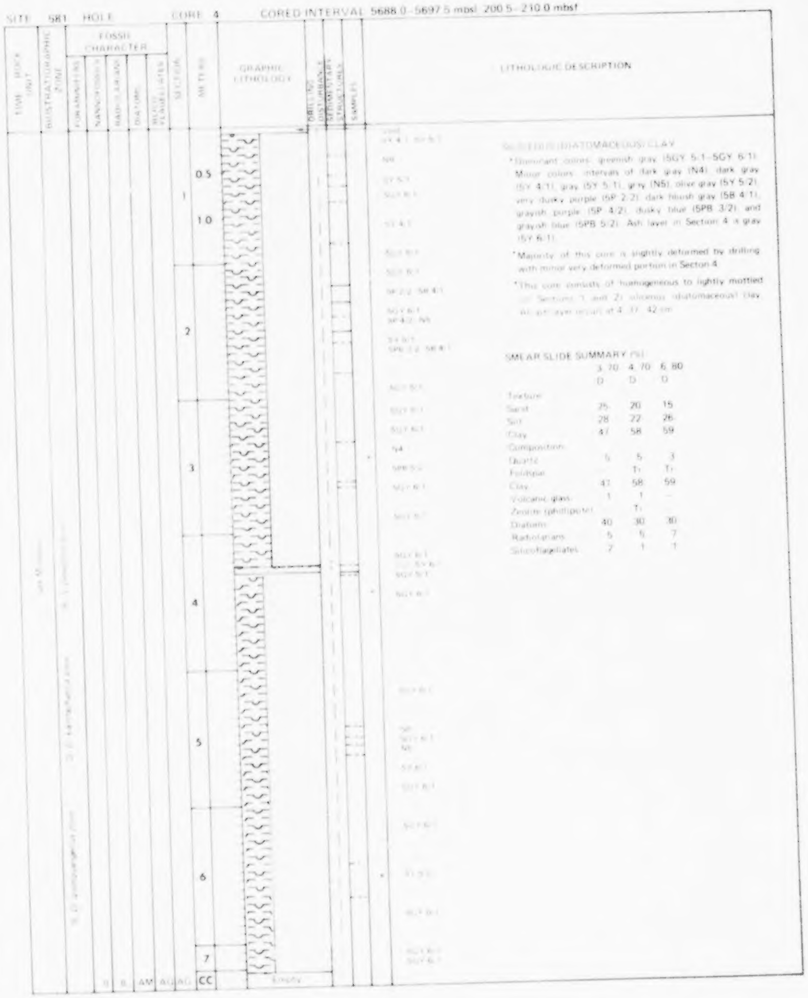
SITE 581 HOLE CORE 4 CORED INTERVAL 5688.0–5697.5 mbsl 200.5–210.0 mbsf
TIME-ROCK UNIT
BIOSTRATIGRAPHIC ZONE
FOSSIL CHARACTER
FORAMINIFERS
NANNOFOSSILS
RADIOLARIANS
DIATOMS
SILICOFLAGELLATES
SECTION
METERS
GRAPHIC LITHOLOGY
DRILLING DISTURBANCE
SEDIMENTARY STRUCTURES
SAMPLES
LITHOLOGIC DESCRIPTION
0.5
1.0
1
2
3
4
5
6
7
CC
B
B
AM
AG
AG
Empty
N4
N5

SILICEOUS (DIATOMACEOUS) CLAY

- Dominant colors: greenish gray (5GY 5/1–5GY 6/1). Minor colors: intervals of dark gray (N4), dark gray (5Y 4/1), gray (5Y 5/1), gray (N5), olive gray (5Y 5/2), very dusky purple (5P 2/2), dark bluish gray (5B 4/1), grayish purple (5P 4/2), dusky blue (5PB 3/2), and grayish blue (5PB 5/2). Ash layer in Section 4 is gray (5Y 6/1).
- Majority of this core is slightly deformed by drilling with minor very deformed portion in Secton 4.
- This core consists of homogeneous to lightly mottled (in Sections 1 and 2) siliceous (diatomaceous) clay. An ash layer occurs at 4, 37–42 cm.

SMEAR SLIDE SUMMARY (%)

	3, 70	4, 70	6, 80
	D	D	D
Texture:			
Sand	25	20	15
Silt	28	22	26
Clay	47	58	59
Composition:			
Quartz	5	5	3
Feldspar	—	Tr	Tr
Clay	47	58	59
Volcanic glass	1	1	—
Zeolite (phillipsite)	—	Tr	—
Diatom	40	30	30
Radiolarians	5	5	7
Silicoflagellates	2	1	1

SITE 581 HOLE CORE 5 CORED INTERVAL 5697.5–5707.0 mbsl; 210.0–219.5 mbsf

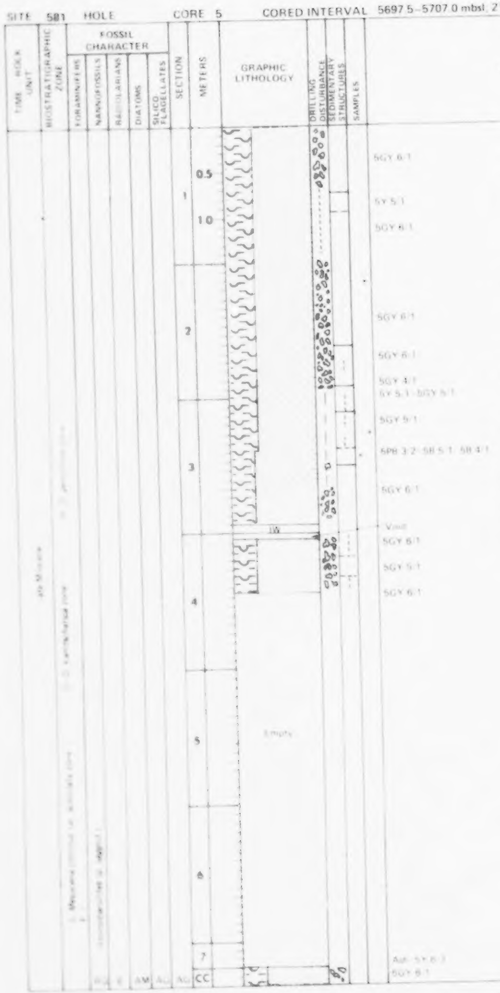
TIME-ROCK UNIT
BIOSTRATIGRAPHIC ZONE
FOSSIL CHARACTER
FORAMINIFERS
NANNOFOSSILS
RADIOLARIANS
DIATOMS
SILICO-FLAGELLATES
SECTION
METERS
GRAPHIC LITHOLOGY
DRILLING DISTURBANCE
SEDIMENTARY STRUCTURES
SAMPLES
0.5
1.0
1
2
3
4
5
6
7
CC
AM
AG
AG
Empty
5GY 6/1
5Y 5/1
5GY 6/1
5GY 6/1
5GY 6/1
5GY 4/1
5Y 5/1–5GY 5/1
5GY 5/1
5PB 3/2–5B 5/1–5B 4/1
5GY 6/1
Void
5GY 6/1
5GY 5/1
5GY 6/1
Ash 5Y 6/3
5GY 6/1

LITHOLOGIC DESCRIPTION

SILICEOUS (DIATOMACEOUS) CLAY

- Dominant colors: greenish gray (5GY 5/1/5GY 6/1). Minor colors: intervals of gray (5Y 5/1), dark greenish gray (5GY 4/1), dusky blue (5PB 3/2), bluish gray (5B 5/1), dark bluish gray (5B 3/1). Several mottles of white (5Y 8/1) diatom ooze in Sections 2 and 4. Ash in the Core Catcher is pale olive (5Y 6/3).
- Most of the core is very deformed to brecciated by drilling. The upper portion of Section 3 is slightly deformed.
- This core consists of homogeneous to lightly mottled siliceous clay. A discontinuous ash layer occurs in the Core Catcher from 12–13 cm. Section 1, 0–8 cm contains two greenstone pebbles and one indurated clay lump.

SMEAR SLIDE SUMMARY (%):

	2, 22 D	3, 40 D	3, 68 D
Texture:			
Sand	0	20	15
Silt	65	27	23
Clay	35	53	62
Composition:			
Quartz	3	5	3
Feldspar	—	—	Tr
Clay	36	53	62
Volcanic glass	—	2	—
Diatoms	60	30	25
Radiolarians	1	7	7
Silicoflagellates	Tr	3	3

SITE 581 HOLE CORE 6 CORED INTERVAL 5707.0–5716.5 mbsl; 219.5–229.0 mbsf

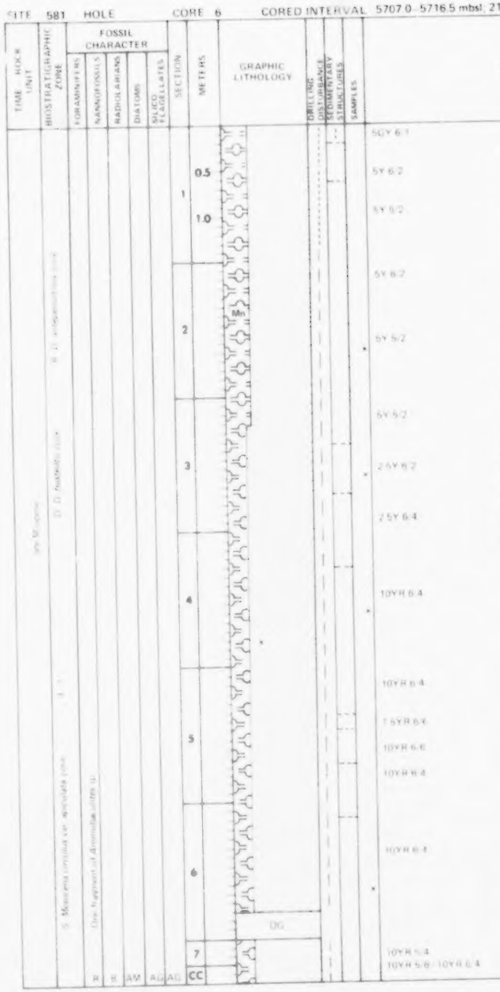
TIME-ROCK UNIT
BIOSTRATIGRAPHIC ZONE
FOSSIL CHARACTER
FORAMINIFERS
NANNOFOSSILS
RADIOLARIANS
DIATOMS
SILICO-FLAGELLATES
SECTION
METERS
GRAPHIC LITHOLOGY
DRILLING DISTURBANCE
SEDIMENTARY STRUCTURES
SAMPLES
0.5
1.0
1
2
3
4
5
6
7
CC
R
B
AM
AG
AG
Mn
OG
5GY 6/1
5Y 6/2
5Y 5/2
5Y 6/2
5Y 5/2
5Y 5/2
2.5Y 6/2
2.5Y 6/4
10YR 6/4
10YR 6/4
7.5YR 6/6
10YR 6/6
10YR 6/4
10YR 6/4
10YR 5/4
10YR 5/6–10YR 6/4

LITHOLOGIC DESCRIPTION

SILICEOUS CLAY

- Dominant colors: olive gray (5Y 5/2), light olive gray (5Y 6/2), and greenish gray (5GY 6/1) in Sections 1, 2, and 3, 0–50 cm. Below 3, 50 cm grades to light brownish gray (2.5Y 6/2) and light yellowish brown (2.5Y 6/4). Below 4, 38 cm grades to light yellowish brown (10YR 6/4) with intervals of yellowish brown (10YR 5/4–10YR 5/6), reddish yellow (7.5YR 6/6), and brownish yellow (10YR 6/6). Minor colors: top of Section 1 is lightly mottled with very dark gray (5Y 3/1).
- Section 1, 0–130 cm is very deformed, rest of the core is slightly deformed by drilling.
- This core consists of homogeneous siliceous clay changing from greenish gray to light yellowish brown in color downcore. Small grapestone manganese nodule at 2, 67–68 cm.

SMEAR SLIDE SUMMARY (%):

	2, 100 D	3, 40 D	4, 90 D	6, 100 D
Texture:				
Sand	15	10	15	15
Silt	19	20	15	19
Clay	66	70	70	66
Composition:				
Quartz	3	3	2	3
Feldspar	Tr	—	Tr	—
Clay	66	70	70	66
Volcanic glass	Tr	1	1	1
Diatoms	25	20	15	7
Radiolarians	5	5	7	20
Silicoflagellates	1	1	5	3

SITE 581 HOLE CORE 7 CORED INTERVAL 5716.5–5726.0 mbsl; 229.0–238.5 mbsf

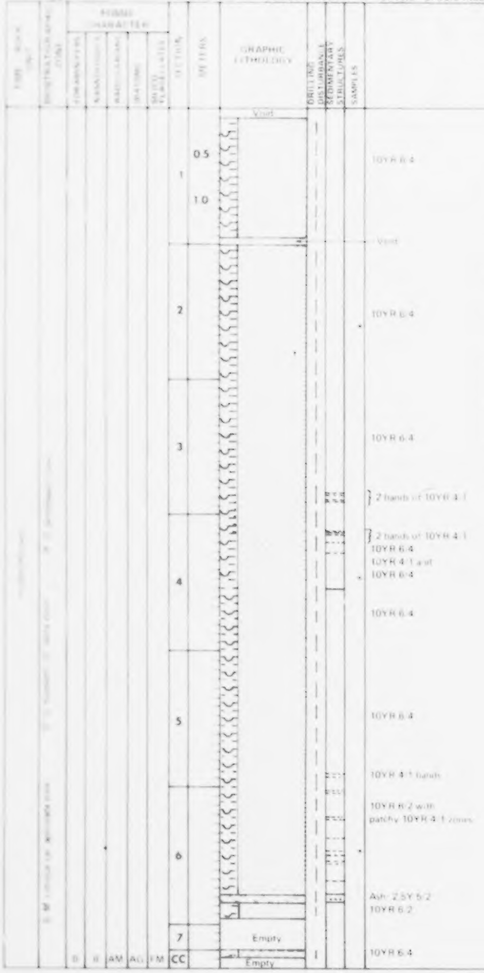
TIME-ROCK UNIT
BIOSTRATIGRAPHIC ZONE
FOSSIL CHARACTER
FORAMINIFERS
NANNOFOSSILS
RADIOLARIANS
DIATOMS
SILICO-FLAGELLATES
SECTION
METERS
GRAPHIC LITHOLOGY
DRILLING DISTURBANCE
SEDIMENTARY STRUCTURES
SAMPLES
Void
0.5
1
1.0
Void
2
3
4
5
6
7
CC
Empty
Empty
B
R
AM
AG
FM
10YR 6/4
10YR 6/4
10YR 6/4
2 bands of 10YR 4/1
2 bands of 10YR 4/1
10YR 6/4
10YR 4/1 ash
10YR 6/4
10YR 6/4
10YR 6/4
10YR 4/1 bands
10YR 6/2 with patchy 10YR 4/1 zones
Ash: 2.5Y 5/2
10YR 6/2
10YR 6/4

LITHOLOGIC DESCRIPTION

SILICEOUS CLAY WITH ONE VOLCANIC ASH LAYER

- Dominant colors: light yellowish brown (10YR 6/2–10YR 6/4). Minor colors: Sections 3 through 6 have thin bands and patchy zones of dark gray (10YR 4/1). Ash in Section 6 is grayish brown (2.5Y 5/2).
- Entire core is slightly deformed by drilling.
- This core consists of homogeneous siliceous clay. A normally graded ash layer occurs at 6, 118–126.6 cm.

SMEAR SLIDE SUMMARY (%)

	2, 90	4, 70	6, 70
	D	D	D
Texture:			
Sand	15	10	10
Silt	19	20	20
Clay	66	70	70
Composition:			
Quartz	5	5	3
Feldspar	Tr	Tr	
Mica	Tr	Tr	
Clay	66	69	68
Volcanic glass	1	1	2
Diatoms	15	10	15
Radiolarians	10	10	10
Silicoflagellates	3	5	2
Opaques		Tr	

SITE 581 HOLE CORE 8 CORED INTERVAL 5726.0–5735.5 mbsl; 238.5–248.0 mbsf

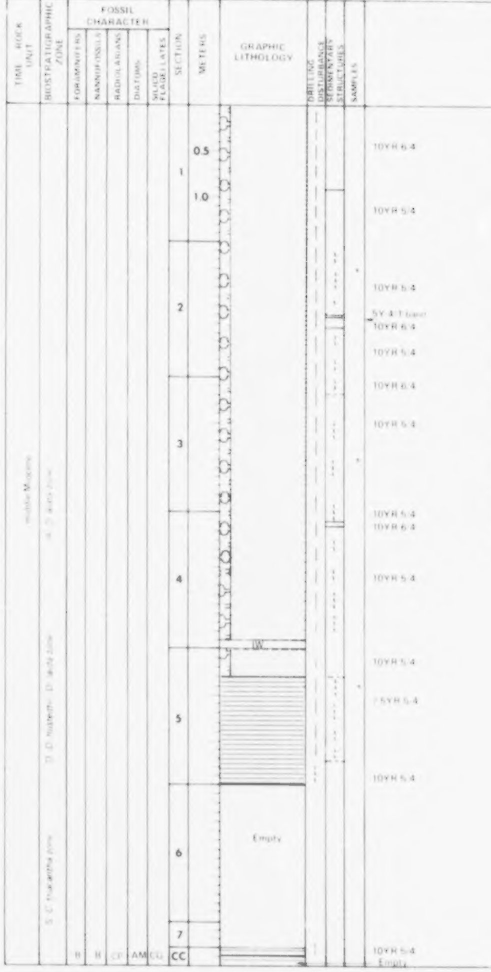
TIME-ROCK UNIT
BIOSTRATIGRAPHIC ZONE
FOSSIL CHARACTER
FORAMINIFERS
NANNOFOSSILS
RADIOLARIANS
DIATOMS
SILICO-FLAGELLATES
SECTION
METERS
GRAPHIC LITHOLOGY
DRILLING DISTURBANCE
SEDIMENTARY STRUCTURES
SAMPLES
middle Miocene
0.5
1
1.0
2
3
4
5
6
7
CC
Empty
B
B
CP
AM
CG
10YR 6/4
10YR 5/4
10YR 6/4
5Y 4/1 band
10YR 6/4
10YR 5/4
10YR 6/4
10YR 5/4
10YR 5/4
10YR 6/4
10YR 5/4
10YR 5/4
7.5YR 5/4
10YR 5/4
10YR 5/4
Empty

LITHOLOGIC DESCRIPTION

SILICEOUS CLAY GRADING DOWNCORE TO PELAGIC CLAY

- Dominant colors: yellowish brown (10YR 5/4) and light yellowish brown (10YR 6/4) grading at 5, 30 cm to brown (7.5YR 5/4). Minor colors: local thin bands and mottles of dark gray (10YR 4/1).
- Section 5, 125–150 cm and the Core Catcher are very deformed, resulting from flow-in. The rest of the core is slightly deformed.
- This core consists of homogeneous to lightly mottled yellowish brown siliceous clay grading to mottled brown pelagic clay at 5, 30 cm.

SMEAR SLIDE SUMMARY (%)

	2, 30	3, 90	5, 90
	D	D	D
Texture:			
Sand	0	5	0
Silt	15	15	6
Clay	85	80	94
Composition:			
Quartz	2	3	2
Feldspar	Tr	Tr	Tr
Clay	84	80	94
Volcanic glass	Tr	Tr	1
Diatoms	7	7	Tr
Radiolarians	7	10	1
Sponge spicules			Tr
Silicoflagellates	Tr	Tr	Tr
Opaques			2

SITE 581 HOLE CORE 9 CORED INTERVAL 5735.5–5745.0 mbsl; 248.0–257.5 mbsf

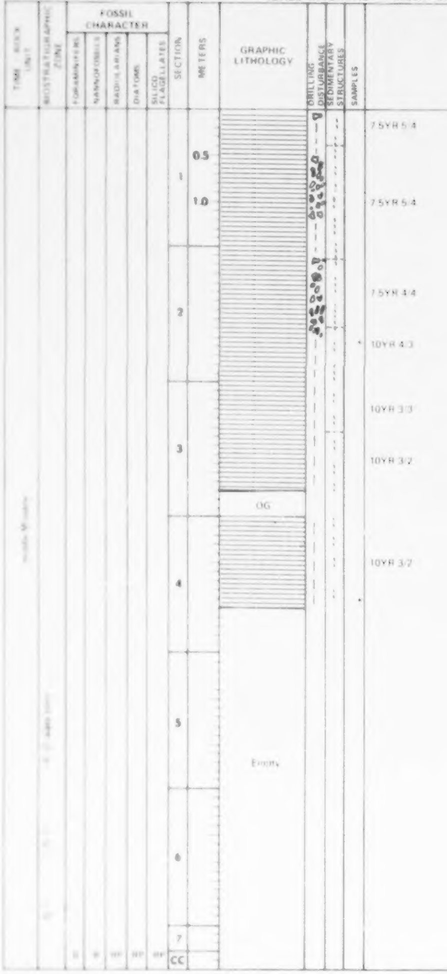
TIME-ROCK UNIT
BIOSTRATIGRAPHIC ZONE
FOSSIL CHARACTER
FORAMINIFERS
NANNOFOSSILS
RADIOLARIANS
DIATOMS
SILICO-FLAGELLATES
SECTION
METERS
GRAPHIC LITHOLOGY
DRILLING DISTURBANCE
SEDIMENTARY STRUCTURES
SAMPLES
0.5
1.0
1
2
3
4
5
6
7
CC
B
B
RP
RP
RP
OG
Empty
7.5YR 5/4
7.5YR 5/4
7.5YR 4/4
10YR 4/3
10YR 3/3
10YR 3/2
10YR 3/2

LITHOLOGIC DESCRIPTION

PELAGIC CLAY

Dominant colors: brown (7.5YR 5/4) and dark brown (7.5YR 4/4) grading to dark brown (10YR 4/3); dark brown (10YR 3/3) below 2, 89 cm and very dark grayish brown (10YR 3/2) below 3, 53 cm. Minor colors: Section 1 has dark grayish brown (10YR 4/2) patches. Sections 2 through 4 are mottled with light brown (7.5YR 6/4) and yellowish brown (10YR 5/4, 10YR 6/4).

Sections 1 and 2 have brecciated intervals; rest of the core is slightly deformed by drilling.

This core consists of mottled brown pelagic clay. There is a pebble at 1, 0–1 cm.

SMEAR SLIDE SUMMARY (%):

	2, 104	4, 90
	D	D
Texture:		
Sand	3	1
Silt	7	8
Clay	90	91
Composition:		
Quartz	2	2
Feldspar	Tr	
Mica		Tr
Clay	90	91
Volcanic glass	Tr	Tr
Micronodules	7	7
Radiolarians	1	

SITE 581 HOLE CORE 10 CORED INTERVAL 5745.0–5754.5 mbsl; 257.5–267.0 mbsf

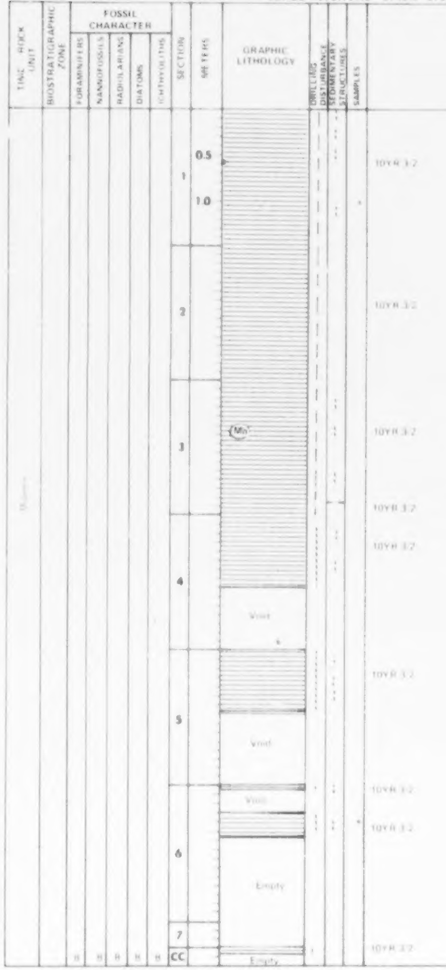
TIME-ROCK UNIT
BIOSTRATIGRAPHIC ZONE
FOSSIL CHARACTER
FORAMINIFERS
NANNOFOSSILS
RADIOLARIANS
DIATOMS
ICHTHYOLITHS
SECTION
METERS
GRAPHIC LITHOLOGY
DRILLING DISTURBANCE
SEDIMENTARY STRUCTURES
SAMPLES
0.5
1.0
1
2
3
4
5
6
7
CC
B
B
B
B
B
Mn
Void
Void
Void
Empty
Empty
10YR 3/2
10YR 3/2
10YR 3/2
10YR 3/2
10YR 3/2
10YR 3/2
10YR 3/2
10YR 3/2
10YR 3/2

LITHOLOGIC DESCRIPTION

PELAGIC CLAY

*Dominant color: very dark grayish brown (10YR 3/2). Minor colors: Section 1 has light reddish brown (5YR 6/4) mottles. Section 3 has very minor brown (7.5YR 5/4) mottles. Sections 4 through 6 have minor brownish yellow (10YR 6/6) mottles.

*Section 3, 136 cm through the Core Catcher are moderately to very deformed. The rest of the core is slightly deformed by drilling.

*This core consists of homogeneous to lightly mottled very dark grayish brown pelagic clay. There is a small (0.5 cm diameter) manganese nodule at 3, 59 cm.

SMEAR SLIDE SUMMARY (%):

	1, 100	6, 40
	D	D
Texture:		
Sand	0	0
Silt	10	20
Clay	90	80
Composition:		
Quartz	3	3
Clay	92	91
Volcanic glass		3
Opaques (hematite and goethite)	5	3

SITE 581 HOLE CORE 11 CORED INTERVAL 5754.5–5764.0 mbsl; 267.0–276.5 mbsf

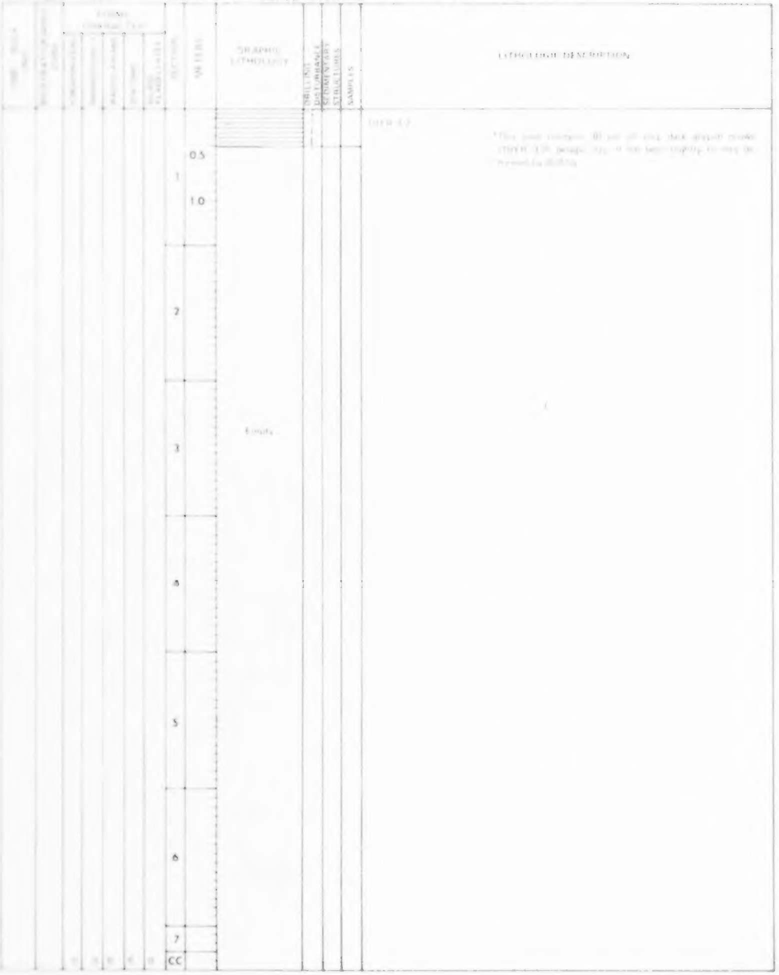
TIME-ROCK UNIT
BIOSTRATIGRAPHIC ZONE
FOSSIL CHARACTER
FORAMINIFERS
NANNOFOSSILS
RADIOLARIANS
DIATOMS
SILICO-FLAGELLATES
SECTION
METERS
GRAPHIC LITHOLOGY
DRILLING DISTURBANCE
SEDIMENTARY STRUCTURES
SAMPLES
LITHOLOGIC DESCRIPTION
0.5
1.0
1
2
3
4
5
6
7
CC
Empty
10YR 3/2

*This core contains 40 cm of very dark grayish brown (10YR 3/2) pelagic clay, it has been slightly to very deformed by drilling.

SITE 581 HOLE CORE 12 CORED INTERVAL 5764.0–5773.5 mbsl; 276.5–286.0 mbsf

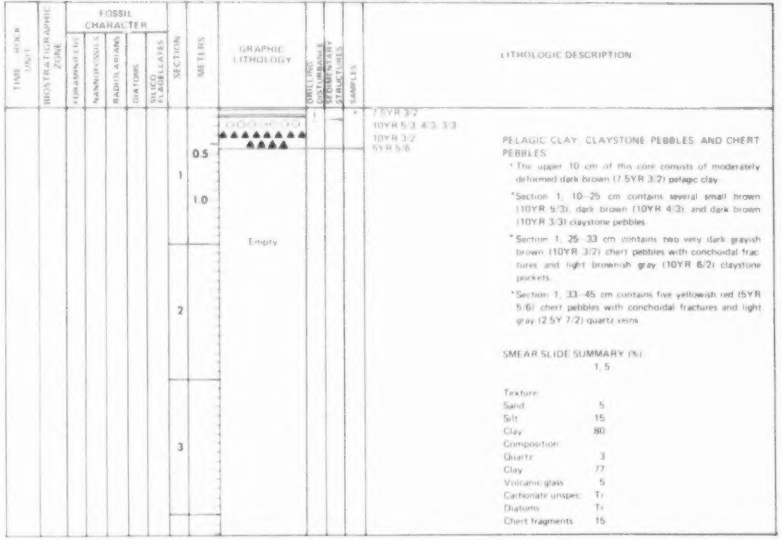
TIME-ROCK UNIT
BIOSTRATIGRAPHIC ZONE
FOSSIL CHARACTER
FORAMINIFERS
NANNOFOSSILS
RADIOLARIANS
DIATOMS
SILICO-FLAGELLATES
SECTION
METERS
GRAPHIC LITHOLOGY
DRILLING DISTURBANCE
SEDIMENTARY STRUCTURES
SAMPLES
LITHOLOGIC DESCRIPTION
0.5
1.0
1
2
3
Empty
*
7.5YR 3/2
10YR 5/3, 4/3, 3/3
10YR 3/2
5YR 5/6

PELAGIC CLAY, CLAYSTONE PEBBLES, AND CHERT PEBBLES

- *The upper 10 cm of this core consists of moderately deformed dark brown (7.5YR 3/2) pelagic clay.
- *Section 1, 10–25 cm contains several small brown (10YR 5/3), dark brown (10YR 4/3), and dark brown (10YR 3/3) claystone pebbles.
- *Section 1, 25–33 cm contains two very dark grayish brown (10YR 3/2) chert pebbles with conchoidal fractures and light brownish gray (10YR 6/2) claystone pockets.
- *Section 1, 33–45 cm contains five yellowish red (5YR 5/6) chert pebbles with conchoidal fractures and light gray (2.5Y 7/2) quartz veins.

SMEAR SLIDE SUMMARY (%)

	1, 5
Texture:	
Sand	5
Silt	15
Clay	80
Composition:	
Quartz	3
Clay	77
Volcanic glass	5
Carbonate unspec.	Tr
Diatoms	Tr
Chert fragments	15

SITE 581 HOLE CORE 13 CORED INTERVAL 5773.5–5783.0 mbsl; 286.0–295.5 mbsf

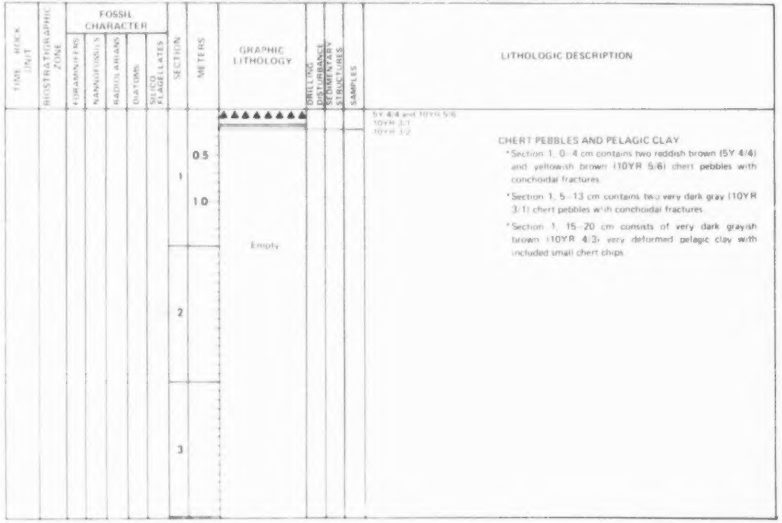
TIME-ROCK UNIT
BIOSTRATIGRAPHIC ZONE
FOSSIL CHARACTER
FORAMINIFERS
NANNOFOSSILS
RADIOLARIANS
DIATOMS
SILICO-FLAGELLATES
SECTION
METERS
GRAPHIC LITHOLOGY
DRILLING DISTURBANCE
SEDIMENTARY STRUCTURES
SAMPLES
LITHOLOGIC DESCRIPTION
0.5
1.0
1
2
3
Empty
5Y 4/4 and 10YR 5/6
10YR 3/1
10YR 3/2

CHERT PEBBLES AND PELAGIC CLAY

- *Section 1, 0–4 cm contains two reddish brown (5Y 4/4) and yellowish brown (10YR 5/6) chert pebbles with conchoidal fractures.
- *Section 1, 5–13 cm contains two very dark gray (10YR 3/1) chert pebbles with conchoidal fractures.
- *Section 1, 15–20 cm consists of very dark grayish brown (10YR 4/3) very deformed pelagic clay with included small chert chips.

SITE 581 HOLE CORE 14 CORED INTERVAL 5783.0–5792.5 mbsl; 295.5–305.0 mbsf

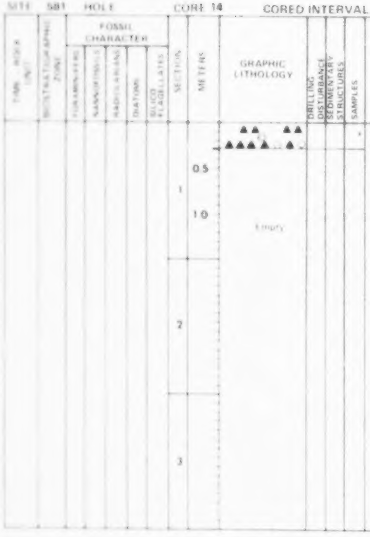
TIME-ROCK UNIT
BIOSTRATIGRAPHIC ZONE
FOSSIL CHARACTER
FORAMINIFERS
NANNOFOSSILS
RADIOLARIANS
DIATOMS
SILICO-FLAGELLATES
SECTION
METERS
GRAPHIC LITHOLOGY
DRILLING DISTURBANCE
SEDIMENTARY STRUCTURES
SAMPLES
0.5
1.0
1
2
3
Empty
*

LITHOLOGIC DESCRIPTION

7.5YR 4/4 and 7.5YR 7/4
10YR 3/1–2/1
10YR 7/4

CHERT AND CLAYSTONE PEBBLES

- Section 1, 0–6 cm contains a medium brown (7.5YR 4/4) and pink (7.5YR 7/4) banded chert cobble with conchoidal fractures.
- Section 1, 7–10 cm contains a very dark gray (10YR 3/1) to black (10YR 2/1) chert cobble with clear quartz veins and conchoidal surface fractures.
- Section 1, 11–13 cm contains a very pale brown (10YR 7/4) soft banded claystone pebble (see smear slide summary below).
- Section 1, 15–28 cm contains a mixture of small pebbles, including banded medium brown (7.5YR 4/4) and pink (7.5YR 7/4) banded chert, very dark gray (10YR 3/1) chert, and very pale brown (10YR 7/4) claystone.

SMEAR SLIDE SUMMARY (%):

	1, 12
	D
Texture:	
Sand	0
Silt	10
Clay	90
Composition:	
Quartz	3
Clay	90
Volcanic glass	7
Diatoms	Tr

SITE 581 HOLE CORE 15 CORED INTERVAL 5792.5–5802.0 mbsl; 305.0–314.5 mbsf

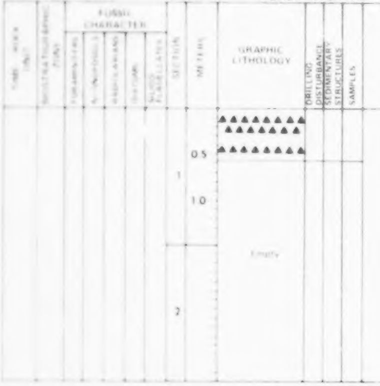
TIME-ROCK UNIT
BIOSTRATIGRAPHIC ZONE
FOSSIL CHARACTER
FORAMINIFERS
NANNOFOSSILS
RADIOLARIANS
DIATOMS
SILICO-FLAGELLATES
SECTION
METERS
GRAPHIC LITHOLOGY
DRILLING DISTURBANCE
SEDIMENTARY STRUCTURES
SAMPLES
0.5
1.0
1
2
Empty

LITHOLOGIC DESCRIPTION

CHERT PEBBLES AND FRAGMENTS

- This core is 55 cm long (including ethafoam spacers) and contains dull to vitreous chert pebbles and fragments.
- The chert pebbles range in size from 2 to 7 cm in diameter. They are of various colors, including: dusky red (10R 3/2), dark reddish gray (10R 3/1), reddish black (10R 2.5/1), black (10YR 2.5/1), very dark gray (10YR 3/1), and very dark grayish brown (10YR 3/2).
- Some of the chert pebbles are laminated. Some contain quartz-filled veins and/or blebs of yellowish brown (10YR 5/4) to very pale (10YR 8/4) porcellanite.

SITE 581 HOLE CORE 16 CORED INTERVAL 5802.0–5811.5 mbsl; 314.5–324.0 mbsf

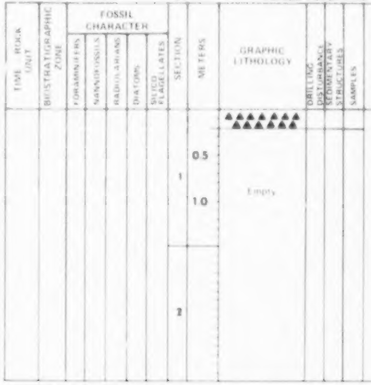
TIME-ROCK UNIT
BIOSTRATIGRAPHIC ZONE
FOSSIL CHARACTER
FORAMINIFERS
NANNOFOSSILS
RADIOLARIANS
DIATOMS
SILICO-FLAGELLATES
SECTION
METERS
GRAPHIC LITHOLOGY
DRILLING DISTURBANCE
SEDIMENTARY STRUCTURES
SAMPLES
0.5
1.0
1
2
Empty

LITHOLOGIC DESCRIPTION

CHERT PEBBLES AND FRAGMENTS

- This core is 19 cm long (including ethafoam spacers) and contains dull to vitreous chert pebbles and fragments.
- The chert pebbles range in size from 2 to 6 cm in diameter. They are of various colors, including: very dark gray (10YR 3/1), very dark grayish brown (10YR 3/2) and black (10YR 2.5/1).

Several of the chert pebbles are laminated with yellowish brown (10YR 5/4–10YR 5/6).

SITE 581 HOLE CORE 17 CORED INTERVAL 5811.5–5821.0 mbsl; 324.0–333.5 mbsf

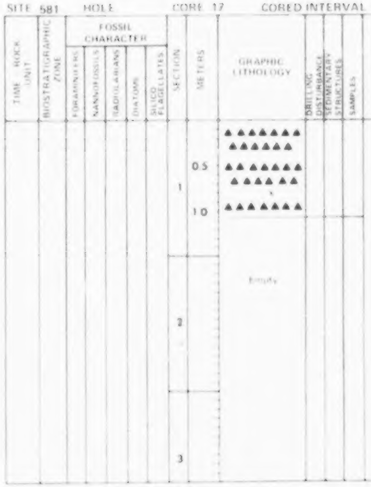
TIME-ROCK UNIT
BIOSTRATIGRAPHIC ZONE
FOSSIL CHARACTER
FORAMINIFERS
NANNOFOSSILS
RADIOLARIANS
DIATOMS
SILICO-FLAGELLATES
SECTION
METERS
GRAPHIC LITHOLOGY
DRILLING DISTURBANCE
SEDIMENTARY STRUCTURES
SAMPLES
0.5
1.0
1
2
3
Empty

LITHOLOGIC DESCRIPTION

CHERT PEBBLES AND FRAGMENTS

- This core is 107 cm long (including ethafoam spacers) and contains dull to vitreous chert pebbles and fragments.
- The chert pebbles range in size from 4 to 7 cm in diameter. They are of various colors, including: yellowish brown (10YR 5/8), banded red (10YR 4/6), yellowish brown (10YR 5/8), and dark yellowish brown (10YR 4/4), red (10YR 4/6), brown (10YR 4/3) or brown (7.5YR 4/4) with yellow (10YR 7/8), reddish yellow (5YR 6/8), weak red (10R 4/4), and/or dusky red (10R 3/4) patches, dark red (2.5Y 3/6), dark brown (10YR 3/3) with very dark gray (10YR 3/1) laminations and dusky red (10Y 3/2) patches, black (10YR 2.5/1), very dark grayish brown (10YR 3/2), and, very dark gray (10YR 3/1).

Some of the black, dark gray, and very dark grayish brown chert pebbles have brownish yellow (10YR 6/6) to dark yellowish brown (10YR 4/4) to yellow (10YR 7/6) indurated clay patches and/or laminations. The yellowish brown and red chert pebbles have small brownish yellow (10YR 6/8) to yellow (10YR 7/8) burrows. Fractures in the pebbles are filled with clear to weak red (10YR 4/4) quartz. Some of the quartz is well crystallized.

SITE 581 HOLE CORE 18 CORED INTERVAL 5821.0–5830.5 mbsl; 333.5–343.0 mbsf

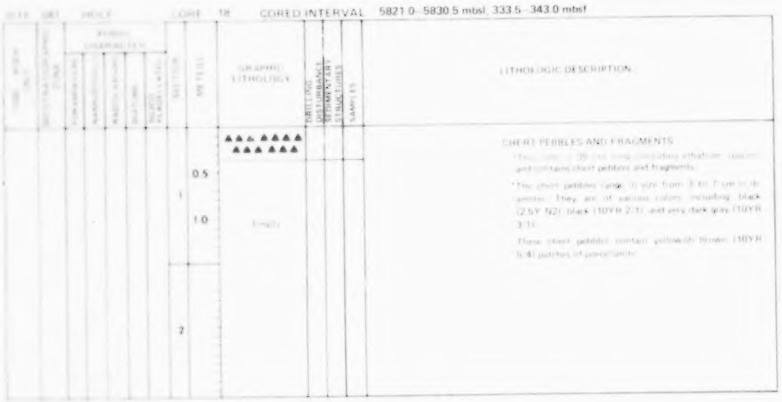
TIME – ROCK UNIT
BIOSTRATIGRAPHIC ZONE
FOSSIL CHARACTER
FORAMINIFERS
NANNOFOSSILS
RADIOLARIANS
DIATOMS
PLANT FRAGMENTS
SECTION
METERS
GRAPHIC LITHOLOGY
DRILLING DISTURBANCE
SEDIMENTARY STRUCTURES
SAMPLES
LITHOLOGIC DESCRIPTION
1
2
0.5
1.0
Empty

CHERT PEBBLES AND FRAGMENTS

- This core is 28 cm long (including ethafoam spacers) and contains chert pebbles and fragments.
- The chert pebbles range in size from 3 to 7 cm in diameter. They are of various colors including black (2.5Y N2), black (10YR 2/1), and very dark gray (10YR 3/1).

These chert pebbles contain yellowish brown (10YR 5/4) patches of porcellanite.

SITE 581 HOLE CORE 19 CORED INTERVAL 5830.5–5840.0 mbsl; 343.0–352.5 mbsf

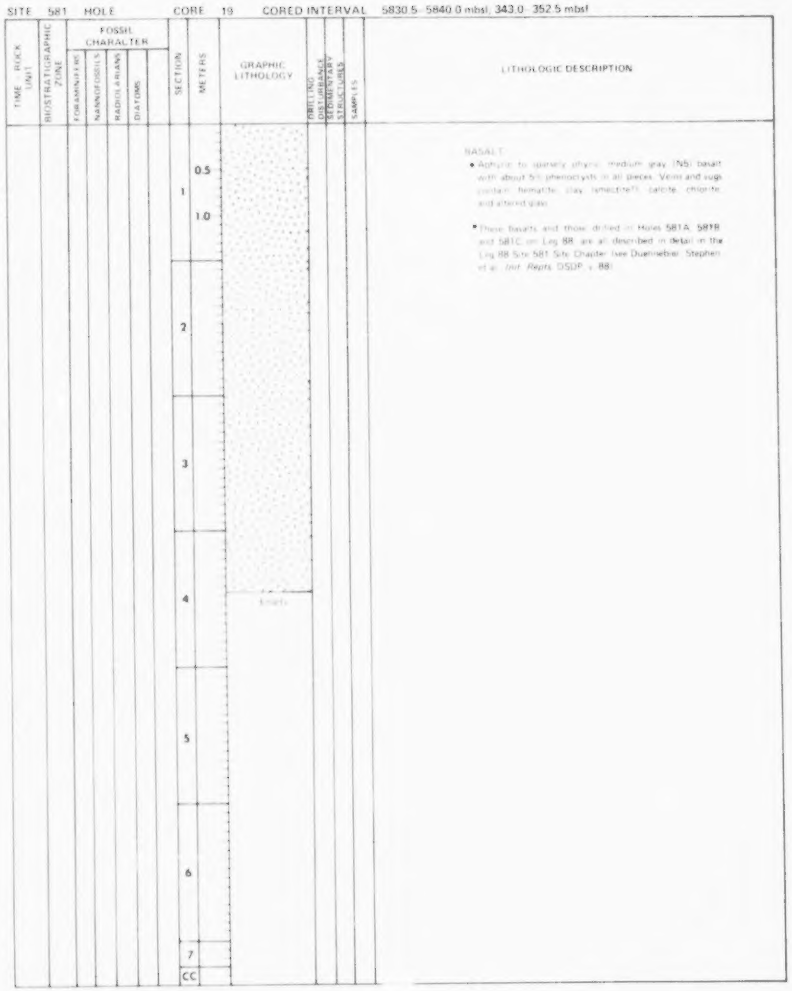
TIME – ROCK UNIT
BIOSTRATIGRAPHIC ZONE
FOSSIL CHARACTER
FORAMINIFERS
NANNOFOSSILS
RADIOLARIANS
DIATOMS
SECTION
METERS
GRAPHIC LITHOLOGY
DRILLING DISTURBANCE
SEDIMENTARY STRUCTURES
SAMPLES
LITHOLOGIC DESCRIPTION
1
2
3
4
5
6
7
CC
0.5
1.0
Empty

BASALT:

- Aphyric to sparsely phyric, medium gray (N5) basalt with about 5% phenocrysts in all pieces. Veins and vugs contain hematite, clay (smectite?), calcite, chlorite, and altered glass.
- These basalts and those drilled in Holes 581A, 581B and 581C on Leg 88, are all described in detail in the Leg 88 Site 581 Site Chapter (see Duennebier, Stephen et al., *Init. Repts.* DSDP, v. 88).

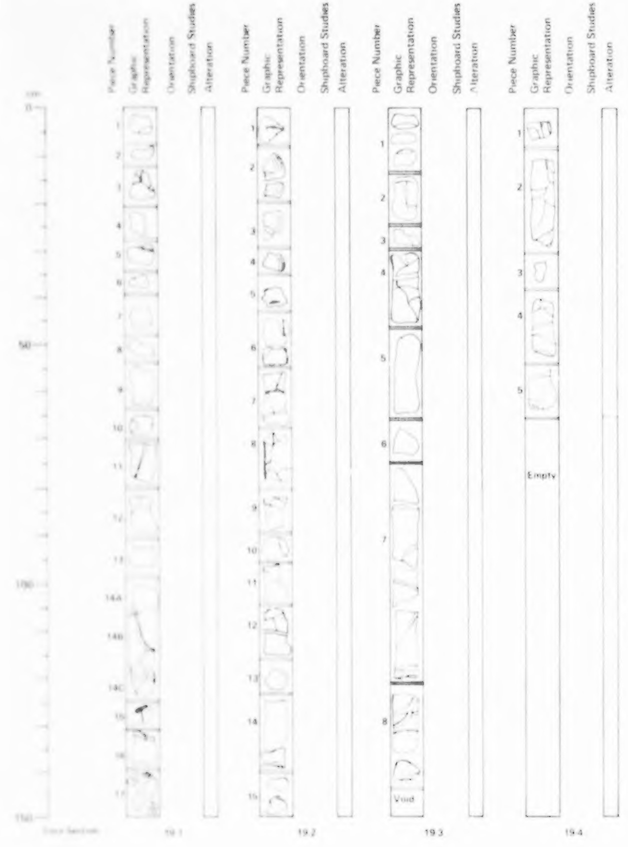

86-581-19-1 Depth: 5830.5–5832.0 mbsl; 343.0–344.5 mbsf

Aphyric to sparsely phyric basalt medium gray (N5) with ≤ 5% phenocrysts in all pieces.

Hematite veins in Pieces 3, 11, 12, 14, 15, 16, and 17 along small cracks.

Veins in Pieces 3, 14, 15, and 16 contain clay (smectite?) (+ alteration products).

Piece 3 contains a calcite vein cross cutting the hematite vein.

Piece 14B also contains a calcite vein.

Pieces 1, 2, and 10 contain calcite and alterations of chlorite and serpentine(?).

Pieces 17A, B, and C contain calcite and similar alterations as Pieces 1 and 2 plus minor glass alteration.

Uncut surfaces show minor alteration to chlorite.

86-581-19-2 Depth: 5832.0–5833.5 mbsl; 344.5–346.0 mbsf

Medium gray (N5) predominantly aphyric to sparsely phyric basalt with < 3% phenocrysts.

Pieces 13 and 15 are cropped, so internal structure and alteration are unknown. Show minor external alteration to chlorite.

Fe_2O_3 alteration products in veins in Pieces 1, 5, 6B, 7, 8, 9, 10, 11, and 12.

Dark green chlorite-altered glass(?) veins in Pieces 2, 3, 4, 7, 9 (very large vein across top of piece), 12, and 14.

Smectite(?) — brownish soft alteration material — contained in the green veins in Pieces 7A and 14.

Pieces 1, 3, 4, and 5 all show transition from external glass/slightly altered glass to fine-grained and aphyric basalt interior, but all pieces were rotated during recovery, so basalt top (glassy surface) is not pointed upwards. Alteration rind includes interlayered calcite and chlorite and slightly altered glass.

86-581-19-3 Depth: 5833.5–5835.0 mbsl; 346.0–347.5 mbsf

Aphyric to sparsely phyric basalt, medium gray (N5) with < 5% visible phenocrysts in all pieces.

Hematite alteration along small cracks and in veins in Pieces 1, 2, 3, 4, 7B, 7C, 7D, 8A, and 8B.

Calcite veins in Pieces 2, 4, 7B, and 7C.

Chlorite(?) (dark green veins) in Pieces 2, 4, 7B, 7C, 7D, and 8A — perhaps altered glass.

86-581-19-4 Depth: 5835.0–5835.6 mbsl; 347.5–348.1 mbsf

Aphyric to sparsely phyric basalt medium gray (N5) with 3–5% phenocrysts in all pieces.

Hematite filling in cracks in Pieces 1, 2, 4, and 5.

Calcite vugs in Pieces 3 and 4 with chlorite (serpentine?) and hematite in Piece 3 with chlorite in Piece 4.

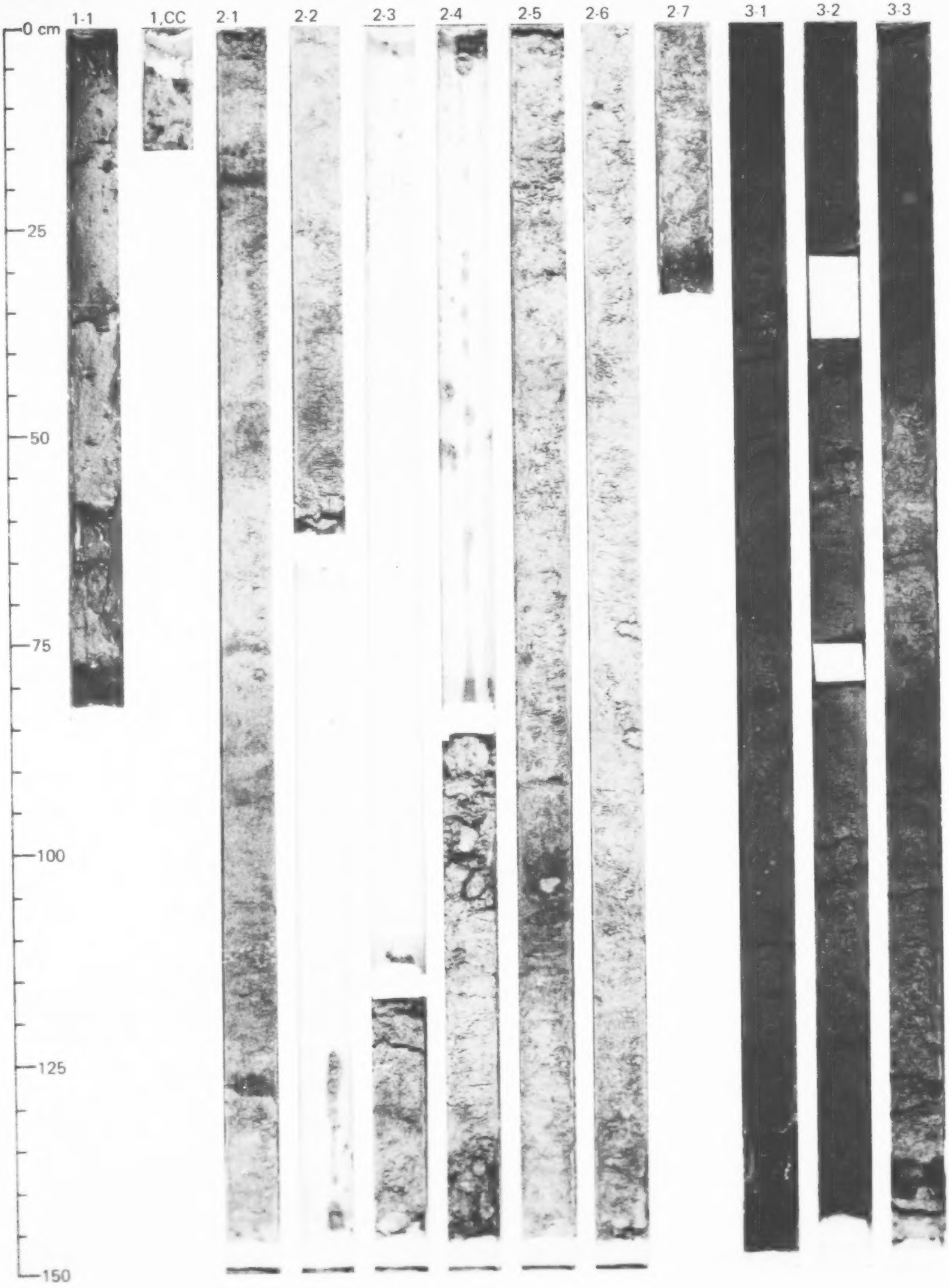
0 cm
25
50
75
100
125
150
1-1
1,CC
2-1
2-2
2-3
2-4
2-5
2-6
2-7
3-1
3-2
3-3

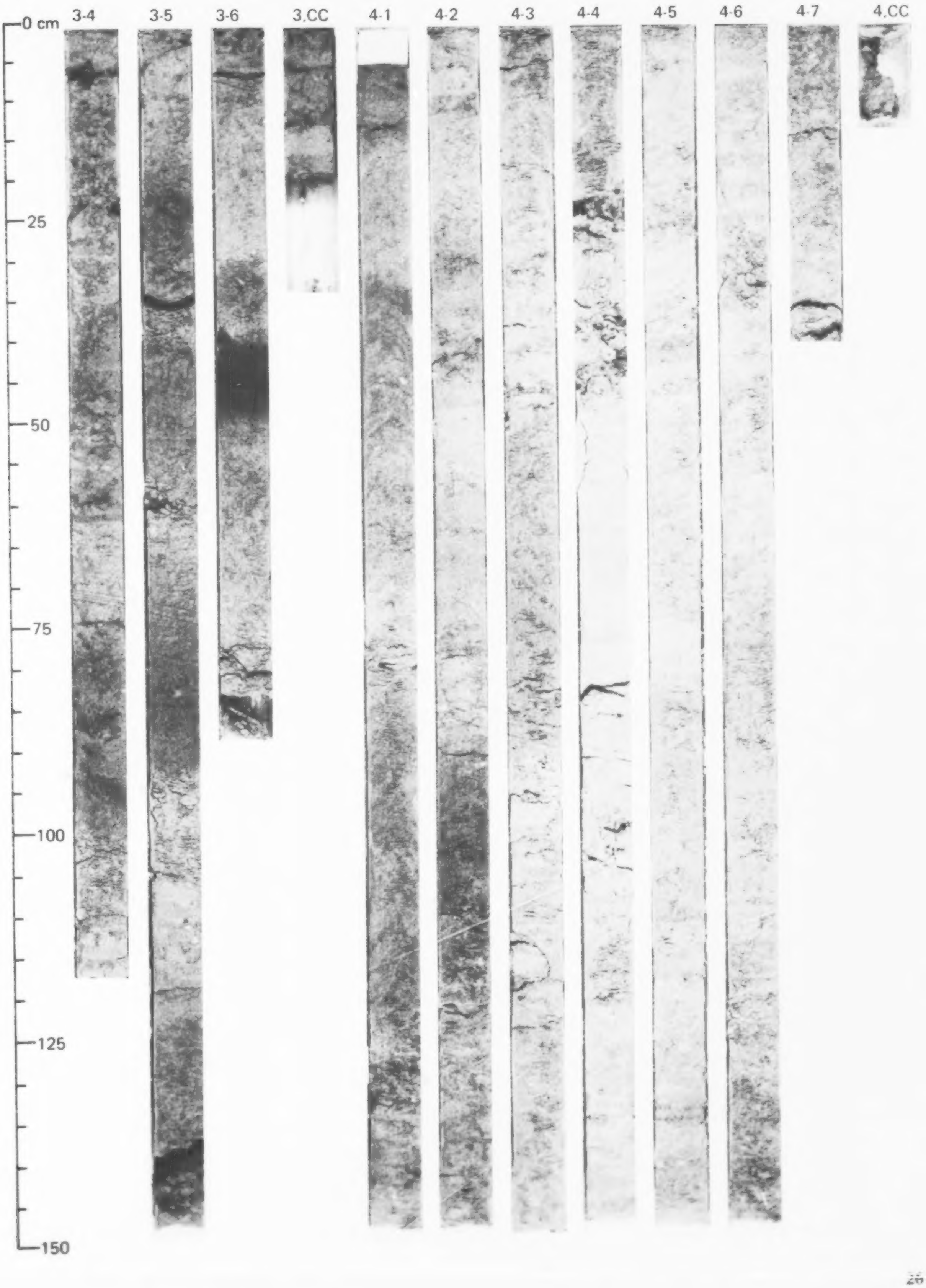
0 cm
25
50
75
100
125
150
3-4
3-5
3-6
3,CC
4-1
4-2
4-3
4-4
4-5
4-6
4-7
4,CC

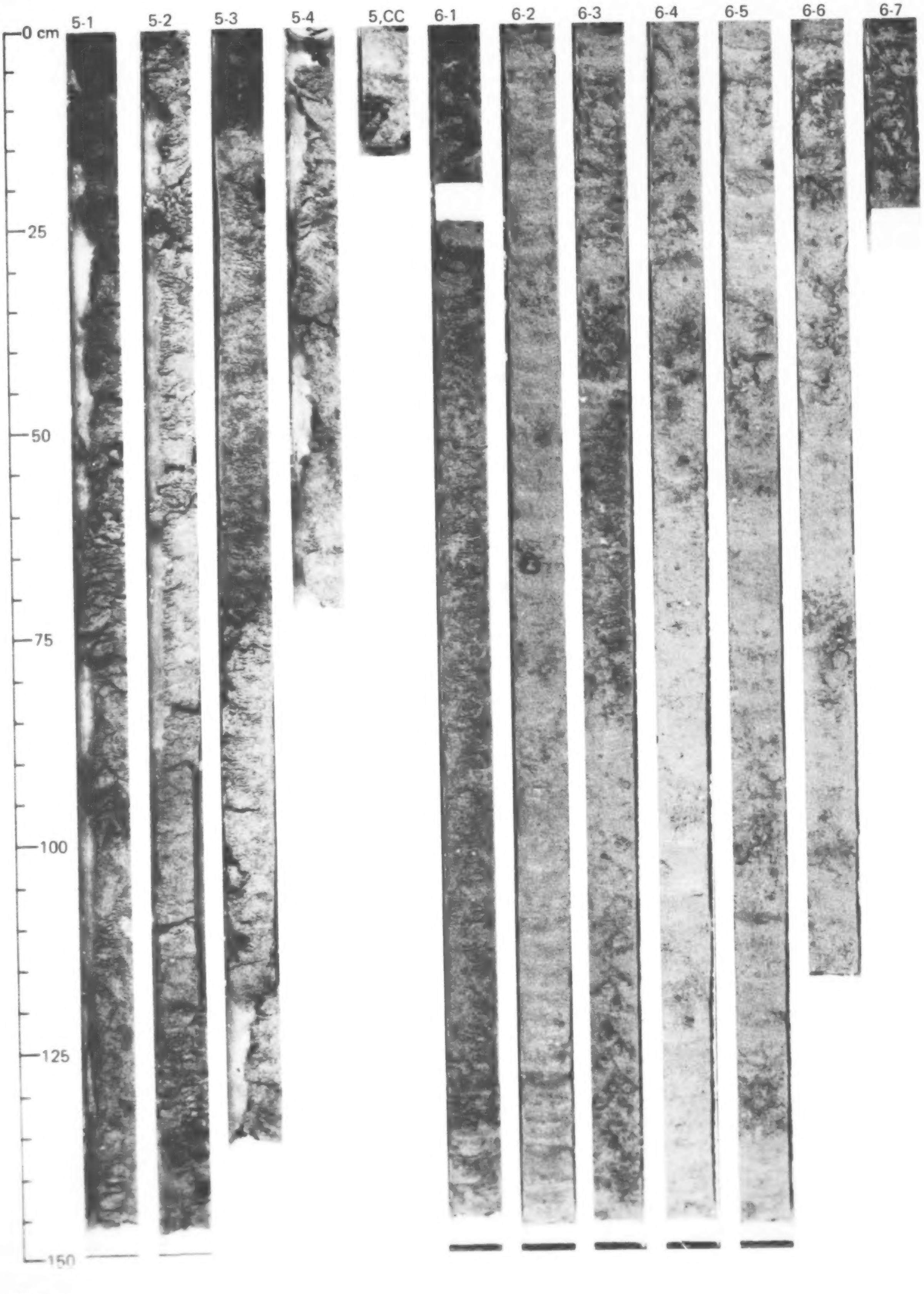
5-1
5-2
5-3
5-4
5,CC
6-1
6-2
6-3
6-4
6-5
6-6
6-7
0 cm
25
50
75
100
125
150

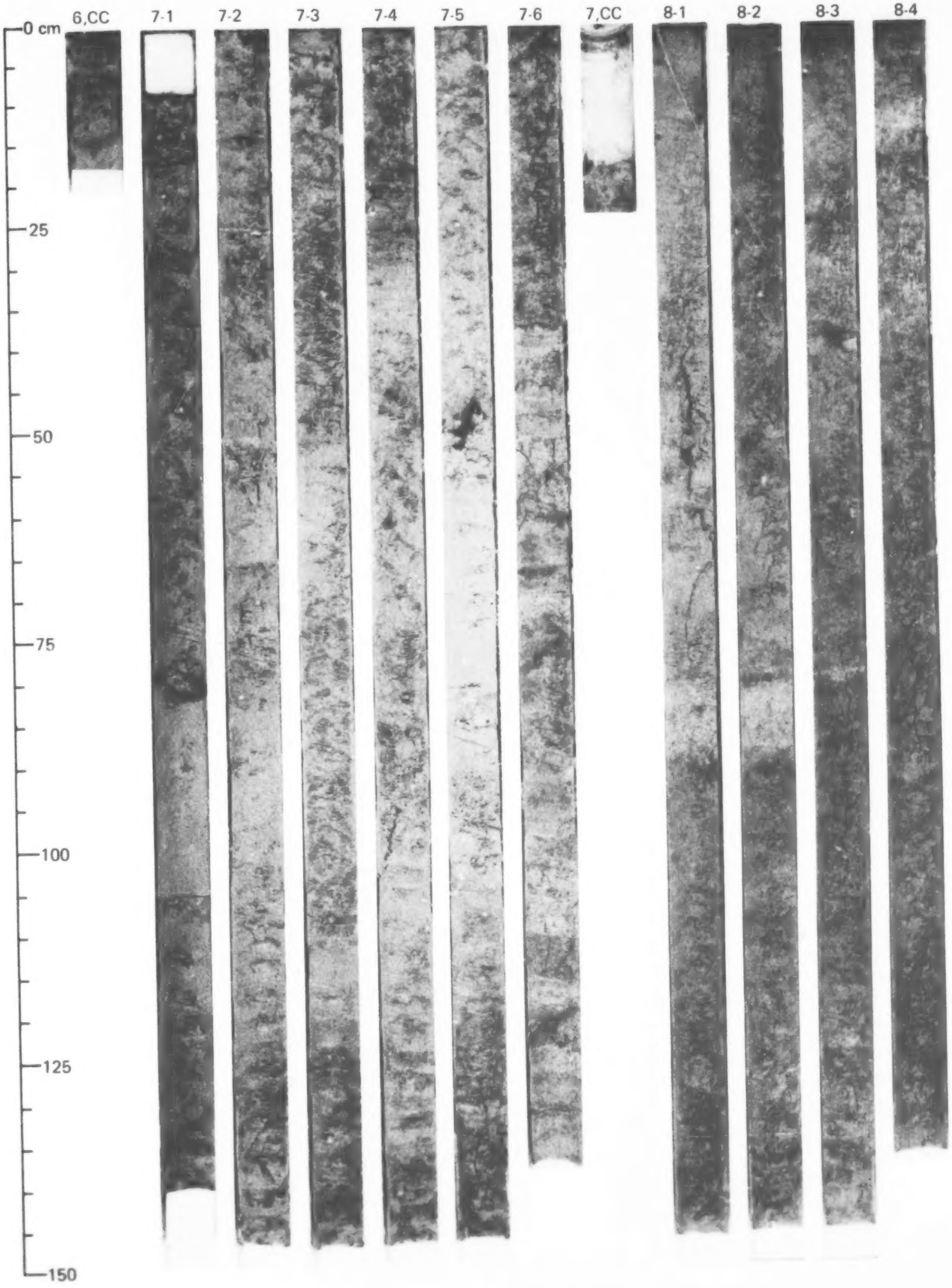
6,CC
7-1
7-2
7-3
7-4
7-5
7-6
7,CC
8-1
8-2
8-3
8-4
0 cm
25
50
75
100
125
150

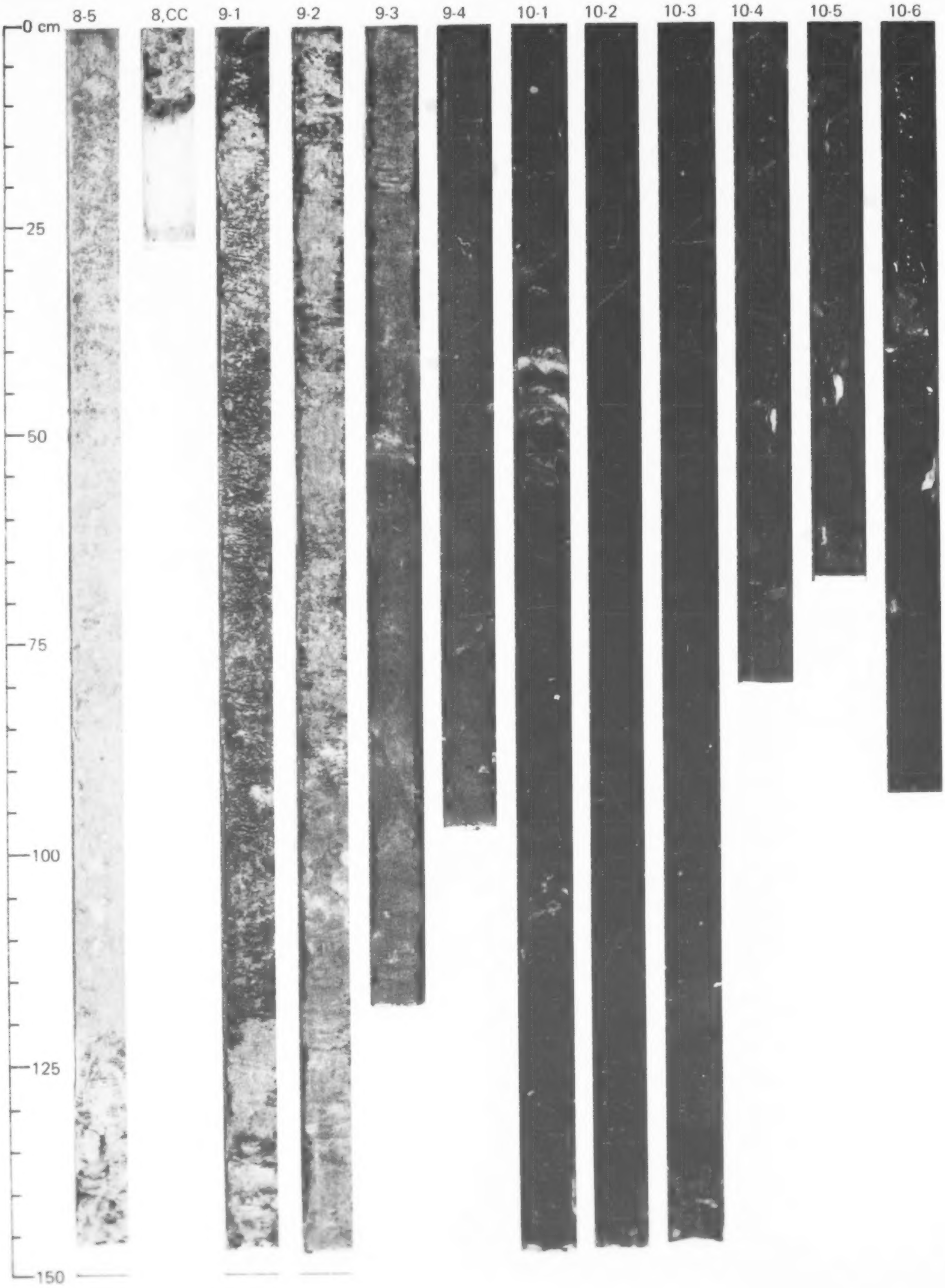
8-5
8,CC
9-1
9-2
9-3
9-4
10-1
10-2
10-3
10-4
10-5
10-6
0 cm
25
50
75
100
125
150

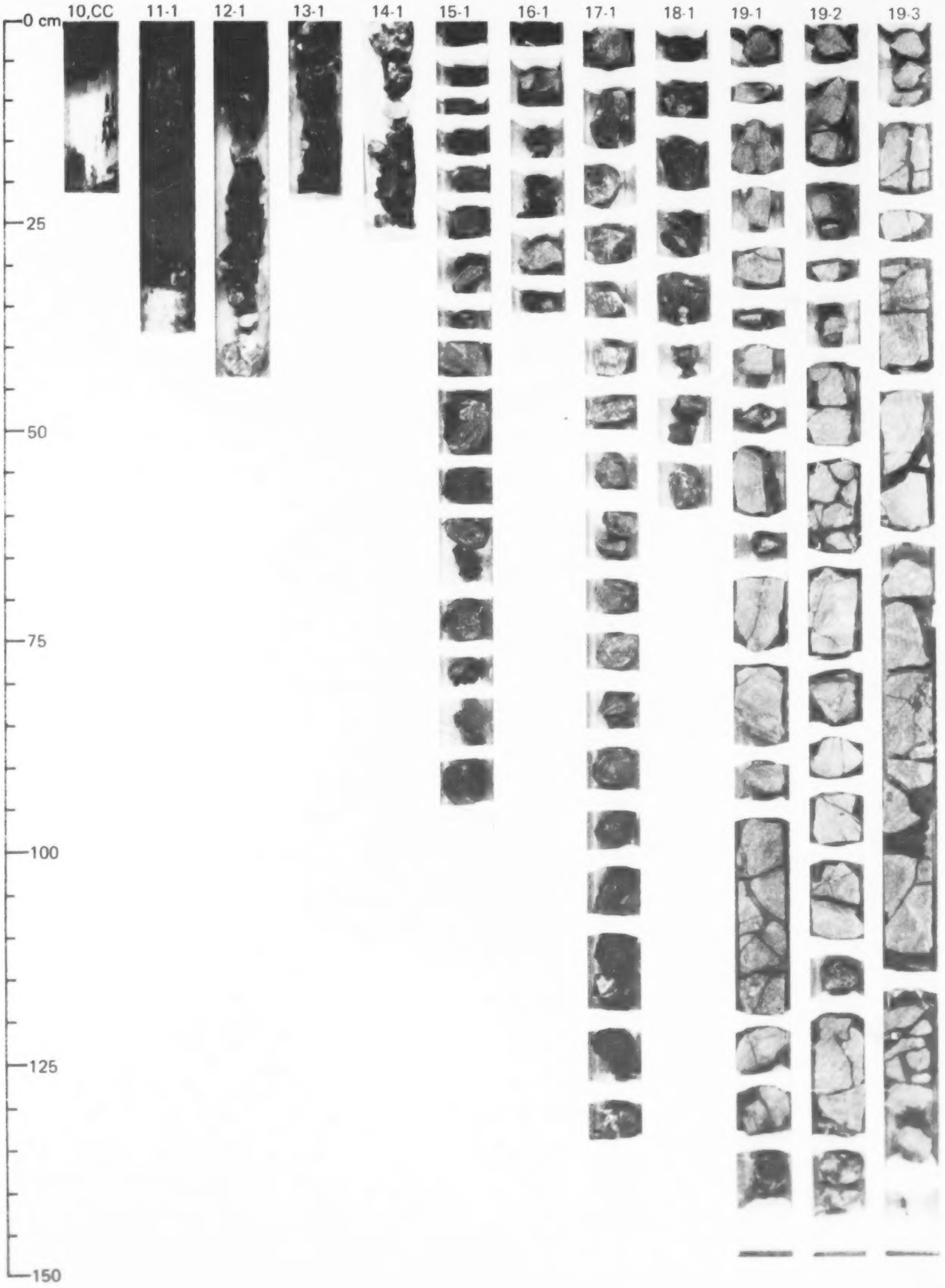
10,CC
11-1
12-1
13-1
14-1
15-1
16-1
17-1
18-1
19-1
19-2
19-3
0 cm
25
50
75
100
125
150

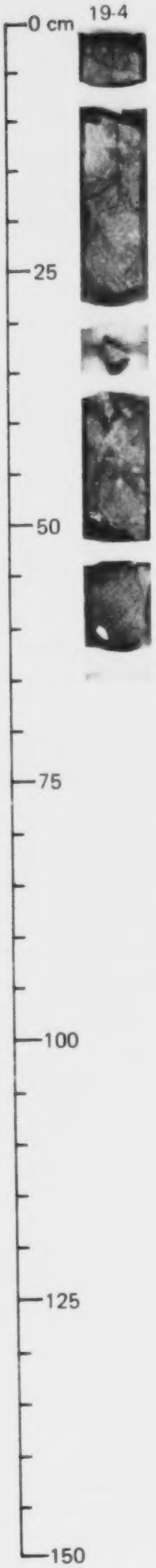
19-4
0 cm
25
50
75
100
125
150

PART II: BIOSTRATIGRAPHIC AND PALEOCEANOGRAPHIC STUDIES

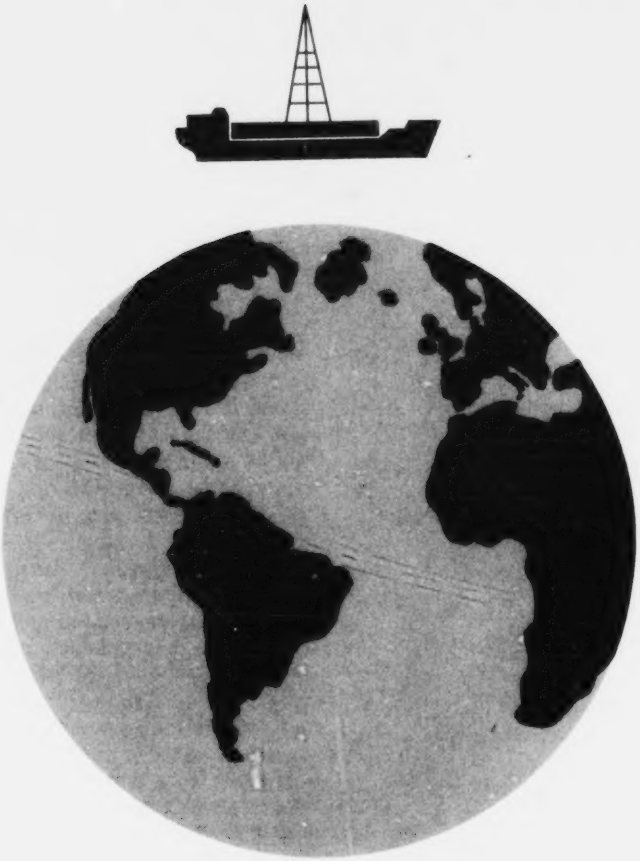

READEX FICHE

9. NEOGENE DIATOM BIOSTRATIGRAPHY OF THE MIDDLE LATITUDE WESTERN NORTH PACIFIC, DEEP SEA DRILLING PROJECT LEG 86[1]

Itaru Koizumi, Osaka University, Osaka, Japan
and
Yoshihiro Tanimura, National Science Museum, Tokyo[2]

ABSTRACT

The Pliocene and Pleistocene sections recovered in a south–north transect (38–42°N, 155°E) in the northwestern Pacific during Leg 86 are largely undeformed, owing to use of the hydraulic piston corer. Twenty-two diatom datum levels are ranked and tied directly to the paleomagnetic reversal record. The following datum levels are biostratigraphically useful: (1) first appearance datum (FAD) *Thalassiosira oestrupii*, 5.10–5.35 m.y. ago, (2) FAD *Nitzschia jouseae*, 4.50 m.y. ago, (3) FAD *Denticulopsis seminae* var. *fossilis*, 3.36–3.70 m.y. ago, (4) last appearance datum (LAD) *Denticulopsis kamtschatica*, 2.50–2.58 m.y. ago, (5) LAD *Thalassiosira convexa*, 2.30 m.y. ago, (6) FAD *Pseudoeunotia doliolus*, 1.89–2.00 m.y. ago, (7) LAD *Actinocyclus oculatus*, 0.93–1.33 m.y. ago, (8) LAD *Nitzschia reinholdii*, 0.47–0.52 m.y. ago, (9) LAD *Rhizosolenia curvirostris*, 0.30–0.35 m.y. ago. A new diatom zonation, based on these first-order datum levels, is proposed for the middle latitude Pliocene and Pleistocene.

The middle to upper Miocene section recovered at Site 581 (44°N, 160°E) provides a new diatom zonation, based on second-order datum levels, for the high latitude Miocene. A late Miocene hiatus spanning the interval from 8.2 to 10.1 m.y. ago is identified at Site 581. The hiatus corresponds to Hiatus NH 5 of Keller and Barron (1983).

INTRODUCTION

A series of excellent biosiliceous sequences from Sites 578, 579, and 580 were recovered on a south–north transect between 34 and 42°N in the western North Pacific (Fig. 1). The Pliocene and Pleistocene sequences were largely undeformed, owing to use of the hydraulic piston corer (HPC). The middle to late Miocene section, recovered at Site 581, contains abundant and well-preserved diatoms.

Through detailed investigations of piston cores, Deep Sea Drilling Project (DSDP) drill cores, and land-exposed marine sections during the past 10 yr., two main problems have appeared: provincialism and accurate age assignment (Koizumi and Burckle, 1984).

Because of provincialism (i.e., the latitudinal dependence of diatom distribution after the Miocene) it is necessary to make up at least two kinds of zonal schemes or datum levels: one for low latitudes and another for high latitudes (Burckle and Opdyke, 1977). The correlation between low and high latitudes was provided by diatom zones (Koizumi, 1975a) and by paleomagnetic reversal records tied to micropaleontological studies (Burckle, 1971; Burckle and Opdyke, 1977). Meanwhile, the sites in middle latitudes allowed a comparison within the same material of zonal boundaries and datum levels in low- and high-latitude diatom zonation (Koizumi, 1975b). The spatial and temporal distribution of zonal boundaries and datum levels have not been discussed in detail because of the lack of suitable and complete sections in middle latitudes.

As concerns age assignment, more than 40 diatom datum levels have been directly tied to the paleomagnet-

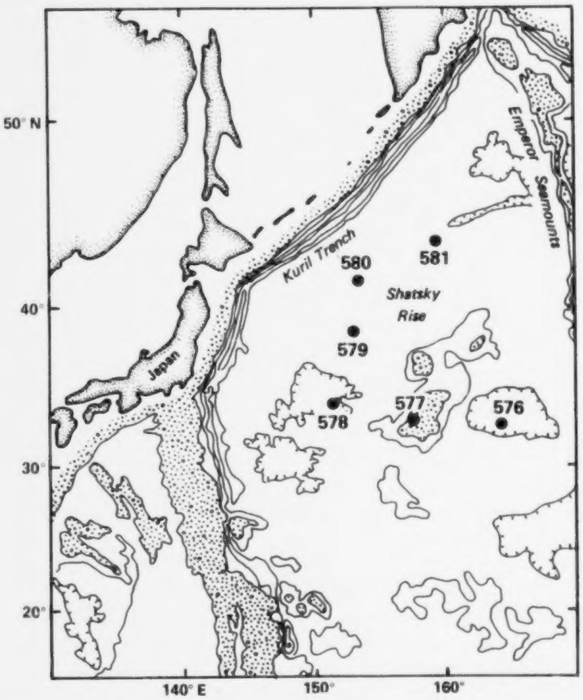

Figure 1. Location of sites occupied on Leg 86 in the western North Pacific Ocean. Areas shallower than 4 km stippled, 5-km contour plain, 6-km contour hachured.

---

[1] Heath, G. R., Burckle, L. H., et al., *Init. Repts. DSDP*, 86: Washington (U.S. Govt. Printing Office).

[2] Addresses: (Koizumi) Institute of Geological Sciences, College of General Education, Osaka University, Toyonaka, Osaka 560, Japan; (Tanimura) Department of Paleontology, National Science Museum, Hyakunin-cho, Shinjuku-ku, Tokyo, Japan.

ic reversal stratigraphy in low latitudes (Burckle, 1972, 1977, 1978; Burckle and Trainer, 1979). In low to middle latitudes, on the other hand, datum levels are tied to the paleomagnetics by such second-order methods as extrapolation from sediment accumulation rate curves based on these paleomagnetic ties in low latitudes (Barron, 1980, 1981; Keller and Barron, 1981; Keller et al., 1982; Barron and Keller, 1983). Datum levels for the Pliocene and Pleistocene in middle to high latitudes are chronologically calibrated against the paleomagnetic stratigraphy in several areas (Donahue, 1970; Koizumi and Kanaya, 1976; Burckle and Opdyke, 1977; Burckle et al., 1978, 1980; Ujiiè et al., 1977). Miocene datum levels in Japan are chronologically tied to K-Ar and fission track dates (Koizumi, 1977).

The purpose of this chapter is (1) to present the distribution of selected diatom datum levels in a south-north transect from 34 to 42°N, (2) to propose a middle latitude diatom zonation for the Pliocene and Pleistocene, (3) to propose a high latitude diatom zonation for the middle to upper Miocene, and (4) to present accurate age assignment for the selected datum levels directly tied to the paleomagnetic stratigraphy (Bleil, this volume) in the same samples.

METHOD OF STUDY

In processing the materials before microscopic examination, Schrader (1974a) and Koizumi's (1980) procedures were modified on two points: (1) wet original material was dried in order to do quantitative analysis of diatoms, and (2) boiling and centrifuging were omitted so as not to destroy the more delicate diatoms. The procedure was as follows: About 1 ml of original wet material was placed in an oven at 60°C for 24 hr., 0.2 g of the dried-up material were placed in a 200-ml beaker of hydrogen peroxide solution (15%) and left to stand for 24 hr. After pouring off the suspension, the residue was diluted with 200 ml of distilled water and homogenized for about 3 s in an ultrasonic washer (Clean Matic; 20 W, 40 kHz). Using a micropipette with disposable plastic tip (Justor-Jv 500 μl), 0.25 ml of this solution was placed on a grease-free cover glass (18 × 18 mm in size), dried on a hot plate at 50°C, and then mounted on a glass slide using Pleurax (refractive index = min. 1.50, alcohol solvent).

All diatoms were identified and counted until the number of individual specimens reached 200 (Sites 577, 578, and 581) or 300 (Sites 579 and 580) total, excluding *Bacteriastrum* spp. and *Chaetoceros* spp. The frequencies of *Coscinodiscus wailesii* and *Ethmodiscus rex*, which were found only as fragments, were excluded from the regular counting although they were larger in number. For the samples from Sites 577 and 578, 400 additional specimens were counted in order to decide the occurrence of stratigraphically important diatoms (a plus sign in Tables 1 and 2). The strewn slides that recorded poor preservation were examined entirely at ×700 (a black dot in Tables 1 and 2).

Abundances for Sites 577 and 578 are graded as follows: B = barren, VR = very rare (<100 individuals on one slide), R = rare (101-1000 individuals), F = few (1001-2000 individuals), C = common (2001-4000 individuals), and A = abundant (>4001 individuals). Quantitative abundance of diatoms was defined for each sample and related to 1 g of dried material for Sites 579 through 581. Estimates of preservation were based on the number of broken and dissolved diatom valves and expressed as follows: p = poor, m = moderate, and g = good.

Diatoms at Sites 577 and 578 were researched by Y. Tanimura and the residues were examined by I. Koizumi.

DIATOMS AT EACH SITE

Site 577

Site 577 is located on the western flank of the Shatsky Rise. Hole 577 (32°26.5'N, 157°43.40'E, depth 2678 m) penetrated to a maximum depth of 118.8 m sub-bottom and terminated in a hard layer. The sediments recovered are nannofossil oozes.

Diatoms are few to very rare and their preservation is poor to moderate from 0.57 through 54.11 m (Samples 577-1-1, 56-57 cm to 577-6-7, 30-31 cm). Diatoms are absent below the core catcher of Core 6.

Diatom assemblages in the interval from Samples 577-1-1, 56-57 cm through 577-3-5, 74-75 cm (0.57-23.05 m below the seafloor) belong to the *Pseudoeunotia doliolus* Zone of Burckle (1972). The *Rhizosolenia praebergonii* Zone in Samples 577-3-6, 74-75 cm to 577-4-2, 61-62 cm (24.14-27.92 m) is followed by the *Nitzschia jouseae* Zone in Samples 577-4-3, 61-62 cm to 577-5,CC (29.42-44.80 m), although it is difficult to examine zonal boundaries because of dissolution of such key species as *Rhizosolenia praebergonii* and *Nitzschia jouseae*. In samples from Core 6 (45.11-54.11 m), because zonal guide species such as *Nitzschia jouseae* and *Thalassiosira convexa* are absent, the corresponding zones can not be assigned (Table 1).

Site 578

Site 578 lies west of the Shatsky Rise in a large area of gently rolling seafloor. A thick section of late Neogene siliceous clay was recovered from Hole 578 (33° 55.56'N, 151°37.74'E; depth 6010 m). The upper 76.8 m of siliceous clay is anoxic, gray and olive gray in color, with many pyrite-cemented layers. On the other hand, siliceous clay and clay from 76.8 to 124.5 m are oxidized, yellow brown and brown in color with rare ferromanganese nodules. From 124.5 to 176 m, the pelagic clay is "slick," predominantly dark to very dark brown, and very homogeneous. Drilling was stopped by chert at 176.8 m below the seafloor.

Diatoms are common to few and preservation is moderate. Sometimes they are very rare and poorly preserved in the upper 52.3 m (down to Sample 578-6,CC). From 53.5 to 116.7 m (between Samples 578-7-1, 121-122 cm and 578-13-5, 135-136 cm), diatoms are abundant to common and moderate to well preserved. They are absent below Core 13 (Table 2, back pocket).

The stratigraphic occurrence of selected diatoms at this site is shown in Figure 2.

The ten diatom zones defined in this chapter were recognized without zonal breaks.

Site 579

Site 579 lies near the southern margin of the transitional zone between the subtropical and subarctic gyres. A total of 149.5 m of siliceous clay was recovered from two holes at Site 579 (Hole 579, 38°37.68'N, 153° 50.17'E, depth 5737 m and Hole 579A, 38°37.61'N, 153°50.28'E, depth 5737 m). Coring was terminated at 149.5 m because of increasingly poor recovery in well-indurated clayey diatom ooze.

Diatoms are generally abundant and well preserved throughout the entire section, except for two samples (579-2-4, 13-14 cm and 579-3-6, 115-116 cm), where they are few and moderately well preserved.

The eight diatom zones ranging from late Pleistocene through early Pliocene were recognized without breaks in Holes 579 and 579A (Table 3, back pocket). Diatom assemblages in both the lower part of Hole 579 (from Sample 579-2-4, 123-124 cm through Sample 579-2-5, 123–124 cm) and the top of Hole 579A (from Sample 579A-1-1, 14–15 cm through Sample 579A-2-2, 13–14 cm) belong to the *Rhizosolenia curvirostris* Zone.

The stratigraphic ranges of diagnostic diatoms at this site are shown in Figure 3.

Site 580

Site 580 lies at the northern margin of the transitional zone between the subarctic and subtropical gyres. A total of 155.3 m of Pleistocene and late Pliocene siliceous gray to dark gray and olive gray clay was recovered from Hole 580 (41°37.47′N, 153°58.58′E, depth 5375 m).

Diatoms are abundant and well preserved throughout the section. Seven diatom zones were recognized without zonal breaks in Hole 580 (Table 4, back pocket).

The stratigraphic ranges of selected diatoms in this hole are shown in Figure 4.

Site 581

Site 581 lies in the modern subarctic gyre, the location proposed for the Leg 88 downhole seismometer experiment. Because of the limited time available and the need to drill to basement to allow Leg 88 to plan their casing program, HPC sampling of the upper part of the sediment section at Site 581 was deferred until Leg 88. Hole 581 (43°55.62′N, 159°47.76′E, depth 5476 m) terminated in basalt recovered from 343 to 352.5 m subbottom depth. After Core 1 was recovered at the mud line (0–1.0 m), an interval of 180.5 m of sediment was washed away. The section from 181.5 to 223.6 m is anoxic, gray and green in color, biosiliceous clay to ooze. On the other hand, the sediments from 223.6 to 244.8 m consist of oxidized, yellow brown, biosiliceous clay. From 244.8 to 276.6 m, the sediment is "slick," fine-grained pelagic clay. From 276.6 to 343.0 m, nothing but chert fragments were recovered.

Diatoms are abundant and well preserved in Cores 1 through 8 (above 248 m), except for one sample (581-8-5, 110–111 cm) where they are very rare. In Core 9 (248.0–257.5 m), diatoms are very rare and only solution-resistant valves were recovered in the shipboard analysis. Diatoms are absent below Core 10.

A hiatus separates the *Denticulopsis katayamae* Zone and the *Thalassionema schraderi* Zone between Section 6 and the core catcher of Core 6 (Fig. 8). The time gap over the zonal boundary is about 1.9 m.y. from 8.2 to 10.1 m.y. ago. This hiatus corresponds with Hiatus NH5 of Keller and Barron (1983).

An early Pliocene to middle Miocene diatom biostratigraphy, typical of the subarctic region, was recovered (Table 5). The stratigraphic ranges of selected species at this site are shown in Figure 5.

DISTRIBUTION OF LATEST MIOCENE TO PLIOCENE AND PLEISTOCENE DATUM LEVELS IN MIDDLE LATITUDES

Twenty-two important middle latitude diatom datum levels based on the data provided from Leg 86 are discussed. Figure 6 gives the temporal and areal distribution of these datum levels, which are defined by first and last occurrence of key species. As was done by Burckle (1977, 1978) and Keller et al. (1982), each datum level is ranked by order of reliability (Table 6), using the criteria of Hornibrook and Edwards (1970), as follows:

First order: "Easily identifiable, common and persistent, either first rapid evolutionary appearance or highly consistent range." Second order: "Easily identifiable, fairly consistently present but not necessarily common, or first gradual evolutionary appearance is fairly consistent range." Third order: "Consistency of identification difficult or rare, or well defined ecologically or local geographic restrictions, or known in very few sections, or limits of range uncertain due to sampling gaps or disconformities."

The datum levels from youngest to oldest are as follows:

1. The last occurrence of *Thalassiosira nidulus* is slightly earlier in low–middle latitudes (0.39 m.y. ago) than in middle–high latitudes (0.28 m.y. ago). This datum levél was first used to define the top of the *Rhizosolenia curvirostris* Zone (Koizumi, 1973). Because of the possible diachrony of this datum level in the middle-high latitude eastern North Pacific (Schrader, 1973) it is assigned to a second-order category.

2. The last occurrence of *Rhizosolenia curvirostris* is almost synchronous at 0.30–0.35 m.y. ago in middle-high latitudes. This datum level defines the top of the *Rhizosolenia curvirostris* Zone. This species is also distributed in the middle latitude eastern North Pacific (Barron, 1981). It is classified as a first-order datum level.

3. The last occurrence of *Nitzschia reinholdii* is almost synchronous at 0.47–0.52 m.y. ago in middle–high latitudes. Koizumi (1975a; Koizumi and Kanaya, 1976) indicated this datum level in the lower part of the Brunhes Epoch in the North Pacific. Burckle (1977) also reported this datum level as a first-order category with an age of approximately 0.63 m.y. in the equatorial regions. It is assigned to a first-order category.

4. The last occurrence of *Nitzschia fossilis* is remarkably synchronous at 0.55 m.y. ago in middle–high latitudes. Koizumi and Kanaya (1976) first reported this datum level in the lowest part of the Brunhes Epoch on the Choshi Peninsula, Central Japan. This species also disappears in the lowest part of the Brunhes Epoch in the equatorial regions (Burckle and Trainer, 1979) and is classified as a first-order datum level.

5. The last occurrence of *Rhizosolenia matuyamai* is slightly later in middle latitudes (0.85 m.y. ago) than in lower and higher latitudes (0.89–0.97 my. ago). Burckle et al. (1978) described this species as ranging consistently from just below the Jaramillo Event to the lower part of the Jaramillo Event over the middle latitude North Pacific. Because of rare and sporadic occurrences it is classified as a second-order datum level.

6. The first occurrence of *Rhizosolenia matuyamai* is slightly earlier in middle latitudes (1.05 m.y. ago) than in lower and higher latitudes (0.91–1.00 m.y. ago). This datum level is put in a second-order category.

7. The last occurrence of *Actinocyclus oculatus* is earlier in lower latitudes (1.33 m.y. ago) than in higher lati-

Table 1. Stratigraphic occurrences of Neogene diatoms in Hole 577.

Core-Section (interval in cm)	Depth below seafloor (m)	Abundance	Preservation	*Bacteriastrum* spp.	*Actinocyclus curvatulus*	*A. ehrenbergii*	*A. ellipticus*	*A. ellipticus* f. *lanceolata*	*A. elongatus*	*A. moronensis*	*A. oculatus*	*Actinocyclus* sp.	*Actinoptychus senarius*	*Actinoptychus* sp.	*Asterolampra marylandica*	*Asterolampra* sp.	*Asteromphalus flabellatus*	*A. heptactis*	*A. imbricatus*	*A. petterssonii*	*A. robustus*	*Asteromphalus* sp.	*Cocconeis costata*	*Coscinodiscus africanus*	*C. nodulifer*	*C. oculus-iridis*	*C. radiatus*	*C. stellaris*	*C. tabularis* v. *egregius*	*C. vetustissimus*	*C. yabei*
1-1, 56-57	0.57	R	p																						●						
1-2, 56-57	2.07	VR	p																						●						
1-3, 56-57	3.57	VR	p																						●						
1-4, 56-57	5.07	R	p																	●					●						
1-5, 56-57	6.57	R	p		●																				●						
1,CC	6.80	F	m	1	4	1							8	1			1		1			1		1	10				7		
2-1, 47-48	7.28	VR	p																						●						
2-2, 47-48	8.78	VR	p										●												●						
2-3, 47-48	10.28	R	p																						●						
2-4, 47-48	11.78	F	m		2																			4	19	1			4		
2-5, 47-48	13.28	R	p																						●				●		
2,CC	16.30	VR	p																												
3-1, 74-75	17.05	F	m		2								2					1							2		1		9		
3-2, 74-75	18.55	VR	p																						●				●		
3-3, 74-75	20.05	C	m								1	1	3		1						1			1				1	7		
3-4, 74-75	21.55	F	m		3											1								2	8				8	1	
3-5, 74-75	23.05	C	m		1																				3				6		
3-6, 74-75	24.14	R	p																						●						
3,CC	25.80	R	m		4	1																			4			1	3		
4-1, 61-62	26.42	VR	p																												
4-2, 61-62	27.92	R	m																											●	r
4-3, 61-62	29.42	R	p																						●						
4-4, 61-62	30.92	R	m	1	5		1	1		1								1						1	18			1	3	1	
4-5, 61-62	32.42	VR	p						●																●						
4-6, 61-62	33.92	R	p		●																				●						
4,CC	35.30	F	g			1																		1	6				2		
5-1, 56-57	35.81	VR	p																						●						
5-2, 56-57	37.31	VR	p																				●								
5-3, 56-57	38.81	VR	p																												
5-4, 56-57	40.31	VR	p	●	●		●																								
5-5, 56-57	41.81	VR	p																						●						
5-6, 56-57	42.86	R	p																						●						
5,CC	44.80	R	p																						●						
6-1, 30-31	45.11	VR	p																												
6-2, 30-31	46.61	VR	p																						●						
6-3, 30-31	48.11	VR	p																												
6-4, 30-31	49.61	VR	p																												
6-5, 30-31	51.11	VR	p																						●						
6-6, 30-31	52.61	B																													
6-7, 30-31	54.11	VR	p																						●						
6,CC	54.30	B																													

Note: A = abundant, C = common, F = few, R = rare, VR = very rare, B = barren, r = reworked, + = found in 600 specimens counted, ● = present in a strewn slide. Preservation: g = good, m = moderate, p = poor. See text for further explanation.

tudes (0.93–1.00 m.y. ago). Donahue (1970) showed that the extinction level of this species in the high latitude North Pacific is near the top of the Jaramillo Event. Because of the diachrony of this datum level, it is assigned to a second-order category.

8. The last occurrence of *Thalassiosira antiqua* is remarkably diachronous from 3.14 m.y. ago in lower latitudes to 1.43 m.y. ago in higher latitudes. This datum level has been used to define the top of the *Thalassiosira zabelinae* Zone (Koizumi, 1973) and the *Denticulopsis seminae* var. *fossilis* Zone (Koizumi, 1975a) in middle-high latitudes. It is a good marker species for high latitudes, but it is assigned to the third-order datum level due to the diachrony.

9. The first occurrence of *Pseudoeunotia doliolus* is slightly earlier in lower latitudes (2.00 m.y. ago) than in higher latitudes (1.89 m.y. ago). Burckle (1972) reported this datum level in the lower part of the Olduvai Event in the equatorial Pacific. This species is broadly distributed over the tropical and middle-high latitudes. It is assigned to a first-order category with an approximate age of 1.90 m.y. in middle latitudes.

10. The last occurrence of *Rhizosolenia praebergonii* is earlier (2.14 m.y. ago) in higher latitudes than in lower latitudes (1.66 m.y. ago). Burckle (1972) reported the extinction level of this species just after the Olduvai Event in the equatorial Pacific. It is a good marker species for low-middle latitudes, but it is classified as a second-order datum level because of the sporadic occurrence and the diachrony between low and high latitudes.

11. The last occurrence of *Thalassiosira convexa* is remarkably synchronous at 2.30 m.y. ago in middle-high latitudes. Burckle (1972) used this datum level to define the top of "B" Subzone of the *Rhizosolenia praebergonii* Zone in the equatorial Pacific. This species is a cosmopolitan species and is assigned to a first-order category.

12. The first occurrence of *Rhizosolenia praebergonii* is slightly earlier in lower latitudes (2.58 m.y. ago) than in higher latitudes (2.40 m.y. ago). It is about 3.0 m.y. old in the equatorial Pacific, according to Burckle (1978). Because of the diachrony between low and high latitudes, it is assigned to a second-order datum level.

13. The last occurrence of *Bogorovia tatsunokuchiensis* is almost synchronous at 2.50–2.55 m.y. ago in middle-high latitudes. This species, described by Koizumi (1972), was the first to be related to the paleomagnetic reversal record. Because this species has only been reported from middle-high latitudes of the western North Pacific, it is assigned to a second-order datum level.

Table 1. (Continued).

Coscinodiscus spp	Cyclotella striata	C. stylorum	Denticulopsis kamtschatica	D. seminae	D. seminae v. fossilis	Diploneis bomboides	D. bombus	Diploneis sp.	Endictia sp.	Hemidiscus cuneiformis	H. simplicissimus	Hemidiscus sp.	Nitzschia bicapitata	N. dietrichii	N. fossilis	N. inflatula	N. interruptestriata	N. jouseae	N. kolaczekii	N. marina	N. reinholdii	N. seriata	N. sicula	Nitzschia spp	Paralia sulcata	Planktoniella sol	Pseudoeunotia doliolus	Rhizosolenia barboi	R. bergonii	R. curvirostris	R. hebetata	R. praebergonii	R. styliformis	Rhizosolenia spp	Roperia tesselata
			r																	●															
●																				●				●											
			r																	●				●	●										
	●	●		●						●							●			●							●		●		●				
	●			●			●			●							●			●			●				●								
2	11	1		1						5							2			11			1	3	3		20		1					2	10
																				●															
●			r																	●	●		●								●				
										●										●	●		●												●
		1						1		7					9			r		13	25		1	3			+	4	5	1				1	2
															●					●	●								●						
										●																									
1								1		2					16	1	3			9	55	1		2			2		1						8
										●					●					●	●														
4						1			2	10	3		1		27					10	26			1			3	1		1			1	1	
					+					9	3				12	1			1	10	40			2			2	4			1				1
2										14		1			31	2	3			10	25		4	1		1	2	3	2			2			3
									●	●					●					●	●		●					●							
					+		1			10				1	17					13	34							+	3				2	3	2
															●					●	●							●						●	
										●					●					●	●		●								●	●			
			●							●					●					●	●														
1			+				2			12					10			20		7	37		1					10	1					1	
			●							●	●				●					●								●							
			●							●					●			●		●	●														
			4							1					5			13		2	15		1					3					2	2	
										●					●			●		●	●														
									●																										
										●											●														
			●												●			●		●	●			●											
																		●			●														
			●							●										●	●														
			●												●			●		●	●							●	●						
										●											●														
			●																	●															
			●																																
										●											●														
										●										●															

14. The last occurrence of *Nitzschia jouseae* is slightly later in middle latitudes (2.58 m.y. ago) than in lower and higher latitudes (2.48–2.50 m.y. ago). Burckle (1972) gave an approximate age of 2.55 m.y. for this datum level. Burckle and Trainer (1979) stated that the last true appearance of this species is older (2.7 m.y. ago) in a higher sedimentation rate core from the equatorial Pacific, and this datum occurs during the onset of a "glacial" event based on the isotopic data. The low Td (diatom temperature) values are observed for this stratigraphic datum at both Sites 579 and 580 (Koizumi, this volume). Because of the wide application of this datum level it is ranked as a first-order category.

15. The last occurrence of *Denticulopsis kamtschatica* is synchronous at 2.50–2.58 m.y. ago in middle–high latitudes. This well-known datum was first used by Koizumi (1973). Burckle and Opdyke (1977) were the first to relate it to the paleomagnetic reversal record. This species is broadly distributed over the middle–high latitude North Pacific. It is assigned to a first-order datum level.

16. The first occurrence of *Denticulopsis seminae* var. *fossilis* is earlier in middle latitudes (3.70 m.y. ago) than in lower latitudes (3.36 m.y. ago). Barron (1980, 1981) reported that this datum level has an absolute age estimated at about 3.1 m.y. by the sediment accumulation rate curves in the middle latitudes of both the western and the eastern North Pacific. Burckle and Opdyke (1977) suggested, however, that this species occurred first at approximately 4.3 m.y. ago in two Lamont–Doherty Geological Observatory piston cores from the middle–high latitude western North Pacific, but they did not indicate the stratigraphic occurrence of this species. This species was not observed in Core 2 of Site 581, which is estimated by the sediment accumulation curve (Fig. 8) to be 3.4–4.4 m.y. old. Because of the diachrony of this datum level, it is classified as a second-order category.

17. The first occurrence of *Nitzschia jouseae* is at 4.50 m.y. ago at Site 578 (34°N). This age also agrees with an age estimated by the sediment accumulation rate curve for Site 581 (44°N). Burckle (1978) indicated that this species appeared in the upper "c" event of the Gilbert Epoch (~4.45 m.y. ago) in the equatorial Pacific. Because of the isochrony and the wide application of this datum level, it is ranked as a first-order category.

18. The first occurrence of *Bogorovia tatsunokuchiensis* is at 5.26 m.y. ago at Site 578, while the first occurrence of the datum is more recent (4.9–5.1 m.y. ago) at Site 581. Because it has only been reported from the middle latitude western North Pacific and is diachronous, it is assigned to the third-order datum.

19. The first occurrence of *Thalassiosira oestrupii* is at 5.35 m.y. ago at Site 578. Barron (1981) used this datum to define the base of his *Thalassiosira oestrupii*

Table 1. (Continued).

Core-Section (interval in cm)	Depth below seafloor (m)	Abundance	Preservation	*Synedra* sp.	*Thalassionema bacillaris*	*T. nitzschioides*	*T. nitzschioides* v. *parva*	*Thalassionema* spp.	*Thalassiosira convexa*	*T. decipiens*	*T. eccentrica*	*T. kryophila*	*T. leptopus*	*T. lineata*	*T. oestrupii*	*T. pacifica*	*T. plicata*	*T. symbolophora*	*T. symmetrica*	*Thalassiosira* spp.	*Thalassiothrix frauenfeldii*	*T. longissima*	*Thalassiothrix* spp.	*Triceratium cinnamomeum*	Diatom zones	Series
1-1, 56-57	0.57	R	p			●					●				●					●		●			*P. doliolus*	
1-2, 56-57	2.07	VR	p			●																●				
1-3, 56-57	3.57	VR	p			●	●															●				
1-4, 56-57	5.07	R	p			●	●								●						●	●				
1-5, 56-57	6.57	R	p			●									●						●	●				
1,CC	6.80	F	m		4	51	5							4	17	1			1	4	1	13				
2-1, 47-48	7.28	VR	p			●									●							●				
2-2, 47-48	8.78	VR	p			●									●							●			*N. reinholdii*	Pleistocene
2-3, 47-48	10.28	R	p			●									●						●	●				
2-4, 47-48	11.78	F	m			46	1	1			2			2	35				1		4	24		1		
2-5, 47-48	13.28	R	p			●									●											
2,CC	16.30	VR	p																							
3-1, 74-75	17.05	F	m		2	47	1			2	2			2	29				1	7	2	11	1			
3-2, 74-75	18.55	VR	p			●									●							●				
3-3, 74-75	20.05	C	m		2	51					1			1	26			1	1	1	5	6				
3-4, 74-75	21.55	F	m		1	56	1	1						1	23					1	5	15				
3-5, 74-75	23.05	C	m		2	47				1	1			6	26		3		1	2	4	13				
3-6, 74-75	24.14	R	p			●									●			●		●		●			*N. jouseae-R. praebergonii*	Pliocene
3,CC	25.80	R	m		2	77					3			2	31					3	1	24				
4-1, 61-62	26.42	VR	p			●															●	●				
4-2, 61-62	27.92	R	m	●		●								●	●						●	●				
4-3, 61-62	29.42	R	p			●			●												●	●				
4-4, 61-62	30.92	R	m		2	58			4				1	1	3			1		4	3	13	1			
4-5, 61-62	32.42	VR	p			●							●		●							●				
4-6, 61-62	33.92	R	p			●			●					●							●	●				
4,CC	35.30	F	g		4	118			2		2	1		1	2				1	1	4	10				
5-1, 56-57	35.81	VR	p			●			●													●				
5-2, 56-57	37.31	VR	p			●																●				
5-3, 56-57	38.81	VR	p			●																●				
5-4, 56-57	40.31	VR	p			●																●				
5-5, 56-57	41.81	VR	p			●																●				
5-6, 56-57	42.86	R	p			●									●							●				
5,CC	44.80	R	p			●			●		●											●				
6-1, 30-31	45.11	VR	p			●																				
6-2, 30-31	46.61	VR	p			●																●				
6-3, 30-31	48.11	VR	p																							
6-4, 30-31	49.61	VR	p			●			●													●			?	?
6-5, 30-31	51.11	VR	p			●																●				
6-6, 30-31	52.61	B																								
6-7, 30-31	54.11	VR	p			●																●				
6,CC	54.30	B																								

Zone in the middle latitude eastern North Pacific and estimated an age of about 5.0–5.1 m.y. for this datum (Barron, 1980; Keller and Barron, 1981; Keller et al., 1982). Because of the possible diachrony of this datum level, it is assigned to a second-order category.

20. The last occurrence of *Rouxia californica* is at 4.40 m.y. ago at Site 578. Harper (1977) pointed out that this datum marks the Miocene/Pliocene boundary. It has since proven to be a useful datum in the middle-high latitude North Pacific (Barron, 1980; Keller and Barron, 1981; Koizumi, 1981, 1983). In this restricted area it is placed in a second-order category and has an age of approximately 5.1 m.y.

21. The last occurrence of *Thalassiosira miocenica* is at 5.35 m.y. ago at Site 578, while an age of 5.25–5.35 m.y. is estimated for this datum by the sediment accumulation rate curve for Site 581 (Fig. 8). It indicates that the last appearance at middle latitudes is isochronous. Burckle (1978) reported that this species disappeared on the Miocene/Pliocene boundary in the equatorial Pacific. It is assigned to a second-order datum level with an approximate age of 5.35 m.y. in middle–high latitudes.

22. The last occurrence of *Asterolampra acutiloba* is at 5.35 m.y. ago at Site 578. The last *Asterolampra acutiloba* has an absolute age estimated at about 5.1–5.2 m.y. by the sediment accumulation rate curve for Site 581. Burckle (1978) indicated that this species disappears at the Gilbert/Epoch 5 boundary (~5.35 m.y. ago) in the equatorial Pacific. Because of the possible diachrony of this datum level, it is assigned to a second-order category.

Figure 6 gives the occurrence of these 22 important datum levels in a south–north transect from 34 to 44°N, centered about 155°E, and Table 6 indicates the stratigraphic occurrence and chronology of these datum levels defined by the first or last occurrence of these diatoms at each site.

PLIOCENE AND PLEISTOCENE DIATOM ZONATION IN MIDDLE LATITUDES

The Pliocene and Pleistocene sections recovered in a south–north transect from Sites 577 to 581 in the middle latitude of the western North Pacific contain a mixture of both subtropical and subarctic diatoms. This fact allows us to propose a new diatom zonation for the Pliocene and Pleistocene (Fig. 7). The zonal boundaries are judged to be first order because the datum levels that define them are tied directly to the paleomagnetic reversal record (Koizumi and Burckle, 1984).

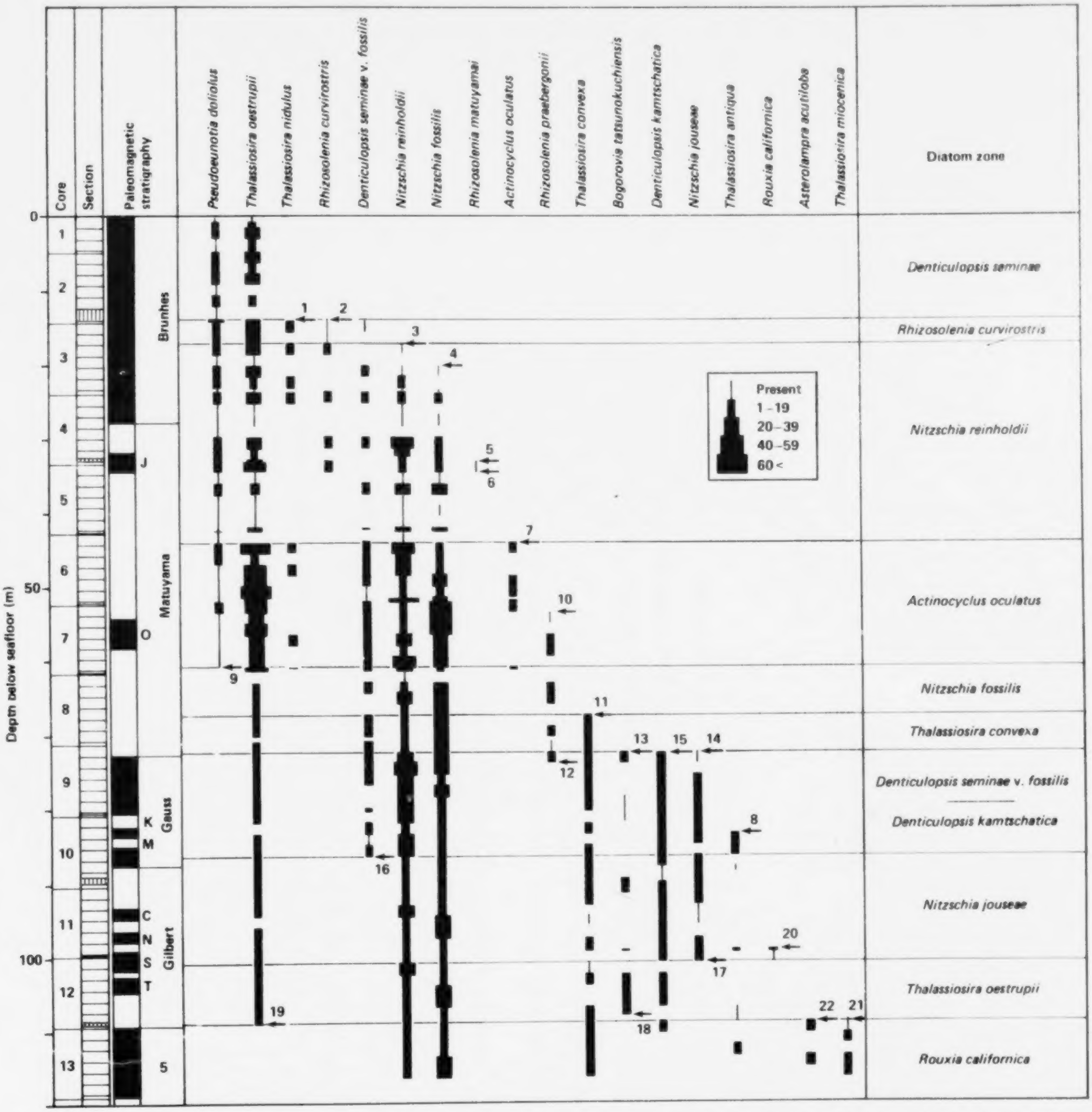

Figure 2. Ranges and abundances of stratigraphically important diatom species at Site 578. Numbers next to ranges indicate selected datum levels as specified in Table 6.

Zonal Definition[3]

Thalassiosira oestrupii Partial Range Zone

Top. First occurrence of *Nitzschia jouseae*.
Base. First occurrence of *Thalassiosira oestrupii*.
Age. Early Pliocene.

Paleomagnetic correlation. The top of the *Thalassiosira oestrupii* Zone is 4.50 m.y. ago and the base is 5.35 m.y. ago (between the base of the Sidufjall Event and the boundary of the Gilbert and Epoch 5 paleomagnetic polarity zone) at Site 578. The base of the *Thalassioria oestrupii* Zone may be correlated with the lowest reversed event of the Gilbert Epoch (~5.1 m.y. ago) in the higher latitudes (Burckle and Opdyke, 1977).

Correlation with other zones. This *Thalassiosira oestrupii* Zone correlates with the lower one-third of the *Thalassiosira oestrupii* Zone of Barron (1981) for the middle latitude eastern North Pacific and with Subzone b of the *Denticulopsis kamtschatica* Zone of Barron

---

[3] Prepared by I. Koizumi.

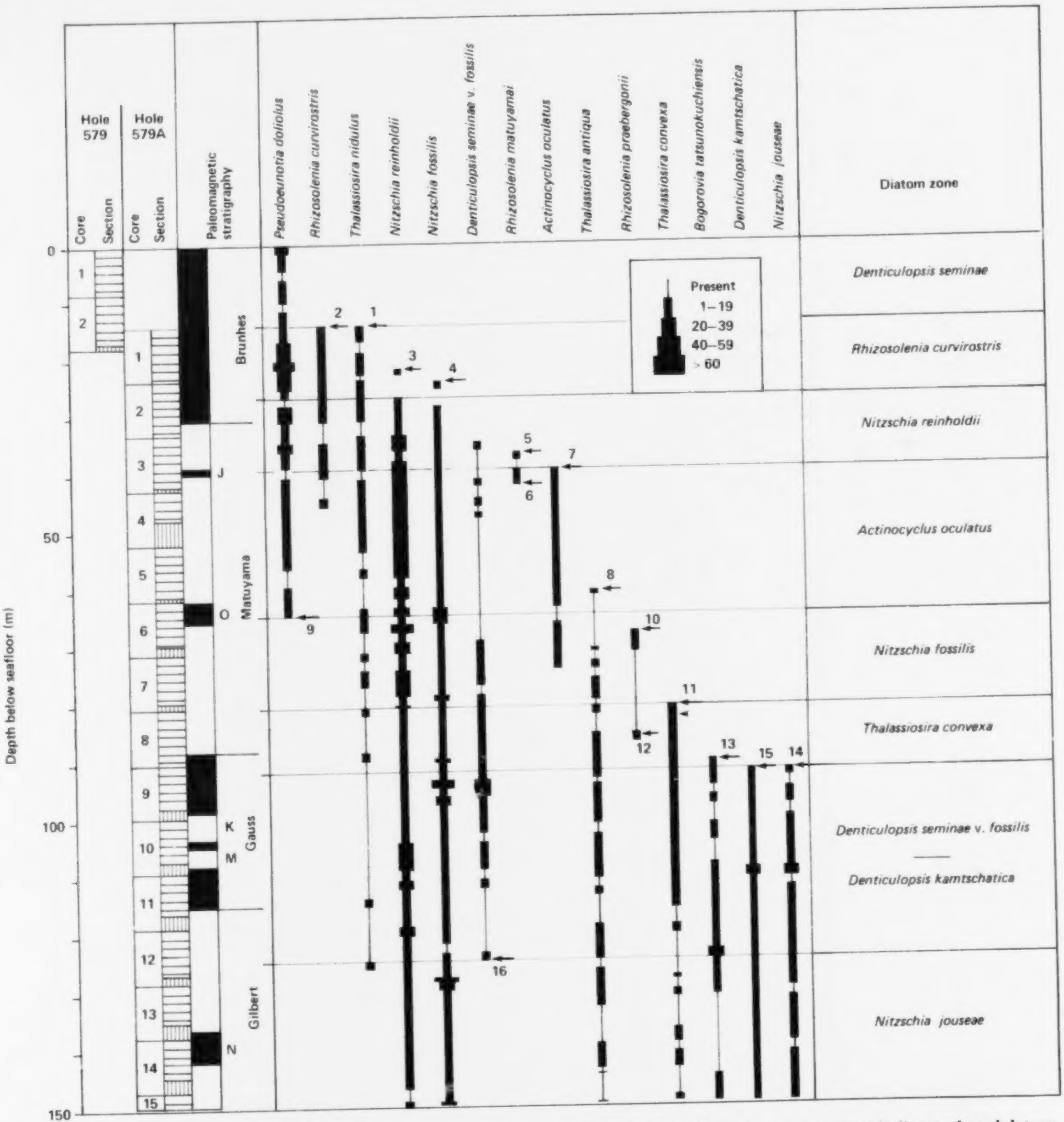

Figure 3. Ranges and abundances of stratigraphically important diatom species at Site 579. Numbers next to ranges indicate selected datum levels, as specified in Table 6.

(1980) for Leg 57, off northeastern Japan. In low-middle latitudes, it correlates to the upper part of the *Thalassiosira convexa* Zone of Burckle (1972).

Important datums. The first occurrence of *Bogorovia tatsunokuchiensis* and the last occurrence of *Asterolampra acutiloba* and *Thalassiosira miocenica* coincides with the base of the *Thalassiosira oestrupii* Zone in middle-high latitudes. In the middle-high latitude western North Pacific, the first occurrence of *Rouxia californica* is used to approximate the base of this zone.

Remarks. The occurrence of *Cosmiodiscus insignis* has not been recognized in the materials from Leg 86.

Original definition. Barron (1980).

Nitzschia jouseae Partial Range Zone

Top. First occurrence of *Denticulopsis seminae* var. *fossilis*.

Base. First occurrence of *Nitzschia jouseae*.

Age. Early Pliocene.

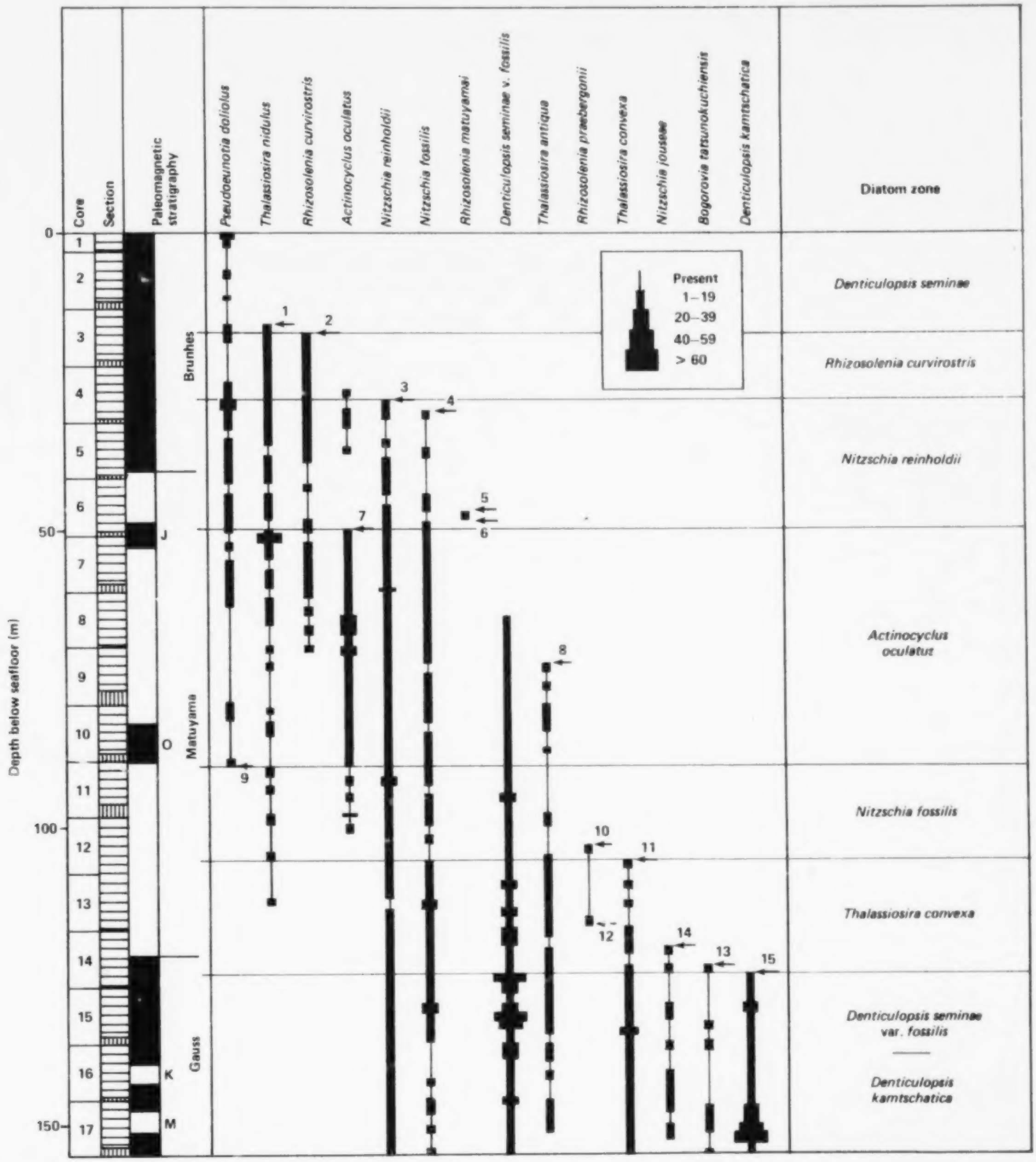

Figure 4. Ranges and abundances of stratigraphically important diatom species at Site 580. Numbers next to ranges indicate selected datum levels, as specified in Table 6.

Paleomagnetic correlation. The top of the *Nitzschia jouseae* Zone is approximately 3.70 m.y. ago and the base 4.50 m.y. ago (between the uppermost reversed event of the Gilbert Epoch and the base of the Sidufjall Event, Gilbert Epoch). The top of the *Nitzschia jouseae* Zone correlates with the base of the Gauss Epoch at Site 578 (Fig. 2) and the upper half of the reversed event of the Gilbert Epoch at Site 579 (Fig. 3), respectively.

Correlation with other zones. The *Nitzschia jouseae* Zone defined herein correlates with the lower half of the *Nitzschia jouseae* Zone of Burckle (1972). This zone also correlates with Subzone c of the *Denticulopsis kamtschatica* Zone of Barron (1980) and the upper part of the *Thalassiosira oestrupii* Zone of Barron (1981).

Original definition. Burckle (1972).

Denticulopsis seminae var. *fossilis*–*Denticulopsis kamtschatica* Concurrent Range Zone

Top. Last occurrence of *Denticulopsis kamtschatica*.

Base. First occurrence of *Denticulopsis seminae* var. *fossilis*.

Age. Late Pliocene.

Table 5. Stratigraphic occurrences of Neogene diatoms in Hole 581.

Core-Section (interval in cm)	Depth below seafloor (m)	Abundance (10^7 per g)	Preservation	*Actinocyclus curvatulus*	*A. ehrenbergii*	*A. ellipticus*	*A. ingens*	*A. ocholensis*	*Actinoptychus senarius*	*Asterolampra acutiloba*	*A. grevillei*	*A. marylandica*	*Asteromphalus brookei*	*A. darwinii*	*A. robustus*	*Bacterosira fragilis*	*Bogorovia praepaleacea*	*B. tatsunokuchiensis*	*Chaetoceros furcellatus*	*Cocconeis costata*	*Coscinodiscus elegans*	*C. endoi*	*C. marginatus*	*C. nodulifer*	*C. obscurus*	*C. oculus-iridis*	*C. plicatus*
1-1, 55-56	0.56	17.7	g	5				1	1							1			2				4			1	
1,CC	1.00	4.7	g	5	1			1								2			1				7				
2-1, 134-135	182.85	12.0	g	2					1									1					9				
2-2, 54-55	183.55	12.0	g	1										1				1					2	3			
2-3, 134-135	185.85	8.0	g	1	2	1			1					1									6	5			
2-4, 134-135	187.35	4.8	g	4	5	2		2	2									2					12	26			
2-5, 134-135	188.85	8.0	g		3				1														11	2			
2-6, 134-135	190.35	3.4	g	1																			42	15		1	
2-7, 25-26	190.76	2.0	g	13	1				3									3					48	2			
3-1, 90-91	191.91	3.2	g	2		1			2						1								40	2		1	
3-2, 90-91	193.41	1.8	g						1									1					32	17			
3-3, 90-91	194.91	2.4	g	3					1		1							1					43	48			
3-4, 90-91	196.41	1.8	g	2	1	1			1														53	13			
3-5, 90-91	197.91	2.2	g						1	1													45	32			
3-6, 75-76	199.26	3.4	g	2	2	1			5	5										1			17	7			
3,CC	200.50	5.3	g		1	2			4	2													12	5		1	
4-1, 98-99	201.49	2.7	g	2	1	9				2													20	4		7	
4-2, 98-99	202.99	3.4	g							2		1			1								18	1		2	
4-3, 98-99	204.49	10.7	g	1		5				2					4								5	7			
4-4, 98-99	205.99	3.2	g	1		5			3						1								26	41			
4-5, 98-99	207.49	6.0	g		5	1			11						1								20	29		1	
4-6, 98-99	208.99	12.0	g						13					1	3								7	2			
4,CC	210.00	5.3	g		7	1			31	2					3								10	19			
5-1, 100-101	211.01	6.0	g		2				2	1					2								2	61			
5-2, 100-101	212.51	16.0	g		3				2														3	10			
5-3, 100-101	214.01	8.0	g	1					4														10	1			
5-4, 64-65	215.14	16.0	g		1				3														4	1		1	
5,CC	219.50	8.0	g						5	1													10				
6-1, 100-101	220.51	3.2	g			1			5	2													34	2			
6-2, 100-101	222.01	3.4	g			1			4		1	2			2								33	1			
6-3, 100-101	223.51	2.2	g			1			1			2											53	4			
6-4, 100-101	225.01	3.2	g			1			6			1											36	2			
6-5, 100-101	226.51	2.3	g				6		16			2			1								61	3			
6-6, 100-101	228.01	5.3	g		2				11			3											27	6		2	
6-7, 10-11	229.21	16.0	g				8		8			1										3	3	6		1	
7-1, 100-101	230.01	4.0	g		1	1	32		9			2										5	9	8	1	1	
7-2, 100-101	231.51	8.0	g			2	3															7	11				
7-3, 100-101	233.01	8.0	g			1	5		3													8	7	3			2
7-4, 100-101	234.51	8.0	g			3	1															6	5	2			2
7-5, 100-101	236.01	8.0	g			1	1		1					1								11	12	4			
7-6, 100-101	237.51	5.3	g			1	12		1													8	4	7		1	1
7,CC	238.50	4.0	g			7	14		2													14	10	3		1	1
8-1, 110-111	239.61	5.3	g		1	3	9			1							4					13	6	3			3
8-2, 110-111	241.11	3.4	g				30		3			4					7					36	3				1
8-3, 110-111	242.61	5.3	g			1	12		1		2		1				4					16	1	13			3
8-4, 110-111	244.11	2.0	g			3	13		1												2	14	24	1			
8-5, 110-111	245.61	0.2	m				2										1					4	2				
8,CC	248.00	5.3	g			1	13		1			1					2					19	11	3			4

Note: See Table 1 for explanation of symbols.

[a] *D.s* = *D. seminae*, *T.o.* = *Thalassiosira oestrupii*, *T.s.* = *T. schraderi*, *D.k.* = *D. katayamae*, *D.d.* = *D. dimorpha*, *D.p.* = *D. praedimorpha*.

Paleomagnetic correlation. The top of the *Denticulopsis seminae* var. *fossilis–Denticulopsis kamtschatica* Zone is 2.58 m.y. ago and the base is 3.70 m.y. ago (between the uppermost reversed event of the Gilbert Epoch and the uppermost part of the normal event of the Gauss Epoch).

Correlation with other zones. The *Denticulopsis seminae* var. *fossilis–Denticulopsis kamtschatica* Zone defined herein is the same zonal definition as Koizumi (1973) and Barron (1980). It correlates to the upper half of the *Nitzschia jouseae* Zone of Burckle (1972).

Important datums. The last occurrence of *Bogorovia tatsunokuchiensis* and *Nitzschia jouseae* coincides with near the top of the *Denticulopsis seminae* var. *fossilis–Denticulopsis kamtschatica* Zone. The first occurrence of *Rhizosolenia praebergonii* is within this zone at Site 578.

Original definition. Koizumi (1973).

Other discussion. Barron (1980, 1981), Burckle and Opdyke (1977), Koizumi (1975a).

Thalassiosira convexa Partial Range Zone

Top. Last occurrence of *Thalassiosira convexa*.

Base. Last occurrence of *Denticulopsis kamtschatica*.

Age. Late Pliocene.

Table 5. (Continued).

C. radiatus	*C. stellaris*	*C. symbolophorus*	*C. tabularis*	*C. tempere v. delicata*	*C. venustissimus*	*C. yabei*	*Cosmiodiscus intersectus*	*Cymatosira lorenziana*	*Cymbella sinuata*	*Delphineis surirelloides*	*Denticulopsis dimorpha*	*D. hustedtii*	*D. hyalina*	*D. kamtschatica*	*D. katayamae*	*D. lauta*	*D. praedimorpha*	*D. punctata*	*D. punctata v. hustedtii*	*D. seminae*	*Hemiaulus polymorphus*	*Hemidiscus cuneiformis*	*Mediaria splendida*	*Nitzschia braarudii*	*N. cylindrus*	*N. fossilis*	*N. grunowii*	*N. heteropolica*	*N. jouseae*	*N. marina*
	1		6						1	1										94				1			1			
	1		8																	82					2		6			
			3		1									98								24					2			1
	2													66								10				1				
							1							76								3								
1														20								2				8	1		1	7
		1												69								23				2			1	1
	2	2												38								6				10			3	3
														18								11				4	1		3	
														25								5					3			1
	1													14								49				2	2			3
														34								10					1			1
														7								33				4	6			
					3									9								8					1			1
														3								12				1	3			
		1												17								19					2			
														39								6								
		2												28																
														19								2	1				1			1
					1									5								6								
	2				33									2								13								
	1				8									8								1								
	2	1			22									5								17						2		1
	1	1			46									2								5								2
	1				12																									1
			14		1									1								4								1
			6		3									1								5				2				
			21		1																	7								
		1	26		1																	11	2							
																					4	13								1
														2							1	10								
																						11				2				
	1		1																		1	17								
				1	1							4			18							1								
		1													4						1	4								
				2	2							1			13						1	1								
				2		1					46				7	11					1	3								
				1	1			1			17	4			6	7					1	2								
				1							12	1			21	5						6								
	1	1									19	2			27	21						3								
	1				2										25	1					2									
				2	1						1	20			13	1						3								
						1						12			9							1								
	1	1										34			8				2		1	2								
					5							30						2	4			9						1		
				1								10	2		1	3	89		2											
												3					2													
					1							45			2	1	14		3			2								

Paleomagnetic correlation. The top of the *Thalassiosira convexa* Zone is 2.30 m.y. ago and the base is 2.58 m.y. ago (between the uppermost part of the normal event of the Gauss Epoch and one third of the lower normal event of the Matuyama Epoch).

Correlation with other zones. The *Thalassiosira convexa* Zone correlates to the lower two-thirds of the *Rhizosolenia praebergonii* Zone of Burckle (1972) and the lower half of the *Denticulopsis seminae* var. *fossilis* Zone of Barron (1980).

Important datums. The first occurrence of *Rhizosolenia praebergonii* occurs within the *Thalassiosira convexa* Zone in middle–high latitudes (e.g., Sites 579 and 580).

Original definition. Burckle (1972).

Other discussion. Koizumi (1975a), Barron (1980, 1981).

Nitzschia fossilis Partial Range Zone

Top. First occurrence of *Pseudoeunotia doliolus*.

Base. Last occurrence of *Thalassiosira convexa*.

Age. Late Pliocene.

Paleomagnetic correlation. The top of the *Nitzschia fossilis* Zone is 1.90 m.y. ago and the base is 2.30 m.y.

Table 5. (Continued).

Core-Section (interval in cm)	Depth below seafloor (m)	Abundance (10^7 per g)	Preservation	N. miocenica	N. porteri	N. praereinholdii	N. reinholdii	N. rolandii	N. suikoensis	Paralia sulcata	Pseudoeunotia doliolus	Rhabdonema japonicum	Rhizosolenia barboi	R. hebetata	R. styliformis	Rhizosolenia spp.	Rouxia californica	R. naviculoides	R. yabei	Stephanopyxis turris	Stephanopyxis spp.	Synedra jouseana	Thalassionema hirosakiensis	T. nitzschioides	T. nitzschioides v. parva	T. nitzschioides vars.	T. schraderi
1-1, 55-56	0.56	17.7	g											6	2					2				3			
1,CC	1.00	4.7	g							1	1			6	6					2	1			10			
2-1, 134-135	182.85	12.0	g				1								1					1				10		4	
2-2, 54-55	183.55	12.0	g										1		1					1				66		4	
2-3, 134-135	185.85	8.0	g										2		2					5				67		2	
2-4, 134-135	187.35	4.8	g				15						1							1				46		7	
2-5, 134-135	188.85	8.0	g				13																	35		3	
2-6, 134-135	190.35	3.4	g				9						3							1	2			29		2	
2-7, 25-26	190.76	2.0	g				2						3		3					2	2			26		4	
3-1, 90-91	191.91	3.2	g				4					4	1		6	2				5				50		6	
3-2, 90-91	193.41	1.8	g				14								8	2				2				10			
3-3, 90-91	194.91	2.4	g				25						1		5									7			
3-4, 90-91	196.41	1.8	g				6	5							1		11	1		3				22		3	
3-5, 90-91	197.91	2.2	g				6	7						3			11			1				46		1	
3-6, 75-76	199.26	3.4	g				36		4					1	3		23	1	1	3				33		3	
3,CC	200.50	5.3	g				21	5	5					4	1		6		7	1				52		14	
4-1, 98-99	201.49	2.7	g				6	2	2				1	3			20			2	1			38		12	
4-2, 98-99	202.99	3.4	g	8			8	5	5				3	2	3		12		2	8				59		3	
4-3, 98-99	204.49	10.7	g	22			7	5	23				5		1		4		1	2				43		16	
4-4, 98-99	205.99	3.2	g				2	2						3	1		8		3	4				47		3	
4-5, 98-99	207.49	6.0	g	6			3	1	3					3			3		1	2				39			
4-6, 98-99	208.99	12.0	g				2		1					1			1							146		2	
4,CC	210.00	5.3	g				4	1	1					1	1		9		4	5				32		2	
5-1, 100-101	211.01	6.0	g			2	6	3									1		1	2		1		45		2	
5-2, 100-101	212.51	16.0	g			1		2					1	1	6		1		2					149			
5-3, 100-101	214.01	8.0	g			2	10	16					1	1	3		2				1			75	4		
5-4, 64-65	215.14	16.0	g			2	7	12	1				3				1		3	1				128			
5,CC	219.50	8.0	g				22	11					2	1	1		1		2			1		93			
6-1, 100-101	220.51	3.2	g			1	6	10					5	1			7		2			2		70	1		
6-2, 100-101	222.01	3.4	g		21	3	8	7	1				1	3	1		1				1	2		71			
6-3, 100-101	223.51	2.2	g		18		1						1				3						12	32	7		47
6-4, 100-101	225.01	3.2	g		10	1	1						6				4		1			1	10	41	2		53
6-5, 100-101	226.51	2.3	g		8		3						4				1		1				8	28	6	7	15
6-6, 100-101	228.01	5.3	g		17	3							6		2		1	2	2				1	25			
6-7, 10-11	229.21	16.0	g		3	1									2				2	1			2	84		10	
7-1, 100-101	230.01	4.0	g		1	1							4						1				3	49		15	
7-2, 100-101	231.51	8.0	g		3								1						1				27	29	31		
7-3, 100-101	233.01	8.0	g										4		2				1				4	93	13	6	
7-4, 100-101	234.51	8.0	g										3				3	6	9				14	56	9	24	
7-5, 100-101	236.01	8.0	g										6					6					3	44	5	16	
7-6, 100-101	237.51	5.3	g			1							5				4	4	3				19	65	8	12	
7,CC	238.50	4.0	g							4			3	1			1		2				11	53	7	11	
8-1, 110-111	239.61	5.3	g										5		4		1	1		1			21	77	14	4	
8-2, 110-111	241.11	3.4	g										3				1		2				6	38		7	
8-3, 110-111	242.61	5.3	g							1			2				2	1					1	70	3	8	
8-4, 110-111	244.11	2.0	g										4										1	17		8	
8-5, 110-111	245.61	0.2	m																				1	6		3	
8,CC	248.00	5.3	g							1					1			1					12	49	6	1	

ago (between one-third of the lower normal event and the bottom of the Olduvai Event of the Matuyama Epoch).

Correlation with other zones. The *Nitzschia fossilis* Zone correlates with the upper part of the *Rhizosolenia praebergonii* Zone of Burckle (1972) and the *Denticulopsis seminae* var. *fossilis* Zone of Barron (1980).

Important datums. The last occurrence of *Rhizosolenia praebergonii* is below the top of the *Nitzschia fossilis* Zone in middle-high latitudes although it is above the first occurrence of *Pseudoeunotia doliolus* in low latitudes (Burckle, 1977; Burckle and Trainer, 1979; Fig. 6).

Original definition. Koizumi, this chapter.

Actinocyclus oculatus Concurrent Range Zone

Top. Last occurrence of *Actinocyclus oculatus*.
Base. First occurrence of *Pseudoeunotia doliolus*.
Age. Early Pleistocene.

Paleomagnetic correlation. The top of the *Actinocyclus oculatus* Zone is 0.95 m.y. ago and the base is 1.90 m.y. ago (between the bottom of the Olduvai Event and the bottom of the Jaramillo Event of the Matuyama Epoch). The top of this zone is 1.33 m.y. ago at the middle part between the Olduvai and Jaramillo Event owing

Table 5. (Continued).

Thalassiosira antiqua	*T. borealis*	*T. burckliana*	*T. convexa*	*T. eccentrica*	*T. gravida*	*T. hyalina*	*T. jacksonii*	*T. lacustris*	*T. leptopus*	*T. lineata*	*T. miocenica*	*T. nativa*	*T. nidulus*	*T. nodulolineata*	*T. nordenskioldii*	*T. oestrupii*	*T. opposita*	*T. praeconvexa*	*T. trifulta*	*Thalassiosira* sp. 1	*Triceratium* spp.	Diatom zone[a]	Subseries
				2	5											14			40			*D.s.*	upper Pliocene
					5	2				1					1	4			39				
				1			4	2	2													*N. jouseae*	lower Pliocene
	2			2			4	2	1							5							
							2		1	1						1							
	1			3			5		1	2		1		1		3			1				
				4			1					13				9			1		1		
				3			1					9				1					1		
				9			2		4	2		10				6					2		
				7			2		7	1		11									1	*T.o.*	
				4	1		2		10	1		7		1									
				4			1			2		8											
				4			3		6	1		11									1	*R. californica*	upper Miocene
				2					11			3											
				4			4		3	1	1	13											
				3			3			1	1	4	1				2						
			3	1			5		3		5												
2	5			1			1		2	2	2						3	1					
	1		2	2					3	2	5							3					
		3	5				1		3	2	3							2					
3	2		2						1		1			4									
		1									1												
1			1						1		6												
			1						2		2												
									2														
	1	27	3	4					4		1							1					
		4	1	4					2														
2		11		3																			
1		2	1	2						1													
		1		3						3													
										1	1											*T.s.*	
		5								2											1		
		1		1						3								1					
		3																		60		*D.k.*	
																				53			
										4	1									27			
										1										3		*D.d.*	
										2										2			
																				3			
																					3		
																				4	3	*C. yabei*	middle Miocene
										1											5		
										1													
										1													
										1												*D.p.*	

to the shorter range of *Actinocyclus oculatus* at Site 578 in lower latitudes.

Correlation with other zones. The *Actinocyclus oculatus* Zone defined herein correlates with the *Actinocyclus oculatus* Zone of Koizumi (1973) and Barron (1980) and the lower part of the *Pseudoeunotia doliolus* Zone of Burckle (1972).

Important datums. The first occurrence of *Rhizosolenia curvirostris* and *Rhizosolenia matuyamai* occurs near the top of this zone in middle-high latitudes.

Remarks. The base of the *Actinocyclus oculatus* Zone is not defined by the last occurrence of *Thalassiosira antiqua*, which is diachronous, but by the first occurrence of *Pseudoeunotia doliolus* (Table 6). The base of this zone is correlated with the Pliocene/Pleistocene boundary. A few *Actinocyclus oculatus* are usually observed in the upper zone with a break after the continuous occurrence in the *Actinocyclus oculatus* Zone in the high latitude region (e.g., Leg 19 and Leg 86, Site 580; Koizumi, 1973).

Original definition. Donahue (1970).

Other discussion. Koizumi (1973, 1975a), Burckle and Opdyke (1977), Barron (1980, 1981).

Nitzschia reinholdii Partial Range Zone

Top. Last occurrence of *Nitzschia reinholdii.*

Base. Last occurrence of *Actinocyclus oculatus.*

Age. Late Pleistocene.

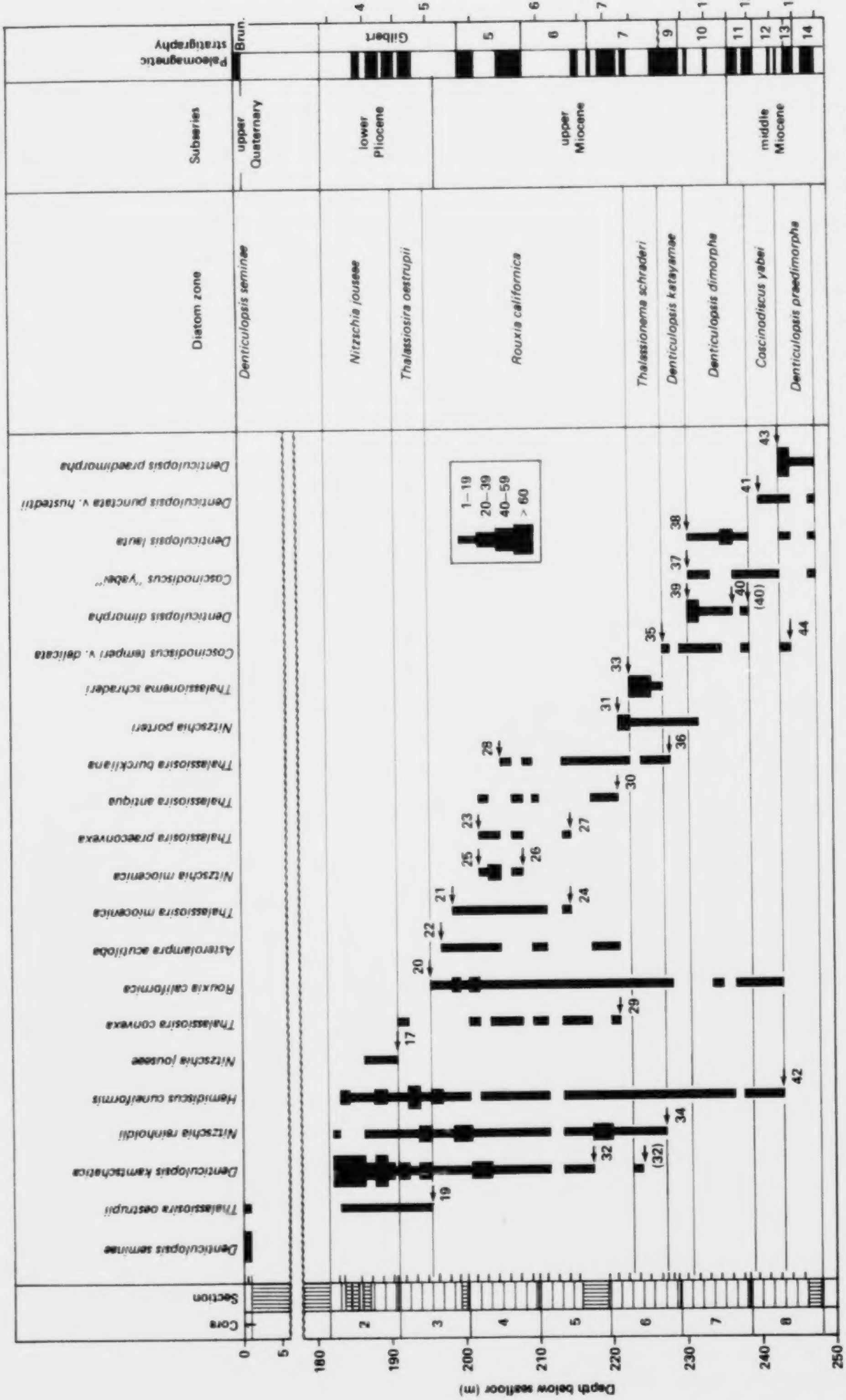

Figure 5. Ranges and abundances of stratigraphically important diatom species at Site 581. Numbers next to ranges indicate selected datums levels, as specified in Table 8.

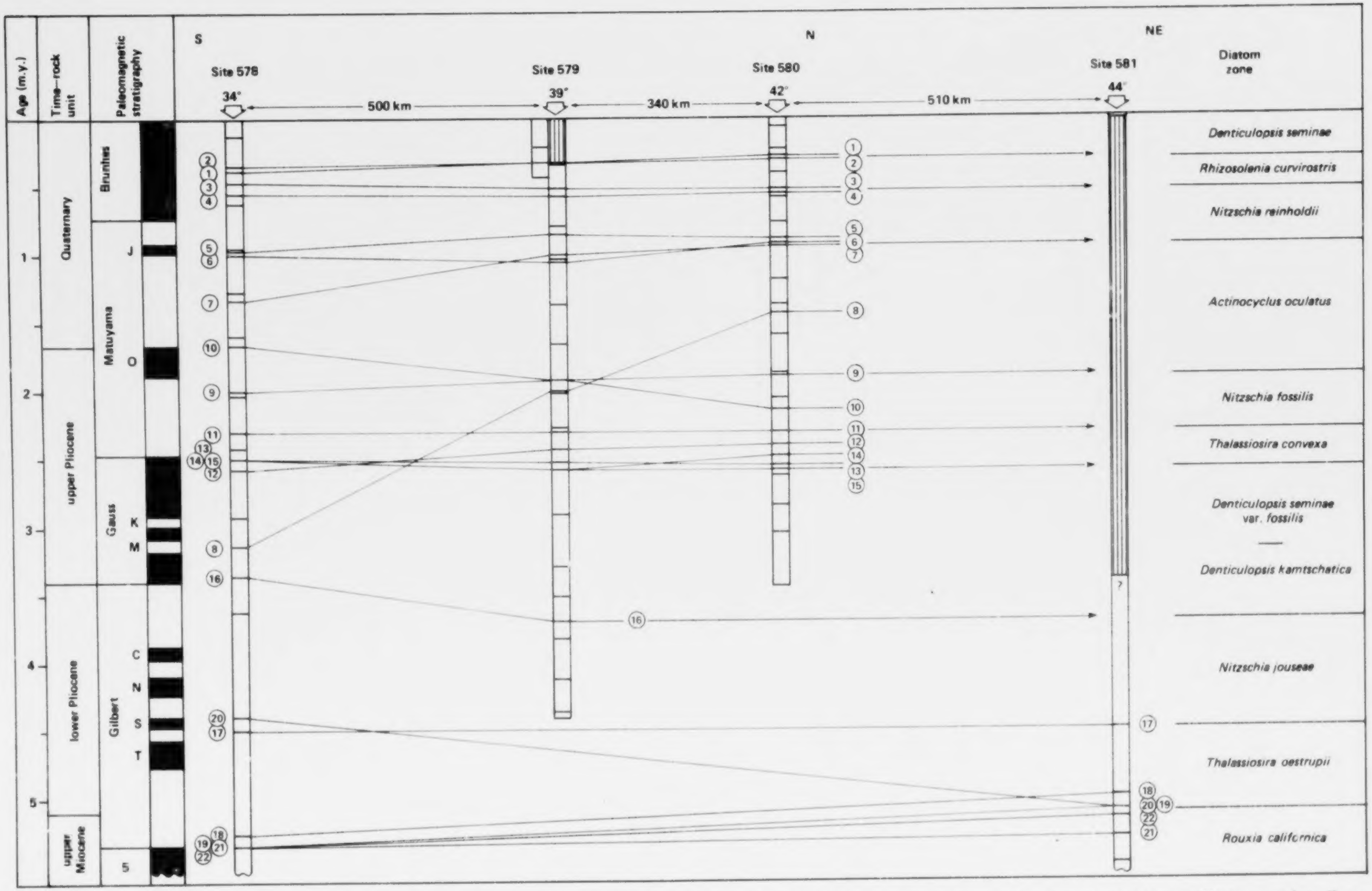

Figure 6. Occurrence of selected datum levels in a south–north transect from 34 to 44°N latitude, centered about 155°E longitude, and proposed middle latitude Neogene diatom zonation. (1 = last *Thalassiosira nidulus*, 2 = last *Rhizosolenia curvirostris*, 3 = last *Nitzschia reinholdii*, 4 = last *Nitzschia fossilis*, 5 = last *Rhizosolenia matuyamai*, 6 = first *Rhizosolenia matuyamai*, 7 = last *Actinocyclus oculatus*, 8 = last *Thalassiosira antiqua*, 9 = first *Pseudoeunotia doliolus*, 10 = last *Rhizosolenia praebergonii*, 11 = last *Thalassiosira convexa*, 12 = first *Rhizosolenia praebergonii*, 13 = last *Bogorovia tatsunokuchiensis*, 14 = last *Nitzschia jouseae*, 15 = last *Denticulopsis kamtschatica*, 16 = first *Denticulopsis seminae* var. *fossilis*, 17 = first *Nitzschia jouseae*, 18 = first *Bogorovia tatsunokuchiensis*, 19 = first *Thalassiosira oestrupii*, 20 = last *Rouxia californica*, 21 = last *Thalassiosira miocenica*, 22 = last *Asterolampra acutiloba*)

Table 6. Stratigraphic occurrences and chronology of datum levels in Holes 578, 579, and 580.

		Datum level[a]	Reliability[b]	Hole 578		Hole 579		Hole 580	
				Stratigraphic level[c]	Age[d] (m.y.)	Stratigraphic level[c]	Age[d] (m.y.)	Stratigraphic level[c]	Age[d] (m.y.)
1.	T	*Thalassiosira nidulus*	2	2,CC/3-1,97	0.39	2-3,124/2-4,123	0.33	3-2,26/3-3,25	0.28
2.	T	*Rhizosolenia curvirostris*	1	2-5,115/2,CC	0.35	2-3,124/2-4,123	0.33	3-3,26/3-4,25	0.30
3.	T	*Nitzschia reinholdii*	1	3-2,96/3-3,97	0.47	1-5,15/1-6,14	0.51	4-4,122/4-5,121	0.52
4.	T	*Nitzschia fossilis*	1	3-4,96/3-5,97	0.55	1-7,15/2-1,33	0.57	4-5,122/4-6,121	0.55
5.	T	*Rhizosolenia matuyamai*	2	4,CC/5-1,117	0.97	3-2,116/3-3,115	0.85	6-4,26/6-5,25	0.89
6.	B	*Rhizosolenia matuyamai*	2	5-1,118/5-2,117	1.00	3-6,116/4-1,12	1.05	6-5,26/6-6,17	0.91
7.	T	*Actinocyclus oculatus*	2	6-1,110/6-2,109	1.33	3-5,116/3-6,115	1.00	6-6,18/6,CC	0.93
8.	T	*Thalassiosira antiqua*	3	10-2,119/10-3,118	3.14	6-6,11/6-6,115	2.00	9-2,24/9-3,23	1.43
9.	B	*Pseudoeunotia doliolus*	1	7-6,122/7-7,47	2.00	6-4,26/6-5,25	1.92	11-1,23/11-2,22	1.89
10.	T	*Rhizosolenia praebergonii*	2	7-1,122/7-2,121	1.66	6-4,26/6-5,25	1.92	12-3,104/12-4,103	2.14
11.	T	*Thalassiosira convexa*	1	8-4,119/8-5,118	2.30	7,CC/8-1,132	2.29	11-5,106/11,CC	2.30
12.	B	*Rhizosolenia praebergonii*	2	9-2,119/9-3,118	2.58	8-4,133/8-5,132	2.43	13-6,16/13,CC	2.40
13.	T	*Bogorovia tatsunokuchiensis*	2	9-1,119/9-2,118	2.50	8-6,133/9-1,30	2.52	14-4,131/14-5,130	2.55
14.	T	*Nitzschia jouseae*	1	9-1,119/9-2,118	2.50	9-1,31/9-2,30	2.58	14-2,131/14-3,130	2.48
15.	T	*Denticulopsis kamtschatica*	1	9-1,119/9-2,118	2.50	9-1,31/9-2,30	2.58	14-5,131/14-6,130	2.58
16.	B	*Denticulopsis seminae* v. *fossilis*	2	10-4,119/10-5,118	3.36	12-4,17/12-5,16	3.70		
17.	B	*Nitzschia jouseae*	1	12-1,101/12-2,100	4.50				
18.	B	*Bogorovia tatsunokuchiensis*	3	12-6,111/12,CC	5.26				
19.	B	*Thalassiosira oestrupii*	2	12,CC/13-1,135	5.35				
20.	T	*Rouxia californica*	2	11-6,131/11-7,20	4.40				
21.	T	*Thalassiosira miocenica*	2	12,CC/13-1,135	5.35				
22.	T	*Asterolampra acutiloba*	2	12,CC/13-1,135	5.35				

[a] B = first occurrence, T = last occurrence.
[b] 1 = most reliable, 2 = reliable, 3 = least reliable.
[c] The highest and lowest stratigraphic levels at each site for each datum level are presented (Core-Section, level in cm) with a slash between them.
[d] Tied to the paleomagnetic time scale of Berggren et al. (in press).

Paleomagnetic correlation. The top of the *Nitzschia reinholdii* Zone is approximately 0.50 m.y. ago and the base is 0.95 m.y. ago (between the bottom of the Olduvai Event of the Matuyama Epoch and the lowest part of the Brunhes Epoch).

Correlation with other zones. The *Nitzschia reinholdii* Zone correlates to Subzone a of the *Rhizosolenia curvirostris* Zone of Barron (1980) and within the *Pseudoeunotia doliolus* Zone of Burckle (1972).

Important datums. The last occurrence of *Nitzschia fossilis* is nearly coincident with the top of the *Nitzschia reinholdii* Zone. The last occurrence of *Rhizosolenia matuyamai* occurs in the bottom of the *Nitzschia reinholdii* Zone.

Original definition. Burckle and Opdyke (1977) described without definition.

Other discussion. Barron (1980, 1981).

Rhizosolenia curvirostris Partial Range Zone

Top. Last occurrence of *Rhizosolenia curvirostris.*

Base. Last occurrence of *Nitzschia reinholdii.*

Age. Late Pleistocene.

Paleomagnetic correlation. The top of the *Rhizosolenia curvirostris* Zone is 0.33 m.y. ago and the base is 0.50 m.y. ago (between the middle part and the lowest part of the Brunhes Epoch).

Correlation with other zones. The *Rhizosolenia curvirostris* Zone defined herein correlates with Subzone b of the *Rhizosolenia curvirostris* Zone of Barron (1980).

Important datums. The last occurrence of *Thalassiosira nidulus* coincides with the top of this zone.

Original definition. Donahue (1970).

Other discussion. Koizumi (1973, 1975a), Burckle and Opdyke (1977), Barron (1980, 1981).

Denticulopsis seminae Partial Range Zone

Top. Present.

Base. Last occurrence of *Rhizosolenia curvirostris.*

Age. Late Quaternary.

Paleomagnetic correlation. The base of the *Denticulopsis seminae* Zone is 0.33 m.y. ago (the base is in the middle part of the Brunhes Epoch).

Correlation with other zones. The *Denticulopsis seminae* Zone defined herein is the same zonal definition as Koizumi (1973) and Barron (1980).

Original definition. Donahue (1970).

Other discussion. Koizumi (1973, 1975a), Barron (1980).

Figure 7 shows the diatom zonation for Leg 86 in middle-high latitudes with primary and secondary datum levels plotted against a paleomagnetic time scale from Berggren and others (1984). Table 7 indicates the diatom zonation of samples from Leg 86, except Sites 576 and 577.

MIOCENE DIATOM ZONATION IN HIGH LATITUDE[4]

The Neogene diatom zonation of Koizumi (1973, 1975a) has been recognized in middle-high latitudes of the North Pacific (Burckle and Opdyke, 1977; Barron, 1980, 1981; Harper, 1980). New subzones and zones were proposed in order to make a critical resolution of stratigraphic problems (Barron, 1980; Koizumi, 1983). The subdivision, recently proposed in Japan (Akiba, 1982, 1983; Maruyama, 1982), was also recognized at

---

[4] Prepared by I. Koizumi.

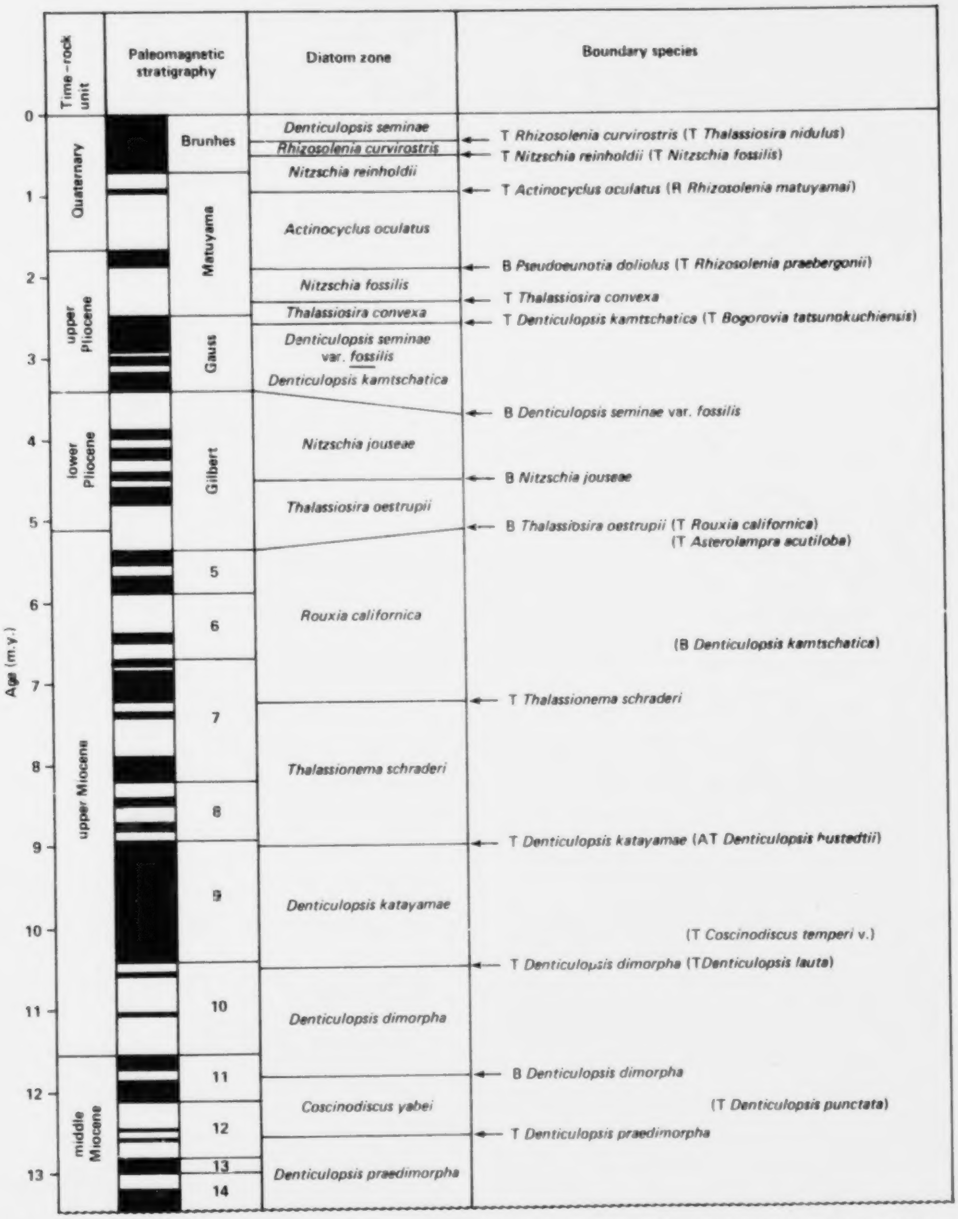

Figure 7. Estimated absolute ages for the Pliocene to Quaternary diatom zones in middle latitudes and the middle to late Miocene in middle-high latitudes. The paleomagnetic time scale is that of Berggren et al. (in press). The Pliocene and Quaternary datum levels are tied directly to the paleomagnetic time scale (Berggren et al., in press). Other datum levels are extrapolated from the sediment accumulation rate curve. (B = first occurrence, T = last occurrence.)

Site 581 in the high latitude North Pacific. These zones, instead of the Miocene zonation of Koizumi (1973, 1975a, 1983) and Barron (1980), are defined by the taxonomic subdivision of "*Denticulopsis lauta*" and "*Denticulopsis hustedtii*."

Sediment accumulation rate curves for many sites show that most of the upper and middle Miocene datum levels (Table 8), which were directly tied to the paleomagnetic stratigraphy of the equatorial Pacific by Burckle (1978), are almost synchronous in the lower-middle latitude regions. The sediment accumulation rate curve based on these secondary datum levels plotted against a paleomagnetic time scale of Berggren et al. (in press) (Fig. 8) and the occurrence chart (Fig. 5) for Site 581 provide the means of estimating the absolute ages of diatom zonal boundaries. In the 202.99 to 228.01 m sub-bottom interval (between Samples 581-4-2, 98-99 cm and 581-6-6, 100-101 cm), the large amount of reworking of

Table 7. Diatom zonation of samples from Leg 86, except Sites 576 and 577.

Age	Diatom zone	Core-Section (interval in cm)				
		Hole 578	Hole 579	Hole 579A	Hole 580	Hole 581
Quaternary	*Denticulopsis seminae*	1-1, 108-109 2-5, 115-116	1-1, 16-17 2-3, 123-124		1-1, 25-26 3-3, 25-26	1-1, 55-56 1,CC
	Rhizosolenia curvirostris	2,CC 3-2, 96-97	2-4, 123-124 2-5, 123-124	1-1, 14-15 1-5, 14-15	3-4, 25-26 4-4, 121-122	
	Nitzschia reinholdii	3-3, 96-97 6-1, 109-110		1-6, 14-15 3-5, 115-116	4-5, 121-122 6-6, 17-18	
	Actinocyclus oculatus	6-2, 109-110 7-6, 121-122		3-6, 115-116 6-4, 25-26	6,CC 11-1, 22-23	
upper Pliocene	*Nitzschia fossilis*	7-7, 47-48 8-4, 118-119		6-5, 25-26 7,CC	11-2, 22-23 11-5, 105-106	
	Thalassiosira convexa	8-5, 118-119 9-1, 118-119		8-1, 132-133 9-1, 30-31	11,CC 14-5, 130-131	
	Denticulopsis seminae v. *fossilis* *Denticulopsis kamtschatica*	9-2, 118-119 10-4, 118-119		9-2, 30-31 12-4, 16-17	14-6, 130-131 17,CC	
lower Pliocene	*Nitzschia jouseae*	10-5, 118-119 12-1, 100-101		12-5, 16-17 15,CC		2-1, 134-135 2-7, 25-26
	Thalassiosira oestrupii	12-2, 100-101 12,CC				3-1, 90-91 3-3, 90-91
upper Miocene	*Rouxia californica*	13-1, 135-136 13,CC				3-4, 90-91 6-2, 100-101
	Thalassionema schraderi					6-3, 100-101 6-5, 100-101
	Denticulopsis katayamae					6-6, 100-101 7-1, 100-101
	Denticulopsis dimorpha					7-2, 100-101 7,CC
middle Miocene	*Coscinodiscus yabei*					8-1, 110-111 8-3, 110-111
	Denticulopsis praedimorpha					8-4, 110-111 8,CC

upper Miocene marker taxa is recognized. This reworking is probably due to a hiatus, as reflected in the sediment accumulation rate curve (Fig. 8) and in the change in lithology from gray to green reduced (pyritic) biosiliceous clay to ooze downhole to yellow brown oxidized biosiliceous clay and a downhole contamination by breccia deformed by drilling.

Zonal Definition

Denticulopsis praedimorpha Range Zone

Top. Last occurrence of *Denticulopsis praedimorpha*.

Base. Not defined herein, but Akiba (1983) proposed the first occurrence of *Denticulopsis praedimorpha* as the base of this zone.

Age. Middle Miocene (12.6–13.6 m.y. ago).

Paleomagnetic correlation. None available.

Correlation with other zones. The *Denticulopsis praedimorpha* Zone correlates to Subzone b of the *Denticulopsis hustedtii–Denticulopsis lauta* Zone of Barron (1980) and Koizumi (1983).

Important datums. The first occurrence of *Hemidiscus cuneiformis* occurs at the top of the *Denticulopsis praedimorpha* Zone.

Original definition. Akiba (1979).

Other discussion. Maruyama (1982), Akiba (1983).

Coscinodiscus yabei Partial Range Zone

Top. First occurrence of *Denticulopsis dimorpha*.

Base. Last occurrence of *Denticulopsis praedimorpha*.

Age. Late middle Miocene (11.9–12.6 m.y. ago).

Paleomagnetic correlation. None available.

Correlation with other zones. The *Coscinodiscus yabei* Zone correlates with Subzone c of the *Denticulopsis hustedtii–Denticulopsis lauta* Zone of Barron (1980).

Important datums. The last occurrence of *Denticulopsis punctata* var. *hustedtii* occurs within this zone. The first occurrence of *Thalassiosira* sp. 1 Barron (1980) occurs in the upper part of the *Coscinodiscus yabei* Zone.

Remarks. A biostratigraphic interval that is correlative with the *Coscinodiscus yabei* Zone defined herein has not been recognized in the zonal subdivisions by Koizumi (1983).

Original definition. Maruyama (1982).

Denticulopsis dimorpha Range Zone

Top. First occurrence of *Denticulopsis dimorpha*.

Base. Last occurrence of *Denticulopsis dimorpha*.

Age. Latest middle Miocene to early late Miocene (10.5–11.9 m.y. ago).

Paleomagnetic correlation. None available.

Correlation with other zones. The *Denticulopsis dimorpha* Zone correlates with Subzone d of the *Denticu-*

Table 8. Estimate of absolute ages of late middle to late Miocene diatom datum levels and stratigraphic occurrences in Hole 581.

		Datum level[a]	Age[b] (m.y.)	Reference[c]	Stratigraphic level[d]
17.	B	*Nitzschia jouseae*	4.45	2	2-7,26/3-1,90
18.	B	*Bogorovia tatsunokuchiensis*	4.9–5.1	3	3-3,91/3-4,90
19.	B	*Thalassiosira oestrupii*	5.0–5.1	3–6	3-3,91/3-4,90
20.	T	*Rouxia californica*	5.1	3,5	3-3,91/3-4,90
21.	T	*Thalassiosira miocenica*	5.1	2,6	3-5,91/3-6,75
22.	T	*Asterolampra acutiloba*	5.35	2,6	3-4,91/3-5,90
23.	T	*Thalassiosira praeconvexa*	5.75	6	4-1,99/4-2,98
24.	B	*Thalassiosira miocenica*	6.1	2,6	5-3,101/5-4,64
25.	T	*Nitzschia miocenica*	5.5–5.75	1–3,6	4-1,99/4-2,98
26.	B	*Nitzschia miocenica*	7.3	1–3,6	4-5,99/4-6,98
27.	B	*Thalassiosira praeconvexa*	6.3	6	5-3,101/5-4,64
28.	T	*Thalassiosira burckliana*	7.95	1,2,5,6	4-3,99/4-4,98
29.	B	*Thalassiosira convexa*	6.6	1–3,6	6-1,101/6-2,100
30.	B	*Thalassiosira antiqua*	8.55–8.75	3–7	6-1,101/6-2,100
31.	T	*Nitzschia porteri*	7.2	1–3	6-1,101/6-2,100
32.	B	*Denticulopsis kamtschatica*	6.5–6.7	3,6	6-3,101/6-4,100
33.	T	*Thalassionema schraderi*	7.2–7.3	5	6-2,101/6-3,100
34.	B	*Nitzschia reinholdii*	6.5–6.9,8.0[e]	2–6	6-5,101/6-6,100
35.	T	*Coscinodiscus temperi* v. *delicata*	10.1	5,6	6-5,101/6-6,100
36.	B	*Thalassiosira burckliana*	9.0	2,5,6	6-6,101/6-7,10
37.	T	*Coscinodiscus yabei*	8.6–8.9	1,3–6	7-1,101/7-2,100
38.	T	*Denticulopsis lauta*	10.5–10.6	3,5	7-1,101/7-2,100
39.	T	*Denticulopsis dimorpha*	10.5–10.6	3–6	7-1,101/7-2,100
40.	B	*Denticulopsis dimorpha*	11.5–11.7	3–6	7,CC/8-1,110
41.	T	*Denticulopsis punctata* v. *hustedtii*	12.3	5,6	8-1,111/8-2,110
42.	B	*Hemidiscus cuneiformis*	12.5–12.7	2,3,6	8-3,111/8-4,110
43.	T	(common) *Denticulopsis praedimorpha*	12.4	7	8-3,111/8-4,110
44.	B	*Coscinodiscus temperi* v. *delicata*	12.85	5,6	8-4,111/8-5,110

[a] B = first occurrence, T = last occurrence.

[b] Tied to the paleomagnetic time scale of Berggren et al. (in press).

[c] (1) Burckle, 1972; (2) Burckle, 1978; (3) Barron, 1980; (4) Barron, 1981; (5) Keller and Barron, 1981; (6) Keller et al., 1982; (7) Barron and Keller, 1983.

[d] The highest and lowest stratigraphic levels of datum levels in Hole 581 are listed (Core-Section, level in cm) with a slash between them.

[e] Barron, pers. comm., 1984.

lopsis hustedtii–Denticulopsis lauta Zone of Barron (1980) and Subzone c of the *Denticulopsis hustedtii–Denticulopsis lauta* Zone of Koizumi (1983).

Important datums. The last occurrence of *Coscinodiscus yabei* and *Denticulopsis lauta* is coincident with the top of this zone. The first occurrence of *Nitzschia porteri* is in the upper part of the *Denticulopsis dimorpha* Zone.

Original definition. Maruyama (1982).

Denticulopsis katayamae Partial Range Zone

Top. Last occurrence of *Denticulopsis katayamae.*

Base. Last occurrence of *Denticulopsis dimorpha.*

Age. Early late Miocene (8.6–10.5 m.y. ago).

Paleomagnetic correlation. None available.

Correlation with other zones. The *Denticulopsis katayamae* Zone correlates with the lower part of the *Denticulopsis hustedtii* Zone of Barron (1980) and Koizumi (1983).

Remarks. The Subzone a/Subzone b boundary of the *Denticulopsis hustedtii* Zone, which correlates with the top of the *Denticulopsis katayamae* Zone, is within the middle part of Epoch 8 (about 8.6 m.y. ago) in the equatorial Pacific (Burckle, 1972) and also in the middle latitude North Pacific (Barron, 1980; Keller et al., 1982) by the last occurrence of *Coscinodiscus yabei.*

Original definition. Maruyama (1982).

Thalassionema schraderi Range Zone

Top. Last occurrence of *Thalassionema schraderi.*

Base. Last occurrence of *Denticulopsis katayamae.*

Age. Middle late Miocene (7.3–8.6 m.y. ago).

Paleomagnetic correlation. None available.

Correlation with other zones. The *Thalassionema schraderii* Zone presumably correlates with the upper part of the *Denticulopsis hustedtii* Zone of Barron (1980) and Koizumi (1983) by the sporadic occurrence of *Denticulopsis kamtschatica* near the top of this zone.

Original definition. Akiba (1982).

Rouxia californica Partial Range Zone

Top. Last occurrence of *Rouxia californica.*

Base. Last occurrence of *Thalassionema schraderi.*

Age. Late Miocene (5.1–7.3 m.y. ago).

Paleomagnetic correlation. None available.

Correlation with other zones. The *Rouxia californica* Zone correlates with Subzone a of the *Denticulopsis kamtschatica* Zone of Barron (1980) and Koizumi (1983).

Important datums. The first occurrence of *Bogorovia tatsunokuchiensis* and *Thalassiosira oestrupii* is coincident with the top of the *Rouxia californica* Zone. Also, the last occurrence of *Asterolampra acutiloba* occurs near the top of this zone. The last occurrence of *Thalassiosira praeconvexa* and *Nitzschia miocenica* is

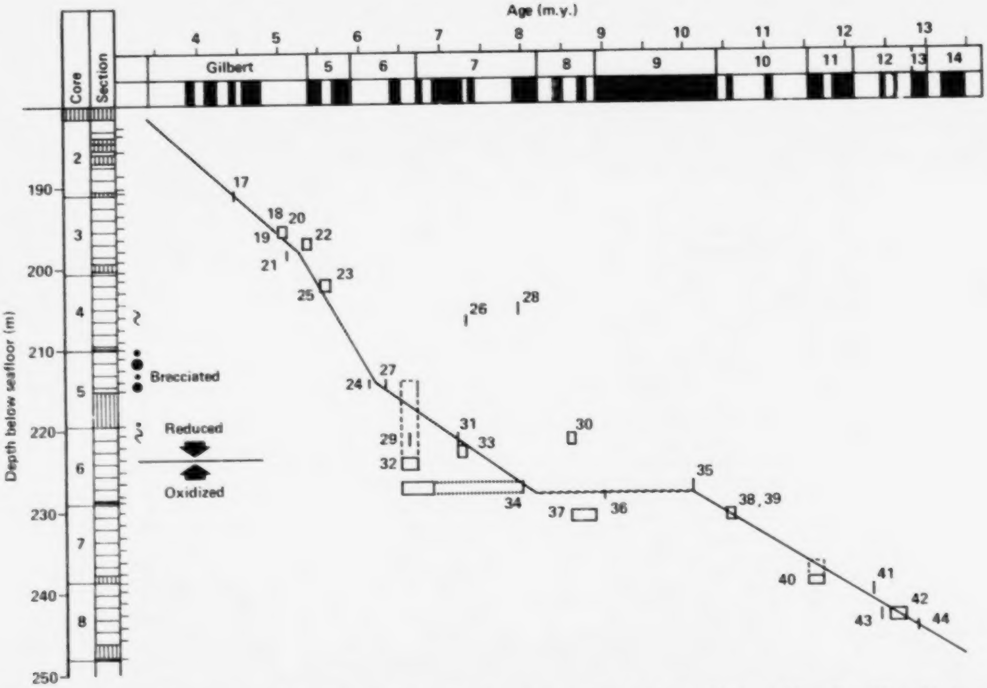

Figure 8. Sediment accumulation rate curve for Site 581 plotted from datum levels listed below. (17 = first *Nitzschia jouseae*, 18 = first *Bogorovia tatsunokuchiensis*, 19 = first *Thalassiosira oestrupii*, 20 = last *Rouxia californica*, 21 = last *Thalassiosira miocenica*, 22 = last *Asterolampra acutiloba*, 23 = last *Thalassiosira praeconvexa*, 24 = first *Thalassiosira miocenica*, 25 = last *Nitzschia miocenica*, 26 = first *Nitzschia miocenica*, 27 = first *Thalassiosira praeconvexa*, 28 = last *Thalassiosira burcklina*, 29 = first *Thalassiosira convexa*, 30 = first *Thalassiosira antiqua*, 31 = last *Nitzschia porteri*, 32 = first *Denticulopsis kamtschatica*, 33 = last *Thalassionema schraderi*, 34 = first *Nitzschia reinholdii*, 35 = last *Coscinodiscus temperi* var. *delicata*, 36 = first *Thalassiosira burckliana*, 37 = last *Coscinodiscus yabei*, 38 = *Denticulopsis lauta*, 39 = last *Denticulopsis dimorpha*, 40 = first *Denticulopsis dimorpha*, 41 = last *Denticulopsis punctata* var. *hustedtii*, 42 = first *Hemidiscus cuneiformis*, 43 = last common *Denticulopsis praedimorpha*, 44 = first *Coscinodiscus temperi* var. *delicata*). Most of Core 5 is very deformed to brecciated and both Section 4 of Core 4 and Section 1 of Core 6 are very deformed by drilling. The lithologic change occurs from reduced biosiliceous clay to ooze downhole to oxidized biosiliceous clay at 223.6 m sub-bottom depth (Sample 581-6-3, 111 cm).

within the upper part of this zone. The first occurrence of *Nitzschia miocenica* occurs within the middle part of this zone.

Original definition. Akiba (1983).

In Figure 9, the proposed diatom zonation is correlated with the lower latitude diatom zonation of Burckle (1972), middle–high latitude diatom zonation of Koizumi (1973, 1975a, 1983), the diatom zonation off northeast Japan of Barron (1980) and Akiba (1983), and the low–middle eastern North Pacific and the California area of Barron (1981; Keller and Barron, 1981; Barron and Keller, 1983).

CONCLUSIONS

Twenty-two diatom datum levels for the latest Miocene to Quaternary, which were defined according to first or last occurrences of a species, are evaluated on the basis of their spatial and temporal distribution in middle latitudes.

Nine diatom zones, based on first-order datum levels, are proposed for the Pliocene and Quaternary in the middle latitudes.

Six diatom zones are proposed for the middle and upper Miocene in high latitudes.

ACKNOWLEDGMENTS

We would like to thank the reviewers, Lloyd H. Burckle, Hans-Joachim Schrader, and John A. Barron, for constructive criticism of this manuscript. John A. Barron was especially helpful and provided the original figure that was modified to Figure 8.

FLORAL REFERENCES

Achnanthes lanceolata (Brébisson) Grunow: Hustedt, 1933, p. 408, fig. 863.

Actinocyclus curvatulus Janisch: Hustedt, 1930b, p. 538, fig. 307; Koizumi, 1973, p. 831, pl. 1, figs. 1–6; Sancetta, 1982, p. 222, pl. 1, figs. 1–3. (Plate 3, Fig. 9)

Actinocyclus ellipticus Grunow: Hustedt, 1930b, p. 533, fig. 303; Koizumi, 1980, pl. 1, fig. 19.

Actinocyclus ellipticus forma *lanceolata* Kolbe, 1954, p. 20, pl. 3, fig. 27; Koizumi, 1980, pl. 1, fig. 20.

Actinocyclus elongatus Grunow: Kolbe, 1954, p. 20, pl. 3, figs. 28, 31; Simonsen, 1974, p. 21, pl. 20, fig. 1–3. (Plate 4, Fig. 16)

Actinocyclus ingens Rattray, 1890, p. 149, pl. 11, fig. 7; Koizumi, 1973, p. 831, pl. 1, figs. 13, 14, pl. 2, figs. 1, 2.

Actinocyclus moronensis Deby: Schrader, 1974b, p. 911, pl. 17, figs. 9–12; Kanaya, 1971, p. 554, pl. 40.2, fig. 7.

Actinocyclus ochotensis Jousé, 1968, p. 17, pl. 2, figs. 2–5; Koizumi, 1973, p. 831, pl. 2, figs. 8, 9.

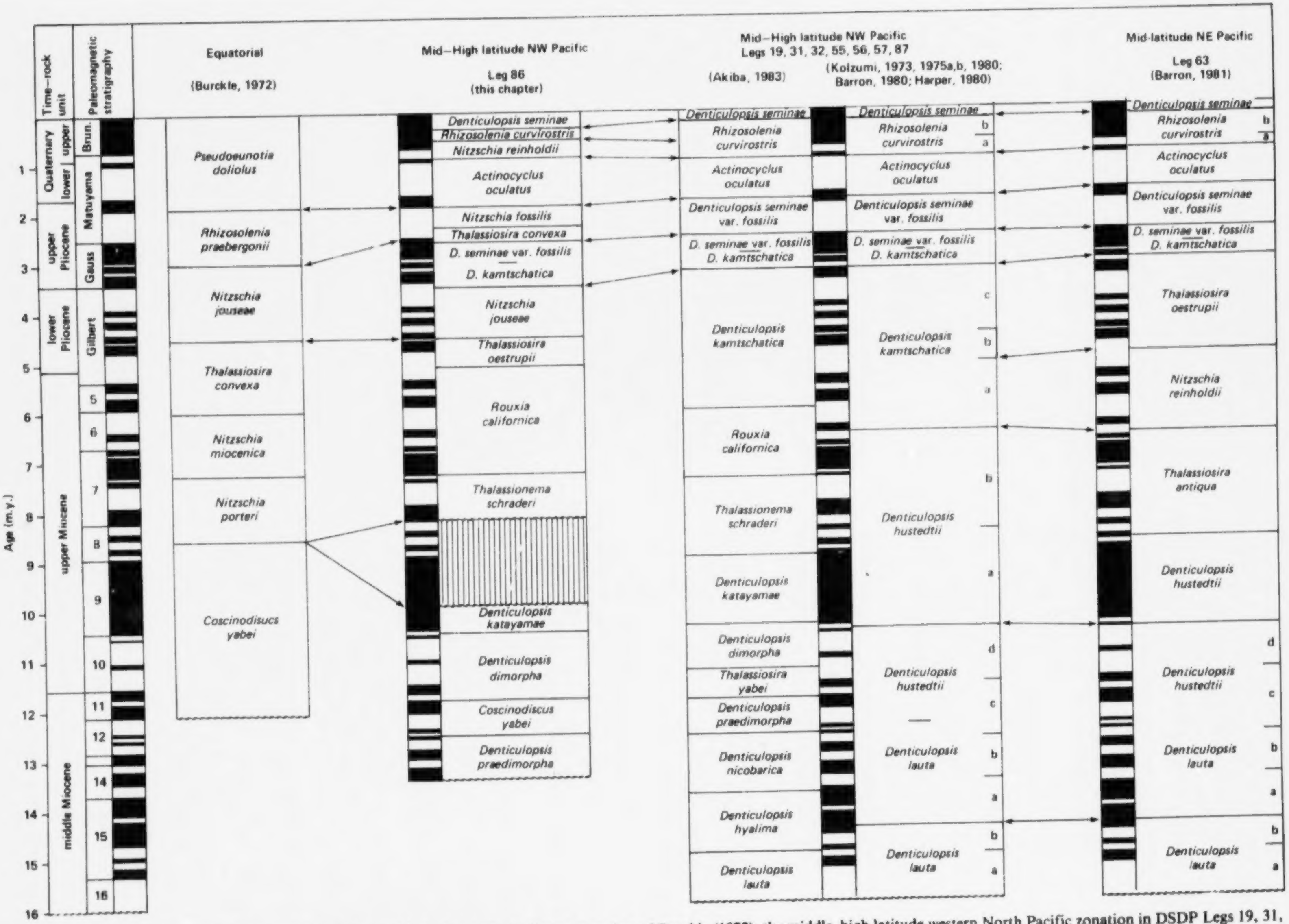

Figure 9. Correlation of the diatom zones in this chapter with the low latitude diatom zonation of Burckle (1972), the middle–high latitude western North Pacific zonation in DSDP Legs 19, 31, 32, and 55 by Koizumi (1973, 1975a, 1975b, 1980), Leg 56 by Harper (1980), Leg 57 by Barron (1980) and Leg 87 by Akiba (1983), and the low–middle eastern North Pacific zonation in Leg 63 by Barron (1981).

Actinocyclus octonarius Ehrenberg: Andrews, 1980a, p. 23, pl. 1, fig. 1, pl. 4, fig. 1.
Actinocyclus oculatus Jousé, 1968, p. 18, pl. 2, figs. 6, 7; Koizumi, 1973, p. 831, pl. 2, figs. 8, 9. (Plate 3, Fig. 12)
Actinoptychus senarius (Ehrenberg) Ehrenberg: Kanaya, 1959, p. 89, pl. 6, figs. 4, 5; Sancetta, 1982, p. 225, pl. 1, fig. 7.
Actinoptychus splendens (Shadbolt) Ralfs: Hustedt, 1930b, p. 478, fig. 265.
Actinoptychus vulgaris Schumann: Sancetta, 1982, p. 223, pl. 1, fig. 8.
Asterolampra acutiloba Forti: Schrader, 1974b, pl. 9, fig. 7, 8; Koizumi, 1980, pl. 1, fig. 18. (Plate 2, Fig. 5)
Asterolampra grevillei (Wallich) Greville: Hustedt, 1930b, p. 489, fig. 274; Schrader, 1974b, pl. 8, fig. 5.
Asterolampra marylandica Ehrenberg: Hustedt, 1930b, p. 485, figs. 270, 271; Koizumi, 1980, pl. 2, fig. 24.
Asteromphalus arachne (Brébisson) Ralfs: Hustedt, 1930b, p. 493, fig. 276; Schrader, 1974b, pl. 9, fig. 11.
Asteromphalus brookei Bailey: Sancetta, 1982, p. 226, pl. 1, fig. 9. (Plate 2, Fig. 7)
Asteromphalus darwinii Ehrenberg: Greville, 1860, p. 116, pl. 4, figs. 12, 13; Koizumi, 1980, p. 397, pl. 2, fig. 26. (Plate 2, Fig. 2)
Asteromphalus flabellatus (Brébisson) Greville: Hustedt, 1930b, p. 498, fig. 279; Schrader, 1974b, p. 912, pl. 8, fig. 3.
Asteromphalus heptactis (Brébisson) Ralfs: Hustedt, 1930b, p. 494, fig. 277; Schrader, 1974b, pl. 8, fig. 1. (Plate 2, Fig. 1)
Asteromphalus hookeri Ehrenberg: Schrader, 1974b, pl. 8, fig. 7.
Asteromphalus imbricatus Wallich: Kolbe, 1957, p. 25, pl. 1, fig. 1; Simonsen, 1974, p. 25, pl. 22, fig. 1.
Asteromphalus petterssonii (Kolbe) Thorrington-Smith, 1970, p. 822, pl. 1, fig. 5; Schrader, 1974b, p. 912, pl. 12, figs. 10–13. (Plate 2, Fig. 3)
Asteromphalus robustus Castracane: Hustedt, 1930b, p. 496, fig. 278; Koizumi, 1975b, pl. 3, fig. 5.
Aulacosira granulata (Ehrenberg) Simonsen, 1979, p. 58; as *Melosira granulata* (Ehrenberg) Ralfs, Hustedt, 1930b, p. 248, fig. 104.
Bacteriosira fragilis (Gran) Gran: Koizumi, 1975a, pl. 2, figs. 5, 6; Sancetta, 1982, p. 227, pl. 2, figs. 1–4.
Biddulphia pulchella Gray: Hustedt, 1930b, p. 832, fig. 490.
Bogorovia praepaleacea (Schrader) Jousé, 1976, p. 1233; Barron, 1981, p. 529, pl. 4, fig. 14.
Bogorovia tatsunokuchiensis (Koizumi) Jousé, 1976, p. 1233; Barron, 1981, p. 529, pl. 4, fig. 17. (Plate 1, Fig. 19)
Chaetoceros furcellatus Bailey: Hustedt, 1930b, p. 749, fig. 433.
Cocconeis californica Grunow: Hustedt, 1933, p. 343, fig. 796.
Cocconeis costata Gregory: Hustedt, 1933, p. 332, fig. 785.
Cocconeis disculus Schumann: Hustedt, 1933, p. 345, fig. 799.
Cocconeis pellucida Grunow: Hustedt, 1933, p. 357, fig. 812.
Cocconeis placentula var. *euglypta* (Ehrenberg) Cleve: Hustedt, 1933, p. 349, fig. 802c.
Cocconeis scutellum Ehrenberg: Hustedt, 1933, p. 337, fig. 790.
Cocconeis scutellum var. *stauroneiformis* Rabenhorst: Hustedt, 1933, p. 339, fig. 792.
Coscinodiscus africanus Janisch: Hustedt, 1930b, p. 428, fig. 231; Koizumi, 1975b, pl. 2, figs. 1, 2; Simonsen, 1974, p. 13, pl. 9, fig. 1.
Coscinodiscus argus Ehrenberg: Hustedt, 1930b, p. 422, fig. 226.
Coscinodiscus asteromphalus Ehrenberg: Hustedt, 1930b, p. 452, fig. 250, 251a.
Coscinodiscus centralis Ehrenberg: Hustedt, 1930b, p. 444, fig. 243.
Coscinodiscus elegans Greville, 1866, p. 3, pl. 1, fig. 6; Kanaya, 1959, p. 75, pl. 3, figs. 6, 7.
Coscinodiscus endoi Kanaya, 1959, p. 76, pl. 3, figs. 8–11; Schrader, 1973, p. 702, pl. 7, figs. 14, 21, pl. 20, figs. 1, 2. (Plate 4, Fig. 12)
Coscinodiscus gigas Ehrenberg: Hustedt, 1930b, p. 456, fig. 254, 256a.
Coscinodiscus marginatus Ehrenberg: Hustedt, 1930b, p. 416, fig. 223; Koizumi, 1975b, pl. 2, fig. 18.
Coscinodiscus nitidus Gregory: Hustedt, 1930b, p. 414, fig. 221.
Coscinodiscus nodulifer Schmidt: Hustedt, 1930b, p. 426, fig. 229; Koizumi, 1975b, p. 1, figs. 3–10. (Plate 3, Fig. 8)
Coscinodiscus obscurus Schmidt: Hustedt, 1930b, p. 418, fig. 224.
Coscinodiscus oculus-iridis Ehrenberg: Hustedt, 1930b, p. 454, fig. 252.
Coscinodiscus perforatus Ehrenberg: Hustedt, 1930b, p. 445, figs. 244, 245.
Coscinodiscus plicatus Grunow: Kanaya, 1971, p. 555, pl. 40.4, figs. 4–6. (Plate 3, Figs. 3, 4)
Coscinodiscus radiatus Ehrenberg: Hustedt, 1930b, p. 240, fig. 225.
Coscinodiscus stellaris Roper: Hustedt, 1930b, p. 395, fig. 207.
Coscinodiscus symbolophorus Grunow: Schrader, 1973, p. 703, pl. 22, figs. 8, 9; as *Coscinodiscus stellaris* Roper var. *symbolophorus* (Grunow) Jørgensen, Koizumi, 1973, p. 832, pl. 4, figs. 5, 6.
Coscinodiscus tabularis Grunow var. *egregius* (Rattray) Hustedt, 1930b, p. 427, fig. 230b; Koizumi, 1975b, pl. 2, figs. 14, 15. (Plate 5, Figs. 13, 14)
Coscinodiscus temperei Brun var. *delicata* Barron, 1981, p. 528, pl. 3, figs. 1, 3, 4.
Coscinodiscus vetustissimus Pantocsek: Hustedt, 1930b, p. 412, fig. 220; Kanaya, 1971, p. 555, pl. 40.2, figs. 1–5; Koizumi, 1975b, pl. 1, figs. 13, 14. (Plate 4, Fig. 11)
Coscinodiscus yabei Kanaya, 1959, p. 86, pl. 5, figs. 6-9. (Plate 3, Figs. 10, 11)
Cosmiodiscus intersectus (Brun) Jousé, 1961, p. 68, pl. 2, figs. 9, 10; Koizumi, 1973, p. 832, pl. 4, figs. 12, 13.
Cyclotella chaetoceras Lemmermann: Hustedt, 1930b, p. 344, fig. 175.
Cyclotella comta (Ehrenberg) Kützing: Hustedt, 1930b, p. 103, fig 69.
Cyclotella kützingiana Thwaites: Hustedt, 1930b, p. 338, fig. 171.
Cyclotella meneghiniana Kützing: Hustedt, 1930b, p. 341, fig. 174.
Cyclotella striata (Kützing) Grunow: Hustedt, 1930b, p. 344, fig. 176.
Cyclotella stylorum Brightwell: Hustedt, 1930b, p. 348, fig. 179.
Cymatodiscus planetophorus (Meister) Hendey, 1958, p. 42, pl. 5, fig. 8.
Cymatosira lorenziana Grunow: Hustedt, 1931, p. 127, fig. 648.
Cymbella leptoceros Kützing: Hustedt, 1930b, p. 353, fig. 645.
Cymbella sinuata Gregory: Hustedt, 1930b, p. 361, fig. 668.
Delphineis surirella (Ehrenberg) Andrews, 1980b, p. 83, pl. 1, 2, figs. 1–7.
Delphineis surirelloides (Simonsen) Andrews, 1980b, p. 86; as *Rhaphoneis surirelloides* Simonsen, 1974, p. 35, pl. 23, figs. 2–8.
Denticulopsis dimorpha (Schrader) Simonsen, 1979, p. 64; Barron, 1981, p. 529, pl. 4, fig. 7. (Plate 1, Fig. 1)
Denticulopsis hustedtii (Kanaya and Simonsen) Simonsen, 1979, p. 64; Barron, 1981, p. 529, pl. 4, fig. 21. (Plate 1, Figs. 7, 8)
Denticulopsis hyalina (Schrader) Simonsen, 1979, p. 64; Barron, 1981, p. 529, pl. 4, figs. 3, 4. (Plate 1, Fig. 3)
Denticulopsis kamtschatica (Zabelina) Simonsen, 1979, p. 64; emend: Koizumi, 1980, p. 396, pl. 2, figs. 1–10. (Plate 6, Fig. 7)
Denticulopsis katayamae Maruyama, 1982: Remarks: This species differs from *Denticulopsis hyalina* (Schrader) Simonsen in the presence of the secondary pseudosepta, and from *Denticulopsis hustedtii* (Kanaya and Simonsen) Simonsen in its heavily silicified and hyaline valve face. (Plate 1, Figs. 5, 6)
Denticulopsis lauta (Bailey) Simonsen, 1979, p. 64; Barron, 1981, p. 529, pl. 4, fig. 5. (Plate 1, Fig. 4)
Denticulopsis praedimorpha (Akiba) Barron, 1981, p. 529, pl. 4, figs. 8–10. (Plate 1, Fig. 2)
Denticulopsis punctata forma *hustedtii* (Schrader) Simonsen, 1979, p. 65; Barron, 1981, pl. 4, fig. 1. (Plate 1, Figs. 9, 10)
Denticulopsis seminae (Simonsen and Kanaya) Simonsen, 1979, p. 65; as *Denticula seminae* Simonsen and Kanaya, Koizumi, 1975a, pl. 1, figs. 1, 2.
Diploneis bomboides (Schmidt) Cleve: Hustedt, 1937, p. 695, fig. 1080.
Diploneis bombus Ehrenberg: Hustedt, 1937, p. 704, fig. 1086a–c, g, h.
Diploneis coffeiformis (Schmidt) Cleve: Hustedt, 1937, p. 611, fig. 1025.
Diploneis interrupta (Kützing) Cleve: Hustedt, 1930a, p. 252, fig. 400.
Diploneis nitescens (Gregory) Cleve: Hustedt, 1937, p. 640, fig. 1047.
Diploneis oculata (Brébisson) Cleve: Hustedt, 1930a, p. 250 fig. 392.
Diploneis ovalis (Hilse) Cleve: Hustedt, 1930a, p. 249, fig. 390.
Diploneis parma Cleve: Hustedt, 1937, p. 673, fig. 1066.
Diploneis smithii (Brebisson) Cleve: Hustedt, 1937, p. 647, fig. 1051.
Diploneis weissflogi (Schmidt) Cleve: Hustedt, 1937, p. 703, fig. 1085.
Epithemia zebra (Ehrenberg) Kützing: Hustedt, 1930a, p. 384, fig. 729.
Eunotia praerupta Ehrenberg: Hustedt, 1932, p. 280, fig. 747a–e.
Eunotia sibirica Cleve: Hustedt, 1932, p. 310, fig. 776.
Fragilaria construens (Ehrenberg) Grunow: Hustedt, 1931, p. 156, fig. 670a–c.
Fragilaria leptostauron (Ehrenberg) Hustedt, 1931, p. 153, fig. 668a–f.
Gomphonema augur Ehrenberg: Hustedt, 1930a, p. 372, fig. 689.
Gomphonema gracile Ehrenberg: Hustedt, 1930a, p. 376, fig. 702.
Grammatophora marina (Lyngbye) Kützing: Hustedt, 1931, p. 43, fig. 569.
Grammatophora oceanica Ehrenberg: Hustedt, 1931, p. 45, fig. 573.

Hemiaulus polymorphus Grunow: Hustedt, 1930b, p. 880, fig. 525.

Hemiaulus sinensis Greville: Hustedt, 1930b, p. 875, fig. 519.

Hemidiscus cuneiformis Wallich: Hustedt, 1930b, p. 904, fig. 542; Koizumi, 1975a, pl. 4, fig. 2. (Plate 5, Fig. 12)

Hemidiscus simplicissimus Hanna and Grant, 1926, p. 147, pl. 16, fig. 13; Schrader, 1973, p. 706, pl. 24, figs. 12, 13.

Hyalodiscus scoticus (Kützing) Grunow: Hustedt, 1930b, p. 293, fig. 133.

Kisseleviella carina Sheshukova-Poretzkaya, 1962, p. 207, fig. 1a–b, 2; Koizumi, 1973, p. 833, pl. 7, figs. 3, 4.

Liriogramma hustedtii Kolbe, 1955, p. 173, pl. 2, fig. 21.

Lithodesmium undulatum Ehrenberg: Hustedt, 1930b, p. 789, fig. 461.

Mediaria splendida Sheshukova-Poretzkaya, 1962, p. 210, fig. 2, 5; Koizumi, 1973, p. 832, pl. 7, figs. 5, 6.

Melosira albicans Sheshukova-Poretzkaya, 1964, p. 69, fig. 1, 2, pl. 2, fig. 3; Koizumi, 1972, p. 351, pl. 43, figs. 1, 2.

Navicula lyra Ehrenberg: Hustedt, 1964, p. 500, figs. 1548–1555; Hendey, 1964, p. 209, pl. 33, fig. 2.

Navicula mutica Kützing: Hustedt, 1966, p. 583, fig. 1592a–f.

Nitzschia bicapitata Cleve: Hustedt, 1958, p. 169, figs. 176–190; Hasle, 1960, p. 21, pl. 6, figs. 53–57; Simonsen, 1974, p. 50, pl. 35, figs. 3–15.

Nitzschia braarudii Hasle, 1960, p. 22, fig. 11, pl. 7, figs. 58–63; Simonsen, 1974, p. 50, pl. 35, fig. 2.

Nitzschia constricta (Gregory) Grunow: Cleve-Euler, 1952, p. 55, pl. 7, fig. 8.

Nitzschia cylindrica Burckle, 1972, p. 239, pl. 2, figs. 1–6; Schrader, 1973, pl. 5, figs. 27, 32, 33.

Nitzschia cylindrus (Grunow) Hasle, 1972, p. 115; Koizumi, 1975a, p. 802, pl. 1, fig. 49; as *Nitzschia cylindra* (Grunow) Hasle, Sancetta, 1982, p. 232, pl. 3, figs. 6, 7.

Nitzschia dietrichii Simonsen, 1974, p. 51, pl. 36, figs. 1–3.

Nitzschia fossilis (Frenguelli) Kanaya: Koizumi and Kanaya, 1976, p. 155, pl. 1, figs. 11–14. (Plate 1, Fig. 18; Plate 6, Fig. 6)

Nitzschia grunowii Hasle, 1972, p. 115; Sancetta, 1982, p. 233, pl. 3, figs. 8–10. (Plate 3, Figs. 5, 6)

Nitzschia heteropolica Schrader, 1973, p. 707, pl. 26, figs. 1, 2. Remarks: Valves heteropolar, one apex broadly rounded, the other acutely rounded. Barron, 1980, pl. 2, fig. 7, pl. 4, fig. 9.

Nitzschia inflatula Hasle, 1965, p. 33, pl. 13, figs. 7–10, pl. 15, figs. 1–8; Simonsen, 1974, p. 52, pl. 36, figs. 7, 8.

Nitzschia interruptestriata Simonsen, 1974, p. 52, pl. 36, figs. 9–11, pl. 37, fig. 1a–7, pl. 38, figs. 1–7. (Plate 6, Fig. 8)

Nitzschia jouseae Burckle, 1972, p. 240, pl. 2, figs. 17–21; Koizumi, 1980, p. 397, pl. 3, figs. 9, 10. (Plate 1, Fig. 12; Plate 6, Fig. 12)

Nitzschia kolaczekii Grunow: Kolbe, 1955, p. 174, pl. 2, figs. 22, 23; Hasle, 1960, p. 24, pl. 5, fig. 50b, c.

Nitzschia marina Grunow: Kolbe, 1954, p. 40, pl. 3, figs. 38–40. (Plate 6, Figs. 1, 2)

Nitzschia miocenica Burckle, 1972, p. 240, pl. 2, figs. 10–15; Schrader, 1974b, p. 915, pl. 5, figs. 10, 11; Koizumi, 1980, p. 397, pl. 3, figs. 15–18. (Plate 1, Fig. 13; Plate 6, Fig. 9)

Nitzschia panduriformis Gregory: Hustedt, 1921, pl. 331, figs. 19, 21.

Nitzschia porteri Frenguelli sensu Burckle, 1972, pl. 2, fig. 16; Barron, 1981, pl. 4, fig. 20. (Plate 1, Fig. 11)

Nitzschia praefossilis Schrader, 1973, p. 708, pl. 5, figs. 19, 21, 22. (Plate 1, Fig. 15)

Nitzschia praereinholdii Schrader, 1973, p. 708, pl. 5, fig. 20, 23–26. (Plate 1, Fig. 16)

Nitzschia reinholdii Kanaya: Koizumi and Kanaya, 1976, p. 155, pl. 1, figs. 15–18. (Plate 6, Figs. 3, 4)

Nitzschia rolandii Schrader emend. Koizumi, 1980, p. 396, pl. 2, figs. 15–20.

Nitzschia seriata Cleve: Hendey, 1964, p. 284, pl. 21, fig. 6.

Nitzschia sicula (Castracane) Hustedt, 1958, p. 180, figs. 128–132; Hasle, 1960, p. 26, pl. 7, figs. 64, 65.

Nitzschia suikoensis Koizumi, 1980, p. 394, pl. 1, figs. 1–6.

Nitzschia trybionella Hantzsch: Hustedt, 1930a, p. 399, fig. 757.

Odontella aurita (Lyngbye) Agardh: Sancetta, 1982, p. 234, pl. 3, figs. 11, 12.

Paralia sulcata (Ehrenberg) Cleve: Andrews, 1976, p. 8, pl. 1, figs. 5, 6; Sancetta, 1982, p. 235, pl. 3, figs. 13–15.

Planktoniella sol (Wallich) Schütt: Hustedt, 1930b, p. 465, fig. 259; Fryxell and Hasle, 1972, figs. 34–36.

Porosira glacialis (Grunow) Jørgensen: Hustedt, 1930b, p. 315, fig. 153; Koizumi, 1973, p. 833, pl. 4, figs. 15–18; Sancetta, 1982, p. 235, pl. 3, figs. 16–18.

Pseudoeunotia doliolus (Wallich) Grunow: Hustedt, 1932, p. 259, fig. 737; Koizumi and Kanaya, 1976, p. 155, pl. 1, figs. 9, 10. (Plate 1, Fig. 17; Plate 6, Fig. 5)

Pseudopodosira elegans Sheshukova-Poretzkaya, 1964, p. 75, pl. 2, figs. 4, 5; Koizumi, 1972, p. 352, pl. 43, figs. 3, 4. (Plate 4, Fig. 10)

Rhabdonema arcuatum (Lyngbye? Agardh) Kützing: Hustedt, 1931, p. 20, fig. 549.

Rhabdonema japonicum Tempère and Brun: Hanna, 1970, p. 192, figs. 47, 92, 93, 95; Schrader, 1973, pl. 12, fig. 10.

Rhaphoneis amphiceros Ehrenberg: Hustedt, 1931, p. 174, fig. 680; Schrader, 1973, pl. 25, figs. 2, 3.

Rhizosolenia alata Brightwell: Hustedt, 1930b, p. 600, fig. 345; Koizumi, 1975a, pl. 1, fig. 38.

Rhizosolenia barboi Brun: Schrader, 1973, p. 709, pl. 24, figs. 4, 7; Koizumi, 1975b, pl. 4, figs. 52, 53. (Plate 6, Fig. 16)

Rhizosolenia bergonii Peragallo: Hustedt, 1930b, p. 575, fig. 327; Koizumi and Kanaya, 1976, p. 155, pl. 1, figs. 20, 21. (Plate 2, Fig. 4; Plate 6, Fig. 14)

Rhizosolenia curvirostris Jousé, 1968, p. 19, pl. 3, fig. 2; Donahue, 1970, p. 135, pl. 1, fig. a; Koizumi, 1973, pl. 5, figs. 29–31. (Plate 4, Fig. 15; Plate 6, Fig. 15)

Rhizosolenia hebetata forma *hiemalis* (Bailey) Gran: Hustedt, 1930b, p. 590, fig. 337; Koizumi, 1973, p. 833, pl. 5, figs. 34, 35; Sancetta, 1982, p. 237, pl. 4, figs. 5, 6.

Rhizosolenia matuyamai Burckle: Burckle et al., 1978, p. 213, figs. 3–6.

Rhizosolenia praebergonii Mukhina, 1965, p. 24, pl. 2, figs. 3, 4: Koizumi, 1968, p. 217, pl. 34, figs. 20a–21b; Burckle, 1972, pl. 3, figs. 1–3. (Plate 6, Fig. 13)

Rhizosolenia setigera Brightwell: Hustedt, 1930b, p. 588, fig. 336.

Rhizosolenia styliformis Brightwell: Hustedt, 1930b, p. 584, fig. 333; Koizumi, 1975a, pl. 1, fig. 33.

Rhoicosphenia curvata (Kützing) Grunow: Hustedt, 1933, p. 430, fig. 879.

Roperia praetesselata Schrader, 1974b, p. 915, pl. 21, figs. 13, 14, pl. 14, figs. 3, 4.

Roperia tesselata (Roper) Grunow: Hustedt, 1930b, p. 524, fig. 297; Koizumi, 1975b, pl. 2, figs. 3, 4. (Plate 5, Figs. 5, 6)

Rouxia californica Peragallo: Hanna, 1930, p. 186, pl. 14, figs. 6, 7; Koizumi, 1975a, p. 802, pl. 1, fig. 52. (Plate 1, Fig. 21)

Rouxia naviculoides Schrader, 1973, p. 710, pl. 3, figs. 27–32.

Rouxia yabei Hanna, 1930, p. 185, pl. 15, figs. 2–4; Schrader, 1973, p. 710, pl. 3, figs. 21, 23. (Plate 1, Fig. 20)

Stephanodiscus astraea (Ehrenberg) Grunow: Hustedt, 1930a, p. 110, fig. 85; Schrader, 1978, p. 863, pl. 2, figs. 7, 11, pl. 3, figs. 11, 12, pl. 4, figs. 15, 22, 23, pl. 8, fig. 13, pl. 12, fig. 15, pl. 13, figs. 2, 8, pl. 16, figs. 5, 6.

Stephanodiscus carconensis Grunow: Van Landingham, 1967, p. 17, pl. 21, fig. 18; Schrader, 1978, p. 863, pl. 4, fig. 24a, pl. 6, figs. 4, 8–10, pl. 7, figs. 6, 9, pl. 9, figs. 5, 8, 11–15, 18–23, 27, pl. 10, figs. 5–8, 10, pl. 11, figs. 9, 14, 15, 20, pl. 12, fig. 14, pl. 16, fig. 4.

Stephanopyxis dimorpha Schrader, 1973, p. 711, pl. 15, figs. 9–11, 19, 20, pl. 16, figs. 1–3, 8–11, pl. 24, fig. 10.

Stephanopyxis horridus Koizumi, 1972, p. 348, pl. 42, figs. 1a–2b; Koizumi, 1973, p. 833, pl. 6, figs. 1–4.

Stephanopyxis turris (Greville and Arnott) Ralfs: Hustedt, 1930b, p. 304, fig. 140; Koizumi, 1973, p. 833, pl. 6, figs. 13–16.

Surirella axmoricana Peragallo: Hendey, 1964, p. 289, pl. 40, fig. 6.

Synedra jouseana Sheshukova-Poretzkaya, 1962, p. 208, fig. 4; Koizumi, 1973, p. 833, pl. 6, fig. 17.

Thalassionema bacillaris (Heiden) Kolbe: Hasle and Mendiola, 1967, p. 109, figs. 1–4, 19, 22–26; Simonsen, 1974, p. 37, pl. 24, fig. 1.

Thalassionema hirosakiensis (Kanaya) Schrader, 1973, p. 711, pl. 23, figs. 31–33; Akiba, 1982, p. 49, figs. 1–5.

Thalassionema schraderi Akiba, 1982, p. 50, figs. 6–11, 16–18. (Plate 1, Fig. 14)

Thalassionema nitzschioides Grunow: Hustedt, 1959, p. 244, fig. 725; Koizumi, 1975a, pl. 1, figs. 50, 51. (Plate 6, Fig. 10)

Thalassionema nitzschioides var. *parva* Heiden and Kolbe, 1928, p. 564, pl. 35, fig. 118; Hasle, 1960, p. 18, fig. 5a. (Plate 6, Fig. 11)

Thalassiosira antiqua (Grunow) Cleve-Euler, 1951, p. 72, fig. 119a; Koizumi, 1973, p. 834, pl. 7, fig. 2. (Plate 4, Fig. 14)

Thalassiosira borealis Koizumi, 1980, p. 395, pl. 1, figs. 7–10 (Plate 4, Fig. 8)

Thalassiosira burckliana Schrader, 1974, p. 916, pl. 1, figs. 21–26; Barron, 1981, p. 530, pl. 5, fig. 2.

Thalassiosira convexa Mukhina, 1965, p. 22, pl. 11, fig. 1, 2; Koizumi, 1975a, pl. 4, figs. 15–20.

Thalassiosira decipiens (Grunow) Jørgensen: Hustedt, 1930b, p. 322, fig. 158; Koizumi, 1973, p. 834, pl. 7, figs. 16–18; Sancetta, 1982, p. 241, pl. 5, figs. 1–3. (Plate 4, Fig. 9)

Thalassiosira eccentrica (Ehrenberg) Cleve: Fryxell and Hasle, 1972, p. 297, pl. 1–4, figs. 1a–18; Simonsen, 1974, p. 9, pl. 2, figs. 1–3; as *Coscinodiscus excentricus* Ehrenberg, Koizumi, 1973, pl. 2, figs. 11, 12.

Thalassiosira gravida Cleve: Hustedt, 1930b, p. 325, fig. 161; Koizumi, 1973, p. 834, pl. 7, figs. 19–21.

Thalassiosira hyalina (Grunow) Gran: Hustedt, 1930b, p. 323, fig. 159; Koizumi, 1973, p. 834, pl. 8, figs. 1, 2; Sancetta, 1982, p. 242, pl. 5, figs. 4, 5.

Thalassiosira jacksonii Koizumi and Barron, 1980, p. 396, pl. 1, figs. 11–14. (Plate 4, Fig. 7)

Thalassiosira kryophila (Grunow) Goerg: Hustedt, 1930b, p. 324, fig. 160; Koizumi, 1973, p. 834, pl. 8, fig. 3.

Thalassiosira lacustris (Grunow) Hasle: Sancetta, 1982, p. 241, pl. 5, figs. 6, 7.

Thalassiosira leptopus (Grunow) Hasle and Fryxell, 1977, p. 20, figs. 1–14; as *Coscinodiscus lineatus* Ehrenberg, Koizumi, 1975b, pl. 2, figs. 5, 6.

Thalassiosira lineata Jousé, 1968, p. 13, pl. 1, figs. 1, 2; Hasle and Fryxell, 1977, p. 22, figs. 15–25; Simonsen, 1974, p. 9, pl. 1, figs. 4–7.

Thalassiosira manifesta Sheshukova-Poretzkaya, 1964, p. 72, pl. 1, figs. 6, 7; Koizumi, 1968, p. 218, pl. 35, figs. 16, 17.

Thalassiosira miocenica Schrader, 1974, p. 916, pl. 22, figs. 1–5, 11–13; Barron, 1981, pl. 5, fig. 3. (Plate 3, Fig. 1, 2)

Thalassiosira nativa Sheshukova-Poretzkaya, 1964, p. 75, pl. 1, figs. 4, 5; Koizumi, 1968, p. 219, pl. 35, figs. 19, 20.

Thalassiosira nidulus (Tempère and Brun) Jousé, 1961, p. 63, pl. 3, figs. 4, 5; Koizumi, 1973, pl. 7, figs. 25, 26. (Plate 2, Fig. 6)

Thalassiosira nodulolineata (Hendey) Hasle and Fryxell, 1977, p. 35, figs. 86–93.

Thalassiosira nordenskioldii Cleve: Hustedt, 1930b, p. 321, fig. 157; Hasle, 1968, p. 196, figs. 2, 4, 8; Koizumi, 1973, p. 834, pl. 8, fig. 4; Sancetta, 1982, p. 243, pl. 5, figs. 8, 9.

Thalassiosira oestrupii (Osterfeld) Proshkina-Lavrenko: Hasle, 1960, p. 8, pl. 1, figs. 5–7; Koizumi, 1973, p. 834, pl. 7, fig. 27. (Plate 4, Figs. 4–6; Plate 5, Figs. 1–4, 11)

Thalassiosira opposita Koizumi, 1980, p. 396, pl. 1, figs. 15–17.

Thalassiosira pacifica Gran and Angst: Schrader, 1973, pl. 14, figs. 13, 14. (Plate 4, Fig. 13)

Thalassiosira plicata Schrader, 1974b, p. 917, pl. 3, figs. 1, 2, 4–9; Koizumi, 1980, p. 398, pl. 3, figs. 22–25. (Plate 3, Fig. 13; Plate 5, Figs. 7, 8)

Thalassiosira praeconvexa Burckle, 1972, p. 242, pl. 2, figs. 7–9; Koizumi, 1975b, p. 878, pl. 3, figs. 21–28.

Thalassiosira symbolophora Schrader, 1974b, p. 917, pl. 4, figs. 1, 2, 4–6, 7, 8. (Plate 5, Figs. 9, 10)

Thalassiosira symmetrica Fryxell and Hasle, 1972, p. 312, figs. 37–46; Simonsen, 1974, p. 11, pl. 6, figs. 1, 2.

Thalassiosira trifulta Fryxell, in Fryxell and Hasle, 1979, p. 16, figs. 1–24; Sancetta, 1982, p. 244, pl. 5, figs. 10–12, pl. 6, figs. 1, 2. (Plate 3, Fig. 7)

Thalassiosira zabelinae Jousé, 1961, p. 66, pl. 2, figs. 1–7; Koizumi, 1973, p. 834, pl. 8, figs. 10–12.

Thalassiosira sp. 1 Barron, 1980, p. 673, pl. 5, figs. 6, 7; Barron, 1981, p. 530, pl. 5, fig. 5. (Plate 4, Figs. 1–3)

Thalassiothrix frauenfeldii Grunow: Hustedt, 1932, p. 247, fig. 727; Hasle and Mendiola, 1967, p. 113, fig. 21a–c.

Thalassiothrix longissima (Cleve) Cleve and Grunow: Hustedt, 1932, p. 247, fig. 726; Hasle and Mendiola, 1967, p. 114, fig. 20; Sancetta, 1982, pl. 6, figs. 3, 4.

Thalassithrix vanhoeffenii Heiden: Simonsen, 1974, p. 38, pl. 25, figs. 1–3.

Trachyneis aspera (Ehrenberg) Cleve: Hendey, 1964, p. 236, pl. 29, fig. 13.

Triceratium alternans Bailey: Hustedt, 1930b, p. 825, fig. 488.

Triceratium cinnamomeum Greville: Kolbe, 1954, p. 47, pl. 2, fig. 18; Schrader, 1974b, pl. 20, figs. 10, 11.

Triceratium reticulum Ehrenberg: Hustedt, 1930b, p. 823, figs. 485, 486.

REFERENCES

Akiba, F., 1979. The morphologies of *Denticula dimorpha* and its related species and the Neogene biostratigraphy of Japan. *Bull. Tech. Lab., JAPEX.*, 22:9–50.

________, 1982. Taxonomy and biostratigraphic significance of a new diatom, *Thalassionema schraderi. Bacillaria*, 5:43–61.

________, 1983. Revised Neogene diatom zonation in middle-high latitude North Pacific. *Mar. Sci.*, 15:717–724.

Andrews, G. W., 1976. Miocene marine diatoms from the Choptank Formation, Calvert County, Maryland. *Geol. Surv. Prof. Pap. (U.S.)*, 910:1–26.

________, 1980a. Neogene diatoms from Petersburg, Virginia. *Micropaleontology*, 26:17–48.

________, 1980b. Revision of the diatom genus *Delphineis* and morphology of *Delphineis surirella* (Ehrenberg) G. W. Andrews, n. comb. *6th Diatom Symposium*, pp. 81–90.

Barron, J. A., 1980. Lower Miocene to Quaternary diatom biostratigraphy of Leg 57, off northeastern Japan, Deep Sea Drilling Project. *In* Scientific Party, *Init. Repts. DSDP*, 56, 57, Pt. 2: Washington (U.S. Govt. Printing Office), 641–685.

________, 1981. Late Cenozoic diatom biostratigraphy and paleoceanography of the middle-latitude eastern North Pacific, Deep Sea Drilling Project Leg 63. *In* Yeats, R. S., Haq, B. U., et al., *Init. Repts. DSDP*, 63: Washington (U.S. Govt. Printing Office), 507–538.

Barron, J. A., and Keller, G., 1983. Paleotemperature oscillations in the Middle and Late Miocene of the northeastern Pacific. *Micropaleontology*, 29:150–181.

Berggren, W. A., Kent, D. V., and Flynn, J. J., in press. Paleogene geochronology and chronostratigraphy. *In* Snelling, N. J. (Ed.), *Geochronology and the Geological Record*, Spec. Publ. Geol. Soc. London.

Burckle, L. H., 1971. Correlation of late Cenozoic marine sections in Japan and the equatorial Pacific. *Trans. Proc. Palaeont. Soc. Japan, N. S.*, 82:117–128.

________, 1972. Late Cenozoic planktonic diatom zones from the eastern equatorial Pacific. *Nova Hedwegia*, 39:217–246.

________, 1977. Pliocene and Pleistocene diatom datum levels from the equatorial Pacific. *Quat. Res.*, 7:330–340.

________, 1978. Early Miocene to Pliocene diatom datum levels from the equatorial Pacific. *Geol. Soc. Indonesia Proc., IGCP Project 114 Meetings, Indonesia, 1977. Geol. Res. Devel. Cent., Spec. Publ.*, 1:25–44.

Burckle, L. H., Dodd, J. R., and Stanton, R. J., Jr., 1980. Diatom biostratigraphy and its relationship to paleomagnetic stratigraphy and molluscan distribution in the Neogene Centerville section, California. *J. Paleontol.*, 54:664–674.

Burckle, L. H., Hammond, S. R., and Seyb, S. M., 1978. A stratigraphically important new diatom from the Pleistocene of the North Pacific. *Pacific*, 32:209–214.

Burckle, L. H., and Opdyke, N. D., 1977. Late Neogene diatom correlations in the circum-Pacific. *In* Saito, T., and Ujiiè, H. (Eds.), *Proceedings of the First International Congress on Pacific Neogene Stratigraphy, Tokyo, 1976:* Tokyo (Kaiyo Shuppan), pp. 255–284.

Burckle, L. H., and Trainer, J., 1979. Middle and late Pliocene diatom datum levels from the central Pacific. *Micropaleontology*, 25: 281–293.

Cleve-Euler, A., 1951–1955. Die Diatomeen von Schweden und Finnland. *K. Sven. Vetenskapsakad. Handl.* (Bibliotheca Phycologica). 5 vols: Bd. 2, no. 1:1–163 (1951); Bd. 3, no. 3:1–153 (1952); Bd. 4, no. 1:1–158 (1953); Bd. 4, no. 5:1–255 (1953); Bd. 5, no. 4:1–232 (1955).

Donahue, J. G., 1970. Pleistocene diatoms as climatic indicators in North Pacific sediments. *In* Hays, L. D. (Ed.), *Geological Investigation of the North Pacific*. Geol. Soc. Amer., Mem., 126:121–138.

Fryxell, G. A., and Hasle, G. R., 1972. *Thalassiosira eccentrica* (Ehrenberg) Cleve, *T. symmetrica* sp. nov., and some related centric diatoms. *J. Phycol.*, 8:297–317.

Greville, R. K., 1860. A monograph of the genus *Asterolampra* including *Asteromphalus* and *Spatangidium*. *Trans. Microsc. Soc. London. N. S.*, 8:102–124.

Hanna, G. D., 1930. Review of the genus *Rouxia*. *J. Paleontol.*, 4: 179–188.

________, 1970. Fossil diatoms from the Pribilof Island, Bering Sea, Alaska. *Proc. Calif. Acad. Sci. Ser. 4*, 37:167–234.

Hanna, G. D., and Grant, W. M., 1926. Expedition to the Revillagigedo Islands, Mexico, in 1925, II. *Proc. Calif. Acad. Sci. Ser. 4*, 15: 115–193.

Harper, H. E., Jr., 1977. Diatom biostratigraphy of the Miocene-Pliocene boundary in marine strata of the Circum-North Pacific [Ph.D. dissert.]. Harvard University, Cambridge, Massachusetts.

________, 1980. Diatom biostratigraphy of Sites 434, 435, and 436, northwestern Pacific, Leg 56, Deep Sea Drilling Project. *In* Scientific Party, *Init. Repts. DSDP*, 56, 57, Pt. 2: Washington (U.S. Govt. Printing Office), 633–640.

Hasle, G. R., 1960. Phytoplankton and ciliate species from the tropical Pacific. *Skr. Nor. Vidensk. Akad. Kl. 1: Mat. Naturvidensk Kl.*, 2:1–50.

________, 1965. *Nitzschia* and *Fragilariopsis* species studied in the light and electron microscopes; III. The genus *Fragilariopsis*. *Skr. Nor. Vidensk. Akad. Kl. 1 Mat. Naturvidensk. Kl., n. ser.*, 21: 1–46.

________, 1968. The valve processes of the centric diatom genus *Thalassiosira*. *Nytt Magasin Botanikk.*, 15:193–201.

________, 1972. *Fragilariopsis* Hustedt as a section of the genus *Nitzschia* Hassall. *Nova Hedwigia*, 39:111–120.

Hasle, G. R., and Fryxell, G. A., 1977. The genus *Thalassiosira;* some species with a linear areola array. *Nova Hedwigia*, 54:15–66.

Hasle, G. R., and Mendiola, de B.R.E., 1967. The fine structure of some *Thalassionema* and *Thalassiothrix* species. *Phycologia*, 6: 107–125.

Heiden, H., and Kolbe, R. W., 1928. Die Marinen Diatomeen der Deutschen Sudpolar-Expedition, 1901–1903. *Dtsch. Sudpolar-Exped. 1901–1903: Berlin (Botanik)*, 8:449–745.

Hendey, N. I., 1958: Marine diatoms from some west African ports. *J. R. Microsc. Soc.*, 77:28–85.

________, 1964. An Introductory Account of the Smaller Algae of British Coastal Waters. Part V: Bacillariophyceae (Diatoms). London (Her Majesty's Stationery Office).

Hornibrook, N. deB., and Edwards, A. R., 1970. Integrated planktonic foraminiferal and calcareous nannoplankton datum levels in the New Zealand Cenozoic. *In* Farinacci, A. (Ed.), *Proc. Planktonic Conf., 2nd, Roma 1970*, pp. 649–657.

Hustedt, F., 1921. *In* Schmidt, A., *Atlas der Diatomaceenkunde*. Continued by Schmidt, M., Fricke, F., Müller, O., Heiden, H., and Hustedt, F. in 1874–1959. Leipzig (R. Reisland).

________, 1930a. Bacillariophyta (Diatomeae), Heft 10. *In* Pascher, A., (Ed.), *Die Süsswasser-Flora Mitteleuropas*. Jena (Gustav Fischer).

________, 1930b–1966. Die Kieselalgen Deutschlands, Österreichs und der Schweiz. *In* Rabenhorst, L. (Ed.), *Kryptogamen-Flora von Deutschland, Osterreichs der Schweiz*. Leipzig (Akad. Verlag), 7: Pt. 1:1–920 (1930b); Pt. 2, No. 1:1–175 (1931); No. 2:177–320 (1932); No. 3–4:321–576 (1933); No. 5:577–736 (1937); No. 6: 737–845 (1959); Pt, 3, No. 1:1–160 (1961); No. 2:161–348 (1962); No. 3:349–556 (1964), No. 4:557–816 (1966).

________, 1958. Diatomeen aus der Antarktis und dem Südatlantik. *Dtsch. Antarktische Exped. 1938–1939, Wiss. Exped. Hamburg*, 2:103–191.

Jousé, A. P., 1961. Miocene and Pliocene marine diatoms from the Far East. *Bot. Mater. Spor. Rast., Bot. Inst., Akad. Nauk SSSR*, 16:59–70.

________, 1968. New species of diatoms in bottom sediments of the Pacific and the Sea of Okhotsk. *Nov. Systemat. Plant. non Vascular 1968, Akad. Nauk SSSR*, 3:12–21.

________, 1976. A review of the genus *Bogorovia* Jousé (Bacillariophyta). *Bot. Mag., Akad. Nauk SSSR.*, 61:1232–1234.

Kanaya, T., 1959. Miocene diatom assemblages from the Onnagawa Formation and their distribution in the correlative formations in northeast Japan. *Sci. Rep. Tohoku Univ., Ser. 2*, 30:1–130.

________, 1971. Some aspects of pre-Quaternary diatoms in the oceans. *In* Funnell, B. M., and Riedel, W. R. (Eds.), *The Micropaleontology of Oceans:* Cambridge (Cambridge Univ. Press), pp. 545–565.

Keller, G., and Barron, J. A., 1981. Integrated planktonic foraminiferal and diatom biochronology for the northeast Pacific and the Monterey Formation. *In* Garrison, R. T., and Douglas, R. G. (Eds.), *The Monterey Formation and Related Siliceous Rocks of California*. Soc. Econ. Paleontol. Mineral., pp. 43–54.

________, 1983. Paleoceanographic implications of Miocene deep-sea hiatuses. *Geol. Soc. Am. Bull.*, 94:590–613.

Keller, G., Barron, J. A., and Burckle. L. H., 1982. North Pacific late Miocene correlations using microfossils, stable isotopes, percent $CaCO_3$, and magnetostratigraphy. *Mar. Micropaleontol.*, 7:327–357.

Koizumi, I., 1968. Tertiary diatom flora of Oga Peninsula, Akita Prefecture, northeast Japan. *Sci. Rep. Tohoku Univ., Ser 2*, 40: 171–225.

________, 1972. Marine diatom flora of the Pliocene Tatsunokuchi Formation in Fukushima Prefecture, northeast Japan. *Trans. Proc. Paleont. Soc. Japan, N. S.*, 86:340–359.

________, 1973. The late Cenozoic diatoms of Sites 183–193, Leg 19, Deep Sea Drilling Project. *In* Creager, J. S., Scholl, D. W., et al., *Init. Repts. DSDP*, 19: Washington (U.S. Govt. Printing Office), 805–856.

________, 1975a. Neogene diatoms from the western margin of the Pacific Ocean, Leg 31, Deep Sea Drilling Project. *In* Karig, D. E., Ingle, J. C., Jr., et al., *Init. Repts. DSDP*, 31: Washington (U.S. Govt. Printing Office), 779–820.

________, 1975b. Neogene diatoms from the northwestern Pacific Ocean, Deep Sea Drilling Project. *In* Larson, R. L., Moberly, R., et al., *Init. Repts. DSDP*, 32: Washington (U.S. Govt. Printing Office), 865–890.

________, 1977. Diatom biostratigraphy in the North Pacific region. *In* Saito, T., and Ujiiê, H. (Eds.), *Proc. First International Congress on Pacific Neogene Stratigraphy, Tokyo, 1976:* Tokyo (Kaiyo Shuppan), pp. 235–253.

________, 1980. Neogene diatoms from the Emperor Seamount Chain, Leg 55, Deep Sea Drilling Project. *In* Jackson, E. D., Koizumi, I., et al., *Init. Repts. DSDP*, 55: Washington (U.S. Govt. Printing Office), 387–408.

________, 1981. The hiatus in the North Pacific ocean-floor based on diatom biostratigraphy. *Mar. Sci.*, 13:95–100.

________, 1983. Sedimentary environments of Neogene diatomaceous sediments, west coast of Japan. *In* Iijima, A., Hein, J. R., and Siever, R. (Eds.), *Siliceous Deposits in the Pacific Region:* Amsterdam (Elsevier), pp. 347–360.

Koizumi, I., and Burckle, L. H., 1984. Evaluation of diatom datum planes of the Pacific Neogene. *In* Ikebe, N., and Tsuchi, R. (Eds.), *Pacific Neogene Datum Planes—Contributions to Biostratigraphy and Chronology:* Tokyo (Univ. Tokyo Press), pp. 41–46.

Koizumi, I., and Kanaya, T., 1976. Late Cenozoic marine diatom sequence from the Choshi district, Pacific coast, central Japan. *In* Takayanagi, Y., and Saito, T. (Eds.), *Progress in Micropaleontology:* New York (Micropaleontology Press), pp. 144–159.

Kolbe, R. W., 1954. Diatoms from equatorial Pacific cores. *Rep. Swed. Deep Sea Exped., 1947–1948*, 6:1–49.

________, 1955. Diatoms from equatorial Atlantic cores. *Rep. Swed. Deep Sea Exped., 1947–1948*, 7:151–184.

Maruyama, T., 1982. Miocene diatom biostratigraphy of onshore sequences on the Pacific side of northeast Japan, with reference to DSDP Hole 438A [Ph.D. dissert.]. Tohoku University, Japan.

Mukhina, V. V., 1965. New species of diatoms from the bottom sediments of the equatorial region of the Pacific. *Nov. Systemat. Plant. non Vascular 1965, Akad. Nauk SSSR*, 11:22–25.

Rattray, J., 1890. A revision of the genus *Actinocyclus* Ehrenberg. *J. Quekett Microsc. Club*, 4:137–212.

Sancetta, C., 1982. Distribution of diatom species in surface sediments of the Bering and Okhotsk seas. *Micropaleontology*, 28: 221–257.

Schrader, H. J., 1973. Cenozoic diatoms from the northeast Pacific, Leg 18. *In* Kulm, L. D., von Huene, R., et al., *Init. Repts. DSDP*, 18: Washington (U.S. Govt. Printing Office), 673–798.

———, 1974a. Proposed for a standardized method of cleaning diatom-bearing deep-sea and land-exposed marine sediments *Nova Hedwegia*, 45:403–409.

———, 1974b. Cenozoic marine planktonic diatom stratigraphy of the tropical Indian Ocean. *In* Fisher, R. L., Bunce, E. T., et al., *Init. Repts. DSDP*, 24: Washington (U.S. Govt. Printing Office), 887–968.

———, 1978. Quaternary through Neogene history of the Black Sea, deduced from the paleoecology of diatoms, silicoflagellates, ebridians, and chrysomonads. *In* Ross, D. A., Neprochnov, Y. P., et al., *Init. Repts. DSDP*, 42, Pt. 2: Washington (U.S. Govt. Printing Office), 789–902.

Sheshukova-Poretzkaya, V. S., 1962. New and rare diatoms from formations of Sakhalin. *Leningrad Gos. Univ., Vest. no. 313, Biol. Inst. Ser. Biol., Nauk Vup.*, 49:203–211.

———, 1964. New and rare marine diatoms of the Neogene of Sakhalin and Kamtchatka. *Nov. Systemat. Plant. non Vascular 1964, Akad Nauk SSSR*, 10:69–77.

Simonsen, R., 1974. The diatom plankton of the Indian Ocean expedition of R/V "Meteor" 1964-1965. *"Meteor" Forschungsergeb., Reihe D*, 19:1–66.

———, 1979. The diatom system: Ideas on phylogeny. *Bacillaria*, 2:9–71.

Thorrington-Smith, M., 1970. Some new and little-known planktonic diatoms from the west Indian Ocean. *Nova Hedwigia*, 31:815–835.

Ujiiè, H., Saito, T., Kent, D. V., Thompson, P. R., Okada, H., Klein, G. deV., Koizumi, I., Harper, H. E., Jr., and Sato, T., 1977. Biostratigraphy, paleomagnetism and sedimentology of late Cenozoic sediments in northwestern Hokkaido, Japan. *Bull. Natl. Sci. Mus., Ser. C: Geol. (Tokyo)*, 3:49–102.

Van Landingham, S. L., 1967. Paleoecology and microfloristics of Miocene diatomites from the Otis Basin–Juntura region of Harney and Malheur Counties, Oregon. *Nova Hedwigia*, 26:1–77.

Date of Initial Receipt: 13 December 1983
Date of Acceptance: 26 March 1984

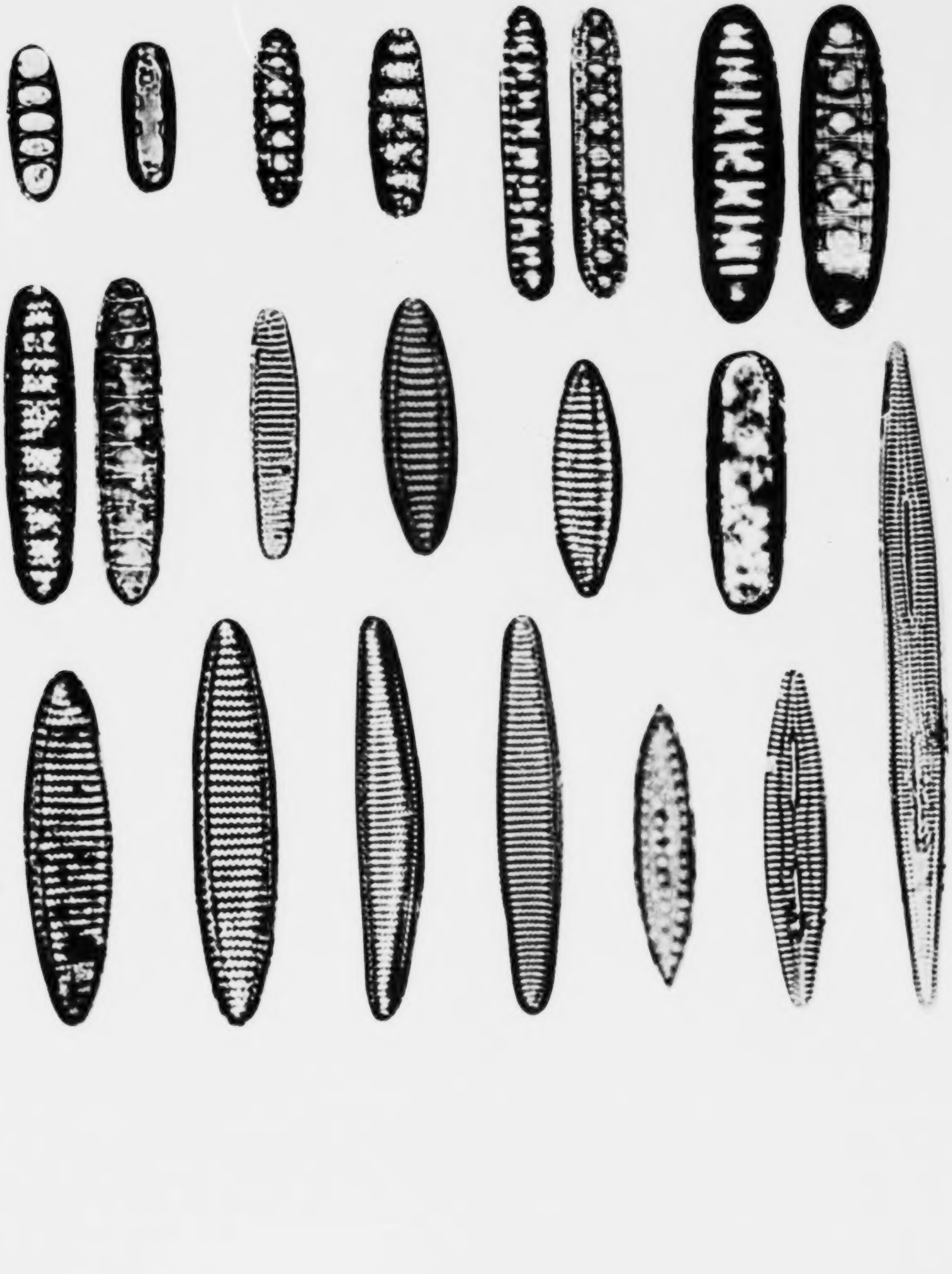

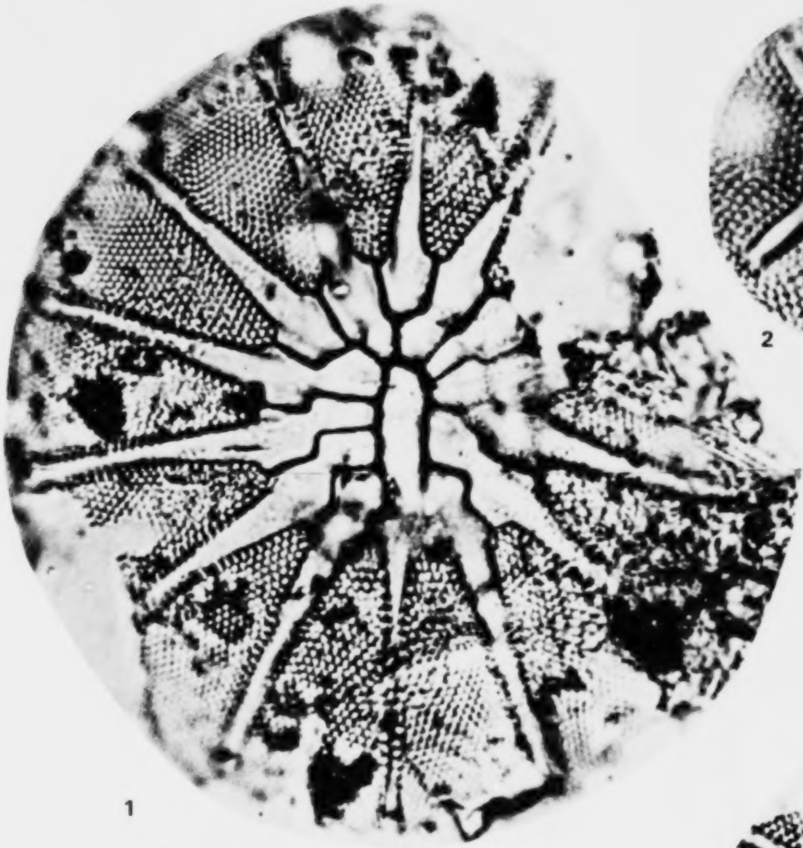
1

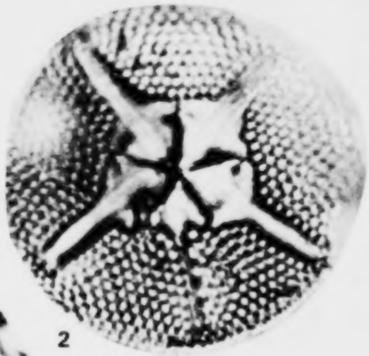
2

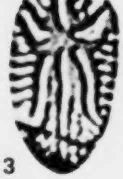
3

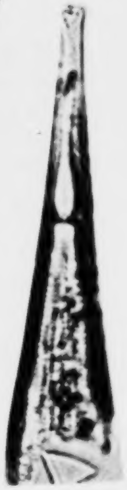
4

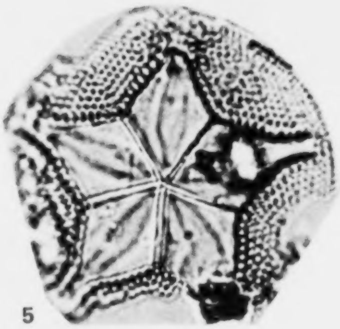
5

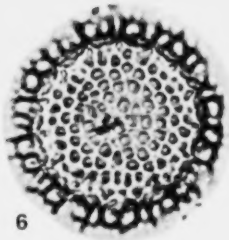
6

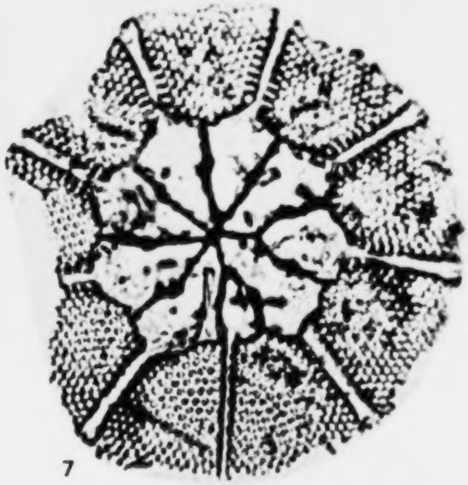
7

Plate 2. (Magnifications are × 1500.) **1.** *Asteromphalus heptactis* (Brebisson) Ralfs. Sample 579A-3-5, 116–117 cm. Diameter 82 μm. **2.** *Asteromphalus darwinii* Ehrenberg. Sample 581-4-6, 98–99 cm. Diameter 35 μm. **3.** *Asteromphalus petterssonii* (Kolbe) Thorrington-Smith. Sample 579A-9-5, 13–131 cm. Length 22 μm. **4.** *Rhizosolenia bergonii* Peragallo. Sample 580-7-1, 8–9 cm. Broken specimen. **5.** *Asterolampra acutiloba* Forti. Sample 581-3-6, 75–76 cm. Diameter 33 μm. **6.** *Thalassiosira nidulus* (Tempere and Brun) Jousé. Sample 580-5-5, 40–41 cm. Diameter 21 μm. **7.** *Asteromphalus brookei* Bailey. Sample 581-8-3, 110–111 cm. Diameter 47 μm.

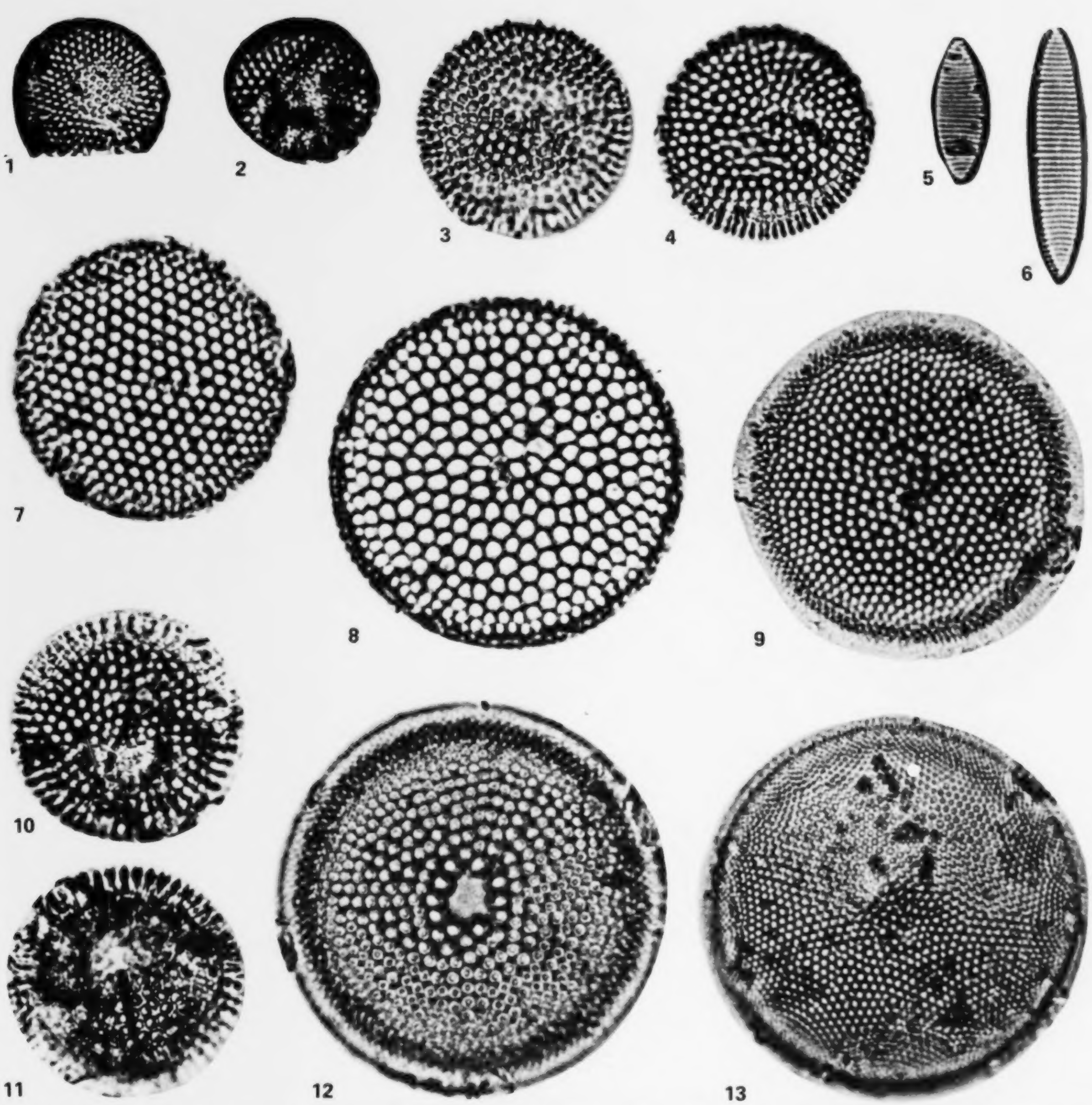

Plate 3. (Magnifications are ×1500.) **1.** *Thalassiosira miocenica* Schrader. Sample 581-4,CC. Diameter 16 μm. **2.** *Thalassiosira miocenica* Schrader. Sample 581-3-6, 75–76 cm. Diameter 17 μm. **3–4.** *Coscinodiscus plicatus* Grunow. Sample 581-7-3, 100–101 cm. Diameter 23 μm. **5–6.** *Nitzschia grunowii* Hasle. (5) Sample 581-4,CC. Length 16 μm. (6) Sample 580-3,CC. Length 28 μm. **7.** *Thalassiosira trifulta* Fryxell. Sample 580-5-1, 40–41 cm. Diameter 30 μm. **8.** *Coscinodiscus nodulifer* Schmidt. Sample 580-5-4, 40–41 cm. Diameter 38 μm. **9.** *Actinocyclus curvatulus* Janisch. Sample 580-9-2, 99–100 cm. Diameter 38 μm. **10–11.** *Coscinodiscus yabei* Kanaya. Sample 581-8-1, 110–111 cm. Diameter 25 μm. **12.** *Actinocyclus oculatus* Jousé. Sample 580-10-1, 25–26 cm. Diameter 42 μm. **13.** *Thalassiosira plicata* Schrader. Sample 580-10-1, 25–26 cm. Diameter 40 μm.

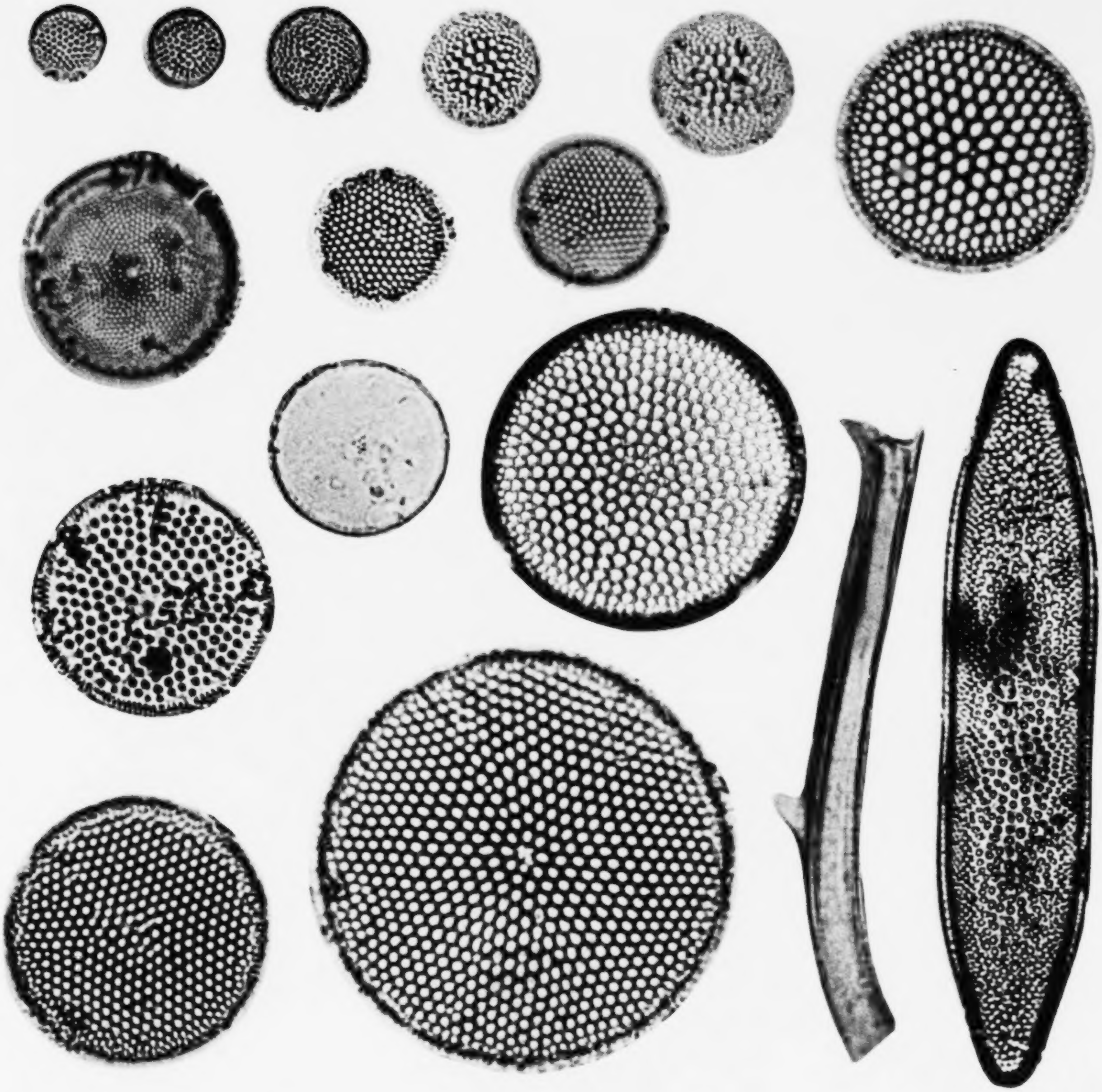

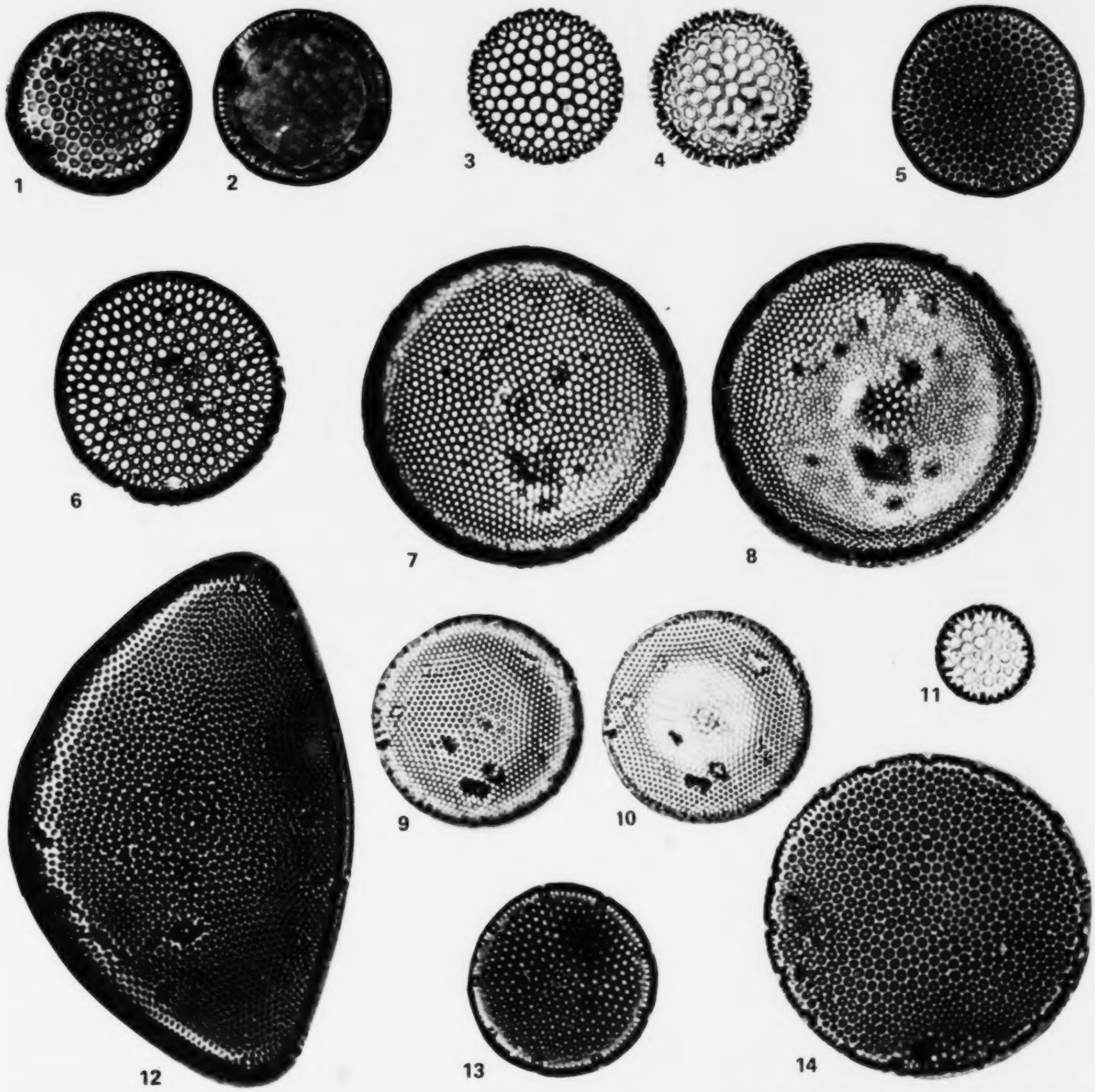

Plate 5. (Magnifications are × 1500.) **1–4.** *Thalassiosira oestrupii* (Ostenfeld) Proshkina-Lavrenko. (1–2) Sample 578-8-2, 118–119cm. Diameter 20 μm. (3–4) Sample 578-7-1, 121–122 cm. Diameter 17 μm. **5–6.** *Roperia tesselata* (Roper) Grunow. (5) Sample 578-8-2, 118–119 cm. Diameter 21 μm. (6) Sample 578-5-1, 117–118 cm. Diameter 26 μm. **7–8.** *Thalassiosira plicata* Schrader. Sample 578-6-6, 121–122 cm. Diameter 34 μm. **9–10.** *Thalassiosira symbolophora* Schrader. Sample 578-3-3, 96–97 cm. Diameter 24 μm. **11.** *Thalassiosira oestrupii* (Ostenfeld) Proshkina-Lavrenko. Sample 578-3-3, 96–97 cm. Diameter 11 μm. **12.** *Hemidiscus cuneiformis* Wallich. Sample 577-3,CC. Length 56 μm. **13–14.** *Coscinodiscus tabularis* var. *egregius* (Rattray) Hustedt. (13) Sample 578-8-2, 118–119 cm. Diameter 21 μm. (14) Sample 577-1,CC. Diameter 35 μm.

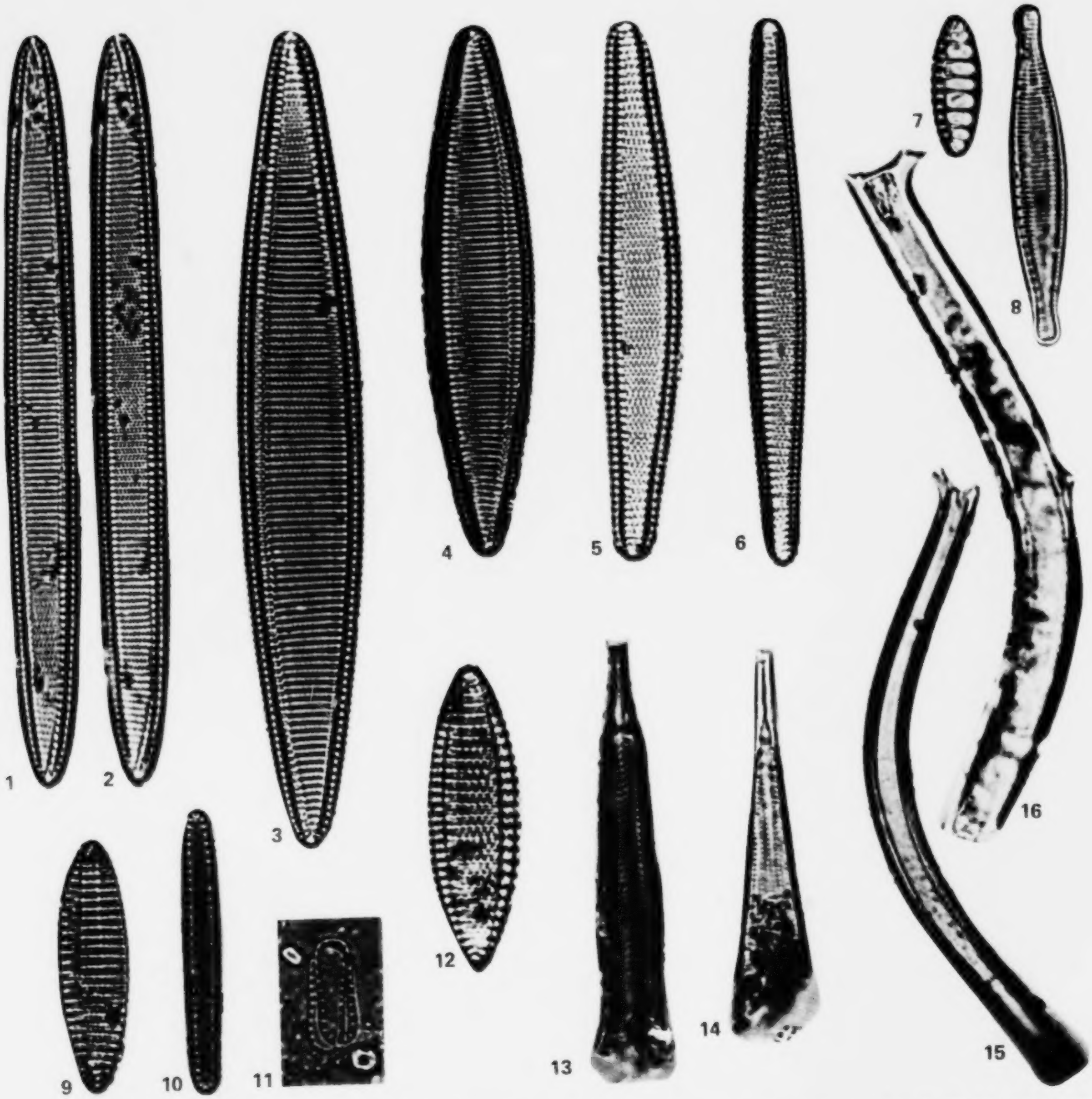

Plate 6. (Magnifications are × 1500, except for Figs. 1, 2, and 15 which are × 1050.) **1–2.** *Nitzschia marina* Grunow. Sample 578-2-5, 115–116 cm. Length 116 μm. **3–4.** *Nitzschia reinholdii* Kanaya and Koizumi. (3) Sample 578-4-5, 95–96 cm. Length 89 μm. (4) Sample 578-6-3, 109–110 cm. Length 58 μm. **5.** *Pseudoeunotia doliolus* (Wallich) Grunow. Sample 578-2,CC. Length 58 μm. **6.** *Nitzschia fossilis* (Frenguelli) Kanaya. Sample 578-6-7, 43–44 cm. Length 59 μm. **7.** *Denticulopsis kamtschatica* (Zabelina) Simonsen. Sample 578-8-1, 118–119 cm. Length 15 μm. **8.** *Nitzschia interruptestriata* Simonsen. Sample 578-2-2, 115–116 cm. Length 37 μm. **9.** *Nitzschia miocenica* Burckle. Sample 578-13-3, 135–136 cm. Length 27 μm. **10.** *Thalassionema nitzschioides* Grunow. Sample 578-11,CC. Length 31 μm. **11.** *Thalassionema nitzschioides* var. *parva* Heiden and Kolbe. Sample 578-1,CC. Length 12 μm. **12.** *Nitzschia jouseae* Burckle. Sample 578-10,CC. Length 33 μm. **13.** *Rhizosolenia praebergonii* Mukhina. Sample 578-9-2, 118–119 cm. Length 45 μm. **14.** *Rhizosolenia bergonii* Peragallo. Sample 578-2,CC. Length 40 μm. **15.** *Rhizosolenia curvirostris* Jousé. Sample 578-5-1, 117–118 cm. Length 75 μm. **16.** *Rhizosolenia barboi* Brun. Sample 578-5-1, 117–118 cm. Length 91 μm.

10. CAMPANIAN TO PLEISTOCENE CALCAREOUS NANNOFOSSIL STRATIGRAPHY FROM THE NORTHWEST PACIFIC OCEAN, DEEP SEA DRILLING PROJECT LEG 86[1]

Simonetta Monechi, Geological Research Division, Scripps Institution of Oceanography[2]

ABSTRACT

During Leg 86, Sites 576–581 were drilled in the northwest Pacific Ocean. Only Sites 576, 577, and 580 contain calcareous nannofossils. The cored stratigraphic sequences range from lower Campanian to Pleistocene, although some of the stratigraphic sequences are discontinuous because of hiatuses or poor core recovery.

Site 576 was drilled at the eastern flank of the Shatsky Rise, and recovered a common and moderately well preserved calcareous nannofossil assemblage of lower Maestrichtian to lower Campanian age. Site 577 was drilled on the southwest flank of the Shatsky Rise. Three holes were hydraulically piston cored. Holes 577 and 577A both recovered a very good late Cenozoic to Late Cretaceous sediment section with a major hiatus from the middle Miocene to the middle Eocene. An undisturbed and extended Cretaceous/Tertiary boundary sequence was recovered. An additional core containing the Cretaceous/Tertiary boundary was recovered from Hole 577B. Coccoliths are generally abundant and diversified. Preservation is moderate to poor. The Cretaceous/Tertiary boundary is located in all three holes at a sub-bottom depth of about 109.6 m.

A detailed investigation of the calcareous nannofossil assemblage was conducted on samples from Site 577, and particular attention was given to the flora at the Cretaceous/Tertiary boundary. Few selected early Tertiary species have been investigated both by light and scanning electron microscope.

At Site 580 only one sample (Core Catcher 3) contains calcareous nannofossils. They are poorly preserved and indicate a probable Pliocene age.

INTRODUCTION

Leg 86 of the Deep Sea Drilling Project (DSDP) drilled six sites in the Pacific (Fig. 1). Only the sediments recovered at Sites 576, 577, and 580 contain calcareous nannofossils. The stratigraphic sequence at these sites ranges from lower Campanian to Pleistocene with some discontinuities. The light microscope (LM) was used to study the nannofossils.

A few selected samples were studied by scanning electron microscope (SEM) for taxonomic and illustrative purposes; special attention was given to the early Tertiary species. A few Paleocene species were investigated using Moskhovitz's (1974) technique, which allows the study of the same specimen in both LM and SEM. Zonal assignments of the cores from Sites 576, 577, and 580 are summarized in Table 1 for the Cretaceous and Table 2 for the Tertiary. The full generic and specific names of all taxa considered in this report and reference to the authors are given in the Appendix.

Abundance, preservation, and stratigraphic distribution of calcareous nannofossils are presented in Tables 3 to 10. Preservation is described as etching and overgrowth following the scheme developed by Roth and Thierstein (1972).

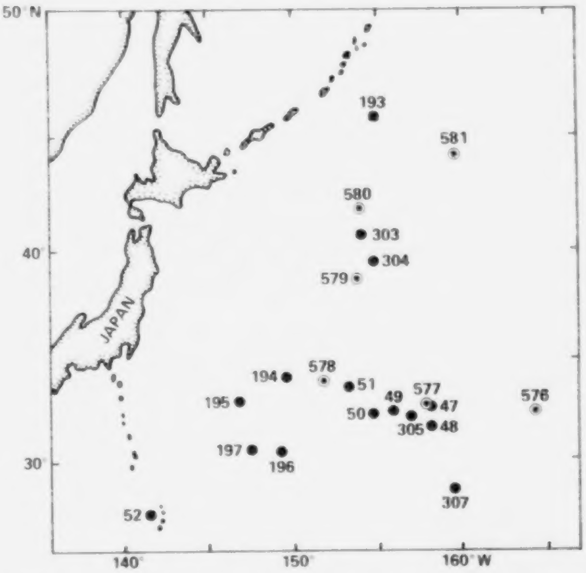

Figure 1. Location of DSDP sites in the Northwest Pacific (◉ = Leg 86, • = other legs).

CALCAREOUS NANNOFOSSIL ZONES

Cretaceous

The zonation used for the Cretaceous sequences recovered on Leg 86 includes zones and ranges given by Bukry and Bramlette (1970), Martini (1976), Thierstein (1976), Verbeek (1977), and Perch-Nielsen (1979). Table 1 shows the zones used and the biostratigraphic distribution of the cores recovered. The definition of the zones is discussed below from the bottom of the recovered sections to the top.

Aspidolithus parcus Zone, Verbeek, 1977

Definition. Interval from the first occurrence (FO) of *A. parcus* to the FO of *Ceratolithoides aculeus*.

---

[1] Heath, G. R., Burckle, L. H., et al., *Init. Repts. DSDP*, 86: Washington (U.S. Govt. Printing Office).

[2] Address: Dipartimento di Scienze della Terra, Università di Firenze, Via G. La Pira n.4, 50121 Firenze, Italy.

Table 1. Calcareous nannofossil zonation of the Cretaceous from Sites 576 and 577.

Age	Zone	Hole 576		Hole 576B		Hole 577		Hole 577A		Hole 577B	
		Sub-bottom depth (m)	Core-Section (level in cm)	Sub-bottom depth (m)	Core-Section (level in cm)	Sub-bottom depth (m)	Core-Section (level in cm)	Sub-bottom depth (m)	Core-Section (level in cm)	Sub-bottom depth (m)	Core-Section (level in cm)
Maestrichtian	*Micula prinsii*	—		—		109.20-110.82	12-5, 130/ 12-6, 142	109.65-111.80	12-4, 75/ 12-5, 146	109.66-111.60	1-4, 76/ 1-5, 120
	Micula murus					111.10-118.80	12-7, 20/ 13,CC	112.107-120.34	12-6, 26/ 13-5, 44	112.00-113.90	1-6, 10/ 1,CC
	Lithraphidites quadratus							120.96-123.4	13-5, 106/ 13,CC		
	Quadrum trifidum	61.3–69.2	8-1, 136-8,CC	51.70-62.05	6-4, 100-7-5, 35						
Campanian	*Quadrum gothicum*	—		63.9–67.47	7-6, 73-8-2, 77						
	Ceratolithoides aculeus			68.75	8-3, 55						
	Aspidolithus parcus			69.15-74.8	8-3, 90-9,CC						

Note: Where a zone or subzone is represented in samples from two or more core sections the highest/lowest occurrences are given. — means barren of calcareous nannoplankton.

Stratigraphic position. Lower Campanian.

Remarks. The *A. parcus* Zone was found only at Hole 576B and it is the oldest Cretaceous zone recovered. The base of this zone was not reached. Rare species of *Quadrum gothicum* were found in the upper part of this zone; they have been considered here as contaminants.

Ceratolithoides aculeus Zone, Čepek and Hay, 1969a,b; emend. Verbeek, 1977

Definition. Interval from the FO of *C. aculeus* to the FO of *Q. gothicum.*

Stratigraphic position. Lower Campanian.

Remarks. The *C. aculeus* Zone was found only in Hole 576B.

Quadrum gothicum Zone, Martini, 1976

Definition. Interval from the FO of *Q. gothicum* to the FO of *Q. trifidum.*

Stratigraphic position. Middle Campanian.

Remarks. The *Q. gothicum* Zone occurs only in Hole 576B.

Quadrum trifidum Zone, Verbeek, 1977

Definition. Interval from the FO to the last occurrence (LO) of *Q. trifidum.*

Stratigraphic position. Upper Campanian to lower Maestrichtian.

Remarks. This zone was found in both holes at Site 576; in Hole 576 it is the oldest Cretaceous zone recovered.

Lithraphidites quadratus Zone, Bukry and Bramlette, 1970

Definition. Interval from the FO of *L. quadratus* to the FO of *Micula murus.*

Stratigraphic position. Middle Maestrichtian.

Remarks. This zone was found only in Hole 577A and the base was not reached. This zone represents the oldest Cretaceous sediments recovered at Site 577.

Micula murus Zone, Bukry and Bramlette, 1970; emend. Perch-Nielsen, 1981

Definition. Interval from the FO of *M. murus* to the FO of *M. prinsii.*

Stratigraphic position. Upper Maestrichtian.

Remarks. This zone was found in all three holes (577, 577A, 577B) at Site 577. It is known from the literature that *M. murus* is probably restricted to tropical regions, while *Nephrolithus frequens* is common in the boreal regions. In our sediments *N. frequens* was not found, but *M. murus* is present.

Micula prinsii Zone, Perch-Nielsen, 1981

Definition. Interval from the FO of *M. prinsii* to the FO (or increased frequency) of *Thoracosphaera* sp.

Stratigraphic position. Very top of the Maestrichtian.

Remarks. *M. prinsii* was found in all three holes recovered at Site 577. It is usually very rare and not well preserved.

Tertiary and Quaternary

The low latitude coccolith zonation of Bukry (1973, 1975) and Okada and Bukry (1980) was used for the Tertiary and Quaternary deep-sea sediments recovered on Leg 86 (Table 2). This zonation is well suited to the biostratigraphic subdivision of the recovered sequences.

A few remarks are made here only for the early Paleocene Zones CP1, CP2, and CP3.

Zygodiscus sigmoides Zone (CP1)

This zone was defined as the interval from the LO of *Micula murus* and other Cretaceous species to the FO of *Chiasmolithus danicus.* It is not possible in a continuous and expanded Cretaceous/Tertiary boundary to identify precisely the lower limit of the *Zygodiscus sigmoides* Zone, because it is impossible to distinguish Cretaceous coccoliths from those nonreworked. Also Cretaceous coccoliths disappear gradually in many lower Tertiary sequences. The criterium used on Leg 86 to define the Cretaceous/Tertiary boundary was the rapid increase in frequency of *Thoracosphaera*, a calcareous dinoflagellate. This increase occurs sharply in the early Tertiary, together with the first occurrence of small *Biscutum* cf. *B. romeinii*. In some sequences the first occurrence of *B. sparsus* was used, but this datum was rare and discontinuous in the recovered sediments.

The upper boundary of CP1 is defined by the FO of *C. danicus*. The FO of *C. danicus* is not easily recognized since intermediate forms between *C. edwardsii* and *C. danicus* occur. Indeed, *C. danicus* seems to evolve gradually from *C. edwardsii*.

Chiasmolithus danicus Zone (CP2) and *Ellipsolithus macellus* Zone (CP3)

Following the definition of Romein (1979), the lower boundary of the *C. danicus* Zone is defined by the FO of *C. danicus* s.s.

The upper boundary of CP2 is defined by the FO of *E. macellus*. This species is rare and discontinuously present in this zone, it becomes common only in the overlying *Fasciculithus tympaniformis* Zone (CP4).

The first occurrence of *Sphenolithus* occurs in Hole 577A at the top of the *C. danicus* Zone (CP2); the FO of *Fasciculithus* occurs slightly higher in the *E. macellus* Zone.

SITE SUMMARIES

Only Sites 576, 577, and 580, which contain calcareous nannofossils, are discussed here. Tables 1 and 2 show the nannofossil zonations found at these sites. Tables 3 to 10 are range charts showing the distribution of calcareous nannofossil species that are recognized in the samples studied. The first and last occurrence of marker species in the above-mentioned tables are underlined, so that it is easier to recognize the markers and the boundaries of the zones.

The reliability of first and last occurrences of the species recorded varies, since it has only been possible to pick up the exact ranges of the markers and some of the most important species in the limited time available.

Site 576 (Holes 576, 576A, and 576B)

Site 576 is located on the east flank of the Shatsky Rise at a water depth of 6227 m (Fig. 1). Three holes were drilled: 576, 576A, and 576B. One complete hole (Hole 576A) was left unopened for shore-based geotechnical studies (Geotechnical Consortium, this volume).

The lithostratigraphic succession observed in Holes 576 and 576B consists of a pelagic clay unit (barren of nannofossils) overlying an interbedded pelagic clay and a nannofossil and nannofossil-foraminifer ooze; some of the nannofossil ooze layers contain graded bedding characteristic of turbidites (Site 576 chapter, this volume).

Tables 3A and 3B contain the nannofossil distribution of Holes 576 and 576B, respectively.

Calcareous nannofossils are not present in the uppermost seven cores of Hole 576 and in the uppermost five cores of Hole 576B. The recovered calcareous nannofossils are common and moderately to poorly preserved below these levels.

The uppermost samples containing nannofossils from each hole (576-8-1, 135 cm and 576B-6-4, 100 cm) indicate deposition close to the carbonate compensation depth (CCD). This is suggested by the presence of only solution-resistant forms such as *Micula staurophora*, *Quadrum gothicum*, *Q. trifidum*, and *Lithastrinus* sp.

All of Core 8 from Hole 576 belongs to the *Q. trifidum* Zone and is assigned to the late Campanian–early Maestrichtian. Few reworked Early Cretaceous nannofossils were noted.

In Hole 576B a lower Campanian to lower Maestrichtian assemblage was recovered. Sections 6-4 to 7-5 belong to the upper Campanian–lower Maestrichtian *Q. trifidum* Zone. The assemblages are characterized by the presence of *Q. trifidum*, *Q. gothicum*, *Aspidolithus parcus*, *Cretarhabdus surrirellus*, *Cribrosphaera ehrenbergii*, *Eiffellithus turriseiffeli*, *Manivitella pemmatoidea*, and *Prediscosphaera cretacea*. Sections 7-6 to 8-2 belong to the late Campanian *Q. gothicum* Zone. Sample 576B-8-3, 55 cm belongs to the *Ceratolithoides aculeus* Zone. The lower part of Cores 8 and 9 belongs to the lower Campanian *A. parcus* Zone.

Few specimens of *Rucinolithus hayii* occurred in this *A. parcus* Zone. A *Braarudosphaera* sp. 1 form was found in the Campanian sediments of Core 8. This species can be related to the species of *Braarudosphaera* (sp. ind.) found by Thierstein and Manivit (1981) in Campanian deep-sea sediments at Site 462.

Various Cretaceous specimens are illustrated in Plate 1. These species are usually overgrown, and this overgrowth appears to occur preferentially along one of the individual calcite crystals of the pentalith. The individual elements are radially asymmetric and the sutures between the elements are inclined relative to the radial symmetry plane of the pentalith. The paleoecological and paleoceanographic implications of these *Braarudosphaera* in Campanian deep-sea sediments are still to be established.

Only one sample (576B-8-3, 55 cm) contains rare specimens of *Kamptnerius magnificus*, a species that is usually found in shallow water sediments. Few specimens of *R. magnus* were found throughout the Campanian (Plate 2, Figs. 1–3). Rare *B. africana*, *R. irregularis*, and *L. floralis* appear to have been reworked from paleo-outcrops of Aptian–Albian sediments nearby.

Site 577

Site 577 is located very close to Site 47 on the flank of the Shatsky Rise (Fig. 1). The relatively shallow water depth (2680 m) yielded a good preservation of the calcareous microfossils. Three holes were hydraulically piston cored: Holes 577 and 577A both recovered a very good late Cenozoic and Paleogene sequence and an undisturbed Cretaceous/Tertiary boundary sequence. Only one core containing the Cretaceous/Tertiary boundary was recovered from Hole 577B.

Calcareous nannofossils recovered at all three holes are abundant and diversified. Their preservation ranges

Table 2. Calcareous nannofossil zonation of the Tertiary from Leg 86 sites.

Age	Zone Bukry (1973, 1975)			Events	Hole 577		Hole 577A		Hole 577B		Hole 580	Zone Martini (1971)
					Sub-bottom depth (m)	Core-Section (level in cm)	Sub-bottom depth (m)	Core-Section (level in cm)	Sub-bottom depth (m)	Core-Section (level in cm)		
Quaternary	CN15	*Emiliania huxleyi*			0.50	1-1, 50	1.0	1-1, 100				NN21
	CN14	*Gephyrocapsa oceanica*	CN14b	*Emiliania huxleyi*	1.25-3.40	1-1, 25/1-3, 40	2.5-4.0	1-2, 100/1-3, 100				NN20
			CN14a	*Emiliana ovata*	5.75-20.26	1-4, 40/3-3, 96	5.5-22.3	1.4, 100/3-2, 90				NN19
	CN13	*Crenalithus doronicoides*	CN13b									
			CN13a	*Discoaster brouweri*								
Pliocene	CN12	*Discoaster brouweri*	CN12d	*Discoaster pentaradiatus*	21.76-26.13	3-4, 96/4-1, 33	22.50-25.50	3-3, 60/3-5, 50			13,CC	NN18
			CN12c	*Discoaster surculus*	26.92-27.60	4-1, 112/4-2, 30	25.90	3,CC				NN17
			CN12b	*Discoaster tamalis*	28.42-29.05	4-2, 112/4-3, 25	29.2	4-1, 80				NN16
			CN12a	*Reticulofenestra pseudoumbilica*	29.92-40.75	4-3, 112/5-4, 95	30.7-44.2	4-2, 80/5-5, 30				
	CN11	*Reticulofenestra pseudoumbilica*	CN11b		42.00-46.90	5-5, 70/6-2, 60	44.9-47.5	5-5, 100/6-1, 15				NN15
			CN11a	*Amaurolithus tricorniculatus*								
	CN10	*Amaurolithus tricorniculatus*	CN10d		47.50-49.90	6-2, 120/6-4, 60	49.05-53.55	6-2, 15/6-5, 15				NN14
			CN10c	*Ceratolithus rugosus*								NN13
Miocene			CN10b									NN12
			CN10a		51.50-55.60	6-4, 120/7-1, 130	55.05-56.55	6-6, 15/6-7, 15				
	CN9	*Discoaster quinqueramus*	CN9b	*Discoaster quinqueramus*	56.00-58.60	7-2, 20/7-3, 130	56.9-60.26	6,CC (30)/7-3, 36				NN11
			CN9a	*Amaurolithus primus*								
	CN8	*Discoaster neohamatus*	CN8b									NN10
			CN8a									
	CN7	*Discoaster hamatus*	CN7b									NN9
			CN7a									NN8
	CN6	*Catinaster coalitus*										NN7
	CN5	*Discoaster exilis*	CN5b									NN6
			CN5a		59.22-60.10	7-4, 42/7-4, 130	62.26	7-4, 86				
	CN4	*Sphenolithus heteromorphus*			60.72	7-5, 42						NN2/NN5
	CN3	*Helicosphaera ampliaperta*										
	CN2	*Sphenolithus belemnos*										
	CN1	*Triquetrorhabdulus carinatus*	CN1c									
			CN1b									NP25/NN1
			CN1a									

	CP19	*Sphenolithus ciperoensis*	CP19b									NP25/NN1
			CP19a									NP24
Oligocene	CP18	*Sphenolithus distentus*										NP23
	CP17	*Sphenolithus predistentus*										NP22
	CP16	*Helicosphaera reticulata*	CP16c									NP21
			CP16b									
			CP16a		61.60–66.50	7-5, 130/8-2, 120	63.16–63.66	7-5, 36/7-5, 86				NP19/NP20
	CP15	*Discoaster barbadiensis*	CP15b									NP18
			CP15a									NP17
				Chiasmolithus grandis ↱								
	CP14	*Reticulofenestra umbilica*	CP14b		67.00	8-3, 20	64.76–65.26	7-6, 36/7-4, 84				NP15/NP16
			CP14a									
	CP13	*Nannotetrina quadrata*	CP13c									
Eocene			CP13b									
			CP13a									
	CP12	*Discoaster sublodoensis*	CP12b		68.00	8-3, 120	65.76	7,CC (2-3)				NP14
			CP12a									
				Discoaster sublodoensis ↳								
	CP11	*Discoaster lodoensis*			69.50–72.50	8-4, 20/8-6, 120	64.85–71.95	8-1, 105/8-4, 105				NP12/NP13
				Coccolithus crassus ↳								
	CP10	*Tribrachiatus orthostylus*			72.91–74.60	8-7, 11/9-1, 130	72.95–74.43	8-5, 15/8,CC				NP11
				Discoaster lodoensis ↳								
	CP9	*Discoaster diastypus*	CP9b		74.90–80.47	9-2, 20/9-5, 117	76.20–79.65	9-1, 30/9,CC				NP10
				Tribrachiatus contortus ↳								
			CP9a		80.90–86.00	9-6, 10/10-3, 20		Not cored				NP9
	CP8	*Discoaster multiradiatus*	CP8b									
			CP8a									
				Discoaster multiradiatus ↳								
	CP7	*Discoaster nobilis*			87.00–88.50	10-3, 120/10-4, 120	85.79–88.10	10-1, 39/10-2, 120				NP7/NP8
				Discoaster nobilis ↳								
	CP6	*Discoaster mohleri*			89.00–95.64	10-5, 20/11-3, 34	88.79–92.78	10-3, 39/10-5, 138				
				Discoaster mohleri ↳								
	CP5	*Heliolithus kleinpellii*					93.00	10-6, 10				NP6
				Heliolithus kleinpellii ↳								
Paleocene	CP4	*Fasciculithus tympaniformis*			95.70–98.00	11-3, 40/11-4, 120	94.90–97.50	10,CC/11-2, 110				NP5
				Fasciculithus tympaniformis ↳								
	CP3	*Ellipsolithus macellus*			98.70–100.20	11-5, 40/11-6, 40	98.29–99.80	11-3, 39/11-4, 40				NP4
				Ellipsolithus macellus ↳								
	CP2	*Chiasmolithus danicus*			101.00–104.66	11-6, 120/12-2, 136	100.50–105.35	11-4, 110/12-1, 95	104.4–105.3	1-1, 10/1-1, 90		NP3
				Chiasmolithus danicus ↳								
	CP1	*Zygodiscus sigmoides*	CP1b		105.06–107.86	12-3, 60/12-5, 60	105.71–108.06	12-1, 126/12-3, 66	105.3–108.0	1-1, 110/1-3, 60		NP2
				Cruciplacolithus tenuis ↳								
			CP1a		108.16–109.10	12-5, 36/12-5, 129	108.46–109.60	12-3, 106/12-4, 70	108.10–109.62	1-3, 70/1-4, 72		NP1
				Thoracosphaera sp. ↳								

Note: Where a zone or subzone is represented in samples from several core sections, the highest/lowest samples are given. ↳ First occurrence, ↱ Last occurrence.

Table 3A. Distribution of Cretaceous calcareous nannofossils in Hole 576.

Age	Nannofossil zone	Core-Section (level in cm)	Sub-bottom depth (m)	Abundance	Preservation	Etching	Overgrowth	Reworking	*Aspidolithus parcus*	*Broinsonia enormis*	*Ceratolithoides aculeus*	*Cretarhabdus conicus*	*C. crenulatus*	*C. surirellus*	*Cribrosphaera ehrenbergii*	*Cyclagelosphaera margereli*	*Cylindralithus serratus*	*Discorhabdus rotatorius*	*Eiffellithus eximius*	*E. turriseiffeli*	*Glaukolithus diplogrammus*	*Kamptnerius magnificus*	*Lithastrinus floralis*	*L. grillii*	*Lithraphidites carniolensis*	*Manivitella pemmatoidea*	*Microrhabdulus decoratus*	*Micula staurophora*	*Parhabdolithus embergeri*	*Prediscosphaera cretacea*	*P. spinosa*	*Quadrum gothicum*	*Q. trifidum*	*Rucinolithus irregularis*	*R. aff. magnus*	*Watznaueria barnesae*	*Zygolithus tarboulensis*
late Campanian/early Maestrichtian	*Quadrum trifidum*	8-1,136	61.06	C	P	2	2																					C				F	F				
		8-2,13	61.33	A	M/P	2	1		R					C	C											C		F		C		F	F			A	
		8-2,50	61.70	A	M/P	2	1		R	R				C	C									R		C	R	F		C		F	F		R	A	
		8-2,91	62.11	A	M/P	2	1			F				C	C									R		C	F	F		C		F	F		R	A	
		8-3,30	63.00	A	M/P	2	1		F	F				C	C											C	F	F		C		F	F	R		A	
		8-3,80	63.50	A	M/P	2	1			F				C	C											C	F			C		RR	C			A	
		8-3,104	63.74	A	M/P	2	1			F				C	C									F		C	F			C		F	F		F	A	
		8-3,136	64.06	A	M/P	1	1	R		F					C					C			RR			C	F			C		F	F	R		A	F
		8-3,142	64.12	A	M/P	2	1			F				C	C											C	F			C		F	F			A	
		8-4,4	64.26	A	M/P	2	1			C				C	C				C	C						C	F	F		C			RR			A	
		8-4,12	64.32	B																																	
		8-4,26	64.46	A	M/P	2	2				R			C	C					C				F		C	R	F		A		F	F			C	
		8-4,50	64.70	A	M/P	2	1	F	F	C				C	C					C			F	F	F	C		F	F	A		F	F		R	C	R
		8.4,53	64.73	A	M/P	2	2		F	C				C	C				F	C					F	C	F	F		A		R	R			C	
		8-4,70	64.90	A	M/P	2	1		F	C	R	F		C	C				F	F				F	F	C			F	A		R	R			C	F
		8-4,79	64.99	A	M/P	2	2		R	C				C	C					C						C	F	F	F	A		R				C	
		8-4,116	65.36	A	M/P	2	1			C				C	C				C	C						C	F	F	F	A		RR	RR			A	R
		8-6,14	67.34	A	M	1	1	R	F	F				C	C					C		1	R	F	F	C	F	F	F	C		R	F			A	
		8-6,64	67.84	A	M/P	2	1		R	C				C	C	F				C	F			F	F	C	F		R	C		R	RR			A	
		8-6,72.5	67.92	A	M/P	1	2		R	C			F	C	C	F	F			C				F		C	F		R	C		R	R			A	
		8-6,148	68.68	A	M/P	1	2		F	R			C	C	C	R	F			C				F		C	F		R	C		R	R			A	
		8-7,35	69.05	A	M/P	1	2		F	F			F	C	C	F	F		F	C	R			F		C	F		R	C		R	F			A	
		8-7,bottom	69.15	A	M/P	1	2		F	C			F	C	C		F			C			F			C	F	F		C			R			A	
		8,CC	69.2	A	M/P	2	1	R		F	F		C	C	C			R	C	C			RR	F		C	F	F	R	C	F	F	F			A	

Note: RR = very rare, R = rare, F = few, C = common, A = abundant. Preservation: M = moderate, P = poor. Etching: 1–3 indicates increase in etching, overgrowth: 1–3 indicates increase in overgrowth in calcareous nannofossils (Roth and Thierstein, 1972).

Table 3B. Distribution of Cretaceous calcareous nannofossils in Hole 576B.

Age	Nannofossil zone	Core-Section (level or interval in cm)	Sub-bottom depth (m)	Abundance	Preservation	Etching	Overgrowth	Reworking	*Aspidolithus parcus*	*Braarudosphaera africana*	*B. bigelowii*	*Braarudosphaera* sp. 1	*Broinsonia enormis*	*Ceratolithoides aculeus*	*Chiastozygus litterarius*	*Cretarhabdus surirellus*	*Cribrosphaera ehrenbergii*	*Cyclagelosphaera margereli*	*Cylindralithus* sp.	*Eiffellithus eximius*	*E. turriseiffeli*	*Kamptnerius magnificus*	*Lithastrinus floralis*	*L. grillii*	*Lithastrinus* sp.	*Lithraphidites carniolensis*	*Manivitella pemmatoidea*	*Microrhabdulus decoratus*	*Micula staurophora*	*Parhabdolithus asper*	*P. embergeri*	*Prediscosphaera cretacea*	*Quadrum gothicum*	*Q. trifidum*	*Rucinolithus irregularis*	*R. aff. magnus*	*Rucinolithus hayii*	*Watznaueria barnesae*	*Zygolithus' tarboulensis*
Campanian late	*Quadrum trifidum*	6-4,100	51.70	F	P	2	2							C											C				A				R	R					
		6-4,130	52.00	A	M/P	2	1		F								C				C			F			F		R			C	F	C				A	
		6,CC	55.43	A	M/P	2	1		F								C				C			F			F				R	C		F				A	
		7-1,25	55.95	A	M/P	2	1		R				F			C	C				C					F	F				R	C	F	R		F		A	
		7-3,70	59.40	A	M/P	2	1		R				F			C	C	R	F		C						F		F		R	C	F	R		R		A	
		7-5,35	62.05	A	M/P	2	1		R							C	C		F		C					F	F				R	C	F	R		F		A	
	Quadrum gothicum	7-6,73	63.9	A	M/P	2	1		F				R	F		C	F	R			C						F		F		R	C	F					A	
		7-7,15	64.78	A	M/P	2	1		R				R	R		C	C		F	RR	C			F		F	C		F			C	F			F		A	
		7,CC	65.2	A	M/P	2	1		R				R	C		C	C			F	C						C		F			C	F			F		A	
		8-1,142	66.62	A	M	1	1		F					C			F		F	F	C						F		R			C	F			R		A	
		8-2,77	67.47	A	M/P	1	1		R			R		C			C		F	F	C						F		F			C	F					A	
	Ceratolithoides aculeus	8-3,55	68.75	A	M	1	1		F				F	C			C			R	C	R					F		R			C						A	
early	*Aspidolithus parcus*	8-3,90–91	69.15	A	M/P	2	1		R		R	R				C	F				C						F		F			C	R				R	A	
		8-3,126–127	69.46	A	M/P	2	1	R	R				R			F	C	F		F	C		F			F	C	F		C	F	C	R					A	R
		8-4,4–5	69.74	A	M/P	2	1	R	R				F			C	F		F	F	F		F				C	R		F		C						A	
		8-4,68–69	70.38	A	M/P	2	1		R			F	F		F	C	F			F	C						F		F		R	C					R	A	
		8-4,95	70.65	A	M/P	2	1	R			R	F			F		C		F	F	C		F			F	F		C			C			R	R	F	A	
		8-5,7	71.22	A	M/P	2	1					F	F				R		F	F	C			R		F	F		F			C				R	F	A	
		8-5,52	71.72	A	M/P	2	1		R			F					F		F		C			R			F	R	F			C					F	A	
		8-5,120	72.40	A	M/P	2	1		R			F					F				C						F	R	F			C					F	A	
		8-5,140	72.60	A	M/P	2	1		R	R		F					F				C						F		F			C						A	
		8-6,7	72.77	A	M/P	2	1			R			R							R	C			R			F		F			C				R		A	
		8-7,5	74.30	A	M/P	2	1																						F			C						A	
		8,CC	74.73	A	M/P	2	1		R			R					C		F		C						F		F			C				F	R	A	
		9,CC	74.8	C	P	2	2		R			R					C				C						F		F			C				F		A	

Note: See footnote to Table 3A for definition of symbols.

from poor to moderate. Calcareous nannofossils are considerably overgrown near the Cretaceous/Tertiary boundary and in the lower middle Eocene. A significant hiatus is noted from the middle Eocene to the upper Miocene.

The calcareous nannofossil assemblages recovered at Site 577 are discussed below. Tables 4 through 10 show the distribution of the calcareous nannofossils in the samples studied. The detailed correlation between calcareous nannofossil events, magnetostratigraphy, and the numerical time scale is discussed by Monechi, Bleil, and Backman (this volume).

Pleistocene

The upper part of Sections 577-1-1 and 577A-1-1 belongs to the *Emiliania huxleyi* Zone (CN15) (Tables 6 and 9). In both holes the last occurrence of *E. ovata* in Sections 577-1-4 and 577A-1-4 marks the *Ceratolithus cristatus* Subzone (CN14b) (Tables 6 and 9). Few reworked discoasters are found.

In both holes the lower parts of Cores 1 and 2 and the upper part of Section 3-2 contain a rich assemblage of *Gephyrocapsa oceanica, G. caribbeanica, Emiliania annula, E. ovata, G. aperta, Calcidiscus leptoporus*, and *Ceratolithus cristatus*. The assemblages can be assigned to the *E. ovata* Subzone (CN14a) and *Crenalithus doronicoides* (CN13) Zone, which correspond to the *Pseudoemiliania lacunosa* Zone (NN19) of Martini (1971) (Tables 6 and 9). The highest occurrence of *Calcidiscus macintyrei* is observed in both holes in Core 3, Section 1, slightly above the last occurrence of *Discoaster brouweri*. Occasionally rare reworked discoasters are found in the upper part of the sequence.

Pliocene

The top of the *Discoaster brouweri* Zone (CN12) is recognized by the last occurrence of *D. brouweri* in Sections 577-3-4 and 577A-3-3. All the subzones of the *D. brouweri* Zone (CN12) were found in both holes (Tables 6 and 9). Section 577-3-4 through the upper part of Sections 577-4-1 and 577A-3-3 through 577A-3-5 belong to the *Calcidiscus macintyrei* Subzone (CN12d); the lower part of Section 577-4-1 and Sample 577A-3,CC belong to the *D. pentaradiatus* Subzone (CN12c); in Hole 577 the lower parts of Sections 577-4-2 and 577A-4-1 belong to the *D. surculus* Subzone; and the lower parts of Sections 577-4-3 through 577-5-4 and 577A-4-2 through the top of 577A-5-4 belong to the *D. tamalis* Subzone (CN12a). With the exception of the marker species the assemblages are similar to those of the early Pleistocene; discoasters are common to abundant.

The top of the *Reticulofenestra pseudoumbilica* Zone (CN11) is recognized in both holes in Core 5, Section 5 (Tables 6 and 9). Preservation is poor down to the top of Core 7 in both holes.

The top of the *Amaurolithus tricorniculatus* Zone (CN10) is defined by the last occurrence of *A. primus* and *A. tricorniculatus* in Section 577A-6-2 (Table 8). The *A. tricorniculatus* found above that level are considered reworked. In Hole 577 the top of the *A. tricorniculatus* Zone is at the bottom of Section 577-6-2 (Table 6).

The first occurrence of *Ceratolithus rugosus* occurs in Sections 577-6-4 and 577A-6-5. The lower part of the *A. tricorniculatus* Zone could not be divided into subzones because of the scarcity or the absence of *Triquetrorhabdulus rugosus* and *C. acutus*. Rare specimens were found only in one sample in both holes. For this reason the Miocene/Pliocene boundary could not be placed accurately.

Miocene

The Miocene sequence recovered at Site 577 is very short because of a major hiatus that occurs from middle Miocene to middle Eocene time. The Miocene is represented only by the upper part of Core 7 in both holes. Sporadic occurrences of marker species in Core 7 in both holes make zonal assignments of individual samples difficult. Sample 577A-6,CC through Section 577A-7-3 and Sections 577-7-2 through 577-7-3 belong to the *Amaurolithus primus* Subzone (CN9b) (Tables 6 and 9). The first occurrence of *A. primus* occurs in both holes in Section 7-3.

A hiatus from the lower part of the *Discoaster quinqueramus* Zone (CN9) to the middle Miocene is present.

Sections 577A-7-4 and 577-7-4 to 577-7-5 contain a mixed assemblage of Eocene and Miocene species. The presence of *Calcidiscus macintyrei, Coccolithus formosus, Sphenolithus heteromorphus, D. aulakos, D. sanmiguelensis*, and *D. variabilis* s.l. suggests that these samples belong to the upper part of the *S. heteromorphus* Zone (CN14) and the lower part of the *D. exilis* Zone (CN5) (Tables 6 and 9).

Eocene

The Eocene sequence is not complete due to a major unconformity in Sections 577-7-5 and 577A-7-4. All of the upper Eocene is missing. Sections 577-7-5 through 577-8-2 and 577B-7-5 belong to the *Discoaster barbadiensis* Zone (CP15) (Tables 5 and 8). Sections 577-8-3, and 577A-7-6 belong to the *Reticulofenestra umbilica* Zone (CP14). A small hiatus is present in the middle Eocene; the *Nannotetrina quadrata* Zone (CP13) and the upper part of the *D. sublodoensis* Zone (CP12) are missing in both holes. The assignment of Sample 577A-7,CC to the *D. sublodoensis* Zone is suggested by the presence of some upper Eocene species together with *D. sublodoensis*. The *D. sublodoensis* Zone is present in only one sample (Sample 577-8-3, 120 cm).

The *D. lodoensis* Zone (CP11), characterized by the first occurrence of *Coccolithus crassus*, was recognized in both holes from Sections 577-8-4 through 577-8-6 and 577A-8-1 through 577A-8-4.

Sections 577-8-7 through 577-9-1 and Section 577A-8-5 through Sample 577A-8,CC contain an assemblage of the *Tribrachiatus orthostylus* Zone (CP10). *T. orthostylus* is present in both holes and it ranges from the *D. diastypus* Zone (CP9) to the middle part of the *D. lodoensis* Zone (CP11). The few *T. orthostylus* species found in the samples above have been considered reworked.

The very lower part of the Eocene, the *D. diastypus* Zone (CP9), seems not to be complete because of the absence of the *Tribrachiatus contortus* Subzone (CP9a).

Table 4. Distribution of Maestrichtian-early Paleocene calcareous nannofossils in Hole 577.

Age	Zone	Core-Section (interval in cm)	Sub-bottom depth (m)	Abundance	Preservation	Etching	Overgrowth	Reworking	Cretaceous species	*Ahmuerella octoradiata*	*Arkhangelskiella cymbiformis*	*Braarudosphaera bigelowii*	*Ceratolithoides aculeus*	*Cretarhabdus conicus*	*C. crenulatus*	*C. surirellis*	*Cretarhabdus* sp.	*Cribrosphaera ehrenbergii*	*Cylindralithus serratus*	*Cylindralithus* sp.	*Eiffellithus turriseiffeli*	*Glaukolithus diplogrammus*	*Lithraphidites carniolensis*	*L. quadratus*
	CP2	12-1,33–34	102.13	A	M	1	1	R								F								
		12-1,73–74	102.53	A	M	1	1	R								F								
		12-1,113–114	102.93	A	M	1	1	R								F								
		12-2,16–17	103.46	A	M	1	1	R								R								
		12-2,76–77	104.06	A	M	1	1	R								R								
		12-2,136–137	104.66	A	M	1	1	R																
early Paleocene	CP1b	12-3,6–7	104.86	A	M	1	1	R									C	F		F				
		12-3,76–77	105.56	A	M	2	1	R			R						C	R		F				
		12-3,116–117	105.96	A	M/P	2	1	R									F	R		R	F			
		12-3,142	106.22	A	M	1	2	R									F		R	R			R	
		12-4,16–17	106.46	A	M/P	2	1	R									F		R					
		12-4,56–57	106.86	A	M	1	1	R																
		12-4,96–97	107.26	A	M	1	1	R																
		12-4,117	107.47	A	M	1	1	R																
		12-5,6–7	107.86	A	M	1	1	R				R					F	R		R				
	CP1a	12-5,36–37	108.16	A	M	1	1	R																
		12-5,76–77	108.56	A	M/P	1	1	F									R							
		12-5,94–95	108.74	C	M	1	1	F								R					R			
		12-5,100–101	108.80	F	M/P	1	2	F									R							
		12-5,105–106	108.83	F	M/P	1	1	F											R					
		12-5,110–111	108.90	C	M/P	2	1	C			F	R				C	C	F	C	F	F		F	
		12–5,115	108.95	C	M/P	2	1	C			R					C	C	C	F	C	C	R	F	R
		12-5,118	108.98	C	M/P	1	1	C			F					C	C	C	F	C	C		C	
		12-5,120	109.00	A	M/P	1	1	C			C					C	C	C	F	C	C		C	F
		12-5,122	109.02	A	M	1	1	A			C				R	C	C	C	C	C	C		C	R
		12-5,124–125	109.05	A	M	1	1	A			F					F	C	C	C	A	C	F	F	R
		12-5,129	109.10	A	M/G		1	A			C				F	C	C	C	C	A	C	C	C	R
Maestrichtian	*Micula prinsii*	12-5,130	109.11	A	M	1	1				C				F	C	C	C	C	C	C	C	C	R
		12-5,136–137	109.17	A	M	1	1				F			F	C	C	C	C	F	C	C	F	C	F
		12-6,36–37	109.67	A	M	1	1				F						C	C		C	C		C	F
		12-6,96–97	110.27	A	M	1	2										C	C	C	C	C	F	A	R
		12-6,142–143	110.72	A	P	2	1										C			C				R
	Micula murus	12-7,20	111.00	A	M/P	2	2				F					C	C	C	C	C	C	F	A	R
		13-1,50	111.80	A	M/P	2	2			F	C		F			C	C	C	C	C	C	F	A	R
		13-1,111	112.41	A	M	1	1				F		C			C	C	C	C	C	C	F	A	
		13-2,111	113.91	A	M	1	1			R			C			C	C	C	C	C	C	F	A	R
		13-3,111	115.41	A	M	1	1						C	R		C	C	C	C	C	C	R	A	
		13-4,48	116.28	A	M	1	1				F		F			C	C	C	C	C	C	F	A	F
		13-4,111	116.91	A	M	1	1						F		F	C	C	C	C	C	C	F	A	
		13-5,14	117.44	A	M	1	1			R	F		C		F	C	C	C	C	C	C	R	A	R
		13,CC(5)	118.8	A	M	1	1			R			F		F	C	C	C	C	C	C		A	F

Note: See footnote to Table 3A for definition of symbols.

Only rare species of *T. contortus* were found in Sample 577-9-5, 117 cm.

Paleocene

All Paleocene zones (Tables 5 and 8) were recognized in the Paleocene sequence at Site 577. The nannofossils are moderately well preserved.

The *Discoaster multiradiatus* Zone (CP8) was not cored in Hole 577A, but it is well represented in Hole 577 from Sections 577-9-6 to 577-10-3.

Sections 577-10-3 through 577-10-4 and 577A-10-1 to 577A-10-2 belong to the *D. nobilis* Zone (CP7). *D. okadai*, a relatively large five-rayed discoaster described by Bukry (1981), was recognized in this zone. Together with this occurrence of *D. okadai*, a smaller *Discoaster* sp.A was found. The latter was reported by Okada and Thierstein (1979) at the same stratigraphic level at Site 384 in the Atlantic Ocean. This species occurs slightly below the first occurrence of *D. okadai*; both species are considered characteristic of the *D. nobilis* Zone; and their transoceanic significance is definitely confirmed.

It was not possible to separate the *D. mohleri* (CP6) and *Heliolithus kleinpellii* (CP5) Zones in Hole 577. In Hole 577A the first occurrences of *D. mohleri* and *H. kleinpellii* were separated by an interval of only a few centimeters.

The *Fasciculithus tympaniformis* Zone (CP4) occurs in Sections 577-11-3 through 577-11-4 and in Sample 577A-10,CC through Section 577A-11-2. The first *Fasciculithus* sp. appear in Hole 577A in the upper part of Section 577A-11-6 together with *Sphenolithus* sp. In Hole 577, the first *Fasciculithus* appear slightly above

Table 4. (Continued).

Manivitella pemmatoidea	*Microrhabdulus decoratus*	*Micula murus*	*M. prinsii*	*M. staurophora*	*Parhabdolithus embergeri*	*Prediscosphaera cretacea*	*P. grandis*	*Stephanolithion mutinum*	*Watznaueria barnesae*	*Zygodiscus spiralis*	*Zygodiscus* sp.	*Zygolithus tarboulensis*	Cenozoic species	*Biantholithus sparsus*	*Biscutum* cf. *romeinii*	*Chiasmolithus bidens*	*C. consuetus*	*C. danicus*	*C. subrotundus*	*Coccolithus pelagicus*	*Cruciplacolithus edwardsii*	*C. primus*	*C. tenuis*	*Cyclagelosphaera reinhardtii*	*Discolithina rimosa*	*Ericsonia cava*	*E. robusta*	*E. subpertusa*	Foraminifer debris	*Markalius astroporus*	*Neochiastozygus concinnus*	*Neocrepidolithus* sp.	*Placozygus sigmoides*	*Prinsius bisulcus*	*P. dimorphosus*	*Thoracosphaera deflandrei*	*T. operculata*	*T. saxea*	*Thoracosphaera* sp.	*Toweius* sp.	*Zygodiscus simplex*
																	F	R		C			C					A		F	F		C	C					F		
																F	F	F		C			C		R	F		A		F			C	C				F	F		
																	C	F	F	C			C			F	C	A		F			C	C					F		
														R			F	F	R	C			C			F	F	A		F			A	F	C			R	F		
														R			R	F		C			C	R		F	R	C		F			C		F						F
																		F		C			C			C		C		F			C		F			F	F	C	
				F		C			C		C			R						A	C		C	F		C	F	C		C	R					F	R	F	C	A	
	F	F		R	R	C					C			R	C					A	F	F	C	F		F		C		C	R					F	R	F	C	A	
		F		R	R	C					C				C					A	R	C	C	F		F		C		F	R					F	F	C	C	A	
	F	F		R		F			F		F			R	C					A	R	C	A	F						R	F	R				R	R	C	C	A	
		F				C			F						A					A		C	C	C						F	F	R				C	F	C	C	F	
		R							C						A					C		A	C	A						C	R	F			F	C	C	A	A		
									R		F				A					F		A	R	C						F		F				C	C	A	A		
									F		F				A							A	C	C						R		C				C	C	A	A		
		F				F			F		R			R	A							A	R	C						C						C	C	A	A		
	R	R				C			C		F	R		F	A							A		C						C		R				C		A	A		
						R			C		R				A							C		A						C						A	R	C	A		
						R			F						A							F		A					R	F						C	C	A	A		
						R			F						A							R		A					F	F						C	C	A	A		
		R							F						A									C					F	R						R	C	A	A		
		C		C		C			A		F				A									F					C	F						F	C	C	A		
	F	C		C	R	A	R		A		C				A														C							R		F	C		
	F	C		C		A			A	F	C				C									R					C							R		F	C		
	C	C		A		A	R		A	F	C	R			C														C										C		
R	C	C		C	R	A		R	A		F	R			C									F					C							C			C		
	F	C		C		A	R		A	F		R			C									R					C							C			C		
	F	C	R	C		A		F	A	C	C	F			R														C										R		
	R	C	R	C		A			A	F	C	F																	C										R		
		C	F	C	R	A	F		A	F	F	F																	C										R		
F	F	C	R	C		A		F	A	F																			F												
F	F	C	R	A		A		F	A	F																															
		A	R	A		C			C																																
	F	C		C		A		F	A			F																													
C	C	C		C		A			A																																
C	C	C		C		A	F		A	F	F																														
	C	C		C		A		F	A		F	R																													
F	C	C		C	R	A	F		A	F		R																													
	C	F		C		A			A		F																														
	C	F		C		A	F	F	A																																
F	C	R		C		A	F	F	A	F																															
F	C			C		A			A			F																													

the first occurrence of *Sphenolithus* sp. in the lower part of Section 577-11-6. The genus *Fasciculithus* is quite common and well diversified in the upper Paleocene. *F. pileatus* was the first species recognized in the upper part of the *Ellipsolithus macellus* Zone (CP3).

The first occurrence of *E. macellus* defining the base of the *E. macellus* Zone (CP3) was recognized in Samples 577-11-6, 40 cm and 577A-11-4, 40 cm. In the lower part of the *E. macellus* Zone this species is very rare and discontinuously present.

The *Chiasmolithus danicus* Zone (CP2), defined at the bottom by the first occurrence of *C. danicus* s.s. as defined by Romein (1979), occurs in Sample 577-12-2, 136 cm (sub-bottom depth 104.86 m), in Sample 577A-12-1, 95 cm (sub-bottom depth 105.35 m), in Sample 577B-1-1, 90 cm (sub-bottom depth 105.3 m) (Table 9). The first occurrence of *Cruciplacolithus edwardsii* occurs slightly below that in Sample 577-12-3, 142 cm (sub-bottom depth 106.22 m), Sample 577A-12-2, 106 cm (sub-bottom depth 106.75 m), Sample 577B-12-2, 115 cm (sub-bottom depth 106.84 m) (Tables 4, 8, and 10). This species, described by Romein (1979), is characterized by a central cross in which the bars make an angle with the axes of the ellipse in clockwise direction. Both species have been grouped together in the literature until recently.

Assemblages of the *Zygodiscus sigmoides* Zone (CP1) occur in Samples 577-12-3, 6 cm through 577-12-5, 129 cm, 577A-12-1, 126 cm through 577A-12-4, 70 cm, and 577B-1-1, 110 cm through 577B-1-4, 72 cm (Tables 4, 8, and 10).

The *C. primus* (CP1a) and the *C. tenuis* (CP1b) subzones are recognized at all three holes. The *C. tenuis* Subzone, identified by the first occurrence of *C. tenuis*

Table 5. Distribution of calcareous nannofossils in the Paleocene-Eocene in Hole 577.

Age	Nannofossil zone	Core-Section (interval in cm)	Sub-bottom depth (m)	Abundance	Preservation	Etching	Overgrowth	Reworking	*Biscutum romeinii*	*Braarudosphaera bigelowii*	*B. discula*	*Bramletteus serraculoides*	*Campylosphaera dela*	*Chiasmolithus bidens*	*C. californicus*	*C. consuetus*	*C. danicus*	*C. expansus*	*C. grandis*	*Coccolithus crassus*	*C. eopelagicus*	*C. formosus*	*C. jugatus*	*C. pelagicus*	*Crepidolithus* sp	*Cruciplacolithus primus*	*C. subrotundus*	*C. tenuis*	*Cyclagelosphaera reinhardtii*	*Cyclicargolithus floridanus*	*Cyclicargolithus* sp	*Cyclococcolithus gammation*	*Cyclolithella kingi*	*C. placitilis*	*Dictyococcites bisecta*	*D. scrippsae*	*Discoaster barbadiensis*	*D. diastypus*	*D. germanicus*	*D. lenticularis*
middle Eocene	CP15/16	75,130–131	61.60	A	M/P	1	1	R				C												C						F					C	F	R			
		7-6,20–21	62.00	A	M/P	2	1	R				F	R									C		C											A	F	C			
		7,CC,7–8	62.40	A	P	2	2	R				F										C		C									F		A	C	C			
		8-1,120–121	65.00	A	M	2	1					C												C									R	F	A	F	C			
		8-2,120–121	66.50	A	M	1	1	R				R						R	F					C									R		A	F	C			
early Eocene	CP14	8-3,20–21	67.00	A	M/P	2	2					R							R					C							C		R		C	C	F			
	CP12	8-3,120–121	68.00	A	M/P	1	2					R	C						R			F		C										F			C			
	CP11	8-4,20–21	68.50	A	M	1	1						A							R		C	R	F									R	F			F			
		8-4,120–121	69.50	A	M/P	1	2					R	C					R	F	C	F	C	F	F									F	C			F			
		8-5,20–21	70.00	A	P	2	2						C								C	C		R									R	F			F			
		8-5,120–121	71.00	A	M/P	1	1					R	C					F	F	C	F	C	C	C								F	F	C			F			
		8-6,20–21	71.50	A	P	2	2						A						R	C	F	F	R									R	F	R			F			
		8-6,120–121	72.50	A	M/P	1	2					R	C			R		F	F	F	F	F	F	F									C	C			F			
	CP10	8-7,11–12	72.91	A	P	2	2						C			F					F	R											R				F			
		8,CC,34–35	73.26	A	M/P	2	2						C			F			F		C												C				F	F	R	
		9-1,20–21	73.50	A	M/P	2	2					R	C			F					F		F	F									F				F	C		
		9-1,130–131	74.60	A	M/P	2	1						C			F					F			R														F		
	CP9b	9-2,20–21	75.00	A	M/P	1	1					F	C			F					F		F	F									C				F	C		
		9-3,20–21	76.50	A	M/P	2	2					R	C			F					C		R	F								F	F				F	F		
		9-3,130–131	77.60	A	M/P	1	2						C			R					C			F													F			
		9-4,19–20	78.01	A	M/P	1	2						C	F		F					C		R	C													C	C		
		9-5,10–11	79.50	A	M/P	2	2	R					F	F		C					C		F	C													C	C		
		9-5,117–118	80.75	A	M	1	1					F	F	F	F	F					C			C													C	C		
late Paleocene	CP8	9-6,10–11	81.00	A	M/P	1	2					F	C	F	F	R		R			C			F																
		9-6,120–121	82.10	A	M/P	1	2						C	F	F	F					C		F	C														R		
		9,CC,8–9	82.28	A	M/P	1	2	R				R	F	F		F					R		C																	
		10-1,50–51	83.30	A	M/P	2	1								R	R								C																
		10-1,120–121	84.00	A	M/P	1	2							F	F									C																R
		10-2,50–51	84.80	A	M/P	2	1								F									C																R
		10-2,120–121	85.50	A	M/P	1	2							C	F		R							C																F
		10-3,20–21	86.00	A	M/P	1	2							F	F									A																F
	CP7	10-3,120–121	87.00	A	M/P	1	2							F	F		R							A																
		10-4,50–51	87.80	A	P	2	2							F	F	F	F							A																
		10-4,120–121	88.50	A	M	1	1							F	C	F								C																R
	CP5/6	10-5,20–21	89.00	A	M/P	1	1							R		F	R							C																
		10-5,120–121	90.00	A	M	1	1							F	C	F								C				R												R
		10-6,20–21	90.50	A	M	1	1							F		F	R							C				R												
		10-6,120–121	91.50	A	M	1	1	R							F	C								C																C
		10-7,30–31	92.10	A	M	1	1	R							F	C								C				F												C
		10,CC,10–11	92.40	A	M/P	2	1	R							F	C								C																C
		11-1,10–11	92.60	A	M	1	1	R							C	C								C																C
		11-1,70–71	93.00	A	M	1	1	R							C	C								C				F												F
		11-1,130–131	93.60	A	M	1	1	R							C	C								C																C
		11-2,40–41	94.20	A	M	1	1								C	C	R							C				R												C
		11-2,120–121	95.00	A	M/P	2	1	R							F	C								C																
		11-3,34–35	95.64	A	M	1	1	R								C								C				F												
	CP4	11-3,120–121	96.50	A	M	1	1	R							C	C								C			F	C												
		11-4,40–41	97.20	A	M	1	1			R					C	C								C			R	F												
		11-4,120–121	98.00	A	M	1	1					F		C	F	F								C				C												
early Paleocene	CP3	11-5,40–41	98.70	A	M	1	1							F	F	F								C				C												
		11-5,120–121	99.50	A	M	1	1							F	F	C	F							C				C	R											
		11-6,40–41	100.20	A	M/P	1	2	C				F		F	F	C	F							C		F		C												
	CP2	11-6,120–121	101.00	A	M/P	1	2	C						F	F	C	F							C		R		C												
		11,CC	101.50	A	M	1	1	C			R			C	F	F	F							C	R	F		C	R											

Note: See footnote to Table 3A for definition of symbols.

s.s., occurs in Samples 577-12-3, 6 cm through 577-12-5, 6 cm, 577A-12-1, 126 cm through 577A-12-3, 66 cm, and 577B-1-1, 110 cm through 577B-1-3, 60 cm. The *C. primus* Subzone (CP1a) yields an assemblage characterized by small *Biscutum romeinii, Z. sigmoides, Zygodiscus* sp., *C. primus, Markalius astroporus*, and *Thoracosphaera* sp. The first occurrence of *C. primus* was recognized in the three holes about 30 cm above the Cretaceous/Tertiary boundary. Reworked Cretaceous nannofossils are rare in the upper part of the *C. primus* Zone, but become more abundant downward and dominate the Tertiary species in the samples just above the Cretaceous/Tertiary boundary.

Cretaceous/Tertiary Boundary

An extended and undisturbed Cretaceous/Tertiary boundary was cored three times at Site 577 in Sections 577-12-5, 577A-12-4, and 577B-1-4 (Tables 4, 8, and 10). The lower Paleocene-upper Maestrichtian sequence is an undisturbed white to light brown nannofossil ooze

Table 5. (Continued).

D. lodoensis	D. mohleri	D. multiradiatus	D. nobilis	D. okadai	D. saipanensis	D. salisburgensis	D. sublodoensis	D. tanii	Discoaster sp. 1	Discoaster sp.	Discoasteroides kuepperi	Discolithina plana	D. rimosa	Ellipsolithus distichus	E. lajollaensis	E. macellus	Ericsonia cava	E. robusta	E. subpertusa	Fasciculithus havii	F. involutus	F. pileatus	F. tympaniformis	F. ulii	Fasciculithus sp.	Heliolithus conicus	H. kleinpellii	Markalius astroporus	Neochiastozygus concinnus	Pedinocyclus larvalis	Prinsius bisulcus	P. dimorphosus	Reticulofenestra samodurovii	R. umbilica	Rhabdosphaera sp.	Sphenolithus anarrhopus	S. heteromorphus	S. moriformis	S. primus	S. radians	S. spiniger	Sphenolithus sp.	Striatococcolithus pacificanus	Thoracosphaera deflandrei	T. operculata	T. saxea	Thoracosphaera sp.	Toweius craticulus	T. eminens	T. magnicrassus	T. tovae	Tribrachiatus contortus	T. orthostylus	Wiseorhabdus inversus	Zygodiscus sigmoides	Z. simplex	Zygodiscus sp.	Zygrhablithus bijugatus
					R																													F			R					C											R					
					C			C		R																								C				R				F																F
					C			C				F																					C									C											R					F
					C			C				R																					F	C								C												R				
					C			F																									F	F								C												R				
					C			C			C																						F	C	R						F	C											F	C				A
C							C			C	C		R																	F											R						F											C
C							R'						R																									R		C	C						R											C
C						F		C			C		R															R		F										C			R				F											C
C																R														F										F			R				F											A
C						F		C			F		R			R													F	C								F		C			R				R			F								C
C						R					R																			F										C			R							F								F
C						F				C	F		R					F										R		F								F		C			F				R						C					C
C						F					R		R					F																				R		F							R			C			C					A
C						C					F		R		R													F										F		C			F				F						F					
C		R				C					C	R			F		F											R										C		C			F							F			F	R				A
R						F					F		R					F																				F		F							F						C					C
			F			C					F		R			R		F																				F		F			F				R			C			C					C
			F			F				F	F		F			F		F	R									R										F		C			F				F			C			F					C
			F			R					F		F			R		F																				R		F			R				F			C			C	F				C
			F								F		R			R	R																						C													C					C
		R	C			F					F		F					F											F							C		C		C							R	F		C			C					
		C	C			F							R			F			F																												R	F				R						
		C	F										F	F		F		C											R							C		C										F	F							C			R
		C	F										R	F				C	F						F				R							C		C										F	R							F			
	C	C	F										R	R				F	F	F	R		R	F	F				R							F		C									R		R	C		R				F			F
	F	C	R										R	R		F		F	F	F	F		C	F	F				F							F		C									R			C										
	C	C	F										R			F		C	C	F			F	F	C				F									C												C										
	C	C	F										F	R		R		C	F		F		R	F	C																							F	C										
	C	C	F										F			F		C	A	F			C		C				F							C		C								F			C										
	C	R	R										F			F		C	A	F			F		C				F									C				C				F			C								F		
			R	C						C	F			F	R		R		C	A	F			F		C				F							C		C								R			C								F		
	C		R	F						F				R			F		C	C	F	F		C		C				F							F		C								R			C		R								
	C		R	F						F							R		C	C				F		C				F							C		C										F	C								R	R	
C				R					R				F	R		R		C	C	F			F		C				F		F					C		F										F	C								R		
C									F				R			R			C				F		C			F	F		R						C		C										C	C								C		
C									R				R	R		F		F	C				C		C				R								C										F	R	F	C						C			
C										C			F	F		C			C				C		C			F	F								C		C										F	F	C						C		F	
C										C						C	F		C				C		C		F	F	F								C		C											F	C		F				C			
C										C						F	F		C				C		C		C		F									A											C	C		F				C		F	
C										C			F			F	F		C				C		C		F		F							A		A						F					C	C		F				C		F	
C										C			F			F		F	C				C		C				C							A		C											C	C		F				C			
C										C				F		C	F	C	C				C		C		R		F							A		A									F		F	C		F				C			
C										C			F	R		C	F	C	C				C		C				F							C		C								F	F		F		F				C		F	
C										C				F		F	F	F	C				C		C		C	F								A		A										F	F		F				C			
C										R							F	F	C				C		A	F	F		F							C		C				C							F		C				C			
																	F	F	C	F			C		A	F			C							F		C							R		F		F		C				C		F	
																	C	F	C			F	C		A	F			C							F		C	C			C						F			C				C	C		
																F	F	F	C				C		A				F										C			C							F		C				C			
																	F	F	C			C			A			F	C		C								C			C						F	F		F				C	F		
																	C	F	C			C			A			R	C		F								C			C							F						C			
													F			R	C	F	C		F	F		F	A			F	C		F	F							C			C						F	F						C			
																	C	F	C			R			A			F	C		C								C			C													C		F	
																	C	R	C			F			A			F	F		F											C						F										

see Site 577 chapter, this volume). Except for a minor olor change from a Maestrichtian white to Tertiary ght brown calcareous ooze, the recovered sediments re essentially featureless with no signs of sedimentation isruption. The upper Maestrichtian is characterized by a rich Cretaceous nannofossil assemblage. This assemblage is dominated by species such as *Arkhangelskiella cymbiformis, Prediscosphaera cretacea, P. grandis, Lithraphidites quadratus, Micula staurophora, Cretarhabdus surrirellus, C. crenulatus,* and *Watznaueria barnesae. M. murus, M. prinsii,* and *L. quadratus* zones were recognized (Tables 3, 6, and 9). *M. prinsii*, a rather delicate form, characteristic of the uppermost Maestrichtian in low latitudes, was found at ~1 m below the Cretaceous/Tertiary boundary.

Preservation of Cretaceous nannofossils is moderate and becomes poor in the very early Paleocene. No significant changes in relative abundances of the Cretaceous taxa were observed from the *L. quadratus* Zone (the oldest Cretaceous sediments recovered) up to the Cretaceous/Tertiary boundary. The Cretaceous/Tertiary boundary was defined in terms of calcareous nanno-

Table 6. Distribution of calcareous nannofossils in the Neogene in Hole 577.

Age	Nannofossil zone	Core-Section (interval in cm)	Sub-bottom depth (m)	Abundance	Preservation	Etching	Overgrowth	Reworking	*Amaurolithus amplificus*	*A. delicatus*	*A. primus*	*A. tricorniculatus*	*Bramletteius serraculoides*	*Calcidiscus leptoporus*	*C. macintyrei*	*Ceratolithus acutus*	*C. cristatus*	*C. rugosus*	*C. telesmus*	*Coccolithus miopelagicus*	*C. pelagicus*	*Coronocyclus nitescens*	*Crenalithus doronicoides*	*C. productellus*	*Cricolithus jonesii*	*Cyclicargolithus* sp.	*Cyclolithella rotula*	*Dictyococcites bisecta*
Pleistocene	CN15	1-1,50–51	0.50	A	M	1	1							C			R				C			C	F			
	CN14b	1-1,125–126	1.25	A	M	1	1	R						C			R		R		F			C	C			
		1-2,40–41	1.90	A	M	1	1							C			R				F		C	C	F			
		1-2,125–126	2.75	A	M	1	1							C			R				F		C	C				
		1-3,40–41	3.40	A	M	1	1							C			R		R		R			C				
		1-4,40–41	4.90	A	M	1	1							C			R				C		C	C				
	CN13/14a	1-5,46–47	5.75	A	M	1	1							C			R				F			C	F			
		1,CC(10–11)	6.81	A	M	1	1							C			R				F		C	C				
		2-1,40–41	7.20	A	M	1	1							C			R				F		C	A				
		2-1,103–104	7.83	A	M	1	1							C			R		R		F		C	C				
		2-2,43–44	8.73	A	M	1	1							C			R		R		F		C					
		2-2,103–104	9.33	A	M	1	1							C			R				F		C					
		2-3,43–44	10.23	A	M	1	1							C			R				F		F					
		2-4,43–44	11.73	A	M	1	1							C			R				F		C		R			
		2-5,35–36	13.15	A	M	1	1							C			R	R			F		C					
		2-6,40–41	14.70	A	M	1	1							A			R				F		C					
		3-1,103–104	17.80	A	M	1	1							C	F		R				C		C					
		3-2,96–97	18.66	A	M	1	1	R						C	F		R		R		F		C		R			
		3-3,96–97	20.76	A	M	1	1							C	C		R				F		C					
Pliocene late	CN12d	3-4,96–97	21.76	A	M	1	1							C	C		R	R			F		C					
		3-5,44–45	22.74	A	M	1	1							C	C		R				F		C					
		3-5,110–111	23.40	A	M/P	2	1							C	C		R		R		F		C		R			
		3-6,30–31	24.10	A	M	1	1							C	C		R	R			F		C					
		3,CC(3–4)	25.8	A	M	1	1							C	R		R				F		A					
		4-1,33–34	26.13	A	M	1	1							C	C		R	R			C		A					
	CN12c	4-1,112–113	26.92	A	M	1	1							C	F		R		R		F		A					
		4-2,30–31	27.60	A	M	1	1							C	F		R				F		A					
	CN12b	4-2,112–113	28.42	A	M	1	1							C	F		R	R			F		A					
		4-3,25–26	29.05	A	M	1	1							C	C		R				C		C					
	CN12a	4-3,112–113	29.92	A	M	1	1							C	C		R	R			F		C					
		4-4,112–113	31.42	A	M	1	1							C	C		R				C							
		4-5,112–113	32.92	A	M	1	1							F	C		R				C							
		4,CC(14–15)	35.30	A	M	1	1							C	R		R				C							
		5-1,120–121	36.50	A	M	1	1							C	F		R	R			F							
		5-3,33–34	38.63	A	M	1	1							C	F		R				F							
		5-4,30–31	40.10	A	M	1	1	R		R				C	C			R			F							
		5-4,95–96	40.76	A	M	1	1							C	C			R			F							
Pliocene early	CN11	5-5,70–71	42.00	A	M	1	1							C	C			R			F							
		6-1,20–21	45.00	A	M	1	1	R		R		R		C	C			R			F						F	
		6-1,120–121	46.00	A	M	1	1	R		R				C	C			R			F						F	
		6-2,60–61	46.90	A	M	1	1							C	C			R			F						F	
	CN10c/d	6-2,120–121	47.50	A	M/P	2	1			R		R̄		C	C			R			F						F	
		6-3,20–21	48.00	A	M/P	2	1			R	R	R		C	C			R			F							
		6-3,120–121	49.00	A	M/P	2	1			R	R	R		C	F			R			C							
		6-4,60–61	49.90	A	M/P	2	1			F	R	R		C	C			R̲			F							
	CN10	6-4,120–121	50.50	A	M/P	2	1			F	R	R		C	C						C							
		6-5,20–21	51.00	A	M/P	2	1			R	R	F		C	C						C							
		6-5,115–116	51.95	A	M/P	2	1			F	R	R		C	C						F							
		6-6,20–21	52.50	A	M/P	2	1			R		R		C	C						F							
		6-6,120–121	53.50	A	M/P	2	1			F		R		C	C						F							
Miocene late		6-7,12–13	53.92	A	M/P	2	1			R	R	F		C	C						C							
		6,CC(15–16)	54.30	A	M/P	2	1			R	R	R		C	F	R					F							
		7-1,20–21	54.50	A	M/P	2	1			R	R	R		C	F						F							
		7-1,130–131	55.60	A	M/P	2	1			R	R	R		C	F						F							
	CN9b	7-2,20–21	56.10	A	M/P	2	1		R	R	R	R		C	F						F							
		7-2,130–131	57.10	A	M/P	2	1			R	R	R		C	F						F							
		7-3,20–21	57.60	A	M/P	1	1			R	R			C	F						C							
		7-3,130–131	58.60	A	M/P	2	1				R̲			C	F						F							
	CN5	7-4,43–44	59.23	A	M/P	2	1							F	F					F	F	R						
		7-4,130–131	60.10	A	M/P	2	1	R						F	F					F	F							
	CN4/5	7-5,42–43	60.72	A	M	2	1	R					F	A	R						F				F			R

Note: See footnote to Table 3A for definition of symbols.

Table 6. (Continued).

D. minutus	*D. asymmetricus*	*Discoaster aulakos*	*D. barbadiensis*	*D. berggreni*	*D. blackstockae*	*D. brouweri*	*D. challengeri*	*D. deflandrei*	*D. exilis*	*D. intercalaris*	*D. multiradiatus*	*D. pentaradiatus*	*D. pseudovariabilis*	*D. quinqueramus*	*D. sanmiguelensis*	*D. surculus*	*D. tamalis*	*D. tanii*	*D. triradiatus*	*D. variabilis*	*Discoaster* sp.	*Discolithina japonica*	*Emiliana annula*	*E. huxleyi*	*E. ovata*	*Gephyrocapsa aperta*	*G. caribbeanica*	*G. oceanica*	*Gephyrocapsa* sp.	*Helicopontosphaera granulata*	*H. kamptneri*	*H. wallichii*	*Pedinocyclus larvalis*	*Reticulofenestra pseudoumbilica*	*Reticulofenestra* sp.	*Rhabdosphaera clavigera*	*Scyphosphaera globulata*	*Sphenolithus abies*	*S. heteromorphus*	*Sphenolithus* sp.	*Striatococcolithus pacificanus*	*Syracosphaera hystrica*	*Thoracosphaera* sp.	*Triquetrorhabdulus rugosus*	*Umbilicosphaera mirabilis*	*U. sibogae*
																								C		A	C	C	C		C												F			
																					R	F				C	C	C	C		C												R			
																						F				C	C	C	C		C	F				F						F	F			F
																						F				F	C	C	C	R	C	R				R							F			F
																										C	C	C	C		C	R										F	F			
																						R				C	C	C	C	R	C					R						F	F			F
																						F	C		C	F	C	C	C		F											R	R			F
																							F		C	C		C	C		C					R							F			R
																						F	C		C	C	C	C	C	F	C					F						F	F			R
																							C		C	C	C	C	C		F					F						R	F			
																							C		C			C	C	R	F												F		R	
																						F	C		C		C	C	C		F												F			
																							C		C		F	C	A		F					F							F		R	
																						F	C		C		F	C	A	R	C												F			
																							C		C			C	A		C					R										
																						F	C		C			C	C		C												F			
																						F	C		C			C	C		F					R							R		R	
																							C		C				C		F												F			
																							C		C				C	F	F															
						F																	C		C				C	F						R										
						F																	C		C				C		F					R										R
						F													R			F	C		C				C		F												F			
						R																									F					R										
						R													F				F						C		F														R	
						F																R	C						C	R	C					R							F			
						F						F							F				C						C	F	F												F			
						F						F										R	C						C		F												F			
						C						C				F			F				C						C	R	F											R	R			
						C						C				F			F				C								R												F			
						C						F				F	F		R				C								R															
						C						C				F	F		R				C						C		R												F			
						C						C				C	C						C							F	R												F			
						C						C				C	F						C						C	F	R												R			
						C						C				C	F						F							R	R												F			
						C						F				C	C					R	C							R	R											R				
C	F					C						F				C	C						C						C													R				
C	F					C	R					F				C	F						C								F											F				
C	R					C	F					F				C	F												C		R			C						R		R				
C	R					C	F					F				F	F			F									C					C		R				F						
C	F					C	F									F				F														C						F			R			
C	C					C	F					R				F				F										R				C		R		R		F			R			
C	C					C	F					C				C				F														C				R		F						
C	C					C	F					C				C				F														C						F						
A	F				R	C	F					C				C				C										R				C						F						
A	C				R	C	F					C				C				F														C						F						
A						C	F					F				C				F														C						F						
A					R	C	F					F				C				C														C						F						
A	F					C	F					C				C				C														C						F						
A						C	F					C				C				C														C						F						
C	F				R	C	C					F				C				C														C						F						
A	R					C	F					F				C				F														C						F						
A						C	F					F				C				C														C						F						
A						C	F					F				C				C														C						F						
A						C	F					F				C				F														C						F						
C	R					C	C	R				F		F		C		F		C														C						F						
C	R					C	F	R				C		C		C				C														C						F						
C						F	F					C		C		F				F														C						F						
C						C	F			R		F	R	F		F				C													1	C						F				1		
F		R		R		C	F		F						F					C														C	R					F						
F		F	1			C	F	F	F						F					C													R	C	R					F						
		F				F	F	C	F		RR				F																			F	R				F	F	R					

Table 7. Distribution of calcareous nannofossils in the Maestrichtian in Hole 577A.

Age	Nannofossil zone	Core-Section (level or interval in cm)	Sub-bottom depth (m)	Abundance	Preservation	Etching	Overgrowth	Reworking	*Ahmuerella octoradiata*	*Arkhangelskiella cymbiformis*	*Ceratolithoides aculeus*	*Cretarhabdus conicus*	*C. crenulatus*	*C. surirellus*	*Cretarhabdus* sp.	*Cribrosphaera ehrenbergii*	*Cylindralithus serratus*	*Cylindralithus* sp.	*Discorhabdus rotatorius*	*Eiffellithus turriseiffeli*	*Glaukolithus diplogrammus*	*Lithraphidites carniolensis*	*L. quadratus*	*Manivitella pemmatoidea*	*Microrhabdulus decoratus*	*Micula murus*	*M. prinsii*	*M. staurophora*	*Parhabdolithus embergeri*	*Prediscosphaera cretacea*	*P. grandis*	*Quadrum gartneri*	*Reinhardtites anthophorus*	*Stephanolithion mutitum*	*Watznaueria barnesae*	*Zygodiscus spiralis*	*Zygodiscus* sp.	*Zygolithus tarboulensis*	Foraminifer debris
Maestrichtian	*Micula prinsii*	12-4,75	109.65	A	M	2	1		F	F			R	C	C	C	C	C		C	R	C	R	R	C	C		C		A	R			R	R	F	C	F	C
		12-4,80	109.70	A	M	2	1		F	F				C	C	A	C	C		C	R	C	R	F	R	C		C	F	A	R				A	C	C	F	F
		12-4,82–83	109.72	A	M	2	1		F	R				C	C	C	C	C		C		C		R	C	C	R	A	R	A	R	F			A	C	C	C	F
		12-4,100	109.90	A	M	2	1		R	F				F	A	A	C	C		C		C	F	C	C	C		A		A	F	F			A	C	C	R	
		12-4,120	110.10	A	M	1	1		F	F				C	C	C	C	C		C	R	C		C	C	C		A		A	F	R			A	F	C		
		12-4,126–127	110.16	A	M	2	1			C			F	C	C	C	A	A		C		A	F	C	C	A	R	A		A									
		12-5,6–7	110.46	A	M/P	2	1			F				F	A	C	A	A		F	F	F	R	C	C	A		A		A	C	C	F		A		F	F	
		12-5,86–87	111.26	A	M/P	2	1			R				C	A	C	A	A		F		A	F	F	C	A	R	A		A	C	C	F		A	F			
		12-5,146–147	111.86	A	M/P	2	1			R		F		C	A	F	A	A		R	F	A	F	F	F	A	R	C		A	C	F			A		F		
	Micula murus	12-6,26–27	112.16	A	M/P	2	1		F	R					A	C	A	A		F	F	A		C	F	C		C		A	C	F			A		F		
		12-6,30–31	112.20	A	M/P	2	1			F				C	A	C	A	A	R	C	C	A	F	C	C	C		C		A		F			A		C		
		12-6,80–81	112.70	A	M/P	2	1			C				C	A	C	A	A		C	C	A	F	F	C	A		C		A	F				A		C		
		12-6,130–131	113.20	A	M/P	2	1		F	C	R		F	C	A	C	A	A		C	F	A		F	C	C		F		A					A		F		
		12-6,140–141	113.40	A	M	2	1			C		C		C	A	C	A	C		C	F	A	R	C	C	A		C		A					C		F		
		12,CC	113.90	A	M	2	1		F	F	F	F	C	C	C	C	C	C		C		C		C	C	A		F		A	F				C				
		13-1,44–45	114.34	A	M	2	1			C	R	F	C	C	C	C	C	F		C	F	F	F	C	C	F		F		A					C	R	R	R	R
		13-1,106–107	114.96	A	M	2	1		F	C	R	C	C	C	C	C	C	F		C		F	F	F	C	F		F	R	A					C	R	R		
		13-2,44	115.84	A	M	2	1		F	C	F	C	C	C		C	C	C	R	C	F	F		C	C	F		C	F	A	R				C	C		R	
		13-2,106–107	116.46	A	M	2	1		F	F	F	C	C	C	F	C	C	C		C	R	C	R	C	C	C		C		A					C	C			
		13-3,44–45	117.34	A	M	2	1		F	C	F	C	C	C	F	C	C	C		C	F	C		C	C	F		C	R	A				R	C	F			
		13-3,106–107	117.96	A	M	2	1		F	C	R	C	A	C		C	C	C	R	C	F	C		C	C	F		C	F	A					C	F			
		13-4,44–45	118.84	A	M	2	1		F	F	C	C	C	C	F	C	C	A		C	F	C	F	C	C	R		C	R	A	F	F		R	C	R			
		13-4,106–107	119.46	A	M	2	1		F	R	R	F	C	C		C	C	C		C	F	C	F	C	C	F		F	R	C	F	F			C	F	R		
		13-5,44–45	120.34	A	M	2	1		F	F			C	F	C	C	F	C		C	C	C	F	C	C	F		F	F	C		F		R	C	F			
	Lithraphidites quadratus	13-5,106–107	120.96	A	M	2	1		F	F		C	C	C	F	A	F	C		C	F	C	F	C	C			F	F	C	F	F			C	F			
		13-6,44–45	121.84	A	M	1	1		F	F		C	C	C	F	A		C		C	F	C	F	C	C			F	F	C					C	C			
		13-6,106–107	122.46	A	M	1	1		F	F		C	C	F	C	A		C		C	F	A		A	C			R	F	C	F	F			C	F	F		
		13,CC	123.4	A	M	1	1		F	F	F	C	C	C		C		F		C	F	A	A	A	C			F	F					F	C	F			

Note: See footnote to Table 3A for definition of symbols.

fossils by the increased frequency of *Thoracosphera*, a calcareous dinoflagellate. *Thoracosphera* was found throughout upper Maestrichtian sediments in low latitude sections like Caravaca and El Kef (Perch-Nielsen, 1981a), but it is not present in high latitude sections such as the North Sea. At Site 577, rare species of *Thoracosphaera* appear at the very top of the Upper Cretaceous samples: 5 cm below the Cretaceous/Tertiary boundary.

The appearance and subsequent increase of *Thoracosphaera* is abrupt and occurs just at the bottom of the color change where the boundary was placed, at about 109.60 m sub-bottom depth. Immediately below the first occurrence of *Thoracosphaera* a sizable portion of "debris of forams" was observed; they have been listed in the range chart because it appears to be a characteristic feature of the Cretaceous/Tertiary boundary interval. Foraminifer fragments decrease and almost disappear about 40 cm above the Cretaceous/Tertiary boundary. The increase of *Thoracosphaera* comes together with the first occurrence of small ~1 to 3 μm *Biscutum* such as *B. romeinii*, a form described by Perch-Nielsen (1981a) in the lowermost Paleocene of the El Kef section. In my samples, these small *Biscutum* always have an empty central area. *Markalius astroporus* and *Cyclagelosphaera reinhardtii* appear slightly above the Cretaceous/Tertiary boundary. Only rare specimens of *B. bigelowi* and *B. sparsus* are found.

The first specimens of *Cruciplacolithus* belong to *C. primus*. Forms of this species vary greatly in size and in the dimensions of the central area.

Very rare forms of small *Prinsius* and *Toweius* were found together with *C. primus*. *C. tenuis, Ericsonia cava,* and *E. subpertusa* become common in the upper part of the *C. tenuis* Subzone (CP1b).

As a conclusion, if we consider the assemblage and the succession of the nannofossil events and compare them with the magnetostratigraphy (Monechi et al., this volume) we can say that the Shatsky Rise provides a well preserved and continuous Cretaceous/Tertiary boundary section. The enrichment in iridium (Michel et al., this volume) and the oxygen isotope values (Zachos et al., this volume) found just at the Cretaceous/Tertiary boundary support the statement that the Shatsky Rise sections are indeed some of the most complete sequences across the Cretaceous/Tertiary boundary.

Maestrichtian

Both Holes 577 and 577A (the lower part of Cores 12 and 13) and Hole 577B (the lower part of Core 1) contain moderately to strongly dissolved Upper Cretaceous nannofossil assemblages.

Micula prinsii, the marker of the uppermost Maestrichtian, was first found in all three holes, in Samples 577-12-6, 142 cm, 577A-12-5, 146 cm, and 577B-1-5, 120 cm (Tables 4, 7, and 10). The specimens are rare and not very well preserved. The *M. murus* Zone was recognized in all three holes. The base of this zone was reached only at Hole 577A (Sample 577A-13-5, 44 cm, Table 7).

Intermediate forms between *M. staurophora* and *M. murus* can be observed in the lower part of Core 13 in Hole 577A.

The oldest recovered nannofossil assemblage was in Hole 577A. This assemblage belongs to the middle Maestrichtian *Lithraphidites quadratus* Zone and is dominated by the following species: *L. quadratus, Arkhangelskiella cymbiformis* (few), *Ahmuerella octoradiata, Cretarhabdus surrirellus, C. crenulatus, Cylindralithus serratus, Eiffellithus turriseiffeli, Prediscosphaera grandis, M. staurophora,* and *Watznaueria barnesae*.

Site 580

Site 580 lies near the present day subarctic front (42°N), marking the northern margin of the transition zone between the subarctic and subtropical gyres (Fig. 1). Coring was intended to provide a detailed paleoceanographic record in the subtropical/subarctic gyre transition zone for the late Miocene to Recent and to document north–south migration of the frontal zone with time.

Calcareous nannofossils are absent in all the cores recovered except the core catcher of Core 13. The poorly preserved assemblage in this sample includes *Crenalithus doronicoides, Coccolithus pelagicus, Calcidiscus leptoporus, Emiliania annula, Discoaster brouweri, Ceratolithus rugosus, Gephyrocapsa* sp., and *Reticulofenestra* sp. This assemblage belongs to the late Pliocene *D. brouweri* Zone (CN12).

REMARKS ON SYSTEMATICS

Braarudosphaera sp. 1
(Plate 1, Figs. 1–10, 12)

Braarudosphaera (sp. ind.) in Thierstein and Manivit, 1981 (plate 7, figs. 1–4).

Remarks. The pentaliths consist of five subradial, imbricate elements having almost straight radial sutures that meet the peripheral margin at the midpoints between adjacent apices. All specimens found are considerably overgrown; in fact the length of the elements of some specimens is doubled or even tripled by overgrowth (see Plate 1, Fig. 4). The overgrowth of the elements of the *Braarudosphaera* gives a typical rotational pattern (see Plate 1, Figs. 5 and 11). This specimen differs from *Braarudosphaera imbricata* by a star-shaped outline. *Bukryaster hayii* differs from *Braarudosphaera* sp. 1 by its central disc with orientated ridges.

Occurrence. Found in Campanian sediments in Core 576B-8 in the *Aspidolithus parcus* Zone. Thierstein and Manivit (1981) found the same forms in the Campanian deep-sea sediments at Site 462, Cores 55 and 9A (Nauru Basin).

Rucinolithus magnus Bukry, 1975
(Plate 2, Figs. 1–3)

Rucinolithus magnus Bukry, 1975 (p. 690, plate 3, figs. 12–14).

Remarks. Specimens composed of large radial rosettes of six equal rhombohedral elements and tapered to points. The elements are slightly imbricate at the center. This species differs from *R. hayii* (Plate 2, Fig. 11) by its larger size and more elongate elements.

Distribution. Common in Campanian sediments in Core 576B-8.

Discoaster sp. A.
(Plate 10, Fig. 2)

Discoaster sp. 1 Okada and Thierstein, 1979 (p. 523, plate 15, fig. 11).

Remarks. Discoaster composed of five to seven thick rhombohedral rays. The sutures are straight and the rays symmetrically arranged.

Distribution. Common in the upper Paleocene, *D. nobilis* Zone, at Site 577. Found at Site 384, Western North Atlantic Ocean, in upper Paleocene sediments.

ACKNOWLEDGMENTS

I would like to thank Katharina Perch-Nielsen and Hans Thierstein for helpful criticism and critical reading of the manuscript and Franca Proto Decima for valuable discussions. Mr. Maurizio Ulivi provided technical assistance at the scanning electron microscope, and Mr. Fabio Cozzini prepared the photographs for the plates. Research was supported by Consiglio Nazionale delle Ricerche—Centro di Studio per la Geologia dell'Appennino e delle Catene Perimediterranee (Publ. 147) and through M.P.I. No. 0071.

APPENDIX
Taxonomic List

Calcareous nannofossil species considered in this report are listed in alphabetical order. The bibliographic references of these species are provided in Loeblich and Tappan (1966, 1968, 1969, 1970a,b, 1971, 1973) and in the bibliography of van Heck (1979–1984).

Mesozoic

Ahmuerella octoradiata (Gorka, 1957) Reinhardt, 1964
Arkhangelskiella cymbiformis Veskina, 1959
Aspidolithus parcus (Stradner, 1963) Noël, 1969
Braarudosphaera africana Stradner, 1961
B. bigelowii (Graan and Braarud) Deflandre, 1947
B. imbricata Bukry, 1969
Braarudosphaera sp. 1
Broinsonia enormis (Shumenko, 1968) Manivit, 1971
Bukryaster hayii (Bukry, 1969) Prins, 1971
Ceratolithoides aculeus (Stradner, 1961) Prins and Sissingh, 1977
Chiastozygus litterarius (Gorka, 1957) Manivit, 1971
Cretarhabdus conicus Bramlette and Martini, 1964
C. crenulatus Bramlette and Martini, 1964
C. surrirellus (Deflandre, 1954) Reinhardt, 1970
Cretarhabdus sp.
Cribrosphaera ehrenbergii (Arkhangelsky, 1912) Deflandre, 1952
Cyclagelosphaera margerelii Noel, 1965
Cylindralithus serratus Bramlette and Martini, 1964
Cylindralithus sp.
Discorhabdus rotatorius (Bukry, 1969) Thierstein, 1973
Eiffellithus eximius (Stover, 1966) Perch-Nielsen, 1968
E. turriseiffeli (Deflandre, 1954) Reinhardt, 1965
Glaukolithus diplogrammus (Deflandre, 1954) Reinhardt, 1964
Kamptnerius magnificus Deflandre, 1959
Lithastrinus floralis Stradner, 1962
L. grillii Stradner, 1962
Lithastrinus sp.

Table 8. Distribution of calcareous nannofossils in the Paleocene-Eocene in Hole 577A.

Age	Nannofossil zone	Core-Section (level or interval in cm)	Sub-bottom depth (m)	Abundance	Preservation	Etching	Overgrowth	Reworking	*Biantholithus sparsus*	*Biscutum romeinii*	*Biscutum* sp.	*Braarudosphaera bigelowii*	*B. discula*	*Bramletteius serraculoides*	*Campylosphaera dela*	*Chiasmolithus bidens*	*C. californicus*	*C. consuetus*	*C. danicus*	*C. expansus*	*C. grandis*	*Coccolithus crassus*	*C. eopelagicus*	*C. formosus*	*C. jugatus*	*C. pelagicus*	*Crepidolithus* sp.	*Cruciplacolithus edwardsii*	*C. primus*	*C. subrotundus*	*C. tenuis*	*Cyclagelosphaera reinhardtii*	*Cyclicargolithus floridanus*	*Cyclicargolithus* sp.	*Cyclococcolithus gammation*	*Cycolithella kingii*	*C. placitis*	*Dictyococcites bisectus*	*D. scrippsae*	*Discoaster barbadensis*	*D. diastypus*	*D. germanicus*	*D. lenticularis*
Eocene middle	CP15	75,36−37	63.26	A	P	2	2	R						C										C		C							R					C		C			
		7-5,86−87	63.76	A	P	1	2	R						C								F		F		F												C		C			
	CP14	7-6,36−37	64.76	A	M/P	1	1							F	F					R	R		C	C	R	F												C		C			
		7-6,87−87	65.26	A	M/P	1	1							F	F						F	C	C	C	F	C								C				A		C			
early	CP12	7,CC,(2−3)	65.76	A	M/P	1	1							F	C		R			F	C	C	C	C	F	F								C	F	F				C			
	CP11	8-1,105−106	67.45	A	M/P	1	1							F	C						C	C	C	C	C	C								C	F				F	C			
		8-2,105−106	68.95	A	M/P	1	1								C		F			F	C	C	C		F	F								C		F			C	F			
		8-3,105−106	70.45	A	P	2	2							F	C		F			C	C	C	C	C	F	C								C					F	F		F	
		8-4,20−21	71.10	A	M/P	1	1							R	C	F	R				F	F	C	F	F	C								C	C	R				F			
		8-4,105−106	72.95	A	P	2	2								C	F	R			C	C	C	A	C	F	C														C			
	CP10	8-5,15−16	73.55	A	P	2	2							R	C	F	F			F	R	R	C	C												C				C		F	
		8-5,105−106	74.45	A	P	2	2							F	C	R	F	F			C		A	C	C	C										F				F			
		8-6,15−16	75.05	A	P	2	2							R	C	F	F	F		F	C		C	C	C	C										F				C			
		8,CC(5−6)	74.43	A	M/P	2	1								F	F	F				F		C	C	F	C										F				C	C		
	CP9b	9-1,30−31	76.20	A	M/P	1	2							F	F	F	F			F	F		C		R	C										F				C	C		
		9-1,97−98	76.88	A	M/P	1	2									F	F							C		C										F				A	C		C
		9-2,30−31	77.70	A	M/P	2	1							F		F	C	C						C		C														C			C
		9-2,97−98	78.38	A	M	1	1							F		F	C	C						C		C														C			C
		9-3,30−31	79.20	A	M	1	2							F		C	F	C						C		C														C	C		C
		9,CC(10−11)	79.65	A	M	1	1	R						F	C	F	F	C								C																	
Paleocene late	CP7	10-1,39−40	85.79	A	M/P	1	2											C								C																	
		10-1,120−121	86.60	A	M/P	1	2									F	F	C								A																	
		10-2,39−400	87.29	A	M/P	2	1										F									C																	
		10-2,120−121	88.10	A	M	1	1										F	C								A																	
	CP6	10-3,33−40	88.79	A	M/P	2	1										F									C																	
		10-3,120−121	89.60	A	M	1	1										F	C								A																	
		10-4,120−121	91.10	A	M	1	1										C	F								A																	
		10-5,39−40	91.79	A	M	1	1										F	C								A																	
		10-5,120−121	92.60	A	M	1	1	R									F	C								A																	
		10-5,128	92.78	A	M/P	2	2											F								C																	
	CP5	10-6,10−11	93.00	A	M	1	1									F	C	C	F							C				F													
	CP4	10,CC	95.38	A	M	1	1									F	C	C	F							C				R	C	R											
		11-1,40	95.30	A	M	1	1											C	F							C			R		C												
		11-1,110−111	96.00	A	M	1	1											C	F							C					C												
		11-2,110−111	97.50	A	M	1	1											F	F							C		R			C												
early	CP3	11-3,39−40	98.29	A	M	1	1	R																				F															
		11-3,110−111	99.80	A	M	1	1	R										F	F							C					C												
		11-4,40	99.80	A	M/P	2	1	R																				F															
	CP2	11-4,110−111	100.50	A	M/P	2	1	C																							C												
		11-5,110−111	102.00	A	M	1	1	C											F							C		F	F		C	R											
		11-6,110−111	103.50	A	M	1	1	C	R										F							C			F		C												
		11-7,5−6	103.85	A	M	1	1	C			F		R						F							C		F	C		C	F											
		12-1,95−96	103.35	A	M/P	2	1	C			C								F							C		F	C		C												
	CP1b	12-1,126−27	105.66	A	M	1	1	C			C															C		F	C		C	C											
		12-2,26−27	106.16	A	M	1	1	C		R	C															C		F	C		C												
		12-2,66−67	106.56	A	M/P	1	1	C		C	C															C	F	F	C		C	C											
		12-2,106−107	106.96	A	M/P	2	1	C		A	C															C	F	F	C		C	C											
		12-2,146−147	107.36	A	M	1	1	C		A	F															C	C		A		C	C											
		12-3,10	107.50	A	M	1	1	C		A	F															F	C		A		C	C											
		12-3,30−31	107.70	A	M	1	1	F	R	A	F																		A		C	C											
		12-3,66−67	108.06	A	M	1	1			A	F															R	C		A		C	C											
	CP1a	12-3,106−107	108.46	A	M	1	1	F		A																			C			F											
		12-3,146−147	108.86	A	M	1	1	F		A																			A			A											
		12-4,7−8	108.97	A	M/P	2	1	F	R	A																			C			A											
		12-4,15	109.05	A	M/P	2	1	F		A																			F			A											
		12-4,26−27	109.16	A	M	1	1	C	R	A																			R			A											
		12-4,30	109.20	A	M	1	1	R	R	A																						C											
		12-4,35−36	109.25	A	P	2	1	R		A																			R			C											
		12-4,38	109.28	A	P	2	1	R	R	A		R																				C											
		12-4,41−42	109.33	A	P	2	1	R	R	A		R																	R			C											
		12-4,44	109.36	A	P	2	1	R		A																						F											
		12-4,48	109.40	A	P	2	1	R		A	R																				R	C											
		12-4,50	108.42	A	P	2	2	R		A																						C											
		12-4,51−52	109.43	R	P	2	2	R		A																					R	F											
		12-4,54−55	109.46	R	P	2	2	C		A																						C											
		12-4,56	109.48	F	P	2	1	A		A																						F											
		12-4,58	109.50	F	P	2	1	A		A	F																					F											
		12-4,59	109.51	C	P	2	1	A		A	C																					R											
		12-4,60	109.52	C	P	2	1	A		A	C																					F											
		12-4,62	109.54	C	M/P	2	1	A		A	C																																
		12-4,63	109.55	A	M/P	2	1	A		R	C																																
		12-4,65	109.57	A	M/P	2	1	A		R	F																																
		12-4,68	106.60	A	M	1	1	A		R	R																																
		12-4,70	109.62	A	M	2	1	A		R	R																																

Note: See footnote to Table 3A for definition of symbols.

Table 8. (Continued).

D. lodoensis	*D. mohleri*	*D. multiradiatus*	*D. nobilis*	*D. okadai*	*D. saipanensis*	*D. salisburgensis*	*D. sublodoensis*	*D. tanii*	*Discoaster* sp. 1	*Discoaster* sp	*Discoasteroides kuepperi*	*Discolithina plana*	*D. rimosa*	*Ellipsolithus distichus*	*E. lajollaensis*	*E. macellus*	*Ericsonia cava*	*E. robusta*	*E. subpertusa*	*Fasciculithus havii*	*F. involutus*	*F. pileatus*	*F. tympaniformis*	*F. ulii*	*Fasciculithus* sp.	*Heliolithus conicus*	*H. kleinpellii*	*Markalius astroporus*	*Neochiastozygus concinnus*	*Neococcolithus dubius*	*Pedinocyclus larvalis*	*Prinsius bisulcus*	*P. dimorphosus*	*Reticulofenestra umbilica*	*Rhabdosphaera perlonga*	*Rhabdosphaera* sp	*Sphenolithus anarrhopus*	*S. heteromorphus*	*S. moriformis*	*Sphenolithus primus*	*S. radians*	*S. spiniger*	*Striatococcolithus pacificanus*	*Thoracosphaera deflandrei*	*T. operculata*	*T. saxea*	*Thoracosphaera* sp	*Toweius craticulus*	*T. eminens*	*T. magnicrassus*	*T. tovae*	*Toweius* sp.	*Tribrachiatus orthostylus*	*Wiseorhabdus inversus*	*Zygodiscus sigmoides*	*Z. simplex*	*Zygodiscus* sp	*Zygrhablithus bijugatus*	Foraminifer debris
R					C			F		F																						A					F				F				R						R	F				R	
F					C			F		F																						R					R																R	R					
																																				C		C					C														C					
R					F																																C	R	F			F		F		F								C						
C							F					C																					F									F			C		F							C				F					C
A										C	R	F		R																			F													F						F			C								A	
C										C	F	R																						R										F		C		C						F			C								C	
A													F																							F														C		C						F			C			R					C	
C																																					F										F		C	F										F			F					A	
A										A		F																							C														C		C						C			C			F					A	
C						C					F	R	R																				F										F		C						F			F			F					A	
C										C	R	F		F																			R											F		C	F	C				F	F		C			C					A	
C										C	F	F			R																															C		C	F	C					F		R			C					C	
C										F		F		C																																F		C	F												C	F				C	
							C							C		F	F												C		R				R			F		C		F				C	F				C	F					C	
		R				C							C			F											F	F										C		C								C						C	C			A	
																																											C															F					A	
															F			C										F											C													C					A	
		C	C									C			F	C		C								C							C		F									C					C					F	
	C	A	C	F						C		F	R		F	C		C						C																					F	C											
	C		C	F					C				F	F		C	C		C										F								C												C											
	C		C	C					C	C			F	F		C	C		C	C					C			F									C												C											
	C		C	R																					C																										F											
	C		F	F				C			C			F	R		F	C		C	C			C													C		C									C								F				
	C																									C																																		C				
	C									F	C			F	R		R	C		C				C		C				F							A		C									C							C				
	C										C				F		C	C		C	C			C		A							C					A		A							F								C				
	C										C				F		C	C		C	F			C		A		R									C		C	C							F		F		F				C				
	C										A				C		C	C		C	F			C		A		C	F									C		C	C												F				C				
	C															R		F	C	C									F											C		C	C													F									
															R	C	C	C	F	F	C	C	F	A	R	F													C								C		C				A	C			
															F	C	F	C	F		C	F		A														C								C		C				A	C			
																C	F	C			C	R	F	A			C												C												C				A	C			
															R	C	F	C		F	C	F	C	A			C	C											C											C				A	C			
															R	C		C		F	C	F	C	A			F	C											C															A	C			
															R												F											C															A	C			
																C		C			F				A			F	F											C															C	C			
															R																										C															C	C			
																C	F	C																					C															C	C			
																C		C																																							C	C			
																C		C										C																									A	C	F		
																C		C										F																			F					F			A		C		
																C		C										R																			F					A			A		C		
																C		C										F															R			F					A			A		C		
																C		C										R																		F	F					A			A		C		
																C		C										R															R	R	R	F								A		C		
																F		C										F	F													R	F	F	F								A		C		
																												R					F											R	C	C	C								C		C		
																				F								F					C											F	C	C	C								C		F		
																												R																F	C	C	C								C		C		
																												F																F	C	C	C								R		F		
																												F																F	C	A	A										F		
																												C																F	F	A	C								R				
																												A																F	C	A	C								F		F		
																												C																C	C	A	C												
																												R																		R	C	C										R		
																												R																F	F	C	C												R
																												R																R	R	C	F												R
																												F																	R	C	C												R
																												F																F	C	C	C												R
																												R																	R	R	C												F
																												R																	F	C	C												F
																												F																	C	C	C										R		F
																												R																		R	C								F		R		F
																																													C	C	C										F		F
																												R																F	C	C	C										R		F
																												R																R	C	A	C										C		F
																																												R			C												C		C
																												R																			C												C		C
																																															C												C		C
																												R																R			C												C		C
																												R																R			C												C		C
																																												R			F												C		C
																																												R			F												C		C

Table 9. Distribution of calcareous nannofossils in the Neogene in Hole 577A.

Age	Nannofossil zone	Core-Section (level or interval in cm)	Sub-bottom depth (m)	Abundance	Preservation	Etching	Overgrowth	Reworking	*Amaurolithus amplificus*	*A. delicatus*	*A. primus*	*A. tricorniculatus*	*Bramletteius serraculoides*	*Calcidiscus leptoporus*	*C. macintyrei*	*Ceratolithus acutus*	*C. cristatus*	*C. rugosus*	*C. telesmus*	*Coccolithus miopelagicus*	*C. pelagicus*	*Coronocyclus nitescens*	*Crenalithus doronicoides*	*C. productellus*	*Cricolithus jonesii*	*Cyclicargolithus* sp.	*Cyclolithella rotula*	*Dictyococcites bisectus*	*D. minutus*
Pleistocene	CN15	1-1,100−101	1.0	A	M	1	1							C			R		R		F			C	C				
		1-2,100−101	2.50	A	M	1	2	R						C							C			C	F				
	CN14b	1-3,100−101	4.00	A	M	1	1							F			R				C		C	C	C				
		1-4,100−101	5.5	A	M	1	1							F			R				C			A					
		1-5,100−101	7.00	A	M	1	1	R						R			F		R		F		C	C					
		1-6,100−101	8.50	A	M	1	1							F			R		R		F		C	A					
		1-2,29−30	9.29	A	M	1	1							F							C		C	C					
		1,CC,4−5	9.40	A	M	1	1							C			R				A		C		F				
		2-1,15	9.55	A	M	1	1	R						C	I		R				C		C						
	CN13/14a	2-2,30−31	11.20	A	M	1	1							C			R				C		A						
		2-3,30−31	12.70	A	M	1	1							C							F		A						
		2-4,30−31	14.20	A	M	1	1							A							R		C						
		2-4,135−136	15.25	A	M	1	1			I				C			R				F		F						
		2-5,100−101	16.40	A	M	1	1							F					R		R		C						
		2-6,95−96	17.35	A	M	1	1							C				R	R		R		C						
		3-1,90−91	19.80	A	M/P	1	1							C	F		RR	R			F		A						
		3-2,90−91	21.30	A	M	1	1							F	C								A		R				
Pliocene late		3-3,60−61	22.50	A	M	1	1							C	F		R	R					A						
		3-4,79−80	24.19	A	M/P	1	1							C	R		RR				C		A						
	CN12d	3-5,50−51	25.40	A	M	1	1	R						C	C		R				C		A						
	CN12c	3,CC,13−14	25.90	A	M	1	1							C	C				R		C		A		R				
	CN12b	4-1,80−81	29.20	A	M	1	1							C	C						F		A						
		4-2,80−81	30.70	A	M	1	1							C	C			R			F		C						
		4-3,80−81	32.20	A	M	1	1							C	C		F				R								
		4-4,80−81	33.70	A	M	1	1							C	C						C								
		4-5,80−81	35.20	A	M	1	1																						
		4-6,80−81	36.70	A	M	1	1																						
		4,CC,17−18	37.87	A	M	1	1							C	A		R	R			C								C
		5-1,30−31	38.20	A	M	1	1			R				C	C						C								C
		5-1,100−101	38.90	A	M	1	1							C	C		R	R			C								C
	CN12a	5-2,100−107	40.40	A	M	1	1			R				C	C						F								C
		5-3,30−31	41.20	A	M	1	1	R				R		C	C			R			F								C
		5-3,100−101	41.90	A	M	1	1							C															C
		5-4,30−41	42.70	A	M	1	1							C	A			R											C
		5-4,100−101	43.40	A	M	1	1							C	C			F											C
		5-5,30−31	44.20	A	M	1	1							C	C			F											C
early		5-5,100−101	44.90	A	M	1	1	R		R				C	C			F	R										C
		5-6,30−31	45.70	A	M	1	1			R				C	C			F											C
		5,CC,16−17	46.56	A	M/P	1	1	R		R				C	C		R	R	R								C		C
	CN11	6-1,15−16	47.55	A	M/P	1	1						F	C	C		F	C			F						F		A
		6-2,15−16	49.05	A	P	2	1			F	R	F		C	C			F			C						F		A
		6-3,15−16	50.55	A	M/P	1	1	R		F	R	F		C	C			C			C	R					F		A
	CN10c/d	6-4,15−16	52.05	A	M/P	2	1	R	R	F	R	F		C	F			R			C								A
		6-5,15−16	53.55	A	M/P	1	1	R		F	R	C		C	F	R		R			C								A
Miocene late		6-6,15−16	55.05	A	M/P	1	1			F	F	F		C	C			R			C								A
	CN10a/b	6-7,15−16	56.55	A	M/P	1	1			F	F	F		C	F						C								A
		6,CC,30−31	57.15	A	M/P	1	1			F	R			F	F						C								C
		7-1,86−87	57.76	A	M/P	1	1			F	F	F		C	F						C	F							C
	CN9b	7-2,86−87	59.26	A	M/P	1	1			F	R			C	F						C								F
		7-3,86−87	60.26	A	M	1	1	F			1			C	F					C	F	F							
	CN5/4	7-4,86−87	62.26	A	M	1	1	R					R	C	F					F	F					F		F	

Note. See footnote to Table 3A for definition of symbols.

Lithraphidites carniolensis Deflandre, 1963
Lithraphidites quadratus Bramlette and Martini, 1964
Manivitella pemmatoidea (Deflandre ex Manivit, 1965) Thierstein, 1971
Microrhabdulus decoratus Deflandre, 1959
Micula murus (Martini, 1961) Bukry, 1973
M. prinsii Perch-Nielsen, 1979
M. staurophora (Gardet, 1955) Stradner, 1963
Parhabdolithus embergeri (Noël, 1959) Stradner, 1963
Prediscosphaera cretacea (Arkhangelsky, 1912) Gartner, 1968
P. grandis Perch-Nielsen, 1979
P. spinosa (Bramlette and Martini, 1964) Gartner, 1968
Quadrum gartneri Prins and Perch-Nielsen, 1977 in Manivit et al.
Q. gothicum (Deflandre, 1959) Prins and Perch-Nielsen, 1977 in Manivit et al.
Q. trifidum (Stradner, 1961) Prins and Perch-Nielsen, 1977 in Manivit et al.
Reinhardtites anthophorus (Deflandre, 1959) Perch-Nielsen, 1968
Rucinolithus hayii Stover, 1966
R. irregularis Thierstein, 1972
R. magnus Bukry, 1975

Table 9. (Continued).

Discoaster asymmetricus	D. aulakos	D. barbadiensis	D. berggreni	D. blackstockae	D. brouweri	D. challengeri	D. deflandrei	D. exilis	D. intercalaris	D. multiradiatus	D. pentaradiatus	D. pseudovariabilis	D. quinqueramus	D. sanmiguelensis	D. surculus	D. tamalis	D. tanii	D. triradiatus	D. variabilis	Discoaster sp. A	Discoaster sp.	Discolithina japonica	Emiliania annula	E. huxleyi	E. ovata	Gephyrocapsa aperta	G. caribbeanica	G. oceanica	Gephyrocapsa sp.	Helicopontosphaera granulata	H. kampneri	H. wallichii	Pednocyclus larvalis	Reticulofenestra pseudoumbilica	R. umbilica	Rhabdosphaera clavigera	Scyphosphaera globulata	Sphenolithus abies	S. heteromorphus	Sphenolithus sp.	Striatococcolithus pacificanus	Syracosphaera hystrica	Thoracosphaera sp.	Triquetrorhabdulus rugosus	Umbilicosphaera mirabilis	U. sibogae	Zygrhablithus bijugatus
																						F		C̲		C	C	A			C																
																					R	F				A	A	C			C												F				
																										C	A	C			F	F				R										C	
																							F		C̄	A	A	A			F					F						F				C	
																					R	R	F		C		A	C			C					R						F	F				
																							A		A	F	F	C	C		C											F	R			F	
																						C	A		A	C	F	C	C		C					C						F	F			F	
																						F	C		C	C	C	C	C		C					C										F	
																					R	F	C		C	C	A	F	C		C					F						F	R			F	
																						C	C		F		C		C		C																
																						F	C		F		F		F		F												F				
																						F	C		C				C		F																
																							C		C				C		F					R							F				
																						R	C		C				C		C					R									F		
																						R	C		C				C		F																
																							C		F				C		F																
																							F		F				C		R																
					F̄													F					C		F				C		F					R							R				
					R													R				R	F						C							R											
					C													R			R		C						F		R																
					F						R̄										R		F								F														C	F	
					F						F				F̄			R					C								F					R									F		
					C						F				C	F̄							F						C		F																
F					C						C				F	R							F						C		R																
R					C						C				F	C							F						C		F																
															C	C							F																								
															F	C							F																								
C					F						C				F	C							C																								
C					C						C				F	C							C							R	R																
C					C						C				C	C							C							R	R																
C					C						F				C	C		F				R	C							R	R															R	
C					C						F				A	C		R				R	C							R	R											R					
C					C						R				C	F							C																								
C					C						F				F	C							F																								
C					C						F				A	F							C						C																		
F					C	R					F				C	F							C						C													F					
F					C	C					C				C						R	R							C					C̄			R					F	F				
C					C	R					C				C															R	R			C			R										
C					C	F					C				C															F	F			C									F				
C					C						C				C	R			F											F				A													
F					C	F					C	F			C															R				C				F									
C					C	F				R	C	F			C				C															A	R		R			R							
C					C	F					C	F			C				C															A													
R				R	C	F					C				C				C	F										F				C													
F				R	C	C					C	F			C				C											F				C						C							F
R				R	F	C					C				F				C											F				C						C				R			
					C	F					C		F̄		F				C															C													
					C	F	R				F		C		R				C											R				C													
					C	C					F		C		F				C											R				A						F				R			
			R		F	F	R	R	R		F		F						C											R			C	C				R									
	F	1					C	C				F		F			R		C														F		R				F		F						

tephanolithion munitum Perch-Nielsen, 1973

atznaueria barnesae (Black, 1959) Perch-Nielsen, 1968

ygodiscus spiralis Bramlette and Martini, 1964

ygodiscus sp.

ygolithus tarboulensis Shafik and Stradner, 1971

enozoic

maurolithus amplificus (Bukry and Percival, 1971) Gartner and Bukry, 1975

. *delicatus* Gartner and Bukry, 1975

. *primus* (Bukry and Percival, 1971) Gartner and Bukry, 1975

A. tricorniculatus (Gartner, 1967) Gartner and Bukry, 1975

Biantholithus sparsus Bramlette and Martini, 1964

Biscutum romeinii Perch-Nielsen, 1981

Biscutum sp.

Braarudosphaera discula Bramlette and Riedel, 1954

Bramletteius serraculoides Gartner, 1969

Calcidiscus leptoporus (Murray and Blackman, 1898) Loeblich and Tappan, 1978

C. macintyrei (Bukry and Bramlette, 1969) Loeblich and Tappan, 1978

Campylosphaera dela (Bramlette and Sullivan, 1961) Hay and Mohler, 1967

Table 10. Distribution of calcareous nannofossils in the late Maestrichtian-early Paleocene in Hole 577B.

Age	Zone	Core-Section (level in in cm)	Sub-bottom depth (m)	Abundance	Preservation	Etching	Overgrowth	Reworking	*Ahmuellerella octoradiata*	*Arkhangelskiella cymbiformis*	*Cretarhabdus crenulatus*	*Cretarhabdus surirellus*	*Cretarhabdus* sp	*Cribrosphaerella ehrenbergii*	*Cylindralithus serratus*	*Cylindralithus* sp	*Eiffellithus turriseiffeli*	*Glaukolithus diplogrammus*	*Lithraphidites carniolensis*	*Lithraphidites quadratus*	*Microrhabdulus decoratus*	*Micula murus*	*Micula staurophora*	*Prediscosphaera cretacea*	*Prediscosphaera grandis*	*Zygodiscus spiralis*	*Zygodiscus* sp	*Watznaueria barnesae*	*Quadrum gartneri*	*Zygolithus tarboulensis*	*Stephanolithion munitum*	*Micula prinsii*	Foraminifer debris	*Thoracosphaera* sp	*Thoracosphaera deflandrei*	*Biscutum romeinii*	*Biscutum* sp	*Markalius astroporus*	*Cyclagelosphaera reinhardtii*	*Thoracosphaera operculata*	*Thoracosphaera saxea*	*Braarudosphaera bigelowi*	*Cruciplacolithus primus*	*Biantholithus sparsus*	*Placozygus sigmoides*	*Coccolithus pelagicus*	*Cruciplacolithus tenuis*	*Ericsonia subpertusa*	*Ericsonia cava*	*Cruciplacolithus edwardsii*	*Prinsius dimorphosus*	*Neochiastozygus concinnus*	*Chiasmolithus danicus*
Paleocene	CP2	1-1,10	104.50	A	M	1	1	F																										F											C	C	C	C	C			F	R
		1-1,30	104.70	A	M	1	1	C																										F	R						F		F		A	C	C	C	C	R		F	F
		1-1,70	105.10	A	M	1	1	C																										F	R		F				F		C		C	C	C	C	C	R			F
		1-1,90	105.30	A	M	1	1	C																										F	R		F				C		C		A	C	C	C	C	F		F	F
	CP1b	1-1,110	105.50	A	M	1		C																										C			F			R	C		C		A	C	C	C	C	R			
		1-2,15	106.05	A	M	1	1	C																										C	R		C			R	C		C		C	C	C	C	C	F			
		1-2,35	106.25	A	M	1	1	C																										C	R		C				C		F		C	C	F	C	C	R			
		1-2,55	106.45	A	M	1	1	C																										C	R	F	C			F	C		F		C	C	C	C	C	F			
		1-2,75	106.65	A	M	1	1	C																										C	R		C			F	F		F		C	C	C	C	C	F	F		
		1-2,85	106.75	A	M	1	1	C																										C	R	F	C			F	F		F		C	C	F	C	C	F	F		
		1-2,95	106.85	A	M	2	1	C																										C	R	F	C			F	C		C		C	C	C	C	A	F	F		
		1-2,115	107.05	A	M	2	1	C																										C		F	C				F		C		C	F	C	C	A	F			
		1-2,135	107.25	A	M	1	1	C																										C	R	F	C		F	F	F		C		C	C	C	C	A				
		1-2,145	107.35	A	M	1	1	C																										C	R	F	C			F	C		C		C	C	C	C	C				
		1-3,10	107.50	A	M	1	1	C																										F	R	F	C			R	C		C		C	C	C	C					
		1-3,20	107.60	A	M	1	1	F																										F	F	F	C				C		C		C	F	F	F					
		1-3,30	107.70	A	M	1	1	R																										F	F	F	C			R	C		C		F	C	C	F					
		1-3,40	107.80	A	M	1	1	R																										C	F	F	C			F	C		C		C	C	F						
		1-3,50	107.90	A	M	1	1																											C	F	C	C				C		C		C	F	F						
		1-3,60	108.00	A	M	1	1	R																										F	F	C	C			F	F		C		C	F	F						
	CP1a	1-3,70	108.10	A	M	1	1	F																										C	R	C	C	F		F	F		C		R	F							
		1-3,80	108.20	A	M	1	1	R																											R	C	C	F		F	F		C			F							
		1-3,90	108.30	A	M	1	1	R																										C		C	C	C		C	C		C		F								
		1-3,100	108.40	A	M	1	1	R																										C		F	C	C	R	C	C		A		F								
		1-3,110	108.50	A	M/P	2	1	R																										C	F	F	C	F		C	C		A		F								
		1-3,120	108.60	A	M	2	1	F																										C	R	C	C	F		F	C		A		R								
		1-3,130	108.70	A	M	1	1	F																										C		C	C	F	F	F	C		C		R								
		1-3,140	108.80	A	M	1	1	F																										F	R	C	C	F	F		F		C										
		1-3,145	108.85	A	M	1	1	R							R																			F		C	C	F	F	R	F		F										
		1-4,10	109.00	A	M	1	1	R							R		R					I		R										F	F	C	A	F	I	F	C		C										
		1-4,20	109.10	A	M	1	1	F							F							R		R				R						C	R	C	A	F	C	F	F		C										
		1-4,30	109.20	A	M	1	1	R							R		R					R		R									R	C		C	A	R	C		C		C										
		1-4,35	109.25	A	M	1	1	R							R							R						R					F	C	R	C	A	F	F	R	C		C										
		1-4,38	109.28	A	M/P	1	1	R							R		R					R		R									F	C		C	A	F	F	F	C		F	R									
		1-4,45	109.35	A	M/P	2	1	R						R	R		R				R	R		R				R					F	A	R	C	A	R	F	C	C		F	R									
		1-4,48	109.38	A	M/P	2	1	F				R			R	R						R		F			F	F			R		F	A		C	C	R	F		C	R	F	R									
		1-4,50	109.40	A	M/P	2	1	F						R	F		R		R					F				F					F	A		C	A	R	R	F	C		F	R									
		1-4,52	109.42	R	P	2	2	C				R			F							R		F			F	F					F	C		C	A	R	R		A												
		1-4,56	109.46	F	P	2	2	C				R	R	F	F	R								F			F	C					F	C		C	A	R	R	F	C			R									
		1-4,58	109.48	C	P	2	2	A				F		F	F		R		R		R	F		F			F	C			R		C	C	R	C	A	R		F	C	I	R										
		1-4,60	109.50	C	P	2	2	A	R			F	F	F	F	R	F				R	F	F	F			F	C					C	C	F	C	A	R	R	R	F												
		1-4,62	109.52	C	M/P	2	2	A				F		F	F		F					F		F			C	C					C	C	R	F	C	R															
		1-4,66	109.56	A	M/P	2	1	A	R			F	F	C	F	R	F		R		R	F	F	C			C	C					C	C	R	F	C	R															
		1-4,68	109.58	A	M/P	2	1	A				C		C	F	C	F					F	F	C			C	C					C	C	R	R	C																
		1-4,70	109.60	A	M/P	2	1	A	R			C	R	C	C	C	F		F		R	F	F	C	R		C	A			R		C	F	R	R	R																
		1-4,72	109.62	A	M/P	2	1	A	R	F		C		C	C	C	C	R	F	R	F	F	C	A	R	F	C	A		R			C	F	R	R	R																
Maestrichtian	*Micula prinsii*	1-4,74	109.64	A	M/P	2	1		R	R	F	C		C	C	C	C	R	C	R	F	C	C	A	R	F	C	A			R		C	F																			
		1-4,75	109.65	A	M/P	2	1		R	R		C		A	F	C	C	R	C	R	F	C	C	A	R	F	C	A		R			F	R																			
		1-4,76	109.66	A	M/P	2	1			R	R	C		C	C	C	F		C		C	C	C	A	R	C	C	A					F																				
		1-4,78	109.68	A	M/P	2	1		F	F		C		C	C	C	F		F	R	F	C	C	C	R	F	C	A		F			R																				
		1-4,80	109.70	A	M/P	2	1		R	R		C		C	F	C	F		C	R	F	C	C	C	F	F	C	A				R																					
		1-4,85	109.75	A	M	1	1			F	R	C		C	C	C	C		C		C	C	A	C	F	C	F	A		F																							
		1-4,90	109.80	A	M	1	1		F	R		C		C	C	C	F		C		C	C	C	C	F	C	C	A				R																					
		1-4,100	109.90	A	M/P	2	1		F	R	R	C		C	C	C	C		F	R	C	C	C	C	F	F	C	A		F		R																					
		1-6,120	110.10	A	M/P	2	1		F			F		C	C	C	F	R	F		C	C	C	C	F		F	A	F	R	R																						
		1-4,140	110.30	A	M/P	2	1			R		C		C	C	C	F	R	C	R	F	C	C	C	C		F	A	F			R																					
		1-5,10	110.50	A	M/P	2	1		R			C		C	C	C	F		C		C	C	C	C	C	F	C	A	F																								
		1-5,60	111.00	A	M/P	2	1		R	R		C		C	C	C	F	F	C		C	C	C	C	F		C	A	F			R																					
		1-5,120	111.60	A	M/P	2	1		R	F	R	C	R	C	C	C	F	F	F	R	R	A	C	C	F	F	C	A	F		I	R																					
	Micula murus	1-6,10	112.00	A	M/P	2	1		R		F	C		C	C	C	F		F	R	F	A	C	C			C	A	F	R																							
		1-6,60	112.50	A	M	1	1			R		C		C	C	C	R	F	C		F	C	F	C	F	F	F	A	F																								
		1-6,130	113.20	A	M/P	2	1		R		R	C	F	C	C	C	R	F	C	R	F	C	F	C	C		F	C	F																								
		1-7,10	113.50	A	M	2	1			R		C		C	C	C	F	F	C		F	C	C	C				C	F																								
		1-7,40	113.80	A	M	2	1				F	C		C	A	C	F	F	C	R	F	C	F	C	F		F	C	F																								
		1-7,CC	113.90	A	M/P	2	2		R	R	F	C	F	C	A	C	F	F	C	R	F	C	F	C	F		F	C	F																								

Note: See footnote to Table 3A for definition of symbols.

Ceratolithus acutus Gartner and Bukry, 1975
C. cristatus Kamptner, 1954
C. rugosus Bukry and Bramlette, 1968
C. telesmus Norris, 1975
Chiasmolithus bidens (Bramlette and Sullivan, 1961) Hay and Mohler, 1967
C. californicus (Sullivan, 1964) Hay and Mohler, 1967
C. consuetus (Bramlette and Sullivan, 1961) Hay and Mohler, 1967
C. danicus (Brotzen, 1959) Hay and Mohler, 1967
C. expansus (Bramlette and Sullivan, 1961) Gartner, 1970
C. grandis (Bramlette and Riedel, 1954) Radomski, 1968
Coccolithus crassus Bramlette and Sullivan, 1961
C. eopelagicus (Bramlette and Riedel, 1954) Bramlette and Sullivan, 1961
C. formosus (Kamptner, 1963) Wise, 1973
C. jugatus (Perch-Nielsen, 1967) Proto Decima et al., 1975
C. miopelagicus Bukry, 1971
C. pelagicus (Wallich, 1877) Schiller, 1930
Coronocyclus nitescens (Kamptner, 1963) Bramlette and Wilcoxon, 1967
Crenalithus doronicoides (Black and Barnes, 1961) Roth, 1973
C. productellus Bukry, 1975
Crepidolithus sp.

Cricolithus jonesii Cohen, 1965
Cruciplacolithus edwardsii Romein, 1979
C. primus Perch-Nielsen, 1977
C. subrotundus (Perch-Nielsen, 1969) Perch-Nielsen, 1972
C. tenuis (Stradner, 1961) Hay and Mohler, 1967
Cyclagelosphaera reinhardtii (Perch-Nielsen, 1968) Romein, 1977
Cyclicargolithus floridanus (Roth and Hay, 1967) Bukry, 1971
Cyclicargolithus sp.
Cyclococcolithus gammation (Bramlette and Sullivan, 1961) Sullivan, 1964
Cyclolithella kingi Roth, 1970
C. plactilis Bukry and Percival, 1971
C. rotula (Kamptner, 1956) Haq and Berggren, 1978
Dictyococcites bisecta (Hay, Mohler, Wade, 1966) Bukry and Percival, 1971
D. minutus (Haq, 1973) Haq, 1976
D. scrippsae Bukry and Percival, 1971
D. asymmetricus Gartner, 1969
Discoaster aulakos Gartner, 1967
D. barbadiensis Tan Sin Hok, 1927
D. berggrenii Bukry, 1971
D. blackstockae Bukry, 1973
D. brouweri Tan Sin Hok, 1927
D. challengeri Bramlette and Riedel, 1954
D. deflandrei Bramlette and Riedel, 1954
D. diastypus Bramlette and Sullivan, 1961
D. exilis Martini and Bramlette, 1963
D. germanicus Martini, 1958
D. intercalaris Bukry, 1971
D. lenticularis Bramlette and Sullivan, 1961
D. lodoensis Bramlette and Riedel, 1954
D. mohleri Bukry and Percival, 1971
D. multiradiatus Bramlette and Riedel, 1954
D. nobilis Martini, 1961
D. okadai Bukry, 1981
D. pentaradiatus Ten Sin Hok, 1927
D. pseudovariabilis Martini and Worsley, 1971
D. quinqueramus Gartner, 1969
D. saipanensis Bramlette and Riedel, 1954
D. salisburgensis Stradner, 1961
D. sanmiguelensis Bukry, 1981
D. sublodoensis Bramlette and Sullivan, 1961
D. surculus Martini and Bramlette, 1963
D. tamalis Kamptner, 1967
D. tanii Bramlette and Riedel, 1954
D. triradiatus Ton Sin Hok, 1927
D. variabilis Martini and Bramlette, 1963
Discoaster sp.A
Discoaster sp.
Discoasteroides kuepperi (Stradner, 1959) Bramlette and Sullivan, 1961
Discolithina japonica Takayama, 1967
D. plana (Bramlette and Sullivan, 1961) Levin, 1965
D. rimosa (Bramlette and Sullivan, 1961) Sullivan, 1964
Ellipsolithus distichus (Bramlette and Sullivan, 1961) Sullivan, 1964
E. lajollensis Bukry and Percival, 1971
E. macellus (Bramlette and Sullivan, 1961) Sullivan, 1964
Emiliania annula (Cohen, 1964) Bukry, 1971
E. huxleyi (Lohmann, 1902) Hay and Mohler, 1967
E. ovata Bukry, 1973
Ericsonia cava (Hay and Mohler, 1967) Perch-Nielsen, 1969
E. robusta (Bramlette and Sullivan, 1961) Perch-Nielsen, 1977
E. subpertusa Hay and Mohler, 1967
Fasciculithus hayii Bukry, 1971
F. involutus Bramlette and Sullivan, 1961
F. pileatus Bukry, 1973
F. tympaniformis Hay and Mohler, 1967
F. ulii Perch-Nielsen, 1971
Fasciculithus sp.
Gephyrocapsa aperta Kamptner, 1963
G. caribbeanica Boudreaux and Hay, 1967
G. oceanica Kamptner, 1943
Gephyrocapsa sp.
Helicopontosphaera granulata Bukry and Percival, 1971
H. kamptneri Hay and Mohler, 1967
H. wallichii (Lohmann, 1902) Okada and McIntyre, 1976
Heliolithus conicus Perch-Nielsen, 1977
H. kleinpellii Sullivan, 1964
Isthmolithus recurvus Deflandre in Deflandre and Fert, 1954
Markalius astroporus (Stradner, 1963) Hay and Mohler, 1967
Neochiastozygus concinnus (Martini, 1961) Perch-Nielsen, 1971
Neococcolithus dubius (Deflandre, 1954) Black, 1967
Neocrepidolithus sp.
Pedinocyclus larvalis (Bukry and Bramlette, 1969) Loeblich and Tappan, 1978
Prinsius bisulcus (Stradner, 1963) Hay and Mohler, 1967
P. dimorphosus (Perch-Nielsen, 1969) Perch-Nielsen, 1977
Reticulofenestra pseudoumbilica (Gartner, 1967) Gartner, 1969
R. samodurovii (Hay, Mohler, and Wade, 1966) Roth, 1960
R. umbilica (Levin, 1965) Martini and Ritzkoski, 1968
Reticulofenestra sp.
Rhabdosphaera clavigera Murray and Blackman, 1898
R. perlonga (Deflandre, 1952) Bramlette and Sullivan, 1961
Rhabdosphaera sp.
Scyphosphaera globulata Bukry and Percival, 1971
Sphenolithus abies Deflandre, 1954
S. anarrhopus Bukry and Bramlette, 1969
S. editus Perch-Nielsen, 1978 in Perch-Nielsen et al.
S. heteromorphus Deflandre, 1953
S. moriformis (Brönnimann and Stradner, 1960) Bramlette and Wilcoxon, 1967
S. primus Perch-Nielsen, 1977
S. radians Deflandre, 1952
S. spiniger Bukry, 1971
Sphenolithus sp.
Striatococcolithus pacificanus Bukry, 1971
Syracosphaera hystrica Kamptner, 1941
Thoracosphaera deflandrei Kamptner, 1953
T. operculata Bramlette and Martini, 1964
T. saxea Stradner, 1961
Thoracosphaera sp.
Toweius craticulus Hay and Mohler, 1967
T. eminens (Bramlette and Sullivan, 1971) Romein, 1979
T. magnicrassus (Bukry, 1971) Romein, 1979
T. tovae Perch-Nielsen, 1971
Toweius sp.
Tribrachiatus contortus (Stradner, 1958) Bukry, 1972
T. orthostylus Shamrai, 1963
Triquetrorhabdulus rugosus Bramlette and Wilcoxon, 1967
Umbilicosphaera mirabilis Lohmann, 1902
U. sibogae (Weber von Bosse, 1901) Gaarder, 1970
Wiseorhabdus inversus (Bukry and Bramlette, 1969; emend. Wise and Constans, 1976) Bukry, 1981
Zygodiscus sigmoides Bramlette and Sullivan, 1961
Z. simplex (Bramlette and Sullivan, 1961) Hay and Mohler, 1967
Zygodiscus spp.
Zygrhablithus bijugatus (Deflandre, 1954) Deflandre, 1959

REFERENCES

Bukry, D., 1973. Low-latitude coccolith biostratigraphic zonation. *In* Edgar, N. T., Saunders, J. B., et al., *Init. Repts. DSDP*, 15:Washington (U.S. Govt. Printing Office), 685-704.

________, 1975. Coccolith and silicoflagellate stratigraphy, northwestern Pacific Ocean, Deep Sea Drilling Project, Leg 32. *In* Larson, R. L., Moberly, R., et al., *Init. Repts. DSDP*, 32: Washington (U.S. Govt. Printing Office), 677-702.

________, 1981. Pacific coast coccolith stratigraphy between Point Conception and Cabo Corrientes, Deep Sea Drilling Project. Leg 63. *In* Yeats, R. S., Haq, B. U., et al., *Init. Repts. DSDP*, 63: Washington (U.S. Govt. Printing Office), 445-472.

Bukry, D., and Bramlette, M. N., 1970. 18 Coccolith age determinations Leg 3 Deep Sea Drilling Project. *In* Maxwell, A. E., Von Herzen, R. P., et al., *Init. Repts. DSDP*, 3: Washington (U.S. Govt. Printing Office), 589-612.

Ćepek, P., and Hay, W. W., 1969a. Calcareous nannoplankton and biostratigraphic subdivision of the Upper Cretaceous. *Trans. Gulf Coast Assoc. Geol. Soc.*, 19:323-336.

________, 1969b. Zonation of the Upper Cretaceous using calcareous nannoplankton. *Int. Geol. Congr. Rep. Sess., 23rd, 1968*, pp. 333-340.

Heck, S. E. van, 1979-1984. Bibliography and taxa of calcareous nannoplankton. *Int. Nannoplankton Assoc. Newsl.*, Vols. 1-6.

Loeblich, A. R., 1968. Annotated index and bibliography of the calcareous nannoplankton III. *J. Paleontol.*, 42:584-598.

———, 1969. Annotated index and bibliography of the calcareous nannoplankton III. *J. Paleontol.*, 43:568-588.

———, 1970a. Annotated index and bibliography of the calcareous nannoplankton IV. *J. Paleontol.*, 44:558-574.

———, 1970b. Annotated index and bibliography of the calcareous nannoplankton VI. *Phycologia*, 9:157-174.

———, 1971. Annotated index and bibliography of the calcareous nannoplankton VI. *Phycologia*, 10:315-339.

———, 1973. Annotated index and bibliography of the calcareous nannoplankton VII. *J. Paleontol.*, 47:715-759.

Loeblich, A. R., Jr., and Tappan, H., 1966. Annotated index and bibliography of the calcareous nannoplankton. *Phycologia*, 5:81-216.

Martini, E., 1971. Standard Tertiary and Quaternary calcareous nannoplankton zonation. *In* Farinacci, A. (Ed.), *Proceedings II Planktonic Conference, Rome, 1970:* Roma (Edizioni Tecnoscienza), pp. 739-785.

———, 1976. Cretaceous to Recent calcareous nannoplankton from the central Pacific Ocean (DSDP Leg 33). *In* Schlanger, S. O., Jackson, E. D., et al., *Init. Repts. DSDP*, 33: Washington (U.S. Govt. Printing Office), 383-424.

Moshkovitz, S., 1974. A new method for observing the same nannofossil specimen both by light microscope and scanning electron microscope and preservation of types. *Isr. J. Earth Sci.*, 23:145-147.

Okada, H., and Bukry, D., 1980. Supplementary modification and introduction of code numbers to the low-latitude coccolith biostratigraphic zonation (Bukry, 1973; 1975). *Mar. Micropaleontol.*, 5: 335-353.

Perch-Nielsen, K., 1979. Calcareous nannofossils from the Cretaceous between North Sea and the Mediterranean. *Aspekte der Kreide Europas, IUGS Ser.*, 6:223-272.

———, 1981a. Les nannofossils calcaires à la limite Crétacé-Tertiare près d'El Kef, Tunisie. *Cah. Micropaléontologie*, 3:25-37.

———, 1981b. New Maestrichtian and Paleocene calcareous nannofossils from Africa, Denmark, the U.S.A. and the Atlantic, and some Paleocene lineages. *Eclogae Geol. Helv.*, 74(3):831-963.

Romein, A. J. T., 1977. Calcareous nannofossils from the Cretaceous/Tertiary boundary interval in the Barranco del Gredero (Caravaca, Prov. Murcia, S.E. Spain), I and II. *Proc. K. Ned. Akad. Wet. Ser. B: Palaeontol., Geol., Phys., Chem.*, 80(4):256-279.

———, 1979. Lineages in early Paleogene calcareous nannoplankton. *Utrecht Micropaleontol. Bull.*, 22:1-231.

Roth, P. H., and Thierstein, H. R., 1972. Calcareous nannoplankton: Leg 14 of the Deep Sea Drilling Project. *In* Hayes, D. E., Pimm, A. C., et al., *Init. Repts. DSDP*, 14: Washington (U.S. Govt. Printing Office), 421-486.

Thierstein, H. R., 1976. Mesozoic calcareous nannoplankton biostratigraphy of marine sediments. *Mar. Micropaleontol.*, 1:325-362.

Thierstein, H. R., and Manivit, H., 1981. Calcareous nannofossil biostratigraphy, Nauru Basin, Deep Sea Drilling Project Site 462, and Upper Cretaceous nannofacies. *In* Larson, R. L., Schlanger, S. O., et al., *Init. Repts. DSDP*, 61: Washington (U.S. Govt. Printing Office), 475-494.

Verbeek, J. W., 1977. Calcareous nannoplankton biostratigraphy of Middle and Upper Cretaceous deposits in Tunisia, southern Spain and France. *Utrecht Micropaleontol. Bull.*, 16:1-157.

Date of Initial Receipt: 21 December 1983
Date of Acceptance: 16 July 1984

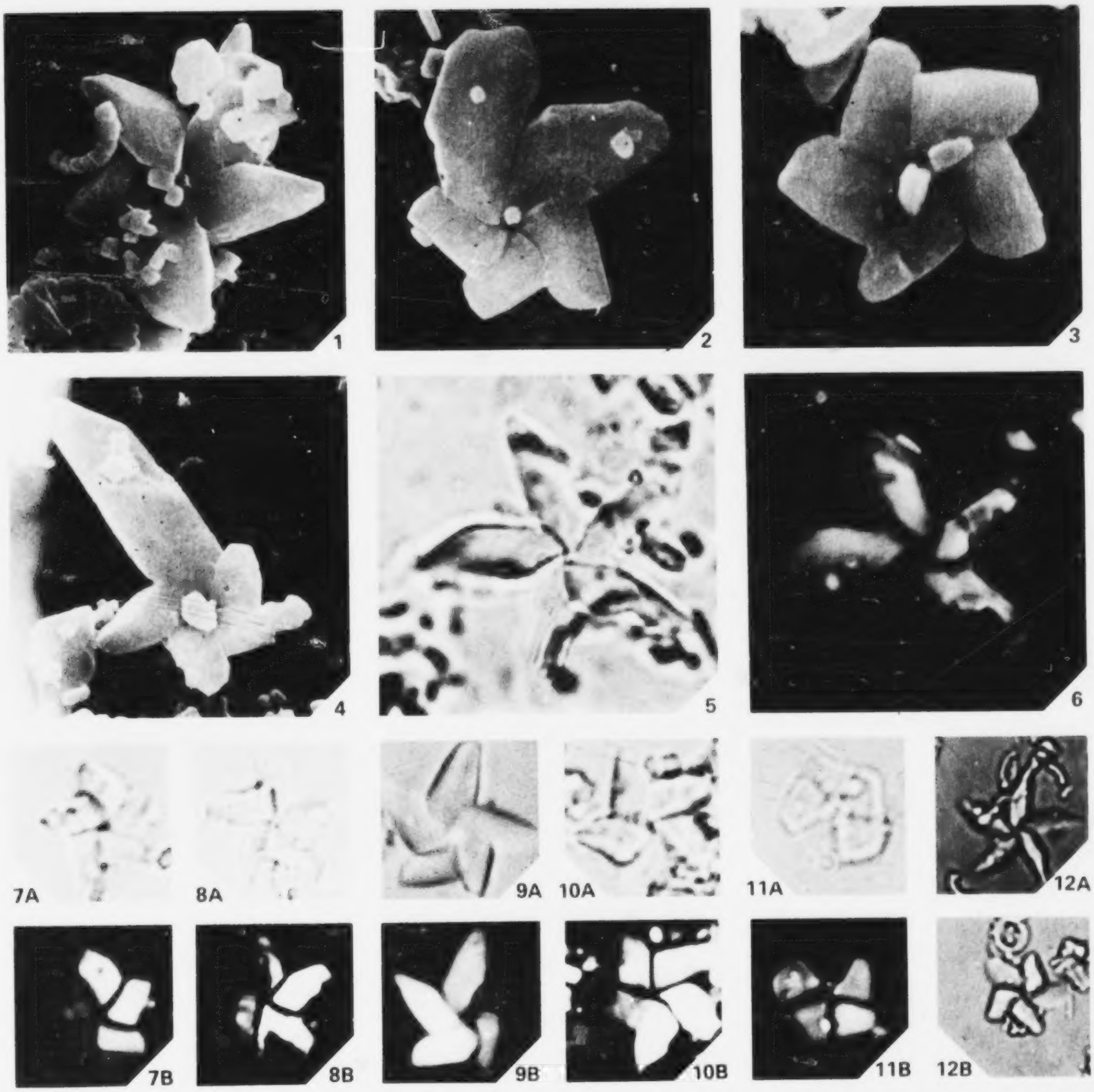

Plate 1. (The abbreviations XN and OL denote cross-polarized and transmitted light.) **1, 3.** *Braarudosphaera* sp. 1, Sample 576B-8-5, 120–121 cm, electron micrograph, × 7000. **2.** *Braarudosphaera* sp. 1, Sample 576B-8-5, 120–121 cm, electron micrograph, × 5000. **4.** *Braarudosphaera* sp. 1, Sample 576B-8-5, 120–121 cm, electron micrograph, × 3500. **5, 6, 7.** *Braarudosphaera* sp. 1, Sample 576B-9,CC (5, 7A) OL, (6, 7B) XN, × 2800. **8.** *Braarudosphaera* sp. 1, Sample 576B-8-4, 95 cm, (8A) OL, (8B) XN × 2260. **9.** *Braarudosphaera* sp. 1, Sample 576B-8-6, 7 cm, (9A) OL, (9B) XN, × 2800. **10.** *Braarudosphaera* sp. 1, Sample 576B-8-7, 35 cm, (10A) OL, (10B) XN, × 2800. **11.** *Braarudosphaera imbricata* Bukry, Sample 576-8,CC (11A) OL, (11B) XN, × 2800. **12.** *Braarudosphaera* sp. 1, Sample 576-8,CC (12A, B) OL, × 2800.

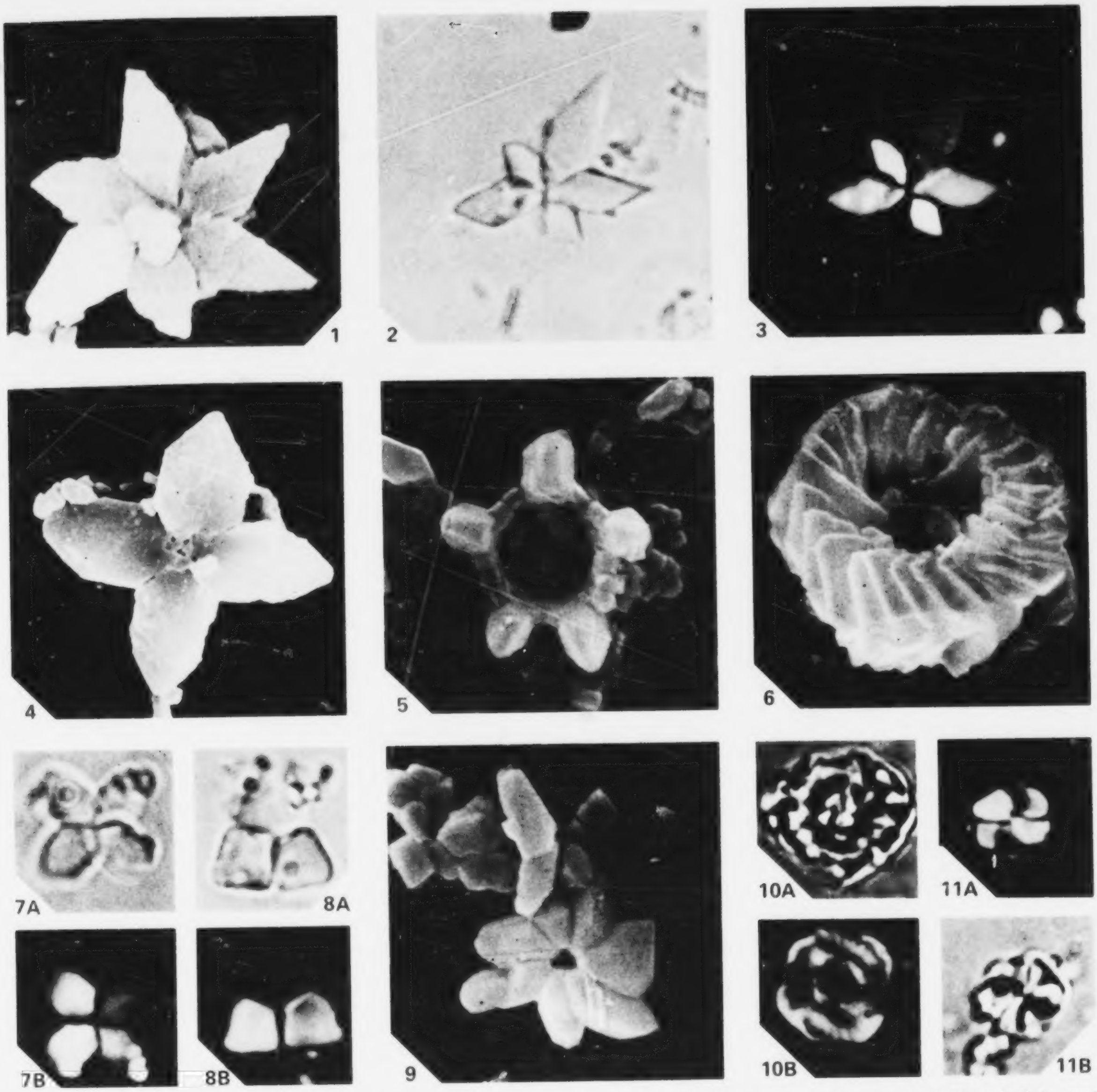

Plate 2. (The abbreviations XN and OL denote cross-polarized and transmitted light. All light microscope pictures are ×2800.) **1, 2, 3.** *Rucinolithus magnus* (Bukry), (1) Sample 576-8-6, 13–14 cm, ×8400, (2) OL, Sample 576-8-7, 35 cm, (3) XN. **4, 7.** *Quadrum gothicum* (Deflandre), Sample 576-8,CC, 16–17 cm, ×4200, (7A) Sample 576-8-7, 35 cm, OL, (7B) XN. **5.** *Stephanolithion munitum* (Perch-Nielsen), Sample 577A-12-4, 57–58 cm, ×7000. **6, 10.** *Cylindralithus* sp., Sample 577A-12-6, 146–147 cm, ×5600, (10A) OL, (10B) XN. **8.** *Quadrum trifidum* (Stradner), Sample 576B-9,CC, (8A) OL, (8B) XN. **9.** *Rucinolithus* sp. Sample 576B-8-5, 120–121 cm, ×7000. **11.** *Rucinolithus hayii* Stover, Sample 576-8,CC, 16–17 cm, (11A) OL, (11B) XN.

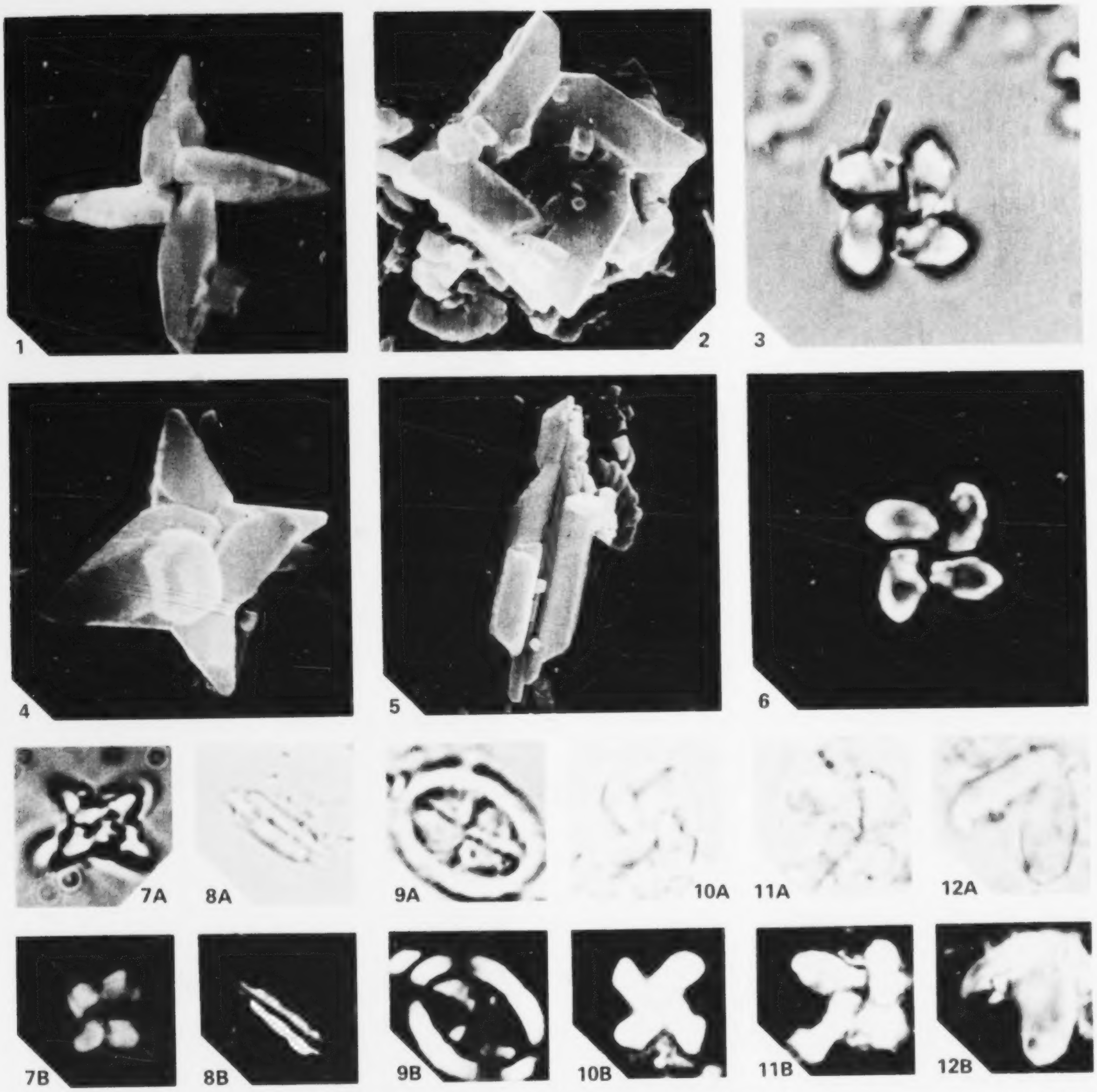

Plate 3. (The abbreviations XN and OL denote cross-polarized and transmitted light. Magnification for light microscope photos is ×2800.) **1.** Distal end of the central process of *Prediscosphaera cretacea*, Sample 577A-12-6, 146–147 cm, ×7000. **2.** *Micula murus* Martini, Sample 577-12-5, 136–137 cm, ×4200. **3, 6.** *Micula murus* Martini, Sample 577-12-5, 136–137 cm, (3) OL, (6) XN. **4, 7.** *Micula staurophora* (Gardet), Sample 577A-12-6, 146–147, (4) ×7000, (7A) OL, same specimen as Fig. 4, (7B) XN. **5, 8.** *Lithraphidites quadratus* (Bramlette and Martini), (5) Sample 577A-12-3, 106–107 cm, ×5000, (8A) Sample 577-12-5, 120–121 cm, OL, (8B) XN. **10.** *Micula murus* (Martini), Sample 577-12-5, 120–121 cm, (10A) OL, (10B) XN. **9.** *Arkhangelskiella cymbiformis* Veskina, Sample 577-12-5, 136–137 cm, (9A) OL, (9B) XL. **11, 12.** *Micula prinsii* Perch-Nielsen, (11A) OL, (11B) XN, Sample 577B-1-4, 68 cm, (12A) OL, (12B) XN, Sample 577-12-5, 120–121 cm.

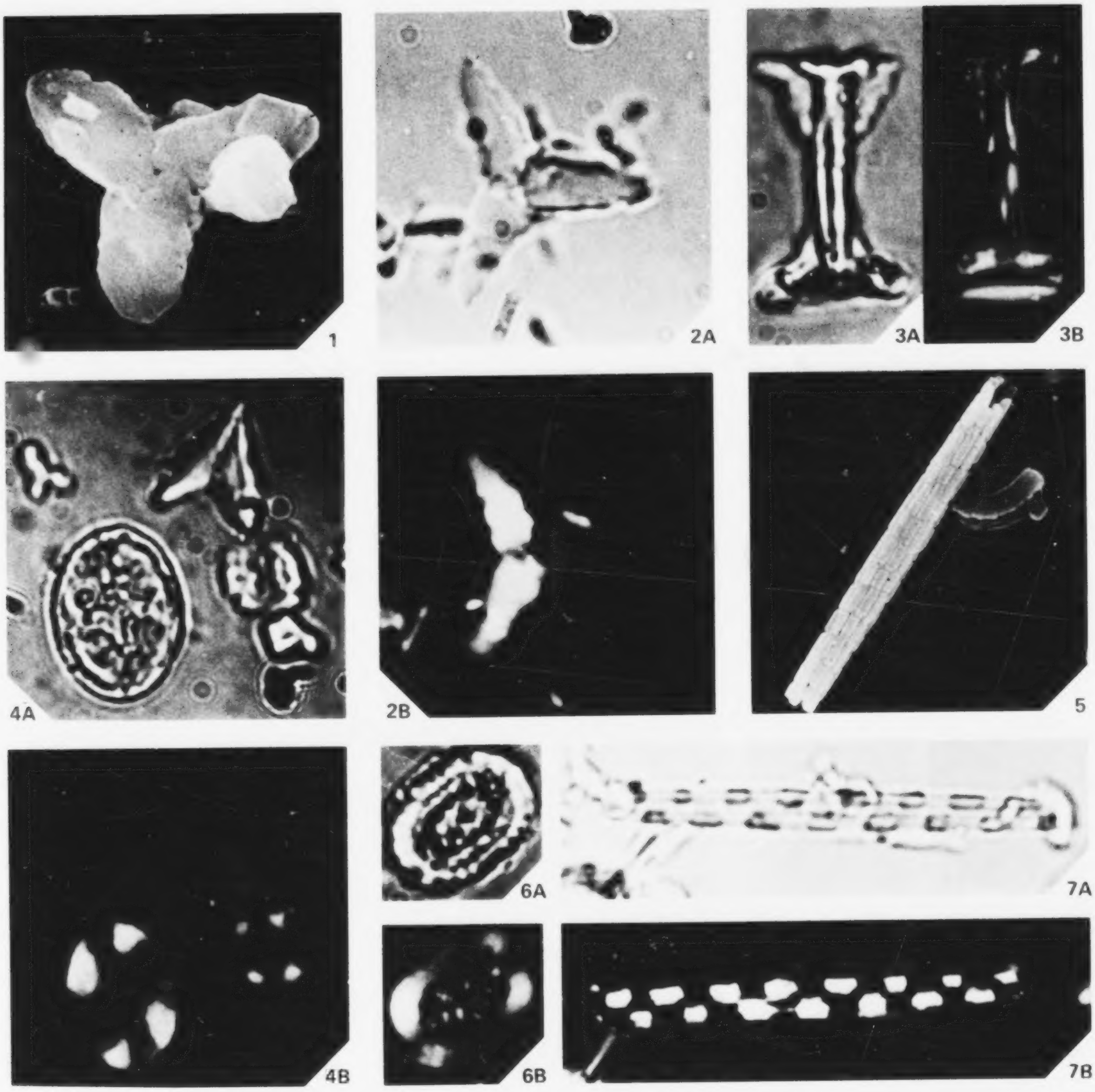

Plate 4. (The abbreviations XN and OL denote cross-polarized and transmitted light. All light microscope pictures are × 2800.) **1, 2A, B.** *Quadrum trifidum* (Stradner), (1) Sample 576-8,CC (16–17 cm), × 5600, (2) Sample 576-8-7, 35 cm, (2A) OL, (2B) XN. **3A, B.** *Prediscosphaera cretacea* (Arkhangelsky), Sample 576-8-6, 13–14 cm, (3A) OL, (3B) XN. **4A, B.** *Ceratolithoides aculeus* (Stradner) and *Eiffellithus eximius* (Stover), Sample 576-8,CC (16–17 cm), (4A) OL, (4B) XN. **6A, B.** *Cretarhabdus surrirellus* (Deflandre), Sample 577A-12-5, 136–137 cm, (6A) OL, (6B) XN. **5, 7A, B.** *Microrhabdulus decoratus* (Deflandre), (5) Sample 577A-12-6, 146–147 cm, × 2800, (7) Sample 576-8-6, 13–14 cm, (7A) OL, (7B) XN.

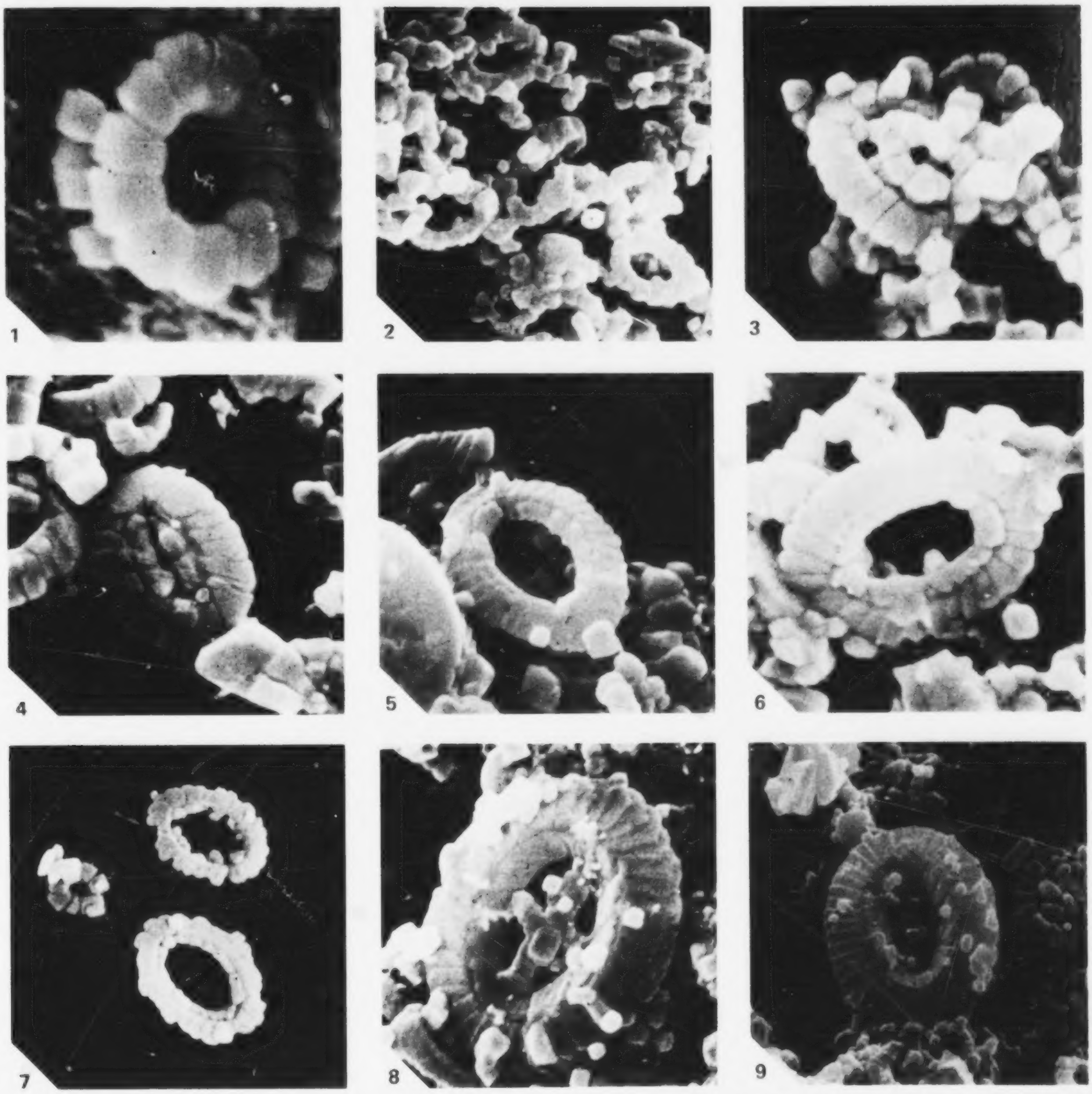

Plate 5. (All electron microscope photographs.) **1.** *Biscutum* sp. Sample 577-12-5, 120–121 cm, × 20,000. **2.** *Biscutum* sp. Sample 577-12-5, 111–112 cm, × 5600. **3.** *Biscutum* sp. Sample 577A-12-4, 57–58 cm, × 14,000. **4.** *Biscutum parvulum* Romein, Sample 577A-12-4, 7–8 cm, × 11,200. **5, 6.** *Biscutum romeinii* Perch-Nielsen, Sample 577A-12-4, 56–57 cm, (5) × 700, (6) × 11,200. **7, 8, 9.** *Cruciplacolithus primus* Perch-Nielsen, (7) Sample 577A-12-4, 7–8 cm, (8) × 7000, (9) × 4200, Sample 577-12-4, 56–57 cm.

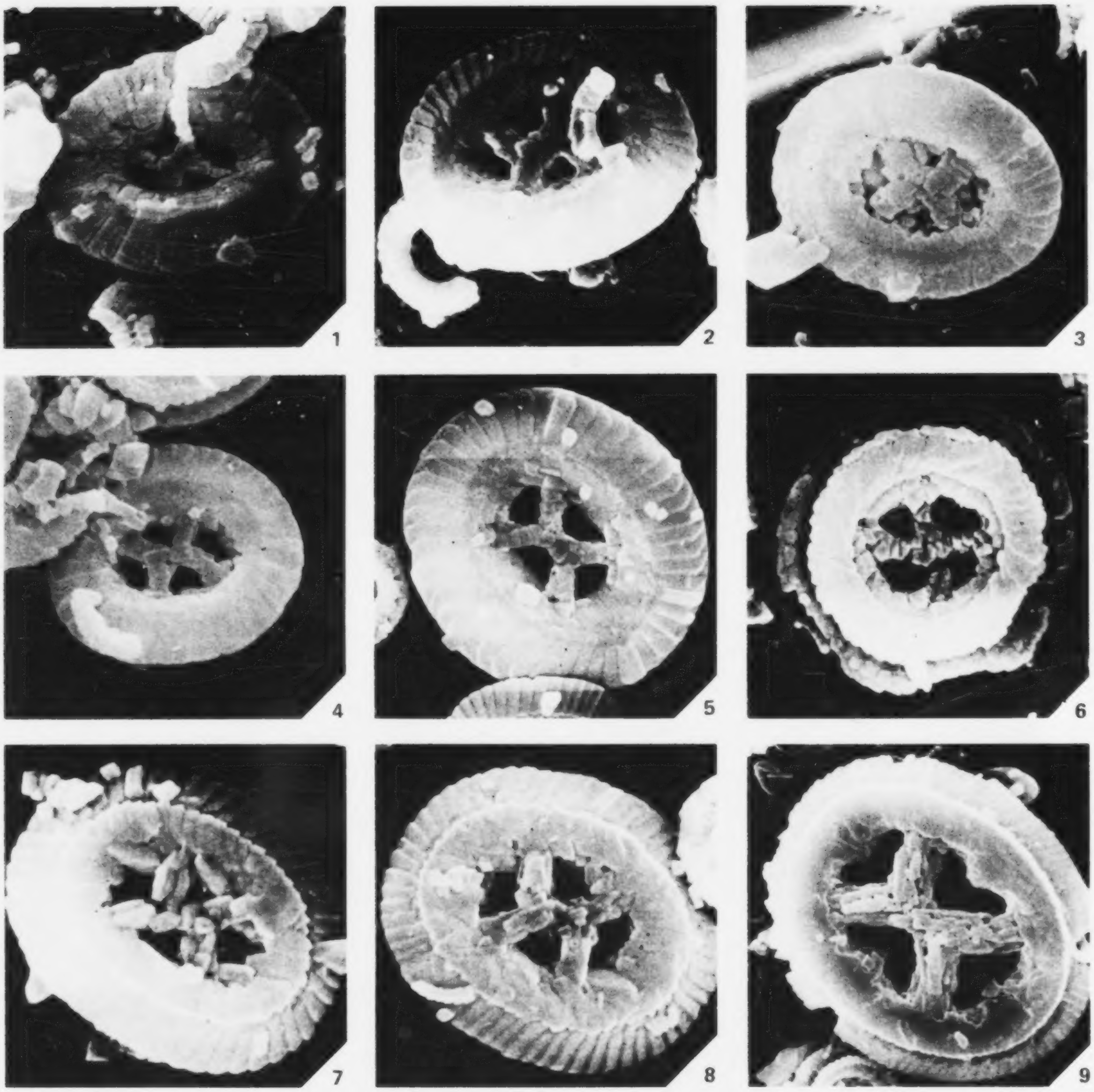

Plate 6. (All electron microscope photographs.) **1.** *Cruciplacolithus edwardsii* Romein, Sample 577A-12-2, 66–67 cm, ×4200. **2.** *Chiasmolithus danicus* (Brotzen), Sample 577-11-2, 18–19 cm, ×4200. **3, 4.** *Chiasmolithus consuetus* (Bramlette and Sullivan), Sample 577A-9,CC (10–11 cm), ×4200. **5.** *Chiasmolithus californicus* (Sullivan), Sample 577-10-4, 140–141 cm, ×4200. **6.** *Cruciplacolithus subrotundus* (Perch-Nielsen), Sample 577-10-1, 110–111 cm, ×4200. **7.** An intermediate form between *Chiasmolithus danicus* and *Chiasmolithus bidens* (Bramlette and Sullivan), Sample 577-10-1, 110–111 cm, ×7000. **8.** *Chiasmolithus bidens*, Sample 577-10-1, 110–111 cm, ×4200. **9.** *Chiasmolithus grandis* (Bramlette and Riedel), Sample 577A-7-6, 86–87 cm, ×2100.

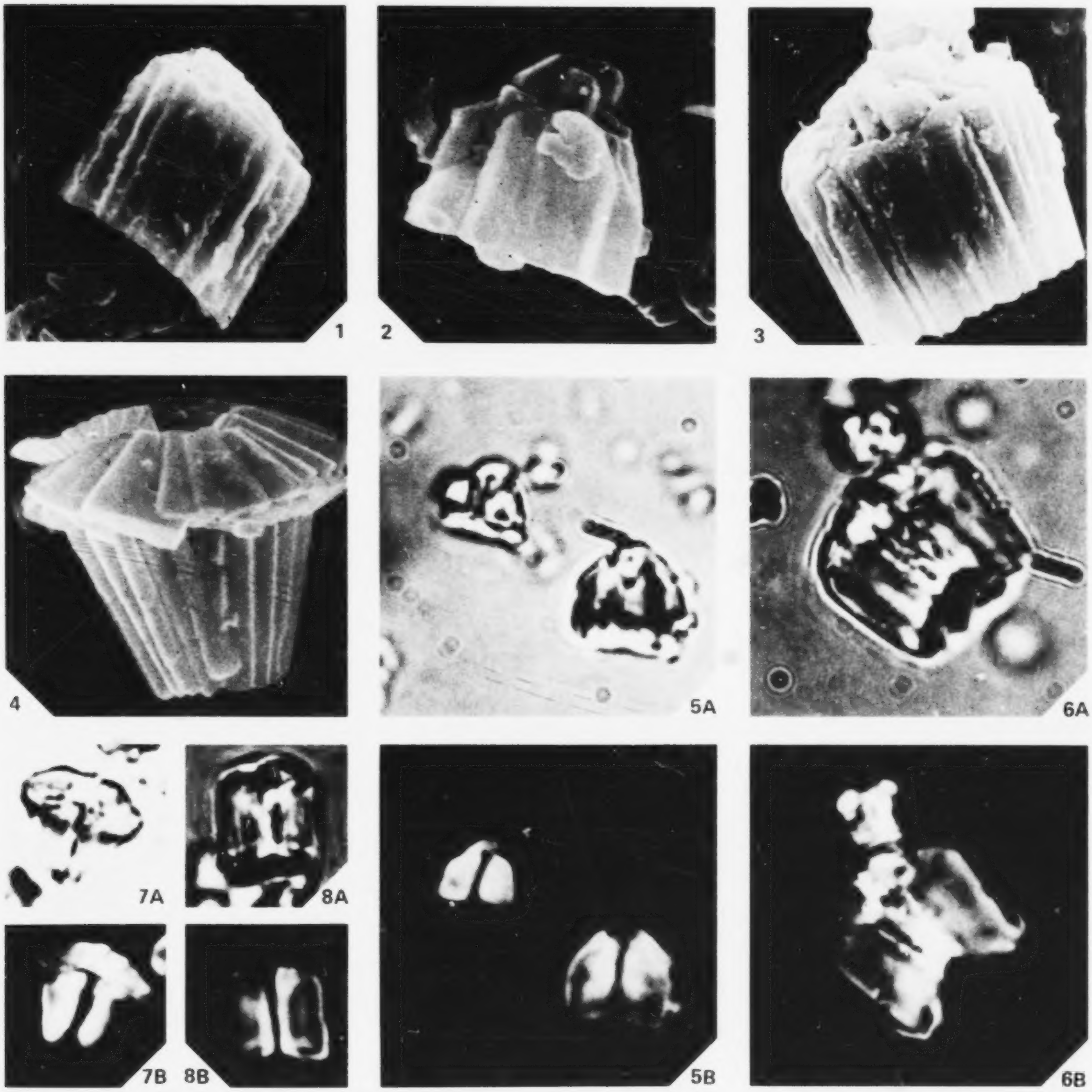

Plate 7. (The abbreviations XN and OL denote cross-polarized and transmitted light. All light microscope photographs are ×2800.) **1, 8.** *Fasciculithus tympaniformis* (Hay and Mohler), Sample 577A-10-6, 39–40 cm, (1) ×5600, (8) same specimen as Fig. 1, (8A) OL, (8B) XN. **2, 5.** *Fasciculithus clinatus* (Bukry) Sample 577-11-2, 18–19 cm, (2) ×9800, (5) same specimen as Fig. 2, (5A) OL, (5B) XN. **3, 6.** *Fasciculithus ulii* (Perch-Nielsen), Sample 577A-10-6, 39–40 cm, (3) ×4200, (6) same specimen as Fig. 3, (6A) OL, (6B) XN. **4, 7.** *Fasciculithus pileatus* (Bukry), Sample 577-10-1, 110–111 cm, (4) ×7000, (7) same specimen as Fig. 4, (7A) OL, (7B) XN.

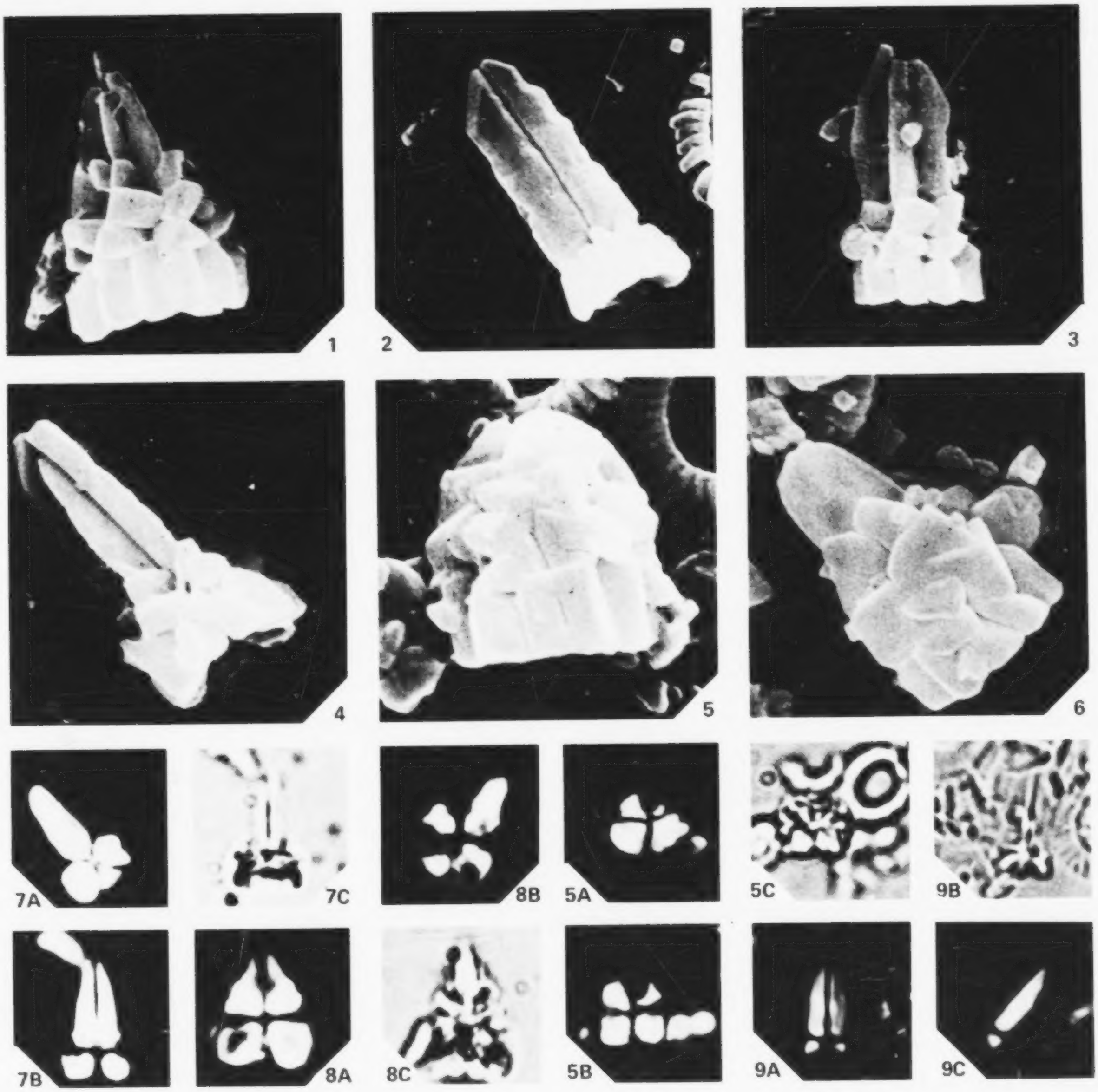

Plate 8. (The abbreviations XN and OL denote cross-polarized and transmitted light.) **1, 8.** *Sphenolithus editus* Perch-Nielsen, Sample 577A-8-6, 15–16 cm, (1) × 5600, (8A) XN, (8B) XN (45°), (8C) OL, same specimen as Fig. 1. **2.** *Sphenolithus* cf. *obtusus* (Bukry), Sample 577A-7-6, 86–87 cm, × 8400. **3, 4, 7.** *Sphenolithus pseudoradians* (Bramlette and Wilcoxon), Sample 577A-7-6, 86–87 cm, (3, 4) × 8400, (7) same specimen as Fig. 4, (7A) OL, (7B) XN. **5, 8.** *Sphenolithus primus* Perch-Nielsen, Sample 577-11-2, 18–19 cm, (8) same specimen as Fig. 5, (8A) XN, (8B) XN (45°), (8C) OL. **6.** *Sphenolithus* cf. *anarrhopus* (Bukry and Bramlette), Sample 577-10-4, 140–141 cm, × 7000. **9.** *Sphenolithus obtusus* (Bukry), Sample 577A-7-6, 86–87 cm, (9A) XN, (9B) XN (45°), (9C) OL.

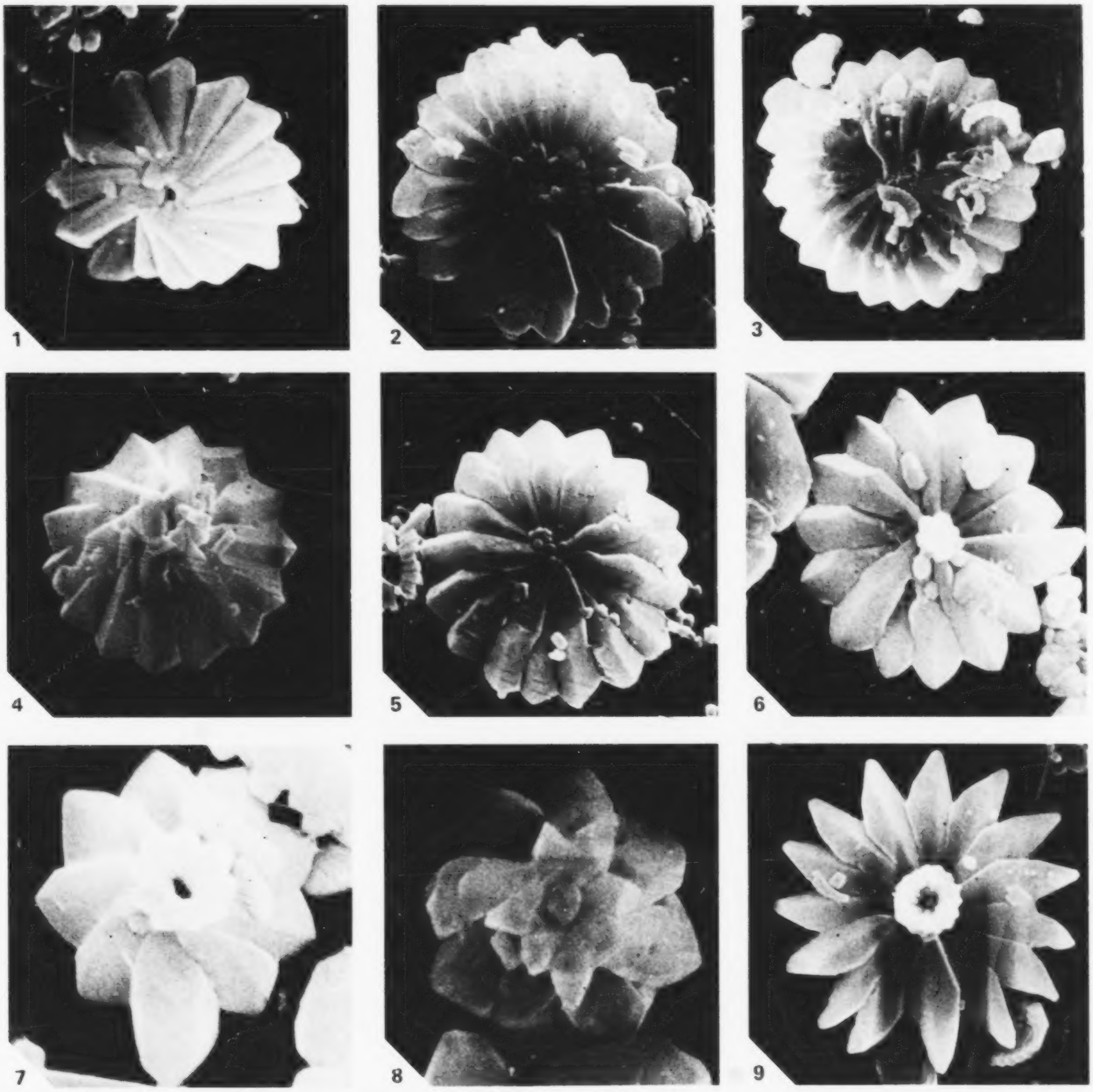

Plate 9. (The abbreviations XN and OL denote cross-polarized and transmitted light.) **1, 4.** *Discoaster mohleri* Bukry and Percival, (1) Sample 577A-9,CC (10–11 cm), ×7000, (4) Sample 577-9-5, 117–118 cm, ×4200. **2, 3, 5.** *Discoaster multiradiatus* Bramlette and Riedel, (2, 5) Sample 577A-9,CC, 10–11 cm, ×4200, (3) Sample 577-9-5, 117–118 cm, ×2100. **6.** *Discoaster barbadiensis* Tan Sin Hok, Sample 577-8-3, 120–121 cm, ×4200. **7, 8.** *Discoasteroides kuepperi* (Stradner), Sample 577-8-3, 120–121 cm, ×7000. **9.** *Discoaster diastypus* Bramlette and Sullivan, Sample 577A-8,CC, ×3500.

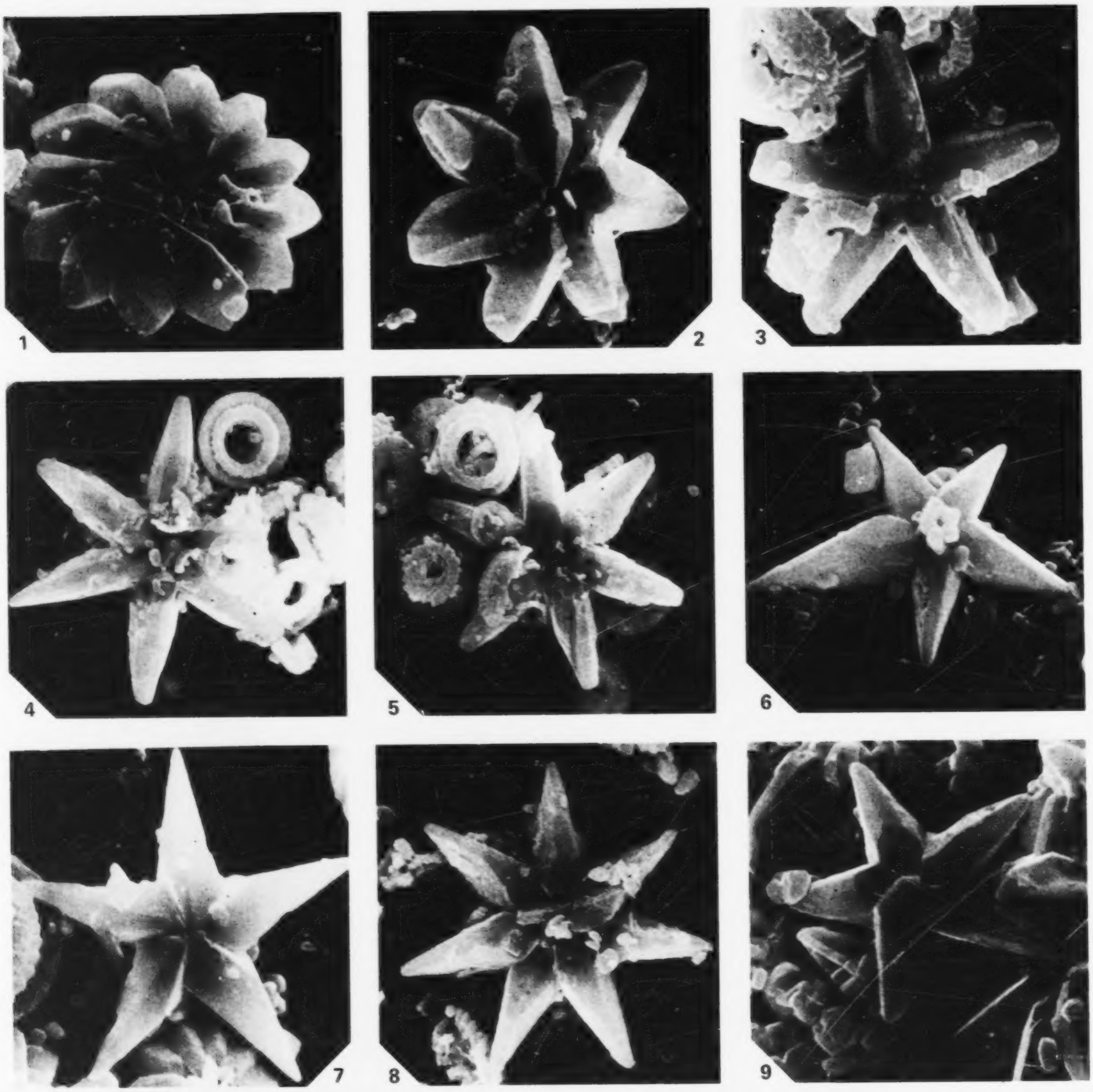

Plate 10. (The abbreviations XN and OL denote cross-polarized and transmitted light.) **1.** ***Discoaster nobilis*** Martini, Sample 577-10-3, 120–121 cm, ×3000. **2.** *Discoaster* sp. 1, Sample 577-10-3, 120–121 cm, ×3000. **3, 4, 5.** *Discoaster okadai* Bukry, (3) Sample 577-10-3, 120–121 cm, ×3000, (4) Sample 577A-10-2, 39–40 cm, ×1960. **6, 7, 8.** *Discoaster lodoensis* Bramlette and Riedel, Sample 577-8-3, 120–121 cm, (6) ×3500, (7, 8) ×2800. **9.** *Discoaster sublodoensis* Bramlette and Sullivan, Sample 577-8-3, 120–121 cm, ×3500.

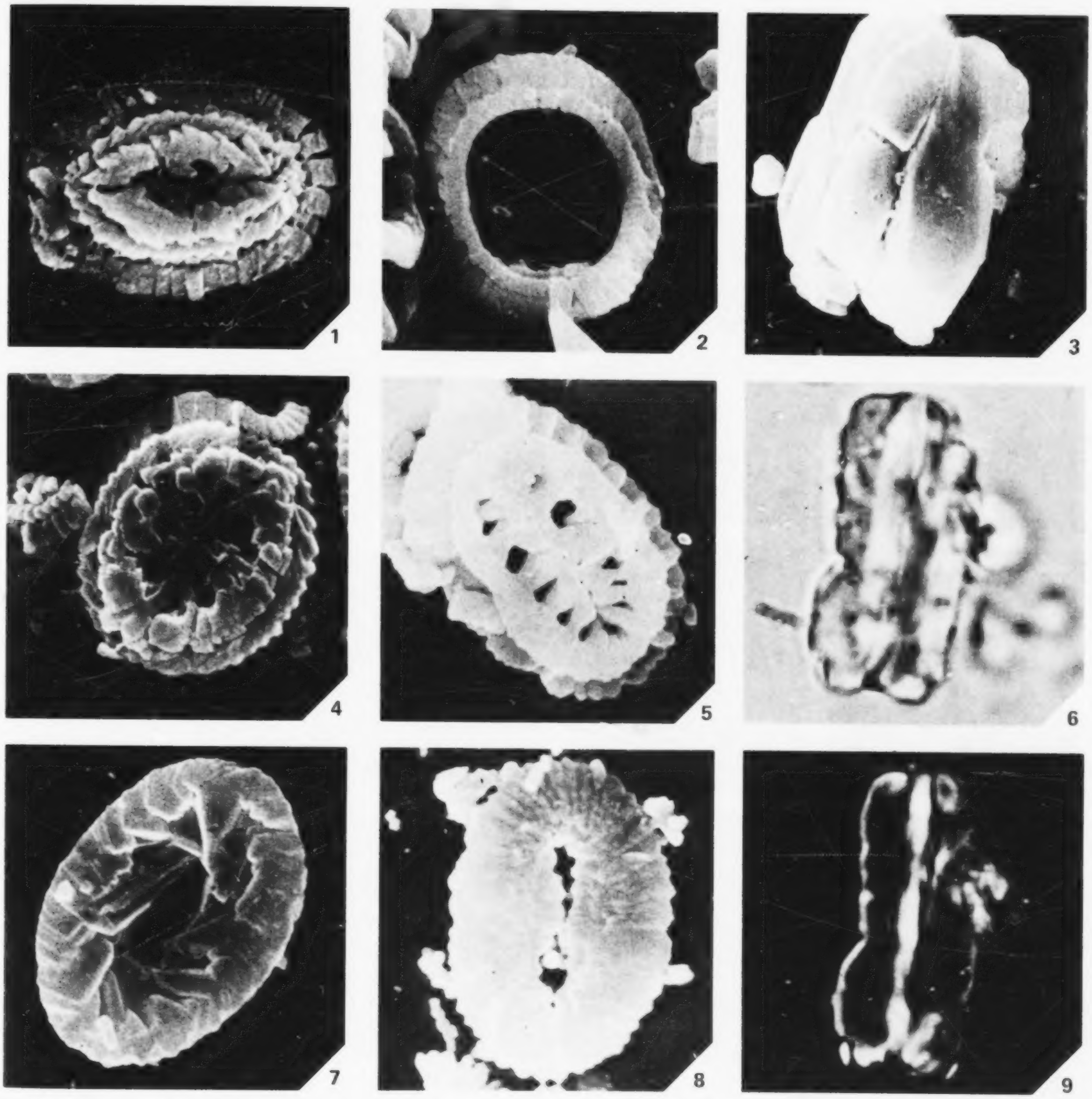

ate 11. (The abbreviations XN and OL denote cross-polarized and transmitted light.) **1.** *Prinsius bisulcus* (Stradner), Sample 577A-10-6, 39-40 cm, ×4900. **2.** *Campylosphaera dela* (Bramlette and Sullivan) Hay and Mohler, Sample 577-8-3, 120-121 cm, ×4200. **3, 6, 9.** *Zygrhablithus* cf. *bijugatus* (Deflandre) Deflandre, (3) Sample 577A-8,CC, ×5600, (6) OL, (9) XN, Sample 577A-9-1, 30-31 cm, overcalcified specimen. **4.** *Toweius tovae* Perch-Nielsen, Sample 577-10-1, 110-111 cm, ×5600. **5.** *Ellipsolithus distichus* (Bramlette and Sullivan), Sample 577-10-3, 120-121 cm, ×4200. **7.** *Discolithina rimosa* (Bramlette and Sullivan), Sample 577-11-2, 18-19 cm, ×5600. **8.** *Ellipsolithus macellus* (Bramlette and Sullivan), Sample 577A-9,CC (10-11 cm), ×4200.

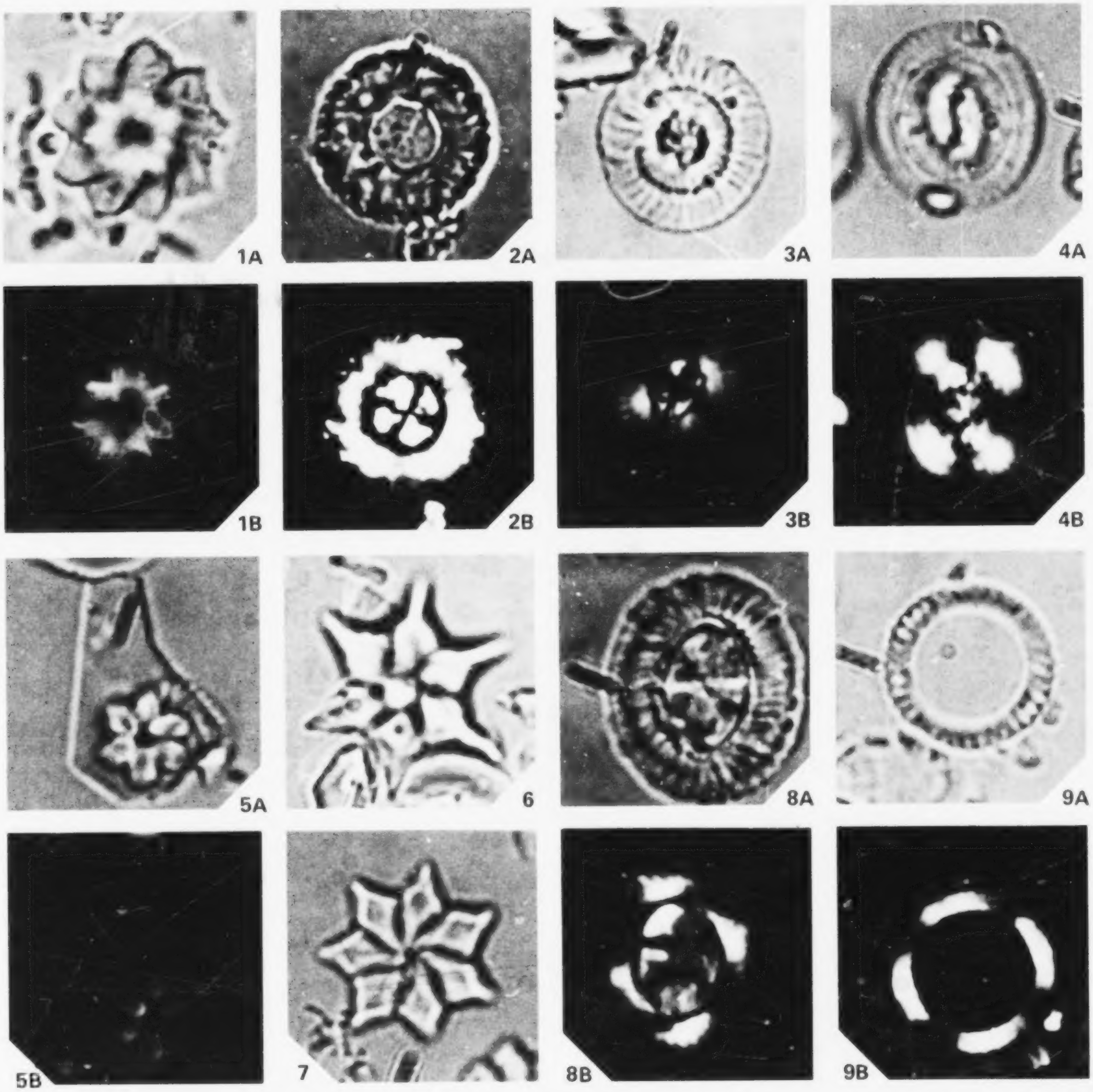

Plate 12. (The abbreviations XN and OL denote cross-polarized and transmitted light.) **1.** *Discoasteroides kuepperi* (Stradner), Sample 577A-8-2, 15–16 cm, (1A) OL, (1B) XN. **2.** *Markalius astroporus* (Stradner), Sample 577A-12-2, 66–67 cm, (2A) OL, (2B) XN. **3.** *Striatococcolithus pacificanus* Bukry, Sample 577A-8-6, 15–16 cm, (3A) OL, (3B) XN. **4.** *Dictyococcites bisecta* (Hay, Mohler, and Wade), Sample 577A-7-6, 86–87 cm, (4A) OL, (4B) XN. **5.** *Bramletteius serraculoides* Gartner, Sample 577A-7-5, 36–37 cm, (5A) OL, (5B) XN. **6.** *Discoaster saipanensis* Bramlette and Riedel, Sample 577A-7-5, 36–37 cm, OL. **7.** *Discoaster* cf. *saipanensis*, Sample 577A-7-5, 36–37 cm. **8.** *Coccolithus jugatus* (Perch-Nielsen), Sample 577A-8-1, 105–106 cm, (8A) OL, (8B) XN. **9.** *Coronocyclus nitescens* (Kamptner), Sample 577A-7-3, 86–87 cm, (9A) OL, (9B) XN.

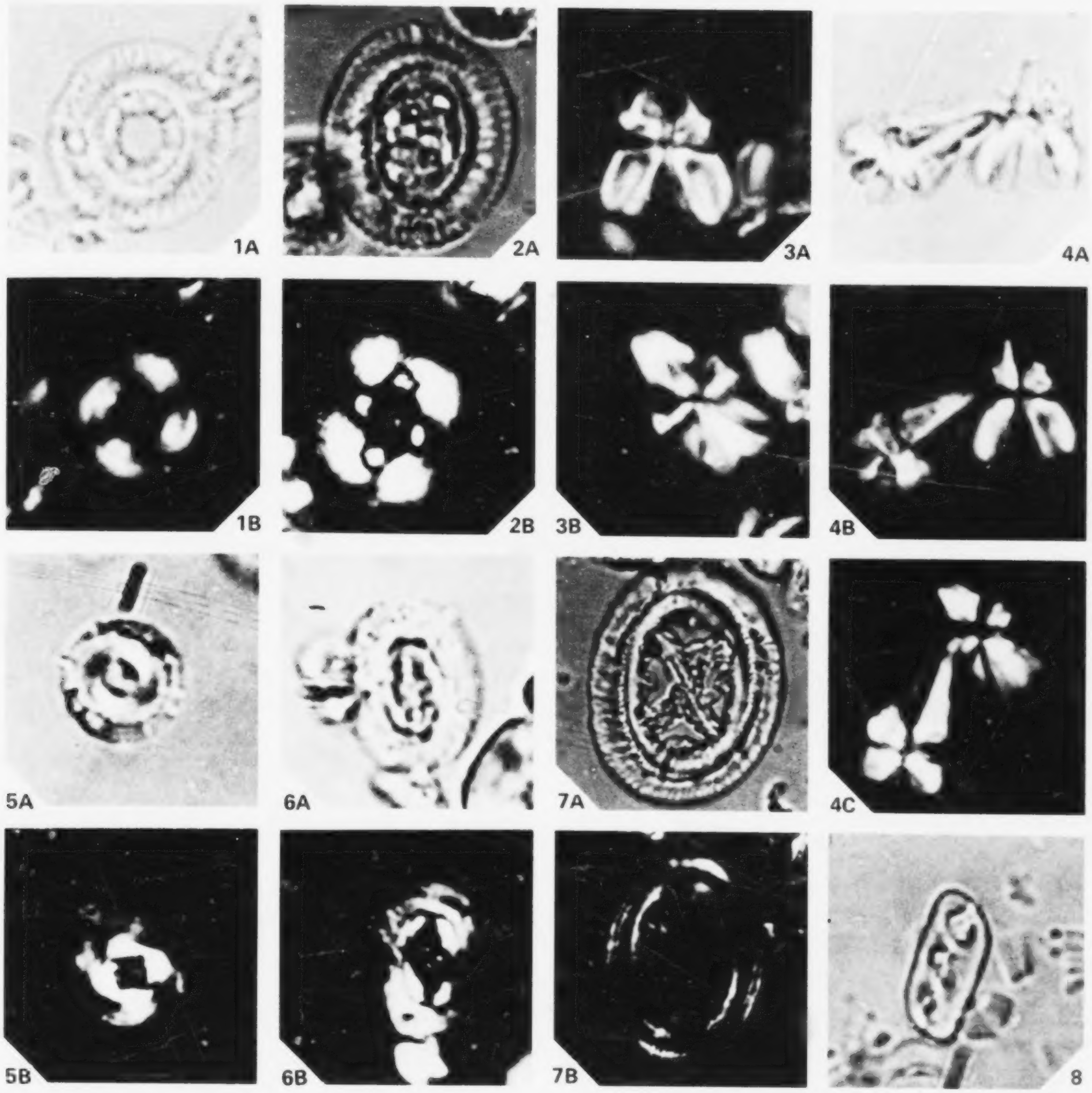

Plate 13. (The abbreviations XN and OL denote cross-polarized and transmitted light. All photographs are ×2800, only Fig. 7 is ×1500.) **1.** *Coccolithus formosus* (Kamptner), Sample 577A-8,CC (5–6 cm). **2.** *Cruciplacolithus tenuis* (Stradner), Sample 577A-8,CC (5–6 cm). **3, 4.** *Sphenolithus spiniger* Bukry, Sample 577-8-4, 120–121 cm. (3A) XN, (3B) XN (45°), (4A) OL, (4B) XN, (4C) XN (45°). **5.** *Toweius craticulus* Hay and Mohler, Sample 577A-9,CC (10–11 cm), (5A) OL, (5B) XN. **6.** *Campylosphaera eodela* Bukry, Sample 577A-9,CC, (6A) OL, (6B) XN. **7.** *Chiasmolithus grandis* (Bramlette and Riedel), Sample 577A-7,CC, (7A) OL, (7B) XN. **8.** *Isthmolithus recurvus* Deflandre, Sample 577A-7-6, 20–21 cm.

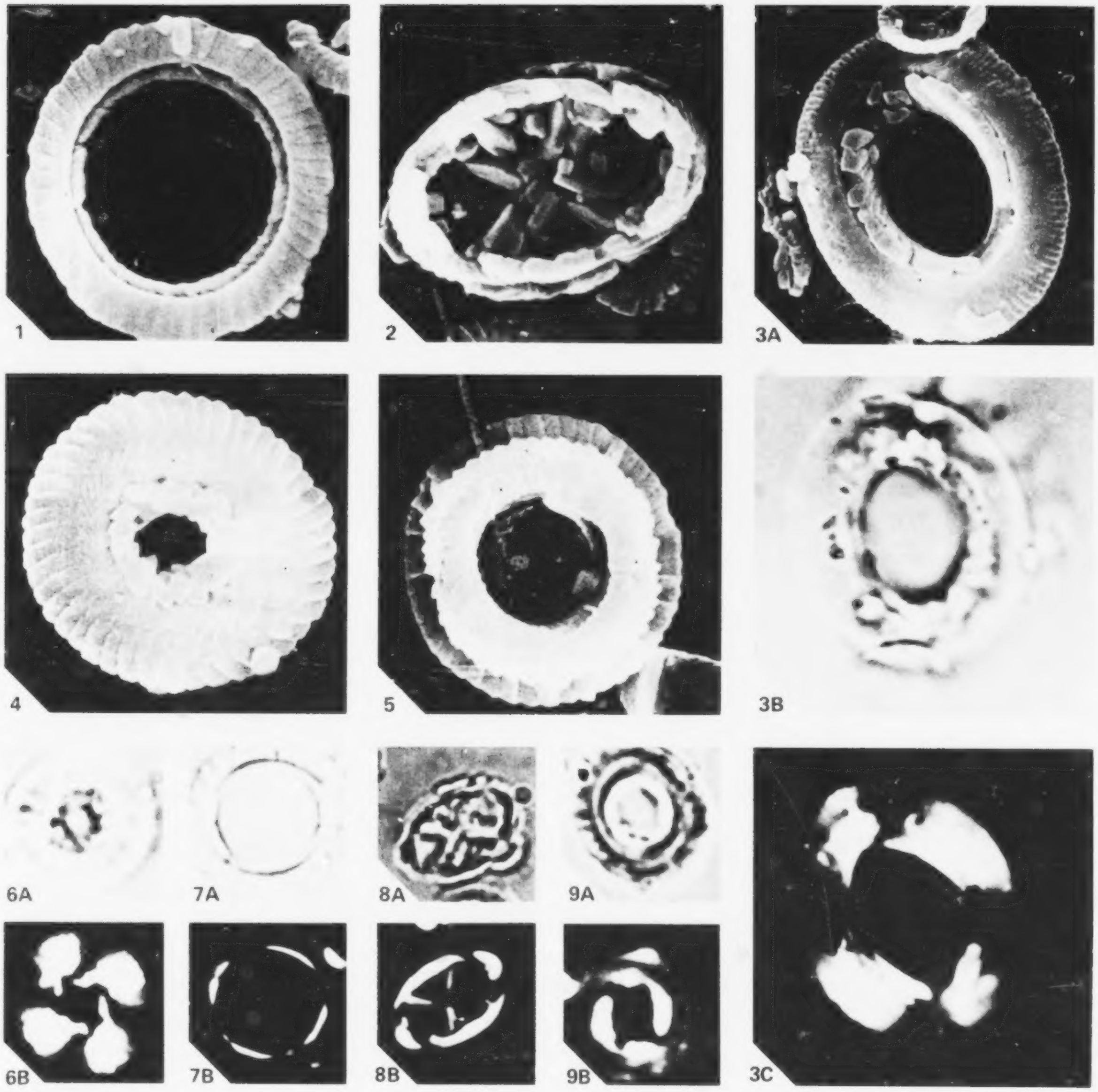

Plate 14. (The abbreviations XN and OL denote cross-polarized and transmitted light. All light microscope photographs are × 2800.) **1, 7.** *Cyclolithella kingi* (Roth), Sample 577A-7,CC, (1) × 5600, (7) same specimen as Fig. 1, (7A) OL, (7B) XN. **2, 8.** *Neochiastozygus concinnus* (Martini), Sample 577-11-2, 18–19 cm, (2) × 7000, (8) same specimen as Fig. 2, (8A) OL, (8B) XN. **3.** *Reticulofenestra umbilica* (Levin), Sample 577A-7-6, 86–87 cm, (3A) × 3500, (3B) OL, (3C) XN. **4, 6.** *Reticulofenestra* cf. *dictyoda* (Deflandre and Fert), Sample 577A-7,CC, (4) × 5600, (6) same specimen as Fig. 4, (6A) OL, (6B) XN. **5, 9.** *Coccolithus formosus* (Kamptner), Sample 577A-8-6, 15–16, (5) × 5600, (9) same specimen as Fig. 5, (9A) OL, (9B) XN.

11. FORAMINIFERS AND COARSE DETRITUS FROM FIVE DEEP-WATER SITES, DEEP SEA DRILLING PROJECT LEG 86, NORTHWEST PACIFIC[1]

Anthony D'Agostino, ARCO Exploration Company[2]

ABSTRACT

Five sites of Leg 86 of the Deep Sea Drilling Project were drilled in water greater than 5000 m deep in the northwest Pacific. The objectives of the coring program at these sites included sampling Cenozoic pelagic sediments, in an effort to define paleoceanographic patterns and boundaries, and assessing the nature of the red clay/chert boundary which is seismically mappable. The biostratigraphy of foraminifers contributes to these objectives in only four short intervals. Cenozoic pelagic sediments contained rare, small, moderately preserved assemblages of planktonic foraminifers. Calcareous sediments below 55.3 m sub-bottom at Site 576 are turbidites of Cretaceous age containing Santonian/Campanian foraminifers. A small assemblage of early Eocene age (P9–P11) was found at 163.28 m at Site 578, corroborating a similar determination based on ichthyoliths. Foraminifers in calcareous sediment immediately above the chert at 176.44 m sub-bottom at Site 578 indicate a Campanian minimum for the age of the chert horizon at that location. At Site 580, a modest assemblage of late Pleistocene (N23) age was recovered above 41.29 m sub-bottom and an early Pleistocene (N22) assemblage found in one sample at 44.89 m sub-bottom. Samples from Sites 579 and 581 were barren of foraminifers.

Examination of the washed residue for foraminifers disclosed abundant volcanic glass, Mn-oxide nodules and tubes, and eolian silt in the greenish and red pelagic clays. Biosiliceous debris and ichthyoliths are also common to abundant. Middle Miocene deposits at Site 581 contain ice-rafted basalt and andesite pebbles.

INTRODUCTION

Five deep-water sites were planned for Leg 86 (Fig. 1). The site objectives were to study the nature and rate of Cenozoic sedimentation and the chert/clay horizon. The Cenozoic sediments were expected to be predominantly biosiliceous, so the importance of calcareous fossil groups was expected to be minimal. The seismically mappable chert layer was, however, thought to be associated with calcareous deposits and foraminifers were expected to be significant in dating this horizon.

The biostratigraphic utility of foraminifers was indeed limited by rare occurrences of planktonic or benthic species in recovered Cenozoic sediments. One Cretaceous calcareous turbidite (Site 576) was penetrated above the chert, and Campanian calcareous sediment was recovered at Site 580, just above the chert. Besides foraminifers, sample examination uncovered manganese-oxide replacement of foraminifers and middle Miocene ice-rafted detritus. Results of the study of Cretaceous and Cenozoic calcareous sediment recovered from Site 577 on the Shatsky Rise will be published elsewhere.

Cored sediment is divided into lithologic units on the basis of color, smear-slide, textural, and compositional data. Three units were designated at Site 576 (see Site 576 chapter, this volume). Lithologic Unit I (0–55 m sub-bottom) consisted of yellowish brown to brown pelagic clay above 28 m sub-bottom (Subunit IA) and dark brown "slick" clay below (Subunit IB). Lithologic Unit II is an interbedded dark brown pelagic clay and pale brown nannofossil ooze. Lithologic Unit III (76 m sub-bottom) is chert and porcellanite. Four units were designated at Site 578 (see Site 578 chapter, this volume). Lithologic Unit I (0–76.6 m sub-bottom) is a gray to olive gray clay and siliceous clay, Lithologic Unit II (76.6–124.5 m sub-

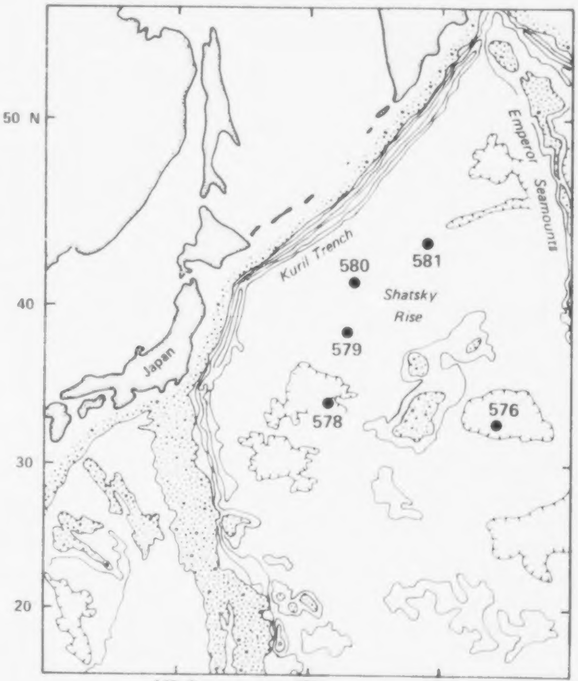

Figure 1. Map showing location of the five deep-water sites: 576, 578, 579, 580, and 581. Areas shallower than 4 km stippled, 5-km contour plain, 6-km contour hachured.

---

[1] Heath, G. R., Burckle, L. H., et al., *Init. Repts. DSDP*, 86: Washington (U.S. Govt. Printing Office).

[2] Address: ARCO Exploration Company, P.O. Box 1346, Houston, TX 77056.

bottom) is a yellowish-brown to brown clay containing minor amounts of siliceous microfossils. Lithologic Unit III (124.5–176 m sub-bottom) is a dark brown pelagic clay. It contains 90% or more clay and biogenic silica is virtually absent. Lithologic Unit IV (176.0–176.8 m sub-bottom) consists of interlaminated brown, yellow, and gray clays over chert. One major unit was designated at Site 579 (see Site 579 chapter, this volume). Lithologic Unit I was subdivided into three subunits (IA, 0–60 m sub-bottom; IB, 60–102.5 m sub-bottom; IC, 102.5–149.5 m sub-bottom) based on the abundance of biogenic silica, quartz, and clay. One lithologic unit was designated at Site 580 (see Site 580 chapter, this volume). Unit I is a siliceous clay subdivided into five subunits (IA, 0–60.3 m sub-bottom; IB, 60.3–79.3 m sub-bottom; IC, 79.3–117.3 m sub-bottom; ID, 117.3–136.3 m sub-bottom; IE, 136.3–155.3 m sub-bottom) based on the content of clay, quartz, biogenic silica, and clay-sized carbonate. Four units were designated at Site 581 (see Site 581 chapter, this volume). Lithologic Unit I (0–244.8 m sub-bottom) is a gray green or yellowish brown biosiliceous clay. Unit II (244.8–276.6 m sub-bottom) is a dark brown "slick" pelagic clay. Unit III (276.7–343 m sub-bottom) is chert and porcellanite. Unit IV (343–352.5 m sub-bottom) is aphyric basalt.

METHODS

Samples were disaggregated in distilled water and occasionally hydrogen peroxide or Calgon was used to aid in dispersal of clays. The sediment was then washed over 149- and 63-μm sieves. The dried residues then placed in separate containers for each size fraction and examined with a binocular microscope.

RESULTS

Site 576: Holes 576 and 576B

Site 576 is located east of the Shatsky Rise in 6220 m of water. The dark brown pelagic clay of Unit I (0–55 m sub-bottom) (Fig. 2) contains no planktonic foraminifers and only rare specimens of *Reophax nodulosus* and *R. difflugiformis*. Mn-oxide replacement of foraminifers was also noted in the sediments of Unit I. This phenomenon was also reported by Thompson (1980) in sediments from the Japan Trench.

Sequences of massive, cross-bedded and normally graded units exhibiting sharp and gradational contacts are common in sediments deposited by turbidity flows. The calcareous sediments of Unit II exhibit these features. The calcareous oozes are also separated by greenish pelagic clay containing Late Cretaceous ichthyoliths (see Site 576 chapter, this volume). Interbedded pelagic sediments characteristically overlie turbidity flows in a deep-sea environment. The calcareous units containing Santonian–Campanian foraminifers can be correlated between the two holes and a sequence of 23 turbidity flows can be recognized (Fig. 3). The reworked nature of the sediments is also indicated by the wide age range indicated by the foraminifers. The specimens found are typical of Late Cretaceous foraminiferal assemblages as reported in the U.S. Gulf Coast (Pessagno, 1967), New Jersey (Olsson, 1960; Petters, 1977), Shatsky Rise (Caron, 1975; Hofker, 1978), the Pacific west of the Shatsky Rise (Krasheninnikov and Hoskins, 1973), the western interior seaway of the U.S. (Frerichs and Dring, 1981), northern California (Trujillo, 1960), and Vancouver, B.C. (McGugan, 1982).

All sub-bottom depths given here and in Appendix B are adjusted according to the factors determined by Ross Heath. Details and techniques used for the adjustments are given in the Site 576 chapter (this volume). Appendix A contains lists of species found in the turbidites and clays recovered at Site 576. Appendix B contains detailed sample information for the two holes.

Site 578: Hole 578

Site 578 was the southernmost site in a northerly transect on Leg 86. It is located west of the Shatsky Rise in 6020 m of water. Foraminifers are rare in the late Pleistocene siliceous clay of Lithologic Subunit IA and in the pelagic clay of Lithologic Unit II. A small assemblage containing two species can be used to date a portion of Lithologic Unit III. A small but diverse assemblage was found just above the chert in Lithologic Unit IV. Sample 578-1-3, 80–82 cm (4.79 m sub-bottom) contained rare specimens of *Reophax difflugiformis* and *Chilostomella* sp. Sample 578-12,CC (109.29 m sub-bottom) contained two specimens of *Massilina tenuis*. Sample 578-18,CC (18–20 cm) (163.28 m sub-bottom) contained rare specimens of *Globorotalia spinulosa* and *G. broedermanni*. These indicate an early Eocene age, but the precise zonation is indeterminate. Their ranges span P9–P11 (the *Globorotalia pentacamerata* Zone to the *Globigerinatheka subconglobata* Zone; Stainforth et al., 1975). Samples 578-20-1, 64–66 cm and 578-20,CC (176.45 m, 176.8 m sub-bottom) contained abundant specimens of *Globotruncana fornicata*; common *G. tricarinata*, *G. lapparenti*, *Pseudotextularia elegans*, and *Heterohelix striata;* and rare to few *Globigerinelloides asperus*, *G. prairiehillensis*, *Hedbergella planispira*, *Globotruncana arca*, *G. stuartiformis*, and *Rugoglobigerina rugosa*. A Late Cretaceous Campanian age is indicated in the *Globotruncana fornicata-stuartiformis* Zone of Pessagno (1967).

Appendix B contains detailed information on the particles observed in these samples including Mn nodules and ichthyoliths.

Site 579: Holes 579, 579A

This site was the second in the north–south paleoceanographic transect and is located in 5746 m of water. No foraminifers were recovered. Appendix B lists observations on the detritus found in the samples examined.

Site 580: Hole 580

Site 580 is located in 5385 m of water and is the third in the series of sites in the north–south transect on Leg 86. Foraminifers were found only in the Pleistocene siliceous clay of lithologic Subunit IA (above 44.9 m sub-bottom). Planktonic and benthic species are typically rare (Table 1). Preservation is moderate to good, with no evident abrasion or breakage, and dissolution effects are light to moderate. The presence of these specimens in the

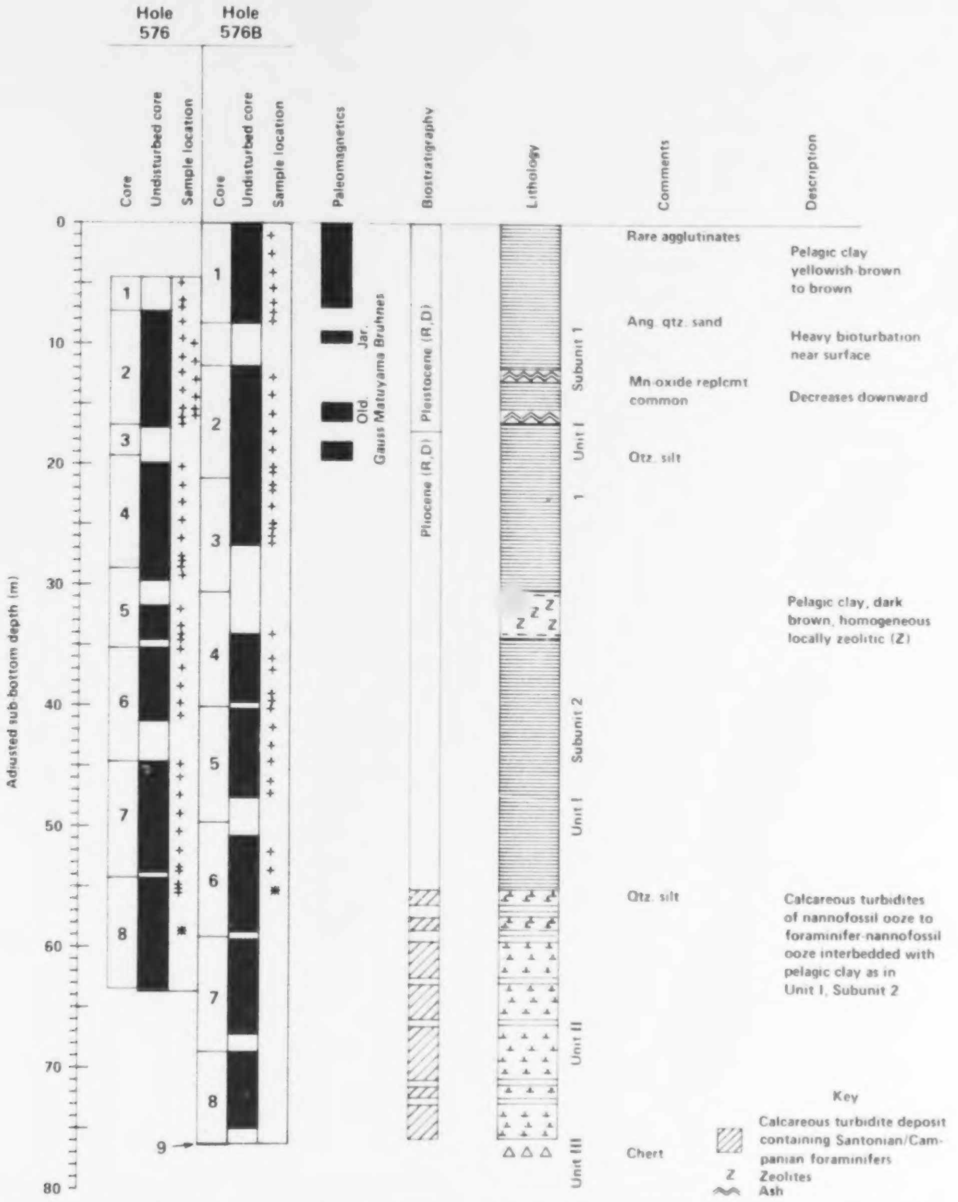

Figure 2. Sample location, paleomagnetics, biostratigraphy, and core description for Holes 576 and 576B. For information on samples below asterisks, see Figure 3.

biosiliceous clay indicates that sedimentation rate alone does not control the preservation of calcareous fossils ince the rate apparently has not changed at that site ince the mid-Pliocene. Appendix B contains detailed ample information for Site 580.

ite 581: Hole 581

This hole was the last and most northerly location drilled on Leg 86. The water depth of 5486 m is reflected by the total absence of foraminifers in recovered sediment. Two samples analyzed from Core 581-9 (middle Miocene, see Site 581 chapter, this volume) contain rounded basalt and andesite pebbles indicative of ice-rafted detritus deposition at this location (Duennebier, Stephen, Gettrust et al., in press).

SUMMARY

The biostratigraphic utility of foraminifers was limited at the five deep-water sites visited in the northwest Pacific during DSDP Leg 86. At Site 576, foraminifers are rare to absent except in the calcareous sediment below 55.3 m sub-bottom. Because of the turbiditic nature of the deposits, foraminifers could not be used to date them. At Sites 579, 580, and 581 foraminifers were either rare or absent and merely supplemented the detailed siliceous biostratigraphy provided by diatoms, radiolarians, and silicoflagellates. The stated objective of dating the chert/clay boundary was accomplished only at Site 578, where a minimum Campanian age can be assigned to the chert. Figure 4 summarizes the foraminiferal biostratigraphy of the deep-water sites of Leg 86.

ACKNOWLEDGMENT

The author wishes to thank ARCO Exploration Co. and Mssrs. G. B. Martin and K. Geitzenaur for the leave of absence required to take part in Leg 86. Gerta Keller reviewed this manuscript.

REFERENCES

Blow, W. H., 1969. Late middle Eocene to Recent planktonic biostratigraphy. *Proc. Int. Conf. Planktonic Microfossils, 1st, Geneva, 1967,* 1:199–422.

Caron, M., 1975. Late Cretaceous planktonic foraminifera from the northwestern Pacific, Leg 32 of the Deep Sea Drilling Project. *In* Larson, R. L., Moberly, R., *Init. Repts. DSDP,* 32: Washington (U.S. Govt. Printing Office), 719–724.

Duennebier, F. K., Stephen, R., Gettrust, J. F., et al., in press. Site 581. *In* Duennebier, F. K., Stephen, R., Gettrust, J. F., et al., *Init. Repts. DSDP,* 88/91: Washington (U.S. Govt. Printing Office).

Frerichs, W. E., and Dring, N. B., 1981. Planktonic foraminifera from the Smoky Hill Shale of West Central Kansas. *J. Foraminiferal Res.,* 11(1):47–69.

Hofker, J., 1978. Analysis of a large succession of samples through the upper Maestrichtian and the lower Tertiary of drill Hole 47.2, Shatsky Rise, Pacific, Deep Sea Drilling Project. *J. Foraminiferal Res.,* 8(1):46–75.

Krasheninnikov, V., and Hoskins, R. H., 1973. Late Cretaceous, Paleogene, and Neogene planktonic foraminifera. *In* Heezen, B. C., MacGregor, I. D., et al., *Init. Repts. DSDP,* 20: Washington (U.S. Govt. Printing Office), 105–203.

McGugan, A., 1982. Upper Cretaceous (Campanian and Maestrichtian) foraminifera from the upper Lambert and Northumberland formations, Gulf Islands, British Columbia, Canada. *Micropaleontology,* 28(4):399–430.

Olsson, R. K., 1960. Foraminifera of the Latest Cretaceous and earliest Tertiary Age in the New Jersey Coastal Plain. *J. Paleontol.,* 34(1):1–58.

Pessagno, E. A., 1967. Upper Cretaceous planktonic foraminifera from the Western Gulf Coastal Plain. *Paleontographica Americana,* V(37):243–445.

Petters, S. W., 1977. Upper Cretaceous planktonic foraminifera from the subsurface of the Atlantic Coastal Plain of New Jersey. *J. Foraminiferal Res.,* 7(3):165–187.

Stainforth, R. M., Lamb, J. L., Luterbacher, H., Beard, J. H., and Jeffords, R. M., 1975. Cenozoic planktonic foraminiferal zonation and characteristics of index forms. *Univ. Kans. Paleontol. Contrib. Pap.,* 62.

Thompson, P. R., 1980. Foraminifers from Deep Sea Drilling Project Sites 434, 435, and 436, Japan Trench. *In* Scientific Party, *Init. Repts. DSDP,* 56, 57, Pt. 2: Washington (U.S. Govt. Printing Office), 775–808.

Trujillo, E. F., 1960. Upper Cretaceous foraminifera near Redding, Shasta County, California. *J. Paleontol.,* 34:290–346.

Date of Initial Receipt: 25 April 1984
Date of Acceptance: 27 July 1984

APPENDIX A
Listing of Species, Holes 576 and 576B

Species found in Hole 576 turbidites

Ammodiscus asperellus (d'Orbigny)
Aragonia velascoensis (Cushman)
Archaeoglobigerina blowi Pessagno
A. tradinghousensis (Pessagno)
Bolivinoides sp.
Bulimina quadrata Plummer
Dentalina colei Cushman & Dusenbury
D. peracuta (Reuss)
D. wilcoxensis Cushman
Dentalina sp.
Eponides bandyi Trujillo
E. simplex (White)
Fissurina sp.
Globigerinelloides asperus (Ehrenberg)
G. prairiehillensis Pessagno
Globotruncana angusticarinata (Gandolfi)
G. bulloides Volger
G. elevata (Brotzen)
G. lapparenti Brotzen
G. stuartiformis Dalbiez
Gyroidina tsablensis McGugan
Haplophragmoides multicameras Krasheninnikov
H. pervagatus Krasheninnikov
Hastigerinoides watersi (Cushman)
Hedbergella planispira (Tappan)
Heterohelix globulosa (Ehrenberg)
H. pulchra (Brotzen)
H. reussi (Cushman)
H. striata (Ehrenberg)
Lagena gracilis (d'Orbigny)
Melonis affinis Reuss
Nodosaria tenuicosta Reuss
Ostracod fragments
Paratrochamminoides intracatus Krasheninnikov
P. semipellucidus Krasheninnikov
P. vitreus Krasheninnikov
Praecystammina globigerinaeformis Krasheninnikov
Pseudotextularia elegans (Rzehak)
Reophax nodulosus Cushman
Reophax sp.
Schackoina multispinata (Cushman & Wickenden)
Stilostomella midwayensis (Cushman & Todd)

Species found in Hole 576B

Aragonia velascoensis (Cushman)
Archaeoglobigerina blowi Pessagno
A. bosquensis Pessagno
A. tradinghousensis (Pessagno)
Bulimina sp.
Dentalina colei Cushman & Dusenbury
D. peracuta (Reuss)
D. semipellucidus Krasheninnikov
Dentalina wilcoxensis Cushman
Dentalina sp.
Eponides bandyi Trujillo
E. simplex (White)
Fissurina sp.
Glandulina pygmaea Reuss
Globigerinelloides asperus (Ehrenberg)
G. prairiehillensis Pessagno
Globotruncana angusticarinata (Gandolfi)
G. bulloides Voiger
G. calcarata Cushman
G. elevata (Brotzen)
G. lapparenti Brotzen
G. stuartiformis Dalbiez
Gyroidina tsablensis McGugan
Haplophragmoides biumbilicalis Krasheninnikov
H. multicamerus Krasheninnikov
H. pervagatus Krasheninnikov
Hastigerinoides watersi (Cushman)
Hedbergella planispira (Tappan)
Heterohelix globulosa (Ehrenberg)
H. pulchra (Brotzen)
H. reussi (Cushman)
H. striata (Ehrenberg)
Lagena gracilis (d'Orbigny)
Lenticulina sp.
Melonis affinis Reuss
Mn-oxide replacements
Nodosaria tenuicosta Reuss
Osangularia sp.
Paratrochamminoides intracatus Krasheninnikov
P. vitreus Krasheninnikov
Praecystammina globigerinaeformis Krasheninnikov
Pseudotextularia elegans (Rzehak)
Schackoina multispinata (Cushman & Wickendam)
Stilostomella midwayensis (Cushman & Todd)

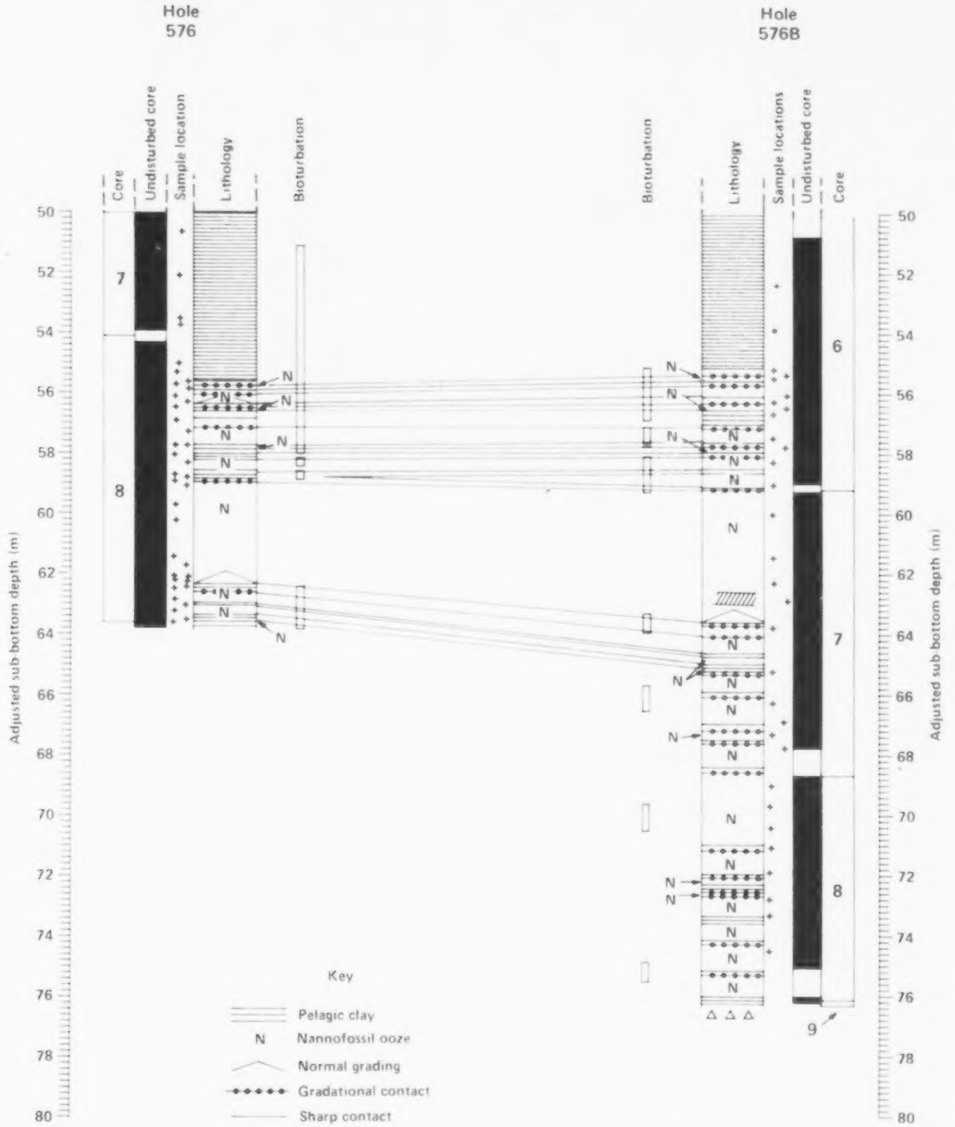
Hole 576
Hole 576B
Core
Undisturbed core
Sample location
Lithology
Bioturbation
Bioturbation
Lithology
Sample locations
Undisturbed core
Core
7
8
6
7
8
9
N
Adjusted sub-bottom depth (m)
Adjusted sub-bottom depth (m)
50
52
54
56
58
60
62
64
66
68
70
72
74
76
78
80
Key
Pelagic clay
Nannofossil ooze
Normal grading
Gradational contact
Sharp contact

Figure 3. Sample location, lithology, bioturbation, and correlation of calcareous turbidites in Holes 576 and 576B.

Table 1. Occurrence and abundance of foraminifers in samples from Hole 580.

Core-Section (interval in cm)	Sub-bottom depth (m)	Age	*Globorotalia humerosa*	*G. inflata*	*G. ronda*	*G. tosaensis*	*G. hirsuta*	*G. praehirsuta*	*G. acostaensis*	*Neogloboquadrina pachyderma* (S)	*Globigerina linaperta*[a]	*Melonis pompilioides*	*Melonis* sp.	*Pyrgo fornasini*	*Fissurina annectens*	*Saccammina sphaerica*
1-1, 112-114	1.13	l. Pleist.										R	R			
1-2, 33-35	1.84		C	F	R					R	A					
2-4, 106-108	8.15					R	F	R			A	R	R	R		
4-3, 80-82	26.11			A	R	R					F					
5-5, 85-87	38.66			R									R			R
5,CC	41.29												R			
6-3, 58-60	44.89	e. Pleist.	A					R	A			F	R		R	

[a] Reworked.

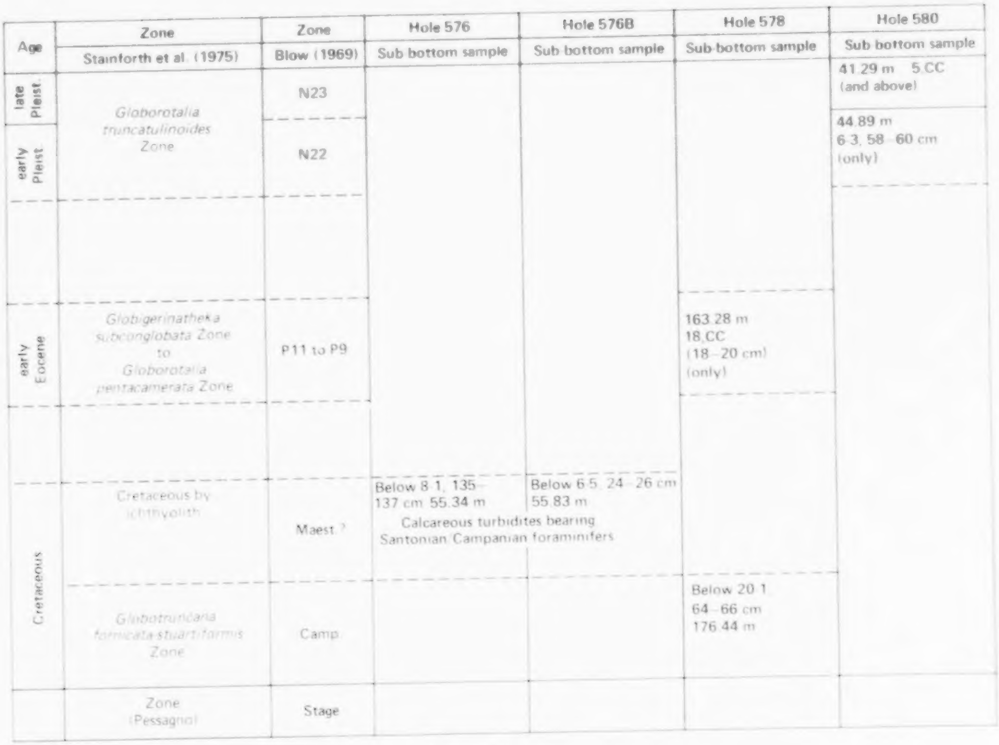
Age
Zone
Stainforth et al. (1975)
Zone
Blow (1969)
Hole 576
Sub bottom sample
Hole 576B
Sub bottom sample
Hole 578
Sub bottom sample
Hole 580
Sub bottom sample
late Pleist.
early Pleist.
Globorotalia truncatulinoides Zone
N23
N22
41.29 m 5,CC (and above)
44.89 m 6-3, 58–60 cm (only)
early Eocene
Globigerinatheka subconglobata Zone to Globorotalia pentacamerata Zone
P11 to P9
163.28 m 18,CC (18–20 cm) (only)
Cretaceous
Cretaceous by ichthyolith
Maest.?
Below 8-1, 135–137 cm 55.34 m
Below 6-5, 24–26 cm 55.83 m
Calcareous turbidites bearing Santonian/Campanian foraminifers
Globotruncana fornicata-stuartiformis Zone
Camp.
Below 20-1 64–66 cm 176.44 m
Zone (Pessagno)
Stage

Figure 4. Summary of biostratigraphy, Sites 576, 578, and 580.

APPENDIX B
Sample Contents of All Material Examined from Sites 576, 578, 579, 580, and 581

		Coarse fraction (>63 μm) components[a]								Foraminifers[b]			
Core-Section (interval in cm)	Depth in hole (m)	Biosiliceous debris	Clay flocs	Mn nodules	Fish teeth, fish debris	Volcanic glass	Pumice fragments	Quartz silt/sand	Phillipsite	Preservation	Planktonic	Benthic	Comments
Hole 576[c]													
1-1, 56-58	5.06-5.08	A	A							G		R	*Rheophax* sp.
1-2, 53-55	6.53-6.55	A	A			C							
1,CC (10-13)	7.17-7.20	A	A			C				G		R	Agglutinates
2-1, 101-102	8.21-8.23	A	A										
2-2, 101-102	9.71-9.73	C	A										
2-3, 101-102	11.21-11.23	C	A										
2-4, 80-82	12.50-12.52	C	A	A	C					R		R	Mn-oxide replacement
2-5, 80-82	14.00-14.02	C	A	A									
2-6, 80-82	15.50-15.52	C	A	A	R								
2-7, 20-22	16.40-16.42	C	A	A	C								
2,CC (8-11)	16.78-16.81	C	A	A	C								
3-1, 50-52	10.10-10.12	C	A	A	C								Repeat of Core 2
3-2, 50-52	11.60-11.62	C	A	A	R								Repeat of Core 2
3-3, 50-52	13.10-13.12	C	A	A	R								Repeat of Core 2
3-4, 50-52	14.60-14.62	C	A	A	R								Repeat of Core 2
3-5, 12-14	15.72-15.74	C	A	A	R								Repeat of Core 2
3,CC (10-13)	16.02-16.05	C	A	A	R					R		P	Repeat of Core 2, Mn-oxide replacement
4-1, 120-122	20.30-20.32	P	A	A	C								
4-2, 120-122	21.80-21.82	P	A	A	R								
4-3, 120-122	23.30-23.32	P	A	A	R								
4-4, 120-122	24.80-24.82	P	A	A	C								
4-5, 120-122	26.30-26.32	P		A	F								
4-6, 120-122	27.80-27.82	P		A	F								

Appendix B. (Continued).

		Coarse fraction (>63 μm) components[a]								Foraminifers[b]			
Core-Section (interval in cm)	Depth in hole (m)	Biosiliceous debris	Clay flocs	Mn nodules	Fish teeth, fish debris	Volcanic glass	Pumice fragments	Quartz silt/sand	Phillipsite	Preservation	Planktonic	Benthic	Comments
Hole 576[c] (Cont.)													
4-7, 20-22	28.30-28.32	P		A									
4,CC (10-13)	28.68-28.71	P		A	A								
5-1, 120-122	29.40-29.42	R	A	A	A								
5-2, 120-122			A	A	A								Flow-in
5-3, 102-104			A	A	A								Flow-in
5-4, 102-104			A	A	A								Flow-in
5-5, 102-104	32.12-32.14	P	A	A	A								
5-6, 102-104	33.62-33.64	P	A	A	A								
5-7, 30-32	34.40-34.42	P	A	A	A								
5,CC (10-13)	34.69-34.72	P	F	A	A								
6-1, 135-136		P	R	F	A								Flow-in
6-2, 112-113		P	R	A	A			A					Flow-in
6-3, 112-113	35.52-35.53	P	R	F	A			A					
6-4, 112-113	37.02-37.03	P			A								
6-5, 112-113	38.52-38.53		F	F	A								
6-6, 112-113	40.02-40.03	P			A								
6-7, 40-42	40.80-40.82		P		A								
6,CC (10-13)	40.95-40.98		P		A								
7-1, 50-52	45.10-45.12		P		A			A					
7-2, 50-52	46.10-46.12				A								
7-3, 50-52	47.60-47.62		A	A	A								
7-4, 50-52	49.10-49.12		F	A	A								
7-5, 50-52	50.60-50.62		R	R	A	A							
7-6, 50-52	52.10-52.12	F	R	R	A								
7-7, 40-42	53.50-53.52		F	R	A								
7,CC (15-18)	53.75-53.78		F		A								
8-1, 90-92	55.00-55.02		A	A	A			A					
8-1, 135-137	55.35-55.37		A	A	A			A		M		R	
8-2, 4-6	55.64-55.66		A	A	A								
8-2, 18-20	55.78-55.80			A	A					M	A	C	Graded nannofossil ooze, tests in 63-149 μm fraction, dissolution, abrasion
8-2, 25-27	55.85-55.87		A	A						M	C	C	Bioturbated clay
8-2, 50-52	56.10-56.12		R	A	A					M	A	F	Dissolution, graded nannofossil ooze
8-2, 71-73	56.31-56.33			A	A			A		G	R	C	Tests stained brown, bioturbated clay
8-2, 88-90	56.48-56.50		R	A	A					M	A	C	Abrasion, dissolution, nannofossil ooze
8-2, 132-134	56.92-56.94			C	A					M	R	C	Brown tests, abrasion, bioturbated clay
8-3, 18-20	57.28-57.30		R	C	A					M	R	F	Bioturbated nannofossil ooze
8-3, 66-68	57.76-57.78			C	C			A					
8-3, 81-83	57.91-57.93		R	F				A					
8-3, 96-98	58.06-68.08			F	A								
8-3, 122-124	58.32-58.34			F	C					M	C	C	Nannofossil ooze
8-4, 10-12	58.78-58.72									M	R	C	Brown-stain, nannofossil ooze, bioturbation?
8-4, 20-22	58.80-58.82			A	A								
8-4, 30-32	58.90-58.92	P								P	A	F	Nannofossil ooze, dissolution, abrasion
8-4, 49-51	59.09-59.11	P		R						P	A	C	Nannofossil ooze, dissolution, abrasion
8-4, 110-112	59.70-59.72	P		R						P	A	C	Nannofossil ooze, dissolution, abrasion
8-5, 12-14	60.22-60.24			R						P	A	C	Nannofossil ooze, dissolution, abrasion
8-5, 132-134	61.42-61.44	P		C						P	A	C	Nannofossil ooze, dissolution, abrasion
8-6, 12-14	61.72-61.74	P		C						P	A	C	Nannofossil ooze, dissolution, abrasion
8-6, 42-44	62.02-62.04			C						P	A	C	Nannofossil ooze, dissolution, abrasion
8-6, 52-54	62.12-62.14	R								P	A	C	Cross-bedding, dissolution, abrasion
8-6, 62-64	62.22-62.24	R								P	A	C	Graded nannofossil ooze
8-6, 72-74	62.32-62.34	R		C	A					P	A	C	Graded nannofossil ooze, bioturbated?
8-6, 84-86	62.44-62.46	R		C	A					P	A	C	Graded nannofossil ooze, bioturbated?
8-6, 98-100	62.58-62.60	P	F	C	R					P	A	C	White tests, dissolution, abrasion, bioturbated nannofossil ooze
8-6, 125-127	62.85-62.87	P	F		A					P	A	C	White tests, dissolution, abrasion, bioturbated clay
8-6, 148-150	62.08-63.10	P		F						P	A	C	White tests, dissolution, abrasion, bioturbated nannofossil ooze
8-7, 16-18	63.26-63.28	P		C						P	A	C	White tests, dissolution, abrasion, bioturbated nannofossil ooze
8,CC (4-7)	63.57-63.59	R	C	C	A			A		P	F	F	Broken tests stained brown
8,CC (15-18)	63.68-63.70			F						P	A	C	White tests, dissolution, abrasion, nannofossil ooze
Foram-bearing													

Appendix B. (Continued).

Core-Section (interval in cm)	Depth in hole (m)	Coarse fraction (>63 µm) components[a]								Foraminifers[b]			Comments
		Biosiliceous debris	Clay flocs	Mn nodules	Fish teeth, fish debris	Volcanic glass	Pumice fragments	Quartz silt/sand	Phillipsite	Preservation	Planktonic	Benthic	
Hole 576[c]													
Shipboard CC's 8,CC										M	A	R	
Hole 576B[c]													
1-1, 108-110	1.08-1.10	A	A										
1-2, 108-110	2.58-2.60	A	A			R							
1-3, 108-110	4.08-4.10	A	A	F									
1-4, 108-110	5.58-5.60	A	A	F									
1-5, 68-70	6.68-6.70	A	A	F	P								
1-6, 20-22	7.70-7.72	A	A	F									
1,CC (7-10)	8.14-8.16	A	A	A				P					Angular quartz sand
2-1, 130-132	12.90-12.92	A	A	A	R								
2-2, 130-132	14.40-14.42	A	A	A	R								
2-3, 130-132	15.90-15.92	A	A	A	R								
2-4, 130-132	17.40-17.42	A	A	A	R					R		P	Mn-oxide replacement
2-5, 130-132	18.90-18.92	R	A	A	R			P					Quartz silt
2-6, 130-132	20.40-20.42	R	A	A	R			P					Quartz silt
2-7, 10-12	20.70-20.72		A	A	R								
2,CC (10-13)	21.08-21.10		A	A	F			P					
3-1, 92-94	22.02-22.04	P	A	A	R			P		R		P	Mn-oxide replacement
3-2, 92-94	23.52-23.54		A	A	R								
3-3, 92-94	25.02-25.04		P	A									
3-4, 92-94			A	A	R			P					Flow-in
3-5, 92-94				A	A								Flow-in
3-6, 92-94	25.41-25.43		A	A	A								
3-7, 10-12	26.09-26.11		C	A	A								
3,CC (10-13)	26.59-26.61		C	A	A								
4-1, 138-140			A	A	A								Flow-in
4-2, 12-14			A	A	A								Flow-in
4-3, 12-14			A	A	A								Flow-in
4-4, 12-14	34.72-34.74		A	A	A								
4-5, 12-14	36.22-36.24			A	A								
4-6, 12-14	37.72-37.74			A	A								
4-7, 12-14	39.22-39.24			A	A								
4,CC (10-13)	39.72-39.74			C	A								
5-1, 130-132			R		A								Flow-in
5-2, 34-36	40.44-40.46		R	R	A								
5-3, 34-36	41.94-41.96		R	R	A								
5-4, 34-36	43.44-43.46		R	R	A								
5-5, 34-36	44.94-44.96		R		A								
5-6, 34-36	46.44-46.46		R	R	A								
5,CC (10-13)	47.43-47.45		R	A	A								
6-1, 110-112			P	C	C								Flow-in
6-2, 110-112	52.20-52.22		R	A	A								
6-3, 110-112	53.70-53.72			R	A								
6-4, 90-92	55.00-55.02			A	A								
6-4, 110-112	55.20-55.22		A	A	A								
6-4, 126-128	55.36-55.38		C	C	C			A					Quartz silt
6-5, 24-26	55.84-55.86		C	C						M	F	F	Dissolution, abrasion, white tests, nannofossil ooze
6-5, 56-58	56.16-56.18			C	R			P		P	C	F	Dissolution, abrasion, white tests, bioturbated clay
6-5, 70-72	56.30-56.32			C	R			P		P	C	F	Dissolution, abrasion, white tests, bioturbated nannofossil ooze
6-5, 96-98	56.56-56.58			A	A					P		R	Tests stained brown, bioturbated clay
6-6, 28-30	57.38-57.40			C	C					M	R	R	
6-6, 58-60	57.68-57.70			R	R	R							
6-6, 100-102	58.10-58.12			R	R					P	R	R	Dissolution, abrasion, white tests, bioturbated nannofossil ooze
6,CC (34-35)	58.86-58.88			P	R					P	A	F	Dissolution, abrasion, nannofossil ooze, white tests
7-1, 76-78	59.84-59.86		R	R						P	A	C	Dissolution, abrasion, nannofossil ooze, white tests
7-2, 76-78	61.34-61.36	P	R	R	R					P	A	C	Dissolution, abrasion, nannofossil ooze, white tests

Appendix B. (Continued).

Core-Section (interval in cm)	Depth in hole (m)	Coarse fraction (>63 μm) components[a]								Foraminifers[b]			Comments
		Biosiliceous debris	Clay flocs	Mn nodules	Fish teeth, fish debris	Volcanic glass	Pumice fragments	Quartz silt/sand	Phillipsite	Preservation	Planktonic	Benthic	
Hole 576B[c] (Cont.)													
7-3, 115-117	62.15-62.17	P	R	R	P					P	A	C	Dissolution, abrasion, nannofossil ooze, white tests
7-4, 24-26	62.74-62.76	C	R							P	A	C	Dissolution, abrasion, nannofossil ooze, white tests
7-4, 115-117	63.65-63.67	R		R	R					P	A	C	Dissolution, abrasion, nannofossil ooze, white tests
7-5, 104-106	65.04-65.06	R	R							P	A	C	Dissolution, abraison, bioturbated nannofossil ooze, white tests
7-6, 68-70	66.18-66.20		R	R						P	R	R	Fragments only
7-6, 120-122	66.70-66.72	P		R						P	F	F	Dissolution, abrasion, nannofossil ooze, white tests
7-7, 10-12	67.10-67.12	P		R						P	A	C	Dissolution, abrasion, nannofossil ooze, white tests
7,CC (30-33)	67.64-67.66	P	R	R						P	A	C	Dissolution, abrasion, nannofossil ooze, white tests
8-1, 135-140	68.80-68.82	P		P						P	A	C	Dissolution, abrasion, nannofossil ooze, white tests
8-2, 58-60	69.53-69.55	P	R	R						P	A	C	Dissolution, abrasion, nannofossil ooze, white tests
8-2, 128-130	70.23-70.25									P	R	R	Dissolution, abrasion, 63-149 μm fraction only, graded nannofossil ooze
8-3, 50-52	70.95-70.97									P	F	R	Dissolution, abrasion, 63-149 μm fraction only
8-3, 124-126	71.69-71.71		R		R					P	F	R	Dissolution, abrasion, 63-149 μm fraction only
8-4, 66-68	72.61-72.63									P	F	R	Dissolution, abrasion, 63-149 μm fraction only
8-4, 124-126	73.19-73.21		R		P					P	F	R	Dissolution, abrasion, 63-149 μm fraction only, graded ooze
8-5, 90-92	74.35-74.37		R							P		R	Tests stained brown, dissolution, bioturbation?
Shipboard CC's													
7,CC										P		R	Agglut. benthics
6,CC										M		R	Agglut. benthics
Hole 578													
1-3, 80-82	3.80-3.82	A	A							G		R	2 calc. benthic, 1 agglut.
1,CC (18-20)	4.78-4.80	C	A		R								
2-3, 80-82	8.60-8.62	A	A										
2,CC (18-20)	14.28-14.30	A	A			A							
3-3, 90-92	18.20-18.22	A	A										
3,CC (18-20)	23.70-23.72	A	A	R									
4-3, 90-92	27.70-27.72	A	A		R								
4,CC (18-20)	33.28-33.30	A	A										
5-4, 90-92	38.70-38.72	A	A										
5,CC (18-20)	42.78-42.80	A	A			A							
6-4, 70-72	48.00-48.02	A	A			A							
6,CC (18-20)	52.58-52.30	A	A			A							
7-2, 70-72	54.50-54.52	A	A			A							
7,CC (18-20)	61.78-61.80	A	A										
8-3, 60-62	65.40-65.42	A	A			C							
8,CC (18-20)	71.28-71.30	A	A			A							Green and clear glassy particles >149 μm in size
9-3, 57-59	74.87-74.89	A	A			A							
9,CC (18-20)	80.78-80.80	A	A			A			A				
10-3, 69-71	84.49-84.51	A	A	C		A							
10,CC (18-20)	90.28-90.30	A	A	C		A	P						
11-3, 60-62	93.90-93.92	A	A						A				
11,CC (18-20)	99.78-99.90	A	A										
12-3, 50-52	103.30-103.32	A	A										
12,CC (18-20)	109.28-109.30	A	A	A					A	G		R	2 calc. benthic
13-4, 80-82	114.60-114.62	A				A							
13,CC (18-20)	118.78-118.80	A	A	A	R				A				
14-3, 90-92	122.70-122.72	A	A	C	R				A				
14,CC (18-20)	128.28-128.30			A	R								

Appendix B. (Continued).

Core-Section (interval in cm)	Depth in hole (m)	Coarse fraction (>63 μm) components[a]								Foraminifers[b]			Comments
		Biosiliceous debris	Clay flocs	Mn nodules	Fish teeth, fish debris	Volcanic glass	Pumice fragments	Quartz silt/sand	Phillipsite	Preservation	Planktonic	Benthic	
Hole 578 (Cont.)													
15-3, 33-35	131.63-131.65	A	A	A	R								
15,CC (18-20)	137.78-137.80		A	A	R								
16-1, 20-22	138.00-138.02		A	A	R								
16-2, 28-30	139.58-139.60		A	A	R								
16-2, 138-139	140.68-140.69		A	A	R								
16-3, 130-131	142.09-142.11		A	A	R								
16-5, 138-139	145.17-145.19					A							Blocky, varicolored glass
16,CC (18-20)	147.28-147.30		A	A	A	C							
17,CC (18-20)	155.28-155.30		R	A	A								
18-3, 50-52	160.30-160.32			C	A								
18,CC (18-20)	163.28-163.30			A	A					M	C	R	late early to early middle Eocene
19-2, 70-72	168.50-168.52			A	A								
20-1, 64-66	176.44-176.46									R	A	C	Silica replacement, Campanian
20,CC	176.78-176.80									R	A	C	Silica replacement, Campanian
Hole 579													
1-4, 41-43	4.91-4.93		A					P					
1,CC (18-20)	8.38-8.40		A					A					
2-3, 95-97	12.35-12.37		A					P					
2,CC (18-20)	17.88-17.99	A	A					R					
Hole 579A													
1-5, 95-97	20.95-20.97	A	A					C					
1,CC (18-20)	23.48-23.50	A	A					C					
2-5, 100-102	30.50-30.52	A	A					C					
2,CC (18-20)	32.98-33.00	A						C					
3-3, 68-70	36.68-36.70	A						C					
3,CC (18-20)	42.48-42.50	C	A					C					
4-3, 118-120	46.68-46.70	A	A			C							
4,CC (18-20)	51.98-51.20	A				A							
5-3, 53-55	55.53-55.55	A	A			C							
5,CC (18-20)	61.48-61.50	A	A			A							
6-3, 50-52	65.00-65.02	A	A										
6,CC (18-20)	70.98-71.00	A	A										
7-3, 94-96	74.94-74.96	A	A			C							
7,CC (18-20)	80.48-80.50	A	A										
8-5, 100-102	87.50-87.52	A	A										
8,CC (18-20)	89.98-90.00	A	A										
9-3, 70-72	93.70-93.72	A	A										
9,CC (18-20)	99.48-99.50	A	A										
10-4, 100-102	105.00-105.02	A	A										
10,CC (18-20)	108.98-109.00	C	A										
11,CC (18-20)	118.48-118.50	A											
12-3, 28-30	121.78-121.80	A				A							
12,CC (18-20)	127.98-128.00	A				A							
13-3, 70-72	131.70-131.72	A	A			C							
13,CC (18-20)	137.48-137.50	A	A										
14-3, 30-32	140.80-140.82	A	A										
14,CC (18-20)	146.98-147.00	A	A										
15-1, 110-112	148.10-148.12	A	A										
15,CC (18-20)	149.48-149.50	A	A										
Hole 580													
1-1, 27-29	0.27-0.29	A				C							
1-1, 112-114	1.12-1.14	A				A	C			G		P	2 calc. benthics, 1 rounded basalt pebble
1-2, 33-35	1.83-1.85	A				A				G	A	A	Rounded basalt pebbles
1-2, 142-144	2.92-2.94	A	A			C							
1-3, 3-5	3.03-3.05	A				C							2 rounded basalt pebbles
1,CC (18-20)	3.28-3.30	A				C							
2-1, 76-80	4.06-4.08	A				A							
2-2, 124-126	6.04-6.06	A				A							
2-3, 108-110	7.38-7.40	A				C							
2-3, 124-126	7.54-7.56	A				C							

Appendix B. (Continued).

Core-Section (interval in cm)	Depth in hole (m)	Coarse fraction (>63 μm) components[a]								Foraminifers[b]			Comments
		Biosiliceous debris	Clay flocs	Mn nodules	Fish teeth, fish debris	Volcanic glass	Pumice fragments	Quartz silt/sand	Phillipsite	Preservation	Planktonic	Benthic	
Hole 580 (Cont.)													
2-4, 34-36	8.14-8.16	A	A			C							
2-4, 106-108	8.86-8.88	A				A				G	A	C	
2-5, 72-74	10.02-10.04	A				A							
2,CC (18-20)	12.78-12.80	A				A							
3-4, 45-47	17.75-17.77	A	A										
3,CC (18-20)	22.28-22.30	A	C			C							Varicolored glassy grains
4-3, 80-82	26.10-26.12	A	A							G	A	R	
4,CC (18-20)	31.78-31.80	A				A							
5-5, 85-87	38.65-38.67	A	A							G	R	R	
5,CC (18-20)	41.28-41.30	A	A							M	R	R	
6-3, 58-60	44.88-44.90	A	A							M	A	C	
6,CC (18-20)	50.78-50.80	A	A										
7-3, 62-64	54.42-54.44	A	A			A							
7,CC (18-20)	60.28-60.30	A	A										
8-3, 43-45	63.73-63.75	A	A										
8,CC (18-20)	69.78-69.80	A				A							
9-3, 32-34	73.12-73.14	A	A			A							
9,CC (18-20)	79.28-79.30	A											
10-3, 60-62	82.90-82.92	A				A							
10,CC (18-20)	88.78-88.80	A	A			A							
11-3, 105-107	92.85-92.87	A	A										
11,CC (18-20)	98.28-98.30	A	A			A							
12-4, 20-22	103.00-103.02	A	A										
12,CC (18-20)	107.78-107.80	A											
13-4, 60-62	112.90-112.92	A											
13,CC (18-20)	117.28-117.30	A											
14-3, 30-32	120.60-120.62	A	A										
14,CC (18-20)	126.78-126.80	A	C										
15-2, 101-103	129.31-129.33	A											
15,CC (18-20)	136.28-136.30	A				A							
16-3, 26-28	139.56-139.58	A	A										
16,CC (18-20)	145.78-145.80	A	A										
17-3, 21-23	149.01-149.03	A	A										
17,CC (18-20)	155.28-155.30	A											
Hole 581													
1-1, 40-42	0.40-0.42	A	C			A	C						Glassy grains of various colors
1,CC (18-20)	0.98-1.00	A	C			A	C						Glassy grains of various colors
2-2, 20-22	183.20-183.22	A											
2,CC (18-20)	190.98-191.00	A	C										
3-4, 33-35	195.83-195.85	A											
3,CC (18-20)	200.48-200.50	A											
4-4, 50-52	205.50-205.52	A	A										
4,CC (18-20)	209.98-210.00	A				C							
5-3, 34-36	213.34-213.36	A	A										
5,CC (18-20)	219.48-219.50	A							A				
6-3, 28-30	222.78-222.80	A	A										
6,CC (18-20)	228.98-229.00	A	A										
7-3, 80-82	232.80-232.82	A							A				
7,CC (18-20)	238.48-238.50	A	A						A				
8-3, 60-62	242.10-242.12	A	A										
8,CC (18-20)	247.98-248.00	A	A										One large, rounded, basalt pebble
9-2, 60-62	250.10-250.12	C	F										
9,CC (18-20)	257.48-257.50	C	F										2 rounded basalt, 1 angular andesite pebble
10-2, 90-92	259.90-259.92		F		P								
10,CC (18-20)	266.98-267.00		F		P								
11-1, 26-28	267.26-267.28		C		R								

---

[a] Abundance: P = present, R = rare, F = few, C = common, A = abundant.

[b] Preservation: G = good, M = moderate, P = poor, R = replaced.

[c] Adjusted sub-bottom depth.

12. ICHTHYOLITH BIOSTRATIGRAPHY OF WESTERN NORTH PACIFIC PELAGIC CLAYS, DEEP SEA DRILLING PROJECT LEG 86[1]

P. S. Doyle and W. R. Riedel, Scripps Institution of Oceanography[2]

ABSTRACT

Pelagic clay sequences representing most of the Cenozoic Era were cored at Sites 576 and 578; the three holes drilled at Site 576 penetrated to Cretaceous sediments. A Cretaceous-Paleogene succession was obtained from Hole 577. The combined results from these holes, and some piston cores from more eastern localities, provide the basis for a synthesis of North Pacific Cenozoic ichthyolith stratigraphy. The synthesis is approached both by conventional biostratigraphic procedures and by a probabilistic interpretation based on events weighted according to their relative reliabilities. Seven new taxa from the Paleocene are described, thus improving the stratigraphic resolution attainable in that epoch.

INTRODUCTION

On Leg 86, ichthyoliths were investigated at four sites:

Site 576: 32°21.36′N, 164°16.54′E; water depth 6217 m,
Site 577: 32°26.51′N, 157°43.40′E; water depth 2675 m,
Site 578: 33°55.56′N, 151°37.74′E; water depth 6010 m, and
Site 581: 43°55.62′N, 159°47.76′E; water depth 5476 m.

Additional information on late Paleogene and Neogene ichthyolith successions, required for probabilistic stratigraphic interpretations, is shown in Table 1 based on the following MPGII piston core samples provided by G. R. Heath of Oregon State University, Corvallis:

Y74-3-62PC: 33°8.7′N, 151°15.8′W; water depth 5329 m,
Y74-3-65PC: 33°13.2′N, 150°59.6′W; water depth 5512 m, and
Y74-3-73PC: 33°26.6′N, 150°54.7′W; water depth 5540 m.

Figure 1 shows the locations of these sites, and of other Pacific sites from which we obtained samples contributing to ichthyolith stratigraphic interpretations.

In addition to providing a time-stratigraphic interpretation of the Leg 86 cores, we improved our understanding of Paleocene ichthyolith stratigraphy (describing seven new subtypes) and continued development of a procedure for probabilistic stratigraphic interpretations by employing a method of indexing the reliability of biostratigraphic events as applied in Gottfried et al. (1984).

Sediment samples treated were of approximately 40 cm^3 from Deep Sea Drilling Project (DSDP) Holes 576, 576B, 577, 578, and 581, of 100 cm^3 from Hole 576A, and of 150 cm^3 from the MPGII cores. Sample and slide preparation techniques followed those detailed by Edgerton et al. (1977). The numbers of ichthyoliths in the fractions coarser than 63 μm commonly ranged from 100 to several thousand per sample. Forms useful for stratigraphic interpretations at present constitute only a very small fraction of the total. Numbers of specimens observed are shown in Tables 1-4.

CONVENTIONAL STRATIGRAPHIC INTERPRETATIONS

Over the past 10 yr., we have built up an ichthyolith stratigraphy by establishing the ranges of approximately 120 taxa (*subtypes*) in sediment sequences in which ages have been determined on the basis of other groups of microfossils, mainly calcareous nannoplankton (Doyle et al., 1974; Dunsworth et al., 1975; Doyle et al., 1977; Gottfried et al., 1985). Application of this ichthyolith stratigraphy to pelagic clay sequences results in age assignments to about the level of epochs within the Cenozoic (Edgerton et al., 1977; Doyle and Riedel, 1979b; Kaneps et al., 1981). These "conventional" procedures are here applied to the Leg 86 sequences, with the results summarized below and shown in the left-hand columns of Tables 2-4.

As the basis for stratigraphic comparisons, we have used only Pacific Ocean samples with ages assigned on the basis of calcareous nannofossils or radiolarians and not Atlantic and Indian Ocean samples (which were taken into account in our earlier correlations—Doyle and Riedel, 1979a). Until sufficient ichthyolith data are accumulated to allow formal zonal definitions, we do not capitalize subepoch designations assigned on the basis of these microfossils. Site 577 is not discussed in the following paragraphs because its stratigraphic interpretation is based on calcareous nannofossils.

Hole 576

Standard samples 40 cm^3 in size were taken from cores in this hole. Concentrations of ichthyoliths and dry weights of samples are given in the right-hand columns of Table 2.

Ichthyoliths in Cores 2 through 4 are late Miocene or younger, based on the presence of *Long ellipse*, *Narrow*

---

[1] Heath, G. R., Burckle, L. H., et al., *Init. Repts. DSDP*, 86: Washington (U.S. Govt. Printing Office).

[2] Address: Scripps Institution of Oceanography, University of California, San Diego, La Jolla, CA 92093.

Table 1. Numbers of observed specimens of taxa in samples from the central North Pacific MPG-II area.

Samples	Subtypes Depth (cm)	*Five peaks flared base*	*Triangle pointed margin ends*	*Triangle inline halfway*	*Triangle with triangular projection*	*Flexed triangle shallow inbase*	*Triangle concave base*	*Triangle medium wing*	*Wide triangle*	*Triangle short wing*	*Triangle broad wing*	*Triangle transverse line across*	*Narrow triangle cross-hachured*	*Tanged triangle*	*Triangle one canal above*	*Broad triangle parallel inline*	*Wide triangle straight inbase*	*Triangle hooked margin*	*Narrow triangle straight inbase*	*Triangle double flex*	*Triangle sigmoid*
Y74-3-62PC	40–60																	4			
	140–160																	5			
	240–260				1											2		2			
	310–330		1	1	5	12		6	1	4		1				13		7	2		2
	380–400			1	20	14		4		4						6		3	4		1
	470–490			1	5	13		3		2		3				5	1		1		
	570–590		1		11	3		3		2		15		1	4	15	2	1	1		1
	660–680		13		51	1	1	12		9		23	1	2	?	4	8	2	2		8
	760–780		6	1	23	1	2	4		2		12	4	3		1		2	1		
	860–880		11		17		2	11		2		8	2	2				2	2		
	960–980		44		46		4	9		2		5				1					
Y74-3-65PC	40–60																				
	140–160				1													1			
	240–260															2		1			
	340–360		9	1						7		1	1			7	1	5	1		1
	410–430				15	16		2		9					2			3	4	2	
	490–510			4	14	12		2							2	1		1	4		
	600–620			1	18	6		3		1		15				4		3	2		
	720–740		1	2	29	1		3	1			6	1		2	4		4	1	1	
	830–850		5		22	1		18		3		19	2			1			1		
	930–950		7		16		2	7	1	1		2	1					2	2		
	1020–1040		5		3			5				2		1		1					
Y74-3-73PC	100–120				1			1								2		2	1		
	200–220																				
	310–330							1				1						1			
	400–420				7			1		4		1				7	2	3	1	3	
	485–505		1		9	2		6		3		3				5		3			1
	650–670		1		26	8	1	8		1		10				18		2	3		
	737–752				10	11		3		3		1	6								
	775–795		1		6	15		4	1			11			1	9	1	2	1		
	880–900		6		15	1		17				4				5		2	3		4
	980–1000		2		19			13	2	1		6		3		3			2	1	6
	1080–1100	1	4		10	1	1	19				4		2	1	1	1		2		1
	1180–1200	3	6		7	1	1	18	1	6		2	1	2	2	5	2	2	2		
	1204–1219	1	27		29	2	2	7			1		43						1	1	

Samples	Subtypes Depth (cm)	*Small dendritic few radiating lines*	*Triangle with parallel inline*	*Pointed triangle short inline*	*Triangle with canals*	*Pointed triangle long margins*	*Curved triangle inline constricted*	*Rounded apex triangle*	*Flexed triangle shallow inbase ≥ 120*	*Triangle with base angle*	*Asymmetrical peak depression*	*Triangle with high inline apex*	*Small circular center*	*Triangle inward angle*	*Small dendritic many radiating lines*	*Large with numerous lines*	*Rectangular saw-toothed*	*Two triangles*	*Short triangle stepped margin*	*Curved triangle pointed margin*	*Elliptical with line across*
Y74-3-62PC	40–60					3		2				3				1	1	1	1	1	7
	140–160							2			1	2					2	1		1	21
	240–260					3		3		1						1	13	1			4
	310–330	8	4	3		1		8	1	4	1	7			2	4	11	3	1	3	1
	380–400	4	2			2		3				1	1		3	1	7			2	
	470–490		1			2		1	1	4				?	2	1				2	
	570–590				1			1	3	2	2	1		1							
	660–680				3	1		1							1		?				
	760–780																				
	860–880																				
	960–980																				
Y74-3-65PC	40–60					1		1				3							2	2	17
	140–160					2		3				10				1			3	2	48
	240–260	1				4		5		1		6	1			1	16	1	1	2	3
	340–360	4				2		10		1	1	2			1		5	1	1	2	1
	410–430	10	2			4		2	1	9					2	15	1	2	3		
	490–510		3			5		3	4	1		20			8	12	3				
	600–620		4	1						1					3	1	1				
	720–740				2	1			1								2			?	
	830–850			3											1	?					
	930–950			1	1																
	1020–1040																				
Y74-3-73PC	100–120					1		4				7			1	1					18
	200–220					1		4				4					6			1	9
	310–330	1				1		1		1		1				1	2	1	1	1	3
	400–420		1			4		3		3	2	3	1		5	3	5		4	2	
	485–505	11				9		4		5		9	1		1	5	1			1	
	650–670	1	2				1	5		6		1				1	1				
	737–752				2			13		?	1		1							1	
	775–795			5	1	1		3	2		1		1							1	
	880–900	2										cf	1				1				
	980–1000				1			1							1						
	1080–1100						1							1							
	1180–1200				6							cf									
	1204–1219																				

Samples	Subtypes Depth (cm)	*Small triangle long striations*	*Circular with line across*	*Short rectangular with striations*	*Long rectangular with striations*	*Triangle sinuous inline*	*Stippled triangle*	*Long triangle short inline*	*Long ellipse*	*Triangle concave first margin*	*Long triangle stepped margin*	*Narrow triangle ragged base*	*Triangle irregular base*
Y74-3-62PC	40–60	23	7		1				4	6		3	2
	140–160	23			1	1		5	4	3		5	1
	240–260	2						9			2		
	310–330	11	1					cf					
	380–400												
	470–490												
	570–590												
	660–680												
	760–780												
	860–880												
	960–980												
Y74-3-65PC	40–60	14		2	1				6	7		1	8
	140–160	30		4	4	1		3	14		4	1	
	240–260	2			1	2		9			1		
	340–360	2				1		6			1		
	410–430	2						?					
	490–510												
	600–620												
	720–740												
	830–850												
	930–950												
	1020–1040												
Y74-3-73PC	100–120	19	6		1				16	3		1	5
	200–220	7	6	2	1	1		6	2				
	310–330	3				1	1				1		
	400–420	3		1				1					
	485–505	2											1
	650–670												
	737–752												
	775–795												
	880–900												
	980–1000												
	1080–1100												
	1180–1200												
	1204–1219												

Note: The total number of ichthyoliths in each sample ranges from several hundred to several thousand.

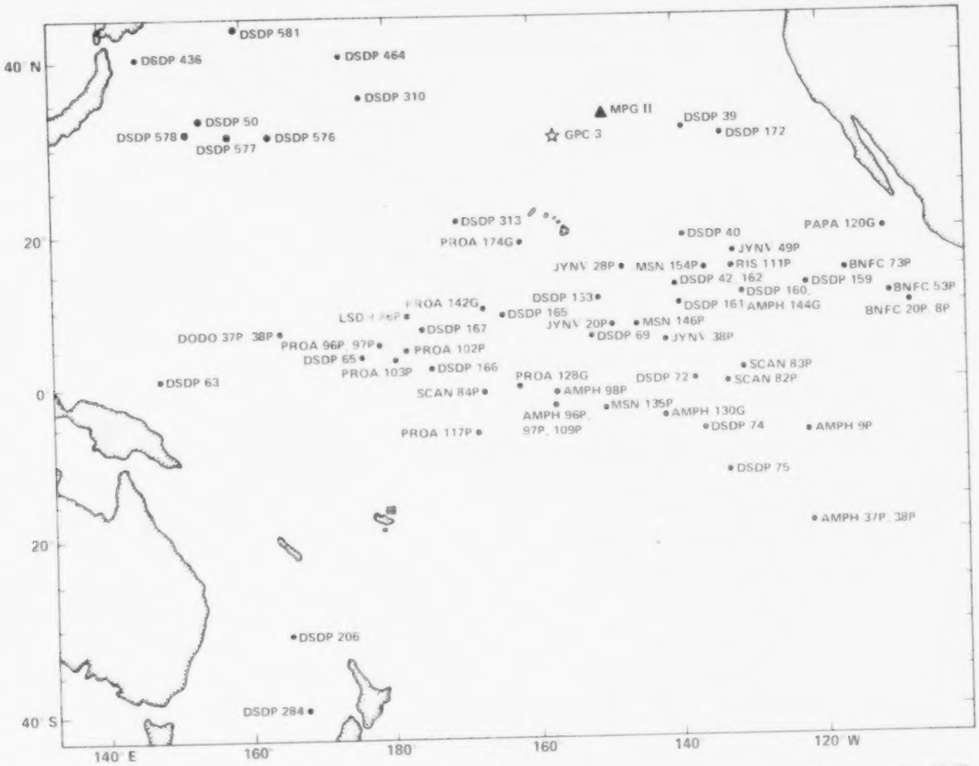
DSDP 581
DSDP 436
DSDP 464
40° N
DSDP 310
DSDP 50
DSDP 578
DSDP 577
DSDP 576
MPG II
GPC 3
DSDP 39
DSDP 172
DSDP 313
PROA 174G
DSDP 40
PAPA 120G
20°
JYNV 49P
JYNV 28P
MSN 154P
RIS 111P
BNFC 73P
DSDP 42, 162
DSDP 159
DSDP 160,
BNFC 53P
DSDP 153
PROA 142G
DSDP 165
DSDP 161
AMPH 144G
BNFC 20P, 8P
LSD
JYNV 20P
MSN 146P
DSDP 167
DODO 37P, 38P
DSDP 69
JYNV 38P
PROA 96P, 97P
DSDP 65
PROA 102P
PROA 103P
DSDP 166
SCAN 83P
DSDP 63
PROA 128G
DSDP 72
SCAN 82P
0°
SCAN 84P
AMPH 98P
MSN 135P
AMPH 96P,
97P, 109P
AMPH 130G
DSDP 74
AMPH 9P
PROA 117P
DSDP 75
AMPH 37P, 38P
20°
DSDP 206
DSDP 284
40° S
140° E
160°
180°
160°
140°
120° W

Figure 1. Location of sites from which samples were used in this study. In pelagic clay sequences from Deep Sea Drilling Project (DSDP) Sites 576, 578, and 581, GPC-3, and the MPG-2 area (location of piston cores Y74-3-62-PC, Y74-3-65PC, Y74-3-73PC) ichthyoliths are the only microfossils available for biostratigraphic control. Samples from the other sites contain both ichthyoliths and other microfossils, permitting intercorrelation of biostratigraphies.

triangle ragged base, and *Long triangle stepped margin*. Although the Miocene/Pliocene boundary cannot yet be distinguished on the basis of ichthyolith events in samples dated by other microfossils, the concurrence of the beginning of the range of *Long ellipse* and the end of the range of *Long triangle short inline* in Core 5, Section 6 indicates a late Miocene age. The ranges of these two taxa consistently overlap at discrete levels and in approximately the same position in relationship to the distribution of the other taxa in the Neogene sections from Holes 576, 576A, and 578, the three cores from the MPGII area, and GPC-3. This co-occurrence is at .50 m in GPC-3. Paleomagnetic stratigraphy indicates an age of 2.4 m.y. (Gilsa–Matuyama/Gauss boundary) at 4.5 m (Corliss et al., 1982, p. 284). At Site 578, these two taxa appear together below sediments with late Miocene radiolarians and diatoms (Table 3).

Core 6, Section 3 is Oligocene, based on the presence of *Rounded apex triangle* and *Flexed triangle shallow nbase ≥120*, and the absence of *Small triangle long striations* which is commonly found in the Neogene (Kaneps et al., 1981, p. 329).

Core 6, Section 6 is most probably late Eocene, or possibly early Oligocene. The Eocene age is based on the absence of *Rounded apex triangle* (which is abundant in the sample immediately above). This taxon occurs in relatively high numbers with a coherent range in Oligocene and Neogene sequences (Kaneps et al., 1981, p. 328). Until more data are obtained, the correlation of the first appearance of *Rounded apex triangle* cannot be used confidently to mark the Eocene/Oligocene boundary, but that event is used in this study as the boundary marker.

The sample from Hole 576B, Core 5, Section 3 was taken to supplement a gap left in the coring of Hole 576. This sample and the first three sections of Core 7 are assigned an Eocene age on the basis of taxa commonly found in the Eocene Epoch (*Triangle broad wing*, *Tanged triangle*, *Triangle pointed margin ends*) and the absence of younger and older taxa.

The Paleocene/Eocene boundary occurs in Core 7, most probably between Sections 3 and 5. Sections 5 and 6 of Core 7 and Section 1 of Core 8 are of Paleocene age, on the basis of the presence of *Beveled triangle concave base* and *Triangle modified margin ends*.

Additional levels of correlation in "red" clay sequences are the two striking peaks in ichthyolith abundances within the Oligocene or latest Eocene and near the Paleocene/Eocene boundary (Doyle and Riedel, 1979b, 1980, 1981). The right-hand column of Table 2 gives the number of triangular ichthyoliths in a gram of dry sample. The Oligocene or latest Eocene peak occurs in Sample 576-6-3, 69–75 cm; the Paleocene/Eocene peak is in Sample 576-7-5, 68–74 cm.

Table 2. Occurrences of previously described taxa in samples from Deep Sea Drilling Project Leg 86.

Other microfossil zones[a]	Age		Sample (interval in cm)	Depth to top of sample (m)	*Centrally striated triangle*	*Spiky palmate*	*Triangle smooth surface*	*Triangle square inline*	*Triangle long inline*	*Triangular toothed*	*Striated blunt triangle*	*Wide triangle projection*	*Narrow triangle sharply pointed*	*Prominent polygon*	*Plain and lined lanceolate*	*Prominence with wire line*	*Pointed and skirted*	*Wide crescent*	*Narrower crescent*	*Two peaks flared base*	*Triangle sigmoid rough*	*Triangle curved base*	*Triangle pointed margin ends*	*Triangle inline halfway*
	Ichthyoliths																							
	Conventionally determined epoch boundaries	Probabilistically determined epoch boundaries																						
			Hole 576, 576B																					
R. *Stylatractus universus* (Quaternary)			576-2-3, 118–125	11.38																				
			576-2-6, 108–114	15.70																				
			576-3-3, 58–65	17.18																				
	Miocene or younger		576-4-1, 8–14	19.88																				
		Mioc.–Plio.	576-4-3, 58–65	22.68										1										
			576-4-6, 98–104	27.58																				
	Mioc.–late Oligocene	Oligo.–Mioc.	576-5-6, 59–65	33.19																				1
			576-6-3, 69–75	35.79											1									2
	Eocene		576-6-6, 59–65	39.49											1								?	
			576B-5-3, 68–74	42.38											1				1					
		Eoc.–Oligo.	576-7-1, 58–64	45.18									1										1	
		Paleoc.–Eoc.	576-7-2, 88–94	46.98																			13	2
			576-7-3, 69–75	47.79																			8	1
			576-7-4, 68–74	49.28										1	1		1						?	
	Paleocene		576-7-5, 68–74	50.78											1								56	
			576-7-6, 15–25	52.28						1			2	1		1								
			576-8-1, 15–25	54.40		2	1							1		1								
			Hole 576A																					
R. *Stylatractus universus* (Quaternary)			576A-1-1, 140–150	3.60																				
			576A-1-3, 140–150	6.60																				
R. Quaternary ?			576A-1-5, 140–150	9.60																				
D. Quaternary Pliocene Miocene			576A-2-1, 140–150	12.30																				
			576A-2-3, 140–150	15.30																			1	
			576A-2-5, 140–150	18.30																				
	Miocene late	Mioc.–Plio.	576A-3-1, 140–150	21.80																				
			576A-3-3, flow-in	24.80																				
			576A-3-5, 140–150	27.80																				
			576A-4-1, 140–150	31.30																				
		Oligo.–Mioc.	576A-4-3, 140–150	34.30																				
	Oligo. late		576A-4-5, 140–150	37.30																1			9	
	Oligo. early	Eoc.–Oligo.	576A-5-1, 140–150	40.80																			?	
	Eocene		576A-5-3, 140–150	43.80											1					1			7	1
		Paleoc.–Eoc.	576A-5-5, 140–150	46.90																			10	
	Paleocene		576A-6-1, 140–150	50.30										2	3	1						1	18	
		Cret.–Paleoc.	576A-6-3, flow-in	53.30			1					2		1	2	1								
N. *Tetralithus trifidus*	Cretaceous		576A-6-5, 140–150	56.30	3	30	29	18	22	1	12	17		18										
N. *Broinsonia parca*–*Eiffellithus eximius*			576A-7-1, 140–150	59.80							cf	1		1										
			576A-7-3, 140–150	62.80					2	1	10	1	1	2	1		1	1	2					
			576A-7-5, 140–150	65.80				1			2													

Note: Subtypes are arranged in order of their earliest occurrence in GPC-3. Numbers in the body of the table represent the total number of specimens found. Numbers in the third column from the right are the total number of triangular ichthyoliths in each sample. In Section 576A-2-1, several hundred ichthyoliths are present, but exact count cannot be made because the preparations are obscured by radiolarians. Question marks represent broken specimens in samples with no complete specimens of the subtype; "cf." indicates specimens that are similar, but do not fit the name description exactly. Age assignments based on microfossils other than ichthyoliths are from site summaries and S. Monechi's nannofossil stratigraphy chapter (this volume).

[a] R = radiolarian, D = diatom, N = nannofossil.

Hole 576A

Samples from this hole were taken as part of a geotechnical study of a "type" red clay section. The cores were cut into sections, but were left unsplit. A 10-cm, whole-round slice was cut from the end of each section and an approximately 100-cm^3 sample for biostratigraphic study was taken within that interval. Concentrations of ichthyoliths and dry weights of samples are given in the right-hand column of Table 2.

Ichthyoliths in Cores 1 and 2 are latest Miocene or younger based on the coherent range of *Narrow triangle ragged base*. Cores 3 and 4, Sections 1 and 3, are Miocene with a rich and diverse assemblage of characteristic Miocene taxa. Representative subtypes are *Two triangles, Triangle sinuous inline, Elliptical with line across*, and *Triangle irregular base*. Core 3, Section 3 contains an aberrant, very sparse assemblage of foraminifers, radiolarians, diatoms, and ichthyoliths. The ichthyoliths indicate only that this sample is Miocene.

Recognition of the Oligocene depends at present on the characteristic order of first appearances of several of the most dependable subtypes. In samples from the Pacific dated by other microfossils, the first appearance of *Rounded apex triangle* corresponds with nannofossil Zone CP16, the first appearance of *Triangle with high inline apex* with nannofossil Zone CP17, and the first appearance of *Small triangle long striations* with Zone CN1. This succession is also present in sequences without other microfossils (Edgerton et al., 1977; Doyle and Riedel, 1979b, Kaneps et al., 1981; Gottfried et al., 1985). In Hole 576A, this places (along with some supporting evidence from less common taxa—*Flexed triangle shallow inbase ≥ 120, Rectangular saw-toothed, Triangle with base angle*) the Oligocene/Miocene boundary between Sections 3 and 5 of Core 4, and the Eocene/Oligocene boundary between Sections 1 and 3 of Core 5. The lower part of Core 4 (Sample 576A-4-5, 140–150 cm) is probably late Oligocene, and the upper part of Core 5 (Sample 576A-5-1, 140–150 cm) probably early Oligocene.

Table 2. (Continued).

Triangle with triangular projection	Flexed triangle shallow inbase	Beveled triangle mid inline	Short triangle bowed inline	Giant lanceolate	Triangle concave base	Triangle medium wing	Wide triangle	Triangle short wing	Triangle broad wing	Triangle transverse line across	Narrow triangle cross hachured	Tanged triangle	Small triangle crenate margin	Triangle one canal above	Broad triangle parallel inline	Wide triangle straight inbase	Triangle hooked margin	Narrow triangle straight inbase	Triangle double flex	Triangle sigmoid	Small dendritic few radiating lines	Triangle with parallel inline	Pointed triangle short inline	Triangle with canals	Pointed triangle long margins	Rounded apex triangle	Flexed triangle shallow inbase >120	Triangle with base angle	Triangle with high inline apex	Triangle inward angle	Small dendritic many radiating lines	Large with numerous lines	Rectangular saw-toothed	Two triangles	Short triangle stepped margin	Asymmetrical peak depression	Curved triangle pointed margin	Elliptical with line across	Small triangle long striations	Circular with line across
	1																												1						1			1	2	
2																													6						1			5	2	1
																													3									3	2	1
	1																												3						1			2		1
																		1								3		1	3					1	3			3	1	1
1	2					1		1							1		1				4			1	1	12		3	<1		1	2	1	1					8	
11	5			1		2		2		1	1		1		12		1			6						11	1									22	1			
12					<1	3		3		1	1				2		1	2																						
13	2					5				2	1				2	2	2		1																					
3	2				1	2		2		1		1			1		1			2																				
9	1				1	3		2				1			1		1	2								3			2											
6	2					1				7				1				10																						
[illegible]					2	3				4			1					2																						
10					5	6				3																														
1																																								
																										2												5	1	
	1															1										6		1	2				1		2			17	1	13
	1															1	1									2			6			1		1	3		5	13	3	5
	2															3		4								2			21					2	2		1	4	15	1
	1																2	1								1			10						1		2	5	12	11
1	1															2	2	5								4			15			1		2	1		1	10	19	1
	1																1									5			4				6		3		1	7	21	6
																																1		1				13	2	
1	6																				1				1	2			10				1		1		1	4	6	1
2	3						2			1						1	1	1			1				2	2			15		1	1	4	2	2		5	2	6	3
11	4					1	2	1						1	1		5	1	1		1				1	6	3	1	6		2	3	2	2	2	1	1		4	
11	3					9	1			2	1				17	1	4	1	2	1	1		13	1		4	4		2				2				1			
14	3				1	3		1		4				1	2				1	2			1	1		4	2			1		[illegible]								
21						4	2	1		3	1	1			1																									
11	1				8	2		1		3		6				1	1																							
17				2	10	22	1	9		[illegible]		3						1																						
						1																																		

Sections 3 and 5 of Core 5 are Eocene, based on the absence of younger taxa and the presence of subtypes characteristically found in abundance in the Eocene: *Triangle with triangular projection, Triangle pointed margin ends*, and *Triangle medium wing*.

The Paleocene/Eocene boundary is placed between Core 5, Section 5, and Core 6, Section 3, on the basis of the presence of *Beveled triangle concave margins* in the sample from Section 3. The first appearance in the sequence of several taxa (*Triangle radiating inline, Narrow straight triangle, Triangle pointed margin ends*) in Section 1 of Core 6 suggests this sample is also Paleocene.

The Cretaceous/Tertiary boundary is between Sections 3 and 5 of Core 6. The Cretaceous assemblages in Core 6, Section 5 and Core 7 include the subtypes *Striated blunt triangle, Triangle long inline, Triangle square inline*, and *Wide triangle projection*.

Concentrations of triangular ichthyoliths in the sequence (right-hand column of Table 2) show a peak of abundance in Sample 576A-6-1, 140–150 cm which is judged, on present evidence, as late Paleocene. While there is an increase in ichthyolith abundance in samples considered Oligocene (Samples 576A-4-5, 140–150 cm and 576A-5-1, 140–150 cm), the typical middle Tertiary concentration of 40–45 triangular ichthyoliths per gram is not detected by our sampling.

Hole 576B

Six channel samples were taken from Core 6, Sections 2 and 3 to determine the location of the Cretaceous/Tertiary boundary. A narrow groove of sediment was scraped from the middle surface of the split core yielding a sample of approximately 40 cm^3.

Both Sections 2 and 3 of Core 6 are Paleocene, placing the Cretaceous/Tertiary boundary between 54.10 m (the top of Section 4 in Core 6) and 55.40 m, the level at which Maestrichtian nannofossils occur (see Site 576 chapter, this volume). A comparison of the distribution of the newly described taxa in Hole 576B with Site 577 and the other sequences shown in Table 4 suggests that Section 3 correlates with nannofossil zones older than Zone CP5.

Concentrations of triangular ichthyoliths show a peak abundance in Sample 576B-6-2, 50–100 cm which corre-

Table 2. (Continued).

Age																		
	Ichthyoliths																	
Other microfossil zones[a]	Conventionally determined epoch boundaries	Probabilistically determined epoch boundaries	Sample (interval in cm)	Depth to top of sample (m)	*Short rectangular with striations*	*Long rectangular with striations*	*Triangle sinuous inline*	*Stippled triangle*	*Long triangle short inline*	*Long ellipse*	*Triangle concave first margin*	*Long triangle stepped margin*	*Narrow triangle ragged base*	*Triangle irregular base*	*Triangle double inline*	Total number of triangular (*a8,9*) ichthyoliths in sample	Total dry weight of sample (g)	Number of triangular (*a8,9*) ichthyoliths in 1 g
			Hole 576, 576B															
R. *Stylatractus universus* (Quaternary)			576-2-3, 118-125	11.38							1					65	21.79	2.98
			576-2-6, 108-114	15.70						1		1		1	1	107	18.88	5.67
			576-3-3, 58-65	13.18			1				1	1		1		56	17.86	3.14
	Miocene or younger		576-4-1, 8-14	19.88	1		1						1			89	19.10	4.66
		Mioc./Plio.	576-4-3, 58-65	22.68	2		1			2		1		1		84	21.98	3.82
			576-4-6, 98-104	27.58												Barren	29.37	Barren
	Mioc.–late Oligocene	Oligo./Mioc.	576-5-6, 59-65	33.19					6	1	1				1	270	25.20	10.17
			576-6-3, 69-75	35.79												907	28.59	31.72
	Eocene		576-6-6, 59-65	39.49												796	25.47	31.25
			576B-5-3, 68-74	42.38												459	24.60	18.66
		Eoc./Oligo.	576-7-1, 58-64	45.18												339	32.81	10.33
		Paleoc./Eoc.	576-7-2, 88-94	46.98												683	30.89	22.11
			576-7-3, 69-75	47.79												512	26.64	19.22
			576-7-4, 68-74	49.28												585	25.46	22.98
			576-7-5, 68-74	50.78												2002	28.98	69.08
	Paleocene		576-7-6, 15-25	52.28												740	33.96	21.18
			576-8-1, 15-25	54.40												38	25.09	1.51
			Hole 576A															
R. *Stylatractus universus* (Quaternary)			576A-1-1, 140-150	3.60						3		2		3	1	93	54.81	1.70
			576A-1-3, 140-150	6.60	2					2	6	1	1	5		150	76.21	1.97
			576A-1-5, 140-150	9.60	2			1		1	4		1	2		179	81.45	2.20
R. Quaternary ?			576A-2-1, 140-150	12.30	2					3	7			4		—	45.26	—
D. Quaternary Pliocene Miocene			576A-2-3, 140-150	15.30	3	3	1			1		1	1	5		225	65.83	3.87
			576A-2-5, 140-150	18.30	2	1	4			2	1	1	2	7		368	73.91	4.98
	Miocene late	Mioc./Plio.	576A-3-1, 140-150	21.80	1		3			2	7	1	1	6	1	389	74.11	5.25
			576A-3-3, flow-in	24.80			1			5	1			1		9	69.10	0.13
			576A-3-5, 140-150	27.80		1			2	1	2	1		9		437	52.72	8.29
			576A-4-1, 140-150	31.30			1				1		cf			462	48.11	9.60
			576A-4-3, 140-150	34.30			1		2							539	38.61	13.96
	Oligo. late	Oligo./Mioc.	576A-4-5, 140-150	37.30												2226	94.81	23.48
	Oligo. early	Eoc./Oligo.	576A-5-1, 140-150	40.80												951	50.79	18.72
	Eocene		576A-5-3, 140-150	43.80												586	79.70	7.35
		Paleoc./Eoc.	576A-5-5, 140-150	46.90												234	66.95	3.50
	Paleocene		576A-6-1, 140-150	50.30												5526	89.44	61.78
			576A-6-3, flow-in	53.30												1130	87.28	12.95
N. *Tetralithus trifidus*	Cretaceous	Cret./Paleoc.	576A-6-5, 140-150	56.30												1250	87.99	14.27
			576A-7-1, 140-150	59.80												61	—	—
N. *Broinsonia parca–Eiffellithus eximius*			576A-7-3, 140-150	62.80												341	101.25	3.37
			576A-7-5, 140-150	65.80												36	154.90	0.23

sponds with abundances found at the late Paleocene, or earliest Eocene, level in other pelagic clay sequences (Table 3; Doyle and Riedel, 1979b; Kaneps et al., 1981).

Site 578

Thirteen standard samples 40 cm^3 in size and two samples (Sections 578-17-4 and 578-19-2) of approximately 80 cm^3 were examined from this hole.

Ichthyoliths in samples from Cores 11–14 are not numerous but are in agreement with the Pliocene and late Miocene ages of the siliceous microfossils. The co-occurrence of *Long ellipse* and *Long triangle short inline* in Core 14, Section 2 indicates that sample is late Miocene (discussed in second paragraph under Hole 576). The presence of *Circular with line across* and *Short rectangular with striations* in Core 16, Section 2 indicates a middle Miocene age.

The Oligocene/Miocene boundary falls between Core 17, Section 4 and Section 5, and the Eocene/Oligocene boundary between Core 17, Section 5, and Core 18, Section 1. The Oligocene is identified by the presence of *Rounded apex triangle* and *Triangle with base angle* and the absence of *Small triangle long striations*. It is not possible for us to tell from the available data whether some part of the Oligocene and early–middle Miocene is missing or if sediment accumulation was very slow.

Cores 18 and 19, Section 1 are Eocene. The absence of *Triangle curved base* (which ranges in samples dated by calcareous nannofossils from Zone CP11 to Zone CP2) from the upper part of this interval, and its presence in the lower, suggests that Sections 1 and 3 of Core 18 are late to middle Eocene and Section 4 of Core 18 and Section 1 of Core 19 are middle to early Eocene.

The Paleocene/Eocene boundary is in Core 19, between Sections 1 and 3. The presence of *Beveled triangle concave margins* in Section 578-19-2, as well as the first appearance of *Triangle radiating inline* and *Narrow straight triangle*, suggests that Section 2 is Paleocene, but the extension of typically Paleocene forms into earliest Eocene has not been studied sufficiently to allow a confident Paleocene age assignment to this sample. Section 3 is Paleocene. *Short triangle bowed inline* and *Bev-*

eled triangle concave margins are present in the sample from this section, both forms restricted to Paleocene assemblages.

Concentrations of triangular ichthyoliths peak in Sample 578-17-5, 69–75 cm, corresponding with an Oligocene age assigned on the basis of ichthyolith biostratigraphic evidence. The characteristic high spike in abundance at the Paleocene/Eocene boundary is not evident in this hole, perhaps due to sample spacing.

Site 581

One standard sample of 40 cm^3 was taken from Core 10 to corroborate the Miocene age of diatoms found within the cherts of Core 12.

Ichthyoliths are sparse, but the presence of *Small triangle long striations* as well as *Rectangular saw-toothed, Triangle with high inline apex*, and *Triangle medium wing* indicates that the sample is Miocene, most probably early or middle (Table 3).

PROBABILISTIC STRATIGRAPHY

Although the conventional procedures employed above for stratigraphic interpretation have served us reasonably well in the past, when the number of known ichthyolith sequences was small and manageable, we are approaching the stage at which the body of data will be so large as to require its automated (computerized) accessing and manipulation. This is true to some extent for all microfossil groups, but the problem is particularly acute for the ichthyoliths. Their commonly sparse and intermittent occurrences in sedimentary sequences make it difficult to make syntheses that take account of the different levels of reliability to be placed on each particular upper or lower stratigraphic limit of a subtype in each sequence in which it is observed.

The procedures of probabilistic stratigraphy, developed first by Hay (1972) and applied, for example, by Blank and Ellis (1982), offer a promising route toward the integration of data from large numbers of sequences, but they have the shortcoming that they depend on the principle of "majority rule." For example, in determining the most-likely-correct stratigraphic succession, three occurrences of a pair of events in one order of succession outweighs two occurrences of those same events in the opposite order, although the evidence for the former three may be very weak and the evidence for the latter two very strong. It is to take account of the inequalities in the strength of the different items of evidence that Riedel (1981), Westberg and Riedel (1982), and Riedel and Westberg (1982) developed a means of indexing the reliability of single biostratigraphic events in single sequences.

This procedure has been applied to ichthyolith data by Gottfried et al. (1984), and a further step is made here by applying the probabilistic procedure of Hay to a substantial body of stratigraphic data from the North Pacific, weighted according to their indices of reliability. We have taken account of three of the four factors used by Gottfried et al. in assessing reliabilities, with only one minor change to the factor scores, as shown in Table 5. The omitted factor concerns the limits of geographic distribution of certain subtypes of ichthyoliths, which we now feel not to be sufficiently well known to provide a reliable multiplier. In better understood fossil groups, the number of factors used in assessing these reliabilities is as high as a dozen or more, and the number applied to ichthyoliths will increase as we gain experience in using the procedure.

As the basis for a probabilistic ichthyolith stratigraphy for the western North Pacific, we have used data from seven sequences—Holes 576, 576A, and 578 from Leg 86, three from the MPGII localities listed in the Introduction, and piston core GPC-3 (Doyle and Riedel, 1979b). In each of these sequences we looked for all of the subtypes that have so far been described (with the exception of *Triangle complex transverse line, Flexed triangle 102–112, Flexed triangle 115–118*, and *Flexed triangle 120–128*, the concepts of which are under revision) and recorded the abundances of all that we encountered (79 subtypes). The upper and lower limits of the ranges of the most dependable of the taxa (58 subtypes) were weighted according to the products of the scores of the three factors used (the right-hand numbers in each of the seven main columns of Table 6) and then arranged in the most probable stratigraphic order (the order in which they appear in Table 6) by the procedure of Hay, modified so that the contribution of each pair of events to the matrix depends on their reliability indices.

The mean of the reliabilities of each event at the seven sites is shown toward the right side of Table 6. The second-last column of that table shows the nannofossil zone in which each event is thought to occur, using the conventional stratigraphic procedures discussed in the previous section. Epoch boundaries are placed against the calcareous nannofossil zones in accordance with the scheme of Okada and Bukry (1980). The extent of uncertainty in placement of boundaries between the Tertiary epochs, against the probabilistically ordered list of ichthyolith events, was derived from the calcareous nannofossil ages of those ichthyolith events that have high mean reliability indices (>0.25). The wide intervals of uncertainty in placing epoch boundaries depends partly on our requiring these high mean reliability indices and partly on the fact that the probabilistically derived succession of ichthyolith events violates to some extent the order of ages indicated by the ties to the calcareous nannofossil zonation. The latter problem will undoubtedly be reduced as more sequences are incorporated into the data base (thereby allowing successions of events with high reliability indices to correct errors), but there will probably remain a residue of inconsistencies due to some calcareous nannofossil age determinations being less soundly based than others and, to that extent, unreliable. If sufficient data were available on the nannofossil occurrences to permit determination of reliability indices, these could be handled probabilistically along with the ichthyolith data to provide a uniform, integrated succession.

The indicated epoch boundaries, with their ranges of uncertainty, were then carried into the body of the table, to determine their levels in each of the Leg 86 sequences (with the results shown in the third column from the left

Table 3. Occurrences of previously described taxa in samples from Deep Sea Drilling Project Leg 86.

Age			Sample (interval in cm)	Depth to top of sample (m)	*Centrally striated triangle*	*Spiky palmate*	*Triangle smooth surface*	*Triangle square inline*	*Triangle long inline*	*Triangular toothed*	*Striated blunt triangle*	*Wide triangle projection*	*Narrow triangle sharply pointed*	*Prominent polygon*	*Plain and lined lanceolate*	*Prominence with wye line*	*Pointed and skirted*	*Wide crescent*	*Narrower crescent*	*Five peaks flared base*	*Triangle sigmoid rough*	*Triangle curved base*
	Ichthyoliths																					
Other microfossil zones[a]	Conventionally determined epoch boundaries	Probabilistically determined epoch boundaries																				
			Hole 576B																			
	Paleocene		576B-6-2, 0-50	51.10											1				1			4
			576B-6-2, 50-100	51.60										2	1		2					2
			576B-6-2, 100-150	52.10												1					1	
			576B-6-3, 0-50	52.60																		1
			576B-6-3, 50-100	53.10															1		2	
			576B-6-3, 100-150	53.60						1						2			1			
			Hole 577																			
N *Discoaster barbadiensis* CP15	Eocene late		577-7-5, 100-107	61.30																		
N *Reticulofenestra umbilica* CP14	mid to		577-8-3, 23-31	67.03											1					3		
N *Discoaster binodosus* CP9b	early		577-9-5, 32-40	79.92																		
N CP7/CP8	Paleocene late		577-10-3, 31-39	87.11																		
N CP5/CP6			577-10-5, 122-130	90.02						1					1	1						2
			577-11-2, 31-39	94.11										1								
N *Fasciculithus tympaniformis* CP4			577-11-4, 122-130	98.02										1								
N *Chiasmolithus danicus* CP2	early		577-11-6, 120-128	101.00																		1
N *Zygodiscus sigmoides* CP1			577-12-3, 82-90	105.62											1	2						
N *Micula mura*	Cretaceous		577-12-6, 82-90	109.12		3	2				1			1								
			Hole 578																			
R *Sphaeropyle langii*			578-11-2, 96-102	92.46																		
R *Stichocorys peregrina*			578-12-2, 108-114	102.38																		
D *Thalassiosira convexa*			578-13-2, 107-114	111.87																		
	Miocene late		578-14-2, 108-114	121.38																		
	middle		578-15-2, 79-85	130.29																		
	to	Mio./Plio.	578-16-2, 77-83	140.07																		
	early		578-17-3, 92-98	151.22														1				
		Oligo./Mio.	578-17-4, 140-150	153.20														1				
	Oligocene		578-17-5, 69-75	154.09																		
	Eocene late to middle		578-18-1, 78-84	157.58																		
			578-18-3, 74-80	160.54																		
F early middle Eocene P9-11	middle to early	Eoc./Oligo.	578-18-4, 79-85	162.09											1					1		1
		Paleoc./Eoc.	578-19-1, 76-82	166.96																		1
			578-19-2, 140-150	169.20									2	1		1						1
	Paleocene		578-19-3, 79-85	170.09									4	1								1
			Hole 581																			
	Miocene		581-10-4, 70-76	262.70																		

Note: Conventions as in Table 2.
[a] N = nannofossil, R = radiolarian, D = diatom, F = foraminifer.

in Tables 2 and 3). This step at present involves a considerable amount of subjective judgement, but we expect in the future to be able to establish rules that will permit it to be done with a degree of objectivity and reproducibility. At present, the placement of each epoch boundary in each sequence depends simply on an *ad hoc* evaluation of the evidence on the levels of occurrence, and the indices of reliability, of the probabilistically ordered events in the core concerned. Because of the sparse occurrence of individual subtypes of ichthyoliths and departures of individual sequences from the most probably correct order of events, the intervals of uncertainty in placement of epoch boundaries in individual cores tend to be larger than those in the placement of those boundaries against the probabilistically ordered list of events.

SYSTEMATIC SECTION

Seven new subtypes that first appear in the Paleocene are described below. The procedure for describing and naming the ichthyoliths involves use of a string of letters and numbers corresponding to objectively defined characters of the image as seen in a transmitted-light microscope. These name descriptions can be decoded in full by reference to Doyle and Riedel (1979a, 1980) and Gottfried et al. (1984). Distinctive features necessary to distinguish each subtype from described and undescribed forms are pointed out in the text. The coded descriptions are frequently long, and therefore colloquial names are coined to act as their surrogates.

In order to differentiate the newly described subtypes, the following changes to the descriptive system are required.

1. Under Type *a8/b1,5*, add the character

    g. Shape of prominent flexure

        1. angle/angle 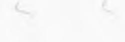

        2. angle/curve

Table 3. (Continued).

Triangle pointed margin ends	Triangle inline halfway	Triangle with triangular projection	Flexed triangle shallow inbase	Beveled triangle mid inline	Short triangle bowed inline	Giant lanceolate	Triangle concave base	Triangle medium wing	Wide triangle	Triangle short wing	Triangle broad wing	Triangle transverse line across	Narrow triangle cross hachured	Tanged triangle	Small triangle crenate margin	Triangle one canal above	Broad triangle parallel inline	Wide triangle straight inbase	Triangle hooked margin	Narrow triangle straight inbase	Triangle double flex	Triangle sigmoid	Small dendritic few radiating lines	Triangle with parallel inline	Pointed triangle short inline	Triangle with canals	Pointed triangle long margins	Rounded apex triangle	Flexed triangle shallow inbase ≥120	Triangle with base angle	Triangle with high inline apex	Triangle inward angle	Small dendritic many radiating lines	Large with numerous lines	Rectangular saw-toothed	Two triangles	Short triangle stepped margin	Asymmetrical peak depression	Curved triangle pointed margin	Elliptical with line across	Small triangle long striations	Circular with line across	Short rectangular with striations	Long rectangular with striations	Triangle sinuous inline	Stippled triangle	Long triangle short inline	Long ellipse
3		9	1				2	3		1		4						1																					2									
4		5					5	3		1		1																																				
2		2			1		1																																									
					1		2	<1													<1																											
				3																																												
		30	1					2		1		1	3	3			1			1							2					1																
1		25	5					[illegible]				2	2				1										1																					
1		6						1																																								
[illegible]		5						2																																								
		3						1																																								
2		6					1					1			1																																	
1		4			1		1	1			<1																																					
<1		1		<1			1	1				1																																				
				1																																												
																																											1							
																																											1				1			
																		1	1												1										2							
																			1												4						1			1	6		1		1		2	1
																			1									1			1				5						3					1		
																		1		4		1						2		1				2	1						2	1	1					
		2	9					1	1	2								1	2		2										1				1						4							
		3	7					3		6		1					2			1		2	2	4			1	15		4	1			1							2							
		6	5			1		2	1			6						2	2			1	1	1				14		2																		
2		8	1					3		1	1		1				1																															
1		17						2				[illegible]						2																														
6		10					2	2	1						1		1	6				2																										
18		11	1				1				4			2	4			2		1																												
62		10					6	10			1																																					
4		4			1		4	7																																								
																				1											1				1						1							

2. Under Type *a8/b1,5*, add the character

h. Shape of transverse line

0. indeterminable

1. straight line terminating at margins at approximately the same level

2. simply curved or straight line terminating at margins at different levels ("perpendicular" distances from apex of outline to the levels at which the transverse line intersects the margins differ by at least 5%)

3. straight or simply curved line extending across sides of inline; one end running through area between inline and outline, the other terminating at the flexed margin

DESCRIPTIONS OF NEW TAXA

a8/b1,5/c1/d1/e0/f23-38/g2/h2 new subtype

Flexed triangle asymmetric

(Plate 1, Figs. 1-5)

Characters: A distinctive triangular form with one margin modified by a prominent flexure. The flexure nearer the apex is sharply angled, that nearer the base smoothly curved. Transverse line, or base when transverse line absent, a simply curved or straight line terminating at margins at different levels. Overall length 360-1100 μm, maximum width 120-300 μm.

Distinction from similar forms: The prominent curved flexure modifying one margin readily distinguishes this taxon from most co-occurring forms. A similar form found in the Cretaceous differs in that the transverse line does not terminate at both margins. In the Cretaceous form the transverse line extends across the sides of the inline, one end

Table 3. (Continued).

Other microfossil zones[a]	Age: Ichthyoliths: Conventionally determined epoch boundaries	Age: Ichthyoliths: Probabilistically determined epoch boundaries	Sample (interval in cm)	Depth to top of sample (m)	*Triangle concave first margin*	*Long triangle stepped margin*	*Narrow triangle ragged base*	*Triangle irregular base*	*Triangle double inline*	Total number of triangular (a8,9) ichthyoliths in sample	Total dry weight of sample (g)	Number of triangular (a8,9) ichthyoliths in 1 g
			Hole 576B									
	Paleocene		576B-6-2, 0-50	51.10						964	26.81	35.95
			576B-6-2, 50-100	51.60						1387	23.90	58.03
			576B-6-2, 100-150	52.10						962	23.09	41.66
			576B-6-3, 0-50	52.60						541	20.19	26.79
			576B-6-3, 50-100	53.10						289	23.14	12.49
			576B-6-3, 100-150	53.60						92	25.06	3.67
			Hole 577									
N. *Discoaster barbadiensis* CP15	Eocene late		577-7-5, 100-107	61.50						836	62.33	13.41
N. *Reticulofenestra umbilica* CP14	mid to		577-8-3, 23-31	67.03						695	72.99	9.52
N. *Discoaster binodosus* CP9b	early		577-9-5, 32-40	79.92						283	90.67	3.12
N. CP7/CP8			577-10-3, 31-39	87.11						572	66.77	8.57
			577-10-5, 122-130	90.02						126	64.14	1.96
N. CP5/CP6	Paleocene late		577-11-2, 31-39	94.11						254	50.19	5.06
N. *Fasciculithus tympaniformis* CP4			577-11-4, 122-130	98.02						260	67.74	3.84
N. *Chiasmolithus danicus* CP2			577-11-6, 120-128	101.00						252	76.96	3.27
N. *Zygodiscus sigmoides* CP1	early		577-12-3, 82-90	105.62						112	53.15	2.11
N. *Micula mura*	Cretaceous		577-12-6, 82-90	109.12						48	58.77	0.82
			Hole 578									
R. *Sphaeropyle langii*			578-11-2, 96-102	92.46	1					21	24.32	0.86
R. *Stichocorys peregrina*			578-12-2, 108-114	102.38	1					14	24.52	0.57
D. *Thalassiosira convexa*			578-13-2, 107-114	111.87						11	28.71	0.38
	Miocene late		578-14-2, 108-114	121.38						82	23.91	3.43
	middle		578-15-2, 79-85	130.29						144	33.43	4.31
	to		578-16-2, 77-83	140.07						123	40.91	3.01
	early	Mio.–Plio.	578-17-3, 92-98	151.22						309	35.47	8.71
			578-17-4, 140-150	153.20						1274	105.16	12.12
	Oligocene	Oligo.–Mio.	578-17-5, 69-75	154.09						1357	31.02	43.75
			578-18-1, 78-84	157.58						356	38.11	9.34
	Eocene late to middle		578-18-3, 74-80	160.54						301	36.03	8.35
			578-18-4, 79-85	162.09						692	46.47	14.89
F. early middle Eocene P9–11	middle to early	Eoc.–Oligo.	578-19-1, 76-82	166.96						966	37.44	25.80
		Paleoc.–Eoc.	578-19-2, 140-150	169.20						2221	139.63	15.90
	Paleocene		578-19-3, 79-85	170.09						330	41.74	7.90
			Hole 581									
	Miocene		581-10-4, 70-76	262.70						161	27.45	5.86

running through the area between inline and outline, the other terminating at the flexed margin. In similar forms in later Cenozoic assemblages (see Doyle et al., 1974, pl. 2H, figs. 5-13), the flexure nearest the base is sharply angled or with a slight curve (see Doyle et al., 1974, pl. 2H, fig. 9) and the transverse line intersects only the flexed margin.

Occurrence: In middle and upper Paleocene and earliest Eocene, in sequences with age assigned on the basis of ichthyoliths (see Table 4). Not present in reference samples from Site 577.

a9/b1,5/c1,13/d1,13/e1/f1/g1/h0,5/i6/j2,3/k3,14/m0.35-0.75/n1.3-2.0/p0/q0,2,6,7/r0,1/s1/t1/z4/cc0/dd0/ee0/ff0/gg0/hh0/jj2/kk2/mm0/nn0 new subtype
Triangle modified margin ends
(Plate 2, Figs. 6-9)

Characters: Curved triangular form (length-to-width ratio 1.3-2.0) with one margin and occasionally both margins modified by a shallow inward angle or base of margins inwardly curved in bottom one-fourth. Apex between sharp and blunt. Sides of inline bowed in, or acuminate with sides below apical portion straight and divergent. Apex of inline in lower two-thirds of tooth. Base, or transverse line when present, an upwardly convex line slightly above the level of margin ends. Overall length 360-600 μm, maximum width 240-340 μm.

Distinction from similar forms: Some superficially similar forms (Doyle and Riedel, 1979b, pl. 7, figs. 16, 32, 35, 36) differ in either greater extension of the margin ends below the base of the inline, a more sharply pointed apex, or in having straight rather than curved margins. Other similar forms (Doyle and Riedel, 1979b, pl. 6, figs. 6, 16) possess canals or striations radiating out from the inline.

Occurrence: In early Paleocene (nannofossil Zone CP2) at Site 577. Occurs in lower part of Paleocene in sequences with ages assigned on the basis of ichthyoliths (Table 4).

a9/b1,5/c1/d1/e1/f4/g1/h0,5/i2,6/j2,3/k8/m0.14-0.25/n2.5-3.0/p0/q0,2/r0,1/s1/t1/z2/cc0/dd0/ee0/ff0/gg0/hh0/jj2/kk2/mm0/nn0 new subtype
Narrow straight triangle
(Plate 2, Figs. 1-5)

Characters: Narrow triangular form (length-to-width ratio 2.5-3.0) with lateral shadows, moderately rounded apex, straight base, and generally straight margins. Occasional specimens with one margin concave, the other convex. Inline approximately same shape as outline, extending into upper third of the outline. Transverse line, though seldom preserved, straight. Overall length 330-800 μm, maximum width 130-260 μm.

Distinction from similar forms: *Narrow straight triangle* is easily distinguished by the large length-to-width ratio, moderately rounded apex, and straight sides.

Occurrence: One broken specimen in late Paleocene (nannofossil Zone CP6) at Site 577. In sequences with ages based on ichthyoliths (see Table 4), ranges from late Paleocene through earliest Eocene.

Table 4. Distribution of newly described Paleogene taxa in Deep Sea Drilling Project Leg 86 sediments and in Giant Piston Core-3 (GPC-3).

	Age									
Nannofossil zone	Ichthyoliths		Samples (interval in cm)	*Triangle modified margin ends*	*Beveled triangle concave margins*	*Triangle curved pointed margins*	*Narrow triangle unequal margins*	*Triangle radiating inline*	*Narrow straight triangle*	*Flexed triangle asymmetric*
			Hole 576							
	Eocene		576-7-1, 58-64						?	
			576-7-2, 88-94			2			1	
			576-7-3, 69-75			1		2		
			576-7-4, 68-74			3		5		
	Paleocene		576-7-5, 68-74		1	7		8	?	
			576-7-6, 68-74	1	27					
			576-8-1, 15-25							
			Hole 576A							
	Paleocene		576A-6-1, 140-150			3		11	2	
			576A-6-3, 140-150		9	1				
			Hole 576B							
	Paleocene		576B-6-2, 0-50			6		14	3	
			576B-6-2, 50-100					10	5	
			576B-6-2, 100-150				2	7	1	5
			576B-6-3, 0-50	1	2		4	3		3
			576B-6-3, 50-100	3	2			3		
			576B-6-3, 100-150	2				1		
			Hole 577							
CP7/8	Paleocene	late	577-10-3, 31-39			8		4		
			577-10-5, 122-130			1		1		
CP5/6			577-11-2, 31-39			1		1	?	
CP4			577-11-4, 122-130		1	5		3		
CP2		early	577-11-6, 120-128			1				
CP1			577-12-3, 82-90	3						
			Hole 578							
	Paleocene		578-19-2, 140-150	?	3	1		9	4	
			578-19-3, 79-85					4		
			Giant Piston Core-3 Depth (cm)							
	Eocene		1691-1708			2		2	3	1
	Paleocene		1750		2	1	1	4	5	1
			1789-1811		11	10	4	14	11	9
			1850		5	4	1	5	9	1
			1893-1912		23		2	6	6	1
			1950	2	15	2				
			1995-2008	8						
			2040							
	Cretaceous		2060							

Note: The new subtypes were searched for in all the Leg 86 samples, but only those samples in which they occur are listed. In GPC-3, samples above the 15-m level were not examined. Subtypes are arranged in order of their earliest occurrence in GPC-3.

Table 5. Factors and weights used to score the reliabilities of ichthyolith biostratigraphic events.

	Multiplier				
Factors	0.10	0.25	0.50	0.75	1.00
Abundance (number of specimens in each sample)		1	2-5		>5
Ease of distinguishing from co-occurring subtypes	Difficult		Moderately easy		Very easy
Constancy of occurrence, above or below the event			Interrupted		Constant

a9/b1,5/c1/d1/e1/f4 + (1,16)/g1/h0,5/i4/j4/k3,8/m0.5-0.75/ n1.6-1.8/p2.2-2.8/q0,3,6/r0,4/s1,2/t1/z4/cc0/dd0/ee0/ff0/gg0/ hh0/jj2/kk2/mm0/nn0 new subtype
Triangle curved margin ends
(Plate 3, Figs. 5-12)

Characters: Triangular form (length-to-width ratio between 1.6 and 1.8) with both margins curved basally and extending below base of inline. Inline approximately same shape as outline, or with sides bowed in, not extending into upper half of outline. Base of inline a straight or smoothly curved line. transverse line, when present, a simply curved line terminating at margins at same level. Lateral shadows present. Overall length, 110-325 μm, maximum width 65-200 μm.

Distinction from similar forms: In *Triangle pointed margin ends*, which co-occurs with *Triangle curved margin ends*, the base of each margin is modified by a shallow simple angle and is pointed (Doyle et al., 1974, pl. 2K, figs. 1,2). In *Triangle transverse line across*, apex of inline extends into upper half of tooth.

Occurrence: In the Paleocene (nannofossil Zone CP6-7) at Site 577. Ranges from late Paleocene through earliest Eocene in sequences correlated by ichthyoliths (see Table 4).

a9/b1,5/c1,13/d1/e1/f21/g1/h0,4,5/i2/j2/k7,8/m0.40-0.75/ n1.0-2.0/pl.0-2.4/q0,2,3,6/r0,1,2/s1,2/t1/z1,4/cc0/dd0/ee0/ff0/ gg0/hh0/jj2/kk2/mm0/nn0 + a8/b1,5/c1/d2/e100-140/f20-30/ g1,2/h0 new subtype
Triangle radiating inline
(Plate 1, Figs. 12-17)

Characters: Generalized group of triangular forms (range of length-to-width ratio 1.0-2.4) with approximately straight margins, one margin frequently modified by a shallow simple angle (not reflexed), or occasionally by a prominent flexure, in bottom quarter. Inline approximately same shape as outline, or parallel sided. Characteristic canals radiate out from inline. Overall length 130-400 μm, maximum width 60-200 μm.

Distinction from similar forms: Distinguished from forms of the same general description (Doyle and Riedel, 1979b, pl. 6, fig. 1, pl. 7, fig. 36) by the canals extending out from both the apex and sides of the inline.

Occurrence: In Paleocene (nannofossil Zones CP6-7) at Site 577. Distribution in sequences without other microfossils indicates a range through late Paleocene and into earliest Eocene (Table 4).

a9/b1,5/c13/d1,13/e1/f1/g1/h0,3,4/i2,3/j6/k8/m0.1-0.4/ ni.8-2.5/p2.2-2.6/q0,6/r0,1,2,3/s1,2/t1/z9/cc0/dd0/ee0/ff0/gg0/ hh0/jj0/kk0/mm0/nn0 new subtype
Narrow triangle unequal margins
(Plate 3, Figs. 1-4)

Characters: Triangular form without lateral shadows, one margin straight or convex and modified by a shallow angle in bottom one-fourth; the other margin concave, moderately to markedly longer, and occasionally modified by a shallow angle at the base. Length-to-width ratio 1.8-2.5. Inline approximately same shape as outline, extending into upper half of outline. Base of inline, or transverse line if present, a curved line, concave downward, terminating at margins at different levels. Overall length, 400-600 μm, maximum width 180-240 μm.

Distinction from similar forms: *Triangle concave base* (Doyle and Riedel, 1979b, pl. 6, fig. 7) has a rather similar name description, but lacks the angle at the base of the shorter margin. The two forms illustrated in figs. 18 and 19 of the plate cited above are narrower (length to width ratio >2.5).

Occurrence: Restricted to the Paleocene in sequences correlated by ichthyoliths (see Table 4). Not present in reference samples from Site 577.

a9/b1,5/c13/d13/e1/f1/g1/h0,5/i6,7/j6,7/k3,8,14/m0.25-0.60/ n1.3-2.0/p0/q0,2,6/r0,1,3/s1,2/t1/z4/cc0/dd0/ee0/ff0/gg0/hh0/ jj2/kk2/mm2/nn0 new subtype
Beveled triangle concave margins
(Plate 1, Figs. 6-11)

Characters: Triangle (length-to-width ratio 1.3-2.0) with both margins concave, usually with most of the curvature toward the base. Both margins modified by a simple angle (not reflexed) in bottom one-fourth. Apex moderately or sharply pointed. Inline in middle one-third of outline and approximately same shape as outline, or with sides bowed in, or acuminate apically and flared basally. Transverse line, or base when

Table 6. Most probable sequence of ichthyolith events derived from their occurrence in seven "unfossiliferous" pelagic clay sequences from the North Pacific

Event		GPC-3		62PC		65PC		73PC		DSDP 576		DSDP 576A		DSDP 578		Rel mean	Age	
		Up Lo	Rel	Up Lo	Rel	Up Lo	Rel	Up Lo	Rel	Up Lo	Rel	Up Lo	Rel	Up Lo	Rel		Nanno. zone	Epoch
► *Small triangle long striations*	T	0-49	0.25	0-60	1.00	0-60	1.00	0-120	1.00	0-1148	0.50	0-370	0.25	0-9246	0.25	0.61	CN15	Pliocene/ Quaternary
► *Elliptical with line across*	T	0-49	0.50	0-60	1.00	0-60	1.00	0-120	1.00	0-1148	0.25	0-370	0.50	11197-12148	0.13	0.63	CN15	
Triangle irregular base	T	49-110	0.13	0-60	0.25	0-60	0.50	0-120	0.13	1148-1580	0.06	0-370	0.25	0-0	0.00	0.19	CN15	
Triangle concave first margin	T	0-49	0.03	0-60	0.10	0-60	0.05	0-120	0.03	0-1148	0.01	370-660	0.05	9256-10248	0.01	0.04	CN15	
► *Long ellipse*	T	49-110	0.50	0-60	0.50	0-60	1.00	0-120	1.00	1148-1580	0.13	0-370	0.50	11197-12148	0.13	0.54	CN15	
Triangle with high inline apes	T	49-110	0.13	0-60	0.13	0-60	0.13	0-120	0.13	0-1148	0.13	370-670	0.06	10248-11197	0.13	0.12	CN15	
► *Rounded apex triangle*	T	49-110	0.13	0-60	0.50	0-60	0.25	0-120	0.50	1993-2278	0.25	0-370	0.25	12148-13039	0.25	0.30	CN15	
► *Circular with line across*	T	49-110	0.25	0-60	0.25	0-0	0.00	0-120	0.50	1148-1580	0.13	370-670	0.50	13039-14017	0.06	0.28	CN15	
► *Short rectangular with striations*	T	0-49	0.13	0-0	0.00	0-60	0.50	120-220	0.25	1328-1993	0.13	370-670	0.50	11197-12238	0.13	0.27	CN15	
Narrow triangle ragged base	T	49-110	0.03	0-60	0.05	0-60	0.03	0-120	0.01	1993-2278	0.13	370-670	0.01	0-0	0.00	0.04	CN15	
► *Short triangle stepped margin*	T	49-110	0.25	0-60	0.13	0-60	0.50	220-330	0.25	0-1148	0.13	370-670	0.50	11197-12148	0.06	0.26	CN15	
Long rectangular with striations	T	49-110	0.25	0-60	0.25	0-60	0.25	0-120	0.25	0-0	0.00	1240-1540	0.25	0-0	0.00	0.25	CN15	
Triangle hooked margin	T	49-110	0.13	0-60	0.13	60-160	0.06	0-120	0.13	2278-3329	0.13	670-970	0.06	11197-12148	0.06	0.10	CN15	
Curved triangle pointed margin	T	150-218	0.06	0-60	0.06	0-60	0.25	220-330	0.06	3329-3589	0.06	670-970	0.06	0-0	0.00	0.09	CN15	
Long triangle stepped margin	T	49-110	0.25	260-330	0.25	60-160	0.25	230-330	0.13	1148-1580	0.13	0-370	0.25	0-9246	0.13	0.20	CN15	
Large with numerous lines	T	250-303	0.06	0-60	0.06	60-160	0.06	0-120	0.06	2768-3329	0.13	670-970	0.06	13039-14017	0.13	0.08	CN15	
Triangle sinuous inline	T	350-408	0.25	60-160	0.13	60-160	0.25	120-220	0.25	1148-1328	0.25	1240-1540	0.13	9256-10248	0.13	0.20	CN15-13	
Two triangles	T	49-110	0.13	0-60	0.25	160-260	0.25	220-330	0.13	1993-2278	0.13	670-970	0.13	0-0	0.00	0.17	CN15	
Pointed triangle long margins	T	350-408	0.01	0-60	0.03	0-60	0.01	0-120	0.01	2768-3329	0.01	2490-2790	0.03	15132-15330	0.01	0.02	CN12-10	
Triangle concave first margin	B	648-694	0.01	140-240	0.05	40-140	0.05	100-200	0.03	3319-3579	0.01	3130-3430	0.01	10238-11187	0.01	0.02	CN19-17	
Narrow triangle ragged base	B	595-648	0.01	240-310	0.05	140-240	0.03	100-200	0.01	2268-3319	0.01	2180-2480	0.01	0-0	0.00	0.02	CN10	
► *Long triangle short inline*	T	607-650	0.50	60-160	0.50	60-160	0.50	120-220	0.50	2278-3329	0.50	2490-2790	0.25	11197-12148	0.25	0.43		
► *Rectangular saw toothed*	T	0-49	0.13	0-60	0.25	160-260	1.00	120-220	0.50	2278-3329	0.13	370-670	0.13	12148-13039	0.13	0.32	CN15	
Stippled triangle	T	49-110	0.13	0-0	0.00	0-0	0.00	330-420	0.13	0-0	0.00	670-970	0.01	12148-13039	0.13	0.10	CN15	
Triangle with base angle	T	450-509	0.06	160-260	0.06	160-260	0.13	220-330	0.13	1993-2278	0.06	370-670	0.06	13039-14017	0.06	0.08	CN15	
Triangle irregular base	B	493-548	0.06	140-240	0.13	140-240	0.25	100-200	0.06	2268-3319	0.06	2780-3130	0.50	0-0	0.00	0.18	CN7-4	
Short rectangular with striations	B	850-894	0.25	0-0	0.00	140-240	0.50	400-485	0.13	2278-3329	0.25	2180-2480	0.25	14007-15122	0.13	0.25	CN5	
► *Long ellipse*	B	648-694	0.13	140-240	0.50	160-260	1.00	100-200	0.50	3319-3579	0.13	2780-3130	0.25	12138-13029	0.13	0.38	CN7	Miocene
Small dendritic few radiating lines	T	49-110	0.01	260-330	0.03	160-260	0.01	220-330	0.01	2278-3329	0.25	2490-2790	0.03	15133-15330	0.01	0.05	CN15	
► *Broad triangle parallel inline*	T	750-809	0.25	160-260	0.25	160-260	0.25	0-120	0.25	2368-3329	0.50	3140-3440	0.25	15128-15326	0.25	0.29	CN7-4	
Long rectangular with striations	B	798-850	0.25	140-240	0.25	240-340	0.25	200-310	0.25	0-0	0.00	2780-3130	0.13	0-0	0.00	0.19	CN5	
Small circular center	T	550-607	0.06	330-400	0.06	160-260	0.06	330-420	0.06	0-0	0.00	0-0	0.00	0-0	0.00	0.06	CN12	
Long triangle stepped margin	B	595-648	0.25	240-310	0.25	340-410	0.25	310-400	0.01	2268-3319	0.13	2780-3130	0.25	13029-14007	0.13	0.18	CN7	
Triangle with triangular projection	T	607-650	0.13	160-260	0.25	360-430	0.13	330-420	0.13	1319-1580	0.25	370-670	0.13	14017-15132	0.50	0.21	CN15	
Small dendritic many radiating lines	T	650-706	0.06	260-330	0.13	260-360	0.06	0-120	0.06	2278-3329	0.13	2790-3190	0.13	0-0	0.00	0.09	CN15	
Stippled triangle	B	798-850	0.13	0-0	0.00	0-0	0.00	310-400	0.13	0-0	0.00	960-1230	0.13	13029-14007	0.13	0.13	CN1	
Circular with line across	B	850-894	0.13	310-380	0.06	0-0	0.00	200-310	0.50	2278-3329	0.13	3130-3430	0.13	14007-15122	0.06	0.17	CN7	
Triangle sinuous inline	B	798-850	0.25	140-240	0.13	340-410	0.25	310-400	0.25	2278-3329	0.25	3430-3730	0.13	12138-13029	0.13	0.20	CN1	
Wide triangle	T	852-906	0.01	260-330	0.01	260-360	0.01	330-420	0.01	2278-3329	0.03	2790-3140	0.03	14017-15123	0.01	0.02	CN15	
Triangle transverse line across	T	852-906	0.06	260-330	0.06	260-360	0.06	220-330	0.13	3324-3589	0.13	2790-3140	0.06	15123-15330	0.06	0.08	CN10	
► *Elliptical with line across*	B	894-995	0.13	310-380	0.25	340-410	0.25	310-400	0.50	2268-3319	0.50	3130-3430	0.50	12138-13039	0.13	0.32	CN7	
Asymmetrical peak depression	T	852-906	0.05	60-160	0.01	260-360	0.01	330-420	0.03	3329-3589	0.01	3140-3440	0.01	0-0	0.00	0.02	CN9	
Triangle short wing	T	809-852	0.06	260-330	0.25	260-360	0.25	330-420	0.13	2278-3329	0.13	3140-3440	0.13	14017-15123	0.13	0.15	CN8	
► *Long triangle short inline*	B	748-798	0.25	240-310	1.00	340-410	1.00	400-485	0.13	3319-3579	0.50	3430-3730	0.25	12138-13029	0.13	0.46		
Triangle sigmoid	T	0-49	0.13	260-330	0.25	260-360	0.13	420-505	0.13	3329-3584	0.50	3440-3740	0.25	13039-14017	0.13	0.21	CN15	
Triangle with parallel inline	T	0-49	0.03	260-330	0.05	360-430	0.05	330-420	0.01	0-0	0.00	0-0	0.00	15123-15330	0.01	0.02	CN15	
Triangle double flex	T	852-906	0.13	0-0	0.00	360-430	0.25	330-420	0.25	3949-4238	0.13	3140-3440	0.25	14017-15123	0.13	0.16	CN2	
Triangle pointed margin ends	T	1215-1250	0.25	260-330	0.06	260-360	0.13	420-505	0.06	3589-3949	0.13	1240-1540	0.06	15415-15764	0.25	0.13	CN2	
Flexed triangle shallow inbase ≥ 120	T	750-809	0.13	260-330	0.13	360-430	0.25	752-795	0.25	3329-3589	0.13	3140-3440	0.50	0-0	0.00	0.23	CN2	
Triangle medium wing	T	852-906	0.50	260-330	0.50	360-430	0.25	0-120	0.06	2278-3329	0.13	3140-3440	0.13	14015-15128	0.13	0.24	CN5	
► *Short triangle stepped margin*	B	995-1048	0.25	310-380	0.13	410-490	0.50	400-485	0.50	2268-3319	0.50	3430-3730	0.25	12138-13029	0.13	0.32	CN1	
► *Two triangles*	B	1048-1103	0.13	310-380	0.50	410-490	0.50	310-400	0.13	3319-3579	0.13	3430-3730	0.25	0-0	0.00	0.27	CN2	
► *Small triangle long striations*	B	894-995	0.13	310-380	1.00	410-490	0.50	485-650	0.50	3319-3579	1.00	3430-3730	0.50	15320-15409	0.50	0.59	CN1	
Triangle with base angle	B	1200-1250	0.06	570-650	0.13	600-720	0.13	737-775	0.50	3319-3579	0.13	3430-3730	0.06	15409-15758	0.25	0.18	CP14	
Pointed triangle short inline	T	650-706	0.01	260-330	0.03	510-620	0.01	752-795	0.03	0-0	0.00	3440-3740	0.10	0-0	0.00	0.03	CP18	

Small circular center	B	1150-1200	0.13	380-470	0.06	240-340	0.06	880-980	0.06	0-0	0.00	0-0	0.00	0-0	0.00	0.08	CP19	
Small dendritic few radiating lines	B	1350-1394	0.06	380-470	0.25	410-490	0.50	880-980	0.13	3319-3579	0.13	3730-4080	0.13	15409-15758	0.06	0.18	CN2	
► Rectangular saw-toothed	B	1103-1150	0.13	380-470	1.00	720-830	0.50	650-737	0.13	3319-3579	0.13	3730-4080	0.25	15122-15320	0.50	0.38	CN2	
Curved triangle pointed margin	B	894-995	0.06	470-570	0.25	720-830	0.25	485-650	0.06	0-0	0.00	3730-4080	0.06	0-0	0.00	0.14	CP17	Oligocene
Triangle with high inline apex	B	1150-1200	0.06	570-650	0.06	490-600	0.25	650-737	0.13	2268-3529	0.25	3730-4080	0.13	15320-15409	0.06	0.13	CP17	
Triangle with canals	T	250-303	0.01	490-590	0.03	620-740	0.03	670-752	0.03	2278-3329	0.01	0-0	0.00	0-0	0.00	0.02	CN15	
Small dendritic many radiating lines	B	1103-1150	0.13	660-760	0.06	830-930	0.06	980-1080	0.06	3319-3579	0.13	3430-3730	0.25	0-0	0.00	0.14	CP15	
Tanged triangle	T	809-850	0.06	490-590	0.13	950-1040	0.06	900-1000	0.25	4248-4528	0.25	4090-4390	0.13	16060-16215	0.06	0.13	CP18	
Triangle inward angle	T	750-809	0.03	490-590	0.01	0-0	0.00	1000-1100	0.01	0-0	0.00	3740-4090	0.01	0-0	0.00	0.01	CN2	
Large with numerous lines	B	1103-1150	0.13	470-570	0.06	830-930	0.06	650-737	0.06	3319-3579	0.13	4080-4380	0.13	15320-15409	0.13	0.10	CP17	
Triangle inward angle	B	1103-1150	0.05	570-660	0.01	0-0	0.00	1080-1180	0.01	0-0	0.00	4080-4380	0.01	0-0	0.00	0.01	CP14	
Asymmetrical peak depression	B	1288-1350	0.01	570-660	0.03	340-410	0.01	775-880	0.01	3579-3949	0.01	3430-3730	0.01	0-0	0.00	0.01	CP14	
► Flexed triangle shallow inbase ≥ 120	B	1200-1250	0.25	570-660	0.25	490-600	0.50	775-880	0.25	3579-3949	0.13	4080-4580	0.50	0-0	0.00	0.31	CP17	
Pointed triangle long margins	B	1288-1350	0.03	660-760	0.01	720-830	0.01	775-880	0.01	3319-3579	0.01	3430-3730	0.03	15320-15409	0.01	0.02	CP14-11	
► Rounded apex triangle	B	1250-1288	0.25	660-760	0.50	490-600	0.50	980-1080	0.13	3579-3949	1.00	4080-4380	0.25	15409-15758	1.00	0.52	CP16	
Triangle with parallel inline	B	1350-1394	0.01	470-570	0.03	600-720	0.05	650-737	0.03	0-0	0.00	0-0	0.00	15409-15758	0.01	0.02	CP16	
Five peaks flared base	T	1252-1288	0.13	0-0	0.00	0-0	0.00	1000-1100	0.13	0-0	0.00	3440-3740	0.06	16060-16215	0.06	0.09	CP17	
Triangle concave base	T	1252-1300	0.06	570-680	0.13	850-950	0.13	670-752	0.06	4248-4528	0.06	3740-4090	0.13	16064-16219	0.25	0.12	CP11	
Pointed triangle short inline	B	1288-1350	0.05	310-380	0.03	930-1020	0.01	775-880	0.03	0-0	0.00	4080-4380	0.03	0-0	0.00	0.03	CP11-6	
► Triangle sigmoid	B	1394-1450	0.13	650-760	0.50	340-410	0.13	1080-1180	0.13	4518-4698	0.25	4080-4380	0.50	16209-16696	0.25	0.31	CP12	Eocene
Triangle with canals	B	1288-1350	0.05	660-760	0.05	930-1020	0.01	1180-1204	0.05	0-0	0.00	4080-4380	0.03	0-0	0.00	0.04	CP13	
Triangle curved base	T	1452-1483	0.50	0-0	0.00	0-0	0.00	0-0	0.00	4789-4938	0.06	4700-5040	0.06	16064-16215	0.13	0.19	CP11	
Triangle double flex	B	1483-1540	0.13	0-0	0.00	720-830	0.13	1204-1220	0.13	4238-4518	0.13	4080-4380	0.03	0-0	0.00	0.11	CP13	
Broad triangle parallel inline	B	1483-1850	0.50	960-990	0.13	1020-1050	0.13	1180-1204	0.25	4698-4779	0.25	4380-4690	0.25	16209-16696	0.13	0.23	CP14-11	
Flexed triangle asymmetric	T	1652-1708	0.25	0-0	0.00	0-0	0.00	0-0	0.00	0-0	0.00	0-0	0.00	0-0	0.00	0.25		
Narrow straight triangle	T	1652-1708	0.06	0-0	0.00	0-0	0.00	0-0	0.00	4248-4528	0.06	4700-5040	0.13	16703-16926	0.13	0.09		
Triangle hooked margin	B	1691-1750	0.13	860-960	0.13	930-1020	0.13	1180-1204	0.13	4698-4779	0.13	4690-5030	0.06	15409-15758	0.13	0.12	CN1	
► Triangle radiating inline	T	1652-1708	0.13	0-0	0.00	0-0	0.00	0-0	0.00	4708-4789	0.25	4700-5040	0.25	16229-17009	0.50	0.28	CP7-6	Paleocene
Prominence with wye-line	T	1498-1540	0.01	0-0	0.00	0-0	0.00	0-0	0.00	5088-5238	0.13	4700-5040	0.25	16703-16926	0.13	0.17	CP6	
Prominent polygon	T	1708-1752	0.25	0-0	0.00	0-0	0.00	0-0	0.00	4789-4938	0.13	4700-5040	0.50	16703-16926	0.13	0.25	CP6	
Narrow triangle unequal margins	T	1708-1752	0.13	0-0	0.00	0-0	0.00	0-0	0.00	0-0	0.00	0-0	0.00	0-0	0.00	0.13		
Giant lanceolate	T	1952-1995	0.01	0-0	0.00	0-0	0.00	0-0	0.00	0-0	0.00	4700-5040	0.03	0-0	0.00	0.02	CP18	
Wide triangle	B	1893-1950	0.01	310-380	0.01	0-930	0.01	1180-1204	0.01	0-0	0.00	5030-5330	0.01	16209-16702	0.04	0.01	CP11-6	
Tanged triangle	B	1483-1995	0.13	860-960	0.25	1020-1050	0.06	1180-1204	0.25	4698-4779	0.06	5030-5330	0.25	16696-16920	0.13	0.16	CP11	
Triangle transverse line across	B	1789-1850	0.25	960-990	0.13	1180-1204	0.25	1180-1204	0.25	5078-5228	0.25	5030-5330	0.25	16054-16209	0.06	0.21	CP2	
Triangle short wing	B	1850-1893	0.06	960-990	0.25	1180-1204	0.25	1180-1204	0.25	4698-4779	0.25	5030-5330	0.50	16920-17009	0.13	0.24	CP12-2	
Beveled triangle mid inline	T	1850-1912	0.13	0-0	0.00	0-0	0.00	0-0	0.00	0-0	0.00	0-0	0.00	0-0	0.00	0.13		
Short triangle bowed inline	T	1852-1912	0.25	0-0	0.00	0-0	0.00	0-0	0.00	0-0	0.00	0-0	0.00	16926-17015	0.13	0.19		
Flexed triangle asymmetric	B	1893-1950	0.13	0-0	0.00	0-0	0.00	0-0	0.00	0-0	0.00	0-0	0.00	0-0	0.00	0.13		
Narrow triangle unequal margins	B	1893-1950	0.06	0-0	0.00	0-0	0.00	0-0	0.00	0-0	0.00	0-0	0.00	0-0	0.00	0.06		
Narrow straight triangle	B	1893-1950	0.25	0-0	0.00	0-0	0.00	0-0	0.00	4698-4779	0.06	5030-5330	0.13	16920-17015	0.13	0.14		
Triangle curved base	B	1990-2040	0.06	0-0	0.00	0-0	0.00	0-0	0.00	5078-5228	0.06	5030-5330	0.06	16229-17009	0.13	0.08	CP2	
► Triangle radiating inline	B	1893-1950	0.25	0-0	0.00	0-0	0.00	0-0	0.00	5078-5228	0.50	5030-5330	0.25	17009-17010	0.50	0.38	CP4-3	
► Triangle concave base	B	1950-1995	0.13	960-990	0.25	930-1020	0.13	1204-1220	0.13	5078-5228	0.50	5030-5330	0.50	17009-17010	0.25	0.27	CP6-3	
Triangle modified margin ends	T	1912-1952	0.06	0-0	0.00	0-0	0.00	0-0	0.00	5088-5238	0.06	0-0	0.00	16702-16926	0.13	0.08	CP1-2	
► Triangle pointed margin ends	B	1995-2040	0.13	960-990	0.25	1020-1050	0.25	1204-1220	0.25	5078-5228	0.50	5030-5330	0.25	16229-17009	0.50	0.30	CP4-3	
► Triangle medium wing	B	1893-1950	0.13	960-990	0.50	1020-1050	0.25	1204-1220	0.25	5078-5228	0.50	5030-5330	0.13	17009-17010	0.50	0.32	CP2	
Giant lanceolate	B	1995-2040	0.01	0-0	0.00	0-0	0.00	0-0	0.00	0-0	0.00	5030-5330	0.03	0-0	0.00	0.01	CP6-3	
► Beveled triangle concave margins	T	1708-1752	0.13	0-0	0.00	0-0	0.00	0-0	0.00	5088-5238	0.25	5040-5340	0.50	16703-16929	0.25	0.28	CP4-5	
► Beveled triangle concave margins	B	1950-1995	0.13	0-0	0.00	0-0	0.00	0-0	0.00	5228-5440	1.00	5330-5630	0.50	16920-17009	0.25	0.47	CP4-3	
Beveled triangle mid inline	B	1995-2040	0.13	0-0	0.00	0-0	0.00	0-0	0.00	0-0	0.00	0-0	0.00	0-0	0.00	0.13	CP1	
► Triangle modified margin ends	B	1995-2040	0.25	0-0	0.00	0-0	0.00	0-0	0.00	5228-5440	1.00	0-0	0.00	16920-17009	0.13	0.46	CP1	
► Triangle with triangular projection	B	1995-2040	0.13	960-990	1.00	1020-1050	0.25	1204-1220	0.50	5228-5440	1.00	5030-5330	0.50	16929-17009	0.50	0.55	CP2	
Short triangle bowed inline	B	1995-2040	0.13	0-0	0.00	0-0	0.00	0-0	0.00	0-0	0.00	0-0	0.00	17009-17010	0.13	0.13	CP4-3	
► Spiky palmate	T	2008-2040	0.25	0-0	0.00	0-0	0.00	0-0	0.00	5238-5450	0.06	5340-5640	0.50	0-0	0.00	0.27		Cretaceous
► Triangle smooth surface	T	2008-2040	1.00	0-0	0.00	0-0	0.00	0-0	0.00	5238-5450	0.06	5340-5640	1.00	0-0	0.00	0.69		
► Wide triangle projection	T	2042-2060	0.25	0-0	0.00	0-0	0.00	0-0	0.00	0-0	0.00	5340-5640	0.50	0-0	0.00	0.38		
Centrally striated triangle	T	2042-2060	0.06	0-0	0.00	0-0	0.00	0-0	0.00	0-0	0.00	5340-5640	0.13	0-0	0.00	0.10		
► Triangle long inline	T	2042-2060	0.13	0-0	0.00	0-0	0.00	0-0	0.00	0-0	0.00	5340-5640	0.50	0-0	0.00	0.32		
Triangle square inline	T	2042-2060	0.13	0-0	0.00	0-0	0.00	0-0	0.00	0-0	0.00	5340-5640	0.25	0-0	0.00	0.19		
Striated blunt triangle	T	2042-2060	0.06	0-0	0.00	0-0	0.00	0-0	0.00	0-0	0.00	5340-5640	0.25	0-0	0.00	0.16		

Note: T indicates latest occurrence of subtype and B the earliest occurrence. The levels in the cores between which an event occurs are in centimeters under the headings "Up" and "Lo." The reliability index (see text) for each event is listed under "Rel," the mean of the reliability scores under "Rel. mean." Events with a reliability score greater than 0.25 are designated by an arrow (►). The nannofossil zone in which the subtype first or last appears in Pacific samples containing other microfossils is shown on the right (based on all previously published co-occurrences of ichthyoliths and nannofossils). For the procedure to determine epoch boundaries, see text.

transverse line absent, a simply curved line terminating at margins at same level. Lateral shadows absent. Overall length 130–650 μm, maximum width 100–400 μm.

Distinction from similar forms: *Beveled triangle concave margins* is readily distinguished by its concave, beveled margins, pointed apex (in a few specimens, such as that illustrated on Plate 1, Fig. 11, the apex is rounded), and lack of lateral shadows.

Occurrence: In late Paleocene (nannofossil Zone CP6) at Site 577. Restricted to Paleocene in sequences correlated by means of ichthyoliths (see Table 4).

LIST OF TAXA USED

Listed below, in alphabetical order, by colloquial name, are the ichthyolith subtypes identified in this study, with bibliographic references to indicate the current concept of each taxon.

Asymmetrical peak depression: Gottfried et al., 1984
Beveled triangle concave margins: new subtype
Beveled triangle mid inline: Doyle et al., 1978
Broad triangle parallel inline: Gottfried et al., 1984
Centrally striated triangle: Doyle et al., 1978
Circular with line across: Doyle et al., 1974; emend. Doyle and Riedel, 1979a
Curved triangle pointed margin: Doyle et al., 1974; emend. Doyle and Riedel, 1979a
Curved triangle inline constricted: Doyle et al., 1974
Elliptical with line across: Doyle et al., 1974; emend. Edgerton et al., 1977
Five peaks flared base: Doyle et al., 1974
Flexed triangle asymmetric: new subtype
Flexed triangle shallow inbase: Doyle et al., 1974
Flexed triangle shallow inbase ≥ 120: Dunsworth et al., 1975; emend. Edgerton et al., 1977
Giant lanceolate: Doyle et al., 1974
Large with numerous lines: Doyle et al., 1974
Long ellipse: Gottfried et al., 1984
Long rectangular with striations: Doyle et al., 1974
Long triangle short inline: Gottfried et al., 1984
Long triangle stepped margin: Doyle et al., 1974; emend. Edgerton et al., 1977
Narrow straight triangle: new subtype
Narrow triangle cross-hachured: Doyle et al., 1974
Narrow triangle ragged base: Dunsworth et al., 1975
Narrow triangle sharply pointed: Gottfried et al., 1984
Narrow triangle straight inbase: Doyle et al., 1974
Narrow triangle unequal margins: new subtype
Narrower crescent: Doyle et al., 1978
Plain and lined lanceolate: Doyle et al., 1974; emend. Doyle et al., 1978
Pointed and skirted: Doyle et al., 1978
Pointed triangle long margins: Gottfried et al., 1984
Pointed triangle short inline: Gottfried et al., 1984
Prominence with wye-line: Doyle et al., 1978
Prominent polygon: Doyle et al., 1978
Rectangular saw-toothed: Doyle et al., 1974; Dunsworth et al., 1975; Doyle and Riedel, 1979a
Rounded apex triangle: Doyle et al., 1974
Short rectangular with striations: Doyle et al., 1974
Short triangle bowed inline: Doyle et al., 1978
Short triangle stepped margin: Doyle et al., 1974; emend. Edgerton et al., 1977
Small circular center: Doyle et al., 1974
Small dendritic few radiating lines: Doyle et al., 1974
Small dendritic many radiating lines: Doyle et al., 1974
Small triangle crenate margin: Dunsworth et al., 1975; emend. Doyle and Riedel, 1979a
Small triangle long striations: Dunsworth et al., 1975; Kaneps et al., 1981
Spiky palmate: Doyle and Riedel, 1980
Stippled triangle: Dunsworth et al., 1975
Striated blunt triangle: Doyle et al., 1978
Tanged triangle: Gottfried et al., 1984
Triangle broad wing: Doyle et al., 1974; emend. Edgerton et al., 1977
Triangle concave base: Dunsworth et al., 1975
Triangle concave first margin: Gottfried et al., 1984
Triangle curved base: Doyle et al., 1978
Triangle curved pointed margins: new subtype
Triangle double flex: Dunsworth et al., 1975; emend. Doyle and Riedel, 1979a
Triangle double inline: Gottfried et al., 1984
Triangle hooked margin: Doyle et al., 1974
Triangle inward angle: Gottfried et al., 1984
Triangle inline halfway: Doyle et al., 1974
Triangle irregular base: Gottfried et al., 1984
Triangle long inline: Doyle et al., 1978
Triangle medium wing: Doyle et al., 1974
Triangle modified margin ends: new subtype
Triangle one canal above: Doyle et al., 1974
Triangle pointed margin ends: Doyle et al., 1974; emend. Doyle and Riedel, 1979a
Triangle radiating inline: new subtype
Triangle short wing: Doyle et al., 1974
Triangle sigmoid: Dunsworth et al., 1975; emend. Edgerton et al., 1977
Triangle sigmoid rough: Ramsey et al., 1976
Triangle sinuous inline: Gottfried et al., 1984
Triangle square inline: Doyle et al., 1978; emend. Edgerton et al., 1977
Triangle smooth surface: Doyle and Riedel, 1980
Triangle transverse line across: Doyle et al., 1974; emend. Doyle and Riedel, 1979a
Triangle with canals: Doyle et al., 1974
Triangle with base angle: Dunsworth et al., 1975
Triangle with high inline apex: Doyle et al., 1974
Triangle with parallel inline: Doyle et al., 1974
Triangle with triangular projection: Doyle et al., 1974
Triangular toothed: Doyle et al., 1978
Two triangles: Doyle et al., 1974
Wide triangle: Dunsworth et al., 1975; emend. Doyle and Riedel, 1979a
Wide crescent: Doyle et al., 1978
Wide triangle projection: Doyle et al., 1978
Wide triangle straight inbase: Doyle et al., 1974

ACKNOWLEDGMENTS

This research was supported partly by Contract 26-6608 from Sandia National Laboratories and NSF Grant OCE82-14587 and partly by the University of California.

Hans Thierstein and an anonymous reviewer reviewed the manuscript and made suggestions that improved it. M. J. Westberg provided the computer program used to determine the most probable order of the biostratigraphic events. Susan Green and Elaine Winfrey helpfully assisted in various aspects of the work. The frequently frustrating task of entering and retrieving the text from the CATT computer system was accomplished by Carol Pittman.

REFERENCES

Blank, R. G., and Ellis, C. H., 1982. The probable range concept applied to the biostratigraphy of marine microfossils. *J. Geol.*, 90: 415–433.

Corliss, B. H., Hollister, C. D., et al., 1982. A paleoenvironmental model for Cenozoic sedimentation in the central North Pacific. *In* Scrutton, R., and Talwani, M. (Eds.), *The Ocean Floor:* New York (Wiley), pp. 277–304.

Doyle, P. S., Dunsworth, M. J., and Riedel, W. R., 1977. Reworking of ichthyoliths in eastern tropical Pacific sediments. *Deep-Sea Res.*, 24:181–198.

________, 1978. Ichthyoliths from some southeast Atlantic sediments, DSDP Leg 40. *In* Bolli, H. M., Ryan, W. B. F., et al., *Init. Repts. DSDP*, Suppl. to Vols. 38, 39, 40, and 41: Washington (U.S. Govt. Printing Office), 743–759.

Doyle, P. S., Kennedy, G. G., and Riedel, W. R., 1974. Stratignathy. *In* Davies, T. A., Luyendyk, B. P., et al., *Init. Repts. DSDP*, 26: Washington (U.S. Govt. Printing Office), 825–905.

Doyle, P. S., and Riedel, W. R., 1979a. Ichthyoliths: Present status of taxonomy and stratigraphy of microscopic fish skeletal debris. Scripps Institution of Oceanography Reference Series, Number 79-

16. National Technical Information Service (Publications), Springfield, Virginia 22161, pp. 1-231.

———, 1979b. Cretaceous to Neogene ichthyoliths in a giant piston core from the central North Pacific. *Micropaleontology*, 25: 337-364.

———, 1980. Ichthyoliths from Site 436, Northwest Pacific, Leg 56, Deep Sea Drilling Project. *In* Scientific Party, *Init. Repts. DSDP*, 56, Pt. 2: Washington (U.S. Govt. Printing Office), 887-893.

———, 1981. Ichthyoliths at Site 464 in the Northwest Pacific, Deep Sea Drilling Project Leg 62. *In* Thiede, J., Vallier, T. L., et al., *Init. Repts. DSDP*, 62: Washington (U.S. Govt. Printing Office), 491-494.

Dunsworth, M. J., Doyle, P. S., and Riedel, W. R., 1975. Ichthyoliths from some NW Pacific Sediments, DSDP Leg 32. *In* Larson, R. L., Moberly, R., et al., *Init. Repts. DSDP*, 32: Washington (U.S. Govt. Printing Office), 853-864.

Edgerton, C. C., Doyle, P. S., and Riedel, W. R., 1977. Ichthyolith age determinations of otherwise unfossiliferous Deep Sea Drilling Project cores. *Micropaleontology*, 23:194-205.

Gottfried, M. D., Doyle, P. S., and Riedel, W. R., 1984. Advances in ichthyolith stratigraphy of the Pacific Neogene and Oligocene. *Micropaleontology*, 30:71-85.

———, 1985. Stratigraphic interpretations of pelagic sequences revised on the basis of ichthyoliths. *Micropaleontology*, 30:426-444.

Hay, W. W., 1972. Probabilistic stratigraphy. *Eclogae Geol. Helv.*, 65: 255-266.

Kaneps, A. G., Doyle, P. S., and Riedel, W. R., 1981. Further ichthyolith age determinations of otherwise unfossiliferous Deep Sea Drilling Project cores. *Micropaleontology*, 27:317-331.

Okada, H., and Bukry, D., 1980. Supplementary modification and introduction of code numbers to the low-latitude coccolith biostratigraphic zonation (Bukry, 1973; 1975). *Mar. Micropaleontol.*, 5: 321-325.

Ramsey, C. A., Doyle, P. S., and Riedel, W. R., 1976. Ichthyoliths in late Mesozoic pelagic sediments, mainly from Italy. *Micropaleontology*, 22:129-142.

Riedel, W. R., 1981. DSDP biostratigraphy in retrospect and prospect. *Spec. Publ. Soc. Econ. Paleontol. Mineral.*, 32:253-315.

Riedel, W. R., and Westberg, M. J., 1982. Neogene radiolarians from the eastern tropical Pacific and Caribbean, DSDP Leg 68. *In* Prell, W. L., Gardner, J. V., et al., *Init. Repts. DSDP*, 68: Washington (U.S. Govt. Printing Office), 289-300.

Westberg, M. J., and Riedel, W. R., 1982. Radiolarians from the Middle America Trench off Guatemala, DSDP Leg 67. *In* Aubouin, J., von Huene, R., et al., *Init. Repts. DSDP*, 67: Washington (U.S. Govt. Printing Office), 401-424.

Date of Initial Receipt: 21 February 1984
Date of Acceptance: 21 May 1984

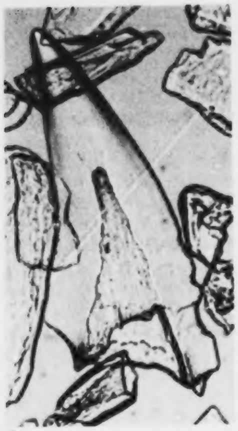
1

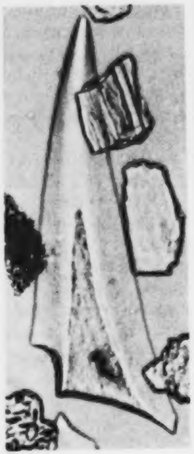
2

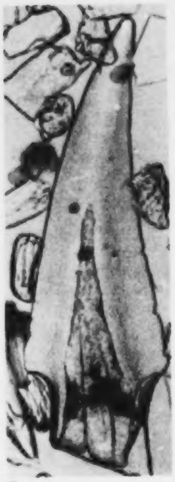
3

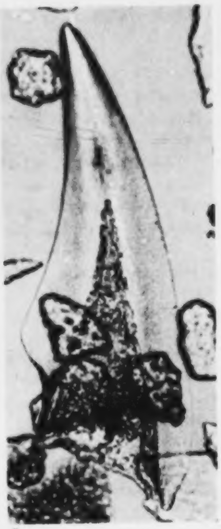
4

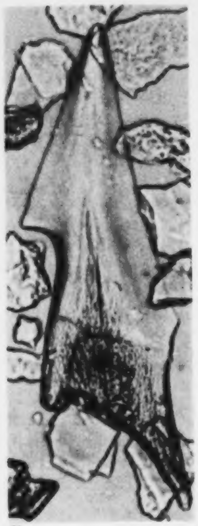
5

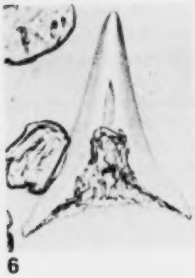
6

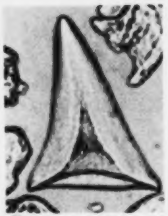
7

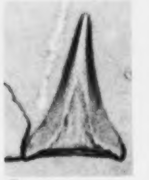
8

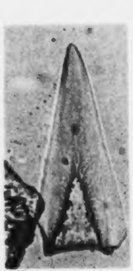
12

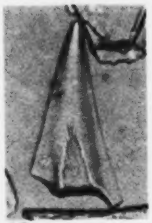
13

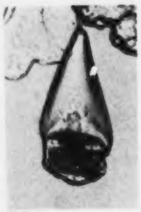
14

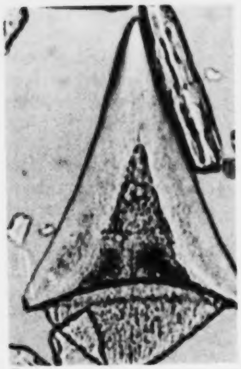
9

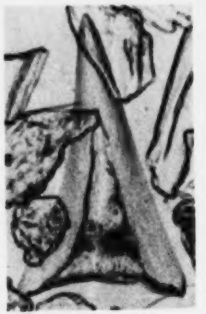
10

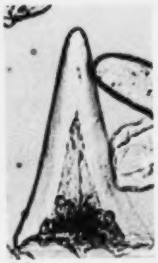
11

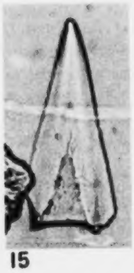
15

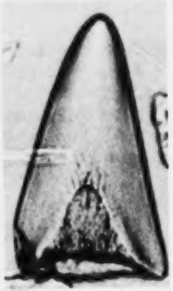
16

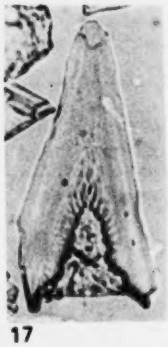
17

Plate 1. Paleocene and early Eocene taxa described herein from DSDP Leg 86 and GPC-3 sequences. Magnifications are ×120, unless otherwise indicated. In the explanations to the figures, the sample numbers and slide designations (in the form "Sl.5", etc.) indicate preparations in our collection at Scripps Institution of Oceanography, and designations in the form "P48" indicate England Finder positions of the illustrated specimens on the slides. **1-5.** *a8/b1,5/c1/d1/e0/f23-38/g2/h2* new subtype. *Flexed triangle asymmetric.* (1) GPC-3, 1789–1811 cm, Sl.5, F31. (2) DSDP 576B-6-2, 100–150 cm, Sl.63-1, C29. (3) DSDP 576B-6-2, 100–150 cm, Sl.63-1, H16. (4) GPC-3, 1789–1811 cm, Sl.1, C8. (5) DSDP 576B-6-2, 100–150 cm, Sl.63-3, M19. Type specimen. **6-11.** *a9/b1,5/c13/d13/e1/f1/g1/h0,5/i6,7/j6,7/k3,8,14/m0.25–0.60/n1.3–2.0/p0/q0,2,6/r0,1,3/s1,2/t1/z4/cc0/dd0/ee0/ff0/gg0/hh0/jj2/kk2/mm0/nn0* new subtype. *Beveled triangle concave margins.* (6) DSDP 578-19-2, 140–150 cm, Sl.63-1, L27. (7) DSDP 576-7-6, 68–74 cm, Sl.63-3, Y33. (8) DSDP 576A-6-3, 140–150 cm, Sl.63-6, J45. (9) DSDP 576-7-6, 68–74 cm, Sl.63-3, R38. Type specimen. (10) DSDP 576B-6-2, 100–150 cm, Sl.63-1, M26. (11) DSDP 576-7-6, 68–74 cm, Sl.63-3, Q34. **12-17.** *a9/b1,5/c1,13/d1/e1/f21/g1/h0,4,5/i2/j2/k7,8/m0.40–0.75/n1.0–2.2/p1.0–2.4/q0,2,3,6/r0,1,2/s1,2/t1/z1,4/cc0/dd0/ee0/ff0/gg0/hh0/jj2/kk2/mm0/nn0* new subtype. *Triangle radiating inline.* (12) GPC-3, 1789–1811 cm, Sl.2, P23. Type specimen. (13) DSDP 577-10-3, 31–39 cm, Sl.63-3, N29. (14) GPC-3, 1850 cm, Sl.3, Q49. (15) GPC-3, 1789–1811 cm, Sl.2, P23. (16) GPC-3, 1893–1912 cm, Sl.1, C29. (17) DSDP 576-7-5, 68–74 cm, Sl.63-1, K24, ×200.

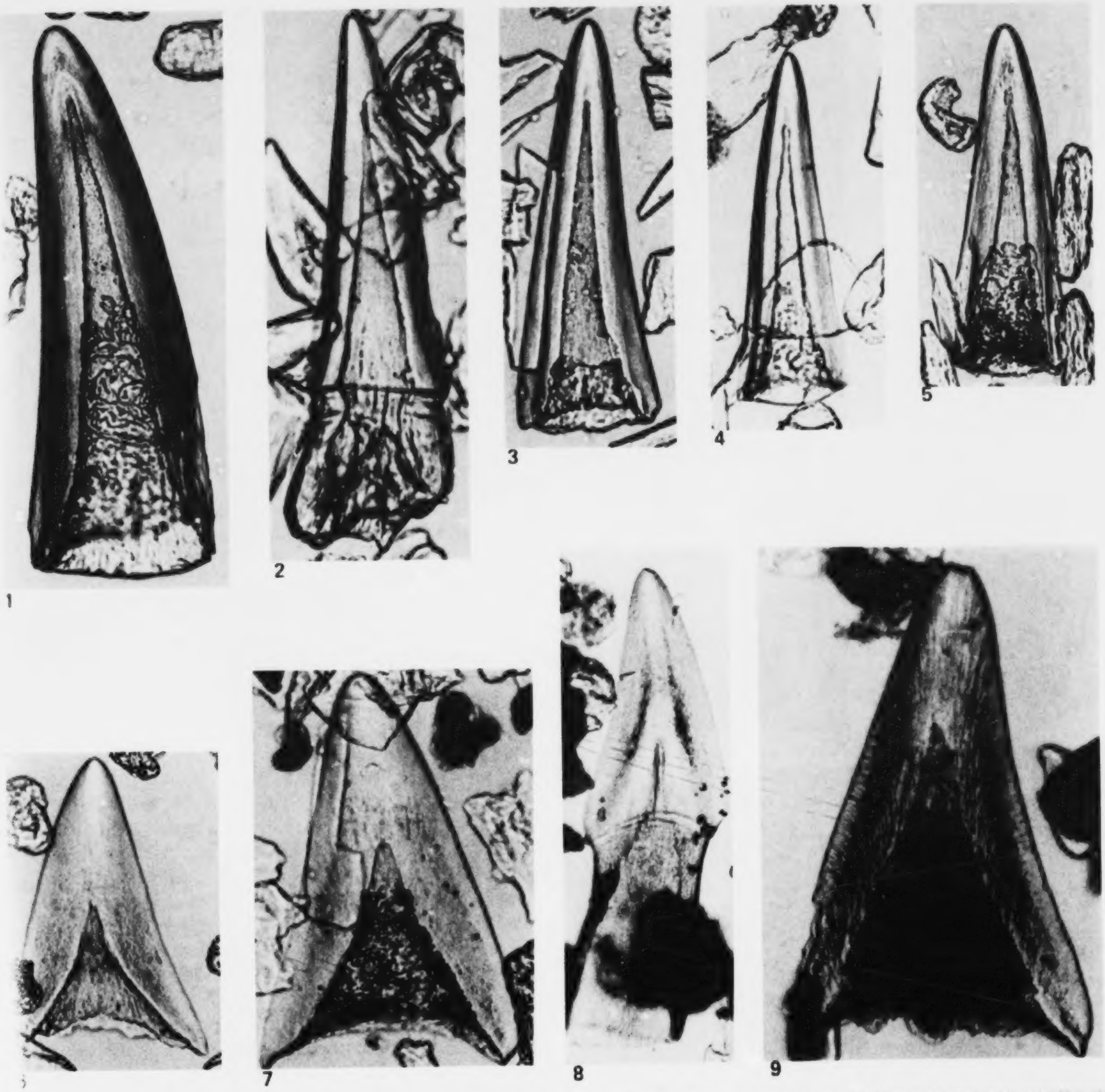

te 2. Magnifications are ×120. **1–5.** ***a9/b1,5/c1/d1/e1/f4/g1/h0,5/i2,6/j2,3/k8/m0.14–0.25/n2.5–3.0/p0/q0,2/r0,1/s1/t1/z2/cc0/dd0/ee0/ff0/gg0/hh0/jj2/kk2/mm0/nn0*** new subtype. *Narrow straight triangle.* (1) GPC-3, 1789–1811 cm, Sl.5, C12. (2) DSDP 578-19-2, 140–150 cm, Sl.63-1, U17. Type specimen. (3) GPC-3, 1789–1811 cm, Sl.5, F31. (4) GPC-3, 1789–1811 cm, Sl.1, M40. (5) DSDP 576-7-6, 59–65 cm, Sl.63-2, J42. **6–9.** ***a9/b1,5/c1,13/d1,13/e1/f1/g1/h0,5/i6/j2,3/k3,14/m0.35–0.75/n1.3–2.0/p0/q0,2,6,7/r0,1/s1/t1/z4/cc0/dd0/ee0/ff0/gg0/hh0/jj2/kk2/mm0/nn0*** new subtype. *Triangle modified margin ends.* (6) GPC-3, 1995–2008 cm, Sl.7, V48. (7) GPC-3, 1995–2008 cm, Sl.7, H42. (8) DSDP 577-11-6, 31–39 cm, Sl.63-1, V39. Type specimen. (9) DSDP 577-12-3, 82–90 cm, Sl.63-1, W39.

READEX FICHE

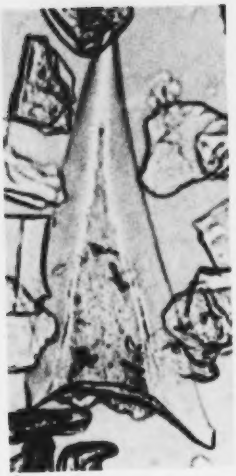
1

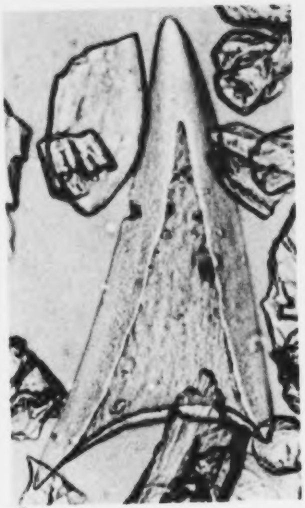
2

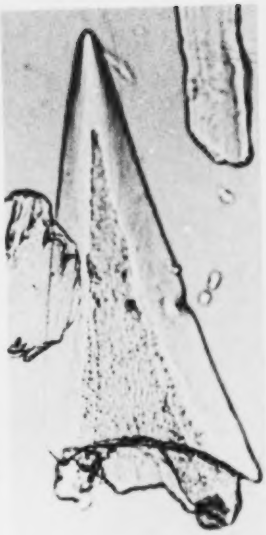
3

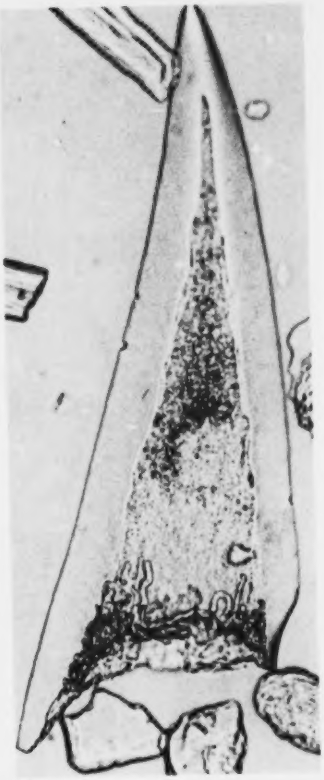
4

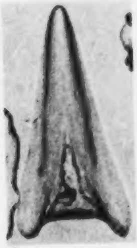
5

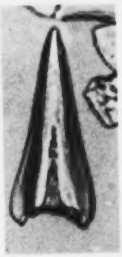
6

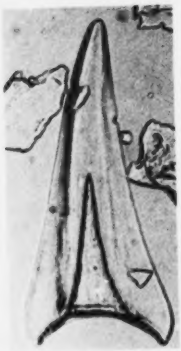
7

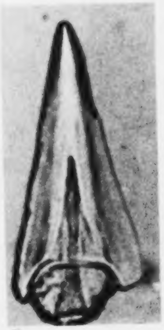
8

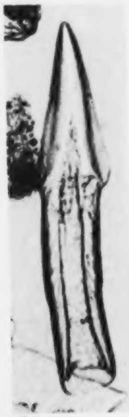
9

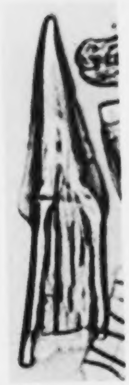
10

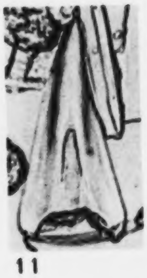
11

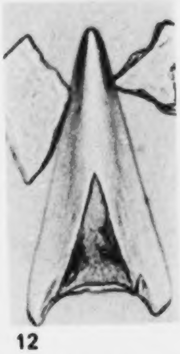
12

Plate 3. Magnifications are ×120. **1–4.** *a9/b1,5/c13/d1,13/e1/f1/g1/h0,3,4/i2,3/j6/k8/m0.1–0.4/n1.8–2.5/p2.2–2.6/q0,6/r0,1,2,3/s1,2/t1/z9 cc0/dd0/ee0/ff0/gg0/hh0/jj0/kk0/mm0/nn0* new subtype. *Narrow triangle unequal margins.* (1) GPC-3. 1893–1912 cm, Sl.2, P25. (2) GPC-3 1789–1811 cm, Sl.5, F39. (3) GPC-3, 1893–1912 cm, Sl.1, Q35. Type specimen. (4) GPC-3, 1789–1811 cm, Sl.6, L35. **5–12.** *a9/b1,5/c1/d1 e1/f4+(1,16)/g1/h0,5/i4/j4/k3,8/m0.50–0.75/n1.6–1.8/p2.2–2.8/q0,3,6/r0,4/s1,2/t1/z4/cc0/dd0/ee0/ff0/gg0/hh0/jj2/kk2/mm0/nn0* new sub type. *Triangle curved margin ends.* (5) DSDP 576-7-4, 69–75 cm, Sl.63-4, K13. (6) DSDP 577-11-4, 122–130 cm, Sl.63-1, Q40. (7) GPC-3, 1789 1811 cm, Sl.7, E30. (8) GPC-3, 1789–1811 cm, Sl.7, B23. (9) DSDP 577-11-4, 122–130 cm, Sl.63-1, F30. (10) DSDP 577-11-4, 122–130 cm, Sl.6 1, K20. (11) GPC-3, 1789–1811 cm, Sl.2, E32. Type specimen. (12) DSDP 576-7-4, 69–75 cm, Sl.63-1, S46.

13. LATE CENOZOIC SILICOFLAGELLATES FROM THE NORTHWEST PACIFIC, DEEP SEA DRILLING PROJECT LEG 86: PALEOTEMPERATURE TRENDS AND TEXTURE CLASSIFICATION[1]

David Bukry, United States Geological Survey and Scripps Institution of Oceanography
and
Simonetta Monechi, Geological Research Division, Scripps Institution of Oceanography[2]

ABSTRACT

A quantitative study of late Cenozoic silicoflagellates from the northwestern Pacific sites of Deep Sea Drilling Project Leg 86 shows a relative paleotemperature (Ts) gradient with lowest values (Ts = 30) in the north. Some new ecostratigraphic relations for the region are indicated, such as the last common occurrence of *Dictyocha brevispina* at 2.6–3.0 m.y. ago during a cool interval. Elements of North Pacific and low-latitude biostratigraphic zonations can be identified, but the mixing of cool- and warm-indicator taxa prompted the definition of the new Miocene *Mesocena hexalitha* Subzone and Pliocene *Distephanus jimlingii* Subzone.

Scanning-electron microscope study of Leg 86 silicoflagellates was done to determine whether various types of skeletal surface texture are temperature dependent. To conduct the study we organized a new surface-texture descriptive code, which characterizes the apical structure/basal ring/spine sequence using new definitions of the terms crenulate (C), linear (L), nodular (N), reticulate (R), and smooth (S).

One new silicoflagellate genus, *Caryocha* Bukry et Monechi, n. gen., is described and several new combinations are made.

INTRODUCTION

The recovery of biosilica-rich sediment from the Northwest Pacific Basin and biosilica-bearing calcareous sediment from Shatsky Rise by Deep Sea Drilling Project (DSDP) Leg 86 provided the opportunity to investigate silicoflagellate relative paleotemperature trends in a region where the warm Kuroshio Current and cool Oyashio Current meet. A comparative interval through the Quaternary and late Pliocene was studied from three holes: Holes 577, 579A, and 580. A Miocene section was studied from Hole 581 (Fig. 1).

Although many assemblages contain cool-water or temperate-water taxa, such as *Dictyocha subarctios* and *Distephanus jimlingii*, and some warm-water taxa (*Octactis pulchra*) are missing, the low-latitude biostratigraphic zonation can be identified for most assemblages. North Pacific zonation is, however, applied to the Quaternary at Site 580 because of the predominance of cool-water taxa.

Relative paleotemperature fluctuations correspond fairly well with the regional disappearances of *Dictyocha brevispina* and *Mesocena circulus* in the Pliocene, providing ecostratigraphic correlations. The highest relative temperature values occur in southern Hole 577 and the lowest in northern Hole 580, supporting the presence of a latitudinal gradient during the late Cenozoic, which also supports the effectiveness of the relative paleotemperature criteria. There is some correspondence between the silicoflagellate and the foraminiferal paleoclimatological scales. For example, Keller's (1979) C_2 cool trough was characterized as intense and brief (3.0–3.2 m.y. ago). This may be related to the *D. brevispina* cool trough (Event c) which is calibrated here at 2.6 to 3.0 m.y. ago. The major foraminiferal cooling between 2.5 and 1.9 m.y. ago (Keller, 1979) is not evident in silicoflagellate assemblages at Leg 86 sites.

Surface textures on Leg 86 silicoflagellates were examined to determine whether the patterns are temperature dependent. The scanning electron microscope (SEM)

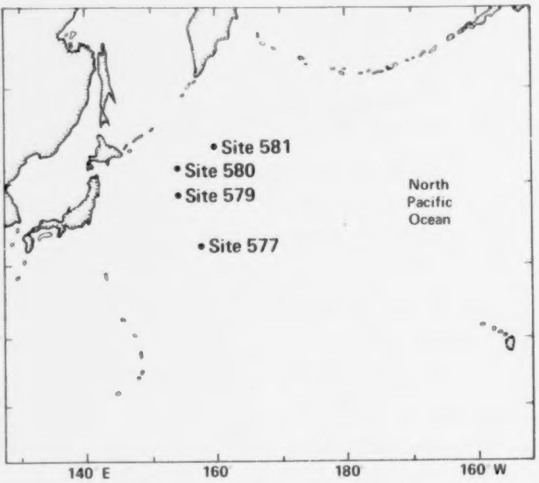

Figure 1. Location of coring sites from DSDP Leg 86 that were studied for silicoflagellates.

---

[1] Heath, G. R., Burckle, L. H., et al., *Init. Repts. DSDP*, 86: Washington (U.S. Govt. Printing Office).

[2] Addresses: (Bukry) United States Geological Survey (A-015), Scripps Institution of Oceanography, La Jolla, California 92093; (Monechi, present address) Dipartimento di Scienze della Terra, Università di Firenze, Via La Pira No. 4, 50121 Firenze, Italy.

study led to the establishment of a new system of descriptive coding in order to compare the results. Clearcut temperature dependence could not be established, but speculation on evolution and preservation is discussed in the context of an analysis of the published literature on silicoflagellate surface textures.

This chapter was not intended to detail nomenclature, so a list of previously cited taxa is provided. One new genus, *Caryocha*, is described and several new combinations are made.

METHODS AND MATERIALS

Light-microscope study at magnification of 200 to 500× was used for biostratigraphic and paleotemperature enumeration of silicoflagellates for Leg 86. Structural details on silicoflagellate surfaces were studied with the scanning-electron microscope at Firenze at magnifications of 720 to 12,000×. Except for the carbonate-rich sediment from Shatsky Rise (Site 577), all samples were studied in smear preparations from unprocessed sediment. Processed acid residues were used for Site 577. The main goal of the study was to establish the pattern of Ts paleotemperature value fluctuations; therefore, counts were done mainly at the level of genus and morphologic group. Only selected species were counted individually.

The Leg 86 material studied includes:

1. Hole 577, Cores 577-1 to 577-7; 32°26.51′N, 157°43.40′E, depth 2675 m.
2. Hole 578, Core 578-12; 33°55.56′N, 151°37.74′E, depth 6010 m.
3. Hole 579A, Cores 579A-1 to 579A-15; 38°37.61′N, 153°50.28′E, depth 5737 m.
4. Hole 580, Cores 580-1 to 580-17;p 41°37.47′N, 153°58.58′E, depth 5375 m.
5. Hole 581, Cores 581-2 to 581-8; 43°55.62′N, 159°47.76′E, depth 5476 m.

A comparative sample from Hole 572A, Core 572-5, 01°26.09′N, 113°50.52′W, depth 3893 m, was also examined.

SILICOFLAGELLATE ZONATION

Low-latitude and North Pacific silicoflagellate zonations are used for biostratigraphic assignment of assemblages from DSDP Leg 86. The greatest differentiation between cool- and warm-water assemblages is in the Quaternary, where the North Pacific *Dictyocha subarctios* Zone (Ling, 1973) and the *Distephanus octangulatus* Zone (Bukry, 1973) are used for northern Site 580. Low-latitude zonation (Bukry, 1981b, 1983) is applied elsewhere, except for two new subzones that are described for northern Site 581 (Fig. 2). The zonal units are briefly characterized below from oldest to youngest.

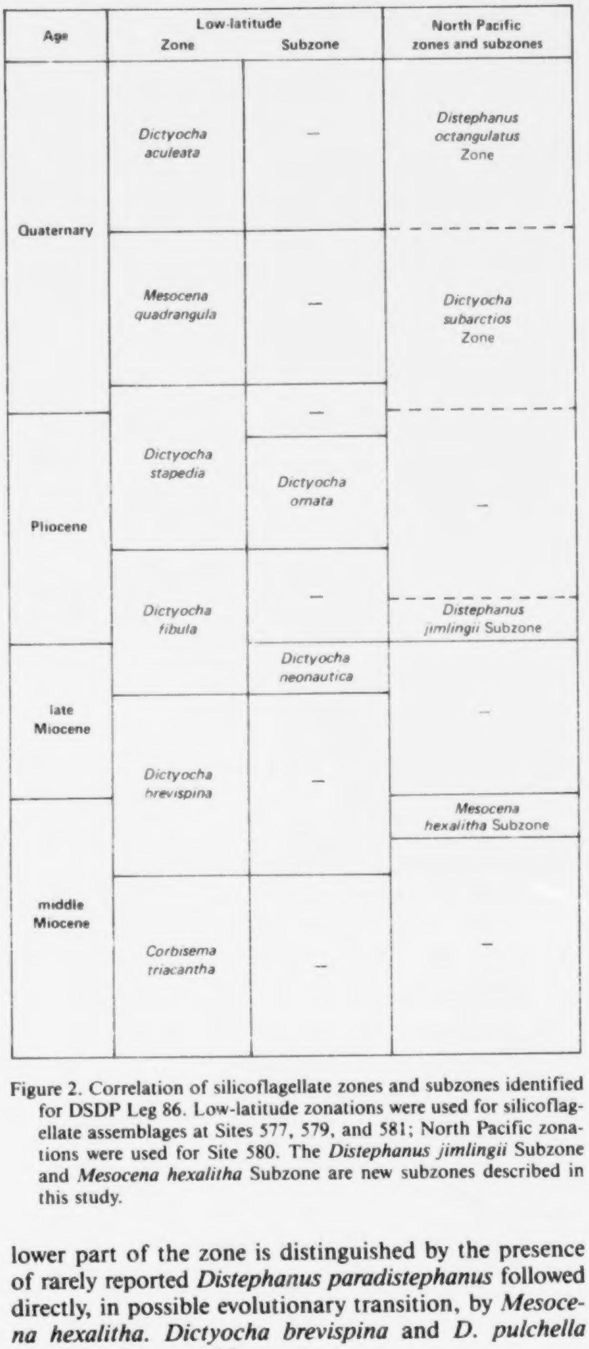

Age	Low-latitude		North Pacific zones and subzones
	Zone	Subzone	
Quaternary	*Dictyocha aculeata*	–	*Distephanus octangulatus* Zone
	Mesocena quadrangula	–	*Dictyocha subarctios* Zone
	Dictyocha stapedia	–	
Pliocene			–
		Dictyocha ornata	
	Dictyocha fibula	–	
			Distephanus jimlingii Subzone
late Miocene		*Dictyocha neonautica*	–
	Dictyocha brevispina	–	
middle Miocene			*Mesocena hexalitha* Subzone
			–
	Corbisema triacantha	–	

Figure 2. Correlation of silicoflagellate zones and subzones identified for DSDP Leg 86. Low-latitude zonations were used for silicoflagellate assemblages at Sites 577, 579, and 581; North Pacific zonations were used for Site 580. The *Distephanus jimlingii* Subzone and *Mesocena hexalitha* Subzone are new subzones described in this study.

Corbisema triacantha Zone

Two samples from Site 581 contain 11 and 16% *Corbisema triacantha* associated with predominant *Dictyocha pulchella.* Some mixing in the core-catcher of Core 581-8 is suggested by the association of *Mesocena hexalitha* with *C. triacantha. M. hexalitha* is typically younger then *C. triacantha* (Bukry, 1981a). *Distephanus longispinus* is sparse in both samples from Site 581, respectively 3% and <1%.

Dictyocha brevispina Zone

The interval between the last *Corbisema triacantha* and the first *Dictyocha neonautica* was used to identify the *D. brevispina* Zone for Site 581 because the primary guide to the top of the zone (*D. longa*) is missing. The lower part of the zone is distinguished by the presence of rarely reported *Distephanus paradistephanus* followed directly, in possible evolutionary transition, by *Mesocena hexalitha. Dictyocha brevispina* and *D. pulchella* dominate the assemblages.

Mesocena hexalitha Subzone (new subzone)

The stratigraphic range of *Mesocena hexalitha* defines the *M. hexalitha* Subzone as a short interval at the boundary between middle and upper Miocene. It is limited to Core 581-8 for Leg 86, but can be identified in the coccolith *Discoaster hamatus* Zone at Site 470 (Bukry, 1981a) and the diatom Subzone c of the *Denticulopsis hustedtii–D. lauta* Zone (Barron, 1980) at Hole 438A and in the Monterey Formation at upper Newport Bay, California (Barron, 1976).

Dictyocha fibula Zone

The interval between the first *Dictyocha neonautica* and the first *D. stapedia stapedia* is assigned to the *D. fibula* Zone at Holes 579A and 581. Fibuloid specimens dominate the assemblages of *Dictyocha* in the upper part of the zone at Hole 579A, but asperoid specimens are dominant in the lower part of the zone at Hole 581.

Dictyocha neonautica Subzone

The range of *Dictyocha neonautica* is used to identify the *D. neonautica* Subzone (Bukry, 1981b). This interval occupies the lower part of the *D. fibula* Zone and is typically latest Miocene in age. At Site 581 the *D. neonautica* Subzone occurs in Cores 3 to 6, where it contains *D. aspera clinata* and *Distephanus quinquangellus*. *Dictyocha neonautica* is missing in the middle of the subzone in Core 4, a relationship that exists at Hole 503A in the eastern Pacific (Bukry, 1982).

Distephanus jimlingii Subzone (new subzone)

A new subzone, based on the first occurrence of *Distephanus jimlingii* s. ampl. is identified at Site 581 in Core 581-2, and probably in Cores 579A-12 and 579A-13 from Hole 579A.

The interval from the first occurrence to the last occurrence of *D. jimlingii* in the *Dictyocha fibula* Zone is used to identify the *Distephanus jimlingii* Subzone. This subzone is correlative with the early Pliocene *Dictyocha pulchella* Subzone and possibly the *D. angulata* Subzone of lower latitude (Bukry, 1983).

Ling's (1973) *Cannopilus hemisphaericus* Zone is based on a species concept that partly includes *Distephanus jimlingii* (Ling, 1973, Plate 1, Figs. 1 and 2). His zone ranges from the last *D. quinquangellus* to the last *D. jimlingii*. Because Ling's taxonomic concept is not directly equivalent to *D. jimlingii* and because *D. quinquangellus* occurs with *D. jimlingii* in the lower Pliocene of Hole 579A, that biostratigraphic unit is not equivalent to the newly defined *D. jimlingii* Subzone.

Ling (1975) illustrated a specimen called *Cannopilus hemisphaericus* (Ehrenberg) which resembles *D. jimlingii* (Bukry). His occurrence charts for Sites 301 and 302 in the Sea of Japan show *C. hemisphaericus* mainly in the late Miocene. A zonal correlation chart, however, lists a *C. hemisphaericus* Zone in the early Pliocene. Ling (1980) adopted the name *D. jimlingii* Zone for the 1973 zone, but used the same definition. However, his broad taxonomic concept for *D. jimlingii*, exemplified in Ling (1973), ranges into taxa with large apical openings, which have different stratigraphic ranges. This, together with the variable range of *D. quinquangellus*, supports definition of the more biostratigraphically circumscribed, new *D. jimlingii* Subzone. See Barron (1976, 1980) for additional information concerning the biostratigraphic significance of *D. jimlingii* near the Miocene/Pliocene boundary.

Dictyocha stapedia Zone

The low- to mid-latitude *Dictyocha stapedia* Zone is defined as the interval between the first *D. stapedia stapedia* and the first *Mesocena quadrangula*. The base can be alternately identified by the first occurrence of *D. flexatella* and *D. ornata*. In the Leg 86 area, *D. ornata* is more sporadic than *D. flexatella* or *D. stapedia stapedia*.

The top of the zone is influenced, here, by the variable association with *D. subarctios*, which defines a regional North Pacific zone that is coeval with the upper part of the *D. stapedia* Zone in the Quaternary. For example, *D. subarctios* first occurs with the *M. quadrangula* acme, above the *D. stapedia* Zone in Hole 579A. But at more northerly Site 580, *D. subarctios* appears earlier than the *M. quadrangula* acme, providing an overlap in the defined limits for the upper *D. stapedia* Zone and lower *D. subarctios* Zone. Mixed cool, cosmopolitan, or warm indicator species in the Northwest Pacific Basin represent the regional meeting of warm- and cool-water masses.

Dictyocha ornata Subzone

The *Dictyocha ornata* Subzone is identified in Holes 577 and 579A mainly by the range of *D. flexatella* which has a range similar to *D. ornata* (= *D. ornata africana* and *D. ornata ornata*) at lower latitudes. *D. ornata* is sparse and sporadic at Leg 86 sites. At low latitude, the first common *D. delicata* marks the top of the subzone, but this species is missing in Leg 86 samples. Therefore, the alternative disappearance of either *D. flexatella* or *D. ornata* is used.

Dictyocha subarctios Zone

The *Dictyocha subarctios* Zone was defined for North Pacific high latitudes (Ling, 1973) as the interval from the last *Ammodochium rectangulare* (an ebridian) to the last *D. subarctios*. An alternate criterion, the local range zone for *D. subarctios* was also provided in the original definition. The alternate definition is used for Site 580. *Mesocena quadrangula* has an acme at the top of the *D. subarctios* Zone of Hole 580, which suggests partial correlation with the low-latitude *M. quadrangula* Zone.

Mesocena quadrangula Zone

The middle Quaternary acme of *Mesocena quadrangula* occurs at Holes 577, 579A, and 580. This acme defines the low-latitude *M. quadrangula* Zone. At Site 580 the *Dictyocha subarctios* Zone encompasses the *M. quadrangula* acme Zone.

Distephanus octangulatus Zone

The original *Distephanus octangulatus* Zone from DSDP Leg 18 (Bukry, 1973) is defined from the first *D. octangulatus* at the base to living assemblages at the top. A second *D. octangulatus* Zone was described for DSDP Leg 19 (Ling, 1973) from the last *D. floridus* to an undefined top. The first *D. octangulatus* is used for

Site 580, but the overlap with *D. floridus* is short, so the original zone is somewhat longer. The assemblages have low diversity with *Dictyocha aculeata, D. stapedia stapedia*, and *Distephanus octangulatus* as the dominant taxa.

Dictyocha aculeata Zone

Low- to mid-latitude assemblages from the end of the acme of *Mesocena quadrangula* to living assemblages are assigned to the *Dictyocha aculeata* Zone. *D. aculeata* and small *D. stapedia stapedia* dominate these assemblages. No warm water *Octactis pulchra* were observed in the *D. aculeata* Zone at either Hole 577 or 579A.

SILICOFLAGELLATE RELATIVE PALEOTEMPERATURE VALUES (Ts)

A latitudinal array of sites was cored by DSDP Leg 86 to the east of Japan and south of Kamchatka in a region where the warm Kuroshio and cool Oyashio oceanic currents converge. The silicoflagellates preserved in the sediment deposited under these currents in the Northwest Pacific Basin and on the Shatsky Rise include variable proportions of cool, warm, and cosmopolitan taxa. Quantitative study of silicoflagellate assemblages from the Leg 86 sites permits comparison of paleotemperature trends through calculation of relative paleotemperature values (Bukry, 1981a, 1983, in press b). The array of sites examined ranges 11° of latitude from 32°26.51′N on Shatsky Rise (Site 577) to 43°55.62′N near the Hokkaido Fracture Zone (Site 581). Coeval stratigraphic successions are available only for the southern three holes—Holes 577, 579A, and 580—which range up to 41°37.47′N. These sections contain coeval silicoflagellates from the late Pliocene (3.4 m.y. ago) to late Pleistocene (0.7 m.y. ago). The northernmost Hole 581 sampled a middle Miocene (14 m.y. ago) to early Pliocene (3.6 m.y. ago) section. Quantitative silicoflagellate results are presented for all four sites as annotated summaries (Tables 1-4) and time-calibrated curves (Figs. 3-6). Chronology for silicoflagellate paleotemperature results is based on paleomagnetic and correlative diatom time scales determined for the northwestern Pacific region (see Barron, 1980, 1981; Koizumi and Tanimura, this volume; Monechi, this volume).

The major horizons of biostratigraphic and relative paleotemperature correlation between the Pliocene and Pleistocene curves for Holes 577 (Fig. 3), 579A (Fig. 4), and 580 (Fig. 5) include the cool trough at approximately 0.95 m.y. ago, during the *Mesocena quadrangula* acme. Other points of correlation are signified by the letters a to e on the paleotemperature curves (Table 5; Fig. 3).

M. circulus disappeared at about 2.4 m.y. ago at all three sites (reference point a; Figs. 3-5). This species had

Table 1. Late Cenozoic silicoflagellate biostratigraphy, relative paleotemperature values (Ts), and percent distribution of various genera and morphologic subgroups with remarks on noteworthy occurrences for Hole 577.

Age	Zone or subzone		Hole 577 sample (interval in cm)	Depth (m)	Total specimens	Ts value	Generic percentages						Noteworthy occurrences
							Dictyocha	*Distephanus* (quadrate)	*Distephanus* (nonquadrate)	*Mesocena* (quadrate)	*Mesocena* (nonquadrate)	*Octactis*	
Quaternary	*D. aculeata*		1-1, 125-126	1	100	100	100						
			1-3, 40-41	3	100	100	100						*Dictyocha stapedia* 40%
			1-4, 40-41	5	100	100	100						*D. aculeata* > *D. stapedia*
			1-5, 46-47	6	50	99	99		1				
	M. quadrangula		2-1, 103-104	8	100	95	94		5	1			Last *Mesocena quadrangula*
			2-3, 43-44	10	100	92	85		1	14			
			2-4, 43-44	12	300	88	79	1	4	16			
			2-4, 103-104	12	100	95	90			10			
	D. stapedia	—	2-6, 103-104	15	50	98	98		2				
			3-1, 140-141	18	100	96	95	1	3	1			
			3-2, 54-55	18	100	95	95		5				
late Pliocene			3-3, 96-97	20	100	93	92		6	2			
			3-5, 44-45	23	300	96	96		4				
		D. ornata	3-5, 110-111	24	200	97	96		2	2			*Dictyocha flexatella* 3%
			3-6, 30-31	24	200	93	93	2	6				
			4-1, 33-34	26	200	92	90	2	4		3		
			4-2, 112-113	28	100	92	91	2	5		2		First *D. ornata*
			4-4, 112-113	31	200	80	78	3	10		8		*Dictyocha flexatella* 25%
			4-6, 25-26	34	100	58	56	4	28		12		Last *D. brevispina*
			5-1, 30-31	36	50	71	68	6	24		2		*Dictyocha flexatella* 20%
			5-2, 30-31	37	50	92	90	4	6				
			5-3, 34-35	39	50	81	80	2	10		8		First *D. flexatella, D. stapedia*
early Pliocene	—		5-6, 20-21	43	50	68	64	6	6	2	22		
			6-1, 120-121	46	100	82	80	4	9		7		
			6-3, 20-21	48	50	91	90	2	6		2		Last *D. pulchella*
			6-7, 12-13	54	200	92	90	3	6		1		*Dictyocha brevispina* 40%
late Miocene			7-1, 86-87	55	80	92	90		7	3			
			7-3, 130-131	59	25	80	80		20				

Table 2. Late Cenozoic silicoflagellate biostratigraphy, relative paleotemperature values (Ts), and percent distribution of various genera and morphologic subgroups with remarks on noteworthy occurrences for Hole 579A.

Age	Zone	Hole 579A sample (interval in cm)	Depth (m)	Total specimens	Ts value	Generic percentages						Noteworthy occurrences
						Dictyocha	*Distephanus* (quadrate)	*Distephanus* (nonquadrate)	*Mesocena* (quadrate)	*Mesocena* (nonquadrate)	*Octactis*	
Quaternary	*D. aculeata*	1-2, 40-42	16	200	99	99		1				*Dictyocha aculeata* 57%
		1-5, 75-77	21	300	96	96		4				*Dictyocha aculeata* 70%
	M. quadrangula	2-4, 115-117	29	200	92	85		2	14			
		3-2, 30-32	35	50	68	50		14	36			*Mesocena quadrangula* acme peak
		3-5, 93-95	40	200	79	69		4	28			*Dictyocha subarctios* 4% (cool water)
		4-2, 14-16	44	100	84	84	1	2	13			*Dictyocha subarctios* 7% (cool water)
		5-5, 38-40	58	200	98	97		2	1			
	D. stapedia	6-5, 28-30	68	300	94	94	<1	7				
late Pliocene		7-2, 20-22	73	100	94	94		6				
		7-5, 20-22	77	200	83	81	3	18				
		8-2, 80-82	83	100	82	81	1	18				
		8-5, 80-82	87	300	64	64		15		20		*Mesocena circulus* 20%
		9-2, 40-42	92	100	73	73		24		3		*D. ornata* 1%, *D. flexatella* 23%
		9-5, 50-52	97	100	66	66		20		14		
		10-2, 75-77	102	100	57	56	1	32		11		Asperoid/fibuloid ratio >1
		10-4, 75-77	105	300	63	62	1	17		20		Asperoid/fibuloid ratio >1 *Dictyocha flexatella* 10%
		11-2, 34-36	111	100	85	84	1	14	1			First *Dictyocha stapedia stapedia*
early Pliocene	*D. fibula*	11-4, 34-36	114	200	66	64		26	4	7		
		12-2, 34-36	120	200	62	54	3	28	13	4		*Distephanus speculum minutus* 2%
		12-5, 34-36	125	200	50	49	1	48	1	3		*Distephanus speculum minutus* 3%
		13-2, 30-32	130	300	78	77	<1	17	1	4		
		13-4, 30-32	133	300	56	54	<1	16	4	26		*Distephanus quinquangellus* 5%
		14-2, 36-38	139	300	85	83	<1	12	3	2		Last *Dictyocha pulchella*
?early Pliocene		14-5, 36-38	144	300	52	41	<1	24	22	13		*Distephanus quinquangellus* 5%
		15-1, 16-18	147	200	68	56	1	18	22	5		
		15-2, 16-18	149	300	74	65	1	15	16	3		Asperoid/fibuloid ratio <1

its most numerous blooms at high southern latitudes (Stadum and Burckle, 1973; Bukry, 1975, 1976a) in the late Miocene. For Leg 86, *M. circulus* is most numerous at Hole 580 where it disappeared at a pronounced cool event (Ts = 58). The coeval cool trough at the intermediate latitude Hole 579A is less pronounced (Ts = 64). At southern latitude Site 577, where *M. circulus* is least numerous, it disappeared during a warm peak. This suggests that the regional disappearance of *M. circulus* was coeval and that a cooling event at the northern location was more intense than to the south. Also, the *M. circulus* disappearance in the region did not result directly from the cold pulse, unless the southern population was exotic and required continual "resettlement" from the more numerous northern population. The disappearance of *M. circulus* at a warm peak at Site 577 shows the removal was not related to cool temperatures at that location. A significant warming occurred at the northern location following 2.4 m.y. ago (Fig. 5).

A warm peak (reference point b) occurs at northern Holes 580 and 579A, but the coeval point (2.6 m.y. ago) at southern Hole 577 appears to be part of a general warming trend. The calculated Ts values are warmest (Ts = 80) in the south and coolest (Ts = 69) at the northern limit (Figs. 3, 4, and 5).

The last common occurrence of *Dictyocha brevispina* (reference point c) in Holes 577, 579A, and 580 correlates with a distinct cool trough between 2.6 and near 3.0 m.y. ago. Cooling across latitude for this event is shown by the relative paleotemperature values which decrease northward from Ts = 58 at Site 577 to Ts = 45 at Site 580.

A short warm peak (reference point d), between 3.0 and 3.3 m.y. ago precedes the *D. brevispina* cool event (c) at all three sites and is near the first occurrence of *D. stapedia stapedia*. The latitudinal order of the sites is shown by the Ts relative paleotemperature values, which range from Ts = 92 for this warm peak at Site 577 to Ts = 60 at Site 580.

The final correlation point between the sites (reference point e) is a warming trend that occurs at about 3.4 m.y. ago (Figs. 3–5). The Ts curves for the sites show lowest values in the north and highest, or warmest, values in the south, which indicates the potential for silicoflagellates to contribute to other more sophisticated paleotemperature analyses for the North Pacific (Barron, in press; Barron and Keller, 1983; Ingle, 1973; Keller, 1979, 1980a,b, 1981a,b; Vincent, 1975, 1981).

In detail these paleotemperature and occurrence events for silicoflagellates are believed to be most effective for local correlations such as the Leg 86 sites; however, comparison to distant Pacific Site 504 suggests some transoceanic similarity, too. At Site 504 off Ecuador (Bukry, 1983), *D. brevispina* disappears at a cool trough (~2.5 m.y. ago) followed by a brief warm peak and then a second cool trough (~2.1 m.y. ago) where *M. circulus* disappears. This sequence matches that described as events (c, b, and a) for Leg 86. The ages for

Table 3. Late Cenozoic silicoflagellate biostratigraphy, relative paleotemperature values (Ts), and percent distribution of various genera and morphologic subgroups with remarks on noteworthy occurrences for Hole 580.

Age	Zone or subzone		Hole 580 sample (interval in cm)	Depth (m)	Total specimens	Ts value	Generic percentages: *Dictyocha*	*Distephanus* (quadrate)	*Distephanus* (nonquadrate)	*Mesocena* (quadrate)	*Mesocena* (nonquadrate)	*Octactis*	Noteworthy occurrences
Quaternary	*D. octangulatus*		1,CC	3	50	84	82	4	16				
			2-2, 42-44	5	100	76	76		24				*Distephanus octangulatus* 13%
			2-5, 42-44	10	50	40	40		60				*Distephanus octangulatus* 52%
			2,CC	12	50	36	32	8	60				
			3-3, 40-42	16	100	58	57	1	42				*Distephanus octangulatus* 11%
			3-6, 110-111	21	50	96	96		4				
			4-5, 20-22	29	50	66	66		34				*D. octangulatus* 4%, last *D. floridus*
			4,CC	31	50	84	84		16				
	—		5,CC	41	300	88	85	5	10				
			6-2, 42-44	43	200	98	98		2				*Dictyocha lingui* 4%
	D. subarctios		6-5, 42-44	48	100	78	90		1	9			*Dictyocha* sp. aff. *D. subarctios* 17%
			6,CC	50	300	86	83		11	6			
			7-2, 49-51	53	100	82	75		2	23			*Dictyocha subarctios* 5%
			7-6, 10-11	58	200	72	96		4				*Dictyocha subarctios* 24%
			8-2, 18-20	62	300	70	84		16	1			*Dictyocha subarctios* 15%
			8-5, 17-19	66	300	22	30		69	1			*D. subarctios* 9%; *D. floridus* 30%
			8,CC	70	300	73	73		26		1		
			9-2, 28-30	72	300	89	91	1	7				*D. subarctios* 3%
			9,CC	77	100	82	82		14		4		
late Pliocene	*D. stapedia*	—	10-5, 90-92	86	200	84	83	2	16				*Dictyocha calida ampliata* 16%
			10,CC	88	100	92	92		8				
			11-3, 60-62	92	100	94	94		6				*Dictyocha perlaevis* predominant
			11,CC	96	100	76	76		24				
		D. ornata	12-3, 20-22	102	300	84	83	1	17				*D. calida ampliata* 22%; *D. ornata* 1%
			12,CC	108	100	79	76	5	19				
			13-3, 54-56	111	200	36	36		65				*Dictyocha flexatella* 3%
			13,CC	117	300	56	55	1	33	<1	10		
			14,CC	127	300	69	69		29		2		
			15-2, 25-27	129	300	53	53		21		26		*Dictyocha flexatella* 13%
			15,CC	135	100	52	47	10	33		10		
			16,CC	145	100	45	44	2	36		18		
			17-2, 27-29	148	100	60	60		6		34		*D. brevispina* 39%; *D. flexatella* 6%
			17,CC	154	300	38	30	2	28	14	26		

the events at both locations are based on diatom chronology and show that the Ecuadorian sequence is 0.1 to 0.3 m.y. younger than in the northwest Pacific. An offset in ages for the sequence could have several causes including diatom and paleomagnetic calibration, lag in latitude transfer, or microclimatics. The local or global significance of ecostratigraphic events will become even clearer as more quantitative data is created for different regions.

Interpretation of the Miocene to early Pliocene paleotemperature trend for Site 581 (Fig. 6) is hindered by a paucity of diatom correlation points and by potential hiatuses. The major features of the record, following about 7 m.y. ago at 225 m (Fig. 6), can be tentatively correlated with Hole 503A in the eastern equatorial Pacific (Bukry, 1982, 1983). A cool trough between 3.9 and 4.4 m.y. ago in the early Pliocene is prominent at both holes, but the Ts = 34 to 41 for Site 581 is markedly cooler than the Ts = 68 to 72 for Hole 503A. The preceding warm peak near the Miocene/Pliocene boundary at about 5 m.y. ago is a widespread feature reported in various areas including the North Atlantic (Bukry, in press a). A cool interval with many fluctuations occurs from about 5.1 to 5.4 m.y. ago at Hole 503A, but a single cool trough is recorded in that interval at Site 581, probably because of the fewer samples examined. Preceding the cooling at 5.1 to 5.4 m.y. ago there are warm peaks at about 5.8 and 6.0 m.y. ago separated by a minor cool trough at 5.9 m.y. ago. A warming trend between 6 and 7 m.y. ago is also noted at both sites. Below these levels the time framework is less definite and trends are not coordinated, because of hiatuses, sparse samples, or local effects. Detailed study of Site 581 between 180 and 230 m may demonstrate whether the broad trends in Ts values shown here are indicative for transoceanic correlation.

In calculating relative paleotemperature values for Leg 86, *D. pentagona* and *D. subarctios* were considered to be cool indicators and therefore not included in the Ts summation.

SURFACE TEXTURE OF SILICOFLAGELLATE SKELETONS

Small structural features on the surface of the opaline rod structure forming a silicoflagellate were noted and illustrated by Lemmermann (1901). In later studies, Deflandre (1950) illustrated silicoflagellate surfaces of several genera (*Dictyocha, Lyramula, Naviculopsis,* and

Table 4. Late Cenozoic silicoflagellate biostratigraphy, relative paleotemperature values (Ts), and percent distribution of various genera and morphologic subgroups with remarks on noteworthy occurrences for Hole 581.

							Generic percentages							
Age	Zone or subzone		Hole 581 sample (interval in cm)	Depth (m)	Total specimens	Ts value	*Corbisema*	*Dictyocha* (pentagonal)	*Dictyocha* (nonpentagonal)	*Distephanus* (quadrate)	*Distephanus* (nonquadrate)	*Mesocena* (quadrate)	*Mesocena* (nonquadrate)	Noteworthy occurrences
early Pliocene	*D. fibula*	*D. jimlingii*	2-1, 46-47	182	200	38		13	34	5	45	3	3	
			2-3, 123-124	186	300	41		20	41	2	37	< 1		A < F
			2-5, 45-46	188	300	34		11	34		55			First *D. jimlingii;* last *D. pulchella*
late Miocene		—	2-7, 8-9	191	300	75		< 1	74		24	1	1	Last *D. aspera clinata;* A > F
		D. neonautica	3-2, 45-46	193	300	77			77		22			*D. aspera clinata* 41%; *D. neonautica* 2%; A > F
			3-6, 45-46	199	200	73			73		27			
			3,CC, 10-11	200	300	73			72	< 1	27			
			4-2, 48-49	203	300	62		1	62		34		2	*D. quinquangellus* 11%; last *M. diodon nodosa;* A < F
			4-4, 48-49	205	200	60			60		37		4	*Distephanus quinquangellus* 21%; A < F
			4,CC, 2-3	210	300	87			85		10	4	1	
			5-2, 69-70	212	200	87			86	1	13		1	A > F
			5-4, 50-51	215	300	92			91		7	1	2	A > F
			5,CC, 4-5	218	300	88			85	1	8	4	2	First *Dictyocha* sp. cf. *D. flexatella*
			6-1, 50-51	220	200	87			79	15	6		1	*D. neonautica* 17%; *D. aspera clinata* 15%
			6-2, 50-51	221	300	96			94	1	< 1	4	1	First *D. neonautica;* first *D. aspera clinata;* A < F
	D. brevispina	—	6-3, 60-61	223	100	86			82	7	7		4	
			6-4, 50-51	225	200	79		2	68	11	6		7	*Mesocena circulus* 7%
			6-6, 50-51	227	300	79			76	6	17		2	
			6,CC, 10-11	229	300	54			52	3	36		9	
			7-1, 55-56	229	200	90			89	2	4		6	Elongate mode in several taxa
			7-4, 55-56	234	300	77			71	11	8		11	*Mesocena diodon nodosa* 10%
			8-1, 55-56	239	200	83			75	16	8		2	*Distephanus longispinus* 10%
middle Miocene		*M. hexalitha*	8-2, 55-56	241	300	69			56	20	4	3	18	*Mesocena hexalitha* 12%
			8-2, 60-62	241	300	67			55	17	2	7	16	*Mesocena hexalitha* 8%
		—	8-3, 55-56	242	300	62			37	49	8	1	5	*Distephanus paradistephanus* 2%
			8-4, 60-62	244	100	74			54	36	6	3	1	
	C. triacantha		8-4, 75-76	244	100	82	11		62	15	10	2		
			8-5, 55-56	245	0	—								
			8,CC, 6-7	248	300	72	16		40	27	10	5	2	

Vallacerta) that have complex reticulate networks of intersecting ridges. Through the use of scanning and transmission electron microscopy (SEM and TEM), the junctions between the linear ridges were shown to be elevated into peaks (Bachmann and Keck, 1969; Jerković, 1969; Mandra and Mandra, 1971; McPherson and Ling, 1973; Wornardt, 1971). These studies also showed that the reticulation was not necessarily constant over the whole surface; instead, some areas had long subparallel ridges (Bachmann and Keck, 1969). Mandra and Mandra (1972) found specimens of *Distephanus* with smooth surfaces. Finally, Martini and Müller (1976) conducted a comprehensive description and analysis of the occurrence of surface textures in silicoflagellates using SEM. They described several major patterns that we have adopted with some modifications in this study. We have classified the patterns into general categories for whole skeleton and separate categories for various areas of the skeleton such as basal ring, apical structures, spines, and pikes. The terminology for the general whole skeleton patterns includes combinations of the following terms which can describe particular areas: crenulate (C), linear (L), nodular (N), reticulate (R), and smooth (S).

To systematically describe the surface texture variation on an individual skeleton the following subsection sequence is used: apical structure/basal ring/spine. Therefore, an individual skeleton can have its complete surface texture characterized for these three areas as reticulate (R)/linear (L)/linear (L), or simply R/L/L. If the distal and proximal surfaces had different textures then the proximal texture could be cited in parentheses: R/R(L)/L. The surface textures on proximal (abapical) surfaces are typically fainter than on distal (apical) surfaces because of lower relief. For example, see the reticulate texture illustrated for *Corbisema disymmetrica communis* (as *C. naviculoidea*) by Perch-Nielsen (1976) and the contrast in apical ring textures for *Distephanus crux* (as *Dictyocha crux*) by Bachmann and Keck (1969). The inequant (i) form of the reticulate pattern with interpeak ridges of disparate lengths could be added when needed: R/Ri(L)/L. A simple dash means that information is not available. Although such a system may be overdetailed, it provides the opportunity for more specific comparisons of structures from different ages and regions.

Definition of the descriptive terms are as follows:

1. *Crenulate* (C). Long subparallel ridges are interrupted by peaks that are aligned to form rows perpendicular to ridge axes. At low magnification these rows resemble periodic crenulations. This is a typical surface texture of *Mesocena diodon nodosa* (Plate 9, Figs. 1-3).

2. *Linear* (L). Long subparallel ridges which are not, or very rarely, interrupted by peaks. The ridges are sub-

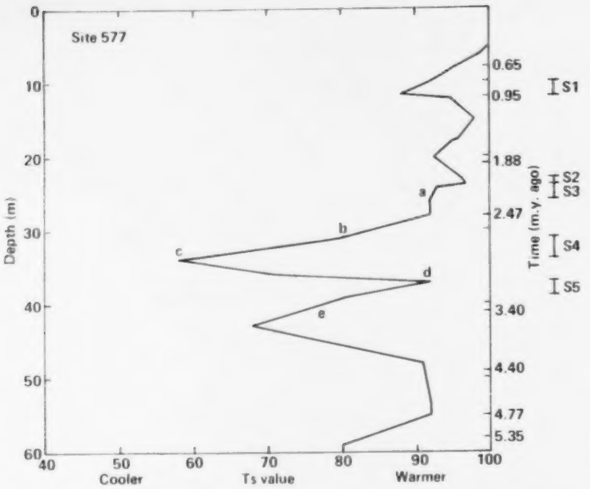

Figure 3. Silicoflagellate relative paleotemperature curve for Site 577 samples. The chronology is based on paleomagnetic correlation (Monechi, this volume). Silicoflagellate data for the curve are available in Table 1. Useful silicoflagellate events include: S1 = Acme of *Mesocena quadrangula*. S2 = Last *Dicytocha flexatella*. S3 = Last common *M. circulus*. S4 = Last common *D. brevispina*. S5 = First *D. stapedia*. The reference points (a to e) are selected correlation points between Leg 86 sites:

a = Disappearance of *M. circulus*, near 2.4 m.y. ago, is associated with a cooling event in Holes 580 and 579A, which is not observed at southern Site 577.
b = A warming event, near 2.6 m.y. ago, is observed in Holes 580 and 579A, but is not observed at Site 577.
c = A distinct cooling event, between 2.6 and 3.0 m.y. ago, is associated with the last common *D. brevispina* at Holes 580 and 579A.
d = A warm peak, between about 3.0 to 3.3 m.y. ago, occurs at Holes 580, 579A, and 577.
e = Part of a distinct warming trend near 3.4 m.y. ago which is least intense (Ts = 50) in northern Hole 580, moderate (Ts = 62) in intermediate Hole 579A, and most intense (Ts = 77) in southern Hole 577.

parallel to the rod axes. For example, see *Distephanus speculum* and *Caryocha ernestinae* in Martini and Müller (1976, plate 6, figs. 1–4).

3. *Nodular* (N). Nodular swellings, or rounded protuberances arising from a smooth rod occur in several taxa of *Distephanus*, especially on the apical structure (Plate 8, Fig. 1).

4. *Reticulate* (R). A network of intersecting ridges that may form peaks at their junctions. Hexagonal arrays occur where peaks are most numerous, such as on apical structures. Pentagonal and triangular arrays also occur. The vertical relief of the ridges and peaks is variable. Martini and Müller (1976) showed that inequant long and short ridge lengths occurred in *Dicytocha pentagona* and *D.* sp. cf. *D. fibula.* Regular reticulate texture with nearly equant ridges occurs in *M. apiculata apiculata, Corbisema apiculata*, and *D. challengeri.*

5. *Smooth* (S). Uniform finely granular surfaces with no nodes, peaks, or ridges are classified as smooth. Mandra and Mandra (1972) showed specimens of binocular *Distephanus* with nodular spines and apical structures, but featureless basal rings. Etching or inhibited ridge formation could account for some smooth rods.

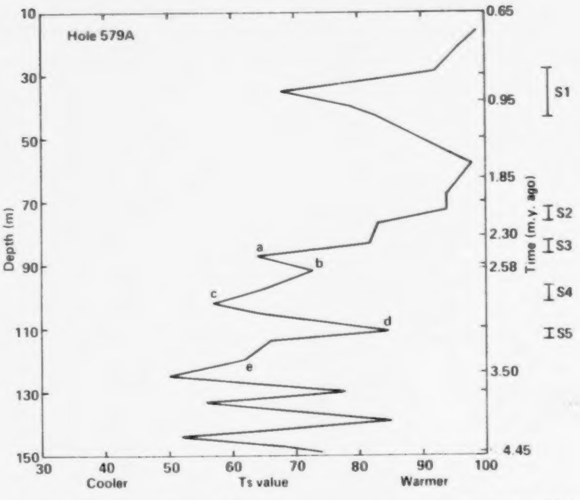

Figure 4. Silicoflagellate relative paleotemperature curve for Hole 579A samples. The chronology is based on diatom and paleomagnetic correlation (Koizumi and Tanimura, this volume). Silicoflagellate data for the curve are available in Table 2. Useful silicoflagellate events include those cited in Figure 3.

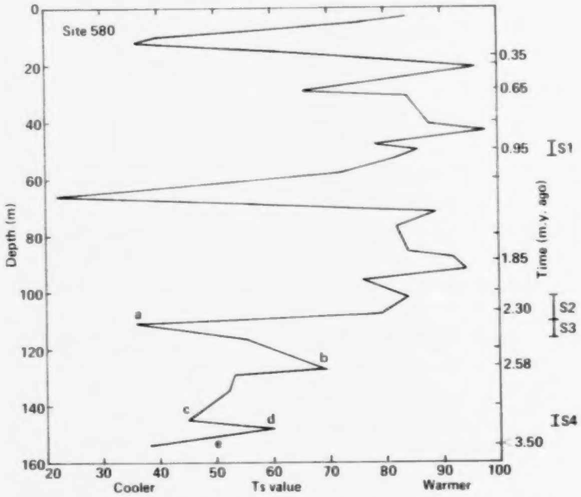

Figure 5. Silicoflagellate relative paleotemperature curve for Hole 580 samples. The chronology is based on diatom and paleomagnetic correlation (Koizumi and Tanimura, this volume). Silicoflagellate data for the curve are available in Table 3. Useful silicoflagellate events (S1 to S4) are described in Figure 3. Reference points (a to e) are described in Figure 3.

Like the larger apical structures and basal rings, the generally smaller spines and pikes can also have noteworthy surface texture. Dumitrică (1973, plate 1, fig. 6) showed clusters of small points at the ends of the spines on *M. quadrangula.* Our studies have shown similar clusters in *Dictyocha* on spines and pikes (Plate 7), but not on *Distephanus.* But specimens of *M. circulus* from Leg 86 have a large well-organized rosette termination to the spines (Plate 10). Rosette spine or pike terminations and other simpler patterns might yield additional insight into silicoflagellate paleoenvironmental responses or evo-

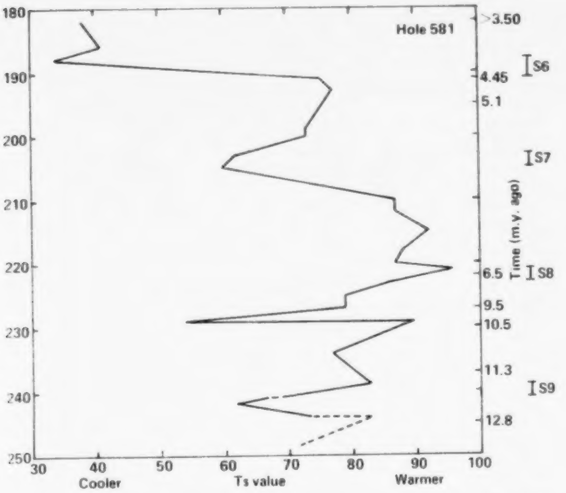

ure 6. Silicoflagellate relative paleotemperature curve for Hole 581 samples. The chronology is based on diatom and paleomagnetic correlation; see Barron (1980, 1981) and Koizumi and Tanimura (this volume). Silicoflagellate data for the curve are available in Table 4. Useful silicoflagellate events include: S6 = First *Distephanus jimlingii.* S7 = Acme of *D. quinquangellus.* S8 = First *Dictyocha neonautica.* S9 = Last *Mesocena hexalitha.* Dashed parts of curve indicate a degree of uncertainty.

Table 5. Ts relative paleotemperature values for correlative events at Leg 86 holes show latitudinal gradients in the Northwest Pacific Basin for the Pliocene.

	Hole (latitude)		
Events	580 (41°37′N)	579A (38°38′N)	577 (32°27′N)
a	36	64	92
b	69	73	80
c	45	57	58
d	60	85	92
e	50	62	77

Note: See Figure 3 for identification of the events.

ionary lineages. Stadum and Burckle (1973) suggest- that the rosettes formed in nutrient enriched waters d smooth spines in less enriched waters.

To help to interpret the surface textures determined Leg 86 specimens, a survey of published SEM and M illustrations of silicoflagellates was made. Most illtrations lack the resolution needed to identify surface uctures, but a few can be characterized for comparis. For example, an illustration of *Distephanus* (like *speculum*) from the late Eocene of New Zealand andra et al., 1973) shows a reticulate/linear/linear /L/L) pattern on distal surfaces. This contrasts with *D. speculum* from the late Miocene of Spain (Bergen et al., 1976), which show a nodular(smooth)/liar(linear)/linear(linear) [N(S)/L(L)/L(L)] pattern. It so differs from our Pliocene specimen (Plate 5, Figs. 2) and late Miocene specimens from California (Worardt, 1971) which are basically smooth (S) with minor nodules on apical and basal surfaces. Several explanations are possible for the differences: (1) temperature and nutrient levels affect surface texture; (2) dissolution and diagenesis can reduce or alter textures, such as reticulate to nodular or linear to smooth; (3) textures may trace polyphyletic origins of long-ranged taxa; (4) SEM metal-coating techniques may vary (we used gold coating with a maximum thickness less than 200 Å which would not alter surface patterns).

Differential dissolution between specimens in the same sample is suggested by comparing two specimens of *Dictyocha deflandrei completa* from Perch-Nielsen (1975b, plate 15, figs. 5 and 6). Reticulate texture is sharply defined on one specimen on the apical structure and down onto the adjoining basal ring area. The second specimen shows no definitive major textures and is more coarsely granular. Inspection of the basal ring adjoining the apical struts does reveal a remnant reticulate pattern, which implies dissolution because the apical structure generally has the highest relief texture. Similar dissolution evidence is suggested by our specimens of *M. quadrangula* (Plate 12) because the typical crenulate texture of long ridges with peaks aligned in rows is not seen in the enlargement of Plate 12, Figure 2. Instead, the rows of peaks remain, but the ridges are missing. Low- and moderate-ridged specimens are recorded on Plates 11 and 12.

Texture-pattern summaries for the most definitive published illustrations are summarized according to genus and age (Table 6). Preliminary determinations based on that information and on the Leg 86 results (Table 7 and Plates 1–17) help to confirm and expand certain observations.

Reticulate spines have only rarely been recorded (see Bukry, 1976c; Mandra and Mandra, 1971; and Martini and Müller, 1976). Although the taxa having this structure belong to several genera, they are all from Eocene strata, and no reticulate spined specimens are recorded from the Neogene. Spines on younger taxa are smooth, nodular, or linear.

Nodular spines are mainly recorded in hexagonal *Distephanus*, a cold-water indicator in the late Cenozoic. Dissolution of the crenulate or reticulate texture, as in *Mesocena diodon nodosa* or some *Dictyocha brevispina* might produce a remnant nodular pattern, but the general restriction to *Distephanus* suggests nodular spines are probably a cold indicator. If this assumption is extended to the Cretaceous genus *Vallacerta*, then *V. siderea* from the Arctic Ocean (McPherson and Ling, 1973), with apparently nodular spines, should represent a colder species than coeval *V. hortonii* with linear spines from lower latitudes. It is difficult to assess smooth spines because of uncertainty over diagenetic alterations. Linear spines are most typical in the Leg 86 assemblages.

Abapical surfaces are predominated by linear or by smooth textures. If the smooth texture is dismissed as partly (on basal ring and spine) a dissolution product, then the linear texture dominates abapical surfaces through time and space. The apical surfaces of the basal ring, especially toward the outer diameter and the strut junctions, are areas where the structurally more com-

Table 6. Summary of published silicoflagellate surface textures arranged by genus and age.

Taxon, textures	Reference	Age	Locality
Caryocha			
C. depressa, Ri/-/L	1	Miocene	California
C. ernestinae, L-Ri/L/L	1	Miocene	California
C. ernestinae, L/L/L	13	Miocene	Norwegian Sea
Corbisema			
C. hastata, R/?R/-	13	Eocene	Norwegian Sea
C. triacantha, R(S)/L-R(L)/L(L-R)	13	Eocene	Norwegian Sea
C. apiculata, (S)/(R)/-	13	Reworked	Norwegian Sea
C. apiculata, R/-/-	13	Eocene	Norwegian Sea
C. sp., R/L/-	6	Eocene	New Zealand
C. disymmetrica communis, R/R/-	14	Paleocene or Eocene	Denmark
C. geometrica, S/S/-	7	Cretaceous	California
Deflandryocha			
D. cymbiformis, L/L/-	2	Miocene	Yugoslavia
Dictyocha			
D. brevispina, N/N/N	5	Miocene	Mexico
D. brevispina, -/L/L	5	Miocene	Mexico
D. fibula (s. ampl.), R/R/L	4	Miocene	California
D. pulchella, -/L/L	12	Miocene	Spain
D. deflandrei completa, (S)/(L)/(L)	10	Oligocene	Tasman Sea
D. deflandrei completa, R(S)/L(L)/L(L)	10	Oligocene	Tasman Sea
Distephanus			
D. jimlingii, N/-/-	13	Pliocene	Norwegian Sea
D. pseudofibula, N/S/S	8	Pliocene	Japan
D. speculum speculum, N/S/S	13	Pliocene	Norwegian Sea
D. crux, R(S)/L(L)/L(L)	1	Miocene	California
D. crux, (S)/(L)/(L)	12	Miocene	Spain
D. schaunislandii, R/R/-	2	Miocene	Yugoslavia
D. quinquangellus, N/S/S	13	Miocene	Norwegian Sea
D. speculum binoculus, N/S/N	5	Miocene	California
D. speculum binoculus, S/S/S	5	Miocene	California
D. speculum speculum, R-N/L/L	13	Miocene	Norwegian Sea
D. speculum speculum, N/S/S	12	Miocene	Spain
D. speculum speculum, N/L/L	12	Miocene	Spain
D. speculum speculum, (S)/(L)/(L)	12	Miocene	Spain
D. speculum speculum, S/S/S	4	Miocene	California
D. speculum triommata, S/S/S	5	Miocene	California
D. stradneri, -/L/L	2	Miocene	Yugoslavia
D. crux, (S)/(L)/(L)	10	Oligocene	Tasman Sea
D. norvegiensis, N/S/S	14	Eocene	Norwegian Sea
D. rosae, (S)/(L)/(L)	14	Eocene	Norwegian Sea
D. sp. (like *D. speculum*), R/L/L	6	Eocene	New Zealand
Lyramula			
L. sp., -/R/R	9	Cretaceous	Southwest Pacific
L. sp., -/S/S	9	Cretaceous	Southwest Pacific
Mesocena			
M. diodon nodosa, -/C/L	13	Miocene	Norwegian Sea
M. quadrangula, -/C/L	13	Miocene	Norwegian Sea
M. quadrangula, -/C/L	13	Miocene	Norwegian Sea
M. apiculata apiculata, -/R/R	13	Eocene	Norwegian Sea
M. oamaruensis, -/R/R	3	Eocene	New Zealand
Naviculopsis			
N. lata, ?N/N/-	13	Miocene	Norwegian Sea
N. punctilia, R/-/-	13	Eocene	Norwegian Sea
N. foliacea, ?S(S)/S(S)/S(S)	14	Eocene	Norwegian Sea
N. aspera, N(S)/N(N)/N(N)	14	Paleocene/Eocene	Denmark
N. constricta, N(S)/S(S)/S(S)	14	Paleocene/Eocene	Denmark
N. minor, N(S)/S(S)/S(S)	14	Paleocene/Eocene	Denmark
Vallacerta			
V. hortonii, R/L/L	7	Cretaceous	California
V. siderea, Ri/L/N?	7	Cretaceous	Arctic Ocean
V. tumidula, S&R/-/-	11	Cretaceous	Southwest Pacific

Note: The texture code is defined in text; the sequence describes: apical structure/basal ring/spine. Reference code is as follows: (1) Bachmann and Keck, 1969; (2) Jerković, 1969; (3) Mandra and Mandra, 1971; (4) Wornardt, 1971; (5) Mandra and Mandra, 1972; (6) Mandra et al., 1973; (7) McPherson and Ling, 1973; (8) Uchio, 1974; (9) Hajós, 1975; (10) Perch-Nielsen, 1975b; (11) Perch-Nielsen, 1975a; (12) Berggren et al., 1976; (13) Martini and Müller, 1976; (14) Perch-Nielsen, 1976.

plex reticulate texture tends to develop. But reticulate structures are most prominent on apical structures in the genera *Corbisema, Dictyocha*, and *Vallacerta*. The occurrence of reticulate texture on the apical structure of *Caryocha depressa* (for example, Bachmann and Keck, 1969) prove it to be a silicoflagellate and also help to demonstrate that more hexagonal species with subdivided apical rings should not be classified there (see Bukry and Foster, 1973, and Mandra and Mandra, 1972).

Nodular apical structures are recorded from Eocene high-latitude *Naviculopsis* (Perch-Nielsen, 1976) and for cool-water Neogene *Distephanus*, suggesting that fur-

Table 7. Summary of Leg 86 surface textures arranged alphabetically by genus.

Taxon, textures	Plate	Age	Hole
Dictyocha			
D. aspera, L/L/L	2	Plio-Pleistocene	579A
D. brevispina, (S)/(N)/(S)*	3	Miocene	581
D. brevispina, C/C/L	4	Pliocene	579A
D. brevispina, (S)/(L)/(L)	4	Pliocene	577
D. brevispina, (-)/(C)/(L)*	4	Pliocene	577
D. brevispina, C/C/C	5	Pliocene	579A
D. brevispina, -/R/L	5	?Miocene	579A
D. brevispina, C/C/-	5	Pliocene	579A
D. calida ampliata, N/N/S	6	Pleistocene	579A
D. sp. cf. *D. concinna*, L/L/L	1	Pliocene	579A
D. flexatella, R/R/L	13	Pliocene	572A
D. flexatella, N/N/L	14	Pliocene	579A
D. hessii, (S)/(S)/(S)	3	Pleistocene	581
D. lingii, S/N/S	3	Pleistocene	581
D. sp. cf. *D. longa*, (S)/(L)/(L)	2	Miocene	581
D. perlaevis, N/N/S*	7	Pleistocene	579A
D. perlaevis, (S)/(S)/(S)*	7	Cenozoic	581
D. subarctios, (S)/(L)/(L)*	1	Pleistocene	581
D. spp., N/N/S	2	Plio-Pleistocene	579A
Distephanus			
D. crux, R/L/L	8	Miocene	581
D. sp. cf. *D. floridus*, S/S/S	5	Pleistocene	581
D. jimlingii s. ampl., N/N/N	8	Pliocene	579A
D. pseudofibula, S/S/S	15	Pliocene	579A
D. quinquangellus, N/S/S	15	Miocene	581
D. speculum minutus, (N)/(N)/(S)	8	Pliocene	579A
D. speculum speculum, S/S/S	5	Pliocene	579A
Mesocena			
M. circulus, -/N/S*	10	Pliocene	579A
M. circulus, -/S/S*	10	Miocene	581
M. diodon nodosa, -/C/L	9	Miocene	581
M. hexalitha, -/R?/L	9	Miocene	581
M. quadrangula, -/C/L	11	Miocene	579A
M. quadrangula, -/C/L	11	Pliocene	580
M. quadrangula, -/C/S*	12	Pleistocene	577

Note: The texture code is defined in text; the sequence describes: apical structure/basal ring/spine. * = star-shaped spine terminations.

ther analysis of surface textures will improve the paleoecologic utility of silicoflagellates.

Martini and Müller (1976) observed that surface textures may have higher relief in colder areas. However, he lack of sufficient comparative materials from different latitudes and the unsolved problems of dissolution nit the interpretations that are possible. For example, e find that specimens showing smooth textures often ave an especially coarse surface granularity, which beuse of sometimes surprising wall thickness (Plate 9, g. 7; Mandra and Mandra, 1972, fig. 26) can imply at the original surface textures could be dissolved without damaging the underlying rod structure. Diagenesis dehydration of the opaline skeletal rods by sediment ore waters could cause surface granularity. Some granarity might also be produced during metal-coating eparation for SEM.

Analysis of the data from Tables 6 and 7 shows perct matches of surface textures between Leg 86 and the orld literature for Miocene *D. crux* (R/L/L), *D. quinuangellus* (N/S/S), *M. diodon nodosa* (-/C/L), and *M. uadrangula* (-/C/L). Two other near matches are indiated for Pliocene *D. pseudofibula* and *D. speculum speculum*. Aside from the typical association of the crenulate texture with cool intervals at Leg 86, there is no marked allocation of textures between cool and warm fluctuations.

The most marked contrast between the texture compilations for Leg 86 and the world literature is in the occurrence of the reticulate texture. In Leg 86 material, reticulate surfaces are very sparse, occurring only in *Dictyocha flexatella, Distephanus crux*, and *M. hexalitha*. There are a higher number of nodular-textured specimens in Leg 86 material than in the previously illustrated assemblages. These two relationships could be accounted for by differential preservation of surface peaks instead of ridges, which would make the reticulate texture appear to be nodular. Either way, there appears to have been a decline in the reticulate texture through time. The world literature compilation (Table 6) shows reticulate textures were typical in the dominant Cretaceous genera *Lyramula* and *Vallacerta*, and even more pervasive in early Cenozoic *Corbisema*. In this same vein, Eocene *M. apiculata apiculata* and *M. oamaruensis* are wholly reticulate, but Miocene to Pleistocene *Mesocena* do not have reticulate texture. Whereas preservation may have skewed our limited data, the Leg 86 results indicate that reticulate texture has declined during the late Cenozoic (Table 8). The younger *Mesocena* often exhibit the crenulate texture, which could have developed from the reticulate texture. Sufficiently detailed and organized study of modern silicoflagellate textures to establish the range of structures and their geographic distribution has not been done.

As part of the examination of possible temperature-dependent variation in surface texture, late Pliocene specimens of *Dictyocha flexatella* from Leg 86 (Plate 14) were compared to tropical specimens from Leg 85 (Plate 13). The tropical specimens are narrower and have greater disparity in minor to major spine length, but surface textures on both are sparse. Very faint reticulate texture characterizes the apical and basal rings of tropical forms (R/R/L). High latitude specimens have nodular apical structures and some specimens have nodular basal rings, whereas others have a very faint linear pattern, which

Table 8. Summary of the average surface textures for silicoflagellate genera derived from compilations in Tables 6 and 7 for the available literature and for Leg 86.

Genus	Literature average texture	Leg 86 average texture
Caryocha	L-Ri/L/L	—
Corbisema	R/R-L/L	—
Deflandryocha	L/L/-	—
Dictyocha	R/L-R/L	N-C/N/L-S
Distephanus	N/L-S/L-S	S-N/S/S
Lyramula	-/R/R	—
Mesocena, Neogene	-/C/L	-/C/L
Mesocena, Paleogene	-/R/R	—
Naviculopsis, Paleogene	N/S/S	—
Vallacerta	R/L/L	—

could be a residual reticulate pattern, because the rod-parallel linear ridges may be more robust than the intersecting ridges (see Jerković, 1969, plate 9, fig. 1).

Other comparisons of possible temperature-dependent texture for Leg 86 include:

1. *Dictyocha.* The surface texture of *Dictyocha* is slightly more marked in cooler intervals. For example, warm conditions produced specimens with smooth to slightly noded texture, whereas cooler conditions produced a more heavily noded specimen (Plate 6). A similar contrast in the higher frequency of nodes and peaks on cool specimens is illustrated by *Dictyocha* spp. (contrast Plate 2, Fig. 7 with Fig. 9). Higher relief texture for cool intervals is also shown by *Dictyocha* sp. cf. *D. concinna* (Plate 1, Figs. 7–9).
2. *Dictyocha brevispina.* There is no particular difference in texture between Miocene and Pliocene specimens. All *D. brevispina* have similar crenulate texture on the apical structure and basal ring. This texture can be very faint or very marked, and does not seem to be related to warm or cold conditions in Leg 86 assemblages (Plate 4, Figs. 1–3, 6–9; Plate 5, Figs. 4–9).
3. *Dictyocha perlaevis.* There are no differences in the texture between Miocene and Pliocene specimens and between warm and cool conditions for Leg 86 (Plate 7, Figs. 1–5, 7, 8). Star-shaped, rosette spine terminations can occur in this species, as well as *Dictyocha brevispina.*
4. *Distephanus.* A wide variety of textures were observed in *Distephanus* including smooth (Plate 5, Figs. 1–3), nodular (Plate 8, Figs. 1–3), reticulate, and linear (Plate 8, Figs. 7–9). No temperature-dependent trend in textures was established for Leg 86. Comparison of higher and lower latitude coeval assemblages is needed. Hexagonal specimens from Leg 86 lack the reticulate texture seen in quadrate specimens (Plate 8). This may be a significant change from the Paleogene, where some hexagonal specimens have reticulate texture (e.g., Mandra et al., 1973).
5. *Mesocena.* Crenulate and smooth structures characterize the Leg 86 specimens.
6. *Mesocena quadrangula.* Pleistocene (warm) specimens show modified crenulate texture with reduced ridges (Plate 12, Fig. 2). The spines may taper to simple points or rosette terminations (Plate 12, Fig. 5; also Dumitrică (1973, plate 1, fig. 6). Although Dumitrică (1973, plate 3, fig. 4) illustrated an *M. quadrangula* having reticulate texture, we found only crenulate texture, reduced crenulate texture, or smooth textures for Leg 86 (Plate 11).
7. *Mesocena circulus.* Leg 86 specimens are smooth or slightly nodular with two kinds of spines—blunt and rosette. Both spine types were found in the Miocene and Pliocene and warm and cool intervals.
8. *Mesocena diodon nodosa.* The degree of relief varies, but all specimens observed have crenulate texture which may approach the regularity of the verticillate pattern of some sponge spicules (see Bukry, 1978, plate 5, fig. 15; plate 13, fig. 9).
9. *Mesocena hexalitha.* This species occurred only at a cold, middle Miocene interval of Leg 86. *M. hexalitha* has a faint reticulate texture (Plate 9, Figs. 5, 7) and possibly(?) a very faint crenulate variation (Plate 7, Figs. 6, 9).

NEW SILICOFLAGELLATE NOMENCLATURE

Genus *CARYOCHA* Bukry et Monechi, n. gen.

Type species. *Halicalyptra depressa* Ehrenberg, 1854. Junior synonym: *Cannopilus sphaericus* Gemeinhardt, 1931.

Description. Silicoflagellates that have globular form, many apical portals, and nearly equant basal spines are classified in genus *Caryocha* Bukry et Monechi. The rounded apical structure is at least as high as the basal ring is wide and may have spires in some species. The apical structure pattern is well integrated with the basal ring. Although the apical portals are generally larger above the basal ring, they are generally rounded instead of polygonal. The basal ring is polygonal to round, but radially symmetric with little or no elongation. The diameter of the basal ring is equal to, or less than, the diameter of the apical structure. Basal spines are short to moderate in length and tilt down out of the plane of the basal ring.

Remarks. The species of globular silicoflagellates now classified in genus *Caryocha* Bukry et Monechi were previously assigned to either genus *Cannopilus* Haeckel or genus *Halicalyptra* Ehrenberg. Locker (1974), during a restudy of Ehrenberg material, found *Halicalyptra* and the proper type specimens to be radiolarians. But *Halicalyptra depressa* was found to be a silicoflagellate. The type species of *Cannopilus* has a fairly flat rosette of seven portals elevated by struts above a hexagonal basal ring with axially elongate spines that do not tilt down out of the plane of the basal ring. These are characteristics typically contained in genus *Distephanus* Stöhr. Because the type species of *Cannopilus* is more readily classified in genus *Distephanus* as *Distephanus speculum hemisphaericus* (Ehrenberg), than with silicoflagellates having globular apical structures, the new genus *Caryocha* is proposed for a more circumscribed classification. Silicoflagellate surface textures were demonstrated to occur on these globular forms by Bachmann and Keck (1969) and Martini and Müller (1976).

A case could be made for recognizing all three genera: *Distephanus*, *Caryocha*, and *Cannopilus*. But the phenotypic array of forms with subdivided rings (from 2 to 3 to 4, and more portals) within the same sample and species of *Distephanus* leads us to continue to include nonglobular specimens of *Cannopilus* in *Distephanus*.

Caryocha depressa (Ehrenberg) Bukry et Monechi, n. comb.

Halicalyptra depressa Ehrenberg, 1854, pl. 18, fig. 111.
Cannopilus sphaericus Gemeinhardt, 1931, p. 105, pl. 10, figs. 3, 4.
Cannopilus sphaericus, in Bachmann and Keck, 1969, p. 205, pl. 2, upper left.
Cannopilus depressus (Ehrenberg) Locker, 1974, p. 639, pl. 4, fig. 3.
Cannopilus depressus (Ehrenberg), Martini and Müller, 1976, p. 868, pl. 3, figs. 11, 12.

Caryocha ernestinae (Bachmann) Bukry et Monechi, n. comb.

Cannopilus ernestinae Bachmann, 1962, p. 255, fig. 1.
Cannopilus ernestinae, in Bachmann and Keck, 1969, p. 205.
Cannopilus ernestinae Bachmann, Bukry, 1976b, p. 696, pl. 1, figs. 1–6.
Cannopilus ernestinae Bachmann, Martini and Müller, 1976, p. 869, pl. 3, figs. 8–10; pl. 6, figs. 2–4; pl. 9, figs. 6, 7.

Caryocha ichikawai (Bachmann) Bukry et Monechi, n. comb.

Cannopilus ichikawai Bachmann *in* Ichikawa et al., 1964, p. 110, pl 6, figs. 59–61.

Caryocha jouseae (Bachmann) Bukry et Monechi, n. comb.

Cannopilus jouseae Bachmann *in* Ichikawa et al., 1964, p. 109, pl. 6 figs. 54–58; figs. 1, 3–4.

Caryocha latifenestrata (Bachmann) Bukry et Monechi, n. comb.

Cannopilus latifenestratus Bachmann *in* Ichikawa et al., 1964, p. 111 pl. 6, figs. 62–64.

Caryocha picassoi (Stradner) Bukry et Monechi, n. comb.

Cannopilus picassoi Stradner, 1961, p. 92, pl. 3, figs. 101–104.

Genus *DISTEPHANUS* Stöhr, 1880

***Distephanus paradistephanus* (Tsumura) Bukry et Monechi, n. comb.**

Dictyocha paradistephanus Tsumura, 1963, p. 57, pl. 11, figs. 6, 7; pl. 24, figs. 6, 7.

OTHER TAXA CITED

Corbisema apiculata (Lemmermann) Hanna
C. disymmetrica communis Bukry
C. geometrica Hanna
C. hastata (Lemmermann) Frenguelli
C. naviculoidea (Frenguelli) Perch-Nielsen (invalid basionym)
C. triacantha (Ehrenberg) Hanna
Deflandryocha cymbiformis Jerković
Dictyocha aculeata (Lemmermann) Dumitrică
D. aspera aspera (Lemmermann) Frenguelli
D. aspera clinata Bukry
D. brevispina (Lemmermann) Bukry
D. calida ampliata Bukry
D. challengeri Martini et Müller
D. concinna Bukry
D. deflandrei completa (Glezer) Bukry
D. fibula Ehrenberg
D. flexatella (Bukry) Bukry
D. hessii Bukry
D. lingii Dumitrică
D. longa Bukry
D. neonautica Bukry
D. ornata ornata (Bukry) Bukry
D. ornata africana Bukry
D. perlaevis Frenguelli
D. pulchella Bukry
D. stapedia stapedia Haeckel
D. subarctios Ling
Distephanus crux (Ehrenberg)
D. floridus Bukry
D. jimlingii (Bukry) Bukry
D. norvegiensis Perch-Nielsen
D. pseudofibula (Schulz) Bukry
D. quinquangellus Bukry et Foster
D. rosae Perch-Nielsen
D. schauinslandii Lemmermann
D. speculum binoculus (Ehrenberg) Bukry
D. speculum hemisphaericus (Ehrenberg) Bukry
D. speculum minutus Bachmann, emend. Bukry
D. speculum speculum (Ehrenberg) Haeckel
D. speculum triommata (Ehrenberg) Bukry
D. stradneri (Jerković) Bukry
Mesocena apiculata apiculata (Schulz) Hanna
M. circulus (Ehrenberg) Ehrenberg
M. diodon nodosa Bukry
M. hexalitha Bukry
M. oamaruensis Schulz
M. quadrangula Ehrenberg ex Haeckel
Naviculopsis aspera (Schulz) Perch-Nielsen
N. constricta (Schulz) emend. Bukry
N. foliacea Deflandre
N. lata (Deflandre) Frenguelli
N. minor (Schulz) Bukry
N. punctilia Perch-Nielsen
Octactis pulchra Schiller
Vallacerta hortonii Hanna
V. siderea (Schulz) Bukry
V. tumidula Glezer

CONCLUSIONS

Quantitative relative paleotemperature values calculated for Leg 86 silicoflagellate assemblages show that a north–south gradient existed between Holes 577 and 580 during the Pliocene. A comparison between selected correlation events at the Leg 86 holes indicates a maximum difference between Ts = 92 at Site 577 and Ts = 36 at Site 580 occurred during the late Pliocene about 2.4 m.y. ago. The widely recorded warming across the Miocene/Pliocene boundary and the subsequent major cooling in the early Pliocene (about 3.9 to 4.4 m.y. ago) are indicated by the silicoflagellates at Site 581. Therefore, transoceanic paleotemperature events may be detected by relative paleotemperature values for Leg 86, but local gradients and fluctuations also appear to be significant.

The relationship of surface texture of silicoflagellates to relative paleotemperature values for Leg 86 is not clear-cut, but cool intervals appear to have specimens with high frequency and high relief texture. Cool-water indicator *Distephanus* (hexagonal) has either smooth or nodular texture in Leg 86 assemblages. No reticulate *Distephanus* (hexagonal) occur, and the reticulate texture is sparse in other taxa, too. Considerably more information on textures from living specimens and from a wider geographic range of fossils are needed to determine the usefulness of surface textures. Together with the DSDP Leg 38 analysis of surface textures from the Atlantic Ocean (Martini and Müller, 1976), the Leg 86 information for the Pacific Ocean should provide a useful step in understanding silicoflagellate textures.

ACKNOWLEDGMENTS

We thank John A. Barron, U.S. Geological Survey, Gerta Keller, U.S. Geological Survey, and Audrey A. Wright, Deep Sea Drilling Project, for constructive reviews of the manuscript. We also thank Fabio Cozzini and Maurizio Ulivi for photographic and technical assistance with the SEM study at Universitá di Firenze. Amy B. Altman, Deep Sea Drilling Project, expedited additional samples to complete the study. The manuscript and figures were excellently typed and proofed by Dorothy L. Blackstock, U.S. Geological Survey. Research was supported by CNR Centro Studi della Geologia dell'Appennino e delle catene Perimediterranee (Publ. 149) and through MPI (60%) No. 0071.

REFERENCES

Bachmann, A., 1962. Eine neu entdeckte Silicoflagellidenart: *Cannopilus ernestinae* Bachmann, nov. spec. *Mikrokosmos*, 51:255.

Bachmann, A., and Keck, A., 1969. Die Oberflächenstruktur der Silicoflagellaten. *Mikrokosmos*, 7:204–207.

Barron, J. A., 1976. Revised Miocene and Pliocene diatom biostratigraphy of Upper Newport Bay, Newport Beach, California. *Mar. Micropaleontol.*, 1:27–63.

________, 1980. Lower Miocene to Quaternary diatom biostratigraphy of Leg 57, off northeastern Japan, Deep Sea Drilling Project. *In* Scientific Party, *Init. Repts. DSDP*, 56, 57, Pt. 2: Washington (U.S. Govt. Printing Office), 641–685.

________, 1981. Late Cenozoic diatom biostratigraphy and paleoceanography of middle-latitude eastern North Pacific, Deep Sea Drilling Project Leg 63. *In* Yeats, R. S., Haq, B. U., et al., *Init. Repts. DSDP*, 63: Washington (U.S. Govt. Printing Office), 507–538.

________, in press. Diatom paleoceanography and paleoclimatology of the central and eastern equatorial Pacific between 18 and 6.2 Ma. *In* Mayer, L., Thayer, F., Thomas, E., et al., *Init. Repts. DSDP*, 85: Washington (U.S. Govt. Printing Office).

Barron, J. A., and Keller, G., 1983. Paleotemperature oscillations in the Middle and Late Miocene of the northeastern Pacific. *Micropaleontology*, 29:150–181.

Berggren, W. A., Benson, R. H., Haq, B. U., Riedel, W. R., Sanfilippo, A., Schrader, H. J., and Tjalsma, R. C., 1976. The El Cuervo Section (Andalusia, Spain): Micropaleontologic anatomy of an early late Miocene lower bathyal deposit. *Mar. Micropaleontol.*, 1: 195–247.

Bukry, D., 1973. Coccolith and silicoflagellate stratigraphy, Deep Sea Drilling Project Leg 18, eastern North Pacific. *In* Kulm, L. D., von Huene, R., et al., *Init. Repts. DSDP*, 18: Washington (U.S. Govt. Printing Office), 817–831.

________, 1975. Silicoflagellate and coccolith stratigraphy, Deep Sea Drilling Project Leg 29. *In* Kennett, J. P., Houtz, R. E., et al., *Init. Repts. DSDP*, 29: Washington (U.S. Govt. Printing Office), 845-872.

________, 1976a. Cenozoic silicoflagellate and coccolith stratigraphy, South Atlantic Ocean, Deep Sea Drilling Project Leg 36. *In* Hollister, C. D., Craddock, C., et al., *Init. Repts. DSDP*, 35: Washington (U.S. Govt. Printing Office), 885-917.

________, 1976b. Comments on some coccoliths and silicoflagellates from Deep Sea Drilling Project Leg 35. *In* Hollister, C. D., Craddock, C., et al., *Init. Repts. DSDP*, 35: Washington (U.S. Govt. Printing Office), 693-699.

________, 1976c. Silicoflagellate and coccolith stratigraphy, southeastern Pacific Ocean, Deep Sea Drilling Project Leg 34. *In* Yeats, R. S., Hart, S. R., et al., *Init. Repts. DSDP*, 34: Washington (U.S. Govt. Printing Office), 715-735.

________, 1978. Cenozoic coccolith, silicoflagellate, and diatom stratigraphy, Deep Sea Drilling Project Leg 44. *In* Benson, W. E., Sheridan, R. E., et al., *Init. Repts. DSDP*, 44: Washington (U.S. Govt. Printing Office), 807-863.

________, 1981a. Silicoflagellate stratigraphy of offshore California and Baja California, Deep Sea Drilling Project Leg 63. *In* Yeats, R. S., Haq, B. U., et al., *Init. Repts. DSDP*, 63: Washington (U.S. Govt. Printing Office), 539-557.

________, 1981b. Synthesis of silicoflagellate stratigraphy for Maestrichtian to Quaternary marine sediment. *Soc. Econ. Paleontol. Mineral. Spec. Publ.*, 32:433-444.

________, 1982. Neogene silicoflagellates of the eastern equatorial Pacific, Deep Sea Drilling Project Hole 503A. *In* Prell, W. L., Gardner, J. V., et al., *Init. Repts. DSDP*, 68: Washington (U.S. Govt. Printing Office), 311-323.

________, 1983. Upper Cenozoic silicoflagellates from offshore Ecuador, Deep Sea Drilling Project Site 504. *In* Cann, J. R., Langseth, M. G., Honnorez, J., Von Herzen, R. P., White, S. M., et al., *Init. Repts. DSDP*, 69: Washington (U.S. Govt. Printing Office), 321-342.

________, in press a. Cenozoic silicoflagellates from Rockall Plateau, Deep Sea Drilling Project Leg 81. *In* Roberts, D. G., Schnitker, D., et al., *Init. Repts. DSDP*, 81: Washington (U.S. Govt. Printing Office).

________, in press b. Tropical Pacific silicoflagellate zonation and paleotemperature trends of the Late Cenozoic. *In* Mayer, L., Theyer, F., Thomas, E., et al., *Init. Repts. DSDP*, 85: Washington (U.S. Govt. Printing Office).

Bukry, D., and Foster, J. H., 1973. Silicoflagellate and diatom stratigraphy, Leg 16, Deep Sea Drilling Project. *In* van Andel, T. H., Heath, G. R., et al., *Init. Repts. DSDP*, 16: Washington (U.S. Govt. Printing Office), 815-871.

Deflandre, G., 1950. Contribution a l'étude des silicoflagellidés actuels et fossiles. *Mikroskopie*, 2:72-108, 117-142, 191-210.

Dumitrică, P., 1973. Miocene and Quaternary silicoflagellates in sediments from the Mediterranean Sea. *In* Ryan, W. B. F., Hsü, K. J., et al., *Init. Repts. DSDP*, 13, Pt. 2: Washington (U.S. Govt. Printing Office), 902-933.

Ehrenberg, C. G., 1854. *Mikrogelogie:* Leipzig (Leopold Voss).

Gemeinhardt, K., 1931. Organismen formen auf der Grenze zwischen Radiolarien und Flagellaten. *Dtsch. Bot. Ges. Ber.*, 49:103-110.

Hajós, M., 1975. Late Cretaceous Archaeomonadaceae, Diatomaceae, and Silicoflagellatae from the South Pacific Ocean, Deep Sea Drilling Project Leg 29, Site 275. *In* Kennett, J. P., Houtz, R. E., et al., *Init. Repts. DSDP*, 29: Washington (U.S. Govt. Printing Office), 913-1009.

Ichikawa, W., Fuji, N., and Bachmann, A., 1964. Fossil diatoms, pollen grains and spores, silicoflagellates and arachaeomonads [sic] in the Miocene Hojuji Diatomaceous Mudstone, Noto Peninsula, central Japan. *Sci Rep. Kanazawa Univ.*, 9:25-118.

Ingle, J. C., Jr., 1973. Neogene foraminifera from the northeastern Pacific Ocean, Leg 18, Deep Sea Drilling Project. *In* Kulm, L. D., von Huene, R., et al., *Init. Repts. DSDP*, 18: Washington (U.S. Govt. Printing Office), 517-567.

Jerković, L., 1969. Les nouvelles recherches de la superficie du squelette des silicoflagellidés. *Univ. Sarajevu Biol. Inst.* Godisnjaka, 22: 129-176.

Keller, G., 1979. Late Neogene paleoceanography of the North Pacific DSDP Sites 173, 310, and 296. *Mar. Micropaleontol.*, 4:159-172.

________, 1980a. Middle to late Miocene planktonic foraminiferal datum levels and paleoceanography of the North and Southeastern Pacific Ocean. *Mar. Micropaleontol.*, 5:249-281.

________, 1980b. Planktonic foraminiferal biostratigraphy and paleoceanography of the Japan Trench, Leg 57, Deep Sea Drilling Project. *In* Scientific Party, *Init. Repts. DSDP*, 56, 57, Pt. 2: Washington (U.S. Govt. Printing Office), 809-833.

________, 1981a. Miocene biochronology and paleoceanography of the North Pacific. *Mar Micropaleontol.*, 6:535-551.

________, 1981b. Planktonic foraminiferal faunas of the equatorial Pacific suggest Early Miocene origin of present oceanic circulation. *Mar. Micropaleontol.*, 6:269-295.

Lemmermann, E., 1901. Silicoflagellatae. *Dtsch. Bot. Ges. Ber.*, 19: 247-271.

Ling, H. Y., 1973. Silicoflagellates and ebridians from Leg 19. *In* Creager, J. S., Scholl, D. W., et al., *Init. Repts. DSDP*, 19: Washington (U.S. Govt. Printing Office), 751-775.

________, 1975. Silicoflagellates and ebridians from Leg 31. *In* Karig, D. E., Ingle, J. C., Jr., et al., *Init. Repts. DSDP*, 31: Washington (U.S. Govt. Printing Office), 763-777.

________, 1980. Silicoflagellates and ebridians from Leg 55. *In* Jackson, E. D., Koizumi, I., et al., *Init. Repts. DSDP*, 55: Washington (U.S. Govt. Printing Office), 375-385.

Locker, S., 1974. Revision der Silicoflagellaten aus der Mikrogeologischen Sammlung von C. G. Ehrenberg. *Eclogae Geol. Helv.*, 67: 631-646.

McPherson, L. M., and Ling, H. Y., 1973. Surface microstructure of selected silicoflagellates. *Micropaleontology*, 19:475-480.

Mandra, Y. T., Brigger, A. L., and Mandra, H., 1973. Temperature fluctuations during the late Eocene in southern ocean waters near South Island, New Zealand. *Antarct. J.*, 8:282-284.

Mandra, Y. T., and Mandra, H., 1971. Upper Eocene silicoflagellates from New Zealand. *U.S. Antarct. J.*, 6:177-178.

________, 1972. Paleoecology and taxonomy of silicoflagellates from an upper Miocene diatomite near San Felipe, Baja California, Mexico. *Occas. Pap. Calif. Acad. Sci.*, 99:1-35.

Martini, E., and Müller, C., 1976. Eocene to Pleistocene silicoflagellates from the Norwegian-Greenland Sea (DSDP Leg 38). *In* Talwani, M., Udintsev, G., et al., *Init. Repts. DSDP*, 38: Washington (U.S. Govt. Printing Office), 857-895.

Perch-Nielsen, K., 1975a. Late Cretaceous to Pleistocene archaemonads, ebridians, endoskeletal dinoflagellates, and other siliceous microfossils from the subantarctic southwest Pacific, DSDP Leg 29. *In* Kennett, J. P., Houtz, R. E., et al., *Init. Repts. DSDP*, 29: Washington (U.S. Govt. Printing Office), 873-907.

________, 1975b. Late Cretaceous to Pleistocene silicoflagellates from the southern southwest Pacific, DSDP Leg 29. *In* Kennett, J. P., Houtz, R. E., et al., *Init. Repts. DSDP*, 29: Washington (U.S. Govt. Printing Office), 677-721.

________, 1976. New silicoflagellates and a silicoflagellate zonation in north European Paleocene and Eocene diatomites. *Bull. Geol. Soc. Den.*, 25:27-40.

Stadum, C. J., and Burckle, L. H., 1973. A silicoflagellate ooze from the east Falkland Plateau. *Micropaleontology*, 19:104-109.

Stradner, H., 1961. Über fossile Silicoflagelliden und die Möglichkeit ihrer Verwendung in der Erdölstratigraphie. *Erdoel Kohle*, 14:87-92.

Tsumura, K., 1963. A systematic study of Silicoflagellatae. *Yokohama Municipal Univ. Jour.*, Ser. C-45, No. 146:1-84.

Uchio, T., 1974. Tertiary nannoplankton stratigraphy of Sado Island, Niigata Prefecture, and a proposal of the *Braarudosphaera bigelowi-Coccolithus pelagicus* Zone for the Pliocene of Japanese oil fields of Japan Sea side. *Jpn Geol. Survey Rept.*, 250-1:235-254.

Vincent, E., 1975. Neogene planktonic foraminifera from the central North Pacific, Leg 32, Deep Sea Drilling Project. *In* Larson, R. L., Moberly, R., et al., *Init. Repts. DSDP*, 32: Washington (U.S. Govt. Printing Office), 765-801.

________, 1981. Neogene planktonic foraminifers from the central North Pacific, Deep Sea Drilling Project Leg 62. *In* Thiede, J., Vallier, T., et al., *Init. Repts. DSDP*, 62: Washington (U.S. Govt. Printing Office), 329-353.

Wornardt, W. W., Jr., 1971. Eocene, Miocene and Pliocene marine diatoms and silicoflagellates studied with the scanning electron microscope. *Proc. Planktonic Conf.*, 2nd, pp. 1277-1300.

Date of Initial Receipt: 22 March 1984
Date of Acceptance: 4 April 1984

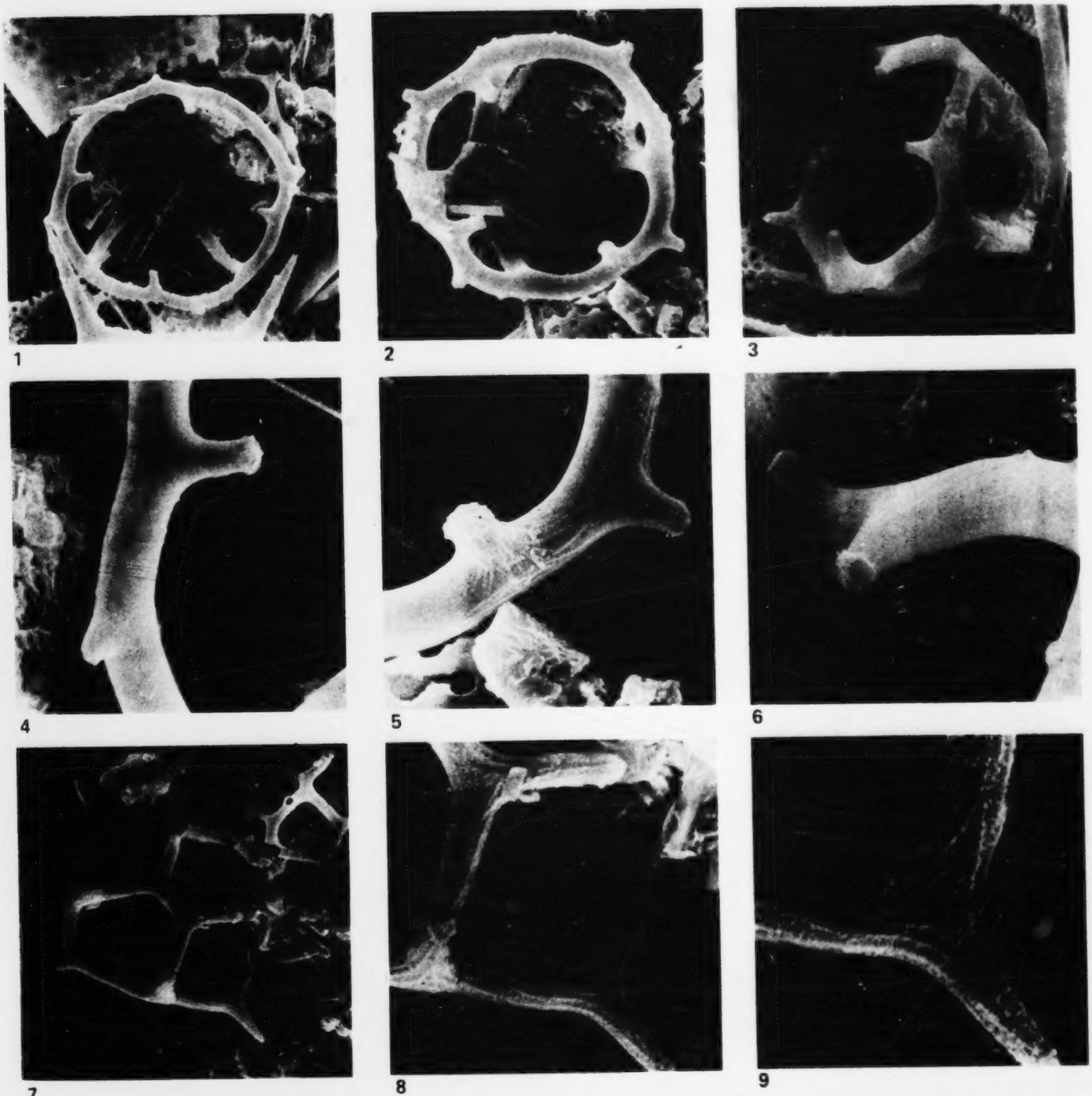

Plate 1. Silicoflagellates from DSDP Leg 86. **1–6.** *Dictyocha subarctios* Ling. Sample 581-8,CC. Quaternary (cool). (1, 4) × 960 and × 3600, negs. SM810–811. (2, 5) × 1080 and × 3000, negs. SM890–891. (3, 6) × 1440 and × 4200, negs. SM892–893. **7–9.** *Dictyocha* sp. cf. *D. concinna* Bukry. Sample 579A-9-2, 40–42 cm. Late Pliocene (cool). (7) × 1440, neg. SM784. (8) × 3600, neg. SM785. (9) × 6000, neg. SM786.

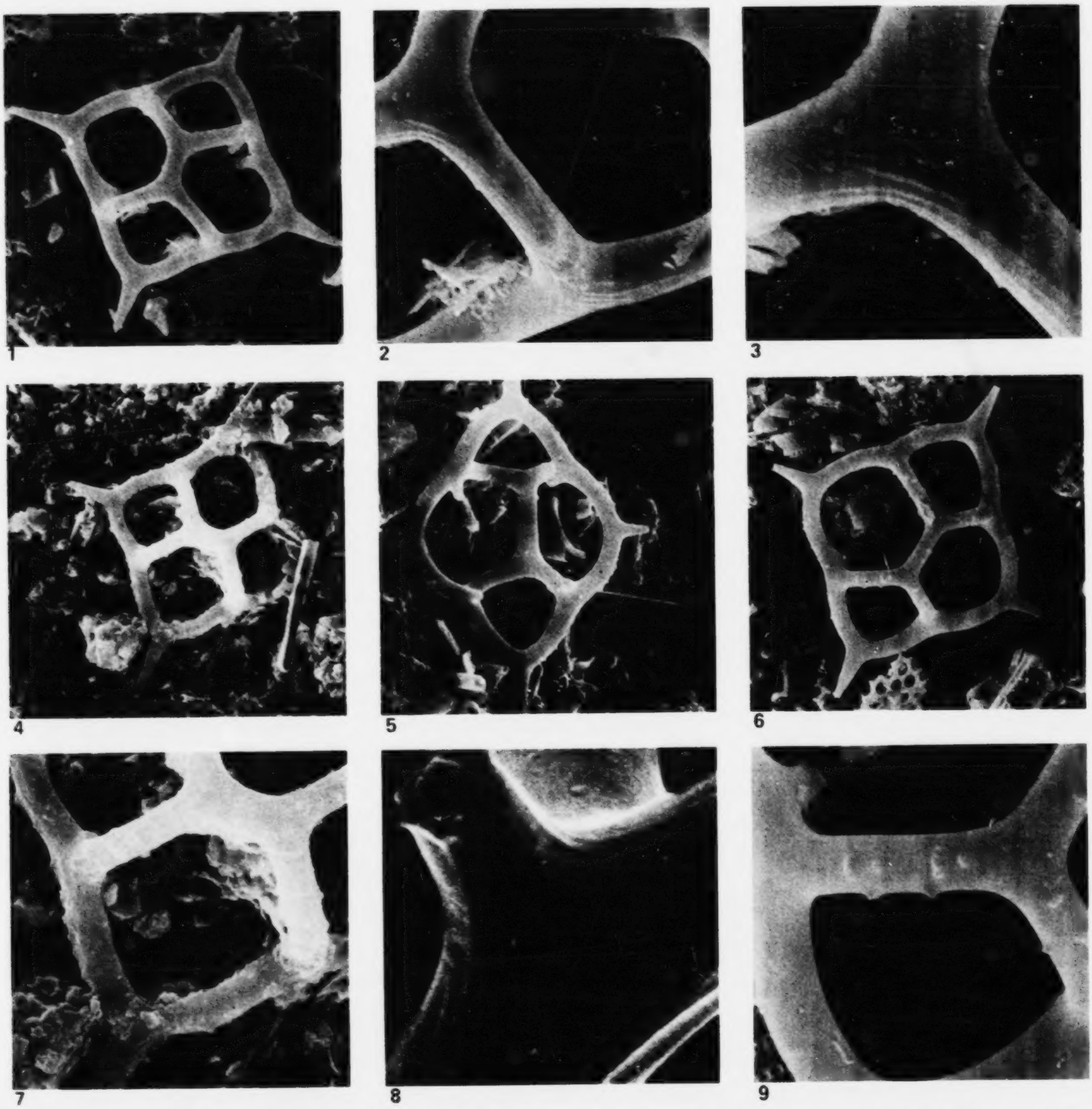

Plate 2. Silicoflagellates from DSDP Leg 86. **1–3.** *Dictyocha aspera* (Lemmermann). Sample 579A-6,CC. Pliocene and Pleistocene (warm). (1) × 1200, neg. SM757. (2) × 4200, neg. SM758. (3) × 7200, neg. SM759. **4, 6, 7, 9.** *Dictyocha* spp. (4, 7) Sample 581-7-3, 30–31 cm. Late Miocene (cool). (4) × 900, neg. SM717. (7) × 1800, neg. SM718. (6, 9) Sample 579A-6,CC. Pliocene and Pleistocene (warm). (6) × 980, neg. SM755. (9) × 3500, neg. SM756. **5, 8.** *Dictyocha* sp. cf. *D. longa* Bukry. Sample 581-3,CC. Late Miocene (cool). (5) × 1200, neg. SM706. (8) × 12,000, neg. SM707.

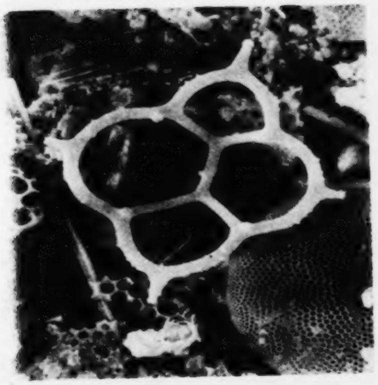

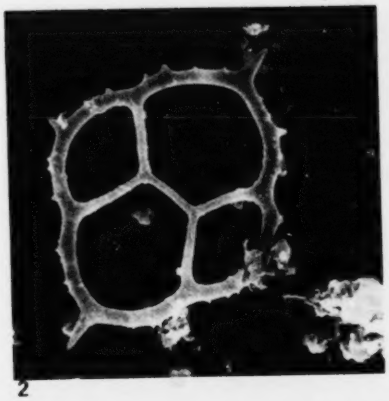

2

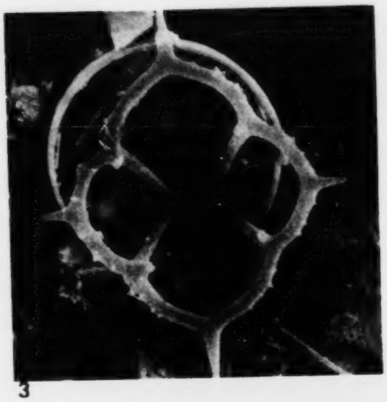

3

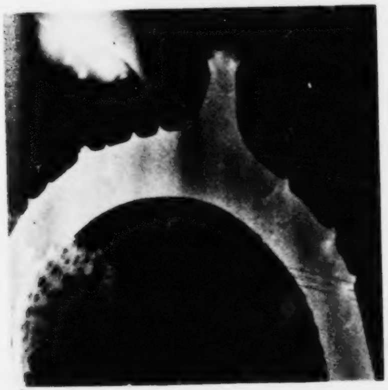

4

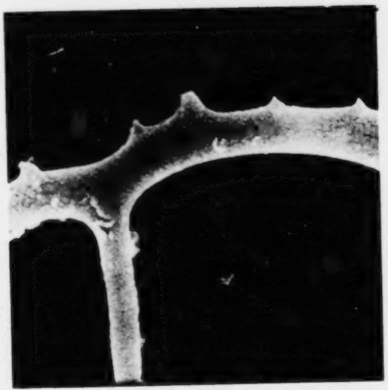

5

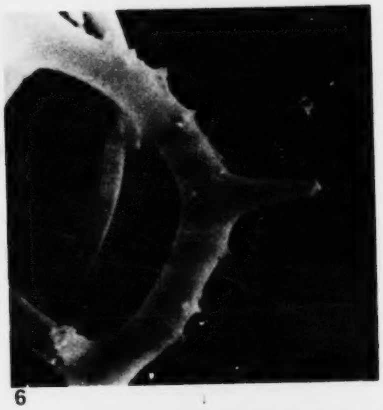

6

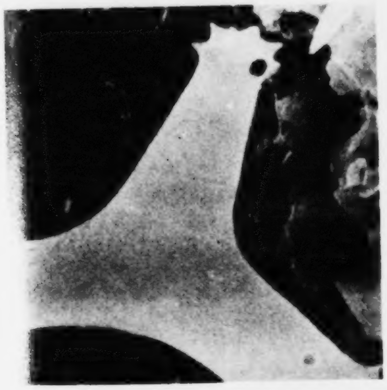

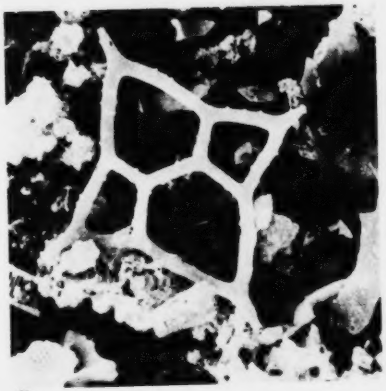

8

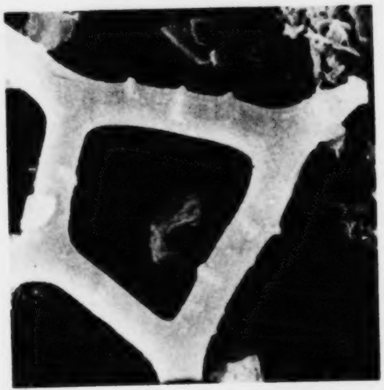

9

te 3. Silicoflagellates from DSDP Leg 86. **1, 4, 7.** *Dictyocha brevispina* (Lemmermann). Sample 581-8,CC. Middle Miocene (cool). (1) ×480, neg. SM806. (4) ×1800, neg. SM809. (7) ×3600, neg. SM807. **2, 5.** *Dictyocha lingii* Dumitrică. Sample 579A-4,CC. Pleistocene (warm). (2) ×1320, neg. SM885. (5) ×3000, neg. SM886. **3, 6.** *Dictyocha hessii* Bukry. Sample 581-8,CC. Quaternary (cool). (3) ×1080, neg. SM896. (6) ×3000, neg. SM897. **8, 9.** *Dictyocha* sp. cf. *D. brevispina* (Lemmermann). Sample 579A-12,CC. Early Pliocene (cold). (8) ×600, neg. SM776. (9) ×1800, neg. SM777.

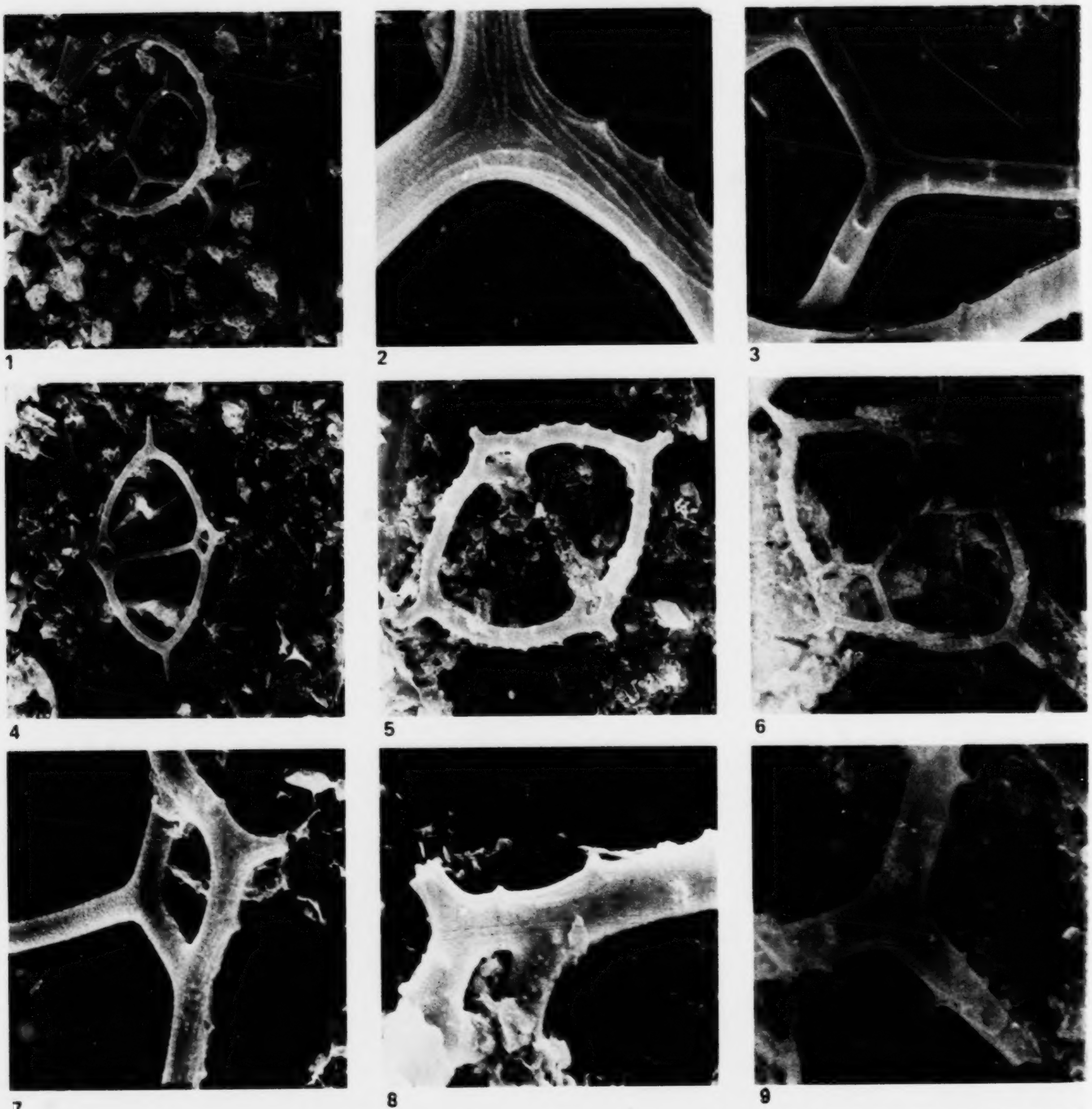

Plate 4. Silicoflagellates from DSDP Leg 86. **1-9.** *Dictyocha brevispina* (Lemmermann). (1-3) Sample 579A-10,CC. Late Pliocene (cold). (1) Wit a *Mesocena;* ×2400, neg. SM865. (2) ×4800, neg. SM867. (3) With *Mesocena* at bottom; ×3000, neg. SM868. (4, 7) Sample 577-6-7, 12-13 cm Early Pliocene (warm). (4) ×600, neg. SM871. (7) ×3000, neg. SM872. (5, 8) Sample 577-6-7, 12-13 cm. Early Pliocene (warm). (5) ×960, neg SM869. (8) ×3000, neg. SM870. (6, 9) Sample 580-17,CC. Late Pliocene (cold). (6) ×960, neg. SM814. (9) ×3600, neg. SM815.

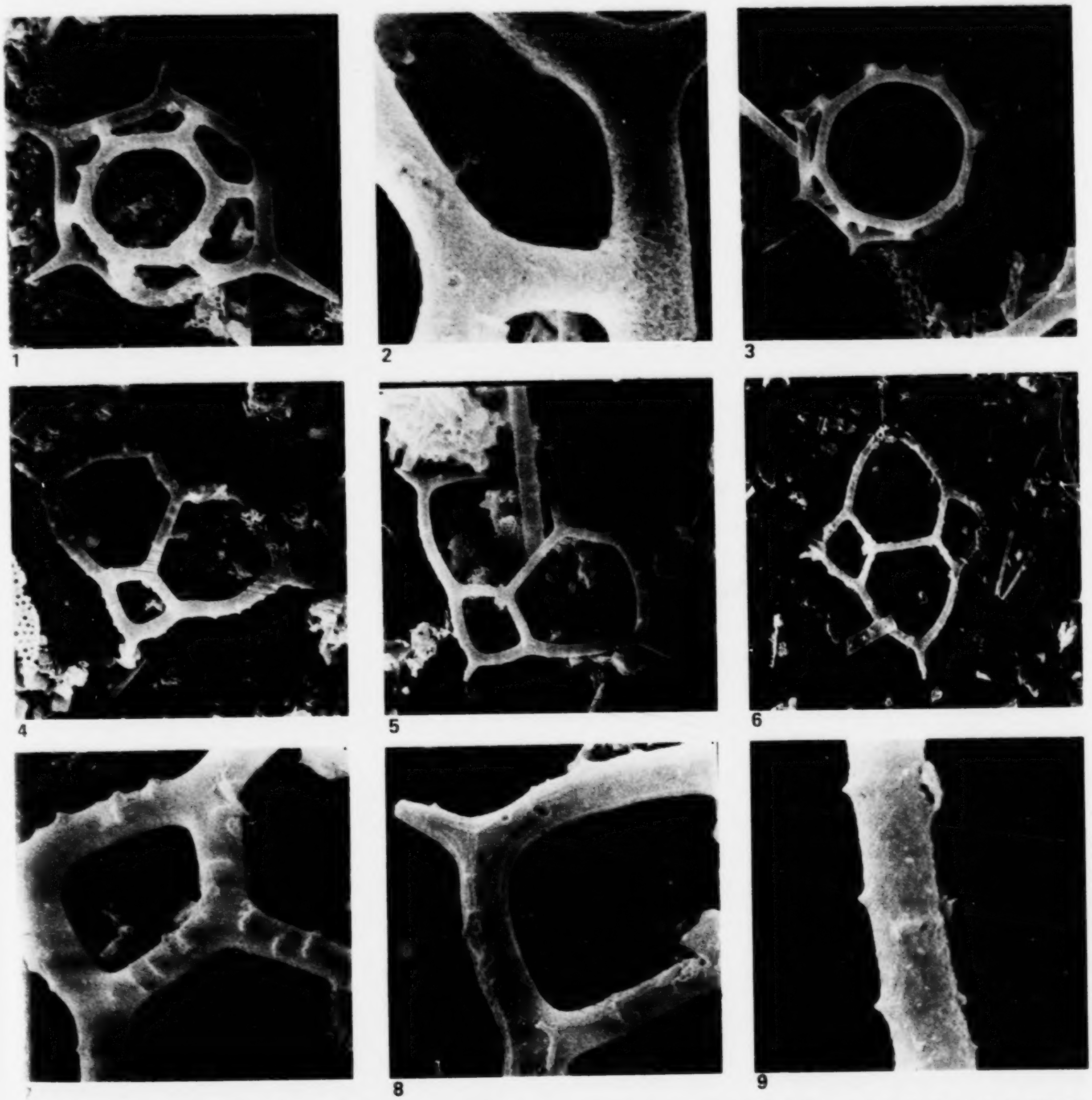

ate 5. Silicoflagellates from DSDP Leg 86. **1, 2.** *Distephanus speculum speculum* (Ehrenberg). Sample 579A-9-2, 40–42 cm. Late Pliocene (warm). (1) × 1600, neg. SM741. (2) × 4800, neg. SM742. **3.** *Distephanus* sp. cf. *D. floridus* Bukry. Sample 581-8,CC. Quaternary (cool). × 1200, neg. SM803. **4–9.** *Dictyocha brevispina* (Lemmermann). (4, 7) Sample 579A-10,CC. Late Pliocene (cool). (4) × 840, neg. SM864. (7) × 2400, neg. SM865. (5, 8) Sample 579A-15,CC. ?Late Miocene. (5) × 840, neg. SM826. (8) × 3000, neg. SM828. (6, 9) Sample 579A-12,CC. Early Pliocene (cool). (6) × 420, neg. SM778. (9) Apical bar; × 3600, neg. SM779.

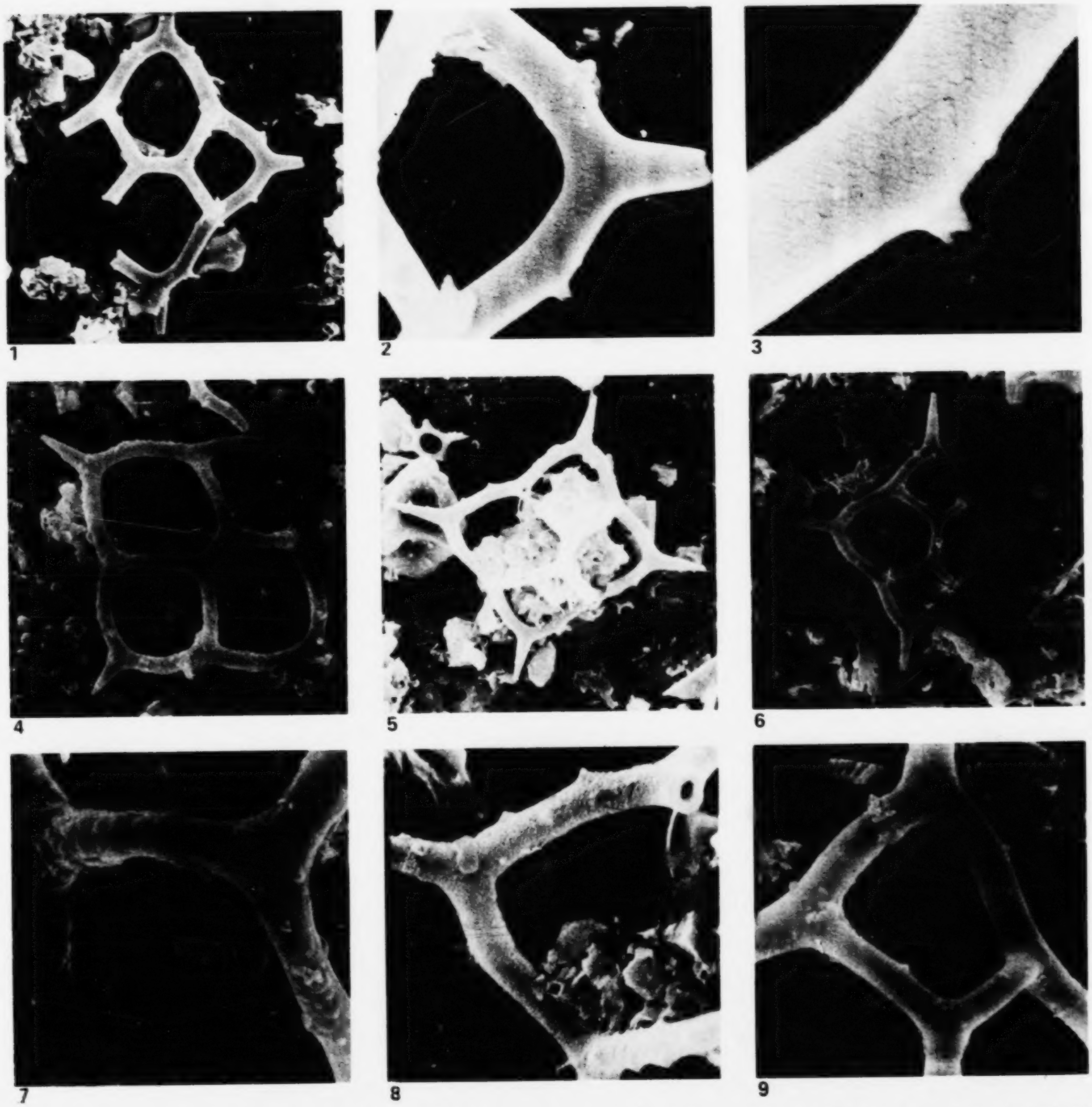

Plate 6. Silicoflagellates from DSDP Leg 86. **1-3, 5, 6, 8, 9.** *Dictyocha calida ampliata* Bukry. (1-3) Sample 579A-4,CC. Pleistocene (warm). (1) ×760, neg. SM878. (2) ×4200, neg. SM879. (3) ×10,800, neg. SM880. (5, 8) Sample 579A-4,CC. Pleistocene (warm). (5) ×1080, neg. SM881. (8) ×3000, neg. SM882. (6, 9) Sample 577-2-4, 43-44 cm. Pleistocene (warm). (6) ×960, neg. SM846. (9) ×3000, neg. SM847. **4, 7.** *Dictyocha* sp. Sample 578-12,CC. Late Miocene (cool). (4) ×900, neg. SM736. (7) ×2400, neg. SM737.

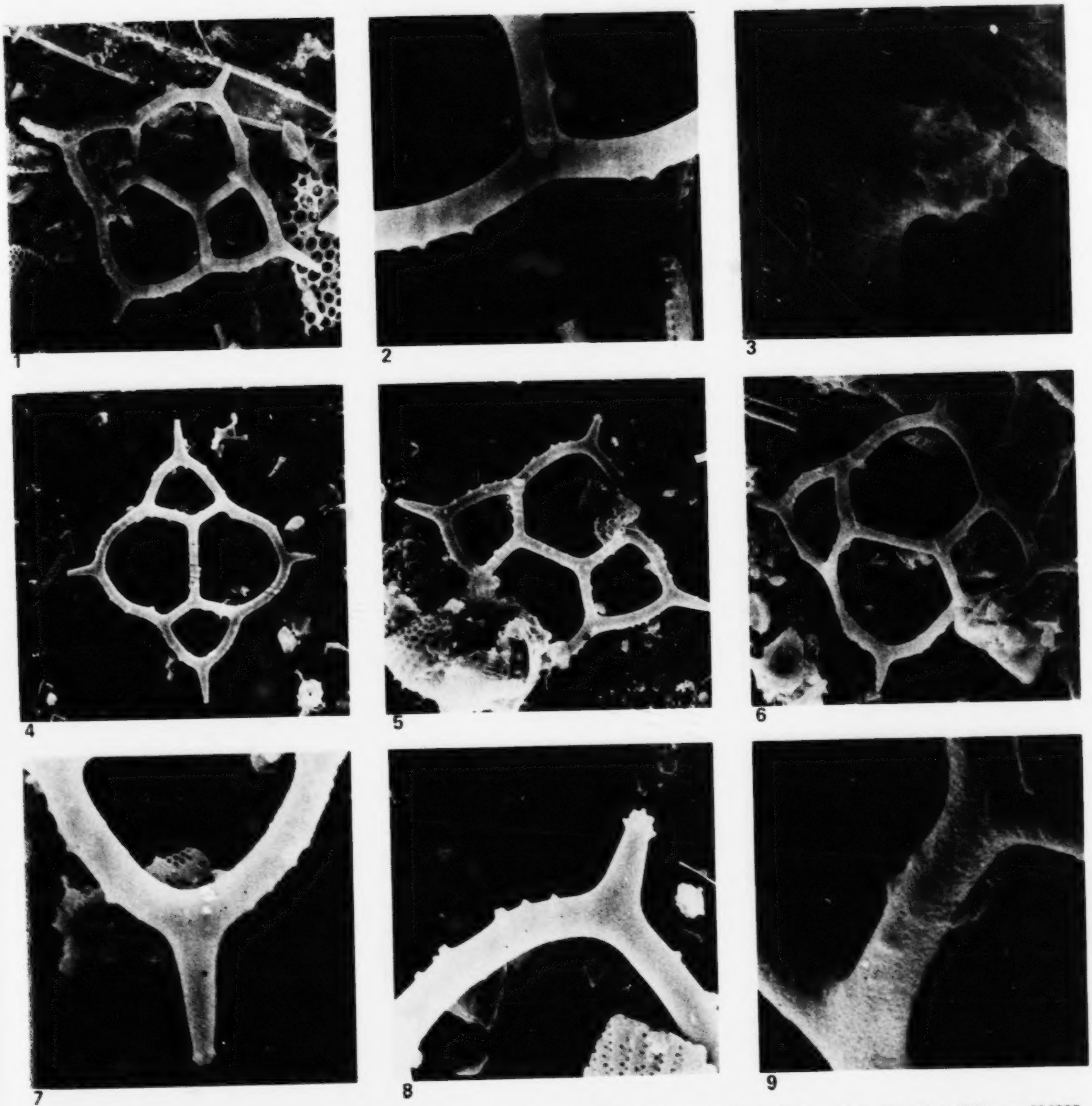

late 7. Silicoflagellates from DSDP Leg 86. **1–9.** *Dictyocha perlaevis* Frenguellii. (1–3) Sample 581-8,CC. Late Cenozoic. (1) ×720, neg. SM887. (2) ×1800, neg. SM889. (3) ×9600, neg. SM888. (4, 7) Sample 579A-4,CC. Pleistocene (warm) (4) ×540, neg. SM883. (7) ×1800, neg. SM884. (5, 8) Sample 579A-4,CC. Pleistocene (warm). (5) ×600, neg. SM875. (8) ×1800, neg. SM876. (6, 9) Sample 579A-6,CC. Near Pliocene/Pleistocene boundary (warm). (6) ×980, neg. SM753. (9) ×4200, neg. SM754.

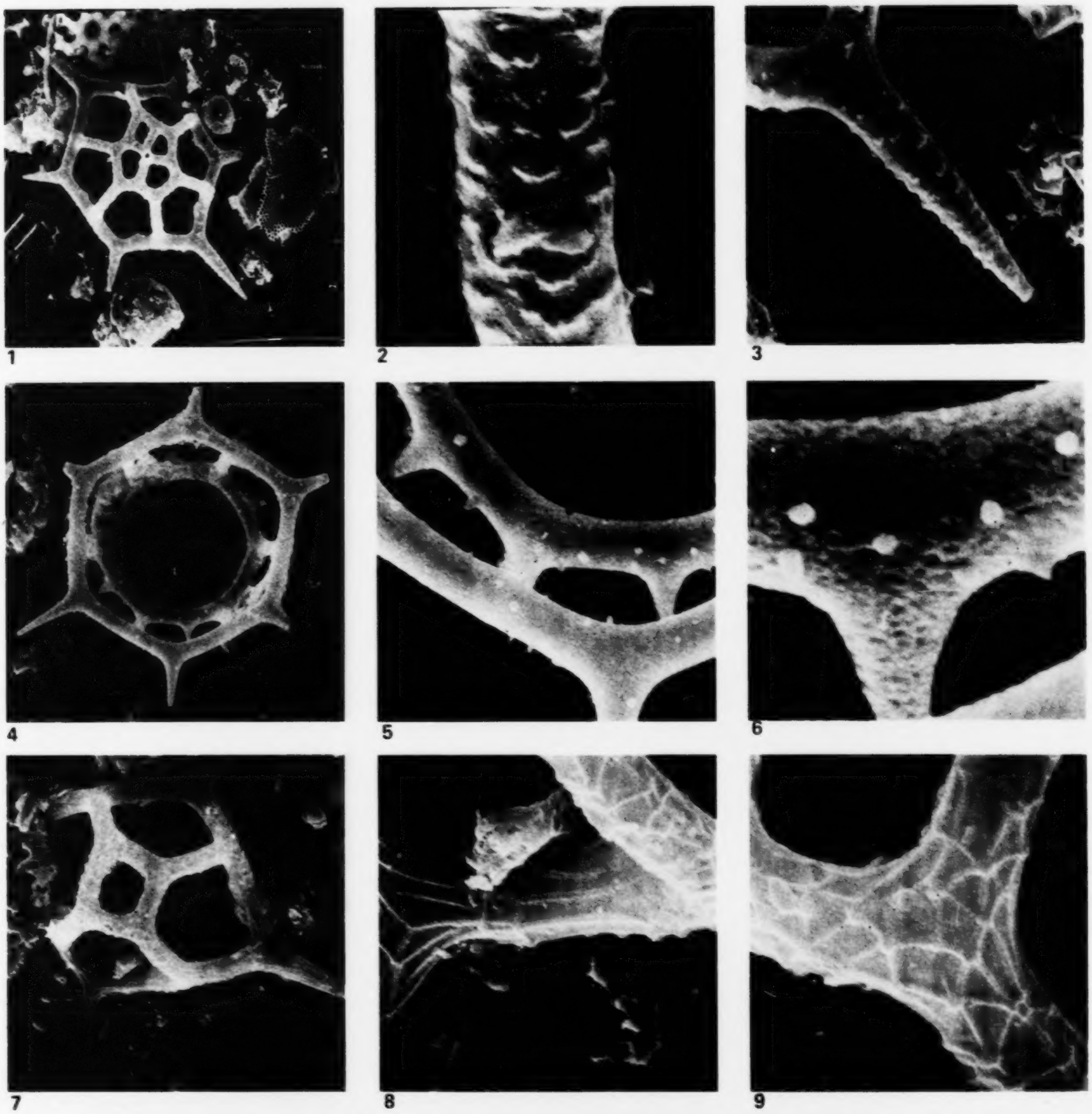

Plate 8. Silicoflagellates from DSDP Leg 86. **1–3.** *Distephanus jimlingii* (Bukry) s. ampl. Sample 579A-9,CC. Late Pliocene (cold). (1) × 840, neg. SM856. (2) × 9600, neg. SM860, strut. (3) × 3000, neg. SM858, spine. **4–6.** *Distephanus speculum minutus* (Bachmann) emend. Sample 579A-9-2, 40–42 cm. Late Pliocene (cool). (4) × 1400, neg. SM746. (5) × 4200, neg. SM749. (6) × 12,000, neg. SM748. **7–9.** *Distephanus crux* (Ehrenberg). Sample 581-7-3, 30–31 cm. Late Miocene (warm). (7) × 1080, neg. SM723. (8) × 3600, neg. SM725, basal ring. (9) × 4800, neg. SM724, apical ring.

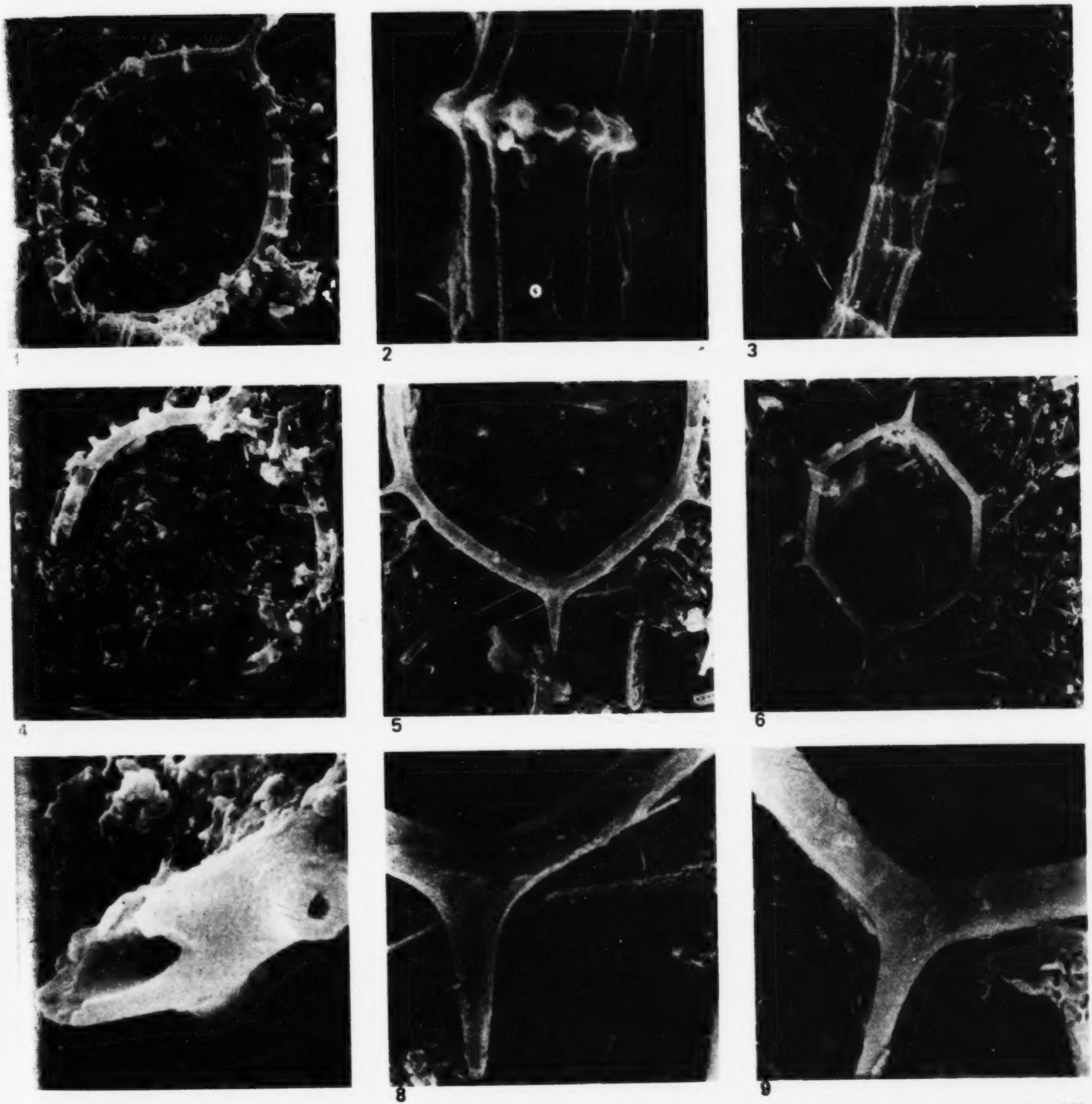

ate 9. Silicoflagellates from DSDP Leg 86. **1, 2.** *Mesocena diodon nodosa* Bukry. Sample 581-7-3, 30–31 cm. Late Miocene (warm). (1) ×840, neg. SM721. (2) ×4800, neg. SM722. **3.** *Mesocena diodon nodosa* Bukry. Sample 581-8-2, 75–76 cm. Middle Miocene (cold). ×3600, neg. SM788. **4, 7.** *Mesocena circulus* (Ehrenberg). Sample 581-7-3, 30–31 cm. Late Miocene (warm). (4) ×840, neg. SM734. (7) ×4800, neg. SM735. **5, 8.** *Mesocena hexalitha* Bukry. Sample 581-8-2, 55–56 cm. Middle Miocene (cold). (5) ×960, neg. SM797. (8) ×3000, neg. SM798. **6, 9.** *Mesocena hexalitha* Bukry. Sample 581-8-2, 75–76 cm. Middle Miocene (cold). (6) ×540, neg. SM789. (9) ×3000, neg. SM790.

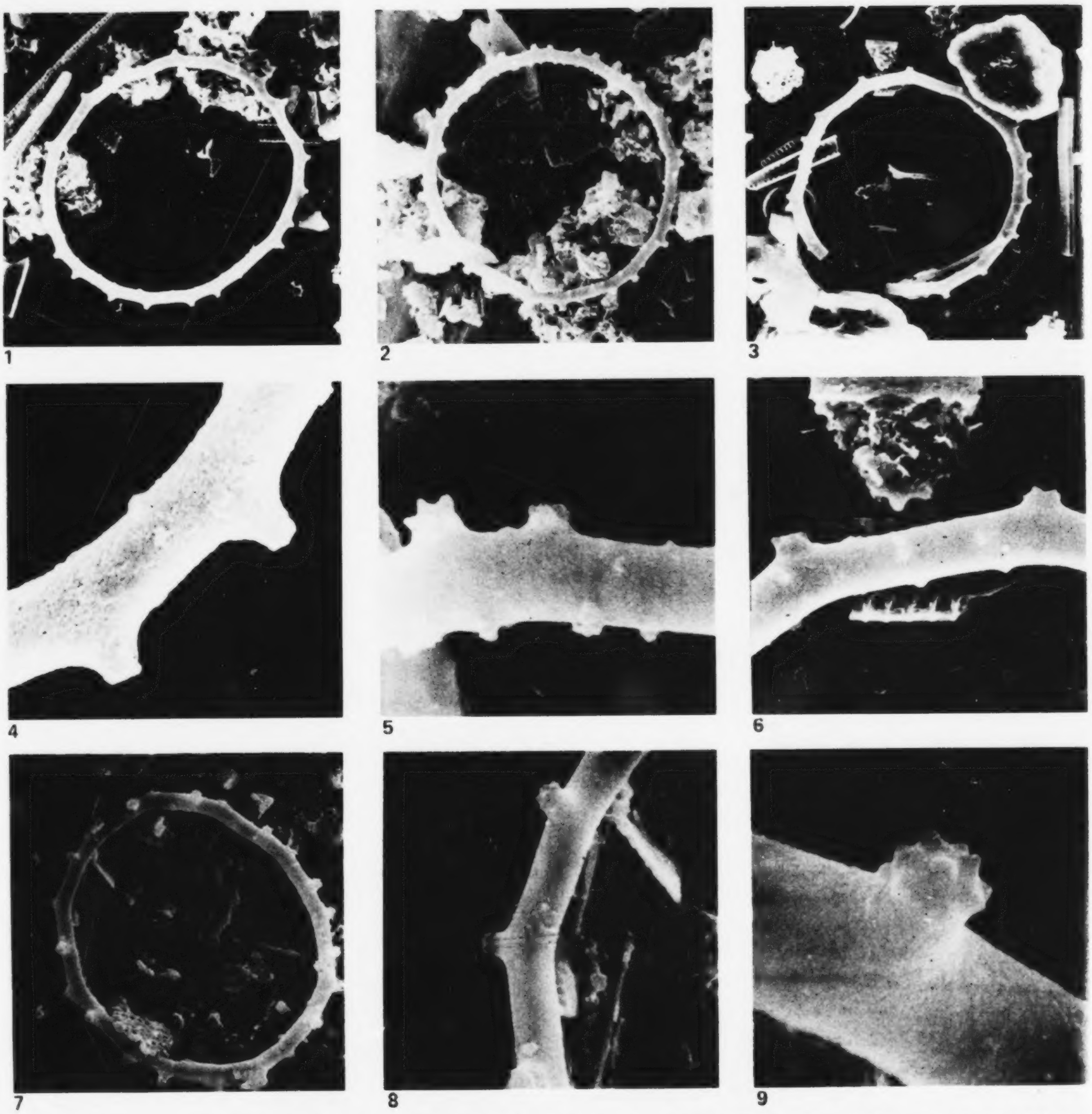

Plate 10. Silicoflagellates from DSDP Leg 86. **1–9.** *Mesocena circulus* (Ehrenberg). (1, 4) Sample 579A-9,CC. Late Pliocene (cold). (1) × 840, neg SM772. (4) × 6000, neg. SM773. (2, 5) Sample 579A-15,CC. Late Miocene? (2) × 840, neg. SM819. (5) × 6000, neg. SM820. (3, 6) Sample 579A 9,CC. Late Pliocene (cold). (3) × 840, neg. SM774. (6) × 3600, neg. SM775. (7–9) Sample 581-7-3, 30–31 cm. Late Miocene (warm). (7) × 840 neg. SM731. (8) × 2400, neg. SM733. (9) × 8400, neg. SM732.

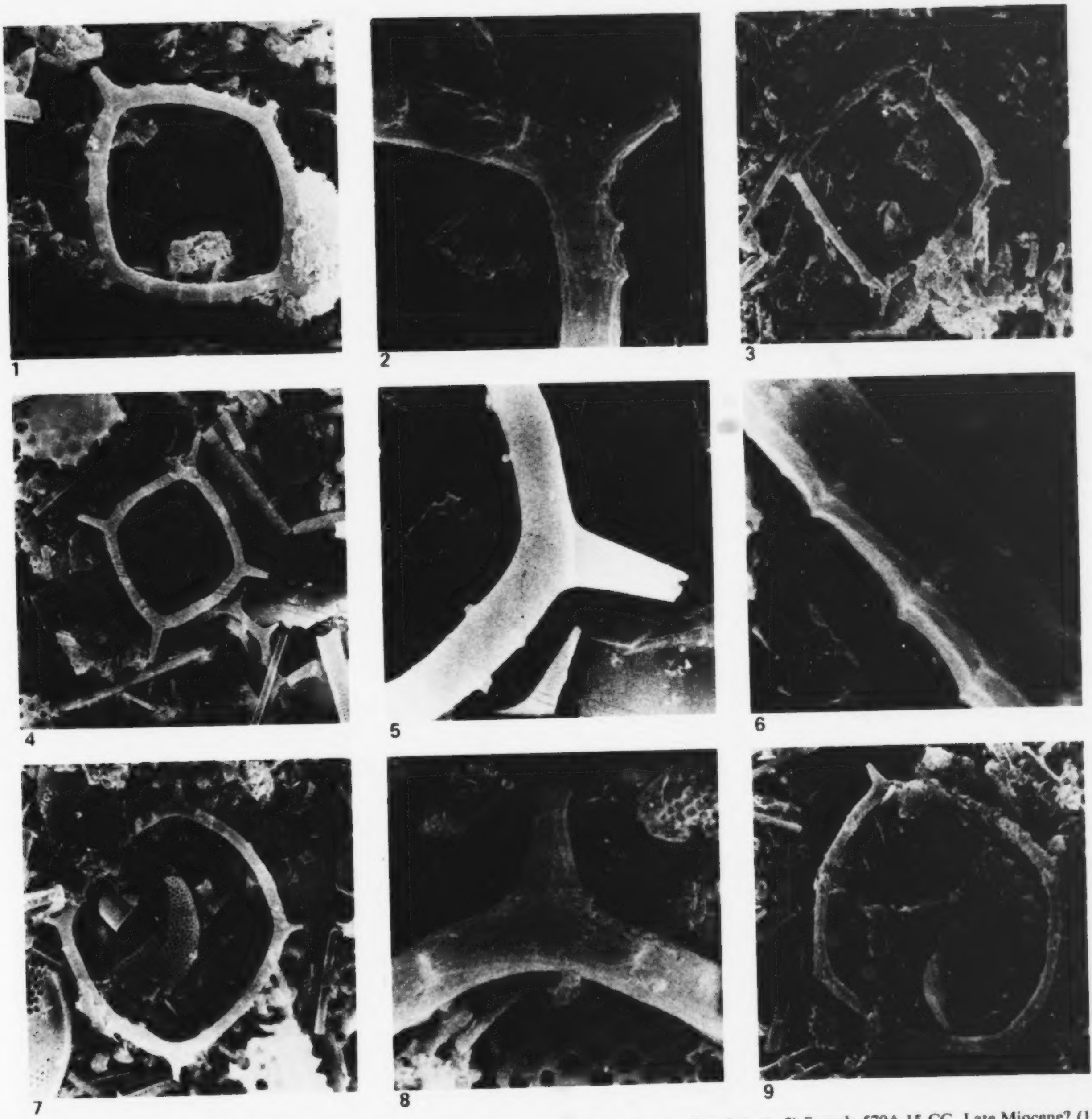

Plate 11. Silicoflagellates from DSDP Leg 86. **1–9.** *Mesocena quadrangula* Ehrenberg ex Haeckel. (1, 2) Sample 579A-15,CC. Late Miocene? (1) ×840, neg. SM824. (2) ×2400, neg. SM825. (3, 6) Sample 581-8-2, 75–76 cm. Middle Miocene (cool). (3) ×540, neg. SM854. (6) ×6000, neg. SM855. (4, 5) Sample 581-8,CC. Late Cenozoic. (4) ×600, neg. SM804. (5) ×3000, neg. SM805. (7, 8) Sample 580-17,CC. Late Pliocene (cold). (7) ×720, neg. SM812. (8) ×3600, neg. SM813. (9) Sample 581-8-2, 75–76 cm. Middle Miocene (cold). ×840, neg. SM795.

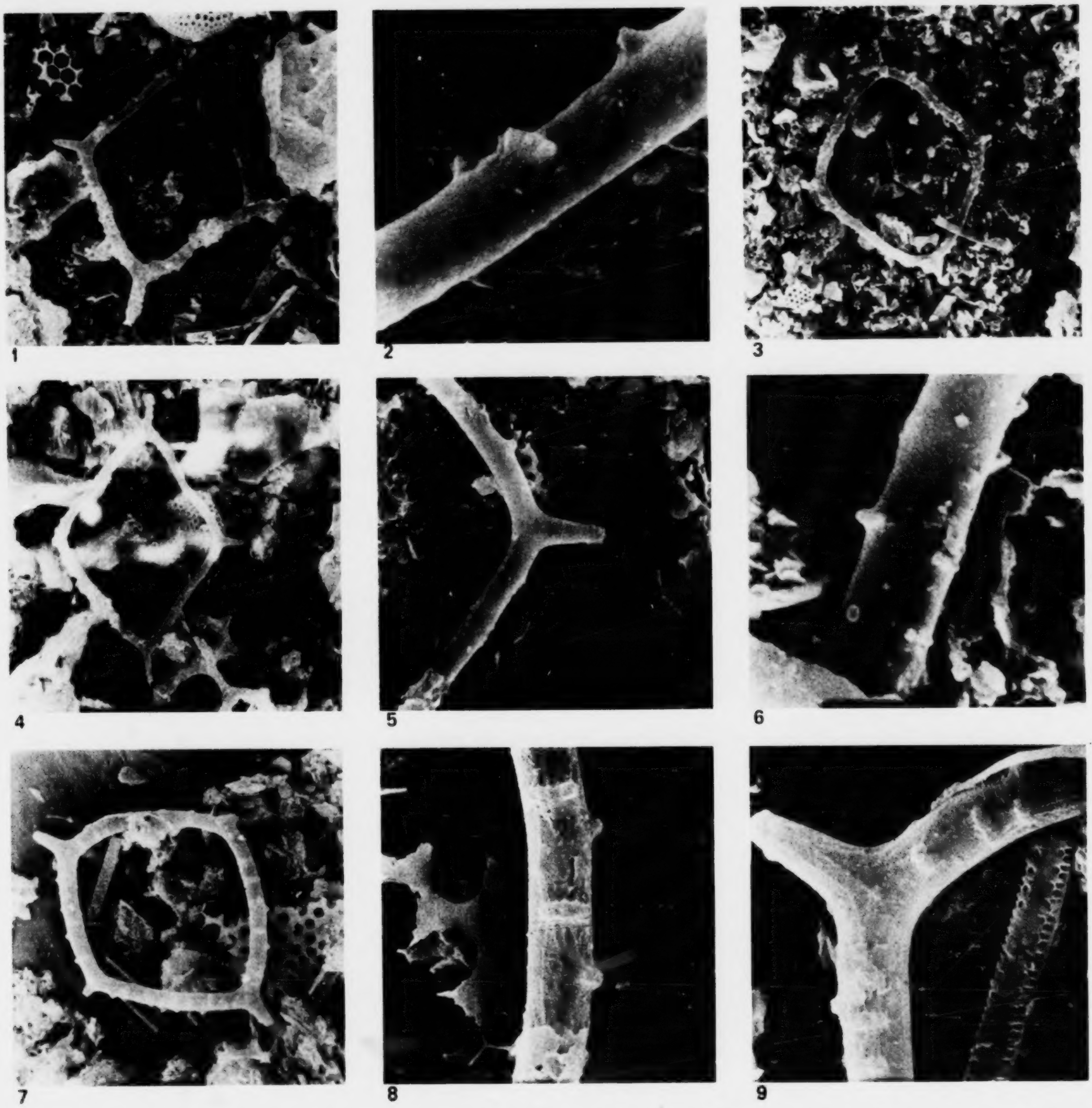

Plate 12. Silicoflagellates from DSDP Leg 86. **1-9.** ***Mesocena quadrangula*** Ehrenberg ex Haeckel. (1-6) Sample 577-2-4, 43-44 cm. Pleistocene (warm). (7-9) Sample 579A-15,CC. Late Miocene? (1, 2) ×840, neg. SM852; ×6000, neg. SM853. (3) ×6000, neg. SM844. (4, 5) ×600, neg. SM841; ×1800, neg. SM842. (6) ×6000, neg. SM844b. (7-9) ×840, neg. SM821; ×3000, neg. SM822; ×3000, neg. SM823.

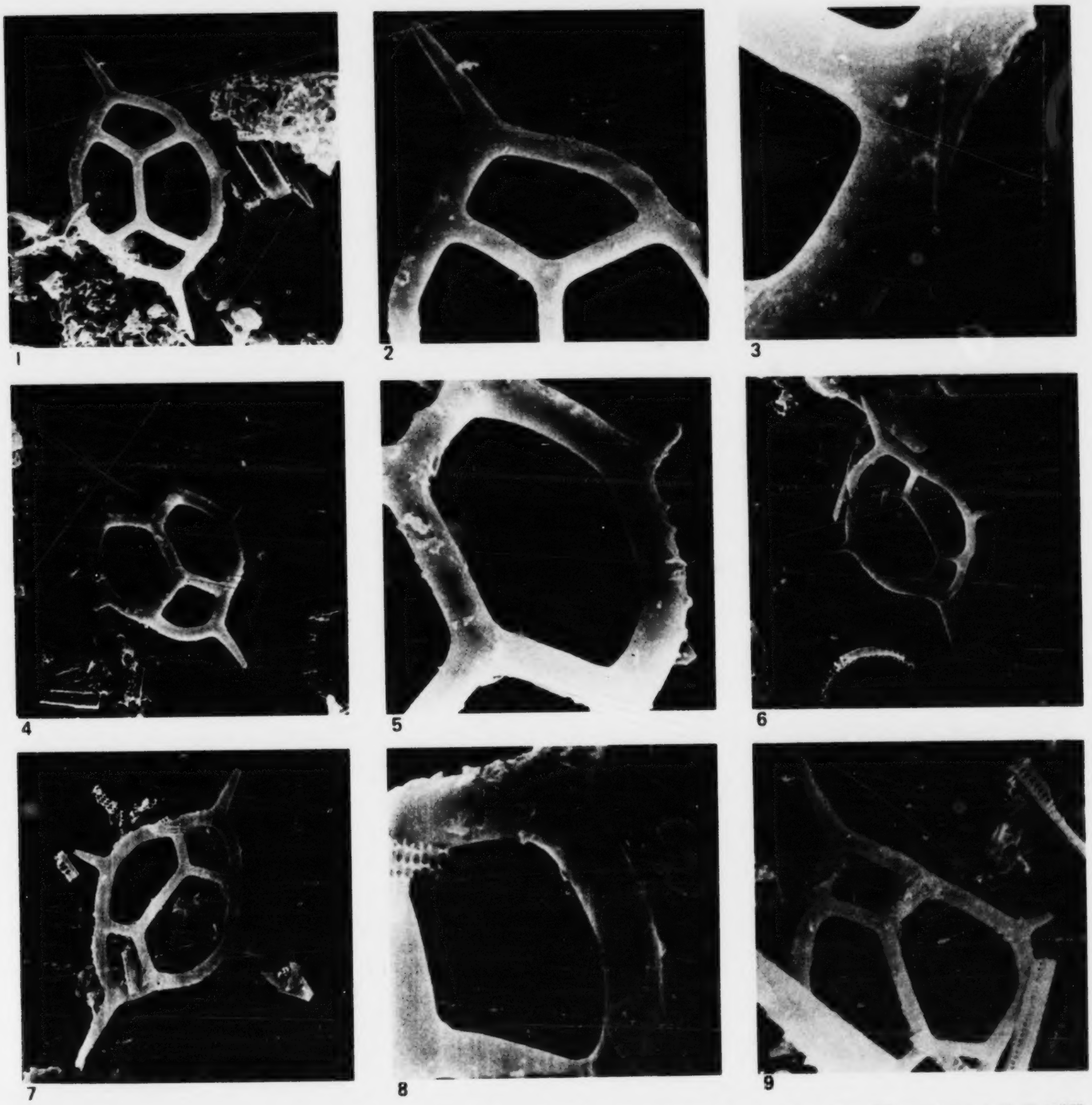

Plate 13. Silicoflagellates from DSDP Leg 85. **1-9.** *Dictyocha flexatella* (Bukry). Sample 572A-5-3, 16-17 cm. Late Pliocene (warm). (1-3) × 960, neg. SM762; × 2400, neg. SM764; × 6000, neg. SM763. (4, 5) × 960, neg. SM767; × 3000, neg. SM768. (6) × 840, neg. SM765. (7, 8) × 840, neg. SM835; × 4200, neg. SM836. (9) × 1320, neg. SM833.

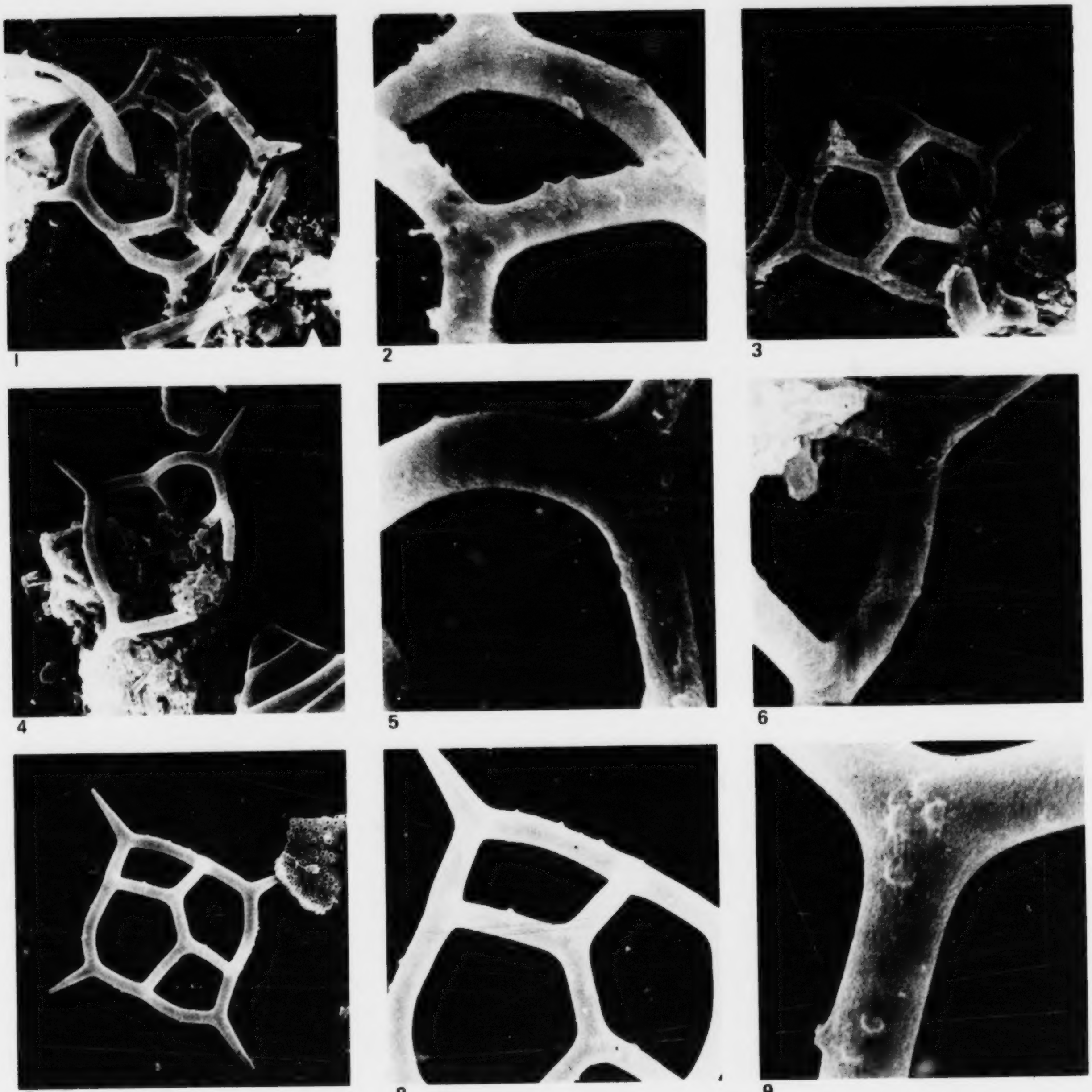

Plate 14. Silicoflagellates from DSDP Leg 86. **1–9.** *Dictyocha flexatella* (Bukry). Sample 579A-9-2, 40–42 cm. Late Pliocene (cool). (1, 2) ×1080, neg. SM780; ×3600, neg. SM781. (3, 6) ×960, neg. SM839; ×3000, neg. SM840. (4, 5) ×840, neg. SM782; ×4200, neg. SM783. (7–9) ×960, neg. SM769; ×1800, neg. SM770; ×6000, neg. SM771.

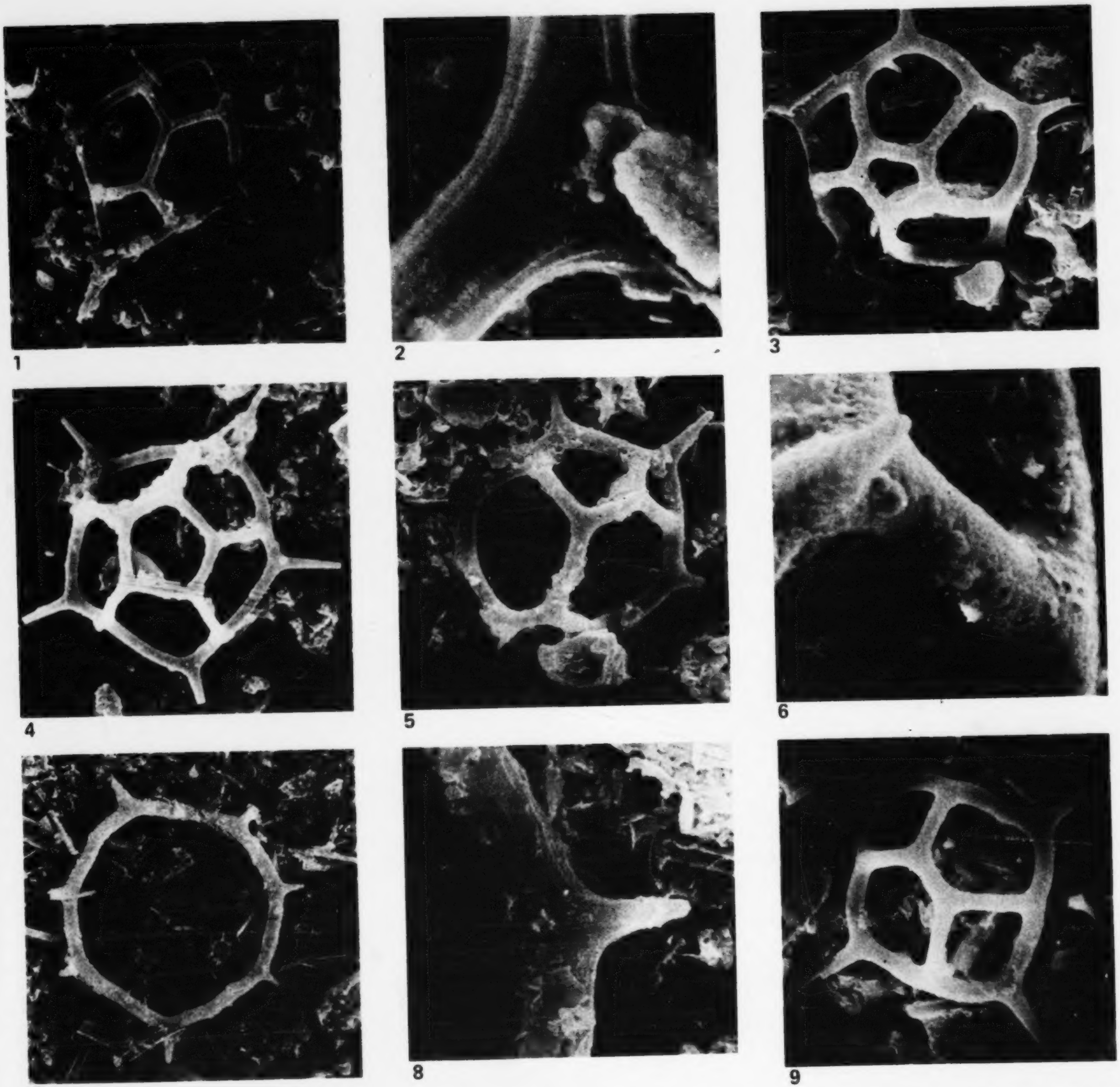

Plate 15. Silicoflagellates from DSDP Leg 86. **1, 2.** *Dictyocha longa* Bukry. Sample 581-7-3, 30–31 cm. Late Miocene (warm). (1) × 900, neg. SM715. (2) × 9000, neg. SM716. **3, 4.** *Distephanus quinquangellus* Bukry et Foster. (3) Sample 581-3,CC. Late Miocene (warm). × 1320, neg. SM709. (4) Sample 579A-9-2, 40–42 cm. Late Pliocene (cool). × 1200, neg. SM745. **5, 6** *Distephanus* sp. cf. *D. pseudofibula* (Schulz). Sample 579A-9-2, 40–42 cm. Late Pliocene (cool). (5) × 1200, neg. SM743. (6) × 7000, neg. SM744. **7, 8.** *Mesocena hexalitha* Bukry. Sample 581-8-2, 75–77 cm. Middle Miocene (cool). (7) × 600, neg. SM791. (8) × 3000, neg. SM792. **9.** *Dictyocha* sp. Sample 581-3,CC. Late Miocene (warm). × 1500, neg. SM702.

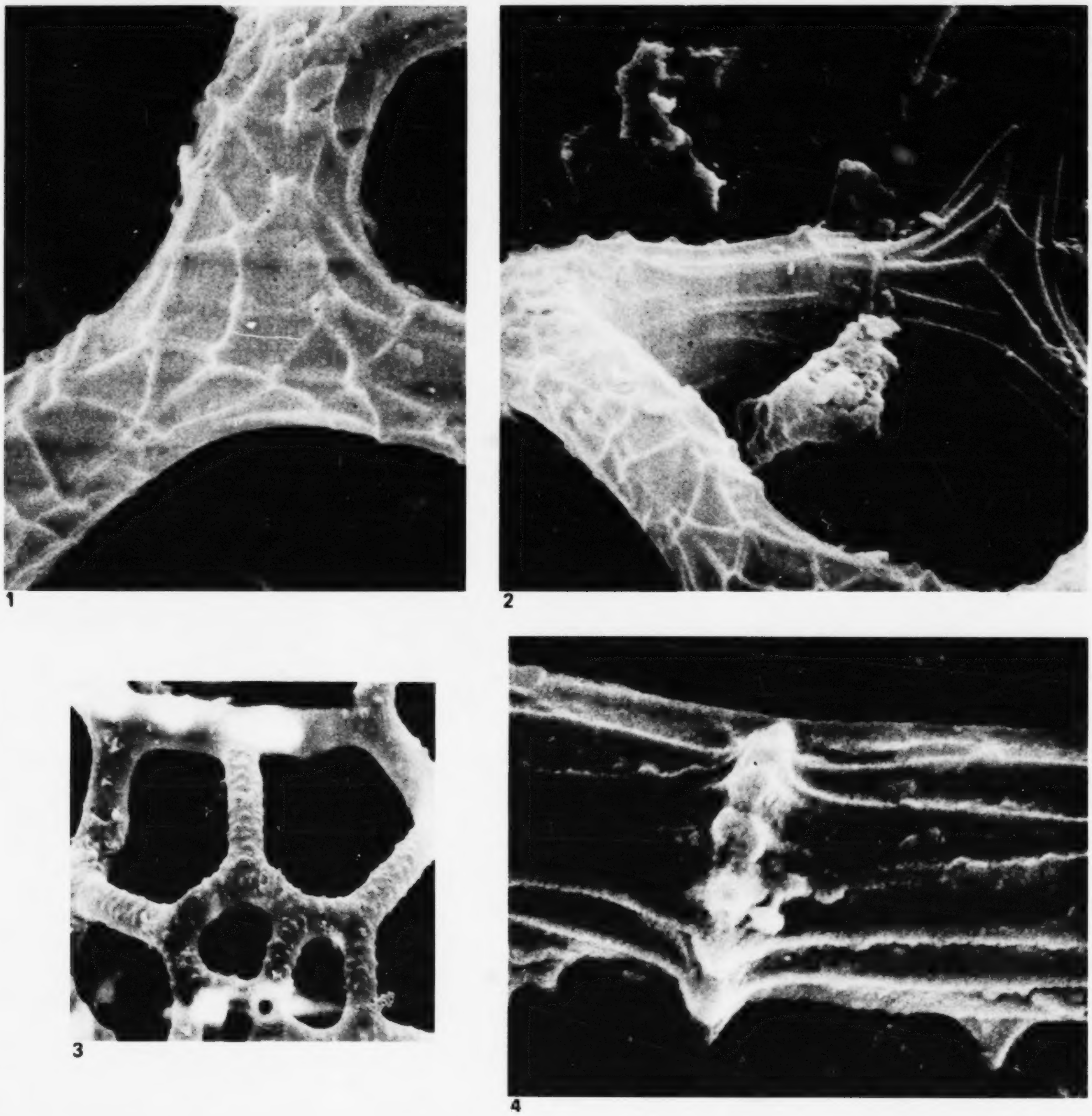

Plate 16. Enlargements of silicoflagellate textures from DSDP Leg 86. **1.** Reticulate texture of intersecting ridges and peaks. Detail of apical ring and strut of *Distephanus crux* Ehrenberg. Sample 581-7-3, 30–31 cm. × 10,000; neg. SM724. **2.** Reticulate texture on strut and linear texture on the basal ring and spine of the same specimen as Fig. 1. × 8000; neg. SM725. **3.** Nodular texture on the apical ring and struts of *Distephanus jimlingii* (Bukry) s. ampl. Sample 579A-9,CC. × 2400; neg. SM859. **4.** Crenulate texture on the ring of *Mesocena diodon nodosa* Bukry. Sample 581-7-3, 30–31 cm. × 10,000; neg. SM722.

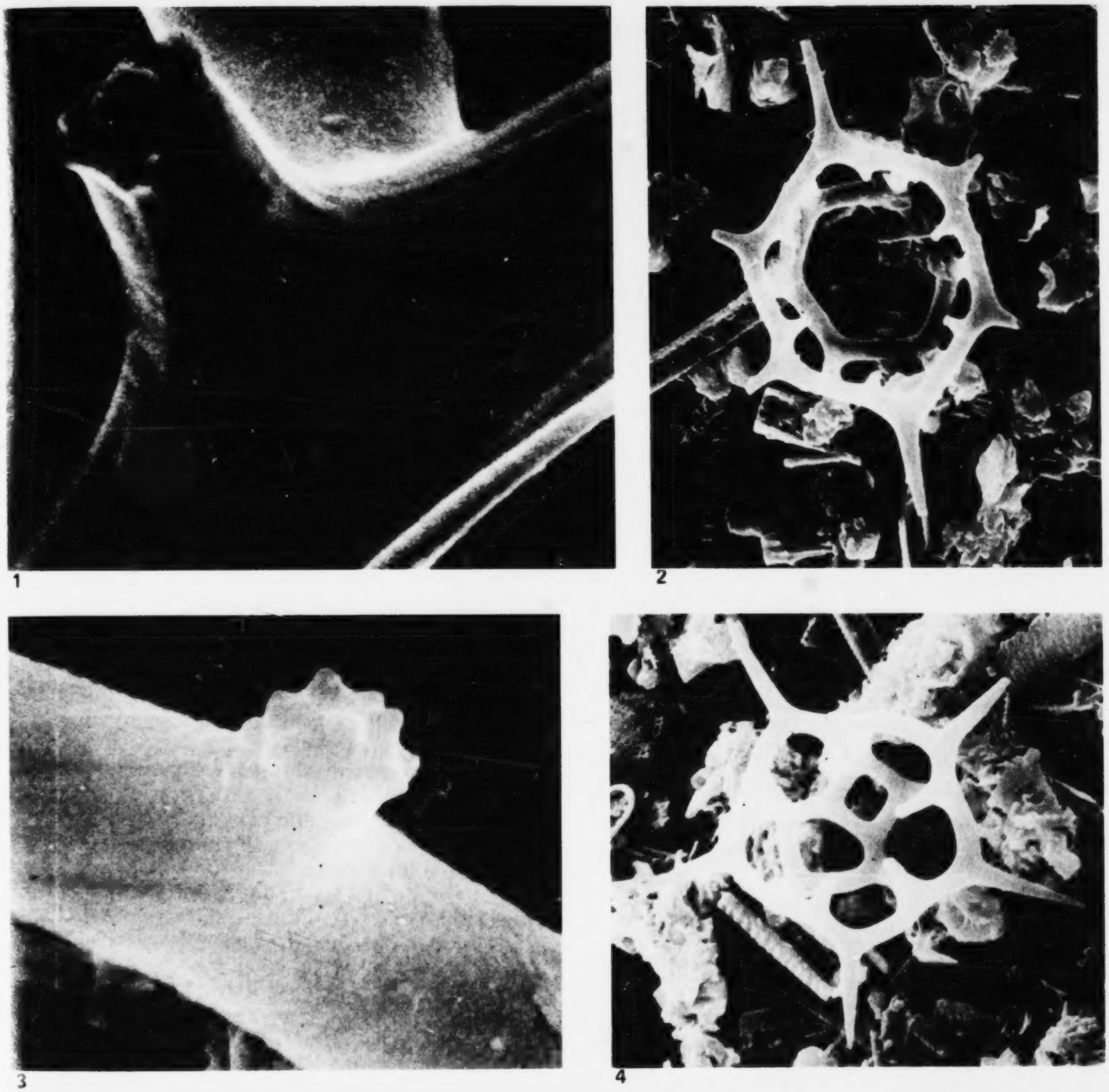

ate 17. Enlargements of silicoflagellate textures from DSDP Leg 86. **1.** Linear texture on basal ring and pike of *Dictyocha* sp. Pike has a semirosette termination. Sample 581-3,CC. × 20,000; neg. SM707. **2.** Smooth texture on basal ring and short spine of *Mesocena circulus* (Ehrenberg). Spine has a rosette termination. Sample 581-7-3, 30–31 cm. × 14,000; neg. SM732. **3.** Smooth texture on all proximal surfaces of *Distephanus speculum minutus* (Bachmann, emend.). Sample 581-3,CC. × 2000, neg. SM708. **4.** Smooth texture on all proximal surfaces of *Distephanus quinquangellus* Bukry and Foster (binocular). Sample 581-3,CC. × 1800; neg. SM714.

14. RADIOLARIANS FROM THE NORTHWEST PACIFIC, DEEP SEA DRILLING PROJECT LEG 86[1]

Joseph J. Morley, Lamont-Doherty Geological Observatory of Columbia University[2]

ABSTRACT

Radiolarians occur in sediments from all northwest Pacific sites drilled on DSDP Leg 86. The oldest radiolarian-bearing sediment was recovered at Site 581, where middle Miocene radiolarians were found. Site 578 recovered late Miocene through Pleistocene radiolarians, while an early Pliocene through Pleistocene radiolarian assemblage was present in sediments at Sites 577 and 579. Site 580 contained radiolarians ranging in age from late Pliocene to Pleistocene. Only Pleistocene radiolarians were preserved in sediments from Site 576.

The onset of Miocene biosiliceous sedimentation in the northwest Pacific is not synchronous, but is dependent upon the time when each specific site exited from the low-productivity central gyre into what appears to be a preexisting, high-productivity gyre-margin region. During this Neogene and Quaternary period of biosiliceous sedimentation in the northwest Pacific, radiolarian productivity increased throughout the early and middle late Pliocene, reaching a maximum between 2.3 and 2.4 m.y. ago. Early Pleistocene productivity levels are lower than late Pliocene values, with indications of minor pulses in the early, middle, and latest Pleistocene.

INTRODUCTION

Deep Sea Drilling Project (DSDP) Leg 86 drilled 11 holes at six sites in the northwest Pacific (Table 1, Fig. 1). The six sites were positioned so that the radiolarians preserved in the sediments from these sites reflected Miocene through Pleistocene conditions in the northwest Pacific along a transect across the Subarctic Convergence, with its end members centered in the southern subarctic gyre and the central subtropical gyre.

Although investigators (Kling, 1971; Ling, 1973; Foreman, 1973a; Foreman, 1975; Ling, 1980; Sakai, 1980; Reynolds, 1980; Schaaf, 1981) have reported on radiolarians in sediments from earlier northwest Pacific DSDP Legs (6, 19, 20, 32, 55, 56, 57, and 62), the sites drilled during Leg 86 represent the first time that sediments from this region have been recovered using the hydraulic piston corer. This technique was utilized at all sites except Site 581, where sediments were recovered using the rota- drill. The relatively undisturbed sediment sequences from these various sites provide a rigorous test of the si- eous faunal biostratigraphy for the North Pacific first proposed by Hays (1970) and then modified by Foreman (1975).

Radiolarians occur at all sites drilled on Leg 86. At Site 581, radiolarians range in age from middle Miocene Pleistocene. Site 578 contains radiolarians characteristic of the late Miocene through Pleistocene. Radiolarians of early Pliocene to Pleistocene age are present at Sites 577 and 579. A late Pliocene to Pleistocene radiolarian assemblage is found in sediments at Site 580. Radiolarians at Site 576 are limited to the Pleistocene.

Table 1. Coordinates and water depths of DSDP Leg 86 sites.

Hole	Latitude	Longitude	Water depth (m)
576	32°21.36′N	164°16.54′E	6217
576A	32°21.38′N	164°16.52′E	6217
576B	32°21.37′N	164°16.52′E	6217
577	32°26.51′N	157°43.40′E	2675
577A	32°26.53′N	157°43.39′E	2675
577B	32°26.48′N	157°43.39′E	2675
578	33°55.56′N	151°37.74′E	6010
579	38°37.68′N	153°50.17′E	5737
579A	38°37.61′N	153°50.28′E	5737
580	41°37.47′N	153°58.58′E	5375
581	43°55.62′N	159°47.76′E	5476

PROCEDURES AND ANALYSES

Up to three samples were taken per core for biostratigraphic analysis. After disaggregation, the sample was sieved at 63 μm. The coarse fraction from sediments at Sites 576 and 577 was strewn on slides. The greater than 63 μm fraction from Sites 578, 579, 580, and 581 was randomly settled onto slides following the technique described by Moore (1973).

Radiolarian preservation is indicated for samples taken at Sites 577 through 581 (Tables 2–6) with abbreviations defined as follows: G (good), signifying that more than half of the specimens are unbroken with minimal dissolution; M (moderate), denoting breakage in more than half the specimens and/or some degree of dissolution; and P (poor), meaning that most specimens were fragmented and/or exhibited a high degree of dissolution. Because samples from Sites 578 through 581 were dried and weighed prior to disaggregation, and slides prepared using the random settling technique, it is possible to calculate the relative abundance of radiolarians per gram of sediment. The abundance values in Tables 3 through 6 are rounded to the nearest thousand radiolarians per gram.

The relative abundance of individual species given in Tables 2 through 6 is based on examination of a minimum of 500 radiolarians per sample with abbreviations defined as follows: r, very rare (0.01–0.10%); R, rare (0.11–1.0%); F, few (1.1–10.0%); C, common (10.1–30.0%); +, one or two specimens present; —, specimens sought but not found.

---

[1] Heath, G. R., Burckle, L. H., et al., *Init. Repts. DSDP*, 86: Washington (U.S. Govt. ng Office).

[2] Address: Lamont-Doherty Geological Observatory of Columbia University, Palisades, 0964.

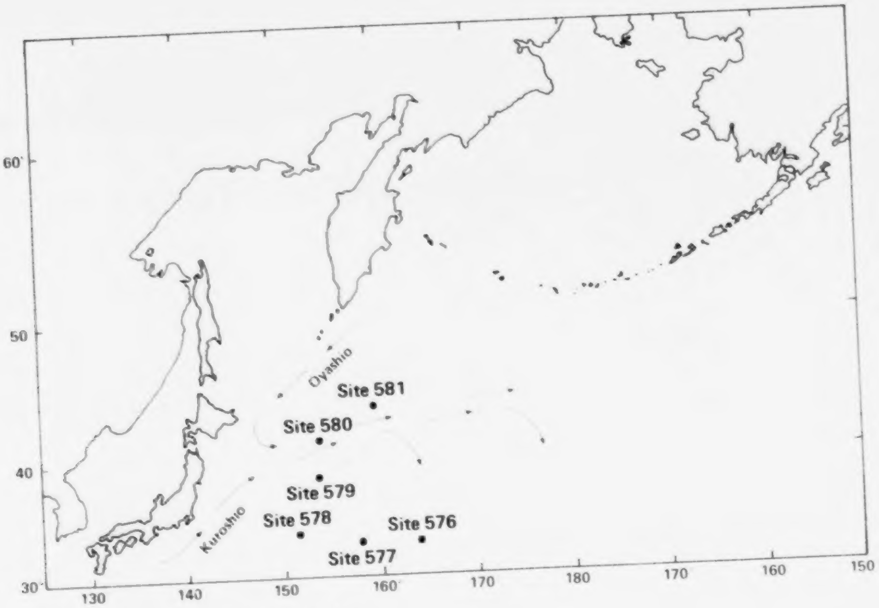

Figure 1. Location of DSDP Leg 86 sites.

BIOSTRATIGRAPHIC FRAMEWORK

The radiolarian zonation proposed by Foreman (1975) was applied to the radiolarian assemblage in the Pliocene through Pleistocene sediment sequence recovered during Leg 86. For the middle to late Miocene radiolarian sequences, the zonation defined by Riedel and Sanfilippo (1978) was appropriate for the radiolarian fauna present. The sites drilled on this leg spanned a wide geographic area of the northwest Pacific, sampling a subtropical to subarctic fauna. Even so, this stratigraphic zonation, with its various datum levels, was easily applied to the sediment sequence from each hole, providing a uniform biostratigraphic framework. The definitions of these zones are as follows:

Botryostrobus aquilonaris Zone, Hays, 1970

The base is defined by the presence of *Botryostrobus aquilonaris* (= *Eucyrtidium tumidulum* of Hays, 1970; = *Artostrobium miralestense* of Kling, 1973; = *Artostrobium tumidulum* of Foreman, 1975) and the absence of *Stylatractus universus* (= *Axoprunum angelium* of Foreman, 1975). The age of the base of this zone is 0.425 m.y. based on the estimated age of the upper limit of *Stylatractus universus* (Hays and Shackleton, 1976; Morley and Shackleton, 1978).

Stylatractus universus Zone, Hays, 1970

The base of this zone is defined by the extinction of *Eucyrtidium matuyamai* and the top by the upper limit of *Stylatractus universus*. The age range of this zone is from 0.97 to 0.425 m.y.

Eucyrtidium matuyamai Zone, Hays, 1970, emend. Foreman, 1973a

This zone is defined by the range of *Eucyrtidium matuyamai* and spans the period from 1.88 to 0.97 m.y.

Lamprocyrtis heteroporos Zone, Hays, 1970, emend. Foreman, 1975

The base of this zone is marked by the extinction of *Stichocorys peregrina*, and the top is defined by the earliest evolutionary appearance of *Eucyrtidium matuyamai*. The zone ranges in age from 2.85 to 1.88 m.y.

Sphaeropyle langii Zone, Foreman, 1975

The base is defined as the first morphological appearance of *Sphaeropyle langii*, and the top is marked by the upper limit of *Stichocorys peregrina*. The age range of this zone is from 4.40 to 2.85 m.y.

Stichocorys peregrina Zone, Riedel and Sanfilippo, 1970, emend. Foreman, 1975

The base is defined by the first evolutionary appearance of *Stichocorys peregrina* and the top by the earliest morphological appearance of *Sphaeropyle langii*. This zone spans the time interval from 6.20 to 4.40 m.y.

Didymocyrtis penultima Zone, Riedel and Sanfilippo, 1970

The base is defined by the first evolutionary appearance of *Didymocyrtis penultima* (= *Ommatartus penultimus* of Riedel and Sanfilippo, 1970) and the top by the first evolutionary appearance of *Stichocorys peregrina*. The age range of this zone is from 7.90 to 6.20 m.y.

Didymocyrtis antepenultima Zone, Riedel and Sanfilippo, 1970, emend. Riedel and Sanfilippo, 1978

The base of this zone is defined by the earliest evolutionary appearance of *Didymocyrtis antepenultima* (= *Ommatartus antepenultimus* of Riedel and Sanfilippo, 1970), and the top is marked by the first evolutionary appearance of *Didymocyrtis penultima*. This zone spans the time interval from 10.80 to 7.90 m.y.

Diartus petterssoni Zone, Riedel and Sanfilippo, 1970, emend. Riedel and Sanfilippo, 1978

The base of this zone is marked by the earliest morphologic appearance of *Diartus petterssoni* (= *Cannartus petterssoni* of Riedel and Sanfilippo, 1970). The top of this zone is defined by the first evolutionary appearance of *Didymocyrtis antepenultima*. The age range of this zone is from 12.50 to 10.80 m.y.

Dorcadospyris alata Zone, Riedel and Sanfilippo, 1970, emend. Riedel and Sanfilippo, 1971

The base of this zone is marked by the first evolutionary appearance of *Dorcadospyris alata*, and the top is delineated by the earliest morphologic appearance of *Diartus petterssoni*. This zone spans the time interval from 15.25 to 12.50 m.y.

RADIOLARIAN SITE SUMMARIES

Site 576

At Site 576, located between the Shatsky Rise and Emperor Seamounts, sediments from three holes (576, 576A, 576B) were recovered using the hydraulic piston corer. Moderately well-preserved late Pleistocene radiolarians are present in the upper few meters of the pelagic lay sequence. The topmost sediments in each of the three ioles contain a fauna characteristic of the *Botryostro- us aquilonaris* Zone, with fauna in the underlying sedi- nents in Core 1 belonging to the *Stylatractus universus* one. Although radiolarians are present in Core 2 from ll three holes, the low abundance and poor preservation revented precise age determination. Radiolarians were bsent from sediments in all three holes below Core 2 ex- pt for Hole 576 which contained traces of a Pleisto- ne(?) fauna in Core 3 (Sample 576-3,CC) and an Up- r Cretaceous(?) fauna in a thin calcareous sequence in ore 8 (Sample 576-8,CC).

te 577

The three holes (577, 577A, 577B) drilled at Site 577 mpled a calcareous sequence on the western flank of e Shatsky Rise. Radiolarians are present in only the rst six cores from Holes 577 (Table 2) and 577A. The ell-preserved fauna in the uppermost sediments from ore 1 is representative of the late Pleistocene *Botryo- robus aquilonaris* Zone. The remainder of Core 1 con- ains a fauna characteristic of the *Stylatractus universus* one. Core 2 through the middle of Core 3 contains good to poorly preserved early Pleistocene radiolarians of the *Eucyrtidium matuyamai* Zone. Some difficulty was encountered in locating the base of this zone in Holes 577 and 577A because of the very low abundance of *E. matuyamai* in Core 3. Radiolarians are moderately to poorly preserved in Cores 4 through 6. Late Pliocene radiolarians of the *Lamprocyrtis heteroporos* Zone are present in sediments from the lower portion of Core 3 through the upper half of Core 4. The remainder of Core 4 through Core 5 contains middle Pliocene radiolarians belonging to the *Sphaeropyle langii* Zone, with the early Pliocene fauna in Core 6 characteristic of the *Stichocorys peregrina* Zone.

Site 578

Hole 578, located west of the Shatsky Rise, sampled thick pelagic clay sequence overlying Cretaceous chert nd chalk. The gray to brown clays in the upper 120 m sediment (Cores 1–14) contain radiolarians (Table 3). adiolarians are not present in the dark brown clays and ert in Cores 15 through 20.

Preservation of the Pleistocene radiolarians in the up- rmost sediments from the first eight cores varies from od to poor. Fauna characteristic of the *Botryostrobus uilonaris* Zone is present in sediments from the tops Cores 1 through 3, with the latest occurrence of *Sty- ractus universus* in Sample 578-3-2, 50–51 cm, mark- g the bottom of this zone (level of datum based on more tensive sampling than shown in Table 3). The remain- r of Core 3 and the uppermost sediments in Cores 4 nd 5 contain radiolarians representative of the *S. uni- rsus* Zone. The presence of *Eucyrtidium matuyamai* sediments at the tops of Cores 6, 7, and 8 indicates at the fauna in these sediments is early Pleistocene in ge, belonging to the *E. matuyamai* Zone.

The fauna in the remainder of Core 8 is characteristic of the late Pliocene *Lamprocyrtis heteroporos* Zone. The top of the *Sphaeropyle langii* Zone is located between Samples 578-8,CC and 578-10-1, 10–11 cm, as marked by the latest occurrence of *Stichocorys peregrina*. The boundary between early and late Pliocene, defined by the upper limit of *S. delmontensis*, occurs within Core 10, with the remainder of Core 11 and the top of Core 12 containing fauna indicative of the middle to lower *Sphaeropyle langii* Zone. Although not delineated by any siliceous faunal marker, the magnetostratigraphy shows that the Miocene/Pliocene boundary occurs near the base of Core 12 (see Site 578 chapter, this volume). Late Miocene radiolarians representative of the *Stichocorys peregrina* Zone are present in sediments from Core 13 and the top of Core 14.

Site 579

Located at the southern limit of the transition zone between subtropical and subarctic gyres, Site 579 contains radiolarians throughout its 150 m of siliceous clays and oozes (Table 4). Radiolarians are well to moderately preserved in late Pliocene through Pleistocene sediments and moderately to poorly preserved in early Pliocene sediments.

The fauna in Hole 579 and in the uppermost sediment from Core 1 in Hole 579A is indicative of the *Botryostrobus aquilonaris* Zone. The top of the *Stylatractus universus* Zone, as marked by the upper limit of *S. universus*, occurs between Samples 579A-1-3, 145–147 cm and 579A-1-4, 5–7 cm (based on more extensive sampling than shown in Table 4). Radiolarians present in sediments from Core 2 from Hole 579A are also representative of this zone. The *Eucyrtidium matuyamai* Zone extends from the lower portion of Core 3 through at least the bottom of Core 5 based on the occurrence of *E. matuyamai* throughout this sediment sequence. Sediments in Cores 6 through 8 from Hole 579A contain a radiolarian fauna characteristic of the *Lamprocyrtis heteroporos* Zone, with the bottom of this zone marked by the latest occurrence of *Stichocorys peregrina* located between Samples 579A-8,CC (25–27 cm) and 579A-9,CC (5–7 cm). The upper limit of *S. delmontensis* occurs between Samples 579A-10,CC (15–17 cm) and 579A-11,CC (5–7 cm), indicating that the boundary between early and late Pliocene is located within Core 11. Radiolarians in sediments in Cores 9 through 12 from Hole 579A are representative of the *Sphaeropyle langii* Zone, while Cores 13 through 15 from Hole 579A contain an early Pliocene radiolarian fauna belonging to the *Stichocorys peregrina* Zone.

Site 580

At Site 580, located near the present-day subarctic front, sediments were recovered to a sub-bottom depth of 155 m. The radiolarians that are present throughout the siliceous clay to clayey diatom ooze sediment sequence are well to moderately preserved (Table 5).

The first three cores contain a late Pleistocene radiolarian fauna representative of the *Botryostrobus aquilonaris* Zone. Examination of closely spaced samples from Cores 4 through 7 (not all shown in Table 5) shows that

Table 2. Abundances of some radiolarians from Hole 577.

Epoch	Zone	Core-Section (interval in cm)	Preservation (poor, moderate, good)	*Lamprocyrtis nigriniae*	*Spongaster tetras irregularis*	*Cycladophora davisiana*	*Theocorythium trachelium trachelium*	*Theocorythium trachelium dianae*	*Spongurus pylomaticus*	*Botryostrobus aquilonaris*	*Sphaeropyle langii*	*Phormostichoartus corbula*	*Euchitonia* sp.	*Larcospira quadrangula*	*Didymocyrtis tetrathalamus*	*Lamprocyclas maritalis*	*Druppatractus acquilonius*	*Pterocorys zancleus*	*Saturnalis circularis*	*Eucyrtidium acuminatum*	*Heliodiscus asteriscus*	*Spongocore puella*	*Clathrocyclas* spp.	*Cycladophora davisiana cornutoides*	*Cornutella profunda*	*Carpocanistrum* spp.	*Actinomma medianum*	*Spongopyle osculosa*	*Spongotrochus venustum*	*Lychnocanoma grande*	*Eucyrtidium calvertense*	*Stylatractus universus*	*Eucyrtidium matuyamai*	*Lamprocyrtis neoheteroporos*	*Lamprocyrtis heteroporos*	*Sphaeropyle robusta*	*Pterocanium prismatium*	*Stichocorys peregrina*	*Stichocorys delmontensis*
Pleistocene	*B. aquilonaris*	1-1, 5-6	G	R	—	R	R	R	R	R	r	R	R	R	F	R	—	F	—	F	R	R	R	—	r	R	R	R	F	—	r	—		—					
	S. universus	1-3, 65-66	M	R	—	F	r	R	r	R	+	+	+	R	R	R	R	R	r	R	R	+	F	r	+	R	R	r	F	R	r	r	—	R					
		1,CC	G	R	r	F	R	R	+	r	R	+	+	R	F	R	r	F	r	R	R	r	F	—	+	F	R	F	F	R	R	R	—	R	—				
	E. matuyamai	2-4, 63-64	G	r	r	F	r	r	R	R	+	R	r	R	F	F	R	F	r	R	R	r	F	+	r	F	R	R	F	+	R	R	r	R	r	—			
		2,CC	P	—	—	F	+	+	+	+	R	+	+	+	+	F	F	+	+	+	R	+	F	—	R	F	R	R	F	+	R	R	+	R	F	R			
		3-4, 67-68	G	—	—	F	R	R	+	R	+	r	R	R	F	R	R	R	R	F	R	R	F	R	R	F	R	R	F	—	r	R	r	+	R	+	—		
Pliocene	*L. heteroporos*	3,CC	G		—	R	R	R	R	R	r	+	+	R	F	R	R	R	R	R	R	R	F	r	+	F	R	R	F	—	R	R	—	r	R	r	+		
		4-4, 25-26	M			R	R	+	R	+	+	—	R	R	R	R	R	+	+	R	R	+	F	R	—	F	R	F	F	+	R	R	—	—	R	R	—	—	
	S. langii	4,CC	M			—	—	—	+	R	+	—	R	R	R	F	+	R	R	F	+	+	F	R	—	F	R	R	F	R	+	+	—	—	+	R	+	F	—
		5-3, 70-71	P			—	—	—	—	—	R	—	—	R	R	R	R	+	R	R	R	R	F	+	R	F	R	R	F	—	R	R	—	—	R	+		R	R
		5,CC	M			—	—	—		—	+		—	r	+	R	—	—	+	R	R	+	R	r	—	F	+	r	F	—	R	R			—	R		F	F
	S. peregrina	6-4, 57-58	P								—			R	—	R	—		R	R	R	+	F	—	R	F	+	R	F	R	R	R			—	R		C	F
		6,CC	P								—			F		R	—		+	F	R	R	F	—	R	F		R	F	—	R	R			—	R		F	F

Note: Cores 7-13 are barren of radiolaria. See Procedures and Analyses for explanation of entries.

Table 3. Abundances of some radiolarians from Hole 578.

Epoch	Zone	Core-Section (interval in cm)	Radiolarian abundance (thousands per gram of sediment)	Preservation (poor, moderate, good)	*Lamprocyrtis nigriniae*	*Spongaster tetras irregularis*	*Cycladophora davisiana*	*Theocorythium trachelium trachelium*	*Theocorythium trachelium dianae*	*Spongurus pylomaticus*	*Botryostrobus aquilonaris*	*Sphaeropyle langii*	*Phormostichoartus corbula*	*Euchitonia* sp.	*Larcospira quadrangula*	*Didymocyrtis tetrathalamus*	*Lamprocyclas maritalis*	*Druppatractus acquilonius*	*Pterocorys zancleus*	*Saturnalis circularis*	*Eucyrtidium acuminatum*	*Heliodiscus asteriscus*	*Spongocore puella*	*Clathrocyclas* spp.	*Cycladophora davisiana cornutoides*	*Cornutella profunda*	*Carpocanistrum* spp.	*Actinomma medianum*	*Spongopyle osculosa*	*Spongotrochus venustum*	*Lychnocanoma grande*	*Eucyrtidium calvertense*	*Stylatractus universus*	*Eucyrtidium matuyamai*	*Lamprocyrtis neoheteroporos*	*Lamprocyrtis heteroporos*	*Sphaeropyle robusta*	*Pterocanium prismatium*	*Stichocorys peregrina*	*Stichocorys delmontensis*
Pleistocene	*B. aquilonaris*	1-1, 10–11	66	M-P	—	—	R	R	R	+	+	+	—	R	—	R	R	—	F	—	R	+	+	R	R	R	R	R	R	F	—	—	—							
		2-1, 1–2	19	P	—	R	F	+	R	+	R	—	—	+	R	F	R	—	F	+	R	R	R	F	R	+	+	R	R	C	—	—	—							
		3-1, 1–2	29	M	—	—	F	R	R	—	+	+	—	+	R	F	R	+	F	R	F	R	R	F	R	R	F	R	R	F	—	—	—		—					
	S. universus	4-1, 1–2	12	P	—	—	F	R	R	—	R	R	—	—	+	F	+	R	F	—	F	R	R	F	+	—	F	R	F	C	—	—	R	—	—	—				
		5-1, 10–12	37	M	—	—	F	+	R	R	R	R		—	R	F	R	+	R	R	F	R	R	F	R	—	F	R	F	F	R	R	+	—	—	—	—			
	E. matuyamai	6-1, 12–14	22	M	+	R	R	R	+	+	+	+		+	+	F	R	R	F	R	R	R	R	F	+	+	F	R	R	C	—	R	+	+	—	R	—	—		
		7-1, 100–102	41	G-M	—	—	F	F	R	R	R	+		R	R	R	R	+	R	R	+	R	R	F	R	R	R	R	R	F	+	R	R	+	+	R	R	+	—	
		8-1, 30–32	25	M	—	—	R	+	+	+	R	+		+	—	R	R	R	R	R	R	R	R	F	R	R	R	R	R	C	—	R	+	R	R	+	R	—	—	
Pliocene	*L. heteroporos*	8,CC	5	M		—	F	R	R	—	R	R		—	—	R	R	R	—	+	R	R	+	F	+	R	F	R	R	F	R	R	R	—	—	—	R	—	—	—
	S. langii	10-1, 10–11	35	M			—	—	R	—	R	R		R	—	F	R	R	—	R	F	R	R	F	R	R	F	—	R	F	+	R	R	—	—	—	R		R	—
		11-1, 15–17	50	G-M			—	—	—	—	—	R		—	R	R	R	R	R	+	R	R	+	R	R	+	F	+	R	F	—	+	R	—	—	—	+		F	R
		12-1, 15–17	46	G			—	—	—		—	R		—	R	R	—	R	—	R	R	R	—	R	R	—	R	R	R	C	—	R	+		R	—		F	R	
late Miocene	*S. peregrina*	13-1, 20–22	44	M			—		—		—	—			—	R	+	R	—	+	R	R	—	R	R	R	R	+	R	F	—	+	R		—	R		F	R	
		14-1, 80–82	6	M-P								—			R	R	R	R	—	R	R	F	F	F	R	R	F	F	F	C	R	R	R		—	+		R	+	

Note: Cores 15–20 are barren of radiolaria. See Procedures and Analyses for explanation of entries.

Table 4. Abundances of some radiolarians from Holes 579 and 579A.

Epoch	Zone	Core-Section (interval in cm)	Radiolarian abundance (thousands per gram of sediment)	Preservation (poor, moderate, good)	*Lamprocyrtis nigriniae*	*Spongaster tetras irregularis*	*Cycladophora davisiana*	*Theocorythium trachelium trachelium*	*Theocorythium trachelium dianae*	*Spongurus pylomaticus*	*Botryostrobus aquilonaris*	*Sphaeropyle langii*	*Phormostichoartus corbula*	*Euchitonia* sp.	*Larcospira quadrangula*	*Didymocyrtis tetrathalamus*	*Lamprocyclas maritalis*	*Druppatractus acquilonius*	*Pterocorys zancleus*	*Saturnalis circularis*	*Eucyrtidium acuminatum*	*Heliodiscus asteriscus*	*Spongocore puella*	*Clathrocyclas* spp.	*Cycladophora davisiana cornutoides*	*Cornutella profunda*	*Carpocanistrum* spp.	*Actinomma medianum*	*Spongopyle osculosa*	*Spongotrochus venustum*	*Lychnocanoma grande*	*Eucyrtidium calvertense*	*Stylatractus universus*	*Eucyrtidium matuyamai*	*Lamprocyrtis neoheteroporos*	*Lamprocyrtis heteroporos*	*Sphaeropyle robusta*	*Pterocanium prismatium*	*Stichocorys peregrina*	*Stichocorys delmontensis*
Pleistocene	*B. aquilonaris*	**Hole 579**																																						
		1-1, 4-6	102	G	+	r	F	r	R	R	R	R	—	R	R	F	r	—	F	r	F	R	R	R	R	r	R	R	R	F	—	—	—							
		1,CC (16-18)	40	G	R	—	F	R	R	+	R	R	—	+	R	R	+	—	F	+	R	R	R	R	R	+	R	R	R	F	R	—	—							
		2,CC (11-13)	35	G	R	—	F	+	+	R	R	R	—	R	R	R	+	—	R	R	R	R	R	R	—	+	R	F	+	C	R	—	—							
		Hole 579A																																						
		1-1, 5-7	63	M	r	—	F	+	+	R	R	R	—	+	+	R	r	—	F	+	R	r	+	F	R	R	R	R	+	C	R	r	—		—					
	S. universus	1,CC (17-19)	42	G	—	R	F	+	+	+	R	—	—	+	R	F	R	R	F	+	R	R	R	R	+	R	R	R	R	F	R	R	R		—					
		2-7, 42-49	49	G	—	R	F	R	—	R	R	+	R	—	R	F	R	+	R	R	F	R	+	R	R	R	R	R	R	F	R	—	R	—	—	—				
	E. matuyamai	3,CC (4-6)	32	M	—	R	F	R	—	+	+	R	—	R	R	R	R	+	R	R	R	R	R	F	R	R	F	R	R	C	+	+	R	R	—	—	—			
		4,CC (10-12)	20	M	—	—	F	R	+	R	R	R	—	+	R	F	R	R	+	R	F	R	R	F	R	+	R	R	F	C	—	R	F	+	—	+	—	—		
		5-6, 126-128	33	M		—	F	R	R	R	R	+	R	—	+	F	+	R	+	R	R	R	+	F	R	R	R	F	R	C	—	R	R	R	+	+	R	—		
Pliocene	*L. heteroporos*	6,CC (15-17)	48	M		—	F	+	—	+	R	+	—	+	—	R	+	R	—	R	R	R	+	F	R	+	R	F	R	C	—	—	R	—	+	R	R	—		
		7-6, 70-72	89	G			F	R	—	R	+	+	—	—	—	R	+	R	—	R	R	R	+	F	F	R	R	F	F	C	—	R	R	—	—	R	R	—	—	
		8,CC (25-27)	72	M			R	+	R	R	R	R	—	+	R	R	R	+	R	R	R	R	R	F	—	+	F	F	R	C	—	R	R	—	—	R	R	—	—	
	S. langii	9,CC (5-7)	53	M			—	—	—	R	R	R	—	+	—	R	R	R	—	R	R	R	R	F	R	F	R	R	R	F	—	+	R	—	—	+	R		R	—
		10,CC (15-17)	40	M-P			—	—	R	+	—	R	—	—	—	R	R	—	—	R	R	R	—	F	R	R	R	+	F	C	R	R	R		—	+	R		+	—
		11,CC (5-7)	44	M-P			—	—	—	R	—	R	—	—	R	R	R	R	—	+	R	—	R	R	R	R	R	R	R	C	R	—	R			R	—		R	R
		12,CC (23-25)	83	M-P			—	—	—	+	—	+	R	—	R	R	R	R		R	R	R	R	R	R	R	R	R	R	C	R	R	F			—	R		R	R
	S. peregrina	13,CC	60	M-P					—	—		—	R	—	F	R	+	—		+	R	+	R	F	F	R	R	—	R	C	—	—	+			—	+		R	R
		14,CC	54	P						—		—	—	R	R	R	—	—		R	R	R	R	R	R	—	R	R	F	F	—	R	R				—		F	R
		15,CC	55	P						—		—	—	—	R	R	+	—		R	R	R	—	R	+	+	R	R	R	F	—	+	+				+		F	F

Note: See Procedures and Analyses for explanation of entries.

Table 5. Abundances of some radiolarians from Hole 580.

Epoch	Zone	Core-Section (interval in cm)	Radiolarian abundance (thousands per gram of sediment)	Preservation (poor, moderate, good)	*Lamprocyrtis nigriniae*	*Spongaster tetras irregularis*	*Cycladophora davisiana*	*Theocorythium trachelium trachelium*	*Theocorythium trachelium dianae*	*Spongurus pylomaticus*	*Botryostrobus aquilonaris*	*Sphaeropyle langii*	*Phormostichoartus corbula*	*Euchitonia* sp.	*Larcospira quadrangula*	*Didymocyrtis tetrathalamus*	*Lamprocyclas maritalis*	*Druppatractus acquilonius*	*Pterocorys zancleus*	*Saturnalis circularis*	*Eucyrtidium acuminatum*	*Heliodiscus asteriscus*	*Spongocore puella*	*Clathrocyclas* spp.	*Cycladophora davisiana cornutoides*	*Cornutella profunda*	*Carpocanistrum* spp.	*Actinomma medianum*	*Spongopyle osculosa*	*Spongotrochus venustum*	*Lychnocanoma grande*	*Eucyrtidium calvertense*	*Stylatractus universus*	*Eucyrtidium matuyamai*	*Lamprocyrtis neoheteroporos*	*Lamprocyrtis heteroporos*	*Sphaeropyle robusta*	*Pterocanium prismatium*	*Stichocorys peregrina*	*Stichocorys delmontensis*
Pleistocene	*B. aquilonaris*	1-1, 3-5	52	G	—	R	R	+	+	R	F	+	—	R	—	R	—	—	F	+	R	—	R	F	R	+	R	F	+	C	—	—	—							
		1,CC (5-7)	20	G	—	—	F	+	R	R	R	R	—	R	R	+	—	—	F	+	R	R	+	R	R	R	—	R	R	C	R	—	—							
		2,CC (5-7)	12	G	—	—	C	+	+	+	+	+	—	+	—	+	—	—	F	+	R	—	R	F	R	R	—	R	+	F	F	—	—							
		3-6, 105-107	18	G	R	R	F	+	+	R	+	R	—	+	—	+	—	R	R	R	R	R	R	F	R	R	R	R	R	C	F	—	—		—					
	S. universus	4,CC (20-22)	21	G	R	R	F	—	—	R	R	R	—	R	R	F	—	R	F	—	R	R	R	F	R	—	R	F	F	F	F	R	+	—	—	—				
		5,CC (30-32)	15	G	—	—	C	—	R	+	R	R	—	—	—	R	—	R	F	—	R	R	—	F	R	+	R	R	F	C	+	—	R	—	—	—	—			
		6,CC (26-28)	23	G	—	—	F	—	R	R	—	R	—	—	R	+	—	R	F	R	R	R	R	F	F	R	R	R	F	F	R	—	R	—	R	—	—			
	E. matuyamai	7-6, 5-7	12	M	—	—	C	R	—	R	—	R	—	—	—	R	+	—	+	R	R	—	—	R	R	—	+	R	F	C	R	+	R	F	—	R	—			
		8,CC (30-32)	16	G	—	—	F	—	—	R	—	R	—	—	—	R	—	R	—	R	R	R	—	R	R	+	—	R	F	C	+	+	R	R	—	—	+			
		9,CC (35-37)	32	G			F	—	—	+	+	+	—	R	—	+	+	R	R	R	R	+	—	F	R	R	R	R	R	C	R	+	F	+	+	R	R	—		
		10,CC (35-37)	39	G			F	+	—	R	—	+	+	—	—	R	+	R	—	R	R	R	R	R	R	R	+	R	F	C	R	+	R	+	R	R	+	+		
Pliocene	*L. heteroporos*	11,CC (20-22)	34	G			F	—	—	+	+	R	—	—	—	+	—	R	—	—	R	+	+	R	R	R	R	F	F	C	R	+	R	—	R	F	R	—		
		12,CC (10-12)	40	G			F	—		+	R	+	R	—		R	—	R	—	—	R	R	+	F	F	R	R	F	F	F	+	+	+	—	—	R	R	—		
		13,CC (5-7)	61	G			F	—		R	—	r	R	r		R	—	+	—	r	R	+	+	R	F	F	R	R	R	F	R	—	R	—	—	R	r			
		14,CC (5-7)	37	G			F	—		+	—	+	R	R		R	—	R	—	R	R	+	+	R	F	R	R	R	F	C	—	+	R	—	—	R	R		—	
		15,CC (5-7)	47	G			R			R	R	R	—	—		+	R	+	R	R	R	R	R	F	F	R	R	—	F	C	+	+	R		—	R	R		—	
	S. langii	16-6, 120-122	44	G			—			+	R	—	—	—		R	—	R	—	R	R	R	+	R	R	R	R	+	F	F	R	+	R			R	R		R	—
		17,CC (13-15)	40	G			—			+	—	R		—		R	R	R	—	R	—	+	—	F	F	R	R	R	F	F	—	+	R			R	R		R	—

Note: See Procedures and Analyses for explanation of entries.

the upper limit of *Stylatractus universus* occurs between Samples 580-4-1, 65–67 cm and 580-4-1, 95–97 cm, with the upper limit of *Eucyrtidium matuyamai* occurring between Samples 580-7-2, 5–7 cm and 580-7-2, 35–37 cm. These two biostratigraphic datum levels define the top and bottom of the *S. universus* Zone. The first occurrence of *E. matuyamai* is found in the uppermost sample from Core 11 (Sample 580-11-1, 10–11 cm, based on more extensive sampling than shown in Table 5), indicating that the early Pleistocene *E. matuyamai* Zone extends from Core 7 through Core 10. Fauna characteristic of the late Pliocene *Lamprocyrtis heteroporos* Zone is present in Cores 11 through 15, with the bottom of this zone coinciding with the latest occurrence of *Stichocorys peregrina* located between Samples 580-15,CC (5–7 cm) and 580-16-6, 120-122 cm. The radiolarians in sediments from Cores 16 and 17 are representative of the *Sphaeropyle langii* Zone. The absence of *Stichocorys delmontensis* from the oldest sediment recovered from Hole 580 in conjunction with the magnetostratigraphy indicates that drilling terminated above the biostratigraphic and paleomagnetic boundary between early and late Pliocene.

Site 581

Site 581 was selected to sample siliceous sediments in a high-deposition subarctic setting. Radiolarians with various states of preservation are preserved in Neogene and Quaternary siliceous clay sediments from this site (Table 6).

The echo character of the seismic profiles from this site suggests that the uppermost sediment may represent a debris-flow deposit. Although a mixed fauna was not detected in Core 1 collected at the mudline, the radiolarians present throughout this core are characteristic of the *Stylatractus universus* Zone, indicating that either latest Pleistocene sediments containing fauna of the *Botryostrobus aquilonaris* Zone were not deposited at this site or these younger sediments were reworked into older late Pleistocene sediments as a result of some bottom-current process. Because of the overall high Neogene and Quaternary siliceous sedimentation rates and the nature of the seismic profiles at this site, the latter hypothesis appears more plausible. Because of time constraints no sediment was recovered from approximately the next 181 m of sediment. Continuous rotary drilling commenced at a sub-bottom depth of 181.5 m. Fauna in the uppermost sediments from Core 2 (Sample 581-2-1, 10-12 cm) is representative of the early Pliocene marked by the presence of *Stichocorys delmontensis* and *Sphaeropyle langii*. Likewise, the radiolarians present in the remainder of Core 2 are characteristic of the early Pliocene *S. langii* Zone. The sediment sequence from Core 3 through the top of Core 5 contains a fauna characteristic of the *Stichocorys peregrina* Zone. The fauna in the remainder of Core 5 through the top of Core 6 is representative of the *Didymocyrtis penultima* Zone. The *Didymocyrtis antepenultima* Zone extends throughout most of Core 6 into the upper portion of Core 7, with the radiolarians in the remainder of Core 7 into the top of Core 8 indicative of the *Diartus petterssoni* Zone. The fauna in most of Core 8 and in that portion of Core 9 where radiolarians are present is characteristic of the *Dorcadospyris alata* Zone.

STRATIGRAPHIC AND GEOGRAPHIC RADIOLARIAN RANGES

A complete stratigraphic range chart for selected Neogene and Quaternary radiolarians in sediments from Sites 577 through 581 is shown in Figure 2. The high recovery rate and quality of radiolarian preservation at the various sites drilled during Leg 86 make it possible to examine various biostratigraphic datum levels across a broad latitudinal band (~12°). These analyses are summarized as follows:

1. The last abundant appearance of *Lychnocanoma grande* occurs near the top of the *Botryostrobus aquilonaris* Zone. Analyses of the correlation of this datum level with the relative abundance pattern of *Cycladophora davisiana* at closely spaced sample intervals at Sites 579 and 580 (not all shown in Tables 4 and 5) shows that this event is synchronous in this region.
2. Correlation of the latest occurrence of *Druppatractus acquilonius* with the relative abundance pattern of *C. davisiana* at closely spaced sample intervals at Sites 579 and 580 (not all shown in Tables 4 and 5) indicates that this datum is synchronous in this region, occurring just above the base of the *B. aquilonaris* Zone.
3. Based on correlation with the relative abundance pattern of *C. davisiana* and specific ash layers in sediments from Sites 579 and 580 (not all samples shown in Tables 4 and 5), the latest occurrence of *Stylatractus universus* appears to be synchronous throughout the region, confirming the results reported by Hays and Shackleton (1976) and Morley and Shackleton (1978).
4. Examination at closely spaced sample intervals at Sites 579 and 580 (not all shown in Tables 4 and 5) indicates that the latest occurrence of *Eucyrtidium matuyamai* occurs just above the base of the Jaramillo Subchronozone. Although samples were not taken at close intervals at Sites 577 or 578, the preliminary findings from these sites are in agreement with those from Sites 579 and 580, indicating that this event is synchronous throughout the northwest Pacific.
5. Because of the scarcity of *E. matuyamai* and close morphological characteristics to *E. calvertense* at the time of its first appearance, it is difficult to define the first occurrence of *E. matuyamai* as precisely as the previous four biostratigraphic markers. Detailed analyses at Sites 579 and 580 (not all samples shown in Tables 4 and 5), however, indicate that this datum level occurs within the Olduvai Subchronozone, which is in agreement with the previous findings of Hays (1970) and Kellogg and Hays (1975). Preliminary analyses of this species throughout its range indicate that the mean shell width of this assemblage is smallest in the southernmost site (Site 578) and largest in the northernmost site (Site 580). Hays (1970) first suggested that such a trend existed from his analyses of samples from several lower-sedimentation-rate cores in the North Pacific.
6. *Pterocanium prismatium* was present in samples from Holes 577, 578, and 580. The latest occurrence of *P. prismatium* in Hole 577 is located between Samples 577-3-4, 67–68 cm and 577-3,CC. The Pliocene/Pleisto-

Table 6. Abundances of some radiolarians from Hole 581.

Epoch	Zone	Core-Section (interval in cm)	Radiolarian abundance (thousands per gram of sediment)	Preservation (poor, moderate, good)	*Cycladophora davisiana*	*Spongurus pylomaticus*	*Botryostrobus aquilonaris*	*Sphaeropyle langii*	*Phormostichoartus corbula*	*Larcospira quadrangula*	*Didymocyrtis tetrathalamus*	*Lamprocyclas maritalis*	*Druppatractus acquilonius*	*Pterocorys zancleus*	*Saturnalis circularis*	*Eucyrtidium acuminatum*	*Heliodiscus asteriscus*	*Spongocore puella*	*Clathrocyclas* spp.	*Cycladophora davisiana cornutoides*	*Cornutella profunda*	*Carpocanistrum* spp.	*Actinomma medianum*	*Spongopyle osculosa*	*Spongotrochus venustum*	*Lychnocanoma grande*	*Eucyrtidium calvertense*	*Stylatractus universus*	*Lamprocyrtis heteroporos*	*Sphaeropyle robusta*	*Stichocorys peregrina*	*Stichocorys delmontensis*	*Didymocyrtis penultima*	*Didymocyrtis antepenultima*	*Diartus hughesi*	*Diartus petterssoni*	*Didymocyrtis laticonus*	*Cyrtocapsella japonica*	*Cyrtocapsella cornuta*	*Cyrtocapsella tetrapera*
Pleistocene	*S. universus*	1-1, 9-10	96	G	F	F	F	R	—	R	+	R	+	F	—	R	—	R	F	R	R	R	R	R	F	F	—	R	—	—										
		1,CC	43	G	C	R	F	R	R	+	R	+	+	F	—	R	—	R	F	F	R	—	R	R	F	F	—	R	—	—										
Pliocene	*S. langii*	2-1, 10-12	36	G	—	+	+	R	—	—	R	R	R	+	R	—	R	R	R	R	R	—	R	R	C	F	—	F	F	R	F	F								
		2,CC	56	G-M	—	—	—	+	—	—	+	—	R	—	—	+	R	R	R	R	R	—	+	R	C	+	+	F	R	+	F	R								
	S. peregrina	3,CC	62	M-P		—	—	—	R	—	R	—	R	R	R	R	R	R	F	R	R	—	R	R	C	R	—	R	—	—	F	R	—							
Late Miocene		5-1, 110-112	85	G-M				—	—		—	—	+	R	—	—	R	+	R	R	+	R	R	R	F	R	—	R	—	R	F	F	—	—						
	D. penultima	6-1, 70-72	150	G-M					—		—		—	R	+	R	+	—	R	R	R	R	R'	R	F	+	+	R		+	R	F	R	—	—					
	D. antepenultima	7-1, 60-62	126	G-M					—				—	—	—	R	R	R	R	R	R	R	R	R	C	—	—	F		R	R	F	—	R	R	—	—	—		
Mid Miocene	*D. petterssoni*	8-1, 70-72	134	M-P										—	—	—	R	+	R	R	R	R	—	F	F	R	+	R		+	+	R	—	—	+	R	R	F	—	—
	D. alata	9-1, 40-42	15	P												—	—	—	—	R	R	R	R	F	F	F	—	F		R	—	+		—	—	—	—	R	F	C

Note: Cores 10-11 are barren of radiolaria. See Procedures and Analyses for explanation of entries.

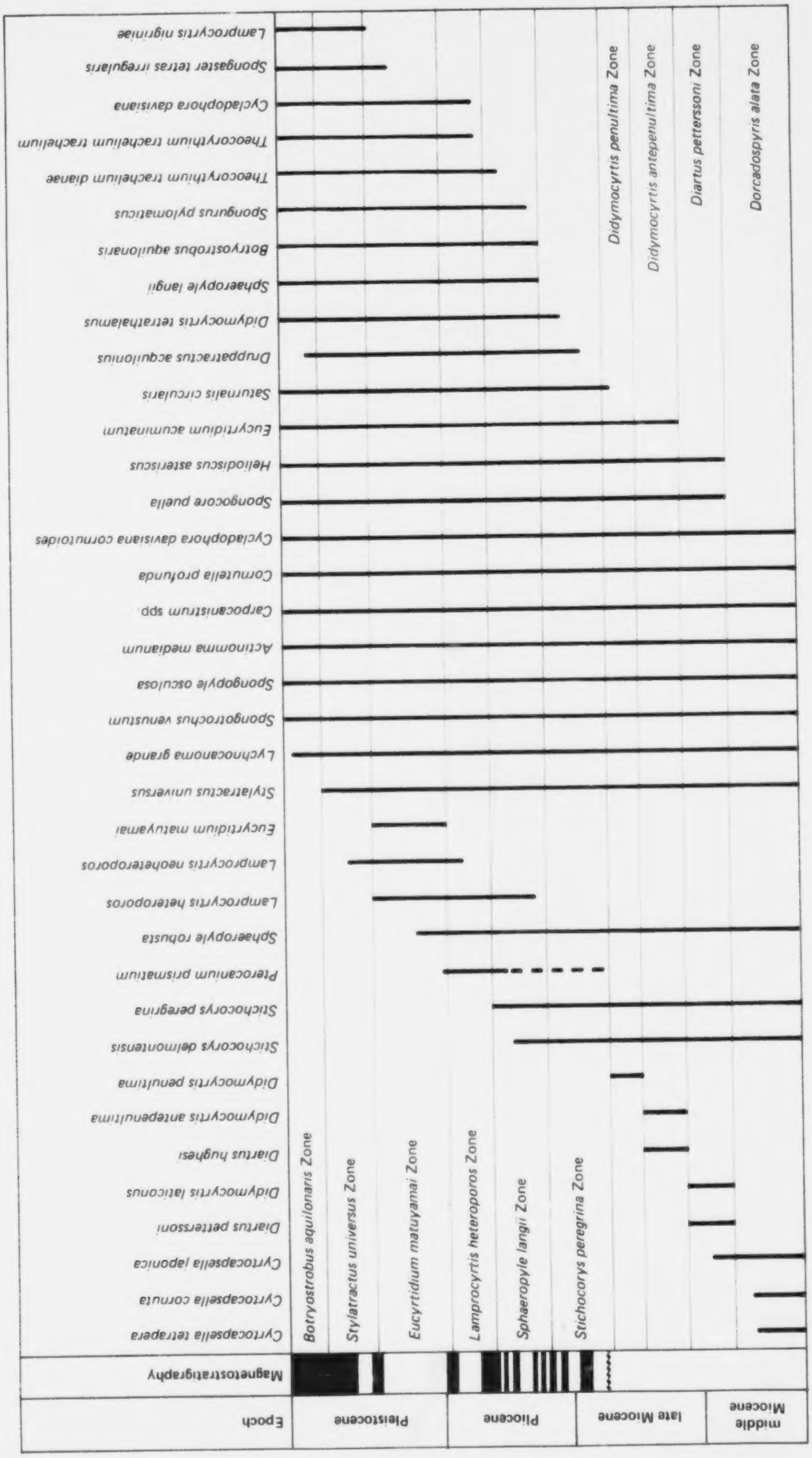

Figure 2. Range chart for Neogene and Quaternary radiolarians from DSDP Leg 86 sites.

cene boundary based on magnetostratigraphy occurs in the middle of Core 3. At Site 578, the latest occurrence of *P. prismatium* is positioned less than a meter above the top of the Olduvai Subchronozone (Pliocene/Pleistocene boundary). This biostratigraphic marker occurs between Samples 580-9,CC (35-37 cm) and 580-10,CC 35-37 cm) in sediments from Hole 580, with the Olduvai Subchronozone spanning the lower 6 m of Core 10 hrough the top meter of Core 11. These data show that *P. prismatium* ranges as far north as 42°N latitude in he Pacific and that although very rare in abundance, its ipper limit occurs near the Pliocene/Pleistocene boundary based on magnetostratigraphy.

7. At most sites drilled on Leg 86, the latest occurrence of *Lamprocyrtis heteroporos* was recorded near the op of the early Pleistocene *Eucyrtidium matuyamai* Zone.

8. Based on examination of samples at closely spaced ntervals at Sites 579 and 580 (not all shown in Tables 4 nd 5), the first occurrence of *Cycladophora davisiana* occurs in the upper Gauss Chronozone near the base of he *Lamprocyrtis heteroporos* Zone approximately 2.7 m.y. ago.

9. Preliminary analyses indicate that *Lamprocyrtis neoheteroporos* ranges from the upper third of the *L. heteroporos* Zone through the lower two-fifths of the *Stylatractus universus* Zone. A similar range for this species in sediments from this region was reported by Foreman (1975).

10. At the sites where *Theocorythium trachelium trachelium* was present in high enough abundances (Sites 577, 578, 579), the first occurrence of this species was detected at or near the base of the *L. heteroporos* Zone, which is in agreement with analyses reported by Foreman (1975).

11. The latest occurrence of *Stichocorys peregrina* was well documented in sediment sequences from all sites drilled during Leg 86 except Site 576 where radiolarians were not present in sediments older than Pleistocene. This event serves as an easily recognizable boundary between the bottom of the *Lamprocyrtis heteroporos* Zone and the op of the *Sphaeropyle langii* Zone throughout the northwest Pacific.

12. The latest occurrence of *Stichocorys delmontensis* coincides with both the Gilbert/Gauss magnetic polarity boundary and the early/late Pliocene boundary. his event is easily identified in samples from sites drilled n Leg 86 which contained siliceous sediments of this ge (Sites 577, 578, 579).

13. The first occurrence of *Lamprocyrtis heteroporos* ccurs near the base of the *Sphaeropyle langii* Zone.

14. Although the first occurrence of *Sphaeropyle langii* as registered in sediments from Sites 577, 578, 579, nd 581 assisted in defining the top of the *Stichocorys peregrina* Zone, it was difficult at times to distinguish nis species from others, such as *Sphaeropyle robusta*. he low abundance of this species in some samples made difficult to identify the boundary between the *Stichocorys peregrina* Zone and the *Sphaeropyle langii* Zone.

15. At Site 581, the range of *Didymocyrtis penultima* was used to delineate the *D. penultima* Zone.

16. The range of *D. antepenultima* was used to define the *D. antepenultima* Zone at Site 581.

17. At Site 581, the ranges of *Diartus petterssoni* and *Didymocyrtis laticonus* were used to define the *Diartus petterssoni* Zone.

18. Preliminary analyses of samples from Site 581 indicate that the latest occurrence of *Cyrtocapsella japonica* occurred somewhere within the *Diartus petterssoni* Zone. This agrees with results from DSDP sites near Japan reported by Sakai (1980).

19. Results from Site 581 agree with that reported by Sakai (1980), placing the latest occurrence of *C. tetrapera* and *C. cornuta* in the upper half of the *Dorcadospyris alata* Zone.

PALEOCEANOGRAPHY

One of the major objectives of Leg 86 was to determine whether the initiation of significant biosiliceous accumulation in the Neogene was synchronous or transitional at the four sites roughly aligned along a north-south transect (Sites 578, 579, 580, and 581) in the northwest Pacific. Although the hydraulic piston core did not penetrate deep enough to recover sediments recording this event at Sites 579 and 580, the onset of biosiliceous sedimentation in the northwest Pacific was recovered in sediments at the southernmost (Site 578) and northernmost (Site 581) sites. At Site 578, biosiliceous sedimentation commenced in the late Miocene with earliest radiolarian fauna characteristic of the *Stichocorys peregrina* Zone, whereas at Site 581, biosiliceous sedimentation began in the middle Miocene with the oldest Neogene radiolarians representative of the *Dorcadospyris alata* Zone. Therefore, the initiation of Miocene biosiliceous sedimentation in the northwest Pacific as recorded in sediments along this north-south transect marks the time when each specific site exited from the low-productivity central gyre and moved into the preexisting high-productivity belt at the gyre margins.

Within the period of biosiliceous sedimentation recorded in sediments from the northwest Pacific, a relative measure of radiolarian productivity can be acquired from calculations of the number of radiolarians per gram of sediment. This value was computed in samples from Sites 578, 579, 580, and 581 (Tables 3 through 6). From comparison of these numbers in each of the holes, regional pulses and/or trends in radiolarian productivity can be detected. Specifically, Sites 579 and 580 record a nearly continuous increase in productivity through the early and middle portion of the late Pliocene coincident with the Gauss Chronozone. This trend toward increasing radiolarian productivity levels reaches a maximum early in the Matuyama Chronozone between 2.3 and 2.4 m.y. ago. Radiolarian productivity decreases from these high late Pliocene values, remaining relatively low throughout the early Pleistocene at Sites 578, 579, and 580. Late Pleistocene biosiliceous productivity is somewhat higher than that recorded for the early Pleistocene, with indications of minor productivity increases in the early, middle, and latest Pleistocene.

SYSTEMATICS

The classification scheme is adapted from Riedel and Sanfilippo (1977) with minor variations following Hays (1970) and Nigrini and Moore (1979). Minimal synonomies of taxa are presented with restriction to original description and those that reflect current usage. Species arranged alphabetically by family.

Subclass RADIOLARIA Müller 1858
Superorder POLYCYSTINA Ehrenberg 1838, emend. Riedel 1967b
Order SPUMELLARIA Ehrenberg 1875
Family ACTINOMMIDAE Haeckel 1862, emend. Riedel 1967b
Subfamily ACTINOMMIDAE Haeckel 1862, emend. Petrushevskaya and Kozlova, 1972
Genus *ACTINOMMA* Haeckel 1860, emend. Nigrini 1967

***Actinomma medianum* Nigrini**
(Plate 1, Figs. 4A, 4B)

Actinomma medianum Nigrini, 1967, p. 27, pl. 2, figs. 2a, 2b; 1970, p. 167, pl. 1, fig. 10; Nigrini and Moore, 1979, p. S31, pl. 3, figs. 5, 6.

Genus *DRUPPATRACTUS* Haeckel 1887

***Druppatractus acquilonius* Hays**
(Plate 4, Figs. 1A, 1B)

Druppatractus acquilonius Hays, 1970, p. 214, pl. 1, figs. 4, 5.

Stylacontarium acquilonium (Hays), Kling, 1973, p. 634, pl. 1, figs. 17-20, pl. 14, figs. 1-4; Ling, 1973, p. 777, pl. 1, figs. 6, 7.

Remarks: Although most recent studies place this species in the genus *Stylacontarium*, this chapter used the original genus description given by Hays.

Genus *SPHAEROPYLE* Dreyer 1889

***Sphaeropyle langii* Dreyer**
(Plate 5, Figs. 3A, 3B)

Sphaeropyle langii Dreyer, 1889, p. 13, pl. 4, fig. 54; Kling, 1973, p. 634, pl. 1, figs. 5-10, pl. 13, figs. 6-8; Foreman, 1975, p. 618, pl. 9, figs. 30, 31.

***Sphaeropyle robusta* Kling emend. Foreman**
(Plate 5, Figs. 4A, 4B)

Sphaeropyle robusta Kling, 1973, p. 634, pl. 1, fig. 12, pl. 6, figs. 6-13; Foreman, 1975, p. 618, pl. 9, figs. 24-26.

Genus *STYLATRACTUS* Haeckel 1887

***Stylatractus universus* Hays**
(Plate 4, Figs. 2A, 2B)

Stylatractus sp. Hays, 1965, p. 167, pl. 1, fig. 6.

Stylatractus universus Hays, 1970, p. 215, pl. 1, figs 1, 2; Kling, 1971, p. 1086, pl. 1, fig. 6.

Axoprunum angelinum (Campbell and Clark), Kling, 1973, p. 634, pl. 1, figs. 14-17; Ling, 1973, p. 777, pl. 1, figs. 1-4; Foreman, 1975, p. 618, pl. 9, figs. 28, 29; Sakai, 1980, p. 704, pl. 2, figs. 1a, 1b.

Remarks: Although most recent studies place this species in the genus *Axoprunum*, this chapter used the genus designation of Hays 1970.

Subfamily ARTISCINAE Haeckel 1881, emend. Riedel 1967b
Genus *DIARTUS* Sanfilippo and Riedel 1980

***Diartus hughesi* (Campbell and Clark)**
(Plate 8, Figs. 3A, 3B)

Ommatocampe hughesi Campbell and Clark, 1944, p. 23, pl. 3, fig. 12.

Ommatartus hughesi (Campbell and Clark), Riedel and Sanfilippo, 1970, p. 521; Kling, 1973, p. 634, pl. 7, fig. 6; Foreman, 1975, p. 619, pl. 8, fig. 3; Sakai, 1980, p. 708, pl. 4, figs. 3a, 3b.

Diartus hughesi (Campbell and Clark), Sanfilippo and Riedel, 1980, p. 1010, pl. 1, fig. i.

***Diartus petterssoni* (Riedel and Sanfilippo)**
(Plate 8, Figs. 4A, 4B)

Cannartus(?) petterssoni Riedel and Sanfilippo, 1970, p. 520, pl. 14, fig. 3; Kling, 1973, p. 634, pl. 7, fig. 8; Sakai, 1980, p. 705, pl. 4, figs. 4a, 4b, 6a, 6b, 7a, 7b.

Diartus petterssoni (Riedel and Sanfilippo), Sanfilippo and Riedel, 1980, p. 1010, pl. 1, fig. h.

Genus *DIDYMOCYRTIS* Haeckel 1860

***Didymocyrtis antepenultima* (Riedel and Sanfilippo)**
(Plate 8, Fig. 2)

Ommatartus antepenultimus Riedel and Sanfilippo, 1970, p. 521, pl. 14, fig. 14; Westberg and Riedel, 1978, p. 22, pl. 2, figs. 4, 5; Sakai, 1980, p. 708, pl. 3, figs. 3a, 3b.

Didymocyrtis antepenultima (Riedel and Sanfilippo), Sanfilippo and Riedel, 1980, p. 1010.

***Didymocyrtis laticonus* (Riedel)**
(Plate 8, Fig. 5)

Cannartus laticonus Riedel, 1959, p. 291, pl. 1, fig. 5; Westberg and Riedel, 1978, p. 20, pl. 2, figs. 1-3.

Didymocyrtis laticonus (Riedel), Sanfilippo and Riedel, 1980, p. 1010, pl. 1, fig. e.

***Didymocyrtis penultima* (Riedel)**
(Plate 8, Fig. 1)

Panarium penultimum Riedel, 1957, p. 76, pl. 1, fig. 1

Ommartartus penultimus (Riedel), Westberg and Riedel, 1978, p. 22, pl. 2, figs. 6-8; Sakai, 1980, p. 708, pl. 3, figs. 3a, 3b, 4a, 4b, 5a, 5b.

Didymocyrtis penultima (Riedel), Sanfilippo and Riedel, 1980, p. 1010, pl. 1, fig. f.

***Didymocyrtis tetrathalamus* (Haeckel)**
(Plate 1, Figs. 2A, 2B)

Panartus tetrathalamus Haeckel, 1887, p. 378, pl. 40, fig. 3.

Ommatartus tetrathalamus (Haeckel), Riedel and Sanfilippo, 1971, p. 1588, pl. 1C, figs. 5-7; Sakai, 1980, p. 708, pl. 3, figs. 1a, 1b.

Didymocyrtis tetrathalamus (Haeckel), Sanfilippo and Riedel, 1980, p. 1010, pl. 1, fig. g.

Subfamily SATURNALINAE Deflandre 1953
Genus *SATURNALIS* Haeckel 1881, emend. Nigrini 1967

***Saturnalis circularis* Haeckel**
(Plate 3, Fig. 1)

Saturnalis circularis Haeckel, 1887, p. 131; Nigrini, 1967, p. 24, pl. 1, fig. 9; Kling, 1973, p. 634, pl. 1, figs. 21-25, pl. 7, figs. 1-5; Ling, 1973, p. 777, pl. 1, fig. 5; Sakai, 1980, p. 709, pl. 6, fig. 14.

Family LITHELIIDAE Haeckel 1862
Genus *LARCOSPIRA* Haeckel 1887

***Larcospira quadrangula* Haeckel**
(Plate 3, Fig. 9)

Larcospira quadrangula Haeckel, 1887, p. 696, pl. 49, fig. 3; Benson, 1966, p. 266, pl. 18, figs. 7, 8; Nigrini and Moore, 1979, p. S133, pl. 17, fig. 2.

Family PHACODISCIDAE Haeckel 1881
Genus *HELIODISCUS* Haeckel 1862, emend. Nigrini 1967

***Heliodiscus asteriscus* Haeckel**
(Plate 3, Fig. 8)

Heliodiscus asteriscus Haeckel, 1887, p. 445, pl. 33, fig. 8; Nigrini, 1967, p. 32. pl. 3, figs. 1a, 1b; Nigrini and Moore, 1979, p. S73, pl. 9, figs. 1, 2.

Family SPONGODISCIDAE Haeckel 1862, emend. Riedel 1967b
Genus *EUCHITONIA* Ehrenberg 1860, emend. Nigrini 1967

***Euchitonia* sp.**
(Plate 2, Fig. 3)

Euchitonia elegans (Ehrenberg), Nigrini, 1967, p. 39, pl. 4, figs. 2a, 2b; Nigrini and Moore, 1979, p. S83, pl. 11, figs. 1a, 1b.

Euchitonia furcata Ehrenberg, 1872a, p. 289, pl. IV, fig. 6; Ling and Anikouchine, 1967, p. 1484, pl. 189, figs. 1, 2, 5–7, pl. 190, figs. 1, 2, 5–7; Nigrini and Moore, 1979, p. S85, pl. 11, figs. 2a, 2b.

Remarks: Most specimens present were *Euchitonia furcata*, with only very rare occurrences of *Euchitonia elegans*.

Genus *SPONGASTER* Ehrenberg 1860, emend. Riedel and Sanfilippo, 1971

Spongaster tetras irregularis Nigrini

(Plate 3, Fig. 5)

Spongaster tetras irregularis Nigrini, 1967, p. 43, pl. 5, fig. 2; Foreman, 1975, p. 619, pl. 9, fig. 27; Sakai, 1980, p. 709, pl. 6, fig. 2.

Genus *SPONGOPYLE* Dreyer 1889

Spongopyle osculosa Dreyer

(Plate 3, Fig. 2)

Spongopyle osculosa Dreyer, 1889, p. 42, pl. 11, figs. 99, 100; Nigrini and Moore, 1979, p. S115, pl. 15, fig. 1.

Genus *SPONGOTROCHUS* Haeckel 1860

Spongotrochus(?) *venustum* (Bailey)

(Plate 2, Figs. 1A, 1B)

Perichlamydium venustum Bailey, 1856, p. 5, pl. 1, figs. 16, 17.

Stylochlamydium venustum (Bailey), Haeckel, 1887, p. 515; Ling, 1973, p. 778, pl. 1, fig. 8.

Spongotrochus(?) *venustum* (Bailey), Nigrini and Moore, 1979, p. S119, pl. 15, figs. 3a, 3b.

Spongotrochus(?) *glacialis* Popofsky, Riedel, 1958, p. 227, pl. 2, figs. 1, 2; Kling, 1973, p. 635, pl. 2, figs. 4–6.

Remarks: Included all the above forms in the counts of *Spongotrochus*(?) *venustum*.

Family SPONGURIDAE Haeckel 1862, emend. Petrushevskaya 1975

Genus *SPONGOCORE* Haeckel 1887

Spongocore puella Haeckel

(Plate 2, Fig. 5)

Spongocore puella Haeckel, 1887, p. 347, pl. 48, fig. 6; Benson, 1964, pl. 1, fig. 21; Kling, 1973, p. 635, pl. 7, figs. 18–22; Nigrini and Moore, 1979, p. S69, pl. 8, figs. 5a–5c.

Genus *SPONGURUS* Haeckel 1860

Spongurus pylomaticus Riedel

(Plate 2, Fig. 4)

Spongurus pylomaticus Riedel, 1958, p. 226, pl. 1, figs. 10, 11; Petrushevskaya, 1967, p. 32, figs. 16I, 16II; Nigrini and Moore, 1979, p. S65, pl. 8, figs. 3a, 3b.

Spongurus(?) pylomaticus Riedel, Petrushevskaya, 1975, p. 577, pl. 7, fig. 4, pl. 37, fig. 7.

ORDER NASSELLARIA Ehrenberg 1875

Suborder CYRTIDA Haeckel 1862, emend. Petrushevskaya 1971

Family ARTOSTROBIIDAE Riedel 1967a, emend. Foreman 1973b

Genus *BOTRYOSTROBUS* Haeckel 1887, emend. Nigrini 1977

Botryostrobus aquilonaris (Bailey)

(Plate 1, Fig. 1)

Eucyrtidium aquilonaris Bailey, 1856, p. 4, pl. 1, fig. 9.

Eucyrtidium tumidulum Bailey(?), Kling, 1971, pl. 1, fig. 2.

Botryostrobus aquilonaris (Bailey), Nigrini, 1977, p. 246, pl. 1, fig. 1; Nigrini and Moore, 1979, p. N99, pl. 27, fig. 1.

Genus *PHORMOSTICHOARTUS* Campbell 1951, emend. Nigrini 1977

Phormostichoartus corbula (Harting)

(Plate 3, Fig. 6)

Lithocampe corbula Harting, 1863, p. 12, pl. 1, fig. 21.

Siphocampe corbula (Harting), Nigrini, 1967, p. 85, pl. 8, fig. 5, pl. 9, fig. 3.

Phormostichoartus corbula (Harting), Nigrini, 1977, p. 252, pl. 1. fig. 10; Nigrini and Moore, 1979, p. N103, pl. 27, fig. 3.

Family CARPOCANIIDAE Haeckel 1881, emend. Riedel 1967b

Genus *CARPOCANISTRUM* Haeckel 1887, emend. Riedel and Sanfilippo, 1971

Carpocanistrum spp.

(Plate 3, Fig. 7)

Carpocanium petalospyris Benson, 1966, p. 434, pl. 29, figs. 9, 10, 25.

Carpocanium spp. Nigrini, 1970, p. 171, pl. 4, figs. 4–6.

Carpocanistrum spp. Riedel and Sanfilippo, 1971, p. 1596, pl. 1G, figs. 1–6, 8-13, pl. 2F, figs. 5, 6, pl. 3D, figs. 1, 2, 6, 7, 9; Nigrini and Moore, 1979, p. N23, pl. 21, figs. 1a–1c.

Family PTEROCORYIDAE Haeckel 1881, emend. Riedel 1967b

Genus *LAMPROCYCLAS* Haeckel 1881, emend. Petrushevskaya and Kozlova, 1972

Lamprocyclas maritalis

(Plate 3, Fig. 3)

Lamprocyclas maritalis Haeckel, 1887, p. 1390, pl. 74, figs. 13, 14.

Lamprocyclas maritalis maritalis Haeckel, Nigrini, 1967, p. 74, pl. 7, fig. 5; Nigrini and Moore, 1979, p. N75, pl. 25, fig. 4.

Lamprocyclas maritalis polypora Nigrini, 1967. p. 76, pl. 7, fig. 6; Nigrini and Moore, 1979, p. N77, pl. 25, fig. 5.

Remarks: Counts of these two subspecies of *Lamprocyclas maritalis* (*maritalis* and *polypora*) were combined in this study.

Genus *LAMPROCYRTIS* Kling 1973

Lamprocyrtis heteroporos (Hays)

(Plate 6, Figs. 3A, 3B)

Lamprocyclas heteroporos Hays, 1965, p. 179, pl. 3, fig. 1.

Lamprocyrtis heteroporos (Hays), Kling, 1973, p. 639, pl. 5, figs. 19, 20; Foreman, 1975, p. 620, pl. 9, fig. 21; Sakai, 1980, p. 711, pl. 9, figs. 9, 10, 11a, 11b.

Lamprocyrtis neoheteroporos Kling

(Plate 6, Fig. 2)

Lamprocyrtis neoheteroporos Kling, 1973, p. 639, pl. 5, figs. 17, 18, pl. 15, figs. 4, 5; Foreman, 1975, p. 620, pl. 9, fig. 12; Sakai, 1980, p. 711, pl 9, figs. 9a, 9b.

Lamprocyrtis nigriniae (Caulet)

(Plate 6, Fig. 1)

Conarchnium nigriniae Caulet, 1971, p. 3, pl. 3, figs. 1–4, pl. 4, figs. 1–4.

Lamprocyrtis haysi Kling, 1973, p. 639, pl. 5, figs. 15, 16, pl. 15, figs. 1–3; Foreman, 1975, p. 620, pl. 9, fig. 22; Sakai, 1980, p. 711, pl. 7, figs. 8a, 8b.

Lamprocyrtis nigriniae (Caulet), Nigrini and Moore, 1979, p. N81, pl. 25, fig. 7.

Genus *PTEROCORYS* Haeckel 1881

Pterocorys zancleus (Müller)

(Plate 3, Fig. 4)

Eucyrtidium zanclaeum Müller, 1858, p. 41, pl. 6, figs. 1–3.

Theoconus zancleus (Müller), Benson, 1966, p. 482, pl. 33, fig. 4; Kling, 1973, p. 639, pl. 5, figs. 9–11.

Pterocorys zancleus (Müller), Nigrini and Moore, 1979, p. N89, pl. 25, figs. 11a, 11b.

Genus *THEOCORYTHIUM* Haeckel

Theocorythium trachelium dianae (Haeckel)

(Plate 5, Fig. 1)

Theocorys dianae Haeckel, 1887, p. 1416, pl. 69, fig. 11.

Theocorythium trachelium dianae (Haeckel), Nigrini, 1967, p. 77, pl. 8, figs. 1a, 1b, pl. 9, figs. 1a, 1b; Foreman, 1975, p. 620, pl. 9, fig. 13; Sakai, 1980, p. 711, pl. 10, figs. 1a, 1b.

Theocorythium trachelium trachelium (Ehrenberg)
(Plate 5, Fig. 2)

Eucyrtidium trachelius Ehrenberg, 1872b, p. 312.
Theorcorythium trachelium trachelium (Ehrenberg), Nigrini, 1967, p. 79, pl. 8, fig. 2, pl. 9, fig. 2; Foreman, 1975, p. 620, pl. 9, fig. 12; Sakai, 1980, p. 711, pl. 10, figs. 2a, 2b.

Family THEOPERIDAE Haeckel 1881, emend. Riedel 1967b
Genus *CLATHROCYCLAS* Haeckel 1881

Clathrocyclas spp.
(Plate 1, Figs. 5A, 5B)

Remarks: The description by Kling (1973) for this group was followed in this study.

Genus *CORNUTELLA* Ehrenberg 1838

Cornutella profunda Ehrenberg
(Plate 1, Fig. 3)

Cornutella clathrata β profunda Ehrenberg, 1856, pl. 35B, fig. 21; Bailey, 1856, p. 2, pl. 1, fig. 23.
Cornutella profunda Ehrenberg, 1858, p. 31; Riedel, 1958, p. 232, pl. 3, figs. 1, 2; Nigrini, 1967, p. 60, pl. 6, figs. 5a–5c; Kling, 1973, p. 635, pl. 3, figs. 1–4, pl. 9, figs. 8–17.

Genus *CYCLADOPHORA* Ehrenberg 1847

Cycladophora davisiana Ehrenberg
(Plate 1, Figs. 6A, 6B)

Cycladophora(?) davisiana Ehrenberg, 1861, p. 297.
Theocalyptra davisiana (Ehrenberg), Riedel, 1958, p. 239, pl. 4, figs. 2, 3; Kling, 1973, p. 638, pl. 3, figs. 9–12; Nigrini and Moore, 1979, p. N59, pl. 24, figs. 2a, 2b.
Cycladophora davisiana Ehrenberg, Petrushevskaya, 1967, p. 122, pl. 69, figs. I–VII; Ling, 1973, p. 780, pl. 2, fig. 2; Sakai, 1980, p. 709, pl. 6, figs. 6, 7a, 7b, 8a, 8b.

Cycladophora davisiana var. *cornutoides* Petrushevskaya
(Plate 2, Figs. 2A, 2B)

Cycladophora davisiana var. *cornutoides* Petrushevskaya, 1967, p. 124, pl. 71, figs. I–III; Ling, 1973, p. 780, pl. 2, fig. 3.

Genus *CYRTOCAPSELLA* Haeckel 1887, emend. Sanfilippo and Riedel 1970

Cyrtocapsella cornuta Haeckel
(Plate 8, Fig. 8)

Cyrtocapsa (Cyrtocapsella) cornuta Haeckel, 1887, p. 1513, pl. 78, fig. 9.
Cyrtocapsella cornuta Haeckel, Sanfilippo and Riedel, 1970, p. 453, pl. 1, figs. 19, 20; Kling, 1973, p. 636, pl. 11, figs. 16–18; Foreman, 1975, p. 620, pl. 8. fig. 8; Sakai, 1980, p. 709, pl. 8, figs. 8a, 8b.

Cyrtocapsella japonica (Nakaseko)
(Plate 8, Fig. 7)

Eusyringium japonicum Nakaseko, 1963, p. 193, pl. 4, figs. 1–3.
Cyrtocapsella japonica (Nakaseko), Sanfilippo and Riedel, 1970, p. 452, pl. 1, figs. 13–15; Kling, 1973, p. 636, pl. 11, figs. 19, 20; Foreman, 1975, p. 620, pl. 8, fig. 7; Sakai, 1980, p. 709, pl. 8, figs. 7a, 7b.

Cyrtocapsella tetrapera Haeckel
(Plate 8, Fig. 6)

Cyrtocapsa (Cyrtocapsella) tetrapera Haeckel, 1887, p. 1512, pl. 78, fig. 5.
Cyrtocapsella tetrapera Haeckel, Sanfilippo and Riedel, 1970, p. 453, pl. 1, figs. 16–18; Kling, 1973, p. 636, pl. 11, figs. 12–15; Ling, 1973, p. 780, pl. 2, fig. 4; Sakai, 1980, p. 709, pl. 8, figs. 5, 6.

Genus *EUCYRTIDIUM* Ehrenberg 1847, emend. Nigrini 1967

Eucyrtidium acuminatum (Ehrenberg)
(Plate 5, Fig. 5)

Lithocampe acuminatum Ehrenberg, 1844, p. 84.
Eucyrtidium acuminatum (Ehrenberg), Nigrini, 1967, p. 81, pl. 8, figs. 3a, 3b; Kling, 1973, p. 636, pl. 4, figs. 20–23; Nigrini and Moore, 1979, p. N61, pl. 24, figs. 3a, 3b.

Eucyrtidium calvertense Martin
(Plate 5, Fig. 6)

Eucyrtidium calvertense Martin, 1904, p. 450, pl. 130, fig. 5; Kling, 1973, p. 636, pl. 4, figs. 16, 18, 19, pl. 11, figs. 1–5; Foreman, 1975, p. 620, pl. 9, fig. 14.

Eucyrtidium matuyamai Hays
(Plate 5, Figs. 7A, 7B)

Eucyrtidium matuyamai Hays, 1970, p. 213, pl. 1, figs. 7–9; Kling, 1971, p. 1088, pl. 1, fig. 4; Kling, 1973, p. 636, pl. 4, fig. 17; Ling, 1973, p. 780, pl. 2, figs. 5, 6; Foreman, 1975, p. 620, pl. 9, fig. 15; Sakai, 1980, p. 710, pl. 7, figs. 1a, 1b.

Genus *LYCHNOCANOMA* Haeckel 1887, emend. Foreman 1973b

Lychnocanoma grande (Campbell and Clark)
(Plate 6, Figs. 4A, 4B)

Lychnocanoma grande Campbell and Clark, 1944, p. 42, pl. 6, figs. 3–6; Kling, 1973, p. 637, pl. 10, figs. 10–14.

Genus *PTEROCANIUM* Ehrenberg 1847

Pterocanium prismatium Riedel
(Plate 7, Figs. 3A, 3B)

Pterocanium prismatium Riedel, 1957, p. 87, pl. 3, figs. 4, 5; Sakai, 1980, p. 711, pl. 8, figs. 15a, 15b.

Genus *STICHOCORYS* Haeckel 1881

Stichocorys delmontensis (Campbell and Clark)
(Plate 7, Fig. 2)

Eucyrtidium delmontense Campbell and Clark, 1944, p. 56, pl. 7, figs. 19, 20.
Stichocorys delmontensis (Campbell and Clark), Sanfilippo and Riedel, 1970, p. 451, pl. 1, fig. 9; Kling, 1973, p. 638, pl. 11, figs. 8–10; Ling, 1973, p. 781, pl. 2, fig. 12; Foreman, 1975, p. 622, pl. 9, figs. 5–7; Sakai, 1980, p. 711, pl. 8. fig. 3.

Stichocorys peregrina Riedel)
(Plate 7, Figs. 1A, 1B)

Eucyrtidium elongatum peregrinum Riedel, 1953, p. 812, pl. 85, fig. 2.
Stichocorys peregrina (Riedel), Sanfilippo and Riedel, 1970, p. 451, pl. 1, fig. 10; Kling, 1973, p. 638, pl. 4, fig. 27, pl. 11, fig. 29, pl. 13, figs. 9, 10; Foreman, 1975, p. 622, pl. 9, figs. 1–4; Sakai, 1980, p. 711, pl. 8, figs. 1, 2.

ACKNOWLEDGMENTS

I thank W. R. Riedel and C. Nigrini for their helpful suggestions for improving an earlier version of this manuscript. A. Wright also reviewed this document, insuring that remarks were in agreement with those stated elsewhere in this volume.

REFERENCES

Bailey, J. W., 1856. Notice of microscopic forms found in the soundings of the Sea of Kamtschatka—with a plate. *Am. J. Sci. Arts*, Ser. 2, 22:1–6.

Benson, R. N., 1964. Preliminary report on Radiolaria in Recent sediments of the Gulf of California. *In* van Andel, T. H., and Shor, G. G., Jr. (Eds.), *Marine Geology of the Gulf of California—A Symposium.* Mem. Am. Assoc. Pet. Geol., 3:398–400.

_______, 1966. Recent radiolaria from the Gulf of California [Ph.D. dissert.]. University of Minnesota.

Campbell, A. S., 1951. New genera and subgenera of radiolaria. *J. Paleontol.*, 25:527–530.

Campbell, A. S., and Clark, B. L., 1944. Miocene radiolarian faunas from southern California. *Spec. Pap. Geol. Soc. Am.*, 51:1–76.

Caulet, J., 1971. Contribution à l'étude de quelques Radiolaires Nassellaires des bous de la Méditerranée et du Pacifique. *Arch. Orig. Centre de Documentation C.N.R.S., Cahiers de Micropaleontologie*, Ser. 2(498), 10:1–10.

Deflandre, G., 1953. Radiolaires fossiles. *In* Grassé, P.-P. (Ed.), *Traite de Zoologie* (Vol. 1): Paris (Masson), 389–436.

Dreyer, F., 1889. Die Pylombildungen in vergleichend-anatomischer und entwicklungsgeschichtlicher Beziehung bei Radiolarien und bei Protisten überhaupt, nebst System und Beschreibung neuer und der bis jetzt bekannten pylomatischen Spumellarien. *Jena. Z. Naturwiss.*, new Ser. 16, 23:1–138.

hrenberg, C. G., 1838. Über die Bildung der Kriedefelsen und des Kriedemergels durch unsichtbare Organismen. *Abh. Kgl. Preuss. Akad. Wiss. Berlin Jahrg.*, pp. 59–147.

_____, 1844. Über 2 neue Lager von Gebirgsmassen aus Infusorien als Meeres-Absatz in Nord-Amerika unde eine Vergleichung derselben mit den organischen Kreide-Gebilden in Europa und Afrika. *Monatsber. Kgl. Preuss. Akad. Wiss. Berlin Jahrg.*, pp. 57–97.

_____, 1847. Über die mikroskopischen kieselschaligen Polycystinen als mächtige Gebirgsmasse von Barbados ünd uber das Verhältnis der aus mehr als 300 neuen Arten bestehenden ganz eigenthümlichen Formengruppe jener Felsmasse zu den lebenden Thieren und zur Kreidebildung. Eine neue Anregung zur Erforschung der Erdlebens. *Monatsber. Kgl. Preuss. Akad. Wiss. Berlin Jahrg.*, pp. 40–60.

_____, 1856. Über 2 neue südamerikanische Gebirgsmassen aus mikroskopischen Organismen, eine aus Meeresorganismen in Chile und eine als mit gefritteten Süfswasserorganismen gemischten vulkanischen efsbaren Tuff aus Honduras in Centro-Amerika. *Monatsber. Kgl. Preuss. Akad. Wiss. Berlin Jahrg.*, pp. 425–431.

_______, 1858. Kurze Characteristik der 9 neuen Genera und der 105 neuen Species des ägäischen Meeres und des Tiefgrundes des Miffel-Meeres. *Monatsber. Kgl. Preuss. Akad. Wiss. Berlin Jahrg.*, pp. 10–40.

_____, 1860. Über den Tiefgrund des stillen Oceans zwischen Californien und den Sandwich-Inseln aus bis 15600' Tiefe nach Lieut. Brooke. *Monatsber. Kgl. Preuss. Akad. Wiss. Berlin Jahrg.*, pp. 819–833.

_____, 1861. Über die Tiefgrund-Verhältnisse des Oceans am Eingange der Davisstrasse und bei Island. Nebst einem Übersichts-Kärtchen. *Monatsber. Kgl. Preuss. Akad. Wiss. Berlin Jahrg.*, pp. 275–315.

_____, 1872a. Mikrogeologische Studien über das kleinste Leben der Meeres-Tiefgründe aller Zonen und dessen geologischen Einfluss. *Abh. Kgl. Preuss. Akad. Wiss. Berlin Jahrg.*, pp. 131–399.

_____, 1872b. Mikrogeologischen Studien als Zusammenfassung seiner Beobachtungen des kleinsten Lebens der Meeres-Tiefgrunde aller Zonen und dessen geologischen Einfluss. *Monatsber. Kgl. Preuss. Akad. Wiss. Berlin Jahrg.*, pp. 265–322.

_____, 1875. Fortsetzung der mikrogeologischen Studien als Gesammt-Uebersicht der mikroskopischen Paläontologie gleichartig analysirter Gebirgsarten der Erde, mit specieller Rücksicht auf den Polycystinen-Mergel von Barbados. *Abh. Kgl. Preuss. Akad. Wiss. Berlin Jahrg.*, pp. 1-226.

reman, H. P., 1973a. Radiolaria from DSDP Leg 20. *In* Heezen, B. C., MacGregor, I. D., et al., *Init. Repts. DSDP*, 20: Washington (U.S. Govt. Printing Office), 249–306.

_____, 1973b. Radiolaria of Leg 10 with systematics and ranges for the families Amphipyndacidae, Artostrobiidae, and Theoperidae. *In* Worzel, J. L., Bryant, W., et al., *Init. Repts. DSDP*, 10: Washington (U.S. Govt. Printing Office), 407–474.

_____, 1975. Radiolaria from the North Pacific, Deep Sea Drilling Project, Leg 32. *In* Larson, R. L., Moberly, R., et al., *Init. Repts. DSDP*, 32: Washington (U.S. Govt. Printing Office), 579–676.

Haeckel, E., 1860. Über neue, lebende Radiolarien des Mittelmeeres und legte die dazu gehörigen Abbildungen. *Monatsber. Kgl. Preuss. Akad. Wiss. Berlin Jahrg.*, pp. 794–817.

_______, 1862. *Die Radiolarien (Rhizopoda Radiaria)*: Berlin (Reimer).

_______, 1881. Entwurf eines Radiolarien-Systems auf Grund von Studien der Challenger-Radiolarien. *Jena. Z. Naturwiss*, 15: 418–472.

_______, 1887. Report on the Radiolaria collected by H.M.S. *Challenger* during the years 1873–76. *Report on the Scientific Results of the Voyage of the H.M.S.* Challenger. *Zoology*, 18:1–1803.

Harting, P., 1863. Bijdrage tot de kennis der mikroskopische faune en flora van de Banda-Zee, naar aanleiding van een onderzoek van eenige door diepzeeloodingen van 990 tot 4000 vademen uit die zee opgebragte gronden. *Verh. K. Akad. Wet. Amsterdam Afd. Natuurkd.*, 10:1–34.

Hays, J. D., 1965. Radiolaria and late Tertiary and Quaternary history of Antarctic seas. *In* Llano, G. A. (Ed.), *Biology of the Antarctic Seas II* (Vol. 5): Washington (Am. Geophys. Union), 125–184.

_______, 1970. Stratigraphy and evolutionary trends of radiolaria in North Pacific deep-sea sediments. *In* Hays, J. D. (Ed.), *Geological Investigations of the North Pacific*. Mem. Geol. Soc. Am., 126: 185–218.

Hays, J. D., and Shackleton, N. J., 1976. Globally synchronous extinction of the radiolarian *Stylatractus universus*. *Geology*, 4: 649–652.

Kellogg, D. E., and Hays, J. D., 1975. Microevolutionary patterns in late Cenozoic radiolaria. *Paleontology*, 1:150–160.

Kling, S. A., 1971. Radiolaria: Leg 6 of the Deep Sea Drilling Project. *In* Fischer, A. G., Heezen, B. C., et al., *Init. Repts. DSDP*, 6: Washington (U.S. Govt. Printing Office), 1069–1117.

_______, 1973. Radiolaria from the eastern North Pacific, Deep Sea Drilling Project, Leg 18. *In* Kulm, L. D., von Huene, R., et al., *Init. Repts. DSDP*, 18: Washington (U.S. Govt. Printing Office), 617–672.

Ling, H.-Y., 1973. Radiolaria: Leg 19 of the Deep Sea Drilling Project. *In* Creager, J. S., Scholl, D. W., et al., *Init. Repts. DSDP*, 19: Washington (U.S. Govt. Printing Office), 777–798.

_______, 1980. Radiolarians from the Emperor Seamounts of the Northwest Pacific: Leg 55 of the Deep Sea Drilling Project. *In* Jackson, E. D., Koizumi, I., et al., *Init. Repts. DSDP*, 55: Washington (U.S. Govt. Printing Office), 365–374.

Ling, H.-Y., and Anikouchine, W. A., 1967. Some Spumellarian radiolaria from the Java, Philippine and Mariana trenches. *J. Paleontol.*, 41:1481–1491.

Martin, G. C., 1904. *Radiolaria*: Baltimore (Maryland Geol. Survey), pp. 447–459.

Moore, T. C., Jr., 1973. Method of randomly distributing grains for microscopic examination. *J. Sediment. Petrol.*, 43:904–906.

Morley, J. J., and Shackleton, N. J., 1978. Extension of the radiolarian *Stylatractus universus* as a biostratigraphic datum to the Atlantic Ocean. *Geology*, 6:309–311.

Müller, J., 1858 Über die Thalassicollen, Polycystinen und Acanthometren des Mittelmeeres. *Abh. Kgl. Preuss. Akad. Wiss. Berlin Jahrg.*, pp. 1–62.

Nakaseko, K., 1963. Neogene Cyrtoidea (Radiolaria) from the Isozaki Formation in Ibaraki Prefecture, Japan. *Osaka Univ., Coll. General Education, Sci. Rept.*, 12:165–198.

Nigrini, C., 1967. Radiolaria in pelagic sediments from the Indian and Atlantic Ocean. *Bull. Scripps. Inst. Oceanogr.*, 11:1–125.

_______, 1970. Radiolarian assemblages in the North Pacific and their application to a study of Quaternary sediments in Core V20-130. *In* Hays, J. D. (Ed.), *Geological Investigations of the North Pacific*. Mem. Geol. Soc. Am., 126:139–184.

_______, 1977. Tropical Cenozoic Artostrobiidae (Radiolaria). *Micropaleontology*, 23:241–269.

Nigrini, C., and Moore, T. C., Jr., 1979. A guide to modern Radiolaria. *Spec. Publ. Cushman Found. Foraminiferal Res. 16*.

Petrushevskaya, M. G., 1967. Radiolyarii otryador Spumellaria i Nassellaria antarkticheskoi oblasti (Antarctic spumelline and nasselline radiolarians). *In* Andriyashev, A. P., and Ushakov, P. V. (Eds.), *Rez. Biol. Issed. Sov. Antarkt. Eksped. 1955–58*, 3:5–187.

_______, 1971. On the natural system of polycystine Radiolaria (Class Sarcodina). *In* Farinacci, A. (Ed.), *Proc. II Plankt. Conf.*: Rome (Tecnoscienza), pp. 981–992.

_______, 1975. Cenozoic radiolarians of the Antarctic, Leg 29, DSDP. *In* Kennett, J. P., Houtz, R. E., et al., *Init. Repts. DSDP*, 29: Washington (U.S. Govt. Printing Office), 541–676.

Petrushevskaya, M. G., and Kozlova, G. E., 1972. Radiolaria: Leg 14, Deep Sea Drilling Project. *In* Hayes, D. E., Pimm, A. C., et al., *Init. Repts. DSDP*, 14: Washington (U.S. Govt. Printing Office), 495–648.

Reynolds, R. A., 1980. Radiolarians from the western North Pacific, Leg 57, Deep Sea Drilling Project. *In* Scientific Party, *Init. Repts. DSDP*, 56, 57, Pt. 2: Washington (U.S. Govt. Printing Office), 735–770.

Riedel, W. R., 1953. Mesozoic and late Tertiary Radiolaria of Rotti. *J. Paleontol.*, 27:805–813.

________, 1957. Radiolaria: a preliminary stratigraphy. *Rep. Swed. Deep Sea Exped. 1947–1948*, 6:59–96.

________, 1958. Radiolaria in Antarctic sediments. *Rep. B.A.N.Z. Antarctic Res. Exped.*, Ser. B., 6:217–255.

________, 1959. Oligocene and Lower Miocene Radiolaria in tropical Pacific sediments. *Micropaleontology*, 5:285–302.

________, 1967a. Some new families of Radiolaria. *Proc. Geol. Soc. London*, 1640:148–149.

________, 1967b. Protozoa [Subclass Radiolaria]. *In* Harland, W. B., Holland, C. H., House, M. R., Hughes, N. F., Reynolds, A. B., et al. (Eds.), *The Fossil Record*: London (Geol. Soc. London), pp. 291–298.

Riedel, W. R., and Sanfilippo, A., 1970. Radiolaria, Leg 4, Deep Sea Drilling Project. *In* Bader, R. G., Gerard, R. D., et al., *Init. Repts. DSDP*, 4: Washington (U.S. Govt. Printing Office), 503–575.

________, 1971. Cenozoic Radiolaria from the western tropical Pacific, Leg 7. *In* Winterer, E. L., Riedel, W. R., et al., *Init. Repts. DSDP*, 7, Pt. 2: Washington (U.S. Govt. Printing Office), 1529–1672.

________, 1977. Cenozoic Radiolaria. *In* Ramsey, A. T. S. (Ed.), *Oceanic Micropaleontology* (Vol. 2): London (Academic Press), 847–912.

________, 1978. Stratigraphy and evolution of tropical Cenozoic radiolarians. *Micropaleontology*, 24:61–96.

Sakai, T., 1980. Radiolarians from Sites 434, 435, and 436, Northwest Pacific, Leg 56, Deep Sea Drilling Project. *In* Scientific Party, *Init. Repts. DSDP*, 56, 57, Pt. 2: Washington (U.S. Govt. Printing Office), 695–734.

Sanfilippo, A., and Riedel, W. R., 1970. Post-Eocene "closed" theoperid radiolarians. *Micropaleontology*, 16:446–462.

________, 1980. A revised generic and suprageneric classification of the Articins (Radiolaria). *J. Paleontol.*, 54: 1008–1012.

Schaaf, A., 1981. Late Early Cretaceous Radiolaria from Deep Sea Drilling Project Leg 62. *In* Thiede, J., Vallier, T. L., et al., *Init. Repts. DSDP*, 62: Washington (U.S. Govt. Printing Office), 419–470.

Westberg, M. J., and Riedel, W. R., 1978. Accuracy of radiolarian correlations in the Pacific Miocene. *Micropaleontology*, 24:1–23.

Date of Initial Receipt: 28 September 1983
Date of Acceptance: 9 April 1984

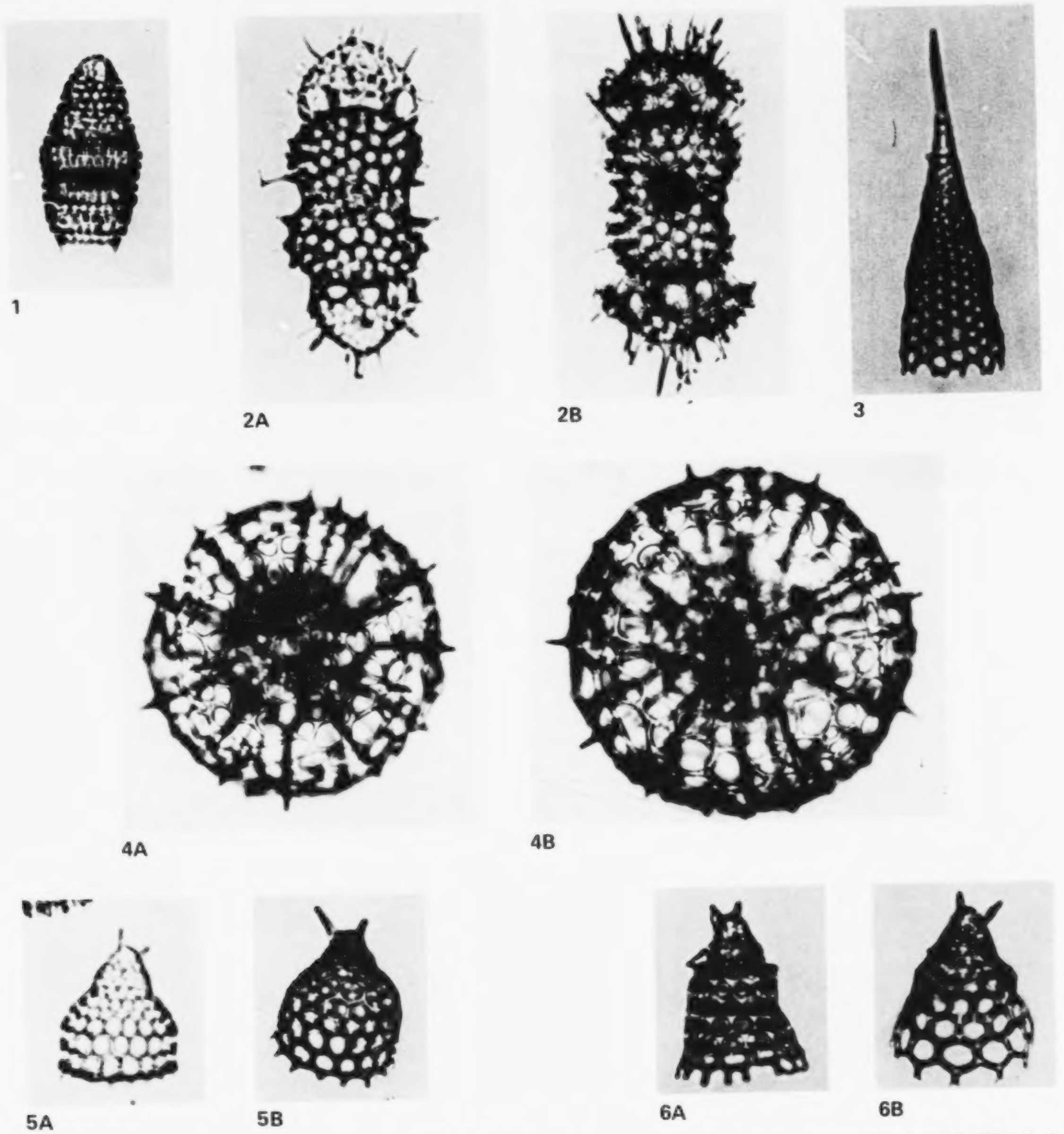

ate 1. **1.** *Botryostrobus aquilonaris* (Bailey), Sample 577-1-1, 5–6 cm. **2A.** *Didymocyrtis tetrathalamus* (Haeckel), Sample 577-1-1, 5–6 cm. **2B.** *Didymocyrtis tetrathalamus* (Haeckel), Sample 578-7-1, 100–102 cm. **3.** *Cornutella profunda* Ehrenberg, Sample 580-11,CC (20–22 cm). **4A.** *Actinomma medianum* Nigrini, Sample 578-1-1, 10–11 cm. **4B.** *Actinomma medianum* Nigrini, Sample 578-7-1, 100–102 cm. **5A.** *Clathrocyclas* spp., Sample 577-1-1, 5–6 cm. **5B.** *Clathrocyclas* spp., Sample 578-7-1, 100–102 cm. **6A.** *Cycladophora davisiana* Ehrenberg, Sample 579A-1,CC (17–19 cm). **6B.** *Cycladophora davisiana* Ehrenberg, Sample 578-7-1, 100–102 cm. (Scale bar equals 100 μm; magnifications are ×200.)

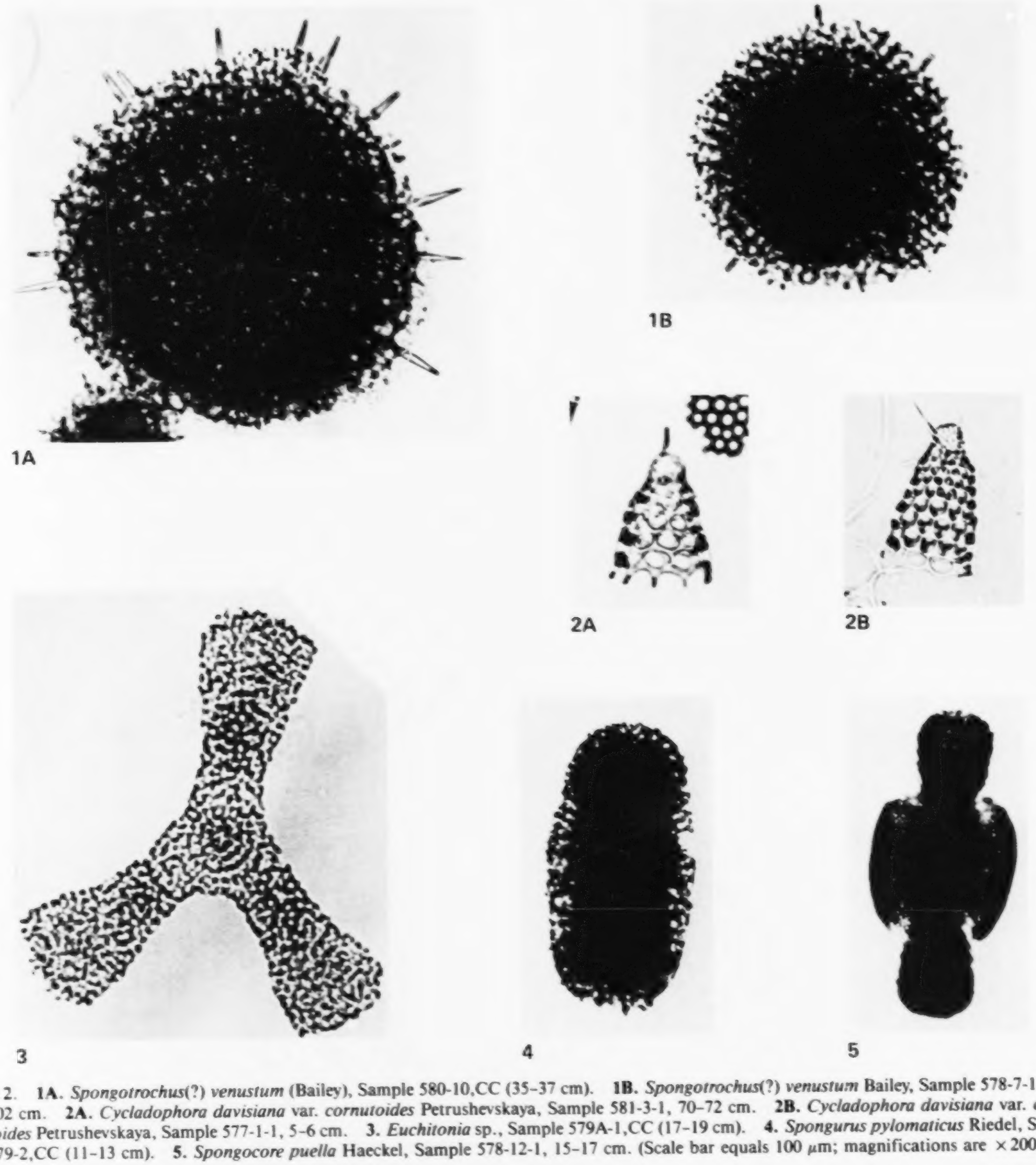

Plate 2. **1A**. *Spongotrochus*(?) *venustum* (Bailey), Sample 580-10,CC (35–37 cm). **1B**. *Spongotrochus*(?) *venustum* Bailey, Sample 578-7-1, 100–102 cm. **2A**. *Cycladophora davisiana* var. *cornutoides* Petrushevskaya, Sample 581-3-1, 70–72 cm. **2B**. *Cycladophora davisiana* var. *cornutoides* Petrushevskaya, Sample 577-1-1, 5–6 cm. **3**. *Euchitonia* sp., Sample 579A-1,CC (17–19 cm). **4**. *Spongurus pylomaticus* Riedel, Sample 579-2,CC (11–13 cm). **5**. *Spongocore puella* Haeckel, Sample 578-12-1, 15–17 cm. (Scale bar equals 100 μm; magnifications are ×200.)

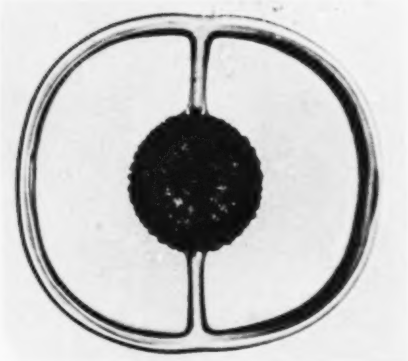

1

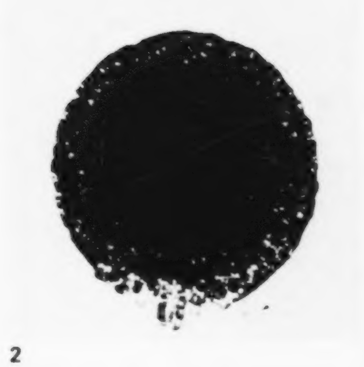

2

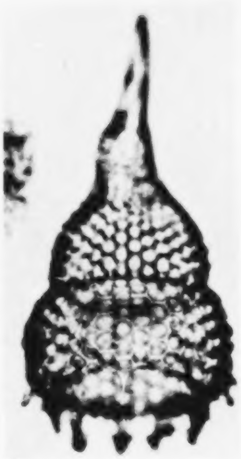

3

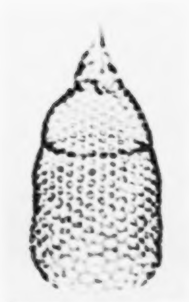

4

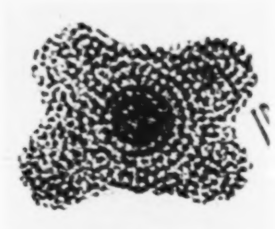

5

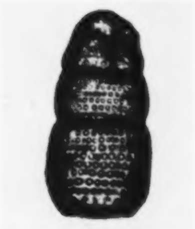

6

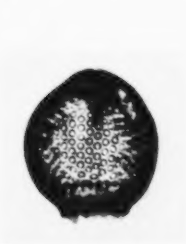

7

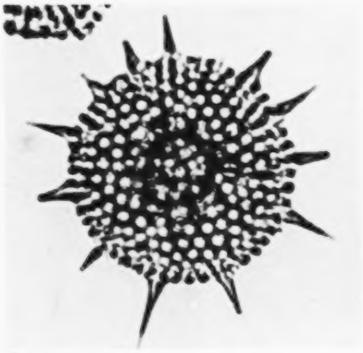

8

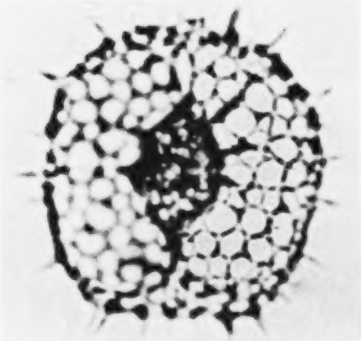

9

late 3. **1.** *Saturnalis circularis* Haeckel, Sample 579-2,CC (11–13 cm). **2.** *Spongopyle osculosa* Dreyer, Sample 578-7-1, 100–102 cm. **3.** *Lamprocyclas maritalis*, Sample 578-7-1, 100–102 cm. **4.** *Pterocorys zancleus* (Müller), Sample 577-1-1, 5–6 cm. **5.** *Spongaster tetras irregularis* Nigrini, Sample 578-1-1, 10–11 cm. **6.** *Phormostichoartus corbula* (Harting), Sample 581-8-1, 70–72 cm. **7.** *Carpocanistrum* spp., Sample 578-7-1, 100–102 cm. **8.** *Heliodiscus asteriscus* Haeckel, Sample 577-1-1, 5–6 cm. **9.** *Larcospira quadrangula* Haeckel, Sample 577-1-1, 5–6 cm. (Scale bar equals 100 μm; magnifications are × 200.)

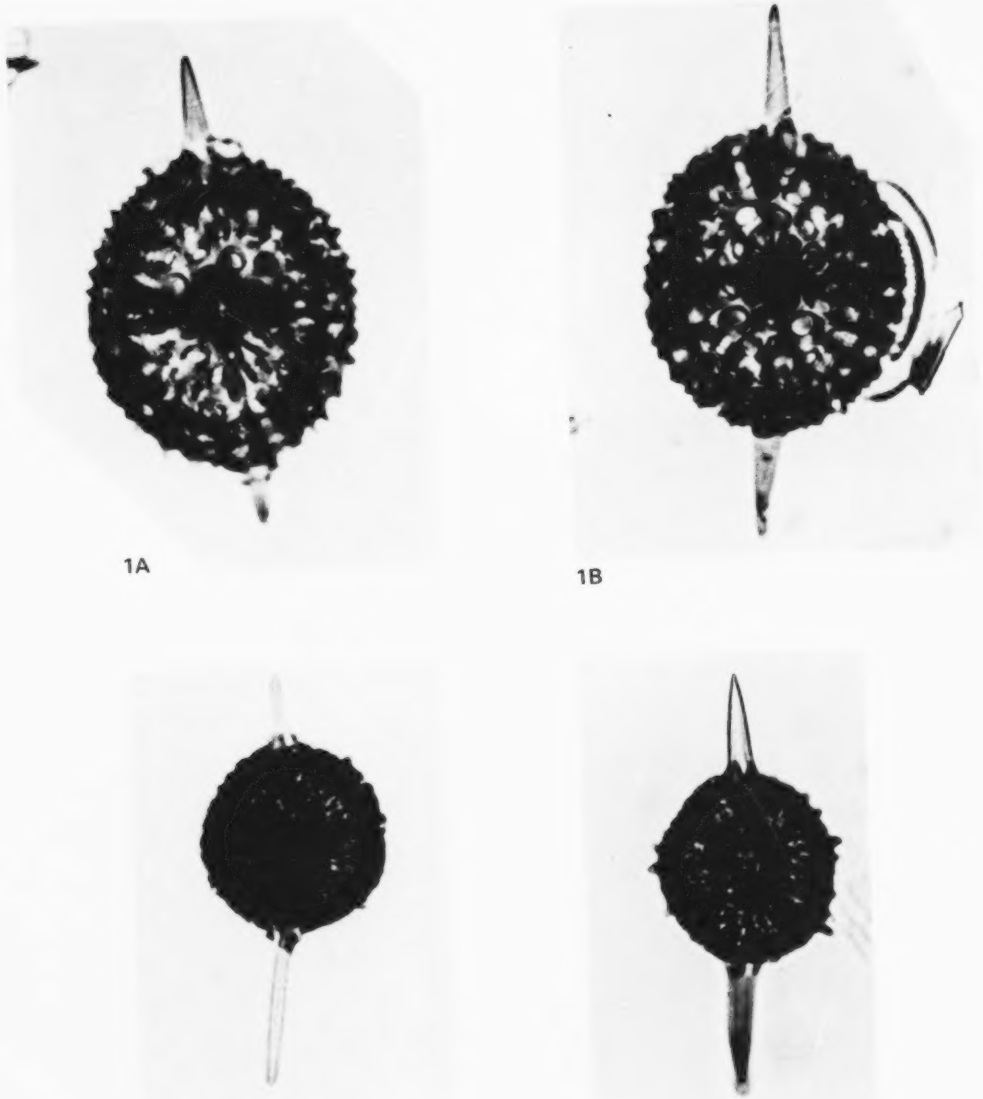

1A

1B

2A

2B

Plate 4. **1A**. *Druppatractus acquilonius* Hays, Sample 580-3-6, 105–107 cm. **1B**. *Druppatractus acquilonius* Hays, Sample 580-3-6, 105–107 cm. **2A**. *Stylatractus universus* Hays, Sample 578-7-1, 100–102 cm. **2B**. *Stylatractus universus* Hays, Sample 579A-4,CC (10–12 cm). (Scale bar equals 100 μm; magnifications are ×200.)

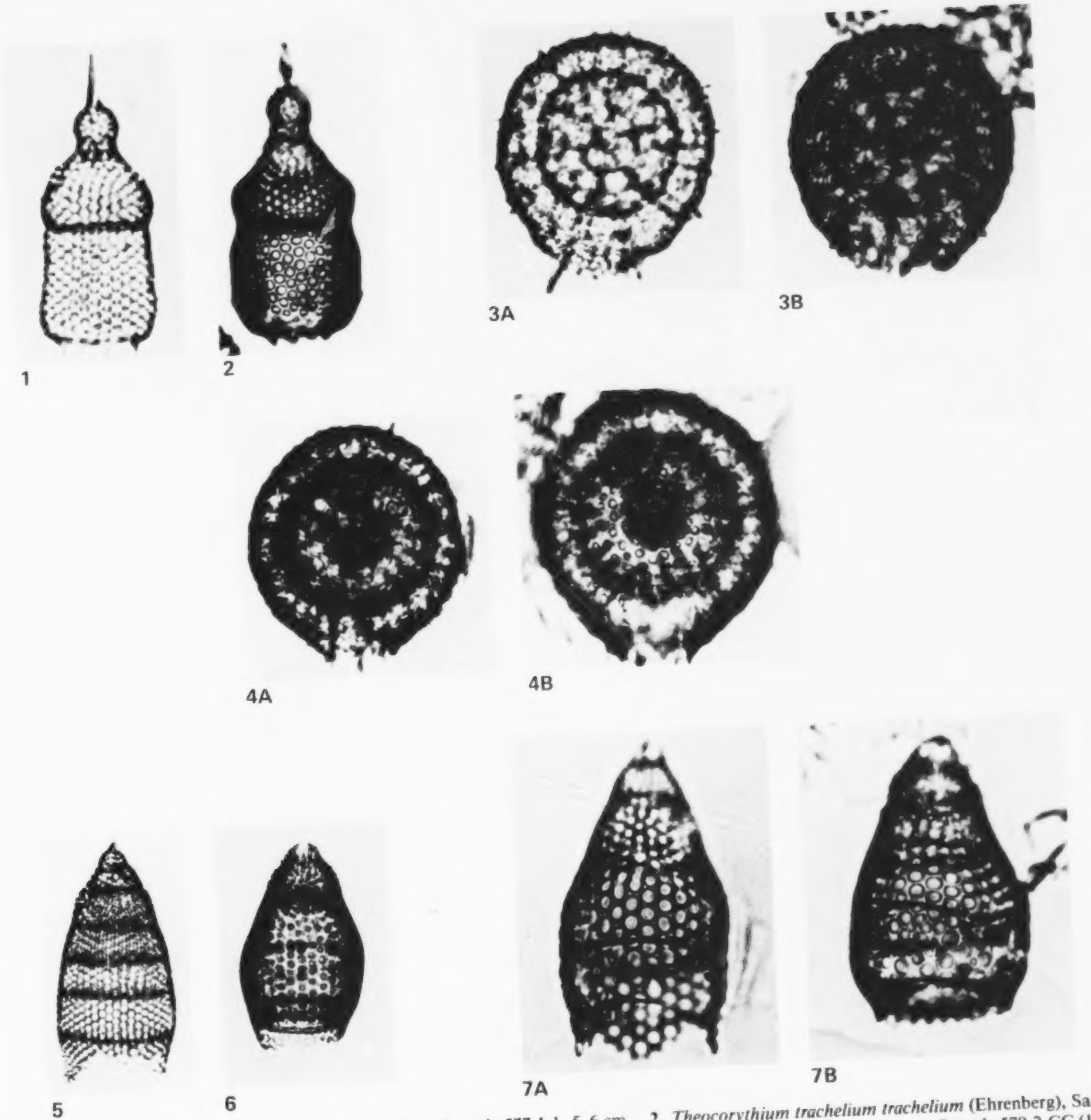

Plate 5. **1.** *Theocorythium trachelium dianae* (Haeckel), Sample 577-1-1, 5–6 cm. **2.** *Theocorythium trachelium trachelium* (Ehrenberg), Sample 578-7-1, 100–102 cm. **3A.** *Sphaeropyle langii* Dreyer, Sample 579A-1,CC (17–19 cm). **3B.** *Sphaeropyle langii* Dreyer, Sample 579-2,CC (11–13 cm). **4A.** *Sphaeropyle robusta* Kling, Sample 579A-7-6, 70–72 cm. **4B.** *Sphaeropyle robusta* Kling, Sample 579A-7-6, 70–72 cm. **5.** *Eucyrtidium acuminatum* (Ehrenberg), Sample 578-1-1, 10–11 cm. **6.** *Eucyrtidium calvertense* Martin, Sample 578-6,CC. **7A.** *Eucyrtidium matuyamai* Hays, Sample 579A-4,CC (10–12 cm). **7B.** *Eucyrtidium matuyamai* Hays, Sample 579A-4,CC (10–12 cm). (Scale bar equals 100 μm; magnifications are ×200.)

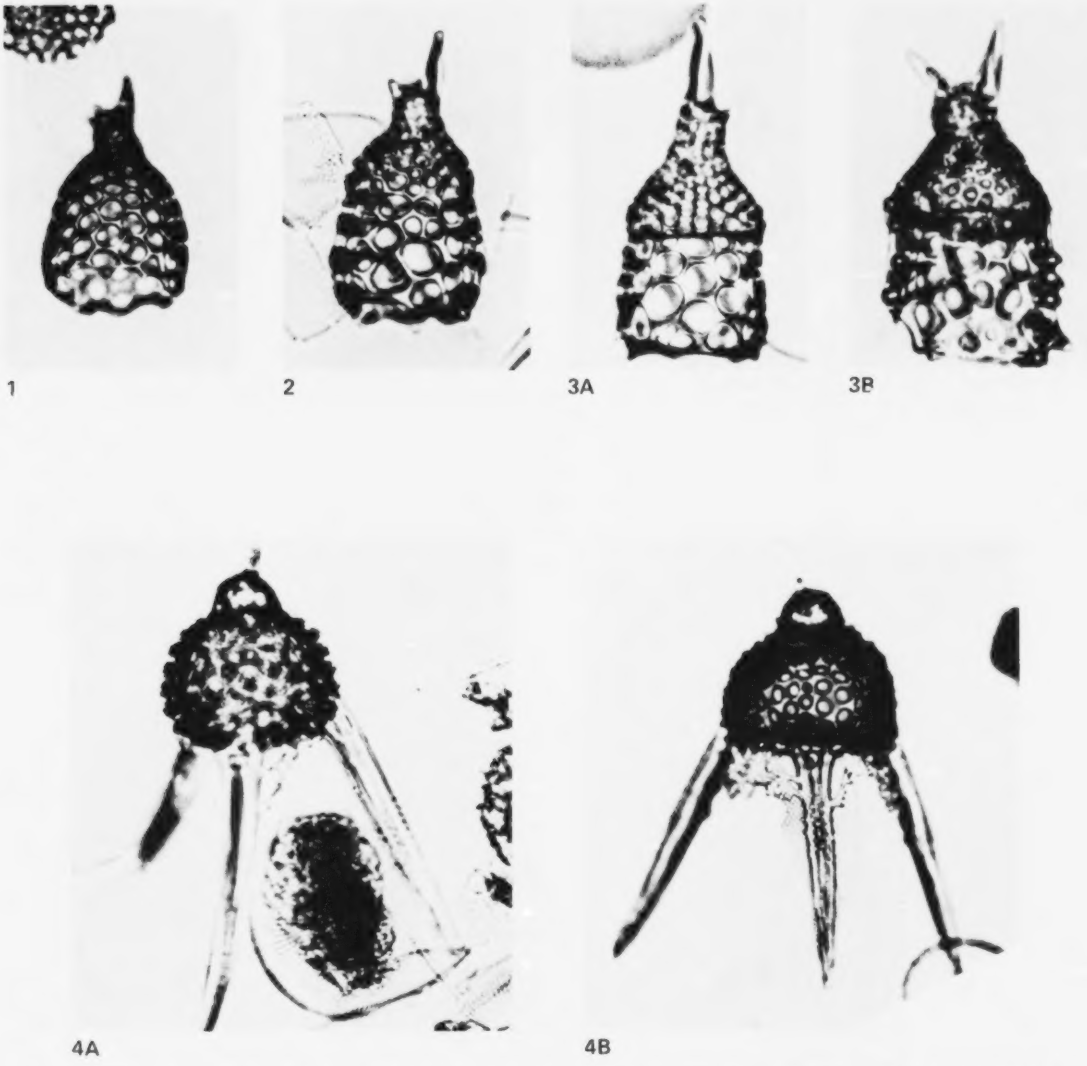

Plate 6. **1.** *Lamprocyrtis nigriniae* (Caulet), Sample 579A-1,CC (17–19 cm). **2.** *Lamprocyrtis neoheteroporos* Kling, Sample 579A-4,CC (10–12 cm). **3A.** *Lamprocyrtis heteroporos* (Hays), Sample 579A-7-6, 70–72 cm. **3B.** *Lamprocyrtis heteroporos* (Hays), Sample 580-11,CC (20–22 cm). **4A.** *Lychnocanoma grande* (Campbell and Clark), Sample 580-3-6, 105–107 cm. **4B.** *Lychnocanoma grande* (Campbell and Clark), Sample 580-3-6, 105–107 cm. (Scale bar equals 100 μm; magnifications are ×200.)

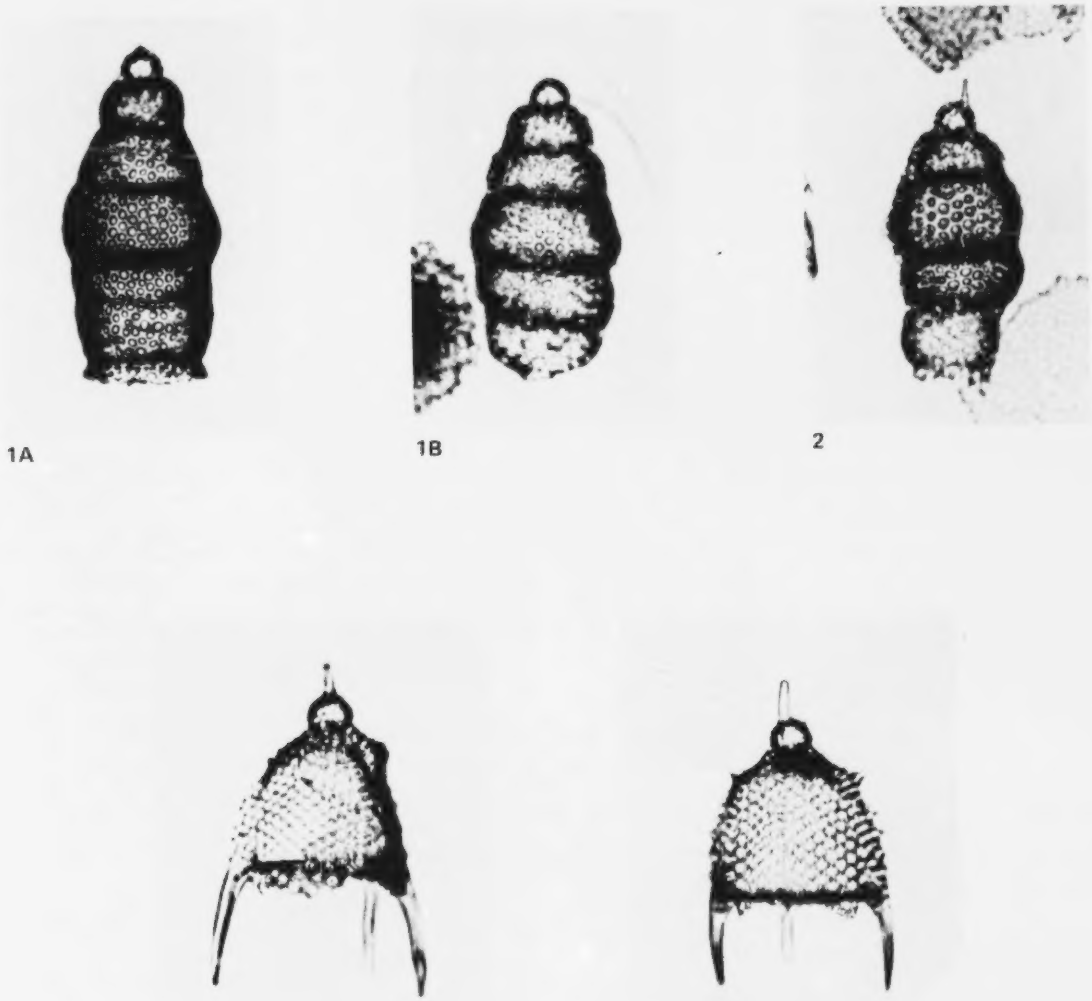

late 7. **1A.** *Stichocorys peregrina* (Riedel), Sample 578-11-1, 15–17 cm. **1B.** *Stichocorys peregrina* (Riedel), Sample 581-3-1, 70–72 cm. **2.** *Stichocorys delmontensis* (Campbell and Clark), Sample 581-7-1, 60–62 cm. **3A.** *Pterocanium prismatium* Riedel, Sample 578-7-1, 100–102 cm. **3B.** *Pterocanium prismatium* Riedel, Sample 578-7-1, 100–102 cm. (Scale bar equals 100 µm; magnifications are ×200.)

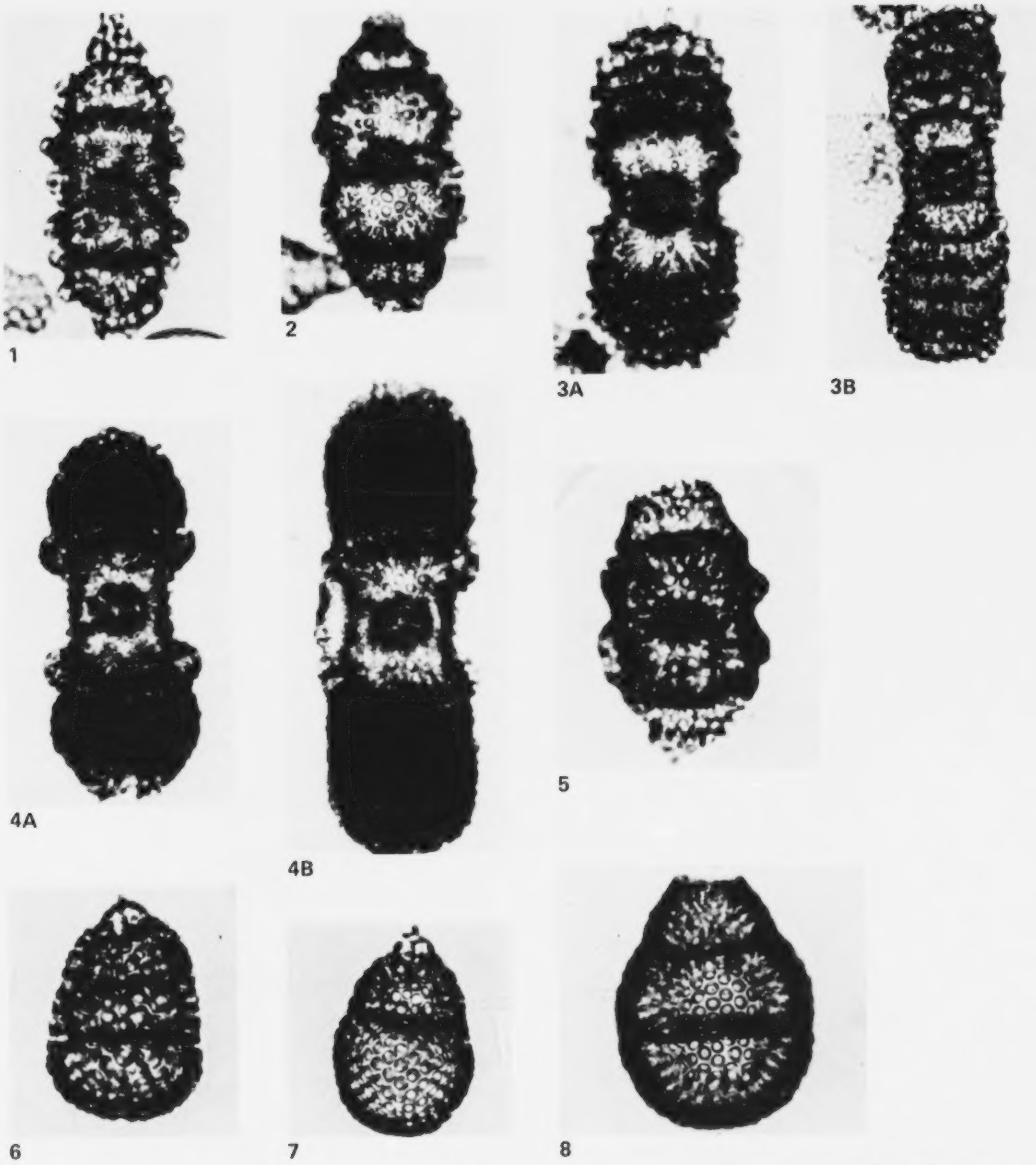

Plate 8. **1.** *Didymocyrtis penultima* (Riedel), Sample 581-6-1, 70–72 cm. **2.** *Didymocyrtis antepenultima* (Riedel and Sanfilippo), Sample 581-7-1, 60–62 cm. **3A.** *Diartus hughesi* (Campbell and Clark), Sample 581-8-1, 70–72 cm. **3B.** *Diartus hughesi* (Campbell and Clark), Sample 581-7-1, 60–62 cm. **4A.** *Diartus petterssoni* (Riedel and Sanfilippo), Sample 581-8-1, 70–72 cm. **4B.** *Diartus petterssoni* (Riedel and Sanfilippo), Sample 581-8-1, 70–72 cm. **5.** *Didymocyrtis laticonus* (Riedel), Sample 581-8-1, 70–72 cm. **6.** *Cyrtocapsella tetrapera* Haeckel, Sample 581-9-1, 40–42 cm. **7.** *Cyrtocapsella japonica* (Nakaseko), Sample 581-8-1, 70–72 cm. **8.** *Cyrtocapsella cornuta* Haeckel, Sample 581-9-1, 40–42 cm. (Scale bar equals 100 μm; magnifications are ×200.)

15. LATE PLEISTOCENE (BRUNHES) DIATOM RECORD AT SITE 580[1]

Constance Sancetta, Lamont-Doherty Geological Observatory of Columbia University[2]

ABSTRACT

The late Quaternary (Brunhes) diatom assemblage at Site 580 is diverse (about 40 species, of which 12 reach abundances >10%) and varies both on the short scale of a single glacial–interglacial cycle and on a longer scale of several hundred thousand years. All of the species show fluctuations in relative abundance which, in many cases, seem to be correlated with glacial–interglacial stages. Superimposed on the basic cyclic record, there is evidence of at least two instances of permanent population readjustment. The early Brunhes was characterized by the presence of true subtropical species, the middle Brunhes by high-amplitude changes in species characteristic of the transition zone, and the late Brunhes by an increase of subarctic species. Since the site itself has not migrated appreciably during this time, the diatom record probably reflects a progressive southward advance of the subarctic gyre at the expense of the subtropical gyre. During the mid-Brunhes, when the Subarctic Front repeatedly crossed the site, the environment was particularly unstable—two radiolarian extinctions (*Druppatractus acquilonius* and *Stylatractus universus*), one diatom extinction (*Rhizosolenia curvirostris*), and the local disappearance of a diatom form (*Actinocyclus ochotensis*) occurred during this time.

INTRODUCTION

Site 580 is located at 41°37′N, 153°58′E, about 600 miles east of northern Honshu, in 5375 m of water. It lies beneath the northern part of the modern Subarctic Front, a transitional zone of temperature and salinity gradients. The site was chosen as the northern end of a latitudinal transect, intended to monitor changes of the front throughout late Neogene time.

A 40-m section representing the Brunhes magnetic interval was recovered by hydraulic piston coring, with excellent recovery (91%, see Site 580 chapter, this volume). Both magneto- and biostratigraphic studies indicate a linear sedimentation rate throughout the interval. Samples at roughly 50-cm intervals (9.2 k.y.) were analyzed or fossil diatoms, to elucidate the history of local ocean-graphic events and the response of the phytoplankton opulation to them.

METHODS

Approximately 1 g of sediment was disaggregated in 50 ml of a ak solution of $Na_4P_2O_7 \cdot 10H_2O$ (sodium pyrophosphate) and subted to 1 min. in an ultrasonic bath. The beaker was then filled to 0 ml with distilled water and the particles allowed to settle for 1 hr., er which the supernatant liquid and suspended particles were poured . The settling procedure, repeated three times, removes most of the y-sized particles. Slides were prepared by placing an aliquot of the naining slurry on the slides and drying them on a hot plate. Perount medium and a cover slip were added and the solvent allowed to aporate.

Diatom population of each sample was analyzed by counting apoximately the first 400 specimens encountered in a series of random verses, at 1250× magnification. Data are expressed as percent abunnce of each taxon relative to the total diatom assemblage.

RESULTS

Cyclic Fluctuations of *Thalassiosira trifulta*

When the species abundance data are plotted against depth below surface (Fig. 1), *Thalassiosira trifulta* Fryxell shows large-amplitude variations which appear to be periodic. A Fourier time-series analysis was done on this record, using the basic age model summarized below.

Depth (m)	Age (k.y.)
0	0
8.00	125
23.26	425
39.60	730

The top of Core 1 (0 m) is assumed to be modern (0 k.y.). This assumption is optimistic; it is likely that deployment of the coring gear disturbed the surface sediments, so that part of the Holocene record was lost. However, the diatom assemblage of the first sample (Sample 580-1-1, 15 cm) is similar to that of neighboring piston-core tops and very different from that typical of Wisconsin-age material (Sancetta, 1979 and unpublished data); thus, no more than 10 k.y. can be missing. Sample 580-2-4, 20 cm (8.0 m) was taken to represent the maximum of the last interglacial (Isotope Stage 5e), 125 k.y., based on the coinciding maxima of *T. oestrupii* (Ostenfeld) Proshkina-Lavrenko and *Pseudoeunotia doliolus* (Wallich) Grunow, two warm-water species. The extinction of the radiolarian *Stylatractus universus* occurs at 23.26 m (Morley, this volume); this event was globally synchronous and occurred at 425 k.y. (Morley and Shackleton, 1978). The Brunhes/Matuyama boundary (730 k.y.) is located at 39.6 m (Site 580 chapter, this volume).

---

[1] Heath, G. R., Burckle, L. H., et al., *Init. Repts. DSDP*, 86: Washington (U.S. Govt. inting Office).

[2] Address: Lamont-Doherty Geological Observatory of Columbia University, Palisades, Y 10964.

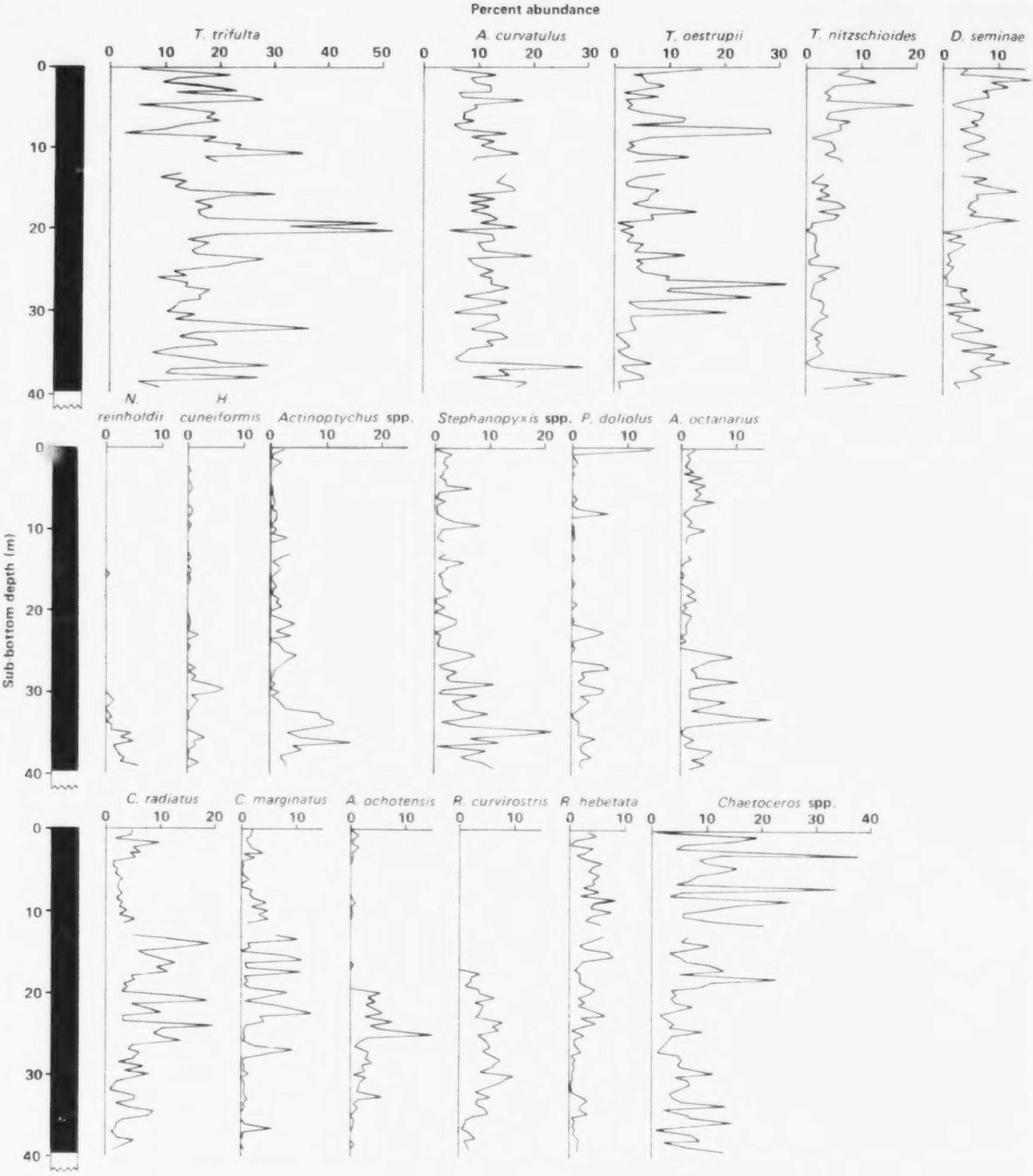

Figure 1. Variation in abundance of diatoms (in percent) at Site 580. Depth scale and paleomagnetic record (from Site 580 chapter, this volume) repeated to the left of each row. The space from 11.5 to 13.0 m in each curve represents an unrecovered interval.

The results of the Fourier analysis show a strong concentration of variance with a period of 41 k.y. and a weak concentration with a period of 23 k.y. (Fig. 2). These are the periods of axial obliquity and equinoctial precession, respectively, which have been identified in time series of other parameters from marine sediments, including oxygen isotopes in foraminiferal tests (Hays e al., 1976). However, when the abundance of *T. trifulta* i plotted together with the global stacked isotope record of Imbrie et al. (1984), subsampled at 10-k.y. intervals (Fig. 3), it is clear that the species record does not reflect the ice-volume record represented by the isotope values.

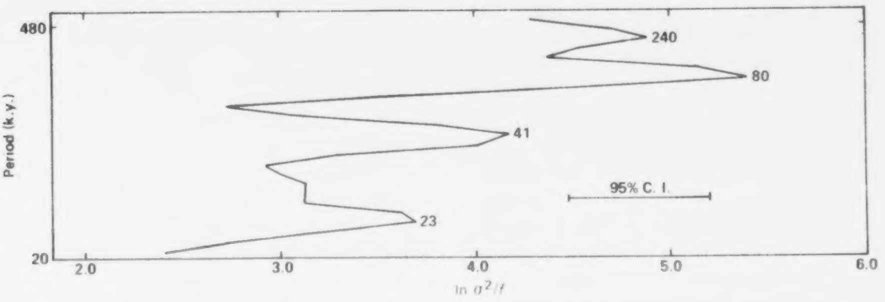

Figure 2. Variance spectrum for *T. trifulta* record. (ln σ^2/f = natural log of variance per frequency; C.I. = confidence interval).

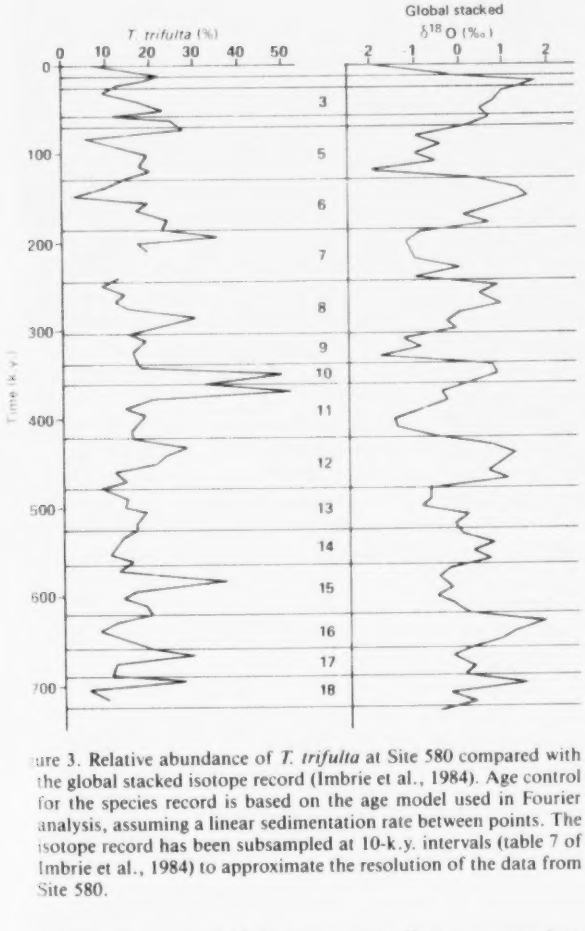

ure 3. Relative abundance of *T. trifulta* at Site 580 compared with the global stacked isotope record (Imbrie et al., 1984). Age control for the species record is based on the age model used in Fourier analysis, assuming a linear sedimentation rate between points. The isotope record has been subsampled at 10-k.y. intervals (table 7 of Imbrie et al., 1984) to approximate the resolution of the data from Site 580.

axima on the *T. trifulta* curve usually correspond to pes on the isotope curve. Thus, maximum abundances this species occurred during times of transition be- een glacial and interglacial conditions.

T. trifulta occurs in low abundances in modern sedi- ents of the subarctic Pacific, with much higher abun- ance in the Sea of Okhotsk (Sancetta, 1982b), a region haracterized by unusually low-temperature and low-sa- nity surface waters (7°C, 32.5‰ in summer) and a strong hick halocline, bounded at 50 and 150 m by thermo- lines (Yasuoka, 1967, 1968). This vertical structure is the result of prolonged winter sea ice and cold Siberian winds. The high abundances of *T. trifulta* at Site 580 imply that similar "cold, fresh" conditions existed in the region of the western Subarctic Front during times of climatic transition.

Other Species

Actinocyclus curvatulus Janisch is also consistently present throughout the Brunhes section (Fig. 1) and shows fluctuations in abundance, although the amplitudes are not as high as for *Thalassiosira trifulta*. The two records show no overall correlation ($r = -0.03$), although the largest maxima of *A. curvatulus* do correspond to some of the *T. trifulta* maxima. *A. curvatulus* is also common in modern sediments of the Sea of Okhotsk, but is present throughout the subarctic Pacific. The record at Site 580 does not show a clearly interpretable pattern; it may be that this species is rather tolerant of environmental change.

T. oestrupii (Ostenfeld) Proskina-Lavrenko is rare during the Brunhes (averaging 5%), but shows several intervals of high abundance, at 0.15, 6.25–6.50, 7.50–8.00, 11.00, 17.50, 22.85, 26.45, 27.95, and 29.95 m, corresponding to Isotope Stages 1, 5, 7, 9, 11, 13, and 14. This suggests that *T. oestrupii* represents warmer, more saline waters typical of the modern interglacial values in the region (15°C, 33.5‰ in summer). Sancetta (1979) found that *T. oestrupii* is characteristic of the assemblage underlying the Subarctic Front in the North Pacific (42–45°N), the transition zone from the cold low-salinity subarctic gyre to the warm saline subtropical gyre. *T. oestrupii* was excluded from the westernmost part of the transition zone during the last glacial maximum and existed only in the central North Pacific (Sancetta, 1979), suggesting that it does not tolerate the extreme temperature and salinity seasonal fluctuations of the western region. Its occasional high abundance at Site 580 may represent interglacial periods in which the effect of subarctic water was particularly low.

Thalassionema nitzschioides (Grunow) H. and M. Peragallo also averages <5% through most of the section, but has maxima at 1.75, 4.50, and 37.20 m, corresponding to Isotope Stages 3, late 5, and 17. The late Stage 5 maximum is associated with the occurrence of rare freshwater diatoms (*Stephanodiscus* spp.) and opaline phytoliths. *T. nitzschioides* is a cosmopolitan species, often common in areas of high productivity, such as the eastern equatorial Pacific (Hasle and de Mendiola, 1967; L. Burckle, pers. comm., 1982). The three maxima at Site 580 may represent times of increased wind stress and upwelling within the transition zone.

The record of *Denticulopsis seminae* (Simonsen and Kanaya) Simonsen does show a trend, but the significance is not clear. During the early part of the Brunhes (Stage 18 to late 13), *D. seminae* averages 5% of the flora. Following this is a prolonged minimum (late Stage 13 to late Stage 11) and then a return to an average of 5% (late Stage 11 through Stage 1) with maxima at 1.22, 14.9, and 18.5 m (Stages 2, 8, and 10). *D. seminae* today is characteristic of the entire subarctic gyre, particularly the eastern and central part, where surface temperature and salinity are intermediate (9-12°C, 32.5-32.75‰ in summer). Site 580 lies outside this biogeographic region (being to the south and west), so that conditions at the site may be presumed to be marginal for the species. The three maxima may represent brief expansions of eastern-subarctic conditions during times of peak glacial advance on land.

A group of species shows markedly higher average abundance during the early Brunhes. These include *Nitzschia reinholdii* Kanaya and Koizumi, *Hemidiscus cuneiformis* Wallich, *Actinoptychus* spp. (*A. senarius* Ehrenberg and *A. vulgaris* Schumann), *Stephanopyxis* spp., *Pseudoeunotia doliolus* (Wallich) Grunow, and, over a shorter interval, *Actinocyclus octonarius* Ehrenberg. With the exception of *Stephanopyxis* spp., these forms are all typical of warm, saline tropical and subtropical waters today. The distribution of *Stephanopyxis* in sediments has not been defined, but personal observations suggest that it is more common along temperate continental margins. The consistent (albeit fluctuating) presence of these species during the early Brunhes, and their virtual absence from the later part of the record, suggest that conditions at Site 580 were generally more "subtropical" during Stages 18-12 than they have been since. The extinction of *N. reinholdii* occurs within this interval, at 550 k.y. (early Stage 14). Barron (1980) estimated an age of 630 k.y. for this event, which corresponds to the small acme ending at 34 m (Stage 16). The event may be time transgressive (Sancetta, 1982a), or Barron may have overlooked the very rare occurrence of the species just prior to its disappearance.

Two species, *Coscinodiscus radiatus* Ehrenberg and *C. marginatus* Ehrenberg, show low values in the early and late Brunhes, and high-amplitude fluctuations during the middle Brunhes (13-28 m, Stages 8-13). Neither species shows consistent maxima or minima corresponding to isotopic stages. *C. marginatus* is more common today in the southern part of the subarctic gyre just north of the Subarctic Front, whereas *C. radiatus* occurs within the transition zone. The high-amplitude fluctuations of these two species suggest an interval of instability in the front, which repeatedly migrated across the site during the mid-Brunhes.

The record of two other species shows that the mid-Brunhes was a time of instability and of a changing (stressful) environment. *A. ochotensis* Jousé, which was a minor member of the floral assemblage during the early Brunhes, increased in average abundance during the middle Brunhes and then disappeared from the region. Subsequently, *Rhizosolenia curvirostris* Jousé suffered extinction during Stage 8 (276 k.y., Morley et al., 1982).

Following the extinction of *R. curvirostris*, a congeneric species, *R. hebetata* Bailey, increased in average abundance and remained consistently more common through the late Brunhes (Stages 8-1). Today this species is limited to the subarctic gyre and does not occur in sediments at or south of the Subarctic Front. The increased occurrence of *R. hebetata* during the late Brunhes suggests that the influence of subarctic waters became more important during that time.

Finally, spores of the genus *Chaetoceros* fluctuate in abundance throughout the Brunhes, with an overall increase in amplitude in the late Brunhes (Stages 7-1). The highest maxima occur at 0.75, 3.08, 7.00, 8.50, 11.50, and 18.00 m, corresponding to Isotope Stages 1/2, 3/4, 6, 7, and 9/10. *Chaetoceros* species are characteristic of high productivity along continental margins today; in the North Pacific they are dominant in sediments underlying the East Kamchatka and Oyashio Currents, regions of maximum productivity in cold, low salinity surface waters. The high-amplitude fluctuations at Site 580 during the late Brunhes suggest short periods of increased input from the productive Oyashio Current, particularly during times of climatic transition.

TAXONOMIC NOTES

Most of the species discussed here have been described and illustrated by numerous workers, and there seems to be little taxonomic confusion in the literature. A review of systematics in this chapter is therefore unnecessary. I have discussed taxonomic identification of subarctic species elsewhere (Sancetta, 1982b); I note here only a few cases that may require clarification.

Actinocyclus octonarius is synonymous with *A. ehrenbergii* Ralfs. The latter epithet is illegitimate, being a junior synonym.

Actinocyclus ochotensis is probably not a true species, but an irregular morphotype of *A. curvatulus*. A complete intergradation can be seen in these forms. Further work is needed to resolve the question.

ACKNOWLEDGMENTS

I am grateful to the technical and scientific staff of Leg 86 for making the samples available for study. The chapter was reviewed by Lloyd Burckle and Joseph Morley, who freely shared their own results from Leg 86, and by John Barron and Nicklas Pisias, who provided helpful criticism. Research was supported by NSF Grant OCE81-09933. This is Lamont-Doherty Contribution No. 3722.

REFERENCES

Barron, J. A., 1980. Lower Miocene to Quaternary diatom biostratigraphy of Leg 57, off northeastern Japan, Deep Sea Drilling Project. *In* Scientific Party, *Init. Repts. DSDP*, 56, 57, Pt. 2, (U.S. Govt. Printing Office), 641-685.

Hasle, G. R., and de Mendiola, B. R. E., 1967. The fine structure of some *Thalassionema* and *Thalassiothrix* species. *Phycologia*, 6: 107-125.

Hays, J. D., Imbrie, J., and Shackleton, N. J., 1976. Variations in the Earth's orbit: pacemaker of the ice ages. *Science*, 194:1121-1132.

Imbrie, J., Hays, J. D., Martinson, D. G., McIntyre, A., Mix, A. C., Morley, J. J., Pisias, N. G., Prell, W. L., and Shackleton, N. J., 1984. The orbital theory of Pleistocene climate: support from a revised chronology of the marine $\delta^{18}O$ record. *In* Berger, A., et al. (Eds.), *Milankovich and Climate:* Dordrecht (D. Riedel), pp. 269-305.

Morley, J. J., Hays, J. D., and Robertson, J. H., 1982. Stratigraphic framework for the late Pleistocene in the northwest Pacific Ocean. *Deep-Sea Res.*, 29:1485-1499.

Morley, J. J., and Shackleton, N. J., 1978. Extension of the radiolarian *Stylatractus universus* as a biostratigraphic datum to the Atlantic Ocean. *Geology*, 7:309-311.

Sancetta, C., 1979. Oceanography of the North Pacific during the last 18,000 years: Evidence from fossil diatoms. *Mar. Micropaleontol.*, 4:103-123.

________, 1982a. Diatom biostratigraphy and paleoceanography, Deep Sea Drilling Project Leg 68. *In* Prell, W. L., Gardner, J. V., et al., *Init. Repts. DSDP*, 68: Washington (U.S. Govt. Printing Office), 301-309.

________, 1982b. Distribution of diatom species in surface sediments of the Bering and Okhotsk seas. *Micropaleontology*, 28:221-257.

Yasuoka, T., 1967. Hydrography in the Okhotsk Sea (1). *Oceanogr.*, 19:61-72.

________, 1968. Hydrography in the Okhotsk Sea (2). *Oceanogr.*, 20: 55-63.

Date of Initial Receipt: 28 October 1984
Date of Acceptance: 11 May 1984

16. LATE NEOGENE PALEOCEANOGRAPHY IN THE WESTERN NORTH PACIFIC[1]

Itaru Koizumi, Institute of Geological Sciences, Osaka University[2]

ABSTRACT

Late Neogene paleoceanographic history in the western North Pacific is discussed on the basis of: (1) Td (diatom temperature) values, (2) species composition, and (3) the structure of diatom assemblages at Sites 579 and 580. These factors provide a record of fluctuations of the past position of the subarctic-subtropic front because these sites lie within the transition zone between the modern day subarctic and central water masses. Changes in species composition during the past 4.0 m.y. are recognized. Major paleoclimatic events are discussed on the basis of Td values. Distinct, large drops in surface water temperature, estimated on the basis of Td values, occurred 2.5, 2.0, and 1.6 m.y. ago. Large fluctuations of surface water temperature are recognized throughout the recovered sediments. The preglacial/glacial boundary occurs 2.50–2.85 m.y. ago at 40°N in the western North Pacific.

INTRODUCTION

The primary objective of Deep Sea Drilling Project (DSDP) Leg 86 was to unravel the late Neogene paleoceanographic history in the western North Pacific by establishing a north-south transect across the Kuroshio Current system. At both Sites 579 and 580, thick sections of Pleistocene and Pliocene biosiliceous clay and ooze were recovered in the transition zone between the modern subarctic and central water masses (Fig. 1). Sediments from both sites are homogeneous in color and texture. These sediments lack any depositional sedimentary structures, although the sediments from Site 579 are burrow mottled. Diatoms are abundant and well preserved throughout much of these sections (see Koizumi and Tanimura, this volume).

The western North Pacific Ocean is divided into three different marine environments (Fig. 1): (1) the subarctic region containing the subarctic water mass, (2) the subtropic region containing the central water mass, and (3) he transition region, which is a mixed zone of both subrctic and central water masses (Fig. 1). The subarctic gion is characterized by an annual precipitation that ceeds evaporation and by cold, low salinity surface ater. A permanent halocline extends between 100 and 0 m below the sea surface. The subtropic region is aracterized by a high annual evaporation that exceeds ecipitation. The surface water salinity maximum deeases to a minimum between 500 and 600 m below the a surface. The transition region located between the barctic and subtropic regions lies between 40 and 42°N itude. This region is at the 34‰ isohaline and coinides with the line along which evaporation equals prepitation (Dodimead et al., 1963). Transition region war is derived from off the coast of Japan, where the ld Oyashio Current, originating in the Bering Sea and the Sea of Okhotsk, converges with the warm Kuroshio Current, originating in the central water mass (Fig. 1). The mixed surface water moves eastward across the Pacific in the West Wind Drift.

Concentration of nutrient salts in the surface waters is higher in the subarctic region than in the subtropic region. Upwelling of nutrient-rich deep water occurs near the center of the gyres in the subarctic region. Primary productivity in the subarctic region is, therefore, greater than in the subtropic region.

Site 579 lies near the southern margin of the transition zone between the subarctic and subtropic water masses, and its sediments should therefore provide a record of extreme southerly excursions of the subarctic-subtropic front. Site 580 lies near the northern margin of the transition zone, and its sediments should provide a record of northward fluctuations of the position of this front.

Donahue (1970) discussed Pleistocene climatic changes on the basis of Td values (Kanaya and Koizumi, 1966) in several northern North Pacific piston cores for which a paleomagnetic time scale is available. The paleoceanographic history of the western North Pacific has not been extended back through the Pliocene. This is the result of a lack of complete sections, since piston corers cannot recover a complete Pliocene section in this region of the North Pacific, where sedimentation rates are relatively high.

Major paleoclimatic and paleoceanographic events have, however, been identified by delineating planktonic foraminiferal biofacies in DSDP cores from the subtropic region (e.g., Vincent, 1975; Keller, 1979) and by establishing oxygen isotope records in both equatorial piston cores (e.g., Shackleton and Opdyke, 1976, 1977) and DSDP cores from the subtropic region of the eastern North Pacific (e.g., Keigwin, 1979).

The Pliocene/Pleistocene boundary is conventionally placed at the top of the Olduvai Event (Burckle and Opdyke, 1977). The early/late Pliocene boundary is placed at about 3.0 m.y. ago (at the base of the Kaena Event); the early/late Pleistocene boundary is at about 0.9 m.y. ago (at the top of the Jaramillo Event).

---

[1] Heath, G. R., Burckle, L. H., et al., *Init. Repts. DSDP*, 86: Washington (U.S. Govt. rinting Office).

[2] Address: Institute of Geological Sciences, College of General Education, Osaka Uniersity, Toyonaka, Osaka 560, Japan.

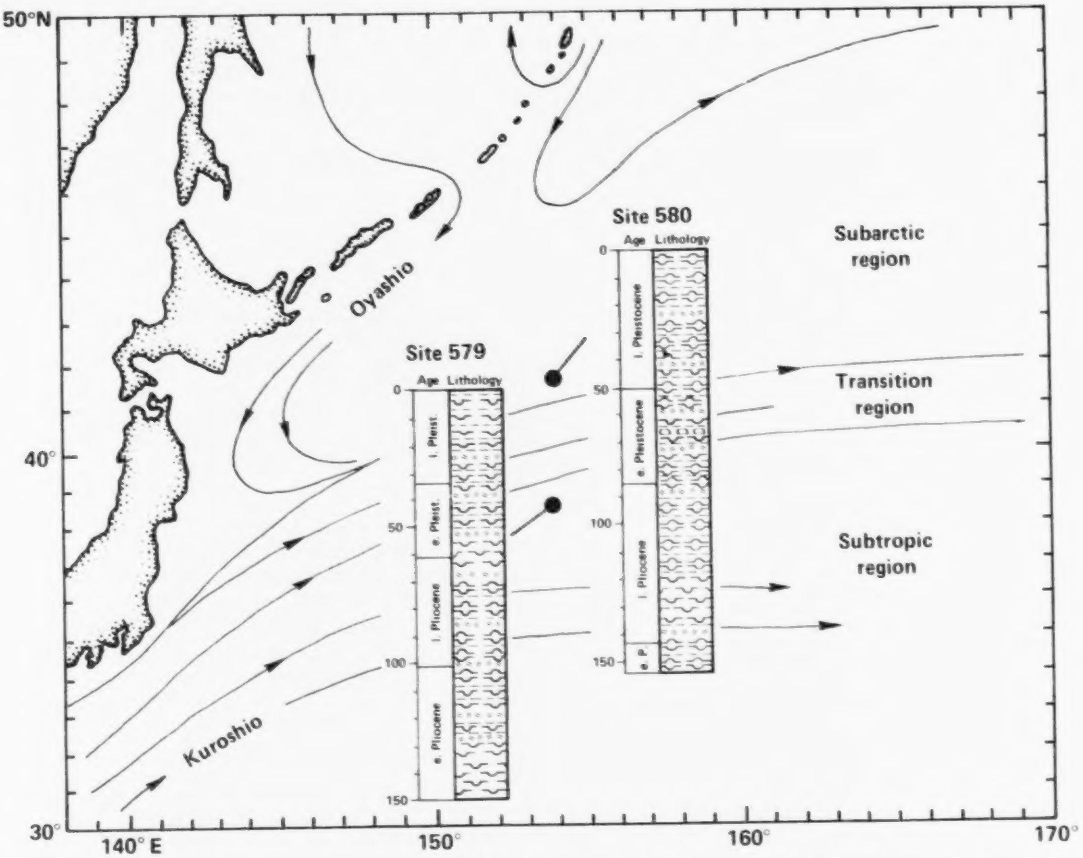

Figure 1. Location and schematic lithologic sections of Sites 579 and 580 studied on DSDP Leg 86. Site locations are shown in relation to the three major ocean regions. Two holes were drilled at Site 579: Hole 579 lies at 38°37.68′N, 153°50.17′E, depth 5737 m; Hole 579A at 38°37.61′N, 153°50.28′E, depth 5737 m. Site 580 is located at 41°37.47′N, 153°58.58′E, depth 5375 m.

This study extends the work of Donahue (1970) back into the Pliocene in a north–south transect across the transition zone of the western North Pacific.

MATERIALS

Samples were taken one per section (one per 150 cm) throughout all the cores recovered at Sites 579 and 580. A detailed chronology, developed through paleomagnetic studies, is available for each of these sections (Bleil, this volume). Age–depth profiles at Sites 579 and 580 indicate that the sedimentation rates increased in the late Pleistocene at both sites (Fig. 2). Sedimentation rates average about 4 cm/10^3 yr. at Site 579, giving a sample spacing of about 38,000 yr. and about 5.4 cm/10^3 yr. at Site 580, giving a sample spacing of about 28,000 yr. Sedimentation rates during the early Pleistocene and Pliocene are about 3.2 cm/10^3 yr. at Site 579, giving rise to a sampling interval of 47,000 yr. and 4.4 cm/10^3 yr. at Site 580, giving rise to a sampling interval of 34,000 yr.

METHOD OF STUDY

Paleoceanographic analysis is undertaken in this chapter on the basis of: (1) Td values, (2) species composition in a given assemblage, and (3) assemblage structure. Td variations are the primary indicator of paleoclimatic events.

Td (diatom temperature) Values

The Td statistic was proposed by Kanaya and Koizumi (1966) to estimate surface water temperature during the accumulation of sediments in the lower levels of a core sequence. Td is defined as $(Xw/Xw + Xc) \times 100$, where Xw is the frequency of warm-water diatoms and Xc is that of cold-water diatoms. Xw and Xc species have been selected according to Kanaya and Koizumi (1966; Table 1). All these diatoms are living species. Td ranges in value from 0 to 100. Going from the subarctic region to the tropic region, Td becomes systematically larger (Kanaya and Koizumi, 1966, fig. 5). Namely, Td values show (in a broad sense) a positive correlation with surface water temperature over a given geographical site in the North Pacific. Correlation of the uppermost sediment Td values with surface water temperature at both Sites 579 and 580 is used to estimate surface water temperature from downhole Td values at both sites (Fig. 3).

Species Composition

1. Selected Species. Quantitative distribution of selected species from the members of Xw and Xc in the Td formula is examined. *Coscinodiscus nodulifer* was chosen as a representative of the central water mass (Xw) and *Denticulopsis seminae* as a representative of the subarctic water mass (Xc). *C. nodulifer* has been classified as a subtropic or tropic (i.e., "warm-water") species in other investigations (e.g., Jousé et al., 1971; Hasle, 1976). *D. seminae* has been classified

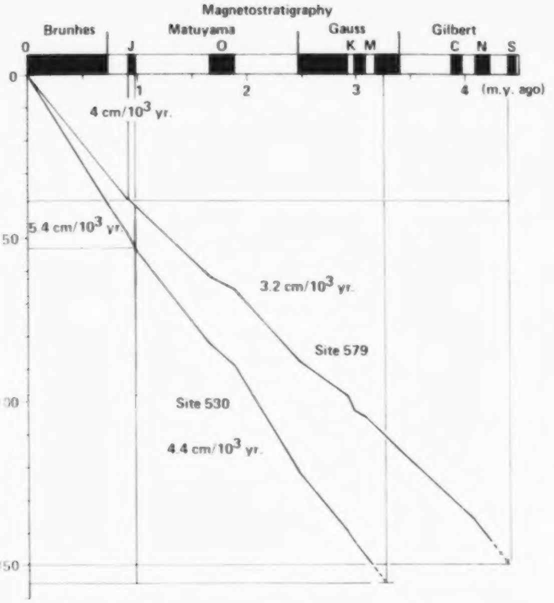

Figure 2. Age-depth plot for Sites 579 and 580. Age is based on magnetostratigraphy (Bleil, this volume). Late Pleistocene sedimentation rates average about 4 cm/10^3 yr. at Site 579 and about 5.4 cm/10^3 yr. at Site 580. Sedimentation rates decrease to about 3.2 cm/10^3 yr. at Site 579 and 4.4 cm/10^3 yr. at Site 580 during the early Pleistocene and Pliocene. See legend of Figure 4 for definition of magnetostratigraphic events.

as "cold-water" (Hasle, 1976) and as "subarctic" (Venrick, 1971) in the North Pacific. The relative frequency of occurrence of these two species changes significantly in the transition zone between the modern subarctic and central water masses.

2. Recurrent Group. Kanaya and Koizumi (1966) determined recurrent groups by using joint occurrences of diatoms that have habitats in the water column of the North Pacific. Group I is composed of planktonic diatoms known to inhabit subtropic and tropic waters, Group II is composed of oceanic diatoms of the boreal zone occurring in subarctic waters, and Group IV is limited to arctic and arctoboreal neritic diatoms. Their species composition at Sites 579 and 580 is given in Table 1.

According to the distribution patterns of recurrent groups (Kanaya Koizumi, 1966, fig. 4), both Groups I and II are identified within geographic range of the transition zone. The distribution of Group losely coincides with the path of the cold Oyashio Current. There-, at all stations where Group IV is identified, Group II is also recized.

Downhole variations in abundances of Group I and Group II dias at Sites 579 and 580 are examined to determine which group was inant at various geologic times in the transition zone. A discusof abundance variations of Group IV diatoms follows.

mblage Structure

. Number of Diatoms. Jousé et al. (1971) counted diatoms per in surface sediments of the Pacific Ocean. The number of dias in a given volume of sediments depends on (1) preservation and/issolution of the diatoms, (2) dilution with terrigenous and/or r organic materials, and (3) diatom productivity. As expected, the iber of diatoms in surface sediments varies considerably in differregions of the Pacific Ocean. High diatom concentrations of 5.0 × 10^7/g occur in the transition region of the western North ific, but in most areas the concentration is less than 2.5 × 10^7/g usé et al., 1971). Quantitative analysis of the number of diatoms mined in this study resulted in much higher diatom concentrations ues than those estimated by Jousé et al. (1971).

Table 1. Species composition of cold-water diatoms, warm-water diatoms, and recurrent groups.

Cold-water diatoms (Xc)

Actinocyclus curvatulus Janisch
Actinocyclus ochotensis Jousé
Asteromphalus robustus Castracane
Bacteriosira fragilis (Gran) Gran
Chaetoceros furcellatus Bailey
Coscinodiscus marginatus Ehrenberg
Coscinodiscus oculus-iridis Ehrenberg
Denticulopsis seminae (Simonsen and Kanaya) Simonsen
Nitzschia cylindrus (Grunow) Hasle
Odontella aurita (Lyngbye) Agardh
Porosira glacialis (Grunow) Jørgensen
Rhizosolenia hebetata forma *hiemalis* (Bailey) Gran
Thalassiosira gravida Cleve
Thalassiosira hyalina (Grunow) Gran
Thalassiosira kryophila (Grunow) Goerg
Thalassiosira nordenskioldii Cleve
Thalassiosira trifulta Fryxell

Warm-water diatoms (Xw)

Coscinodiscus africanus Janisch
Coscinodiscus nodulifer Schmidt
Coscinodiscus perforatus Ehrenberg
Hemidiscus cuneiformis Wallich
Nitzschia marina Grunow
Planktoniella sol (Wallich) Schütt
Pseudoeunotia doliolus (Wallich) Grunow
Rhizosolenia bergonii Peragallo
Ropertia tesselata (Roper) Grunow
Thalassiosira leptopus (Grunow) Hasle and Fryxell
Thalassiosira lineata Jousé

Group I (Subtropic diatoms)

Coscinodiscus africanus Janisch
Coscinodiscus nodulifer Schmidt
Coscinodiscus perforatus Ehrenberg
Coscinodiscus tabularis Grunow var. *egregius* (Rattry) Hustedt
Hemidiscus cuneiformis Wallich
Nitzschia marina Grunow
Planktoniella sol (Wallich) Schütt
Pseudoeunotia doliolus (Wallich) Grunow
Rhizosolenia bergonii Peregallo
Roperia tesselata (Roper) Grunow
Thalassionema nitzschioides Grunow
Thalassionema nitzschioides Grunow vars.
Thalassiosira decipiens (Grunow) Jørgensen
Thalassiosira eccentrica (Ehrenberg) Cleve
Thalassiosira leptopus (Grunow) Hasle and Fryxell
Thalassiosira lineata Jousé
Thalassiosira oestrupii (Ostfeld) Proskina-Lavrenko

Group II (Subarctic diatoms)

Actinocyclus curvatulus Janisch
Actinocyclus ochotensis Jousé
Asteromphalus robustus Castracane
Coscinodiscus marginatus Ehrenberg
Coscinodiscus oculus-iridis Ehrenberg
Denticulopsis seminae (Simonsen and Kanaya) Simonsen
Odontella aurita (Lyngbye) Agardh
Rhizosolenia hebetata forma *hiemalis* (Bailey) Gran
Thalassiosira gravida Cleve
Thalassiosira trifulta Fryxell

Group IV (Arctic and arcto-boreal neritic diatoms)

Bacteriosira fragilis (Gran) Gran
Chaetoceros furcellatus Bailey
Nitzschia cylindrus (Grunow) Hasle
Porosira glacialis (Grunow) Jørgensen
Thalassiosira hyalina (Grunow) Gran
Thalassiosira kryophila (Grunow) Goerg
Thalassiosira nordenskioldii Cleve

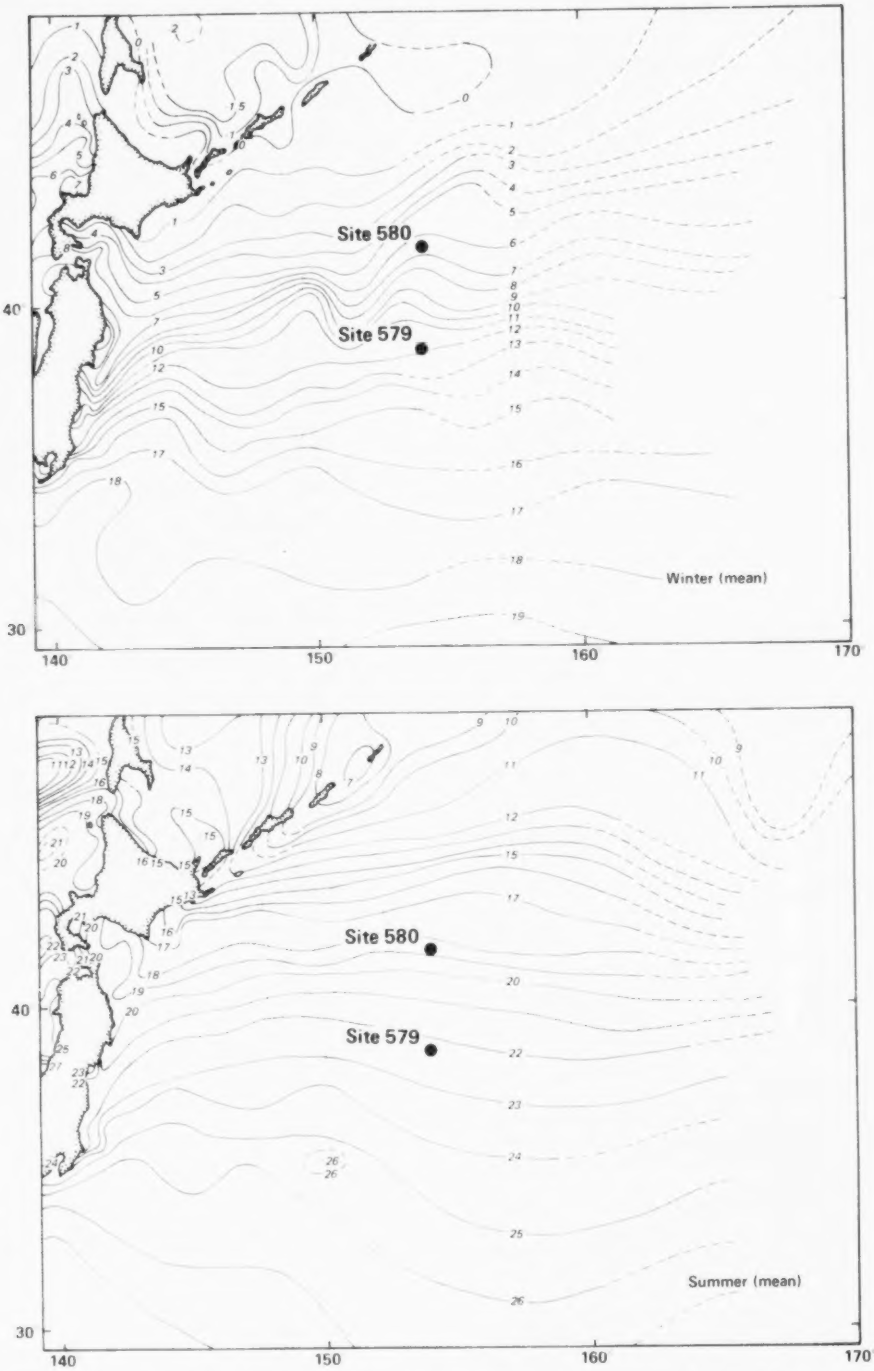

Figure 3. Location of Sites 579 and 580 in relation to surface water temperatures in winter and summer (Japan Oceanographic Data Center, 1978).

2. Productivity. A close relationship between high concentrations of *Chaetoceros* spores, high productivity, and intensive upwelling has been recognized in the surface sediments of the Bering and Okhotsk seas (Sancetta, 1982). On the basis of this observation, the number of *Chaetoceros* spores was examined in order to estimate the level of diatom productivity at Sites 579 and 580.

3. Species Diversity. Characteristics of the assemblage structure, which should vary with changing environments, may be expressed by the diversification of species constituting the assemblages (Ikeya, 1971). A numerical diversity index showing the degree of balance in the structure of assemblages, Simpson's diversity index, was adopted in this study (Simpson, 1949). The diversity index is defined as

$$N(N-1) \quad \sum_{i=1}^{S} n_i(n_i - 1),$$

where N is total number of specimens, s is total number of species, and n_i is the number of specimens of the ith species. This diversity index is high when the assemblage structure is complex or highly diversified and low when the structure is simple or less diversified.

RESULTS OF PALEOCEANOGRAPHIC ANALYSIS

d (diatom temperature) Value

Site 579

Td values generally decrease from the bottom to the op of Site 579 (Fig. 4). This decrease probably indicates overall decline in temperature toward the present day. his general trend is punctuated by large fluctuations in d value throughout the section.

The high Td values observed in the lower Pliocene sult both from the absence of cold-water diatoms, such *Denticulopsis seminae*, and from the abundance of arm-water diatoms, such as *Coscinodiscus nodulifer* and *emidiscus cuneiformis*. A large decrease in Td value ccurs during the upper Pliocene; late Pliocene Td values are lower than the present-day value for the site. This ecrease in Td value occurs at about 100 m sub-bottom (between Cores 9 and 10) within the Kaena Event, coinciding with the lithologic change from a clayey diatom ooze to a clayey siliceous ooze. The sharp decrease in Td value at this point indicates the transition from a preglacial to glacial age. The first Td minimum, which is equivalent to the low Td values observed in the Brunhes Epoch, occurs between 67.76 and 71.00 m sub-bottom (Samples 579A-6-5, 25–26 cm to 579A-6,CC), below the Olduvai Event. The beginning of the Pleistocene is marked by a sharp drop in Td values occurring at about 60 m sub-bottom (from Sample 579A-5-6, 94–95 cm to Sample 579A-5-7, 25–26 cm). The Td curve is fairly stable, with only small fluctuations in the lower Pleistocene. The large Td fluctuations during the upper Pleistocene suggest repeated north–south shifts of the subarctic-subtropic front in response to climatic fluctuations. Remarkably high Td values occur in the interval from 17.15 to 23.15 m sub-bottom (Samples 579A-1-3, 3–14 cm to 579A-1-7, 13–14 cm), indicative of a large nterglacial stage.

Site 580

Fluctuations in the Td curve at Site 580 correlate very ell with those at Site 579 (Fig. 5). Two sharp drops are pparent: one at about 140 m sub-bottom (Samples 0-16-2, 83–84 cm to 580-16-4, 83–84 cm) within the aena Event and the other at about 121 m sub-bottom amples 580-14-1, 130–131 cm to 580-14-5, 130–131 cm) tween the Matuyama and Gauss Epoch. Td values durg the Matuyama and Brunhes Epoch are generally wer than the present value for Site 580, although high d values occur at 102 m sub-bottom (Sample 580-12-3, 3–104 cm), between the Olduvai Event and the Gauss/atuyama boundary, and at 29.52 m sub-bottom (Same 580-4-5, 121–122 cm), in the lower part of the Brunes Epoch. Nine Td minima are seen during the Brunes Epoch, as indicated by Donahue (1970) in LDGO Lamont–Doherty Geological Observatory) piston core V20-108 (45°27′N, 179°14′W). Donahue (1970) also discussed two major subdivisions of the Pleistocene on the basis of Td values in deep-sea cores from the North Pacific: one from 1.7 to 0.7 m.y. ago, which was a time of relatively stable Td values, the other from 0.7 m.y. ago to the present, which was a time of lower average Td values than in the former interval but of greater fluctuation.

Large fluctuations in Td value occur at Site 579. These fluctuations probably represent significant north–south shifts of the subarctic–subtropic front. Lower Td values with smaller fluctuations, on the other hand, are observed throughout most of Site 580. These Td shifts may reflect changes in the surface water temperature of the subarctic region.

Species Composition

Site 579

1. Selected Species. *Coscinodiscus nodulifer* is abundant in the lower part of the lower Pliocene, but its abundance sharply decreases coincident with the appearance of *Denticulopsis seminae* in the upper part of the Gilbert Epoch (Fig. 4). Upsection, *C. nodulifer* becomes a minor element in the assemblages. Fluctuations in the frequency of *D. seminae* mirror fluctuations in Td values during the upper Pliocene and Pleistocene. Two frequency peaks are seen: one at 9.64 m sub-bottom (Sample 579-2-1, 123–124 cm) and the other at 25.14 m sub-bottom (Sample 579A-2-2, 13–14 cm) in the Brunhes Epoch.

2. Recurrent Group. Group I is more abundant than Group II throughout the site, except for these three levels (Fig. 4): 59.76 m sub-bottom (Sample 579A-5-6, 25–26 cm) just above the Olduvai Event, and 9.64 and 25.14 m sub-bottom as mentioned earlier.

The shape of the Group I abundance curve is similar to the Td value curve (i.e., decreasing toward the top of the site). Group IV appears at 53.76 m sub-bottom (Sample 579A-5-2, 25–26 cm), although absent between the Olduvai and Jaramillo events, but it is never more than a minor component in the assemblages.

Site 580

1. Selected Species. *Coscinodiscus nodulifer* is nil or scarce throughout the Pleistocene and is only slightly more abundant in the Pliocene (Fig. 5). *Denticulopsis seminae* shows large abundance fluctuations throughout the section (Fig. 5). The overall abundance of *D. seminae* is greatest in the lower Pleistocene and in the lower part of the upper Pleistocene. This variation in abundance is generally concordant with that of Group II, which is composed of subarctic diatoms (Table 1).

Two sharp abundance decreases of *D. seminae* are recognized: one at 26.52 m sub-bottom (Sample 580-4-3, 121–122 cm) and the other at 4.59 m sub-bottom (Sample 580-2-1, 128–129 cm) in the Brunhes Epoch. At these two points, Group I, which is composed of the subtropic diatoms, is of greater abundance than Group II, but the assemblage is otherwise different. At the deeper point, decreases in the abundances of Group II diatoms,

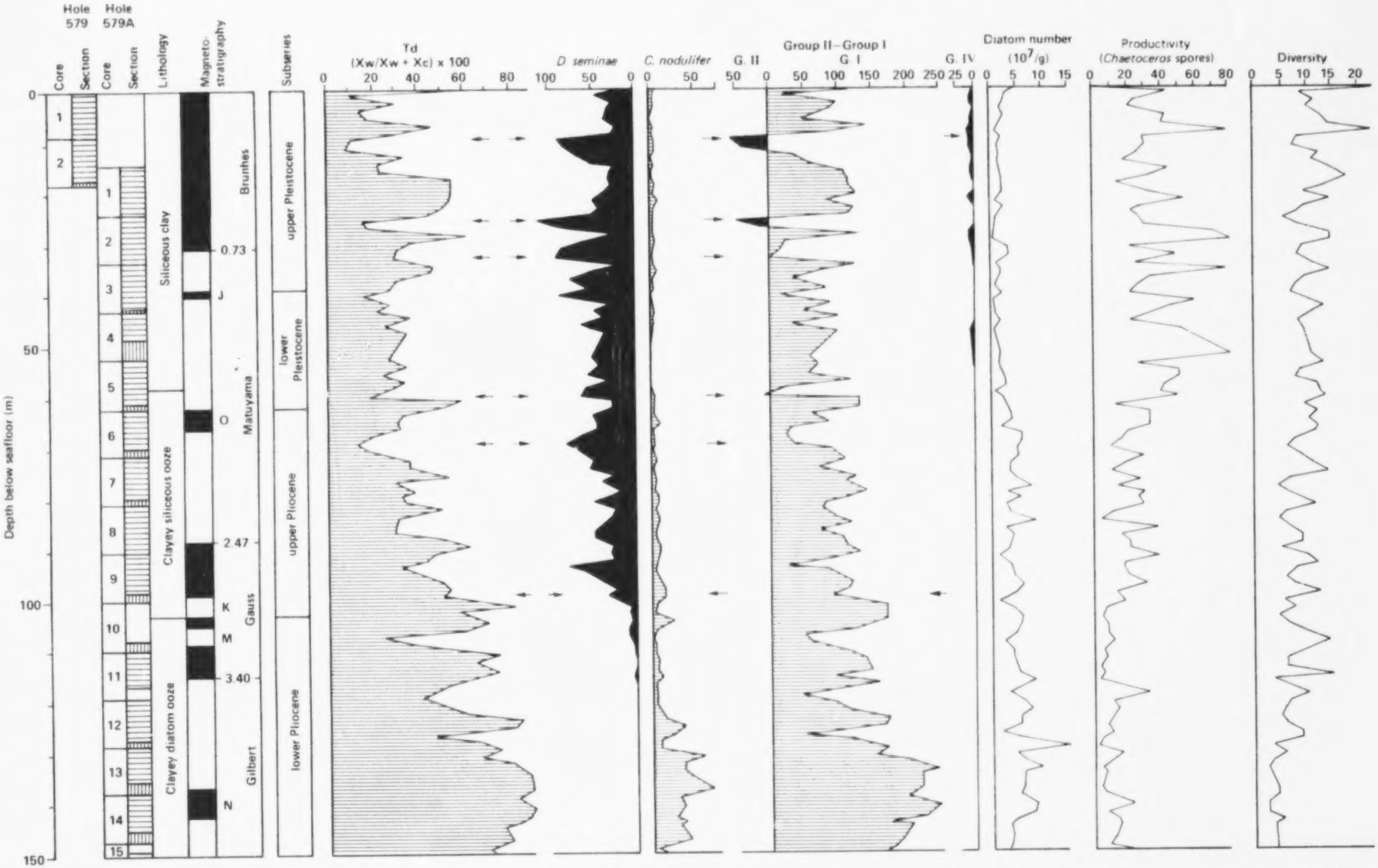

Figure 4. Site 579: Stratigraphic variations of Td (diatom temperature) values, frequencies of the cold-water diatom *Denticulopsis seminae* and the warm-water diatom *Coscinodiscus nodulifer*, discrepancies in frequencies between recurrent Groups I and II, frequencies of recurrent Group IV, concentration of diatoms, productivity on the basis of numbers of *Chaetoceros* spores, and Simpson's diversity index. Arrows indicate locations of major paleoceanographic changes as suggested by Td values and the composition of species as follows: 9.64 m sub-bottom (Sample 579-2-1, 123–124 cm), 25.14 m sub-bottom (Sample 579A-2-2, 13–14 cm), 32.64 m sub-bottom (Sample 579A-2-7, 13–14 cm), 59.76 m sub-bottom (Sample 579A-5-6, 25–26 cm), 67.76 m sub-bottom (Sample 579A-6-5, 25–26 cm), and about 100 m sub-bottom (between Samples 579A-9,CC and 579A-10,CC). Magnetostratigraphy: J = Jaramillo Event, O = Olduvai Event, K = Kaena Event, M = Mammoth Event, C = Cochiti Event, N = Nunivak Event, S = Sidufjall Event.

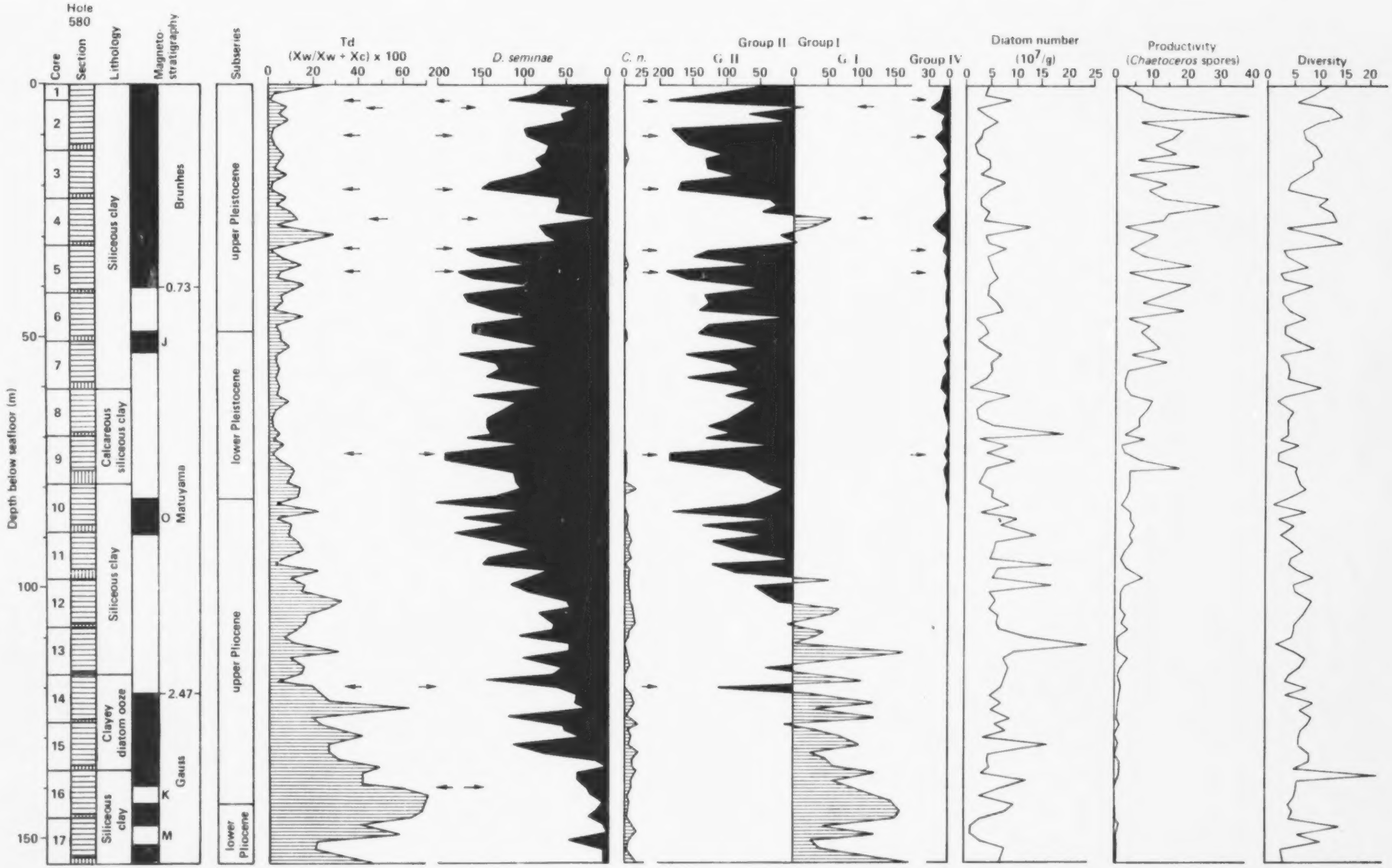

Figure 5. Site 580: Stratigraphic variations of Td (diatom temperature) values, frequencies of the cold-water diatom *Denticulopsis seminae* and the warm-water diatom *Coscinodiscus nodulifer*, discrepancies in frequencies between recurrent Groups I and II, frequencies of recurrent Group IV, concentration of diatoms, productivity on the basis of numbers of *Chaetoceros* spores, and Simpson's diversity index. Arrows indicate location of major paleoceanographic changes as suggested by Td values and the composition of species as follows: 3.02 m sub-bottom (Sample 580-1-3, 2–3 cm), 10.59 m sub-bottom (Sample 580-2-5, 128–129 cm), 26.52 m sub-bottom (Sample 580-4-3, 121–122 cm), 20.56 m sub-bottom (Sample 580-3-6, 25–26 cm), 32.21 m sub-bottom (Sample 580-5-1, 40–41 cm), 36.71 m sub-bottom (Sample 580-5-4, 40–41 cm), 73.04 m sub-bottom (Sample 580-9-3, 23–24 cm), 120.10 m sub-bottom (Sample 580-14-2, 130–131 cm), and about 140 m sub-bottom (between Samples 580-16-2, 83–84 cm and 580-16-4, 83–84 cm). See legend to Figure 4 for definition of magnetostratigraphic events.

especially of *D. seminae* and *Thalassiosira trifulta*, are recognizable; the sharp drops at the upper point are apparently the result of both decreases of Group II diatoms (*D. seminae*, *T. trifulta*, and *C. marginatus*) and increases of Group I diatoms (mainly of *T. eccentrica* and *Thalassionema nitzschioides*).

2. Recurrent Group. Group I is dominant in the lower Pliocene and the lower part of the upper Pliocene with two peaks shifted to Group II, at 113.96 m sub-bottom (Sample 580-13-5, 15–16 cm) and 120.60 m sub-bottom (Sample 580-14-2, 130–131 cm) (Fig. 5). From 100.84 m sub-bottom (Sample 580-12-2, 103–104 cm), between the Gauss/Matuyama boundary and the Olduvai Event, upward, Group II dominates over Group I, except for a short interval at about 26.52 m sub-bottom (Samples 580-4-3, 121–122 cm and 580-4-4, 121–122 cm) in the lower part of the Brunhes Epoch (Fig. 5). Group II shows a cyclic abundance variation with large fluctuations throughout the Pleistocene.

Group IV occurs almost continuously from 84.91 m sub-bottom (Sample 580-10-4, 110–111 cm) upward. Its abundance fluctuates and increases during the Brunhes Epoch, but these fluctuations do not coincide with those observed in either the Td values or abundances of *D. seminae*, except at 10.59 m sub-bottom (Sample 580-2-5, 128–129 cm). At 28.02 m (Sample 580-4-4, 121–122 cm), a Group IV peak corresponds to low Td values, but at this level Group I dominates over Group II as mentioned before.

All these changes in species composition are likely caused by a drop in surface water temperature during a glacial period, except for changes at 4.59 and 26.52 m sub-bottom, where high temperatures are dominant.

Assemblage Structure

Site 579

1. Number of Diatoms. The number of diatoms observed at this site varies with lithologic type (Fig. 4). High concentrations of diatoms, about 5.0×10^7/g, are generally recognized within the Pliocene clayey siliceous (diatom) ooze. Lower concentrations, generally less than 5.0×10^7/g, occur throughout the Pleistocene siliceous clay.

2. Productivity. At Site 579, *Chaetoceros* spores are rare (~3%) in the lower Pliocene and increase to a maximum of about 7% in the upper Pliocene (Fig. 4). The number of *Chaetoceros* spores fluctuates widely between 6 and 21% throughout the Pleistocene (Fig. 4).

3. Species Diversity. The diversity increases from about 3.8 in the Nunivac Event to about 13 in the upper part of the Brunhes Epoch, with large fluctuations throughout (Fig. 4). The amplitude of these fluctuations increases from bottom to top of the holes. High diversity values generally correspond to peaks in productivity, as seen in the number of *Chaetoceros* spores. The maximum diversity value is 22.9 at 8.40 m sub-bottom (Sample 579-1,CC), whereas the minimum diversity is 2.4 at 140.53 m sub-bottom (Sample 579A-14-3, 2–3 cm).

Site 580

1. Number of Diatoms. The number of diatoms varies throughout the site (Fig. 5). Generally speaking, the number of diatoms averages about 6.0×10^7/g in the upper Pliocene and about 5.0×10^7/g in the Pleistocene. The number of diatoms does not seem to vary with lithologic type.

2. Productivity. Fluctuations in the concentration of *Chaetoceros* spores at Site 580 are similar to those observed at Site 579 (Fig. 5), but the absolute values are only half to one-third of that recognized at Site 579.

3. Species Diversity. Diversity values at Site 580 do not show downhole fluctuations coincident with other assemblage structure parameters. Diversity is generally lowest in the lower Pleistocene and increases from the lower part of the upper Pleistocene upward, resulting in an average diversity value of 9.4 within most of the Brunhes Epoch (Fig. 5).

The concentration of *Chaetoceros* spores at both sites shows a trend of upward increase in abundance. The varying concentration of diatoms, on the other hand, describes a different curve. Therefore, diatom productivity is only partially explained by *Chaetoceros* productivity (Oyashio Current).

The number of diatoms fluctuates more at Site 580 than at Site 579, whereas productivity and the diversity index both fluctuate more at Site 579 than at Site 580. In particular, the productivity at Site 579 is two to three times that at Site 580. Accordingly, upwelling caused by the shift of the front between the subarctic and subtropic water masses seems to have had a more important effect on the productivity at Site 579 than at Site 580, especially during glacial periods.

MAJOR PALEOCLIMATIC EVENTS

Td values fluctuate in similar ways at both Sites 579 and 580 (Fig. 6). These Td values help unravel the paleoceanographic history of the western North Pacific.

A sharp and large drop in Td value at both Site 579 and Site 580 occurred 3.0 m.y. ago (Fig. 6). This decrease in Td value indicates that the winter surface water temperature fell about 8.9°C in 0.3 m.y. at Site 579 and about 11.0°C in 0.2 m.y. at Site 580. This Td drop marks the boundary between the preglacial and glacial Pliocene previously proposed by Berggren (1972) and Keigwin (1979). No change, however, occurs in recurrent group at this level (Figs. 4 and 5). It is at 2.85 m.y. ago at Site 579, and at 2.50 m.y. ago at Site 580, that the surface water temperature falls below that of the present day. Shackleton and Opdyke (1977) also indicated that the scale of glaciations increased about 2.5 m.y. ago. Since then the surface water temperature has never risen to the present level, except at 2.12 m.y. ago when a short-lived comparable surface water temperature is recognized at both sites (Fig. 6). Presumably this level is recognizable as the preglacial/glacial boundary in the western North Pacific. The temperature 2.12 m.y. ago was about 0.5°C warmer than today at Site 580.

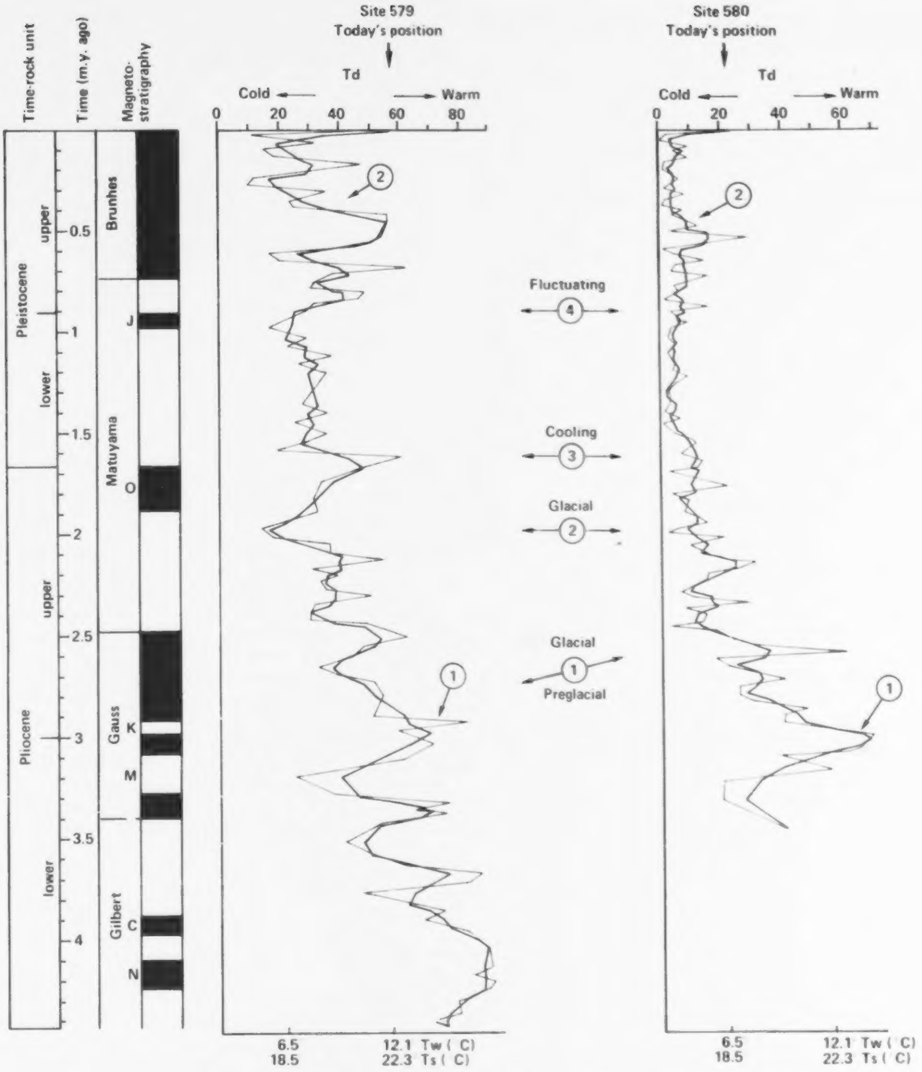

Figure 6. Major paleoclimatic events at Sites 579 and 580. (1) Initiation of glaciation 2.5–2.8 m.y. ago; (2) major glacial event, which is a match for the glacial stages of the Brunhes Epoch, about 2.0 m.y. ago; (3) remarkable cooling about 1.6 m.y. ago (at the Pliocene/Pleistocene boundary); and (4) beginning of cycles of glacial/interglacial stages about 0.9 m.y. ago (at the early/late Pleistocene boundary). Arrows indicate (1) the beginning of the critical levels where surface water temperature falls below that of the present day about 3.0 m.y. ago, and (2) the beginning of the smaller amplitude and more rhythmic temperature fluctuations about 0.4 m.y. ago. See legend to Figure 4 for definition of magnetostratigraphic events.

Through the late Pliocene, the surface water temper-
re kept declining at both sites. At Site 579, the tem-
ature fell an estimated 4.8°C from 3.0 to 2.0 m.y.
; at Site 580, about 6.7°C (Fig. 6). At Site 579, 5.4°C
the temperature drop occurs immediately before the
duvai Event 2.0 m.y. ago (Fig. 6). At Site 580, a simi-
fall in surface water temperature is recognized at the
ne time. Keigwin (1979) suggested that a major glaci-
on or bottom-water cooling event occurred between
and 2.3 m.y. ago on the basis of a significant varia-
n observed in $\delta^{18}O$ record.

At about the same time as the Olduvai Event, the
rface water temperature increased about 7.5°C at Site 579. The temperatures at Site 580 seem to stabilize at about 3.2°C throughout this period, with some minor fluctuations (Fig. 6).

About 1.6 m.y. ago (at the Pliocene/Pleistocene boundary), a third drop in surface water temperature is recognized. At Site 579, surface water temperature is estimated to have fallen about 5.6°C within a short 0.1 m.y. period. Similarly, the temperature decreased about 2.8°C in 0.2 m.y. at Site 580. After this drop, the surface water temperature did not fluctuate to any recognizable degree. Fluctuations of $\delta^{18}O$ in oxygen isotope records (Williams et al., 1981) confirm the drop and leveling off of surface water temperature.

The surface water temperature fluctuates again after a small temperature increase at the Jaramillo Event. This temperature increase begins at about halfway between the Jaramillo Event and the Brunhes Epoch and marks the fourth climatic event (Fig. 6). Note that cycles of glacial/interglacial stages begin at about this level in middle latitudes (Hays and Berggren, 1971). At Site 580, significant decreases in Td values (i.e., a drop in surface water temperature) are recognized nine times during the Brunhes Epoch. The largest of these decreases occurred at 0.05, 0.16–0.19, 0.38, 0.59, and 0.70 m.y. ago. Similarly, at Site 579, large Td decreases occurred at 0.25, 0.63, and 0.78 m.y. ago.

After a sudden increase in Td value near 0.5 m.y. ago at both sites, the Td values show small amplitude, somewhat rhythmic fluctuations to the present day. This pattern corresponds to that observed in the North Atlantic by Berggren (1972).

CONCLUSIONS

Both productivity estimated on the basis of the number of *Chaetoceros* spores and species diversity fluctuate greatly at Site 579 (Fig. 4). Both paleoclimate indexes increase in overall value and in fluctuation amplitude upsection.

A major Td value decrease and the alternation from warm-water diatom *Coscinodiscus nodulifer* to cold-water diatom *Denticulopsis seminae* occurred 3.0 m.y. ago at both Sites 579 and 580, but no change in recurrent group occurred (Figs. 4 and 5).

The preglacial/glacial boundary occurred 2.50–2.85 m.y. ago at about 40°N latitude in the western North Pacific (Fig. 6). Since then the surface water temperature has never risen to the present-day level.

The second surface water temperature drop occurred 2.0 m.y. ago at both sites (Fig. 6).

The third drop of temperature occurred about 1.6 m.y. ago (at the Pliocene/Pleistocene boundary; Fig. 6). Recurrent Group IV appears approximately from this level upward.

The surface water temperature did not fluctuate significantly during the lower Pleistocene interval.

Cycles of glacial/interglacial stages begin about halfway between the Jaramillo Event and the Brunhes Epoch. At Site 580, surface water temperature decreases occurred nine times during the Brunhes Epoch (Figs. 5 and 6). An interglacial stage occurred about 0.5 m.y. ago at both Sites 579 and 580 (Fig. 6).

Td values from 0.5 m.y. ago to the present show smaller amplitudes and more rhythmic fluctuation than before (Fig. 6).

ACKNOWLEDGMENTS

This study builds on the fundamental work on diatoms initiated by Dr. Taro Kanaya, who had to retire in the middle of his active academic career, which had such a promised start.

I would like to thank the reviewers, Drs. Constance A. Sancetta and Howard E. Harper, and especially Drs. Audrey A. Wright, Lloyd H. Burckle, and Tsunemasa Saito, who made suggested English revisions and scientific comments.

REFERENCES

Berggren, W. A., 1972. Late Pliocene–Pleistocene glaciation. *In* Laugh ton, A. S., Berggren, W. A., et al., *Init. Repts. DSDP*, 12: Wash ington (U.S. Govt. Printing Office), 953–963.

Burckle, L. H., and Opdyke, N. D., 1977. Late Neogene diatom co relations in the circum-Pacific. *In* Saito, T. and Ujiié, H. (Eds. *Proceedings of the First International Congress on Pacific Ne gene Stratigraphy, Tokyo, 1976:* Tokyo (Kaiyo Shuppan), p 255–284.

Dodimead, A. J., Favorite, F., and Hirano, T., 1963. Review of ocea ography of the subarctic Pacific region. *International North Paci ic Fisheries Commission, Bull.*, Pt. II, 13:1–195.

Donahue, J. G., 1970. Pleistocene diatom as climatic indicators North Pacific sediments. *In* Hays, J. D. (Ed.), *Geological Inve tigation of the North Pacific*. Mem. Geol. Soc. Am., 126:121–13

Hasle, G. R., 1976. The biogeography of some marine planktonic di toms. *Deep-Sea Res.*, 23:319–338.

Hays, J. D., and Berggren, W. A., 1971. Quaternary boundaries an correlations. *In* Funnell, B. M., and Riedel, W. R. (Eds.), *Th Micropaleontology of Oceans:* London (Cambridge Univ. Press pp. 669–692.

Ikeya, N., 1971. Species diversity of benthonic foraminifera, off th Shimokita Peninsula, Pacific coast of north Japan. *Rec. Oceanog Works in Japan*, 11:27–37.

Japan Oceanographic Data Center, 1978. *Marine Environment Atla Northwestern Pacific Ocean* (Vol II) (Seasonal and Monthly): To kyo (Japan Hydrogr. Assoc.).

Jousé, A. P., Kozlova, O. G., and Muhina, V. V., 1971. Distributio of diatoms in the surface layer of sediment from the Pacific Ocean *In* Funnell, B. M. and Riedel, W. R. (Eds.), *The Micropaleontology of Oceans:* London (Cambridge Univ. Press), pp. 263–269.

Kanaya, T., and Koizumi, I. 1966. Interpretation of diatom thanatocenoses from the North Pacific applied to a study of core V20-13 (Studies of a deep-sea core V20-130. Part IV). *Sci. Rep. Tohok Univ. Ser. 2*, 37:89–130.

Keigwin, L. D., Jr., 1979. Late Cenozoic stable isotope stratigraph and paleoceanography of DSDP sites from the east equatorial an central North Pacific Ocean. *Earth Planet. Sci. Lett.*, 45:361–382

Keller, G., 1979. Late Neogene paleoceanography of the North Pacifi DSDP Sites 173, 310, and 296. *Mar. Micropaleontol.*, 4:159–172

Sancetta, C., 1982. Distribution of diatom species in surface sediments of the Bering and Okhotsk seas. *Micropaleontology*, 28 221–257.

Shackleton, N. J., and Opdyke, N. D., 1976. Oxygen-isotope and paleomagnetic stratigraphy of Pacific core V28-239: Late Pliocene t latest Pleistocene. *In* Cline, R. M., and Hays, J. D. (Eds.), *Investigation of Late Quaternary Paleoceanography and Paleoclimatology*, Geol. Soc. Am. Mem., 145:449–464.

________, 1977. Oxygen isotope and paleomagnetic evidence for earl Northern Hemisphere glaciation. *Nature (London)*, 270:216–219

Simpson, E. H., 1949. Measurement of diversity. *Nature (London)* 163:688

Venrick, E. L., 1971. Recurrent groups of diatom species in the Nort Pacific. *Ecology*, 52:614–625.

Vincent, E., 1975. Neogene planktonic foraminifera from the Centra North Pacific Leg 32, Deep Sea Drilling Project. *In* Larson, R. L Moberly, R., et al., *Init. Repts. DSDP*, 32: Washington (U.S. Gov Printing Office), 765–791.

Williams, D. F., Moore, W. S., and Fillon, R. H., 1981. Role of gla cial Arctic Ocean ice sheets in Pleistocene oxygen isotope and se level records. *Earth Planet. Sci. Lett.*, 56:157–166.

Date of Initial Receipt: 4 January 1984
Date of Acceptance: 14 May 1984

PART III: PALEOMAGNETIC AND GEOCHEMICAL STRATIGRAPHIC STUDIES

17. THE MAGNETOSTRATIGRAPHY OF NORTHWEST PACIFIC SEDIMENTS, DEEP SEA DRILLING PROJECT LEG 86[1]

Ulrich Bleil, Institut für Geophysik, Ruhr-Universität Bochum[2]

ABSTRACT

Results of paleomagnetic analyses of pelagic sediment sequences recovered in the Northwest Pacific during Deep Sea Drilling Project Leg 86 are presented. On the basis of these data, almost complete late Cenozoic magnetostratigraphies are established for each drill site.

At Site 577, on the Shatsky Rise, a stratigraphic duplication of Late Cretaceous to middle Eocene sequences was achieved using the hydraulic piston coring technique. For the first time, a detailed paleomagnetic study of this period using largely undisturbed and complete sedimentary columns from the Pacific region was possible. Available biostratigraphy and stable isotope stratigraphy data allowed a positive correlation of the downhole magnetic reversal patterns with a calibrated geomagnetic polarity time scale. In general, the results obtained are in remarkable agreement with other recently published magnetostratigraphies from various parts of the world. Therefore, they represent a high quality framework for an early Tertiary magnetobiochronology including the Cretaceous/Tertiary boundary interval.

INTRODUCTION

Scientific objectives of Deep Sea Drilling Project (DSDP) Leg 86 were focused on the late Cenozoic paleoceanographic history of the western North Pacific. Four sites (Sites 578–581) were drilled on a north–south profile from subtropical to subarctic waters across the Kuroshio Current system. Additional operations included the recovery of a Late Cretaceous to Recent sedimentary sequence, containing the Cretaceous/Tertiary boundary, on the Shatsky Rise (Site 577) and a "type" red clay section east of this geologic structure (Site 576). Sites 576 to 580 were cored with the hydraulic piston corer (HPC), which allowed retrieval of mostly complete and undisturbed sediment sections. These materials provided high stratigraphic resolution for detailed biostratigraphic, magnetostratigraphic, and stable-isotope stratigraphic analyses.

The northern Pacific is one of the classic areas for paleomagnetic work on pelagic sediments; some of the pio- er paleomagnetic investigations using conventional pis- n cores (e.g., Opdyke, 1972) were done there. Because the limited penetration capacity of this sampling tech- ue, however, paleomagnetic studies typically have been tricted to the late Cenozoic period. A giant piston core ntaining pelagic red clay deposited during the entire nozoic was recently recovered in the mid-oceanic gyre ion, but its magnetic record was inadequate to estab- a magnetostratigraphy because the remanent mag- ization became highly unstable only a few meters be- the seafloor (Prince et al., 1980).

Despite relatively frequent DSDP operations in the thern Pacific, only sparse paleomagnetic results from ary-cored materials have been published. Moreover, the specific constraints imposed by this drilling method often reduced the quality and amount of the retrieved sediments and, consequently, the resolution of their magnetostratigraphies. On the other hand, very successful paleomagnetic studies have been completed on HPC materials recovered in the Caribbean (Kent and Spariosu, 1982a), the South Atlantic (Tauxe et al., 1984; Chave, 1984) and the Equatorial Pacific (Kent and Spariosu, 1982b; Weinreich and Theyer, in press).

This chapter includes magnetostratigraphic analyses of the predominantly calcareous nannofossil oozes penetrated in two holes at Site 577 (Holes 577 and 577A) and of the biosiliceous sediments of Sites 579 and 580 (Fig. 1). At all of these sites, the late Cenozoic is represented in extended sections, for which mostly complete and detailed magnetostratigraphic records were obtained. The Late Cretaceous to middle Eocene sequences, including the Cretaceous/Tertiary boundary epoch, recovered in the lower parts of Holes 577 and 577A made possible the first paleomagnetic study of this period on Pacific sedimentary suites.

The downhole patterns of magnetic reversals are correlated with the recently revised geomagnetic polarity time scale of Berggren et al. (in press). For pre-Neogene time, biostratigraphic and stable-isotope criteria had to be employed in places to positively identify a number of polarity intervals. In turn, the magnetostratigraphic data were used to elaborate numerical ages for coccolith event zonations calibrated on the basis of geomagnetic reversal boundary dates (Monechi et al., this volume). The results of detailed paleomagnetic work on the red clay sections encountered at Sites 576 and 578 are reported by Heath et al. (this volume).

METHODS AND MATERIALS

An extensive shipboard paleomagnetic sampling program was used for the sedimentary columns recovered at five drill sites (Sites 576 through 580) during Leg 86. Vertically oriented specimens of about 7 cm^3 were taken at intervals ranging from 10 to 50 cm. The sample spacing typically represented time intervals on the order of 10^4 yr. or less; in parts

---

[1] Heath, G. R., Burckle, L. H., et al., *Init. Repts. DSDP*, 86: Washington (U.S. Govt. nting Office).

[2] Address: Institut für Geophysik, Ruhr-Universität Bochum, Postfach 102148, 4630 Bo- m 1, Federal Republic of Germany.

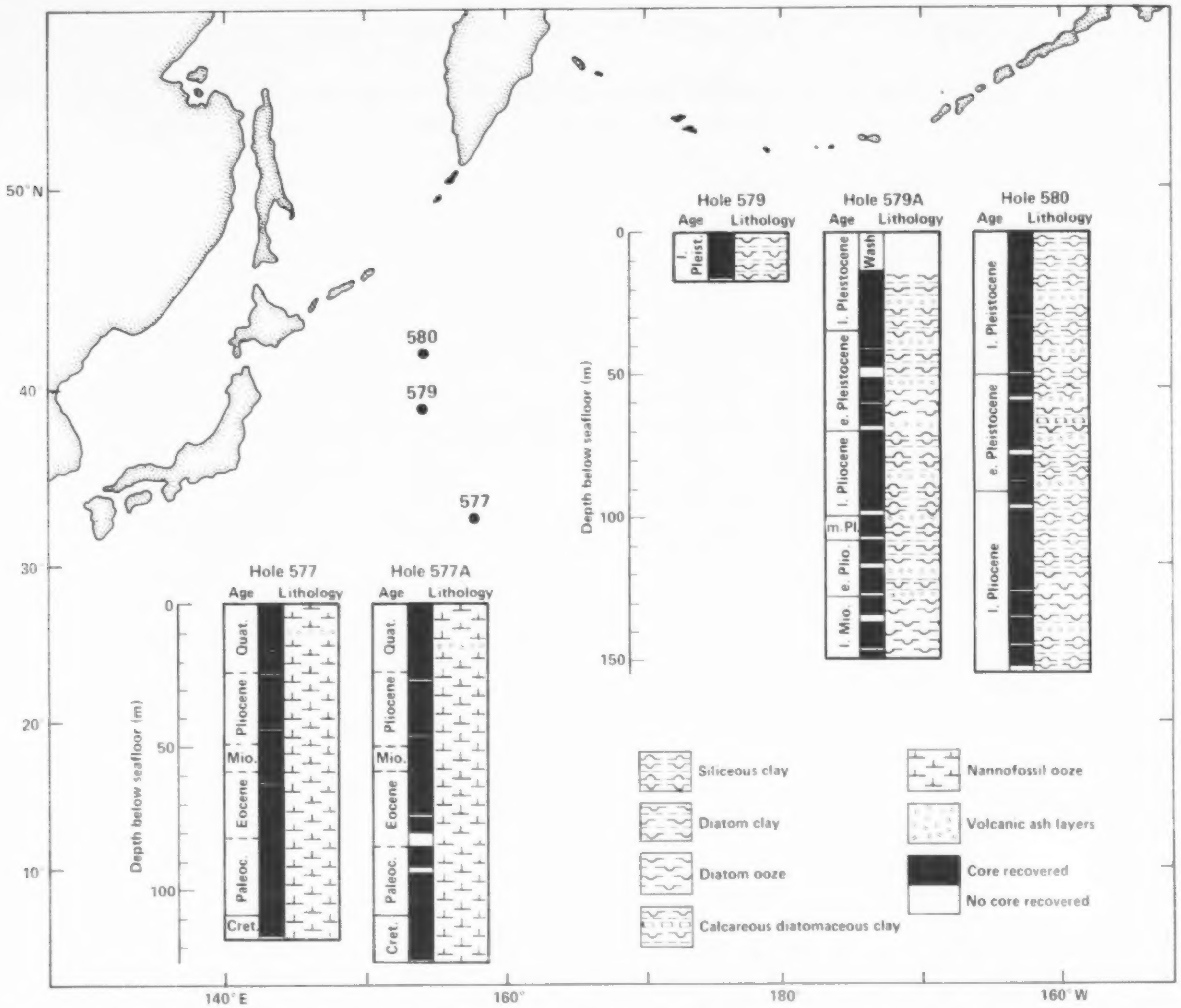
50°N
40°
30°
20°
10°
140°E
160°
180°
160°W
580
579
577
Hole 579
Hole 579A
Hole 580
Age
Lithology
l. Pleist.
Wash
l. Pleistocene
e. Pleistocene
l. Pliocene
m. Pl.
e. Plio.
l. Mio.
Depth below seafloor (m)
0
50
100
150
Hole 577
Hole 577A
Quat.
Pliocene
Mio.
Eocene
Paleoc.
Cret.
Siliceous clay
Diatom clay
Diatom ooze
Calcareous diatomaceous clay
Nannofossil ooze
Volcanic ash layers
Core recovered
No core recovered

Figure 1. Location map of DSDP Leg 86 Sites 577, 579, and 580 together with schematic age, core recovery, and lithostratigraphy of sediments recovered by HPC.

of Sites 576 and 577 it increased to almost 10^5 yr. The individual cubic samples, about 2 cm on edge, thus contain a paleomagnetic record of some 2×10^2 to approximately 10^4 yr.

Because of the inadequate sensitivity of the Digico spinner magnetometer, shipboard paleomagnetic analyses had to be restricted to measurements of the natural remanent magnetization (NRM) direction without performing any demagnetization treatments. Depending on the sediment type, highly variable NRM intensities were encountered (see site reports, this volume). In general, clay and biosiliceous sediments carry a predominantly strong remanent magnetism, whereas increasing amounts of calcareous components result in a drastic reduction of the NRM intensity. A preliminary shipboard magnetostratigraphy, therefore, could be established only for the upper parts of Holes 576, 576B, and 578 and for the complete sediment sequences in Holes 579, 579A, and 580.

Shore-based paleomagnetic work on clay sediments recovered at Sites 576 and 578 was completed by Heath et al. (this volume). Preliminary shipboard paleomagnetic results from these sites are reported in their respective site chapters (this volume). It is interesting to note that, even on the basis of the shipboard NRM data, meaningful magnetostratigraphies could be derived to appreciable depths (~ 20 and 110 m sub-bottom at Sites 576 and 578, respectively). This clearly contrasts with the observation made during previous studies that the magnetization of red clays in the central northern Pacific is generally unstabl below a depth of about 5 m (Foster and Opdyke, 1970; Kent and Lowrie, 1974; Prince et al., 1980).

Samples from Sites 577, 579, and 580 were analyzed for their paleomagnetic properties at the Ruhr-University Bochum. Measurement of magnetization intensity and direction were made on a cryogeni magnetometer (Cryogenic Consultants, Model GM 400). A Schonste GSD-1 single axis demagnetizer was used for the alternating field (A demagnetization.

In addition to remeasurements of the NRM, systematic stepwis demagnetization treatments were carried out on each sample. For th bulk of the material, the demagnetization was taken to the 500 Oerste (Oe) level, which mostly exceeds the median destructive fields (MD Steps of 25 or 50 Oe were typically applied up to 100 Oe, followed 50-Oe steps up to 200 or 300 Oe and 100-Oe steps beyond that stag Characteristic stable magnetization directions were evaluated from di ferent graphic representations of the demagnetization data. The p leolatitudes of all drill sites permitted direct determination of the p larity sequence from the downhole pattern of stable inclinations. A though the "Kuster single-shot" orientation device was frequently en ployed during HPC operations on Leg 86, onshore paleomagnet work revealed that the absolute azimuthal orientation data are bas cally useless. The instrument photographically fixes the position of double-line mark on the core liner relative to a compass needle immediately before the stroke-out of the HPC barrel. However, any amount of random rotation is apparently possible between the position in this instantaneous photograph and the orientation of the azimuthal sediment magnetization finally found in the top part of the core liner. Moreover, downcore clockwise or counterclockwise rotations, sometimes even offsets of different magnitudes, are observed in the declination data (see also Weinreich and Theyer, in press). They are obviously produced by relative motions between sediment, core liner, or perhaps also the HPC barrel itself during stroke-out. As in former DSDP reports, therefore, only relative declinations could be defined with reference to the surface of the split core.

Shifts of 180° in stable relative declinations were almost always found to coincide exactly with changes in sign of stable inclinations, further substantiating the identification of reversal boundaries. In the lower part of Holes 577 and 577A, however, only minor variations in declination are generally observed where stable inclinations indicate a polarity transition. Here, a uniform, presumably artificial magnetic overprinting could not be destroyed sufficiently by AF demagnetization. The spurious magnetization component is obviously approximately perpendicular to the split core surface, but any explanation of its origin seems speculative at present. Despite the likelihood that the individual inclination value may also be affected to varying degrees, the downhole variation in inclination polarity appears essentially to be preserved and a reliable magnetostratigraphy can be established, which is confirmed by the magnetostratigraphic duplication in the two adjacent holes drilled at Site 577.

The recently revised geomagnetic polarity time scale of Berggren et al. (in press) was used as a basis for the interpretation of the downhole polarity sequences and to define numerical ages for the reversal boundaries. In the late Cenozoic, the series of Earth's magnetic paleofield polarity intervals are specified according to the traditional "epoch" and "event" nomenclature (McDougall, 1977). The pre-Neogene magnetic time units are denoted as "chrons," following the recommendation of the Subcommission on Stratigraphic Classifications (Hedberg et al., 1979). In the terminology developed by Tauxe et al. (1984), a chron extends between the youngest reversal boundaries of a numbered marine magnetic anomaly as defined by Heirtzler et al. (1968) and revised by LaBrecque et al. (1977). The widely used number system for the anomaly pattern is thereby incorporated into this magnetostratigraphic time scale, and the chron unit is distinguished only by a prefix C. As to its definition, a chron includes not only the time interval of normal polarity corresponding to the respective anomaly number but also the preceding period of reversed polarity (see Fig. 7B). In order to denote the polarity zone, the suffix N (normal) or R (reversed) is added. Further subdivision into subchrons is needed where a chron comprises more than one normal or reversed polarity interval; for example C-23N-2 indicates the second (older) normal period within Chron 23.

RESULTS

Before discussing results[3] for the different drill sites, some typical examples of the AF demagnetization response of the sediment types encountered during Leg 86 are briefly reviewed. At the same time, a general outline of the sediments' magnetization characteristics and the paleomagnetic methods used in this study is made.

At Sites 579 and 580, predominantly biosiliceous sediments were recovered (Fig. 1). As anticipated from the shipboard NRM data, their shore-based demagnetization treatment revealed a simple and uniform remanent magnetization structure (Type I behavior). Independent of their respective polarity, most of the samples showed a monotonous decrease in remanent magnetization intensity upon progressive AF demagnetization (Fig. 2A) with MDFs typically on the order of 250 Oe. The resultant vectors of magnetization, that is, the directions remaining after each demagnetization step, form a close cluster (Fig. 2B). Very minor scatter is also observed in the difference vectors (Hoffman and Day, 1978; Fig. 2C), that is, the magnetization directions removed by stepwise progressive demagnetization. In general, after a demagnetization to 50 or rarely to 100 Oe, the directions of resultant and difference vectors on average coincide, indicating the presence of an essentially single-component stable remanence. Additional proof for this interpretation was always obtained from Zijderveld (1967) vector diagrams. The characteristic stable inclination and de-

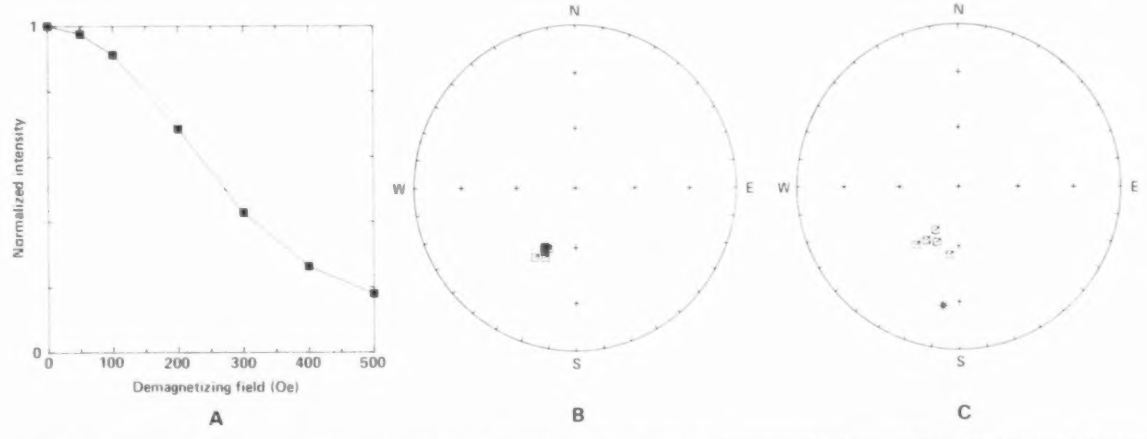

Figure 2. Demagnetization behavior of Sample 580-14-4, 139-141 cm. The results are characteristic of almost all the biosiliceous sediments penetrated at Sites 579 and 580 carrying a stable remanent magnetization (Type I behavior). A. NRM-normalized remanent magnetization intensity as a function of the applied demagnetizing field (in Oersted.) Dotted lines denote the MDF. B. Stereographic projection of the resultant vectors of magnetization. The asterisk indicates the NRM direction. Consecutive demagnetization steps are connected by great-circles. The respective AF increments may be read from Figure 2A. Open symbols represent negative inclinations. C. Stereographic projection of the difference vectors. The asterisk indicates the first demagnetization step, consecutive demagnetization steps are connected by great-circles. Open symbols represent negative inclinations.

---

[3] Data on a sample-by-sample basis are available from the author on request.

clination are determined for each sample from the demagnetization interval yielding the least directional scatter. A few samples from Sites 579 and 580 showed erratic characteristic directions. However, this is not because of an insufficient magnetic stability, but presumably results from disturbances introduced by the coring process.

In clear contrast, the predominantly calcareous oozes recovered in two holes at Site 577 frequently carry a multicomponent remanent magnetism. Here samples of reversed polarity typically show an increase of normalized magnetization intensity upon progressive AF demagnetization to 100 to 200 Oe, followed by a monotonous decrease beyond this stage (Fig. 3A). At the same time the resultant vectors gradually approach a consistent stable direction (Fig. 3B). Difference vector plots (Fig. 3C) show most clearly that two roughly antiparallel magnetization components are present in these samples. A magnetically less-stable fraction of normal polarity apparently results from a viscous magnetic overprinting during the Brunhes Epoch. It is mostly destroyed by alternating fields of 200 to 250 Oe after which the average resultant and difference vectors fall together, allowing determination of characteristic stable remanence directions. Again these results are always checked using Zijderveld (1967) diagrams. Note that in Figures 2 through 4, the declination data have been corrected by means of their respective core mean values to, on average, 180° or 360°, thereby yielding a plausible relationship to the variations in sign of inclinations.

Many of the samples at Site 577 contain minor spurious unstable magnetization components, which do not show any directional consistency, however. Their magnetic stability is mostly even lower than the stability of those components tentatively identified as being of viscous origin. The unstable components may have been acquired, therefore, during handling, transport, or storage of the samples. Any multicomponent remanent magnetism from which characteristic stable directions can be discriminated is denoted as Type II behavior in this study.

An example of the Type III demagnetization response is shown in Figure 4. The demagnetization curve of these samples typically shows unsystematic variations in normalized remanent intensity (Fig. 4A). Both the resultant and difference vectors usually exhibit large directional changes upon progressive AF demagnetization, without ever attaining a clear-cut stable direction (Figs. 4B, 4C). These features have only been observed for a few samples in the calcareous oozes recovered at Site 577. They may not always reflect intrinsic magnetic properties of the sediments, however, since some physical disturbance is mostly indicated in the respective sampling intervals.

As mentioned before, detailed shore-based paleomagnetic analyses of the red clay sediments encountered at Sites 576 and 578 are presented by Heath et al. (this volume). In this chapter, therefore, only the preliminary shipboard magnetostratigraphies from those sites, based on NRM data, are listed in Tables 1 and 2. A brief discussion of these results is given in the appropriate site chapters (this volume).

Site 577

In two adjacent holes at Site 577, on the Shatsky Rise, a late Cenozoic and (separated by a major hiatus) a Maestrichtian to middle Eocene sequence of nannofossil oozes, including an undisturbed Cretaceous/Tertiary boundary interval were recovered. The upper ~60 m of the sedimentary column comprising the latest Miocene to Quaternary stratigraphic record contains subordinate amounts of volcanic ash and biosiliceous components (Fig. 1).

The paleomagnetic properties of almost 500 samples from Holes 577 and 577A were analyzed. On average, the NRM intensities are distinctly lower than those at the more northern sites of Leg 86. On the other hand, their variability, both between and within cores, is less pronounced. The NRM intensity systematically decreases from about 15 × 10^{-6} G near the top to about 10^{-6} G in the lower parts of both holes (Figs. 5 and 6). The overall geometric means amount to 2.7 × 10^{-6} and 2.3

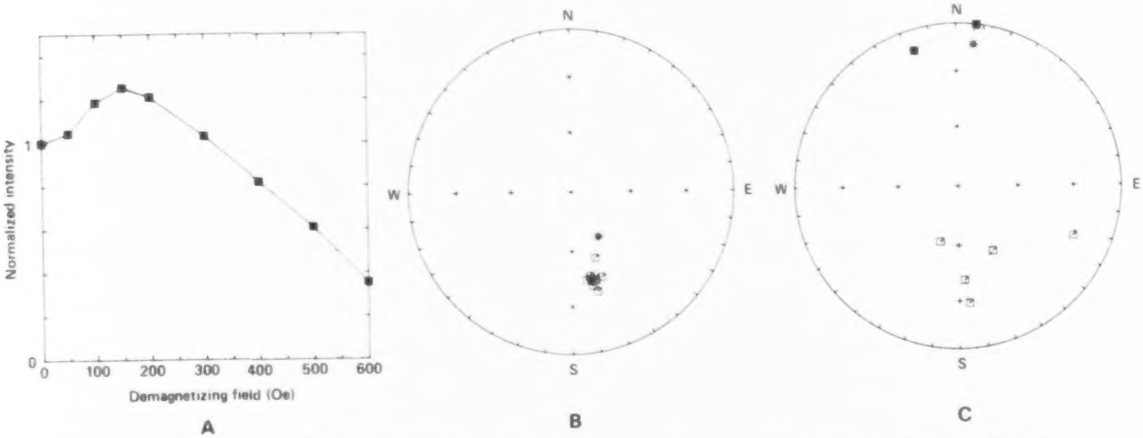

Figure 3. Demagnetization behavior of Sample 577-2-3, 38–40 cm. The results are characteristic of the majority of predominantly calcareous sediments recovered at Site 577 on the Shatsky Rise (Type II behavior). See caption of Figure 2 for details. Closed and open symbols in (A) and (B) represent positive and negative inclinations, respectively.

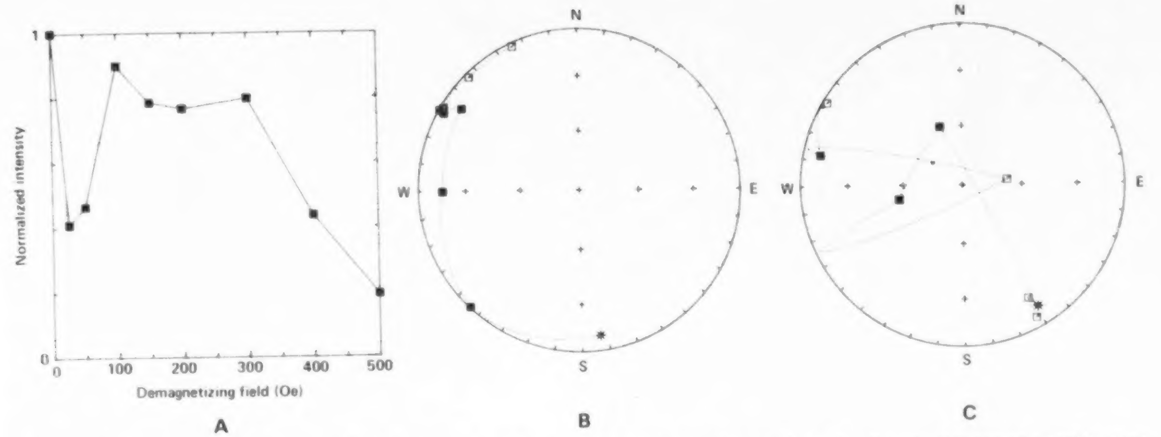

Figure 4. Demagnetization behavior of Sample 577A-5-3, 39–41 cm. The results are characteristic of sediments carrying an unstable remanent magnetization (Type III behavior). These features were only observed for a relatively small number of samples at Site 577. See caption of Figure 2 for details. Closed and open symbols in (A) and (B) represent positive and negative inclinations, respectively.

Table 1. Magnetostratigraphy of Holes 576 and 576B.

Boundary	Age[a] (m.y.)	Polarity transition[b] (Core, Section, level in cm)	Corrected sub-bottom depth[c] (m)
Brunhes/Matuyama	0.73	1-5, 85 to 1-5, 106[d]	6.95
Jaramillo			
top	0.91	2-2, 26 to 2-2, 36[e]	9.01
bottom	0.98	2-2, 106 to 2-2, 116[e]	9.81
Olduvai			
top	1.66	2-6, 26 to 2-6, 46[e]	15.06
bottom	1.88	2-7, 16 to 2-7, 36[e]	16.46
Matuyama/Gauss	2.47	2-5, 56 to 2-5, 66[d]	18.21

[a] Berggren et al. (in press).
[b] Range reflects uncertainty in determination.
[c] See Site 576 chapter (this volume) for details.
[d] Hole 576B.
[e] Hole 576.

10^{-6} G in Holes 577 and 577A, respectively. A signif-
ant difference of roughly a factor of two in the aver-
es for normal and reversed polarities is observed in
late Cenozoic period, but not in the older sediment
quences. The magnetic stability characterized by the
DF displays the opposite trends. These findings re-
ct the negative interaction of bipolar magnetization
nponents reducing the NRM intensity. In turn, MDF
ched at 50% NRM (Fig. 3) is too high as compared
an MDF at 50% of the sum of all magnetization
ounts initially present. However, because of the com-
x magnetization structure in many samples of Site
, no attempt has been made to quantify this latter,
ysically more rational parameter from the demagnet-
tion curves. In the upper ~60 m, although extremely
riable, the MDFs yield a geometric mean of 295 Oe,
ore than twice that of the Late Cretaceous to Paleo-
ne period (132 Oe).

AF demagnetization frequently resulted in large di-
ctional changes in remanent magnetization directions.
the latest Cenozoic portion, secondary magnetization
omponents could mostly be identified as originating
om a viscous overprinting in the Brunhes Epoch, at least for samples carrying a reversed polarity (Fig. 3). In contrast, in the older sedimentary sequences, unstable magnetization components typically did not show much directional consistency (Fig. 4). In the older sediments, the poor magnetic stability mentioned obviously led to the acquisition of spurious remanences during and/or after recovery of the cores. The relatively large scatter in directional data likely indicates that the stable directions defined are not always true primary, single-component magnetizations, but also include some secondary com-

Table 2. Magnetostratigraphy of Hole 578.

Boundary[a]	Age[b] (m.y.)	Polarity transition[c] (Core, Section, level in cm)	Sub-bottom depth[d] (m)
Brunhes/Matuyama	0.73	4-3, 65 to 4-3, 105	27.66
Jaramillo			
top	0.91	4-6, 46 to 4-6, 66	31.86
bottom	0.98	5-1, 106 to 5-1, 126	34.46
Olduvai			
top	1.66	7-2, 28 to 7-2, 46	54.17
bottom	1.88	7-4, 126 to 7-4, 146	58.16
Matuyama/Gauss	2.47	9-1, 126 to 9-1, 146	72.66
Kaena			
top	2.92	9-7, 26 to 9-7, 48	80.67
bottom	2.99	10-2, 6 to 10-2, 24	82.45
Mammoth			
top	3.08	10-2, 126 to 10-2, 146	83.66
bottom	3.18	10-3, 106 to 10-3, 146	85.06
Gauss/Gilbert	3.40	10-5, 66 to 10-5, 106	87.66
Cochiti			
top	3.88	11-2, 146 to 11-3, 26	93.41
bottom	3.97	11-3, 126 to 11-4, 6	94.71
Nunivak			
top	4.10	11-5, 6 to 11-5, 46	96.56
bottom	4.24	11-5, 116 to 11-6, 6	97.66
Sidufjall			
top	4.40	11-6, 126 to 11-7, 6	99.21
bottom	4.47	12-2, 4 to 12-2, 51	101.58
Thvera			
top	4.57	12-2, 106 to 12-2, 146	102.56
bottom	4.77	12-4, 6 to 12-4, 46	104.56
Gilbert/Epoch 5	5.35	12-6, 140 to 13-1, 46	109.23

[a] Terminology according to McDougall (1977).
[b] Berggren et al. (in press).
[c] Range reflects uncertainty in determination.
[d] From coring summary, see Table 1 of Site 578 chapter (this volume).

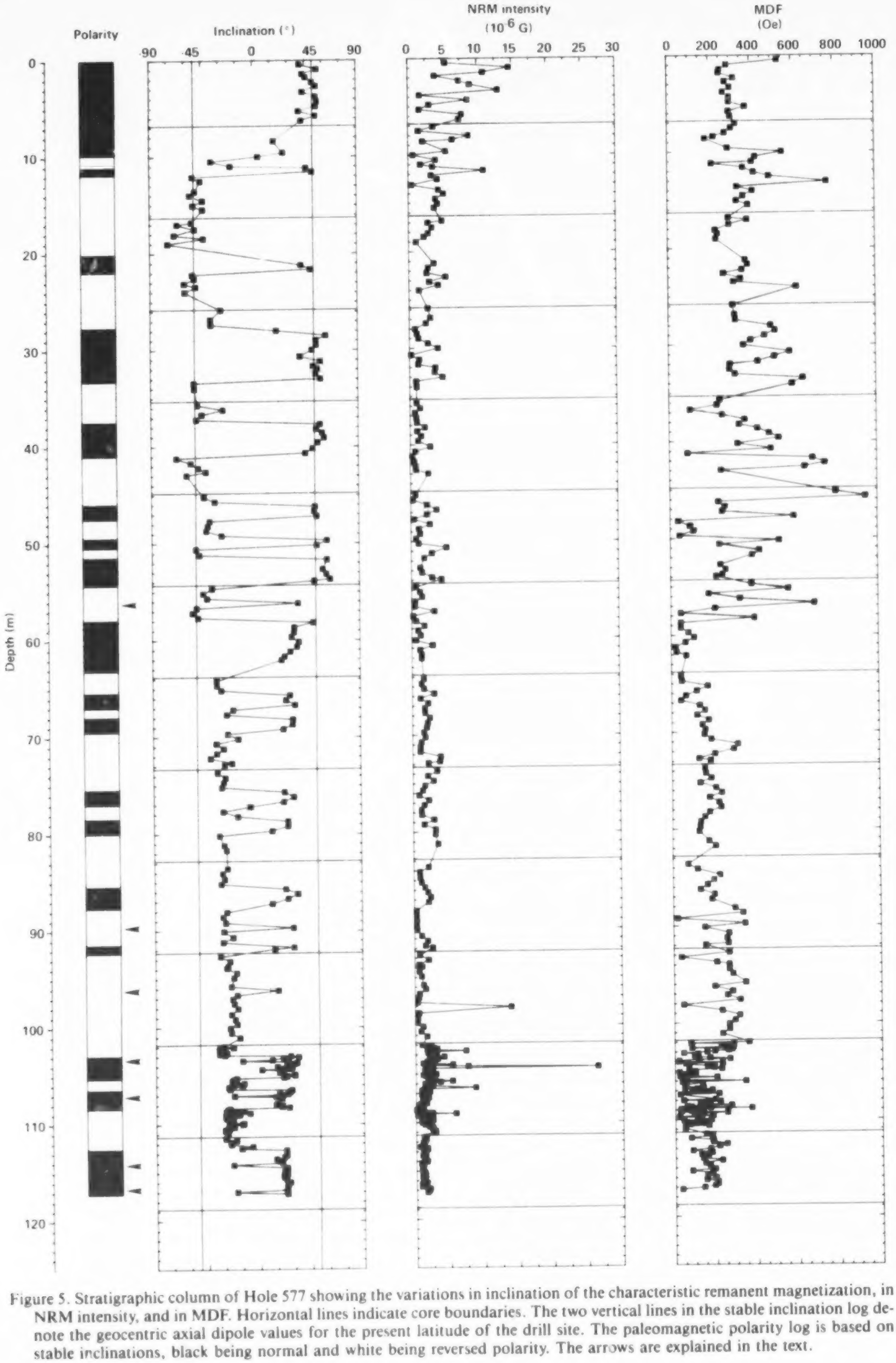

Figure 5. Stratigraphic column of Hole 577 showing the variations in inclination of the characteristic remanent magnetization, in NRM intensity, and in MDF. Horizontal lines indicate core boundaries. The two vertical lines in the stable inclination log denote the geocentric axial dipole values for the present latitude of the drill site. The paleomagnetic polarity log is based on stable inclinations, black being normal and white being reversed polarity. The arrows are explained in the text.

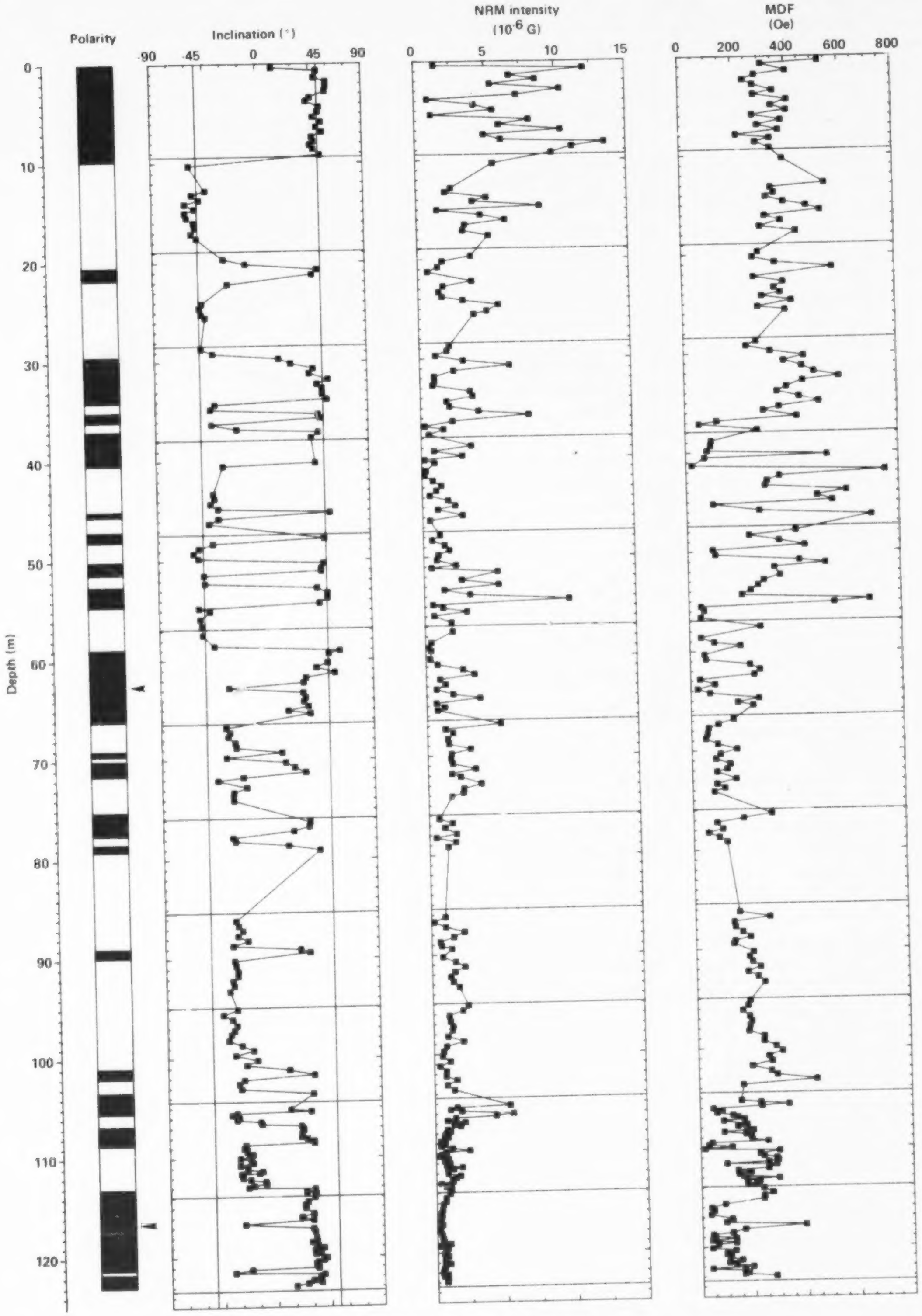

Figure 6. Stratigraphic column of Hole 577A. See caption of Figure 5 for details.

ponents that could not be erased completely by AF demagnetization. Such effects should not greatly reduce the quality of the magnetostratigraphies derived, but make the results a rather poor choice for paleosecular variation and paleolatitude analyses.

In the upper part of the cored sections, the downhole pattern of characteristic remanent magnetization inclination yields an almost unequivocal reversal stratigraphy for about the last 5.5 m.y. (Figs. 5, 6, and 7A). That stratigraphy includes all major transitions of the Earth's magnetic field since the beginning of the Gilbert Epoch. However, because of limited recovery or badly disturbed sediments in some cores of both holes, appreciable uncertainty exists in defining exact depth positions for a number of reversal boundaries (Table 3). For the same reason, the following short polarity events are missing in one hole but can be recognized in the other: in Hole 577 the normal interval separating the Kaena and Mammoth events in the middle of the Gauss Epoch and the Cochiti Event in the Gilbert Epoch, and in Hole 577A, the Jaramillo Event in the late Matuyama Epoch.

A comparison of depth positions for several well-defined reversals in both holes reveals variable degrees of mutual offsets amounting to at least ±1 m downhole (Fig. 7A). Although this could effectively be the result of real fluctuations in paleotopography, it can also be explained by the standard DSDP procedure of accounting for any material loss at the base of each cored interval.

The depth position for the last occurrence of the calcareous nannofossil *Discoaster quinqueramus* in the early part of the Gilbert Epoch (Monechi et al., this volume) disagrees with most other published results. In general, this coccolith datum level has been observed near the middle of Epoch 5. There is a possibility, therefore, that the normal polarity interval identified as the Thvera Event here could be the late part of Epoch 5. Without further evidence, this interpretation was rejected mainly because it requires both a drastic change in sedimentation rate and rather complicated arguments concerning the remaining magnetobiostratigraphic sequence around this level.

To about 60 m below seafloor, the sedimentary column apparently accumulated at a remarkably constant average rate of about 11 m/m.y. The sedimentation rates were slightly higher in the Brunhes and Gauss Epochs and lower in the Gilbert Epoch, but any shift is limited to within 30% of the average (Fig. 7A).

At around 62 m sub-bottom, a major hiatus separates latest Miocene from middle Eocene sediments (Monechi, this volume; Site 577 report, this volume). Calcareous nannofossils suggest additional shorter hiatuses in the early Eocene and near the Paleocene/Eocene boundary (Monechi, this volume). Detailed correlations of biostratigraphic and paleomagnetic marker horizons in the sedimentary columns of both holes also revealed missing intervals at the boundary of Cores 8 and 9 of Hole 577 and within Core 10 of Hole 577A, each about 2.6-m long, that are not listed in the coring record (Monechi et al., this volume). Further complicated by an incomplete or badly disturbed recovery at several levels, for the lower halves of both holes and in particular for the Eocene period, magnetostratigraphies could only be established in the framework of biostratigraphic and stable-isotope stratigraphy (Shackleton et al., this volume) data.

The first positively identified magnetic polarity zone beneath the major unconformity is the C-22N subchron in Hole 577, corresponding to the marine magnetic Anomaly 22. In this hole, with the exception of the two normal polarity intervals of the C-23 and C-27N subchrons, a virtually complete reversal sequence was identified ending in the Late Cretaceous C-30N subchron near the base of the hole (Figs. 5 and 7B). In Hole 577A, only the C-22N and C-25N subchrons could not be recognized (Figs. 6 and 7B), which was evidently the result of a lack of recovery in the relevant intervals. At the base of this slightly deeper hole, the magnetostratigraphic record reaches into the C-31N subchron. The above-described difficulties caused relatively large ranges of uncertainty in defining the depth of a number of reversal boundaries in both holes (Table 3).

At different levels in Holes 577 and 577A, short polarity events are indicated in the downhole patterns of the characteristic remanent magnetization inclinations. They are denoted by small arrows at the magnetostratigraphic columns in Figures 5 and 6. As no consistency exists in these data between the two holes, no attempt was made for a correlation with similar paleomagnetic results from Site 524 in the South Atlantic (Tauxe et al., 1984) or with the "tiny wiggles" in the polarity time scale of LaBrecque et al. (1977).

On the basis of biostratigraphic evidence, the Cretaceous/Tertiary boundary was recognized at 109.10 and 109.62 m depth below seafloor in Holes 577 and 577A, respectively. In both holes the boundary is located within the interval of reversed polarity that separates the marine magnetic Anomalies 29 and 30, denoted as the C-29R subchron in the presently used nomenclature. Worldwide, the same result was obtained from analyses of various marine sections (Alvarez et al., 1977; Alvarez and Lowrie, 1978; Hsü et al., 1982; Shackleton et al., 1984; Thierstein, 1982 and references therein). As pointed out by Thierstein (1982), the relative position of the paleontological boundary within the magnetic C-29R subchron is highly variable in different pelagic sequences, indicating major changes in sedimentation rate and/or the possible presence of hiatuses. Similar to the situation in most of these sections, the C-29R subchron is expanded in the sedimentary column recovered at Site 577 relative to the preceding C-30N and the following C-29N normal polarity subchrons. A numerical age determined for the Cretaceous/Tertiary boundary horizon by interpolation from the magnetic C-29R boundaries and by extrapolation downward using the C-29N and upward using the C-30N boundary varies between about 66.3 and 66.5 m.y. This is in complete agreement with other recent estimates based on the same time scale (Berggren et al., in press; Shackleton et al., 1984).

Since it was only possible to elaborate a rather crude magnetostratigraphy for the Eocene, the apparent sedimentation rates derived from the paleomagnetic data for this period are of relatively poor quality (Fig. 7B). They

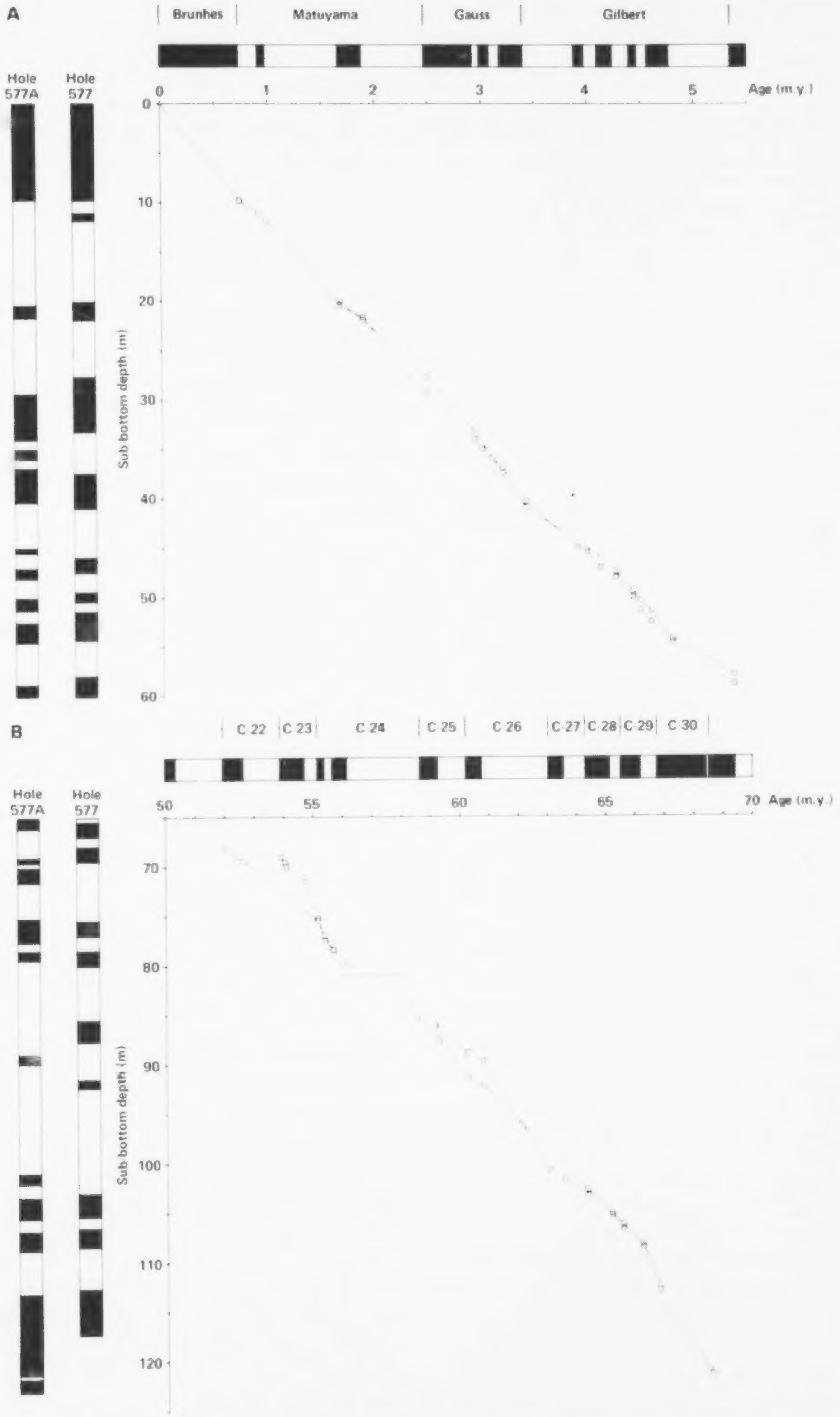

Figure 7. Apparent sediment accumulation at Site 577. ⊙ Hole 577, ▣ Hole 577A. The downhole pattern in remanent magnetization polarity is correlated to the geomagnetic polarity time scale of Berggren et al. (in press). A. Late Cenozoic. Geomagnetic time units (epochs, events) according to McDougall (1977). B. Late Cretaceous to middle Eocene. Geomagnetic time units (chrons) according to Tauxe et al. (1984).

Table 3. Magnetostratigraphy of Holes 577 and 577A.

		Hole 577		Hole 577A	
Boundary[a]	Age[b] (m.y.)	Polarity transition[c] (Core, Section, level in cm)	Sub-bottom depth[d] (m)	Polarity transition[c] (Core, Section, level in cm)	Sub-bottom depth[d] (m)
Brunhes/Matuyama	0.73	2-2, 130 to 2-3, 20	9.80	1-7, 22 to 2-1, 89	9.76
Jaramillo					
top	0.91	2-3, 119 to 2-3, 140	11.10	—	—
bottom	0.98	2-4, 30 to 2-4, 80	11.85	—	—
Olduvai					
top	1.66	3-2, 120 to 3-4, 41	20.11	3-1, 129 to 3-2, 35	20.47
bottom	1.88	3-4, 85 to 3-4, 140	21.93	3-2, 85 to 3-3, 30	21.73
Matuyama/Gauss	2.47	4-2, 10 to 4-2, 70	27.70	4-1, 79 to 4-1, 130	29.45
Kaena					
top	2.92	4-5, 120 to 4-6, 14	33.22	4-4, 90 to 4-4, 140	34.05
bottom	2.99	—	—	4-5, 40 to 4-5, 90	35.05
Mammoth					
top	3.08	—	—	4-5, 130 to 4-6, 40	36.00
bottom	3.18	5-2, 41 to 5-2, 90	37.46	4-6, 90 to 4-6, 120	36.95
Gauss/Gilbert	3.40	5-4, 90 to 5-4, 140	40.95	5-2, 80 to 5-2, 110	40.35
Cochiti					
top	3.88	—	—	5-5, 90 to 5-5, 130	45.00
bottom	3.97	—	—	5-5, 130 to 5-6, 40	45.50
Nunivak					
top	4.10	6-1, 90 to 6-1, 140	45.95	5-6, 90 to 6-1, 40	47.05
bottom	4.24	6-2, 90 to 6-2, 140	47.45	6-1, 40 to 6-1, 90	48.05
Sidufjall					
top	4.40	6-3, 140 to 6-4, 40	49.45	6-2, 90 to 6-2, 140	50.05
bottom	4.47	6-4, 90 to 6-4, 130	50.40	6-3, 70 to 6-3, 110	51.30
Thvera					
top	4.57	6-5, 40 to 6-5, 90	51.45	6-4, 40 to 6-4, 90	52.55
bottom	4.77	6-7, 9 to 7-1, 40	54.30	6-5, 90 to 6-5, 140	54.55
Gilbert/Epoch 5	5.35	7-3, 40 to 7-3, 90	57.95	7-2, 20 to 7-2, 70	58.85
? (N/R)	?	7-6, 26 to 8-1, 40	63.13	—	—
C-17 or C-18					
(R/N)	?	8-1, 140 to 8-2, 40	65.45	—	—
(N/R)	?	8-2, 140 to 8-3, 40	66.95	7-6, 100 to 8-1, 40	66.10
?/C-22N	51.95	8-3, 90 to 8-3, 140	67.95	—	—
C-22N/C-22R	52.62	8-4, 90 to 8-4, 140	69.45	—	—
C-22R/C-23N-1	53.88	—	—	8-2, 90 to 8-2, 140	69.05
C-23N-1/C-23R-1	54.03	—	—	8-2, 140 to 8-3, 40	69.55
C-23R-1/C-23N-2	54.09	—	—	8-3, 40 to 8-3, 90	70.05
C-23N-2/C-23R-2	54.70	—	—	8-4, 40 to 8-4, 90	71.55
C-23R-2/C-24N-1	55.14	9-2, 40 to 9-2, 90	75.45	8-6, 20 to 9-1, 41	75.21
C-24N-1/C-24R-1	55.37	9-3, 40 to 9-3, 90	76.95	9-1, 131 to 9-2, 44	77.53
C-24R-1/C-24N-2	55.66	9-4, 40 to 9-4, 90	78.45	9-2, 82 to 9-2, 125	78.44
C-24N-2/C-24R-2	56.14	9-5, 40 to 9-5, 90	79.95	—	—
C-24R-2/C-25N	58.64	10-2, 90 to 10-2, 140	85.45	—	—
C-25N/C-25R	59.24	10-3, 140 to 10-4, 80	87.65	—	—
C-25R/C-26N	60.21	10-6, 92 to 10-6, 142	91.47	10-3, 30 to 10-3, 71	88.91
C-26N/C-26R	60.75	10-7, 11 to 11-1, 39	92.30	10-3, 100 to 10-4, 31	89.81
C-26R/C-27N	63.03	—	—	11-4, 130 to 11-5, 30	100.95
C-27N/C-27R	63.54	—	—	11-5, 80 to 11-5, 130	101.95
C-27R/C-28N	64.29	12-1, 110 to 12-1, 120	102.95	11-6, 70 to 11-6, 120	103.35
C-28N/C-28R	65.12	12-3, 40 to 13-3, 50	105.25	12-1, 96 to 12-1, 116	105.46
C-28R/C-29N	65.50	12-4, 10 to 12-4, 20	106.45	12-2, 76 to 12-2, 94	106.75
C-29N/C-29R	66.17	12-5, 50 to 12-5, 60	108.35	12-3, 116 to 12-3, 135	108.66
C-29R/C-30N	66.74	13-1, 120 to 13-1, 140	112.60	12-6, 111 to 12-6, 126	113.09
C-30N/C-30R	68.42	—	—	13-5, 119 to 13-5, 137	121.18
C-30R/C-31N	68.52	—	—	13-6, 15 to 13-6, 35	121.65

Note: — means not recovered.

[a] Terminology according to McDougall (1977) and Tauxe et al. (1984).

[b] Berggren et al. (in press).

[c] Range reflects uncertainty in determination.

[d] From coring summary, see Table 1 of Site 577 chapter (this volume).

yield an average sedimentation rate of 3.5 m/m.y. in Hole 577 and 5.3 m/m.y. in Hole 577A. During the Paleocene, the sediments accumulated at an average rate of about 3 m/m.y. (3.0 m/m.y. and 3.3 m/m.y. in Holes 577 and 577A, respectively). In detail, the magnetostratigraphic record indicates that the variability in sedimentation rate during the early Tertiary was mostly within a factor of two. The apparent accumulation rate increases to about 7.6 m/m.y. in the C-29R subchron containing the Cretaceous/Tertiary boundary horizon. According t the data from Hole 577A, on average it amounts to 4. m/m.y. in the Late Cretaceous.

Site 579

At Site 579, 149 m of early Pliocene to Quaternar biosiliceous clays with numerous interlayered volcani ashes were penetrated in two holes using the HPC (Fig 1). Because of marginal weather conditions, the sediments were frequently distorted, stretched, or otherwise disturbed. The recovery was distinctly below the average for Leg 86, only about 80% in many cores.

About 300 vertically oriented samples were analyzed for their paleomagnetic properties. The NRM intensity was extremely variable throughout the section. Continuous downhole trends of decreasing NRM intensity from about 4×10^{-5} to about 4×10^{-6} G occur in the uppermost ~60 m spanning the Brunhes and the latter half of the Matuyama epochs, and from about 3×10^{-5} to about 10^{-6} G below 95 m sub-bottom to the base of Hole 579A extending between the Gauss and the late part of the Gilbert epochs (Fig. 8). The overall geometric mean amounts to 1.1×10^{-5} G. On average, distinctly higher NRM intensities are observed for samples of normal magnetization polarity (1.7×10^{-5} G) than for those carrying a reversed polarity (8.6×10^{-6} G). The viscous magnetization components resulting from the present Brunhes field are a plausible explanation for this difference. With a few exceptions, the magnetic stability characterized by the MDF is high (Fig. 8). MDF geometric means for the entire sample collection (278 Oe), normal polarities (270 Oe), and reversed polarities (284 Oe) are essentially identical. Low NRM and MDF values are more abundant in core sections showing clear evidence for intensive drilling disturbance.

The downhole pattern in characteristic remanent magnetization inclination (Fig. 8) reveals a rather high degree of "noise" over various intervals. The variation appears to exceed the normal range of secular field variation in the region during late Cenozoic (see also results of Site 580), but seemingly also reflects the limited quality of the materials retrieved at Site 579. Although these effects did not cause specific ambiguities in recognizing magnetic boundaries, in the lower part of Hole 579A gaps in the recovery repeatedly resulted in comparatively large ranges of uncertainty in determining their depth.

The polarity sequence derived from stable inclinations is shown in Figure 8. The two cores recovered in Hole 579 acquired their remanent magnetization during the normal Brunhes Epoch. Therefore, the sediments at the base of this hole (17.9 m sub-bottom) are less than 0.73 m.y. old. An almost complete reversal series for the last about .5 m.y. was obtained in Hole 579A. The Brunhes/Matuyama boundary was recognized at a sub-bottom depth of 30.65 m; the Matuyama/Gauss boundary at 87.95 m, and the Gauss/Gilbert boundary at 115.01 m. In addition to the Jaramillo and Olduvai events, a third short normal polarity zone is recorded within the reversed Matuyama Epoch. Its interpolated numerical age of about .14 m.y. suggests a correlation to the "X" event (McDougall, 1977), which was previously identified in marine magnetic anomaly data (Heirtzler et al., 1968; Emi-a and Heinrichs, 1972). Both the Kaena and Mammoth events are present in the Gauss Epoch, indicating that the paleomagnetic record is also continuous and complete in this part of the hole. The deepest unequivocally identifiable magnetic boundary is the Gauss/Gilbert transition. Beneath, only one additional zone of normal polarity occurs. The interpretation given in Table 4 and Figure 9 relates this interval to the Nunivak Event, assuming that the Cochiti Event was lost in the 2.5-m gap in recovery between Cores 13 and 14. The alternative solution, its correlation to the Cochiti Event, would require a major change in sedimentation rate around this level. The average apparent accumulation rate at Site 579 is about 34.0 m/m.y. It gradually decreases from 42.0 m/m.y. during the Brunhes to 32.9 m/m.y. and 29.1 m/m.y. in the Matuyama and Gauss epochs, respectively. Compared to other sites drilled on Leg 86, the late Cenozoic sedimentation rates at Site 579 are somewhat more variable, apparently a result of real fluctuations in the sediment supply.

Site 580

At Site 580 about 155 m of Quaternary to late Pliocene biosiliceous clays containing numerous ash layers over the entire sedimentary column were penetrated (Fig. 1). A high percentage recovery was achieved with comparatively minor coring disturbances.

The paleomagnetic sampling program provided approximately 360 vertically oriented specimens. In the upper ~120 m comprising the record of the geomagnetic Brunhes and Matuyama epochs, there is a systematic decrease in the NRM intensity from about 4×10^{-5} to some 5×10^{-6} G (Fig. 10). Below this level to the base of the hole, in the Gauss Epoch, on average slightly higher NRM intensities of about 10^{-5} G were encountered again. The NRM values vary by at least one order of magnitude within virtually all of the cores. Their overall geometric mean amounts to 1.7×10^{-5} G. The conspicuous difference in normal (2.4×10^{-5} G) and reversed (1.2×10^{-5} G) polarities should mainly reflect contributions of viscous magnetization components acquired in the Brunhes Epoch of normal Earth's field configuration. Detailed shore-based analyses using progressive stepwise demagnetization in alternating fields revealed a remarkably high constant magnetic stability throughout. The overall geometric mean for the MDF is 278 Oe and almost the same values were obtained for normal (268 Oe) and reversed (289 Oe) polarities, indicating that the magnetic mineral assemblage should be essentially uniform in composition and grain size. Only minor directional changes are observed between NRM and stable inclinations and declinations upon AF demagnetization. This is practically independent of the respective magnetization polarity (Fig. 2). The general variation in the inclination data throughout the hole apparently results from a normal range of secular paleofield variation. In contrast, the stable declination pattern is much more complex, as it frequently includes variable amounts of disturbances introduced by the coring process.

All magnetic reversal boundaries could be recognized unequivocally. As none of the major polarity transitions coincides with a core boundary and almost no magnetization directions appear to have recorded true transitional Earth field states, it was possible to define an accurate depth position for each reversal boundary. Therefore, the magnetostratigraphic sequence obtained (Table 5) is superior in quality to the other Leg 86 paleomagnetic results. The polarity pattern derived from the down-

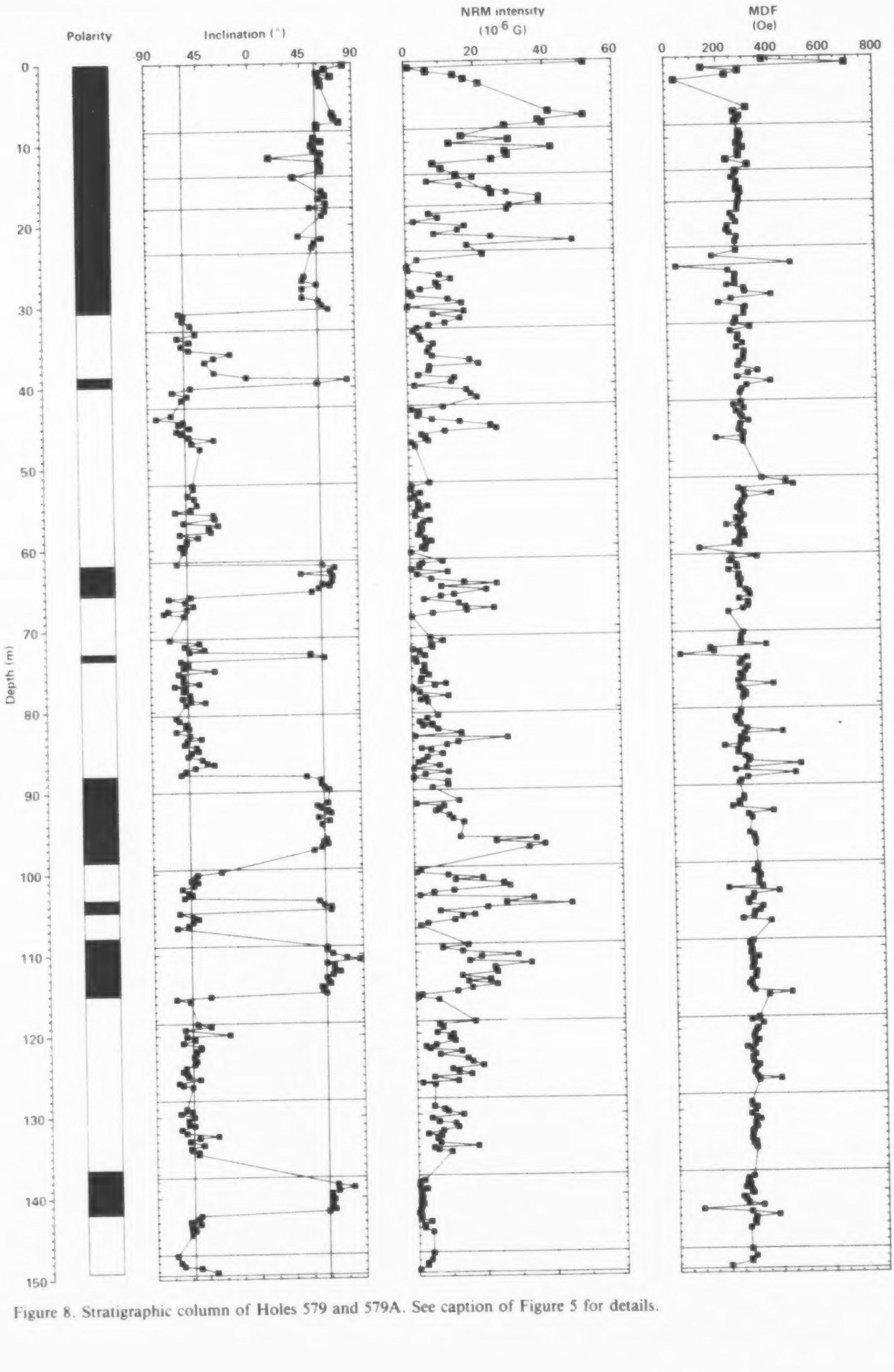

Figure 8. Stratigraphic column of Holes 579 and 579A. See caption of Figure 5 for details.

Table 4. Magnetostratigraphy of Holes 579 and 579B.

Boundary	Age[a] (m.y.)	Polarity transition[b] (Core, Section, level in cm)	Sub-bottom depth[c] (m)
Brunhes/Matuyama	0.73	2-5, 90 to 2-5, 140	30.65
Jaramillo			
top	0.91	3-4, 70 to 3-5, 10	38.65
bottom	0.98	3-5, 60 to 3-5, 110	39.85
Olduvai			
top	1.66	6-1, 31 to 6-1, 55	61.93
bottom	1.88	6-3, 85 to 6-3, 140	65.63
Matuyama/Gauss	2.47	8-5, 131 to 8-6, 9	87.95
Kaena			
top	2.92	9-5, 120 to 10-1, 33	98.52
bottom	2.99	10-3, 51 to 10-3, 91	103.21
Mammoth			
top	3.08	10-4, 51 to 10-4, 91	104.71
bottom	3.18	10-5, 121 to 11-1, 13	107.92
Gauss/Gilbert	3.40	11-4, 130 to 11-5, 21	115.01
Cochiti			
top	3.88	—	—
bottom	3.97	—	—
Nunivak			
top	4.10	13-5, 61 to 14-1, 64	136.38
bottom	4.24	14-3, 121 to 14-4, 18	141.95

Note: — means not recovered.

[a] Berggren et al. (in press).

[b] Range reflects uncertainty in determination.

[c] From coring summary, see Table 1 of Site 579 chapter (this volume).

hole variation in stable inclination is shown in Figure 10. It spans most of the last three geomagnetic epochs (Fig. 11). The Brunhes/Matuyama boundary was recognized at 40.00 m sub-bottom, the Matuyama/Gauss boundary at 121.44 m below seafloor. In addition to the Jaramillo and Olduvai events, the reversed Matuyama Epoch also comprises the recording of two short polarity events. However, they are both documented by only one data point at present. Although each reversal is clearly indicated in stable inclination and declination, this does not exclude the possibility of an accidental misorientation during sampling. The younger event at about 58 m sub-bottom, corresponding to an age of about 1.1 m.y., could not be identified in any other Leg 86 sedimentary column. However, there are indications of such a short reversal or possibly field excursion in pelagic sediments from the Central Pacific (e.g., Forster and Opdyke, 1970), and it is apparently also recorded in a piston core (V36-51P) recovered near Site 576 during the *Vema*-36 presite survey cruise (C. Barton, pers. comm., 1981).

For the event at about 98 m sub-bottom between the Olduvai and the Matuyama/Gauss boundary, an age of about 2.05 m.y. is interpolated assuming a constant sedimentation rate in this interval. It therefore should represent the Réunion Event (McDougall and Watkins, 1973). In the normal Gauss Epoch, both the Kaena and Mammoth events are clearly recognizable in the magnetostra-

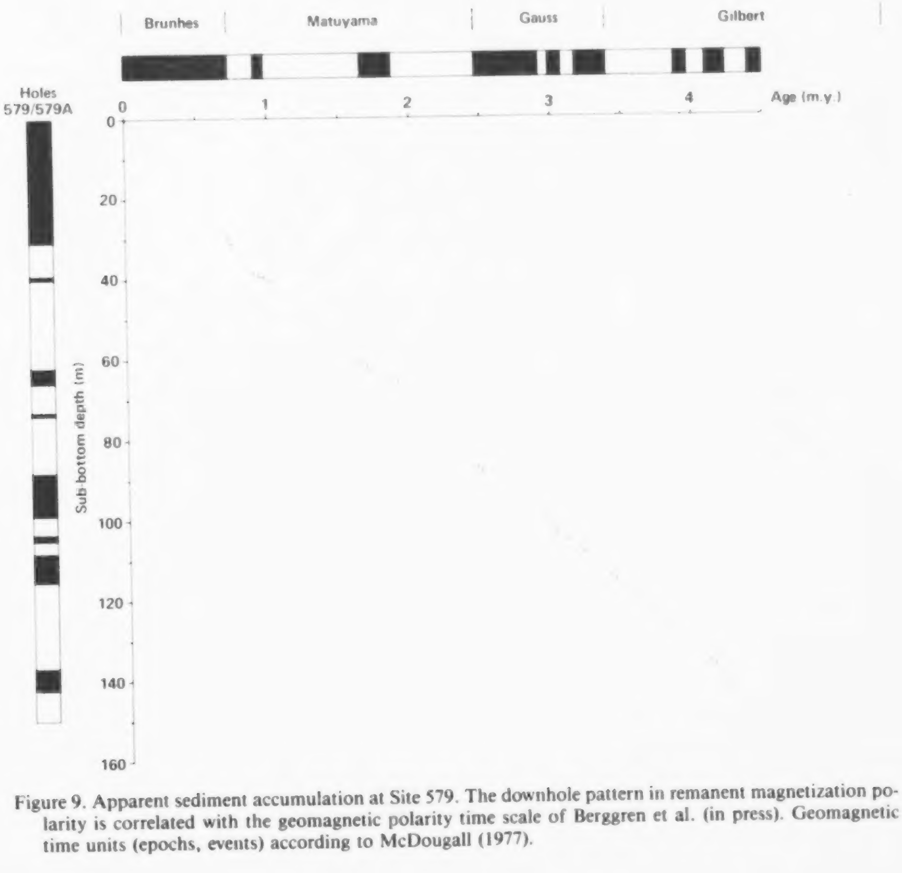

Figure 9. Apparent sediment accumulation at Site 579. The downhole pattern in remanent magnetization polarity is correlated with the geomagnetic polarity time scale of Berggren et al. (in press). Geomagnetic time units (epochs, events) according to McDougall (1977).

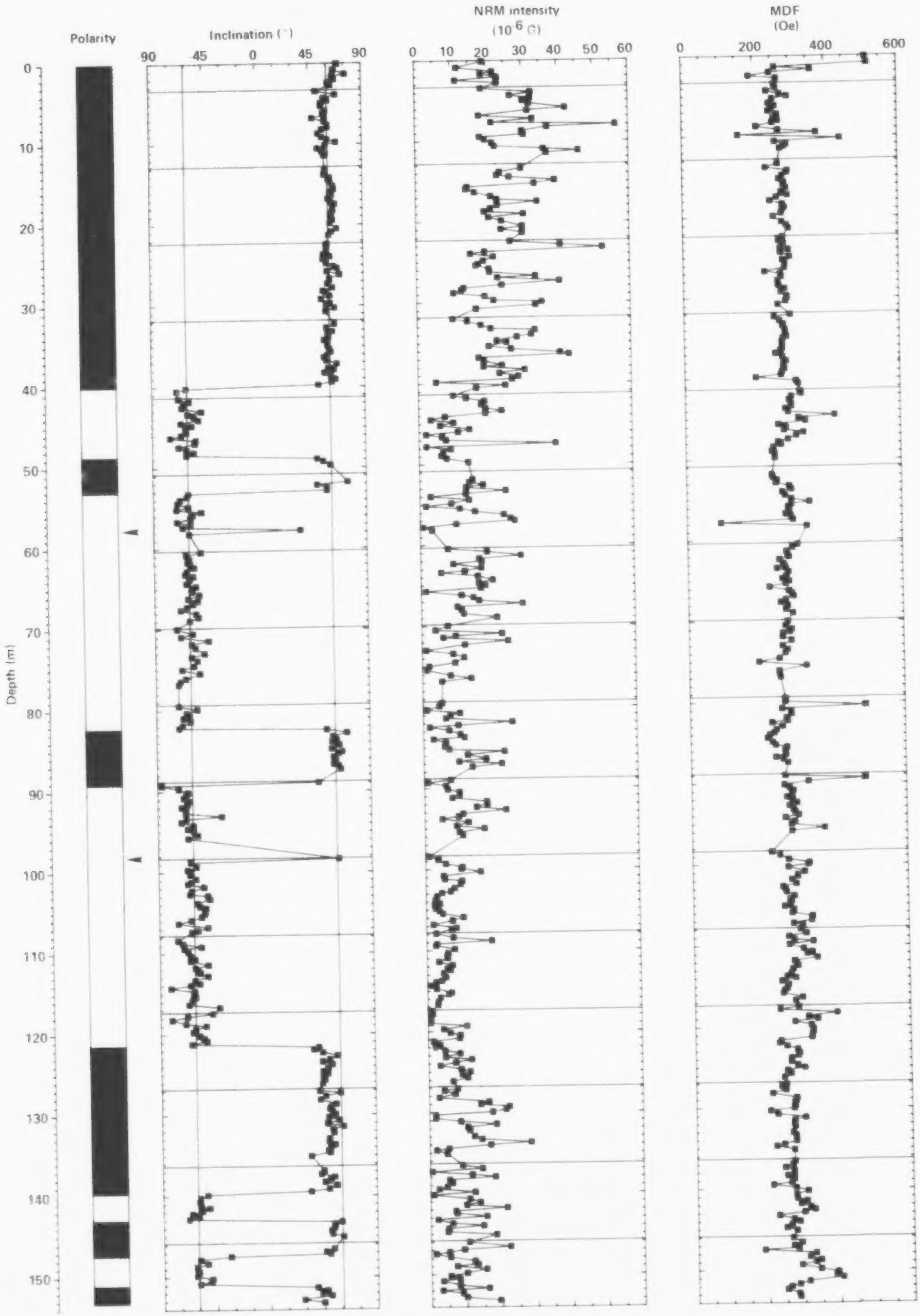

Figure 10. Stratigraphic column of Hole 580. See caption of Figure 5 for details.

Table 5. Magnetostratigraphy of Hole 580.

Boundary	Age[a] (m.y.)	Polarity transition[b] (Core, Section, level in cm)	Sub-bottom depth[c] (m)
Brunhes/Matuyama	0.73	5-6, 50 to 5-6, 90	40.00
Jaramillo			
top	0.91	6-5, 114 to 6-6, 13	48.69
bottom	0.98	7-2, 54 to 7-2, 92	53.03
Olduvai			
top	1.66	10-2, 140 to 10-3, 15	82.33
bottom	1.88	11-1, 15 to 11-1, 50	89.13
Matuyama/Gauss	2.47	14-3, 91 to 14-3, 136	121.44
Kaena			
top	2.92	16-3, 15 to 16-3, 51	139.63
bottom	2.99	16-5, 51 to 16-5, 91	143.01
Mammoth			
top	3.08	17-1, 141 to 17-2, 15	147.33
bottom	3.18	17-4, 51 to 17-4, 101	151.06

Berggren et al. (in press).

Range reflects uncertainty in determination.

From coring summary, see Table 1 of Site 580 chapter (this volume).

graphic record. The base of the hole at 155.30 m below afloor did not reach the Gauss/Gilbert reversal boundary.

The entire sediment column at Site 580 accumulated at a remarkably constant average rate of about 47.5 m./m.y. (Fig. 11). Downhole, it only decreases from about 54.8 m/m.y. during the Brunhes Epoch to 46.8 m/m.y. in the Matuyama Epoch and 41.7 m/m.y. in the Gauss Epoch. Extrapolation yields an age of about 3.30 m.y. at the base of the hole. The high sedimentation rates facilitate determination of a detailed sequence of transitional configurations of the Earth's magnetic field during several reversals. The results of this study will be reported elsewhere.

PALEOLATITUDES

Any evaluation of paleolatitudes from paleomagnetic data of DSDP drill cores is known to have specific limitations (Pierce, 1976). Those limitations mainly result from the drilling process (disturbed or incomplete recovery and undetected oblique coring) and also from the statistical problem of accounting appropriately for the lack in azimuthal orientation of the cores. The development of the HPC technique has reduced these difficulties to some extent and, although no direct measurements were performed during Leg 86, according to all previous experience, DSDP drill cores should not deviate by more than 2 to 3° from the vertical. Exactly this same amount of inaccuracy would apply to the inclinations and, at about 30 to 40° latitude, also to the paleolatitudinal data. Other potential error sources, such as the depositional mode or a compaction of the sediments and an inappropriately averaged secular field variation, should be negligible in the present case. As in most other recent studies on DSDP materials (Tauxe et al., 1984; Weinreich and Theyer, in press), the method developed by Briden

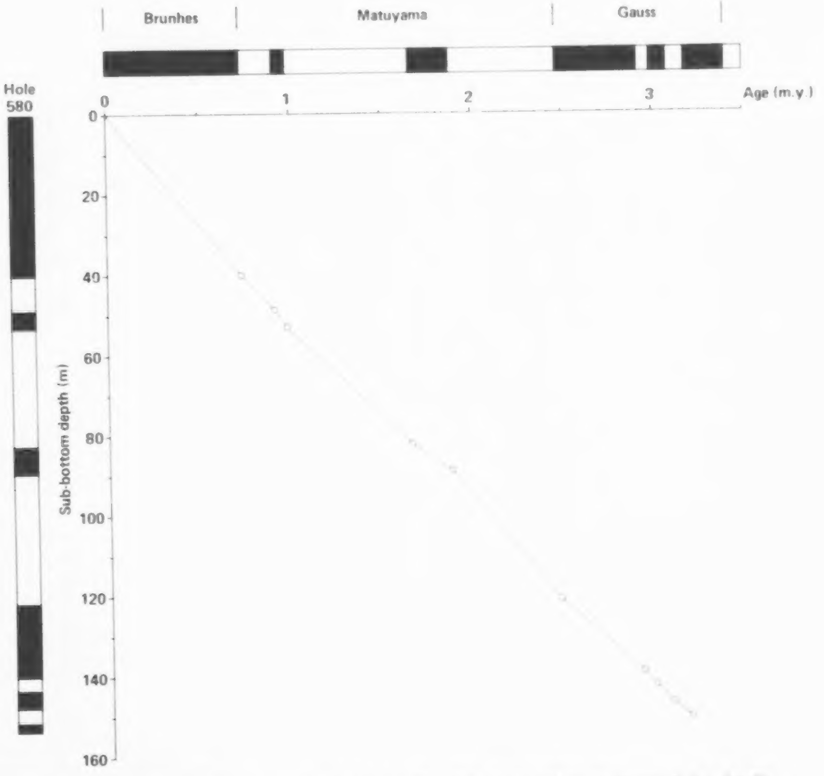

Figure 11. Apparent sediment accumulation at Site 580. See caption of Figure 9 for details.

and Ward (1966) and refined by Kono (1980) has been used to estimate true mean inclinations from the paleomagnetic data.

The results for the different drill sites are shown in Figures 12 through 14. In the late Cenozoic, average paleolatitudes were determined for each geomagnetic epoch. The 95% errors of the paleolatitudes, as resulting from the Kono (1980) statistics, are typically on the order of ±2-3°. At none of the sites do mean values indicate simple continuous trends, which could unequivocally be interpreted in terms of plate motions.

According to plate tectonic models derived from hotspot analysis (Epp, 1978), the north component of the Pacific plate motion has been about 0.3°/m.y. during the last about 15 m.y. The Pliocene to Quaternary paleomagnetic records obtained at Sites 577, 579, and 580, therefore, obviously extend over too short a period of time to allow any significant contribution to this problem, in view of their inherent statistical accuracy and even without additional systematic errors.

A puzzling and as yet unexplained feature is the remarkable difference in inclination and thus in paleolatitude for normal and reversed magnetizations in the deepest four cores of Hole 580 (Fig. 10). It evidently can no be caused by a nonvertical drill hole. Also, because of th high magnetic stability and the well-defined demagnetiz

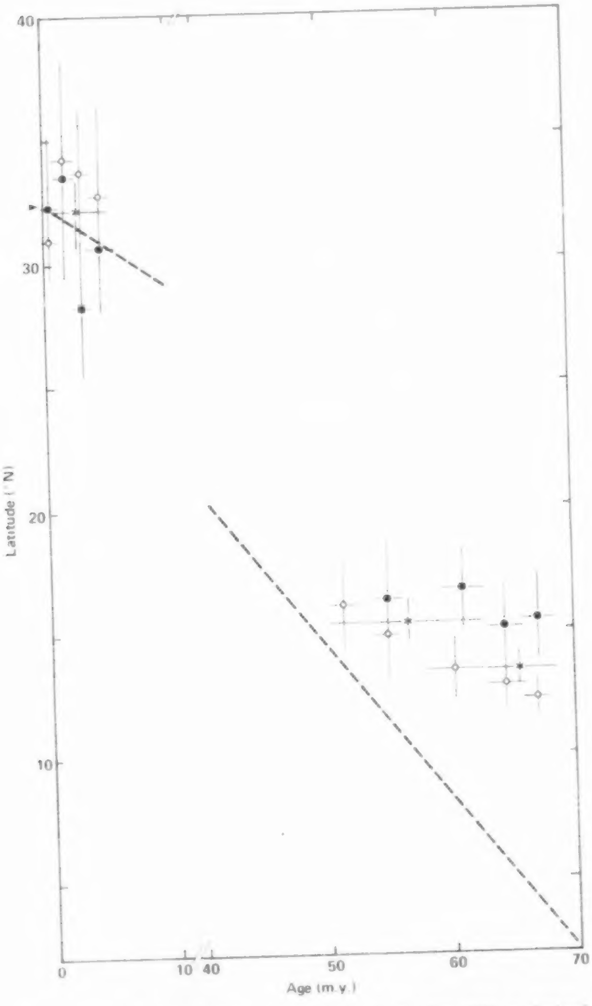

Figure 12. Age dependence of paleolatitude for Site 577 as derived from the downhole variation in inclination of the characteristic remanent magnetization of sediments. ○ Hole 577, ● Hole 577A, • Holes 577/577A combined. Vertical error bars represent the latitudinal dispersion as resulting from the Kono (1980) statistics, horizontal error bars denote the averaged time intervals corresponding to geomagnetic epochs in the late Cenozoic. The arrow indicates the present latitude of Site 577, the broken line its progressive northward motion since the Late Cretaceous as quantified by plate tectonic reconstructions (Epp, 1978).

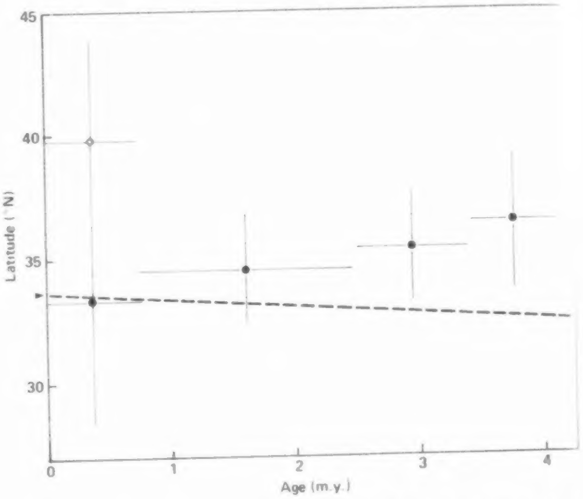

Figure 13. Age dependence of paleolatitude for Site 579 as derived from the downhole variation in inclination of the characteristic remanent magnetization of sediments. ○ Hole 579, ● Hole 579A. See caption of Figure 12 for details.

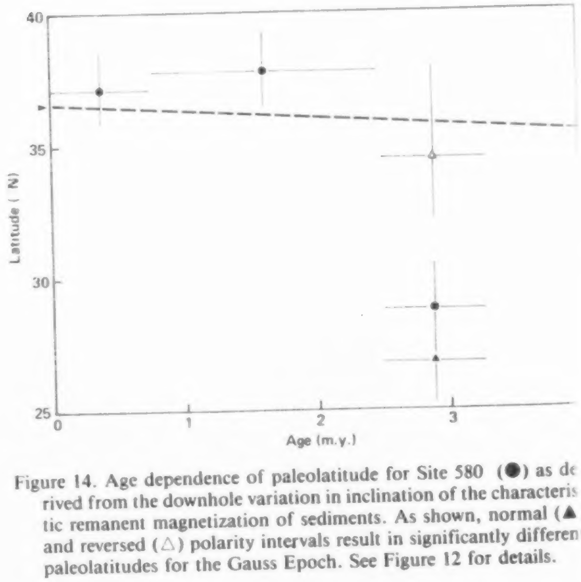

Figure 14. Age dependence of paleolatitude for Site 580 (●) as derived from the downhole variation in inclination of the characteristic remanent magnetization of sediments. As shown, normal (▲ and reversed (△) polarity intervals result in significantly differen paleolatitudes for the Gauss Epoch. See Figure 12 for details.

tion characteristics of these samples, an undetected overprinting by secondary components appears rather unlikely. On the other hand, similar behavior is not observed in the relevant intervals at the other sites.

For Late Cretaceous to middle Eocene sequences recovered in the lower halves of both holes at Site 577, the characteristic remanent magnetization inclination is disinctly shallower than the centered axial dipole value for he present latitude of the site (Figs. 5 and 6), providing lear evidence for the major unconformity at around 60 m ub-bottom. They suggest a northward motion of this art of the Pacific plate of about 17° between about 50 nd 5 m.y. ago. The same order of magnitude is inferred rom a hot-spot analysis (Epp, 1978), the most elaboate basis for a plate tectonic reconstruction of the reion at present (J. Morgan, pers. comm., 1983). Howver, according to the latter data, the Pacific plate has oved with an average north component of 0.75°/m.y. the period between 70 and 50 m.y. ago, whereas the resent results would give less than half this value (Fig. 2). As discussed in detail before, there are some indicaions that the paleomagnetic data may not be of prime uality in this interval. Nevertheless, the altogether convincing magnetostratigraphy obtained is not really compatible with an almost equatorial position of Site 577 in the Late Cretaceous and early Tertiary. A more complete treatment of the various aspects of these problems will be given elsewhere.

CONCLUSIONS

The paleomagnetic analyses of biosiliceous and calcareous sedimentary columns recovered on DSDP Leg 86 in the Northwest Pacific are a valuable aid in resolving the stratigraphic record of the deep sea in this area. Detailed Pliocene to Recent magnetostratigraphies were established at all drill sites, comprising major parts or the complete sequences of Earth's magnetic field reversals during the last four geomagnetic epochs. The magnetostratigraphies of Late Cretaceous to middle Eocene ediments penetrated in stratigraphic duplication at Site 77 (on the Shatsky Rise) using HPC could successfully e correlated to marine magnetic anomaly series and reent paleomagnetic results on pelagic sections from difrent parts of the world. These data constitute the first pportunity to elaborate a magnetobiochronology for is period, including the Cretaceous/Tertiary boundary terval, in the Pacific (Monechi et al., this volume).

For each site a diagrammatic apparent sedimentation te based on the magnetostratigraphy is presented. Paolatitudes derived from the variations in characteristic manent magnetization inclination with age have a bearg on the northward motion of the Pacific plate. The ata, however, show rather large discrepancies with exting plate tectonic models, presumably reflecting the till limited suitability of DSDP materials for such studies.

ACKNOWLEDGMENTS

I am very grateful to the many people responsible for the success f DSDP Leg 86, in particular to my scientific colleagues for their riendly cooperation. Special appreciation is given to V. Spiess and N. Weinreich for their help with the laboratory work, discussions, and valuable comments. W. Lowrie and an anonymous reviewer critically reviewed drafts, materially improving the manuscript.

The financial support of the Deutsche Forschungsgemeinschaft both toward the Deep Sea Drilling Project and the paleomagnetic laboratory in Bochum is gratefully acknowledged.

REFERENCES

Alvarez, W., Arthur, M. S., Fischer, A. F., Lowrie, W., Napoleone, G., Premoli Silva, I., and Roggenthen, W. M., 1977. Type section for the Late Cretaceous-Paleocene geomagnetic reversal time scale. *Geol. Soc. Am. Bull.*, 88:383-389.

Alvarez, W., and Lowrie, W., 1978. Upper Cretaceous paleomagnetic stratigraphy at Moria (Umbrian Apennines, Italy): Verification of the Gubbio section. *Geophys. J. R., Astron. Soc.*, 55:1-17.

Berggren, W. A., Kent, D. V., and Flynn, J. J., in press. Paleogene geochronology and chronostratigraphy. *In* Snelling, N. J. (Ed.), *Geochronology and the Geological Record*. Geol. Soc. London, Spec. Publ.

Briden, J. C., and Ward, M. A., 1966. Analysis of magnetic inclinations in bore cores. *Pure Appl. Geophys.*, 63:133-152.

Chave, A., 1984. Lower Paleocene-Upper Cretaceous magnetostratigraphy, Sites 525, 527, 528, and 529, Deep Sea Drilling Project Leg 74. *In* Moore, T. C., Jr. Rabinowitz, P. D., et al., *Init. Repts. DSDP*, 74: Washington (U.S. Govt. Printing Office), 525-531.

Emilia, D. A., and Heinrichs, D. F., 1972. Palaeomagnetic events in the Brunhes and Matuyama epochs identified from magnetic profiles reduced to the pole. *Mar. Geophys. Res.*, 1:436-444.

Epp, D., 1978. Age and tectonic relationship among volcanic chains on the Pacific plate. [Ph. D. dissert.]. University of Hawaii, Honolulu.

Foster, J. H., and Opdyke, N. D., 1970. Upper Miocene to Recent magnetic stratigraphy in deep-sea sediments. *J. Geophys. Res.*, 75: 4465-4473.

Hedberg, H. D., Salvador, A., and Opdyke, N. D., 1979. Magnetostratigraphic polarity units—A supplement chapter of the ISSC International Stratigraphic Guide. *Geology*, 7:578-583.

Heirtzler, J. R., Dickson, G. O., Herron, E. M., Pitman, W. C., III, and Le Pichon, X., 1968. Marine magnetic anomalies, geomagnetic field reversals and motions of the ocean floor and continents. *J. Geophys. Res.*, 73:2119-2136.

Hoffman, K. A., and Day, R., 1978. Separation of multi-component NRM, a general method. *Earth Planet. Sci. Lett.*, 40:433-438.

Hsü, K. J., He, Q., McKenzie, J. A., Weissert, H., Perch-Nielsen, K., Oberhänsli, H., Kelts, K., LaBrecque, J., Tauxe, L., Krähenbühl, U., Percival, S. F., Jr., Wright, R., Karpoff, A. M., Petersen, N., Tucker, P., Poore, R. Z., Gombos, A. M., Pisciotto, K., Carman, M. F., Jr., and Schreiber, E., 1982. Mass mortality and its environmental and evolutionary consequences. *Science*, 216:249-256.

Kent, D. V., and Lowrie, W., 1974. Origin of magnetic instability in sediment cores from the central north Pacific. *J. Geophys. Res.*, 79:2987-3000.

Kent, D. V., and Spariosu, D. J., 1982a. Magnetostratigraphy of Caribean Site 502 hydraulic piston cores. *In* Prell, W. L., Gardner, J. V., et al., *Init. Repts. DSDP*, 68: Washington (U.S. Govt. Printing Office), 419-433.

________, 1982b. Magnetostratigraphy of equatorial Pacific Site 503 hydraulic piston cores. *In* Prell, W. L., Gardner, J. V., et al., *Init. Repts. DSDP*, 68: Washington (U.S. Govt. Printing Office), 435-440.

Kono, M., 1980. Statistics of paleomagnetic inclination data. *J. Geophys. Res.*, 85:3878-3882.

LaBrecque, J. L., Kent, D. V., and Cande, S. C., 1977. Revised magnetic polarity time scale for Late Cretaceous and Cenozoic time. *Geology*, 5:330-335.

McDougall, I., 1977. The present status of the geomagnetic polarity time scale. Research School of Earth Sciences, A.N.U., Publ. No. 1288.

McDougall, I., and Watkins, N. D., 1973. Age and duration of the Réunion geomagnetic polarity event. *Earth Planet. Sci. Lett.*, 19: 443-452.

Opdyke, N. D., 1972. Paleomagnetism of deep-sea cores. *Rev. Geophys. Space Phys.*, 10:213-249.

Pierce, J. W., 1976. Assessing the reliability of DSDP paleolatitudes. *J. Geophys. Res.*, 81:4173-4187.

Prince, R. A., Heath, G. R., and Kominz, M., 1980. Paleomagnetic studies of central North Pacific sediment cores: Stratigraphy, sedimentation rates, and the origin of magnetic instability. *Geol. Soc. Am. Bull.*, 91(Part II):1789-1835.

Shackleton, N. J., and Shipboard Scientific Party, 1984. Accumulation rates in Leg 74 sediments. *In* Moore, T. C., Jr., Rabinowitz, P. D., et al., *Init. Repts. DSDP*, 74: Washington (U.S. Govt. Printing Office), 621-644.

Tauxe, L., Tucker, P., Petersen, N., and LaBrecque, J. L., 1984. Magnetostratigraphy of Leg 73 sediments. *In* Hsü, K. J., LaBrecque, J. L., et al., *Init. Repts. DSDP*, 73: Washington (U.S. Govt. Printing Office), 609-622.

Thierstein, H. R., 1982. Terminal Cretaceous plankton extinction: A critical assessment. *Geol. Soc. Am. Spec. Pap.*, 190:385-399.

Weinreich, N., and Theyer, F., in press. Paleomagnetism of the Leg 85 sediments: Neogene magnetostratigraphy and tectonic history of the Central Equatorial Pacific. *In* Mayer, L., Theyer, F., et al., *Init. Repts. DSDP*, 85: Washington (U.S. Govt. Printing Office).

Zijderveld, J. D. A., 1967. A.C. demagnetization of rocks: analysis of results. *In* Collison, D. W., Creer, K. M., and Runcorn, S. K. (Eds.) *Methods in Palaeomagnetism*: Amsterdam (Elsevier), pp. 254-286

Date of Initial Receipt: 3 January 1984
Date of Acceptance: 18 June 1984

18. PALEOMAGNETISM AND ACCUMULATION RATES OF SEDIMENTS AT SITES 576 AND 578, DEEP SEA DRILLING PROJECT LEG 86, WESTERN NORTH PACIFIC[1]

G. Ross Heath, Donna H. Rea, and Shaul Levi, Oregon State University[2]

ABSTRACT

The upper sections of Deep Sea Drilling Project Sites 576 (32°21.4′N, 164°16.5′E) and 578 (33°55.6′N, 151°37.7′E) both have stable detrital remanence that can be correlated with the standard reversal stratigraphy. Site 576 contains all reversals above the base of the Gilbert Epoch (5 m.y.) at about 25 m, whereas Site 578 contains a remarkable section of about 60 reversals extending to Anomaly 5B (15 m.y.) at about 150 m sub-bottom depth. In both cases, the paleomagnetic stratigraphy breaks down when accumulation rates drop below 2 m/m.y. At both sites, authigenic manganiferous clays deposited from 70 to 16 m.y. ago accumulated at about 0.4 m/m.y. Similarly, at both sites, the Pleistocene pulse of eolian debris increased accumulation rates by about 6 m/m.y.^{2}. From 16 to 2 m.y. ago, however, sediment accumulated at Site 578 about five times as rapidly as at Site 576, apparently because of augmented input to the western site by bottom currents.

INTRODUCTION

Geologic Setting

Prior paleomagnetic studies of the sediments in the vicinity of Deep Sea Drilling Project (DSDP) Site 576, based on piston cores collected during cruise *Vema*-36 (Barton and Sopher, 1982), have shown that deposition has been extremely uniform (core to core variations in sedimentation rates are only about 6% over 10,000 km^2). In contrast, Site 578 lies close to an east/west boundary across which there is a several-fold increase in sedimentation rate from south to north (Jacobi et al., this volume). Because of the stable remanence of the *Vema*-36 samples and the generally poor preservation of siliceous microfossils, we anticipated that dating of the Leg 86 sections would depend heavily on paleomagnetic stratigraphy. In addition, we were interested in the degree to which the paleomagnetic results from giant piston core LL44-GPC-3, taken north of Hawaii (Fig. 1; Prince et al., 1980) would resemble those at the lithologically similar Site 576, some 40° of longitude to the west.

The lithology of the Site 576 sediments is relatively mple. Above 27 m, the section is dominated by yellow-own pelagic clay rich in quartz (Leinen, this volume). is clay is terrigenous debris derived from Asia and rried to the site by upper atmosphere westerlies (Jane-k, this volume). Similar material dominates late Ceno-ic pelagic clays across the Pacific (Leinen and Heath, 81; Moore and Heath, 1978).

The sediments between 27 and 56 m are very dark own "slick" clays depleted in quartz and enriched in romanganese oxyhydroxides. These clays accumulated ry slowly (less than 1 m/m.y.; Doyle and Riedel, this lume) and are dominated by authigenic components licates as well as oxyhydroxides). Below 56 m, the clays are interbedded with carbonate ooze derived either from fluctuations in the width of the Late Cretaceous equatorial carbonate zone or from turbidites originating on nearby topographic highs.

The deeper part of the section at Site 578 is comparable to Site 576. Above 77 m, however, the section consists of gray green clay with variable amounts of biogenic silica and numerous thin layers of volcanic ash and dark greenish gray indurated clay that may be altered basic ash. These sediments are reduced (authigenic pyrite is common) and are richer in organic carbon than are the Site 576 deposits.

The yellow-brown clays analogous to the surficial deposits at Site 576 extend from 77 to 125 m. The dark brown "slick" clays complete the section from 125 to 176 m, terminating against chert overlain by a few silicified foraminifers. Unlike Site 576, the basal sediments are not calcareous, suggesting that at Site 578, biogenic sediments (now silicified to chert) gave way abruptly to pelagic clay.

Methodology

Magnetic samples were taken at 10- or 20-cm intervals in visually undisturbed sections of core using a new sampling system designed by R. Karlin. This sampler produces strikingly less disturbance of the magnetic samples and of the surrounding sediment left behind in the core, particularly in stiff clays, than does the conventional technique of pressing 2 × 2 × 2 cm plastic boxes into the split sediment surface. Each sample was extracted from the core with a thin-walled, sharpened, 2 × 2 cm stainless-steel tube. The bottom of the resultant square sample was trimmed of disturbed sediment and extruded into a standard 2 × 2 × 2 cm plastic cube by means of a tightly fitting plastic piston. The cube was trimmed to a flat surface and capped. Sample cubes were grouped into packages of 50, each package being individually wrapped in Saran® wrap, then seawater-saturated paper toweling, then another layer of Saran® wrap to minimize water loss. Packages were shipped back to

---

[1] Heath, G. R. Burckle, L. H., et al., *Init. Repts. DSDP*, 86: Washington (U.S. Govt. nting Office).

[2] Address: (Heath) College of Ocean and Fishery Sciences, University of Washington, attle, WA 98195; (Rea, Levi) College of Oceanography, Oregon State University, Corvallis, R 97331.

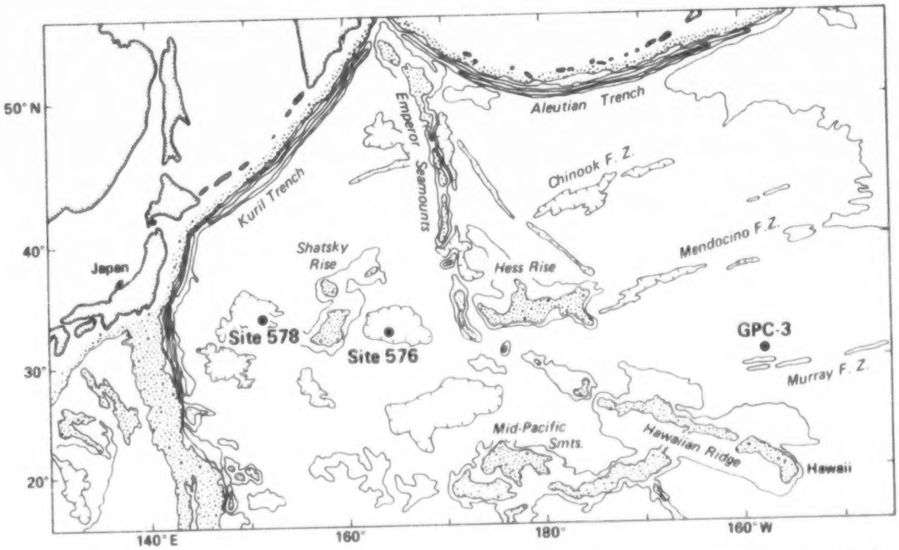

Figure 1. Location of Sites 576 and 578 and giant piston core LL44-GPC-3 relative to the generalized bathymetry of the western North Pacific (after Chase, 1975). Areas shallower than 4 km stippled; 5 km contour plain; 6 km contour hachured.

Oregon State University in carrying cases lined with mu-metal to minimize exposure to extraneous magnetic fields.

Samples were weighed wet (for later water-content determinations) before being subjected to paleomagnetic analysis on a Digico magnetometer. Most samples were run for natural remanent magnetization (NRM), and again after alternating field (AF) demagnetization at 100 and 200 Oe. Where the remanence appeared unstable, additional measurements at higher demagnetization levels (up to 800 Oe in some cases) were taken in an effort to characterize the original detrital remanence. The reported inclinations and declinations are based on the 100-Oe data, or on vector averages of higher demagnetization levels, depending on the behavior of intensities and directions as a function of demagnetization intensity.

RESULTS

Site 576

Tables 1 to 4 list the magnetic data for Holes 576 and 576B. Figure 2 and Table 5 show the polarity profile based on the combined results, versus the latest standard polarity scale of Berggren et al. (in press). The reversal stratigraphy is interpretable through most of the Gilbert Epoch, the base of the Thvera Event being the last reliable boundary.

Most of the reversals were picked on the basis of the inclination data, although confirmed by 180° declination changes. The absolute declinations are unknown because of difficulties with the shipboard core-orienting device and rotation of the hydraulic piston core (HPC) barrel as it is driven ahead of the bit (Fig. 3).

A much more serious problem in constructing Figure 2 arose from the depth discrepancies and the condition of HPC cores from Holes 576 and 576B. The alignment of lithologic as well as magnetic boundaries suggests that Cores 576-2 and 576-3 sampled the same interval and that the top 4 m in Hole 576B was not recovered in Hole 576 (see Site 576 chapter, this volume). In addition, the normally magnetized intervals below the Kaena and Mammoth events are repeated in Core 576B-3, suggesting that the HPC "bounced" while sampling this interval. Such an occurrence, like the presence of "flow-in" structures in some of the cores, is indicative of significant piston motion as the HPC penetrated the sediment. We estimate that about 20% of the core recovered is so deformed as to be stratigraphically suspect. Based on the magnetic and lithologic correlations between Holes 576 and 576B, however, we believe that the composite section of Figure 2 approaches the *in situ* stratigraphy. There is some residual uncertainty about the thickness of the reversed section between the Olduvai Event and the base of the Matuyama Epoch (due to a small interval that lies in the gap between Cores 576-2 and 576-4 and in a disturbed section of Core 576B-2).

Based on the radiolarian stratigraphy (Morley, this volume), neither hole recovered the surficial sediments. The core-top age of 280,000 yr. (Core 576B-1), obtained by extrapolating the polarity stratigraphy (Fig. 2), agrees well with Morley's estimate of 200,000–300,000 yr.

Below 25 m, the reversal stratigraphy becomes uninterpretable. At this depth, the lithology changes from brown to very dark brown clay, and the sedimentation rate drops below 1 m/m.y. The average J_{100}/J_0 value also decreases abruptly (Fig. 4), suggesting that the ratio of magnetically unstable authigenic oxyhydroxides to stable detrital magnetic minerals has become so large that the detrital remanence is submerged in the "noise" of chemical remanence. A similar breakdown in stable remanence at this lithologic boundary has been recorded in other North Pacific cores (Opdyke and Foster, 1970; Kent and Lowrie, 1974; Prince et al., 1980).

The NRM profile (Fig. 4) is noisy at all depths, with a tendency to higher values below about 29 m and more

Table 1. Magnetic properties of samples from Hole 576.

Sample	Core	Section	Depth in Section (cm)	Depth in Hole (cm)	Declination (deg)	Inclination (deg)	NRM (emu)	J_{100} (emu)	J_{100}/J_0	J_{200} (emu)	J_{200}/J_0	Note
1	1	1	11	415	299	58	0.4230E-04	0.3750E-04	0.887	0.3193E-04	0.755	A1-2
3	1	1	31	435	322	49	0.3368E-04	0.2584E-04	0.767	0.2353E-04	0.699	A1-2
5	1	1	51	455	301	53	0.2309E-04	0.2153E-04	0.932	0.1843E-04	0.798	A1-2
6	1	1	61	465	292	46	0.3882E-04	0.2892E-04	0.745	0.3160E-04	0.814	A1-4
7	1	1	71	475	300	58	0.4271E-04	0.3785E-04	0.886	0.3269E-04	0.765	A1-2
9	1	1	91	495	277	57	0.3416E-04	0.2769E-04	0.811	0.2254E-04	0.660	A1-2
1	1	1	111	515	305	48	0.2838E-04	0.2542E-04	0.896	0.2078E-04	0.732	A1-2
3	1	1	131	535	300	56	0.3474E-04	0.3488E-04	1.004	0.2855E-04	0.822	A1-2
4	1	1	141	545	300	58	0.4269E-04	0.3895E-04	0.912	0.3424E-04	0.802	A1-2
5	1	2	6	555	298	-24	0.5103E-04	0.4962E-04	0.972	0.3957E-04	0.776	A1-2
6	1	2	16	565	313	66	0.4576E-04	0.3802E-04	0.831	0.3414E-04	0.746	A1-2
7	1	2	22	575	330	60	0.4128E-04	0.3667E-04	0.888	0.3102E-04	0.751	A1-2
9	1	2	41	595	310	68	0.3731E-04	0.3434E-04	0.920	0.2829E-04	0.758	A1-2
1	1	2	61	615	360	62	0.3926E-04	0.3524E-04	0.897	0.3011E-04	0.767	A1-2
3	1	2	81	635	3	62	0.5004E-04	0.4405E-04	0.880	0.3716E-04	0.743	A1-2
4	1	2	91	645	33	63	0.4049E-04	0.3579E-04	0.884	0.2935E-04	0.725	A1-2
26	1	2	101	655	40	66	0.1771E-04	0.1446E-04	0.816	0.1215E-04	0.686	A1-3
5	1	*	7	668	186	-35	0.2550E-04	0.1928E-04	0.756	0.1476E-04	0.579	A1-2
27	2	1	6	701	263	-54	0.1146E-04	0.1382E-04	1.206	0.1246E-04	1.088	A1-2
29	2	1	26	721	297	-56	0.1599E-04	0.2161E-04	1.351	0.1818E-04	1.137	A1-2
31	2	1	46	741	339	-42	0.2154E-04	0.2321E-04	1.078	0.1857E-04	0.862	A1-2
33	2	1	66	761	21	-53	0.1397E-04	0.1635E-04	1.170	0.1383E-04	0.990	A1-2
35	2	1	86	781	30	-50	0.1191E-04	0.1252E-04	1.051	0.1037E-04	0.871	A1-2
36	2	1	96	791	47	-51	0.2534E-04	0.2473E-04	0.976	0.2016E-04	0.796	A1-4
37	2	1	106	801	44	-47	0.2758E-04	0.2896E-04	1.050	0.2484E-04	0.901	A1-2
39	2	1	126	821	65	-53	0.1371E-04	0.1548E-04	1.129	0.1408E-04	1.027	A1-2
41	2	1	146	841	68	-52	0.2097E-04	0.2631E-04	1.254	0.2079E-04	0.991	A1-2
43	2	2	16	861	97	-51	0.2348E-04	0.2940E-04	1.252	0.2628E-04	1.119	A1-2
44	2	2	26	871	99	-51	0.1848E-04	0.1897E-04	1.026	0.1587E-04	0.859	A1-2
45	2	2	36	881	263	19	0.6239E-05	0.1639E-05	0.263	0.1123E-05	0.180	L3
46	2	2	46	891	292	47	0.1105E-04	0.8203E-05	0.742	0.5910E-05	0.535	A1-2
47	2	2	56	901	273	53	0.2331E-04	0.1953E-04	0.838	0.1553E-04	0.666	A1-2
49	2	2	76	921	278	54	0.2681E-04	0.2425E-04	0.904	0.2130E-04	0.794	A1-4
51	2	2	96	941	302	54	0.4001E-04	0.3572E-04	0.893	0.2886E-04	0.721	A1-2
53	2	2	116	961	267	-38	0.2869E-05	0.6663E-06	0.232	0.5597E-06	0.194	A3-4
55	2	2	136	981	143	-57	0.1954E-04	0.2169E-04	1.110	0.1744E-04	0.893	A1-2
57	2	3	6	1001	163	-53	0.1966E-04	0.2029E-04	1.032	0.1705E-04	0.868	A1-2
59	2	3	26	1021	158	-45	0.2738E-04	0.2710E-04	0.990	0.2090E-04	0.763	A1-2
61	2	3	46	1041	172	-52	0.2014E-04	0.2078E-04	1.032	0.1792E-04	0.890	A1-2
63	2	3	66	1061	173	-65	0.1663E-04	0.1853E-04	1.115	0.1531E-04	0.921	A1-2
65	2	3	86	1081	183	-49	0.1428E-04	0.1609E-04	1.126	0.1311E-04	0.918	A1-2
67	2	3	106	1101	174	-50	0.1109E-04	0.1149E-04	1.037	0.1006E-04	0.907	A1-2
9	2	3	126	1121	171	-49	0.2528E-04	0.2484E-04	0.982	0.2173E-04	0.860	A1-2
1	2	3	146	1141	196	-59	0.2699E-04	0.2627E-04	0.973	0.2315E-04	0.858	A1-2
3	2	4	16	1161	166	-43	0.2324E-04	0.2224E-04	0.957	0.1925E-04	0.828	A1-2
5	2	4	36	1181	170	-51	0.3210E-04	0.3216E-04	1.002	0.2697E-04	0.840	A1-2
7	2	4	56	1201	171	-53	0.1760E-04	0.1838E-04	1.044	0.1541E-04	0.875	A1-2
9	2	4	76	1221	177	-49	0.2970E-04	0.2775E-04	0.934	0.2457E-04	0.827	A1-2
1	2	4	96	1241	180	-56	0.2503E-04	0.2525E-04	1.009	0.2141E-04	0.855	A1-2
3	2	4	116	1261	182	-48	0.2596E-04	0.2720E-04	1.048	0.1986E-04	0.765	A1-2
5	2	4	136	1281	174	-50	0.1689E-04	0.1946E-04	1.152	0.1533E-04	0.907	A1-2
7	2	5	6	1301	172	-46	0.2641E-04	0.2578E-04	0.977	0.2275E-04	0.862	A1-2
9	2	5	26	1321	168	-59	0.2302E-04	0.2427E-04	1.054	0.2055E-04	0.892	A1-2
1	2	5	46	1341	156	-48	0.1699E-04	0.1856E-04	1.092	0.1477E-04	0.869	A1-2
3	2	5	66	1361	159	-51	0.2477E-04	0.2514E-04	1.015	0.2028E-04	0.819	A1-2
5	2	5	86	1381	158	-59	0.1651E-04	0.1850E-04	1.121	0.1448E-04	0.877	A1-2
6	2	5	96	1391	162	-67	0.1218E-04	0.1443E-04	1.185	0.1066E-04	0.875	A1-2
7	2	5	106	1401	287	-69	0.7365E-05	0.1077E-04	1.463	0.8607E-05	1.169	A1-2
8	2	5	116	1411	289	-71	0.2168E-04	0.2138E-04	0.986	0.1733E-04	0.799	A1-2
99	2	5	126	1421	154	-67	0.2143E-04	0.2139E-04	0.998	0.1799E-04	0.840	A1-3

Table 1. (Continued).

Sample	Core	Section	Depth in Section (cm)	Depth in Hole (cm)	Declination (deg)	Inclination (deg)	NRM (emu)	J_{100} (emu)	J_{100}/J_0	J_{200} (emu)	J_{200}/J_0	Note
101	2	5	146	1441	185	-84	0.2224E-04	0.1966E-04	0.884	0.1736E-04	0.781	A1-4
102	2	6	6	1451	249	-68	0.2032E-04	0.2167E-04	1.066	0.1792E-04	0.882	A1-2
103	2	6	16	1461	75	-79	0.2178E-04	0.2120E-04	0.973	0.1739E-04	0.798	A1-3
104	2	6	26	1471	13	-61	0.2460E-04	0.2551E-04	1.037	0.2191E-04	0.891	A1-2
105	2	6	36	1481	254	-43	0.1296E-04	0.1201E-04	0.927	0.1035E-04	0.799	A1-2
106	2	6	46	1491	6	29	0.5678E-05	0.3672E-05	0.647	0.2996E-05	0.528	A1-2
107	2	6	56	1501	343	38	0.5924E-05	0.5729E-05	0.967	0.3919E-05	0.662	A1-2
108	2	6	66	1511	4	34	0.4720E-05	0.4060E-05	0.860	0.2946E-05	0.624	A1-2
109	2	6	76	1521	22	14	0.3792E-05	0.4242E-05	1.119	0.3337E-05	0.880	A1-3
110	2	6	86	1531	20	-20	0.1421E-04	0.1262E-04	0.888	0.9781E-05	0.688	A1-3
111	2	6	96	1541	6	28	0.1448E-04	0.1215E-04	0.839	0.9639E-05	0.666	A1-3
113	2	6	116	1561	329	19	0.9358E-05	0.8217E-05	0.878	0.7149E-05	0.764	A1-3
114	2	6	126	1571	335	19	0.5845E-05	0.5615E-05	0.961	0.3800E-05	0.650	A1-4
115	2	6	136	1581	32	51	0.9028E-05	0.6818E-05	0.755	0.5357E-05	0.593	A1-2
117	2	7	6	1601	352	45	0.1968E-05	0.8114E-06	0.412	0.2353E-06	0.120	A1-2
118	2	7	16	1611	185	-53	0.6332E-05	0.7110E-05	1.123	0.6297E-05	0.994	A1-2
119	2	7	26	1621	198	-56	0.7243E-05	0.6263E-05	0.865	0.3012E-05	0.416	A1-2
121	2	7	46	1641	153	-24	0.2754E-05	0.2717E-05	0.098	0.2156E-05	0.076	A1-2
123	3	1	36	1021	288	-58	0.6702E-05	0.7439E-05	1.110	0.6139E-05	0.916	A1-2
125	3	1	56	1041	285	-49	0.1256E-04	0.2136E-04	1.701	0.2377E-04	1.893	A1-2
127	3	1	76	1061	291	-45	0.6494E-05	0.1676E-04	2.582	0.1343E-04	2.068	A1-2
129	3	1	96	1081	281	-62	0.6616E-05	0.9555E-05	1.444	0.7800E-05	1.179	A1-2
131	3	1	116	1101	278	-38	0.7595E-05	0.1097E-04	1.444	0.8743E-05	1.151	A1-2
133	3	1	136	1121	281	-50	0.2430E-04	0.2407E-04	0.991	0.1989E-04	0.818	A1-2
135	3	2	6	1141	311	-46	0.2001E-04	0.2085E-04	1.042	0.1888E-04	0.944	A1-2
137	3	2	26	1161	296	-57	0.2485E-04	0.2500E-04	1.006	0.2058E-04	0.828	A1-2
139	3	2	46	1181	296	-52	0.2369E-04	0.2498E-04	1.054	0.2210E-04	0.933	A1-2
141	3	2	66	1201	284	-48	0.2149E-04	0.2268E-04	1.055	0.1729E-04	0.804	A1-2
143	3	2	86	1221	291	-47	0.2528E-04	0.2862E-04	1.132	0.2192E-04	0.867	A1-2
145	3	2	106	1241	291	-54	0.1870E-04	0.1957E-04	1.047	0.1581E-04	0.845	A1-2
147	3	2	126	1261	281	-42	0.1428E-04	0.1431E-04	1.003	0.1286E-04	0.901	A1-2
149	3	2	146	1281	261	-58	0.2827E-04	0.2562E-04	0.906	0.2274E-04	0.804	A1-2
151	3	3	16	1301	288	-46	0.2253E-04	0.2372E-04	1.053	0.1883E-04	0.836	A1-2
153	3	3	36	1321	276	-48	0.2109E-04	0.2098E-04	0.995	0.1740E-04	0.825	A1-2
155	3	3	56	1341	268	-57	0.7469E-05	0.1003E-04	1.343	0.7404E-05	0.991	A1-2
157	3	3	76	1361	299	-46	0.1794E-04	0.1956E-04	1.090	0.1515E-04	0.844	A1-2
159	3	3	96	1381	271	-47	0.1753E-04	0.1999E-04	1.140	0.1584E-04	0.904	A1-2
161	3	3	116	1401	275	-50	0.1284E-04	0.1509E-04	1.175	0.1207E-04	0.940	A1-2
163	3	3	136	1421	273	-43	0.1145E-04	0.1195E-04	1.044	0.1064E-04	0.929	A1-2
165	3	4	6	1441	284	-51	0.2897E-04	0.2705E-04	0.934	0.2599E-04	0.897	A1-2
167	3	4	26	1461	273	-53	0.2879E-04	0.2950E-04	1.024	0.2461E-04	0.855	A1-2
169	3	4	56	1491	290	-53	0.1133E-04	0.1379E-04	1.217	0.1078E-04	0.951	A1-2
171	3	4	76	1511	108	42	0.2170E-04	0.1729E-04	0.797	0.1243E-04	0.573	A1-2
173	3	4	46	1481	284	-57	0.1582E-04	0.1582E-04	1.000	0.1309E-04	0.827	A1-2
175	3	4	106	1541	100	56	0.2849E-04	0.2340E-04	0.821	0.1776E-04	0.623	A1-2
177	3	4	126	1561	106	50	0.3383E-04	0.2742E-04	0.811	0.2310E-04	0.683	A1-2
179	3	4	146	1581	162	40	0.5520E-05	0.8473E-06	0.154	0.4673E-06	0.085	A1-3
181	3	5	16	1601	281	-54	0.1680E-04	0.1852E-04	1.102	0.1589E-04	0.946	A1-2
183	3	*	6	1623	187	-68	0.1342E-04	0.1490E-04	1.111	0.1166E-04	0.869	A1-2
185	3	*	26	1643	190	-66	0.2706E-04	0.2808E-04	1.038	0.2276E-04	0.841	A1-2
186	4	1	6				0.9634E-05	0.6745E-05	0.700	0.5242E-05	0.544	F
187	4	1	16				0.1172E-04	0.8100E-05	0.691	0.6435E-05	0.549	F
188	4	1	26				0.1736E-04	0.1196E-04	0.689	0.8915E-05	0.514	F
189	4	1	76	1856			0.6859E-05	0.4927E-05	0.718	0.3259E-05	0.475	U
190	4	1	86	1866	152	38	0.1306E-04	0.5822E-05	0.446	0.4637E-05	0.355	A1-2
191	4	1	96	1876	152	58	0.3089E-04	0.1915E-04	0.620	0.1481E-04	0.479	A1-2
192	4	1	106	1886	146	51	0.3843E-04	0.2746E-04	0.715	0.1952E-04	0.508	A1-4
193	4	1	116	1896	146	55	0.2768E-04	0.2053E-04	0.742	0.1586E-04	0.573	A1-2
194	4	1	126	1906	155	56	0.21100-04	0.13500-04	0.639	0.10100-04	0.478	A1-2
195	4	1	136	1916	143	54	0.2888E-04	0.1922E-04	0.665	0.1410E-04	0.488	A1-2

Table 1. (Continued).

Sample	Core	Section	Depth in Section (cm)	Depth in Hole (cm)	Declination (deg)	Inclination (deg)	NRM (emu)	J_{100} (emu)	J_{100}/J_0	J_{200} (emu)	J_{200}/J_0	Note
196	4	1	146	1926	211	-54	0.3501E-04	0.2311E-04	0.660	0.1693E-04	0.484	A1-3
97	4	2	5	1935	148	56	0.3125E-04	0.2284E-04	0.731	0.1657E-04	0.530	A1-2
198	4	2	16	1946	151	55	0.3050E-04	0.1868E-04	0.612	0.1340E-04	0.439	A1-2
99	4	2	26	1956	154	52	0.3490E-04	0.2103E-04	0.603	0.1454E-04	0.417	A1-2
00	4	2	36	1966	150	48	0.3636E-04	0.2664E-04	0.733	0.1837E-04	0.505	A1-2
01	4	2	46	1976	149	55	0.3557E-04	0.2171E-04	0.610	0.1592E-04	0.447	A1-2
02	4	2	56	1986	341	-49	0.6369E-05	0.8841E-05	1.388	0.7515E-05	1.180	A1-2
03	4	2	66	1996	324	-39	0.2436E-05	0.9928E-05	4.076	0.7875E-05	3.233	A1-2
04	4	2	76	2006	305	-58	0.6574E-05	0.1216E-04	1.850	0.1046E-04	1.591	A1-2
05	4	2	86	2016	157	47	0.2272E-04	0.1103E-04	0.486	0.6830E-05	0.301	A1-2
06	4	2	96	2026	151	54	0.2405E-04	0.1227E-04	0.510	0.8846E-05	0.368	A1-2
07	4	2	106	2036	210	-49	0.2257E-04	0.1092E-04	0.484	0.7020E-05	0.311	A1-2
08	4	2	116	2046	343	-44	0.6619E-05	0.2276E-05	0.344	0.2285E-05	0.345	A1-2
09	4	2	126	2056	334	-59	0.4080E-05	0.1040E-04	2.549	0.7921E-05	1.941	A1-2
10	4	2	136	2066	347	-54	0.5506E-05	0.3833E-05	0.696	0.3293E-05	0.598	A1-2
11	4	2	146	2076	158	47	0.1404E-04	0.2948E-05	0.210	0.2137E-05	0.152	A1-2
212	4	3	6	2086	169	45	0.3105E-04	0.1817E-04	0.585	0.1303E-04	0.420	A1-2
213	4	3	16	2096	163	51	0.2662E-04	0.1681E-04	0.631	0.1244E-04	0.467	A1-2
14	4	3	26	2106	171	48	0.3024E-04	0.1541E-04	0.510	0.1088E-04	0.360	A1-2
215	4	3	36	2116	165	54		0.1710E-04		0.1140E-04		A1-4
216	4	3	46	2126	163	52	0.3315E-04	0.2047E-04	0.617	0.1452E-04	0.438	A1-2
217	4	3	56	2136	187	61	0.1248E-04	0.5346E-05	0.428	0.3171E-05	0.254	A1-2
218	4	3	66	2146	348	-47	0.2933E-05	0.6702E-05	2.285	0.5799E-05	1.977	A1-2
219	4	3	76	2156	7	51	0.2546E-05	0.7828E-05	3.074	0.6733E-05	2.644	A1-6
220	4	3	86	2166	345	-52	0.3696E-05	0.1145E-04	3.098	0.9502E-05	2.571	A1-2
221	4	3	96	2176	354	-55	0.6523E-05	0.1544E-04	2.367	0.1260E-04	1.938	A1-5
222	4	3	106	2186	348	-57	0.5785E-05	0.1478E-04	2.555	0.1156E-04	1.998	A1-2
223	4	3	116	2196	339	-48	0.3430E-05	0.1190E-04	3.465	0.9210E-05	2.685	A1-2
224	4	3	126	2206	353	-54	0.1057E-04	0.1896E-04	1.793	0.1440E-04	1.362	A1-2
225	4	3	136	2216	338	-54	0.5295E-05	0.1374E-04	2.596	0.1036E-04	1.957	A1-2
226	4	3	146	2226	353	-55	0.1046E-04	0.1750E-04	1.673	0.1270E-04	1.214	A1-2
227	4	4	6	2236	333	-55	0.3953E-05	0.1127E-04	2.851	0.9036E-05	2.286	A1-2
228	4	4	16	2246	339	-54	0.9072E-05	0.1442E-04	1.590	0.1062E-04	1.171	A1-2
229	4	4	26	2256	343	-54	0.2693E-05	0.1048E-04	3.892	0.7503E-05	2.787	A1-2
230	4	4	36	2266	338	-56	0.5151E-05	0.1200E-04	2.329	0.9650E-05	1.873	A1-2
231	4	4	46	2276	187	54	0.1424E-04	0.4159E-05	0.292	0.2403E-05	0.169	A1-2
232	4	4	56	2286	164	57	0.1982E-04	0.6372E-05	0.322	0.4415E-05	0.223	A1-2
233	4	4	66	2296	314	-54	0.6774E-05	0.5122E-05	0.756	0.4154E-05	0.613	A1-2
234	4	4	76	2306	350	-61	0.7140E-05	0.6034E-05	0.845	0.4683E-05	0.656	A1-2
235	4	4	86	2316	339	-56	0.4620E-05	0.6371E-05	1.379	0.4772E-05	1.033	A1-2
236	4	4	96	2326	351	-59	0.5325E-05	0.1091E-04	2.048	0.9025E-05	1.695	A1-2
237	4	4	106	2336	182	50	0.1510E-04	0.3310E-05	0.220	0.2470E-05	0.164	A1-2
238	4	4	116	2346	174	57	0.2218E-04	0.1051E-04	0.474	0.7074E-05	0.319	A1-2
39	4	4	126	2356	336	-56	0.3885E-05	0.3880E-05	0.999	0.3063E-05	0.788	A1-2
40	4	4	136	2366	354	-57	0.2981E-05	0.8204E-05	2.753	0.6701E-05	2.248	A1-2
41	4	4	146	2376	308	- 4	0.2554E-05	0.1005E-04	3.935	0.7620E-05	2.983	L5
42	4	5	6	2386	355	-52	0.6994E-05	0.3390E-05	0.485	0.3337E-05	0.477	A1-2
43	4	5	16	2396	182	47	0.1863E-04	0.8131E-05	0.436	0.5263E-05	0.283	A1-2
44	4	5	26	2406	361	-44	0.6492E-05	0.7039E-05	1.084	0.5456E-05	0.840	A1-2
45	4	5	36	2416	356	-53	0.1844E-05	0.9002E-05	4.881	0.6547E-05	3.550	A1-2
46	4	5	46	2426	354	-58	0.9185E-05	0.5570E-05	0.606	0.4489E-05	0.489	A1-2
47	4	5	56	2436	177	51	0.2542E-04	0.1321E-04	0.520	0.9302E-05	0.366	A1-2
48	4	5	66	2446	175	57	0.2300E-04	0.1023E-04	0.445	0.7020E-05	0.305	A1-2
49	4	5	76	2456	174	52	0.1862E-04	0.8785E-05	0.472	0.5941E-05	0.319	A1-2
50	4	5	86	2466	185	52	0.2713E-04	0.1023E-04	0.377	0.6835E-05	0.252	A1-2
51	4	5	96	2476	338	-68	0.7109E-05	0.3792E-05	0.533	0.2859E-05	0.402	A1-2
52	4	5	106	2486	304	- 3	0.5865E-05	0.4772E-05	0.814	0.3833E-05	0.654	A1-2
253	4	5	116	2496	5	-53	0.6473E-05	0.3784E-05	0.585	0.2994E-05	0.462	A1-2
254	4	5	126	2506	3	-52	0.5017E-05	0.1350E-04	2.692	0.9285E-05	1.851	A1-2
255	4	5	136	2516	3	-54	0.4274E-05	0.1013E-04	2.370	0.8197E-05	1.918	A1-2

READEX FICHE

Table 1. (Continued).

Sample	Core	Section	Depth in Section (cm)	Depth in Hole (cm)	Declination (deg)	Inclination (deg)	NRM (emu)	J_{100} (emu)	J_{100}/J_0	J_{200} (emu)	J_{200}/J_0	Note
256	4	5	146	2526	360	-52	0.6473E-05	0.8143E-05	1.258	0.7055E-05	1.090	A1-2
257	4	6	6	2536	341	-53	0.4195E-05	0.8681E-05	2.070	0.6251E-05	1.490	A1-2
258	4	6	16	2546	349	-53	0.7811E-05	0.1071E-04	1.371	0.8373E-05	1.072	A1-3
259	4	6	26	2556	351	-50	0.3809E-05	0.1025E-04	2.692	0.7322E-05	1.922	A1-2
260	4	6	36	2566	350	-48	0.7718E-05	0.1255E-04	1.626	0.9998E-05	1.295	A1-2
261	4	6	46	2576	333	-21	0.1197E-04	0.9133E-05	0.763	0.6255E-05	0.523	A1-2
262	4	6	56	2586	353	-45	0.1070E-04	0.1026E-04	0.959	0.7739E-05	0.723	A1-3
263	4	6	66	2596	333	-30	0.1940E-04	0.4439E-05	0.229	0.3402E-05	0.175	A1-3
264	4	6	76	2606	340	-20	0.2007E-04	0.7299E-05	0.364	0.5903E-05	0.294	A1-4
265	4	6	86	2616	9	-66	0.1018E-04	0.1165E-04	1.145	0.1042E-04	1.024	A1-4
266	4	6	96	2626	335	-45	0.2680E-04	0.4657E-05	0.174	0.3894E-05	0.145	A1-3
267	4	6	106	2636	286	-38	0.2784E-04	0.1506E-05	0.054	0.1220E-05	0.044	A2-3
268	4	6	116	2646	21	-13	0.2460E-04	0.5160E-05	0.210	0.3871E-05	0.157	A1-4
269	4	6	126	2656	294	-24	0.8764E-06	0.3429E-06	0.391	0.2684E-06	0.306	L3
270	4	6	136	2666	281	-10	0.3355E-04	0.1105E-05	0.033	0.1019E-05	0.030	L3
271	4	6	146	2676	309	-48	0.2471E-05	0.1155E-06	0.047	0.1431E-06	0.058	L3
272	4	7	6	2686	282	- 7	0.3009E-04	0.4030E-05	0.134	0.2337E-05	0.078	L3
273	4	7	16	2696	265	-20	0.1983E-05	0.3099E-06	0.156	0.2335E-06	0.118	A1-3
274	4	7	26	2706	357	-40	0.2575E-04	0.1507E-05	0.059	0.1591E-05	0.062	L3
275	4	7	36	2716	275	-14	0.1873E-05	0.2403E-06	0.128	0.9944E-07	0.053	L2.5
276	4	7	46	2726	77	17		0.2343E-05		0.2260E-05		A2-4
277	5	1	36				0.2222E-04	0.1094E-04	0.492	0.7064E-05	0.318	F
278	5	1	46	2866	148	-78	0.9231E-05	0.8187E-05	0.887	0.6140E-05	0.665	A1-4
279	5	1	56	2876	243	-66	0.7358E-05	0.1463E-04	1.988	0.9413E-05	1.279	A1-2
280	5	1	66	2886	220	-69	0.1049E-04	0.1135E-04	1.082	0.7999E-05	0.763	A1-3
281	5	1	76	2896	225	-71	0.5771E-05	0.1108E-04	1.919	0.3188E-04	5.525	A1-3
282	5	1	86	2906	233	-78	0.8572E-05	0.8915E-05	1.040	0.6218E-05	0.725	A1-3
283	5	1	96	2916	228	-64	0.8385E-05	0.9506E-05	1.134	0.6085E-05	0.726	A1-2
284	5	1	106	2926	64	13	0.1837E-04	0.4820E-05	0.262	0.3260E-05	0.178	A1-3
285	5	1	116	2936	71	6	0.1356E-04	0.4475E-05	0.330	0.2375E-05	0.175	A1-4
286	5	1	126	2946	95	-37	0.1402E-04	0.2451E-05	0.175	0.1442E-05	0.103	A1.5-3
287	5	1	136	2956	87	- 4	0.1056E-04	0.2350E-05	0.223	0.1409E-05	0.133	A1-4
288	5	1	146	2966	48	3	0.1463E-04	0.3212E-05	0.220	0.2140E-05	0.146	A1-3
289	5	2	56				0.4445E-05	0.5173E-05	1.164	0.3192E-05	0.718	F
290	5	2	116				0.8428E-05	0.5912E-05	0.701	0.3551E-05	0.421	F
291	5	3	23				0.3968E-05	0.3047E-05	0.768	0.1970E-05	0.496	F
292	5	3	99				0.1196E-04	0.4016E-05	0.336	0.2296E-05	0.192	F
293	5	4	76				0.4096E-05	0.5938E-05	1.450	0.4248E-05	1.037	F
294	5	5	46				0.1002E-04	0.1023E-04	1.021	0.7204E-05	0.719	F
295	5	5	56	3166	230	-45	0.1377E-04	0.1717E-05	0.125	0.1124E-05	0.082	L2
296	5	5	66	3176	321	45	0.1507E-04	0.1925E-05	0.128	0.6429E-06	0.043	A1-2
297	5	5	76	3186	305	-50	0.1102E-04	0.9520E-06	0.086	0.4319E-06	0.039	L2
298	5	5	86	3196	352	-53	0.2570E-04	0.3604E-05	0.140	0.1510E-05	0.059	L2
299	5	5	96	3206	360	52	0.2001E-04	0.5148E-05	0.257	0.3276E-05	0.164	A1-2
300	5	5	106	3216	316	-38	0.1751E-04	0.1240E-05	0.071	0.4285E-06	0.024	L2
301	5	5	119	3229	352	43	0.3900E-04	0.4930E-05	0.126	0.2595E-05	0.067	A1-2
302	5	5	130	3240	308	- 5	0.2796E-04	0.9760E-05	0.349	0.5360E-05	0.192	A1-4
303	5	5	146	3256	4	50	0.4197E-04	0.9771E-05	0.233	0.6490E-05	0.155	A1-2
304	5	6	6	3266	330	55	0.2569E-04	0.5202E-05	0.202	0.3078E-05	0.120	A1-2
305	5	6	16	3276	287	4	0.2975E-04	0.3134E-05	0.105	0.2204E-05	0.074	L3
306	5	6	26	3286	255	14	0.2359E-04	0.3432E-05	0.145	0.2357E-05	0.100	L3
307	5	6	36	3296	352	48	0.3866E-04	0.8010E-05	0.207	0.4833E-05	0.125	A1-2
308	5	6	46	3306	305	30	0.2188E-04	0.4753E-05	0.217	0.2879E-05	0.132	L2
309	5	6	56	3316	315	-14	0.2352E-04	0.3845E-05	0.163	0.2694E-05	0.115	A3-4
310	5	6	66	3326	336	36	0.1820E-04	0.4230E-05	0.230	0.2320E-05	0.127	A1-2
311	5	6	76	3336	294	-22	0.2021E-04	0.2613E-05	0.129	0.2189E-05	0.108	L3
312	5	6	86	3346	293	- 9	0.1467E-04	0.1967E-05	0.134	0.1028E-05	0.070	L3
313	5	6	96	3356	301	26	0.2851E-04	0.3488E-05	0.122	0.1993E-05	0.070	L3
314	5	6	107	3367	265	- 9	0.1136E-04	0.1953E-05	0.172	0.1395E-05	0.123	A3-4
315	5	6	116	3376	303	21	0.2381E-04	0.3597E-05	0.151	0.2165E-05	0.091	L3

Table 1. (Continued).

Sample	Core	Section	Depth in Section (cm)	Depth in Hole (cm)	Declination (deg)	Inclination (deg)	NRM (emu)	J_{100} (emu)	J_{100}/J_0	J_{200} (emu)	J_{200}/J_0	Note
16	5	6	126	3386	346	18	0.1622E-04	0.3762E-05	0.232	0.2371E-05	0.146	A2-3
17	5	6	135	3395	339	39	0.2411E-04	0.5267E-05	0.218	0.3423E-05	0.142	L2
18	5	7	145	3405	325	38	0.1594E-04	0.4964E-05	0.311	0.2478E-05	0.155	L2
19	5	7	6	3416	305	31	0.1947E-04	0.2338E-05	0.120	0.1538E-05	0.079	L2
20	5	7	16	3426	345	39	0.1970E-04	0.3460E-05	0.176	0.1680E-05	0.085	L2
21	5	7	26	3436	296	- 6	0.2181E-04	0.2481E-05	0.114	0.2162E-05	0.099	L2
22	5	7	36	3446	342	55	0.2310E-04	0.3881E-05	0.168	0.1804E-05	0.078	A1-2
23	5	7	45	3455	295	37	0.2354E-04	0.1720E-05	0.073	0.1031E-05	0.044	A1-2
24	6	1	131				0.3565E-04	0.3462E-04	0.971	0.2303E-04	0.646	F
25	6	1	141				0.6250E-04	0.3430E-04	0.549	0.2305E-04	0.369	F
26	6	2	121				0.3568E-04	0.1145E-04	0.321	0.6468E-05	0.181	F
27	6	2	131				0.4555E-04	0.7762E-05	0.170	0.4799E-05	0.105	F
28	6	2	141				0.2656E-04	0.8816E-05	0.332	0.6023E-05	0.227	F
29	6	3	6				0.4077E-04	0.9182E-05	0.225	0.5860E-05	0.144	F
30	6	3	26				0.1941E-04	0.9594E-05	0.494	0.6622E-05	0.341	F
331	6	3	16				0.4196E-04	0.1013E-04	0.241	0.6475E-05	0.154	F
332	6	3	36				0.2396E-04	0.9235E-05	0.385	0.5967E-05	0.249	F
333	6	3	46				0.1408E-04	0.8356E-05	0.594	0.5899E-05	0.419	F
334	6	3	56				0.2239E-04	0.1019E-04	0.455	0.6452E-05	0.288	F
335	6	3	66				0.3231E-04	0.9009E-05	0.279	0.5245E-05	0.162	F
336	6	3	76	3516	121	47	0.2965E-04	0.9127E-05	0.308	0.5950E-05	0.201	A1-2
337	6	3	86	3526	215	-54	0.2608E-04	0.8938E-05	0.343	0.6089E-05	0.233	A1-2
338	6	3	96	3536	139	58	0.3078E-04	0.9072E-05	0.295	0.7191E-05	0.234	A1-2
339	6	3	106	3546	135	59	0.3198E-04	0.9718E-05	0.304	0.5934E-05	0.186	A1-2
340	6	3	116	3556	260	-47	0.2477E-04	0.2257E-05	0.090	0.2091E-05	0.080	A1-4
341	6	3	126	3566	129	37	0.4301E-04	0.7775E-05	0.181	0.4456E-05	0.104	A1-2
342	6	3	136	3576	164	29	0.2916E-04	0.8587E-05	0.294	0.5498E-05	0.189	A1-4
343	6	3	146	3586	205	-37	0.2061E-04					L4
344	6	4	6	3596	210	-34	0.1946E-04	0.8571E-05	0.440	0.6303E-05	0.324	A1-3
345	6	4	16	3606	219	-56	0.1685E-04					A4-5
346	6	4	26	3616	212	-52	0.2229E-04	0.2921E-05	0.131	0.2902E-05	0.130	L2
347	6	4	36	3626	46	8	0.4372E-04					A5-8
348	6	4	46	3636	65	45	0.4285E-04	0.1491E-04	0.348	0.1045E-04	0.244	A1-2
349	6	4	56	3646	106	13	0.5334E-04					L6
350	6	4	66	3656	44	50	0.2894E-04	0.6069E-05	0.210	0.3759E-05	0.130	A1-3
351	6	4	76	3666	47	49	0.2629E-04			0.6424E-05	0.244	A1-2
352	6	4	86	3676	72	52	0.1697E-04	0.4195E-05	0.247	0.3609E-05	0.213	A1-3
353	6	4	96	3686	50	11	0.2631E-04			0.2778E-05	0.106	A4-6
354	6	4	106	3696	223	-65	0.1374E-04	0.3249E-05	0.236	0.3811E-05	0.277	A1-2
355	6	4	116	3706	245	-50	0.2596E-04	0.1581E-05	0.061	0.1215E-05	0.047	L2
56	6	4	126	3716	54	20	0.3331E-04	0.1284E-04	0.385	0.5776E-05	0.173	A1-2
57	6	4	136	3726			0.2235E-04	0.7593E-05	0.340	0.3136E-05	0.140	U
58	6	4	146	3736	86	32	0.3487E-04	0.1454E-04	0.417	0.6639E-05	0.190	A1-2
59	6	5	6	3746	81	40	0.3313E-04	0.1510E-04	0.456	0.8913E-05	0.269	A1-2
60	6	5	16	3756	91	47	0.2421E-04	0.1288E-04	0.532	0.7700E-05	0.318	A1-2
61	6	5	26	3766	111	60	0.1194E-04	0.9041E-05	0.757	0.6631E-05	0.555	A1-2
62	6	5	36	3776	96	41	0.2617E-04	0.1176E-04	0.449	0.7313E-05	0.279	A1-2
63	6	5	46	3786	93	57	0.1470E-04	0.6693E-05	0.455	0.4401E-05	0.299	A1-2
64	6	5	56	3796	73	64	0.1527E-04	0.8660E-05	0.567	0.5476E-05	0.359	A1-2
65	6	5	66	3806	88	62	0.1876E-04	0.8318E-05	0.443	0.5693E-05	0.303	A1-2
66	6	5	76	3816	83	45	0.1874E-04	0.3066E-05	0.164	0.2315E-05	0.123	A1-2
67	6	5	86	3826	90	36	0.1490E-04	0.1050E-04	0.704	0.7100E-05	0.476	A1-2
68	6	5	96	3836	109	14	0.1858E-04	0.3941E-05	0.212	0.2326E-05	0.125	A1-2
69	6	5	106	3846	116	36	0.1315E-04	0.5332E-05	0.406	0.3974E-05	0.302	A1-2
70	6	5	116	3856	121	51	0.1423E-04	0.7534E-05	0.529	0.5212E-05	0.366	A1-2
71	6	5	126	3866	123	44	0.1203E-04	0.6856E-05	0.570	0.4613E-05	0.384	A1-2
72	6	5	136	3876	142	34	0.2162E-04	0.4798E-05	0.222	0.2556E-05	0.118	A1-2
373	6	5	146	3886	125	-13	0.2207E-04	0.9216E-05	0.418	0.1544E-05	0.070	L3
374	6	6	6	3896	183	-43	0.2958E-04	0.1074E-04	0.363	0.4622E-05	0.156	A1-2
375	6	6	16	3906	211	-68	0.1659E-04	0.6864E-05	0.414	0.2950E-05	0.178	A1-2

Table 1. (Continued).

Sample	Core	Section	Depth in Section (cm)	Depth in Hole (cm)	Declination (deg)	Inclination (deg)	NRM (emu)	J_{100} (emu)	J_{100}/J_0	J_{200} (emu)	J_{200}/J_0	Note
376	6	6	26	3916			0.1122E-04			0.2300E-05	0.205	U
377	6	6	36	3926	183	33	0.1956E-04	0.5581E-05	0.285	0.2387E-05	0.122	L3
378	6	6	46	3936	216	-43	0.3572E-04			0.1265E-04	0.354	A2-3
379	6	6	56	3946	52	34	0.1379E-04	0.3150E-05	0.228	0.3120E-05	0.226	A1-2
380	6	6	66	3956	42	61	0.2211E-04	0.7257E-05	0.328	0.4665E-05	0.211	A1-2
381	6	6	76	3966	245	-32	0.1268E-04	0.2535E-05	0.200	0.3233E-05	0.255	L2
382	6	6	86	3976	31	46	0.3564E-04	0.1418E-04	0.398	0.5887E-05	0.165	A1-2
383	6	6	96	3986	299	48	0.2244E-04	0.4701E-05	0.209	0.1306E-05	0.058	L2
384	6	6	106	3996	290	27	0.3123E-04	0.9583E-05	0.307	0.3512E-05	0.112	L3
385	6	6	116	4006	30	11	0.3396E-04	0.1887E-04	0.556	0.1142E-04	0.336	L2
386	6	6	126	4016	230	-39	0.1473E-04	0.2056E-04	1.396	0.1435E-04	0.975	A1-2
387	6	6	136	4026	203	-29	0.1920E-04	0.1439E-04	0.744	0.1043E-04	0.540	A1-2
388	6	6	146	4036	3	15	0.2742E-04	0.9641E-05	0.352	0.4577E-05	0.167	A1-3
389	6	6	6	4046	255	12	0.2650E-04	0.3628E-05	0.137	0.3440E-05	0.130	L2
390	6	7	16	4056	347	25	0.2430E-04	0.9680E-05	0.405	0.7570E-05	0.311	A1-2
391	6	7	26	4066	306	27	0.2366E-04	0.7786E-05	0.329	0.6185E-05	0.261	A2-4
392	6	7	36	4076	347	34	0.3143E-04	0.1367E-04	0.435	0.9233E-05	0.294	A2-4
393	6	7	44	4084	324	38	0.3131E-04	0.9476E-05	0.303	0.7151E-05	0.228	A2-4
394	7	1	9	4469			0.8808E-05	0.1392E-04	1.580	0.9591E-05	1.089	U
395	7	1	16	4476	295	-39	0.2573E-04	0.2447E-04	0.951	0.1837E-04	0.714	A4-5
396	7	1	26	4486	357	-52	0.8892E-04	0.7187E-04	0.808	0.4567E-04	0.514	A5-6
397	7	1	36	4496	167	-61	0.1068E-03	0.8434E-04	0.789	0.5411E-04	0.506	A5-6
398	7	1	46	4506	211	-45	0.2037E-03	0.1447E-03	0.711	0.9858E-04	0.484	A5-6
399	7	1	56	4516	93	-44	0.3678E-04	0.4122E-04	1.121	0.2398E-04	0.652	A1-2
400	7	1	66	4526	130	-25	0.4627E-04	0.4419E-04	0.955	0.2555E-04	0.552	L3
401	7	1	76	4536	280	44	0.3339E-04	0.1212E-04	0.363	0.7511E-05	0.225	A1-2
402	7	1	86	4546	274	39	0.4174E-04	0.1323E-04	0.317	0.6274E-05	0.150	A1-2
403	7	1	96	4556	270	-49	0.1960E-04	0.3944E-05	0.201	0.2179E-05	0.111	L2
404	7	1	106	4566	302	14	0.4700E-04	0.2210E-04	0.470	0.1286E-04	0.274	A1-2
405	7	1	116	4576	137	-20	0.1791E-04	0.9119E-05	0.509	0.6864E-05	0.383	L3
406	7	1	126	4586	261	28	0.3095E-04	0.7115E-05	0.230	0.2435E-05	0.079	A1-2
407	7	1	136	4596	101	-28	0.2165E-04	0.1298E-05	0.060	0.2576E-05	0.119	A1-2
408	7	1	146	4606	283	1	0.2701E-04			0.1100E-04	0.407	A2-5
409	7	2	5				0.6749E-05	0.1857E-04	2.752	0.1284E-04	1.903	F
410	7	2	26				0.2066E-04					F
411	7	2	36				0.1528E-04			0.9085E-06	0.059	F
412	7	2	56	4616	98	-26	0.2455E-04	0.3002E-04	1.223	0.1400E-04	0.570	A1-2
413	7	2	66	4626	118	-25	0.2412E-04	0.3141E-04	1.302	0.1570E-04	0.651	A1-2
414	7	2	76	4636	119	-19	0.5188E-04	0.4247E-04	0.819	0.2067E-04	0.398	A1-2
415	7	2	86	4646	114	-25	0.4050E-04	0.4293E-04	1.060	0.1960E-04	0.484	A1-3
416	7	2	96	4656	111	-38	0.3891E-04	0.5095E-04	1.310	0.2686E-04	0.690	A1-2
417	7	2	108	4666	272	57	0.3520E-04	0.1056E-04	0.300	0.4709E-05	0.134	A1-2
418	7	2	116	4676	290	33	0.7185E-04	0.3360E-04	0.468	0.1624E-04	0.226	A1-2
419	7	2	126	4686	253	35	0.3001E-04	0.6461E-05	0.215	0.2698E-05	0.090	A1-2
420	7	2	136	4696	272	36	0.8055E-04	0.3507E-04	0.435	0.1888E-04	0.234	A1-2
421	7	2	146	4706	279	20	0.4221E-04	0.1507E-04	0.357	0.8146E-05	0.193	L4
422	7	3	5	4716	258	23	0.3232E-04	0.4115E-05	0.127	0.1594E-05	0.049	L3
423	7	3	14	4726	116	-32	0.1249E-04	0.1113E-04	0.891	0.6438E-05	0.515	A1-2
424	7	3	26	4736	242	12	0.3523E-04	0.3187E-05	0.090	0.2027E-05	0.058	A2-4
425	7	3	36	4746	159	-23	0.1756E-04	0.5638E-05	0.321	0.3156E-05	0.180	A4-5
426	7	3	46	4756	223	-18	0.2423E-04	0.2587E-05	0.107	0.1738E-05	0.072	A4-5
427	7	3	56	4766	286	-23	0.1939E-04	0.2133E-05	0.110			L5
428	7	3	66	4776	109	-38	0.9600E-05	0.2186E-04	2.277	0.1527E-04	1.590	L2
429	7	3	76	4786	272	25	0.2820E-04	0.3801E-05	0.135	0.1908E-05	0.068	A2-4
430	7	3	86	4796	89	-33	0.2947E-04	0.8012E-05	0.272	0.4910E-05	0.167	A1-2
431	7	3	96	4806	99	-46	0.2420E-04	0.1178E-04	0.487	0.8743E-05	0.361	L2
432	7	3	106	4816	305	-40	0.2269E-04	0.6747E-05	0.297	0.6384E-05	0.281	A3-5
433	7	3	116	4826	280	32	0.4513E-04	0.1747E-04	0.387	0.1185E-04	0.263	A1-2
434	7	3	126	4836	283	31	0.7154E-04	0.2876E-04	0.402	0.1846E-04	0.258	A1-3
435	7	3	136	4846	277	34	0.6464E-04	0.2780E-04	0.430	0.1811E-04	0.280	A1-2

Table 1. (Continued).

Sample	Core	Section	Depth in Section (cm)	Depth in Hole (cm)	Declination (deg)	Inclination (deg)	NRM (emu)	J_{100} (emu)	J_{100}/J_0	J_{200} (emu)	J_{200}/J_0	Note
6	7	3	146	4856	275	36	0.7666E-04	0.2546E-04	0.332	0.1650E-04	0.215	A1-3
7	7	4	6	4866	272	30	0.7949E-04	0.4434E-04	0.558	0.2997E-04	0.377	A1-2
8	7	4	16	4876	266	34	0.8817E-04	0.3812E-04	0.432	0.2467E-04	0.280	A1-3
9	7	4	26	4886	263	42	0.4568E-04	0.1264E-04	0.277	0.6944E-05	0.152	A1-2
0	7	4	36	4896	278	40	0.4744E-04	0.3458E-05	0.073	0.1792E-05	0.038	A1-3
1	7	4	46	4906	270	36	0.3890E-04	0.6610E-05	0.170	0.4413E-05	0.113	A1-2
2	7	4	56	4916	251	49	0.3745E-04	0.3025E-05	0.081	0.1678E-05	0.045	L3
3	7	4	66	4926	242	46	0.3315E-04	0.5658E-05	0.171	0.3795E-05	0.114	A1-2
4	7	4	76	4936	114	-24	0.3124E-04	0.1617E-04	0.518	0.9588E-05	0.307	A1-3
5	7	4	86	4946	231	39	0.3617E-04	0.2662E-05	0.074	0.2148E-05	0.059	A1-2
6	7	4	96	4956	61	-25	0.2977E-04	0.5545E-05	0.186	0.4708E-05	0.158	A2-3
7	7	4	106	4966	71	-26	0.2411E-04	0.8078E-05	0.335	0.6789E-05	0.282	L3
448	7	4	116	4976	238	26	0.4212E-04	0.5385E-05	0:128	0.2747E-05	0.065	A1-2
449	7	4	126	4986	265	42	0.3993E-04	0.7597E-05	0.190	0.4415E-05	0.111	A1-2
450	7	4	136	4996	62	17	0.3510E-04	0.5517E-05	0.157	0.3309E-05	0.094	A1-2
451	7	4	146	5006	91	-36	0.3113E-04	0.1585E-04	0.509	0.9317E-05	0.299	L3
452	7	5	6	5016	76	- 6	0.1980E-04	0.1011E-04	0.510	0.5986E-05	0.302	A1-2
453	7	5	16	5026	115	-16	0.2974E-04	0.4024E-05	0.135	0.3274E-05	0.110	A2-3
454	7	5	26	5036	274	40	0.3521E-04	0.7357E-05	0.209	0.4495E-05	0.128	A1-2
455	7	5	36	5046	260	51	0.4453E-04	0.1006E-04	0.226	0.7554E-05	0.170	A1-2
456	7	5	46	5056	255	24	0.5667E-04	0.2457E-04	0.434	0.1618E-04	0.286	A1-2
457	7	5	56	5066	267	48	0.4358E-04	0.1309E-04	0.300	0.9436E-05	0.216	A1-2
458	7	5	66	5076	272	62	0.3938E-04	0.6974E-05	0.177	0.4282E-05	0.109	A1-2
459	7	5	76	5086	229	27	0.3146E-04	0.4568E-05	0.145	0.3060E-05	0.097	A3-4
460	7	5	86	5096	242	34	0.3861E-04	0.6251E-05	0.162	0.3807E-05	0.099	L3
461	7	5	96	5106	238	46	0.1746E-04	0.5472E-05	0.313	0.3847E-05	0.220	A3-4
462	7	5	106	5116	76	-40	0.2549E-04	0.5681E-05	0.223	0.3550E-05	0.139	A1-2
463	7	5	116	5126	250	55	0.2939E-04	0.6566E-05	0.223	0.4987E-05	0.170	A1-2
464	7	5	126	5136	238	48	0.4695E-04	0.7424E-05	0.158	0.4708E-05	0.100	A1-2
465	7	5	136	5146	79	-18	0.1764E-04	0.1472E-04	0.834	0.9101E-05	0.516	L3
466	7	5	146	5156	100	-40	0.2715E-04	0.9809E-05	0.361	0.4623E-05	0.170	L2
467	7	6	6	5166	258	70	0.4191E-04	0.5377E-05	0.128	0.3572E-05	0.085	A1-2
468	7	6	16	5176	216	64	0.3050E-04	0.3661E-05	0.120	0.2663E-05	0.087	L2
469	7	6	26	5186	119	-17	0.3454E-04	0.7383E-05	0.214	0.3726E-05	0.108	L3
470	7	6	36	5196	268	55	0.3569E-04	0.6023E-05	0.169	0.5321E-05	0.149	L2
471	7	6	46	5206	102	8	0.3202E-04	0.4401E-05	0.137	0.2805E-05	0.088	A1-2.5
472	7	6	56	5216	94	-28	0.2095E-04	0.1016E-04	0.485	0.7101E-05	0.339	L3
473	7	6	66	5226	296	42	0.3216E-04	0.5130E-05	0.159	0.1616E-05	0.050	A1-2
474	7	6	76	5236	83	26	0.3417E-04	0.2891E-05	0.085	0.1348E-05	0.039	L2
475	7	6	86	5246			0.3473E-04	0.2459E-05	0.071	0.1863E-05	0.054	U
6	7	6	96	5256	242	45	0.3718E-04	0.5498E-05	0.148	0.2318E-05	0.062	A1-2
7	7	6	106	5266	283	35	0.4264E-04	0.9500E-05	0.220	0.4776E-05	0.112	A2-4
8	7	6	116	5276	284	33	0.4412E-04	0.1057E-04	0.240	0.6171E-05	0.140	A1-2
9	7	6	126	5286	48	-19	0.3240E-04	0.6910E-05	0.213	0.3890E-05	0.120	L3
0	7	6	136	5296	94	-29	0.2153E-04	0.1346E-04	0.625	0.9467E-05	0.440	L3
1	7	6	146	5306	108	-15	0.3452E-04	0.2821E-04	0.817	0.2102E-04	0.609	A1-4
2	7	7	6	5316	100	-21	0.2115E-04	0.1512E-04	0.715	0.1201E-04	0.568	L2
3	7	7	16	5326	127	-26	0.3797E-04	0.3838E-05	0.101	0.4624E-05	0.122	L2
4	7	7	26	5336	293	51	0.4167E-04	0.4277E-05	0.103	0.1615E-05	0.039	L1
5	7	7	36	5346	259	45	0.3958E-04	0.6848E-05	0.173	0.3565E-05	0.090	A2-3
6	7	7	46	5356	37	-35	0.3210E-04	0.2581E-05	0.080	0.2309E-05	0.072	L2
7	8	1	26	5436	146	-51	0.2103E-04	0.2761E-04	1.313	0.1900E-04	0.904	L5
8	8	1	36	5446	118	-67	0.3259E-04	0.1314E-04	0.403	0.9773E-05	0.300	A1-5
9	8	1	46	5456	143	-18	0.7447E-04	0.3549E-04	0.477	0.2502E-04	0.336	L5
0	8	1	56	5466	318	-53	0.2850E-04	0.1308E-04	0.459	0.1030E-04	0.361	A1-5
1	8	1	66	5476	312	-41	0.3130E-04			0.1094E-04	0.349	A1-3
2	8	1	76	5486	319	-40	0.4522E-04	0.2089E-04	0.462	0.1554E-04	0.344	A1-2
3	8	1	86	5496	327	-45	0.3797E-04	0.1550E-04	0.408	0.1266E-04	0.334	A1-2
4	8	1	96	5506	190	1	0.8664E-04	0.1168E-04	0.135	0.5045E-05	0.058	L2
495	8	1	106	5516	327	-13	0.3277E-04	0.2405E-04	0.734	0.1807E-04	0.352	A1-3

Table 1. (Continued).

Sample	Core	Section	Depth in Section (cm)	Depth in Hole (cm)	Declination (deg)	Inclination (deg)	NRM (emu)	J_{100} (emu)	J_{100}/J_0	J_{200} (emu)	J_{200}/J_0	Note
496	8	1	116	5526	328	-34	0.4651E-04	0.2001E-04	0.430	0.1615E-04	0.347	A1-2
497	8	1	126	5536	340	-18	0.1956E-04	0.3853E-04	1.969	0.2857E-04	1.460	A1-2
498	8	1	136	5546	190	- 3	0.6552E-04	0.1249E-04	0.191	0.8773E-05	0.134	A1-3
499	8	1	146	5556	321	-20	0.2987E-04	0.2493E-04	0.835	0.1628E-04	0.545	A1-3
500	8	2	5	5565	137	15	0.9755E-04	0.4520E-04	0.463	0.3423E-04	0.351	A1-4
501	8	2	22	5582	319	-12	0.3062E-04	0.1543E-04	0.504	0.1151E-04	0.376	A1-2
502	8	2	32	5592	141	17	0.7556E-04	0.2639E-04	0.349	0.2145E-04	0.284	A1-4
503	8	2	67	5627	178	49	0.4953E-04	0.5108E-05	0.103	0.3312E-05	0.067	A1-3
504	8	2	78	5638	312	-35	0.3043E-04	0.1294E-04	0.425	0.8765E-05	0.288	A1-2
505	8	2	106	5666	140	19	0.7197E-04	0.2976E-04	0.413	0.2353E-04	0.327	A1-3
506	8	2	116	5676	317	-19	0.1928E-04	0.3857E-04	2.000	0.2609E-04	1.353	A1-2
507	8	2	126	5686	292	- 9	0.5458E-04	0.5365E-05	0.098	0.3738E-05	0.068	L3
508	8	2	136	5696	313	-17	0.3127E-04	0.5674E-04	1.814	0.3803E-04	1.216	A1-2
509	8	2	146	5706	304	54	0.3881E-04	0.3727E-05	0.096	0.2555E-05	0.066	L2
510	8	3	4	5714	132	21	0.6602E-04	0.2373E-04	0.360	0.1600E-04	0.242	A1-2
511	8	3	66	5776	123	-20	0.3812E-04	0.6045E-05	0.159	0.2732E-05	0.072	L3
512	8	3	92	5802	249	-27	0.5272E-04	0.9811E-05	0.186	0.4145E-05	0.079	A1-2
513	8	3	101	5811	146	18	0.5164E-04			0.3351E-05	0.065	A2.5-3
514	8	3	147	5857	311	-14	0.3123E-04	0.1034E-04	0.331	0.9479E-05	0.304	L1
515	8	4	3	5863	132	-18	0.1948E-04	0.1337E-04	0.686	0.1121E-04	0.576	L2
516	8	4	13	5873	318	27	0.5460E-04	0.2600E-04	0.476	0.1740E-04	0.318	A1-2
517	8	4	23	5883	114	9	0.2491E-04	0.9294E-05	0.373	0.5722E-05	0.230	L4
519	8	5	84	6094			0.78160-05	0.5142E-05	0.658	0.3232E-05	0.414	U
521	8	6	77	6237				0.5670E-04		0.4068E-04		U
522	8	6	90	6250	345	-14	0.3189E-04	0.4845E-04	1.519	0.3403E-04	1.067	A1-4
523	8	7	39	6349	157	-12	0.2280E-04	0.2657E-05	0.117	0.2048E-05	0.090	A2-3
524	8	*	6	6359	328	- 6	0.3526E-04	0.7382E-05	0.209	0.6771E-05	0.192	L2

Note: A = vector average of declination and inclination values at demagnetization levels (x 100) shown.
L = demagnetization level (x 100) used to define declination and inclination. U = magnetically unstable sample.
F = flow-in material (based on shipboard visual descriptions).

variable values below about 45 m. In contrast, J_{100} values tend to decrease downcore, but again with a marked increase in variance below about 45 m. The J_{100}/J_0 ratio (Fig. 4) emphasizes the contrast, with a major trend from values near 1 above about 18 m to close to zero below about 29 m. Demagnetization curves above (Fig. 5A, B, C) and below (Fig. 5D, E, F) the lithologic change illustrate the marked change in magnetic properties. The shallower samples show a steady decrease in intensity with increasing AF strength, with little change in the direction of magnetization. Even at 400 Oe, J_{400}/J_0 values exceed 0.25. In contrast, the deeper samples show marked intensity changes (Fig. 5D) or a rapid J/J_0 decrease to values of 0.1 or less at AF strengths of 100 Oe or more (Fig. 5E, F).

The coincidence of the transitional change in lithology, loss of paleomagnetic stratigraphy, and decrease in J_{100} (both absolute and relative to NRM) point to a common sedimentological cause for these phenomena.

Site 578

Site 578 yielded an excellent magnetic record (Tables 6 and 7). Even on the *Challenger*, it was clear that all the magnetic events in the first four chrons were present (see Site 578 chapter, this volume; Fig. 6). Subsequent shore-based laboratory studies suggest that, with the exception of a 600,000-yr. hiatus from 8.2 to 8.8 m.y. ago, all reversals from 15 m.y. ago to the present were recovered (Table 8). In the complex interval from the base of the Gilbert Epoch to Anomaly 5B (Fig. 7), only five samples from Site 578 (indicated by asterisks in Table 8) do not fit the standard stratigraphy.

The sequence of 60 identifiable reversals yields an extremely detailed age-depth curve (Fig. 8), the upper par of which is generally similar in form to the Site 57 curve (Fig. 2).

As at Site 576, the reversal stratigraphy is based pri marily on inclination data. The declinations support thes picks, but the absolute values are unknown and rota tions within a single HPC can exceed 120° (Fig. 9). Th depth at which the reversal stratigraphy breaks dow (~145 m) again corresponds to the level at which th sedimentation rate drops below about 2 m/m.y. At Sit 578, this level lies well within a dark brown unit that i magnetically uninterpretable at Site 576, suggesting tha sedimentation rate has a greater influence on the stabili ty of detrital remanence than does gross lithology. Th brown to dark brown boundary at about 125 m mark the point at which the sedimentation rate drops belov about 4 m/m.y., but the detrital sedimentation rate wa

Table 2. Magnetic properties of samples from Hole 576B.

Sample	Core	Section	Depth in Section (cm)	Depth in Hole (cm)	Declination (deg)	Inclination (deg)	NRM (emu)	J_{100} (emu)	J_{100}/J_0	J_{200} (emu)	J_{200}/J_0	Note
51	1	1	6	6	230	44	0.2352E-04	0.2050E-04	0.872	0.1564E-04	0.665	L1-2
53	1	1	26	26	231	49	0.3669E-04	0.3131E-04	0.853	0.2903E-04	0.791	L1-2
55	1	1	46	46	234	43	0.3506E-04	0.2647E-04	0.755	0.2207E-04	0.630	L1-2
57	1	1	66	66	230	51	0.3593E-04	0.3210E-04	0.893	0.2375E-04	0.661	L1-2
59	1	1	86	86	254	57	0.3930E-04	0.3476E-04	0.884	0.3009E-04	0.766	L1-2
61	1	1	106	106	260	62	0.3764E-04	0.3352E-04	0.891	0.2432E-04	0.646	L1-2
63	1	1	126	126	228	49	0.2240E-04	0.1724E-04	0.770	0.1362E-04	0.608	L1-2
65	1	2	146	146	265	50	0.3510E-04	0.2973E-04	0.847	0.2397E-04	0.683	L1-2
67	1	2	16	166	272	47	0.3218E-04	0.2940E-04	0.913	0.2502E-04	0.778	L1-2
69	1	2	36	186	267	49	0.2631E-04	0.2488E-04	0.946	0.1917E-04	0.729	L1-2
1	1	2	56	206	260	54	0.3129E-04	0.2721E-04	0.870	0.2439E-04	0.780	L1-2
73	1	2	76	226	270	45	0.2212E-04	0.2129E-04	0.962	0.1625E-04	0.735	L1-2
75	1	2	116	266	274	58	0.3380E-04	0.2795E-04	0.827	0.2424E-04	0.717	L1-2
77	1	2	96	246	269	58	0.2500E-04	0.2136E-04	0.854	0.1889E-04	0.755	L1-2
79	1	2	136	286	256	60	0.2554E-04	0.2104E-04	0.824	0.1585E-04	0.621	L1-2
581	1	3	6	306	278	60	0.2005E-04	0.1854E-04	0.924	0.1460E-04	0.728	L1-2
583	1	3	26	326	293	62	0.7175E-05	0.5257E-05	0.733	0.4895E-05	0.682	L1-2
585	1	3	47	347	262	41	0.3212E-04	0.2195E-04	0.684	0.1716E-04	0.534	L1-2
587	1	3	66	366	248	44	0.2489E-04	0.2149E-04	0.863	0.1796E-04	0.722	L1-2
589	1	3	86	386	240	39	0.1582E-04	0.1328E-04	0.839	0.1101E-04	0.696	L1-2
591	1	3	106	406	274	74	0.1839E-04	0.1492E-04	0.812	0.1302E-04	0.708	L1-2
593	1	3	126	426	233	59	0.2469E-04	0.1791E-04	0.726	0.1486E-04	0.602	L1-2
595	1	3	146	446	225	55	0.2510E-04	0.2241E-04	0.893	0.1856E-04	0.740	L1-2
597	1	4	16	466	213	34	0.2199E-04	0.1767E-04	0.803	0.1431E-04	0.651	L1-2
599	1	4	36	486	218	45	0.2335E-04	0.2144E-04	0.918	0.1918E-04	0.821	L1-2
601	1	4	56	506	204	41	0.2787E-04	0.2181E-04	0.782	0.1887E-04	0.677	L1-2
603	1	4	76	526	249	30	0.2734E-04	0.2301E-04	0.841	0.1897E-04	0.694	L1-2
605	1	4	96	546	212	41	0.2244E-04	0.1948E-04	0.868	0.1540E-04	0.686	L1-2
607	1	4	116	566	221	41	0.3107E-04	0.2849E-04	0.917	0.2339E-04	0.753	L1-2
609	1	4	136	586	214	47	0.2882E-04	0.2566E-04	0.890	0.2029E-04	0.704	L1-2
610	1	4	146	596	213	42	0.3409E-04	0.2821E-04	0.828	0.2206E-04	0.647	L1-2
617	1	5	6	606	217	12	0.2261E-04	0.1863E-04	0.824	0.1502E-04	0.664	L1-3
619	1	5	26	626	190	38	0.1320E-04	0.1115E-04	0.845	0.9069E-05	0.687	L1-2
620	1	5	36	636	209	- 3	0.2120E-04	0.1424E-04	0.672	0.1094E-04	0.516	L1-2
621	1	5	46	646	207	28	0.2362E-04	0.1662E-04	0.703	0.1419E-04	0.601	L1-2
622	1	5	56	656	201	25	0.3032E-04	0.2318E-04	0.765	0.2028E-04	0.669	L1-2
623	1	5	66	666	204	-12	0.2282E-04	0.2111E-04	0.925	0.1811E-04	0.794	L1-2
624	1	5	76	676	207	-24	0.1960E-04	0.1571E-04	0.801	0.1300E-04	0.663	L1-2
625	1	5	86	686	230	- 2	0.7069E-05	0.8025E-05	1.135	0.5878E-05	0.832	L5
626	1	5	96	696	276	-45	0.4260E-05	0.5473E-05	1.285	0.5042E-05	1.184	L1-3
627	1	5	106	706	257	-51	0.7136E-05	0.8119E-05	1.138	0.8212E-05	1.151	L1-2
29	1	5	126	726	249	-28	0.6293E-05	0.7374E-05	1.172	0.6298E-05	1.001	L1-2
31	1	5	146	746	263	-38	0.5295E-05	0.5652E-05	1.067	0.4454E-05	0.841	L1-2
11	1	6	6	756	271	-50	0.1245E-04	0.1510E-04	1.213	0.1173E-04	0.942	L1-3
3	1	6	26	776	271	-50	0.1867E-04	0.1914E-04	1.025	0.1469E-04	0.787	L1-2
5	1	6	46	796	287	-51	0.1865E-04	0.2002E-04	1.073	0.1543E-04	0.827	L1-2
6	1	6	54	804	282	-48	0.1572E-04	0.1477E-04	0.939	0.1338E-04	0.851	L1-2
2	2	1	11	1171	27	-31	0.1078E-04	0.1050E-04	0.974	0.1013E-04	0.939	L1-2,F
3	2	1	19	1179	29	-44	0.1477E-04	0.1693E-04	1.146	0.1391E-04	0.942	L1-2
5	2	1	36	1196	34	-57	0.2128E-04	0.2088E-04	0.981	0.1750E-04	0.822	L1-2
7	2	1	56	1216	21	-42	0.2047E-04	0.2182E-04	1.066	0.1770E-04	0.865	L1-2
9	2	1	76	1236	24	-56	0.1025E-04	0.9172E-05	0.895	0.1001E-04	0.977	L1-2
1	2	1	96	1256	29	-50	0.2546E-04	0.2589E-04	1.017	0.1962E-04	0.770	L1-2
13	2	1	116	1276	31	-40	0.1574E-04	0.1830E-04	1.163	0.1358E-04	0.863	L1-2
15	2	1	136	1296	26	-34	0.1232E-04	0.1390E-04	1.128	0.1150E-04	0.933	L1-2
17	2	2	6	1316	19	-31	0.1191E-04	0.1376E-04	1.156	0.1191E-04	1.001	L1-2
19	2	2	26	1336	37	-48	0.9595E-05	0.1018E-04	1.061	0.9212E-05	0.960	L1-2
51	2	2	46	1356	32	-39	0.1742E-04	0.1991E-04	1.143	0.1521E-04	0.873	L1-2
53	2	2	66	1376	19	-53	0.1250E-04	0.1145E-04	0.916	0.1021E-04	0.817	L1-2
55	2	2	86	1396	27	-48	0.2542E-04	0.2544E-04	1.001	0.2083E-04	C.819	L1-2

Table 2. (Continued).

Sample	Core	Section	Depth in Section (cm)	Depth in Hole (cm)	Declination (deg)	Inclination (deg)	NRM (emu)	J_{100} (emu)	J_{100}/J_0	J_{200} (emu)	J_{200}/J_0	Note
657	2	2	106	1416	25	-49	0.1801E-04	0.2198E-04	1.220	0.1756E-04	0.975	L1-2
659	2	2	126	1436	29	-49	0.2017E-04	0.2135E-04	1.059	0.1770E-04	0.877	L1-2
661	2	2	146	1456	26	-51	0.1156E-04	0.1279E-04	1.106	0.1156E-04	0.999	L1-2
663	2	3	15	1475	357	-46	0.5785E-05	0.8371E-05	1.447	0.6624E-05	1.145	L1-2
664	2	3	26	1486	10	-47	0.1105E-04	0.1287E-04	1.165	0.9473E-05	0.857	L1-2
665	2	3	36	1496	168	13	0.8638E-05	0.4473E-05	0.518	0.3425E-05	0.396	L1-2
667	2	3	56	1516	189	49	0.2157E-04	0.1943E-04	0.900	0.1406E-04	0.652	L1-2
669	2	3	76	1536	181	13	0.2631E-04	0.2115E-04	0.804	0.1806E-04	0.687	L1-2
673	2	4	46	1656	196	-48	0.2022E-04	0.2223E-04	1.099	0.1728E-04	0.855	L1-2
674	2	4	56	1666	193	-46	0.1308E-04	0.1492E-04	1.141	0.1037E-04	0.793	L1-2
675	2	4	66	1676	189	-49	0.1750E-04	0.2045E-04	1.168	0.1697E-04	0.970	L1-2
676	2	4	76	1686	182	-54	0.1505E-04	0.1475E-04	0.981	0.1231E-04	0.818	L1-2
677	2	4	86	1696	184	-41	0.1552E-04	0.1962E-04	1.265	0.1449E-04	0.934	L1-2
678	2	4	96	1706	163	-49	0.2233E-04	0.2051E-04	0.918	0.1735E-04	0.777	L1-2
679	2	4	106	1716	188	-53	0.1512E-04	0.1487E-04	0.984	0.1183E-04	0.782	L1-2
680	2	4	116	1726	188	-44	0.2453E-04	0.2465E-04	1.005	0.1914E-04	0.780	L1-2
681	2	4	126	1736	184	-51	0.1784E-04	0.1833E-04	1.028	0.1521E-04	0.853	L1-2
682	2	4	136	1746	194	-68	0.2104E-04	0.1764E-04	0.838	0.1417E-04	0.674	L1-2
683	2	4	146	1756	171	-48	0.1604E-04	0.1551E-04	0.967	0.1305E-04	0.814	L1-2
684	2	5	6	1766	164	-68	0.8324E-05	0.9673E-05	1.162	0.7930E-05	0.953	L1-2
685	2	5	16	1776	158	-87	0.3707E-05	0.6104E-05	1.647	0.4410E-05	1.190	L1-3
686	2	5	25	1786	200	-36	0.7980E-05	0.9018E-05	1.130	0.6499E-05	0.814	L1-2
687	2	5	36	1796	188	-53	0.1391E-04	0.1539E-04	1.107	0.1239E-04	0.891	L1-2
688	2	5	46	1806	299	-72	0.1354E-04	0.1666E-04	1.230	0.1155E-04	0.853	L1-3
689	2	5	56	1816	298	-71	0.1067E-04	0.1317E-04	1.235	0.1127E-04	1.056	L1-2
690	2	5	66	1826	139	-80	0.1002E-04	0.1309E-04	1.306	0.8905E-05	0.889	L1-2
691	2	5	76	1836	131	-63	0.1352E-05	0.1759E-05	1.300	0.1262E-05	0.933	L1-2
692	2	5	86	1846	30	46	0.1361E-04	0.9511E-05	0.699	0.7171E-05	0.527	L1
693	2	5	96	1856	5	40	0.2262E-04	0.1549E-04	0.685	0.1261E-04	0.557	L1-2
694	2	5	106	1866	3	49	0.1896E-04	0.1098E-04	0.579	0.9542E-05	0.503	L1-2
695	2	5	116	1876	4	47	0.1756E-04	0.1239E-04	0.706	0.1070E-04	0.609	L1-2
696	2	5	126	1886	13	36	0.2871E-04	0.2372E-04	0.826	0.1633E-04	0.569	L1-2
697	2	5	136	1896	357	50	0.2859E-04	0.2381E-04	0.833	0.1962E-04	0.686	L1-2
698	2	5	146	1906	5	50	0.1472E-04	0.1212E-04	0.823	0.6915E-05	0.470	L1-2
699	2	6	6	1916	3	51	0.2533E-04	0.1826E-04	0.721			L1-2
700	2	6	16	1926	6	55	0.2626E-04	0.2161E-04	0.823	0.1568E-04	0.597	L1-2
701	2	6	26	1936	3	41	0.2142E-04	0.1668E-04	0.779	0.1250E-04	0.584	L1-2
702	2	6	36	1946	8	41	0.2510E-04	0.1921E-04	0.765	0.1393E-04	0.555	L1-2
703	2	6	46	1956	5	42	0.2327E-04	0.1834E-04	0.788	0.1253E-04	0.538	L1-2
704	2	6	56	1966	4	47	0.2256E-04	0.1510E-04	0.669	0.1198E-04	0.531	L1-2
705	2	6	66	1976	360	51	0.3137E-04	0.2370E-04	0.756	0.1902E-04	0.606	L1-2
706	2	6	76	1986	4	46	0.1875E-04	0.1141E-04	0.608	0.8260E-05	0.441	L1-2
707	2	6	86	1996	168	-47	0.3568E-05	0.4439E-05	1.244	0.4510E-05	1.264	L1-2
708	2	6	96	2006	179	-47	0.7811E-05	0.1175E-04	1.505	0.9735E-05	1.246	L1-2
709	2	6	106	2016	7	49	0.1830E-04	0.1102E-04	0.602	0.6503E-05	0.355	L1-2
710	2	6	116	2026	0	52	0.2458E-04	0.1520E-04	0.619	0.9541E-05	0.388	L1-2
711	2	6	126	2036	119	-19	0.7439E-05	0.8339E-06	0.112	0.5363E-06	0.072	L3
712	2	6	136	2046	170	-53	0.6789E-05	0.1039E-04	1.531	0.9320E-05	1.373	L1-2
713	2	6	146	2056	56	-62	0.5867E-05	0.6582E-06	0.112	0.4942E-06	0.084	L2-3
714	2	7	6	2066	341	66	0.1066E-04	0.7012E-05	0.658	0.4429E-05	0.416	L1-5
715	2	7	16	2076	346	48	0.7562E-05	0.5553E-05	0.734	0.4033E-05	0.533	L1-2
716	2	7	26	2086	288	77	0.1425E-04	0.9334E-05	0.655	0.6670E-05	0.468	L1-7
717	2	7	36	2096	347	66	0.2024E-04	0.1377E-04	0.681	0.9337E-05	0.461	L1-2
718	3	1	6	2116	298	33	0.9963E-05	0.4398E-05	0.441	0.2794E-05	0.280	L1-2
719	3	1	16	2126	309	42	0.1476E-04	0.6263E-05	0.424	0.4549E-05	0.308	L1-2
720	3	1	26	2136	120	-65	0.3283E-05	0.4179E-05	1.273	0.2981E-05	0.908	L1-2
721	3	1	36	2146	128	-54	0.8681E-06	0.5440E-05	6.266	0.3948E-05	4.548	L1-2
722	3	1	86	2196	329	45	0.9741E-05	0.6017E-05	0.618	0.3296E-05	0.338	L1-2
723	3	1	46	2156	146	-50	0.2864E-05	0.6617E-05	2.310	0.5712E-05	1.994	L1-2
724	3	1	56	2166	142	-56	0.2264E-05	0.6562E-05	2.898	0.5742E-05	2.536	L1-2

Table 2. (Continued).

Sample	Core	Section	Depth in Section (cm)	Depth in Hole (cm)	Declination (deg)	Inclination (deg)	NRM (emu)	J_{100} (emu)	J_{100}/J_0	J_{200} (emu)	J_{200}/J_0	Note
5	3	1	66	2176	140	-53	0.2922E-05	0.6975E-05	2.387	0.5628E-05	1.926	L1-2
6	3	1	76	1996	169	-73	0.5738E-05	0.3001E-06	0.052	0.3689E-06	0.064	L1-2
7	3	1	96	2016	342	42	0.9242E-05	0.4551E-05	0.492	0.2827E-05	0.306	L1-2
8	3	1	106	2026	134	-53	0.3855E-05	0.2564E-05	0.665	0.2377E-05	0.617	L1-2
9	3	1	116	2036	152	-54	0.1359E-05	0.5320E-05	3.915	0.3883E-05	2.858	L1-2
0	3	1	126	2046	149	-42	0.2032E-05	0.7549E-05	3.715	0.5870E-05	2.889	L1-2
1	3	1	136	2056	154	-54	0.2386E-05	0.6185E-05	2.592	0.4220E-05	1.769	L1-2
2	3	1	146	2066	332	37	0.1283E-04	0.5884E-05	0.459	0.4390E-05	0.342	L1-2
3	3	2	6	2076	351	41	0.1747E-04	0.9174E-05	0.525	0.5492E-05	0.314	L1-2
4	3	2	16	2086	337	45		0.6428E-05		0.4346E-05		L1-2
5	3	2	26	2096	347	53	0.1141E-04	0.6032E-05	0.529	0.3613E-05	0.317	L1-2
6	3	2	36	2106	345	39	0.1153E-04	0.6126E-05	0.531	0.4434E-05	0.385	L1-2
7	3	2	46	2116	352	47	0.1324E-04	0.7074E-05	0.534	0.5032E-05	0.380	L1-2
8	3	2	56	2126	351	52	0.1262E-04	0.7451E-05	0.590	0.3827E-05	0.303	L1-2
739	3	2	66	2136	161	-49	0.4161E-05	0.1638E-05	0.394	0.1438E-05	0.346	L1-2
740	3	2	76	2206	153	-49	0.4359E-05	0.2628E-05	0.603	0.2410E-05	0.553	L1-2
741	3	2	86	2216	146	-52	0.2801E-05	0.5005E-05	1.787	0.3587E-05	1.281	L1-2
742	3	2	96	2226	153	-49	0.1209E-05	0.3176E-05	2.627	0.2650E-05	2.192	L1-2
743	3	2	106	2236	162	-43	0.1169E-05	0.3787E-05	3.241	0.3408E-05	2.916	L1-2
744	3	2	116	2246	169	-56	0.1089E-05	0.5882E-05	5.403	0.4196E-05	3.854	L1-2
745	3	2	126	2256	161	-36	0.1544E-05	0.4406E-05	2.854	0.3693E-05	2.392	L1-2
746	3	2	136	2266	161	-37	0.2920E-05	0.6511E-05	2.230	0.4978E-05	1.705	L1-2
747	3	2	146	2276	162	-38	0.2444E-05	0.6976E-05	2.855	0.5204E-05	2.129	L1-2
748	3	3	6	2286	186	41	0.5170E-05	0.9350E-05	1.808	0.5610E-05	1.085	L1-2
749	3	3	16	2296	182	-47	0.2157E-05	0.2741E-05	1.271	0.2042E-05	0.947	L1-2
750	3	3	26	2306	161	-37	0.2856E-05	0.1763E-05	0.617	0.1365E-05	0.478	L1-2
751	3	3	36	2316	158	-33	0.4506E-05	0.7157E-05	1.588	0.5529E-05	1.227	L1-2
752	3	3	46	2326	106	16	0.9670E-05	0.6476E-05	0.670	0.4699E-05	0.486	L1-4
765	3	6	26	2452	355	54	0.1255E-04	0.1671E-05	0.133	0.6691E-06	0.053	L1
766	3	6	46	2462	131	-44	0.3928E-05	0.5506E-05	1.402	0.4631E-05	1.179	L1-2
767	3	6	66	2492	63	74	0.1237E-04	0.9983E-06	0.081	0.3768E-06	0.030	L1
768	3	6	86	2512	316	55	0.1670E-04	0.5049E-05	0.302	0.3067E-05	0.184	L1-2
769	3	6	106	2532	134	-46	0.7143E-05	0.5366E-05	0.751	0.4295E-05	0.601	L1-2
770	3	6	126	2552	139	4	0.1578E-04	0.1296E-05	0.082	0.9644E-06	0.061	L3-4
771	3	6	146	2572	117	-25	0.7950E-05	0.2499E-05	0.314	0.2611E-05	0.328	L1-2
772	3	7	6	2582	120	66	0.1303E-04	0.1070E-05	0.082	0.3924E-06	0.030	L1-2
773	3	7	26	2602	345	63	0.1582E-04	0.1490E-05	0.094	0.5079E-06	0.032	L1
774	3	7	46	2622	324	52	0.1407E-04	0.3479E-05	0.247	0.1844E-05	0.131	L1-2
775	4	3	106	3416	12	18	0.1480E-04	0.6264E-05	0.423	0.3760E-05	0.254	L1-3
776	4	3	126	3436	7	-11	0.8827E-05	0.5145E-05	0.583	0.3506E-05	0.397	L1-3
777	4	3	146	3456	7	19	0.1344E-04	0.3097E-05	0.230	0.1580E-05	0.118	L1-3
778	4	4	6	3466	2	16	0.1704E-04	0.4060E-05	0.238	0.2065E-05	0.121	L1-3
9	4	4	26	3486	3	12	0.1450E-04	0.3586E-05	0.247	0.1824E-05	0.126	L1-3
0	4	4	46	3506	353	23	0.1517E-04	0.3571E-05	0.235	0.1805E-05	0.119	L1-3
1	4	4	66	3526	5	22	0.1199E-04	0.2473E-05	0.206	0.1354E-05	0.113	L1-3
2	4	4	86	3546	337	32	0.1223E-04	0.3474E-05	0.284	0.1906E-05	0.156	L1-3
3	4	4	106	3566	342	29	0.1447E-04	0.3357E-05	0.232	0.1996E-05	0.138	L1-3
4	4	4	126	3586	342	37	0.1759E-04	0.4362E-05	0.248	0.2146E-05	0.122	L1-2
5	4	4	146	3606	11	17	0.1496E-04	0.3091E-05	0.207	0.1777E-05	0.119	L1-3
6	4	5	6	3616	327	-15	0.1456E-04	0.5362E-05	0.368	0.3025E-05	0.208	L1-2
7	4	5	26	3636	355	17	0.1528E-04	0.3090E-05	0.202	0.1789E-05	0.117	L1-3
8	4	5	46	3656	349	24	0.2030E-04	0.2924E-05	0.144	0.1784E-05	0.088	L1-3
9	4	5	66	3676	18	-18	0.1606E-04	0.2439E-05	0.152	0.1842E-05	0.115	L1-3
0	4	5	86	3696	27	-25	0.1653E-04	0.4022E-05	0.243	0.3460E-05	0.209	L1-3
1	4	5	106	3716	5	-18	0.1594E-04	0.6014E-05	0.377	0.4083E-05	0.256	L1-3
2	4	5	126	3736				1.5229E-05		2.3684E-05		U
3	4	5	146	3756	354	16	0.1007E-04	0.5496E-05	0.546	0.3969E-05	0.394	L1-3
4	4	6	6	3766	360	-11	0.1045E-04	0.5869E-05	0.562	0.3308E-05	0.317	L1-3
5	4	6	26	3786	6	-14	0.8672E-05	0.5609E-05	0.647	0.3583E-05	0.413	L1-3
96	4	6	46	3806	352	-10	0.8328E-05	0.7404E-05	0.889	0.4629E-05	0.556	L1-4

Table 2. (Continued).

Sample	Core	Section	Depth in Section (cm)	Depth in Hole (cm)	Declination (deg)	Inclination (deg)	NRM (emu)	J_{100} (emu)	J_{100}/J_0	J_{200} (emu)	J_{200}/J_0	Note
797	4	6	66	3826	2	-49	0.8676E-05	0.8458E-05	0.975	0.5881E-05	0.678	L1-2
798	4	6	86	3846	10	-33	0.1688E-05	0.5970E-05	3.536	0.4756E-05	2.817	L1-2
799	4	6	106	3866	31	-15	0.6964E-05	0.6753E-05	0.970	0.4012E-05	0.576	L1-2
800	4	6	126	3886	26	- 5	0.1244E-04	0.1066E-04	0.857	0.6970E-05	0.560	L1-2
801	4	6	146	3906	270	12	0.3239E-04	0.1363E-04	0.421	0.9374E-05	0.289	L1-7
802	4	7	6	3916	269	56	0.3634E-04	0.1803E-04	0.496	0.1285E-04	0.353	L1-2
803	4	7	26	3936	336	37	0.2354E-04	0.5384E-05	0.229	0.3126E-05	0.133	L1-2
804	4	7	46	3957	54	42	0.1938E-04	0.6843E-05	0.353	0.5074E-05	0.262	L1-2
806	5	2	6	4016	103	29	0.1632E-04	0.8228E-05	0.504	0.6278E-05	0.385	L1-3
807	5	2	26	4036	105	46	0.3435E-04	0.1370E-04	0.399	0.9721E-05	0.283	L1-2
808	5	2	46	4056	97	49	0.3040E-04	0.1011E-04	0.333	0.5747E-05	0.189	L1-2
809	5	2	67	4077	90	16	0.2331E-04	0.8137E-05	0.349	0.4794E-05	0.206	L1-2
810	5	2	87	4097	110	18	0.2265E-04	0.7602E-05	0.336	0.5233E-05	0.231	L1-3
811	5	2	107	4117	105	32	0.1540E-04	0.6051E-05	0.393	0.3511E-05	0.228	L1-2
812	5	2	126	4136	121	28	0.1724E-04	0.3696E-05	0.214	0.2494E-05	0.145	L1-2
813	5	2	146	4156	98	60	0.2646E-04	0.6526E-05	0.247	0.4259E-05	0.161	L1-2
814	5	3	6	4166	103	58	0.2998E-04	0.9982E-05	0.333	0.6253E-05	0.209	L1-2
815	5	3	26	4186	3	64	0.1633E-04	0.5688E-05	0.348	0.3578E-05	0.219	L1-2
816	5	3	46	4206	79	-23	0.1483E-04	0.5437E-05	0.367	0.2913E-05	0.196	L1
817	5	3	66	4226	261	2	0.1789E-04	0.9223E-05	0.516	0.2755E-05	0.154	L1-3
818	5	3	86	4246	89	-13	0.1618E-04	0.5585E-05	0.345	0.3848E-05	0.238	L1-3
819	5	3	106	4266	97	20	0.4027E-04	0.1294E-04	0.321	0.5921E-05	0.147	L1-2
820	5	3	126	4286	289	44	0.1613E-04	0.5407E-05	0.335	0.5262E-05	0.326	L1-2
821	5	3	146	4306	74	24	0.1564E-04	0.1270E-04	0.812	0.9839E-05	0.629	L1-2
822	5	4	6	4316	293	-21	0.1226E-04	0.1508E-04	1.230	0.1150E-04	0.939	L1-2
823	5	4	26	4336	107	32	0.4144E-04	0.1154E-04	0.278	0.5199E-05	0.125	L1-2
824	5	4	46	4356	85	36	0.2586E-04	0.9017E-05	0.349	0.4917E-05	0.190	L1-2
825	5	4	66	4376			0.1242E-04	1.1595E-05	0.128	2.8791E-06	0.071	U
826	5	4	86	4396	273	-13	0.2668E-04	0.2576E-04	0.965	0.1256E-04	0.471	L1-2
827	5	4	106	4416	96	13	0.2650E-04	0.4960E-05	0.187	0.7229E-06	0.027	L1
828	5	4	126	4436	96	41	0.3056E-04	0.8733E-05	0.286	0.2449E-05	0.080	L1-2
829	5	4	146	4456	315	44	0.2864E-04	0.5956E-05	0.208	0.4706E-05	0.164	L1-2
830	5	5	6	4466	61	43	0.2244E-04	0.2971E-05	0.132	0.8105E-06	0.036	L1
831	5	5	26	4486	94	53	0.2914E-04	0.1132E-04	0.389	0.4192E-05	0.144	L1-2
832	5	5	46	4506	301	2	0.7380E-05	0.3889E-05	0.527	0.3905E-05	0.529	L1-2
833	5	5	66	4526	8	-46	0.1286E-04	0.1913E-05	0.149	0.2087E-05	0.162	L1-2
834	5	5	86	4546	273	- 6	0.1232E-04	0.1129E-04	0.917	0.6796E-05	0.552	L1-2
835	5	5	107	4567	109	13	0.4942E-04	0.2692E-04	0.545	0.1636E-04	0.331	L1-3
836	5	5	126	4586	257	- 9	0.1268E-04	0.3407E-05	0.269	0.2177E-05	0.172	L1-4
837	5	5	146	4606	281	-34	0.9651E-05	0.1212E-04	1.256	0.5552E-05	0.575	L1-2
838	5	6	6	4616	262	-17	0.1514E-04	0.1603E-04	1.059	0.1013E-04	0.669	L1-3
839	5	6	26	4636	259	1	0.1811E-04	0.1821E-04	1.006	0.1091E-04	0.603	L1-3
840	5	6	46	4656	283	0	0.1976E-04	0.2064E-04	1.045	0.1061E-04	0.537	L1-2
841	5	6	66	4676	280	- 6	0.2812E-04	0.2301E-04	0.818	0.1517E-04	0.540	L1-2
842	5	6	86	4696	243	- 3	0.1420E-04	0.9403E-05	0.662	0.4469E-05	0.315	L1-2
843	5	6	106	4716	57	19	0.2690E-04	0.6006E-05	0.223	0.4380E-05	0.163	L1-2
844	6	1	126	5122	26	-57	0.2155E-04	0.8238E-05	0.382	0.6188E-05	0.287	L1-2
845	6	1	146	5142	263	-22	0.3091E-04	0.6020E-05	0.195	0.3932E-05	0.127	L1-2
846	6	2	6	5162	312	- 8	0.2003E-04	0.5521E-05	0.276	0.3436E-05	0.171	L1-2
847	6	2	26	5182	47	-12	0.3040E-04	0.7982E-05	0.263	0.4810E-05	0.158	L1-2
848	6	2	46	5202	232	30	0.5203E-04	0.1352E-04	0.260	0.8374E-05	0.161	L1-2
849	6	2	66	5222	237	17	0.5246E-04	0.1408E-04	0.268	0.1014E-04	0.193	L1-2
850	6	2	86	5242	278	-13	0.3722E-04	0.4717E-05	0.127	0.2590E-05	0.070	L1-2
851	6	2	106	5262	244	46	0.3808E-04	0.5654E-05	0.148	0.3243E-05	0.085	L1-2
852	6	2	126	5282	261	20	0.3825E-04	0.3968E-05	0.104	0.2852E-05	0.075	L1-4
853	6	2	146	5302	52	7	0.3257E-04	0.3611E-05	0.111	0.2009E-05	0.062	L1-2
854	6	3	6	5312	27	-19	0.2570E-04	0.7921E-05	0.308	0.5690E-05	0.221	L1-2
855	6	3	26	5322	257	40	0.3434E-04	0.4186E-05	0.122	0.3185E-05	0.093	L1-2
856	6	3	46	5342	131	58	0.3327E-04	0.3897E-05	0.117	0.2475E-05	0.074	L1-2
857	6	3	67	5363	260	20	0.4743E-04	0.1023E-04	0.216	0.6504E-05	0.137	L1-2

Table 2. (Continued).

Sample	Core	Section	Depth in Section (cm)	Depth in Hole (cm)	Declination (deg)	Inclination (deg)	NRM (emu)	J_{100} (emu)	J_{100}/J_0	J_{200} (emu)	J_{200}/J_0	Note
858	6	3	86	5382	32	2	0.3146E-04	0.6622E-05	0.211	0.3959E-05	0.126	L1-2
859	6	3	106	5402	48	-13	0.2716E-04	0.7798E-05	0.287	0.5935E-05	0.219	L1-2
860	6	3	126	5422	70	-25	0.2424E-04	0.1590E-04	0.656	0.1150E-04	0.474	L1-2
861	6	3	146	5442	262	-55	0.3211E-04	0.5615E-05	0.175	0.2364E-05	0.074	L1-2
862	6	4	6	5452	324	13	0.2343E-04	0.4006E-05	0.171	0.2551E-05	0.109	L1
863	6	4	26	5472	215	38	0.3452E-04	0.3926E-05	0.114	0.1129E-05	0.033	L1
864	6	4	46	5492	258	12	0.5312E-04	0.1479E-04	0.278	0.1070E-04	0.201	L1-2
865	6	4	66	5512	87	-22	0.3780E-04	0.8017E-06	0.021	0.2888E-05	0.076	L1-3
866	6	4	86	5532	253	- 5	0.4840E-04	0.4384E-05	0.091	0.1542E-05	0.032	L1
867	6	4	106	5552	304	27	0.4988E-04	0.1199E-04	0.240	0.8632E-05	0.173	L1-2
868	6	4	146	5592	275	17	0.7992E-04	0.4446E-04	0.556	0.3180E-04	0.398	L1-2
869	6	5	55	5651	273	22	0.5306E-04	0.1666E-04	0.314	0.1231E-04	0.232	L1-2
870	6	5	86	5682	275	19	0.7436E-04	0.3535E-04	0.475	0.2620E-04	0.352	L1-2
871	6	5	106	5702	306	27	0.3562E-04	0.5017E-05	0.141	0.2708E-05	0.076	L1-2
872	6	5	126	5722	83	-11	0.2257E-04	0.1265E-04	0.561	0.9275E-05	0.411	L1-2
873	6	5	144	5740	290	7	0.3917E-04	0.1761E-04	0.450	0.1277E-04	0.326	L1-2
874	6	6	47	5793	278	4	0.4097E-04	0.1252E-04	0.306	0.6730E-05	0.164	L1-3
875	6	6	76	5822	57	- 6	0.3526E-04	0.1775E-05	0.050	0.3466E-05	0.098	L1-2
876	6	6	136	5882	69	-24	0.2648E-04	0.3838E-05	0.145	0.4448E-05	0.168	L1-2
877	7	3	145	6245	162	-21	0.3007E-04	0.4494E-04	1.494	0.3157E-04	1.050	L1-2
878	7	4	91	6341	152	- 4	0.2487E-04	0.6307E-05	0.254	0.6090E-05	0.245	L1-2
879	7	4	128	6378	339	12	0.3786E-04	0.5319E-05	0.140	0.2401E-05	0.063	L1
880	7	5	79	6479	119	-14	0.2868E-04	0.2459E-04	0.858	0.1776E-04	0.619	L1-2
881	7	6	26	6576	103	-17	0.1395E-04	0.2372E-04	1.701	0.1821E-04	1.305	L1-2
882	7	6	46	6596	115	70	0.1495E-04	0.1041E-04	0.697	0.9306E-05	0.623	L1-2
883	7	6	89	6639	275	5	0.3872E-04	0.1461E-04	0.377	0.8647E-05	0.223	L1-2
884	7	7	30	6730	260	- 5	0.1769E-04	0.1442E-04	0.815	0.1187E-04	0.671	L1-2
885	8	2	81	6976	293	3	0.4411E-04	0.2268E-04	0.514	0.1260E-04	0.286	L1-2
886	8	3	29	7074	318	- 2	0.3063E-04	0.8459E-05	0.276	0.4129E-05	0.135	L1-2
887	8	3	65	7110	316	5	0.3969E-04	0.1472E-04	0.371	0.7835E-05	0.197	L1-2
888	8	3	96	7141	310	13	0.5152E-04	0.2096E-04	0.407	0.1303E-04	0.253	L1-2
889	8	4	21	7216	333	8	0.6136E-04	0.3187E-04	0.519	0.1644E-04	0.268	L1-2
890	8	4	41	7236	326	13	0.4531E-04	0.1506E-04	0.332	0.7976E-05	0.176	L1-2
891	8	4	99	7294	132	- 6	0.1723E-04	0.3324E-05	0.193	0.2161E-05	0.125	L1-2
892	8	5	58	7403	142	-20	0.3787E-04	0.3818E-04	1.008	0.2331E-04	0.615	L1-2
893	8	5	142	7487	136	-15	0.1176E-04	0.7574E-05	0.644	0.5679E-05	0.483	L1-2
894	8	6	44	7539	330	13	0.1350E-04	0.2052E-04	1.520	0.1207E-04	0.894	L1-2

Note: L = demagnetization level or levels (x 100; vector averages) used to define declination and inclination.
U = magnetically unstable samples. F = flow-in, based on shipboard visual descriptions.

ill high enough to prevent the "swamping" of detrital manence by chemical remanence, as appears to have ccurred at Site 576.

The NRM (J_0) and J_{100} values correlate very well for e magnetically stable samples above about 145 m (Fig.)). At greater depths, however, NRM values increase, hereas J_{100} values approach zero. The J_{100}/J_0 ratio ig. 10) shows a tight clustering of values above about 0 m, where sedimentation rates exceed 12 m/m.y., inreased scatter but a good continuation of the shallower end to about 145 m, then scattered, very low values to e base of the section.

DISCUSSION

The magnetic data at both Sites 576 and 578 yield deailed age-depth curves (Figs. 2, 8). Differentiation of these curves yields sedimentation rates as a function of time (Fig. 11).

In both cases, the past 2 m.y. has been a period of increased sedimentation, a phenomenon that has been observed across the North Pacific and that has been attributed to eolian transport of fine-grained glacial debris from Asia and, to a lesser extent, from North America. This explanation is supported by the remarkable similarity of the rate increases at Sites 576 and 578 (about 5-6 m/m.y.^{2} during the Quaternary, in each case). Such a uniform increase is unlikely to reflect either changes in bottom transport, given the separation of the two sites by Shatsky Rise, or changes in surface transport, given the upstream distance to source areas, particularly at Site 576. The uniformity of the increase also is in striking contrast to the very different accumulation rate his-

Table 3. Magnetization of Site 576 samples after AF demagnetization at intensities above 200 Oe.

Sample	Core	Section	Depth in Section (cm)	Depth in Hole (cm)	Declination (deg)	Inclination (deg)	Demagnetization Level (OE)	J (emu)	J/J_0
36	2	1	96	791	47	-51	300	0.1745E-04	0.689
							400	0.1310E-04	0.517
45	2	2	36	881	263	19	300	0.1244E-05	0.199
49	2	2	76	921	278	54	300	0.1560E-04	0.582
							400	0.1185E-04	0.442
53	2	2	116	961	267	-38	250	0.6133E-06	0.214
							300	0.3696E-06	0.129
							400	0.6096E-06	0.212
97	2	5	106	1401	287	-69	300	0.5571E-05	0.756
99	2	5	126	1421	154	-67	300	0.1380E-04	0.644
101	2	5	146	1441	185	-84	300	0.1349E-04	0.606
							400	0.1066E-04	0.479
103	2	6	16	1461	75	-79	300	0.1429E-04	0.656
109	2	6	76	1521	22	14	300	0.1893E-05	0.499
110	2	6	86	1531	20	-20	300	0.7121E-05	0.501
111	2	6	96	1541	6	28	300	0.6299E-05	0.435
113	2	6	116	1561	329	19	300	0.5379E-05	0.575
114	2	6	126	1571	335	19	300	0.2906E-05	0.497
							400	0.1669E-05	0.286
179	3	4	146	1581	162	40	300	0.3612E-06	0.065
189	4	1	76	1856			300	0.2121E-05	0.309
							400	0.1489E-04	2.171
							500	0.1091E-05	0.159
							600	0.1138E-05	0.166
							700	0.8307E-06	0.121
							800	0.6931E-06	0.101
192	4	1	106	1886	146	51	300	0.1328E-04	0.346
							400	0.8800E-05	0.229
196	4	1	146	1926	211	-54	300	0.1115E-04	0.319
215	4	3	36	2116	165	54	300	0.68200-05	
							400	0.40900-05	
219	4	3	76	2156	7	51	300	0.4559E-05	1.791
							400	0.2523E-05	0.991
							500	0.1432E-05	0.562
							600	0.1092E-05	0.429
221	4	3	96	2176	354	-55	300	0.7906E-05	1.212
							400	0.4623E-05	0.709
							500	0.3139E-05	0.481
241	4	4	146	2376	308	- 4	300	0.5650E-05	2.212
							400	0.3054E-05	1.196
							500	0.2011E-05	0.787
							600	0.1389E-05	0.544
							700	0.1316E-05	0.515
252	4	5	106	2486	304	- 3	300	0.2457E-05	0.419
254	4	5	126	2506	3	-52	300	0.5584E-05	1.113
256	4	5	146	2526	360	-52	300	0.4065E-05	0.628
258	4	6	16	2546	349	-53	300	0.5221E-05	0.668
262	4	6	56	2586	353	-45	300	0.4812E-05	0.450
263	4	6	66	2596	333	-30	300	0.2324E-05	0.120
264	4	6	76	2606	340	-20	300	0.3839E-05	0.191
							400	0.1731E-05	0.086
265	4	6	86	2616	9	-66	300	0.5058E-05	0.497
							400	0.3182E-05	0.313
266	4	6	96	2626	335	-45	300	0.2418E-05	0.090
267	4	6	106	2636	286	-38	300	0.1486E-05	0.053
268	4	6	116	2646	21	-13	300	0.2102E-05	0.085
							400	0.7508E-06	0.031
269	4	6	126	2656	294	-24	300	0.2051E-06	0.234

Table 3. (Continued).

Sample	Core	Section	Depth in Section (cm)	Depth in Hole (cm)	Declination (deg)	Inclination (deg)	Demagnetization Level (OE)	J (emu)	J/J0
270	4	6	136	2666	281	-10	300	0.9917E-06	0.030
271	4	6	146	2676	309	-48	300	0.1365E-06	0.055
272	4	7	6	2686	282	- 7	300	0.2052E-05	0.068
273	4	7	16	2696	265	-20	300	0.2310E-06	0.116
274	4	7	26	2706	357	-40	300	0.1101E-05	0.043
275	4	7	36	2716	284	-14	300	0.1790E-05	0.097
							250	0.1656E-06	0.088
							300	0.8989E-06	0.480
276	4	7	46	2726	77	17	300	0.1772E-05	0.064
							400	0.1774E-05	0.064
							400	0.2038E-05	0.073
							500	0.1865E-05	0.067
							500	0.1994E-05	0.072
278	5	1	46	2866	148	-78	300	0.3144E-05	0.341
							400	0.1339E-05	0.145
280	5	1	66	2886	220	-69	300	0.4670E-05	0.445
281	5	1	76	2896	225	-71	300	0.5182E-05	0.898
282	5	1	86	2906	233	-78	300	0.4674E-05	0.545
284	5	1	106	2926	64	13	300	0.1790E-05	0.097
285	5	1	116	2936	71	6	300	0.1225E-05	0.090
							300	0.1729E-05	0.128
							400	0.1133E-05	0.084
286	5	1	126	2946	95	-37	300	0.7718E-06	0.055
287	5	1	136	2956	87	- 4	300	0.7589E-06	0.072
							400	0.6077E-06	0.058
288	5	1	146	2966	48	3	300	0.9601E-06	0.066
302	5	5	130	3240	308	- 5	300	0.2997E-05	0.107
							400	0.1415E-05	0.051
305	5	6	16	3276	287	4	300	0.8436E-06	0.028
306	5	6	26	3286	255	14	300	0.1515E-05	0.064
308	5	6	46	3306	305	30	300	0.1280E-05	0.058
							400	0.9700E-06	0.044
309	5	6	56	3316	315	-14	300	0.1652E-05	0.070
							400	0.5543E-06	0.024
							500	0.1300E-05	0.055
311	5	6	76	3336	294	-22	300	0.1126E-05	0.056
312	5	6	86	3346	293	- 9	300	0.6740E-06	0.046
313	5	6	96	3356	301	26	300	0.8159E-06	0.029
314	5	6	107	3367	265	- 9	300	0.6934E-06	0.061
							400	0.3996E-06	0.035
							400	0.7917E-06	0.070
315	5	6	116	3376	303	21	300	0.1054E-05	0.044
316	5	6	126	3386	346	18	300	0.1258E-05	0.078
317	5	6	135	3395	339	39	300	0.1257E-05	0.052
321	5	7	26	3436	296	- 6	300	0.9003E-06	0.041
325	6	1	141				300	0.1166E-04	0.187
							400	0.4557E-05	0.073
							450	0.2356E-05	0.038
340	6	3	116	3556	260	-47	300	0.9980E-06	0.040
							400	0.1341E-05	0.050
342	6	3	136	3576	164	29	300	0.2420E-05	0.083
							400	0.1561E-05	0.054
343	6	3	146	3586	205	-37	400	0.1929E-05	0.094
							500	0.1308E-05	0.063
							600	0.1188E-05	0.058
344	6	4	6	3596	210	-34	300	0.3350E-05	0.172
345	6	4	16	3606	219	-56	400	0.3452E-05	0.205
							500	0.2173E-05	0.129

Table 3. (Continued).

Sample	Core	Section	Depth in Section (cm)	Depth in Hole (cm)	Declination (deg)	Inclination (deg)	Demagnetization Level (OE)	J (emu)	J/J_0
347	6	4	36	3626	46	8	500	0.2490E-05	0.057
							600	0.2787E-05	0.064
							700	0.2872E-05	0.066
							800	0.2223E-05	0.051
349	6	4	56	3646	106	13	500	0.2871E-05	0.054
							600	0.2915E-05	0.055
							700	0.2339E-05	0.044
351	6	4	76	3666	47	49	300	0.4827E-05	0.184
353	6	4	96	3686	50	11	300	0.2240E-05	0.085
							400	0.2622E-05	0.100
							500	0.2168E-05	0.082
							600	0.1755E-05	0.067
355	6	4	116	3706	245	-50	300	0.1180E-05	0.045
357	6	4	136	3726			300	0.1233E-05	0.055
							400	0.1212E-05	0.054
							400	0.6656E-06	0.030
							500	0.9008E-06	0.040
373	6	5	146	3886	125	-13	300	0.1312E-05	0.059
							400	0.1856E-05	0.084
							500	0.3103E-05	0.141
							600	0.3332E-05	0.151
							800	0.3900E-05	0.177
							1000	0.4200E-05	0.190
							1000	0.4400E-05	0.199
376	6	6	26	3916			300	0.4524E-06	0.040
							300	0.7400E-06	0.066
							400	0.1510E-05	0.135
							400	0.5800E-06	0.052
377	6	6	36	3926	183	33	300	0.9439E-06	0.048
378	6	6	46	3936	216	-43	300	0.7285E-05	0.204
381	6	6	76	3966	245	-32	300	0.3289E-05	0.259
							400	0.4064E-05	0.321
							500	0.5379E-05	0.424
383	6	6	96	3986	299	48	300	0.3170E-05	0.141
							400	0.4420E-05	0.197
384	6	6	106	3996	290	27	300	0.3155E-05	0.101
385	6	6	116	4006	30	11	300	0.4908E-05	0.145
							400	0.2875E-05	0.085
388	6	6	146	4036	3	15	300	0.3472E-05	0.127
389	6	6	6	4046	255	12	300	0.5214E-05	0.197
							400	0.6814E-05	0.257
							500	0.7657E-05	0.289
							600	0.8285E-05	0.313
391	5	7	26	4066	306	27	300	0.5510E-05	0.233
							400	0.5310E-05	0.224
							500	0.6320E-05	0.267
							600	0.6830E-05	0.289
392	6	7	36	4076	347	34	300	0.6526E-05	0.208
							400	0.4423E-05	0.141
							500	0.5433E-05	0.173
							600	0.5203E-05	0.166
							800	0.5731E-05	0.182
							1000	0.6848E-05	0.218
393	6	7	44	4084	324	38	300	0.5410E-05	0.173
							400	0.5470E-05	0.175
							500	0.4140E-05	0.132
							600	0.5430E-05	0.173
							700	0.6590E-05	0.210

Table 3. (Continued).

Sample	Core	Section	Depth in Section (cm)	Depth in Hole (cm)	Declination (deg)	Inclination (deg)	Demagnetization Level (OE)	J (emu)	J/J_0
							800	0.7850E-05	0.251
							900	0.5600E-05	0.179
395	7	1	16	4476	295	-39	300	0.1054E-04	0.410
							400	0.4661E-05	0.181
							500	0.3836E-05	0.149
396	7	1	26	4486	357	-52	300	0.2593E-04	0.292
							400	0.1020E-04	0.115
							500	0.6990E-05	0.079
							600	0.4430E-05	0.050
							800	0.3700E-05	0.042
							1000	0.3980E-05	0.045
397	7	1	36	4496	167	-61	300	0.2738E-04	0.256
							400	0.1313E-04	0.123
							500	0.7683E-05	0.072
							600	0.4709E-05	0.044
398	7	1	46	4506	211	-45	300	0.4884E-04	0.240
							400	0.2141E-04	0.105
							500	0.1352E-04	0.066
							600	0.1124E-04	0.055
400	7	1	66	4526	130	-25	300	0.1252E-04	0.271
							400	0.5118E-05	0.111
405	7	1	116	4576	137	-20	300	0.3051E-05	0.170
							400	0.4553E-06	0.025
							400	0.6295E-06	0.035
							500	0.1274E-05	0.071
							500	0.1924E-05	0.107
408	7	1	146	4606	283	1	300	0.2743E-05	0.102
							400	0.3182E-05	0.118
							400	0.4367E-05	0.162
							500	0.3784E-05	0.140
							500	0.3832E-05	0.142
410	7	2	26				300	0.8580E-06	0.042
411	7	2	36				300	0.1439E-05	0.094
							400	0.2103E-05	0.138
415	7	2	86	4646	114	-25	300	0.8551E-05	0.211
421	7	2	146	4706	279	20	300	0.5011E-05	0.119
							400	0.3785E-05	0.090
422	7	3	5	4716	258	23	300	0.8281E-06	0.026
424	7	3	26	4736	242	12	150	0.2683E-05	0.076
							300	0.1263E-05	0.036
							300	0.1614E-05	0.046
							400	0.1120E-05	0.032
							400	0.9046E-06	0.026
425	7	3	36	4746	159	-23	300	0.1095E-05	0.062
							400	0.2421E-05	0.138
							400	0.3064E-05	0.174
							450	0.2350E-05	0.134
							500	0.2334E-05	0.133
426	7	3	46	4756	223	-18	300	0.2127E-05	0.088
							400	0.1170E-05	0.048
							500	0.2343E-05	0.097
							600	0.1267E-05	0.052
							600	0.1842E-05	0.076
427	7	3	56	4766	286	-23	400	0.1429E-05	0.074
							400	0.9473E-06	0.049
							500	0.1382E-05	0.071
							500	0.1553E-05	0.080
429	7	3	76	4786	272	25	300	0.2087E-05	0.074

Table 3. (Continued).

Sample	Core	Section	Depth in Section (cm)	Depth in Hole (cm)	Declination (deg)	Inclination (deg)	Demagnetization Level (OE)	J (emu)	J/J_0
							400	0.1667E-05	0.059
432	7	3	106	4816	305	-40	300	0.3527E-05	0.155
							400	0.1460E-05	0.064
							500	0.1589E-05	0.070
434	7	3	126	4836	283	31	300	0.1023E-04	0.143
436	7	3	146	4856	275	36	300	0.9860E-05	0.129
438	7	4	16	4876	266	34	300	0.1225E-04	0.139
440	7	4	36	4896	278	40	300	0.1338E-05	0.028
442	7	4	56	4916	251	49	300	0.7719E-06	0.021
444	7	4	76	4936	114	-24	300	0.5653E-05	0.181
446	7	4	96	4956	61	-25	300	0.1366E-05	0.046
							400	0.1862E-05	0.063
							500	0.3275E-05	0.110
							600	0.3413E-05	0.115
447	7	4	106	4966	71	-26	300	0.2589E-05	0.107
450	7	4	136	4996	62	17	300	0.6054E-06	0.017
							300	0.9025E-06	0.026
							400	0.1403E-05	0.040
							500	0.3012E-05	0.086
451	7	4	146	5006	91	-36	300	0.4135E-05	0.133
453	7	5	16	5026	115	-16	300	0.9808E-06	0.033
459	7	5	76	5086	229	27	300	0.2097E-05	0.067
							400	0.1594E-05	0.051
460	7	5	86	5096	242	34	300	0.2234E-05	0.058
461	7	5	96	5106	238	46	300	0.1666E-05	0.095
							400	0.2485E-05	0.142
							500	0.2982E-05	0.171
465	7	5	136	5146	79	-18	250	0.6459E-05	0.366
							300	0.4089E-05	0.232
466	7	5	146	5156	100	-40	300	0.1431E-05	0.053
							400	0.2179E-05	0.080
							400	0.6568E-06	0.024
							500	0.1013E-05	0.037
469	7	6	26	5186	119	-17	300	0.1176E-05	0.034
471	7	6	46	5206	102	8	250	0.1576E-05	0.049
							300	0.4906E-06	0.015
472	7	6	56	5216	94	-28	300	0.3531E-05	0.169
475	7	6	86	5246			300	0.1829E-05	0.053
							400	0.2760E-05	0.079
							500	0.2992E-05	0.086
477	7	6	106	5266	283	35	300	0.2785E-05	0.065
							400	0.2138E-05	0.050
479	7	6	126	5286	48	-19	300	0.1420E-05	0.040
480	7	6	136	5296	94	-29	300	0.3077E-05	0.143
							400	0.8370E-06	0.039
							500	0.2507E-05	0.116
481	7	6	146	5306	108	-15	300	0.1290E-04	0.374
							400	0.4970E-05	0.144
482	7	7	6	5316	100	-21	300	0.6480E-05	0.306
							400	0.2221E-05	0.105
483	7	7	16	5326	127	-26	300	0.1830E-05	0.048
							400	0.1830E-05	0.048
							400	0.2130E-05	0.056
484	7	7	26	5336	293	51	300	0.1230E-05	0.030
							300	0.9400E-06	0.023
485	7	7	36	5346	259	45	300	0.2310E-05	0.058
							400	0.1940E-05	0.049
							500	0.2960E-05	0.075

Table 3. (Continued).

Sample	Core	Section	Depth in Section (cm)	Depth in Hole (cm)	Declination (deg)	Inclination (deg)	Demagnetization Level (OE)	J (emu)	J/J_0
							600	0.2810E-05	0.071
							800	0.3370E-05	0.085
							1000	0.3340E-05	0.084
							1000	0.3510E-05	0.089
487	8	1	26	5436	146	-51	300	0.1048E-04	0.498
							400	0.3773E-05	0.179
							500	0.3590E-05	0.171
							500	0.3828E-05	0.182
							600	0.3740E-05	0.178
488	8	1	36	5446	118	-67	300	0.6513E-05	0.200
							400	0.4304E-05	0.132
							500	0.4006E-05	0.123
489	8	1	46	5456	143	-18	300	0.1440E-04	0.193
							400	0.7524E-05	0.101
							500	0.4269E-05	0.057
							600	0.3166E-05	0.043
490	8	1	56	5466	318	-53	300	0.5509E-05	0.193
							400	0.1884E-05	0.066
							500	0.2255E-05	0.079
491	8	1	66	5476	312	-41	300	0.5083E-05	0.162
494	8	1	96	5506	190	1	300	0.2642E-05	0.030
							300	0.2751E-05	0.032
495	8	1	106	5516	327	-13	300	0.9768E-05	0.298
498	8	1	136	5546	190	- 3	300	0.4784E-05	0.073
							400	0.1724E-05	0.026
499	8	1	146	5556	321	-20	300	0.9775E-05	0.327
500	8	2	5	5565	137	15	300	0.2161E-04	0.222
							400	0.1064E-04	0.109
							500	0.4788E-05	0.049
							500	0.4807E-05	0.049
502	8	2	32	5592	141	17	300	0.1069E-04	0.142
							400	0.6719E-05	0.089
							500	0.2200E-05	0.029
503	8	2	67	5627	178	49	300	0.2262E-05	0.046
505	8	2	106	5666	140	19	300	0.1180E-04	0.164
507	8	2	126	5686	292	- 9	300	0.3371E-05	0.062
							400	0.1210E-05	0.022
509	8	2	146	5706	304	54	300	0.1592E-05	0.041
							400	0.8995E-06	0.023
511	8	3	66	5776	123	-20	300	0.1494E-05	0.039
513	8	3	101	5811	146	18	250	0.2269E-05	0.044
							300	0.1811E-05	0.035
514	8	3	147	5857	311	-14	300	0.4948E-05	0.158
							400	0.1063E-05	0.034
515	8	4	3	5863	132	-18	300	0.6623E-05	0.340
							400	0.2348E-05	0.121
517	8	4	23	5883	114	9	300	0.3409E-05	0.137
							400	0.2093E-05	0.084
521	8	6	77	6237			300	0.2245E-04	1.029
							400	0.9355E-05	0.429
							500	0.4326E-05	0.198
							500	0.4334E-05	0.199
522	8	6	90	6250	345	-14	300	0.2051E-04	0.643
							400	0.8676E-05	0.272
523	8	7	39	6349	157	-12	300	0.9922E-06	0.044

Table 4. Magnetization of Hole 576B samples after AF demagnetization at intensities above 100 Oe.

Sample	Core	Section	Depth in Section (cm)	Depth in Hole (cm)	Demagnetization Level (OE)	J (emu)	J/J_0
617	1	5	6	606	300	0.1255E-04	0.555
624	1	5	76	676	201	0.1309E-04	0.668
625	1	5	86	686	300	0.6085E-05	0.861
				686	301	0.4694E-05	0.664
				686	400	0.4220E-05	0.597
				686	500	0.3285E-05	0.465
				686	600	0.2845E-05	0.402
611	1	6	6	756	300	0.9197E-05	0.739
632	2	1	11	1171	201	0.9128E-05	0.846
635	2	1	36	1196	201	0.1590E-04	0.747
685	2	5	16	1776	300	0.3081E-05	0.831
688	2	5	46	1806	300	0.8236E-05	0.608
707	2	6	86	1996	201	0.4483E-05	1.257
711	2	6	126	2036	202	0.5460E-06	0.073
				2036	300	0.5960E-06	0.080
713	2	6	146	2056	300	0.4284E-06	0.073
714	2	7	6	2066	201	0.6357E-05	0.596
				2066	300	0.4061E-05	0.381
				2066	400	0.2057E-05	0.193
				2066	500	0.1327E-05	0.125
				2066	600	0.1174E-05	0.110
716	2	7	26	2086	300	0.4193E-05	0.294
				2086	301	0.5282E-05	0.371
				2086	400	0.2936E-05	0.206
				2086	500	0.1678E-05	0.118
				2086	600	0.1240E-05	0.087
				2086	700	0.7874E-06	0.055
752	3	3	46	2326	300	0.2409E-05	0.249
				2326	400	0.1547E-05	0.160
770	3	6	126	2552	300	0.6193E-06	0.039
				2552	400	0.3523E-06	0.022
775	4	3	106	3416	300	0.1801E-05	0.122
				3416	400	0.9116E-06	0.062
776	4	3	126	3436	300	0.1672E-05	0.189
777	4	3	146	3456	300	0.4622E-06	0.034
778	4	4	6	3466	300	0.1027E-05	0.060
779	4	4	26	3486	300	0.7908E-06	0.055
780	4	4	46	3506	300	0.7645E-06	0.050
781	4	4	66	3526	300	0.7230E-06	0.060
782	4	4	86	3546	300	0.7836E-06	0.064
783	4	4	106	3566	300	0.8954E-06	0.062
785	4	4	146	3606	300	0.7728E-06	0.052
786	4	5	6	3616	300	0.1445E-05	0.099
				3615	401	0.6454E-06	0.044
787	4	5	26	3636	300	0.6849E-06	0.045
788	4	5	46	3656	300	0.8751E-06	0.043
789	4	5	66	3676	300	0.9333E-06	0.058
790	4	5	86	3696	300	0.1566E-05	0.095
791	4	5	106	3716	300	0.2116E-05	0.133
792	4	5	126	3736	300	0.1622E-05	0.000
				3736	400	0.9335E-06	0.000
793	4	5	146	3756	300	0.1806E-05	0.179
				3756	400	0.8306E-06	0.082
794	4	6	6	3766	300	0.1663E-05	0.159
795	4	6	26	3786	300	0.1433E-05	0.165
796	4	6	46	3806	300	0.2593E-05	0.311
				3806	400	0.1095E-05	0.132
800	4	6	126	3886	300	0.3337E-05	0.268

Table 4. (Continued).

Sample	Core	Section	Depth in Section (cm)	Depth in Hole (cm)	Demagnetization Level (OE)	J (emu)	J/J₀
801	4	6	146	3906	300	0.5924E-05	0.183
				3906	400	0.3753E-05	0.116
				3906	500	0.3010E-05	0.093
				3906	600	0.3041E-05	0.094
				3906	700	0.2625E-05	0.081
806	5	2	6	4016	300	0.3072E-05	0.188
809	5	2	67	4077	300	0.1872E-05	0.080
810	5	2	87	4097	300	0.1948E-05	0.086
817	5	3	66	4226	300	0.7327E-06	0.041
				4226	301	0.1094E-05	0.061
818	5	3	86	4246	300	0.2446E-05	0.151
820	5	3	126	4286	201	0.5567E-05	0.345
821	5	3	146	4306	201	0.1076E-04	0.688
835	5	5	107	4567	300	0.5734E-05	0.116
836	5	5	126	4586	300	0.3053E-05	0.241
				4586	400	0.4037E-05	0.318
838	5	6	6	4616	300	0.7755E-05	0.512
839	5	6	26	4636	300	0.9557E-05	0.529
850	6	2	86	5242	300	0.1668E-05	0.045
852	6	2	126	5282	300	0.1843E-05	0.048
				5282	400	0.1406E-05	0.037
865	6	4	66	5512	300	0.1478E-05	0.039
874	6	6	47	5793	300	0.3731E-05	0.091
				5793	400	0.2211E-05	0.054
				5793	500	0.2332E-05	0.057
893	8	5	142	7487	300	0.3206E-05	0.273
894	8	6	44	7539	300	0.5708E-05	0.423

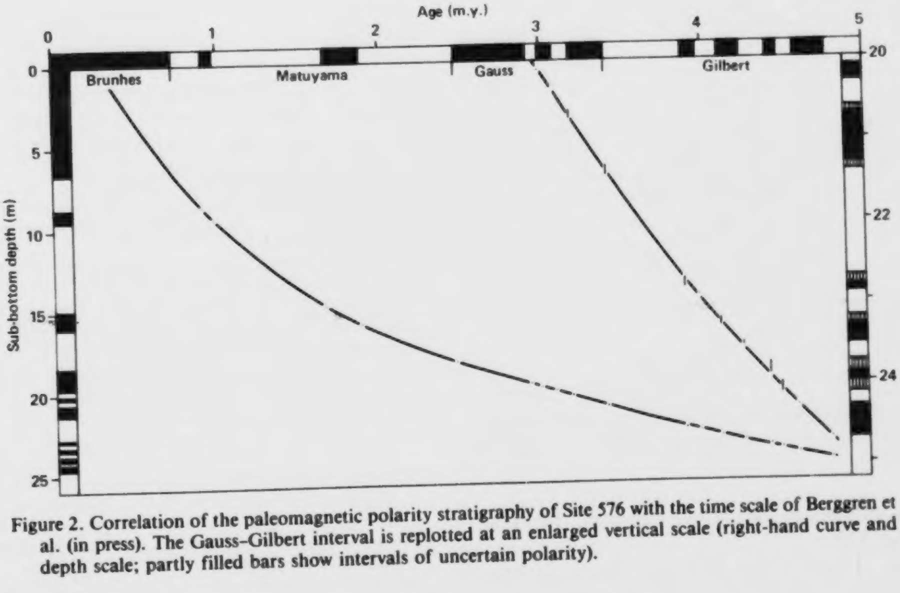

Figure 2. Correlation of the paleomagnetic polarity stratigraphy of Site 576 with the time scale of Berggren et al. (in press). The Gauss-Gilbert interval is replotted at an enlarged vertical scale (right-hand curve and depth scale; partly filled bars show intervals of uncertain polarity).

Table 5. Magnetostratigraphy for Site 576.

Age[a] (m.y.)	Depth (m)		Boundary or event
	Hole 576	Hole 576B	
0.73	6.61 ± 0.05	6.61 ± 0.04	Brunhes/Matuyama
0.91	8.76 ± 0.04	—	Jaramillo
0.98	9.51 ± 0.09	—	
1.66	14.91 ± 0.04	14.91 ± 0.04	Olduvai
1.88	16.01 ± 0.04	—	
2.47	—	18.41 ± 0.04	Matuyama/Gauss
2.92	19.81 ± 0.04	19.91 ± 0.04	Kaena
2.99	20.11 ± 0.04	20.11 ± 0.04	
3.08	20.31 ± 0.04	20.31 ± 0.04	Mammoth
3.18	20.71 ± 0.04	20.61 ± 0.04	
3.40	21.41 ± 0.04	21.31 ± 0.04	Gauss/Gilbert
3.88	22.71 ± 0.04	22.81 ± 0.04	Cochiti
3.97	22.91 ± 0.04	22.91 ± 0.04	
4.10	23.31 ± 0.04	—	Nunivak
4.24	23.51 ± 0.04	—	
4.40	23.91 ± 0.04	—	Sidufjall
4.47	24.01 ± 0.04	—	
4.57	24.31 ± 0.04	—	Thvera
4.77	24.71 ± 0.04	24.61 ± 0.04	

Note: — means not recovered.
[a] From Berggren et al. (in press).

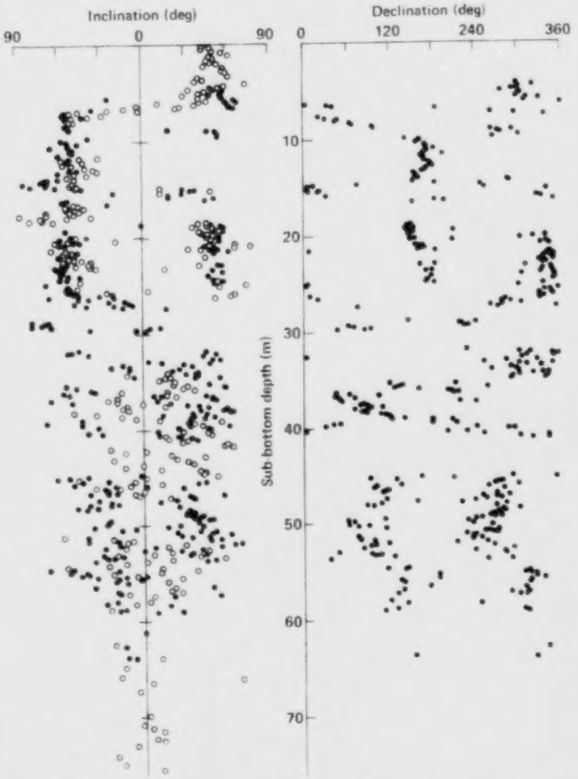

Figure 3. Inclination (filled circles, Hole 576; open circles, Hole 576B) and declination (Hole 576 only) of magnetic samples as a function of depth at Site 576.

tories at the two sites from the middle Miocene through the Pliocene (Fig. 11).

Prior to 16 m.y. ago at Site 578 and 5 m.y. at Site 576, the age-depth curves are constrained only by ichthyolith (see Doyle and Riedel, this volume) and limited foraminiferal (see D'Agostino, this volume) stratigraphy. The uncertainties in age assignments and relatively wide spacings of the control points conceal any short-term rate changes (i.e., <5-10 m.y.).

Within the uncertainties of the initial ichthyolith stratigraphies, the accumulation rates at the two sites from 16 to 70 m.y. ago are identical and uniform at about 0.4 m/m.y.

From about 16 to 2 m.y. ago, sediment accumulated at Site 578 about five times as fast as at Site 576. The process responsible for this difference has not been identified, but the sharpness of the isopach gradient near Site 578 (see Jacobi et al., this volume) suggests that transport by bottom currents to this site, rather than introduction of excess sediment at the sea surface, is a likely explanation.

CONCLUSIONS

Sites 576 and 578 both appear to contain essentially complete Cenozoic sections of pelagic clay. At Site 576, the accumulation rate increases gradually from about 0.4 m/m.y. prior to 15 m.y. ago to about 4 m/m.y. at 2 m.y. ago. An influx of Pleistocene eolian debris then results in a rapid increase to a rate in excess of 15 m/m.y. today. Stable detrital remanence yields a good paleomagnetic record for the past 5 m.y., during which period the accumulation rate has exceeded 2 m/m.y.

At Site 578, the accumulation rate prior to 16 m.y. ago was 0.3-0.4 m/m.y. It then increased abruptly to 2-4 m/m.y. for the interval from 16 to 9 m.y. ago. Following a hiatus from 8.2 to 8.8 m.y. ago, the rate increased fairly uniformly to the surface, reaching a maximum value of about 38 m/m.y. The rate increase during the Quaternary is very similar to the pattern at Site 576.

Site 578 contains a remarkable record of detrital remanence spanning the past 16 m.y. About 60 reversals can be correlated to the standard paleomagnetic stratigraphic section, yielding a detailed age-depth curve for the site. As at Site 576, the magnetic stratigraphy breaks down when the accumulation rate drops below about 2 m/m.y., owing, apparently, to "swamping" of the detrital remanence by the unstable chemical remanence of authigenic oxyhydroxides.

ACKNOWLEDGMENTS

We are grateful to the members of the scientific party of Leg 86 for many stimulating discussions. Bob Karlin, Dennis Schultz, Dave Rea, Carlos Lopez, Chris Dymond, and Dick Kovar helped enter, plot, and cross-check data. Bob Karlin designed the sampler that worked so well at sea, and built the mu-metal boxes. Ronald Merrill and Dennis Kent reviewed this manuscript. To all these people, our sincere thanks.

Support for the shore-based studies came from Sandia National Laboratories Contract SAN26-6611.

REFERENCES

Barton, C., and Sopher, C., 1982. Paleomagnetic study of areas B1, C1 and E3. *In* Hinga, K. R. (Ed.), *Subseabed Disposal Program Annual Report January to September 1981* (Vol. II, App. L): Albuquerque, NM (Sandia National Laboratories), Rept. SAND82-0664/II, 235-334.

Berggren, W. A., Kent, D. V., and Flynn, J. J., in press. Paleogene geochronology and chronostratigraphy. *In* Snelling, N. J. (Ed.), *Geochronology and the Geological Record*. Spec. Publ. Geol. Soc. London.

Chase, T. E., 1975. Topography of the oceans. Univ. Calif. San Diego, Scripps Inst. Oceanog., *Inst. Mar. Resources Tech. Rept.*, Ser. TR57.

Kent, D. V., and Lowrie, W., 1974. Origin of magnetic instability in sediment cores from the central North Pacific. *J. Geophys. Res.*, 79:2987–3000.

einen, M., and Heath, G. R., 1981. Sedimentary indicators of atmospheric circulation in the northern hemisphere during the Cenozoic. *Palaeogeogr., Palaeoclimat., Palaeoecol.*, 36:1–21.

cDougall, I., 1977. The present status of the geomagnetic polarity time scale. Publ. Aust. Natl. Univ., Res. Sch. Earth Sci., 1288.

oore, T. C., Jr., and Heath, G. R., 1978. Sea-floor sampling techniques. *In* Riley, J. P., and Chester, R. (Eds.), *Chemical Oceanography* (Vol. 7): New York (Academic Press), 75–126.

Ness, G., Levi, S., and Couch, R., 1980. Marine magnetic anomaly timescales for the Cenozoic and Late Cretaceous: a precis, critique, and synthesis. *Rev. Geophys. Space Phys.*, 18:753–770.

Opdyke, N. D., and Foster, J. H., 1970. Paleomagnetism of cores from the North Pacific. *In* Hays, J. D. (Ed.), *Geological Investigations of the North Pacific*. Mem. Geol. Soc. Am., 126:83–119.

Prince, R. A., Heath, G. R., and Kominz, M., 1980. Paleomagnetic studies of central North Pacific sediment cores: stratigraphy, sedimentation rates, and the origin of magnetic instability. *Geol. Soc. Am. Bull.*, 91(II):1789–1835.

Date of Initial Receipt: 7 November 1984
Date of Acceptance: 14 June 1984

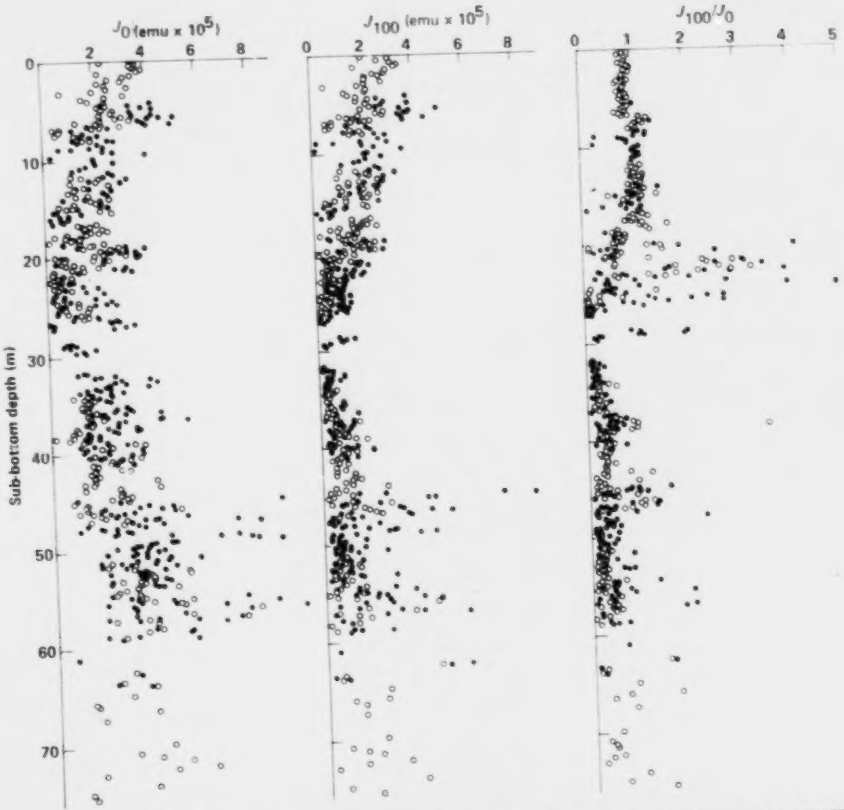

Figure 4. Natural remanent magnetization (J_0), remanent intensity after AF demagnetization at 100 Oe (J_{100}), and J_{100}/J_0 for samples from Site 576. Filled circles, Hole 576; open circles, Hole 576B.

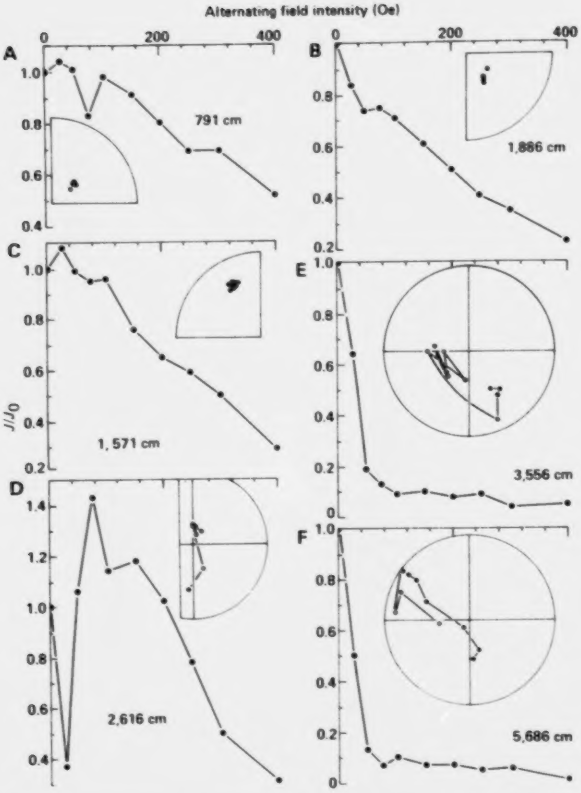

Figure 5. Demagnetization curves for typical samples from Site 576. (A) Sample 576-2-1, 96 cm, (B) Sample 576-4-1, 106 cm and (C) Sample 576-2-6, 126 cm yield stable estimates of detrital remanence, whereas (D) Sample 576-4-6, 86 cm, (E) Sample 576-6-3, 116 cm, and (F) Sample 576-8-2, 126 cm from the dark brown manganese-rich clays do not yield reliable detrital remanence values.

Table 6. Magnetic properties of samples from Site 578.

Sample	Core	Section	Depth in Section (cm)	Depth in Hole (cm)	Declination (deg)	Inclination (deg)	NRM (emu)	J_{100} (emu)	J_{100}/J_0	Note
901	1	1	16	16	173	47	0.9823E-04	0.8813E-04	0.897	L1
903	1	1	53	53	150	53	0.8811E-04	0.7592E-04	0.862	L1
905	1	1	86	86	116	44	0.1419E-04	0.1039E-04	0.732	L1
906	1	1	106	106	96	52	0.4563E-04	0.3943E-04	0.864	L1
907	1	1	126	126			0.5234E-04			
908	1	1	146	146	91	55	0.6319E-04	0.5353E-04	0.847	L1
909	1	2	6	156	97	55	0.5295E-04	0.4980E-04	0.940	L1
911	1	2	50	200	79	50	0.5279E-04	0.3896E-04	0.738	L1
913	1	2	86	236	96	55	0.2965E-04	0.2809E-04	0.948	L1
915	1	2	126	276	112	64	0.4481E-04	0.3993E-04	0.891	L1
916	1	2	146	296	82	54	0.4955E-04	0.3969E-04	0.801	L1
917	1	3	6	306	117	48		0.5108E-04		L1
918	1	3	27	327	136	47	0.7817E-04	0.6858E-04	0.877	L1
919	1	3	46	346	126	51		0.7448E-04		L1
920	1	3	66	366	130	30	0.5894E-04	0.4499E-04	0.763	L1
921	1	3	86	386	149	41	0.5645E-04	0.4376E-04	0.775	L1
923	1	3	126	426	153	44	0.6618E-04	0.5542E-04	0.837	L1
925	2	1	6	486	201	40	0.6386E-04	0.5296E-04	0.829	L1
927	2	1	43	523	219	56	0.5751E-04	0.4656E-04	0.810	L1
929	2	1	86	566	218	30	0.3148E-04	0.2548E-04	0.809	L1
931	2	1	126	606	251	62	0.5760E-04	0.5276E-04	0.916	L1
932	2	1	146	626	232	48	0.5948E-04	0.5291E-04	0.890	L1
933	2	2	5	635	232	-28	0.3430E-04	0.2636E-04	0.768	L1
934	2	2	26	656	237	42	0.5290E-04	0.4363E-04	0.825	L1
935	2	2	46	676	222	54	0.4485E-04	0.3730E-04	0.832	L1
937	2	2	86	716	242	54	0.5689E-04	0.4919E-04	0.865	L1
939	2	2	126	756	235	64	0.5176E-04	0.4532E-04	0.876	L1
941	2	3	16	796	243	37	0.2839E-04	0.2359E-04	0.831	L1,F
942	2	3	41	821	234	48	0.1158E-03	0.8305E-04	0.717	L1
943	2	3	66	846	189	19	0.6138E-04	0.5086E-04	0.829	L1
944	2	3	86	866	176	55	0.5493E-04	0.4996E-04	0.909	L1
945	2	3	106	886	178	51	0.6649E-04	0.5105E-04	0.768	L1
947	2	3	144	924	172	54	0.4597E-04	0.3624E-04	0.788	L1
949	2	4	26	956	167	59	0.8649E-04	0.7093E-04	0.820	L1
951	2	4	64	994	159	61	0.8073E-04	0.6583E-04	0.815	L1
953	2	4	106	1036	174	49	0.5319E-04	0.4363E-04	0.820	L1
955	2	4	146	1076	178	49	0.5833E-05	0.4645E-05	0.796	L1
957	2	5	26	1106	177	59	0.6167E-04	0.5225E-04	0.847	L1
959	2	5	66	1146	187	60	0.7992E-04	0.6815E-04	0.853	L1
961	2	5	106	1186	180	59	0.8308E-04	0.6693E-04	0.806	L1
963	2	6	6	1236	186	55	0.9513E-04	0.7451E-04	0.783	L1
965	3	1	4	1434	351	45	0.1195E-03	0.9947E-04	0.832	L1
967	3	1	46	1476	3	64	0.8910E-05	0.7434E-05	0.834	L1
969	3	1	86	1516	355	54	0.2057E-04	0.1716E-04	0.834	L1
970	3	1	106	1536	5	53	0.4809E-04	0.4028E-04	0.838	L1
971	3	1	126	1556	5	-58	0.3841E-04	0.3398E-04	0.885	L1
972	3	1	146	1576	357	47	0.4986E-04	0.4115E-04	0.825	L1
973	3	2	6	1586	9	55	0.4534E-04	0.3737E-04	0.824	L1
975	3	2	46	1626	358	51	0.2706E-04	0.2394E-04	0.885	L1
977	3	2	86	1666	8	60	0.6184E-04	0.5196E-04	0.840	L1
979	3	2	126	1706	18	58	0.5784E-04	0.4808E-04	0.831	L1
980	3	2	146	1726	23	54	0.5837E-04	0.4957E-04	0.849	L1
981	3	3	6	1736	52	-13	0.5258E-04	0.4256E-04	0.809	L1
982	3	3	26	1756	15	53	0.8643E-04	0.7252E-04	0.839	L1
983	3	3	46	1776	28	55	0.5266E-04	0.4174E-04	0.793	L1
985	3	3	83	1813	22	56	0.6009E-04	0.5335E-04	0.888	L1
987	3	3	126	1856	38	54	0.7511E-04	0.6474E-04	0.862	L1
989	3	4	6	1886	34	52	0.6767E-04	0.5842E-04	0.863	L1
991	3	4	46	1926	44	54	0.5153E-C4	0.4372E-04	0.848	L1
993	3	4	86	1966	43	54	0.5618E-04	0.5377E-04	0.957	L1

Table 6. (Continued).

Sample	Core	Section	Depth in Section (cm)	Depth in Hole (cm)	Declination (deg)	Inclination (deg)	NRM (emu)	J_{100} (emu)	J_{100}/J_0	Note
995	3	4	126	2006	49	57	0.7995E-04	0.7084E-04	0.886	L1
997	3	5	6	2036	50	48	0.9282E-04	0.8056E-04	0.868	L1
999	3	5	46	2076	48	54	0.7261E-04	0.6503E-04	0.896	L1
1001	3	5	86	2116	58	58	0.7631E-04	0.6187E-04	0.811	L1
1003	3	5	126	2156	67	52	0.1058E-03	0.9329E-04	0.882	L1
1005	3	6	6	2186	79	48	0.4716E-04	0.3893E-04	0.825	L1
1007	3	6	50	2230	79	66	0.8473E-05	0.6610E-05	0.780	L1
1009	3	6	86	2266	63	56	0.2053E-05	0.1705E-05	0.830	L1
1011	3	7	6	2336	67	49	0.4198E-04	0.3244E-04	0.773	L1
1013	3	7	46	2376	66	53	0.3954E-04	0.3326E-04	0.841	L1
1015	4	1	26	2405	333	75	0.9327E-05	0.7909E-05	0.848	L1
1017	4	1	66	2446	329	47	0.4799E-04	0.4128E-04	0.860	L1
1019	4	1	113	2493	340	47	0.4362E-04	0.3854E-04	0.883	L1
1021	4	1	145	2525	329	53	0.4006E-04	0.3469E-04	0.866	L1
1023	4	2	25	2555	328	46	0.4658E-04	0.3951E-04	0.848	L1
1025	4	2	66	2596	321	51	0.6295E-04	0.5487E-04	0.872	L1
1027	4	2	108	2638	329	58	0.6493E-04	0.5450E-04	0.839	L1
1029	4	2	146	2676	332	56	0.5844E-04	0.5307E-04	0.908	L1
1039	4	3	26	2706	312	50	0.4358E-04	0.3634E-04	0.834	L1
1041	4	3	66	2746	314	29	0.7841E-04	0.6466E-04	0.825	L1
1042	4	3	86	2766	266	49	0.4281E-04	0.3593E-04	0.839	L1
1043	4	3	105	2785	116	-12	0.6468E-05	0.8880E-05	1.373	A2-3
1031	4	4	25	2855	99	-58	0.4112E-04	0.4355E-04	1.059	L1
1033	4	4	65	2895	65	-29	0.5159E-06	0.6415E-06	1.243	L1
1035	4	4	110	2940	65	-50	0.9491E-06	0.9051E-06	0.954	A3-4
1037	4	4	146	2976	68	-52	0.6026E-05	0.5643E-05	0.937	L1
1044	4	3	126	2806	95	-61	0.3614E-04	0.3452E-04	0.955	L1
1045	4	3	146	2826	79	-52	0.5822E-04	0.6056E-04	1.040	L1
1047	4	5	32	3012	50	-50	0.2102E-04	0.2156E-04	1.026	L1
1049	4	5	66	3046	49	-46	0.9623E-05	0.9706E-05	1.009	L1
1051	4	5	106	3086	41	-59	0.1535E-04	0.1903E-04	1.240	L1
1053	4	5	146	3126	22	-54	0.4646E-04	0.5007E-04	1.078	L1
1055	4	6	26	3156	10	-55	0.3728E-04	0.4142E-04	1.111	L1
1056	4	6	46	3176	10	-51	0.3980E-04	0.4380E-04	1.101	L1
1057	4	6	66	3196	2	57	0.2730E-04	0.3323E-04	1.217	L1
1059	4	6	114	3244	161	56	0.5555E-04	0.4381E-04	0.789	L1
1061	5	1	47	3377	330	48	0.5012E-04	0.4458E-04	0.889	L1
1062	5	1	106	3436	2	67	0.1931E-04	0.1509E-04	0.781	L1
1063	5	1	126	3456	154	-57	0.3798E-04	0.3878E-04	1.021	L1
1065	5	2	6	3486	162	-47	0.6264E-04	0.5965E-04	0.952	L1
1067	5	2	51	3531	156	-42	0.4311E-04	0.4515E-04	1.047	L1
1069	5	2	85	3565	143	-39	0.1035E-04	0.1277E-04	1.234	L1
1071	5	2	126	3606	167	-49	0.5329E-04	0.5386E-04	1.011	L1
1073	5	3	6	3636	165	-49	0.6879E-04	0.6906E-04	1.004	L1
1075	5	3	45	3675	168	-51	0.4353E-04	0.4475E-04	1.028	L1
1077	5	3	86	3716	167	-52	0.3510E-04	0.3907E-04	1.113	L1
1078	5	3	105	3735	178	-44	0.1619E-04	0.1990E-04	1.230	L1
1079	5	3	128	3758	356	44	0.2183E-04	0.1661E-04	0.761	L1
1080	5	3	146	3776	46	-45	0.4044E-04	0.4543E-05	0.112	L1
1081	5	4	6	3786	167	-38	0.1102E-04	0.1270E-04	1.153	L1
1083	5	4	46	3826	176	-46	0.3321E-04	0.3177E-04	0.957	L1
1085	5	4	86	3866	174	-48	0.3601E-04	0.3666E-04	1.018	L1
1087	5	4	126	3906	181	-52	0.1873E-04	0.1999E-04	1.067	L1
1089	5	5	6	3936	151	-52	0.6993E-06	0.5485E-06	0.784	L1
1091	5	5	46	3976	184	-54	0.9561E-05	0.8065E-05	0.844	L1
1093	5	5	86	4016	197	-52	0.2632E-04	0.2318E-04	0.881	L1
1095	5	5	128	4058	175	-51	0.1753E-04	0.1544E-04	0.881	L1
1097	5	6	6	4086	188	-52	0.2485E-04	0.2129E-04	0.857	L1
1099	5	6	46	4126	177	-52	0.6102E-04	0.5938E-04	0.973	L1
1101	5	6	86	4166	191	-54	0.7963E-04	0.7240E-04	0.909	L1

Table 6. (Continued).

Sample	Core	Section	Depth in Section (cm)	Depth in Hole (cm)	Declination (deg)	Inclination (deg)	NRM (emu)	J_{100} (emu)	J_{100}/J_0	Note
1103	5	6	126	4206	194	-55	0.7699E-04	0.7254E-04	0.942	L1
1105	5	7	22	4252	190	-56	0.4073E-04	0.3743E-04	0.919	L1
1107	6	1	6	4286			0.4570E-05	0.2415E-05	0.529	F
1109	6	1	67	4347	31	-51	0.3309E-04	0.3485E-04	1.053	L1
1111	6	1	106	4386	43	-57	0.4049E-04	0.3598E-04	0.889	L1
1113	6	1	146	4426	63	-56	0.1237E-04	0.1056E-04	0.854	L1
1115	6	2	26	4456	35	-48	0.3326E-04	0.3226E-04	0.970	L1
1117	6	2	66	4496	53	-51	0.3450E-04	0.3643E-04	1.056	L1
1119	6	2	106	4536	56	-41	0.5831E-04	0.5671E-04	0.972	L1
1121	6	2	146	4576	71	-46	0.7053E-04	0.7330E-04	1.039	L1
1123	6	3	26	4606	66	-55	0.5079E-04	0.4799E-04	0.945	L1
1125	6	3	63	4643	81	-54	0.7311E-04	0.7222E-04	0.988	L1
1127	6	3	102	4682	88	-53	0.3394E-04	0.3314E-04	0.976	L1
1129	6	3	146	4726	63	-57	0.6839E-06	0.6920E-06	1.012	L1
1131	6	4	24	4756	81	-48	0.2404E-05	0.2218E-05	0.923	L1
1133	6	4	66	4796	86	-52	0.1841E-04	0.1699E-04	0.923	L1
1135	6	4	106	4836	83	-51	0.2761E-04	0.2668E-04	0.966	L1
1137	6	4	146	4876	99	-55	0.2893E-04	0.3367E-04	1.164	L1
1139	6	5	26	4906	90	-55	0.6737E-04	0.6803E-04	1.010	L1
1141	6	5	66	4946	68	-59	0.3964E-04	0.4335E-04	1.094	L1
1143	6	5	106	4986	67	-52	0.2143E-04	0.2457E-04	1.146	L1
1145	6	5	146	5026	79	-49	0.2629E-04	0.2353E-04	0.895	L1
1147	6	6	34	5064	72	-37	0.1374E-05	0.1244E-05	0.906	L1
1149	6	6	86	5116	75	-50	0.2321E-04	0.2111E-04	0.910	L1
1151	6	7	3	5183	73	-56	0.4278E-04	0.4016E-04	0.939	L1
1153	6	7	43	5223	70	-57	0.2653E-04	0.2431E-04	0.916	L1
1155	7	1	46	5266	301	-38	0.3578E-04	0.3165E-04	0.884	L1
1157	7	1	86	5306	298	-60	0.7281E-04	0.6341E-04	0.871	L1
1159	7	1	126	5346	298	-61	0.1145E-04	0.1157E-04	1.011	L1
1160	7	1	146	5366	122	50	0.3663E-04	0.3182E-04	0.869	L1
1161	7	2	6	5376	123	58	0.3285E-04	0.2974E-04	0.905	L1
1162	7	2	28	5398	263	-44	0.1595E-04	0.1418E-04	0.889	L1
1163	7	2	46	5416	114	47	0.3948E-04	0.3696E-04	0.936	L1
1165	7	2	86	5456	133	47	0.6829E-04	0.5882E-04	0.861	L1
1167	7	2	131	5501	122	49	0.5317E-04	0.4489E-04	0.844	L1
1169	7	3	6	5526	116	46	0.4255E-04	0.3519E-04	0.827	L1
1171	7	3	46	5566	129	46	0.4265E-04	0.3646E-04	0.855	L1
1173	7	3	86	5606	122	58	0.6792E-04	0.6968E-04	1.026	L1
1175	7	3	126	5646	125	58	0.6372E-04	0.5330E-04	0.836	L1
1177	7	4	6	5676	143	57	0.8232E-04	0.7665E-04	0.931	L1
1179	7	4	26	5717	140	52	0.5154E-04	0.4050E-04	0.786	L1
1181	7	4	86	5756	148	58	0.8095E-04	0.7638E-04	0.944	L1
1183	7	4	126	5796	160	50	0.2698E-04	0.2158E-04	0.800	L1
1184	7	4	146	5816	325	-56	0.2340E-04	0.2715E-04	1.160	L1
1185	7	5	6	5826	328	-55	0.3487E-04	0.3819E-04	1.095	L1
1187	7	5	46	5866	316	-78	0.1187E-04	0.1923E-04	1.619	L1
1189	7	5	66	5906	321	-49	0.6215E-04	0.6744E-04	1.085	L1
1191	7	5	126	5946	312	-56	0.6257E-04	0.6426E-04	1.027	L1
1193	7	6	6	5976	306	-46	0.4563E-04	0.4633E-04	1.015	L1
1195	7	6	45	6015	315	-48	0.5123E-04	0.5166E-04	1.008	L1
1197	7	6	86	6056	323	-47	0.4669E-04	0.5263E-04	1.127	L1
1199	7	6	126	6096	308	-50	0.4198E-04	0.4282E-04	1.020	L1
1201	7	7	11	6131	304	-58	0.5380E-04	0.5343E-04	0.993	L1
1202	7	7	46	6166	295	-59	0.4657E-04	0.4697E-04	1.009	L1
1203	8	1	26	6206	165	54	0.1504E-04	0.1333E-04	0.886	L1
1204	8	1	46	6226	315	-62	0.1115E-05	0.1064E-05	0.954	L1
1205	8	1	66	6246	272	42	0.1202E-04	0.1035E-04	0.861	L1
1206	8	1	87	6267	75	-59	0.7472E-06	0.6568E-06	0.879	L1
1207	8	1	92	6272	92	-50	0.1924E-05	0.1868E-05	0.971	L1
1209	8	1	126	6306	81	-53	0.1483E-05	0.1404E-05	0.947	L1

Table 6. (Continued).

Sample	Core	Section	Depth in Section (cm)	Depth in Hole (cm)	Declination (deg)	Inclination (deg)	NRM (emu)	J_{100} (emu)	J_{100}/J_0	Note
1211	8	2	6	6336	73	-45	0.2489E-05	0.2406E-05	0.967	L1
1213	8	2	46	6376	61	-51	0.4387E-04	0.3952E-04	0.901	L1
1215	8	2	86	6416	64	-49	0.6411E-04	0.5885E-04	0.918	L1
1217	8	2	126	6456	54	-55	0.6024E-04	0.5416E-04	0.899	L1
1219	8	3	6	6486	68	-56	0.6618E-04	0.6401E-04	0.967	L1
1221	8	3	46	6526	64	-56	0.7144E-04	0.6561E-04	0.918	L1
1223	8	3	86	6566	65	-50	0.5553E-04	0.5890E-04	1.061	L1
1225	8	3	126	6606	65	-46	0.4465E-04	0.4530E-04	1.014	L1
1227	8	4	6	6636	48	-43	0.4288E-04	0.4636E-04	1.081	L1
1229	8	4	48	6678	52	-51	0.6347E-04	0.6089E-04	0.959	L1
1231	8	4	86	6716	59	-34	0.4446E-04	0.4295E-04	0.966	L1
1233	8	4	126	6756	64	-44	0.4565E-04	0.4579E-04	1.003	L1
1235	8	5	6	6786	61	-41	0.4855E-04	0.4737E-04	0.976	L1
1237	8	5	46	6826	70	-43	0.4080E-04	0.4001E-04	0.981	L1
1239	8	5	86	6866	73	-45	0.1511E-04	0.1806E-04	1.195	L1
1241	8	5	123	6903	78	-50	0.5791E-04	0.6302E-04	1.088	L1
1243	8	6	6	6936	82	-49	0.3933E-04	0.4270E-04	1.086	L1
1245	8	6	46	6976	73	-56	0.1046E-03	0.1023E-03	0.977	L1
1247	8	6	91	7021	83	-60	0.7549E-04	0.7968E-04	1.056	L1
1249	8	6	126	7056	75	-47	0.6629E-04	0.6296E-04	0.950	L1
1251	8	7	5	7085	75	-49	0.8053E-04	0.7936E-04	0.985	L1
1253	8	7	36	7116	88	-55	0.8628E-04	0.9006E-04	1.044	L1
1255	9	1	31	7161	77	-43	0.1602E-04	0.1723E-04	1.076	L1
1257	9	1	66	7196	61	-56	0.4017E-04	0.4508E-04	1.122	L1
1258	9	1	86	7216	67	32	0.5689E-04	0.6237E-04	1.096	L1
1259	9	1	106	7236	71	-42	0.6136E-04	0.6231E-04	1.015	L1
1260	9	1	126	7256	58	-45	0.1512E-04	0.1930E-04	1.276	L1
1261	9	2	146	7276	249	50	0.4425E-04	0.3795E-04	0.858	L1
1263	9	2	26	7306	61	48	0.7538E-04	0.7155E-04	0.949	L1
1265	9	2	67	7347	49	55	0.6244E-04	0.5327E-04	0.853	L1
1267	9	2	106	7386	78	61	0.3821E-04	0.3532E-04	0.924	L1
1269	9	2	146	7426	61	49	0.1010E-03	0.8029E-04	0.795	L1
1271	9	3	26	7456	112	42	0.8663E-04	0.8172E-04	0.943	L1
1273	9	3	66	7496	99	49	0.4996E-04	0.4038E-04	0.808	L1
1275	9	3	106	7536	104	37	0.6787E-04	0.6201E-04	0.914	L1
1277	9	3	146	7576	117	45	0.1579E-04	0.1211E-04	0.767	L1
1279	9	4	26	7606	297	50	0.1086E-03	0.1057E-03	0.974	L1
1281	9	4	66	7646	312	41	0.7633E-04	0.6769E-04	0.887	L1
1283	9	4	106	7686	313	48	0.6943E-04	0.5788E-04	0.834	L1
1285	9	4	146	7726	314	50	0.5620E-04	0.4888E-04	0.870	L1
1287	9	5	25	7755	327	53	0.1161E-03	0.1040E-03	0.895	L1
1289	9	5	66	7796	322	57	0.7050E-04	0.5330E-04	0.756	L1
1291	9	5	100	7830	334	51	0.8589E-04	0.7122E-04	0.829	L1
1293	9	6	6	7886	316	47	0.6791E-04	0.6092E-04	0.897	L1
1295	9	6	46	7926	315	54	0.5598E-04	0.5325E-04	0.951	L1
1297	9	6	86	7966	325	54	0.5560E-04	0.4729E-04	0.851	L1
1299	9	6	126	8006	340	48	0.8341E-04	0.7401E-04	0.887	L1
1301	9	7	6	8036	336	50	0.8154E-04	0.7387E-04	0.906	L1
1302	9	7	26	8056	305	59	0.1581E-04	0.1061E-04	0.671	L1
1303	9	7	48	8078	141	-42	0.1182E-04	0.1174E-04	0.993	L1
1304	10	1	28	8108	31	55	0.4943E-04	0.4307E-04	0.871	L1
1305	10	1	46	8126	34	38	0.3978E-04	0.3666E-04	0.922	L1
1306	10	1	78	8158	235	-46	0.6801E-04	0.7009E-04	1.031	L1
1307	10	1	96	8176	221	-37	0.2774E-04	0.3139E-04	1.131	L1
1309	10	1	130	8210	223	-45	0.5719E-04	0.6044E-04	1.057	L1
1310	10	1	146	8226	217	-49	0.5144E-04	0.5110E-04	0.993	L1
1311	10	2	6	8236	196	-43	0.3538E-04	0.3561E-04	1.007	L1
1312	10	2	24	8254	11	48	0.4338E-04	0.3761E-04	0.867	L1
1313	10	2	46	8276	11	45	0.8454E-04	0.6420E-04	0.759	L1
1315	10	2	86	8316	8	52	0.7406E-04	0.6796E-04	0.918	L1

Table 6. (Continued).

Sample	Core	Section	Depth in Section (cm)	Depth in Hole (cm)	Declination (deg)	Inclination (deg)	NRM (emu)	J_{100} (emu)	J_{100}/J_0	Note
1317	10	2	126	8356	19	50	0.4981E-04	0.4010E-04	0.805	L1
1318	10	2	146	8376	183	-53	0.1745E-04	0.2662E-04	1.525	L1
1319	10	3	6	8386	180	-45	0.4050E-04	0.4079E-04	1.007	L1
1321	10	3	46	8426	176	-38	0.3214E-04	0.3143E-04	0.978	L1
1323	10	3	86	8466	178	-42	0.7631E-04	0.6928E-04	0.908	L1
1324	10	3	106	8486	170	-47	0.1547E-04	0.1733E-04	1.121	L1
1325	10	3	126	8506	354	54	0.6684E-04	0.6042E-04	0.904	L1
1327	10	4	6	8536	299	45	0.4472E-04	0.3356E-04	0.750	L1
1329	10	4	46	8576	311	48	0.6309E-04	0.5494E-04	0.871	L1
1331	10	4	86	8616	318	50	0.6750E-04	0.5654E-04	0.838	L1
1333	10	4	126	8656	307	46	0.6016E-04	0.4713E-04	0.783	L1
1335	10	5	6	8686	297	44	0.6861E-04	0.5820E-04	0.848	L1
1337	10	5	46	8726	294	46	0.5962E-04	0.5166E-04	0.866	L1
1338	10	5	66	8746	294	45	0.2063E-04	0.1487E-04	0.721	L1
1339	10	5	86	8766	123	-44	0.3724E-04	0.3765E-04	1.011	L1
1340	10	5	106	8786	108	-46	0.5225E-04	0.4965E-04	0.950	L1
1341	10	5	126	8806	108	-46	0.3914E-04	0.4185E-04	1.069	L1
1343	10	6	6	8836	76	-47	0.5016E-04	0.4799E-04	0.957	L1
1345	10	6	46	8876	64	-41	0.3957E-04	0.4588E-04	1.159	L1
1347	10	6	86	8916	62	-37	0.4167E-04	0.4665E-04	1.120	L1
1349	11	1	26	9056	199	-54	0.6015E-04	0.5868E-04	0.976	L1
1351	11	1	66	9096	196	-55	0.5362E-04	0.5684E-04	1.060	L1
1353	11	1	106	9136	196	-52	0.5078E-04	0.5196E-04	1.023	L1
1355	11	1	143	9176	192	-49	0.2599E-04	0.2794E-04	1.075	L1
1357	11	2	26	9206	196	-51	0.2544E-04	0.2501E-04	0.983	L1
1359	11	2	66	9246	198	-33	0.3502E-04	0.3362E-04	0.960	L1
1361	11	2	106	9286	200	-43	0.4665E-04	0.4971E-04	1.066	L1
1363	11	2	146	9326	203	-58	0.4504E-04	0.4817E-04	1.069	L1
1364	11	3	6	9336	225	-53	0.3167E-04	0.3390E-04	1.070	L1
1365	11	3	26	9356	26	55	0.4916E-04	0.3987E-04	0.811	L1
1367	11	3	66	9396	22	47	0.4220E-04	0.3502E-04	0.830	L1
1369	11	3	106	9436	17	47	0.6359E-04	0.5831E-04	0.917	L1
1370	11	3	126	9456	14	54	0.3733E-04	0.3120E-04	0.836	L1
1371	11	3	146	9476	200	-29	0.6256E-05	0.7830E-05	1.252	L1
1373	11	4	26	9506	205	-47	0.4083E-04	0.4364E-04	1.069	L1
1375	11	4	66	9546	210	-42	0.2594E-04	0.2678E-04	1.033	L1
1377	11	4	106	9586	208	-52	0.2329E-04	0.2467E-04	1.059	L1
1379	11	4	146	9626	199	-52	0.2965E-04	0.3123E-04	1.053	L1
1380	11	5	6	9636	196	-57	0.8611E-05	0.1054E-04	1.223	L1
1381	11	5	26	9656	42	51	0.2645E-04	0.2101E-04	0.794	L1
1383	11	5	66	9696	42	47	0.3562E-04	0.2986E-04	0.838	L1
1385	11	5	97	9727	41	49	0.4141E-04	0.3415E-04	0.825	L1
1386	11	5	116	9746	85	4	0.8046E-05	0.3718E-05	0.462	A2,4
1387	11	5	134	9764	207	-48	0.4231E-04	0.4279E-04	1.011	L1
1389	11	6	26	9806	228	-53	0.2945E-04	0.3219E-04	1.093	L1
1391	11	6	66	9846	228	-42	0.3202E-04	0.3241E-04	1.012	L1
1393	11	6	106	9886	225	-47	0.4696E-04	0.4246E-04	0.904	L1
1394	11	6	126	9906	217	-44	0.2680E-04	0.2554E-04	0.953	L1
1395	11	6	146	9926	45	56	0.3465E-04	0.2612E-04	0.754	L1
1397	11	7	21	9951	44	45	0.4694E-04	0.3983E-04	0.849	L1
1399	12	1	96	10013	160	32	0.3709E-04	0.3111E-04	0.839	L1
1401	12	1	146	10054	145	36	0.1900E-04	0.1476E-04	0.777	L1
1402	12	2	4	10062	169	28	0.6665E-05	0.4931E-05	0.740	L1
1403	12	2	34	10092	306	-27	0.3246E-04	0.3797E-04	1.170	L1
1405	12	2	67	10125	311	-22	0.8694E-05	0.7190E-05	0.827	A3-4
1407	12	2	106	10164	314	-49	0.2826E-04	0.3213E-04	1.137	L1
1408	12	2	126	10184	142	55	0.3917E-04	0.2985E-04	0.762	L1
1409	12	2	146	10204	142	47	0.5624E-04	0.4447E-04	0.791	L1
1411	12	3	26	10234	133	49	0.4837E-04	0.4022E-04	0.832	L1
1413	12	3	66	10274	136	50	0.4737E-04	0.3580E-04	0.756	L1

Table 6. (Continued).

Sample	Core	Section	Depth in Section (cm)	Depth in Hole (cm)	Declination (deg)	Inclination (deg)	NRM (emu)	J_{100} (emu)	J_{100}/J_0	Note
1415	12	3	111	10319	139	52	0.4742E-04	0.3598E-04	0.759	L1
1416	12	4	6	10364	145	44	0.2173E-04	0.1056E-04	0.486	L1
1417	12	4	26	10384	313	-51	0.2152E-04	0.2701E-04	1.255	L1
1419	12	4	66	10424	327	-38	0.2076E-04	0.2413E-04	1.163	L1
1421	12	4	106	10464	307	-58	0.1631E-04	0.2127E-04	1.304	L1
1423	12	4	146	10504	313	-49	0.2302E-04	0.2513E-04	1.092	L1
1425	12	5	26	10534	310	-44	0.1929E-04	0.2299E-04	1.192	L1
1427	12	5	66	10574	320	-51	0.2865E-04	0.3227E-04	1.126	L1
1429	12	5	106	10614	316	-31	0.1219E-04	0.1674E-04	1.373	L1
1431	12	5	146	10654	307	-44	0.1968E-04	0.2228E-04	1.132	L1
1433	12	6	86	10744	289	-52	0.2139E-04	0.2317E-04	1.083	L1
1435	12	6	123	10781	274	-51	0.1586E-04	0.1749E-04	1.103	L1
1437	13	1	26	10956	353	-49	0.8239E-05	0.1239E-04	1.503	L1
1438	13	1	46	10976	159	48	0.3311E-04	0.2597E-04	0.784	L1
1439	13	1	66	10996	168	49	0.3535E-04	0.2780E-04	0.786	L1
1440	13	1	86	11016	164	52	0.4564E-04	0.3470E-04	0.760	L1
1441	13	1	106	11036	156	48	0.2597E-04	0.1777E-04	0.684	L1
1442	13	1	126	11056	161	40	0.3100E-04	0.2218E-04	0.715	L1
1443	13	1	146	11076	169	59	0.1494E-04	0.9174E-05	0.614	L1
1444	13	2	6	11086	154	36	0.2060E-04	0.1534E-04	0.745	L1
1445	13	2	26	11106	160	47	0.3059E-04	0.2351E-04	0.768	L1
1446	13	2	46	11126	165	45	0.3959E-04	0.2761E-04	0.697	L1
1447	13	2	66	11146	167	44	0.3294E-04	0.2547E-04	0.773	L1
1448	13	2	86	11166	159	46	0.3418E-04	0.2715E-04	0.794	L1
1449	13	2	106	11186	172	-60	0.7371E-05	0.1523E-05	0.207	A1-3
1450	13	2	126	11206	340	-51	0.1065E-04	0.1448E-04	1.359	L1
1451	13	2	146	11226	8	-49	0.1968E-04	0.2173E-04	1.104	L1
1452	13	3	6	11236	340	-44	0.1294E-04	0.1516E-04	1.171	L1
1453	13	3	26	11256	3	-33	0.1418E-05	0.3569E-05	2.517	L1
1454	13	3	46	11276	351	-44	0.1449E-04	0.1711E-04	1.181	L1
1455	13	3	66	11296	356	-33	0.9721E-05	0.1608E-04	1.655	L1
1456	13	3	86	11316	358	-47	0.1185E-04	0.1465E-04	1.237	L1
1457	13	3	106	11336	177	32	0.1770E-04	0.9773E-05	0.552	L1
1458	13	3	126	11356	187	44	0.2936E-04	0.1979E-04	0.674	L1
1459	13	3	146	11376	192	47	0.3660E-04	0.2497E-04	0.682	L1
1460	13	4	6	11386	204	51	0.3511E-04	0.2531E-04	0.721	L1
1461	13	4	26	11406	196	45	0.2804E-04	0.2018E-04	0.720	L1
1462	13	4	46	11426	162	-41	0.4035E-04	0.3189E-04	0.790	L1
1463	13	4	66	11446	208	40	0.1956E-04	0.1505E-04	0.769	L1
1464	13	4	86	11466	13	15	0.4203E-05	0.3235E-05	0.770	A1-3
1465	13	4	106	11486	212	47	0.3481E-04	0.2337E-04	0.671	L1
1466	13	4	126	11506	211	45	0.2380E-04	0.1755E-04	0.737	L1
1467	13	4	146	11526	213	49	0.2796E-04	0.1977E-04	0.707	L1
1468	13	5	6	11536	210	46	0.4190E-04	0.3183E-04	0.760	L1
1469	13	5	26	11556	214	49	0.2937E-04	0.2102E-04	0.716	L1
1470	13	5	46	11576	212	41	0.2836E-04	0.1905E-04	0.672	L1
1471	13	5	66	11596	56	64	0.8749E-05	0.2183E-05	0.250	A2-3
1472	13	5	86	11616	35	-43	0.1354E-04	0.1816E-04	1.341	L1
1473	13	5	106	11636	30	-44	0.1729E-04	0.2430E-04	1.405	L1
1474	13	5	126	11656	32	-45	0.1740E-04	0.2217E-04	1.274	L1
1475	13	5	146	11676	24	-39	0.1543E-04	0.1915E-04	1.241	L1
1476	13	6	6	11686	27	-34	0.1514E-04	0.1852E-04	1.223	L1
1477	13	6	26	11706	28	-41	0.1792E-04	0.2364E-04	1.319	L1
1478	13	6	46	11726	30	-45	0.2548E-04	0.2866E-04	1.125	L1
1479	13	6	66	11746	30	-44	0.1807E-04	0.2376E-04	1.315	L1
1480	13	6	86	11766	30	-49	0.1385E-04	0.1780E-04	1.284	L1
1481	13	6	106	11786	16	-44	0.1404E-04	0.2264E-04	1.613	L1
1482	13	6	126	11806	173	-10	0.2589E-05	0.5176E-05	1.999	L1
1483	13	6	146	11826	29	-39	0.1924E-04	0.2846E-04	1.479	L1
1484	13	7	6	11836	27	-47	0.1312E-04	0.1708E-04	1.302	L1

Table 6. (Continued).

Sample	Core	Section	Depth in Section (cm)	Depth in Hole (cm)	Declination (deg)	Inclination (deg)	NRM (emu)	J_{100} (emu)	J_{100}/J_0	Note
1485	13	7	26	11856	22	-48	0.1200E-04	0.1936E-04	1.614	L1
1486	14	1	31	11866	189	53	0.2533E-04	0.1723E-04	0.680	L1
1487	14	1	56	11891	246	41	0.4624E-04	0.3475E-04	0.752	L1
1488	14	1	86	11921	36	-60	0.8273E-05	0.1264E-04	1.528	L1
1489	14	1	106	11941	217	46	0.4058E-04	0.2765E-04	0.681	L1
1490	14	1	146	11981	37	-54	0.1463E-05	0.7047E-05	4.817	L1
1491	14	2	6	11991	39	-50	0.1304E-04	0.2080E-04	1.594	L1
1492	14	2	26	12011	33	-46	0.9752E-05	0.1474E-04	1.511	L1
1493	14	2	46	12031	35	-47	0.1231E-04	0.1918E-04	1.558	L1
1494	14	2	66	12051	235	50	0.2119E-04	0.1194E-04	0.563	L1
1495	14	2	86	12071	207	54	0.1477E-04	0.7275E-05	0.493	L1
1496	14	2	106	12091	31	-47	0.9361E-05	0.1369E-04	1.462	L1
1497	14	2	126	12111	210	50	0.2554E-04	0.1493E-04	0.585	L1
1498	14	2	146	12131	208	48	0.3486E-04	0.2417E-04	0.693	L1
1499	14	3	6	12141	215	44	0.4112E-04	0.2663E-04	0.648	L1
1500	14	3	26	12161	21	-45	0.3142E-05	0.8150E-05	2.594	L1
1501	14	3	46	12181	214	45	0.1590E-04	0.7077E-05	0.445	L1
1502	14	3	66	12201	216	48	0.2341E-04	0.1442E-04	0.616	L1
1503	14	3	86	12221	221	46	0.3661E-04	0.2373E-04	0.648	L1
1504	14	3	106	12241	209	48	0.5163E-04	0.4087E-04	0.792	L1
1505	14	3	126	12261	218	45	0.5122E-04	0.3340E-04	0.652	L1
1506	14	3	146	12281	217	49	0.4075E-04	0.2651E-04	0.650	L1
1507	14	4	6	12291	220	40	0.4312E-04	0.3129E-04	0.726	L1
1508	14	4	26	12311	213	47	0.3900E-04	0.3051E-04	0.782	L1
1509	14	4	46	12331	206	47	0.3678E-04	0.2183E-04	0.594	L1
1510	14	4	66	12351	211	37	0.3144E-04	0.2271E-04	0.722	L1
1511	14	4	86	12371	210	42	0.4121E-04	0.2822E-04	0.685	L1
1512	14	4	106	12391	32	-51	0.7912E-05	0.1485E-04	1.877	L1
1513	14	4	126	12411	23	-47	0.6006E-05	0.6313E-05	1.051	L1
1514	14	4	146	12431	8	-43	0.2324E-04	0.2954E-05	0.127	A2-4
1515	14	5	6	12441	238	74	0.3502E-04	0.1038E-04	0.296	L1
1516	14	5	26	12461	200	42	0.3547E-04	0.2018E-04	0.569	L1
1517	14	5	46	12481	24	-40	0.2395E-04	0.3157E-04	1.318	L1
1518	14	5	66	12501	24	-41	0.1698E-04	0.2228E-04	1.312	L1
1519	14	5	86	12521	28	-41	0.2309E-04	0.3141E-04	1.360	L1
1520	14	5	106	12541	21	-41	0.2972E-04	0.3448E-04	1.160	L1
1521	14	5	126	12561	21	-43	0.2532E-04	0.3161E-04	1.248	L1
1522	14	5	146	12581	18	-46	0.2950E-04	0.3579E-04	1.213	L1
1523	14	6	6	12591	18	-39	0.2763E-04	0.3340E-04	1.209	L1
1524	14	6	26	12611	177	46	0.1797E-04	0.9230E-05	0.514	L1
1525	14	6	46	12631	15	-35	0.1206E-04	0.2111E-04	1.750	L1
1526	14	6	66	12651	197	53	0.5247E-04	0.3329E-04	0.634	L1
1527	14	6	86	12671	201	44	0.6367E-04	0.4145E-04	0.651	L1
1528	14	6	106	12691	200	43	0.5489E-04	0.3569E-04	0.650	L1
1529	14	6	126	12711	203	45	0.4876E-04	0.3162E-04	0.649	L1
1530	14	6	138	12723	197	48	0.4790E-04	0.2892E-04	0.604	L1
1531	14	7	6	12741	351	-26	0.9530E-05	0.4193E-05	0.440	L1
1532	14	7	26	12761	31	-38	0.1018E-04	0.2033E-05	0.200	L1
1533	14	7	44	12779	242	47	0.1644E-04	0.2298E-05	0.140	L1
1538	15	1	44	12844	10	35	0.3002E-04	0.1502E-04	0.500	L1
1539	15	1	66	12866	12	50	0.2763E-04	0.1818E-04	0.658	L1
1540	15	1	86	12886	5	46	0.3703E-04	0.2156E-04	0.582	L1
1541	15	1	108	12908	6	48	0.4506E-04	0.3042E-04	0.675	L1
1542	15	1	126	12926	8	38	0.3070E-04	0.1880E-04	0.612	L1
1543	15	1	146	12946	7	44	0.2548E-04	0.1646E-04	0.646	L1
1544	15	2	6	12956	18	45	0.3706E-04	0.2395E-04	0.646	L1
1545	15	2	26	12976	21	40	0.3596E-04	0.2036E-04	0.566	L1
1546	15	2	46	12996	17	43	0.5665E-04	0.3519E-04	0.621	L1
1547	15	2	66	13016	22	44	0.3196E-04	0.2053E-04	0.642	L1
1548	15	2	86	13036	25	43	0.3378E-04	0.1933E-04	0.572	L1

Table 6. (Continued).

Sample	Core	Section	Depth in Section (cm)	Depth in Hole (cm)	Declination (deg)	Inclination (deg)	NRM (emu)	J_{100} (emu)	J_{100}/J_0	Note
1549	15	2	106	13056	30	39	0.3428E-04	0.2187E-04	0.638	L1
1550	15	2	126	13076	18	43	0.4259E-04	0.2585E-04	0.607	L1
1551	15	2	146	13096	28	43	0.4667E-04	0.3579E-04	0.767	L1
1552	15	3	6	13106	216	-40	0.9441E-05	0.1392E-04	1.474	L1
1553	15	3	26	13126	215	-45	0.3001E-04	0.3488E-04	1.162	L1
1554	15	3	46	13146	39	39	0.4376E-04	0.3294E-04	0.753	L1
1555	15	3	66	13166	224	-42	0.1235E-04	0.1592E-04	1.289	L1
1556	15	3	86	13186	42	45	0.2121E-04	0.1063E-04	0.501	L1
1557	15	3	106	13206	229	-38	0.4946E-05	0.1014E-04	2.050	L1
1558	15	3	126	13226	223	-39	0.6896E-05	0.1248E-04	1.809	L1
1559	15	3	146	13246	220	-47	0.2387E-04	0.2887E-04	1.210	L1
1560	15	4	6	13256	226	-46	0.1605E-04	0.1657E-04	1.032	L1
1561	15	4	26	13275	228	-46	0.1456E-04	0.1803E-04	1.239	L1
1562	15	4	46	13296	54	47	0.3137E-04	0.2054E-04	0.655	L1
1563	15	4	66	13316	189	-35	0.7430E-05	0.1533E-05	0.206	L1
1564	15	4	86	13336	246	-42	0.3972E-05	0.1167E-04	2.939	L1
1565	15	4	106	13356	231	-42	0.1475E-04	0.2004E-04	1.358	L1
1566	15	4	126	13376	243	-36	0.8419E-05	0.1491E-04	1.771	L1
1567	15	4	146	13396	236	-39	0.7604E-05	0.1191E-04	1.566	L1
1568	15	5	6	13406	244	-41	0.1656E-04	0.2228E-04	1.345	L1
1569	15	5	26	13426	244	-39	0.1789E-04	0.2333E-04	1.304	L1
1570	15	5	46	13446	64	47	0.2998E-04	0.1630E-04	0.544	L1
1571	15	5	66	13466	68	48	0.3657E-04	0.2274E-04	0.622	L1
1572	15	5	84	13484	258	-36	0.4662E-05	0.3502E-05	0.751	L1
1573	15	5	100	13500	248	-46	0.1232E-04	0.1737E-04	1.410	L1
1574	15	5	116	13516	70	42	0.1740E-04	0.6583E-05	0.378	L1
1575	15	6	6	13556	72	43	0.4046E-04	0.2943E-04	0.727	L1
1576	15	6	26	13576	109	13	0.1144E-04	0.3175E-05	0.278	A2-3
1577	15	6	46	13596	241	-42	0.7020E-05	0.9208E-05	1.312	L1
1578	15	6	66	13616	254	-48	0.1224E-04	0.1810E-04	1.479	L1
1579	15	6	86	13636	202	-71	0.1065E-04	0.1399E-04	1.314	L1
1580	15	6	106	13656	249	-43	0.1101E-04	0.1888E-04	1.715	L1
1581	15	6	116	13666	74	51	0.2254E-04	0.1406E-04	0.624	L1
1582	15	6	146	13696	254	-30	0.7919E-05	0.1259E-04	1.591	L1
1583	15	7	6	13706	250	-39	0.7291E-05	0.1148E-04	1.574	L1
1584	15	7	26	13726	65	43	0.3110E-04	0.1872E-04	0.602	L1
1585	15	7	45	13745	137	-72	0.8058E-05	0.4334E-05	0.538	L1
1586	16	1	36	13811	175	-58	0.2041E-04	0.1981E-04	0.971	L1
1587	16	1	56	13831	180	-69	0.1941E-04	0.2104E-04	1.084	L1
1588	16	1	76	13851			0.2368E-04	0.1437E-04	0.607	F
1589	16	1	96	13871			0.1852E-04	0.1454E-04	0.785	F
1590	16	1	116	13891			0.9501E-05	0.7753E-06	0.082	F
1591	16	1	136	13911	127	-36	0.4586E-05	0.1184E-04	2.581	L1
1592	16	2	6	13931	130	-41	0.8434E-05	0.1075E-04	1.274	L1
1593	16	2	26	13951	310	42	0.3245E-04	0.1746E-04	0.538	L1
1594	16	2	46	13971	306	35	0.1881E-04	0.6758E-05	0.359	L1
1595	16	2	66	13991	311	47	0.2391E-04	0.1421E-04	0.595	L1
1596	16	2	86	14011	116	-34	0.5894E-05	0.1342E-04	2.277	L1
1597	16	2	106	14031	115	-39	0.1061E-05	0.9290E-05	8.760	L1
1598	16	2	126	14051	122	-39	0.7173E-05	0.6423E-05	0.895	L1
1599	16	2	146	14071	307	38	0.2429E-04	0.1301E-04	0.536	L1
1600	16	3	6	14081	292	48	0.3254E-04	0.1882E-04	0.578	L1
1601	16	3	26	14101	300	52	0.2697E-04	0.1707E-04	0.633	L1
1602	16	3	46	14121	296	44	0.3104E-04	0.1657E-04	0.534	L1
1603	16	3	66	14141	299	43	0.2920E-04	0.1614E-04	0.553	L1
1604	16	3	86	14161	299	48	0.3069E-04	0.1672E-04	0.545	L1
1605	16	3	106	14181	118	-40	0.4671E-05	0.7214E-05	1.544	L1
1606	16	3	126	14201	295	54	0.2012E-04	0.7350E-05	0.365	L1
1607	16	3	146	14221	304	49	0.3431E-04	0.1978E-04	0.576	L1
1608	16	4	6	14231	288	57	0.3891E-04	0.1945E-04	0.500	L1

Table 6. (Continued).

Sample	Core	Section	Depth in Section (cm)	Depth in Hole (cm)	Declination (deg)	Inclination (deg)	NRM (emu)	J_{100} (emu)	J_{100}/J_0	Note
1609	16	4	26	14251	295	49	0.2588E-04	0.1419E-04	0.548	L1
1610	16	4	46	14271	302	52	0.3367E-04	0.1291E-04	0.383	L1
1611	16	4	66	14291	304	47	0.1854E-04	0.8913E-05	0.481	L1
1612	16	4	86	14311	305	53	0.3482E-04	0.2341E-04	0.672	L1
1613	16	4	106	14331	307	55	0.2479E-04	0.1343E-04	0.542	L1
1614	16	4	126	14351	113	-52	0.7806E-05	0.1519E-04	1.946	L1
1615	16	4	146	14371	121	-48	0.5035E-05	0.1095E-04	2.175	L1
1616	16	5	6	14381	122	-39	0.3309E-05	0.7869E-05	2.378	L1
1617	16	5	26	14401	108	-51	0.7526E-05	0.1389E-04	1.845	L1
1618	16	5	46	14421	297	58	0.4191E-04	0.1792E-04	0.428	L1
1619	16	5	66	14441	120	-51	0.9065E-05	0.5156E-05	0.569	L1
1620	16	5	86	14461	264	53	0.3941E-04	0.1885E-04	0.478	L1
1621	16	5	106	14481	295	54	0.3171E-04	0.1877E-04	0.592	L1
1622	16	5	126	14501	90	-56	0.9104E-05	0.1775E-05	0.195	L1
1623	16	5	146	14521	101	-56	0.3760E-05	0.1319E-04	3.507	L1
1624	15	6	7	14532	97	-53	0.2974E-05	0.1194E-04	4.016	L1
1625	16	6	21	14546	120	-55	0.3110E-05	0.8721E-05	2.804	L1
1626	17	1	32	14734	11	-27	0.5588E-05	0.1171E-04	2.096	L1
1627	17	1	48	14750	8	-35	0.3507E-05	0.1355E-04	3.864	L1
1628	17	1	67	14769	358	-27		0.5876E-05		L1
1629	17	1	86	14788	189	41	0.2875E-04	0.8843E-05	0.308	L1
1630	17	1	106	14808	188	32	0.3565E-04	0.1142E-04	0.320	L1
1631	17	1	126	14828	190	35	0.3124E-04	0.1310E-04	0.419	L1
1632	17	1	146	14848	8	-23	0.1519E-04	0.3254E-05	0.214	L1
1633	17	2	11	14863	28	-23	0.1430E-04	0.4898E-05	0.342	L1
1634	17	2	43	14895	208	41	0.2591E-04	0.7429E-05	0.287	L1
1635	17	2	55	14907	209	33	0.3334E-04	0.1251E-04	0.375	L1
1636	17	2	71	14923	209	34	0.2936E-04	0.7848E-05	0.267	L1
1637	17	2	86	14938	212	31	0.3446E-04	0.1332E-04	0.386	L1
1638	17	2	106	14958	216	32	0.3100E-04	0.8913E-05	0.288	L1
1639	17	2	116	14978	213	36	0.2674E-04	0.7604E-05	0.284	L1
1640	17	2	146	14998	24	-37	0.1304E-04	0.4397E-05	0.337	L1
1641	17	3	6	15008	35	- 4	0.1532E-04	0.2212E-05	0.144	L1
1642	17	3	26	15028	36	-26	0.9142E-05	0.4795E-05	0.525	L1
1643	17	3	46	15048	223	39	0.2501E-04	0.7120E-05	0.285	L1
1644	17	3	66	15068	224	69	0.2510E-04	0.1935E-05	0.077	L1
1645	17	3	82	15084	230	39	0.2861E-04	0.4050E-05	0.142	L1
1646	17	3	99	15101	222	26	0.2749E-04	0.2729E-05	0.099	L1
1647	17	3	118	15120	221	57	0.2796E-04	0.2341E-05	0.084	L1
1648	17	3	134	15136	236	68	0.2665E-04	0.2439E-05	0.092	L1
1649	17	4	6	15158			0.2442E-04			
1650	17	4	26	15178	80	53	0.3638E-04	0.2573E-05	0.071	L1
1651	17	4	46	15198	66	38	0.3047E-04	0.4412E-05	0.145	L1
1652	17	4	66	15218	65	44	0.3240E-04	0.4173E-05	0.129	L1
1653	17	4	82	15234	60	40	0.4795E-04	0.9313E-05	0.194	L1
1654	17	4	100	15252	52	50	0.5287E-04	0.8289E-05	0.157	L1
1655	17	4	118	15270	227	-53	0.2877E-04	0.4426E-05	0.154	L1
1656	17	4	136	15288	65	44	0.3212E-04	0.7608E-05	0.237	L1
1657	17	5	6	15308	161	-41	0.3230E-04	0.1493E-05	0.046	L1
1658	17	5	26	15328	26	43	0.4083E-04	0.5451E-05	0.134	L1
1659	17	5	46	15348	170	-61	0.4079E-04	0.1871E-05	0.046	L1
1660	17	5	66	15368	26	47	0.5119E-04	0.3999E-04	0.781	L1
1661	17	5	86	15388	77	- 3	0.3779E-04	0.9297E-06	0.025	L1
1662	17	5	106	15408	32	30	0.3819E-04	0.6601E-05	0.173	L1
1663	17	5	126	15428	29	38	0.4074E-04	0.6990E-05	0.172	L1
1664	18	1	26	15686	108	19	0.3434E-04	0.1357E-04	0.395	L1
1665	18	1	46	15706	127	30	0.3803E-04	0.1626E-04	0.428	L1
1666	18	1	66	15726	294	-38	0.1403E-04	0.9060E-05	0.646	L1
1667	18	1	86	15746	292	-35	0.1273E-04	0.1168E-04	0.918	L1
1668	18	1	106	15766	69	-62	0.2475E-04	0.7350E-06	0.030	L1

Table 6. (Continued).

Sample	Core	Section	Depth in Section (cm)	Depth in Hole (cm)	Declination (deg)	Inclination (deg)	NRM (emu)	J_{100} (emu)	J_{100}/J_0	Note
1669	18	1	126	15786	123	56	0.3054E-04	0.3829E-05	0.125	L1
1670	18	1	146	15806	273	-32	0.2734E-04	0.1124E-05	0.041	L2
1671	18	2	6	15816	109	55	0.2195E-04	0.2413E-05	0.110	L1
1672	18	2	29	15839	279	-26	0.2490E-04	0.1746E-05	0.070	L1
1673	18	2	46	15856	112	44	0.4851E-04	0.1534E-04	0.316	L1
1674	18	2	66	15876	285	-39	0.1673E-04	0.9543E-05	0.570	L1
1675	18	2	86	15896	280	-29	0.0000E+00	0.2565E-04	0.000	L1
1676	18	2	106	15916	284	-28	0.1403E-04	0.1146E-04	0.816	L1
1677	18	2	126	15936	290	-48	0.1991E-04	0.2438E-05	0.122	L1
1678	18	2	146	15956	102	35	0.4185E-04	0.9439E-05	0.226	L1
1679	18	3	6	15966	104	29	0.5050E-04	0.2155E-04	0.427	L1
1680	18	3	26	15986	95	29	0.4334E-04	0.1840E-04	0.425	L1
1681	18	3	46	16006	93	43	0.3608E-04	0.1092E-04	0.303	L1
1682	18	3	66	16026	101	36	0.4690E-04	0.1932E-04	0.412	L1
1683	18	3	86	16046	267	15	0.2479E-04	0.5041E-05	0.203	L1
1684	18	3	106	16066	99	26	0.4028E-04	0.9549E-05	0.237	L1
1685	18	3	117	16077	307	-46	0.2291E-04	0.2266E-05	0.099	L1
1686	18	4	6	16116	293	-31	0.3353E-04	0.1276E-05	0.038	L2
1687	18	4	26	16136	5	-61	0.3110E-04	0.3020E-05	0.097	L2
1688	18	4	46	16156	309	1	0.2732E-04	0.1373E-05	0.050	A2-8
1689	18	4	66	16176	260	-54	0.2371E-04	0.7729E-05	0.326	L1
1690	18	4	86	16196	107	57	0.3912E-04	0.5386E-05	0.138	L1
1691	18	4	106	16216	272	-11	0.2585E-04	0.1773E-05	0.069	L2
1692	18	4	126	16236	288	-15	0.4435E-04	0.1109E-05	0.025	A2,2,3
1693	18	*	5	16248	27	30	0.3709E-04	0.3847E-05	0.104	L1
1694	18	*	30	16273	354	36	0.4899E-04	0.1875E-04	0.383	L1
1695	19	1	47	16634	54	-38	0.2905E-04	0.1927E-04	0.663	L1
1696	19	1	66	16653	196	-68	0.1914E-04	0.4100E-05	0.214	L1
1697	19	1	86	16673	225	-28	0.2365E-04	0.6389E-05	0.270	L1
1698	19	1	106	16693	254	-18	0.3959E-04	0.1108E-05	0.028	L2
1699	19	1	126	16713	87	31	0.3263E-04	0.2728E-05	0.084	L1
1700	19	1	146	16733	66	38	0.5360E-04	0.1249E-04	0.233	L1
1741	19	2	32	16769	134	-58	0.3322E-04	0.3195E-05	0.096	L1
1742	19	2	48	16785	220	-24	0.3112E-04	0.1861E-04	0.598	L1
1743	19	2	66	16803	61	37	0.7116E-04	0.2620E-04	0.368	L1
1744	19	2	86	16823	73	52	0.5539E-04	0.1618E-04	0.292	L1
1701	19	2	99	16836	58	38	0.6668E-04	0.2130E-04	0.319	L1
1702	19	2	111	16848	236	-24	0.3478E-04	0.3144E-05	0.090	A2-3
1703	19	2	125	16862	67	50	0.4658E-04	0.9889E-05	0.212	L1
1704	19	2	138	16875	53	40	0.6065E-04	0.1456E-04	0.240	L1
1705	19	3	6	16893	65	60	0.5155E-04	0.8085E-05	0.157	L1
1706	19	3	26	16913	40	48	0.6502E-04	0.1873E-04	0.288	L1
1707	19	3	46	16933	40	42	0.5965E-04	0.1962E-04	0.329	L1
1708	19	3	66	16953	58	45	0.7369E-04	0.1264E-04	0.172	L1
1709	19	3	86	16973	36	52	0.1058E-03	0.4526E-04	0.428	L1
1710	19	3	106	16993	48	47	0.7406E-04	0.2157E-04	0.291	L1
1711	19	*	5	17012	131	38	0.6046E-04	0.2648E-04	0.438	L1
1712	19	*	29	17036	335	-51	0.7116E-04	0.2450E-04	0.344	L1
1534	20	1	6	17586	21	-60	0.3479E-04	0.2473E-04	0.711	L1
1535	20	1	22	17602	85	-82	0.2995E-04	0.2995E-04	1.000	L1
1536	20	1	46	17626	19	- 2	0.4952E-04	0.6246E-05	0.126	L1
1537	20	1	71	17651	170	-59	0.3531E-04	0.7584E-05	0.215	L1

Note: A = vector average of declination and inclination at demagnetization levels (x100) shown. L = demagnetization level (x 100) used to define declination and inclination.
F = flow-material (based on shipboard visual descriptions).

Table 7. Magnetization of Site 578 samples after AF demagnetization at intensities above 100 Oe.

Sample	Core	Section	Depth in Section (cm)	Depth in Hole (cm)	Demagnetization Level (OE)	J (emu)	J/J_0
932	2	1	146	626	200	0.4132E-04	0.695
					300	0.2687E-04	0.452
					400	0.1937E-04	0.326
933	2	2	5	635	200	0.2073E-04	0.604
					300	0.1406E-04	0.410
934	2	2	26	656	200	0.3296E-04	0.623
					300	0.2351E-04	0.444
					400	0.1602E-04	0.303
943	2	3	66	846	200	0.3776E-04	0.615
970	3	1	106	1536	200	0.2907E-04	0.604
					300	0.1972E-04	0.410
					400	0.1318E-04	0.274
971	3	1	126	1556	200	0.2268E-04	0.590
					300	0.1500E-04	0.391
					400	0.1078E-04	0.281
972	3	1	146	1576	200	0.3206E-04	0.643
					300	0.2194E-04	0.440
					400	0.1430E-04	0.287
980	3	2	146	1726	200	0.3292E-04	0.564
					300	0.2160E-04	0.370
					400	0.1529E-04	0.262
981	3	3	6	1736	200	0.3145E-04	0.598
					300	0.2066E-04	0.393
					400	0.1282E-04	0.244
982	3	3	26	1756	200	0.5557E-04	0.643
					300	0.3565E-04	0.413
					400	0.2460E-04	0.285
1015	4	1	26	2406	200	0.5280E-05	0.566
					300	0.3119E-05	0.334
					400	0.1905E-05	0.204
1043	4	3	105	2785	200	0.8119E-05	1.255
					300	0.6588E-05	1.019
1033	4	4	65	2895	200	0.4803E-06	0.931
					300	0.4005E-06	0.776
					400	0.3983E-06	0.772
1035	4	4	110	2940	200	0.7180E-06	0.757
					300	0.6649E-06	0.701
					400	0.4490E-06	0.473
1057	4	6	66	3196	200	0.2376E-04	0.870
					300	0.1644E-04	0.602
1062	5	1	106	3436	200	0.8516E-05	0.441
1079	5	3	128	3758	200	0.8811E-05	0.404
					300	0.6265E-05	0.287
					400	0.3528E-05	0.162
1080	5	3	146	3776	200	0.4987E-05	0.123
					300	0.4579E-05	0.113
					400	0.3042E-05	0.075
					401	0.2945E-05	0.073
					500	0.2658E-05	0.066
					600	0.1237E-05	0.031
1107	6	1	6	4286	200	0.2013E-05	0.441
					300	0.1515E-05	0.332
1129	6	3	146	4726	200	0.5970E-06	0.873
					300	0.4529E-06	0.662
1160	7	1	146	5366	200	0.2766E-04	0.755
					300	0.1873E-04	0.511
1161	7	2	6	5376	200	0.2213E-04	0.674
					300	0.1601E-04	0.487

Table 7. (Continued).

Sample	Core	Section	Depth in Section (cm)	Depth in Hole (cm)	Demagnetization Level (OE)	J (emu)	J/J_0
1187	7	5	46	5866	200	0.1821E-04	1.534
1203	8	1	26	6206	200	0.1086E-04	0.722
					300	0.6289E-05	0.418
					400	0.3930E-05	0.261
1204	8	1	46	6226	200	0.9682E-06	0.868
1258	9	1	86	7216	200	0.4474E-04	0.786
					300	0.3401E-04	0.598
					400	0.2137E-04	0.376
					500	0.1347E-04	0.237
					600	0.9747E-05	0.171
					700	0.6455E-05	0.113
					800	0.4818E-05	0.085
					900	0.3515E-05	0.062
					1000	0.1613E-04	0.284
					1001	0.2339E-04	0.411
1261	9	1	146	7276	200	0.2555E-04	0.578
					300	0.1791E-04	0.405
					400	0.1125E-04	0.254
1277	9	3	146	7576	200	0.9401E-05	0.595
					300	0.7193E-05	0.456
					400	0.5297E-05	0.335
1281	9	4	66	7646	200	0.5498E-04	0.720
					300	0.3802E-04	0.498
					400	0.2789E-04	0.365
1303	9	7	6	8078	200	0.9738E-05	0.824
1386	11	4	86	9746	200	0.1749E-05	0.217
					400	0.5929E-06	0.074
1402	12	2	4	10062	200	0.3298E-05	0.495
1403	12	2	34	10092	200	0.2829E-04	0.872
1405	12	2	67	10125	200	0.7830E-05	0.901
					300	0.6293E-05	0.724
					400	0.4484E-05	0.516
1449	13	2	106	11186	200	0.9654E-06	0.131
					300	0.7596E-06	0.103
1453	13	3	6	11256	200	0.3595E-05	2.535
					300	0.3129E-05	2.207
1462	13	4	46	11426	200	0.2352E-04	0.583
					201	0.2211E-04	0.548
					300	0.1453E-04	0.360
					400	0.1051E-04	0.260
1464	13	4	86	11466	200	0.2320E-05	0.552
					300	0.1696E-05	0.403
					400	0.1069E-05	0.254
					401	0.1206E-05	0.287
					500	0.8130E-06	0.193
					500	0.8707E-06	0.207
1471	13	5	6	11596	200	0.1755E-05	0.201
					300	0.9173E-06	0.105
1488	14	1	86	11921	200	0.9574E-05	1.157
					300	0.6095E-05	0.737
1490	14	1	146	11981	200	0.5393E-05	3.686
1500	14	3	26	12161	200	0.6505E-05	2.071
1513	14	4	126	12411	200	0.5417E-05	0.902
1514	14	4	146	12431	200	0.2876E-05	0.124
					400	0.2151E-05	0.093
					401	0.1955E-05	0.084
1515	14	5	6	12441	200	0.3592E-05	0.103
					300	0.1548E-05	0.044

Table 7. (Continued).

Sample	Core	Section	Depth in Section (cm)	Depth in Hole (cm)	Demagnetization Level (OE)	J (emu)	J/J_0
1524	14	6	26	12611	200	0.4682E-05	0.261
1531	14	7	6	12741	200	0.3566E-05	0.374
1532	14	7	26	12761	200	0.2050E-05	0.201
1538	15	1	44	12844	200	0.1030E-04	0.343
1554	15	3	46	13146	200	0.2130E-04	0.487
1557	15	3	106	13206	200	0.7991E-05	1.616
1563	15	4	66	13316	200	0.2058E-05	0.277
1566	15	4	126	13376	200	0.1473E-04	1.749
1567	15	4	146	13396	200	0.9878E-05	1.299
1572	15	5	84	13484	200	0.2857E-05	0.613
1576	15	6	26	13576	200	0.1087E-05	0.095
					300	0.8085E-06	0.071
					400	0.3896E-06	0.034
1577	15	6	46	13596	200	0.7011E-05	0.999
1579	15	6	86	13636	200	0.9886E-05	0.928
					300	0.5618E-05	0.528
					400	0.3977E-05	0.373
1582	15	6	146	13696	200	0.8980E-05	1.134
1585	15	7	45	13745	200	0.3341E-05	0.415
					300	0.2223E-05	0.276
					400	0.1102E-05	0.137
					500	0.9358E-06	0.116
1586	16	1	36	13811	200	0.1333E-04	0.653
1587	15	1	56	13831	200	0.1439E-04	0.741
					300	0.7812E-05	0.402
1590	16	1	116	13891	200	0.3516E-06	0.037
1592	16	2	6	13931	200	0.8549E-05	1.014
1596	16	2	86	14011	200	0.9364E-05	1.589
1597	16	2	106	14031	200	0.7786E-05	7.340
1605	16	3	105	14181	200	0.5042E-05	1.079
1616	16	5	6	14381	200	0.6133E-05	1.854
1619	16	5	66	14441	200	0.4128E-05	0.455
1622	16	5	126	14501	200	0.2322E-05	0.255
					300	0.1419E-05	0.156
					400	0.1134E-05	0.125
1624	16	6	7	14532	200	0.7615E-05	2.560
1625	16	6	21	14546	200	0.6492E-05	2.087
1626	17	1	32	14734	200	0.7998E-05	1.431
					300	0.5865E-05	1.050
1627	17	1	48	14750	200	0.9433E-05	2.689
1628	17	1	67	14769	200	0.4391E-05	
1632	17	1	146	14848	200	0.3200E-05	0.211
1633	17	2	6	14863	200	0.3618E-05	0.253
					300	0.2515E-05	0.176
1635	17	2	55	14907	200	0.7296E-05	0.219
1637	17	2	86	14938	200	0.7611E-05	0.221
1640	17	2	146	14998	200	0.3495E-05	0.268
1641	17	3	6	15008	200	0.1972E-05	0.129
1642	17	3	26	15028	200	0.4236E-05	0.463
1644	17	3	66	15068	200	0.4656E-06	0.019
1646	17	3	99	15101	200	0.6381E-06	0.023
1648	17	3	134	15136	200	0.8466E-06	0.032
1649	17	4	6	15158	200	0.8036E-06	0.033
1651	17	4	46	15198	200	0.1333E-05	0.044
1655	17	4	118	15270	200	0.4578E-05	0.159
1656	17	4	136	15288	200	0.3553E-05	0.111
1657	17	5	6	15308	200	0.2679E-05	0.083
1659	17	5	46	15348	200	0.3254E-05	0.080

Table 7. (Continued).

Sample	Core	Section	Depth in Section (cm)	Depth in Hole (cm)	Demagnetization Level (OE)	J (emu)	J/J$_0$
1660	17	5	66	15368	200	0.7063E-05	0.138
1661	17	5	86	15388	200	0.1627E-05	0.043
1664	18	1	26	15686	200	0.7207E-05	0.210
					300	0.4591E-05	0.134
					400	0.2686E-05	0.078
1666	18	1	66	15726	200	0.7451E-05	0.531
1670	18	1	146	15806	200	0.1248E-05	0.046
					300	0.8684E-06	0.032
1672	18	2	29	15839	200	0.2420E-05	0.097
					300	0.2190E-05	0.088
1674	18	2	66	15876	200	0.8124E-05	0.486
1675	18	2	86	15896	200	0.1892E-04	0.000
1676	18	2	106	15916	200	0.9851E-05	0.702
1677	18	2	126	15936	200	0.3407E-05	0.171
1680	18	3	26	15986	200	0.1291E-04	0.298
					300	0.6404E-05	0.148
1682	18	3	66	16026	200	0.1205E-04	0.257
1683	18	3	86	16046	200	0.3223E-05	0.130
					201	0.3684E-05	0.149
					300	0.1944E-05	0.078
					400	0.1801E-05	0.073
					500	0.2234E-05	0.090
					600	0.2448E-05	0.099
1684	18	3	106	16066	200	0.4631E-05	0.115
1685	18	3	117	16077	200	0.2795E-05	0.122
1686	18	4	6	16116	200	0.1562E-05	0.047
1687	18	4	26	16136	200	0.1360E-05	0.044
					201	0.1098E-05	0.035
1688	18	4	46	16156	200	0.1122E-05	0.041
					201	0.1096E-05	0.040
					300	0.1169E-05	0.043
					400	0.2011E-05	0.074
					500	0.1770E-05	0.065
					600	0.3131E-05	0.115
					700	0.2435E-05	0.089
					800	0.2655E-05	0.097
1689	18	4	66	16176	200	0.5579E-05	0.235
1690	18	4	86	16196	200	0.2713E-05	0.069
1691	18	4	106	16216	200	0.2695E-05	0.104
					201	0.2972E-05	0.115
					300	0.1169E-05	0.045
1692	18	4	126	16236	200	0.1328E-05	0.030
					200	0.1290E-05	0.029
1693	18	*	5	16248	200	0.4618E-05	0.125
					201	0.4476E-05	0.121
					300	0.1837E-05	0.050
1694	18	*	30	16273	200	0.1270E-04	0.259
					300	0.7325E-05	0.150
					400	0.3993E-05	0.082
					500	0.2557E-05	0.052
					600	0.2264E-05	0.046
1696	19	1	47	16653	200	0.2600E-05	0.136
					300	0.1071E-05	0.056
1697	19	1	86	16673	200	0.5269E-05	0.223
1698	19	1	106	16693	200	0.2138E-05	0.054
1741	19	2	32	16769	200	0.3776E-05	0.114
1743	19	2	66	16803	200	0.1326E-04	0.186
1702	19	2	111	16848	200	0.4169E-05	0.120

Table 7. (Continued).

Sample	Core	Section	Depth in Section (cm)	Depth in Hole (cm)	Demagnetization Level (OE)	J (emu)	J/J_0
					300	0.2160E-05	0.062
1534	20	1	6	17586	200	0.1453E-04	0.418
1535	20	1	22	17602	200	0.1834E-04	0.612
					300	0.9067E-05	0.303
					400	0.4177E-05	0.139
					500	0.3763E-05	0.126
1536	20	1	46	17626	200	0.2795E-05	0.056
					300	0.1223E-05	0.025
1537	20	1	71	17651	200	0.6546E-05	0.185

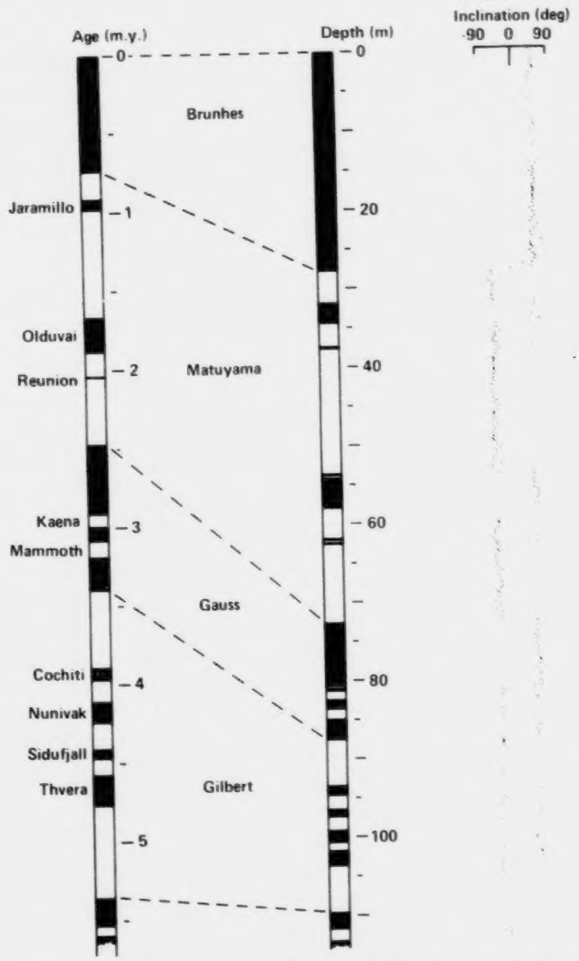

Figure 6. Correlations of the inclination data and paleomagnetic polarity stratigraphy of the upper part of Site 578 with the time scale of Berggren et al. (in press) and the age of the Reunion Event from MacDougall (1977).

Table 8. Magnetostratigraphy for Hole 578.

Age[a] (m.y.)	Depth in hole (m)	Note[b]	Boundary or event
0.73	27.86 ± 0.19		Brunhes/Matuyama
0.91	31.86 ± 0.09		Jaramillo
0.98	34.46 ± 0.09		
	37.46 ± 0.10	(+)[c]	
	37.67 ± 0.08		
1.66	53.56 ± 0.09		
	53.07 ± 0.20	(−)[c]	Olduvai
	54.07 ± 0.09		
1.88	58.06 ± 0.09		
2.01[d]	61.86 ± 0.19		
	62.16 ± 0.09	(−)[c]	Reunion
	62.36 ± 0.09		
2.04[d]	62.56 ± 0.09		
2.47	72.66 ± 0.09		Matuyama/Gauss
	80.67 ± 0.10	(−)[c]	
	80.93 ± 0.14		
2.92	81.43 ± 0.15		Kaena
2.99	82.45 ± 0.08		
3.08	83.66 ± 0.09		Mammoth
3.18	84.96 ± 0.09		
3.40	87.56 ± 0.09		Gauss/Gilbert
3.88	93.46 ± 0.09		Cochiti
3.97	94.66 ± 0.09		
4.10	96.46 ± 0.09		Nunivak
4.24	97.46 ± 0.18		
4.40	99.16 ± 0.09		Sidufjall
4.47	100.77 ± 0.14		
4.57	101.74 ± 0.09		Thvera
4.77	103.74 ± 0.09		
5.35	109.66 ± 0.09		Base of Gilbert
	111.76 ± 0.09		Anomaly 3.1
5.68	113.26 ± 0.09		
	114.16 ± 0.09	(−)[c]	Anomaly 3.2
5.89	115.96 ± 0.19		
6.37	118.61 ± 0.04		
	119.06 ± 0.14	(−)[c]	Anomaly 3.3
	119.31 ± 0.09	(+)	
6.50	119.61 ± 0.19		
6.70	120.41 ± 0.09		
6.78	120.81 ± 0.09	(−)	
6.85	121.01 ± 0.09		
	121.51 ± 0.09	(−)[c]	Anomaly 4
	121.71 ± 0.09		
7.28	123.81 ± 0.09		
7.35	124.36 ± 0.04		
7.41	124.71 ± 0.09		
7.90	126.01 ± 0.09		
	126.21 ± 0.09	(−)[c]	Anomaly 4.1
8.21, 8.80	127.32 ± 0.08		
8.92	127.70 ± 0.08		Anomaly 5
10.42	131.01 ± 0.04		
10.54	131.36 ± 0.09	(+)	Anomaly 5′
10.59	131.56 ± 0.09		
	131.76 ± 0.09	(−)	
	131.96 ± 0.09	(+)[c]	
11.03	132.86 ± 0.09	(+)	
11.09	133.06 ± 0.09		
11.55	134.36 ± 0.09		
11.73	134.75 ± 0.09		
11.86	135.08 ± 0.07		Anomaly 5A
12.12	135.86 ± 0.09		
12.46	136.61 ± 0.04	(+)	
12.49	136.81 ± 0.14		
12.58	137.16 ± 0.09	(+)	
12.62	137.36 ± 0.09		
12.83	138.41 ± 0.09		
13.01	139.01 ± 0.09		
13.20	139.41 ± 0.09		
13.46	140.01 ± 0.09		
13.69	140.61 ± 0.09		
14.08	141.71 ± 0.09	(−)	
14.20	141.91 ± 0.09		
14.66	143.41 ± 0.09		
14.87	144.11 ± 0.09		
14.96	144.31 ± 0.09	(−)	Anomaly 5B
15.13	144.51 ± 0.09		
15.27	144.91 ± 0.09		

[a] From Berggren et al. (in press).
[b] (+) or (−) indicate normal or reversed intervals defined by single samples.
[c] Polarity interval not shown by Berggren et al. (in press).
[d] Reunion age from MacDougall (1977).

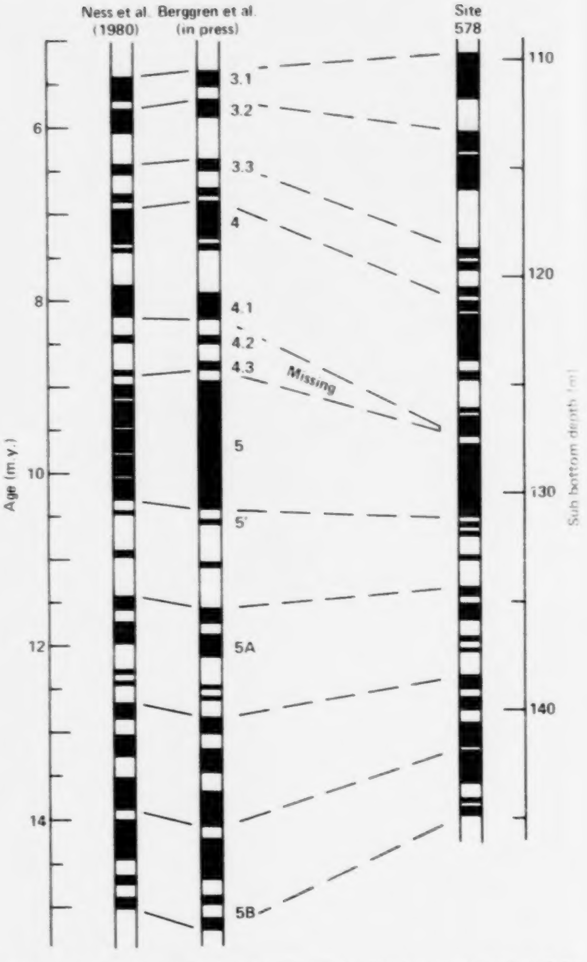

Figure 7. Correlation of the paleomagnetic polarity stratigraphy of th deeper part of Site 578 with the scales of Berggren et al. (in press and Ness et al. (1980) and marine magnetic Anomalies 3.1 to 5B

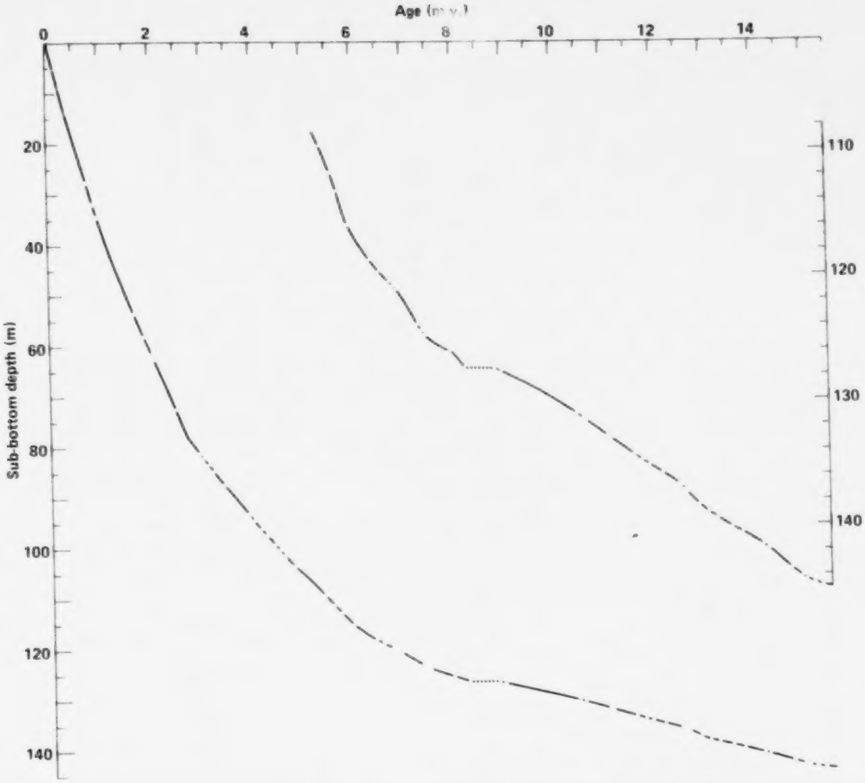

Figure 8. Age-depth curve for Site 578 based on the paleomagnetic correlations of Figures 6 and 7 and the time scale of Berggren et al. (in press). The vertical scale of the 5- to 15-m.y. section (right curve and axis) have been enlarged to show the sedimentation rate changes in more detail.

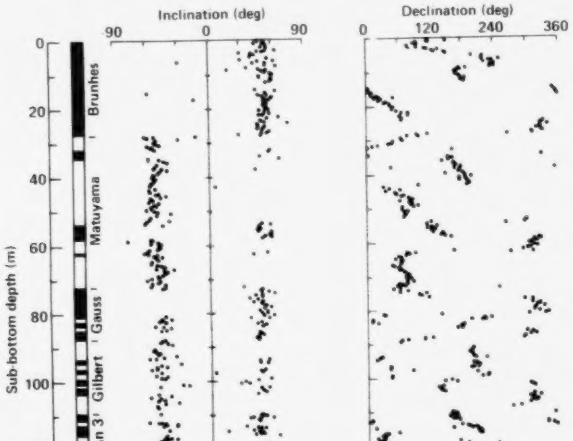

Figure 9. Inclination and declination as a function of depth at Site 578. Rotation of the hydraulic piston core as it cores the sediment is apparent in the declinations for the upper part of the section.

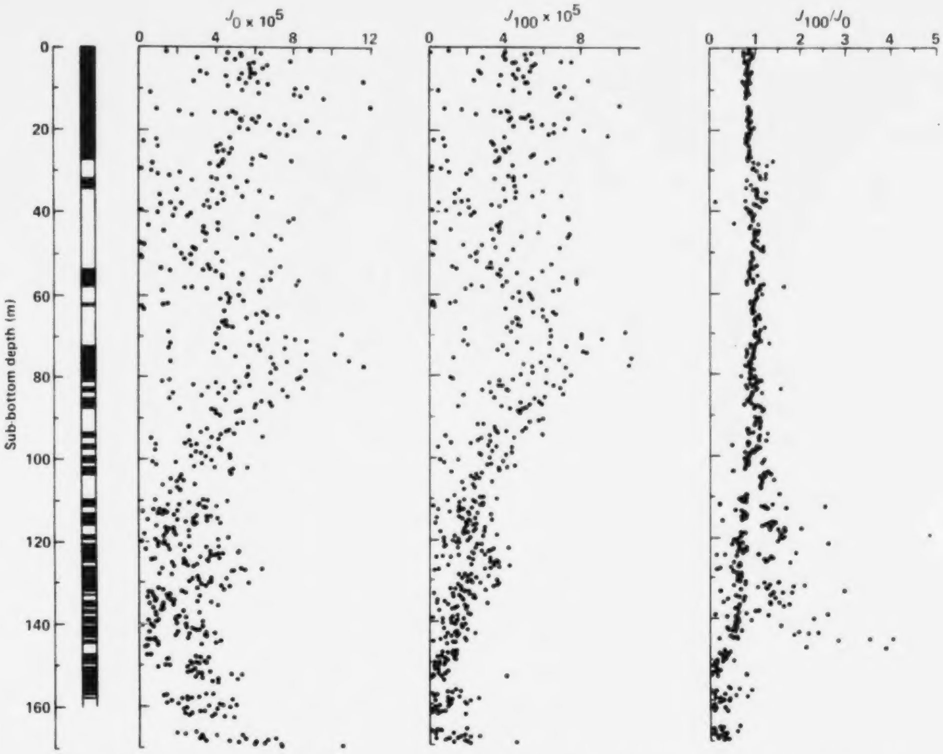

Figure 10. Natural remanent magnetization (J_0), remanent intensity after AF demagnetization at 100 Oe (J_{100}), and J_{100}/J_0 as a function of sub-bottom depth at Site 578.

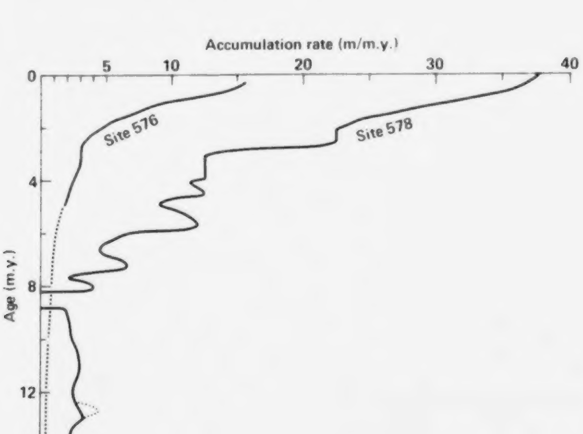

Figure 11. Sediment-accumulation rate as a function of age for the 0- to 16-m.y. sections of Sites 576 and 578. These profiles are obtained by differentiating the curves of Figures 2 and 8 against age. Note the similar rates below 16 m.y. and the similar Quaternary rate accelerations at the two sites. The dotted peak at 12.5 m.y. on the Site 578 curve is believed to be an artifact caused by stretching of the sediment section during the coring process.

19. CARBON-ISOTOPE STRATIGRAPHY, SITE 577[1]

N. J. Shackleton and M. A. Hall, University of Cambridge
and
U. Bleil, Institut für Geophysik, Ruhr-Universität Bochum[2]

ABSTRACT

We have obtained a detailed carbon-isotope stratigraphy of the Paleocene sections recovered from Deep Sea Drilling Project (DSDP) Holes 577 and 577A. This ^{13}C record is useful in stratigraphically correlating the two holes and in interpreting the magnetostratigraphic data. Comparison with the published data for Site 527 (Southeast Atlantic Ocean) shows that ^{13}C stratigraphy is also valuable for long-distance correlation.

INTRODUCTION

It has been known for many years that substantial fluct itions in the level of oceanic ^{13}C occurred during the I anerozoic. For the Cenozoic, the fluctuations were first n ticed in the ^{13}C content of foraminifers (Douglas and Savin, 1971; Shackleton and Kennett, 1975). Scholle and Arthur (1980) first demonstrated important ^{13}C variations in the Mesozoic by analyzing bulk carbonate. Shackleton and Hall (1984) obtained a detailed ^{13}C stratigraphy from bulk sediment at the Leg 74 sites.

It is important to gather information on the ^{13}C stratigraphy of marine carbonates in order to understand the history of the global organic carbon budget (Scholle and Arthur, 1980; Shackleton, in press). In this context, the anomalously high ^{13}C values apparent in the late Paleocene are of particular interest because they are comparable with the ^{13}C values observed by Scholle and Arthur (1980) in association with Cretaceous ocean anoxic events. It was interest in this late Paleocene ^{13}C maximum that was the original motive for analyzing carbonates from the Paleocene section recovered at Site 577 on Leg 86.

Site 577 was cored using the hydraulic piston corer (HPC) (Site 577 chapter, this volume). The site is located on the Shatsky Rise at 32°36.51′N, 157°43.40′E in 2675 m water depth. The paleolatitude of Site 577 during the Paleocene would have been within the tropics at a out 15°N, according to the reconstruction of Firstb ook, et al. (1979); paleomagnetic data for the sedi nts of Site 577 (Bleil, this volume) are consistent with t s reconstruction. The site experienced erosion or non osition during most of mid-Eocene to mid-Miocene e, but the Paleocene and lower Eocene are well repre ted and have provided a good magnetostratigraphic ord (Bleil, this volume) and a detailed nannofossil tigraphy (Monechi, this volume; Monechi, Bleil, and ckman, this volume). The cored section consists of foraminifer–nannofossil ooze that is not lithified and was easily cored through the Cretaceous/Tertiary boundary using the HPC (Site 577 chapter, this volume); the early Paleogene section has probably never been at a significantly deeper burial depth than it is today (Schultheiss, this volume). The Cretaceous/Tertiary boundary is located at 109.6 m below the seafloor.

Methods

Samples were obtained at approximately 30-cm intervals throughout the recovered Paleocene and Eocene sections (apart from the earliest Paleocene, which is the subject of another study; Zachos et al., this volume). This sampling interval provides several samples per million years. At present, the ultimate useful resolution for ^{13}C-stratigraphic studies in bulk sediment is not known. Both Holes 577 and 577A were sampled. This was initially done in order to maximize coverage by duplicating in Hole 577A those intervals missed in Hole 577, but it subsequently became evident that the ^{13}C record is a valuable tool for determining accurate stratigraphic correlations between the two holes.

Isotope analyses were made in a VG Isogas 903 triple collector mass spectrometer using the reaction system shown in Shackleton, Hall, and Boersma (1984). Measurements are expressed with reference to the PDB (PeeDee belemnite) standard (Epstein et al., 1951) using the calibrations in Shackleton, Imbrie, and Hall (1983). The chief limitation on analytical reproducibility is that the system used is designed for small numbers of foraminifers; because of the inhomogeneity of the sediment samples it would be preferable to use larger amounts of sediment (~100 mg) for each analysis rather than about 1 mg, the amount used in this study. In the present study reproducibility is about ±0.1 per mil; reproducibility at least a factor of two better is possible with homogeneous samples.

RESULTS

Carbon- and oxygen-isotope analyses are listed in Table 1. Before discussing their wider significance, it is appropriate to discuss their use in understanding the stratigraphic relationship between the two holes drilled at Site 577. The carbon- and oxygen-isotope data are plotted against reported depth below the seafloor in Figure 1. When one examines either the stable-isotope data (Fig. 1) or the biostratigraphic or magnetostratigraphic data (Monechi, Bleil, and Backman, this volume), it is readily apparent that events are not observed at precisely the same reported depth in the two holes. This discrepancy is partly the consequence of the convention by which depth is assigned to the sediment contained in an incompletely filled core barrel (Introduction and Explanatory Notes, this volume) and partly a result of uncertainty of the ex-

---

[1] Heath, G. R., Burckle, L. H., et al., *Init. Repts. DSDP*, 86: Washington (U.S. Govt. ting Office).

[2] Addresses: (Shackleton and Hall) University of Cambridge, Godwin Laboratory for aternary Research, Free School Lane, Cambridge CB2 3RS, United Kingdom; (Bleil) Institut für Geophysik, Ruhr-Universität, 4630 Bochum, Federal Republic of Germany.

Table 1. Carbon- and oxygen-isotope data for bulk sediment carbonate from Holes 577 and 577A.

Sample (interval in cm)	Depth (m)	Adjusted depth (m)	Age (m.y.)	$\delta^{18}O$ (‰)	$\delta^{13}C$ (‰)
Hole 577					
8-4, 0-1	68.30	67.00	52.106	0.12	2.13
8-4, 30-31	68.60	67.30	52.240	0.00	2.13
8-4, 60-61	68.90	67.60	52.374	0.32	2.30
8-4, 90-91	69.20	67.90	52.508	−0.07	2.16
8-4, 120-121	69.50	68.20	52.642	−0.27	2.09
8-5, 0-1	69.80	68.50	52.775	−0.09	2.07
8-5, 30-31	70.10	68.80	52.908	−0.24	2.04
8-5, 60-61	70.40	69.10	53.040	−0.67	1.95
8-5, 90-91	70.70	69.40	53.173	−0.41	1.97
8-5, 120-121	71.00	69.70	53.306	−0.29	2.00
8-6, 0-1	71.30	70.00	53.439	−0.59	1.86
8-6, 30-31	71.60	70.30	53.571	−0.68	1.60
8-6, 60-61	71.90	70.60	53.704	−0.42	1.98
8-6, 90-91	72.20	70.90	53.837	−0.54	1.77
8-6, 120-121	72.50	71.20	53.970	−0.79	1.41
8-7, 0-1	72.80	71.50	54.103	−0.58	1.90
8,CC (17-18)	72.97	71.67	54.178	−0.35	1.71
9-1, 0-1	73.30	73.30	54.776	−0.67	1.18
9-1, 30-31	73.60	73.60	54.827	−0.58	1.53
9-1, 60-61	73.90	73.90	54.878	−0.52	1.42
9-1, 90-91	74.20	74.20	54.928	−0.46	1.20
9-1, 120-121	74.50	74.50	54.979	−0.49	1.33
9-2, 0-1	74.80	74.80	55.030	−0.45	1.39
9-2, 30-31	75.10	75.10	55.081	−0.48	1.43
9-2, 60-61	75.40	75.40	55.132	0.09	1.45
9-2, 90-91	75.70	75.70	55.183	−0.42	1.29
9-2, 120-121	76.00	76.00	55.235	−0.19	1.35
9-3, 0-1	76.30	76.30	55.287	−0.67	0.83
9-3, 30-31	76.60	76.60	55.339	−0.60	1.12
9-3, 60-61	76.90	76.90	55.391	−0.44	1.26
9-3, 90-91	77.20	77.20	55.443	−0.65	1.45
9-3, 120-121	77.50	77.50	55.495	−0.42	1.33
9-4, 0-1	77.80	77.80	55.547	−0.68	1.64
9-4, 30-31	78.10	78.10	55.599	−0.45	1.55
9-4, 60-61	78.40	78.40	55.651	−0.41	1.31
9-4, 90-91	78.70	78.70	55.740	−0.32	1.55
9-4, 120-121	79.00	79.00	55.836	−0.27	1.61
9-5, 0-1	79.30	79.30	55.932	−0.46	1.09
9-5, 30-31	79.60	79.60	56.028	−0.22	1.21
9-5, 60-61	79.90	79.90	56.124	−0.54	1.58
9-5, 90-91	80.20	80.20	56.332	−0.62	1.72
9-5, 113-114	80.43	80.43	56.509	−0.68	2.08
9-6, 0-1	80.80	80.80	56.793	−0.61	2.07
9-6, 30-31	81.10	81.10	57.024	−0.81	1.90
9-6, 60-61	81.40	81.40	57.254	−0.87	2.08
9-6, 90-91	81.70	81.70	57.485	−0.86	2.17
9-6, 120-121	82.00	82.00	57.643	−0.81	2.20
9,CC (8-9)	82.08	82.08	57.686	−0.74	2.17
10-1, 30-31	83.10	83.10	57.961	−0.76	3.28
10-1, 60-61	83.40	83.40	58.048	−0.67	3.10
10-1, 90-91	83.70	83.70	58.134	−0.81	3.22
10-1, 120-121	84.00	84.00	58.221	−0.49	3.42
10-2, 0-1	84.30	84.30	58.308	−0.75	3.24
10-2, 30-31	84.60	84.60	58.394	−0.65	3.59
10-2, 60-61	84.90	84.90	58.481	−1.08	3.53
10-2, 90-91	85.20	85.20	58.568	−0.96	3.61
10-2, 120-121	85.50	85.50	58.654	−0.94	3.45
10-3, 0-1	85.80	85.80	58.735	−0.96	3.49
10-3, 30-31	86.10	86.10	58.817	−1.03	3.07
10-3, 60-61	86.40	86.40	58.899	−0.99	3.40
10-3, 90-91	86.70	86.70	58.981	−0.93	3.79
10-3, 120-121	87.00	87.00	59.063	−0.99	3.72
10-4, 0-1	87.30	87.30	59.145	−1.13	3.66
10-4, 30-31	87.60	87.60	59.226	−1.15	3.50
10-4, 60-61	87.90	87.90	59.310	−1.13	3.52
10-4, 90-91	88.20	88.20	59.394	−1.02	3.78
10-4, 120-121	88.50	88.50	59.478	−0.92	3.80
10-5, 0-1	88.80	88.80	59.561	−1.05	3.69
10-5, 30-31	89.10	89.10	59.645	−0.85	3.85
10-5, 60-61	89.40	89.40	59.729	−1.04	3.71
10-5, 90-91	89.70	89.70	59.813	−0.86	3.76
10-5, 120-121	90.00	90.00	59.897	−0.83	3.79
10-6, 0-1	90.30	90.30	59.981	−0.78	3.90
10-6, 30-31	90.60	90.60	60.065	−0.56	3.60
Hole 577 (Cont.)					
10-6, 60-61	90.90	90.90	60.148	−0.49	3.44
10-6, 90-91	91.20	91.20	60.232	−0.67	3.62
10-6, 120-121	91.50	91.50	60.316	−0.71	3.33
10-7, 0-1	91.80	91.80	60.400	−0.87	3.41
10-7, 30-31	92.10	92.10	60.484	−1.05	3.62
10,CC (17-18)	92.27	92.27	60.531	−1.02	3.39
11-1, 0-1	92.30	92.30	60.540	−0.96	3.82
11-1, 30-31	92.60	92.60	60.624	−0.88	3.91
11-1, 60-61	92.90	92.90	60.707	−0.87	3.65
11-1, 90-91	93.20	93.20	60.791	−0.76	3.59
11-1, 120-121	93.50	93.50	60.875	−0.62	3.55
11-2, 0-1	93.80	93.80	60.959	−0.45	3.75
11-2, 30-31	94.10	94.10	61.043	−0.47	3.29
11-2, 60-61	94.40	94.40	61.127	−1.02	3.29
11-2, 90-91	94.70	94.70	61.210	−0.37	2.78
11-2, 120-121	95.00	95.00	61.294	−0.85	3.23
11-3, 0-1	95.30	95.30	61.378	−0.54	3.18
11-3, 30-31	95.60	95.60	61.462	−0.71	3.12
11-3, 60-61	95.90	95.90	61.546	−0.86	3.04
11-3, 90-91	96.20	96.20	61.630	−0.71	2.99
11-3, 120-121	96.50	96.50	61.714	−0.58	2.98
11-4, 0-1	96.80	96.80	61.797	−0.58	3.04
11-4, 30-31	97.10	97.10	61.881	−0.88	3.08
11-4, 60-61	97.40	97.40	61.965	−0.73	2.79
11-4, 90-91	97.70	97.70	62.049	−0.62	3.05
11-4, 120-121	98.00	98.00	62.133	−0.66	2.87
11-5, 0-1	98.30	98.30	62.217	−0.46	2.91
11-5, 30-31	98.60	98.60	62.301	−0.82	2.81
11-5, 60-61	98.90	98.90	62.384	−0.59	2.89
11-5, 90-91	99.20	99.20	62.468	−0.49	2.84
11-5, 120-121	99.50	99.50	62.552	−0.55	2.59
11-6, 0-1	99.80	99.80	62.636	−0.54	2.46
11-6, 30-31	100.10	100.10	62.720	−0.40	2.59
11-6, 60-61	100.40	100.40	62.804	−0.91	2.61
11-6, 90-91	100.70	100.70	62.887	−0.81	2.70
11-6, 120-121	101.00	101.00	62.971	−0.98	2.43
11,CC (0-1)	101.30	101.30	63.090	−0.66	2.67
Hole 577A					
9-1, 4-5	75.94	75.94	55.225	−0.14	1.36
9-1, 30-31	76.20	76.20	55.272	−0.51	1.36
9-1, 60-61	76.50	76.50	55.324	−0.51	1.49
9-1, 90-91	76.80	76.80	55.374	−0.15	1.48
9-1, 120-121	77.10	77.10	55.426	−0.18	1.45
9-2, 0-1	77.40	77.40	55.478	−0.45	1.91
9-2, 30-31	77.70	77.70	55.530	−0.32	1.72
9-2, 60-61	78.00	78.00	55.582	−0.59	1.83
9-2, 90-91	78.30	78.30	55.634	−0.47	1.97
9-2, 120-121	78.60	78.60	55.708	−0.42	1.64
9-3, 0-1	78.90	78.90	55.804	−0.16	1.80
9-3, 30-31	79.20	79.20	55.900	−0.52	1.76
9-3, 60-61	79.50	79.50	55.996	−0.45	1.74
9,CC (5-6)	79.76	79.76	56.079	−0.82	1.84
10-1, 2-3	85.42	85.42	58.631	−0.92	3.58
10-1, 30-31	85.70	85.70	58.708	−0.94	3.27
10-1, 60-61	86.00	86.00	58.790	−0.96	3.57
10-1, 79-81	86.20	86.20	58.845	−0.57	3.81
10-1, 90-91	86.30	86.30	58.872	−1.12	3.69
10-1, 120-121	86.60	86.60	58.954	−0.92	3.74
10-1, 129-131	86.70	86.70	58.981	−0.88	3.74
10-2, 0-1	86.90	86.90	59.035	−0.98	3.45
10-2, 29-31	87.20	87.20	59.117	−0.84	3.77
10-2, 32-33	87.22	87.22	59.123	−0.96	3.62
10-2, 60-61	87.50	87.50	59.199	−1.06	3.33
10-2, 79-81	87.70	87.70	59.254	−1.06	3.55
10-2, 90-91	87.80	87.80	59.282	−1.06	3.51
10-2, 120-121	88.10	88.10	59.366	−0.92	3.66
10-2, 129-131	88.20	88.20	59.394	−0.96	3.88
10-3, 0-1	88.40	88.40	59.450	−0.92	3.75
10-3, 29-30	88.69	88.69	59.531	−0.76	3.86
10-3, 29-31	88.70	88.70	59.533	−1.11	3.74
10-3, 58-59	88.98	88.98	59.612	−0.88	3.83
10-3, 70-72	89.11	89.11	59.648	−1.02	3.85

Table 1. (Continued).

Sample (interval in cm)	Depth (m)	Adjusted depth (m)	Age (m.y.)	$\delta^{18}O$ (‰)	$\delta^{13}C$ (‰)
Hole 577A (Cont.)					
10-3, 90-91	89.30	89.30	59.701	−0.89	3.77
10-3, 99-101	89.40	89.40	59.729	−0.85	3.89
10-3, 120-121	89.60	89.60	59.785	−0.82	3.79
10-4, 0-1	89.90	89.90	59.869	−0.82	3.74
10-4, 28-29	90.18	90.18	59.950	−0.77	3.52
10-4, 30-32	90.21	90.21	59.956	−0.70	3.61
10-4, 60-61	90.50	90.50	60.037	−0.56	3.39
10-4, 80-82	90.71	90.71	60.095	−0.62	2.48
10-4, 90-91	90.80	90.80	60.120	−0.56	3.52
10-4, 118-119	91.08	91.08	60.199	−0.56	3.39
10-4, 129-131	91.20	91.20	60.232	−0.39	3.58
10-5, 0-1	91.40	91.40	60.288	−0.93	3.50
10-5, 30-31	91.70	91.70	60.372	−0.96	3.40
10-5, 31-33	91.72	91.72	60.378	−1.02	3.38
10-5, 60-61	92.00	92.00	60.456	−0.96	3.48
10-5, 80-82	92.21	94.85	61.252	−0.92	3.49
10-5, 90-91	92.30	94.92	61.272	−0.84	3.52
10-5, 120-121	92.60	95.14	61.333	−0.84	3.36
10-5, 129-131	92.70	95.21	61.353	−0.79	3.20
10-6, 0-1	92.90	95.35	61.392	−0.71	3.11
10-6, 30-31	93.20	95.57	61.454	−0.65	3.02
10-6, 34-46	93.25	95.61	61.465	−0.80	3.03
10-6, 60 61	93.50	95.79	61.515	−0.76	3.12
11-1, 0-1	94.90	96.81	61.800	−0.61	2.88
11-1, 30-31	95.20	97.03	61.862	−0.68	2.74
11-1, 60-61	95.50	97.25	61.920	−0.70	2.75
11-1, 90-91	95.80	97.46	61.982	−0.54	2.85
11-1, 120-121	96.10	97.68	62.041	−0.58	2.81
11-2, 0-1	96.40	97.90	62.105	−0.52	2.81
11-2, 30-31	96.70	98.12	62.166	−0.32	2.78
11-2, 60-61	97.00	98.34	62.225	−0.50	2.43
11-2, 90-91	97.30	98.55	62.287	−0.60	2.34
11-2, 120-121	97.59	98.76	62.345	−0.75	2.63
11-3, 0-1	97.90	98.99	62.410	−0.77	2.64
11-3, 30-31	98.20	99.21	62.471	−0.61	2.53
11-3, 60-61	98.49	99.42	62.530	−0.72	2.48
11-3, 90-91	98.80	99.64	62.591	−0.77	2.32
11-3, 120-121	99.10	99.86	62.653	−0.62	2.36
11-4, 0-1	99.40	100.08	62.714	−0.80	2.16
11-4, 30-31	99.70	100.30	62.776	−0.58	2.45
11-4, 60-61	100.00	100.51	62.834	−0.86	2.43
11-4, 90-91	100.30	100.73	62.896	−0.64	2.42
11-4, 120-121	100.60	100.95	62.957	−0.85	2.31
11-5, 0-1	100.90	101.17	63.019	−0.64	1.97
11-5, 30-31	101.20	101.39	63.136	−0.67	2.54
11-5, 60-61	101.50	101.61	63.288	−0.77	2.52
11-5, 90-91	101.80	101.82	63.434	−1.03	2.36
11-5, 120-121	102.10	102.10	63.607	−0.69	2.38
11-6, 0-1	102.40	102.40	63.773	−0.83	2.20
11-6, 30-31	102.70	102.70	63.940	−0.87	2.33
11-6, 60-61	103.00	103.00	64.101	−0.89	1.91
11-6, 90-91	103.30	103.30	64.273	−0.74	1.98
11-6, 120-121	103.60	103.60	64.396	−1.09	2.13
11-7, 0-1	103.90	103.90	64.513	−0.96	1.96
11,CC (5-6)	104.15	104.15	64.603	−1.00	2.08

Note: Both reported depth below sea level and depth as adjusted according to Table 2 are given (see text). Note that "reported depth" is consistent with DSDP records and should be used to collate these data with those contained in other chapters in this volume. Ages are also given as estimated by linear interpolation between the control points in Table 3.

t depth of the corer below the seafloor at the moment deployment. Until the advent of the HPC, little conderation was given to the problems involved in making precise stratigraphic correlation between two adjacent oles other than in terms of reported depth below seaoor. It is now becoming important to do this, especial in order to obtain accurate accumulation-rate data, as attempted by Shackleton and Members of the Shipboard Scientific Party (1984).

Both carbonate content (within a limited geographical area; e.g., Arrhenius, 1952; Crowley, 1981) and oxygen-isotope stratigraphy (globally; e.g., CLIMAP, 1976; Shackleton, 1977) have been used for many years to correlate accurately Pleistocene deep-sea records. Varying carbonate content provides a good signal only if carbonate content is well below 100%, and conventional isotope stratigraphy is labor intensive because much time is spent picking the appropriate species for analysis. In any case, the use of oxygen-isotope variations for stratigraphic correlation is dependent on substantial ocean-isotope variations resulting from ice-volume variations and hence would not apply in the Paleocene. Carbon-isotope stratigraphy in bulk sediment can be performed more rapidly because less time is required to prepare the samples; for this reason it is interesting to explore its potential for use in correlation studies.

In the case of Site 577, when the ^{13}C data for the two holes were plotted using the paleomagnetic stratigraphy as it was first interpreted, it became apparent that an inconsistency had arisen. The two measurements of normal polarity that were originally interpreted as representing Chron C-26N in Hole 577 (Samples 577-10-6, 141 cm and 577-10-7, 10 cm; 91.72 to 91.91 m sub-bottom) and the two that were interpreted as representing Chron C-26N in Hole 577A (Samples 577A-10-3, 70 cm and 577A-10-3, 91 cm; 89.11 to 89.40 m sub-bottom) fall at different points in the ^{13}C record. Moreover, these events occur in sediments with significantly different ^{13}C contents. An additional normally magnetized interval was found in Hole 577 (Sample 577-10-5, 89 cm; 89.70 m sub-bottom); since this was observed only in a single sample it would usually be ignored by a conservative magnetostratigrapher. However, the ^{13}C stratigraphy suggests that it is this event, and not the deeper normal event in Hole 577 (Samples 577-10-6, 141 cm and 577-10-7, 10 cm; 91.72 to 91.91 m sub-bottom), that is precisely correlated with the normal event recorded in Hole 577A (Samples 577A-10-3, 70 cm and 577A-10-3, 91 cm; 89.11 to 89.40 m sub-bottom).

Inspection of the ^{13}C data shown in Figure 1 indicates that the peak of isotopically heavy values in the top of Core 577-11 between 92.3 and 93.8 m sub-bottom is not present in Hole 577A. The detailed biostratigraphic studies of Monechi, Bleil, and Backman (this volume) suggest that, if the reason is that some sediment is missing in Hole 577A, the sediment must be missing from just above the base of Core 577A-10, because the detailed biostratigraphic analysis of Site 577 shows that the missing section is above the *Heliolithus kleinpellii* peak that is present at the bottom of Core 577A-10. Close inspection of the two ^{13}C records leads us to the same conclusion. We have therefore attempted to estimate the position below the seafloor at which the sediment in each core barrel most probably lay (assuming that the strata were horizontal between the two holes), using only features in the ^{13}C record and magnetic reversals to estimate the offsets.

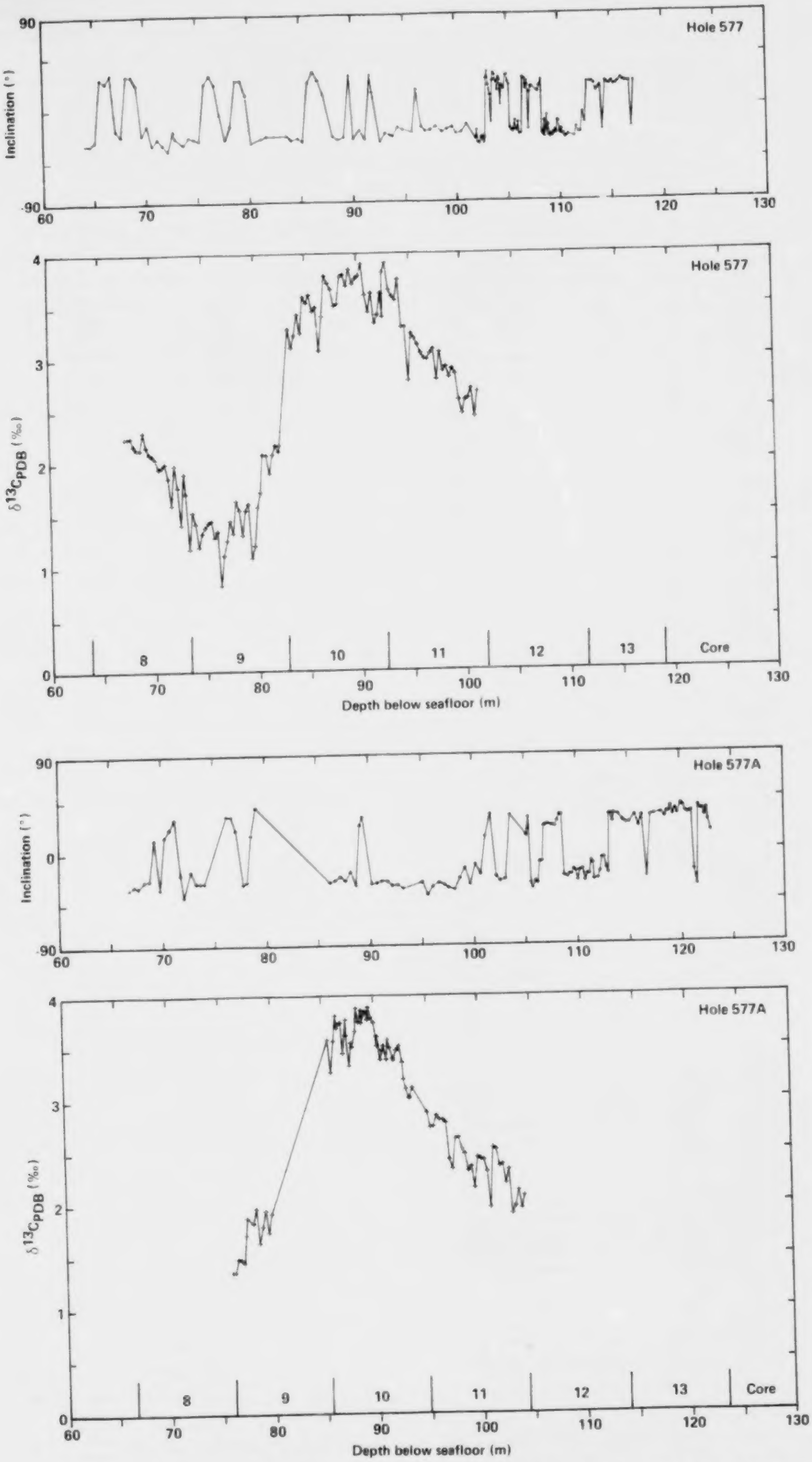

Figure 1. Carbon isotope and magnetic inclination records plotted against reported depth below seafloor.

Table 2 gives the adjusted sub-bottom depth figures assigned. In order to minimize the amount of distortion of reported depths, we have assumed that the chief problem is a stretching of Core 577A-11. We have therefore made a downward adjustment of the top of Core 577A-11, as well as a small section of Core 10, while holding the base of Core 11 fixed. Aside from this distortion, the same depth adjustment is applied to the top and bottom of each sediment core recovered.

In Table 1, each sample is assigned two depths: that used in DSDP records and a second depth that repre-ents our estimate of the most likely depth at which the ample actually lay below the seafloor (using the adjustments in Table 2). Since most of the cores in Hole 577 ad a high recovery, it is the Hole 577A cores that are more likely to require adjustment; however, one has to onsider the continuity of the whole column when making such adjustments. For this reason, the discrepancy as been distributed equally between Core 577-8 and ore 577A-8. As will be seen, comparison with the ^{13}C ata from Site 527 suggests that the Hole 577 record at his point is correct and that there is indeed a section of over 1.5 m thickness missing in Core 577A-10.

The adjusted carbon-isotope data are plotted against estimated age in Figures 2 and 3 by assigning ages (Berggren et al., in press) to the magnetic boundaries at their newly assigned depths, as shown in Table 3. In view of potential uncertainty as to the identification of Chron C-26N, the sections were interpolated over the interval between Chrons C-25N to C-27N. Using this procedure, the normal event that (according to the ^{13}C stratigraphy) is common to both sites has an interpolated age of about 59.7 m.y.; in Hole 577 two additional magnetically normal events were observed with interpolated ages of about 60.4 and 61.7 m.y. For convenience, the magnetic data are replotted in Figures 2 and 3 according to this age model.

Table 2. Control points for converting reported depths to adjusted depths for the purpose of reporting data from both holes on a common depth scale (m).

Hole 577			Hole 577A		
Control point	Depth		Control point	Depth	
	Reported	Adjusted		Reported	Adjusted
Core 8			Core 8		
Top	63.8	62.5	Top	66.4	67.7
Base	73.29	71.99	8-5, 140 cm	73.8	75.1
Core 9			Core 9		
Top	73.3	73.3	Top	75.9	75.9
Core 11			Base	85.4	85.4
Base	101.59	101.59	Core 10		
Core 12			Top	85.4	85.4
Top	101.6	101.95	10-5, 60 cm	92.0	92.0
Core 13			10-5, 62 cm	92.02	94.72
Base	118.8	119.15	Core 11		
			11-5, 100 cm	101.9	101.9
			Base	104.4	104.4
			Core 12		
			Top	104.4	104.4
			Core 13		
			Base	123.4	123.4

Note: In Hole 577A we have assumed that there was some loss of sediment at about Sample 577A-10-5, 60 cm and that there was some stretching in Core 11; the model we have used compresses the recovered sediment linearly between 92.02 m and 101.9 m.

Although it has no bearing on the present discussion, it should be noted that the lowest control point has been taken at the first appearance of *Micula mura* since the proximity of this datum to the samples interpreted as correlative with the base of Chron C-30N appears to be inconsistent with the age estimate in Shackleton et al. (1984), suggesting the possibility of a hiatus at this point. Before we can use Site 577 material to estimate tropical productivity in the Late Cretaceous, the viability of this interpretation of the Maestrichtian record, as opposed to the more inherently likely one proposed by Bleil (this volume), must be investigated further.

DISCUSSION

The preceding data suggest that the identification of Chron C-26N may prove more difficult than expected. According to the time scale of Berggren et al. (in press), Chron C-26N had a duration of 0.54 m.y. (60.75–60.21 m.y. ago). The normal event at an interpolated age of 59.7 m.y.) is bounded above and below by reversed samples (in both holes) and has an estimated duration of less than 0.5 m.y. (Hole 577, one sample) and between 0.1 and 0.5 m.y. (Hole 577A, two samples). The normal event at the interpolated age of 60.4 m.y. in Hole 577 is at the bottom of a core and can only be assigned a minimum duration of about 0.2 m.y. (2 samples); the oldest unidentified normal event can again only be assigned a duration of less than 0.5 m.y., being represented by only a single normally magnetized sample.

Which of these three normal events should be correlated with Chron C-26N cannot be decided definitively merely by stating that the middle of the three best fits the assigned for Chron C-26N, since there is no particular reason to believe that the sediment accumulated at a uniform rate. The marine magnetic anomaly sequence should perhaps be reinspected for evidence of more than one normal event in this interval. If there was not, in fact, a single normal event with a duration as long as is usually assigned to Anomaly 26, this would explain why some sites have not detected a normal event between Chrons C-25N and C-27N (Berggren et al., in press, table 4) although the marine magnetic records suggest that Anomaly 26 is a clear entity (Dan Mackenzie, pers. comm., 1984).

It is uncertain whether any of the three normal events just mentioned should be correlated with the one found in Sites 527 and 529 and interpreted there as C-26N (Shackleton et al., 1984). Figure 4 shows the ^{13}C bulk sediment record of Site 527 plotted using the age control points of Shackleton et al. (1984, table 1). Although the reliability of long-distance ^{13}C correlations has not been established, comparison of Figures 2 and 4 suggests that this may prove to be a valuable tool. The position of the magnetically normal event in Site 527 (which was assumed to represent the base of Chron C-26 for the purpose of constructing Fig. 4) in the ^{13}C record suggests that it is not correlative with any of the three magnetic normal events in Hole 577. It may be noticed that there are oth-

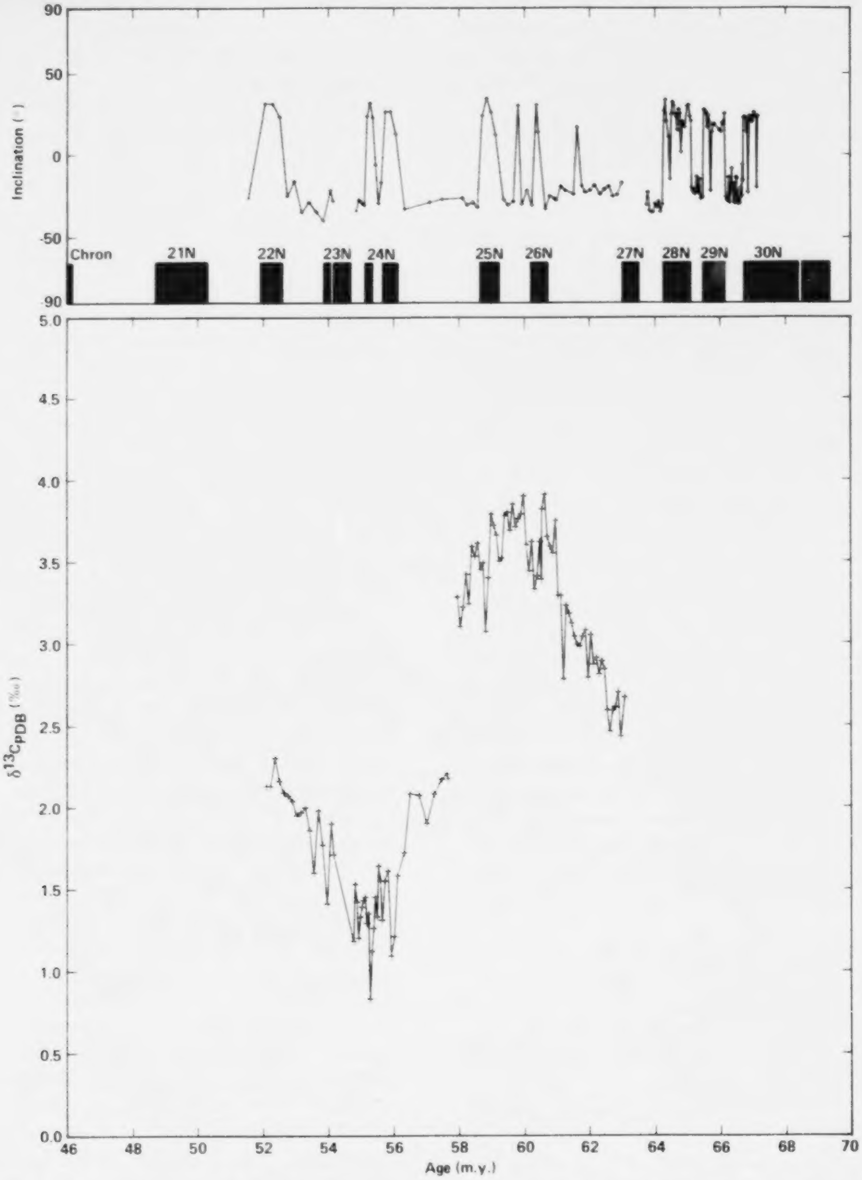

Figure 2. Magnetic record (above) and carbon-isotope record (below) of Hole 577 plotted on a time scale using linear interpolation between the control points in Table 3. The marine magnetic anomaly time scale of Berggren et al. (in press) that was used to create the time scale is shown in the center.

er sections in which three normal events have been recognized in the region of C-26N: the Contessa Highway Section (Lowrie et al., 1982), Site 524 (Tauxe et al., 1984) and the Pietralata Section (Alvarez and Lowrie, 1984).

Comparison of Figures 2 and 3 with Figure 4 shows not only that two sites in different oceans and water masses show similar features in their ^{13}C records, but that the absolute ^{13}C values are also remarkably similar. This implies that a global bulk sediment ^{13}C record should be available on the basis of data from only a few sites. Only further work will reveal whether the subtle differences between the records of Sites 577 and 527 should be interpreted as implying gaps in one or the other record, o as an indication of the limits of detailed ^{13}C correlation

The cause of the ^{13}C peak during the Paleocene is no known. The unusually high ^{13}C values may be explaine as a compensation for the global extinctions and drop i productivity at the Cretaceous/Tertiary boundary, whic must have led to an imbalance in the effectiveness wit which nutrients in the oceans were utilized. There ma have been a buildup in oceanic nutrient levels so that th subsequent increase in diversity a few million years int the Tertiary may have led to the recolonization of an ocea that was anomalously rich in nutrients, permitting an in-

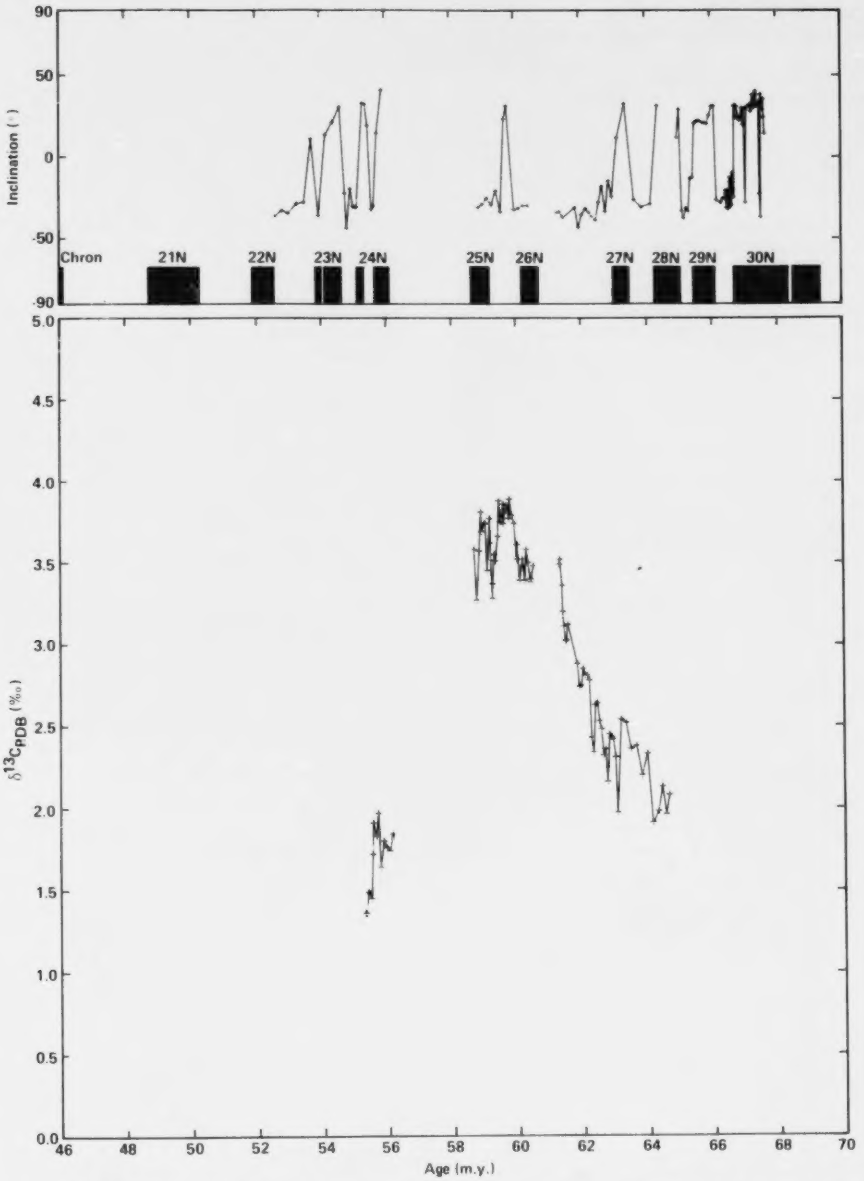

Figure 3. Magnetic record (above) and carbon-isotope record (below) of Hole 577A plotted on a time scale using linear interpolation between the control points in Table 3. The marine magnetic anomaly time scale of Berggren et al. (in press) that was used to create the time scale is shown in the center.

ased burial rate for organic matter. There is certainly ope for developing a model along these lines. How- er, the drop in ^{13}C very close to the top of the Paleo- ne is not predicted by such a model; this seems to im- y an even more dramatic crash in marine productivity an at the Cretaceous/Tertiary boundary, whereas in re- ity the end of the Paleocene was probably a time of atively modest faunal turnover.

CONCLUSIONS

Carbon-isotope measurements in bulk sediment from oles 577 and 577A have been useful in aiding detailed orrelation between these two holes. A very close similarity between the ^{13}C record of Site 577 and that of Site 527 (South Atlantic) suggests that the ^{13}C history of global oceanic carbonate can be quite well characterized by a single ^{13}C record. Moreover the development of a standard ^{13}C record for the Cenozoic will be of considerable value in elucidating the stratigraphy of individual sites, perhaps to a better resolution than that afforded by biostratigraphic methods.

ACKNOWLEDGMENTS

Isotope analysis in Cambridge is supported by NERC grant GR3/3606. We are grateful to Jan Backman for helpful discussion on these sediments, and to Richard Corfield, Jan Backman, Michael Arthur,

Table 3. Control points for conversion of adjusted depths to ages using magnetostratigraphic time scale of Berggren et al. (in press).

Adjusted depth (m)	Assigned age (m.y.)	Identification
64.15	48.75	Top Chron C-21N
65.65	50.34	Base Chron C-21N
66.65	51.95	Top Chron C-22N
68.15	52.62	Base Chron C-22N
72.85	54.7	Base Chron C-23N
75.45	55.14	Top Chron C-24N-2
78.45	55.66	Top Chron C-24N-1
79.95	56.14	Base Chron C-24N-1
82.6	57.8	^{13}C change
85.45	58.64	Top Chron C-25N
87.65	59.24	Base Chron C-25N
101.21	63.03	Top Chron C-27N
101.98	63.54	Base Chron C-27N
103.33	64.29	Top Chron C-28N
105.53	65.12	Base Chron C-28N
106.78	65.50	Top Chron C-29N
108.68	66.17	Base Chron C-29N
109.4	66.46	Cretaceous/Tertiary boundary
113.02	66.74	Top Chron C-30N
121.0	67.5	Base *Micula mura*

Note: Control points for the Cretaceous/Tertiary boundary and the first appearance of *Micula mura* as estimated by Shackleton et al. (1984) have been inserted to facilitate future comparison with the older part of the records from DSDP Leg 74. Also, an age of 57.8 m.y. has been assigned to the midpoint of the major ^{13}C change.

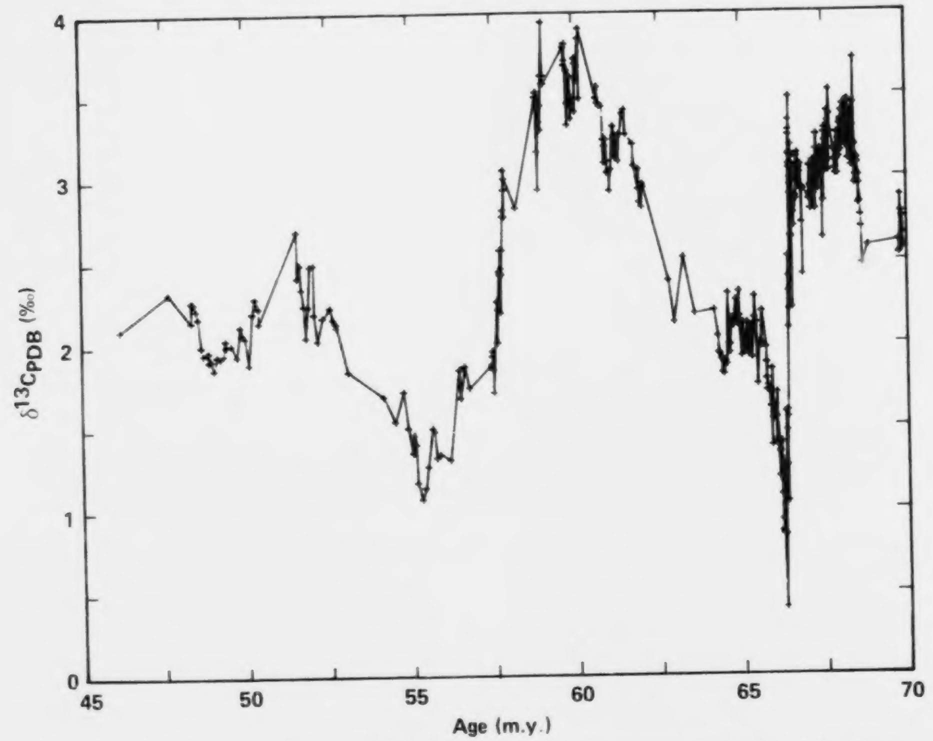

Figure 4. Carbon-isotope record of Site 527 (Shackleton and Hall, 1984, and additional unpublished measurements) using the time scale of Shackleton et al. (1984).

Peter Scholle, and Audrey Wright for reviewing an earlier draft of the manuscript.

REFERENCES

Alvarez, W., and Lowrie, W., 1984. Magnetic stratigraphy applied to synsedimentary slumps, turbidites, and basin analysis: the Scaglia Limestone at Furlo (Italy). *Geol. Soc. Am. Bull.*, 95:324–336.

Arrhenius, G., 1952. Sediment cores from the East Pacific. *Swedish Deep-Sea Exped. Repts.*, 5:6–227

Berggren, W. A., Kent, D. V., and Flynn, J. J., in press. Paleogene geochronology and chronostratigraphy. *In* Snelling, N. J. (Eds.), *Geochronology and the Geological Record*. Spec. Publ. Geol. Soc. London.

CLIMAP project members, 1976. The surface of the ice-age earth. *Science*, 191:1131–1137.

Crowley, T. J., 1981. Temperature and circulation changes in the eastern North Atlantic during the last 150,000 years: evidence from the planktonic foraminiferal record. *Mar. Micropaleontol.*, 6:97–129.

Douglas, R. G., and Savin, S. M., 1971. Isotopic analyses of planktonic foraminifera from the Cenozoic of the Northwest Pacific, Leg 6. *In* Fischer, A. G., Heezen, B. C., et al., *Init. Repts. DSDP*, 6: Washington (U.S. Govt. Printing Office), 1123–1130.

Epstein, S. M., Buchsbaum, R., Lowenstam, H. A., and Urey, H. C., 1951. Carbonate-water isotopic temperature scale. *Geol. Soc. Am. Bull.*, 62:417–426.

Firstbrook, P. L., Funnell, B. M., Hurley, A. M., and Smith, A. G., 1979. *Paleoceanic Reconstructions 160–0 Ma*: La Jolla, California (Deep Sea Drilling Project).

Lowrie, W., Alvarez, W., Napoleone, G., Perch-Nielsen, K., Premoli Silva, I., and Toumarkine, M., 1982. Paleogene magnetic stratigraphy in Umbrian pelagic carbonate rocks: the Contessa sections, Gubbio. *Geol. Soc. Am. Bull.*, 93:414–432.

Scholle, P. A., and Arthur, M., 1980. Carbon isotope fluctuations in Cretaceous pelagic limestones: potential stratigraphic and petroleum exploration tool. *Am. Assoc. Pet. Geol. Bull.*, 64:67–87.

Shackleton, N. J., 1977. The oxygen isotope stratigraphic record of the Late Pleistocene. *Philos. Trans. R. Soc. London Ser.* B,280: 169–179.

________, in press. The carbon isotope record of the Cenozoic. *In* Brooks, J., and Fleet, A. J. (Eds.), *Petroleum Source Rocks*: Oxford (Blackwells).

Shackleton, N. J., and Hall, M. A., 1984. Carbon isotope data from Leg 74 sediments. *In* Moore, T. C., Jr., Rabinowitz, P. D., et al., *Init. Repts. DSDP,* 74: Washington (U.S. Govt. Printing Office), 613–619.

Shackleton, N. J., Hall M. A., and Boersma, A., 1984. Oxygen and carbon isotope data from Leg 74 foraminifers. *In* Moore, T. C., Jr., Rabinowitz, et al., *Init. Repts. DSDP*, 74: Washington (U.S. Govt. Printing Office), 599–612.

Shackleton, N. J., Imbrie, J., and Hall, M. A., 1983. Oxygen and carbon isotope record of East Pacific core V19-30: implications for the formation of deep water in the late Pleistocene North Atlantic. *Earth Planet. Sci. Lett.*, 65:233–244.

Shackleton, N. J., and Kennett, J. P., 1975. Paleotemperature history of the Cenozoic and the initiation of Antarctic glaciation: oxygen and carbon isotope analyses in DSDP Sites 277, 279, and 281. *In* Kennett, J. P., Houtz, R. E., et al., *Init. Repts. DSDP*, 29: Washington (U.S. Govt. Printing Office), 743–756.

Shackleton, N. J., and Shipboard Scientific Party, 1984. Accumulation rates in Leg 74 sediments. *In* Moore, T. C., Jr., Rabinowitz, P. D., et al., *Init. Repts. DSDP*, 74: Washington (U.S. Govt. Printing Office), 621–644.

Tauxe, L., Tucker, P., Petersen, N. P., and LaBrecque, J. L., 1984. Magnetostratigraphy of Leg 73 sediments. *In* Hsü, K. J., LaBrecque, J. L., et al., *Init. Repts. DSDP*, 73: Washington (U.S. Govt. Printing Office), 609–621.

Date of Initial Receipt: 29 February 1984
Date of Acceptance: 6 August 1984

20. STABLE ISOTOPE AND TRACE ELEMENT GEOCHEMISTRY OF CARBONATE SEDIMENTS ACROSS THE CRETACEOUS/TERTIARY BOUNDARY AT DEEP SEA DRILLING PROJECT HOLE 577, LEG 86[1]

James C. Zachos and Michael A. Arthur, University of Rhode Island
Robert C. Thunell, Douglas F. Williams, and Eric J. Tappa, University of South Carolina[2]

ABSTRACT

Detailed analyses of well-preserved carbonate samples from across the Cretaceous/Tertiary boundary in Hole 577 have revealed a significant decline in the $\delta^{13}C$ values of calcareous nannoplankton from the Maestrichtian to the Danian Age accompanied by a substantial reduction in carbonate accumulation rates. Benthic foraminifers, however, do not exhibit a shift in carbon composition similar to that recorded by the calcareous nannoplankton, but actually increase slightly over the same time interval. These results are similar to the earlier findings at two North Pacific Deep Sea Drilling Project locations, Sites 47.2 and 465, and are considered to represent a dramatic decrease in oceanic phytoplankton production associated with the catastrophic Cretaceous/Tertiary boundary extinctions. In addition, the change in carbon composition of calcareous nannoplankton across the Cretaceous/Tertiary boundary at Hole 577 is accompanied by only minor changes in the oxygen isotope trends of both calcareous nannoplankton and benthic foraminifers, suggesting that temperature variations in the North Pacific from the late Maestrichtian to the early Danian Age were insignificant.

INTRODUCTION

The uncertain origin of the biotic extinctions at the Cretaceous/Tertiary boundary is one of the more intriguing problems in paleoceanography. A plethora of models have been proposed to account for the pattern and timing of the extinctions (e.g., Silver and Schultz, 1982), but many of the published papers are based on relatively few data. A recently popular explanation is that of an extraterrestrial cause for the extinctions. An early paper by Alvarez et al. (1980) reported the discovery of anomalous concentrations of iridium and other platinum group metals (siderophile elements) in a clay layer at the Cretaceous/Tertiary boundary at Gubbio, Italy. Since that time, they and a number of other workers have recorded similar enriched zones at the boundary in at least 19 other globally distributed sites, including several terrestrial (nonmarine) sequences (Alvarez et al., 1982). It appears that, on the basis of the distribution of the Ir anomalies and the ratios of platinum group metals to one another, there as an impact of an extraterrestrial object with the earth t the end of the Maestrichtian Age. However, the sig-ificance of the iridium anomaly as evidence of an im-act signature has been questioned (e.g., Officer and 'rake, 1983; McLean, 1982). Abrupt extinctions of many xa of Cretaceous marine plankton occur in conjunc-on with the Ir anomaly, but the relationship that the ajor impact (or other) event had to the biotic extinc-ons is not yet clear.

Alvarez et al. (1980, 1982) proposed a "lights out" enario, whereby the dust or ejecta thrown up into the mosphere by the impact would lead to a period of dark-ess lasting several years. This episode of darkness is proposed to have led to cessation of photosynthesis, extinction of most phytoplankton, and resulting effects on down the marine and terrestrial food chains. More recent modeling suggests that the period of darkness would have been much shorter, on the order of 3 to 6 months (Toon et al., 1982; Thierstein, 1982). Other authors have proposed variants of the impact hypothesis, including extinction by chemical poisoning related to the impact of a cometary body (Hsü, 1980), catastrophic warming related to drastic increases in atmospheric water vapor as the result of an ocean impact and resulting thermal stress on organisms (Emiliani et al., 1981), and sudden cooling as the result of global albedo increases from high concentrations of atmospheric dust (Toon et al., 1982). These hypotheses are not mutually exclusive and the suggested mechanisms could have, in combination, affected the terrestrial and marine biotas.

Other workers (e.g., Bramlette, 1965; Tappan, 1968; Fischer and Arthur, 1977; Vogt, 1972; McLean, 1980, 1982) have provided models for the biotic extinctions at the Cretaceous/Tertiary boundary that require causes internal to the earth. Vogt (1972), McLean (1980, 1982), and Zoller et al. (1983) suggested increased rates of volcanism at the end of the Cretaceous. The biotic extinctions would therefore be related to either trace metal poisoning, increased atmospheric pCO_2 and sudden global climatic warming, and/or decreased oceanic surface water pH. Others (Bramlette 1965; Tappan, 1968; Fischer and Arthur, 1977) suggested that increased extinction rates at the end of the Cretaceous were the result of marine regression, oceanic nutrient deficiencies, and global cooling. Needless to say, the variety of mechanisms proposed and the often contradictory hypotheses (e.g., warming vs. cooling) point to the need for much more data bearing on rates of extinction, environmental tolerances, and paleoclimate and paleoproductivity estimates. Thus, high resolution studies of complete marine Cretaceous/Tertiary boundary sequences are needed.

---

[1] Heath, G. R., Burckle, L. H., et al., *Init. Repts. DSDP*, 86: Washington (U.S. Govt. 'rinting Office).

[2] Addresses: (Zachos, Arthur) Graduate School of Oceanography, University of Rhode sland, Kingston, RI 02882; (Thunell, Williams, Tappa) Department of Geology, University f South Carolina, Columbia, SC 29208.

We have examined geochemical and stable isotopic compositions of sediment and calcareous microfossils in pelagic-hemipelagic sequences across the Cretaceous/Tertiary boundary at a number of sites in the Pacific, the North Atlantic, and the South Atlantic Ocean basins (Zachos et al., unpubl. data; Williams et al., 1983). Our intent is to provide high resolution chemical and stable-isotopic profiles across the Cretaceous/Tertiary boundary in order to evaluate possible changes in carbonate preservation, which might affect the stable-isotope signals from calcareous plankton, and to evaluate climatic, paleoceanographic or oceanic chemical changes that may have occurred at the boundary.

In this chapter we present stable isotopic and geochemical data from Cretaceous/Tertiary boundary sequences recovered at two Deep Sea Drilling Project (DSDP) sites in the Pacific, Sites 47.2 and 577 (Fig. 1). The Site 47.2 sequence is apparently disturbed by drilling. Site 577, which was hydraulically piston cored during Leg 86 (Site 577 chapter, this volume), offers an undisturbed Cretaceous/Tertiary boundary transition in a pelagic carbonate facies deposited at relatively high sedimentation rates. Preservation of calcareous microfossils is good as we show in scanning electron micrographs and trace element geochemical data (Sr/Ca, Mn) presented in this chapter. We compare our stable-isotope results with those from Boersma and Shackleton (198 from Pacific Site 465 (Figs. 4 and 5). We also discuss t implications of stable-isotopic data from carbonate fin fraction, planktonic and benthic foraminifers and chang in carbonate accumulation rates across the boundary paleoceanographic events at the end of the Cretaceo through the early Paleocene.

ANALYTICAL METHODS

Bulk samples were weighed, disaggregated, and wet sieved throu a 63-μm screen. The less than 63-μm fraction was then thoroug washed with deionized water through 0.45-μm metricel filters in a v uum apparatus. The washed specimens were then prepared for stab

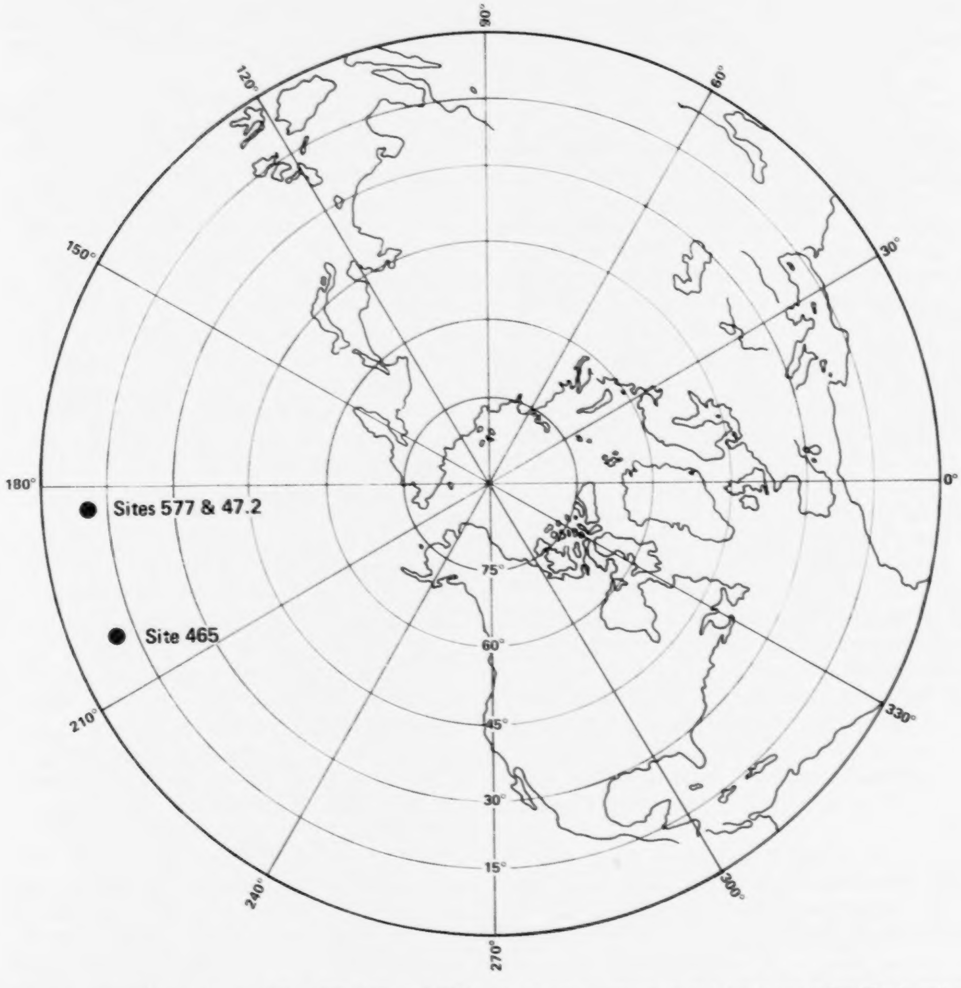

Figure 1. The paleopositions of Sites 577, 465, and 47.2 in the Northern Hemisphere 70 m.y. ago (after Firstbrook et al., 1979; Lancelot and Larson, 1975). Sites 577 and 47.2 are located on the Shatsky Rise. Site 465 is located on the nearby Hess Rise.

isotope analysis in the following manner. The samples were first roasted at 400°C under vacuum for 1 hr. and then reacted in 100% orthophosphoric acid at 50°C. Isotopic analyses were preformed on a VG Micromass 602D isotope ratio mass spectrometer. All samples were measured relative to a laboratory standard reference gas and are reported in notation as per mil deviations from PDB.

$$\delta(‰) = \left(\frac{\text{R sample}}{\text{R standard}} - 1\right) \times 10^3$$

libration of the reference gas was achieved by analysis of B-1 stan-rd, which has a measured value of +0.06‰ for $\delta^{18}O$ and +0.64‰ $\delta^{13}C$ relative to PDB (Keigwin, 1980). Precision of isotopic analy-is better than +0.11 per mil for oxygen and +0.08 per mil for carbon. Trace-element measurements were conducted on the less than 63 carbonate fraction. Each sample was thoroughly washed with de-ized water to remove sea salts, dried, and finely ground. The sam- (0.1 g) were then dissolved in 0.7 *N* acetic acid to avoid stripping ons from clay minerals as much as possible, filtered, and diluted to ml. Magnesium, strontium, and manganese concentrations were n determined with a Perkins Elmer Model 503 Atomic Absorbtion ctrophotometer. All results are reported in ppm. Analytical preci-n for Mg is ±5%, for Mn ±3%, and for Sr ±8%. Although we al-analyzed the same samples for Ca, the analytical precision was much er (±20%) than for the other elements. We have used calculated values from carbonate contents, assuming pu CaCO$_3$. This tech-ue has worked well for other Cretaceous pelagic carbonate sequences ere analytical Ca and total CaCO$_3$ contents were obtained (Dean d Arthur, unpubl. data) and introduces less variation due to poor ecision than the atomic absorption method. Percent calcium car-nate was determined by the bomb method (Müller and Gastner, 71).

Carbonate accumulation rates (CAR) (Table 4) were determined ing the following equation:

$$\text{CAR} = (\%\text{CaCO}_3/100)\{[(W\ \text{g/cm}^3) - (P/100)(1.01\ \text{g/cm}^3)](S\ \text{cm/yr.})\}$$

where *P* is porosity and *W* is wet bulk density. Sedimentation rates (*S*) were determined from magneto- and biostratigraphies.

STABLE-ISOTOPE RESULTS

Planktonic Calcareous Microfossils

Results of oxygen- and carbon-isotope analyses of Maestrichtian and Danian fine fraction (<63 μm) CaCO$_3$ and benthic foraminifers from Hole 577[3] and whole rock CaCO$_3$ from Site 47.2 are given in Tables 1 and 2 and shown in Figures 2 and 3. Carbon- and oxygen-isotope analyses were performed on samples of carbonate fine fraction from the top of Section 577-12-2 (*Chiasmolith- s danicus*, nannofossil Zone CP2, 101–106 m sub-bot- m depth) to the bottom of Section 577-13-4 (*Micula urus* nannofossil Zone, 109–117.6 m sub-bottom depth) Hole 577 and from the top of Section 47.2-10-6 (*Cru- placolithus tenuis*, CP1b Subzone) to the bottom of ection 47.2-12-2 (*M. murus* Zone) at Site 47.2. Sample acing ranged from 10- to 20-cm intervals although the acing interval was reduced to 5 cm near the Cretaceous/ rtiary boundary at each site.

Oxygen-isotope values of Hole 577 carbonate fine- action samples from the *M. murus* zone varied only slightly upcore, averaging −1.0 ± 0.05‰ throughout (Fig. 2). Values begin to increase slightly near the top of this zone several centimeters below the Cretaceous/Tertiary boundary, reaching a peak of −0.49‰ at Sample 577-12-5, 99 cm. Above this level, through the *Markalius inversus* and *C. tenuis* zones (106 to 109 m sub-bottom depth), $\delta^{18}O$ values vary considerably, fluctuating between a low of −1.45‰ in Sample 577-12-3, 110 cm and high value of −0.16‰ in Sample 577-12-4, 110 cm.

Site 47.2 Maestrichtian $\delta^{18}O$ values are only an average of 0.1‰ heavier than the $\delta^{18}O$ values of corresponding samples from Hole 577 (Figs. 3 and 4). Similarly, the Danian oxygen-isotope ratios are also just slightly heavier than the corresponding values from Hole 577.

$\delta^{13}C$ values of carbonate fine-fraction samples from the *M. murus* Zone are relatively constant, averaging 2.65 ± 0.2‰ (Fig. 2). At the Cretaceous/Tertiary boundary, there is a sharp decrease of 1.0‰ over a 10-cm interval which coincides with a layer of slightly lower than average carbonate content. Further upcore, through the *C. tenuis* nannofossil Zone, $\delta^{13}C$ values remain relatively low between 1.7 and 2.3‰. A similar shift in $\delta^{13}C$ is recorded in the Site 47.2 bulk CaCO$_3$ samples (Fig. 3). Maestrichtian samples at Site 47.2 yield average $\delta^{13}C$ values of 2.6 ±0.2‰ compared to values of 1.75 ± 0.1‰ for Danian samples, with the actual carbon-isotope shift occurring somewhere between Samples 47.2-11-5, 25 cm and 47.2-11-3, 100 cm. The major shift apparently coincides with the Cretaceous/Tertiary boundary determined from calcareous nannofossils (Thierstein, 1981). Anomalous points in both the Maestrichtian and Danian sections are probably an artifact of displaced or mixed sediments resulting from coring disturbances.

Stable carbon-isotope compositions of planktonic foraminifers from Site 465 (Boersma and Shackleton, 1981) on the Hess Rise have been plotted against an absolute time framework in Figure 5 along with the data from Sites 577 and 47.2 for comparison using the chronology shown in Figure 6. Boersma and Shackleton (1981) determined Maestrichtian and Danian near-surface-water carbon-isotope values at Site 465 by analyzing *Rugoglobigerina* and *Guembelitria*, respectively. The absolute shift in $\delta^{13}C$ (surface water) at Site 465 as recorded in the tests of these planktonic foraminifers is greater (2.2‰) than the shifts found at Sites 577 and 47.2 as measured in the fine fraction CaCO$_3$ (Fig. 5). However, because the carbon-isotope anomalies at Hole 465 were not determined on a single species across the boundary, this rather large shift may be partially a function of differences in species vital effects, although it is unlikely that the entire shift could be attributed to this. A further possibility is that the measured values reflect actual differences in the carbon composition of surface waters overlying these two locations; however, given the relative proximity of the Shatsky and Hess rises and their central paleoposition in the Pacific, this also seems unlikely.

Benthic Foraminiferal Isotope Records

Since many species of benthic foraminifers survived the Cretaceous/Tertiary boundary extinctions (Douglas and Woodruff, 1981), one may assume that it would be

---

[3] Subsequent to completion of this manuscript a recalibration of standard values was nducted at the Graduate School of Oceanography stable-isotope lab which affects the con-rsion of measured values to PDB. As a result, Hole 577 oxygen and carbon stable-isotope lues reported here in tables, text, and illustrations should be corrected by adding 0.42‰ and 13‰ respectively. The change in oxygen-isotope values amounts to less than 2°C in paleo-mperature estimates.

Table 1. Stable-isotope results from Hole 577.

Core-Section (interval in cm)	Depth (m)	% $CaCO_3$	% >63 μm	Sample type	$\delta^{18}O_{PDB}$	$\delta^{13}C_{PDB}$
12-2, 49-51	103.8	93	7	Fine fraction	−1.30	2.03
12-2, 69-71	104	91.9	1	Fine fraction	−1.42	1.95
12-2, 89-91	104.2	91.6	1	Fine fraction	−1.37	2.13
12-2 99-101	104.3	92.8	3	Fine fraction	−0.90	2.09
12-2, 129-131	104.6	94.5	3	Fine fraction	−1.27	2.02
12-3, 9-11	104.9	89.7	3	Fine fraction	−1.24	1.89
12-3, 29-31	105.1	93.9	1	Fine fraction	−0.97	2.04
12-3, 49-51	105.3	91.3	1	Fine fraction	−1.08	2.18
12-3, 69-71	105.5	92.5	1	Fine fraction	−0.95	2.27
12-3, 89-91	105.7	87.9	1	Fine fraction	−1.37	2.06
12-3, 109-111	105.9	94.85	3	Fine fraction	−1.45	1.92
12-3, 129-131	106.1	92.7	11	Fine fraction	−1.30	2.04
12-4, 9-11	106.4	95.4	14	Fine fraction	−1.09	2.00
12-4, 29-31	106.6	95.6	18	Fine fraction	−1.13	1.98
12-4, 49-51	106.8	93.1	20	Fine fraction	−1.24	1.73
12-4, 69-71	107	95.6	27	Fine fraction	−0.85	1.75
12-4, 89-91	107.2	94.5	25	Fine fraction	−0.34	1.87
12-4, 109-111	107.4	95.2	23	Fine fraction	−0.16	1.85
12-5, 19-21	108	93.1	20	Fine fraction	−0.85	1.78
12-5, 39-41	108.2	91.3	28	Fine fraction	−0.95	1.83
12-5, 59-61	108.4	93.1	25	Fine fraction	−0.90	1.84
12-5, 79-81	108.6	93.7	24	Fine fraction	−0.87	1.98
12-5, 91-93	108.72	93	14	Fine fraction	−0.70	2.19
12-5, 98-100	108.89	91.5	16	Fine fraction	−0.49	2.15
12-5, 108-109	108.99	93.2	15	Fine fraction	−0.83	2.02
12-5, 113-114	109.44	93.5	13	Fine fraction	−0.63	2.02
12-5, 117-119	109.09	89.5	9	Fine fraction	−0.65	1.91
12-5, 125-126	109.16	88.2	6	Fine fraction	−0.73	2.03
12-5, 128-130	109.19	88.8	3	Fine fraction	−0.74	2.49
12-5, 131-132	109.22	94.8	1	Fine fraction	−0.82	2.83
12-5, 134-136	109.26	95.7	<1	Fine fraction	−0.64	2.94
12-5, 144-145	109.35	96	<1	Fine fraction	−0.97	2.87
12-6, 19-21	109.6	95.2	<1	Fine fraction	−0.81	2.76
12-6, 39-41	109.8	96.1	<1	Fine fraction	−0.85	2.55
12-6, 59-61	110	94.8	<1	Fine fraction	−0.87	2.55
12-6, 99-101	110.4	95.2	<1	Fine fraction	−0.93	2.50
12-7, 9-11	111	93.6	<1	Fine fraction	−0.94	2.64
13-4, 59-61	111.8	87.4	<1	Fine fraction	−1.08	2.48
13-1, 99-101	112.2	94	<1	Fine fraction	−1.05	2.49
13-1, 139-141	112.6	95.38	<1	Fine fraction	−0.99	2.83
13-2, 39-41	113.1	96.3	<1	Fine fraction	−1.10	2.80
13-2, 79-81	113.5	94.5	<1	Fine fraction	−1.03	2.78
13-2, 119-121	113.9	94.8	<1	Fine fraction	−1.05	2.76
13-3, 19-21	114.4	94	<1	Fine fraction	−0.97	2.72
13-3, 59-61	114.8	94.6	<1	Fine fraction	−0.94	2.80
13-3, 99-101	115.2	90.9	<1	Fine fraction	−0.95	2.65
13-3, 139-141	115.6	95.1	<1	Fine fraction	−0.93	2.86
13-4, 39-41	116.1	94.1	<1	Fine fraction	−0.99	2.71
13-4, 99-101	116.7	94.9	<1	Fine fraction	−0.87	2.64
12-2, 89-91				*Aragonia*	−0.05	0.81
12-2, 129-131				*Aragonia*	0.08	0.88
12-3, 9-11				*Aragonia*	−0.08	0.60
12-4, 89-91				*Aragonia*	0.05	1.21
12-5, 59-61				*Aragonia*	0.48	1.98
12-5, 79-81				*Aragonia*	0.39	1.90
12-5, 117-119				*Aragonia*	0.20	1.65
12-5, 125-126				*Aragonia*	0.15	1.61
12-5, 108-109				*Aragonia*	0.45	1.82
12-5, 128-130				*Aragonia*	0.04	1.65
12-6, 19-21				*Aragonia*	0.31	1.36
12-6, 59-61				*Aragonia*	−0.33	0.82

fairly easy to reconstruct monospecific benthic stable-isotope records across the boundary. However, species of benthic foraminifers that are abundant in Danian samples are often present but not abundant in Maestrichtian samples and vice versa. In addition, the dilution of coarse-fraction foraminifers by calcareous nannofossils (predominance of fine fraction) in Maestrichtian sediments makes it extremely difficult to find the necessary number of a specific benthic foraminifer from the small sample sizes available at the closely spaced intervals needed to conduct stable-isotope analyses. In this case, analyses of mixed benthic assemblages, which provide less reliable data, must be performed instead. At Hole 577 w were fortunate enough to find one genus of benthic foraminifer, *Aragonia* (Plate 2, Figs. 1, 3, and 4), that wa both relatively plentiful and present in a few sample from either side of the boundary. The measured δ^{13} values of late Maestrichtian *Aragonia* indicate a carbo isotope trend toward heavier values just below the boundary, increasing from +0.83‰ a meter below the boundary (Sample 577-12-6, 79 cm) to +1.38‰ at the boundary (Sample 577-12-5, 125 cm). This trend continues i

Table 2. Stable-isotope results from Site 47.2.

Core-Section (interval in cm)	% >63 μm	Sample type	$\delta^{18}O_{PDB}$	$\delta^{13}C_{PDB}$
10-6, 50-51	4	Whole rock	−0.97	2.05
10-6, 100-101	8	Whole rock	−1.13	2.04
10-6, 127-128	4	Whole rock	−1.31	1.99
1, 25-26	16	Whole rock	−1.15	1.38
1, 75-77	19	Whole rock	−0.86	1.39
, 125-126	20	Whole rock	−0.98	1.62
2, 30-31	18	Whole rock	−0.72	1.66
2, 50-51	20	Whole rock	−0.76	1.71
2, 100-101	18	Whole rock	−0.61	1.93
, 30-31	1	Whole rock	−0.74	2.80
, 60-61	7	Whole rock	−0.74	2.19
, 100-101	15	Whole rock	−0.76	1.96
, 125-126	16	Whole rock	−0.70	1.90
, 138-139	14	Whole rock	−0.67	1.90
, 30-31	1	Whole rock	−0.97	2.66
, 60-61	4	Whole rock	−0.92	2.66
, 80-81	3	Whole rock	−0.88	2.64
, 98-99	10	Whole rock	−0.83	2.10
, 120-121	4	Whole rock	−0.85	2.14
138-139	9	Whole rock	−0.91	2.28
10-11	5	Whole rock	−0.94	2.48
20-21	5	Whole rock	−0.91	2.52
, 27-28	<1	Whole rock	−0.90	2.43
, 30-31	<1	Whole rock	−0.90	2.76
, 48-49	<1	Whole rock	−1.01	2.42
, 70-71	<1	Whole rock	−0.78	2.69
, 90-91	<1	Whole rock	−0.85	2.73
, 110-111	<1	Whole rock	−0.87	2.75
, 127-128	<1	Whole rock	−0.92	2.65
5, 140-141	<1	Whole rock	−0.77	2.65
11-6, 23-24	<1	Whole rock	−0.89	2.58
11-6, 40-41	<1	Whole rock	−0.78	2.57
11-6, 60-61	<1	Whole rock	−0.84	2.74
11-6, 80-81	<1	Whole rock	−0.70	2.72
11-6, 125-126	<1	Whole rock	−0.89	2.74
12-1, 25-26	<1	Whole rock	−0.92	2.52
12-1, 75-76	<1	Whole rock	−1.10	2.39
12-1, 125-126	<1	Whole rock	−0.98	2.79
12-2, 25-26	<1	Whole rock	−0.93	2.81
12-2, 68-69	<1	Whole rock	−1.01	2.73
12-2, 100-101	<1	Whole rock	−1.02	2.75
12-2, 125-127	<1	Whole rock	−1.07	2.75

the Danian section, reaching a maximum value of 1.98‰ in Sample 577-12-5, 60 cm. Further upcore, in Sections 577-12-2 and 577-12-3, *Aragonia* values return to preboundary levels, decreasing by as much as 1.2‰.

A similar trend across the Cretaceous/Tertiary boundary, but of lesser magnitude, is exhibited in the Site 465 arbon-isotope values of another benthic foraminifer, *Bu- mina* (Fig. 4; Boersma and Shackleton, 1981). The $\delta^{13}C$ lues of Maestrichtian *Bulimina* become enriched by 5‰, relative to earlier late Maestrichtian values, prior the boundary. Above this point, the carbon isotopic mposition of *Bulimina* decreases by about 0.4‰ up to .5 m.y. ago (above the Cretaceous/Tertiary boundary). ere appears to be a slight discrepancy between the o benthic isotope records in both the overall trend and ne of change, although the overall magnitude of the otope values are similar. Because the analyses of benic foraminifers at these two sites were performed on fferent species, *Bulimina* and *Aragonia*, the discrepncies between the two isotope records may be attributle to differences in species vital effects. In fact, differnt species of modern benthic foraminifers from the same mples have been found to possess significantly different $\delta^{13}C$ values and may also show considerable intraspecific variation between various size fractions (Woodruff et al., 1980; Belanger et al., 1981; Savin and Yeh, 1981).

Oxygen-isotope analyses of *Aragonia* in Hole 577 show no prominent trends (range ~0.5‰) although additional analyses of Core 13 samples should be conducted in order to determine whether the anomalous Maestrichtian value (Sample 577-12-6, 70 cm) is significant (Fig. 2). Overall, the $\delta^{18}O$ values are 0.8–1.5‰ heavier than the values obtained for planktonic organisms and roughly equivalent to the values obtained for Site 465 *Bulimina* (Fig. 4).

TRACE-ELEMENT GEOCHEMISTRY

Mineralogic stabilization of carbonate sediment occurs through solution–recrystallization processes. These processes also result in carbon- and oxygen-isotope stabilization. The stable-isotope values of altered carbonate sediments, therefore, may not represent the isotopic composition of the originally precipitated calcite, but rather some average of the isotopic composition of the original calcite and the reprecipitated calcite cements and overgrowths. In order to determine the extent of recrystallization, early investigators generally examined the downhole changes of various textural parameters such as porosity and cementation. However, more recently, chemical criteria have been considered in conjunction with textural studies, providing investigators with a quantitative as well as a qualitative measure of diagenesis (e.g., Matter et al., 1975). The distribution and concentration of certain trace elements such as strontium, magnesium, and manganese are known to change with increasing grades of diagenesis (e.g., Veizer, 1978; Baker et al., 1982). The direction of change is generally dependent upon the distribution coefficient of the element in question. Although contamination by noncarbonate fractions may prevent precise measurement of some elements such as Mn, the overall downhole trends and their signs provide us with important information for evaluating oxygen-isotope data that may have been influenced by diagenesis. The concentrations of the trace elements strontium, magnesium, and manganese in fine-fraction carbonates from across the Cretaceous/Tertiary boundary at Hole 577 are therefore reported and evaluated here (Table 3, Fig. 7).

The average measured value of magnesium for Site 577 samples falls within the typical range of values expected for a nannofossil ooze (Bathurst, 1981). From 116 to 109 m (the Cretaceous/Tertiary boundary) sub-bottom depth Mg concentrations range from 800 to 1300 ppm, varying very little throughout. From 109 to 108 m sub-bottom depth Mg concentrations increase sharply, reaching a peak value of 2100 ppm in Sample 577-12-5, 20 cm. This increase in Mg concentration coincides with an increase in fine-fraction insoluble residue contents (Fig. 7) over the same interval, suggesting that some Mg ions were leached from the clays during sample preparation. Above the Cretaceous/Tertiary bound-

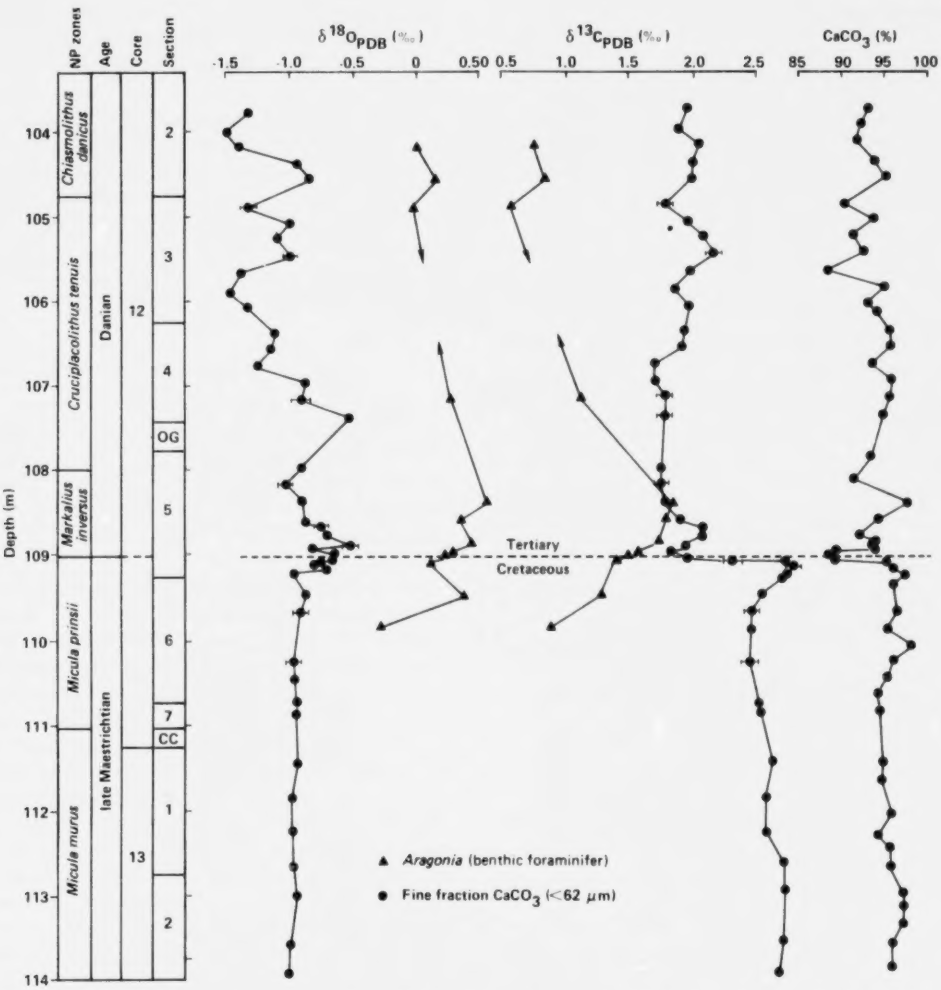

Figure 2. Carbon- and oxygen-isotope values of Hole 577 fine-fraction $CaCO_3$ and benthic foraminifer *Aragonia* and the carbonate content of whole rock. The Cretaceous/Tertiary boundary is located at Sample 577-12-5, 130 cm (see Monechi, this volume). OG = organic geochemistry sample, CC = core catcher.

ary (108 to 105 m) Mg concentrations decline to values of 1100 ppm, similar to those for the Maestrichtian samples.

Manganese concentrations are generally low throughout the entire sequence, ranging between 50 and 200 ppm (Fig. 7). Higher concentrations in Danian samples correspond to higher levels of insoluble residue, again suggesting that the measured concentrations of Mn were probably inflated by additional leached ions from manganese micronodules or other particles associated with the insoluble residue fraction.

Strontium content (and Sr/Ca ratio) varies very little in samples from below the boundary, ranging from 950 (Sample 577-12-6, 100 cm) to 1230 ppm (Sample 577-13-4, 100 cm) (Fig. 7). A sharp increase in Sr occurs just above the boundary between Samples 577-12-5, 109 cm and 577-12-5, 92 cm, with concentrations reaching 1700 ppm. Sr content declines rapidly upcore and, unlike Mg or Mn, exhibits no correspondence with the insoluble residue concentration. The Sr values and the Sr/Ca ratios are those expected for moderately preserved pelagic carbonates (Matter et al., 1975; Scholle, 1977).

CARBONATE PRESERVATION

In order to evaluate further the degree of preservatio of Site 577 carbonates, scanning electron microscop (SEM) photographs were taken of foraminifer and co colith tests and ultrastructure in conjunction with trac element studies.

Adelseck et al. (1973) have demonstrated in labor tory experiments that calcite overgrowths and dissol tion etching occur with greater frequency with increa ing burial conditions (i.e., increased temperature and pre sure). The dissolution and recrystallization of calcite a calcareous ooze is such that cement overgrowths o the low magnesium calcite of large coccoliths and disco asters occur at the expense of planktonic foraminife and small coccoliths, which usually disaggregate wit

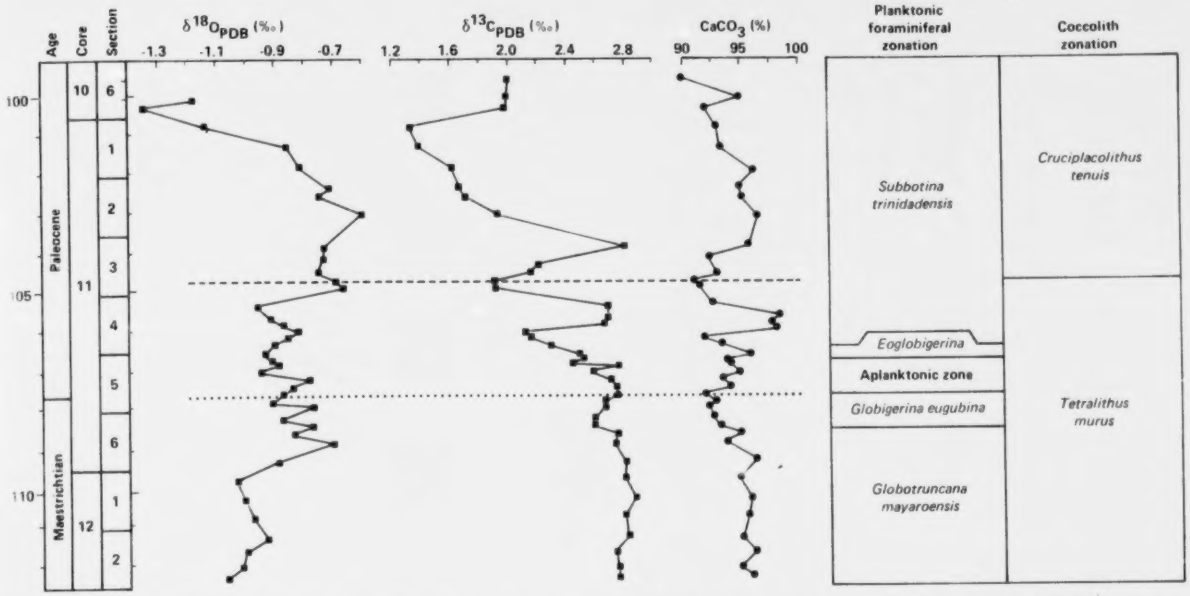

Figure 3. Site 47.2 carbon- and oxygen-isotope values and carbonate content of whole rock samples. Included are Cretaceous/Tertiary boundary locations based on planktonic foraminifer (dots; Hofker, 1978) and coccolith (dashed; Thierstein, 1981) biostratigraphy.

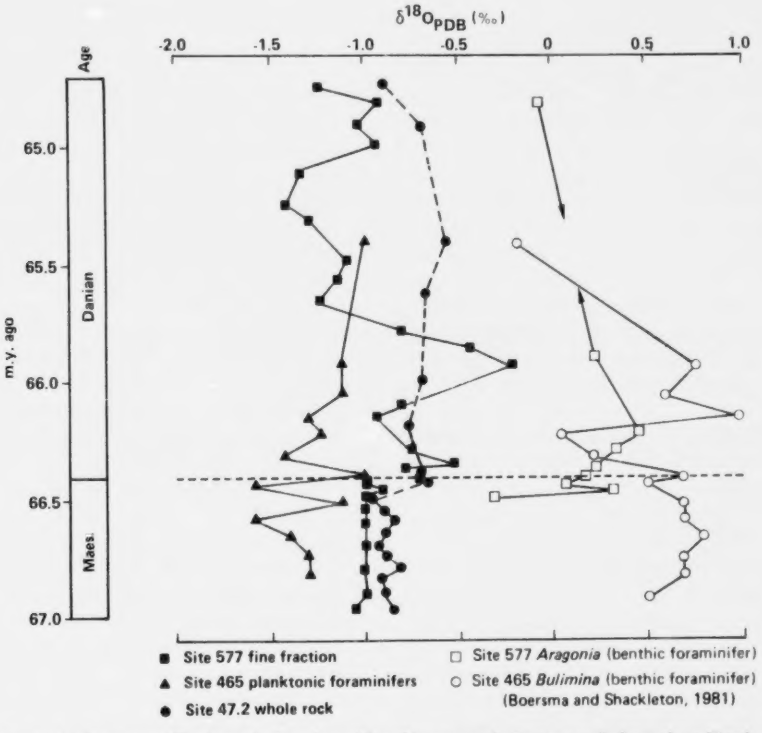

Figure 4. Cretaceous/Tertiary planktonic and benthic oxygen-isotope records from three North Pacific DSDP sites: 465 (data from Boersma and Shackleton, 1981), 47.2, and 577. Site 465 is located on the Hess Rise and 47.2 and 577 on the Shatsky Rise (see Fig. 1).

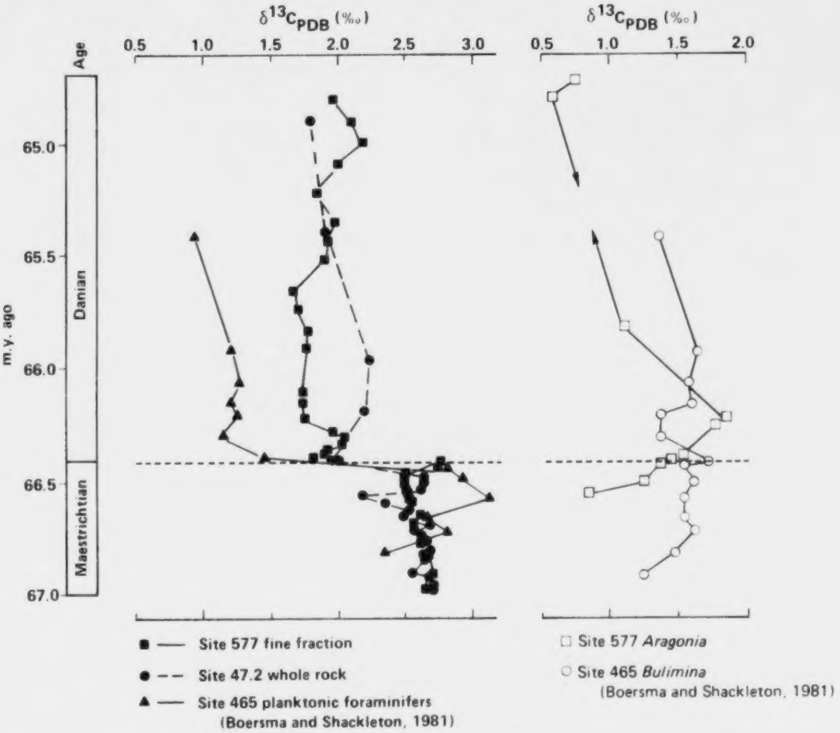

Figure 5. Compilation of planktonic and benthic carbon-isotope records from Sites 465 (data from Boersma and Shackleton, 1981), 47.2, and 577.

increasing dissolution (e.g., Douglas and Savin, 1971; Schlanger and Douglas, 1974; Roth and Berger, 1975; Berger, 1975; Thierstein, 1980; Thunell, 1982). As diagenesis progresses, cementation of grains generally follows, resulting in a transition from ooze to chalk to limestone. A well-preserved calcareous fossil assemblage should, therefore, exhibit the following physical characteristics: (1) individual specimens of foraminifers and nannofossils are essentially unbroken and free of extensive etchings or overgrowths, and (2) cementation between grains is absent. If signs of extensive diagenetic alteration do exist, then stable-isotope values must be considered suspect.

SEM photographs of Site 577 Danian and Maestrichtian samples show moderately to well-preserved calcareous microfossil specimens. Coccoliths from Maestrichtian samples in Hole 577 (Plate 4, Figs. 5-8) exhibit some signs of incipient dissolution and recrystallization.

Overall, the preservation of Maestrichtian calcareous nannofossils is moderate at Site 577. Euhedral calcite overgrowths are present on some coccoliths and some specimens are etched or partially dissolved and disaggregated (Plate 4, Figs. 7 and 8). Similar structures have been found on coccoliths from Site 47.2 (Plate 1, Fig. 3 and 4). Earlier calcareous nannofloral work at Site 47.2 (Thierstein, 1981) revealed a large increase in the proportions of dissolution-resistant taxa, such as *Micula staurophora* and *M. murus* in the middle sections of Core 11, suggesting either slight pre- or postburial dissolution. However, because the sediments at Site 47.2 have been mechanically displaced and mixed, it is difficult to determine exactly where stratigraphically, relative to the Cretaceous/Tertiary boundary, the dissolution may have occurred.

Danian samples from both Sites 577 and 47.2 (Plate 1, Fig. 2; Plate 2, Figs. 1-4) also contain moderately to well-preserved specimens of calcareous nannofossils. Overgrowths are notably absent on many coccoliths from Sample 577-12-2, 50 cm (Plate 3), although some coccoliths at that level are overgrown and/or etched, especially on the inner regions of the proximal side of coccolith shields (Plate 3, Fig. 3). Calcareous nannofossils at the Cretaceous/Tertiary boundary appear to be just as well, if not better, preserved than those from above and below the boundary (Plate 4, Figs. 1-4), as was observed at Site 384 by Thierstein and Okada (1979). In addition, unlike *Aragonia* from other sections of the core (Plate 2, Fig. 5), the tests of *Aragonia* from the Cretaceous/Tertiary boundary samples show fewer adhering cemented carbonate fragments and/or coccoliths (Plate 2, Fig. 6). Further examination of the carbonate trace-element data reveals that Sr/Ca ratios increase over a short interval across the Cretaceous/Tertiary boundary (Fig. 7). This provides more substantial empirical evidence on the state of preservation of the fine-fraction carbonates. During dissolution-reprecipitation of calcite, Sr ions are preferentially removed from the carbonate matrix (because the Sr partition coefficient is less than 1) so that with progressive recrystallization, cementation, or replacement the Sr/Ca ratio of the calcite should decrease (Lawrence,

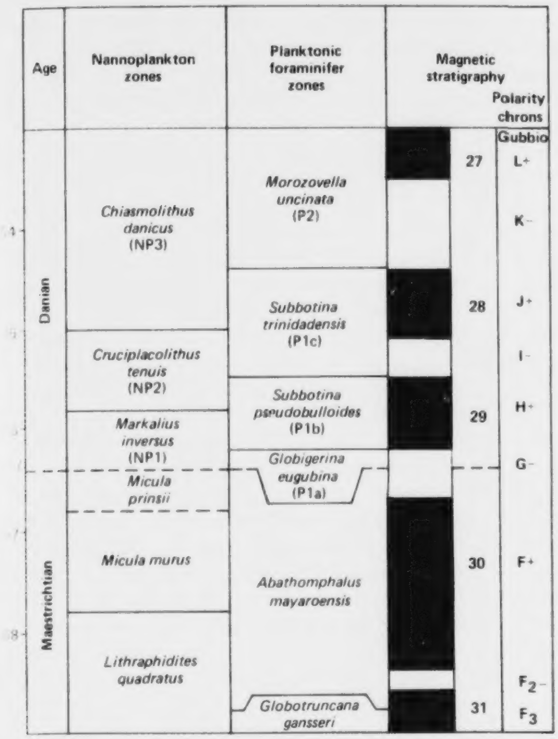
Age
Nannoplankton zones
Planktonic foraminifer zones
Magnetic stratigraphy
Polarity chrons
Gubbio
Danian
Maestrichtian
Chiasmolithus danicus (NP3)
Cruciplacolithus tenuis (NP2)
Markalius inversus (NP1)
Micula prinsii
Micula murus
Lithraphidites quadratus
Morozovella uncinata (P2)
Subbotina trinidadensis (P1c)
Subbotina pseudobulloides (P1b)
Globigerina eugubina (P1a)
Abathomphalus mayaroensis
Globotruncana gansseri
27
28
29
30
31
L+
K−
J+
I−
H+
G−
F+
F2−
F3

Figure 6. The Cretaceous/Tertiary boundary time scale and zonations utilized in this investigation. After van Hinte (1976), Martini (1976), Palmer (1983), Poore et al. (1983), and Berggren, Kent, and Flynn (in press). Polarity chrons are defined in Alvarez et al. (1977).

Table 3. Site 577 trace-element concentrations (<63 μm carbonate).

Core-Section (interval in cm)	% $CaCO_3$ (bulk)	Sr (ppm)	Mg (ppm)	Mn (ppm)
12-2, 49-51	90.3	1050	1010	145
12-2, 129-131	90.5	1030	950	168
12-3, 49-51	87.4	1190	1220	201
12-2, 129-131	92.8	1000	1260	139
12-4, 49-51	90.5	1030	1610	112
12-4, 89-91	87.1	1010	1820	148
12-5, 19-21	84.3	1260	2080	149
12-5, 59-61	87.1	1260	2000	149
12-5, 91-93	94.2	1640	1840	126
12-5, 108-109	94.1	1670	1760	118
12-5, 125-126	85.4	1030	1590	150
12-5, 128-130	88.4	1130	1200	101
12-5, 131-132	95.1	1080	1010	159
12-5, 144-145	95.8	1130	890	122
12-6, 39-41	95.8	1010	960	54
12-6, 99-101	96.5	940	1180	53
13-1, 59-61	95	1190	1380	79
13-1, 139-141	95	1110	1680	53
13-2, 79-81	96.4	1150	1310	49
13-3, 59-61	94.2	1140	1390	54
13-3, 139-141	93.7	1210	1570	68
13-4, 99-101	93	1230	1500	113

1971; Matter et al., 1975; Sayles and Manheim, 1975; Scholle, 1977; Brand and Veizer, 1980; Bathurst, 1981; Baker et al., 1982). However, it is difficult to imagine why the Cretaceous/Tertiary boundary carbonate would be better preserved than the carbonates in overlying sequences, considering that sedimentation rates were apparently lower, and other workers have suggested a major dissolution pulse at the boundary (e.g., Worsley, 1974). Some workers suggest that chemical preservation of

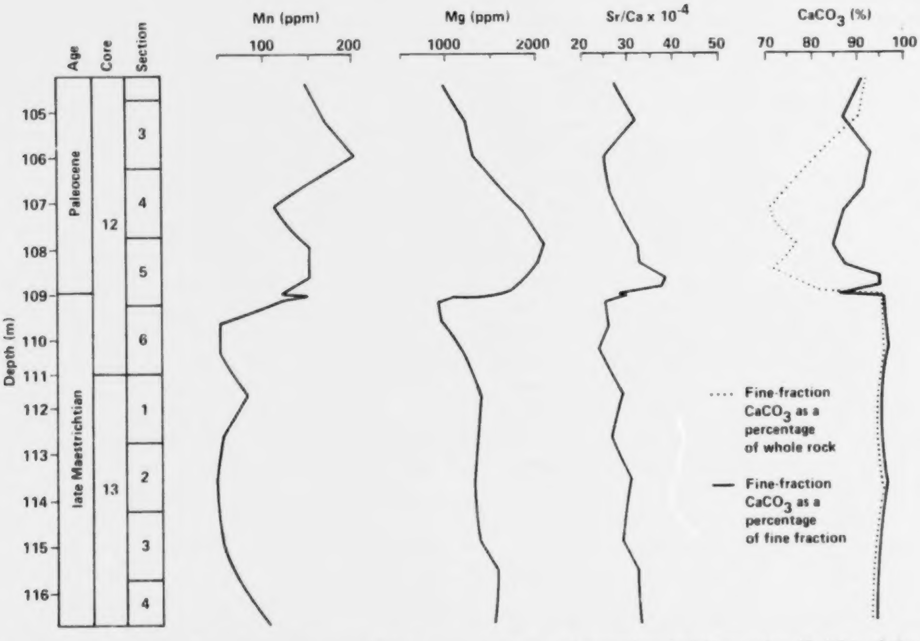

Figure 7. Manganese (Mn) and magnesium (Mg) concentrations and strontium/calcium ratios (Sr/Ca) of the fine-fraction (<63 μm) carbonates from Cores 12 and 13 of Hole 577. Fine-fraction carbonate content of whole fine-fraction and whole rock are included. The boundary is located at 109 m sub-bottom depth.

$CaCO_3$ may be enhanced if the lithology of the sediment sequence is not conducive to cementation (i.e., low porosity, high clay content, etc., Schlanger and Douglas, 1974; Matter et al., 1975). Downhole variations in preservation, therefore, may often be a function of changes in insoluble residue content. The increase in insoluble residue at the boundary represents a slight change in lithology, one which may have improved the resistance of the boundary sequence to postburial overgrowth and cementation. This is in contrast to reports of poorly preserved calcareous microfossils at some other Cretaceous/Tertiary boundary sequences (Worsley, 1974; Monechi, 1977).

An important consideration is whether or not there is any relationship between the changes in the state of preservation and the anomalies in the oxygen-isotope record. The slight enrichment in $\delta^{18}O$ at the boundary may be interpreted as improved preservation (no addition of isotopically lighter cement) rather than as a decrease in the temperature of the surface water mass in which the calcite was precipitated. Downhole changes in Sr/Ca ratios and preservation have been correlated previously with changes in oxygen-isotope records (Matter et al., 1975), whereas others have developed simple mathematical models attributing decreasing trends in $\delta^{18}O$ records through time to progressively greater diagenetic reactions with increasing age and burial depth (Killingley, 1983). Ignoring temperature effects for the moment, the somewhat anomalous $\delta^{18}O$ values of the Hole 577 boundary samples may be a function of the degree of diagenesis. If so, similar enrichments in oxygen-isotope signals at other marine boundary sequences (Site 524, Hsü et al., 1982a; Site 516, Williams et al., 1984) may also be a function of differential preservation (due to high clay content) rather than the result of real changes in oceanic temperatures.

CARBONATE ACCUMULATION RATES

Barring severe diagenesis and/or preburial dissolution, carbonate accumulation rates on the seafloor should reflect the magnitude of productivity in overlying surface waters. One would therefore expect that a postulated decrease in phytoplankton production associated with the Cretaceous/Tertiary boundary extinctions would be accompanied by a similar decrease in carbonate accumulation rates. At Hole 577 total and fine-fraction carbonate accumulation and rates decline significantly across the Cretaceous/Tertiary boundary (Table 4) (Fig. 8). Preboundary rates are stable at 1.10 g/cm²/1000 yr., with fine-fraction carbonate accumulation contributing a major portion to the total (>99%). Just above the boundary, total carbonate accumulation rates decrease to 0.3 g/cm²/1000 yr., with fine-fraction carbonate contributing far less as a percentage of the total (75–85%). This may imply that the decline in fine-fraction carbonate accumulation was more severe relative to the decline in foraminifer accumulation, that the recovery of foraminifer production occurred earlier than that of nannofossil (phytoplankton) production, or that current winnowing of fine-fraction carbonate occurred relative to coarse fraction.

There do not appear to be any significant variations in carbonate accumulation rates during the early Paleocene because values generally remain constant. However, accumulation rates for the entire *Cruciplacolithus tenuis* and *Markalius inversus* zones (Samples 577-12-5, 128 cm to 577-12-4, 70 cm) were determined by utilizing a single sedimentation rate of 2.9 m/m.y. This rate was determined by using the lowest datable biostratigraphic marker (first appearance datum *Chiasmolithus danicus*) available. It is probable, however, that actual sedimentation rates varied considerably over this interval. For example the 10–20 cm of sediment lying just above the boundary may have accumulated at a much slower rate than the calculated rate of 2.9 m/m.y., by inference from the higher insoluble residue contents and the possibility that sediments higher in the *C. tenuis* Zone may have accumulated at a greater rate. This may explain why calculations reveal an increase in foraminifer accumulation rate across the boundary whereas, given the magnitude of the biotic extinctions, one might expect a decline. However unless datable biostratigraphic markers lower than the one used to determine the average 2.9 m/m.y. rate are located, the aforementioned rate must, for the moment be considered the best obtainable. Sedimentation rates as determined with preliminary paleomagnetic stratigraphy (Fig. 9) (Bleil, this volume) are similar to the above rates.

We believe that the magnitude of the decrease in the carbonate accumulation rate is real and not only a function of the absolute time scale used. First of all, the accumulation rate of insoluble residue (Fig. 7) does not decrease across the Cretaceous/Tertiary boundary by the same factor as the carbonate accumulation rate. Second, the insoluble residue accumulation rate decreases only gradually from Maestrichtian through Danian time.

DISCUSSION

As reported at Site 465 (Boersma and Shackleton, 1981) there appears to be little if any temperature change in surface waters across the Cretaceous/Tertiary boundary at Hole 577. The slight enrichment in the $CaCO_3$ fine-fraction $\delta^{18}O$ in Hole 577 is perhaps an artifact of preservation–diagenesis rather than a function of surface water temperature changes. However, if one were to interpret this 0.5‰ enrichment in terms of a temperature change, such an enrichment in $\delta^{18}O$ would represent a 2°C decrease in surface water temperatures at most. A second enrichment occurs in the lower part of Section 577-12-4 and may represent a slightly greater temperature decrease (3–3.5°C). Higher in the core, $\delta^{18}O$ values show significant fluctuations and are difficult to interpret. In Section 577-12-3, $\delta^{18}O$ values are slightly enriched, identical to average Maestrichtian values. However, the $\delta^{13}C$ ratios and the ratios of coarse-fraction (<63 μm) to fine-fraction carbonate over this interval are also similar to ratios in Maestrichtian sediments, indicating a possible lateral reworking of sediments through some sections at this location. The presence of poorly preserved fragments of Maestrichtian foraminifers in Section 577-12-3 is confirmation that reworking occurred.

Table 4. Site 577 accumulation rates.

Core-Section (interval in cm)	Depth (m)	Age (m.y.)	WBD (g/cm^3)	Poros.	CaCO$_3$ (%)	DBD (g/cm^3)	Sed. rate (cm/1000 yr.)	MAR	CAR	Wt. % <63 μm	FFAR (g/cm^2/1000 yr.)
12-2, 49–51	103.8	64.55	1.65	0.5	0.93	1.15	0.29	0.33	0.31	0.93	0.287
12-2, 69–71	104	64.62	1.65	0.5	0.919	1.15	0.29	0.33	0.31	0.99	0.302
12-2, 89–91	104.2	64.69	1.65	0.5	0.916	1.15	0.29	0.33	0.30	0.99	0.301
12-2, 109–111	104.4	64.76	1.65	0.5	0.938	1.15	0.29	0.33	0.31	0.97	0.302
12-2, 129–131	104.6	64.83	1.65	0.5	0.945	1.15	0.29	0.33	0.31	0.97	0.304
12-3, 9–11	104.9	64.93	1.65	0.5	0.897	1.15	0.29	0.33	0.30	0.97	0.289
12-3, 29–31	105.1	65	1.65	0.5	0.939	1.15	0.29	0.33	0.31	0.99	0.309
12-3, 49–51	105.3	65.07	1.65	0.5	0.913	1.15	0.29	0.33	0.30	0.99	0.300
12-3, 69–71	105.5	65.14	1.65	0.5	0.925	1.15	0.29	0.33	0.31	0.99	0.304
12-3, 89–91	105.7	65.21	1.65	0.5	0.879	1.15	0.29	0.33	0.29	0.99	0.289
12-3, 109–111	105.9	65.28	1.65	0.5	0.9485	1.15	0.29	0.33	0.31	0.97	0.306
12-3, 129–131	106.1	65.34	1.65	0.5	0.927	1.15	0.29	0.33	0.31	0.89	0.274
12-4, 9–11	106.4	65.45	1.65	0.5	0.954	1.15	0.29	0.33	0.32	0.86	0.272
12-4, 29–31	106.6	65.52	1.65	0.5	0.956	1.15	0.29	0.33	0.32	0.82	0.260
12-4, 49–51	106.8	65.59	1.65	0.5	0.931	1.15	0.29	0.33	0.31	0.8	0.247
12-4, 69–71	107	65.66	1.65	0.5	0.956	1.15	0.29	0.33	0.32	0.73	0.232
12-4, 89–91	107.2	65.72	1.65	0.5	0.945	1.15	0.29	0.33	0.31	0.75	0.235
12-4, 99–101	107.3	65.76	1.65	0.5	0.99	1.15	0.29	0.33	0.33	0.77	0.253
12-5, 19–21	108	66	1.65	0.5	0.931	1.15	0.29	0.33	0.31	0.8	0.247
12-5, 39–41	108.2	66.07	1.65	0.5	0.913	1.15	0.29	0.33	0.30	0.72	0.218
12-5, 59–61	108.4	66.14	1.65	0.5	0.931	1.15	0.29	0.33	0.31	0.75	0.232
12-5, 79–81	108.6	66.21	1.65	0.5	0.937	1.15	0.29	0.33	0.31	0.76	0.236
12-5, 83–85	108.64	66.22	1.65	0.5	0.93	1.15	0.29	0.33	0.31	0.83	0.256
12-5, 98–100	108.89	66.31	1.65	0.5	0.915	1.15	0.29	0.33	0.30	0.84	0.255
12-5, 108–109	108.99	66.34	1.65	0.5	0.932	1.15	0.29	0.33	0.31	0.85	0.263
12-5, 113–114	109.44	66.50	1.65	0.5	0.935	1.15	0.29	0.33	0.31	0.87	0.270
12-5, 117–119	109.09	66.38	1.65	0.5	0.895	1.15	0.29	0.33	0.30	0.91	0.270
12-5, 125–126	109.16	66.4	1.65	0.5	0.882	1.15	1	1.1	1.0	0.94	0.949
12-5, 128–130	109.19	66.40	1.65	0.5	0.888	1.15	1	1.1	1.0	0.99	1.01
12-5, 131–132	109.22	66.41	1.65	0.5	0.948	1.15	1	1.1	1.1	0.99	1.07
12-5, 134–136	109.26	66.41	1.65	0.5	0.957	1.15	1	1.1	1.1	0.99	1.08
12-5, 139–140	109.29	66.41	1.65	0.5	0.959	1.15	1	1.1	1.1	0.99	1.09
12-5, 144–145	109.35	66.42	1.65	0.5	0.96	1.15	1	1.1	1.1	0.99	1.09
12-6, 9–11	109.5	66.43	1.65	0.5	0.952	1.15	1	1.1	1.1	0.99	1.08
12-6, 19–21	109.6	66.44	1.65	0.5	0.952	1.15	1	1.1	1.1	0.99	1.08
12-6, 29–31	109.7	66.45	1.65	0.5	0.958	1.15	1	1.1	1.1	0.99	1.09
12-6, 39–41	109.8	66.46	1.65	0.5	0.961	1.15	1	1.1	1.1	0.99	1.09
12-6, 49–51	109.9	66.47	1.65	0.5	0.939	1.15	1	1.1	1.1	0.99	1.06
12-6, 59–61	110	66.48	1.65	0.5	0.948	1.15	1	1.1	1.1	0.99	1.07
12-6, 69–71	110.1	66.49	1.65	0.5	0.95	1.15	1	1.1	1.1	0.99	1.08
12-6, 79–81	110.2	66.50	1.65	0.5	0.969	1.15	1	1.1	1.1	0.99	1.10
12-6, 89–91	110.3	66.51	1.65	0.5	0.964	1.15	1	1.1	1.1	0.99	1.09
12-6, 99–101	110.4	66.52	1.65	0.5	0.952	1.15	1	1.1	1.1	0.99	1.08
12-6, 109–111	110.5	66.53	1.65	0.5	0.944	1.15	1	1.1	1.1	0.99	1.07
12-6, 119–121	110.6	66.54	1.65	0.5	0.945	1.15	1	1.1	1.1	0.99	1.07
12-6, 129–131	110.7	66.55	1.65	0.5	0.924	1.15	1	1.1	1.1	0.99	1.05
12-6, 139–141	110.8	66.56	1.65	0.5	0.944	1.15	1	1.1	1.1	0.99	1.07
12-7, 9–11	111	66.58	1.65	0.5	0.936	1.15	1	1.1	1.1	0.99	1.06
13-1, 19–21	111.4	66.62	1.65	0.5	0.946	1.15	1	1.1	1.1	0.99	1.07
13-1, 39–41	111.6	66.64	1.65	0.5	0.943	1.15	1	1.1	1.1	0.99	1.07
13-1, 59–61	111.8	66.66	1.65	0.5	0.874	1.15	1	1.1	1.0	0.99	0.991
13-1, 79–81	112	66.68	1.65	0.5	0.951	1.15	1	1.1	1.1	0.99	1.08
13-1, 99–101	112.2	66.70	1.65	0.5	0.94	1.15	1	1.1	1.1	0.99	1.07
13-1, 119–121	112.4	66.72	1.65	0.5	0.952	1.15	1	1.1	1.1	0.99	1.08
13-1, 139–141	112.6	66.74	1.65	0.5	0.9538	1.15	1	1.1	1.1	0.99	1.08
13-2, 19–21	112.9	66.77	1.65	0.5	0.904	1.15	1	1.1	1.0	0.99	1.02
13-2, 39–41	113.1	66.79	1.65	0.5	0.963	1.15	1	1.1	1.1	0.99	1.09
13-2, 59–61	113.3	66.81	1.65	0.5	0.961	1.15	1	1.1	1.1	0.99	1.09
13-2, 79–81	113.5	66.83	1.65	0.5	0.945	1.15	1	1.1	1.1	0.99	1.07
13-2, 99–101	113.7	66.85	1.65	0.5	0.949	1.15	1	1.1	1.1	0.99	1.08
13-2, 119–121	113.9	66.87	1.65	0.5	0.948	1.15	1	1.1	1.1	0.99	1.07
13-2, 139–141	114.1	66.89	1.65	0.5	0.95	1.15	1	1.1	1.1	0.99	1.08
13-3, 19–21	114.4	66.92	1.65	0.5	0.94	1.15	1	1.1	1.1	0.99	1.07
13-3, 39–41	114.6	66.94	1.65	0.5	0.953	1.15	1	1.1	1.1	0.99	1.08
13-3, 59–61	114.8	66.96	1.65	0.5	0.946	1.15	1	1.1	1.1	0.99	1.07
13-3, 79–81	115	66.98	1.65	0.5	0.974	1.15	1	1.1	1.1	0.99	1.10
13-3, 99–101	115.2	67.00	1.65	0.5	0.909	1.15	1	1.1	1.0	0.99	1.03
13-3, 119–121	115.4	67.02	1.65	0.5	0.964	1.15	1	1.1	1.1	0.99	1.09
13-3, 139–141	115.6	67.04	1.65	0.5	0.951	1.15	1	1.1	1.1	0.99	1.08
13-4, 19–21	115.9	67.07	1.65	0.5	0.924	1.15	1	1.1	1.1	0.99	1.05
13-4, 39–41	116.1	67.09	1.65	0.5	0.941	1.15	1	1.1	1.1	0.99	1.07
13-4, 59–61	116.3	67.11	1.65	0.5	0.95	1.15	1	1.1	1.1	0.99	1.08
13-4, 79–81	116.5	67.13	1.65	0.5	0.948	1.15	1	1.1	1.1	0.99	1.07
13-4, 99–101	116.7	67.15	1.65	0.5	0.949	1.15	1	1.1	1.1	0.99	1.08
13-4, 119–121	116.9	67.17	1.65	0.5	0.928	1.15	1	1.1	1.1	0.99	1.05
13-4, 139–141	117.1	67.19	1.65	0.5	0.952	1.15	1	1.1	1.1	0.99	1.08

Note: WBD = wet bulk density, DBD = dry bulk density, MAR = mass accumulation rate (g/cm^2/1000 yr.), CAR = carbonate accumulation rate (g/cm^2/1000 yr.), FFAR = fine fraction accumulation rate (g/cm^2/1000 yr.).

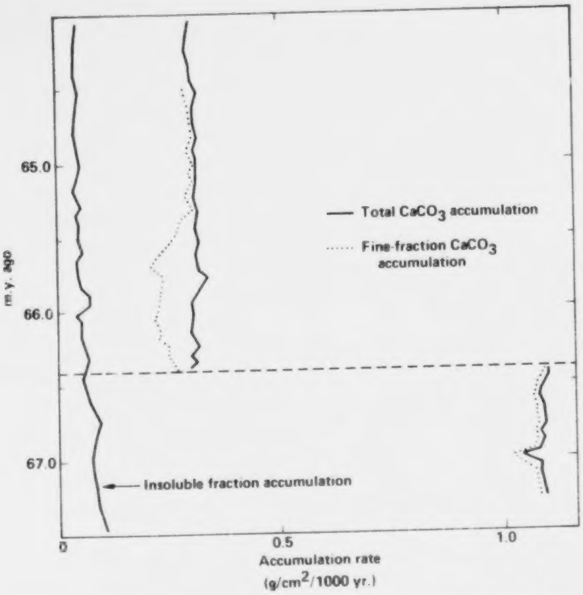

Figure 8. Total carbonate, fine-fraction carbonate, and insoluble fraction accumulation rates prior to and following the Cretaceous/Tertiary boundary.

Nonetheless, overall δ^{18}O values in uncontaminated Danian sections at Hole 577 tend to be lighter than Maestrichtian values. Because preservation changes relatively little, this implies a slight warming in surface waters. A slight cooling was apparently recorded by the whole rock values at Site 47.2 and by planktonic foraminifers from Site 465 where the δ^{18}O values of Danian foraminifers are somewhat heavier (Fig. 4) than the values of their Maestrichtian counterparts. Isotopic paleotemperature estimates for surface waters at the studied sites average near 15–18°C for the Maestrichtian and 14–18°C for the Danian. These temperatures appear to be rather cool for the estimated paleolatitude of about 15°N (Fig. 8) (Lancelot and Larson, 1975), but are in line with those calculated from other published data (Boersma and Shackleton, 1981).

The benthic oxygen-isotope stratigraphy from Site 465 and Hole 577 suggests that bottom water temperatures did not change systematically from the Maestrichtian to the Danian. At Site 465, δ^{18}O values of *Bulimina* showed variations amounting to about 4°C in paleotemperature estimates. The range of δ^{18}O values of *Aragonia* in Hole 577 was somewhat less. Because different species of benthic foraminifers were analyzed at each location, we can only speculate on the relative bottom-water temperatures of these two sites. However, considering the relatively small difference (0.5‰) in δ^{18}O between these two sections, it may be reasonable to assume that bottom-water temperatures at Sites 465 and 577 were very similar if not equal. The estimated isotopic paleotemperatures of deep water at the sites are between 8 and 12°C both above and below the Cretaceous/Tertiary boundary. These values fall within the range for shallow intermediate waters (< 1500 m) determined for inoceramids for the Late Cretaceous at other DSDP sites (Saltzman and Barron, 1982). There appears to have been relatively little change in the vertical temperature gradient across the Cretaceous/Tertiary boundary at either Site 465 or 577, but δ^{18}O values of *Aragonia* from Hole 577 suggest cooling across the boundary whereas δ^{18}O values of *Bulimina* from Site 465 apparently record a brief warming episode. The estimated paleodepths of Sites 465 and 577 are about 1500 and 2400 m, respectively (using subsidence curves and assumptions of Thiede et al., 1982). The estimated paleotemperatures at Hole 577 appear to be too warm fo the deeper paleodepth.

The negative δ^{13}C shift of about 1.0‰ recorded in th fine-fraction carbonate at the Cretaceous/Tertiary boundary at Hole 577 has been found in varying magnitude at nearly every Cretaceous/Tertiary boundary sequenc studied (e.g., Arthur et al., 1979; Scholle and Arthur 1980; Hsü et al., 1982a; Perch-Nielsen et al., 1982). Th negative shift detected in our data from Hole 577 occur within a few centimeters of the Cretaceous/Tertiary boundary determined by calcareous nannofossil stratigraphy (Monechi, this volume) and the major iridium spike and highest Ir/Fe ratio (Michel et al., this volume). The close correspondence of the δ^{13}C anomaly and the iridium anomaly in most other sections (Hsü et al., 1982a Zachos et al., unpubl. data) across the Cretaceous/Tertiary boundary suggest that the δ^{13}C shift is an excellent stratigraphic marker for the boundary (barring significant hiatuses). Some investigators have interpreted this anomaly to represent a decrease in oceanic surface water phytoplankton production (Boersma et al., 1979; Boersma and Shackleton, 1981; Arthur and Dean, 1982; Hsü et al., 1982a, b). While a number of authors have speculated on the cause of the catastrophy that brought about the extinctions and what effects the event and accompanying phytoplankton extinctions may have had on global climate, few have attempted to quantify the magnitude of the decline in marine productivity or its duration. Boersma and Shackleton (1981) and Hsü et al. (1982a) determined the δ^{13}C of benthic foraminifers as well as measuring the δ^{13}C of corresponding planktonic organisms, recognizing that the abrupt decline in δ^{13}C across the boundary might only have been a surface-water phenomenon. Benthic foraminifers tend to record the δ^{13}C of deep water (Woodruff et al., 1980, Belanger et al., 1981; Savin and Yeh, 1981) although, as mentioned earlier, some interspecies fractionation effects exist. By comparing the benthic and planktonic foraminifer carbon isotope records, Boersma and Shackleton (1981) were able to establish rough estimates of surface to deep-water carbon-isotope gradients prior to and following th Cretaceous/Tertiary boundary. Surface to deep-water carbon-isotope gradients of the modern oceans have been correlated with nutrient gradients (Broecker, 1974, Broecker and Peng, 1982) and dissolved oxygen or apparent oxygen utilization (Kroopnick et al., 1970; Williams et al. 1977; Kroopnick, 1974, 1980) and, hence, with primary productivity in surface waters and carbon oxidation in deep-water masses. Therefore, variations in primary productivity and consequent transfer and oxidation of organic matter in deeper waters should be reflected in

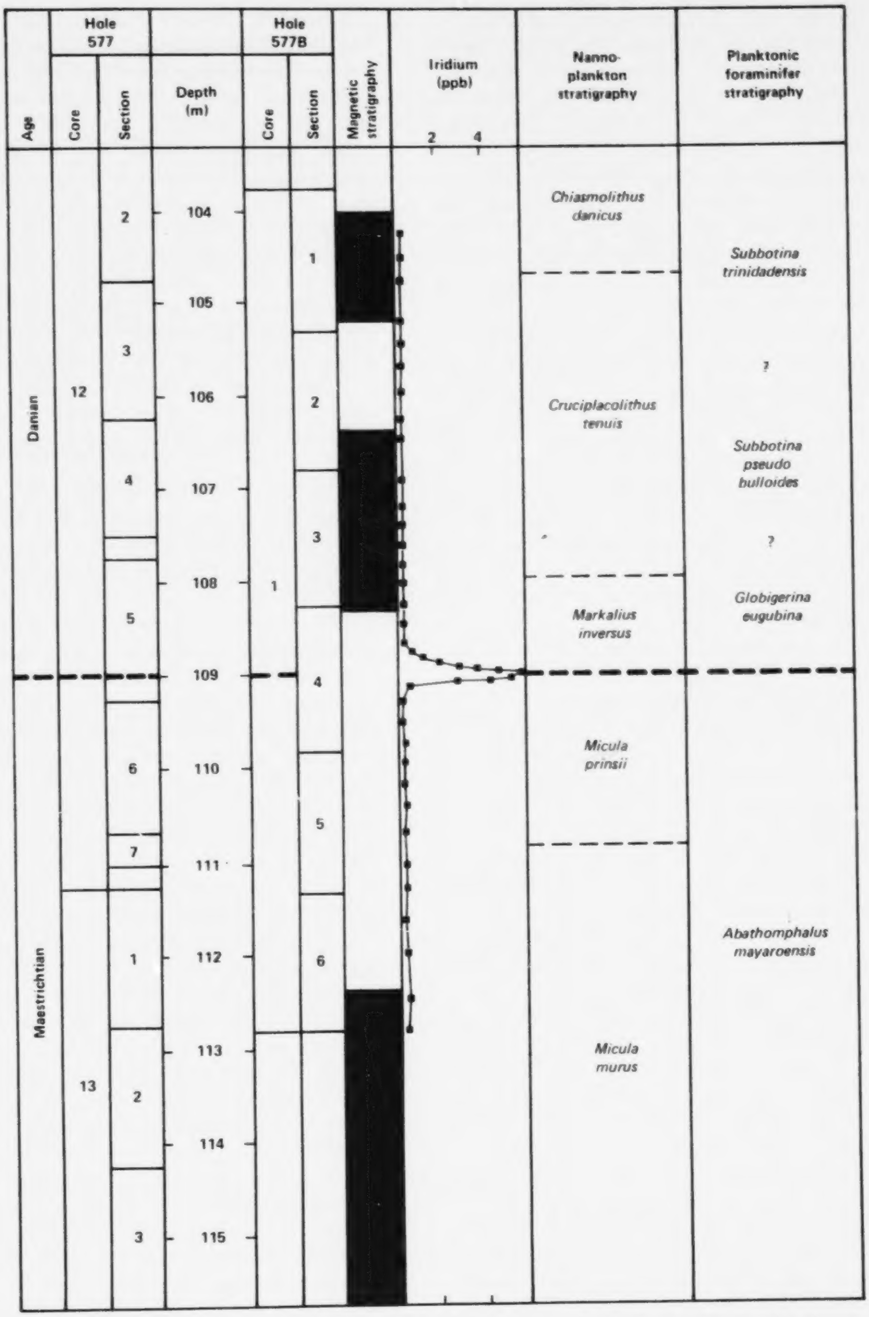

Figure 9. Correlation between Holes 577 and 577B showing magnetic stratigraphy (Bleil, this volume) and iridium concentrations as measured in Hole 577B (Michel et al., this volume). Cretaceous/Tertiary boundary was chosen at both holes on the basis of calcareous nannofossil biostratigraphy (Monechi, this volume). The nannoplankton and planktonic foraminifer stratigraphies in the right two columns are those of Hole 577.

anges in the surface to deep water $\delta^{13}C$ gradients in-rred from calcareous planktonic and benthic organisms. rom the Maestrichtian to the Danian at Site 465, there as a decrease in the surface to deep water $\delta^{13}C$ gradient rom 1.5 to 0‰ which was interpreted to represent an al-nost complete cessation of total dissolved CO_2 utilization for organic carbon production in surface waters (Boersma and Shackleton, 1981). The change in Maestrichtian to Danian surface- to deep-water carbon-isotope gradients at Hole 577, as the difference between the $\delta^{13}C$ of fine-fraction carbonate and of the benthic foraminifer *Aragonia*, was similar in magnitude to the change measured at Site 465 (Fig. 4). The decrease in the $\delta^{13}C$ gradient of 1.5‰ at Site 465, however, was a direct result of the decrease in planktonic carbon-isotope ratios because the carbon-isotope values of the benthic foraminifer *Bulimina* remained more or less constant. The change in surface to deep gradients at Hole 577 was partially a function of both an approximate 0.8‰ enrichment in benthic carbon-isotope values and a decrease of 0.8 to 1.0‰ in fine-fraction $\delta^{13}C$. This reduction of the surface to deep $\delta^{13}C$ gradient at the Cretaceous/Tertiary boundary is similar in some respects to the reduction of the $\delta^{13}C$ gradients in some freshwater lakes during the summer to winter transition when surface water productivity declines and summer thermal stratification is removed by vertical mixing (e.g., McKenzie, 1982). Following a fairly abrupt decline in surface organic productivity at the Cretaceous/Tertiary boundary that might have accompanied extinction of the majority of calcareous nannoplankton species, the flux of organic matter to deep-water masses would rapidly decrease. The amount of isotopically light CO_2 released from the decaying detritus would therefore decrease and $\delta^{13}C$ values for Danian deep-water masses may be more positive relative to those of the Late Cretaceous.

Further upcore at Hole 577, benthic $\delta^{13}C$ values decrease, reaching preboundary levels within the *Cruciplocolithus tenuis* zone. In addition, surface- to deep-carbon isotope gradients also return to preboundary levels by 2 m.y. following the event. If we assume that a positive surface to deep $\delta^{13}C$ gradient is produced by normally operating transfer mechanisms, such as the preferred extraction of isotopically light carbon from surface water in the organic flux to deep waters resulting from higher primary productivity, then these data may be interpreted to suggest that primary production recovered to near preboundary levels about 2 m.y. after the extinction event. However, the equilibrium levels of both surface and deep $\delta^{13}C$ were apparently much lighter in the Danian than in the Maestrichtian, perhaps because the overall rate of organic carbon burial was still somewhat lower in the Danian than during the late Maestrichtian (e.g., Scholle and Arthur, 1980) following the Cretaceous/Tertiary "event." The lighter average $\delta^{13}C$ values would therefore be a whole-reservoir signal.

On the basis of the change in planktonic foraminifer/nannofossil ratios, it appears that the rate of production of calcareous nannofossils decreased relative to the production of planktonic foraminifers or that planktonic foraminifers were able to recover much more quickly. Berger (1976), however, suggested that increases in the foraminifer/nannofossil ratio were the result of increased winnowing. This seems unlikely given the thickness of the section with higher foraminifer ratios (200 cm) and the absence of apparent current-induced laminations or other primary sedimentary structures indicative of current action. Foraminifers have a greater depth stratification than nannofossils, which generally inhabit only the photic zone, and as a group may have been able to maintain higher levels of productivity. The transition from nannofossil to relatively foraminifer-rich sediment occurs gradually across the Cretaceous/Tertiary boundary. Coarse fraction percentages increase from less than 1% to as much as 24% of the total sediment weight over a 60-cm interval above the boundary (Table 1). This suggests that the inferred productivity decrease may not have occurred instantly, geologically speaking, or that bioturbation mixed out the originally sharp change (e.g., Thierstein and Okada, 1979). Perch-Neilsen et al. (1982) and Hsü et al. (1982a) have presented evidence indicating that the extinction of calcareous nannoplankton may have occurred over a longer period than previously believed. However, in light of the sudden shift in carbon-isotope records across the boundary in the apparently continuou pelagic sequence at Site 577, it would be difficult to suggest that the decline in productivity was a slow and gradual process. It must have occurred in a period of less than 28,000 yr.

CONCLUSIONS

On the basis of available biostratigraphic and geochemical evidence (Monechi, this volume; Michel et al. this volume), we assume that the pelagic carbonate sequence at Hole 577 is continuous across the Cretaceous Tertiary boundary. Our trace-element and SEM studies of closely spaced samples across the Cretaceous/Tertiary boundary suggest that there are relatively small changes in preservation of calcareous microplankton and nannoplankton assemblages across the boundary. Oxygen-isotope determinations of the calcareous fine-fraction (representing surface-water masses) and benthic foraminifers in Hole 577 suggest relatively little temperature change in surface or deep-water masses across the boundary. Similar results were obtained in studies of DSDP Site 47.2 on the Shatsky Rise and Site 465 on nearby Hess Rise. The $\delta^{13}C$ gradient, inferred from analyses of planktonic and benthic calcareous groups, decreased abruptly at the Cretaceous/Tertiary boundary in conjunction with nannofossil and foraminifer extinctions and an increase in Ir concentrations and the Ir/Fe ratio. We attribute the change in the $\delta^{13}C$ gradient to a sudden decrease in surface productivity associated with the extinction event. Further substantiation of this is given by a significant reduction of carbonate accumulation rates across the Cretaceous/Tertiary boundary at Hole 577 and other localities without apparent significant changes in carbonate preservation. The decline in carbonate production/accumulation apparently lasted at least 2 m.y. The relationship to a postulated meteoritic impact, however, is not clear. Previously hypothesized temperature and carbonate preservational changes at the boundary are not evident at Pacific DSDP sites analyzed so far. The mechanism(s) for the extinctions and for decreased plankton productivity at the Cretaceous/Tertiary boundary remain(s) obscure.

ACKNOWLEDGMENTS

The authors would like to thank Hans Thierstein, Nick Shackleton, James Kennett, and Audrey Wright for reviewing this manuscrip and offering helpful criticism and Maria Burdett for drafting origina figures. This work was supported by NSF Grant EAR-8306561.

REFERENCES

Adelseck, C. G., Geehan, G. W., and Roth, P. H., 1973. Experimenta evidence for the selective dissolution and overgrowth of calcareous nannofossils during diagenesis. *Geol. Soc. Am. Bull.*, 84(8): 2755-2762.

Alvarez, L. W., Alvarez, W., Asaro, F., and Michel, H., 1980. Extraterrestrial cause for the Cretaceous-Tertiary extinctions. *Science*, 208:1095-1108.

lvarez, W., Alvarez, L. W., Asaro, F., and Michel, H. V., 1982. Current status of the impact theory for the terminal Cretaceous extinction. *In* Silver, L. T., and Shultz, P. H. (Eds.)., *Geologic Implications of Impacts of Large Asteroids and Comets on the Earth*. Geol. Soc. Am. Spec. Pap., 190:305-315.

rez, W., Arthur, M., Fischer, A. G., Lowrie, W., Giovanni, N., remoli Silva, I., and Roggenthen, W. N., 1977. The upper Cretaeous-Paleocene magnetic stratigraphy at Gubbio, Italy. *Geol. Soc. m. Bull.*, 88:367-389.

ur, M. A., and Dean, W. E., 1982. Changes in deep ocean circu- ation and carbon cycling at the Cretaceous-Tertiary boundary *In* erschmen, A., (Ed.), *Abstracts of Papers of the 148th Natl. Meet- g of the Amer. Assoc. for the Advance. of Sci.* AAAS Public., o. 82-2, p. 48. (Abstract)

ur, M. A., Scholle, P. A., and Hasson, P., 1979. Stable isotopes f oxygen and carbon in carbonates from Sites 398 and 116 of the eep Sea Drilling Project. *In* Sibuet, J.-C. Ryan, W. B. F., et al., *nit. Repts. DSDP*, 47, Pt. 2: Washington (U.S. Govt. Printing Of- ice), 477-492.

r, P. A., Gieskes, J. M., and Elderfield, H., 1982. Diagenesis of arbonates in deep sea sediments—evidence from Sr/Ca ratios and nterstitial dissolved Sr data. *J. Sediment. Petrol.*, 52(1):0071-0082.

hurst, R. G. C., 1981. *Carbonate Sediments and Their Diagenesis*: Amsterdam (Elsevier).

anger, P. E., Curry, W. B., and Matthews, R. K., 1981. Core-top evaluation of benthic foraminiferal isotopic ratios for paleo-ocean- ographic interpretations. *Paleogeogr. Paleoclimatol., Paleoecol.*, 33:205-220.

Berger, W. H., 1975. Deep sea carbonates. Dissolution profiles from foraminiferal preservation. *In* Sliter, W. V., Bé, A. W. H., and Berger, W. H., (Eds.), *Dissolution of Deep-Sea Carbonate*. Spec. Publ. Cushman Found. Foraminiferal Res., 13:82-86.

________, 1976. Biogenous deep sea sediments: Production, preservation, and interpretation. *In* Riley, J. P., and Chester, R. (Eds.) *Treatise on Chemical Oceanography* (Vol. 5): New York (Academic Press), 265-388.

Berggren, W. A., Kent, D. V., and Flynn, J. J., in press. Paleogene geochronology and chronostratigraphy. *In Geochronology and the Geological Record*: London (Geol. Soc. London).

Boersma, A., and Shackleton, N. J., 1981. Oxygen and carbon isotope variations and planktonic-foraminifer depth habitats, Late Cretaceous to Paleocene, Central Pacific. *In* Thiede, J., Vallier, T. L., et al., *Init. Repts. DSDP*, 62: Washington (U.S. Govt. Printing Office), 513-526.

Boersma, A., Shackleton, N. J., Hall, M., and Given, Q., 1979. Carbon and oxygen isotope records at DSDP Site 384 (North Atlantic) and some Paleocene paleotemperatures and carbon isotope variations in the Atlantic Ocean. *In* Tucholke, B. E., Vogt, P. R., et al., *Init. Repts. DSDP*, 43: Washington (U.S. Govt. Printing Office), 695-717.

amlette, M. N., 1965. Massive extinctions of biota at the end of Mesozoic time. *Science*, 148:1696-1699.

nd, U., and Veizer, J., 1980. Chemical diagenesis of a multicomponent carbonate system—1: Trace elements. *J. Sediment. Petrol.*, 50:1219-1236.

ecker, W. S., 1974. *Chemical Oceanography*: New York (Harcourt Brace Jovanovich).

ecker, W. S., and Peng, T.-H., 1982. *Tracers in the Sea*: New York (Lamont-Doherty Geological Observatory, Columbia University).

uglas, R., and Savin, S., 1971. Isotopic analyses of planktonic fo- aminifera from the Cenozoic of the Northwest Pacific, Leg 6. *In* Fischer, A. G., Heezen, B. C., et al., *Init. Repts. DSDP*, 6: Wash- ington (U.S. Govt. Printing Office), 1123-1127.

uglas, R., and Woodruff, F., 1981. Deep sea benthic Foraminifera. *In* Emiliani, C. (Ed.), *The Oceanic Lithosphere*: New York (Wi- ley), pp. 1233-1327.

iliani, C., Kraus, E. B., and Shoemaker, E. M., 1981. Sudden death at the end of the Mesozoic. *Earth Planet. Sci. Lett.*, 55: 317-334.

Firstbrook, P. L., Funnel, B. M., Hurley, A. M., and Smith, A. G., 1979. Paleoceanic reconstructions 160-0 Ma. Univ. of California, *National Science Foundation National Ocean Sediment Coring Program*, p. 22.

Fischer, A. G., and Arthur, M. A., 1977. Secular variations in the pelagic realm. *Spec. Publ. Soc. Econ. Paleontol. Mineral.*, 25:19-50.

Hofker, J., 1978. Analysis of a large succession of samples through the upper Maestrichtian and the lower Tertiary of drill Hole 47.2, Shatsky Rise, Pacific, DSDP. *J. Foraminiferal Res.*, 8:46-75.

Hsü, K. J., 1980. Terrestrial catastrophe by cometary impact at the end of the Cretaceous. *Nature*, 285:201-203.

Hsü, K. J., He, Q., McKenzie, J. A., Weissert, H., Perch-Nielsen, K., Oberhansli, H., Kelts, K., LaBrecque, J., Tauxe, L., Krahenbuhl, U., Percival, S. F., Wright, R., Karpoff, A. M., Petersen, N., Tucker, P., Poore, R. Z., Gombod, A. M., Pisciotto, K., Carman, M. F., and Schreiber, E., 1982a. Mass mortality and its environmental and evolutionary consequences. *Science*, 216:249-256.

Hsü, K. J., McKenzie, J. A., He, Q. X., 1982b. Terminal Cretaceous environmental and evolutionary changes. *In* Silver, L. T., and Shultz, P. H., (Eds.), *Geological Implications of Large Asteriods and Comets on the Earth*. Geol. Soc. Am. Spec. Pap. 190:317-328.

Keigwin, L. D., 1980. Paleoceanographic change in the Pacific at the Eocene-Oligocene boundary. *Nature*, 287:722-725.

Killingley, J. S., 1983. Effects of diagenetic recrystallization on $^{18}O/^{16}O$ values of deep sea sediments. *Nature*, 301:594-597.

Kroopnick, P.$_1$ 1974. Modeling the dissolved O_2-CO_2-^{13}C system in the eastern equatorial Pacific *Deep Sea Res.*, 21:211-229.

________, 1980. The distribution of ^{13}C in the Atlantic Ocean. *Earth Planet. Sci. Lett.*, 49:469-484.

Kroopnick, P., Deuser, W. G., Craig, H., 1970. Carbon-13 measurements on dissolved inorganic carbon at the North Pacific (1969) GEOSECS station. *J. Geophys. Res.*, 75:7668-7671.

Lancelot, Y., and Larson, R. L., 1975. Sedimentary and tectonic evolution of Northwestern Pacific. *In* Larson, R. L., Moberly, R., et al., *Init. Repts. DSDP*, 32: Washington (U.S. Govt. Printing Office), 925-940.

Lawrence, J. R., 1971. Interstitial water studies, Leg 15-Stable oxygen and carbon isotope variations in water, carbonates, and silicates from the Venezuela Basin (Site 149) and the Aves Rise (Site 148). *In* Heezen, B. C., MacGregor, I. D., et al., *Init. Repts. DSDP*, 20: Washington (U.S. Govt. Printing Office), 891-900.

McKenzie, J. A., 1982. Carbon-13 cycle in Lake Greifen: a model for restricted ocean basins. *In* Schlanger, S. O., and Cita, M. B. (Eds.), *Nature and Origin of Cretaceous Carbon Rich Facies*: New York (Academic Press), pp. 197-208.

McLean, D. M., 1980. Terminal Cretaceous catastrophe. *Nature*, 287: 760.

________, 1982. Flood basalt volcanism and global extinctions at the Cretaceous-Tertiary transition. *In* Herschmen, A. (Ed.), *Abstracts of Papers of the 148th National Meeting of the Amer. Assoc. for the Advance. of Sci.* AAAS Publ., No. 82-2, p. 47. (Abstract)

Martini, E., 1976. Cretaceous to Recent calcareous nannoplankton from the Central Pacific Ocean (DSDP Leg 33). *In* Schlanger, S. O., Jackson, E. D., et al., *Init. Repts. DSDP*, 33: Washington (U.S. Govt. Printing Office), 383-423.

Matter, A., Douglas, R. G., and Perch-Nielsen, K., 1975. Fossil preservation, geochemistry and diagenesis of pelagic carbonates from Shatsky Rise, N.W. Pacific. *In* Larson, R. L., Moberly, R., et al., *Init. Repts. DSDP*, 32: Washington (U.S. Govt. Printing Office), pp. 891-922.

Monechi, S., 1977. Upper Cretaceous and Early Tertiary nannoplankton from the Scaglia Umbra Formation (Gubbio, Italy). *Riv. Ital. Paleontol.*, 83:754-802.

Müller, G., and Gastner, M., 1971. The "Karbonate Bombe," a simple device for the determination of the carbonate content in sediments, soils, and other materials. *Neves Jahrb. Mineral. Monatsh.*, 10: 466-469.

Officer, C. B., and Drake, C. L., 1983. The Cretaceous-Tertiary transition. *Science*, 219:1383-1390.

Palmer, A. R., 1983. The decade of North American geology, 1983 geologic time scale. *Geology*, 11:503-504.

Perch-Nielsen, K., McKenzie, J., and He, Q., 1982. Biostratigraphy and isotope stratigraphy and the "Catastrophic" extinction of calcareous nannoplankton at the Cretaceous/Tertiary boundary. *In*

Silver, L. T., and Schultz, P. H. (Eds.), *Geological Implications of Impacts of Large Asteriods and Comets on the Earth*. Geol. Soc. Am. Spec. Pap., 190:353–371.

Poore, R. A., Tauxe, L., Percival, S. F., LaBrecque, J. L., Wright, R., Petersen, N. P., Smith, C. C., Tucker, P., and Hsü, K. J., 1983. Late Cretaceous-Cenozoic magnetostratigraphic and biostratigraphic correlations of the South Atlantic Ocean: DSDP Leg 73. *Paleogeogr., Paleoclimatol., Paleoecol.*, 42:127–148.

Roth, P. H., and Berger, W. H., 1975. Distribution and dissolution of coccoliths in the South and Central Pacific. *In* Sliter, W. V., Bé, A. W. H., and Berger, W. H. (Eds.), *Dissolution of Deep Sea Carbonates*. Spec. Publ. Cushman Found. Foraminiferal Res. 13: 87–113.

Saltzman, E. S., Barron, E. J., 1982. Deep circulation in the Late Cretaceous; oxygen isotope paleotemperatures from *Inocermus* remains in DSDP cores. *Paleogeogr., Paleoclimatol., Paleoecol.*, 40: 167–181.

Savin, S. M., and Yeh, H. W., 1981. Stable isotopes in ocean sediments. *In* Emiliani, C. (Ed.), *The Sea* (Vol. 7): New York (Wiley-Interscience), 1521–1554.

Sayles, F. L., and Manheim, F. T., 1975. Interstitial solutions and diagenesis in deeply buried marine sediments: Results from the Deep Sea Drilling Project. *Geochim. Cosmochim. Acta.*, 39:103–127.

Schlanger, S. O., and Douglas, R. G., 1974. The pelagic ooze-chalk-limestone transition and its implications for marine stratigraphy. *In* Hsü, K. J., and Jenkyns, H. C. (Eds.), *Pelagic Sediments on Land and under the Sea*. Int. Assoc. Sed. Spec. Public., 1:177–210.

Scholle, P. A., 1977. Chalk diagenesis and its relation to petroleum exploration: Oil from chalks a modern miracle? *Am. Assoc. Pet. Geol. Bull.*, 61:982–1009.

Scholle, P. A., and Arthur, M. A., 1980. Carbon isotope fluctuations in Cretaceous pelagic limestones; potential stratigraphic and petroleum exploration tool. *Am. Assoc. Pet. Geol. Bull.*, 64:67–87.

Silver, L. T., and Schultz, P. H. (Eds.), 1982. Geological implications of impacts of large asteroids and comets on the Earth. *Geol. Soc. Am. Spec. Pap.*, 190.

Tappan, H., 1968. Primary production, isotopes, extinctions and the atmosphere. *Paleogeogr., Paleoclimatol., Paleoecol.*, 4:187–210.

Thiede, J., Dean, W. E., and Claypool, G. E., 1982. Oxygen deficient depositional environments in the Mid-Cretaceous tropical to subtropical Pacific Ocean. *In* Schlanger, S. O., and Cita, M. B. (Eds.), *Nature and Origin of Cretaceous Carbon-Rich Facies*: New York (Academic Press), pp. 79–100.

Thierstein, H. R., 1980. Selective dissolution of Late Cretaceous and earliest Tertiary calcareous nannofossils: Experimental evidence. *Cretaceous Res.*, 2:165–176.

________, 1981. Late Cretaceous nannoplankton and the Cretaceous/Tertiary boundary. *Soc. Econ. Paleontol. Mineral.*, 32:355–394.

________, 1982. Terminal Cretaceous plankton extinctions: A critical assessment. *In* Silver, L. T., and Schultz, P. H. (Eds.), *Geological Implications of Impacts of Large Asteriods and Comets on the Earth*. Geol. Soc. Am. Spec. Paper, 190:385–400.

Thierstein, H. R., and Okada, H., 1979. The Cretaceous/Tertiary boundary event in the North Atlantic. *In* Tucholke, B. E., Vogt, P. R., et al., *Init. Repts. DSDP*, 43: Washington (U.S. Govt. Printin Office), 601–616.

Thunell, R. C., 1982. Carbonate dissolution and abyssal hydrograph in the Atlantic Ocean. *Mar. Geol.*, 47:165–180.

Toon, O. B., Pollack, J. B., Ackerman, T. P., Turco, R. P., McKay, C P., and Liu, M. S., 1982. Evolution of an impact-generated du cloud and its effects on the atmosphere. *In* Silver, L. T., an Schultz, P. H. (Eds.), *Geological Implications of Impacts of Lar Asteroids and Comets on the Earth*. Geol. Soc. Am. Spec. Pap 190:187–200.

van Hinte, J. E., 1976. A Cretaceous time scale. *Am. Assoc. Petro Geol. Bull.*, 60:498–516.

Veizer, J., 1978. Simulation of limestone diagenesis—a model base on strontium depletion: Discussion. *Can. J. Earth. Sci.*, 1 1683–1686.

Vogt, P. R., 1972. Evidence for global synchronism in mantle plum convection, and possible significance for geology. *Nature*, (*London*) 240:338–342.

Williams, D. F., Healy-Williams, N., Thunell, R. C., and Levente A., 1983. Detailed stable isotope and carbonate records from th late Maestrichtian early Paleocene section of Site 516F (Leg 72) including the Cretaceous/Tertiary boundary. *In* Barker, P. F., Carlson, R. L., Johnson, D. A., et al., *Init. Repts. DSDP*, 72: Washington (U.S. Govt. Printing Office), 921–930.

Williams, D. F., Sommer, M. A., and Bender, M. L., 1977. Carbon isotopic composition of recent planktonic foraminifera of the Indian Ocean. *Earth Planet. Sci. Lett.*, 36:391–403.

Woodruff, F., Savin, S., and Douglas, R., 1980. Biological fractionation of oxygen and carbon isotopes by recent benthic foraminifera. *Mar. Micropaleontol.*, 5:3–11.

Worsley, T., 1974. The Cretaceous-Tertiary boundary event in the ocean. *Soc. Econ. Paleontol. Mineral., Spec. Publ.*, 20:94–125.

Zoller, W. H., Parrington, J. R., and Phelan Kotra, J. M., 1983. Iridium enrichment in airborne particles from Kilauea volcano: January 1983. *Science*, 222:1118–1121.

Date of Initial Receipt: 17 January 1984
Date of Acceptance: 17 August 1984

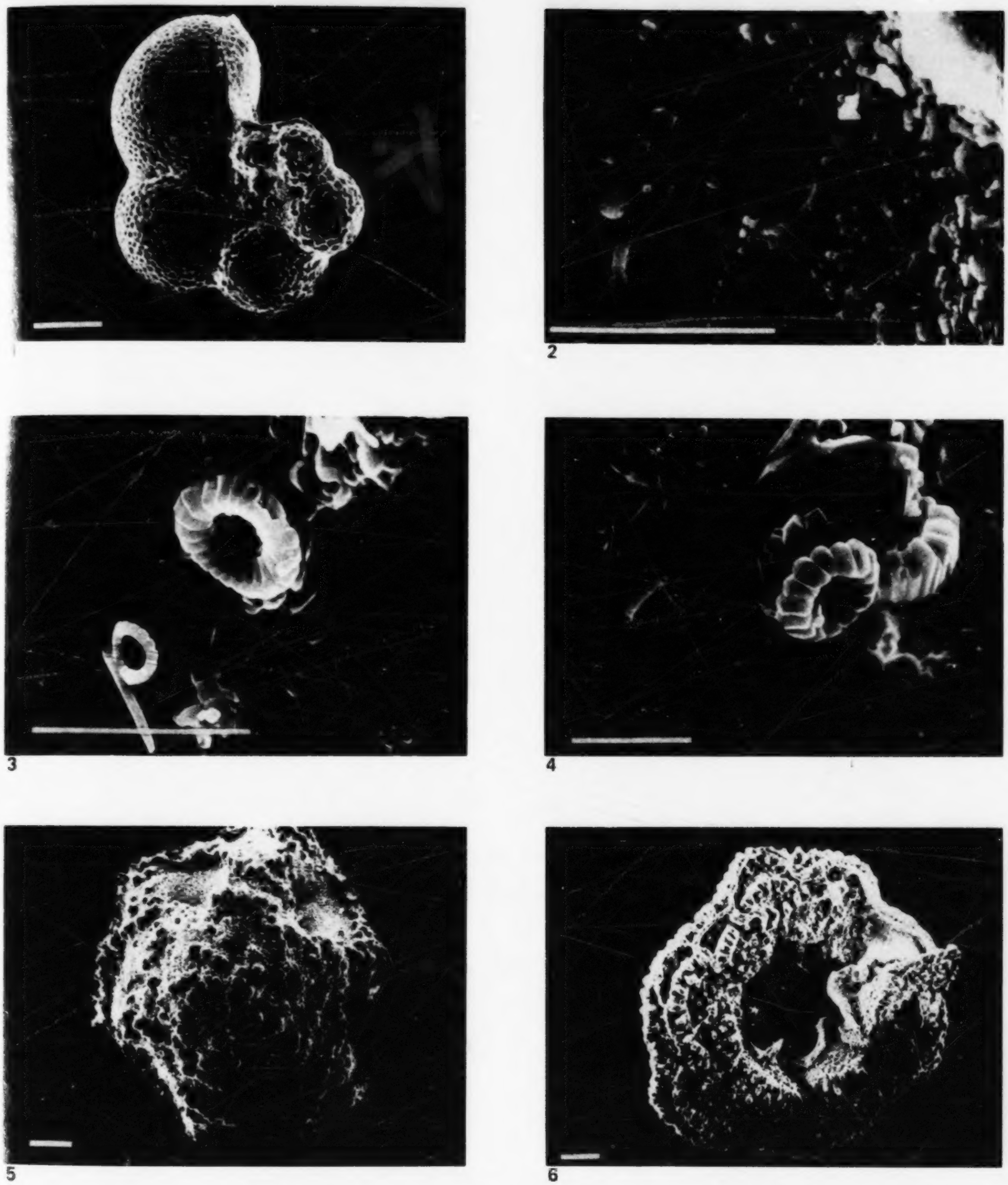

te 1. Site 47.2. **1.** *Globorotalia trinidadensis* (Bolli), Sample 47.2-11-2, 45 cm. Bar = 100 μm. **2.** Danian calcareous nannofossil ooze, Sample 47.2-11-2, 45 cm. Bar = 10 μm. **3, 4.** Maestrichtian calcareous nannofossils, Sample 47.2-12-1, 28 cm. Bar = 10 μm. **5, 6.** Spiral and umbilical views of *Globotruncana contusa* (Cushman), Sample 47.2-11-1, 28 cm. Bar = 100 μm.

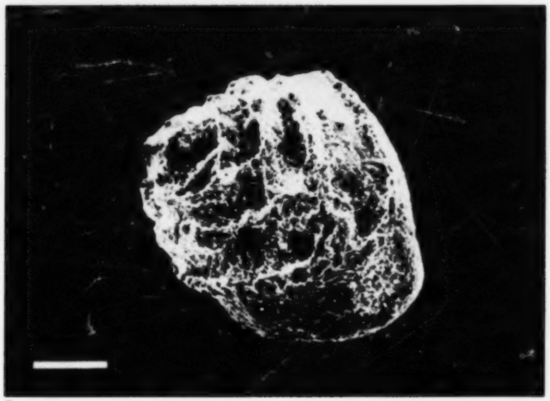

1

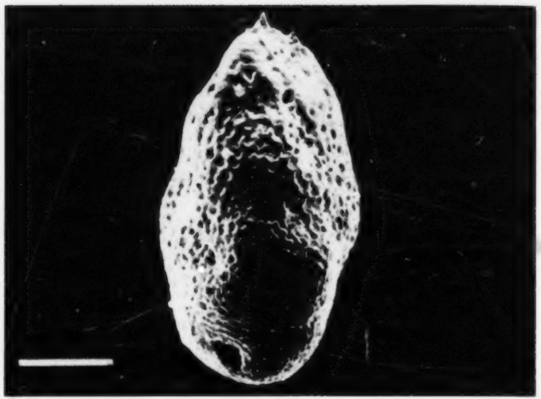

2

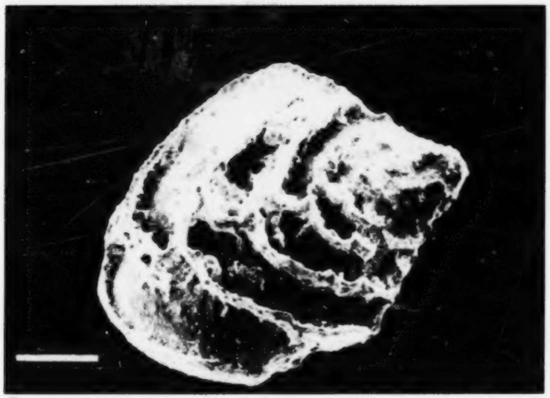

3

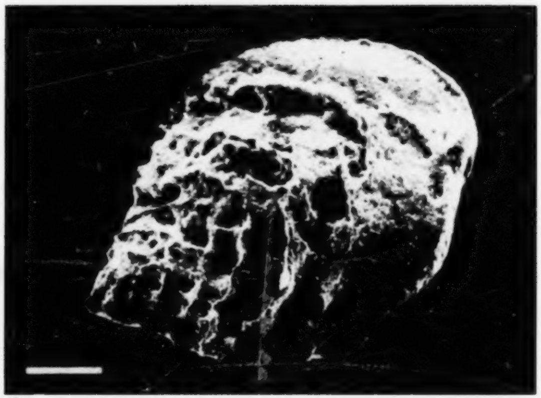

4

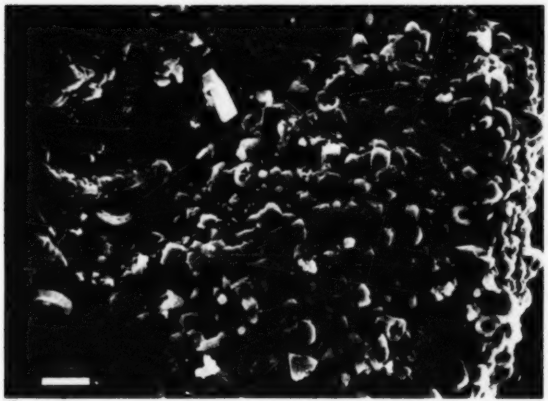

5

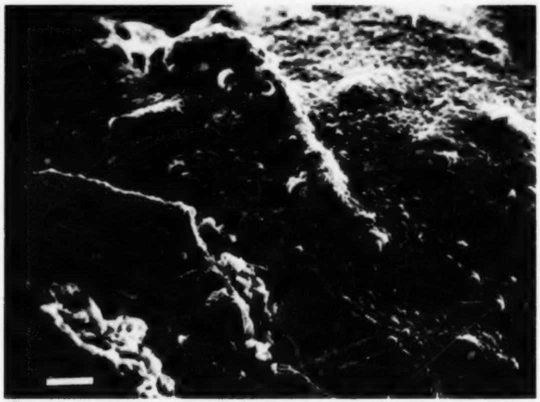

6

Plate 2. Site 577. **1.** *Aragonia* (Finlay), Sample 577-12-5, 80 cm. Bar = 100 μm. **2.** *Bulimina* (Cushman), Sample 577-12-5, 80 cm. Bar = 100 μm. **3, 4.** *Aragonia* (Finlay), Samples 577-12-5, 80 cm and 577-12-5, 128 cm. Bar = 100 μm. **5, 6.** Contrasting surface textures of two *Aragonia*, Sample 577-12-5, 128 cm. Bar = 10 μm.

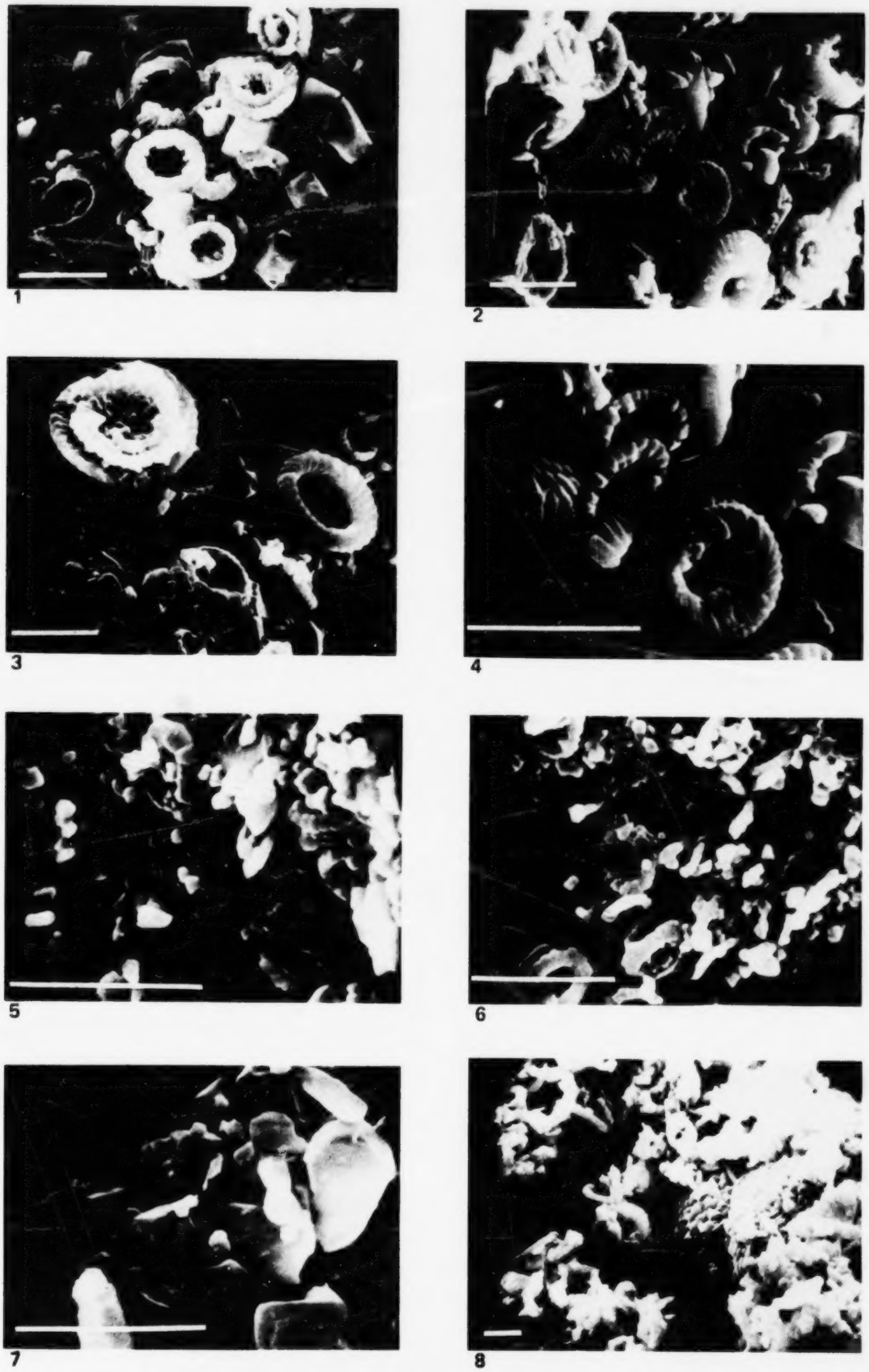

te 3. (Bar represents 10 μm.) **1–4.** Moderate to well preserved Danian calcareous nannofossil assemblage. Note the lack of overgrowths and etchings on the coccolith shields, Sample 577-12-2, 50 cm. **5, 6.** Coccoliths and coccolith fragments from Zone NP2. Calcite overgrowths are present on some specimens, Sample 577-12-5, 80 cm. **7.** Surface of a planktonic foraminifer from the boundary, sample 577-12-5, 125 cm. **8.** Coccolith ooze with foraminifer test in background, Sample 577-12-5, 125 cm.

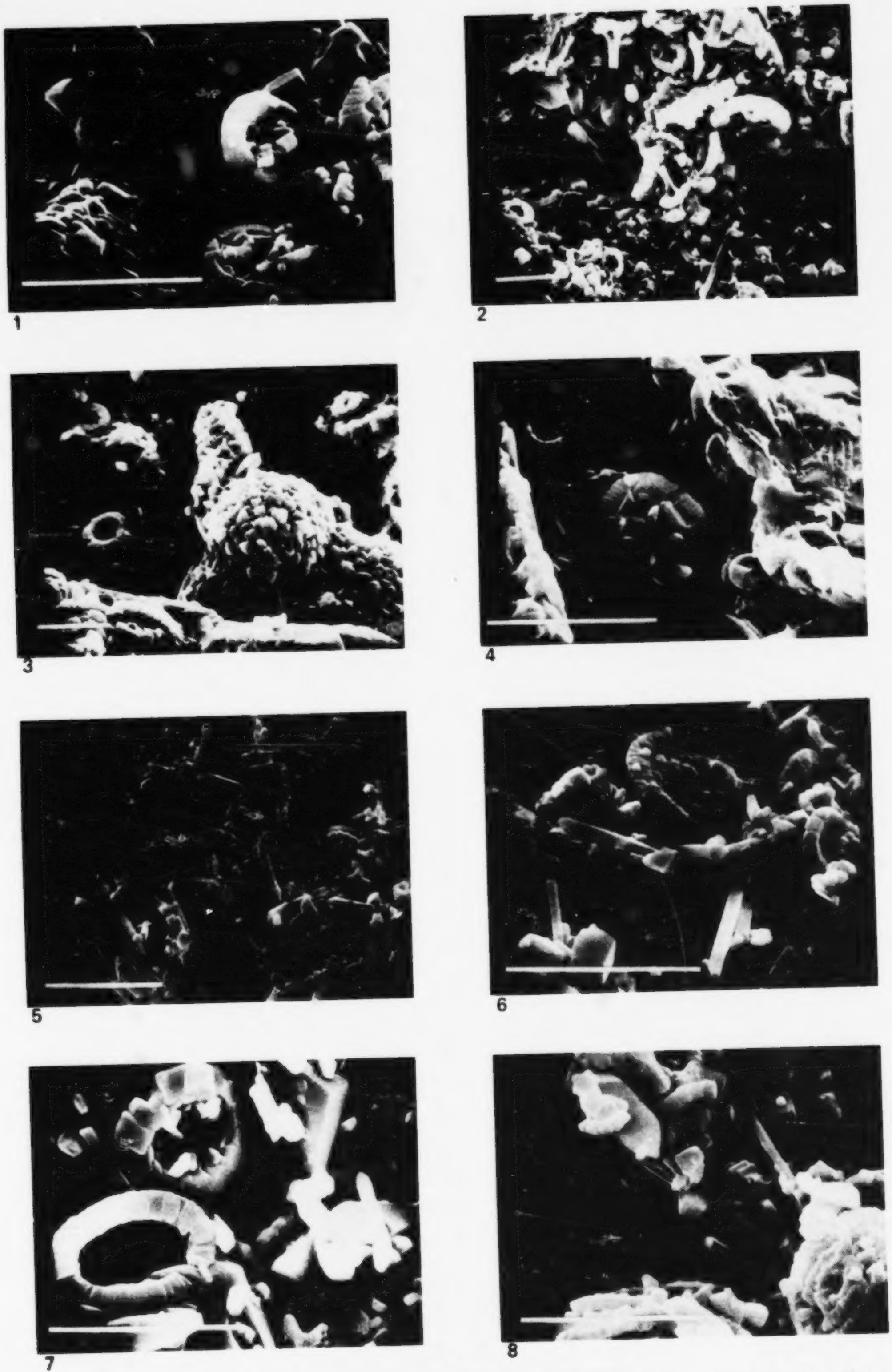

Plate 4. (Bar represents 10 μm.) **1–4.** Various calcareous nannofossils from boundary samples. Most specimens are moderately to well preserved. Overgrowths can be seen on several coccolith shields. Sample 577-12-5, 128 cm. **5–8.** Coccolith ooze of Maestrichtian age. Euhedral calcite overgrowths are present on most coccolith specimens. Partially disaggregated shields and fragments are also present.

21. ELEMENTAL PROFILE OF IRIDIUM AND OTHER ELEMENTS NEAR THE CRETACEOUS/TERTIARY BOUNDARY IN HOLE 577B[1]

Helen V. Michel and Frank Asaro, Lawrence Berkeley Laboratory
Walter Alvarez, University of California, Berkeley
and
Luis W. Alvarez, Lawrence Berkeley Laboratory[2]

ABSTRACT

An Ir anomaly of 61 ng/cm^2 was found in Deep Sea Drilling Project Hole 577B at the same stratigraphic level as the Cretaceous/Tertiary boundary defined by nannoplankton. This close correspondence supports the asteroid-impact theory for the Cretaceous/Tertiary boundary extinctions.

INTRODUCTION

An iridium anomaly associated with the Cretaceous/Tertiary boundary has been identified at more than 50 sites worldwide (Alvarez et al., 1984). The most viable explanation for this worldwide anomaly is that an asteroid or other extraterrestrial body about 10 km in diameter impacted the Earth 65 m.y. ago, exploded, and distributed a dust cloud of terrestrial and extraterrestrial material which encircled the Earth and settled in a few months. Samples from Hole 577B were examined using neutron-activation analysis (NAA) to test this prediction and to search for other geochemical anomalies that would shed light on the mechanisms of boundary deposition.

A single core containing seven sections and a core catcher was taken at Hole 577B and an intact Cretaceous/Tertiary boundary was recovered. The sediment is an undeformed white to light brown nannofossil ooze (see Site 577 chapter, this volume). The boundary region is light brown (in the midst of a slightly whiter region); this colored region extends from about Sample 577B-1-4, 58 cm to 577B-1-4, 72 cm. This boundary area is slightly firmer and more clay rich than the surrounding whiter regions.

METHODS

Continuous 1-cm samples were taken from 577B-1-4, 50 cm to B-1-4, 85 cm. Above and below this interval, spot samples were en about every 5 cm. The sampling interval was increased farther n the boundary, eventually to a 50-cm interval in Sections 1 and 6 Core 577B-1.

A total of 77 samples were first dried at 110°C and then measured high-precision methods of NAA (Perlman and Asaro, 1969). Iridi- was calibrated against the Danish boundary clay standard "DINO-1" varez et al., 1982a). Calcium was calibrated against a primary stan- d, $CaCO_3$. All other elements were calibrated against "Standard tery" (Perlman and Asaro, 1971).

The data from the NAA are shown in Table 1. The listed errors are one sigma values of the counting error or 1%, whichever is larger, and are about equal to the precision of measurement.

The iridium near the boundary (Samples 577B-1-4, 56 cm to 577B-1-4, 77 cm) could be measured precisely without any postirradiation chemistry. Farther from the boundary (as the level of Ir dropped), high temperature radiochemical separations were made in order to purify the Ir fraction without adding Ir carrier. In our procedure (which was inspired by the work of Rammensee and Palme, 1982) the same samples used for the regular NAA measurements (which each contained 100 mg of rock and 50 mg of cellulose binder) were heated to 1000°C in an oxidizing atmosphere to remove CO_2 and oxidizable carbon. The residues were then each mixed in a boron nitride crucible with 200 mg of powdered Fe, 100 mg of Hawaiian basalt (which served as a silicate flux), and a few milligrams of graphite (which provided a reducing environment). The crucibles (which were covered with a graphite plate) were slowly brought up to a temperature of 1477°C in a Deltech furnace under an argon atmosphere. The furnace was held at that temperature for 1 hr. and then slowly cooled. The slow speed was necessary to prevent the mulite dome, which permitted the controlled atmosphere, from fracturing.

The iron fraction in each crucible was in the form of a ball imbedded in a silicate glass. Each crucible was crushed, and the Fe ball was removed and then cleaned of residual glass with pliers. In the oxidizing firing step, the yield of Ir and other elements was 99 ± 1%. In the reduction firing step the yields were 100.0 ± 0.2, 99.85 ± 0.01, and 98.6 ± 0.2% for Ir, Co, and Fe radioactivities, respectively. Only 0.1 to 1% of the lithophile elements in the whole rock samples was extracted with the iron fraction.

This procedure provides a quantitative method of separating Ir radioactivity from the intense lithophile element radiations produced in NAA without adding Ir carrier, which can enhance the risk of laboratory contamination with Ir. The limits of detection for Ir were lowered to ~0.015 ppb for each sample, with a 1-day measurement time. As these low concentrations were considered to be background level Ir, four or more samples were analyzed simultaneously, resulting in a detection limit of 0.007 ppb in a 1-day measurement for highly calcareous samples.

RESULTS

Iridium Abundances

The Ir abundance profile at Hole 577B is plotted as a function of stratigraphic position in Figure 1. One major peak is seen (in Section 4), along with five smaller ones. To determine which of these peaks is most likely associated with an impacting meteorite and which with the normal iridium background resulting from meteorit-

---

[1] Heath, G. R., Burckle, L. H., et al., *Init. Repts. DSDP*, 86: Washington (U.S. Govt. ting Office).

[2] Addresses: (Michel, Asaro, L. Alvarez) Lawrence Berkeley Laboratory, University of fornia, Berkeley, CA 94720; (W. Alvarez) Department of Geology and Geophysics, Unity of California, Berkeley, CA 94720.

Table 1. Elemental abundances in Core 577B-1.

Section	Interval (cm)	Al (%)	Ca (%)	Dy (ppm)	Mn (ppm)	U (ppm)	Ba (ppm)	Ir (ppb)	Cr (ppm)	Th (ppm)	Ni (ppm)	Tb (ppm)	Fe (%)
1	10-11	0.33 ± 0.02	37.21 ± 0.83	9.22 ± 0.11	865 ± 9	0.241 ± 0.020	700 ± 18	0.039 ± 0.008	2.2 ± 0.4	0.97 ± 0.03	21 ± 4	1.457 ± 0.044	0.25 ± 0.01
	50-51	0.31 ± 0.03	38.72 ± 0.88	8.95 ± 0.11	834 ± 8	0.232 ± 0.020	960 ± 21		6.0 ± 0.4	2.28 ± 0.03	29 ± 4	1.419 ± 0.043	0.24 ± 0.01
	87-88	0.42 ± 0.04	40.51 ± 0.94	8.52 ± 0.11	897 ± 9	0.221 ± 0.019	884 ± 20		3.8 ± 0.4	1.09 ± 0.03	25 ± 4	1.324 ± 0.041	0.26 ± 0.01
	100-101	0.21 ± 0.05	39.12 ± 0.95	7.09 ± 0.10	747 ± 7	0.193 ± 0.018	723 ± 18		2.4 ± 0.3	0.79 ± 0.03	21 ± 4	1.170 ± 0.036	0.20 ± 0.01
	140-141	0.46 ± 0.08	36.80 ± 0.99	13.73 ± 0.14	1104 ± 11	0.376 ± 0.023	656 ± 19		3.8 ± 0.4	1.24 ± 0.03	39 ± 5	2.273 ± 0.066	0.34 ± 0.01
2	10-11	0.43 ± 0.02	36.70 ± 0.83	13.25 ± 0.13	1066 ± 11	0.294 ± 0.023	662 ± 19	0.073 ± 0.009	3.4 ± 0.4	1.15 ± 0.03	32 ± 5	2.137 ± 0.063	0.31 ± 0.01
	31-32	0.55 ± 0.03	37.82 ± 0.88	13.70 ± 0.15	1342 ± 13	0.339 ± 0.022	624 ± 19		4.3 ± 0.4	1.37 ± 0.03	30 ± 5	2.179 ± 0.064	0.43 ± 0.01
	70-71	0.34 ± 0.04	37.43 ± 0.89	7.20 ± 0.10	707 ± 7	0.167 ± 0.017	514 ± 15		2.3 ± 0.3	0.72 ± 0.02	22 ± 4	1.165 ± 0.036	0.20 ± 0.01
	120-121	0.25 ± 0.05	35.78 ± 0.92	6.99 ± 0.10	718 ± 7	0.172 ± 0.017	528 ± 15		2.0 ± 0.3	0.58 ± 0.02	24 ± 4	1.076 ± 0.034	0.19 ± 0.01
3	20-21	0.19 ± 0.06	38.40 ± 0.97	5.18 ± 0.08	241 ± 2	0.099 ± 0.016	312 ± 12	0.016 ± 0.006	1.5 ± 0.3	0.40 ± 0.02	10 ± 3	0.783 ± 0.025	0.09 ± 0.01
	40-41	0.10 ± 0.02	38.86 ± 0.84	4.73 ± 0.07	181 ± 2	0.113 ± 0.015	358 ± 13		0.6 ± 0.3	0.29 ± 0.02	4 ± 3	0.737 ± 0.024	0.06 ± 0.01
	60-61	0.02 ± 0.02	37.24 ± 0.84	3.93 ± 0.06	124 ± 1	0.081 ± 0.014	350 ± 12		0.7 ± 0.2	0.26 ± 0.02	5 ± 3	0.627 ± 0.021	0.05 ± 0.01
	80-81	0.08 ± 0.03	37.58 ± 0.87	5.12 ± 0.07	147 ± 1	0.109 ± 0.015	368 ± 13		1.0 ± 0.3	0.35 ± 0.02	5 ± 3	0.820 ± 0.026	0.07 ± 0.01
	100-101	0.09 ± 0.05	37.59 ± 0.93	6.36 ± 0.08	233 ± 2	0.100 ± 0.017	229 ± 13		0.8 ± 0.3	0.49 ± 0.02	9 ± 3	1.038 ± 0.032	0.10 ± 0.01
	120-121	0.14 ± 0.06	37.48 ± 0.97	4.78 ± 0.07	177 ± 2	0.086 ± 0.016	335 ± 13		0.5 ± 0.3	0.36 ± 0.02	10 ± 3	0.787 ± 0.025	0.07 ± 0.01
	140-141	0.08 ± 0.02	38.21 ± 0.86	4.28 ± 0.07	195 ± 2	0.134 ± 0.016	157 ± 11		0.4 ± 0.2	0.34 ± 0.02	10 ± 3	0.709 ± 0.023	0.08 ± 0.01
4	1-2	0.11 ± 0.02	38.98 ± 0.90	4.14 ± 0.07	156 ± 2	0.123 ± 0.015	270 ± 12	0.019 ± 0.006	1.5 ± 0.2	0.30 ± 0.02	5 ± 3	0.633 ± 0.021	0.05 ± 0.01
	10-11	0.07 ± 0.03	38.79 ± 0.92	3.95 ± 0.06	118 ± 1	0.105 ± 0.015	328 ± 12		1.0 ± 0.2	0.25 ± 0.02	6 ± 3	0.641 ± 0.021	0.05 ± 0.01
	20-21	0.12 ± 0.04	37.84 ± 0.94	3.98 ± 0.07	129 ± 1	0.082 ± 0.015	350 ± 12		0.4 ± 0.2	0.21 ± 0.02	5 ± 3	0.621 ± 0.021	0.04 ± 0.01
	30-31	0.14 ± 0.06	37.83 ± 0.99	3.58 ± 0.07	153 ± 2	0.079 ± 0.014	297 ± 11		0.6 ± 0.2	0.16 ± 0.02	9 ± 2	0.550 ± 0.019	0.04 ± 0.01
	35-36	0.04 ± 0.01	36.52 ± 0.86	3.58 ± 0.06	90 ± 1	0.098 ± 0.016	254 ± 11	0.058 ± 0.014	0.0 ± 0.2	0.35 ± 0.02	2 ± 2	0.512 ± 0.018	0.04 ± 0.01
	40-41	0.07 ± 0.01	38.51 ± 0.90	3.83 ± 0.08	137 ± 2	0.090 ± 0.014	267 ± 12	0.048 ± 0.007	0.6 ± 0.2	0.21 ± 0.02	8 ± 2	0.568 ± 0.018	0.03 ± 0.01
	45-46	0.04 ± 0.02	39.36 ± 0.92	3.98 ± 0.07	99 ± 1	0.080 ± 0.016	278 ± 11	0.117 ± 0.016	0.4 ± 0.2	0.13 ± 0.02	3 ± 2	0.555 ± 0.019	0.05 ± 0.01
	50-51	0.07 ± 0.01	39.01 ± 0.96	4.26 ± 0.08	89 ± 2	0.093 ± 0.013	339 ± 13	0.110 ± 0.014	0.3 ± 0.2	0.20 ± 0.02	1 ± 2	0.633 ± 0.020	0.04 ± 0.01
	51-52	0.04 ± 0.03	38.87 ± 0.95	4.51 ± 0.07	115 ± 1	0.085 ± 0.016	350 ± 13	0.194 ± 0.033	0.6 ± 0.3	0.25 ± 0.02	6 ± 3	0.585 ± 0.020	0.05 ± 0.01
	52-53	0.03 ± 0.04	38.35 ± 0.99	4.85 ± 0.07	117 ± 1	0.069 ± 0.016	457 ± 14	0.272 ± 0.029	1.2 ± 0.3	0.23 ± 0.02	14 ± 3	0.715 ± 0.024	0.06 ± 0.01
	53-54	0.10 ± 0.05	35.74 ± 0.99	4.40 ± 0.07	83 ± 1	0.080 ± 0.016	406 ± 13	0.166 ± 0.025	0.2 ± 0.3	0.17 ± 0.02	7 ± 3	0.648 ± 0.022	0.04 ± 0.01
	54-55	0.07 ± 0.01	36.87 ± 0.80	5.36 ± 0.07	136 ± 1	0.121 ± 0.017	541 ± 15	0.261 ± 0.023	1.3 ± 0.3	0.18 ± 0.02	8 ± 3	0.809 ± 0.026	0.08 ± 0.01
	55-56	0.11 ± 0.02	38.78 ± 1.00	5.36 ± 0.09	163 ± 2	0.096 ± 0.015	536 ± 16	0.443 ± 0.044	2.0 ± 0.3	0.21 ± 0.02	13 ± 3	0.849 ± 0.026	0.09 ± 0.01
	56-57	0.11 ± 0.02	37.88 ± 0.84	5.84 ± 0.07	164 ± 2	0.111 ± 0.018	629 ± 16	0.59 ± 0.05	2.0 ± 0.3	0.29 ± 0.02	15 ± 3	0.863 ± 0.028	0.11 ± 0.01
	57-58	0.10 ± 0.03	39.02 ± 0.89	6.19 ± 0.08	183 ± 2	0.109 ± 0.018	660 ± 16	0.83 ± 0.05	2.4 ± 0.3	0.35 ± 0.02	4 ± 3	0.901 ± 0.029	0.11 ± 0.01
	58-59	0.13 ± 0.04	39.77 ± 0.92	6.24 ± 0.08	191 ± 2	0.112 ± 0.018	712 ± 17	0.85 ± 0.04	3.3 ± 0.3	0.33 ± 0.02	9 ± 3	0.891 ± 0.029	0.12 ± 0.01
	59-60	0.17 ± 0.05	37.54 ± 0.94	6.34 ± 0.08	169 ± 2	0.104 ± 0.018	709 ± 17	1.21 ± 0.06	4.3 ± 0.3	0.31 ± 0.02	15 ± 3	0.961 ± 0.031	0.14 ± 0.01
	60-61	0.14 ± 0.03	37.88 ± 1.03	6.38 ± 0.10	215 ± 2	0.132 ± 0.016	779 ± 19	1.68 ± 0.07	4.9 ± 0.3	0.45 ± 0.02	19 ± 3	0.985 ± 0.029	0.19 ± 0.01
	61-62	0.20 ± 0.01	37.68 ± 0.79	6.66 ± 0.08	217 ± 2	0.097 ± 0.018	768 ± 17	1.95 ± 0.10	5.0 ± 0.3	0.48 ± 0.02	20 ± 3	1.001 ± 0.032	0.20 ± 0.01
	62-63	0.22 ± 0.02	38.31 ± 0.82	6.80 ± 0.08	232 ± 2	0.107 ± 0.017	792 ± 18	2.74 ± 0.12	6.3 ± 0.3	0.40 ± 0.02	20 ± 4	1.027 ± 0.033	0.24 ± 0.01
	63-64	0.28 ± 0.05	37.69 ± 1.08	6.50 ± 0.10	239 ± 2	0.140 ± 0.016	777 ± 19	3.05 ± 0.13	7.9 ± 0.3	0.47 ± 0.02	24 ± 3	1.049 ± 0.031	0.29 ± 0.01
	64-65	0.28 ± 0.02	36.26 ± 0.88	6.64 ± 0.09	230 ± 2	0.136 ± 0.016	834 ± 19	3.64 ± 0.16	12.0 ± 0.4	0.52 ± 0.02	33 ± 4	1.057 ± 0.031	0.38 ± 0.01
	65-66	0.28 ± 0.02	35.01 ± 0.90	6.80 ± 0.09	253 ± 3	0.123 ± 0.016	828 ± 19	4.55 ± 0.20	13.5 ± 0.4	0.63 ± 0.02	39 ± 4	1.106 ± 0.033	0.46 ± 0.01
	66-67	0.30 ± 0.03	36.30 ± 0.96	6.76 ± 0.09	248 ± 2	0.142 ± 0.017	762 ± 19	4.75 ± 0.19	15.0 ± 0.4	0.60 ± 0.02	43 ± 4	1.066 ± 0.032	0.50 ± 0.01
	67-68	0.41 ± 0.05	35.35 ± 0.99	6.46 ± 0.09	285 ± 3	0.131 ± 0.016	697 ± 18	4.97 ± 0.21	15.0 ± 0.4	0.59 ± 0.02	31 ± 4	1.023 ± 0.031	0.48 ± 0.01
	68-69	0.35 ± 0.06	35.18 ± 1.02	6.43 ± 0.09	240 ± 2	0.133 ± 0.016	671 ± 17	4.96 ± 0.21	16.5 ± 0.4	0.62 ± 0.02	37 ± 4	0.977 ± 0.029	0.55 ± 0.01
	69-70	0.31 ± 0.01	36.59 ± 0.73	6.05 ± 0.08	230 ± 2	0.115 ± 0.016	523 ± 15	5.33 ± 0.21	22.8 ± 0.4	0.60 ± 0.02	42 ± 4	0.981 ± 0.030	0.54 ± 0.01
	70-71	0.33 ± 0.02	37.51 ± 0.80	5.63 ± 0.07	202 ± 7	0.121 ± 0.016	457 ± 14	5.61 ± 0.22	16.6 ± 0.4	0.55 ± 0.02	37 ± 4	0.912 ± 0.028	0.53 ± 0.01
	71-72	0.21 ± 0.02	34.30 ± 0.78	3.95 ± 0.06	135 ± 1	0.122 ± 0.014	272 ± 12	4.55 ± 0.18	12.1 ± 0.3	0.42 ± 0.02	28 ± 3	0.626 ± 0.021	0.39 ± 0.01
	72-73*	0.24 ± 0.03	35.84 ± 0.83	4.00 ± 0.06	125 ± 1	0.124 ± 0.014	245 ± 11	5.35 ± 0.21	18.5 ± 0.4	0.48 ± 0.02	36 ± 3	0.655 ± 0.021	0.46 ± 0.01
	73-74	0.24 ± 0.04	37.62 ± 0.88	3.86 ± 0.06	173 ± 2	0.086 ± 0.013	255 ± 11	2.50 ± 0.08	6.4 ± 0.3	0.26 ± 0.02	22 ± 3	0.593 ± 0.019	0.17 ± 0.01
	74-75	0.15 ± 0.01	38.51 ± 0.79	3.72 ± 0.06	115 ± 1	0.093 ± 0.014	247 ± 11	1.57 ± 0.05	4.0 ± 0.2	0.27 ± 0.02	10 ± 2	0.568 ± 0.018	0.10 ± 0.01
	75-76	0.07 ± 0.01	39.39 ± 0.82	3.23 ± 0.06	158 ± 2	0.062 ± 0.013	248 ± 10	0.670 ± 0.034	1.1 ± 0.2	0.21 ± 0.01	11 ± 2	0.477 ± 0.016	0.05 ± 0.01
	76-77	0.05 ± 0.02	38.79 ± 0.84	3.40 ± 0.06	102 ± 1	0.056 ± 0.013	185 ± 10	0.601 ± 0.036	0.4 ± 0.2	0.29 ± 0.02	7 ± 2	0.484 ± 0.016	0.04 ± 0.01
	77-78	0.10 ± 0.03	38.32 ± 0.88	3.50 ± 0.06	120 ± 1	0.090 ± 0.014	233 ± 11	1.07 ± 0.08	1.6 ± 0.2	0.21 ± 0.02	7 ± 2	0.537 ± 0.018	0.08 ± 0.01
	78-79	0.03 ± 0.04	37.21 ± 0.89	3.16 ± 0.06	108 ± 1	0.070 ± 0.013	234 ± 10	0.83 ± 0.08	1.9 ± 0.2	0.14 ± 0.01	7 ± 2	0.484 ± 0.016	0.05 ± 0.01
	79-80	0.03 ± 0.02	39.14 ± 0.86	3.07 ± 0.06	97 ± 1	0.045 ± 0.014	213 ± 10	0.465 ± 0.044	0.5 ± 0.2	0.19 ± 0.02	4 ± 2	0.473 ± 0.017	0.05 ± 0.01
	80-81	0.11 ± 0.03	37.83 ± 0.88	3.32 ± 0.06	123 ± 1	0.081 ± 0.014	289 ± 11	0.557 ± 0.050	0.5 ± 0.2	0.21 ± 0.02	5 ± 2	0.509 ± 0.018	0.04 ± 0.01
	81-82	0.10 ± 0.05	38.39 ± 0.91	3.50 ± 0.06	139 ± 1	0.095 ± 0.015	286 ± 10	0.87 ± 0.06	1.9 ± 0.2	0.20 ± 0.02	10 ± 2	0.536 ± 0.019	0.08 ± 0.01
	82-83	0.10 ± 0.01	41.23 ± 0.85	3.29 ± 0.06	140 ± 1	0.097 ± 0.015	291 ± 11	0.82 ± 0.06	2.3 ± 0.2	0.22 ± 0.02	10 ± 2	0.498 ± 0.018	0.07 ± 0.01
	83-84	0.12 ± 0.02	39.37 ± 0.85	3.25 ± 0.06	113 ± 1	0.100 ± 0.014	247 ± 10	0.53 ± 0.04	1.2 ± 0.2	0.24 ± 0.02	2 ± 2	0.476 ± 0.017	0.06 ± 0.01
	84-85	0.08 ± 0.02	40.38 ± 0.89	2.99 ± 0.06	118 ± 1	0.090 ± 0.014	224 ± 10	0.257 ± 0.030	0.7 ± 0.2	0.11 ± 0.02	5 ± 2	0.467 ± 0.017	0.04 ± 0.01
	85-86	0.05 ± 0.03	40.45 ± 0.92	2.98 ± 0.06	112 ± 1	0.054 ± 0.014	261 ± 10	0.229 ± 0.020	0.2 ± 0.2	0.16 ± 0.02	3 ± 2	0.446 ± 0.016	0.04 ± 0.01
	90-91	0.15 ± 0.04	38.89 ± 0.95	2.92 ± 0.05	90 ± 1	0.055 ± 0.014	236 ± 10	0.102 ± 0.013	0.7 ± 0.2	0.12 ± 0.02	4 ± 2	0.452 ± 0.016	0.03 ± 0.01
	100-101	0.10 ± 0.01		3.21 ± 0.06	105 ± 1	0.101 ± 0.012	259 ± 8	0.059 ± 0.011	0.4 ± 0.2	0.17 ± 0.01	3 ± 2	0.456 ± 0.014	0.03 ± 0.01
	110-111	0.11 ± 0.02		3.52 ± 0.06	126 ± 1	0.069 ± 0.012	312 ± 9	0.297 ± 0.025	1.2 ± 0.2	0.17 ± 0.01	7 ± 2	0.506 ± 0.015	0.06 ± 0.01
	120-121	0.14 ± 0.03		3.42 ± 0.06	117 ± 1	0.066 ± 0.012	289 ± 8	0.019 ± 0.003	0.4 ± 0.2	0.22 ± 0.02	3 ± 2	0.493 ± 0.015	0.03 ± 0.01
	130-131	0.13 ± 0.04		3.34 ± 0.06	131 ± 1	0.083 ± 0.012	332 ± 9		0.3 ± 0.2	0.13 ± 0.02	4 ± 2	0.503 ± 0.015	0.05 ± 0.01
	140-141	0.19 ± 0.05		3.54 ± 0.07	154 ± 2	0.099 ± 0.012	387 ± 9		0.8 ± 0.2	0.20 ± 0.02	4 ± 2	0.495 ± 0.015	0.04 ± 0.01
	150-151	0.13 ± 0.02		3.69 ± 0.06	158 ± 2	0.090 ± 0.012	310 ± 9		0.6 ± 0.2	0.21 ± 0.02	8 ± 2	0.506 ± 0.015	0.05 ± 0.01
5	20-21	0.14 ± 0.03		3.90 ± 0.07	184 ± 2	0.079 ± 0.013	399 ± 9	0.012 ± 0.004	0.6 ± 0.2	0.23 ± 0.02	4 ± 2	0.601 ± 0.017	0.05 ± 0.01
	40-41	0.08 ± 0.05		3.76 ± 0.07	176 ± 2	0.073 ± 0.013	368 ± 9		0.7 ± 0.2	0.24 ± 0.02	8 ± 2	0.528 ± 0.016	0.05 ± 0.01
	60-61	0.19 ± 0.07		3.73 ± 0.07	228 ± 2	0.064 ± 0.013	316 ± 9		0.9 ± 0.2	0.23 ± 0.02	9 ± 3	0.554 ± 0.016	0.06 ± 0.01
	80-81	0.29 ± 0.09		4.22 ± 0.07	293 ± 3	0.069 ± 0.012	524 ± 10		2.2 ± 0.2	0.26 ± 0.02	9 ± 3	0.589 ± 0.017	0.07 ± 0.01
	100-101	0.15 ± 0.01		4.62 ± 0.07	293 ± 3	0.098 ± 0.013	289 ± 8		1.0 ± 0.2	0.32 ± 0.02	11 ± 3	0.708 ± 0.019	0.06 ± 0.01
	120-121	0.75 ± 0.02		18.72 ± 0.21	2149 ± 21	0.362 ± 0.024	500 ± 14	0.14 ± 0.05	4.2 ± 0.4	1.33 ± 0.03	78 ± 6	3.416 ± 0.078	0.52 ± 0.01
	140-141	0.15 ± 0.02		5.48 ± 0.08	366 ± 4	0.086 ± 0.014	215 ± 8	0.010 ± 0.006	1.0 ± 0.2	0.29 ± 0.02	14 ± 3	0.787 ± 0.021	0.08 ± 0.01
6	30-31	0.12 ± 0.03		4.11 ± 0.07	209 ± 2	0.080 ± 0.013	426 ± 9		0.9 ± 0.2	0.24 ± 0.02	7 ± 2	0.628 ± 0.018	0.06 ± 0.01
	48-49	0.16 ± 0.04		4.29 ± 0.07	240 ± 2	0.089 ± 0.013	442 ± 10		0.7 ± 0.2	0.25 ± 0.02	10 ± 3	0.655 ± 0.018	0.06 ± 0.01
	90-91	0.18 ± 0.01		5.65 ± 0.08	363 ± 4	0.120 ± 0.014	323 ± 9		1.0 ± 0.2	0.31 ± 0.02	13 ± 3	0.861 ± 0.022	0.08 ± 0.01
	140-141	0.12 ± 0.01		4.17 ± 0.06	158 ± 2	0.072 ± 0.013	224 ± 8		0.6 ± 0.2	0.23 ± 0.02	4 ± 2	0.586 ± 0.017	0.04 ± 0.01

Note: Asterisk indicates location of Cretaceous/Tertiary boundary as determined by nannofossil biostratigraphy.

ic dust, the following model was used: During any brief interval of geological time, both the clay deposition rate and the Ir deposition rate from meteorite dust in the area of Hole 577B would be approximately constant. The rate of $CaCO_3$ deposition, however, could change as the biological productivity fluctuated or the calcite compensation depth varied. Changes in rates of $CaCO_3$ deposition would affect the abundances of clay and iridium, but not their ratios. For the present analysis, Fe rather than Al was taken as a measure of the clay abundance because Fe was measured with comparably high sensitiv ity throughout the section studied while Al was not.

Ir/Fe ratios are also shown in Figure 1. The back ground value is 2×10^{-8} in both the Cretaceous an Tertiary regions even though the Ir abundance varies b an order of magnitude. Thus, the broad Ir peak in Sec tions 1 and 2 (Peak E, Fig. 1) and the relatively shar peak in Section 5 (Peak A, Fig. 1) may have been cause simply by changes in the deposition rate of $CaCO_3$. O the other hand, the main Ir peak and the three smalle

Table 1. (Continued).

Sm (ppm)	La (ppm)	Lu (ppm)	Co (ppm)	Sc (ppm)	Sb (ppm)	Eu (ppm)	Ce (ppm)	Hf (ppm)	Ta (ppm)	Yb (ppm)	Nd (ppm)
8.576 ± 0.086	34.76 ± 0.67	0.750 ± 0.019	10.15 ± 0.19	6.63 ± 0.07	0.17 ± 0.05	2.151 ± 0.022	18.28 ± 0.50	0.21 ± 0.04	0.043 ± 0.003	5.427 ± 0.054	40.1 ± 1.1
8.430 ± 0.084	34.56 ± 0.67	0.716 ± 0.018	10.49 ± 0.20	6.05 ± 0.06	0.26 ± 0.05	2.389 ± 0.024	18.68 ± 0.51	0.29 ± 0.04	0.038 ± 0.003	5.246 ± 0.053	40.3 ± 1.1
8.078 ± 0.081	33.15 ± 0.66	0.661 ± 0.017	11.46 ± 0.21	6.06 ± 0.06	0.22 ± 0.05	2.079 ± 0.021	19.75 ± 0.50	0.23 ± 0.04	0.044 ± 0.003	4.888 ± 0.051	39.0 ± 1.1
6.659 ± 0.067	27.98 ± 0.60	0.560 ± 0.015	8.95 ± 0.18	5.44 ± 0.05	0.17 ± 0.05	1.736 ± 0.017	15.84 ± 0.46	0.27 ± 0.04	0.037 ± 0.002	4.071 ± 0.044	32.3 ± 0.9
3.059 ± 0.131	50.77 ± 0.84	1.016 ± 0.024	14.17 ± 0.24	8.11 ± 0.08	0.25 ± 0.06	3.340 ± 0.033	27.30 ± 0.59	0.33 ± 0.04	0.062 ± 0.003	7.513 ± 0.075	62.8 ± 1.5
2.609 ± 0.126	50.75 ± 0.84	0.995 ± 0.023	13.64 ± 0.23	7.92 ± 0.08	0.27 ± 0.06	3.202 ± 0.032	24.45 ± 0.58	0.39 ± 0.04	0.058 ± 0.003	7.387 ± 0.074	58.2 ± 1.4
2.835 ± 0.128	49.78 ± 0.83	0.923 ± 0.022	16.29 ± 0.26	7.79 ± 0.08	0.28 ± 0.06	3.259 ± 0.033	28.05 ± 0.58	0.51 ± 0.04	0.067 ± 0.003	6.900 ± 0.069	58.3 ± 1.4
.891 ± 0.069	26.75 ± 0.59	0.520 ± 0.014	8.82 ± 0.17	4.30 ± 0.04	0.11 ± 0.04	1.752 ± 0.018	16.14 ± 0.44	0.17 ± 0.03	0.037 ± 0.002	3.846 ± 0.042	33.1 ± 0.9
505 ± 0.065	26.06 ± 0.58	0.496 ± 0.014	9.06 ± 0.17	4.06 ± 0.04	0.15 ± 0.04	1.624 ± 0.016	14.82 ± 0.43	0.14 ± 0.03	0.034 ± 0.002	3.634 ± 0.040	30.7 ± 0.9
855 ± 0.049	22.98 ± 0.53	0.352 ± 0.011	3.03 ± 0.10	2.64 ± 0.03	0.11 ± 0.03	1.220 ± 0.013	6.81 ± 0.34	0.13 ± 0.03	0.022 ± 0.002	2.688 ± 0.033	25.2 ± 0.8
167 ± 0.042	20.65 ± 0.54	0.329 ± 0.010	2.19 ± 0.08	2.48 ± 0.02	0.09 ± 0.03	1.064 ± 0.012	5.46 ± 0.33	0.08 ± 0.03	0.013 ± 0.002	2.483 ± 0.031	20.2 ± 0.7
520 ± 0.035	20.20 ± 0.52	0.278 ± 0.008	1.61 ± 0.07	2.01 ± 0.02	0.13 ± 0.03	0.902 ± 0.011	3.90 ± 0.30	0.07 ± 0.03	0.009 ± 0.002	2.181 ± 0.029	17.4 ± 0.6
782 ± 0.048	23.47 ± 0.55	0.340 ± 0.010	1.97 ± 0.08	2.61 ± 0.03	0.08 ± 0.03	1.223 ± 0.013	5.99 ± 0.32	0.08 ± 0.03	0.017 ± 0.002	2.623 ± 0.032	24.2 ± 0.7
091 ± 0.061	28.13 ± 0.63	0.409 ± 0.011	2.92 ± 0.09	3.20 ± 0.03	0.08 ± 0.03	1.572 ± 0.016	9.03 ± 0.37	0.12 ± 0.03	0.026 ± 0.002	3.155 ± 0.036	30.4 ± 0.9
699 ± 0.047	21.77 ± 0.56	0.322 ± 0.010	2.21 ± 0.08	2.53 ± 0.03	0.05 ± 0.03	1.220 ± 0.013	5.51 ± 0.33	0.08 ± 0.03	0.016 ± 0.002	2.553 ± 0.032	24.2 ± 0.8
919 ± 0.039	18.74 ± 0.55	0.278 ± 0.008	2.52 ± 0.09	2.43 ± 0.02	0.09 ± 0.03	1.020 ± 0.012	5.48 ± 0.33	0.09 ± 0.03	0.016 ± 0.002	2.264 ± 0.030	19.8 ± 0.7
745 ± 0.037	18.38 ± 0.53	0.272 ± 0.008	2.06 ± 0.08	2.19 ± 0.02	0.10 ± 0.03	0.965 ± 0.011	4.51 ± 0.31	0.07 ± 0.03	0.011 ± 0.002	2.141 ± 0.029	18.7 ± 0.7
576 ± 0.036	19.25 ± 0.52	0.260 ± 0.008	1.74 ± 0.07	2.06 ± 0.02	0.05 ± 0.02	0.929 ± 0.011	4.06 ± 0.29	0.04 ± 0.03	0.012 ± 0.002	2.114 ± 0.029	17.3 ± 0.7
515 ± 0.035	18.57 ± 0.52	0.262 ± 0.008	1.76 ± 0.07	2.00 ± 0.02	0.10 ± 0.03	0.907 ± 0.011	3.12 ± 0.30	0.03 ± 0.03	0.008 ± 0.002	2.108 ± 0.027	18.3 ± 0.7
970 ± 0.030	17.38 ± 0.49	0.255 ± 0.007	1.98 ± 0.08	1.78 ± 0.02	0.07 ± 0.03	0.783 ± 0.010	3.17 ± 0.28	0.06 ± 0.02	0.009 ± 0.002	2.011 ± 0.026	14.8 ± 0.6
910 ± 0.029	16.72 ± 0.53	0.260 ± 0.010	1.16 ± 0.06	1.67 ± 0.02	0.06 ± 0.03	0.762 ± 0.010	2.31 ± 0.30	0.01 ± 0.03	0.011 ± 0.002	2.028 ± 0.030	15.0 ± 0.7
071 ± 0.031	17.84 ± 0.43	0.281 ± 0.007	1.70 ± 0.07	1.78 ± 0.02	0.09 ± 0.03	0.797 ± 0.010	2.28 ± 0.26	0.02 ± 0.02	0.012 ± 0.002	2.078 ± 0.025	16.1 ± 0.5
62 ± 0.031	19.24 ± 0.55	0.273 ± 0.010	1.33 ± 0.07	1.72 ± 0.02	0.06 ± 0.03	0.769 ± 0.010	2.71 ± 0.30	0.05 ± 0.03	0.009 ± 0.002	2.144 ± 0.031	14.1 ± 0.7
79 ± 0.034	20.36 ± 0.44	0.316 ± 0.007	1.29 ± 0.06	1.83 ± 0.02	0.07 ± 0.03	0.857 ± 0.010	2.42 ± 0.26	0.04 ± 0.02	0.010 ± 0.002	2.306 ± 0.026	17.5 ± 0.5
551 ± 0.036	19.38 ± 0.57	0.320 ± 0.011	1.58 ± 0.07	1.88 ± 0.02	0.06 ± 0.03	0.900 ± 0.011	2.66 ± 0.31	0.07 ± 0.03	0.017 ± 0.002	2.336 ± 0.033	17.3 ± 0.7
03 ± 0.040	22.71 ± 0.60	0.318 ± 0.011	1.58 ± 0.07	2.07 ± 0.02	0.10 ± 0.03	1.036 ± 0.012	3.35 ± 0.32	0.04 ± 0.03	0.016 ± 0.002	2.576 ± 0.034	20.5 ± 0.8
01 ± 0.036	20.02 ± 0.57	0.306 ± 0.011	1.13 ± 0.06	1.90 ± 0.02	0.01 ± 0.03	0.956 ± 0.012	2.66 ± 0.32	0.07 ± 0.03	0.014 ± 0.002	2.387 ± 0.033	18.5 ± 0.7
527 ± 0.045	24.89 ± 0.64	0.346 ± 0.012	1.82 ± 0.08	2.30 ± 0.02	0.05 ± 0.03	1.191 ± 0.013	3.16 ± 0.34	0.04 ± 0.03	0.015 ± 0.002	2.756 ± 0.037	24.3 ± 0.9
785 ± 0.048	25.57 ± 0.50	0.383 ± 0.010	2.45 ± 0.08	2.44 ± 0.02	0.08 ± 0.03	1.231 ± 0.013	3.87 ± 0.30	0.03 ± 0.03	0.015 ± 0.002	2.819 ± 0.031	23.7 ± 0.6
162 ± 0.052	27.42 ± 0.66	0.383 ± 0.013	2.72 ± 0.10	2.62 ± 0.03	0.08 ± 0.03	1.329 ± 0.014	4.01 ± 0.36	0.08 ± 0.03	0.017 ± 0.002	3.045 ± 0.038	27.1 ± 0.9
06 ± 0.054	28.70 ± 0.67	0.381 ± 0.013	2.83 ± 0.10	2.78 ± 0.03	0.03 ± 0.04	1.402 ± 0.015	4.02 ± 0.37	0.04 ± 0.03	0.019 ± 0.002	3.126 ± 0.039	27.1 ± 0.9
09 ± 0.054	28.22 ± 0.67	0.398 ± 0.014	3.03 ± 0.10	2.80 ± 0.03	0.09 ± 0.04	1.387 ± 0.014	4.40 ± 0.36	0.16 ± 0.03	0.019 ± 0.002	3.107 ± 0.039	27.1 ± 0.9
536 ± 0.055	29.35 ± 0.69	0.404 ± 0.014	2.81 ± 0.10	2.91 ± 0.03	0.12 ± 0.04	1.404 ± 0.015	4.44 ± 0.37	0.08 ± 0.03	0.017 ± 0.002	3.161 ± 0.040	27.4 ± 1.0
671 ± 0.057	28.85 ± 0.53	0.417 ± 0.011	4.17 ± 0.11	3.09 ± 0.03	0.09 ± 0.03	1.4[illegible] 0.015	5.01 ± 0.32	0.14 ± 0.03	0.018 ± 0.002	3.189 ± 0.034	29.9 ± 0.7
696 ± 0.057	29.73 ± 0.69	0.414 ± 0.014	4.40 ± 0.12	3.12 ± 0.03	0.10 ± 0.04	1.46[illegible] 0.015	4.39 ± 0.37	0.11 ± 0.03	0.022 ± 0.002	3.202 ± 0.039	29.2 ± 1.0
775 ± 0.058	30.85 ± 0.69	0.414 ± 0.014	4.76 ± 0.12	3.19 ± 0.03	0.12 ± 0.04	1.466 ± 0.015	4.71 ± 0.38	0.16 ± 0.03	0.023 ± 0.002	3.233 ± 0.040	29.2 ± 1.0
837 ± 0.058	31.58 ± 0.55	0.418 ± 0.011	6.18 ± 0.14	3.37 ± 0.03	0.15 ± 0.04	1.533 ± 0.015	5.77 ± 0.33	0.12 ± 0.03	0.024 ± 0.002	3.182 ± 0.034	29.6 ± 0.7
264 ± 0.063	32.10 ± 0.57	0.417 ± 0.011	6.47 ± 0.14	3.61 ± 0.04	0.17 ± 0.04	1.601 ± 0.016	5.61 ± 0.35	0.22 ± 0.03	0.030 ± 0.002	3.219 ± 0.034	31.3 ± 0.7
361 ± 0.064	33.05 ± 0.58	0.435 ± 0.011	7.53 ± 0.16	3.68 ± 0.04	0.17 ± 0.04	1.638 ± 0.016	5.50 ± 0.36	0.20 ± 0.03	0.035 ± 0.002	3.197 ± 0.034	32.7 ± 0.7
086 ± 0.061	31.20 ± 0.57	0.396 ± 0.011	7.74 ± 0.16	3.64 ± 0.04	0.22 ± 0.04	1.568 ± 0.016	5.48 ± 0.35	0.17 ± 0.03	0.038 ± 0.002	3.032 ± 0.033	31.9 ± 0.7
789 ± 0.058	29.57 ± 0.56	0.394 ± 0.011	8.99 ± 0.17	3.56 ± 0.04	0.17 ± 0.04	1.477 ± 0.015	5.21 ± 0.35	0.24 ± 0.03	0.040 ± 0.002	2.908 ± 0.032	29.3 ± 0.7
689 ± 0.057	28.26 ± 0.54	0.372 ± 0.010	7.97 ± 0.16	3.39 ± 0.03	0.22 ± 0.04	1.442 ± 0.014	5.75 ± 0.34	0.31 ± 0.03	0.035 ± 0.002	2.793 ± 0.032	27.8 ± 0.7
476 ± 0.055	27.84 ± 0.54	0.362 ± 0.010	7.77 ± 0.15	3.10 ± 0.03	0.17 ± 0.04	1.383 ± 0.014	5.56 ± 0.34	0.22 ± 0.03	0.036 ± 0.002	2.762 ± 0.031	28.6 ± 0.7
147 ± 0.051	26.42 ± 0.53	0.327 ± 0.008	6.55 ± 0.14	2.87 ± 0.03	0.23 ± 0.04	1.295 ± 0.013	4.70 ± 0.33	0.27 ± 0.03	0.036 ± 0.002	2.639 ± 0.030	26.2 ± 0.6
3.495 ± 0.035	20.51 ± 0.47	0.275 ± 0.007	4.53 ± 0.11	2.48 ± 0.02	0.13 ± 0.04	0.892 ± 0.011	3.59 ± 0.30	0.15 ± 0.03	0.030 ± 0.002	2.108 ± 0.025	17.4 ± 0.5
3.498 ± 0.035	19.03 ± 0.45	0.278 ± 0.007	4.45 ± 0.11	2.10 ± 0.02	0.18 ± 0.04	0.893 ± 0.011	3.29 ± 0.30	0.18 ± 0.03	0.026 ± 0.002	2.151 ± 0.025	19.3 ± 0.5
3.280 ± 0.033	18.70 ± 0.44	0.273 ± 0.007	4.21 ± 0.10	1.69 ± 0.02	0.09 ± 0.03	0.866 ± 0.010	2.99 ± 0.26	0.06 ± 0.02	0.019 ± 0.002	2.090 ± 0.025	17.1 ± 0.5
3.119 ± 0.031	17.71 ± 0.44	0.257 ± 0.006	2.67 ± 0.08	1.49 ± 0.01	0.17 ± 0.03	0.806 ± 0.010	2.14 ± 0.27	0.08 ± 0.02	0.014 ± 0.002	1.947 ± 0.024	15.9 ± 0.5
2.714 ± 0.027	16.01 ± 0.40	0.235 ± 0.006	2.88 ± 0.08	1.26 ± 0.01	0.07 ± 0.03	0.681 ± 0.009	2.04 ± 0.24	0.05 ± 0.02	0.014 ± 0.002	1.815 ± 0.023	14.0 ± 0.5
2.803 ± 0.028	16.46 ± 0.41	0.243 ± 0.006	1.82 ± 0.07	1.28 ± 0.01	0.08 ± 0.02	0.711 ± 0.009	2.42 ± 0.24	0.02 ± 0.02	0.011 ± 0.002	1.866 ± 0.023	13.2 ± 0.5
2.943 ± 0.029	16.16 ± 0.43	0.228 ± 0.006	2.09 ± 0.07	1.37 ± 0.01	0.02 ± 0.03	0.748 ± 0.009	2.52 ± 0.26	0.06 ± 0.02	0.014 ± 0.002	1.756 ± 0.023	14.9 ± 0.5
2.729 ± 0.027	14.56 ± 0.41	0.228 ± 0.006	1.88 ± 0.07	1.28 ± 0.01	0.07 ± 0.03	0.681 ± 0.009	2.21 ± 0.25	0.05 ± 0.02	0.014 ± 0.002	1.715 ± 0.022	13.6 ± 0.5
2.478 ± 0.025	14.73 ± 0.49	0.215 ± 0.008	1.59 ± 0.07	1.22 ± 0.01	0.04 ± 0.02	0.629 ± 0.009	1.82 ± 0.27	0.04 ± 0.02	0.012 ± 0.002	1.689 ± 0.026	13.0 ± 0.7
2.761 ± 0.028	15.54 ± 0.51	0.221 ± 0.008	1.89 ± 0.07	1.25 ± 0.01	0.05 ± 0.03	0.697 ± 0.009	2.00 ± 0.28	0.01 ± 0.02	0.015 ± 0.002	1.768 ± 0.026	14.9 ± 0.7
3.014 ± 0.030	16.43 ± 0.52	0.227 ± 0.008	2.25 ± 0.08	1.35 ± 0.01	0.07 ± 0.03	0.756 ± 0.010	2.35 ± 0.28	0.08 ± 0.03	0.011 ± 0.002	1.815 ± 0.027	17.8 ± 0.7
2.869 ± 0.029	16.03 ± 0.52	0.226 ± 0.008	2.23 ± 0.08	1.26 ± 0.01	0.06 ± 0.03	0.719 ± 0.009	2.36 ± 0.29	0.05 ± 0.02	0.014 ± 0.002	1.751 ± 0.026	14.6 ± 0.7
2.728 ± 0.027	14.78 ± 0.50	0.214 ± 0.008	1.59 ± 0.07	1.19 ± 0.01	0.39 ± 0.05	0.667 ± 0.009	2.56 ± 0.27	0.04 ± 0.02	0.017 ± 0.002	1.684 ± 0.025	14.4 ± 0.7
2.534 ± 0.025	14.95 ± 0.50	0.198 ± 0.008	1.43 ± 0.07	1.21 ± 0.01	0.10 ± 0.03	0.639 ± 0.009	1.97 ± 0.27	0.07 ± 0.02	0.009 ± 0.002	1.629 ± 0.025	14.6 ± 0.7
2.579 ± 0.026	13.68 ± 0.50	0.200 ± 0.008	1.44 ± 0.06	1.18 ± 0.01	0.02 ± 0.02	0.654 ± 0.009	2.25 ± 0.26	0.11 ± 0.02	0.011 ± 0.002	1.609 ± 0.025	13.5 ± 0.7
2.619 ± 0.026	15.24 ± 0.51	0.191 ± 0.007	1.06 ± 0.06	1.19 ± 0.01	0.01 ± 0.02	0.642 ± 0.009	1.84 ± 0.27	0.05 ± 0.02	0.009 ± 0.002	1.589 ± 0.025	14.1 ± 0.7
		0.192 ± 0.005	1.01 ± 0.05	1.13 ± 0.01	0.03 ± 0.02	0.644 ± 0.009	1.44 ± 0.26	0.02 ± 0.02	0.010 ± 0.002	1.563 ± 0.021	12.6 ± 0.4
		0.215 ± 0.006	1.66 ± 0.07	1.14 ± 0.01	0.06 ± 0.02	0.784 ± 0.010	2.05 ± 0.26	0.08 ± 0.02	0.610 ± 0.002	1.646 ± 0.022	15.8 ± 0.4
		0.220 ± 0.006	1.22 ± 0.06	1.15 ± 0.01	0.01 ± 0.02	0.721 ± 0.009	2.62 ± 0.25	0.03 ± 0.02	0.012 ± 0.002	1.736 ± 0.022	15.5 ± 0.4
		0.215 ± 0.006	1.35 ± 0.06	1.25 ± 0.01	0.00 ± 0.02	0.731 ± 0.010	2.23 ± 0.25	0.00 ± 0.02	0.032 ± 0.002	1.624 ± 0.021	15.6 ± 0.4
		0.219 ± 0.006	1.51 ± 0.06	1.24 ± 0.01	0.02 ± 0.02	0.723 ± 0.010	3.06 ± 0.25	0.03 ± 0.02	0.011 ± 0.002	1.720 ± 0.022	15.5 ± 0.4
		0.236 ± 0.006	1.52 ± 0.06	1.28 ± 0.01	0.04 ± 0.02	0.782 ± 0.010	2.85 ± 0.26	0.06 ± 0.02	0.013 ± 0.002	1.781 ± 0.023	15.8 ± 0.4
		0.242 ± 0.006	1.55 ± 0.07	1.41 ± 0.01	0.09 ± 0.03	0.890 ± 0.011	2.74 ± 0.27	0.03 ± 0.02	0.013 ± 0.002	1.845 ± 0.023	18.4 ± 0.5
		0.247 ± 0.006	1.52 ± 0.06	1.40 ± 0.01	0.03 ± 0.02	0.792 ± 0.010	2.99 ± 0.26	0.03 ± 0.02	0.009 ± 0.002	1.885 ± 0.023	16.3 ± 0.4
		0.237 ± 0.006	2.24 ± 0.08	1.55 ± 0.02	0.10 ± 0.03	0.845 ± 0.010	3.54 ± 0.26	0.04 ± 0.02	0.014 ± 0.002	1.830 ± 0.023	16.8 ± 0.4
		0.280 ± 0.007	2.27 ± 0.08	1.73 ± 0.02	0.07 ± 0.03	0.919 ± 0.011	3.36 ± 0.26	0.06 ± 0.02	0.012 ± 0.002	2.121 ± 0.024	18.8 ± 0.5
		0.287 ± 0.007	2.75 ± 0.09	1.99 ± 0.02	0.08 ± 0.03	1.116 ± 0.012	4.58 ± 0.28	0.05 ± 0.02	0.015 ± 0.002	2.235 ± 0.025	21.9 ± 0.5
		0.855 ± 0.018	22.11 ± 0.29	6.00 ± 0.06	0.31 ± 0.06	5.456 ± 0.055	29.22 ± 0.54	0.46 ± 0.04	0.080 ± 0.003	6.961 ± 0.070	106.6 ± 16.0
		0.318 ± 0.008	3.67 ± 0.10	2.07 ± 0.02	0.06 ± 0.03	1.220 ± 0.013	4.45 ± 0.29	0.08 ± 0.03	0.020 ± 0.002	2.467 ± 0.027	24.5 ± 0.5
		0.250 ± 0.007	2.18 ± 0.08	1.59 ± 0.02	0.04 ± 0.02	0.927 ± 0.011	2.91 ± 0.25	0.04 ± 0.02	0.012 ± 0.002	1.979 ± 0.024	19.8 ± 0.5
		0.255 ± 0.007	2.40 ± 0.08	1.58 ± 0.02	0.10 ± 0.03	0.953 ± 0.011	3.52 ± 0.26	0.04 ± 0.02	0.015 ± 0.002	1.985 ± 0.024	19.4 ± 0.5
		0.316 ± 0.008	3.73 ± 0.10	1.82 ± 0.02	0.09 ± 0.03	1.283 ± 0.013	4.59 ± 0.29	0.09 ± 0.03	0.017 ± 0.002	2.462 ± 0.027	26.4 ± 0.6
		0.280 ± 0.007	1.69 ± 0.07	1.34 ± 0.01	0.04 ± 0.02	0.830 ± 0.010	2.61 ± 0.25	0.05 ± 0.02	0.012 ± 0.002	2.099 ± 0.024	16.5 ± 0.4

aks in Section 4 (Peak B at 110 cm, Peak C at 81–83 cm, eak D at 77–78 cm) have Ir/Fe ratios that are one to vo orders of magnitude higher than background (Fig. 1), nd they should, therefore, have a different origin. The evated tail in the lower part of Section 4 is also not kely to be due to background (Fig. 1).

The rise of the main Ir peak is steepest between Sam- les 577B-1-4, 74 cm and 577B-1-4, 73 cm, which is in lose agreement with the location of the Cretaceous/Ter- iary boundary at 577B-1-4, 72 cm defined by nannofos- il studies (Site 577 chapter, this volume; Monechi, this volume). Similar agreements between biostratigraphic and geochemically defined Cretaceous/Tertiary boundary levels (Asaro et al., 1982) have been found in many marine sections, and these would be expected from the asteroid-impact theory. The three smaller peaks below the main peak (Peaks B, C, and D in Fig. 1) and the elevated tail, however, should not be primary deposits in Cretaceous sediment if the asteroid-impact theory is correct.

Bioturbation can cause smearing of sharp boundaries, but it is not clear that it would produce the two well-shaped peaks (C and D) seen in Figure 1. Also the

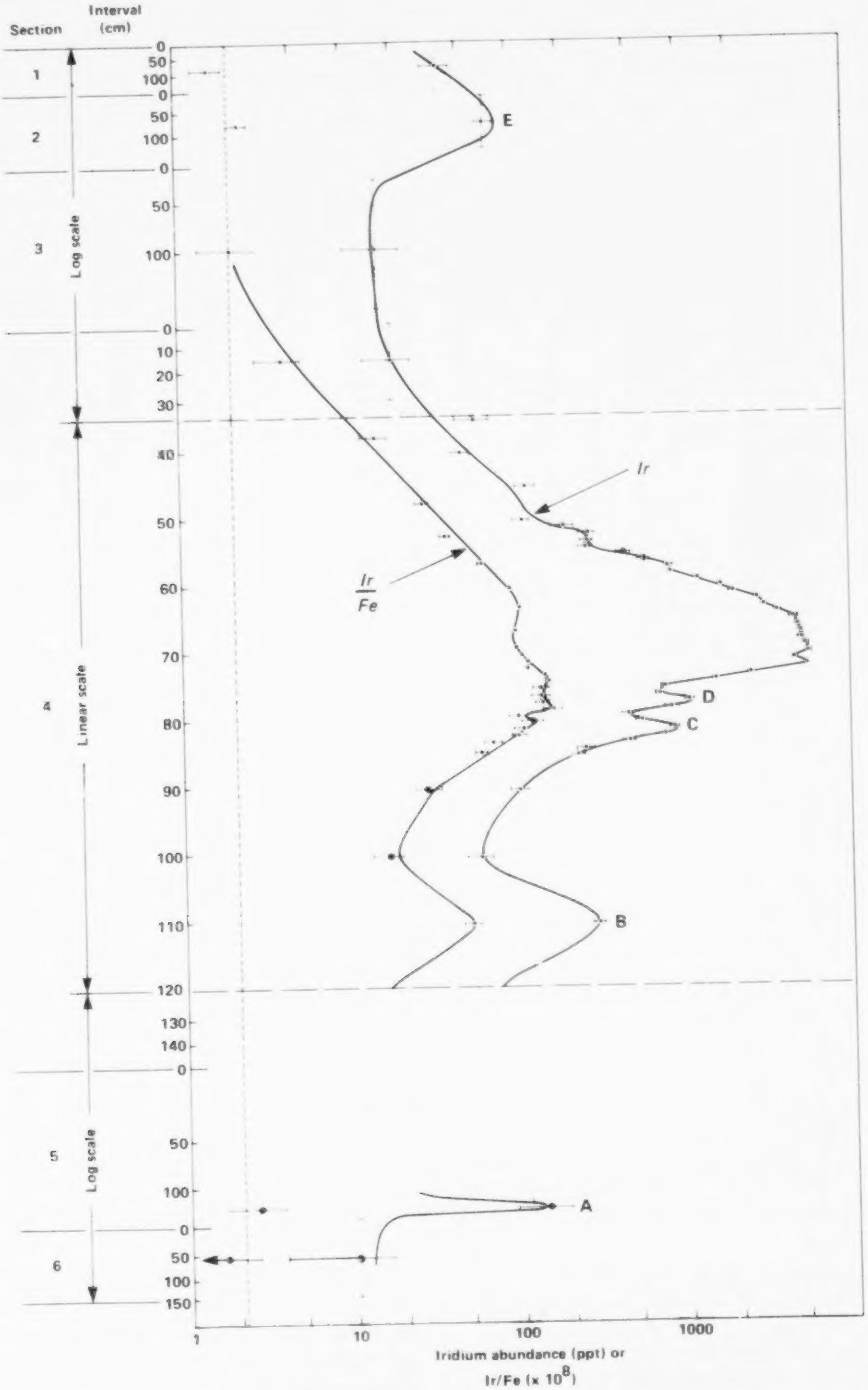

Figure 1. Stratigraphic position in Core 577B-1 versus abundance of iridium (ppt) and (Ir/Fe) × 10^{-8}. The main Ir anomaly is located between 65 and 73 cm in Section 4. Five smaller anomalies, labeled A–E occur in Samples 577B-1-5, 120–121 cm (Peak A) 577B-1-4, 110–111 cm (Peak B), 577B-1-4, 81–83 cm (Peak C), 577-1-4, 77–78 cm (Peak D) and 577B-1-1, 10 cm to 577B-1-2, 121 cm (Peak E). The depth over which a sample was collected for the Ir measurements is shown by a vertical bar. A dashed vertical bar indicates the collection was not continuous.

extent of penetration of the tail into the Cretaceous sediment (over a meter) and the depth of Peak B below the main Ir distribution (38 cm) are greater than would be expected from bioturbation. Iridium in Cretaceous/Tertiary sediments is to some extent soluble in acids (L. W. Alvarez et al., 1980) and the observed tail may be due to bility of the Ir. It is also possible that Peak B is due ontamination or to another impact (Davis et al., 1984, itmire and Jackson, 1984). A method of checking ne of these suppositions would be to resample the erial below the sliced surface. As neither bioturba- n nor contamination is likely to reproduce Peaks B, and D in measurements of such samples, another cause uld be likely if the peaks are still observed.

erophile Element Abundances

Cobalt, Ni, Cr, and Fe all show abundance profiles ilar to that of Ir (Table 1) near the Cretaceous/Ter- y boundary, as do the lithophile elements Al and Ta g. 3). The Ni/Ir ratio is about a factor of 3 lower than chondritic value and the Cr/Ir ratio is about a factor 1.5 lower.

At Stevns Klint, Denmark and at Deep Sea Drilling Project (DSDP) Hole 465A in the Central Pacific Ocean, siderophile elements measured have ratios consistent with mixtures of terrestrial and meteoritic (chondritic) components (F. Asaro, W. Alvarez, H. V. Michel, L. W. Alvarez, M. Kastner, and J. Thiede, unpubl. data). The anoxic environment in which sediments from these sections were deposited may have preserved the ratios of these siderophile elements, as these elements form insoluble sulfides.

Sulfur was not measured in the Hole 577B sediments. As none of the sediments contain measurable amounts of Se (<0.7 ppm), which is normally associated with sulfide deposits, the environment of deposition at Site 577 was probably not anoxic, and some siderophile elements may have been lost during diagenesis.

Rare-Earth Patterns

Hole 577B rare-earth element abundance patterns divided by the chondritic values (Masuda et al., 1973) are shown in Figure 2. The large negative Ce anomaly (cha- cteristic of seawater) indicates that the predominant rare-earth elements were originally dissolved in seawater. s seen in Figure 3, Ce (over and above the amount that associated with Sm in the region directly above and low the boundary) has the same abundance profile as in the boundary region. This excess Ce may be due to detrital component from the impact site. In addition excess Ce, the ratio of heavy to light rare-earth elements is smaller in the Ir-rich region than above and be- w this region.

DISCUSSION

dimentation Rate

Barker and Anders (1968) measured the content of Ir Pacific red clays as a maximum of 140 ppt, for a de- osition rate of 1 mm per thousand years and a density f 0.5 g of solid per cubic centimeter of wet sediment. About half of this Ir was attributed to an extraterrestrial source and half to sources independent of the deposition rate, but the uncertainties were such that all of the Ir could have come from the extraterrestrial source. Kyte and Wasson (1982) found a somewhat higher abundance of Ir, when normalized to the same deposition rate. With the Barker and Anders (1968) maximum Ir deposition value, a 1.9 m/m.y. average sedimentation rate given in the Site 577 chapter (this volume) for the Cretaceous/Tertiary boundary region, and a density of 0.8 g/cm^3, the background Ir should be about 46 ppt. This is consistent with the present work as it is about midway between the highest (73 ppt) and lowest (10 ppt) values of the measured Ir background. Assuming the Barker and Anders (1968) maximum meteorite Ir deposition rate and a density of 0.8 g/cm^3, the rate of sedimentation at any stratigraphic level in this section, where the "background" Ir abundance from normal meteoritic dust can be measured, would therefore be 46 (m/m.y.)/background Ir abundance (ppt).

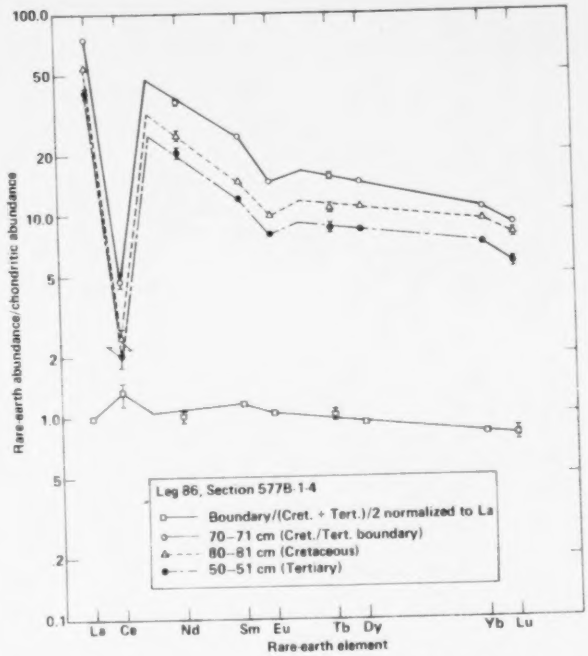

Figure 2. Rare-earth element abundances divided by those of Leedy chondrite (Masuda et al., 1973) as a function of atomic number.

Integrated Amount of Ir

If the products of the Ir abundance in each stratigraphic interval and the stratigraphic height of the interval are summed over the boundary region, and a background of 0.015 ppb times the total stratigraphic height is removed, and the net value is multiplied by a density of 0.8 g/cm^3, there are found to be 61 ng/cm^2 of anomalous Ir in the boundary region. This is comparable to the average amount found at other studied Cretaceous/Tertiary sections worldwide (50 ng/cm^2) (W. Alvarez et al., 1982b).

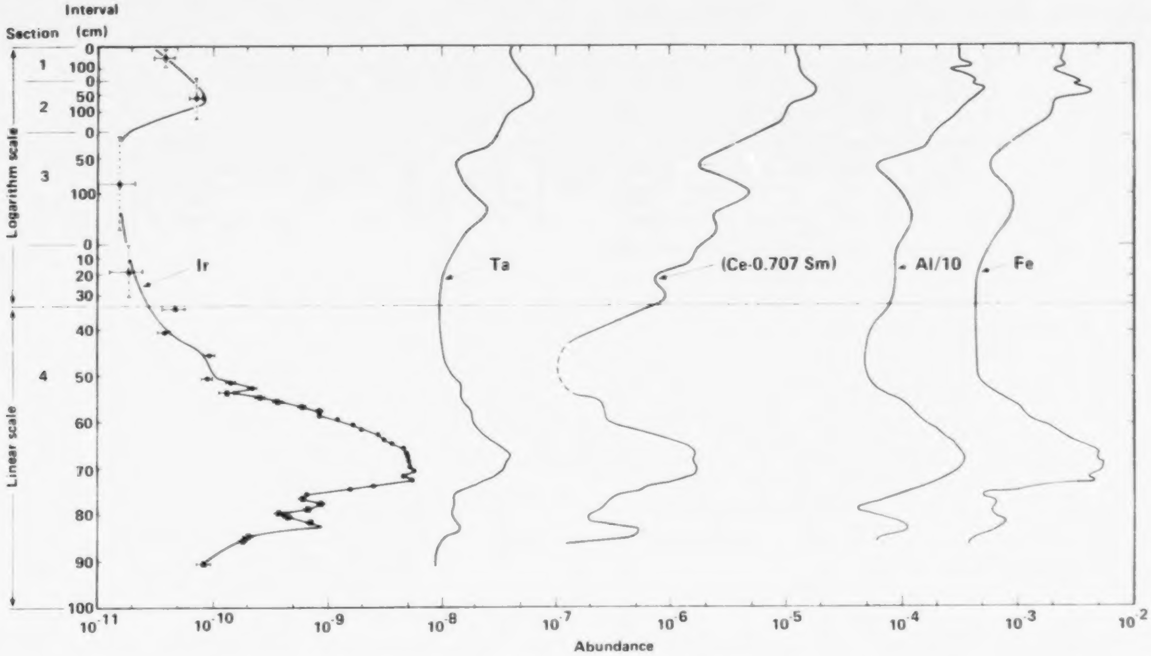

Figure 3. Abundances of Ir, Ta, (Ce − 0.707Sm), Al/10 and Fe as a function of stratigraphic position in Core 577B-1, Shatsky Rise.

CONCLUSION

The Ir anomaly predicted by the asteroid-impact theory was found in the Cretaceous/Tertiary boundary region of Hole 577B and its magnitude was 61 ng/cm^2. The sharp rise of the main Ir peak occurs within 2 cm of the Cretaceous/Tertiary boundary as defined by nannoplankton (Monechi, this volume). Five other small Ir peaks as well as an elevated tail are also observed near the main Ir peak. Two of the small peaks are probably related to changes in the $CaCO_3$ deposition rate, while two others and the elevated tail may be due to perturbations of the main peak. One small Ir peak remains unexplained. Siderophile element (Cr/Ir and Ni/Ir) ratios are somewhat different from chondritic values in the Cretaceous/Tertiary region, but this may be due to loss of elements in the oxidizing marine environment.

ACKNOWLEDGMENTS

We are grateful to Audrey Wright and Amy Altman for their assistance in obtaining the samples, to Audrey Wright for her help in editing the manuscript, and to Charles J. Orth and Frank T. Kyte for reviewing the manuscript. We thank Tek Lim and his staff at the Berkeley Triga Reactor for the neutron irradiations. We also appreciate the assistance of Raphael Zamora and Jon Bechtel in sample preparation and data reduction. Jonathan Stebbins was most helpful in the development of the high-temperature Ir separations.

Funding for this work was provided by the Director, Office of Energy Research, Office of Basic Sciences Division of Engineering, Mathematical and Geosciences of U.S. Department of Energy under Contract No. DE-AC03-76SF00098, the U.S. National Science Foundation under Grant EAR-81-15858, and the National Aeronautics and Space Administration Ames Research Center under Contract A-71683B. DSDP samples were provided through the assistance of the National Science Foundation.

REFERENCES

Alvarez, L. W., Alvarez, W., Asaro, F., and Michel, H. V., 1980. Extraterrestrial cause for the Cretaceous-Tertiary extinction. *Science*, 208:1095-1108.

Alvarez, W., Alvarez, L. W., Asaro, F., and Michel, H. V., 1982a. Iridium anomaly approximately synchronous with terminal Eocene extinctions. *Science*, 216:868-888.

________, 1982b. Current status of impact theory for the terminal Cretaceous extinction. *Spec. Pap. Geol. Soc. Am.*, 190:305-315.

________, 1984. The end of the Cretaceous: Sharp boundary or gradual transition. *Science*, 223:1183-1186.

Asaro, F., Alvarez, L. W., Michel, H. V., and Alvarez, W., 1982. Letter to Editor. *Am. Sci.*, 70:567-568.

Barker, J. L., and Anders, E., 1968. Accretion rate of cosmic matter from iridium and osmium contents of deep sea sediments. *Geochim. Cosmochim. Acta*, 32:627-645.

Davis, M., Hut, P., and Muller, R. A., 1984. Extinctions of species b periodic comet showers. *Nature*, 308:715-717.

Kyte, F., and Wasson, J. T., 1982. A search for iridium anomalies i sediments deposited during the past 70 Ma. *Lunar Planet. Sci* XIII:411-412. (Abstract)

Masuda, A., Nakamura, N., Tanaka, T., 1973. Fine structures of m tually normalized rare-earth patterns of chondrites. *Geochim. Co mochim. Acta*, 37:239-248.

Perlman, I., and Asaro, F., 1969. Pottery analysis by neutron activ tion. *Archaeometry*, 11:21-52.

________, 1971. Pottery analysis by neutron activation. *In* Brill, R. I (Ed.), *Science and Archaeology*: Cambridge (M.I.T. Press), p 182-195.

Rammensee, W., and Palme, H., 1982. "Metal-silicate extractio technique for the analysis of geological and meteoritic samples *J. Radioanal. Chem.*, 71:401-418.

Whitmire, D. P., and Jackson, A. A., IV, 1984. Are periodic mass e tinctions driven by a distant solar companion? *Nature*, 30 713-715.

Date of Initial Receipt: 30 January 1984
Date of Acceptance: 6 June 1984

22. ^{10}Be DISTRIBUTIONS IN DEEP SEA DRILLING PROJECT SITE 576 AND SITE 578 SEDIMENTS STUDIED BY ACCELERATOR MASS SPECTROMETRY[1]

T. L. Ku, University of Southern California
J. R. Southon and J. S. Vogel, Simon Fraser University
Z. C. Liang and M. Kusakabe, University of Southern California
and
D. E. Nelson, Simon Fraser University[2]

ABSTRACT

Extension of the ^{10}Be geochronology for deep-sea sediments beyond the limit of late Pliocene age found in published works has been attempted. The results obtained on sediments from Deep Sea Drilling Project (DSDP) Sites 576 and 578 of Leg 86 suggest the feasibility of dating sediments as old as 12 to 15 m.y. At both sites, there have been large changes in sedimentation rate, with the Pleistocene sediments accumulating several times faster than those of the Pliocene, which in turn were deposited several times more rapidly than the late Miocene sediments. The Pleistocene–Pliocene section is considerably thicker in Hole 578 than in Hole 576B: the respective depths for the 7-m.y. time boundary in the two holes are ~125 and ~25 m. These ^{10}Be-based age estimates are in agreement with the paleomagnetic stratigraphies established for the two sites. The suggested enhancement in the oceanic deposition of ^{10}Be before 7 to 9 m.y. ago, as noticed in manganese crusts, has found tentative support from the present sedimentary records. A preliminary search for ^{10}Be production variation during a geomagnetic field reversal has been conducted. In Hole 578, an enhanced ^{10}Be concentration is found in a sample close to the Brunhes/Matuyama reversal boundary. More detailed and systematic measurements are required to confirm this observation, which bears on the detailed behavior of the geomagnetic field during the reversal.

INTRODUCTION

The potential of using the long-lived ^{10}Be (half-life 1.5 m.y.) to study cosmic-ray intensity variations and deep ocean sedimentation rates was first suggested by Peters (1955). The detection of this cosmogenic radionuclide in marine sediments soon followed (Arnold, 1956; Goel et al., 1957). Since then, many papers on ^{10}Be in deep-sea sediments have been written (Amin et al., 1975; Inoue and Tanaka, 1976, 1979; Tanaka and Inoue, 1979, 1980; Tanaka et al., 1977, 1982; Somayajulu, 1977; Finkel et al., 1977; Raisbeck et al., 1979), contributing handsomely toward the realization of that potential. Most of these works have measured the beta activities of ^{10}Be. Although state-of-the-art low-level beta counting techniques have been used, the sensitivities in the measurements remain relatively low. Few such measurements give desirable precisions for samples with ages beyond one or two half-lives of ^{10}Be. And, since over 100 g of sediment are often required for each radio-counting assay, the minimum analyzed depth intervals from a conventional piston core (5-cm diameter) are larger than 10 cm. With a typical deep-sea accumulation rate on the order of 0.5 g/cm^2 per 1000 yr., these sampled intervals correspond to a time resolution of $>10^4$ yr.

The nuclear accelerator mass spectrometry developed in recent years (e.g., Muller, 1977; Raisbeck et al., 1978; SAMS, 1981) enables us to improve on the situation. It attains a measurement sensitivity for ^{10}Be of 10^7 atoms or less, which is about three orders of magnitude smaller than that achieved by the decay counting methods. It is clear that the ^{10}Be chronology of pelagic deposits can be greatly extended with the accelerator technique. The ^{10}Be chronology of sediments recovered from the Deep Sea Drilling Project (DSDP) should be particularly valuable as a supplement to the age information based on paleomagnetism and biostratigraphy.

The study presented here gives the first accelerator measurements of ^{10}Be in DSDP sediments. Measurements were made on samples from two DSDP sites in the western North Pacific: Sites 576 and 578. Site 576 (32°21.4′N, 164°16.5′E; 6217 m), which has been proposed by JOIDES panels as a "type" North Pacific red clay site, lies in an area of apparently uniform pelagic sedimentation between Shatsky Rise and the Emperor Seamounts. Site 578 is farther to the west (33°55.6′N, 151°37.7′E; 6010 m) and is located in an area covered with a thick section of late Neogene siliceous clays. Paleomagnetic studies carried out on samples from both sites give good to excellent reversal records for the last 5 m.y. (Heath et al., this volume). At Site 578, the magnetostratigraphy extends to about 15 m.y. ago, although data control for the extension is of lesser quality. Three holes were drilled at Site 576: 576, 576A, and 576B. The analyzed ^{10}Be samples are from Hole 576B, except for the two samples at sub-bottom depths of 29.68 and 40.00 m, which are from Hole 576 (material from these two depths in Hole 576B was not recovered in the coring operation). It should be noted that drilling records indicate that the sub-bottom depth of the base of the clay unit in

---

[1] Heath, G.R., Burckle, L.H., et al., *Init. Repts. DSDP*, 86: Washington (U.S. Govt. Printing Office).

[2] Addresses: (Ku, Kusakabe) Department of Geological Sciences, University of Southern California, Los Angeles, CA 90089-0741; (Southon, Vogel, Nelson) Archeology Department, Simon Fraser University, Burnaby, British Columbia, Canada; (Liang, permanent address) Institute of Geochemistry, Academia Sinica, Guiyang, People's Republic of China.

Hole 576 (~55 m) is more than 10 m deeper than in Hole 576B. Adjustments of sub-bottom depth assignment have been made to correct for this discrepancy (see Site 576 chapter, this volume). The adjusted depths are used in this chapter.

The primary purpose of this study was to establish ^{10}Be geochronologies for Sites 576 and 578 and to compare these chronologies with ages obtained from magneto- or biostratigraphy. Another purpose was to check the possible deviation from constancy in the oceanic precipitation rate of ^{10}Be about 7 to 9 m.y. ago, as observed in ferromanganese crusts (Ku, Kusakabe, Nelson, et al., 1982). In addition, we examined the extent of variations in the ^{10}Be concentration in sediment layers close to a geomagnetic reversal. Information thus acquired may bear on the detailed behavior of the geomagnetic field during a geomagnetic reversal. Because of the great lengths of the cores involved (~70 m at Site 576 and ~165 m at Site 578), the number of ^{10}Be measurements made so far constitutes only a fraction of the number needed to completely fulfill the aforementioned objectives. We are currently trying to fill in the data gaps, which will become evident in the following discussion.

EXPERIMENTAL PROCEDURES

Samples were taken from the hydraulic piston cores retrieved in Holes 576, 576B, and 578. The sampled depth intervals varied from 1 to 3 cm. The sediments arrived at the lab in wet condition. After being dried at 110°C, they were homogenized in powdered form. Aliquots of about 150 mg and about 1 g were taken from each sample for analyses of $CaCO_3$ content and ^{10}Be, respectively.

The carbonate aliquots were leached with hot acetic acid. Their $CaCO_3$ percentages were estimated from calcium determinations made on the leachates using atomic absorption spectrophotometry. The accuracy was about ±10%. The ^{10}Be samples were completely dissolved with successive treatments of HCl, HF + $HClO_4$, and aqua regia. To each sample solution was added 0.9492 mg of ^{9}BeO (in the form of $BeSO_4$ solution) as Be carrier. The extraction and purification procedures for Be followed those of Ku et al. (1979) with some simplifications, since the BeO prepared for the accelerator runs does not have to be radiochemically pure. Dowex-1 anion resins were used to first separate out iron. Beryllium was then purified against Al on a Dowex-50 cation-exchange column using 0.5 *M* oxalic acid (for Al) and 4 *M* HCl (for Be) as eluants. After heating over a Bunsen burner in a covered Pt crucible to convert $Be(OH)_2$ to BeO, the BeO was mixed with a few milligrams of ultra-pure Ag powder (as a binder) and impacted into stainless steel sample holders, ready for insertion into the accelerator's ion source.

The technical details of ^{10}Be analysis, including adaptations of the McMaster University FN tandem Van de Graaff accelerator used for the analysis, have been described by Southon et al. (1983). The primary standard consists of ultra-pure ^{9}BeO irradiated with thermal neutrons to produce ^{10}Be/^{9}Be ratios of 10^{-9}. (A neutron capture cross section of 9.2 mb [Mughabghab and Garber, 1973] was used.) Several similarly prepared secondary standards with ^{10}Be/^{9}Be ratios of 10^{-10}, 10^{-11}, etc. were used for consistency check. Each measurement consisted of three separate ^{10}Be/^{9}Be determinations: one on the standard, one on the unknown, and a second on the standard. The measured ratio of the standard (the mean of the results from the two runs) was then used with the measured ratio for the unknown to determine the absolute ratio for the latter. Each sample was measured several times. After every second unknown run, a check was made of a secondary standard or a blank. The blank consisted of the reagents used (including 0.9492 mg of BeO carrier) which had undergone all the preparation chemistry.

RESULTS

Table 1 lists the ^{10}Be and $CaCO_3$ data of Sites 576 and 578. The measured ^{10}Be/^{9}Be ratios refer to the atom ratio of natural ^{10}Be to the carrier ^{9}Be added (^{9}Be in samples is negligible), before correction for the blank. The blank has a ^{10}Be/^{9}Be ratio of $(1.7 \pm 0.2) \times 10^{-13}$, which is small compared to the ratios for most of the samples, and it is the same as that of Sample 576-6-6, 110 cm, which has the lowest measured ratio of the samples analyzed. According to magnetic and ichthyolith studies (Heath et al., this volume; Doyle and Riedel, this volume), this sample has an age of about 30 m.y., so it should be ^{10}Be free. The quoted uncertainties in the tables are one standard deviations derived from the scatter of the several ^{10}Be/^{9}Be measurements on each sample.

Semilog plots of the ^{10}Be concentrations versus depth in Holes 576B and 578 are shown in Figures 1 and 2, respectively. The closely spaced data points near the Brunhes/Matuyama boundaries in both holes are plotted on an expanded depth scale in the upper part of each of the figures; their average values (and standard deviations) are plotted in the lower diagram. Sedimentation rates are derived from the slopes of the straight lines fitting the data points. The assumption is made that deposition rates of both ^{10}Be and the sediment remain constant (to within the data scatter) over the time period represented by a given straight-line segment. If zero age is taken to be the sediment/water interface, the age for a particular depth in the holes can be calculated from the sedimentation rates. A few such ages are indicated in parentheses.

DISCUSSION OF RESULTS

Measurement Precision and Sensitivity—Extending the Deep-Sea ^{10}Be Geochronology

The analytical precision of <5% in this study is a significant improvement over that of >15% generally reported in the earlier studies. The validity of the error limits is supported by the two sets of duplicate results shown in Table 1. The sensitivity of the present analyses can be estimated from ^{10}Be/^{9}Be ratios of $(1.7 \pm 0.2) \times 10^{-13}$ and $(1.9 \pm 0.4) \times 10^{-13}$ obtained for the blank and for the oldest sample, respectively. With the amount of the ^{9}Be carrier used, these ratios correspond to about 4×10^6 atoms of ^{10}Be, a quantity that is typically found in 1 mg of abyssal sediments of modern age. Thus, our measurement sensitivity should potentially allow the deep-sea ^{10}Be chronology to be extended beyond 15 m.y., well into the Miocene Epoch. There is no reason to discount the feasibility of ^{10}Be dating of even earlier Neogene deposits. Since accelerator mass spectrometry is capable of detecting ^{10}Be/^{9}Be ratios of 10^{-14} to 10^{-15} (e.g., Gove, 1981), and since the sample/carrier proportion can be readily maximized (increased) over those used in this study, one only has to reduce the blank values associated mostly with the extraction chemistry. Of course, knowledge must also be secured on the long-term constancy of ^{10}Be or ^{10}Be/^{9}Be of the oceanic reservoirs prior to 7 to 9 m.y. ago (Ku, Kusakabe, Nelson, et al., 1982). In this regard, cross-checks of ^{10}Be ages with K-Ar or fission-track ages obtained on intercalated volcanic ash deposits commonly found in the deep sea, as well as with magneto- and biostratigraphic ages, would be useful.

Table 1. ^{10}Be and $CaCO_3$ data for Holes 576B, 576, and 578.

Core-Section (level in cm)	Sub-bottom depth (m)	$CaCO_3$ (%)	Measured[a] $^{10}Be/^{9}Be \times 10^{-11}$	^{10}Be (10^9 atoms/g)
Hole 576B				
1-1, 49	0.49	0.39	15.1 ± 0.8	3.30 ± 0.17
1-4, 57	5.07	0.39	13.6 ± 0.8	3.01 ± 0.18
1-5, 59	6.60	—	22.5 ± 0.3	3.11 ± 0.04
1-5, 79	6.79	0.37	15.0 ± 0.4	3.38 ± 0.08
1-5, 98	6.98[b]	0.35	15.3 ± 0.3	3.12 ± 0.06
1-5, 108	7.08[b]	—	19.1 ± 0.3	2.31 ± 0.04
1-5, 120	7.20	0.31	11.2 ± 0.3	2.30 ± 0.06
1-5, 149	7.49	0.38	16.7 ± 0.6	2.75 ± 0.10
1-6, 50	8.00	0.34	14.3 ± 0.4	2.36 ± 0.07
2-1, 40	12.00	0.41	12.4 ± 0.3	2.21 ± 0.05
2-3, 40	15.00	—	15.8 ± 0.3	2.33 ± 0.05
2-4, 140	17.50	—	10.9 ± 0.2	1.50 ± 0.03
2-6, 90	20.00	0.45	4.3 ± 0.4	0.63 ± 0.06
3-6, 50	24.99	—	0.90 ± 0.02	0.127 ± 0.003
Hole 576				
5-1, 148[c]	29.68	0.60	1.9 ± 0.2	0.20 ± 0.02
5-1, 148[c]	29.68	—	1.28 ± 0.05	0.18 ± 0.01
6-6, 110	40.00	1.22	0.019 ± 0.004	0.0003 ± 0.0006
Hole 578				
1-1, 50	0.50	0.39	13.2 ± 0.4	2.96 ± 0.09
3-4, 120	20.00	0.49	9.6 ± 0.5	1.81 ± 0.09
4-1, 120	25.00	0.46	10.6 ± 0.2	1.58 ± 0.03
4-2, 103	26.33	0.34	14.8 ± 1.0	2.27 ± 0.15
4-2, 130	26.60	0.37	12.2 ± 1.0	1.94 ± 0.16
4-3, 10	26.90[d]	0.44	20.0 ± 1.8	3.18 ± 0.29
4-3, 20	27.00	0.39	11.7 ± 0.3	2.20 ± 0.06
4-3, 50[c]	27.30	0.19	2.7 ± 0.1	0.56 ± 0.02
4-3, 50[c]	27.30	—	2.9 ± 0.1	0.60 ± 0.02
4-3, 70	27.50	0.35	13.2 ± 0.5	2.08 ± 0.08
4-3, 92	27.72	0.36	9.5 ± 0.1	1.84 ± 0.02
4-3, 120	28.00	0.34	10.4 ± 0.3	1.77 ± 0.05
6-5, 120	50.00	0.29	6.4 ± 0.2	1.16 ± 0.04
11-6, 20	98.00	0.38	2.85 ± 0.06	0.435 ± 0.009
12-6, 143	108.73	—	1.89 ± 0.05	0.265 ± 0.007
14-5, 64	125.44	0.34	0.82 ± 0.02	0.113 ± 0.003
16-2, 75	140.05	—	0.087 ± 0.008	0.009 ± 0.001
17-2, 148	150.28	0.56	0.061 ± 0.012	0.005 ± 0.002

Note: — means not measured.

[a] Atom ratios before correction for blank which has a ratio of $(1.7 \pm 0.2) \times 10^{-13}$.

[b] Brunhes/Matuyama magnetic reversal found near these two levels at 7.05 m.

[c] Duplicate analyses made on two different aliquots of the sample.

[d] Location of Brunhes/Matuyama reversal.

onstancy of ^{10}Be Deposition

The temporal variations in the oceanic deposition of Be have been assessed to be within ± 10% when the :position is integrated over time periods of 2 to 7 × 10^5 . (Inoue and Tanaka, 1979; Tanaka and Inoue, 1980). or shorter intervals of 10^4 to 10^5 yr. corresponding ap- roximately to glacial–interglacial cycles, the limits have een placed at ±(25–30)% (Tanaka and Inoue, 1980; u, Kusakabe, Huh, et al., 1982). These assessments are ased on the ^{10}Be distributions in sediment cores cover- ıg time spans up to 2.5 m.y. ago. The time coverage has een extended by the records in two ferromanganese rusts from the seafloor of the Pacific and the Atlantic Ku, Kusakabe, Nelson, et al., 1982). Measurements on hese crusts, when averaged over time intervals of about m.y., record a variation of ±6% in ^{10}Be deposition luring the last 7 to 9 m.y. Further back in time, the crustal records indicate a possible two- or threefold increase of ^{10}Be influx.

The average sedimentation rates shown in Figures 1 and 2 are derived with the above background information in mind. As will be seen, a comparison between the ^{10}Be-based ages and the magnetic reversal ages supports the general consistency of ^{10}Be precipitation since about 7 m.y. ago.

Tantalizing evidence exists for the possible increase of ^{10}Be input in the late Miocene. At Site 576, the "anomalously high" ^{10}Be concentration in Sample 576-5-1, 148 cm at 29.68 m (Fig. 1) appears to reflect a threefold increase of ^{10}Be flux before 7 m.y. ago. At Site 578, the check for high ^{10}Be influx is complicated by the fact that a rapid slowdown of sediment accumulation occurred earlier than 7 m.y. ago, as shown by the magnetic record (Heath et al., this volume) as well as our ^{10}Be data (Fig. 2). The ^{10}Be age of Sample 578-16-2, 75 cm (at

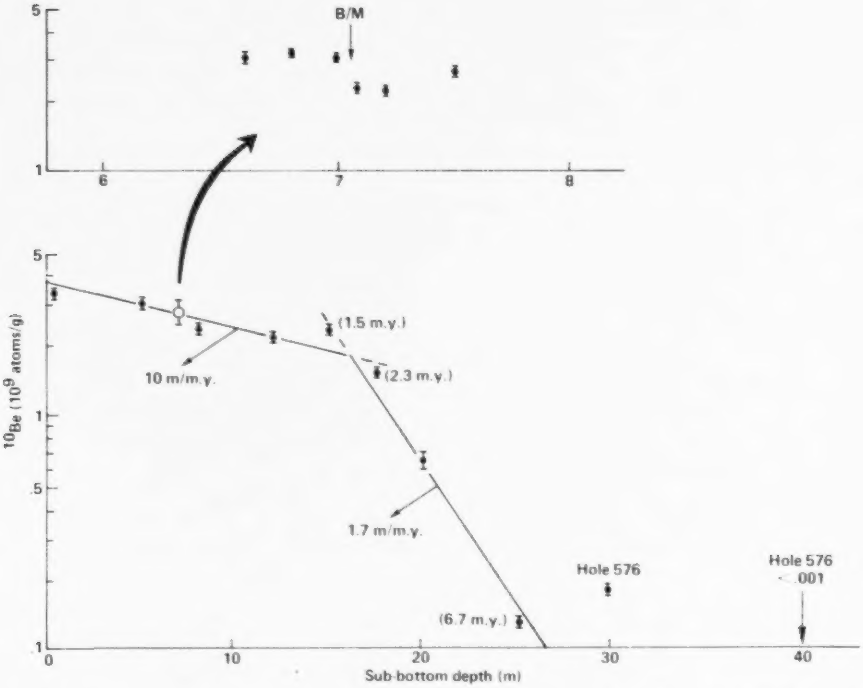

Figure 1. ^{10}Be concentrations versus depth in Site 576 sediments. All samples are from Hole 576B, except for the two deepest ones from Hole 576 as noted. Estimated average sedimentation rates and ages are shown, as is the position of the Brunhes/Matuyama reversal boundary (B/M). See text for further explanation.

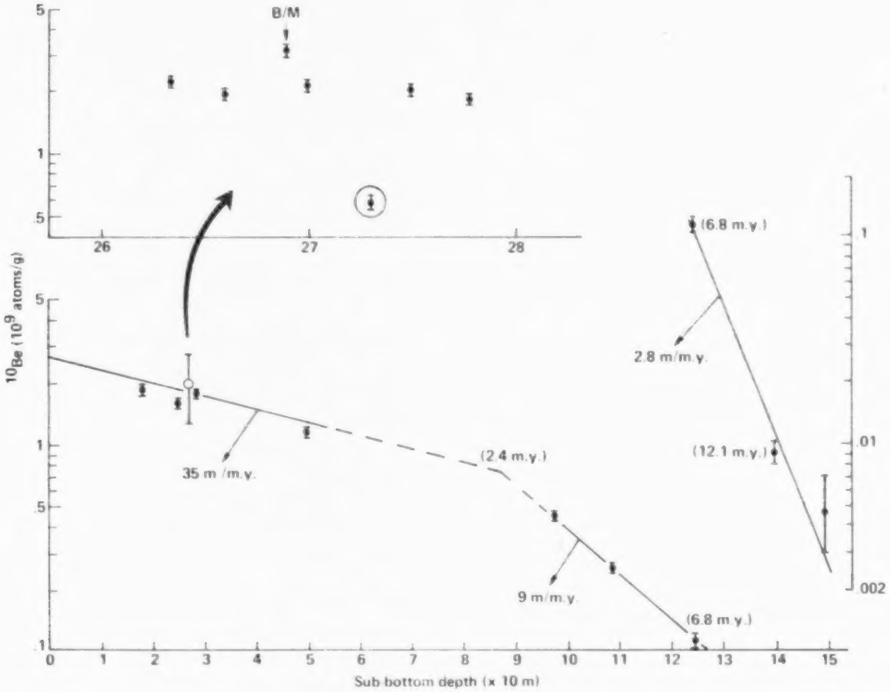

Figure 2. ^{10}Be concentrations versus depth in Site 578 sediments, with estimated average sedimentation rates and ages shown. The position of the Brunhes/Matuyama reversal boundary (B/M) is indicated. Note a shift in the ^{10}Be concentration scale for the three deepest samples on the right-hand side of the graph. The encircled data point is from a sample with abundant volcanic material. See text for further explanation.

140.05 m) is younger than its magnetic age by one half-life of ^{10}Be (12.1 versus 13.6 m.y.), a discrepancy consistent with a late Miocene higher ^{10}Be input. However, the uncertainties of these ages render their difference inconsequential.

Although evidence appears to be present in support a higher ^{10}Be deposition rate before 7 to 9 m.y. ago, it uld be viewed with qualification at this time. A firm-check would require a series of closely spaced mea-ements on sediments of uniform accumulation rate r and below the 7 m.y. boundary. It should also be ed that a factor of two uncertainty in the ^{10}Be input ses an age uncertainty of 1.5 m.y., which becomes serious for older samples. Interest in the 7–9 m.y. narcation lies more in the realm of paleoceanography n of geochronology, since the ^{10}Be fluxes near the undary may reflect a major change in the global abys-circulation (Ku, Kusakabe, Nelson, et al., 1982).

e Chronologies at the Two Sites

The sedimentation rates derived from the rate of decrease in ^{10}Be concentration with depth permit the establishment of absolute chronologies for the two sites. It is apparent from Figures 1 and 2 that in both holes drastic changes in sedimentation rate have taken place. The Pleistocene rates are several times more rapid than those of earlier times. In Hole 576B, the change occurred between 15 and 17.5 m, about 1.5 to 2.3 m.y. ago (Fig. 1). In Hole 578, relative sparsity of data brackets the change between 50 and 98 m. As shown in Figure 2, extrapolations of the two rate-determining lines would place the beginning of accelerated sedimentation near 2.4 m.y. ago (86 m depth), in late Pliocene/early Pleistocene times. Farther down the hole, another major change occurred around 7 m.y. ago (Fig. 2), with earlier deposits having accumulated considerably more slowly. The slow accumulation rate is also suggested by the large difference in ^{10}Be concentrations between 30 and 40 m in Hole 576 (Fig. 1). The data density precludes precise definition of the time intervals involved in the changes—they could have spanned millions of years. But the changes themselves and their magnitudes are clearly apparent from the data.

The paleomagnetic records for the two sites have been thoroughly examined (Heath et al., this volume) and can e correlated with the ^{10}Be age results. Figure 3 shows e correlation between the interpolated magnetic ages d the ^{10}Be ages estimated from the mean sedimenta-on rates for each of the data points shown in the lower ots of Figures 1 and 2. The two dashed lines represent 20% deviations from the 1:1 correlation denoted by e solid line.

The linear regression line of the data set gives a *y*-in-ercept (magnetic age) of −0.1 m.y. and a slope of 1.06, nd it has a correlation coefficient of 0.985. The average f the percent standard deviation of the means for the 9 pairs of data is ±5.4%. All these statistics are better han expected, in view of the errors involved in the de-ermination of both the ^{10}Be and the magnetic ages. In any case, the following implications can be drawn from Figure 3:

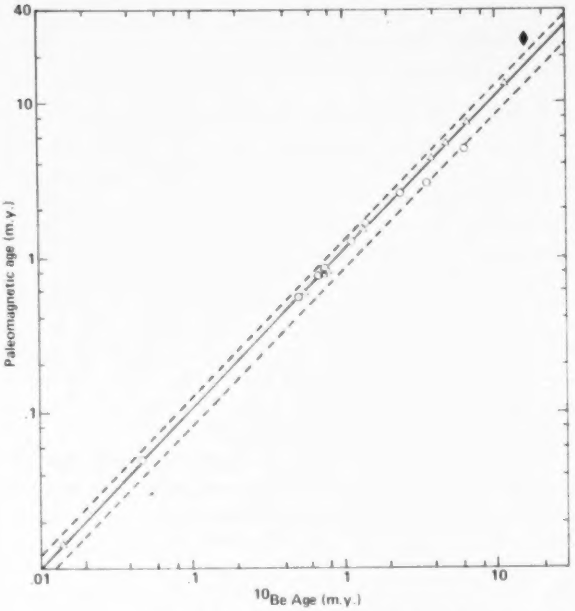

Figure 3. A correlation plot between ^{10}Be ages derived from the sedimentation rate data shown in Figures 1 and 2 (open circles, Site 576, open triangles, Site 578) and the paleomagnetic ages of Heath et al. (this volume). The two dashed lines bracket the ±20% deviations from a 1:1 correlation (solid line). The solid diamond-shaped data point represents the ^{10}Be age of Sample 578-17-2, 148 cm plotted against age based on ichthyoliths (Doyle et al., this volume). The ^{10}Be ages of this sample and the ~12 m.y. old sample may be 1.5 to 3 m.y. too young, because of the possible two- to threefold higher ^{10}Be flux before 7–9 m.y. ago.

1. The ^{10}Be geochronology in deep-sea sediments can be applied at least to the last 7 m.y., with an excellent prospect of being extended to 15 m.y. ago.
2. The two sites are located near or in an area of the western North Pacific where occurrence of large-scale depositional hiatuses during Cenozoic times is suspected (van Andel et al., 1975). The Figure 3 data imply continuous deposition at the two sites for the last 12 m.y. or thereabout. Were the large decrease in sedimentation rates caused by hiatus, one might expect stepwise patterns in ^{10}Be concentration versus depth plots. On the other hand, it could be that the hiatuses are too brief and our data are too sparse for the hiatuses to show up as steps in the depth distribution of ^{10}Be. More detailed ^{10}Be analyses in the future should provide further information on the matter.
3. The ^{10}Be ages are obtained on samples from Hole 576B only, whereas the magnetic records are based on samples from both Hole 576 and Hole 576B. It would seem that the adjustments made to correct for the ~10 m sub-bottom depth offset between the two holes in the drilling records (Site 576 chapter, this volume) might have largely restored the *in situ* stratigraphy.

4. The data represent as good a "geological" calibration for the ^{10}Be half-life of 1.5 m.y. (Yiou and Raisbeck, 1972) as presently exists over a 7-m.y. span.

^{10}Be Input Variation near Geomagnetic Reversal

Earlier workers (Raisbeck et al., 1979) have searched for an increased ^{10}Be flux into the marine sediments during a geomagnetic reversal. The search is based on the belief that a geomagnetic reversal is accompanied by the lowering of the dipole intensity to a near-zero level. During this zero-field period, which has been variously estimated to last for about 1000 yr. (Kawai et al., 1975) to 5000 yr. (Harrison and Somayajulu, 1966; Cox et al., 1975), cosmogenic isotope production would be increased two- or threefold (Black, 1967; O'Brian, 1979). If so, a change in ^{10}Be concentration might be found in sediments deposited during that period.

The Hole 578 sediments may be used to test this hypothesis. Assume that the zero-field period lasted 1000 yr. During the Brunhes/Matuyama transition, 3.5 cm of sediments would have been deposited having, say, twice the ^{10}Be concentration of those deposited during the normal field intensity. If mixing due to bioturbation is assumed to affect a 7-cm sediment interval, this 7-cm interval at the Brunhes/Matuyama boundary would have a ^{10}Be concentration 50% higher than normal. If we apply the above conditions to sediments at the Brunhes/Matuyama boundary in Hole 576B, we find only a 14% increase of ^{10}Be concentration in the zero-field period. The smaller increase is due to the slower sediment accumulation at Hole 576B, where accumulation was 3.5 times slower than at Hole 578.

These scenarios are in agreement with our observations. In Hole 576B, the ^{10}Be near the reversal (i.e., the six data points shown in the upper part of Fig. 1) show variations no greater that those of the age-corrected concentrations for all the data points above 25 m: the standard deviations from the means in both cases are about ±15%. Hence, we either have yet to obtain or are unable to identify the signals we search for. In Hole 578, the ^{10}Be concentration found at 26.90 m is about 54% higher than concentrations nearby. This may be of significance, because the standard deviation from the average ^{10}Be concentration of the five points adjacent to the reversal (see upper Fig. 2; the data at 27.30 m are excluded) is about ±9%, and this value is also the scatter about the age-corrected mean ^{10}Be concentration for all the data points (the sample at 27.30 m is again excluded) down to 125.44 m. We exclude the data for the sample at 27.30 m in our discussion because microscopic examination shows this sample to contain abundant volcanic glass fragments. It could well be from one of the many ash layers present in the hole, and its low ^{10}Be concentration results from dilution by the ash material.

Before accepting the above interpretations, one should also be aware of the following complications. First, variations in ^{10}Be concentration due to variations in sediment composition and sedimentation rate must be considered. Volcanic sediments and biogenic carbonates are two types of material that act as a dilutant for ^{10}Be contents (Tanaka et al., 1977; Ku, Kusakabe, Huh, et al., 1982). Data in Table 1 shows that the effect of $CaCO_3$ dilution should be minimal. We also need biogenic silica data for Hole 578, but those data are currently unavailable. One further notices that the ^{10}Be concentration varies rather weakly with sedimentation rate; namely, the surface concentrations in the two holes differ by about 30%, whereas sedimentation rates differ by a factor of 3.5. This dependence of ^{10}Be scavenging efficiency on sedimentation rate, which has been noted previously (e.g., Tanaka et al., 1982), and the generally uniform lithologies of the samples studied do tend to reduce the "noise" attributable to the composition–rate factor. Nevertheless, composition and sedimentation rate should be considered when small differences in ^{10}Be concentration (e.g., $<20\%$) are compared among adjacent layers.

The second complication, as pointed out by Raisbeck et al. (1979), is the so-called depth-lag. Depth-lag is the depth below the sediment/water interface where the magnetic grains become held firmly enough in position so that changes in the Earth's magnetic polarity do not result in movements of the grains. Estimates of the depth-lag vary from a few centimeters (hence within the bioturbated zone of 5–10 cm) to over 1 m (Dymond, 1969). Therefore, search for the ^{10}Be input variations should be conducted on sediments above as well as at the level where the magnetic reversal is found.

The examples given above assume that the average residence time of Be in the ocean is negligible compared with the zero-field period. Available data on Be in seawater point to a residence time of about 1000 yr. (Yokoyama et al., 1978; Measures and Edmond, 1982). Therefore we must also consider the "damping" effect of ocean mixing (as well as of bioturbation) on the amplitude of the ^{10}Be concentration variations in sediments relative to that of the atmospheric ^{10}Be input changes due to geomagnetic field variation. This effect can be explained mathematically as follows.

The time variation of the amount of ^{10}Be in seawater, $M(t)$, depends on the input and removal rates of ^{10}Be.

$$dM/dt \text{ (atoms/cm}^2 \cdot \text{yr.)} = P - RM. \qquad (1)$$

Here, the removal is expressed in terms of first-order rate constant R, the value of which can be taken as 10^{-3}/yr.

The stationary ^{10}Be standing crop in the water column is thus:

$$M\text{(atoms/cm}^2\text{)} = P/R. \qquad (2)$$

Let the production rate P increase by a factor of n over a time period t:

$$dM/dt = nP - RM. \qquad (3)$$

If Eq. (3) is solved with the initial condition $M(0) \equiv M_0 = P/R$,

$$M/M_0 = (1 - n) \exp(-Rt) + n. \qquad (4)$$

This relationship depicts the change of water-column ^{10}Be inventory in response to the input change. It is illustrated in Figure 4 by the example cited earlier: a twofold increase ($n = 2$) of ^{10}Be input over a zero-field period of 1000 yrs. This increase results in an increase of 1.6 times M at the end of the period.

What are the corresponding changes of ^{10}Be concentration in sediments? The flux of ^{10}Be in sediments can be written

$$F = RM. \tag{5}$$

If it is assumed that bioturbational mixing is rapid compared to sediment accumulation (so that within the mixing zone of L cm, the ^{10}Be concentration C is uniform), it becomes possible to use the following equation from Berger and Heath (1968):

$$dC/dt = (F - wC)/L, \tag{6}$$

where w is sedimentation rate (cm/yr).

At steady state,

$$C = F/w = P/w. \tag{7}$$

Again, let the system be initially at steady state (i.e., $C(0) \equiv C_0 = P/w$) and solve Eq. (6) for the zero-field period with a ^{10}Be production nP:

$$C/C_0 = w(1 - n)/(w - RL) \exp(-Rt) + (1 - n)[1 - w/(w - RL)] \exp(-wt/L) + n. \tag{8}$$

As shown in Figure 4, if $L = 7$ cm, $n = 2$, and $R = 10^{-3}$/yr., a zero-field period of 1000 yr. gives rise to a merely 16% increase of the ^{10}Be concentration in Hole 578 sediments near the Brunhes/Matuyama boundary ($w = 3.5$ cm/10^3 yr.). Matching the 54% increase as observed requires (with the given values for L and R) a zero-field period of 1500 yr. with $n = 3$, or of 3000 yr. with $n = 2$ (Fig. 4).

In light of the discussion above, further detailed measurements at intervals of 5 to 10 cm near and above the level of 26.90 m in Hole 578 are warranted to determine whether the high ^{10}Be signal at that level has indeed recorded the geomagnetic reversal event. We believe that it may be possible to infer from these measurements information regarding the intensity and duration of the geomagnetic field at reversal, depth-lag, and/or the thickness of the bioturbated zone.

CONCLUSIONS

Use of ^{10}Be as a geochronometer for marine sediments has been successfully tested against the paleomagnetic reversal time scale for the past 2.5 m.y. (Tanaka et al., 1977; Inoue and Tanaka, 1979). The high-sensitivity ^{10}Be analysis afforded by nuclear accelerator mass spectrometry enables us to demonstrate that the ^{10}Be geochronology can be extended to about 15 m.y. ago. Our measurements on sediments from Sites 576 and 578 show a correlation between ^{10}Be ages and magnetostratigraphy of ±15% or better. The high ^{10}Be concentration found in Sample 576-5-1, 148 cm may be evidence of an elevated oceanic ^{10}Be flux prior to ~7 m.y. ago; high concentrations have also been found in manganese crusts. The potential of this long-lived radioberyllium as a tracer for cosmic-ray intensity changes during a geomagnetic field reversal is explored. The data on hand are somewhat too limited to permit any except tentative conclusions. Nevertheless, they strongly suggest that the search for an increase of ^{10}Be concentration in marine sediments recording geomagnetic reversals is warranted. If the high ^{10}Be concentration found at 26.90 m in Hole 578 proved to record a higher production of the isotope during the Brunhes/Matuyama reversal, then the data would imply that the duration of the reduction in dipole intensity during the reversal was not much longer than a few thousand years and that the depth-lag for the "freezing" of magnetization in Hole 578 sediments is no more than the normal bioturbated interval of 5 to 10 cm.

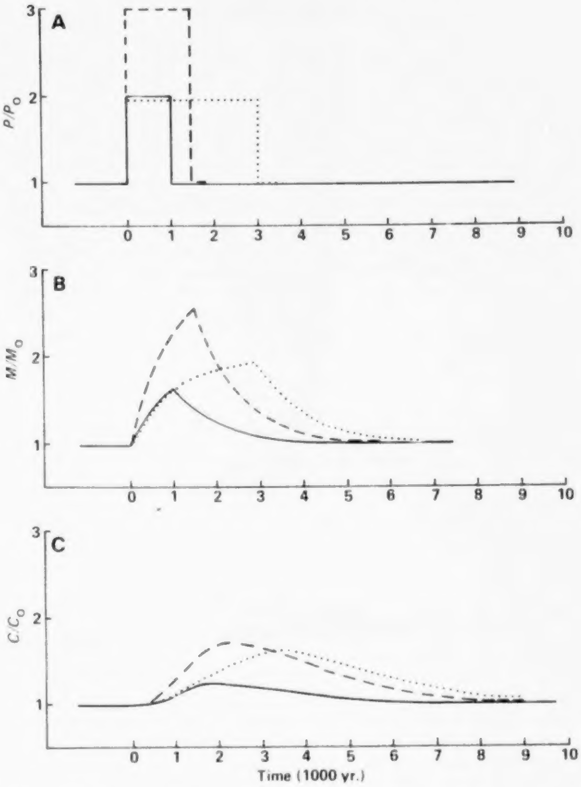

Figure 4. Relationship among changes in (A) ^{10}Be input P, (B) water-column ^{10}Be inventory M, and (C) ^{10}Be in sediments C. Calculations are done using oceanic ^{10}Be scavenging constant $R = 10^{-3}$ per year, sedimentation rate $w = 3.5$ cm/1000 yr. and bioturbated mixed layer thickness $L = 7$ cm. Three cases with respect to the duration (Δt) and increase (n) in ^{10}Be production are shown: solid line: $\Delta t = 1000$ yr., $n = 2$; dashed line: $\Delta t = 1500$ yr., $n = 3$; and dotted line: $\Delta t = 3000$ yr., $n = 2$. The latter two cases will give rise to the observed 54% increase in ^{10}Be concentration in Hole 578 sediments near the Brunhes/Matuyama boundary. Note a time lag of about 500 yr. for the peaks in Figure 4C relative to those of Figure 4B. The lag is mainly a function of L. The zero-subscripts for P, M, and C denote the unperturbed conditions, that is, the steady-state properties prior to the ^{10}Be production increase.

ACKNOWLEDGMENTS

We are grateful to Dr. G. Ross Heath for his encouragement and assistance on the project. We also thank the McMaster University Tandem Accelerator Laboratory for technical support, Emil W. Jalajas for the Ca analyses and microscopic and X-ray examination of Sample 578-4-3, 50 cm, the DSDP personnel (particularly Amy B. Altman) for sampling the cores, and Pamela Ku for assistance in drafting. This manuscript was reviewed by Kirk Cochran and David Kadko. Funding was provided by the NSF (Grants OCE-8217914 and -8303031) and the Canadian NSERC. In addition, TLK is indebted to the John Simon Guggenheim Foundation for fellowship support and to the Franco-American Commission for Educational Exchange for a Fulbright Senior Scholarship while in residence at Centres des Faibles Radioactivités, (CFR), where the manuscript was prepared. To Dr. Claude Lalou and Dr. Jacques Labeyrie of CFR: a word of deep appreciation for their hospitality.

REFERENCES

Amin, B. S., Lal, D., and Somayajulu, B. L. K., 1975. Chronology of marine sediments using the ^{10}Be method: Intercomparison with other methods. *Geochim. Cosmochim. Acta*, 39:1187–1192.

Arnold, J. R., 1956. Beryllium-10 produced by cosmic rays. *Science*, 124:584–585.

Berger, W. H., and Heath, G. R., 1968. Vertical mixing in pelagic sediment. *J. Mar. Res.*, 26:134–143.

Black, D. I., 1967. Cosmic ray effects and faunal extinctions at geomagnetic field reversals. *Earth Planet. Sci. Lett.*, 3:225–236.

Cox, A., Hillhourse, J., and Fuller, M., 1975. Paleomagnetic records of polarity transitions, excursions, and secular variations. *Rev. Geophys. Space Phys.*, 13:185–189.

Dymond, J., 1969. Age determination of deep-sea sediments: A comparison of three methods. *Earth Planet. Sci. Lett.*, 6:9–14.

Finkel, R., Krishnaswami, S., and Clark, D. L., 1977. ^{10}Be in Arctic Ocean sediments. *Earth Planet. Sci. Lett.*, 35:199–204.

Goel, P. S., Kharkar, D. P., Lal, D., Narasappaya, N., Peters, B., and Yatirajam, V., 1957. The beryllium-10 concentration of deep sea sediments. *Deep-Sea Res.*, 4:202–210.

Gove, H. E., 1981. Ultrasensitive mass spectrometry with a tandem Van de Graaff accelerator. *Proc. Symp. Accelerator Mass Spectrom.*: Argonne, Ill. (Argonne Natl. Lab.), pp. 16–22.

Harrison, C. G. A., and Somayajulu, B. L. K., 1966. Behavior of earth's magnetic field during a reversal. *Nature* (London), 212: 1193–1195.

Inoue, T., and Tanaka, S., 1976. ^{10}Be in marine sediments. *Earth Planet. Sci. Lett.*, 29:155–160.

________, 1979. ^{10}Be in marine sediments, earth's environment and cosmic rays. *Nature* (London), 277:209–210.

Kawai, N., Yaskawa, K., Nakajima, T., Torii, M., and Natsuheva, N., 1975. Voice of geomagnetism from Lake Biwa. *In* Horie, S. (Ed.), *Paleolimnology and the Japanese Pleistocene*, (Vol. 3): Kyoto (Kyoto Univ. Press), 143–158.

Ku, T. L., Kusakabe, M., Huh, C. A., Nelson, D. E., Southon, J. R., Vogel, J., Korteling, R. G., Reyss, J. L., and Duplessy, J. C., 1982. Studies of beryllium-10 in the marine environment. *Abs. 5th Internat. Conf. on Geochronology, Cosmochronology, Isotope Geology* (Nikko Natl. Park, Japan): Geochem. Soc. Japan, pp. 196–197.

Ku, T. L., Kusakabe, M., Nelson, D. E., Southon, J. R., Korteling, R. G., Vogel, J., and Nowikow, I., 1982. Constancy of oceanic deposition of ^{10}Be as recorded in manganese crusts. *Nature* (London), 299:240–242.

Ku, T. L., Omura, A., and Chen, P. S., 1979. Be^{10} and U-series isotopes in manganese nodules from the central North Pacific. *In* Bischoff, J. L., and Piper, D. Z. (Eds.), *Marine Geology and Oceanography of the Pacific Manganese Nodule Province*: New York (Plenum), pp. 791–814.

Measures, C. I., and Edmond, J. M., 1982. Beryllium in the water column of the central North Pacific. *Nature* (London), 297:51–5

Mughabghab, S. F., and Garber, D. I., 1973. Neutron cross-sect
Brookhaven National Laboratory Report 325, 3rd ed., Vol. 1

Muller, R. A., 1977. Radioisotope dating with a cyclotron. *Scie*
196:489–494.

O'Brian, K., 1979. Secular variation in the production of cosmog
isotopes in the earth's atmosphere. *J. Geophys. Res.*, 84:423-4

Peters, B., 1955. Radioactive beryllium in the atmosphere and on
earth. *Proc. Indian Acad. Sci., Sect. A*, 41:67–71.

Raisbeck, G. M., Yiou, F., Fruneau, M., and Loiseaux, J. M., 19
Beryllium-10 mass spectrometry with a cyclotron. *Science*, 2
215–217.

Raisbeck, G. M., Yiou, F., Fruneau, M., Loiseaux, J. M., Lieu
M., Ravel, J. C., and Hays, J., 1979. A search in a marine se
ment core for ^{10}Be concentration variations during a geomagn
field reversal. *Geophys. Res. Lett.*, 6:717–719.

SAMS, 1981. *Proc. Symposium on Accelerator Mass Spectromet*
Argonne, Ill. (Argonne Natl. Lab).

Somayajulu, B. L. K., 1977. Analysis of causes for the beryllium-
variations in deep-sea sediments. *Geochim. Cosmochim. Acta*, 4
909–913.

Southon, J. R., Vogel, J. S., Nowikow, I., Nelson, D. E., Kortelin
R. G., Ku, T. L., Kusakabe, M., and Huh, C. A., 1983. The me
surement of ^{10}Be concentrations with a tandem accelerator. *Nuc*
Instrum. Methods, 205:251–257.

Tanaka, S., and Inoue, T., 1979. ^{10}Be dating of North Pacific sediment cores up to 2.5 million years B. P. *Earth Planet. Sci Lett.*, 45:
181–187.

________, 1980. ^{10}Be evidence for geochemical events in the North Pacific during the Pliocene. *Earth Planet. Sci. Lett.*, 49:34–38.

Tanaka, S., Inoue, T., and Huang, Z. Y., 1982. ^{10}Be and ^{10}Be/^{9}Be in near Antarctica sediment cores. *Geochem. J.*, 16:321–325.

Tanaka, S., Inoue, T., and Imamura, M., 1977. The ^{10}Be method of dating marine sediments — comparison with the paleomagnetic method. *Earth Planet. Sci. Lett.*, 37:55–60.

van Andel, T. H., Heath, G. R., and Moore, T. C., Jr., 1975. Cenozoic history and paleoceanography of the central equatorial Pacific Ocean. *Mem. Geo. Soc. Am.*, 143.

Yiou, F., and Raisbeck, G. M., 1972. Half life of ^{10}Be. *Phys. Rev. Lett.*, 29:372–375.

Yokoyama, Y., Guichard, F., Reyss, J. L., and Van, N. H., 1978. Oceanic residence times of dissolved beryllium and aluminum deduced from cosmogenic tracers ^{10}Be and ^{26}Al. *Science*, 201:1016–1017.

Date of Initial Receipt: 10 January 1984
Date of Acceptance: 6 June 1984

PART IV: SEDIMENTOLOGIC AND GEOCHEMICAL STUDIES

23. MINERALOGY AND DIAGENESIS: THEIR EFFECT ON ACOUSTIC AND ELECTRICAL PROPERTIES OF PELAGIC CLAYS, DEEP SEA DRILLING PROJECT LEG 86[1]

J. Schoonmaker, F. T. Mackenzie, M. Manghnani, R. C. Schneider, D. Kim, A. Weiner, and J. To,
University of Hawaii[2]

ABSTRACT

Analysis of pelagic clay samples from Sites 576, 578, and 581 shows that physical, acoustic, and electrical trends with increasing burial depth are related to mineralogical and diagenetic changes. The properties of interest are bulk density (ρ), porosity (Φ), compressional-wave velocity (V_p) and velocity anisotropy (A_p), and electrical resistivity (R_o) and resistivity anisotropy (A_r). In general, as demonstrated in particular for the brown pelagic clay, the increase in ρ, V_p, R_o, and to a lesser extent A_p and A_r, with increasing depth is primarily caused by decreasing Φ (and water content) as a result of compaction.

The mineralogy and chemistry of the pelagic clays vary as a function of burial depth at all three sites. These variations are interpreted to reflect changes in the relative importance of detrital and diagenetic components. Mineralogical and chemical variations, however, play minor roles in determining variations in acoustic and electrical properties of the clays with increasing burial depth.

INTRODUCTION

This chapter is part of a continuing effort to relate sedimentary and diagenetic conditions of deposition and lithification of sediments to the physical, acoustic, and electrical properties of the sediments (e.g., Manghnani, et al., 1980). Our main purpose is to develop predictive physical-property models of sediment sequences in ocean basins and to correlate these with available seismic measurements. Both geological and geophysical approaches must be applied to the development of predictive models for ocean sediment. By a predictive model we mean one in which the important geophysical parameters, namely density (ρ), porosity (Φ), compressional velocity (V_p), shear velocity (V_s), Poisson's ratio (σ), velocity anisotropy (A_p, A_s), attenuation (Q_p^{-1}, Q_s^{-1}), electrical resistivity (R_o), and resistivity anisotropy (A_r), can be estimated along a depth axis in a sediment sequence between the seafloor and the basaltic basement for a given latitude and longitude. These geophysical parameters are a function of the sedimentologic, paleoceanographic, and diagenetic processes leading to the formation of these sediment sequences.

In this chapter, laboratory measurements are reported for density, compressional velocity and velocity anisotropy, resistivity and resistivity anisotropy, chemistry, and mineralogy of Leg 86 sediment samples, particularly pelagic clays. Although values for some of these parameters are reported elsewhere in this volume, our purpose was to determine physical, chemical, and mineralogical properties by a cooperative group of investigators in the same laboratory on the same samples. Some measurements, such as shear velocity, are still in progress at the time of this writing. The measured geophysical parameters of the sedimentary sequences at Deep Sea Drilling Project (DSDP) Sites 576, 578, and 581 are evaluated in light of sediment burial depth (compaction), age, and diagenetic stage as interpreted from sediment chemistry and mineralogy. Emphasis is placed on the pelagic clay within these sequences.

On Leg 86, a series of sites were sampled in the Northwest Pacific Basin, which is essentially an abyssal plain removed from significant riverine terrigenous sediment input (Fig. 1). Hydraulic piston coring at Site 576 was designed to sample the regional, laterally uniform, surface, acoustically "transparent" layer for studies of the origin and geotechnical properties of the pelagic clay making up the layer. Hole 576 penetrated a 55-m section of Tertiary pelagic clay underlain by Cretaceous interbedded calcareous ooze and pelagic clay (Fig. 2). The "type" pelagic clay section can be subdivided into two subunits, the upper having a considerable eolian component and the lower having a significant authigenic component (see Site 576 chapter, this volume).

Holes 578 and 581 penetrated thicker sections of Tertiary pelagic sediment, including interbedded siliceous clay, volcanic ash, and "type" pelagic clay overlying Cretaceous chert. Hole 578 was sampled by hydraulic piston coring; Hole 581 was cored using conventional rotary drilling methods. The fact that all three holes penetrated a section of relatively homogeneous pelagic clay, termed "slick" in the initial DSDP Hole Summary (unpublished data), is of particular interest. This unit is found at increasing stratigraphic depth from Site 576 to 578 to 581. Thus, it is a particularly useful horizon for study of the effects of physical compaction on acoustic and electrical properties, as opposed to effects of sediment mineralogy and diagenesis. It was anticipated that

---

[1] Heath, G. R., Burckle, L. H., et al., *Init. Repts. DSDP*, 86: Washington (U.S. Govt. Printing Office).

[2] Addresses: (Schoonmaker) Hawaii Institute of Geophysics, University of Hawaii, Honolulu, HI 96822; (Mackenzie) Hawaii Institute of Geophysics and Department of Oceanography, University of Hawaii, Honolulu, HI 96822; (Manghnani) Hawaii Institute of Geophysics and Department of Geology and Geophysics, University of Hawaii, Honolulu, HI 96822; (Schneider) Department of Oceanography, University of Hawaii, Honolulu, HI 96822; (Kim, Weiner, To) Department of Geology and Geophysics, University of Hawaii, Honolulu, HI 96822.

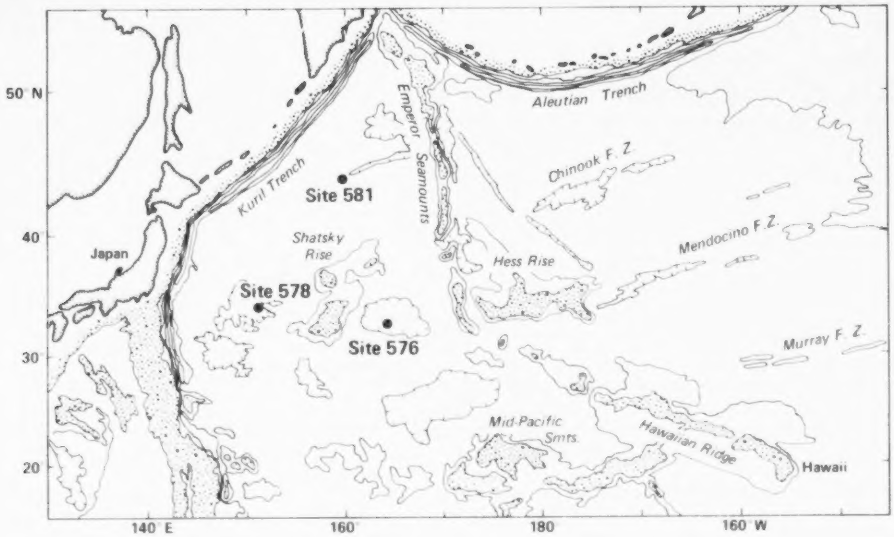

Figure 1. Location of Sites 576, 578, and 581 visited during DSDP Leg 86.

the sedimentary sequences of Holes 576, 578, and 581, including the "slick" clay layer, might be dominated by eolian and current-transported fine-grained detritus. If so, the "slick" pelagic clay would be an ideal unit to determine the effects of simple compaction on deep-sea muds. To our knowledge, there are no hiatuses within the sediment sequences studied that could complicate the interpretation of depth trends as discussed in this chapter.

It is generally known that the porosity of sediment increases with decreasing grain size. As shown by Hamilton et al. (1982) for pelagic and hemipelagic sediments, this relationship shows a large amount of scatter. This scatter is due to other factors (e.g., sorting, grain shape, grain packing, and mineralogy) that are interrelated and that all influence porosity. It appears that the primary reason for the high initial porosity of muds is their microstructure or fabric. In clay-rich sediments, clay mineral platelets adhere to one another in a face-to-face arrangement forming books or packets. Depending on the amount of clay, the initial sediment depositional fabric will vary somewhat. In most hemipelagic and pelagic mudstones, however, the plates, packets, and clay flocs will be randomly oriented and interlinked in a "house of cards" fashion leading to initially high porosities. Upon burial and compaction, the links or chains between clay packets fail and the particles orient under the overburden pressure with long axes normal to pressure. This preferred orientation of clay minerals with increasing burial depth should lead to increasing anisotropy in acoustic velocity and electrical resistivity of the sediment with increase in depth.

It will be shown that the mineralogy and chemistry of the sedimentary sequences of Holes 576, 578, and 581 vary with burial depth and that there is evidence for diagenetic reactions occurring, particularly in the "slick" clay zone. Regardless, it appears that most variations in the acoustic and electrical properties of the pelagic clay can be attributed to compactional effects such as reo ganization of clay platelets.

METHODS

Sampling

The cores were sampled by cutting a 50-cm^3piece from the cente of the working half of the core. The samples were extracted with spatulas, wrapped carefully with plastic wrap, and stored in sealed bag with wet sponges to prevent dehydration. In our laboratory, cube were cut for acoustic and electrical property measurements. The trimmings from these cubes were used to determine chemistry and mineralogy.

Samples were taken at intervals of 5 to 10 m in Hole 576. The calcareous oozes from the hole were not sampled. Four samples were taken from the upper 110 m of Hole 578; the remainder of the hole wa sampled at 5- to 10-m intervals. Three samples were taken from the pelagic clay of Hole 581.

Mineralogy

Mineralogy was determined by X-ray diffraction. Samples for bulk mineralogy were dried at 70°C for 24 hr., gently crushed to homogeneity, and packed into an aluminum holder. For clay mineralogy, sample were first treated with 5% sodium hypochlorite (Chlorox) buffered t pH 9.5 with HCl to remove organic matter (Anderson, 1963). The les than 2-μm fraction was then separated by centrifugation. A slurry o the sample was settled on a glass slide and dried at room temperatur to produce an oriented sample. These slides were placed in an ethylen glycol atmosphere at 40°C for 24 hr. prior to X-ray diffraction to in sure full expansion of expandable clay minerals. An additional aliquo of the <2-μm sample was treated to remove amorphous Fe-oxyhydrox ides with the Na citrate–Na dithionite method of Mehra and Jackso (1960). The presence of amorphous Fe-oxyhydroxides has been show to interfere with detection of clay minerals by X-ray diffraction, espe cially at very low 2θ angles (Risvet, 1978). Slides were prepared an glycolated as described above. All samples were analyzed on a Phillip Norelco X-ray diffractometer using Ni-filtered, CuKα radiation. Sam ples were scanned from 2 to 32°2θ at a rate of 2°2θ/min. The >2-μ fraction of selected samples was analyzed for zeolites, and the >20-μ fraction of a few samples was analyzed for feldspars by X-ray diffrac tion. To distinguish kaolinite and chlorite, and palygorskite and illit samples were scanned at 1/4°2θ/min. over the intervals 23–26°2θ an 7-10°2θ, respectively. Smectite, identified by its 17-Å (001) peak an the series of higher order peaks, was found in all cases to contain in terlayered illite. It is therefore referred to as mixed-layer illite/smectite or simply illite/smectite.

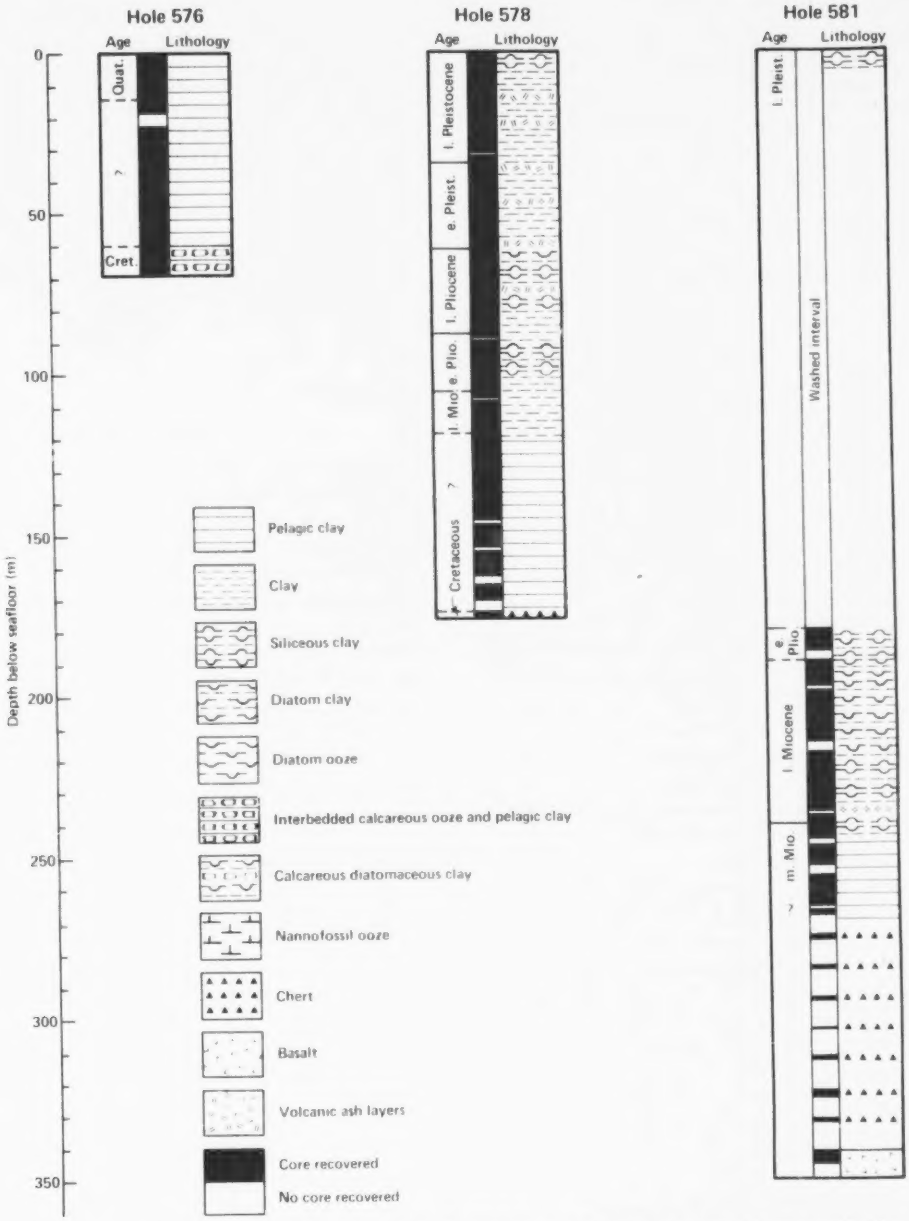
Hole 576
Age
Lithology
Quat.
?
Cret.
Hole 578
Age
Lithology
l. Pleistocene
e. Pleist.
l. Pliocene
e. Plio.
l. Mio.
?
Cretaceous
Hole 581
Age
Lithology
l. Pleist.
Washed interval
e. Plio.
l. Miocene
m. Mio
?
Depth below seafloor (m)
0
50
100
150
200
250
300
350
Pelagic clay
Clay
Siliceous clay
Diatom clay
Diatom ooze
Interbedded calcareous ooze and pelagic clay
Calcareous diatomaceous clay
Nannofossil ooze
Chert
Basalt
Volcanic ash layers
Core recovered
No core recovered

Figure 2. Age, core recovery, and lithostratigraphy for Holes 576, 578, and 581 (adapted from Introduction and Explanatory Notes, this volume).

Semiquantitative analysis of bulk-mineral composition followed the ethod of Schultz (1964). Using peak heights, and the factors for iartz, plagioclase + K-feldspar, total clay, and clinoptilolite, the sum these components was normalized to 100%. Minor constituents mitted from this calculation included halite (from seawater contamiition) and pyroxenes.

Clay-mineral abundances were calculated from peak areas measured y "the triangle method" of Mann and Fischer (1982). The weighting ictors of Mann and Müller (1979) were used, and the weighted areas f all clay peaks were summed to 100%. Quartz peaks, present in evry sample, were omitted in this calculation, as was clinoptilolite which as present in one sample. The percentages of kaolinite and chlorite ere determined by measuring the peak area at 12.3°2θ (kaolinite 001, hlorite 002), and using the peak heights at 24.9°2θ (kaolinite 002) and 25.2°2θ (chlorite 003) to assess the relative contribution of the two minerals (Biscaye, 1965; Mann and Müller, 1979).

The abundances of mixed-layer illite/smectite, discrete illite, and the summation of kaolinite + chlorite were also determined by the method of Hoffman (1976). In this method, peak heights rather than areas are used. In addition, the intensity of the illite/smectite 003/005 peak at about 3.35 Å, corrected using an empirical relationship between intensity and mixed-layer composition, is used to estimate percent mixed-layer clay. This is in contrast to the method of Mann and Müller (1979), which uses the area of the (001) smectite peak and a weighting factor which is a linear combination of the individual illite and smectite factors. Composition of the mixed-layer illite/smectite was determined by the methods of Hoffman (1976) and Reynolds and Hower (1970).

Chemistry

Bulk samples (2.5 g) were dried (70°C, 24 hr.), ground to a homogeneous powder, and rinsed and centrifuged three times in distilled water to remove sea-salt contamination. Major and trace elements (except silicon) were analyzed by inductively coupled plasma (ICP) after hydrofluoric-acid digestion. Silicon was analyzed by ICP after fusion with lithium metaborate.

Scanning Electron Microscopy

Pieces of bulk untreated samples were dried (70°C, 24 hr.), and small fragments were broken off to reveal fresh surfaces. These were mounted on scanning electron microscopy (SEM) sample holders and coated with carbon and gold-palladium before analysis.

Physical Properties

Bulk Density

The bulk densities of the sediments were determined from their weights and volumes. Sediment samples were cut by a slow-speed saw and ground to well-shaped cuboids with three sets of parallel faces for ultrasonic velocity measurements. The three dimensions of the cuboid were measured with a vernier gauge or micrometer to an accuracy of 0.001 cm.

Ultrasonic Velocity Measurements

The pulse-transmission technique (Birch, 1960) was used to measure compressional-wave velocities of the sediment. The apparatus, similar to the Hamilton-frame system (Boyce, 1976), consisted of a pulse generator, amplifier, and filter. A calibrated mercury delay line was used to measure transmission time of pulses in the specimen. 1-MHz lead zirconium titanate (PZT-4) transducers mounted in holders were placed against the sediment surfaces. Dow Resin 276-V9 was used as the acoustic coupler. A small weight (25 g) was placed on the transducer holder to provide good acoustic contact. The reported compressional velocity values are accurate to ± 2%.

Electrical Resistivity

The four-electrode resistivity method (Olhoeft, 1980), which has the advantage of eliminating electrode electrochemical polarization, was used for electrical resistivity measurements. Current leakage around the saturated sample was prevented by proper jacketing. The plexiglas sample holder was rectangular in shape to allow measurements of cuboid specimens. Two pairs of faces parallel and one pair of faces perpendicular to the bedding plane were prepared.

The resistivity of saturated samples (as received) was measured at 100 Hz with the Hewlett-Packard 4375B LCR meter. The applied current density was in the range 10^{-8} to 10^{-9} amp/m^2, within the linear range of measurement. The sensitivity of the resistivity measurements is up to three decimal places. The measured values are reproducible to ± 5%.

DATA

Mineralogy

Bulk Mineralogy

The pelagic clays of Sites 576, 578, and 581 are broadly similar in mineralogy and consist of varying amounts of clay minerals (mixed-layer illite/smectite, discrete illite, kaolinite, chlorite), quartz, feldspar, frequent palygorskite, rare zeolites, and amorphous material, probably primarily opaline silica. The quantitative bulk mineralogy, determined by X-ray diffraction, is given in Table 1; plots versus depth of percent total clay minerals, quartz, and feldspar are shown in Figure 3, and plots versus depth of clay to quartz ratio are shown in Figure 4. All depths for Hole 576 have been corrected following the format given in the Site 576 chapter (this volume).

Table 1. Mineralogy as determined by x-ray diffraction of bulk samples from DSDP Holes 576, 578, and 581.

Sample (interval in cm)	Sub-bottom depth (m)	Total clay (%)	Quartz (%)	Feldspar (%)	Clinoptilolite (%)	Phillipsite	X-ray amorphous material
576-1-1, 46-50	4.96-5.00	65	25	10			x
576-2-1, 109-116	8.29-8.36	74	19	7			x
576-2-6, 99-106	15.69-15.76	71	21	8			x
576-3-3, 109-115	13.69-13.75	69	22	9			x
576-4-2, 88-95	21.48-21.55	76	18	6			
576-4-5, 98-104	26.08-26.14	76	17	7			
576-5-1, 108-115	29.28-29.35	77	16	7			
576-5-6, 18-25	32.78-32.85	80	11	10		x	x
576-6-4, 37-44	36.27-36.34	86	9	5			
576-7-2, 130-137	46.90-46.97	85	10	6			
576-7-6, 19-26	51.79-51.86	83	11	6			
576-8-1, 98-105	55.08-55.15	82	11	7			
576-8-6, 81-84	62.41-62.44	85	10	6			
578-2-4, 38-45	9.68-9.75	65	20	15			x
578-5-3, 91-98	37.21-37.28	71	19	10			x
578-10-3, 91-98	87.71-87.78	70	21	9			x
578-13-1, 78-85	110.08-110.15	73	19	8			x
578-14-4, 53-60	123.83-123.90	79	15	6			x
578-15-2, 53-60	130.33-130.40	80	13	7			x
578-15-7, 28-34	137.58-137.64	81	13	6			
578-16-5, 67-74	144.47-144.54	84	10	6			x
578-17-2, 72-79	149.52-149.59	82	12	6			x
578-17-5, 61-68	153.91-153.98	85	9	6			
578-18-3, 38-45	160.18-160.25	81	14	5			
578-19-1, 57-64	166.87-166.94	82	12	6			
578-19-3, 53-60	169.83-169.90	81	14	6			
581-8-5, 65-72	245.15-245.22	83	11	6			
581-9-4, 33-40	252.83-252.90	81	10	6	3		
581-10-3, 44-51	260.94-261.01	83	11	6			

Note: x indicates mineral is present.

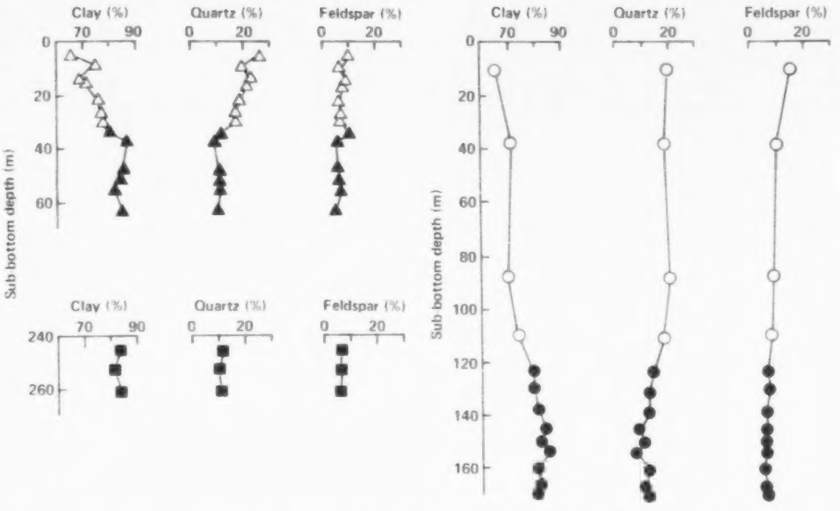

Figure 3. Bulk mineralogy of clay samples from Holes 576 (△), 578 (○), and 581 (□). Solid symbols indicate samples within the brown pelagic clay unit defined in the discussion section.

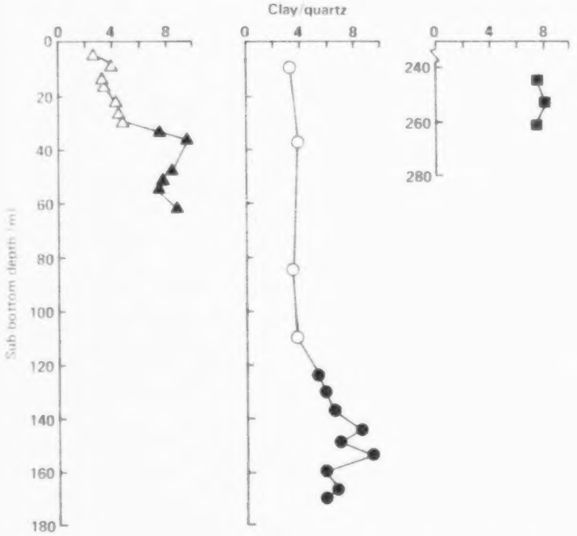

gure 4. Clay/quartz ratios of samples collected from DSDP Holes 576, 578, and 581. Symbols as in Figure 3.

anning-electron photomicrographs illustrating some of e minerals and their textures are shown in Plate 1.

Total clay-mineral contents of samples from Holes 576 d 578 increase with depth from near-surface values of 65% to high values of 80–85% at depth (Fig. 3). Quartz d feldspar contents vary inversely with clay mineral ntent. Near-surface pelagic clay samples contain about 0% quartz and between 8 and 15% feldspar, whereas e deeper pelagic clays generally contain about 10–12% uartz and 5–6% feldspar. The three samples analyzed om Hole 581 have bulk mineralogies very similar to amples from the deeper portions of Holes 576 and 578; hat is, they are rich in clay minerals and poor in quartz nd feldspar (Fig. 3). The depth trends of the clay/quartz ratios for the three sites (Fig. 4) emphasize the bulk mineralogical differences between pelagic clays of the upper and lower parts of the sites.

Clay Mineralogy

Mineralogies of the <2-μm size fraction of the samples are given in Table 2. We report the data for the samples from which amorphous Fe-oxyhydroxides were not removed to facilitate comparison of our results with those of other workers, the majority of whom do not remove amorphous iron compounds. The effect of Fe removal will be discussed later. Figures 5, 6, and 7 show the trends with depth of the relative amounts of the clay minerals (mixed-layer illite/smectite, illite, kaolinite, chlorite, and palygorskite) normalized to 100%. Although the amounts of non-clay minerals were not determined quantitatively, it is important to note that significant amounts of quartz and lesser amounts of feldspar are present in virtually every <2-μm sample (see Table 2).

X-ray diffractograms were quantified using two methods. The solid lines in Figures 5, 6, and 7 indicate the values obtained using measured peak areas and the factors of Mann and Müller (1979). These are also the data given in Table 2. The dashed lines for percent illite/smectite and illite in Figures 5, 6, and 7 indicate data obtained by using the quantification technique of Hoffman (1976), modified to account for the presence of quartz in the clay samples. Depth trends obtained by using the two methods are generally quite similar, although the Hoffman technique usually results in lower estimates of percent mixed-layer illite/smectite.

Samples of the <2-μm fraction were also analyzed after amorphous Fe-oxyhydroxide removal. These patterns were quantified according to both the Mann and Müller (1979) and the Hoffman (1976) techniques and the results compared to those shown in Figures 5, 6, and 7. With very few exceptions, the removal of Fe-oxyhydroxides enhanced the illite/smectite peaks, resulting in

Table 2. Mineralogy of the <2-μm size fraction.

Sample (interval in cm)	Sub-bottom depth (m)	ML (%)	Illite (%)	Kaolinite (%)	Chlorite (%)	Palygorskite (%)	Quartz	Feldspar	Clinoptilolite	X-ray amorphous material	*Z*
576-1-1, 46-50	4.96-5.00	43	37	7	13		x	x		x	48
576-2-1, 109-116	8.29-8.36	52	37	4	7		x	x			43
576-2-6, 99-106	15.69-15.76	61	31	4	5		x	x		x	30
576-3-3, 109-115	13.69-13.75	57	35	3	5		x	x		x	33
576-4-2, 88-95	21.48-21.55	52	36	5	7		x	x			35
576-4-5, 98-104	26.08-26.14	48	37	6	9		x	x			33
576-5-1, 108-115	29.28-29.35	60	30	4	6		x	x			38
576-5-6, 18-25	32.78-32.85	61	28	4	6		x	x			28
576-6-4, 37-44	36.27-36.34	66	24	4	5	1	x			x	20
576-7-2, 130-137	46.90-46.97	64	28	3	4	2	x				30
576-7-6, 19-26	51.79-51.86	65	25	4	4	3	x	x		x	33
576-8-1, 98-105	55.08-55.15	59	31	3	4	3	x	x		x	40
576-8-6, 81-84	62.41-62.44	61	32	2	2	3	x	x		x	35
578-2-4, 38-45	9.68-9.75	65	23	4	8		x	x		x	40
578-5-3, 91-98	37.21-37.28	54	32	5	9		x	x		x	38
578-10-3, 91-98	87.71-87.78	57	31	4	8		x	x			33
578-13-1, 78-85	110.08-110.15	70	24	3	3		x	x		x	43
578-14-4, 53-60	123.83-123.90	71	22	3	3		x	x			28
578-15-2, 53-60	130.33-130.40	71	24	2	2		x	x			18
578-15-7, 28-34	137.58-137.64	72	19	5	4		x	x			23
578-16-5, 67-74	144.47-144.54	65	17	8	10		x	x			23
578-17-2, 72-79	149.52-149.59	68	19	7	6	1	x	x			33
578-17-5, 61-68	153.91-153.98	59	24	7	9	1	x	x		x	25
578-18-3, 38-45	160.18-160.25	47	37	5	5	6	x	x			40
578-19-1, 57-64	166.87-166.94	48	34	5	6	6	x	x			40
578-19-3, 53-60	169.83-169.90	62	29	3	3	4	x	x			38
581-8-5, 65-72	245.15-245.22	77	20	2	1		x	x			28
581-9-4, 33-40	252.83-252.90	78	19	2	1		x	x	x		25
581-10-3, 44-51	260.94-261.01	54	35	0	11		x	x			30

Note: Values obtained using measured peak areas and the factors of Mann and Muller (1979). ML = mixed-layer illite/smectite, x indicates mineral is present, *Z* = percentage of illite interlayers in illite/smectite.

increased calculated percentages of illite/smectite and correspondingly lower percentages of all other clay minerals present. Similar effects of chemical pretreatment on X-ray intensities have been noted by Brewster (1980). This effect was more dramatic when the Mann and Müller quantification method was used because of the significant enhancement of the low 2θ (001) peak for illite/smectite. Values of percent illite/smectite were increased by 15 to 20% for the Mann and Müller method and by 0 to 10% for the Hoffman method when amorphous Fe-oxyhydroxides were removed. Although all methods are admittedly semiquantitative, the significant influence of chemical pretreatments on the results makes interpretation of clay data even more difficult. It is interesting to note, however, that the removal of amorphous Fe-oxyhydroxides did not affect the interpretation of the amount of illite layers in the mixed-layer illite/smectite phase. Comparison of the various results presented here illustrates the need for standardized procedures in quantification of clay mineralogy, especially for mixed-layer clay minerals, from X-ray diffraction data.

There is a very general trend of increasing percent illite/smectite with depth in Hole 576 (Fig. 5). Two regions of particularly high mixed-layer clay mineral content (about 16 m and 36-52 m sub-bottom) are superimposed on this general trend. Furthermore, samples of high mixed-layer content tend to have illite/smectite with fewer illite interlayers.

Discrete illite content declines with depth in Hole 576 and mirrors the pattern of mixed-layer content. Kaolinite and chlorite percentages both decrease with depth in Hole 576 (Fig. 5). Palygorskite was first detected in X-ray diffractograms of samples from a depth of about 36 m sub-bottom, and increases in concentration were detected to the base of Hole 576.

The percentage of mixed-layer illite/smectite appears to oscillate somewhat with depth at Site 578, with a pronounced zone of maximum percent mixed-layer clay from about 110 to 145 m sub-bottom. The composition of the mixed-layer clay mineral (given as % illite interlayers, Fig. 6) again tends to reflect the quantity of illite/smectite, as in Hole 576. In general, mixed-layer, clay-mineral-rich sediment samples have fewer illite interlayers in the illite/smectite. As was also the case for Hole 576, the depth trend of discrete illite mirrors that of mixed-layer illite/smectite (Fig. 6). Kaolinite and chlorite percentages decrease slightly with depth down to about 130 m sub-bottom. Below this depth the concentrations of both minerals increase sharply to roughly 8% kaolinite and 10% chlorite and then decline again to the bottom of the hole. Palygorskite first appears in X-ray patterns of sediments at a depth of about 150 m and increases in percentage downhole (Fig. 6).

The relative percentages of mixed-layer illite/smectite, illite, kaolinite, and chlorite at Site 581 are similar to those found in samples from Holes 576 and 578 (cf. Figs. 5, 6, and 7). The shift from high mixed-layer and low illite content to the reverse with depth in Hole 581 is similar to the depth profile of Hole 578 between 140 and 150 m. The high chlorite content of the sample from Section 581-10-3 (the deepest sample from Hole 581) is also consistent with the depth variations in Hole 578, al-

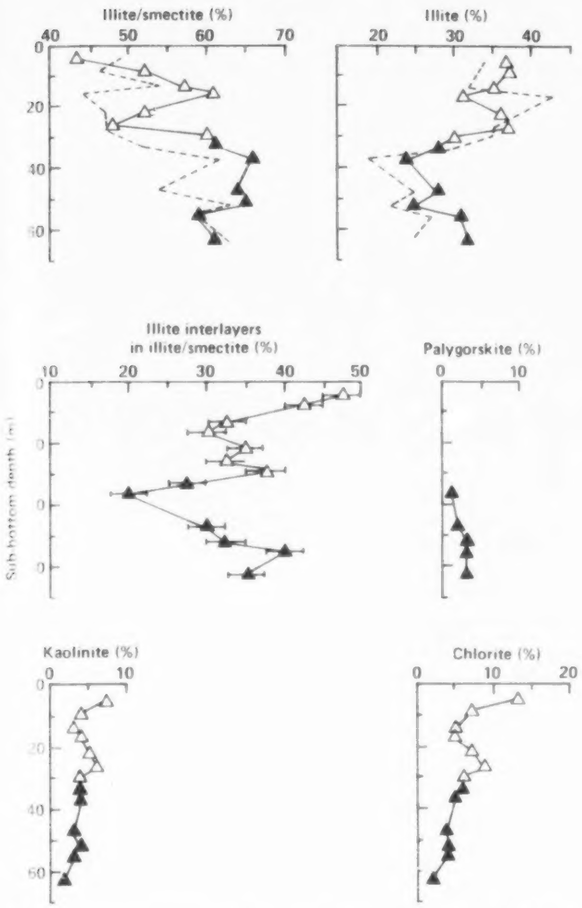

Figure 5. Clay mineralogy of the < 2-μm size fraction of samples from Hole 576. Symbols as in Figure 3. Significance of solid and dashed lines is discussed in text.

though the disappearance of kaolinite in Hole 581 is different. No palygorskite was detected in X-ray diffraction patterns of samples from Hole 581.

Chemistry

Analyses of major and trace-element concentrations were made for selected samples; these data are given in Table 3. In general, the chemical compositions of all pelagic clays from the three sites studied are similar, although significant depth trends are evident for nearly all elements in Holes 576 and 578. The chemistry of the two samples from Hole 581 is similar to that of samples from below about 130 m sub-bottom in Hole 578.

The depth profiles of weight percent Al_2O_3 and SiO_2 in Holes 576 and 578 are shown in Figure 8. The percent SiO_2 after subtraction of the SiO_2 in quartz as determined by X-ray diffraction represents SiO_2 in other silicate minerals. No attempt was made to quantify the percent SiO_2 in opaline silica, although it appears to be a minor component in all but a few samples.

In Hole 576, Al_2O_3 decreases slightly downhole from about 16.5 to 14%, with a maximum of over 17% in the intermediate depth range of 20–30 m sub-bottom. Total SiO_2 decreases downhole from about 58 to 48% in Hole 576, although *non-quartz* SiO_2 initially increases, then decreases slightly, with depth. The depth trends of decreasing percent Al_2O_3 and increasing percent non-quartz SiO_2 are consistent with the trends in clay mineralogy noted earlier (Fig. 5). Smectite has a higher Si/Al ratio than illite, and the general increase in percent illite/smectite and decline of percent illite with depth in Hole 576 are reflected in the changes in percent Al_2O_3 and percent non-quartz SiO_2.

In Hole 578, Al_2O_3 increases slightly with depth to a maximum of 17.5% at about 138 m sub-bottom, then decreases to the bottom of the hole (Fig. 8). SiO_2 decreases downhole from about 60 to 40%, then increases near the base of the hole. Corrected for quartz, the SiO_2 profile appears fairly uniform with depth, perhaps decreasing slightly downhole (Fig. 8). The presence of small amounts of volcanic glass and siliceous microfossils in the upper 120 m of Hole 578, as noted in smear slides (see Site 578 chapter, this volume), would result in higher SiO_2 and lower Al_2O_3 percentages. If a correction to the percent SiO_2-profile were made to account for these components, the depth trends would probably be more similar to those from Hole 576. Without corrections for volcanic glass and siliceous microfossils, it is difficult to relate the SiO_2 and Al_2O_3 contents to clay mineralogy, although the zone of high illite/smectite content between 110 and 150 m sub-bottom (Fig. 6) is also a region of relatively high percent non-quartz SiO_2 (Fig. 8).

The depth trends of other major elements are similar in Holes 576 and 578 (Table 3). Percentages of Fe_2O_3, K_2O, MgO, and MnO increase with depth at both sites. Several trace elements (Cu, Co, and Ni in both holes; Sr, Pb, and Zr in Hole 578 only) covary with MnO. Cr shows an antithetical relationship with MnO in Hole 578. The high percentages of Fe_2O_3, MnO, and associated trace elements probably reflect authigenic Fe and Mn oxyhydroxides. The increase of percent K_2O with depth is related to the changing abundance of illite. Illite is present both as a discrete phase and as illite interlayers in the mixed-layer illite/smectite. Percentage K_2O reflects the summation of percent discrete and interlayered illite (Fig. 9). The percentage of CaO initially decreases slightly with depth and then increases downhole in both holes. P_2O_5 in Hole 576 and Sr in Hole 578 tend to covary with CaO. The trends of percentage CaO are probably due to variable contents of biogenic calcite, and perhaps trace amounts of phillipsite in some samples, and to decreasing plagioclase feldspar contents with depth. Na_2O decreases in percentage downhole in both holes, reflecting the decline of feldspar content with depth.

The downhole variations of chemistry at all three sites are possibly most clearly demonstrated by the increase in metals associated with authigenic oxyhydroxides (Fe, Mn, Cu, Co, and Ni) and the decreases in Si. The trends with depth of these two parameters are indicated in Figure 10 by arrows pointing in the downhole direction for each site.

Physical Properties

Emphasis in this study was on the clay mineral-rich sediment of Sites 576, 578, and 581 and on evaluation

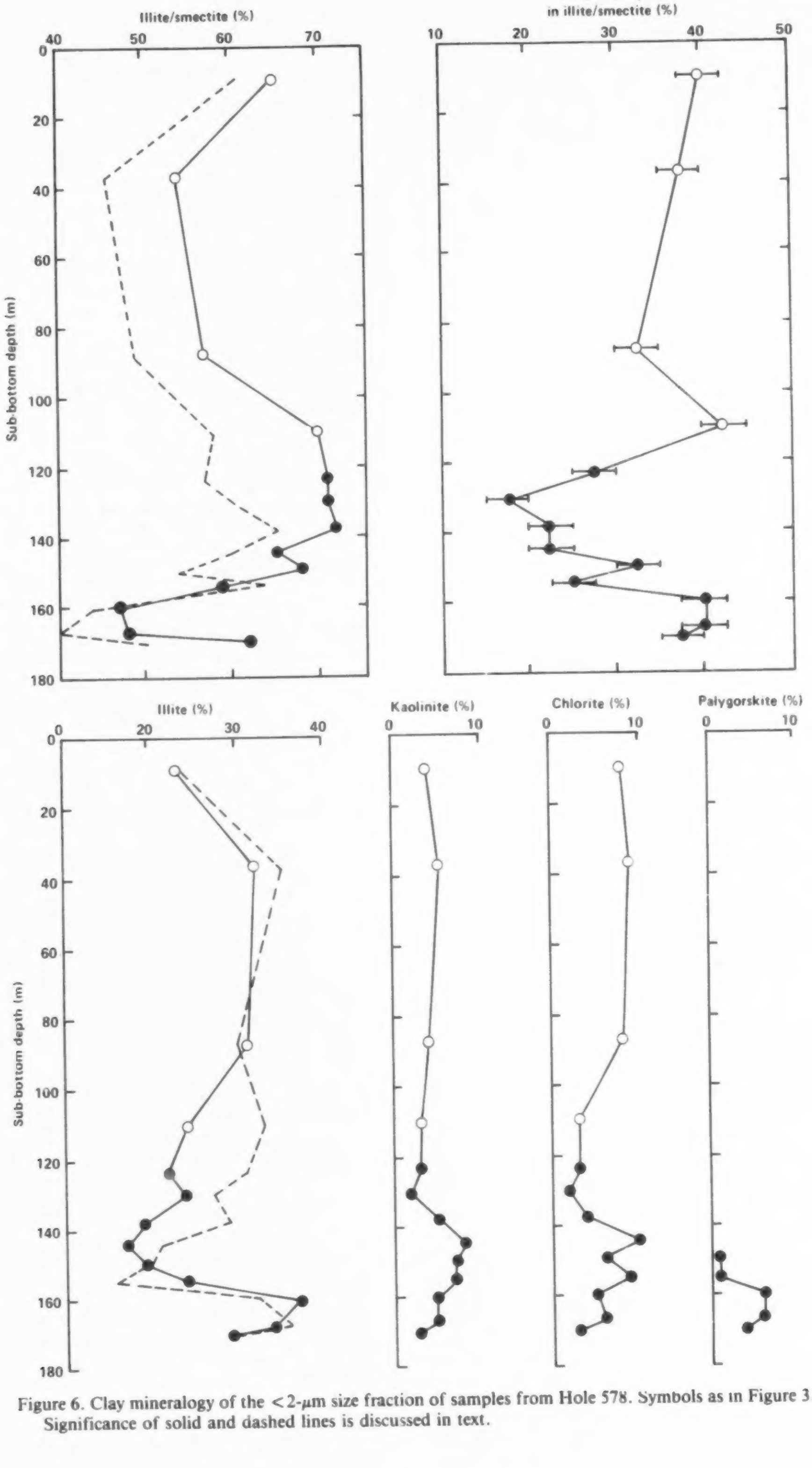

Figure 6. Clay mineralogy of the <2-μm size fraction of samples from Hole 578. Symbols as in Figure 3. Significance of solid and dashed lines is discussed in text.

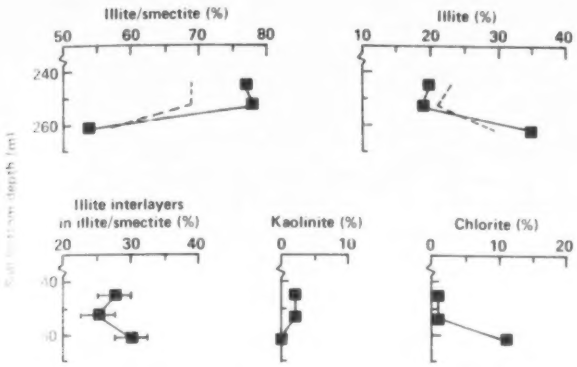

7. Clay mineralogy of the < 2-μm size fraction of samples from ole 581. Symbols as in Figure 3. Significance of solid and dashed es is discussed in text.

of vertical gradients in physical properties as a function of compaction of the pelagic clay sequences. Consequently, most of the data in this section are portrayed as a function of burial depth of the sediments. Futhermore, we will be concerned mainly with a unit of relatively homogeneous brown pelagic clay which is described in detail in the discussion section.

Bulk Density

Laboratory-determined saturated bulk densities of the clay samples are given in Table 4 and shown as a function of sub-bottom depth (equivalent to burial depth) in Figure 11. In general, bulk density increases with burial depth in all three holes. This density increase reflects a decrease in porosity, and thus water content, of the pelagic clay sediments with increasing burial depth (Schultheiss, this volume). The density variation of brown pelagic clay from Hole 576 to 578 to 581 is of particular interest. There appears to be within each hole, and be-

3. Concentrations of major and trace elements in selected bulk samples from Holes 576, 578, and 581.

mple l in cm)	Sub-bottom depth (m)	Major elements (%)										Trace elements (ppm)														
		Al_2O_3	Fe_2O_3	CaO	MgO	TiO_2	MnO	Na_2O	K_2O	P_2O_5	SiO_2	Be	Cr	Co	Cu	Pb	Ni	Ba	Sr	Th	Zr	V	Zn	Cd	Mo	Ag
46-50	4.96-5.00	16.4	7.45	0.96	2.93	0.743	0.445	1.78	3.30	0.11	57.2	2.2	56.4	42	143	35	66	619	140	35	113	134	113	< 7	< 30	< 5
99-106	15.69-15.76	16.1	7.08	0.30	3.12	0.729	0.703	1.50	3.16	0.10	58.3	2.3	70.0	59	205	80	98	735	126	21	109	129	117	< 7	< 30	< 5
88-95	21.48-21.55	17.1	7.77	0.78	3.14	0.768	0.943	1.53	3.46	0.10	53.4	2.5	70.9	84	246	40	121	594	130	26	133	145	134	< 7	< 30	< 5
108-115	29.28-29.35	17.3	8.23	0.76	3.27	0.806	1.35	1.42	3.51	0.16	54.0	2.4	55.8	148	280	50	192	525	137	34	160	143	168	< 7	< 30	< 5
18-25	32.78-32.85	16.2	8.21	1.12	3.04	0.791	2.48	1.59	3.40	0.37	50.5	2.2	39.0	297	418	55	388	438	173	41	180	135	178	< 7	< 30	< 5
19-26	51.79-51.86	15.3	8.19	2.31	3.29	0.721	1.89	0.868	4.05	1.35	49.4	2.1	31.6	164	226	50	242	481	173	38	180	132	184	< 7	< 30	< 5
98-105	55.08-55.15	14.0	8.61	2.27	3.33	0.751	3.41	0.875	4.36	1.25	47.7	2.4	29.7	298	300	75	463	611	241	53	219	168	249	< 7	< 30	6
38-45	9.68-9.75	14.3	6.60	1.49	2.57	0.656	0.104	1.91	2.71	0.08	59.7	1.7	66.6	< 3	75.8	15	41	741	137	< 6	83	122	96	< 7	< 30	< 5
91-98	37.21-37.28	14.8	6.76	1.31	2.52	0.641	0.0994	1.80	2.61	0.08	61.0	1.7	61.2	< 3	76.8	20	45	606	124	< 6	84	102	98	< 7	< 30	< 5
91-98	87.71-87.78	15.3	6.73	1.49	2.42	0.652	1.19	2.12	2.78	0.10	58.3	1.9	48.7	12	174	40	62	607	130	< 6	98	125	136	< 7	< 30	< 5
78-85	110.08-110.15	15.3	6.41	0.84	2.35	0.635	0.362	1.79	3.23	0.09	60.1	2.2	71.7	< 3	155	30	62	606	109	6	112	121	117	< 7	< 30	< 5
14-4, 53-60	123.83-123.90	17.0	7.08	0.73	3.06	0.695	0.663	1.48	2.86	0.09	55.0	2.2	65.7	10	168	30	81	551	104	6	114	111	126	< 7	< 30	< 5
15-2, 28-34	137.58-137.64	17.5	7.51	0.50	2.95	0.743	1.01	1.26	3.10	0.11	53.3	2.4	55.5	53	238	35	112	606	116	< 6	126	148	121	< 7	< 30	< 5
17-5, 61-68	153.91-153.98	15.9	8.65	1.35	2.98	0.749	3.69	0.926	3.08	0.62	46.6	2.0	30.6	356	309	70	469	426	262	< 6	197	142	217	< 7	< 30	< 5
38-45	160.18-160.25	16.4	7.38	0.70	3.66	0.703	1.20	0.750	3.91	0.33	53.6	2.2	67.3	36	134	45	207	378	132	< 6	137	119	133	< 7	< 30	< 5
53-60	169.83-169.90	15.4	7.46	1.93	3.14	0.691	1.53	0.896	3.99	1.05	52.1	2.0	40.6	125	218	50	264	524	190	10	179	129	172	< 7	< 30	< 5
581-8-5, 65-72	245.15-245.22	15.0	6.84	0.52	3.02	0.262	0.782	1.12	2.82	0.06	57.3	3.1	44.5	63	252	30	141	1700	106	32	59	108	140	< 7	< 30	< 5
44-51	260.94-261.01	17.5	6.98	0.60	3.28	0.629	2.44	1.25	3.67	0.23	51.5	2.7	37.7	243	331	50	364	736	214	51	170	123	174	< 7	< 30	< 5

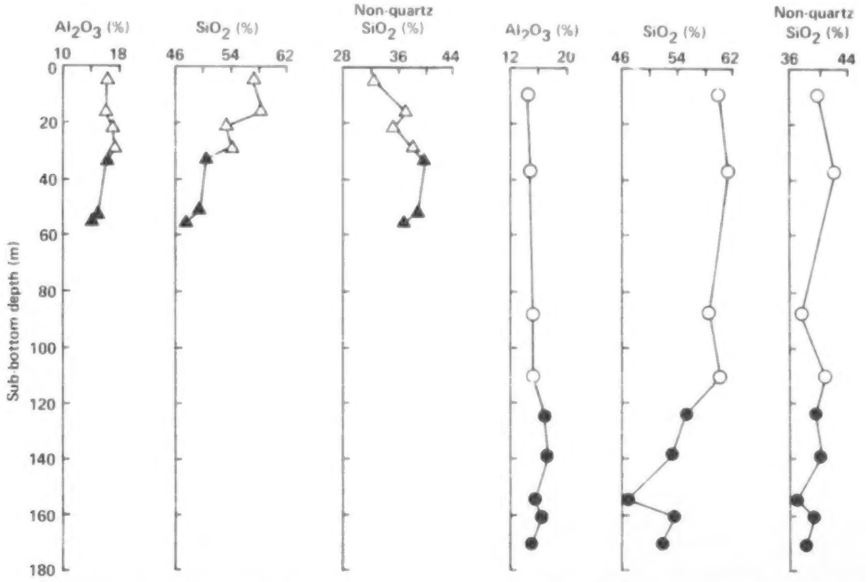

Figure 8. Percentage Al_2O_3, SiO_2, and non-quartz SiO_2 of samples from Holes 576 and 578. Symbols as in Figure 3.

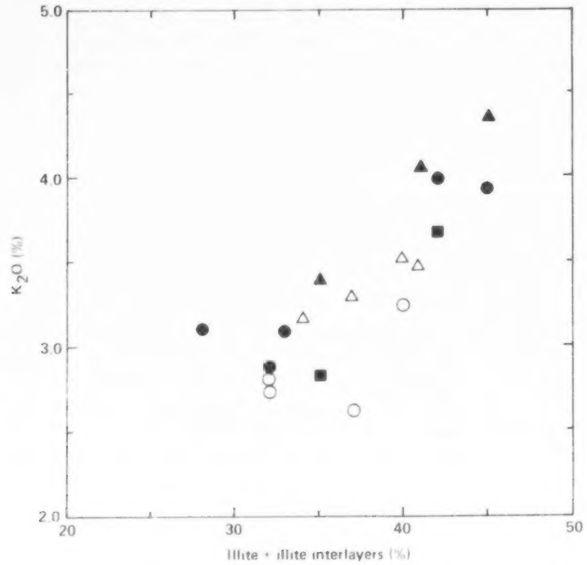

Figure 9. Percentage K_2O plotted versus the sum of percentage discrete illite and percentage illite interlayers in illite/smectite mixed-layer clay for bulk samples of clay-rich sediments from Leg 86. Symbols as in Figure 3.

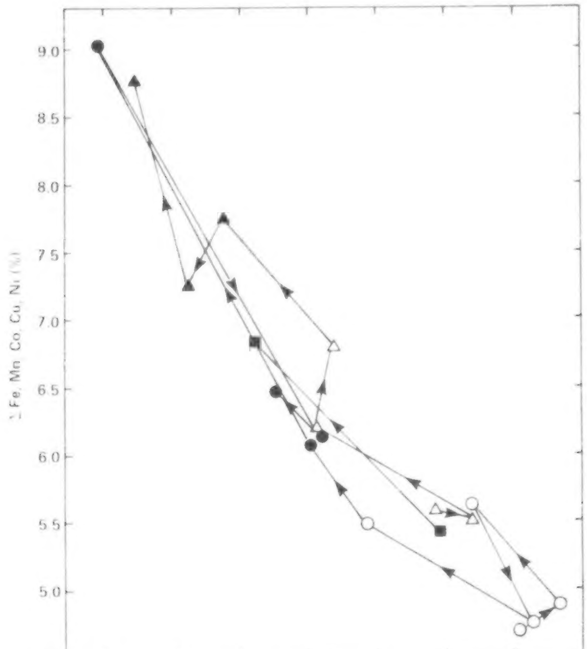

Figure 10. Summation of the metals Fe, Mn, Co, Cu, and Ni plotted versus percentage Si for the clay samples of Holes 576, 578, and 581. Lines with arrows connect data points for each hole; arrows point in a downhole direction, indicating the general increase in metal content and decrease in percentage Si downhole at all three sites. Symbols as in Figure 3.

tween holes, a general increase, perhaps non-linear, in density in this unit with increasing burial depth (Fig. 11). In Hole 581, however, the saturated bulk density of the brown pelagic clay at 245–255 m sub-bottom is nearly the same as that from 130–155 m sub-bottom in Hol 578. Also, the water content in the brown pelagic clay i Hole 581 at 262 m is 75%, whereas at Sites 576 and 57 water contents 20% less than this value are found depths of 60 and 170 m sub-bottom, respectively (Schul heiss, this volume). Possible reasons for this apparent anomalous situation in density will be discussed later.

Electrical Resistivity

The major purpose of this section is to present the r sistivity data obtained for the pelagic clays from Sit 576, 578, and 581. It is worthwhile initially, however, consider some concepts concerning the relationship b tween electrical conductivity and sediment characteri tics. Details are given in a number of publications sur marized for DSDP studies by Boyce (1980, 1981).

Electricity will pass through marine sediments becau an electrolyte-rich water is present in the pores and a sorbed on clay particles; dry sediment generally is a po conductor of electricity. Conduction of electricity in saturated sediment is complicated because of the pre ence of a granular framework. If the framework mi erals are nonconductive, then the passage of electricit is through the interstitial water. In pelagic clay, whe clay minerals exchange ions with the interstitial water, i would be anticipated that the conduction of electricity would be more complicated. Clay minerals with differing ion-exchange capacities may act as conductors or resistors of electricity relative to different pore-water resistivities.

The electrical resistivity of any material is the resistance in ohms between opposite faces of a unit cube of the material and is defined as

$$R_o = rA/L \text{ (ohm m}^2\text{m}^{-1}\text{ or ohm-m)},$$

where R_o is the resistivity, and r is the resistance of a conducting cube with cross-sectional area A and length L. To a first approximation, it is likely that in the shallowly buried clay sediments of Sites 576, 578, and 581, the *in situ* resistivity of the interstitial water is nearly constant with burial depth. Neither pore-water salinitie nor sediment temperatures change significantly with buria depth (see Site 576, 578, and 581 chapters, this volume Laboratory sediment resistivities were measured at a cor stant temperature of 23°C. Thus, the laboratory dete minations of resistivity of the sediments from these sit will depend primarily on the amount of water prese (i.e., the porosity) and on the fabric of the sedime (i.e., the size, shape, and arrangement of detrital grai and authigenic minerals).

For a homogeneous sediment completely saturated wi seawater, its resistivity, R_o, is proportional to the resi tivity of the seawater, R_{sw}, at the same temperature a pressure,

$$R_o = FR_{sw};$$

Table 4. Measured bulk densities and compressional-wave velocities for samples from Holes 576, 578, and 581.

Sample (interval in cm)	Sub-bottom depth (m)	Bulk density (g/cm^3)	Compressional velocity V_p (km/sec)				Anisotropy A_p (%)
			Vertical V_{pv}	Horizontal V_{ph} A	Horizontal V_{ph} B	$\overline{X}$ V_{ph}	
576-1-1, 46-50	4.96-5.00	1.474	1.527	1.566	1.543	1.554	+1.75
576-2-1, 109-116	8.29-8.36	1.455	1.533	1.510	1.506	1.508	−1.65
576-2-6, 99-106	15.69-15.76	1.362	1.531	1.581	1.524	1.553	+1.42
576-3-3, 109-115	13.69-13.75	1.375	1.485	1.507	1.497	1.502	+1.14
576-4-2, 88-95	21.48-21.55	1.378	1.460	1.526	1.513	1.520	+4.00
576-4-5, 98-104	26.08-26.14	1.403	1.492	1.488	1.507	1.498	+0.40
576-5-1, 108-115	29.28-29.35	1.398	1.496	1.489	1.495	1.492	−0.27
576-5-6, 18-25	32.78-32.85	1.363	1.502	1.509	1.521	1.515	+0.86
576-6-4, 37-44	36.27-36.34	1.421	1.503	1.507	1.495	1.501	−0.13
576-7-2, 130-137	46.90-46.97	1.397	1.477	1.488	1.498	1.493	+1.08
576-7-6, 19-26	51.79-51.86	1.462	1.497	1.504	1.510	1.507	+0.67
576-8-1, 98-105	55.08-55.15	1.411	1.508	1.502	1.508	1.505	−0.20
576-8-6, 81-84	62.41-62.44	1.398	1.513	1.501	1.545	1.523	+0.66
578-2-4, 38-45	9.68-9.75	1.319	1.613	1.562	1.532	1.547	−4.21
578-5-3, 91-98	37.21-37.28	1.346	1.513	1.519	1.526	1.523	+0.66
578-10-3, 91-98	87.71-87.78	1.351	1.532	1.535	1.541	1.538	+0.39
578-13-1, 78-85	110.08-110.15	1.364	1.534	1.520	1.514	1.517	−1.12
578-14-4, 53-60	123.83-123.90	1.407	1.521	1.530	1.532	1.531	+0.65
578-15-2, 53-60	130.33-130.40	1.464	1.524	1.536	1.549	1.543	+1.24
578-15-7, 28-34	137.58-137.64	1.467	1.509	1.530	1.545	1.538	+1.90
578-16-5, 67-74	144.47-144.54	1.497	1.535	1.538	1.542	1.540	+0.33
578-17-2, 72-79	149.52-149.59	1.508	1.513	1.510	1.536	1.523	+0.66
578-17-5, 61-68	153.91-153.98	1.453	1.512	1.524	1.530	1.527	+0.99
578-18-3, 38-45	160.18-160.26	1.620	1.520	1.552	1.567	1.560	+2.59
578-19-1, 57-64	166.87-166.94	1.575	1.516	1.530	1.544	1.537	+1.37
578-19-3, 53-60	169.83-169.90	1.603	1.526	1.568	1.566	1.567	+2.64
581-8-5, 65-72	245.15-245.22	1.471	1.519	1.541	1.538	1.540	+1.37
581-9-4, 33-40	252.83-252.90	1.517	1.526	1.541	1.559	1.550	+1.56
581-10-3, 44-51	260.94-261.01	1.543	1.541	1.542	1.553	1.548	+0.45

F is commonly called the formation factor (Archie, 1942, 1950). The formation factor is a parameter that accounts for the tortuous path electricity follows through a sediment of varying grain size and shape, mineral arrangement, and porosity. Thousands of laboratory determinations on thousands of samples (mainly sandstones and carbonates) (Schlumberger, 1958) have shown that an empirical relationship for F and porosity is

$$F = a\Phi^{-m},$$

where Φ is porosity, and a and m are constants.

It is possible that the passage of electricity through freshly deposited marine sediment is isotropic. In pelagic clays, however, where clay minerals of flat or elongated shape are deposited and during compaction are preferentially oriented with their least size dimension perpendicular to bedding, bedding planes will offer a favorable path for the conduction of electricity. Thus, resistivity parallel to bedding is typically less than that perpendicular to bedding in clay mineral-bearing sediments. sistivity anisotropy with horizontal resistivity less than rtical resistivity should develop in these sediments with reasing burial depth. Resistivity anisotropy is defined

$$A_r = 100(R_v - R_h)/\overline{R}$$

ere R_v is vertical resistivity, R_h is horizontal resistivi-, and $\overline{R}$ is mean sample resistivity. In later sections, llowing presentation of the physical property data, we will employ some of these concepts in interpretation of the resistivity data.

Figures 12 and 13 show vertical gradients in laboratory-determined horizontal and vertical resistivities and resistivity anisotropy, respectively. Table 5 gives the data for these parameters. Emphasis in resistivity measurements was placed on the brown pelagic clay samples. In general, the resistivity of the brown pelagic clay increases irregularly with increasing burial depth. Vertical (R_v) resistivities tend to be greater than horizontal (R_h) and resistivity anisotropy (A_r) appears to increase with increasing burial depth. Site 581 brown pelagic clay appears anomalous once more, based on very limited data; resistivities and resistivity anisotropies seem less than anticipated for the depth of burial of the clay sequence at this site.

It is difficult to determine whether some of the scatter, specifically the large single point deviations in resistivity and resistivity anisotropy, is a result of disturbances in core samples (e.g., deformation during coring or subsequent dessication), errors in laboratory measurement, or real changes in sediment properties. If we include all the measurements, the sediments exhibit resistivity values ranging from about 0.5 to slightly greater than 1.3 ohm and resistivity anisotropies of about −15 to +47%. Below a depth of about 30 m, the resistivity anisotropy is positive, whereas above that depth some pelagic clay samples show negative anisotropy values. Most samples of the brown pelagic clay exhibited positive resistivity anisotropy ($R_v > R_h$), with values ranging from about 2 to 47%. It is possible that some of the

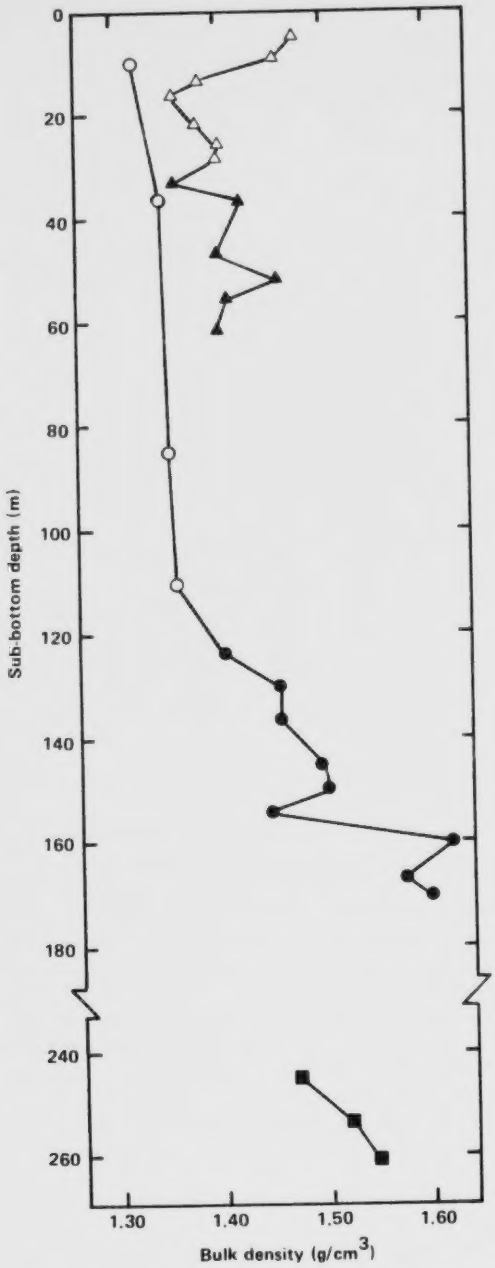

Figure 11. Bulk density as a function of depth for Holes 576, 578, and 581. Symbols as in Figure 3.

irregularities in sediment resistivity properties may be related to changes in sediment mineralogy. We will discuss this possibility in a later section, as well as the significance of the resistivity changes in the pelagic clay sediment with increasing burial depth.

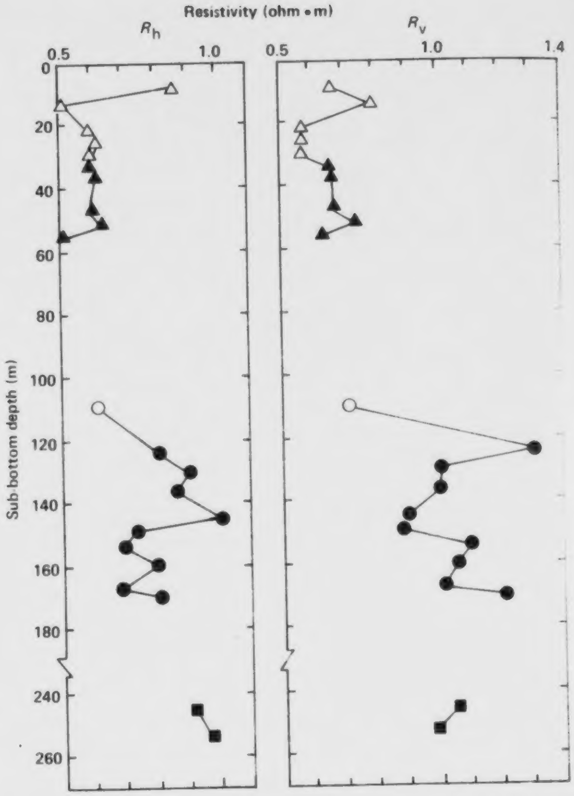

Figure 12. Electrical resistivity in both horizontal (R_h) and vertical (R_v) directions as a function of depth for Holes 576, 578, and 581. Symbols as in Figure 3.

Acoustic Properties

In this section we present vertical and horizontal compressional-wave velocity data and velocity anisotropy data for the clay mineral-rich sediments of Holes 576, 578, and 581. Compressional velocity in isotropic material is related to bulk and shear moduli by the following equation (e.g., Birch, 1961; Boyce, 1981):

$$V_p = \left(\frac{K + 4\mu/3}{\rho_b}\right)^{1/2},$$

where V_p is compressional velocity, ρ_b is wet-bulk density, K is incompressibility or bulk modulus, and μ is shear modulus (rigidity). K and μ may vary with direction in the sediment; therefore, sound traveling in the vertical and horizontal directions will have different velocities in an anisotropic sediment. Compressional velocity anisotropy is defined as

$$A_p\ (\%) = (100)\ \frac{V_{ph} - V_{pv}}{\overline{V}_p}$$

where V_{ph} designates horizontal compressional-wave velocity, V_{pv} denotes vertical compressional-wave velocity, and $\overline{V}_p$ is the mean compressional-wave velocity. It is anticipated, for a clay-size sediment undergoing compaction and collapse of fabric, that sound anisotropy may develop with velocity greater in the horizontal direction (Hamilton and Bachman, 1982).

Compressional-wave velocities and anisotropies in sediment and rock are related to a number of factors, usu-

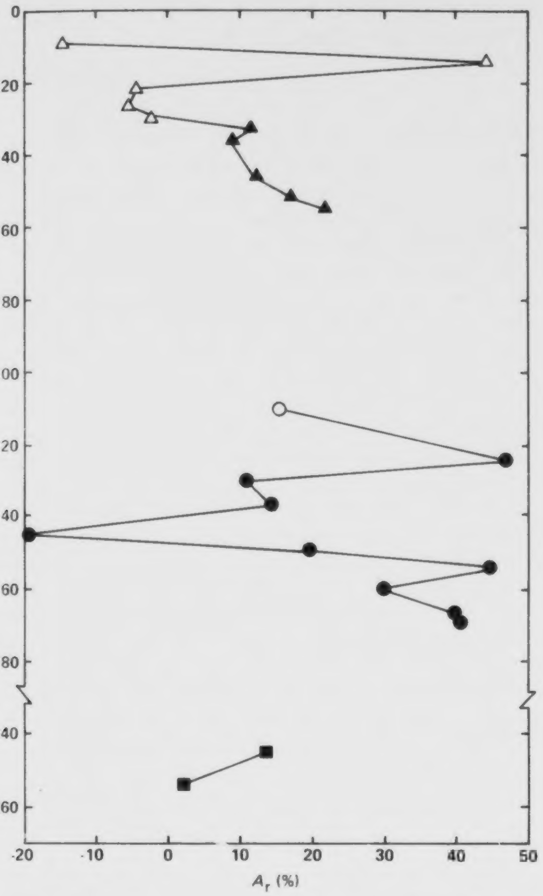

Figure 13. Resistivity anisotropy, A_r (%), as a function of depth for Holes 576, 578, and 581. Symbols as in Figure 3.

Table 5. Electrical resistivity values for selected samples from Holes 576, 578, and 581.

Sample (interval in cm)	Sub-bottom depth (m)	R_h (ohm-m)	R_v (ohm-m)	A_r (%)
576-2-1, 109-116	8.29-8.36	0.760	0.656	−14.7
576-3-3, 109-115	13.69-13.75	0.512	0.798	43.7
576-4-2, 88-95	21.48-21.55	0.587	0.565	−3.82
576-4-5, 98-104	26.08-26.14	0.605	0.569	−6.13
576-5-1, 108-115	29.28-29.35	0.586	0.574	−2.07
576-5-6, 18-25	32.78-32.85	0.579	0.647	11.1
576-6-4, 37-44	36.27-36.34	0.605	0.659	8.54
576-7-2, 130-137	46.90-46.97	0.591	0.667	12.1
576-7-6, 19-26	51.79-51.86	0.628	0.744	16.9
576-8-1, 98-105	55.08-55.15	0.503	0.628	22.1
578-13-1, 78-85	110.08-110.15	0.614	0.720	15.9
578-14-4, 53-60	123.83-123.90	0.809	1.311	47.4
578-15-2, 53-60	130.33-130.40	0.909	1.018	11.3
578-15-7, 28-34	137.58-137.64	0.872	1.004	14.1
578-16-5, 67-74	144.47-144.54	1.087	0.901	−18.7
578-17-2, 72-79	149.52-149.59	0.728	0.888	19.8
578-17-5, 61-68	153.91-153.98	0.696	1.100	45.0
578-18-3, 38-45	160.18-160.25	0.800	1.068	28.7
578-19-1, 57-64	166.87-166.94	0.685	1.024	39.6
578-19-3, 53-60	169.83-169.90	0.809	1.222	40.6
581-8-5, 65-72	245.15-245.22	0.918	1.050	13.4
581-9-4, 33-40	252.83-252.90	0.967	0.986	1.9

ally not independent, including pressure, temperature, mineralogical composition, fluid content, pore-water saturation, grain size, shape, and arrangement, and other variables (Press, 1966; Boyce, 1981). In a later section, we will discuss the effect of some of these variables on sound velocity in pelagic clay sediments from Holes 576, 578, and 581.

Figures 14 and 15 show laboratory-determined values of horizontal and vertical compressional-wave velocities and compressional-wave anisotropies, respectively. Table 4 gives data for these variables. In general, compressional-wave velocities, except for irregular velocities at depths shallower than about 20 m, exhibit little change with increasing burial depth of the clay mineral-rich sediment sampled. There is, however, a slight, nearly linear, increase in V_{ph} in the brown pelagic clay with increasing burial depth: mean V_{ph} ($\bar{x}$) increases from about 1.49 km/sec at 30 m sub-bottom depth to about 1.55 km/sec at a depth of 260 m, equivalent to a V_{ph} gradient of 0.26/sec (Table 4). A poorly defined positive gradient of

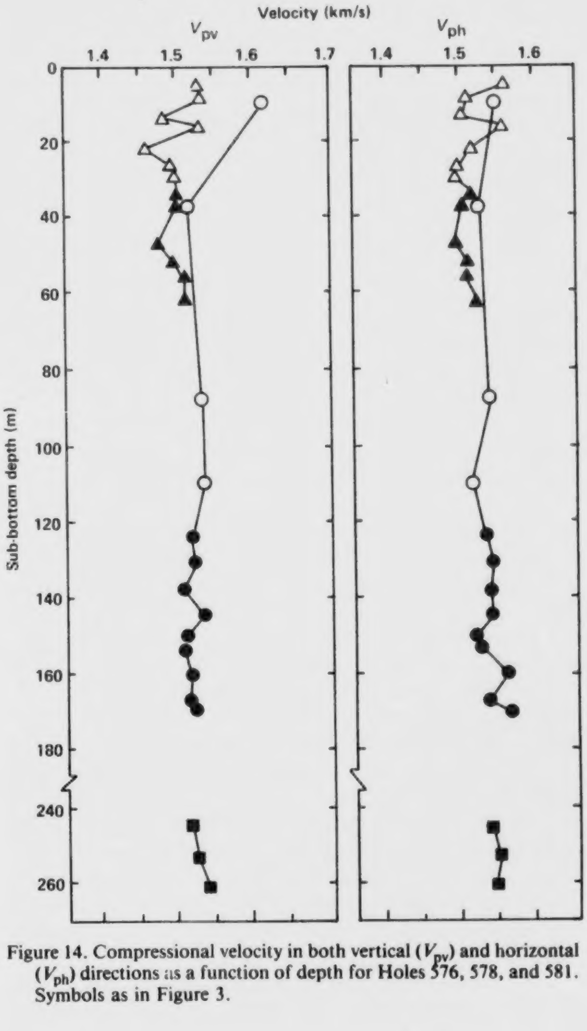

Figure 14. Compressional velocity in both vertical (V_{pv}) and horizontal (V_{ph}) directions as a function of depth for Holes 576, 578, and 581. Symbols as in Figure 3.

READEX FICHE

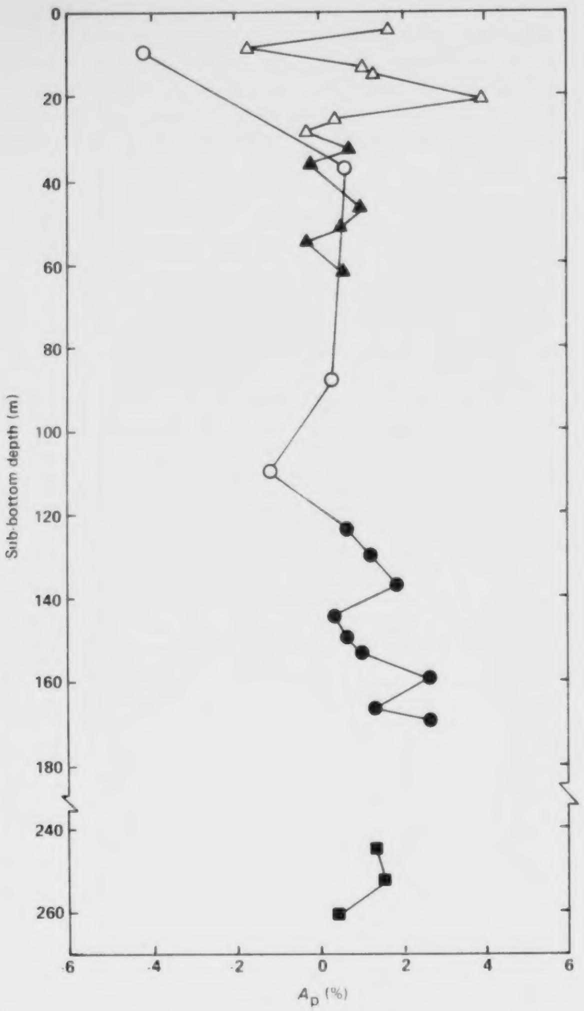

Figure 15. Compressional velocity anisotropy, A_p (%), as a function of depth for Holes 576, 578, and 581. Symbols as in Figure 3.

V_{pv} exists as a function of increasing burial depth of the brown pelagic clay. At Site 578, however, the change in V_{pv} with increasing depth of the brown pelagic clay is small.

Compressional-wave velocity anisotropy for these clay mineral-rich sediments is not large, varying from about −4 to +4% (Fig. 15). Most anisotropy values tend to be positive or slightly negative. The observation that the brown pelagic clay develops velocity anisotropy at relatively shallow depths is of greater interest. Definite and persistent anisotropy starts at a saturated bulk density of 1.45 g/cm^3 at a sub-bottom depth of 130 m. Stratigraphically higher pelagic clay samples show some anisotropy but the trend in A_p is not clear as in deeper sediment. There appears to be, at least in Hole 578, a general increase in sound velocity anisotropy with increasing depth of burial.

The three samples of brown pelagic clay from Site 581 again seem different. The values of V_{pv}, V_{ph}, and A_p for these samples are less than anticipated for the depth of burial of the samples.

DISCUSSION

Characteristics of the Brown Pelagic Clay Unit

As noted in the introduction, one goal of this stud was to assess the effects of compaction on acoustic an electrical properties of pelagic clay. We have identified unit of brown pelagic clay present at progressively deepe burial depths at Sites 576, 578, and 581. Because of thi unit's chemical and mineralogical homogeneity, it is particularly well suited for evaluation of the changes in acoustic and electrical properties of pelagic clay resulting primarily from compaction. This homogeneous brown pelagic clay is characterized by: (1) a high clay mineral t quartz ratio, (2) a relatively high percentage of mixed layer illite/smectite and low content of discrete illite, (3 the presence of palygorskite (at levels detectable b X-ray diffraction) in more than 50% of the samples, (4 high concentrations of Fe, Mn, Cu, Co, and Ni, (5) few microfossils except ichthyoliths (see Doyle and Riedel this volume), and (6) relatively high shear-wave velocity and vane-shear strength (see Schultheiss, this volume).

The upper boundary of this brown pelagic clay unit i transitional at all three sites, with the clay grading upward to a slightly silty mud that in some places is siliceous or contains abundant volcanic ash layers. The lower boundary is different at the three sites (see Site 576, 578, and 581 chapters, this volume). In Hole 576, the brown pelagic clay unit is underlain by interbedded pelagic clay and carbonate ooze. The lower boundary of the brown pelagic clay unit at Site 578 appears to be at the base of the hole, where chert and foraminiferal mud were recovered in the core catcher of the stratigraphically lowest core. At Site 581, the brown pelagic clay unit is underlain by a mixture of pelagic clay and chert pebbles that grades downward to chert.

The approximate boundaries of the homogeneous brown pelagic clay unit are indicated on the stratigraphic cross section in Figure 16. These boundaries have been selected primarily on the basis of lithology and bulk mineralogy. Because of the transitional nature of the upper boundaries, precise locations are difficult to pick. It was felt that a criterion based on the clay/quartz ratio is a useful guide, and a cut-off of clay/quartz >5 was chosen (Fig. 4). Note that the depths of the boundaries chosen on this basis are similar, but do not correspond precisely, to lithologic boundaries based on color changes and smear-slide data noted in the site chapters (this volume).

The clay mineralogy and chemical data support the differentiation of the brown clay unit from overlying sediment. Because the upper boundaries are transitional and the distinction of the brown pelagic clay unit from overlying sediment probably reflects both original detrital and subsequent diagenetic differences, the precise location of the upper unit boundaries would vary somewhat if clay mineralogy or chemistry were used as selection criteria. In addition, the mineralogical and chemical data for Site 578 (Fig. 6; Table 3) suggest that the lower

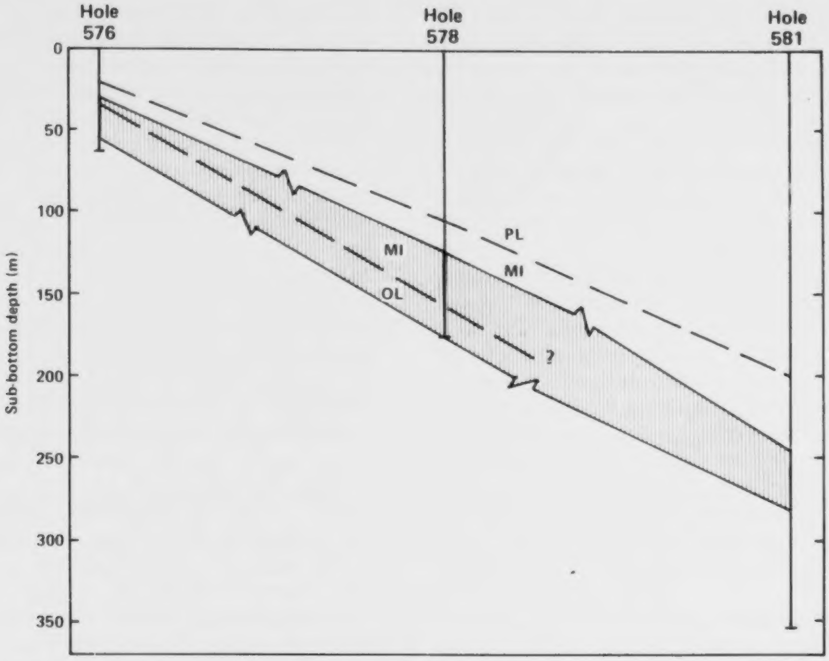

Figure 16. Cross-section depicting boundaries (solid lines) of the brown pelagic clay unit (hachured) at Sites 576, 578, and 581. Dashed lines are time lines indicating approximate locations of the Pliocene/Miocene (PL/MI) and Miocene/Oligocene (MI/OL) boundaries.

boundary of the brown pelagic clay unit may also be transitional and that, with more detailed study, an additional unit could be defined near the base of that site. Because our clay/quartz criterion does not support differentiation of an additional unit, however, we extend the lower boundary of the brown pelagic clay unit in Hole 578 to the core catcher of the deepest core.

The time lines indicated on Figure 16 were approximately located using paleomagnetic data (see Heath, Rea, and Levi, this volume), ichthyolith data (Doyle and Riedel, this volume), and microfossil data (Site 576, 578, and 581 chapters, this volume). At Sites 576 and 578, the homogeneous brown pelagic clay unit is underlain by Upper Cretaceous sediment, and the transition from deposition of pelagic clay to deposition of more silty mud occurred sometime in the Miocene. The sparse age data for the brown pelagic clay at Site 581 indicate a Miocene or older age. Thus, the brown pelagic clay units at each of the three sites appear to be roughly age equivalent.

The transition from the silty, sometimes siliceous, mud to the brown pelagic clay unit below probably represents both a change in original detrital mineralogy and an overprint of diagenesis. Thus, this transition provides an opportunity for evaluation of the possible effects of mineralogy, chemistry, and diagenesis on the electrical and acoustic properties of pelagic clay, a second goal of this project. The evidence for changes in detrital mineralogy and diagenetic imprint across the lithologic transition will be reviewed next. We will then consider the influence of compaction (i.e., depth of burial), mineralogy, chemistry, and degree of diagenetic alteration on acoustic and electrical properties of pelagic clay.

Detrital versus Diagenetic Imprint

Leinen (this volume) and Janecek (this volume) provide independent estimates of mass-accumulation rates of quartz and other eolian material, respectively, for Site 576. Their data indicate low eolian mass-accumulation rates for sediment below about 30 m sub-bottom depth, with a rapid rise to high values for sediment in the upper 10–12 m. They suggest the rapid increase in eolian mass-accumulation rates corresponds to movement of Site 576 into the zone of prevailing westerlies. Our bulk mineralogy data for Site 576 (see Fig. 3) reflect the change in eolian mass-accumulation rates. The homogeneous brown pelagic clay unit, having high total clay mineral content and low quartz and feldspar contents, was deposited during the period of low eolian mass-accumulation rates. As Site 576 moved northwest into the zone of the westerlies, the relative percentages of quartz and feldspar increased. Bulk mineralogical data for Site 578 (Fig. 3) indicate an analogous situation.

Clay mineralogy data for Site 576 are also consistent with an increase in eolian mass-accumulation rates at relatively shallow burial depths. The percentages of illite, kaolinite, and chlorite, all of which probably reflect a detrital signal, increase upsection (Fig. 5). The case for Site 578 appears more complicated. Although changes in sample compositions expressed in percentages do not necessarily indicate variations in mass-accumulation rates for all components, the relatively high contents of illite, kaolinite, and chlorite in the basal 20–25 m of Hole 578 *may* indicate an early period of high eolian mass-accumulation rates (Fig. 6). Immediately above this basal zone, the presumed detrital minerals are present in low concentrations and then their percentages increase upsection. Thus, it appears that the low contents of quartz and other probable eolian minerals in the homogeneous brown pelagic clay unit compared to overlying muds reflect original detrital differences related to changes in eolian mass-accumulation rates.

In addition to changes in mass-accumulation rates, the eolian flux of material to the sites may have changed in composition as the sites moved north and northwest with time. Oscillations in the relative proportions of mixed-layer illite/smectite and illite at Sites 576 and 578 (Figs. 5 and 6), for example, could possibly reflect variations in the composition of the eolian flux of clay minerals to the sites, as has been suggested by Lenotre et al. (this volume). Various lines of evidence suggest, however, that diagenetic alteration of the sediments has influenced their clay mineralogy and chemistry and may be responsible for some of the observed compositional variations.

For example, it was noted earlier (Figs. 5 and 6) that the composition of the mixed-layer illite/smectite varies downsection in Holes 576 and 578, and that samples with high percentages of illite/smectite tend to have fewer illite interlayers in the mixed-layer clay. Hein et al. (1976), Hein and Scholl (1978), and Vallier and Kidd (1977) presented guidelines for determining whether or not fine-grained sediment has had a significant volcanogenic source. In general, muds or mudstones derived from alteration of volcanic debris are likely to contain high percentages of smectite which has relatively few (< 15–20) illite interlayers. A clay mineral-rich sediment made up of >75% smectite is thought to be mostly volcanogenic in origin; one containing 50–75% smectite is suspected of having a significant volcanogenic component. Furthermore, Hein et al. (1976) noted that as the percentage of smectite in Bering Sea sediment declined, the number of illite interlayers increased to the background level of 45–50% illite interlayers, a composition representative of the terrigenous input in that area. Following these guidelines, a number of the samples analyzed in this study are thought to have a significant volcanogenic component. Figures 5, 6, and 7 show that many samples contain more than 50% illite/smectite and several more than 70%. If the samples containing the least amount of illite/smectite are considered representative of the terrigenous input, that illite/smectite contains about 40–50% illite interlayers. In most places, the samples richest in illite/smectite contain fewer than 25% illite interlayers. Thus, these samples, although not dominantly volcanogenic, probably contain a significant volcanic component. Almost all the samples with suspected volcanic origins fall within the brown pelagic clay unit. The more silty muds overlying this unit contain dominantly terrigenous illite/smectite. Disseminated volcanic glass and volcanic ash layers were noted in smear-slide examinations of sediments from Sites 576 and 578 (see Site 576 and 578 chapters, this volume), particularly from the silty mud overlying the brown clay unit. The presence of this material documents the volcanic influx to the sediment and suggests that in the younger sediment, diagenesis has not yet altered the volcanic debris to smectite and associated minerals.

Additional evidence of a diagenetic imprint on the brown pelagic clay unit can be seen in the chemical data. As was noted earlier, Fe_2O_3, MnO, and associated trace metals typical of authigenic amorphous Fe- and Mn-oxyhydroxides are more abundant in the brown clay unit than in overlying deposits (see Table 3). The changing influence of detrital versus diagenetic components in the sediments of Leg 86 is shown in Figure 17. As one moves downhole at each site, the detrital component (represented by the sum of quartz plus feldspar) declines in abundance whereas the authigenic metal phases increase.

Palygorskite, which may be another diagenetically produced phase, was detected in samples from the brown pelagic clay units of Holes 576 and 578. As shown in Figures 5 and 6, palygorskite increases in abundance downhole at these two sites. Although palygorskite may be detrital, in many deep-sea sediments it is believed to have formed authigenically either by the action of Mg-rich hydrothermal solutions on sediments overlying basalt or by the low temperature alteration of volcanic debris, perhaps with smectite as an intermediate product (Elderfield, 1976; Couture, 1977). Phillipsite, another common product of alteration of volcanic debris, was noted in one sample (Sample 576-5-6, 18–25 cm; see Plate 1).

It should be noted that, in general, the results of our mineralogical analyses are very similar to those of Lenotre et al. (this volume), who studied the clay stratigraphy of Sites 576 and 578. Those authors favor a changing detrital supply, with minimal diagenetic effects, as an explanation of the observed mineralogical variations. Their conclusion is drawn primarily on the bases of transmission electron microscope observations of clay morphology and mineral associations. We feel, however, that

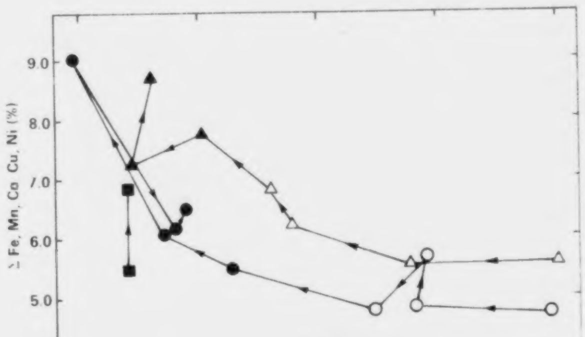

Figure 17. Metal content (summation of Fe, Mn, Co, Cu, and Ni in %) plotted versus the summation of quartz plus feldspar content for samples from Holes 576, 578, and 581. Arrows point in a downhole direction for each hole, indicating the downhole enrichment in metals and depletion in quartz plus feldspar. Symbols as in Figure 3.

our observations of the correlation of abundance and composition of illite/smectite mixed-layer clay; the abundance of Fe, Mn, and associated trace metals; and the presence of palygorskite suggest that the diagenetic imprint on sediment composition is significant, particular-y in the brown pelagic clay unit identified in Holes 576, 78, and 581.

elationships between Resistivity and Other Sediment operties

In this section we discuss relationships between resis- ity, acoustic velocity, and clay sediment chemistry and neralogy. Emphasis is on the brown pelagic clay unit. will demonstrate that it is primarily the physical pro- s of compaction that affects the depth-related acous- and electrical response of the brown pelagic clay unit; tial detrital mineralogy and subsequent diagenesis play nor roles.

Resistivity Correlations

Sediment resistivity can be expressed as the product a formation factor, F, and the resistivity of the inter- tial water, R_w. Measured resistivities, therefore, will flect changes in variables affecting F (e.g., porosity, bric, texture, mineralogy) and R_w (e.g., salinity, tem- erature). For marine sediment, the assumption is usu- lly made that pore waters have constant salinities equal o that of the overlying bottom water. Although this is certainly not always the case, it appears to be a good approximation for Sites 576, 578, and 581. The pore-water data (see Site 576, 578, and 581 chapters, this volume) show that all salinities measured at these three sites fall between 34.5 and 35.5‰. At the temperature of measurement (23°C), a 1‰ salinity variation would result in less than a 0.01 ohm-m change in resistivity of the pore water. We have, therefore, assumed a constant value of 0.19 ohm-m for R_w (Schlumberger, 1958; Boyce, 1968). Observed variations in measured sediment resistivity can therefore be assumed to reflect changes in the sediment (i.e., changes in the formation factor, F).

Porosity, and therefore water content, should vary inversely with resistivity. Although porosity was not measured in our laboratory, these data are available from Schultheiss (this volume). To investigate correlations between resistivity and porosity, we used porosity data for samples from the same core, and whenever possible the same section, as the samples on which resistivity mea- urements were made. Resistivity parallel to bedding (R_h) nd perpendicular to bedding (R_v) is roughly correlated ith porosity (Figure 18). As expected, this relationship eems better developed for R_v than for R_h. During bur- l, the reduction in porosity and the reorientation of lay mineral particles both act to increase resistivity in he vertical direction. On the other hand, the alignment f grains and pore spaces with long axes lying in a hori- ontal plane lowers resistivity somewhat in the horizon- al direction and tends to counterbalance some of the esistivity increase owing to porosity reduction. Similar elationships were found between resistivity and water con- ent (data from Schultheiss, this volume). Resistivity anisotropy shows only a weak inverse correlation with porosity.

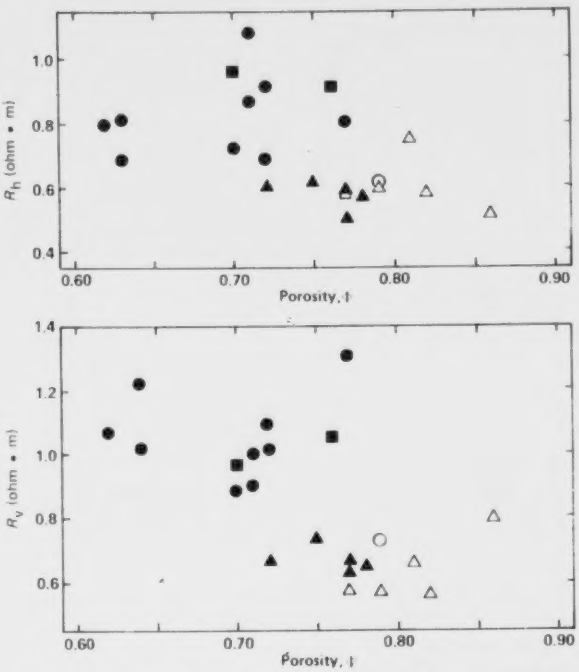

Figure 18. Horizontal (R_h) and vertical (R_v) resistivity as a function of porosity (Φ) for samples from Holes 576, 578, and 581. Symbols as in Figure 3.

The resistivity–porosity relationship is shown on a log-log plot in Figure 19. A linear fit to these data yields the following expression:

$$R_o = 0.46\ \Phi^{-1.65}.$$

Division of the above expression for R_o by the resistivity of the pore water ($R_{sw} = 0.19$) yields the formation factor:

$$\frac{R_o}{R_{sw}} = F = 2.4\ \Phi^{-1.65}.$$

The value of the constant, m (1.65), is slightly less than values obtained by Boyce (1968) and Kermabon et al. (1969) for silty muds and marine muds and turbidite sands. Separate regressions for R_v and R_h yield similar expressions with the constant, m, equal to 1.98 and 1.33, respectively. Note that the linear fit to the data does not fulfill a boundary condition required by physical considerations (Fig. 19). That is, for a porosity of 100% ($\log \phi = 0$) the resistivity should be that of the interstitial water. In other words, at $\log \phi = 0$, $\log R_o$ should equal -0.7 ($\log R_{sw}$). This discrepancy perhaps indicates that the linear fit cannot be extended to high porosities and that the data should properly be fit with a curvilinear expression. Another possible explanation for the discrepancy centers on the two sources of the data

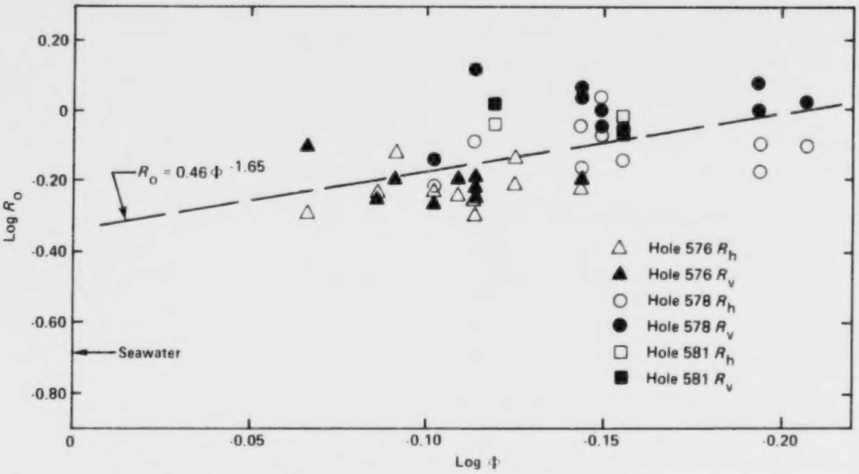

Figure 19. Log resistivity, R_o, (both horizontal and vertical) as a function of log porosity (Φ). Dashed line gives the least squares fit to the data ($r^2 = 0.533$). Log R_o for seawater is indicated by the arrow.

involved. Porosities were obtained from measurements made on shipboard, soon after core recovery. The resistivities, however, were measured in our laboratory approximately 1.5 yr. after Leg 86 took place. It is possible that partial dehydration of the cores during that time period resulted in increased resistivities and, when those data are plotted against shipboard porosities, an offset results.

Another factor that influences the resistivity of a sediment is its fabric; the size, shape, and nature of packing of grains affect how electricity will flow through a sediment. The ratio of clay/quartz can be used as a general indicator of changes in fabric, as well as changes in mineralogy. There are two roughly parallel trends of decreasing R_v with increasing clay/quartz ratio, one established by the samples within the brown pelagic clay unit and the other for the overlying mud (Fig. 20). The existence of two separate trends is difficult to explain. Depth of burial does not appear to be responsible because the two trends have overlapping depth ranges. The explanation presumably lies in compositional differences (either mineralogical or chemical) between the two types of sediment. The brown pelagic clay unit samples have higher contents of Fe and other metallic elements. The presence of metallic minerals, however, tends to decrease resistivity (Boyce, 1981; Keller, 1966), which would not explain the separate trends of Figure 20. Because the mineralogical variations between the two types of clay are transitional, it is unlikely that concentration of a particular mineral could cause the separate trends. More likely, a combination of factors, perhaps including content of water, microfossils, volcanic debris, and mineralogical and chemical make-up, results in separation of the trends of R_v versus clay/quartz ratio. It is also possible that analysis of more samples would lead to delineation of a transition between the two trends of Figure 20.

The relationships between R_h and resistivity anisotropy and the clay/quartz ratio are not so well established. The weak correlations are similar, however, to that of R_v versus clay/quartz, with R_h and A_r decreasing with increasing clay/quartz ratio. Separate trends for the brown clay unit and the overlying clays may exist.

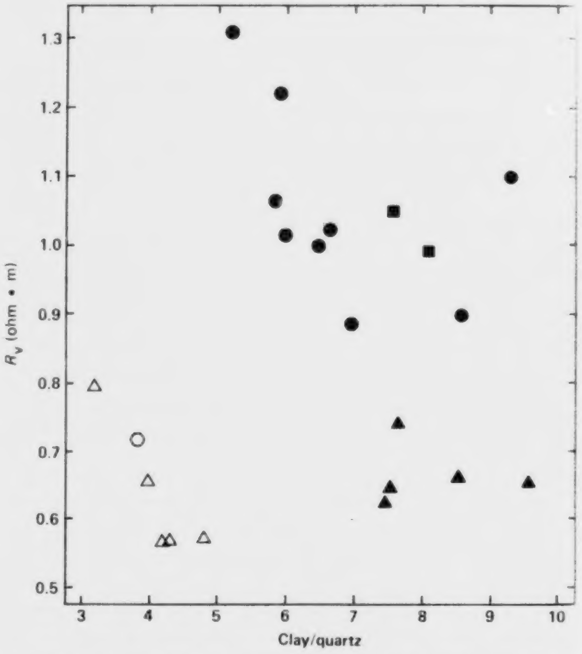

Figure 20. Vertical resistivity (R_v) as a function of the clay/quartz ratio for samples from Holes 576, 578, and 581. Symbols as in Figure 3.

Different clay minerals are known to have different electrical resistivities. This variability is due largely to their cation exchange capacities. Clay minerals that exchange or remove ions from solution surround themselves with an ionic cloud that can be highly conductive. Smectite, because of its net negative layer charge and high water content, would tend to have lower electrical resistivity than many other clay minerals. With this in mind, we attempted to determine if resistivity is correlated with specific clay mineralogy. No correlations with mineralogy (other than with clay/quartz as already discussed) could be found. Perhaps the observed mineralogical variations are not of significant magnitude to generate a response in resistivity properties, or such response is overshadowed by the dominant effects of compaction (porosity loss) and texture change (clay/quartz ratio).

Acoustic Property Correlations

The incompressibility (bulk modulus) of surficial deep-
sediments varies with porosity and therefore with den-
y (Hamilton, 1971). Sediment bulk moduli increase
th decreasing porosity and increasing bulk density. Be-
use compressional-wave sound velocity V_p is directly
ated to the sediment bulk modulus by

$$\rho V_p^2 = K + 4\mu/3,$$

ositive correlation between V_p and ρ, and a negative
rrelation between V_p and Φ, would be anticipated for
e clay mineral-rich sediment of this study. Furthermore,
e observed general trends of porosity and density with
creasing burial depth (negative gradient of porosity,
sitive gradient of density) should lead to an increase
bulk moduli and rigidity (Hamilton, 1971) with increasing depth. That the sediment has rigidity is demonstrated by the observation that it transmits shear waves
en at high porosities (shallow depths). Shear-wave velocities tend to increase, somewhat irregularly, with increasing burial depth (Schultheiss, this volume). Thus, a positive gradient of V_p would be anticipated for the clay mineral-rich sediment as a function of depth (Fig. 14).

Correlations of V_{pv} and V_{ph} with porosity are not strong, probably accounting in part for the small gradient in V_p as a function of burial depth (Fig. 21). It is apparent that the $V_p - \Phi$ relationship is poor at high porosities (shallow depths), but is fair in the brown pelagic clay at lower porosities (deeper depths). The trend of V_{ph} with porosity for the brown pelagic clay is more apparent than that of V_{pv}. Thus, the positive gradient of V_{ph} with burial depth is steeper than that of V_{pv} (Fig. 14).

V_p anisotropy, particularly in the brown pelagic clay, with V_{ph} generally greater than V_{pv}, is also weakly correlated to porosity; decreasing porosity generally results in
ncreasing positive anisotropy (Fig. 22). In general a decrease in sediment porosity is reflected in an increase in
ensity. Thus, there are weak positive correlations between density and velocity (Fig. 23) and density and anisotropy (cf. Figs. 11 and 15). The trend with density is
ore apparent for V_{ph} than V_{pv}. The two regression lines
n Figure 23 are those calculated by Hamilton (1978)
r surficial seafloor sediments and for soft sediment
uried to depths less than 500 m. The trend for seafloor
ediment is very similar to that for all the velocity data
btained by us in the laboratory.

Sound velocity in seawater at laboratory conditions
f 23°C and 1 atm. pressure is 1.53 km/sec. Many of
he clay mineral-rich sediments have velocities less than
hat in seawater (Fig. 21). Also, as mentioned above,
here appears to be greater scatter of velocities at higher porosities than at lower, with velocities ranging from
% greater than to 5% less than that of seawater at porosities greater than 80%. The low-velocity effect is probably a result of the low rigidity of the high porosity sediment and the high compressibility (low bulk modulus) of seawater relative to mineral moduli (Hamilton, 1971).

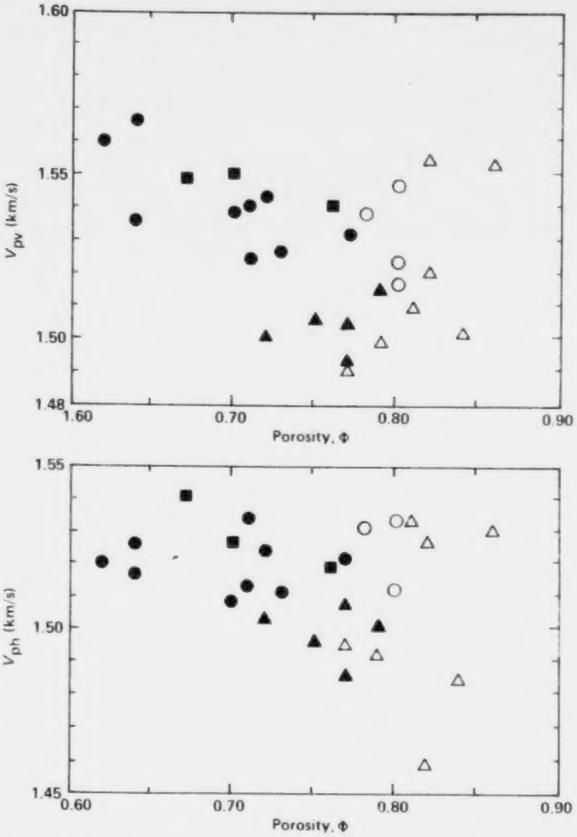

Figure 21. Horizontal (V_{ph}) and vertical (V_{pv}) compressional velocity versus porosity (Φ). Symbols as in Figure 3.

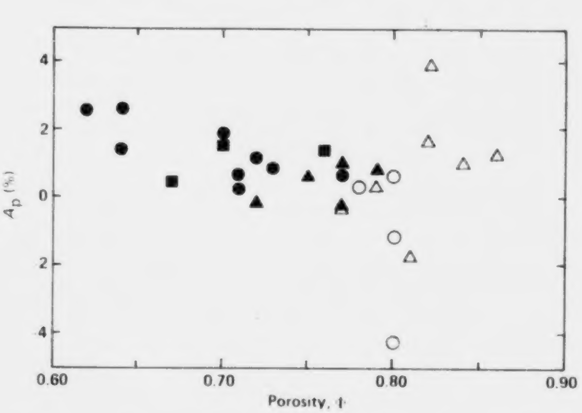

Figure 22. Compressional velocity anisotropy (A_p) as a function of porosity (Φ). Symbols as in Figure 3.

Aside from the correlations shown in Figures 21, 22, and 23, no definitive correlation was obtained for V_{pv}, V_{ph}, or A_p as a function of chemical or mineralogical independent variables. Perhaps some of the scatter in sound

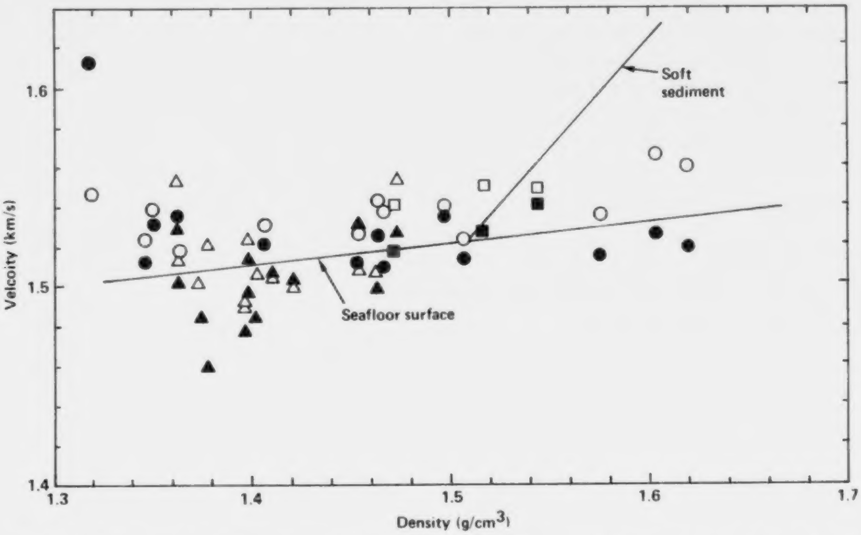

Figure 23. Compressional velocity versus density. Lines indicating trends for seafloor surface and soft sediments are from Hamilton (1978). Symbols as in Figure 3.

properties of the clay mineral-rich sediment at high porosities is due to minor admixtures of opaline silica and volcanogenic material. Certainly volcanic ash layers, not sampled by us, exhibit relatively high compressional-wave velocities (Schultheiss, this volume).

We believe that the changes in acoustic properties of the brown pelagic clay with burial depth are principally due to physical processes. Increasing overburden pressure results in preferred reorientation of the clay mineral particles with long axes normal to the pressure, reduction in porosity (water content), and increasing bulk density. Because of these changes, with increasing depth of burial, sound velocity increases and velocity anisotropy develops with velocity greater parallel to the seafloor.

Correlations between Resistivity and Acoustic Properties

This discussion will be restricted to the brown pelagic clay unit, for which reasonably well-defined relationships exist between resistivity and acoustic properties and burial depth. In general the positive gradient of V_{ph} with burial depth is correlated with a positive gradient of R_v. Although values of V_{pv} and R_h also seem to increase with burial depth, the trend is not as definite or as steep. To a first approximation these gradients are related to a decrease in porosity, and thus increase in bulk density, of the clay mineral-rich sediment with increasing burial depth.

Of particular interest is the positive correlation between resistivity anisotropy and compressional-wave velocity anisotropy (Fig. 24). In general anisotropies increase with porosity decrease and bulk density increase, hence burial depth. There are exceptions to the general trend. It appears to be true, however, that with increasing burial depth positive anisotropies of increasing magnitude become more the rule than the exception. Thus, with increasing burial depth the brown pelagic clay develops anisotropies with sound velocity and electrica conductivity greater parallel to the seafloor than norma to it. This is the situation predicted if the collapse of th "house of cards" clay mineral structure, because of increased overburden pressure, is the main cause of th acoustic and electrical response of the brown pelagic cla sediment.

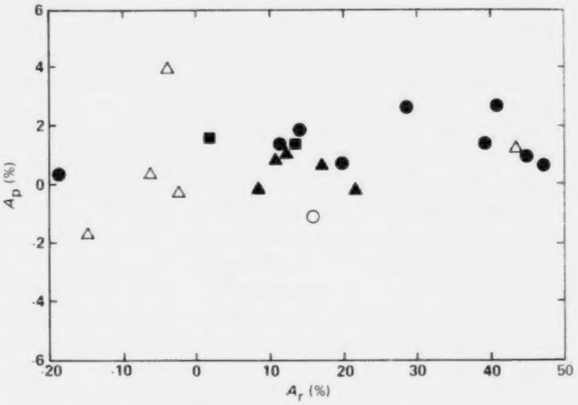

Figure 24. Compressional velocity anisotropy (A_p) versus resistivity anisotropy (A_r). Symbols as in Figure 3.

Throughout the discussion we have alluded to the di ferent properties of the brown pelagic clay unit at Sit 581. It has a higher water content, lower density, lowe compressional-wave velocity, and lower resistivity tha would be anticipated for its depth of burial. The reasor for this anomalous situation are not clear. There doe not appear to be a substantially large difference in the l thology of this unit from location to location, althoug Hole 581 brown pelagic clay may be less silty than th brown pelagic clays of Holes 576 and 578. It is possibl that because of the high depositional rate of the overly ing biosiliceous muds in Hole 581, the expulsion of water from the underlying brown pelagic clay was not able to keep pace with pressure loading. The brown pelagic clay pore waters may be supporting some of the weight of the overlying sediments. It is also possible that the change in drilling technique between Holes 576 and 578 (HPC) and Hole 581 (conventional rotary drilling) influenced the properties of Site 581 brown pelagic clay differently than the brown pelagic clay from Sites 576 and 578. Whatever the cause, the apparent different physical properties of Site 581 brown pelagic clay complicate the picture relating burial depth, porosity, and density to resistivity and elastic properties.

CONCLUSIONS

The measurement of a number of properties (mineralogy, chemistry, bulk density, acoustic velocity, and electrical resistivity) on the same samples has allowed us to draw the following conclusions concerning (1) the depth variations of these properties at Sites 576, 578, and 581 and (2) the role of composition and diagenesis in determining the physical properties and acoustic and electrical response of pelagic clays.

1. A relatively homogeneous brown pelagic clay unit of similar age can be identified at all three sites studied. This unit is characterized by a high clay/quartz ratio, a high trace-metal content, generally a high content of smectite-rich mixed-layer illite/smectite, and the presence of palygorskite in many samples.

2. These characteristics reflect both the diminished importance of detrital input and an enhanced diagenetic signal in the brown pelagic clay unit relative to overlying muds.

3. Variations in bulk density, acoustic velocity, and electrical resistivity primarily reflect the effects of compaction and loss of porosity accompanying burial.

4. Resistivity, especially in the vertical direction, varies with clay/quartz ratio. The trend in the brown pelagic clay unit is separate and approximately parallel to that defined by overlying muds. The separate trends cannot be explained by any single factor (depth, porosity, mineralogy, or chemistry), but must reflect a combination of factors that influence resistivity.

5. Other than the influence of clay/quartz ratio on resistivity, no correlations of mineralogy or chemistry with physical, acoustic, or electrical properties were noted. It is likely that the observed compositional variations are not large enough to generate a response in these properties, or such response is overshadowed by the dominant effects of compaction (porosity loss) and textural change (clay/quartz ratio).

6. Development of preferred orientation of clay platelets upon burial and loss of porosity and water content during compaction result in development of anisotropy in both acoustic and electrical properties with depth.

ACKNOWLEDGMENTS

We gratefully acknowledge DSDP and the scientists of Leg 86 for permitting us early access to samples. An early draft of the manuscript was improved because of the reviews of James Hein, Seymour Schlanger, and Audrey Wright. We thank Carol Koyanagi and Pat Sexton for typing the manuscript. This research was supported by ONR N00014-82-C-0380. Hawaii Institute of Geophysics Contribution No. 1599.

REFERENCES

Anderson, J. U., 1963. An improved pretreatment for the mineralogical analysis of samples containing organic matter. *Clays Clay Miner.*, 10:380–388.

Archie, G. E., 1942. The electrical resistivity log as an aid in determining some reservoir characteristics. *Trans. Am. Inst. Min., Metall. Pet. Eng.*, 146:54–62.

________, 1950. Introduction to petrophysics of reservoir rocks. *Am. Assoc. Pet. Geol. Bull.*, 34:943–961.

Birch, F., 1960. The velocity of compressional waves in rocks to 10 kilobars, Part 1. *J. Geophys. Res.*, 65:1083–1103.

________, 1961. The velocity of compressional waves in rocks to 10 kilobars, Part 2. *J. Geophys. Res.*, 66:2199.

Biscaye, P. E., 1965. Mineralogy and sedimentation of Recent deep-sea clay in the Atlantic Ocean and adjacent seas and oceans. *Geol. Soc. Am. Bull.*, 76:803–832.

Boyce, R. E., 1968. Electrical resistivity of modern marine sediments from the Bering Sea. *J. Geophys. Res.*, 73:4759–4766.

________, 1976. Sound velocity-density parameters of sediment and rock from DSDP drill Sites 315–318 on the Line Islands Chain, Manihiki Plateau, and Tuamotu Ridge in the Pacific Ocean. *In* Schlanger, S. O., Jackson, E. D., et al., *Init. Repts. DSDP*, 33: Washington (U.S. Govt. Printing Office), 695–728.

________, 1980. Determination of the relationships of electrical resistivity, sound velocity, and density/porosity of sediment and rock by laboratory techniques and well logs from Deep Sea Drilling Project Sites 415 and 416 off the coast of Morocco. *In* Lancelot, Y., Winterer, E. L., et al., *Init. Repts. DSDP*, 50: Washington (U.S. Govt. Printing Office), 305–318.

________, 1981. Electrical resistivity, sound velocity, thermal conductivity, density-porosity, and temperature, obtained by laboratory techniques and well logs: Site 462 in the Nauru Basin of the Pacific Ocean. *In* Larson, R. L., Schlanger, S. O., et al., *Init. Repts. DSDP*, 61: Washington (U.S. Govt. Printing Office), 743–761.

Brewster, G. R., 1980. Effect of chemical pretreatment on x-ray powder diffraction characteristics of clay minerals derived from volcanic ash. *Clays Clay Miner.*, 28:303–310.

Couture, R. A., 1977. Composition and origin of palygorskite-rich and montmorillonite-rich zeolite-containing sediments from the Pacific Ocean. *Chem. Geol.*, 19:113–130.

Elderfield, H., 1976. Hydrogenous material in marine sediments; excluding manganese nodules. *In* Riley, J. P., and Chester, R. (Eds.), *Chemical Oceanography* (Vol. 5, 2nd ed.): New York (Academic Press), 137–215.

Hamilton, E. L., 1971. Elastic properties of marine sediments. *J. Geophys. Res.*, 76:579–604.

________, 1978. Sound velocity-density relations in seafloor sediments and rocks. *J. Acoust. Soc. Am.*, 63:366–377.

Hamilton, E. L., and Bachman, R. T., 1982. Sound velocity and related properties of marine sediments. *J. Acoust. Soc. Am.*, 72: 1891–1904.

Hamilton, E. L., Bachman, R. T., Berger, W. H., Johnson, T. C., and Mayer, L. A., 1982. Acoustic and related properties of calcareous deep-sea sediments. *J. Sediment. Petrol.*, 52:733–753.

Hein, J. R., and Scholl, D. W., 1978. Diagenesis and distribution of late Cenozoic volcanic sediment in the southern Bering Sea. *Geol. Soc. Am. Bull.*, 89:197–210.

Hein, J. R., Scholl, D. W., and Gutmacher, C. E., 1976. Neogene clay minerals of the far NW Pacific and southern Bering Sea. *In* Bailey, S. W. (Ed.), *A.I.P.E.A. Proceedings, 1975 International Clay Conference, Mexico City:* Illinois (Applied Publishing), pp. 71–80.

Hoffman, J., 1976. Regional metamorphism and K-Ar dating of clay minerals in Cretaceous sediments of the Disturbed Belt of Montant [Ph.D. dissert.]. Case Western Reserve University, Cleveland.

Keller, G. V., 1966. Electrical properties of rocks and minerals. *In* Clark, S. P. Jr., (Ed.), *Handbook of Physical Constants* (revised ed.). Mem. Geol. Soc. Am., 97:553–577.

Kermabon, A., Gehin, C., and Blavier, P., 1969. A deep-sea electrical resistivity probe for measuring porosity and density of unconsolidated sediment. *Geophysics*, 34:554–571.

Manghnani, M. H., Schlanger, S. O., and Milholland, P. D., 1980. Elastic properties related to depth of burial, strontium content, and age and diagenetic stage in pelagic carbonate sediments. *In* Kuperman, W. A., and Jensen, F. B. (Eds.), *Bottom Interacting Ocean Acoustics:* New York (Plenum Press), pp. 44–51.

Mann, U., and Fischer, K., 1982. The triangle method—semiquantitative determination of clay minerals. *J. Sediment. Petrol.*, 52: 654–657.

Mann, U., and Müller, G., 1979. X-ray mineralogy of Deep Sea Drilling Project Legs 51 through 53, Western North Atlantic, *In* Donnelly, T., Francheteau, J., Bryan, W., Robinson, P., Flower, M., Salisbury, M., et al., *Init. Repts. DSDP*, 51, 52, 53, Pt. 2: Washington (U.S. Govt. Printing Office), 721–729.

Mehra, O. P., and Jackson, M. L., 1960. Iron oxide removal from soils and clays by a dithionite-citrate system buffered with sodium bicarbonate. *Clays Clay Miner.*, 7:317–327.

Olhoeft, G. R., 1980. Initial report of the petrophysics laboratory. 1977–1979 Addendum, *U.S. Geol. Survey Open File*, Rept. 80-522.

Press, F., 1966. Seismic velocities. *In* Clark, S. P., Jr. (Ed.), *Handbook of Physical Constants* (revised ed.). Mem. Geol. Soc. Am., 97:195–218.

Reynolds, R. C., and Hower, J., 1970. The nature of interlayering in mixed-layer illite-montmorillonites. *Clays Clay Miner.*, 18:25–36.

Risvet, B. L., 1978. *Reverse Weathering Reactions within Recent Nearshore Marine Sediments, Kaneohe Bay, Oahu.* Test Directorate Fiel Command, Kirtland AFB, New Mexico.

Schlumberger, 1958. *Introduction to Schlumberger Well Loggin* (Schlumberger Document No. 8): New York (Schlumberger We Surveying Corp.).

Schultz, L. G., 1964. Quantitative interpretation of mineralogical con position from x-ray and chemical data for the Pierre Shale. *Geo Surv. Prof. Pap. U.S.*, 391-C:1–31.

Vallier, T. L., and Kidd, R. B., 1977. Volcanogenic sediments in th Indian Ocean. *In* Heirtzler, J. R. (Ed.), *Indian Ocean Geology a Biostratigraphy:* Washington (Am. Geophys. Union), pp. 87–11

Date of Initial Receipt: 26 April 1984
Date of Acceptance: 26 August 1984

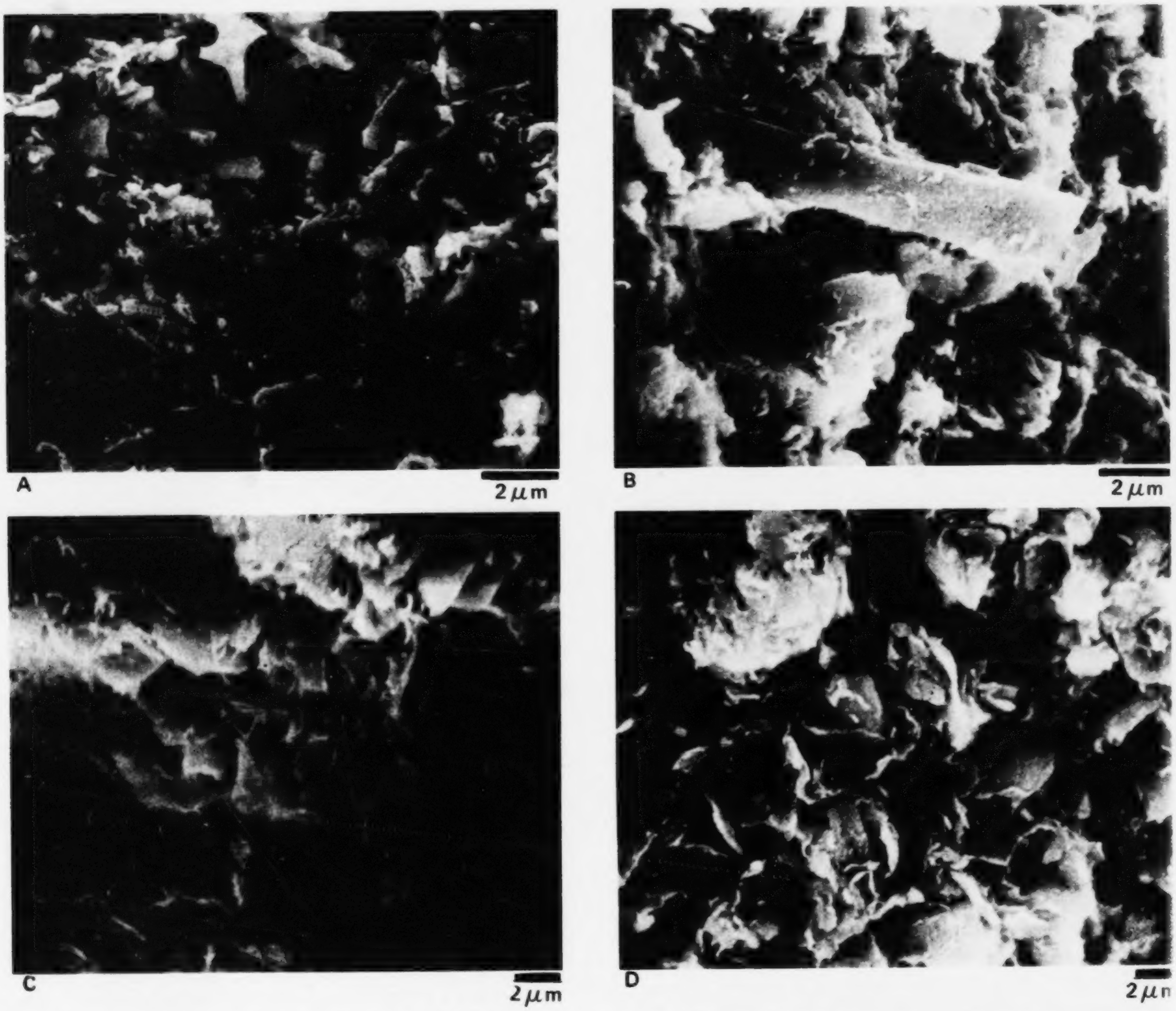

Plate 1. Scanning electron photomicrographs of pelagic clay textures. **A.** Smectite (Sample 576-8-6, 81–84 cm). **B.** Fibrous palygorskite (Sam ple 578-18-3, 38–45 cm). **C.** Authigenic phillipsite crystal (Sample 576-5-6, 18–25 cm). **D.** Opaline silica-rich clay (Sample 576-8-1, 98–105 cm

24. CLAY STRATIGRAPHY AT DEEP SEA DRILLING PROJECT SITES 576 AND 578, LEG 86 (WESTERN NORTH PACIFIC)[1]

Nicole Lenôtre, Bureau de Recherches Géologiques et Minières, Orléans, France
Hervé Chamley, Université de Lille I, Villeneuve d'Ascq, France
and
Michel Hoffert, Université de Bretagne Occidentale, Brest, France[2]

ABSTRACT

Late Cretaceous and Cenozoic sediments deposited on the eastern and western sides of the Shatsky Rise show similar clay assemblages of chlorite, illite, mixed layers, smectite, kaolinite, and palygorskite, and a similar vertical differentiation into three units. The deep-sea pelagic red clay is dominated by terrigenous components, which suggests that diagenesis is minor in this part of the western North Pacific and that eolian supply is very important. The role of the Shatsky Rise as a submarine barrier is of minor importance. The volcanic contribution to the clay component appears very small, as in some other parts of the Pacific Ocean. Stratigraphic correlations between Sites 576 and 578, which can be made from mineralogical data, partly offset the rareness of biostratigraphic markers.

INTRODUCTION

During Deep Sea Drilling Project (DSDP) Leg 86, one site was drilled on either side of the Shatsky Rise in the northwest Pacific basin (Fig. 1). Site 576, located east of the Shatsky Rise in 6220 m water depth, recovered a typical northwestern Pacific pelagic "red" clay section. Holes 576 and 576B penetrated about 55 m of pelagic red clay overlying 20 m of interbedded Campanian–Maestrichtian carbonate turbidites and pelagic clay before bottoming in chert at 76 m sub-bottom (see Site 576 chapter, this volume).

Site 578, located west of the Shatsky Rise in 6010 m water depth, was cored continuously to Campanian-Maestrichtian chert, 176 m below the seafloor. Hole 578 penetrated 76 m of olive gray anoxic clay grading downhole to radiolarian–diatom ooze that contains at least 55 ash beds. The ooze overlies 38 m of yellow brown clay with locally abundant radiolarians and 19 ash beds decreasing in abundance downhole, overlying 52 m of dark brown homogeneous pelagic clay with rare ferromanganese micronodules and chert (see Site 578 chapter, this volume).

Detailed sedimentologic studies of Sites 576 and 578 can resolve (1) whether or not the Shatsky Rise is a barrier to sediment transport and (2) the relative roles of terrigenous autochtonous sedimentation in these typical "red" clay areas.

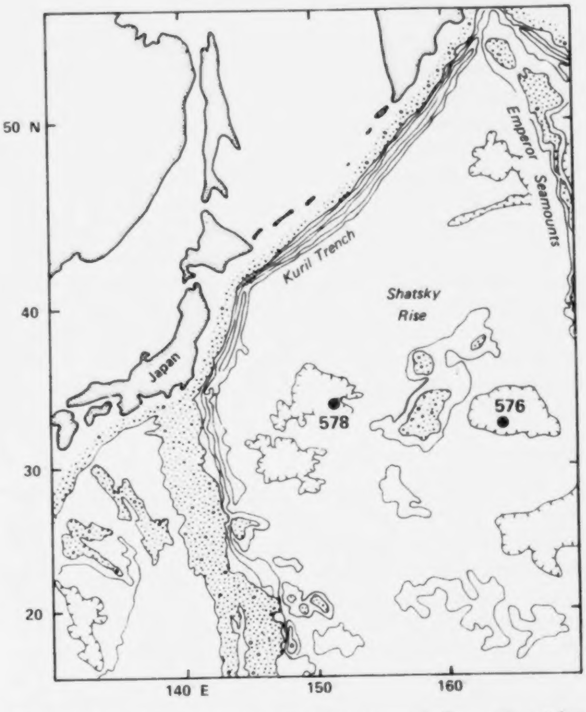

Figure 1. Location of Sites 576 and 578. Areas shallower than 4 km stippled, 5-km contour plain, 6-km contour hachured.

ANALYTICAL PROCEDURES

In our X-ray diffraction method, the samples were dissociated in water, then decarbonated in 5*N* hydrochloric acid. Excess acid was removed by successive centrifuging. Microhomogenization effects deflocculation. Fractions smaller than 2 μm were collected by decantation, using Stokes's law; then oriented pastes were made on glass slides. A Philips 1730 diffractometer (copper radiation) was used to run the X-ray diffraction scans at 2°2Θ/min. Three scans were carried out: (1) from 2.5° to 28.5°2Θ on natural (unglycolated) samples, (2) from 2.5° to 14.5°2Θ on glycolated samples, and (3) from 2.5° to 14.5°2Θ on samples heated for 2 hr. at 490°C. Semiquantitative evaluations were based on peak heights and areas (Chamley, 1971). The height of illite and chlorite 001 peaks on the scan of the glycolated sample were taken as references. By comparison with these values, values for smectite, palygorskite, and irregular mixed-layer clays were corrected by addition of peak height, whereas values for well-crystallized kaolinite were corrected by subtraction. The relative proportions of chlorite and kaolinite were determined from the ratio of peak heights (3.54 and 3.58 Å, respectively); when this ratio was 1:1, the amount of chlorite was assumed to be twice that of kaolinite. Data were given in percentages, the relative error being about ±5%.

---

[1] Heath, G. R., Burckle, L. H., et al., *Init. Repts. DSDP*, 86: Washington (U.S. Govt. Printing Office).

[2] Addresses: (Lenôtre) Bureau de Recherches Géologiques et Minières, Département Géologie Marine, B.P. 6009, 45060 Orléans Cedex, France; (Chamley) Sédimentologie et Géochimie, E.R.A. 764, Université de Lille I, 59655 Villeneuve d'Ascq, Cedex, France; (Hoffert) Océanologie et Géodynamique, G.I.S. Océanographie, Université de Bretagne Occidentale, 29273 Brest, France.

Electron-microscopic observations were made with a Siemens transmission microscope on less than 8-μm particles deposited on copper grids covered by a collodion film, after carbonate removal and physical deflocculation.

The geochemical procedure was as follows: the samples were dried at 105°C, then crushed and homogenized. Samples of 0.2 g were subjected to alkaline fusion, solubilized by HCl, and diluted to 100 ml; 0.2 g were then subjected to fluoronitric treatment in a bomb at 150°C and 50 bars for SiO_2 and Al_2O_3 determination. Also, 1 g was submitted to fluoroperchloric treatment, then solubilized by HCl and diluted to 100 ml. The dilutions were used for colorimetric analysis of TiO_2 and P_2O_5 and spectrophotometric analysis of other major and trace elements by atomic absorption in flame, with a type 5000 Perkin Elmer automatized spectrophotometer.

RESULTS

Smear Slide Data

Smear slides analyses have been carried out on each sample (selected results are shown in Table 1). Most sediments contain large amounts of clay-sized particles that are dominated by clay minerals. The sand fraction is significant in the late Pleistocene only (a few percent of quartz, feldspars, and heavy minerals). The silt fraction is generally not important and consists chiefly of siliceous biogenic debris (mainly diatoms). Nannofossils are absent, except in the Latest Cretaceous calcareous oozes, sometimes as graded beds. Volcanic glass and palagonite, as well as micronodules and opaque minerals, are dispersed in small amounts (0–10%) throughout the sedimentary column. Phillipsite occurs rarely, except in Cores 576-4 and 5 (up to 15%) and Sections 576B-3-6 and 4-6, and 578-17-1 and 17-3.

Nature of Clay Minerals

The clay assemblage identified in sediments from Sites 576 and 578 includes a fairly large range of minerals (Figs. 2 and 3). Well-crystallized illite (5–45% of clay minerals) and medium-crystallized smectites (15–90%) are the most abundant phases. They are accompanied by medium-crystallized chlorite (traces to 25%) and kaolinite (traces to 10%) and by noticeable amounts (traces to 30%) of irregular mixed-layer minerals (chiefly of chlorite–smectite and illite–smectite types). Palygorskite (traces to 30%) is easily recognizable on electron micrographs as abundant fibers, broken or whole (Plates 1 and 2). Associate minerals in the clay fraction consist of ubiquitous quartz, frequent feldspars, and opal CT.

Stratigraphic Distribution

Except for the palygorskite, the clay minerals identified occur throughout the stratigraphic column, extending from Late Cretaceous to latest Pleistocene. Three major mineralogical units can be distinguished (Figs. 2–4). The upper unit is characterized by comparable amounts of illite and smectite, and smaller amounts of chlorite, irregular mixed layers and kaolinite (Hole 576, Cores 1–5; Hole 576B, Cores 1–4; Hole 578, Cores 1–13). Separation between the upper unit and the middle unit is well marked by a sudden change in the proportions of clay minerals. The middle unit is characterized by high amounts of smectite and often of quartz, small amounts of palygorskite, and relatively low amounts of other clay minerals (Hole 576, Core 6 to Section 8-3; Hole 576B, Core 5 to Section 6-5; Hole 578, Cores 14–20 The lowest unit corresponds to the Late Cretaceous sediments recovered at Holes 576 (Section 8-3) and 576 (Sections 6-5 to 8-3) and is characterized by fairly abundant palygorskite (up to 30%) and abundant smectite There is no relationship between the clay mineralogy and the lithological units described in the site chapter (this volume). The clay assemblages do not change when the abundance of clay, volcanic glass, zeolites, nannofossils, or biogenic silica varies (Table 1). The upper mineralogical unit is fairly homogeneous, the relative abundance of each species varying by about 5 to 10% only. The middle mineralogical unit beneath the well dated Neogene sediments shows important quantitative variations of the different species, especially illite and smectite. Palygorskite forms less than 5% of these dark brown pelagic clays and can be clearly identified by electron microscopy only. Palygorskite appears in increased amounts on the X-ray diagrams corresponding to the Site 576 Maestrichtian–Campanian carbonates and pelagic clays (lowest unit).

Clay Morphology

Three major morphological facies can be identified from transmission electron microscopic observations. (1) The first facies is restricted to the upper part of the drill holes (Neogene to Quaternary pelagic clay and radiolarian–diatom ooze) and is characterized by abundant well-shaped and rather broad sheets, mainly of illite and chlorite (Plate 1, Figs. 1, 2). Illite and chlorite are accompanied by variable amounts of fleecy and small particles (smectite and irregular mixed layers) and a few kaolinite hexagons. Isolated fibers of palygorskite, not identifiable on X-ray diffractograms, are sparse in all the levels. More or less dissolved diatom and radiolarian debris is frequently present, and corresponds to the opal recognized by X-ray diffraction. (2) The second facies occurs chiefly in the lower part of the sedimentary columns (brown pelagic clay and nannofossil ooze) and is distinguished by fairly abundant to abundant palygorskite, which increases downward (Plate 1, Figs. 3, 4; Plate 2, Figs. 1, 2). Associated with the palygorskite in this facies are smectite, variable amounts of illite, chlorite, and kaolinite, and some strongly dissolved siliceous debris. The palygorskite occurs as well-shaped but often broken fibers, either isolated or grouped into small bundles. The abundance of the fibrous clays on electron micrographs appears higher than on X-ray diffractograms, especially in Sample 576B-8-3, 82 cm where these minerals occupy nearly 50% of the total clay surface. (3) The third morphological facies consists of very abundant smectite (up to 80%) and corresponds to the brown pelagic clay in the lower, barren part of the drilled sections. Smectite

Table 1. Clay mineralogy and smear slide data (%) of selected samples from Sites 576 and 578.

	Smear slide												X-ray diffractograms					
	Grain size			Bulk petrography									Clay mineralogy					
Sample (interval in cm)	Sand	Silt	Clay	Clay minerals	Quartz	Zeolites	Other minerals	Volcanic glass	Palagonite	Opaques	Micro-nodules	Siliceous debris	Chlorite	Illite	Mixed layers	Smectite	Kaolinite	Palygor-skite
Hole 576																		
1-1, 26-28	1	39	60	70	20	—	2	2	2	1	1	3	25	40	15	15	5	—
2-3, 130-132	0	5	95	90	5	—	tr	1	1	tr	2	1	5	35	15	35	10	—
6-3, 20-22	1	4	95	95	tr	5	—	—	—	—	—	—	5	20	5	65	5	—
Hole 576B																		
1-6, 10-13	7	13	80	75	15	—	—	5	2	—	1	2	10	35	15	35	5	—
5-2, 100-103	1	5	94	94	1	—	tr	1	—	2	2	—	5	10	5	80	tr	tr
8-3, 30-33	1	8	91	91	1	—	tr	1	—	2	5	—	tr	10	10	55	tr	25
Hole 578																		
2-3, 20-22	15	40	45	44	20	—	1	10	—	—	—	25	10	25	15	40	10	—
5-2, 78-80	3	17	80	80	3	—	1	1	2	—	—	13	15	35	15	25	10	—
6-6, 78-80	10	25	65	65	3	—	tr	22	—	—	—	10	15	35	20	25	5	—
11-2, 30-32	2	20	78	78	3	—	tr	tr	tr	5	—	14	5	30	15	40	10	—
15-6, 33-35	0	7	93	93	2	—	tr	tr	1	3	1	—	tr	10	5	80	5	—
16-6, 10-12	0	5	95	93	2	—	tr	tr	1	3	1	—	tr	10	5	80	5	tr
18-1, 56-58	0	5	95	81	1	—	tr	tr	tr	15	3	tr	5	15	tr	75	5	—

Note: tr = trace, — = not present.

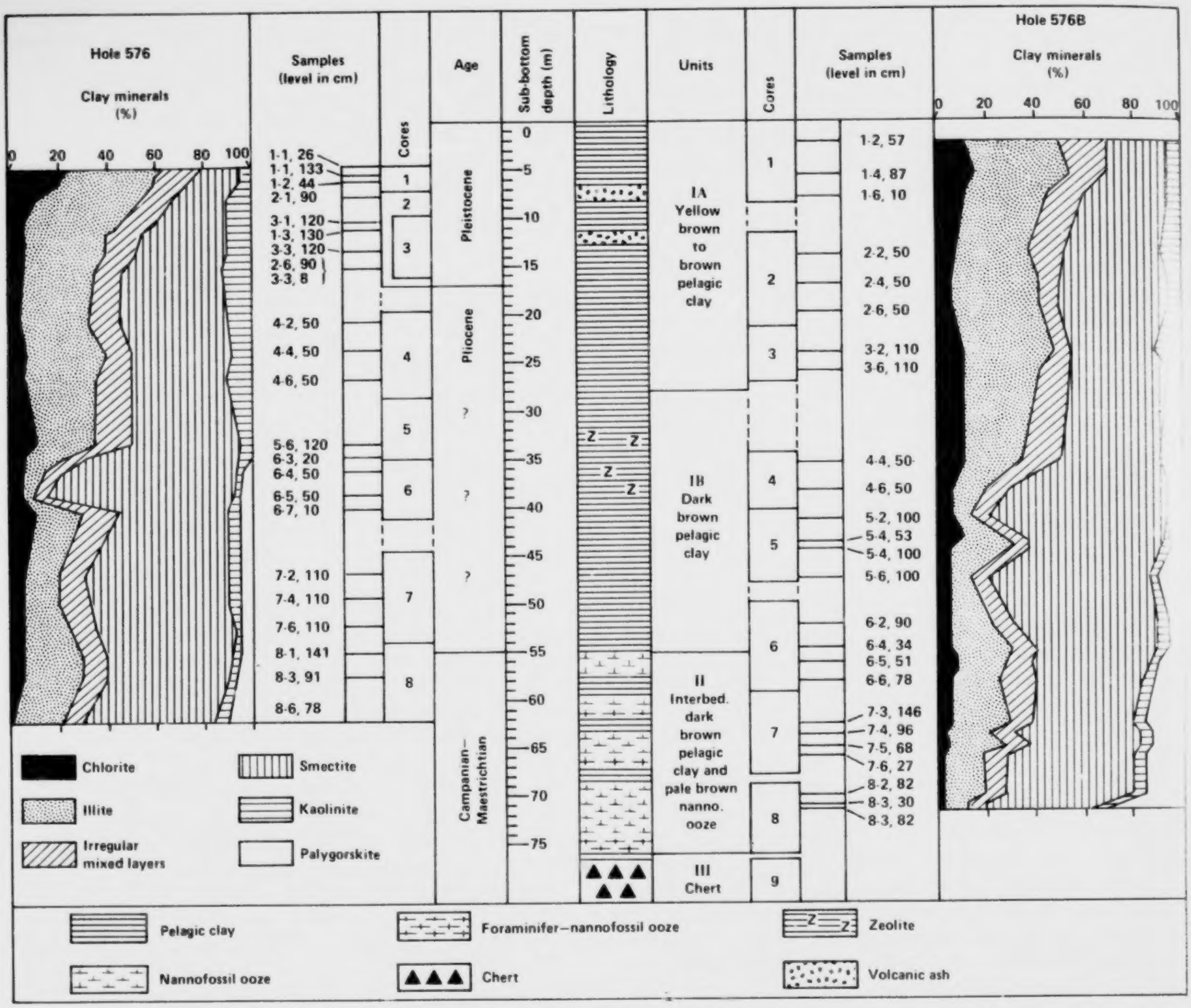

Figure 2. Lithology and clay mineralogy of Site 576 plotted versus adjusted sub-bottom depth. Tables used to compute adjusted depths are given in the Site 576 chapter (this volume).

typically occurs as cloudy and fleecy particles of variable size and is accompanied by small amounts of illite, palygorskite, and other clay minerals (Plate 2, Figs. 3, 4).

All the facies identified and all the levels studied are characterized by the total morphological independence of the different clay minerals. In particular, smectite does not show any transition from fleecy to lathed particles, and palygorskite fibers or bundles are completely isolated and dispersed among the other minerals.

Comparison between Sites 576 and 578

In addition to the similarities in the clay stratigraphy described above, the percentages of the different clay species at the two drilling sites are similar (Figs. 2 and 3). There are no major differences in the relative abundances of chlorite, illite, irregular mixed layers, smectite, and kaolinite on the eastern and the western sides of the Shatsky Rise. Only three minor differences can be noticed. (1) The relative abundances of illite and chlorite tend to increase slightly, and of smectite to decrease, toward the top of the Pleistocene sediments, east of the Shatsky Rise (Holes 576 and 576B). (2) Palygorskite is significantly more abundant in the lowest part of Hole 576B (Cores 6–8), in sediments of Campanian–Maestrichtian age that were only poorly recovered at Site 578 (Core 20). (3) Variations in the abundance of illite in the lower mineralogical zone are greater at Site 578 (e.g., Samples 578-18-4, 86 cm and 56 cm, 578-17-3, 36 cm, and 578-16-2, 10 cm) than at Site 576.

DISCUSSION

Origin of Clay Minerals

The large number of clay species, the abundance of minerals typically derived from land masses (illite, irregular mixed layers, kaolinite, quartz), the parallel variations of illite and chlorite, the medium crystallinity of smectite, the absence of continuous mineralogical evo-

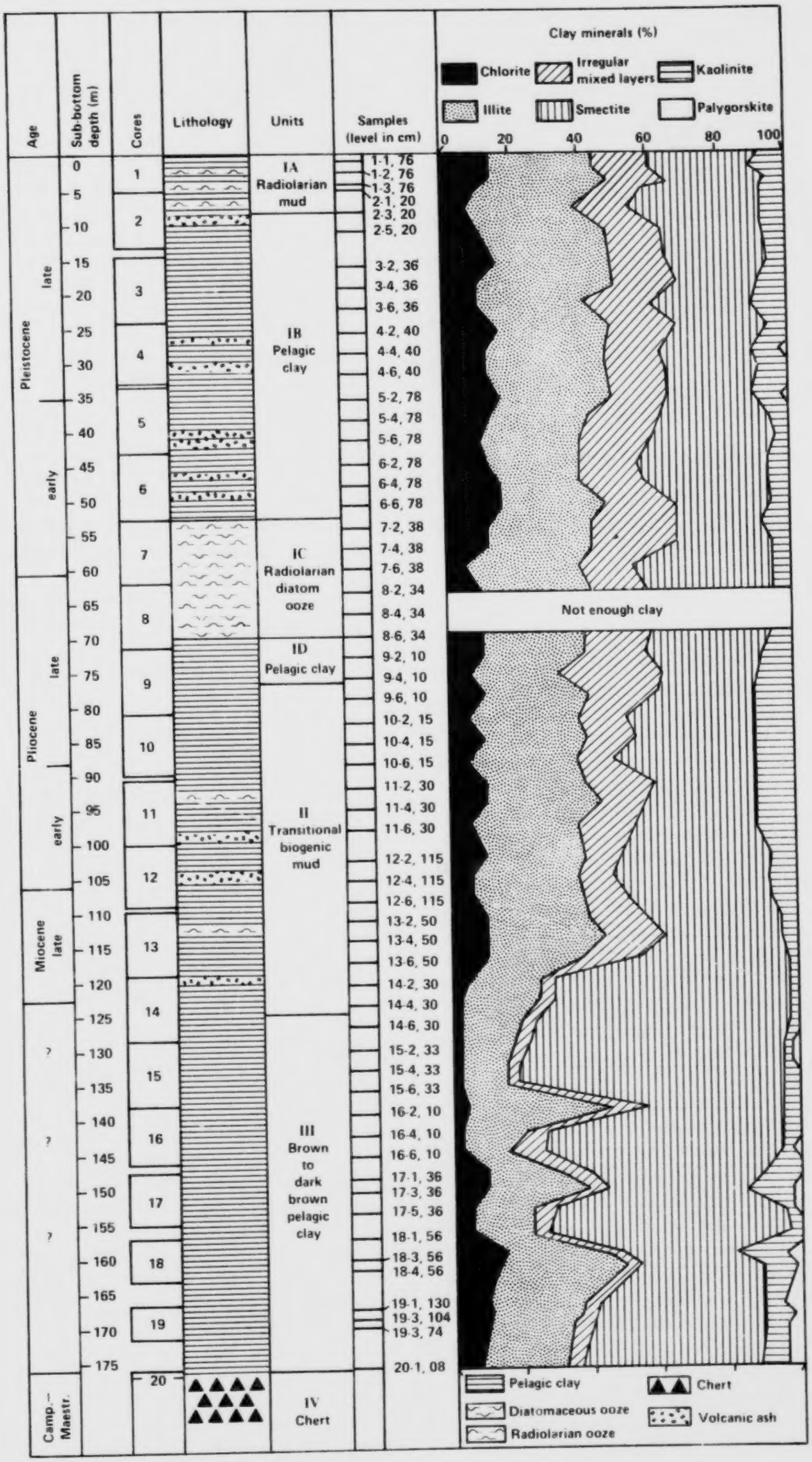

Figure 3. Lithology and clay mineralogy of Site 578.

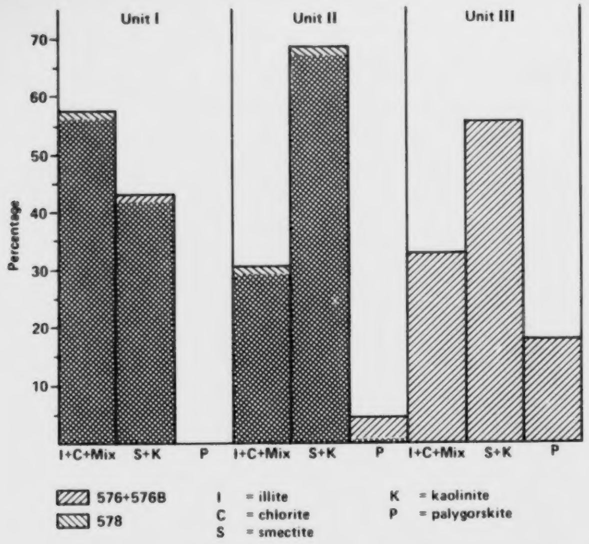

Figure 4. Comparison of clay stratigraphy in Sites 576 and 578. Results are averages of all sample compositions from each unit. Amounts of smectite and palygorskite are individualized because they vary a lot from one unit to another.

lution with increasing depth of burial, the lack of relationships between clay assemblages, lithology, and associated minerals such as zeolites or micronodules (see smear slide data in site chapters), and the morphological independence of each clay species from the others, clearly point to the importance of detrital supply to Sites 576 and 578 during the Cenozoic. Such a result is in agreement with the data of Hein et al. (1975) and Leinen and Heath (1981), who have shown the importance of detrital minerals in North Pacific sediments, especially during the past 25 m.y. The clay assemblages identified at Sites 576 and 578 are similar to those encountered farther west in the North Pacific (Legs 57, 58, and 87), where the Neogene clays are chiefly derived from the erosion of rocks and soils in Japan and Eastern Asia (Chamley, 1981; Chamley et al., in press). The main difference at Sites 576 and 578 is the larger amount of illite, which is a typical detrital mineral that is more abundant at the more northern location of the Leg 86 drill sites (Griffin et al., 1968). Clay minerals appear to be transported from Asia by marine currents, especially the prolongation of the Kuroshio and Oyashio currents and by atmospheric circulation (Leinen and Heath, 1981).

The importance of detrital supply in the northwestern Pacific is a result of the relative proximity of the Asiatic land mass. The fairly high sedimentation rates (~ 3 cm/10^3 yr. during the Pleistocene at Site 578; 1 cm/10^3 yr. at Site 576) inhibit reactions between aluminosilicates and seawater and diminish the possibility of *in situ* clay genesis. This situation contrasts with other parts of the Pacific, especially in the central eastern zone, where very low sedimentation rates and the absence of significant detrital supply allow the autochtonous formation of large amounts of smectite (Hoffert, 1980).

Volcanic Influence on the Clay Composition

The relative abundance and good crystallinity of smectite, partly associated with significant amounts of palygorskite, in the lower part of the sedimentary columns at Sites 576 and 578 could result from the alteration of volcanic materials or from increased volcanohydrothermal activity during the early Cenozoic and the Latest Cretaceous. Such a possibility is not supported by the facts. Electron micrographs do not show the large smectite laths or tufts typically developed from the alteration of volcanic lava, ash, or glass (e.g., Chamley, 1981). Palygorskite and smectite are not developed in nodules, concretions, or specific levels and are completely dispersed among the detrital minerals (Plates 1 and 2). Moreover, there is no relationship between the abundance of smectite or palygorskite and the presence or abundance of morphologically distinct volcanic particles, zeolites such as phillipsite, or palagonite (Table 1). Similarly, the smectite abundance and morphology are not correlated with the presence or abundance of opaque minerals, micronodules, iron oxides, or siliceous debris. All of these observations argue against autochtonous clay genesis due to volcanism or *in situ* conditions. If diagenetic processes occur in the Shatsky Rise area, they have had little impact on the clay mineralogical budget since the end of the Cretaceous. This is analogous to the situation in the Atlantic Ocean which also has fairly high sedimentation rates (Chamley, 1979).

Influence of the Shatsky Rise on Clay Sedimentation

A significant finding from the mineralogical study is the absence of differences across the Shatsky Rise. The types and proportions of clay minerals identified are the same and show similar proportions on the eastern (Site 576) and on the western (Site 578) sides of the Rise. Palygorskite is more abundant in the lower part of Site 576B (from Cores 576-8 and 576B-6 downward) than at the base of Site 578 (Figs. 2 and 3), but this is probably due to a slight difference in age: Hole 578 bottomed in late Maestrichtian deposits, whereas Holes 576 and 576B penetrated into Campanian–Maestrichtian sediments.

The first consequence of the mineralogical similarity between the two sites is that the Shatsky Rise did not act as a significant barrier to the detrital supply from Asiatic land masses. This is especially true for minerals of unequivocal terrigenous origin such as illite, chlorite, mixed layers, and kaolinite. The transport of land-derived minerals has occurred either by surficial and intermediate water masses little affected by submarine barriers, or by air masses as shown by Bonatti and Arrhenius (1965), Windom (1975), Leinen and Heath (1981), Rea and Janecek (1981, 1982). The Shatsky Rise may have limited the amounts, but not the nature, of detrital materials issued from Asia. This is suggested by the lower sedimentation rates at Site 576 than at Site 578. Such a decreased terrigenous supply could also result solely from the increased distance of the source land masses.

The second consequence of the homogeneous influence of the land supply across the whole Shatsky Rise area is that the clay successions identified at Sites 576 and 578 can be used for stratigraphic correlations (Figs. 2, 3, and 4). Mineralogical correlations between the two sites are particularly useful when the sediments are devoid of common microfossils, as is the case for the brown to dark brown pelagic clays located below the well-dated Neogene sediments. The general stratigraphic correlations based on clay mineralogical data are summarized in Table 2. More precise stratigraphic correlations might be possible but they would necessitate more dense sampling. For example, the increase in illite and chlorite in samples 576-6-7, 576B-5-4, and 578-16-2 (Figs. 2 and 3) could be an identifying marker. The inverse variations of the illite group (illite, chlorite, irregular mixed layers), and of the smectite during the Neogene and the Quaternary at Site 578 (Fig. 3), probably reflect climatic variations on land (soils development) and in the sea (location and intensity of currents).

The influence of the Shatsky Rise on clay sedimentation during the Latest Cretaceous and the early Cenozoic remains questionable. The sources of the large amounts of smectite and, locally, of palygorskite in the sediments could be Asia, where these minerals could have formed massively in soils and perimarine basins of the world during the warm and humidity-contrasted climate of this geologic period (e.g., Millot, 1964; Chamley, 1979). Eolian transport is possible, given the parallel increases of smectite, palygorskite, and quartz often observed in sediments from Sites 576 and 578 (see also Leinen and Heath, 1981; and Leinen, this volume). Alternatively, the Shatsky Rise itself could have been a source if this volcanic area was emergent and exposed to weathering and erosion during the early Cenozoic. The large oscillations in the abundance of illite, chlorite, and kaolinite, which are particularly well recorded in pre-Miocene sediments at Site 578, could perhaps record major stages of subsidence of the rise toward its present position. There is, however, no hard evidence to support the hypothesis of an emergence of the Shatsky Rise: Late Cretaceous and Cenozoic sequences sampled by DSDP Legs 6 and 32 consist of pelagic nannofossil ooze and some zeolite clay (Fisher et al., 1971; Larson, Moberly, et al., 1975), but no minerals derived from subaerial weathering of volcanic rocks comparable to those recognized in the Emperor Seamount area (Karpoff, 1980).

Table 2. Main stratigraphic correlations between Sites 576 and 578, from clay mineralogical data.

Clay mineralogical units (significant minerals)	Unit depth (Core-Section)		
	Hole 576	Hole 576B	Hole 578
I (chlorite, illite, mixed layers)	1-1 to 5-6	1-1 to 4-4	1-1 to 13-6
II (smectite)	6-3 to 8-1	4-6 to 6-4	14-2 to 20-1
III (palygorskite, smectite)	8-3 to 8-6	6-5 to 8-3	—

Note: — = not reached.

ACKNOWLEDGMENTS

We are grateful to the Leg 86 shipboard party for helpful sampling and stimulating discussions, and to M. Bocquet, J. Carpentier, F. Dujardin, and P. Recourt for efficient technical assistance. This manuscript was improved by the helpful reviews of Margaret Leinen and Jane Schoonmaker. The financial support of ATP GGO 1983 (CNRS) and BRGM (France) is gratefully acknowledged.

REFERENCES

Bonatti, W. P., and Arrhenius, G., 1975. Eolian sedimentation in the Pacific off northern Mexico. *Mar. Geol.*, 3:337–348.

Chamley, H., 1971. Recherches sur la sédimentation argileuse en Méditerranée. *Sci. Geol. Mem., Strasbourg (France)*, 35:1–215.

________, 1979. North Atlantic clay sedimentation and paleoenvironment since the Late Jurassic. *In* Talwani, M., Hay, W., Ryan, W. B. F. (Eds.), *Deep Drilling Res. Atlantic Ocean: Continental Margins and Paleoenvironment*, Maurice Ewing Ser. (Am. Geophys. Un.), 3:342–361.

________, 1981. Clay sedimentation and paleoenvironment in the Shikoku Basin since the middle Miocene (Deep Sea Drilling Project Leg 58, North Phillippine Sea). *In* Klein, G. deV., Kobayashi, K., et al., *Init. Repts. DSDP*, 58: Washington (U.S. Govt. Printing Office), 669–681.

Chamley, H., Cadet, J.-P., and Charvet, J., in press. Paleoenvironmental significance of Pacific clay assemblages off the Japan since the Miocene. *In* Kagami, H., Karig, D. E., Coulbourn, W. T., et al., *Init. Repts. DSDP*, 87: Washington (U.S. Govt. Printing Office).

Fisher, A. G., Heezen, B. C., et al., 1971. *Init. Repts. DSDP*, 6: Washington (U.S. Govt. Printing Office).

Griffin, J. J., Windom, H., and Goldberg, E. D., 1968. The distribution of clay minerals in the World Ocean. *Deep-Sea Res.*, 15: 433–459.

Hein, J. R., Schall, D. W., and Gutmacher, C. E., 1975. Neogene clay minerals of the far NW Pacific and southern Bering Sea: sedimentation and diagenesis. *Proc. Int. Clay Conf.*, 1975, pp. 71–80.

Hoffert, M., 1980. Les "Argiles rouges des grands fonds" dans le Pacifique Centre-Est. Authigenèse, transport, diagenèse. *Sci. Geol. Mem.*, 61:1–231.

Karpoff, A. M., 1980. The claystone layer between two basalt flows in Hole 432A: an argument for the emergence of Nintoku Seamount. *In* Jackson, E. D., Koizumi, I., et al., *Init. Repts. DSDP*, 55: Washington (U.S. Govt. Printing Office), 707–711.

Larson, R. L., Moberly, R., et al., 1975. *Init. Repts. DSDP*, 32: Washington (U.S. Govt. Printing Office).

Leinen, M., and Heath, G. R., 1981. Sedimentary indicators of atmospheric activity in the Northern Hemisphere during the Cenozoic. *Palaeogeogr. Paleoclimatol. Paleoecol.*, 36:1–21.

Millot, G., 1964. *Géologie des Argiles*: Paris (Masson).

Rea, D. K., Janecek, T. R., 1981. Late Cretaceous history of eolian deposition in the mid-Pacific mountains, central north Pacific Ocean. *Paleogeogr., Paleoclimatol., Paleoecol.*, 36(1/2):55–67.

________, 1982. Late Cenozoic changes in atmospheric circulation deduced from north Pacific eolian sediments. *Mar. Geol.*, 49:149–167.

Windom, H. L., 1975. Eolian contributions to marine sediments. *J. Sediment. Petrol.*, 45:520–529.

Date of Initial Receipt: 6 December 1983
Date of Acceptance: 2 October 1984

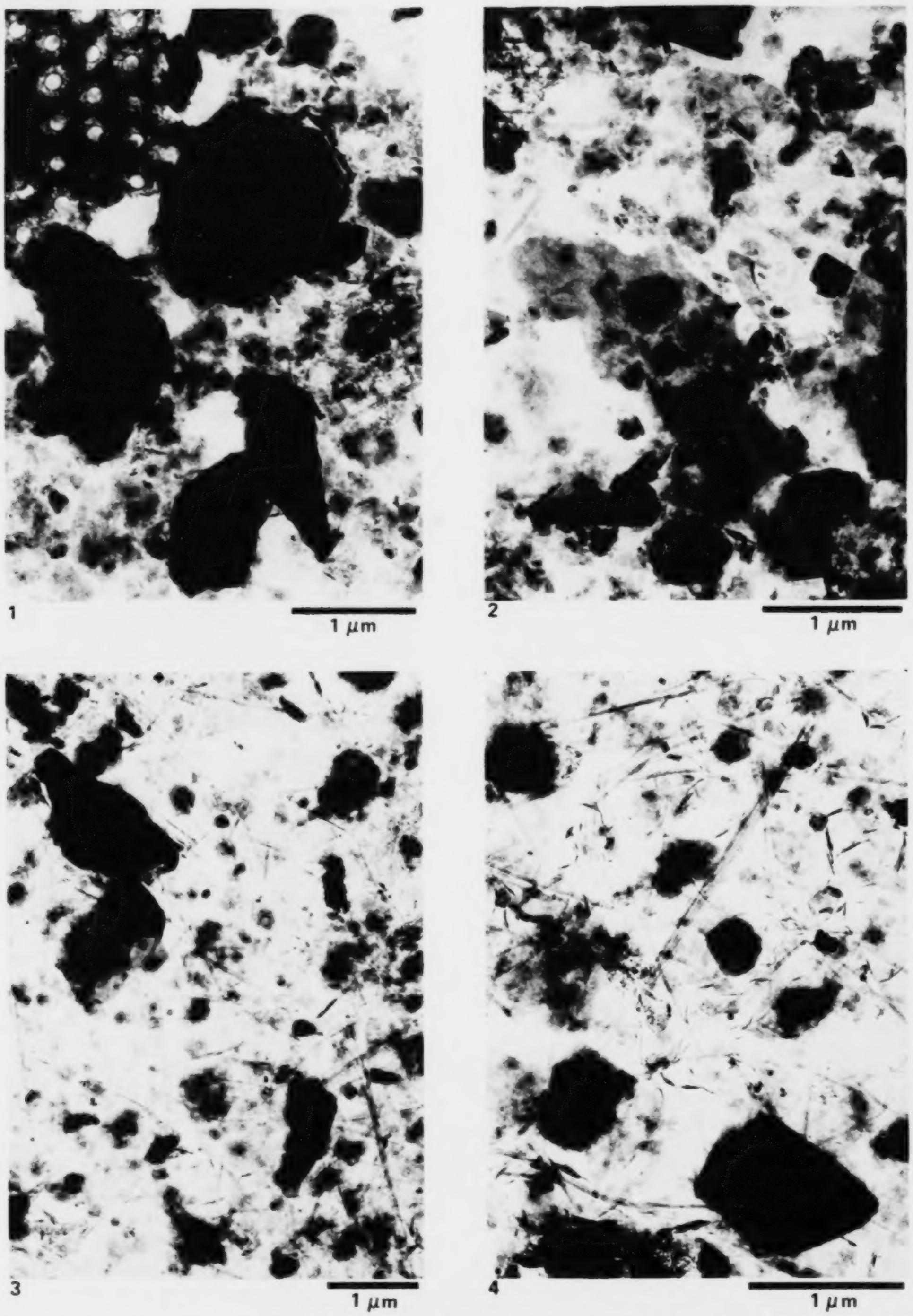

Plate 1. Electron micrographs—transmission electron microscopy. **1,2.** Illite and chlorite-rich assemblage. Sample 576-1-1, 135 cm, yellowis brown to brown pelagic clay. Abundant well-shaped illite and chlorite sheets, small fleecy smectite particles, rare hexagonal kaolinite and fibers c palygorskite. Siliceous biogenic debris. **3,4.** Assemblage with fairly abundant palygorskite. Sample 576-8-6, 78 cm, Upper Cretaceous, dar brown pelagic clay. Isolated palygorskite fibers or bundles, sometimes broken. Illite, chlorite, and smectite. Strongly dissolved siliceous debri

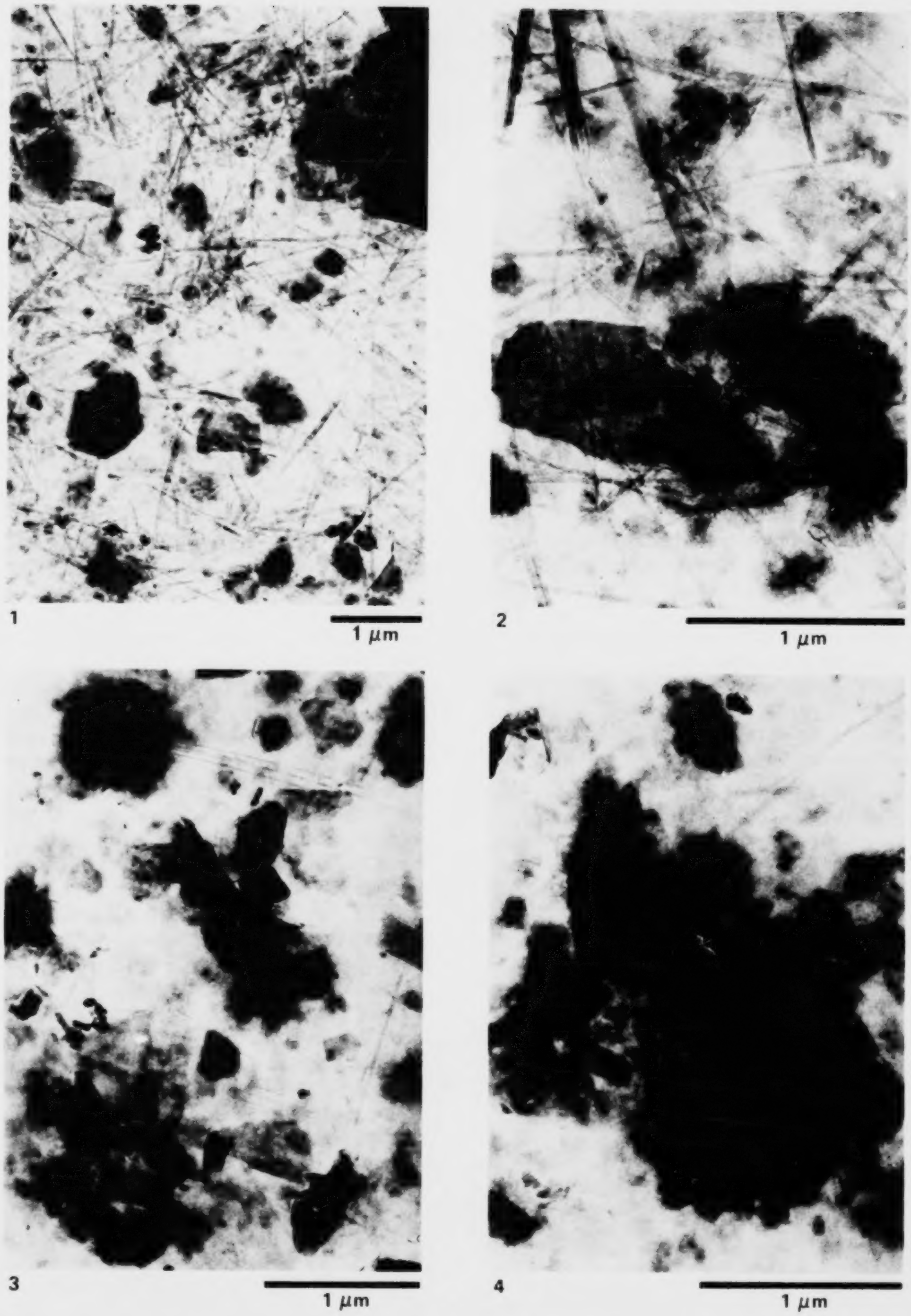

ate 2. Electron micrographs. **1,2.** Palygorskite-rich assemblage. Sample 576B-8-3, 82 cm, upper Cretaceous, dark brown pelagic clay. Abundant palygorskite, as isolated fibers or bundles, often broken, dispersed among fleecy smectite and well-shaped illite. **3,4.** Smectite-rich assemblage. Sample 578-15-4, 33 cm, early Cenozoic (?), brown pelagic clay. Abundant fleecy and cloudy smectite, associated with low amounts of illite and palygorskite.

25. QUARTZ CONTENT OF NORTHWEST PACIFIC HOLE 576A AND IMPLICATIONS FOR CENOZOIC EOLIAN TRANSPORT[1]

Margaret Leinen, University of Rhode Island[2]

ABSTRACT

The amount and the accumulation rate of quartz were measured in 33 samples from Hole 576A. The amount and source of mineral aerosol being deposited in the northwest Pacific during the Cenozoic are evaluated using these data. When Hole 576A is compared to a Cenozoic record in the central North Pacific, a strong uniformity in the composition of the mineral aerosol across the North Pacific is seen. The data suggest that Hole 576A entered the influence of the westerlies about 15 m.y. ago and that since that time the rates of sediment deposition have increased. Only the dramatic change in quartz accumulation 2.5 m.y. ago can be clearly related to a climatic event, but a gradual increase in quartz accumulation through the Miocene and early Pliocene is probably a result of increasing Northern Hemisphere aridity and intensified atmospheric activity associated with global cooling during the interval.

INTRODUCTION

Since quartz does not precipitate authigenically in the deep sea, variations in its accumulation rate in unlithified oceanic sediments must result from changes in detrital sedimentation. At sites remote from land and protected from turbidite deposition, the quartz content of sediments reflects eolian transport of terrigenous mineral aerosol to the oceans (Rex and Goldberg, 1958; Rex et al., 1969; Windom, 1969, 1975). The distribution of quartz in surface sediments mirrors present-day atmospheric circulation patterns (Heath et al., 1973; Kolla and Biscaye, 1977; Molina-Cruz and Price, 1977; Thiede, 1979), and its variation in Pleistocene sediments has been shown to reflect changes in wind intensity, wind-belt position, and continental weathering in areas removed from the influence of continental runoff and transport down the continental slope in areas closer to shore (Kolla and Biscaye, 1977; Pisias and Leinen, 1983; Schramm, 1983).

Only one long, continuous, and unequivocally eolian pre-Pleistocene record of deep-sea quartz content has been available previously to study Cenozoic eolian deposition in the Pacific Ocean (Core LL44-GPC3, Leinen and Heath, 1981). Without others it has been difficult to evaluate the relative importance of changing rates of eolian input and changing composition of mineral aerosol from changes in deposition due to migration of the te into and out of wind belts (caused by rotation of the acific plate).

By examining the long, continuous red-clay sediment cord from Hole 576A, we can constrain the previous odels of Cenozoic eolian deposition in the North acific. Site 576 is presently located at 32°21.4′N, 64°16.5′E, beneath the core of the Northern Hemihere westerlies (Fig. 1). About 53 m of pelagic clay verlying about 13 m of interbedded Late Cretaceous arbonate turbidites and pelagic clay were recovered from Hole 576A. A companion hole, Hole 576, terminated on chert at 76 m. The uppermost clays are yellowish brown and slightly silty. Below about 12 m the clays are dark brown, finer grained, and somewhat "slick" when cut. The lithologic column from Hole 576A is very similar to, but thicker than, that recovered in a long piston core, Core LL44-GPC3, from the central North Pacific. Thus, the quartz content of Hole 576A can be used to study Cenozoic eolian deposition in the western North Pacific.

METHODS

The quartz content of 33 samples from Hole 576A was measured using a modification of the techniques of Till and Spears (1969) and Ellis and Moore (1973). Freeze-dried samples were leached with acetic acid buffered to pH 5.6 with sodium acetate to remove calcium carbonate. This procedure and subsequent washing of the sample in deionized water also removed sea salt from interstitial pore water in the sample. An amount of alpha Al_2O_3 equal to one-half the sample weight was added to each sample as an internal standard. The samples were ground for 2 hr. in an automatic mortar and pestle to achieve a uniform grain size, dried, and fired at 1000°C in alumina crucibles for 24 hr. to eliminate interference caused by clay minerals. The samples were subsequently ground briefly in alumina mortars under acetone and the dried, powdered samples were pressed into duplicate X-ray planchettes using 40-mesh granulated zinc as a backing medium. The samples were X-rayed on a Phillips diffractometer using Ni-filtered, monochromatized CuK alpha radiation at 45 kV and 35 mA. Each sample was scanned from 25.11° to 25.94° 2θ at 0.004° 2θ/s (200 s) over the 3.48-Å (012) alumina peak and from 26.17° to 27.00° 2θ at the same rate and for the same time interval over the 3.34-Å (101) quartz peak. To correct the X-ray peaks for background, 200-s background counts were made at 25°, 26°, and 27° 2θ. The total X-ray counts over the 200-s intervals were collected digitally by an interfaced microprocessor and used to calculate peak areas of alumina and quartz. The ratio of quartz/alumina peak areas was converted to weight percent quartz in the sample by reference to a calibration curve determined by standard additions of quartz to a central North Pacific red clay from 2500 to 2550 cm depth in Core LL44-GPC3 that has been homogenized and is used as a standard for geochemical and mineralogical analyses in our laboratory.

RESULTS AND DISCUSSION

Quartz Content of Hole 576A Samples

The quartz contents of Hole 576A samples are listed in Table 1. The average of the duplicate determinations of quartz concentration is plotted versus depth in Fig-

---

[1] Heath, G. R., Burckle, L. H., et al., *Init. Repts. DSDP*, 86: Washington (U.S. Govt. rinting Office).

[2] Address: Graduate School of Oceanography, University of Rhode Island, Narraganett, RI 02882.

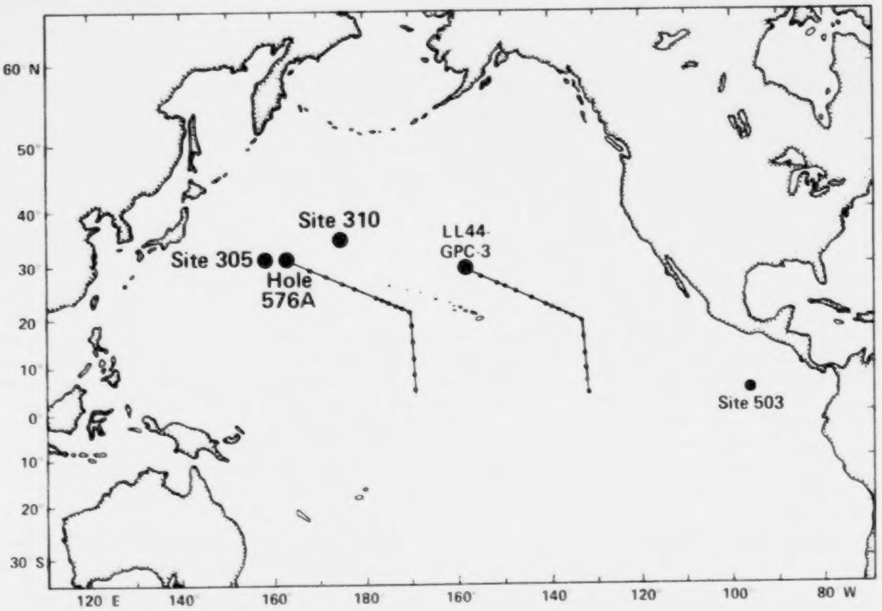

Figure 1. Location of DSDP Hole 576A and Core LL44-GPC-3. DSDP Sites 305, 310, and 503 are also shown. The backtrack paths along which the sites traveled in response to seafloor spreading are also shown. Dots along these paths correspond to 5-m.y. time intervals. 20°N latitude is the approximate present-day boundary between the Northern Hemisphere westerlies and northeast trade winds.

Table 1. Quartz content of Hole 576A samples.

Core-Section (interval in cm)	Sub-bottom depth (cm)	Quartz (wt %)		
		1	2	Average
1-1, 21-25	23	16.94	16.31	16.63
1-3, 81-85	383	18.39	17.82	18.11
1-6, 80-83	831	15.57	15.48	15.52
2-3, 47-50	1219	17.79	16.91	17.35
3-1, 47-50	1869	13.05	13.06	13.06
3-3, 70-73	2191	8.46	9.27	8.87
3-4, 117-120	2389	11.20	12.11	11.66
3-5, 127-130	2549	9.07	8.97	9.02
3-6, 110-113	2681	14.05	15.23	14.64
4-1, 50-53	2821	10.91	10.93	10.92
4-2, 103-106	3025*	8.62	8.52	8.57
4-3, 98-101	3169	6.02	5.60	5.81
4-4, 104-107	3325	5.81	5.91	5.86
4-5, 20-23	3391	4.36	4.15	4.25
4-6, 60-63	3581	5.16	5.47	5.31
5-1, 87-90	3809	5.17	5.15	5.16
5-2, 40-43	3911*	1.68	1.84	1.76
5-3, 30-33	4051	2.64	2.63	2.64
5-5, 137-140	4459	4.72	4.63	4.67
5-6, 130-133	4601	2.85	2.91	2.88
5-7, 25-28	4646	6.22	6.14	6.18
6-1, 90-93	4761	3.92	4.00	3.96
6-2, 47-50	4869	4.35	4.06	4.21
6-3, 93-96	5065*	4.74	4.87	4.81
6-4, 11-14	5132	6.29	5.95	6.12
6-5, 12-15	5283	5.46	5.36	5.41
6-5, 127-130	5399	4.54	4.54	4.54
6-6, 17-20	5439	5.53	5.05	5.29
6-7, 22-25	5593	4.03	3.80	3.91
7-1, 137-140	5759	4.18	4.14	4.16
7-2, 22-25	5793	5.48	5.51	5.50
7-3, 17-20	5939	7.15	5.77	6.46
7-3, 35-38	5946	3.51		3.51

Note: All sub-bottom depths were calculated by G. R. Heath on the basis of correlation with Holes 576 and 576B. Samples with asterisks are from intervals that show some evidence of flow-in.

ure 2. The sample spacing in the upper portion of the core was intentionally larger than that in the middle and lower portion of the core because it was anticipated that sedimentation rates for the upper (late Neogene) portion of the sedimentary record would be much greater than those for earlier time intervals.

Comparison of Hole 576A and Core LL44-GPC3 Quartz Content

Also plotted for comparison on Figure 2 is the quartz content of samples from Core LL44-GPC3, the central North Pacific (30°19.9′N, 157°49.9′W) red clay core that has been used by Leinen and Heath (1981) to infer Cenozoic eolian deposition. The age at the bottom of Core LL44-GPC3 is roughly equivalent to that at the base of Hole 576A.

The stratigraphy for Core LL44-GPC3 has been revised and additional quartz-content determinations have been made since it was first published. The original stratigraphy was based on paleomagnetic reversal stratigraphy in the upper 4 m (2.47 m.y. ago) of the core (Prince et al., 1980) and ichthyolith stratigraphy for the remaining 20 m of the core (Doyle and Riedel, 1979). Additional ichthyolith age determinations (Doyle, 1980) and identification of an Ir anomaly associated with the Cretaceous/Tertiary boundary (Kyte and Wasson, in press) ha resulted in a new stratigraphy that is discussed in deta in Leinen and Heath (in press) and is used in this cha ter. The stratigraphy for Hole 576A is based on correl tion with that of Holes 576 and 576B. Holes 576 an 576B were dated using paleomagnetic reversal stratigraphy (Heath et al., 1983; Heath, Rea, and Levi, this vo ume), ichthyolith stratigraphy (Doyle, 1983; Doyle an

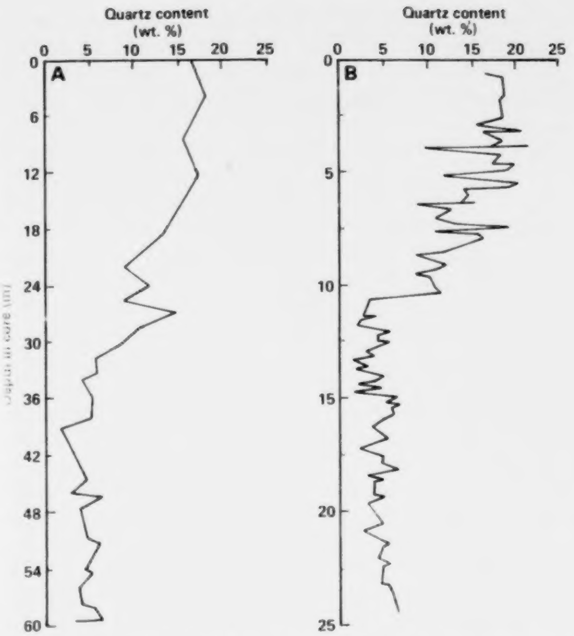

Figure 2. Quartz contents of (A) Hole 576A and (B) Core LL44-GPC-3 in weight percent plotted versus depth in core. (All data are calcium carbonate and biogenic opal-free values.) Because of differences in sedimentation rates, the plots are essentially age equivalent (i.e., bottom of both cores are approximately time equivalent).

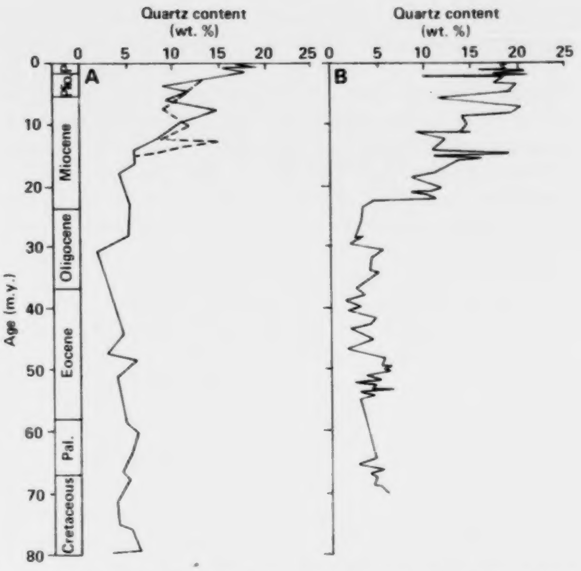

Figure 3. Quartz content of (A) Hole 576A and (B) Core LL44-GPC-3 in weight percent plotted versus age. All data are calcium carbonate and biogenic opal-free values. Dotted line on the curve for Hole 576A indicates age determinations for the Miocene Epoch based solely on ichthyolith stratigraphy.

Riedel, this volume), and nannofossil stratigraphy for the interbedded pelagic clay and carbonate turbidite section.

The remarkable similarity of the two North Pacific quartz records is less striking when they are plotted versus age rather than depth in the core (Fig. 3). Plotted versus age, the absolute amount of quartz in the sediments and the time series of quartz variation are very similar for all but the Miocene and early Pliocene (2.5–22 m.y. ago) portions of the record. A major difference in the stratigraphies of the two sediment columns is the lack of a stable magnetic signal for paleomagnetic reversal stratigraphy below about 4 m (2.47 m.y. ago) in Core LL44-GPC3. This has been attributed to a decrease in the ratio of stable detrital magnetic minerals to unstable authigenic iron oxide and oxyhydroxides (Prince et al., 1980; Heath et al., 1983; Heath, Rea, and Levi, this volume). Thus, although high-quality magnetic-reversal stratigraphy is available back to the Miocene in Holes 576 and 576B, it ends in the early Pliocene in Core LL44-GPC3. This factor is important in evaluating the differences between the temporal quartz record at the two sites during the Miocene and Pliocene epochs. Ichthyolith age determinations for Holes 576 and 576B are quite different from paleomagnetic ages in the Miocene sediments (Doyle, 1983; Doyle and Riedel, this volume). To evaluate the effect of this difference on the quartz curves in Figure 3, a second temporal quartz record is plotted (dotted line) based on paleomagnetic stratigraphy to 2.47 m.y. ago (Heath, Rea, and Levi, this volume) and on ichthyolith ages for the rest of the hole. Obviously, the superior paleomagnetic data indicate this alternate stratigraphy is wrong. However, we can see from this curve that the differences between the two sites during the Miocene are at least partly a function of stratigraphy.

In spite of uncertainties in the Miocene, a comparison of the quartz-content curves from Hole 576A and Core LL44-GPC3 suggests long-term changes in the abundance of mineral aerosol being carried to the North Pacific. In order to determine whether any of these changes are solely caused by the position of the sites with respect to the major wind belts, the sites have been rotated along the paths they have followed as a result of seafloor spreading from Pacific spreading centers. The rotation model used was developed by Prince (1978) and Prince et al. (1980) and is very similar to that of van Andel et al. (1975). The backtrack paths are indicated on Figure 1. Because the sites are at nearly the same latitude, their temporal positions relative to the margin of Northern Hemisphere westerlies are very similar.

Leinen and Heath (1981) interpreted the large change in quartz content of Core LL44-GPC3 at roughly 23 m.y. ago as a result of rotation of that core site into the westerlies. They also found a difference in the chemistry of the sediments (quartz/Al ratio) and in the mineralogy (quartz/illite) before and after the change in quartz content. They attributed both to a change in source material from quartz-poor, more basic dust transported from the developing western North American cordillera by the trade winds before the Miocene to more quartz-rich, acidic material from the Asian continent after the site rotated into the westerlies. Although the general features of this model are confirmed by Hole 576A, the details remain unclear because of the stratigraphic uncertainty. The Neogene increase in quartz content from 5 to 14%

in Hole 576A occurs gradually between 8 and 18 m.y. ago, 5 m.y. after the dramatic increase in quartz content in Core LL44-GPC3 23 m.y. ago. Both stratigraphies suggest that the gradual increase in quartz content in Hole 576A is correlated with the gradual increase between 8 and 22 m.y ago, not with the sharp increase at 23 m.y. ago in Core LL44-GPC3. The sites are at similar latitudes, and their angle of rotation along the backtrack paths is very flat relative to lines of latitude. Therefore, the sites must have traveled north at a rate of about 1° latitude/5 m.y. during the Neogene period. The southern margin of material deposited from the westerlies is very sharp (Moore and Heath, 1978). The difference in timing of the major quartz increase (23 m.y. ago in Core LL44-GPC3 vs. 18 m.y. ago in Hole 576A) could therefore be because of the small difference in their latitudes (1°1.5′). Thus, the rotation data do not help to constrain the ambiguities in age of the large increase in quartz content at the sites. Both records are very similar prior to 30 m.y. ago and suggest great uniformity in the source and nature of mineral aerosol being deposited across the North Pacific during the early Tertiary.

Implications of Quartz Content for Depositional Processes

It has been assumed that the mineral aerosol injected into the atmosphere has a complicated vertical distribution and undergoes complex mixing and depositional processes near its site of injection (Windom, 1975). It has further been assumed that these mixing and depositional processes continue over continents and the ocean/continent boundary (Windom, 1975; Pewe et al., 1981). This is confirmed by a growing number of studies of present-day dust storms (e.g., Gillette, 1981; McCauley et al., 1981; Pewe et al., 1981). Once injected into the stratosphere and transported over the oceans, the mineral aerosol is assumed to achieve some sort of equilibrium grain-size distribution (Windom, 1975; Rea and Janecek, 1982; Janecek and Rea, in press); the grain size of material deposited from this equilibrium assemblage is representative of the average atmospheric circulation "intensity" or "vigor" (e.g., Parkin, 1974; Parkin and Padgham, 1975). These assumptions have implications for the mineralogy of the aerosol: since clay minerals are concentrated in the smaller size fractions and silt-sized particles are enriched in quartz and feldspars (e.g., Griffin et al., 1968), changes in grain size along a dust storm or dust transport trajectory should result in changes in the mineral assemblage along the trajectory. Thus, only the assumption of an "equilibrium" grain-size assemblage allows the direct comparison of quartz contents from cores at different distances from the continent. This assumption is especially important of paleoclimatic studies of Cenozoic sediments, such as those of Rea and his co-workers (Rea and Janecek, 1982) since they were forced to compare grain-size data from a small number of widely separated drilling locations, all of which had incomplete sedimentary records.

Recent work by Dauphin (1983) has suggested that the assumption of a uniform "equilibrium" grain-size distribution across the central Pacific wind belts is incorrect. He analyzed the grain size of only the quartz in the surface sediments to insure that he was not looking at material formed authigenically or transported to the sample sites by other means. His analyses show a linear decrease in quartz grain size from 10.3 m to 7.3 μm across 7000 km in the North Pacific. These results suggest a nonequilibrium mineral aerosol and imply that mineralogy might also change with distance. Although fine-grained, the quartz was concentrated in the silt range (2–20 μm) rather than in the clay range (<2 μm). Stu ies by Rea and his co-workers and studies of presen accumulating mineral aerosols (Rea and Janecek, 19 R. A. Duce, personal communication, 1984) suggest t the average size of North Pacific dust is in the clay ran Unless all of this material is deposited as aggregat Dauphin's (1983) grain-size data may not be represen tive of the bulk of the mineral aerosol. If particles transported as aggregates, techniques that include grai size analysis of clay particles that have become disagg gated are not representative.

The uniformity of quartz concentration between H 576A and Core LL44-GPC3 (Fig. 2) suggests a very h mogeneous mineral aerosol composition across 5000 k of the North Pacific. Although this might also be i ferred from the fairly uniform quartz and illite conte of surface sediments in samples analyzed by Heath ar his co-workers (Moore and Heath, 1978; Heath and P sias, 1979), the two cores discussed here established that this has been the case for most, if not all of the Cenozoic Era.

Quartz Accumulation Rates

Changes in the quartz content of deep-sea sediments in the North Pacific have been attributed primarily to changes in the mineral assemblage resulting from different source regions (Leinen and Heath, 1981). The mass accumulation of quartz in the sediments is influenced by source regions, but is also influenced by the proximity of source regions, the amount of material available for transport, and the vigor of long-distance transport. The last factor is probably a complex function of the mean atmospheric circulation intensity and the intensity of the large storms that transport the bulk of mineral aerosol carried to the oceans (e.g., Duce et al., 1980; Gillette, 1981). If differences caused by the proximity of a depositional site can be evaluated, the remaining record should contain a paleoclimatic signal. The two sites discussed here, because of their similar source regions and latitudinal positions, provide a unique opportunity to evaluate the differences in quartz accumulation caused by distance along a transport path.

Mass sediment-accumulation rates for the two sediment columns have been constructed using the paleomagnetic reversal stratigraphies and ichthyolith stratigraphies, together with bulk-density data (Table 2). The mass sediment-accumulation rate is $R = \rho S$ where ρ is the dry-bulk density in g/cm^3 and S is the linear sedimentation rate between two datums in cm/m.y. Quartz accumulation rates (Table 3, Fig. 4) were calculated from the mass sediment-accumulation rates and the analytical quartz percentages. The quartz accumulation rate record

Table 2. Mass sediment-accumulation rates of Hole 576A samples and parameters used for their calculation.

Sample depth[a] (cm)	Water content[a] (%)	Dry-bulk density[b] (g/cm^3)	Sedimentation rate[c] (cm/m.y.)	Mass accumulation rate[d] (g/cm^2/m.y.)
245	60.47	1.035	1377	1425
452	62.41	1.008	1377	1388
727	62.55	1.022	1194	1220
754	63.64	0.978	1194	1168
767	66.89	0.911	794	1088
1025	69.04	0.858	794	681
1111	67.21	0.885	794	703
1165	66.10	0.936	794	743
1243	66.10	0.936	794	743
1352	64.16	0.968	499	768
1554	64.91	0.972	407	485
1622	63.50	0.982	322	400
1952	60.16	1.155	318	372
2076	54.34	1.247	167	397
2288	52.61	1.308	167	218
2434	54.54	1.245	175	218
2602	54.75	1.226	76	93
2939	59.51	1.073	76	82
3009	57.98	1.105	76	84
3065	60.94	1.094	76	83
3247	61.69	1.050	76	80
3443	57.45	1.166	41.5	48
3529	56.52	1.191	41.5	49
3937	58.68	1.145	41.5	48
4036	58.68	1.153	41.5	48
4102	55.96	1.189	41.5	49
4202	53.49	1.288	41.5	53
4278	52.61	1.313	41.5	55
4338	51.46	1.350	41.5	56
4461	53.05	1.254	41.5	52
4997	55.16	1.220	41.5	51
4560	55.16	1.238	41.5	51
4720	59.18	1.122	41.5	47
4821	56.90	1.134	41.5	47
4965	57.26	1.188	41.5	49
5136	54.55	1.250	41.5	52
5369	54.55	1.277	41.5	53
5422	32.43	1.838	Carbonate turbidites	
5710	36.31	1.745	Carbonate turbidites	
5872	33.77	1.795	Carbonate turbidites	
6009	41.86	1.634	Carbonate turbidites	
6070	35.90	1.750	Carbonate turbidites	
6277	34.21	1.816	Carbonate turbidites	
6361	33.77	1.788	Carbonate turbidites	

[a] Dadey, 1983.

[b] Calculated from water contents and wet-bulk density data (Dadey, 1983):

$$\rho_D = \rho_W (1 - X_W)/100$$

when ρ_D is the dry-bulk density, ρ_W is the wet-bulk density, and X_W is the water content.

[c] Heath et al., 1983.

[d] Calculated from dry-bulk densities and sedimentation rates, see text.

Hole 576A shows low and nearly constant accumula-on rates until the middle Neogene Period. About 15 .y. ago, quartz accumulation began to increase slight-. Two large increases in accumulation took place about and 2.5 m.y. ago. The timing of the increases is very milar to increases in quartz accumulation in Core LL44-PC3 (Fig. 4, Leinen and Heath, in press). The princi-al difference between the two sites is in the absolute alue of the accumulation rate. In Hole 576A quartz as accumulated at roughly four times the rate in Core L44-GPC3 for most of the Pliocene and Pleistocene pochs (5 m.y. ago to present).

The initial increase in quartz accumulation from the ow mid-Tertiary values in Core LL44-GPC3 occurred bout 20 m.y. ago. Because age determinations are necessary for the accumulation-rate calculation, the values are dependent on stratigraphy. Correlation of ichthyolith ranges suggests that the increase in quartz accumulation in Core LL44-GPC3 is actually coincident with that in Hole 576. These increases could be caused by changes in the positions of the sites with respect to the westerlies (i.e., source mineralogy) or changes in the amount or efficiency of transport from land, but their association with changes in the quartz content and clay mineralogy (see Leinen and Heath, 1981; Lenotre et al., this volume) argues strongly that they reflect the passage of the core sites into the influence of the westerlies rather than solely a change in transport efficiency.

During the late Neogene, the quartz accumulation rate in Hole 576A increased markedly between 4 and 6 m.y.

Table 3. Quartz accumulation rates of Hole 576A samples.

Core-Section (interval in cm)	Sample depth (cm)	Quartz (%)	Age[a] (m.y.)	Quartz accumulation rate[b] (g/cm²/m.y.)
1-1, 21-25	23	16.63	0.26	237.0
1-3, 81-85	383	18.11	0.53	254.0
1-6, 80-83	831	15.52	0.87	166.0
2-3, 47-50	1219	17.35	1.32	129.0
3-1, 47-50	1869	13.06	2.56	47.0
3-3, 70-73	2191	8.87	3.59	33.0
3-4, 117-120	2389	11.66	4.39	37.0
3-5, 127-130	2549	9.02	5.86	8.3
3-6, 110-113	2681	14.64	7.60	14.0
4-1, 50-53	2821	10.92	9.44	10.0
4-2, 103-106	3025	8.57	12.13	7.2
4-3, 98-101	3169	5.81	14.03	4.8
4-4, 104-107	3325	5.86	16.35	2.7
4-5, 20-23	3391	4.25	17.94	2.0
4-6, 60-63	3581	5.31	25.00	2.6
5-1, 87-90	3809	5.16	28.00	2.5
5-2, 40-43	3911	1.76	31.00	0.8
5-3, 30-33	4051	2.64	34.00	1.3
5-5, 137-140	4459	4.67	44.00	2.4
5-6, 130-133	4601	2.88	47.00	1.4
5-7, 25-28	4646	6.18	48.00	3.0
6-1, 90-93	4761	3.96	51.00	1.9
6-2, 47-50	4869	4.21	54.00	2.0
6-3, 93-96	5065	4.81	58.00	2.4
6-4, 11-14	5132	6.12	60.00	3.2
6-5, 12-15	5283	5.41	64.00	2.8
6-5, 127-13	5399	4.54	66.00	2.4
6-6, 17-20	5439	5.29	Carbonate turbidites	
6-7, 22-25	5593	3.91	Carbonate turbidites	
7-1, 137-140	5759	4.16	Carbonate turbidites	
7-2, 22-25	5793	5.50	Carbonate turbidites	
7-3, 17-20	5939	6.46	Carbonate turbidites	
7-3, 35-38	5946	3.51	Carbonate turbidites	

[a] Determined by interpolation between paleomagnetic datums for 0-24.76 m and by interpolation between ichthyolith datums for 24.76-54.0 m.

[b] Mass accumulation rates for sample depths were interpolated from data in Table 2.

ago. Similar increases in eolian accumulation over this interval have been calculated by Rea and Janecek (1982) from DSDP Sites 305 and 310 (Fig. 1). They attributed the increase to an influx of volcanic ash and pumice associated with the late Miocene to early Pliocene volcanic episode (Kennett and Thunell, 1975; Kennett, 1977). There is, however, no significant ash component in sediments of that age in either Core LL44-GPC3 or Hole 576A. Therefore, the increase cannot be attributed to volcanic activity in these cores.

It is likely that there is aliasing in the temporal record of quartz concentration. Two Neogene samples have a much lower quartz content than those above and below them. If these points are ignored, the late Neogene record simply records an accelerating increase in mineral-aerosol accumulation with increasing Miocene and Pliocene aridity (Wolfe and Hopkins, 1967) caused by global cooling (Savin, 1977; Kennett, 1977; Woodruff et al., 1981) or movement of the core site into the influence of the westerlies.

The Hole 576A quartz accumulation does highlight the dramatic increase in mineral-aerosol accumulation that occurred after the onset of Northern Hemisphere glaciation 2.5 m.y. ago (Shackleton et al., 1983; Prell, 1982). Quartz accumulation increased from about 50 to 130 g/cm²/m.y., and total sediment accumulation increased from about 400 to 700 g/cm²/m.y. at that time. Late Pleistocene quartz accumulation rates are about 250 g/cm²/m.y., five times their preglacial rates. The rather small changes in grain size of both the total eolian mineral assemblage in Hole 576 (Janecek, this volume) and the quartz in Core LL44-GPC3 (Janecek and Rea, in press) suggest that these changes are due primarily to changes in climate, which made more material available for transport, rather than to changes in wind "vigor."

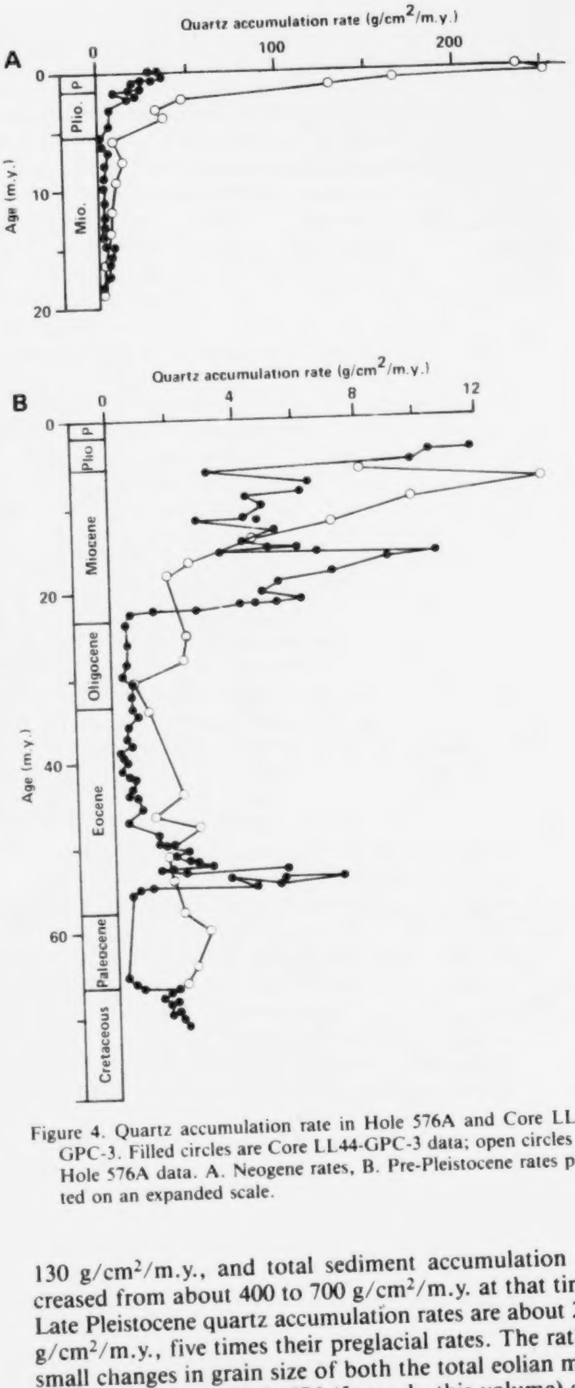

Figure 4. Quartz accumulation rate in Hole 576A and Core LL44-GPC-3. Filled circles are Core LL44-GPC-3 data; open circles are Hole 576A data. A. Neogene rates, B. Pre-Pleistocene rates plotted on an expanded scale.

CONCLUSIONS

The quartz record in Hole 576A reflects changes in the source and amount of mineral aerosol being deposited in the northwest Pacific with time. When the Hole 576A quartz record is compared with other long records of mineral-aerosol deposition (Core LL44-GPC3), a strong uniformity in the composition of the mineral aerosol across the North Pacific and an equilibrium mineral assemblage in the aerosol are indicated. The temporal record of quartz content and accumulation rate suggests that Hole 576A entered the influence of material transported by the westerlies about 15 m.y ago and that rates of sediment deposition have increased since then. Only a dramatic change in quartz accumulation about 2.5 m.y. ago can be clearly related to a climatic event, but it is likely that the gradual increase in quartz accumulation through the Miocene and early Pliocene epochs is a result of increasing Northern Hemisphere aridity and intensified atmospheric activity associated with global cooling and an increase in the equator-to-pole temperature gradient.

ACKNOWLEDGMENTS

The careful X-ray diffraction analyses for this study were performed by Tammy King Walsh and Sandra Furda. The work was supported by the Subseabed Disposal Program of the Department of Energy (Contract No. SAN 26-6610) administered by Sandia National Laboratories. I would like to thank Les Shephard for sampling the cores and G. Ross Heath for providing the paleomagnetic reversal stratigraphy before publication and for reviewing the manuscript. The manuscript was typed by Kathy Hazard. It benefited from reviews by Thomas Janecek and Ted Moore.

REFERENCES

Dadey, K., 1983. Consolidation parameters of a northwest Pacific clay site, DSDP Site 576A [M. S. thesis]. University of Rhode Island, Kingston.

Dauphin, J. P., 1983. Eolian quartz granulometry as a paleowind indicator in the northeast equatorial Atlantic, north Pacific , and southeast equatorial Pacific [Ph.D. dissert.]. University of Rhode Island, Kingston.

Doyle, P., 1980. Seabed disposal program: improvement of ichthyolith stratigraphy for giant piston Core 3, progress report for period November 1, 1979–September 30, 1980. *In* Hinga, K. (Ed.), *Subseabed Disposal Program Annual Report*, January to December, 1980, Vol. 2, Pt. 2, Appendices, SAN81-1095/II , July 1981, pp. 325–341.

______, 1983. Ichthyolith stratigraphy in the Pacific. *EOS, Trans. Am. Geophys. Union* (Fall 1983 Ann. Mtg.). (Abstract)

Doyle, P., and Riedel, W. R., 1979. Cretaceous to Neogene ichthyoliths in a giant piston core from the Central North Pacific. *Micropaleontology*, 25:337–364.

Duce, R. A., Unni, C. K., Ray, B. J., Prospero, J. M., and Merrill, J. T., 1980. Long-range atmospheric transport of soil dust from Asia to the tropical North Pacific: Temporal variability. *Science*, 209: 1522–1524.

Ellis, D. B., and Moore, T. C., Jr., 1973. Calcium carbonate opal and quartz in Holocene pelagic sediments and the calcite compensation level in the south Atlantic Ocean. *J. Mar. Res.*, 31:210–227.

Gillette, D. A., 1981. Production of dust that may be carried great distances. *In* Pewe, T. L. (Ed.), *Desert Dust: Origin, Characteristics, and Effects on Man*. Geol. Soc. Am. Spec. Pap., 186:11–26.

Griffin, J. J., Windom, H., and Goldberg, E. D., 1968. The distribution of clay minerals in the world ocean. *Deep-Sea Res.*, 15:433–459.

Heath, G. R., Moore, T. C., Jr., Opdyke, N. D., and Dauphin, J. P., 1973. Distribution of quartz, opal, calcium carbonate and organic carbon in Holocene, 600,000 and Brunhes/Matuyama age sediments of the north Pacific. *Geol. Soc. Am. Abstr. Prog.*, 5:662 (Abstract)

Heath, G. R., and Pisias, N. G., 1979. A method for the quantitative estimation of clay mineral in north Pacific deep-sea sediments. *Clays Clay Mineral.*, 27(3):175–184.

Heath, G. R., Rea, D. K., and Pisias, N. G., 1983. Paleomagnetic stratigraphy and sedimentation rates of pelagic clays from the western North Pacific. *EOS, Trans. Am. Geophys. Union*, Fall 1983 Ann. Mtg., 741.

Janecek, T., and Rea, D. K., in press. Variations in atmospheric circulation associated with the onset of Northern Hemisphere glaciation. *Mar. Geol.*

Kennett, J. P., 1977. Cenozoic evolution of Antarctic glaciation, the circum-Antarctic Ocean, and their impact on global paleoceanography. *J. Geophys. Res.*, 82(27):3843–3860.

Kennett, J. P., and Thunell, R. C., 1975. Global increase in Quaternary explosive volcanism. *Science*, 187:497–503.

Kolla, V., and Biscaye, P. E., 1977. Distribution and origin of quartz in the sediments of the Indian Ocean. *J. Sediment. Petrol.*, 47(2): 642–649.

Kyte, F. T., and Wasson, J., in press. The Cretaceous-Tertiary boundary in GPC3, an abyssal clay section. *Geochim. Cosmochim. Acta.*

Leinen, M., and Heath, G. R., 1981. Sedimentary indicators of atmospheric circulation in the Northern Hemisphere during the Cenozoic. *Paleogeogr., Paleoclimatol., Paleoecol.*, 36:1–21.

________, in press. Chemical signatures in Cenozoic sediments from the central North Pacific and their oceanographic significance. *Geochim. Cosmochim. Acta.*

McCauley, J. F., Breed, C. S., Grolier, M. J., and MacKinnon, D. J., 1981. The U.S. dust storm of February 1977. *In* Pewe, T. L. (Ed.), *Desert Dust: Origin, Characteristics, and Effect on Man*. Geol. Soc. Am., Spec. Pap., 186:123–148.

Molina-Cruz, A., and Price, P., 1977. Distribution of opal and quartz on the ocean floor of the subtropical southeastern Pacific. *Geology*, 5:81–84.

Moore, T. C., Jr., and Heath, G. R., 1978. Sea-floor sampling techniques. *In* Riley, J. P., and Chester, R. (Eds.), *Chemical Oceanography*, (2nd ed., Vol. 7, Chap. 36): New York (Academic Press), 75–126.

Parkin, D. W., 1974. Trade winds during the glacial cycles. *Proc. R. Soc. London, Ser. A*, 337:73–100.

Parkin, D. W., and Padgham, R. C., 1975. Further studies on trade winds during the glacial cycles. *Proc. R. Soc. London, Ser. A*, 346: 245–260.

Pewe, T. L., Pewe, E. A., Pewe, R. H., Journaux, A., and Slatt, R. M., 1981. Desert dust: Characteristics and rates of deposition in central Arizona, U.S.A. *In* Pewe, T. L., (Ed.), *Desert Dust: Origin, Characteristics, and Effect on Man*. Geol. Soc. Am. Spec. Pap., 186:169–190.

Pisias, N. G., and Leinen, M., 1983. Late Pleistocene variability of the northwest sector of the Pacific Ocean. *In* Berger, A., and Imbrie, J. (Co-chairmen), *Int. Symp. Milankovitch and Climate: Understanding the Response to Orbital Forcing*, Pt. 1, 307–330.

Prell, W., 1982. A reevaluation of the initiation of Northern Hemisphere glaciation at 3.2 m.y.: New isotopic evidence. *Geol. Soc. Am. Abstr. Progr.*, 14(7):592. (Abstract)

Prince, R. A., 1978. Southward motion of the Hawaiian hotspot between 42 and 25 MYPB. *Geol. Soc. Am. Abstr. Progr.*, 10:474. (Abstract)

Prince, R. A., Heath, G. R., and Kominz, M., 1980. Paleomagnetic stratigraphies of central north Pacific sediment cores: Stratigraphy sedimentation rates and the origin of magnetic instability. *Geol. Soc. Am. Bull.*, 91(II):1789–1835.

Rea, D. K., and Janecek, T. R., 1981. Late Cretaceous history of Eolian deposition in the Mid-Pacific mountain, central North Pacific Ocean. *Paleogeogr., Paleoclimatol., Paleoecol.*, 36:55–67.

________, 1982. Late Cenozoic changes in atmospheric circulation deduced from North Pacific eolian sediments. *Mar. Geol.*, 49:149–167.

Rex, R. W., and Goldberg, E. D., 1958. Quartz content of pelagic sediments of the Pacific Ocean. *Tellus*, 10:153–159.

Rex, R. W., Syers, J. K., Jackson, M. L., and Clayton, R. N., 1969. Eolian origin of quartz in soils of Hawaiian Islands and in Pacific pelagic sediments. *Science*, 163:277–279.

Savin, S. M., 1977. The history of the Earth's surface temperature during the past 100 million years. *Annu. Rev. Earth Planet. Sci.*, 5:319–355.

Schramm, C. T., 1983. Changes in atmospheric and oceanic circulation in the east equatorial Pacific during the late Quaternary [M.S. thesis]. University of Rhode Island, Kingston.

Shackleton, N. J., Backman, J., Kent, D., Imbrie, J., Pestiaux, P., et al., 1983. The evolution of climate response to orbital forcing: Results over three million years from DSDP Site 552A. *In* Berger, A., and Imbrie, J. (Co-chairmen), *Internat. Symp. Milankovitch and Climate: Understanding the Response to Orbital Forcing.* (abstract)

Thiede, J., 1979. Wind regimes over the late Quaternary southwest Pacific Ocean. *Geology*, 7:259–262.

Till, R., and Spears, D. A., 1969. The determination of quartz in sedimentary rocks using an X-ray diffraction method. *Clays Clay Mineral.*, 17:323–327.

van Andel, T. H., Heath, G. R., and Moore, T. C., Jr., 1975. Cenozoic history and paleoceanography of the Central Equatorial Pacific Ocean. *Mem. Geol. Soc. Am.*, 143:134.

Windom, H. L., 1969. Atmospheric dust records in permanent snowfields: Implications to marine sedimentation. *Geol. Soc. Am. Bull.*, 80:761–782.

________, 1975. Eolian contributions to marine sediments. *J. Sediment. Petrol.*, 45:520–529.

Wolfe, J. A., and Hopkins, D. M., 1967. Climatic changes recorded by Tertiary land floras in northwestern North America: Tertiary correlations and climatic changes in the Pacific. *11th Pacific Science Congr., Tokyo, Symp.*, 25:67–76.

Woodruff, F., Savin, S. M., and Douglas, R. G., 1981. Miocene stable isotope record: A detailed deep Pacific Ocean study and its paleoclimatic implications. *Science*, 212:665–668.

Date of Initial Receipt: 3 November 1983
Date of Acceptance: 14 June 1984

26. EOLIAN SEDIMENTATION IN THE NORTHWEST PACIFIC OCEAN: A PRELIMINARY EXAMINATION OF THE DATA FROM DEEP SEA DRILLING PROJECT SITES 576 AND 578[1]

Thomas R. Janecek, Lamont-Doherty Geological Observatory of Columbia University[2]

ABSTRACT

The mass-accumulation rate and grain size of the total eolian component of North Pacific pelagic clays at Deep Sea Drilling Project Sites 576 and 578 have been used to evaluate changes in eolian sedimentation and the intensity of atmospheric circulation that have occurred during the past 70 m.y. Eolian deposition, an indicator of source area aridity, was low in the Paleocene, Eocene, and Oligocene, apparently reflecting the humid environments of that time as well as the lack of glacial erosion products. A general increase in eolian accumulation in the Miocene apparently reflects the relative increase in global aridity during the latter part of the Cenozoic. A dramatic increase in eolian accumulation rates in the Pliocene reflects the increased aridity and availability of glacial erosion products associated with Northern Hemisphere glaciation 2.5 m.y. ago. Eolian grain size, an indicator of wind intensity, suggests that Late Cretaceous wind strength was comparable to present-day wind strength. A sharp decrease in eolian grain size across the Paleocene/Eocene boundary is not readily interpreted, but may indicate a significant reduction in the intensity of atmospheric circulation at that time. Fine eolian grain size and low accumulation rates in the Eocene and early Oligocene are in agreement with low early Tertiary thermal gradients and less vigorous atmospheric circulation. Large increases in grain size during the Oligocene, mid-to-late Miocene, and Pliocene appear to be a response to steepening thermal gradients resulting from increasing polar isolation.

INTRODUCTION

Background and Objectives

One of the objectives of Leg 86 of the Deep Sea Drilling Project (DSDP) was to recover a long-term record of North Pacific pelagic sedimentation in order to determine the Late Cretaceous and Cenozoic history of eolian input in the region. Until recently, the only continuous record of Cenozoic eolian deposition in the North Pacific was that of LL44-GPC-3 (Leinen and Heath, 1981; Janecek and Rea, 1983), located in the northeastern Pacific (Fig. 1). The recovery of an essentially continuous Cenozoic section at Site 576 (Figs. 1 and 2), at a similar latitude to LL44-GPC-3, provides an opportunity to evaluate differences in the accumulation rate and grain size of dust with distance of transport across the North Pacific. If plate movement and changing source reas can be accounted for, then the eolian records can interpreted in terms of a paleoclimatic signal.

In addition to the long-term record of Site 576, a ick late Neogene siliceous clay section was recovered Site 578 (Figs. 1 and 2). The high sedimentation rates this site provide an opportunity to evaluate high freency changes in terrigenous (eolian) input in the northstern Pacific Ocean during the late Cenozoic.

olian Sedimentation

Nonbiogenic pelagic sediments recovered seaward of e realm of hemipelagic sedimentation and away from rbidites and ice-rafted debris are composed primarily terrigenous material (mostly quartz and clays) transported to the sea surface by wind. Rapid settling of these particles from surface waters by fecal pellets and large amorphous aggregates (Honjo, 1980, 1983) minimizes surface current smearing of atmospheric input patterns and thus sedimentary patterns mimic surface input patterns (Berger, 1976).

The distribution of eolian material in surface sediments has been shown to reflect present-day atmospheric circulation patterns (Rex and Goldberg, 1958; Molina-Cruz and Price, 1977; Kolla et al., 1979; Thiede, 1979; Leinen and Heath, 1981). Variations in the distribution, accumulation rate, and grain size of eolian material in Pleistocene sediments reflect changes in wind intensity, latitudinal position of the zonal winds, and continental climate (Kolla et al., 1979; Pisias and Leinen, 1984; Janecek and Rea, in press).

The flux of wind-borne dust to the oceans depends, in part, on the strength of the zonal winds, on distance to source, and on the annual number of dust-transporting episodes, but is mainly dependent upon the climate of the source area (Prospero and Nees, 1977; Gillette, 1981; Rea and Janecek, 1981a). Humid climates tend to promote vegetation, thereby reducing the amount of material available for wind erosion, transport, and subsequent deposition in the deep sea. High precipitation rates also increase the scavenging of dust by rain thus decreasing the amount of deposition downwind (Windom, 1975, Parkin and Padgham, 1975). Therefore, variations in the accumulation rate of eolian material will primarily reflect changes in continental climate.

Both air-sampling (Johnson, 1976; Glaccum and Prospero, 1980) and theoretical calculations (Gillette et al., 1974; Schutz, 1979) suggest that beyond 1000 km distance from the source, eolian material is in equilibrium with the transporting wind. That is, the settling velocities of the particles are some small fraction of the verti-

---

[1] Heath, G. R., Burckle, L. H., et al., *Init. Repts. DSDP*, 86: Washington (U.S. Govt. rinting Office).

[2] Address: Lamont-Doherty Geological Observatory of Columbia University, Palisades, NY 10964.

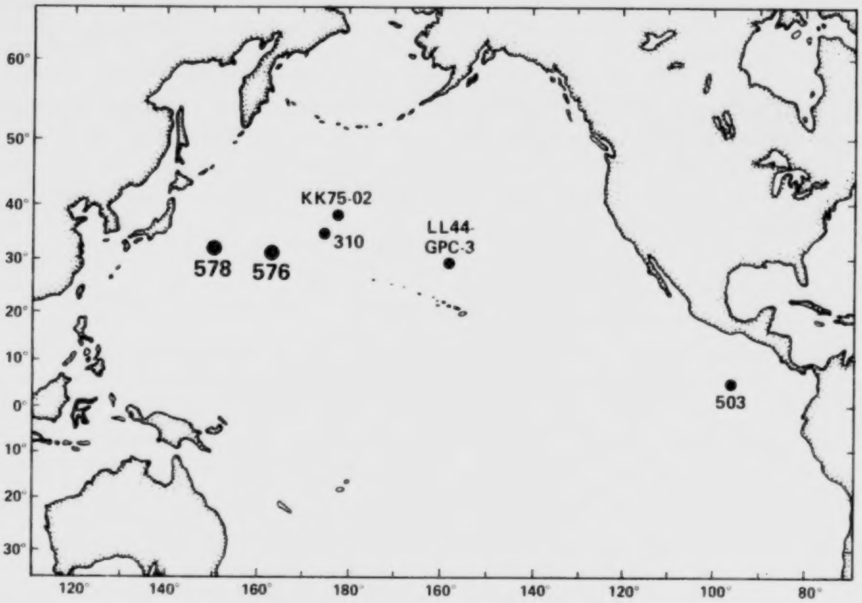

Figure 1. Location map showing DSDP Sites 578 and 576. DSDP Sites 503 and 310 (Janecek, 1983) and piston cores KK75-02 (Janecek and Rea, in press) and LL44-GPC-3 (Janecek and Rea, 1983) are also shown for reference.

cal velocity component of atmospheric motions. These equilibrium grains, which can remain in suspension indefinitely (Gillette et al., 1974), are carried global distances in the upper troposphere (Windom, 1969; Schutz, 1979) and are generally removed by rain (Jackson et al., 1973). A change in the size of the equilibrium grain represents a change in the intensity of the transporting wind, with stronger winds carrying larger particles (Parkin, 1974). Thus, the independent nature of the grain-size and accumulation-rate data allow us to determine the intensity of past atmospheric circulation and the amount of dust input to the seafloor from the same samples.

Geologic Setting

Site 576 was hydraulically piston cored to a depth of 74 m sub-bottom east of the Shatsky Rise. The site lies in over 6200 m of water beneath the central Pacific water mass (Fig. 1). Site 576 was chosen to be in an area of uniform pelagic "red clay" sedimentation between the Shatsky Rise and the Emperor Seamounts, but far enough east to minimize the fraction of the section occupied by ash layers. The area around Site 576 is characterized by gently rolling topography with less than 50 m of local relief (see Site 576 chapter, this volume). Three major lithologic units are recognized at Site 576 and are shown in Figure 2. Basal lithologic Unit III, consisting of chert and porcellanite fragments, forms the prominent reflector at the base of the "transparent layer" in the North Pacific.

Site 578 was drilled to 176.8 m sub-bottom in 6010 m of water west of the Shatsky Rise (Fig. 1) in an area of gently rolling seafloor with local relief of tens of meters. The seafloor is underlain by a section several hundred meters thick lying above Cretaceous chert and chalk and characterized by continuous parallel sub-bottom reflectors. The late Neogene section was divided into four lithologic units (Fig. 2; see Site 578 chapter, this volume).

METHODS

The samples for Site 576 were taken primarily from Hole 576B at approximately 1.5-m intervals (one per section) to a depth of 58 m. Coring gaps in Hole 576B were filled with samples from Hole 576 (Table 1). Samples for Site 578 were taken at 30- to 50-cm intervals to a depth of 100 m (Table 2).

The basic data set for this study includes (1) the weight percent of the total eolian load rather than just the weight percent of quartz, which comprises only 20 to 40% or less of the total eolian load (Windom, 1969; Prospero and Bonatti, 1969; Johnson, 1979; Prospero et al., 1981) and (2) the grain size of the eolian material. The detrital mineral or eolian component is isolated b a series of selective extractions to remove calcium carbonate, opaline silica, Fe and Mn oxides, and hydroxides and zeolites. The amount of residual eolian material, predominantly fine-grained quartz and clays, determines the eolian weight percentage (see Rea and Janecek 1981b for details of the chemical procedures).

Grain-size analysis of the eolian component was carried out on the 6- to 10-ϕ (16 to 1 μm) size fraction a 0.5-ϕ intervals using a Coulter Counter model Zb particle-size analyzer. This procedure is described in detail b Graham and Rea (1980), and the precision of the resulting size determinations is ± 0.03 ϕ (average of difference between duplicate samples).

Linear Sedimentation Rates

At Site 576, paleomagnetic reversal stratigraphy (se Heath, Rea, and Levi, this volume) was used to calculate sedimentation rates from 25 m sub-bottom to the

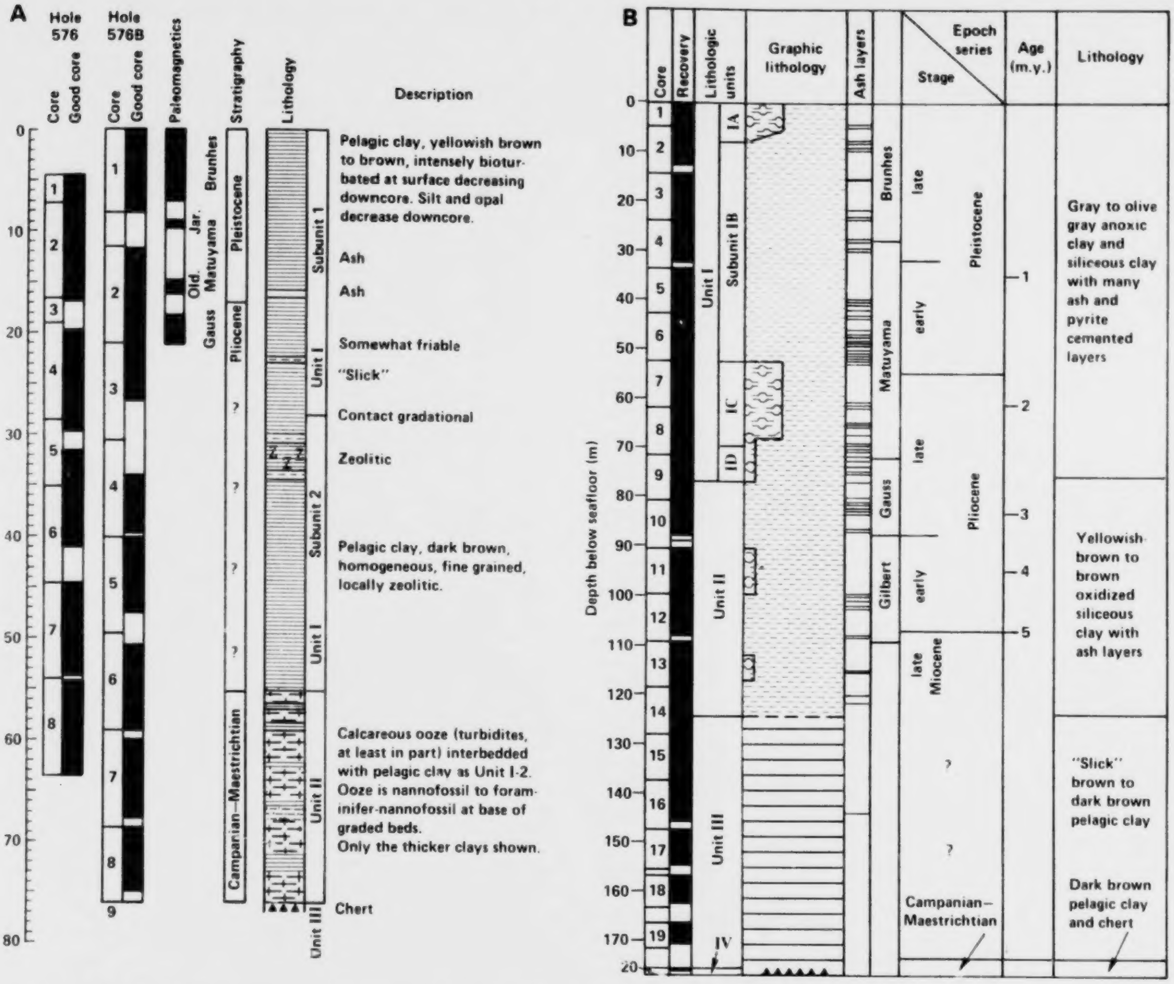
A
Hole 576
Hole 576B
Core
Good core
Paleomagnetics
Stratigraphy
Lithology
Description
Brunhes
Jar.
Old.
Matuyama
Gauss
Pleistocene
Pliocene
Campanian–Maestrichtian
Subunit 1
Unit I
Subunit 2
Unit II
Unit III
Pelagic clay, yellowish brown to brown, intensely bioturbated at surface decreasing downcore. Silt and opal decrease downcore.
Ash
Ash
Somewhat friable
"Slick"
Contact gradational
Zeolitic
Pelagic clay, dark brown, homogeneous, fine grained, locally zeolitic.
Calcareous ooze (turbidites, at least in part) interbedded with pelagic clay as Unit I-2. Ooze is nannofossil to foraminifer-nannofossil at base of graded beds. Only the thicker clays shown.
Chert
B
Core
Recovery
Lithologic units
Graphic lithology
Ash layers
Epoch series
Stage
Age (m.y.)
Lithology
Depth below seafloor (m)
IA
Subunit IB
Unit I
IC
ID
Unit II
Unit III
IV
Brunhes
Matuyama
Gauss
Gilbert
late
early
late
early
late Miocene
Pleistocene
Pliocene
Campanian–Maestrichtian
Gray to olive gray anoxic clay and siliceous clay with many ash and pyrite cemented layers
Yellowish brown to brown oxidized siliceous clay with ash layers
"Slick" brown to dark brown pelagic clay
Dark brown pelagic clay and chert

Figure 2. Lithologic columns constructed for (A) Site 576 and (B) Site 578. Paleomagnetic data from Heath, Rea, and Levi (this volume).

surface (4.77 m.y. ago to present). Below 25 m ichthyolith stratigraphic ranges constrain ages in the least-fossiliferous clays (Doyle and Riedel, this volume). Further age constraints are provided by foraminiferal and nannofossil datums in the carbonate oozes at the base of the hole (D'Agostino, this volume; Monechi, this volume). A smooth sedimentation-rate curve was constructed using the paleomagnetic data and microfossil age ranges (Fig. 3). Sedimentation rates were determined from the slope of the curve at 5-m.y. intervals and are included in Table 1. Through the upper 25 m the sedimentation rates decrease from 15 m/m.y. during the Brunhes Epoch to about 2 m/m.y. in the Gilbert Epoch. Sedimentation rates between 4.77 and 70 m.y. ago range from m/m.y. at 5 m.y. ago to 0.3 m/m.y. at 35 m.y. ago. Linear sedimentation rates increase slightly to about .6 m/m.y. in the Late Cretaceous.

Paleomagnetic reversal stratigraphy (see Heath, Rea, and Levi, this volume) was used at Site 578 to calculate sedimentation rates. Sedimentation rates were calculated between the paleomagnetic reversal horizons (Fig. 3) and are included in Table 2. Sedimentation rates drop from 40 m/m.y. at the surface to about 25 m/m.y. around 2.0 m.y. ago. Sedimentation rates decreased to less than 12 m/m.y. around 3.0 m.y. ago and to about 8 m/m.y. 4.5 m.y. ago.

Mass-Accumulation Rate Calculations

To calculate the mass-accumulation rate of a sedimentary unit the actual dry mass of sediment per unit volume must be determined. The mass-accumulation rate is then the product of the linear sedimentation rate and this dry-bulk density. The dry-bulk density was determined by weighing, freeze-drying, and reweighing a known volume of original sample. Details of the procedures and calculations are found in Rea and Janecek (1981b). The calculated dry-bulk densities and mass-accumulation rates for Sites 576 and 578 are included in Tables 1 and 2, respectively. Eolian mass-accumulation rates were calculated by multiplying the eolian weight percentage by the total mass-accumulation rate and are presented in Tables 1 and 2 and Figures 4 and 5.

Table 1. Data generated for the calculation of eolian mass-accumulation rates and grain size at Site 576.

Sample (interval in cm)	Depth (m)	Age (m.y.)	LSR (m/m.y.)	DBD (gm/cm^3)	MAR (mg/cm^2 1000 yr.)	Eolian wt. %	Eolian MAR (mg/cm^2 1000 yr.)	Eolian size (ϕ_{50})
1-6, 30-33	7.80	0.830	11.94	0.606	723	83.4	603	8.52
2-1, 90-93	12.50	1.360	7.94	0.489	388	86.0	334	8.50
2-2, 90-93	14.00	1.55	7.94	0.497	395	99.8	394	8.45
2-3, 90-93	15.50	1.78	5.0	0.489	245	84.2	206	8.44
3-5, 20-23[a]	15.80	1.84	5.0	0.521	261	79.3	207	8.34
2-4, 90-93	17.00	2.12	4.07	0.575	234	88.0	206	8.37
2-5, 90-93	18.50	2.50	3.11	0.553	172	87.7	151	8.43
2-6, 90-93	20.00	2.96	4.28	0.569	244	93.8	229	8.35
2-7, 20-23	20.80	3.21	3.18	0.616	200	84.4	169	8.37
3-1, 40-43	21.50	3.43	2.71	0.593	212	86.8	184	8.52
3-2, 40-43	23.00	3.99	3.08	0.614	189	87.9	166	8.54
3-3, 40-43	24.50	4.66	2.00	0.694	139	87.1	121	8.60
3-6, 40-43	24.89	4.80	1.00	0.689	69	85.8	59	8.59
3-7, 40-43	26.39	6.3	1.00	0.671	67	81.6	55	8.58
4-6, 30-33[a]	26.90	6.8	1.00	0.651	65	82.0	53	8.60
4-6, 130-133[a]	27.90	7.8	1.00	0.686	68	81.1	55	8.67
5-1, 40-43[a]	28.60	9.3	0.6	0.670	40	79.8	32	8.73
5-5, 112-115[a]	32.22	16.8	0.4	0.589	25	82.1	21	8.62
5-6, 30-33[a]	32.90	18.5	0.4	0.681	27	87.1	24	8.61
5-6, 140-143[a]	34.00	21.7	0.3	0.649	19	83.1	16	8.59
5-7, 20-23[a]	34.30	22.7	0.3	0.540	16	85.1	14	8.54
4-4, 40-43	35.00	25.0	0.3	0.579	17	81.6	14	8.59
4-5, 40-43	36.50	29.0	0.3	0.601	18	79.5	14	8.78
4-6, 40-43	38.00	34.5	0.3	0.606	18	79.8	15	8.93
4-7, 40-43	39.50	36.7	0.4	0.660	20	84.7	17	8.98
5-2, 50-53	40.60	40.0	0.4	0.592	18	88.2	16	8.94
5-3, 50-53	42.10	43.8	0.4	0.588	23	90.3	21	8.80
5-4, 50-53	43.60	47.5	0.4	0.579	37	99.9	37	8.90
5-5, 50-53	45.10	51.5	0.45	0.780	35	98.7	35	8.41
5-6, 50-53	46.60	55.00	0.5	0.775	39	99.9	39	8.42
7-3, 40-43[a]	47.50	56.80	0.5	0.779	39	91.0	35	8.60
7-4, 40-43[a]	49.00	59.80	0.5	0.790	40	89.7	35	8.60
7-4, 130-133[a]	49.90	61.50	0.6	0.775	46	93.0	43	8.59
6-1, 130-133	50.90	63.00	0.6	0.760	45	87.6	40	8.64
6-2, 130-133	52.50	65.50	0.6	0.780	47	85.3	40	8.50
6-3, 130-133	53.90	68.00	0.6	0.780	47	86.1	40	8.66
6-4, 50-53	54.60	69.20	0.6	0.787	47	88.3	41	8.65
6-5, 110-113	56.70	72.70	0.6	0.767	46	84.3	38	8.69
6-6, 75-78	57.85	74.62	0.6	0.793	48	79.9	38	8.67

Note: Depths are corrected according to the scheme outlined in the Site 576 chapter (this volume). LSR = linear sedimentation rate, DBD = dry-bulk density of the sample, MAR = mass-accumulation rate of the bulk sample. See text for an explanation of the calculations.

[a] Samples are from Hole 576. All other samples are from Hole 576B.

The precision of the chemical techniques was determined by replicate analyses and is less than ±3%. The accuracy of the final values for the mass-accumulation rates of the eolian component is determined largely by the accuracy of the stratigraphy. The placement of zonal boundaries, assuming constant linear sedimentation rates between boundaries and assignment of absolute ages to those boundaries almost certainly results in errors larger than the few percent that are the result of the laboratory work. Therefore, geological significance is not attached to changes in mass-accumulation rate of less than 10% of the values.

RESULTS

Eolian Mass-Accumulation Rates

In the Late Cretaceous, Paleocene, and early Eocene the eolian mass-accumulation rates at Site 576 (Fig. 4) remain relatively constant, averaging about 40 mg/cm^2/10^3 yr. Eolian accumulation rates then decline through the middle and late Eocene to about 15 mg/cm^2/10^3 yr., where they remain until the early Miocene. Eolian mass-accumulation rates increase in the early Miocene to almost 30 mg/cm^2/10^3 yr., then increase by more than a factor of two in the middle to late Miocene to 60 mg/cm^2/10^3 yr. In the Pliocene, eolian accumulation rates increase dramatically to values over 400 mg/cm^2/10^3 yr.

Eolian accumulation rates at Site 578 (Fig. 5) are relatively low and constant during the interval from 4.5 to 3.0 m.y. ago, averaging 500 mg/cm^2/10^3 yr. A peak in eolian accumulation rates at 2000 mg/cm^2/10^3 yr. occurs around 3.0 m.y. ago, followed by a permanent increase in eolian accumulation rates around 2.5 m.y. ago to values in the range of 1500 to 2500 mg/cm^2/10^3 yr. Samples younger than 2.5 m.y. appear to exhibit greater variability, although this may be an artifact of the greater sample density in the upper portion of the core.

Eolian Grain Size

The size of the wind-borne grains at Site 576 increases from 8.70 ϕ in the Late Cretaceous to 8.40 ϕ in the Paleocene (Fig. 4), representing a 50% increase in grain mass. Eolian size decreases sharply to 8.85 ϕ in the early Eocene and declines further to a low of 8.98 ϕ in the earliest Oligocene, equivalent to an overall decrease in grain mass by a factor of 2.7. From this low in the early

Table 2. Data generated for the calculation of eolian mass-accumulation rates and grain size at Site 578.

Sample (interval in cm)	Depth (m)	Age (m.y.)	LSR (m/m.y.)	DBD (gm/cm^3)	MAR (mg/cm^2 1000 yr.)	Eolian wt. %	Eolian MAR (mg/cm^2 1000 yr.)	Eolian size (ϕ_{50})
1-1, 28-31	0.28	0.007	37.4	0.583	2180	82.1	1790	7.89
1-1, 56-59	0.56	0.015	37.4	0.517	1934	71.6	1385	7.94
1-1, 88-91	0.88	0.024	37.4	0.520	1645	78.1	1519	8.12
1-1, 115-118	1.15	0.031	37.4	0.541	2023	76.1	1539	8.40
1-1, 140-143	1.40	0.037	37.4	0.512	1915	79.4	1521	8.13
1-2, 28-31	1.78	0.048	37.4	0.580	2169	77.6	1683	8.30
1-2, 56-59	2.06	0.055	37.4	0.593	2218	74.6	1655	7.93
1-2, 88-89	2.38	0.064	37.4	0.525	1964	75.6	1485	8.07
1-2, 116-119	2.66	0.071	37.4	0.546	2042	77.8	1589	8.05
1-2, 140-143	3.00	0.080	37.4	0.553	2068	82.2	1699	8.06
1-3, 28-31	3.28	0.088	37.4	0.520	1948	77.2	1504	8.30
1-3, 56-59	3.56	0.096	37.4	0.616	2303	74.0	1704	7.85
1-3, 88-91	3.88	0.104	37.4	0.723	2704	77.9	2106	7.94
1-3, 116-119	4.16	0.111	37.4	0.671	2509	82.9	2080	8.00
1-3, 141-144	4.41	0.118	37.4	0.619	2315	82.9	1919	8.10
2-1, 9-12	4.89	0.131	37.4	0.559	2091	74.6	1559	8.16
2-1, 59-62	5.39	0.144	37.4	0.666	2491	71.7	1786	8.14
2-1, 100-103	5.80	0.155	37.4	0.538	2012	77.6	1561	7.94
2-2, 9-12	6.39	0.171	37.4	0.593	2218	83.4	1850	7.93
2-2, 59-62	6.89	0.184	37.4	0.556	2079	76.9	1599	7.85
2-2, 100-103	7.30	0.195	37.4	0.632	2364	79.9	1888	8.16
2-3, 2-12	7.89	0.211	37.4	0.601	2248	74.2	1668	8.30
2-3, 59-62	8.39	0.225	37.4	0.588	2199	75.8	1667	7.66
2-3, 100-103	8.80	0.236	37.4	0.634	2370	80.6	1910	7.75
2-4, 9-12	9.39	0.251	37.4	0.697	2607	82.6	2153	7.59
2-4, 59-62	9.89	0.265	37.4	0.723	2704	80.5	2176	7.60
2-4, 100-103	10.30	0.276	37.4	0.707	2644	88.4	2337	7.64
2-5, 9-12	10.89	0.291	37.4	0.606	2266	82.5	1869	8.24
2-5, 59-62	11.39	0.305	37.4	0.640	2394	84.1	2013	7.74
2-5, 100-103	11.80	0.316	37.4	0.624	2334	79.7	1860	7.80
2-6, 9-12	12.39	0.332	37.4	0.572	2151	78.9	1697	7.77
3-1, 8-11	14.38	0.385	37.4	0.694	2596	85.8	2227	8.14
3-1, 55-58	14.85	0.397	37.4	0.654	2446	86.0	2103	8.07
3-1, 115-118	15.45	0.414	37.4	0.627	2345	65.4	1534	7.86
3-2, 8-11	15.88	0.425	37.4	0.615	2302	80.2	1846	7.90
3-2, 55-58	16.35	0.438	37.4	0.606	2266	74.6	1690	8.02
3-2, 115-118	16.95	0.454	37.4	0.598	2237	74.9	1675	8.11
3-3, 8-11	17.38	0.465	37.4	0.627	2345	80.0	1876	8.21
3-3, 55-58	17.85	0.478	37.4	0.608	2274	80.2	1824	7.63
3-3, 115-118	18.45	0.494	37.4	0.627	2345	79.2	1857	7.60
3-4, 8-11	18.88	0.505	37.4	0.671	2510	79.4	1993	8.35
3-4, 52-55	19.32	0.517	37.4	0.653	2442	82.3	2009	8.02
3-4, 115-118	19.95	0.534	37.4	0.666	2491	84.4	2102	7.65
3-5, 8-11	20.38	0.545	37.4	0.733	2741	76.0	2083	7.53
3-5, 55-55	20.82	0.557	37.4	0.675	2525	82.5	2084	7.97
3-5, 115-118	21.45	0.575	37.4	0.640	2394	83.9	2002	7.66
3-6, 8-11	21.88	0.586	37.4	0.790	2955	80.7	2385	8.14
3-6, 52-55	22.32	0.597	37.4	0.762	2850	83.2	2371	8.08
3-6, 115-118	22.95	0.614	37.4	0.655	2450	80.5	1972	7.77
3-7, 8-11	23.38	0.626	37.4	0.624	2334	87.3	2037	7.70
4-1, 8-11	23.88	0.639	37.4	0.832	3112	83.7	2604	7.70
4-1, 56-59	24.36	0.652	37.4	0.732	2704	78.2	2115	7.99
4-1, 99-102	24.79	0.644	37.4	0.806	3014	76.4	2302	8.32
4-2, 8-11	25.38	0.678	37.4	0.647	3420	87.1	2108	7.98
4-2, 48-51	25.78	0.690	37.4	0.798	2973	84.9	2525	7.94
4-2, 99-102	26.29	0.704	37.4	0.694	2596	83.9	2178	7.55
4-3, 1-4	26.81	0.718	37.4	0.718	2685	77.2	2072	7.90
4-3, 56-59	27.36	0.736	28.8	0.694	2000	95.8	1916	7.70
4-3, 99-102	27.79	0.751	28.8	0.655	1886	81.6	1543	8.27
4-4, 8-11	28.38	0.771	28.8	0.671	1932	78.6	1519	7.80
4-4, 56-59	28.86	0.788	28.8	0.679	1956	83.7	1637	7.73
4-4, 99-102	29.29	0.803	28.8	0.757	2180	83.2	1813	7.86
4-5, 8-11	29.88	0.823	28.8	0.751	2163	77.8	1683	8.00
4-5, 56-59	30.36	0.840	28.8	0.668	1924	88.5	1703	8.04
4-5, 99-102	30.79	0.855	28.8	0.619	1783	73.4	1309	8.05
4-6, 9-12	31.39	0.876	28.8	0.829	2388	94.0	2245	7.64
5-1, 100-103	34.30	0.936	54.0	0.624	3370	76.7	2584	8.09
5-1, 140-143	34.70	0.947	29.0	0.744	2156	77.7	1677	8.07
5-2, 54-57	35.34	0.969	29.0	0.707	2050	79.4	1628	8.15
5-2, 100-103	35.80	0.985	29.0	0.707	2050	87.2	1789	8.01
5-2, 140-143	36.20	0.999	29.0	0.679	1969	81.9	1613	7.86
5-3, 54-57	36.84	1.021	29.0	0.655	1899	77.8	1477	8.13
5-3, 100-103	37.30	1.037	29.0	0.621	1801	65.4	1178	7.94
5-3, 140-143	37.70	1.050	29.0	0.673	1952	71.4	1394	7.93
5-4, 54-57	38.34	1.073	29.0	0.707	2050	57.5	1179	8.16
5-4, 100-103	38.80	1.088	29.0	0.749	2172	83.3	1809	7.80
5-5, 8-11	39.38	1.108	29.0	0.679	1969	87.2	1717	7.85

Table 2. (Continued).

Sample (interval in cm)	Depth (m)	Age (m.y.)	LSR (m/m.y.)	DBD (gm/cm^3)	MAR (mg/cm^2 1000 yr.)	Eolian wt. %	Eolian MAR (mg/cm^2 1000 yr.)	Eolian size (ϕ_{50})
5-5, 60-63	39.90	1.126	29.0	0.621	1801	89.0	1602	7.92
5-5, 100-103	40.30	1.140	29.0	0.645	1871	85.5	1600	7.70
5-6, 33-36	41.13	1.169	29.0	0.723	2097	91.9	1927	8.04
5-6, 100-103	41.80	1.192	29.0	0.692	2007	91.3	1832	7.75
5-7, 33-36	42.63	1.221	29.0	0.673	1952	86.6	1690	7.48
6-1, 57-60	43.37	1.246	29.0	0.564	1636	83.4	1364	7.60
6-1, 100-103	43.80	1.261	29.0	0.564	1636	86.1	1408	7.37
6-1, 140-143	44.20	1.275	29.0	0.650	1885	81.3	1533	8.03
6-2, 52-55	44.82	1.296	29.0	0.772	2239	82.9	1856	7.55
6-2, 100-103	45.30	1.313	29.0	0.601	1743	77.4	1349	7.90
6-2, 140-143	45.70	1.327	29.0	0.590	1711	81.7	1398	7.40
6-3, 30-33	46.10	1.340	29.0	0.663	1923	89.1	1713	7.90
6-3, 95-98	46.75	1.363	29.0	0.559	1621	81.6	1322	8.04
6-4, 15-18	47.45	1.387	29.0	0.738	2140	86.7	1855	7.98
6-4, 90-93	48.20	1.413	29.0	0.601	1743	81.7	1424	7.54
6-4, 140-143	48.70	1.430	29.0	0.702	2036	84.0	1710	7.86
6-5, 50-53	49.30	1.451	29.0	0.582	1688	99.0	1671	7.75
6-5, 90-93	49.70	1.465	29.0	0.707	2050	90.3	1851	7.25
6-5, 140-143	50.20	1.482	29.0	0.564	1636	79.9	1307	7.69
6-6, 47-50	50.77	1.502	29.0	0.564	1636	82.8	1354	7.51
6-6, 100-103	51.30	1.520	29.0	0.554	1607	81.7	1312	7.70
6-7, 37-40	52.17	1.550	29.0	0.767	2224	85.9	1910	7.68
7-1, 12-15	52.42	1.559	29.0	0.790	2291	80.5	1844	7.97
7-1, 60-63	52.90	1.575	29.0	0.733	2126	74.1	1612	7.65
7-1, 110-113	53.40	1.592	29.0	0.679	1969	87.8	1729	7.30
7-2, 10-13	53.90	1.610	29.0	0.842	2442	82.6	2017	7.52
7-2, 60-63	54.40	1.635	20.4	0.749	1535	82.6	1260	7.79
7-2, 135-138	55.15	1.693	20.4	0.642	1316	75.0	987	7.74
7-3, 10-13	55.40	1.711	20.4	0.655	1343	80.9	1086	7.43
7-3, 60-63	55.90	1.750	20.4	0.702	1439	76.5	1100	7.67
7-3, 110-113	56.40	1.788	20.4	0.975	1999	85.5	1709	7.41
7-4, 10-13	56.90	1.826	20.4	0.772	1583	74.3	1176	7.80
7-4, 60-63	57.40	1.864	20.4	0.603	1236	80.4	993	7.82
7-4, 110-113	57.90	1.902	20.4	0.780	1599	95.7	1530	7.71
7-5, 10-13	58.40	1.925	26.6	0.728	1936	83.4	1614	8.22
7-5, 60-63	58.90	1.944	26.6	0.975	2594	85.0	2205	7.78
7-5, 110-113	59.40	1.963	26.6	0.975	2594	82.7	2145	7.95
7-6, 10-13	59.90	1.981	26.2	0.619	1647	79.4	1308	8.14
7-6, 60-63	60.40	2.000	26.6	0.663	1764	81.8	1442	8.24
7-6, 110-113	60.90	2.019	26.6	0.650	1729	82.9	1433	8.07
7-7, 12-15	61.42	2.039	26.6	0.866	2304	91.8	2115	7.84
8-1, 20-23	62.00	2.060	26.6	0.584	1553	81.0	1258	7.75
8-1, 74-77	62.54	2.081	26.6	0.580	1543	84.4	1302	7.98
8-1, 120-123	63.00	2.098	26.6	0.957	2546	88.5	2253	7.67
8-2, 20-23	63.54	2.118	26.6	0.668	1777	77.1	1370	8.25
8-2, 74-77	64.04	2.137	26.6	0.559	1487	83.9	1248	7.78
8-2, 120-123	64.50	2.154	26.6	0.660	1756	82.5	1449	7.61
8-3, 20-23	65.00	2.173	26.6	0.866	2304	86.0	1981	7.49
8-3, 74-77	65.54	2.193	26.6	0.718	1910	83.7	1599	7.77
8-3, 120-123	66.00	2.211	26.6	0.686	1826	95.0	1734	7.80
8-4, 20-23	66.50	2.229	26.6	0.647	1721	87.2	1500	7.45
8-4, 75-78	67.06	2.250	26.6	0.611	1625	79.2	1287	7.48
8-4, 130-133	67.60	2.271	26.6	0.646	1718	83.5	1434	8.20
8-5, 20-23	68.00	2.286	26.6	0.671	1785	76.4	1364	7.83
8-5, 74-77	68.54	2.306	26.6	0.842	2240	81.3	1821	8.22
8-5, 123-128	69.05	2.325	26.6	0.985	2620	83.3	2183	7.53
8-6, 20-23	69.50	2.342	26.6	1.118	2974	79.4	2361	8.13
8-6, 60-63	69 90	2.357	26.6	0.772	2054	84.5	1736	8.19
8-6, 114-117	70.44	2.378	26.6	0.803	2136	83.7	1788	8.26
8-7, 24-27	71.04	2.400	26.6	0.816	2171	88.4	1919	8.20
9-1, 17-20	71.47	2.416	26.6	0.842	2240	79.9	1789	7.86
9-1, 67-70	71.97	2.435	26.6	0.881	2343	81.4	1907	7.95
9-1, 114-117	72.44	2.453	26.6	0.723	1923	81.7	1571	8.06
9-2, 17-20	72.97	2.474	17.0	1.069	1817	88.4	1606	8.05
9-2, 71-74	73.51	2.506	17.0	0.780	1326	77.1	1022	7.83
9-2, 114-117	73.95	2.531	17.0	0.774	1265	82.1	1038	8.45
9-3, 17-20	74.47	2.562	17.0	0.889	1511	84.0	1269	7.83
9-3, 67-70	74.97	2.591	17.0	0.629	1069	81.2	868	8.20
9-3, 114-117	75.44	2.619	17.0	0.655	1114	81.0	902	8.03
9-4, 17-20	75.97	2.650	17.0	0.842	1431	72.0	1030	8.07
9-4, 47-50	76.27	2.668	17.0	0.897	1525	89.0	1369	8.23
9-4, 114-117	76.95	2.707	17.0	0.650	1105	78.3	865	8.29
9-5, 30-33	77.63	2.747	17.0	0.634	1078	78.7	848	7.95
9-5, 67-70	77.97	2.767	17.0	0.642	1091	78.7	859	8.22
9-5, 105-108	78.35	2.790	17.0	0.874	1486	72.8	1082	8.05
9-6, 14-17	78.94	2.824	17.0	0.874	1486	85.9	1277	8.31
9-6, 54-57	79.34	2.848	17.0	0.702	1193	76.6	914	8.20

Table 2. (Continued).

Sample (interval in cm)	Depth (m)	Age (m.y.)	LSR (m/m.y.)	DBD (gm/cm^3)	MAR (mg/cm^2 1000 yr.)	Eolian wt. %	Eolian MAR (mg/cm^2 1000 yr.)	Eolian size (ϕ_{50})
9-6, 97-100	79.77	2.873	17.0	0.794	1351	83.3	1113	7.86
9-7, 14-17	80.44	2.912	22.2	0.939	2085	82.1	1712	7.90
10-1, 9-12	80.89	2.932	22.2	1.048	2327	80.4	1871	7.72
10-1, 56-59	81.36	2.953	22.2	1.009	2220	81.3	1805	8.20
10-1, 108-111	81.88	2.977	22.2	0.975	2165	73.8	1598	8.37
10-2, 9-12	82.39	3.000	17.1	0.858	1461	81.8	1195	8.04
10-2, 62-65	82.92	3.030	17.1	0.744	1272	83.8	1066	8.20
10-2, 108-111	83.38	3.057	17.1	0.647	1106	82.4	911	8.16
10-3, 9-12	83.89	3.091	14.0	0.702	983	80.0	786	8.30
10-3, 56-59	84.36	3.124	14.0	0.718	1005	84.1	845	8.53
10-3, 108-111	84.88	3.161	14.0	0.728	1019	87.0	886	8.42
10-4, 9-12	85.30	3.197	11.3	0.728	823	79.4	653	8.53
10-4, 56-59	85.86	3.246	11.3	0.738	834	81.2	677	7.95
10-4, 102-105	86.32	3.287	11.3	0.650	735	83.2	611	8.46
10-5, 9-12	86.89	3.338	11.3	0.827	935	75.6	707	8.36
10-5, 56-59	87.36	3.380	11.3	0.640	723	79.5	575	8.40
10-5, 108-111	87.88	3.423	13.9	0.718	998	82.6	824	8.05
10-6, 9-12	88.39	3.460	13.9	0.874	1215	78.2	950	8.03
10-6, 56-59	88.86	3.493	13.9	0.660	917	85.3	754	8.44
11-1, 40-43	90.70	3.626	13.9	0.686	954	75.0	715	8.00
11-1, 80-83	91.10	3.655	13.9	0.670	931	76.8	715	8.14
11-1, 134-137	91.64	3.693	13.9	0.640	890	77.2	687	8.09
11-2, 40-42	92.20	3.734	13.9	0.661	919	75.1	690	8.19
11-2, 80-83	92.60	3.762	13.9	0.772	1073	93.3	1001	8.01
11-2, 138-141	93.18	3.804	13.9	0.881	1225	79.9	979	8.20
11-3, 30-33	93.60	3.835	13.0	0.707	919	78.2	719	8.20
11-3, 77-80	94.07	3.872	13.0	0.749	974	75.3	733	8.25
11-3, 122-125	94.52	3.906	13.0	0.738	959	74.5	714	8.30
11-4, 40-43	95.20	3.964	11.3	0.837	946	85.5	809	8.13
11-4, 80-83	95.60	3.999	11.3	0.697	788	81.8	645	8.17
11-4, 122-125	96.02	4.036	11.3	0.707	799	81.0	647	8.37
11-5, 40-43	96.70	4.112	7.2	0.733	528	82.7	436	8.25
11-5, 77-80	97.07	4.163	7.2	0.749	539	85.4	460	8.43
11-5, 122-125	97.52	4.225	7.4	0.785	565	86.5	489	7.90
11-6, 41-44	98.21	4.319	7.4	0.692	512	85.0	435	8.35
11-6, 122-125	99.02	4.429	7.4	0.767	568	79.8	453	8.33

Note: Abbreviations are as in Table 1.

Oligocene, the size of the eolian material steadily increases to 8.55 ϕ in the early Miocene. Following a decrease in size to 8.73 ϕ in the middle Miocene, eolian size increases through the late Miocene and Pliocene to 8.35 ϕ. The increases in size during the Oligocene and late Miocene/Pliocene are equivalent to changes in grain mass by a factor of 2.4 and 2.1, respectively.

Between 4.5 and 2.5 m.y. ago the average eolian grain size at Site 578 (Fig. 5) was relatively small, generally less than 8.00 ϕ. The size of the eolian material increases from an average of 8.20 ϕ at 2.5 m.y. ago to an average of 7.7 ϕ at 1.5 m.y. ago, then decreases to an average of 8.00 ϕ over the last million years.

DISCUSSION

omparison of DSDP Site 576 and LL44-GPC-3

The record of eolian accumulation and grain size DSDP Site 576 provides an excellent complement to the record at LL44-GPC-3 (Leinen and Heath, 1981, anecek and Rea, 1983; Leinen, this volume), located 500 km to the east at approximately the same latitude Fig. 1). The eolian mass-accumulation rate and the grain size for both sites are plotted in Figure 6.

During the Late Cretaceous and Paleocene, Site 576 was moving northward on the Pacific plate under the northeast trade winds (Fig. 7). Eolian accumulation rates were relatively low, averaging about 40 mg/cm^2/10^3 yr. Low eolian input is in agreement with independent data suggesting warmer (Savin, 1977; Frakes, 1979) and wetter (Wolfe and Hopkins, 1967; Wolfe, 1978; Kemp, 1978) climatic conditions during the early Cenozoic than at the present. In addition, the lack of glacial erosion products would mean less material was available for erosion and transportation. Eolian accumulation rates decreased further to less than 20 mg/cm^2/10^3 yr. during the middle and late Eocene and may be indicative of the humid climates that characterized that time (cf. Frakes, 1979) and/or the passage of the site out of the core of the trade winds (Leinen and Heath, 1981). The low accumulation rates in the Oligocene contrast with other climatic data (cf. Frakes, 1979) that suggest drier conditions in the Oligocene than in the Paleocene and Eocene.

The eolian accumulation records at Site 576 and LL44-GPC-3 are very similar for the Late Cretaceous and early Cenozoic; both are characterized by relatively low rates. However, eolian accumulation rates at Site 576 are two to three times greater than at LL44-GPC-3. In addition, the record at LL44-GPC-3 is marked by an accumulation rate maximum in the early Eocene that is not present at Site 576 (Fig. 6).

The early Eocene accumulation maximum at LL44-GPC-3 has been interpreted by Leinen and Heath (1981) to be the result of the site moving through the zone of

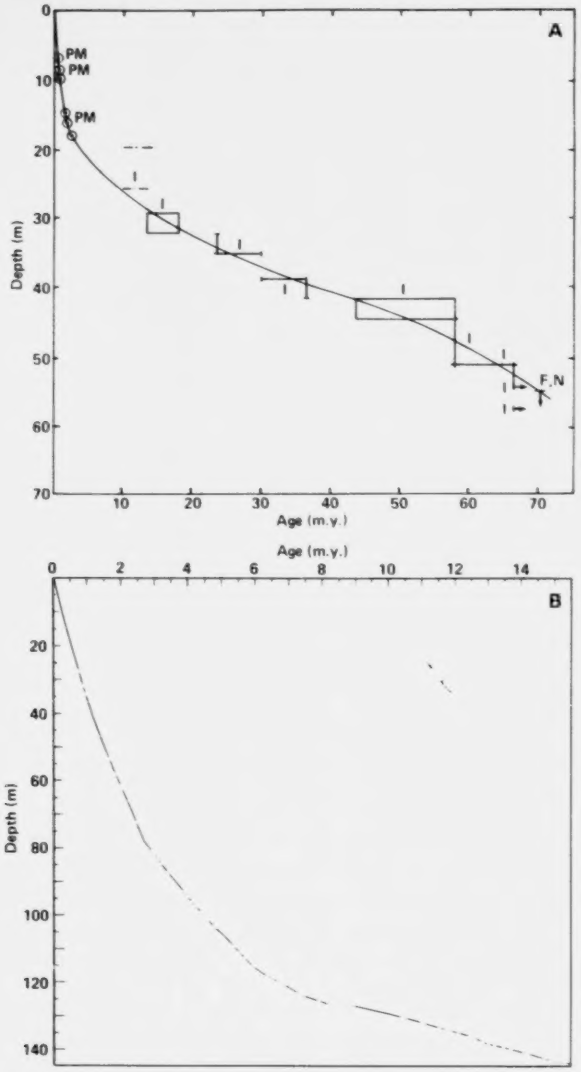

Figure 3. Depth versus age plot. A. Site 576. B. Site 578. Paleomagnetic (PM) data from Heath, Rea, and Levi (this volume). Foraminiferal (F) age ranges from D'Agostino (this volume). Nannofossil (N) age ranges from Monechi (this volume). Ichthyolith (I) age ranges from Doyle and Riedel (this volume).

the maximum northeast trade wind influence in the eastern Pacific. The lack of similar pattern at Site 576 may be the result of poorly constrained biostratigraphy.

The higher early Cenozoic eolian accumulation rates at Site 576 relative to LL44-GPC-3 are interesting in that LL44-GPC-3 is 3500 km closer to the predominant source regions in Central America and Mexico and might be expected to have greater eolian accumulation rates. The difference, again, may be the result of poorly constrained biostratigraphy at both sites. Another possible explanation, however, is that Site 576 was receiving significant input from Asia as well as from Central America. Duce et al. (1980) have shown that Asian dust can contribute significantly to the total marine aerosol at locations in the trade winds. At present, dust originating in Asia is carried eastward by the high-level westerlies, injected below the trade-wind inversion by subsidence associated with anticyclones moving off of Japan in the spring of the year, and carried westward by the trade winds. If such trajectories occurred in the early Cenozoic, Site 576 would have been influenced more by these circulation patterns than LL44-GPC-3 and, thus, would record higher eolian input.

Distinct changes in eolian accumulation rates and the mineralogy of bulk sediment (Leinen, this volume; Schoonmaker et al., this volume) at 25 m.y. ago may be the result of the two sites moving into the influence of the westerlies at this time. Schoonmaker et al. (this volume) record an increase in quartz and feldspar content as well as an increase in mixed layer illite to smectite ratio at Site 576 around 20–25 m.y. ago. Leinen (this volume) shows an increase in quartz content at 28 m.y. ago and a gradual increase between 18 and 8 m.y. ago at Site 576. Leinen and Heath (1981) recorded a large change in the quartz content and chemistry of the sediments at LL44-GPC-3 approximately 23 m.y. ago. In addition, they report a gradual increase in quartz content between 18 and 8 m.y. ago. The temporal difference in the initial increase in quartz content at Site 576 is probably the result of the greater sample density used by Leinen in her study. Thus, the mineralogy data suggest a change in source material from quartz-poor, more basic dust before the Miocene to a more quartz-rich material from the Asian continent after the sites moved into the influence of the westerlies between 20 and 28 m.y. ago (Leinen and Heath, 1981). The details of that transition time remain unclear, however, because of stratigraphic uncertainty.

Eolian accumulation rates underwent another increase at both sites between 15 and 10 m.y. ago (Fig. 6), a time coincident with the onset of rapid ice-volume increase in Antarctica (Savin, 1977; Brewster, 1980; Woodruff et al., 1981). This increase in the mid-to-late Miocene, along with a factor of six increase in accumulation rates in Pliocene/Pleistocene time, supports the general correlation between glacial ages, global aridity, and an increase in glacial erosion products for dust transport (Rea and Janecek, 1982).

Eolian Grain Size and Atmosphere Circulation

The size of wind-borne grains at Site 576 (Fig. 4) increased from the Late Cretaceous into the Paleocene, suggesting a slight increase in the intensity of atmospheric circulation across the Cretaceous/Tertiary boundary. An increase in quartz grain size (Janecek and Rea, 1983) is also seen at LL44-GPC-3 over this same time interval although the trend in the total eolian component is less obvious (Fig. 6). Thus, there may not be a significant change in atmospheric circulation across the Cretaceous/Tertiary boundary. The sampling interval in these cores, however, was not designed to resolve short-duration phenomena.

The eolian grain size at Site 576 in the Late Cretaceous and Paleocene is equivalent to that in the Pliocene and Pleistocene, two very different climatic intervals.

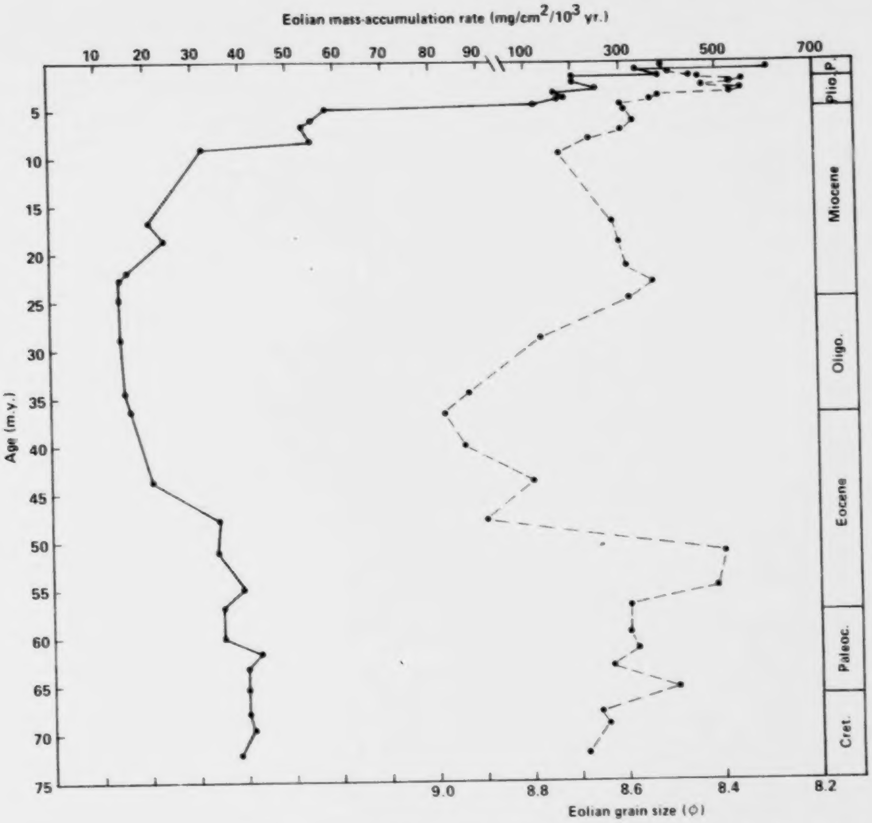

Figure 4. Eolian mass-accumulation rates (solid line) and eolian grain size (dashed line) for Site 576.

Global atmospheric circulation models developed by Barron and Washington (1982) that incorporate Cretaceous paleogeography suggest that Cretaceous wind speeds may have been increased relative to the present and were much greater than would be inferred from Cretaceous pole-to-equator temperature gradients. The eolian size data from Site 576 and LL44-GPC-3 are in agreement with relatively high Cretaceous wind intensities.

A sharp reduction in the eolian grain size at Site 576 near the Paleocene/Eocene boundary could represent a significant reduction in the intensity of atmospheric circulation. Over this relatively short time span, the eolian grain mass is reduced by a factor of three at Site 576; a change on the order of the one that occurs between the glacial-to-interglacial oscillations in the late Pleistocene (Janecek and Rea, in press). A similar, although larger, size decrease occurs at LL44-GPC-3 (Fig. 6) at this time (Janecek and Rea, 1983). Diagenetic effects resulting in increased grain size in the older sediments are not the cause of the size change, since scanning electron microscopy of the eolian material at LL44-GPC-3 (Janecek and Rea, 1983) and at Site 576 shows no grain overgrowths or cementation in the older sediments. Since the eolian material is in equilibrium with the transporting wind because of the large transport distances involved, the introduction of material from a more distant source area should have little, if any, effect on the size of the eolian grains. This sharp decrease in grain size might be associated with a reduction in pole-to-equator temperature gradients at this time, although there is little other independent paleoclimatic information to suggest such a large change in climate in the early Eocene.

The relatively low grain-size values in the Eocene and early Oligocene imply that the vigor of atmospheric circulation was lower at that time than at any other time in the Cenozoic. This scenario is supported by planktonic and benthic ^{18}O data (Savin, 1977), which indicate low latitudinal thermal gradients and hence sluggish atmospheric circulation during the Eocene and early Oligocene. Following the low in eolian grain size in the late Eocene and early Oligocene, eolian grain size at both sites increased steadily into the early Miocene. The increase in wind intensity suggested by this information corresponds well with the sudden onset of polar cooling and cold bottom-water formation about 38 m.y. ago (Kennett and Shackleton, 1976).

The decrease in grain size at both sites in the early Miocene (Fig. 6) may be the result of a slight warming trend at that time. Oxygen isotopes (Woodruff et al., 1981) indicate an increase in temperature in the early Miocene and thus, possibly a reduction in pole-to-equator temperature gradients and in the intensity of the zonal winds. The reduction in grain size also may be, in part, the result of the light and variable winds associated with

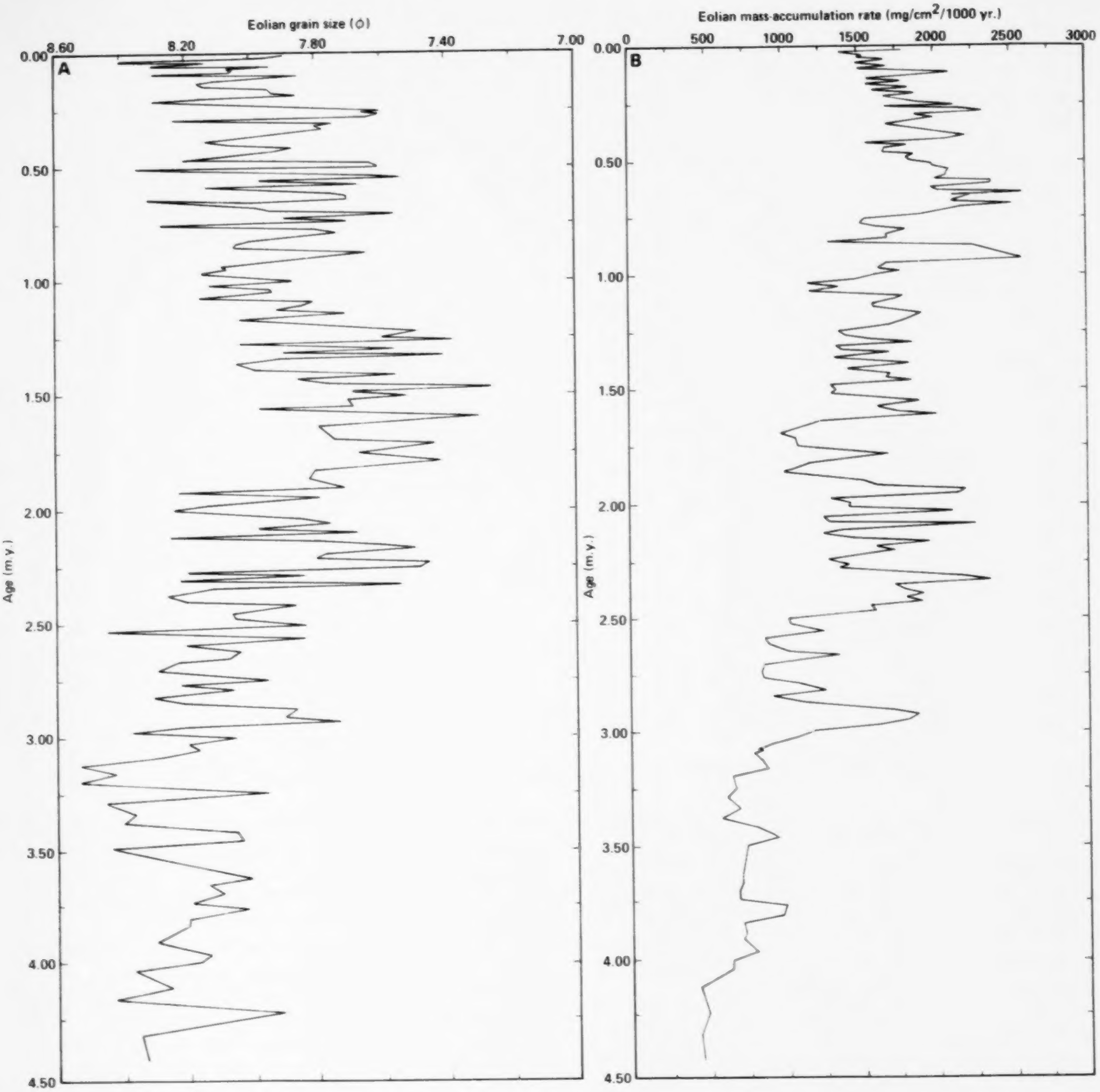

Figure 5. (A) Eolian grain size and (B) eolian mass-accumulation rates for Site 578.

the transition zone between the prevailing westerlies and the trade winds.

The size of the wind-borne material at LL44-GPC-3 (Fig. 6) increased during the Miocene, suggesting an intensification of atmospheric circulation, apparently the result of polar cooling (Bandy et al., 1969; Savin, 1977; Woodruff et al., 1981). However, the record at Site 576 shows an overall decrease in grain size between 10 and 20 m.y. ago. Because the record at Site 576 over this time interval is constrained by only three points, it is unclear to what degree the data actually conflict. Both sites exhibit generally coarsening grain-size trends in samples younger than 10 m.y. A relatively smaller increase in grain size in the Pliocene than in the Miocene and Oligocene suggests that larger increases in atmospheric circulation occurred during the Oligocene and possibly the Miocene than during the onset of Northern Hemisphere glaciation.

The Onset of Northern Hemisphere Glaciation

The eolian accumulation rate and grain-size data for Site 576 and LL44-GPC-3 increase dramatically in the mid-Pliocene, coincident with the onset of Northern Hemisphere glaciation. However, the low sedimentation rates in these cores make it difficult to establish the timing of the changes in eolian deposition with the onset of North-

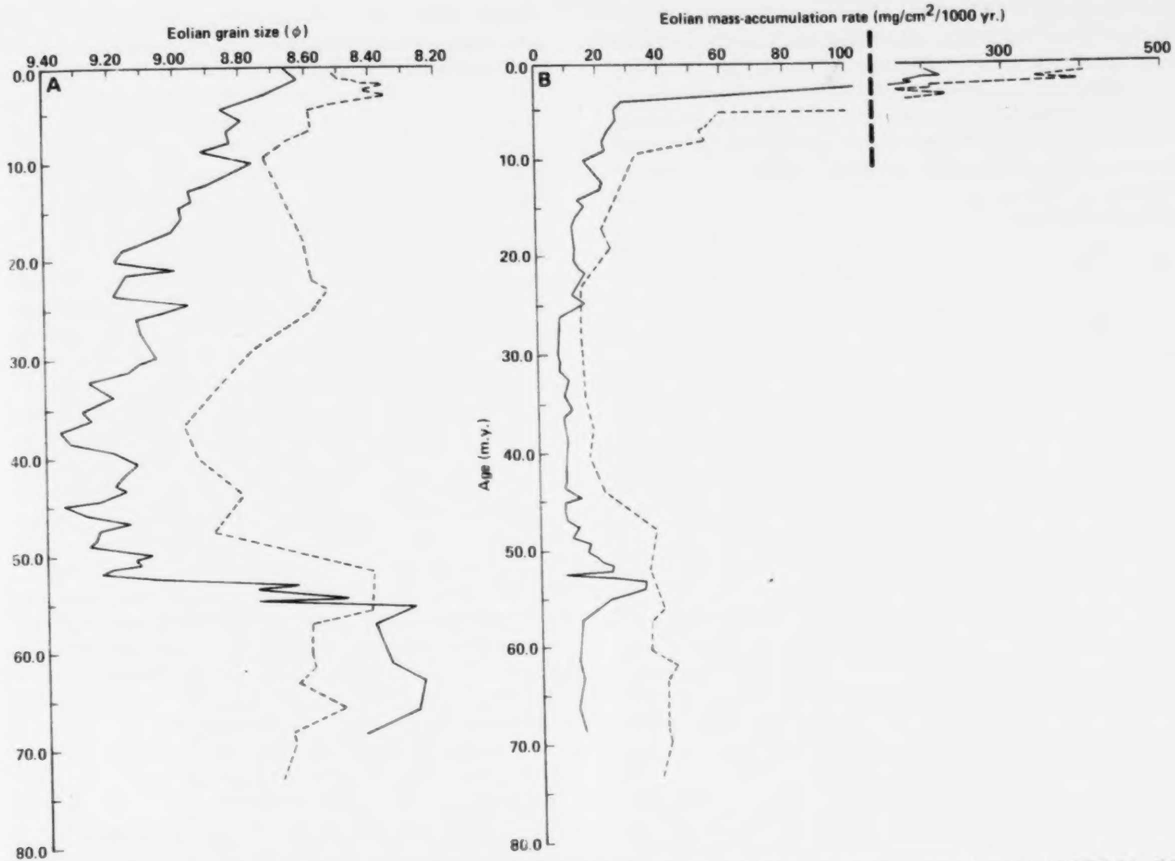

Figure 6. (A) Site 576 (dashed line) eolian grain size and (B) mass-accumulation rates plotted with respective components from LL44-GPC-3 (solid line) (Janecek and Rea 1983).

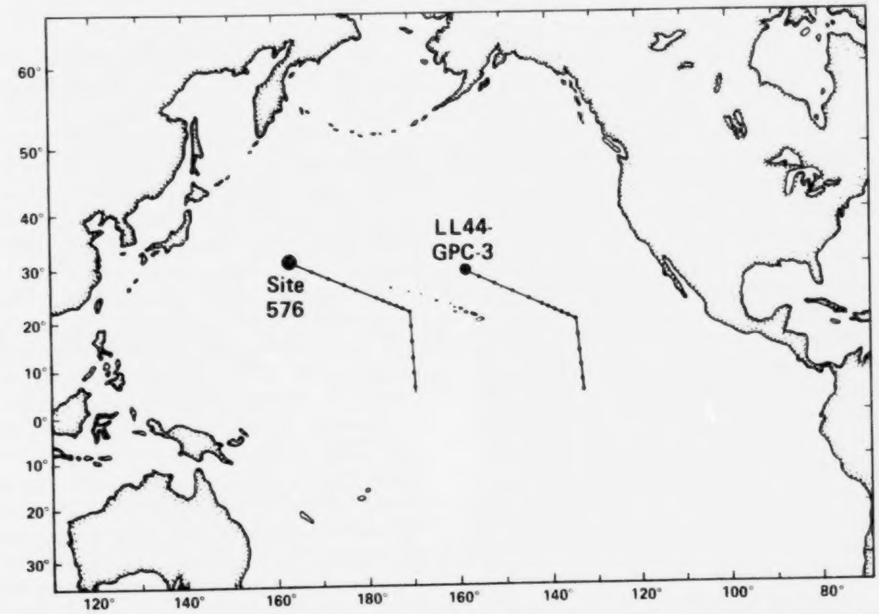
60°
50°
40°
30°
20°
10°
0°
10°
20°
30°
LL44-GPC-3
Site 576
120°
140°
160°
180°
160°
140°
120°
100°
80°

Figure 7. Backtrack path of DSDP Site 576 and LL44-GPC-3 (Leinen and Heath, 1981). Points on the backtrack path mark 5 m.y. intervals along the path.

ern Hemisphere glaciation. The high sedimentation rates at Site 578 allow increased resolution to evaluate better the changes in eolian input and atmospheric circulation with the onset of Northern Hemisphere glaciation.

Until recently, the onset of major Northern Hemisphere glaciation was thought to have occurred around 3.2 m.y. ago. Much of the evidence supporting this date has come from low-resolution rotary-drilled DSDP cores and widely spaced samples. The inception of ice-rafting observed in rotary-drilled cores in the North Atlantic (DSDP Sites 111 and 116) was thought to occur about 3.0 m.y. ago (Berggren, 1972). In rotary-drilled cores in the Mediterranean Sea, Thunell (1979) found foraminiferal evidence for significant cooling around 3.2 m.y. ago. Oxygen-isotope analyses from foraminifers in the same sediments suggest a surface-water cooling at 3.2 m.y. ago followed by an ice-volume increase between 3.1 and 3.0 m.y. ago (Keigwin and Thunell, 1979). These results are in agreement with those of Saito (1976) and Keigwin (1979), which date the final closing of the Isthmus of Panama between 3.5 and 3.1 m.y. ago.

However, other evidence, including the eolian data presented here, suggest a later date for the onset of major ice buildup. In the Atlantic Ocean, off northwest Africa at Site 397, a significant increase in the variability of oxygen-isotope data occurs around 2.5 m.y. ago (Shackleton and Cita, 1979). Herman (1974) recorded a distinct change in sediment characteristics and microfaunal abundances in the Arctic about 2.4 m.y. ago. More recent work (Shackleton et al., 1984) from Site 552 in the North Atlantic, shows that the onset of Northern Hemisphere glaciation, as marked by the appearance of an alternating sequence of nannofossil-foraminifer oozes and ice-rafted debris, occurred about 2.4 m.y. ago. A reexamination of the sediment from Sites 111 and 116 by Bachman (1979) resulted in an age of 2.5 m.y. for the earliest onset of ice-rafted debris at those sites.

Several data sets from the Pacific Ocean also suggest a later date for the onset of Northern Hemisphere glaciation. Conolly and Ewing (1970) recorded the beginning of ice-rafted debris about 2.5 m.y. ago from evidence in piston cores. Rea and Schrader (in press) came to a similar conclusion based upon the reexamination of ice-rafting in North Pacific cores. Shackleton and Opdyke (1977) analyzed oxygen isotopes in foraminifers in equatorial Pacific sediments which recorded a permanent change in isotopic composition around 3.1 m.y. ago. However, they also showed a major change in the variability of the oxygen isotopes around 2.5 m.y. ago, indicating glacial ice volume of a magnitude at least two-thirds that of the later Pleistocene glaciations.

The eolian mass-accumulation rates and grain size at Site 578 support the later date of 2.4 to 2.5 m.y. ago for the onset of major ice buildup in the Northern Hemisphere. At Site 578, the eolian accumulation rates increase by more than a factor of two and appear to become highly variable around 3.0 m.y. ago, near the time previously associated with the onset of Northern Hemisphere glaciation. However, following this temporary increase, eolian input decreases between 2.9 and 2.5 m.y. ago, then increases sharply at 2.5 m.y. ago, and remains high and variable until the present. A similar pattern is seen in the eolian record at Sites 310 and 503 in the North Pacific. The accumulation rates at these two sites record a relative maximum around 2.9 to 2.75 m.y. ago and an increase to higher rates around 2.5 m.y. ago (Janecek, 1983).

This later age for the major climate change is also supported by the grain-size records at Sites 578, 310, and 503 (Janecek, 1983). All three sites record the largest grain size and hence wind vigor after 2.5 m.y. ago. In addition, the grain-size record at Site 578 also suggests a maximum in wind intensity occurred around 1.5 to 1.0 m.y. ago.

Combined, these data suggest that the significant change in Northern Hemisphere continental climate occurred as late as 2.5 to 2.4 m.y. ago. The increased eolian accumulation apparently is the result of the general increase in global aridity associated with stronger surface outflow of air from the continents, which enhances sinking motions and thus reduces rainfall (Manabe and Hahn, 1977). The changes in grain size would be a natural consequence of large ice expansion in the Northern Hemisphere as albedo feedback at high latitudes would result in steepened thermal gradients, increased wind intensity (Gates, 1976; Berger et al., 1981; CLIMAP, 1981), and hence larger grains transported to the deep sea.

The eolian records at Sites 578, 503, and 310 suggest that a "cooling event" or dry period may have occurred about 2.9 to 3.0 m.y. ago. The eolian accumulation records at all three sites record peaks in accumulation at this time and suggest dryer (colder?) conditions in Asia, central America, and northern South America. The eolian grain size, however, does not change significantly at this time, suggesting the dryer (colder?) conditions were not accompanied by an increase in the intensity of atmospheric circulation.

Recent studies of oxygen isotopes in the Mediterranean and South Atlantic also suggest that a temporary global cooling occurred around 3.0 m.y. ago, prior to the onset of Northern Hemisphere glaciation. Isotopic records from the Mediterranean (Thunell and Williams, 1983) show that the interval between 4.2 and 2.5 m.y. ago was marked by relatively warm and stable conditions. However, a short-term enrichment of ^{18}O occurred about 3.2 m.y. ago, which Thunell and Williams (1983) interpreted to reflect a cooling of surface water rather than a buildup of continental ice. A permanent shift in ^{18}O is recorded in the Mediterranean at 2.5 m.y. ago, indicating the initial large buildup of permanent continental ice (Thunell and Williams, 1983).

Isotopic records from the South Atlantic (Hodell et al., 1983) indicate no ^{18}O enrichment in the planktonic foraminifers at 3.2 m.y. ago, although each site studied contained an enrichment in the benthic foraminifers that increased in magnitude with depth. Hodell et al., (1983) suggested that the event 3.2 m.y. ago does not necessarily represent an increase in ice volume but rather a fun damental change in deep-water ocean circulation patterns resulting from a global cooling event and/or the closing of the Central American Seaway.

Implications for Long-Distance Transport

The late Pleistocene eolian records at Sites 576 and 78 can be compared with other late Pleistocene North acific records from similar latitudes to constrain models long-distance dust transport. Late Pleistocene eolian cumulation and grain size records from Sites 576 and 8 (this manuscript and unpublished data), University Hawaii piston Core KK75-02 (Janecek and Rea, in ess), and LL44-GPC-3 (Janecek and Rea, 1983) were eraged and plotted versus longitudinal distance (Fig. to determine trends in accumulation and grain size th distance of transport. The reader is referred to the aforementioned references for a compilation and a more comprehensive analysis of the data for these cores. Both the accumulation rates and grain size decrease sharply between Sites 578 and 576 and then decrease very slowly farther to the east between Site 576 and LL44-GPC-3. This information suggests that the eolian material reaching Site 578 is influenced to a large extent by gravitational settling and thus records more and larger material. By the time that the eolian grains reach Site 576 in the central North Pacific, they have a size distribution that is nearly in equilibrium with the transporting wind. That is, the settling velocity of the grains is balanced by the lifting effects of atmospheric motions (Gillette et al., 1974; Gillette, 1981) and the grain size remains constant with further transport.

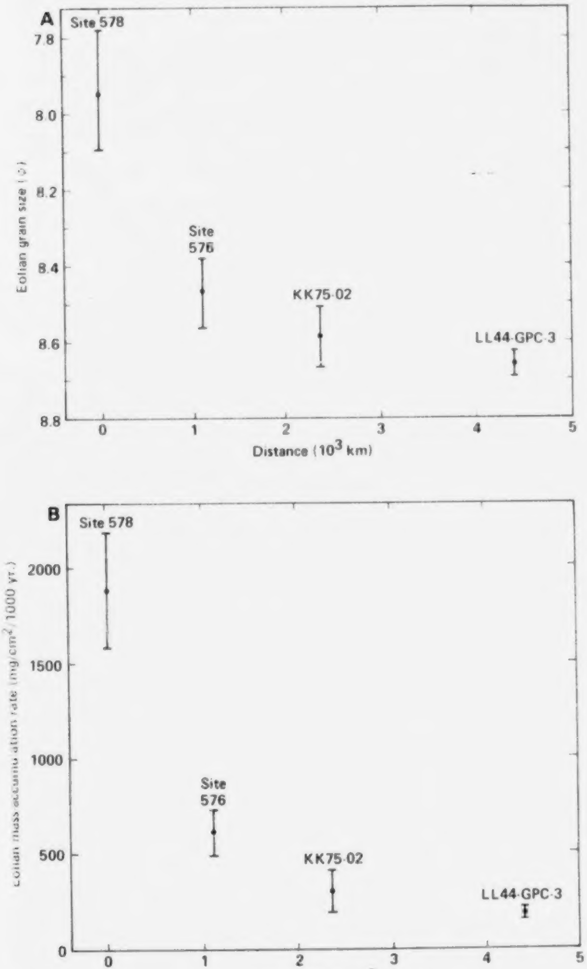

igure 8. Distance of transport versus (A) eolian grain size and (B) eolian mass-accumulation rate for late Pleistocene samples from Site 578 (71 samples, this manuscript), Site 576 (64 samples, unpublished data), KK75-02 (90 samples, Janecek and Rea, in press), and LL44-GPC-3 (3 samples, Janecek and Rea, 1983). Error bars indicate one standard deviation.

Recent work by Dauphin (1983) on quartz grains in the North Pacific has shown that there is a linear decrease in quartz size across the North Pacific. This implies a heterogeneous or continually changing mineral aerosol across the North Pacific. The grain-size and accumulation-rate data presented here, as well as the uniformity of quartz concentration between Site 576 and LL44-GPC-3 (Leinen, this volume), suggest that a very homogeneous dust composition is present after several thousand kilometers of transport. The data in Figure 8 suggest that Site 576 is not quite at the equilibrium point, which might explain why the grain size and accumulation rates for Site 576, while it has been under the influence of the westerlies, are greater than those of LL44-GPC-3.

Intensity of Atmospheric Circulation

The atmospheric motions that support this equilibrium grain size can be quantified by using Stokes's settling law to calculate the settling velocity of dust grains in the air. Thus, changes in wind intensities in the past can be determined by comparing, in ratio form, the settling velocities calculated from the grain size from two different samples. As all terms except the grain size in Stoke's law will remain constant, the ratio of wind intensities between two different time horizons is given by the ratio of the squares of the larger, D_L^2, and smaller, D_S^2, grain diameters (Janecek and Rea, in press).

These ratios can be applied to grain-size data sets from sites far enough from the source for grain size to be nearly in equilibrium with the transporting wind. Application of this ratio to the eolian grain-size record at Site 576 suggests that atmospheric circulation was reduced by at least a factor of 2.2 across the Paleocene/Eocene boundary. Increases in wind intensity in the Oligocene and Pliocene are by factors of 1.8 and 1.4, respectively. In comparison, at LL44-GPC-3 wind intensity decreases by a factor of 3.8 at the Paleocene/Eocene boundary. At this same site, wind intensity increases by a factor of 1.5 for the Oligocene, 1.8 for the Miocene, and 1.3 for the Pliocene.

SUMMARY

The grain size and mass-accumulation rate of eolian material isolated from Sites 576 and 578 in the Northwest Pacific have been used to evaluate changes in eolian sedimentation rate and the intensity of atmospheric circulation that have occurred during the past 70 m.y. The similarity in source regions and latitudinal positions of DSDP Site 576 and LL44-GPC-3 (located 3500 kilometers to the east) provides an opportunity to evaluate differences in long-distance transport of dust to the North Pacific during the Cenozoic. The temporal pattern of eolian accumulation rate and grain size is very similar in both cores. The eolian accumulation rate, an indicator of source area climate, is relatively low in the Late Cretaceous and early Cenozoic, in agreement with the humid conditions that characterized that time period. Increased eolian accumulation occurred at 25 m.y. ago, 15–10 m.y. ago, and around 3.0 m.y. ago. The increase around 25 m.y. ago is probably the result of the two sites moving into the westerlies, whereas the increase 15–10 m.y. ago coincides with the expansion of ice in Antarctica and a general increase in global aridity. An order of magnitude increase in accumulation rates in the Pliocene coincides with the onset of Northern Hemisphere glaciation. Eolian grain size, an indicator of wind intensity, suggests that Late Cretaceous and Paleocene time are characterized by wind intensities comparable to the present, a scenario supported by recent computer models of atmospheric circulation. A large decrease in grain size at the Paleocene/Eocene boundary is not readily explainable but suggests that a significant decrease in the intensity of atmospheric circulation may have occurred at that time. The lowest grain-size values occur in the middle Cenozoic and are in agreement with other proxy indicators of climate suggesting low thermal gradients and sluggish atmospheric circulation. The grain-size records indicate that relatively larger increases in atmospheric circulation occurred in the Oligocene (38 to 25 m.y. ago) and Miocene (20 to 10 m.y. ago) than with the onset of Northern Hemisphere glaciation in the Pliocene.

High-resolution samples from Site 578 record a temporary increase in grain size and accumulation rate around 3.0 m.y. ago and a permanent increase in both parameters 2.5 m.y. ago. These records lend support to the idea that Northern Hemisphere glaciation occurred 2.4 to 2.5 m.y. ago and that the earlier event (3.0 m.y. ago) was a temporary global cooling.

Differences in accumulation rate and grain size with transport distance suggest that these indicators decrease exponentially, not linearly, with transport distance across the North Pacific and do not reach an equilibrium state until at least 3000 km distance from source areas.

ACKNOWLEDGMENTS

This chapter represents work the author conducted while at the University of Michigan. This manuscript benefitted from discussions with David K. Rea and Joseph Morley. In addition, the manuscript was reviewed by Margaret Leinen and an anonymous reviewer who provided helpful suggestions for its improvement. This work was supported, in part, by the National Science Foundation, Grant OCE80-24368.

REFERENCES

Bachman, J., 1979. Pliocene biostratigraphy of DSDP Sites 111 and 116 from the North Atlantic Ocean and the age of northern hemisphere glaciation. *Stockholm Contrib. Geol.*, 32:113–137.

Bandy, O. L., Butler, E. A., and Wright, R. C., 1969. Alaskan upper Miocene marine glacial deposits and the *Turborotalia pachyderma* datum plane. *Science*, 166:607–609.

Barron, E. J., and Washington, W. M., 1982. The atmospheric circulation during warm geologic periods: Is the equator to pole surfac temperature gradient the controlling factor? *Geology*, 10:633–636.

Berger, W. H., 1976. Biogenous deep sea sediments: Production preservation and interpretation. *In* Riley, J. P., and Chester, R. (Eds.), *Chemical Oceanography* (Vol. 5): New York (Academic Press 265–388.

Berger, W. H., Vincent, E., and Theirstein, H. R., 1981. The deep-se record: Major steps in Cenozoic ocean evolution. *In* Warme, J. E Douglas, R. G., and Winterer, E. L. (Eds.), *The Deep Sea Drillin Project: A Decade of Progress*. Soc. Econ. Paleontol. Minera Spec. Publ., 32:489–504.

Berggren, W. A., 1972. Late Pliocene–Pleistocene glaciation. *In* Laughton, A. S., Berggren, W. A., et al., *Init. Repts. DSDP*, 12: Washington (U.S. Govt. Printing Office), 953–963.

Brewster, N. A., 1980. Cenozoic biogenic silica sedimentation in th Antarctic Ocean. *Geol. Soc. Am. Bull.*, 91(1):337–347.

CLIMAP Project Members, 1981. *Seasonal Reconstruction of th Earth's Surface at the Last Glacial Maximum*. Map and Chart Series 36 (Text, Map, and Microfiche), Geol. Soc. Am., Boulde Colorado.

Conolly, J. R., and Ewing, M., 1970. Ice-rafted detritus in northwes Pacific sediments. *In* Hays, J. D. (Ed.), *Geological Investigatio of the North Pacific*. Mem. Geol. Soc. Am., 126:219–232.

Dauphin, J. P., 1983. Eolian quartz granulometry as a paleowind indicator in the northeast Atlantic, North Pacific, and southwes equatorial Pacific [Ph. D. dissert.]. University of Rhode Island Kingston.

Duce, R. A., Unni, C. K., Ray, B. J., Prospero, J. M., and Merrill, J T., 1980. Long-range atmospheric transport of soil dust from Asia to the tropical North Pacific: Temporal variability. *Science*, 209 1522–1524.

Frakes, L. A., 1979. *Climates Throughout Geologic Time*: New York (Elsevier).

Gates, W. L., 1976. Modelling the ice age climate. *Science*, 191: 1138–1144.

Gillette, D. A., 1981. Production of dust that may be carried great distances, *In* Pewe, T. L. (Ed.), *Desert Dust: Origin, Characteristics, and Effect on Man*. Geol. Soc. Am. Spec. Pap., 186:11–26.

Gillette, D. A., Blifford, I. H., Jr., and Fryrear, D. W., 1974. The influence of wind velocity on the size distributions of aerosols generated by wind erosion of soils. *J. Geophys. Res.*, 79:4068–4075.

Glaccum, R. A., and Prospero, J. M., 1980. Saharan aerosols over the tropical North Atlantic-mineralogy. *Mar. Geol.*, 37:295–321.

Graham, E. J., and Rea, D. K., 1980. Grain size and mineralogy of sediment cores from western Lake Huron. *J. Great Lakes Res.*, 6: 129–140.

Herman, Y., 1974. Arctic Ocean sediments, microfauna, and the climatic record of the late Cenozoic, *In* Herman, Y. (Ed.), *Marine Geology and Oceanography of the Arctic Sea*: New York (Springer-Verlag), pp. 283–348.

Hodell, D. A., Williams, D. F., and Kennett, J. P., 1983. Fundamental changes in deep and intermediate water circulation patterns in the Western South Atlantic at 3.2 Ma. *Geol. Soc. Am. Abstracts with Program*, 15:596.

Honjo, S., 1983. Transport mechanism of pelagic particles in time and space. *Trans. Am. Geophys. Union*, 65:225.

________, 1980. Material fluxes and modes of sedimentation in the mesopelagic and bathypelagic zones. *J. Mar. Res.*, 38:53–97.

Jackson, M. L., Gillette, D. A., Danielson, E. F., Blifford, I. H., Bryson, R. A., and Syers, J. K., 1973. Global dustfall during the Quaternary as related to environments. *Soil Sci.*, 116:135–145.

Janecek, T. R., 1983. The history of eolian sedimentation and atmospheric circulation during the Late Cenozoic [Ph. D. dissert.]. University of Michigan, Ann Arbor.

Janecek, T. R., and Rea, D. K., 1983. Eolian deposition in the northeast Pacific Ocean: Cenozoic history of atmospheric circulation. *Geol. Soc. Am. Bull.*, 94:730–738.

________, in press. Quaternary fluctuations in the northern hemisphere westerlies and tradewind. *Quat. Res.*

Johnson, L. R., 1976. Particle-size fractionation of eolian dusts during transport and sampling. *Mar. Geol.*, 21:M17–M21.

_______, 1979. Mineralogical dispersal patterns of North Atlantic deep-sea sediments with particular reference to eolian dust. *Mar. Geol.*, 29:335-345.

Keigwin, L. D., 1979. Late Cenozoic stable isotope stratigraphy and paleoceanography of DSDP sites from the east equatorial and north central Pacific Ocean. *Earth Planet. Sci. Lett.*, 45:361-382.

Keigwin, L. D., and Thunnell, R. 1979. Middle Pliocene climatic change in the western Mediterranean from faunal and oxygen isotopic trends. *Nature (London)*, 282:294-296.

Kemp, E. M., 1978. Tertiary climatic evolution and vegetation history in the southeast Indian Ocean region. *Palaeogeogr., Palaeoclimatol., Palaeoecol.*, 24:169-208.

Kennett, J. P., and Shackleton, N. J., 1979. Oxygen isotopic evidence for the development of the psychrosphere 38 mya. *Nature (London)*, 260:169-208.

Kolla, V., Biscaye, P. E., and Hanley, A. F., 1979. Distribution of quartz in late Quaternary Atlantic sediments in relation to climate. *Quat. Res.*, 11:261-277.

Leinen, M., and Heath, G. R., 1981. Sedimentary indicators of atmospheric circulation in the Northern Hemisphere during the Cenozoic. *Palaeogeogr., Palaeoclimatol., Palaeoecol.*, 36:1-21.

Manabe, S., and Hahn, D. C., 1977. Simulation of the tropical climate of the ice age. *J. Geophys. Res.*, 82:3889-3912.

Molina-Cruz, A., and Price, P., 1977. Distribution of opal and quartz on the ocean floor of the subtropical southeastern Pacific. *Geology*, 5:81-84.

Parkin, D. W., 1974. Trade winds during the glacial cycles. *Proc. R. Soc. London, Ser. A*, 337:73-100.

Parkin, D. W., and Padgham, R. C., 1975. Further studies on trade winds during the glacial cycles. *Proc. R. Soc. London Ser. A*, 346: 245-260.

Pisias, N. G., and Leinen, M., 1984. Milankovitch forcing of the oceanic system: evidence from the Northwest Pacific. *In* Berger, A., and Imbrie, J. (Eds.), *Milankovitch and Climate*, Part 1: Dordrecht (Reidel), pp. 307-330.

Prospero, J. M., and Bonatti, E., 1969. Continental dust in the atmosphere of the eastern Equatorial Pacific. *J. Geophys. Res.*, 74: 3362-3371.

Prospero, J. M., Glaccum, R. A., and Nees, R. T., 1981. Atmospheric transport of soil dust from Africa to South America. *Nature (London)*, 289:570-572.

Prospero, J. M., and Nees, R. T., 1977. Dust concentrations in the atmosphere of the equatorial North Atlantic; Possible relationships to the Sahalian droughts. *Science*, 196:1196-1198.

Rea, D. K., and Janecek, T. R., 1981a. Late Cretaceous history of eolian deposition in the Mid-Pacific Mountains, central North Pacific Ocean. *Palaeogeogr., Palaeoclimatol., Palaeoecol.*, 36:55-67.

_______, 1981b. Mass accumulation rates of the non-authigenic, inorganic, crystalline (eolian) component of deep sea sediments from the western Mid-Pacific Mountains, DSDP Site 463. *In* Thiede, J., Vallier, T. L., et al., *Init. Repts. DSDP*, 62: Washington (U.S. Govt. Printing Office), 653-659.

_______, 1982. Late Cenozoic changes in atmospheric circulation deduced from North Pacific eolian sediments. *Mar. Geol.*, 49: 149-167.

Rea, D. K., and Schrader, H., in press. Late Pliocene onset of glaciation: Ice-rafting and diatom stratigraphy of North Pacific DSDP cores. *Palaeogeogr., Palaeoclimatol., Palaeoecol.*

Rex, R. W., and Goldberg, E. D., 1958. Quartz content of pelagic sediments of the Pacific Ocean. *Tellus*, 10:153-159.

Saito, T., 1976. Geological significance of coiling direction in Planktonic foraminifera, "Pulleniatina." *Geology*, 4:305-309.

Savin, S. M., 1977. The history of the earth's surface temperature during the past 100 million years. *Ann. Rev. Earth Planet. Sci.*, 5: 319-335.

Shackleton, N. J., Backman, J., Zimmerman, H. B., Kent, D., Hall, M. A., Roberts, D. G., Schnitker, D., Baldauf, J. G., Desprairies, A., Homringhausen, R., Huddlestun, P., Keene, J. B., Kaltenback, A. J., Krumsiek, K. A. O. Morton, A. C., Murray, J. W., and Wertberg-Smith, J., 1984. Oxygen isotope calibration of the onset of ice-rafting and history of glaciation in the North Atlantic region. *Nature (London)*, 307:620-623.

Shackleton, N. J., and Cita, M. B., 1979. Oxygen and carbon isotope stratigraphy of benthic foraminifers at Site 397: detailed history of climatic change during the Late Neogene. *In* von Rad, U., Ryan, W. B. F., et al., *Init. Repts. DSDP*, 47: Washington (U.S. Govt. Printing Office), 433-444.

Shackleton, N. J., and Opdyke, N. D., 1977. Oxygen isotope and paleomagnetic evidence for early Northern Hemisphere glaciation. *Nature (London)*, 270:216-219.

Schultz, L., 1979. Saharan dust transport over the Atlantic, model calculations and measurements. *In* Morales, C. (Ed.), *Saharan Dust Mobilization, Transport and Deposition*: New York (Wiley), pp. 267-277.

Thiede, J., 1979. Wind regimes over the Late Quaternary southwest Pacific Ocean. *Geology*, 7:259-262.

Thunell, R. C., 1979. Pliocene-Pleistocene paleotemperatures and paleosalinity history of the Mediterranean Sea, results from Deep Sea Drilling Project Sites 125 and 132. *Mar. Micropaleontol.*, 4: 173-177.

Thunell, R. C., and Williams, R. F., 1983. The stepwise development of Pliocene-Pleistocene paleoclimatic conditions in the Mediterranean based on high resolution oxygen isotopic studies. *Geol. Soc. Am. Abstracts with Program*, 15:706.

Windom, H. L., 1969. Atmospheric dust records in permanent snow fields: Implications to marine sedimentation. *Geol. Soc. Am. Bull.*, 80:761-782.

_______, 1975. Eolian contributions to marine sediments *J. Sediment. Petrol.*, 45:520-529.

Wolfe, J. A., 1978. A paleobotanical interpretation of Tertiary climates in the northern hemisphere. *Am. Sci.*, 66:694-703.

Wolfe, J. A., and Hopkins, D. M., 1967. Climatic changes recorded by Tertiary land floras in northwestern North America. *In* Hatai, K. (Ed.), *Tertiary Correlations and Climatic Changes in the Pacific*. Pacific Science Congress, 11th, Tokyo, Symposium 25:67-76.

Woodruff, F., Savin, S. M., and Douglas, R. G., 1981. Miocene stable isotope record: A detailed deep Pacific Ocean study and its paleoclimatic implications. *Science*, 212:665-668.

Date of Initial Receipt: 23 October 1983
Date of Acceptance: 20 August 1984

27. ELEMENTAL COMPOSITION OF CENOZOIC PELAGIC CLAYS FROM DEEP SEA DRILLING PROJECT SITES 576 AND 578, WESTERN NORTH PACIFIC[1]

G. Ross Heath, Richard B. Kovar, Carlos Lopez, and Gregory L. Campi, Oregon State University[2]

ABSTRACT

X-ray fluorescence analyses of 1143 samples from Site 576 (32°21.4'N, 164°16.5'E) and 539 samples from Site 578 (33°55.6'N, 151°37.7'E) for the elements Na, Mg, Al, Si, P, K, Ca, Ti, Mn, Fe, Ba, and S show consistent trends from Si-rich surficial deposits to dark brown clays rich in Mn, Fe, P, and Ti in early Cenozoic sections. These data sets form the basis for a detailed paleogeochemical stratigraphy of North Pacific "red" clays.

INTRODUCTION

Deep Sea Drilling Project (DSDP) Sites 576 (between the Shatsky Rise and Emperor Seamounts at 32°21.4'N, 164°16.5'E) and 578 (between the Japan, French, and Shatsky Rise at 33°55.6'N, 151°37.7'E; Fig. 1) were sampled continuously from the seafloor to chert (at 76 and 176 m, respectively, below the seafloor) by means of the hydraulic piston core (HPC) during DSDP Leg 86.

At Site 576, we recovered 27 m of buff clay over 29 m (27–56 m sub-bottom) of dark brown clay, which in turn overlay 20 m (56–76 m sub-bottom) of interbedded calcareous ooze and dark brown clay resting on chert of Campanian–Maestrichtian age.

At Site 578, we recovered a similar section of buff (77–125 m sub-bottom) and dark brown clay (125–176 m sub-bottom), overlain by 77 m of gray green, intermittently biosiliceous clay and ooze with numerous thin ash layers. At Site 578, the dark brown clay rests directly on Campanian chert at 176 m sub-bottom; the cored section contains no carbonate.

METHODOLOGY

Both sites were sampled at 10- to 20-cm intervals for paleomagnetic analysis (Heath, Rea, and Levi, this volume). After determination of remanent magnetization before and after alternating-field demagnetization, the 2 × 2 × 2 cm cubes of sediment were weighed, freeze-dried, weighed again (to yield water contents), and disaggregated by shaking with methacrylate spheres in polycarbonate sample tubes.

The resulting fine powder required no further grinding before being pressed at 10 tons pressure into X-ray fluorescence (XRF) discs. The XRF analyses were carried out on a Phillips PW1600 simultaneous spectrometer. This instrument has 25 detectors, one per element, distributed around the sample and X-ray tube. Each detector–crystal system is optimized for the element it is measuring, leading to high signal/noise ratios for all elements. The system is controlled by a DEC PDP 11/34 computer system which manages sample manipulation, data collection and archiving, data reduction through a fundamental parameters program (Chriss et al., 1978), and tabulation and plotting of elemental concentrations. The system has been calibrated by a set of 60 rock and sediment standards from the U.S. Geological Survey, National Bureau of Standards, Canada, and France, as well as by in-house pelagic clay standards that have been analyzed repeatedly by atomic absorption spectrophotometry and instrumental neutron activation analysis. These analyses indicate no systematic errors for the elements discussed.

SUB-BOTTOM DEPTH OF SITE 576 SAMPLES

Even at sea, visual examination and preliminary paleomagnetic analyses indicated that the nominal 100% recovery and sub-bottom depths reported for Holes 576 and 576B by the drillers were not consistent with the sections recovered (see Site 576 chapter, this volume). Several problems were identified:

1. Incorrectly cored interval. Cores 2 and 3 of Hole 576A sampled the same interval. The reason is unknown, but may indicate a 1-stand drill pipe miscount on the drill floor.
2. Closure of the bumper subs as the sediments became stiffer with depth. This appears to have occurred in Core 6 of Hole 576, with a resultant reduction of the interval cored.
3. Uncertainties as to the location of "good" core within 9-m cored intervals.
4. Stretching ("flow-in") or compression of ductile clays within a core. Stretching is visually apparent due to elongation of sedimentary structures. Compression is difficult to demonstrate, but is the logical complement to stretching. These effects imply that the HPC piston was moving more slowly than the heave of the ship, suggesting malfunction of the HPC due either to premature failure of the shear pins or the stiffness of the clays.
5. Double cored sections (e.g., in Core 576B-3) also suggest heave velocities greater than piston velocities.

These problems led to actual recoveries of good ("undisturbed") sediment of about 80% in Holes 576 and

---

[1] Heath, G. R., Burckle, L. H., et al., *Init. Repts. DSDP*, 86: Washington (U.S. Govt. Printing Office).

[2] Addresses: (Heath, present address) College of Ocean and Fishery Sciences, University of Washington, Seattle, WA 98195; (Kovar, Lopez, Campi) College of Oceanography, Oregon State University, Corvallis, OR 97331.

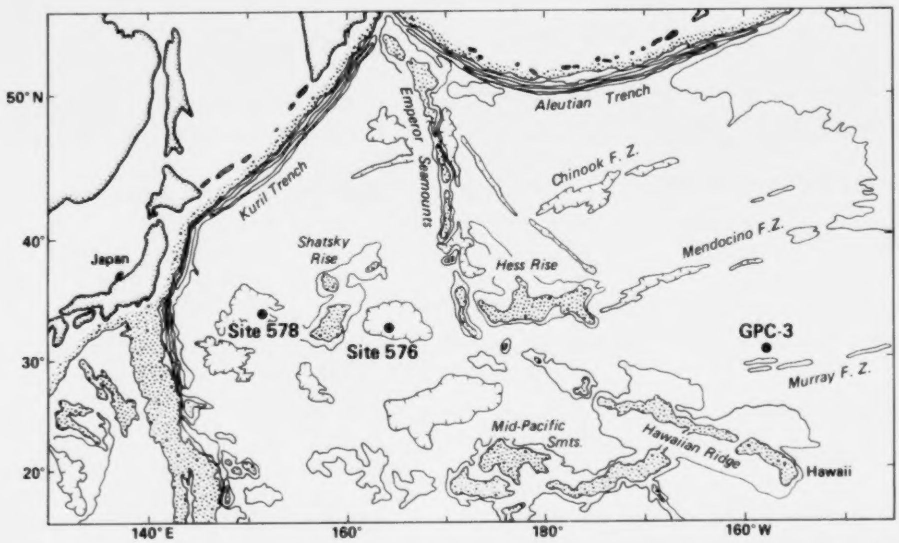

Figure 1. Location of DSDP Sites 576 and 578 relative to major physiographic features of the western North Pacific, and to LL44-GPC-3, a 24-m piston core studied in detail by Leinen (1979). Areas shallower than 4 km stippled; 5 km contour plain; 6 km contour hachured.

576B, rather than the nominal 100% recorded as the core was received on board. Because most of the Hole 576A sediment was taken in unopened sections of core liner for geotechnical measurements, the condition of this clay sequence is not well known. The presence of flow-in structures in several of the intervals remaining after geotechnical sampling suggests that the character of cores from Hole 576A is similar to that of the cores from the other two sites.

Based on detailed correlations of visual logs, paleomagnetic profiles, carbonate and intervening clay layers below 54 m sub-bottom, and profiles of elemental abundances, it has been possible to align the sediments recovered in the three holes, and create a composite section that represents virtually a complete sequence of the clay section at Site 576.

Table 1 lists the sub-bottom depths of sections of good core from the three holes drilled. We emphasize that the Hole 576A corrections are much less certain than the Hole 576 and 576B corrections, because of the absence of paleomagnetic data and the unavailability of much of the cored material from Hole 576A. We also emphasize that the depths in Table 1 replace those presented in the Site 576 chapter, which were compiled before shore-based magnetic data or any geochemical profiles were available. Because Table 1 could not be prepared until late in the Leg 86 *Initial Report* production schedule, articles in the second part of this *Initial Report* volume that plot data versus *adjusted depth* have used adjusted depths from the Site 576 chapter that differ from those of Table 1 by as much as 4 m.

The composite section contains only one notable gap, from 36.96 to 38.06 m sub-bottom. The discontinuities in a number of elemental profiles, particularly that of Ti, across the gap suggest that it may be larger than the 1.1 m indicated. Because corrected depths for Hole 576B are deeper than driller's depths, whereas depths for Hole 576 below Core 2 are shallower, we have no real constraints on the magnitude of the missing section; 1.1 m is our best estimate, however.

RESULTS

Tables 2 to 6 list the analytical results from Holes 576, 576A, and 576B, the 576 composite section based on the corrected depths of Table 1 and Hole 578, respectively. Except for Na and S, which have uncertainties of 10 and 15%, respectively, the precision of the tabulated values is within 2%, and the accuracies within 5%. For Hole 576A, the Na values are much noisier, resulting from detector problems, and are presented only to show general trends. Individual values should not be considered reliable.

Because of the length of time required to resolve the depth corrections for the Site 576 holes and the tight production schedule for the Leg 86 *Initial Report* volume, a full interpretation of the compositional data has been deferred to a future publication.

ACKNOWLEDGMENTS

We are grateful to Chris Dymond and Kerry O'Shea for preparing many of the XRF discs and for plotting and checking data. Donna Rea determined most of the water contents. Discussions with colleagues from the Leg 86 scientific party, particularly Joe Morley, Bob Jacobi, and Ulrich Bleil helped resolve some of the problems in assigning sub-bottom depths to cores from Holes 576 and 576B.

REFERENCES

Chriss, J. W., Birks, L. S., and Gilfrich, J. V., 1978. A versatile X-ray analysis program combining fundamental parameters and empirical coefficients. *Anal. Chem.*, 50:33.

Leinen, M., 1979. Paleochemical signatures in Cenozoic Pacific sediments [Ph.D. dissert.]. Univ. Rhode Island, Kingston.

Date of Initial Receipt: 28 August 1984
Date of Acceptance: 25 September 1984

Table 1. Key to convert section depths in Holes 576, 576A, and 576B to sub-bottom depths in centimeters.

Section	Depth (cm)	Adjusted sub-bottom depth (cm)	Comments
Hole 576			
1-1	0	64	0–64 cm not recovered
1-2	0	214	
1,CC	0	321	
			334–695 cm not recovered
2-1	0	695	
2-2	0	845	
2-3	0	995	
2-4	0	1145	
2-5	0	1295	
2-5	110	1445	1405–1445 cm missing
2-6	0	1485	
2-7	0	1635	
2,CC	0	1685	
			1708–1850 cm not recovered
3-1	0	1025	
3-2	0	1175	
3-3	0	1325	
3-4	0	1475	
3-5	0	1625	
3,CC	0	1657	1025–1689 cm overlap
4-1	70	1890	
4-2	0	1970	
4-3	0	2120	
4-4	0	2270	
4-5	0	2420	
4-6	0	2570	
4-7	0	2720	
4,CC	0	2768	
			2788–2800 cm not recovered
5-1	40	2800	
5-5	48	3098	2910–3098 cm not recovered
5-6	0	3200	
5-7	0	3350	
5,CC	0	3399	
			3435–3800 cm not recovered
6-3	70	3800	
6-4	0	3880	
6-5	0	4030	
6-6	0	4180	
6-7	0	4330	
6,CC	0	4375	
	41	4405	
			4340–4412 cm overlap
7-1	0	4340	
7-2	50	4640	
7-3	0	4740	
7-4	0	4890	
7-5	0	5040	
7-6	0	5190	
7-7	0	5340	
7,CC	0	5390	
			5415–5425 cm not recovered
8-1	15	5425	
8-2	0	5560	
8-3	0	5710	
8-4	0	5860	
8-5	0	6010	
8-6	0	6160	
8-7	0	6310	
8,CC	0	6353	
	4	6355	
			Hole 576, 6379 cm total depth sampled
Hole 576A			
1-1	12	132	
1-2	0	270	
1-3	0	420	
1-4	0	570	
1-5	0	720	
1-6	0	872	
1,CC	0	972	
			989–1075 cm not recovered
2-1	45	1075	
2-2	0	1180	
2-3	0	1330	
2-4	0	1480	
2-5	0	1630	
2-6	0	1780	
2-7	0	1930	
2,CC	0	1936	
			1951–2300 cm not recovered
3-1	0	2300	
3-2	0	2450	
3-3	0	2600	
3-4	0	2750	2700-cm region disturbed
			2755–2960 cm disturbed
3-6	100	2960	
3-7	0	3010	
3,CC	10	3040	
			2890–3065 cm overlap
4-1	0	2890	
4-2	0	3040	3090–3290 cm (approx.) disturbed
4-3	0	3190	
4-4	0	3340	
4-5	0	3490	
4-6	0	3640	3690–3808 cm (approx.) disturbed
4,CC	0	3768	
			3808–3910 cm not recovered
5-1	0	3910	
5-2	0	4060	4080–4220 cm (approx.) disturbed
5-3	0	4210	
5-4	0	4360	
5-5	0	4510	
5-6	0	4660	
5-7	0	4810	
5,CC	15	4840	
			4825–4863 cm overlap
6-1	0	4825	
6-2	0	4975	5075–5270 cm (approx.) disturbed
6-3	0	5125	
6-4	0	5275	
6-5	0	5425	
6-6	0	5575	
6-7	0	5725	
6,CC	0	5775	5775–5798 cm disturbed
7-1	0	5795	5795–5845 cm (approx.) disturbed
7-2	0	5945	
7-3	0	6095	
7-4	0	6245	
7-5	0	6385	
7-6	0	6535	
7-7	0	6675	
7,CC	8	6745	

Table 1. (Continued).

Section	Depth (cm)	Adjusted sub-bottom depth (cm)	Comments
Hole 576A (Cont.)			
			Hole 576A, 6778 cm total depth sampled
Hole 576B			
1-1	0	0	
1-2	0	150	
1-3	0	300	
1-4	0	450	
1-5	0	600	
1-6	0	750	
1,CC	0	807	
			821-1205 cm not recovered
2-1	5	1205	
2-2	0	1350	
2-3	0	1500	
			1600-1685 cm disturbed
2-4	35	1685	
2-5	0	1800	
2-6	0	1950	
2-7	0	2100	
2,CC	0	2148	
			2041-2160 cm overlap
3-1	0	2150	
3-1	71	2041	2041-2181 cm repeated
3-2	0	2110	
3-2	71	2271	2221-2271 cm not recovered
3-3	0	2350	
3-6	21	2787	
3-7	0	2916	
3,CC	0	2666	
			2988-3150 cm not recovered
4-3	100	3150	
4-4	0	3200	
4-5	0	3350	
4-6	0	3500	
4-7	0	3650	
4,CC	0	3702	

Table 1. (Continued).

Section	Depth (cm)	Adjusted sub-bottom depth (cm)	Comments
Hole 576B (Cont.)			
			3724-3930 cm not recovered
5-2	0	3930	
5-3	0	4080	
5-3	20	4140	4100-4140 cm not recovered
5-3	75	4255	4195-4255 cm not recovered
5-4	0	4330	
5-5	0	4480	
5-6	0	4630	
5,CC	2	4755	
			4775-4940 cm not recovered
6-1	110	4940	
6-2	0	4980	
6-3	0	5130	5220-5300 cm missing
6-3	90	5300	
6-4	0	5360	5430-5516 cm missing
6-4	70	5516	
6-5	0	5596	
6-6	0	5746	
6,CC	10	5888	
			5901-5913 cm not recovered
7-1	5	5913	
7-2	0	6058	
7-3	108	6208	
7-4	0	6250	
7-5	0	6400	
7-6	0	6550	
7-7	0	6700	
7,CC	0	6734	
			6771-6860 cm not recovered
8-1	115	6860	
8-2	0	6895	
8-3	0	7045	
8-4	0	7195	
8-5	0	7345	
8-6	0	7495	
			7500-7610 cm not recovered
9,CC	0	7610	Hole 576B, 7610 cm total depth sampled

Table 2. Elemental abundance (wt.%) and water content (% dry wt.) of Hole 576 sediment samples.

Lab ID	Core	Section	Depth in Section (m)	Depth in hole (m)	Na	Mg	Al	Si	P	K	Ca	Ti	Mn	Fe	Ba	S	H_2O
DP14294	1	1	0.11	0.75	0.62	1.86	7.43	26.3	0.062	2.50	0.46	0.412	0.47	4.77	0.091	0.020	141
DP14295	1	1	0.21	0.85	0.58	1.88	7.31	26.3	0.067	2.52	0.53	0.409	0.45	4.74	0.098	0.061	130
DP14296	1	1	0.31	0.95	0.52	1.90	7.50	26.3	0.058	2.59	0.45	0.416	0.21	4.86	0.086	0.035	142
DP14297	1	1	0.41	1.05	0.59	1.85	7.48	26.4	0.059	2.56	0.53	0.415	0.31	4.71	0.087	0.044	139
DP14298	1	1	0.51	1.15	0.60	1.89	7.59	26.4	0.060	2.57	0.51	0.418	0.33	4.82	0.090	0.026	146
DP14299	1	1	0.61	1.25	0.56	1.91	7.58	26.1	0.060	2.59	0.49	0.419	0.35	4.86	0.093	0.030	132
DP14300	1	1	0.71	1.35	0.56	1.89	7.44	25.9	0.059	2.57	0.52	0.423	0.37	4.81	0.085	0.040	141
DP14301	1	1	0.81	1.45	0.49	1.89	7.50	26.2	0.059	2.57	0.54	0.422	0.42	4.69	0.086	0.053	152
DP14302	1	1	0.91	1.55	0.53	1.93	7.68	26.2	0.062	2.57	0.53	0.427	0.56	4.83	0.088	0.038	139
DP14303	1	1	1.01	1.65	0.56	1.95	7.60	26.1	0.061	2.57	0.59	0.420	0.81	4.75	0.090	0.076	139
DP14304	1	1	1.11	1.75	0.52	1.91	7.43	26.6	0.056	2.48	0.43	0.409	0.74	4.66	0.097	0.026	174
DP14305	1	1	1.21	1.85	0.40	1.91	7.37	26.8	0.053	2.52	0.45	0.414	0.38	4.65	0.092	0.050	177
DP14306	1	1	1.31	1.95	0.44	1.89	7.36	26.8	0.053	2.50	0.39	0.410	0.34	4.66	0.091	0.023	192
DP14307	1	1	1.41	2.05	0.49	1.87	7.34	26.8	0.054	2.48	0.41	0.409	0.26	4.63	0.092	0.026	170
DP14309	1	2	0.16	2.30	0.42	1.89	7.31	26.9	0.051	2.58	0.42	0.410	0.14	4.65	0.087	0.051	174
DP14310	1	2	0.22	2.36	0.44	1.88	7.42	27.0	0.052	2.56	0.38	0.409	0.29	4.65	0.086	0.031	177
DP14311	1	2	0.31	2.45	0.41	1.87	7.21	26.9	0.051	2.57	0.44	0.406	0.22	4.58	0.089	0.063	189
DP14312	1	2	0.41	2.55	0.41	1.87	7.32	27.0	0.050	2.51	0.36	0.400	0.36	4.53	0.092	0.031	220
DP14313	1	2	0.51	2.65	0.43	1.91	7.32	27.0	0.051	2.59	0.43	0.408	0.27	4.61	0.087	0.058	185
DP14314	1	2	0.61	2.75	0.44	1.89	7.39	26.9	0.052	2.60	0.43	0.417	0.43	4.61	0.086	0.052	179
DP14315	1	2	0.71	2.85	0.51	1.87	7.30	26.9	0.051	2.62	0.48	0.412	0.25	4.62	0.083	0.059	162
DP14316	1	2	0.81	2.95	0.64	2.06	8.20	29.9	0.059	2.90	0.49	0.469	0.22	5.35	0.110	0.035	164
DP14317	1	2	0.91	3.05	0.49	1.88	7.44	26.9	0.053	2.60	0.46	0.419	0.24	4.74	0.089	0.045	165
DP14319	1	2	1.01	3.15	0.52	1.87	7.52	26.8	0.053	2.60	0.46	0.424	0.39	4.74	0.089	0.033	162
DP14318	1	C	0.07	3.28	0.63	2.02	8.30	30.7	0.062	2.87	0.57	0.470	0.58	5.48	0.129	0.041	170
DP14320	2	1	0.06	7.01	0.53	2.01	7.61	26.1	0.051	2.69	0.45	0.425	0.63	4.79	0.091	0.060	134
DP14321	2	1	0.16	7.11	0.55	2.03	7.60	26.4	0.047	2.73	0.49	0.430	0.28	4.80	0.085	0.091	149
DP14322	2	1	0.26	7.21	0.52	1.97	7.59	26.4	0.050	2.66	0.44	0.417	0.36	4.70	0.088	0.050	159
DP14323	2	1	0.36	7.31	0.59	1.98	7.48	26.2	0.050	2.67	0.51	0.417	0.44	4.68	0.096	0.088	145
DP14324	2	1	0.46	7.41	0.51	2.01	7.56	26.4	0.053	2.69	0.50	0.417	0.38	4.70	0.091	0.091	158
DP14325	2	1	0.56	7.51	0.57	2.04	7.59	26.3	0.052	2.75	0.48	0.431	0.33	4.80	0.092	0.088	144
DP14326	2	1	0.66	7.61	0.48	2.03	7.63	26.1	0.051	2.77	0.43	0.428	0.28	4.82	0.086	0.076	143
DP14327	2	1	0.76	7.71	0.56	2.08	7.61	26.3	0.053	2.77	0.48	0.431	0.27	4.83	0.091	0.095	146
DP14328	2	1	0.86	7.81	0.52	2.01	7.67	26.3	0.050	2.72	0.41	0.430	0.25	4.86	0.086	0.052	144
DP14329	2	1	0.96	7.91	0.46	2.01	7.53	26.1	0.051	2.68	0.42	0.418	0.29	4.76	0.090	0.058	159
DP14330	2	1	1.06	8.01	0.44	2.04	7.58	26.1	0.050	2.70	0.42	0.414	0.31	4.75	0.095	0.067	159
DP14331	2	1	1.16	8.11	0.59	2.07	7.64	26.3	0.051	2.78	0.50	0.430	0.32	4.87	0.095	0.095	146
DP14332	2	1	1.26	8.21	0.43	2.05	7.62	26.2	0.053	2.67	0.44	0.417	0.38	4.77	0.089	0.065	168
DP14333	2	1	1.36	8.31	0.39	2.01	7.49	26.4	0.052	2.61	0.46	0.408	0.39	4.65	0.088	0.073	178
DP14334	2	1	1.46	8.41	0.48	1.98	7.58	26.2	0.057	2.59	0.42	0.413	0.39	4.71	0.088	0.036	154
DP14335	2	2	0.06	8.51	0.49	2.00	7.61	26.3	0.055	2.65	0.45	0.418	0.34	4.77	0.089	0.049	145
DP14336	2	2	0.16	8.61	0.46	1.99	7.58	26.2	0.054	2.61	0.47	0.418	0.39	4.79	0.087	0.049	147
DP14337	2	2	0.26	8.71	0.45	1.96	7.59	26.4	0.053	2.58	0.46	0.414	0.39	4.77	0.087	0.032	159
DP14338	2	2	0.36	8.81	0.47	2.01	7.58	26.2	0.055	2.61	0.43	0.416	0.41	4.75	0.094	0.048	156
DP14339	2	2	0.46	8.91	0.46	1.99	7.60	26.5	0.054	2.60	0.41	0.413	0.42	4.74	0.096	0.029	161
DP14340	2	2	0.56	9.01	0.46	2.00	7.54	26.3	0.053	2.61	0.40	0.414	0.29	4.74	0.094	0.041	165
DP14341	2	2	0.66	9.11	0.46	2.06	7.54	26.3	0.048	2.68	0.47	0.418	0.39	4.78	0.090	0.072	161
DP14342	2	2	0.76	9.21	0.45	1.98	7.48	26.3	0.049	2.59	0.42	0.410	0.39	4.72	0.092	0.043	170
DP14343	2	2	0.86	9.31	0.32	2.03	7.36	26.7	0.050	2.58	0.42	0.398	0.26	4.73	0.087	0.070	207
DP14344	2	2	0.96	9.41	0.37	1.96	7.48	26.5	0.056	2.55	0.43	0.411	0.26	4.68	0.087	0.043	194
DP14345	2	2	1.06	9.51	0.49	2.02	7.51	26.4	0.058	2.64	0.55	0.422	0.46	4.72	0.085	0.082	163
DP14346	2	2	1.16	9.61	0.47	1.96	7.46	26.2	0.056	2.55	0.44	0.406	0.40	4.65	0.085	0.041	170
DP14347	2	2	1.26	9.71	0.53	2.03	7.46	26.2	0.053	2.67	0.54	0.418	0.36	4.75	0.093	0.081	149
DP14348	2	2	1.36	9.81	0.48	1.97	7.46	26.2	0.054	2.61	0.46	0.412	0.37	4.71	0.094	0.055	154
DP14349	2	2	1.46	9.91	0.69	2.04	7.53	26.1	0.050	2.76	0.51	0.429	0.39	4.83	0.098	0.107	154
DP14350	2	3	0.06	10.01	0.50	2.03	7.56	26.0	0.051	2.69	0.41	0.422	0.39	4.75	0.099	0.088	176
DP14351	2	3	0.16	10.11	0.50	2.05	7.44	26.1	0.050	2.72	0.47	0.414	0.38	4.70	0.101	0.118	185
DP14352	2	3	0.26	10.21	0.40	1.98	7.40	26.4	0.051	2.55	0.36	0.396	0.30	4.55	0.095	0.051	218
DP14353	2	3	0.36	10.31	0.29	1.83	6.98	27.3	0.052	2.43	0.39	0.389	0.52	4.40	0.095	0.056	218
DP14354	2	3	0.46	10.41	0.55	1.90	7.44	26.4	0.057	2.52	0.43	0.409	0.49	4.64	0.086	0.033	180
DP14355	2	3	0.56	10.51	0.51	1.95	7.37	26.3	0.053	2.59	0.53	0.410	0.44	4.62	0.089	0.074	163
DP14356	2	3	0.66	10.61	0.55	1.94	7.41	26.2	0.051	2.60	0.50	0.408	0.41	4.67	0.087	0.059	142
DP14357	2	3	0.76	10.71	0.60	1.91	7.31	26.5	0.048	2.63	0.57	0.402	0.37	4.48	0.087	0.073	138

Table 2. (Continued).

Lab ID	Core	Section	Depth in Section (m)	Depth in hole (m)	Na	Mg	Al	Si	P	K	Ca	Ti	Mn	Fe	Ba	S	H_2O
DP14358	2	3	0.86	10.81	0.59	1.78	7.15	26.6	0.046	2.55	0.57	0.373	0.35	4.13	0.089	0.042	122
DP14359	2	3	0.96	10.91	0.61	1.77	7.05	26.6	0.043	2.67	0.54	0.358	0.38	3.95	0.083	0.075	12
DP14360	2	3	1.06	11.01	0.53	1.98	7.50	26.0	0.050	2.65	0.45	0.417	0.56	4.70	0.092	0.065	146
DP14361	2	3	1.16	11.11	0.57	2.07	7.58	26.1	0.050	2.71	0.48	0.431	0.46	4.81	0.089	0.085	149
DP14362	2	3	1.26	11.21	0.56	2.03	7.61	26.3	0.045	2.70	0.40	0.421	0.38	4.73	0.090	0.062	157
DP14363	2	3	1.36	11.31	0.46	2.05	7.52	26.3	0.048	2.67	0.44	0.421	0.28	4.74	0.095	0.081	16
DP14364	2	3	1.46	11.41	0.55	2.00	7.58	26.1	0.047	2.70	0.38	0.424	0.28	4.81	0.092	0.050	14
DP14365	2	4	0.06	11.51	0.51	2.04	7.61	26.4	0.053	2.68	0.49	0.420	0.43	4.76	0.094	0.072	15
DP14366	2	4	0.16	11.61	0.45	2.01	7.58	26.3	0.056	2.61	0.42	0.415	0.47	4.69	0.091	0.052	16
DP14367	2	4	0.26	11.71	0.37	1.98	7.39	26.4	0.054	2.58	0.41	0.401	0.51	4.51	0.092	0.046	18
DP14368	2	4	0.36	11.81	0.48	2.02	7.57	26.4	0.052	2.62	0.38	0.406	0.46	4.64	0.095	0.031	16
DP14369	2	4	0.46	11.91	0.49	1.99	7.48	26.5	0.054	2.62	0.45	0.397	0.46	4.51	0.092	0.050	14
DP14370	2	4	0.56	12.01	0.54	1.98	7.45	26.4	0.054	2.62	0.43	0.405	0.41	4.55	0.095	0.044	14
DP14371	2	4	0.66	12.11	0.65	1.48	6.64	27.5	0.045	3.02	0.44	0.275	0.32	3.25	0.090	0.042	11
DP14372	2	4	0.76	12.21	0.49	2.00	7.60	26.4	0.049	2.65	0.30	0.399	0.37	4.54	0.091	0.015	17
DP14373	2	4	0.86	12.31	0.37	2.06	7.46	26.5	0.053	2.61	0.41	0.402	0.47	4.52	0.092	0.052	17
DP14374	2	4	0.96	12.41	0.47	2.03	7.58	26.4	0.050	2.66	0.39	0.411	0.30	4.67	0.087	0.039	165
DP14375	2	4	1.06	12.51	0.38	2.03	7.54	26.2	0.053	2.59	0.42	0.411	0.42	4.66	0.093	0.041	17
DP14376	2	4	1.16	12.61	0.45	1.97	7.41	26.3	0.054	2.47	0.45	0.400	0.46	4.59	0.092	0.031	180
DP14377	2	4	1.26	12.71	0.42	2.01	7.42	26.4	0.055	2.56	0.43	0.405	0.48	4.62	0.089	0.053	175
DP14378	2	4	1.36	12.81	0.37	2.03	7.53	26.2	0.051	2.59	0.35	0.411	0.49	4.70	0.090	0.035	176
DP14379	2	4	1.46	12.91	0.33	2.11	7.59	26.4	0.054	2.62	0.39	0.411	0.48	4.67	0.096	0.057	185
DP14380	2	5	0.06	13.01	0.39	2.03	7.63	26.4	0.055	2.54	0.32	0.411	0.52	4.64	0.099	0.021	202
DP14381	2	5	0.16	13.11	0.32	2.06	7.50	26.4	0.056	2.55	0.39	0.404	0.51	4.56	0.089	0.048	198
DP14382	2	5	0.26	13.21	0.42	2.00	7.47	26.3	0.055	2.53	0.39	0.404	0.52	4.58	0.089	0.038	176
DP14383	2	5	0.36	13.31	0.40	2.02	7.48	26.7	0.056	2.55	0.41	0.405	0.50	4.56	0.093	0.049	183
DP14384	2	5	0.46	13.41	0.45	2.00	7.51	26.8	0.054	2.55	0.33	0.400	0.48	4.59	0.090	0.013	192
DP14385	2	5	0.56	13.51	0.35	2.06	7.50	26.4	0.053	2.62	0.36	0.400	0.42	4.58	0.090	0.045	181
DP14386	2	5	0.66	13.61	0.40	2.02	7.53	26.6	0.052	2.55	0.29	0.396	0.41	4.57	0.096	0.011	195
DP14387	2	5	0.76	13.71	0.28	2.04	7.41	26.8	0.053	2.48	0.40	0.396	0.43	4.52	0.093	0.042	220
DP14388	2	5	0.86	13.81	0.42	1.98	7.39	26.6	0.053	2.46	0.41	0.396	0.41	4.59	0.091	0.018	192
DP14389	2	5	0.96	13.91	0.44	1.99	7.42	26.7	0.051	2.51	0.44	0.408	0.38	4.67	0.091	0.021	171
DP14390	2	5	1.05	14.00	0.46	1.99	7.38	26.5	0.052	2.48	0.41	0.396	0.41	4.63	0.089	0.019	178
DP14391	2	5	1.16	14.51	0.46	2.02	7.46	26.6	0.050	2.56	0.43	0.412	0.38	4.70	0.092	0.033	154
DP14392	2	5	1.26	14.61	0.43	2.09	7.62	26.4	0.046	2.61	0.35	0.415	0.40	4.71	0.093	0.026	172
DP14393	2	5	1.36	14.71	0.42	2.09	7.60	26.6	0.050	2.64	0.42	0.416	0.43	4.63	0.099	0.058	172
DP14394	2	5	1.46	14.81	0.47	2.04	7.64	26.3	0.052	2.58	0.31	0.409	0.45	4.65	0.100	0.014	178
DP14395	2	6	0.06	14.91	0.41	2.07	7.63	26.4	0.053	2.63	0.38	0.409	0.50	4.64	0.100	0.039	172
DP14396	2	6	0.16	15.01	0.36	2.03	7.58	26.6	0.054	2.62	0.37	0.399	0.42	4.54	0.100	0.029	175
DP14397	2	6	0.26	15.11	0.40	2.01	7.50	26.8	0.055	2.59	0.38	0.395	0.41	4.44	0.104	0.024	178
DP14398	2	6	0.36	15.21	0.40	2.03	7.57	26.4	0.053	2.56	0.32	0.399	0.41	4.51	0.097	0.018	197
DP14399	2	6	0.46	15.31	0.41	2.08	7.64	26.5	0.056	2.56	0.36	0.409	0.46	4.65	0.095	0.020	172
DP14400	2	6	0.56	15.41	0.43	2.06	7.52	26.3	0.057	2.44	0.33	0.404	0.52	4.55	0.098	0.012	182
DP14401	2	6	0.66	15.51	0.35	2.04	7.57	26.7	0.057	2.49	0.35	0.407	0.53	4.55	0.097	0.011	196
DP14402	2	6	0.76	15.61	0.34	2.07	7.52	26.3	0.055	2.46	0.33	0.398	0.50	4.53	0.095	0.021	194
DP14403	2	6	0.86	15.71	0.29	2.07	7.58	26.6	0.056	2.51	0.37	0.407	0.48	4.56	0.094	0.027	200
DP14404	2	6	0.96	15.81	0.42	2.04	7.54	26.2	0.058	2.43	0.36	0.401	0.49	4.59	0.094	0.014	204
DP14405	2	6	1.06	15.91	0.24	2.09	7.59	26.4	0.058	2.45	0.40	0.404	0.45	4.58	0.095	0.040	202
DP14406	2	6	1.16	16.01	0.39	2.08	7.52	26.2	0.056	2.44	0.41	0.406	0.49	4.59	0.095	0.042	191
DP14407	2	6	1.26	16.11	0.39	2.08	7.57	26.4	0.057	2.43	0.39	0.403	0.49	4.61	0.096	0.020	190
DP14408	2	6	1.36	16.21	0.44	2.10	7.67	26.3	0.053	2.52	0.36	0.416	0.46	4.69	0.092	0.022	176
DP14409	2	6	1.46	16.31	0.38	2.13	7.60	26.2	0.054	2.56	0.43	0.418	0.40	4.68	0.092	0.057	165
DP14410	2	7	0.06	16.41	0.45	2.10	7.66	26.3	0.054	2.56	0.39	0.418	0.43	4.72	0.094	0.039	165
DP14411	2	7	0.16	16.51	0.44	2.09	7.69	26.6	0.056	2.62	0.41	0.419	0.43	4.72	0.094	0.037	163
DP14412	2	7	0.26	16.61	0.41	2.12	7.60	26.2	0.054	2.49	0.38	0.406	0.49	4.67	0.091	0.032	186
DP14413	2	7	0.36	16.71	0.33	2.15	7.62	26.3	0.057	2.49	0.43	0.410	0.46	4.66	0.093	0.047	181
DP14414	2	7	0.46	16.81	0.42	2.13	7.62	26.2	0.056	2.46	0.41	0.410	0.51	4.70	0.093	0.033	181
DP14415	3	1	0.26	10.51	0.47	2.00	7.50	26.3	0.057	2.61	0.51	0.417	0.41	4.73	0.088	0.058	148
DP14416	3	1	0.36	10.61	0.45	1.97	7.48	26.2	0.053	2.55	0.41	0.405	0.39	4.68	0.092	0.026	165
DP14417	3	1	0.46	10.71	0.37	2.02	7.57	26.3	0.052	2.65	0.42	0.419	0.38	4.70	0.097	0.051	171
DP14418	3	1	0.56	10.81	0.42	2.02	7.69	26.5	0.052	2.61	0.31	0.412	0.36	4.69	0.098	0.017	183
DP14419	3	1	0.66	10.91	0.31	1.88	7.36	27.0	0.052	2.46	0.31	0.391	0.45	4.52	0.098	0.012	214
DP14420	3	1	0.76	11.01	0.39	1.90	7.40	26.6	0.055	2.47	0.39	0.399	0.47	4.51	0.086	0.025	196

Table 2. (Continued).

Lab ID	Core	Section	Depth in Section (m)	Depth in hole (m)	Na	Mg	Al	Si	P	K	Ca	Ti	Mn	Fe	Ba	S	H_2O
DP14421	3	1	0.86	11.11	0.48	1.97	7.50	26.6	0.053	2.61	0.50	0.413	0.43	4.67	0.087	0.054	150
DP14422	3	1	0.96	11.21	0.52	1.86	7.30	26.5	0.047	2.55	0.52	0.387	0.37	4.42	0.088	0.038	133
DP14423	3	1	1.06	11.31	0.48	1.87	7.34	26.8	0.045	2.68	0.46	0.378	0.33	4.14	0.085	0.047	133
DP14424	3	1	1.16	11.41	0.49	2.02	7.64	26.3	0.050	2.62	0.42	0.422	0.58	4.78	0.088	0.040	149
DP14425	3	1	1.26	11.51	0.55	2.05	7.62	26.2	0.049	2.69	0.44	0.427	0.49	4.81	0.092	0.065	132
DP14426	3	1	1.36	11.61	0.50	1.97	7.54	26.7	0.046	2.65	0.43	0.408	0.13	4.58	0.086	0.042	143
DP14427	3	1	1.46	11.71	0.35	2.03	7.56	26.5	0.048	2.61	0.36	0.421	0.24	4.72	0.092	0.047	177
DP14428	3	2	0.06	11.81	0.47	2.02	7.58	26.2	0.046	2.64	0.37	0.415	0.33	4.74	0.094	0.042	146
DP14429	3	2	0.16	11.91	0.47	2.05	7.64	26.3	0.049	2.74	0.41	0.422	0.30	4.79	0.095	0.056	147
DP14430	3	2	0.26	12.01	0.44	2.03	7.65	26.4	0.052	2.64	0.39	0.423	0.38	4.74	0.098	0.040	161
DP14431	3	2	0.36	12.11	0.52	2.02	7.62	26.2	0.052	2.69	0.44	0.422	0.36	4.77	0.092	0.049	136
DP14432	3	2	0.46	12.21	0.44	2.02	7.67	26.4	0.054	2.62	0.39	0.418	0.43	4.75	0.096	0.034	157
DP14433	3	2	0.56	12.31	0.43	1.99	7.47	26.3	0.055	2.61	0.44	0.412	0.48	4.63	0.090	0.050	159
DP14434	3	2	0.66	12.41	0.39	2.01	7.57	26.4	0.052	2.60	0.38	0.412	0.43	4.66	0.095	0.038	173
DP14435	3	2	0.76	12.51	0.37	1.97	7.39	26.5	0.054	2.59	0.42	0.404	0.42	4.54	0.094	0.055	184
DP14436	3	2	0.86	12.61	0.46	1.97	7.43	26.4	0.051	2.62	0.40	0.397	0.38	4.57	0.090	0.040	157
DP14437	3	2	0.96	12.71	0.44	2.01	7.52	26.6	0.052	2.65	0.43	0.415	0.44	4.65	0.095	0.053	164
DP14438	3	2	1.06	12.81	0.46	1.97	7.45	26.4	0.054	2.63	0.45	0.402	0.45	4.53	0.092	0.055	151
DP14439	3	2	1.16	12.91	0.50	2.01	7.46	26.6	0.053	2.69	0.46	0.403	0.41	4.54	0.100	0.061	144
DP14440	3	2	1.26	13.01	0.51	1.69	6.96	26.9	0.052	2.76	0.41	0.321	0.42	3.75	0.088	0.034	151
DP14441	3	2	1.36	13.11	0.75	1.32	6.40	27.7	0.042	3.09	0.46	0.254	0.27	3.06	0.092	0.045	115
DP14442	3	2	1.46	13.21	0.41	2.08	7.52	26.0	0.050	2.70	0.43	0.409	0.38	4.61	0.089	0.091	177
DP14443	3	3	0.06	13.31	0.47	2.07	7.41	26.5	0.051	2.67	0.47	0.403	0.38	4.52	0.089	0.090	175
DP14444	3	3	0.16	13.41	0.47	2.07	7.49	26.3	0.051	2.68	0.49	0.413	0.33	4.69	0.093	0.083	159
DP14445	3	3	0.26	13.51	0.46	2.02	7.57	26.7	0.055	2.50	0.41	0.413	0.43	4.64	0.094	0.022	198
DP14446	3	3	0.36	13.61	0.32	2.04	7.36	26.3	0.056	2.51	0.43	0.401	0.50	4.55	0.091	0.075	204
DP14447	3	3	0.46	13.71	0.42	1.99	7.51	26.6	0.054	2.58	0.38	0.407	0.47	4.66	0.090	0.032	176
DP14448	3	3	0.56	13.81	0.40	2.09	7.49	26.1	0.052	2.67	0.47	0.416	0.42	4.69	0.090	0.128	177
DP14449	3	3	0.66	13.91	0.35	2.04	7.60	26.6	0.056	2.55	0.36	0.404	0.51	4.59	0.092	0.048	204
DP14450	3	3	0.76	14.01	0.46	2.06	7.42	26.3	0.056	2.61	0.49	0.408	0.50	4.59	0.090	0.097	176
DP14451	3	3	0.86	14.11	0.45	2.01	7.50	26.8	0.056	2.55	0.40	0.408	0.53	4.61	0.091	0.035	174
DP14452	3	3	0.96	14.21	0.40	2.02	7.34	26.4	0.052	2.62	0.45	0.395	0.44	4.51	0.091	0.084	169
DP14453	3	3	1.06	14.31	0.36	2.04	7.51	26.6	0.051	2.61	0.36	0.405	0.39	4.59	0.093	0.036	188
DP14454	3	3	1.16	14.41	0.38	2.03	7.33	26.7	0.053	2.54	0.47	0.389	0.38	4.51	0.093	0.082	204
DP14455	3	3	1.26	14.51	0.38	2.01	7.47	27.0	0.052	2.51	0.41	0.402	0.39	4.63	0.089	0.022	192
DP14456	3	3	1.36	14.61	0.55	2.00	7.33	26.5	0.051	2.59	0.55	0.406	0.40	4.68	0.095	0.078	148
DP14457	3	3	1.46	14.71	0.45	2.03	7.51	26.6	0.047	2.63	0.41	0.413	0.33	4.69	0.094	0.041	164
DP14458	3	4	0.06	14.81	0.41	2.06	7.54	26.2	0.052	2.64	0.44	0.407	0.33	4.63	0.095	0.066	168
DP14459	3	4	0.16	14.91	0.43	2.01	7.54	26.9	0.053	2.59	0.38	0.400	0.43	4.48	0.100	0.027	180
DP14460	3	4	0.26	15.01	0.42	2.09	7.56	26.4	0.055	2.66	0.47	0.417	0.36	4.61	0.098	0.076	167
DP14461	3	4	0.36	15.11	0.38	2.06	7.58	26.8	0.056	2.54	0.39	0.402	0.17	4.57	0.092	0.029	186
DP14466	3	4	0.46	15.21	0.37	2.11	7.52	26.3	0.056	2.59	0.44	0.404	0.37	4.61	0.097	0.066	173
DP14462	3	4	0.56	15.31	0.44	2.16	7.60	26.4	0.055	2.62	0.44	0.407	0.40	4.66	0.101	0.073	181
DP14463	3	4	0.66	15.41	0.40	2.09	7.66	26.5	0.055	2.60	0.39	0.416	0.52	4.66	0.099	0.041	210
DP14464	3	4	0.76	15.51	0.35	2.07	7.42	26.4	0.056	2.50	0.42	0.403	0.44	4.52	0.097	0.056	206
DP14465	3	4	0.86	15.61	0.37	2.09	7.58	26.5	0.054	2.55	0.41	0.408	0.36	4.61	0.095	0.048	208
DP14467	3	4	0.96	15.71	0.39	2.10	7.61	26.6	0.057	2.55	0.44	0.413	0.48	4.63	0.095	0.044	182
DP14468	3	4	1.06	15.81	0.46	2.12	7.47	26.2	0.056	2.57	0.54	0.412	0.45	4.63	0.094	0.107	188
DP14469	3	4	1.16	15.91	0.37	2.06	7.48	26.2	0.057	2.49	0.43	0.402	0.45	4.58	0.095	0.038	124
DP14470	3	4	1.26	16.01	0.54	2.16	7.56	26.3	0.049	2.67	0.51	0.429	0.36	4.72	0.092	0.109	170
DP14471	3	4	1.36	16.11	0.40	2.11	7.62	26.4	0.053	2.58	0.42	0.416	0.41	4.70	0.091	0.042	171
DP14472	3	4	1.46	16.21	0.58	2.14	7.60	26.2	0.055	2.70	0.51	0.426	0.38	4.74	0.095	0.103	164
DP14473	3	5	0.06	16.31	0.43	2.12	7.64	26.3	0.054	2.62	0.41	0.417	0.41	4.68	0.093	0.047	163
DP14474	3	5	0.16	16.41	0.52	2.17	7.60	26.3	0.058	2.65	0.51	0.423	0.44	4.70	0.090	0.105	175
DP14475	3	5	0.26	16.51	0.41	2.14	7.66	26.5	0.059	2.57	0.43	0.422	0.43	4.68	0.097	0.046	162
DP14476	3	C	0.06	16.63	0.48	2.18	7.57	26.2	0.056	2.54	0.54	0.421	0.48	4.71	0.090	0.100	182
DP14477	3	C	0.16	16.73	0.38	2.16	7.64	26.4	0.056	2.49	0.44	0.411	0.46	4.69	0.093	0.041	182
DP14478	3	C	0.26	16.83	0.61	2.15	7.61	26.2	0.049	2.80	0.47	0.429	0.30	4.75	0.095	0.104	156
DP14479	4	1	0.06		0.47	2.26	7.68	26.2	0.053	2.33	0.40	0.396	0.39	4.39	0.086	0.035	
DP14480	4	1	0.16		0.36	2.14	7.82	26.5	0.060	2.57	0.37	0.429	0.55	4.75	0.100	0.034	
DP14481	4	1	0.26		0.42	2.10	7.65	26.1	0.060	2.50	0.42	0.414	0.51	4.72	0.093	0.031	
DP14482	4	1	0.76	18.96	0.45	2.17	7.79	26.4	0.054	2.62	0.46	0.425	0.49	4.81	0.094	0.072	168
DP14483	4	1	0.86	19.06	0.38	2.12	7.65	25.7	0.058	2.38	0.51	0.406	0.56	4.82	0.089	0.037	195

Table 2. (Continued).

Lab ID	Core	Section	Depth in Section (m)	Depth in hole (m)	Na	Mg	Al	Si	P	K	Ca	Ti	Mn	Fe	Ba	S	H_2O
DP14484	4	1	0.96	19.16	0.40	2.15	7.87	26.3	0.058	2.43	0.52	0.428	0.55	4.93	0.088	0.031	184
DP14485	4	1	1.06	19.26	0.43	2.12	7.76	26.0	0.059	2.45	0.49	0.410	0.55	4.86	0.088	0.028	173
DP14486	4	1	1.16	19.36	0.44	2.11	7.73	25.8	0.059	2.53	0.44	0.415	0.55	4.80	0.088	0.038	175
DP14487	4	1	1.26	19.46	0.40	2.12	7.88	26.3	0.058	2.59	0.44	0.439	0.57	4.94	0.088	0.038	173
DP14488	4	1	1.36	19.56	0.42	2.09	7.74	25.9	0.055	2.57	0.44	0.422	0.54	4.88	0.088	0.042	171
DP14489	4	1	1.46	19.66	0.47	2.11	7.82	26.0	0.056	2.60	0.44	0.429	0.57	4.94	0.092	0.045	159
DP14490	4	2	0.05	19.75	0.41	2.10	7.85	26.0	0.056	2.61	0.46	0.424	0.55	4.91	0.087	0.042	164
DP14491	4	2	0.16	19.86	0.44	2.10	7.80	25.9	0.058	2.58	0.44	0.425	0.55	4.87	0.086	0.048	166
DP14492	4	2	0.26	19.96	0.43	2.10	7.82	26.0	0.056	2.62	0.41	0.427	0.54	4.91	0.092	0.044	155
DP14493	4	2	0.36	20.06	0.45	2.07	7.81	25.8	0.054	2.61	0.40	0.421	0.52	4.87	0.089	0.046	155
DP14494	4	2	0.46	20.16	0.48	2.07	7.85	26.0	0.057	2.67	0.43	0.431	0.50	4.96	0.091	0.054	148
DP14495	4	2	0.56	20.26	0.45	2.06	7.79	25.7	0.055	2.58	0.45	0.424	0.55	4.93	0.088	0.049	160
DP14496	4	2	0.66	20.36	0.47	2.11	7.92	26.0	0.058	2.61	0.46	0.432	0.58	5.00	0.087	0.064	165
DP14497	4	2	0.76	20.46	0.43	2.07	7.83	25.6	0.058	2.57	0.45	0.422	0.59	4.95	0.089	0.051	155
DP14498	4	2	0.86	20.56	0.47	2.06	7.92	25.8	0.060	2.61	0.47	0.434	0.60	5.01	0.087	0.057	153
DP14499	4	2	0.96	20.66	0.45	2.02	7.83	25.5	0.060	2.57	0.46	0.424	0.61	4.97	0.085	0.048	160
DP14500	4	2	1.06	20.76	0.53	2.01	7.92	25.7	0.059	2.60	0.49	0.442	0.61	5.08	0.082	0.046	144
DP14501	4	2	1.16	20.86	0.47	2.01	7.93	25.7	0.057	2.60	0.49	0.432	0.60	5.04	0.083	0.048	148
DP14502	4	2	1.26	20.96	0.47	1.99	7.80	25.6	0.054	2.66	0.43	0.426	0.59	4.93	0.088	0.057	150
DP14503	4	2	1.36	21.06	0.44	2.00	7.72	25.3	0.057	2.60	0.43	0.418	0.62	4.89	0.088	0.053	157
DP14504	4	2	1.46	21.16	0.50	2.02	7.84	25.7	0.059	2.63	0.45	0.432	0.62	4.97	0.088	0.054	152
DP14505	4	3	0.06	21.26	0.51	2.01	7.59	25.0	0.058	2.56	0.47	0.412	0.61	4.89	0.085	0.066	148
DP14506	4	3	0.16	21.36	0.47	2.05	7.77	25.5	0.060	2.59	0.46	0.436	0.67	4.98	0.086	0.057	149
DP14507	4	3	0.26	21.46	0.49	2.05	7.82	25.6	0.063	2.62	0.46	0.436	0.71	4.99	0.085	0.059	155
DP14508	4	3	0.36	21.56	0.46	2.07	7.78	25.3	0.063	2.60	0.44	0.427	0.71	4.99	0.085	0.057	152
DP14509	4	3	0.46	21.66	0.53	2.05	7.83	25.5	0.058	2.63	0.45	0.426	0.67	5.01	0.085	0.058	146
DP14510	4	3	0.56	21.76	0.48	2.05	7.85	25.6	0.054	2.63	0.45	0.434	0.67	5.04	0.084	0.056	148
DP14511	4	3	0.66	21.86	0.50	2.03	7.82	25.5	0.053	2.58	0.49	0.429	0.66	5.07	0.079	0.052	151
DP14512	4	3	0.76	21.96	0.50	2.03	7.82	25.4	0.053	2.57	0.49	0.434	0.66	5.08	0.081	0.048	141
DP14513	4	3	0.86	22.06	0.46	2.02	7.84	25.5	0.059	2.63	0.42	0.438	0.70	5.00	0.086	0.045	144
DP14514	4	3	0.96	22.16	0.50	2.06	7.97	25.8	0.061	2.70	0.44	0.447	0.66	5.04	0.086	0.057	144
DP14515	4	3	1.06	22.26	0.51	2.07	7.83	25.4	0.061	2.64	0.44	0.433	0.67	4.98	0.086	0.062	146
DP14516	4	3	1.16	22.36	0.49	2.06	7.99	26.0	0.059	2.69	0.43	0.447	0.71	5.08	0.088	0.047	140
DP14517	4	3	1.26	22.46	0.47	2.04	7.88	25.6	0.061	2.66	0.43	0.442	0.68	5.02	0.085	0.063	146
DP14518	4	3	1.36	22.56	0.44	2.04	7.86	25.4	0.060	2.63	0.42	0.439	0.69	5.01	0.085	0.074	154
DP14519	4	3	1.46	22.66	0.40	2.05	7.87	25.5	0.059	2.57	0.41	0.439	0.69	5.03	0.083	0.070	158
DP14520	4	4	0.06	22.76	0.49	2.04	7.85	25.6	0.060	2.65	0.43	0.443	0.78	5.04	0.087	0.060	146
DP14521	4	4	0.16	22.86	0.49	2.04	7.86	25.5	0.063	2.65	0.43	0.444	0.74	5.03	0.086	0.065	143
DP14522	4	4	0.26	22.96	0.47	2.01	7.89	25.5	0.065	2.65	0.44	0.433	0.73	4.96	0.085	0.061	143
DP14523	4	4	0.36	23.06	0.48	2.03	7.81	25.3	0.064	2.66	0.44	0.432	0.70	4.95	0.083	0.066	138
DP14524	4	4	0.46	23.16	0.49	2.02	7.80	25.4	0.065	2.70	0.43	0.435	0.70	4.98	0.084	0.069	134
DP14525	4	4	0.56	23.26	0.48	2.02	7.78	25.4	0.063	2.70	0.42	0.440	0.68	4.97	0.084	0.068	135
DP14526	4	4	0.66	23.36	0.53	2.01	7.75	25.2	0.061	2.72	0.41	0.437	0.70	4.99	0.087	0.074	127
DP14527	4	4	0.76	23.46	0.51	1.98	7.75	25.2	0.058	2.72	0.40	0.432	0.64	4.96	0.080	0.070	131
DP14528	4	4	0.86	23.56	0.53	1.98	7.87	25.4	0.063	2.74	0.42	0.438	0.64	4.99	0.083	0.071	127
DP14529	4	4	0.96	23.66	0.51	1.99	7.85	25.3	0.068	2.73	0.43	0.431	0.68	4.92	0.081	0.074	134
DP14530	4	4	1.06	23.76	0.47	1.96	7.81	25.3	0.069	2.70	0.43	0.432	0.69	4.91	0.079	0.066	131
DP14531	4	4	1.16	23.86	0.47	1.98	7.84	25.3	0.067	2.71	0.42	0.437	0.64	4.92	0.079	0.073	138
DP14532	4	4	1.26	23.96	0.45	1.98	7.86	25.4	0.069	2.69	0.43	0.434	0.65	4.94	0.080	0.064	140
DP14533	4	4	1.36	24.06	0.45	1.97	7.85	25.4	0.064	2.69	0.41	0.437	0.65	4.97	0.079	0.056	135
DP14534	4	4	1.46	24.16	0.48	1.98	7.93	25.6	0.063	2.67	0.45	0.448	0.63	5.07	0.078	0.065	137
DP14535	4	5	0.06	24.26	0.46	1.95	7.91	25.5	0.060	2.65	0.44	0.444	0.64	5.06	0.076	0.049	138
DP14536	4	5	0.16	24.36	0.44	1.98	7.91	25.6	0.060	2.68	0.40	0.440	0.66	5.00	0.077	0.046	139
DP14537	4	5	0.26	24.46	0.43	1.99	7.93	25.6	0.067	2.66	0.41	0.443	0.68	4.98	0.079	0.048	140
DP14538	4	5	0.36	24.56	0.47	2.00	7.86	25.5	0.070	2.68	0.42	0.444	0.71	4.98	0.080	0.056	133
DP14539	4	5	0.46	24.66	0.49	2.01	7.91	25.6	0.072	2.69	0.43	0.451	0.72	5.04	0.082	0.054	132
DP14540	4	5	0.56	24.76	0.46	2.02	7.95	25.7	0.075	2.70	0.42	0.446	0.70	5.02	0.087	0.051	136
DP14541	4	5	0.66	24.86	0.43	1.98	7.90	25.5	0.071	2.66	0.39	0.437	0.72	4.97	0.081	0.036	135
DP14542	4	5	0.76	24.96	0.44	1.99	7.87	25.4	0.071	2.68	0.41	0.444	0.71	4.96	0.080	0.049	134
DP14543	4	5	0.86	25.06	0.41	2.00	7.96	25.6	0.072	2.71	0.40	0.442	0.75	4.99	0.077	0.049	141
DP14544	4	5	0.96	25.16	0.41	2.00	7.94	25.5	0.071	2.71	0.38	0.440	0.72	4.97	0.081	0.053	143
DP14545	4	5	1.06	25.26	0.45	1.99	7.89	25.4	0.067	2.70	0.36	0.430	0.67	4.92	0.077	0.049	134
DP14546	4	5	1.16	25.36	0.45	2.01	7.93	25.4	0.070	2.72	0.40	0.434	0.72	4.91	0.078	0.069	137

Table 2. (Continued).

Lab ID	Core	Section	Depth in Section (m)	Depth in hole (m)	Na	Mg	Al	Si	P	K	Ca	Ti	Mn	Fe	Ba	S	H_2O
DP14547	4	5	1.26	25.46	0.46	2.01	7.84	25.4	0.067	2.73	0.39	0.437	0.71	4.93	0.080	0.063	129
DP14548	4	5	1.36	25.56	0.49	2.00	7.88	25.6	0.068	2.80	0.39	0.445	0.54	5.01	0.077	0.059	121
DP14549	4	5	1.46	25.66	0.50	1.99	7.81	25.5	0.066	2.83	0.39	0.447	0.60	4.98	0.079	0.062	117
DP14550	4	6	0.06	25.76	0.51	2.01	7.89	25.7	0.066	2.83	0.39	0.450	0.67	5.05	0.080	0.053	117
DP14551	4	6	0.16	25.86	0.53	2.00	7.78	25.4	0.069	2.83	0.40	0.446	0.61	5.02	0.079	0.063	110
DP14552	4	6	0.26	25.96	0.51	2.01	7.83	25.6	0.073	2.83	0.39	0.451	0.61	5.06	0.076	0.057	116
DP14553	4	6	0.36	26.06	0.45	2.03	7.86	25.7	0.079	2.81	0.39	0.456	0.69	5.14	0.082	0.045	117
DP14554	4	6	0.46	26.16	0.51	2.03	7.72	25.5	0.094	2.79	0.42	0.468	0.79	5.21	0.084	0.041	109
DP14555	4	6	0.56	26.26	0.50	2.10	7.51	25.1	0.124	2.80	0.52	0.482	0.85	5.40	0.092	0.057	115
DP14556	4	6	0.66	26.36	0.45	2.18	7.42	25.3	0.163	2.77	0.59	0.522	0.99	5.63	0.110	0.045	124
DP14557	4	6	0.76	26.46	0.47	2.16	7.27	25.0	0.167	2.75	0.63	0.515	0.99	5.57	0.110	0.056	124
DP14558	4	6	0.86	26.56	0.46	2.14	7.34	25.1	0.157	2.76	0.58	0.511	0.91	5.54	0.106	0.045	123
DP14559	4	6	0.96	26.66	0.46	2.17	7.28	25.1	0.174	2.76	0.64	0.523	0.99	5.61	0.115	0.054	129
DP14560	4	6	1.06	26.76	0.45	2.18	7.18	24.9	0.173	2.73	0.64	0.511	0.98	5.55	0.117	0.059	131
DP14561	4	6	1.16	26.86	0.46	2.17	7.19	24.8	0.174	2.74	0.64	0.514	0.97	5.54	0.115	0.057	127
DP14562	4	6	1.26	26.96	0.44	2.18	7.23	25.0	0.176	2.74	0.64	0.518	0.98	5.58	0.114	0.057	128
DP14563	4	6	1.36	27.06	0.48	2.19	7.25	25.1	0.183	2.78	0.68	0.525	0.97	5.59	0.115	0.070	129
DP14564	4	6	1.46	27.16	0.46	2.17	7.13	24.7	0.178	2.74	0.67	0.507	0.96	5.52	0.112	0.069	132
DP14565	4	7	0.06	27.26	0.45	2.17	7.20	24.9	0.189	2.75	0.70	0.522	0.98	5.55	0.117	0.066	128
DP14566	4	7	0.16	27.36	0.44	2.17	7.27	25.1	0.186	2.76	0.68	0.527	1.01	5.59	0.116	0.062	130
DP14567	4	7	0.26	27.46	0.47	2.17	7.25	24.9	0.181	2.76	0.68	0.523	1.01	5.58	0.117	0.066	129
DP14568	4	7	0.36	27.56	0.49	2.19	7.21	24.9	0.193	2.77	0.73	0.532	1.00	5.55	0.115	0.082	127
DP14569	4	7	0.46	27.66	0.45	2.15	7.13	24.6	0.196	2.73	0.72	0.514	1.00	5.50	0.117	0.076	128
DP14570	5	1	0.36		0.50	2.03	8.04	25.5	0.070	2.81	0.41	0.456	0.70	5.23	0.079	0.062	
DP14571	5	1	0.46	28.06	0.46	2.02	8.00	25.2	0.076	2.76	0.42	0.448	0.81	5.21	0.077	0.056	119
DP14572	5	1	0.56	28.16	0.45	2.00	7.94	25.0	0.079	2.74	0.41	0.440	0.81	5.16	0.079	0.049	121
DP14573	5	1	0.66	28.26	0.46	2.04	7.93	25.1	0.082	2.72	0.44	0.446	0.92	5.21	0.079	0.052	121
DP14574	5	1	0.76	28.36	0.46	2.05	7.84	24.9	0.085	2.69	0.45	0.447	0.89	5.24	0.080	0.057	126
DP14575	5	1	0.86	28.46	0.47	2.06	7.84	25.0	0.084	2.68	0.47	0.453	0.88	5.29	0.079	0.058	121
DP14576	5	1	0.96	28.56	0.44	2.08	7.83	25.0	0.086	2.67	0.44	0.447	0.90	5.25	0.082	0.051	127
DP14577	5	1	1.06	28.66	0.46	2.07	7.86	25.0	0.083	2.69	0.46	0.449	0.89	5.28	0.081	0.059	132
DP14578	5	1	1.16	28.76	0.47	2.06	7.77	24.7	0.084	2.63	0.46	0.431	0.93	5.20	0.077	0.057	135
DP14579	5	1	1.26	28.86	0.47	2.09	7.93	25.2	0.086	2.69	0.46	0.449	0.91	5.23	0.077	0.060	136
DP14580	5	1	1.36	28.96	0.46	2.06	7.90	25.1	0.085	2.71	0.45	0.438	0.94	5.15	0.079	0.059	138
DP14581	5	1	1.46	29.06	0.51	2.07	7.81	24.9	0.086	2.72	0.46	0.440	0.94	5.17	0.077	0.066	133
DP14582	5	2	0.56		0.48	2.07	7.90	25.2	0.084	2.71	0.47	0.460	0.89	5.32	0.080	0.063	
DP14583	5	2	1.16		0.45	2.06	7.75	25.0	0.090	2.74	0.44	0.451	0.97	5.22	0.079	0.057	
DP14584	5	3	0.23		0.51	2.06	7.75	24.7	0.106	2.77	0.50	0.455	1.01	5.25	0.077	0.062	
DP14585	5	3	0.99		0.55	2.04	7.78	24.8	0.112	2.82	0.51	0.461	1.04	5.25	0.076	0.059	
DP14586	5	4	0.76		0.62	1.96	7.92	25.6	0.124	2.88	0.57	0.461	1.28	5.29	0.075	0.070	
DP14587	5	5	0.46		0.55	2.09	7.95	24.4	0.125	2.72	0.55	0.478	1.32	5.51	0.071	0.071	
DP14588	5	5	0.56	31.06	0.54	2.06	7.88	24.0	0.150	2.65	0.61	0.444	1.49	5.37	0.074	0.073	134
DP14589	5	5	0.66	31.16	0.51	2.06	7.89	23.8	0.156	2.63	0.61	0.447	1.56	5.37	0.074	0.064	134
DP14590	5	5	0.76	31.26	0.57	2.02	7.93	24.0	0.155	2.72	0.61	0.446	1.47	5.34	0.072	0.057	129
DP14591	5	5	0.86	31.36	0.65	1.91	7.83	23.6	0.151	2.73	0.61	0.418	1.40	5.05	0.067	0.059	139
DP14592	5	5	0.96	31.46	0.54	2.02	7.79	23.8	0.172	2.60	0.67	0.438	1.61	5.32	0.068	0.060	146
DP14593	5	5	1.06	31.56	0.57	2.04	7.87	24.0	0.186	2.61	0.71	0.444	1.77	5.39	0.071	0.061	146
DP14594	5	5	1.19	31.69	0.57	1.97	7.82	24.0	0.193	2.66	0.72	0.441	1.68	5.29	0.074	0.064	143
DP14595	5	5	1.30	31.80	0.53	2.00	7.72	23.8	0.194	2.67	0.74	0.449	1.70	5.32	0.074	0.070	136
DP14596	5	5	1.46	31.96	0.61	1.97	7.69	23.8	0.198	2.69	0.75	0.445	1.67	5.29	0.072	0.059	134
DP14597	5	6	0.06	32.06	0.64	2.01	7.68	23.7	0.197	2.65	0.78	0.447	1.84	5.32	0.072	0.070	139
DP14598	5	6	0.16	32.16	0.62	2.01	7.70	23.8	0.202	2.64	0.78	0.452	1.65	5.38	0.072	0.071	145
DP14599	5	6	0.26	32.26	0.61	2.02	7.69	23.9	0.187	2.63	0.73	0.456	1.58	5.44	0.074	0.066	137
DP14600	5	6	0.36	32.36	0.60	2.01	7.63	23.8	0.172	2.63	0.69	0.455	1.53	5.45	0.073	0.063	140
DP14601	5	6	0.46	32.46	0.60	2.00	7.61	23.7	0.174	2.62	0.69	0.446	1.58	5.43	0.070	0.061	142
DP14602	5	6	0.56	32.56	0.60	1.99	7.73	23.8	0.176	2.66	0.69	0.451	1.68	5.45	0.073	0.061	143
DP14603	5	6	0.66	32.66	0.59	1.98	7.72	23.7	0.169	2.68	0.67	0.450	1.56	5.45	0.071	0.063	143
DP14604	5	6	0.76	32.76	0.59	1.99	7.83	23.9	0.173	2.74	0.68	0.446	1.53	5.41	0.072	0.060	141
DP14605	5	6	0.86	32.86	0.58	1.99	7.87	24.0	0.158	2.79	0.66	0.449	1.51	5.36	0.074	0.065	136
DP14606	5	6	0.96	32.96	0.59	1.98	7.88	24.0	0.169	2.81	0.67	0.445	1.48	5.32	0.074	0.062	133
DP14607	5	6	1.07	33.07	0.60	1.94	7.76	23.6	0.180	2.76	0.68	0.428	1.45	5.25	0.071	0.059	139
DP14608	5	6	1.16	33.16	0.57	1.97	7.86	23.9	0.196	2.74	0.73	0.453	1.64	5.43	0.074	0.065	145
DP14609	5	6	1.26	33.26	0.55	1.95	7.74	23.6	0.201	2.68	0.73	0.438	1.65	5.39	0.074	0.060	148

Table 2. (Continued).

Lab ID	Core	Section	Depth in Section (m)	Depth in hole (m)	Na	Mg	Al	Si	P	K	Ca	Ti	Mn	Fe	Ba	S	H_2
DP14610	5	6	1.35	33.35	0.56	1.99	7.84	23.9	0.192	2.71	0.72	0.458	1.74	5.53	0.074	0.061	1
DP14611	5	6	1.45	33.45	0.58	1.96	7.74	23.5	0.200	2.70	0.74	0.439	1.70	5.43	0.073	0.067	1
DP14612	5	7	0.06	33.56	0.61	1.96	7.73	23.5	0.200	2.70	0.76	0.445	1.74	5.44	0.073	0.074	1
DP14613	5	7	0.16	33.66	0.54	1.99	7.74	23.5	0.204	2.70	0.77	0.453	1.80	5.52	0.074	0.074	1
DP14614	5	7	0.26	33.76	0.57	2.00	7.72	23.4	0.211	2.66	0.78	0.452	1.78	5.53	0.074	0.084	1
DP14615	5	7	0.36	33.86	0.52	2.04	7.67	23.3	0.211	2.61	0.79	0.452	1.76	5.57	0.070	0.086	1
DP14616	5	7	0.45	33.95	0.47	2.04	7.79	23.7	0.222	2.60	0.79	0.470	1.88	5.66	0.072	0.082	1
DP14617	6	1	1.31		0.37	2.00	7.72	23.4	0.279	2.54	0.87	0.466	2.09	5.33	0.075	0.064	
DP14618	6	1	1.41		0.38	1.98	7.54	23.0	0.295	2.54	0.91	0.448	2.02	5.32	0.073	0.064	
DP14619	6	2	1.21		0.35	2.05	7.36	22.6	0.518	2.54	1.57	0.442	2.14	5.48	0.076	0.089	
DP14620	6	2	1.31		0.39	2.10	7.38	22.6	0.545	2.55	1.62	0.432	2.25	5.54	0.075	0.110	
DP14621	6	2	1.41		0.37	2.05	7.33	22.5	0.591	2.52	1.69	0.433	2.20	5.48	0.074	0.094	
DP14622	6	3	0.06		0.39	2.10	7.49	22.8	0.502	2.59	1.51	0.413	2.27	5.45	0.074	0.097	
DP14624	6	3	0.16		0.37	2.06	7.43	22.6	0.520	2.56	1.51	0.408	2.25	5.44	0.073	0.086	
DP14623	6	3	0.26		0.34	2.13	7.35	22.5	0.502	2.56	1.55	0.403	2.21	5.38	0.076	0.109	
DP14625	6	3	0.36		0.35	2.10	7.56	23.0	0.481	2.61	1.43	0.393	2.19	5.32	0.073	0.085	
DP14626	6	3	0.46		0.33	2.10	7.54	22.9	0.523	2.59	1.44	0.394	2.16	5.29	0.074	0.090	
DP14627	6	3	0.56		0.34	2.10	7.55	22.9	0.503	2.61	1.45	0.394	2.17	5.32	0.073	0.087	
DP14628	6	3	0.66		0.35	2.09	7.47	22.6	0.485	2.59	1.44	0.386	2.13	5.24	0.073	0.093	
DP14629	6	3	0.76	38.06	0.37	2.06	7.98	23.9	0.313	3.01	0.88	0.379	1.50	4.98	0.072	0.082	1
DP14630	6	3	0.86	38.16	0.35	2.05	8.01	23.9	0.315	3.01	0.88	0.378	1.51	4.99	0.073	0.073	12
DP14631	6	3	0.96	38.26	0.35	2.03	7.94	23.9	0.300	2.99	0.85	0.375	1.49	4.98	0.072	0.065	12
DP14632	6	3	1.06	38.36	0.38	2.06	8.00	23.9	0.302	3.01	0.86	0.381	1.50	4.98	0.074	0.071	12
DP14633	6	3	1.16	38.46	0.38	2.07	8.01	24.0	0.319	3.02	0.88	0.393	1.53	5.02	0.072	0.079	12
DP14634	6	3	1.26	38.56	0.34	2.07	7.97	24.0	0.289	2.96	0.82	0.384	1.53	4.98	0.072	0.066	12
DP14635	6	3	1.36	38.66	0.37	2.06	7.95	23.8	0.297	2.92	0.86	0.392	1.66	4.96	0.071	0.073	12
DP14636	6	3	1.46	38.76	0.36	2.02	7.88	23.6	0.294	2.86	0.85	0.390	1.70	4.91	0.073	0.069	12
DP14637	6	4	0.06	38.86	0.34	2.11	7.84	23.5	0.301	2.90	0.87	0.440	1.58	5.15	0.071	0.070	12
DP14638	6	4	0.16	38.96	0.33	2.14	7.94	23.7	0.292	2.92	0.81	0.473	1.74	5.28	0.076	0.061	11
DP14639	6	4	0.26	39.06	0.36	2.15	7.83	23.4	0.311	2.84	0.84	0.487	1.50	5.33	0.073	0.070	121
DP14640	6	4	0.36	39.16	0.36	2.13	7.96	23.6	0.290	2.82	0.80	0.490	1.51	5.32	0.072	0.071	122
DP14641	6	4	0.46	39.26	0.37	2.10	7.94	23.6	0.311	2.77	0.87	0.500	1.53	5.31	0.072	0.074	124
DP14642	6	4	0.56	39.36	0.39	2.04	7.91	23.4	0.360	2.64	0.99	0.532	1.57	5.40	0.071	0.076	129
DP14643	6	4	0.66	39.46	0.40	1.98	7.89	23.4	0.352	2.68	0.95	0.550	1.45	5.53	0.071	0.078	128
DP14644	6	4	0.76	39.56	0.38	1.95	7.92	23.6	0.325	2.81	0.91	0.544	1.48	5.56	0.072	0.069	13
DP14645	6	4	0.86	39.66	0.37	2.02	7.90	23.5	0.364	2.65	0.98	0.595	1.59	5.66	0.073	0.076	139
DP14646	6	4	0.96	39.76	0.34	2.01	7.81	23.0	0.327	2.55	0.91	0.590	1.64	5.65	0.075	0.069	140
DP14647	6	4	1.06	39.86	0.38	2.01	7.87	23.1	0.350	2.59	0.94	0.615	1.74	5.80	0.076	0.065	13
DP14648	6	4	1.16	39.96	0.35	2.03	7.88	23.1	0.345	2.64	0.88	0.628	1.66	5.90	0.072	0.068	13
DP14649	6	4	1.26	40.06	0.34	2.01	7.86	23.2	0.301	2.69	0.83	0.622	1.68	5.88	0.077	0.063	140
DP14650	6	4	1.36	40.16	0.36	2.03	7.89	23.2	0.324	2.62	0.86	0.621	1.74	5.92	0.077	0.075	140
DP14651	6	4	1.46	40.26	0.39	2.05	7.87	23.1	0.325	2.65	0.89	0.611	1.74	5.95	0.078	0.081	144
DP14652	6	5	0.06	40.36	0.43	2.03	7.70	22.7	0.319	2.63	0.89	0.583	1.66	5.85	0.075	0.092	140
DP14653	6	5	0.16	40.46	0.40	2.04	7.79	23.0	0.303	2.63	0.88	0.597	1.67	5.93	0.076	0.076	13
DP14654	6	5	0.26	40.56	0.39	2.07	7.90	23.3	0.314	2.67	0.89	0.608	1.68	6.01	0.077	0.083	13
DP14655	6	5	0.36	40.66	0.43	2.07	7.92	23.3	0.312	2.69	0.89	0.612	1.73	6.02	0.075	0.086	14
DP14656	6	5	0.46	40.76	0.39	2.04	7.87	23.2	0.335	2.64	0.90	0.608	1.69	6.03	0.075	0.072	13
DP14657	6	5	0.56	40.86	0.40	2.05	7.82	23.0	0.308	2.65	0.89	0.599	1.68	5.98	0.075	0.083	14
DP14658	6	5	0.66	40.96	0.41	2.07	7.89	23.3	0.309	2.66	0.88	0.607	1.70	6.03	0.075	0.079	13
DP14659	6	5	0.76	41.06	0.41	2.07	7.86	23.2	0.301	2.66	0.86	0.598	1.67	6.02	0.076	0.086	13
DP14660	6	5	0.86	41.16	0.41	2.04	7.85	23.2	0.298	2.68	0.85	0.593	1.57	5.93	0.075	0.083	13
DP14661	6	5	0.96	41.26	0.36	2.01	7.93	23.5	0.294	2.77	0.79	0.598	1.36	5.80	0.072	0.064	13
DP14662	6	5	1.06	41.36	0.36	2.04	7.94	23.6	0.292	2.78	0.81	0.595	1.34	5.77	0.070	0.074	13
DP14663	6	5	1.16	41.46	0.37	2.04	7.93	23.5	0.293	2.79	0.82	0.599	1.35	5.81	0.070	0.080	13
DP14664	6	5	1.26	41.56	0.35	2.02	7.96	23.6	0.290	2.77	0.80	0.598	1.40	5.80	0.070	0.062	13
DP14665	6	5	1.36	41.66	0.34	2.05	7.86	23.3	0.299	2.77	0.80	0.615	1.38	5.88	0.072	0.071	13
DP14666	6	5	1.46	41.76	0.25	2.15	7.71	23.1	0.332	2.74	0.84	0.677	1.46	6.21	0.075	0.074	13
DP14667	6	6	0.06	41.86	0.35	2.11	7.69	23.1	0.316	2.75	0.85	0.721	1.44	6.40	0.075	0.067	140
DP14668	6	6	0.16	41.96	0.34	2.11	7.67	23.0	0.360	2.72	0.89	0.723	1.40	6.50	0.075	0.068	140
DP14669	6	6	0.26	42.06	0.37	2.10	7.66	23.0	0.319	2.74	0.87	0.727	1.40	6.50	0.074	0.077	139
DP14670	6	6	0.36	42.16	0.42	2.09	7.63	22.9	0.322	2.72	0.86	0.724	1.36	6.50	0.074	0.062	141
DP14671	6	6	0.46	42.26	0.39	2.08	7.73	23.2	0.314	2.84	0.87	0.748	1.36	6.56	0.075	0.059	138
DP14672	6	6	0.56	42.36	0.44	2.08	7.79	23.5	0.311	3.03	0.85	0.741	1.29	6.32	0.075	0.064	130

Table 2. (Continued).

Lab ID	Core	Section	Depth in Section (m)	Depth in hole (m)	Na	Mg	Al	Si	P	K	Ca	Ti	Mn	Fe	Ba	S	H_2O
DP14673	6	6	0.66	42.46	0.43	2.07	7.76	23.6	0.287	3.12	0.81	0.742	1.21	6.28	0.074	0.067	127
DP14674	6	6	0.76	42.56	0.43	2.08	7.78	23.8	0.295	3.16	0.81	0.751	1.18	6.26	0.075	0.066	125
DP14675	6	6	0.86	42.66	0.40	2.12	7.70	23.7	0.302	3.17	0.81	0.730	1.17	6.22	0.074	0.069	128
DP14676	6	6	0.96	42.76	0.38	2.08	7.53	23.3	0.248	3.12	0.69	0.656	1.14	5.85	0.072	0.054	119
DP14677	6	6	1.06	42.86	0.41	2.18	7.63	23.8	0.230	3.20	0.65	0.710	1.10	6.17	0.073	0.057	115
DP14678	6	6	1.16	42.96	0.37	2.17	7.73	24.0	0.253	3.18	0.70	0.658	1.17	6.01	0.074	0.064	115
DP14679	6	6	1.26	43.06	0.34	2.17	7.72	24.0	0.256	3.18	0.72	0.604	1.21	5.74	0.075	0.054	111
DP14680	6	6	1.36	43.16	0.33	2.18	7.65	23.9	0.264	3.16	0.71	0.569	1.15	5.63	0.078	0.054	106
DP14681	6	6	1.46	43.26	0.31	2.26	7.71	24.1	0.248	3.21	0.69	0.593	1.18	5.72	0.076	0.059	109
DP14682	6	7	0.06	43.36	0.31	2.23	7.50	23.7	0.281	3.12	0.75	0.573	1.13	5.73	0.075	0.059	114
DP14683	6	7	0.16	43.46	0.30	2.27	7.67	23.9	0.282	3.13	0.76	0.544	1.20	5.59	0.077	0.054	107
DP14684	6	7	0.26	43.56	0.32	2.24	7.68	24.1	0.266	3.19	0.72	0.587	1.15	5.74	0.076	0.052	109
DP14685	6	7	0.36	43.66	0.30	2.31	7.77	24.4	0.272	3.16	0.74	0.624	1.13	5.91	0.075	0.056	105
DP14686	6	7	0.44	43.74	0.32	2.31	7.72	24.1	0.258	3.13	0.70	0.609	1.07	5.85	0.076	0.062	104
DP14687	7	1	0.09	43.49	0.26	2.23	7.53	23.8	0.269	3.16	0.74	0.584	1.14	5.72	0.076	0.066	127
DP14688	7	1	0.16	43.56	0.28	2.26	7.61	24.1	0.272	3.16	0.75	0.590	1.13	5.78	0.075	0.064	119
DP14689	7	1	0.26	43.66	0.31	2.27	7.66	24.2	0.264	3.18	0.76	0.576	1.19	5.74	0.077	0.064	114
DP14690	7	1	0.36	43.76	0.37	2.28	7.66	24.0	0.265	3.15	0.78	0.561	1.18	5.66	0.075	0.074	111
DP14691	7	1	0.46	43.86	0.32	2.24	7.65	24.0	0.259	3.14	0.72	0.595	1.14	5.81	0.075	0.056	117
DP14692	7	1	0.56	43.96	0.37	2.17	7.75	23.9	0.233	3.15	0.63	0.647	0.99	6.01	0.073	0.053	114
DP14693	7	1	0.66	44.06	0.42	2.12	7.72	23.9	0.268	3.28	0.72	0.671	0.92	5.99	0.073	0.062	108
DP14694	7	1	0.76	44.16	0.35	2.20	7.80	24.1	0.247	3.13	0.64	0.654	1.00	6.02	0.075	0.046	116
DP14695	7	1	0.86	44.26	0.33	2.24	7.81	23.9	0.238	3.02	0.64	0.628	1.08	6.11	0.075	0.058	123
DP14696	7	1	0.96	44.36	0.28	2.26	7.73	23.7	0.249	3.00	0.66	0.601	1.07	5.89	0.074	0.062	127
DP14697	7	1	1.06	44.46	0.32	2.31	7.87	24.1	0.265	3.01	0.67	0.626	1.04	5.99	0.073	0.059	121
DP14698	7	1	1.16	44.56	0.32	2.33	7.83	24.1	0.285	3.02	0.73	0.649	1.06	6.12	0.074	0.067	116
DP14699	7	1	1.26	44.66	0.28	2.32	7.84	24.1	0.287	3.00	0.73	0.615	1.13	6.06	0.074	0.056	117
DP14700	7	1	1.36	44.76	0.29	2.27	7.63	23.6	0.316	2.97	0.80	0.618	1.09	6.11	0.075	0.059	118
DP14701	7	1	1.46	44.86	0.32	2.21	7.70	23.8	0.270	3.13	0.72	0.624	1.03	6.11	0.074	0.062	117
DP14702	7	2	0.05		0.32	2.20	7.74	23.7	0.299	3.02	0.77	0.600	1.06	6.10	0.075	0.060	
DP14703	7	2	0.26		0.31	2.25	7.75	23.5	0.283	2.92	0.75	0.589	1.07	6.06	0.071	0.057	
DP14704	7	2	0.36		0.33	2.20	7.82	23.6	0.304	2.90	0.77	0.603	1.04	6.23	0.074	0.056	
DP14705	7	2	0.56	46.46	0.37	2.17	7.78	23.6	0.287	2.99	0.74	0.646	1.08	6.57	0.076	0.056	115
DP14706	7	2	0.66	46.56	0.41	2.13	7.66	23.3	0.264	2.98	0.72	0.672	1.00	6.70	0.074	0.063	116
DP14707	7	2	0.76	46.66	0.38	2.13	7.72	23.0	0.336	2.76	0.83	0.692	1.01	6.95	0.073	0.060	123
DP14708	7	2	0.86	46.76	0.38	2.18	7.85	23.3	0.386	2.81	0.97	0.708	1.11	6.78	0.073	0.068	121
DP14709	7	2	0.96	46.86	0.35	2.22	7.66	23.5	0.348	2.96	0.91	0.653	1.16	6.41	0.072	0.063	119
DP14710	7	2	1.08	46.98	0.41	2.07	7.80	23.2	0.383	2.83	0.88	0.709	1.13	6.89	0.074	0.045	126
DP14711	7	2	1.16	47.06	0.33	2.17	7.68	22.9	0.429	2.73	1.01	0.652	1.17	6.65	0.074	0.077	128
DP14712	7	2	1.26	47.16	0.34	2.26	7.74	23.5	0.442	2.83	1.04	0.641	1.26	6.53	0.074	0.076	125
DP14713	7	2	1.36	47.26	0.30	2.31	7.43	23.4	0.509	2.96	1.19	0.622	1.39	6.46	0.077	0.069	130
DP14714	7	2	1.46	47.36	0.31	2.30	7.35	23.2	0.500	3.05	1.24	0.614	1.56	6.03	0.082	0.074	121
DP14715	7	3	0.05	47.45	0.27	2.31	7.30	23.2	0.531	3.09	1.31	0.627	1.43	6.00	0.080	0.073	125
DP14716	7	3	0.14	47.54	0.27	2.31	7.36	23.5	0.446	3.18	1.17	0.649	1.34	6.10	0.078	0.067	126
DP14717	7	3	0.26	47.66	0.28	2.24	7.32	23.1	0.518	3.04	1.28	0.573	1.32	5.93	0.080	0.056	119
DP14718	7	3	0.36	47.76	0.28	2.23	7.39	23.2	0.546	3.07	1.38	0.600	1.35	5.93	0.077	0.074	118
DP14719	7	3	0.46	47.86	0.31	2.23	7.37	23.3	0.591	3.09	1.52	0.601	1.30	5.94	0.078	0.081	119
DP14720	7	3	0.56	47.96	0.29	2.25	7.30	23.3	0.561	3.12	1.43	0.607	1.45	5.97	0.077	0.074	126
DP14721	7	3	0.66	48.06	0.32	2.19	7.06	22.9	0.699	3.18	1.85	0.572	1.35	5.99	0.075	0.085	126
DP14722	7	3	0.76	48.16	0.28	2.19	7.17	23.0	0.620	3.12	1.62	0.541	1.42	5.73	0.079	0.086	128
DP14723	7	3	0.86	48.26	0.31	2.17	7.15	22.8	0.659	3.05	1.69	0.569	1.34	5.92	0.076	0.088	127
DP14724	7	3	0.96	48.36	0.35	2.15	7.16	22.7	0.645	3.04	1.68	0.578	1.25	5.91	0.076	0.084	124
DP14725	7	3	1.06	48.46	0.37	2.10	7.14	22.6	0.720	3.02	1.77	0.605	1.17	6.03	0.074	0.086	126
DP14726	7	3	1.16	48.56	0.35	2.11	7.37	23.1	0.662	3.08	1.66	0.567	1.27	6.04	0.077	0.089	125
DP14727	7	3	1.26	48.66	0.39	2.12	7.42	22.9	0.695	3.03	1.73	0.538	1.30	6.02	0.077	0.090	123
DP14728	7	3	1.36	48.76	0.38	2.09	7.41	22.9	0.642	3.04	1.64	0.546	1.27	5.96	0.078	0.089	123
DP14729	7	3	1.46	48.86	0.39	2.08	7.40	22.9	0.705	3.05	1.70	0.555	1.17	6.00	0.074	0.096	121
DP14730	7	4	0.06	48.96	0.47	2.12	7.48	23.2	0.847	3.15	2.08	0.529	1.21	5.89	0.074	0.120	117
DP14731	7	4	0.16	49.06	0.40	2.07	7.24	22.8	0.809	3.12	2.03	0.473	1.22	5.56	0.075	0.110	115
DP14732	7	4	0.26	49.16	0.41	2.05	7.11	22.5	0.789	3.07	2.03	0.474	1.26	5.53	0.075	0.091	121
DP14733	7	4	0.36	49.26	0.38	2.11	7.20	22.8	0.796	3.10	2.10	0.478	1.34	5.60	0.076	0.091	125
DP14734	7	4	0.46	49.36	0.37	2.11	7.14	22.8	0.836	3.20	2.18	0.463	1.33	5.44	0.074	0.092	127
DP14735	7	4	0.56	49.46	0.31	2.10	7.10	22.8	0.840	3.25	2.18	0.445	1.35	5.34	0.072	0.097	128

Table 2. (Continued).

Lab ID	Core	Section	Depth in Section (m)	Depth in hole (m)	Na	Mg	Al	Si	P	K	Ca	Ti	Mn	Fe	Ba	S	H_2O
DP14736	7	4	0.66	49.56	0.35	2.14	6.96	22.6	0.886	3.25	2.25	0.433	1.40	5.42	0.078	0.105	125
DP14737	7	4	0.76	49.66	0.39	2.16	6.84	22.9	0.744	3.37	2.04	0.468	1.35	5.78	0.076	0.075	125
DP14738	7	4	0.86	49.76	0.36	2.26	6.86	23.1	0.858	3.43	2.25	0.495	1.37	5.97	0.076	0.098	122
DP14739	7	4	0.96	49.86	0.34	2.18	7.05	22.8	0.845	3.27	2.16	0.415	1.51	5.29	0.074	0.107	130
DP14740	7	4	1.06	49.96	0.34	2.16	7.07	22.9	0.832	3.29	2.15	0.406	1.55	5.19	0.078	0.096	125
DP14741	7	4	1.16	50.06	0.33	2.16	7.05	22.7	0.853	3.25	2.10	0.414	1.54	5.21	0.078	0.104	128
DP14742	7	4	1.26	50.16	0.40	2.16	7.10	22.9	0.779	3.26	2.03	0.415	1.54	5.25	0.077	0.081	129
DP14743	7	4	1.36	50.26	0.35	2.10	6.86	22.5	0.810	3.36	2.07	0.437	1.36	5.46	0.073	0.102	128
DP14744	7	4	1.46	50.36	0.35	2.12	6.89	22.9	0.686	3.50	1.85	0.472	1.33	5.75	0.074	0.084	131
DP14745	7	5	0.06	50.46	0.31	2.11	7.12	22.7	0.835	3.35	2.16	0.379	1.51	4.94	0.072	0.100	131
DP14746	7	5	0.16	50.56	0.34	2.14	7.18	22.6	0.905	3.27	2.23	0.388	1.51	4.97	0.073	0.112	125
DP14747	7	5	0.26	50.66	0.33	2.14	7.27	23.0	0.734	3.30	1.95	0.393	1.38	4.95	0.076	0.090	118
DP14748	7	5	0.36	50.76	0.33	2.15	7.26	22.9	0.803	3.31	2.02	0.403	1.34	5.08	0.075	0.102	116
DP14749	7	5	0.46	50.86	0.33	2.11	7.24	22.9	0.760	3.29	1.97	0.398	1.35	5.08	0.076	0.095	119
DP14750	7	5	0.56	50.96	0.33	2.13	7.30	23.0	0.809	3.30	2.11	0.398	1.41	5.08	0.076	0.096	117
DP14751	7	5	0.66	51.06	0.34	2.14	7.32	23.2	0.790	3.34	2.12	0.405	1.44	5.10	0.077	0.095	118
DP14752	7	5	0.76	51.16	0.33	2.12	7.24	22.9	0.916	3.32	2.30	0.399	1.46	5.15	0.076	0.105	120
DP14753	7	5	0.86	51.26	0.34	2.10	7.12	22.5	1.028	3.25	2.63	0.386	1.39	5.02	0.075	0.112	116
DP14754	7	5	0.96	51.36	0.35	2.09	7.14	22.6	1.023	3.30	2.56	0.392	1.39	5.10	0.076	0.114	116
DP14755	7	5	1.06	51.46	0.36	2.06	7.15	22.7	0.962	3.35	2.48	0.388	1.38	5.05	0.074	0.111	118
DP14756	7	5	1.16	51.56	0.38	2.06	7.14	22.7	0.979	3.39	2.50	0.380	1.46	4.97	0.074	0.122	119
DP14757	7	5	1.26	51.66	0.38	1.98	6.92	21.8	1.138	3.31	2.86	0.362	1.42	4.82	0.074	0.126	116
DP14758	7	5	1.36	51.76	0.36	2.07	7.26	22.9	0.864	3.38	2.23	0.378	1.42	5.09	0.077	0.101	118
DP14759	7	5	1.46	51.86	0.38	2.07	7.15	22.4	0.931	3.34	2.37	0.371	1.34	5.05	0.077	0.114	117
DP14760	7	6	0.06	51.96	0.37	2.09	7.10	22.4	0.949	3.23	2.32	0.391	1.27	5.20	0.074	0.112	115
DP14761	7	6	0.16	52.06	0.35	2.16	7.17	22.8	0.786	3.20	2.04	0.415	1.28	5.38	0.077	0.096	111
DP14762	7	6	0.26	52.16	0.34	2.17	7.22	23.0	0.672	3.23	1.78	0.428	1.30	5.48	0.080	0.098	112
DP14763	7	6	0.36	52.26	0.34	2.19	7.31	23.3	0.666	3.27	1.79	0.428	1.38	5.57	0.078	0.089	116
DP14764	7	6	0.46	52.36	0.34	2.19	7.32	23.2	0.756	3.28	1.99	0.410	1.37	5.34	0.079	0.092	112
DP14765	7	6	0.56	52.46	0.34	2.15	7.22	22.9	0.802	3.26	2.08	0.393	1.32	5.25	0.076	0.097	114
DP14766	7	6	0.66	52.56	0.35	2.17	7.19	22.9	0.838	3.29	2.12	0.390	1.28	5.17	0.075	0.107	110
DP14767	7	6	0.76	52.66	0.38	2.16	7.17	22.8	0.898	3.27	2.20	0.389	1.28	5.21	0.075	0.115	111
DP14768	7	6	0.86	52.76	0.35	2.17	7.22	22.9	0.731	3.27	1.95	0.390	1.31	5.27	0.078	0.091	112
DP14769	7	6	0.96	52.86	0.35	2.19	7.23	22.9	0.734	3.24	1.84	0.393	1.29	5.33	0.076	0.098	111
DP14770	7	6	1.06	52.96	0.33	2.22	7.39	23.4	0.656	3.33	1.74	0.403	1.35	5.38	0.078	0.094	112
DP14771	7	6	1.16	53.06	0.36	2.18	7.27	23.1	0.612	3.29	1.62	0.390	1.24	5.34	0.073	0.087	110
DP14772	7	6	1.26	53.16	0.35	2.18	7.45	23.6	0.520	3.37	1.37	0.403	1.21	5.48	0.075	0.076	109
DP14773	7	6	1.36	53.26	0.38	2.16	7.49	23.5	0.617	3.34	1.55	0.389	1.21	5.30	0.074	0.085	114
DP14774	7	6	1.46	53.36	0.35	2.14	7.39	23.4	0.558	3.33	1.44	0.398	1.26	5.30	0.077	0.085	111
DP14775	7	7	0.06	53.46	0.36	2.17	7.48	23.7	0.345	3.42	1.00	0.401	1.27	5.36	0.074	0.071	109
DP14776	7	7	0.16	53.56	0.36	2.17	7.60	24.1	0.349	3.46	0.98	0.402	1.31	5.28	0.073	0.062	110
DP14777	7	7	0.26	53.66	0.36	2.17	7.49	23.7	0.362	3.43	1.00	0.394	1.35	5.21	0.076	0.072	109
DP14778	7	7	0.36	53.76	0.37	2.18	7.51	23.8	0.337	3.46	0.96	0.395	1.36	5.18	0.074	0.075	110
DP14779	7	7	0.46	53.86	0.35	2.20	7.58	24.2	0.345	3.52	0.99	0.408	1.46	5.29	0.078	0.068	113
DP14780	8	1	0.26	54.36	0.34	2.18	7.38	23.5	0.385	3.43	1.06	0.390	1.42	5.19	0.077	0.076	119
DP14781	8	1	0.36	54.46	0.35	2.19	7.36	23.5	0.451	3.47	1.20	0.389	1.35	5.19	0.076	0.081	120
DP14782	8	1	0.46	54.56	0.32	2.20	7.19	23.3	0.471	3.46	1.31	0.403	1.71	5.43	0.082	0.084	128
DP14783	8	1	0.56	54.66	0.32	2.12	7.17	23.3	0.594	3.53	1.60	0.397	1.71	5.09	0.080	0.086	123
DP14784	8	1	0.66	54.76	0.34	2.08	6.97	22.6	0.768	3.48	1.93	0.389	1.81	4.99	0.077	0.105	124
DP14785	8	1	0.76	54.86	0.35	2.09	7.08	23.1	0.653	3.49	1.81	0.397	1.95	5.11	0.083	0.084	124
DP14786	8	1	0.86	54.96	0.33	2.22	6.85	23.0	0.453	3.42	1.25	0.429	2.08	6.08	0.089	0.081	128
DP14787	8	1	0.96	55.06	0.33	2.16	6.76	22.5	0.686	3.45	1.86	0.430	2.23	5.53	0.090	0.098	121
DP14788	8	1	1.06	55.16	0.32	2.30	6.68	22.8	0.533	3.32	1.41	0.419	2.11	6.03	0.090	0.081	128
DP14789	8	1	1.16	55.26	0.35	2.26	6.38	22.4	0.523	3.32	2.46	0.386	1.72	6.13	0.089	0.079	115
DP14790	8	1	1.26	55.36	0.32	2.21	6.82	22.7	0.640	3.49	1.74	0.423	2.10	5.67	0.089	0.088	123
DP14791	8	1	1.36	55.46	0.26	1.17	3.09	9.9	0.176	1.56	23.92	0.220	1.01	3.32	0.067	0.038	58
DP14792	8	1	1.46	55.56	0.33	2.22	6.78	22.7	0.721	3.42	2.37	0.417	1.80	5.50	0.081	0.081	116
DP14793	8	2	0.05	55.65	0.32	2.28	6.56	22.7	0.508	3.32	2.06	0.394	1.62	5.87	0.079	0.063	118
DP14794	8	2	0.22	55.82	0.27	1.92	5.87	19.5	0.460	3.09	6.71	0.376	1.63	5.28	0.077	0.068	109
DP14795	8	2	0.32	55.92	0.32	2.32	6.54	22.5	0.394	3.21	1.11	0.358	1.85	6.88	0.084	0.065	133
DP14796	8	2	0.67	56.27	0.26	2.17	6.67	22.6	0.446	3.35	2.42	0.386	1.58	5.53	0.080	0.071	121
DP14797	8	2	0.78	56.38	0.29	2.14	6.29	21.2	0.348	3.11	3.60	0.353	1.75	6.42	0.083	0.058	122
DP14798	8	2	1.06	56.66	0.29	2.18	6.86	23.0	0.419	3.37	1.64	0.371	1.54	5.62	0.078	0.075	123

Table 2. (Continued).

Lab ID	Core	Section	Depth in Section (m)	Depth in hole (m)	Na	Mg	Al	Si	P	K	Ca	Ti	Mn	Fe	Ba	S	H_2O
DP14799	8	2	1.16	56.76	0.29	2.24	7.11	23.8	0.359	3.42	0.96	0.390	1.52	5.71	0.081	0.064	122
DP14800	8	2	1.26	56.86	0.27	2.20	6.95	23.3	0.339	3.34	1.60	0.390	1.40	5.90	0.079	0.068	118
DP14801	8	2	1.36	56.96	0.29	2.23	6.93	23.5	0.383	3.33	0.97	0.376	1.43	5.94	0.082	0.059	120
DP14802	8	2	1.46	57.06	0.30	2.23	6.31	21.9	0.373	3.03	3.29	0.356	1.51	6.83	0.089	0.063	120
DP14803	8	3	0.04	57.14	0.34	2.45	6.38	23.0	0.491	3.02	1.38	0.355	1.53	7.42	0.101	0.067	130
DP14804	8	3	0.66	57.76	0.32	2.40	6.71	22.7	0.285	3.08	0.84	0.356	1.76	8.19	0.090	0.064	126
DP14805	8	3	0.92	58.02	0.28	2.33	7.00	24.1	0.296	3.40	0.80	0.394	1.21	5.95	0.076	0.062	117
DP14806	8	3	1.01	58.11	0.27	2.40	6.48	22.9	0.339	3.10	0.96	0.351	1.61	7.81	0.091	0.068	133
DP14807	8	3	1.47	58.57	0.30	2.31	7.02	24.2	0.380	3.38	1.01	0.416	1.14	5.77	0.074	0.070	116
DP14808	8	4	0.03	58.63	0.27	2.32	6.91	23.7	0.393	3.32	1.08	0.392	1.40	5.98	0.083	0.066	112
DP14809	8	4	0.13	58.73	0.31	2.35	6.89	23.6	0.558	3.36	1.43	0.391	0.97	6.23	0.073	0.071	108
DP14810	8	4	0.23	58.83	0.28	2.46	6.28	23.0	0.430	3.13	1.96	0.358	1.41	6.50	0.088	0.062	124
DP14811	8	5	0.74	60.84	0.08	0.42	0.58	2.1	0.031	0.26	35.69	0.057	0.20	0.78	0.054	0.016	53
DP14812	8	5	0.84	60.94	0.10	0.42	0.58	2.1	0.030	0.26	35.87	0.057	0.20	0.78	0.053	0.015	54
DP14813	8	5	0.95	61.05	0.06	0.42	0.57	2.1	0.029	0.27	35.65	0.057	0.20	0.80	0.055	0.016	53
DP14814	8	6	0.77	62.37	0.30	2.38	6.92	24.0	0.431	3.34	1.09	0.382	1.52	5.86	0.159	0.055	113
DP14815	8	6	0.90	62.50	0.26	2.46	6.84	24.4	0.295	3.35	0.80	0.389	1.21	5.36	0.102	0.042	118
DP14816	8	7	0.39	63.49	0.20	2.53	6.99	24.7	0.339	3.46	0.81	0.394	1.16	5.09	0.083	0.044	121
DP14817	8	C	0.06	63.59	0.22	2.56	6.86	24.7	0.286	3.38	0.76	0.377	1.22	5.19	0.084	0.043	124

Note: Depth in hole omitted for disturbed samples.

Table 3. Elemental abundance (wt.%) and water content (% dry wt.) of Hole 576A samples.

Lab ID	Core	Section	Depth in Section (m)	Depth in hole (m)	Na	Mg	Al	Si	P	K	Ca	Ti	Mn	Fe	Ba	S	H_2O
DP19732	1	1	0.24	1.44	0.32	1.75	7.10	26.8	0.053	2.49	0.31	0.394	0.18	4.56	0.086	0.046	149
DP19733	1	1	0.24	1.44	0.44	1.78	7.40	26.5	0.052	2.43	0.64	0.411	0.51	4.92	0.096	0.043	149
DP19734	1	1	0.27	1.47	0.50	1.78	7.40	26.4	0.052	2.40	0.70	0.412	0.48	4.98	0.092	0.039	
DP19735	1	1	0.33	1.53	0.50	1.80	7.54	26.2	0.056	2.53	0.46	0.413	0.56	4.83	0.099	0.033	
DP19736	1	1	0.45	1.65	0.58	1.80	7.53	26.2	0.054	2.59	0.44	0.417	0.55	4.82	0.095	0.037	
DP19737	1	1	0.49	1.69	0.53	1.83	7.53	26.2	0.054	2.61	0.44	0.421	0.45	4.82	0.094	0.046	120
DP19738	1	1	0.55	1.75	0.51	1.86	7.60	26.2	0.051	2.67	0.41	0.429	0.20	4.88	0.091	0.041	
DP19739	1	1	0.65	1.85	0.47	1.84	7.56	26.0	0.052	2.61	0.45	0.427	0.32	4.85	0.087	0.043	
DP19740	1	1	0.74	1.94	0.46	1.86	7.52	26.0	0.054	2.57	0.49	0.416	0.51	4.80	0.096	0.060	145
DP19741	1	1	0.89	2.09	0.75	1.99	7.85	24.6	0.124	2.77	0.48	0.461	1.13	5.33	0.074	0.036	140
DP19742	1	2	0.14	2.84	0.30	1.76	7.14	26.9	0.049	2.54	0.24	0.393	0.09	4.54	0.098	0.012	201
DP19743	1	2	0.20	2.90	0.38	1.74	7.31	27.1	0.050	2.52	0.33	0.403	0.11	4.67	0.098	0.014	
DP19744	1	2	0.30	3.00	0.30	1.68	7.03	26.8	0.049	2.42	0.27	0.380	0.11	4.42	0.097	0.022	
DP19745	1	2	0.39	3.09	0.26	1.65	7.11	27.1	0.053	2.38	0.27	0.378	0.22	4.43	0.099	0.014	232
DP19746	1	2	0.48	3.18	0.31	1.65	6.96	26.5	0.052	2.42	0.34	0.379	0.26	4.46	0.091	0.032	
DP19747	1	2	0.58	3.28	0.45	1.75	7.28	26.2	0.054	2.54	0.42	0.398	0.34	4.64	0.088	0.041	
DP19748	1	2	0.64	3.34	0.53	1.77	7.38	26.3	0.055	2.59	0.43	0.412	0.42	4.73	0.089	0.037	138
DP19749	1	2	0.67	3.37	0.47	1.75	7.41	26.4	0.054	2.56	0.39	0.405	0.44	4.70	0.093	0.025	
DP19750	1	2	0.75	3.45	0.50	1.79	7.39	26.2	0.054	2.61	0.42	0.411	0.37	4.76	0.087	0.037	
DP19751	1	2	0.85	3.55	0.42	1.82	7.54	26.4	0.054	2.61	0.41	0.410	0.35	4.72	0.091	0.035	
DP19752	1	2	0.94	3.64	0.43	1.75	7.46	26.3	0.058	2.56	0.48	0.399	0.51	4.57	0.088	0.030	143
DP19753	1	2	1.09	3.79	0.48	1.82	7.51	26.1	0.057	2.58	0.48	0.403	0.39	4.72	0.088	0.041	134
DP19754	1	2	1.34	4.04	0.43	1.91	7.58	26.2	0.054	2.67	0.42	0.418	0.27	4.86	0.088	0.056	134
DP19755	1	3	0.34	4.54	0.46	1.84	7.56	26.2	0.055	2.60	0.44	0.411	0.33	4.72	0.090	0.044	134
DP19756	1	3	0.84	5.04	0.46	1.92	7.60	26.0	0.050	2.66	0.37	0.419	0.44	4.81	0.086	0.035	129
DP19757	1	3	1.03	5.23	0.41	1.88	7.52	26.0	0.050	2.57	0.37	0.409	0.42	4.66	0.087	0.038	
DP19758	1	4	0.17	5.87	0.39	1.98	7.63	26.1	0.052	2.67	0.38	0.418	0.33	4.81	0.094	0.052	
DP19759	1	4	0.23	5.93	0.51	1.95	7.70	26.0	0.053	2.66	0.34	0.421	0.33	4.87	0.090	0.027	
DP19760	1	4	0.35	6.05	0.51	1.87	7.52	26.3	0.054	2.55	0.36	0.408	0.44	4.65	0.089	0.024	
DP19761	1	4	0.44	6.14	0.44	1.91	7.58	26.2	0.054	2.59	0.39	0.411	0.41	4.75	0.090	0.033	143
DP19762	1	4	0.74	6.44	0.39	1.91	7.57	26.1	0.054	2.58	0.36	0.416	0.41	4.75	0.092	0.029	155
DP19763	1	5	0.05	7.25	0.46	1.95	7.60	26.4	0.052	2.59	0.30	0.412	0.40	4.69	0.097	0.025	
DP19764	1	5	0.15	7.35	0.46	1.96	7.57	26.1	0.052	2.61	0.36	0.409	0.32	4.78	0.098	0.035	
DP19765	1	5	0.24	7.44	0.29	1.83	7.31	26.5	0.052	2.49	0.33	0.395	0.46	4.58	0.099	0.025	182
DP19766	1	5	0.49	7.69	0.44	1.90	7.44	26.2	0.050	2.57	0.44	0.408	0.43	4.70	0.084	0.044	135
DP19767	1	5	0.53	7.73	0.50	1.89	7.44	26.2	0.051	2.57	0.45	0.406	0.40	4.68	0.084	0.039	
DP19768	1	5	0.74	7.94	0.55	1.59	6.86	26.5	0.044	2.56	0.49	0.337	0.35	3.71	0.082	0.037	113
DP19769	1	5	0.99	8.19	0.44	1.97	7.54	26.0	0.049	2.63	0.36	0.409	0.35	4.77	0.090	0.042	148
DP19770	1	5	1.05	8.25	0.61	1.94	7.56	26.2	0.047	2.64	0.35	0.413	0.24	4.73	0.085	0.027	
DP19771	1	5	1.15	8.35	0.52	1.91	7.58	26.4	0.048	2.56	0.26	0.416	0.28	4.73	0.092	0.018	
DP19772	1	5	1.24	8.44	0.41	1.97	7.56	26.3	0.049	2.61	0.33	0.415	0.41	4.76	0.092	0.037	157
DP18564	1	5	1.27	8.47	0.34	1.99	7.61	26.3	0.048	2.67	0.30	0.416	0.25	4.82	0.090	0.020	
DP19773	1	6	0.33	9.03	0.36	1.93	7.52	26.1	0.055	2.55	0.34	0.410	0.47	4.67	0.090	0.031	
DP19774	1	6	0.35	9.05	0.53	1.91	7.51	26.1	0.054	2.59	0.35	0.410	0.45	4.69	0.092	0.036	
DP19775	1	6	0.45	9.15	0.49	1.91	7.49	26.2	0.054	2.57	0.34	0.414	0.45	4.71	0.095	0.031	
DP19776	1	6	0.54	9.24	0.30	1.85	7.27	26.2	0.052	2.49	0.30	0.399	0.51	4.53	0.089	0.023	192
DP19777	1	6	0.60	9.30	0.44	1.86	7.31	26.2	0.054	2.54	0.35	0.392	0.51	4.52	0.088	0.028	
DP19778	1	6	0.70	9.40	0.60	1.90	7.52	26.4	0.051	2.57	0.31	0.406	0.45	4.67	0.097	0.030	
DP19779	1	6	0.79	9.49	0.43	1.91	7.47	26.4	0.053	2.61	0.38	0.410	0.46	4.65	0.094	0.039	147
DP10802	1	C		9.80	0.54	1.90	7.36	26.3	0.055	2.65	0.44	0.403	0.38	4.64	0.095	0.038	
DP19780	2	1	0.55	10.85	0.32	1.96	7.55	26.5	0.055	2.58	0.32	0.405	0.37	4.56	0.102	0.035	
DP19781	2	1	0.65	10.95	0.52	1.93	7.54	26.6	0.054	2.57	0.30	0.399	0.39	4.55	0.100	0.023	
DP19782	2	1	0.74	11.04	0.40	1.95	7.53	26.5	0.056	2.53	0.31	0.397	0.45	4.56	0.097	0.020	179
DP19783	2	1	0.78	11.08	0.39	2.00	7.53	26.3	0.059	2.50	0.32	0.399	0.45	4.61	0.094	0.022	
DP19784	2	1	0.85	11.15	0.57	1.94	7.46	25.4	0.058	2.47	0.26	0.386	0.38	4.61	0.094	0.017	
DP19785	2	1	0.95	11.25	0.53	2.00	7.51	25.9	0.056	2.55	0.34	0.405	0.42	4.64	0.099	0.034	
DP19786	2	1	0.99	11.29	0.42	1.99	7.51	26.0	0.055	2.58	0.37	0.411	0.40	4.71	0.098	0.041	143
DP19787	2	1	1.24	11.54	0.32	1.98	7.54	26.0	0.054	2.48	0.35	0.408	0.47	4.66	0.095	0.033	171
DP19788	2	1	1.30	11.60	0.56	2.00	7.60	26.1	0.054	2.48	0.30	0.406	0.44	4.69	0.097	0.029	
DP19789	2	1	1.39	11.69	0.41	1.96	7.46	26.2	0.056	2.41	0.34	0.398	0.49	4.61	0.099	0.034	184
DP18565	2	2	0.05	11.85	0.37	1.98	7.50	26.1	0.055	2.48	0.37	0.409	0.43	4.72	0.095	0.011	
DP19790	2	2	0.58	12.38	0.67	1.97	7.65	26.2	0.062	2.42	0.28	0.402	0.49	4.71	0.091	0.010	
DP19791	2	2	0.69	12.49	0.36	2.01	7.58	26.1	0.059	2.50	0.34	0.410	0.48	4.69	0.092	0.028	167

Table 3. (Continued).

Lab ID	Core	Section	Depth in Section (m)	Depth in hole (m)	Na	Mg	Al	Si	P	K	Ca	Ti	Mn	Fe	Ba	S	H_2O
DP19792	2	2	0.73	12.53	0.34	1.97	7.53	25.9	0.059	2.50	0.33	0.406	0.44	4.66	0.090	0.023	
DP19793	2	2	0.89	12.69	0.50	2.01	7.60	26.1	0.058	2.40	0.31	0.398	0.52	4.65	0.090	0.016	183
DP19794	2	2	1.24	13.04	0.44	1.99	7.57	26.1	0.048	2.63	0.32	0.415	0.36	4.73	0.090	0.032	144
DP18566	2	2	1.42	13.22	0.31	2.05	7.57	26.1	0.047	2.57	0.29	0.421	0.42	4.76	0.093	0.025	
DP19795	2	3	0.28	13.58	0.41	2.02	7.55	25.8	0.048	2.70	0.34	0.421	0.40	4.84	0.097	0.046	
DP19796	2	3	0.36	13.66	0.52	2.00	7.66	26.0	0.048	2.74	0.31	0.420	0.33	4.84	0.094	0.038	
DP19797	2	3	0.46	13.76	0.48	1.99	7.58	25.9	0.053	2.55	0.25	0.404	0.39	4.65	0.096	0.018	
DP19798	2	3	0.49	13.79	0.50	2.05	7.61	26.4	0.056	2.47	0.26	0.409	0.40	4.58	0.092	0.022	166
DP18567	2	3	0.67	13.97	0.34	2.06	7.60	26.1	0.054	2.56	0.34	0.421	0.39	4.72	0.093	0.017	
DP19799	2	4	0.03	14.83	0.50	2.15	7.59	26.1	0.054	2.41	0.31	0.383	0.39	4.49	0.081	0.034	
DP19800	2	4	0.10	14.90	0.50	2.32	7.48	26.0	0.052	2.11	0.31	0.336	0.43	3.97	0.075	0.036	
DP19801	2	4	0.15	14.95	0.62	2.36	7.41	26.6	0.051	1.91	0.35	0.284	0.32	3.38	0.069	0.040	
DP19802	2	4	0.20	15.00	0.53	2.19	7.55	26.3	0.059	2.28	0.33	0.376	0.49	4.33	0.085	0.032	
DP19803	2	4	0.29	15.09	0.75	1.97	7.70	26.2	0.065	2.44	0.26	0.414	0.50	4.78	0.093	0.008	162
DP19804	2	5	0.10	16.40	0.59	2.07	7.73	26.1	0.052	2.57	0.35	0.418	0.46	4.79	0.095	0.042	
DP19805	2	5	0.20	16.50	0.68	2.00	7.64	25.9	0.058	2.51	0.37	0.419	0.49	4.83	0.094	0.031	
DP19806	2	5	0.29	16.59	0.43	1.96	7.57	25.8	0.062	2.48	0.40	0.417	0.53	4.79	0.094	0.034	157
DP18568	2	5	0.41	16.71	0.27	2.04	7.65	25.4	0.057	2.38	0.47	0.410	0.56	4.89	0.088	0.031	
DP19807	2	6	1.19	18.99	0.69	1.87	7.93	25.5	0.062	2.52	0.42	0.427	0.63	5.10	0.080	0.022	136
DP19808	2	6	1.23	19.03	0.53	1.89	7.87	25.4	0.057	2.51	0.45	0.420	0.61	5.06	0.081	0.034	
DP19809	2	6	1.49	19.29	0.46	1.93	7.82	25.5	0.062	2.59	0.39	0.419	0.65	4.98	0.088	0.039	134
DP19810	2	7	0.03	19.33	0.52	1.90	7.77	25.3	0.058	2.58	0.37	0.421	0.62	4.93	0.084	0.036	
DP10803	2	C		19.50	0.43	1.98	7.90	25.5	0.055	2.62	0.41	0.439	0.67	5.12	0.084	0.040	
DP19811	3	1	0.05	23.05	0.59	1.92	7.84	25.3	0.060	2.67	0.30	0.424	0.71	4.99	0.081	0.031	
DP19812	3	1	0.15	23.15	0.67	1.89	7.93	25.4	0.062	2.65	0.27	0.427	0.70	4.98	0.079	0.022	
DP19813	3	1	0.24	23.24	0.51	1.91	7.90	25.4	0.064	2.68	0.34	0.430	0.69	4.93	0.081	0.040	124
DP19814	3	1	0.49	23.49	0.49	1.90	7.94	25.5	0.069	2.66	0.33	0.429	0.65	4.92	0.080	0.034	131
DP19815	3	1	0.74	23.74	0.51	1.91	7.85	25.2	0.064	2.64	0.34	0.431	0.65	4.95	0.080	0.037	138
DP19816	3	1	0.78	23.78	0.64	1.85	7.90	25.2	0.069	2.59	0.30	0.422	0.73	4.95	0.079	0.028	
DP19817	3	1	0.83	23.83	0.68	1.90	7.94	25.4	0.064	2.62	0.32	0.437	0.68	5.07	0.078	0.027	
DP19818	3	1	0.93	23.93	0.68	1.88	7.91	25.2	0.059	2.54	0.40	0.431	0.64	5.17	0.075	0.027	
DP19819	3	1	0.99	23.99	0.75	1.86	7.94	25.3	0.061	2.55	0.33	0.433	0.63	5.10	0.077	0.019	124
DP19820	3	1	1.10	24.10	0.80	1.86	7.96	25.4	0.066	2.63	0.30	0.430	0.68	5.03	0.077	0.022	
DP19821	3	1	1.20	24.20	0.69	1.89	7.95	25.3	0.070	2.60	0.30	0.430	0.71	4.99	0.080	0.020	
DP19822	3	1	1.24	24.24	0.63	1.90	7.86	25.3	0.073	2.61	0.34	0.440	0.69	5.01	0.079	0.033	126
DP19823	3	2	0.91	25.41	0.55	1.94	7.80	25.3	0.069	2.78	0.33	0.435	0.62	4.99	0.077	0.038	108
DP19824	3	2	0.97	25.47	0.70	1.93	7.81	25.3	0.066	2.76	0.29	0.437	0.59	4.99	0.077	0.031	
DP19825	3	2	1.04	25.54	0.56	1.95	7.82	25.3	0.068	2.80	0.33	0.436	0.74	5.00	0.077	0.040	
DP19826	3	3	0.94	26.94	0.51	2.15	7.15	24.5	0.195	2.72	0.68	0.512	0.98	5.51	0.111	0.066	122
DP19827	3	3	1.04	27.04	0.52	2.13	7.20	24.6	0.188	2.72	0.65	0.515	0.97	5.53	0.116	0.057	
DP19828	3	3	1.14	27.14	0.60	2.14	7.26	24.8	0.197	2.72	0.63	0.516	0.99	5.57	0.113	0.047	
DP19829	3	3	1.19	27.19	0.51	2.11	7.20	24.6	0.190	2.72	0.66	0.514	0.98	5.53	0.114	0.060	120
DP19830	3	3	1.23	27.23	0.48	2.15	7.21	24.6	0.188	2.74	0.66	0.515	0.99	5.55	0.112	0.068	
DP19831	3	3	1.39	27.39	0.57	2.14	7.24	24.7	0.198	2.72	0.66	0.521	1.04	5.57	0.114	0.053	117
DP19832	3	4	0.04	27.54	0.58	2.09	7.22	24.7	0.229	2.71	0.73	0.523	1.00	5.55	0.115	0.050	
DP19833	3	4	0.12		0.60	1.93	7.85	25.2	0.063	2.94	0.33	0.433	0.49	4.98	0.072	0.038	
DP19834	3	4	0.14		0.61	1.92	7.86	25.2	0.065	2.94	0.36	0.434	0.50	4.97	0.074	0.053	96
DP18569	3	4	0.26		0.50	1.98	7.92	25.1	0.065	2.88	0.34	0.431	0.65	5.00	0.077	0.040	
DP19835	3	4	1.08		0.52	1.99	7.98	25.1	0.068	2.75	0.34	0.441	0.82	5.12	0.076	0.044	
DP19836	3	4	1.19		0.59	1.93	8.02	25.0	0.073	2.72	0.33	0.444	0.77	5.18	0.079	0.033	108
DP19837	3	5	0.05		0.68	2.00	7.95	24.9	0.085	2.67	0.38	0.448	0.91	5.30	0.078	0.031	
DP19838	3	5	0.11		0.54	2.02	7.84	24.8	0.086	2.65	0.44	0.446	0.88	5.29	0.079	0.053	113
DP19839	3	5	1.24		0.56	1.98	7.68	24.4	0.091	2.66	0.39	0.438	0.93	5.19	0.074	0.036	
DP19840	3	5	1.29		0.58	2.01	7.78	24.8	0.098	2.68	0.40	0.438	0.95	5.22	0.076	0.040	113
DP19841	3	6	0.04		0.40	1.84	7.42	26.0	0.053	2.52	0.44	0.404	0.64	4.72	0.097	0.047	
DP19842	3	6	0.22		0.76	2.01	7.82	24.4	0.120	2.72	0.46	0.463	1.12	5.36	0.072	0.033	
DP19843	3	6	0.29		0.58	1.97	7.75	24.3	0.129	2.72	0.52	0.461	1.13	5.32	0.071	0.050	105
DP19844	3	6	0.88		0.65	1.95	7.85	24.4	0.139	2.74	0.53	0.454	1.24	5.35	0.073	0.042	
DP19845	3	6	1.09	29.69	0.65	2.00	7.82	24.8	0.096	2.73	0.39	0.453	0.93	5.32	0.082	0.028	106
DP19846	3	6	1.19	29.79	0.62	2.00	7.79	24.6	0.105	2.71	0.41	0.449	0.99	5.26	0.077	0.033	
DP19847	3	6	1.29	29.89	0.60	2.00	7.83	24.8	0.109	2.73	0.42	0.453	0.96	5.32	0.082	0.033	
DP19848	3	6	1.34	29.94	0.59	2.00	7.79	24.6	0.111	2.79	0.45	0.453	1.03	5.30	0.077	0.045	110
DP19849	3	6	1.49	30.09	0.49	2.01	7.81	24.6	0.112	2.79	0.49	0.459	1.10	5.29	0.074	0.044	114

Table 3. (Continued).

Lab ID	Core	Section	Depth in Section (m)	Depth in hole (m)	Na	Mg	Al	Si	P	K	Ca	Ti	Mn	Fe	Ba	S	H_2O
DP10804	3	C		30.50	0.89	1.86	7.84	24.2	0.120	2.80	0.56	0.455	1.28	5.31	0.074	0.020	
DP19850	4	1	0.24	29.14	0.58	2.01	7.87	24.8	0.097	2.69	0.39	0.447	1.00	5.27	0.075	0.033	127
DP19851	4	1	0.45	29.35	0.67	1.92	7.84	24.0	0.132	2.70	0.49	0.445	1.27	5.26	0.072	0.039	
DP19852	4	1	0.49	29.39	0.67	1.91	7.89	24.1	0.132	2.71	0.48	0.440	1.24	5.23	0.072	0.042	124
DP19853	4	1	0.65	29.55	1.01	1.86	8.05	24.3	0.129	2.76	0.43	0.444	1.30	5.30	0.075	0.026	
DP19854	4	1	0.74	29.64	0.67	1.90	7.95	24.2	0.137	2.74	0.50	0.445	1.30	5.27	0.073	0.037	127
DP19855	4	1	0.78	29.68	0.71	1.88	7.94	24.0	0.133	2.72	0.49	0.447	1.33	5.29	0.072	0.046	
DP19856	4	1	0.99	29.89	0.80	1.89	7.98	24.1	0.136	2.73	0.50	0.447	1.41	5.36	0.071	0.041	121
DP19857	4	1	1.39	30.29	0.65	1.94	8.01	24.4	0.123	2.72	0.43	0.454	1.32	5.36	0.071	0.042	129
DP18570	4	2	0.19	30.59	0.69	2.02	7.88	23.9	0.127	2.79	0.61	0.462	1.39	5.41	0.073	0.085	
DP19858	4	2	1.06	31.46	0.74	1.97	8.01	23.8	0.168	2.58	0.53	0.444	1.59	5.40	0.071	0.038	
DP19859	4	2	1.14	31.54	0.80	1.96	8.02	23.9	0.170	2.58	0.49	0.438	1.53	5.41	0.071	0.037	
DP19860	4	2	1.22	31.62	0.74	1.96	7.93	23.7	0.166	2.58	0.52	0.441	1.53	5.38	0.071	0.045	128
DP19861	4	3	0.52	32.42	0.72	1.93	7.86	23.6	0.199	2.57	0.67	0.433	1.71	5.34	0.071	0.051	138
DP19862	4	3	0.76	32.66	0.69	1.97	7.79	23.5	0.197	2.57	0.67	0.434	1.67	5.33	0.073	0.048	
DP19863	4	3	0.81	32.71	0.87	1.93	7.87	23.8	0.195	2.59	0.64	0.435	1.70	5.38	0.073	0.041	
DP19864	4	3	0.93	32.83	1.15	1.91	7.80	23.8	0.217	2.56	0.63	0.447	1.63	5.45	0.071	0.034	
DP19865	4	3	0.97	32.87	0.84	1.98	7.71	23.8	0.205	2.61	0.71	0.450	1.58	5.41	0.071	0.064	132
DP19866	4	3	1.12	33.02	0.95	1.91	7.80	23.6	0.195	2.61	0.63	0.442	1.68	5.46	0.071	0.049	134
DP19867	4	4	0.11	33.51	0.81	1.92	7.62	22.9	0.205	2.52	0.68	0.443	1.85	5.48	0.073	0.051	
DP19868	4	4	0.26	33.66	0.73	1.96	7.74	23.3	0.223	2.54	0.70	0.446	1.84	5.60	0.070	0.066	143
DP19869	4	4	0.67	34.07	0.77	1.99	7.48	23.0	0.362	2.58	1.05	0.463	2.24	5.50	0.077	0.057	
DP19870	4	4	0.76	34.16	0.65	1.95	7.85	23.9	0.164	2.76	0.54	0.439	1.48	5.14	0.072	0.062	120
DP19871	4	4	0.87	34.27	0.70	1.97	7.92	24.0	0.168	2.76	0.52	0.433	1.47	5.13	0.073	0.045	
DP19872	4	4	0.99	34.39	0.93	1.88	7.79	23.4	0.235	2.59	0.67	0.447	1.96	5.30	0.073	0.048	
DP19873	4	4	1.06	34.46	0.73	1.92	7.77	23.3	0.238	2.61	0.73	0.441	2.03	5.23	0.074	0.061	95
DP19874	4	4	1.35	34.75	1.01	1.92	7.68	23.1	0.347	2.51	0.90	0.453	2.09	5.42	0.076	0.065	
DP19875	4	5	0.07	34.97	0.84	1.95	7.90	23.8	0.187	2.65	0.59	0.454	1.79	5.36	0.073	0.046	
DP19876	4	5	0.26	35.16	0.60	2.04	7.37	22.8	0.388	2.57	1.12	0.450	2.16	5.49	0.075	0.072	
DP19877	4	5	0.37	35.27	0.69	1.99	7.31	22.6	0.518	2.58	1.40	0.440	2.09	5.42	0.076	0.079	
DP19878	4	5	0.47	35.37	0.61	1.98	7.28	22.4	0.566	2.57	1.52	0.440	2.04	5.38	0.076	0.085	134
DP19880	4	5	0.69	35.59	0.44	2.04	7.60	22.6	0.510	2.66	1.36	0.380	2.03	5.15	0.073	0.076	122
DP18571	4	5	0.73	35.63	0.57	2.11	7.68	22.8	0.488	2.90	1.41	0.392	1.66	5.05	0.074	0.114	
DP19881	4	6	0.21	36.61	0.58	1.95	7.82	23.2	0.312	2.84	0.79	0.382	1.66	4.88	0.071	0.059	
DP19882	4	6	0.34	36.74	0.55	2.01	7.90	23.4	0.318	2.84	0.82	0.388	1.77	4.95	0.072	0.071	116
DP19883	4	6	0.63	37.03	0.43	2.03	7.82	23.4	0.339	2.88	0.90	0.413	1.70	5.04	0.074	0.064	
DP19884	4	6	0.77	37.17	0.46	2.08	7.86	23.5	0.318	2.91	0.85	0.439	1.64	5.13	0.071	0.068	111
DP19885	4	6	1.03	37.43	0.52	2.05	7.92	23.4	0.322	2.73	0.84	0.502	1.56	5.28	0.073	0.067	110
DP19886	4	6	1.16	37.56	0.47	2.09	7.95	23.4	0.270	2.82	0.73	0.483	1.56	5.34	0.071	0.055	
DP10805	4	C		37.75	1.21	2.02	8.13	23.9	0.298	2.87	0.69	0.451	1.69	5.21	0.074	0.000	
DP19887	5	1	0.09	39.19	0.65	2.02	8.03	23.7	0.326	3.03	0.81	0.380	1.59	5.07	0.074	0.063	
DP19888	5	1	0.24	39.34	0.37	2.04	7.81	23.4	0.310	2.37	0.83	0.407	1.71	4.98	0.072	0.068	128
DP19889	5	1	0.75	39.85	0.46	2.13	7.85	23.2	0.274	2.78	0.71	0.477	1.53	5.30	0.072	0.058	
DP19890	5	1	0.89	39.99	0.39	2.07	7.92	23.3	0.278	2.80	0.73	0.479	1.53	5.29	0.073	0.060	
DP19891	5	1	0.95	40.05	0.47	2.09	7.97	23.5	0.285	2.80	0.74	0.488	1.54	5.31	0.072	0.065	
DP19892	5	1	1.14	40.24	0.42	2.05	7.89	23.3	0.335	2.69	0.87	0.505	1.55	5.29	0.072	0.068	120
DP19893	5	1	1.39	40.49	0.43	2.03	7.93	23.4	0.346	2.65	0.89	0.519	1.58	5.36	0.072	0.068	120
DP19894	5	2	0.24	40.84	0.44	1.98	7.85	23.1	0.360	2.59	0.93	0.522	1.60	5.40	0.072	0.070	120
DP19895	5	2	0.43	41.03	0.48	1.96	7.80	23.0	0.355	2.57	0.89	0.534	1.57	5.42	0.070	0.066	
DP19896	5	2	0.50	41.10	0.62	1.98	7.99	23.5	0.360	2.65	0.90	0.544	1.58	5.50	0.070	0.083	
DP19897	5	2	0.64	41.24	0.55	1.95	7.88	23.2	0.354	2.59	0.91	0.542	1.57	5.48	0.072	0.068	122
DP19898	5	2	1.04	41.64	0.47	1.95	7.85	23.3	0.365	2.64	0.95	0.551	1.50	5.52	0.070	0.074	119
DP19899	5	2	1.30	41.90	0.62	1.93	7.89	23.3	0.335	2.64	0.87	0.541	1.48	5.52	0.071	0.061	
DP19900	5	2	1.49	42.09	0.48	1.94	7.83	23.2	0.356	2.64	0.92	0.543	1.48	5.48	0.071	0.067	120
DP19901	5	3	0.88	42.98	0.45	2.08	7.63	23.7	0.257	3.19	0.71	0.588	1.19	5.71	0.076	0.051	
DP19902	5	5	0.03	45.13	0.58	2.09	7.79	24.0	0.226	3.31	0.60	0.657	0.92	6.00	0.074	0.041	
DP19903	5	5	0.09	45.19	0.51	2.08	7.64	23.7	0.241	3.26	0.66	0.661	0.94	5.95	0.074	0.047	94
DP18572	5	5	0.12	45.22	0.58	2.13	7.66	23.7	0.232	3.33	0.70	0.672	0.94	6.01	0.076	0.079	
DP19904	5	5	0.28	45.38	0.47	2.15	7.71	23.9	0.243	3.18	0.66	0.652	0.99	6.02	0.075	0.049	
DP19905	5	5	0.34	45.44	0.46	2.20	7.80	23.9	0.241	3.11	0.63	0.637	1.06	6.02	0.075	0.046	
DP19906	5	5	0.39	45.49	0.44	2.21	7.73	23.7	0.225	3.07	0.61	0.615	1.06	5.99	0.073	0.051	97
DP19907	5	5	1.39	46.49	0.43	2.24	7.69	23.4	0.292	2.99	0.75	0.571	1.11	6.02	0.074	0.056	99
DP19908	5	6	0.10	46.70	0.58	2.20	7.79	23.4	0.315	2.88	0.76	0.612	1.12	6.32	0.073	0.053	

Table 3. (Continued).

Lab ID	Core	Section	Depth in Section (m)	Depth in hole (m)	Na	Mg	Al	Si	P	K	Ca	Ti	Mn	Fe	Ba	S	H_2O
P19909	5	6	0.24	46.84	0.52	2.09	7.69	23.1	0.303	2.91	0.76	0.681	1.03	6.86	0.071	0.056	101
P19910	5	6	0.89	47.49	0.37	2.20	7.34	23.0	0.555	3.07	1.37	0.575	1.33	5.86	0.078	0.081	88
P19911	5	6	1.08	47.68	0.37	2.18	7.16	22.9	0.557	3.09	1.44	0.578	1.46	5.90	0.078	0.074	
P19912	5	6	1.29	47.89	0.37	2.14	7.13	22.8	0.639	3.12	1.63	0.530	1.44	5.72	0.080	0.079	114
P19913	5	6	1.39	47.99	0.54	2.13	7.14	22.7	0.641	3.07	1.57	0.585	1.33	6.01	0.075	0.086	
19914	5	6	1.49	48.09	0.44	2.12	7.18	22.7	0.711	3.08	1.70	0.590	1.29	6.01	0.076	0.092	111
19915	5	7	0.15	48.25	0.53	2.11	7.15	22.5	0.741	3.04	1.79	0.582	1.29	5.95	0.077	0.091	
19916	5	7	0.24	48.34	0.46	2.06	7.19	22.6	0.759	3.06	1.81	0.584	1.27	5.99	0.076	0.095	114
19917	5	7	0.28	48.38	0.42	2.08	7.19	22.6	0.756	3.05	1.82	0.564	1.29	5.96	0.075	0.095	
19918	5	7	0.49	48.59	0.47	2.07	7.24	22.7	0.696	3.06	1.70	0.555	1.29	5.95	0.076	0.092	109
10806	5	C		48.70	0.36	2.05	7.21	22.6	0.591	3.05	1.69	0.552	1.26	5.88	0.076	0.094	
19919	6	1	0.24	48.49	0.44	2.02	7.18	22.5	0.811	3.09	1.93	0.457	1.23	5.45	0.073	0.098	131
19920	6	1	0.68	48.93	0.66	2.09	7.18	22.7	0.781	3.11	1.94	0.479	1.31	5.68	0.074	0.088	
19921	6	1	0.72	48.97	0.50	2.05	7.06	22.3	0.871	3.08	2.05	0.495	1.26	5.71	0.072	0.109	
19922	6	1	0.89	49.14	0.37	2.08	7.08	22.5	0.890	3.13	2.13	0.469	1.34	5.57	0.074	0.106	122
P19923	6	1	1.00	49.25	0.47	2.07	7.07	22.5	0.913	3.20	2.19	0.447	1.35	5.38	0.072	0.103	
P19924	6	2	0.24	49.99	0.36	2.06	6.77	22.3	0.758	3.47	1.91	0.463	1.35	5.69	0.072	0.099	120
P19925	6	2	0.28	50.03	0.36	2.10	6.84	22.6	0.732	3.50	1.88	0.470	1.36	5.74	0.071	0.094	
P19926	6	2	0.35	50.10	0.59	2.08	7.11	22.4	0.886	3.32	2.10	0.378	1.54	4.93	0.072	0.102	
P19927	6	2	0.49	50.24	0.36	2.10	7.25	22.9	0.700	3.32	1.77	0.391	1.38	4.97	0.075	0.089	108
P19928	6	2	1.20	50.95	0.55	2.05	7.26	22.8	0.841	3.38	2.12	0.383	1.33	5.08	0.075	0.094	
P19929	6	2	1.39	51.14	0.42	2.09	7.17	22.6	0.870	3.28	2.18	0.390	1.35	5.17	0.076	0.104	104
P18573	6	2	1.42	51.17	0.45	2.17	7.24	22.9	0.753	3.34	2.18	0.392	1.32	5.19	0.077	0.122	
DP19930	6	3	0.18	51.43	0.40	2.08	7.13	22.5	0.825	3.23	2.07	0.396	1.32	5.27	0.074	0.100	
DP19931	6	3	0.24	51.49	0.44	2.10	7.19	22.7	0.804	3.25	2.04	0.396	1.32	5.30	0.079	0.095	
DP19932	6	3	0.37	51.62	0.44	2.11	7.13	22.6	0.766	3.19	1.93	0.414	1.30	5.44	0.078	0.088	104
DP19933	6	3	0.56	51.81	0.45	2.14	7.19	22.9	0.723	3.22	1.87	0.425	1.33	5.48	0.078	0.095	
DP19934	6	3	0.64	51.89	0.44	2.14	7.20	22.9	0.726	3.23	1.84	0.428	1.32	5.51	0.079	0.089	102
DP19935	6	3	1.00	52.25	0.41	2.12	7.12	22.6	0.840	3.26	2.15	0.387	1.30	5.18	0.076	0.106	
DP19936	6	3	1.16	52.41	0.37	2.15	7.23	22.9	0.782	3.32	1.97	0.390	1.31	5.18	0.075	0.097	106
DP19937	6	3	1.29	52.54	0.46	2.12	7.17	22.6	0.769	3.26	1.91	0.384	1.33	5.28	0.076	0.094	
DP19938	6	3	1.39	52.64	0.37	2.11	7.15	22.6	0.728	3.27	1.88	0.384	1.32	5.27	0.075	0.092	101
DP19939	6	4	0.04	52.79	0.47	2.15	7.24	22.8	0.714	3.25	1.76	0.398	1.29	5.34	0.075	0.085	
DP19940	6	4	0.13	52.88	0.39	2.19	7.38	23.2	0.647	3.28	1.65	0.402	1.32	5.40	0.077	0.086	103
DP19941	6	4	1.04	53.79	0.35	2.14	7.44	23.6	0.377	3.45	0.99	0.398	1.40	5.26	0.075	0.068	
DP19942	6	4	1.09	53.84	0.44	2.12	7.38	23.4	0.355	3.43	1.00	0.391	1.41	5.21	0.076	0.065	
DP19943	6	4	1.29	54.04	0.42	2.11	7.37	23.4	0.385	3.45	1.03	0.389	1.44	5.20	0.077	0.064	101
DP19944	6	5	0.03	54.28	0.40	2.12	7.42	23.4	0.344	3.45	0.96	0.393	1.32	5.32	0.076	0.068	
DP19945	6	5	0.14	54.39	0.43	2.14	7.34	23.2	0.437	3.47	1.15	0.386	1.36	5.22	0.075	0.080	102
DP18574	6	5	1.06	55.31	0.49	2.27	6.82	22.7	0.505	3.56	1.50	0.419	2.06	5.83	0.087	0.101	
DP19946	6	5	1.13	55.38	0.36	1.85	5.49	18.2	0.378	2.85	8.76	0.351	1.71	5.36	0.079	0.061	
DP19947	6	5	1.17	55.42	0.29	0.82	2.07	6.4	0.109	1.01	29.18	0.158	0.72	2.28	0.063	0.032	
DP19948	6	5	1.29	55.54	0.37	2.24	6.78	22.7	0.643	3.39	1.85	0.418	1.50	5.61	0.068	0.077	95
DP19949	6	6	0.10	55.85	0.25	0.43	0.76	2.5	0.035	0.33	34.99	0.067	0.30	1.10	0.055	0.018	
DP19950	6	6	0.19	55.94	0.25	0.43	0.76	2.5	0.038	0.33	35.33	0.066	0.30	1.11	0.057	0.016	45
DP19951	6	6	1.38	57.13	0.24	0.83	1.69	5.8	0.098	0.75	30.12	0.127	0.51	2.41	0.069	0.024	
DP19952	6	6	1.40	57.15	0.31	0.80	1.67	5.7	0.094	0.74	30.55	0.126	0.50	2.35	0.068	0.021	
DP19953	6	6	1.49	57.24	0.26	1.31	3.43	11.5	0.159	1.71	19.61	0.242	1.03	4.21	0.075	0.034	79
DP19954	6	7	0.24	57.49	0.31	2.29	6.74	23.1	0.381	3.23	1.01	0.365	1.55	6.79	0.085	0.061	110
DP19955	6	7	0.28	57.53	0.32	2.30	6.98	23.8	0.313	3.38	0.83	0.392	1.33	6.02	0.081	0.055	
DP19956	6	7	0.42	57.67	0.21	0.48	0.84	2.8	0.039	0.37	34.44	0.072	0.34	1.58	0.059	0.019	
DP19957	6	7	0.51	57.76	0.33	2.33	6.71	22.8	0.288	3.19	0.82	0.351	1.67	7.50	0.085	0.055	117
DP19958	7	1	0.24	58.19	0.21	0.95	2.19	7.1	0.096	1.01	26.60	0.162	0.76	3.46	0.070	0.034	87
DP19959	7	1	0.49	58.44	0.20	0.96	2.28	7.7	0.125	1.15	24.88	0.190	0.75	3.38	0.071	0.030	81
DP18575	7	1	0.90	58.85	0.00	0.43	0.59	2.1	0.034	0.25	36.48	0.058	0.20	0.79	0.055	0.033	
DP19960	7	1	1.13	59.08	0.20	0.40	0.56	2.0	0.030	0.25	35.84	0.057	0.20	0.76	0.059	0.016	
DP19961	7	1	1.33	59.28	0.19	0.39	0.54	2.0	0.030	0.24	35.90	0.056	0.19	0.75	0.057	0.017	
DP19962	7	1	1.39	59.34	0.21	0.39	0.54	2.0	0.031	0.24	36.11	0.056	0.20	0.75	0.059	0.014	50
DP19963	7	2	0.04	59.49	0.29	0.40	0.57	2.1	0.031	0.25	36.07	0.056	0.20	0.77	0.056	0.016	
DP19964	7	2	0.24	59.69	0.16	0.38	0.51	1.9	0.029	0.23	36.18	0.054	0.19	0.73	0.057	0.016	53
DP19965	7	2	1.35	60.80	0.27	0.38	0.53	2.0	0.029	0.23	35.94	0.054	0.19	0.73	0.057	0.015	
DP19966	7	2	1.49	60.94	0.17	0.38	0.52	1.9	0.029	0.23	36.04	0.055	0.19	0.74	0.057	0.017	47
DP19967	7	3	0.10	61.05	0.25	0.40	0.57	2.1	0.030	0.25	35.66	0.057	0.18	0.76	0.058	0.015	

Table 3. (Continued).

Lab ID	Core	Section	Depth in Section (m)	Depth in hole (m)	Na	Mg	Al	Si	P	K	Ca	Ti	Mn	Fe	Ba	S	H_2O
DP19968	7	3	0.19	61.14	0.19	0.39	0.56	2.1	0.030	0.25	35.57	0.057	0.18	0.75	0.057	0.017	49
DP19969	7	3	0.38	61.33	0.19	0.39	0.54	2.0	0.029	0.24	35.74	0.056	0.18	0.76	0.059	0.016	
DP19970	7	3	0.45	61.40	0.22	0.40	0.56	2.1	0.029	0.25	35.80	0.056	0.19	0.76	0.059	0.016	
DP19971	7	3	0.59	61.54	0.20	0.39	0.54	2.0	0.030	0.24	35.93	0.055	0.16	0.72	0.057	0.017	48
DP18576	7	3	1.32	62.27	0.25	0.54	0.87	3.7	0.144	0.42	33.49	0.096	0.10	1.11	0.071	0.033	
DP19972	7	4	0.43	62.88	0.21	0.63	1.23	4.2	0.066	0.60	31.76	0.114	0.48	1.71	0.061	0.023	
DP19973	7	4	0.45	62.90	0.27	0.50	0.86	2.9	0.033	0.39	34.28	0.072	0.31	1.04	0.056	0.019	
DP19974	7	4	0.54	62.99	0.21	0.42	0.64	2.2	0.027	0.29	35.50	0.056	0.23	0.75	0.056	0.016	50
DP19975	7	4	1.06	63.51	0.23	0.45	0.71	2.4	0.028	0.31	35.41	0.061	0.25	0.80	0.057	0.016	50
DP19976	7	5	0.44	64.39	0.59	2.43	6.53	24.0	0.389	3.36	1.10	0.353	1.52	5.31	0.098	0.046	
DP19977	7	5	0.64	64.59	0.21	0.35	0.47	1.7	0.024	0.21	36.13	0.048	0.17	0.53	0.055	0.016	49
DP18577	7	5	1.13	65.08	0.02	0.44	0.66	2.5	0.046	0.31	36.68	0.066	0.18	0.78	0.066	0.034	
DP19978	7	5	1.27	65.22	0.27	0.37	0.55	2.0	0.025	0.25	36.17	0.051	0.21	0.63	0.054	0.015	
DP19979	7	5	1.39	65.34	0.24	0.37	0.54	1.9	0.026	0.24	35.96	0.051	0.21	0.63	0.055	0.015	46
DP19980	7	6	0.18	65.63	0.15	0.40	0.58	2.1	0.027	0.27	35.97	0.055	0.22	0.67	0.071	0.023	
DP19981	7	6	0.21	65.66	0.30	0.38	0.57	2.0	0.028	0.25	35.75	0.053	0.21	0.65	0.074	0.018	
DP19982	7	6	0.29	65.74	0.26	0.40	0.64	2.3	0.027	0.29	35.30	0.059	0.23	0.72	0.072	0.018	47
DP19983	7	6	1.14	66.59	0.25	0.30	0.35	1.4	0.025	0.16	36.65	0.043	0.14	0.44	0.055	0.015	48
DP19984	7	6	1.18	66.63	0.21	0.32	0.40	1.5	0.025	0.18	36.50	0.046	0.15	0.49	0.056	0.018	
DP19985	7	6	1.39	66.84	0.21	0.32	0.40	1.5	0.025	0.18	36.69	0.046	0.15	0.49	0.056	0.017	44
DP19986	7	7	0.05	67.00	0.27	0.32	0.39	1.5	0.025	0.18	36.65	0.045	0.14	0.48	0.055	0.018	
DP19987	7	7	0.19	67.14	0.19	0.34	0.43	1.6	0.028	0.20	36.50	0.049	0.15	0.53	0.066	0.018	45
DP19988	7	7	0.55	67.50	0.57	2.60	6.44	24.3	0.291	3.15	0.83	0.364	1.21	5.40	0.086	0.045	
DP19989	7	7	0.69	67.64	0.27	1.00	2.12	7.8	0.102	1.08	25.76	0.177	0.66	2.73	0.068	0.031	48

Note: Depth in hole omitted for disturbed samples.

Table 4. Elemental abundance (wt.%) and water content (% dry wt.) of Hole 576B samples.

Lab ID	Core	Section	Depth in Section (m)	Depth in hole (m)	Na	Mg	Al	Si	P	K	Ca	Ti	Mn	Fe	Ba	S	H_2O
DP19212	1	1	0.06	0.06	0.37	1.75	7.20	26.8	0.049	2.51	0.40	0.407	0.24	4.66	0.095	0.031	169
DP19213	1	1	0.16	0.16	0.28	1.74	7.15	26.8	0.049	2.51	0.40	0.400	0.28	4.57	0.093	0.040	179
DP19214	1	1	0.26	0.26	0.28	1.76	7.18	27.2	0.048	2.51	0.43	0.405	0.33	4.65	0.099	0.047	177
DP19215	1	1	0.36	0.36	0.24	1.70	7.02	27.3	0.048	2.42	0.46	0.393	0.31	4.62	0.105	0.040	184
DP19216	1	1	0.46	0.46	0.42	1.77	7.29	26.5	0.053	2.40	0.66	0.410	0.45	4.87	0.094	0.039	149
DP19217	1	1	0.56	0.56	0.50	1.84	7.53	26.7	0.054	2.46	0.77	0.434	0.50	5.08	0.097	0.050	134
DP19218	1	1	0.66	0.66	0.48	1.87	7.57	26.4	0.054	2.61	0.47	0.425	0.65	4.85	0.098	0.042	132
DP19219	1	1	0.76	0.76	0.46	1.88	7.66	26.7	0.053	2.68	0.43	0.438	0.24	4.93	0.093	0.038	130
DP19220	1	1	0.86	0.86	0.43	1.90	7.64	26.4	0.051	2.67	0.41	0.425	0.28	4.87	0.089	0.037	137
DP19221	1	1	0.96	0.96	0.46	1.85	7.61	26.4	0.052	2.62	0.46	0.426	0.36	4.87	0.087	0.033	137
DP19222	1	1	1.06	1.06	0.43	1.85	7.62	26.3	0.055	2.56	0.48	0.421	0.47	4.87	0.098	0.032	150
DP19223	1	1	1.16	1.16	0.43	1.84	7.54	26.4	0.053	2.57	0.48	0.425	0.52	4.84	0.100	0.041	145
DP19224	1	1	1.26	1.26	0.39	1.82	7.46	26.2	0.054	2.54	0.44	0.407	0.58	4.75	0.106	0.043	146
DP19225	1	1	1.36	1.36	0.42	1.87	7.52	26.5	0.055	2.55	0.44	0.419	0.83	4.75	0.103	0.040	146
DP19226	1	1	1.46	1.46	0.44	1.84	7.41	26.4	0.055	2.55	0.47	0.413	0.49	4.74	0.096	0.048	136
DP19227	1	2	0.06	1.56	0.40	1.88	7.40	26.5	0.053	2.60	0.43	0.422	0.37	4.78	0.097	0.043	138
DP19228	1	2	0.16	1.66	0.38	1.85	7.34	26.9	0.052	2.56	0.45	0.414	0.27	4.77	0.095	0.035	155
DP19229	1	2	0.26	1.76	0.16	1.69	6.71	27.7	0.050	2.38	0.30	0.383	0.27	4.41	0.104	0.031	200
DP19230	1	2	0.36	1.86	0.16	1.67	6.70	27.8	0.050	2.35	0.25	0.374	0.51	4.31	0.105	0.012	219
DP19231	1	2	0.46	1.96	0.28	1.71	6.82	27.6	0.050	2.36	0.23	0.374	0.61	4.30	0.103	0.000	226
DP19232	1	2	0.56	2.06	0.27	1.70	6.74	27.3	0.050	2.37	0.25	0.371	0.47	4.27	0.099	0.010	217
DP19233	1	2	0.66	2.16	0.11	1.79	6.98	27.7	0.049	2.50	0.30	0.393	0.33	4.46	0.099	0.037	228
DP19234	1	2	0.76	2.26	0.13	1.75	6.82	27.5	0.049	2.45	0.36	0.386	0.28	4.47	0.093	0.035	214
DP19237	1	2	0.86	2.36	0.40	1.77	7.15	26.9	0.050	2.49	0.37	0.397	0.14	4.66	0.096	0.007	195
DP19238	1	2	0.96	2.46	0.18	1.76	6.86	27.3	0.047	2.37	0.43	0.385	0.14	4.56	0.097	0.021	225
DP19235	1	2	1.06	2.56	0.17	1.76	7.01	27.5	0.049	2.53	0.26	0.389	0.12	4.53	0.097	0.019	210
DP19236	1	2	1.16	2.66	0.29	1.77	7.05	26.9	0.048	2.53	0.33	0.391	0.13	4.52	0.100	0.030	201
DP19239	1	2	1.26	2.76	0.29	1.76	7.25	27.0	0.050	2.52	0.37	0.407	0.12	4.64	0.093	0.022	188
DP19240	1	2	1.36	2.86	0.32	1.75	7.23	26.8	0.050	2.51	0.34	0.396	0.18	4.59	0.102	0.025	181
DP19241	1	2	1.46	2.96	0.10	1.66	6.89	27.3	0.049	2.34	0.22	0.367	0.17	4.33	0.107	0.006	252
DP19242	1	3	0.06	3.06	0.00	1.62	6.69	27.3	0.051	2.28	0.22	0.358	0.20	4.19	0.101	0.019	274
DP19243	1	3	0.16	3.16	0.29	1.74	7.23	26.5	0.053	2.48	0.38	0.396	0.26	4.60	0.089	0.033	189
DP19244	1	3	0.26	3.26	0.30	1.75	7.26	26.6	0.053	2.50	0.35	0.401	0.23	4.61	0.093	0.020	185
DP19245	1	3	0.36	3.36	0.36	1.76	7.31	26.5	0.054	2.53	0.41	0.405	0.34	4.64	0.089	0.037	166
DP19246	1	3	0.47	3.47	0.35	1.78	7.32	26.7	0.055	2.55	0.43	0.406	0.42	4.66	0.091	0.044	165
DP19247	1	3	0.56	3.56	0.39	1.76	7.26	26.4	0.054	2.54	0.44	0.403	0.34	4.66	0.093	0.051	153
DP19248	1	3	0.66	3.66	0.43	1.78	7.31	26.2	0.054	2.56	0.42	0.402	0.45	4.65	0.091	0.042	150
DP19249	1	3	0.76	3.76	0.43	1.77	7.31	26.3	0.054	2.57	0.42	0.408	0.37	4.70	0.090	0.033	144
DP19250	1	3	0.86	3.86	0.38	1.81	7.33	25.9	0.053	2.58	0.40	0.404	0.33	4.72	0.084	0.030	152
DP19251	1	3	0.96	3.96	0.40	1.79	7.44	26.2	0.055	2.56	0.43	0.409	0.34	4.70	0.092	0.024	157
DP19252	1	3	1.06	4.06	0.37	1.79	7.39	26.1	0.057	2.56	0.46	0.404	0.43	4.60	0.087	0.040	160
DP19253	1	3	1.16	4.16	0.34	1.78	7.42	26.1	0.056	2.53	0.44	0.403	0.38	4.62	0.088	0.031	152
DP19254	1	3	1.26	4.26	0.42	1.74	7.28	26.1	0.057	2.56	0.50	0.395	0.48	4.46	0.092	0.040	141
DP19255	1	3	1.36	4.36	0.39	1.74	7.33	26.5	0.054	2.60	0.51	0.394	0.27	4.50	0.095	0.046	144
DP19256	1	3	1.46	4.46	0.38	1.81	7.52	26.3	0.058	2.55	0.47	0.409	0.47	4.68	0.091	0.032	151
DP19257	1	4	0.06	4.56	0.37	1.78	7.42	26.1	0.058	2.55	0.50	0.400	0.48	4.61	0.094	0.045	144
DP19258	1	4	0.16	4.66	0.44	1.76	7.35	26.7	0.057	2.60	0.52	0.395	0.38	4.47	0.094	0.043	140
DP19259	1	4	0.26	4.76	0.35	1.88	7.41	25.8	0.054	2.58	0.44	0.412	0.30	4.75	0.098	0.055	148
DP19260	1	4	0.36	4.86	0.33	1.84	7.36	26.0	0.053	2.57	0.43	0.402	0.31	4.66	0.093	0.044	
DP19261	1	4	0.46	4.96	0.37	1.89	7.52	26.3	0.054	2.62	0.43	0.422	0.36	4.81	0.099	0.050	144
DP19262	1	4	0.56	5.06	0.33	1.91	7.52	26.3	0.053	2.65	0.42	0.422	0.29	4.81	0.099	0.055	145
DP19263	1	4	0.66	5.16	0.33	1.91	7.48	26.0	0.052	2.63	0.39	0.420	0.23	4.84	0.092	0.040	152
DP19264	1	4	0.76	5.26	0.31	1.92	7.50	26.0	0.054	2.65	0.43	0.414	0.26	4.79	0.087	0.059	151
DP19265	1	4	0.86	5.36	0.35	1.89	7.48	26.1	0.056	2.62	0.43	0.413	0.28	4.80	0.089	0.050	143
DP19266	1	4	0.96	5.46	0.35	1.92	7.56	26.2	0.053	2.64	0.41	0.421	0.24	4.83	0.090	0.042	153
DP19267	1	4	1.06	5.56	0.35	1.92	7.55	26.0	0.052	2.65	0.41	0.414	0.24	4.82	0.093	0.042	144
DP19268	1	4	1.16	5.66	0.37	1.97	7.69	26.4	0.052	2.70	0.42	0.438	0.24	4.93	0.097	0.047	142
DP19269	1	4	0.26	5.76	0.37	1.94	7.62	26.1	0.051	2.68	0.43	0.429	0.23	4.87	0.091	0.047	139
DP19270	1	4	1.36	5.86	0.42	1.93	7.61	26.0	0.051	2.68	0.45	0.428	0.26	4.83	0.093	0.058	138
DP19271	1	4	1.46	5.96	0.38	1.93	7.63	26.1	0.052	2.66	0.46	0.429	0.28	4.84	0.092	0.055	136
DP19278	1	5	0.06	6.06	0.38	1.92	7.73	26.3	0.054	2.65	0.46	0.433	0.34	4.90	0.091	0.050	139
DP19279	1	5	0.16	6.16	0.39	1.88	7.59	26.0	0.055	2.60	0.47	0.422	0.35	4.79	0.092	0.051	143
DP19280	1	5	0.26	6.26	0.36	1.90	7.67	26.2	0.054	2.63	0.44	0.422	0.32	4.82	0.093	0.047	147

Table 4. (Continued).

Lab ID	Core	Section	Depth in Section (m)	Depth in hole (m)	Na	Mg	Al	Si	P	K	Ca	Ti	Mn	Fe	Ba	S	H_2O
DP19281	1	5	0.36	6.36	0.32	1.88	7.62	26.4	0.055	2.61	0.47	0.419	0.35	4.76	0.091	0.048	154
DP19282	1	5	0.46	6.46	0.41	1.84	7.53	26.2	0.056	2.59	0.49	0.414	0.35	4.74	0.093	0.051	138
DP19283	1	5	0.56	6.56	0.46	1.86	7.56	26.5	0.056	2.62	0.51	0.419	0.34	4.75	0.094	0.060	133
DP19284	1	5	0.66	6.66	0.39	1.90	7.60	26.4	0.054	2.66	0.45	0.428	0.30	4.80	0.097	0.054	139
DP19285	1	5	0.76	6.76	0.41	1.91	7.58	26.4	0.054	2.65	0.46	0.427	0.31	4.79	0.096	0.054	137
DP19286	1	5	0.86	6.86	0.38	1.95	7.50	26.3	0.054	2.60	0.45	0.414	0.38	4.77	0.095	0.046	152
DP19287	1	5	0.96	6.96	0.38	1.89	7.43	26.6	0.048	2.58	0.45	0.407	0.36	4.58	0.083	0.032	147
DP19288	1	5	1.06	7.06	0.52	1.71	7.04	26.9	0.047	2.45	0.61	0.375	0.31	4.10	0.086	0.043	125
DP19289	1	5	1.16	7.16	0.47	1.74	7.16	26.7	0.045	2.65	0.48	0.371	0.27	4.12	0.085	0.045	119
DP19290	1	5	1.26	7.26	0.35	1.94	7.51	26.0	0.047	2.62	0.40	0.415	0.41	4.70	0.089	0.048	148
DP19291	1	5	1.36	7.36	0.40	1.99	7.51	25.9	0.049	2.63	0.41	0.415	0.54	4.77	0.089	0.056	141
DP19292	1	5	1.46	7.46	0.30	1.96	7.46	25.8	0.047	2.56	0.35	0.399	0.36	4.67	0.083	0.035	174
DP19272	1	6	0.06	7.56	0.49	1.97	7.43	25.7	0.047	2.66	0.43	0.408	0.42	4.73	0.093	0.069	132
DP19273	1	6	0.16	7.66	0.32	2.04	7.67	26.7	0.047	2.71	0.41	0.438	0.32	4.84	0.089	0.062	160
DP19274	1	6	0.26	7.76	0.31	1.99	7.64	26.6	0.049	2.62	0.32	0.426	0.32	4.80	0.095	0.029	177
DP19275	1	6	0.36	7.86	0.27	1.97	7.56	26.6	0.049	2.58	0.32	0.413	0.36	4.70	0.093	0.030	186
DP19276	1	6	0.46	7.96	0.36	1.98	7.52	26.2	0.047	2.63	0.37	0.418	0.43	4.74	0.093	0.053	155
DP19277	1	6	0.54	8.04	0.38	2.02	7.57	26.2	0.047	2.69	0.38	0.421	0.34	4.80	0.093	0.054	144
DP19293	2	1	0.11	12.11	0.31	1.99	7.55	26.5	0.054	2.58	0.34	0.407	0.42	4.66	0.089	0.025	177
DP19294	2	1	0.19	12.19	0.31	1.99	7.56	26.3	0.052	2.62	0.38	0.417	0.39	4.73	0.089	0.040	171
DP19295	2	1	0.27	12.27	0.28	2.00	7.55	26.3	0.054	2.55	0.39	0.412	0.44	4.70	0.093	0.036	180
DP19296	2	1	0.36	12.36	0.23	1.98	7.43	26.1	0.054	2.51	0.36	0.402	0.44	4.63	0.097	0.041	200
DP19297	2	1	0.46	12.46	0.29	1.94	7.40	26.2	0.056	2.47	0.33	0.400	0.63	4.58	0.091	0.023	193
DP19298	2	1	0.56	12.56	0.30	1.93	7.33	26.2	0.054	2.49	0.39	0.396	0.49	4.58	0.093	0.045	180
DP19299	2	1	0.66	12.66	0.28	1.98	7.56	26.3	0.051	2.57	0.31	0.414	0.48	4.71	0.093	0.025	181
DP19300	2	1	0.76	12.76	0.26	2.03	7.60	26.4	0.054	2.58	0.33	0.416	0.50	4.73	0.097	0.037	182
DP19301	2	1	0.86	12.86	0.19	2.01	7.54	26.1	0.054	2.53	0.31	0.405	0.47	4.66	0.094	0.035	198
DP19302	2	1	0.96	12.96	0.23	2.03	7.53	26.3	0.055	2.55	0.36	0.407	0.43	4.66	0.088	0.047	194
DP19303	2	1	1.06	13.06	0.26	1.99	7.36	26.0	0.054	2.50	0.38	0.397	0.51	4.56	0.086	0.054	182
DP19304	2	1	1.16	13.16	0.30	1.96	7.32	26.0	0.055	2.50	0.39	0.393	0.49	4.55	0.091	0.052	181
DP19305	2	1	1.26	13.26	0.27	1.94	7.27	25.9	0.053	2.47	0.37	0.389	0.51	4.49	0.092	0.047	183
DP19306	2	1	1.36	13.36	0.26	1.97	7.31	26.3	0.054	2.49	0.37	0.389	0.49	4.48	0.090	0.047	195
DP19307	2	1	1.46	13.46	0.08	1.97	7.38	26.2	0.051	2.57	0.31	0.402	0.41	4.56	0.093	0.050	196
DP19308	2	2	0.06	13.56	0.10	2.01	7.51	26.4	0.051	2.60	0.31	0.411	0.43	4.64	0.096	0.045	193
DP19309	2	2	0.16	13.66	0.08	1.95	7.30	26.0	0.051	2.47	0.31	0.394	0.47	4.51	0.097	0.040	207
DP19310	2	2	0.26	13.76	0.12	1.91	7.19	25.9	0.052	2.42	0.35	0.382	0.42	4.45	0.097	0.042	213
DP19311	2	2	0.36	13.86	0.14	1.95	7.31	26.4	0.052	2.46	0.41	0.400	0.39	4.59	0.091	0.047	190
DP19312	2	2	0.46	13.96	0.28	1.97	7.31	26.1	0.049	2.52	0.47	0.406	0.36	4.69	0.088	0.061	160
DP19313	2	2	0.56	14.06	0.34	1.99	7.37	26.3	0.049	2.59	0.45	0.416	0.36	4.72	0.091	0.069	150
DP19314	2	2	0.66	14.16	0.28	1.99	7.28	25.7	0.046	2.56	0.43	0.404	0.35	4.64	0.093	0.080	164
DP19315	2	2	0.76	14.26	0.26	2.03	7.55	26.3	0.047	2.64	0.39	0.424	0.37	4.73	0.094	0.067	158
DP19316	2	2	0.86	14.36	0.18	2.01	7.55	26.0	0.051	2.59	0.34	0.410	0.38	4.64	0.103	0.052	185
DP19317	2	2	0.96	14.46	0.12	2.01	7.55	26.1	0.052	2.60	0.33	0.412	0.40	4.63	0.099	0.049	188
DP19318	2	2	1.06	14.56	0.20	1.96	7.34	26.0	0.053	2.58	0.38	0.390	0.42	4.41	0.096	0.057	174
DP19319	2	2	1.16	14.66	0.20	2.03	7.48	26.2	0.053	2.62	0.39	0.410	0.31	4.63	0.103	0.068	174
DP19320	2	2	1.26	14.76	0.22	2.01	7.46	25.8	0.053	2.60	0.39	0.402	0.35	4.60	0.100	0.064	166
DP19321	2	2	1.36	14.86	0.18	2.01	7.44	26.1	0.056	2.59	0.40	0.402	0.36	4.55	0.098	0.063	172
DP19322	2	2	1.46	14.96	0.12	2.02	7.38	26.1	0.055	2.52	0.37	0.391	0.45	4.47	0.096	0.057	194
DP19323	2	3	0.06	15.06	0.16	2.08	7.51	26.1	0.056	2.56	0.39	0.404	0.45	4.63	0.097	0.066	179
DP19324	2	3	0.15	15.15	0.18	2.07	7.62	26.2	0.055	2.58	0.34	0.415	0.39	4.71	0.097	0.044	178
DP19325	2	3	0.26	15.26	0.20	2.02	7.46	26.2	0.056	2.53	0.39	0.402	0.44	4.66	0.101	0.056	179
DP19326	2	3	0.36	15.36	0.13	2.02	7.55	26.3	0.054	2.52	0.37	0.414	0.46	4.69	0.099	0.054	173
DP19327	2	3	0.46	15.46	0.16	2.01	7.51	26.4	0.055	2.48	0.35	0.404	0.45	4.61	0.092	0.041	192
DP19328	2	3	0.56	15.56	0.20	2.06	7.58	26.1	0.055	2.56	0.37	0.414	0.51	4.68	0.095	0.050	194
DP19329	2	3	0.66	15.66	0.12	2.05	7.55	26.5	0.056	2.51	0.38	0.414	0.50	4.64	0.098	0.053	184
DP19330	2	3	0.76	15.76	0.19	2.01	7.58	26.2	0.053	2.51	0.35	0.415	0.42	4.68	0.095	0.039	178
DP19331	2	3	0.86	15.86	0.15	2.01	7.59	26.4	0.057	2.47	0.35	0.417	0.50	4.66	0.094	0.030	193
DP19332	2	3	1.01		0.21	2.02	7.56	26.4	0.055	2.47	0.35	0.411	0.47	4.67	0.096	0.031	
DP19333	2	4	0.16		0.24	2.05	7.60	26.3	0.053	2.55	0.35	0.419	0.42	4.71	0.094	0.040	
DP19334	2	4	0.46	16.96	0.28	2.04	7.67	26.2	0.052	2.63	0.39	0.436	0.35	4.83	0.096	0.052	162
DP19335	2	4	0.56	17.06	0.24	2.03	7.63	26.1	0.052	2.56	0.36	0.424	0.40	4.79	0.093	0.031	166
DP19336	2	4	0.66	17.16	0.28	2.06	7.66	26.0	0.048	2.62	0.37	0.429	0.36	4.89	0.098	0.055	154
DP19337	2	4	0.76	17.26	0.34	2.04	7.65	26.0	0.048	2.58	0.37	0.429	0.35	4.89	0.092	0.041	156

Table 4. (Continued).

Lab ID	Core	Section	Depth in Section (m)	Depth in hole (m)	Na	Mg	Al	Si	P	K	Ca	Ti	Mn	Fe	Ba	S	H_2O
DP19338	2	4	0.86	17.36	0.31	2.10	7.63	26.0	0.050	2.54	0.41	0.428	0.38	4.82	0.096	0.057	155
DP19339	2	4	0.96	17.46	0.20	2.06	7.64	25.9	0.051	2.60	0.34	0.419	0.43	4.75	0.108	0.044	169
DP19340	2	4	1.06	17.56	0.28	2.09	7.62	25.9	0.048	2.65	0.35	0.415	0.35	4.75	0.101	0.060	156
DP19341	2	4	1.16	17.66	0.31	2.07	7.60	25.9	0.046	2.71	0.35	0.422	0.33	4.78	0.100	0.065	146
DP19342	2	4	1.26	17.76	0.33	2.06	7.70	26.2	0.045	2.74	0.33	0.428	0.31	4.85	0.105	0.055	141
DP19343	2	4	1.36	17.86	0.28	2.11	7.81	26.4	0.046	2.69	0.32	0.427	0.34	4.81	0.126	0.049	155
DP19344	2	4	1.46	17.96	0.25	2.14	7.74	26.3	0.044	2.52	0.33	0.417	0.37	4.61	0.098	0.054	173
DP19345	2	5	0.06	18.06	0.21	2.21	7.71	26.3	0.048	2.37	0.33	0.407	0.44	4.44	0.098	0.052	180
DP19346	2	5	0.16	18.16	0.20	2.28	7.67	26.2	0.050	2.20	0.35	0.391	0.40	4.24	0.083	0.053	193
DP19347	2	5	0.25	18.25	0.24	2.36	7.83	26.6	0.049	2.01	0.36	0.381	0.36	3.99	0.075	0.044	190
DP19348	2	5	0.36	18.36	0.39	2.31	7.74	26.3	0.048	1.87	0.42	0.356	0.31	3.74	0.073	0.051	169
DP19349	2	5	0.46	18.46	0.35	2.25	7.68	26.1	0.051	2.11	0.39	0.386	0.42	4.18	0.076	0.051	166
DP19350	2	5	0.56	18.56	0.35	2.23	7.73	26.3	0.052	2.34	0.40	0.408	0.42	4.48	0.085	0.057	159
DP19351	2	5	0.66	18.66	0.30	2.10	7.63	25.9	0.051	2.47	0.36	0.409	0.42	4.61	0.088	0.053	249
DP19352	2	5	0.76	18.76	0.38	2.10	7.82	26.3	0.051	2.67	0.39	0.434	0.42	4.87	0.093	0.064	136
DP19353	2	5	0.86	18.86	0.27	2.06	7.72	26.0	0.049	2.60	0.37	0.427	0.45	4.83	0.097	0.054	164
DP19354	2	5	0.96	18.96	0.25	2.05	7.68	26.0	0.057	2.53	0.41	0.422	0.52	4.81	0.094	0.051	170
DP19355	2	5	1.06	19.06	0.28	2.05	7.70	26.2	0.060	2.56	0.43	0.433	0.50	4.85	0.094	0.060	165
DP19356	2	5	1.16	19.16	0.24	2.07	7.67	26.1	0.059	2.54	0.36	0.424	0.50	4.73	0.093	0.051	174
DP19357	2	5	1.26	19.26	0.29	2.07	7.61	25.8	0.054	2.54	0.36	0.407	0.40	4.68	0.095	0.059	161
DP19358	2	5	1.36	19.36	0.33	2.03	7.78	26.0	0.051	2.68	0.34	0.423	0.42	4.91	0.099	0.044	151
DP19359	2	5	1.46	19.46	0.28	2.03	7.64	25.7	0.059	2.37	0.47	0.411	0.57	4.89	0.088	0.039	181
DP19360	2	6	0.06	19.56	0.22	2.05	7.74	25.8	0.059	2.41	0.45	0.422	0.61	4.91	0.091	0.038	186
DP19361	2	6	0.16	19.66	0.35	2.00	7.69	25.7	0.059	2.48	0.41	0.414	0.57	4.86	0.089	0.038	162
DP19362	2	6	0.26	19.76	0.32	2.00	7.73	25.8	0.056	2.55	0.44	0.428	0.56	4.92	0.088	0.053	161
DP19363	2	6	0.36	19.86	0.31	2.00	7.68	25.6	0.053	2.54	0.43	0.421	0.54	4.93	0.089	0.060	157
DP19364	2	6	0.46	19.96	0.30	2.00	7.74	25.6	0.055	2.55	0.41	0.427	0.54	4.97	0.086	0.051	160
DP19365	2	6	0.56	20.06	0.29	2.02	7.81	25.8	0.058	2.59	0.39	0.429	0.57	4.93	0.090	0.054	245
DP19366	2	6	0.66	20.16	0.33	2.01	7.72	25.6	0.054	2.61	0.41	0.423	0.47	4.87	0.089	0.073	157
DP19367	2	6	0.76	20.26	0.34	1.98	7.74	25.6	0.058	2.60	0.42	0.430	0.52	4.96	0.091	0.059	149
DP19368	2	6	0.86	20.36	0.35	1.99	7.76	25.6	0.056	2.56	0.46	0.437	0.53	5.05	0.088	0.063	147
DP19369	2	6	0.96	20.46	0.30	1.98	7.74	25.5	0.058	2.55	0.44	0.429	0.55	5.00	0.086	0.058	162
DP19370	2	6	1.06	20.56	0.31	1.98	7.84	25.6	0.061	2.59	0.44	0.433	0.61	5.03	0.088	0.060	155
DP19371	2	6	1.16	20.66	0.35	1.95	7.78	25.2	0.060	2.56	0.46	0.426	0.62	4.99	0.084	0.062	149
DP19372	2	6	1.26	20.76	0.43	1.92	7.74	25.1	0.057	2.56	0.49	0.426	0.61	5.02	0.083	0.065	135
DP19373	2	6	1.36	20.86	0.39	1.96	7.80	25.5	0.052	2.67	0.42	0.431	0.52	5.02	0.085	0.065	136
DP19374	2	6	1.46	20.96	0.37	1.96	7.67	25.0	0.057	2.60	0.42	0.414	0.60	4.89	0.087	0.069	147
DP19375	2	7	0.06	21.06	0.35	1.99	7.76	25.4	0.058	2.60	0.42	0.427	0.56	4.94	0.084	0.061	144
DP19376	2	7	0.16	21.16	0.32	2.00	7.84	25.5	0.058	2.59	0.42	0.431	0.61	4.95	0.086	0.059	153
DP19377	2	7	0.26	21.26	0.35	1.99	7.73	25.3	0.058	2.57	0.42	0.427	0.64	4.92	0.086	0.065	147
DP19378	2	7	0.36	21.36	0.37	2.00	7.81	25.4	0.060	2.58	0.42	0.436	0.67	4.99	0.086	0.060	147
DP19379	3	1	0.06	21.56	0.35	1.93	7.85	25.2	0.068	2.67	0.38	0.426	0.63	4.89	0.078	0.056	141
DP19380	3	1	0.16	21.66	0.33	1.94	7.95	25.6	0.068	2.67	0.36	0.442	0.68	4.95	0.080	0.048	143
DP19381	3	1	0.26	21.76	0.33	1.92	7.87	25.3	0.067	2.65	0.35	0.430	0.62	4.92	0.079	0.046	144
DP19382	3	1	0.36	21.86	0.37	1.96	7.96	25.7	0.066	2.70	0.38	0.446	0.64	5.00	0.079	0.055	139
DP19384	3	1	0.46	21.96	0.36	1.93	7.90	25.5	0.064	2.67	0.37	0.441	0.64	4.99	0.078	0.053	136
DP19385	3	1	0.56	22.06	0.35	1.92	7.85	25.3	0.062	2.63	0.40	0.436	0.64	5.01	0.075	0.051	143
DP19386	3	1	0.66	22.16	0.39	1.94	7.90	25.5	0.061	2.64	0.42	0.443	0.64	5.08	0.078	0.060	146
DP19387	3	1	0.76		0.39	1.93	7.76	25.0	0.060	2.61	0.42	0.428	0.64	4.98	0.078	0.056	144
DP19383	3	1	0.86		0.37	1.94	7.89	25.3	0.060	2.64	0.37	0.432	0.60	4.98	0.077	0.048	140
DP19388	3	1	0.96		0.39	1.95	7.86	25.2	0.060	2.69	0.39	0.432	0.56	4.96	0.076	0.069	144
DP19389	3	1	1.06		0.35	1.94	7.86	25.2	0.067	2.63	0.39	0.435	0.66	4.98	0.078	0.056	142
DP19390	3	1	1.16		0.38	1.96	7.85	25.3	0.069	2.63	0.39	0.440	0.68	4.98	0.078	0.051	141
DP19391	3	1	1.26		0.39	1.96	7.90	25.6	0.071	2.67	0.39	0.451	0.67	5.01	0.079	0.052	140
DP19392	3	1	1.36		0.35	1.98	7.87	24.9	0.068	2.64	0.36	0.432	0.70	5.04	0.080	0.048	134
DP19393	3	1	1.46		0.36	1.95	7.89	25.4	0.073	2.60	0.35	0.433	0.70	4.95	0.081	0.030	142
DP19394	3	2	0.06		0.35	1.95	7.84	25.3	0.073	2.62	0.38	0.431	0.68	4.94	0.082	0.046	142
DP19395	3	2	0.16		0.31	1.93	7.78	25.0	0.074	2.59	0.34	0.424	0.68	4.90	0.082	0.032	148
DP19396	3	2	0.26		0.37	1.97	7.93	25.4	0.071	2.69	0.40	0.444	0.75	4.99	0.082	0.059	141
DP19397	3	2	0.36		0.38	1.98	7.92	25.4	0.071	2.66	0.39	0.440	0.74	4.98	0.082	0.054	138
DP19398	3	2	0.46		0.36	1.95	7.90	25.4	0.071	2.69	0.38	0.439	0.72	5.00	0.079	0.056	137
DP19399	3	2	0.56		0.35	2.00	7.97	25.5	0.073	2.71	0.40	0.444	0.76	5.01	0.079	0.067	140
DP19400	3	2	0.66		0.36	2.01	8.09	25.8	0.072	2.73	0.38	0.448	0.76	5.03	0.080	0.057	141

Table 4. (Continued).

Lab ID	Core	Section	Depth in Section (m)	Depth in hole (m)	Na	Mg	Al	Si	P	K	Ca	Ti	Mn	Fe	Ba	S	H_2O
DP19401	3	2	0.76	22.76	0.42	2.06	8.03	25.6	0.073	2.78	0.41	0.447	0.71	5.04	0.081	0.085	142
DP19402	3	2	0.86	22.86	0.34	1.97	8.00	25.5	0.066	2.71	0.33	0.438	0.68	4.97	0.078	0.046	142
DP19403	3	2	0.96	22.96	0.35	1.96	7.87	25.1	0.066	2.68	0.35	0.425	0.67	4.89	0.078	0.054	142
DP19404	3	2	1.06	23.06	0.39	1.97	7.90	25.1	0.065	2.68	0.35	0.426	0.67	4.88	0.080	0.061	140
DP19405	3	2	1.16	23.16	0.37	1.99	7.99	25.4	0.066	2.72	0.35	0.439	0.67	4.97	0.080	0.060	137
DP19406	3	2	1.26	23.26	0.38	1.99	7.92	25.5	0.067	2.76	0.36	0.444	0.68	5.02	0.081	0.053	132
DP19407	3	2	1.36	23.36	0.40	1.98	7.85	25.4	0.067	2.76	0.36	0.440	0.65	4.99	0.079	0.049	127
DP19408	3	2	1.46	23.46	0.39	1.97	7.86	25.5	0.068	2.78	0.35	0.439	0.63	4.98	0.082	0.049	128
DP19409	3	3	0.06	23.56	0.41	1.96	7.87	25.6	0.066	2.82	0.35	0.444	0.58	5.01	0.080	0.046	121
DP19410	3	3	0.16	23.66	0.40	1.96	7.88	25.5	0.067	2.81	0.34	0.444	0.62	5.02	0.080	0.047	128
DP19411	3	3	0.26	23.76	0.40	1.98	7.83	25.5	0.067	2.83	0.37	0.442	0.62	5.00	0.079	0.063	124
DP19412	3	3	0.36	23.86	0.45	1.99	7.75	25.2	0.068	2.81	0.37	0.435	0.62	5.00	0.077	0.062	118
DP19413	3	3	0.46	23.96	0.47	2.15	7.30	24.7	0.153	2.78	0.61	0.503	0.93	5.50	0.105	0.082	131
DP19414	3	3	0.56		0.40	2.18	7.25	24.9	0.179	2.76	0.66	0.527	0.99	5.58	0.117	0.070	
DP19415	3	3	0.66		0.38	2.16	7.28	24.9	0.182	2.77	0.67	0.526	1.03	5.61	0.120	0.067	
DP19416	3	3	0.96		0.48	2.13	7.23	25.1	0.236	2.75	0.84	0.550	0.95	5.56	0.121	0.071	
DP19417	3	3	1.16		0.86	1.57	6.32	26.3	0.569	2.43	1.87	0.711	0.32	4.69	0.133	0.073	
DP19418	3	3	1.41		0.53	1.97	7.96	25.5	0.063	2.98	0.36	0.444	0.52	5.04	0.077	0.056	
DP19422	3	4	0.26		0.51	1.97	7.90	25.2	0.065	2.90	0.38	0.436	0.65	5.01	0.080	0.061	
DP19423	3	4	0.81		0.48	1.97	7.90	25.2	0.067	2.87	0.37	0.438	0.66	5.01	0.078	0.052	
DP19424	3	4	1.46		0.42	2.01	7.98	25.1	0.069	2.79	0.38	0.447	0.89	5.07	0.081	0.063	
DP19419	3	5	0.26		0.43	2.00	7.94	25.0	0.068	2.79	0.38	0.443	0.85	5.05	0.080	0.063	
DP19420	3	5	0.76		0.47	2.02	7.92	24.9	0.070	2.78	0.40	0.437	0.84	5.07	0.077	0.075	
DP19421	3	5	1.26		0.42	2.02	8.04	25.4	0.067	2.79	0.37	0.451	0.83	5.14	0.078	0.058	
DP19425	3	6	0.06		0.43	1.99	7.96	25.2	0.067	2.76	0.35	0.446	0.81	5.10	0.076	0.049	
DP19426	3	6	0.26	27.92	0.44	2.06	7.86	25.1	0.093	2.77	0.44	0.473	0.95	5.35	0.082	0.053	118
DP19427	3	6	0.46	28.12	0.49	2.08	7.78	24.7	0.109	2.78	0.50	0.459	0.96	5.26	0.080	0.076	119
DP19428	3	6	0.66	28.32	0.48	2.08	7.85	24.9	0.103	2.82	0.50	0.464	1.04	5.35	0.078	0.062	118
DP19429	3	6	0.86	28.52	0.48	2.03	7.77	24.8	0.100	2.80	0.47	0.450	0.99	5.23	0.079	0.058	113
DP19430	3	6	1.06	28.72	0.51	2.07	7.85	24.9	0.107	2.85	0.49	0.465	1.03	5.34	0.081	0.067	113
DP19431	3	6	1.26	28.92	0.50	2.03	7.77	24.8	0.114	2.84	0.52	0.466	1.05	5.29	0.072	0.068	115
DP19432	3	6	1.46	29.12	0.50	2.01	7.71	24.4	0.117	2.75	0.53	0.461	1.05	5.28	0.072	0.065	119
DP19433	3	7	0.06	29.22	0.51	2.01	7.75	24.5	0.122	2.76	0.53	0.462	1.01	5.34	0.075	0.060	119
DP19434	3	7	0.26	29.42	0.54	2.01	7.77	24.3	0.129	2.76	0.57	0.461	1.22	5.26	0.074	0.072	124
DP19435	3	7	0.46	29.62	0.54	1.98	7.80	24.3	0.128	2.75	0.55	0.457	1.21	5.27	0.072	0.061	124
DP19436	4	3	1.06	31.56	0.46	2.00	7.76	23.7	0.180	2.58	0.66	0.435	1.57	5.31	0.070	0.063	151
DP19437	4	3	1.26	31.76	0.52	1.96	7.69	23.7	0.198	2.69	0.74	0.446	1.68	5.31	0.074	0.072	139
DP19438	4	3	1.46	31.96	0.42	1.99	7.72	23.4	0.203	2.56	0.70	0.454	1.83	5.61	0.071	0.061	159
DP19439	4	4	0.06	32.06	0.44	2.01	7.73	23.4	0.205	2.61	0.75	0.455	1.77	5.61	0.073	0.084	149
DP19440	4	4	0.26	32.26	0.40	1.97	7.74	23.4	0.215	2.59	0.71	0.443	1.86	5.46	0.072	0.058	152
DP19441	4	4	0.46	32.46	0.42	1.98	7.75	23.4	0.205	2.65	0.69	0.439	1.70	5.31	0.072	0.068	138
DP19442	4	4	0.66	32.66	0.43	1.97	7.79	23.7	0.172	2.77	0.58	0.430	1.45	5.07	0.072	0.060	128
DP19443	4	4	0.86	32.86	0.43	2.02	7.87	24.0	0.158	2.81	0.55	0.442	1.42	5.15	0.071	0.067	127
DP19444	4	4	1.06	33.06	0.43	1.98	7.73	23.6	0.170	2.70	0.62	0.446	1.61	5.22	0.070	0.074	142
DP19445	4	4	1.26	33.26	0.44	1.98	7.72	23.5	0.193	2.62	0.68	0.450	1.83	5.31	0.074	0.067	148
DP19446	4	4	1.46	33.46	0.42	1.95	7.71	23.3	0.232	2.62	0.77	0.446	2.04	5.25	0.074	0.073	154
DP19447	4	5	0.06	33.56	0.42	1.99	7.77	23.5	0.214	2.67	0.75	0.457	2.01	5.26	0.074	0.076	153
DP19448	4	5	0.26	33.76	0.40	1.99	7.59	23.0	0.262	2.55	0.90	0.462	2.19	5.33	0.074	0.083	148
DP19449	4	5	0.46	33.96	0.41	1.96	7.79	23.4	0.250	2.53	0.76	0.458	2.07	5.46	0.075	0.043	157
DP19450	4	5	0.66	34.16	0.40	1.99	7.54	22.9	0.288	2.57	0.95	0.455	2.03	5.33	0.073	0.094	153
DP19451	4	5	0.86	34.36	0.34	2.03	7.57	23.1	0.289	2.61	0.97	0.463	2.05	5.40	0.074	0.086	150
DP19452	4	5	1.06	34.56	0.35	2.04	7.54	23.1	0.312	2.62	1.01	0.468	2.15	5.46	0.077	0.081	149
DP19453	4	5	1.26	34.76	0.31	2.07	7.38	23.0	0.443	2.59	1.28	0.457	2.20	5.54	0.077	0.086	154
DP19454	4	5	1.46	34.96	0.32	2.07	7.29	22.7	0.458	2.59	1.37	0.455	2.13	5.47	0.076	0.095	151
DP19455	4	6	0.06	35.06	0.33	2.06	7.35	22.8	0.449	2.61	1.36	0.454	2.12	5.48	0.076	0.096	148
DP19456	4	6	0.26	35.26	0.34	2.07	7.30	22.7	0.457	2.61	1.39	0.452	2.12	5.47	0.075	0.100	149
DP19457	4	6	0.46	35.46	0.34	2.01	7.11	22.2	0.446	2.55	1.36	0.430	2.00	5.35	0.074	0.093	151
DP19458	4	6	0.66	35.66	0.36	2.08	7.32	22.8	0.466	2.61	1.41	0.452	2.11	5.47	0.075	0.097	144
DP19459	4	6	0.86	35.86	0.33	2.08	7.31	22.8	0.465	2.61	1.41	0.451	2.10	5.47	0.075	0.093	148
DP19460	4	6	1.06	36.06	0.34	2.06	7.29	22.7	0.467	2.61	1.41	0.449	2.07	5.45	0.076	0.094	144
DP19461	4	6	1.26	36.26	0.32	2.06	7.32	22.8	0.446	2.61	1.39	0.454	2.07	5.45	0.076	0.085	147
DP19462	4	6	1.46	36.46	0.32	2.09	7.90	23.5	0.295	2.78	0.83	0.497	1.54	5.29	0.074	0.071	125
DP19463	4	7	0.06	36.56	0.34	2.01	7.88	23.2	0.376	2.63	1.00	0.536	1.58	5.42	0.073	0.081	129

Table 4. (Continued).

Lab ID	Core	Section	Depth in Section (m)	Depth in hole (m)	Na	Mg	Al	Si	P	K	Ca	Ti	Mn	Fe	Ba	S	H_2O
DP19464	4	7	0.26	36.76	0.38	1.94	7.89	23.4	0.337	2.71	0.90	0.550	1.45	5.57	0.072	0.074	129
DP19465	4	7	0.46	36.96	0.37	1.94	7.85	23.4	0.328	2.82	0.89	0.539	1.46	5.54	0.074	0.079	129
DP19466	5	1	1.36		0.29	2.12	8.01	23.7	0.257	2.85	0.75	0.497	1.52	5.32	0.075	0.075	
DP19467	5	2	0.06	39.36	0.32	2.09	7.97	23.7	0.307	2.78	0.88	0.509	1.55	5.32	0.073	0.075	131
DP19468	5	2	0.26	39.56	0.34	2.03	7.98	23.6	0.350	2.66	0.99	0.542	1.61	5.46	0.071	0.079	137
DP19469	5	2	0.46	39.76	0.35	1.99	7.96	23.6	0.343	2.65	0.96	0.552	1.52	5.53	0.070	0.076	135
DP19470	5	2	0.67	39.97	0.33	1.95	7.92	23.6	0.300	2.76	0.86	0.551	1.43	5.55	0.071	0.074	139
DP19471	5	2	0.87	40.17	0.32	1.93	7.91	23.6	0.295	2.82	0.85	0.540	1.44	5.51	0.070	0.071	141
DP19472	5	2	1.07	40.37	0.35	1.95	7.94	23.6	0.326	2.83	0.93	0.555	1.52	5.57	0.074	0.081	137
DP19473	5	2	1.26	40.56	0.34	1.98	7.91	23.6	0.341	2.76	0.94	0.574	1.58	5.59	0.075	0.080	142
DP19474	5	2	1.46	40.76	0.32	1.99	7.89	23.4	0.303	2.65	0.88	0.590	1.61	5.63	0.073	0.072	146
DP19475	5	3	0.06	40.86	0.30	2.00	7.93	23.5	0.302	2.65	0.88	0.609	1.66	5.71	0.076	0.073	147
DP19476	5	3	0.26	41.46	0.22	2.05	7.87	23.3	0.320	2.59	0.91	0.605	1.64	5.66	0.076	0.087	154
DP19477	5	3	0.46	41.66	0.30	2.10	7.79	23.3	0.284	2.80	0.81	0.673	1.50	6.24	0.075	0.067	141
DP19478	5	3	0.66	41.86	0.35	2.06	7.57	22.7	0.313	2.72	0.84	0.714	1.38	6.46	0.073	0.073	143
DP19479	5	3	0.86	42.66	0.38	2.07	7.69	23.4	0.314	3.10	0.84	0.733	1.18	6.22	0.074	0.071	130
DP19480	5	3	1.06	42.86	0.34	2.13	7.65	23.7	0.238	3.18	0.67	0.688	1.16	6.06	0.074	0.060	120
DP19481	5	3	1.26	43.06	0.30	2.17	7.80	24.1	0.258	3.19	0.71	0.633	1.23	5.90	0.075	0.060	114
DP19482	5	3	1.46	43.26	0.27	2.22	7.66	24.0	0.255	3.13	0.69	0.561	1.18	5.63	0.075	0.055	109
DP19483	5	4	0.06	43.36	0.27	2.25	7.73	24.1	0.254	3.17	0.70	0.586	1.21	5.70	0.076	0.058	108
DP19484	5	4	0.26	43.56	0.26	2.24	7.59	24.0	0.266	3.16	0.75	0.602	1.20	5.89	0.075	0.061	114
DP19485	5	4	0.46	43.76	0.26	2.25	7.73	24.2	0.275	3.18	0.77	0.556	1.25	5.68	0.076	0.056	108
DP19486	5	4	0.66	43.96	0.28	2.26	7.67	24.0	0.248	3.15	0.70	0.593	1.16	5.83	0.076	0.059	109
DP19487	5	4	0.86	44.16	0.37	2.11	7.75	24.0	0.231	3.30	0.65	0.674	0.93	5.98	0.074	0.053	103
DP19488	5	4	1.06	44.36	0.29	2.26	7.79	23.9	0.240	3.04	0.67	0.616	1.09	5.95	0.073	0.060	108
DP19489	5	4	1.26	44.56	0.28	2.27	7.82	24.0	0.264	3.03	0.70	0.642	1.05	6.10	0.073	0.059	108
DP19490	5	4	1.46	44.76	0.29	2.29	7.67	23.7	0.296	3.02	0.78	0.618	1.09	6.08	0.074	0.066	163
DP19491	5	5	0.06	44.86	0.30	2.28	7.74	23.9	0.302	3.06	0.81	0.628	1.13	6.18	0.075	0.067	111
DP19492	5	5	0.26	45.06	0.36	2.19	7.74	23.9	0.264	3.17	0.71	0.628	1.04	6.17	0.074	0.062	109
DP19493	5	5	0.46	45.26	0.29	2.27	7.80	23.7	0.298	3.01	0.79	0.580	1.12	6.07	0.075	0.070	106
DP19494	5	5	0.66	45.46	0.31	2.22	7.81	23.6	0.269	2.97	0.74	0.599	1.07	6.15	0.073	0.066	108
DP19495	5	5	0.86	45.66	0.29	2.28	7.85	23.7	0.287	2.94	0.79	0.602	1.13	6.18	0.076	0.065	107
DP19496	5	5	1.07	45.87	0.32	2.22	7.83	23.5	0.307	2.90	0.79	0.615	1.11	6.32	0.074	0.070	108
DP19497	5	5	1.26	46.06	0.32	2.21	7.78	23.3	0.287	2.89	0.75	0.630	1.14	6.47	0.074	0.072	114
DP19498	5	5	1.46	46.26	0.35	2.16	7.77	23.6	0.267	3.06	0.73	0.653	1.07	6.61	0.073	0.066	110
DP19499	5	6	0.06	46.36	0.38	2.12	7.74	23.5	0.270	3.07	0.74	0.669	1.03	6.67	0.073	0.065	110
DP19500	5	6	0.26	46.56	0.38	2.14	7.77	23.2	0.312	2.87	0.80	0.728	1.04	7.05	0.073	0.074	114
DP19501	5	6	0.46	46.76	0.36	2.16	7.78	23.1	0.320	2.80	0.83	0.702	1.08	7.02	0.073	0.070	115
DP19502	5	6	0.66	46.96	0.35	2.15	7.87	23.1	0.319	2.77	0.84	0.726	1.04	7.01	0.073	0.067	113
DP19503	5	6	0.86	47.16	0.32	2.18	7.80	23.2	0.350	2.83	0.91	0.698	1.09	6.70	0.072	0.068	118
DP19504	5	6	1.06	47.36	0.27	2.11	7.28	22.9	0.674	3.08	1.78	0.560	1.27	5.95	0.076	0.096	125
DP19505	6	1	1.26	49.92	0.25	2.17	7.09	22.8	0.819	3.26	2.14	0.410	1.53	5.22	0.074	0.101	129
DP19506	6	1	1.46	50.12	0.26	2.18	7.13	22.9	0.781	3.30	2.04	0.419	1.56	5.21	0.077	0.102	126
DP19507	6	2	0.06	50.22	0.18	2.19	7.19	23.1	0.773	3.30	2.02	0.426	1.55	5.25	0.079	0.106	150
DP19508	6	2	0.26	50.42	0.24	2.12	7.17	22.7	0.789	3.35	2.08	0.379	1.51	4.92	0.072	0.103	133
DP19509	6	2	0.46	50.62	0.25	2.14	7.37	23.2	0.725	3.36	1.93	0.407	1.37	5.06	0.077	0.090	119
DP19510	6	2	0.66	50.82	0.28	2.14	7.27	22.9	0.823	3.30	2.09	0.399	1.40	5.13	0.078	0.108	117
DP19511	6	2	0.86	51.02	0.28	2.09	7.08	22.4	0.882	3.27	2.31	0.384	1.40	5.06	0.075	0.115	115
DP19512	6	2	1.06	51.22	0.29	2.11	7.16	22.6	0.950	3.31	2.47	0.393	1.39	5.08	0.078	0.120	114
DP19513	6	2	1.26	51.42	0.32	2.04	7.12	22.5	1.033	3.37	2.57	0.383	1.45	5.00	0.075	0.135	121
DP19514	6	2	1.46	51.62	0.33	2.02	7.03	22.0	1.218	3.33	2.97	0.366	1.46	4.92	0.076	0.147	119
DP19515	6	3	0.06	51.72	0.32	2.07	7.18	22.5	0.958	3.37	2.40	0.370	1.41	5.02	0.075	0.125	115
DP19516	6	3	0.26	51.92	0.31	2.11	7.20	22.8	0.914	3.30	2.32	0.389	1.30	5.19	0.077	0.118	116
DP19517	6	3	0.46	52.12	0.33	2.17	7.17	22.9	0.733	3.23	1.92	0.428	1.30	5.47	0.078	0.106	111
DP19518	6	3	0.67	53.13	0.33	2.20	7.48	23.7	0.569	3.42	1.51	0.417	1.20	5.53	0.076	0.095	108
DP19519	6	3	0.86	53.32	0.34	2.16	7.42	23.5	0.544	3.41	1.46	0.392	1.20	5.31	0.075	0.094	110
DP19520	6	3	1.06	53.52	0.34	2.16	7.48	23.5	0.516	3.36	1.38	0.416	1.24	5.46	0.074	0.089	107
DP19521	6	3	1.26	53.72	0.35	2.16	7.45	23.6	0.414	3.43	1.15	0.397	1.29	5.28	0.076	0.087	112
DP19522	6	3	1.46	53.92	0.34	2.14	7.43	23.6	0.354	3.43	1.02	0.388	1.25	5.25	0.075	0.085	96
DP19523	6	4	0.06	54.02	0.34	2.14	7.48	23.8	0.355	3.47	1.02	0.401	1.35	5.24	0.077	0.079	121
DP19524	6	4	0.26	54.22	0.33	2.15	7.43	23.7	0.337	3.45	0.99	0.400	1.40	5.24	0.076	0.076	109
DP19525	6	4	0.46	54.92	0.32	2.15	7.10	23.2	0.473	3.49	1.35	0.402	1.67	5.40	0.079	0.092	118
DP19526	6	4	0.66	55.12	0.29	2.21	6.81	23.0	0.424	3.46	1.29	0.415	2.05	6.06	0.087	0.090	121

Table 4. (Continued).

Lab ID	Core	Section	Depth in Section (m)	Depth in hole (m)	Na	Mg	Al	Si	P	K	Ca	Ti	Mn	Fe	Ba	S	H_2
DP19527	6	4	0.86	55.32	0.31	2.18	6.76	22.8	0.578	3.51	2.12	0.429	2.05	5.63	0.087	0.093	11
DP19528	6	4	1.06	55.52	0.31	2.21	6.74	22.5	0.774	3.49	2.53	0.425	1.93	5.45	0.084	0.106	10
DP19529	6	4	1.46	55.92	0.29	2.29	6.74	22.9	0.426	3.41	1.56	0.387	1.91	6.25	0.084	0.088	11
DP19530	6	5	0.55	56.51	0.29	2.30	6.86	23.2	0.348	3.36	0.99	0.374	1.86	6.61	0.086	0.085	12
DP19531	6	5	0.86	56.82	0.31	2.18	6.94	23.2	0.398	3.43	1.60	0.379	1.46	5.62	0.075	0.086	11
DP19532	6	5	1.06	57.02	0.30	2.17	7.00	23.4	0.324	3.36	1.14	0.379	1.43	5.85	0.078	0.074	118
DP19533	6	5	1.26	57.22	0.29	2.32	6.78	23.3	0.384	3.23	1.27	0.376	1.58	6.63	0.087	0.078	119
DP19534	6	5	1.44	57.40	0.17	1.19	2.68	9.2	0.166	1.23	24.64	0.187	0.82	3.99	0.076	0.041	70
DP19535	6	6	0.47	57.93	0.27	2.39	6.74	23.0	0.291	3.20	0.86	0.356	1.74	7.84	0.091	0.076	125
DP19536	6	6	0.76	58.22	0.24	2.31	6.87	23.5	0.393	3.35	1.12	0.381	1.69	6.45	0.086	0.077	121
DP19537	6	6	1.36	58.82	0.26	2.33	6.90	23.7	0.374	3.36	1.00	0.397	1.27	5.83	0.079	0.076	115
DP19538	7	3	1.45	62.45	0.27	2.47	6.97	24.4	0.364	3.38	0.94	0.410	1.23	5.46	0.118	0.087	109
DP19539	7	4	0.91	63.41	0.17	2.51	6.82	24.3	0.303	3.41	0.81	0.376	1.23	5.05	0.084	0.059	121
DP19540	7	4	1.28	63.78	0.22	2.42	6.91	24.1	0.451	3.50	1.28	0.383	1.30	5.13	0.085	0.065	111
DP19541	7	5	0.79	64.79	0.21	2.49	6.77	24.6	0.378	3.41	1.02	0.395	1.24	5.08	0.089	0.066	110
DP19542	7	6	0.26	65.76	0.20	2.32	6.26	22.4	0.267	3.13	4.07	0.376	1.05	4.81	0.082	0.059	112
DP19543	7	6	0.46	65.96	0.07	2.84	6.50	24.8	0.348	3.09	0.82	0.388	0.95	4.89	0.088	0.056	138
DP19544	7	6	0.89	66.39	0.06	2.86	6.61	25.3	0.305	3.18	0.72	0.400	0.76	4.75	0.079	0.055	133
DP19545	7	7	0.30	67.30	0.06	2.92	6.52	24.9	0.426	3.05	0.99	0.382	0.93	4.75	0.088	0.051	139
DP19546	8	2	0.81	69.76	0.27	2.39	6.51	24.0	0.358	3.52	2.09	0.385	1.00	4.82	0.090	0.052	102
DP19547	8	3	0.29	70.74	0.12	2.76	6.61	25.1	0.286	3.22	0.70	0.393	0.99	4.86	0.096	0.044	126
DP19548	8	3	0.65	71.10	0.16	2.61	6.60	24.8	0.507	3.37	1.17	0.399	1.03	4.88	0.093	0.070	117
DP19549	8	3	0.96	71.41	0.19	2.57	6.18	23.5	0.345	3.12	2.66	0.384	0.96	4.88	0.087	0.057	116
DP19550	8	4	0.21	72.16	0.25	2.65	6.52	24.7	0.466	3.27	1.20	0.388	1.23	5.95	0.087	0.059	108
DP19551	8	4	0.41	72.36	0.38	2.50	6.24	23.7	0.479	3.36	1.33	0.347	1.59	6.22	0.094	0.075	103
DP19552	8	4	0.99	72.94	0.37	2.46	6.00	23.4	0.575	3.25	2.41	0.363	1.32	6.01	0.093	0.070	100
DP19553	8	5	0.58	74.03	0.24	2.73	6.36	25.6	0.337	3.39	0.84	0.400	0.77	5.52	0.083	0.057	109
DP19554	8	5	1.42	74.87	0.20	2.98	6.50	25.5	0.302	3.19	0.78	0.405	0.85	5.38	0.084	0.056	113
DP19555	8	6	0.44	75.39	0.19	3.03	6.33	25.3	0.266	3.16	1.10	0.397	0.82	5.18	0.086	0.052	112

Note: Depth in hole omitted for disturbed samples.

Table 5. Elemental abundance (wt.%) and water content (% dry wt.) of samples making up the composite section of Site 576.

Hole	Core	Section	Depth in Section (m)	Depth in hole (m)	Na	Mg	Al	Si	P	K	Ca	Ti	Mn	Fe	Ba	S	H_2O
76B	1	1	0.06	0.06	0.37	1.75	7.20	26.8	0.049	2.51	0.40	0.407	0.24	4.66	0.095	0.031	169
76B	1	1	0.16	0.16	0.28	1.74	7.15	26.8	0.049	2.51	0.40	0.400	0.28	4.57	0.093	0.040	179
76B	1	1	0.26	0.26	0.28	1.76	7.18	27.2	0.048	2.51	0.43	0.405	0.33	4.65	0.099	0.047	177
76B	1	1	0.36	0.36	0.24	1.70	7.02	27.3	0.048	2.42	0.46	0.393	0.31	4.62	0.105	0.040	184
76B	1	1	0.46	0.46	0.42	1.77	7.29	26.5	0.053	2.40	0.66	0.410	0.45	4.87	0.094	0.039	149
76B	1	1	0.56	0.56	0.50	1.84	7.53	26.7	0.054	2.46	0.77	0.434	0.50	5.08	0.097	0.050	134
76B	1	1	0.66	0.66	0.48	1.87	7.57	26.4	0.054	2.61	0.47	0.425	0.65	4.85	0.098	0.042	132
76B	1	1	0.76	0.76	0.46	1.88	7.66	26.7	0.053	2.68	0.43	0.438	0.24	4.93	0.093	0.038	130
76B	1	1	0.86	0.86	0.43	1.90	7.64	26.4	0.051	2.67	0.41	0.425	0.28	4.87	0.089	0.037	137
76B	1	1	0.96	0.96	0.46	1.85	7.61	26.4	0.052	2.62	0.46	0.426	0.36	4.87	0.087	0.033	137
76B	1	1	1.06	1.06	0.43	1.85	7.62	26.3	0.055	2.56	0.48	0.421	0.47	4.87	0.098	0.032	150
76B	1	1	1.16	1.16	0.43	1.84	7.54	26.4	0.053	2.57	0.48	0.425	0.52	4.84	0.100	0.041	145
76B	1	1	1.26	1.26	0.39	1.82	7.46	26.2	0.054	2.54	0.44	0.407	0.58	4.75	0.106	0.043	146
76B	1	1	1.36	1.36	0.42	1.87	7.52	26.5	0.055	2.55	0.44	0.419	0.83	4.75	0.103	0.040	146
76B	1	1	1.46	1.46	0.44	1.84	7.41	26.4	0.055	2.55	0.47	0.413	0.49	4.74	0.096	0.048	136
76B	1	2	0.06	1.56	0.40	1.88	7.40	26.5	0.053	2.60	0.43	0.422	0.37	4.78	0.097	0.043	138
76B	1	2	0.16	1.66	0.38	1.85	7.34	26.9	0.052	2.56	0.45	0.414	0.27	4.77	0.095	0.035	155
576B	1	2	0.26	1.76	0.16	1.69	6.71	27.7	0.050	2.38	0.30	0.383	0.27	4.41	0.104	0.031	200
576B	1	2	0.36	1.86	0.16	1.67	6.70	27.8	0.050	2.35	0.25	0.374	0.51	4.31	0.105	0.012	219
576B	1	2	0.46	1.96	0.28	1.71	6.82	27.6	0.050	2.36	0.23	0.374	0.61	4.30	0.103	0.000	226
576B	1	2	0.56	2.06	0.27	1.70	6.74	27.3	0.050	2.37	0.25	0.371	0.47	4.27	0.099	0.010	217
576B	1	2	0.66	2.16	0.11	1.79	6.98	27.7	0.049	2.50	0.30	0.393	0.33	4.46	0.099	0.037	228
576B	1	2	0.76	2.26	0.13	1.75	6.82	27.5	0.049	2.45	0.36	0.386	0.28	4.47	0.093	0.035	214
576B	1	2	0.86	2.36	0.40	1.77	7.15	26.9	0.050	2.49	0.37	0.397	0.14	4.66	0.096	0.007	195
576B	1	2	0.96	2.46	0.18	1.76	6.86	27.3	0.047	2.37	0.43	0.385	0.14	4.56	0.097	0.021	225
576B	1	2	1.06	2.56	0.17	1.76	7.01	27.5	0.049	2.53	0.26	0.389	0.12	4.53	0.097	0.019	210
576B	1	2	1.16	2.66	0.29	1.77	7.05	26.9	0.048	2.53	0.33	0.391	0.13	4.52	0.100	0.030	201
576B	1	2	1.26	2.76	0.29	1.76	7.25	27.0	0.050	2.52	0.37	0.407	0.12	4.64	0.093	0.022	188
576B	1	2	1.36	2.86	0.32	1.75	7.23	26.8	0.050	2.51	0.34	0.396	0.18	4.59	0.102	0.025	181
576B	1	2	1.46	2.96	0.10	1.66	6.89	27.3	0.049	2.34	0.22	0.367	0.17	4.33	0.107	0.006	252
576B	1	3	0.06	3.06	0.00	1.62	6.69	27.3	0.051	2.28	0.22	0.358	0.20	4.19	0.101	0.019	274
576B	1	3	0.16	3.16	0.29	1.74	7.23	26.5	0.053	2.48	0.38	0.396	0.26	4.60	0.089	0.033	189
576B	1	3	0.26	3.26	0.30	1.75	7.26	26.6	0.053	2.50	0.35	0.401	0.23	4.61	0.093	0.020	185
576B	1	3	0.36	3.36	0.36	1.76	7.31	26.5	0.054	2.53	0.41	0.405	0.34	4.64	0.089	0.037	166
576B	1	3	0.47	3.47	0.35	1.78	7.32	26.7	0.055	2.55	0.43	0.406	0.42	4.66	0.091	0.044	165
576B	1	3	0.56	3.56	0.39	1.76	7.26	26.4	0.054	2.54	0.44	0.403	0.34	4.66	0.093	0.051	153
576B	1	3	0.66	3.66	0.43	1.78	7.31	26.2	0.054	2.56	0.42	0.402	0.45	4.65	0.091	0.042	150
576B	1	3	0.76	3.76	0.43	1.77	7.31	26.3	0.054	2.57	0.42	0.408	0.37	4.70	0.090	0.033	144
576B	1	3	0.86	3.86	0.38	1.81	7.33	25.9	0.053	2.58	0.40	0.404	0.33	4.72	0.084	0.030	152
576B	1	3	0.96	3.96	0.40	1.79	7.44	26.2	0.055	2.56	0.43	0.409	0.34	4.70	0.092	0.024	157
576B	1	3	1.06	4.06	0.37	1.79	7.39	26.1	0.057	2.56	0.46	0.404	0.43	4.60	0.087	0.040	160
576B	1	3	1.16	4.16	0.34	1.78	7.42	26.1	0.056	2.53	0.44	0.403	0.38	4.62	0.088	0.031	152
576B	1	3	1.26	4.26	0.42	1.74	7.28	26.1	0.057	2.56	0.50	0.395	0.48	4.46	0.092	0.040	141
576B	1	3	1.36	4.36	0.39	1.74	7.33	26.5	0.054	2.60	0.51	0.394	0.27	4.50	0.095	0.046	144
576B	1	3	1.46	4.46	0.38	1.81	7.52	26.3	0.058	2.55	0.47	0.409	0.47	4.68	0.091	0.032	151
576B	1	4	0.06	4.56	0.37	1.78	7.42	26.1	0.058	2.55	0.50	0.400	0.48	4.61	0.094	0.045	144
576B	1	4	0.16	4.66	0.44	1.76	7.35	26.7	0.057	2.60	0.52	0.395	0.38	4.47	0.094	0.043	140
576B	1	4	0.26	4.76	0.35	1.88	7.41	25.8	0.054	2.58	0.44	0.412	0.30	4.75	0.098	0.055	148
576B	1	4	0.36	4.86	0.33	1.84	7.36	26.0	0.053	2.57	0.43	0.402	0.31	4.66	0.093	0.044	
576B	1	4	0.46	4.96	0.37	1.89	7.52	26.3	0.054	2.62	0.43	0.422	0.36	4.81	0.099	0.050	144
576B	1	4	0.56	5.06	0.33	1.91	7.52	26.3	0.053	2.65	0.42	0.422	0.29	4.81	0.099	0.055	145
576B	1	4	0.66	5.16	0.33	1.91	7.48	26.0	0.052	2.63	0.39	0.420	0.23	4.84	0.092	0.040	152
576B	1	4	0.76	5.26	0.31	1.92	7.50	26.0	0.054	2.65	0.43	0.414	0.26	4.79	0.087	0.059	151
576B	1	4	0.86	5.36	0.35	1.89	7.48	26.1	0.056	2.62	0.43	0.413	0.28	4.80	0.089	0.050	143
576B	1	4	0.96	5.46	0.35	1.92	7.56	26.2	0.053	2.64	0.41	0.421	0.24	4.83	0.090	0.042	153
576B	1	4	1.06	5.56	0.35	1.92	7.55	26.0	0.052	2.65	0.41	0.414	0.24	4.82	0.093	0.042	144
576B	1	4	1.16	5.66	0.37	1.97	7.69	26.4	0.052	2.70	0.42	0.438	0.24	4.93	0.097	0.047	142
576B	1	4	0.26	5.76	0.37	1.94	7.62	26.1	0.051	2.68	0.43	0.429	0.23	4.87	0.091	0.047	139
576B	1	4	1.36	5.86	0.42	1.93	7.61	26.0	0.051	2.68	0.45	0.428	0.26	4.83	0.093	0.058	138
576B	1	4	1.46	5.96	0.38	1.93	7.63	26.1	0.052	2.66	0.46	0.429	0.28	4.84	0.092	0.055	136
576B	1	5	0.06	6.06	0.38	1.92	7.73	26.3	0.054	2.65	0.46	0.433	0.34	4.90	0.091	0.050	139

Table 5. (Continued).

Hole	Core	Section	Depth in Section (m)	Depth in hole (m)	Na	Mg	Al	Si	P	K	Ca	Ti	Mn	Fe	Ba	S	H_2O
576B	1	5	0.16	6.16	0.39	1.88	7.59	26.0	0.055	2.60	0.47	0.422	0.35	4.79	0.092	0.051	143
576B	1	5	0.26	6.26	0.36	1.90	7.67	26.2	0.054	2.63	0.44	0.422	0.32	4.82	0.093	0.047	147
576B	1	5	0.36	6.36	0.32	1.88	7.62	26.4	0.055	2.61	0.47	0.419	0.35	4.76	0.091	0.048	154
576B	1	5	0.46	6.46	0.41	1.84	7.53	26.2	0.056	2.59	0.49	0.414	0.35	4.74	0.093	0.051	138
576B	1	5	0.56	6.56	0.46	1.86	7.56	26.5	0.056	2.62	0.51	0.419	0.34	4.75	0.094	0.060	133
576B	1	5	0.66	6.66	0.39	1.90	7.60	26.4	0.054	2.66	0.45	0.428	0.30	4.80	0.097	0.054	139
576B	1	5	0.76	6.76	0.41	1.91	7.58	26.4	0.054	2.65	0.46	0.427	0.31	4.79	0.096	0.054	137
576B	1	5	0.86	6.86	0.38	1.95	7.50	26.3	0.054	2.60	0.45	0.414	0.38	4.77	0.095	0.046	152
576B	1	5	0.96	6.96	0.38	1.89	7.43	26.6	0.048	2.58	0.45	0.407	0.36	4.58	0.083	0.032	147
576	2	1	0.06	7.01	0.53	2.01	7.61	26.1	0.051	2.69	0.45	0.425	0.63	4.79	0.091	0.060	134
576	2	1	0.16	7.11	0.55	2.03	7.60	26.4	0.047	2.73	0.49	0.430	0.28	4.80	0.085	0.091	149
576	2	1	0.26	7.21	0.52	1.97	7.59	26.4	0.050	2.66	0.44	0.417	0.36	4.70	0.088	0.050	159
576	2	1	0.36	7.31	0.59	1.98	7.48	26.2	0.050	2.67	0.51	0.417	0.44	4.68	0.096	0.088	145
576	2	1	0.46	7.41	0.51	2.01	7.56	26.4	0.053	2.69	0.50	0.417	0.38	4.70	0.091	0.091	158
576	2	1	0.56	7.51	0.57	2.04	7.59	26.3	0.052	2.75	0.48	0.431	0.33	4.80	0.092	0.088	144
576	2	1	0.66	7.61	0.48	2.03	7.63	26.1	0.051	2.77	0.43	0.428	0.28	4.82	0.086	0.076	143
576	2	1	0.76	7.71	0.56	2.08	7.61	26.3	0.053	2.77	0.48	0.431	0.27	4.83	0.091	0.095	146
576	2	1	0.86	7.81	0.52	2.01	7.67	26.3	0.050	2.72	0.41	0.430	0.25	4.86	0.086	0.052	144
576	2	1	0.96	7.91	0.46	2.01	7.53	26.1	0.051	2.68	0.42	0.418	0.29	4.76	0.090	0.058	159
576	2	1	1.06	8.01	0.44	2.04	7.58	26.1	0.050	2.70	0.42	0.414	0.31	4.75	0.095	0.067	159
576	2	1	1.16	8.11	0.59	2.07	7.64	26.3	0.051	2.78	0.50	0.430	0.32	4.87	0.095	0.095	146
576	2	1	1.26	8.21	0.43	2.05	7.62	26.2	0.053	2.67	0.44	0.417	0.38	4.77	0.089	0.065	168
576	2	1	1.36	8.31	0.39	2.01	7.49	26.4	0.052	2.61	0.46	0.408	0.39	4.65	0.088	0.073	178
576	2	1	1.46	8.41	0.48	1.98	7.58	26.2	0.057	2.59	0.42	0.413	0.39	4.71	0.088	0.036	154
576	2	2	0.06	8.51	0.49	2.00	7.61	26.3	0.055	2.65	0.45	0.418	0.34	4.77	0.089	0.049	145
576	2	2	0.16	8.61	0.46	1.99	7.58	26.2	0.054	2.61	0.47	0.418	0.39	4.79	0.087	0.049	147
576	2	2	0.26	8.71	0.45	1.96	7.59	26.4	0.053	2.58	0.46	0.414	0.39	4.77	0.087	0.032	159
576	2	2	0.36	8.81	0.47	2.01	7.58	26.2	0.055	2.61	0.43	0.416	0.41	4.75	0.094	0.048	156
576	2	2	0.46	8.91	0.46	1.99	7.60	26.5	0.054	2.60	0.41	0.413	0.42	4.74	0.096	0.029	161
576	2	2	0.56	9.01	0.46	2.00	7.54	26.3	0.053	2.61	0.40	0.414	0.29	4.74	0.094	0.041	165
576	2	2	0.66	9.11	0.46	2.06	7.54	26.3	0.048	2.68	0.47	0.418	0.39	4.78	0.090	0.072	161
576	2	2	0.76	9.21	0.45	1.98	7.48	26.3	0.049	2.59	0.42	0.410	0.39	4.72	0.092	0.043	170
576	2	2	0.86	9.31	0.32	2.03	7.36	26.7	0.050	2.58	0.42	0.398	0.26	4.73	0.087	0.070	207
576	2	2	0.96	9.41	0.37	1.96	7.48	26.5	0.056	2.55	0.43	0.411	0.26	4.68	0.087	0.043	194
576	2	2	1.06	9.51	0.49	2.02	7.51	26.4	0.058	2.64	0.55	0.422	0.46	4.72	0.085	0.082	163
576	2	2	1.16	9.61	0.47	1.96	7.46	26.2	0.056	2.55	0.44	0.406	0.40	4.65	0.085	0.041	170
576	2	2	1.26	9.71	0.53	2.03	7.46	26.2	0.053	2.67	0.54	0.418	0.36	4.75	0.093	0.081	149
576	2	2	1.36	9.81	0.48	1.97	7.46	26.2	0.054	2.61	0.46	0.412	0.37	4.71	0.094	0.055	154
576	2	2	1.46	9.91	0.69	2.04	7.53	26.1	0.050	2.76	0.51	0.429	0.39	4.83	0.098	0.107	154
576	2	3	0.06	10.01	0.50	2.03	7.56	26.0	0.051	2.69	0.41	0.422	0.39	4.75	0.099	0.088	176
576	2	3	0.16	10.11	0.50	2.05	7.44	26.1	0.050	2.72	0.47	0.414	0.38	4.70	0.101	0.118	185
576	2	3	0.26	10.21	0.40	1.98	7.40	26.4	0.051	2.55	0.36	0.396	0.30	4.55	0.095	0.051	218
576	2	3	0.36	10.31	0.29	1.83	6.98	27.3	0.052	2.43	0.39	0.389	0.52	4.40	0.095	0.056	218
576	2	3	0.46	10.41	0.55	1.90	7.44	26.4	0.057	2.52	0.43	0.409	0.49	4.64	0.086	0.033	180
576	2	3	0.56	10.51	0.51	1.95	7.37	26.3	0.053	2.59	0.53	0.410	0.44	4.62	0.089	0.074	163
576	2	3	0.66	10.61	0.55	1.94	7.41	26.2	0.051	2.60	0.50	0.408	0.41	4.67	0.087	0.059	142
576	2	3	0.76	10.71	0.60	1.91	7.31	26.5	0.048	2.63	0.57	0.402	0.37	4.48	0.087	0.073	138
576	2	3	0.86	10.81	0.59	1.78	7.15	26.6	0.046	2.55	0.57	0.373	0.35	4.13	0.089	0.042	122
576	2	3	0.96	10.91	0.61	1.77	7.05	26.6	0.043	2.67	0.54	0.358	0.38	3.95	0.083	0.075	127
576	2	3	1.06	11.01	0.53	1.98	7.50	26.0	0.050	2.65	0.45	0.417	0.56	4.70	0.092	0.065	146
576	2	3	1.16	11.11	0.57	2.07	7.58	26.1	0.050	2.71	0.48	0.431	0.46	4.81	0.089	0.085	149
576	2	3	1.26	11.21	0.56	2.03	7.61	26.3	0.045	2.70	0.40	0.421	0.38	4.73	0.090	0.062	157
576	2	3	1.36	11.31	0.46	2.05	7.52	26.3	0.048	2.67	0.44	0.421	0.28	4.74	0.095	0.081	168
576	2	3	1.46	11.41	0.55	2.00	7.58	26.1	0.047	2.70	0.38	0.424	0.28	4.81	0.092	0.050	147
576	2	4	0.06	11.51	0.51	2.04	7.61	26.4	0.053	2.68	0.49	0.420	0.43	4.76	0.094	0.072	155
576	2	4	0.16	11.61	0.45	2.01	7.58	26.3	0.056	2.61	0.42	0.415	0.47	4.69	0.091	0.052	165
576	2	4	0.26	11.71	0.37	1.98	7.39	26.4	0.054	2.58	0.41	0.401	0.51	4.51	0.092	0.046	181
576	2	4	0.36	11.81	0.48	2.02	7.57	26.4	0.052	2.62	0.38	0.406	0.46	4.64	0.095	0.031	164
576	2	4	0.46	11.91	0.49	1.99	7.48	26.5	0.054	2.62	0.45	0.397	0.46	4.51	0.092	0.050	149
576	2	4	0.56	12.01	0.54	1.98	7.45	26.4	0.054	2.62	0.43	0.405	0.41	4.55	0.095	0.044	140
576	2	4	0.66	12.11	0.65	1.48	6.64	27.5	0.045	3.02	0.44	0.275	0.32	3.25	0.090	0.042	119

Table 5. (Continued).

Hole	Core	Section	Depth in Section (m)	Depth in hole (m)	Na	Mg	Al	Si	P	K	Ca	Ti	Mn	Fe	Ba	S	H_2O
76	2	4	0.76	12.21	0.49	2.00	7.60	26.4	0.049	2.65	0.30	0.399	0.37	4.54	0.091	0.015	178
76	2	4	0.86	12.31	0.37	2.06	7.46	26.5	0.053	2.61	0.41	0.402	0.47	4.52	0.092	0.052	177
76	2	4	0.96	12.41	0.47	2.03	7.58	26.4	0.050	2.66	0.39	0.411	0.30	4.67	0.087	0.039	165
76	2	4	1.06	12.51	0.38	2.03	7.54	26.2	0.053	2.59	0.42	0.411	0.42	4.66	0.093	0.041	174
76	2	4	1.16	12.61	0.45	1.97	7.41	26.3	0.054	2.47	0.45	0.400	0.46	4.59	0.092	0.031	180
76	2	4	1.26	12.71	0.42	2.01	7.42	26.4	0.055	2.56	0.43	0.405	0.48	4.62	0.089	0.053	175
76	2	4	1.36	12.81	0.37	2.03	7.53	26.2	0.051	2.59	0.35	0.411	0.49	4.70	0.090	0.035	176
76	2	4	1.46	12.91	0.33	2.11	7.59	26.4	0.054	2.62	0.39	0.411	0.48	4.67	0.096	0.057	185
76	2	5	0.06	13.01	0.39	2.03	7.63	26.4	0.055	2.54	0.32	0.411	0.52	4.64	0.099	0.021	202
76	2	5	0.16	13.11	0.32	2.06	7.50	26.4	0.056	2.55	0.39	0.404	0.51	4.56	0.089	0.048	198
76	2	5	0.26	13.21	0.42	2.00	7.47	26.3	0.055	2.53	0.39	0.404	0.52	4.58	0.089	0.038	176
76	2	5	0.36	13.31	0.40	2.02	7.48	26.7	0.056	2.55	0.41	0.405	0.50	4.56	0.093	0.049	183
76	2	5	0.46	13.41	0.45	2.00	7.51	26.8	0.054	2.55	0.33	0.400	0.48	4.59	0.090	0.013	192
76	2	5	0.56	13.51	0.35	2.06	7.50	26.4	0.053	2.62	0.36	0.400	0.42	4.58	0.090	0.045	181
76	2	5	0.66	13.61	0.40	2.02	7.53	26.6	0.052	2.55	0.29	0.396	0.41	4.57	0.096	0.011	195
76	2	5	0.76	13.71	0.28	2.04	7.41	26.8	0.053	2.48	0.40	0.396	0.43	4.52	0.093	0.042	220
76	2	5	0.86	13.81	0.42	1.98	7.39	26.6	0.053	2.46	0.41	0.396	0.41	4.59	0.091	0.018	192
76	2	5	0.96	13.91	0.44	1.99	7.42	26.7	0.051	2.51	0.44	0.408	0.38	4.67	0.091	0.021	171
76	2	5	1.05	14.00	0.46	1.99	7.38	26.5	0.052	2.48	0.41	0.396	0.41	4.63	0.089	0.019	178
76B	2	2	0.56	14.06	0.34	1.99	7.37	26.3	0.049	2.59	0.45	0.416	0.36	4.72	0.091	0.069	150
576B	2	2	0.66	14.16	0.28	1.99	7.28	25.7	0.046	2.56	0.43	0.404	0.35	4.64	0.093	0.080	164
576B	2	2	0.76	14.26	0.26	2.03	7.55	26.3	0.047	2.64	0.39	0.424	0.37	4.73	0.094	0.067	158
576B	2	2	0.86	14.36	0.18	2.01	7.55	26.0	0.051	2.59	0.34	0.410	0.38	4.64	0.103	0.052	185
576B	2	2	0.96	14.46	0.12	2.01	7.55	26.1	0.052	2.60	0.33	0.412	0.40	4.63	0.099	0.049	188
576	2	5	1.16	14.51	0.46	2.02	7.46	26.6	0.050	2.56	0.43	0.412	0.38	4.70	0.092	0.033	154
576	2	5	1.26	14.61	0.43	2.09	7.62	26.4	0.046	2.61	0.35	0.415	0.40	4.71	0.093	0.026	172
576	2	5	1.36	14.71	0.42	2.09	7.60	26.6	0.050	2.64	0.42	0.416	0.43	4.63	0.099	0.058	172
576	2	5	1.46	14.81	0.47	2.04	7.64	26.3	0.052	2.58	0.31	0.409	0.45	4.65	0.100	0.014	178
576	2	6	0.06	14.91	0.41	2.07	7.63	26.4	0.053	2.63	0.38	0.409	0.50	4.64	0.100	0.039	172
576	2	6	0.16	15.01	0.36	2.03	7.58	26.6	0.054	2.62	0.37	0.399	0.42	4.54	0.100	0.029	175
576	2	6	0.26	15.11	0.40	2.01	7.50	26.8	0.055	2.59	0.38	0.395	0.41	4.44	0.104	0.024	178
576	2	6	0.36	15.21	0.40	2.03	7.57	26.4	0.053	2.56	0.32	0.399	0.41	4.51	0.097	0.018	197
576	2	6	0.46	15.31	0.41	2.08	7.64	26.5	0.056	2.56	0.36	0.409	0.46	4.65	0.095	0.020	172
576	2	6	0.56	15.41	0.43	2.06	7.52	26.3	0.057	2.44	0.33	0.404	0.52	4.55	0.098	0.012	182
576	2	6	0.66	15.51	0.35	2.04	7.57	26.7	0.057	2.49	0.35	0.407	0.53	4.55	0.097	0.011	196
576	2	6	0.76	15.61	0.34	2.07	7.52	26.3	0.055	2.46	0.33	0.398	0.50	4.53	0.095	0.021	194
576	2	6	0.86	15.71	0.29	2.07	7.58	26.6	0.056	2.51	0.37	0.407	0.48	4.56	0.094	0.027	200
576	2	6	0.96	15.81	0.42	2.04	7.54	26.2	0.058	2.43	0.36	0.401	0.49	4.59	0.094	0.014	204
576	2	6	1.06	15.91	0.24	2.09	7.59	26.4	0.058	2.45	0.40	0.404	0.45	4.58	0.095	0.040	202
576	2	6	1.16	16.01	0.39	2.08	7.52	26.2	0.056	2.44	0.41	0.406	0.49	4.59	0.095	0.042	191
576	2	6	1.26	16.11	0.39	2.08	7.57	26.4	0.057	2.43	0.39	0.403	0.49	4.61	0.096	0.020	190
576	2	6	1.36	16.21	0.44	2.10	7.67	26.3	0.053	2.52	0.36	0.416	0.46	4.69	0.092	0.022	176
576	2	6	1.46	16.31	0.38	2.13	7.60	26.2	0.054	2.56	0.43	0.418	0.40	4.68	0.092	0.057	165
576	2	7	0.06	16.41	0.45	2.10	7.66	26.3	0.054	2.56	0.39	0.418	0.43	4.72	0.094	0.039	165
576	2	7	0.16	16.51	0.44	2.09	7.69	26.6	0.056	2.62	0.41	0.419	0.43	4.72	0.094	0.037	163
576	2	7	0.26	16.61	0.41	2.12	7.60	26.2	0.054	2.49	0.38	0.406	0.49	4.67	0.091	0.032	186
576	2	7	0.36	16.71	0.33	2.15	7.62	26.3	0.057	2.49	0.43	0.410	0.46	4.66	0.093	0.047	181
576	2	7	0.46	16.81	0.42	2.13	7.62	26.2	0.056	2.46	0.41	0.410	0.51	4.70	0.093	0.033	181
576B	2	4	0.46	16.96	0.28	2.04	7.67	26.2	0.052	2.63	0.39	0.436	0.35	4.83	0.096	0.052	162
576B	2	4	0.56	17.06	0.24	2.03	7.63	26.1	0.052	2.56	0.36	0.424	0.40	4.79	0.093	0.031	166
576B	2	4	0.66	17.16	0.28	2.06	7.66	26.0	0.048	2.62	0.37	0.429	0.36	4.89	0.098	0.055	154
576B	2	4	0.76	17.26	0.34	2.04	7.65	26.0	0.048	2.58	0.37	0.429	0.35	4.89	0.092	0.041	156
576B	2	4	0.86	17.36	0.31	2.10	7.63	26.0	0.050	2.54	0.41	0.428	0.38	4.82	0.096	0.057	155
576B	2	4	0.96	17.46	0.20	2.06	7.64	25.9	0.051	2.60	0.34	0.419	0.43	4.75	0.108	0.044	169
576B	2	4	1.06	17.56	0.28	2.09	7.62	25.9	0.048	2.65	0.35	0.415	0.35	4.75	0.101	0.060	156
576B	2	4	1.16	17.66	0.31	2.07	7.60	25.9	0.046	2.71	0.35	0.422	0.33	4.78	0.100	0.065	146
576B	2	4	1.26	17.76	0.33	2.06	7.70	26.2	0.045	2.74	0.33	0.428	0.31	4.85	0.105	0.055	141
576B	2	4	1.36	17.86	0.28	2.11	7.81	26.4	0.046	2.69	0.32	0.427	0.34	4.81	0.126	0.049	155
576B	2	4	1.46	17.96	0.25	2.14	7.74	26.3	0.044	2.52	0.33	0.417	0.37	4.61	0.098	0.054	173
576B	2	5	0.06	18.06	0.21	2.21	7.71	26.3	0.048	2.37	0.33	0.407	0.44	4.44	0.098	0.052	180
576B	2	5	0.16	18.16	0.20	2.28	7.67	26.2	0.050	2.20	0.35	0.391	0.40	4.24	0.083	0.053	193

Table 5. (Continued).

Hole	Core	Section	Depth in Section (m)	Depth in hole (m)	Na	Mg	Al	Si	P	K	Ca	Ti	Mn	Fe	Ba	S	H_2
576B	2	5	0.25	18.25	0.24	2.36	7.83	26.6	0.049	2.01	0.36	0.381	0.36	3.99	0.075	0.044	19
576B	2	5	0.36	18.36	0.39	2.31	7.74	26.3	0.048	1.87	0.42	0.356	0.31	3.74	0.073	0.051	16
576B	2	5	0.46	18.46	0.35	2.25	7.68	26.1	0.051	2.11	0.39	0.386	0.42	4.18	0.076	0.051	16
576B	2	5	0.56	18.56	0.35	2.23	7.73	26.3	0.052	2.34	0.40	0.408	0.42	4.48	0.085	0.057	15
576B	2	5	0.66	18.66	0.30	2.10	7.63	25.9	0.051	2.47	0.36	0.409	0.42	4.61	0.088	0.053	24
576B	2	5	0.76	18.76	0.38	2.10	7.82	26.3	0.051	2.67	0.39	0.434	0.42	4.87	0.093	0.064	13
576B	2	5	0.86	18.86	0.27	2.06	7.72	26.0	0.049	2.60	0.37	0.427	0.45	4.83	0.097	0.054	16
576	4	1	0.76	18.96	0.45	2.17	7.79	26.4	0.054	2.62	0.46	0.425	0.49	4.81	0.094	0.072	16
576	4	1	0.86	19.06	0.38	2.12	7.65	25.7	0.058	2.38	0.51	0.406	0.56	4.82	0.089	0.037	19
576	4	1	0.96	19.16	0.40	2.15	7.87	26.3	0.058	2.43	0.52	0.428	0.55	4.93	0.088	0.031	18
576	4	1	1.06	19.26	0.43	2.12	7.76	26.0	0.059	2.45	0.49	0.410	0.55	4.86	0.088	0.028	17
576	4	1	1.16	19.36	0.44	2.11	7.73	25.8	0.059	2.53	0.44	0.415	0.55	4.80	0.088	0.038	17
576	4	1	1.26	19.46	0.40	2.12	7.88	26.3	0.058	2.59	0.44	0.439	0.57	4.94	0.088	0.038	17
576	4	1	1.36	19.56	0.42	2.09	7.74	25.9	0.055	2.57	0.44	0.422	0.54	4.88	0.088	0.042	17
576	4	1	1.46	19.66	0.47	2.11	7.82	26.0	0.056	2.60	0.44	0.429	0.57	4.94	0.092	0.045	15
576	4	2	0.05	19.75	0.41	2.10	7.85	26.0	0.056	2.61	0.46	0.424	0.55	4.91	0.087	0.042	16
576	4	2	0.16	19.86	0.44	2.10	7.80	25.9	0.058	2.58	0.44	0.425	0.55	4.87	0.086	0.048	16
576	4	2	0.26	19.96	0.43	2.10	7.82	26.0	0.056	2.62	0.41	0.427	0.54	4.91	0.092	0.044	155
576	4	2	0.36	20.06	0.45	2.C7	7.81	25.8	0.054	2.61	0.40	0.421	0.52	4.87	0.089	0.046	155
576	4	2	0.46	20.16	0.48	2.07	7.85	26.0	0.057	2.67	0.43	0.431	0.50	4.96	0.091	0.054	148
576	4	2	0.56	20.26	0.45	2.06	7.79	25.7	0.055	2.58	0.45	0.424	0.55	4.93	0.088	0.049	160
576	4	2	0.66	20.36	0.47	2.11	7.92	26.0	0.058	2.6'	0.46	0.432	0.58	5.00	0.087	0.064	165
576	4	2	0.76	20.46	0.43	2.07	7.83	25.6	0.058	2.57	0.45	0.422	0.59	4.95	0.089	0.051	159
576	4	2	0.86	20.56	0.47	2.06	7.92	25.8	0.060	2.61	0.47	0.434	0.60	5.01	0.087	0.057	153
576	4	2	0.96	20.66	0.45	2.02	7.83	25.5	0.060	2.57	0.46	0.424	0.61	4.97	0.085	0.048	160
576	4	2	1.06	20.76	0.53	2.01	7.92	25.7	0.059	2.60	0.49	0.442	0.61	5.08	0.082	0.046	144
576	4	2	1.16	20.86	0.47	2.01	7.93	25.7	0.057	2.60	0.49	0.432	0.60	5.04	0.083	0.048	148
576	4	2	1.26	20.96	0.47	1.99	7.80	25.6	0.054	2.66	0.43	0.426	0.59	4.93	0.088	0.057	150
576	4	2	1.36	21.06	0.44	2.00	7.72	25.3	0.057	2.60	0.43	0.418	0.62	4.89	0.088	0.053	157
576	4	2	1.46	21.16	0.50	2.02	7.84	25.7	0.059	2.63	0.45	0.432	0.62	4.97	0.088	0.054	152
576	4	3	0.06	21.26	0.51	2.01	7.59	25.0	0.058	2.56	0.47	0.412	0.61	4.89	0.085	0.066	148
576	4	3	0.16	21.36	0.47	2.05	7.77	25.5	0.060	2.59	0.46	0.436	0.67	4.98	0.086	0.057	149
576	4	3	0.26	21.46	0.49	2.05	7.82	25.6	0.063	2.62	0.46	0.436	0.71	4.99	0.085	0.059	155
576	4	3	0.36	21.56	0.46	2.07	7.78	25.3	0.063	2.60	0.44	0.427	0.71	4.99	0.085	0.057	152
576	4	3	0.46	21.66	0.53	2.05	7.83	25.5	0.058	2.63	0.45	0.426	0.67	5.01	0.085	0.058	146
576	4	3	0.56	21.76	0.48	2.05	7.85	25.6	0.054	2.63	0.45	0.434	0.67	5.04	0.084	0.056	148
576	4	3	0.66	21.86	0.50	2.03	7.82	25.5	0.053	2.58	0.49	0.429	0.66	5.07	0.079	0.052	151
576	4	3	0.76	21.96	0.50	2.03	7.82	25.4	0.053	2.57	0.49	0.434	0.66	5.08	0.081	0.048	141
576	4	3	0.86	22.06	0.46	2.02	7.84	25.5	0.059	2.63	0.42	0.438	0.70	5.00	0.086	0.045	144
576	4	3	0.96	22.16	0.50	2.06	7.97	25.8	0.061	2.70	0.44	0.447	0.66	5.04	0.086	0.057	144
576	4	3	1.06	22.26	0.51	2.07	7.83	25.4	0.061	2.64	0.44	0.433	0.67	4.98	0.086	0.062	146
576	4	3	1.16	22.36	0.49	2.06	7.99	26.0	0.059	2.69	0.43	0.447	0.71	5.08	0.088	0.047	140
576	4	3	1.26	22.46	0.47	2.04	7.88	25.6	0.061	2.66	0.43	0.442	0.68	5.02	0.085	0.063	146
576	4	3	1.36	22.56	0.44	2.04	7.86	25.4	0.060	2.63	0.42	0.439	0.69	5.01	0.085	0.074	154
576	4	3	1.46	22.66	0.40	2.05	7.87	25.5	0.059	2.57	0.41	0.439	0.69	5.03	0.083	0.070	158
576	4	4	0.06	22.76	0.49	2.04	7.85	25.6	0.060	2.65	0.43	0.443	0.78	5.04	0.087	0.060	146
576	4	4	0.16	22.86	0.49	2.04	7.86	25.5	0.063	2.65	0.43	0.444	0.74	5.03	0.086	0.065	143
576	4	4	0.26	22.96	0.47	2.01	7.89	25.5	0.065	2.65	0.44	0.433	0.73	4.96	0.085	0.061	143
576	4	4	0.36	23.06	0.48	2.03	7.81	25.3	0.064	2.66	0.44	0.432	0.70	4.95	0.083	0.066	138
576	4	4	0.46	23.16	0.49	2.02	7.80	25.4	0.065	2.70	0.43	0.435	0.70	4.98	0.084	0.069	134
576	4	4	0.56	23.26	0.48	2.02	7.78	25.4	0.063	2.70	0.42	0.440	0.68	4.97	0.084	0.068	135
576	4	4	0.66	23.36	0.53	2.01	7.75	25.2	0.061	2.72	0.41	0.437	0.70	4.99	0.087	0.074	127
576	4	4	0.76	23.46	0.51	1.98	7.75	25.2	0.058	2.72	0.40	0.432	0.64	4.96	0.080	0.070	131
576	4	4	0.86	23.56	0.53	1.98	7.87	25.4	0.063	2.74	0.42	0.438	0.64	4.99	0.083	0.071	127
576	4	4	0.96	23.66	0.51	1.99	7.85	25.3	0.068	2.73	0.43	0.431	0.68	4.92	0.081	0.074	134
576	4	4	1.06	23.76	0.47	1.96	7.81	25.3	0.069	2.70	0.43	0.432	0.69	4.91	0.079	0.066	131
576	4	4	1.16	23.86	0.47	1.98	7.84	25.3	0.067	2.71	0.42	0.437	0.64	4.92	0.079	0.073	138
576	4	4	1.26	23.96	0.45	1.98	7.86	25.4	0.069	2.69	0.43	0.434	0.65	4.94	0.080	0.064	140
576	4	4	1.36	24.06	0.45	1.97	7.85	25.4	0.064	2.69	0.41	0.437	0.65	4.97	0.079	0.056	135
576	4	4	1.46	24.16	0.48	1.98	7.93	25.6	0.063	2.67	0.45	0.448	0.63	5.07	0.078	0.065	137
576	4	5	0.06	24.26	0.46	1.95	7.91	25.5	0.060	2.65	0.44	0.444	0.64	5.06	0.076	0.049	138

Table 5. (Continued).

Hole	Core	Section	Depth in Section (m)	Depth in hole (m)	Na	Mg	Al	Si	P	K	Ca	Ti	Mn	Fe	Ba	S	H_2O
576	4	5	0.16	24.36	0.44	1.98	7.91	25.6	0.060	2.68	0.40	0.440	0.66	5.00	0.077	0.046	139
576	4	5	0.26	24.46	0.43	1.99	7.93	25.6	0.067	2.66	0.41	0.443	0.68	4.98	0.079	0.048	140
576	4	5	0.36	24.56	0.47	2.00	7.86	25.5	0.070	2.68	0.42	0.444	0.71	4.98	0.080	0.056	133
576	4	5	0.46	24.66	0.49	2.01	7.91	25.6	0.072	2.69	0.43	0.451	0.72	5.04	0.082	0.054	132
576	4	5	0.56	24.76	0.46	2.02	7.95	25.7	0.075	2.70	0.42	0.446	0.70	5.02	0.087	0.051	136
576	4	5	0.66	24.86	0.43	1.98	7.90	25.5	0.071	2.66	0.39	0.437	0.72	4.97	0.081	0.036	135
576	4	5	0.76	24.96	0.44	1.99	7.87	25.4	0.071	2.68	0.41	0.444	0.71	4.96	0.080	0.049	134
576	4	5	0.86	25.06	0.41	2.00	7.96	25.6	0.072	2.71	0.40	0.442	0.75	4.99	0.077	0.049	141
576	4	5	0.96	25.16	0.41	2.00	7.94	25.5	0.071	2.71	0.38	0.440	0.72	4.97	0.081	0.053	143
576	4	5	1.06	25.26	0.45	1.99	7.89	25.4	0.067	2.70	0.36	0.430	0.67	4.92	0.077	0.049	134
576	4	5	1.16	25.36	0.45	2.01	7.93	25.4	0.070	2.72	0.40	0.434	0.72	4.91	0.078	0.069	137
576	4	5	1.26	25.46	0.46	2.01	7.84	25.4	0.067	2.73	0.39	0.437	0.71	4.93	0.080	0.063	129
576	4	5	1.36	25.56	0.49	2.00	7.88	25.6	0.068	2.80	0.39	0.445	0.54	5.01	0.077	0.059	121
576	4	5	1.46	25.66	0.50	1.99	7.81	25.5	0.066	2.83	0.39	0.447	0.60	4.98	0.079	0.062	117
576	4	6	0.06	25.76	0.51	2.01	7.89	25.7	0.066	2.83	0.39	0.450	0.67	5.05	0.080	0.053	117
576	4	6	0.16	25.86	0.53	2.00	7.78	25.4	0.069	2.83	0.40	0.446	0.61	5.02	0.079	0.063	110
576	4	6	0.26	25.96	0.51	2.01	7.83	25.6	0.073	2.83	0.39	0.451	0.61	5.06	0.076	0.057	116
576	4	6	0.36	26.06	0.45	2.03	7.86	25.7	0.079	2.81	0.39	0.456	0.69	5.14	0.082	0.045	117
576	4	6	0.46	26.16	0.51	2.03	7.72	[illegible].5	0.094	2.79	0.42	0.468	0.79	5.21	0.084	0.041	109
576	4	6	0.56	26.26	0.50	2.10	7.51	25.1	0.124	2.80	0.52	0.482	0.85	5.40	0.092	0.057	115
576	4	6	0.66	26.36	0.45	2.18	7.42	25.3	0.163	2.77	0.59	0.522	0.99	5.63	0.110	0.045	124
576	4	6	0.76	26.46	0.47	2.16	7.27	25.0	0.167	2.75	0.63	0.515	0.99	5.57	0.110	0.056	124
576	4	6	0.86	26.56	0.46	2.14	7.34	25.1	0.157	2.76	0.58	0.511	0.91	5.54	0.106	0.045	123
576	4	6	0.96	26.66	0.46	2.17	7.28	25.1	0.174	2.76	0.64	0.523	0.99	5.61	0.115	0.054	129
576	4	6	1.06	26.76	0.45	2.18	7.18	24.9	0.173	2.73	0.64	0.511	0.98	5.55	0.117	0.059	131
576	4	6	1.16	26.86	0.46	2.17	7.19	24.8	0.174	2.74	0.64	0.514	0.97	5.54	0.115	0.057	127
576	4	6	1.26	26.96	0.44	2.18	7.23	25.0	0.176	2.74	0.64	0.518	0.98	5.58	0.114	0.057	128
576	4	6	1.36	27.06	0.48	2.19	7.25	25.1	0.183	2.78	0.68	0.525	0.97	5.59	0.115	0.070	129
576	4	6	1.46	27.16	0.46	2.17	7.13	24.7	0.178	2.74	0.67	0.507	0.96	5.52	0.112	0.069	132
576	4	7	0.06	27.26	0.45	2.17	7.20	24.9	0.189	2.75	0.70	0.522	0.98	5.55	0.117	0.066	128
576	4	7	0.16	27.36	0.44	2.17	7.27	25.1	0.186	2.76	0.68	0.527	1.01	5.59	0.116	0.062	130
576	4	7	0.26	27.46	0.47	2.17	7.25	24.9	0.181	2.76	0.68	0.523	1.01	5.58	0.117	0.066	129
576	4	7	0.36	27.56	0.49	2.19	7.21	24.9	0.193	2.77	0.73	0.532	1.00	5.55	0.115	0.082	127
576	4	7	0.46	27.66	0.45	2.15	7.13	24.6	0.196	2.73	0.72	0.514	1.00	5.50	0.117	0.076	128
576B	3	6	0.26	27.92	0.44	2.06	7.86	25.1	0.093	2.77	0.44	0.473	0.95	5.35	0.082	0.053	118
576B	3	6	0.46	28.12	0.49	2.08	7.78	24.7	0.109	2.78	0.50	0.459	0.96	5.26	0.080	0.076	119
576B	3	6	0.66	28.32	0.48	2.08	7.85	24.9	0.103	2.82	0.50	0.464	1.04	5.35	0.078	0.062	118
576B	3	6	0.86	28.52	0.48	2.03	7.77	24.8	0.100	2.80	0.47	0.450	0.99	5.23	0.079	0.058	113
576B	3	6	1.06	28.72	0.51	2.07	7.85	24.9	0.107	2.85	0.49	0.465	1.03	5.34	0.081	0.067	113
576B	3	6	1.26	28.92	0.50	2.03	7.77	24.8	0.114	2.84	0.52	0.466	1.05	5.29	0.072	0.068	115
576B	3	6	1.46	29.12	0.50	2.01	7.71	24.4	0.117	2.75	0.53	0.461	1.05	5.28	0.072	0.065	119
576B	3	7	0.06	29.22	0.51	2.01	7.75	24.5	0.122	2.76	0.53	0.462	1.01	5.34	0.075	0.060	119
576B	3	7	0.26	29.42	0.54	2.01	7.77	24.3	0.129	2.76	0.57	0.461	1.22	5.26	0.074	0.072	124
576B	3	7	0.46	29.62	0.54	1.98	7.80	24.3	0.128	2.75	0.55	0.457	1.21	5.27	0.072	0.061	124
576A	4	1	0.74	29.64	0.67	1.90	7.95	24.2	0.137	2.74	0.50	0.445	1.30	5.27	0.073	0.037	127
576A	4	1	0.78	29.68	0.71	1.88	7.94	24.0	0.133	2.72	0.49	0.447	1.33	5.29	0.072	0.046	
576A	4	1	0.99	29.89	0.80	1.89	7.98	24.1	0.136	2.73	0.50	0.447	1.41	5.36	0.071	0.041	121
576A	4	1	1.39	30.29	0.65	1.94	8.01	24.4	0.123	2.72	0.43	0.454	1.32	5.36	0.071	0.042	129
576A	4	2	0.19	30.59	0.69	2.02	7.88	23.9	0.127	2.79	0.61	0.462	1.39	5.41	0.073	0.085	
576	5	5	0.56	31.06	0.54	2.06	7.88	24.0	0.150	2.65	0.61	0.444	1.49	5.37	0.074	0.073	134
576	5	5	0.66	31.16	0.51	2.06	7.89	23.8	0.156	2.63	0.61	0.447	1.56	5.37	0.074	0.064	134
576	5	5	0.76	31.26	0.57	2.02	7.93	24.0	0.155	2.72	0.61	0.446	1.47	5.34	0.072	0.057	129
576	5	5	0.86	31.36	0.65	1.91	7.83	23.6	0.151	2.73	0.61	0.418	1.40	5.05	0.067	0.059	139
576	5	5	0.96	31.46	0.54	2.02	7.79	23.8	0.172	2.60	0.67	0.438	1.61	5.32	0.068	0.060	146
576B	4	3	1.06	31.56	0.46	2.00	7.76	23.7	0.180	2.58	0.66	0.435	1.57	5.31	0.070	0.063	151
576B	4	3	1.26	31.76	0.52	1.96	7.69	23.7	0.198	2.69	0.74	0.446	1.68	5.31	0.074	0.072	139
576B	4	3	1.46	31.96	0.42	1.99	7.72	23.4	0.203	2.56	0.70	0.454	1.83	5.61	0.071	0.061	159
576B	4	4	0.06	32.06	0.44	2.01	7.73	23.4	0.205	2.61	0.75	0.455	1.77	5.61	0.073	0.084	149
576B	4	4	0.26	32.26	0.40	1.97	7.74	23.4	0.215	2.59	0.71	0.443	1.86	5.46	0.072	0.058	152
576B	4	4	0.46	32.46	0.42	1.98	7.75	23.4	0.205	2.65	0.69	0.439	1.70	5.31	0.072	0.068	138
576B	4	4	0.66	32.66	0.43	1.97	7.79	23.7	0.172	2.77	0.58	0.430	1.45	5.07	0.072	0.060	128

Table 5. (Continued).

Hole	Core	Section	Depth in Section (m)	Depth in hole (m)	Na	Mg	Al	Si	P	K	Ca	Ti	Mn	Fe	Ba	S	H_2O
576B	4	4	0.86	32.86	0.43	2.02	7.87	24.0	0.158	2.81	0.55	0.442	1.42	5.15	0.071	0.067	127
576B	4	4	1.06	33.06	0.43	1.98	7.73	23.6	0.170	2.70	0.62	0.446	1.61	5.22	0.070	0.074	142
576B	4	4	1.26	33.26	0.44	1.98	7.72	23.5	0.193	2.62	0.68	0.450	1.83	5.31	0.074	0.067	148
576B	4	4	1.46	33.46	0.42	1.95	7.71	23.3	0.232	2.62	0.77	0.446	2.04	5.25	0.074	0.073	154
576B	4	5	0.06	33.56	0.42	1.99	7.77	23.5	0.214	2.67	0.75	0.457	2.01	5.26	0.074	0.076	153
576B	4	5	0.26	33.76	0.40	1.99	7.59	23.0	0.262	2.55	0.90	0.462	2.19	5.33	0.074	0.083	148
576B	4	5	0.46	33.96	0.41	1.96	7.79	23.4	0.250	2.53	0.76	0.458	2.07	5.46	0.075	0.043	157
576B	4	5	0.66	34.16	0.40	1.99	7.54	22.9	0.288	2.57	0.95	0.455	2.03	5.33	0.073	0.094	153
576B	4	5	0.86	34.36	0.34	2.03	7.57	23.1	0.289	2.61	0.97	0.463	2.05	5.40	0.074	0.086	150
576B	4	5	1.06	34.56	0.35	2.04	7.54	23.1	0.312	2.62	1.01	0.468	2.15	5.46	0.077	0.081	149
576B	4	5	1.26	34.76	0.31	2.07	7.38	23.0	0.443	2.59	1.28	0.457	2.20	5.54	0.077	0.086	154
576B	4	5	1.46	34.96	0.32	2.07	7.29	22.7	0.458	2.59	1.37	0.455	2.13	5.47	0.076	0.095	151
576B	4	6	0.06	35.06	0.33	2.06	7.35	22.8	0.449	2.61	1.36	0.454	2.12	5.48	0.076	0.096	148
576B	4	6	0.26	35.26	0.34	2.07	7.30	22.7	0.457	2.61	1.39	0.452	2.12	5.47	0.075	0.100	149
576B	4	6	0.46	35.46	0.34	2.01	7.11	22.2	0.446	2.55	1.36	0.430	2.00	5.35	0.074	0.093	151
576B	4	6	0.66	35.66	0.36	2.08	7.32	22.8	0.466	2.61	1.41	0.452	2.11	5.47	0.075	0.097	144
576B	4	6	0.86	35.86	0.33	2.08	7.31	22.8	0.465	2.61	1.41	0.451	2.10	5.47	0.075	0.093	148
576B	4	6	1.06	36.06	0.34	2.06	7.29	22.7	0.467	2.61	1.41	0.449	2.07	5.45	0.076	0.094	144
576B	4	6	1.26	36.26	0.32	2.06	7.32	22.8	0.446	2.61	1.39	0.454	2.07	5.45	0.076	0.085	147
576B	4	6	1.46	36.46	0.32	2.09	7.90	23.5	0.295	2.78	0.83	0.497	1.54	5.29	0.074	0.071	125
576B	4	7	0.06	36.56	0.34	2.01	7.88	23.2	0.376	2.63	1.00	0.536	1.58	5.42	0.073	0.081	129
576B	4	7	0.26	36.76	0.38	1.94	7.89	23.4	0.337	2.71	0.90	0.550	1.45	5.57	0.072	0.074	129
576B	4	7	0.46	36.96	0.37	1.94	7.85	23.4	0.328	2.82	0.89	0.539	1.46	5.54	0.074	0.079	129
576	6	3	0.76	38.06	0.37	2.06	7.98	23.9	0.313	3.01	0.88	0.379	1.50	4.98	0.072	0.082	122
576	6	3	0.86	38.16	0.35	2.05	8.01	23.9	0.315	3.01	0.88	0.378	1.51	4.99	0.073	0.073	122
576	6	3	0.96	38.26	0.35	2.03	7.94	23.9	0.300	2.99	0.85	0.375	1.49	4.98	0.072	0.065	124
576	6	3	1.06	38.36	0.38	2.06	8.00	23.9	0.302	3.01	0.86	0.381	1.50	4.98	0.074	0.071	125
576	6	3	1.16	38.46	0.38	2.07	8.01	24.0	0.319	3.02	0.88	0.393	1.53	5.02	0.072	0.079	121
576	6	3	1.26	38.56	0.34	2.07	7.97	24.0	0.289	2.96	0.82	0.384	1.53	4.98	0.072	0.066	125
576	6	3	1.36	38.66	0.37	2.06	7.95	23.8	0.297	2.92	0.86	0.392	1.66	4.96	0.071	0.073	123
576	6	3	1.46	38.76	0.36	2.02	7.88	23.6	0.294	2.86	0.85	0.390	1.70	4.91	0.073	0.069	127
576	6	4	0.06	38.86	0.34	2.11	7.84	23.5	0.301	2.90	0.87	0.440	1.58	5.15	0.071	0.070	123
576	6	4	0.16	38.96	0.33	2.14	7.94	23.7	0.292	2.92	0.81	0.473	1.74	5.28	0.076	0.061	119
576	6	4	0.26	39.06	0.36	2.15	7.83	23.4	0.311	2.84	0.84	0.487	1.50	5.33	0.073	0.070	121
576	6	4	0.36	39.16	0.36	2.13	7.96	23.6	0.290	2.82	0.80	0.490	1.51	5.32	0.072	0.071	122
576	6	4	0.46	39.26	0.37	2.10	7.94	23.6	0.311	2.77	0.87	0.500	1.53	5.31	0.072	0.074	124
576	6	4	0.56	39.36	0.39	2.04	7.91	23.4	0.360	2.64	0.99	0.532	1.57	5.40	0.071	0.076	129
576	6	4	0.66	39.46	0.40	1.98	7.89	23.4	0.352	2.68	0.95	0.550	1.45	5.53	0.071	0.078	128
576	6	4	0.76	39.56	0.38	1.95	7.92	23.6	0.325	2.81	0.91	0.544	1.48	5.56	0.072	0.069	132
576	6	4	0.86	39.66	0.37	2.02	7.90	23.5	0.364	2.65	0.98	0.595	1.59	5.66	0.073	0.076	139
576	6	4	0.96	39.76	0.34	2.01	7.81	23.0	0.327	2.55	0.91	0.590	1.64	5.65	0.075	0.069	140
576	6	4	1.06	39.86	0.38	2.01	7.87	23.1	0.350	2.59	0.94	0.615	1.74	5.80	0.076	0.065	137
576	6	4	1.16	39.96	0.35	2.03	7.88	23.1	0.345	2.64	0.88	0.628	1.66	5.90	0.072	0.068	138
576	6	4	1.26	40.06	0.34	2.01	7.86	23.2	0.301	2.69	0.83	0.622	1.68	5.88	0.077	0.063	140
576	6	4	1.36	40.16	0.36	2.03	7.89	23.2	0.324	2.62	0.86	0.621	1.74	5.92	0.077	0.075	140
576	6	4	1.46	40.26	0.39	2.05	7.87	23.1	0.325	2.65	0.89	0.611	1.74	5.95	0.078	0.081	144
576	6	5	0.06	40.36	0.43	2.03	7.70	22.7	0.319	2.63	0.89	0.583	1.66	5.85	0.075	0.092	140
576	6	5	0.16	40.46	0.40	2.04	7.79	23.0	0.303	2.63	0.88	0.597	1.67	5.93	0.076	0.076	138
576	6	5	0.26	40.56	0.39	2.07	7.90	23.3	0.314	2.67	0.89	0.608	1.68	6.01	0.077	0.083	139
576	6	5	0.36	40.66	0.43	2.07	7.92	23.3	0.312	2.69	0.89	0.612	1.73	6.02	0.075	0.086	141
576	6	5	0.46	40.76	0.39	2.04	7.87	23.2	0.335	2.64	0.90	0.608	1.69	6.03	0.075	0.072	139
576	6	5	0.56	40.86	0.40	2.05	7.82	23.0	0.308	2.65	0.89	0.599	1.68	5.98	0.075	0.083	141
576	6	5	0.66	40.96	0.41	2.07	7.89	23.3	0.309	2.66	0.88	0.607	1.70	6.03	0.075	0.079	137
576	6	5	0.76	41.06	0.41	2.07	7.86	23.2	0.301	2.66	0.86	0.598	1.67	6.02	0.076	0.086	137
576	6	5	0.86	41.16	0.41	2.04	7.85	23.2	0.298	2.68	0.85	0.593	1.57	5.93	0.075	0.083	137
576	6	5	0.96	41.26	0.36	2.01	7.93	23.5	0.294	2.77	0.79	0.598	1.36	5.80	0.072	0.064	132
576	6	5	1.06	41.36	0.36	2.04	7.94	23.6	0.292	2.78	0.81	0.595	1.34	5.77	0.070	0.074	130
576	6	5	1.16	41.46	0.37	2.04	7.93	23.5	0.293	2.79	0.82	0.599	1.35	5.81	0.070	0.080	132
576	6	5	1.26	41.56	0.35	2.02	7.96	23.6	0.290	2.77	0.80	0.598	1.40	5.80	0.070	0.062	130
576	6	5	1.36	41.66	0.34	2.05	7.86	23.3	0.299	2.77	0.80	0.615	1.38	5.88	0.072	0.071	133
576	6	5	1.46	41.76	0.25	2.15	7.71	23.1	0.332	2.74	0.84	0.677	1.46	6.21	0.075	0.074	138

Table 5. (Continued).

Hole	Core	Section	Depth in Section (m)	Depth in hole (m)	Na	Mg	Al	Si	P	K	Ca	Ti	Mn	Fe	Ba	S	H_2O
576	6	6	0.06	41.86	0.35	2.11	7.69	23.1	0.316	2.75	0.85	0.721	1.44	6.40	0.075	0.067	140
576	6	6	0.16	41.96	0.34	2.11	7.67	23.0	0.360	2.72	0.89	0.723	1.40	6.50	0.075	0.068	140
576	6	6	0.26	42.06	0.37	2.10	7.66	23.0	0.319	2.74	0.87	0.727	1.40	6.50	0.074	0.077	139
576	6	6	0.36	42.16	0.42	2.09	7.63	22.9	0.322	2.72	0.86	0.724	1.36	6.50	0.074	0.062	141
576	6	6	0.46	42.26	0.39	2.08	7.73	23.2	0.314	2.84	0.87	0.748	1.36	6.56	0.075	0.059	138
576	6	6	0.56	42.36	0.44	2.08	7.79	23.5	0.311	3.03	0.85	0.741	1.29	6.32	0.075	0.064	130
576	6	6	0.66	42.46	0.43	2.07	7.76	23.6	0.287	3.12	0.81	0.742	1.21	6.28	0.074	0.067	127
576	6	6	0.76	42.56	0.43	2.08	7.78	23.8	0.295	3.16	0.81	0.751	1.18	6.26	0.075	0.066	125
576	6	6	0.86	42.66	0.40	2.12	7.70	23.7	0.302	3.17	0.81	0.730	1.17	6.22	0.074	0.069	128
576	6	6	0.96	42.76	0.38	2.08	7.53	23.3	0.248	3.12	0.69	0.656	1.14	5.85	0.072	0.054	119
576	6	6	1.06	42.86	0.41	2.18	7.63	23.8	0.230	3.20	0.65	0.710	1.10	6.17	0.073	0.057	115
576	6	6	1.16	42.96	0.37	2.17	7.73	24.0	0.253	3.18	0.70	0.658	1.17	6.01	0.074	0.064	115
576	6	6	1.26	43.06	0.34	2.17	7.72	24.0	0.256	3.18	0.72	0.604	1.21	5.74	0.075	0.054	111
576	6	6	1.36	43.16	0.33	2.18	7.65	23.9	0.264	3.16	0.71	0.569	1.15	5.63	0.078	0.054	106
576	6	6	1.46	43.26	0.31	2.26	7.71	24.1	0.248	3.21	0.69	0.593	1.18	5.72	0.076	0.059	109
576	6	7	0.06	43.36	0.31	2.23	7.50	23.7	0.281	3.12	0.75	0.573	1.13	5.73	0.075	0.059	114
576	6	7	0.16	43.46	0.30	2.27	7.67	23.9	0.282	3.13	0.76	0.544	1.20	5.59	0.077	0.054	107
576	7	1	0.09	43.49	0.26	2.23	7.53	23.8	0.269	3.16	0.74	0.584	1.14	5.72	0.076	0.066	127
576	6	7	0.26	43.56	0.32	2.24	7.68	24.1	0.266	3.19	0.72	0.587	1.15	5.74	0.076	0.052	109
576	7	1	0.26	43.66	0.31	2.27	7.66	24.2	0.264	3.18	0.76	0.576	1.19	5.74	0.077	0.064	114
576	6	7	0.44	43.74	0.32	2.31	7.72	24.1	0.258	3.13	0.70	0.609	1.07	5.85	0.076	0.062	104
576	7	1	0.36	43.76	0.37	2.28	7.66	24.0	0.265	3.15	0.78	0.561	1.18	5.66	0.075	0.074	111
576	7	1	0.46	43.86	0.32	2.24	7.65	24.0	0.259	3.14	0.72	0.595	1.14	5.81	0.075	0.056	117
576	7	1	0.56	43.96	0.37	2.17	7.75	23.9	0.233	3.15	0.63	0.647	0.99	6.01	0.073	0.053	114
576	7	1	0.66	44.06	0.42	2.12	7.72	23.9	0.268	3.28	0.72	0.671	0.92	5.99	0.073	0.062	108
576	7	1	0.76	44.16	0.35	2.20	7.80	24.1	0.247	3.13	0.64	0.654	1.00	6.02	0.075	0.046	116
576	7	1	0.86	44.26	0.33	2.24	7.81	23.9	0.238	3.02	0.64	0.628	1.08	6.11	0.075	0.058	123
576	7	1	0.96	44.36	0.28	2.26	7.73	23.7	0.249	3.00	0.66	0.601	1.07	5.89	0.074	0.062	127
576	7	1	1.06	44.46	0.32	2.31	7.87	24.1	0.265	3.01	0.67	0.626	1.04	5.99	0.073	0.059	121
576	7	1	1.16	44.56	0.32	2.33	7.83	24.1	0.285	3.02	0.73	0.649	1.06	6.12	0.074	0.067	116
576	7	1	1.26	44.66	0.28	2.32	7.84	24.1	0.287	3.00	0.73	0.615	1.13	6.06	0.074	0.056	117
576	7	1	1.36	44.76	0.29	2.27	7.63	23.6	0.316	2.97	0.80	0.618	1.09	6.11	0.075	0.059	118
576	7	1	1.46	44.86	0.32	2.21	7.70	23.8	0.270	3.13	0.72	0.624	1.03	6.11	0.074	0.062	117
576B	5	5	0.26	45.06	0.36	2.19	7.74	23.9	0.264	3.17	0.71	0.628	1.04	6.17	0.074	0.062	109
576B	5	5	0.46	45.26	0.29	2.27	7.80	23.7	0.298	3.01	0.79	0.580	1.12	6.07	0.075	0.070	106
576B	5	5	0.66	45.46	0.31	2.22	7.81	23.6	0.269	2.97	0.74	0.599	1.07	6.15	0.073	0.066	108
576B	5	5	0.86	45.66	0.29	2.28	7.85	23.7	0.287	2.94	0.79	0.602	1.13	6.18	0.076	0.065	107
576B	5	5	1.07	45.87	0.32	2.22	7.83	23.5	0.307	2.90	0.79	0.615	1.11	6.32	0.074	0.070	108
576B	5	5	1.26	46.06	0.32	2.21	7.78	23.3	0.287	2.89	0.75	0.630	1.14	6.47	0.074	0.072	114
576B	5	5	1.46	46.26	0.35	2.16	7.77	23.6	0.267	3.06	0.73	0.653	1.07	6.61	0.073	0.066	110
576B	5	6	0.06	46.36	0.38	2.12	7.74	23.5	0.270	3.07	0.74	0.669	1.03	6.67	0.073	0.065	110
576	7	2	0.56	46.46	0.37	2.17	7.78	23.6	0.287	2.99	0.74	0.646	1.08	6.57	0.076	0.056	115
576	7	2	0.66	46.56	0.41	2.13	7.66	23.3	0.264	2.98	0.72	0.672	1.00	6.70	0.074	0.063	116
576	7	2	0.76	46.66	0.38	2.13	7.72	23.0	0.336	2.76	0.83	0.692	1.01	6.95	0.073	0.060	123
576	7	2	0.86	46.76	0.38	2.18	7.85	23.3	0.386	2.81	0.97	0.708	1.11	6.78	0.073	0.068	121
576	7	2	0.96	46.86	0.35	2.22	7.66	23.5	0.348	2.96	0.91	0.653	1.16	6.41	0.072	0.063	119
576	7	2	1.08	46.98	0.41	2.07	7.80	23.2	0.383	2.83	0.88	0.709	1.13	6.89	0.074	0.045	126
576	7	2	1.16	47.06	0.33	2.17	7.68	22.9	0.429	2.73	1.01	0.652	1.17	6.65	0.074	0.077	128
576	7	2	1.26	47.16	0.34	2.26	7.74	23.5	0.442	2.83	1.04	0.641	1.26	6.53	0.074	0.076	125
576	7	2	1.36	47.26	0.30	2.31	7.43	23.4	0.509	2.96	1.19	0.622	1.39	6.46	0.077	0.069	130
576	7	2	1.46	47.36	0.31	2.30	7.35	23.2	0.500	3.05	1.24	0.614	1.56	6.03	0.082	0.074	121
576	7	3	0.05	47.45	0.27	2.31	7.30	23.2	0.531	3.09	1.31	0.627	1.43	6.00	0.080	0.073	125
576	7	3	0.14	47.54	0.27	2.31	7.36	23.5	0.446	3.18	1.17	0.649	1.34	6.10	0.078	0.067	126
576	7	3	0.26	47.66	0.28	2.24	7.32	23.1	0.518	3.04	1.28	0.573	1.32	5.93	0.080	0.056	119
576	7	3	0.36	47.76	0.28	2.23	7.39	23.2	0.546	3.07	1.38	0.600	1.35	5.93	0.077	0.074	118
576	7	3	0.46	47.86	0.31	2.23	7.37	23.3	0.591	3.09	1.52	0.601	1.30	5.94	0.078	0.081	119
576	7	3	0.56	47.96	0.29	2.25	7.30	23.3	0.561	3.12	1.43	0.607	1.45	5.97	0.077	0.074	126
576	7	3	0.66	48.06	0.32	2.19	7.06	22.9	0.699	3.18	1.85	0.572	1.35	5.99	0.075	0.085	126
576	7	3	0.76	48.16	0.28	2.19	7.17	23.0	0.620	3.12	1.62	0.541	1.42	5.73	0.079	0.086	128
576	7	3	0.86	48.26	0.31	2.17	7.15	22.8	0.659	3.05	1.69	0.569	1.34	5.92	0.076	0.088	127
576	7	3	0.96	48.36	0.35	2.15	7.16	22.7	0.645	3.04	1.68	0.578	1.25	5.91	0.076	0.084	124

Table 5. (Continued).

Hole	Core	Section	Depth in Section (m)	Depth in hole (m)	Na	Mg	Al	Si	P	K	Ca	Ti	Mn	Fe	Ba	S	H_2
576	7	3	1.06	48.46	0.37	2.10	7.14	22.6	0.720	3.02	1.77	0.605	1.17	6.03	0.074	0.086	12
576	7	3	1.16	48.56	0.35	2.11	7.37	23.1	0.662	3.08	1.66	0.567	1.27	6.04	0.077	0.089	12
576	7	3	1.26	48.66	0.39	2.12	7.42	22.9	0.695	3.03	1.73	0.538	1.30	6.02	0.077	0.090	12
576	7	3	1.36	48.76	0.38	2.09	7.41	22.9	0.642	3.04	1.64	0.546	1.27	5.96	0.078	0.089	12
576	7	3	1.46	48.86	0.39	2.08	7.40	22.9	0.705	3.05	1.70	0.555	1.17	6.00	0.074	0.096	12
576	7	4	0.06	48.96	0.47	2.12	7.48	23.2	0.847	3.15	2.08	0.529	1.21	5.89	0.074	0.120	11
576	7	4	0.16	49.06	0.40	2.07	7.24	22.8	0.809	3.12	2.03	0.473	1.22	5.56	0.075	0.110	11
576	7	4	0.26	49.16	0.41	2.05	7.11	22.5	0.789	3.07	2.03	0.474	1.26	5.53	0.075	0.091	12
576	7	4	0.36	49.26	0.38	2.11	7.20	22.8	0.796	3.10	2.10	0.478	1.34	5.60	0.076	0.091	12
576	7	4	0.46	49.36	0.37	2.11	7.14	22.8	0.836	3.20	2.18	0.463	1.33	5.44	0.074	0.092	12
576	7	4	0.56	49.46	0.31	2.10	7.10	22.8	0.840	3.25	2.18	0.445	1.35	5.34	0.072	0.097	12
576	7	4	0.66	49.56	0.35	2.14	6.96	22.6	0.886	3.25	2.25	0.433	1.40	5.42	0.078	0.105	12
576	7	4	0.76	49.66	0.39	2.16	6.84	22.9	0.744	3.37	2.04	0.468	1.35	5.78	0.076	0.075	12
576	7	4	0.86	49.76	0.36	2.26	6.86	23.1	0.858	3.43	2.25	0.495	1.37	5.97	0.076	0.098	12
576	7	4	0.96	49.86	0.34	2.18	7.05	22.8	0.845	3.27	2.16	0.415	1.51	5.29	0.074	0.107	13
576	7	4	1.06	49.96	0.34	2.16	7.07	22.9	0.832	3.29	2.15	0.406	1.55	5.19	0.078	0.096	12
576	7	4	1.16	50.06	0.33	2.16	7.05	22.7	0.853	3.25	2.10	0.414	1.54	5.21	0.078	0.104	128
576	7	4	1.26	50.16	0.40	2.16	7.10	22.9	0.779	3.26	2.03	0.415	1.54	5.25	0.077	0.081	129
576	7	4	1.36	50.26	0.35	2.10	6.86	22.5	0.810	3.36	2.07	0.437	1.36	5.46	0.073	0.102	128
576	7	4	1.46	50.36	0.35	2.12	6.89	22.9	0.686	3.50	1.85	0.472	1.33	5.75	0.074	0.084	131
576	7	5	0.06	50.46	0.31	2.11	7.12	22.7	0.835	3.35	2.16	0.379	1.51	4.94	0.072	0.100	131
576	7	5	0.16	50.56	0.34	2.14	7.18	22.6	0.905	3.27	2.23	0.388	1.51	4.97	0.073	0.112	125
576	7	5	0.26	50.66	0.33	2.14	7.27	23.0	0.734	3.30	1.95	0.393	1.38	4.95	0.076	0.090	118
576	7	5	0.36	50.76	0.33	2.15	7.26	22.9	0.803	3.31	2.02	0.403	1.34	5.08	0.075	0.102	116
576	7	5	0.46	50.86	0.33	2.11	7.24	22.9	0.760	3.29	1.97	0.398	1.35	5.08	0.076	0.095	119
576	7	5	0.56	50.96	0.33	2.13	7.30	23.0	0.809	3.30	2.11	0.398	1.41	5.08	0.076	0.096	117
576	7	5	0.66	51.06	0.34	2.14	7.32	23.2	0.790	3.34	2.12	0.405	1.44	5.10	0.077	0.095	118
576	7	5	0.76	51.16	0.33	2.12	7.24	22.9	0.916	3.32	2.30	0.399	1.46	5.15	0.076	0.105	120
576	7	5	0.86	51.26	0.34	2.10	7.12	22.5	1.028	3.25	2.63	0.386	1.39	5.02	0.075	0.112	116
576	7	5	0.96	51.36	0.35	2.09	7.14	22.6	1.023	3.30	2.56	0.392	1.39	5.10	0.076	0.114	116
576	7	5	1.06	51.46	0.36	2.06	7.15	22.7	0.962	3.35	2.48	0.388	1.38	5.05	0.074	0.111	118
576	7	5	1.16	51.56	0.38	2.06	7.14	22.7	0.979	3.39	2.50	0.380	1.46	4.97	0.074	0.122	119
576	7	5	1.26	51.66	0.38	1.98	6.92	21.8	1.138	3.31	2.86	0.362	1.42	4.82	0.074	0.126	116
576	7	5	1.36	51.76	0.36	2.07	7.26	22.9	0.864	3.38	2.23	0.378	1.42	5.09	0.077	0.101	118
576	7	5	1.46	51.86	0.38	2.07	7.15	22.4	0.931	3.34	2.37	0.371	1.34	5.05	0.077	0.114	117
576	7	6	0.06	51.96	0.37	2.09	7.10	22.4	0.949	3.23	2.32	0.391	1.27	5.20	0.074	0.112	115
576	7	6	0.16	52.06	0.35	2.16	7.17	22.8	0.786	3.20	2.04	0.415	1.28	5.38	0.077	0.096	111
576	7	6	0.26	52.16	0.34	2.17	7.22	23.0	0.672	3.23	1.78	0.428	1.30	5.48	0.080	0.098	112
576	7	6	0.36	52.26	0.34	2.19	7.31	23.3	0.666	3.27	1.79	0.428	1.38	5.57	0.078	0.089	116
576	7	6	0.46	52.36	0.34	2.19	7.32	23.2	0.756	3.28	1.99	0.410	1.37	5.34	0.079	0.092	112
576	7	6	0.56	52.46	0.34	2.15	7.22	22.9	0.802	3.26	2.08	0.393	1.32	5.25	0.076	0.097	114
576	7	6	0.66	52.56	0.35	2.17	7.19	22.9	0.838	3.29	2.12	0.390	1.28	5.17	0.075	0.107	110
576	7	6	0.76	52.66	0.38	2.16	7.17	22.8	0.898	3.27	2.20	0.389	1.28	5.21	0.075	0.115	111
576	7	6	0.86	52.76	0.35	2.17	7.22	22.9	0.731	3.27	1.95	0.390	1.31	5.27	0.078	0.091	112
576	7	6	0.96	52.86	0.35	2.19	7.23	22.9	0.734	3.24	1.84	0.393	1.29	5.33	0.076	0.098	111
576	7	6	1.06	52.96	0.33	2.22	7.39	23.4	0.656	3.33	1.74	0.403	1.35	5.38	0.078	0.094	112
576	7	6	1.16	53.06	0.36	2.18	7.27	23.1	0.612	3.29	1.62	0.390	1.24	5.34	0.073	0.087	110
576	7	6	1.26	53.16	0.35	2.18	7.45	23.6	0.520	3.37	1.37	0.403	1.21	5.48	0.075	0.076	109
576	7	6	1.36	53.26	0.38	2.16	7.49	23.5	0.617	3.34	1.55	0.389	1.21	5.30	0.074	0.085	114
576	7	6	1.46	53.36	0.35	2.14	7.39	23.4	0.558	3.33	1.44	0.398	1.26	5.30	0.077	0.085	111
576	7	7	0.06	53.46	0.36	2.17	7.48	23.7	0.345	3.42	1.00	0.401	1.27	5.36	0.074	0.071	109
576	7	7	0.16	53.56	0.36	2.17	7.60	24.1	0.349	3.46	0.98	0.402	1.31	5.28	0.073	0.062	110
576	7	7	0.26	53.66	0.36	2.17	7.49	23.7	0.362	3.43	1.00	0.394	1.35	5.21	0.076	0.072	109
576	7	7	0.36	53.76	0.37	2.18	7.51	23.8	0.337	3.46	0.96	0.395	1.36	5.18	0.074	0.075	110
576	7	7	0.46	53.86	0.35	2.20	7.58	24.2	0.345	3.52	0.99	0.408	1.46	5.29	0.078	0.068	113
576	8	1	0.26	54.36	0.34	2.18	7.38	23.5	0.385	3.43	1.06	0.390	1.42	5.19	0.077	0.076	119
576	8	1	0.36	54.46	0.35	2.19	7.36	23.5	0.451	3.47	1.20	0.389	1.35	5.19	0.076	0.081	120
576	8	1	0.46	54.56	0.32	2.20	7.19	23.3	0.471	3.46	1.31	0.403	1.71	5.43	0.082	0.084	128
576	8	1	0.56	54.66	0.32	2.12	7.17	23.3	0.594	3.53	1.60	0.397	1.71	5.09	0.080	0.086	123
576	8	1	0.66	54.76	0.34	2.08	6.97	22.6	0.768	3.48	1.93	0.389	1.81	4.99	0.077	0.105	124
576	8	1	0.76	54.86	0.35	2.09	7.08	23.1	0.653	3.49	1.81	0.397	1.95	5.11	0.083	0.084	124

Table 5. (Continued).

Hole	Core	Section	Depth in Section (m)	Depth in hole (m)	Na	Mg	Al	Si	P	K	Ca	Ti	Mn	Fe	Ba	S	H_2O
576B	6	4	0.46	54.92	0.32	2.15	7.10	23.2	0.473	3.49	1.35	0.402	1.67	5.40	0.079	0.092	118
576	8	1	0.86	54.96	0.33	2.22	6.85	23.0	0.453	3.42	1.25	0.429	2.08	6.08	0.089	0.081	128
576	8	1	0.96	55.06	0.33	2.16	6.76	22.5	0.686	3.45	1.86	0.430	2.23	5.53	0.090	0.098	121
576B	6	4	0.66	55.12	0.29	2.21	6.81	23.0	0.424	3.46	1.29	0.415	2.05	6.06	0.087	0.090	121
576	8	1	1.06	55.16	0.32	2.30	6.68	22.8	0.533	3.32	1.41	0.419	2.11	6.03	0.090	0.081	128
576	8	1	1.16	55.26	0.35	2.26	6.38	22.4	0.523	3.32	2.46	0.386	1.72	6.13	0.089	0.079	115
576B	6	4	0.86	55.32	0.31	2.18	6.76	22.8	0.578	3.51	2.12	0.429	2.05	5.63	0.087	0.093	114
576	8	1	1.26	55.36	0.32	2.21	6.82	22.7	0.640	3.49	1.74	0.423	2.10	5.67	0.089	0.088	123
576B	6	4	1.06	55.52	0.31	2.21	6.74	22.5	0.774	3.49	2.53	0.425	1.93	5.45	0.084	0.106	107
576A	6	5	1.29	55.54	0.37	2.24	6.78	22.7	0.643	3.39	1.85	0.418	1.50	5.61	0.068	0.077	95
576	8	1	1.46	55.56	0.33	2.22	6.78	22.7	0.721	3.42	2.37	0.417	1.80	5.50	0.081	0.081	116
576	8	2	0.05	55.65	0.32	2.28	6.56	22.7	0.508	3.32	2.06	0.394	1.62	5.87	0.079	0.063	118
576B	6	4	1.46	55.92	0.29	2.29	6.74	22.9	0.426	3.41	1.56	0.387	1.91	6.25	0.084	0.088	115
576	8	2	0.67	56.27	0.26	2.17	6.67	22.6	0.446	3.35	2.42	0.386	1.58	5.53	0.080	0.071	121
576	8	2	0.78	56.38	0.29	2.14	6.29	21.2	0.348	3.11	3.60	0.353	1.75	6.42	0.083	0.058	122
576B	6	5	0.55	56.51	0.29	2.30	6.86	23.2	0.348	3.36	0.99	0.374	1.86	6.61	0.086	0.085	126
576	8	2	1.06	56.66	0.29	2.18	6.86	23.0	0.419	3.37	1.64	0.371	1.54	5.62	0.078	0.075	123
576	8	2	1.16	56.76	0.29	2.24	7.11	23.8	0.359	3.42	0.96	0.390	1.52	5.71	0.081	0.064	122
576B	6	5	0.86	56.82	0.31	2.18	6.94	23.2	0.398	3.43	1.60	0.379	1.46	5.62	0.075	0.086	113
576	8	2	1.26	56.86	0.27	2.20	6.95	23.3	0.339	3.34	1.60	0.390	1.40	5.90	0.079	0.068	118
576	8	2	1.36	56.96	0.29	2.23	6.93	23.5	0.383	3.33	0.97	0.376	1.43	5.94	0.082	0.059	120
576B	6	5	1.06	57.02	0.30	2.17	7.00	23.4	0.324	3.36	1.14	0.379	1.43	5.85	0.078	0.074	118
576	8	2	1.46	57.06	0.30	2.23	6.31	21.9	0.373	3.03	3.29	0.356	1.51	6.83	0.089	0.063	120
576	8	3	0.04	57.14	0.34	2.45	6.38	23.0	0.491	3.02	1.38	0.355	1.53	7.42	0.101	0.067	130
576B	6	5	1.26	57.22	0.29	2.32	6.78	23.3	0.384	3.23	1.27	0.376	1.58	6.63	0.087	0.078	119
576A	6	7	0.24	57.49	0.31	2.29	6.74	23.1	0.381	3.23	1.01	0.365	1.55	6.79	0.085	0.061	110
576A	6	7	0.28	57.53	0.32	2.30	6.98	23.8	0.313	3.38	0.83	0.392	1.33	6.02	0.081	0.055	
576	8	3	0.66	57.76	0.32	2.40	6.71	22.7	0.285	3.08	0.84	0.356	1.76	8.19	0.090	0.064	126
576B	6	6	0.47	57.93	0.27	2.39	6.74	23.0	0.291	3.20	0.86	0.356	1.74	7.84	0.091	0.076	125
576	8	3	0.92	58.02	0.28	2.33	7.00	24.1	0.296	3.40	0.80	0.394	1.21	5.95	0.076	0.062	117
576	8	3	1.01	58.11	0.27	2.40	6.48	22.9	0.339	3.10	0.96	0.351	1.61	7.81	0.091	0.068	133
576B	6	6	0.76	58.22	0.24	2.31	6.87	23.5	0.393	3.35	1.12	0.381	1.69	6.45	0.086	0.077	121
576	8	3	1.47	58.57	0.30	2.31	7.02	24.2	0.380	3.38	1.01	0.416	1.14	5.77	0.074	0.070	116
576	8	4	0.03	58.63	0.27	2.32	6.91	23.7	0.393	3.32	1.08	0.392	1.40	5.98	0.083	0.066	112
576	8	4	0.13	58.73	0.31	2.35	6.89	23.6	0.558	3.36	1.43	0.391	0.97	6.23	0.073	0.071	108
576B	6	6	1.36	58.82	0.26	2.33	6.90	23.7	0.374	3.36	1.00	0.397	1.27	5.83	0.079	0.076	115
576	8	4	0.23	58.83	0.28	2.46	6.28	23.0	0.430	3.13	1.96	0.358	1.41	6.50	0.088	0.062	124
576	8	6	0.77	62.37	0.30	2.38	6.92	24.0	0.431	3.34	1.09	0.382	1.52	5.86	0.159	0.055	113
576B	7	3	1.45	62.45	0.27	2.47	6.97	24.4	0.364	3.38	0.94	0.410	1.23	5.46	0.118	0.087	109
576	8	6	0.90	62.50	0.26	2.46	6.84	24.4	0.295	3.35	0.80	0.389	1.21	5.36	0.102	0.042	118
576B	7	4	0.91	63.41	0.17	2.51	6.82	24.3	0.303	3.41	0.81	0.376	1.23	5.05	0.084	0.059	121
576	8	7	0.39	63.49	0.20	2.53	6.99	24.7	0.339	3.46	0.81	0.394	1.16	5.09	0.083	0.044	121
576	8	C	0.06	63.59	0.22	2.56	6.86	24.7	0.286	3.38	0.76	0.377	1.22	5.19	0.084	0.043	124
576B	7	4	1.28	63.78	0.22	2.42	6.91	24.1	0.451	3.50	1.28	0.383	1.30	5.13	0.085	0.065	111
576B	7	5	0.79	64.79	0.21	2.49	6.77	24.6	0.378	3.41	1.02	0.395	1.24	5.08	0.089	0.066	110
576B	7	6	0.46	65.96	0.07	2.84	6.50	24.8	0.348	3.09	0.82	0.388	0.95	4.89	0.088	0.056	138
576B	7	6	0.89	66.39	0.06	2.86	6.61	25.3	0.305	3.18	0.72	0.400	0.76	4.75	0.079	0.055	133
576B	7	7	0.30	67.30	0.06	2.92	6.52	24.9	0.426	3.05	0.99	0.382	0.93	4.75	0.088	0.051	139
576B	8	2	0.81	69.76	0.27	2.39	6.51	24.0	0.358	3.52	2.09	0.385	1.00	4.82	0.090	0.052	102
576B	8	3	0.29	70.74	0.12	2.76	6.61	25.1	0.286	3.22	0.70	0.393	0.99	4.86	0.096	0.044	126
576B	8	3	0.65	71.10	0.16	2.61	6.60	24.8	0.507	3.37	1.17	0.399	1.03	4.88	0.093	0.070	117
576B	8	3	0.96	71.41	0.19	2.57	6.18	23.5	0.345	3.12	2.66	0.384	0.96	4.88	0.087	0.057	116
576B	8	4	0.21	72.16	0.25	2.65	6.52	24.7	0.466	3.27	1.20	0.388	1.23	5.95	0.087	0.059	108
576B	8	4	0.41	72.36	0.38	2.50	6.24	23.7	0.479	3.36	1.33	0.347	1.59	6.22	0.094	0.075	103
576B	8	4	0.99	72.94	0.37	2.46	6.00	23.4	0.575	3.25	2.41	0.363	1.32	6.01	0.093	0.070	100
576B	8	5	0.58	74.03	0.24	2.73	6.36	25.6	0.337	3.39	0.84	0.400	0.77	5.52	0.083	0.057	109
576B	8	5	1.42	74.87	0.20	2.98	6.50	25.5	0.302	3.19	0.78	0.405	0.85	5.38	0.084	0.056	113
576B	8	6	0.44	75.39	0.19	3.03	6.33	25.3	0.266	3.16	1.10	0.397	0.82	5.18	0.086	0.052	112

Table 6. Elemental abundance (wt.%) and water content (% dry wt.) of Hole 578 sediment samples.

Lab ID	Core	Section	Depth in Section (m)	Depth in hole (m)	Na	Mg	Al	Si	P	K	Ca	Ti	Mn	Fe	Ba	S	H_2O
DP17319	1	1	0.16	0.16	0.46	1.51	6.72	27.2	0.068	1.95	0.86	0.360	0.59	4.28	0.107	0.061	167
DP17321	1	1	0.53	0.53	0.50	1.57	6.81	26.6	0.067	2.02	0.97	0.363	0.31	4.44	0.109	0.080	151
DP17323	1	1	0.86	0.86	0.31	1.76	6.92	27.1	0.053	2.23	0.65	0.370	0.14	3.99	0.094	0.036	206
DP17324	1	1	1.06	1.06	0.22	1.78	6.94	26.8	0.053	2.26	0.67	0.379	0.20	3.95	0.091	0.061	215
DP17325	1	1	1.26	1.26	0.26	1.83	7.05	27.0	0.053	2.35	0.58	0.386	0.18	4.24	0.092	0.062	188
DP17326	1	1	1.46	1.46	0.33	1.81	7.04	27.0	0.053	2.35	0.62	0.391	0.15	4.27	0.088	0.062	175
DP17327	1	2	0.06	1.56	0.32	1.84	7.03	26.7	0.053	2.34	0.68	0.395	0.14	4.40	0.084	0.062	170
DP17329	1	2	0.50	2.00	0.38	1.73	6.98	27.0	0.053	2.28	0.78	0.386	0.11	4.44	0.089	0.067	166
DP17333	1	2	1.26	2.76	0.84	0.95	5.92	27.9	0.043	1.98	1.13	0.238	0.11	2.42	0.084	0.034	105
DP17334	1	2	1.46	2.96	0.36	1.73	7.10	27.0	0.052	2.33	0.75	0.393	0.10	4.19	0.093	0.079	169
DP17335	1	3	0.06	3.06	0.40	1.69	7.04	27.0	0.052	2.24	0.84	0.388	0.10	4.26	0.094	0.070	167
DP17336	1	3	0.27	3.27	0.40	1.70	7.12	26.9	0.053	2.25	0.85	0.392	0.10	4.41	0.100	0.063	158
DP17337	1	3	0.46	3.46	0.51	1.77	7.12	26.8	0.056	2.25	0.98	0.401	0.11	4.74	0.100	0.061	133
DP17338	1	3	0.66	3.66	0.44	1.72	7.03	26.7	0.056	2.20	0.91	0.391	0.10	4.64	0.102	0.055	156
DP17339	1	3	0.86	3.86	0.51	1.82	7.10	26.5	0.056	2.12	1.32	0.410	0.10	5.04	0.086	0.056	136
DP17343	2	1	0.06	4.86	0.29	1.69	6.68	27.4	0.049	2.14	0.87	0.381	0.25	4.19	0.078	0.054	200
DP17345	2	1	0.43	5.23	0.38	1.73	6.74	27.1	0.052	2.18	0.90	0.378	0.63	4.14	0.079	0.058	183
DP17347	2	1	0.86	5.66	0.29	1.72	6.81	27.0	0.050	2.31	0.65	0.376	0.18	4.19	0.087	0.175	171
DP17349	2	1	1.26	6.06	0.31	1.77	6.96	27.3	0.050	2.39	0.66	0.392	0.20	4.16	0.085	0.069	166
DP17353	2	2	0.46	6.76	0.24	1.68	6.69	27.4	0.049	2.19	0.80	0.368	0.14	4.04	0.088	0.117	194
DP17355	2	2	0.86	7.16	0.33	1.72	6.88	27.0	0.051	2.27	0.80	0.385	0.17	4.22	0.083	0.364	173
DP17357	2	2	1.26	7.56	0.44	1.70	6.85	27.1	0.048	2.11	1.17	0.375	0.10	4.44	0.091	0.060	169
DP17359	2	3	0.16	7.96	0.56	1.43	6.44	27.9	0.050	1.83	1.33	0.374	0.09	4.10	0.099	0.055	172
DP17361	2	3	0.66	8.46	0.61	1.37	6.30	27.3	0.049	1.93	1.15	0.346	0.10	4.01	0.093	0.053	152
DP17362	2	3	0.86	8.66	0.41	1.79	7.04	26.9	0.049	2.28	0.93	0.412	0.11	4.58	0.080	0.056	160
DP17363	2	3	1.06	8.86	0.52	1.62	6.84	27.2	0.047	2.12	1.06	0.392	0.10	4.16	0.091	0.065	143
DP17365	2	3	1.44	9.24	0.41	1.70	6.84	27.0	0.048	2.26	0.83	0.369	0.12	4.45	0.087	0.067	164
DP17367	2	4	0.26	9.56	0.46	1.61	6.74	27.4	0.046	2.26	0.83	0.377	0.09	4.16	0.095	0.066	148
DP17369	2	4	0.64	9.94	0.49	1.68	6.81	26.9	0.048	2.21	0.87	0.376	0.11	4.65	0.094	0.065	151
DP17371	2	4	1.06	10.36	0.50	1.64	6.78	27.3	0.051	2.38	0.84	0.370	0.10	4.30	0.097	0.065	134
DP17373	2	4	1.46	10.76	0.40	1.73	6.97	27.0	0.050	2.35	0.84	0.392	0.18	4.02	0.090	0.091	145
DP17375	2	5	0.26	11.06	0.39	1.78	6.99	26.3	0.049	2.35	0.77	0.387	0.12	4.22	0.098	0.119	151
DP17377	2	5	0.66	11.46	0.46	1.77	7.16	26.7	0.050	2.32	0.93	0.405	0.10	4.34	0.084	0.079	145
DP17379	2	5	1.06	11.86	0.48	1.67	7.10	27.0	0.051	2.18	1.00	0.403	0.10	4.36	0.092	0.061	148
DP17381	2	6	0.06	12.36	0.48	1.65	6.82	26.8	0.049	2.12	1.10	0.363	0.10	4.48	0.097	0.076	153
DP17383	3	1	0.04	14.34	0.84	1.47	6.40	27.0	0.054	1.69	1.59	0.378	0.13	4.73	0.086	0.059	119
DP17385	3	1	0.46	14.76	0.43	1.77	6.94	26.9	0.052	2.31	0.90	0.408	0.34	4.05	0.088	0.066	139
DP17387	3	1	0.86	15.16	0.34	1.81	7.00	26.9	0.049	2.38	0.70	0.404	0.13	4.27	0.087	0.080	154
DP17391	3	2	0.06	15.86	0.57	1.52	6.46	27.3	0.049	1.94	1.23	0.356	0.26	3.87	0.081	0.059	126
DP17393	3	2	0.46	16.26	0.43	1.70	6.82	27.0	0.052	2.28	0.85	0.382	0.44	3.91	0.084	0.052	152
DP17395	3	2	0.86	16.66	0.54	1.76	6.63	26.0	0.191	2.08	1.47	0.363	2.13	3.85	0.087	0.063	150
DP17397	3	2	1.26	17.06	0.42	1.62	6.83	27.0	0.047	2.13	1.05	0.395	0.09	4.21	0.086	0.064	160
DP17398	3	2	1.46	17.26	0.45	1.70	7.09	26.8	0.049	2.26	0.94	0.398	0.09	4.25	0.085	0.067	141
DP17399	3	3	0.06	17.36	0.45	1.54	6.65	27.1	0.049	2.20	0.86	0.338	0.10	3.84	0.089	0.060	150
DP17400	3	3	0.26	17.56	0.53	1.39	6.33	27.3	0.047	1.87	1.10	0.338	0.09	3.91	0.089	0.055	164
DP17401	3	3	0.46	17.76	0.62	1.43	6.61	27.4	0.047	1.75	1.51	0.359	0.11	4.44	0.081	0.058	136
DP17403	3	3	0.83	18.13	0.45	1.51	6.69	27.0	0.050	2.10	0.84	0.344	0.10	4.05	0.093	0.055	159
DP17405	3	3	1.26	18.56	0.54	1.23	6.35	27.6	0.046	2.29	0.77	0.305	0.09	3.23	0.085	0.045	137
DP17407	3	4	0.06	18.86	0.54	1.38	6.72	27.5	0.049	2.26	0.84	0.335	0.09	3.71	0.087	0.047	149
DP17409	3	4	0.46	19.26	0.44	1.77	7.12	26.8	0.052	2.41	0.69	0.396	0.10	4.67	0.086	0.064	145
DP17411	3	4	0.86	19.66	0.60	1.61	7.07	26.4	0.065	2.28	1.16	0.412	0.11	4.31	0.085	0.051	134
DP17413	3	4	1.26	20.06	0.52	1.55	6.99	27.2	0.055	2.14	0.97	0.383	0.09	4.08	0.090	0.051	144
DP17415	3	5	0.06	20.36	0.79	1.37	6.59	26.8	0.063	2.01	1.34	0.373	0.10	3.89	0.084	0.053	120
DP17417	3	5	0.46	20.76	0.58	1.64	7.03	26.9	0.051	2.29	0.91	0.384	0.09	4.34	0.091	0.065	122
DP17419	3	5	0.86	21.16	0.57	1.61	6.59	27.1	0.051	2.11	1.10	0.358	0.11	4.63	0.089	0.048	147
DP17421	3	5	1.26	21.56	0.59	1.45	6.69	27.2	0.049	2.12	1.04	0.350	0.09	3.92	0.092	0.085	137
DP17423	3	6	0.06	21.86	0.61	1.36	6.60	27.3	0.051	2.51	0.96	0.316	0.08	3.49	0.084	0.054	118
DP17425	3	6	0.50	22.30	0.33	1.72	7.01	27.0	0.049	2.38	0.71	0.389	0.09	3.96	0.096	0.063	156
DP17427	3	6	0.86	22.66	0.45	1.54	6.66	27.2	0.046	2.54	0.69	0.351	0.11	3.35	0.091	0.073	130
DP17429	3	7	0.06	23.36	0.34	1.73	7.00	27.0	0.050	2.33	0.78	0.398	0.18	4.00	0.088	0.066	151
DP17431	3	7	0.46	23.76	0.32	1.77	7.11	26.9	0.047	2.37	0.72	0.402	0.13	4.26	0.093	0.081	162
DP17433	4	1	0.26	24.06	0.35	1.79	6.89	27.1	0.048	2.34	0.71	0.390	0.17	4.20	0.088	0.065	152
DP17435	4	1	0.66	24.46	0.38	1.76	6.99	27.0	0.049	2.35	0.81	0.402	0.15	4.09	0.088	0.082	149
DP17437	4	1	1.13	24.93	0.32	1.73	6.96	26.8	0.049	2.32	0.77	0.394	0.13	4.33	0.086	0.071	160

Table 6. (Continued).

Lab ID	Core	Section	Depth in Section (m)	Depth in hole (m)	Na	Mg	Al	Si	P	K	Ca	Ti	Mn	Fe	Ba	S	H_2O
DP17439	4	1	1.45	25.25	0.29	1.84	7.01	26.8	0.049	2.42	0.71	0.399	0.20	4.44	0.091	0.086	160
DP17443	4	2	0.66	25.96	0.45	1.80	7.12	26.9	0.048	2.35	0.79	0.399	0.11	4.62	0.090	0.071	135
DP17445	4	2	1.08	26.38	0.58	1.69	7.11	26.7	0.051	2.21	1.00	0.409	0.11	4.30	0.082	0.075	121
DP17447	4	2	1.46	26.76	0.51	1.59	7.07	27.0	0.048	2.20	0.91	0.385	0.09	4.20	0.091	0.070	133
DP17457	4	3	0.26	27.06	0.57	1.63	6.88	27.0	0.050	2.26	0.98	0.390	0.09	4.19	0.087	0.055	119
DP17459	4	3	0.66	27.46	0.44	1.68	7.08	27.4	0.048	2.25	0.86	0.390	0.11	4.43	0.093	0.074	154
DP17463	4	3	1.46	28.26	0.56	1.64	6.71	27.2	0.051	2.25	0.77	0.358	0.11	4.70	0.092	0.058	134
DP17465	4	5	0.32	30.12	0.40	1.90	7.09	26.3	0.048	2.53	0.57	0.395	0.12	4.48	0.088	0.079	134
DP17467	4	5	0.66	30.46	0.47	1.80	7.23	26.6	0.049	2.44	0.76	0.400	0.09	4.32	0.090	0.067	127
DP17469	4	5	1.06	30.86	0.48	1.62	6.77	26.8	0.048	2.18	0.89	0.361	0.10	4.32	0.094	0.055	147
DP17471	4	5	1.46	31.26	0.55	1.68	6.91	27.0	0.054	2.30	0.76	0.373	0.12	4.43	0.089	0.061	131
DP17473	4	6	0.26	31.56	0.54	1.65	6.98	27.0	0.053	2.26	0.79	0.371	0.16	4.42	0.086	0.055	130
DP17474	4	6	0.46	31.76	0.51	1.68	7.08	26.9	0.053	2.41	0.76	0.374	0.09	4.27	0.089	0.057	126
DP17477	4	6	1.14	32.44	0.52	1.72	7.05	26.8	0.055	2.35	0.81	0.394	0.12	4.73	0.090	0.062	129
DP17479	5	1	0.47	33.77	0.49	1.77	7.18	27.2	0.052	2.44	0.69	0.402	0.44	4.50	0.082	0.053	130
DP17481	5	1	1.26	34.56	0.52	1.58	6.68	27.6	0.050	2.24	0.82	0.355	0.10	4.44	0.096	0.062	143
DP17483	5	2	0.06	34.86	0.56	1.65	6.93	26.7	0.055	2.37	0.74	0.374	0.12	4.49	0.085	0.058	123
DP17485	5	2	0.51	35.31	0.57	1.58	6.88	26.9	0.055	2.18	1.02	0.379	0.10	4.34	0.085	0.058	133
DP17487	5	2	0.85	35.65	0.57	1.79	7.06	27.0	0.058	2.45	0.74	0.416	0.15	4.73	0.095	0.061	108
DP17489	5	2	1.26	36.06	0.46	1.77	7.19	26.7	0.054	2.44	0.69	0.401	0.10	4.47	0.093	0.064	129
DP17491	5	3	0.06	36.36	0.46	1.63	6.85	27.4	0.052	2.30	0.76	0.382	0.10	4.39	0.094	0.052	142
DP17493	5	3	0.45	36.75	0.56	1.49	6.76	27.3	0.053	2.18	0.98	0.356	0.10	4.19	0.086	0.059	163
DP17495	5	3	0.86	37.16	0.55	1.60	7.01	27.1	0.053	2.22	0.91	0.387	0.09	4.44	0.094	0.062	131
DP17499	5	4	0.06	37.86	0.49	1.69	7.13	26.7	0.051	2.21	1.15	0.397	0.10	4.64	0.082	0.051	134
DP17503	5	4	0.86	38.66	0.51	1.59	6.90	27.3	0.051	2.05	1.14	0.377	0.09	4.17	0.090	0.059	114
DP17509	5	5	0.46	39.76	0.49	1.70	7.11	27.4	0.050	2.52	0.92	0.400	0.09	3.95	0.089	0.055	123
DP17511	5	5	0.86	40.16	0.43	1.59	6.77	27.4	0.046	2.10	0.95	0.359	0.10	4.04	0.088	0.052	153
DP17513	5	5	1.28	40.58	0.33	1.83	7.28	26.8	0.044	2.52	0.59	0.413	0.10	4.16	0.093	0.076	155
DP17515	5	6	0.06	40.86	0.44	1.88	7.32	26.5	0.045	2.62	0.58	0.408	0.10	4.14	0.087	0.081	126
DP17517	5	6	0.46	41.26	0.41	1.65	6.95	27.1	0.051	2.35	0.72	0.365	0.09	4.00	0.095	0.049	153
DP17519	5	6	0.86	41.66	0.49	1.77	7.08	26.5	0.051	2.43	0.69	0.394	0.12	4.59	0.087	0.061	131
DP17521	5	6	1.26	42.06	0.46	1.78	7.13	26.7	0.051	2.46	0.66	0.390	0.09	4.35	0.101	0.069	138
DP17523	5	7	0.22	42.52	0.62	1.27	6.11	27.6	0.045	2.57	0.69	0.277	0.10	3.43	0.095	0.053	119
DP17525	6	1	0.06	42.86	0.45	1.49	6.67	27.8	0.048	2.40	0.67	0.342	0.12	3.90	0.102	0.046	152
DP17527	6	1	0.67	43.47	0.45	1.62	6.10	27.2	0.045	2.21	0.63	0.316	0.14	4.74	0.108	0.064	168
DP17529	6	1	1.06	43.86	0.44	1.77	6.91	26.9	0.048	2.46	0.63	0.374	0.37	4.15	0.086	0.071	149
DP17531	6	1	1.46	44.26	0.57	1.32	6.51	27.6	0.055	2.55	0.91	0.303	0.15	3.07	0.092	0.055	125
DP17533	6	2	0.26	44.56	0.45	1.62	6.83	27.6	0.052	2.30	0.79	0.357	0.12	4.07	0.091	0.059	153
DP17535	6	2	0.66	44.96	0.58	1.47	6.51	27.4	0.045	2.54	0.64	0.326	0.12	3.58	0.090	0.061	109
DP17537	6	2	1.06	45.36	0.44	1.45	6.32	27.5	0.047	2.29	0.79	0.336	0.10	3.72	0.094	0.045	150
DP17539	6	2	1.46	45.76	0.51	1.51	6.74	27.7	0.051	2.07	1.19	0.363	0.10	4.19	0.093	0.049	156
DP17541	6	3	0.26	46.06	0.52	1.63	6.83	27.0	0.051	2.51	0.79	0.366	0.12	4.37	0.097	0.055	128
DP17543	6	3	0.63	46.43	0.46	1.77	7.15	26.7	0.050	2.46	0.74	0.403	0.08	4.44	0.088	0.064	133
DP17549	6	4	0.24	47.54	0.54	1.63	6.99	27.1	0.047	2.17	1.30	0.386	0.09	4.07	0.083	0.050	119
DP17551	6	4	0.66	47.96	0.52	1.45	6.49	27.1	0.048	2.22	0.79	0.328	0.09	3.56	0.086	0.072	136
DP17553	6	4	1.06	48.36	0.55	1.99	5.78	26.7	0.044	2.07	0.59	0.308	0.20	6.36	0.077	0.062	159
DP17555	6	4	1.46	48.76	0.58	1.49	6.74	26.9	0.051	2.25	0.94	0.349	0.08	3.84	0.093	0.049	119
DP17557	6	5	0.26	49.06	0.52	1.57	6.75	27.4	0.054	2.16	0.80	0.367	0.09	4.24	0.084	0.050	151
DP17559	6	5	0.66	49.46	0.57	1.73	6.57	26.8	0.051	2.20	0.74	0.353	0.12	4.98	0.083	0.057	139
DP17563	6	5	1.46	50.26	0.33	1.73	6.68	27.1	0.046	2.30	0.59	0.360	0.11	4.55	0.092	0.082	178
DP17565	6	6	0.34	50.64	0.68	1.94	7.11	26.0	0.058	2.15	0.99	0.341	4.38	3.56	0.094	0.056	123
DP17567	6	6	0.86	51.16	0.52	1.36	6.43	27.3	0.048	2.28	0.87	0.336	0.08	3.32	0.095	0.054	139
DP17569	6	7	0.03	51.83	0.50	1.66	6.74	26.7	0.047	2.23	0.88	0.378	0.11	4.25	0.088	0.057	134
DP17571	6	7	0.43	52.23	0.52	1.69	6.97	26.9	0.045	2.27	1.00	0.400	0.13	4.03	0.090	0.080	133
DP17573	7	1	0.46	52.66	0.44	1.82	7.12	26.6	0.050	2.41	0.81	0.396	0.10	4.45	0.088	0.065	145
DP17577	7	1	1.26	53.46	0.42	1.62	6.76	27.3	0.052	2.19	0.89	0.378	0.11	4.26	0.094	0.057	164
DP17581	7	2	0.46	54.16	0.37	1.83	7.16	26.5	0.050	2.46	0.64	0.393	0.10	4.41	0.094	0.075	147
DP17583	7	2	0.86	54.56	0.63	1.49	6.55	27.2	0.047	1.80	1.43	0.363	0.11	4.38	0.084	0.052	130
DP17585	7	2	1.31	55.01	0.45	1.66	6.75	27.3	0.051	2.23	0.80	0.377	0.11	4.56	0.088	0.057	164
DP17589	7	3	0.46	55.66	0.50	1.56	6.82	27.4	0.051	2.13	0.98	0.378	0.11	3.82	0.091	0.053	139
DP17591	7	3	0.86	56.06	0.46	1.52	6.66	27.4	0.050	1.95	1.12	0.369	0.11	4.33	0.089	0.047	174
DP17593	7	3	1.26	56.46	0.56	1.48	6.56	27.2	0.049	1.88	1.39	0.366	0.11	4.60	0.090	0.051	151
DP17595	7	4	0.06	56.76	0.52	1.57	6.34	27.3	0.052	2.03	0.96	0.343	0.13	4.77	0.086	0.058	160
DP17599	7	4	0.86	57.56	0.47	1.71	6.96	26.4	0.051	2.32	0.78	0.388	0.12	4.40	0.089	0.054	137

Table 6. (Continued).

Lab ID	Core	Section	Depth in Section (m)	Depth in hole (m)	Na	Mg	Al	Si	P	K	Ca	Ti	Mn	Fe	Ba	S	H_2O
DP17601	7	4	1.26	57.96	0.70	1.30	6.53	27.7	0.054	2.07	1.22	0.328	0.11	3.63	0.090	0.053	124
DP17602	7	4	1.46	58.16	0.55	1.56	6.73	26.6	0.051	2.25	0.85	0.363	0.11	4.36	0.089	0.056	128
DP17603	7	5	0.06	58.26	0.62	1.48	6.64	27.2	0.052	2.16	0.91	0.348	0.11	4.22	0.084	0.053	122
DP17605	7	5	0.46	58.66	0.59	1.44	6.45	27.2	0.052	1.96	1.29	0.340	0.10	4.22	0.082	0.052	138
DP17609	7	5	1.26	59.46	0.62	1.43	6.47	27.3	0.053	2.03	1.08	0.343	0.11	4.11	0.084	0.056	133
DP17611	7	6	0.06	59.76	0.54	1.42	6.54	27.4	0.052	1.99	1.06	0.354	0.13	4.25	0.091	0.055	141
DP17613	7	6	0.45	60.15	0.83	1.05	5.89	28.0	0.047	1.78	1.07	0.279	0.11	3.08	0.080	0.040	104
DP17615	7	6	0.86	60.56	0.60	1.53	6.32	27.5	0.048	2.02	0.99	0.344	0.11	4.72	0.102	0.060	137
DP17617	7	6	1.26	60.96	0.53	1.73	7.08	27.0	0.052	2.44	0.71	0.399	0.09	4.56	0.089	0.062	127
DP17619	7	7	0.11	61.31	0.66	1.47	6.51	27.6	0.045	2.32	0.70	0.338	0.09	4.01	0.081	0.053	114
DP17620	7	7	0.46	61.66	0.46	1.71	6.97	26.9	0.049	2.38	0.73	0.399	0.11	4.37	0.087	0.065	146
DP17625	8	1	0.92	62.72	0.38	1.94	6.49	27.0	0.046	2.31	0.61	0.365	0.16	5.19	0.100	0.074	165
DP17627	8	1	1.26	63.06	0.47	1.97	7.30	26.7	0.050	2.53	0.69	0.393	1.40	4.05	0.091	0.076	128
DP17629	8	2	0.06	63.36	0.52	1.54	6.82	27.1	0.045	2.55	0.75	0.360	0.09	3.47	0.088	0.062	122
DP17631	8	2	0.46	63.76	0.57	1.59	6.24	27.2	0.045	2.30	0.74	0.318	0.14	4.34	0.091	0.068	144
DP17633	8	2	0.86	64.16	0.39	1.73	7.02	27.0	0.047	2.43	0.79	0.400	0.10	4.08	0.093	0.070	147
DP17635	8	2	1.26	64.56	0.53	1.30	6.94	31.0	0.050	3.06	0.81	0.349	0.11	3.88	0.120	0.030	132
DP17637	8	3	0.06	64.86	0.81	0.89	6.21	31.0	0.044	2.76	1.35	0.248	0.11	2.71	0.116	0.027	89
DP17639	8	3	0.46	65.26	0.47	1.90	7.28	26.5	0.049	2.53	0.61	0.404	0.30	4.34	0.092	0.072	129
DP17641	8	3	0.86	65.66	0.47	1.50	6.64	27.6	0.048	2.19	0.78	0.353	0.10	4.02	0.097	0.055	157
DP17643	8	3	1.26	66.06	0.52	1.83	7.07	26.9	0.049	2.56	0.68	0.401	0.16	4.87	0.096	0.070	131
DP17645	8	4	0.06	66.36	0.40	1.81	7.28	26.7	0.048	2.46	0.67	0.400	0.22	4.45	0.087	0.048	148
DP17647	8	4	0.48	66.78	0.72	1.03	5.98	27.9	0.041	2.53	0.91	0.255	0.10	3.01	0.097	0.047	107
DP17649	8	4	0.86	67.16	0.47	1.50	6.54	27.2	0.050	2.24	0.78	0.358	0.11	4.26	0.091	0.052	148
DP17651	8	4	1.26	67.56	0.47	1.72	6.96	26.7	0.050	2.38	0.76	0.386	0.15	4.47	0.093	0.064	137
DP17653	8	5	0.06	67.86	0.46	1.60	6.82	27.1	0.051	2.26	0.89	0.386	0.11	4.39	0.090	0.046	146
DP17655	8	5	0.46	68.26	0.53	1.68	6.87	26.5	0.050	2.43	0.69	0.375	0.14	4.55	0.089	0.060	123
DP17657	8	5	0.86	68.66	0.87	0.61	5.36	28.5	0.037	3.11	0.62	0.154	0.09	1.97	0.090	0.019	74
DP17659	8	5	1.23	69.03	0.54	1.49	6.54	27.0	0.054	2.17	0.89	0.356	0.11	4.19	0.091	0.051	135
DP17661	8	6	0.06	69.36	0.58	1.45	6.46	26.7	0.051	2.01	1.06	0.339	0.12	4.19	0.079	0.052	139
DP17663	8	6	0.46	69.76	0.59	1.69	7.08	26.6	0.137	2.42	1.03	0.400	0.23	4.50	0.087	0.059	107
DP17665	8	6	0.91	70.21	0.63	1.47	6.65	26.8	0.053	1.97	1.28	0.358	0.11	4.14	0.086	0.050	129
DP17667	8	6	1.26	70.56	0.61	1.60	6.73	26.5	0.052	2.23	0.95	0.370	0.13	4.60	0.093	0.055	112
DP17669	8	7	0.05	70.85	0.57	1.68	6.94	26.3	0.046	2.37	0.80	0.383	0.14	4.63	0.097	0.052	111
DP17671	8	7	0.36	71.16	0.82	1.24	6.17	27.1	0.047	1.50	1.69	0.327	0.12	4.00	0.085	0.044	104
DP17673	9	1	0.31	71.61	0.53	1.77	7.81	30.3	0.060	2.58	0.98	0.435	0.28	4.75	0.111	0.048	123
DP17678	9	1	1.26	72.56	0.56	1.53	6.75	26.6	0.050	2.17	0.92	0.367	0.13	4.24	0.084	0.053	131
DP17679	9	1	1.46	72.76	0.54	1.54	6.87	27.0	0.050	2.26	0.90	0.379	0.12	4.41	0.091	0.050	123
DP17681	9	2	0.26	73.06	0.47	1.78	7.33	26.6	0.051	2.48	0.74	0.416	0.18	4.58	0.096	0.061	123
DP17683	9	2	0.67	73.47	0.57	1.56	6.68	27.1	0.050	1.93	1.38	0.379	0.12	4.82	0.078	0.042	139
DP17685	9	2	1.06	73.86	0.49	1.62	6.94	26.9	0.051	2.31	0.73	0.385	0.17	4.33	0.090	0.054	130
DP17687	9	2	1.46	74.26	0.65	1.20	6.03	27.3	0.047	2.06	0.93	0.312	0.10	3.59	0.082	0.037	121
DP17689	9	3	0.26	74.56	0.82	1.21	6.38	27.5	0.047	2.47	0.86	0.351	0.11	3.66	0.093	0.043	112
DP17693	9	3	1.06	75.36	0.49	1.61	6.98	26.5	0.050	2.53	0.66	0.362	0.14	4.35	0.099	0.054	128
DP17695	9	3	1.46	75.76	0.50	1.46	6.68	27.3	0.048	2.15	0.93	0.358	0.10	4.20	0.097	0.047	151
DP17699	9	4	0.66	76.46	0.60	1.51	6.78	27.5	0.051	2.02	1.37	0.369	0.11	4.69	0.087	0.045	136
DP17701	9	4	1.06	76.86	0.60	1.35	6.43	26.9	0.051	2.12	0.87	0.334	0.12	3.93	0.095	0.047	117
DP17703	9	4	1.46	77.26	0.62	1.46	6.58	27.0	0.057	1.94	1.19	0.366	0.13	4.53	0.081	0.045	142
DP17705	9	5	0.25	77.55	0.78	1.56	6.70	26.2	0.064	1.67	2.02	0.417	0.17	5.39	0.076	0.041	112
DP17707	9	5	0.66	77.96	0.62	1.54	6.76	26.7	0.053	1.94	1.31	0.377	0.22	4.80	0.079	0.047	133
DP17709	9	5	1.00	78.30	0.48	1.52	6.79	26.7	0.052	2.15	0.93	0.369	0.16	4.54	0.089	0.045	149
DP17713	9	6	0.46	79.26	0.75	1.14	6.00	27.4	0.044	2.05	1.22	0.292	0.11	3.59	0.077	0.031	99
DP17715	9	6	0.86	79.66	0.60	1.47	6.77	26.9	0.051	2.37	0.89	0.348	0.15	4.19	0.084	0.045	117
DP17717	9	6	1.26	80.06	0.58	1.65	6.89	26.6	0.049	2.26	1.05	0.389	0.14	4.67	0.084	0.054	124
DP17719	9	7	0.06	80.36	0.62	1.49	6.80	27.3	0.050	2.27	0.88	0.363	0.17	4.13	0.090	0.052	113
DP17722	10	1	0.28	81.08	0.59	1.49	6.93	27.5	0.052	2.39	0.90	0.360	0.16	4.32	0.085	0.051	121
DP17723	10	1	0.46	81.26	0.58	1.42	6.67	27.0	0.051	2.40	0.84	0.335	0.15	4.06	0.083	0.049	126
DP17724	10	1	0.78	81.58	0.58	1.58	6.85	26.8	0.048	2.06	1.14	0.372	0.17	4.64	0.093	0.051	125
DP17725	10	1	0.96	81.76	0.58	1.51	6.70	26.9	0.049	2.03	1.04	0.358	0.15	4.52	0.086	0.057	143
DP17727	10	1	1.30	82.10	0.54	1.52	6.74	27.3	0.050	2.08	0.93	0.365	0.13	4.41	0.081	0.052	144
DP17728	10	1	1.46	82.26	0.55	1.58	6.79	27.0	0.050	2.03	1.10	0.373	0.13	4.71	0.082	0.057	140
DP17729	10	2	0.06	82.36	0.58	1.48	6.70	27.1	0.050	1.91	1.22	0.368	0.24	4.61	0.083	0.033	136
DP17730	10	2	0.24	82.54	0.72	1.33	6.46	26.8	0.052	1.89	1.26	0.353	0.27	4.19	0.079	0.042	111
DP17731	10	2	0.46	82.76	1.02	1.41	6.65	26.3	0.067	1.45	2.13	0.427	0.55	4.55	0.086	0.045	90

Table 6. (Continued).

Lab ID	Core	Section	Depth in Section (m)	Depth in hole (m)	Na	Mg	Al	Si	P	K	Ca	Ti	Mn	Fe	Ba	S	H_2O
DP17733	10	2	0.86	83.16	0.58	1.48	6.74	27.0	0.052	1.96	1.09	0.376	0.16	4.43	0.082	0.044	129
DP17735	10	2	1.26	83.56	0.65	1.53	6.96	26.5	0.053	1.84	1.31	0.379	0.16	4.63	0.078	0.045	119
DP17736	10	2	1.46	83.76	0.74	1.59	7.09	26.2	0.054	1.58	2.06	0.398	0.19	5.16	0.077	0.038	113
DP17737	10	3	0.06	83.86	0.65	1.57	6.87	26.5	0.054	1.83	1.37	0.381	0.17	4.85	0.080	0.047	121
DP17739	10	3	0.46	84.26	0.52	1.56	7.05	27.0	0.051	2.21	0.89	0.383	0.18	4.61	0.085	0.049	133
DP17741	10	3	0.86	84.66	0.48	1.65	7.23	26.5	0.052	2.34	0.74	0.389	0.47	4.69	0.093	0.041	129
DP17742	10	3	1.06	84.86	0.58	1.51	6.86	26.2	0.053	2.01	1.06	0.352	0.61	4.40	0.087	0.051	129
DP17743	10	3	1.26	85.06	0.55	1.56	7.06	26.7	0.053	2.14	0.98	0.375	0.27	4.62	0.089	0.048	131
DP17745	10	4	0.06	85.36	0.55	1.58	7.14	26.8	0.053	2.26	0.85	0.377	0.37	4.57	0.090	0.043	127
DP17747	10	4	0.46	85.76	0.52	1.51	6.89	27.1	0.050	2.27	0.81	0.364	0.21	4.35	0.084	0.049	132
DP17749	10	4	0.86	86.16	0.72	1.37	6.62	26.5	0.072	1.96	1.29	0.376	0.37	4.12	0.091	0.042	117
DP17751	10	4	1.26	86.56	0.67	1.43	6.66	26.7	0.055	1.96	1.28	0.389	0.14	4.41	0.085	0.035	125
DP17753	10	5	0.06	86.86	0.57	1.41	6.66	26.9	0.053	2.14	0.96	0.363	0.15	4.16	0.094	0.033	131
DP17755	10	5	0.46	87.26	0.52	1.55	7.00	27.1	0.063	2.23	0.80	0.365	0.40	4.48	0.088	0.051	137
DP17756	10	5	0.66	87.46	0.50	1.52	6.80	26.6	0.055	2.17	0.82	0.354	0.33	4.39	0.083	0.056	139
DP17757	10	5	0.86	87.66	0.56	1.49	6.81	26.3	0.049	1.97	1.09	0.348	0.47	4.37	0.080	0.040	123
DP17758	10	5	1.06	87.86	0.60	1.46	6.80	26.8	0.047	2.09	0.96	0.365	0.18	4.44	0.076	0.049	129
DP17759	10	5	1.26	88.06	0.55	1.58	6.95	26.5	0.044	2.00	1.20	0.381	0.18	4.84	0.072	0.041	131
DP17761	10	6	0.06	88.36	0.60	1.48	6.73	26.8	0.049	2.05	1.04	0.358	0.50	4.35	0.085	0.034	132
DP17763	10	6	0.46	88.76	0.53	1.65	7.02	26.4	0.049	2.12	1.02	0.368	0.34	4.57	0.083	0.048	142
DP17765	10	6	0.86	89.16	0.51	1.54	6.95	26.5	0.050	2.20	0.79	0.361	0.17	4.48	0.083	0.043	138
DP17767	11	1	0.26	90.56	0.48	1.44	6.75	27.1	0.047	2.24	0.80	0.352	0.24	4.28	0.095	0.048	131
DP17769	11	1	0.66	90.96	0.55	1.21	6.31	27.1	0.044	2.53	0.61	0.274	0.24	3.46	0.084	0.037	121
DP17771	11	1	1.06	91.36	0.57	1.47	7.00	29.1	0.057	2.10	1.12	0.393	0.19	4.90	0.096	0.030	128
DP17773	11	1	1.43	91.73	0.51	1.50	6.71	26.7	0.048	2.20	0.76	0.358	0.63	4.37	0.095	0.046	143
DP17775	11	2	0.26	92.06	0.48	1.47	6.75	26.5	0.047	2.12	0.83	0.350	0.27	4.40	0.076	0.045	139
DP17777	11	2	0.66	92.46	0.69	1.60	7.40	30.0	0.060	2.01	1.77	0.454	0.33	5.54	0.092	0.033	115
DP17779	11	2	1.06	92.86	0.52	1.33	6.62	27.4	0.047	2.10	0.86	0.332	0.16	4.11	0.081	0.033	136
DP17781	11	2	1.46	93.26	0.47	1.42	6.82	27.2	0.050	2.28	0.77	0.341	0.16	4.21	0.080	0.035	136
DP17782	11	3	0.06	93.36	0.48	1.48	6.78	27.2	0.047	2.13	0.85	0.347	0.36	4.26	0.086	0.049	142
DP17783	11	3	0.26	93.56	0.49	1.48	6.86	26.9	0.048	2.27	0.71	0.353	0.18	4.40	0.089	0.043	136
DP17785	11	3	0.66	93.96	0.45	1.45	6.90	27.1	0.053	2.27	0.68	0.357	0.29	4.38	0.086	0.041	139
DP17787	11	3	1.06	94.36	0.54	1.29	6.60	27.4	0.048	2.05	1.04	0.334	0.27	4.13	0.082	0.036	129
DP17788	11	3	1.26	94.56	0.36	1.59	7.53	31.2	0.055	2.59	0.69	0.401	0.30	5.18	0.107	0.044	150
DP17789	11	3	1.46	94.76	0.57	1.43	6.72	27.0	0.050	2.15	0.83	0.350	0.76	4.32	0.094	0.040	137
DP17791	11	4	0.26	95.06	0.48	1.45	6.69	26.8	0.047	2.20	0.66	0.344	0.19	4.20	0.101	0.051	136
DP17793	11	4	0.66	95.46	0.47	1.51	6.97	26.4	0.047	2.32	0.66	0.359	0.15	4.42	0.090	0.051	129
DP17795	11	4	1.06	95.86	0.48	1.52	7.22	26.8	0.050	2.38	0.63	0.364	0.17	4.42	0.085	0.046	123
DP17797	11	4	1.46	96.26	0.49	1.48	7.10	26.8	0.051	2.40	0.59	0.352	0.18	4.30	0.084	0.052	123
DP17798	11	5	0.06	96.36	0.47	1.41	6.97	26.7	0.051	2.41	0.59	0.340	0.20	4.06	0.086	0.048	116
DP17799	11	5	0.26	96.56	0.44	1.50	7.23	26.7	0.054	2.45	0.53	0.364	0.23	4.33	0.085	0.056	130
DP17801	11	5	0.66	96.96	0.52	1.53	7.32	26.8	0.054	2.41	0.62	0.374	0.24	4.39	0.085	0.051	115
DP17807	11	6	0.26	98.06	0.54	1.48	6.97	26.6	0.051	2.13	0.85	0.373	0.21	4.43	0.082	0.045	121
DP17809	11	6	0.66	98.46	0.72	1.24	6.51	26.3	0.051	2.01	1.08	0.323	0.19	3.96	0.069	0.037	104
DP17811	11	6	1.06	98.86	0.77	0.93	6.05	28.1	0.045	2.38	1.11	0.279	0.17	2.88	0.078	0.028	84
DP17812	11	6	1.26	99.06	0.58	1.54	6.80	26.4	0.047	2.00	1.16	0.375	0.61	5.02	0.079	0.054	132
DP17813	11	6	1.46	99.26	0.50	1.47	6.95	26.6	0.048	2.33	0.71	0.356	0.39	4.35	0.081	0.045	131
DP17815	11	7	0.21	99.51	0.73	0.90	5.86	28.0	0.039	2.55	0.90	0.255	0.14	2.88	0.081	0.020	86
DP17817	12	1	0.96	100.04	0.58	1.08	6.19	28.1	0.040	2.46	0.76	0.275	0.13	3.13	0.084	0.029	108
DP17819	12	1	1.46	100.54	0.66	0.86	5.86	28.0	0.038	2.52	0.95	0.244	0.12	2.84	0.082	0.023	103
DP17820	12	2	0.04	100.62	0.80	0.63	5.40	28.3	0.034	2.65	1.09	0.206	0.10	2.21	0.085	0.029	75
DP17821	12	2	0.34	100.92	0.43	1.54	7.08	26.8	0.049	2.30	0.66	0.373	0.58	4.50	0.084	0.043	142
DP17823	12	2	0.67	101.25	0.62	1.74	6.92	26.3	0.046	1.80	1.92	0.438	0.14	5.53	0.071	0.050	118
DP17825	12	2	1.06	101.64	0.52	1.58	6.95	26.4	0.048	2.19	0.83	0.364	0.17	4.54	0.080	0.050	129
DP17826	12	2	1.26	101.84	0.50	1.60	7.03	26.5	0.050	2.28	0.71	0.375	0.15	4.51	0.086	0.057	126
DP17827	12	2	1.46	102.04	0.46	1.50	6.95	26.7	0.051	2.31	0.61	0.364	0.14	4.38	0.088	0.047	139
DP17829	12	3	0.26	102.34	0.44	1.40	6.81	26.8	0.049	2.26	0.74	0.344	0.15	4.23	0.083	0.039	136
DP17831	12	3	0.66	102.74	0.49	1.48	6.94	26.9	0.051	2.17	0.88	0.375	0.19	4.59	0.085	0.048	138
DP17833	12	3	1.11	103.19	0.47	1.58	7.25	26.7	0.054	2.40	0.66	0.393	0.21	4.58	0.089	0.059	125
DP17834	12	4	0.06	103.64	0.49	1.52	7.21	26.6	0.054	2.13	1.12	0.379	0.22	4.67	0.080	0.042	124
DP17835	12	4	0.26	103.84	0.44	1.55	7.21	26.4	0.056	2.38	0.60	0.372	0.29	4.37	0.084	0.056	129
DP17837	12	4	0.66	104.24	0.44	1.47	6.87	26.4	0.051	2.26	0.76	0.360	0.21	4.38	0.085	0.049	139
DP17839	12	4	1.06	104.64	0.52	1.62	7.18	26.5	0.053	2.32	0.72	0.385	0.33	4.54	0.077	0.051	125
DP17841	12	4	1.46	105.04	0.62	1.18	6.29	27.4	0.043	2.79	0.52	0.262	0.26	2.91	0.088	0.027	80

Table 6. (Continued).

Lab ID	Core	Section	Depth in Section (m)	Depth in hole (m)	Na	Mg	Al	Si	P	K	Ca	Ti	Mn	Fe	Ba	S	H_2O
DP17843	12	5	0.26	105.34	0.51	1.58	7.26	26.7	0.058	2.45	0.57	0.366	0.34	4.30	0.076	0.048	119
DP17845	12	5	0.66	105.74	0.54	1.63	7.17	26.7	0.057	2.42	0.60	0.362	0.33	4.24	0.079	0.044	112
DP17847	12	5	1.06	106.14	0.46	1.60	7.12	26.8	0.063	2.39	0.61	0.366	0.40	4.24	0.081	0.043	131
DP17849	12	5	1.46	106.54	0.50	1.75	7.39	26.4	0.061	2.47	0.54	0.382	0.58	4.45	0.088	0.051	126
DP17851	12	6	0.86	107.44	0.58	1.25	6.60	27.3	0.046	2.78	0.54	0.288	0.28	3.34	0.085	0.034	100
DP17853	12	6	1.23	107.81	0.48	1.67	7.37	26.3	0.055	2.40	0.55	0.381	0.95	4.48	0.093	0.044	123
DP17855	13	1	0.26	109.56	0.42	1.37	6.89	26.7	0.049	2.46	0.47	0.338	0.18	3.97	0.082	0.038	125
DP17856	13	1	0.46	109.76	0.39	1.53	7.29	26.8	0.051	2.43	0.45	0.380	0.51	4.43	0.085	0.035	138
DP17857	13	1	0.66	109.96	0.40	1.45	7.11	26.8	0.050	2.39	0.47	0.365	0.29	4.32	0.085	0.033	135
DP17858	13	1	0.86	110.16	0.41	1.43	6.93	26.9	0.049	2.44	0.47	0.352	0.22	4.17	0.083	0.037	136
DP17859	13	1	1.06	110.36	0.36	1.44	6.98	26.9	0.049	2.37	0.43	0.363	0.21	4.30	0.083	0.030	142
DP17860	13	1	1.26	110.56	0.43	1.46	6.98	26.9	0.051	2.45	0.45	0.358	0.27	4.20	0.087	0.031	125
DP17861	13	1	1.46	110.76	0.45	1.35	6.76	27.2	0.048	2.44	0.47	0.330	0.39	3.90	0.086	0.032	131
DP17862	13	2	0.06	110.86	0.38	1.48	7.02	27.0	0.051	2.41	0.44	0.365	0.44	4.28	0.089	0.033	146
DP17863	13	2	0.26	111.06	0.41	1.46	7.02	27.2	0.051	2.38	0.49	0.364	0.32	4.25	0.086	0.039	145
DP17864	13	2	0.46	111.26	0.42	1.50	7.07	26.8	0.050	2.42	0.47	0.375	0.27	4.37	0.084	0.038	138
DP17865	13	2	0.66	111.46	0.40	1.49	7.12	26.9	0.051	2.37	0.52	0.374	0.23	4.46	0.084	0.034	140
DP17866	13	2	0.86	111.66	0.42	1.56	7.31	26.9	0.051	2.41	0.56	0.382	0.23	4.58	0.077	0.040	134
DP17867	13	2	1.06	111.86	0.44	1.55	7.16	26.1	0.049	2.38	0.48	0.369	0.22	4.47	0.085	0.044	131
DP17868	13	2	1.26	112.06	0.38	1.52	7.17	26.9	0.049	2.33	0.46	0.372	0.23	4.40	0.089	0.037	138
DP17869	13	2	1.46	112.26	0.38	1.52	7.17	26.7	0.048	2.36	0.47	0.369	0.23	4.42	0.087	0.037	137
DP17870	13	3	0.06	112.36	0.40	1.58	7.36	26.9	0.049	2.43	0.49	0.396	0.24	4.57	0.087	0.033	129
DP17871	13	3	0.26	112.56	0.38	1.50	7.07	26.4	0.049	2.35	0.52	0.372	0.32	4.54	0.079	0.027	140
DP17872	13	3	0.46	112.76	0.34	1.52	7.19	26.8	0.048	2.37	0.49	0.378	0.26	4.55	0.083	0.033	141
DP17873	13	3	0.66	112.96	0.45	1.81	7.49	26.2	0.049	2.34	0.49	0.392	0.32	4.71	0.087	0.043	120
DP17874	13	3	0.86	113.16	0.42	1.52	7.21	26.3	0.049	2.35	0.52	0.375	0.19	4.53	0.078	0.041	135
DP17875	13	3	1.06	113.36	0.37	1.60	7.33	26.5	0.051	2.43	0.47	0.385	0.30	4.57	0.082	0.040	136
DP17876	13	3	1.26	113.56	0.41	1.50	7.09	26.8	0.048	2.30	0.58	0.376	0.30	4.57	0.078	0.045	146
DP17877	13	3	1.46	113.76	0.38	1.55	7.23	27.0	0.049	2.42	0.52	0.385	0.22	4.60	0.076	0.036	138
DP17878	13	4	0.06	113.86	0.38	1.51	6.92	26.2	0.048	2.27	0.60	0.364	0.27	4.54	0.077	0.038	143
DP17879	13	4	0.26	114.06	0.40	1.51	7.13	26.7	0.048	2.32	0.63	0.378	0.20	4.63	0.080	0.034	130
DP17880	13	4	0.46	114.26	0.36	1.45	6.95	26.9	0.047	2.34	0.51	0.363	0.25	4.40	0.082	0.030	141
DP17881	13	4	0.66	114.46	0.39	1.34	6.69	27.0	0.045	2.43	0.60	0.323	0.16	3.99	0.085	0.027	129
DP17882	13	4	0.86	114.66	0.40	1.31	6.72	27.2	0.046	2.50	0.55	0.320	0.23	3.75	0.083	0.026	116
DP17883	13	4	1.06	114.86	0.46	1.54	7.22	26.6	0.049	2.40	0.50	0.390	0.34	4.53	0.084	0.050	131
DP17884	13	4	1.26	115.06	0.40	1.54	7.25	26.5	0.051	2.39	0.53	0.388	0.23	4.63	0.076	0.053	136
DP17885	13	4	1.46	115.26	0.47	1.68	7.34	26.5	0.051	2.39	0.60	0.405	0.18	4.76	0.082	0.057	124
DP17886	13	5	0.06	115.36	0.44	1.66	7.14	26.6	0.048	2.22	0.77	0.400	0.16	4.97	0.078	0.044	139
DP17887	13	5	0.26	115.56	0.47	1.53	7.09	26.9	0.049	2.42	0.58	0.360	0.16	4.30	0.084	0.047	123
DP17888	13	5	0.46	115.76	0.50	1.62	7.16	26.6	0.048	2.32	0.66	0.387	0.18	4.65	0.077	0.053	131
DP17889	13	5	0.66	115.96	0.45	1.58	7.32	26.7	0.051	2.36	0.58	0.392	0.18	4.59	0.079	0.036	126
DP17890	13	5	0.86	116.16	0.42	1.56	7.14	26.6	0.049	2.31	0.63	0.372	0.17	4.48	0.079	0.040	128
DP17891	13	5	1.06	116.36	0.47	1.77	7.43	26.3	0.050	2.32	0.63	0.406	0.20	4.95	0.083	0.053	131
DP17892	13	5	1.26	116.56	0.41	1.56	7.25	26.6	0.052	2.33	0.52	0.381	0.18	4.57	0.079	0.042	142
DP17893	13	5	1.46	116.76	0.45	1.61	7.21	26.4	0.054	2.36	0.55	0.381	0.20	4.64	0.082	0.051	133
DP17894	13	6	0.06	116.86	0.36	1.55	7.20	26.7	0.053	2.30	0.59	0.383	0.21	4.67	0.078	0.036	143
DP17895	13	6	0.26	117.06	0.47	2.08	7.42	26.1	0.052	2.13	0.56	0.385	0.39	4.57	0.078	0.062	138
DP17896	13	6	0.46	117.26	0.38	1.54	7.07	26.7	0.053	2.18	0.82	0.376	0.22	4.73	0.078	0.029	145
DP17897	13	6	0.66	117.46	0.43	1.54	7.20	26.7	0.055	2.44	0.60	0.368	0.26	4.48	0.084	0.035	129
DP17898	13	6	0.86	117.66	0.49	1.48	7.01	26.5	0.052	2.52	0.61	0.339	0.25	4.16	0.080	0.042	112
DP17899	13	6	1.06	117.86	0.57	1.65	7.12	26.3	0.053	2.14	1.08	0.405	0.21	5.19	0.082	0.046	115
DP17900	13	6	1.26	118.06	0.55	1.75	7.34	25.9	0.057	2.15	1.02	0.427	0.23	5.39	0.074	0.050	110
DP17901	13	6	1.46	118.26	0.48	1.70	7.17	25.9	0.054	2.05	1.17	0.417	0.24	5.27	0.086	0.047	116
DP17902	13	7	0.06	118.36	0.43	1.72	7.19	25.9	0.053	2.11	1.05	0.426	0.27	5.31	0.084	0.042	123
DP17903	13	7	0.26	118.56	0.44	1.72	7.33	26.2	0.057	2.17	0.91	0.415	0.31	5.11	0.088	0.050	125
DP17904	14	1	0.31	118.66	0.38	1.66	7.08	26.1	0.053	1.96	1.23	0.402	0.27	5.24	0.081	0.049	142
DP17905	14	1	0.56	118.91	0.51	1.63	6.99	26.5	0.052	2.01	1.31	0.401	0.23	5.09	0.084	0.055	118
DP17906	14	1	0.86	119.21	0.45	1.66	7.15	26.0	0.057	2.28	0.74	0.375	0.41	4.66	0.083	0.053	124
DP17907	14	1	1.06	119.41	0.56	1.38	6.64	26.8	0.047	2.35	1.27	0.324	0.28	4.57	0.076	0.043	120
DP17908	14	1	1.46	119.81	0.35	1.82	7.41	25.7	0.062	2.27	0.51	0.393	0.45	4.81	0.088	0.055	139
DP17909	14	2	0.06	119.91	0.42	1.84	7.45	25.7	0.063	2.30	0.52	0.398	0.48	4.88	0.086	0.053	191
DP17910	14	2	0.26	120.11	0.40	1.86	7.34	25.6	0.059	2.23	0.57	0.396	0.41	4.87	0.081	0.054	134
DP17911	14	2	0.46	120.31	0.42	1.80	7.33	26.1	0.057	2.30	0.59	0.388	0.37	4.67	0.079	0.057	133
DP17912	14	2	0.66	120.51	0.39	1.66	7.04	26.2	0.054	2.06	0.80	0.377	0.32	4.62	0.077	0.043	132

Table 6. (Continued).

Lab ID	Core	Section	Depth in Section (m)	Depth in hole (m)	Na	Mg	Al	Si	P	K	Ca	Ti	Mn	Fe	Ba	S	H_2O
DP17913	14	2	0.86	120.71	0.71	1.20	6.16	27.5	0.048	1.99	1.08	0.306	0.20	3.30	0.074	0.031	92
DP17914	14	2	1.06	120.91	0.33	1.88	7.24	25.9	0.053	2.15	0.55	0.378	0.38	4.72	0.091	0.061	152
DP17915	14	2	1.26	121.11	0.27	1.88	7.35	26.0	0.059	2.17	0.55	0.395	0.49	4.91	0.098	0.053	158
DP17916	14	2	1.46	121.31	0.46	1.88	7.39	25.8	0.064	2.21	0.61	0.400	0.51	5.00	0.101	0.061	132
DP17917	14	3	0.06	121.41	0.45	1.88	7.37	25.7	0.060	2.22	0.60	0.402	0.43	5.01	0.100	0.058	130
DP17918	14	3	0.26	121.61	0.39	1.91	7.35	26.0	0.059	2.23	0.55	0.406	0.42	5.15	0.101	0.069	138
DP17919	14	3	0.46	121.81	0.36	1.90	7.35	25.7	0.062	2.24	0.53	0.405	0.45	5.08	0.101	0.054	137
DP17920	14	3	0.66	122.01	0.44	1.87	7.40	25.7	0.064	2.24	0.62	0.408	0.41	5.11	0.096	0.055	126
DP17921	14	3	0.86	122.21	0.46	1.86	7.41	25.8	0.065	2.28	0.59	0.405	0.42	5.07	0.103	0.052	118
DP17922	14	3	1.06	122.41	0.40	1.93	7.41	25.9	0.057	2.17	0.70	0.413	0.33	5.33	0.103	0.060	141
DP17923	14	3	1.26	122.61	0.58	1.93	7.38	26.1	0.057	2.31	0.59	0.409	0.37	4.99	0.108	0.053	103
DP17924	14	3	1.46	122.81	0.57	1.85	7.26	26.0	0.053	2.20	0.68	0.386	0.35	4.93	0.113	0.054	104
DP17925	14	4	0.06	122.91	0.53	1.86	7.30	26.0	0.056	2.34	0.44	0.393	0.54	4.76	0.108	0.050	106
DP17926	14	4	0.26	123.11	0.53	1.91	7.28	25.9	0.058	2.27	0.48	0.393	0.49	4.86	0.093	0.058	109
DP17927	14	4	0.46	123.31	0.55	1.98	7.26	26.1	0.055	2.13	0.57	0.378	0.46	4.73	0.078	0.055	114
DP17928	14	4	0.66	123.51	0.56	1.90	7.37	25.9	0.055	2.26	0.53	0.397	0.51	4.91	0.083	0.052	112
DP17929	14	4	0.86	123.71	0.61	1.95	7.39	26.1	0.060	2.28	0.53	0.396	0.58	4.88	0.089	0.064	105
DP17930	14	4	1.06	123.91	0.62	2.15	7.19	26.2	0.049	2.06	0.57	0.404	0.38	4.86	0.076	0.054	116
DP17931	14	4	1.26	124.11	0.61	1.94	7.30	25.8	0.056	2.31	0.57	0.410	0.39	5.29	0.084	0.049	99
DP17932	14	4	1.46	124.31	0.59	2.01	7.15	25.4	0.044	1.66	1.30	0.479	0.19	5.37	0.071	0.045	137
DP17933	14	5	0.06	124.41	0.70	1.88	7.30	25.3	0.047	1.82	1.37	0.448	0.25	5.86	0.071	0.055	122
DP17934	14	5	0.26	124.61	0.64	1.86	7.32	25.8	0.056	2.31	0.57	0.408	0.48	5.09	0.091	0.051	93
DP17935	14	5	0.46	124.81	0.63	1.95	7.27	25.9	0.055	2.26	0.52	0.398	0.53	4.94	0.085	0.049	99
DP17936	14	5	0.66	125.01	0.70	1.92	7.38	26.1	0.060	2.32	0.65	0.410	0.44	5.10	0.092	0.060	92
DP17937	14	5	0.86	125.21	0.61	1.90	7.13	26.0	0.057	2.13	0.52	0.367	0.62	4.72	0.079	0.048	107
DP17938	14	5	1.06	125.41	0.61	1.86	7.13	26.1	0.060	2.18	0.48	0.385	0.58	4.75	0.089	0.038	102
DP17939	14	5	1.26	125.61	0.66	1.84	7.14	25.9	0.070	2.23	0.55	0.393	0.57	4.80	0.095	0.051	94
DP17940	14	5	1.46	125.81	0.70	1.87	7.25	25.9	0.070	2.20	0.66	0.401	0.51	5.07	0.089	0.051	94
DP17941	14	6	0.06	125.91	0.66	1.87	7.20	25.8	0.062	2.33	0.48	0.396	0.57	4.91	0.095	0.046	89
DP17942	14	6	0.26	126.11	0.67	1.81	7.27	25.8	0.061	2.42	0.52	0.411	0.54	4.99	0.099	0.045	83
DP17943	14	6	0.46	126.31	0.65	1.82	7.35	25.8	0.068	2.32	0.63	0.408	0.60	5.15	0.086	0.041	89
DP17944	14	6	0.66	126.51	0.67	1.78	7.25	25.4	0.065	2.34	0.60	0.403	0.64	5.09	0.085	0.038	85
DP17945	14	6	0.86	126.71	0.74	1.88	7.35	25.6	0.061	2.38	0.53	0.406	0.67	5.18	0.084	0.053	90
DP17946	14	6	1.06	126.91	0.59	1.87	7.34	26.0	0.068	2.29	0.52	0.390	0.44	4.84	0.071	0.035	96
DP17947	14	6	1.26	127.11	0.65	1.93	7.34	25.7	0.062	2.30	0.43	0.384	0.63	4.83	0.086	0.044	97
DP17948	14	6	1.38	127.23	0.67	1.80	7.40	25.7	0.064	2.45	0.51	0.411	0.64	5.05	0.086	0.042	85
DP17949	14	7	0.06	127.41	0.66	1.81	7.39	25.7	0.065	2.42	0.54	0.410	0.65	5.08	0.084	0.050	87
DP17950	14	7	0.26	127.61	0.66	1.79	7.39	25.7	0.068	2.46	0.47	0.403	0.70	4.97	0.089	0.042	86
DP17951	14	7	0.44	127.79	0.69	1.81	7.45	25.8	0.067	2.43	0.53	0.408	0.73	5.08	0.089	0.048	89
DP17956	15	1	0.44	128.44	0.61	1.84	7.34	25.2	0.064	2.25	0.51	0.394	0.82	5.03	0.092	0.033	103
DP17957	15	1	0.66	128.66	0.51	2.04	7.41	25.7	0.063	2.04	0.43	0.365	0.67	4.46	0.086	0.043	122
DP17958	15	1	0.86	128.86	0.63	1.85	7.36	25.2	0.064	2.17	0.52	0.398	0.80	4.95	0.090	0.042	107
DP17959	15	1	1.08	129.08	0.64	1.86	7.44	25.6	0.073	2.06	0.58	0.451	0.66	5.15	0.081	0.046	123
DP17960	15	1	1.26	129.26	0.60	1.84	7.51	25.6	0.078	2.23	0.48	0.423	0.83	5.00	0.095	0.036	104
DP17961	15	1	1.46	129.46	0.65	1.86	7.47	25.2	0.072	2.37	0.42	0.402	0.81	5.01	0.093	0.043	93
DP17962	15	2	0.06	129.56	0.59	1.87	7.42	25.6	0.068	2.22	0.46	0.395	0.65	4.82	0.083	0.043	105
DP17963	15	2	0.26	129.76	0.64	1.86	7.45	25.4	0.069	2.31	0.49	0.408	0.80	5.09	0.092	0.045	96
DP17964	15	2	0.46	129.96	0.67	1.80	7.42	25.7	0.062	2.37	0.45	0.402	0.73	4.85	0.088	0.046	97
DP17965	15	2	0.66	130.16	0.65	1.80	7.50	25.6	0.066	2.38	0.45	0.401	0.75	4.89	0.092	0.040	93
DP17966	15	2	0.86	130.36	0.59	1.81	7.42	25.5	0.066	2.17	0.50	0.394	0.71	5.08	0.087	0.033	106
DP17967	15	2	1.06	130.56	0.61	1.76	7.49	25.7	0.066	2.41	0.39	0.403	0.69	4.90	0.087	0.033	88
DP17968	15	2	1.26	130.76	0.63	1.79	7.44	25.5	0.071	2.36	0.44	0.402	0.68	4.91	0.087	0.040	91
DP17969	15	2	1.46	130.96	0.60	1.84	7.45	25.7	0.069	2.29	0.42	0.402	0.65	5.00	0.087	0.028	102
DP17970	15	3	0.06	131.06	0.61	1.85	7.42	25.6	0.070	2.40	0.40	0.413	0.62	4.98	0.089	0.031	92
DP17971	15	3	0.26	131.26	0.60	1.83	7.44	25.6	0.065	2.37	0.38	0.403	0.65	4.94	0.084	0.032	92
DP17972	15	3	0.46	131.46	0.64	1.84	7.49	25.7	0.068	2.40	0.41	0.410	0.68	4.95	0.086	0.045	92
DP17973	15	3	0.66	131.66	0.63	1.84	7.51	25.6	0.069	2.35	0.40	0.407	0.81	5.05	0.089	0.046	97
DP17974	15	3	0.86	131.86	0.63	1.83	7.53	25.5	0.070	2.32	0.40	0.404	0.82	4.93	0.091	0.047	99
DP17975	15	3	1.06	132.06	0.62	1.84	7.53	25.2	0.075	2.31	0.40	0.404	0.85	5.07	0.093	0.052	98
DP17976	15	3	1.26	132.26	0.62	1.84	7.50	25.4	0.067	2.32	0.40	0.416	0.81	5.15	0.089	0.048	98
DP17977	15	3	1.46	132.46	0.53	1.93	7.52	25.7	0.065	2.30	0.32	0.389	0.72	4.84	0.081	0.037	101
DP17978	15	4	0.06	132.56	0.53	2.33	7.41	26.1	0.050	1.57	0.33	0.278	0.46	3.79	0.060	0.044	138
DP17979	15	4	0.26	132.76	0.51	1.92	7.35	25.2	0.053	2.04	0.40	0.412	0.73	5.62	0.076	0.029	122
DP17980	15	4	0.46	132.96	0.55	1.84	7.51	25.3	0.063	2.31	0.35	0.406	0.72	5.21	0.085	0.045	104

Table 6. (Continued).

Lab ID	Core	Section	Depth in Section (m)	Depth in hole (m)	Na	Mg	Al	Si	P	K	Ca	Ti	Mn	Fe	Ba	S	H_2O
DP17981	15	4	0.66	133.16	0.56	1.77	7.61	25.3	0.068	2.41	0.33	0.411	0.85	5.11	0.091	0.035	92
DP17982	15	4	0.86	133.36	0.56	1.79	7.62	25.4	0.067	2.51	0.31	0.417	0.76	5.13	0.086	0.041	88
DP17983	15	4	1.06	133.56	0.55	1.84	7.57	25.4	0.060	2.45	0.32	0.423	0.65	5.29	0.080	0.040	92
DP17984	15	4	1.26	133.76	0.55	1.90	7.50	25.3	0.058	2.21	0.43	0.433	0.68	5.65	0.077	0.046	111
DP17985	15	4	1.46	133.96	0.54	1.97	7.37	25.3	0.054	1.96	0.45	0.428	0.65	5.96	0.074	0.042	127
DP17986	15	5	0.06	134.06	0.57	1.85	7.63	25.4	0.066	2.57	0.33	0.429	0.63	5.23	0.081	0.050	86
DP17987	15	5	0.26	134.26	0.56	1.85	7.67	25.6	0.072	2.49	0.33	0.416	0.74	5.04	0.084	0.047	91
DP17988	15	5	0.46	134.46	0.53	1.96	7.54	25.4	0.066	2.18	0.33	0.419	0.65	5.20	0.077	0.051	113
DP17989	15	5	0.66	134.66	0.50	1.95	7.52	25.2	0.061	2.02	0.39	0.422	0.65	5.73	0.075	0.044	123
DP17990	15	5	0.84	134.84	0.52	1.91	7.66	25.5	0.070	2.23	0.33	0.403	0.75	4.95	0.081	0.042	107
DP17991	15	5	1.00	135.00	0.58	1.87	7.78	25.4	0.070	2.15	0.36	0.415	0.72	5.08	0.079	0.042	109
DP17992	15	5	1.16	135.16	0.58	1.84	7.80	25.3	0.067	2.17	0.40	0.418	0.73	5.31	0.080	0.035	109
DP17993	15	6	0.06	135.56	0.60	1.81	7.83	25.3	0.074	2.34	0.32	0.408	0.83	5.04	0.090	0.047	95
DP17994	15	6	0.26	135.76	0.55	1.93	7.75	25.5	0.065	1.99	0.34	0.406	0.69	5.04	0.076	0.040	115
DP17995	15	6	0.46	135.96	0.62	1.83	7.86	25.5	0.072	2.34	0.30	0.391	0.86	4.88	0.087	0.051	92
DP17996	15	6	0.66	136.16	0.60	1.85	7.84	25.4	0.064	2.41	0.28	0.396	0.72	4.89	0.083	0.048	90
DP17997	15	6	0.86	136.36	0.64	1.84	7.84	25.5	0.066	2.39	0.30	0.403	0.83	4.89	0.088	0.052	89
DP17998	15	6	1.06	136.56	0.64	1.82	7.82	25.4	0.064	2.47	0.28	0.412	0.71	5.00	0.084	0.050	85
DP17999	15	6	1.16	136.66	0.61	1.82	7.82	25.4	0.064	2.33	0.30	0.411	0.68	5.16	0.086	0.045	95
DP18000	15	6	1.46	136.96	0.63	1.84	7.77	25.3	0.065	2.30	0.31	0.409	0.68	5.17	0.082	0.057	95
DP18002	15	7	0.26	137.26	0.59	1.82	7.82	25.2	0.073	2.35	0.32	0.416	0.77	5.14	0.089	0.052	94
DP18003	15	7	0.45	137.45	0.60	1.80	7.85	25.2	0.072	2.28	0.31	0.416	0.81	5.18	0.086	0.048	100
DP18004	16	1	0.36	138.11	0.57	1.88	7.86	25.3	0.071	2.25	0.33	0.424	0.75	5.27	0.088	0.055	112
DP18005	16	1	0.56	138.31	0.56	1.91	7.93	25.1	0.073	2.25	0.32	0.420	0.74	5.24	0.086	0.058	108
DP18006	16	1	0.76	138.51	0.50	1.89	7.75	25.2	0.075	2.19	0.29	0.410	0.76	5.03	0.088	0.049	120
DP18007	16	1	0.96	138.71	0.58	1.86	7.80	25.4	0.072	2.33	0.31	0.418	0.70	5.09	0.084	0.059	111
DP18008	16	1	1.16	138.91	0.60	1.81	7.85	25.1	0.073	2.38	0.31	0.418	0.72	5.11	0.087	0.064	105
DP18009	16	1	1.36	139.11	0.65	1.81	7.93	25.3	0.077	2.39	0.31	0.411	0.77	5.03	0.095	0.060	91
DP18010	16	2	0.06	139.31	0.61	1.82	7.91	25.2	0.069	2.36	0.30	0.420	0.65	5.18	0.086	0.050	93
DP18011	16	2	0.26	139.51	0.60	1.79	7.93	25.3	0.072	2.50	0.30	0.422	0.60	5.17	0.083	0.047	84
DP18012	16	2	0.46	139.71	0.61	1.80	8.00	25.4	0.071	2.51	0.30	0.427	0.61	5.36	0.085	0.048	82
DP18013	16	2	0.66	139.91	0.61	1.79	7.89	25.2	0.074	2.39	0.30	0.421	0.73	5.28	0.087	0.047	88
DP18014	16	2	0.86	140.11	0.64	1.80	8.02	25.3	0.071	2.50	0.31	0.430	0.68	5.24	0.087	0.052	82
DP18015	16	2	1.06	140.31	0.61	1.76	7.94	25.2	0.078	2.39	0.31	0.414	0.66	5.19	0.084	0.053	86
DP18016	16	2	1.26	140.51	0.62	1.79	7.82	24.9	0.071	2.31	0.31	0.422	0.67	5.58	0.087	0.056	94
DP18017	16	2	1.46	140.71	0.63	1.78	7.92	25.1	0.077	2.37	0.31	0.414	0.73	5.21	0.089	0.058	87
DP18018	16	3	0.06	140.81	0.62	1.78	7.95	25.2	0.073	2.32	0.31	0.408	0.71	5.20	0.086	0.055	90
DP18019	16	3	0.26	141.01	0.65	1.78	8.00	25.2	0.081	2.50	0.31	0.419	0.59	5.25	0.084	0.057	79
DP18020	16	3	0.46	141.21	0.65	1.75	8.05	25.0	0.085	2.33	0.33	0.408	0.76	5.12	0.089	0.059	88
DP18021	16	3	0.66	141.41	0.65	1.74	8.14	24.9	0.085	2.43	0.35	0.422	0.78	5.36	0.097	0.058	81
DP18022	16	3	0.86	141.61	0.64	1.74	8.14	24.9	0.082	2.27	0.36	0.426	0.81	5.54	0.092	0.056	89
DP18023	16	3	1.06	141.81	0.64	1.69	8.20	25.0	0.095	2.43	0.37	0.417	0.83	5.17	0.098	0.056	77
DP18024	16	3	1.26	142.01	0.66	1.70	8.19	25.0	0.087	2.46	0.35	0.423	0.77	5.25	0.094	0.060	79
DP18025	16	3	1.46	142.21	0.64	1.78	8.00	24.9	0.080	2.36	0.33	0.425	0.65	5.42	0.085	0.056	85
DP18026	16	4	0.06	142.31	0.65	1.76	8.07	24.9	0.078	2.46	0.33	0.430	0.67	5.34	0.088	0.054	80
DP18027	16	4	0.26	142.51	0.64	1.78	8.22	25.2	0.080	2.47	0.32	0.425	0.67	5.21	0.086	0.057	83
DP18028	16	4	0.46	142.71	0.57	1.81	8.10	25.0	0.077	2.29	0.31	0.404	0.65	4.98	0.083	0.049	97
DP18029	16	4	0.66	142.91	0.60	1.80	8.18	25.1	0.080	2.43	0.31	0.409	0.72	5.06	0.087	0.046	86
DP18030	16	4	0.86	143.11	0.55	1.90	8.15	25.3	0.076	2.13	0.30	0.388	0.61	4.72	0.075	0.047	107
DP18031	16	4	1.06	143.31	0.63	1.79	8.10	25.0	0.083	2.37	0.35	0.415	0.68	5.10	0.084	0.058	89
DP18032	16	4	1.26	143.51	0.58	1.93	7.97	25.1	0.078	2.15	0.33	0.433	0.66	5.24	0.078	0.052	106
DP18033	16	4	1.46	143.71	0.56	2.00	7.94	25.1	0.074	2.06	0.30	0.387	0.71	4.80	0.077	0.048	114
DP18034	16	5	0.06	143.81	0.43	2.10	8.20	25.4	0.060	1.53	0.31	0.339	0.63	3.81	0.062	0.055	141
DP18035	16	5	0.26	144.01	0.62	1.93	7.82	24.9	0.092	2.09	0.40	0.407	0.85	5.03	0.087	0.059	108
DP18036	16	5	0.46	144.21	0.64	1.88	7.94	24.6	0.081	2.27	0.38	0.424	1.07	5.31	0.089	0.061	95
DP18037	16	5	0.66	144.41	0.64	1.79	7.98	24.5	0.102	2.41	0.42	0.418	1.13	5.33	0.090	0.061	86
DP18039	16	5	1.06	144.81	0.62	1.95	7.80	25.1	0.095	2.16	0.40	0.418	0.86	5.00	0.077	0.059	99
DP18040	16	5	1.26	145.01	0.63	1.96	7.78	25.0	0.101	2.05	0.42	0.414	1.08	5.11	0.083	0.067	106
DP18041	16	5	1.46	145.21	0.65	1.86	7.73	25.0	0.105	2.13	0.41	0.412	0.91	5.30	0.078	0.060	95
DP18042	16	6	0.07	145.32	0.65	1.83	7.89	25.3	0.110	2.23	0.41	0.394	0.94	4.90	0.082	0.064	91
DP18043	16	6	0.21	145.46	0.64	1.91	7.91	25.3	0.079	2.19	0.33	0.393	0.80	4.87	0.074	0.059	95
DP18044	17	1	0.32	147.34	0.62	1.80	8.18	24.0	0.114	2.47	0.47	0.429	1.23	5.30	0.074	0.067	94
DP18045	17	1	0.48	147.50	0.67	1.79	8.14	24.1	0.123	2.55	0.49	0.434	1.23	5.31	0.073	0.063	89
DP18046	17	1	0.67	147.69	0.69	1.78	8.13	24.0	0.137	2.56	0.53	0.443	1.24	5.45	0.071	0.068	88

Table 6. (Continued).

Lab ID	Core	Section	Depth in Section (m)	Depth in hole (m)	Na	Mg	Al	Si	P	K	Ca	Ti	Mn	Fe	Ba	S	H_2O
DP18047	17	1	0.86	147.88	0.65	1.76	8.12	24.2	0.135	2.61	0.52	0.431	1.38	5.32	0.072	0.060	86
DP18048	17	1	1.06	148.08	0.61	1.75	8.03	23.9	0.133	2.54	0.49	0.435	1.54	5.43	0.069	0.052	91
DP18049	17	1	1.26	148.28	0.57	1.77	8.00	23.9	0.134	2.49	0.49	0.446	1.51	5.56	0.070	0.048	90
DP18050	17	1	1.46	148.48	0.59	1.76	8.06	23.9	0.132	2.53	0.47	0.450	1.52	5.59	0.072	0.055	88
DP18051	17	2	0.11	148.63	0.55	1.77	8.09	23.9	0.124	2.50	0.44	0.457	1.57	5.63	0.073	0.052	88
DP18052	17	2	0.43	148.95	0.51	1.82	7.85	23.3	0.121	2.45	0.44	0.436	2.20	5.50	0.079	0.052	95
DP18053	17	2	0.55	149.07	0.61	1.72	7.99	24.2	0.123	2.59	0.44	0.444	0.41	5.79	0.061	0.061	81
DP18054	17	2	0.71	149.23	0.61	1.76	8.07	23.9	0.126	2.53	0.47	0.440	1.62	5.61	0.075	0.067	88
DP18055	17	2	0.86	149.38	0.60	1.79	8.03	24.0	0.123	2.55	0.48	0.446	1.63	5.60	0.070	0.064	88
DP18056	17	2	1.06	149.58	0.58	1.77	8.02	24.0	0.113	2.61	0.42	0.438	1.46	5.44	0.071	0.061	83
DP18057	17	2	1.16	149.78	0.59	1.76	7.97	24.1	0.098	2.67	0.38	0.429	1.36	5.22	0.073	0.059	75
DP18058	17	2	1.46	149.98	0.61	1.77	8.04	24.3	0.104	2.67	0.39	0.420	1.24	5.09	0.070	0.060	77
DP18059	17	3	0.06	150.08	0.59	1.82	7.96	24.3	0.096	2.71	0.36	0.430	1.18	5.15	0.070	0.054	73
DP18060	17	3	0.26	150.28	0.63	1.77	8.01	24.3	0.107	2.70	0.40	0.424	1.26	5.13	0.074	0.059	75
DP18061	17	3	0.46	150.48	0.63	1.77	7.96	23.9	0.118	2.58	0.47	0.431	1.59	5.36	0.072	0.063	79
DP18062	17	3	0.66	150.68	0.63	1.78	7.99	24.1	0.100	2.69	0.40	0.430	1.47	5.17	0.071	0.061	92
DP18063	17	3	0.82	150.84	0.66	1.73	7.93	23.7	0.127	2.59	0.49	0.429	1.68	5.23	0.068	0.064	90
DP18064	17	3	0.99	151.01	0.65	1.75	8.01	23.8	0.132	2.62	0.51	0.435	1.83	5.35	0.071	0.068	90
DP18065	17	3	1.18	151.20	0.56	1.74	8.10	24.0	0.141	2.61	0.51	0.428	1.95	5.30	0.071	0.058	93
DP18066	17	3	1.34	151.36	0.54	1.75	8.04	23.7	0.138	2.59	0.50	0.431	1.95	5.32	0.071	0.056	91
DP18067	17	4	0.06	151.58	0.60	1.69	7.97	23.3	0.159	2.53	0.58	0.422	2.17	5.31	0.069	0.064	103
DP18068	17	4	0.26	151.78	0.67	1.68	7.94	23.4	0.176	2.57	0.62	0.426	2.08	5.23	0.068	0.059	103
DP18069	17	4	0.46	151.98	0.58	1.78	7.89	23.3	0.200	2.54	0.67	0.432	2.27	5.32	0.071	0.061	98
DP18070	17	4	0.66	152.18	0.50	1.82	7.73	23.0	0.227	2.52	0.75	0.436	2.49	5.38	0.075	0.067	94
DP18071	17	4	0.82	152.34	0.56	1.86	7.52	22.6	0.274	2.53	0.88	0.448	2.62	5.55	0.075	0.075	92
DP18072	17	4	1.00	152.52	0.59	1.87	7.41	22.6	0.276	2.56	0.89	0.445	2.69	5.63	0.075	0.072	86
DP18073	17	4	1.18	152.70	0.55	1.90	7.44	22.7	0.276	2.59	0.91	0.433	2.76	5.57	0.075	0.078	96
DP18074	17	4	1.36	152.88	0.52	1.87	7.49	22.8	0.262	2.60	0.85	0.421	2.48	5.41	0.071	0.074	101
DP18075	17	5	0.06	153.08	0.52	1.91	7.49	22.8	0.256	2.58	0.86	0.435	2.50	5.52	0.071	0.071	97
DP18076	17	5	0.26	153.28	0.51	1.91	7.49	22.7	0.266	2.52	0.89	0.434	2.63	5.62	0.072	0.073	103
DP18077	17	5	0.46	153.48	0.49	1.89	7.41	22.4	0.286	2.52	0.95	0.430	2.80	5.86	0.073	0.076	103
DP18078	17	5	0.66	153.68	0.50	1.89	7.41	22.4	0.295	2.56	0.98	0.427	2.75	5.83	0.073	0.075	101
DP18079	17	5	0.86	153.88	0.50	1.90	7.49	22.4	0.288	2.58	0.94	0.406	2.63	5.70	0.071	0.073	102
DP18080	17	5	1.06	154.08	0.52	1.84	7.79	22.8	0.231	2.72	0.78	0.371	2.36	5.21	0.068	0.074	97
DP18081	17	5	1.26	154.28	0.51	1.87	7.85	23.0	0.206	2.84	0.67	0.368	2.07	5.24	0.070	0.064	87
DP18082	18	1	0.26	156.86	0.58	1.75	7.91	24.0	0.142	2.93	0.50	0.388	1.06	5.37	0.062	0.054	73
DP18083	18	1	0.46	157.06	0.57	1.74	7.88	24.0	0.160	2.87	0.54	0.428	1.13	5.46	0.065	0.051	75
DP18084	18	1	0.66	157.26	0.56	1.79	7.88	23.9	0.185	2.91	0.62	0.421	1.26	5.48	0.066	0.054	75
DP18085	18	1	0.86	157.46	0.56	1.80	7.84	23.9	0.176	2.92	0.60	0.419	1.27	5.50	0.067	0.054	75
DP18086	18	1	1.06	157.66	0.53	1.82	7.82	23.8	0.146	2.87	0.51	0.464	1.09	5.80	0.067	0.050	77
DP18087	18	1	1.26	157.86	0.53	1.80	7.94	24.0	0.134	2.92	0.47	0.467	1.07	5.74	0.066	0.049	75
DP18088	18	1	1.46	158.06	0.51	1.82	7.91	23.9	0.128	2.93	0.46	0.472	1.10	5.75	0.067	0.049	77
DP18089	18	2	0.06	158.16	0.52	1.84	7.87	23.9	0.138	2.92	0.49	0.476	1.15	5.74	0.068	0.057	81
DP18091	18	2	0.46	158.56	0.48	1.95	7.45	23.5	0.234	2.93	0.74	0.473	1.35	5.71	0.069	0.063	79
DP18092	18	2	0.66	158.76	0.45	2.03	7.62	24.3	0.188	3.04	0.60	0.451	1.14	5.53	0.069	0.059	75
DP18093	18	2	0.86	158.96	0.44	2.07	7.59	24.5	0.176	3.09	0.56	0.403	1.03	5.20	0.068	0.053	66
DP18094	18	2	1.06	159.16	0.37	2.15	7.47	24.6	0.166	3.07	0.52	0.410	0.89	5.11	0.068	0.048	66
DP18095	18	2	1.26	159.36	0.36	2.20	7.49	24.6	0.176	3.08	0.55	0.416	0.93	5.14	0.070	0.053	69
DP18096	18	2	1.46	159.56	0.37	2.18	7.36	24.4	0.183	3.07	0.57	0.400	0.99	5.01	0.070	0.054	66
DP18097	18	3	0.06	159.66	0.38	2.20	7.38	24.7	0.185	3.08	0.56	0.412	0.96	5.03	0.070	0.049	63
DP18098	18	3	0.26	159.86	0.40	2.20	7.34	24.5	0.174	3.08	0.53	0.405	0.92	4.97	0.070	0.049	60
DP18099	18	3	0.46	160.06	0.43	2.21	7.35	24.6	0.174	3.11	0.54	0.413	0.95	5.00	0.071	0.054	60
DP18100	18	3	0.66	160.26	0.39	2.20	7.22	24.4	0.169	3.08	0.53	0.406	0.90	4.94	0.070	0.048	60
DP18101	18	3	0.86	160.46	0.41	2.18	7.23	24.5	0.170	3.11	0.53	0.410	0.88	4.89	0.068	0.049	59
DP18102	18	3	1.06	160.66	0.40	2.19	7.37	24.7	0.153	3.12	0.48	0.412	0.86	5.03	0.068	0.044	60
DP18103	18	3	1.17	160.77	0.39	2.18	7.36	24.5	0.151	3.11	0.48	0.403	0.93	4.98	0.071	0.047	62
DP18104	18	4	0.06	161.16	0.40	2.18	7.32	24.4	0.156	3.11	0.49	0.401	0.94	4.93	0.069	0.043	61
DP18105	18	4	0.26	161.36	0.40	2.24	7.42	24.8	0.158	3.16	0.50	0.409	0.92	5.02	0.070	0.050	62
DP18106	18	4	0.46	161.56	0.40	2.21	7.38	24.5	0.171	3.10	0.53	0.402	0.95	5.02	0.068	0.048	61
DP18107	18	4	0.66	161.76	0.40	2.28	7.48	24.7	0.161	3.13	0.51	0.404	1.09	5.03	0.071	0.050	63
DP18108	18	4	0.86	161.96	0.40	2.21	7.36	24.6	0.230	3.14	0.69	0.407	1.03	5.06	0.070	0.055	62
DP18109	18	4	1.06	162.16	0.42	2.15	7.26	24.2	0.254	3.10	0.76	0.412	1.10	4.98	0.071	0.056	63
DP18110	18	4	1.26	162.36	0.41	2.15	7.20	24.3	0.282	3.10	0.82	0.407	0.99	4.96	0.070	0.062	63
DP18111	18	C	0.05	162.48	0.39	2.21	7.27	24.6	0.318	3.07	0.91	0.429	1.34	4.99	0.076	0.060	66

Table 6. (Continued).

Lab ID	Core	Section	Depth in Section (m)	Depth in hole (m)	Na	Mg	Al	Si	P	K	Ca	Ti	Mn	Fe	Ba	S	H_2O
DP18112	18	C	0.30	162.73	0.38	2.18	7.02	23.8	0.342	3.00	0.97	0.419	1.26	4.96	0.082	0.064	66
DP18113	19	1	0.47	166.34	0.38	2.29	7.51	24.7	0.162	3.14	0.51	0.405	1.04	5.05	0.071	0.053	69
DP18114	19	1	0.66	166.53	0.39	2.21	7.31	24.4	0.244	3.14	0.72	0.407	1.11	4.99	0.072	0.055	67
DP18115	19	1	0.86	166.73	0.41	2.18	7.35	24.5	0.271	3.12	0.79	0.412	1.10	4.99	0.070	0.061	67
DP18116	19	1	1.06	166.93	0.38	2.16	7.16	24.1	0.276	3.06	0.79	0.395	1.14	4.91	0.072	0.057	66
DP18117	19	1	1.26	167.13	0.37	2.21	7.09	24.2	0.292	3.04	0.83	0.425	1.10	4.93	0.072	0.059	67
DP18118	19	1	1.46	167.33	0.37	2.17	7.03	23.8	0.346	2.99	0.98	0.418	1.19	4.93	0.072	0.065	68
DP18131	19	2	0.32	167.69	0.50	1.94	6.78	24.0	0.642	3.02	1.74	0.413	1.23	5.13	0.081	0.083	82
DP18132	19	2	0.48	167.85	0.53	1.97	7.00	23.2	0.735	2.90	2.05	0.435	1.50	5.17	0.074	0.102	98
DP18133	19	2	0.66	168.03	0.50	1.92	7.06	23.4	0.695	2.96	1.89	0.419	1.29	5.21	0.075	0.087	68
DP18134	19	2	0.86	168.23	0.50	1.97	7.04	23.5	0.677	3.02	1.78	0.414	1.38	5.15	0.075	0.085	68
DP18119	19	2	0.99	168.36	0.52	1.94	7.03	23.6	0.660	3.06	1.75	0.414	1.37	5.16	0.075	0.086	66
DP18120	19	2	1.11	168.48	0.49	1.94	7.08	23.6	0.654	3.02	1.72	0.404	1.32	5.10	0.073	0.081	65
DP18121	19	2	1.25	168.62	0.48	1.94	7.14	23.8	0.568	3.09	1.53	0.406	1.23	5.02	0.075	0.080	64
DP18122	19	2	1.38	168.75	0.47	1.94	7.07	23.7	0.557	3.08	1.55	0.401	1.19	5.08	0.075	0.074	65
DP18123	19	3	0.06	168.93	0.48	1.94	7.11	23.9	0.522	3.11	1.47	0.412	1.24	5.14	0.076	0.074	64
DP18124	19	3	0.26	169.13	0.49	1.95	7.03	23.9	0.490	3.12	1.45	0.412	1.30	5.15	0.078	0.072	65
DP18125	19	3	0.46	169.33	0.46	1.95	7.03	24.0	0.490	3.12	1.44	0.411	1.30	5.21	0.078	0.068	65
DP18126	19	3	0.66	169.53	0.51	1.93	6.97	24.0	0.601	3.10	1.68	0.419	1.25	5.15	0.078	0.081	64
DP18127	19	3	0.86	169.73	0.55	1.85	6.92	23.7	0.637	3.06	1.77	0.410	1.38	5.14	0.078	0.085	66
DP18128	19	3	1.06	169.93	0.52	1.89	6.84	23.8	0.699	3.06	1.89	0.410	1.30	5.11	0.077	0.089	64
DP18129	19	C	0.05	170.12	0.53	1.92	6.80	23.9	0.667	3.03	1.84	0.410	1.25	5.11	0.077	0.088	65
DP18130	19	C	0.29	170.36	0.37	2.10	7.05	23.9	0.470	2.94	1.32	0.428	1.32	5.05	0.074	0.072	64
DP17952	20	1	0.06	175.86	0.36	2.17	6.15	23.7	0.574	3.08	1.68	0.354	1.77	5.38	0.113	0.076	101
DP17953	20	1	0.22	176.02	0.58	2.08	5.97	23.4	0.995	3.07	2.60	0.353	1.39	4.70	0.112	0.097	73
DP17954	20	1	0.46	176.26	0.71	1.90	5.94	24.1	0.803	3.21	2.14	0.337	1.02	4.10	0.084	0.086	63
DP17955	20	1	0.71	176.51	0.67	2.07	5.74	23.1	1.282	2.88	3.24	0.346	1.32	4.40	0.091	0.110	61

28. THE OCCURRENCE, ABUNDANCE, AND COMPOSITION OF ICE-RAFTED DEBRIS IN SEDIMENTS FROM DEEP SEA DRILLING PROJECT SITES 579 AND 580, NORTHWEST PACIFIC[1]

Lawrence A. Krissek, Oregon State University
Joseph J. Morley, Lamont-Doherty Geological Observatory of Columbia University
and
Darlene K. Lofland, Washington State University[2]

ABSTRACT

The abundance and composition of the coarse-sand fraction (250 μm–2 mm) of samples from Deep Sea Drilling Project Sites 579 and 580 were investigated to determine the chronology of ice rafting at these locations.

The ice-rafting signal at these sites is reduced relative to the generalized ice-rafting chronology of the North Pacific (Kent et al., 1971) because of increased distance to the ice-rafting source areas. These data, however, do record the general increase in ice-rafting importance as sediment age decreases, especially between 0 and 1.0 m.y. ago. In addition, peaks in ice-rafting importance since 1.0 m.y. ago at Sites 579 and 580 are generally synchronous with periods of major ice-rafting influence throughout the North Pacific. The first occurrence of ice-rafted debris at the Matuyama/Gauss magnetic boundary supports a proposed age of approximately 2.47 m.y. for the onset of major Northern Hemisphere glaciation.

The coarse-sand fraction at Sites 579 and 580 contains a significant component of non-ice-rafted material, particularly biogenic particles and volcanic pumice. Under these conditions, the standard assumption that the weight percent of the coarse-sand fraction reflects variations in ice-rafting importance may not be valid. For samples taken at some distance from the source of ice-rafted debris, both the abundance and the composition of the coarse-sand fraction must be considered to obtain a valid measure of the influence of sediment transport via ice rafting.

INTRODUCTION

A series of studies of the coarse-sediment fraction (>63 μm) from a number of Deep Sea Drilling Project (DSDP) sites and piston cores (Griggs and Kulm, 1969; Conolly and Ewing, 1970; Kent et al., 1971; von Huene et al., 1973, 1976) have outlined in some detail the lateral and temporal distribution of ice-rafted debris (IRD) in the North Pacific Ocean. These studies have used the abundance of a particular sand-size fraction as an indicator of the relative importance of transport via ice-rafting at the time of deposition (see the Methods section). Downcore variations in the abundance of that size fraction, and therefore in the importance of ice rafting, were interpreted as indicators of general hemispheric climatic conditions. Increases in the abundance of IRD indicate times of continental glaciation, whereas decreases in IRD abundance reflect periods of climatic warming. In addition, IRD composition was determined qualitatively to reveal sediment source areas; these data were used to outline paleoceanographic circulation patterns.

Of direct importance to this study are the works of Conolly and Ewing (1970) and Kent et al. (1971). Conolly and Ewing (1970) used coarse-fraction data from 22 *Vema* piston cores to delineate the horizontal and vertical distribution of IRD in the northwest Pacific Ocean. In these samples, the first IRD is younger than approximately 2.2 m.y.; IRD becomes common in sediments younger than 1.5 m.y. and abundant in horizons younger than 1.0 m.y. Up to six major IRD zones occur within the Brunhes Normal Epoch (Conolly and Ewing, 1970), but limited magnetostratigraphic control prevented the development of a more detailed IRD chronology. Horizontal distribution and composition of the IRD suggests source areas in the Kurile–Kamchatka–Aleutian arc, with dispersal by a Pleistocene current system similar to the one now in existence (Fig. 1).

Coarse-fraction samples from three of the *Vema* cores studied by Conolly and Ewing (1970), three additional *Vema* cores, and three *Robert Conrad* cores were investigated further by Kent et al. (1971). In combination with detailed paleomagnetic, biostratigraphic, and tephrochronologic age control, IRD abundances in these cores were converted into a generalized chronology of relative ice-rafting importance in the North Pacific. Four periods of increased rafting were identified between 1.2 and 2.5 m.y. ago, whereas at least 11 such intervals were identified from 1.2 m.y. ago to the present. Included in these 11 are the 6 IRD-rich zones identified by Conolly and Ewing (1970).

More recent studies of ice-rafting in the North Pacific have concentrated on sediments obtained during DSDP Leg 18 at Sites 178, 179, 180, and 183 in the Gulf of Alaska (von Huene et al., 1973, 1976). Age control for these samples was very good, but the establishment of an ice-rafting chronology was hampered by core recovery of less than 50% of the drilled sections (von Huene et al., 1976). As a result, the major conclusions of von

---

[1] Heath, G. R., Burckle, L. H., et al., *Init. Repts. DSDP*, 86: Washington (U.S. Govt. Printing Office).

[2] Addresses: (Krissek, present address) Department of Geology and Mineralogy, Ohio State University, Columbus, OH 43210; (Morley) Lamont-Doherty Geological Observatory of Columbia University, Palisades, NY 10964; (Lofland) Department of Geology, Washington State University, Pullman, WA 99163.

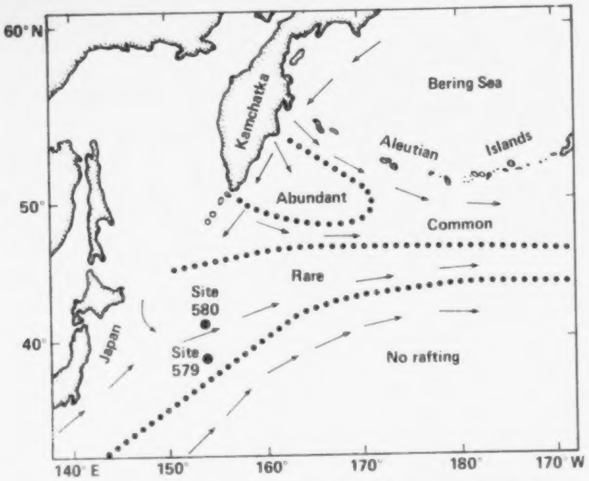

Figure 1. Map of the northwest Pacific Ocean, showing the locations of Sites 579 and 580. Major surface currents (northward-flowing Kuroshio, southward-flowing Oyashio, eastward-flowing West Wind Drift) and zones of occurrence of ice-rafted debris modified from Conolly and Ewing (1970).

Huene et al. (1973) were that (1) the coarse-sand fraction (250 μm–2 mm) is ice transported in origin and (2) the duration of periods of ice erratic influx is approximately 10,000 to 20,000 yr. Further work with these data, in conjunction with data from one of the *Vema* cores, allowed the generation of an IRD chronology curve for the past 300,000 yr. in the Gulf of Alaska (von Huene et al., 1976); this curve showed a positive correspondence with variations in other Northern Hemisphere climatic indicators during the same period.

In summary, the studies outlined above have:

1. Concluded that abundances of continentally derived sand-sized material in deep-sea sediments of the North Pacific do indicate relative importance of transport via ice rafting at the time of deposition,
2. Concluded that the coarse-sand fraction (250 μm–2 mm) is transported predominantly by icebergs (at least near source areas, e.g., the Gulf of Alaska),
3. Established a generalized chronology of IRD abundance for the North Pacific which can be interpreted as a climatic record back to approximately 2.5 m.y. ago, and
4. Concluded that general paleocirculation patterns in the North Pacific have been relatively constant from at least the Pleistocene to the present.

Additional sediments with a potential North Pacific IRD signal were recovered during DSDP Leg 86. As shown in Figure 1, Sites 579 and 580 were located within the zone of "rare" IRD occurrence as outlined by Conolly and Ewing (1970). However, the high recovery rate (86–94% at Site 579, 91% at Site 580; see Site 579 and Site 580 chapters, this volume) of relatively undisturbed sediments with the hydraulic piston corer (HPC), combined with detailed paleomagnetic and biostratigraphic age control, suggested that the IRD signal, although weak, should be discernible at these sites. As a result, this study was undertaken with two major objectives. The first objective was to determine the temporal abundance of IRD in sediments recovered at Sites 579 and 580, in order to establish an IRD chronology for the northwest Pacific Ocean. This chronology was then compared to the generalized North Pacific chronology of ice-rafting influence published by Kent et al. (1971); the two chronologies generally show synchronous variations, although the signal from Sites 579 and 580 is less complete because of increased transport distance. The second objective was to evaluate the use of the coarse sand (250 μm–2 mm) weight percent as an indicator of IRD abundance. Although this approach may be valid near IRD source areas (i.e., the Gulf of Alaska; von Huene et al., 1973), our data suggest that such an assumption may not be valid near the boundaries of ice-rafting influence.

METHODS AND ANALYSES

Samples were taken for IRD analysis at intervals of approximately 100 cm, from Cores 1 through 12 at Site 579 and from Cores 1 through 17 at Site 580. A total of 121 samples from Site 579 were analyzed and 142 samples from Site 580 were analyzed. On the basis of sedimentation rates of 40 to 50 m/m.y. (see Site 579 and Site 580 chapters, this volume), the sampling interval is estimated at approximately 20,000 yr. (Table 1). This interval is equivalent to that used by Conolly and Ewing (1970) and Kent et al. (1971). Because of the 20,000-yr. sampling interval, these data are not suitable for the examination of high-frequency climatic fluctuations; they are valuable, however, in delineating major, long-term changes.

In order to be most consistent with previous investigations, the 250 μm–2 mm grain-size interval was chosen as the indicator of IRD abundance in sediments from Sites 579 and 580 (Table 1). Samples were dried at 60°C, weighed, disaggregated ultrasonically, and wet-sieved at 2 mm and 250 μm. The 250 μm–2 mm grain-diameter fraction was then dried, weighed, and examined under a binocular microscope to determine qualitatively the abundances of various sediment components. The grains were classified as biogenic (predominantly radiolarians), volcanic, or ice rafted in origin on the basis of appearance and gross surface texture. Several samples from Site 580 were not successfully dispersed by the ultrasonic technique following initial weighing, so an additional group of undisaggregated particles ("mudballs") was also recognized. A major problem in classifying grains was the discrimination of pumice grains transported solely by wind from those transported by a combination of wind and ice. In this study, the occurrence of pumice independent of other IRD grains, the fresh appearance of the pumice grains, and the location of these sites several hundred kilometers downwind from a major volcanic chain all support an interpretation of direct eolian transport for most of the pumice grains observed at Sites 579 and 580. As a result, the coarse sands were subdivided into biogenic, volcanic, ice-rafted, and undisaggregated components. Compositionally, grains classified as IRD included quartz, feldspar, and lithic fragments of mudstones, granite, andesite, and basalt.

RESULTS AND DISCUSSION

The coarse-sand fraction abundance and compositional data are tabulated in the Appendix. Porosity and bulk-density data for these samples are given elsewhere in this

Table 1. Summary of analytical techniques (size fraction and sampling intervals) employed in various studies of ice-rafted debris in the North Pacific.

Coarse fraction measured	Sampling interval (cm)	Approximate sampling interval (yr.)	Reference
>62 μm multiplied by IRD % in >62 μm fraction from point count data	10–30	20,000–100,000	Conolly and Ewing (1970)
250 μm–7 mm	10	17,000	Kent et al. (1971)
250 μm–2 mm	20–50	3,000	von Huene et al. (1973)
250 μm–2 mm	20–50	3,000	von Huene et al. (1976)
250 μm–2 mm	100	20,000	This study

volume (see Site 579 and Site 580 chapters and Schultheiss, this volume). Relative abundance data for the coarse-sand fraction (wt.% in the 250 μm–2 mm interval) in samples from Sites 579 and 580 are plotted in Figure 2 as a function of sub-bottom depth. Values from Site 579 range from 0 to 6.5% with an average of 0.12%; values from Site 580 range from 0 to 1.18%, with an average of 0.15%. The patterns of coarse-fraction abundance are fairly irregular in both cases, with many highs and lows defined by single data points. Several general observations, however, can be made:

1. Above-average coarse-fraction abundances at Site 579 are most common between 10 and 28 m sub-bottom, with other major abundance peaks at 42 m, 67–76 m, and 87–104 m sub-bottom.
2. Coarse-fraction abundance at Site 579 shows no long-term trend of increase or decrease downcore.
3. Most of the coarse sand sampled at Site 579 is biogenic or volcanic in origin; zones containing IRD occur at 17–25, 42, 61, and possibly 90 m downcore.
4. Within the zones at Site 579 where IRD does occur, the relative importance of the IRD within the coarse fraction generally decreases downcore.
5. Above-average coarse-fraction abundances at Site 580 are most common in the intervals 0–24 m, 37–56 m, 70-90 m, and 102–113 m sub-bottom.
6. Data from Site 580 samples show a long-term decrease in coarse-fraction abundance downcore, interrupted by the shorter intervals of increase listed above.
7. Composition of the coarse fraction changes downcore, from an IRD–biogenic–pumice assemblage above 45 m sub-bottom to a predominantly biogenic–pumice–undisaggregated material assemblage with minor IRD below that level.

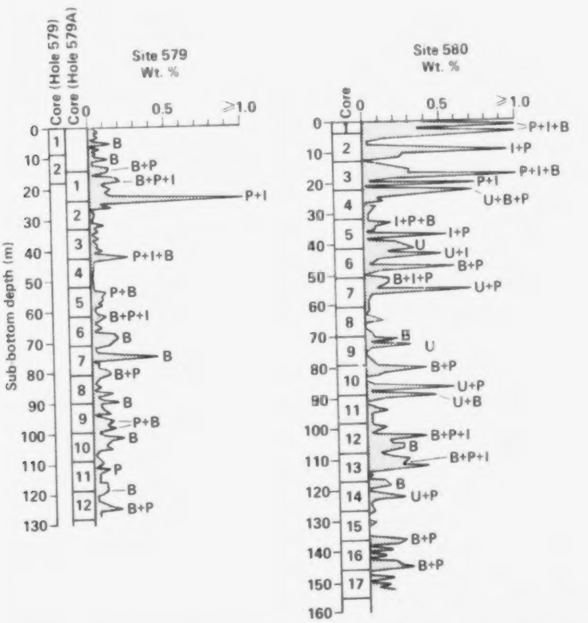

Figure 2. Abundance and composition of the coarse-sand fraction (wt.% of the 250 μm–2 mm size fraction) downcore at Sites 579 and 580. Coarse sands are classified as biogenic particles (B), pumice (P), ice-rafted debris (I), or undisaggregated clays (U) and are listed in order of decreasing importance for each peak.

A major point illustrated by Figure 2 is the predominance of non-IRD grains in the 250 μm–2 mm fraction of these samples. Based on point counts, volcanic pumice and biogenic particles form the majority of grains present (see Appendix). Although this analysis does not consider differences in density between volcanic, biogenic, and ice-rafted particles, the data presented in Figure 2 indicate that many of the samples with abundant coarse sand contain essentially no IRD grains. These results suggest that a detailed study considering coarse-sand abundance, mode of particle origin, and particle density will be needed to determine quantitatively the abundance of IRD (measured as wt.% of the sample) in these sediments. The data presently available, however, do indicate that non-ice-transported grains form a significant component of the coarse sands; as such, the conclusion of von Huene et al. (1973) that the weight percent of the 250 μm–2 mm fraction serves as a reliable indicator of ice-rafting importance may not be valid away from the source areas of ice rafting.

By combining the IRD abundance data contained in Figure 2 with the linear sedimentation rates calculated for Sites 579 and 580 from paleomagnetic and biostratigraphic data (see Site 579 and Site 580 chapters and Bleil, this volume), qualitative chronologies of ice-rafting influence at these sites can be constructed. These chronologies are shown in Figure 3, with the generalized North Pacific chronology of Kent et al. (1971) for comparison. Since the uncertainty of an age assignment increases as the total age increases, discrepancies between chronologies are not unexpected, especially for the older horizons.

Three general conclusions may be drawn from the data presented in Figure 3. The first conclusion is that the IRD records at Sites 579 and 580 agree well with the generalized ice-rafting curve of Kent et al. (1971) for sediments younger than approximately 1.0 m.y. Within the limits of age determinations based on shipboard paleomagnetic and biostratigraphic data, the times of increased ice-rafting importance at Sites 579 and 580 can be correlated with times of increased rafting in the general North Pacific curve for sediments younger than 1.0 m.y. In fact, the increases at Site 580 reflect the major events of the generalized chronology. The record at Site 579, however, is lower in amplitude and does not correlate quite as well with the general North Pacific chronology for sediments less than 1 m.y. old. A significant loss of information occurs between both the northern North Pacific (where Kent et al. [1971] obtained their data) and Site 580 and between Sites 580 and 579. Such a loss is expected because of increased distance from the proposed IRD source in the Kurile–Kamchatka–Aleutian region. Estimates of the paleopositions of Sites 579 and 580 for the past 1 m.y. suggest a WNW movement of approximately 78 km during this time (Table 2). Backtracking these two sites places Site 579 very close to the boundary between "rare" and "no rafting" regions established by Conolly and Ewing (1970; Fig. 1),

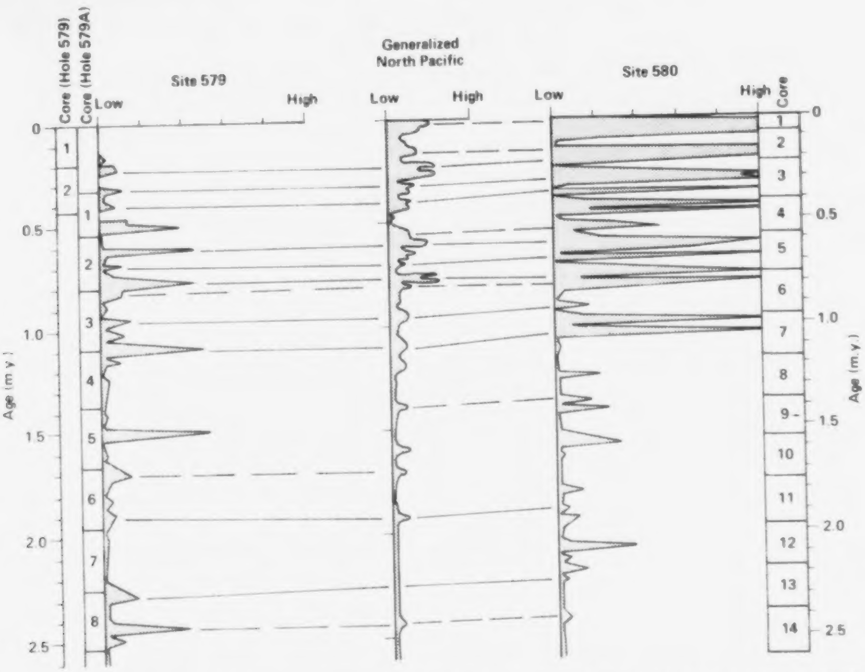

Figure 3. Chronologies of relative ice-rafting influence at Sites 579 and 580, with the generalized North Pacific chronology of Kent et al. (1971) for comparison. Ages were determined using sedimentation rates given in the Site 579 and Site 580 chapters and Bleil (this volume). Dashed lines are preliminary correlations based on the age data. Solid lines are preliminary correlations based on age data and supported by radiolarian abundances (Morley, this volume).

Table 2. Estimates of paleopositions of Sites 579 and 580 for the past 2.5 m.y.

	Site 579			Site 580	
Age (m.y.)	Latitude (°N)	Longitude (°E)	Distance from present position (km)	Latitude (°N)	Longitude (°E)
0	38.63	153.84	0	41.62	153.98
0.5	38.48	154.24	38.8	41.32	154.40
1.0	38.33	154.64	77.6	41.02	154.82
1.5	38.18	155.04	116.4	40.87	155.24
2.0	38.03	155.44	155.2	40.72	155.66
2.5	37.88	155.84	194.0	40.57	156.08

Note: Estimates based on rates of motion northward = 33.35 km/m.y. and westward = 70.04 km/m.y. (van Andel et al., 1975; Leinen and Heath, 1981; Bleil, this volume).

while Site 580 remains well within the region of rare rafting. As a result, the better IRD record upcore at Site 579 may reflect both climatic variations and the change in location of Site 579 through time, while climatic variations are the sole control on the IRD record at Site 580. In summary, the IRD chronologies at Site 579 and 580, for sediments younger than 1.0 m.y., are incomplete relative to the general North Pacific chronology; the chronology at Site 580, however, appears to record the major events that influenced the region.

The second observation about the data in Figure 3 is that the IRD record at Sites 579 and 580 is relatively poor before 1.0 m.y. ago. Fewer IRD increases occur between 1.0 and 2.0 m.y. ago than in the younger sediments, and the peaks in the Site 580 and Site 579 sequences that do occur are generally weaker than the peaks in sequences younger than 1.0 m.y. As such, they may reflect rare or random rafting influence or may be the result of misidentification of detrital grain origin. The generalized North Pacific chronology also indicates a significant decrease in ice-rafting importance at this time; the decrease observed closer to the source by Kent et al. (1971) is synchronous with the major loss of IRD further to the south at Sites 579 and 580. Estimates of paleopositions suggest that Sites 579 and 580 moved WNW from approximately 194 to 78 km away from their present positions during the interval from 2.5 to 1.0 m.y. ago (Table 2). Backtracking these two sites places Site 579 essentially at the boundary between the "rare" and "no rafting" regions of Conolly and Ewing (1970; Fig. 1), while Site 580 moves close to that boundary. As a result, the decreased IRD signal at Site 579 may reflect both site location and climatic variation controls during this time, while the decreased IRD signal at Site 580 is controlled predominantly by climatic fluctuations. At this point, it is necessary to emphasize again the 20,000-yr. sampling interval for the data. If intervals of IRD influx have a duration of only 10,000 to 20,000 yr. (von Huene et al., 1973), then short-duration increases may be missed totally by the samples used in this study. In addition, the relatively long sampling period eliminates much of the detail seen throughout the generalized North Pacific curve.

The final conclusion based on these data is that ice rafting in the North Pacific began at or before approximately 2.4 to 2.5 m.y. ago. The earliest IRD occurrence at Site 579 is dated at approximately 2.49 m.y. ago using sedimentation-rate data; this horizon can be correlated biostratigraphically (Morley, this volume) with the 2.41 m.y. old IRD-rich horizon at Site 580. Given uncertainties in the sedimentation rates used to determine ages for these samples, these two earliest occurrences may both reflect the ice-rafting increase shown at approximately 2.45 m.y. ago on the general North Pacific curve (Kent et al., 1971). In fact, the first IRD at Sites 579 and 580 occurs near the Gauss/Matuyama magnetic boundary (see Site 579 and Site 580 chapters, this volume). The paleoposition estimates (Table 2) suggest that Site 579 entered the zone of "rare" ice-rafting (Conolly and Ewing, 1970; Fig. 1) approximately 2.5 m.y. ago; as a result, the first appearance of IRD at Site 579 at this time may be controlled by either site location, climatic variation, or both. Site 580 entered the zone of "rare" ice rafting prior to 2.5 m.y. ago, however, so that the first appearance of IRD at Site 580 2.5 m.y. ago suggests the importance of climatic variation as the primary control at this time. Similar paleomagnetic ages of first IRD occurrence were reported by Kent et al. (1971) in the North Pacific, and by various investigators in the North Atlantic (Roberts et al., 1982; Shackleton et al., 1982; Schnitker, 1982). For these reasons, the first occurrence of IRD at Sites 579 and 580 appears to reflect a climatic, rather than a site paleoposition, control; as such, these data support a conclusion, also based on North Pacific ice-rafting data, that the onset of major Northern Hemisphere glaciation took place approximately 2.47 m.y. ago (the time of the Matuyama/Gauss reversal boundary; Rea and Schrader, in press).

CONCLUSIONS

On the basis of the abundance and composition of the 250 μm–2 mm size fraction in samples from Sites 579 and 580, the following conclusions can be reached:

1. The records of ice rafting at Sites 579 and 580 reflect the major variations in ice-rafting importance observed elsewhere in the North Pacific. These variations include both a long-term increase in ice-rafting importance as sediment age decreases and eight short-term increases between 1.0 m.y. ago and the present. The less-detailed nature of the record is a result of the long distance from the ice-rafting source areas to Sites 579 and 580.

2. Biostratigraphic and paleomagnetic data place the first occurrence of ice-rafted debris at Sites 579 and 580 at the Matuyama/Gauss reversal boundary (approximately 2.47 m.y. ago). Similar ages of first IRD occurrence have been reported in the North Atlantic and elsewhere in the North Pacific. These data support a proposed age of approximately 2.47 m.y. for the onset of major Northern Hemisphere glaciation (Rea and Schrader, in press).

3. The coarse-sand fraction at Sites 579 and 580 contains a significant component of non-ice-rafted grains, suggesting that the weight percent of the coarse-sand fraction alone may not be a valid indicator of ice-rafting importance at these sites. The mode of origin and transport of the coarse sand grains must be considered, therefore, in studies of IRD. Near sources of ice rafting, the coarse-sand fraction may be dominated by IRD, as concluded by von Huene et al. (1973). At more distal locations, however, other components may become important within the coarse-sand fraction; their influence on the weight percent values must be removed in order to obtain an accurate measure of ice-rafting influence.

ACKNOWLEDGMENTS

The authors thank G. Ross Heath for suggesting this project, and D. K. Rea for helpful discussions of other ice-rafting studies. D. Bernosky assisted in analysis of the Site 579 samples. D. K. Rea and LaVerne Kulm provided helpful comments on the manuscript.

REFERENCES

Conolly, J. R., and Ewing, M., 1970. Ice-rafted detritus in northwest Pacific deep-sea sediments. *In* Hays, J. D. (Ed.), *Geological Investigations of the North Pacific*. Mem. Geol. Soc. Am., 126:219–231.

Griggs, G. B., and Kulm, L. D., 1969. Glacial marine sediments from the northeast Pacific. *J. Sediment. Petrol.*, 39:1142–1148.

Kent, D., Opdyke, N. D., and Ewing, M., 1971. Climate change in the north Pacific using ice-rafted detritus as a climatic indicator. *Geol. Soc. Am. Bull.*, 82:2741–2754.

Leinen, M., and Heath, G. R., 1981. Sedimentary indicators of atmospheric activity in the northern hemisphere during the Cenozoic. *Paleogeogr., Paleoclimatol., Paleoecol.*, 36:1–11.

Rea, D. K., and Schrader, H., in press. Late Pliocene onset of glaciation: Ice rafting and diatom stratigraphy of North Pacific DSDP cores. *Paleogeogr., Paleoclimatol., Paleoecol.*

Roberts, D. G., Schnitker, D., Backman, J., Baldauf, J. G., Desprairies, A., et al., 1982. Leg 81 drills west margin Rockall Plateau. *Geotimes*, 27:21–23.

Shackleton, N. J., Backman, J., Kent, D., Imbrie, J., Pestiaux, P., Pisias, N. G., and Zimmerman, H. B., 1982. The evolution of climate response to orbital forcing: Results over three million years from DSDP Site 522A. (Paper presented at the International Symposium on Milankovitch and Climate: Understanding the Response to Orbital Forcing, Lamont-Doherty Geological Observatory, New York).

Schnitker, D., 1982. Regular fluctuations of northeast Atlantic environments—Miocene to Recent. *EOS Trans. Am. Geophys. Union*, 63:984. (Abstract)

van Andel, T. H., Heath, G. R., and Moore, T. C., Jr., 1975. Cenozoic history and paleoceanography of the central equatorial Pacific. *Mem. Geol. Soc. Am.*, 143:1–134.

von Huene, R., Crouch, J., and Larson, E., 1976. Glacial advance in the Gulf of Alaska implied by ice-rafted material. *In* Cline, R. M., and Hays, J. D. (Eds.), *Investigation of Late Quaternary Paleoceanography and Paleoclimatology*. Mem. Geol. Soc. Am., 145: 411–422.

von Huene, R., Larson, E., and Crouch, J., 1973. Preliminary study of ice-rafted erratics as indicators of glacial advances in the Gulf of Alaska. *In* Kulm, L. D., von Huene, R., et al., *Init. Repts. DSDP*, 18: Washington (U.S. Govt. Printing Office), 835–842.

Date of Initial Receipt: 10 November 1983
Date of Acceptance: 2 October 1984

APPENDIX
Coarse-Sand Fraction Abundance and Compositional Data

Core-Section (level in cm)	Sub-bottom depth (m)	Interpolated age (1000 yr.)	Wt. % 250 μm–2 mm	Percent in 250 μm–2 mm fraction[a]		
				% IRD	% Volcanics	% Biogenic
Hole 579						
1-1, 14	0.14	3.3	0.02	1.0	3.0	96.0
1-1, 114	1.14	27.1	0.06	0	6.5	93.5
1-2, 64	2.14	51.0	0.04	0	0	100.0
1-3, 14	3.14	74.8	0.05	0	30.9	69.1
1-3, 114	4.14	98.6	0.01	0	1.0	99.0
1-4, 64	5.14	122.4	0.14	0	0	100.0
1-5, 14	6.14	146.2	0.01	0	0	100.0
1-5, 107	7.07	168.3	0.07	1.2	5.8	93.0
1-6, 44	7.94	189.0	0.03	1.4	7.0	91.6
2-1, 14	8.54	203.3	0.04	9.1	9.1	81.8
2-1, 114	9.54	227.1	0.04	9.6	13.5	76.9
2-2, 64	10.54	251.0	0:12	0	0	100.0
2-3, 13	11.53	274.5	0.02	0	1.0	99.0
2-3, 114	12.54	298.6	0.03	0	21.7	78.3
2-4, 64	13.54	322.4	0.13	4.0	26.0	70.0
2-5, 15	14.55	346.4	0.12	0	1.0	99.0
2-5, 114	15.54	370.0	0.02	1.0	6.0	93.0
2-6, 76	16.66	396.7	0.17	2.0	2.0	96.0
Hole 579A						
1-1, 51	14.51	345.5	0.12	0	39.1	60.9
1-1, 136	15.36	365.7	0.10	0	5.0	95.0
1-2, 91	16.41	390.7	0.08	0	100.0	0
1-3, 51	17.51	416.9	0.19	0	94.1	5.9
1-3, 136	18.36	437.1	0.08	0	50.0	50.0
1-4, 96	19.46	463.3	0.11	0	20.0	80.0
1-5, 51	20.51	488.3	0.14	4.2	10.4	85.4
1-5, 136	21.36	509.0	0.11	16.7	66.7	16.7
1-6, 81	22.31	531.7	0.15	0	50.0	50.0
2-1, 31	23.81	567.4	6.50	0	100.0	0
2-1, 131	24.81	591.2	0.08	0	75.0	25.0
2-2, 81	25.81	615.1	0.14	16.7	56.2	37.5
2-3, 31	26.81	638.9	0.01	8.8	91.2	0
2-3, 131	27.81	662.7	0.02	50.0	50.0	0
2-4, 71	28.71	684.2	0.03	15.4	53.8	30.8
2-5, 31	29.81	710.4	0.02	0	40.0	60.0
2-5, 131	30.81	734.9	0.02	11.1	11.1	77.8
2-6, 81	31.81	765.2	0.10	23.1	46.2	30.8
2-7, 31	32.81	795.6	0.03	16.7	33.3	50.0
3-1, 2	33.02	802.0	0.06	0	100.0	0
3-1, 101	34.01	832.1	0.05	10.0	80.0	10.0
3-2, 51	35.01	862.5	0.01	0	100.0	0
3-3, 9	36.09	895.3	0.07	2.2	19.6	78.3
3-3, 109	37.09	925.7	0.01	0	0	100.0
3-4, 59	38.09	956.1	0.05	13.3	60.0	26.7
3-5, 13	39.13	987.8	0.05	0	50.0	50.0
3-5, 113	40.13	1018.1	0.06	10.0	90.0	0
3-6, 65	41.15	1049.1	0.03	0	4.9	95.1
4-1, 2	42.52	1090.8	0.25	10.0	80.0	10.0
4-1, 116	43.66	1125.4	0.01	0	70.0	30.0
4-2, 49	44.49	1150.7	0.02	20.0	80.0	0
4-3, 2	45.52	1182.0	0.01	9.5	90.5	0
4-3, 102	46.54	1213.0	0.01	1.0	2.0	97.0
4-4, 43	47.43	1240.0	0.01	16.0	0	84.0
5-1, 7	52.07	1381.1	0.01	0	0	100.0
5-1, 107	53.07	1411.4	0.01	6.7	46.7	46.6
5-2, 69	54.19	1445.5	0.09	0	90.9	9.1
5-3, 11	55.11	1473.5	0.00	—	—	—
5-3, 98	55.98	1499.9	0.07	37.5	37.5	25.0
5-4, 65	57.15	1535.5	0.06	0	60.0	40.0
5-5, 21	58.21	1567.7	0.07	0	0	100.0
5-5, 115	59.15	1596.3	0.03	2.0	4.0	94.0
5-6, 65	60.15	1626.6	0.03	0	0	100.0
6-1, 18	61.68	1673.2	0.09	5.2	30.1	64.7
6-1, 126	62.76	1706.0	0.07	10.0	50.0	40.0
6-2, 57	63.57	1730.6	0.04	4.8	11.9	83.3
6-3, 8	64.58	1761.3	0.03	4.4	8.8	86.8
6-3, 107	65.57	1791.4	0.07	0	25.0	75.0
6-4, 48	66.48	1819.0	0.02	9.1	45.4	45.4
6-5, 7	67.57	1852.2	0.14	0	2.0	98.0
6-5, 115	68.65	1885.0	0.17	1.8	5.4	92.8
7-1, 21	71.21	1962.8	0.11	0	25.0	75.0
7-1, 121	72.21	1993.2	0.01	2.0	4.0	94.0

Appendix. (Continued).

Core-Section (level in cm)	Sub-bottom depth (m)	Interpolated age (1000 yr.)	Wt. % 250 μm–2 mm	Percent in 250 μm–2 mm fraction[a]		
				% IRD	% Volcanics	% Biogenic
Hole 579A (Cont.)						
7-2, 71	73.21	2023.6	0.03	2.0	1.0	97.0
7-3, 31	74.31	2057.0	0.17	0	40.0	60.0
7-3, 131	75.31	2087.4	0.44	0	0	100.0
7-4, 82	76.32	2118.1	0.00	—	—	—
7-5, 31	77.31	2148.2	0.04	0	27.3	72.7
7-5, 131	78.31	2178.6	0.05	0	33.3	66.7
7-6, 69	79.19	2205.4	0.09	0	1.6	98.4
8-1, 23	80.73	2252.2	0.12	4.0	31.0	65.0
8-1, 123	81.73	2282.6	0.06	13.3	52.0	34.7
8-2, 75	82.75	2313.6	0.02	0	0	100.0
8-3, 23	3.73	2343.4	0.01	0	3.0	97.0
8-3, 123	84.73	2373.7	0.05	0	10.0	90.0
8-4, 73	85.73	2404.2	0.01	11.8	29.4	58.8
8-5, 23	86.73	2434.6	0.14	14.0	3.0	83.0
8-5, 115	87.65	2462.5	0.04	0	20.0	80.0
8-6, 73	88.73	2489.3	0.07	6.2	25.0	68.8
8-7, 23	89.73	2523.7	0.14	0	0	100.0
9-1, 19	90.19	2539.5	0.05	0	74.0	26.0
9-1, 119	91.19	2573.8	0.06	0	30.0	70.0
9-2, 61	92.11	2605.4	0.08	0	4.0	96.0
9-3, 19	93.19	2642.6	0.11	0	5.0	95.0
9-3, 111	94.11	2674.2	0.02	0	77.7	22.2
9-4, 131	95.81	2732.6	0.14	0	85.7	14.3
9-5, 19	96.19	2745.7	0.10	0	54.5	45.5
9-5, 11	97.11	2777.3	0.14	0	46.7	53.3
10-1, 21	99.71	2866.6	0.03	0	83.3	16.7
10-1, 121	100.71	2901.0	0.06	0	6.2	93.8
10-2, 71	101.71	2935.4	0.19	0	0	100.0
10-3, 21	102.71	2969.7	0.12	0	100.0	0
10-3, 121	103.71	3004.1	0.09	0	48.0	52.0
10-4, 71	104.71	3039.5	0.12	0	75.0	25.0
10-5, 21	105.71	3072.8	0.02	0	4.4	85.6
10-5, 116	106.66	3105.4	0.01	0	40.0	60.0
11-1, 21	109.21	3193.1	0.05	0	0	100.0
11-1, 121	110.21	3227.4	0.06	0	6.7	93.3
11-2, 71	111.21	3261.8	0.03	0	46.7	53.3
11-3, 21	112.21	3296.2	0.10	0	3.0	97.0
11-3, 121	113.21	3330.5	0.05	0	3.2	96.8
11-4, 69	114.19	3364.2	0.04	0	27.3	72.7
11-5, 39	115.39	3393.8	0.04	0	12.2	87.8
11-5, 76	115.76	3404.7	0.08	0	14.9	85.1
12-1, 10	118.60	3488.2	0.09	0	28.6	71.4
12-1, 113	119.63	3518.5	0.06	0	6.0	94.0
12-2, 56	120.56	3545.9	0.02	0	33.3	66.7
12-3, 14	121.64	3577.6	0.02	0	27.8	72.2
12-3, 113	122.63	3606.8	0.06	0	2.5	97.5
12-4, 56	123.56	3634.1	0.10	0	33.3	66.7
12-5, 10	124.60	3664.7	0.17	0	0	100.0
12-5, 113	125.63	3695.0	0.03	0	18.8	81.2
12-6, 34	126.34	3715.9	0.03	0	7.1	92.9
Hole 580						
1-1, 20	0.21	3.8	0.12	7.5	4.1	88.4
1-1, 120	1.21	22.1	1.02	21.5	65.1	13.4
1-2, 70	2.21	40.3	0.35	26.0	52.2	21.8
2-1, 32	3.63	66.2	1.18	7.0	89.4	3.6
2-1, 130	4.61	84.1	0.69	49.9	50.0	0.0
2-2, 80	5.61	102.4	0.14	10.5	5.0	84.5
2-3, 30	6.61	120.6	0.02	4.6	1.5	93.9
2-3, 130	7.61	138.9	0.02	0.0	1.0	99.0
2-4, 76	8.57	156.4	0.39	41.8	34.4	23.8
2-5, 30	9.61	175.4	0.93	43.0	50.4	6.6
2-5, 135	10.66	194.5	0.26	32.5	45.5	22.0
2-6, 40	11.21	204.6	0.24	30.5	43.9	25.6
3-1, 45	13.26	242.0	0.01	2.0	33.4	64.6
3-1, 145	14.26	260.2	0.12	14.7	28.4	56.9
3-2, 100	15.31	279.4	0.30	22.5	15.5	62.0
3-3, 45	16.26	296.7	0.30	15.5	44.3	40.2
3-3, 145	17.26	315.0	1.03	25.0	54.9	20.1
3-4, 80	18.11	330.5	0.13	3.0	4.5	92.5
3-5, 45	19.26	351.5	0.04	0.0	1.0	99.0
3-5, 110	19.91	363.3	0.58	25.4	71.1	3.5
3-6, 80	21.11	385.2	0.02	3.8	26.8	69.4

Appendix. (Continued).

Core-Section (level in cm)	Sub-bottom depth (m)	Interpolated age (1000 yr.)	Wt. % 250 μm–2 mm	Percent in 250 μm–2 mm fraction[a]		
				% IRD	% Volcanics	% Biogenic
Hole 580 (Cont.)						
4-1, 28	22.59	412.2	0.65	1.2	36.8	62.0
4-1, 130	23.61	430.8	0.26	28.1	32.7	39.2
4-2, 70	24.51	447.3	0.09	9.1	4.5	86.4
4-3, 28	25.59	467.0	0.11	49.6	22.2	28.1
4-3, 130	26.61	485.6	0.00	5.6	38.8	55.6
4-4, 70	27.51	502.0	0.07	2.5	5.0	92.5
4-5, 28	28.59	521.7	0.05	34.8	7.4	57.8
4-5, 130	29.61	540.3	0.03	80.9	12.4	6.7
4-6, 74	30.55	557.5	0.03	13.4	14.5	72.0
5-1, 28	32.09	585.6	0.03	37.0	63.0	0.0
5-1, 135	33.16	605.1	0.15	35.0	36.1	28.9
5-2, 70	34.04	621.2	0.07	58.8	32.9	8.3
5-3, 28	35.09	640.3	0.07	47.7	41.2	11.1
5-3, 135	36.16	659.8	0.02	6.2	31.2	62.6
5-4, 83	37.14	677.7	0.48	51.0	49.0	0.0
5-5, 28	38.09	695.1	0.00	—	—	—
5-5, 110	38.91	710.0	0.17	2.9	5.2	92.0
6-1, 9	41.40	760.1	0.33	15.3	28.3	56.4
6-1, 106	42.37	780.6	0.17	3.8	1.3	94.9
6-2, 60	43.41	802.9	0.50	78.8	15.8	5.4
6-3, 9	44.40	824.0	0.11	32.0	67.0	1.0
6-3, 106	45.37	844.7	0.07	2.4	10.7	86.9
6-4, 52	46.33	865.3	0.04	2.9	17.4	79.7
6-5, 9	47.40	888.1	0.55	0.0	21.0	79.0
6-5, 106	48.37	908.8	0.12	7.0	10.2	82.8
6-6, 60	49.41	931.1	0.00	—	—	—
7-1, 13	50.94	963.8	0.15	4.4	12.3	83.3
7-1, 115	51.96	985.6	0.15	50.6	38.0	11.4
7-2, 86	53.17	1011.4	0.13	3.3	95.7	1.3
7-3, 29	54.10	1031.3	0.08	50.0	40.6	9.4
7-3, 110	54.91	1048.6	0.67	20.9	56.9	22.2
7-4, 56	55.87	1069.1	0.04	0.0	48.9	51.1
7-5, 22	57.03	1184.7	0.02	0.0	20.2	79.8
7-5, 107	57.88	1112.1	0.02	2.1	7.2	90.7
8-1, 32	60.63	1170.8	0.02	0.0	1.0	99.0
8-1, 110	61.41	1187.5	0.02	0.0	36.0	64.0
8-2, 60	62.41	1208.8	0.00	—	—	—
8-3, 24	63.55	1233.2	0.04	0.0	1.0	99.0
8-3, 110	64.41	1251.6	0.10	10.7	29.9	59.4
8-4, 68	65.49	1274.7	0.00	—	—	—
8-5, 24	66.55	1297.3	0.00	—	—	—
8-5, 120	67.51	1317.8	0.01	0.0	2.6	97.4
8-6, 60	68.41	1337.1	0.04	0.0	1.0	99.0
9-1, 19	70.00	1371.0	0.06	13.1	47.5	39.4
9-1, 102	70.83	1388.8	0.19	0.0	1.0	99.0
9-2, 56	71.87	1411.0	0.04	31.6	41.9	26.5
9-3, 19	73.00	1435.1	0.29	0.0	4.8	95.2
9-3, 90	73.71	1450.3	0.00	—	—	—
9-4, 73	75.04	1478.7	0.00	—	—	—
9-5, 31	76.01	1499.4	0.00	—	—	—
9-5, 73	76.44	1508.6	0.02	0.4	1.2	98.4
10-1, 30	79.61	1576.4	0.07	21.4	31.6	47.0
10-1, 130	80.61	1597.7	0.35	0.0	11.0	89.0
10-2, 80	81.61	1619.1	0.13	0.0	1.0	99.0
10-3, 30	82.61	1640.5	0.09	1.3	4.8	93.9
10-3, 130	83.61	1661.8	0.00	—	—	—
10-4, 90	84.71	1685.3	0.00	—	—	—
10-5, 30	85.61	1704.6	0.05	0.0	14.1	85.9
10-5, 145	86.76	1729.1	0.57	0.0	80.2	19.8
10-6, 45	87.26	1739.8	0.02	0.0	1.0	99.0
11-1, 30	89.11	1779.4	0.41	0.0	7.5	92.5
11-1, 120	90.01	1789.6	0.12	5.0	3.8	91.2
11-2, 80	91.11	1822.1	0.00	—	—	—
11-3, 30	92.11	1843.5	0.00	—	—	—
11-3, 140	93.21	1867.0	0.04	0.0	0.0	100.0
11-4, 80	94.11	1886.2	0.11	2.0	3.6	94.4
11-5, 30	95.11	1907.6	0.03	1.6	5.5	92.9
11-5, 110	95.91	1924.7	0.03	13.3	13.4	73.3
12-1, 40	98.71	1984.5	0.03	0.0	81.5	18.5
12-1, 145	99.76	2006.9	0.12	0.0	0.0	100.0
12-2, 90	100.71	2027.2	0.08	0.0		100.0
12-3, 40	101.71	2048.6	0.04	5.6	2.2	92.2
12-3, 145	102.76	2071.0	0.37	4.8	31.4	63.8
12-4, 90	103.71	2091.3	0.13	0.0	4.3	95.7
12-5, 40	104.71	2112.7	0.15	0.0	1.0	99.0

Appendix. (Continued).

Core-Section (level in cm)	Sub-bottom depth (m)	Interpolated age (1000 yr.)	Wt. % 250 μm–2 mm	Percent in 250 μm–2 mm fraction[a]		
				% IRD	% Volcanics	% Biogenic
Hole 580 (Cont.)						
12-5, 105	105.36	2126.6	0.23	0.8	0.5	98.7
12-6, 90	106.71	2155.4	0.23	0.0	8.9	91.1
13-1, 20	108.01	2183.2	0.08	7.4	11.1	81.5
13-1, 120	109.01	2204.6	0.12	0.0	0.0	100.0
13-2, 70	110.01	2225.9	0.28	0.4	4.4	95.2
13-3, 20	111.01	2247.3	0.24	0.0	1.0	99.0
13-3, 120	112.01	2273.9	0.22	0.0	2.0	98.0
13-4, 70	113.01	2295.3	0.40	0.0	0.0	100.0
13-5, 20	114.01	2316.7	0.00	—	—	—
13-5, 120	115.01	2338.2	0.02	0.0	1.1	98.9
13-6, 70	116.01	2359.6	0.00	—	—	—
14-1, 8	117.39	2389.2	0.11	0.0	0.0	100.0
14-1, 108	118.39	2410.6	0.15	0.1	0.0	99.9
14-2, 80	119.61	2436.8	0.00	—	—	—
14-3, 8	120.39	2453.5	0.00	—	—	—
14-3, 108	121.39	2475.0	0.09	0.0	1.5	98.5
14-4, 60	122.41	2498.3	0.25	0.0	3.0	97.0
14-5, 8	123.39	2521.8	0.04	0.0	27.0	73.0
14-5, 108	124.39	2545.7	0.00	0.0	18.6	81.4
14-6, 60	125.41	2570.2	0.02	0.0	3.5	96.5
15-1, 18	126.99	2608.1	0.03	0.0	8.0	92.0
15-1, 114	127.95	2631.0	0.00	—	—	—
15-2, 61	128.92	2654.4	0.00	—	—	—
15-3, 1	129.82	2676.0	0.00	—	—	—
15-3, 101	130.82	2699.9	0.04	0.0	28.9	71.1
15-4, 61	131.92	2726.3	0.00	—	—	—
15-5, 1	132.82	2747.9	0.00	—	—	—
15-5, 102	133.83	2772.1	0.00	—	—	—
15-6, 52	134.83	2796.1	0.01	0.0	31.0	69.0
16-1, 10	136.41	2834.0	0.24	2.1	25.7	72.2
16-1, 110	137.41	2858.0	0.18	0.0	15.6	84.4
16-2, 57	138.38	2881.2	0.00	—	—	—
16-3, 10	139.41	2905.9	0.16	0.0	4.0	96.0
16-3, 110	140.41	2929.9	0.00	—	—	—
16-4, 57	141.38	2953.2	0.11	0.0	0.0	100.0
16-5, 10	142.41	2977.9	0.00	0.0	100.0	0.0
16-5, 110	143.41	3001.9	0.17	0.0	0.0	100.0
16-6, 57	144.38	3025.1	0.20	0.0	14.0	86.0
17-1, 1	145.82	3059.7	0.28	0.0	19.1	80.9
17-1, 103	146.84	3084.1	0.00	—	—	—
17-2, 57	147.88	3109.1	0.00	—	—	—
17-3, 1	148.82	3131.6	0.15	0.0	0.8	99.2
17-3, 103	149.84	3156.1	0.00	—	—	—
17-4, 57	150.88	3181.0	0.13	0.0	10.4	89.6
17-5, 1	151.82	3203.5	0.07	0.0	1.1	98.9
17-5, 106	152.87	3228.7	0.14	0.0	14.5	85.5

[a] Point count data recalculated on a "mudball"-free basis.

29. GEOCHEMISTRY OF SEDIMENTS AT SITES 579, 580, AND 581, DEEP SEA DRILLING PROJECT LEG 86, WESTERN NORTH PACIFIC[1]

G. Ross Heath, Richard B. Kovar, and Carlos Lopez, Oregon State University[2]

ABSTRACT

The elemental composition of sediments from Sites 579 (38°38′N, 153°50′E) and 580 (41°37′N, 153°59′E) is dominated by contributions from terrigenous detritus (including numerous thin ash beds) and opal-rich biogenic debris, with the terrigenous component increasing in dominance in the youngest sediments as the flux of Pleistocene eolian debris associated with Northern Hemisphere glaciation has increased. Diagenesis related to redox-sensitive reactions in near-surface sediments has had a marked impact on the distributions of Mn and S.

At Site 581 (43°56′N, 159°48′E), the reduced biosiliceous clays corresponding to the sections at Sites 579 and 580 are underlain by a normal oxidized North Pacific "red clay" sequence. As at other North Pacific sites, the concentrations of Mn and Fe (as oxyhydroxides), Ba (as barite), and P (as fish debris) vary inversely with the accumulation rates of the clays. The cherts underlying the clays at Site 581 are noteworthy for their high P contents (comparable to values for biosiliceous clays) and high Fe and Mn relative to Ti and Al, suggestive of derivation from well-oxidized pelagic sediments.

INTRODUCTION

Setting

During Deep Sea Drilling Project (DSDP) Leg 86, holes were drilled in pure calcareous ooze (Site 577), pelagic "red" clay (Site 576), and carbonate-free pelagic clay with variable contents of biogenic silica and volcanic ash (Sites 578–581). This chapter focuses on the elemental composition of sediments from Sites 579 (38°38′N, 153°50′E), 580 (41°37′N, 153°59′E), and 581 (43°56′N, 159°48′E) (Fig. 1) in order to assess the roles of temporally varying biogenic and ash inputs and of *in situ* redox conditions in establishing the geochemical character of such deposits. The soft sediments at Sites 579 and 580 were cored continuously by hydraulic piston corer. The more indurated Site 581 sediments were recovered by conventional wire-line rotary coring. Because the upper section (0–181.5 m sub-bottom) of Hole 581 was not sampled, we report only on deeper portions of the section at this site.

The descriptions of the sediments at Sites 579 and 580 (see Site 579 and 580 chapters, this volume) show them to be uniform gray and greenish gray siliceous clay and siliceous ooze that accumulated at rates of about 35 and 50 m/m.y., respectively, interrupted by 61 (Site 579) and 89 (Site 580) identifiable ash beds and numerous dark greenish gray indurated layers that may be altered basic ash layers. Our samples, taken approximately 1.5 m apart, were placed so as to avoid both ashes and indurated layers. The color of the sediment and the presence of fine pyrite grains point to strongly reduced conditions (Fe^{3+} and SO_4^{2-} reduction) throughout both sections.

The section from 0 to 224 m at Site 581 (0-9 m.y. ago) is assumed to resemble the sections at Sites 579 and 580, although only the interval below 181 m (with an accumulation rate decreasing downcore from ~12 to ~4 m/m.y.) was cored continuously. From 224 to 245 m (9 to ~14 m/m.y. ago), the sediments are brown and light brown pelagic clays (that accumulated at about 4 m/m.y.), with small but variable concentrations of biogenic silica that decrease downcore and are rare at the base of the interval. The deepest clays (245–276 m) are very dark brown "slick" pelagic deposits typical of early to middle Tertiary deposits from vast areas of the North Pacific. Below 276 m, only small fragments of porcellaneous chert were recovered. From the behavior of the drill, the chert is believed to form thin beds in pelagic clay. The intense circulation of seawater required to keep chert fragments away from the bit washed away all the soft sediment, however.

Methodology

Samples were freeze-dried, disaggregated by shaking with methacrylate spheres in polycarbonate sample tubes, pressed into pellets, and analyzed by X-ray fluorescence using a Phillips PW-1600 simultaneous spectrometer. Raw counts for each element were ratioed to U.S. Geological Survey (USGS) standard SY3, which was run before and after each sample, and then converted to concentrations using a fundamental parameters program (Criss et al., 1978). Analyses of standard rocks and sediments indicate no systematic errors for the elements discussed. Analytical precision (counting statistics) is better than 2% for the elements reported, but sample to sample variability at the same level in a core is closer to 5% of the reported concentrations.

In order to determine the number of components in the Leg 86 sediments, we analyzed the elemental data using Q-mode factor analysis (Klovan and Imbrie, 1971). The empirical orthogonal functions (factors) generated

---

[1] Heath, G. R., Burckle, L. H., et al., *Init. Repts. DSDP*, 86: Washington (U.S. Govt. Printing Office).

[2] Address: (Heath, present address) College of Ocean and Fishery Sciences, University of Washington, Seattle, WA 98195; (Kovar, Lopez) College of Oceanography, Oregon State University, Corvallis, OR 97331.

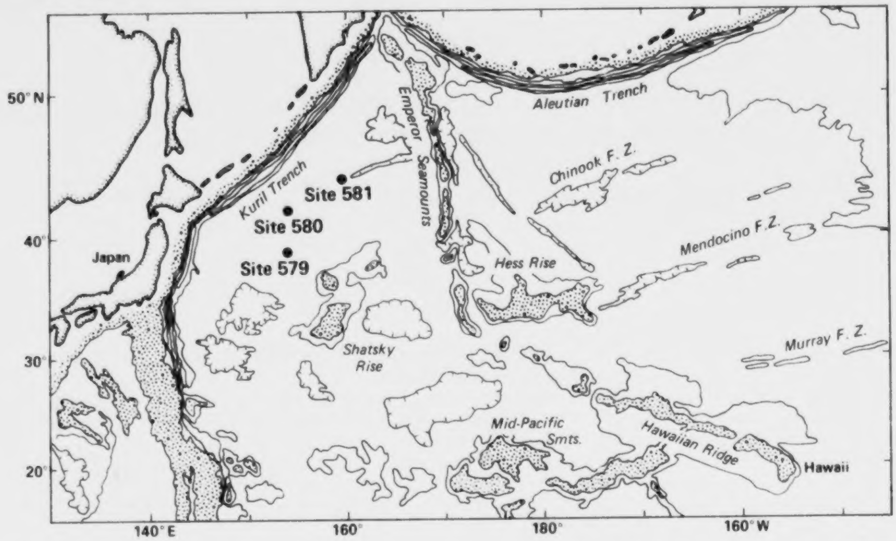

Figure 1. Location of Sites 579, 580, and 581 relative to major physiographic features of the western North Pacific (after Chase, 1975). Areas shallower than 4 km stippled; 5-km contour plain; 6-km contour hachured.

by this technique distribute the variance in the raw data as equally as possible between a subjectively selected number of "factors." We chose three factors in all of our analyses because this number accounted for 97% or more of the variance in the data sets.

RESULTS

The major-element analytical results for Sites 579, 580, and 581 are summarized in Tables 1 to 3. Figures 2 to 4 show downhole plots of elemental abundances that illustrate the major compositional variations at the three sites.

Titanium, which is typical of elements supplied in detritus, shows similar distributions in the sections at Sites 579 and 580 (Fig. 2). For the past 1 m.y., values have been relatively high (0.36 and 0.35%, respectively), with standard deviations of 8 to 10%. Concentrations decrease downhole by about a third in the deposits older than 2 m.y., apparently due to dilution of the terrigenous component by biogenic opal. At the base of Hole 579, which is older than the base of Hole 580, Ti and several other elements (Fig. 2) increase slightly.

The profile at Site 581, which is older than the two preceding sites, shows higher Ti values prior to 5 m.y. ago (Fig. 4). The concentration increases downhole in steps, with an increase of approximately 0.05% at 9 m.y. (225 m) and a similar 0.05% increase at about 14 m.y. (245 m). These increases correspond to the downhole changes in lithology from gray green siliceous clay to light brown pelagic clay to dark brown pelagic clay, respectively (see Site 581 chapter, this volume).

Below 270 m, only chert was recovered from the sedimentary section at Site 581. Ti values for the cherts are three to five times lower than in the overlying sediments (due to dilution by silica), but decrease downhole suggesting a reversal of the lithologic trend observed from 180 to 270 m (Fig. 4). Because the time duration of the interval represented by the chert section is unknown, we can only infer that the low Ti values at the base of the section are indicative of biogenic dilution of terrigenous debris at the time when the site lay beneath the equatorial zone of high biological productivity.

Other elements with distributions similar to Ti, particularly at Sites 579 and 580, are Al, Mg, K, and Fe (Fig. 2). At Site 581, Fe diverges from Ti in the deeper cherts, reaching up to 50% of the detrital values below 300 m (Fig. 4). One possible explanation for such a divergence would be the deposition of excess hydrothermal Fe beneath the equator (Leinen and Stakes, 1979).

Si, much of which is supplied as biogenic opal, varies almost inversely with the terrigenous elements. Short-term variability is again about 10%, with the more northerly (and more productive) Site 580 showing more variability than Site 579, particularly during the past 1 m.y. (Fig. 2).

At Site 581, the light brown (224–245 m) and gray green (above 224 m) sections and the chert samples (below 276 m) are all silica rich (Fig. 4). In fact, the chert values (32.8 ± 1.3%) are indistinguishable from those for the light brown pelagic clays (31.8 ± 1.4%). In contrast, the dark brown pelagic clays (245–276 m) are silica depleted, with a mean value of only 24.2% (and a standard deviation of 2.4%).

Mn and S are both redox-sensitive elements. Mn is reduced from the insoluble $+4$ to soluble $+2$ state under mildly reducing (suboxic) conditions (Froelich et al., 1979), whereas S is reduced from $+6$ to -2 (SO_4^{2-} to S^{2-}) only when O_2, NO_3^-, Mn^{4+}, and Fe^{3+} have been consumed.

At Site 579, virtually all the oxyhydroxide Mn has been reduced and has diffused out of the sediments (Fig. 3). Spikes near the base of the section and near the surface are the only indicators of more oxidized conditions. In contrast, the more rapidly deposited sediments at Site

Table 1. Elemental composition (wt.%) of Site 579 sediment samples.

OSU Lab Sample	Core	Section	Depth in Section (cm)	Depth in Hole (cm)	Mn	Fe	Si	Al	K	Ca	Mg	Ti	P	Ba	S
DP10808	1	1	0.35	0.35	0.38	4.47	30.6	8.07	2.02	0.90	1.62	0.370	0.067	0.114	0.084
DP10809	1	2	0.35	1.85	0.01	5.19	31.7	8.01	2.26	0.65	1.97	0.373	0.053	0.058	0.162
DP10810	1	3	0.35	3.35	0.03	2.92	31.9	6.75	2.19	0.80	1.09	0.240	0.041	0.079	0.139
DP10811	1	4	0.35	4.85	0.39	4.35	31.2	7.85	2.26	0.64	1.84	0.339	0.052	0.084	0.171
DP10812	1	5	0.35	6.35	0.07	5.36	30.4	8.69	2.03	1.81	2.04	0.425	0.052	0.064	0.061
DP10813	1	6	0.35	7.85	0.04	3.71	30.9	7.89	2.08	1.03	1.45	0.348	0.050	0.090	0.084
DP10814	2	1	0.71	9.11	0.02	4.27	32.4	7.83	2.23	0.76	1.82	0.370	0.051	0.063	0.186
DP10815	2	2	0.71	10.61	0.02	3.99	31.3	8.03	2.09	0.96	1.58	0.371	0.049	0.085	0.083
DP10816	2	3	0.71	12.11	0.01	3.78	31.3	7.90	2.23	0.80	1.51	0.352	0.048	0.094	0.095
DP10817	2	4	0.71	13.61	0.02	4.63	32.9	7.86	2.29	0.82	1.81	0.393	0.051	0.085	0.206
DP10818	2	5	0.71	15.11	0.02	3.79	30.0	7.97	2.14	0.82	1.55	0.366	0.047	0.084	0.309
DP10819	2	6	0.71	16.61	0.01	4.01	30.9	8.15	2.23	0.80	1.65	0.369	0.048	0.108	0.131
DP10820	1	1	1.15	15.15	0.03	5.36	30.7	7.97	2.23	0.70	1.89	0.359	0.046	0.086	0.146
DP10821	1	2	1.15	16.65	0.04	4.08	30.8	8.12	1.94	1.29	1.50	0.388	0.053	0.088	0.065
DP10822	1	3	1.15	18.15	0.02	3.90	30.6	7.70	2.02	0.88	1.45	0.334	0.046	0.100	0.134
DP10823	1	4	1.15	19.65	0.03	4.27	30.7	8.44	2.46	0.91	1.90	0.407	0.052	0.069	0.166
DP10824	1	5	1.15	21.15	0.02	4.05	30.7	7.76	2.03	0.86	1.50	0.337	0.045	0.089	0.158
DP10825	1	6	1.15	22.65	0.02	3.71	30.4	8.05	2.18	0.95	1.51	0.358	0.048	0.074	0.107
DP10826	1	7	0.13	23.13	0.01	3.85	31.1	7.93	2.11	0.94	1.47	0.351	0.047	0.077	0.084
DP10827	2	1	0.59	24.09	0.03	4.07	30.9	7.64	2.13	0.88	1.54	0.328	0.047	0.069	0.127
DP10828	2	2	0.59	25.59	0.01	4.20	31.2	7.78	2.39	0.63	1.77	0.328	0.048	0.065	0.094
DP10829	2	3	0.59	27.09	0.01	4.21	31.5	8.00	2.22	0.82	1.55	0.356	0.049	0.080	0.061
DP10830	2	4	0.51	28.51	0.01	4.55	30.5	8.03	2.41	0.78	1.85	0.366	0.052	0.063	0.146
DP10831	2	5	0.59	30.09	0.02	4.24	31.6	8.40	2.34	0.87	1.70	0.386	0.049	0.080	0.078
DP10832	2	6	0.59	31.59	0.02	3.92	30.2	7.88	2.25	0.80	1.51	0.354	0.046	0.075	0.511
DP10833	2	7	0.19	32.69	0.01	3.44	30.7	7.56	2.20	0.76	1.46	0.334	0.044	0.079	0.146
DP10834	3	1	0.65	33.65	0.03	4.57	30.3	8.34	2.47	0.65	1.90	0.387	0.049	0.078	0.072
DP10835	3	2	0.65	35.15	0.05	4.91	31.5	8.04	2.29	0.74	1.81	0.369	0.049	0.062	0.094
DP10836	3	3	0.65	36.65	0.03	3.26	30.2	6.59	1.55	1.26	1.03	0.275	0.041	0.049	0.021
DP10837	3	4	0.65	38.15	0.02	4.39	30.2	8.18	2.32	0.72	1.83	0.375	0.049	0.063	0.066
DP10838	3	5	0.65	39.65	0.02	3.37	29.9	7.37	2.50	0.71	1.40	0.298	0.043	0.059	0.031
DP10839	3	6	0.51	41.01	0.03	4.16	30.0	7.76	2.19	0.91	1.62	0.359	0.048	0.074	0.096
DP10840	4	1	0.36	42.86	0.05	3.10	29.5	6.89	2.35	0.63	1.23	0.255	0.046	0.058	0.076
DP10841	4	2	0.36	44.36	0.02	3.40	30.2	7.72	2.28	0.83	1.52	0.336	0.046	0.058	0.136
DP10842	4	3	0.36	45.86	0.03	6.36	31.3	7.73	2.42	0.38	2.20	0.344	0.046	0.079	0.341
DP10843	4	4	0.21	47.21	0.02	3.57	30.2	7.07	2.82	0.56	1.35	0.260	0.040	0.074	0.104
DP10844	5	1	0.31	52.31	0.01	3.77	31.0	7.80	2.30	0.95	1.52	0.361	0.047	0.071	0.100
DP10845	5	2	0.31	53.81	0.02	3.76	32.0	7.08	2.14	0.71	1.46	0.318	0.044	0.085	0.233
DP10846	5	3	0.31	55.31	0.06	3.39	31.1	6.64	1.63	1.09	1.06	0.268	0.041	0.052	0.201
DP10847	5	4	0.31	56.81	0.03	3.85	30.7	7.25	1.77	1.09	1.39	0.327	0.045	0.061	0.152
DP10848	5	5	0.31	58.31	0.02	4.11	32.2	6.98	2.14	0.38	1.73	0.321	0.043	0.081	0.161
DP10849	5	6	0.31	59.81	0.02	6.29	30.8	7.92	2.39	0.64	2.17	0.350	0.047	0.060	1.335
DP10850	6	1	0.35	61.85	0.02	3.38	30.9	6.64	1.98	0.73	1.27	0.298	0.045	0.075	0.067
DP10851	6	2	0.35	63.35	0.02	3.25	32.8	6.66	2.08	0.62	1.29	0.293	0.042	0.086	0.080
DP10852	6	3	0.35	64.85	0.02	3.90	29.7	7.26	2.18	0.71	1.47	0.349	0.044	0.078	0.110
DP10853	6	4	0.35	66.35	0.02	3.64	31.5	7.88	2.36	0.75	1.58	0.363	0.046	0.072	0.063
DP10854	6	5	0.35	67.85	0.02	3.26	32.3	6.72	2.07	0.65	1.21	0.293	0.042	0.073	0.074
DP10855	6	6	0.15	69.15	0.01	2.84	31.8	6.30	1.90	0.74	1.04	0.254	0.040	0.076	0.046
DP10856	7	1	0.56	71.56	0.03	4.41	32.6	7.26	2.19	0.54	1.65	0.335	0.043	0.080	0.248
DP10857	7	2	0.56	73.06	0.02	4.07	33.4	6.82	2.21	0.63	1.56	0.314	0.042	0.082	0.255
DP10858	7	3	0.56	74.56	0.02	3.87	30.9	7.89	2.45	0.73	1.76	0.376	0.045	0.067	0.289
DP10859	7	4	0.56	76.06	0.01	3.35	32.1	7.04	2.35	0.48	1.45	0.312	0.042	0.091	0.223
DP10860	7	5	0.56	77.56	0.02	4.19	34.2	8.45	2.66	0.68	1.90	0.403	0.048	0.073	0.292
DP10861	7	6	0.56	79.06	0.02	3.98	31.9	6.85	1.85	1.10	1.43	0.328	0.041	0.072	0.338
DP10862	8	1	0.57	81.07	0.01	3.28	34.2	6.57	1.94	0.74	1.28	0.314	0.046	0.078	0.077
DP10863	8	2	0.57	82.57	0.01	2.71	33.7	6.63	1.92	0.89	1.01	0.283	0.043	0.084	0.106
DP10864	8	3	0.57	84.07	0.01	1.96	31.4	6.32	2.51	0.79	0.75	0.199	0.033	0.070	0.068

READEX FICHE

Table 1. (Continued).

OSU Lab Sample	Core	Section	Depth in Section (m)	Depth in Core (m)	Mn	Fe	Si	Al	K	Ca	Mg	Ti	P	Ba	S
DP10865	8	4	0.57	85.57	0.03	4.88	30.9	8.11	2.51	0.62	2.09	0.374	0.047	0.074	0.260
DP10866	8	5	0.57	87.07	0.01	2.53	33.7	5.66	1.70	0.86	0.85	0.255	0.038	0.075	0.102
DP10867	8	6	0.57	88.57	0.02	3.59	30.7	7.86	2.26	0.79	1.66	0.377	0.047	0.074	0.051
DP10868	8	7	0.37	89.87	0.02	3.51	32.6	6.92	2.06	0.53	1.39	0.327	0.043	0.077	0.037
DP10869	9	1	1.23	91.23	0.04	3.19	32.5	7.21	2.21	0.63	1.27	0.304	0.041	0.077	0.022
DP10870	9	2	0.91	92.41	0.04	3.34	32.3	6.52	1.89	0.65	1.16	0.288	0.039	0.076	0.019
DP10871	9	3	0.91	93.91	0.01	3.25	32.5	6.86	2.22	0.55	1.16	0.275	0.041	0.087	0.031
DP10872	9	4	1.19	95.69	0.05	3.73	33.5	7.02	2.07	0.99	1.16	0.309	0.043	0.075	0.047
DP10873	9	5	0.91	96.91	0.02	3.83	32.9	6.74	2.07	0.65	1.26	0.308	0.042	0.073	0.014
DP10874	10	1	0.55	100.05	0.07	3.73	32.9	6.57	2.04	0.49	1.34	0.292	0.040	0.085	0.026
DP10875	10	2	0.55	101.55	0.04	3.07	30.4	5.78	1.55	0.61	1.03	0.253	0.037	0.067	0.013
DP10876	10	3	0.55	103.05	0.05	3.32	32.7	6.43	1.97	0.67	1.21	0.287	0.040	0.079	0.023
DP10877	10	4	0.55	104.55	0.04	4.21	32.6	7.15	2.07	0.59	1.41	0.324	0.039	0.091	0.033
DP10878	10	5	0.55	106.05	0.03	3.65	32.0	6.36	1.99	0.64	1.23	0.291	0.037	0.071	0.051
DP10879	11	1	0.99	109.99	0.08	3.86	32.2	7.68	2.16	0.46	1.53	0.324	0.042	0.072	0.023
DP10880	11	2	0.99	111.49	0.05	3.67	33.1	6.85	1.94	0.47	1.35	0.299	0.039	0.085	0.027
DP10881	11	3	0.99	112.99	0.08	3.11	33.8	5.76	1.76	0.29	1.16	0.256	0.036	0.065	0.035
DP10882	11	4	0.99	114.49	0.05	3.20	33.7	6.68	2.04	0.43	1.29	0.279	0.039	0.065	0.064
DP10883	11	5	0.71	115.71	0.12	2.87	35.6	5.26	1.61	0.31	1.05	0.239	0.037	0.072	0.020
DP10884	12	1	0.87	119.37	0.06	2.75	33.3	5.42	1.95	0.28	0.94	0.221	0.035	0.064	0.012
DP10885	12	2	0.87	120.87	0.03	3.52	34.3	6.50	2.11	0.22	1.33	0.294	0.039	0.090	0.019
DP10886	12	3	0.87	122.37	0.02	3.26	33.0	6.05	1.89	0.30	1.25	0.279	0.036	0.093	0.059
DP10887	12	4	0.87	123.87	0.02	3.71	33.1	6.64	1.94	0.45	1.29	0.295	0.038	0.070	0.013
DP10888	12	5	0.85	125.35	0.01	3.27	32.2	6.41	1.88	0.48	1.28	0.294	0.036	0.086	0.039
DP10889	12	6	0.07	126.07	0.04	4.09	31.5	6.32	1.83	0.95	1.30	0.306	0.041	0.065	0.051
DP10890	13	1	0.42	128.42	0.02	2.29	32.4	5.66	2.23	0.29	0.88	0.192	0.034	0.067	0.120
DP10891	13	2	0.42	129.92	0.07	3.35	33.4	5.65	1.74	0.27	1.15	0.254	0.035	0.095	0.012
DP10892	13	3	0.42	131.42	0.07	3.49	32.7	6.33	1.87	0.29	1.29	0.274	0.036	0.070	0.087
DP10893	13	4	0.42	132.92	0.02	3.24	33.4	6.15	1.88	0.31	1.20	0.280	0.036	0.069	0.055
DP10894	13	5	0.42	134.42	0.03	3.46	33.2	6.30	1.82	0.38	1.24	0.287	0.035	0.063	0.060
DP10895	14	1	0.81	138.31	0.01	2.63	31.9	5.30	1.83	0.25	0.90	0.238	0.033	0.071	0.051
DP10896	14	2	0.81	139.81	0.05	3.02	33.6	5.89	1.80	0.40	1.08	0.263	0.035	0.072	0.189
DP10897	14	3	0.81	141.31	0.02	3.01	33.8	5.95	1.84	0.28	1.12	0.265	0.035	0.075	0.192
DP10898	14	4	0.81	142.81	0.01	2.13	28.5	4.14	1.45	0.25	0.70	0.162	0.026	0.053	0.190
DP10899	14	5	0.81	144.31	0.23	3.21	36.3	7.07	2.09	0.36	1.30	0.315	0.041	0.082	0.030
DP10900	15	1	0.89	147.89	0.01	4.08	34.7	8.42	2.48	0.31	1.60	0.350	0.044	0.097	0.020
DP10901	15	2	0.21	148.71	0.03	3.60	32.2	7.55	2.26	0.41	1.36	0.304	0.038	0.080	0.022

Note: Samples DP10808–10819 are from Hole 579, subsequent samples are from Hole 579A.

580 contain higher and more variable amounts of Mn (Fig. 3). Given the gray green color of the Site 580 sediments, which implies Fe^{3+} reduction (Lyle, 1983), we are more inclined to assign the higher Mn values to the presence of $MnCO_3$ than to oxyhydroxides. We have not been able to identify $MnCO_3$ in X-ray diffractograms, because of its low concentration, but Coleman et al.'s (1982) description of $MnCO_3$ in similar reduced sediments collected on Leg 68 (Pedersen and Price, 1982) and the availability of CO_3^{2-} at Site 580 (inferred from the Ca concentrations) add credibility to this hypothesis.

At Site 581, the Mn profile can be divided into three segments (Fig. 4). Above 224 m, in the gray green sediments, Mn values (with one exception) are very low, comparable to those at Sites 579 and 580. In this interval, oxyhydroxide Mn has been reduced and lost from the sediments. The residual detrital Mn is somewhat diluted by biogenic opal. From 224 to 245 m, in the light brown siliceous clay, some reduction may have taken place, but there is less opal dilution. From 245 to 276 m, authigenic Mn oxyhydroxides form a much larger fraction of the dark brown pelagic clay, which accumulated more slowly and is strongly oxidizing. The Mn contents of the Site 581 cherts (276–343 m) are variable, but generally fairly high (comparable to the light brown siliceous clays), suggesting that the silicified clays were more like the sediments below 224 m than the shallower deposits at Site 581.

The elements Ba, P, and Ca, which, like Si, are associated with biogenic deep-sea deposition, have distributions intermediate between those of Ti–Al and Si. At Sites 579 and 580, P resembles Ti, whereas Ba resembles Si (although values at Site 580 are distinctly higher and more variable than those at Site 579; Fig. 3). Ca has its own distribution, with high variability at both sites, and

Table 2. Elemental composition (wt.%) of Site 580 sediment samples.

OSU Lab Sample	Core	Section	Depth in Section (m)	Depth in Core (m)	Mn	Fe	Si	Al	K	Ca	Mg	Ti	P	Ba	S
DP10902	1	1	0.19	0.19	1.45	3.73	30.6	7.27	1.51	1.12	1.37	0.311	0.066	0.160	0.082
DP10903	1	1	0.91	0.91	0.19	4.11	31.2	7.04	1.91	1.08	1.90	0.338	0.054	0.104	0.086
DP10904	1	2	0.21	1.71	0.17	4.15	30.8	7.15	1.75	1.29	1.79	0.343	0.052	0.067	0.099
DP10905	2	1	0.56	3.86	0.18	4.42	30.8	7.56	2.16	0.82	1.95	0.355	0.054	0.119	0.072
DP10906	2	2	0.56	5.36	0.14	4.85	31.6	6.81	1.91	0.74	1.86	0.308	0.049	0.105	0.251
DP10907	2	3	0.56	6.86	0.08	4.10	31.8	7.71	2.06	0.78	1.70	0.353	0.049	0.138	0.169
DP10908	2	4	0.56	8.36	0.18	5.67	28.0	6.51	1.82	1.15	2.10	0.317	0.047	0.081	0.101
DP10909	2	5	0.56	9.86	0.16	4.02	31.0	7.46	2.05	1.30	1.79	0.368	0.053	0.086	0.110
DP10910	2	6	0.56	11.36	0.16	4.65	30.6	7.56	2.21	0.85	1.91	0.358	0.052	0.080	0.137
DP10911	3	1	0.81	13.61	0.10	4.19	30.2	8.31	2.28	0.88	1.91	0.383	0.051	0.109	0.126
DP10912	3	2	0.81	15.11	0.12	4.16	30.5	7.80	2.20	0.77	1.90	0.361	0.050	0.121	0.072
DP10913	3	3	0.91	16.71	0.13	4.21	30.0	8.37	2.39	1.22	1.99	0.401	0.054	0.075	0.220
DP10914	3	4	0.76	18.06	0.20	3.93	31.1	8.25	2.34	0.75	1.80	0.365	0.053	0.089	0.068
DP10915	3	5	0.91	19.71	0.05	3.56	31.1	7.92	2.61	0.90	1.63	0.332	0.053	0.106	0.043
DP10916	3	6	0.76	21.06	0.10	5.03	30.6	8.41	2.40	0.69	2.10	0.381	0.052	0.065	0.330
DP10917	4	1	0.45	22.75	0.07	4.03	32.4	7.33	1.80	1.29	1.40	0.324	0.046	0.135	0.066
DP10918	4	2	0.45	24.25	0.20	4.23	30.6	7.92	2.32	0.88	1.99	0.361	0.049	0.077	0.269
DP10919	4	3	0.45	25.75	0.10	4.60	30.2	8.42	2.46	0.74	2.05	0.378	0.052	0.082	0.255
DP10920	4	4	0.45	27.25	0.09	4.01	32.1	7.32	2.01	0.72	1.59	0.331	0.045	0.130	0.076
DP10921	4	5	0.45	28.75	0.28	4.15	30.5	8.14	2.34	1.01	1.96	0.369	0.052	0.102	0.101
DP10922	4	6	0.45	30.25	0.06	3.98	31.2	8.03	2.10	0.87	1.73	0.357	0.048	0.121	0.080
DP10991	5	1	1.06	32.86	0.17	3.28	30.0	6.82	1.86	1.15	1.51	0.307	0.044	0.075	0.152
DP10992	5	2	1.06	34.36	0.14	3.00	29.5	7.00	2.38	0.95	1.43	0.297	0.047	0.083	0.141
DP10993	5	3	1.06	35.86	0.07	4.10	30.4	8.46	2.42	0.62	1.94	0.397	0.050	0.084	0.069
DP10994	5	4	1.06	37.36	0.20	4.28	29.2	7.98	2.28	1.11	1.94	0.370	0.053	0.076	0.279
DP10995	5	5	1.06	38.86	0.08	3.61	30.5	7.74	2.19	0.79	1.61	0.325	0.048	0.079	0.214
DP10923	6	1	0.31	41.61	0.14	4.36	30.6	7.84	2.17	1.60	1.82	0.358	0.052	0.082	0.373
DP10924	6	2	0.31	43.11	0.05	3.77	32.7	7.52	2.15	0.69	1.61	0.333	0.044	0.135	0.158
DP10925	6	3	0.31	44.61	0.20	3.69	29.7	7.51	2.45	0.92	1.88	0.334	0.048	0.088	0.215
DP10926	6	4	0.31	46.11	0.09	3.77	29.8	7.94	2.40	0.70	1.85	0.365	0.047	0.084	0.105
DP10927	6	5	0.31	47.61	0.17	5.46	30.4	6.94	2.09	1.01	1.77	0.327	0.049	0.072	0.197
DP10928	6	6	0.31	49.11	0.06	4.28	31.2	8.26	2.45	0.79	1.86	0.382	0.051	0.101	0.088
DP10929	7	1	0.20	51.00	0.13	4.75	31.9	7.83	2.21	0.66	1.90	0.331	0.048	0.121	0.170
DP10930	7	2	0.20	52.50	0.11	4.24	31.3	8.11	2.29	0.60	1.99	0.366	0.049	0.076	0.359
DP10931	7	3	0.20	54.00	0.11	4.06	30.8	8.55	2.38	0.90	1.99	0.401	0.052	0.081	0.050
DP10932	7	4	0.20	55.50	0.13	3.92	31.0	8.10	2.24	0.91	1.90	0.366	0.049	0.082	0.241
DP10933	7	5	0.20	57.00	0.07	4.08	32.3	7.22	1.69	1.10	1.48	0.290	0.046	0.124	0.664
DP10934	8	1	0.42	60.72	0.24	5.24	37.0	9.03	2.66	1.31	2.04	0.476	0.067	0.102	0.073
DP10935	8	2	0.42	62.22	0.16	3.20	31.9	6.63	1.77	0.85	1.38	0.286	0.042	0.085	0.169
DP10936	8	3	0.42	63.72	0.09	3.50	33.3	6.76	1.88	0.84	1.45	0.304	0.045	0.145	0.129
DP10937	8	4	0.42	65.22	0.01	2.81	32.6	6.64	2.51	0.48	1.13	0.235	0.038	0.124	0.035
DP10938	8	5	0.42	66.72	0.06	3.31	32.0	6.82	1.89	1.06	1.32	0.323	0.045	0.093	0.085
DP10939	8	6	0.42	68.22	0.05	3.75	31.6	7.68	2.36	0.61	1.73	0.351	0.046	0.089	0.128
DP10940	9	1	0.54	70.34	0.17	4.96	30.9	7.10	2.13	0.62	1.97	0.322	0.044	0.088	0.470
DP10941	9	2	0.54	71.84	0.06	2.88	30.8	6.48	2.22	0.84	1.14	0.265	0.040	0.082	0.161
DP10942	9	3	0.54	73.34	0.13	3.78	30.9	7.55	2.29	0.69	1.79	0.346	0.046	0.081	0.193
DP10943	9	4	0.54	74.84	0.16	4.06	32.9	6.76	1.97	0.86	1.54	0.294	0.043	0.102	0.104
DP10944	9	5	0.54	76.34	0.19	3.29	32.4	6.97	2.00	0.62	1.50	0.321	0.045	0.120	0.059
DP10945	10	1	0.41	79.71	0.07	3.73	31.1	7.28	2.18	0.59	1.70	0.344	0.046	0.101	0.267
DP10946	10	2	0.41	81.21	0.10	3.82	34.6	5.92	1.81	0.48	1.49	0.283	0.042	0.092	0.898
DP10947	10	3	0.41	82.71	0.24	4.97	30.3	7.36	2.25	0.68	2.16	0.335	0.045	0.095	0.241
DP10948	10	4	0.41	84.21	0.08	3.04	32.9	5.82	1.71	0.55	1.31	0.261	0.040	0.112	0.023
DP10949	10	5	0.41	85.71	0.40	6.14	32.6	5.97	1.84	0.49	2.12	0.260	0.040	0.117	0.260
DP10950	10	6	0.41	87.21	0.28	4.17	33.2	7.82	2.31	0.72	1.86	0.362	0.050	0.116	0.133
DP10951	11	1	0.44	89.24	0.06	2.94	32.9	5.63	1.54	0.89	1.11	0.265	0.041	0.101	0.264
DP10952	11	2	0.44	90.74	0.07	3.36	33.5	6.37	1.84	0.55	1.38	0.287	0.041	0.124	0.275
DP10953	11	3	0.44	92.24	0.06	5.31	32.8	6.81	1.97	0.58	1.58	0.288	0.041	0.093	3.040

Table 2. (Continued).

OSU Lab Sample	Core	Section	Depth in Section (m)	Depth in Core (m)	Mn	Fe	Si	Al	K	Ca	Mg	Ti	P	Ba	S
DP10954	11	4	0.44	93.74	0.07	3.60	32.4	6.66	2.13	0.61	1.58	0.322	0.043	0.088	0.351
DP10955	11	5	0.44	95.24	0.22	3.19	34.8	6.15	1.89	0.54	1.43	0.290	0.041	0.131	0.124
DP10956	12	1	1.11	99.41	0.07	2.56	33.9	5.01	1.71	0.43	1.03	0.227	0.036	0.087	0.231
DP10957	12	2	1.11	100.91	0.13	2.82	33.5	4.34	1.43	1.49	1.14	0.219	0.035	0.093	0.486
DP10958	12	3	0.81	102.11	0.09	2.58	34.2	5.23	2.01	0.49	1.10	0.226	0.037	0.111	0.144
DP10959	12	4	1.11	103.91	0.03	2.83	33.8	5.29	1.64	0.37	1.12	0.242	0.038	0.127	0.132
DP10960	12	5	0.96	105.26	0.14	4.05	32.3	7.43	2.29	0.67	1.85	0.352	0.045	0.071	0.525
DP10961	12	6	1.11	106.91	0.14	3.19	33.8	6.12	1.92	0.78	1.32	0.279	0.042	0.108	0.145
DP10962	13	1	1.11	108.91	0.06	3.42	33.6	4.78	1.56	0.33	1.14	0.224	0.035	0.116	0.516
DP10963	13	2	1.11	110.41	0.09	2.89	36.4	4.25	1.43	0.26	1.04	0.202	0.038	0.119	0.103
DP10964	13	3	1.11	111.91	0.08	2.72	35.3	4.37	1.46	0.28	1.07	0.214	0.038	0.121	0.089
DP10965	13	4	1.11	113.41	0.09	3.38	34.0	5.66	1.49	1.22	1.13	0.256	0.042	0.062	0.315
DP10966	13	5	1.11	114.91	0.12	3.02	34.0	5.42	1.71	0.45	1.27	0.238	0.038	0.126	0.255
DP10967	13	6	1.11	116.41	0.12	3.44	31.6	6.02	1.89	1.39	1.44	0.280	0.040	0.082	0.532
DP10968	14	1	1.16	118.46	0.14	3.83	33.7	5.32	1.64	0.64	1.39	0.252	0.038	0.120	1.450
DP10969	14	2	1.16	119.96	0.11	2.38	33.6	4.84	1.65	0.90	0.86	0.204	0.035	0.085	0.117
DP10970	14	3	1.16	121.46	0.05	3.65	32.9	6.31	1.96	0.46	1.49	0.280	0.040	0.130	0.202
DP10971	14	4	1.16	122.96	0.15	3.21	35.2	4.87	1.55	0.29	1.24	0.233	0.036	0.130	0.231
DP10972	14	5	1.16	124.46	0.09	3.12	34.0	5.73	1.80	0.42	1.29	0.278	0.039	0.103	0.243
DP10973	14	6	1.16	125.96	0.12	3.10	33.4	5.66	1.85	0.32	1.43	0.267	0.037	0.116	0.099
DF10974	15	1	0.58	127.38	0.10	3.53	32.3	6.65	2.12	0.41	1.57	0.302	0.039	0.103	0.151
DP10975	15	2	0.58	128.88	0.05	2.54	33.7	5.16	1.71	0.53	0.91	0.212	0.035	0.105	0.002
DP10976	15	3	0.58	130.38	0.08	2.70	33.7	5.13	1.60	0.40	1.07	0.225	0.034	0.089	0.044
DP10977	15	4	0.58	131.88	0.10	3.09	33.9	5.49	1.74	0.33	1.19	0.255	0.037	0.114	0.196
DP10978	15	5	0.58	133.38	0.08	2.82	33.4	5.61	1.77	0.60	1.05	0.253	0.037	0.083	0.012
DP10979	15	6	0.58	134.88	0.10	2.59	32.7	5.57	2.10	0.71	0.95	0.185	0.033	0.075	0.019
DP10980	16	1	0.81	137.11	0.14	3.70	33.5	5.76	1.75	0.24	1.42	0.251	0.036	0.112	0.005
DP10981	16	2	0.81	138.61	0.13	3.20	41.2	5.43	1.84	0.35	1.32	0.277	0.045	0.113	0.150
DP10982	16	3	0.81	140.11	0.12	2.53	35.4	4.72	1.53	0.30	1.11	0.221	0.034	0.103	0.033
DP10983	16	4	0.81	141.61	0.05	2.94	34.7	5.48	1.69	0.33	1.18	0.239	0.037	0.092	0.012
DP10984	16	5	0.81	143.11	0.05	2.45	35.3	3.06	1.06	0.08	0.72	0.152	0.030	0.092	0.212
DP10985	16	6	0.81	144.61	0.05	2.27	34.8	4.18	1.44	0.21	0.90	0.203	0.031	0.080	0.032
DP10986	17	1	0.78	146.58	0.06	2.31	34.5	4.37	1.59	0.39	0.77	0.190	0.035	0.111	0.000
DP10987	17	2	0.78	148.08	0.05	2.88	33.8	4.85	1.53	0.27	1.11	0.229	0.031	0.123	0.079
DP10988	17	3	0.78	149.58	0.03	2.59	34.5	4.93	1.67	0.27	1.03	0.220	0.033	0.129	0.038
DP10989	17	4	0.78	151.08	0.04	2.79	33.3	6.01	2.11	0.48	1.14	0.236	0.034	0.096	0.065
DP10990	17	5	0.78	152.58	0.11	2.96	33.3	5.76	1.73	0.53	1.22	0.262	0.035	0.096	0.103

a well-defined decrease in concentration below about 3.2 m.y. (110 m) at Site 579 and about 2.3 m.y. (100 m) at Site 580.

At Site 581, Ba, P, and Ca all resemble Ti rather than Si in the clay section. In the basal dark brown pelagic clay (245–276 m) and in the upper and lower cherts (below 276 m), however, P has clear peaks that are matched by Ca peaks, suggesting abundant fish debris. Ba also peaks in the lower cherts, but not the upper ones. Ba peaks in the oxidized (light and dark brown) pelagic clays, as it does elsewhere in the Pacific (Dymond, 1981; Leinen, 1979).

Because elements like silicon are derived from more than one source (detrital aluminosilicates and biogenic opal, for example), we have carried out a Q-mode factor analysis of the data. In its conventional form (Klovan and Imbrie, 1971), such a factor analysis expresses each sample in terms of a number of orthogonal functions that share the variance of the data set as equally as possible. This procedure simplifies the interpretation of large data sets, but the factors may be difficult to interpret physically because they can contain negative contributions of some elements.

Figure 5 shows the downhole variation in three factors derived from the data sets for both Sites 579 and 580. Overall, it is clear that the sediments at Site 579 are markedly less variable than those at Site 580. The variability is due primarily to Mn (Factor 2), which is relatively uniform at Site 579 (particularly above 80 m), but fluctuates markedly at Site 580 (Fig. 3). In contrast, the biogenically dominated Factor 3 (loaded in Si and Ba; Fig. 5) is of comparable importance at the two sites. In fact, this factor is slightly more variable at Site 579.

The factors are easier to interpret if the Q-mode axes are rotated toward the mean of the data set until they enter the positive quadrant (i.e., until their projections

Table 3. Elemental composition (wt.%) of Site 581 sediment samples.

OSU Lab Sample	Core	Section	Depth in Section (m)	Depth in Core (m)	Mn	Fe	Si	Al	K	Ca	Mg	Ti	P	Ba	S
DP10996	1	1	0.51	0.51	0.08	3.73	32.3	6.43	1.61	1.19	1.43	0.320	0.048	0.113	0.094
DP10997	2	1	0.37	181.87	0.09	2.71	34.3	4.69	1.51	0.41	1.09	0.212	0.034	0.174	0.137
DP10998	2	2	0.37	183.37	0.13	3.40	35.8	3.53	1.24	0.05	1.31	0.172	0.030	0.157	0.149
DP10999	2	3	1.28	185.78	0.08	3.34	40.3	5.72	1.90	0.15	1.43	0.274	0.039	0.157	0.085
DP11000	2	4	1.28	187.28	0.04	2.26	35.8	3.24	1.15	0.02	0.82	0.161	0.029	0.167	0.065
DP11001	2	5	0.37	187.87	0.11	2.65	35.3	4.17	1.43	0.22	1.01	0.214	0.033	0.162	0.050
DP11002	2	6	0.35	189.35	0.06	3.19	33.5	4.96	1.66	0.13	1.19	0.227	0.032	0.115	0.045
DP11003	2	7	0.16	190.66	0.01	2.84	35.5	4.95	1.71	0.20	1.15	0.238	0.032	0.124	0.059
DP11004	3	1	0.22	191.22	0.05	2.34	34.1	4.53	1.62	0.17	1.12	0.221	0.031	0.118	0.109
DP11005	3	2	0.22	192.72	0.08	2.76	32.4	5.55	1.88	0.16	1.28	0.244	0.034	0.128	0.142
DP11006	3	3	0.22	194.22	0.13	2.07	34.9	3.73	1.31	0.03	0.92	0.187	0.032	0.095	0.096
DP11007	3	4	0.22	195.72	0.05	2.84	34.4	4.88	1.69	0.12	1.17	0.233	0.031	0.107	0.044
DP11008	3	5	0.22	197.22	0.07	4.34	35.2	3.48	1.26	0.01	1.27	0.159	0.030	0.096	0.040
DP11009	3	6	0.22	198.72	0.00	2.26	35.5	3.83	1.35	0.02	0.83	0.186	0.031	0.114	0.030
DP11010	4	1	0.17	200.67	0.01	1.50	37.7	2.69	1.05	0.00	0.57	0.154	0.031	0.116	0.081
DP11011	4	2	0.17	202.17	0.08	2.62	35.7	4.10	1.40	0.06	1.00	0.196	0.034	0.130	0.033
DP11012	4	3	0.17	203.67	0.07	2.57	34.9	3.62	1.30	0.00	0.90	0.187	0.032	0.141	0.052
DP11013	4	4	0.17	205.17	0.07	3.94	34.2	4.97	1.84	0.20	1.45	0.226	0.034	0.108	0.050
DP11014	4	5	0.17	206.67	0.04	3.04	35.6	5.09	1.75	0.14	1.19	0.235	0.034	0.140	0.058
DP11015	4	6	0.17	208.17	0.06	3.56	33.1	5.59	1.86	0.15	1.33	0.256	0.033	0.122	0.036
DP11016	4	7	0.17	209.67	0.04	3.96	35.6	4.37	1.60	0.05	1.30	0.206	0.032	0.126	0.050
DP11017	5	1	0.41	210.41	0.04	3.06	36.7	4.82	1.58	0.07	1.04	0.224	0.034	0.138	0.028
DP11018	5	2	0.41	211.91	1.31	2.19	36.7	3.72	1.28	0.10	0.82	0.173	0.031	0.114	0.029
DP11019	5	3	0.41	213.41	0.01	1.94	35.1	3.64	1.39	0.02	0.85	0.194	0.029	0.142	0.055
DP11020	5	4	0.41	214.91	0.10	2.09	35.1	4.22	1.41	0.07	0.88	0.196	0.030	0.111	0.039
DP11021	6	1	0.91	220.41	0.06	3.33	32.4	5.03	1.66	0.14	1.04	0.224	0.037	0.121	0.024
DP11022	6	2	0.45	221.45	0.07	3.60	34.9	5.12	1.73	0.16	1.11	0.241	0.038	0.119	0.029
DP11023	6	2	1.18	222.18	0.07	3.10	33.8	4.50	1.53	0.15	0.93	0.209	0.034	0.128	0.039
DP11024	6	3	0.45	222.95	0.07	4.08	30.8	6.51	2.08	0.34	1.31	0.286	0.047	0.118	0.030
DP11025	6	3	1.18	223.68	0.11	4.11	31.2	6.54	2.09	0.30	1.31	0.294	0.048	0.110	0.018
DP11026	6	4	0.45	224.45	0.15	4.04	31.3	6.71	2.08	0.40	1.25	0.298	0.044	0.125	0.021
DP11027	6	4	1.18	225.18	0.14	3.93	33.3	6.16	2.01	0.31	1.16	0.284	0.042	0.119	0.018
DP11028	6	5	0.45	225.95	0.14	4.18	31.6	7.01	2.22	0.34	1.30	0.303	0.046	0.091	0.023
DP11029	6	5	1.18	226.68	0.21	3.77	30.3	6.46	2.01	0.35	1.20	0.287	0.046	0.112	0.021
DP11030	6	6	0.45	227.45	0.16	3.69	32.7	6.35	2.00	0.30	1.18	0.269	0.044	0.146	0.052
DP11031	6	6	1.06	228.06	0.29	3.42	32.1	5.95	1.90	0.26	1.11	0.253	0.040	0.141	0.044
DP11032	7	1	0.49	229.49	0.36	3.44	34.6	5.89	1.86	0.19	1.09	0.259	0.042	0.144	0.025
DP11033	7	1	1.11	230.11	0.40	3.65	33.0	6.25	1.98	0.24	1.19	0.270	0.042	0.195	0.059
DP11034	7	2	0.49	230.99	0.22	3.89	32.5	7.04	2.19	0.28	1.27	0.293	0.044	0.178	0.039
DP11035	7	2	1.11	231.61	0.21	3.75	31.7	6.31	2.00	0.22	1.14	0.277	0.039	0.170	0.029
DP11036	7	3	0.49	232.49	0.33	3.99	31.4	6.89	2.15	0.32	1.29	0.300	0.039	0.149	0.046
DP11037	7	3	1.11	233.11	0.20	3.82	30.5	6.54	2.08	0.21	1.16	0.288	0.037	0.143	0.024
DP11038	7	4	0.49	233.99	0.35	3.81	30.5	6.63	2.09	0.21	1.19	0.283	0.035	0.152	0.030
DP11039	7	4	1.11	234.61	0.23	3.82	31.0	6.50	2.12	0.23	1.15	0.283	0.038	0.159	0.025
DP11040	7	5	0.49	235.49	0.42	3.19	33.7	5.13	1.77	0.14	1.03	0.249	0.035	0.227	0.073
DP11041	7	5	1.11	236.11	0.28	3.79	31.2	6.46	2.06	0.26	1.20	0.286	0.040	0.199	0.053
DP11042	7	6	0.49	236.99	0.32	3.55	30.6	6.32	1.98	0.23	1.11	0.266	0.039	0.132	0.032
DP11043	7	6	1.11	237.61	0.18	3.46	30.7	6.54	2.30	0.31	1.08	0.253	0.037	0.109	0.019
DP11044	8	1	0.29	238.79	0.28	4.05	30.0	7.01	2.20	0.34	1.28	0.301	0.045	0.211	0.054
DP11045	8	1	1.01	239.51	0.21	4.01	30.4	6.95	2.16	0.32	1.28	0.292	0.049	0.203	0.053
DP11046	8	2	0.29	240.29	0.30	4.13	30.1	7.04	2.21	0.34	1.28	0.302	0.046	0.218	0.048
DP11047	8	2	1.01	241.01	0.32	3.79	33.5	6.39	2.10	0.26	1.20	0.286	0.044	0.182	0.042
DP11048	8	3	0.29	241.79	0.27	3.31	33.4	5.72	1.86	0.19	1.03	0.248	0.036	0.183	0.055
DP11049	8	3	1.01	242.51	0.40	3.81	31.3	6.97	2.15	0.23	1.18	0.282	0.039	0.163	0.032
DP11050	8	4	0.29	243.29	0.41	3.62	34.3	6.37	2.03	0.17	1.16	0.271	0.041	0.236	0.057
DP11051	8	4	1.01	244.01	0.55	4.53	29.9	8.12	2.33	0.31	1.65	0.335	0.046	0.160	0.047
DP11052	8	5	0.29	244.79	0.64	4.74	27.0	8.18	2.31	0.31	1.86	0.350	0.050	0.109	0.021

Table 3. (Continued).

OSU Lab Sample	Core	Section	Depth in Section (m)	Depth in Core (m)	Mn	Fe	Si	Al	K	Ca	Mg	Ti	P	Ba	S
DP11053	8	5	1.01	245.51	0.61	4.86	23.8	7.19	2.06	0.30	1.71	0.342	0.043	0.174	0.036
DP11054	9	1	0.25	248.25	0.60	4.97	25.5	7.81	2.21	0.32	1.93	0.357	0.051	0.198	0.045
DP11055	9	1	0.73	248.73	0.90	4.66	24.9	7.62	2.02	0.27	1.90	0.327	0.043	0.162	0.033
DP11056	9	1	1.29	249.29	0.75	4.73	23.8	7.37	2.07	0.29	1.81	0.332	0.051	0.121	0.016
DP11057	9	2	0.25	249.75	0.87	4.97	23.8	7.29	2.09	0.33	1.79	0.343	0.047	0.149	0.030
DP11058	9	2	0.73	250.23	0.93	4.84	27.6	8.51	2.24	0.31	2.14	0.352	0.055	0.194	0.042
DP11059	9	2	1.29	250.79	0.77	4.86	24.9	7.55	2.22	0.30	1.92	0.346	0.044	0.218	0.042
DP11060	9	3	0.25	251.25	0.99	4.83	24.2	7.52	2.17	0.33	1.85	0.330	0.065	0.232	0.041
DP11061	9	3	0.73	251.73	1.06	4.77	23.2	7.24	2.11	0.27	1.80	0.320	0.057	0.212	0.017
DP11062	9	4	0.25	252.75	1.30	4.97	25.9	8.09	2.33	0.43	1.85	0.339	0.077	0.171	0.026
DP11063	9	4	0.73	253.23	1.13	4.75	24.6	7.77	2.15	0.35	1.80	0.332	0.063	0.156	0.026
DP11064	10	1	0.11	257.61	1.35	5.03	23.6	8.18	2.27	0.30	1.81	0.349	0.061	0.113	0.006
DP11065	10	1	0.81	258.31	1.56	4.85	23.4	8.06	2.18	0.41	1.81	0.353	0.082	0.130	0.016
DP11066	10	1	1.41	258.91	1.73	4.99	19.7	6.94	1.96	0.31	1.46	0.343	0.058	0.102	0.007
DP11067	10	2	0.11	259.11	1.66	4.29	22.2	7.93	2.01	0.40	1.48	0.292	0.078	0.120	0.014
DP11068	10	2	0.81	259.81	2.61	4.73	22.3	8.10	2.43	0.57	1.55	0.317	0.174	0.112	0.023
DP11069	10	2	1.41	260.41	2.35	4.77	21.4	7.81	2.25	0.38	1.67	0.343	0.107	0.103	0.000
DP11070	10	3	0.11	260.61	2.91	5.20	21.7	8.21	2.41	0.58	1.71	0.355	0.181	0.085	0.021
DP11071	10	3	0.81	261.31	2.05	4.67	21.9	7.92	2.58	0.59	1.90	0.341	0.178	0.041	0.021
DP11072	10	3	1.31	261.81	1.62	5.47	20.1	7.08	2.07	0.76	1.72	0.493	0.229	0.044	0.025
DP11073	10	4	0.11	262.11	1.39	4.96	22.8	7.66	2.08	0.29	1.76	0.340	0.059	0.128	0.023
DP11074	10	4	0.61	262.61	1.82	5.18	28.1	9.28	2.34	0.33	2.29	0.380	0.070	0.189	0.025
DP11075	10	5	0.11	263.61	1.25	5.02	26.1	8.74	2.38	0.32	2.06	0.371	0.062	0.130	0.026
DP11076	10	5	0.61	264.11	0.99	4.83	23.8	7.96	2.25	0.29	1.84	0.353	0.056	0.110	0.022
DP11077	10	6	0.11	265.11	1.29	4.94	27.2	8.78	2.32	0.32	2.07	0.358	0.069	0.162	0.032
DP11078	11	1	0.17	267.17	1.85	5.07	24.1	8.60	2.79	0.55	2.12	0.392	0.186	0.044	0.026
DP11079	12	1	0.21	276.71	0.11	1.16	33.9	1.08	0.47	0.68	0.42	0.085	0.248	0.003	0.023
DP11080	12	1	0.37	276.87	0.00	1.40	33.3	1.15	0.56	0.49	0.45	0.091	0.186	0.000	0.016
DP11081	13	1	0.04	286.04	0.00	0.32	31.3	0.21	0.17	0.23	0.04	0.091	0.117	0.000	0.016
DP11082	14	1	0.22	295.72	0.34	1.71	33.5	0.77	0.42	0.28	0.33	0.059	0.117	0.029	0.008
DP11083	15	1	0.34	305.34	0.51	2.35	33.5	0.19	0.17	0.25	0.07	0.040	0.086	0.035	0.006
DP11084	15	1	0.95	305.95	0.37	2.11	31.3	0.27	0.22	0.21	0.07	0.031	0.080	0.024	0.005
DP11085	16	1	0.23	314.72	0.68	2.58	34.2	0.61	0.42	0.53	0.30	0.051	0.182	0.119	0.022
DP11086	17	1	0.12	324.12	0.15	1.67	33.3	0.19	0.24	0.19	0.09	0.026	0.089	0.095	0.041
DP11087	17	1	0.30	324.30	0.00	1.76	34.0	0.22	0.25	0.10	0.11	0.026	0.051	0.000	0.000
DP11088	17	1	1.10	325.10	0.31	2.24	32.6	0.14	0.11	0.04	0.03	0.037	0.031	0.000	0.000
DP11089	18	1	0.19	333.69	0.44	1.93	29.9	0.13	0.10	0.05	0.02	0.020	0.033	0.000	0.000

on all elemental abundance axes are positive). These rotated axes can then be converted to actual elemental compositions and can be treated as physical end members of the population. This technique was developed by Leinen and Pisias (1984). We have used their algorithm to analyze the Leg 86 data.

Table 4 shows the compositions of the reference (rotated) axes for the combined Site 579 and 580 data sets. Figure 6 shows how these factors load on to the downhole samples.

Factor 1 is primarily terrigenous detritus with some biogenic opal. The Site 580 samples are slightly depleted in this factor and are markedly more variable than the Site 579 samples (Fig. 6). In contrast, Factor 3, which is dominated by biogenic opal and Mn, is much more abundant in the Site 580 samples from the more productive northern site. Factor 2 is a mixture of authigenic iron sulfide and terrigenous detritus. Its greater abundance at Site 580 is consistent with a greater influx of organic carbon, which has served as the energy source for sulfate-reducing bacteria at this site.

If sulfur is excluded from the factor analysis, three simpler end members emerge (Table 5, Fig. 7). Factor 1 is again dominated by terrigenous debris, in this case with a smaller addition of biogenic opal. The downhole patterns at Sites 579 and 580 are very similar, with the abundance of factor 1 roughly doubling from the oldest (Pliocene) to youngest (Quaternary) samples. The opal-rich Factor 3 shows almost the inverse pattern, with a marked decrease from older to younger samples. At Site 580, the transition is continuous, with a lot of variability throughout the section. In contrast, the abundance of

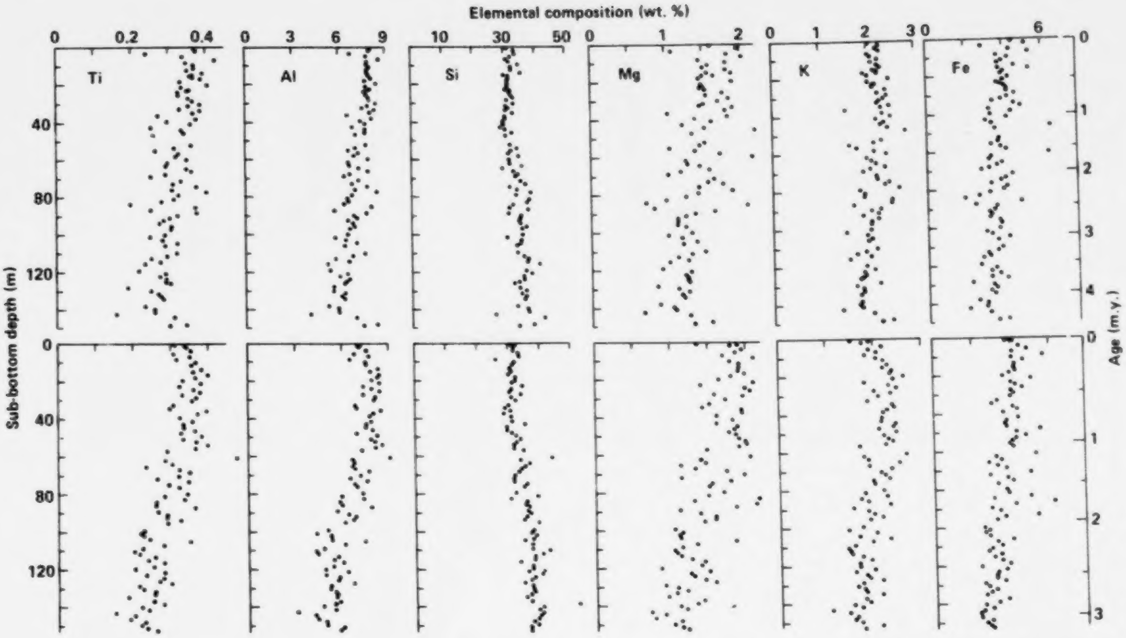

Figure 2. Downhole profiles of elemental abundances in samples from Sites 579 (upper) and 580 (lower). Analyses by X-ray fluorescence, salt corrected. The data are given in Tables 1 and 2.

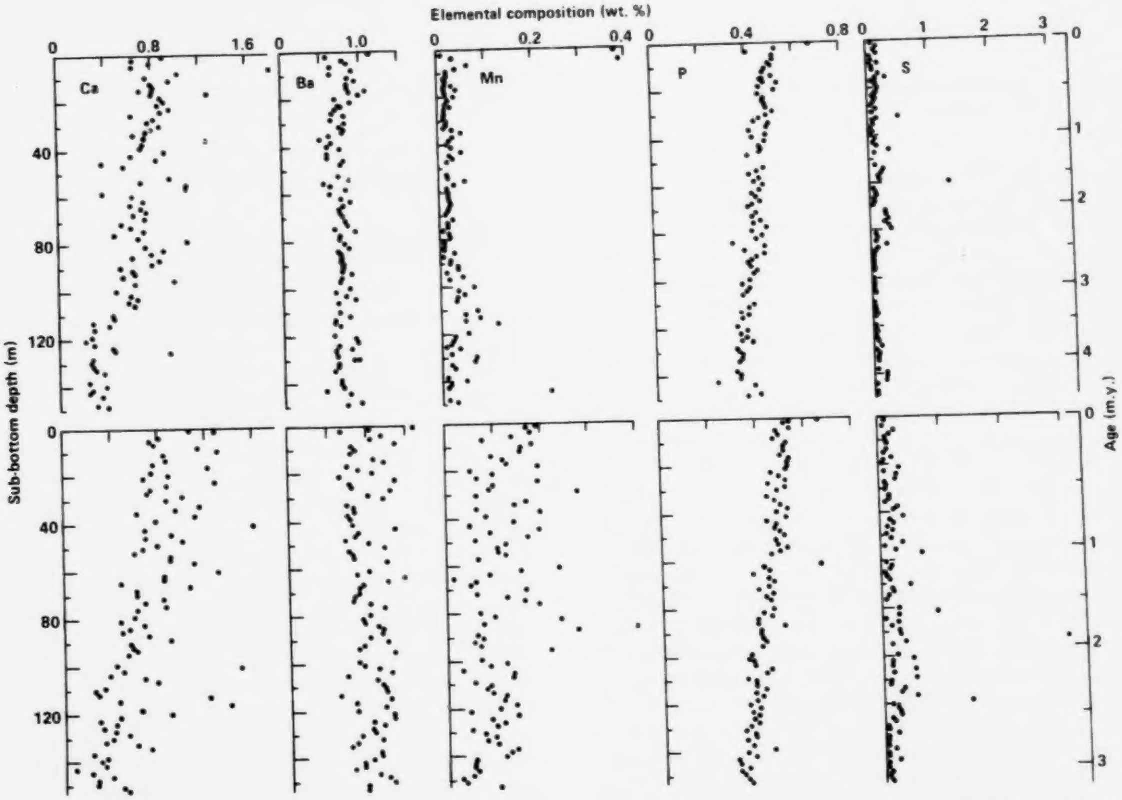

Figure 3. Downhole profiles of minor element abundances in samples from Sites 579 (upper) and 580 (lower). Analyses by X-ray fluorescence, salt corrected. The data are given in Tables 1 and 2.

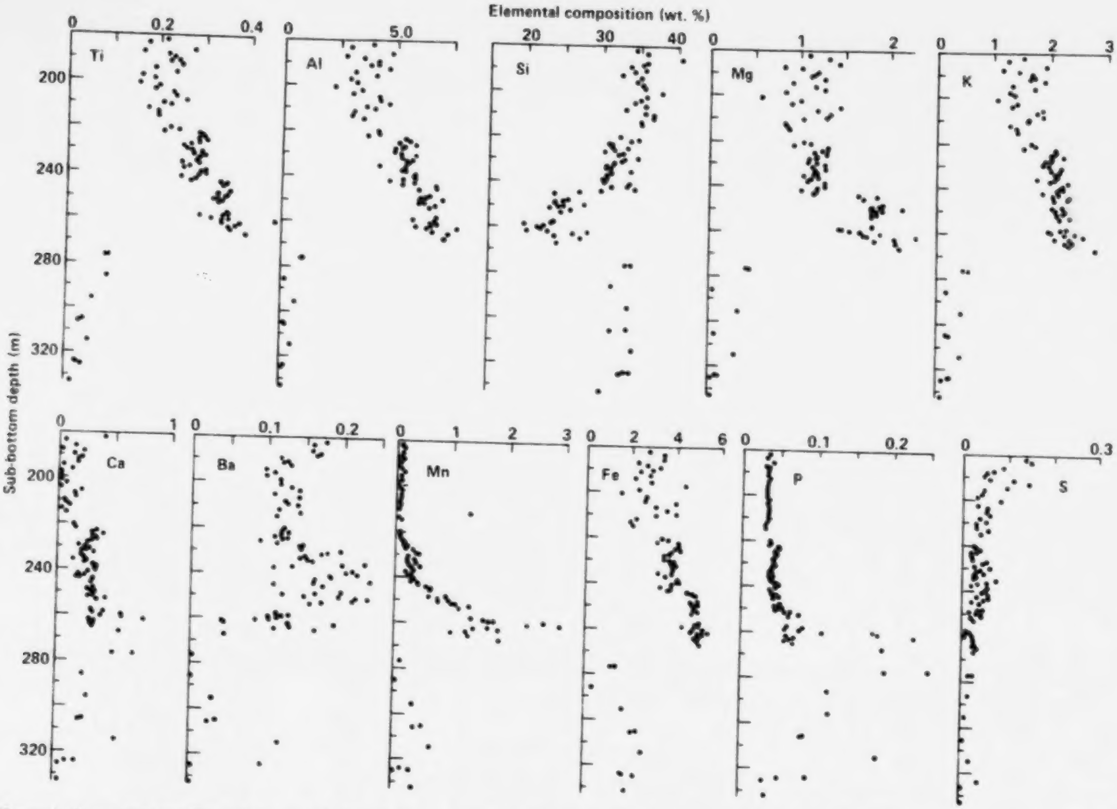

Figure 4. Downhole profiles of elemental abundances in samples from Site 581. Analyses by X-ray fluorescence, salt corrected. The data are given in Table 3.

Factor 3 at Site 579 decreases abruptly near 110 m, corresponding to an age of about 3.2 m.y. Factor 2, which consists of terrigenous detritus enriched in authigenic (?) iron and manganese, is more abundant at Site 580 than at Site 579, but shows little variation downhole.

The results of factor analysis of the Site 581 samples are shown in Figure 8. The Q-mode analysis (Table 6) distinguishes detrital, Mn-rich, and biogenic factors (Factors 1, 2, and 3, respectively). The detrital factor decreases continuously in importance from the basal clays to the cherts below 276 m. The other two factors show sharp discontinuities at this boundary.

The rotated factors (Table 7), in contrast, vary much more smoothly across the clay/chert boundary. The detrital-rich Factor 1 decreases to very low values in the chert, with only three elevated values near 325 m. Factor 3, dominated by opal and minor fish debris, is uniformly high in the chert, decreases to a minimum in the dark brown clays (245–276 m), and increases slightly in the less oxidized clays. Factors 2, which is dominated by an authigenic ferromanganese component with subordinate fish debris and detritus, is concentrated in the dark brown clays (245–276 m). Lower but still significant levels are evident in the light brown clays (224–245 m) and chert (below 276 m). Only the reduced (gray green) clays above 224 m are depleted in this factor.

DISCUSSION AND CONCLUSIONS

The elemental composition of sediments at Sites 579, 580, and 581 is dominated by contributions from terrigenous detritus and opal-rich biogenic debris. Redox-driven diagenetic reactions (mobilization and redistribution of manganese and precipitation of iron sulfide) and the deposition of authigenic ferromanganese oxyhydroxides in mid-Tertiary dark brown clays at Site 581 modify the abundances of some elements.

From a geochemical perspective, Sites 579 and 580 are almost indistinguishable. A slight enrichment of the biogenically associated elements Si, Ca, Ba, and P at Site 580, which lies beneath more biologically productive waters than Site 579, is the major difference. At both sites, the ratio of detrital to biogenic debris increases uphole from the late Pliocene to the late Quaternary portions of the profiles. It seems unlikely that this trend resulted from a decrease in biogenic input, given the northward drift of the sites and more vigorous oceanic circulation during the Quaternary in this region. Rather, the trend probably reflects the accelerated eolian deposition of continental debris from loess deposits in Asia that accompanied the development of Northern Hemisphere glaciation and that has been recognized elsewhere in the North Pacific (Heath, 1969; Leinen and Heath, 1981).

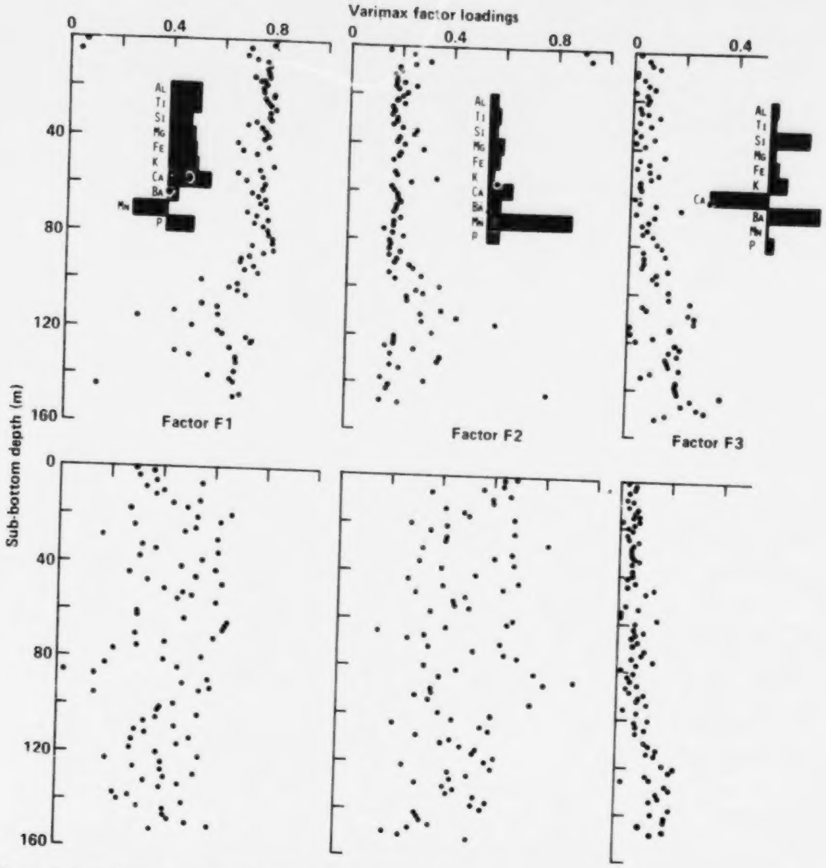

Figure 5. Downhole profiles of loadings of Q-mode varimax factors on samples from Sites 579 (upper) and 580 (lower). Histograms show contributions of elements to each factor.

Table 4. Composition (wt.%) of the rotated Q-mode factors for Sites 579 and 580 plotted in Figure 6.

Element	Factor 1	Factor 2	Factor 3
Ti	0.31	0.35	0.25
Al	7.09	6.53	5.18
Si	32.4	25.3	34.3
Mg	1.35	2.65	1.62
K	2.14	1.83	1.53
Fe	3.51	6.36	3.48
Ca	0.65	1.39	0.62
Ba	0.08	0.07	0.14
Mn	0.00	0.005	0.48
P	0.04	0.05	0.04
S	0.03	3.08	0.00

A feature deserving of additional study is the enhanced deposition of Mn at Site 580 relative to Site 579. We suspect that the excess Mn is preserved as a carbonate, but the depositional conditions responsible for such preservation have not been identified.

The record at Site 581 captures the basal part of the sequence cored at Sites 579 and 580 (reduced, opal-bearing detrital clays), as well as oxidized detrital-rich clays and highly oxidized pelagic clays rich in authigenic ferromanganese oxyhydroxides. This section overlies porcellaneous chert.

The oxidized clays are reminiscent of "red clay" sequences elsewhere in the North Pacific (see Site 576 and 578 chapters, this volume; Leinen, 1979). Both P and Ba are enriched in the darkest brown clays, reflecting the concentration of the most refractory biogenic debris (phosphatic fish fragments and barite) in the least rapidly accumulating sediments.

The porcellaneous cherts at Site 581 contain some surprises. They contain about the same concentration of silica as the oxidized detrital clays and markedly less than the biosiliceous clays at Site 580. The relatively high Mn contents and red to yellow colors also point to fairly slow deposition in a well-oxygenated environment. The high P contents of the cherts, particularly the youngest ones, also is suggestive of slow deposition (i.e., greater relative abundance of phosphatic fish debris). The possibility that precipitation of the chert layers concentrates fish debris (perhaps by physically displacing the finer clay particles) cannot be excluded, however.

Overall, the chemical data are consistent with the paleoceanographic interpretations derived from lithologic and paleontologic descriptions of the sections at Sites

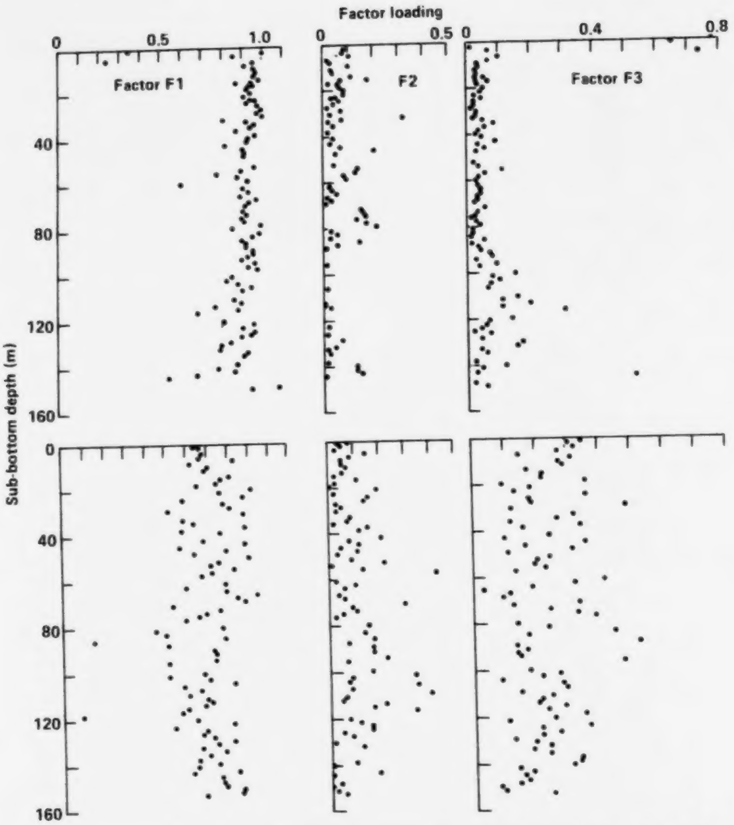

Figure 6. Downhole profiles of loadings of rotated varimax factors (see text for explanation) on samples from Sites 579 (upper) and 580 (lower). Compositions of rotated factors are listed in Table 4. All elements, including sulfur, are included.

Table 5. Composition (wt.%) of the rotated Q-mode factors (S omitted) for Sites 579 and 580 plotted in Figure 7.

Element	Factor 1	Factor 2	Factor 3
Ti	0.34	0.35	0.23
Al	7.75	6.57	5.16
Si	30.7	28.2	36.0
Mg	1.52	2.63	1.10
K	2.22	1.38	1.81
Fe	3.91	5.15	2.90
Ca	0.94	2.10	0.00
Ba	0.07	0.14	0.11
Mn	0.00	0.90	0.06
P	0.05	0.06	0.03

579, 580, and 581. The sets of closely spaced analyses presented here yield a measure of both the general trends and variability of deposition at the three sites. This data set should also be useful for future studies of the comparative geochemistry of North Pacific pelagic clays.

ACKNOWLEDGMENTS

We are grateful to the members of the scientific party of Leg 86 for discussions concerning the deposition of western North Pacific pelagic sediments. We also acknowledge the assistance of Ivan Pavlov and Greg Campi in preparing and analyzing samples, and helping to plot the results. This manuscript was improved by the reviews of Miriam Kastner and Mitchell Lyle.

REFERENCES

Chase, T. E., 1975. Topography of the oceans. Univ. Calif. San Diego, Scripps Inst. Oceanog., *Inst. Mar. Resources Tech. Rept.*, Ser. TR57.

Coleman, M., Fleet., A., and Donson, P., 1982. Preliminary studies of manganese-rich carbonate nodules from Leg 68, Site 503, eastern equatorial Pacific. *In* Prell, W. L., Gardner, J. V., et al., *Init. Repts. DSDP*, 68: Washington (U.S. Govt. Printing Office), 481–489.

Criss, J. W., Birks, L. S., and Gilfrich, J. V., 1978. A versatile x-ray analysis program combining fundamental parameters and empirical coefficients. *Anal. Chem.*, 50:33.

Dymond, J., 1981. The geochemistry of Nazca Plate surface sediments: an evaluation of hydrothermal, biogenic, detrital and hydrogenous sources. *Mem. Geol. Soc. Am.*, 154:133–173.

Froelich, P., Klinkhammer, G., Bender, M., Luedtke, N., Heath, R., Cullen, D., Dauphin, P., Hammond, D., Hartman, B., and Maynard, V., 1979. Early oxidation of organic matter in pelagic sediments of the eastern equatorial Atlantic: suboxic diagenesis. *Geochim. Cosmochim. Acta*, 43:1075–1090.

Heath, G. R., 1969. Mineralogy of Cenozoic deep-sea sediments from the equatorial Pacific Ocean. *Geol. Soc. Am. Bull.*, 80:1997–2018.

Klovan, J. E., and Imbrie, J., 1971. An algorithm and FORTRAN IV program for large scale Q-mode factor analysis. *J. Int. Assoc. Math. Geol.*, 3:61–77.

Leinen, M., 1979. Paleochemical signatures in Cenozoic Pacific sediments [Ph.D. dissert.]. University of Rhode Island, Narragansett.

Leinen, M., and Heath, G. R., 1981. Sedimentary indicators of atmospheric activity in the northern hemisphere during the Cenozoic. *Palaeogeogr., Palaeoclimatol., Palaeoecol.*, 36:1–21.

Leinen, M., and Pisias, N. G., 1984. An objective technique for determining end-member compositions and for partitioning sediments according to their sources. *Geochim. Cosmochim. Acta*, 48:47–63.

Leinen, M., and Stakes, D., 1979. Metal accumulation rates in the central equatorial Pacific during Cenozoic time. *Geol. Soc. Am. Bull.*, 90:357–375.

Lyle, M. W., 1983. The brown-green color transition in marine sediments: a marker of the Fe(III)-Fe(II) redox boundary. *Limnol. Oceanogr.*, 28:1026–1033.

Pederson, T. F., and Price, N. B., 1982. The geochemistry of manganese carbonate in Panama Basin sediments. *Geochim. Cosmochim. Acta*, 46:59–68.

Date of Initial Receipt: 1 May 1984
Date of Acceptance: 25 September 1984

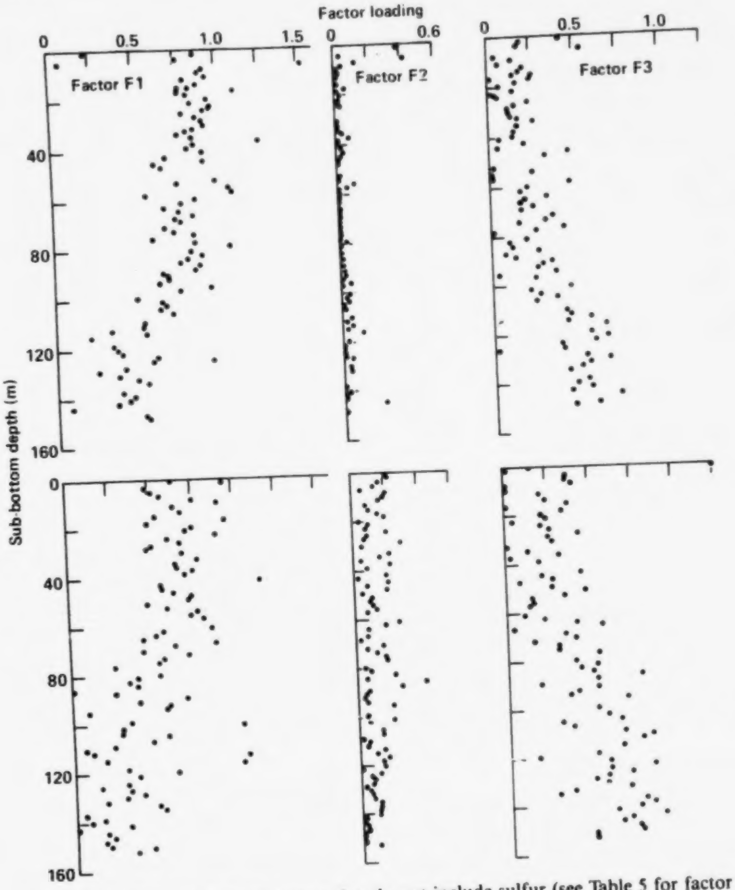

Figure 7. As Figure 6, but for factors that do not include sulfur (see Table 5 for factor compositions).

Table 6. Elemental contributions (factor scores) to Q-mode varimax factors for Site 581 analyses (Fig. 8).

Element	Factor 1	Factor 2	Factor 3
Ti	1.04	0.54	−0.20
Al	1.05	0.68	−0.45
Si	1.27	−0.01	1.37
Mg	1.02	0.66	−0.36
K	1.17	0.43	−0.27
Ca	0.16	0.70	1.19
Ba	1.49	0.10	−0.33
Mn	−0.87	2.72	0.02
Fe	0.88	0.51	0.23
P	−0.11	0.26	2.48

Table 7. Composition (wt.%) of the rotated Q-mode factors for Site 581 plotted in Figure 8.

Element	Factor 1	Factor 2	Factor 3
Ti	0.23	0.01	0.04
Al	5.15	15.0	0.00
Si	32.4	14.6	41.2
Mg	1.12	3.24	0.23
K	1.71	3.76	0.23
Ca	0.13	0.73	0.32
Ba	0.15	0.19	0.01
Mn	0.01	3.72	0.19
Fe	3.07	8.49	1.80
P	0.02	0.11	0.13

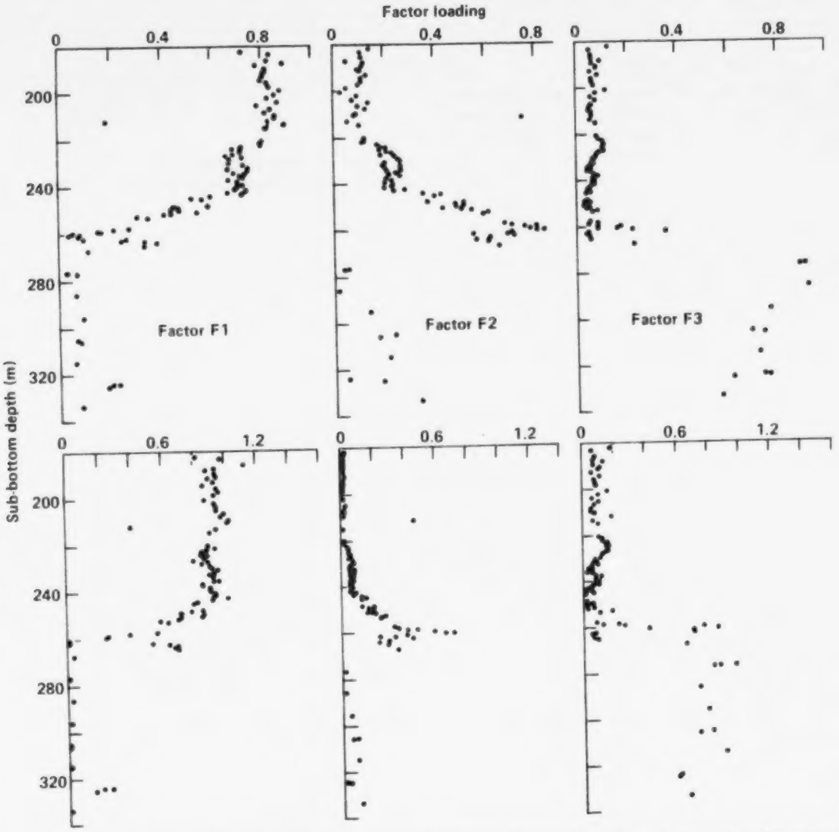

Figure 8. Downhole profiles of loadings of Q-mode varimax factors (upper), and rotated varimax factors (lower) on samples from Site 581. Elemental contributions to Q-mode factors are listed in Table 6. Compositions of rotated factors are listed in Table 7.

30. LIPID GEOCHEMISTRY OF THE CRETACEOUS/TERTIARY BOUNDARY SEDIMENTS, HOLE 577, DEEP SEA DRILLING PROJECT LEG 86[1]

Bernd R. T. Simoneit and Harry R. Beller, Oregon State University[2]

ABSTRACT

Core samples of calcareous sediments taken from above and below the proposed Cretaceous/Tertiary boundary (Sample 577-12-5, 130 cm) were examined for geochemical evidence of the mass extinctions and faunal successions that marked this period. The lipid compositions of the six core samples examined were virtually identical and were characterized by a large component of unresolved naphthenic hydrocarbons and a homologous series of *anteiso*-alkanes, both presumably of bacterial origin. The results of this preliminary study suggest that the lipids of sediments deposited over a several million year period encompassing the Cretaceous–Tertiary extinctions have been almost completely recycled by bacterial metabolism, which occurred under oxic depositional and/or diagenetic conditions and which left a unique bacterial signature with only minor traces of the original sedimentary lipids.

INTRODUCTION

The Cretaceous/Tertiary boundary is marked by major extinctions of both marine and terrestrial species. These extinctions were probably caused by the impact of a massive extraterrestrial body (Alvarez et al., 1980, 1984), which was of meteoritic origin according to current data on Ir and Os anomalies (Alvarez et al., 1982, 1984; Luck and Turekian, 1983). A major meteoritic impact could have had extensive biogeochemical consequences, such as the cessation or dramatic reduction of photosynthetic biomass production on a regional to global scale and the scouring of continents by tidal waves. Presumably, a reduction of biogenesis, a possible hiatus or facies change at the Cretaceous/Tertiary boundary, and a subsequent, gradual buildup of extant and new species should have left a molecular fossil record in the sediments. The purpose of this preliminary analysis is to evaluate such a possibility.

The samples for this study are derived from Hole 577, Core 12, located on the Shatsky Rise in the western Pacific Ocean (32°26.51′N, 157°43.40′E, 2675 m water depth) (Site 577 chapter, this volume). The sediment of Core 12 consists of white calcareous nannofossil ooze with very low organic carbon content. The Cretaceous/Tertiary boundary was tentatively assigned at Sample 577-12-5, 118 cm on board ship and was more accurately determined by shore-based work to be at Sample 577-12-5, 130 cm (Monechi, this volume; Site 577 chapter, this volume). No iridium measurements were made in Hole 577, Core 12 sediments, but an iridium anomaly has been determined to occur in adjacent Hole 577B at the Cretaceous/Tertiary boundary (Sample 577B-1-4, 72 cm) (Michel et al., this volume). The samples for this work were chosen prior to the readjustment of the Cretaceous/Tertiary boundary and the two samples from below the boundary were combined.

METHODS

The samples were freeze-dried and then exhaustively extracted with methylene chloride using ultrasonic agitation. The extracts were concentrated on a rotary evaporator and treated with diazomethane in diethyl ether to derivatize free fatty acids. These total extracts were then subjected directly to gas chromatography (GC) and gas chromatography-mass spectrometry (GC-MS).

The GC analyses were carried out on a Varian Vista 44 gas chromatography system using a 30 m × 0.25 mm fused silica capillary column coated with DB-1701 (J and W Scientific, Inc.) and programmed from 65 to 275°C at 10°C/min. Helium was the carrier gas.

The GC-MS analyses were performed on a Finnigan 4021 quadrupole mass spectrometer interfaced directly to a Finnigan 9610 gas chromatograph, equipped with a 30 m × 0.25 mm fused silica capillary column coated with DB-5. The GC for the GC-MS analyses was programmed from 60 to 310°C at 4°C/min. The mass spectrometric data were acquired and processed with a Finnigan-Incos 2300 data system.

Total organic carbon values were determined for samples above and below the Cretaceous/Tertiary boundary (Samples 577-12-5, 120–121 cm and 132–134 plus 147–149 cm) by the phosphoric acid/dichromate oxidation technique (procedure described in Weliky et al., 1983).

RESULTS AND DISCUSSION

The total extract yields, the total concentrations of *anteiso*-alkanes and the lithologies and ages of the samples are given in Table 1. The total organic carbon contents of the samples tested were below 0.05% (as % dry wt. of sediment) and were thus considered too low for meaningful quantitative comparison among samples. The extract yields are low and consist mainly of unresolvable naphthenic hydrocarbons (hump), as indicated in the gas chromatograms of Figure 1. There is no major change in the lipid data across the Cretaceous/Tertiary boundary, although the sample below has a relatively low total extract yield. The GC traces are essentially identical for all samples (i.e., the same peaks are present), with only minor differences in relative peak concentrations. Not all of the minor peaks could be identified by GC-MS analyses.

The major resolved compounds are *anteiso*-alkanes (some sample distributions are shown in Fig. 2) with lesser amounts of *iso*-alkanes. Normal alkanes are not detectable and pristane (Pr) and phytane (Ph) are present as minor components, with Pr > Ph. This ratio of Pr/

---

[1] Heath, G. R., Burckle, L. H., et al., *Init. Repts. DSDP*, 86: Washington (U.S. Govt. Printing Office).

[2] Address: College of Oceanography, Oregon State University, Corvallis, OR 97331.

Table 1. Lipid yields for samples across the Cretaceous/Tertiary boundary in Hole 577.

Sample (interval in cm)	Age[a]	Lithology	Total extract yield ($\mu g/g$)[b]	Total *anteiso*-alkanes (% of total extract)
577-12-1, 21-23	early Paleocene	Nannofossil ooze	11.7	9.7
577-12-5, 72-74	early Paleocene	Nannofossil ooze	5.6	7.5
577-12-5, 100-102	early Paleocene	Nannofossil ooze	8.1	6.8
577-12-5, 111-113	early Paleocene	Nannofossil ooze	8.8	6.8
577-12-5, 120-121	early Paleocene	Nannofossil ooze	9.3	5.6
577-12-5, 132-134 + 147-149	Late Cretaceous	Nannofossil ooze	2.1	11

[a] Monechi (this volume).
[b] Based on dry weight of sediment.

Ph > 1, coupled with the absence of elemental sulfur, appears to indicate an oxic depositional environment or at least oxidizing diagenetic conditions (Didyk et al., 1978). The overall compound distribution patterns and the range of the hump indicate that these extracts represent a residue of relatively unaltered bacterial lipids superimposed on degraded algal lipid detritus (Simoneit, 1981, 1982). This microbial lipid origin is further supported by the *n*-fatty acid distributions (Fig. 2), which range from C_{14} to C_{18} with a strong even carbon number predominance, typical for microbial sources (Simoneit, 1981, 1982).

The molecular markers are sparse in these samples. Triterpenoids, extended tricyclic terpanes and acyclic isoprenoids ($>C_{20}$), all of microbial origin (Simoneit, 1978; Aquino Neto et al., 1982; Chappe et al., 1982), are not detectable in these samples. Traces of steranes are identifiable in two samples above the Cretaceous/Tertiary boundary (Samples 577-12-5, 100-102 cm and 120-121 cm), where the dominant homologs are diasteranes, with a minor series of steranes. 20*S*-β,α-diacholestane 20*R*-β,α-diacholestane are the dominant homologs and occur in a ratio of $S/R = 1.4$, indicating that these samples are quite mature (Ensminger et al., 1978). The dominance of the various C_{27} homologs may indicate an origin from marine algal detritus (Huang and Meinschein, 1979; Simoneit et al., 1980). In addition, there are various diterpenoid residues and alkyl phenanthrenes present, which could be derived from terrestrial higher plant resins or possibly from algal diterpenoids (Simoneit, 1977, and unpublished data). Methyl-, dimethyl- (possibly pimanthrene), and a C_4-phenanthrene are present as major components in all samples and dehydroabietic acid, 4α- and 4β-dehydroabietin, and a nordehydroabietin are found as minor constituents only in samples above the Cretaceous/Tertiary boundary. The low degree of structural preservation of these diterpenoid residues again indicates an oxic depositional environment.

The overall compound distributions in these lipids indicate an origin from bacteria with minor detrital residues from algae and possibly resinous vascular plants. However, we can offer no explanation for the absence of *n*-alkanes and hopanoids or for the low observed concentrations of *n*-fatty acids, which are all normally significant constituents of bacterial lipids. The possibility of contamination by petroleum product lubricants is unlikely, based mainly on the predominance of the *anteiso*-alkanes and additional specific molecular markers indicative of a syngenetic and biological origin for the lipids.

CONCLUSIONS

The lipid compositions for all samples examined across the Cretaceous/Tertiary boundary are essentially the same. Trace molecular markers are present that indicate a component from algae and, above the Cretaceous/Tertiary boundary, possibly also from terrestrial resinous plants. However, a definitive assignment of the original lipid sources (i.e., algal communities, terrestrial influx) of these samples is not possible, since the residues preserved in the sediments are derived predominantly from bacteria, which efficiently metabolized the other lipids in an oxic environment. Thus, molecular stratigraphy cannot be applied definitively across the Cretaceous/Tertiary boundary because bacterial alteration of the organic detritus has resulted in the preservation of its own unique lipid signature throughout the interval examined here. Changes in ecosystem lipid signatures may be better observed in sediments with enhanced preservation of organic matter and less microbial alteration, that is, in sediments deposited under more euxinic conditions.

ACKNOWLEDGMENTS

We thank James M. Brooks and an anonymous reviewer for reviewing this manuscript.

REFERENCES

Alvarez, L. W., Alvarez, W., Asaro, F., and Michel, H. V., 1980. Extraterrestrial cause for the Cretaceous-Tertiary extinction. *Science*, 208:1095-1108.

Alvarez, W., Alvarez, L. W., Asaro, F., and Michel, H. V., 1982. Current status of the impact theory for the terminal Cretaceous extinction. *Geol. Soc. Am., Spec. Pap.*, 190:305-315.

Alvarez, W., Kauffman, E. G., Surlyk, F., Alvarez, L. W., Asaro, F., and Michel, H. V., 1984. Impact theory of mass extinctions and the invertebrate fossil record. *Science*, 223(4641):1135-1141.

Aquino Neto, F. R., Restle, A., Connan, J., Albrecht, P., and Ourisson, G., 1982. Novel tricyclic terpanes (C_{19}, C_{20}) in sediments and petroleums. *Tetrahedron Lett.*, pp. 2027–2030.

Chappe, B., Albrecht, P., and Michaelis, W., 1982. Polar lipids of archaebacteria in sediments and petroleums. *Science*, 217:65–66.

Didyk, B. M., Simoneit, B. R. T., Brassell, S. C., and Eglinton, G., 1978. Organic geochemical indicators of paleoenvironmental conditions of sedimentation. *Nature (London)*, 272:216–222.

Ensminger, A., Joly, G., and Albrecht, P., 1978. Rearranged steranes in sediments and crude oils. *Tetrahedron Lett.*, pp. 1575–1578.

Huang, W. Y., and Meinschein, W. G., 1979. Sterols as ecological indicators. *Geochim. Cosmochim. Acta*, 43:739–745.

Luck, J. M., and Turekian, K. K., 1983. Osmium 187/Osmium 186 in manganese nodules and the Cretaceous-Tertiary boundary. *Science*, 222:613–615.

Simoneit, B. R. T., 1977. Diterpenoid compounds and other lipids in deep-sea sediments and their geochemical significance. *Geochim. Cosmochim. Acta*, 41:463–476.

________, 1978. The organic chemistry of marine sediments. *In* Riley, J. P., and Chester, R. (Eds.), (Vol. 7, 2nd ed.): *Chemical Oceanography*, New York (Academic Press), 233–311.

________, 1981. Utility of molecular markers and stable isotope compositions in the evaluation of sources and diagenesis of organic matter in the geosphere. *In* Prashnowsky, A. A. (Ed.), *The Impact of the Treibs' Porphyrin Concept on the Modern Organic Geochemistry*: Würzburg (Universität Würzburg), pp. 133–158.

________, 1982. The composition, sources, and transport of organic matter to marine sediments—The organic geochemical approach. *In* Thompson, J. A. J., and Jamieson, W. D. (Eds.), *Proc. of the Symposium Marine Chemistry into the Eighties:* Ottawa (Nat. Res. Council of Canada), pp. 82–112.

Simoneit, B. R. T., Halpern, H. I., and Didyk, B. M., 1980. Lipid productivity of a high Andean Lake. *In* Trudinger, P. A., Walter, M. R., and Ralph, B. J. (Eds.), *Biogeochemistry of Ancient and Modern Environments:* New York (Springer Verlag), pp. 201–210.

Weliky, K., Suess, E., Ungerer, C. A., Muller, P. J., and Fischer, K., 1983. Problems with accurate carbon measurements in marine sediments and particulate matter in seawater: A new approach. *Limnol. Oceanogr.*, 28:1252–1259.

Date of Initial Receipt: 11 May 1984
Date of Acceptance: 11 July 1984

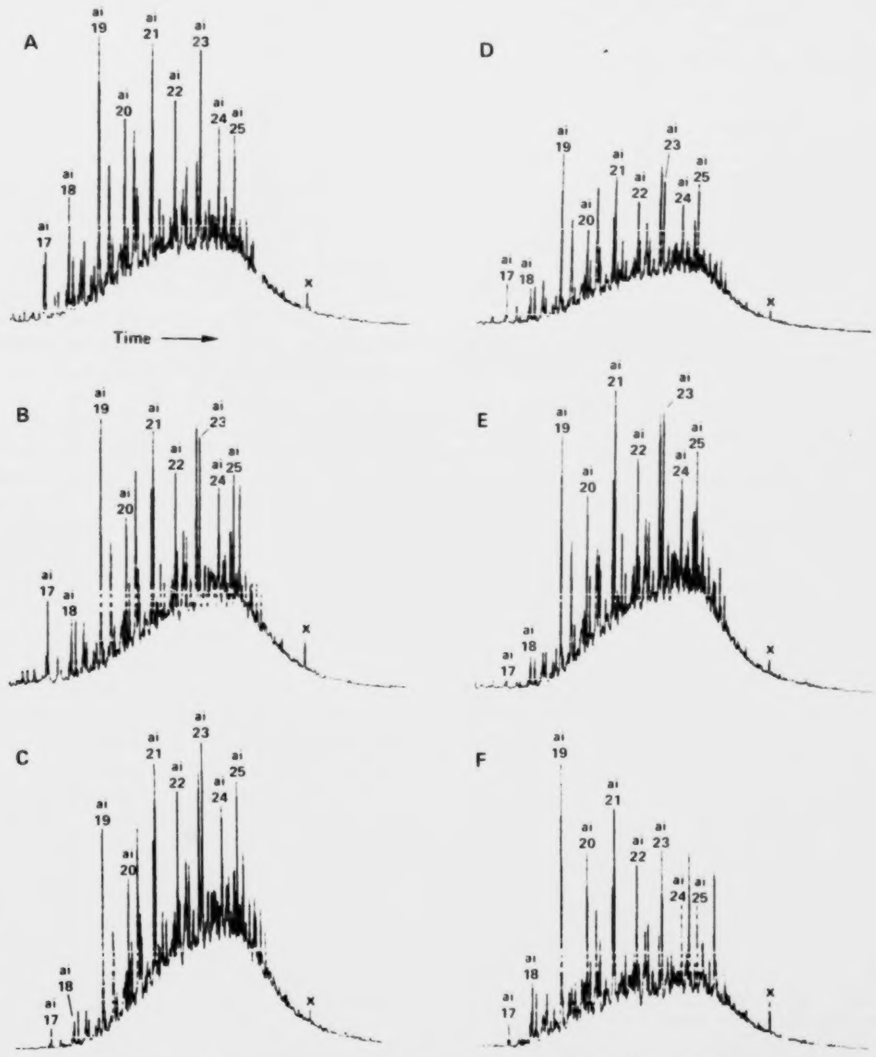

Figure 1. Capillary gas chromatograms of total extract fractions (GC conditions as in text). (A) Sample 577-12-1, 21–23 cm; (B) Sample 577-12-5, 72–74 cm; (C) Sample 577-12-5, 100–102 cm; (D) Sample 577-12-5, 111–113 cm; (E) Sample 577-12-5, 120–121 cm; (F) Sample 577-12-5, 132–134 and 147–149 cm. (Arabic numerals indicate carbon number of *anteiso*-alkanes, x = C_8-phthalate contaminant).

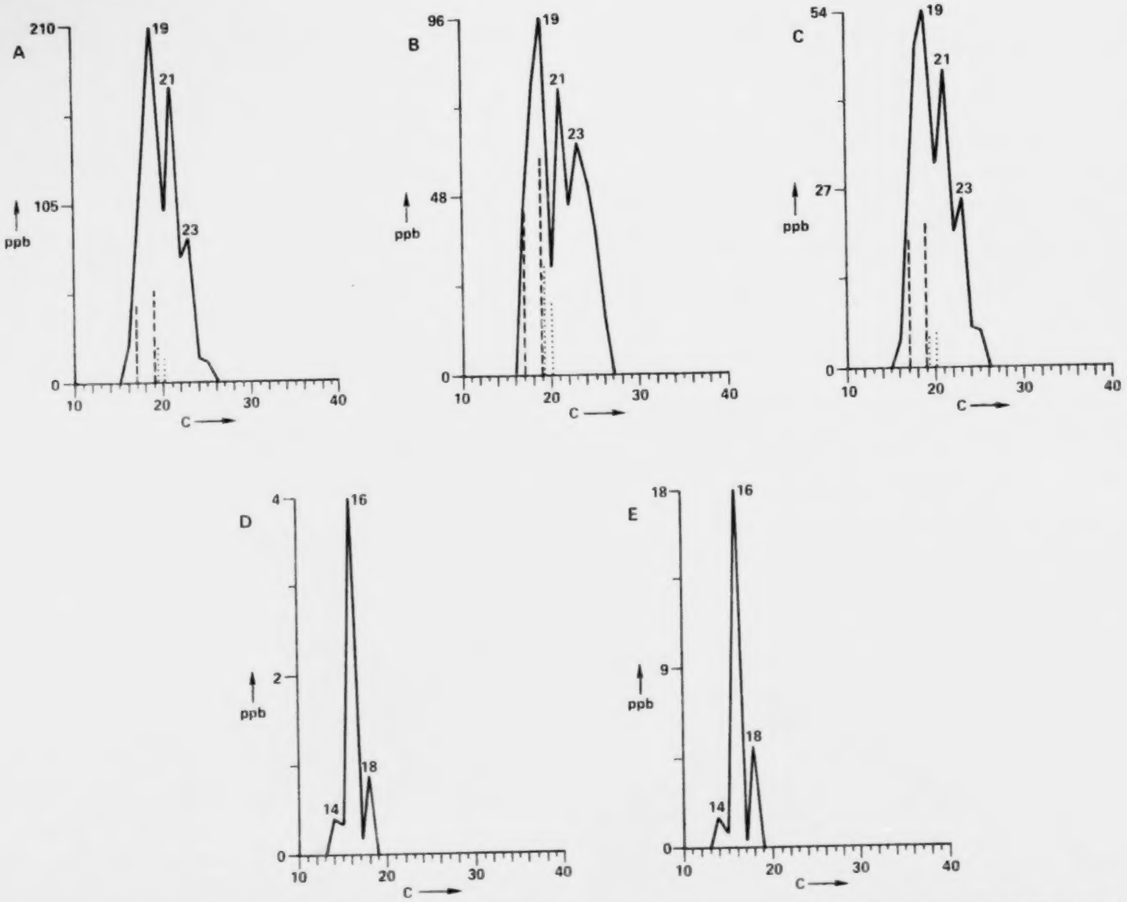

Figure 2. Distribution diagrams of typical hydrocarbon and fatty acid series in the extracts. (A–C) *Anteiso*-alkanes (dashed line, *iso*-alkanes, dotted line, isoprenoids) and (D, E) *n*-fatty acids: (A) Sample 577-12-1, 21–23 cm; (B) Sample 577-12-5, 120–121 cm; (C) Sample 577-12-5, 132–134 and 147–149 cm; (D) Sample 577-12-5, 100–102 cm; (E) Sample 577-12-5, 132–134 and 147–149 cm.

31. THE CHEMISTRY OF INTERSTITIAL WATERS, DEEP SEA DRILLING PROJECT LEG 86[1]

Russell E. McDuff, University of Washington[2]

ABSTRACT

Interstitial water samples from Leg 86 were analyzed for Cl^-, SO_4^{2-}, Ca^{2+}, Mg^{2+}, K^+, Li^+, Sr^{2+}, Mn^{2+}, Si, NO_3^-, NH_4^+, and $\delta^{18}O$. The principal findings are as follows. (1) The chloride profiles consistently show a ~1.5% downcore increase to about 40 m sub-bottom depth. This increase is consistent with model profiles generated by considering the effects of variations in seawater salinity resulting from Pleistocene glaciation on pore-water composition. $\delta^{18}O$ profiles support this model. This agreement of model and observation precludes advection of the pore fluids at rates greater than 1 mm/yr. (2) Ca^{2+} and Mg^{2+} gradients are small relative to other Deep Sea Drilling Project sites, likely resulting from low diffusive fluxes through underlying chert horizons. (3) Other constituents exhibit profiles consistent with previous observations.

INTRODUCTION

Under what conditions does advection of pore fluids in deep-sea sediments occur? Flow has been convincingly documented in young ridge-flank sediments by using various thermal and chemical tracers (Maris and Bender, 1982; Sayles and Jenkins, 1982). Anderson et al. (1979) proposed on the basis of thermal data that flow occurs even in very old sediments. The global distribution of chemical anomalies in Deep Sea Drilling Project (DSDP) cores is consistent with a model in which flow is active until the upper basalts are capped by a sufficient thickness (~100 m) of relatively impermeable sediment (McDuff, 1981).

With the question of advection in mind, we analyzed pore fluids sampled during Leg 86 of DSDP in the northwest Pacific. We investigated the chemistry of the sediments at sites of similar crustal age but of varying sediment type and thickness, in order to refine the model of McDuff (1981). The geologic settings of the sites occupied are summarized in Table 1. All sites except Site 577 are below the carbonate-compensation depth (CCD) and consist mainly of pelagic clays, siliceous clays, and siliceous oozes (see Site chapters, this volume). Site 577 consists of nannofossil oozes. Sedimentation rates vary widely between the sites and increased with the onset of Pleistocene glaciation. Leg 86 samples were attractive for two other reasons. First, if flow occurs, one would expect rather small chemical anomalies because of the limited time available for chemical reaction to take place. It is difficult to document these small anomalies in rotary drill cores because of contamination by surface seawater, the drilling fluid. The samples from Leg 86 were collected with a hydraulic piston corer (HPC). Second, at Sites 576 and 578, multiple complete sequences were cored by HPC. These sequences provided sufficient material to allow much more closely spaced sampling (~ every 10 m) than the 30- to 50-m spacing more typical in DSDP drill holes.

METHODS

Samples were collected aboard the *Glomar Challenger* during Leg 86 by expressing pore fluids in a Manheim-type stainless steel squeezer. No special precautions were taken with respect to temperature of squeezing artifacts (Sayles and Manheim, 1975). Three samples were taken at Site 576 with the Barnes *in situ* sampler; however, these samples were excessively contaminated with seawater and are not considered further.

Samples were analyzed aboard ship for alkalinity, Cl, Ca, Mg, salinity, and pH following the standard protocol (see Introduction and Explanatory Notes, this volume). In our laboratory we repeated the analyses of Cl, Ca, and Mg. In addition, we determined K, Li, Sr, Mn, SO_4^{2-}, Si, NO_3^-, and NH_4^+ and, for Sites 576 and 578, $\delta^{18}O$ of the water. The analytical methods used are summarized in Table 2.

The method for chloride analysis requires some explanation. Chloride was determined by titration with $AgNO_3$ with electrochemical endpoint detection. The electrochemical cell used was $Ag,AgCl | Ag^+ || Ag^+ (0.165\ M) | Ag(s)$. The Ag,AgCl electrode is placed in the sample and the Ag wire electrode is imbedded in the reservoir of a micrometer buret. The liquid junction is established across the buret tip, which is submersed in the sample, with Ag^+ controlled by the titrant strength on one side of the junction and by the progress of the titration on the other. The potential of the cell is balanced by means of a potentiometer. The course of the titration is followed in terms of $\Delta mV/\Delta$ volume versus volume added. Control of quantities is the ultimate limit to precision; the 0.2-g sample is gravimetrically controlled to ±0.0001 g and the delivery of ~0.7 ml titrant is known to ±0.0002 ml. Precisions of ±0.05% (1σ) are routinely obtained. The titer is determined by titration of IAPSO standard seawater.

The shipboard (Site chapters, this volume) and shore-based chloride and calcium determinations agreed within the precision of the methods employed. Our shore-based magnesium data are offset +0.9% relative to the shipboard values, which have been converted to gravimetric units assuming a density of 1.022 g/cm^3. The reason for the offset is not readily apparent. The correction equations of Gieskes and Lawrence (1976) for reducing Ca and Mg data have not been applied to our data. The uncertainty in the correction is large for the small differences that exist in these samples relative to the composition of the standard. We found that for standards containing 46.0 mmol/kg Mg and 15.0 mmol/kg Ca we obtain better accuracy using the IAPSO titer than if we had applied the Gieskes and Lawrence correction. However, the correction is small relative to the observed offset and is of the wrong sign.

RESULTS AND DISCUSSION

Shore-based data are summarized in Table 3 and shown for Sites 576–580 in Figures 1–5.

---

[1] Heath, G. R., Burckle, L. H., et al., *Init. Repts. DSDP*, 86: Washington (U.S. Govt. Printing Office).

[2] Address: School of Oceanography, University of Washington, Seattle, WA 98195.

Table 1. Geologic settings, Leg 86 sites.

Site	Location	Water depth (m)	Sediments	Pliocene-Pleistocene sedimentation rate (m/m.y.)	Cenozoic sedimentation rate (m/m.y.)
576	32°21.4′N, 164°16.5′E	6217	Cenozoic pelagic clay Cretaceous carbonate turbidite/pelagic clay	7	0.9
577	32°26.5′N, 157°43.4′E	2675	Cenozoic and Cretaceous nannofossil ooze (Miocene hiatus)	13	1.8
578	33°55.6′N, 151°37.7′E	6010	Pleistocene siliceous clay Pliocene siliceous ooze, clay Miocene clay Paleogene pelagic clay	27	3
579	38°37.7′N, 153°50.3′E	5737	Miocene-Pliocene-Pleistocene siliceous clay and ooze, with ash layers, pyrite zones	34	Not reached
580	41°37.5′N, 153°56.6′E	5375	Pliocene-Pleistocene siliceous clay and ooze	48	Not reached
581	43°55.6′N, 159°47.8′E	5476	Washed to 181 m Pliocene-Miocene siliceous clay and ooze overlying chert Basaltic basement at 344 m	65	4

Table 2. Methods used in Leg 86 interstitial water analyses.

Component	Method	Reference
Cl^-	Titration, electrometric end point	Methods section, this chapter
SO_4^{2-}	Titration	Gieskes, 1974
Ca^{2+}	Titration	Gieskes and Lawrence, 1976
Mg^{2+}	Titration	Gieskes and Lawrence, 1976
K^+	Atomic absorption	Gieskes, 1974
Li^+	Atomic absorption	Gieskes, 1974
Sr^{2+}	Atomic absorption	Gieskes, 1974
Mn^{2+}	Atomic absorption	Gieskes, 1974
Si	Colorimetric	Mann and Gieskes, 1975
NO_3^-	Colorimetric	Gardner et al., 1976
NH_4^+	Colorimetric	Gieskes, 1974
$\delta^{18}O$	Mass spectrometry	Epstein and Mayeda, 1953

Chloride

Background

Chloride is normally thought of as a conservative constituent of the interstitial waters of marine sediments. Yet, beginning with the onset of distinct glacial–interglacial cycles in the late Pliocene–early Pleistocene, sea level has fluctuated considerably as a consequence of water storage in continental ice sheets. Concomitantly, mean seawater chlorinity must have changed, perhaps as much as 5% if one accepts the upper end of the range of estimated sea-level variations (~200 m). How would such chloride fluctuations be recorded in deep-sea sediments?

Model

To model the potential influence of changes in deep-water chloride concentrations on interstitial-water profiles, we have adopted the following assumptions.

Assumption 1. The history of deep-water chlorinity can be represented by the pattern shown in Figure 6, which parallels the $\delta^{18}O$ record and assumes chloride is 3.7% elevated at maximum glaciation.

Assumption 2. Initially (2 m.y. ago), chloride is constant with depth.

Assumption 3. Transport of chloride in the sediments is by diffusion alone.

Assumption 4. Chloride is considered to be unreactive in the sediment column.

With these assumptions, the mathematical model that follows is a simple one:

$$\frac{\partial c}{\partial t} = D\frac{\partial^2 c}{\partial z^2} \tag{1}$$

subject to the initial condition:

$$c(z, 0) = c_0 \tag{2}$$

and the boundary conditions:

$$c(0,t) = f(t) \tag{3}$$

$$c(z_b,t) = c_b \tag{4}$$

where $c(z,t)$ is the chloride concentration, t is time, z is sub-bottom depth, and $f(t)$ is defined by Figure 6. The depth z_b corresponds to the depth of the sediment section and is taken as 200 m although any value will do as long as it is large relative to the depth to which the signal propagates. The parameter c_b, the concentration of chloride at the base of the sediment, is an additional variable as moderate increases in chloride are occasionally observed in drill cores, apparently supported by a flux from basaltic basement (McDuff, 1978). This set of equations is solved by a Crank–Nicholson scheme to yield chloride versus sub-bottom depth curves every 2000 yr. on a 10-m grid.

Plots of chloride versus time at sub-bottom depths of 10, 30, and 60 m are shown in Figure 7 for a case with c_b

Table 3. Interstitial water data, Leg 86.

Sample (interval in cm)	Sub-bottom depth (m)	K^+ (mmol/kg)	Mg^{2+} (mmol/kg)	Ca^{2+} (mmol/kg)	Sr^{2+} (µmol/kg)	Li^+ (µmol/kg)	Mn^{2+} (µmol/kg)	Cl^- (mmol/kg)	SO_4^{2-} (mmol/kg)	Si (µmol/kg)	NH_4^+ (µmol/kg)	NO_3^- [a] (µmol/kg)	$\delta^{18}O$ (‰)
Site 576													
576A-1-4, 140–150	6	11.3	51.57	10.22	90	28	52	540.4	28.9	450	5	55	+0.13
576A-2-4, 140–150	15	12.0	51.90	10.35	90	32	30	541.7	28.0	—	0	44	+0.26
576A-3-5, 130–140	26	11.6	51.44	10.62	90	31	0	542.7	28.4	260	0	55	+0.27
576A-4-4, 140–150	34	11.8	51.01	10.78	90	33	0	545.4	27.4	215	24	58	+0.14
576A-5-4, 140–150	43	10.7	51.19	10.80	90	33	0	546.6	27.8	180	6	58	+0.19
576A-6-5, 130–140	54	12.4	—	—	90	37	2	543.9	26.0	—	0	60	0.00
576A-7-4, 130–140	62	11.6	51.59	10.60	90	37	0	539.8	27.1	190	3	52	+0.05
Site 577													
577-2-5,140–140	14	12.5	51.94	9.79	115	25	11	543.9	29.1	185	26	3	—
577-6-4, 140–150	50	11.8	52.27	10.38	155	23	3	545.6	27.7	200	27	8	—
577-10-5, 140–150	90	10.0	53.06	10.45	125	22	0	541.9	27.3	155	0	11	—
577A-4-5, 140–150	36	11.9	52.35	9.97	125	22	3	544.6	27.5	195	27	4	—
577A-8-5, 140–150	74	10.0	52.90	10.80	145	22	0	543.0	27.7	205	20	3	—
577A-13-5, 140–150	121	10.1	52.06	10.78	135	25	0	540.2	27.3	225	0	0	—
Site 578													
578-2-5, 140–150	12	13.4	50.44	10.95	90	25	155	542.6	28.4	520	135	10	+0.13
578-5-6, 140–150	42	12.4	49.27	11.81	95	27	130	544.7	28.0	275	160	0	+0.11
578-8-5, 140–150	69	11.6	48.76	12.45	90	30	24	540.9	27.7	430	125	4	—
578-11-6, 140–150	99	10.7	—	—	90	39	26	542.8	27.2	500	92	1	−0.43
578-14-3, 140–150	128	8.7	49.63	13.93	90	45	235	533.4	25.3	425	41	18	−0.68
578-17-3, 140–150	152	9.5	47.66	14.59	90	46	245	539.0	23.2	215	3	34	−0.77
Site 579													
579-2-5, 140–150	16	12.4	51.05	10.58	90	27	135	545.6	27.0	290	160	5	—
579A-5-5, 140–150	59	11.3	49.55	11.31	90	44	110	551.2	25.9	410	—	0	—
579A-8-5, 140–150	88	12.2	48.50	11.74	95	53	110	547.6	25.2	470	265	13	—
579A-11-4, 140–150	115	12.2	47.80	12.08	90	63	92	550.2	24.9	425	275	9	—
579A-14-4, 140–150	143	11.1	47.64	12.44	90	71	120	548.3	24.1	535	225	6	—
Site 580													
580-2-5, 140–150	11	13.2	50.39	10.40	90	27	200	540.4	27.0	335	200	7	—
580-5-5, 140–150	39	13.0	48.73	10.84	90	30	120	546.1	24.9	385	395	6	—
580-8-5, 140–150	68	12.3	47.82	11.06	90	35	97	547.0	23.8	595	475	8	—
580-11-4, 140–150	95	11.9	46.45	11.42	90	41	93	549.0	22.4	485	525	4	—
580-14-5, 140–150	124	11.8	46.61	11.65	95	49	87	546.1	22.3	500	530	7	—
580-17-5, 140–150	153	11.7	45.42	11.80	90	63	77	546.1	21.	540	515	11	—
Site 581													
581-5-3, 140–150	214	12.0	47.58	11.48	90	60	81	545.3	23.9	670	275	16	—
581-8-4, 140–150	244	10.3	48.30	11.58	90	68	180	542.1	22.9	725	160	10	—

Note: — means not determined.

[a] NO_3^- determinations when NH_4^+ is appreciable are considered unreliable.

set to the present interglacial chloride concentration. Three regimes are evident. Near the sediment surface (10 m), the forcing function is quite obvious. At intermediate depths (30 m), the concentration is dampened somewhat and has achieved a value near the mean of the forcing function. At greater depth (60 m), the concentration is considerably dampened and has a value somewhat below the mean value of the forcing function, that is, the signal has just begun to arrive.

Thus, in a present-day profile, one would expect to find a maximum at about 30 m depth (Fig. 8). Also shown are cases in which c_b has been increased and decreased 10%. With c_b increased, at present chloride is predicted to increase monotonically with depth. With c_b decreased, a subsurface maxium is still predicted; however, the shift relative to bottom water is smaller than in the case with c_b at the present interglacial chloride concentration.

I emphasize here that, although the signal is caused by glacial-interglacial cycles, it is not stratigraphic. Rather, it has penetrated from the sediment/water interface to a depth characteristic of a diffusive process acting over ~1 m.y.

Observations

The Leg 86 chloride data, normalized to the present-day sediment/seawater interfacial values, are shown in Figure 9. The pattern predicted by the model is evident. Chloride increases by about 1.5% by 40 m depth. Below that depth the concentration levels are variable, consistent with various c_b values.

Isotopic data confirm that this agreement is the result of glacial-interglacial phenomena. Profiles of $\delta^{18}O$ of the pore fluids at Sites 576 and 578 are shown in Figure 10. A maxium is apparent in both profiles. It is somewhat attenuated at Site 578. This attenuation is caused by the gradient of $\delta^{18}O$ supporting a flux toward basement (Lawrence and Gieskes, 1981), analogous to the low chloride case shown in Figure 8.

Pore-Water Migration

Steady pore-water movement should displace the peak. Some model curves incorporating an advective term in Equation 1 are shown in Figure 11. The position of the peak is sensitive to velocities on the order of 0.1 mm/yr., and the existence of the signal at Leg 86 sites sug-

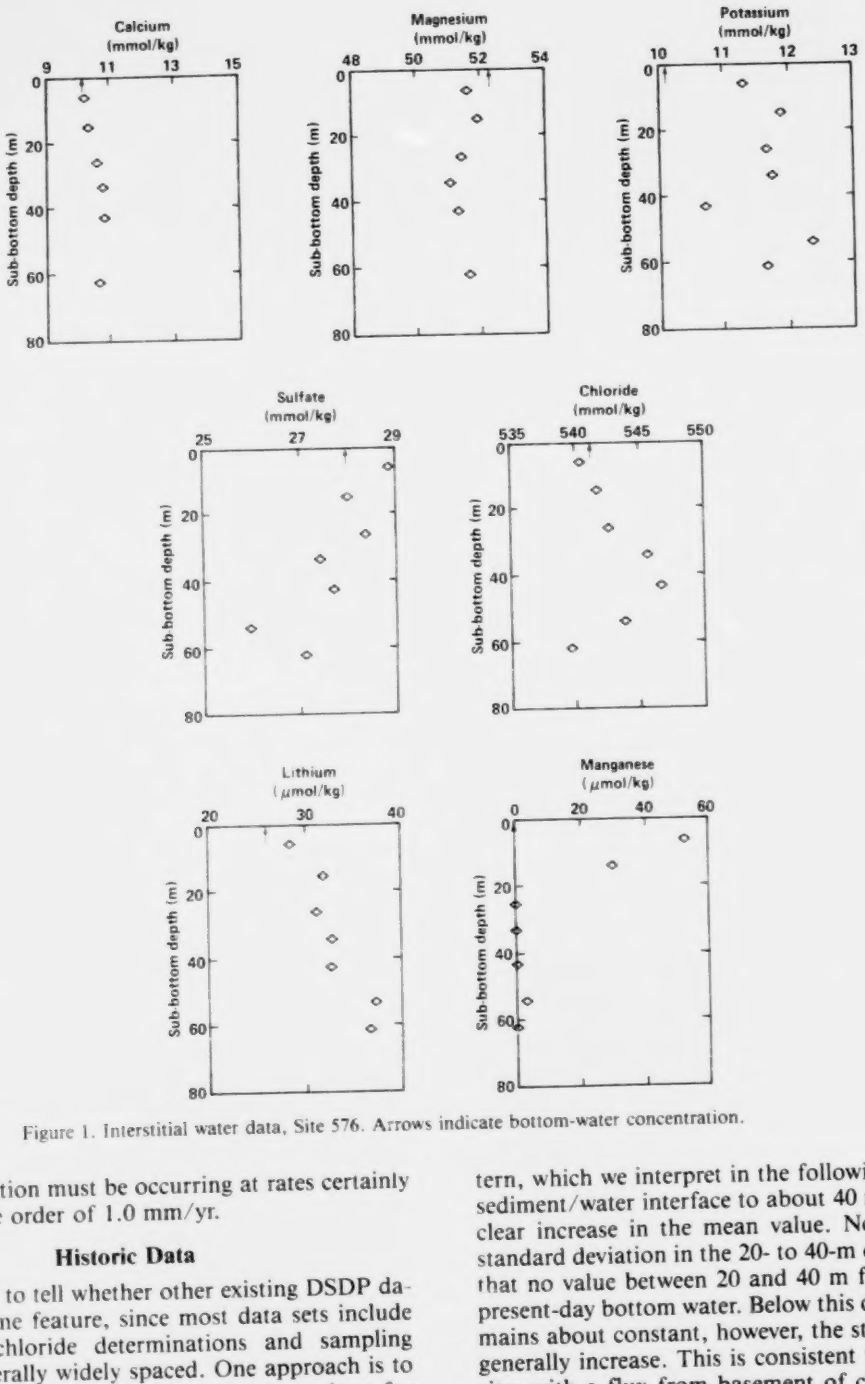

Figure 1. Interstitial water data, Site 576. Arrows indicate bottom-water concentration.

gests that advection must be occurring at rates certainly less than on the order of 1.0 mm/yr.

Historic Data

It is difficult to tell whether other existing DSDP data show the same feature, since most data sets include low-precision chloride determinations and sampling depths are generally widely spaced. One approach is to construct a composite profile. This has been done for the subset of sites identified by McDuff (1981) as having gradients of calcium and magnesium indicative of no fluid advection. Figure 12 shows the data displayed in two forms. The primary data (Fig. 12A) appear at first glance to form a shotgun pattern. However, averages over various depth intervals (Fig. 12B) show a distinct pattern, which we interpret in the following way. From the sediment/water interface to about 40 m depth there is a clear increase in the mean value. Note the very tight standard deviation in the 20- to 40-m depth interval and that no value between 20 and 40 m falls within 1% of present-day bottom water. Below this depth the mean remains about constant, however, the standard deviations generally increase. This is consistent with inclusions of sites with a flux from basement of chloride; that is, a profile of the mean less standard deviation corresponds to the no basement flux case (Fig. 8) and a profile of the mean plus the standard deviation corresponds to the basement flux case (Fig. 8). A similar result is found for $\delta^{18}O$ (Fig. 13), although the subset of sites considered is different (those included in table 1 of Lawrence and Gies-

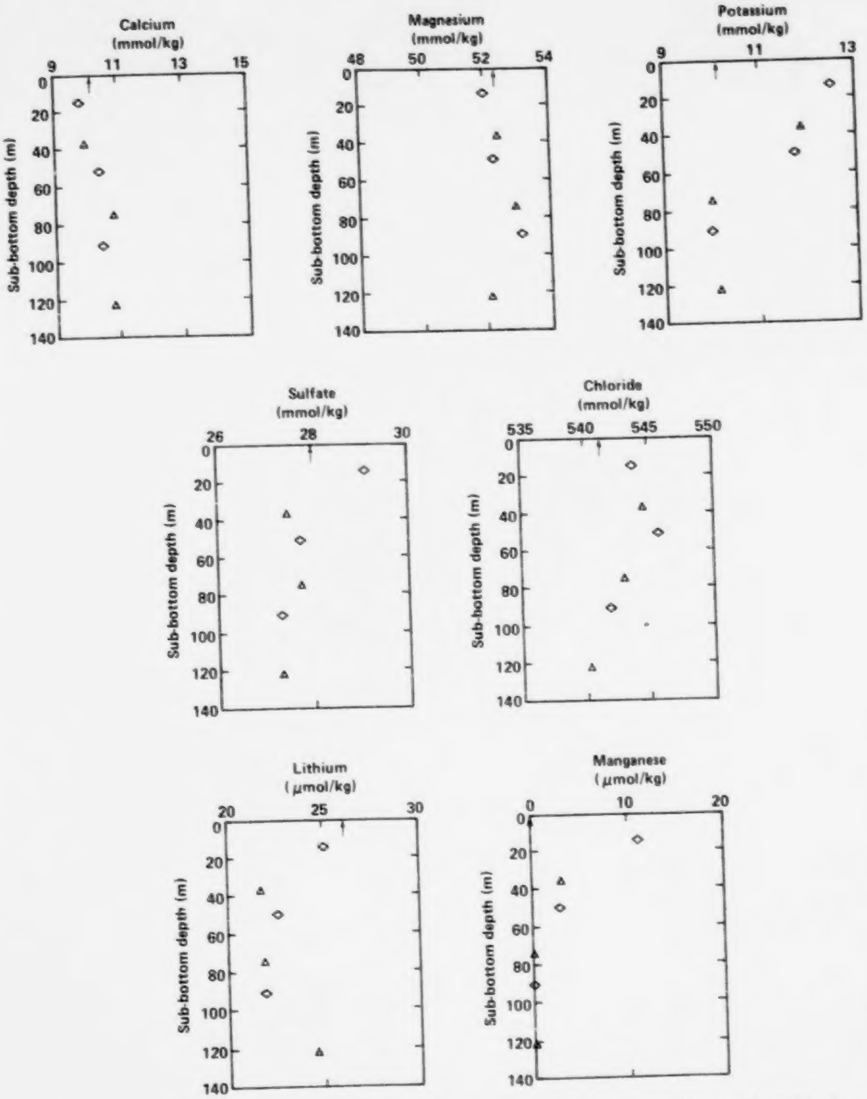

Figure 2. Interstitial water data, Site 577. Symbols: diamond = Hole 577, triangle = Hole 577A. Arrows indicate bottom-water concentration.

kes, 1981). A more comprehensive synthesis, including the implications for excess ice volume-$\delta^{18}O$ coupling, is being prepared.

Calcium and Magnesium

The gradients of calcium and magnesium encountered during Leg 86 are small relative to the range observed in DSDP cores. Site 578 exhibits the largest value, ~0.03 mmol/m, which can be contrasted with gradients as high as 0.2 mmol/m at other DSDP sites (McDuff, 1981).

Changes in the concentrations of calcium and magnesium with sub-bottom depth are generally indicative of reaction of volcanic material, either basement basalts or volcanic ash that is dispersed within the sediment column (Gieskes and Lawrence, 1981; McDuff, 1981). At the three sites with measurable gradients (Sites 578–580, Site 581 is excluded because of lack of data), Ca and Mg are linearly correlated, a feature usually resulting from conservative behavior of calcium and magnesium within the sediment column and gradients supported by diffusive fluxes from Layer 2 (McDuff and Gieskes, 1976; McDuff, 1978).

McDuff (1981) has presented a model for control of Ca and Mg gradients. To summarize, Ca is added to and Mg removed from the pore fluids of the basalts of Layer 2 by chemical reaction and lost or gained, respectively, by exchange with seawater. The thickness of sediment accumulated is critical in determining the mechanism of this exchange. One regime is characterized by thin sediment cover and lack of a Ca gradient. Two possible mechanisms can be imagined. One, previously presented, is that circulation of seawater through the sediment con-

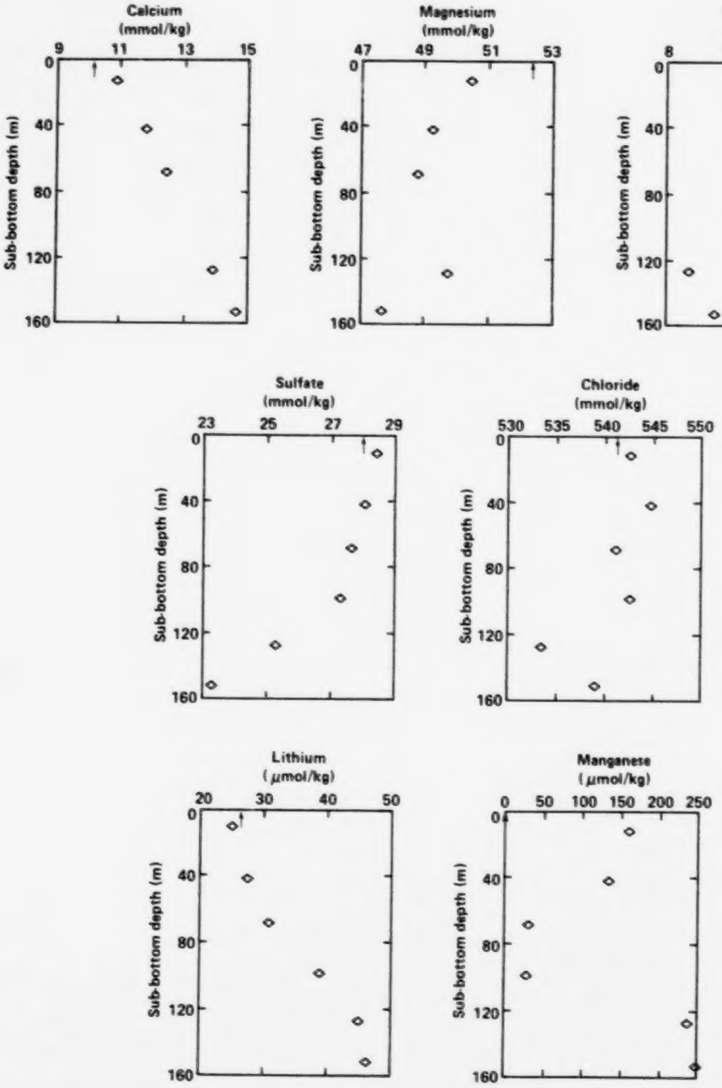

Figure 3. Interstitial water data, Site 578. Arrows indicate bottom-water concentration.

tinues at rates sufficient to obliterate gradients. There is strong evidence that this occurs in very thin sediment sections (Maris and Bender, 1982; Sayles and Jenkins, 1982). Although a moderately thin sediment cover may be sufficiently impermeable to stop fluid movement, another possible mechanism is that Layer 2 pore fluids may continue to be exchanged with seawater at basement outcrops. The profile of Ca in the sediment pore waters would then be controlled by diffusion between two seawater-dominated end members. The other regime is characterized by thicker sediments and the presence of Ca gradients. Transport through the sediment column is by diffusion (McDuff and Gieskes, 1976). Oxygen-isotope mass balances (Lawrence and Gieskes, 1981) and physical factors (McDuff, 1981) suggest that convection within Layer 2 continues to support these diffusive fluxes.

Some aspects of Leg 86 results are difficult to interpret within this framework. Relevant parameters are summarized in Table 4. Drilling generally penetrated a small fraction of the sediment cover inferred from seismic results, with the exception of Site 579. The seismic results commonly contain evidence of chert horizons, sampled at several of the sites. The very low rate of diffusion of solutes through these horizons makes meaningful comparison of the observed fluxes to DSDP sites difficult. To some extent the concentration of solute in deeper layers will increase in response to the reduced transport through chert horizons stabilizing the flux; however, solubility prevents this concentration feedback from occurring on a compensating basis. The net result is a lower gradient in the upper sediments relative to sites without silicification. A good example of this phenomenon is the Ca profile at Site 356 (McDuff, 1978).

The chemistry observed at Leg 86 sites is quite similar to that of other DSDP sites. Figure 14 shows the values of $\Delta Ca/\Delta Mg$ as a function of the Ca gradient and, for

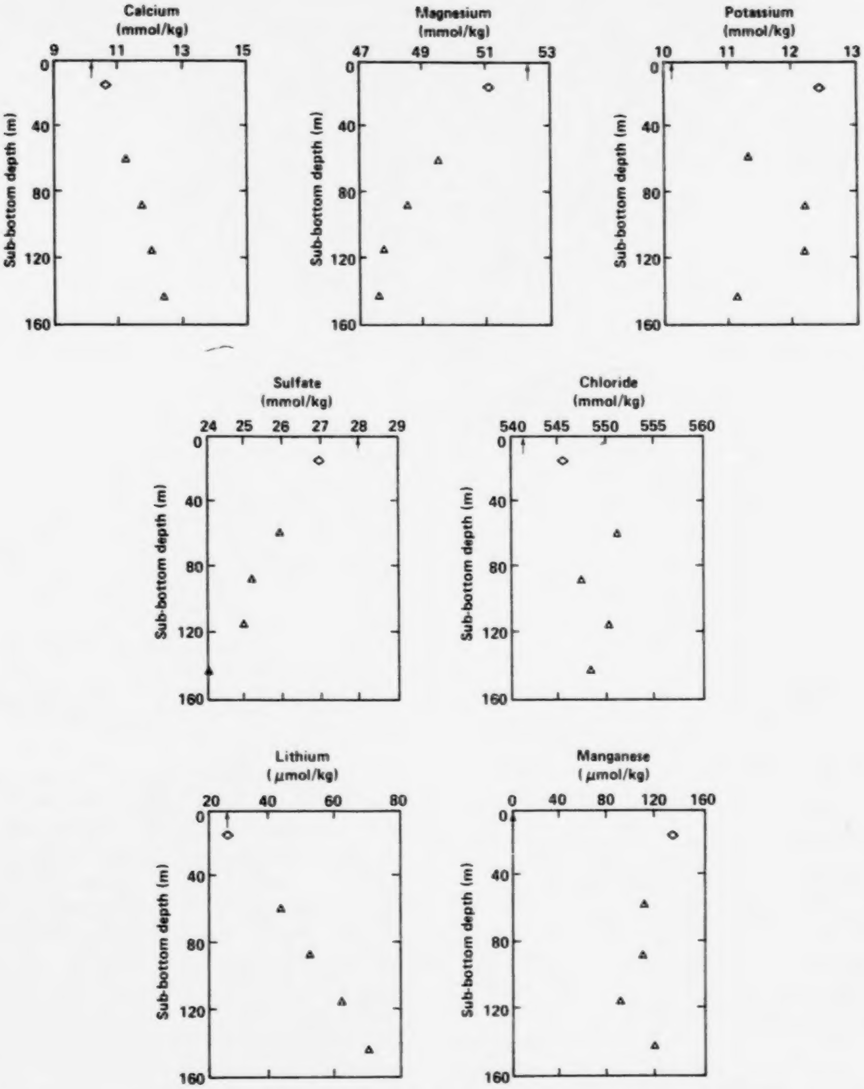

Figure 4. Interstitial water data, Site 579. Symbols: diamond = Hole 579, triangle = Hole 579A. Arrows indicate bottom-water concentration.

comparison, the linear relation found for Legs 1-53 (McDuff, 1981). At the extremely low fluxes characteristic of Leg 86 sites, Ca increases are much smaller than Mg decreases. This is consistent with the concept that, at low rates of basalt hydrolysis, magnesium must be supplied to counterbalance release of both excess calcium and sodium (McDuff, 1981).

Redox Species

The discussion of redox species is necessarily limited since shipboard participation would be required to produce reliable data for the full suite of important redox species. Our results include measurement of NO_3^-, NH_4^+, Mn^{2+}, and SO_4^{2-}. Some artifacts may be introduced by analyzing for NO_3^- and NH_4^+ approximately 1 yr. after sample collection. There is no visual evidence for extensive biological uptake in the samples; however, some bacterial oxidation of NH_4^+ present at several hundred micromoles per kilogram in many of the samples is the probable source of non-zero NO_3^- determinations.

Recently there has been much progress in understanding the sequence of redox reactions that occurs in the upper tens of centimeters of marine sediments (Froelich et al., 1979; Jahnke et al., 1982). This sequence is driven by the relatively constant flux of organic carbon to the sediments. Generally the utilization of terminal electron acceptors follows the order of free energy that can be derived, that is O_2 before NO_3^-, before or concurrent with MnO_2, before FeOOH, before SO_4^{2-}, before CO_2. At high sedimentation rates, the complete sequence can be found in a short core, whereas at lower sedimentation rates O_2 may be present even to the base of the sam-

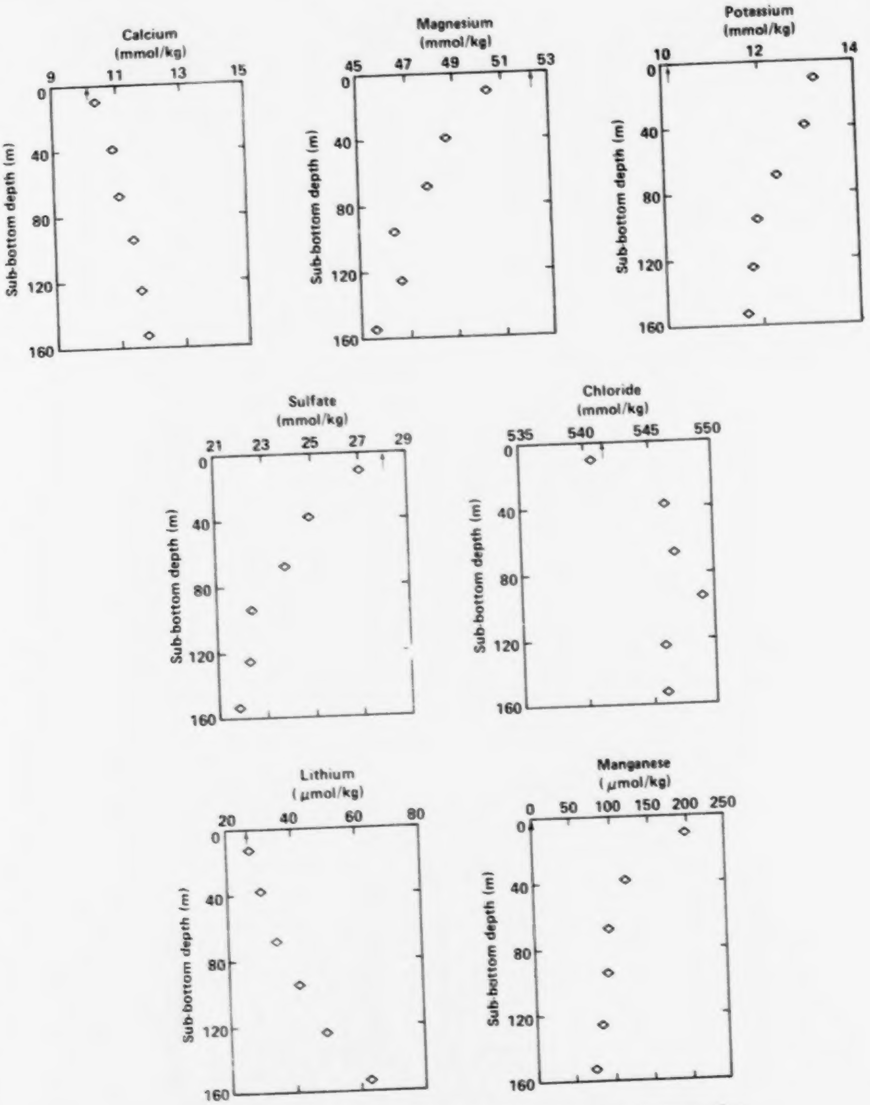

Figure 5. Interstitial water data, Site 580. Arrows indicate bottom-water concentration.

pled interval. In cores of similar sedimentation rate, secondary processes such as bioturbation can play an important role (Emerson et al., 1985).

The rate of sedimentation, and proportionally the supply of organic material, varies significantly in drill cores. Accordingly, while this sequence of utilization will be followed at a particular horizon, historic variations in sedimentation rate will influence the level within the sequence attained. At most Leg 86 sites, sedimentation has increased dramatically in Pliocene–Pleistocene times, as indicated in Table 1. Thus, one would expect the greatest progress through the sequence in the youngest sediments. An additional factor in older sediments is diffusion from either above or below, which may modify the signal. Other factors may also be of importance, especially for manganese. Gieskes (1981) noted a dissolved manganese-dissolved silica correlation which he attributes to either association of Mn-oxides with siliceous material or availability of organic carbon in siliceous horizons. Boyle (1983) discussed the role of carbonate coatings in Mn cycling, especially in immobilizing Mn^{2+} released during suboxic diagenesis.

Most features of the Leg 86 results can be understood in the above context. (1) NO_3^- is enriched relative to bottom seawater in Site 576 sediments, a sign of oxic diagenesis and consistent with the slow rate of sedimentation. At all other sites NO_3^- is depleted in the uppermost sediments. Because of the high NH_4^+ concentration at deeper levels, it would be hazardous to assign significance to other results except to note that concentrations are probably very low *in situ*. (2) Mn^{2+} is strongly enriched in the upper sediments at all sites except Site 577. This is consistent with the suggestion of Boyle (1983) that carbonates can serve to immobilize Mn^{2+}. At deeper

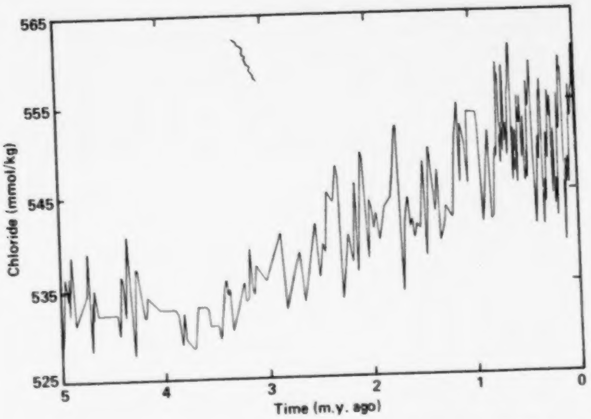

Figure 6. Chloride as a function of time used in model calculations. The curve parallels $\delta^{18}O$ as a function of time assuming that chloride is elevated 3.7‰ at maximum glaciation (~150 m of sea-level change). The $\delta^{18}O$ record used is a composite of the smoothed stacked record of SPECMAP (Imbrie et al., 1984) for the interval 0–0.8 m.y. ago and the measurements of Shackleton and Cita (1979) for the interval 5.0–0.8 m.y. ago. The Shackleton and Cita measurements have been converted to the standard deviation scale using the mean and standard deviation of their measurements in the interval 0–0.8 m.y. ago and have been interpolated between points to give a spacing of 2000 yr. No correction has been made for possible bottom-water temperature differences, which may be significant in the early parts of the record. These will have little effect on the computed chloride profiles, however.

levels Mn^{2+} enrichment is generally lower or absent, the exception being the substantial increase in Mn^{2+} concentration at the base of Site 578. Note at this horizon the very sharp gradient of sulfate. There are few data to support the Mn–Si association noted by Gieskes (1981). For example, at Site 578 the lowest Mn^{2+} concentrations occur at the level with the highest Si concentrations. (3) The SO_4^{2-} profiles are unremarkable. Gradients are generally steeper at sites with higher sedimentation rates. An interesting feature appears in the sulfate profiles at Sites 576 and 577. The sedimentation rate is lowest at these two sites. Sulfate values at both sites are in excess of bottom water in the uppermost sample. This may represent the same kind of effect as seen in the chloride data, recognizing that the diffusivity of sulfate is much lower so that the maximum is found closer to the sediment/water interface and will decay more slowly from the latest influence of glacial conditions. This requires conservative behavior of sulfate in these shallow sediments, consistent with the low sedimentation rate.

Other Constituents

Strontium

Only carbonate-bearing sediments from Site 577 exhibit a gradient of Sr, reaching a maximum value ~1.8 × seawater at 50 m depth. This shallow maximum does not conform to the models of Gieskes (1981) and Baker et al. (1982). First, the maximum occurs nearly a factor of ten shallower than the communication length (ratio diffusion coefficient to sedimentation rate, Gieskes, 1981). To some extent this may be the result of the Pliocene-Pleistocene increase in sedimentation rate. Second, the Sr/Ca ratio achieved is much below the equilibrium ratio of ~5 × seawater for these pore waters (Baker et al., 1982).

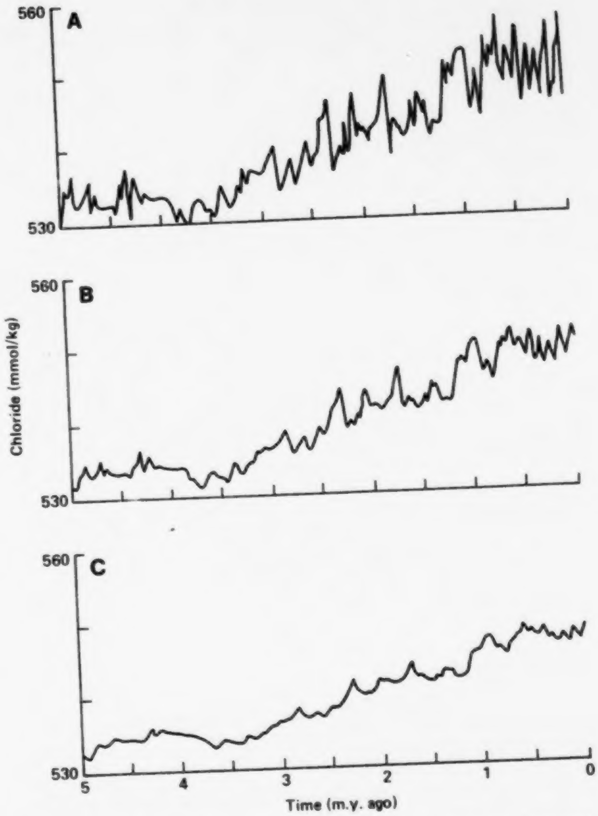

Figure 7. Model chloride curves versus time at (A) 10 m, (B) 30 m, and (C) 60 m sub-bottom depth computed as described in text. Note that the magnitude of the shift depends on the assumption made as to sea level. See caption of Figure 6.

Lithium

Gieskes (1981) noted an association of Li enrichment with Si enrichment and has commented on the contrasting chemistries of Li and K. The data for Sites 578–580 generally agree with these ideas. Site 577, with predominantly carbonate sediment, shows no significant Si enrichment and slightly decreasing Li values. Site 576 exhibits a much different pattern. Si is significantly elevated in the upper sediment with little influence on Li. As depth increases, Si decreases while Li increases. Drilling was terminated at a chert horizon, perhaps supporting a downward flux of Si and exclusion of Li as silicification proceeds.

ACKNOWLEDGMENTS

I thank Ms. Barbara Paul and Mr. Ron Citterman for assistance in the laboratory. Dr. Peter Grootes and Dr. Paul Quay of the Quaternary Isotope Laboratory, University of Washington facilitated the oxygen-isotope determinations. Ms. Trudy Rasp and Ms. Shirley Patterson prepared versions of the manuscript. This manuscript was reviewed by James Lawrence and Joris Gieskes. This research was

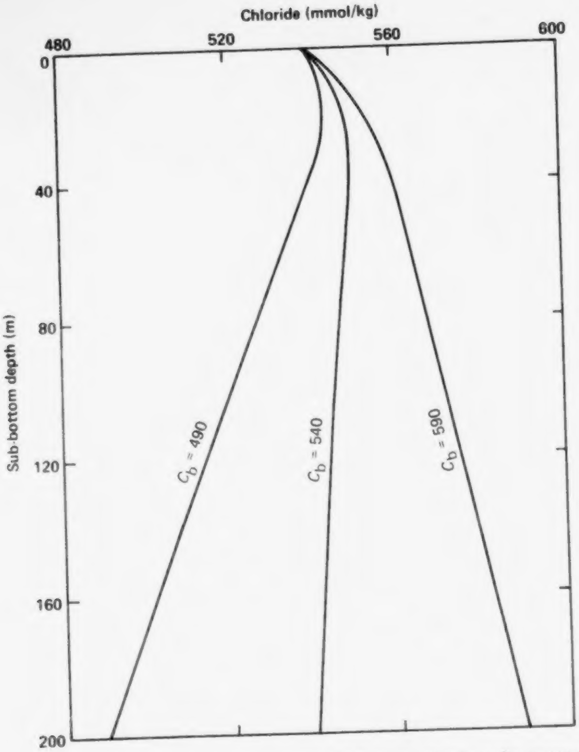

Figure 8. Model chloride curves versus sub-bottom depth at the present time for three different values of c_b. Note that the magnitude of the shift depends on the assumption made as to sea level. See caption of Figure 6.

supported by Sandia National Laboratories (Contracts 26-6612 and 47-5696). This is University of Washington School of Oceanography Contribution No. 1427.

REFERENCES

Anderson, R. N., Hobart, M. A., and Langseth, M. G., 1979. Geothermal convection through oceanic crust and sediments in the Indian Ocean. *Science*, 204:828–832.

Baker, P. A., Gieskes, J. M., and Elderfield, H., 1982. The distribution of Sr^{2+} during diagensis of pelagic carbonate rocks—isotopic, chemical, and experimental evidence. *J. Sediment. Petrol.*, 52: 71–82.

Boyle, E. A., 1983. Manganese carbonate overgrowth on foraminifera tests. *Geochim. Coschim. Acta*, 47:1815–1819.

Emerson, S., Fischer, K., Reimers, C., and Heggie, D., 1985. Organic carbon dynamics and preservation in deep sea sediments. *Deep Sea Res.*, 32:1–22.

Epstein, S., and Mayeda, T., 1953. Variations in the ^{18}O content of water from natural sources. *Geochim. Cosmochim. Acta*, 4: 213–224.

Froelich, P. N., Klinkhammer, G. P., Bender, M. L., Luedtke, N. A., Heath, G. R., Cullen, D., Dauphin, P., Hammond, D., and Hartman, B., 1979. Early oxidation of organic matter in pelagic sediments of the eastern equatorial Atlantic: suboxic diagenesis. *Geochim. Cosmochim. Acta*, 43:1075–1090.

Gardner, W. S., Wynne, D. S., and Dunstan, W. M., 1976. Simplified procedure for the manual analysis of nitrate in seawater. *Mar. Chem.*, 5:393–396.

Gieskes, J. M., 1974. Interstitial water studies, Leg 25. *In* Simpson, E. S. W., Schlich R., et al., *Init. Repts. DSDP*, 25: Washington (U.S. Govt. Printing Office), 361–394.

________, 1981. Deep-sea drilling interstitial water studies: implications for chemical alteration of the oceanic crust, layers I and II. *Soc. Econ. Paleontol. Mineral. Spec. Publ.*, 32:149–167.

Gieskes, J. M., and Lawrence, J. R., 1976. Interstitial water studies, Leg 35. *In* Hollister, C. D., Craddock, C., et al., *Init. Repts. DSDP*, 35: Washington (U.S. Govt. Printing Office), 407–424.

________, 1981. Alteration of volcanic matter in deep sea sediments: evidence from the chemical composition of deep sea drilling cores. *Geochim. Cosmochim. Acta*, 45:1687–1703.

Imbrie, J., Hays, J. D., McIntyre, A., Mix, C., Morley, J. J., Martinson, D. G., Pisias, N. G., Prell, W. L., and Leinen, M., 1984. The orbital theory of Pleistocene climate: support from a revised chronology of the marine $\delta^{18}O$ record. *In* Berger A., Imbrie, J., Hays, J., Kukla, G., and Saltzman, B. (Eds.), *Milankovitch and Climate*: Dordrecht (Reidel).

Jahnke, R., Emerson, S., and Murray, J. W., 1982. A model of oxygen reduction, denitrification, and organic matter mineralization in marine sediments. *Limnol. Oceanogr.*, 27:610–623.

Lawrence, J. R., and Gieskes, J. M., 1981. Constraints on water transport and alteration in the oceanic crust from the isotopic composition of pore water. *J. Geophys. Res.*, 86:7924–7934.

McDuff, R. E., 1978. Conservative behavior of calcium and magnesium in the interstitial waters of marine sediments: identification and interpretation [Ph.D. dissert.]. University of California, San Diego.

________, 1981. Major cation gradients in DSDP interstitial waters: the role of diffusive exchange between seawater and upper oceanic crust. *Geochim. Cosmochim. Acta*, 45:1705–1713.

McDuff, R. E., and Gieskes, J. M., 1976. Calcium and magnesium profiles in DSDP interstitial waters: diffusion or reaction. *Earth Planet. Sci. Lett.*, 33:1–10.

Mann, R., and Gieskes, J. M., 1975. Interstitial water studies, Leg 28. *In* Hayes, D. E., Frakes, L. A., et al., *Init. Repts. DSDP*, 28: Washington (U.S. Govt. Printing Office), 805–814.

Maris, C. R. P., and Bender, M. L., 1982. Upwelling of hydrothermal solutions through ridge flank sediments shown by pore water profiles. *Science*, 216:623–626.

Sayles, F. L., and Jenkins, W. J., 1982. Advection of pore fluids through sediments in the equatorial east Pacific. *Science*, 217:245–248.

Sayles, F. L., and Manheim, F. T., 1975. Interstitial solutions and diagenesis in deeply buried marine sediments: results from the Deep Sea Drilling Project. *Geochim. Cosmochim. Acta*, 39:102–127.

Shackleton, N. J., and Cita, M. B., 1979. Oxygen and carbon isotope stratigraphy of benthic foraminifers at Site 397: detailed history of climatic change during the late Neogene. *In* von Rad, U., Ryan, W. B. F., et al., *Init. Repts. DSDP*, 47, Pt 1: Washington (U.S. Govt. Printing Office), 433–445.

Date of Initial Receipt: 23 November 1983
Date of Acceptance: 13 July 1984

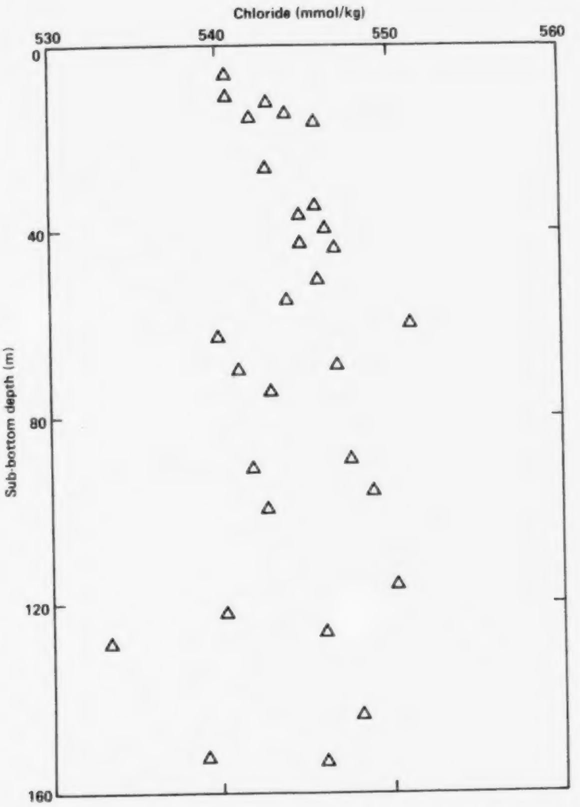

Figure 9. Composite of chloride versus sub-bottom depth for Leg 86. In accord with the model curves (Fig. 8), chloride increases ~1% by 40 m depth before assuming values controlled by diffusion from below. Note that the concentration scale is considerably expanded as compared to Figure 8.

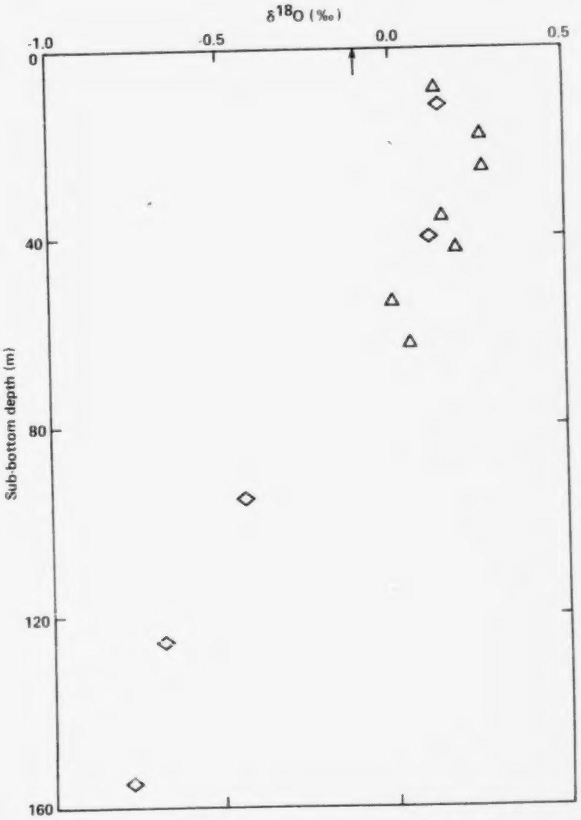

Figure 10. $\delta^{18}O$ versus sub-bottom depth for Sites 576 and 578. Symbols: diamond = Site 578, triangle = Site 576. Arrow indicates bottom-water value.

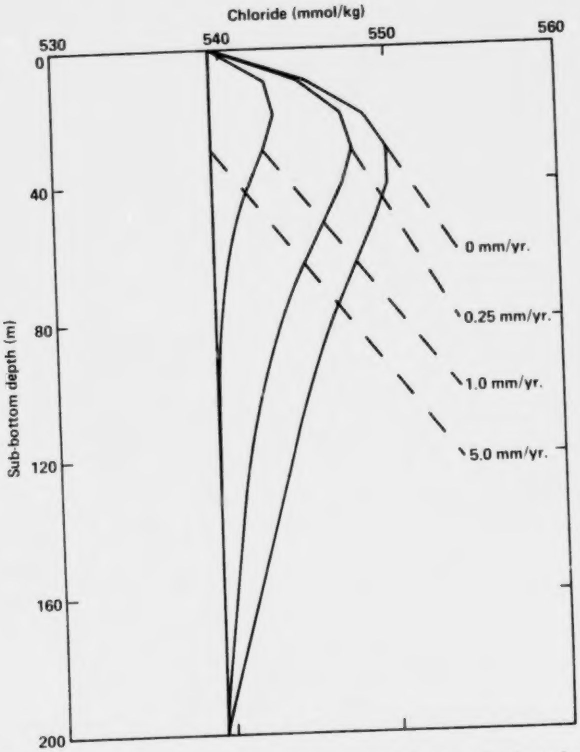

Figure 11. Model curves of chloride versus sub-bottom depth at the present time for different values of upward advection rate. Velocities of the order 1.0 mm/yr. shift the maximum upward and reduce its magnitude. Higher velocities eliminate the signal entirely.

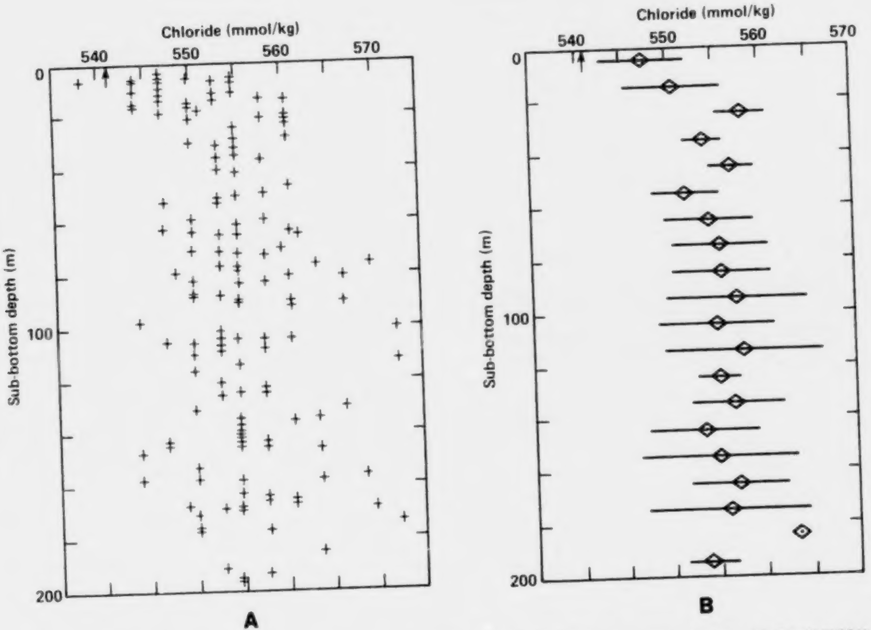

Figure 12. Composite of chloride versus sub-bottom depth for DSDP sites summarized by McDuff (1981) (A) Raw data. (B) Means and standard deviations in 10-m depth intervals. Note especially the tight standard deviation at about 40 m depth and that no value falls below 550 mmol/kg between 20 and 50 m depth. Typical deep waters have Cl = 541 mmol/kg (arrow).

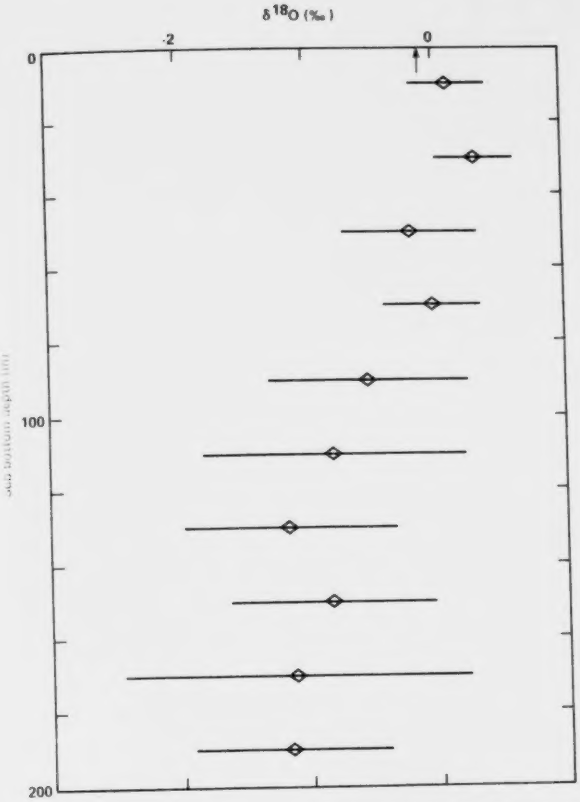

Figure 13. Composite of $\delta^{18}O$ versus sub-bottom depth for DSDP sites summarized by Lawrence and Gieskes (1981) and expressed as means and standard deviations in 20-m depth intervals. Note the slight maximum at 20–40 m depth. Arrow indicates bottom-water value.

Table 4. Parameters relating to Ca and Mg, Leg 86.

Site	Deepest sample (m)	ΔCa (mmol/kg)	ΔMg (mmol/kg)	$-\Delta$Ca/ΔMg	Ca gradient (mmol/kg/m)
576	62	0	0	—	0
577	121	0	0	—	0
578	152	+5	−5	1.0	0.03
579	143	+2	−5	0.4	0.02
580	153	+2	−7	0.3	0.01

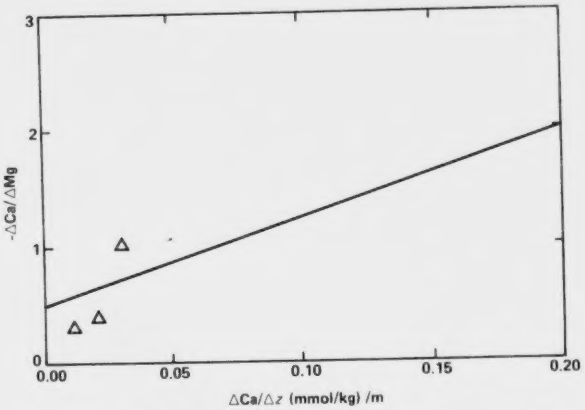

Figure 14. $-\Delta Ca/\Delta Mg$ versus $\Delta Ca/\Delta z$. Points are for sites with gradients, see Table 4. Line is trend for DSDP Legs 1–53 summarized by McDuff (1981) (sites with gradients, Ca and Mg linearly correlated).

PART V: IGNEOUS PETROLOGY

32. PETROLOGY AND GEOCHEMISTRY OF BASALTS FROM DEEP SEA DRILLING PROJECT LEG 86, SITE 581[1]

John C. Fountain, Robert D. Jacobi, and Timothy J. Fahey, State University of New York at Buffalo[2]

ABSTRACT

Approximately 5 m of aphyric to sparsely phyric basalt was recovered from Hole 581, the only hole on Leg 86 where basement was cored. The occurrence of samples with altered glassy rinds indicates that at least three cooling units (pillows or thin flows) were sampled. The samples were moderately to intensely altered; groundmass crystals are generally fresh, but all glass is altered. Alteration is greatest in vesicular samples, but most of the samples have fractures filled with iron oxyhydroxide, clay, and/or calcite.

All 13 samples analyzed are moderately fractionated aluminous N-type mid-ocean ridge basalts. The samples can be divided into two groups based on TiO_2 and FeO contents. The least-evolved group may be derived from a more primitive mid-ocean ridge basalt by the crystallization of 18% plagioclase, 24% clinopyroxene, and 3% olivine. The more evolved group may be derived from the first group by the fractionation of 18% plagioclase, 11% clinopyroxene, and 3% olivine. However, higher Ce/Yb ratios in the more evolved group cannot be produced by fractionation and thus we must invoke a more complex process such as dynamic melting to relate the two groups to a common source.

INTRODUCTION

Igneous basement was cored in only one hole on Deep Sea Drilling Project (DSDP) Leg 86, at Site 581 (Fig. 1). On the basis of magnetic lineations at this site, the basement age has been estimated to be 116 m.y. (see Site 581 chapter, this volume). Southwest of Site 581, slightly older basalts were recovered at Sites 303, 304, and 307 during Leg 32 (Marshall, 1975). The crust at both Site 581 and the Leg 32 sites was generated by the Japanese spreading center, which has since been subducted (Larson and Chase, 1972). The three Leg 32 sites provide the only published data on the composition of ridge-generated basaltic ocean crust in the Northwest Pacific.

Site 581 was drilled again on Leg 88 (Holes 581A, 581B, and 581C) and more basalt was recovered. This chapter includes data only for the Leg 86 samples (Hole 581).

Cores recovered from Site 581 include about 5 m of aphyric to sparsely phyric basalt in Core 19, from a subbottom depth of about 343 m. Several vesicular samples with altered glassy rinds and fine-grained interiors were recovered from the central portion of this core; elsewhere the samples were generally fine grained. The presence of samples with chilled rinds suggests that at least three cooling units were sampled; J. Natland, from examination of other samples of this core, has identified at least eight cooling units (J. Natland, written communication, 1984). Representative samples, spanning the entire igneous portion of the core, were examined in thin section and analyzed for major-element composition and for selected trace-element abundances.

EXPERIMENTAL METHODS

Abundances of major elements were determined using the U.S. Geological Survey (USGS) "rapid" analysis techniques (Shapiro, 1975). Accuracy and precision of these analyses have been reported by Clemency and Borden (1978). Concentrations of rare-earth elements were determined by isotope-dilution mass spectrometry on a 12-in. radius-of-curvature National Bureau of Standards-type mass spectrometer. Samples were dissolved with lithium metaborate and the rare-earth elements isolated by ion exchange using procedures developed at State University of New York, Stony Brook (Vocke, 1983). Precision of rare-earth element determinations is better than 2%.

Abundances of all other trace elements were determined by X-ray fluorescence using pressed-powder pellets. Empirical matrix-correction factors were derived from a suite of international reference standards.

RESULTS

The samples from Hole 581 are aphyric to sparsely phyric tholeiitic basalts. Plagioclase (An 65-70) is the most common microphenocryst (Table 1). Augite microphenocrysts are present in a few samples, while olivine microphenocrysts are rare. Minor amounts of iddingsite, presumably a product of the alteration of olivine, were found in most samples, but there is no evidence that olivine was a major phenocryst phase in any sample.

Groundmass crystals are generally fresh; however, the high water contents and high ferric iron to ferrous iron ratios indicate that all samples have been significantly altered. Alteration is greatest in vesicular samples, but most of the samples have fractures filled with iron oxyhydroxide, clay, and/or calcite. These veins are extensive in several samples, contributing several percent to their bulk composition.

Chemical analyses were performed on the least-altered portions of each sample; generally only the interior por-

---

[1] Heath, G. R., Burckle, L. H., et al., *Init. Repts. DSDP*, 86: Washington (U.S. Govt. Printing Office).

[2] Address: (Fountain, Jacobi, Fahey) Department of Geological Sciences, State University of New York at Buffalo, 4240 Ridge Lea Road, Amherst, NY 14226.

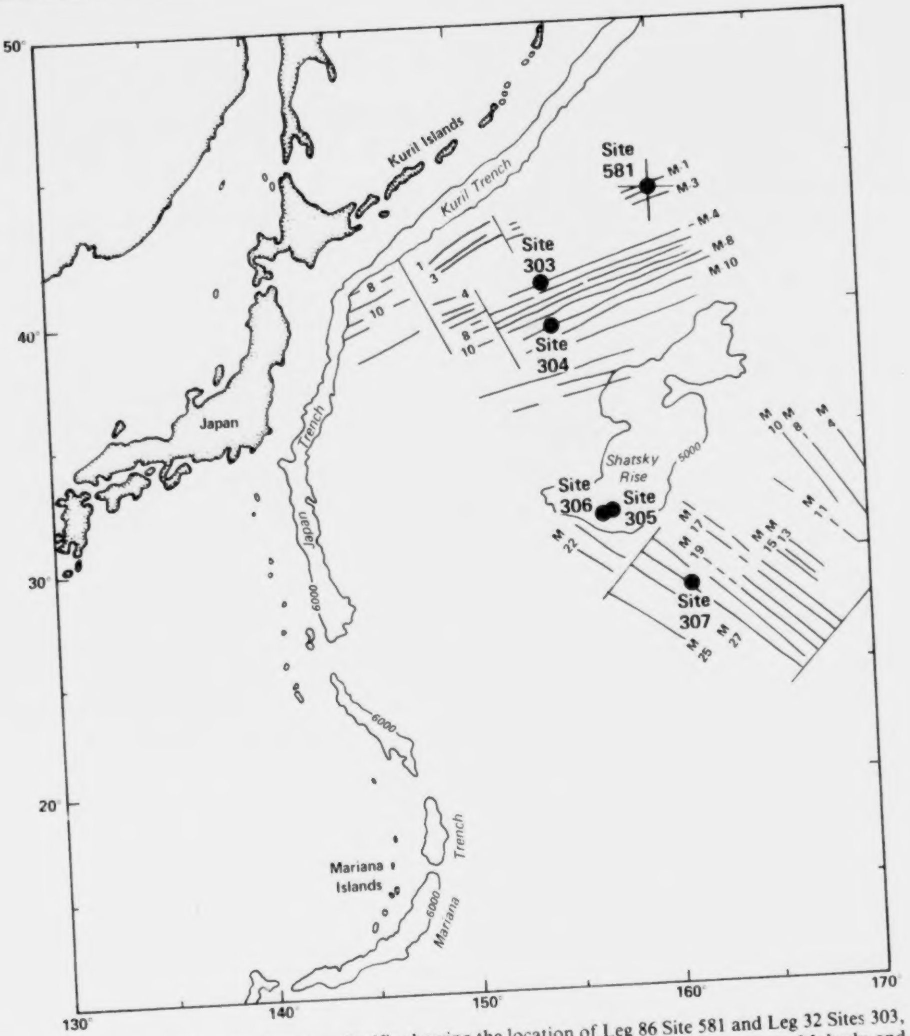

Figure 1. Chart of the northwestern Pacific showing the location of Leg 86 Site 581 and Leg 32 Sites 303, 304, 305, 306, and 307, magnetic lineations and major physiographic features. From Moberly and Larson (1975).

tions of the samples were analyzed since the glassy margins were significantly altered.

The major-element compositions of the samples are typical for slightly fractionated mid-ocean ridge basalts (MORBs), with slightly higher than average Al_2O_3 contents (Table 2). The samples can be divided into two distinct groups based on composition. Group I consists of Samples A and B (the uppermost samples in the core); Group II includes the other 11 samples. The Group II samples are very similar in composition, considering the extent of alteration of the samples. Group I samples have lower levels of TiO_2, FeO^*, and P_2O_5, and hence are more primitive than Group II samples. There are no systematic variations in composition within Group II. Elements with similar geochemical behavior do not show parallel variations, nor is there any regularity in variation in composition with stratigraphic position within the group. The lack of coherence among elements in Group II samples indicates that any variation in composition due to magmatic differentiation is so small that it either is obscured by alteration or is less than the precision of the analyses.

All samples analyzed show typical N-type MORB light-rare-earth element depletion (Fig. 2), and all are within the range of N-type MORBs reported by Sun et al. (1979). The Group I samples have lower rare-earth element abundances and a lower Ce/Yb ratio than the more evolved Group II samples. As with the major elements, all Group II samples have similar rare-earth element abundances.

The distribution of Ni, Cr, Zr, and Rb is also consistent with the previously developed hypothesis that Group I samples are more primitive than Group II samples. The incompatible elements Zr and Rb are higher in Group II samples, while the compatible elements Ni and Cr are higher in the more primitive Group I samples. The average Sr content of Group I is lower than the average of Group II samples; however, the range of the two groups

Table 1. Petrographic summary of samples from Hole 581, DSDP Leg 86.

Sample	DSDP sample no.	Description
A	581-19-1, 23–27 cm	Aphanatic basalt with sparse plagioclase microphenocrysts and one olivine microphenocryst. Intersertal devitrified brown glass contains ~15% plagioclase microlites.
B	581-19-1, 54–63 cm	Aphanitic basalt with ~1% plagioclase microphenocrysts (<0.5 mm), plus rare olivine and clinopyroxene microphenocrysts. An intersertal matrix of brown glass contains ~40% plagioclase microlites and sparse pyroxene.
C	581-19-1, 126–131 cm	Aphanitic basalt containing 15% plagioclase microlites and 1% relict olivine in a matrix of brown glass.
D	581-19-2, 10–17 cm	Fine grained vesicular basalt; 5% plagioclase microlites and 1% olivine in an extremely weathered matrix of brown glass.
E	581-19-2, 23–26 cm	Fine grained basalt containing sparse plagioclase microphenocrysts (<0.5 mm) and 5% plagioclase microlites in a matrix of red–brown glass.
F	581-19-2, 49–53 cm	Fine grained vesicular basalt with an intersertal matrix of brown glass containing 10% plagioclase microlites.
G	581-19-2, 83–88 cm	Aphanitic basalt containing 4% plagioclase phenocrysts (0.5 mm) in a groundmass of 5% plagioclase microlites, and scattered relict olivine microlites. A red devitrified glassy matrix contains a large calcite-filled vein.
H	581-19-2, 93–103 cm	Aphanitic vesicular basalt with sparse plagioclase microphenocrysts in a groundmass of plagioclase microlites and weathered brown glass.
I	581-19-3, 3–7 cm	Aphanitic intersertal basalt with 5% plagioclase microphenocrysts and <1% olivine microphenocrysts (now altered) in a brown glass matrix.
J	581-19-3, 48–58 cm	Aphanitic basalt consisting of 70% plagioclase and clinopyroxene microlites and brown glass.
K	581-19-3, 66–71 cm	Aphanitic basalt containing 1% plagioclase microphenocrysts (<1 mm), in a groundmass of plagioclase and rare clinopyroxene microlites.
L	581-19-3, 104–111 cm	Fine grained intersertal basalt containing 15% plagioclase crystals, and some clinopyroxene, in brown glass.
M	581-19-4, 48–54 cm	Aphanitic intersertal basalt with 70% plagioclase microlites and clinopyroxene in a brown–green glass matrix.

Note: The glass in all samples was altered, and most samples contained minor iddingsite. Note that the sample designation used in this study (A–M) is arranged by increasing depth in the core.

overlaps. The considerable range in the Sr and Rb abundances is much greater than that of other trace elements and thus is most likely due to alteration.

DISCUSSION

Comparison of Group I and Group II samples shows exactly the differences expected from low-pressure fractionation (Clague and Bunch, 1976, and the references therein). Since the stratigraphically highest samples (and hence presumably the youngest) are the least fractionated, it is unlikely that the entire suite of samples were derived by fractionation of a single magma batch. Furthermore, there are no large phenocrysts in the suite.

Calculation of major-element fractional crystallization models (Table 3) indicates that a magma with the composition of an average Group II sample can be derived from a magma of Group I composition by the removal of 18% plagioclase, 10% clinopyroxene, and 3% olivine. Plagioclase and pyroxene are also the most abundant microphenocrysts in the suite. Similar results have been reported for other fractionated MORB suites (Clague and Bunch, 1976; Mattey and Muir, 1980).

The Group I samples clearly have also undergone significant fractionation prior to their eruption. Model results indicate that a magma of the composition of Group I could be derived from the least-evolved basalt associated with the Siqueros Fracture Zone (an area with a well-documented ferrobasalt suite; Batiza et al., 1977) by the removal of 3% olivine, 24% augite, and 18% plagioclase (Table 3).

In view of the extent of alteration of our samples, the numerical solutions to the fractional crystallization models are not as significant as the general pattern of fractionation. Alteration has clearly affected the major-element compositions, and relatively small changes in the composition of the parent and daughter compositions used in a least-squares fractionation model can produce comparatively large changes in the calculated models.

To investigate the variation in model results caused by the alteration of the samples, models for the derivation of each of the samples in Group II were calculated. Models with acceptable correspondence could not be calculated for all flows. Samples with high CaO generally could not be modeled successfully because of large errors in the calculated Ca content since both plagioclase and clinopyroxene have high Ca contents. The proportion of plagioclase to pyroxene in the calculated models varied from about 1:1 to 2:1 as the olivine component increased. Olivine was never a major fractionating phase because removal of olivine results in rapid MgO depletion. The extent of MgO depletion is reduced if plagioclase (a MgO-free phase) is also removed. However, calculations indicate that no more than 5% olivine removal can be involved in the evolution of any of the Group II samples from a magma of Group I composition.

The extent of crystallization required by the models is dependent on all oxides. However, since TiO_2 shows the largest relative change between the groups and is highly resistant to alteration, the fit of TiO_2 was considered the best indicator of fractionation. Since TiO_2 increased by between 30 and 40% between Groups I and II, a minimum 20 to 30% crystallization is required to derive the Group II compositions.

Trace-element variations between Group I and Group II are generally qualitatively consistent with the fractional crystallization model derived from the major-element abundances, but the increase in Ce/Yb ratio between Groups I and II is not. Because Ce and Yb crystal/liquid partition coefficients are small, fractional crystallization will not induce large changes in the Ce/Yb ratio (Gast, 1968, Langmuir et al., 1977). In typical fractionated MORB suites, rare-earth element abundances increase smoothly with fractionation, with little change in the Ce/Yb ratio (Schilling et al., 1976; Humphris et al.,

Table 2. Chemical analyses of basalt samples from DSDP Leg 86, Hole 581.

Oxide (%)	A	B	C	D	E	F	G	H	I	J	K	L	M
SiO_2	49.94	50.16	49.81	49.45	49.68	50.07	49.94	49.81	50.47	49.90	49.91	49.05	49.19
TiO_2	1.33	1.34	1.83	1.74	1.82	1.81	1.85	1.76	1.81	1.82	1.79	1.84	1.79
Al_2O_3	16.12	16.17	15.85	15.53	15.61	15.85	15.89	15.38	16.22	15.75	15.85	16.51	15.52
Fe_2O_3	4.26	3.64	5.11	5.37	4.95	4.25	5.42	5.38	4.79	3.72	3.95	4.94	5.26
FeO	4.37	4.43	4.92	5.93	5.76	4.99	4.25	5.12	4.97	5.36	4.67	4.71	4.66
MnO	0.15	0.15	0.21	0.22	0.21	0.19	0.17	0.21	0.19	0.18	0.20	0.22	0.15
MgO	8.15	8.38	7.36	7.08	7.32	7.62	7.26	7.02	7.36	7.68	8.18	7.92	7.64
CaO	10.85	11.01	10.40	10.58	10.05	10.79	9.66	10.91	10.66	11.03	10.71	9.66	10.54
Na_2O	2.85	2.77	2.98	2.89	3.02	2.98	3.13	2.83	3.01	2.93	3.00	3.01	2.92
K_2O	0.30	0.20	0.36	0.48	0.49	0.30	0.53	0.55	0.36	0.22	0.12	0.17	0.33
P_2O_5	0.11	0.10	0.17	0.16	0.16	0.17	0.19	0.17	0.18	0.17	0.17	0.17	0.18
H_2O^+	2.15	2.05	2.05	nd	1.97	1.87	2.41	1.99	nd	1.89	2.23	2.27	2.19
CO_2	0.09	0.08	0.08	0.04	0.05	0.08	0.11	0.05	0.07	0.03	0.43	0.10	0.13
Mg′	64	66	58	54	56	61	59	56	59	61	64	61	59
Trace-element abundance (ppm)													
Cr	335	335	258	255	269	257	242	259	268	246	236	262	231
Sr	108	126	123	108	135	140	128	124	112	128	131	141	135
Zr	70	75	101	99	112	112	113	106	103	119	111	103	102
Rb	1	1	5	8	9	2	10	6	3	1	1	4	1
Ni	115	113	100	79	106	99	101	90	88	93	202	102	104
Ce		7.1	12.4	11.6					12.5				
Nd		7.7	11.7	11.2					11.7				
Sm		2.9	4.0	3.9					3.9				
Eu		1.1	1.5	1.4					1.5				
Dy		5.3	7.0	6.9					7.2				
Er		3.3	4.4	4.4					4.6				
Yb		3.4	4.6	4.4					4.7				

Note: Sample numbers from Table 1. Mg′ = atomic ratio Mg/(Mg + Fe), Fe = total iron as FeO.

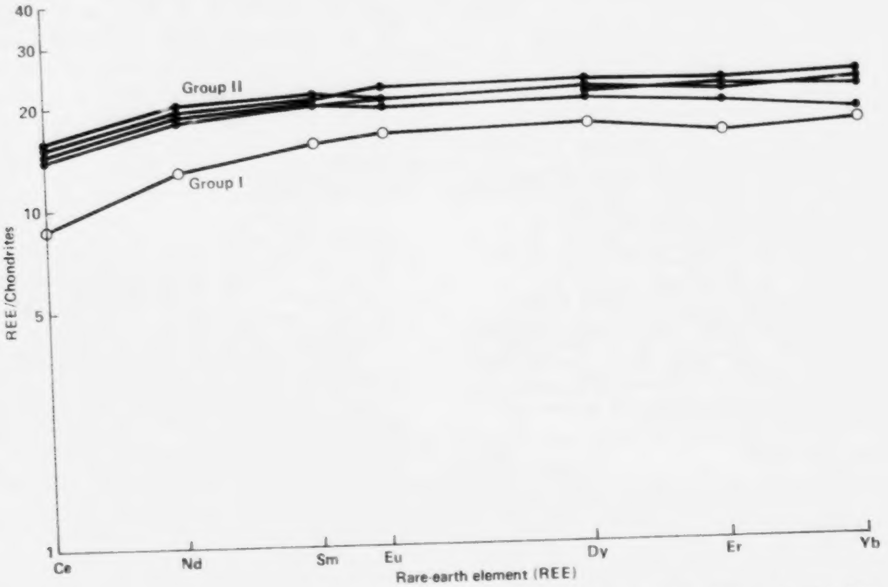

Figure 2. Chondrite normalized rare-earth element (REE) abundances of samples from Hole 581. The Group II samples have been separated slightly for clarity (REE abundances are given in Table 2). Note the lower Ce/Yb ratio of Sample B, a Group I sample, than the Group II samples.

1980; Langmuir et al., 1977). Fractionation of Ce/Yb ratios of the magnitude found in this study have been reported for basalts from the Franco-American Mid Ocean Undersea Study (FAMOUS) area by Langmuir et al. (1977). Although such fractionation cannot be produced by batch melting, Langmuir et al. (1977) have shown it may be produced by dynamic melting, a process that involves multistage melting of a mantle source with partial retention of the initial melt in the source.

The abundance of Ce and Zr predicted by the model is slightly lower than the observed abundances, while the depletion calculated for Ni and Cr is in good agree-

Table 3. Summary of fractional crystallization models.

Parent	Daughter	Minerals	Percent removed	Sum of the residuals
Group I	Group II*	Olivine (Fo 86)	3.08	0.01
		Augite (#1)	10.69	
		Plagioclase (An 71)	18.48	
Primitive MORB	Group I	Olivine (Fo 86)	2.7	0.5
		Augite (#2)	24.32	
		Plagioclase (An 85)	17.63	
Group II	Site 304	Olivine (Fo 83)	5.75	0.87
		Augite (#1)	3.81	
		Plagioclase (An 71)	26.57	

Mineral compositions used in models.

Oxide	Olivine (Fo 86)	Olivine (Fo 83)	Augite #1	Augite #2	Plagioclase (An 71)	Plagioclase (An 85)
SiO_2	39.87	40.8	52.68	50.90	53.78	49.33
TiO_2	0.0	0.0	0.52	0.9	0.0	0.0
Al_2O_3	0.0	0.0	2.29	2.86	28.35	33.00
FeO	13.97	14.6	10.39	15.03	0.0	0.47
MnO	0.23	0.14	0.0	0.32	0.7	0.0
MgO	45.38	46.0	16.95	16.12	0.2	0.0
CaO	0.18	0.3	17.08	13.08	12.82	16.50
Na_2O	0.0	0.0	0.0	0.54	4.2	1.78
K_2O	0.0	0.0	0.0	0.0	0.0	0.0
P_2O_5	0.0	0.0	0.0	0.0	0.0	0.0
Source:	Clague and Bunch (1976)	Average of several	Mattey and Muir (1980)	Thompson and Humphris (1980)	Thompson and Humphris (1980)	Mattey and Muir (1980)

Rock compositions.

Oxide	Group I	Group II*	Primitive	Site 304
SiO_2	50.05	49.67	50.3	49.56
TiO_2	1.34	1.83	0.93	2.07
Al_2O_3	16.14	15.92	15.6	13.05
FeO	7.95	9.38	8.59	12.68
MnO	0.15	0.20	0.14	0.22
MgO	8.27	7.50	9.80	6.57
CaO	10.93	10.16	12.77	10.6
Na_2O	2.81	3.01	2.41	2.78
K_2O	0.25	0.35	0.05	0.08
P_2O_5	0.11	0.17	0.09	0.22
Source:			Batiza et al. (1977)	Marshall (1975)

Note: Group II* is an average of Samples C, E, G, H, and L, the Group II samples with the highest TiO_2. Results for an average of the entire Group II yields nearly identical results, with higher residuals due to CaO, which is always low in the calculated models. The error of TiO_2 is also larger using the average of the entire group, thus we believe the average of the high TiO_2 samples, which are presumably the most fractionated, is more appropriate for modeling the extent of fractionation. The "primitive" analysis represents the least-fractionated MORB found associated with the ferrobasalts of the Siqueros Fracture Zone (Batiza et al., 1977). Models were calculated using the least-squares method of Wright and Doherty (1970).

Table 4. Comparison of the average composition of Hole 581 samples to other MORB suites.

Oxide	Group I, Hole 581	Group II, Hole 581	Site 303, Hole 303A	Site 304, Hole 304	Site 307, Hole 307	Average EPR	Average MORB
SiO_2	50.82	50.32	51.35	50.65	52.04	50.19	50.53
TiO_2	1.36	1.82	3.26	2.11	1.66	1.77	1.56
Al_2O_3	16.39	15.99	15.11	13.33	15.74	14.86	15.27
FeO	8.08	9.49	9.10	12.96	9.75	11.33	10.46
MnO	0.15	0.20	0.19	0.22	0.16	—	—
MgO	8.40	7.58	6.39	6.71	5.66	7.10	7.47
CaO	11.10	10.57	10.59	10.83	11.36	11.44	11.49
Na_2O	2.85	3.00	3.22	2.84	2.85	2.66	2.62
K_2O	0.25	0.36	0.40	0.08	0.62	0.16	0.16
P_2O_5	0.11	0.17	0.33	0.22	0.18	0.14	0.13
Source:	This paper	This paper	Marshall (1975)	Marshall (1975)	Marshall (1975)	Melson et al. (1976)	Melson et al (1976)

Note: All samples have been recalculated on an anhydrous basis, with total iron as FeO. Group I includes Samples A and B, Group II is the average of all other samples in this study. Site 303, 304, and 307 analyses are representative analyses, not averages, because of the extensive alteration of most samples from these holes (Marshall, 1975). Average EPR is an average of basaltic glasses from the East Pacific Rise, Average MORB is an average of over 500 MORB glasses (Melson et al. 1976).

ment with observed values. The scatter in Rb and Sr data is too large for meaningful numerical evaluation.

Comparison of Hole 581 samples to other MORBs from the Northwest Pacific (Sites 303, 304, and 307) is complicated by the considerable alteration of all samples from the other sites (Table 4). The least altered sample from Site 303 has nearly 4% total water, the least altered sample from Site 307 has 3%, and both have a highly altered groundmass (Marshall, 1975). Site 304 samples are clearly more fractionated than Hole 581 samples, and the differences in composition (higher FeO and TiO_2 and lower MgO) are those expected from fractionation. Only the lower Al_2O_3 contents of Site 304 samples would not be expected from fractionation. A magma of the composition of the Site 304 sample may be derived from a magma with the average composition of Group II samples by the removal of 26% plagioclase, 6% olivine, and 4% augite (Table 3), although the validity of such models, considering the extent of alteration of the Site 304 samples, is problematic. Samples from Sites 303 and 307 differ from Hole 581 samples only in lower MgO and Al_2O_3 contents, and the higher TiO_2 content in samples from Site 303. The differences in MgO are attributable to alteration, and the high TiO_2 values in Site 303 samples are not observed at Sites 304 and 307. Thus, the only consistent differences in composition between Hole 581 samples and samples from Sites 303, 304, and 307 that are not attributable to fractionation or alteration are the Al_2O_3 contents. In view of the extreme alteration of the samples from Sites 303 and 307, no fractionation models were calculated for these sites.

Comparison to samples from the East Pacific Rise (EPR) and to average MORBs (Table 4) shows that the average composition of Hole 581 rocks is typical for slightly fractionated MORBs, with a slightly higher than average Al_2O_3 content. The composition of each of the samples in this study is within the range of EPR basalts (Melson et al. 1976). However, the FeO*/MgO ratio is slightly lower than samples with the same TiO_2 content from other areas (Fig. 3).

CONCLUSIONS

The samples from Hole 581 are slightly fractionated MORBs with higher than average Al_2O_3 contents. The more evolved Group II samples could have been derived from a magma with the average composition of the more primitive Group I samples by the crystallization of 18% plagioclase, 10% augite, and 3% olivine. However, trace-element models require a greater amount of fractionation to produce the observed enrichment of Ce and Zr in

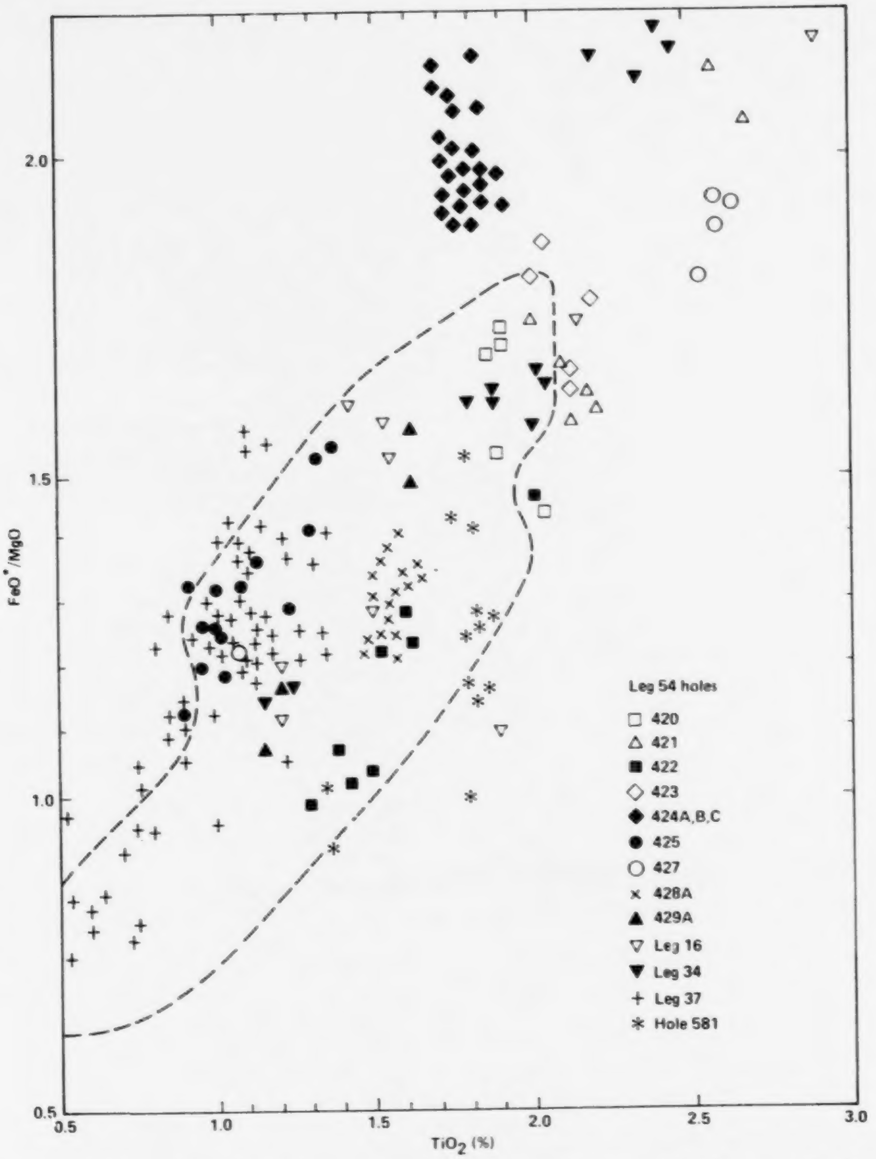

Figure 3. A plot of FeO*/MgO versus TiO_2 comparing Hole 581 samples to other MORBs from the Pacific Ocean (the figure, including all data points other than Hole 581 samples, is from Srivastava et al., 1980). Note the generally lower FeO*/MgO ratios for the Hole 581 samples than for other MORBs. The presence of several of the Hole 581 samples on the main trend is believed to be due to alteration, since the samples that are near the main trend are among the most altered of the samples, while the least altered samples all lie well below the main trend. Alteration would be expected to move samples nearly vertically on the plot, since alteration will increase FeO*, decrease MgO, and not significantly change TiO_2 (Marshall, 1975; Humphris et al., 1980).

Group II samples. The large increase in Ce/Yb ratios between Group I and Group II samples could not have resulted from fractional crystallization, nor could it have been produced by different amounts of partial melting of a homogeneous source. The change in Ce/Yb ratio requires a more complex process such as dynamic melting, if all Hole 581 samples were derived from the same source. The Hole 581 rocks are thus typical slightly fractionated basalts such as are common at fast-spreading ridges and propagating rifts (Melson et al., 1976; Natland, 1980; Christie and Sinton, 1981).

REFERENCES

Arth, J. G., and Hanson, G. N., 1975. Geochemistry and origin of the early Precambrian crust of northeastern Minnesota. *Geochim. Cosmochim. Acta*, 39:325-362.

Batiza, R., Rosendahl, B. R., and Fisher, R. L., 1977. Evolution of Oceanic Crust, 3, Petrology and chemistry of basalts from the East

Pacific Rise and the Siqueiros Transform Fault. *J. Geophys. Res.*, 82:265–277.

Christie, D. M., and Sinton, J. M., 1981. Evolution of abyssal lavas along propagating segments of the Galapagos Spreading Center. *Earth Planet. Sci. Lett.*, 56:321–335.

Clague, D. A., and Bunch, T. E., 1976. Formation of ferrobasalt at East Pacific midocean spreading centers. *J. Geophys. Res.*, 81: 4247–4256.

Clemency, C. V., and Borden, D. L., 1978. The precision of "rapid" rock analyses and the homogeneity of new U.S.G.S. standard rock samples. *Geostandards Newsl.*, 2:147–155.

Gast, P. W., 1968. Trace element fractionation and the origin of tholeiitic and alkaline magma types. *Geochim, Cosmochim, Acta*, 32: 1057–1086.

Humphris, S. E., Thompson, R. N., Gibson, I. L, and Marriner, G. F., 1980. Comparison of geochemistry of basalts from the East Pacific Rise, OCP Ridge and Siqueiros Fracture Zone, Deep Sea Drilling Project Leg 54. *In* Rosendahl, B. R., Hekinian, R., et al., *Init. Repts. DSDP*, 54: Washington (U.S. Govt. Printing Office), 635–650.

Langmuir, C. H., Bender, J. F., Bence, A. E., and Hanson, G. N., 1977. Petrogenesis of basalts from the FAMOUS area; Mid-Atlantic Ridge. *Earth Planet. Sci. Lett.*, 36:133–156.

Larson, R. L., and Chase, C. G., 1972. Late Mesozoic evolution of the Western Pacific Ocean. *Geol. Soc. Am. Bull.*, 83:3627–3644.

Marshall, M., 1975. Petrology and chemical composition of basaltic rocks recovered on Leg 32, Deep Sea Drilling Project. *In* Larson, R. L., Moberly, R., et al., *Init. Repts. DSDP*, 32: Washington (U.S. Govt. Printing Office), 563–570.

Mattey, D. P., and Muir, I. D., 1980. Geochemistry and mineralogy of basalts from the Galapagos Spreading Center, Deep Sea Drilling Project Leg 54. *In* Rosendahl, B. R., Hekinian, R., et al., *Init. Repts. DSDP*, 54: Washington (U.S. Govt. Printing Office), 755–772.

Melson, W. G., Vallier, T. L., Wright, T. L., Byerly, G., and Nelsen, J., 1976. Chemical diversity of abyssal volcanic glass erupted along Pacific, Atlantic and Indian Ocean sea-floor spreading centers. *In* Sutton, G. H., Manghnani, M. H., and Moberly, R. (Eds.), *The Geophysics of the Pacific Ocean Basin and its Margins:* Washington D.C. (American Geophysical Union), 19:351–367.

Moberly, R., and Larson, R. L., 1975. Mesozoic magnetic anomalies, ocean plateaus and seamount chains in the northwestern Pacific Ocean. *In* Larson, R. L., Moberly, R., et al., *Init. Repts. DSDP*, 32: Washington (U.S. Govt. Printing Office), 945–957.

Natland, J. H., 1980. Effects of axial magma chambers beneath spreading centers on the compositions of basaltic rocks. *In* Rosendahl, B. R., Hekinian, R., et al., *Init. Repts. DSDP*, 54: Washington (U.S. Govt. Printing Office, 833–850.

Schilling, J.-G., Anderson, R. N., and Vogt P., 1976. Rare earth, Fe and Ti variations along the Galapagos spreading center, and their relationship to the Galapagos mantle plume. *Nature (London)*, 261: 108–113.

Shapiro, L., 1975. Rapid analysis of silicate, carbonate and phosphate rocks, revised edition. *Geol. Surv. Bull.* (U.S.), 1401:1–76.

Srivastava, R. K., Emmerman, R., and Puchelt, H., 1980. Petrology and geochemistry of basalts from Deep Sea Drilling Project Leg 54. *In* Rosendahl, B. R., Hekinian, R., et al., *Init. Repts DSDP*, 54, Washington (U.S. Govt. Printing Office), 671–694.

Sun, S.-S., Nesbitt, R. G., and Sharaskin, A. Y., 1979. Geochemical characteristics of mid-ocean ridge basalts. *Earth Planet. Sci. Lett.*, 44:119–138.

Thompson, R. N., and Humphris, S. E., 1980. Silicate mineralogy of basalts from the East Pacific Rise, OCP Ridge, and Siqueiros Fracture Zone: Deep Sea Drilling Project Leg 54. *In* Rosendahl, B. R., Hekinian, R., et al., *Init. Repts. DSDP*, 54: Washington (U.S. Govt. Printing Office), 651–667.

Vocke, R. D., 1983. Petrogenetic modelling in an archean gneiss terrain, Saglek, northern Labrador [Ph.D. dissert.]. State University of New York, Stony Brook, New York.

Wright, T. L., and Doherty, P. C., 1970. A linear programming and least squares computer method for solving petrologic mixing problems. *Geol. Soc. Am. Bull.*, 81:1995–2007.

Date of Initial Receipt: 21 February 1984
Date of Acceptance: 12 November 1984

PART VI: PHYSICAL PROPERTIES AND GEOTHERMAL STUDIES

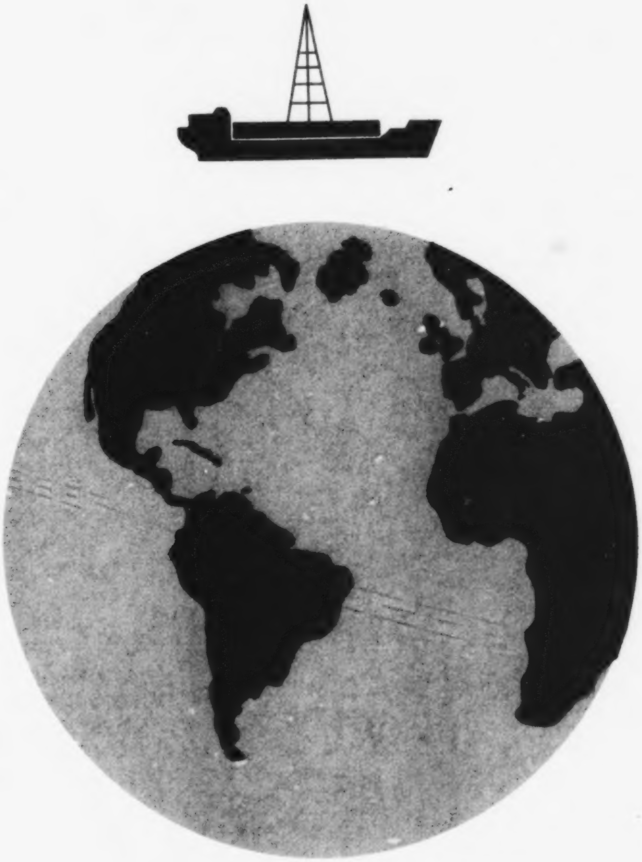

33. PHYSICAL AND GEOTECHNICAL PROPERTIES OF SEDIMENTS FROM THE NORTHWEST PACIFIC: DEEP SEA DRILLING PROJECT LEG 86[1]

P. J. Schultheiss, Institute of Oceanographic Sciences, Wormley[2]

ABSTRACT

A wide variety of sediment types (red clays, carbonate oozes, and siliceous clays) were cored using the hydraulic piston corer on Leg 86 of the Deep Sea Drilling Project in the Northwest Pacific. Physical property data for all these sediments are presented in the form of tables and graphs. Measurements include bulk density, water content, gamma ray attenuation porosity evaluation (GRAPE), shear strength, compressional and shear wave velocities, consolidation, and permeability. Sample quality for the most part was considered good; however, some systematic downcore disturbance was found in the red clays. A significant difference between shipboard and shore-based gravimetric measurements was found and was correlated with sea state. The siliceous clays exhibited little progressive consolidation downhole, whereas the red clays were found to be normally consolidated below 20 m. Vane shear strengths ranged from zero to 1700 g/cm^2 in red clay at a sub-bottom depth of 170 m. Shear wave velocity correlated with vane shear strength and ranged up to 160 m/s in the red clay.

INTRODUCTION

Leg 86 of the Deep Sea Drilling Project (DSDP) was primarily aimed at studying the oceanic paleoenvironment in the Western Pacific. The sites cored using the hydraulic piston corer (HPC) contained a wide variety of sediment types including thick sequences of red clays (Sites 576 and 578), calcareous oozes (Site 577), and siliceous clays (Sites 579 and 580). It was, therefore, a particularly good opportunity to examine and compare the physical properties of these different sediment types during a single cruise. In addition, at Site 576, a complete hole (Hole 576A) was recovered and stored unsplit for geotechnical studies. The large amount of data produced by these studies is presented by the Geotechnical Consortium (this volume).

Data concerning physical and geotechnical properties of deep-sea sediments could substantially aid our understanding of depositional and post-depositional processes if "relatively undisturbed" samples are available. Prior to the introduction of the HPC, the rotary coring process was used to obtain sediment samples in the upper 200 m of unlithified sediments. The sample disturbance in these cores (Demars and Nacci, 1978) made the assessment and interpretation of some of the physical property data problematic. However, use of physical property data has greatly aided our understanding of sediment deposition and consolidation to great depths below the seafloor (e.g., Bennett and Keller, 1973; Lee, 1973; Rocker, 1974). DSDP Leg 68 (Prell, W. L., Gardner, J. V., et al., 1982) was the first cruise devoted to using the then newly developed HPC, which recovered sediment sections of ~4 m length. Before this, the HPC had been successfully used only once (Leg 64, Site 480; Curray et al., 1979; Schrader et al., 1980).

Mayer (1982) presented the first detailed physical property measurements made on HPC samples from depths of more than 200 m and provided an account of the problems of disturbance and the extent to which the HPC overcomes these problems. The observations that Mayer made with regard to the quality of HPC samples are equally applicable to the samples recovered on Leg 86 using the increased coring length (9.5 m) facility of the variable length hydraulic piston corer (VLHPC) and will not be repeated here in any detail.

The purpose of this chapter is to present all of the shipboard physical and geotechnical measurements made on Leg 86 as well as some of the shore-based data. Measurements made on board and on shore included bulk density, water content, shear strength, consolidation, permeability, and both compressional and shear wave velocities. After the techniques used have been described, the data are presented and discussed for each site before a comparison of the different sediment types is made.

TECHNIQUES

Apart from Site 581, all the measurements were made on cores obtained by the HPC. Each core, after having been sectioned at 1.5-m intervals, was allowed to lie unsplit in the rack for at least 4 hr. in order to bring the temperature to equilibrium. This was nominally 21°C in the shipboard laboratory and all measurements were carried out close to this temperature. The only set of data corrected for temperature differences was the compressional wave velocity, which was corrected to 20°C. The following measurements were carried out at varying intervals throughout the recovered cores.

GRAPE

All cores were passed through the Gamma Ray Attenuation and Porosity Evaluator (GRAPE) to assess the saturated bulk density (see Introduction and Explanatory Notes, this volume). The calibration and calculation procedures were explained by Boyce (1976). Samples used for the 2-min. GRAPE count were subsequently used for shipboard gravimetric analyses.

Gravimetric Analysis

Two adjacent samples were normally taken using thin stainless steel sampling cylinders (see Introduction and Explanatory Notes, this volume). One sample was subjected to the 2-min. GRAPE before being weighed wet, dried to constant weight at 105°C, and then weighed dry.

---

[1] Heath, G. R., Burckle, L. H., et al., *Init. Repts. DSDP*, 86: Washington (U.S. Govt. Printing Office).

[2] Address: Institute of Oceanographic Sciences, Wormley, Godalming, Surrey GU8 5UB, United Kingdom.

The second sample was sealed in a plastic vial which was then returned for a shore-based check on the data.

Water content (WC) was calculated from the wet and dry weights. WC = Wt. of salt water/Wt. of solids, using a salt correction of 35‰.

$$\mathrm{WC}\ (\%) = \frac{103.5(W - D)}{D - 0.036(W - D)},$$

where W = wet weight of sediment and D = dry weight of sediment. Estimates of porosity, void ratio, and bulk density were obtained by assuming that the density of seawater is 1.024 g/cm^3 and the solid density is 2.7 g/cm^3.

Compressional Wave Velocity

The velocity of compressional waves was measured at around 400 kHz using the Hamilton frame velocimeter. This equipment and the techniques for using and calibrating it were described by Boyce (1973, 1976). Most measurements were obtained by measuring across a split core section and through half of the liner (TTL). It was found that for HPC cores, where the sediments completely fill the liner, a resolution of better than ±2% is possible; most measurements were probably accurate to within ±1%. Temperature was recorded at the time of each measurement, and the velocities were corrected to 20°C using tables of seawater velocity versus temperature.

Shear Wave Velocity

The general paucity of shear wave data to date has not been caused by a lack of interest but by a lack of suitable techniques for propagating and receiving shear waves in low velocity materials such as unconsolidated sediments. Although resonant column tests, as used by Hardin and Richart (1963), provide most of the shear wave data available, the technique is not suitable as a logging tool for split cores.

Over the last few years shear wave measurements in sediments have progressed significantly with the introduction of piezoelectric bender crystals being used as the transducers (Shirley and Hampton, 1978; Schultheiss, 1981, 1983). To transmit and receive shear waves in sediments, piezoelectric transducers have been constructed using thin bender elements, which are composite sheets consisting of two piezoelectric transverse expander plates bonded together face-to-face so that an applied voltage across the plates causes it to bend, as shown in Figure 1. This bending motion causes a shear stress that propagates as a shear wave and is detected in a reciprocal manner to develop in the surrounding sediment. The relatively large displacements that can be obtained for small applied voltages, coupled with the low resonant frequencies, make bender elements suitable as shear wave transducers for sediments under low effective stresses. For logging cores, a pair of transducers were built that were stiff enough to be pushed into the split core as shown in Figure 2. A perspex frame was used to push the transducers into the sediment. This enabled the elements to be inserted with the correct orientation and at a known separation. The frame was removed before readings were taken in order to decouple mechanically the transmitter and receiver. They were inserted both parallel and normal to the core axis to look for any anisotropic effects. The rising edge of a 10-V square wave was used to drive the transmitter, which had a resonant frequency around 5 kHz. After passing through a high-pass filter, the received signal was displayed on a delay time base oscilloscope which was used to measure the transit time. The accuracy of the velocity measurements depended primarily on the signal quality and was estimated at around ±5%.

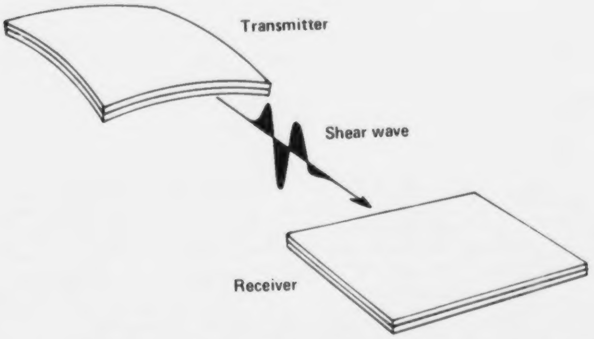

Figure 1. Schematic diagram of piezoelectric bender elements used to transmit and receive shear waves in unconsolidated sediments.

Shear Strength Measurements

Two vane devices were routinely used to measure shear strength: the motorized Wykeham Farrance "Laboratory Vane Apparatus" and the Torvane hand-held vane. The theory, operation, and calculation procedures as used by DSDP for the motorized vane were well documented by Boyce (1977). Briefly, the motorized laboratory vane equipment has a motor that rotates (89°/minute) one end of a calibrated, coiled spring about its axis, with the other end of the spring being connected to a shaft that incorporates a cruciform vane. A mechanical pointer system is used to indicate the amount of rotation of the vane and, in addition, the amount of rotational stress applied to the spring. At some maximum torque the vane begins to rotate more rapidly as the sediment shears around a cylinder described by the rotating vane. The shearing force is related to the maximum torque applied to this cylindrical shearing surface. It is assumed that, at fast rates of strain in clayey sediment with low permeabilities, the calculated shear strength is an undrained value. It should be emphasized here that it is most imperative to clamp rigidly the split core section to the vane apparatus to prevent any relative motions that would invalidate the results.

The Torvane hand-held vane operates on the same principles as the motorized vane except that the degree of control is much more limited and a full stress–strain graph cannot be produced. Only the maximum torque required to produce the failure is recorded. A great deal of care must be taken when using this device; the incorporation of well-engineered ball joints in the operator's wrist would be advantageous.

RESULTS

The data are presented in the form of a table and a series of graphs for each of the six sites (Sites 576–581). The columns in the tables are defined as follows:

Core-Section is self-explanatory; it refers to the core number followed by the section number (see Introduction and Explanatory Notes, this volume). Interval (cm) refers to the range of depths, within a given section, at which all the measurements were taken. Although each measurement was taken at a precisely known depth, they were all generally taken within 30 cm of one another in each section. Consequently, for ease of presentation and to allow parameters to be easily plotted against each other, most of the data within each section have been assigned an average sub-bottom depth (Av. sbd [m]) in meters below the seafloor. This value has been taken at the average of the depth intervals. In some cases, when data have been obtained from a part of the section outside a 50-cm range or in an obviously different lithology, they have been assigned a unique interval and sub-bottom depth. The sub-bottom depth is the adjusted value which takes into account discrepancies that arose from the driller's log; in particular, for Site 576 (see Site 576 chapter, this volume).

Shear strength is separated into two columns; the first is for the hand-held Torvane and the second is for the Wykeham Farrance motorized vane device (W.F.). These are given in g/cm^2 for ease of comparison with other DSDP data. However, the preferred SI units are kilopascals (kPa), where 10 g/cm^2 = 0.918 kPa.

P-wave velocity is the primary or compressional wave velocity measured at 400 kHz and corrected to 20°C and given in m/s.

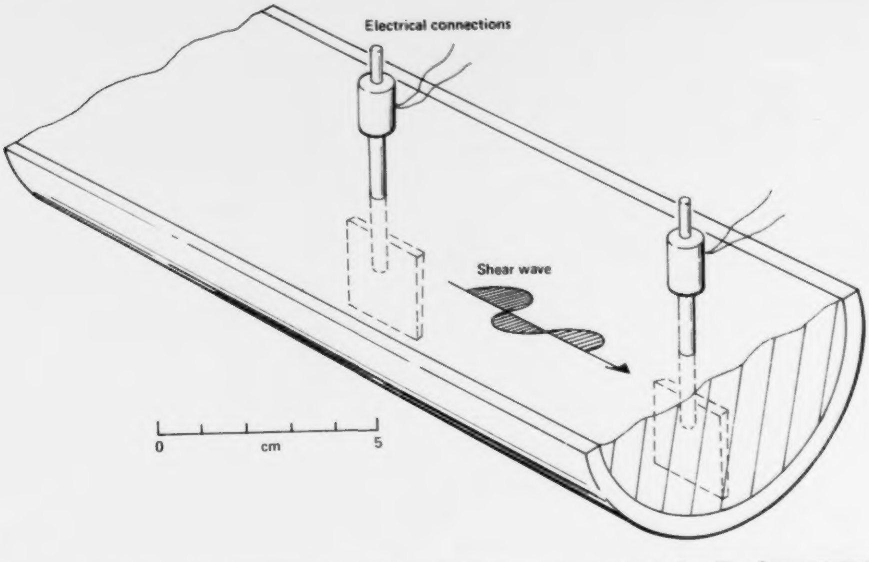

Figure 2. The shear wave transducers inserted into the split core section with the handling frame removed.

S-wave velocity is the secondary or shear wave velocity also given in m/s.

GRAPE bulk density is given in g/cm^3 and refers to the calculated density from the 2-min. GRAPE count.

Bulk Density, Water content, Porosity, and Void ratio have two sets of values; the first is from those measured on board ship (Shipboard) and the second is from those measured at the shore-based laboratory (Laboratory). Where more than one hole was drilled at a site, only the first hole has both sets of data; the other holes have just the shore-based laboratory data.

Most of the graphs have been plotted for each site with the data merged from all the holes at that site. The exception is Site 576, where Hole 576A was dedicated for geotechnical studies (Geotechnical Consortium, this volume). Bulk density data are plotted using the shore-based laboratory data unless stated. For each site, graphs of bulk density, water content, GRAPE bulk density, compressional wave velocity, shear wave velocity, and vane shear strength versus depth have been plotted (Figs. 3–8).

Site 576

This site consists of about 55 m of pelagic clay overlying 20 m of interbedded carbonate turbidites and pelagic clay before terminating in chert at 76 m sub-bottom. The thick pelagic clay is considered to be a "type" northwestern Pacific pelagic (red) clay section with continuous deposition throughout the past 65 m.y. Data for Holes 576 and 576B are presented in Table 1. A large amount of physical property and geotechnical data is presented by the Geotechnical Consortium (this volume) for Hole 576A.

The graphical representation of the data for this site is shown in Figure 3. The carbonate data points that lie between 55 and 72 m are indicated. The water content profile for this site exhibits high-frequency fluctuations which, although not yet understood, may reflect subtle changes in lithology and deposition. Water content overall increases from around 150% near the surface to over 200% between 11 and 20 m before it gradually decreases to around 110% at 20 m. It is suspected that the variations reflect changes in mineralogy similar to that found in LL44-GPC3 where the high water content is caused by increased amounts of authigenic components (probably smectite).

The compressional wave velocity profile (Fig. 3) shows no obvious trend through the brown clay section and is always less than the water velocity because of the high water content. Peaks in the profile correspond to ash layers and, toward the bottom of the core, the carbonate layers. The high velocity carbonates (coupled with their higher bulk densities) provide a large impedance contrast which explains the good acoustic reflector at the clay/ooze boundary (see Site 576 chapter, this volume).

The shear wave velocity profile for the brown clay shows an increase from around 10 m/s at the surface to around 120 m/s at a depth of 70 m (Fig. 3). Shear wave velocities in the carbonates around 60 m have only about half the value (40 m/s) of the velocities in the adjacent clays (80 m/s). A similar profile is shown for shear strength, which increases from less than 50 g/cm^2 at the surface to over 1000 g/cm^2 at 70 m. Once again, the carbonates have much lower values than the adjacent clays. It is thought that the large differences in shear strength and shear wave velocity between the brown clay and the adjacent carbonates is probably caused by the stress disturbance that occurs during the coring operation rather than implying that the *in situ* values vary to a similar degree. The shear strength of a water-saturated sediment may be expressed by the Mohr–Coulomb relationship:

$$s = \bar{c} + \bar{\delta}\tan\bar{\phi}$$

where $\bar{c}$ = cohesion, $\bar{\phi}$ = effective angle of internal friction, and $\bar{\delta}$ = effective normal stress. To a large extent, the shear vane is measuring the cohesion only as

Table 1. Physical property data for Holes 576, 576B, 577, 577A, 578, 579, 579A, 580, and 581.

		Shipboard										Laboratory			
		Shear strength (g/cm²)												
Core-Section (interval or level in cm)	Av. sbd (m)	Torvane	W.F.	P-wave velocity (m/s)	S-wave velocity (m/s)	GRAPE bulk density (g/cm³)	Bulk density (g/cm³)	Water content (%)	Porosity	Void ratio	Bulk density (g/cm³)	Water content (%)	Porosity	Void ratio
Hole 576														
1-1, 58-84	5.21	34	14	—	—	1.56	—	—	—	—	1.28	169	0.82	4.69
1-2, 64-78	6.71	26	—	—	—	1.41	1.28	170	0.82	4.70	1.26	181	0.83	5.04
2-1, 21-79	7.70	56	56	1439	4	1.46	1.31	151	0.81	4.18	1.31	151	0.81	4.20
2-1, 63	7.83	—	32	—	—	—	—	—	—	—	—	—	—	—
2-1, 119	8.39	—	54	—	—	—	—	—	—	—	—	—	—	—
2-1, 131	8.51	—	39	—	—	—	—	—	—	—	—	—	—	—
2-2, 42-69	9.25	46	54	1444	6	1.41	1.27	177	0.83	4.90	1.27	176	0.83	4.88
2-2, 91	9.61	—	—	1443	—	—	—	—	—	—	—	—	—	—
2-3, 60-79	10.89	74	82	1452	10	1.47	1.30	157	0.81	4.34	1.39	113	0.76	3.15
2-4, 12	11.82	—	67	—	—	—	—	—	—	—	—	—	—	—
2-4, 42	12.12	—	131	—	—	—	—	—	—	—	—	—	—	—
2-4, 90-109	12.70	94	81	1445	12	1.39	1.27	173	0.83	4.79	1.27	176	0.83	4.87
2-5, 42-90	13.86	88	91	1441	21	1.29	1.26	221	0.86	6.13	1.21	234	0.87	6.50
2-6, 12-69	15.11	42	51	1440	12	1.33	1.22	216	0.86	5.98	1.22	218	0.86	6.05
2-6, 52	15.22	—	37	—	—	—	—	—	—	—	—	—	—	—
2-6, 121	15.91	—	11	—	—	—	—	—	—	—	—	—	—	—
3-1, 80-99	10.50	96	60	1437	10	1.46	1.32	145	0.80	4.02	1.29	160	0.82	4.45
3-2, 60-79	11.79	80	59	1435	13	1.34	1.22	214	0.86	5.92	1.23	212	0.85	5.89
3-3, 70-90	13.40	104	67	1447	17	1.33	1.25	195	0.84	5.39	1.24	199	0.85	5.52
3-4, 40-80	14.70	120	49	1424	16	1.38	1.27	175	0.83	4.85	1.26	179	0.83	4.98
4-1, 89-109	20.08	92	68	1464	16	1.34	1.23	217	0.85	5.74	1.25	192	0.84	5.32
4-2, 32-80	21.16	108	90	1445	17	1.36	1.28	166	0.82	4.60	1.27	172	0.83	4.77
4-3, 52-79	22.76	128	111	1439	20	1.37	1.31	152	0.81	4.19	1.41	108	0.75	2.99
4-4, 40-80	24.20	168	168	1479	—	1.45	1.35	131	0.78	3.62	1.33	137	0.79	3.80
4-4, 62-69	24.26	—	137	1439	—	—	—	—	—	—	—	—	—	—
4-5, 52-79	25.76	162	191	1433	26	1.55	1.33	138	0.79	3.83	1.33	140	0.80	3.89
4-5, 112	26.22	190	—	—	—	—	—	—	—	—	—	—	—	—
4-6, 62-89	27.36	280	227	1438	45	1.54	1.36	128	0.78	3.54	1.35	131	0.78	3.64
5-1, 52-99	28.95	170	173	1425	44	1.50	1.36	125	0.77	3.45	1.33	137	0.79	3.80
5-2, 50-90	30.40	95	—	—	34	—	—	—	—	—	—	—	—	—
5-2, 80	30.50	120	—	—	—	—	—	—	—	—	—	—	—	—
5-2, 110	30.80	110	—	—	—	—	—	—	—	—	—	—	—	—
5-3, 60-88	31.94	110	—	—	37	—	—	—	—	—	—	—	—	—
5-3, 120	32.40	150	—	—	—	—	—	—	—	—	—	—	—	—
5-4, 40	33.10	120	—	—	—	—	—	—	—	—	—	—	—	—
5-4, 105	33.75	110	—	—	—	—	—	—	—	—	—	—	—	—
5-5, 10-83	37.57	130	100	1454	33	1.48	1.33	137	0.79	3.80	1.34	136	0.79	3.79
5-5, 52-79	37.76	270	241	1415	51	—	—	—	—	—	1.33	142	0.80	3.94
5-5, 88	37.98	260	—	—	—	—	—	—	—	—	—	—	—	—
5-6, 50-79	39.24	220	205	1440	45	1.50	1.33	138	0.79	3.83	1.30	155	0.81	4.30
6-3, 59-93	38.16	230	214	1427	55	1.42	1.37	122	0.77	3.37	1.36	127	0.78	3.54
6-3, 99	38.39	230	—	—	—	—	—	—	—	—	—	—	—	—
6-4, 50-89	39.59	340	205	1421	63	—	1.45	93	0.72	2.59	1.35	131	0.78	3.63
6-5, 70-90	41.20	280	—	1424	58	—	—	—	—	—	1.33	139	0.79	3.85
6-5, 83	41.23	—	—	—	—	—	—	—	—	—	1133	139	0.80	3.87
6-6, 62-89	42.66	310	291	1431	63	1.47	1.38	119	0.77	3.29	1.35	128	0.78	3.56
7-1, 61-90	45.36	260	275	1426	52	1.53	1.39	116	0.76	3.20	—	—	—	—
7-2, 61-94	47.88	320	287	1428	75	1.44	1.37	122	0.77	3.37	1.41	108	0.75	3.00
7-2, 69-102	47.95	—	—	—	65	—	—	—	—	—	1.36	125	0.78	3.46
7-3, 79-102	49.51	380	469	—	—	1.40	1.35	129	0.78	3.56	1.33	141	0.80	3.93
7-4, 60-101	50.91	420	419	1431	68	1.39	1.36	124	0.77	3.44	1.27	179	0.83	4.96
7-5, 30-70	52.10	390	320	—	65	1.42	1.39	114	0.76	3.15	1.38	120	0.77	3.32
7-6, 71-99	53.95	420	420	—	67	1.48	1.41	107	0.75	2.96	1.39	115	0.76	3.20
8-1, 30-70	54.60	360	250	1428	60	1.31	1.37	122	6.77	3.37	1.36	128	0.78	3.54
8-1, 135	55.45	—	—	1451	—	—	—	—	—	—	—	—	—	—
8-2, 47-101	56.34	400	114	1464	59	1.62	1.62	61	0.63	1.69	1.65	55	0.61	1.55
8-2, 110-132	56.81	510	453	1429	—	—	—	—	—	—	1.36	128	0.78	3.55
8-3, 20-139	57.89	330	272	1448	62	1.69	1.59	66	0.65	1.81	1.57	68	0.66	1.90
8-5, 45-84	60.74	150	59	1474	30	1.84	1.67	54	0.60	1.49	1.61	62	0.63	1.74
8-6, 15-63	61.99	—	66	1508	31	—	—	—	—	—	1.66	54	0.60	1.51
8-6, 25-85	62.15	—	552	1426	34	—	—	—	—	—	1.51	80	0.69	2.24
8-6, 80-109	62.55	—	—	1480	75	—	—	—	—	—	—	—	—	—
Hole 576B														
1-1, 72-99	0.85	56	27	1444	11	—	—	—	—	—	1.29	159	0.82	4.42
1-2, 61-79	2.20	14	1	1470	—	—	—	—	—	—	1.17	278	0.88	7.71
1-3, 60-89	3.75	56	68	1452	15	—	—	—	—	—	1.30	154	0.81	4.28
1-4, 41-69	5.05	44	27	1449	12	—	—	—	—	—	1.29	159	0.81	4.41
1-5, 82-109	6.95	102	55	1458	14	—	—	—	—	—	1.28	169	0.83	4.70
2-1, 48-80	12.24	70	57	1461	9	—	—	—	—	—	1.18	262	0.88	7.27
2-2, 60-102	13.91	68	59	—	7	—	—	—	—	—	1.24	197	0.84	5.46

Table 1. (Continued).

		Shipboard									Laboratory			
		Shear strength												
Core-Section (interval or level in cm)	Av. sbd (m)	Torvane (g/cm^2)	W.F. (g/cm^2)	P-wave velocity (m/s)	S-wave velocity (m/s)	GRAPE bulk density (g/cm^3)	Bulk density (g/cm^3)	Water content (%)	Porosity	Void ratio	Bulk density (g/cm^3)	Water content (%)	Porosity	Void ratio
Hole 576B (Cont.)														
2-3, 69-102	15.46	58	43	1465	21	—	—	—	—	—	1.23	212	0.85	5.87
2-4, 41-96	21.29	82	62	1457	15	—	—	—	—	—	1.28	167	0.82	4.63
2-5, 31-89	22.70	115	142	1521	63	—	—	—	—	—	1.28	167	0.82	4.64
2-5, 79-80	22.89	—	—	1471	—	—	—	—	—	—	1.30	158	0.81	4.37
2-6, 62-89	24.36	125	146	1459	62	—	—	—	—	—	1.30	156	0.81	4.34
3-1, 42-69	21.65	140	107	1451	41	—	—	—	—	—	1.31	152	0.81	4.23
3-1, 69-73	21.81	—	109	1448	—	—	—	—	—	—	—	—	—	—
3-2, 51-81	23.26	122	—	—	41	—	—	—	—	—	1.32	146	0.80	4.04
3-3, 12-43	24.38	138	105	1451	33	—	—	—	—	—	1.36	127	0.78	3.52
3-4, 101-146	26.84	142	—	1444	30	—	—	—	—	—	1.37	122	0.77	3.40
3-4, 128	26.88	—	—	1446	—	—	—	—	—	—	—	—	—	—
3-5, 44	27.54	—	—	—	35	—	—	—	—	—	—	—	—	—
3-5, 83	27.93	—	—	—	14	—	—	—	—	—	—	—	—	—
3-5, 57-115	27.96	126	—	1445	41	—	—	—	—	—	—	—	—	—
3-6, 14	28.74	140	—	—	—	—	—	—	—	—	—	—	—	—
3-6, 36-79	29.17	230	209	1449	47	—	—	—	—	—	1.38	119	0.77	3.32
4-4, 61-78	38.30	240	198	1448	50	—	—	—	—	—	1.34	132	0.79	3.68
4-5, 41-59	39.60	260	227	1453	50	—	—	—	—	—	1.29	162	0.82	4.50
4-6, 61-81	41.31	250	232	1444	51	—	—	—	—	—	1.31	150	0.81	4.17
5-2, 70-113	42.51	240	237	1516	49	—	—	—	—	—	1.33	139	0.79	3.85
5-2, 100	42.60	—	—	—	51	—	—	—	—	—	—	—	—	—
5-3, 70-91	43.91	370	—	1463	58	—	—	—	—	—	1.35	129	0.78	3.59
5-4, 61-82	45.32	410	337	1435	68	—	—	—	—	—	1.42	103	0.74	2.86
5-5, 62-81	46.82	340	318	1452	65	—	—	—	—	—	1.40	110	0.75	3.05
5-6, 57-80	48.28	320	318	1456	65	—	—	—	—	—	1.38	119	0.77	3.30
6-2, 61-82	51.82	440	409	1453	68	—	—	—	—	—	1.36	127	0.78	3.53
6-3, 62-81	53.32	390	—	1455	68	—	—	—	—	—	1.40	111	0.76	3.09
6-4, 61-82	54.82	550	519	1456	72	—	—	—	—	—	1.35	130	0.78	3.61
6-5, 34 76	56.15	—	141	1504	38	—	—	—	—	—	1.68	52	0.59	1.45
6-5, 95	56.55	—	—	—	72	—	—	—	—	—	—	—	—	—
7-1, 59-82	59.78	190	55	1492	41	—	—	—	—	—	1.64	58	0.62	1.61
7-5, 106-124	68.15	250	—	1505	40	—	—	—	—	—	1.68	51	0.59	1.44
8-2, 73-98	69.81	900	707	1512	121	—	—	—	—	—	1.73	45	0.56	1.27
8-2, 89	69.84	—	—	1474	—	—	—	—	—	—	1.37	122	0.77	3.38
8-3, 69-84	71.22	1000	1060	1480	127	—	—	—	—	—	1.26	182	0.84	5.05
Hole 577														
1-1, 20-66	0.43	36	—	1506	—	1.72	1.48	88	0.71	2.44	1.47	90	0.72	2.51
1-1, 72	0.72	94	—	—	—	—	—	—	—	—	—	—	—	—
1-3, 74-100	3.87	121	184	1472	39	1.63	1.42	104	0.74	2.88	1.46	93	0.72	2.58
1-4, 12-26	4.69	380	147	1470	—	1.66	1.51	79	0.69	2.21	1.50	82	0.70	2.28
2-2, 69-77	9.04	210	—	1502	36	—	—	—	—	—	1.51	80	0.69	2.22
2-4, 54-74	11.95	380	140	1520	35	1.53	1.46	92	0.72	2.55	1.55	72	0.67	2.00
2-6, 58-94	15.07	330	191	1492	36	1.63	1.51	80	0.69	2.21	1.60	63	0.64	1.75
3-2, 78-84	18.62	130	—	1477	—	—	—	—	—	—	1.47	89	0.71	2.48
3-4, 60-80	21.51	480	169	1480	53	1.72	1.56	71	0.66	1.97	1.59	64	0.64	1.79
3-5, 60	22.91	—	—	1477	—	—	—	—	—	—	—	—	—	—
3-5, 56-73	22.95	420	206	1480	44	1.67	1.58	66	0.65	2.69	1.55	72	0.67	2.00
4-3, 79-100	29.70	450	276	1476	53	1.69	—	—	—	—	—	—	—	—
4-4, 66-85	31.07	340	213	1486	35	1.50	1.59	66	0.64	1.81	1.57	68	0.66	1.90
4-6, 49-68	33.89	400	133	1467	34	1.67	1.54	74	0.67	2.16	1.54	74	0.67	2.07
5-2, 66-85	37.57	400	280	1470	41	1.75	1.58	66	0.65	1.83	1.57	68	0.66	1.91
5-4, 68-82	40.56	580	339	1467	64	1.66	1.57	69	0.66	1.91	1.58	66	0.65	1.84
5-5, 67-85	42.07	550	317	1473	69	1.76	1.58	66	0.65	1.83	1.55	72	0.67	2.00
6-1, 69-85	45.58	410	—	1472	44	1.65	1.55	72	0.67	1.99	1.56	70	0.66	1.95
6-3, 33-85	48.40	410	294	1472	43	1.59	1.59	65	0.64	1.80	1.55	72	0.67	2.01
6-5, 66	51.47	—	—	1479	—	—	—	—	—	—	—	—	—	—
6-5, 56-79	51.49	560	427	1479	67	1.69	1.56	71	0.66	1.97	1.56	70	0.66	1.95
6-6, 69-87	53.09	380	—	1484	43	1.67	1.60	63	0.64	1.75	1.59	65	0.65	1.82
7-1, 62-86	55.05	300	258	—	57	1.72	1.55	73	0.67	2.01	1.53	77	0.68	2.14
7-3, 62-81	58.03	320	302	—	55	1.69	1.58	68	0.65	1.87	1.57	68	0.65	1.89
7-5, 55-81	60.99	260	250	1516	—	1.82	1.72	48	0.57	1.33	1.70	49	0.58	1.38
8-1, 68-87	64.59	250	52	1492	—	1.83	1.66	55	0.60	1.51	1.66	55	0.61	1.54
8-3, 78-95	67.68	180	29	1506	—	1.92	1.72	48	0.57	1.32	1.68	52	0.59	1.45
8-5, 62-98	70.61	110	35	1605	—	1.82	1.72	48	0.57	1.32	1.67	53	0.60	1.48
9-1, 64-100	74.13	96	27	1607	—	1.79	1.72	47	0.57	1.31	1.72	47	0.57	1.31
9-3, 66-98	77.13	115	43	1533	—	1.81	1.71	49	0.57	1.34	1.68	51	0.59	1.44
9-6, 51-87	81.50	88	18	—	58	1.93	1.66	56	0.61	1.54	1.66	54	0.60	1.52
10-1, 70	83.51	—	—	—	—	1.78	—	—	—	—	—	—	—	—
10-2, 66-96	85.12	112	31	1525	—	—	1.71	48	0.57	1.33	1.69	51	0.59	1.42
10-4, 55-88	88.02	142	16	—	64	1.45	1.72	48	0.57	1.33	1.73	46	0.56	1.30
10-6, 57-100	91.07	142	16	1510	61	1.78	1.72	48	0.57	1.33	1.69	51	0.59	1.42

Table 1. (Continued).

Core-Section (interval or level in cm)	Av. sbd (m)	Shipboard									Laboratory			
		Shear strength (g/cm^2)		P-wave velocity (m/s)	S-wave velocity (m/s)	GRAPE bulk density (g/cm^3)	Bulk density (g/cm^3)	Water content (%)	Porosity	Void ratio	Bulk density (g/cm^3)	Water content (%)	Porosity	Void ratio
		Torvane	W.F.											
Hole 577 (Cont.)														
11-1, 71–101	93.17	180	—	1529	39	1.79	1.72	47	0.56	1.30	1.72	48	0.57	1.33
11-4, 100–117	97.90	200	—	1516	—	—	1.72	47	0.57	1.32	1.69	50	0.58	1.40
11-5, 110–122	99.47	200	—	1502	—	—	—	—	—	—	1.67	53	0.60	1.48
Hole 577A														
1-4, 3–16	4.60	420	125	1524	41	—	—	—	—	—	1.51	80	0.69	2.23
1-6, 122–136	8.79	310	18	1471	55	—	—	—	—	—	1.39	113	0.76	3.14
2-4, 3–18	14.00	435	118	1485	49	—	—	—	—	—	1.49	85	0.70	2.37
3-2, 5–19	20.52	150	74	1494	30	—	—	—	—	—	1.51	80	0.69	2.23
3-4, 128–137	24.72	355	—	1483	50	—	—	—	—	—	1.55	73	0.67	2.03
4-4, 3–28	33.05	550	98	1491	43	—	—	—	—	—	1.57	69	0.66	1.91
4-6, 114–137	37.16	290	74	1485	32	—	—	—	—	—	1.59	65	0.64	1.81
5-2, 122–137	40.70	215	51	1474	28	—	—	—	—	—	1.58	66	0.65	1.84
5-6, 4–20	45.52	580	297	1465	55	—	—	—	—	—	1.55	72	0.67	2.00
6-3, 124–137	51.70	500	431	1468	65	—	—	—	—	—	1.53	77	0.68	2.13
6-6, 122–136	56.19	350	261	1482	42	—	—	—	—	—	1.56	70	0.66	1.94
7-2, 109–133	59.61	250	86	1464	41	—	—	—	—	—	1.54	73	0.67	2.04
7-6, 107–128	65.57	124	41	1521	58	—	—	—	—	—	1.69	51	0.59	1.43
8-1, 118–135	67.66	100	33	1537	—	—	—	—	—	—	1.69	50	0.58	1.40
8-4, 104–135	72.10	92	29	1524	46	—	—	—	—	—	1.70	50	0.58	1.39
9-2, 120–135	78.68	62	8	1607	—	—	—	—	—	—	1.69	50	0.58	1.40
10-3, 114–133	89.64	68	3	1531	—	—	—	—	—	—	1.73	46	0.56	1.28
10-6, 2–6	92.94	370	—	1513	36	—	—	—	—	—	1.67	54	0.60	1.50
11-4, 4–19	99.52	104	14	1524	23	—	—	—	—	—	1.68	52	0.59	1.46
11-6, 128–136	103.72	152	62	1504	36	—	—	—	—	—	1.65	56	0.61	1.57
12-3, 12–29	107.60	114	103	1595	27	—	—	—	—	—	1.54	73	0.67	2.03
12-5, 120–142	111.71	126	27	1522	46	—	—	—	—	—	1.72	47	0.57	1.31
13-4, 7–23	118.55	116	16	1515	28	—	—	—	—	—	1.68	51	0.59	1.43
13-6, 114–130	122.62	108	16	1507	43	—	—	—	—	—	1.67	53	0.60	1.49
Hole 578														
1-1, 120–140	1.30	28	21	1460	—	1.56	1.25	189	0.84	5.22	1.34	134	0.79	3.72
1-3, 112–138	4.25	54	55	1461	—	1.59	1.31	151	0.81	4.19	1.30	158	0.81	4.39
2-2, 77–100	7.19	60	37	1563	—	1.56	1.28	166	0.82	4.59	1.26	179	0.83	4.98
2-2, 93	7.23	—	—	1485	—	—	—	—	—	—	—	—	—	—
2-2, 111	7.41	—	—	1562	—	—	—	—	—	—	—	—	—	—
2-3, 50–71	8.40	120	231	1474	28	1.44	1.29	164	0.82	4.55	1.25	188	0.84	5.21
2-3, 93	8.73	—	—	1485	—	—	—	—	—	—	—	—	—	—
2-4, 73–97	10.15	410	199	1468	51	1.49	1.31	149	0.80	4.12	1.30	159	0.81	4.41
2-4, 122	10.52	110	—	—	—	—	—	—	—	—	—	—	—	—
3-2, 89–110	16.80	165	156	1468	43	1.57	1.25	192	0.84	5.30	1.25	191	0.84	5.31
3-3, 70–71	18.01	—	—	1490	—	—	—	—	—	—	1.30	157	0.81	4.37
3-3, 90	18.20	—	—	1470	—	—	—	—	—	—	—	—	—	—
3-3, 110	18.40	—	—	1524	—	—	—	—	—	—	—	—	—	—
3-3, 113	18.43	—	—	1653	—	—	—	—	—	—	—	—	—	—
3-3, 134	18.64	—	—	1505	—	—	—	—	—	—	—	—	—	—
3-4, 102–122	19.92	235	277	1465	43	1.53	1.33	141	0.80	3.90	1.32	144	0.80	4.00
3-5, 63	20.93	—	—	1770	—	—	—	—	—	—	—	—	—	—
3-6, 81–102	22.71	190	154	1468	39	1.50	1.32	144	0.80	3.99	1.33	142	0.80	3.94
3-6, 113	22.93	—	—	1653	—	—	—	—	—	—	1.77	42	0.54	1.18
3-6, 117	22.97	—	—	1462	—	—	—	—	—	—	—	—	—	—
4-2, 49–70	25.89	270	133	—	41	1.45	1.33	139	0.79	3.84	1.32	143	0.80	3.96
4-3, 20–141	27.61	310	283	1642	73	1.59	—	—	—	—	1.39	112	0.76	3.11
4-3, 129	28.09	—	—	1475	—	—	—	—	—	—	—	—	—	—
4-5, 60–82	30.51	370	197	1460	58	1.49	1.34	137	0.79	3.78	1.33	140	0.80	3.88
5-2, 21–42	35.11	210	131	1469	39	1.48	1.33	138	0.79	3.81	1.36	123	0.77	3.43
5-3, 58–82	37.00	390	353	1478	—	1.36	1.34	135	0.80	3.72	1.34	133	0.79	3.70
5-5, 70–98	40.14	285	320	1468	46	—	—	—	—	—	1.35	130	0.78	3.62
5-5, 74–104	40.19	—	343	—	—	—	—	—	—	—	1.32	146	0.80	4.05
5-6, 77	41.57	—	—	—	55	—	—	—	—	—	—	—	—	—
6-2, 61–94	45.07	450	308	1468	91	1.40	1.32	145	0.80	4.02	1.32	146	0.80	4.05
6-3, 16	45.96	—	—	1671	—	—	—	—	—	—	—	—	—	—
6-3, 53	46.33	—	—	1630	—	—	—	—	—	—	—	—	—	—
6-3, 69	46.49	—	—	1431	—	—	—	—	—	—	—	—	—	—
6-3, 116	46.96	—	—	1569	—	—	—	—	—	—	—	—	—	—
6-3, 123	47.03	—	—	1470	—	—	—	—	—	—	—	—	—	—
6-3, 129	47.09	—	—	1554	—	—	—	—	—	—	—	—	—	—
6-3, 144	47.24	—	—	1463	—	—	—	—	—	—	—	—	—	—
6-4, 72–100	48.16	415	466	1473	38	1.35	1.26	181	0.83	5.00	1.27	179	0.83	4.97
6-6, 61–82	51.01	315	279	1469	39	1.39	1.29	160	0.81	4.42	1.28	170	0.83	4.73
7-2, 81–97	54.69	275	168	—	—	1.30	1.27	173	0.83	4.78	1.28	165	0.82	4.58

Table 1. (Continued).

		Shipboard									Laboratory			
		Shear strength												
Core-Section (interval or level in cm)	Av. sbd (m)	Torvane (g/cm^2)	W.F. (g/cm^2)	P-wave velocity (m/s)	S-wave velocity (m/s)	GRAPE bulk density (g/cm^3)	Bulk density (g/cm^3)	Water content (%)	Porosity	Void ratio	Bulk density (g/cm^3)	Water content (%)	Porosity	Void ratio
Hole 578 (Cont.)														
7-4, 60-80	57.50	260	421	1470	—	1.37	1.28	170	0.83	4.71	1.27	179	0.83	4.96
7-6, 69-101	60.65	380	412	1468	—	1.43	1.32	144	0.80	3.00	1.29	161	0.82	4.46
8-2, 89-101	64.25	345	—	1461	—	1.37	1.29	161	0.82	4.45	1.30	154	0.81	4.29
8-4, 111-122	67.47	350	431	1486	—	1.73	1.43	100	0.73	2.76	1.38	117	0.76	3.24
8-6, 62-80	70.01	305	242	1508	57	1.42	1.42	105	0.74	2.90	1.48	86	0.71	2.40
9-2, 110-133	74.02	420	232	1463	49	1.41	1.34	134	0.79	3.71	1.33	140	0.80	3.89
9-4, 109-132	77.01	400	261	1454	51	1.38	1.32	144	0.80	3.97	1.33	142	0.80	3.94
9-6, 69-582	82.06	430	332	1470	53	1.46	1.35	123	0.77	3.40	1.35	129	0.78	3.59
10-2, 90-111	83.31	460	283	1448	64	1.37	1.35	132	0.78	3.65	1.34	136	0.79	3.78
10-4, 99-122	86.40	510	523	1464	64	1.36	1.32	144	0.80	3.99	1.31	152	0.81	4.23
10-4, 131	86.61	—	449	—	—	—	—	—	—	—	—	—	—	—
10-6, 50-72	88.91	520	375	1469	61	1.35	1.33	138	0.79	3.83	1.32	142	0.80	3.95
11-2, 110-130	93.00	530	346	1462	64	1.29	1.33	138	0.79	3.82	1.32	143	0.80	3.96
11-2, 137	93.17	—	324	—	—	—	—	—	—	—	—	—	—	—
11-4, 90-113	95.81	—	431	—	64	1.46	1.33	137	0.79	3.79	1.33	142	0.80	3.94
11-6, 69-93	98.61	640	441	1466	64	1.40	1.36	126	0.78	3.49	1.37	122	0.77	3.39
12-2, 27-113	102.00	605	443	1463	65	1.34	1.34	134	0.79	3.71	1.64	57	0.61	1.58
12-2, 90	102.20	—	—	—	—	—	—	—	—	—	1.33	138	0.79	3.84
12-5, 90-113	106.81	720	632	1465	85	1.34	1.35	129	0.78	3.56	1.34	133	0.79	3.69
13-2, 77-112	111.74	700	464	1459	64	1.40	1.31	148	0.80	4.09	1.31	149	0.81	4.15
13-4, 110-124	114.97	550	449	1459	62	1.27	1.33	141	0.80	3.91	1.32	143	0.80	3.98
13-6, 73-110	117.72	575	497	1480	65	1.50	1.38	117	0.76	3.24	1.38	116	0.76	3.24
14-2, 60-114	121.17	775	479	1469	85	2.01	1.35	130	0.78	3.60	1.32	143	0.80	3.97
14-4, 80-114	124.27	1025	1104	1467	98	1.98	1.38	117	0.77	3.25	1.38	117	0.76	3.24
14-6, 59-106	127.13	850	1237	1471	91	2.10	1.47	90	0.71	2.49	1.40	110	0.75	3.05
15-2, 79-112	130.75	888	1023	1469	128	1.93	1.45	94	0.72	2.60	1.43	99	0.73	2.77
15-4, 77-112	133.75	—	1082	1479	121	2.04	1.48	88	0.71	2.44	1.47	90	0.71	2.50
15-6, 77-112	136.75	900	1001	1482	128	2.00	1.47	89	0.71	2.47	1.47	89	0.71	2.49
16-2, 78-116	140.27	625	982	1484	128	—	1.51	81	0.69	2.23	1.52	77	0.68	2.15
16-3, 95	141.75	—	—	—	—	1.69	—	—	—	—	—	—	—	—
16-4, 90-112	143.31	950	913	1477	128	1.65	1.47	91	0.72	2.51	1.44	96	0.73	2.67
17-1, 90-112	148.31	1025	994	1474	—	1.48	1.49	86	0.70	2.37	1.47	91	0.72	2.53
17-3, 88-114	151.31	975	1001	1468	—	1.45	1.47	89	0.71	2.47	1.47	88	0.71	2.46
17-5, 89-116	154.33	1050	1215	1468	—	1.49	1.44	99	0.73	2.75	1.42	103	0.74	2.87
18-3, 90-113	160.82	1500	1413	1510	134	1.79	1.64	58	0.62	1.61	1.61	61	0.63	1.70
18-4, 92-113	162.33	1600	1539	1468	—	—	—	—	—	—	1.60	63	0.64	1.77
19-1, 90-111	167.31	1650	1200	1491	21	1.71	1.60	64	0.64	1.78	1.57	69	0.66	1.91
19-3, 89-111	170.30	1700	1325	1519	159	1.66	1.60	63	0.64	1.75	1.59	65	0.64	1.81
20-1, 24-41	176.13	1700	1303	1527	—	2.17	1.59	66	0.65	1.82	1.56	70	0.66	1.94
20-4, 36	180.66	—	—	—	142	—	—	—	—	—	—	—	—	—
Hole 579														
1-2, 112-122	2.67	24	23	1484	—	—	1.22	220	0.86	6.09	1.21	231	0.87	6.40
1-5, 114-123	7.19	44	41	1485	—	—	1.26	186	0.84	5.08	1.27	1.75	0.83	4.85
2-2, 124-145	11.25	96	86	1493	18	—	1.30	157	0.81	4.34	1.28	169	0.82	4.70
2-5, 85-88	15.26	—	—	1475	—	—	1.28	167	0.82	4.62	1.30	159	0.81	4.40
Hole 579A														
1-3, 60-105	17.83	210	265	1474	43	1.38	1.29	184	0.84	5.08	1.27	173	0.83	4.80
1-5, 84-116	21.00	200	125	1472	41	1.41	1.31	150	0.81	4.14	1.31	153	0.81	4.24
2-3, 68-122	27.45	250	96	1488	46	1.50	1.35	131	0.78	3.62	1.28	167	0.82	4.63
2-5, 64-96	30.30	220	193	1477	40	1.45	1.32	145	0.80	4.00	1.31	148	0.80	4.11
3-2, 57-84	35.20	160	107	1488	32	—	1.34	132	0.79	3.66	1.40	111	0.76	3.09
3-5, 42-78	39.60	240	304	1499	44	1.45	1.40	111	0.77	3.07	1.38	118	0.77	3.28
4-1, 69-110	43.39	160	176	1474	35	1.35	1.27	176	0.83	4.88	—	—	—	—
4-2, 69	44.69	—	—	—	—	—	—	—	—	—	1.27	173	0.83	4.80
4-3, 77-109	46.43	200	193	1480	40	—	1.27	175	0.73	4.83	1.27	174	0.83	4.83
5-2, 80-96	54.38	80	47	1462	—	1.39	1.29	164	0.72	4.63	1.28	165	0.82	4.59
5-5, 8	58.08	—	—	1606	—	—	—	—	—	—	—	—	—	—
5-5, 19	58.19	—	—	1500	—	—	—	—	—	—	—	—	—	—
5-5, 69-88	58.78	410	332	1484	46	1.42	1.29	162	0.82	4.49	1.26	183	0.84	5.08
6-3, 74-109	65.41	460	328	1484	53	1.39	1.27	175	0.83	4.85	1.28	169	0.82	4.68
6-5, 14-57	67.85	380	380	1491	46	1.41	1.30	157	0.81	4.33	1.28	166	0.82	4.61
6-5, 83-99	68.41	100	107	1473	—	—	1.33	140	0.80	3.89	1.29	161	0.82	4.46
7-2, 99-117	73.58	240	185	1484	40	1.40	1.24	197	0.84	5.46	1.25	190	0.84	5.26
7-4, 120-136	76.78	380	—	1486	—	1.42	1.30	157	0.71	4.35	1.29	164	0.82	4.55
8-1, 98	81.48	—	—	1478	—	—	—	—	—	—	—	—	—	—
8-1, 102-114	81.58	470	250	1462	—	1.39	1.31	151	0.81	4.17	1.31	152	0.81	4.23
8-5, 121-137	87.79	470	349	1488	—	—	1.28	166	0.72	4.60	1.28	172	0.83	4.76
9-2, 67-76	92.22	425	293	1472	—	1.33	1.25	195	0.84	5.40	1.25	188	0.84	5.22
9-5, 48-73	96.60	1000	807	1491	—	1.35	1.24	200	0.85	5.54	1.24	195	0.84	5.42

Table 1. (Continued).

		Shipboard									Laboratory			
Core-Section (interval or level in cm)	Av. sbd (m)	Shear strength		P-wave velocity (m/s)	S-wave velocity (m/s)	GRAPE bulk density (g/cm^3)	Bulk density (g/cm^3)	Water content (%)	Porosity	Void ratio	Bulk density (g/cm^3)	Water content (%)	Porosity	Void ratio
		Torvane (g/cm^2)	W.F.											
Hole 579A (Cont.)														
10-3, 100–112	103.56	750	604	1483	—	1.33	1.24	228	0.86	6.32	1.23	212	0.85	5.89
10-5, 57–67	106.12	500	559	1495	—	1.39	1.26	181	0.83	5.01	1.24	199	0.85	5.53
11-2, 104–126	111.65	575	633	1480	—	—	1.23	213	0.85	5.89	1.22	216	0.86	5.98
11-4, 73–100	114.36	725	670	1474	—	—	1.34	199	0.85	5.49	1.23	212	0.85	5.88
12-2, 97–114	121.06	650	456	1476	—	1.36	1.24	201	0.85	5.56	1.22	222	0.86	6.16
12-4, 79–111	123.95	688	788	1480	—	—	1.22	214	0.86	5.93	1.23	206	0.85	5.73
13-2, 91–115	130.53	750	434	1477	—	1.33	1.22	223	0.86	6.18	1.21	228	0.86	6.33
13-4, 79–114	133.47	650	456	1481	—	1.32	1.21	228	0.86	6.30	—	—	—	—
14-2, 70–104	139.87	525	339	1478	—	1.30	1.23	208	0.85	5.76	—	—	—	—
14-4, 66–107	142.86	575	471	1485	—	1.37	1.25	194	0.84	5.38	1.23	205	0.85	5.68
15-2, 43–57	149.00	625	552	1476	—	1.44	1.30	158	0.81	4.38	1.28	165	0.82	4.59
Hole 580														
1-2, 105–117	2.61	72	41	1473	—	1.40	1.24	203	0.85	5.62	1.27	173	0.83	4.79
1-2, 137	2.87	—	—	1646	—	—	—	—	—	—	—	—	—	—
2-2, 60–85	5.52	48	34	1479	—	1.39	1.21	232	0.86	6.42	1.27	174	0.83	4.84
2-4, 107–125	8.96	74	51	1479	—	1.34	1.19	251	0.87	6.94	1.25	193	0.84	5.35
3-3, 70–84	16.57	92	50	1486	—	1.43	1.30	157	0.81	4.31	1.30	156	0.81	4.33
3-6, 82–94	21.18	128	83	1470	—	1.45	1.27	176	0.83	4.88	1.27	175	0.83	4.85
4-2, 59–108	24.63	102	68	1465	—	1.44	1.26	181	0.83	5.02	1.26	181	0.83	5.02
4-4, 78–115	27.77	164	119	1488	—	1.30	1.24	199	0.85	5.51	1.25	195	0.84	5.40
5-1, 67	32.47	—	—	—	—	1.55	—	—	—	—	—	—	—	—
5-2, 80–109	34.24	240	121	1464	—	1.42	1.28	172	0.83	4.75	1.28	169	0.82	4.70
5-4, 67–102	37.14	260	193	1486	—	—	1.34	134	0.79	3.69	1.29	162	0.82	4.50
6-2, 91–121	43.86	250	152	1479	—	1.47	1.32	146	0.80	4.04	—	—	—	—
6-5, 62–89	48.05	330	209	1472	—	1.39	1.31	152	0.81	4.20	1.27	178	0.83	4.94
7-2, 72–115	53.24	380	277	1476	—	1.41	1.25	191	0.84	5.29	1.27	177	0.83	4.92
7-4, 70–120	56.25	440	285	1467	—	1.41	1.32	145	0.80	4.02	1.30	158	0.81	4.39
8-2, 83–94	62.68	400	258	1488	—	1.56	1.38	117	0.76	3.23	1.31	152	0.81	4.22
8-5, 94–105	67.30	550	368	1489	—	1.47	1.33	141	0.80	3.91	1.30	153	0.81	4.26
8-5, 103	67.33	—	—	1512	—	—	—	—	—	—	—	—	—	—
8-5, 111	67.41	—	—	1586	—	—	—	—	—	—	—	—	—	—
8-5, 115	67.45	—	—	1473	—	—	—	—	—	—	—	—	—	—
9-2, 29–55	71.72	300	236	1486	—	—	1.22	214	0.86	5.92	1.27	176	0.83	4.88
9-2, 57	71.87	—	—	1486	—	—	—	—	—	—	—	—	—	—
9-2, 59	71.89	—	—	1543	—	—	—	—	—	—	—	—	—	—
9-2, 61	71.91	—	—	1477	—	—	—	—	—	—	—	—	—	—
9-2, 63	71.93	—	—	1476	—	—	—	—	—	—	—	—	—	—
9-2, 65	71.95	—	—	1474	—	—	—	—	—	—	—	—	—	—
9-2, 67	71.97	—	—	1493	—	—	—	—	—	—	—	—	—	—
9-2, 69	71.99	—	—	1492	—	—	—	—	—	—	—	—	—	—
9-2, 71	72.01	—	—	1489	—	—	—	—	—	—	—	—	—	—
9-2, 73	72.03	—	—	1497	—	—	—	—	—	—	—	—	—	—
9-2, 75	72.05	—	—	1507	—	—	—	—	—	—	—	—	—	—
9-2, 77	72.07	—	—	1524	—	—	—	—	—	—	—	—	—	—
9-2, 79	72.09	—	—	1559	—	—	—	—	—	—	—	—	—	—
9-2, 81	72.11	—	—	1600	—	—	—	—	—	—	—	—	—	—
9-2, 83	72.13	—	—	1603	—	—	—	—	—	—	—	—	—	—
9-2, 85	72.15	—	—	1616	—	—	—	—	—	—	—	—	—	—
9-2, 87	72.17	—	—	1614	—	—	—	—	—	—	—	—	—	—
9-3, 32	73.12	—	—	—	—	1.40	—	—	—	—	—	—	—	—
9-5, 73–86	76.60	465	361	1484	—	1.43	1.24	200	0.72	5.53	1.28	163	0.82	4.68
10-2, 112–122	81.97	650	471	1486	—	1.39	1.26	185	0.84	5.13	1.28	168	0.82	4.65
10-5, 108–120	86.44	575	567	1491	—	1.41	1.28	169	0.82	4.69	1.28	167	0.82	4.63
11-4, 112–122	94.47	520	353	1477	—	1.39	1.29	160	0.82	4.43	1.27	173	0.83	4.79
12-2, 74–92	100.63	475	375	1508	—	1.37	1.25	189	0.84	5.24	—	—	—	—
12-5, 66–76	105.01	550	545	1482	—	1.45	1.28	165	0.82	4.58	1.27	174	0.83	4.82
13-2, 39–96	109.98	475	464	1479	—	1.38	1.23	209	0.85	5.78	1.28	171	0.83	4.73
13-5, 71–85	114.58	520	449	1484	—	1.41	1.26	183	0.84	5.06	1.28	168	0.82	4.65
14-2, 101–119	119.90	380	368	1485	—	1.35	1.33	139	0.79	3.84	1.27	174	0.83	4.83
14-5, 76–85	124.10	450	795	1506	—	1.39	1.29	165	0.82	4.56	1.31	149	0.81	4.14
15-2, 74–115	129.25	600	699	1488	—	1.41	1.26	184	0.84	5.10	1.28	172	0.83	4.77
15-5, 66–83	133.55	680	596	1494	—	1.41	1.27	177	0.83	4.89	1.27	178	0.83	4.94
16-2, 82–159	139.00	655	567	1498	—	1.38	1.23	207	0.85	5.73	1.27	178	0.83	4.93
16-5, 110–121	143.45	715	714	1507	—	1.34	1.22	217	0.86	6.00	1.28	169	0.82	4.68
17-2, 125–133	148.59	860	891	1490	—	1.42	1.23	207	0.85	5.72	1.27	178	0.83	4.93
17-5, 121–129	153.05	570	589	1490	—	1.34	1.24	203	0.85	5.63	1.30	154	0.81	4.27
Hole 581														
2-6, 90–123	190.07	525	243	1495	—	1.35	1.25	193	0.84	5.33	1.21	229	0.86	6.36
2-6, 107–129	190.18	250	169	1500	—	—	—	—	—	—	—	—	—	—

Table 1. (Continued).

		Shipboard									Laboratory			
Core-Section (interval or level in cm)	Av. sbd (m)	Shear strength (g/cm²) Torvane	Shear strength (g/cm²) W.F.	P-wave velocity (m/s)	S-wave velocity (m/s)	GRAPE bulk density (g/cm³)	Bulk density (g/cm³)	Water content (%)	Porosity	Void ratio	Bulk density (g/cm³)	Water content (%)	Porosity	Void ratio
Hole 581 (Cont.)														
3-5, 124–135	198.30	200	221	1510	—	1.39	1.24	200	0.85	5.52	1.26	184	0.84	5.11
4-2, 60–70	202.65	600	692	1509	—	1.34	1.23	205	0.85	5.66	1.27	174	0.83	4.84
4-2, 122	203.22	—	—	1514	—	—	—	—	—	—	—	—	—	—
6-2, 95–114	222.05	1025	744	1513	—	1.41	1.28	171	0.83	4.72	1.25	187	0.84	5.18
6-5, 66–86	226.26	1275	640	1501	—	1.39	1.31	148	0.80	4.10	1.29	162	0.82	4.50
7-5, 60–78	235.69	750	655	1519	—	1.43	1.30	155	0.81	4.28	1.28	165	0.82	4.58
8-5, 11–100	245.06	1225	699	1484	—	1.56	1.39	115	0.76	3.18	1.29	161	0.82	4.46
8-5, 95	245.45	—	—	1478	—	—	—	—	—	—	—	—	—	—
9-4, 45–63	253.04	1038	780	1472	—	1.60	1.49	85	0.70	2.35	1.31	152	0.81	4.23
10-3, 100–114	261.57	913	1156	1474	—	1.63	1.54	75	0.67	2.08	1.32	146	0.80	4.06

Note: See Results for further explanation of column heads. — means not measured.

the effective normal stress has been reduced to nearly zero by the sampling process. It is not surprising, therefore, that the shear strength as measured by the vane is higher in clay sediments, which have higher values of cohesion. In addition, it is thought that the more brittle nature of the interparticle bonds in the carbonates compared with the clays will result in more structural disturbance during coring and recovery.

Two interesting aspects of the shear wave velocities should be mentioned here. First, measurements made parallel and perpendicular to the core axis indicate a total lack of anisotropy within any of the lithologies. Second, the large increase in both the shear strength and the shear wave velocities in the brown clay below 65 m (while interbedded with carbonates) may be indicative of the onset of diagenesis. The shear strength measurements also often display a systematic decrease in strength between the bottom of one core and the top of the next. This occurred even though the sediments appeared undisturbed. It is thought that this may reflect a decreasing disturbance factor for clays down the length of each hydraulic piston core. A "flow-in" section exists at around 30–38 m sub-bottom depth in Hole 576, which unfortunately coincides with a highly disturbed region in Hole 576B. Shear strength values in this section are much reduced (a factor of 1/2) indicating an *in situ* remolding sensitivity of 2. The shear wave velocity is also reduced in this section, but not as prominently.

Site 577

This site consists of about 120 m of nannofossil oozes which were divided into three lithologic units based on color changes (see Site 577 chapter, this volume). Physical property data for this site are presented for Holes 577 and 577A in Table 1. These data are presented graphically in Figure 4.

The water content profile shows some fluctuations near the surface but generally decreases from around 90 to 75% at 60 m. At this point there is a dramatic decrease to around 50% which is maintained down to 120 m. Note that the GRAPE bulk density does not show this important discontinuity in the data. A similar discontinuity is exhibited at 60 m in both the compressional wave velocity profile and in the shear strength profile; however, it is not clearly defined in the shear wave velocity profile. The compressional wave velocity fluctuates around 1475 m/s down to 60 m and then increases to around 1525 m/s for the remaining length of the holes with a few high-velocity layers around 1600 m/s. The shear strength profile exhibits a great deal of fluctuation down to 60 m with values ranging up to 600 g/cm². The shear strength is very low from 60 m down to the bottom of the holes at 120 m with values around 100 g/cm². For this site there was a distinct difference between values obtained from the hand-held Torvane and from the motorized vane, with the Torvane giving much higher readings. The shear wave velocity profile shows no definite trend and fluctuates around 50 m/s throughout the hole. Poor signal quality in most of these cores limits the accuracy of these measurements to ± 10 m/s.

The discontinuity exhibited by the water content, compressional wave velocity, and shear strength profiles at 60 m occurs just below the boundary between lithologic Units I and II. It corresponds to a possible 30 m.y. missing section in the mid-Tertiary (see Site 577 chapter, this volume) which, at sedimentation rates of 3.0 m/m.y., would represent 90 m of missing sediment. The rapid change in water content suggests that this may have been an erosional event because the material may be overconsolidated. However, the subtle (but distinct) increase in carbonate content across the boundary could mean that the different water contents are simply a function of the different types of skeletal material; in which case it could be argued that the hiatus was a nondepositional event. The increase in compressional wave velocity at the discontinuity is consistent with the decrease in water content. However, the decrease in shear strength is not so easily explained. It is suggested that the relatively subtle change in carbonate content from 90% above the boundary to 95% below is enough to reduce drastically the strength as a result of increased coring disturbance caused by an increase in the brittle nature of the bonds. Alternatively, it may simply reflect the change in cohesion caused by the small reduction in clay content. This is an

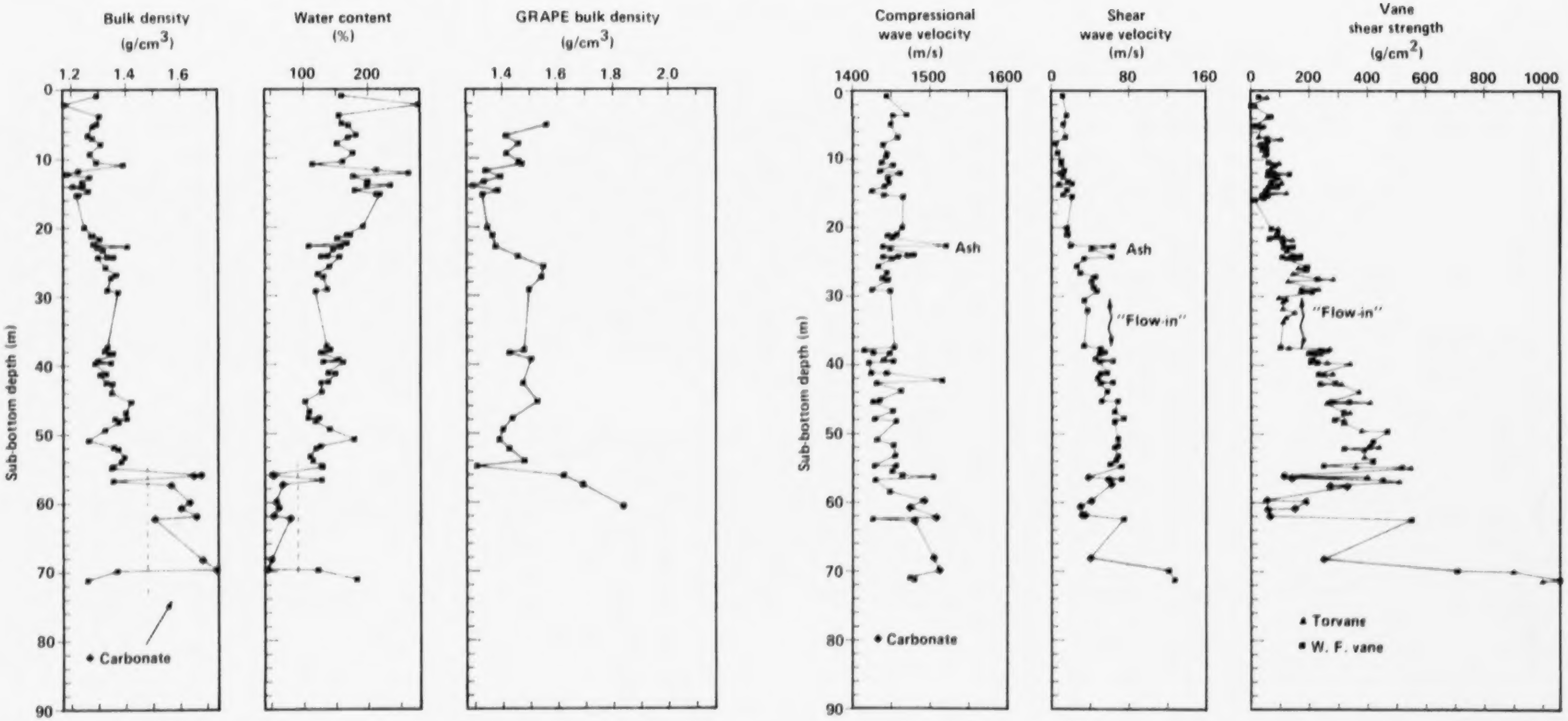

Figure 3. Gravimetric, GRAPE, velocity, and shear strength data for Site 576 (Holes 576 and 576B).

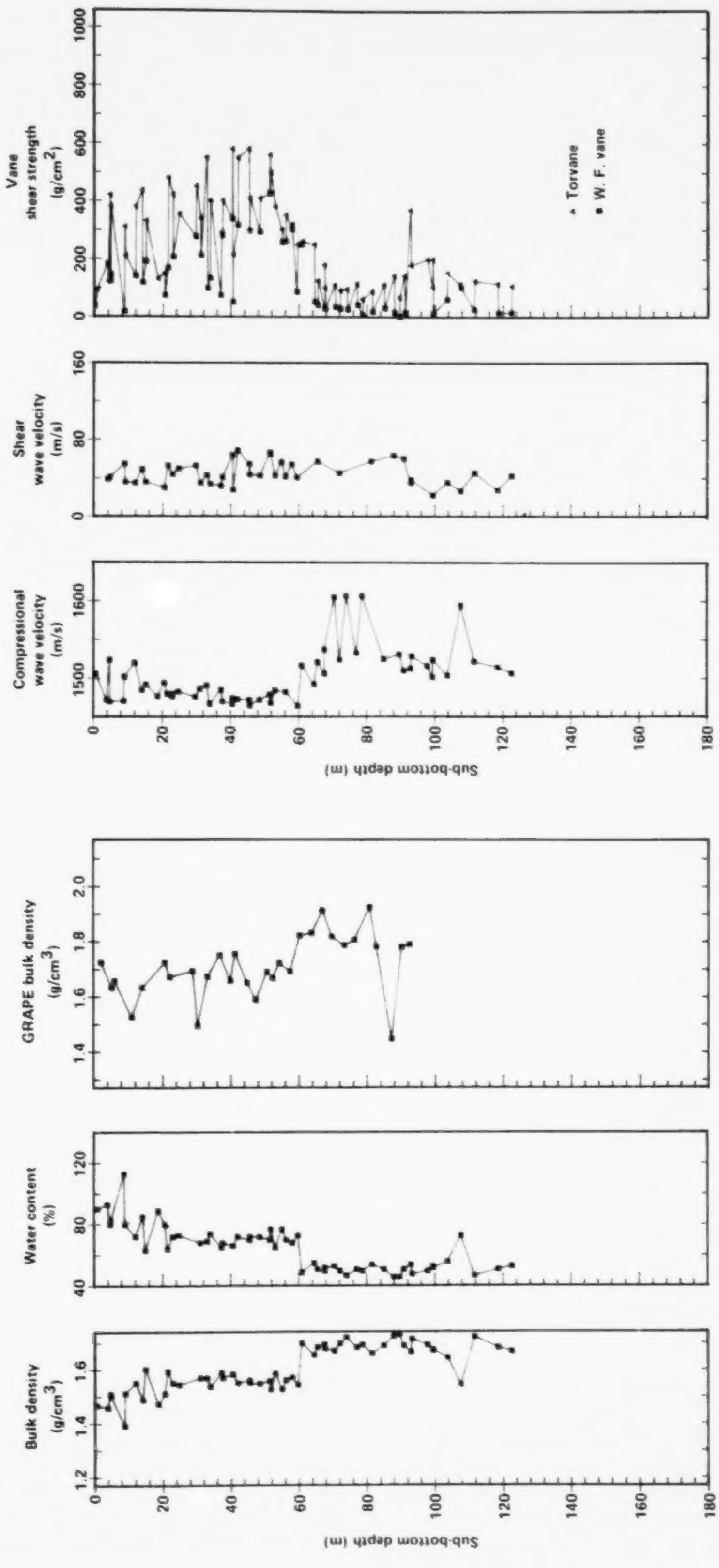

Figure 4. Gravimetric, GRAPE, velocity, and shear strength data for Site 577 (Holes 577 and 577A).

extension of the argument presented to explain the differences reported between clays and carbonates for Site 576.

Site 578

This site consists of a thick section of siliceous clays, (lithologic Units I and II) down to 124.5 m, below which a dark brown pelagic clay extends to 176 m (lithologic Unit III) (see Site 578 chapter, this volume). Within the siliceous clays numerous pyrite-cemented layers and ash layers occur. The data for Site 578 are presented in Table 1 and in Figure 5.

Some fluctuations occur in the water content profile but, generally, the water content decreases from around 175% near the surface to around 125% at the base of lithologic Unit II (124.5 m). Below this, the water content in the dark brown clay decreases more rapidly until at 170 m it is around 70%. The GRAPE bulk density profile shows a major discontinuity at around 120 m, which illustrates the sensitivity of the measurement to the mineral attenuation coefficient. The compressional wave profile is dominated by high-velocity layers of pyrite-indurated clay and ash beds superimposed on a constant velocity profile (around 1469 m/s) down to 160 m (Fig. 5). Only a few of the numerous higher velocity layers were measured but it can be assumed that they all have much higher velocities (between 1600 and 1800 m/s). This corresponds (where measurements were taken) to higher bulk densities (Fig. 5). Below 160 m there is some indication that a positive velocity gradient is developing in the very dark pelagic clay which is not consistent with an increase in bulk density. This may represent an early stage of diagenesis.

Shear wave velocities increase slowly from 40 m/s near the surface to 65 m/s at a depth of 120 m (Fig. 5). A rapid increase occurs between lithologic Units II and III with velocities reaching around 150 m/s at 170 m in the dark brown pelagic clay. Shear strength values exhibit some scatter but generally increase from less than 100 g/cm^2 near the surface to about 600 g/cm^2 at the base of lithologic Unit II (124.5 m). Below this, the value jumps to around 1000 g/cm^2 and increases to above 1600 g/cm^2 at 170 m in the dark brown pelagic clay. Recovery from hydraulically pistoned Cores 17, 18, 19, and 20 in the brown clay were progressively poorer, with Core 20 being only 0.81 m long. Shear strengths at around 1700 g/cm^2 in these pelagic brown clays obviously represent the operational limits of the HPC in its present configuration. It is also interesting to note that no flow-in occurred in these cores. Presumably, water must have flowed around the piston during pull-out as a result of the high lateral stresses plugging the core barrel.

Site 579

A thick section of siliceous clay with numerous ash and thin indurated layers occurs at this site. This single lithologic unit was divided into three subunits: a siliceous clay (0–60 m), a clayey siliceous ooze (60–102.5 m), and a clayey diatom ooze (102.5–149.5 m) (see Site 579 chapter, this volume). The data for this site are presented in Table 1 and in Figure 6.

The water content profile (Fig. 6) can be split into three units. Unit I (0–42 m) shows a decreasing water content from around 230 to 110% which may be the result of normal consolidation processes. There is a discontinuity between 40 and 42 m, where the water content suddenly increases from 110 to 175%. Unit II (42–134 m) exhibits an increased water content downcore from 175 to 228%. Below this, Unit III (134–149 m) shows the water content decreasing to 158%. These units do not correlate with any of the lithological subunits based on visual inspection and smear slide analyses. However, it could be inferred that the increase in water content from 40 to 134 m correlates with an increase in the siliceous microfossil content.

The compressional wave velocity profile (Fig. 6) is dominated by many (61) high-velocity ash layers and numerous (~325), thin (<0.5 cm), stiff-to-indurated, dark greenish grey layers. Velocities measured in a few ash layers are typically about 1600 m/s. The thin, indurated, green layers also have higher velocities (these values are not shown in Fig. 6) but they tend to be variable (one was as high as 1770 m/s). Velocities in the siliceous clay and ooze are remarkably uniform throughout the site at around 1480 m/s.

Shear wave velocity measurements (Fig. 6) were prematurely terminated at this site as one of the transducers broke on insertion. Despite being pushed into some very stiff sediments a large number of times, the somewhat fragile design had proved satisfactory until this time. The data obtained between 18 and 73 m show no distinct trends with depth, the velocity remaining nearly constant at around 45 m/s.

Shear strength measurements, although exhibiting a large amount of scatter, show increasing strength down the hole (Fig. 6). A major discontinuity occurs at 95 m with very high shear strengths below (up to 1000 g/cm^2) compared with shear strengths of about 400 g/cm^2 in shallower sections. This discontinuity does not correlate with any of the lithologic changes. A good example of "flow-in" is found at 68 m (the bottom of Section 579A-6-5). Measurement with both the hand-held and motorized vane shows that the remolded "flow-in" section had decreased in strength from 380 g/cm^2 in the "undisturbed" region to 100 g/cm^2 in the section containing "flow-in." This provides an *in situ* remolding sensitivity of about 4. A small reduction in the compressional wave velocity can also be seen at this point, although the remolding did not change the water content.

Site 580

The sediments cored at Site 580 are similar to those cored at Site 579 and consist of a thick section of siliceous clays with a large number of volcanic ash layers (89) and numerous, thin, stiff-to-indurated, dark greenish-grey layers (see Site 580 chapter, this volume). The data for this site are presented in Table 1 and in Figure 7.

The water content profile shows a remarkably high and constant value (~175%) throughout the entire hole with no variation resulting from changing microfossil content (Fig. 7). As at Sites 578 and 579, the compressional wave velocity profile is dominated by the high ve-

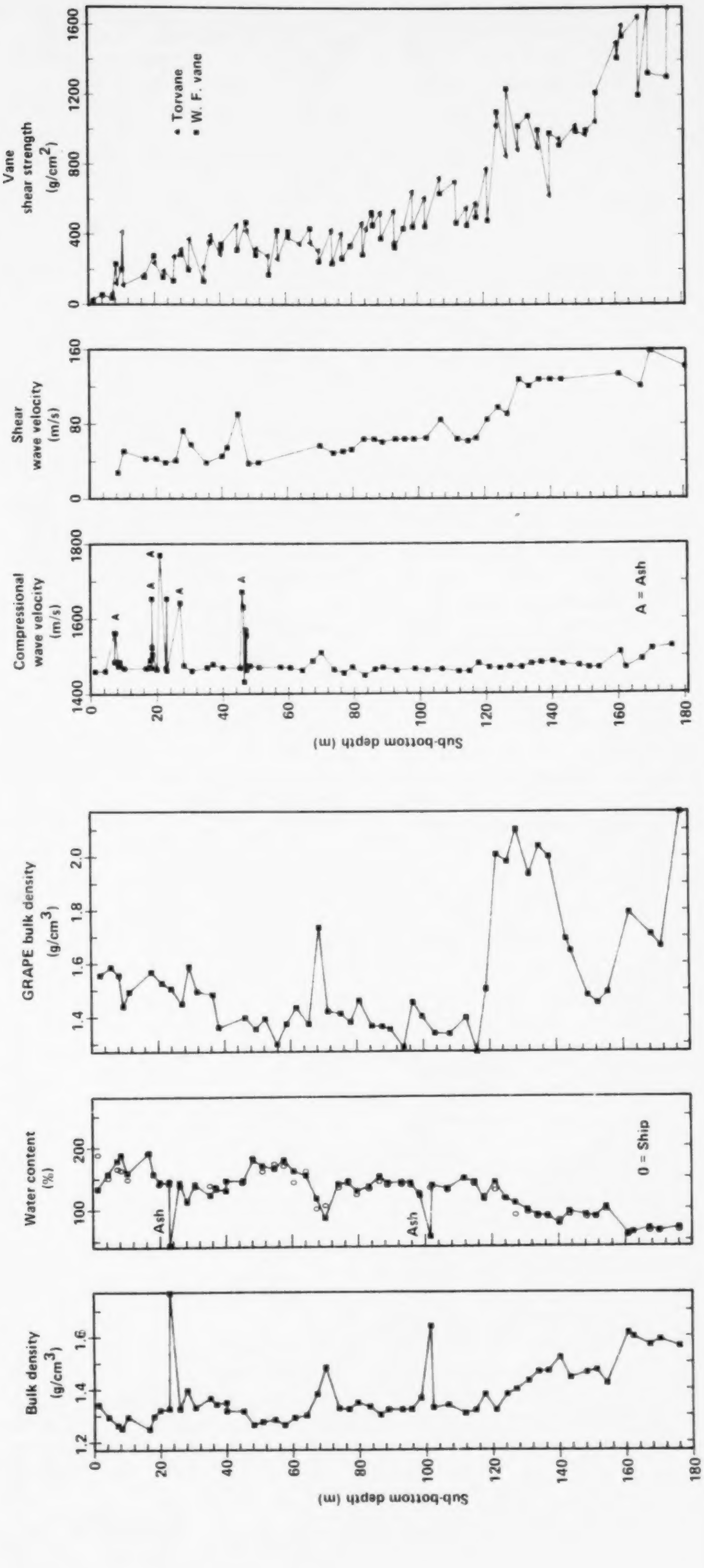

Figure 5. Gravimetric, GRAPE, velocity, and shear strength data for Site 578.

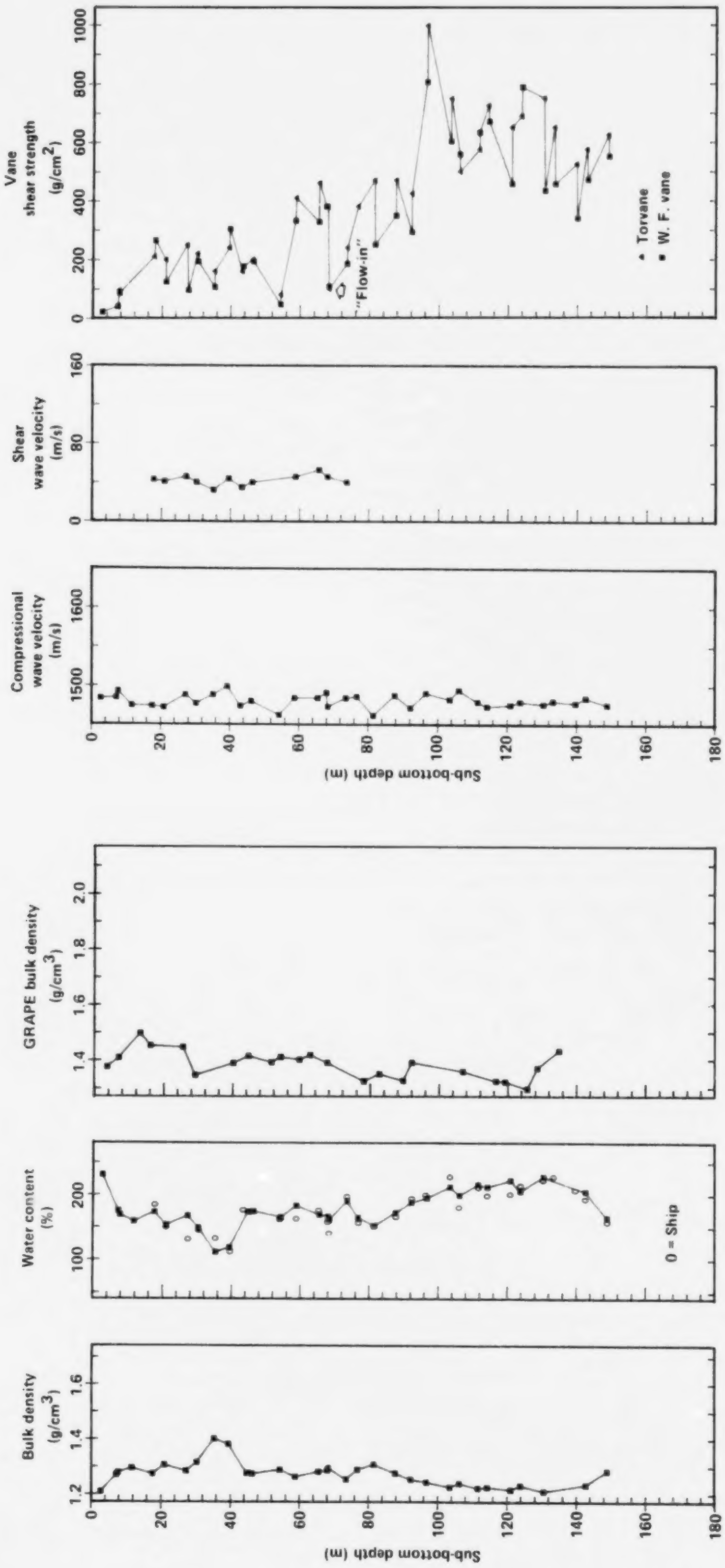

Figure 6. Gravimetric, GRAPE, velocity, and shear strength data for Site 579 (Holes 579 and 579A).

locity, indurated clay and ash layers. Only two of the ash layers are shown in Figure 7. Velocities in the siliceous clays and oozes rise gradually downhole from about 1470 m/s at the surface to about 1490 m/s at a depth of 150 m. The shear strength measurements show a nearly linear increase with depth ranging from only 20 g/cm^2 near the surface to over 800 g/cm^2 at 150 m (Fig. 7).

Site 581

Limited time restricted the coring program at this site. Consequently, sediments were only recovered between 181.5 and 276.6 m using the rotary core (see Site 581 chapter, this volume). Lithologic Unit I extends from 181.5 to 245 m and consists of a biosiliceous clay with some ash and indurated layers. This unit is similar to the siliceous clay found at Sites 579 and 580. Lithologic Unit II is a brown to dark brown pelagic clay similar and probably of comparable age to that found at Sites 576 and 578.

The physical properties data for Site 581 are presented in Table 1 and in Figure 8. The water content profile shows a decrease from 229% at 190 m to 146% at 261 m (Fig. 8). It should be noted that there is a large discrepancy toward the bottom of the hole between the shipboard data and the laboratory data that will be discussed later. Compressional wave velocity measurements show a constant profile in the siliceous clay unit at around 1505 m/s but this decreases to 1475 m/s in the brown pelagic clay (Fig. 8). Some compressional wave measurements were made on selected samples of chert and basalt (lithologic Units III and IV) and these varied between 4000 and 5500 m/s and are not shown in Figure 8.

The shear strength measurements (Fig. 8) should be viewed with even more caution than usual. Rotary coring causes significantly more structural disturbance than the HPC. This is true even when the stratigraphic sequence looks undisturbed. Much of the material in Cores 1-7 consists of alternating layers of soft and stiff sediments, a pattern that is probably caused by intermittent "rotation" and "punch" coring (rotation causing the most disturbance and hence the softer layers). Measurement sites were carefully selected in the largest sections of stiff material that could be found in each core. Even in the stiff sediments the shear strength measurements were hampered by the brittle nature of the semi-indurated sediments. This resulted in major cracks developing either upon initial insertion of the vane or during the test. The test is not valid unless the failure plane is cylindrical. In an attempt to overcome this problem, a slight pressure was applied to either side of the split core by using two strips of aluminium held together by G-clamps. This eliminated the gap between the liner and the sediment and prevented the major cracking.

The first few shear strength readings (between 190 and 210 m) were taken without the G-clamp modification and show low shear strengths (200–600 g/cm^2) because of cracking. All of the remaining measurements were made with the G-clamp and show higher but fluctuating values around 1000 g/cm^2. These values are not as high as those found in the similar dark brown pelagic clays at Site 578 ($>$1600 g/cm^2) despite being subjected to a much higher overburden stress. It is probable that these lower values can be mainly attributed to increased disturbance at Site 581 caused by the rotary drilling process.

DISCUSSION

Effective Stress Profiles

From the bulk density data, the vertical effective stress or overburden stress can be calculated down each hole. The total vertical pressure or effective stress (P) is given by

$$P = \Sigma(\gamma \Delta z)$$

where Δz is the incremental depth and γ is the submerged unit weight. Calculating γ from the bulk density, effective stress profiles for all six sites have been plotted in Figure 9. The position of the profile for Site 581 has been estimated assuming the upper sediments were similar to Sites 579 and 580. Figure 9 illustrates the large differences in effective stress character between the different sediment types. Site 577 has the smallest gradient caused by the most dense carbonate sediments (i.e., effective stress increases rapidly with sub-bottom depth). It also shows the change in gradient at 60 m where the mid-Tertiary hiatus occurs. Site 576 shows a decrease in gradient below 55 m where the sediment increases in density (brown clay to carbonate ooze). The siliceous clays at Sites 579 and 580 are very similar showing a complete lack of any significant consolidation throughout 150 m. At Site 581, the decreasing gradient indicates that some consolidation is occurring when the depth approaches 250 m.

Water Content

There is some discrepancy between the values of water content calculated from the shipboard measurements and those from the laboratory measurements. For Sites 578, 579, 580, and 581, the shipboard measurements have been plotted alongside the shore-based laboratory measurements (Figs. 5, 6, 7, and 8, respectively). For Sites 576 and 577, the shipboard measurements are almost identical to the laboratory measurements (see Table 1), hence only the laboratory values have been plotted. This situation is similar for Sites 578 and 579 (see Figs. 5 and 6). However, the discrepancy arises for Sites 580 and 581 (see Figs. 7 and 8). For Site 580, the shipboard measurements show approximately the same values as the laboratory measurements but they exhibit more scatter (Fig. 7). For Site 581, the shipboard measurements below 240 m are substantially less than the laboratory values (Fig. 8). The only variable that can be attributed to these differences is ship motion and the resulting inaccuracy of the shipboard weighings on the triple beam balance. Ship motion during Leg 86 was marginally worse during op-

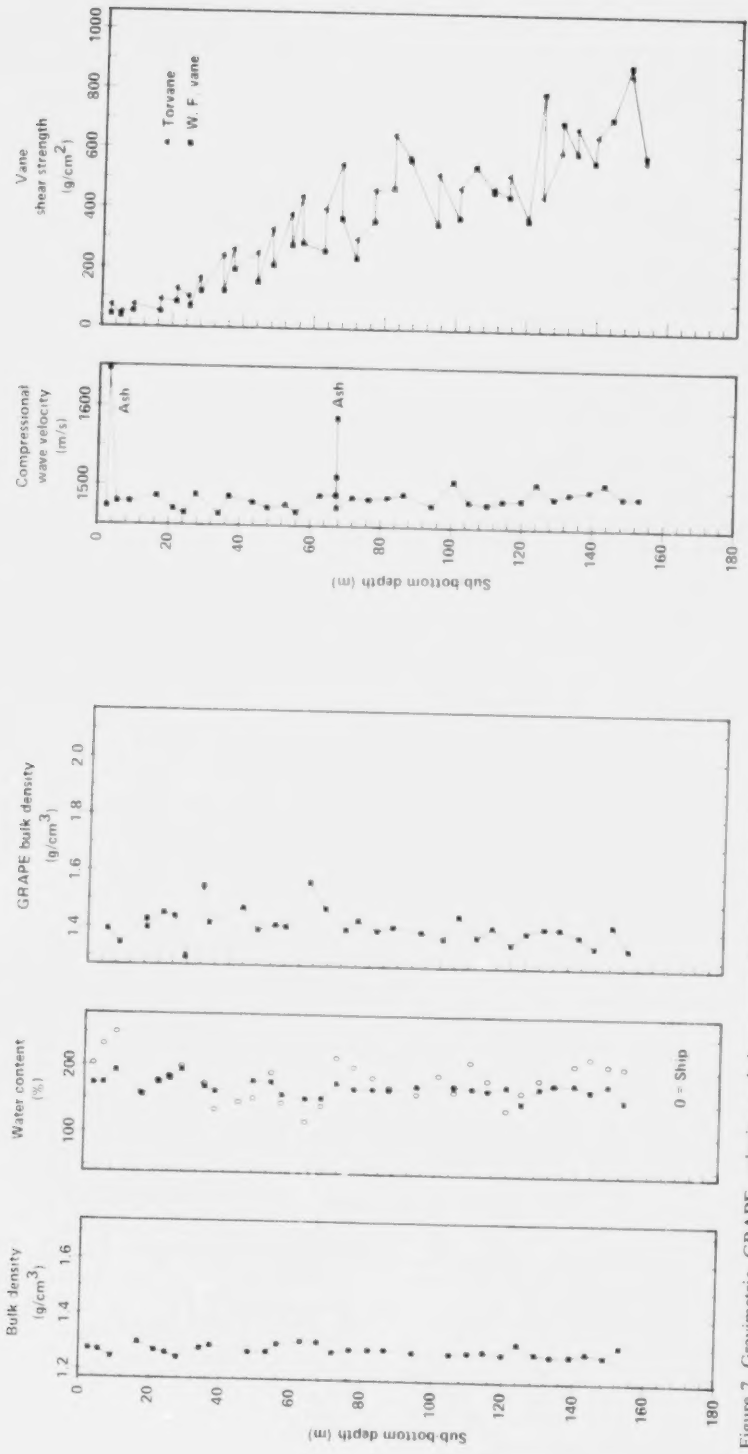

Figure 7. Gravimetric, GRAPE, velocity, and shear strength data for Site 580.

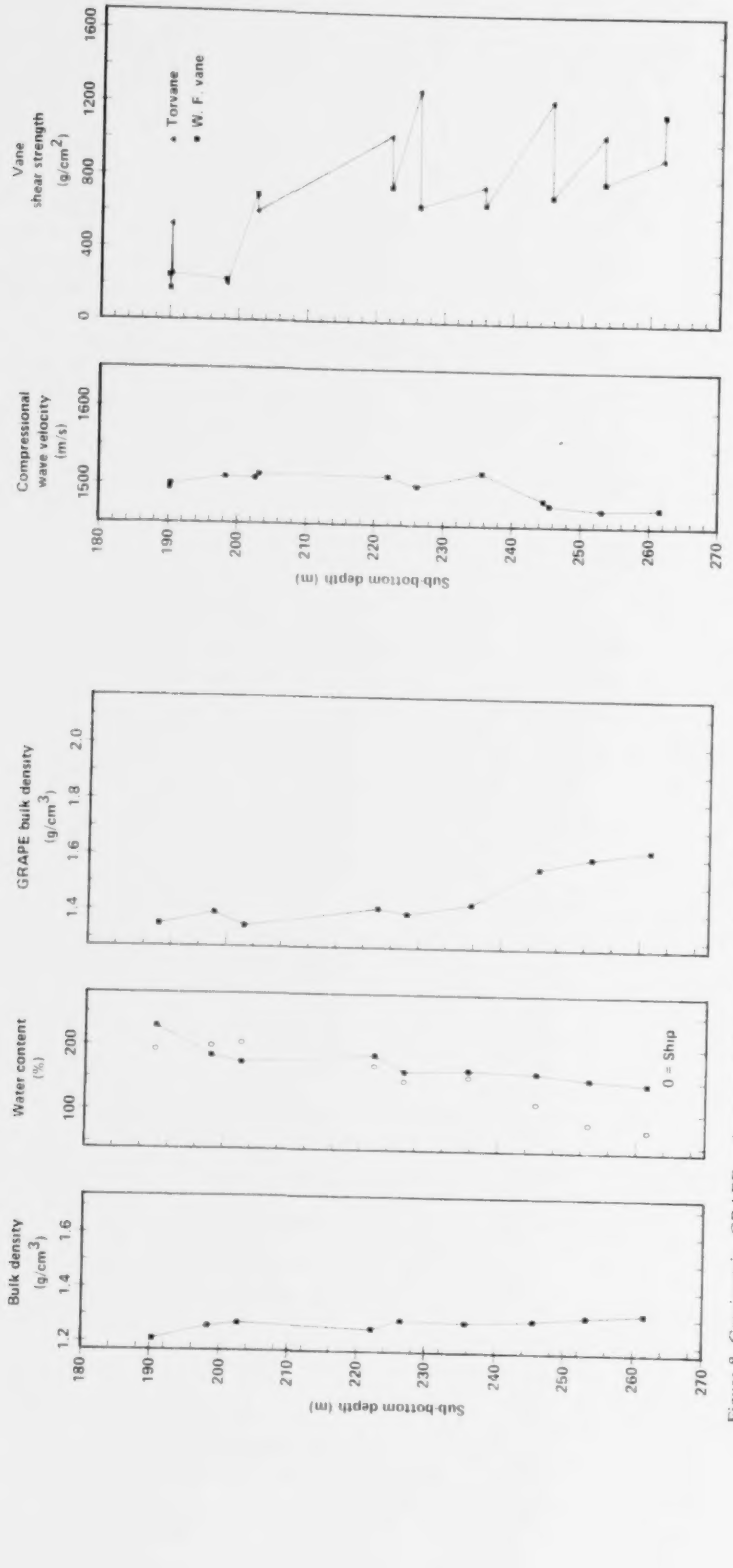

Figure 8. Gravimetric, GRAPE, velocity, and shear strength data for Site 581.

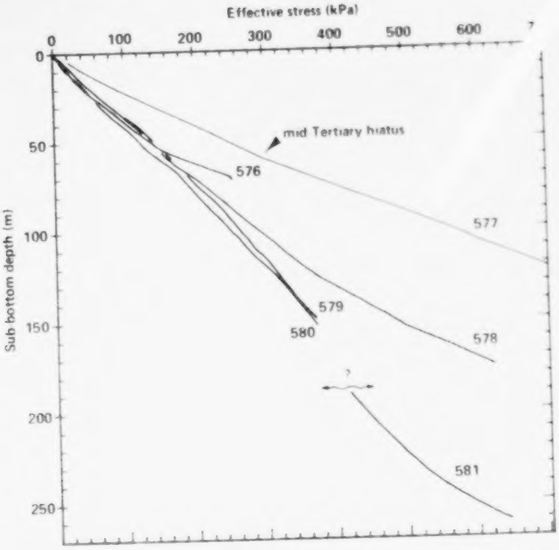

Figure 9. Effective stress (overburden stress) versus depth, calculated from the bulk density profiles for Sites 576–581.

erations at Sites 580 and 581 compared with the earlier sites, consequently the shore-based laboratory values are considered to be the most reliable.

Shear Strength and Shear Wave Velocities

Two sets of shear strength measurements (one using the hand-held Torvane and one using the motorized Wykeham Farrance vane) were conducted throughout the leg. The Torvane measurement is normally considered to provide a much more approximate estimate of undrained shear strength than the more controlled motorized vane. It is interesting, therefore, to examine whether there is any consistent difference between the two devices in different sediment types. Figure 10 shows a plot of Torvane shear strength versus vane shear strength (W.F. motorized vane) for all of the Leg 86 sediments. It is clear that, despite a significant amount of scatter, the overall trend from Figure 10 shows the Torvane shear strength (T_u) to be greater, on average, than the W.F. motorized vane shear strength (M_u) where $T_u = 1.13M_u$. In the carbonate sediments at Site 577, the difference between M_u and T_u was even greater than in the brown clays and siliceous clays at the other sites. For these carbonates, $T_u \approx 2M_u$.

Shear wave velocities ranged from only a few meters per second to over 150 m/s and correlated approximately with the shear strength data. Figure 11 is a scatter plot of the Torvane strength versus the shear wave velocity for all the data.

Consolidation and Permeability Profiles of Red Clay

Whole core samples of red clay from Sites 576 and 578 were tested to determine their consolidation and permeability characteristics. The back-pressurized consolidation/permeability technique used is described by Schultheiss and Gunn (1985). The data are plotted in Figures 12 and 13. Figure 12 shows the data for the individual samples tested (void ratio, vertical effective stress, and permeability relationships). Figure 13 shows the permeability profile through the red clay (permeabilities are taken from the individual plots at the calculated overburden stress) and the overconsolidation ratio profile. It can be seen that the permeability–void ratio relationship lies within a narrow band ranging from 10^{-4} mm/s at a void ratio of 6 down to 5×10^{-9} mm/s at a void ratio of 1. The permeability, therefore, decreases rapidly in the first 40 m of sediment (two-and-a-half orders of magnitude) but relatively little (only another order of magnitude) at a sub-bottom depth of 170 m.

The overconsolidation ratio reveals essentially normal consolidation below a depth of 20 m but with considerable "apparent overconsolidation" between 0 and 20 m. The Hole 576A data are included in the large geotechnical data set reported and fully discussed by the Geotechnical Consortium (this volume). The purpose of including it here is to show how the data from the deep red clay found at Site 578 fit into the overall pattern.

CONCLUSIONS

Leg 86 of the Deep Sea Drilling Project provided HPC cores of red clays, carbonate oozes, and siliceous clays from the Northwest Pacific. Some physical property measurements were made on these sediments (bulk density, water content, shear strength, compressional wave and shear wave velocity, consolidation, and permeability) which illustrate the behavior of the different sediment types. Progressive consolidation is observed in the water content profiles of the red clay and carbonate ooze (Sites 576 and 577) but little if any progressive consolidation is observed in the thick sequence of siliceous clays at Sites 579 and 580. Despite this lack of consolidation at Sites 579 and 580, the vane shear strength increases progressively downhole. The compressional wave profiles are similar in nature to the water content profiles illustrating that, in unconsolidated sediments, the velocity is essentially a function of the bulk density. The high water contents at all the sites, apart from Site 577, produced compressional wave velocities lower than water velocities except in the ash and pyrite-indurated layers. In these numerous layers the velocity was higher but only a few measurements were made. It would be a significant improvement if compressional wave velocity were logged continuously and automatically, similar to the GRAPE technique. In this way detailed velocity profiles could be obtained, enabling the seismic stratigraphy to be examined in detail and correlated with seismic reflection profiles.

The red clays exhibit a significant amount of "apparent" overconsolidation in the upper 20 m. Below this depth, they behave normally. Permeabilities in the red clays fall by three-and-a-half orders of magnitude in the top 170 m as the void ratio decreases.

The discrepancy between shipboard and shore-based laboratory determinations of water content was found to correlate with ship motion. It was concluded that laboratory water contents were the most reliable. The GRAPE bulk density determinations do not reveal importan changes in bulk density. In fact, the GRAPE bulk densi

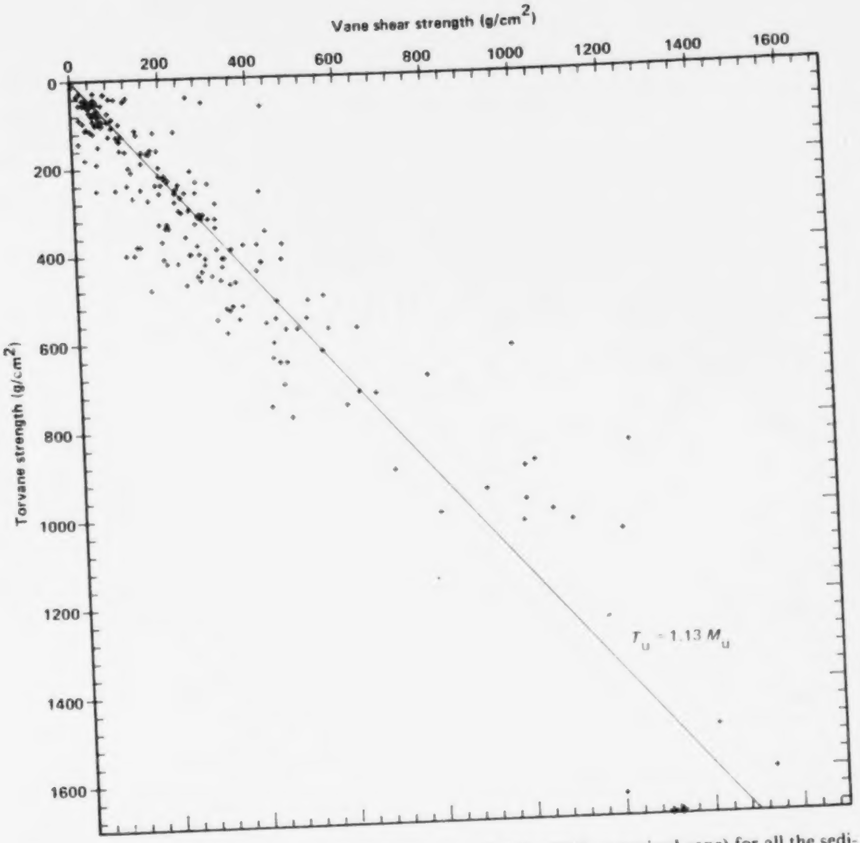

Figure 10. Torvane strength (T_u) versus vane shear strength (M_u) (W.F. motorized vane) for all the sediments from Leg 86.

ty profiles for all the sites correlate very poorly with the reliable laboratory-determined values of bulk density.

ACKNOWLEDGMENTS

The author would like to thank Larry Mayer and Bill Levy for reviewing this paper and for providing some constructive comments. I would also like to thank Tom Janecek, who helped with some of the on board measurements.

REFERENCES

Bennett, R. H., and Keller, G. H., 1973. Physical properties evaluation. *In* Van Andel, T. H., Heath, G. R., et al., *Init. Repts. DSDP*, 16: Washington (U.S. Govt. Printing Office), 513-520.

Boyce, R. E., 1973. Appendix I: Physical property methods. *In* Edgar, N. T., Saunders, J. B., et al., *Init. Repts. DSDP*, 15: Washington (U.S. Govt. Printing Office), 1115-1128.

________, 1976. Appendix I: Definitions and laboratory techniques of compressional sound velocity parameters and wet-water content, wet-bulk density and porosity parameters by gravimetric and gamma ray attenuation techniques. *In* Schlanger, S. O., Jackson, E. D., et al., *Init. Repts. DSDP*, 33: Washington (U.S. Govt. Printing Office), 931-958.

________, 1977. Deep Sea Drilling Project procedures for shear strength measurement of clayey sediment using modified Wykeham Farrance laboratory vane apparatus. *In* Barker, P., Dalziel, I. W. D., et al., *Init. Repts. DSDP*, 36: Washington (U.S. Govt. Printing Office), 1059-1068.

Curray, J. R., Moore, D. G., et al., 1979. Leg 64 seeks evidence on development of basins. *Geotimes*, 24:18-20.

Demars, K. R., and Nacci, V. A., 1978. Significance of Deep Sea Drilling Project sediment physical property data. *Mar. Geotechnol.*, 3(2):151-170.

Hardin, B. O., and Richart, F. E., 1963. Elastic wave velocities in granular soils. *J. Soil Mech. Found. Div., Am. Soc. Civ. Eng.* 89: 33-65.

Lee, H. J., 1973. Measurements and estimates of engineering and other physical properties, Leg 19. *In* Creager, J. S., Scholl, D. W., et al., *Init. Repts. DSDP*, 19: Washington (U.S. Govt. Printing Office), 701-720.

Mayer, L. A., 1982. Physical properties of sediment recovered on Deep Sea Drilling Project Leg 68 with the hydraulic piston corer. *In* Prell, W. L., Gardner, J. V., et al., *Init. Repts. DSDP*, 68: Washington (U.S. Govt. Printing Office), 365-382.

Prell, W. L., Gardner, J. V., et al., 1982. *Init. Repts. DSDP*, 68: Washington (U.S. Govt. Printing Office).

Rocker, K., 1974. Physical properties measurements and test procedures for Leg 27. *In* Veevers, J. J., Heirtzler, J. R., et al., *Init. Repts. DSDP*, 27: Washington (U.S. Govt. Printing Office), 433-444.

Schrader, H.-J., Kelts, K., Curray, J,. et al., 1980. Laminated diatomaceous sediment from the Guaymas Basin slope (central Gulf of California): 250,000-year climate record. *Science*, 207:1207-1209.

Schultheiss, P. J., 1981. Simultaneous measurement of P and S wave velocities during conventional laboratory soil testing procedures. *Mar. Geotechnol.*, 4(4):343-367.

________, 1983. The influence of packing structure and effective stress on V_s, V_p and the calculated dynamic and static moduli in sediments. *Proc. Int. Conf. Acoustics and the Sea-bed*, Bath, pp. 19-27.

Schultheiss, P. J., and Gunn, D. E., 1985. The consolidation and permeability of deep sea sediments. IOS report (in press).

Shirley, D. J., and Hampton, L. D., 1978. Shear wave measurements in laboratory sediments. *J. Acoust. Soc. Am.*, 63:607-613.

Date of Initial Receipt: 3 November 1983
Date of Acceptance: 10 October 1984

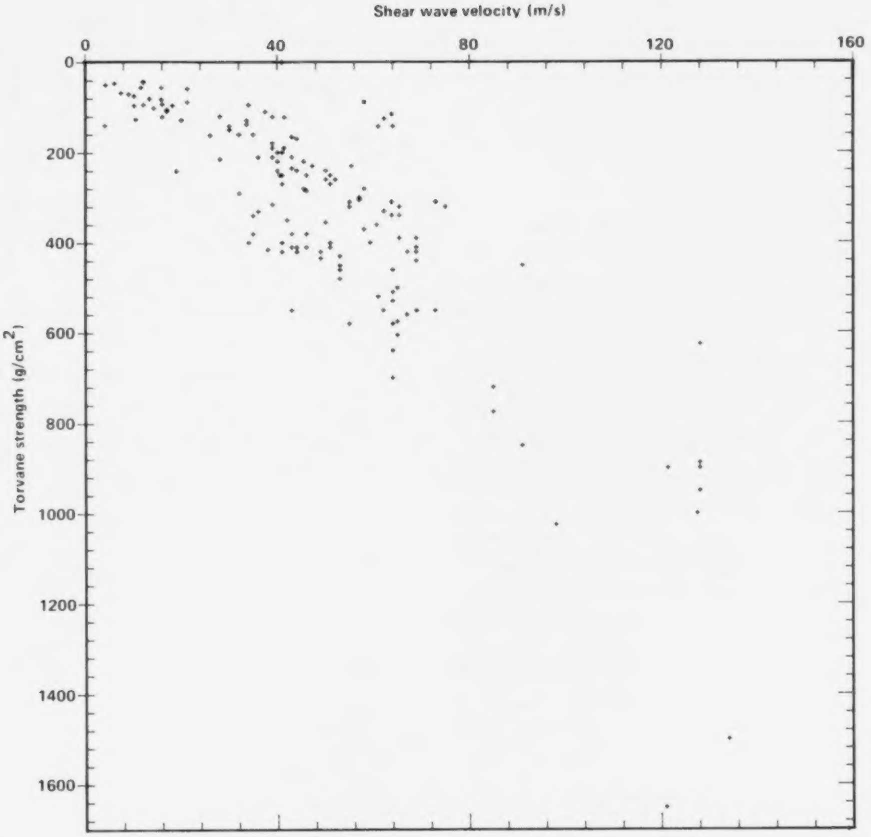

Figure 11. Torvane strength versus shear wave velocity for Sites 576, 577, 578, and 579.

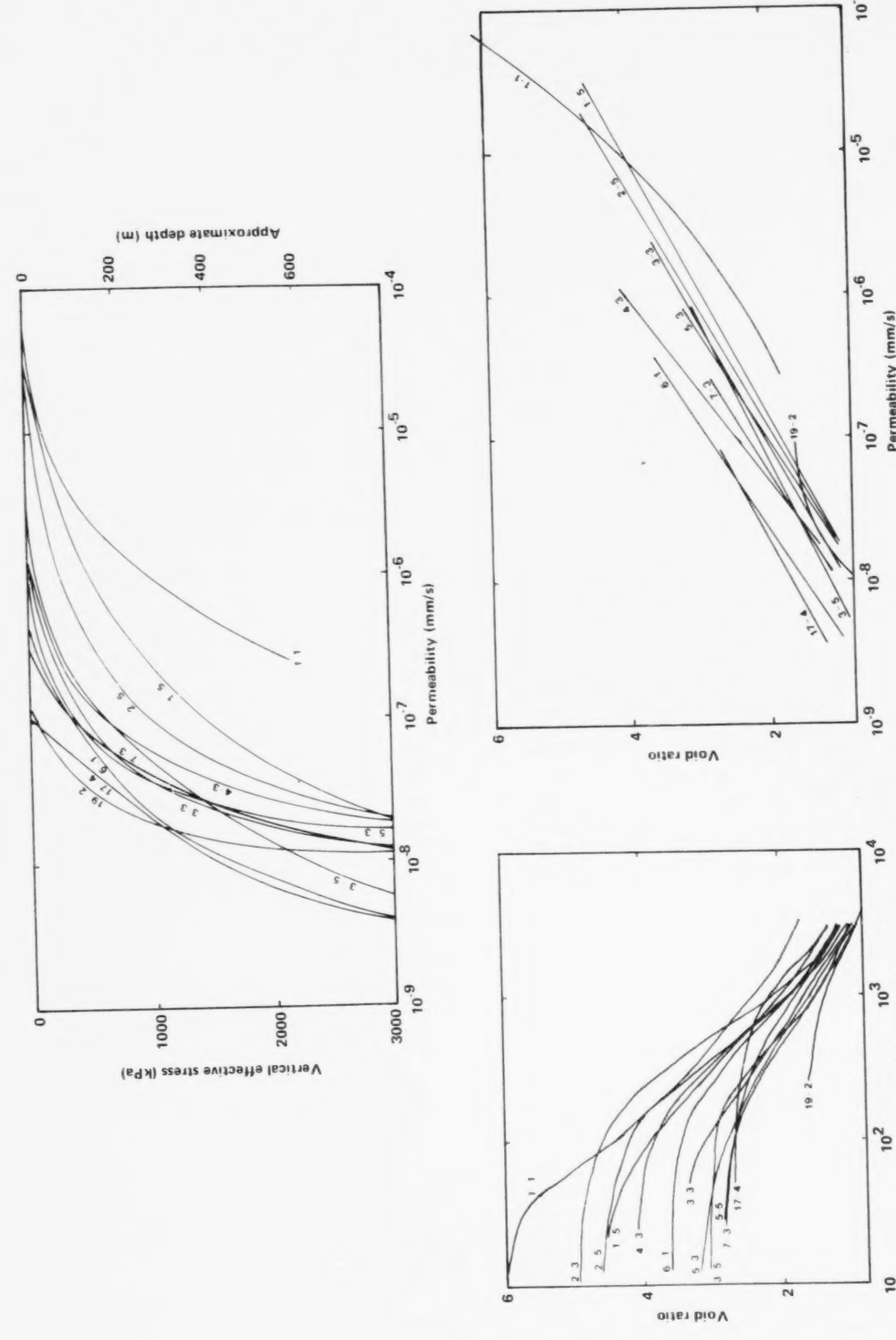

Figure 12. Consolidation and permeability data for red clay. Samples are from Holes 576A (Sections 1-1 to 7-3) and 578 (Sections 17-4 and 19-2).

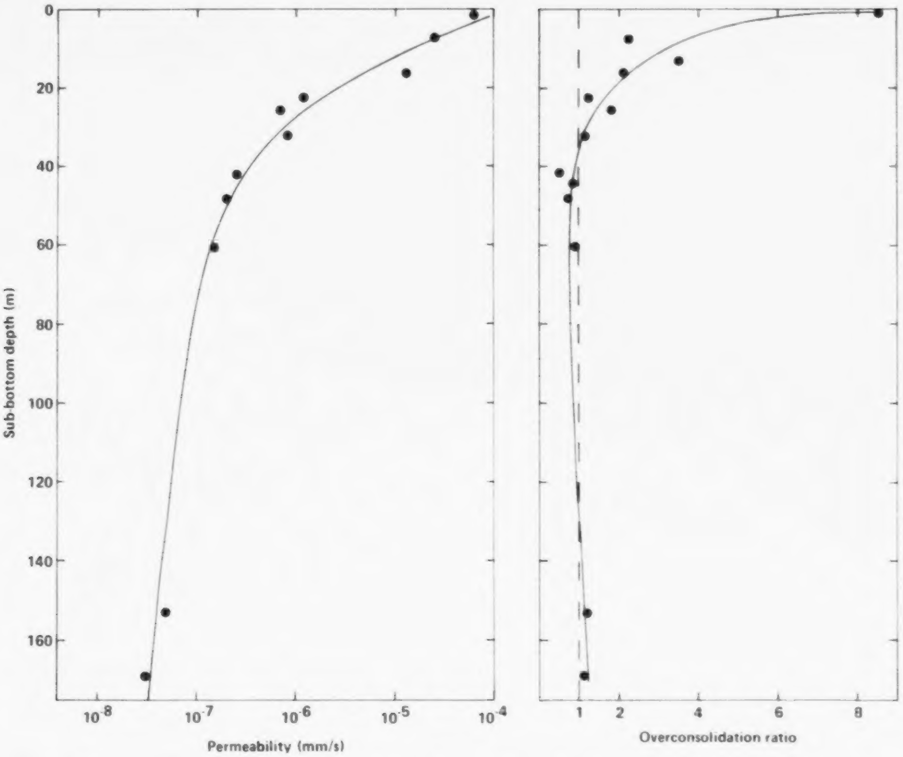

Figure 13. Permeability and overconsolidation ratio profiles in the red clay from Holes 576A and 578.

34. GEOTECHNICAL PROPERTIES OF NORTHWEST PACIFIC PELAGIC CLAYS: DEEP SEA DRILLING PROJECT LEG 86, HOLE 576A[1]

The Marine Geotechnical Consortium[2]

ABSTRACT

Geotechnical property results from Deep Sea Drilling Project Hole 576A sediments represent the most complete data set ever compiled for a continuously depositional, sedimentary section that spans 65 m.y. Geotechnical analyses included index-property and sediment characterization, and consolidation, permeability, and triaxial testing. Excellent agreement exists between test data generated in this multilaboratory effort.

Sediment characterization and index-property data delineate three well-defined units that conform with major lithologic divisions. Within Subunit IA these data appear inconsistent with accepted geotechnical relationships, showing water content, plasticity, and grain size increasing over similar intervals. These unusual relationships are attributed, in part, to silt-sized bonded clay aggregates. Within Subunit IB geotechnical properties become more uniform, and a marked increase in X-ray amorphous material occurs below 28 m sub-bottom. A pronounced change in the geotechnical behavior of Hole 576A sediments occurs in Unit II and corresponds to the presence of calcareous oozes.

Consolidation test results show overconsolidated sediments in the upper 28 m and normally consolidated sediments between 28 and 55 m sub-bottom. Mechanisms to explain the state of overconsolidation that are consistent with the geological history of the area include cementation and interparticle bonding, the release of high hydrostatic pressures during core recovery, and artifacts resulting from the consolidation test process. Additionally, the relevance of the preconsolidation stress determined using consolidation test results may be limited.

Variations in the shear strength gradient with depth are consistent with the consolidation test results. The gradient for the overconsolidated interval (0 and 28 m sub-bottom) is significantly higher than between 28 and 55 m sub-bottom, where the sediments become normally consolidated.

INTRODUCTION

The constraints of standard coring techniques have limited most studies of the geotechnical properties of marine sediments to samples recovered from less than 15 m sub-bottom. Many of these studies have tried to relate variations in geotechnical properties to variations in geological processes. In many instances, however, the relative geological complexity of the area or an insufficient geotechnical data base have precluded the development of such relationships. At Deep Sea Drilling Project (DSDP) Site 576, we were able to evaluate these relationships for a fairly simple, continuously depositional, pelagic clay environment whose geological history is well substantiated over the last 65 m.y.

Site 576 was triple cored (Holes 576, 576A, 576B) to get enough sediment samples for detailed sedimentological, stratigraphic, geochemical, and geotechnical analyses. At the request of the Marine Geological Consortium, Hole 576A was continuously cored and preserved in the full-round for detailed shore-based geotechnical property analyses. These analyses were intended to evaluate the interrelationships between the geotechnical properties and the geological processes of an abyssal hill environment, specifically as they pertain to variations in the sediment stress history, consolidation–permeability relationships, and shear strength.

GEOLOGIC SETTING

Site 576 is located east of Shatsky Rise in the western North Pacific red clay province (Fig. 1) very near magnetic Anomaly M13, which indicates a basement age of 129 m.y. (Site 576 chapter, this volume). Regional seafloor morphology and near-surface seismic profile characteristics have been mapped and discussed by Damuth et al. (1983). The location of Site 576 is characterized by a smooth to gently rolling seafloor. Seafloor bathymetry gradually deepens from southwest to northeast at a gradient of approximately 1:1000, reflecting an abyssal hill oceanic basement covered by pelagic sediments. Water depth at Site 576 is 6127 m.

The sedimentary section of Hole 576A can be divided into three general lithologic units on the basis of macroscopic descriptions and smear-slide analyses (Site 576 chapter, this volume; Fig. 2). Unit I consists of pelagic, brown clay extending to 55 m sub-bottom that can be divided into two subunits. Subunit IA (0 to 28 m sub-bottom) is a pelagic, yellowish brown, burrowed clay. The abundance of burrows and the silt-sized fraction generally decrease down through Subunit IA. Subunit IB (28 to 55 m sub-bottom) is an unburrowed, homogeneous, dark brown, pelagic clay generally containing less than 20% silt. The contact between these subunits is gradational over several meters. Unit II is composed of interbedded carbonate oozes and brown pelagic clays (55 to

---

[1] Heath, G. R., Burckle, L. H., et al., *Init. Repts. DSDP*, 86: Washington (U.S. Govt. Printing Office).

[2] The Marine Geotechnical Consortium for Deep Sea Drilling Project Leg 86 consisted of the University of Colorado (CU), Boulder, Colorado; Humboldt State University (HSU), Arcata, Cailfornia; Institute of Oceanographic Sciences (IOS), Wormley, Godalming, United Kingdom; Oregon State University (OSU), Corvallis, Oregon; San Diego State University (SDSU), San Diego, California; Sandia National Laboratories (SNL), Albuquerque, New Mexico; Texas A&M University (TAMU), College Station, Texas; University of Rhode Island (URI), Narragansett, Rhode Island; and United States Geological Survey (USGS), Denver, Colorado. The following persons contributed to this study. CU: Robert Schiffman, Andrew Dean; HSU: Ronald Chaney, J. Suehanek, B. Vega, T. McFarland; IOS: Peter J. Schultheiss, David Gunn; OSU: George Keller; SDSU: Iraj Noorany, M. Faghihi; SNL: Les Shephard, Joel Lipkin, Jean Kinker; TAMU: William Bryant, Elliot Taylor, Mark Johns; URI: Armand Silva, William Levy, Ricci Siciliano, Kathleen Dadey; USGS: Harold Olsen.

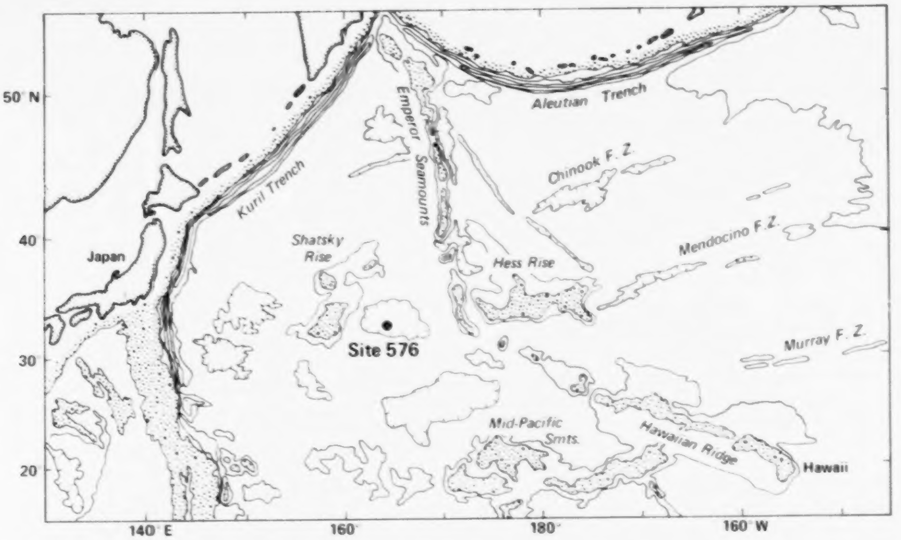

Figure 1. Location of Site 576 in the northwest Pacific. Areas shallower than 4 km stippled, 5-km contour plain, 6-km contour hachured.

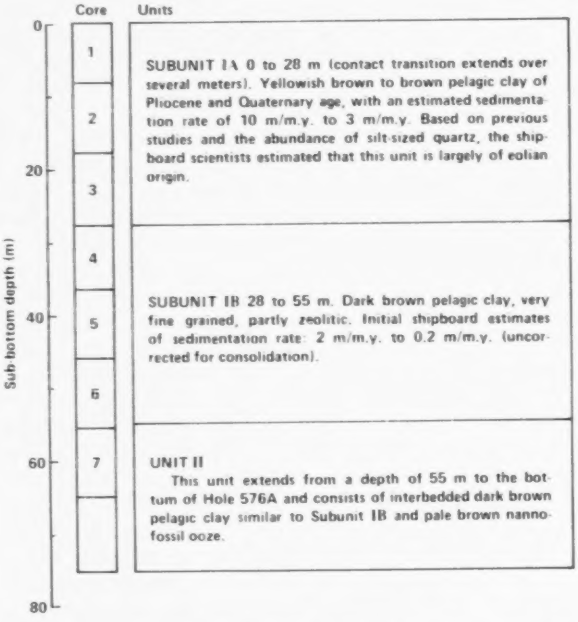

SUBUNIT IA 0 to 28 m (contact transition extends over several meters). Yellowish brown to brown pelagic clay of Pliocene and Quaternary age, with an estimated sedimentation rate of 10 m/m.y. to 3 m/m.y. Based on previous studies and the abundance of silt-sized quartz, the shipboard scientists estimated that this unit is largely of eolian origin.

SUBUNIT IB 28 to 55 m. Dark brown pelagic clay, very fine grained, partly zeolitic. Initial shipboard estimates of sedimentation rate: 2 m/m.y. to 0.2 m/m.y. (uncorrected for consolidation).

UNIT II

This unit extends from a depth of 55 m to the bottum of Hole 576A and consists of interbedded dark brown pelagic clay similar to Subunit IB and pale brown nannofossil ooze.

Figure 2. Generalized description of the lithologic section recovered at Hole 576A.

66 m sub-bottom). Evidence of graded bedding and cross-bedding in some of the carbonate ooze layers and sharp basal contacts between the carbonates and interbedded pelagic clays suggest a turbidite origin for at least some of the oozes. The base of Unit II was penetrated only in Hole 576B, at a sub-bottom depth of 76 m. Unit III, recovered only at the base of Hole 576B, consists of a chert or silicified clay unit.

Sedimentation rates (uncorrected for consolidation) decrease downcore in Unit I from 10 m/m.y. at the surface to less than 3 m/m.y. at the base of the Matuyama Epoch (~20 m sub-bottom; Heath, Rea, and Levi, this volume). This downcore decrease in sedimentation rate reflects the change from primarily eolian material in Subunit IA to an increased authigenic sediment component in Subunit IB. The change in dominant sediment components results from changes in depositional patterns as the location of Site 576 moved north and west in and out of various wind belts in response to seafloor spreading (Leinen, this volume).

GEOTECHNICAL CORE PROCESSING

Hole 576A cores were obtained by the *Glomar Challenger* on Leg 86 using the hydraulic piston corer. Immediately after recovery each full-round core was cut into 1.5-m-long sections, capped, taped, annotated, and stored upright at 4°C in the ship's cold room. Upon arrival in Japan the cores were air-freighted to the DSDP repository at Scripps Institution of Oceanography (SIO), where they were again stored upright at 4°C prior to geotechnical sampling in September 1982.

Members of the consortium institutions and laboratories were present for all geotechnical sampling. Prior to sub-sampling, each core section was examined visually through the core liner to identify areas of obvious disturbance and to note major changes in lithology. These lithologic changes were correlated with shipboard core descriptions for Holes 576 and 576B to develop a core-processing plan that would adequately sample each major lithologic unit.

The core-processing procedure involved cutting the 1.5-m full-round sections into shorter, full-round sections (15 to 40 cm) that were capped, taped, and waxed for subsequent detailed geotechnical analyses. Consortium members hand-carried these sections from SIO to their respective laboratories, where they were radiographed, described, and stored in a cold room prior to being tested.

Analyses performed on the ends of the shorter, full-round sections before capping and sealing at SIO included visual core descriptions and measurements of vane shear strength, water content, bulk density, and compressional velocity. Compressional-velocity measurements were performed parallel to bedding; the vane shear shaft was oriented normal to bedding. In addition, clay mineralogy and fabric samples were obtained from the core section ends for laboratory analyses. All full-round core sections not selected for laboratory analyses at that time were cut into 25-cm full-round sections and stored vertically in the DSDP repository cold room for possible future sample requests.

Additional core processing and sampling were performed by the consortium in June 1983. At that time, a number of remaining full-round sections were distributed to interested consortium laboratories before longitudinally splitting and describing the remaining full-round sections. Geotechnical measurements were performed on the split sections in the manner described above, except that in the vane shear measurements the vane shaft was oriented parallel to bedding.

TEST PROCEDURES AND METHODS

Sediment Characterization and Index Properties

Table 1 summarizes the tests performed during this study. For most of the standard geotechnical tests (e.g., index properties, sediment classification), the appropriate American Society for Testing and Materials (ASTM) Annual Book of Standards is referenced (Table 1). For nonstandardized tests (e.g., consolidation, triaxial tests), suitable references in the geotechnical literature are cited. Variations from standard procedures (e.g., salt corrections) are also noted. Lambe (1951) defines the standard geotechnical terminology (e.g., plastic limit, activity) used throughout this chapter.

All samples hand-carried to the individual laboratories were X-rayed prior to subsampling to assess the degree of core disturbance or flow-in. If any visible signs of disturbance or flow-in were observed, the sample was not tested. Tabulated results include data obtained during both sample processing sessions at SIO and further analyses at the individual consortium laboratories.

Consolidation and Permeability Tests

One-dimensional consolidation tests were performed using three different laboratory procedures. The standard consolidation test involves the incremental loading of a relatively thin, laterally confined sediment sample. Axial strain–time relationships are obtained by measuring the change in sample height during the test. A complete description of this technique can be found in Lambe (1951). A variation of this method involves the application of sufficient back pressure to redissolve gas bubbles and completely saturate the consolidation sample. Lowe et al. (1964) describe the benefits of this method. A serious drawback to both of the above methods is that more than 15 days are required to complete a test. Another test used was the constant rate of deformation (CRD) test, which only requires a few hours per test. The CRD test imposes a uniaxial deformation at a prescribed constant rate and provides a continuous record of the changes of consolidation parameters with respect to the applied effective stress. Gorman et al. (1978), Znidarcic (1982), and Znidarcic and Schiffman (1983) describe the CRD method in detail.

Two fundamental properties that contribute directly to the consolidation process are compressibility and permeability. Compressibility is defined as the amount of sediment volume compression per unit increment of stress. The compression index (C_c) is calculated from the slope of the void ratio–effective stress (e versus log σ') curve obtained from consolidation test results as follows:

$$C_c = \frac{-\Delta e}{(\Delta \log \sigma')}$$

where Δe is the void ratio change over a corresponding log increment of the effective stress (σ') (Lambe, 1951). The compression index is reserved for a loading sequence. If an unloading sequence is being analyzed, the companion term is the expansion index, C_e.

Permeability is defined as the capacity of a sediment to transmit fluid and is calculated by the ratio of the volumetric rate of flow to the gradient that drives fluid through a cross-sectional area of sediment. Three methods available to measure permeability directly include: (1) constant head, (2) falling head, and (3) flow pump. The constant-head method measures the flow rate under an applied pressure gradient. The falling-head method, which is the conventional method used for fine-grained sediments, relates the flow rate to a constantly changing hydraulic gradient. These conventional tests are described in Lambe (1951). The flow-pump method measures the pressure gradient while maintaining a controlled flow rate (Olsen, 1966). A critical assessment of each of these methods (Pane et al., 1983) has shown that permeability results for soft clays may be biased by seepage-induced consolidation unless very small pressure gradients are used.

In addition to measuring permeability directly, two indirect methods were used to deduce the coefficient of permeability from the theoretical consolidation relationships (Znidarcic and Schiffman, 1983). The first method uses the results from the standard consolidation test and is based on linear, infinitesimal strain consolidation theory. The second method uses CRD test results and nonlinear, finite strain, consolidation theory to calculate the coefficient of permeability.

Strength Tests

Several different types of strength tests were performed on Hole 576A sediments. In addition to the laboratory vane shear tests performed during the core processing, three other types of strength tests were completed: (1) unconsolidated-undrained triaxial compression (UU); (2) isotropically consolidated, undrained triaxial compression (CIU); and (3) anistropically consolidated-undrained triaxial compression (CAU; Table 1). Samples for these tests were prepared by cutting a length of core (typically 100 mm) contained in a plastic core-liner tube

Table 1. Summary of referenced procedures used in the geotechnical property analysis of Hole 576A sediments.

Test	Reference for test procedure	Variations from standard procedure
Sediment characterization		
Index properties		
Clay mineralogy	Heath and Pisias (1979)	Talc internal standard
Water content	ASTM D2216	Salt corrected, Noorany (1984)
Liquid limit	ASTM D423	Salt corrected, Noorany (1984)
Plastic limit	ASTM D424	Salt corrected, Noorany (1984)
Specific gravity	ASTM D854	Some tests done using air-comparison pycnometers
Wet-bulk density	ASTM D2937	Small rings (1-in. diam. and less) and piston subsamplers used in core
Grain size (pipette method)	Folk (1974)	Desalinated
Compressional wave velocity	Hamilton (1965)	Measurements made directly in the sediment, not through the core liner
Consolidation		
Consolidation (standard)	ASTM D2435	Load increment ratio of 0.5 used in some tests
Consolidation (back-pressured)	Lowe et al. (1964)	
Consolidation (constant rate of strain)	Znidarcic and Schiffman (1983)	
Permeability		
Constant head	Olsen (1966)	
Falling head	Silva et al. (1981)	
Flow pump	Pane et al. (1983)	
Strength Tests		
Vane shear		Rotation rate = 60°/min. Vane diameter and height 12.7 mm
Unconsolidated-undrained	ASTM D2850	
Consolidated-undrained		
isotropically	Bishop and Henkel (1962)	
anistropically (K_0)	Silva et al. (1983)	

Note: Variations from the referenced standard procedures are also noted in the text.

with either a hand saw or a high-speed saw. After cutting, the sample was extruded directly from the core liner or the liner was split longitudinally and a wire saw was then used to separate and remove the sample from the core-liner halves. The sample was then trimmed to a final diameter of 35 mm and a height of 70 to 85 mm using a vertical sample lathe and a wire saw.

SEDIMENT CHARACTERIZATION AND INDEX PROPERTIES

Clay Mineralogy

Quantitative clay mineralogy results on sediments obtained with piston cores close to Site 576 are consistent with known clay mineral distribution patterns in the North Pacific (Leinen and King, in press; Heath and Pisias, 1979; Griffin et al., 1968). Leinen and King reported data from samples located at the Brunhes/Matuyama boundary (ranging in sub-bottom depth from 3.84 to 5.92 m) within a 10^4-km^2 area around Site 576 and found virtually no variation in the $<20\ \mu$m opal-free mineral assemblage. Illite is the dominant clay mineral present (~39%), with lesser amounts of chlorite (~19%) and minor amounts of kaolinite and smectite (~10%). Detailed downcore clay mineral analysis on a piston core located approximately 10 km from Site 576 shows a slight increase in smectite (5-6% to 12-15%) and decrease in chlorite (~38% to 20-25%) with depth to 12 m sub-bottom. Leinen and King (1985) indicate that these subtle changes suggest either a change in the weathering regime in the continental source areas for the eolian material or a change in the dominant wind patterns that transport the mineral aerosol to the northwest Pacific.

Preliminary clay mineral analyses on Hole 576A sediments have emphasized sediments in Subunit IB below 30 m (Table 2, M. Leinen, pers. comm., 1984). Results from one near-surface sample obtained within Subunit IA are very similar to the piston core mineralogical results summarized above, except for a slightly higher illite component (50% as opposed to 39%) and a lower kaolinite component (trace amounts as opposed to ~10%). Using a talc internal standard, clay mineral results from Subunit IB indicate the single most important factor influencing the mineralogy is the pronounced downhole increase in the ratio of amorphous to crystalline material. This increase is particularly evident below 45 m sub-bottom (Table 2) and is attributed to a probable increase in the amount of iron oxides, manganese oxides, and very fine-grained material with insufficient crystal size to produce good diffractions. Another possible cause contributing to this marked increase in X-ray amorphous material may be related to the effects of grain size on the

Table 2. Preliminary mineralogy results from Hole 576A sediment.[a]

Core-Section	Sub-bottom depth (m)	Smectite (%)	Illite (%)	Kaolinite (%)	Chlorite (%)	Plagioclase (%)	Quartz (%)	Total (%)	Percent amorphous	Smectite:illite ratio
1-1	0.23	8	50	1	22	3	17	100	0	0.16
4-2	30.25	9	23	5	6	3	9	55	45	0.39
4-5	33.91	13	31	6	6	1	4	61	39	0.42
4-6	35.81	6	46	3	4	1	5	65	35	0.13
5-5	44.59	14	30	10	10	1	3	68	32	0.47
6-1	47.61	3	8	3	2	1	4	26	74	0.38
6-3	50.65	7	11	2	4	1	5	30	70	0.64
6-4	53.99	2	7	1	2	2	5	20	80	0.29

Note: Relative percentages of each component were determined using a talc internal standard and weighting factors developed for North Pacific sediments by Heath and Pisias (1979).

[a] M. Leinen, unpublished observations.

standardization procedure (M. Leinen, pers. comm., 1984).

Mineralogical analyses on Hole 576A sediments used for consolidation testing (E. Taylor, pers. comm., 1984) reveal a downhole increase in the relative percentage of smectite over illite in the crystalline clay-sized fraction. However, the much larger increase in the amount of X-ray amorphous material present in the clay-sized fraction (up to 80%, Table 2) over the same intervals would be the controlling mineralogical factor influencing the geotechnical behavior of Hole 576A sediments.

Electron Microscopy

Scanning and transmission electron microscopy (SEM and TEM) and energy dispersion X-ray spectrometry (EDS) were performed on select Hole 576A samples to evaluate particle-to-particle relationships, orientations, and arrangements. These relationships may prove critical to enhancing our understanding of the geotechnical behavior of these sediments.

SEM micrographs within Unit I (Fig. 3) show an open, flocculated structure consisting of a series of linked clay aggregates. Intergrown clay particle domains evident as locally continuous particle arrangements are apparent in several micrographs. The origin of these intergrown domains is uncertain, although they may result from the incipient growth of authigenic clay minerals, silica compounds, or iron oxides. Indications of cementation between clay-particle contacts are evident in Figure 3D. EDS analyses on the contacts between a silt grain and other particles show an enrichment of potassium and iron that suggests cementation (Fig. 4) although, because of the limited resolution of the EDS system, no definite conclusions can be reached.

Transmission electron micrographs from Subunit IA (22.17 m sub-bottom) and Subunit IB (46.02 m sub-bottom) show a very complex clay microstructure consisting of fine-grained, high void ratio clays occurring as clay floccules or as domains oriented face-to-face (Fig. 5). Authigenic minerals and larger opaque particles are often present.

Water Content

Water contents are quite variable within all of the sediments in Subunit IA (Fig. 6 and Table 3). At the sediment surface (< 50 cm sub-bottom) water content values range from 130 to 164%. In general, water content then increases with depth to approximately 10 m sub-bottom where the values range from 156 to 223%. Below 10 m sub-bottom both the absolute values and the range of water-content values decrease down to and through the transition zone (~20 to 28 m sub-bottom) as the sedimentary section gradually changes to Subunit IB. Values range from 102 to 142% over this interval. At 28 m, water content is significantly higher than in the immediately overlying transition zone.

Throughout Subunit IB (28–55 m sub-bottom) water contents generally decrease (Fig. 6). Distinct intervals (~5 m) of increasing and decreasing water-content values probably reflect subtle lithologic changes within Subunit IB and are not a result of variations in interlaboratory test procedures. These cyclic variations are also evident in many of the other properties discussed below.

A pronounced change in water content occurs at the contact between the overlying pelagic clay section (Unit I) and the interbedded carbonates and pelagic clays of Unit II (Fig. 6). Values at the base of Unit I (55 m sub-bottom) range from 110 to 120%; whereas within Unit II below 55 m, water content values decrease to near 50% within the carbonate oozes. Water content within Unit II decreases slightly with depth. The occasional high water-content values observed in Unit II are associated with the interbedded pelagic clay layers in this unit. These high values are similar to those reported at the base of Subunit IB.

Atterberg Limits

Small, local downcore variability in both liquid and plastic limit values (Fig. 7 and Table 3) probably results from minor procedural differences between laboratories. This variability does not, however, obscure the important downcore trends. Liquid limit exhibits a general increasing trend from 131% very near the seafloor to 186% at approximately 16 m sub-bottom, while the plastic limit fluctuates about an average value of 54% over the same interval. Liquid limits above 20 m sub-bottom are generally less than the natural water contents resulting in liquidity indices (I_L) of greater than 1.0 (Fig. 8). Below 20 m sub-bottom, I_L values decrease gradually throughout the remainder of Subunit IA to a minimum of ap-

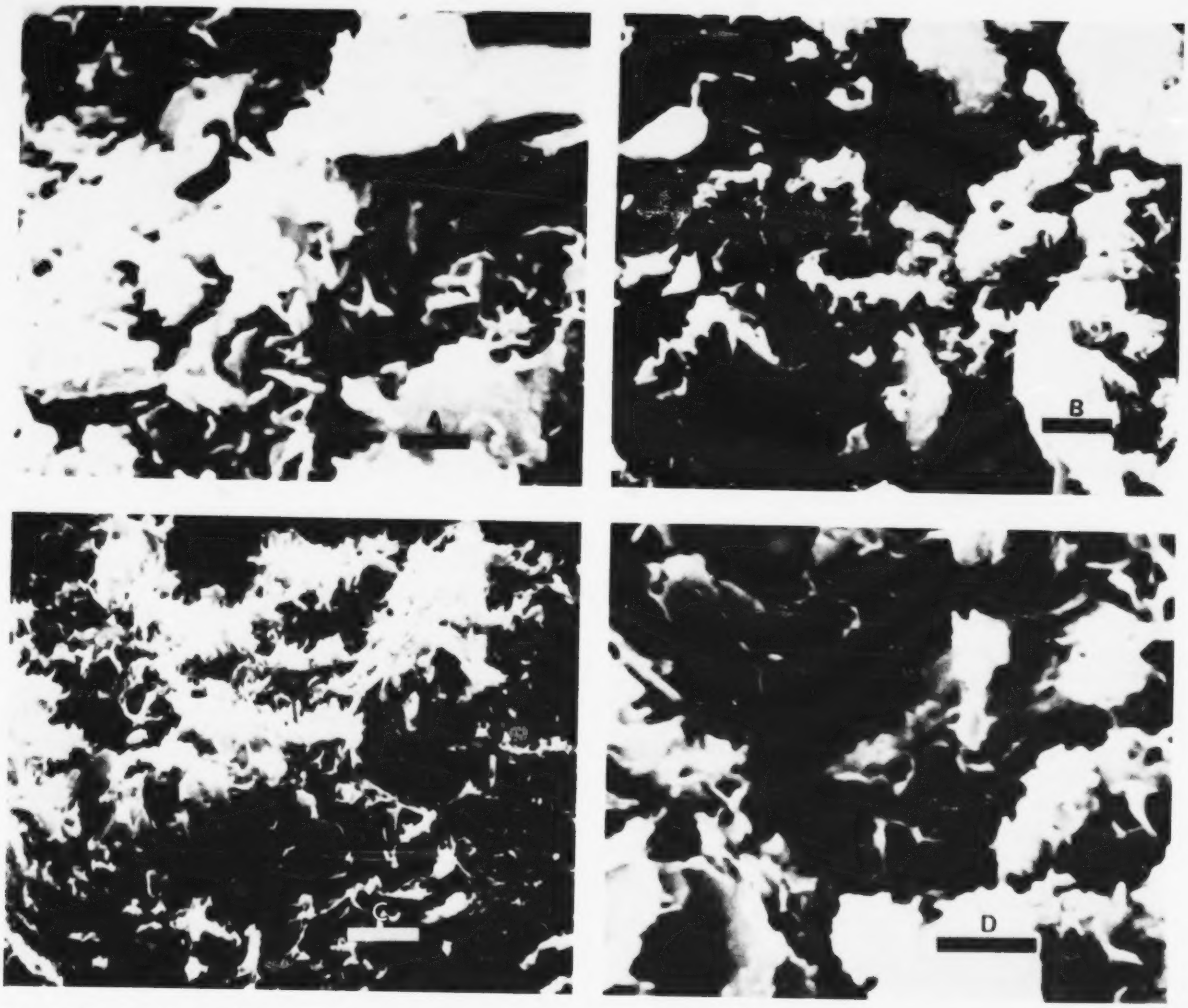

Figure 3. Scanning electron micrographs of sediments located at 11.6 m (A), 15.6 m (B), and 43.3 m (C) sub-bottom showing intergrown clay particle domains (A, B, C), a flocculent microstructure (B), and authigenic material (C). Arrows on micrograph D (11.6 m sub-bottom) show possible indications of interparticle cementation. Bar scale on micrographs A and D equals 1 μm and on B and C it equals 2 μm.

proximately 0.4. Plastic limits remain relatively constant about an average value of 54%, whereas the liquid limits decrease to a low of 140% at 23 m sub-bottom and then begin to increase again through the transitional zone to Subunit IB.

Liquid and plastic limit as well as plasticity index (I_P) values are consistently higher in Subunit IB than in either Subunit IA above or Unit II below (Fig. 7). This is also evident on the standard plasticity chart (Fig. 9; Casagrande, 1948) which shows that the changes in Atterberg limits correspond with the major lithologic divisions. As in Subunit IA, increases and decreases in liquid and plastic limit values in Subunit IB correspond with zones of increasing and decreasing water content. Liquid and plastic limit values average 205 and 82%, respectively.

Liquidity indices (Fig. 8) are quite uniform within Subunit IB, averaging 0.32. This region of uniform I_L values coincides almost exactly with the depth interval represented by Subunit IB (28 to 55 m sub-bottom), suggesting that Subunit IB can be clearly distinguished using the liquidity index.

Atterberg limit data clearly define the contact between Unit I and the underlying carbonate ooze of Unit II. Liquid and plastic limit values for the oozes, averaging 54 and 30%, respectively, are lower in Unit II than in Unit I. Unit II carbonate sediments occur in the low-plasticity region of the standard plasticity chart (Fig. 9), which reflects the difference in the geotechnical behavior between the lower plasticity carbonate oozes and the higher plasticity pelagic clays. One Atterberg limit test on an interbedded pelagic clay interval at 64 m indicates

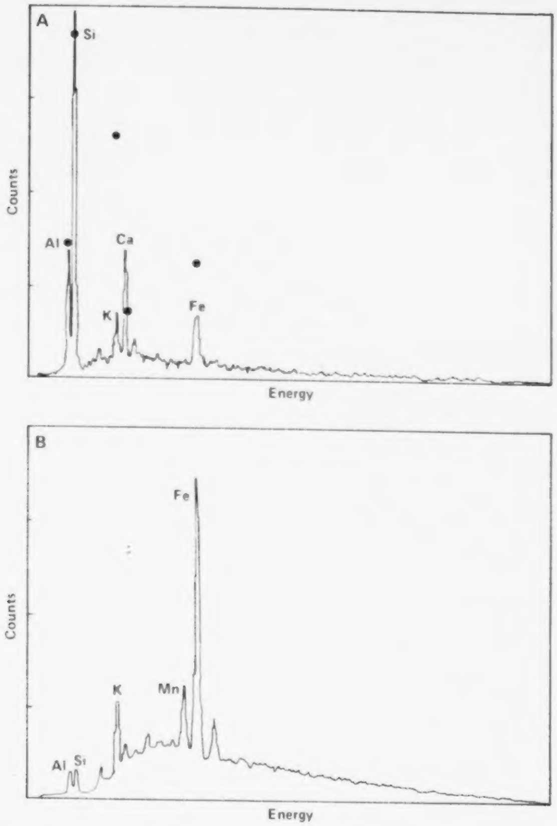

Figure 4. Electron dispersive X-ray spectrometry (EDS) results. (A) EDS results obtained on individual particles present at 7.25 m (solid line) and at the particle contacts (dots) which suggest interparticle cementation. (B) EDS results from intergrown domains present at 15.56 m sub-bottom showing iron enrichment which also suggests possible interparticle cementation.

that these interbedded clays are very similar to the pelagic clays tested in Subunit IB. Liquid limits, for the most part, do not exceed the natural water content, resulting in higher liquidity indices for Unit II sediments than for the overlying Subunit IB sediments.

Grain Size and Activity

Grain-size data vary ± 10% around the mean for Hole 576A sediments (Fig. 10). This variability is attributed to natural variations in the sediment components accumulating in this area and slight differences in interlaboratory test procedures. From the seafloor to approximately 12 m sub-bottom, the silt content increases from about 34 to 45%; whereas sand percentages vary between 0 and 7%. This general downward coarsening trend to 12 m sub-bottom appears anomalous because water content and liquid limit increase over this same interval. The normal trend generally shows water content increasing as grain size decreases. This coarsening trend, plus increasing values of activity over this interval (Fig. 11, ~ 0.9 to 2.7), suggest that the mineralogy may vary significantly from that reported in the preliminary mineralogical analyses. An alternative explanation may be that the clay-sized fraction was not completely dispersed prior to obtaining aliquots for size analysis. In either case, these unusual trends are consistent with consolidation and shear-strength results presented later in this chapter.

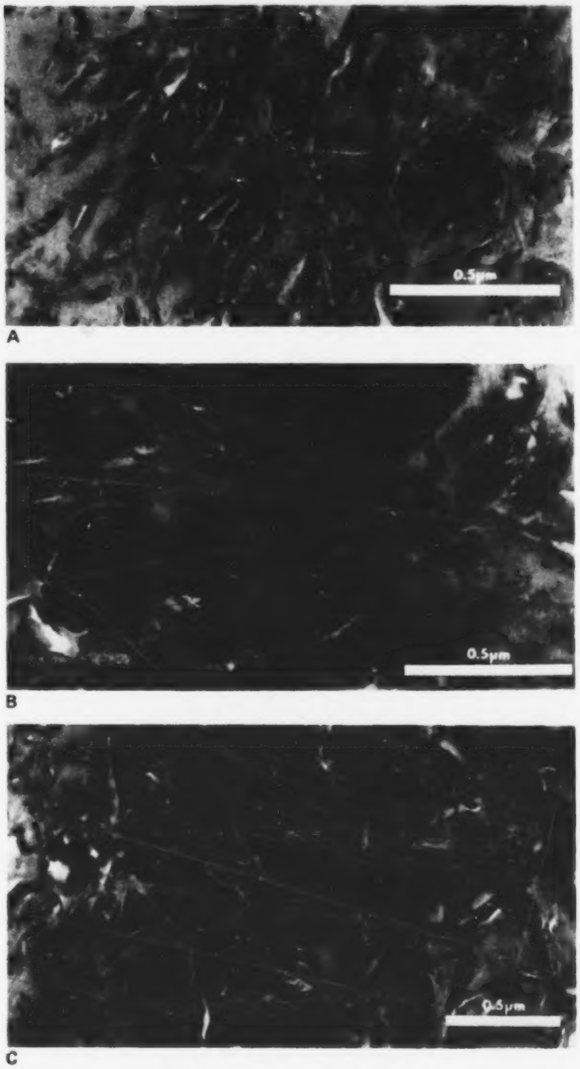

Figure 5. Transmission electron micrographs of sediments located at 22.17 m (A) and 46.02 m (B and C) sub-bottom showing a complex clay microstructure of particle domains, floccules, and zeolitic material. Large semispherical feature at the top of B is microcrystalline zeolitic material.

From approximately 12 m to the base of Subunit IA at 28 m sub-bottom (Fig. 10), the clay-sized fraction gradually increases as the silt-sized fraction decreases. The gradual increase in the clay-sized fraction probably reflects a decrease in eolian input to this area and marks the transition from Subunit IA to Subunit IB (Site 576 chapter, this volume). Activity becomes less variable through this transition interval with values approaching those evident near the seafloor (~ 1.1). These values are more typical of the relationship one normally expects between grain size and plasticity.

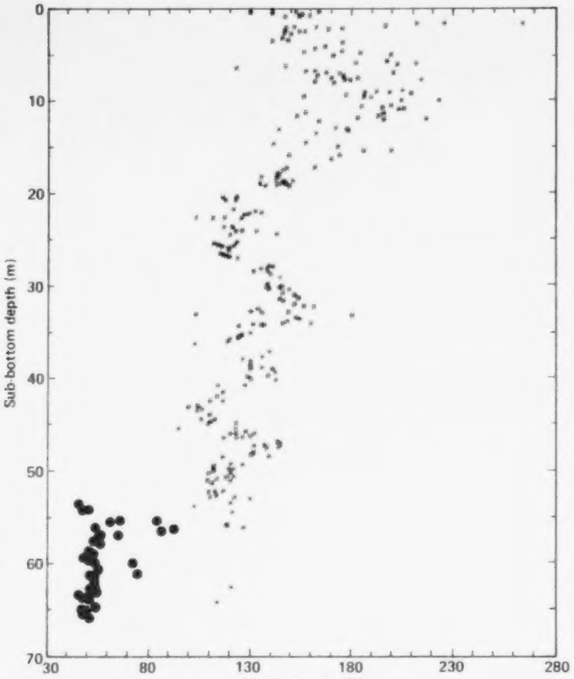

Figure 6. Water content-depth profile for Hole 576A sediments. Solid circles (•) below 55 m represent values obtained in carbonate ooze (% dry weight; salt corrected for 35‰).

From the transitional material of Subunit IA (20 to 28 m sub-bottom) to the pelagic clay in Subunit IB, the amount of clay-sized material reaches a maximum and then remains relatively constant (Fig. 10; ~85% clay-sized fraction). Although some scatter in the grain-size data exist, within certain intervals of Subunit IB the anomalous correlation between grain size, water content, and plasticity identified in Subunit IA is also evident. This is most apparent between 40 and 50 m sub-bottom. As the likelihood of a large silt- and sand-sized fraction is minimal within these authigenic clays, the most likely explanation for these relationships is that the coarse fraction consists of bonded or cemented clay aggregates and that the dispersion technique used in the size analyses (Folk, 1974) is not adequate for these aggregates. As mentioned earlier, clay-fabric analyses show indications of cementation in these sediments.

A large increase in the silt-sized fraction occurs at the contact between Subunit IB and Unit II. Below this contact, the grain-size profile in the carbonate sediments becomes more uniform with an average of 54% silt. Interbedded pelagic clay layers contain approximately 75% clay, with the remainder being silt. Activity values clearly define the carbonates and clays within Unit II (Fig. 11). In general, the carbonate activity values are the lowest observed in Hole 576A sediments.

Bulk Density

Increasing water content normally corresponds with decreasing bulk density in sediments having constant specific gravity. However, no clear decreasing trend is evident in the upper 12 m of Subunit IA (Fig. 12 and Table 3). This may result from variable mineralogy or specific gravity related to the increasing grain size through the interval. From 12 m sub-bottom depth to the base of Subunit IA, increases in bulk density correspond to decreases in water content. This general trend continues down through Subunit IB where bulk density increases to a maximum of 1.50 Mg/m^3.

A large break in the bulk-density profile marks the top of Unit II at 55 m sub-bottom (Fig. 12). Values in this unit are variable but are the highest observed in Hole 576A, averaging 1.71 Mg/m^3. No trend with depth is readily apparent in Unit II, possibly because of the difficulty in obtaining an undisturbed sample in calcareous sediments. The higher bulk-density values occur in the carbonate oozes.

The measured bulk-density values were used to calculate the effective overburden stress-depth profile for Hole 576A sediments, assuming hydrostatic conditions (Fig. 13; Shephard et al., 1978). This profile was used with consolidation test results to determine the state of consolidation.

Compressional Velocity

Compressional velocity data display a large degree of scatter throughout the recovered sedimentary section (Fig. 14 and Table 3). Values average 1489 m/s ($\sigma = \pm 5.5$ m/s) in Subunit IA and 1496 m/s ($\sigma = \pm 4.0$ m/s) in Subunit IB. These velocities approximate the velocity of seawater. Velocity data in Unit II show a pronounced increase to 1536 m/s ($\sigma = \pm 15.50$ m/s), corresponding to the change in lithology from the overlying pelagic clays to the underlying carbonate oozes.

Summary

Sediment characterization and index-property data delineate three well-defined units that appear to be consistent with the major lithologic divisions delineated in the Site 576 chapter (this volume). Sediments from Subunit IA (0–28 m sub-bottom) have water contents that increase from the seafloor to approximately 12 m sub-bottom and then gradually decrease to 28 m sub-bottom. Over this same interval (0–28 m) grain size and activity display similar trends, resulting in anomalous index-property relationships. Although inconsistent with accepted geotechnical relationships, these results are supported by the consolidation and shear strength data presented later. Liquidity indices are generally greater than 1.0 in the upper 20 m, indicating possible overconsolidation to at least that depth. Limited mineralogy results indicate that illite is the dominant clay mineral present.

Results from Subunit IB (28–55 m sub-bottom) display a marked change from the overlying sediments in Subunit IA. Water contents gradually decrease with depth and grain size appears much more uniform. Changes in bulk density are well correlated with the changes in water content. Atterberg limit results show much higher plasticity indices and lower liquidity indices than in the overlying sediments in Subunit IA. Mineralogy results show the amount of X-ray amorphous material in Subunit IB increases markedly over that present in Subunit IA.

Table 3. Summary of sediment characterization and index-property analyses performed on Hole 576A sediments.

Core-Section	Sub-bottom depth (m)	Water content (%)	Bulk density (Mg/m^3)	Compress. velocity (m/s)	Shear strength (kPa)	Liquid limit (%)	Plastic limit (%)	Liquidity index
1-1	0.14				1.96			
1-1	0.17				1.18			
1-1	0.23				1.86			
1-1	0.24	163	1.33					
1-1	0.26	164		1482				
1-1	0.33	152			6.37			
1-1	0.42			1496				
1-1	0.45	130						
1-1	0.47				4.5			
1-1	0.49	130	1.38					
1-1	0.55	140			8.13			
1-1	0.58			1483				
1-1	0.65	155			5.68			
1-1	0.74	159	1.33		5.29			
1-1	0.89	153	1.34		5.88			
1-1	0.93	147						
1-1	1.34				5.29			
1-2	1.64	225	1.25					
1-2	1.65				3.63			
1-2	1.67			1487				
1-2	1.70	211						
1-2	1.75				4.21			
1-2	1.80	211						
1-2	1.84			1502	2.65			
1-2	1.89	263	1.24					
1-2	1.94			1491				
1-2	1.98	196			6.96			
1-2	2.08	162			10			
1-2	2.09			1484				
1-2	2.14	151	1.36		7.74			
1-2	2.16	175	1.34	1482				
1-2	2.20			1485				
1-2	2.25	147			14.41			
1-2	2.35	168			8.43			
1-2	2.39			1486				
1-2	2.44	156	1.37		5.29			
1-2	2.45	153	1.34			131	74	1.39
1-2	2.59	146	1.37		9.6			
1-2	2.84	146	1.36					
1-3	3.00	149				127	47	1.3
1-3	3.24				10.39			
1-3	3.34	146	1.36		7.74			
1-3	3.58							
1-3	3.60					150	49	0.93
1-3	3.84	140	1.37		6.37			
1-3	3.86	149						
1-3	3.93					135	67	1.37
1-3	4.02	175	1.29	1484				
1-3	4.14				10.68			
1-4	4.52	166	1.34					
1-4	4.66			1476				
1-4	4.71			1478				
1-4	4.73	161			9.31			
1-4	4.85	175			13.62			
1-4	4.88			1498				
1-4	4.94	156	1.34		12.25			
1-4	4.98					121	44	1.46
1-4	5.24	170	1.32		8.23			
1-4	5.25	183						
1-4	5.50	199				148	75	1.7
1-4	6.01			1485				
1-4	6.05	197			11.17			
1-4	6.15	181			9.02			
1-4	6.18			1483				
1-4	6.24	202	1.29		7.15			
1-4	6.30	211					51	1.9
1-4	6.49	147	1.36		14.41			
1-4	6.52			1489				
1-4	6.74	122	1.41		6.37			
1-4	6.99	162	1.34		9.6			
1-5	7.03			1496				
1-5	7.05	157			15.68			
1-5	7.15	200			8.53			
1-5	7.21			1488				
1-5	7.24	173	1.33		9.31			

Table 3. (Continued).

Core-Section	Sub-bottom depth (m)	Water content (%)	Bulk density (Mg/m^3)	Compress. velocity (m/s)	Shear strength (kPa)	Liquid limit (%)	Plastic limit (%)	Liquidity index
1-5	7.27	167				135	39	1.33
1-5	7.28							
1-5	7.36	163						
1-5	7.54	175	1.35					
1-5	7.67					118	42	
1-5	7.70	170						
1-5	7.82	183	1.37	1482				
1-5	7.85	176			5.88			
1-5	7.95	176			16.27			
1-5	8.01			1486				
1-5	8.04	214	1.27		5.88			
1-5	8.07			1486				
1-5	8.10	179			13.82			
1-5	8.20	171			18.62			
1-5	8.25			1483				
1-5	8.29	161	1.35		8.23			
1-5	8.49				21.85			
2-1	9.25	205		1490	4.31			
2-1	9.35	192			7.45			
2-1	9.40			1496				
2-1	9.44	198	1.3		8.82			
2-1	9.47	209	1.35	1488				
2-1	9.49			1494				
2-1	9.55	186			16.56			
2-1	9.65	177			9.9			
2-1	9.67			1497				
2-1	9.69	156	1.36		9.1			
2-1	9.94	189	1.3		9.02			
2-1	10.00	186			14.41			
2-1	10.09	204	1.28		11.17			
2-2	10.22							
2-2	10.26	223				154	43	1.62
2-2	10.78	198			12.84			
2-2	10.89	184	1.31		9.6			
2-2	10.92	195	1.37	1487				
2-2	11.09	203	1.28		8.53			
2-2	11.11	205	1.29					
2-2	11.44	157	1.34		10.09			
2-2	11.65	195						
2-3	11.86	153						
2-3	11.96	193						
2-3	11.97	153	1.4	1478				
2-3	12.06				12.25			
2-3	12.16				8.82			
2-3	12.19	183	1.29		5.88			
2-3	12.24	216						
2-3	12.42	195				176	36	1.13
2-3	12.63	163						
2-3	12.80					167	56	0.98
2-3	12.83							
2-4	13.30	171			49.29			
2-4	13.35	144						
2-4	13.40	178			29.3			
2-4	13.49	178	1.3		10.09			
2-4	13.52	179	1.33					
2-4	13.68	162						
2-4	13.73							
2-4	14.00					170	87	0.83
2-5	14.80	141			38.02			
2-5	14.90	157			28.22			
2-5	14.94			1488				
2-5	14.99	173	1.31		11.76			
2-5	15.53							
2-5	15.54	185				186	43	0.99
2-5	15.61	199						
2-6	16.22	174	1.34					
2-6	16.23	149						
2-6	16.42	170				162	44	1.07
2-6	16.44							
2-6	16.80					173	62	1.1
2-6	17.39	148	1.36		19.5			
2-6	17.42	161	1.41	1493				
2-6	17.69	146	1.35		13.62			
2-6	17.73				11.96			
3-1	18.22			1488				
3-1	18.25	143			15.97			

Table 3. (Continued).

Core-Section	Sub-bottom depth (m)	Water content (%)	Bulk density (Mg/m³)	Compress. velocity (m/s)	Shear strength (kPa)	Liquid limit (%)	Plastic limit (%)	Liquidity index
3-1	18.35	144			18.62			
3-1	18.36			1505				
3-1	18.44	135	1.38					
3-1	18.69	143	1.36		11.96			
3-1	18.94	151	1.35		11.96			
3-1	18.97	147	1.42	1479				
3-1	19.00			1490				
3-1	19.03	146			20.29			
3-1	19.13	147			23.42			
3-1	19.14			1489				
3-1	19.19	135	1.37		16.27			
3-1	19.30	143			19.99			
3-1	19.34			1490				
3-1	19.40	148			20.68			
3-1	19.44	137	1.36		11.76			
3-1	19.52							
3-1	19.53	150				145	47	1.05
3-2	20.61	116	1.41					
3-2	20.64			1484				
3-2	20.67	123			18.03			
3-2	20.69			1492				
3-2	20.73	118	1.48	1478				
3-2	20.74				13.03			
3-2	20.76	119	1.42			162	93	0.37
3-2	20.93	123						
3-2	20.97					163	80	0.51
3-3	21.80	121				153	98	0.4
3-3	22.14	132	1.37		14.9			
3-3	22.24	135			21.07			
3-3	22.34	135			21.36			
3-3	22.35			1491				
3-3	22.39	130			14.11			
3-3	22.42			1481				
3-3	22.59	127	1.39		15.68			
3-4	22.72			1490				
3-4	22.74	126			24.89			
3-4	22.80			1486				
3-4	22.82	102			23.62			
3-4	22.84	103	1.44		15.48			
3-4	22.88							
3-4	22.89	111				140	42	0.7
3-4	22.96	117						
3-4	23.77	121	1.46	1485				
3-4	23.89	116	1.4		14.9			
3-5	24.25	125			19.99			
3-5	24.27			1483				
3-5	24.31	122	1.4		15.19			
3-5	24.34	132	1.42					
3-5	24.64	142						
3-5	24.80	119				149	50	0.7
3-5	25.42			1487				
3-5	25.44	123			22.83			
3-5	25.49	122	1.39		16.27			
3-6	25.74	111			26.66			
3-6	25.75			1485				
3-6	25.92	115			28.03			
3-6	25.96			1490				
3-6	25.99	113	1.41		15.48			
3-6	26.02	121	1.43			168	75	0.49
3-6	26.23					167	64	0.54
3-6	26.33	119						
3-6	26.57	119	1.5	1486				
3-6	26.79	114	1.42		16.56			
3-6	26.85			1488				
3-6	26.89	117			25.28			
3-6	26.99	116			24.7			
3-6	27.00			1488				
3-6	27.04	119	1.4		16.56			
3-6	27.19	123	1.41		17.35			
4-1	27.94	138	1.34		3.23			
4-1	28.00			1488				
4-1	28.15	141		1492	13.03			
4-1	28.19	134	1.36		9.6			
4-1	28.35	135			17.64			
4-1	28.39			1494				
4-1	28.44	138	1.36		10.39			

Table 3. (Continued).

Core-Section	Sub-bottom depth (m)	Water content (%)	Bulk density (Mg/m^3)	Compress. velocity (m/s)	Shear strength (kPa)	Liquid limit (%)	Plastic limit (%)	Liquidity index
4-1	28.47			1490				
4-1	28.50					182	71	0.7
4-1	28.69	131	1.37		10.68			
4-1	28.94				11.96			
4-1	29.09	140	1.35		9.02			
4-2	29.37							
4-2	29.39							
4-2	29.46	144				185	48	0.7
4-2	29.47							
4-2	29.53							
4-2	29.75	139						
4-2	30.09	138	1.4			186	77	0.56
4-2	30.25	146	1.36					
4-2	30.34	143			18.62	220	112	0.29
4-2	30.38			1492				
4-2	30.40	137				213	101	0.3
4-2	30.42	139			10.39			
4-2	30.65	149						
4-3	30.73	145						
4-3	31.22	150	1.33		11.96			
4-3	31.46	153	1.31					
4-3	31.51				18.62			
4-3	31.52	154						
4-3	31.54			1494				
4-3	31.63	153			24.79			
4-3	31.67	144	1.35		15.68			
4-3	31.82	146	1.35		15.48			
4-4	32.24			1499				
4-4	32.31	151			34.01			
4-4	32.39			1498				
4-4	32.46	156	1.34		18.62			
4-4	32.47	161	1.35					
4-4	32.75			1497				
4-4	32.87	134			33.32			
4-4	32.96	130	1.38		20.48			
4-4	33.01			1495				
4-4	33.07	148			32.83			
4-4	33.19	136			35.28			
4-4	33.21			1495				
4-4	33.26	102	1.33		22.34			
4-4	33.31			1494				
4-4	33.55	180			35.97			
4-5	33.77	152			39.69			
4-5	33.81			1502				
4-5	33.92				22.34			
4-5	33.95	155	1.4	1492				
4-5	34.03			1494				
4-5	34.07	148			36.26			
4-5	34.17	146	1.34		21.85			
4-5	34.24			1497				
4-5	34.29	159			33.32			
4-5	34.39		1.36		54			
4-5	34.43							
4-5	34.47	135				236	82	0.34
4-5	34.50	136				209	73	0.5
4-5	34.54	131						
4-5	34.56	124						
4-5	34.62					217	105	0.23
4-6	35.29	130	1.42			211	81	0.38
4-6	35.41	127			38.61			
4-6	35.47			1500				
4-6	35.54	125	1.39		60			
4-6	35.82	124	1.43	1493				
4-6	35.97	120	1.4		21.85			
4-6	36.21				37			
4-6	36.23	119	1.41					
4-6	36.29			1496				
4-6	36.34				24.3			
4-6	36.36	102						
4-6	36.42			1495				
5-1	37.29	139						
5-1	37.30				17.35			
5-1	37.32			1492				
5-1	37.44	139	1.35		28			
5-1	37.86				33			
5-1	37.95				24.89			

Table 3. (Continued).

Core-Section	Sub-bottom depth (m)	Water content (%)	Bulk density (Mg/m^3)	Compress. velocity (m/s)	Shear strength (kPa)	Liquid limit (%)	Plastic limit (%)	Liquidity index
5-1	37.97	136						
5-1	38.08	127	1.46	1482				
5-1	38.15				22.93			
5-1	38.17	130						
5-1	38.28			1494				
5-1	38.34	130	1.37		44			
5-1	38.59	130	1.37		29			
5-1	38.73				30.67			
5-2	38.94	130	1.37		34			
5-2	39.10				25.09			
5-2	39.12	136	1.37					
5-2	39.20	141						
5-2	39.23			1493				
5-2	39.24				36			
5-2	39.37	142	1.38			224	96	0.36
5-2	39.74	129	1.38		30			
5-2	40.00	139			23.72			
5-2	40.09			1493				
5-2	40.19	130			40.19			
5-3	40.28							
5-3	40.36	142	1.37			229	96	0.35
5-3	40.74				54			
5-3	41.02	127	1.42			210	74	0.39
5-3	41.07	114	1.48	1485				
5-3	41.29				49			
5-3	41.59				49			
5-4	41.73	116						
5-4	41.94					208	83	0.26
5-4	42.02	115	1.45			205	85	0.25
5-4	42.25				34.69			
5-4	42.65	117						
5-4	42.73	110				166	64	0.45
5-4	42.78							
5-4	42.89							
5-4	42.91							
5-5	43.23	104						
5-5	43.25			1501				
5-5	43.29	101	1.46		38			
5-5	43.37							
5-5	43.38	106				170	58	0.43
5-5	43.39	105	1.5	1487				
5-5	43.52			1504				
5-5	43.54	104			37.34			
5-5	43.59	104	1.46		46			
5-5	43.79					184	61	0.38
5-5	44.00	111				197	73	0.31
5-5	44.43							
5-5	44.57				81			
5-5	44.59	106	1.44					
5-5	44.61	113	1.46			184	74	0.35
5-6	44.80	111			36.65			
5-6	44.86			1498				
5-6	44.94	109	1.44		17			
5-6	44.97	123	1.43			202	79	0.36
5-6	45.59	94	1.3		86			
5-6	45.60	123	1.41			218	88	0.27
5-6	45.77	128	1.47	1490				
5-6	45.99	123	1.4		94			
5-6	46.09	132			39.3			
5-6	46.13			1496				
5-6	46.19	120	1.41		81			
5-7	46.35	130		1495				
5-7	46.44	123	1.4		26.66			
5-7	46.47	125	1.44	1493				
5-7	46.69	118	1.41		36			
6-1	46.94	142	1.29		22			
6-1	46.98	144						
6-1	47.20	145	1.37			246	91	0.35
6-1	47.37	137	1.37	1492				
6-1	47.42	144			26.66			
6-1	47.52			1491				
6-1	47.59	132	1.37		33			
6-1	47.60	138						
6-1	47.67			1495				
6-2	47.70				31.75			
6-2	47.84				65			

Table 3. (Continued).

Core-Section	Sub-bottom depth (m)	Water content (%)	Bulk density (Mg/m^3)	Compress. velocity (m/s)	Shear strength (kPa)	Liquid limit (%)	Plastic limit (%)	Liquidity index
6-2	48.21	132	1.42			226	97	0.27
6-2	48.44	130	1.38		81			
6-2	48.47	131	1.43					
6-2	48.55	139			30.97			
6-2	48.61			1497				
6-2	48.69	116	1.42		89			
6-2	48.80					227	71	0.3
6-2	48.95							
6-2	49.40	121			35.48			
6-2	49.48			1497				
6-2	49.59	112			54			
6-2	49.65	127						
6-3	49.78					207	83	0.31
6-3	49.87	119	1.48					
6-3	49.93				29.69			
6-3	49.94	121						
6-3	50.00			1503				
6-3	50.07	112			52			
6-3	50.26	120			26.95			
6-3	50.31			1493				
6-3	50.34	110	1.43		44			
6-3	50.70	122			24.01			
6-3	50.78			1493				
6-3	50.86	114	1.4		26			
6-3	50.95			1490				
6-3	50.99	118			19.31			
6-3	51.09	109	1.43		26			
6-4	51.24	121			35.97			
6-4	51.33	111	1.44		65			
6-4	51.36	120	1.43			206	96	0.22
6-4	52.23	113	1.47	1490				
6-4	52.29	116			46.35			
6-4	52.42			1506				
6-4	52.49	109	1.43		105			
6-5	52.73	113			44			
6-5	52.76			1499				
6-5	52.84	110	1.43		108			
6-5	53.05	122						
6-5	53.09	130						
6-5	53.10					194	86	0.35
6-5	53.38							
6-5	53.65			1564				
6-5	53.68							
6-5	53.69	120				186	84	0.35
6-5	53.82	102	1.48	1502				
6-5	53.87	46			55.96			
6-5	53.99	102	1.45					
6-6	54.22	48	1.78			59	29	0.63
6-6	54.30	50			36.26			
6-6	54.32			1504				
6-6	54.39	47	1.77					
6-6	54.58	121						
6-6	54.62					72	31	2.13
6-6	55.57	66	1.7	1515				
6-6	55.60	62		1543				
6-6	55.64				45.96			
6-6	55.69	84	1.53					
6-7	55.94	119	1.43					
6-7	55.97	118	1.48	1506				
6-7	56.05				22.15			
6-7	56.12	54						
6-7	56.17			1524	42.83			
7-1	56.21	127	1.39					
7-1	56.44	93	1.49		13			
7-1	56.65				11.37			
7-1	56.69	86	1.53		4.8			
7-1	56.97	65						
7-1	57.08	57						
7-1	57.10							
7-1	57.32	55	1.78	1510				
7-1	57.59	53	1.74		5.59			
7-2	57.74	56			8.53			
7-2	57.86			1525				
7-2	57.94	56	1.74		4.02			
7-2	58.72	51	1.74			54	31	0.87
7-2	59.02	52	1.79	1515				

Table 3. (Continued).

Core-Section	Sub-bottom depth (m)	Water content (%)	Bulk density (Mg/m^3)	Compress. velocity (m/s)	Shear strength (kPa)	Liquid limit (%)	Plastic limit (%)	Liquidity index
7-2	59.04	53			5.29			
7-2	59.13			1546				
7-2	59.19	49	1.76		7.45			
7-3	59.30	49			19.5			
7-3	59.32			1553				
7-3	59.39	52	1.73		5.29			
7-3	59.57	52	1.78	1518				
7-3	59.61			1538				
7-3	59.65				11.17			
7-3	59.79	51	1.76		5.59			
7-3	59.98	53						
7-3	60.03	71						
7-3	60.09	72						
7-3	60.54							
7-3	60.60							
7-4	60.70	56	1.71					
7-4	61.15	74	1.84	1528	14.7			
7-4	61.17	51						
7-4	61.20			1546				
7-4	61.24	53	1.73		8.82			
7-4	61.40							
7-4	61.53					33	31	0.99
7-4	61.59	53						
7-4	61.76	53	1.71		17			
7-4	61.99				86			
7-5	62.23							
7-5	62.43	54						
7-5	62.50							
7-5	62.55							
7-5	62.63	121			9.02			
7-5	62.70					56	28	1
7-5	62.78	54		1539				
7-5	62.83					49		1.15
7-5	62.84	52	1.74		5.88			
7-5	63.02	53						
7-5	63.08					40	30	2.31
7-5	63.17							
7-5	63.18	52				45	32	1.51
7-5	63.41			1518				
7-5	63.47	46			17.64			
7-5	63.53			1546				
7-5	63.59	48	1.75		9.31			
7-5	63.61	51	1.72					
7-6	63.87	51	1.8	1522				
7-6	63.91	50			17.84			
7-6	68.95			1544				
7-6	63.99	49	1.8		7.74			
7-6	64.22	113						
7-6	64.28					240	88	0.13
7-6	64.84	51	1.76		4.02			
7-6	64.87	53	1.78	1520				
7-6	65.09	46	1.79		8.23			
7-7	65.25	49			11.96			
7-7	65.34			1546				
7-7	65.39	47	1.79		6.37			
7-7	65.75			1516	70.66			
7-7	65.89	51	1.66		129			

Results from Unit II (55–64 m sub-bottom) reflect the lithologic change from predominantly pelagic clays to carbonate ooze interbedded with pelagic clays. Water content and activity values for the carbonates are the lowest observed in Hole 576A; whereas bulk density and compressional velocity values are the highest observed. Atterberg limit data show low plasticity and liquidity indices in the carbonates.

CONSOLIDATION AND PERMEABILITY CHARACTERISTICS

Skempton (1970) defined consolidation as the result of all processes causing the progressive transformation of an argillaceous sediment from a soft clay to a shale. These processes include: (1) interparticle bonding, (2) dessication, (3) cementation, and (4) the squeezing out of pore water under the increasing weight of overburden. The effect of each process on consolidation varies through time.

Consolidation tests are used to evaluate the sediment response to an applied load. These results provide insight to the relative degree of consolidation the sediment has experienced *in situ* under the imposed load of the sedimentary column. The state of consolidation is determined using the ratio of preconsolidation stress (σ_c') to the present effective overburden stress (σ_0'). Preconsoli-

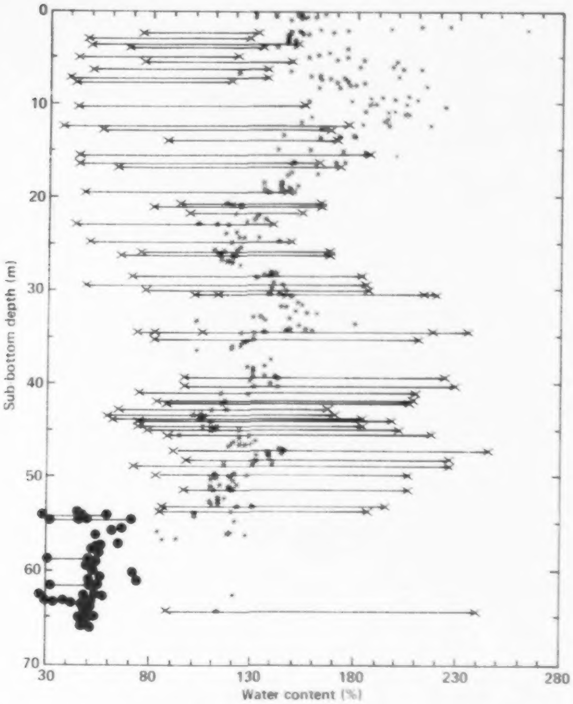

Figure 7. Atterberg limit and water-content results obtained from Hole 576A sediments. Liquid and plastic limit values fall on the right and left side of the profile, respectively. Solid circles (•) below 55 m represent values obtained in carbonate ooze.

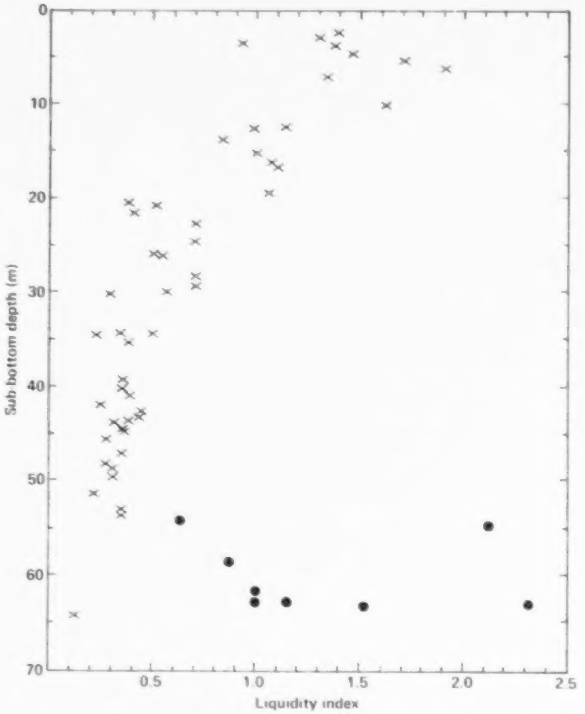

Figure 8. Liquidity index–depth profile for Hole 576A sediments. Values greater than 1.0 indicate material with natural water contents greater than the liquid limit. Solid circles (•) below 55 m represent values obtained in carbonate ooze.

dation stress, defined as the maximum effective stress the sediment has experienced, was calculated using the graphical reconstruction technique of Casagrande (1936). The value of σ_o' is calculated assuming hydrostatic conditions. The ratio of the preconsolidation stress to the effective overburden stress yields the overconsolidation ratio (OCR $= \sigma_c'/\sigma_o'$).

A sediment is considered normally consolidated if the present effective overburden stress is the greatest ever imposed. Thus, for a normally consolidated sediment the preconsolidation stress equals or closely approximates the effective overburden stress ($\sigma_c' = \sigma_o'$). A sediment is overconsolidated if it has been consolidated under a stress that exceeds the present effective overburden stress ($\sigma_c' > \sigma_o'$). Sediment that has not fully consolidated under the present overburden stress is underconsolidated. For underconsolidated sediments the pore-water pressure exceeds the hydrostatic pressure and the preconsolidation stress will be less than the effective overburden stress ($\sigma_c' < \sigma_o'$). Thus, sediments with overconsolidation ratios of approximately 1.0 are considered normally consolidated, greater than 1.0 are overconsolidated, and less than 1.0 are underconsolidated.

Consolidation Test Results

Consolidation test results from Hole 576A sediments probably represent the most extensive suite of consolidation data for any marine sedimentary section (80 consolidation tests performed on 63.70 m of sediment; ≈ 1 test every 0.80 m). This extensive testing program was initiated because the geological history of the area near Site 576 is well-understood and the principles of consolidation theory suggested that such data may be used to define a model of the consolidation process for "a perfect marine clay section" that has been continuously depositional over the last 65 m.y. (Heath, Rea and Levi, this volume). All geological and geotechnical information available prior to beginning the testing program indicated that these sediments would be normally consolidated below the upper few meters. However, test results indicate that the sediments at Hole 576A are overconsolidated in the upper 28 m, normally consolidated in the interval between 28 and 39 m sub-bottom, and normally to underconsolidated in the interval between 39 and 55 m sub-bottom (Fig. 15; Tables 4 and 5). The carbonate-ooze consolidation test results are included in the data compilation for comparison with the pelagic clay results even though these results are not emphasized in the following discussion because of their differences in geotechnical behavior and mode of deposition.

Typical e versus log σ' curves for tests performed in both Subunit IA (0–28 m sub-bottom) and Subunit IB (28–55 m sub-bottom) reveal significant differences in initial void ratios and the sediment response to both an applied load and an unloading sequence (Fig. 16). These differences are also reflected in the average values of several consolidation parameters and the permeability val-

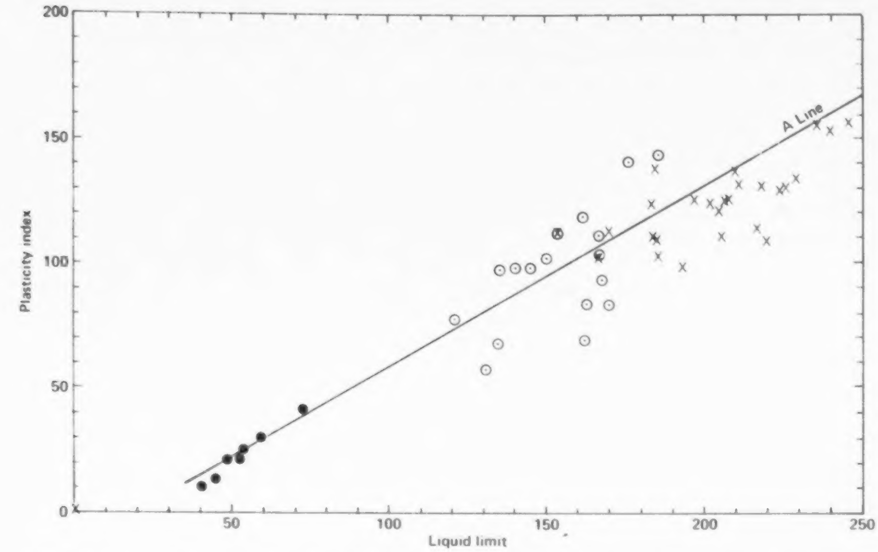

Figure 9. Standard plasticity chart used for classifying fine-grained sediments (Casagrande, 1948). Casagrande's A line is shown. Subunit IB sediments (X) are generally much more plastic than Subunit IA sediments (⊙) or the carbonate oozes (•).

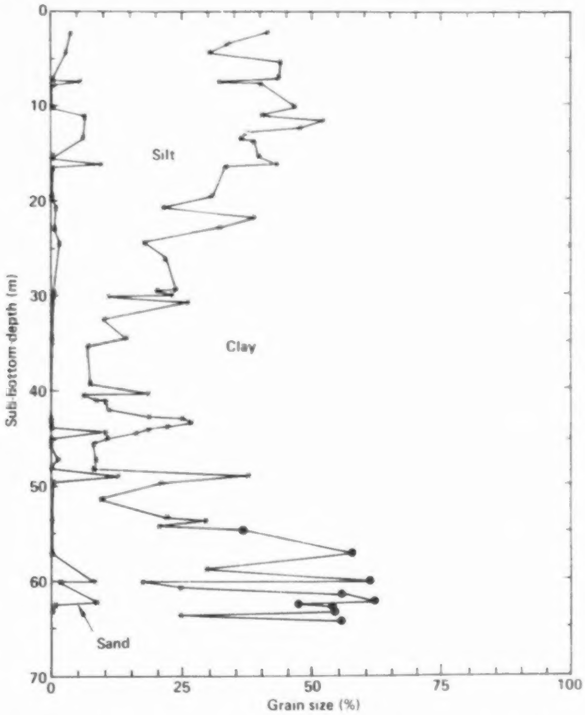

Figure 10. Grain size-depth profile for Hole 576A sediments. Solid circles (•) below 55 m represent values obtained in carbonate ooze.

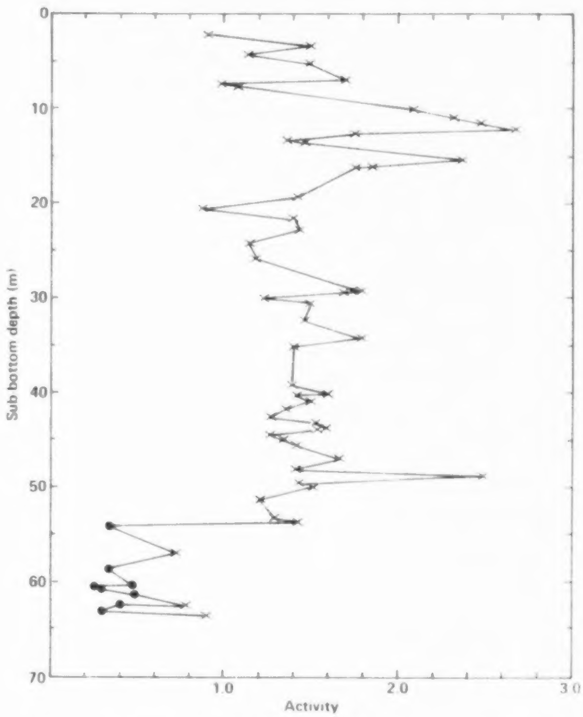

Figure 11. Activity-depth profile for Hole 576A sediments. Solid circles (•) below 55 m represent values obtained in carbonate ooze.

ues reported for each of the major lithologic units (Tables 4 and 5). A compilation of the consolidation test results is illustrated in Figure 17, which shows the void ratios at applied loads of 50, 100, 300, and 1000 kPa plotted versus sub-bottom depth.

The overconsolidated surficial sediments from Hole 576A were not totally unexpected. Consolidation test results from many different marine geological environments indicate that most near-surface sediments are in a state of "apparent overconsolidation' (Hamilton, 1964; She-

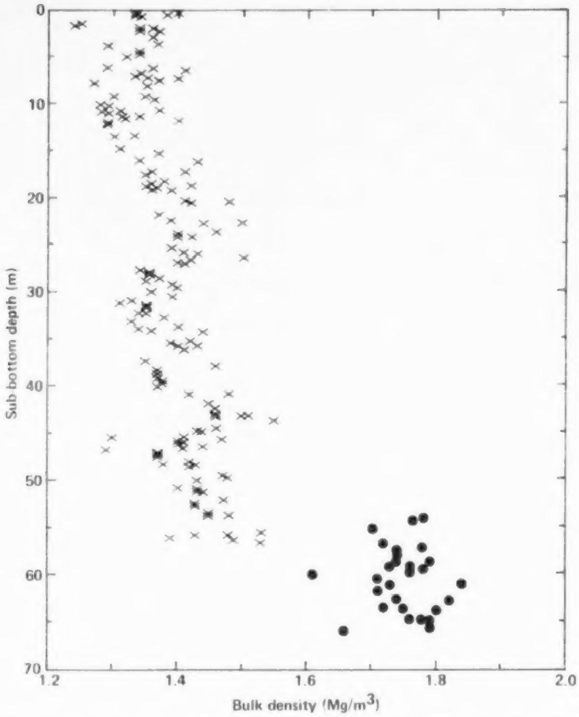

Figure 12. Bulk density-depth profile for Hole 576A sediments. Solid circles (•) below 55 m represent values obtained in carbonate ooze.

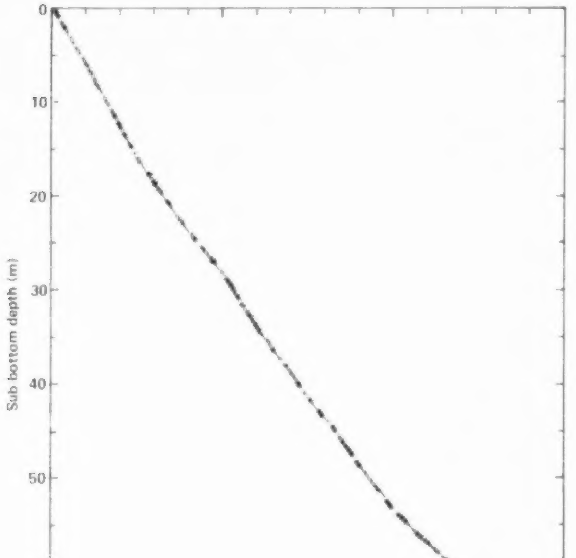

Figure 13. Effective overburden stress-depth profile computed using bulk-density values for Hole 576A sediments. Effective overburden stress was calculated assuming hydrostatic pore-water pressure conditions using the equation of Shephard et al. (1978).

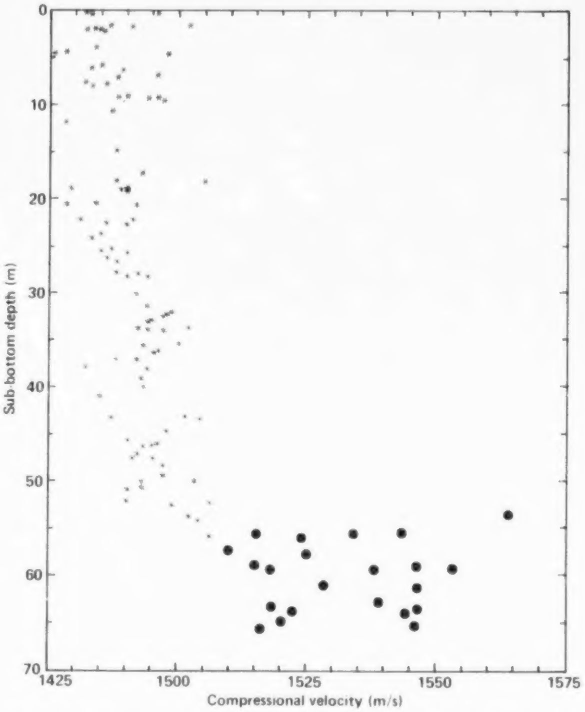

Figure 14. Compressional velocity-depth profile for Hole 576A sediments. Solid circles (•) below 55 m represent values obtained in carbonate ooze.

phard et al., 1978; Silva et al., 1980). Apparent overconsolidation is generally attributed to the cohesion that results from the molecular interaction between solid particles (Terzaghi, 1956). For clay sediments, Terzaghi suggested these cohesive forces are at least 5 kPa. In near-surface sediments these forces are large relative to the small overburden stress, resulting in a calculated preconsolidation stress value that is much larger than the effective overburden stress and, consequently, an overconsolidation ratio that is significantly greater than unity.

A number of mechanisms or processes can influence the state of consolidation (Brumund et al., 1976). The most probable mechanisms responsible for the overconsolidation of the Subunit IA sediments are (1) changes in soil structure due to chemical alterations in the form of cementing agents and interparticle bonds, (2) the effects of high hydrostatic pressure release during core recovery, and (3) artifacts arising from the consolidation test process. Dadey (1983) assumed that the effects of cementation and interparticle bonding on the sediment microstructure would be relatively constant with depth; thus, its significance would be gradually diminished with increasing overburden. Consequently, as is evident in Figure 15, the overconsolidation ratio will decrease with depth, eventually reaching a value that fluctuates around one. This occurs at approximately 25 to 30 m sub-bottom in Hole 576A sediments.

Brumund and Callender (1975) concluded that the apparent overconsolidation present in near-surface sediments was related to the release of high hydrostatic pressures during sampling. Lee (1984) however, suggests that

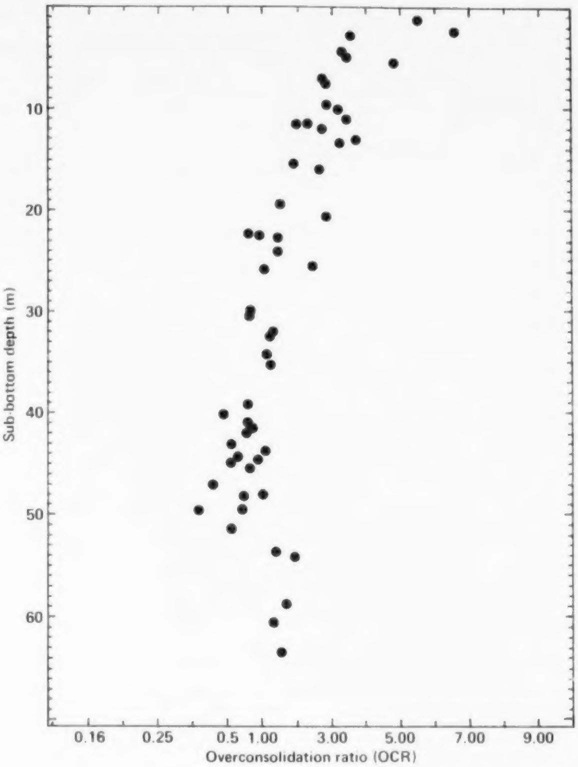

Figure 15. Overconsolidation ratio–depth profile computed using static-load consolidation test results from Hole 576A sediments. Overconsolidation scale reciprocal below 1.00, linear above 1.00.

clays exposed to hydrostatic pressures of 75 to 100 MPa would have an induced effective stress of only 2 to 5 kPa. This is not of sufficient magnitude to affect significantly the preconsolidation stress values determined using the Casagrande method for Hole 576A sediments.

Scully et al. (1984) have shown that completely remolded, normally consolidated sediments develop a fictitious preconsolidation stress, which they attribute to seating of the porous stones and loading platens during initial testing and possibly to wall fraction developed during the consolidation test. This artificial preconsolidation stress is of uncertain magnitude, but may contribute to the apparent overconsolidation observed in Hole 576A sediments.

The sediments between 28 and 39 m sub-bottom appear normally consolidated while those between 38 and 55 m sub-bottom appear normally to underconsolidated. In fact, OCR results indicate that in some instances the sediments between 39 and 55 m sub-bottom are as underconsolidated as the sediments between the seafloor and 28 m sub-bottom are overconsolidated (Fig. 15). The mechanisms generally responsible for underconsolidation include high rates of sediment accumulation, chemical alterations, and coring disturbance (Sangrey, 1977). Sediment accumulation rates at Hole 576A are generally much less than 10 m/m.y. This rate is sufficiently slow to permit the dissipation of any excess pore water pressures that may have developed during the sedimentation process. Available geochemical data for Site 576A (McDuff, this volume) suggest that any chemical alteration effects should be prevalent within all of Subunit IB and not limited to only select intervals. Although coring and sampling disturbance may have contributed to the observed state of underconsolidation, this effect is very difficult to quantify.

The discrepancy between the expected normal state of consolidation and the consolidation test results strongly indicates that the technique employed for determining the preconsolidation stress (Casagrande, 1936) should be carefully evaluated. Various investigators, including Cooling and Skempton (1942), Bishop et al. (1965), and Schmertmann (1955), have concluded that the Casagrande method is inadequate to define the preconsolidation stress under certain circumstances. Other methods used to determine the preconsolidation stress (Burmister, 1951; Schmertmann, 1955) require a rebound and reloading cycle.

Examination of the e versus log σ' curves (Fig. 16) and the profile of expansion index versus sub-bottom depth (Fig. 18) shows that the amount of sediment expansion or rebound that occurs during unloading increases with depth below the seafloor. As the expansion index increases, the error in the determination of the preconsolidation stress, as determined by the Casagrande method, also appears to increase. An examination of the unloading and reloading portions of the e versus log σ' curve at 32.47 m sub-bottom (Fig. 16) shows that the unloading portion of the hysteresis loop in this example started at 400 kPa. Thus, the actual preconsolidation stress of the hysteresis-loop curve is 400 kPa. However, when the preconsolidation stress is determined using the Casagrande method on the hysteresis loop the preconsolidation stress is underestimated by 140 kPa (35%).

These results and the subsequent analysis of 16 e versus log σ' curves containing a hysteresis loop have been used to develop a relationship between the expansion index and the preconsolidation stress as determined by the Casagrande method (Fig. 19). This relationship was used to adjust the values of the preconsolidation stress determined using the Casagrande method. The adjusted values are listed in Table 6 as σ_{c4}.

Another method to determine the preconsolidation stress is based on the characteristics of the rebound curve and the assumption that these characteristics are constant for a given sediment sample (Fig. 20). An examination of all the Site 576A e versus log σ' curves with rebound portions substantiates this assumption. The rebound method for determining the preconsolidation stress utilizes a point on the constant or maximum void ratio line that occurs prior to the maximum point of curvature on the e versus log σ' curve. This point (point B in Fig. 20) should be located at the maximum effective stress occurring on the line of constant void ratio. If that point appears ambiguous, a point one complete log cycle before the point of maximum curvature on the e versus log σ' curve can be used. From that point, a line parallel to the rebound portion of the e versus log σ' curve is extended to intersect the virgin curve. That intersection is

Table 4. Summary of incrementally loaded consolidation test results performed on Hole 576A sediments.

Sub-bottom depth (m)	Initial void ratio (e_0)	Void ratio at σ_c'	Overburden pressure σ_0' (kPa)	Preconsolidation pressure σ_c' (kPa)	Overconsolidation ratio (OCR)	Compression index (C_c)	Expansion index (C_e)	Permeability (indirect) (cm/sec)	Permeability (direct) (cm/sec)
1.40	6.12	5.83	4.48	25	5.58	2.00	0.06	6.48E-5	
2.45	3.77	3.25	7.52	76	10.11	1.25	0.07	5.40E-6	1.30E-5
2.55	3.78	3.36	7.86	52	6.62	1.37	0.06		
3.00	4.70	4.34	9.44	34	3.60	2.20			
4.52	4.34	3.94	14.67	49	3.34	1.99	0.09	6.30E-6	1.49E-5
5.00	4.19	3.79	16.40	57	3.48	1.63		1.68E-6	
5.60	4.46	4.05	18.10	88	4.86	2.30			
7.40	4.56	4.17	23.90	67	2.79	2.25	0.09		
7.54	4.62	4.08	24.27	69	2.84	2.34	0.15	1.93E-6	2.40E-5
9.72	4.77	4.18	30.81	89	2.89	2.30		8.70E-7	
10.23	5.64	4.81	32.39	106	3.27	2.75	0.11	1.04E-6	
11.11	5.16	4.52	34.74	121	3.48	3.04	0.15	9.40E-7	3.40E-6
11.60	5.27	4.36	36.22	84	2.32				
11.66	4.91	4.41	36.39	74	2.03	2.67	0.10	1.69E-6	
12.21	5.74	4.97	38.12	106	2.78	3.01		1.52E-6	
13.15	5.04	4.35	40.96	152	3.71	3.08	0.14		
13.52	4.77	3.82	42.12	140	3.23	2.70	0.12	3.82E-7	7.80E-7
15.50	4.58	3.77	48.80	94	1.93	2.50	0.15	3.25E-7	5.33E-7
16.15	4.61	4.07	50.65	135	2.67	2.58	0.16		
16.22	4.48	3.71	50.85	135	2.65	2.45	0.20	6.10E-7	9.70E-7
19.54	4.22	3.81	63.00	96	1.52	2.19	0.14	3.01E-7	
20.76	2.97	2.68	67.87	195	2.87	1.67	0.13	2.60E-7	3.30E-7
22.43	3.81	3.39	74.64	61	0.82	1.57	0.22	7.30E-8	
22.65	3.65	3.28	75.53	73	0.97	1.45	0.13		
22.86	2.75	2.23	76.40	113	1.48	0.97		3.25E-7	1.32E-7
24.34	3.66	3.12	82.70	120	1.45	1.53	0.12	6.40E-8	2.35E-7
25.65	3.10	2.86	88.04	218	2.48	2.10			
26.02	3.24	2.89	89.63	96	1.07	1.25	0.13	1.15E-7	1.15E-7
Average values (Unit IA)					3.10	2.12	0.13	4.66E-6	7.42E-6
30.09	3.24	2.80	106.13	90	0.85	1.23	0.12	2.70E-8	9.60E-8
30.40	4.33	3.89	107.65	88	0.82	1.70			
30.60	4.13	3.48	108.02	88	0.81	1.56	0.20	1.24E-7	
32.15	4.11	3.65	113.51	145	1.28	1.86	0.17		
32.47	4.32	3.66	114.62	140	1.22	1.84	0.22	5.20E-8	2.20E-7
34.40	3.66	3.08	121.58	140	1.15	1.95	0.26	4.45E-8	
35.29	3.56	3.25	125.09	155	1.24	1.62	0.23	6.20E-9	6.60E-8
39.37	4.00	3.70	141.52	113	0.80	1.69		2.90E-8	1.09E-7
40.36	3.84	3.52	145.35	70	0.48	1.48	0.23	3.85E-8	1.42E-7
41.04	3.32	3.00	147.86	120	0.81	1.33	0.25	3.00E-8	1.11E-7
41.65	3.22	2.69	150.46	130	0.86	1.43			
42.02	3.18	2.88	152.05	120	0.79	1.33	0.25	4.10E-8	1.41E-7
43.30	2.80	2.50	157.78	90	0.57	0.91	0.16	3.90E-8	
44.61	2.67	2.51	163.66	109	0.66	1.16	0.16	4.25E-8	7.80E-8
44.65	2.88	2.53	163.83	155	0.95	1.40	0.28		
44.97	3.26	2.96	165.23	92	0.56	1.40	0.28	2.09E-8	7.00E-8
45.60	3.31	2.92	168.50	140	0.83	1.39	0.27	1.92E-8	
47.20	3.74	3.22	174.47	75	0.43	1.40	0.34	2.20E-8	1.08E-7
48.15	3.62	3.19	177.93	183	1.03	1.89			
48.21	3.14	2.85	178.15	130	0.73	1.52	0.33	3.10E-8	6.70E-8
49.60	3.76	3.34	183.95	130	0.71	1.60			
49.65	3.40		184.21	67	0.36	1.19			
51.36	3.20	2.77	191.45	110	0.57	1.36	0.33	1.47E-8	
53.65	3.09	2.64	201.40	280	1.39	1.73			
Average values (Unit IB)					0.82	1.49	0.22	3.13E-8	1.10E-7
54.22	1.36	1.20	204.70	385	1.88	0.45	0.03	1.80E-6	1.30E-6
58.72	1.37	1.13	232.28	400	1.72	0.30	0.03	3.90E-7	2.40E-6
60.65	2.84	2.40	246.22	320	1.30	1.35	0.15	2.81E-7	
63.61	1.37	1.04	267.50	400	1.50	0.35	0.01	2.50E-7	2.30E-6
Average values (Unit II)					1.60	0.61	0.06	6.80E-7	2.00E-6

determined to be the preconsolidation stress. Values derived by this method are listed in Table 6 as σ_{c5}.

The interpretation of the consolidation test results can vary significantly depending on the technique employed for determining the preconsolidation stress (Table 6). Results using the Casagrande technique (σ_{c1}') indicate that Subunit IA sediments are overconsolidated and Subunit IB sediments are normally to underconsolidated. The second technique used for determining the preconsolidation stress (σ_{c4}') results in almost all Hole 576A sediments being overconsolidated. The third technique, which uses point B (σ_{c5}'), results in the upper sediment (0–28 m sub-bottom) being, in essence, less overconsolidated than the results using σ_{c1}, and the lower sediment (28 to 55 m sub-bottom) normally consolidated. This third technique appears to reflect best the anticipated state of consolidation of Subunit IB based on the geological history of this area.

Table 5. Summary of constant rate of deformation consolidation tests performed on Hole 576A sediments.

Sub-bottom depth (m)	Initial void ratio (e_0)	Void ratio at σ_c'	Overburden pressure σ_0' (kPa)	Preconsolidation pressure σ_c' (kPa)	Overconsolidation ratio (OCR)	Compression index (C_c)	Expansion index (C_e)	Permeability (indirect) (cm/sec)	Permeability (direct) (cm/sec)
4.60	3.58	4.12	14.93	69	4.62	1.71	0.15		1.70E-7
7.60	4.05	3.58	24.46	100	4.09	2.02	0.14		5.10E-7
11.20	4.74	4.02	35.01	105	3.00	2.42	0.26		6.70E-7
13.60	4.40	3.62	42.26	120	2.84	2.04	0.07		4.45E-7
16.30	4.49	3.55	51.13	160	3.13	2.70	0.02		1.65E-7
20.85	3.01	2.44	68.60	179	2.61	2.11		5.19E-8	
24.40	3.69	2.73	82.92	172	2.07	2.12		4.85E-8	
26.10	3.38	2.49	89.97	215	2.40	2.10		3.15E-8	
30.20	3.18	2.83	107.28	88	0.82	1.97		5.35E-8	
32.55	3.99	3.55	114.91	118	1.03	2.56		5.65E-8	
35.25	3.32	3.07	124.92	90	0.72	2.45		4.50E-8	
39.45	3.21	2.81	141.83	100	0.70	2.23		3.21E-8	
40.44	4.19	3.73	145.63	48	0.33	1.73	0.40		7.20E-8
41.04	3.07	2.62	147.90	120	0.81	1.15		3.95E-8	
42.10	2.92	2.61	152.40	115	0.75	1.86		5.40E-8	
43.70	2.57	2.26	159.89	115	0.72	1.76		3.55E-8	
45.10	2.97	2.81	165.84	65	0.39	1.83		4.60E-8	
45.70	3.10	2.88	168.81	88	0.52	2.16		4.50E-8	
49.30	2.97	2.59	182.67	166	0.91	2.25		2.36E-8	
52.40	2.99	2.70	203.28	118	0.58	2.09		2.55E-8	
54.50	1.61	1.43	206.65	223	1.08	1.18		1.55E-7	
58.80	1.27	0.86	232.87	675	2.90			1.83E-6	
61.70	1.16	0.80	253.89	700	2.76			3.05E-7	
63.70	1.08	0.75	270.35	700	2.59			6.30E-7	

The predicted field consolidation curve for Hole 576A pelagic sediments (Fig. 21) was constructed using the void ratio at the preconsolidation stress and the calculated *in situ* vertical effective stress. This curve can be used to interpolate *in situ* porosity-permeability-depth relationships for any portion of the sedimentary section. The quadratic line of best fit defines an *e* versus log σ' curve that has a compression index of 2.2 as compared to an average C_c of 2.12 for Subunit IA sediments (Table 4) and an initial void ratio of 5 to 5.4.

Permeability

As indicated earlier, several means of measuring or calculating the coefficient of permeability were employed. All direct measurements were performed during the course of the consolidation test. The indirect determinations were calculated using either conventional consolidation theory or CRD test results. All reported permeability values were determined at the preconsolidation stress (Fig. 22). The permeability profile is characteristic of other results reported for fine-grained marine sediments and shows decreasing permeability with depth.

Summary

Detailed analysis of Hole 576A consolidation test results indicate that the accepted methodology for interpreting the geological significance of consolidation data is deficient. Sediments in the upper 28 m are overconsolidated regardless of how the preconsolidation stress is determined. Sediments between 28 and 39 m sub-bottom are normally consolidated; whereas sediments between 39 and 55 m sub-bottom appear normally to underconsolidated. A number of mechanisms have been proposed to explain the variation in consolidation behavior, although many of these mechanisms do not appear consistent with the well-substantiated geological history of this area. Much of the apparent discrepancy between the expected consolidation state of Hole 576A sediments based on available geological and geotechnical information and the actual consolidation test results may result from the Casagrande technique employed to determine the preconsolidation stress. An alternative method for calculating σ_c', based on the characteristics of the rebound portion of the *e* versus log σ' curve, yields σ_c' values for Subunit IB that are more consistent with the known geology in the area.

SHEAR STRENGTH

Shear strength tests were performed on Hole 576A sediments to determine the characteristics of the undrained shear strength profile with depth and to evaluate the significance of this profile relative to the observed consolidation state of Hole 576A sediments. The shear strength tests performed included: (1) laboratory vane shear; (2) unconsolidated, undrained triaxial compression; (3) isotropically consolidated, undrained triaxial compression; and (4) anistropically consolidated, undrained triaxial compression (Table 7). Results of these tests and their relationships to the observed geotechnical behavior of Hole 576A sediments are summarized in the following sections.

Undrained Shear Strength

The undrained shear strength of Hole 576A sediments was determined using the laboratory vane shear and the results from unconsolidated-undrained triaxial (UU) compression tests. Results of the vane shear tests are summarized in Figure 23 and Table 3. Table 8 summarizes the results of the UU triaxial tests. These data have been normalized using the ratio of the undrained shear strength to the effective overburden stress calculated for the sub-bottom depth at which the strength measurement was

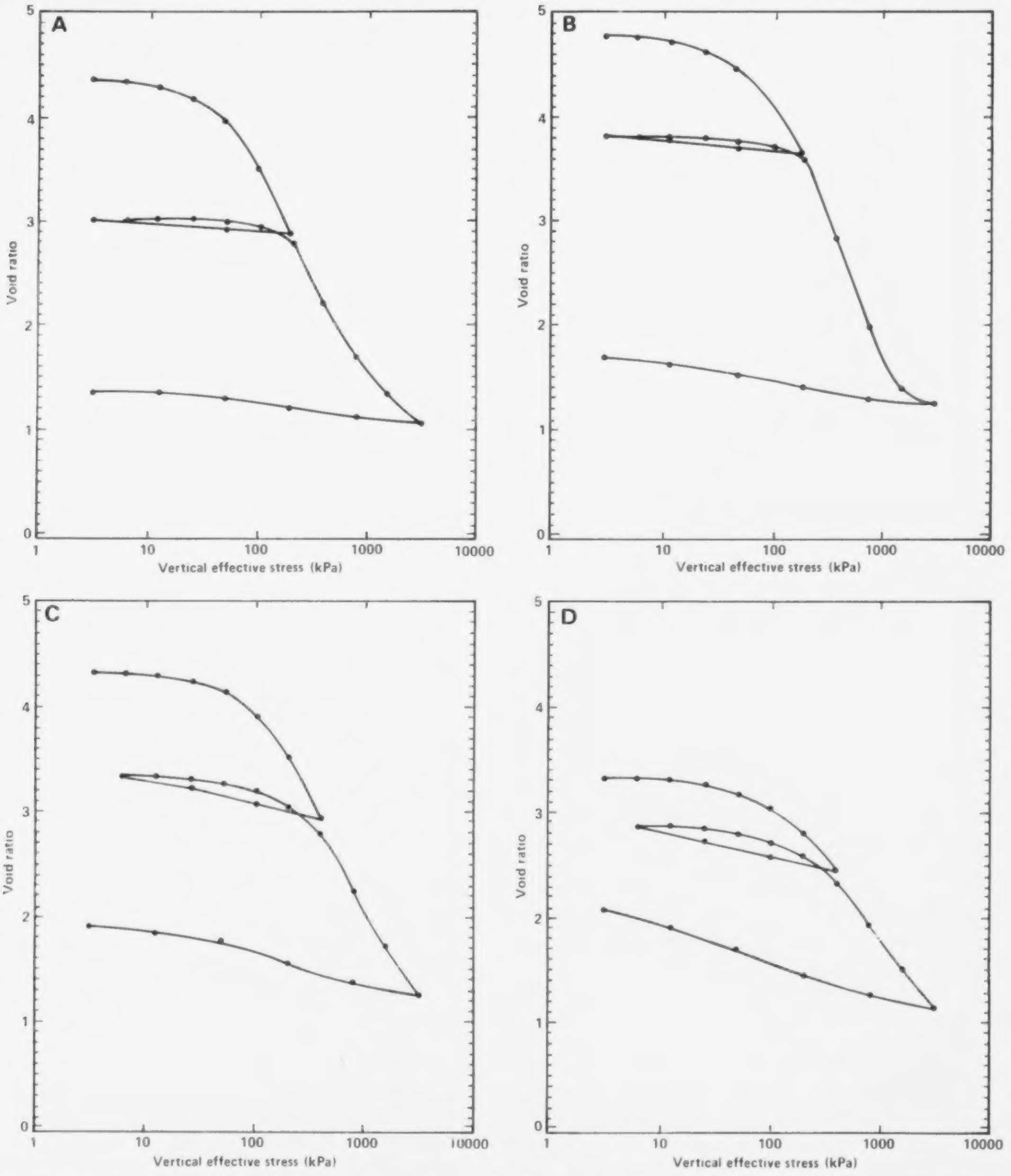

Figure 16. Void ratio versus log of effective stress curves (e versus log σ') obtained from Hole 576A sediments located in Subunit IA (A, 4.20 and B, 13.52 m sub-bottom) and Subunit IB (C, 32.47 and D, 45.60 m sub-bottom).

made (s_u/σ_o'; Fig. 24) for comparison to a computed *in situ* profile presented later. The values of σ_o' were obtained from Figure 13.

Shear Strength Parameters

Effective stress and undrained shear strength parameters were determined from consolidated-undrained triaxial tests for both isotropic and anistropic loading conditions. Table 7 lists the samples tested and the test conditions employed for each specimen. Examples of the stress paths and the effective stress parameters for both the isotropic and anisotropic condition are presented in Figures 25 and 26 with the corresponding shear-strength parameter values derived from the tests summarized in Tables 9 through 11.

Calculated Undrained Shear Strength Profiles

The shear strength parameters measured on Hole 576A sediments provide a basis for calculating an *in situ* undrained shear strength profile. The calculations involve the use of the SHANSEP method (Ladd and Foott, 1976; Ladd et al., 1977), which relates the *in situ* normalized

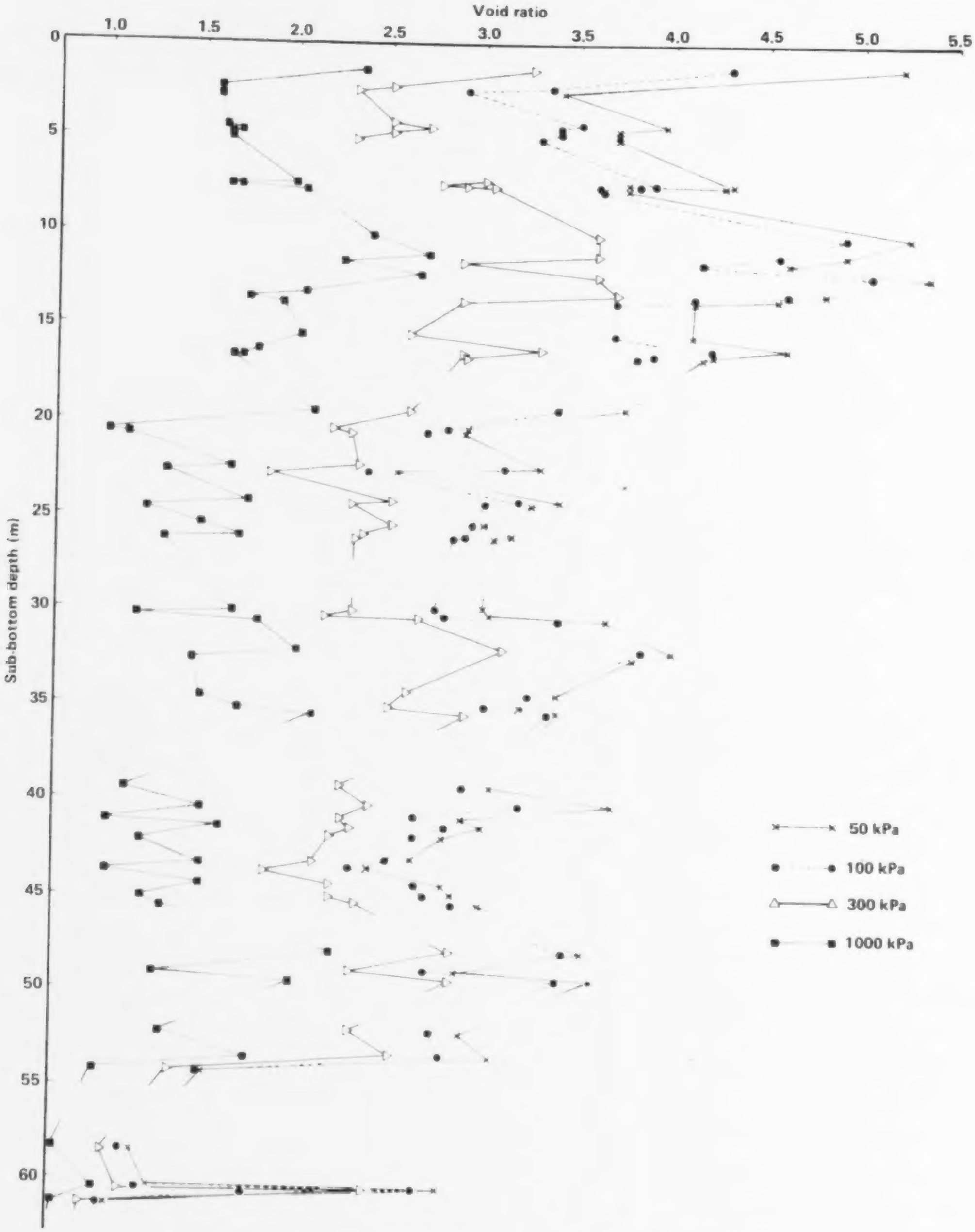

Figure 17. Summary of consolidation test results for Hole 576A sediments. Sediment response to increasing applied stress for each sample tested is displayed as changing void ratio at the same depth. A pronounced change in compressibility with depth at four applied stress levels occurs between Subunits IA and IB.

undrained shear strength to the measured shear strength parameters as follows:

$$s_u/\sigma_o' = (s_u/\sigma_o')_{NC}\mathrm{OCR}^m$$

where s_u is undrained shear strength, σ_o' is effective overburden stress, NC represents the normally consolidated condition, OCR is the overconsolidated ratio, and m is a constant that depends on the type of sediment. On the basis of the results of CIU triaxial tests on overconsolidated samples (Fig. 27 and Table 10), a value of m = 0.5 was computed. This value is lower than the typical m value of 0.8 suggested by Ladd et al. (1977) based on CAU simple shear tests. The discrepancy between m val-

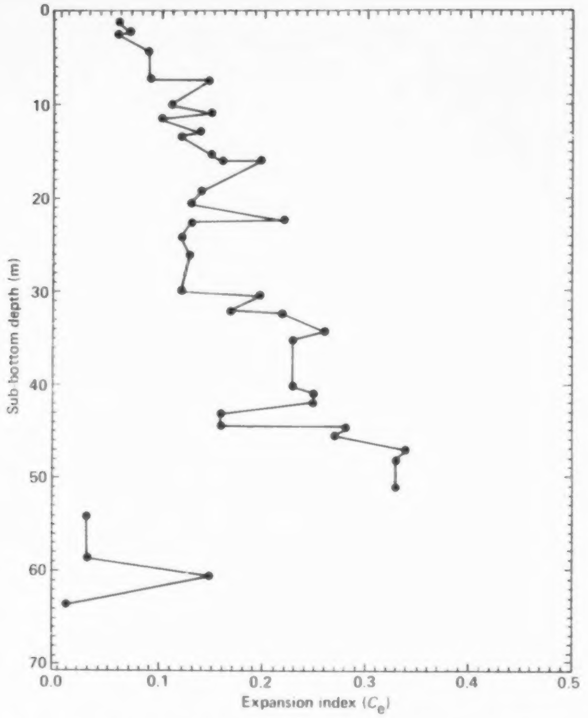

Figure 18. Expansion index-depth profile determined using the rebound portion of the *e* versus log σ' curve generated from consolidation-test results completed on Hole 576A sediments.

ues is due partly to the differences between CIU and CAU tests and partly to the differences between triaxial and simple shear tests.

In order to apply the SHANSEP method to the sediment conditions at Hole 576A, it is first necessary to convert the s_u/σ_o' values from the CIU tests to the *in situ* coefficient of earth pressure at rest condition, K_o, as determined by the CAU test. A study of the data in Tables 9 and 11 indicates that the s_u/σ_o' values from the CIU tests should be multiplied by 0.89 to obtain the estimated values for the CAU condition. The adjusted values are summarized in Table 12.

The values of s_u/σ_o' reported for the upper 28 m of sediment in Table 12 must be further adjusted to account for the apparent *in situ* overconsolidated condition determined on the basis of consolidation test results. This was completed using the SHANSEP equation and a value of $m = 0.5$ (Table 13) together with the OCR values determined from consolidation test results in Figure 13. The computed values of normalized *in situ* strength, s_u/σ_o', and the *in situ* strength, s_u, computed using SHANSEP are plotted versus depth in Figures 28 and 29, respectively.

Interpretation of Shear Strength Profiles

Interpretation of the normalized shear strength profiles presented in Figures 24 and 28 requires consideration of two factors: (1) the effects of sample disturbance and (2) the *in situ* state of consolidation.

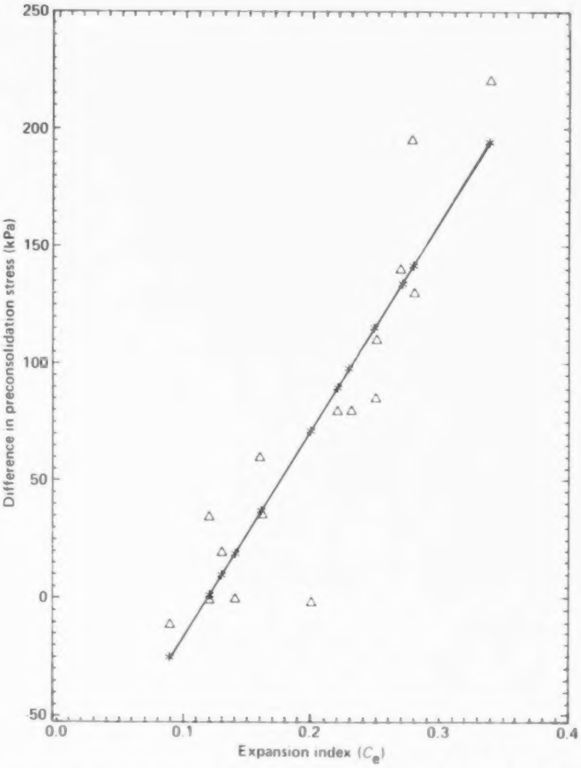

Figure 19. Relationship between the expansion index and the difference between a known preconsolidated stress determined using a hysteresis loop and the preconsolidation stress determined graphically using the Casagrande technique (see test for explanation). As the expansion index increases the difference between the known and calculated preconsolidation stress values also increase. Asterisks(*) represent regression analysis results ($\sigma = 0.83$).

The effects of disturbance are evident from a comparison of the normalized strength-depth profiles in Figures 24 and 28. At all depths, the undrained strengths obtained by both the vane shear and UU triaxial tests are considerably lower than those computed for the *in situ* condition. This decrease in shear strength is consistent with the known effects of sample disturbance on sediment shear strength.

The influence of the *in situ* sediment consolidation state on the undrained shear strength at Hole 576A is clearly demonstrated by the data presented in Figures 24 and 28. Results of consolidation tests summarized in Figure 15 indicate that the sediments are overconsolidated to a depth of 28 m sub-bottom. The normalized shear strength values (Fig. 28), as well as the computed *in situ* values (Fig. 29) are consistent with the consolidation test results from the upper 28 m. The shear strength results show a much higher gradient over this interval than the gradient that exists in the normally consolidated sediments between 28 and 55 m sub-bottom.

An examination of the computed undrained strength profile (Fig. 29) reveals the difference between the sediment strength characteristics of Subunits IA and IB. It also demonstrates the usefulness of the SHANSEP meth-

Table 6. Summary of preconsolidation stress values calculated using Casagrande's technique and the modified techniques incorporating the sediment expansion characteristics described in the text.

Sub-bottom depth (m)	σ_{c1} (kPa)	OCR	σ_{c4} (kPa)	OCR	σ_{c5} (kPa)	OCR
1.40	25	5.58	25	5.58	70	15.6
2.45	76	10.11	76	10.11		
2.55	52	6.62	52	6.62		
3.00	34	3.60				
4.52	49	3.34	49	3.34	45	3.06
5.00	57	3.38			54	
5.60	88	4.86				
7.40	67	2.79	67			
7.54	69	2.84	96	3.95	64	2.84
9.72	89	2.89	89	2.89		
10.23	106	3.27	106	3.27	85	2.62
11.11	121	3.48	136	3.91	110	3.16
11.30					105	
11.60	84	2.32			68	1.87
11.66	74	2.03	74	2.03		
12.21	106	2.78				
13.15	152	3.71	170	4.15		
13.52	140	3.23	140	3.23	85	2.01
15.50	94	1.93	121	2.48	75	1.53
16.15	135	2.67	171	3.37	110	2.17
16.22	135	2.65	207	4.07	97	1.90
19.54	96	1.52	114	1.80	83	1.31
20.76	195	2.87	208	3.06	190	2.79
22.43	61	0.82	151	2.02	115	1.54
22.65	73	0.97	82	1.08		
22.86	113	1.48				
24.34	120	1.45	120	1.45	74	0.89
25.65	218	2.48				
26.02	96	1.07	105	1.17	85	0.95
30.09	90	0.85	90	0.85	80	0.75
30.40	88	0.82				
30.60	88	0.81	160	1.48	61	0.56
32.15	145	1.28	190	1.67	125	1.10
32.47	140	1.22	230	2.00		
34.40	140	1.15	281	2.31	180	1.48
32.29	155	1.24	254	2.03	210	1.67
39.37	113	0.80			110	0.77
40.36	70	0.48	169	1.16	78	0.54
41.04	120	0.81	237	1.60	180	
41.65	130					
42.02	120	0.78	237	1.56	180	1.18
43.30	90	0.57	126	0.79	140	0.88
44.16	109	0.66	145	0.88	180	1.10
44.65	155	0.95	299	1.82	340	2.07
44.97	92	0.56	236	1.43	200	1.21
45.60	140	0.83	275	1.63	200	1.18
47.20	75	0.43	273	1.56	185	1.06
48.15	183	1.03				
48.21	130	0.73	319	1.79	250	1.40
49.60	130	0.71			250	1.36
49.65	67	0.36				
51.36	110	0.57	299	1.56	170	0.88
53.65	280	1.39			330	1.64
54.22	385	1.88			360	1.76
58.72	400	1.72			150	0.64
60.65	320	1.30			240	0.97
63.61	400	1.50				

Note: The overconsolidation ratios reported are those calculated using the adjusted preconsolidation stress. Blanks indicate no data available.

od for estimation of the *in situ* strength from the results of laboratory tests on partially disturbed samples. This profile also represents our best estimate of the *in situ* undrained strength of Subunits IA and IB in Hole 576A.

The sediment cores obtained from the depths of 55 to 64 m sub-bottom were highly disturbed and did not provide enough data for an adequate SHANSEP analysis of the carbonate-ooze sediments in Unit II.

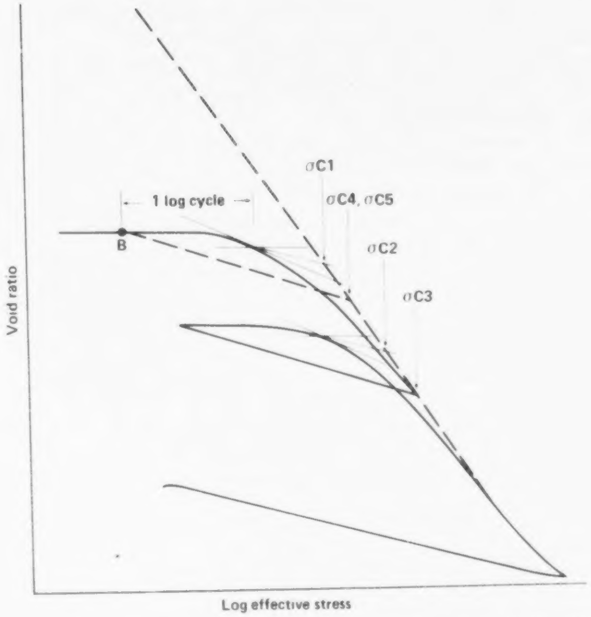

Figure 20. Hypothetical void ratio–log effective stress (e versus log σ') curve showing how the calculated preconsolidation stress varies depending on the technique used (see explanation in text). σ_{c1} is the preconsolidation stress calculated using the Casagrande (1936) technique. σ_{c2} is the preconsolidation stress calculated using the Casagrande technique on the hysteresis loop on the e log σ' curve. σ_{c3} is the actual preconsolidation stress for the hysteresis loop. σ_{c4} is the preconsolidation pressure determined using the rebound characteristics (Fig. 19) and the hysteresis loop. σ_{c5} is the preconsolidation pressure determined using point B and the slope of the rebound curve.

DISCUSSION OF RESULTS

The geotechnical property results for Hole 576A sediments represent the most complete geotechnical data set ever compiled for a continuously depositional sedimentary section that spans 65 m.y. Excellent agreement exists between index property, consolidation, permeability, and shear strength test data generated during the initial sampling at SIO and at the various geotechnical laboratories participating in the analyses. These results are also valuable because they demonstrate the degree of interlaboratory variation one can expect from each type of test performed provided that similar techniques are adopted.

Predicted geotechnical property results (i.e., based on the geological and geotechnical information available prior to drilling) and actual geotechnical property measurements show significant differences. Several important factors or combination of factors have influenced the geotechnical property results observed in Hole 576A sediments. These primary factors include: (1) core disturbance, (2) time, (3) cementation and interparticle bonding, (4) mineralogy, and (5) grain size.

The term core disturbance includes a number of processes. Any sampling method will result in stress relief and expansion. In addition, mechanical alteration of the sediment fabric results from the coring, handling, and

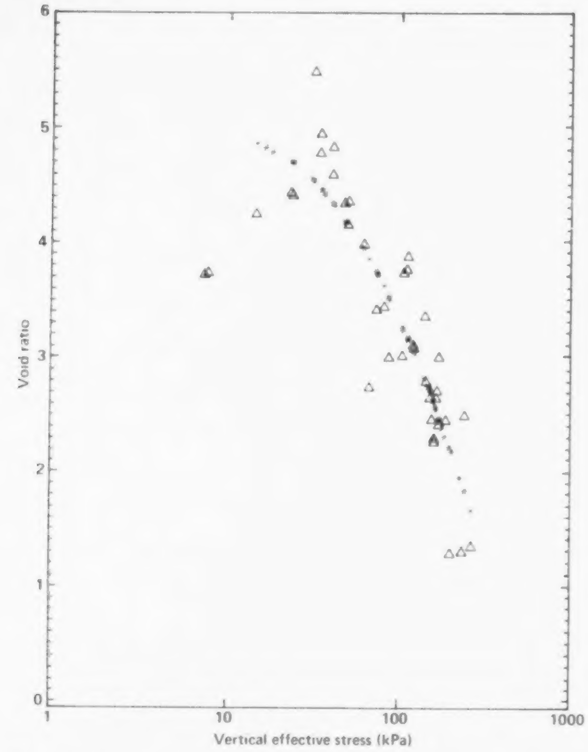

Figure 21. Void ratio-log effective stress curve determined using the void ratios calculated at the preconsolidation stress and the effective overburden stress calculated for each consolidation sample depth. The curve is representative of *in situ* field conditions. Asterisks(*) represent a quadratic fit to the field data (σ = 0.74).

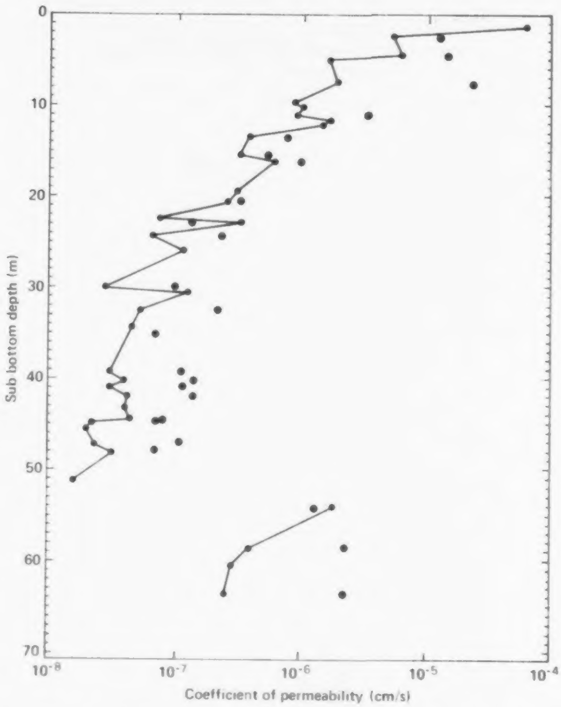

Figure 22. Coefficient of permeability-depth profile for Hole 576A sediments. Permeability values determined by direct measurement (falling head, constant head, and flow pump) are illustrated by connected dots. Permeability values calculated using consolidation theory are illustrated by solid circles (●). All permeability values were obtained at the preconsolidation stress.

initial testing procedures. Such effects disturb the sediment fabric and generally reduce both the shear strength and the preconsolidation stress as determined in the laboratory for a particular sample. Although difficult to quantify, a comparison of the s_u/σ_0' ratios determined using the results of laboratory tests and results corrected for *in situ* conditions using SHANSEP clearly demonstrates the effects of disturbance (Figs. 24 and 28).

Time has a significant effect on the geotechnical behavior of fine-grained sediments. Sedimentation rates at Site 576 were generally less than 10 m/m.y. over the last 65 m.y. These rates are sufficiently slow to allow complete dissipation of any excess pore pressures resulting from the sedimentation process. Thus, the time-dependent physical processes, (i.e., primary and secondary consolidation) have been completed or are continuing at such a slow rate that the Site 576 sediments should be very near a state of physical equilibrium.

Temporal variations in chemical processes (i.e., diagenesis, cementation, and interparticle bonding) could also influence the geotechnical behavior of fine-grained sediments. Dadey (1983) has proposed clay-particle cementation as the primary factor responsible for the overconsolidation evident in Subunit IA sediments. The cementation effect may be more pronounced in high void ratio shallow sediments where the influence of accumulated overburden relative to the effects of cementation is not as significant as in more deeply buried sediments. Similar reasoning suggests that cementation effects should be reflected in the near-surface sediment shear strength. The variations observed in the shear strength gradient evident in the SHANSEP results between Subunits IA and IB may reflect these effects. However, the variability in near-surface shear strength values precludes any definitive assessment of the cementation effects on shear strength.

The most common clay minerals present in Hole 576A sediments are illite, smectite, chlorite, and kaolinite. Illite comprises approximately 50% of the clay minerals present. The quartz content ranges between approximately 3 and 17% (Table 2). The largest mineralogical variation in Hole 576A sediments is the pronounced increase in X-ray amorphous material at depth and the variable quartz content. The higher expansion indices and increased plasticity of Subunit IB sediments suggest that the geotechnical behavior of the X-ray amorphous component is similar to smectite.

Examination of the relationships between void ratio at 50 kPa (Fig. 17), silt content (Fig. 30), and the compression index (Fig. 31) show very unusual relationships with depth, particularly in Subunit IA. As void ratio and compression index increase over this interval, silt content also increases. Examination of scanning electron micrographs obtained from the silt-size fraction revealed this component was made up of quartz grains and clay

Table 7. Shear strength test program completed on Hole 576A sediments.

Core-Section	Sub-bottom depth (m)	Test type			
		UU	$(CIU)_{nc}$	$(CIU)_{oc}$	$(CAU)_{nc}$
1-2	2.9	x			
1-3	3.0	x			
1-3	3.9	x			
1-4(2)	5.5		x		
1-4(1)	5.6		x		
1-5(1)	6.3		x		
1-5(2)	6.4		x		
2-1	10.0	x			
2-4	13.7	x			
2-6	16.8	x			
2-6(1)	17.3		x		
2-6(2)	17.4		x		
2-6(3)	17.5		x		
3-2	21.8	x			
3-5	21.6		x		
3-4(3)	24.7		x		
3-4(2)	24.7		x		
3-4(1)	24.8		x		
3-6	26.7	x			
4-1(1)	29.2			x	
4-2(2)	29.3				x
4-1(2)	29.5			x	
4-2(3)	29.5				x
4-1(3)	29.6			x	
4-2(4)	29.6				x
4-2(1)	29.7				x
5-3	40.2	x	x		
5-3(1)	40.5		x		
5-4	40.7	x	x		
5-4(2)	42.3		x		
5-4(3)	42.4		x		
5-4(1)	42.6				x
5-4(2)	42.7				x
5-4(3)	42.9				x
5-4(4)	43.0				x
5-5	44.0	x			
6-2	48.3	x			
6-2(1)	48.8		x		
6-2(2)	49.0		x		
6-3	49.7	x			
6-3	49.8	x			
6-4	51.8	x			
7-6	64.3	x			

Note: Subscripts nc and oc stand for normally consolidated and overconsolidated sediments, respectively. The test series number is shown in parentheses in the core-section column.

aggregates. No other silt-size components were identified. At 13 m sub-bottom quartz accounts for only 17% of the total 52% sand and silt-size fraction present. Given these relative proportions, the quartz grains are probably dispersed within the sediments and will have little or no effect on the sediments geotechnical behavior. The bonded clay aggregates comprising 35% of the coarse fraction at 13 m sub-bottom are sufficiently bonded to resist deflocculation. If the clays have not undergone extensive diagenetic alterations with time, then these aggregates probably result from clay particle cementation, possibly by iron oxides. In either case, these aggregates must form a high void ratio, porous structure that is dispersed among a clay particle matrix in a manner so as not to decrease the overall soil compressibility. The concept of bonded clay aggregates is not new; however, this study does present indications that clay aggregates do exist and can influence the geotechnical behavior of fine-grained sediments.

In conclusion, the geotechnical property results from Hole 576A sediments, in particular the consolidation test results, appear inconsistent with the known geological history of the area. The consolidation test results are substantiated by both the anomalous relationships occurring between index properties (i.e., grain size increases as void ratio increases) and the shear-strength results. A number of possibilities have been presented to explain these observations, including core disturbance, particle cementation, formation of bonded clay aggregates, and inadequate techniques for determining the preconsolidation stress. Available information precludes definitive conclusions as to which of these possibilities is most significant, although it is likely that each process has influenced the results to some degree. These results do show conclusively, however, that conventional geotechnical relationships developed largely from terrestrial studies should not be applied to the marine environment without very careful consideration and analysis.

ACKNOWLEDGMENTS

We are indebted to the DSDP Leg 86 scientific party and operational personnel for providing the time and patience necessary to successfully complete Hole 576A. This study would not have been possible without the gracious assistance of Amy Altman and the DSDP curatorial staff during the core processing. Sally Frew politely persevered while typing and retyping this report. Phil Valent, Mike Riggins, and Bob Prindle kindly agreed to review this manuscript and provided innumerable helpful comments. Partial financial support was provided by the Department of Energy through contracts with Sandia National Laboratories (DOE-AC04-76DP00789) and Argonne National Laboratory (DOE-31-109-ENG-38).

REFERENCES

American Society for Testing and Materials, 1984. *Annual Book of ASTM Standards, Part 19, Natural Building Stones; Soil and Rock:* Philadelphia (ASTM).

Bishop, A. W., Webb, D. L., and Lewin, P. I., 1965. Undisturbed samples of London clay from the Ashford common shaft: Strength-effective stress relationship. *Geotechnique*, 15:1–31.

Bishop, A. W., and Henkel, D. J., 1962. *The Measurement of Soil Properties in The Triaxial Test:* London (Edward Arnold, Ltd.).

Brumund, W. F., and Callender, G. W., Jr., 1975. Compressibility of undisturbed submarine sediments. *Proc. Civ. Eng. Oceans/III, Am. Soc. Civ. Eng.*, 1:363–379.

Brumund, W. F., Jonas, E., and Ladd, C. C., 1976. Estimating in situ maximum past (preconsolidation) pressure of saturated clays from results of laboratory consolidometer tests. *Transp. Res. Board, Spec. Rept.* 163:4–12.

Burmister, B. M., 1951. The application of controlled test methods in consolidation testing. *Consolidation Testing of Soils, ASTM Spec. Tech. Publ.* 126:83–91.

Casagrande, A., 1936. The determination of the preconsolidation load and its practical significance. *Proc. Int. Conf. Soil Mech. Found. Eng., 1st*, 3:60–64.

________, 1948. Classification and identification of soils. *Trans. Am. Soc. Civ. Eng.*, 113:901.

Cooling, L. F., and Skempton, A. W., 1942. A laboratory study of London clay. *J. Inst. Civ. Eng.*, 17:251–256.

Dadey, K. A., 1983. Stress history of unlithified marine sediments in the northwest Pacific [M.S. thesis]. University of Rhode Island, Kingston.

Damuth, J. E., Jacobi, R. D., and Hayes, D. E., 1983. Sedimentation processes in the Northwest Pacific basin revealed by echo-character mapping studies. *Geol. Soc. Am. Bull.*, 94:381–395.

Folk, R. L., 1974. *Petrology of Sedimentary Rocks:* Austin (Hemphill Publ. Co.).

Gorman, C. T., Hopkins, T. C., Deep, R. C., and Drnevich, V. P., 1978. Constant-rate of strain and controlled gradient consolidation testing. *Geotech. Test. J.*, 1:3–15.

Griffin, J. J., Windom, H., and Goldberg, E. D., 1968. The distribution of clay minerals in the world ocean. *Deep Sea Res.*, 15: 433–459.

Hamilton, E. L., 1964. Consolidation characteristics and related properties of sediments from experimental mohole (Guadalupe site). *J. Geophys. Res.*, 69:4257–4269.

________, 1965. Sound speed and related physical properties of sediments of experimental mohole (Guadalupe site). *Geophysics*, 30: 257–261.

Heath, G. R., and Pisias, N. G., 1979. A method for the quantitative estimation of clay minerals in North Pacific deep-sea sediments. *Clays Clay Miner.*, 27:175–184.

Ladd, C. C., and Foott, R., 1976. New design procedure for stability of soft clays. *J. Geotech. Eng. Div. Am. Soc. Civ. Eng.*, pp. 763–786.

Ladd, C. C., Foott, R., Ishikara, K., Schlosser, S., and Paulos, H. G., 1977. Stress-deformation and strength characteristics, state of art report. *Int. Conf. Soil Mech. Found. Eng., 9th, ISSMFE*, Tokyo.

Lambe, T. W., 1951. *Soil Testing for Engineers*. New York (Wiley).

Lee, H. J., 1984. State of the art: Laboratory determination of the strength of marine soils. Presented at *ATSM Symp. Lab. In Situ Deter. Strength Mar. Soils, San Diego*.

Leinen, M., and King, T. W., 1985. Mineralogy of North Pacific sediments from North Pacific candidate sites. *In* Shephard, L. E. (Ed.), 1983 Subseabed Disposal Program Annual Report: Site Assessment, Sandia National Laboratories, pp. 113–140.

Lowe, J., III., Zaccheo, P. F., and Feldman, H. S., 1964. Consolidation with back pressure. *J. Soil Mech. Found. Div., Am. Soc. Civ. Eng.*, 90:69–86.

Noorany, I., 1984. Phase relations in marine soils. *J. Geotech. Eng. Div., Am. Soc. Civ. Eng.*, 110: 539–543.

Olsen, H. W., 1966. Darcy's Law in saturated kaolinite. *Water Resour. Res.*, 2:287–295.

Pane, V., Croce, P., Znidarcic, D., Ko, H.-Y., Olsen, H. W., and Schiffman, R. L., 1983. Effects of consolidation on permeability measurements for soft clay. *Geotechnique*, 33:67–72.

Sangrey, D., 1977. Marine geotechnology: State of the art. *Mar. Geotechnol.*, 2:45–80.

Scully, R. W., Schiffman, R. L., Olson, H. W., and Ko, H.-Y., 1984. Validation of consolidation properties of phosphatic clay at very high void ratios. *Am. Soc. Civ. Eng. Symp. Consol. Settling*, pp. 158–181.

Schmertmann, J. H., 1955. The undisturbed consolidation behavior of clay. *Trans. Am. Soc. Civ. Eng.*, 120:1201–1227.

Shephard, L. E., Bryant, W. R., and Dunlap, W. A., 1978. Consolidation characteristics and excess pore water pressures of Mississippi Delta sediments. *Proc. Annu. Offshore Technol. Conf.*, Pap. 3167:1037–1048.

Silva, A. J., Hetherman, J. R., and Calnan, D. I., 1981. Low gradient permeability testing of fine-grained marine sediments. *ASTM Spec. Tech. Publ.*, 746:121–136.

Silva, A. J., Jordon, S. A., and Levy, W. P., 1983. Geotechnical Studies for Subseabed Disposal High Level Radioactive Wastes, Progress Report No. 9, Contract No. 37-2235. Albuquerque (Sandia National Laboratories).

Silva, A. J., Laine, E. P., Lipkin, J., Heath, G. R., and Akers, S. A., 1980. Geotechnical properties of sediments from North Pacific and Northern Bermuda Rise. *Proc. Mar. Technol. Soc.*, pp. 491–499.

Skempton, A. W., 1970. The consolidation of clays by gravitational compaction. *Q. J. Geol. Soc. London*, 125:373–411.

Terzaghi, K., 1956. Varieties of submarine slope failures. *Proc. Conf. Soil Mech. Found. Eng., 8th Texas*, pp. 1–41.

Znidarcic, D., 1982. Laboratory determination of consolidation properties of cohesive soil [Ph.D. Dissert.]. University of Colorado, Boulder, Colorado.

Znidarcic, D., and Schiffman, R. L., 1983. Constant rate of deformation consolidation testing. Boulder (Department of Civil Engineering, University of Colorado).

Date of Initial Receipt: 23 May 1984
Date of Acceptance: 25 September 1984

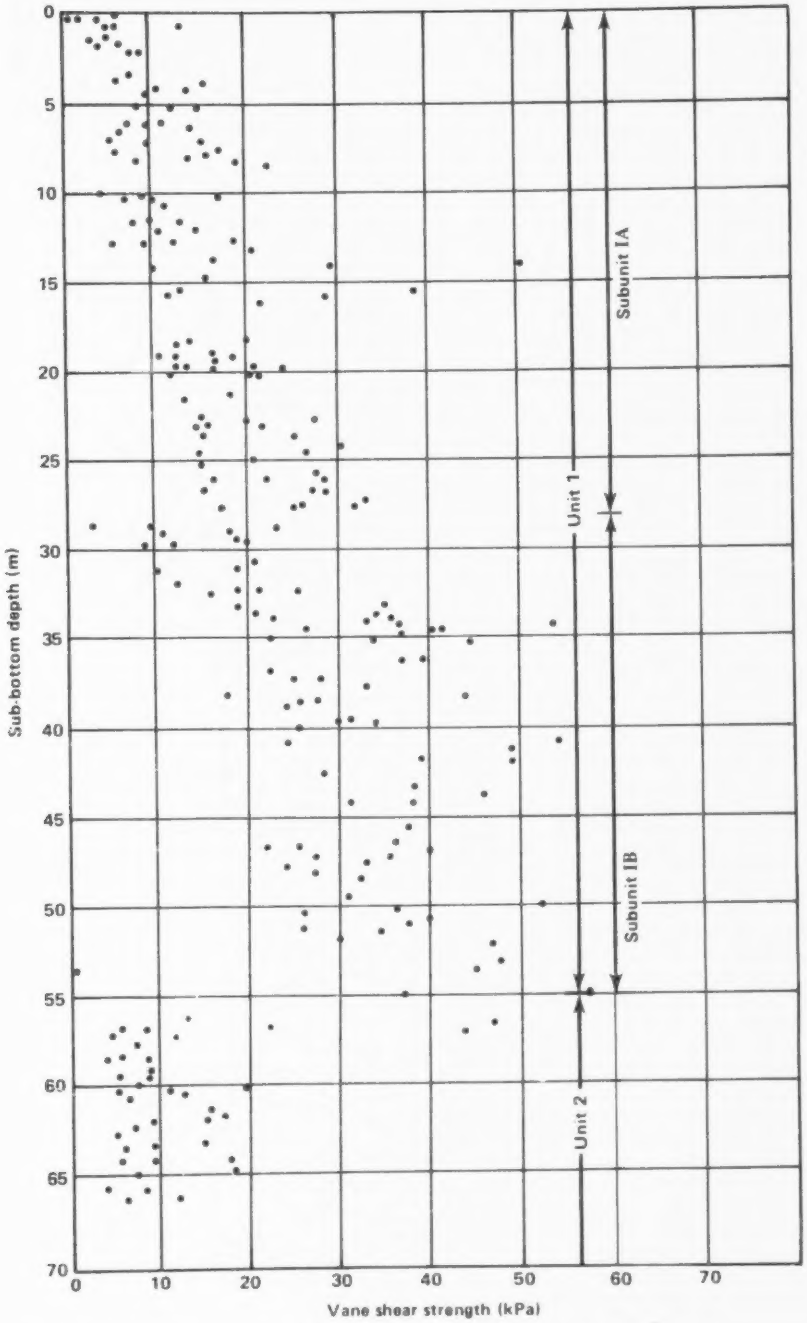

Figure 23. Laboratory vane shear strength-depth profile for Hole 576A sediments.

Table 8. Summary of unconsolidated–undrained (UU) triaxial test results for Hole 576A sediments.

Core-Section	Sub-bottom depth (m)	σ_o' (kPa)	Water content (%)	Triaxial shear strength (kPa)	s_u/σ_o'
1-2	2.9	10.9	153	14.7	1.34
1-3	3.0	11.3	155	13.7	1.21
1-3	3.9	14.7	154	14.3	0.97
2-1	10.0	37.7	191	12.8	9.34
2-4	13.7	51.7	160	11.4	0.22
2-6	16.8	63.4	182	15.6	0.25
3-2	21.8	82.3	121	17.6	0.21
3-5	24.5	92.5	140	18.9	0.20
3-6	26.7	100.8	114	29.6	0.29
4-2	30.4	114.7	147	16.7	0.15
4-3	31.0	116.9	158	18.3	0.16
4-5	34.6	130.6	123	26.6	0.20
4-5	34.7	130.9	130	42.1	0.32
5-3	40.2	151.7	145	26.6	0.18
5-4	40.7	153.6	105	39.3	0.26
5-5	44.0	166	109	32.8	0.20
6-2	48.3	182	101	33.0	0.18
6-3	49.7	187.5	126.4	24.2	0.13
6-3	49.8	188	114	30.0	0.16
6-4	51.8	195	99	29.0	0.15
7-6	64.3	243	117.7	38.0	0.16

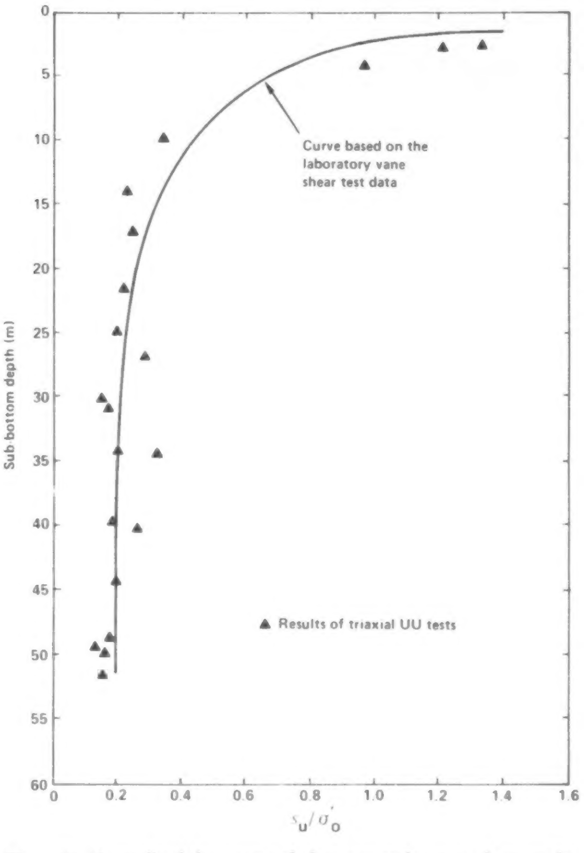

Figure 24. Normalized shear strength data comparing vane shear results with UU test results for Hole 576A sediments.

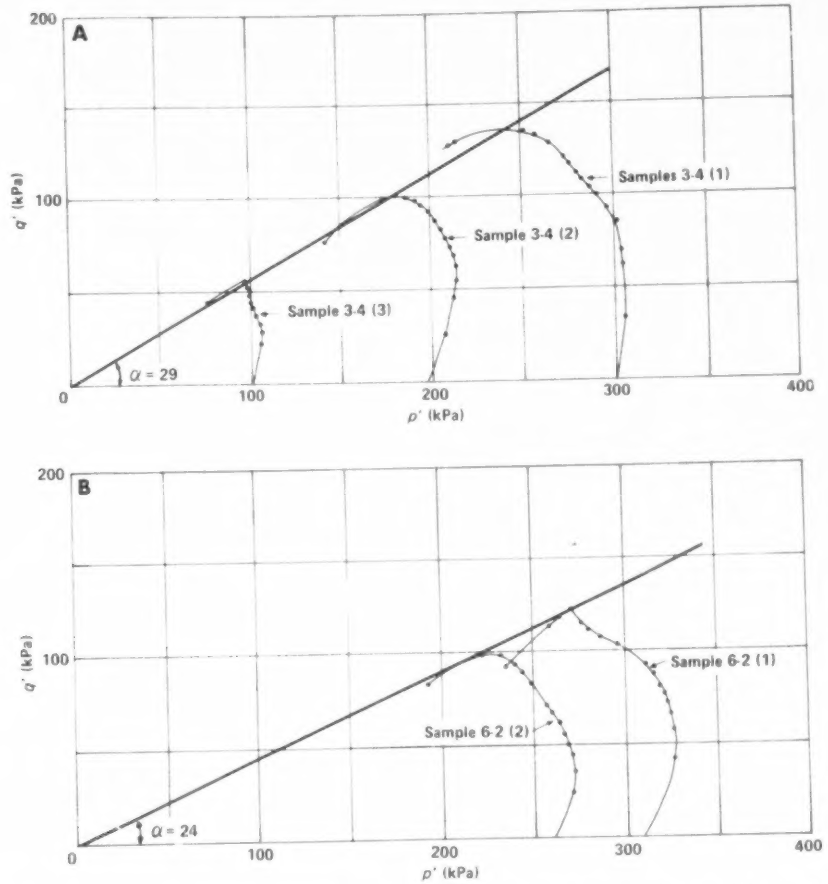

Figure 25. Example of isotropic consolidated undrained (CIU) triaxial test results from Hole 576A sediments located in Subunit IA (A, 24.70 m sub-bottom, $c = 0$, $\phi = 34°$) and Subunit IB (B, 48.90 m sub-bottom, $c' = 0$, $\phi = 26°$). Other CIU test results are summarized in Table 9.

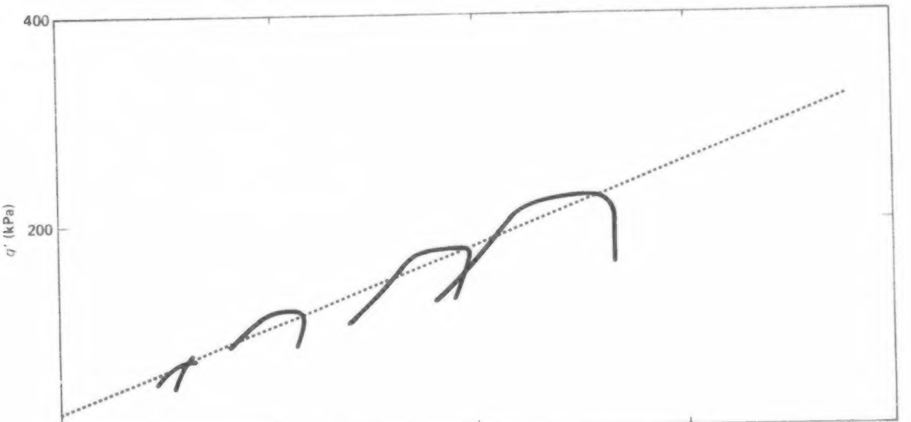

Figure 26. Results of consolidated, anisotropic undrained (CAU) K_0 triaxial test results from sediment located at 30.50 m sub-bottom ($C' = 17.6$ kPa, $\phi = 23°$). Other CAU-K_0 test results are summarized in Table 8.

Table 9. Summary of CIU triaxial test results for Hole 576A sediments.

Test no.	Core-Section	Sub-bottom depth (m)	w_o (%)	w_f (%)	σ_o' (kPa)	σ_3 (kPa)	u_i (kPa)	σ_c' (kPa)	B	OCR	s_u (kPa)	s_u/σ_o'
1	1-4(1)	5.6	192	138	20	392	294	98	0.98	1	60.8	0.62
2	1-4(2)	5.5	199	131	20	441	294	147	0.98	1	70.6	0.48
3	1-5(1)	6.3	216	164	22	392	294	98	0.99	1	59.8	0.61
4	1-5(2)	6.4	189	164	22	353	294	59	0.99	1	45.1	0.76
5	2-6(1)	17.3	154	122	57	540	393	147	0.98	1	73.5	0.50
6	2-6(2)	17.4	153	137	57	491	393	98	0.98	1	48.0	0.49
7	2-6(3)	17.5	155	105	57	601	393	208	0.99	1	84.0	0.40
8	3-4(1)	24.8	113	76	85	588	294	94	0.99	1	132.3	0.45
9	3-4(2)	24.7	115	89	85	490	294	196	0.99	1	98.0	0.50
10	3-4(3)	24.6	127	121	85	392	294	98	0.98	1	53.9	0.55
11	5-3(1)	40.5	134	130	145	621	442	179	0.99	1	62.5	0.35
12	5-4(2)	42.3	103	78	155	690	306	384	0.99	1	145.0	0.38
13	5-4(3)	42.4	103	91	155	414	228	186	0.98	1	83.0	0.45
14	6-2(1)	48.8	124	102	180	598	294	304	0.98	1	117.6	0.39
15	6-2(2)	49.0	125	109	180	549	294	255	0.99	1	95.1	0.37

Note: w_o = initial water content (assuming 35 ppm dissolved salt in pore fluid); w_f = water content at failure; σ_o' = *in situ* effective stress; σ_3 = cell pressure; u_i = back pressure; $\sigma_c' = \sigma_3 - u_i$ = consolidation pressure; B = pore-pressure coefficient; OCR = overconsolidation ratio; $s_u = 1/2\,(\sigma_1 - \sigma_3)_{max}$ = shear strength.

Table 10. Summary of CIU triaxial test results on overconsolidated samples from Hole 567A sediments.

Sample	Sub-bottom depth (m)	w_o (%)	w_f (%)	σ_o' (kPa)	σ_3 (kPa)	u_i (kPa)	σ_c' (kPa)	B	OCR	s_u (kPa)	s_u/σ_o'
4-1(1)	29.2	145	101	100	442	393	49	0.97	8	94.1	1.92
4-1(2)	29.5	148	101	105	559	393	98	0.96	4	108.8	1.11
4-1(3)	29.6	144	96	105	589	393	196	0.98	2	134.3	0.69

Note: See Table 9 for explanation of symbols used in column headings.

Table 11. Summary of CAU triaxial test results for Hole 576A sediments.

Test no.	Sample	Sub-bottom depth (m)	σ_1' (kPa)	σ_{3f}' (kPa)	Multiple of over-burden	w_o (%)	w_f (%)	σ_o' (kPa)	q_f (kPa)	p_f' (kPa)	u_f (kPa)	A_f	s_u/σ_o'
					$\phi' = 23°\ C' = 17.6$ kPa								
1	4-2(1)	29.8	143	67	1.5	146	118	149	65	121	10.4	0.08	0.44
2	4-2(2)	29.4	300	144	3.2	144	103	305	113	232	26.7	0.12	0.37
3	4-2(3)	29.5	498	249	5.3	144	93	495	173	384	41.5	0.12	0.35
4	4-2(4)	29.6	694	376	7.3	138	82	682	223	521	81.3	0.18	0.33
					$\phi' = 21°\ C' = 29.8$ kPa								
5	5-4(1)	42.6	200	93	1.5	112	98.5	202	82	150	27.0	0.16	0.41
6	5-4(2)	42.8	338	170	2.5	111	89.9	331	120	244	45.9	0.19	0.36
7	5-4(3)	42.9	475	276	4	110	81.6	475	164	356	80.7	0.25	0.35
8	5-4(4)	43.0	766	490	8	111		766	237	582	141.0	0.30	0.31

Note: See Table 9 for explanation of symbols used in column headings. q_f = deviation stress at failure; p_f' = mean effective stress at failure; u_f = pore pressure at failure; A_f = pore-pressure coefficient at failure.

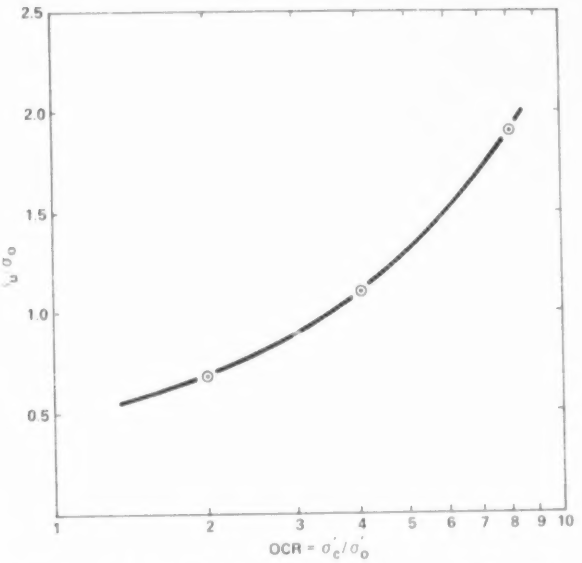

Figure 27. Relationship of the normalized shear strength with varying overconsolidation ratios developed using the results of CIU tests on sediments at 28.70 m sub-bottom.

Table 12. Summary of s_u/σ_o' values determined from CIU triaxial tests and adjusted for the *in situ* K_o condition.

Core-Section	Sub-bottom depth (m)	OCR	CIU tests s_u/σ_o'	s_u/σ_o' K_o condition
Data from CIU test results				
1-4	5.5	1	0.55	0.49
1-5	6.3	1	0.61	0.54
2-6	17.4	1	0.46	0.41
3-4	24.7	1	0.50	0.44
5-3	42.3	1	0.39	0.35
6-2	48.9	1	0.38	0.34
Data from CAU test results				
4-2	29.6	1		0.37
5-4	42.8	1		0.36

Table 13. Summary of s_u/σ_o' values for both the normally consolidated condition and after correcting for the state of overconsolidation.

Sub-bottom depth (m)	$(s_u/\sigma_o')_{NC}$	OCR	(s_u/σ_o')	s_u (kPa)
5.5	4.9	5.0	1.1	22
6.3	0.54	4.0	1.1	24
17.4	0.41	2 5	0.65	37
24.7	0.44	1.5	0.53	45
29.6	0.37	1.0	0.46	48
42.3	0.35	1.0	0.35	54
42.8	0.36	1.0	0.36	56
48.9	0.34	1.0	0.34	61

Note: For comparison with data in Figure 23, the shear strength values (s_u) corrected for *in situ* conditions using SHANSEP are also shown.

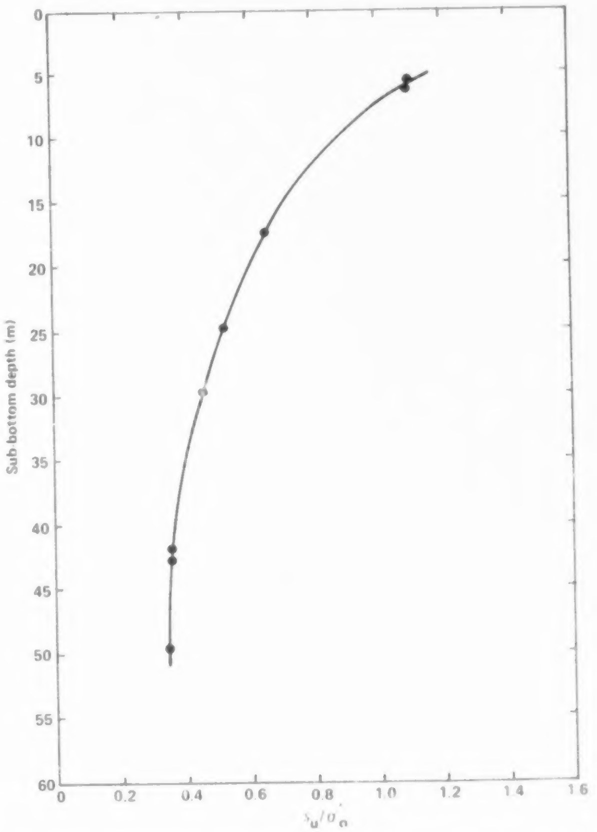

Figure 28. Variations in the ratio of s_u/σ_o' with depth corrected for the K_o condition. Profile developed using normally consolidated triaxial test results.

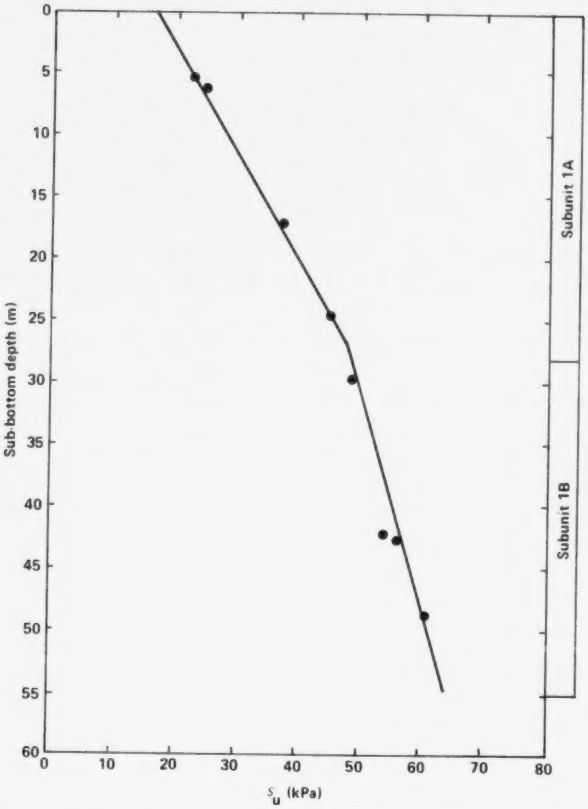

Figure 29. *In situ* shear strength-depth profile for Hole 576A sediments calculated using the SHANSEP technique.

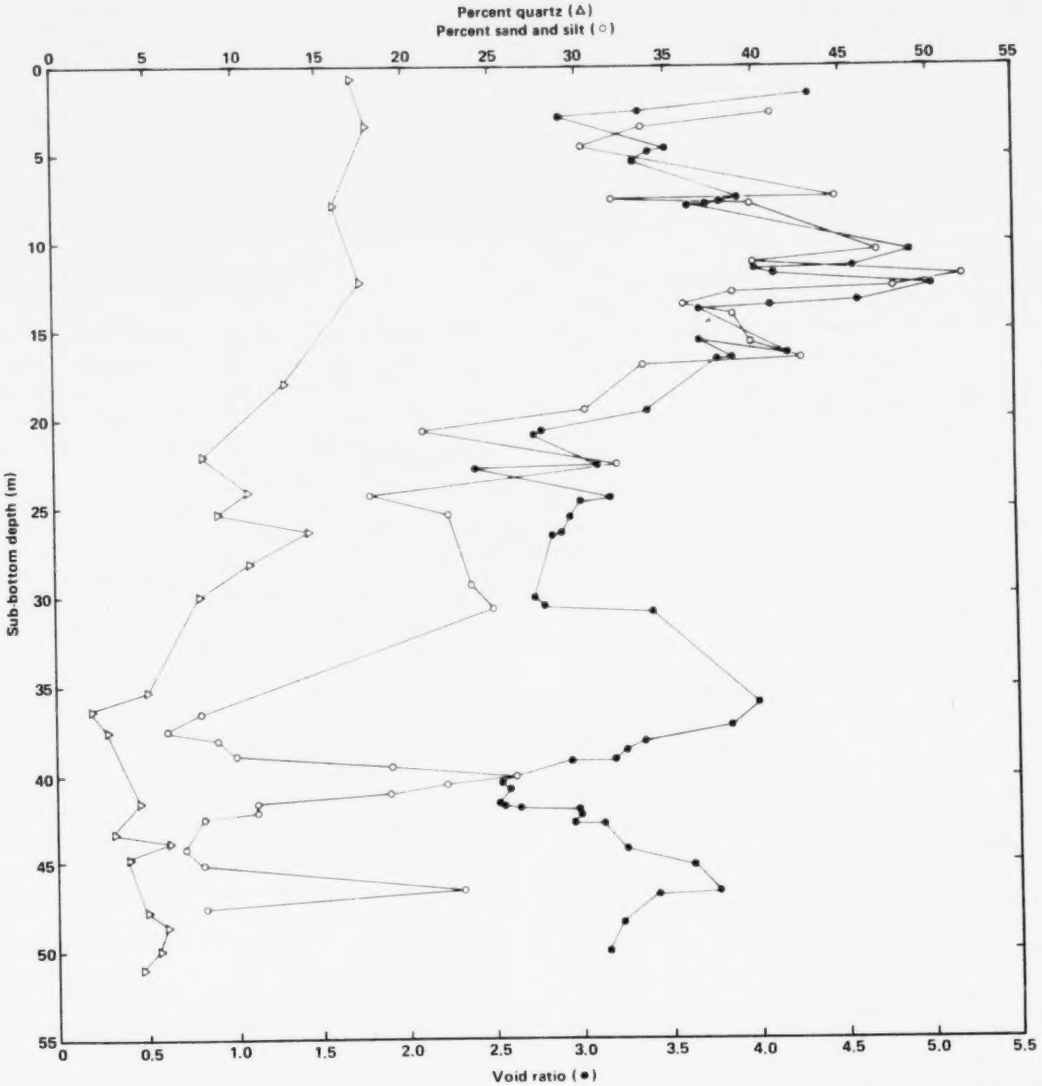

Figure 30. Variations in void ratio (•), sand- and silt-sized fraction (o) and percent quartz (Δ) with depth in Hole 576A sediments.

READEX FICHE

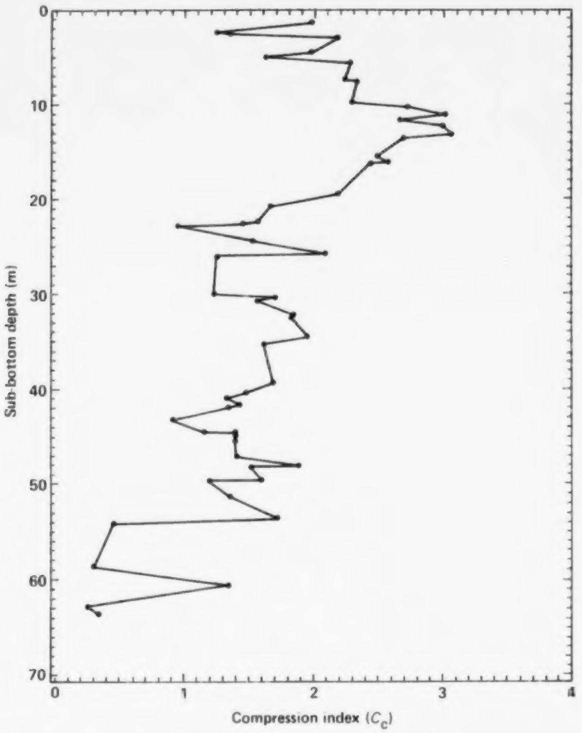

Figure 31. Compression index-depth profile determined using consolidation test results from Hole 576A sediments.

35. MEASUREMENT OF HEAT FLOW ON LEG 86 OF THE DEEP SEA DRILLING PROJECT[1]

Ki-iti Horai, Lamont-Doherty Geological Observatory of Columbia University
and
R. P. Von Herzen, Woods Hole Oceanographic Institution[2]

ABSTRACT

Using a new temperature recording instrument recently developed at the Woods Hole Oceanographic Institution, downhole temperature measurements were made at five sites during Deep Sea Drilling Project Leg 86. The instrument, which can be installed in the shoe of the hydraulic piston corer, allows measurements of sediment temperature to be made simultaneously with the collection of sediment cores. A numerical procedure was applied to correct the temperature disturbance caused by the corer's friction with the sediment. Detailed temperature profiles constructed from the data were combined with the measurement of thermal conductivity to calculate heat flow. Heat flow values were generally low at all sites of Leg 86, consistent with the age of the lithosphere (≥ 100 m.y.) in the Northwestern Pacific Basin.

INTRODUCTION

Since the earliest phase of the Deep Sea Drilling Project (DSDP), measurement of heat flow has been one of the major objectives of the project. The DSDP heat flow program was initiated by Burns (1970) on Leg 5 and was continued by Von Herzen et al. (1971) on Leg 8. Following these preliminary experiments, a self-contained heat flow instrument was developed at the Woods Hole Oceanographic Institution (WHOI). A series of successful measurements were obtained on Leg 19 (Erickson, 1973) and subsequent legs until Leg 46 (Von Herzen, 1973; Sclater and Erickson, 1974; Girdler et al., 1974; Marshall and Erickson, 1974; Hyndman et al., 1974; Watanabe et al., 1975; Hyndman et al., 1977; Erickson and Hyndman, 1979), except for occasional renovations to the instrumentation.

The program was revitalized by Uyeda and Horai (1982) on Leg 60 using a new solid-state recording temperature probe developed by the Earthquake Research Institute of the University of Tokyo (Yokota et al., 1980), and several successful measurements ensued. Overall, however, the opportunity of fully utilizing a deep-drilled DSDP hole for the purpose of heat flow study has not been realized.

The primary obstacle that prevented extensive use of deep-sea drilling holes for heat flow studies lay in the method of using the heat flow instrumentation. Drilling and coring had to be halted for 1 to 2 hr. to lower the heat flow instrument into the drilled hole and take a temperature measurement. A hiatus in the core sampling program for sediment temperature measurements proved intolerable to many shipboard scientists eager to gather and analyze sediment samples.

A new temperature recording instrument developed at the Woods Hole Oceanographic Institution in 1982 is much improved in that respect. Its miniature size enabled it to be inserted into the cutting shoe of the hydraulic piston corer (HPC). This allowed sediment temperatures to be measured simultaneously with the core sampling procedure. The instrument was tested and used for the first time on Leg 86; this chapter summarizes the data and results from that leg.

TEMPERATURE MEASUREMENT METHOD

Figure 1 illustrates the shoe of the HPC that contains the temperature recording instrument. The instrument consists of a temperature sensor, a recorder, and a battery pack that are installed in the slots located in the wall of the shoe. The temperature sensor is a thermistor encased in a stainless steel tube of 3-mm diameter with a tip smeared with heat sink compound to ensure thermal contact with the wall. The recorder is a preprogrammable miniature computer (microprocessor), energized by the battery pack, with memory for storing the measured temperature data. Prior to the coring operation, the recorder is connected to a shipboard computer. Parameters such as the starting time of the recorder, the time interval between measurements, and the total number of measurements are loaded as a command. The computer is disconnected and the recorder then proceeds to execute the program as specified by the parameters. Upon completion of the coring operation, the recorder is recovered along with the HPC core, removed from the HPC shoe, and connected to the computer again to dump the data. The data are then ready for visual display and the numerical analysis required to obtain undisturbed *in situ* temperatures.

Temperature measurements were made at all sites except Site 581 during Leg 86. The HPC was equipped with the temperature recording instrument and lowered in the drill hole every few cores to obtain data at intervals appropriate for delineating a sediment temperature pro-

---

[1] Heath, G. R., Burckle, L. H., et al., *Init. Repts. DSDP*, 86: Washington (U.S. Govt. Printing Office).

[2] Addresses: (Horai, present address) Meteorological College, Asahicho, Kashiwa. Chiba 277, Japan; (Von Herzen) Woods Hole Oceanographic Institution, Woods Hole, MA 02543.

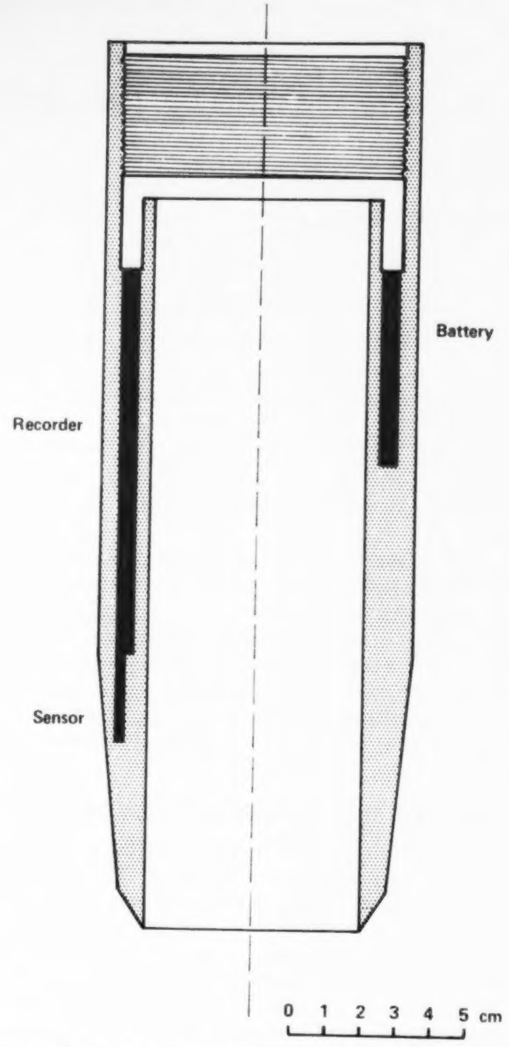

Figure 1. Shoe of the HPC equipped with temperature recorder, sensor, and battery pack.

file. For most instruments, the recorder was programmed so that sediment temperature values were recorded every 20 s while the instrument was in the sediment. The recorded sediment temperature data contain a disturbance that results from frictional heating to which the HPC is subjected as it is thrust into the sediment. This disturbance component in the data is removed numerically to obtain an estimate of undisturbed sediment temperature.

DATA ANALYSIS

Figure 2 shows the temperature data collected from Core 578-14, which was one of the best examples from Leg 86. As the temperature sensor of the recording device was placed within 5 mm of the outer surface of the metallic (thermal conductive) HPC, the measured temperature reflected the changing thermal environment around the HPC due to the conduction of frictional heating.

From a temperature record such as that obtained in Figure 2, the undisturbed sediment temperature can be estimated by the least-square fitting of a theoretical cooling curve to the portion of the temperature data showing the HPC's cooling (c in Fig. 2).

The theoretical cooling curve was obtained by solving the thermal conduction equation for composite circular cylinders simulating the HPC in the sediment (Fig. 3). The HPC is subject to frictional heating as it thrusts into the sediment. The heat of friction between the HPC and the sediment is partly accumulated in the HPC and reaches a maximum when the penetration is completed and the HPC comes to a stop. The distribution of the frictional heat is not uniform in the HPC. Radially, the heating is restricted near the HPC's inner and outer boundaries where it contacts the sediment. Due to high thermal conductivity of the metal composing the HPC, it can be regarded radially isothermal after several tens of seconds of its penetration into the sediment. The thermal conduction equation was solved for the initial condition that, at time $t = 0$, temperature V is uniform in the HPC (middle cylinder) and is zero in the sediment (inner and outer cylinders). If the solution of this equation is obtained for $V = 1.0°C$, its time dependence $V(t)$ evaluated at the outer boundary of the middle cylinder is the HPC's theoretical cooling temperature from an initial value of unity. The observed cooling curve is adequately described by a formula $\alpha V(t) + \beta$ with two adjustable constants α and β (Fig. 4). The value of α and β determined from the least square fitting of the formula to the data are estimates of, respectively, the initial HPC temperature and the undisturbed sediment temperature.

Unlike the oceanic heat flow probe discussed by Bullard (1954), the axial dissipation of heat by conduction through the conductive HPC may not be negligible. For the Bullard probe, the axial thermal constant of 18 days was large enough to confirm the adequacy of treating the problem of a 2.70-cm-diameter probe as two-dimensional radial thermal conduction. In the present case, the location of the temperature sensor in the core cutter near the lower end of the HPC indicates that axial heat flow by conduction will be more important. The corer's frictional heating is probably maximal in the shoe, or the lowermost part of the HPC, decreasing upward along the corer. If the conductive heat loss in the axial direction is nonnegligible, the actual cooling of the HPC must be faster than that given by the two-dimensional theory of thermal conduction, and the equilibrium sediment temperature will be reached within a shorter period of time. In this case, the value of β extrapolated theoretically from the cooling curve is a lower limit (T_{min}) for the estimation of undisturbed sediment temperature.

On the other hand, the last undisturbed part of the cooling curve (D in Fig. 2) can be considered an upper limit (T_{max}). The undisturbed sediment temperature lies between these bounds, probably closer to the lower. In the

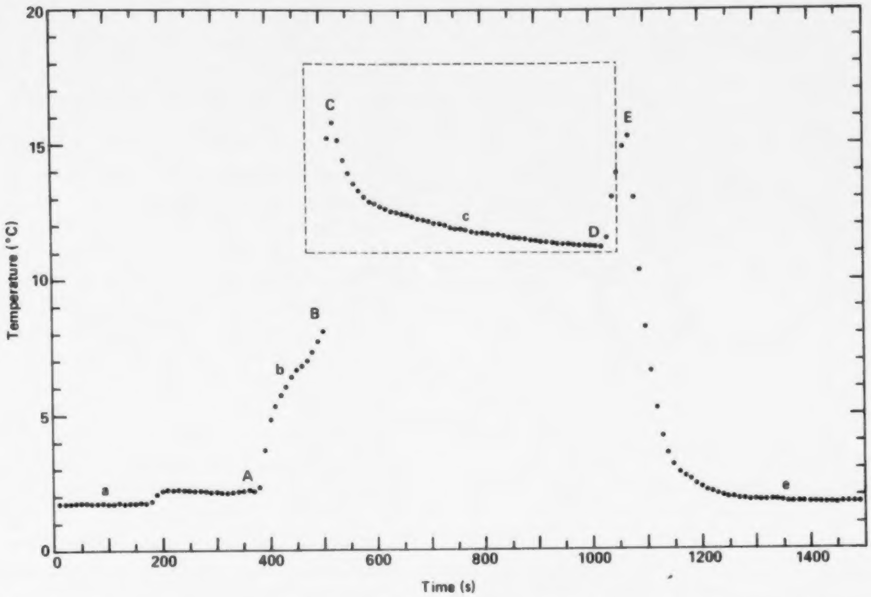

Figure 2. Example of temperature record taken with Core 578-14 at 128.3 m sub-bottom depth. The HPC is lowered into the drill pipe with a wire cable connected to a shipboard winch. By the time the corer approaches the seafloor, the temperature of the HPC is nearly equilibrated with the seawater temperature immediately above the seafloor (a). Upon entering the hole (A), the temperature rises, sensing an increasing temperature with depth (b). The corer is seated at the bottom of the drill pipe (B) and then thrust into the virgin sediment layer below the drilled hole by hydraulic pressure in the drill pipe controlled on the ship (C). The temperature rises rapidly, sensing the frictional heat generated at the contact surface of the corer with the sediment. The temperature then drops gradually as the corer remains stable and the frictional heat dissipates by conduction (c). The temperature of the HPC should eventually come to equilibrium with the surrounding sediment. The corer is retrieved (D), however, before the equilibrium temperature is reached. The temperature rises again, sensing the frictional heat of the extraction (E), and then subsides rapidly to the temperature of the bottom water (e) as the corer is raised.

following analysis of Leg 86 data, both bounds will be considered for each measurement whenever possible.

MEASUREMENT RESULTS

Site 576

The new temperature recording device was tested for the first time at Site 576. A total of 11 runs were made: 5 in Hole 576, 3 in Hole 576A, and 3 in Hole 576B. Seven runs were successful: 2 in Hole 576, 3 in Hole 576A, and 2 in Hole 576B. Run failures were due either to malfunctioning of the instrument or to mishandling in operation.

Even for the successful runs, the data quality was not as satisfactory as the example shown in Figure 2. In some of the data from Site 576, the frictional heating of the HPC at the time of probe penetration and extraction was not apparent, although the correction procedure of obtaining $T_{\min}$ appears applicable to these data. For the data from Core 576-4, the duration of the HPC in the sediment was too short (< 2 min) to apply any meaningful correction to the data. Therefore, only $T_{\max}$ was read from the temperature record.

The results of temperature measurements at Site 576 are summarized in Table 1. The temperature at the sediment surface was estimated from the average of bottom water temperatures recorded by the HPC prior to the hole entry. Figure 5 is a plot of $T_{\max}$ and $T_{\min}$ against sub-bottom sediment depth. The true undisturbed sediment temperature is believed to lie between $T_{\max}$ and $T_{\min}$, probably closer to the latter in most cases.

Site 577

At Site 577, 15 runs were attempted (6 in Hole 577 and 9 in Hole 577A); 10 were successful (4 in Hole 577 and 6 in Hole 577A, Fig. 6). Generally, the quality of the temperature data was much improved over that recorded at Site 576. Based on the suggestion of the shipboard marine technicians, it was decided to release the tension in the cable suspending the HPC during operation of the heat flow instrument in the sediment. This appeared to eliminate transmission of much of the ship's motion to the HPC, which probably caused the small temperature fluctuations appearing in the otherwise smoothly varying cooling curves of the temperature record at Site 576.

For the data showing a monotonic gradual cooling, application of the correction procedure for obtaining $T_{\min}$ by fitting a theoretical cooling curve to the measured temperature was straightforward. However, in the records obtained with Cores 577-8 (Fig. 7) and 577-12, a slight increase in temperature toward the end of the cooling

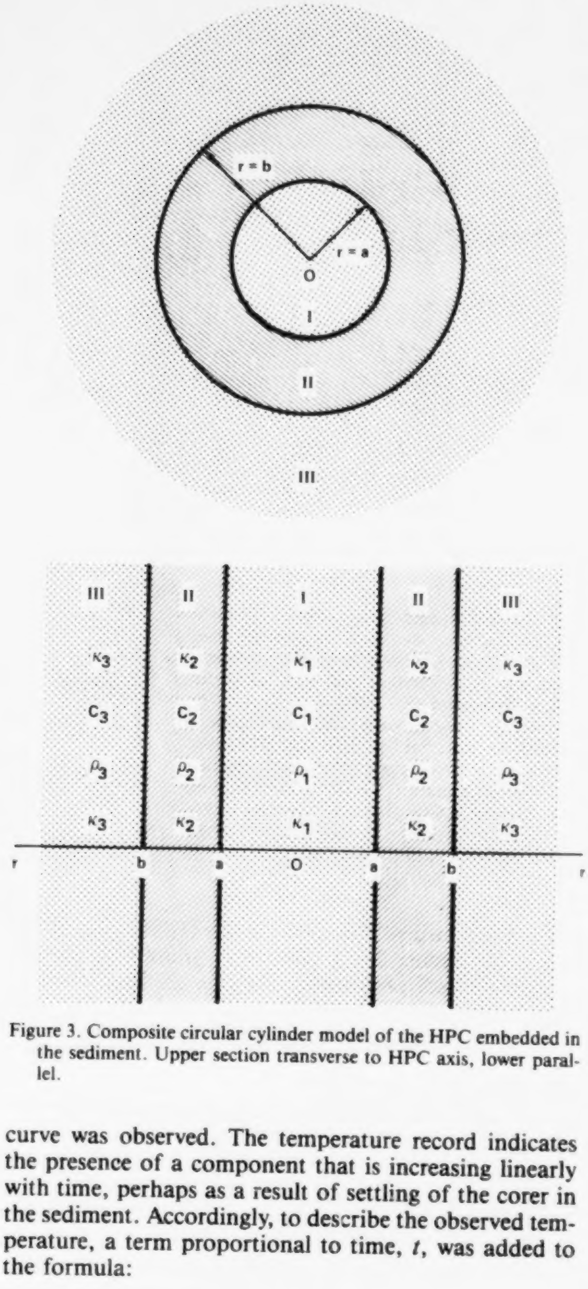

Figure 3. Composite circular cylinder model of the HPC embedded in the sediment. Upper section transverse to HPC axis, lower parallel.

curve was observed. The temperature record indicates the presence of a component that is increasing linearly with time, perhaps as a result of settling of the corer in the sediment. Accordingly, to describe the observed temperature, a term proportional to time, t, was added to the formula:

$$\alpha V(t) + \beta + \gamma t$$

The values of β obtained from the least-square fitting of the formula to the data are indicated as $T_{\min}$ in parentheses in Table 1. The values of γ obtained by the same analysis were 0.211×10^{-3}°C/s for Core 577-8 and 0.582×10^{-4}°C/s for Core 577-12, that is, a total linear increase of temperature over the entire decay time in the bottom of 0.2 and 0.06°C, respectively.

As suggested above, the presence of the linear component in the data can be interpreted as indicating a gradual sinking of the HPC in the sediment. The release of the cable tension during the operation of the heat flow instrument seems to favor this hypothesis. Assuming a linear vertical thermal gradient in the sediment of 0.04°C/m, the rates correspond to a respective sinking velocity of the HPC of 5.0 and 1.4 mm/s, respectively, not unreasonable for the heavy drill collars resting on a moderately soft sediment.

At the depth of Core 577A-8, the new HPC temperature recording device was operated with the conventional ERI-type temperature probe (Uyeda and Horai, 1981), the thermistor for the latter located about 20 cm below the HPC cutter tip. The sediment temperature measured by the ERI probe was 3.5°C higher than $T_{\max} = 4.39$°C recorded by the WHOI device. In the temperature record obtained by the latter, the HPC's temperature rises resulting from the frictional heating at core penetration and extraction were totally missing. The probe configuration is largely responsible for it. For the combined run, the ERI instrument was fixed inside the HPC with its temperature probe protruding from the shoe of the HPC. Therefore, the ERI probe should have made a better contact with the sediment. The run was made, however, without core sampling; that is, in the drilled section of the hole with the ERI probe contacting the unsampled sediment, while the contact of the HPC's shoe with the sediment might not have been complete. It is possible that both of the measured temperatures contain disturbances due to drilling that had not been removed completely. The result of temperature measurement made by the WHOI device, prior to the combined run, with the sampling of Core 577A-8 was $T_{\max} = 4.25$ and $T_{\min} = 4.19$°C (Table 1).

Site 578

One of the most successful series of heat flow measurements were made at Site 578 (Table 1). HPC temperature data taken at every two cores, or at an interval of 19 m, yielded an excellent profile for the range of sediment temperatures at the site. In Figure 8 are plotted $T_{\max}$ and $T_{\min}$ against the sub-bottom depth for Site 578.

For the data obtained with Core 578-2, the cooling curve was recorded for a relatively short period of time of 200 s. However, the data could still be fit satisfactorily to the theoretical cooling curve to obtain an estimate of $T_{\min}$ with the least-square criterion. For other runs, the quality of data was generally satisfactory. Data collected with Cores 578-4 and 578-12 were, however, unsatisfactory because the HPC was mechanically unstable in the sediment as inferred from the discordant variation of the HPC temperature in the middle of cooling. The portion of the cooling curves before the disturbances was used to obtain an estimate of $T_{\min}$ from the data. These different procedures may explain the anomalous gradient inferred between the measurements made on Cores 4 and 6 (Fig. 8).

Site 579

Bad weather prevented operation of the downhole temperature measurement for the first half of the drilling at

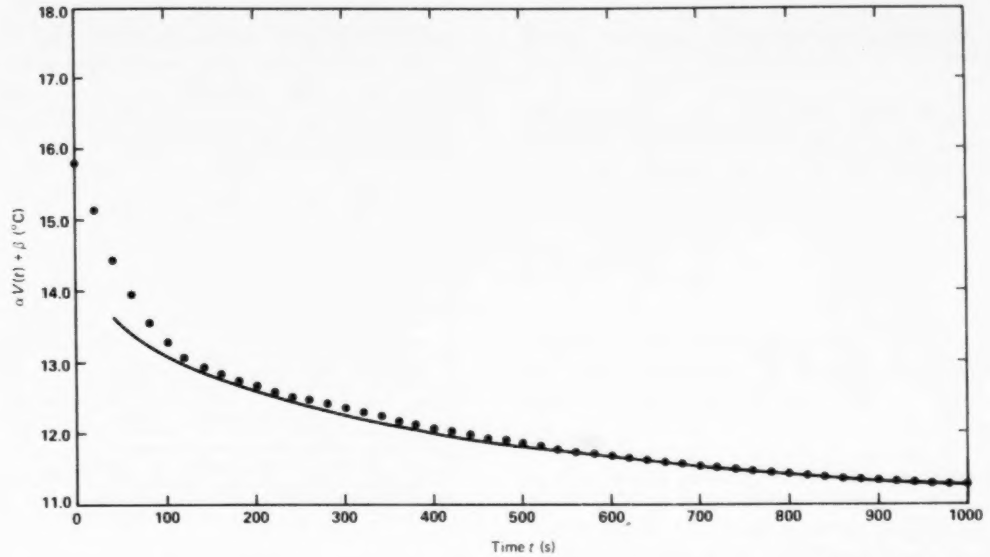

Figure 4. Fitting of theoretical formula $\alpha V(t) + \beta$ to the cooling HPC temperature of Figure 2 (α = 6.53°C, β = 9.31°C).

Site 579. Better weather and moderated sea-surface conditions allowed the operation to resume at Core 9 and at every ensuing core to the bottom of the hole. All runs were successful (Table 1).

The temperature records were generally satisfactory. Only occasional breaks in the otherwise smooth-varying cooling curves suggest movement of the HPC corer in the drill pipe while the HPC was in the sediment. Undisturbed sediment temperatures could be estimated, however, from the portion of the cooling curves devoid of the breaks. The HPC's penetration into the sediment was incomplete with Core 579-15. Therefore, the validity of sediment temperature measured with that core is somewhat doubtful, even though the thermal decay was long and undisturbed.

A plot of T_{max} and T_{min} against the sub-bottom depths defines generally a linear increase of sediment temperature in the lower half of the drilled hole (Fig. 9).

Site 580

At Site 580, a total of 11 runs were attempted, all of which were successful (Table 1). Most of the recorded temperature data showed the HPC temperature smoothly decreasing with time after a rapid increase at the time of the HPC's penetration into the sediment. Therefore, estimates of T_{max} and T_{min} were not difficult to make. For the data obtained with Core 580-14, however, no significant variation of the temperature with time was observed to allow an estimation of T_{min}. In Figure 10, the estimated sediment temperatures versus depth are plotted.

THERMAL CONDUCTIVITY RESULTS

Thermal conductivity was measured on 1056 soft sediment samples collected at Sites 576 to 580, in conjunction with the downhole temperature studies. A needle probe apparatus was used on board ship for measurement of thermal conductivity. Detailed profiles of thermal conductivity versus depth through the soft sediment section recovered at each site are shown in Figures 11 to 15. The data were combined with the sediment temperature data to provide a value of heat flow (see below).

Calcite ($CaCO_3$) is among the rock-forming minerals that have the highest thermal conductivities. Accordingly, the thermal conductivity of the sediment increases with increasing calcium carbonate content if the sediment's water content is the same. At Site 577, the water depth (2675 m) is shallower than the Northwestern Pacific carbonate compensation depth of 3500–4000 m (Broecker and Takahashi, 1977). Probably, for this reason, Site 577 sediments have thermal conductivities that are generally higher than sediments from other sites of Leg 86 where the water depth exceeds the carbonate compensation depth.

The calcium carbonate content of the Site 577 sediments was determined on board ship on 38 selected samples from Hole 577 by the carbonate bomb method (see Site 577 chapter, this volume; Müller and Gastner, 1971). In Figure 16, on the plot of thermal conductivity versus porosity relationship, the calcium carbonate content of the sample is indicated by symbols. In order to show more clearly the increase of thermal conductivity with increasing calcium carbonate content, the range classification (Table 2) is compared (Fig. 17) with the grain thermal conductivity of the sample derived from the sample's water content by a formula adopted from Hashin and Shtrikman (Horai, 1981). The best fitting linear relationship indicates that the grain thermal conductivity of biogenic pelagic calcium carbonate is 4.5 W/m · K.

HEAT FLOW RESULTS

From the sediment temperature data collected by the WHOI temperature recording device and the thermal conductivity data collected on board ship, heat flow was

Table 1. Results of temperature and thermal conductivity measurements at Sites 576, 577, 578, 579, and 580.

Core	Depth z (m)	Depth interval Δz (m)	Average thermal conductivity $\bar{k}$ (W/m·°K)	$\frac{\Delta z}{\bar{k}}$	$\Sigma \frac{\Delta z}{\bar{k}}$	Sediment temperature (°C) T_w[a]	T_{min}	T_{max}
Hole 576								
0	0[b]							
		31.2	0.754	41.39				
4	31.2				41.39	1.59	—	5.38
		19.0	0.756	25.13				
6	50.2				66.52	1.58	5.38	6.29
Hole 576A								
		18.2	0.743	24.50				
2	18.2				24.50	—	3.21	3.54
		19.0	0.806	23.57				
4	37.2				48.07	1.66	4.65	5.56
		28.5	0.970	29.38				
7	65.7				77.45	1.65	5.89	6.41
Hole 576B								
		55.7	0.821	67.84				
6	55.7				67.84	1.66	(5.79)	5.99
		9.5	1.061	8.95				
7	65.2				76.80	1.67	6.05	6.70
Hole 577								
0	0							
		35.3	0.979	36.06				
4	35.3				36.06	1.73	(3.97)	4.66
		19.0	1.062	17.89				
6	54.3				53.95	1.77	4.04	5.47
		19.0	1.199	15.85				
8	73.3				69.80	1.82	(4.90)	(5.40)
		38.0	1.238	30.695				
12	111.3				100.49	1.77	(6.23)	6.87
Hole 577A								
		37.9	1.040	36.44				
4	37.9				36.44	1.74	(3.39)	4.63
		19.0	1.095	17.35				
6	56.9				53.79	1.78	(3.70)	5.91
		19.0	1.138	16.70				
8	75.9				70.49	1.76	4.19	4.25
		19.0	1.267	15.00				
10	94.9				85.49	1.79	5.73	6.29
		19.0	1.165	16.31				
12	113.9				101.80	1.85	(6.38)	7.28
Hole 578								
0								
		14.3	0.745	19.20				
2	14.3				19.20	1.69	(3.15)	3.46
		19.0	0.777	24.45				
4	33.3				43.65	1.68	(4.53)	4.95
		19.0	0.722	26.32				
6	52.3				69.96	1.66	4.79	6.37
		19.0	0.778	24.42				
8	71.3				94.39	1.65	6.00	7.79
		19.0	0.791	24.02				
10	90.3				118.41	1.76	7.09	7.74
		19.0	0.766	23.43				
12	109.3				143.21	1.73	(8.06)	9.64
		19.0	0.811	23.43				
14	128.3				166.64	1.77	9.31	11.24
Hole 579								
0	0							
		99.5	0.733	135.74				
9	99.5				135.74	1.70	7.76	9.05
		9.5	0.696	13.65				
10	109.0				149.39	1.74	8.96	9.67
		9.5	0.695	13.67				
11	118.5				163.06	1.78	9.18	10.29
		9.5	0.690	13.77				
12	128.0				176.83	1.76	9.65	11.10
		9.5	0.669	14.20				
13	137.5				191.03	1.82	9.99	11.75
		9.5	0.710	13.38				
14	147.0				204.41	1.83	11.30	12.43
		9.5	0.730	13.01				
15	156.5				217.43	1.82	(11.08)	(11.89)
Hole 580								
0	0							
		22.3	0.754	29.58				
3	22.3				29.58	1.60	3.08	3.29
		19.0	0.792	23.99				
5	41.3				53.57	1.66	4.13	4.30
		19.0	0.736	25.82				
Hole 580 (Continued)								
7	60.3				79.38	1.63	5.21	5.66
		9.5	0.795	11.95				
8	69.8				91.33	1.65	5.73	6.93
		9.5	0.776	12.24				
9	79.3				103.57	1.62	6.54	7.32
		9.5	0.803	11.83				
10	88.8				115.40	1.59	6.80	7.51
		9.5	0.780	12.18				
11	98.3				127.58	1.65	7.16	8.43
		19.0	0.779	24.39				
13	117.3				151.97	1.71	8.39	9.26
		9.5	0.869	10.93				
14	126.8				162.91	1.71	—	9.88
		9.5	0.859	11.06				
15	136.3				173.96	1.68	9.55	10.61
		19.0	0.785	24.20				
17	155.3				198.17	1.71	10.51	11.85

[a] Bottom water temperature recorded by the HPC prior to the hole entry.

[b] Sediment surface temperature estimated as an average of T_w is 1.64°C at Site 576, 1.78°C at Site 577, 1.71°C at Site 578, 1.78°C at Site 579, and 1.65°C at Site 580. Data points of questionable quality are in parentheses. — indicates lack of appropriate data to estimate T_{min}.

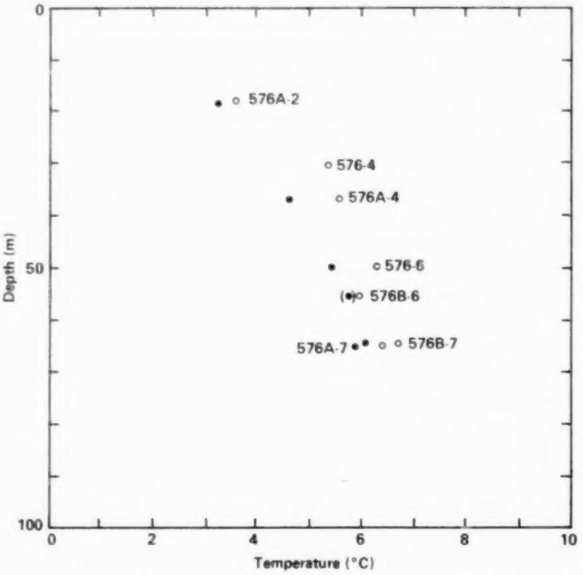

Figure 5. Results of sediment temperature measurements at Site 576. Open circles for T_{max}; filled circles for T_{min}. Data points of questionable quality are in parentheses.

obtained by the method of Bullard (1939). In the subbottom depth interval from z_0 to z, sediment temperature $T(z)$ is related to thermal conductivity $k(z)$ as

$$T(z) = T_0 + Q \int_{z_0}^{z} k(z)^{-1} dz$$

where T_0 is the temperature at the depth z_0 and Q is the steady-state conducted heat flow. If the measured sediment temperature $T_i = T(z_i)$, $i = 1, 2, \ldots, n$ is plotted against the cumulative thermal resistance

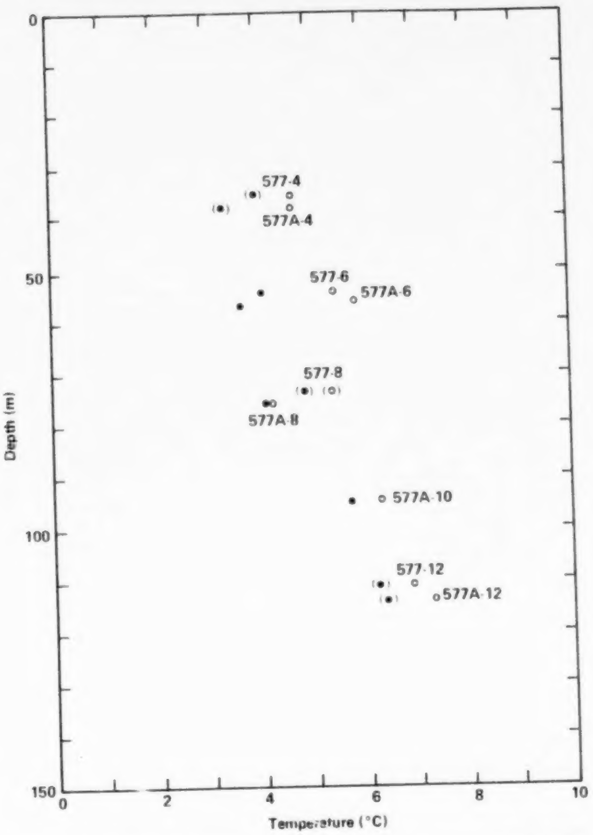

Figure 6. Results of sediment temperature measurements at Site 577. Data points of questionable quality are in parentheses. For symbols, see caption of Figure 5.

$$R_i = \sum_{j=1}^{i} \Delta z_j/\bar{k}_j, \; i = 1, 2, \ldots n,$$

then the slope will give an estimate of Q. A geometric mean of the measured sample thermal conductivities in the depth interval $\Delta z_j = z_j - z_{j-1}$ was used for an estimate of

$$\bar{k}_j^{-1} = \int_{z_{j-1}}^{z} k(z)^{-1} dz.$$

Upper and lower bounds of heat flow, $Q_{\max}$ and $Q_{\min}$, were calculated from the bounds of sediment temperature, $T_{\max}$ and $T_{\min}$, for each site.

Site 576

The concave downward temperature distribution (Fig. 5) observed at Site 576 may indicate a decrease of thermal gradient with depth, and/or the presence of hydrothermal circulation in the sediment on young crust (Anderson and Skilbeck, 1981). At the present site, however, the change of thermal gradient is largely accounted for by the distribution of thermal conductivity, which is markedly different above and below a sub-bottom depth of 55 m (Fig. 11). A plot of sediment temperature against the cumulative thermal resistivity showed a more uniform distribution of heat flow, $Q_{\max} = 61.2$ mW/m^2 and $Q_{\min} = 56.0$ mW/m^2 (Fig. 18). A more detailed and accurate measurement of sediment temperature is necessary to confirm any convective motion of water in the sediment.

Site 577

The temperature reversal apparent in the plot of $T_{\max}$ against the cumulative thermal resistance is less conspic-

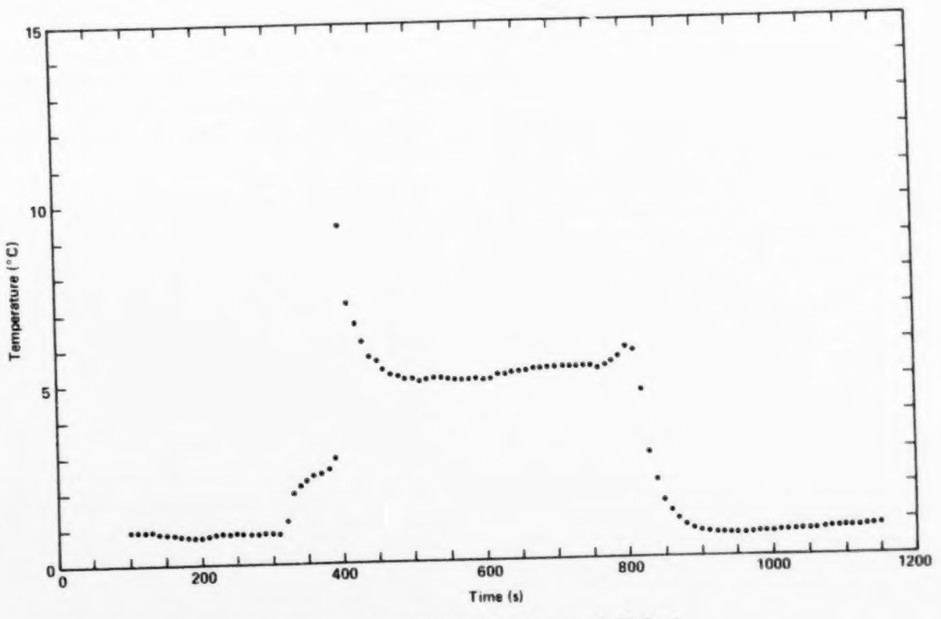

Figure 7. Temperature record taken with Core 577-8 (sub-bottom depth 73.3 m).

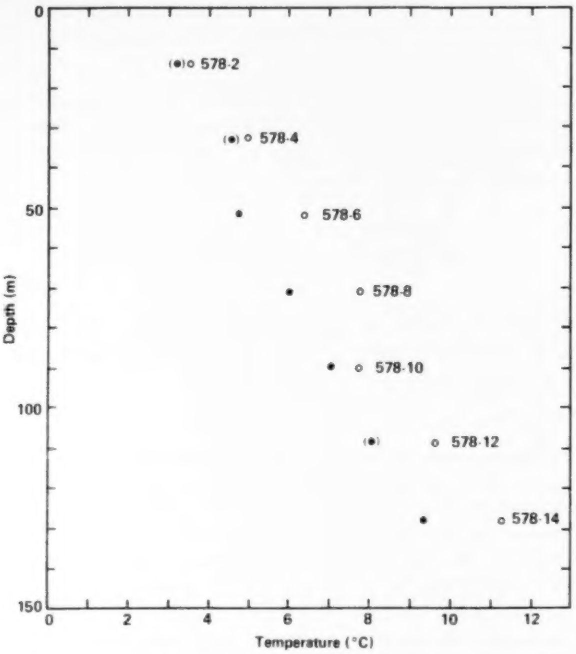

Figure 8. Results of sediment temperature measurements at Site 578. For symbols, see caption of Figure 5.

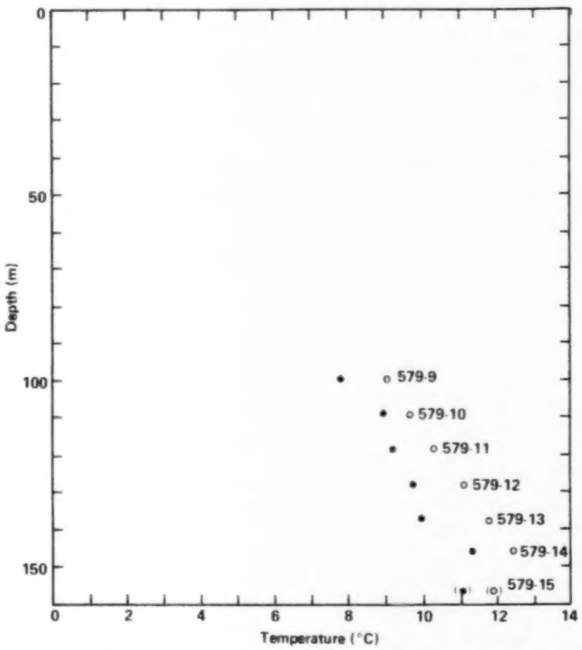

Figure 9. Results of sediment temperature measurements at Site 579. For symbols, see caption of Figure 5.

uous in the plot of T_{min} (Fig. 19). A straight line fit to the data gave Q_{max} = 44.1 mW/m^2 and Q_{min} = 39.2 mW/m^2. This will not be very far from the range of present heat flow at Site 577.

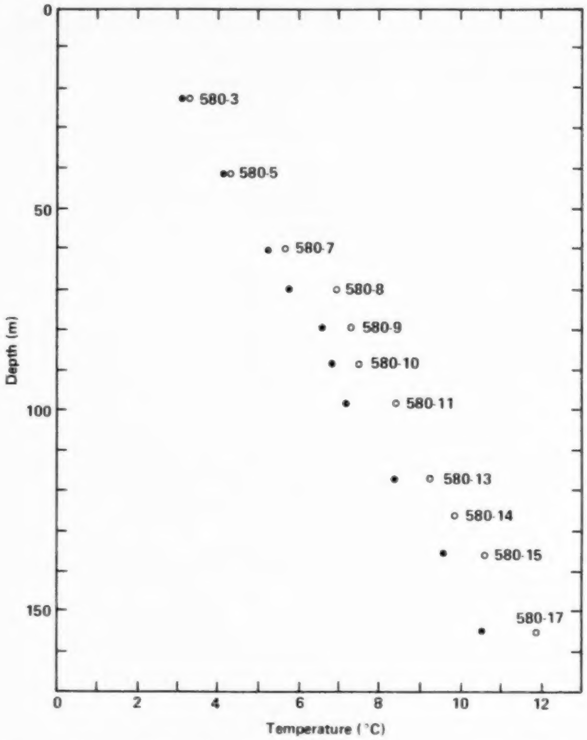

Figure 10. Results of sediment temperature measurements at Site 580. For symbols, see caption of Figure 5.

Site 578

Q_{max} = 52.9 mW/m^2 and Q_{min} = 42.7 mW/m^2 are indicated by the temperature versus cumulative thermal resistivity plot (Fig. 20).

Site 579

A constant heat flow of Q_{max} = 49.7 mW/m^2 and Q_{min} = 44.1 mW/m^2 is indicated from the data (Fig. 21). This is only representative, however, of the lower section of the drilled hole, from the depth of 120 to 220 m sub-bottom.

Site 580

The data (Fig. 22) indicate Q_{max} = 51.4 and Q_{min} = 44.4 mW/m^2 that are almost uniform over the entire length of the hole to a sub-bottom depth of 200 m.

Table 3 is a summary of heat flow results. The lithospheric ages of the sites determined from Mesozoic magnetic lineations of the Northwestern Pacific were taken from Hilde et al. (1976). Figure 23 summarizes the heat flow results at the different sites. A plot of the heat flow range versus lithospheric age in Figure 24 agrees, within the range of data uncertainty, with the average heat flow versus age relationship in the North Pacific (Sclater et al., 1980) and with recent field work designed to test that relationship (J. Sclater, personal communication, 1984). Probably, the lithospheric thermal structure under DSDP Leg 86 sites is not very far from that deduced

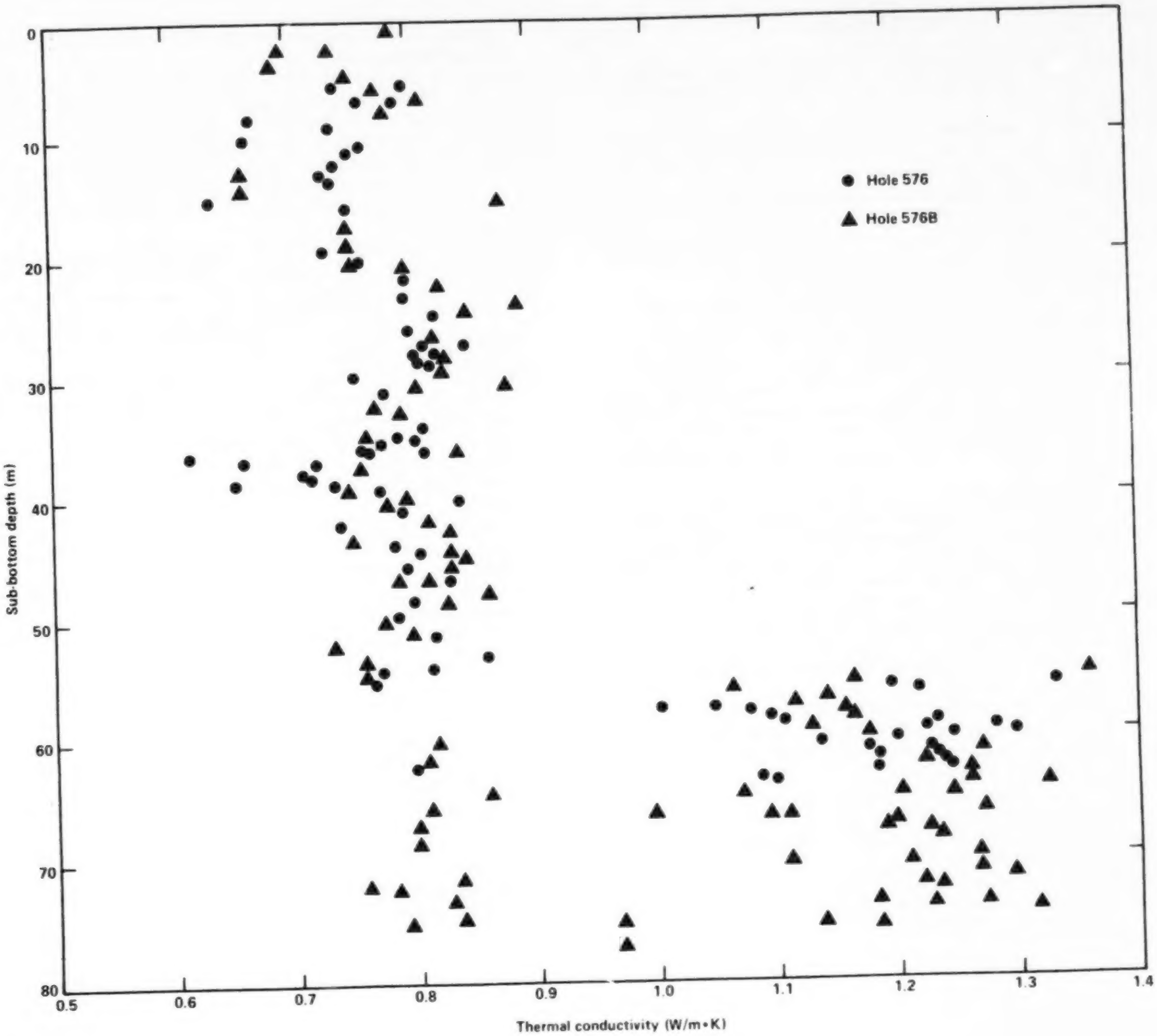

Figure 11. Sediment thermal conductivity versus sub-bottom depth at Site 576.

by the thermal boundary layer model (Parsons and McKenzie, 1978).

CONCLUSION

The new temperature recording device recently designed and constructed at Woods Hole Oceanographic Institution proved useful in recording the temperature measured in DSDP drill holes during Leg 86. The measured temperature data were used to estimate the possible range of undisturbed sediment temperature. These data were then combined with the thermal conductivity of sediment samples for calculation of heat flow. We expect to refine the theory of correcting the temperature data for the disturbance caused by the drilling to improve the estimation of undisturbed sediment temperature.

In general, where the quality of data is good, the new technique of downhole temperature measurements in conjunction with HPC operations demonstrated linear conductive temperature gradients (Sites 578 and 580) as expected for these old well-sedimented sites in the western Pacific. However, even when the measurements are disturbed or otherwise not as satisfactory (Sites 577 and 579), the ability to obtain relatively numerous measurements during coring operations allowed estimation of gradients with relatively small uncertainties (Table 3). The method appears to be capable of providing significantly improved heat flow estimates during HPC operations, with much less time than previously used techniques (Erickson, 1973; Yokota et al., 1980).

ACKNOWLEDGMENTS

This paper was improved by the helpful reviews of V. Vacquier and E. Davis. The development of instrumentation was supported initially by the U.S. Geological Survey (Marine Geology) at Woods Hole, the Ocean Industry Program of the Woods Hole Oceanographic Institution, and DSDP; subsequent funding was from U.S. National Science Foundation Grants OCE82-14658 and 83-00073. We are grateful to the officers, crew, and technical staff aboard the *Glomar Challenger* whose skills and assistance made these measurements possible.

REFERENCES

Anderson, R. N., and Skilbeck, J. N., 1981. Oceanic heat flow. *In* Emiliani, C. (Ed.), *The Sea* (Vol. 7): New York (Wiley-Interscience), 489-523.

Broecker, W. S., and Takahashi, T., 1977. The solubility of calcite in sea water. *In* Frazer, D. Z. (Ed.), *Thermodynamics in Geology:* Dordrecht (D. Reidel), pp. 365-379.

Bullard, E. C., 1939. Heat flow in South Africa. *Proc. R. Soc. London, Ser. A*, 173:474-502.

Burns, R. E., 1970. Heat flow operations at Holes 35.0 and 35.1 *In* McManus, D. A., Burns, R. E., et al., *Init. Repts. DSDP*, 5: Washington (U.S. Govt. Printing Office), 551-554.

Erickson, A., 1973. Initial report on downhole temperature and shipboard thermal conductivity measurements, Leg 19, Deep Sea Drilling Project. *In* Creager, J. S., Scholl, D, W., et al., *Init. Repts. DSDP*, 19: Washington (U.S. Govt. Printing Office), 643-656.

Erickson, J. A., and Hyndman, R. D., 1979. Downhole temperature measurements and thermal conductivities of samples, Site 396 Deep Sea Drilling Project Leg 46. *In* Dmitriev, L., Heirtzler, J., et al., *Init. Repts. DSDP*, 46: Washington (U.S. Govt. Printing Office), 389-400.

Girdler, R. W., Erickson, A. J., and Von Herzen, R. P., 1974. Downhole temperature and shipboard thermal conductivity measurements aboard D/V *Glomar Challenger* in the Red Sea. *In* Whitmarsh, R. B., Weser, O. E., Ross, D. A., et al., *Init. Repts. DSDP*, 23: Washington (U.S. Govt. Printing Office), 879-886.

Hilde, T. W. C., Isezaki, N., and Wageman, J. M., 1975. Mesozoic sea-floor spreading in the North-Pacific. *In* Sutton, G. H., Manghnani, M. H., and Moberly, R. (Eds.), *The Geophysics of the Pacific Ocean Basin and Its Margin*: Washington (American Geophysical Union), pp. 205-226.

Horai, K., 1981. Thermal conductivity of sediments and igneous rocks recovered during Deep Sea Drilling Project Leg 60. *In* Hussong, D. M., Uyeda, S., et al., *Init. Repts. DSDP*, 60: Washington (U.S. Govt. Printing Office), 807-834.

Hyndman, R. D., Erickson, A. J., and Von Herzen, R. P., 1974. Geothermal measurements on DSDP Leg 26. *In* Davies, T. A., Luyendyk, B. P., et al., *Init. Repts. DSDP*, 26: Washington (U.S. Govt. Printing Office), 451-464.

Hyndman, R. D., Von Herzen, R. P., Erickson, A. J., and Jolivet, J., 1977. Heat flow measurements, DSDP Leg 37. *In* Aumento, F., Melson, W. G., et al., *Init. Repts. DSDP*, 37: Washington (U.S. Govt. Printing Office), 347-362.

Marshall, B. V., and Erickson, A. J., 1974. Heat flow and thermal conductivity measurements, Leg 25, Deep Sea Drilling Project. *In* Simpson, E. S. W., Schlich, R., et al., *Init. Repts. DSDP*, 25: Washington (U.S. Govt. Printing Office), 349-355.

Müller, G., and Gastner, M., 1971. The "Karbonate Bombe", a simple device for determination of the carbonate content in sediments, soils, and other materials. *Neues. Jahrb. Mineral. Monatsh.*, 10: 466-469.

Parsons, B., and McKenzie, D. P., 1978. Mantle convection and the thermal structure of the plates. *J. Geophys. Res.*, 83:4485-4496.

Sclater, J. G., and Erickson, A. J., 1974. Geothermal measurements on Leg 22 of the D/V Glomar Challenger. *In* von der Borch, C. C., Sclater, J. G., et al., *Init. Repts. DSDP*, 22: Washington (U.S. Govt. Printing Office), 387-396.

Sclater, J. G., Jaupart, C., and Galson, D., 1980. The heat flow through oceanic and continental crust and the heat loss of the earth. *Rev. Geophys. Space Phys.*, 18:269-311.

Uyeda, S., and Horai, K., 1982. Heat flow measurements on Deep Sea Drilling Project Leg 60. *In* Hussong, D. M., Uyeda, S., et al., *Init. Repts. DSDP*, 60: Washington (U.S. Govt. Printing Office), 789-800.

Von Herzen, R. P., 1973. Geothermal measurements, Leg 21. *In* Burns, R. E., Andrews, J. E., et al., *Init. Repts. DSDP*, 21: Washington (U.S. Govt. Printing Office), 443-458.

Von Herzen, R. P., Fiske, R. J., and Sutton, G., 1971. Geothermal measurements on Leg 8. *In* Tracey, J. I., Jr., Sutton, G. H., et al., *Init. Repts. DSDP*, 8: Washington (U.S. Govt. Printing Office), 837-849.

Watanabe, T., Von Herzen, R. P., and Erickson, A. J., 1975. Geothermal studies Leg 31, Deep Sea Drilling Project. *In* Karig, D. E., Ingle, J. C., Jr., et al., *Init. Repts. DSDP*, 31: Washington (U.S. Govt. Printing Office), 573-576.

Yokota, T., Kinoshita, H., and Uyeda, S., 1980. New DSDP (Deep Sea Drilling Project) downhole temperature probe utilizing IC RAM (Memory) elements. *Bull. Earthquake Res. Inst., Univ. Tokyo*, 55: 75-88.

Date of Initial Receipt: 19 March 1984
Date of Acceptance: 2 October 1984

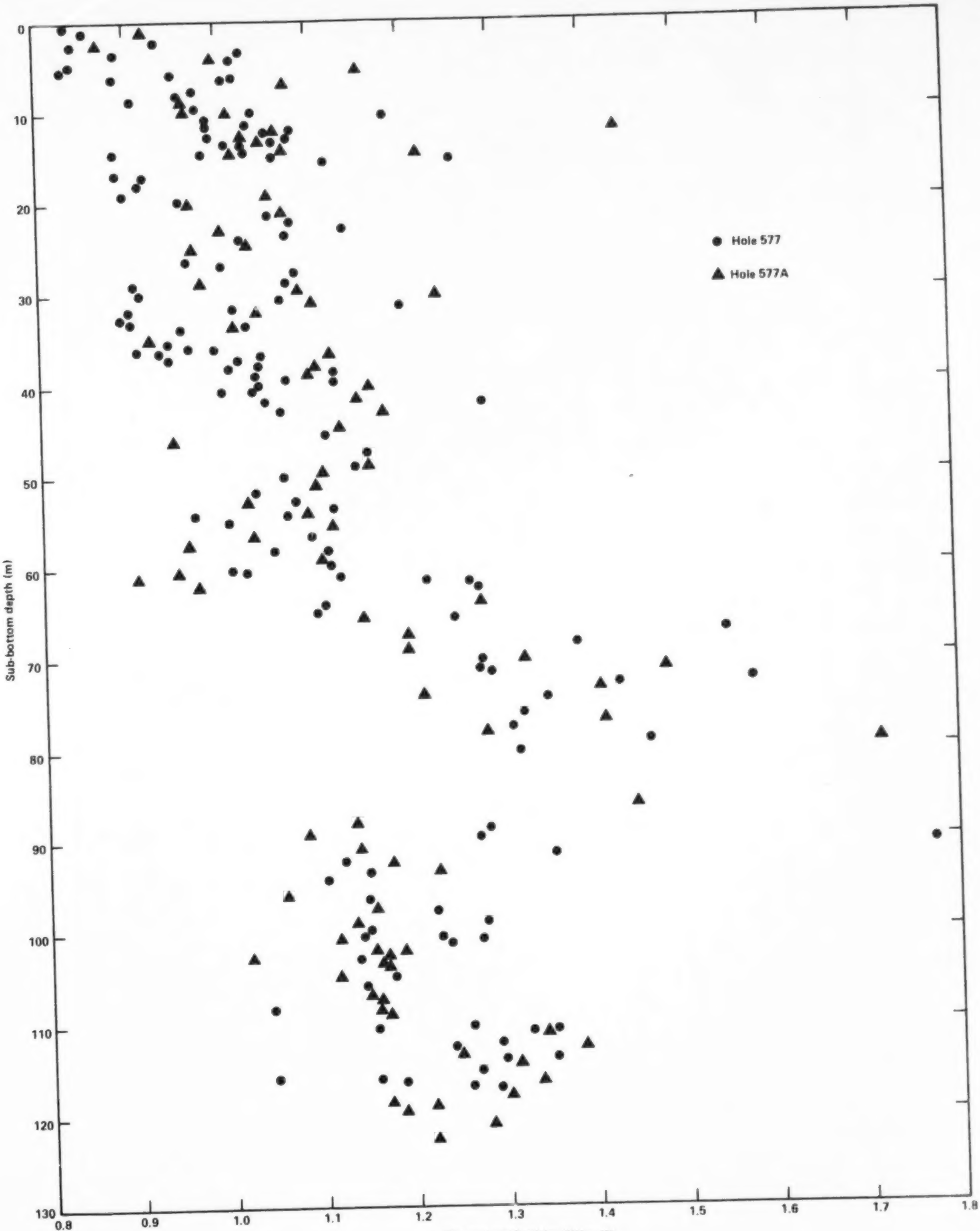

Figure 12. Sediment thermal conductivity versus sub-bottom depth at Site 577.

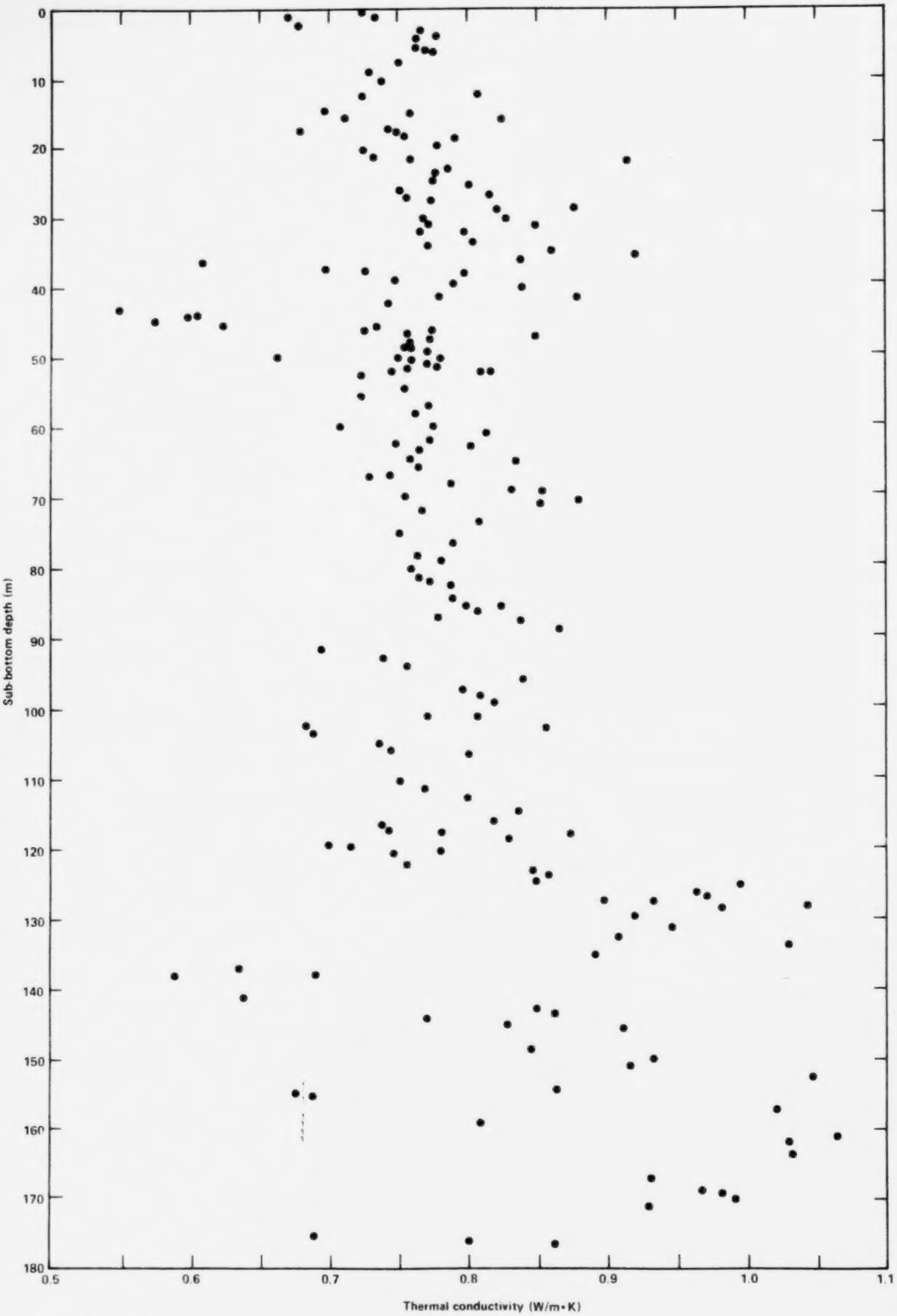

Figure 13. Sediment thermal conductivity versus sub-bottom depth at Site 578.

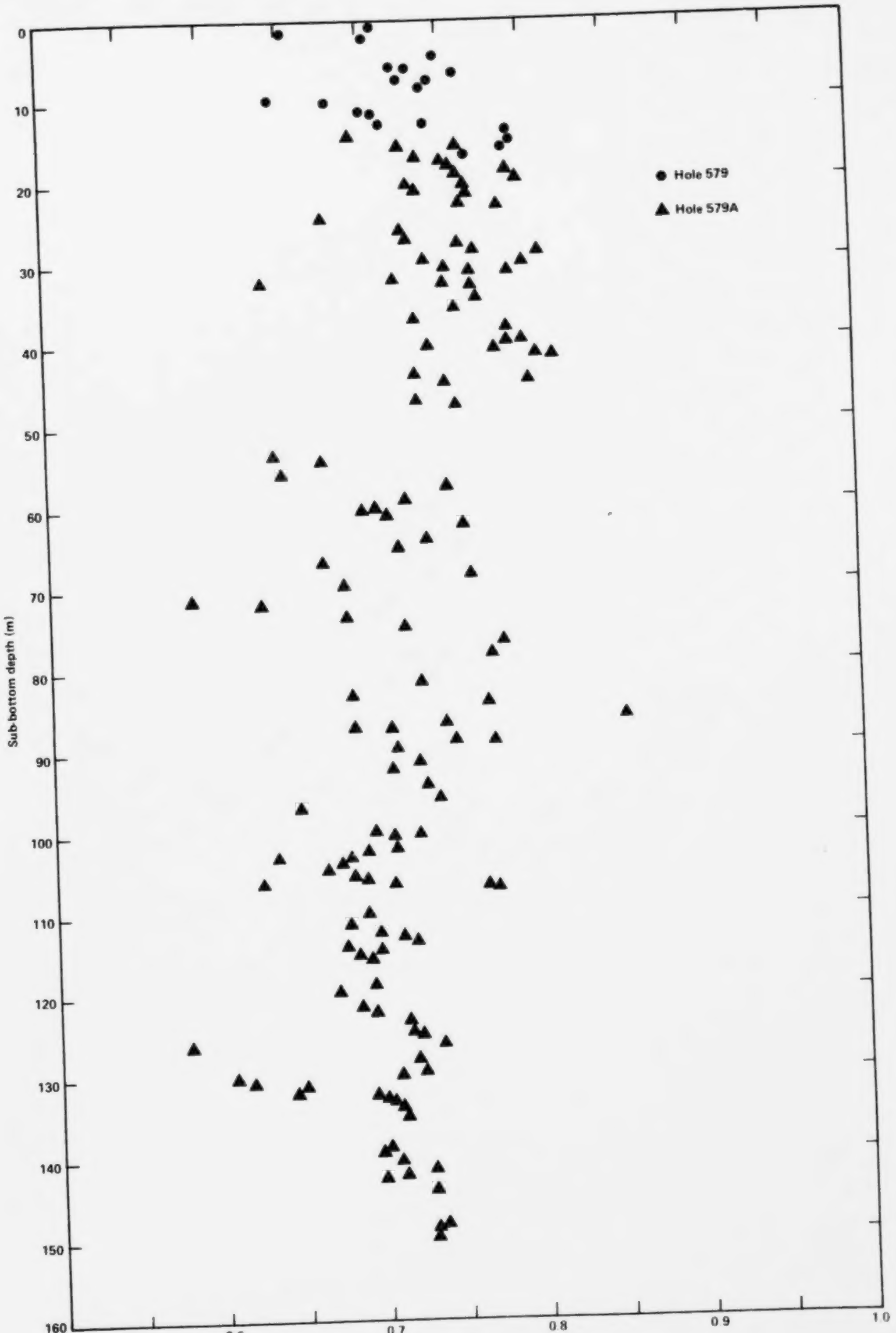

Figure 14. Sediment thermal conductivity versus sub-bottom depth at Site 579.

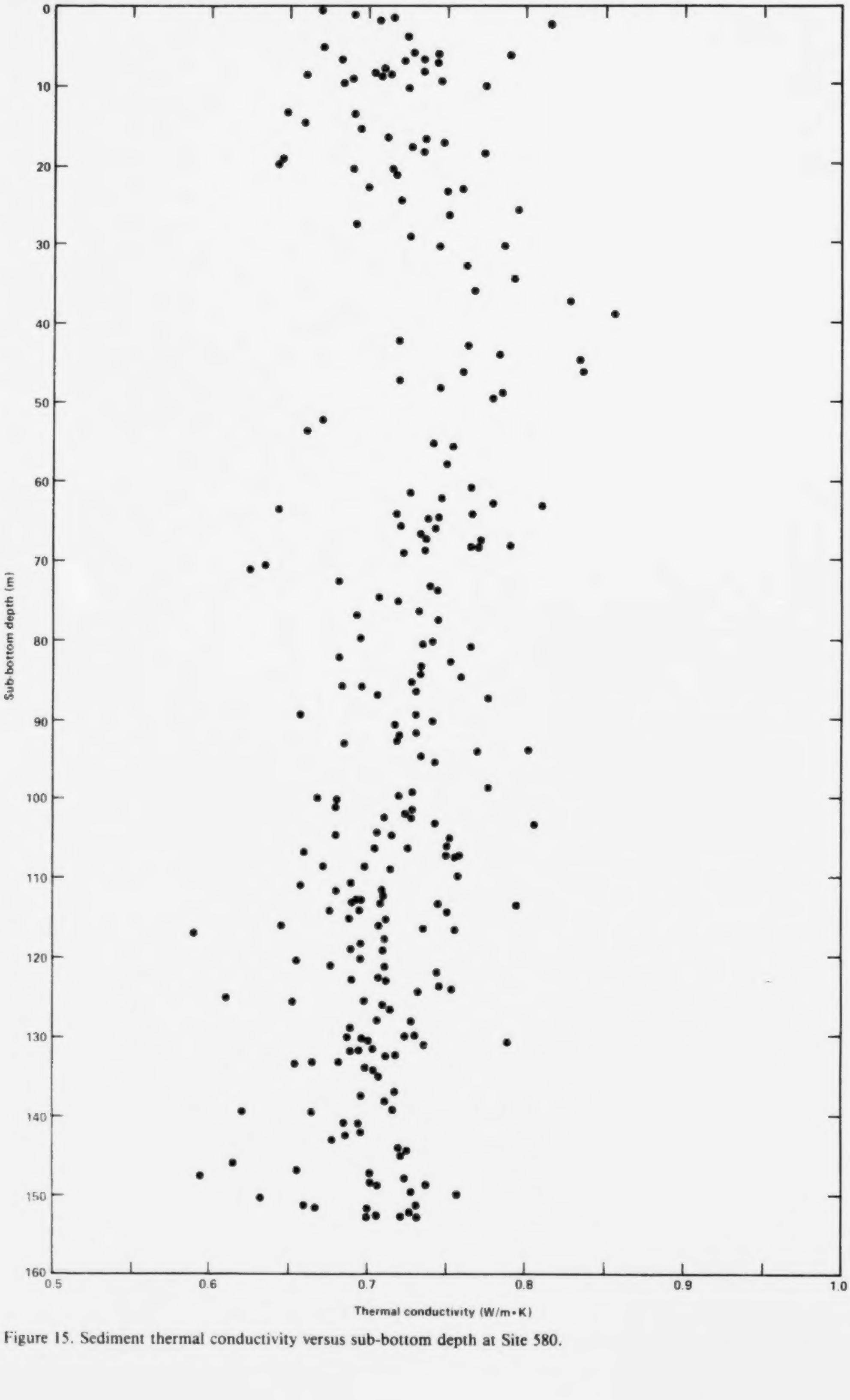

Figure 15. Sediment thermal conductivity versus sub-bottom depth at Site 580.

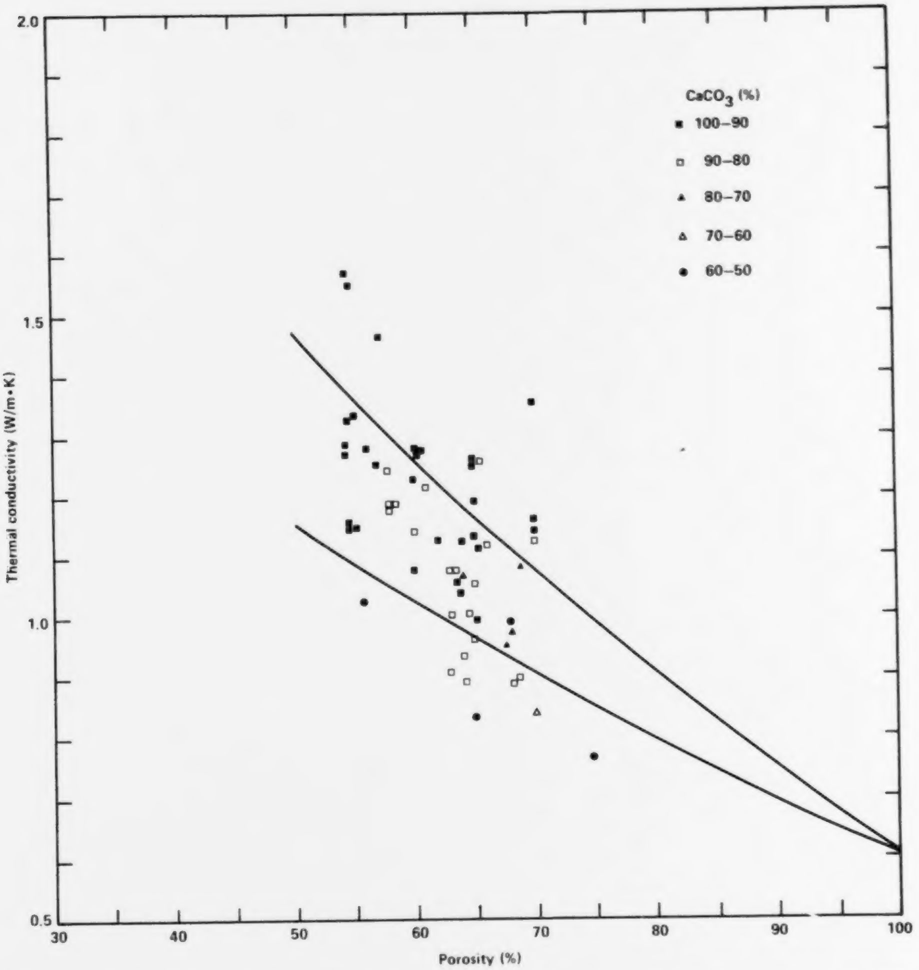

Figure 16. Sediment thermal conductivity versus porosity relationship for various calcium carbonate ($CaCO_3$) contents.

Table 2. Calcium carbonate content and thermal conductivity of Site 577 sediment samples, Leg 86.

Range of $CaCO_3$ content by weight (%)	Thermal conductivity $k + \Delta k$ (s.d.) (W/m·K)	Sample size
90–100	4.37 ± 0.63	12
80–90	3.84 ± 0.54	18
70–80	4.30 ± 0.70	3
60–70	3.70 ± 0.50	2
50–60	3.21 ± 0.84	3

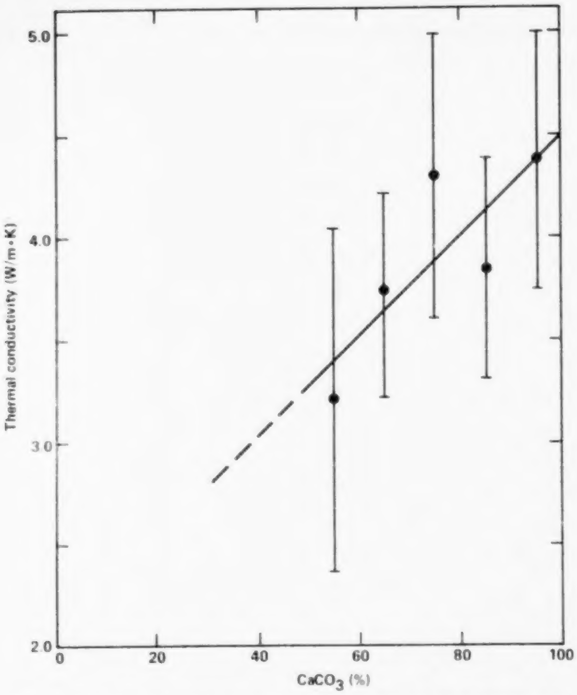

Figure 17. Grain thermal conductivity of sediment as a function of calcium carbonate content by weight.

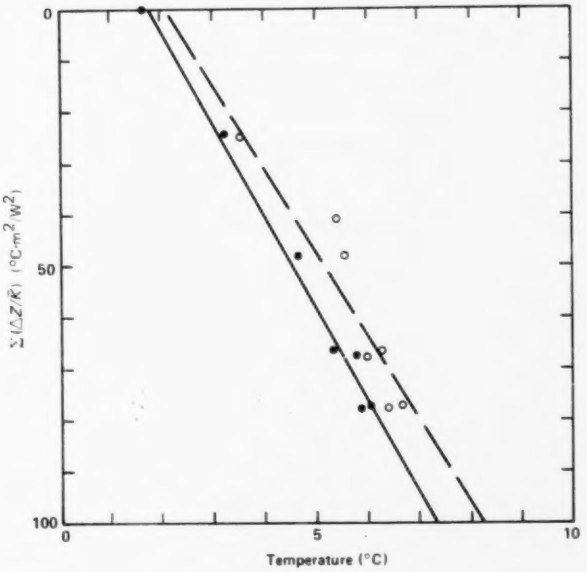

Figure 18. Plot of sediment temperatures, T_{max} and T_{min}, against cumulative thermal resistance at Site 576.

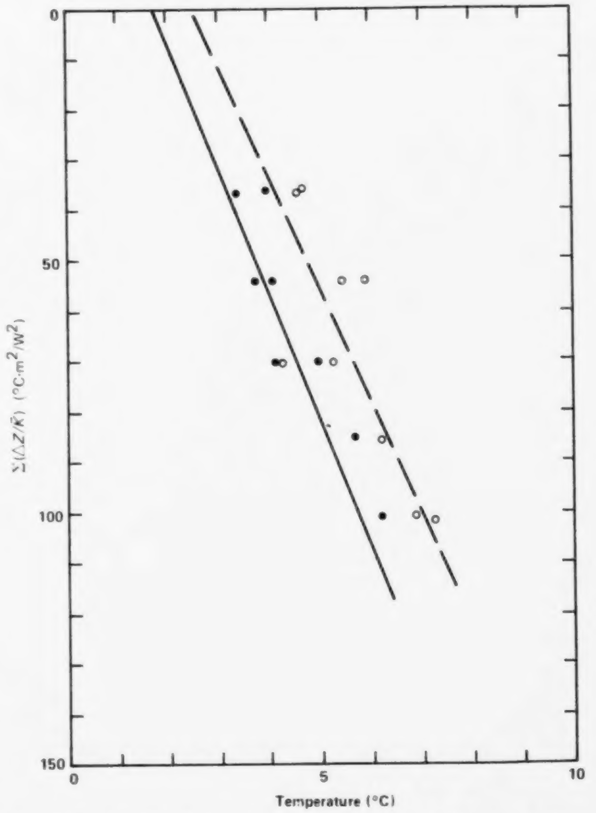

Figure 19. Plot of sediment temperatures, T_{max} and T_{min}, against cumulative thermal resistance at Site 577.

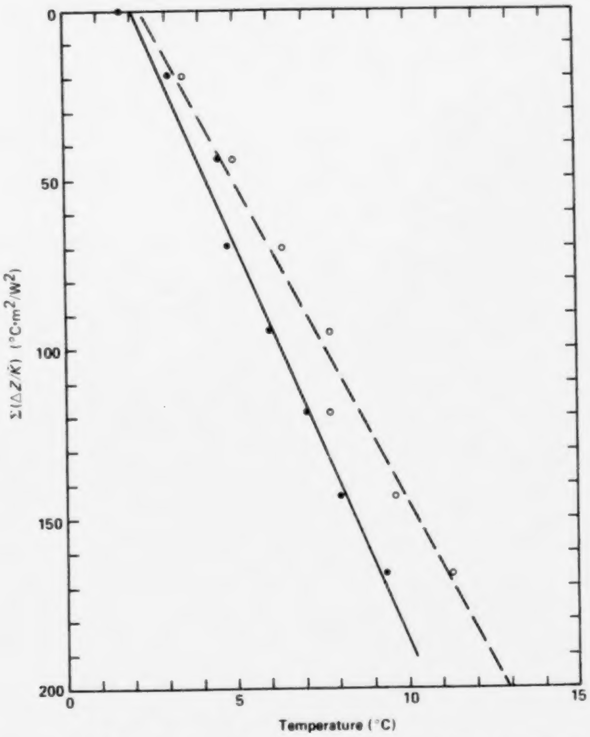

Figure 20. Plot of sediment temperatures, T_{max} and T_{min}, against cumulative thermal resistance at Site 578.

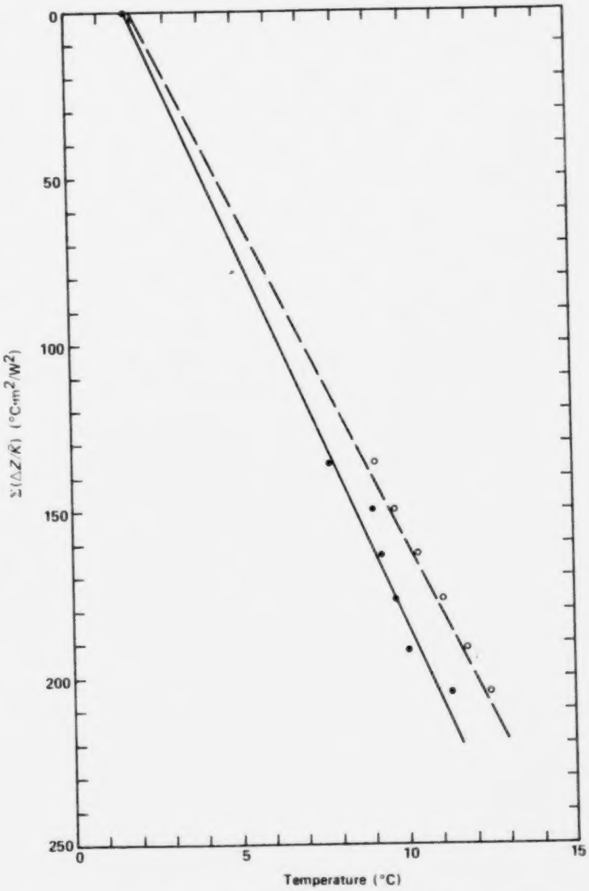

Figure 21. Plot of sediment temperatures, T_{max} and T_{min}, against cumulative thermal resistance at Site 579.

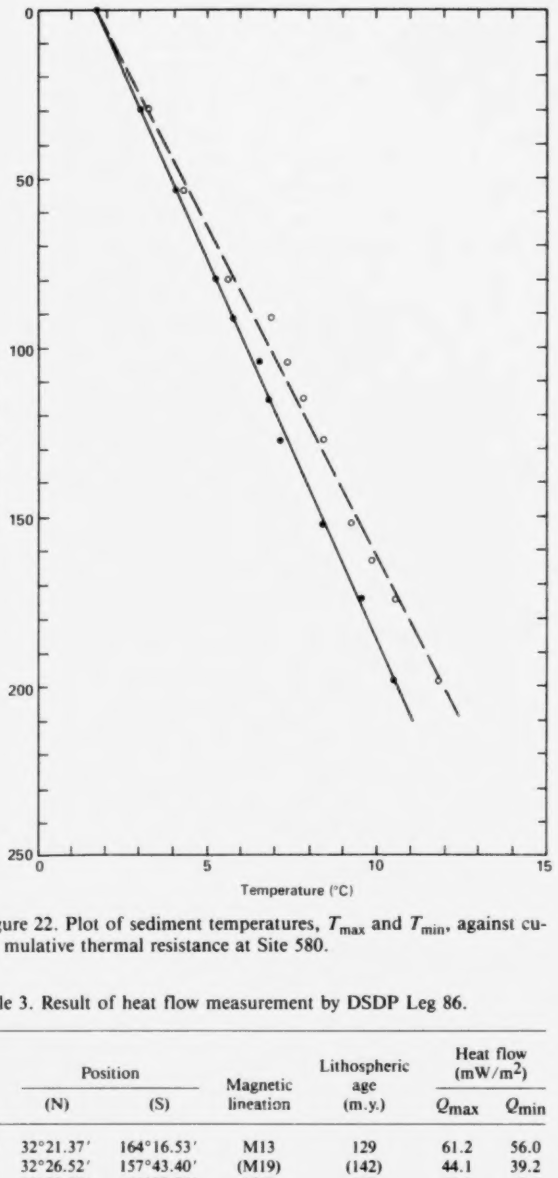

Figure 22. Plot of sediment temperatures, T_{max} and T_{min}, against cumulative thermal resistance at Site 580.

Table 3. Result of heat flow measurement by DSDP Leg 86.

	Position			Lithospheric	Heat flow (mW/m^2)	
Site	(N)	(S)	Magnetic lineation	age (m.y.)	Q_{max}	Q_{min}
576	32°21.37′	164°16.53′	M13	129	61.2	56.0
577	32°26.52′	157°43.40′	(M19)	(142)	44.1	39.2
578	33°55.56′	151°37.74′	M17	137	52.9	42.7
579	38°37.68′	153°50.17′	M10	122	49.7	44.1
580	41°37.47′	153°58.58′	M 3	114	51.4	44.4

Note: Data of questionable quality are in parentheses.

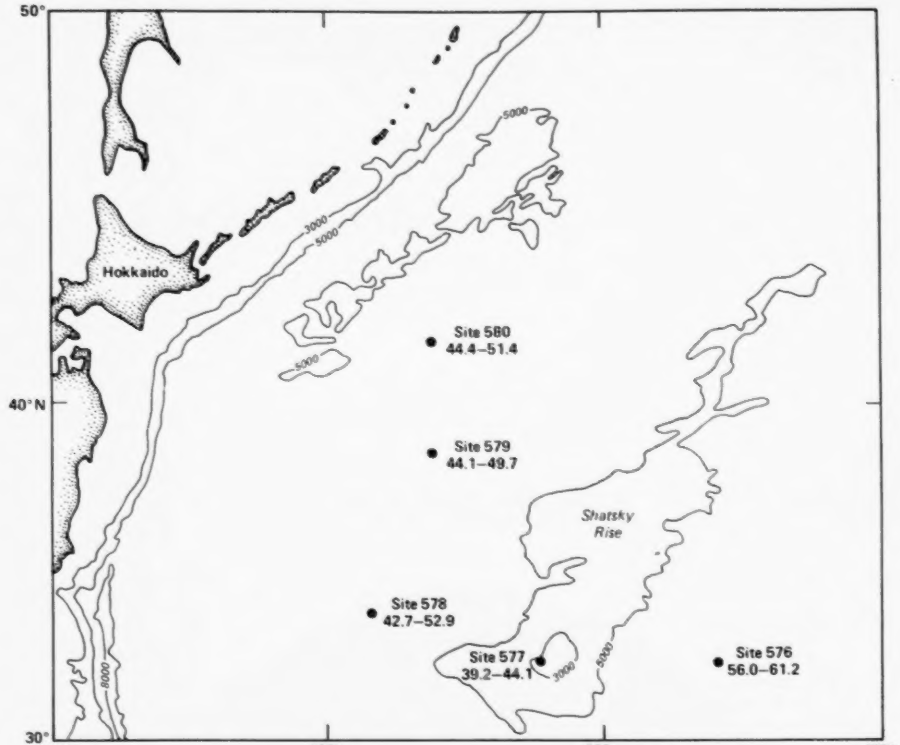
50°
40°N
30°
140°E
150°
160°
170°
Hokkaido
3000
5000
8000
Site 580
44.4–51.4
Site 579
44.1–49.7
Site 578
42.7–52.9
Site 577
39.2–44.1
Site 576
56.0–61.2
Shatsky Rise

Figure 23. Geographical distribution of heat flow stations of Leg 86. Values of heat flow, $Q_{min} - Q_{max}$, in mW/m^2; bathymetry in meters.

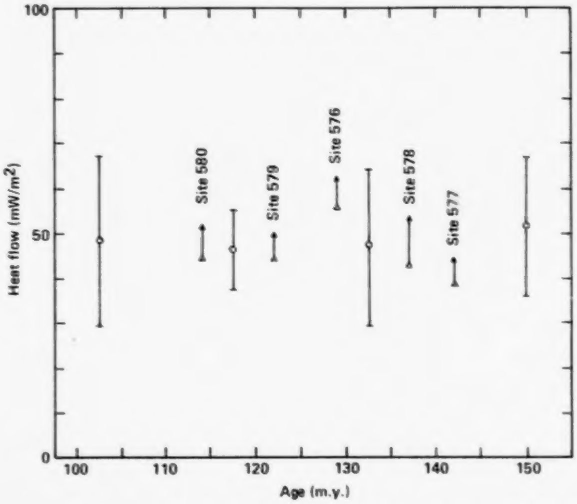

Figure 24. Heat flow versus lithospheric age relation for Leg 86 data compared with the average for North Pacific (Sclater et al., 1980).

PART VII: SYNTHESES AND SUMMARIES

Reprinted from Heath, G. R., Burckle, L. H., et al., 1985
Initial Reports of the Deep Sea Drilling Project, Volume LXXXVI, Washington (U.S. Government Printing Office)

36. ASSESSMENT OF DIATOM AND RADIOLARIAN HIGH- AND LOW-LATITUDE ZONATIONS IN NORTHWEST PACIFIC SEDIMENTS: COMPARISON BASED UPON MAGNETOSTRATIGRAPHY[1]

Lloyd H. Burckle and J. J. Morley, Lamont-Doherty Geological Observatory
I. Koizumi, Osaka University
and
U. Bleil, Ruhr-Universität Bochum[2]

ABSTRACT

Sediments recovered by the hydraulic piston corer at three northwest Pacific sites (Sites 578, 579, and 580; Fig. 1) have a relatively high accumulation rate (> 30 m/m.y.) and contain a detailed paleomagnetic record. This makes it possible to examine the various biostratigraphic datum levels used in low- and high-latitude siliceous floral/faunal zonations in this transitional setting in order to determine which zonal scheme or combination of schemes provides the most reliable biostratigraphic information for the Neogene and Quaternary in this region of the North Pacific. Most high-latitude diatom species do not penetrate the equatorial regions, although they do occur in subarctic to transitional and occasionally subtropical waters. Significant diachroneity is observed in middle Pleistocene sediments. Long-ranging equatorial Pacific forms are found in the northwest Pacific and their first and last appearances are usually isochronous with the equatorial record. However, both first and last appearances tend to be diachronous for species that have short ranges in low latitudes. All of the biostratigraphic marker species associated with the North Pacific radiolarian zonation are present in sediments at the three Deep Sea Drilling Project sites with each event synchronous with its counterpart in high-latitude sediments. Therefore, the North Pacific faunal zonation can be reliably applied to siliceous sediments across a broad region of the northwest Pacific extending from the subarctic to intermediate latitudes.

INTRODUCTION

A persistent problem in biostratigraphy is our uncertainty in correlating between high and low latitudes, across major oceanic (water mass) boundaries, and between northern and southern high latitude sites. It is easy to understand why such a problem exists. Few stratigraphically useful species are so cosmopolitan that they can be used for long-distance correlation. Indeed, most species that are found useful in biostratigraphy have a regional distribution. A way of solving this problem of long-distance correlation presented itself with the advent of magnetostratigraphy as a supporting tool in biostratigraphy (Opdyke et al., 1966; Hays and Opdyke, 1967). Magnetic reversals are isochronous and therefore are not subject to the vagaries of paleoclimate, paleoceanography, or to changing spatial distributions of microfossils.

In spite of these advances in high-resolution biostratigraphy, there were certain limitations that made it difficult to resolve correlation problems for much of the Tertiary. Chief among these limitations was that conventional piston cores used in these studies rarely penetrated more than 25 m of sediment. This meant that, unless several cores were pieced together, it was not possible to obtain good, continuous records for even the Neogene, much less the Paleogene. For this reason, the technology provided by the hydraulic piston core (HPC) is very important, with recovery an order of magnitude greater than that with the wire-line-supported piston corer. Thus, with such cores a continuous magnetostratigraphy for correlation with floral/faunal datums can be acquired, spanning several million years, in regions with relatively high accumulation rates (>30 m/m.y.).

Within this context, the northwest Pacific is a unique area—it is transitional between the tropical Pacific and the subarctic North Pacific, a meeting ground for floral and faunal elements from high and low latitudes, and a crucial area for establishing high-resolution correlation between the equatorial Pacific and the North Pacific. Furthermore, study of this area is essential in establishing a late Neogene correlation scheme for such nearby land areas as Japan, Sakhalin, and Kamchatka.

This chapter uses magnetostratigraphy to determine the relationship of various diatom and radiolarian biostratigraphic datum levels used in low- and high-latitude zonal schemes in late Neogene and Quaternary sedimentary sequences from the northwest Pacific. For the equatorial Pacific, we draw largely from the work of Hays et al. (1969), Opdyke and Foster (1970), Burckle (1972, 1977, 1978), Burckle and Opdyke (1977), Burckle and Trainer (1979), and Theyer et al. (1978). Correlations of magnetostratigraphy with biostratigraphic datum levels were presented by Koizumi (1975a, b) and Hays (1970) for the North Pacific and Barron (1980) for the northwest Pacific. The sedimentary sequences at Sites 578–580 provide a data set for determining which zonal scheme is appropriate for sediments from this transitional zone in the North Pacific.

---

[1] Heath, G. R., Burckle, L. H., et al., *Init. Repts. DSDP*, 86: Washington (U.S. Govt. Printing Office).

[2] Addresses: (Burckle, Morley) Lamont-Doherty Geological Observatory, Palisades, NY 10964; (Koizumi) College of General Education, Osaka University, Osaka 560, Japan; (Bleil) Institut für Geophysik, Ruhr-Universität, 4630 Bochum, Federal Republic of Germany.

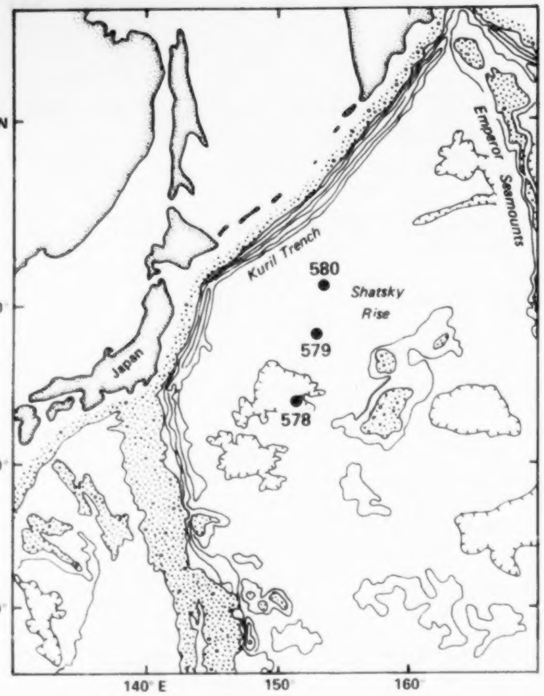

Figure 1. Map of northwest Pacific showing the location of DSDP sites (578–580) used in this study. Areas shallower than 4 km stippled, 5-km contour plain, 6-km contour hachured.

PALEOMAGNETICS

Vertically oriented samples of about 7 cm^3 were taken at intervals ranging from 10 to 50 cm. All Leg 86 materials, with the exceptions noted in Bleil (this volume), were analyzed for their paleomagnetic properties at the Ruhr University, Bochum. Measurements of magnetization intensity and direction were made on a cryogenic magnetometer. The recently revised geomagnetic polarity time scale of Berggren et al. (in press) was used as the basis for interpretation of the downhole polarity sequences and to determine numerical ages for the reversal boundaries (Fig. 2).

DIATOMS

Figure 2 shows the equatorial Pacific diatom zonation of Burckle (1972, 1978), the North Pacific diatom zonation of Koizumi (1975a), and the diatom zonation proposed by Koizumi and Tanimura (this volume) for northwest Pacific Sites 578–580. Key datum levels for both the equatorial Pacific and North Pacific zonations (Table 1) are shown in their stratigraphic position and, using the paleomagnetic stratigraphy for principle time control, we have shown the relative position of these datum levels at Sites 578–580.

In the equatorial Pacific, the oldest datum levels [1(T) = top of *Asterolampra acutiloba* and 2(B) = base of *Nitzschia jouseae*] appear to be isochronous between low latitudes and Site 578. However, Sites 579 and 580 did not penetrate sediments of equivalent age. Koizumi (1975a) does not report either of these diatoms in his North Pacific zonation.

The next equatorial Pacific datum level [3(B) = base of *Rhizosolenia praebergonii*] is diachronous between low latitudes and Site 578. Datum level 3 occurs in the middle of the Gauss Chron in the equatorial Pacific (Burckle, 1972) and in the upper part of the Gauss Chron at Site 578. It occurs in even younger sediments (lower part of the Matuyama) at Site 579 but is isochronous between Sites 579 and 580. Koizumi (1975a) does not report this datum level in his North Pacific zonation.

The last appearance of *Nitzschia jouseae* [= 4(T)] occurs in the upper part of the Gauss Chron in equatorial Pacific sediments. This datum is isochronous between low latitudes and Sites 578–580 and is more or less coincidental with the last occurrence of the high latitude form, *Denticulopsis kamtschatica* (high latitude North Pacific datum level 2(T); Koizumi, 1975a; Koizumi and Tanimura, this volume).

The next youngest datum [5(T) = top of *Thalassiosira convexa*] occurs midway between the top of the Gauss Chron and the base of the Olduvai Event. This datum is isochronous between low latitudes and Sites 578–580. However, in the subarctic North Pacific, Koizumi (1975a) records the last appearance of this form some 200,000 yr. earlier, just above the top of the Gauss Chron. This is consistent with the results of Donahue (1970), who also found that the disappearance of this species in high latitudes precedes that at lower and intermediate latitudes.

One first appearance datum [6(B) = base of *Pseudoeunotia doliolus*] occurs within the Olduvai Event. This datum is not isochronous between low latitudes and any of the northwest Pacific sites. This may be due to the rarity of the species in the early part of its range; it does not become common to abundant until later in the record. Thus, the level at which the first appearance is drawn may be strictly a function of how much time is spent searching the slide.

The last appearance of *Rhizosolenia praebergonii* [= 7(T)] occurs just above the Olduvai Event in low latitudes. This datum becomes progressively older in the northwest Pacific until, at Site 580, it is near the last appearance of *Thalassiosira convexa* [= 5(T)]. The last appearance of *Nitzschia reinholdii* [= 8(T)] appears to be isochronous between low latitudes and the higher latitude North Pacific. In an earlier paper, Koizumi (1975b) suggested that this datum may be slightly diachronous but it is not possible to determine this within the resolution provided by the present paleomagnetic measurements (but see Sancetta, this volume).

Eleven datum levels from the subarctic North Pacific zonation were selected for comparison with Sites 578–580 and the equatorial Pacific (Fig. 2). The first appearance of *Denticulopsis seminae* var. *fossilis* [= 1(B)] occurs in the middle of the Gilbert Chron in the North Pacific. However, this first appearance is diachronous with respect to transitional and subtropical waters (Sites 578 and 579) and is entirely absent from the equatorial regions. The *Denticulopsis kamtschatica* last appearance datum [= 2(T)] is isochronous between the North Pacific and Sites 578–580. It does not occur in low latitudes.

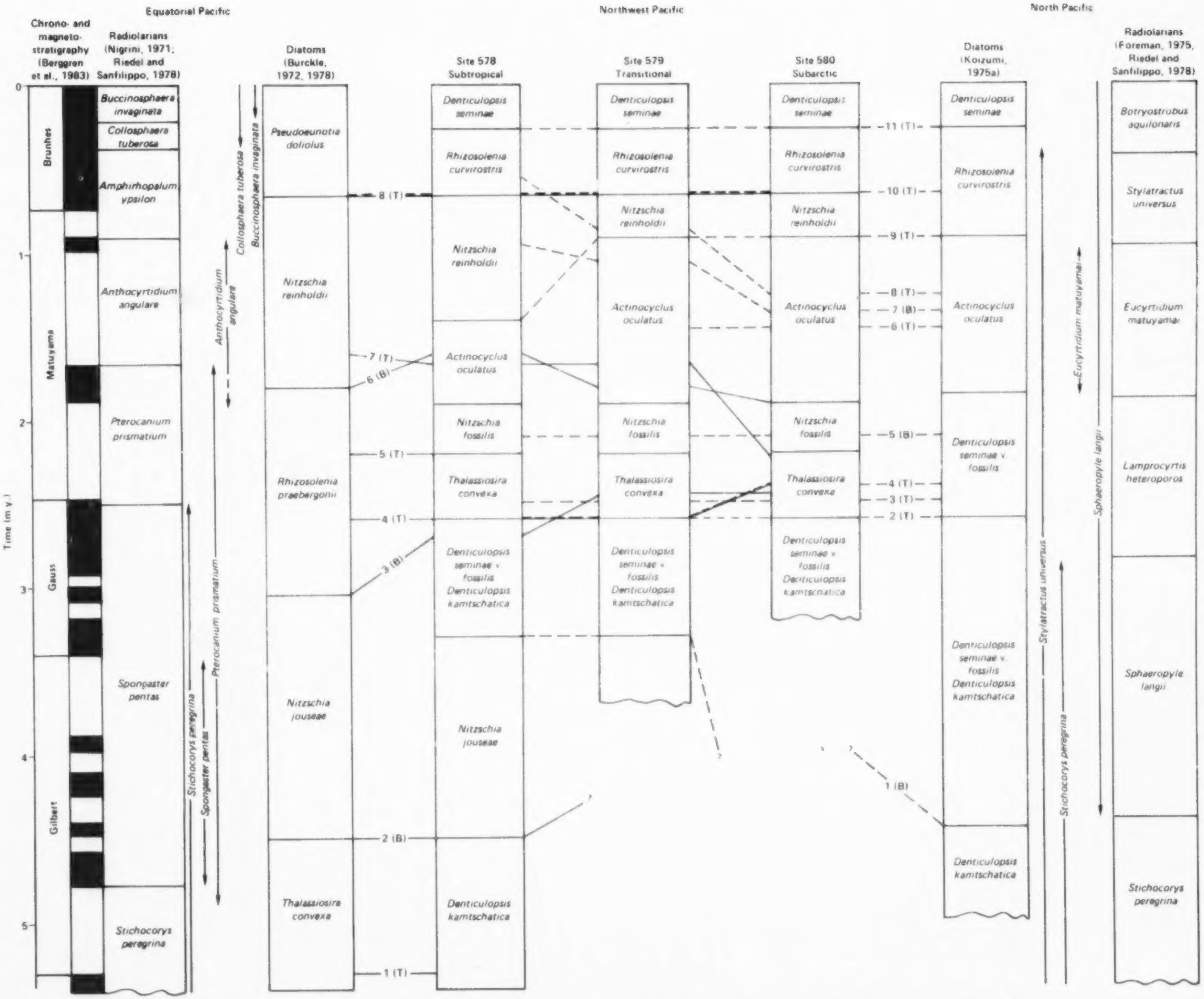

Figure 2. Diatom and radiolarian correlation between the equatorial, northwest, and North Pacific using paleomagnetics as a control (see Bleil, this volume for paleomagnetic stratigraphies of Sites 578–580). Numbers and letters (B and T) represent first appearance (B) and last occurrence (T) of diatom datum levels. These datum levels are explained in the text. Solid lines between sites represent diatom datum levels that originated in the equatorial Pacific; dashed lines between sites represent diatom datum levels that originated in the North Pacific. Diatom zonations at Sites 578–580 proposed by Koizumi and Tanimura (this volume).

Table 1. Diatom datum levels used in Figure 2.

	Equatorial Pacific datum levels
1(T)	Disappearance of *Asterolampra acutiloba*
2(B)	Appearance of *Nitzschia jouseae*
3(B)	Appearance of *Rhizosolenia praebergonii*
4(T)	Disappearance of *Nitzschia jouseae*
5(T)	Disappearance of *Thalassiosira convexa*
6(B)	Appearance of *Pseudoeunotia doliolus*
7(T)	Disappearance of *Rhizosolenia praebergonii*
8(T)	Disappearance of *Nitzschia reinholdii*
	High latitude North Pacific datum levels
1(B)	Appearance of *Denticulopsis seminae* var. *fossilis*
2(T)	Disappearance of *Denticulopsis kamtschatica*
3(T)	Disappearance of *Bogorovia tatsunokuchiensis*
4(T)	Disappearance of *Nitzschia jouseae*
5(B)	Appearance of *Actinocyclus oculatus*
6(T)	Disappearance of *Thalassiosira antiqua*
7(B)	Appearance of *Rhizosolenia curvirostris*
8(T)	Disappearance of *Denticulopsis seminae* var. *fossilis*
9(T)	Disappearance of *Actinocyclus oculatus*
10(T)	Disappearance of *Nitzschia reinholdii*
11(T)	Disappearance of *Rhizosolenia curvirostris*

This datum is nearly coincidental with the last occurrence of *N. jouseae* [equatorial Pacific datum level 4(T)] (Fig. 2).

The last occurrence of *Bogorovia tatsunokuchiensis* [= 3(T)] occurs just above the Gauss Chron at Site 580 and appears to be isochronous at both Sites 578 and 579. This species is not reported from the equatorial Pacific. The next datum level above this is the last occurrence of *N. jouseae* [= 4(T)].

The first occurrence of *Actinocyclus oculatus* [= 5(B)] occurs midway between the top of the Gauss Chron and the base of the Olduvai Event. This datum appears to be isochronous between subarctic and subtropical sites, although it does not penetrate into the equatorial regions. The last occurrence of *Thalassiosira antiqua* [= 6(T)] is found only at Sites 579 and 580; the species did not extend into the subtropical gyre or the equatorial regions. Although Figure 2 shows this datum to be isochronous between Sites 579 and 580, there is some suggestion in our data (Koizumi and Tanimura, this volume) that the last occurrence of *T. antiqua* at Site 579 is earlier than at Site 580.

The next two datum levels are both diachronous with respect to lower latitudes. The first occurrence of *Rhizosolenia curvirostris* [= 7(B)] occurs midway between the Olduvai and Jaramillo events in the northern transition zone (Site 580), just below the Jaramillo Event in southern transitional waters (Site 579), and directly below the Jaramillo Event in the subtropics (Site 578). The next youngest datum level [disappearance of *Denticulopsis seminae* var. *fossilis* = 8(T)] persisted longer in the subtropics. At Site 580, this datum level occurs midway between the Olduvai and Jaramillo events while in the subtropics (Site 578) it occurs in the middle of the Brunhes Chron. It is not observed in equatorial regions. It should also be pointed out that there is frequently some difficulty in differentiating *D. seminae* from *D. seminae* var. *fossilis* near the extinction level of the latter form. This may account for differences in the literature on the placement of this datum level.

The last appearance of *Actinocyclus oculatus* [= 9(T)] is isochronous between Sites 580 and 579 but occurs earlier at Site 578. The difference in this datum level between Sites 579 and 578 is quite significant (Fig. 2). The last two datum levels are isochronous within the limits of the paleomagnetic method. *N. reinholdii* [= 10(T)] last occurs in the lower part of the Brunhes Chron in both high and low latitudes while *R. curvirostris* [= 11(T)] disappears in the upper part of the Brunhes Chron at all three sites, never extending into the equatorial Pacific.

RADIOLARIANS

Separate radiolarian zonations have been devised for the equatorial and North Pacific sediments of Neogene through Quaternary age (Fig. 2). The zonation for the equatorial Pacific is based on work by Nigrini (1971) and Riedel and Sanfilippo (1978), while that for the North Pacific is from Foreman (1975) and Riedel and Sanfilippo (1978).

Although a majority of the species that define the high latitude zonation are present in low-latitude sediments, the two zonal schemes are based almost entirely upon different biostratigraphic datum levels. Specific zones under the equatorial Pacific scheme occupy intervals of geologic time relatively similar to those in the North Pacific zonation, except for the latest Quaternary (last 400,000 yr.) where the low-latitude zonation contains two zones versus only one in the high-latitude zonation. The one exception to the similar placement of zonal boundaries occurs in the late Pliocene sequence where *Stichocorys peregrina* defines a boundary in both zonal systems. In the equatorial Pacific zonation, the top of the *S. pentas* zone is based on the last appearance of *S. peregrina* which occurs in tropical Pacific sediments near the top of the Gauss Chron (Theyer et al., 1978). In North Pacific sediments, however, this same event, which marks the boundary between the *Sphaeropyle langii* and *Lamprocyrtis heteroporos* zones occurs at approximately 2.85 m.y. ago (Berggren et al., 1983). Therefore, *Stichocorys peregrina* appears to have inhabited tropical Pacific waters for several thousand years after it disappeared from the North Pacific.

The sediments recovered at Sites 578–580 contain an abundant siliceous fauna with biostratigraphic species diagnostic of the North Pacific zonation. Based upon correlation with magnetostratigraphy, the biostratigraphic events defining specific zones of the North Pacific zonation are synchronous at all three sites. Of the species that define the equatorial Pacific zonation, only *S. peregrina* was present in any abundance in sediments at all sites. A few specimens of *Pterocanium prismatium* were identified in sediments near the top of its range at Sites 578 and 580. These data indicate that the North Pacific zonation, with its associated datum levels, can be consistently applied to sediments across a broad latitudinal range in the Pacific extending from high-latitude subarctic regions into the mid-latitude subtropics.

CONCLUSIONS

Using magnetostratigraphy for time control, a comparison was made of various diatom and radiolarian zonations and their associated datum levels for the equatorial Pacific, the northwest Pacific, and the North Pacific in sediment sequences at three northwest Pacific sites (578–580). Few North Pacific diatoms penetrated into the equatorial regions and vice versa. Species with a short range in equatorial regions tend to show the greatest degree of diachroneity into higher latitudes. Interestingly, at least one species (*D. seminae* var. *fossilis*), has its longest range in subtropical and transitional waters. The radiolarian biostratigraphic datum levels at all three sites are synchronous with their counterparts in higher latitude sediments, indicating that the North Pacific radiolarian zonation can be applied to sediments in this transitional region.

ACKNOWLEDGMENTS

We thank Constance Sancetta and Audrey Wright for carefully reviewing the manuscript and offering many useful suggestions, both as to style and content. This work was supported by NSF Grant OCE 78-20885 (LHB) and the Deutsche Forschungsgemeinschaft (UB).

REFERENCES

Barron, J. A., 1980. Lower Miocene to Quaternary diatom biostratigraphy of Leg 57, off northeastern Japan, Deep Sea Drilling Project. *In* Scientific Party, *Init. Repts. DSDP*, 56, 57, Pt. 2:Washington (U.S. Govt. Printing Office), 641–685.

Berggren, W. A., Kent, D. V., and Flynn, J. J., in press. Paleogene geochronology and chronostratigraphy. *In* Snelling, N. J. (Ed.), *Geochronology and the Geological Record*. Geological Society of London, Spec. Pap.

Burckle, L. H., 1972. Late Cenozoic planktonic diatom zones from the eastern equatorial Pacific. *Nova Hedwigia*, 39:217–248.

________, 1977. Pliocene and Pleistocene diatom datum levels from the equatorial Pacific. *Quat. Res.*, 7:330–340.

________, 1978. Early Miocene to Pliocene diatom datum levels for the equatorial Pacific. *Proc. Working Group on Biostratigraphic Datum Planes of the Pacific Neogene, 2nd, Bandung, Indonesia*, pp. 25–44.

Burckle, L. H., and Opdyke, N. D., 1977. Late Neogene diatom correlations in the circum-Pacific. *Proc. Int. Congr. Pacific Neogene Strat., 1st, Tokyo*, pp. 255–284.

Burckle, L. H., and Trainer J., 1979. Late Pliocene diatom datum levels in the central Pacific. *Micropaleontology*, 25:281–293.

Donahue, J., 1970. Diatoms as Quaternary biostratigraphic and paleoclimatic indicators in high latitudes of the Pacific ocean [Ph.D. dissert.]. Columbia University, New York.

Foreman, H. P., 1975. Radiolaria from the North Pacific, Deep Sea Drilling Project, Leg 32. *In* Larson, R. L., Moberly, R., et al, *Init. Repts. DSDP*, 32: Washington (U.S. Govt. Printing Office), 579–676.

Hays, J. D., 1970. Stratigraphy and evolutionary trends of radiolaria in north Pacific deep-sea sediments. *In* Hays, J. D. (Ed.), *Geological Investigations of the North Pacific*. Mem. Geol. Soc. Am., 126:185–218.

Hays, J. D., and Opdyke, N. D., 1967. Antarctic radiolaria, magnetic reversals and climatic change. *Science*, 158:1001–1011.

Hays, J. D., Saito, T., Opdyke, N. D., and Burckle, L. H., 1969. Pliocene-Pleistocene sediments of the equatorial Pacific: Their paleomagnetic, biostratigraphic and climatic record. *Geol. Soc. Am. Bull.*, 80:1481–1513.

Koizumi, I., 1975a. Late Cenozoic diatom biostratigraphy in the circum-north Pacific region. *J. Geol. Soc. Japan*, 81:611–627.

________, 1975b. Diatom events in late Cenozoic deep-sea sequences in north Pacific, *J. Geol. Soc. Japan*, 81:567–577.

Nigrini, C., 1971. Radiolarian zones in the Quaternary of the equatorial Pacific ocean. *In* Riedel, W. R., and Funnell, B. M. (Eds.), *The Micropaleontology of the Oceans*: London (Cambridge Univ. Press), pp. 443–461.

Opdyke, N. D., and Foster, J., 1970. The paleomagnetism of cores from the north Pacific, *In* Hays, J. D. (Ed.), *Geological Investigations of the North Pacific*. Mem. Geol. Soc. Am., 126:83–119.

Opdyke, N. D., Glass, B., Hays, J. D., and Foster, J., 1966. A paleomagnetic study of Antarctic deep-sea cores. *Science*, 154:349–357.

Riedel, W. R., and Sanfilippo, A., 1978. Stratigraphy and evolution of tropical Cenozoic radiolarians. *Micropaleontology*, 24:61–96.

Theyer, F., Mato, G. Y., and Hammond, S. R., 1978. Paleomagnetic and geochronologic calibration of latest Oligocene to Pliocene radiolarian events. *Mar. Micropaleontol.*, 3:377–395.

Date of Initial Receipt: 21 February 1984
Date of Acceptance: 20 August 1984

Reprinted from Heath, G. R., Burckle, L. H., et al., 1985
Initial Reports of the Deep Sea Drilling Project, Volume LXXXVI, Washington (U.S. Government Printing Office)

37. MAGNETOBIOCHRONOLOGY OF LATE CRETACEOUS–PALEOGENE AND LATE CENOZOIC PELAGIC SEDIMENTARY SEQUENCES FROM THE NORTHWEST PACIFIC (DEEP SEA DRILLING PROJECT, LEG 86, SITE 577)[1]

Simonetta Monechi, Scripps Institution of Oceanography
Ulrich Bleil, Ruhr-Universität Bochum
and
Jan Backman, University of Stockholm[2]

ABSTRACT

A synthesis of paleomagnetic and calcareous nannofossil stratigraphies for the sedimentary sequences recovered at Deep Sea Drilling Project (DSDP) Site 577 on the Shatsky Rise is presented. Numerical ages are estimated for a series of nannofossil datum levels from the late Maestrichtian to middle Eocene period (~68 to ~52 m.y. ago) and the late Cenozoic (last ~5 m.y.). Absolute age control is obtained on the basis of the revised geomagnetic polarity time scale of Berggren et al. (in press).

The results are compared with various sets of data reported in the literature, in particular to magnetobiochronologies derived from marine sections accessible on land in Italy and from recent DSDP boreholes in the South Atlantic, and with the summary by Berggren et al. (in press). Although a number of minor discrepancies remain to be resolved, the remarkable general agreement of the data validates the basic concept of this approach to the elaboration of a calibrated geologic time scale.

INTRODUCTION

At Site 577 on the Shatsky Rise, fairly complete and undisturbed sedimentary sequences of predominantly nannofossil oozes were recovered using the hydraulic piston corer (HPC), in two adjacent holes (Holes 577 and 577A) (Fig. 1). An upper extended late Cenozoic sequence unconformably overlies middle Eocene to Upper Cretaceous sediments (see site chapters, this volume). High resolution stratigraphy of this material was obtained from paleomagnetic and biostratigraphic analyses (Bleil, this volume; Monechi, this volume). On the basis of these results, this study pursues a number of recent research efforts to elaborate numerical ages for biostratigraphic event zonations.

It is well known that standard radiometric methods have only a very limited application to sediments. For this reason, only a few biostratigraphic datum levels have been dated radiometrically. Moreover, as the majority of these measurements have been made on adjacent magmatic rock bodies, among other problems, there is some uncertainty about the exact stratigraphic relationship to the respective sedimentary unit. On the other hand, paleomagnetic analyses have been very successfully applied to pelagic sediments and used to numerically date biostratigraphic zones and datum levels. For the late Neogene, pioneer work in this field was performed on material recovered by conventional piston coring (e.g., Foster and Opdyke, 1970) and by studies of marine sections exposed on land (e.g., Berggren and Van Couvering, 1974). Theyer and Hammond (1974a, b) correlated magnetostratigraphies with radiolarian zonations to about the base of the Neogene from work on a series of equatorial Pacific piston cores. Late Cretaceous (Alvarez et al., 1977) and Paleogene (Lowrie et al., 1982) magnetobiostratigraphies were established from several sections at Gubbio, Italy. To some extent, however, all these studies were subject to specific constraints. In the pelagic environment they are typically restricted to the Neogene period and to lower accumulation rates because of the limited penetration capacity of conventional piston coring. On the other hand, most marine sections accessible on land have been affected to varying degrees by dissolution or diagenesis, casting some doubt on the accuracy of their paleomagnetic and/or biostratigraphic records.

Until recently, rather sparse contributions to this topic came from work on DSDP materials, since rotary drilling frequently results in limited recovery and extensive disturbance of the penetrated sedimentary columns. With the advent of the HPC system, these problems were drastically reduced although not completely solved. The successful operation of this new tool during several DSDP legs in the South Atlantic has provided a wealth of magnetobiochronologic data (Hsü et al., 1984; Berggren et al., in press). For the first time, the Leg 86 HPC material gives the opportunity for a detailed magnetostratigraphic and biostratigraphic study of the Late Cretaceous, the Cretaceous/Tertiary boundary, and much of the Paleogene period on Pacific deep-sea cores.

MAGNETOBIOSTRATIGRAPHY

From analyses of well preserved calcareous nannofossil assemblages, the positions of the first (FO) and last occurrence (LO) of numerous Cretaceous and Ce-

---

[1] Heath, G. R., Burckle, L. H., et al., *Init. Repts. DSDP*, 86: Washington (U.S. Govt. Printing Office).

[2] Addresses: (Monechi, present address) Dipartimento di Scienze della Terra, Università di Firenze, Via G. La Pira n.4, 50121 Firenze, Italy; (Bleil) Institute für Geophysik, Ruhr-Universität Bochum, Postfach 102148, 4630 Bochum, Federal Republic of Germany; (Backman) Department of Geology, University of Stockholm, Stockholm, Sweden.

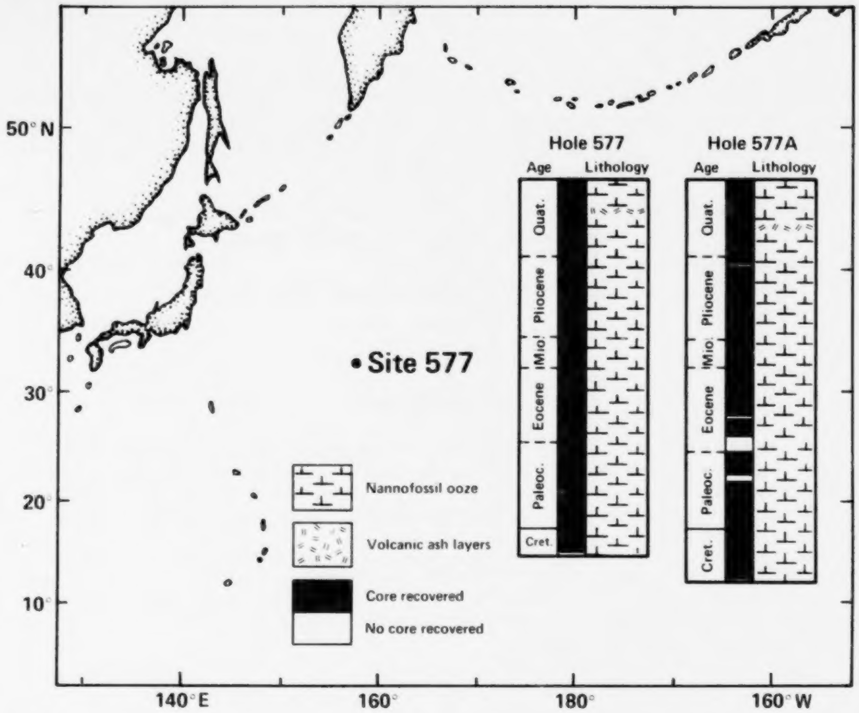

Figure 1. Location of DSDP Site 577 and schematic age, core recovery, and lithostratigraphy of sediments recovered in Holes 577 and 577A using the HPC technique.

nozoic marker events have been recognized in the sedimentary columns recovered at Site 577 in the Northwest Pacific (Monechi, this volume). The coccolith zonation scheme of Bukry (1975) and Okada and Bukry (1980) is used in this chapter.

An almost complete magnetostratigraphy could be established for the entire sequence of Site 577 sediments (Bleil, this volume). The newly revised polarity time scale of Berggren et al. (in press) was used to assign numerical ages to the reversal boundaries. In the late Cenozoic, the series of Earth's magnetic paleofield polarity intervals is specified according to the traditional "epoch" and "event" nomenclature. The pre-Neogene magnetic time units are denoted as "chrons," following the recommendation of the Subcommission on Stratigraphic Classifications (Hedberg et al., 1979). In the terminology developed by Tauxe et al. (1984), a chron extends between the youngest reversal boundaries of a numbered marine magnetic anomaly as defined by Heirtzler et al. (1968) and revised by LaBrecque et al. (1977). The widely used numbering system for the anomaly pattern is thereby incorporated into this magnetostratigraphic time scale and the chron unit distinguished only by prefixing a "C." By its definition, each chron includes not only the time interval of normal polarity corresponding to the respective anomaly number but also the preceding period of reversed polarity (Fig. 2). In order to denote the polarity, the suffix N (normal) or R (reversed) is added. Further subdivision into subchrons is needed where a chron comprises more than one normal or reversed polarity interval, for example, C-23N-2 indicates the second normal period within Chron 23.

A graphical representation of the magneto- and biostratigraphic results for the Cretaceous and Paleogene is given in Figure 2 and for the late Cenozoic in Figure 3. Using the dates of the Berggren et al. (in press) geomagnetic polarity time scale, numerical ages for the nannofossil datum events were determined by interpolation or extrapolation from the reversal boundaries and are presented in Tables 1 and 2, respectively. The paleomagnetic and biostratigraphic studies did not use the same sample set, except in a few cases. Nevertheless, a sample spacing of on average less than 50 cm should introduce small inaccuracies as compared to other potential error sources such as incomplete or disturbed recovery and downhole contamination.

We will discuss the individual datum levels starting with the Cretaceous (i.e., proceeding from the base to the top of the holes). The data are compared to the relevant literature. However, as many of these publications are presently available as preprints, it would be inappropriate to go into complicated arguments about specific discrepancies at this stage. Instead, we simply report the actual findings, which are finally summarized in Table 3.

CRETACEOUS

From the lowest parts of Holes 577 and 577A, 9.7 and 13.0 m, respectively, of Late Cretaceous sediments were

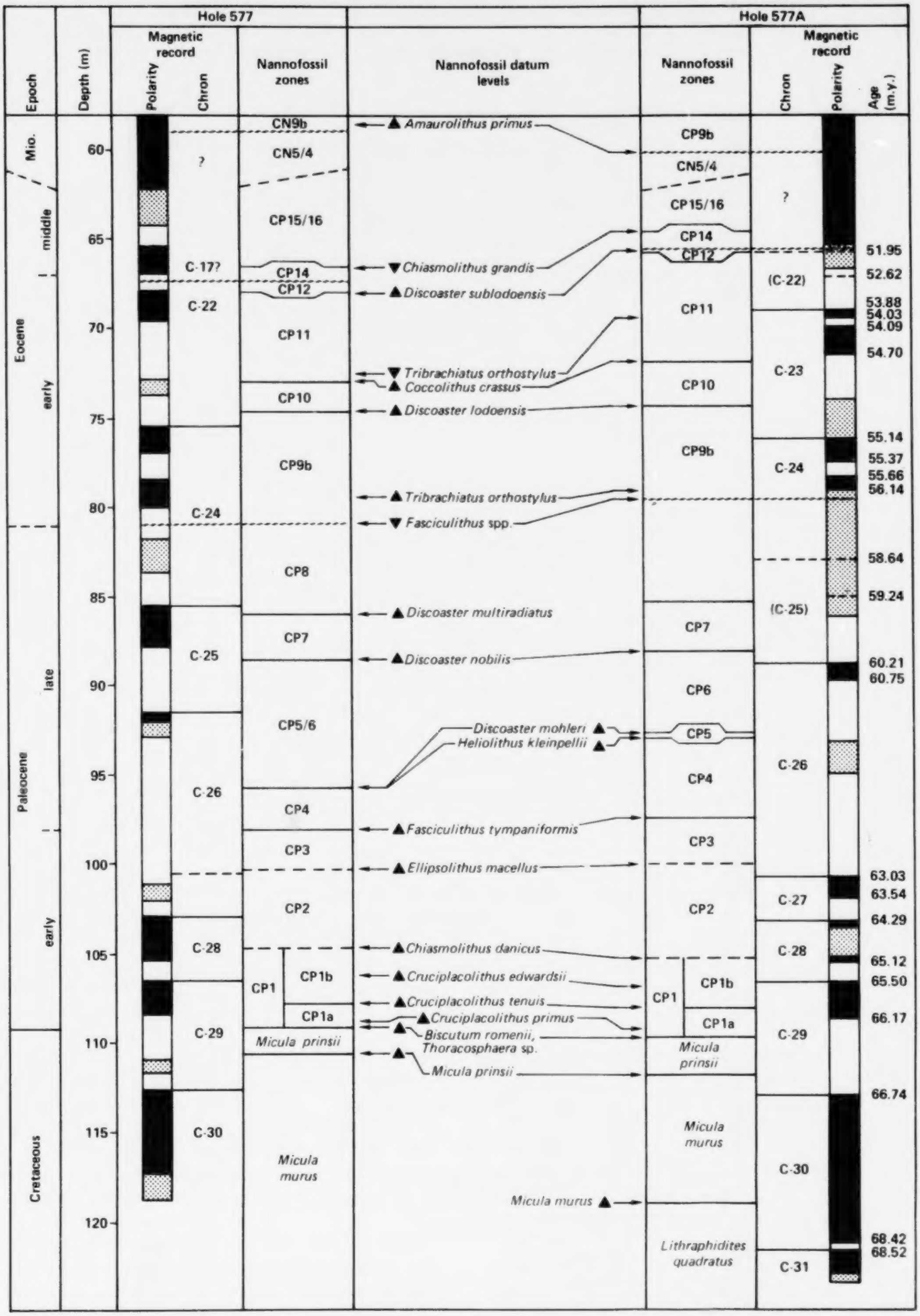

Figure 2. Late Cretaceous–Paleogene nannofossil stratigraphies and magnetostratigraphies in Holes 577 and 577A. Dotted areas in magnetic record refer to gaps in the sample record. The sequence of geomagnetic polarity intervals is defined by the "chron" nomenclature of Tauxe et al. (1984). See caption of Figure 3 for further details.

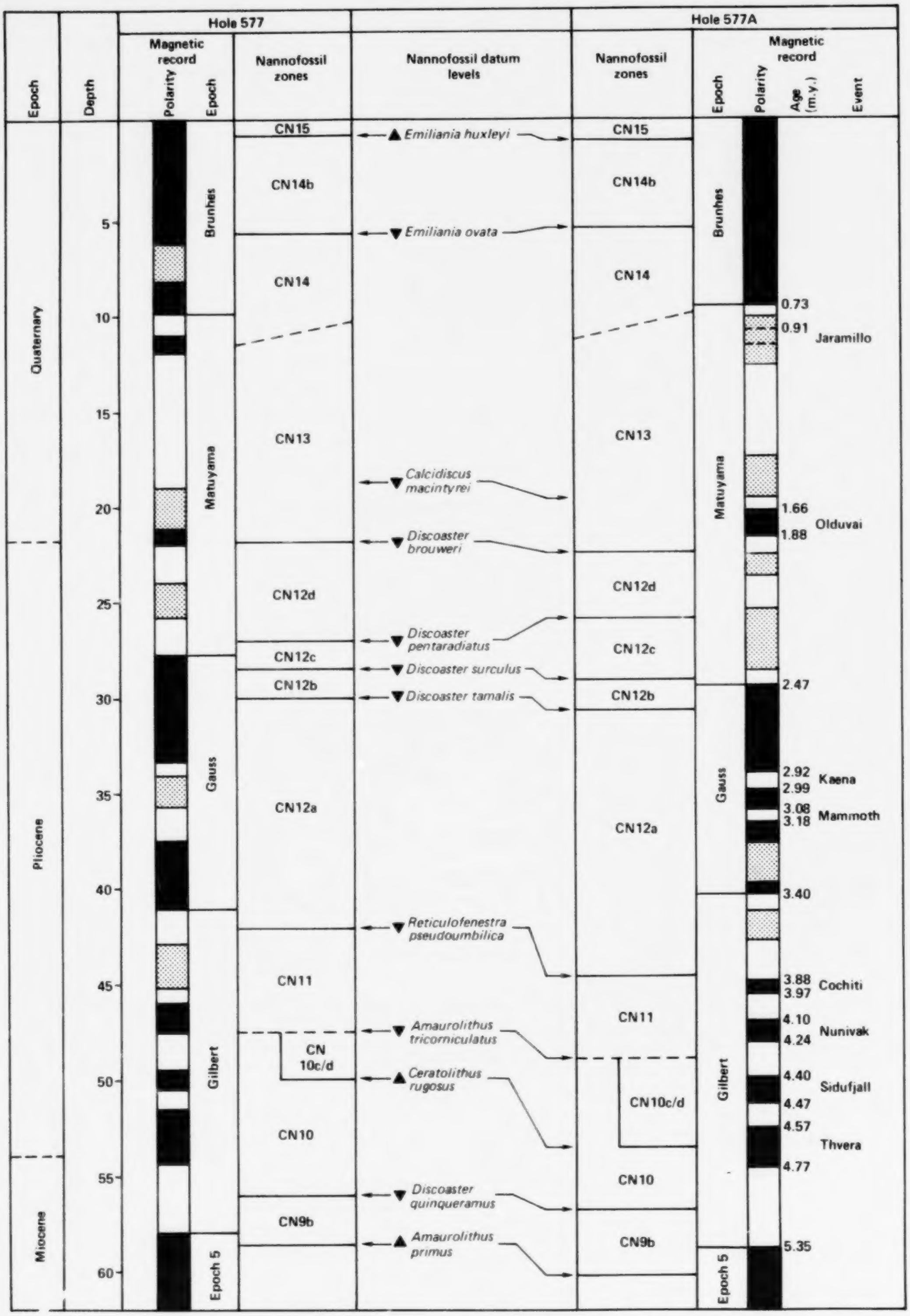

Figure 3. Neogene coccolith stratigraphies and magnetostratigraphies in Holes 577 and 577A. Dotted areas in magnetic record refer to gaps in the sample record. Symbols ▲ and ▼ denote first and last occurrences; calcareous nannofossil zonations according to Bukry (1975) and Okada and Bukry (1980). Black and white sections indicate normal and reversed polarity intervals of the Earth's paleofield configuration. The nomenclature of McDougall (1977) is used for geomagnetic epochs and events, the polarity time scale of Berggren et al. (in press) to assign numerical ages to reversal boundaries. See text for a discussion of alternative interpretations of geomagnetic reversal sequence.

Table 1A. Numerical ages of Paleogene nannofossil events as inferred from the magnetostratigraphic record in Hole 577.

Nannofossil		Sub-bottom depth (m)	Chron	Age (m.y.)	Time basis[a]
Zone	Event				
CP12	FO *Discoaster sublodoensis*	68.00	C-22N	51.97	C-22N
	LO *Tribrachiatus orthostylus*	72.50	?	(53.98)	C-22N
CP11	FO *Coccolithus crassus*	72.91	?	(54.17)	C-22N
CP10	FO *Discoaster lodoensis*	74.60	C-23R-2	55.01	C-24N-1
	FO *Tribrachiatus orthostylus*	79.40	C-24N-2	55.96	C-24N-2
CP8	FO *Discoaster multiradiatus*	86.00	C-25N	58.79	C-25N
CP7	FO *Discoaster nobilis*	88.50	C-25R	59.46	C-25R
CP4	FO *Fasciculithus tympaniformis*	98.00	C-26R	(62.58)	C-28
CP3	FO *Ellipsolithus macellus*	100.20	C-26R	(63.34)	C-28
CP2	FO *Chiasmolithus danicus* s.s.	104.66	C-28N	64.91	C-28N
CP1b	FO *Cruciplacolithus edwardsii*	106.22	C-28R	65.43	C-28R
CP1b	FO *Cruciplacolithus tenuis*	107.86	C-29N	66.00	C-29N
	FO *Cruciplacolithus primus*	108.80	C-29R	66.23	C-29R
	Cretaceous/Tertiary boundary	109.10	C-29R	66.43	C-29N
			C-29R	66.27	C-29R
	FO *Micula prinsii*	110.72	C-29R	66.50	C-29R

Note: Parentheses in age column indicate reduced quality of data.

[a] Magnetostratigraphic data by Bleil (this volume) using the geomagnetic polarity time scale of Berggren et al. (in press).

Table 1B. Numerical ages of Paleogene nannofossil events as inferred from the magnetostratigraphic record in Hole 577A.

Nannofossil		Sub-bottom depth (m)	Chron	Age (m.y.)	Time basis[a]
Zone	Event				
	LO *Tribrachiatus orthostylus*	69.80	C-23R-1	54.06	C-23R-1
CP11	FO *Coccolithus crassus*	71.95	C-23R-2	54.86	C-23R-2
CP10	FO *Discoaster lodoensis*	74.43	(C-23R-2)	(55.02)	C23R-2/C-24N-1
	FO *Tribrachiatus orthostylus*	79.20	(C-24N-2)	(55.90)	C-24R-1
CP7	FO *Discoaster nobilis*	88.10	C-25R	59.72	C-26N
CP6	FO *Discoaster mohleri*	92.78	C-26R	61.12	C-26
CP5	FO *Heliolithus kleinpellii*	93.00	C-26R	61.17	C-26
CP4	FO *Fasciculithus tympaniformis*	97.50	C-26R	62.22	C-26
CP3	FO *Ellipsolithus macellus*	99.80	C-26R	62.76	C-26
CP2	FO *Chiasmolithus danicus* s.s.	105.35	C-28N	65.08	C-28N
CP1b	FO *Cruciplacolithus edwardsii*	106.96	C-29N	65.57	C-29N
CP1b	FO *Cruciplacolithus tenuis*	108.06	C-79N	65.96	C-29N
	FO *Cruciplacolithus primus*	109.31	C-29R	66.25	C-29R
	Cretaceous/Tertiary boundary	109.62	C-29R	66.51	C-29N
				66.29	C-29R
				(66.02)	C-30
	FO *Micula prinsii*	111.86	C-29R	66.58	C-29R
	FO *Micula murus*	120.34	C-30N	68.25	C-30

Note: Parentheses in age column indicate reduced quality of data.

[a] Magnetostratigraphic data by Bleil (this volume) using the geomagnetic polarity time scale of Berggren et al. (in press).

recovered. According to the calcareous nannofossil and planktonic foraminifer stratigraphies, these sediments belong to the Maestrichtian Stage.

Hole 577 ends at 118.80 m below seafloor in the nannofossil *Micula murus* zone within the magnetic Subchron C-30N. At its base, therefore, an age of less than 68.42 m.y. is attained. The C-30/C-29 reversal boundary (66.74 m.y. ago) occurs at 112.60 m.

The lowest magnetic reversal in Hole 577A is recognized at 121.65 m sub-bottom and identified as the C-31/C-30 boundary (68.52 m.y. ago). This also gives a minimum age for the base of the hole at 123.40 m. The C-30R/C-30N (121.18 m; 68.42 m.y. ago) and C-30/C-29 (113.09 m; 66.74 m.y. ago) boundaries allow the interpolation of a numerical age of 68.25 m.y. for the FO of *M. murus* (120.34 m) assuming a constant sedimentation rate of 4.82 m/m.y. in the interval between these two dates. In general, the youngest Cretaceous calcareous nannofossil assemblage characterized by the presence of *M. murus* appears about 1 m.y. before the beginning of the Tertiary (Thierstein, 1982). The best estimate for this time span from the present data would be about 1.5 m.y. Similar to the present result, Monechi and Thierstein (in press) have recognized the *M. murus* zonal boundary in the lower part of C-30N in the Bottaccione section near Gubbio, Italy. At DSDP sites in the South Atlantic it was found either in slightly lower (near the C-30N/C-30R boundary: Leg 73, Hsü et al., 1984) or in higher levels (mid C-30N: Leg 74, Shackleton et al., 1984).

Table 2A. Numerical ages of Neogene nannofossil events as inferred from the magnetostratigraphic record in Hole 577.

Nannofossil			Sub-bottom depth (m)	Magnetostratigraphic position of event		Age (m.y.)	Time basis[a]
Zone		Event		Epoch	Level		
CN15	FO	*Emiliania huxleyi*	0.50	Brunhes	Late Brunhes	(0.04)	Brunhes
CN14b	LO	*Emiliania ovata*	5.75	Brunhes	Mid-Brunhes	(0.43)	Brunhes
	LO	*Calcidiscus macintyrei*	18.66	Matuyama	Mid-Matuyama	1.59	Base of Jaramillo-base of Olduvai
CN13	LO	*Discoaster brouweri*	21.76	Matuyama	Base of Olduvai	1.86	Base of Olduvai-Matuyama/Gauss boundary
CN12d	LO	*Discoaster pentaradiatus*	26.92	Matuyama	Near Matuyama/Gauss boundary	2.39	Base of Olduvai-Matuyama/Gauss boundary
CN12c	LO	*Discoaster surculus*	28.42	Gauss	Near Matuyama/Gauss boundary	2.53	Matuyama/Gauss boundary-top of Kaena
CN12b	LO	*Discoaster tamalis*	29.92	Gauss	Late Gauss	2.65	Matuyama/Gauss boundary-top of Kaena
CN12a	LO	*Reticulofenestra pseudoumbilica*	42.00	Gilbert	Near Gauss/Gilbert boundary	3.55	Gauss/Gilbert boundary-top of Nunivak
CN11	LO	*Amaurolithus tricorniculatus*	47.50	Gilbert	Just below Nunivak	4.24	Base of Nunivak-top of Sidufjall
CN10c	FO	*Ceratolithus rugosus*	49.90	Gilbert	Mid-Sidufjall	4.43	Sidufjall
CN10	LO	*Discoaster quinqueramus*	56.00	Gilbert	Early Gilbert	5.04	Base of Thvera-Gilbert/Epoch 5 boundary
CN9b	FO	*Amaurolithus primus*	58.60	Epoch 5	Near Gilbert/Epoch 5 boundary	5.45	Base of Thvera-Gilbert/Epoch 5 boundary

Note: Parentheses in age column indicate reduced quality of data.

[a] Magnetostratigraphic data by Bleil (this volume) using the geomagnetic polarity time scale of Berggren et al. (in press).

Table 2B. Numerical ages of Neogene nannofossil events as inferred from the magnetostratigraphic record in Hole 577A.

Nannofossil			Sub-bottom depth (m)	Magnetostratigraphic position of event		Age (m.y.)	Time basis[a]
Zone		Event		Epoch	Level		
CN15	FO	*Emiliania huxleyi*	1.00	Brunhes	Late Brunhes	(0.07)	Brunhes
CN14b	LO	*Emiliania ovata*	5.50	Brunhes	Mid-Brunhes	(0.41)	Brunhes
	LO	*Calcidiscus macintyrei*	19.50	Matuyama	Mid-Matuyama	1.58	Brunhes/Matuyama boundary-top of Olduvai
CN13	LO	*Discoaster brouweri*	22.50	Matuyama	Just below Olduvai	1.94	Base of Olduvai-Matuyama/Gauss boundary
CN12d	LO	*Discoaster pentaradiatus*	25.90	Matuyama	Early Matuyama	2.20	Base of Olduvai-Matuyama/Gauss boundary
CN12c	LO	*Discoaster surculus*	29.20	Matuyama	Near Matuyama/Gauss boundary	2.45	Base of Olduvai-Matuyama/Gauss boundary
CN12b	LO	*Discoaster tamalis*	30.70	Gauss	Near Matuyama/Gauss boundary	2.59	Matuyama/Gauss boundary-top of Kaena
CN12a	LO	*Reticulofenestra pseudoumbilica*	44.90	Gilbert	Just above Cochiti	3.87	Gauss/Gilbert boundary-top of Cochiti
CN11	LO	*Amaurolithus tricorniculatus*	49.05	Gilbert	Between Nunivak and Sidufjall	4.32	Base of Nunivak-top of Sidufjall
CN10c	FO	*Ceratolithus rugosus*	53.55	Gilbert	Mid-Thvera	4.67	Thvera
CN10	LO	*Discoaster quinqueramus*	56.90	Gilbert	Early Gilbert	5.09	Base of Thvera-Gilbert/Epoch 5 boundary
CN9b	FO	*Amaurolithus primus*	60.26	Epoch 5	Late Epoch 5	5.54	Base of Thvera-Gilbert/Epoch 5 boundary

[a] Magnetostratigraphic data by Bleil (this volume) using the geomagnetic polarity time scale of Berggren et al. (in press).

CRETACEOUS/TERTIARY BOUNDARY

Based on biostratigraphic evidence, the Cretaceous/Tertiary boundary was identified at 109.10 and 109.62 m depth below seafloor in Holes 577 and 577A, respectively. It is characterized by an abrupt extinction of Mesozoic forms of marine microfauna and microflora, the first appearance of several Tertiary nannofossil taxa (*Biscutum romeinii, Thoracosphaera, Cyclagelosphaera*), and the FO of *Globigerina eugubina*. Details of the calcareous nannofossil stratigraphy are presented in a separate chapter (Monechi, this volume).

In both holes the boundary is located within the interval of reversed magnetic polarity that separates marine magnetic Anomalies 29 and 30, denoted as the C-29R subchron in the presently used nomenclature (Tauxe et al., 1984). Worldwide, the same result was obtained from analyses of various marine sections (Alvarez et al., 1977; Alvarez and Lowrie, 1978; Hsü et al., 1982; Shackleton et al., 1984; Monechi and Thierstein, in press; Thierstein, 1982, and references therein). However, these findings conflict with interpretations of biostratigraphic and magnetostratigraphic studies of the Cretaceous/Tertiary boundary in continental sections (Butler et al., 1977;

Table 3. Late Cretaceous to Eocene numerical ages of nannofossil datum levels for Leg 86, Site 577 as compared to age estimates for Leg 74 (Shackleton et al., 1984), a summary by Berggren et al. (in press) using data from South Atlantic Legs 72–74 and results from marine sections in Italy.[a]

Datum	This chapter (best estimates)	Shackleton et al.	Berggren et al.
FO *Micula murus*	68.3	67.5	—
Cretaceous/Tertiary boundary	66.3–66.5	66.46	—
FO *Cruciplacolithus primus*	66.2	66.1	—
FO *Cruciplacolithus tenuis*	66.0	65.9	65.9
FO *Cruciplacolithus danicus*	65.0	64.9	64.8
FO *Ellipsolithus macellus*	62.8	63.0	62.9
FO *Fasciculithus tympaniformis*	62.2	62.0	62.6
FO *Heliolithus kleinpellii*	61.2	61.6	61.6
FO *Discoaster mohleri*	61.1	60.5	60.4
FO *Discoaster multiradiatus*	58.8	59.0	59.2
LO *Fasciculithus* spp.	57.2	57.6	57.4
FO *Tribrachiatus contortus*	56.3	56.8	—
LO *Tribrachiatus contortus*	56.0	56.3	—
FO *Tribrachiatus orthostylus*	55.9	56.3	56.5
FO *Discoaster lodoensis*	55.0	55.4	55.3
LO *Tribrachiatus orthostylus*	54.1	54.0	54.4
LO *Discoaster sublodoensis*	52.0	51.7	—

[a] All ages listed are determined by interpolation from magnetostratigraphies on the basis of the revised geomagnetic polarity time scale of Berggren et al. (in press).

Lindsay et al., 1981). A detailed discussion of this problem is given by Berggren et al. (in press).

As pointed out by Thierstein (1982), the relative position of the paleontological boundary within the magnetic C-29R subchron is highly variable in different pelagic sequences, indicating major changes in sedimentation rates and/or the possible presence of hiatuses. Similar to the situation in most of these sections, the C-29R subchron is expanded in the sedimentary columns recovered at Site 577 relative to the preceding C-30N and the following C-29N normal polarity subchron. Irrespective of potential inaccuracies resulting from a variable or even discontinuous accumulation at the Cretaceous/Tertiary boundary, a numerical age has been determined for this horizon both by interpolating linearly from the magnetic C-29R boundaries and extrapolating downward using the C-29N boundaries and upward using C-30N (Table 1). The latter calculation was only possible in Hole 577A and yielded an obviously irrelevant datum. The other estimates vary from about 66.3 to 66.5 m.y., in complete agreement with other recent evaluations based on the same time scale (Shackleton et al., 1984).

PALEOGENE

In both holes the FO of *Cruciplacolithus tenuis* (CP1b zonal boundary) falls within the magnetic C-29N subchron; an identical position was found in the South Atlantic DSDP drill holes (Hsü et al,. 1984; Shackleton et al., 1984). The FO of *C. edwardsii* is recorded in the upper part of the same geomagnetic interval in Hole 577, whereas in Hole 577A it is located just above the C-29N/C-28R reversal boundary. The *C. edwardsii* form, characterized by a slightly tilted central cross, has been incorporated here into the *Chiasmolithus danicus* species (Monechi, 1977; Monechi and Thierstein, in press). The FO of *C. danicus* s.s. (Zone CP2) as described by Romein (1979) occurs in the lower part of C-28N in both holes. Again, this agrees with results from the South Atlantic.

The C-27N subchron (marine magnetic Anomaly 27) could only be recognized in the sedimentary column recovered from Hole 577A. In the Hole 577 sequence this interval was presumably lost in between Cores 11 and 12. Furthermore, in places the Core 11 sediments of this hole showed an atypical degree of drilling disturbance. Severe downhole contamination was observed in some intervals, therefore, the nannofossil datum levels and their position relative to magnetostratigraphic boundaries may be of reduced quality here. In the C-26R subchron a series of four marker events was identified in both holes (Fig. 2): FO of *Ellipsolithus macellus* (Zone CP3), FO of *Fasciculithus tympaniformis* (Zone CP4), FO of *Heliolithus kleinpellii* (Zone CP5), and FO of *Discoaster mohleri* (Zone CP6).

E. macellus shows a discontinuous presence in Zones CP3 and CP4. In both the Bottaccione and Contessa profiles near Gubbio, Italy, where this zonal marker is also very rare, its FO was found deeper in the C-28R subchron. This discrepancy is likely to reflect preservational or environmental problems. As in the present case, in the South Atlantic the first appearance level of *E. macellus* was consistently recorded just above the C-27N/C-26R reversal boundary (Berggren et al., in press). These results indicate that the FO of *E. macellus* represents an inaccurate datum event. The FO of *F. tympaniformis* in the lower half of the C-26R subchron coincides reasonably well with all available results from Italy and the South Atlantic.

According to the South Atlantic data summarized by Berggren et al. (in press), the nannofossil Zone CP5 should span about 1.2 m.y. At Site 577 this interval appears to be very compressed. In fact, downhole contamination prevents any detailed conclusions about its stratigraphic distribution. In Hole 577A the FO levels of *H. kleinpellii* and *D. mohleri* are observed in the upper half of C-26R. They are separated by a little more than 20 cm and could be distinguished only on the basis of a very dense sampling around this horizon. In Hole 577 the FO of the two species could not be discriminated.

The lowest occurrence of *H. kleinpellii* in the Contessa and Bottaccione sections is within one of several normal magnetic polarity intervals, which have all been correlated with the marine magnetic Anomaly 26. However, from Leg 74 analyses, Shackleton et al. (1984) have reported a position in the mid C-26R subchron in agreement with the present result. The FO of *D. mohleri* was recorded within the C-26N subchron in the Gubbio sections and in the Leg 74 material, but in the South Atlantic also below the C-26N/C-26R boundary (Legs 72 and 73, see summary by Berggren et al., in press), as now in the Northwest Pacific (Fig. 2).

The FO of *Discoaster nobilis* (Zone CP7) is found in the upper half of the C-25R subchron in Hole 577, in agreement with this datum level in the Contessa profile (Monechi and Thierstein, in press). In Hole 577A it has a position closer to the C-26N/C-26R boundary. The FO of *Discoaster multiradiatus* (Zone CP8) falls within the C-25N subchron (marine magnetic Anomaly 25) in

Hole 577. As Core 9 of Hole 577A has a recovery of only 3.80 m (or 40%) and since the sediments are badly disturbed, we could not identify either the base of the CP8 zone or the C-25N subchron. In all available reports, the base of the CP8 zonal boundary has been found within the C-25N subchron, although there exist some discrepancies as to its exact position within this period of normal polarity.

The LO of *Fasciculithus* that was recorded in the C-24R-2 subchron in the Hole 577 sediments (Core 9/10 transition) agrees with observations in the South Atlantic (Leg 74, Shackleton et al., 1984) and in the Contessa section (Lowrie et al., 1982). This marker level was frequently thought to coincide with the CP8/CP9 nannofossil zonal boundary and therefore to represent the Paleocene/Eocene boundary. However, according to Shackleton et al. (1984), the LO of *Fasciculithus* occurs stratigraphically lower (within Zone CP8) than the FO of *Discoaster diastypus* (top of Zone CP8). In Hole 577 the FO of *Tribrachiatus nunnii/Tribrachiatus contortus* occurs shortly above the LO of *Fasciculithus*, thus corroborating the results of Shackleton et al. (1984). The stratigraphic position for the Paleocene/Eocene boundary between marine magnetic Anomalies 24 and 25 (C-24R-2 subchron) indicated here is the same as in all other analyzed pelagic sections.

The FO of *Tribrachiatus orthostylus* is located in the lower part of the geomagnetic C-24N-2 subchron in Hole 577. The previously mentioned lack of recovery in Core 9 prevented us from successfully correlating its position with the magnetostratigraphic record in Hole 577A. Compared with data from the South Atlantic (DSDP Legs 72 and 73) and Italy (Lowrie et al., 1982; Monechi and Thierstein, in press), the datum level in Hole 577 appears to lie slightly too high since the FO of *T. orthostylus* in the South Atlantic and Italy was always found just below the C-24N-2/C-24R-2 reversal boundary.

The FO of *Discoaster lodoensis* (Zone CP10) is recorded in the reversed magnetic interval following Anomaly 24 (C-23R-2 subchron) in both holes at Site 577. This datum level has been described as occurring in about the same stratigraphic horizon in the Contessa section at Gubbio (Monechi and Thierstein, in press) and in the South Atlantic (Shackleton et al., 1984). According to other reports, however, the FO of *D. lodoensis* is already found in the C-24N-1 subchron (see review by Berggren et al., in press).

The identification of the geomagnetic C-24 chron in the Site 577 sediments is strongly supported by carbon isotope stratigraphy results (Shackleton, this volume). These data further indicate a "hiatus" between Cores 8 and 9 in Hole 577. In fact, a very detailed correlation of the two holes suggests that about 2.6 m of sediments have not been recovered at this level in Hole 577 (see below and Fig. 4).

The base of the nannofossil Zone CP11, as defined by the FO of *Coccolithus crassus*, is situated in the magnetic C-23R-2 subchron in Hole 577A, but was recorded at different levels in normal polarity intervals related to the marine magnetic Anomaly 23 in the Gubbio sections (Monechi and Thierstein, in press). Apparently some dis-

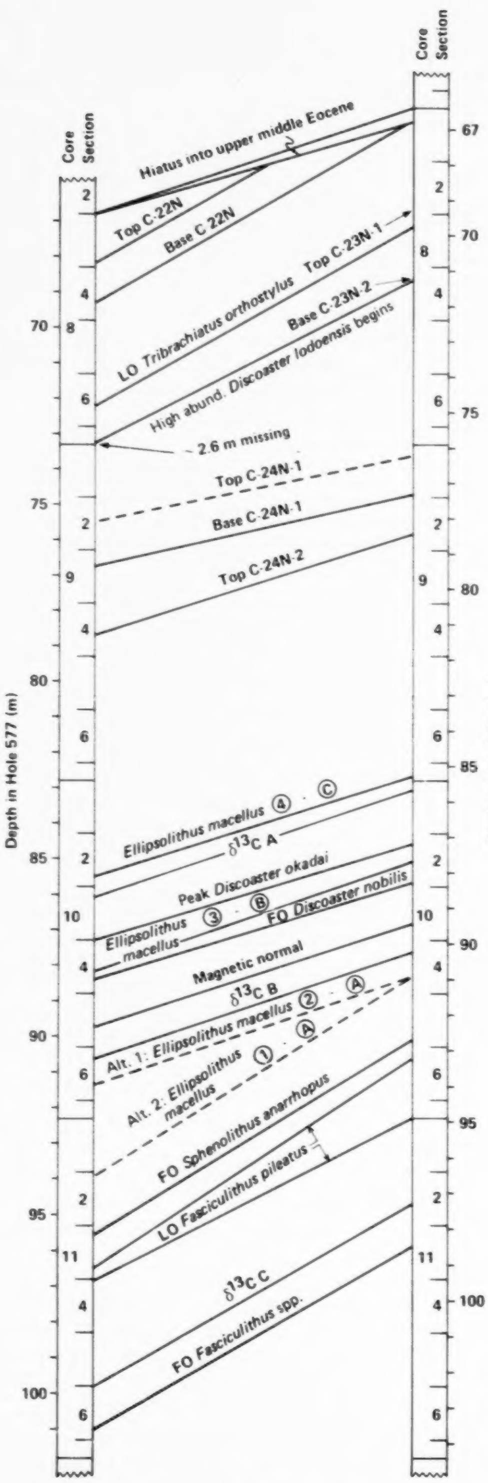
Core
Section
Core
Section
Depth in Hole 577 (m)
Depth in Hole 577A (m)
70
75
80
85
90
95
100
67
70
75
80
85
90
95
100
8
9
10
11
Hiatus into upper middle Eocene
Top C-22N
Base C 22N
Top C-23N-1
LO Tribrachiatus orthostylus
Base C-23N-2
High abund. Discoaster lodoensis begins
~2.6 m missing
Top C-24N-1
Base C-24N-1
Top C-24N-2
Ellipsolithus macellus ④ · ©
δ^{13}C A
Peak Discoaster okadai
Ellipsolithus macellus ③ · Ⓑ
FO Discoaster nobilis
Magnetic normal
δ^{13}C B
Alt. 1: Ellipsolithus macellus ② · Ⓐ
Alt. 2: Ellipsolithus macellus ① · Ⓐ
FO Sphenolithus anarrhopus
LO Fasciculithus pileatus
δ^{13}C C
FO Fasciculithus spp.

Figure 4. Detailed correlations of nannofossil data, geomagnetic reversal boundaries, and carbon isotope data (Shackleton, this volume) in Cores 8 through 11 of Holes 577 and 577A allowing quantification of apparent gaps in core recovery (see text for details).

crepancies also exist regarding the LO of *T. orthostylus*. In Hole 577A this species disappears within the C-23R-1 magnetic subchron, in agreement with results from Leg 74 (Shackleton et al., 1984). Lowrie et al. (1982) reported this datum event in the C-23N-2 subchron in the Contessa section at Gubbio. However, in the same profile Monechi and Thierstein (in press) report a LO for *T. orthostylus* shortly after the C-23/C-22 reversal boundary. The reason for this difference is not known.

The C-22N subchron could only be recognized in Hole 577 and was identified on the basis of the FO of *Discoaster sublodoensis* (base of CP12 zonal boundary), which was reported at this level in the Contessa section in Gubbio (Monechi and Thierstein, in press) and in the South Atlantic (Shackleton et al., 1984).

A hiatus is observed at around 65 m sub-bottom between the CP12 and CP14 nannofossil zones, and a major unconformity separates middle Eocene from late Miocene sediments at around 60 m below seafloor in both holes. Paleomagnetic analyses in this interval yielded no useful results. The correlation of a normal polarity section in Hole 577 to the marine magnetic Anomaly 17 (Fig. 2), therefore, is tentative and only justified because Hsü et al. (1984) have recognized the LO of *Chiasmolithus grandis* in this magnetostratigraphic position in the South Atlantic. In the different Gubbio sections, the LO of *C. grandis* is located within marine magnetic Anomaly 18 (Monechi and Thierstein, in press).

One of us (JB) has made a quantitative nannofossil study of Cores 8 through 11 from Holes 577 and 577A, results which will be presented elsewhere. Nevertheless, we consider it worthwhile to show the resulting correlations between the two holes (Fig. 4). Compared with the present results, the only discrepancies in positions of datum levels are those caused by different sample spacing, implying that consistent taxonomic concepts were applied.

If perfect recoveries had been achieved from the two holes, one would expect, by assuming an identical depositional history, the complete set of correlations of bio-, magneto-, and stable isotope stratigraphy indications to become displayed as parallel lines. Figure 4A shows that lines of correlation are in fact parallel, but also reveals two levels showing imperfect recovery or disturbance. The first occurs between Cores 8 and 9 in Hole 577, where 2.6 m of sediment is missing as indicated by the shift in relative abundance of *D. lodoensis* (J. Backman, unpublished observations).

In Hole 577, the relative abundance of *D. lodoensis* increases by a factor of two between Cores 8 and 9. The corresponding increase in Hole 577A occurs at the base of the C-23N-2 subchron. Referring to this level in the two holes and that indicated by the top of C-24N-1, it becomes obvious that Hole 577 suffers a loss of material in the pertinent interval, presumably at the core boundary. This observation provides a plausible explanation as to why the C-23N subchrons were not identified in Hole 577.

The second level of imperfect recovery or disturbance occurs at the transition between Cores 10 and 11 in Hole 577, which correlates to mid-Core 10 in Hole 577A. Abundance plots of *E. macellus* are of particular importance for the latter problem (Fig. 5). Figure 5 shows that there are two ways of correlating the two holes: alternative one suggests that the uppermost part of Core 11 in Hole 577 is recored, and alternative two suggests that approximately 2.7 m of sediment is missing in mid-Core 10 in Hole 577A. We do not possess any definitive evidence regarding which of these alternatives is the valid one (see also discussion by Shackleton, this volume). This study emphasizes, on one hand, the importance of repeated coring of important sections, evidently the HPC does not necessarily recover the complete section at every deployment. On the other hand, it is clear that detailed biostratigraphy is extremely beneficial.

Finally, it may be of interest to note that the closer spaced sampling intervals in the study of JB revealed the presence of *T. contortus* in Hole 577, Core 9, Section 5, 30–115 cm (4 samples). Rare specimens of *T. nunnii* were also observed in the lowest of these samples. Since members of the genus *Fasciculithus* are abundant up to Sample 577-10-1, 30 cm and not present in Core 9, Section 6, we may conclude that the FO of *T. contortus* and the LO of *Fasciculithus* are separated by not less than 1.5 m of sediment, which in this case probably represents a period of time in excess of 0.2 m.y. (this estimate is based on unpublished work by JB both from Site 577 and Leg 74 material).

NEOGENE

Two interrelated problems characterize the lowest part of the Neogene sequence (Fig. 3, Table 2). The first is that relatively large differences exist in numerical age estimates for two nannofossil datum levels when Hole 577 and Hole 577A are compared, and the other concerns whether the geomagnetic reversal succession is correctly identified. However, the succession of the nannofossil datum events agrees well with all available literature data: FO of *Amaurolithus primus*, LO of *Discoaster quinqueramus*, FO of *Ceratolithus rugosus*, LO of *Amaurolithus tricorniculatus*, and LO of *Reticulofenestra pseudoumbilica*.

Regarding interhole comparisons and age estimates of datum levels, two species are problematic: the FO level of *C. rugosus* and the LO level of *R. pseudoumbilica*. In both holes the LO level of the latter species occurs within the uppermost reversed magnetic interval of the Gilbert Epoch, but the relative positions within this reversed interval give age estimates that differ by approximately 0.3 m.y. Literature data (e.g., Backman and Shackleton, 1983) suggest that the age derived from Hole 577 (3.55 m.y.) represents a more consistent estimate for the *R. pseudoumbilica* extinction event, although our data do not reveal the cause for the older age estimate (3.87 m.y.) obtained from Hole 577A.

The FO level of *C. rugosus* is particularly troublesome since this marker level is associated with different geomagnetic events in the two holes and therefore causes an uncertainty as to the correct identification of the geomagnetic reversal sequence. A difference in age estimate of more than 0.2 m.y. is evident, and our data do not reveal the cause for this discrepancy.

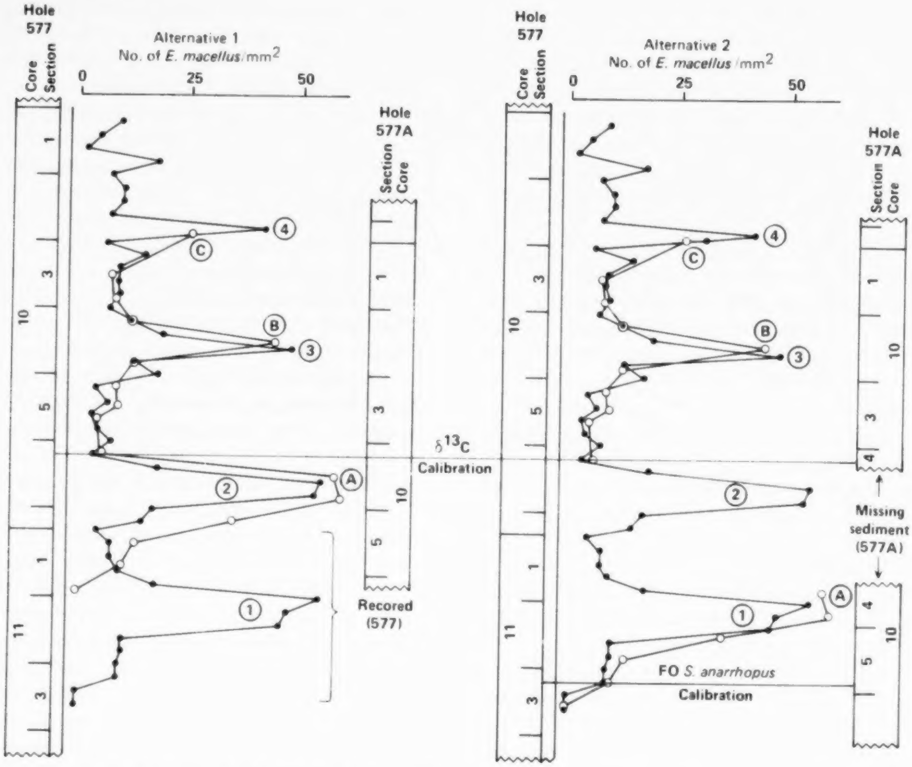

Figure 5. Plots of relative abundance variations of *E. macellus* in Holes 577 (●) and 577A (○). The $\delta^{13}C$ calibration is from Shackleton (this volume) and the *Sphenolithus anarrhopus* calibration is from Backman (unpublished). See text for discussion of these results.

Previous data from the Pacific Ocean (Gartner, 1973; Backman and Shackleton, 1983) and from the South Atlantic (Hsü et al., 1984) unequivocally indicate that the FO level of *C. rugosus* occurs within the lowest normal event (Thvera) of the reversed Gilbert Epoch. Furthermore, according to literature data (Gartner, 1973; Hsü et al., 1984), the LO of *D. quinqueramus* occurs in mid-Epoch 5, within a reversed polarity event separating the two normals of this geomagnetic time unit. Our interpretation places the LO of *D. quinqueramus* higher in the geomagnetic reversal sequence (Fig. 3), in the lowest reversed interval of the Gilbert Epoch. Consequently, the interpretation of the lower Gilbert and Epoch 5 (Fig. 3) must be considered as tentative. Several other interpretations are possible and we would like briefly to discuss two of these, which may be regarded to be as tenable as the one shown in Figure 3.

If referring to Hole 577 and assuming that the FO level of *C. rugosus* is correct in this hole and associated with the Thvera Event, it follows (1) that the LO level of *D. quinqueramus* indeed has a position in mid-Epoch 5, in accord with literature data (see above) and (2) that our interpretation of the geomagnetic reversal sequences is erroneous.

If referring to Hole 577A and assuming that the FO level of *C. rugosus* is correct in this hole and associated with the Thvera Event, we can either conclude that the LO level of *D. quinqueramus* occurs stratigraphically higher than recorded from other areas, or that a hiatus encompassing the upper half of Epoch 5 and the lowest part of the Gilbert Epoch is present between the LO level of *D. quinqueramus* and the base of the Thvera Event.

There are quite a number of disturbed or unrecovered intervals in the uppermost parts of Holes 577 and 577A; however, only very minor inconsistencies in the correlations of nannofossil datum levels with the magnetostratigraphies are observed in the geomagnetic Gauss, Matuyama, and Brunhes epochs (Fig. 3, Table 2). Results obtained from the LO levels of *Discoaster tamalis, D. pentaradiatus, D. brouweri, Calcidiscus macintyrei*, and *Emiliania ovata* as well as for the FO of *E. huxleyi* are all in reasonable agreement with various data from the literature (Haq et al., 1977; Gartner, 1977; Backman and Shackleton, 1983; Hsü et al., 1984).

Because of the absence of generally accepted calcareous nannofossil criteria to correlate with geologic boundaries in the late Cenozoic, we have not discussed this topic in this chapter.

CONCLUSIONS

The magnetobiochronology derived from paleomagnetic and calcareous nannofossil stratigraphic analyses of sedimentary sequences recovered at Site 577 in the Northwest Pacific reveals a remarkable consistency with DSDP data sets from recent South Atlantic legs and with results obtained from marine sections in Italy. Calibrated on the same geomagnetic polarity time scale deduced from oceanic anomaly lineations, the differences in numerical ages of individual nannofossil datum events are typically less than 0.5 m.y. in the Late Cretaceous and Paleogene. Despite these positive correlations, the presently available data do not yet allow any conclusive interpretations in terms of global synchroneity or regional differentiations in evolutionary patterns for this period. Although the HPC technique has greatly improved the quality of materials retrieved by DSDP, the stratigraphic duplication in the adjacent holes at Site 577 still resulted in almost the same amount of mutual discrepancies in the two magnetobiochronologies as their comparison to distant areas in the South Atlantic or Mediterranean.

ACKNOWLEDGMENTS

We thank A. Wright, N. J. Shackleton, and W. A. Berggren for their constructive criticism. The financial support by the Deutsche Forschungsgemeinschaft (UB), by Naturvetenskapliga forskningsrådet (JB), and by CNR Centro Studi per la Geologia dell'Appennino e delle Catene Perimediterranee (Publ. 148) and MPI (SM) is gratefully acknowledged.

REFERENCES

Alvarez, W., Arthur, M. S., Fischer, A. F., Lowrie, W., Napoleone, G., Premoli-Silva, I., and Roggenthen, W. M., 1977. Type section for the Late Cretaceous-Paleocene geomagnetic reversal time scale. *Geol. Soc. Am. Bull.*, 88:383-389.

Alvarez, W., and Lowrie, W., 1978. Upper Cretaceous paleomagnetic stratigraphy at Moria (Umbrian Apennines, Italy): Verification of the Gubbio section. *Geophys. J. R. Astron. Soc.*, 55:1-17.

Backman, J., and Shackleton, N. J., 1983. Quantitative biochronology of Pliocene and early Pleistocene calcareous nannofossils from the Atlantic, Indian and Pacific oceans. *Mar. Micropaleontol.*, 8: 141-170.

Berggren, W. A., Kent, D. V., and Flynn, J. J., in press. Paleogene geochronology and chronostratigraphy. *In* Snelling, N. J. (Ed.), *Geochronology and the Geological Record*. Spec. Publ. Geol. Soc. London.

Berggren, W. A., and Van Couvering, J. A., 1974. The Late Neogene. *Palaeogeogr., Palaeoclimatol., Palaeoecol.*, 16:1-216.

Bukry, D., 1975. Coccolith and silicoflagellate stratigraphy, northwestern Pacific Ocean, Deep Sea Drilling Project Leg 32. *In* Larson, R. L., Moberly, R., et al., *Init. Repts. DSDP*, 32: Washington (U.S. Govt. Printing Office), 677-702.

Butler, R. F., Lindsay, E. H., Jacobs, L. L., and Johnson, N. M., 1977. Magnetostratigraphy of the Cretaceous-Tertiary boundary in the San Juan Basin, New Mexico. *Nature (London)*, 267:318-323.

Foster, J. M., and Opdyke, N. D., 1970. Upper Miocene to Recent magnetic stratigraphy in deep-sea sediments. *J. Geophys. Res.*, 75: 4465-4473.

Gartner, S., 1973. Absolute chronology of the late Neogene calcareous nannofossil succession in the Equatorial Pacific. *Geol. Soc. Am. Bull.*, 84:2021-2034.

________, 1977. Calcareous nannofossil stratigraphy and revised zonation of the Pleistocene. *Marine Micropaleontol.*, 2:1-25.

Haq, B. U., Berggren, W. A., and Van Couvering, J. A., 1977. Corrected age of the Pliocene/Pleistocene boundary. *Nature (London)*, 269:483-488.

Hedberg, H. D., Salvador, A., and Opdyke, N. D., 1979. Magnetostratigraphic polarity units—A supplementary chapter of the ISSC International Stratigraphic Guide. *Geology*, 7:578-583.

Heirtzler, J. R., Dickson, G. O., Herron, E. M., Pitman, W. C., III, and LePichon, X., 1968. Marine magnetic anomalies, geomagnetic field reversals and motions of the ocean floor and continents. *J. Geophys. Res.*, 73:2119-2136.

Hsü, K. J., He, Q., McKenzie, J. A., Weissert, H., Perch-Nielsen, K., Oberhänsli, H., Kelts, K., LaBrecque, J., Tauxe, L., Krähenbühl, U., Percival, S. F., Jr., Wright, R., Karpoff, A. M., Petersen, N., Tucker, P., Poore, R. Z., Gombos, A. M., Pisciotto, K., Carman, M. F., Jr., and Schreiber, E., 1982. Mass mortality and its environmental and evolutionary consequences. *Science*, 216:249-256.

Hsü, K. J., Percival, S. F., Wright, R. C., and Petersen, N., 1984. Numerical ages of magnetostratigraphically calibrated biostratigraphic zones. *In* Hsü, K. J., LaBrecque, J. L., et al., *Init. Repts. DSDP*, 73: Washington (U.S. Govt. Printing Office), 623-636.

LaBrecque, J., Kent, D. V., and Cande, S. C., 1977. Revised magnetic polarity time scale for Late Cretaceous and Cenozoic time. *Geology*, 5:330-335.

Lindsay E. H., Butler, R. F., and Johnson, N. M., 1981. Magnetic polarity zonation and biostratigraphy of Late Cretaceous and Paleocene continental deposits, San Juan Basin, New Mexico. *Am. J. Sci.*, 282:390-435.

Lowrie, W., Alvarez, W., Napoleone, G., Perch-Nielsen, K., Premoli-Silva, I., and Toumarkine, M., 1982. Paleogene magnetic stratigraphy in Umbrian pelagic carbonate rocks: The Contessa sections, Gubbio. *Geol. Soc. Am. Bull.*, 93:414-432.

McDougall, I., 1977. The present status of the geomagnetic polarity time scale. Research School of Earth Sciences, A.N.U., Publ. No. 1288.

Monechi, S., 1977. Upper Cretaceous and Early Tertiary nannoplankton from the Scaglia Umbra Formation (Gubbio, Italy). *Riv. Ital. Paleont.*, 83:759-802.

Monechi, S., and Thierstein, H. R., in press. Late Cretaceous-Paleogene nannofossil and magneto-stratigraphic correlation in the Umbrian Apennines. *Mar. Micropaleontol.*

Okada, H., and Bukry, D., 1980. Supplementary modification and introduction of code numbers to the low-latitude coccolith biostratigraphic zonation (Bukry, 1973, 1975). *Mar. Micropaleontol.*, 5: 321-325.

Romein, A. J. T., 1979. Lineages in Early Paleogene calcareous nannoplankton. *Utrecht Micropal. Bull.*, 22:1-231.

Shackleton, N. J. and Members of the Shipboard Scientific Party, 1984. Accumulation rates in Leg 74 sediments. *In* Moore, T. C., Jr., Rabinowitz, P. D., et al., *Init. Repts. DSDP*, 74: Washington (U.S. Govt. Printing Office), 621-644.

Tauxe, L., Tucker, P., Petersen, N. P., and LaBrecque, J. L., 1984. Magnetostratigraphy of Leg 73 sediments. *In* Hsü, K. J., LaBrecque, J. L., et al., *Init. Repts. DSDP*, 73: Washington (U.S. Govt. Printing Office), 609-621.

Theyer, F., and Hammond, S. R., 1974a. Cenozoic magnetic time scale in deep sea cores: Completion of the Neogene. *Geology*, 2: 487-492.

________, 1974b. Paleomagnetic polarity sequence and radiolarian zones, Brunhes to Epoch 20. *Earth Planet. Sci. Lett.*, 22:307-319.

Thierstein, H. R., 1982. Terminal Cretaceous plankton extinctions: A critical assessment. *Spec. Pap. Geol. Soc. Am.*, 190:385-399.

Date of Initial Receipt: 12 December 1983
Date of Acceptance: 20 July 1984

Reprinted from Heath, G. R., Burckle, L. H., et al., 1985
Initial Reports of the Deep Sea Drilling Project, Volume LXXXVI, Washington (U.S. Government Printing Office)

38. SUMMARY OF CRETACEOUS/TERTIARY BOUNDARY STUDIES, DEEP SEA DRILLING PROJECT SITE 577, SHATSKY RISE[1]

Audrey A. Wright, Ulrich Bleil, Simonetta Monechi, Helen V. Michel, N. J. Shackleton, Bernd R. T. Simoneit, and James C. Zachos[2]

ABSTRACT

Continuous, expanded, and undisturbed Cretaceous/Tertiary boundary sequences were recovered in three holes drilled at Deep Sea Drilling Project Site 577 (32°26.51′N, 157°43.40′E) on Shatsky Rise. The Cretaceous/Tertiary boundary lies at a sub-bottom depth of approximately 109.6 m in a white calcareous ooze. It was identified biostratigraphically within the magnetic C-29R subchron using nannofossils and is characterized by an iridium anomaly of 61 ng/cm^2 and a sharp 1% decrease in ^{13}C. Limited organic geochemical samples suggest that molecular stratigraphy cannot be applied definitively across the boundary.

INTRODUCTION

Deep Sea Drilling Project (DSDP) Site 577 is located at 32°26.51′N and 157°43.40′E in 2678 m of water on the flank of the Shatsky Rise, close to DSDP Site 47 (Fig. 1). Primary drilling objectives at Site 577 were to obtain a detailed paleoceanographic record for the western edge of the subtropical gyre during the late Neogene Period, to establish a high-resolution stratigraphy for the Neogene and Quaternary periods using paleomagnetics, stable isotopes, and biostratigraphy, and to recover the Cretaceous/Tertiary boundary for midlatitude calcareous biostratigraphic, paleomagnetic, and geochemical studies. Three holes were hydraulically piston cored at Site 577; two of them penetrated Quaternary to Upper Cretaceous sediments (Holes 577 and 577A) including Cretaceous/Tertiary boundary sequences. The third hole was washed to basal Paleocene sediments and a third Cretaceous/Tertiary boundary sequence was recovered, providing enough material for all the scientific studies of the boundary that were planned.

This summary chapter briefly details the primary results of shipboard and shore-based studies of the Site 577 Cretaceous/Tertiary boundary sequences. Other Site 577 results from shipboard investigations are given in the Site 577 chapter (this volume). Site 577 shore-based studies not focused on the Cretaceous/Tertiary boundary sequence include radiolarian biostratigraphy (Morley, this volume), diatom biostratigraphy (Koizumi and Tanimura, this volume), heat flow and thermal conductivity (Horai and Von Herzen, this volume), physical and geotechnical properties (Schultheiss, this volume), and interstitial water chemistry (McDuff, this volume).

Site 577 Lithostratigraphy

All of the sediments recovered at Site 577 are lightly mottled nannofossil oozes (Fig. 1), divided into three lithologic units on the basis of color variations.

Lithologic Unit I (0–53.5 m sub-bottom) is a white to light gray nannofossil ooze. It is divided into two subunits on the basis of a downcore decrease in the percentage of foraminifers, radiolarians, and diatoms. The upper subunit contains 60–95% nannofossils, with common foraminifers (0–20%) and rare radiolarians (0–7%) and diatoms (0–3%). The lower subunit contains 90–97% nannofossils, only a few percent foraminifers, and traces of radiolarians and diatoms.

Lithologic Unit II (53.5–111.9 m sub-bottom) is a white to pale brown nannofossil ooze. It is divided into two subunits, the upper one being pale brown in color and containing 80–90% nannofossils and only trace amounts of foraminifers. The lower subunit is characterized by alternating white and pale brown colors, 65–95% nannofossils, and 0–35% foraminifers.

Lithologic Unit III (111.9–123.4 m sub-bottom) is a white calcareous nannofossil ooze containing 80–90% nannofossils.

An undisturbed Cretaceous/Tertiary boundary has been located at a sub-bottom depth of 109.10 m in Hole 577 and 109.62 m in Holes 577A and 577B, in all cases within the lower subunit of Lithologic Unit II. Except for a minor color change from a Maestrichtian white to a Tertiary light brown calcareous ooze, the Cretaceous/Tertiary boundary sediments are essentially featureless with no signs of sedimentation disruption (see frontispiece, this volume).

BIOSTRATIGRAPHY OF THE CRETACEOUS/TERTIARY BOUNDARY

Sediments recovered throughout Site 577 are rich in calcareous microfossils that provide a high-resolution late Cenozoic, Paleogene, and Upper Cretaceous biostratigraphy. Site 577 nannofossil stratigraphy is detailed in Monechi (this volume); results from the Cretaceous and lower Paleogene section close to the Cretaceous/Tertiary

---

[1] Heath, G. R., Burckle, L. H., et al., *Init. Repts. DSDP*, 86: Washington (U.S. Govt. Printing Office).

[2] Addresses: (Wright) Ocean Drilling Program, Texas A&M University, College Station, TX 77843; (Bleil) Institut für Geophysik, Ruhr-Universität Bochum, Postfach 102148, D-4630 Bochum, Federal Republic of Germany; (Monechi) Dipartimento di Scienze della Terra, Università di Firenze, Via G. La Pira n. 4, 50121 Firenze, Italy; (Michel) Lawrence Berkeley Laboratory, University of California at Berkeley, Berkeley, CA 94720; (Shackleton) University of Cambridge, Godwin Laboratory for Quaternary Research, Free School Lane, Cambridge CB2 3RS, England; (Simoneit) College of Oceanography, Oregon State University, Corvallis, OR 97331; (Zachos) Graduate School of Oceanography, University of Rhode Island, Kingston, RI 02882.

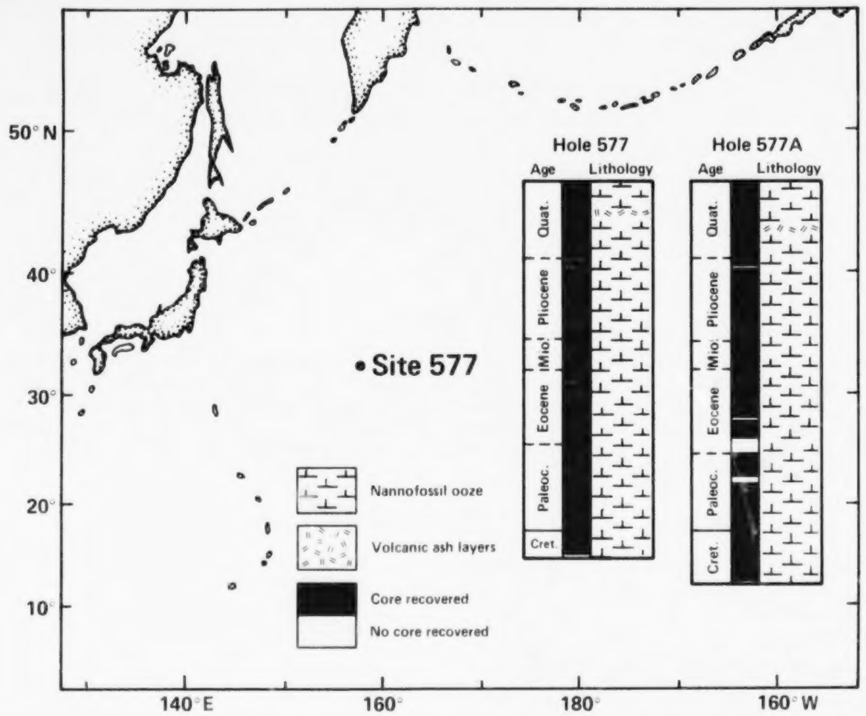

Figure 1. Location of Site 577 on the Shatsky Rise and generalized age, core recovery, and lithology of the sediments recovered in Holes 577 and 577A (from Monechi et al., this volume).

boundary are summarized below. All sediments recovered below Cores 577-6 and 577A-6 are barren of radiolarians and diatoms (Morley, this volume; Koizumi and Tanimura, this volume).

Nannofossils

The Upper Cretaceous (Maestrichtian) section at Site 577 is characterized by a rich nannofossil assemblage. The *Micula prinsii, M. murus*, and *Lithraphidites quadratus* zones were recognized, the latter penetrated only at Hole 577A (Fig. 2). Preservation of Cretaceous nannofossils is moderate and becomes poor in the very early Paleogene; calcareous nannofossils are considerably overgrown near the Cretaceous/Tertiary boundary. No significant changes in relative abundances of the Cretaceous taxa were observed from the *L. quadratus* Zone up to the boundary.

The Cretaceous/Tertiary boundary is located at Sample 577-12-5, 130 cm, Sample 577A-12-4, 72 cm, and Sample 577B-1-4, 72 cm (Fig. 2). The boundary is defined in terms of calcareous nannofossils by the first occurrence of *Thoracosphaera*, a calcareous dinoflagellate, which occurs just at the bottom of the lithologic color change that marks the boundary. The rapid increase in frequency of *Thoracosphaera* occurs simultaneously with the first occurrence of small *Biscutum* such as *B. romeinii* and the extinction of most Mesozoic nannofossils. At Site 577, rare species of *Thoracosphaera* appear sporadically in the topmost Upper Cretaceous samples, about 5 cm below the Cretaceous/Tertiary boundary. Almost complete substitution (90–95%) of the Mesozoic forms by Tertiary ones occurs about 10 cm above the Cretaceous/Tertiary boundary. In this interval, the assemblage is characterized by *Thoracosphaera*, small *Biscutum*, and foraminiferal debris.

The Paleogene *Cruciplacolithus primus* (CP1a) and the *C. tenuis* (CP1b) subzones are recognized at all three holes drilled at Site 577 (Fig. 2). Reworked Cretaceous nannofossils are rare in the upper part of the *C. primus* Subzone, but become more abundant downward and dominate the Tertiary species in the samples just above the Cretaceous/Tertiary boundary.

Planktonic Foraminifers

Only very preliminary results from shipboard study of foraminifers contained in core-catcher samples were available at the time of this writing (Site 577 chapter, this volume), and those results are not adequate to carefully characterize the Cretaceous/Tertiary boundary. The first occurrence of *Globigerina eugubina* is located at the Cretaceous/Tertiary boundary (Monechi et al., this volume). Common to abundant foraminifer fragments occur immediately below the appearance of *Thoracosphaera*, which is a characteristic feature of Cretaceous/Tertiary boundary sequences (Monechi, this volume). These fragments decrease and almost disappear about 40 cm above the boundary.

MAGNETOSTRATIGRAPHY OF THE CRETACEOUS/TERTIARY BOUNDARY

Paleomagnetic results obtained from Holes 577 and 577A are detailed in Bleil (this volume). Because magnetic intensities of the Paleogene and Cretaceous section were near the noise level of the shipboard spinner magnetometer, the results summarized here are based entirely on shore-based study with a cryogenic magnetometer. These results are synthesized with Site 577 calcareous nannofossil stratigraphic results and compared with results from other marine sections and DSDP data sets from recent South Atlantic legs in Monechi et al. (this volume).

Biostratigraphic and stable-isotope stratigraphic control facilitated correlation of the downhole magnetic reversal patterns with the recently revised geomagnetic polarity time scale of Berggren et al. (in press). Virtually complete reversal sequences were identified ending in the latest Cretaceous C-30N subchron and C-31N subchron at Holes 577 and 577A, respectively. In the vicinity of the Cretaceous/Tertiary boundary, the C-27N normal polarity subchron could not be recognized in Hole 577 (Fig. 2), presumably because of loss of material between Cores 577-11 and -12 or drilling disturbance in Core 577-11.

The Cretaceous/Tertiary boundary in both Holes 577 and 577A is located within the C-29R subchron, the interval of reversed polarity that separates marine magnetic Anomalies 29 and 30 (Fig. 2), and is expanded relative to the preceding C-30N and the following C-29N normal polarity subchrons. These results are in agreement with those obtained at various other marine sections (Alvarez et al., 1977; Alvarez and Lowrie, 1978; Hsü et al., 1982; Shackleton et al., in press; Thierstein, 1982). A numerical age determined for the Cretaceous/Tertiary boundary by interpolation from the magnetic C-29R boundaries and by extrapolating downward using the C29-N and upward using the C-30N boundaries varies between about 66.3 and 66.5 m.y., in agreement with other recent estimates using the same time scale (Berggren et al., in press; Shackleton et al., in press).

Based on paleomagnetic results, average sedimentation rates during the Late Cretaceous were 4.8 m/m.y. The sedimentation rate increased to about 7.6 m/m.y. in the Hole 577 and 577A C-29R subchrons that contain the Cretaceous/Tertiary boundary. Paleocene sedimentation rates averaged about 3 m/m.y.

IRIDIUM ANOMALY AT THE CRETACEOUS/TERTIARY BOUNDARY

Samples from Hole 577B were collected to measure iridium levels across the Cretaceous/Tertiary boundary by neutron-activation analysis. The sampling, analysis methods, and detailed results are given in Michel et al. (this volume). A major Ir anomaly of 61 ng/cm^2 occurs at the same level as the Cretaceous/Tertiary boundary defined biostratigraphically by nannofossils (Fig. 2), comparable to the average anomaly (50 ng/cm^2) observed at other Cretaceous/Tertiary boundaries (Alvarez et al., 1982).

Five smaller anomalies occur at Sample 577B-1-5, 120–121 cm, Sample 577B-1-4, 110–111 cm, Sample 577B-1-4, 81–83 cm, Sample 577B-1-4, 77–78 cm, and Samples 577B-1-1, 10 cm to 577B-1-2, 121 cm (Fig. 2; see also fig. 1 of Michel et al., this volume). The two smaller anomaly peaks observed in Section 5 and Sections 1 through 2 are probably related to changes in the $CaCO_3$ deposition rate; the two peaks closest to the main peak may be perturbations of that peak possibly caused by bioturbation; the final small peak in Section 4 remains unexplained, although it may have resulted from contamination of the samples or another extraterrestrial impact (Davis et al., 1984; Whitmire and Jackson, 1984). Resampling of the Cretaceous/Tertiary boundary interval is necessary to differentiate between these possibilities.

OXYGEN- AND CARBON-ISOTOPE RESULTS

Oxygen- and carbon-isotope data from Site 577 are available from two sources: (1) bulk fraction oxygen and carbon-isotope data from the Paleocene section above the Cretaceous/Tertiary boundary in both Holes 577 and 577A in Shackleton et al. (this volume) and (2) Hole 577 fine fraction and benthic foraminifer oxygen- and carbon-isotope data across the Cretaceous/Tertiary boundary in Zachos et al. (this volume).

Although the Shackleton et al. study was originally undertaken to examine the anomalously positive Paleocene ^{13}C event, the detailed carbon-isotope stratigraphy obtained proved useful in making accurate stratigraphic correlations between Holes 577 and 577A. Comparison of carbon-isotope, nannofossil, and paleomagnetic stratigraphies at Holes 577 and 577A allowed adjustment of the sub-bottom depths of the top and bottom of the cored intervals, so that the adjusted depths of these data agree between both holes. Depths plotted in Figure 2 are drilled (unadjusted) depths; control points for adjusting core depths are given in Shackleton et al. (this volume) and may be useful in plotting results from future Site 577 studies.

The Shackleton et al. study suggests that the ^{13}C Paleocene event may represent compensation for the global extinctions and drop in productivity observed at the Cretaceous/Tertiary boundary, because these led to an increased nutrient level in the oceans and burial rate of organic matter. In addition, close similarity between the carbon-isotope records at Sites 577 and 527 (South Atlantic Ocean) suggests that it may be possible to develop a standard ^{13}C record for the Cenozoic that would have worldwide stratigraphic value, perhaps with a resolution better than that available from biostratigraphic methods.

The high-resolution stable-isotope and geochemical study completed by Zachos et al. (this volume) across the Cretaceous/Tertiary boundary at Holes 577 and 47.2 was aimed at evaluating changes in carbonate preservation affecting the stable-isotope signals from calcareous plankton and paleoceanographic changes that may have occurred at the boundary. Oxygen-isotope values of Hole 577 carbonate fine-fraction (<63 μm) samples show only minor fluctuations in the Cretaceous *Micula murus* Zone averaging $-1.0 \pm 0.5‰$, increase slightly near the Cretaceous/Tertiary boundary, and fluctuate between $-1.45‰$ and $-0.16‰$ in the early Paleocene Epoch (Fig. 2). This relatively minor enrichment of ^{18}O at the Cretaceous/Tertiary boundary may be a result of improved microfaunal preservation rather than a decrease in surface water temperature; even if the enrichment is a result of a temperature decrease in the North Pacific

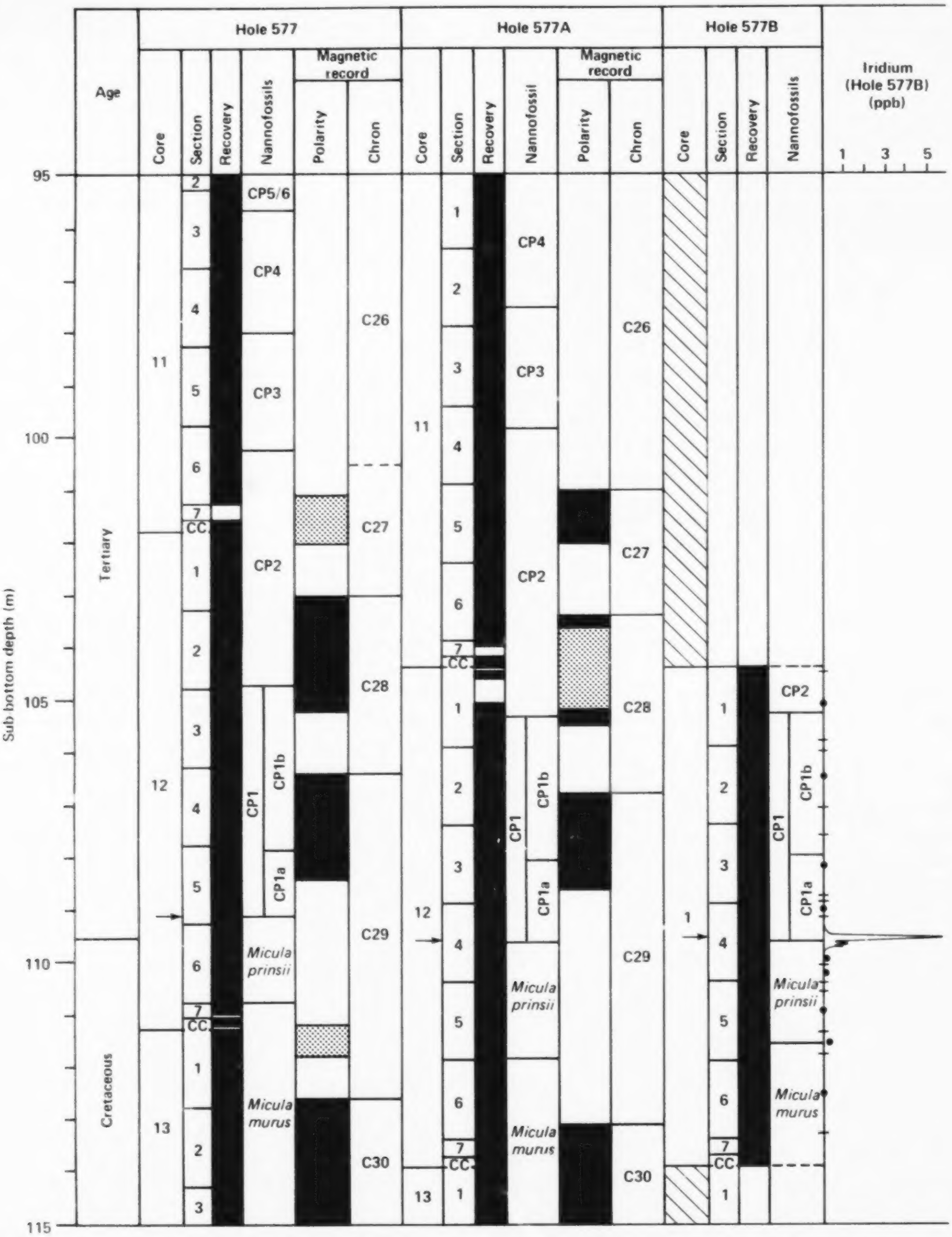

Figure 2. Summary diagram of Hole 577, 577A, and 577B age, cores, recovery, nannofossil stratigraphy, magnetostratigraphy, iridium, bulk fraction and fine fraction ^{18}O and ^{13}C stable isotopes, calcium-carbonate percentages, and lipid geochemistry data versus sub-bottom depth near the Cretaceous/Tertiary boundary (95–115 m sub-bottom). All data are plotted versus unadjusted depths (see Shackleton et al., this volume for adjusted depth explanation and control points). Dotted areas in magnetic record refer to gaps in the sample record (Monechi et al., this volume). Nannofossil stratigraphy is from Monechi (this volume). Magnetostratigraphy is given in Bleil (this volume) and Monechi et al. (this volume). Iridium data are from Michel et al. (this volume). Bulk-fraction stable-isotope data are from Shackleton et al. (this volume); fine-fraction stable-isotope data are from Zachos et al. (this volume). Calcium-carbonate contents are from shipboard carbonate-bomb results (see Site 577 chapter, this volume) and from Zachos et al. (this volume). Hole 577 lipid geochemical results are from Simoneit and Beller (this volume). Arrows in the core columns indicate locations of the Cretaceous/Tertiary boundary (Sample 577-12-5, 130 cm, Sample 577A-12-4, 72 cm, and Sample 577B-1-4, 72 cm).

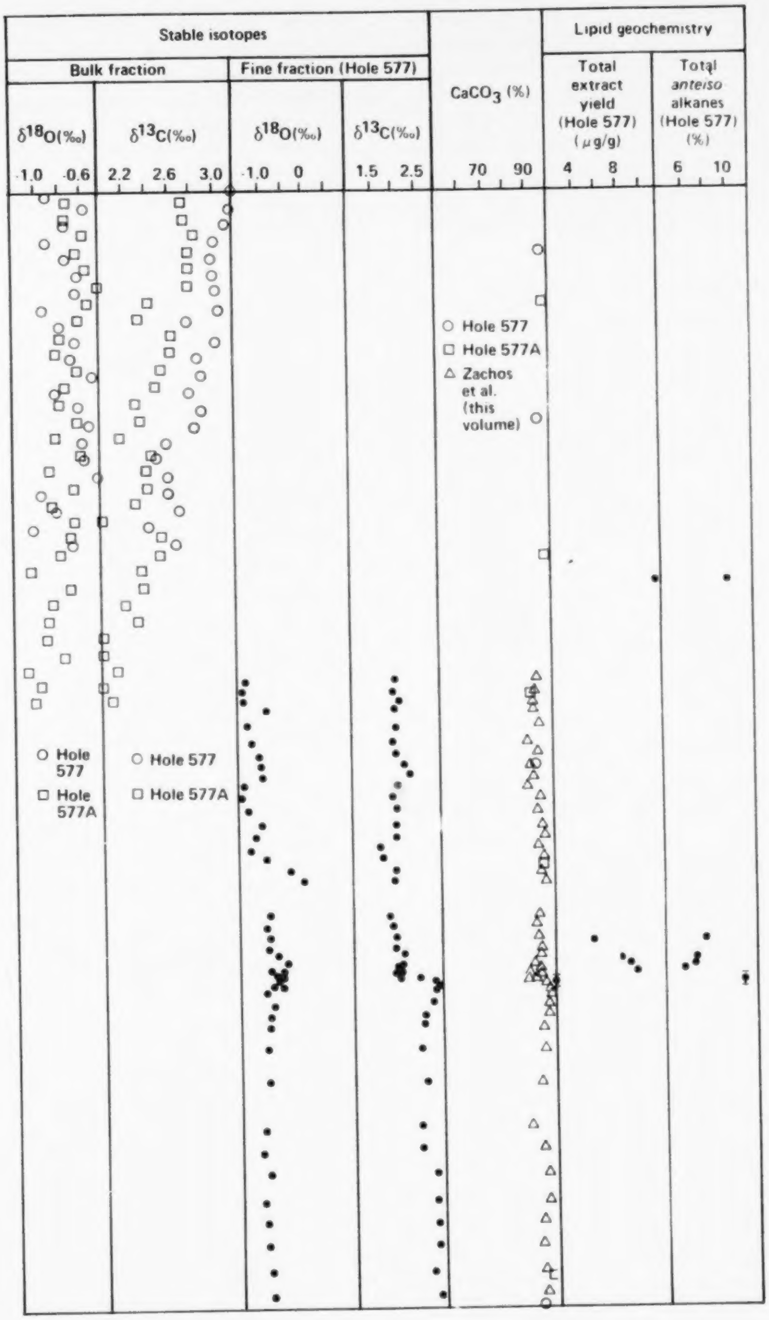

Figure 2. (Continued).

from Cretaceous to Tertiary time, the data suggest a 2°C temperature decrease at most.

Carbonate fine-fraction ^{13}C results indicate relatively constant values for the *M. murus* Zone, averaging 2.65 ± 0.2‰. There is an abrupt decrease of 1.0‰ over a 10-cm interval at the Cretaceous/Tertiary boundary, coinciding with an interval of slightly lower carbonate content (Fig. 2). ^{13}C values remain relatively low throughout the measured Paleocene samples, between 1.7 and 2.3‰. The negative ^{13}C shift observed at the Hole 577 Cretaceous/Tertiary boundary has been found in varying magnitudes at nearly every Cretaceous/Tertiary boundary sequence studied, suggesting that, barring significant hiatuses, this shift is an excellent stratigraphic marker for the boundary. The ^{13}C shift is interpreted to represent an abrupt decrease in oceanic surface water productivity associated with the Cretaceous/Tertiary extinction event. This interpretation is supported by the observed reduction of total carbonate accumulation rates from an average 1.10 g/cm^2/1000 yr. during the Maestrichtian to 0.3 g/cm^2/1000 yr. immediately above the Cretaceous/Tertiary boundary with no apparent changes in carbonate preservation (see table 4 and fig. 8 in Zachos et al., this volume). ^{13}C-isotopic gradients derived by comparing planktonic fine-fraction data and benthic data suggest that primary productivity recovered to pre-Cretaceous/Tertiary boundary levels by 2 m.y. following the extinction event.

LIPID GEOCHEMISTRY ACROSS THE CRETACEOUS/TERTIARY BOUNDARY

Six samples from above and just below the Cretaceous/Tertiary boundary at Hole 577 were analyzed by gas chromatography and gas chromatography-mass spectrometry to look for geochemical evidence of the mass extinctions and faunal successions characteristic of this period (Simoneit and Beller, this volume). Lipid compositions of all these samples are very similar, but the yields may indicate a trend at the Cretaceous/Tertiary boundary (Fig. 2). Trace molecular markers indicate an algal and, above the Cretaceous/Tertiary boundary, possibly a terrestrial resinous plant component. Definitive assignment of the original lipid sources of these samples is not possible since these residues are derived predominantly from bacteria, which efficiently metabolized the other lipids in an oxic depositional environment or at least oxidizing diagenetic conditions. Therefore, molecular stratigraphy cannot be applied definitely across the Cretaceous/Tertiary boundary at Site 577 with these limited samples.

CONCLUSIONS

Three continuous, expanded, and undisturbed Cretaceous/Tertiary boundary sequences were recovered at the three holes hydraulically piston cored at Site 577 on the Shatsky Rise. Based on nannofossil biostratigraphy, the boundary is located at Sample 577-12-5, 130 cm, Sample 577A-12-4, 72 cm, and Sample 577B-1-4, 72 cm, within the magnetic C-29R subchron. At this same level, an iridium anomaly of 61 ng/cm^2 and a sharp decrease of 1.0‰ ^{13}C were observed. These results are characteristic of other marine Cretaceous/Tertiary boundary sections and add support to the extraterrestrial-impact theory offered as explanation for the microfaunal and microfloral extinctions observed at the boundary.

REFERENCES

Alvarez, W., Alvarez, L. W., Asaro, F., and Michel, H. V., 1982. Current status of the impact theory for the terminal Cretaceous extinction. *Geol. Soc. Am. Spec. Pap.*, 190:305-315.

Alvarez, W., Arthur, M. S., Fischer, A. F., Lowrie, W., Napoleone, G., Premoli Silva, I., and Roggenthen, W. M., 1977. Type section for the Late Cretaceous-Paleocene geomagnetic reversal time scale. *Geol. Soc. Am. Bull.*, 88:383-389.

Alvarez, W., and Lowrie, W., 1978. Upper Cretaceous paleomagnetic stratigraphy at Moria (Umbrian Apennines, Italy): verification of the Gubbio section. *Geophys. J. R. Astron. Soc.*, 55:1-17.

Berggren, W. A., Kent, D. V., and Flynn, J. J., in press. Paleogene geochronology and chronostratigraphy. *In* Snelling, N. J. (Ed.), *Geochronology and the Geological Record.* Geol. Soc. London Special Paper.

Davis, M., Hut, P., and Muller, R. A., 1984. Extinctions of species by periodic comet showers. *Nature (London)*, 308:715-717.

Hsü, K. J., He, Q., McKenzie, J. A., Weissert, H., Perch-Nielsen, K., et al., 1982. Mass mortality and its environmental and evolutionary consequences. *Science*, 216:249-256.

Shackleton, N. J., and Shipboard Scientific Party, 1984. Accumulation rates in Leg 74 sediments. *In* Moore, T. C., Jr., Rabinowitz, P. D., et al., *Init. Repts. DSDP*, 74: Washington (U.S. Govt. Printing Office), 621-644.

Thierstein, H. R., 1982. Terminal Cretaceous plankton extinction: a critical assessment. *Geol. Soc. Am. Spec. Pap.*, 190:385-399.

Whitmire, D. P., and Jackson, A. A., IV, 1984. Are periodic mass extinctions driven by a distant solar companion? *Nature (London)*, 308:713-715.

Date of Initial Receipt: 9 January 1985
Date of Acceptance: 6 February 1985

Drilling locations

Leg	Location	Sites
Phase 1 1968–1970		
1	North Atlantic	1–7
2	North Atlantic	8–12
3	South Atlantic	13–22
4	Central Atlantic	23–31
5	North Pacific	32–43
6	North Pacific	44–60
7	Central Pacific	61–67
8	Central Pacific	68–75
9	Central Pacific	76–84
Phase 2 1970–1972		
10	Gulf of Mexico	85–97
11	North Atlantic	98–108
Re-entry trials		109–110
12	North Atlantic	111–119
13	Mediterranean	120–134
14	Central Atlantic	135–144
15	Caribbean	146–154
16	Central Pacific	155–163
17	Central Pacific	164–171
18	North Pacific	172–182
19	North Pacific	183–193
20	North Pacific	194–202
21	Coral Sea	203–210
22	Indian Ocean	211–218
23	Arabian Sea	219–230
24	Indian Ocean	231–238
25	Indian Ocean	239–249
Phase 3 1972–1975		
26	Indian Ocean	250–258
27	Indian Ocean	259–263
28	Antarctic	264–274
29	Tasman Sea	275–284
30	South Pacific	285–289
31	North Pacific	290–302
32	North Pacific	303–313
33	North Pacific	314–318
34	South Pacific	319–321
35	South Pacific	322–325
36	South Atlantic	326–331
37	North Atlantic	332–335
38	Arctic	336–352
39	Atlantic	353–359
40	South Atlantic	360–365
41	South Atlantic	366–370
42A	Mediterranean	371–378
42B	Black Sea	379–381
43	North Atlantic	382–387
44	North Atlantic	388–392
44A	North Atlantic	393–394
IPOD I 1975–present		
45	North Atlantic	395–396
46	North Atlantic	396A–396B
47	North Atlantic	397–398
48	North Atlantic	399–406
49	North Atlantic	407–414
50	North Atlantic	415–416
51A	North Atlantic	417–417A
51B	North Atlantic	417B–417D
52	North Atlantic	417D–418A
53	North Atlantic	418A–418B
54	Central Pacific	419–429
55	North Pacific	430–433
56	North Pacific	434–437
57	North Pacific	438–441
58	North Pacific	442–446
59	North Pacific	447–451
60	North Pacific	452–461
61	Central Pacific	462
62	North Pacific	463–466
63	North Pacific	467–473
64	Gulf of California	474–481
65	Gulf of California	482–485
66	Central Pacific	486–493
67	Central Pacific	494–500
68	Central Pacific	502–503
69	Central Pacific	504–505, 501
70	Central Pacific	506–510, 504B
71	South Atlantic	511–514
72	South Atlantic	515–518
73	South Atlantic	519–524
74	South Atlantic	525–529
75	South Atlantic	530–532
76	North Atlantic	533–534
77	Caribbean	535–540
78	North Atlantic	541–543, 395A, B
79	North Atlantic	544–547
80	North Atlantic	548–551
81	North Atlantic	552–555
82	North Atlantic	556–564
83	Central Pacific	504B
84	Central Pacific	565–570
85	Central Pacific	571–575
86	North Pacific	576–581

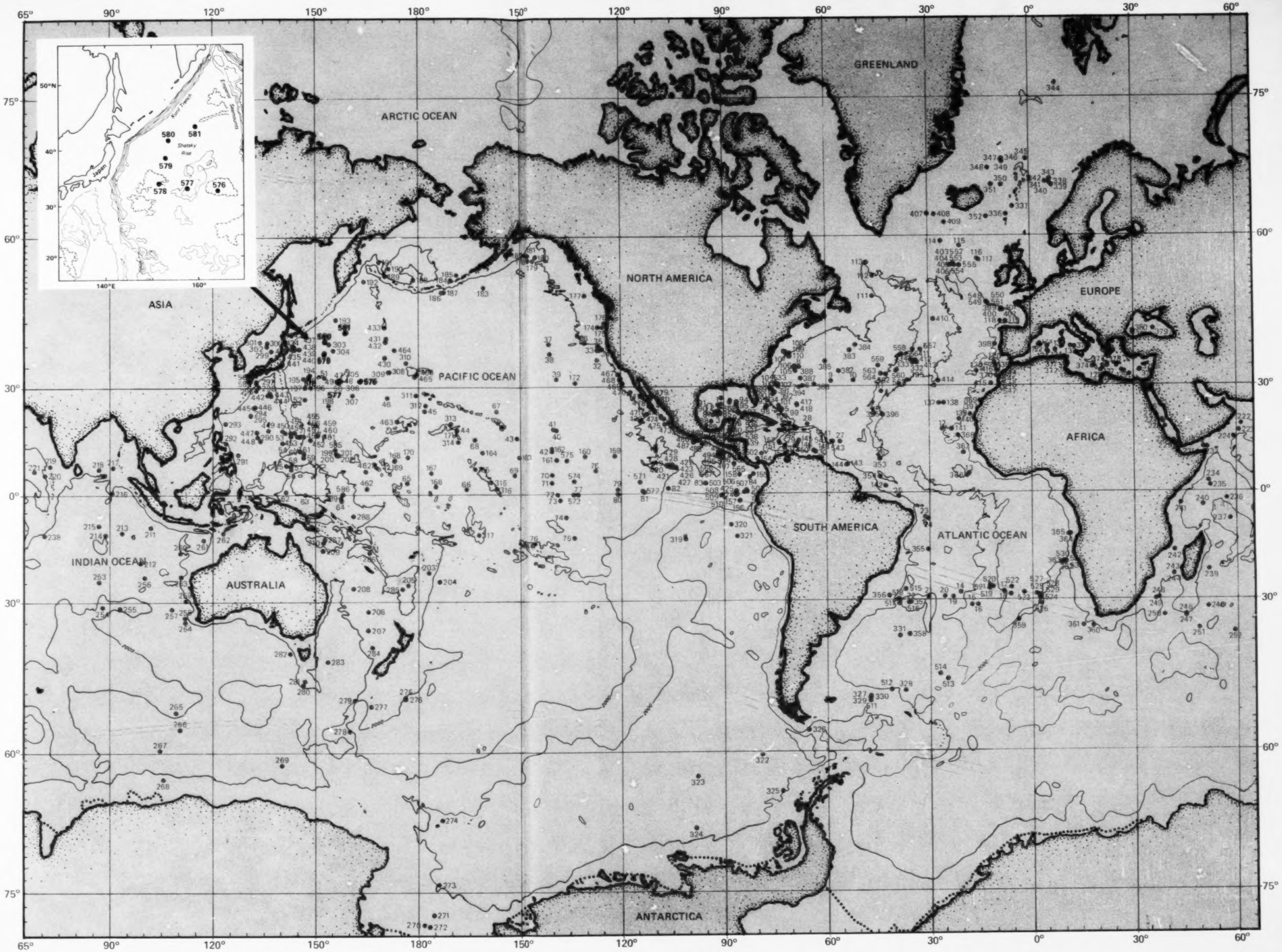
65°
90°
120°
150°
180°
150°
120°
90°
60°
30°
0°
30°
60°
75°
60°
30°
0°
30°
60°
75°
50°N
40°
30°
20°
140°E
160°
Japan
Kuril Trench
Emperor Seamounts
Shatsky Rise
580
581
579
577
578
576
GREENLAND
ARCTIC OCEAN
ASIA
NORTH AMERICA
EUROPE
PACIFIC OCEAN
AFRICA
SOUTH AMERICA
ATLANTIC OCEAN
INDIAN OCEAN
AUSTRALIA
ANTARCTICA

DEEP SEA DRILLING PROJECT

Volume 86: Chapter 9: Table 2. Stratigraphic occurrences of Neogene diatoms in Hole 578.

Core-Section (interval in cm)	Depth below seafloor (m)	Abundance	Preservation	*Bacteriastrum* spp.	*Actinocyclus curvatulus*	*A. ehrenbergii*	Diatom zone[a]	Subseries
1-1, 108-109	1.09	C	g	5		7	*D. seminae*	upper Pleistocene
1-2, 108-109	2.59	F	m	1		8		
1-3, 108-109	4.09	R	m	1	2	6		
1,CC	4.80	C	m		3	4		
2-1, 115-116	5.96	F	m	1		9		
2-2, 115-116	7.46	F	m	2		2		
2-3, 115-116	8.95	F	m		1	7		
2-4, 115-116	10.46	VR	p					
2-5, 115-116	11.96	F	g	1	1	4		
2,CC	14.30	F	m	1	2	2		
3-1, 96-97	15.27	F	m	1	3			
3-2, 96-97	16.77	F	m	6		6		
3-3, 96-97	18.27	C	g	3	1	4	*R.c.*	
3-4, 96-97	19.77	VR	p			●		
3-5, 96-97	21.77	F	g		1	1		
3-6, 96-97	22.77	F	m			12	*N. reinholdii*	
3,CC	23.80	R	p					
4-1, 95-96	24.76	F	m	1	5	11		
4-2, 95-96	26.26	VR	p			●		
4-3, 95-96	27.76	R	p					
4-4, 95-96	29.26	VR	p					
4-5, 95-96	30.76	F	g			4		
4-6, 95-96	32.26	F	m		2	4		
4,CC		F	p	1	7	3		
5-1, 117-118	34.48	C	m		2	1		
5-2, 117-118	35.98	VR	p					
5-3, 117-118	37.48	F	m		3	1		
5-4, 117-118	38.98	VR	p					
5-5, 117-118	40.48	VR	p		●			
5-6, 117-118	41.98	VR	p					
5-7, 38-39	42.69	F	m		3			
5,CC	42.80	R	g		3	1		
6-1, 109-110	43.90	VR	p					
6-2, 109-110	45.40	F	m		4		*A. oculatus*	lower Pleistocene
6-3, 109-110	46.90	C	g	2	6			
6-4, 109-110	48.40	F	m		6			
6-5, 109-110	49.90	C	m					
6-6, 109-110	51.40	C	m		4			
6-7, 43-44	52.24	C	m	1				
6,CC	52.30	F	p		1	4		
7-1, 121-122	53.52	A	g		2			
7-2, 121-122	55.02	C	m	1	2			
7-3, 121-122	56.52	A	g		2			
7-4, 121-122	58.02	A	g	1		1		
7-5, 121-122	59.52	A	g	1	3	2	*N. fossilis*	upper Pliocene
7-6, 121-122	61.02	F	m		3			
7-7, 47-48	61.78	F	m		4	1		
7,CC	61.80	C	m		3			
8-1, 118-119	62.99	VR	p					
8-2, 118-119	64.49	A	m		1	1		
8-3, 118-119	65.98	C	m	1	2	1		
8-4, 118-119	67.48	A	m			2		
8-5, 118-119	68.78	A	g	1	1	1	*T.c.*	
8-6, 118-119	70.48	A	m	1	6	1		
8,CC	71.30	C	m		8			
9-1, 118-119	72.48	C	m	1	6	3		
9-2, 118-119	73.98	A	m		2	2	*D.s. v. f.-D.k.*	
9-3, 118-119	75.48	C	m		6	3		
9-4, 118-119	76.98	C	m		4	2		
9-5, 110-111	78.41	A	g		1			
9-6, 118-119	79.98	A	m		2	3		
9-7, 51-52	80.81	A	m		2	1		
9,CC	80.80	A	m	1	2	2		
10-1, 118-119	81.98	A	m		3	1		
10-2, 118-119	83.48	A	m		3	2		
10-3, 118-119	84.98	A	g		4	1		
10-4, 118-119	86.48	C	m		2	4		
10-5, 118-119	87.98	C	m		1	2	*N. jouseae*	lower Pliocene
10-6, 82-83	89.13	A	m					
10,CC	90.30	A	g			2		
11-1, 130-131	91.60	A	g	1	2	2		
11-2, 130-131	93.10	A	g			2		
11-3, 130-131	94.60	A	g		1			
11-4, 130-131	96.10	A	m		5	4		
11-5, 130-131	97.60	A	m	1	3	1		
11-6, 130-131	99.10	A	g	2	2	2		
11-7, 20-21	99.51	A	g	2	2	1		
11,CC	99.80	A	m	2				
12-1, 100-101	100.81	A	m	2		3		
12-2, 100-101	102.31	A	m	1	4	5	*D.k.*	
12-3, 100-101	103.81	A	g		3	3		
12-4, 100-101	105.31	C	m		9	5		
12-5, 100-101	106.81	C	m		2			
12-6, 110-111	108.41	C	m		2	1		
12,CC	109.30	A	m		2	1		
13-1, 135-136	110.66	A	g			1	*N. miocenica*	upper Miocene
13-2, 135-136	112.16	A	m	1	3	2		
13-3, 135-136	113.66	A	g	1	3	2		
13-4, 135-136	115.16	A	g	13	2	5		
13-5, 135-136	116.66	A	g	2	2	5		
13-6, 135-136	118.16	R	p					
13,CC	118.80	VR	p			●		

Note: See Table 1 for explanation of symbols.

[a] *R.c.* = *R. curvirostris*, *T.c.* = *T. convexa*, *D.s. v. f.-D.k.* = *D. seminae* v. *fossilis*-*D. kamtschatica*, *D.k.* = *D. kamtschatica*.

Volume 86: Chapter 9: Table 3. Stratigraphic occurrences of Neogene diatoms in Holes 579 and 579A.

Core-section (interval in cm)	Depth below seafloor (m)	Abundance (10^7/g)	Preservation	*Bacteriastrum* spp.	*Chaetoceros* spp. (with filament)	*Chaetoceros* spp. (without filament)
Hole 579						
1-1, 16-17	0.17	4.8	g	3	2	
1-1, 97-98	0.98	3.1	g	4	23	20
1-2, 97-98	2.48	2.5	g	2	15	10
1-3, 97-98	3.98	1.8	g		19	3
1-4, 97-98	5.48	2.6	g	1	34	9
1-5, 97-98	6.98	1.7	g	5	35	6
1,CC	8.40	1.1	m	5	71	7
2-1, 123-124	9.64	2.0	g	3	23	7
2-2, 123-124	11.14	1.4	g	3	28	3
2-3, 123-124	12.64	1.6	g	1	20	7
2-4, 123-124	14.14	0.9	m	2	16	1
2-5, 123-124	15.64	2.2	g		59	6
Hole 579A						
1-1, 14-15	14.15	1.7	g		16	2
1-2, 14-15	15.65	1.2	g	1	22	4
1-3, 14-15	17.15	2.4	g	2	25	5
1-4, 14-15	18.65	2.2	g		13	1
1-5, 14-15	20.15	2.4	g	3	33	1
1-6, 14-15	21.65	0.9	m		47	7
1-7, 14-15	23.15	2.5	g	1	27	1
2-1, 33-34	23.84	1.8	g	1	23	
2-2, 13-14	25.14	1.0	g	1	25	3
2-3, 13-14	26.64	0.8	m	2	29	2
2-4, 13-14	28.14	0.4	m		67	4
2-5, 13-14	29.64	0.5	m		68	12
2-6, 13-14	31.14	3.5	g	3	21	1
2-7, 13-14	32.64	3.5	g	2	44	5
3-1, 115-116	34.16	1.2	g	6	21	4
3-2, 115-116	35.66	2.2	g	3	77	2
3-3, 115-116	37.16	1.7	g	2	28	7
3-4, 115-116	38.66	0.8	m	1	25	1
3-5, 115-116	40.16	2.2	g	1	19	3
3-6, 115-116	41.66	0.4	m	1	47	10
4-1, 12-13	42.63	0.8	m		45	1
4-2, 12-13	44.13	1.0	g	1	37	1
4-3, 12-13	45.63	2.0	g	2	21	2
4-4, 12-13	47.13	0.7	m	4	50	2
5-1, 25-26	52.26	2.1	g	1	72	9
5-2, 25-26	53.76	1.6	g	1	26	
5-3, 25-26	55.26	1.9	g	3	51	
5-4, 25-26	56.76	2.8	g	1	47	4
5-5, 25-26	58.26	3.0	g	4	40	2
5-6, 25-26	59.76	0.9	m		39	1
5-6, 94-95	60.45	2.1	g	3	42	8
6-1, 25-26	61.76	3.3	g	1	12	2
6-2, 25-26	63.26	3.7	g	1	27	6
6-3, 25-26	64.76	4.0	g	2	30	3
6-4, 25-26	66.26	1.8	g		32	1
6-5, 25-26	67.76	5.9	g	3	18	2
6-6, 10-11	69.11	5.8	g		15	1
6,CC	71.00	5.0	g	1	7	3
7-1, 114-115	72.14	5.3	g		24	6
7-2, 114-115	73.64	3.6	g	1	15	5
7-3, 114-115	75.14	3.7	g		9	2
7-4, 114-115	76.64	4.9	g	1	21	6
7-5, 114-115	78.14	7.6	g	2	13	2
7-6, 23-24	78.74	3.3	g	2	30	
7,CC	80.50	5.6	g	1	24	2
8-1, 132-133	81.83	3.0	g		24	6
8-2, 132-133	83.83	3.6	g	5	9	3
8-3, 132-133	84.83	8.2	g	5	2	3
8-4, 132-133	86.33	3.0	g		32	6
8-5, 132-133	87.83	4.3	g	4	13	3
8-6, 132-133	89.33	3.6	g	1	20	1
9-1, 30-31	90.31	3.3	g	1	20	2
9-2, 30-31	91.81	1.5	g	2	36	1
9-3, 30-31	93.31	3.8	g		18	
9-3, 95-96	93.96	3.8	g	1	16	2
9-4, 122-123	95.72	4.3	g		21	
9-5, 130-131	97.31	6.3	g	4	31	
9,CC	99.50	5.1	g	3	13	1
10-1, 112-113	100.63	1.5	g	1	16	2
10-2, 112-113	102.13	4.7	g		4	3
10-3, 112-113	103.63	6.1	g	1	1	4
10-4, 112-113	105.13	5.5	g	2	8	
10-5, 112-113	106.63	4.5	g		4	5
10,CC	109.00	2.5	g	2	6	5
11-1, 135-136	110.36	4.1	g	1	1	5
11-2, 135-136	111.86	4.1	g		3	4
11-3, 135-136	113.36	4.9	g	4	3	1
11-4, 135-136	114.86	5.4	g		4	2
11-5, 90-91	115.91	8.1	g		2	2
12-1, 3-4	118.54	3.3	g		28	4
12-2, 16-17	120.17	6.2	g		12	
12-3, 16-17	121.67	7.6	g	3	14	
12-4, 16-17	123.17	5.3	g	1	9	2
12-5, 16-17	124.67	5.7	g	1	6	2
12-6, 16-17	126.17	1.8	g		10	1
12,CC	128.00	6.1	g		5	
13-1, 91-92	128.92	15.1	g	1		3
13-2, 91-92	130.42	4.5	g	1	16	
13-3, 91-92	131.92	6.2	g		6	5
13-4, 91-92	133.42	9.2	g	1	2	3
13-5, 16-17	134.17	6.2	g	5	7	
14-1, 2-3	137.53	6.1	g		3	1
14-2, 2-3	139.03	5.3	g	4	7	
14-3, 2-3	140.53	8.8	g	6	23	
14-4, 2-3	142.03	8.2	g		8	
14-5, 2-3	143.53	4.2	g	2	14	
14-5, 102-103	144.53	3.4	g	3	10	5
15-1, 6-7	147.07	3.8	g	1	13	
15-2, 6-7	148.57	3.5	g	1	9	
15,CC	149.50	3.1	g	7	20	

Note: See Table 1 for explanation of symbols.

Volume 86: Chapter 9: Table 4. Stratigraphic occurrences of Neogene diatoms in Hole 580.

Core-Section (interval in cm)	Depth below seafloor (m)	Abundance (10^7 per g)	Preservation	*Bacteriastrum* spp.	*Chaetoceros* spp. (with filament)	*Chaetoceros* spp. (without filament)	*Achnanthes lanceolata*	*Actinocyclus curvatulus*	*A. ehrenbergii*	*A. ellipticus*	*A. ochotensis*	*A. oculatus*	*Actinoptychus senarius*
1-1, 25-26	0.25	4.2	g	3	15			7					10
1-2, 30-31	1.81	3.6	g	1	71			13	2		2		1
1-3, 2-3	3.02	8.5	g		71			21			2		
2-1, 128-129	4.59	2.0	g	1	129			9	12		1		
2-2, 128-129	6.09	3.9	g	3	385		1	12	5		1		
2-3, 128-129	7.59	6.3	g	1	67		1	6	2		1		
2-4, 128-129	9.09	3.3	g	2	188			4			14		
2-5, 128-129	10.59	3.1	g		162			15	7		8		
2-6, 69-70	11.50	1.8	g		110			19	3		2		1
3-1, 25-26	13.06	2.2	g	1	170			9			6		1
3-2, 25-26	14.56	4.8	g	1	62			10			2		
3-3, 25-26	16.06	4.9	g	1	234	3		5	1		1		1
3-4, 25-26	17.56	2.7	g		29	7		6	6		2		2
3-5, 25-26	19.06	7.5	g		133	10		13	2		3		
3-6, 25-26	20.56	4.7	g		82	9		4	3		5		
3,CC	22.30	3.0	g		130	1		8			11		
4-1, 121-122	23.52	2.9	g	2	277	7		3			11		
4-2, 121-122	25.02	4.5	g	3	139	10		7	8		2		
4-3, 121-122	26.52	3.5	g	1	132	6		7	14		1		4
4-4, 121-122	28.02	12.9	g		15	7		3	2		3	2	
4-5, 121-122	29.52	3.9	g	1	102	15		6	4		1		
4-6, 112-113	30.93	4.2	g		40	29		4	7		2	2	6
5-1, 40-41	32.21	8.1	g		37	2		8	1		1	1	3
5-2, 40-41	33.71	4.2	g	1	67	11		4	6				12
5-3, 40-41	35.21	5.1	g		211	3					1		
5-4, 40-41	36.71	5.3	g		31	3		2	2			1	5
5-5, 40-41	38.21	6.4	g	1	97	4		9	10				
5-5, 120-121	39.01	4.6	g	2	196	18		14	2		1		5
6-1, 25-26	41.56	4.2	g		115	10		5	3		1		
6-2, 25-26	43.06	6.1	g		64	5		6			3		8
6-3, 25-26	44.56	7.4	g		188	6		11	6				5
6-4, 25-26	46.06	2.0	g	6	23	10		4			1		7
6-5, 25-26	47.56	4.0	g	1	96	4		1	1				6
6-6, 17-18	48.98	4.2	g	1	66	3		4	1		3		1
6,CC	50.80	2.4	g		100			6	4			2	3
7-1, 116-117	51.97	4.2	g		116	8		15	7			1	
7-2, 116-117	53.47	6.9	g		39	4		2	2			6	
7-3, 116-117	54.97	5.0	g		145			2				1	
7-4, 116-117	56.47	5.3	g	1	28	5		9			1	5	3
7-5, 116-117	57.97	3.9	g		27			2			1	8	2
7,CC	60.30	1.8	g		15	7		8			1	5	13
8-1, 116-117	61.47	9.1	g		34	8		3			1	14	1
8-2, 116-117	62.97	4.1	g		87	18		11	2		2	12	2
8-3, 116-117	64.47	2.3	g	2	83	5		7	1			10	
8-4, 116-117	65.97	2.7	g		64			10			4	21	3
8-5, 116-117	67.47	5.8	g		64			7				26	4
8-6, 116-117	68.97	19.5	g	1	24				1			7	3
9-1, 23-24	70.04	3.1	g	2	79	4		5			3	26	1
9-2, 23-24	71.54	8.4	g		15			2			2	13	2
9-3, 23-24	73.04	4.3	g	1	23			6				11	2
9-4, 23-24	74.54	9.9	g	2	71			14			1	4	6
9-5, 23-24	76.04	4.4	g	1	187			11	7		3	2	6
9-5, 89-90	76.69	3.9	g		41			11	1		1	4	8
9,CC	79.30	2.7	g	2	21	17		1	2		2	5	4
10-1, 110-111	80.41	5.5	g	3	40			12	3		3	8	6
10-2, 110-111	81.91	5.3	g		31			1	1			13	5
10-3, 110-111	83.41	8.4	g		14			10	3		4	6	
10-4, 110-111	84.91	3.1	g	2	43			9	1		3	11	2
10-5, 110-111	86.41	10.3	g	1	41							2	1
10-6, 25-26	87.06	7.1	g	4	53			2			1	4	3
11-1, 22-23	89.02	13.6	g		38	1		3				3	1
11-2, 22-23	90.52	6.2	g	2	44	5		5			4		13
11-3, 22-23	92.02	5.8	g	1	25			14			2	4	4
11-4, 22-23	93.52	5.0	g		15			18			6		
11-5, 22-23	95.02	17.3	g	1	21	3		10	1		5	2	
11-5, 105-106	95.85	6.7	g	1	31	1		10			3	1	
11,CC	98.30	5.7	g		56	24		8	1		14	28	3
12-1, 103-104	99.34	17.5	g		24	4		8			4		
12-2, 103-104	100.84	5.1	g	2	14			12			4	2	
12-3, 103-104	102.34	6.3	g	1	15			5			1		
12-4, 103-104	103.84	5.0	g		10	3		15	1		1		1
12-5, 103-104	105.34	6.6	g		22	6		9	2		3		1
12-6, 103-104	106.84	6.3	g	1	14	2		8			3		
13-1, 15-16	107.96	6.8	g	2	29	8		6			6		
13-2, 15-16	109.46	12.2	g		4	2		3	1				
13-3, 15-16	110.96	24.6	g	2	5	1		2			1		1
13-4, 15-16	112.46	10.1	g	3	12			3					1
13-5, 15-16	113.96	7.7	g		34			8	2		4		3
13-6, 15-16	115.46	8.5	g		20			5			4		
13,CC	117.30	8.3	g	1		9		4					2
14-1, 130-131	118.60	7.6	g		15			4	3		1		1
14-2, 130-131	120.10	7.3	g		18			4	4		1		
14-3, 130-131	121.60	5.0	g	1	14				3		1		5
14-4, 130-131	123.10	7.5	g	4	10				3		3		7
14-5, 130-131	124.60	5.3	g	1	10				6				4
14-6, 130-131	126.10	9.2	g	1	5			1	2				1
15-1, 22-23	127.02	6.3	g		16								3
15-2, 10-11	128.41	8.2	g		6			2	3				2
15-3, 10-11	129.91	3.6	g			2		3	2				1
15-4, 10-11	131.41	16.5	g		10			2	1				2
15-5, 10-11	132.91	4.9	g		5			3	3				1
15-6, 10-11	134.41	4.7	g		14			1	1				
15,CC	136.30	5.0	g			13			3				18
16-1, 83-84	137.14	3.5	g		11			2	3				1
16-2, 83-84	138.64	12.3	g	1		7		1			2		2
16-3, 83-84	140.14	7.2	g	1		1					1		
16-4, 83-84	141.64	3.3	g	2		2		1			1		5
16-5, 83-84	143.14	9.7	g			2		3		1			
16-6, 83-84	144.64	8.1	g			4		3	4	1			
17-1, 8-9	145.89	3.4	g	1		3		1		1			
17-2, 8-9	147.39	1.5	g			14		4	1	2			1
17-3, 8-9	148.89	1.4	g			7		2	4	1			12
17-4, 8-9	150.39	3.4	g	1		4			1				15
17-5, 8-9	151.89	8.2	g			8		1	2		1		1
17,CC	155.30	7.3	g	1		4		1	2				2

Note: See Table 1 for explanation of symbols.